

Gurdeep Singh Hura
Ashutosh Kumar Singh
Lau Siong Hoe *Editors*

Advances in Communication and Computational Technology

Select Proceedings of ICACCT 2019

Lecture Notes in Electrical Engineering

Volume 668

Series Editors

Leopoldo Angrisani, Department of Electrical and Information Technologies Engineering, University of Napoli Federico II, Naples, Italy

Marco Arteaga, Departament de Control y Robótica, Universidad Nacional Autónoma de México, Coyoacán, Mexico

Bijaya Ketan Panigrahi, Electrical Engineering, Indian Institute of Technology Delhi, New Delhi, Delhi, India

Samarjit Chakraborty, Fakultät für Elektrotechnik und Informationstechnik, TU München, Munich, Germany

Jiming Chen, Zhejiang University, Hangzhou, Zhejiang, China

Shanben Chen, Materials Science and Engineering, Shanghai Jiao Tong University, Shanghai, China

Tan Kay Chen, Department of Electrical and Computer Engineering, National University of Singapore, Singapore, Singapore

Rüdiger Dillmann, Humanoids and Intelligent Systems Laboratory, Karlsruhe Institute for Technology, Karlsruhe, Germany

Haibin Duan, Beijing University of Aeronautics and Astronautics, Beijing, China

Gianluigi Ferrari, Università di Parma, Parma, Italy

Manuel Ferre, Centre for Automation and Robotics CAR (UPM-CSIC), Universidad Politécnica de Madrid, Madrid, Spain

Sandra Hirche, Department of Electrical Engineering and Information Science, Technische Universität München, Munich, Germany

Faryar Jabbari, Department of Mechanical and Aerospace Engineering, University of California, Irvine, CA, USA

Limin Jia, State Key Laboratory of Rail Traffic Control and Safety, Beijing Jiaotong University, Beijing, China

Janusz Kacprzyk, Systems Research Institute, Polish Academy of Sciences, Warsaw, Poland

Alaa Khamis, German University in Egypt El Tagamoa El Khames, New Cairo City, Egypt

Torsten Kroeger, Stanford University, Stanford, CA, USA

Qilian Liang, Department of Electrical Engineering, University of Texas at Arlington, Arlington, TX, USA

Ferran Martín, Departament d'Enginyeria Electrònica, Universitat Autònoma de Barcelona, Bellaterra, Barcelona, Spain

Tan Cher Ming, College of Engineering, Nanyang Technological University, Singapore, Singapore

Wolfgang Minker, Institute of Information Technology, University of Ulm, Ulm, Germany

Pradeep Misra, Department of Electrical Engineering, Wright State University, Dayton, OH, USA

Sebastian Möller, Quality and Usability Laboratory, TU Berlin, Berlin, Germany

Subhas Mukhopadhyay, School of Engineering & Advanced Technology, Massey University, Palmerston North, Manawatu-Wanganui, New Zealand

Cun-Zheng Ning, Electrical Engineering, Arizona State University, Tempe, AZ, USA

Toyoaki Nishida, Graduate School of Informatics, Kyoto University, Kyoto, Japan

Federica Pascucci, Dipartimento di Ingegneria, Università degli Studi "Roma Tre", Rome, Italy

Yong Qin, State Key Laboratory of Rail Traffic Control and Safety, Beijing Jiaotong University, Beijing, China

Gan Woon Seng, School of Electrical & Electronic Engineering, Nanyang Technological University, Singapore, Singapore

Joachim Speidel, Institute of Telecommunications, Universität Stuttgart, Stuttgart, Germany

Germano Veiga, Campus da FEUP, INESC Porto, Porto, Portugal

Haitao Wu, Academy of Opto-electronics, Chinese Academy of Sciences, Beijing, China

Junjie James Zhang, Charlotte, NC, USA

The book series *Lecture Notes in Electrical Engineering* (LNEE) publishes the latest developments in Electrical Engineering—quickly, informally and in high quality. While original research reported in proceedings and monographs has traditionally formed the core of LNEE, we also encourage authors to submit books devoted to supporting student education and professional training in the various fields and applications areas of electrical engineering. The series cover classical and emerging topics concerning:

- Communication Engineering, Information Theory and Networks
- Electronics Engineering and Microelectronics
- Signal, Image and Speech Processing
- Wireless and Mobile Communication
- Circuits and Systems
- Energy Systems, Power Electronics and Electrical Machines
- Electro-optical Engineering
- Instrumentation Engineering
- Avionics Engineering
- Control Systems
- Internet-of-Things and Cybersecurity
- Biomedical Devices, MEMS and NEMS

For general information about this book series, comments or suggestions, please contact leontina.dicecco@springer.com.

To submit a proposal or request further information, please contact the Publishing Editor in your country:

China

Jasmine Dou, Associate Editor (jasmine.dou@springer.com)

India, Japan, Rest of Asia

Swati Meherishi, Executive Editor (Swati.Meherishi@springer.com)

Southeast Asia, Australia, New Zealand

Ramesh Nath Premnath, Editor (ramesh.premnath@springernature.com)

USA, Canada:

Michael Luby, Senior Editor (michael.luby@springer.com)

All other Countries:

Leontina Di Cecco, Senior Editor (leontina.dicecco@springer.com)

**** Indexing: The books of this series are submitted to ISI Proceedings, EI-Compendex, SCOPUS, MetaPress, Web of Science and Springerlink ****

More information about this series at <http://www.springer.com/series/7818>

Gurdeep Singh Hura · Ashutosh Kumar Singh ·
Lau Siong Hoe
Editors

Advances in Communication and Computational Technology

Select Proceedings of ICACCT 2019

 Springer

Editors

Gurdeep Singh Hura
Department of Mathematics
and Computer Science
University of Maryland Eastern Shore
Princess Anne, MD, USA

Ashutosh Kumar Singh
Department of Master of Computer
Applications
National Institute of Technology
Kurukshetra
Kurukshetra, Haryana, India

Lau Siong Hoe
Department of Information Science
and Technology
Multimedia University
Jalan Ayer Keroh Lama, Melaka, Malaysia

ISSN 1876-1100

ISSN 1876-1119 (electronic)

Lecture Notes in Electrical Engineering

ISBN 978-981-15-5340-0

ISBN 978-981-15-5341-7 (eBook)

<https://doi.org/10.1007/978-981-15-5341-7>

© Springer Nature Singapore Pte Ltd. 2020

This work is subject to copyright. All rights are reserved by the Publisher, whether the whole or part of the material is concerned, specifically the rights of translation, reprinting, reuse of illustrations, recitation, broadcasting, reproduction on microfilms or in any other physical way, and transmission or information storage and retrieval, electronic adaptation, computer software, or by similar or dissimilar methodology now known or hereafter developed.

The use of general descriptive names, registered names, trademarks, service marks, etc. in this publication does not imply, even in the absence of a specific statement, that such names are exempt from the relevant protective laws and regulations and therefore free for general use.

The publisher, the authors and the editors are safe to assume that the advice and information in this book are believed to be true and accurate at the date of publication. Neither the publisher nor the authors or the editors give a warranty, express or implied, with respect to the material contained herein or for any errors or omissions that may have been made. The publisher remains neutral with regard to jurisdictional claims in published maps and institutional affiliations.

This Springer imprint is published by the registered company Springer Nature Singapore Pte Ltd. The registered company address is: 152 Beach Road, #21-01/04 Gateway East, Singapore 189721, Singapore

Contents

A Drug Recommendation System for Multi-disease in Health Care Using Machine Learning	1
N. Komal Kumar and D. Vigneswari	
Smart Mobility: Understanding Handheld Device Adoption	13
Latika Kharb, Deepak Chahal, and Vagisha	
An Efficient Numerical Technique for Solving the Time-Fractional Cahn–Allen Equation	31
Amit Prakash and Hardish Kaur	
Image Colorization with Deep Convolutional Neural Networks	45
Sudesh Pahal and Preeti Sehrawat	
Electroencephalogram Based Biometric System: A Review	57
Kaliraman Bhawna, Priyanka, and Manoj Duhan	
Improved Neural Network-Based Plant Diseases Identification	79
Ginni Garg and Mantosh Biswas	
Maximum Power Extraction Using Random Binary Searching Algorithm Under Non-uniform Insolation	91
Kusum Lata Agarwal and Avdhesh Sharma	
Prevention Against Internal Attack via Trust-Based Detection for Wireless Mesh Networks	109
Amit Kumar Roy and Ajoy Kumar Khan	
Sensor-Based Alarm System for Preventing Crop Vandalization by Birds in Agricultural Regions	119
Siddhanta Borah, Ankush Kumar Gaur, and J. Arul Valan	
Pricing Mechanisms for Fair Bills and Profitable Revenue Share in Cloud Federation	133
Sameera Dhuria, Anu Gupta, and R. K. Singla	

Higher Order Squeezing in Pump Mode in Multi-wave Mixing Process	149
Priyanka and Savita Gill	
Active Power Loss Diminution by Chaotic-Based Adaptive Butterfly Mating Optimization Algorithm	163
Kanagasabai Lenin	
Mobile-Based Signature Database (MOBSIGN DB): A New Signature Database	171
Sudhir Rohilla, Anuj Sharma, and R. K. Singla	
Mining of Association Rules in R Using Apriori Algorithm	181
Anjali Mehta and Deepa Bura	
Comprehensive and Comparative Analysis of Different Files Using CP-ABE	189
Sahil Jalwa, Vardaan Sharma, Abdur Rehman Siddiqi, Ishu Gupta, and Ashutosh Kumar Singh	
Efficient Data Cube Materialization	199
Raghu Prashant, Mann Suman, and Raghu Eashwaran	
Ontology-Based Full-Text Searching Using Named Entity Recognition	211
Krishna Kumar, Md. Tanwir Uddin Haider, and Shamsh Sameed Ahsan	
Recognition of Online Handwritten Gurmukhi Characters Through Neural Networks	223
Sukhdeep Singh and Anuj Sharma	
Optimizing Stream Data Classification Using Improved Hoeffding Bound	235
Arvind Pillania, Pardeep Singh, and Vrinda Gupta	
Outline of Lattice Structures: Morphology, Manufacturing, and Material Aspect	245
Sakshi Kokil Shah, Mohanish Shah, Anirban Sur, and Sanjay Darvekar	
Image-Based Recommendation Engine Using VGG Model	257
Smrithi Vasudevan, Nishtha Chauhan, Vergin Sarobin, and S. Geetha	
Stable Optimized Link Heuristic Using Cross-Layering for QoS of Secured HANETs	267
Anita Sethi, Sandip Vijay, and Vishal Gupta	
Use of EEG as a Unique Human Biometric Trait for Authentication of an Individual	277
Bhawna Kaliraman, Priyanka Singh, and Manoj Duhan	

Performance of Feature Extracted on Leaf Images by Discriminant Analysis on Various Classifiers	287
Anjali Pathak, Bhawna Vohra, and Kapil Gupta	
Graph Isomorphism Using Locality Sensitive Hashing	305
R. Vinit Kaushik and Kadiresan Nalinadevi	
Comparative Analysis of Image Segmentation Techniques	317
Snehil Saxena, Sidharth Jain, Saurabh Tripathi, and Kapil Gupta	
Levels and Classification Techniques for Sentiment Analysis: A Review	333
Devendra Sharma and Anoj Kumar	
Breast Cancer Recurrence Prediction in Biopsy Using Machine Learning Framework	347
Akriti Sharma, Nishtha Hooda, and Nidhi Rani Gupta	
Realization of Grounded Inductance Circuit Using Bulk-Driven Current Conveyors	359
Anu Tonk and Neelofer Afzal	
Neural Network Ensemble-Based Prediction System for Chemotherapy Pathological Response: A Case Study	375
Raghvi Bhardwaj and Nishtha Hooda	
Outage and ABER Analysis for L-MRC on OWDP Fading Channels	387
Suparna Goswami, Laishram Mona Devi, and Aheibam Dinamani Singh	
Performance Evaluation of Incremental PCA and Its Variants in Face Recognition	397
Nitin Kumar and Suresh Madhavan	
3-Axis Robot Arm Using Micro-Stepping with Closed-Loop Control	409
G. A. Rathy, P. Sivasankar, Aravind Balaji, and K. Gunasekaran	
False-Positive-Free and Geometric Robust Digital Image Watermarking Method Based on IWT-DCT-SVD	423
Priyanka Singh, Ashok Kumar Pradhan, and Subhash Chandra	
Fair Fit—A Load Balance Aware VM Placement Algorithm in Cloud Data Centers	437
Bhavesh N. Gohil, Sachin Gamit, and Dhiren R. Patel	
Computationally Efficient and Secure Session Key Agreement Techniques for Vehicular Cloud Computing	453
Saurabh Rana, Dheerendra Mishra, and Saurabh Gupta	

Recent Trends in Image Processing Using Granular Computing	469
Shankar Shambhu and Deepika Koundal	
Enveloped Inverted Tree Recursive Hashing: An Efficient Transformation for Parallel Hashing	481
Neha Kishore and Priya Raina	
The Techniques of Vedic Mathematics for ECC Over Weierstrass Elliptic Curve $Y^2 = X^3 + Ax + B$	501
Ankur Kumar, Pratik Gupta, and Manoj Kumar	
EEHCR: Energy-Efficient Hierarchical Cluster-Based Routing Protocol for Wireless Sensor Networks	517
Sakshiwala and M. P. Singh	
Current-Controlled Chaotic Chua's Circuit Using CCCII	535
Manoj Joshi and Ashish Ranjan	
Phishing URL Detection Using Machine Learning	547
Preeti, Rainu Nandal, and Kamaldeep Joshi	
Sybil-Free Hybrid Localization Scheme in Wireless Sensor Networks	561
Narendra Dodwaria and Naveen Chauhan	
Hybrid-RPL: A Step Toward Ensuring Scalable Routing in Internet of Things	583
K. V. Amal, J. Jaisooraj, Priya Chandran, and S. D. Madhu Kumar	
Linear Interpolation-Based Fuzzy Clustering Approach for Missing Data Handling	597
Sonia Goel and Meena Tushir	
Dynamic Web View Materialization	605
Akshay Kumar and T. V. Vijay Kumar	
A Multi-Hop Bit-Map-Assisted Energy-Efficient MAC Protocol for Wireless Sensor Networks	617
Kumar Debasis, M. P. Singh, and Rajat Gupta	
PID Control of a Quadrotor	633
Ritika Thusoo, Sheilza Jain, and Sakshi Bangia	
Levy Flight-Based White Wolf Algorithm for Solving Optimal Reactive Power Problem	647
Kanagasabai Lenin	
Performance of MIMO System—A Review	655
Sweta Sanwal, Aman Kumar, Md. Arib Faisal, and Mohammad Irfanul Hassan	

Incremental Weighted Linear Discriminant Analysis for Face Recognition	677
Nitin Kumar and Suresh Madhavan	
Capacity Using <i>L</i>-Branch Channel MRC System Over Weibull Fading Channels—A Review	689
Adarsh Joshi, Aditya Narayan, Mohammad Irfanul Hasan, and Shalini Singh	
Classification of Static Signature Based on Distance Measure Using Feature Selection	707
Subhash Chandra and Priyanka	
Computational Technique for Fractional Model of Electrical Circuits	719
Amit Prakash and Vijay Verma	
Steganographic Method Based on Interpolation and Cyclic LSB Substitution of Digital Images	731
Jyoti Pandey, Kamaldeep Joshi, Mangal Sain, Gurdiyul Singh, and Mohit Jangra	
Ensuring Food Safety Through Blockchain	745
Ashish Singh, Vineet Kumar, Alok Kumar Ravi, and Kakali Chatterjee	
Design of Observer-Controller Digital Phase-Locked Loop Using Kalman Filter	757
Rachana Arya, B. K. Singh, and Lalit Garia	
Supervised Machine Learning Algorithms for Fake News Detection	767
Ankit Kesarwani, Sudakar Singh Chauhan, Anil Ramachandra Nair, and Gaurav Verma	
Vehicle Tracking System Using GPS and GSM	779
Shreya Verma, Abhay Singh Jamwal, Surabhi Chauhan, and Sribidhya Mohanty	
Multi-factor Authentication Scheme Using Mobile App and Camera	787
Sajal Jindal and Manoj Misra	
Speech Emotion Recognition: A Review	815
Anuja Thakur and Sanjeev Dhull	
CDMA-Based Security Against Wormhole Attack in Underwater Wireless Sensor Networks	829
Nitin Goyal, Jasminder Kaur Sandhu, and Luxmi Verma	

Sensing Performance of Ionic Polymer Metal Nanocomposite Sensors with Pressure and Metal Electrolytes for Energy Harvesting Applications	837
Priya Khanduri, Alankrita Joshi, Lokesh Singh Panwar, Anant Goyal, and Varij Panwar	
Privacy Preserving on Searchable Encrypted Data in Cloud	847
Deepak Sharma and Avtar Singh	
Adaptive Approximate Community Detection Algorithm for Bubble Rap Routing Protocol	865
Sweta Jain, Neerali Chauhan, and Pruthviraj Choudhari	
Automatic Control of Electrical Loads Based on the Atmospheric Conditions	879
T. Ramachandran, Sanjiv Kumar, and Savita	
A Comprehensive Study on Vehicular Ad Hoc Networks: Architecture, Security and Privacy Challenges, and Future Trends . . .	891
Upendra Singh	
Performance Analysis of Hybrid Diversity Combiner Over Nakagami-<i>m</i> Fading Channels—A Review	905
Prabhat Kumar, Karan Arora, Mohammad Irfanul Hasan, and Shalini Singh	
Epileptic Seizure Detection Using Machine Learning Techniques	919
Akshay Sreekumar, A. N. Sasidhar Reddy, D. Udaya Ravikanth, M. Chaitanya Chowdary, G. Nithin, and P. S. Sathidevi	
Comparative Analysis Among Various Soft Computing Classifiers for Nutrient Removal from Wastewater	927
Suresh Kumar and Surinder Deswal	
Automatic Keyphrase Extraction Using SVM	945
Ankit Guleria, Radhika Sood, and Pardeep Singh	
Linearity Analysis of Line Tunneling Based TFET for High-Performance RF Applications	957
Neha Paras and Sudakar Singh Chauhan	
Selection of Optimal Renewable Energy Resources Using TOPSIS-Z Methodology	967
Nisha Rathore, Kumar Debasis, and M. P. Singh	
Routing Algorithms for Hybrid Nodes in WSNs	979
Isha Pant and Shashi Kant Verma	
Extended Security in Heterogeneous Distributed SDN Architecture	991
Sugandhi Midha and Khushboo Tripathi	

Evaluation of SC-FDMA Physical Link Using USRP	1003
Shweta Y. Kukade, M. S. Sutaone, and R. A. Patil	
Real-Time Simulation and Analysis of Energy Storage System in Standalone PV-Based DC Microgrid	1019
Prashant Singh and J. S. Lather	
Intelligent Method for Detection of Coronary Artery Disease with Ensemble Approach	1033
Luxmi Sapra, Jasminder Kaur Sandhu, and Nitin Goyal	
Competitive Study of Various Task-Scheduling Algorithm in Cloud Computing	1043
Nishant Vaishla and Avtar Singh	
Internet of Things for Healthcare: Research Challenges and Future Prospects	1055
Garima Verma and Shiva Prakash	
An Animal Detection and Collision Avoidance System Using Deep Learning	1069
Atri Saxena, Deepak Kumar Gupta, and Samayveer Singh	
Outcome Prediction of Patients for Different Stages of Sepsis Using Machine Learning Models	1085
Pankaj Chaudhary, Deepak Kumar Gupta, and Samayveer Singh	
Existence Result of HIV Model by Employing Mahgoub Adomian Decomposition Procedure	1099
Yogesh Khandelwal, Pawan Chanchal, and Rachana Khandelwal	
Industry 4.0 Manufacturing Based on IoT, Cloud Computing, and Big Data: Manufacturing Purpose Scenario	1109
Arun Kumar Rana and Sharad Sharma	
Preprocessing Techniques for Colon Histopathology Images	1121
Manju Dabass and Jyoti Dabass	
Analysis of Energy Deposition in Hadrontherapy Using Monte Carlo Simulation Toolkit GEANT4	1139
Nitika Sangwan, Summit Jalota, and Ashavani Kumar	
Impact of Optimized Value for Relative Humidity at Cathode in PEMFC for Improved Stack Performance	1145
S. Dhanya, Varghese Paul, and Rani Thottungal	
Denosing, Edge Correction, and Enhancement of Breast Cancer Ultrasound Images	1153
Jyoti Dabass and Manju Dabass	

U-FIN: Unsupervised Feature Integration Approach for Salient Object Detection	1173
Vivek Kumar Singh and Nitin Kumar	
Input Image-Based Dictionary Formation in Super-Resolution for Online Image Streaming	1189
Garima Pandey and Umesh Ghanekar	
Feature Selection Using Genetic Algorithm for Cancer Prediction System	1197
Rupali, Rupali Verma, Rohit Handa, and Veena Puri	
A Hybrid Approach for Diabetes Prediction and Risk Analysis Using Data Mining	1213
Bhavna, Rupali Verma, Rohit Handa, and Veena Puri	
Performance Analysis of Classification Methods for Cardio Vascular Disease (CVD)	1231
N. Komal Kumar, R. Lakshmi Tulasi, and D. Vigneswari	
Secure Data Deduplication (SD^2eDup) in Cloud Computing: Threats, Techniques and Challenges	1239
Basappa B. Kodada and Demian Antony D'Mello	
Analyzing Ensemble Methods for Software Fault Prediction	1253
Nitin, Kuldeep Kumar, and Santosh Singh Rathore	
Porting of eChronos RTOS on RISC-V Architecture	1269
Shubhendra Pal Singhal, M. Sridevi, N. Sathya Narayanan, and M. J. Shankar Raman	
Development of Multi-band MIMO Antenna with Defected Ground Structure	1281
Shrenik S. Sarade and Sachin D. Ruikar	
Reliability Evaluation of Environmentally Affected Mobile Ad Hoc Wireless Networks	1297
N. Padmavathy	
Design of Tunable Miniaturized Frequency Selective Surface Based on Miura-Ori Pattern	1311
Sailabala Soren and Ashwin Kothari	
Vulnerability Assessment, Risk, and Challenges Associated with Automated Vehicles Based on Artificial Intelligence	1323
Aditya Raj Singh, Harbhajan Singh, and Abhineet Anand	
A Review to Forest Fires and Its Detection Techniques Using Wireless Sensor Network	1339
Roopali Dogra, Shalli Rani, and Bhasham Sharma	

The Need for Virtualization: When and Why Virtualization Took Over Physical Servers 1351
 Abhineet Anand, Amit Chaudhary, and M. Arvindhan

A Comparative Analysis on Online Handwritten Strokes Classification Using Online Learning 1361
 Charanjeet, Sukhdeep Singh, and Anuj Sharma

Segmentation of Noisy Mammograms Using Hybrid Techniques 1371
 Jyoti Dabass and Manju Dabass

An Empirical Comparison of Generative Adversarial Network (GAN) Measures 1383
 Pradnyawant Kokate, Amit D. Joshi, and P. S. Tamizharasan

The Fusion of Local and Global Descriptors in Face Recognition Application 1397
 Ali Mohammed Sahan and Ali Sami Al-Itbi

ANFIS-Based Reactive Strategy for uRLLC and eMBB Traffic Multiplexing in 5G New Radio 1409
 Naveen Kumar and Anwar Ahmad

Lexicon-Based Sentiment Analysis 1421
 Kavleen Kour, Jaspreet Kour, and Parminder Singh

Early Prediction of Childhood Obesity Using Machine Learning Techniques 1431
 Kakali Chatterjee, Upendra Jha, Priya Kumari, and Dhatri Chatterjee

A Review on Automatic Epilepsy Detection from EEG Signals 1441
 Satyender, Sanjeev Kumar Dhull, and Krishna Kant Singh

Energy Aware Resource Efficient-(EARE) Server Consolidation Framework for Cloud Datacenter 1455
 Deepika Saxena and Ashutosh Kumar Singh

Ambient Environment Monitoring and Air-Sound Pollution Analyzer on Wi-Fi Network 1465
 Rahul, O. P. Sahu, and Gaurav Verma

Modified Decision Tree Learning for Cost-Sensitive Credit Card Fraud Detection Model 1479
 Sudhansu R. Lenka, Rabindra K. Barik, Sudhashu S. Patra, and Vinay P. Singh

Doha Water Treatment Plant: Interval Modeling and Its Reduced-Order Modeling 1495
 V. P. Singh

Extreme Event Forecasting Using Machine Learning Models 1503
Manish Kumar, Deepak Kumar Gupta, and Samayveer Singh

**Enhancing Mist Assisted Cloud Computing Toward Secure
and Scalable Architecture for Smart Healthcare 1515**
Arijit Dutta, Chinmaya Misra, Rabindra K. Barik, and Sushruta Mishra

**Analysis of YouTube Channel Analytics and Affiliate Marketing
with Operating System 1527**
Kanika Singhal and Abhineet Anand

About the Editors

Dr. Gurdeep Singh Hura is an esteemed researcher and professor in the Department of Mathematics and Computer Science, UMES, Princess Anne, Maryland. He completed his B. S. degree in Electronics and Telecommunication Engineering in 1972 from Jabalpur University, India. He completed M.S. degree in Electronics and Tele-Communications Engineering in 1975 and Ph.D. in Computer Engineering in 1985, from Indian Institute of Technology, Roorkee, India. His research area includes Cyber security, GIS and E-portfolio, Distributed Algorithms, Network forensics, Software Engineering, Modeling and Simulation, Wireless Communication Security, Routing and Scheduling Strategies in High-speed Networks, Resource Allocation and Load Balancing. He is an author/co-author of over hundred technical papers, which were published, in International IEEE journals and refereed conferences. He guest edited three special issues on “Petri nets and related graph models: Past, Present and Future”, 1991, “The Practice of Performance modeling and reliability analysis”, 1996, and “Internet: The state of the art”, Computer Communication (Elsevier, UK), 1998. He is co-author of a book on “Data and Computer Communications: Networking and internetworking”, CRC Press, 2001 and written six chapters in computer networks, terrestrial networks, dynamicity in social networks, and related areas. He received an external funding of over \$5M for his research projects in US. He is a co-author of Best paper award on “Dynamic load balancing in Heterogeneous Computing system with Node Model”, 3rd International Conference in Industry and Engg (CAINE 2018), New Orleans, Oct 8-10, 2018. He is a senior member of IEEE and was elevated to Fellow of Society for Design and Process Science in 2002. He has organized tutorials on Computer Networks, Modeling and analysis, Software engineering, Cyber infrastructure, Cyber security and Accreditation Board of Engineering and Technology (ABET) accreditation in the countries: Singapore, India, Australia, Malaysia, Indonesia, China, and others. He is CAC ABET National and International Program evaluator. He was a consultant to NEC, Inc., Japan on load balancing aspect of its operating system for parallel machine (2000-2004). He received many awards such as Post-Tenure Review award of Excellence in recognition of outstanding achievement

of exemplary Research/Scholarship, UMES, 2018, Distinguished Scholar Award, School of Graduate Studies, UMES, 2015, Achievement award, World Congress of Computer and Engineering, Las Vegas, July 2016, etc.

Dr. Ashutosh Kumar Singh is an esteemed researcher and academician in the domain of Electrical and Computer engineering. Currently, he is working as a Professor and Head; Department of Computer Applications; National Institute of Technology; Kurukshetra, India. He has more than 18 years research, teaching and administrative experience in various University systems of the India, UK, Australia and Malaysia. Dr. Singh obtained his Ph. D. degree in Electronics Engineering from Indian Institute of Technology-BHU, India; Post Doc from Department of Computer Science, University of Bristol, United Kingdom and Chartered Engineer from United Kingdom. He is the recipient of Japan Society for the Promotion of Science (JSPS) fellowship for short term visit in University of Tokyo and other Universities and another university of Japan. His research area includes Verification, Synthesis, Design and Testing of Digital Circuits, Predictive Data Analytics, Data Security in Cloud, Web Technology. He has published more than 240 research papers till now in peer reviewed journals, conferences and news magazines and in these areas. He has also co-authored eight books including “Web Spam Detection Application using Neural Network”, “Digital Systems Fundamentals” and “Computer System Organization & Architecture”. Prof. Singh has worked as principal investigator/investigator for six sponsored research projects and was a key member on a project from EPSRC (United Kingdom) entitled “Logic Verification and Synthesis in New Framework”. Dr. Singh has visited several countries including Australia, United Kingdom, South Korea, China, Thailand, Indonesia, Japan and USA for collaborative research work, invited talks and to present his research work. He had been entitled for 13 awards such as Merit Awards-2003 (Institute of Engineers), Best Poster Presenter-99 in 86th Indian Science Congress held in Chennai, INDIA, Best Paper Presenter of NSC’99 INDIA and Bintulu Development Authority Best Postgraduate Research Paper Award for 2010, 2011, 2012. He has served as an Editorial Board Member of International Journal of Networks and Mobile Technologies, International journal of Digital Content Technology and its Applications. Also he has shared his experience as a Guest Editor for Pertanika Journal of Science and Technology, Chairman of CUTSE International Conference 2011, Conference Chair of series of International Conference on Smart Computing and Communication (ICSCC), and as editorial board member of UNITAR e-journal. He is involved in reviewing process in different journals and conferences of repute including IEEE transaction of computer, IET, IEEE conference on ITC, ADCOM etc.

Dr. Lau Siong Hoe serves as a Professor at the Faculty of Information Science and Technology, Multimedia University, Malaysia. Presently he is the Dean of Faculty of Information Science and Technology. Dr. Lau research interest is in the area of Big Data Visualization, Educational Data Mining & Learning Analytics, Educational Computing & Technology and Human-Computer Interaction. Over the past few

years, he has been doing research focusing on Business Intelligence & Analytics in Education and Human-Computer Interaction Security (HCISec). He has over 100 scientific papers and projects either presented or published. Dr. Lau is a Senior Member of IEEE, USA and certified as a MATRIZ level 3 practitioner. He is regularly sought after and requested lecturer at the majority of major IT/Computer Science schools. He also speaks regularly at workshops/conferences/seminars on Business Intelligence & Analytics with self-service BI solution and how to accelerate innovation and solve problems creatively in a scientific way with Design Thinking and TRIZ approaches for technology, engineering and management fields. Dr. Lau Siong Hoe received his degree in Electrical Engineering with Education (Hons) from University of Technology, Malaysia (UTM). He then completed his study in M. Sc. (IT) from University Putra Malaysia (UPM) and PhD from Multimedia University, Malaysia (MMU).

A Drug Recommendation System for Multi-disease in Health Care Using Machine Learning



N. Komal Kumar and D. Vigneswari

Abstract The remarkable technological advancements in the health care industry have improved recently for the betterment of patients' life and providing better clinical decisions. Applications of machine learning and data mining can change the available data to valuable information that can be used for recommending appropriate drugs by analyzing symptoms of the disease. In this work, a machine learning approach for multi-disease with drug recommendation is proposed to provide accurate drug recommendations for the patients suffering from various diseases. This approach generates appropriate recommendations for the patients suffering from cardiac, common cold, fever, obesity, optical, and ortho. Supervised machine learning approaches such as Support Vector Machine (SVM), Random Forest, Decision Tree, and K-nearest neighbors were used for generating recommendations for patients. The experimentation and evaluation of the study was carried out on a sample dataset created only for testing purpose and is not obtained from any source (medical practitioner). This experimental evaluation shows that the Random Forest classifier approach yields a very good recommendation accuracy of 96.87% than the other classifiers under comparison. Thus, the proposed approach is considered as a promising tool for reliable recommendations to the patients in the health care industry.

Keywords Drug · Data mining · Machine learning · Prescription · Health care

N. Komal Kumar (✉)

Department of Computer Science and Engineering, St. Peter's Institute of Higher Education and Research, Avadi, Chennai, India

e-mail: komalkumarnapa@gmail.com

D. Vigneswari

Department of Information Technology, KCG College of Technology, Karapakkam, Chennai, India

e-mail: vigneswari121192@gmail.com

© Springer Nature Singapore Pte Ltd. 2021

G. S. Hura et al. (eds.), *Advances in Communication and Computational*

Technology, Lecture Notes in Electrical Engineering 668,

https://doi.org/10.1007/978-981-15-5341-7_1

1 Introduction

An Electronic Health Record (EHR) holds the digital version of the patients' medical paper report. They are real-time and instantly available to the users in a secured manner. It contains the medical and treatment histories of the patient right from the entry. This information includes demographics of the patient, medical history, medical diagnosis, medications, treatments, radiology images and test results of disease [1]. The main feature of the EHR is that it can track the medical history of the patient and can be shared among different medical organizations to yield a better diagnosis and treatment of the disease. The data stored in the EHR enable the practitioners to take better decisions on the disease. The Electronic Health Record (EHR) improves the treatment of the patient by reducing medical errors, duplicate treatment approaches, and delay in treatments. With the data stored in the database, a medical practitioner can apply machine learning algorithms to make effective decisions on treatments and medications. Classification approaches intelligently work to provide many accurate recommendations for short-term disease risks. Several reasons have made the authors work on an ensemble classifier to predict disease. Recent work in [2] has proposed an ensemble approach for predicting diabetes mellitus using Random Forest classifiers optimized with a genetic algorithm. Accurate recommendations are needed in the healthcare industry to provide a way better living to the people. Machine learning classifiers can be used in the analysis of predicting lung cancer among patients [3]. Machine learning algorithms with ensemble approaches have yielded good accuracy with success [4]. This paper totally focuses on providing a recommendation of drugs required by the patient to be taken for appropriate medication.

The proposed research is organized in the following sections. Section 2 discussed the related work in machine learning and recommendation systems, Sect. 3 describes the proposed methodology for drug recommendation, Sect. 4 describes the experimental evaluation and findings and finally concluded in Sect. 5.

2 Related Work

This section briefly discusses the recent works of machine learning and data mining approaches in health care.

Recent advances in biotechnology have led to the production of genetic data and medical information which are generated from the Electronic Health Records (EHR). Such data can be converted into valuable information using machine learning and data mining approaches. Kavakiotis et al. [5] investigated the applications of machine learning and data mining approaches for predicting, detecting, complications, and management. In the analysis, Support Vector Machine (SVM) outperformed in predicting and detecting diabetes complications. A technique for predicting the health of a fetal based on maternal medical history using machine learning

approaches was presented in [6], the work comprised of gathering dataset from 96 pregnant women and applying the data to the machine learning classifiers. In the predictive analysis Decision Tree achieved higher accuracy than the other supervised and unsupervised classifiers under clinical analysis. Similar work is done in [7], where a health monitoring system is established to monitor the health of pregnant women to avoid future complications in health. The proposed hybrid machine learning technique established relationships between the physical and mental factors to prevent health complications in women during pregnancies. Kuteesa et al. [8] surveyed machine learning techniques in HIV clinical research; the study concluded that there is a steady increase in the production of genetic data which needs machine learning techniques for translating information to knowledge. Kaur [9] proposed a novel and smart healthcare framework using machine learning with advanced security features such as monitoring daily activity, access control, dynamic data encryption standards and validation at endpoints, the proposed was more effective in diagnosing disease. A machine learning technique for detecting type-2 diabetes was presented in [10], where a data-informed framework is proposed using machine learning via feature engineering, the proposed was found effective in identifying medical subjects from an Electronic Health Record (EHR). Darabi et al. [11] applied supervised machine learning algorithms to estimate the risk mortality of patients admitted in Intensive Care Units (ICUs), the model outperformed in predicting the mortality of patients admitted in ICUs. A recommendation system involves presenting the appropriate data or information to the user using data analysis, such work is represented in [12], where a recommendation system was proposed for recommending most appropriate news to the user using a novel news utility model, the proposed model outperformed the existing models in recommending news to the user. Guan [13] proposed a recommendation model using multiple view information for addressing content heterogeneity; the proposed model outperformed using ample experiments and visuals demonstration. A comparison of machine learning tree classifiers for diabetic mellitus is proposed in [14], where the classifiers such as Random Forest, C4.5, Random Tree, REP tree and Logistic Model Tree accuracies were compared in prediction. A multi-model technique for predicting chronic kidney disease was proposed by Kumar [15], which involves two-stage, such as genetic algorithm and machine learning for its disease prediction. A hybrid machine learning classifier was proposed in [16], which involves a multi-swarm optimization and a multi-layer perceptron for the prediction of DENV serotypes.

3 Proposed Methodology

We worked on a sample EHR dataset created only for testing purposes and not obtained from any source (medical practitioner), the dataset contained admission ID, Sex, Age, disease symptoms, and its prescriptions. First, the dataset is subjected to pandas tool for cleaning, which is then subjected to train various machine learning

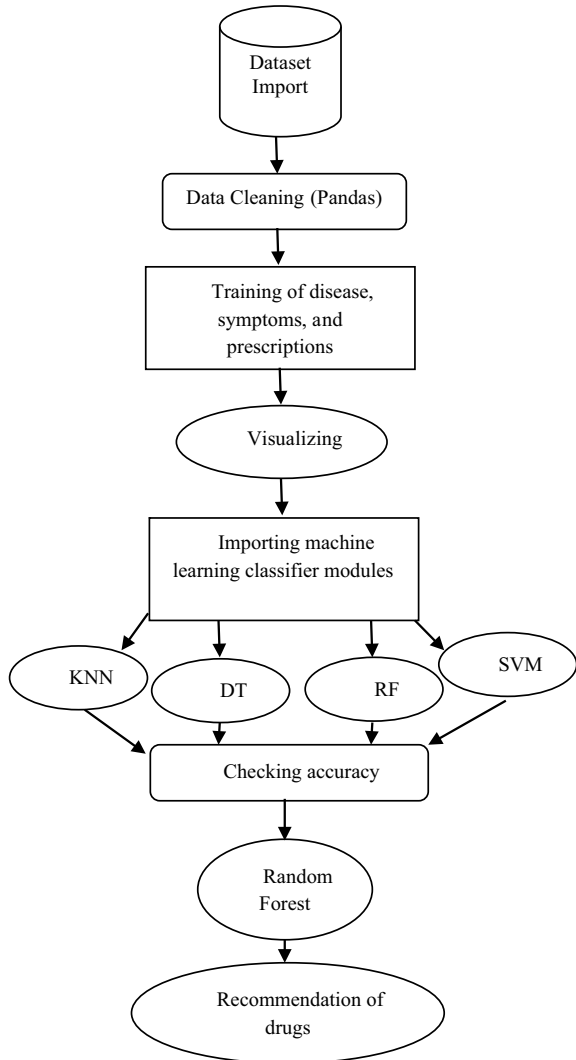
models for prediction, with the help of confusion matrix, the accuracy of the classifiers were calculated, and the classifier with high accuracy were applied to the test dataset for predicting and recommending drugs to the patients. The proposed framework is shown in Fig. 1.

The main steps in providing the recommendation for the disease are as follows:

Step 1: Importing and cleaning Dataset

In this step, the dataset was imported and cleaned using pandas, a python based data analysis tool.

Fig. 1 Proposed framework



Step 2: Training and visualizing of data.

In this step, the dataset is trained with its associated parameters and visualized using mathematical plotting functions to check the feasibility of data values.

A total of 891 testing records were visualized. Data visualizations help the data scientist to check the feasibility of the dataset attributes and its values. Figure 2 shows the relationship between males and female patients under analysis. The disease relationship between males and females is shown in Fig. 3. Symptom relationship between male and female is shown in Figs. 4 and 5, a prescription relationship between male and female is shown in Figs. 6 and 7. The scatter diagram for age and disease is shown in Fig. 8 and finally, the relationship between prescription and disease is shown in Fig. 9 respectively.

Step 3: Applying supervised machine learning classifiers

In this step, the cleansed data are subjected to machine learning classifiers such as Support Vector Machine (SVM), Random Forest, Decision Tree, and K-nearest neighbor.

Fig. 2 Male versus female

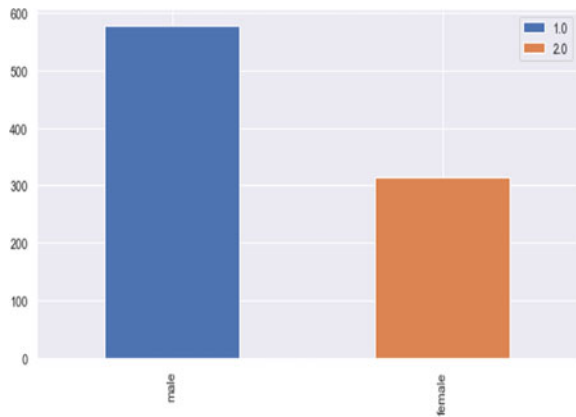


Fig. 3 Disease: male versus female

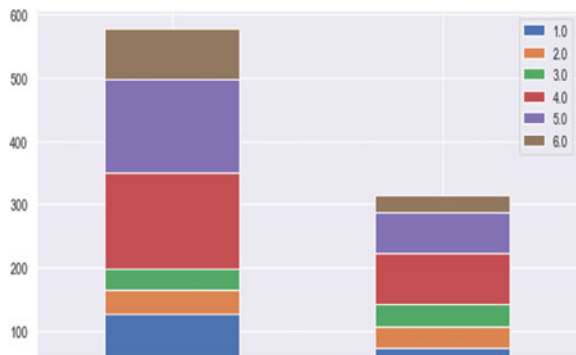


Fig. 4 Symptom 1: male versus female

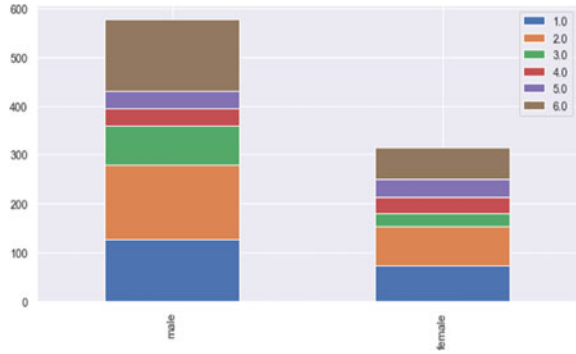


Fig. 5 Symptom 2: male versus female

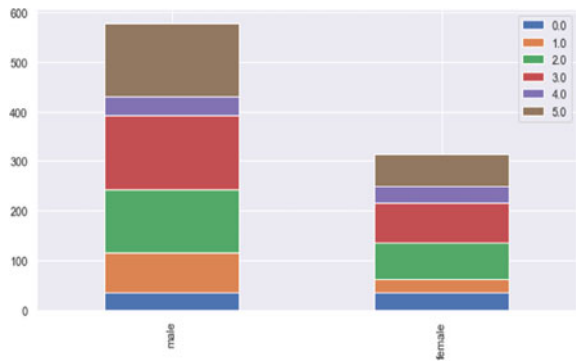
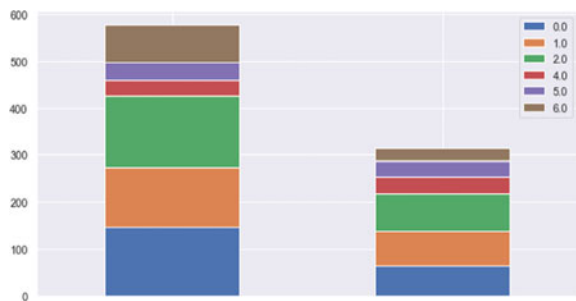


Fig. 6 Prescription 1: male versus female



Step 4: Accuracy measurement

In this step, the classifiers were tested for its accuracy in recommending prescriptions for certain medical symptoms.

Step 5: Termination

Terminate the process when the machine learning classifier model is built for a recommendation.

Fig. 7 Prescription 2: male versus female

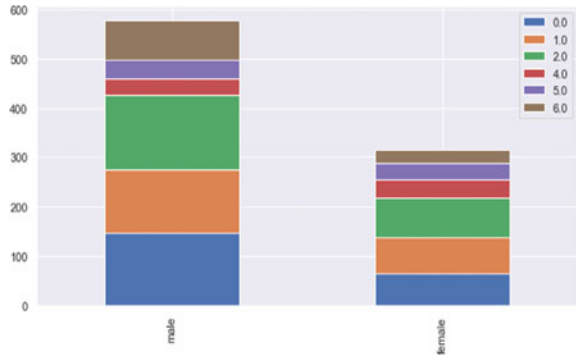


Fig. 8 Age versus disease

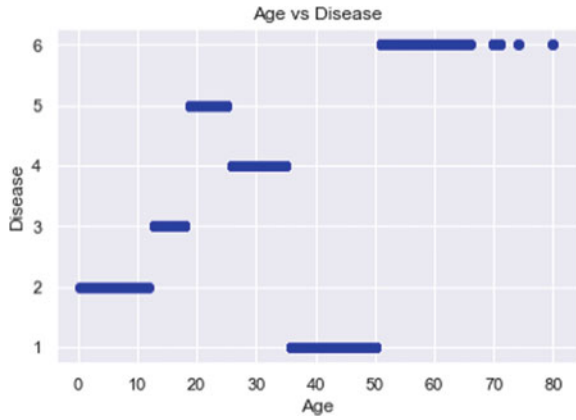
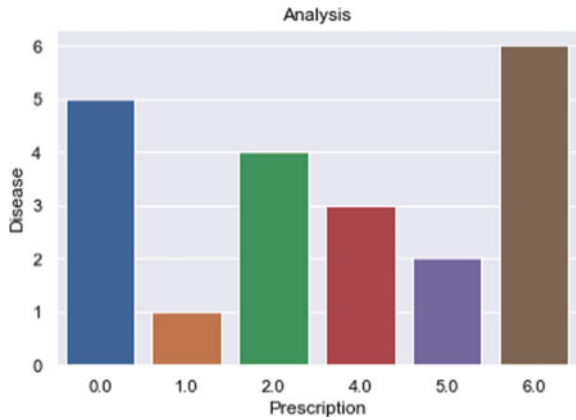


Fig. 9 Prescription versus disease



Algorithm 1: Training

```

1  Input: Dataset D
2  Output: Training Dataset for disease  $D_{T1}$ , symptom  $D_{T2}$ ,  $D_{T3}$ 
    and prescription  $P_1$  and  $P_2$ 
3  begin
4   $D_1 = \text{read}(\text{patientdata})$ 
5  Check if  $D_1.isnull()$ 
6  ExecuteMap(Sex)=  $D_1['Sex'].map(\{'male':1,'female':2\})$ 
7   $D_{T1} = \text{train}(\text{Disease}, D_1).map(\text{Cardiac}=1, \text{cold}=2, \text{fever}=3, \text{obesity}$ 
     $=4, \text{optical}=5, \text{Ortho}=6)$ 
8   $D_{T2} = \text{train}(\text{sympt1}, D_1).map(\text{ChestDiscomfort}=1, \text{fat}=2, \text{pain in}$ 
     $\text{bone}=3, \text{Running nose}=4, \text{Temperature increase}=5, \text{Vision}$ 
     $\text{problems}:6)$ 
9   $D_{T3} = \text{train}(\text{sympt1}, D_1).map(\text{decrease in bone density}=1, \text{heart}$ 
     $\text{burn}=2, \text{lack of physical activity}=3, \text{mild}$ 
     $\text{fever}=4, \text{myopia}=5, \text{nil}=0)$ 
10  $P_1 = \text{train}(\text{pres1}, D_1).map(\text{Aceinhibitors}=1, \text{Physicalactivity}=2,$ 
     $\text{Contactlens}=3, \text{Paracetamol}=4, \text{ibuprofen}=5, \text{Antidepressants}=6)$ 
11  $P_2 = \text{train}(\text{pres2}, D_1).map(\text{Aldosterone}=1, \text{bupropionnaltrexone} =$ 
     $2, \text{contact lens}=3, \text{ibuproifn}=4, \text{acetaminophen}=5,$ 
     $\text{Corticosteroids} =6)$ 
12 end

```

Algorithm 2: Classifier modeling

```

1 Input: Training Dataset for disease  $D_{T1}$ , symptom  $D_{T2}$ ,  $D_{T3}$  and
  prescription  $P_1$  and  $P_2$ , cross validation  $K, K$  nearest neighbour  $Kn$ 
2 Output: Classifier models  $C_1, C_2, C_3,$  and  $C_4$ 
3 begin
   $C_1 = KNeighborsClassifier(n\_neighbors = 13)$ 
4 Calculate score = cross_val_score(clf, train, target, cv=k_fold,
  n_jobs=1, scoring=scoring)
   $C_2 = SVC()$ 
6 Calculate score = cross_val_score(clf, train, target, cv=k_fold,
  n_jobs=1, scoring=scoring)
   $C_3 = RandomForestClassifier(n\_estimators=13)$ 
7 Calculatescore = cross_val_score(clf, train, target, cv=k_fold,
  n_jobs=1, scoring=scoring)
   $C_4 = DecisionTreeClassifier()$ 
8 Calculate score = cross_val_score(clf, train, target, cv=k_fold,
  n_jobs=1, scoring=scoring)
9 end

```

Algorithm 3: Predicting and recommendation

```

1 Input: RandomForestClassifier(n_estimators=13)
2 Output: Prediction P, Prescription  $P_i$ 
3 begin
4  $C_3 = RandomForestClassifier(n\_estimators=13)$ 
5  $C_3.fit(train, target)$ 
6 prediction =  $C_3.predict(test)$ 
7 out (Prediction P, Prescription  $P_{i1}$  or  $P_{i2}$ )
8 end

```

The training algorithm is given in Algorithm 1 deals with training dataset which will then be given to the classifiers for generating appropriate drug recommendation, classifiers modeling algorithm in Algorithm 2 deals with producing classifier models for predicting disease, and finally, prediction and recommendation in Algorithm 3 deals with predicting disease and recommending suitable medication to the patient (Fig. 10).

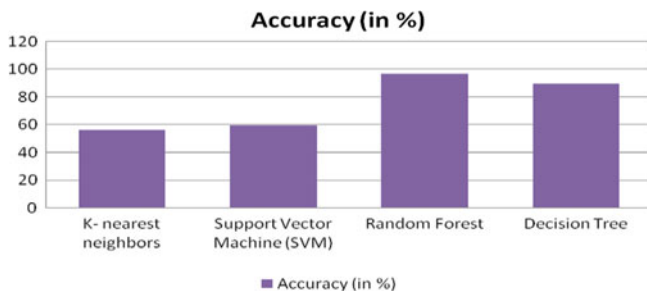


Fig. 10 Accuracy of the classifiers

Table 1 Accuracy of classifiers

Classifier	Accuracy (in %)
K-nearest neighbors	56.52
Support Vector Machine (SVM)	59.65
Random Forest	96.87
Decision Tree	89.68

4 Experimental Analysis and Findings

This section contains the experimental results and analysis of a recommendation system for multi-disease. A dual-core i3 system with 4 GB of RAM, pandas, NumPy, Ipython, SciKit_Learn, SciPy, StatsModels, and Matplotlib libraries was used in the experimental analysis for generating recommendations. Machine learning classifier algorithms were evaluated for its accuracy in recommending appropriate drug recommendations to overcome certain medical issues. The experimental analysis takes place in two steps. In the first step, the dataset is imported and cleansed using pandas tool, the second step involves in training machine learning models for the recommendation system where the test data is subjected to various classifiers such as SVM, Random Forest, Decision Tree, and K-NN and accuracy is measured, then the classifier with high accuracy is used in predicting disease with various symptoms taken into consideration, with the trained symptoms and prescriptions, the Random Forest classifier provides recommendations to the patients (Table 1).

5 Conclusion and Future Directions

In this work, a drug recommendation system for multi-disease using machine learning for healthcare was developed using a sample dataset which was created only for testing purposes and not obtained from any source (medical practitioner). The proposed method using Random Forest machine learning classifier showed that it

can be an effective drug recommendation tool in healthcare. The machine learning classifiers used in the analysis include K-nearest neighbors, Support Vector Machine (SVM), Random Forest, and Decision Tree to achieve accuracy and provide drug recommendations for the patients suffering from short-term disease. The experimental results showed that the proposed method using the Random Forest classifier yielded a higher predictive performance compared with the other classifiers under analysis. Based on the experimental results obtained, the proposed method is found to be effective in improving the quality of drug recommendation, whereby improving the healthcare industry. In the future, we are interested in applying ensemble machine learning algorithms for predicting and generating drug prescriptions for multi-disease.

References

1. <https://www.healthit.gov/faq/what-electronic-health-record-ehr>
2. Komal Kumar N, Vigneswari D, Vamsi Krishna M, Phanindra Reddy V (2019) An optimized random forest classifier for diabetes mellitus. In: Abraham A, Dutta P, Mandal J, Bhattacharya A, Dutta S (eds) Emerging technologies in data mining and information security. Advances in intelligent systems and computing, vol 813. Springer, Singapore. https://doi.org/10.1007/978-981-13-1498-8_67
3. Komal Kumar N, Vigneswari D, Kavya M, Ramya K, Lakshmi Druthi T (2018) Predicting non-small cell lung cancer: a machine learning paradigm. *J Comput Theor Nanosci* 15(6/7):2055–2058. <https://doi.org/10.1166/jctn.2018.7406>
4. Das R, Turkoglu I, Sengur A (2009) Effective diagnosis of heart disease through neural networks ensembles. *Expert Syst Appl* 36:7675–7680
5. Kavakiotis I, Tsave O, Salifoglou A, Maglaveras N, Vlahavas I, Chouvarda I (2017) Machine learning and data mining methods in diabetes research. *Comput Struct Biotechnol J* 15:104–116
6. Akbulut A, Ertugrul E, Topcu V (2018) Fetal health status prediction based on maternal clinical history using machine learning techniques. *Comput Methods Programs Biomed* 163:87–100
7. Lakshmi BN, Indumathi TS, Ravi N (2016) An hybrid approach for prediction based health monitoring in pregnant women. *Procedia Technol* 24:1635–1642
8. Bisaso KR, Anguzu GT, Karungi SA, Kiragga A, Castelnuovo B (2017) A survey of machine learning applications in HIV clinical research and care. *Comput Biol Med* 91:366–371
9. Kaur P, Sharma M, Mittal M (2018) Big data machine learning based secure healthcare framework. *Procedia Comput Sci* 132:1049–1059
10. Zheng T, Xie W, Xu L, He X, Zhang Y, You M, Yang G, Chen Y (2017) A machine learning-based framework to identify type 2 diabetes through electronic health records. *Int J Med Inf* 97:120–127
11. Darabi HR, Tsinis D, Zecchini K, Whitcomb WF, Liss A (2018) Forecasting mortality risk for patients admitted to intensive care units using machine learning. *Procedia Comput Sci* 140:306–313
12. Zihayat M, Ayanso A, Zhao X, Davoudi H, An A (2019) A utility-based news recommendation system. *Decis Support Syst* 117:14–27
13. Guan Y, Wei Q, Chen G (2019) Deep learning based personalized recommendation with multi-view information integration. *Decis Support Syst* 118:58–69
14. Vigneswari D, Komal Kumar N, Ganesh Raj V, Gagan A, Vikash SR (2019) Machine learning tree classifiers in predicting diabetes mellitus. In: IEEE-2019 5th international conference on advanced computing and communication systems (ICACCS), pp 84–87. <https://doi.org/10.1109/icaccs.2019.8728388>

15. Komal Kumar N, Lakshmi Tulasi R, Vigneswari D (2019) An ensemble multi-model technique for predicting chronic kidney disease. *Int J Electr Comput Eng* 9(2):1321–1326
16. Komal Kumar N, Roopa VD, Devi BAS (2018) MSO—MLP diagnostic approach for detecting DENV serotypes. *Int J Pure Appl Math* 118(5):1–6

Smart Mobility: Understanding Handheld Device Adoption



Latika Kharb , Deepak Chahal, and Vagisha

Abstract In recent years, the mobile in one's pocket has become a multifunctional device and is no longer a device used just for making calls or sending text messages. People make use of their mobiles either to take pictures and videos, or to play games or to listen to music. An increasing number of people today have an autonomous Internet connection and they get online using a mobile device to share text, image, games, or applications as new applications are constantly being available. Mobile computing devices including smart phones provide us the capability to access information/make calls and interact using communication methods that can be insecure also. Moreover, redesigning smart phones resulted in a technology that can keep us involved for most of the time and also oblivious to events around us. In this paper, we will cover how mobility in terms of smart phones evolved, its effects on our lives: both positive and negative, various users of mobility and its benefits to casual users, professional users, and transactional users. Then, we will cover effects of mobility on human wellness and existence & solutions for it, security threats to mobility along with future of mobilization with reference to need of mobile cloud. This paper investigates the usage patterns of various mobility devices. We have taken a dataset of 300 people of different countries from UCI repository and analyzed various important patterns of the available smart mobility devices. To sum up, smart phones are remarkably affecting in both positive and negative ways in our world. Since all smart phones are improving in technical specifications, we have to redesign future smart phones by reducing the negatives and increasing the positive impacts on the globe.

Keywords Autonomous Internet connection · Mobility · Mobilization · Security threats

L. Kharb (✉) · D. Chahal
Jagan Institute of Management Studies, Sector-5, Rohini, Delhi 110085, India
e-mail: latika.kharb@jimsindia.org

Vagisha
Banasthali Vidyapeeth, Newai, Rajasthan, India

© Springer Nature Singapore Pte Ltd. 2021
G. S. Hura et al. (eds.), *Advances in Communication and Computational Technology*, Lecture Notes in Electrical Engineering 668,
https://doi.org/10.1007/978-981-15-5341-7_2

1 The Evolution of Cell Phones/Smart Phones

Many of the early cell phones were bulky and it was cumbersome to carry them along with you all the time. Motorola DynaTAC 8000x was launched in 1983; it was the first true mobile phone because it was portable than before and easy enough to carry. However, they were primarily used by business personnel rather than for personal usage. When the technology advanced, numerous cell phone companies came in market: They worked hard on how to embed more features that are demanded by customers' viz. smaller size for making it portable and undoubtedly to be more affordable. Eventually, many manufacturers realized their limitations while integrating the demanded features and technologies. The preliminary smart phones allowed its users to access e-mails, and also make use of the phone as scanners, fax machines, bar code readers, and business address book. Gradually, the work area of the cell phones shifted from a communication device to a multi-versatile device by names of PDA and Handhelds.

In modern years, phone style and pattern have really altered significantly. Today, we use our smart phones for browsing the Web, read-through e-mails, click photo, and for updating their status on social media than actually making calls only. One of the recent developments in the world of wireless technology is the use of mobile ad hoc networks which was initially developed for military applications but now has expanded to include many commercial applications [1].

2 Mobile Technologies Impact on Human Existence

Since the revolutionary event of discovery of the mobile phone and its technology, our lives have changed extensively. Today, most of the people read news over their mobile phone instead of a newspaper, make to-do lists in mobiles instead of paper, and play songs and movies in mobiles instead of iPods/music players. A short message service can facilitate group interaction by providing a context-aware environment with shared calendars, documents, and events anytime and anywhere [2]. So, no matter where you are, you can get information about anything you want in a host of different ways through one device called your mobile; this is mobility. Nearly, all students nowadays own a mobile device and about half of them own more than one [3]. The increasing usage of mobile computing is evident by the study by Juniper Research, which states that the consumer and enterprise market for cloud-based mobile applications is expected to rise to \$9.5 billion by 2014 [4].

Before, taking it in detail, let us firstly discuss how mobile affects our life in positive as well as negative aspects every day in a brief manner.

2.1 Access for All

Internet access has become essential part of our modern life. In general, mobile phones are less costly than our conventional desktops and they have many usages like: they consume less power, are faster, quite portable, and do not require any monitor and/or keyboard. In America alone, 1 in 5 depends on a cell phone for reliable Internet access while 1 in 10 has access to a mobile phone only, choosing not to purchase a home computer [5].

2.2 Stay Connected Always

From getting aid in a crisis to initiate any activity, mobile phones have proved to be the spirit of a number of significant events. In everyday life, we probably use phones for sending a professional e-mail and side by side, meet/interact our friends and family through social media and also make shopping through mobile apps and navigate the path to required locations through our mobile apps.

2.3 Blooming New Businesses

Mobile has reformed the way clients and business interrelate with each other: from replacing the usual methods and devices with new valuable ways viz. relatively planning every shopping list on paper, now you can discover the information you require while shopping; if your car breaks down, you have the option to call engineer rather than recall the figure. Internet has made us to stay connected and share the information in useful ways as and when it is needed. Various businesses like app makers have originated in the previous year's specializing in mobile communications field.

2.4 Personalized Experience

Users expect anytime/anywhere communication with information systems and enjoy a one-to-many relationship with the devices they use [2] as mobile device is a personal device and it is more portable than a desktop/laptop. Misplacing your phone can be distressing as all the individual information could now be unprotected to whoever discovers it.

2.5 “Mobility” Devices

Many businesses use the mobile technologies; there is ample merchandise that has been become obsolete like music players, alarm clocks, wrist watches, navigation systems, calculators, non-digital cameras, paper calendar, and many more. Today, our phone has become sole method of payment and is also replacing our car stereos, and has the ability to control every device at home through IOT.

2.6 Get Information at Anytime

Access to any information is easily possible through smart phones and they can be used for making your living safe. In the way, applications for mobile technologies can suggest you with further faster and significant detail. Mobiles not only authorize us to access facts but also make it feasible to support it entirely in one place.

2.7 Distractions by Mobiles

In today’s culture, developments in technological skills have provided us advanced intensities of technical knowledge through the discovery of different devices and thus made our life stress-free. As mobile expertise has become so widespread in today’s world, research relates it with numeral side effects—majority of which contain anxiety or apprehension related disorders, reduced efficiency, bright displays, and incorrect positions have instigated eye- and neck-related illnesses that have become part of lives of numerous people. In a set of places, it is a common view to see everybody busy in their mobile devices even when they are surrounded by abundant people: By staying connected all the time leads to development of diversion conduct also. On the other hand, each modernization has the prospective of some concealed threats to its users like theft of personal facts and/or information. In the mobile age, where personal information is available via multiple points of entry, there are a number of ways for hackers to get to someone’s information like name, phone number, address, credit card numbers, bank account information, or even their personal files [6].

3 Users of the Mobile Community

Mobility has an inseparable role for the life of businesses by providing mobile community the required flexibility that proves to be great stimulus for business that likes to transform to new strategies. Most of us have a good and positive experience

of smart phones and their in-built/available apps and we expect the similar in business applications also. The chief driver behind the enterprise mobility trend is their workers who desire to make use of their private recent devices to access company assets and not the company. This business community is much manifold and has three kinds of user groups:

- **Casual user:** User who makes use of industry apps on their stylish phones while roaming;
- **Professional user:** User for whom mobile devices are company significant;
- **Transactional user:** User who want to access their complete company workload from their smart devices.

4 Benefits to Users of the Mobile Community

4.1 *Benefits for Casual Users*

Casual users are people who use mobile as a solution to complement all the services that are offered by their laptops and want to accomplish tasks of their daily life in the same way through the phone as they are waiting at airports, traveling in taxis, or in-between meetings. Casual users form the majority of the mobility trend as they make use of smart phone apps in private for accessing data over Internet or social media status. All this was impossible before the smart phone and their apps evolved, but now, it is far easier and entertaining now. Various benefits to casual users include:

- Access critical information about friends or family at any time.
- All necessary information like photographs, e-mails, contacts is accessible while at move.
- Users cannot be bored by being alone as smart phone provides access to world around them.
- Make transactions (e-bills, recharges) on move.

4.2 *Benefits for Professional Users*

Mobility is crucial for this group and it includes field engineers, maintenance workers, and warehouse staff, i.e., these people need acquisition of facts immediately on a mobile device as they cover access to mobile tools for another decade. By advent of mobility, performing tasks like travel expense reporting and authorization of invoices is very easy and quick. Although the functionality has been accessible in business applications in a smart phone or tablet but they facilitate you to execute it from anyplace. One feature of a business app is its easy deployment and it requires zero training to recognize how to utilize it. The user experiences comfort with device

features and they are designed in a way to handle quickly all kind of tasks. Various benefits to professional users include:

- Minimizes admin overloads
- Makes better use of the ERP solution
- More time for customer value-added work
- Information is centrally located to get increased access by all.

4.3 Benefits for Transactional Users

Transactional users who utilize the business application every day require the capabilities to query and enter new information every time. This user group gathers a variety of devices together with laptops, tablets and ultra-books and requires open access to their business purpose. The introduction of Microsoft Windows 8 followed by 10, with a touch-first experience empowers to explore the application on the touch screen and utilize the implanted console to sort in information.

In any case, the business applications as of now keep running by most organizations on their portable workstations have design impediments which confine client operation to mouse only. To give users a chance to utilize the tablets for information, creation and utilization, along with business applications need to change the client encounter, transfer route to history and move to a touch experiences. Different advantages to value-based clients include:

- Touch-based innovation influences the client to be wealthier
- Always-on expands speed of access to fundamental business data
- Greater utilization of full ERP capacity
- Great chance to present new business rehearses
- More expert level of client related administrations.

5 Effects of Mobile Devices on Human Wellbeing and Existence

The smart phone combines different sophisticated features in one place viz. take pictures, save your memories, store and access personal and professional information, watch video, do e-commerce, use social and financial apps and therefore has become an inherent part of our life. Modern telecommunications facilities have also become an integral part of smart phones and are one of the most reliable assistant as they allow people to maintain continuous communication without interruption in spite of their movements and distances proving to be the best for smart phone mobilization. This developing population of advanced mobile phones and its proprietors has raised a negative impact on human well-being.

The main key points are:

- Adverse outcome of electromagnetic wave on human brain;
- Adverse outcome of handheld gadgets over utilization on human higher body parts;
- Adverse consequence of the mobile handset on the driver;
- Weaknesses and advantages of utilizing sophisticated mobile phones;
- Solutions how to relieve impact of cell phones on human well-being.

In the battle to grasp more current advances, we regularly overlook or disregard its negative side and do not understand its impact until late. A pervasive computing system is one such illustration, which presents more up to date, shorter, convenient, ubiquitous devices for supplanting the huge-sized PCs. These frameworks turn up as normal metropolitan waste. They contain numerous risky substances like substantial metals, non-biodegradable materials, and bio-accumulative poisons. Different end-of-life alternatives need to be considered for such devices. While great measure of advance has been made toward this path, scientists and specialists are wearing down the obstacles. In a race to grasp more up-to-date technology, we are ignoring the evil impacts of the innovation and do not consider it until the point when it is past and there is point of no return. Electromagnetic waves highly affect human brain waves and lead to cancer development. The advanced mobile phone is a cause of the effectiveness of electromagnetic waves. A variety of tests have been conducted in the previous years to identify the impact of electromagnetic waves transmitted from the smart devices on humans. Indeed, actions have to be taken to protect humans from harmful waves. In the present day, there is no certified justification acknowledged by research center or medicinal counter to respond this investigation. The irregularity of the realistic information makes it complicated for researchers.

• ***Extensive usage of smart phones affects on Human Body Parts:***

Broad utilization of advanced cells affects human's body parts like back and neck; there exists a critical relationship between the aggregate time spent on usage of cell phone every day and causes pain in shoulder and the wrist.

• ***Effect of smart phones on the Drivers:***

A man who drives an automobile: car/jeep/truck/bus, etc., utilizes its 90% concentration on using smart phone and is at high risk to be affected by technical hazard. According to the National Safety Council (NSC), 27% of car crashes—or 1,535,490 in 2013—were caused by cell phone use and six percent of cell phone-related crashes were texting related [7]. Diverted driving is on the rise because of the use of cell phones while driving. The main challenge to stop this is to discover a solution so that drivers do not get distracted: may be some more strict laws, or usage of some device inside cars while driving and so on. Based on many reviews and surveys, it is found that messaging took less effort and concentration than the voice calls or Web surfing; however, the driver's involvement was similarly distracting.

- ***Lack of Socialism***

Further extension to the issues specified above, it is also having a huge impact on our social lives, people are getting more detached from reality, they place their mobiles in front of human communication, thus it has become harder to see people conversing with each other and opening their feelings; however, they are commonly and extremely occupied with their cell phones, either in checking the chats and sending messages or simply sharing another chat or audio/video. It is a condition that closely resembles an addiction, and it is somewhat transforming individuals into machines.

6 Security Threats to Mobility

Mobile computing devices/smart phones provide the ability to access information remotely and as they are designed for convenience, and they can also be very insecure. The rapid change occurring in the present era of information technology includes the use of computers by persons involved in the commission of crimes. Age or stage in life seemed to influence the manner in which the mobile device users balanced the expenses and convenience associated with mobility [8]. Today, people face three kinds of security threats: general, communications, and Software and Application Security.

6.1 General Security Threats to Mobility

In modern days, applications targeted at mobile devices have started becoming abundant with application in a range of categories such as entertainment, health, business, and news. The popularity of these is evident by browsing through mobile app download centers [9].

- Mobile devices are more insecure than standard computers and they can be easily misplaced or stolen due to the aspect of portability. It is advisable not to use a mobile device for storage of sensitive data and if sensitive data has to be accessed on a mobile device, it should be done with security.
- We must activate screen locks and/or use the pass code protection; however, they do not protect the device in case of theft, but it will prevent immediate access to your mobile.
- In case of theft or misplacement, wipe out the phone through remote access systems.

6.2 *Communications Security Threats to Mobility*

- Avoid syncing of your device through Bluetooth/Wi-Fi in public places. They are extremely insecure gateways and can be easily hacked. We should sync our devices with computer using a USB cable for better safety or in ways like:
 - Turn off all the wireless connection when not required any more. This will not only save battery life but also prevents your device unsecured wireless networks.
 - Use wireless encryption, instead of free and insecure networks.

6.3 *Software and Application Security Threats to Mobility*

- Always make use of secured connections especially while accessing your e-mail. Configure your personal communications through encryption whenever possible.
- It is recommended that never store your e-mail ID on any device as they contain sensitive information that could be hacked easily from your mobile device.
- While installing third-party software, we have to be very cautious as the applications may also install vulnerable software.
- Avoid leaving your device on a synchronized connection as it forms an insecure partnership with other devices used by hacker to steal information.

7 **Mobility Trend Check Analysis Across World**

In the paper, the records on mobile/smart device users are collected from the UC Irvine Machine Learning Repository (also called UCI repository). Dataset contains user records from various countries; it contains 300 records, stating attributes like age, gender, country, employment status, most-used device, marital status, purpose, and Internet accessibility (Figs. 1 and 2).

We have used Python to sort the attributes/features of users from dataset of 300 entries.

In Fig. 3, we have given age-wise usage of smart devices and in Fig. 4, we have compared its survival probability. Every customer set has its own vitality that is defined through its mobility level. For this, each user's boundaries of usage are determined by its device of choice because the diversity of devices is quite vast and everyone has its own preferences. Where some users want a big screen, others prefer a compact sized screen; some prefer touch screens while others are comfortable with traditional keypad style phones. Similarly, some companies want to work on their premises, whereas others would like to work all the way through a cloud; some demand a high-speed Internet connection while others work comfortably with off-line mode. For example:

```
In [14]: dataset.head(10)
```

	User_ID	Country	Employment_status	Age	Gender	Most_Used_Device	Purpose	Marital_Status	internet_accessibility
0	1	United Kingdom	Unemployed	81	Female	Smartphones	Health Tracking	Divorced	Excellent
1	2	United Kingdom	Service	44	Female	Desktop	Banking	Divorced	Average
2	3	United States	Unemployed	58	Female	Tablet	Health Tracking	Single	Average
3	4	United Kingdom	Business	87	Male	Smartwatch	Health Tracking	Common-Law	Excellent
4	5	United States	Retired	86	Female	Laptops	Education	Common-Law	Poor
5	6	India	Student	40	Female	Smartphones	Health Tracking	Common-Law	Below Average
6	7	United States	Student	26	Female	Netbook	Shopping	Single	Poor
7	8	Australia	Student	41	Female	Tablet	Shopping	Common-Law	Below Average
8	9	United States	Retired	67	Female	Desktop	Banking	Divorced	Poor
9	10	Australia	Service	34	Male	Smartwatch	Health Tracking	Single	Below Average

Fig. 1 Head info of dataset

Fig. 2 Features information

```
In [15]: dataset.info()

<class 'pandas.core.frame.DataFrame'>
RangeIndex: 300 entries, 0 to 299
Data columns (total 9 columns):
User_ID          300 non-null int64
Country          300 non-null object
Employment_status 300 non-null object
Age              300 non-null int64
Gender           300 non-null object
Most_Used_Device 300 non-null object
Purpose          300 non-null object
Marital_Status   300 non-null object
internet_accessibility 300 non-null object
dtypes: int64(2), object(7)
memory usage: 12.9+ KB
```

- A particular part of metropolitan computing is mobile participatory sensing, relating the tasking of mobile devices to form interactive systems,
- The Metro Sense mission aim at transformation of the mobile device into a social-sensing stage.
- Goldman et al. show the worth of participatory sensing for our everyday lives and its impact on climate change.
- During the Noise Tube project, mobile phones are used as sound sensors, to calculate the individual contact of citizens to sound, in their daily surroundings.

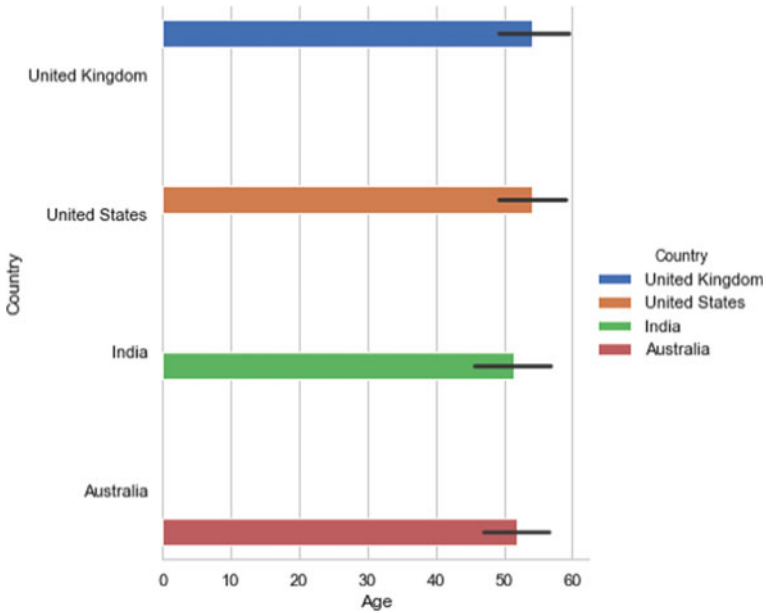


Fig. 3 Age-wise usage of smart devices

The global popularity of smart phones and a minor knowledge about their ill effects forced us to look at its impact on human well-being (Figs. 5, 6, 7 and 8).

8 Proposed Solutions for Fixing the Ill Effects on Human Life

Today, the advancements in technology have provided us advanced levels of technical awareness through the innovation of different devices and thus made our life easier. On the other hand, each technical advancements has the prospective of some concealed threats to its users like stealing/hacking of their personal data that they carry in their device or they share over network. In the mobile age, where personal information is available via multiple points of entry, there are a number of ways for hackers to get to one’s personal/private information like name of bank, aadhar number, bank details as saved as contact list, home address, credit or debit card detail, other e-commerce or insurance policy information, etc. We do not feel that we are going to the correct track with this handy improvement; phones were invented to fetch relaxation and freedom into our lives, and let people linked with each other by using the online applications; however, what we really detect is the contrary (Figs. 9, 10, 11, 12 and 13).

```
In [17]: sns.set(style="whitegrid")

g = sns.catplot(x="Age", y="Country", hue="Country", data=dataset,
               height=6, kind="bar", palette="muted")
g.despine(left=True)
g.set_y_labels("survival probability")

Out[17]: <seaborn.axisgrid.FacetGrid at 0x148fcd0>
```

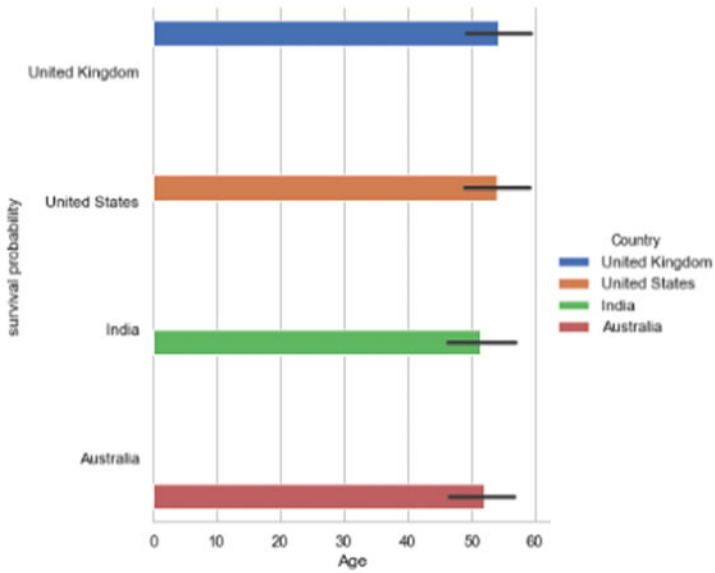


Fig. 4 Age-wise survival probability

```
In [16]: sns.countplot(data=dataset, x = 'Country', label = 'Most_Used_Device')

Out[16]: <matplotlib.axes._subplots.AxesSubplot at 0x148fd70>
```

Fig. 5 Dataset inputs

Fig. 6 Countries using number of smart devices

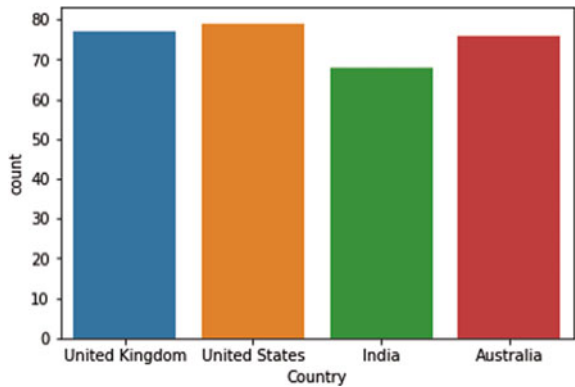
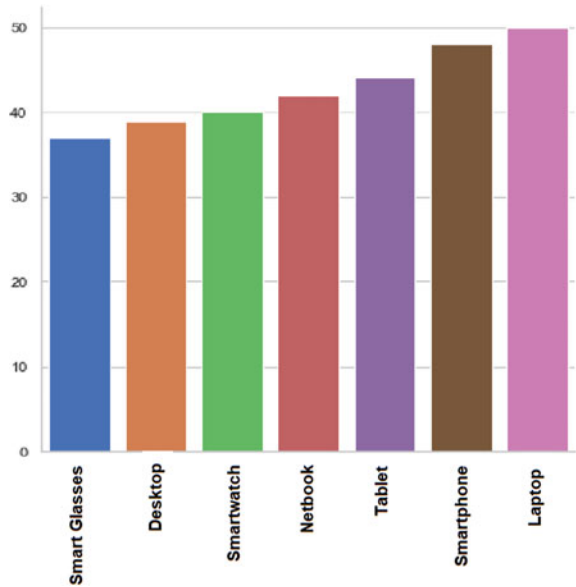




Fig. 7 Most used device

Fig. 8 Number of users for each mobility device



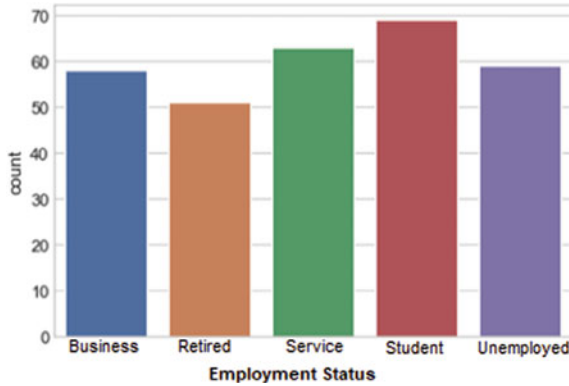


Fig. 9 Mobility usage according employment status

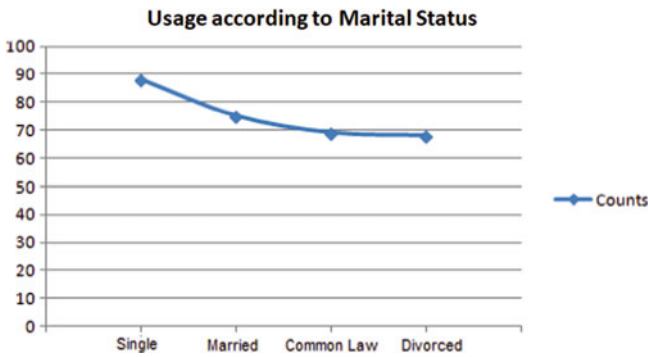


Fig. 10 Usage according to marital status

Fig. 11 Dataset for mobility usage according marital status

Index	Marital_Status
Single	88
Married	75
Common-Law	69
Divorced	68

9 Future of Mobilization: The Need for a Mobile Cloud

The trend of mobility in business enterprises is now moving to an advanced phase. Today, Bring Your Device (BYD) is at hype among employees at work. The world of smart phones/tablets and apps is extremely moving at high pace and new hardware/software innovations have started appearing. The pressure is not only on the

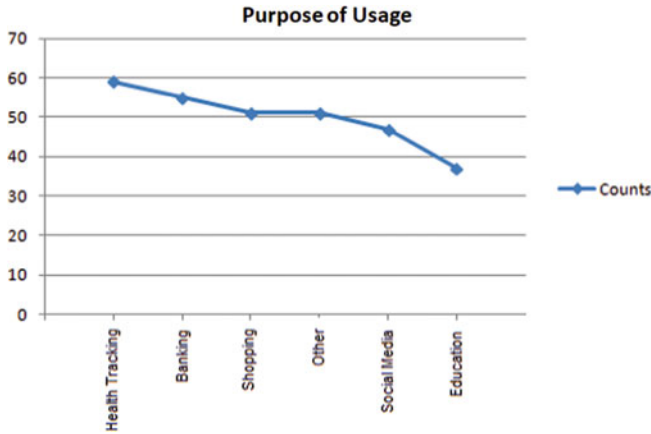


Fig. 12 Purpose of usage

Fig. 13 Dataset for usage of mobility devices by various employers and their tasks

Index	Purpose
Health Tracking	59
Banking	55
Shopping	51
Others	51
Social Media	47
Education	37

hardware and software companies but also on businesses that need the latest and fastest of them. Cloud computing consists of hardware/software resources available on the worldwide Web, i.e., cloud computing will act as a link amid the hardware/software companies and business and bring profit to clients. These services rely on advanced software applications and high-end networks of server computers [10]. This unique approach provides:

- Self-provision of updating the apps that are secretly handled through the app stores and are prepared centrally by cloud.
- Strong security is in-built i.e.no business data are stored without encryption in the Cloud.

A cloud framework keeps its basic information on Internet servers rather than circulating duplicates of information documents to all customers individually. Customers must be linked with the Internet so as to utilize cloud services. Some industry observers expect cloud computing to keep increasing in popularity in coming years [11]. A large series of mobile cloud applications have been familiar today in area

Table 1 Applications of cloud computing

Image processing	Sensor data application
Natural language processing	Crowd computing
Sensor data application	Sharing GPS data
Multimedia searches	Social networking

such as image/video processing, natural language processing, Geo-location sharing, sharing Internet access and its apps, group computing and multimedia sharing. Generally, the term mobile cloud computing means to run an application on a remote server. Some providers offer cloud computing services for free while others require a paid subscription [10, 11]: Amazon EC2—virtual IT, Google App Engine, Google Apps, Apple iCloud, etc (Table 1).

10 Conclusion

Mobility has become an inseparable part in lives of humans when we talk of advancements in computing system. Technically speaking, it has made reasonably small, cheaper but powerful, and wireless communication devices. Each successive development either claims to make the software development process easier or to extend the complexity of applications that can feasibly be built [11]. We have taken a dataset of 300 of people from various countries and analyzed their usage of smart devices. To conclude with, we can say that when we want to be in touch whenever we need to, mobile technology is there; may be in the form of smart phones, tablets, and notebooks, thereby making our lives better than before. We can send and receive important documents almost anywhere in the world and thus mobile technology has helped us to collaborate in real time. Our gadgets also help us to get the right information in time of need and it is the duty of smart phone companies, the app builders, and the Internet providers to keep up with the competition in order to improve this technology. Development of smart phone is extremely shifting our world but it has both positive and negative impacts on the culture; so, it is recommended that designing of future smart phones must comprise of some new features that help in reducing the negative impacts on the society and also increase the positive features. All the investigations on our dataset thus proved the facts given in paper.

References

1. Singh S (2012) Simulation based study of routing protocols in MANET using different scenarios and traffic pattern. http://www.ijetae.com/files/Volume2Issue5/IJETAE_0512_33.pdf
2. Peiper C, Chan E, Campbell R, Bresler J, Al-Muhtad J (2004) Expanding education through active space collaboration. In: Proceedings second annual conference on pervasive computing and communications workshop. IEEE, p 236

3. Klimova B (2018) Mobile phones and/or smartphones and their apps for teaching English as a foreign language. *Educ Inf Technol* 23(3):1091–1099
4. Fernando N, Seng SW, Rahayu W (2013) Mobile cloud computing: a survey. *Future Gener Comput Syst* 29:84–106. <https://doi.org/10.1016/j.future.2012.05.023>
5. <https://www.rocksdigital.com/mobile-technology-changed-lives/>
6. Kharb L, Biometric personal data security systems: trustworthy yet? *Int J Recent Eng Res Dev* 01(06), pp 01–08. ISSN 2455-8761. www.ijrerd.com
7. Nikolaou AA, Nikolaou N (2008) Evaluation of handheld devices for mobile learning. *Int J Eng Educ*. <https://www.researchgate.net/publication/288966917>
8. Sarker S, Wells JD (2003) Understanding mobile handheld device use and adoption. *Commun ACM* 46(12)
9. Xhafa F, Bessis N (eds.) (2014) Inter-cooperative collective intelligence: techniques and applications. *Studies in computational intelligence*, vol 495. Springer, Heidelberg https://doi.org/10.1007/978-3-642-35016-0_2
10. <https://www.lifewire.com/what-is-cloud-computing-817770>
11. Kharb L (2017) Routing mechanisms in ad hoc networks. *J Netw Commun Emerg Technol (JNCET)* 7(3). www.jncet.org

An Efficient Numerical Technique for Solving the Time-Fractional Cahn–Allen Equation



Amit Prakash and Hardish Kaur

Abstract In this paper, we investigate the time-fractional Cahn–Allen equation (CAE) with a novel homotopy-based numerical technique, namely homotopy perturbation transform technique in which homotopy perturbation method and Laplace transform (LT) are combined. In order to verify the reliability and accuracy of the proposed technique, the numerical results are also presented graphically.

Keywords Cahn–Allen equation · Caputo fractional derivative · Homotopy perturbation technique · Homotopy polynomials · Laplace transform

1 Introduction

Fractional differential equations (FDE) have become a topic of interest for the researchers due to their wide applications in different areas of science and engineering. Fractional-order mathematical models [1, 2] are more realistic and most of the complex phenomena like memory dependent phenomena, groundwater flow problems, control theory, mechanical properties of materials, and anomalous diffusion are described more efficiently by using fractional derivatives and equations. Numerous powerful analytical and numerical techniques [3–7] have been developed to investigate the FDEs. Due to wide applications of FDEs, we here study the CAE which has many applications in different disciplines as quantum mechanics and plasma physics, is written as follows

$$D_{\xi} u(\tau, \xi) - u_{\tau\tau}(\tau, \xi) + u^3(\tau, \xi) - u(\tau, \xi) = 0, \quad \tau > 0. \quad (1)$$

A. Prakash · H. Kaur (✉)
Department of Mathematics, National Institute of Technology, Kurukshetra 136119, India
e-mail: harrynanda12@gmail.com

A. Prakash
e-mail: amitmath0185@gmail.com

The CAE is connected with various physical motivated problems such as phase separation, crystal growth, image analysis and has also been widely studied by several researchers. Here, we investigate the following nonlinear time-fractional CAE

$$D_{\xi}^{\alpha} u(\tau, \xi) - u_{\tau\tau}(\tau, \xi) + u^3(\tau, \xi) - u(\tau, \xi) = 0, \tau > 0, 0 < \alpha \leq 1, \quad (2)$$

where $D_{\xi}^{\alpha} u(\tau, \xi)$ is fractional derivative of u w.r.t ξ . Different approaches such as Haar wavelet method [8], homotopy analysis method [9], residual power series method [10], and fractional reduced differential transform method [11] have been employed to investigate the CAE. In this work, the time-fractional CAE of reaction–diffusion is investigated numerically via homotopy perturbation transform technique (HPTT). Homotopy perturbation method (HPM) [12] is a strong computational technique and the Laplace transform (LT) is very effective to solve various nonlinear problems [13–15].

The positivity of HPTT lies in its potential that it requires just a few iterations to yield an accurate solution.

2 Preliminaries

Definition 2.1 A real function $g(\mu)$, $\mu > 0$, in the space C_{ζ} , $\zeta \in \mathbb{R}$ if \exists a $p \in \mathbb{R}$, $p > \zeta$ such that $g(\mu) = \mu^p g_1(\mu)$ where $g_1(\mu) \in C[0, \infty)$ and in the space C_{ζ}^l if $g^l \in C_{\zeta}$, $l \in \mathbb{N}$.

Definition 2.2 The Caputo fractional derivative [1] of $g(\mu)$, $g \in C_{-1}^m$, $m \in \mathbb{N}$, $m > 0$, is defined as

$$D^{\beta} g(\mu) = I^{m-\beta} D^m g(\mu) = \frac{1}{\Gamma(m-\beta)} \int_0^{\mu} (\mu-\eta)^{m-\beta-1} g^{(m)}(\eta) d\eta,$$

where $m-1 < \beta \leq m$.

The operator D^{β} has following basic properties

1. $D^{\beta} I^{\beta} g(\mu) = g(\mu)$,
2. $I^{\beta} D^{\beta} g(\mu) = g(\mu) - \sum_{k=0}^{m-1} g^{(k)}(0^+) \frac{\mu^k}{\Gamma(k+1)}$, $m > 0$.

Definition 2.3 The LT of the Caputo fractional derivative [1] $D_{\mu}^{\beta} g(\mu)$ is given by

$$L[D_{\mu}^{\beta} g(\mu)] = s^{\beta} L[g(\mu)] - \sum_{k=0}^{l-1} s^{\beta-k-1} g^{(k)}(0), \quad l-1 < \beta \leq l.$$

3 Basic Idea of HPTT

Consider the following nonlinear fractional differential equation of order β

$$D_t^\beta u(x, t) + Ru(x, t) + Nu(x, t) = f(x, t), \quad r - 1 < \beta \leq r, \tag{3}$$

with the condition

$$u^m(x, 0) = f_m(x), \quad m = 0, 1, 2, \dots, r - 1, \tag{4}$$

where $D_t^\beta u(x, t)$ is temporal fractional derivative, R and N are the linear and nonlinear differential operators, and $f(x, t)$ is the source term.

Taking LT on Eq. (3) and simplifying, it gives

$$L[u(x, t)] - \sum_{k=0}^{l-1} s^{-k-1} u^k(x, 0) + \frac{1}{s^\beta} \{L[Ru(x, t) + Nu(x, t)] - L[f(x, t)]\} = 0. \tag{5}$$

Exerting inverse LT

$$u(x, t) = L^{-1} \left(\sum_{k=0}^{l-1} s^{-k-1} u^k(x, 0) + L[f(x, t)] \right) - L^{-1} \left\{ \frac{1}{s^\beta} \{L[Ru(x, t) + Nu(x, t)]\} \right\}. \tag{6}$$

By HPM, solution is represented as

$$u(x, t) = \sum_{i=0}^{\infty} p^i u_i(x, t), \tag{7}$$

and the nonlinear term is expressed as

$$Nu(x, t) = \sum_{i=0}^{\infty} p^i H_i(u), \tag{8}$$

here $H_i(u)$ represents the homotopy polynomial defined as:

$$H_i(u) = \frac{1}{i!} \frac{\partial^i}{\partial p^i} \left[N \left(\sum_{j=0}^{\infty} p^j u_j \right) \right]_{p=0}, \quad i = 0, 1, 2, 3, \dots \tag{9}$$

From Eqs. (6)–(8), it gives

$$\sum_{i=0}^{\infty} p^i u_i(x, t) = L^{-1} \left(\sum_{k=0}^{l-1} s^{-k-1} u^k(x, 0) + L[f(x, t)] \right) - p \left[L^{-1} \left\{ \frac{1}{s^\beta} L \left[\left[R \sum_{i=0}^{\infty} p^i u_i(x, t) \right] + \sum_{i=0}^{\infty} p^i H_i(u) \right] \right\} \right]. \quad (10)$$

Comparing the coefficients of similar powers of p , we get

$$\begin{aligned} p^0 : u_0(x, t) &= L^{-1} \left(\sum_{k=0}^{l-1} s^{-k-1} u^k(x, 0) + L[f(x, t)] \right), \\ p^1 : u_1(x, t) &= -L^{-1} \left\{ \frac{1}{s^\beta} L \{ [\mathbf{R}u_0(x, t)] + H_0(u) \} \right\}, \\ p^2 : u_2(x, t) &= -L^{-1} \left\{ \frac{1}{s^\beta} L \{ [\mathbf{R}u_1(x, t)] + H_1(u) \} \right\}, \\ p^3 : u_3(x, t) &= -L^{-1} \left\{ \frac{1}{s^\beta} L \{ [\mathbf{R}u_2(x, t)] + H_2(u) \} \right\}, \end{aligned}$$

in this way, we can find the remaining components. Hence, the solution is given as

$$\begin{aligned} u(x, t) &= \lim_{p \rightarrow 1} \lim_{N \rightarrow \infty} \sum_{i=0}^N p^i u_i(x, t) \\ &= \lim_{N \rightarrow \infty} \sum_{i=0}^N u_i(x, t). \end{aligned} \quad (11)$$

4 Convergence and Error Estimation

Theorem 4.1 Let $u_i(\tau, \xi)$ and $u(\tau, \xi)$ be in the Banach space $(C[0, 1], \|\cdot\|)$. If $\exists 0 < \gamma < 1$ for which $\|u_{i+1}(\tau, \xi)\| \leq \gamma \|u_i(\tau, \xi)\|, \forall i \in N$, then the HPTT solution $\sum_{i=0}^{\infty} u_i(\tau, \xi)$ converges to the solution $u(\tau, \xi)$ of Eq. (2).

Proof Let us consider a sequence $\{s_i\}$ of partial sums of the series $\sum_{i=0}^{\infty} u_i(\tau, \xi)$. Then,

$$\|s_{i+1} - s_i\| = \|u_{i+1}\| \leq \gamma \|u_i\| \leq \gamma^2 \|u_{i-1}\| \leq \cdots \leq \gamma^{i+1} \|u_0\|.$$

For $i, j \in N, i \geq j$,

$$\|s_i - s_j\| = \|(s_i - s_{i-1}) + (s_{i-1} - s_{i-2}) + \cdots + (s_{j+1} - s_j)\|$$

$$\begin{aligned}
 &\leq \|(s_i - s_{i-1})\| + \|(s_{i-1} - s_{i-2})\| + \dots + \|(s_{j+1} - s_j)\| \\
 &\leq \gamma^i \|u_0(\tau, \xi)\| + \gamma^{i-1} \|u_0(\tau, \xi)\| + \dots + \gamma^{j+1} \|u_0(\tau, \xi)\| \\
 &\leq \gamma^{j+1} (1 + \gamma + \gamma^2 + \dots + \gamma^{i-j-1}) \|u_0(\tau, \xi)\| \\
 &\leq \frac{1 - \gamma^{i-j}}{1 - \gamma} \gamma^{j+1} \|u_0(\tau, \xi)\|.
 \end{aligned}$$

Since $0 < \gamma < 1$, we have $1 - \gamma^{i-j} < 1$, then

$$\|s_i - s_j\| \leq \frac{\gamma^{j+1}}{1 - \gamma} \|u_0(\tau, \xi)\|. \tag{12}$$

So, $\|s_i - s_j\| \rightarrow 0$ as $i, j \rightarrow \infty$. So, $\{s_i\}$ being a Cauchy sequence in the Banach space is convergent. So, $\exists u(\tau, \xi) \in B$ for which $\sum_{i=0}^{\infty} u_i(\tau, \xi) = u(\tau, \xi)$.

Theorem 4.2 *If $\exists 0 < \gamma < 1$ in such a way that $\|u_{i+1}(\tau, \xi)\| \leq \gamma \|u_i(\tau, \xi)\|, \forall i \in N$, then the truncated error is estimated as*

$$\left| u(\tau, \xi) - \sum_{i=0}^j u_i(\tau, \xi) \right| \leq \frac{\gamma^{j+1}}{(1 - \gamma)} \|u_0(\tau, \xi)\|.$$

Proof From Eq. (12) and above theorem, taking $i \rightarrow \infty, s_i \rightarrow u(\tau, \xi)$, we have

$$\left| u(\tau, \xi) - \sum_{i=0}^j u_i(\tau, \xi) \right| \leq \frac{\gamma^{j+1}}{(1 - \gamma)} \|u_0(\tau, \xi)\|.$$

5 Application

In this section, HPTT solution for the time-fractional CAE is presented.

Example 5.1 Consider Eq. (2) subject to the initial condition given by

$$u(\tau, 0) = \frac{1}{1 + e^{\left(\frac{\tau}{\sqrt{2}}\right)}}, \tag{13}$$

The solution in closed form as in [9] is $\frac{1}{1 + e^{\left(\frac{\tau}{\sqrt{2}} - \frac{3\xi}{2}\right)}}$.

Following the same steps as in the proposed scheme and after applying HPM, we arrive at the following equation

$$\sum_{n=0}^{\infty} p^n u_n(\tau, \xi) = \frac{1}{\left(1 + e^{\left(\frac{\tau}{\sqrt{2}}\right)}\right)} - p \left[L^{-1} \left\{ \left(\sum_{n=0}^{\infty} p^n u_n(\tau, \xi) \right)_{\tau\tau} - \sum_{n=0}^{\infty} p^n H_n(u) \right\} \right] - p \left[L^{-1} \left\{ \sum_{n=0}^{\infty} p^n u_n(\tau, \xi) \right\} \right],$$

where

$$\sum_{n=0}^{\infty} p^n H_n(u) = u^3.$$

The components of homotopy polynomials are given by

$$\begin{aligned} H_0(u) &= u_0^3, \\ H_1(u) &= 3u_0^2 u_1, \\ H_2(u) &= 3u_0^2 u_2 + 3u_1^2 u_0. \end{aligned}$$

Solving the above equations, we have

$$\begin{aligned} u_0(\tau, \xi) &= \frac{1}{1 + e^{\left(\frac{\tau}{\sqrt{2}}\right)}}, \\ u_1(\tau, \xi) &= \frac{3e^{\left(\frac{\tau}{\sqrt{2}}\right)} \xi^\alpha}{2 \left(1 + e^{\left(\frac{\tau}{\sqrt{2}}\right)}\right)^2 \Gamma(\alpha + 1)}, \\ u_2(\tau, \xi) &= \frac{\xi^{2\alpha}}{\Gamma(2\alpha + 1)} \left\{ \frac{9e^{\left(\frac{\tau}{\sqrt{2}}\right)}}{4 \left(1 + e^{\left(\frac{\tau}{\sqrt{2}}\right)}\right)^2} - \frac{9 \left(e^{\left(\frac{\tau}{\sqrt{2}}\right)}\right)^2}{2 \left(1 + e^{\left(\frac{\tau}{\sqrt{2}}\right)}\right)^3} \right. \\ &\quad \left. + \frac{9 \left(e^{\left(\frac{\tau}{\sqrt{2}}\right)}\right)^3}{2 \left(1 + e^{\left(\frac{\tau}{\sqrt{2}}\right)}\right)^4} - \frac{9e^{\left(\frac{\tau}{\sqrt{2}}\right)}}{2 \left(1 + e^{\left(\frac{\tau}{\sqrt{2}}\right)}\right)^4} \right\}, \\ u_3(\tau, \xi) &= \frac{\xi^{3\alpha}}{\Gamma(3\alpha + 1)} \left\{ \frac{27e^{\left(\frac{\tau}{\sqrt{2}}\right)}}{8 \left(1 + e^{\left(\frac{\tau}{\sqrt{2}}\right)}\right)^2} - \frac{81 \left(e^{\left(\frac{\tau}{\sqrt{2}}\right)}\right)^2}{4 \left(1 + e^{\left(\frac{\tau}{\sqrt{2}}\right)}\right)^3} + \frac{261 \left(e^{\left(\frac{\tau}{\sqrt{2}}\right)}\right)^3}{4 \left(1 + e^{\left(\frac{\tau}{\sqrt{2}}\right)}\right)^4} \right\} \end{aligned}$$

$$\begin{aligned}
 & \left. - \frac{90 \left(e^{\left(\frac{\tau}{\sqrt{2}} \right)} \right)^4}{\left(1 + e^{\left(\frac{\tau}{\sqrt{2}} \right)} \right)^5} \right\} + \frac{\xi^{3\alpha}}{\Gamma(3\alpha + 1)} \left\{ \frac{45 \left(e^{\left(\frac{\tau}{\sqrt{2}} \right)} \right)^5}{\left(1 + e^{\left(\frac{\tau}{\sqrt{2}} \right)} \right)^6} - \frac{27 e^{\left(\frac{\tau}{\sqrt{2}} \right)}}{2 \left(1 + e^{\left(\frac{\tau}{\sqrt{2}} \right)} \right)^4} \right. \\
 & \left. + \frac{81 \left(e^{\left(\frac{\tau}{\sqrt{2}} \right)} \right)^2}{2 \left(1 + e^{\left(\frac{\tau}{\sqrt{2}} \right)} \right)^5} - \frac{117 \left(e^{\left(\frac{\tau}{\sqrt{2}} \right)} \right)^3}{2 \left(1 + e^{\left(\frac{\tau}{\sqrt{2}} \right)} \right)^6} + \frac{27 e^{\left(\frac{\tau}{\sqrt{2}} \right)}}{2 \left(1 + e^{\left(\frac{\tau}{\sqrt{2}} \right)} \right)^6} \right\} \\
 & - \frac{\Gamma(2\alpha + 1) \xi^{3\alpha}}{\Gamma(3\alpha + 1)} \left\{ \frac{27 \left(e^{\left(\frac{\tau}{\sqrt{2}} \right)} \right)^2}{4 \left(1 + e^{\left(\frac{\tau}{\sqrt{2}} \right)} \right)^5} \right\},
 \end{aligned}$$

in the same way, all $u_n(\tau, \xi)$ can be obtained. Thus, the approximate solution is

$$u(\tau, \xi) = u_0(\tau, \xi) + u_1(\tau, \xi) + u_2(\tau, \xi) + \dots .$$

Example 5.2 Consider Eq. (2) subject to the initial condition given as

$$u(\tau, 0) = \frac{1}{1 + e^{\left(-\frac{\tau}{\sqrt{2}} \right)}}. \tag{14}$$

The solution in closed form as in [9] is $\frac{1}{1 + e^{\left(-\frac{\tau}{\sqrt{2}} - \frac{3\xi}{2} \right)}}$.

Following the process as in Example 5.1, the components of homotopy polynomials are given by

$$\begin{aligned}
 H_0(u) &= u_0^3, \\
 H_1(u) &= 3u_0^2 u_1, \\
 H_2(u) &= 3u_0^2 u_2 + 3u_1^2 u_0,
 \end{aligned}$$

we have the following iterates of solution

$$\begin{aligned}
 u_0(\tau, \xi) &= \frac{1}{1 + e^{\left(-\frac{\tau}{\sqrt{2}} \right)}}, \\
 u_1(\tau, \xi) &= \frac{3e^{\left(-\frac{\tau}{\sqrt{2}} \right)} \xi^\alpha}{2 \left(1 + e^{\left(-\frac{\tau}{\sqrt{2}} \right)} \right)^2 \Gamma(\alpha + 1)},
 \end{aligned}$$

$$\begin{aligned}
u_2(\tau, \xi) &= \frac{\xi^{2\alpha}}{\Gamma(2\alpha + 1)} \left\{ \frac{9e^{(-\frac{\tau}{\sqrt{2}})}}{4\left(1 + e^{(-\frac{\tau}{\sqrt{2}})}\right)^2} - \frac{9\left(e^{(-\frac{\tau}{\sqrt{2}})}\right)^2}{2\left(1 + e^{(-\frac{\tau}{\sqrt{2}})}\right)^3} \right. \\
&\quad \left. + \frac{9\left(e^{(-\frac{\tau}{\sqrt{2}})}\right)^3}{2\left(1 + e^{(-\frac{\tau}{\sqrt{2}})}\right)^4} - \frac{9e^{(-\frac{\tau}{\sqrt{2}})}}{2\left(1 + e^{(-\frac{\tau}{\sqrt{2}})}\right)^4} \right\}, \\
u_3(\tau, \xi) &= \frac{\xi^{3\alpha}}{\Gamma(3\alpha + 1)} \left\{ \frac{27e^{(-\frac{\tau}{\sqrt{2}})}}{8\left(1 + e^{(-\frac{\tau}{\sqrt{2}})}\right)^2} - \frac{81\left(e^{(-\frac{\tau}{\sqrt{2}})}\right)^2}{4\left(1 + e^{(-\frac{\tau}{\sqrt{2}})}\right)^3} + \frac{261\left(e^{(-\frac{\tau}{\sqrt{2}})}\right)^3}{4\left(1 + e^{(-\frac{\tau}{\sqrt{2}})}\right)^4} \right. \\
&\quad \left. - \frac{90\left(e^{(-\frac{\tau}{\sqrt{2}})}\right)^4}{\left(1 + e^{(-\frac{\tau}{\sqrt{2}})}\right)^5} \right\} - \frac{\Gamma(2\alpha + 1)\xi^{3\alpha}}{\Gamma(3\alpha + 1)} \left\{ \frac{27\left(e^{(-\frac{\tau}{\sqrt{2}})}\right)^2}{4\left(1 + e^{(-\frac{\tau}{\sqrt{2}})}\right)^5} \right\}
\end{aligned}$$

in this way, all $u_n(\tau, \xi)$ can be obtained. Thus, the approximate solution is

$$u(\tau, \xi) = u_0(\tau, \xi) + u_1(\tau, \xi) + u_2(\tau, \xi) + \dots$$

6 Results and Discussion

In Figs. 1a–c and 3a–c, the three-dimensional behavior of solutions is presented for Examples 5.1 and 5.2, respectively. The graphical results show the accuracy of the suggested technique. The accuracy of the results can be improved by finding more approximations. We can see from Figs. 2 and 4 that the fractional-order affects Eq. (2). Figures 2 and 4 demonstrate the nature of $u(\tau, \xi)$ w.r.t ξ for different values of α for Examples 5.1 and 5.2, respectively, and we notice that as α increases $u(\tau, \xi)$ decreases for Example 5.1 and for Example 5.2, in beginning on increasing the value of α , $u(\tau, \xi)$ decreases but soon, the distance starts increasing on increasing the value of α .

Fig. 1 **a** Exact solution for Example 5.1. **b** Approximate solution at $\alpha = 1$ for Example 5.1. **c** Absolute error for Example 5.1

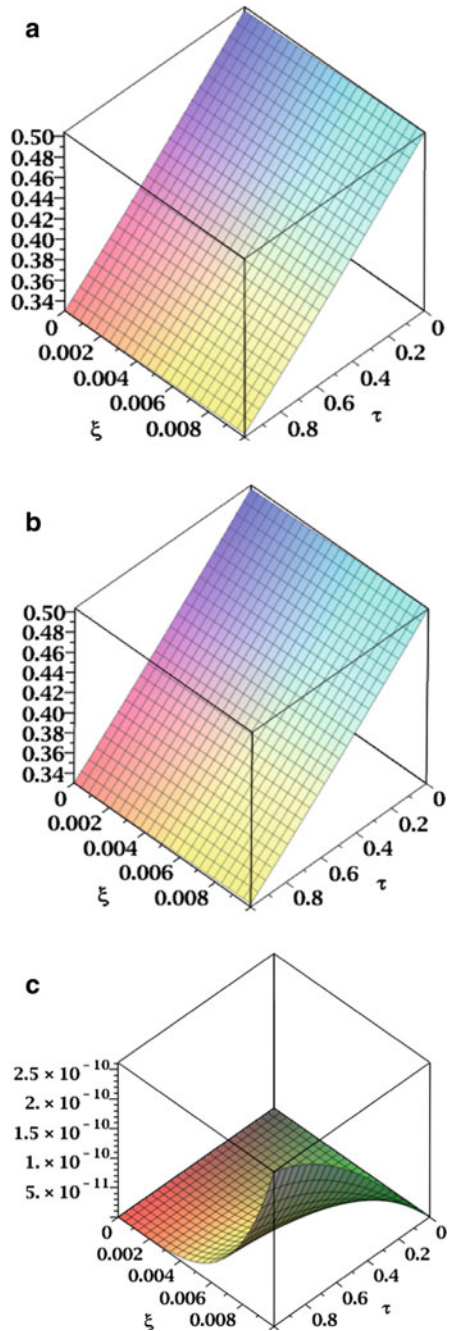
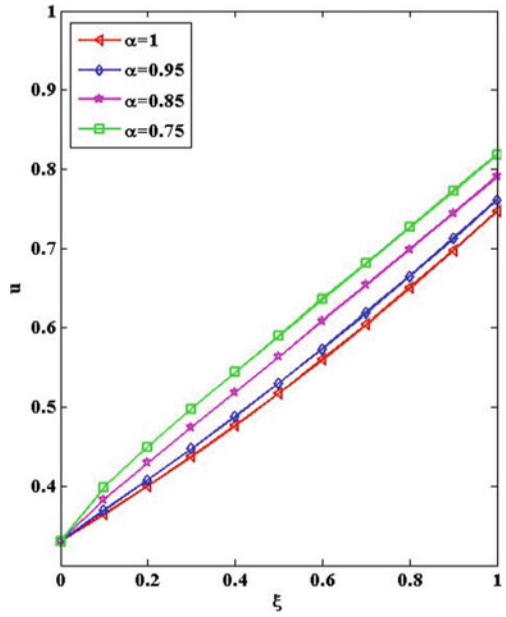


Fig. 2 Plots of the approximate solution w.r.t time ξ for different α for Example 5.1



7 Conclusion

In this work, HPTT is used to study the time-fractional CAE and to handle the computational difficulties which emerge due to the nonlocality of the fractional-order mathematical models. It can be concluded that the investigated fractional CAE and other similar dynamical models efficiently describe the natural phenomena. The proposed technique is a novel powerful technique with high accuracy to investigate various real-world problems.

Fig. 3 **a** Exact solution for Example 5.2. **b** Approximate solution at $\alpha = 1$ for Example 5.2. **c** Absolute error for Example 5.2

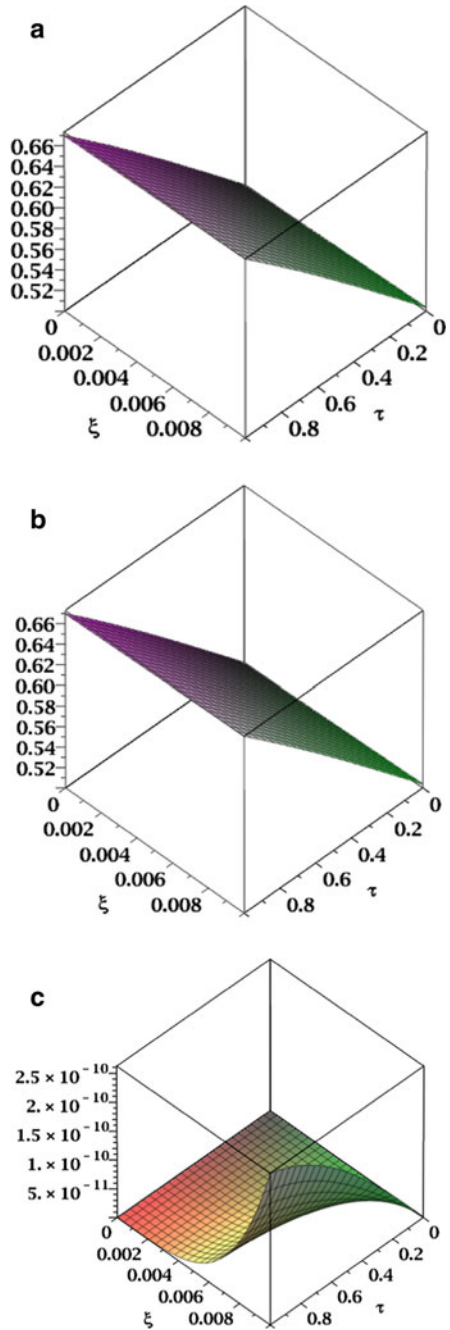
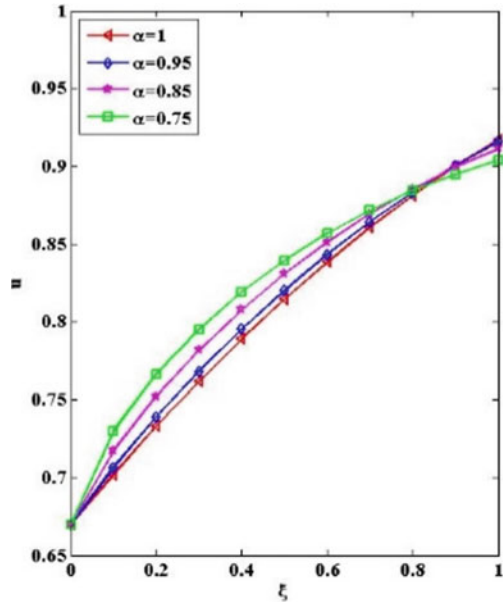


Fig. 4 Plots of the approximate solution w.r.t time ξ for different α for Example 5.2



References

1. Podlubny I (1999) Fractional differential equations. Academic Press, San Diego
2. Kilbas A, Srivastava HM, Trujillo JJ (2006) Theory and applications of fractional differential equations. North-Holland mathematical studies. Elsevier Publications, p 204
3. Jingtang M, Liu J, Zhou Z (2014) Convergence analysis of moving finite element methods for space fractional differential equations. J Comput Appl Math 255:661–670
4. Gupta PK (2011) Approximate analytical solutions of fractional Benney-Lin equation by reduced differential transform method and the homotopy perturbation method. Comput Math Appl 58:2829–2842
5. Hammouch Z, Mekkaoui T (2013) Approximate analytical and numerical solutions to fractional KPP-like equations. Gen. Math Notes. 14(2):1–9
6. Hammouch Z, Mekkaoui T (2012) A Laplace-Variational Iteration method for solving the homogeneous Smoluchowski coagulation equation. Appl Math Sci 6(18):879–886
7. Prakash A, Kumar M, Baleanu D (2018) A new iterative technique for a fractional model of nonlinear Zakharov-Kuznetsov equations via Sumudu transform. Appl Math Comput. 334:30–40
8. Hariharan G (2009) Haar wavelet method for solving Cahn-Allen equation. Appl Math Sci 3:2523–2533
9. Esen A, Yagmurlu NM, Tasbozan O (2013) Approximate analytical solution to time-fractional damped Burger and Cahn-Allen equations. Appl Math Inf Sci 7(5):1951–1956
10. Tariq H, Akram G (2017) New travelling wave exact and approximate solutions for the nonlinear Cahn Allen equation: evolution of nonconserved quantity. Nonlinear Dyn 88:581–594
11. Rawashdeh, MS (2017) A reliable method for the space-time fractional Burgers and time-fractional Cahn-Allen equations via the FRDTM. Adv Diff Equ 99
12. He JH (1999) Homotopy perturbation technique. Comput Methods Appl Mech Eng 178:257–262
13. Sakar MG, Uludag F, Erdogan F (2016) Numerical solution of time-fractional nonlinear PDEs with proportional delays by homotopy perturbation method. Appl Math Model 40:6639–6649

14. Prakash A, Kaur H (2017) Numerical solution for fractional model of Fokker-Planck equation by using q-HATM. *Chaos Solitons Fractals* 105:99–110
15. Gomez-Aguilar JF, Yopez-Martinez H, Torres-Jimenez J, Cordova-Fraga T, Escobar-Jimenez RF, Olivares-Peregrino VH (2017) Homotopy perturbation transform method for nonlinear differential equations involving to fractional operator with exponential kernel. *Adv Differ Equ* 68

Image Colorization with Deep Convolutional Neural Networks



Sudesh Pahal and Preeti Sehrawat

Abstract Colorization, a task of coloring monochrome images or videos, plays an important role in the human perception of visual information, to black and white pictures or videos. Colorizing, when done manually in Photoshop, a single picture might take months to get exactly correct. Understanding the tediousness of the task and inspired by the benefits of artificial intelligence, we propose a mechanism to automate the coloring process with the help of convolutional neural networks (CNNs). Firstly, an Alpha version is developed which successfully works on trained images but fails to colorize images, and the network has never seen before. Subsequently, a Beta version is implemented which is able to overcome the limitations of Alpha version and works well for untrained images. To further enhance the network, we fused the deep CNN with a classifier called Inception ResNet V2 which is a pre-trained model. Finally, the training results are observed for all the versions followed by a comparative analysis for trained and untrained images.

Keywords Colorization · Image classification · Convolutional neural networks · Resnet · Keras

1 Introduction

Colorization is the process of introducing hues black and white images or videos. There exist a large number of historic photographs and videos which contain insufficient amount of colors and luminance information. Colorizing those images will help us in recreating those moments and a better perception of the old times. The rapid progress in multimedia application computer technology has resulted in a rapid increase in digital image use. The rich knowledge contained a wide range of uses including crime prevention, military, home entertainment, education, and cultural heritage are used in this data collection and medical diagnosis. It is a very challenging task to make efficient use of this information, to explore and analyze the vast

S. Pahal (✉) · P. Sehrawat
Maharaja Surajmal Institute of Technology, New Delhi 110058, India
e-mail: sudeshpahal@msit.in

© Springer Nature Singapore Pte Ltd. 2021
G. S. Hura et al. (eds.), *Advances in Communication and Computational Technology*, Lecture Notes in Electrical Engineering 668,
https://doi.org/10.1007/978-981-15-5341-7_4

volume of image data. Although the human visual system can interpret hue information more accurately than the monochrome information, the colorization process can add value to the monochrome images and TV programs. Up until now, colorizing has been done manually by Photoshop which is not so effective and time consuming as well.

With the help of deep learning and convolutional neural networks (CNN), this process is automated by providing more information and context about the image. CNNs are deep artificial networks that are primarily used for object classification and recognition. The layered architecture of CNN helps us in recognizing object patterns. The deeper we move into the network more the patterns are detected and objects get recognized [1]. There are many methods which have been successfully able to colorize grayscale images. Such approaches can be loosely categorized into two groups: one in which an individual pixel is assigned a color based on its brightness, as derived from a color image of relevant content, and the other in which the image is fragmented into regions, that are each then allocated a single color. This paper is based on a previous approach: We evaluate the color material of the training image and then try to anticipate colorized version on a per-pixel basis for a single target grayscale image. Whereas segmentation methods have an inherent attraction and could consequence in more coherent colorization, and these methods depend on accurate image segmentation, which can be discarded by shadows, lighting effects, or color gradients. Furthermore, training color sets are selected for manual identification of the objects in a scene.

One of the major problems in the colorization is that two objects with different colors may appear to have the same color in grayscale mode. One simple solution for this problem is to seek user inputs for colors. However, doing so will make this solution very tedious as it requires the user to repaint all the segments of the image. Most of the automatic colorization techniques are computationally expensive. The objective of our approach is to efficiently automate the process by training a machine learning model on a relatively small corpus of training images. For this research work, we work in the LAB color space instead of RGB, where L stands for luminance, A and B for chrominance. Hence, the input to our algorithm is the grayscale image which is L and the output would be A and B.

This paper is structured as follows: Sect. 1 discusses the history of CNN and its importance to colorization. Section 2 provides a comprehensive of the work concerned in this field. The planned work is explained in detail in Sect. 3. First, we have introduced the Alpha version to colorize grayscale images, then we have enhanced the Beta version by adding a function extractor to it, and in our final version, we have loaded the weights from the inception resnet template to boost our image classifier. Section 4 describes the findings presented followed by the interpretation and possible context in Sect. 5.

2 Literature Survey

A number of researchers are doing research in this field to provide effective solutions for colorizing grayscale images. Welsh et al. [2] suggested a quasi-automatic shading process images using reference images and providing variations to the luminance values of images. This method uses the luminance values of the adjacent pixels into the focus picture and fills colors from the corresponding location in the reference image, but the user must find a reference image containing colors in the desired regions. Matching quality is enhanced by taking advantage of the qualities and structures of the luminance of the surrounding pixels. These color exchange strategies provide adequate coloring productivity, stipulated that the input image has unique luminance standards or graphics around the edge of the element. An alternative solution is to enable the client to allocate colors to certain pixels and to perpetuate those colors to the surviving pixels. The propagation problem is formulated by reducing the polynomial value function, which means that neighboring pixels with similar intensity should have similar shades [3]. Here, the user chooses colors directly and is able to refine the results by scribbling more colors in the image. This methodology was particularly helpful in colorizing animation and cartoon movies.

In [4], the colors of the reference pixels are mixed to decorate the destination pixel centered on the geodesic range from the outlet pixels to the destination pixel. Geode range tests the variance of the luminance from either the reference pixel to the destination pixel across the route. However, spread basic schemes could generate obscuring mistakes in color and their performance is significantly affected by the location of color sources. Deshpande et al. [5] presented the colorizing as linear problem.

Another significant approach is used in [6] where a user is asked for color values onto specific pixels and these are then used to colorize the image. Although effective, this is very tedious task as it asks for user to help again and again. While image segmentation is an intriguing approach which can lead to erroneous results when dealing with background clutter, dissimilar patterns, and non-identical hues. The task of colorizing the images can be automated using machine learning [7]. By automating this process not only computational cost and time is reduced but it also is known to decrease the error rate by half. Inspired by the above-mentioned issues related to colorization and benefits of machine learning,

We design a system that incorporates a deep convolutionary neural network recruited from ground up with strong-level characteristics extracted from a pre-trained Inception ResNet-v2 model. Our approach aims to efficiently transfer the machine learning output to colorize the image. It is done by training our machine on small training data and thereby reducing computational cost of the system.

3 Proposed Models

3.1 Alpha Model

This is the most basic version of our neural network that effectively colorizes trained images (Fig. 1). First, we changed the color channels from RGB to LAB using a pre-defined algorithm. L holds for brightness, as well as a and b for hues of red and blue, yellow. Its laboratory encrypted image has one layer of grayscale and three layers of shadow have been packed into two layers. It implies that we could use the first grayscale picture in our final expectations. Convolutional filters are used between input and output values to tie them together, a convolutionary neural network [8, 9]. Each filter extracts some of the information from the picture.

The system could either make a new picture from either a filter or incorporate a range of filters into a single picture. Throughout the case of a convolutionary neural network, each filter is adjusted instantly to assist with just the expected result.

Hundreds of filters are then stacked and narrowed down to two layers, namely a and b. The neural network then predicts values based on the grayscale input. The predicted values are then mapped with the real values. The real color parameters are from -128 to 128 , that is the preferred period for just the LAB color space. We use the Tanh activation function to map the predicted values. You offer the Tanh function for a certain value, it returns -1 to 1 . This allows us to compare our prediction error. The network keeps revising the filters to reduce the final error and keeps iterating until the error is minimum. The convolutional network then produces colorized version based on images learned from past.

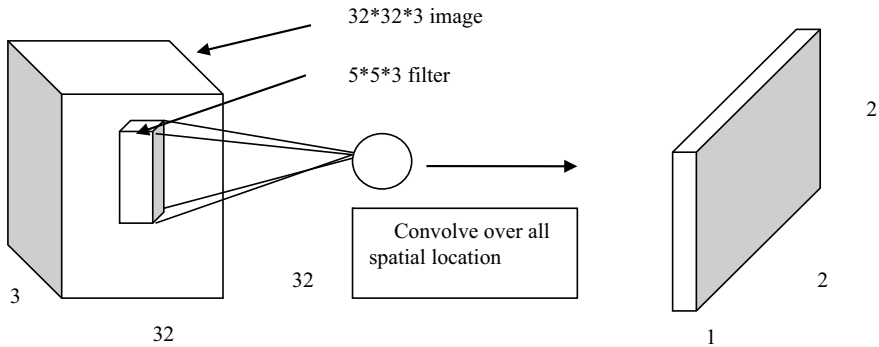


Fig. 1 Process of convolution

3.2 *Beta Model*

In Alpha colorization, we have been successful to colorize an image that network has been trained on. However, for the images that it has not been trained on it shows a poor result. In the development of the beta version, the objective is to generalize our network and teach the network to color the image that you have not seen before. For this process, feature extractor [10] is used which find the link between the grayscale images and their colored images.

Firstly, simple patterns including a diagonal line, all black pixels and other similar patterns are considered. In each square (filter), we look for similar patterns and will remove the pixels that do not match. By doing this, we will generate as many images as number of filters. Scanning those images will yield similar patterns that are already detected by the network. Reducing image size will also be helpful in detecting patterns. With these filters, a nine pixel (3 * 3 filters) layer is obtained. Combining these with low-level filters, we will be able to detect more complex patterns. Many shapes like half circle, a small dot, or a line will be formed and it will generate 128 new filtered images. First, low-level features like edges, curved are formed, and these are then combined into patterns, details, and will eventually result into output. Our network is operating in a trial and error manner. Initially, random estimates are made for each pixel. On the assumption of an error for per each pixel, it operates backwards through the network to improve the extraction of the functionality. In this case, the source of largest errors is in locating the pixels and deciding whether to color it or not. Then all items are colored brown, because this color is most identical to any other color and produces the smallest error. Since most of the training dataset is identical, the system is trying to deal with different objects. More tones of brown would be there in the colorized version and it will fail to generate more nuanced colors as shown in Fig. 2. The major difference from certain visual networks is the significance of pixel positioning. For coloring networks, the width or proportion

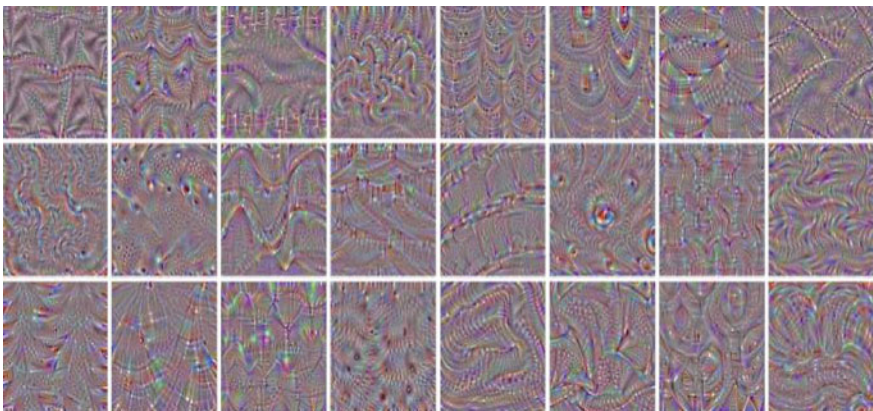


Fig. 2 Deep visualization

of the picture remains the same across the network. Coloring does not cause any distortion in the final image created while the image becomes blurred the closer it moves to the final layer in traditional networks.

In classification networks, the max-pooling layers increase the density of information but also distort the image. It values are only the information, but not an image's layout. Instead, we use a step of 2 in these networks to reduce the width and height by half. This increases the density of information, but does not distort the image. Only the final classification is concerned with classification networks. They therefore continue to reduce the size and quality of the image as it traverses through the network. The ratio of the image is maintained by appending the white padding as shown above; otherwise, each convolutionary layer cuts the images.

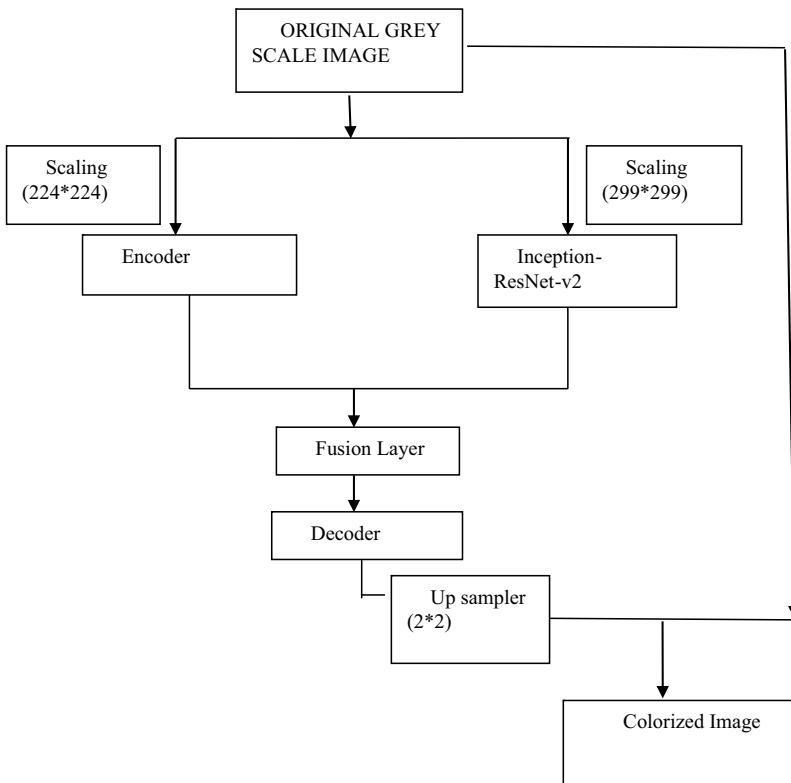


Fig. 3 System model

3.3 Full Model

The final colorization neural network is depicted in Fig. 3 which is built of four main components—encoder, decoder, fusion layer in between and a classifier running in parallel. The classification layer is extracted from the Inception ResNet V2 [11, 12] and fused with the output of encoder.

Our deep CNN is built from scratch whereas the classifier is a pre-trained model. Thus, the classifier helps in identifying objects in the picture well and thus matching the object representation to the corresponding color scheme. We use **E**, the one with the fusion layer which is easy to understand and reproduce in Keras. While the deep CNN is trained from scratch, Inception ResNet-v2 is used as a high-level extractor of features that provides information about the content of images that can help colorize them. The pictures considered in the CIE $L^*a^*b^*$ color space are of size H/W . Starting with the luminance component $XL/RH \times W \times 1$, our model aims to get estimate of the remaining components in order to result into a fully colored version $X^{\sim} \in RH \times W \times 3$. In short, it is assumed that there is a mapping of F such that $F: XL \rightarrow (X^{\sim} a, X^{\sim} b)$, (1) where $X^{\sim} a, X^{\sim} b$ are the a^*, b^* components of the reconstructed image, which combined with the input provide the approximate colored image $X^{\sim} = (XL, X^{\sim} a, X^{\sim} b)$. The proposed architecture is based entirely on CNNs, an effective model that has been extensively used by researchers in the literature, to be independent of the size of the input. In short, a convolutionary layer is a set of short, learnable filters in the input image that fit specific local patterns. Near-input layers search for simple patterns such as contours, while those closer to the output extract more complex characteristics.

We select the CIE $L^*a^*b^*$ color space to represent the input images as it distinguishes the characteristics of color from the luminance comprising the main image characteristics. The combination of the luminance with the color components is guaranteed that the final reconstructed picture has a high level of detail. The model estimates that it is a^*b^* component given the luminance component of an image and combines it with the input to obtain the final approximation of the colored image. We use an Inception-ResNetv2 (referred to as Inception) network instead of training a feature extraction branch from scratch in order to get the grayscale image embedded from its last layer. The network is logically divided into four major components. The feature's encoding and extraction components, respectively, obtain mid-level and high-level features which are then fused into the fusion layer. Lastly, to estimate output, these features are exploited by decoder. The function of each component is given below.

Preprocessing The pixel values are centered and scaled depending on their respective ranges for all three image components. The values are achieved within the interval of $[-1, 1]$ in order to ensure correct learning.

Encoder The encoder processes grayscale images from $H \times W$ and gives output in form of a representation of features from $H/8 \times W/8 \times 512$. It makes use of 8 convolutionary layers with 3×3 kernels for this purpose. Padding is used to preserve

the layer's input width. In addition, the first, third and fifth layers implement a step of 2, thus reduce their output dimension by half and decrease the total number of computations needed.

Feature Extractor High-level elements, e.g., underwater or indoor scene, convey information about objects that can be used in the coloring process. We have used a pre-trained model of Inception to extract an image embedding. First, the image of the input is scaled to 299×299 . Instead, we have stacked the image with it to get a three-channel image to fulfill the dimensional requirements of Inception. First, we feed into the network the resulting image and extract the final layer output prior to the softmax function. It gives output in an embedding of $1001 \times 1 \times 1$.

Fusion The fusion layer takes the function vector from Inception, replicates it twice in $HW/8$ and adds it to the encoder's volume of features along the axis of depth. This approach provides a single volume with the encoded image and the mid-level characteristics of the shape $H/8 \times H/8 \times 1257$. By concatenating and mirroring the feature vector multiple times, it is guaranteed that the semantic information transmitted by the feature vector has uniform distribution across the entire image's spatial region. In addition, this approach also makes arbitrary input image sizes robust, increasing the versatility of the model. Ultimately, we apply 256 size 1×1 , convolution kernels, effectively producing a $H/8 \times W/8 \times 256$ feature dimension.

Decoder Lastly, the decoder applies a sequence of convolutionary and up-sampling layers to the volume $H/8 \times W/8 \times 256$ to have final layer with dimensions $H \times W \times 2$. Up-sampling is achieved by the use of the closest basic approach to the neighbor in order to get twice height and width of the output when compared with the source.

By minimizing an objective function specified over the estimated output and the target output, the optimal model parameters are determined. We use the mean square error metric between the predicted pixel colors in $a * b *$ space and the actual values to measure the design loss. For a particular picture X , the mean square error is given by,

$$C(X, \theta) = \frac{1}{2HW} \sum_{k \in (a,b)} \sum_{i=1}^H \sum_{j=1}^W \left(X_{k,i,j} - \tilde{X}_{k,i,j} \right)^2$$

where θ represents all model parameters, $X_{k,i,j}$ and $\tilde{X}_{k,i,j}$ denote the i, j th pixel values of the k th component of the target and the reconstructed image, respectively. This can easily be extended to a batch B by averaging the cost among all images in the batch, i.e., $1/|B| \sum_{X \in B} C(X, \theta)$. This loss is propagated back during learning to update the parameters of the model using Adam optimizer with an initial learning rate of $\eta = 0.001$. We enforce a fixed image size during training to allow batch processing.

4 Simulation Results

The proposed architecture is implemented with Keras and Tensorflow backend (with Python 3.0 version). The implementation details for the CNN are as follows:

- Model: Convolutional neural network
- Dataset: Public dataset imported from unsplash
- Optimizer: RMSProp(alpha and beta version) and Adam optimizer(full version).
- Activation function: RELU
- Loss: MSE
- Colorspace: Lab
- Layers: Kernels of size 2×2 with stride of 2(beta version) and Kernel of size 1×1 (full version).

4.1 Alpha Model

The output for trained and untrained images for Alpha model is illustrated in Fig. 4 which implies that in case of colorizing trained images; Alpha version successfully recreates the exact colors as in the original image.

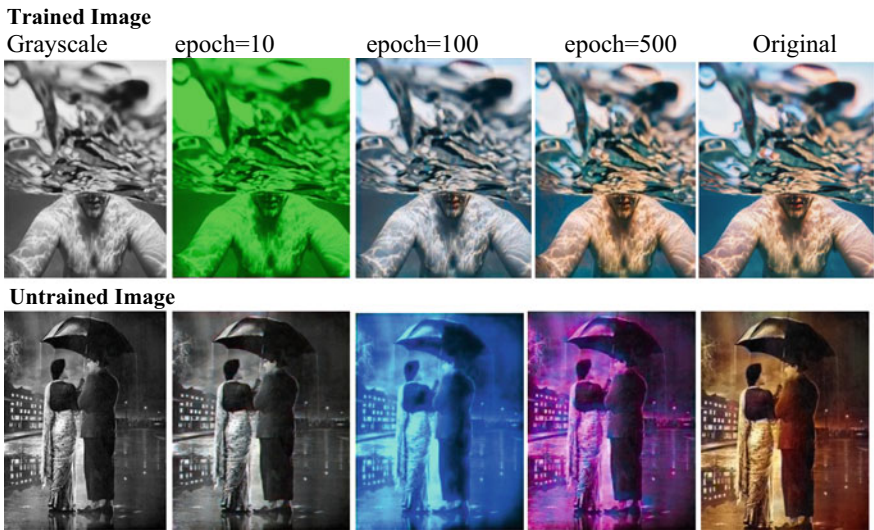


Fig. 4 Output for Alpha model

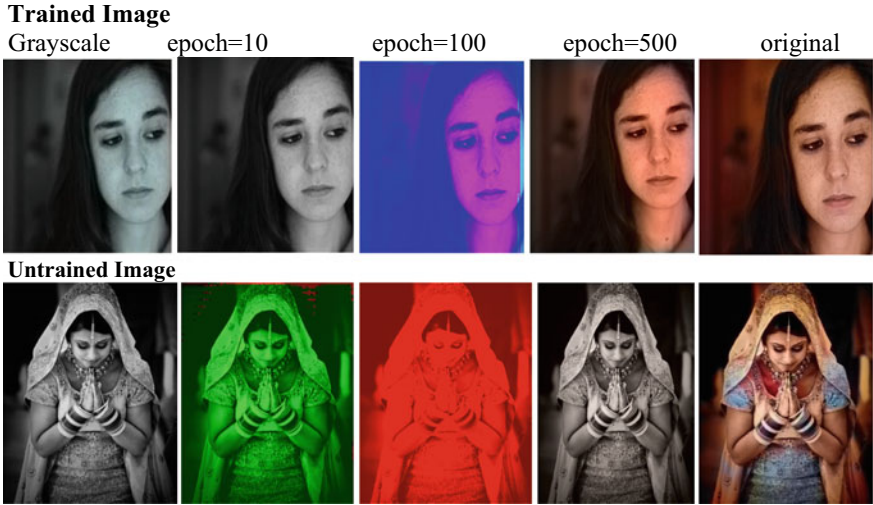


Fig. 5 Output for Beta model

4.2 Beta Model

The output for trained and untrained images for Beta model is illustrated in Fig. 5. In case of trained images, the Beta version correctly colorizes the image even though the input given to the network was black and white.

4.3 Proposed Full Model

We have applied a 254-filtered convolutional network with a 1×1 kernel, the final output of the fusion layer. To prevent the overflowing of memory, we have run 500 iterations with a batch size of 20 images at a time. Although our validation set was quite small, however, running it on larger and more diverse datasets will give more consistent and evolved results. The output for trained and untrained images for proposed model is illustrated in Fig. 6.

5 Conclusion

This paper implements deep learning convolutional neural architecture which is suitable for colorizing black and white images. The proposed model has been successfully able to colorize back and white images up to a perceptive ability of around 80%. However, there is still room for improvement in coloring the image with great

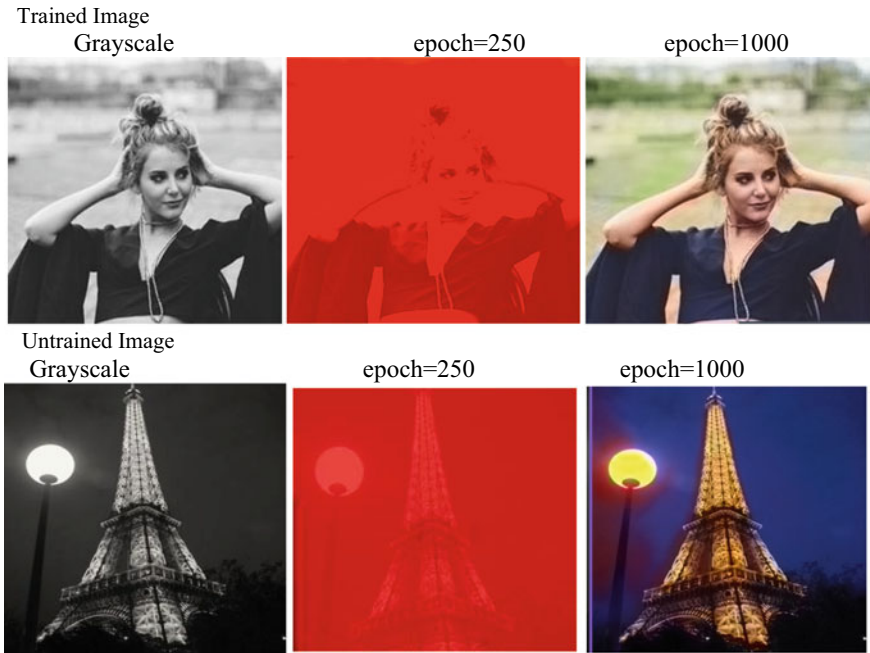


Fig. 6 Output for proposed model

details and background clutter. For the future work, we would recommend running this model on other pre-trained models and different datasets. Also it would be interesting to see its application on video segments. Various changes and hybridization of technologies in the architecture of neural networks is still a field to be explored.

References

1. Burns G, Colorization. Museum of broadcast communications: The Encyclopedia of Television. <http://www.museum.tv/archives/etv/index.html>
2. Welsh T, Ashikhmin M, Mueller K (2002) Transferring color to greyscale images. *ACM Trans Graph* 21(3):277–280
3. Levin A, Lischinski D, Weiss Y (2004) Colorization using optimization. In: *Proceedings ACM SIGGRAPH conference*, pp 689–694
4. Yatziv L, Sapiro G (2006) Fast image and video colorization using chrominance blending. *Trans Img Proc* 15(5):1120–1129
5. Deshpande A, Rock J, Forsyth D (2015) Learning large-scale automatic image colorization. In: *Proceedings of the IEEE international conference on computer vision*, pp 567–575
6. Chia AYS, Zhuo S, Gupta RK, Tai YW, Cho SY, Tan P, Lin S (2011) Semantic colorization with internet images. In: *TOG*, vol. 30 no 6, ACM, p 156
7. He K, Zhang X, Ren S, Sun J (2015) Delving deep into rectifiers: Surpassing human-level performance on imagenet classification. In: *Proceedings of the IEEE international conference on computer vision*, pp 1026–1034

8. Simonyan K, Zisserman A (2014) Very deep convolutional networks for large-scale image recognition. CoRR abs/1409.1556
9. Zeiler MD, Fergus R (2014) Visualizing and understanding convolutional networks. In: European conference on computer vision, Springer, pp 818–833
10. Iizuka S, Simo-Serra E, Ishikawa H (2016) Let there be color!: joint end-to-end learning of global and local image priors for automatic image colorization with simultaneous classification. *ACM Trans Graph (TOG)* 35(4):110
11. Szegedy C, Ioffe S, Vanhoucke V, Alemi AA (2017) Inception-v4, inception-resnet and the impact of residual connections on learning. In: *AAAI*, vol. 4, p 12
12. He K, Zhang X, Ren S, Sun J (2016) Deep residual learning for image recognition. In: *Proceedings of the IEEE conference on computer vision and pattern recognition*, pp 770–778

Electroencephalogram Based Biometric System: A Review



Kaliraman Bhawna, Priyanka, and Manoj Duhan

Abstract EEG signals can be preferred as a biometric trait because of their uniqueness, robustness to spoof attacks, and many other advantages as compared to other commonly used identifiers such as finger print, palm print, and face recognition. A complete overview of biometric systems based on EEG signals, their acquisition, pre-processing, feature extraction, and classification at different frequency bands is presented in this paper. Comparison is made between various techniques and their efficiencies used in EEG-based biometric systems. Different signal acquisition methods (resting state, visual stimuli, cognitive activities) used in previous works have been discussed with their pros and cons. Nowadays researchers focus on low-cost EEG acquisition systems with a smaller number of electrodes with better accuracy. Databases used in this area are also discussed, some of them are public and some authors acquire their personal data. A table is provided which compares the results of different signal acquisition methods, pre-processing techniques, feature extraction, and classification techniques.

Keywords Electroencephalogram (EEG) · Biometrics · Biomedical signal processing · Resting state with eyes closed (REC) · Resting state with eyes open (REO)

K. Bhawna (✉) · Priyanka · M. Duhan
Department of Electronics and Communication Engineering, Deenbandhu Chhotu Ram Institute of Science and Technology, Murthal, Haryana 131039, India
e-mail: bhawna.kaliraman5@gmail.com

Priyanka
e-mail: priyankaiit@yahoo.co.in

M. Duhan
e-mail: duhan.manoj@gmail.com

1 Introduction

Nowadays, with the increasing demand of security, biometric traits are used in personal identification instead of other conventional methods such as ID cards, keys, and passwords which can be easily lost, stolen, and forged. For this purpose, different kinds of biometrics have been proposed such as fingerprint, palmprint, hand geometry, iris, face, voice, electroencephalogram (EEG), and electrocardiogram (ECG). The EEG signals are brain signals which are used as a biometric trait for personal identification because of their uniqueness (i.e., different persons have different EEG patterns while performing same activity), robustness against spoofing attacks, hard to mimic, and people having physical disabilities are not excluded in this kind of system [1]. Active EEG recordings can be acquired from living subject with the normal mental condition and no one can force the subject to provide desired EEG signals which was obtained in the normal state. Further EEG's are recorded non-invasively from the scalp. EEGs are recorded from voltage differences on the scalp which is produced by currents spreading on the scalp. This current is produced by the electrical activity of active nerve cells in the brain. Some standard EEG wave frequency bands are discussed in Table 1. Researches have proved that Alpha and Beta rhythms contain pertinent individual-specific characteristic.

This paper has been organized in five sections as shown in Fig. 1. Section 1 gives introduction. In Sect. 2, different signal acquisition protocols are discussed which include three subfields, i.e., signals acquired in resting state, signals acquired by exposure of visual stimuli, and signals acquired by performing different cognitive activities. In Sect. 3, different pre-processing techniques are presented. Fourth section emphasises on different feature extraction techniques and the last section covers different classification techniques that are used for EEG-based processing.

Table 1 Standard EEG frequency bands

Rhythm	Frequency band (Hz)	Description
Delta(δ)	<4	Concerned with deep sleep or loss of body awareness
Theta (θ)	<7	Waking state of young children, deep meditation, and in dreaming sleep
Alpha (α)	8–15	Relaxed state, awake with eyes closed
Beta (β)	16–31	Concerned with active or anxious thinking, alert state
Gamma (γ)	>32	Shows event brain synchronization and associated with cognitive or motor activities



Fig. 1 EEG-based biometric system

2 EEG Signal Acquisition

Signal acquisition is the first step used in any biometric system. This paper discusses different EEG signal acquisition protocols. EEG recordings are non-invasive, i.e., electrodes are located over the scalp to acquire EEG signals. Basically, in medical grade sensor systems, large number of electrodes are used for capturing the data while in low-cost sensor systems, the number of electrodes is relatively less. The actual number of electrodes may vary from system to system such as some system only consists of a single electrode and others may have four electrodes, eight electrodes, 16 electrodes, etc. Some of the low-cost EEG sensors and number of electrodes used are shown in Table 2.

Electrodes can be distributed as either the 10–20 system [2] or the 10–10 system [3]. Figure 2 shows the electrodes placement using 10–20 system (a) and 10–10 system (b). In 10–20 system, maximum 21 electrodes can be used. Nasion to theinion distance is measured, starting electrodes are at 10% distance, and the remaining electrodes are at 20% of the distances. In 10–10 system, electrodes can be increased from 21 to 74, and all electrodes are at 10% distance. So, this is also known as 10% system or extended 10–20 system.

In case of EEG signal acquisition for biometric identification of person, the main aspect is state of brain and type of its activity. Here, we considered three main types of brain stimulation, i.e., resting state, with eyes closed (REC), and eyes opened (REO). Other is visual stimuli, where subjects were exposed to pictures and then their EEG signals were recorded and the last state is cognitive activities, and in this, subjects were asked to perform serval imagery task.

Table 2 Portable EEG sensors

Device	Electrodes
NeuroSky MindSet	1
Mindflex	1
MindWave	1
XWave Headset	1
HiBrain	1
iFocusBand	1
Aurora Dream Headband	1
Neural Impulse Actuator	3
Melon Headband	4
Muse	4
Emotiv Insight	5
OpenBCI	8 or 16
Emotiv EPOC	14

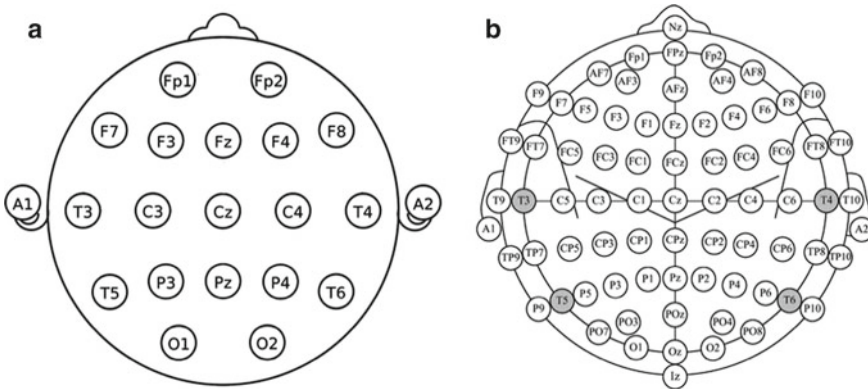


Fig. 2 Electrode placement according to the international 10–20 (a) and 10–10 (b) system [3]

2.1 Resting State (REC, REO)

Various researchers [4–9] used resting state as signal acquisition protocol in their studies and got satisfactory results. In this state subject sits in the quiet room in resting state either with eyes closed (REC) or with eyes open (REO). In this state subject don't need any additional information for signal acquisition and they just relax. Poulos et al. [4, 5, 10], acquired data when subjects were in resting state with eyes closed; 4 subjects and 75 imposters were considered for data acquisition, and voltage difference between O2 and Cz was calculated and EEG signals were recorded for continuous 3 min. In [4], correct classification rate (CRR) was obtained between the range 72 and 80%. In [5], CRR up to 80–100% was obtained. Paranjape et al. [11] collected data from 40 subjects using eight-channel EEG recording device. EEG was recorded during REC and REO. Results show 100% classification accuracy using all data, and 80% when half the data is used. Parisa et al. [12] acquired data from 10 subjects. Data was taken using 100 channels in 24 s duration in REO and the sampling rate was 170 Hz. CRR of 80–95% was achieved using single channel method and 85–100% using multi-channel method. Su et al. [13] recorded EEG signals using HXD-I portable equipment using only FP1 electrode, sampling rate was 200 Hz. Forty healthy volunteers were considered for data acquisition under quiet environment. Data was recorded in two periods and each subject provided 60 min recording in total, and whole data was divided into two halves, first one was used for training and other one for testing. Accuracy up to 97.5% was achieved.

Resting state is advantageous condition because it does not require any involvement of subject in EEG recording, i.e., subject just has to sit and relax with eyes open or closed, and this can reduce artifact occurrences, fatigue, and inconvenience. Also, the ambiguity of instruction to subjects can result in incommensurable of data as it may be interpreted by subjects in different way.

2.2 Visual Stimuli

Another approach used by researchers to acquire data is visual stimuli. In this approach, EEG signals are recorded when some pictures are exposed to subjects, and these recorded signals are called event-related potential (ERP), or visual evoked potential (VEP). ERP are very small voltages in the brain which evoked in response to specific event or stimuli. P300 is an ERP waveform; it is one kind of VEP. To acquire VEP, fast/moving picture series are shown to subject. When VEP data is used during the feature extraction, the presumed waveforms could be accurately measured. Snodgrass and Vandermart picture set [14] is used by most of the researchers [15–19] for their study.

Ferreira et al. [20] acquired VEP from 13 female subjects. Faces of 16 volunteers (8 males and 8 females) were selected to be used as 48 different face stimuli. Images of 16 different house fronts were superimposed on each of the faces. The images were divided into two experimental blocks. In first, the participants were asked to pay attention to houses while ignoring the faces and in second to focus on faces while ignoring the houses. The task for subjects was to find that whether the presented faces or houses are same or not. Stimuli arrive in sequence and lasting for 300 ms each. Twenty electrodes were used to acquire EEG, that were placed according to 10–20 electrode placement system.

In [21], Gui et al. acquired raw EEG signals from 32 volunteers (11 female and 21 male) using EASY CAP device having six electrodes and the sampling rate was 500 Hz. EEG signals were recorded for 1.1 s, so total of 550 samples for each channel. VEP signals were acquired when subjects silently read the text shown to them, which consist of unconnected list of texts having 75 words (such as FISH, BAG), 75 pseudowords (such as TRAT, MOG), 75 acronyms (like TNT, MTV), 75 illegal strings (like PPS, BPW), and 150 instances of their own name. To acquire training and testing set, subjects had to perform same task two times, i.e., first time for training and next time for testing. Four different scenarios were performed; the results shows that classification rates of scenario 4 can reach around 90%. And the classification rate of scenario 3 has worst performance which is less than 11%. Scenario 2 shows improvement, i.e., around 40% classification rate.

Koike-Akino et al. [22] acquired EEG data using 14-channel Emotiv EPOC. Sampling rate was used 128 samples per second and 25 healthy volunteers were considered as subjects. Electrodes were placed using 10–20 electrode placement system. Data was acquired in naturalistic setting. VEP signals were acquired from card counting task, in which five zener cards were shown in random order. Before data acquisition, subjects had to choose one zener card from cards displayed earlier, and that card was named as a target card. To perform the task, subjects had to calculate the total number of time target card was shown on screen. To verify that subjects performed the counting task, each subject was asked at the end of task, the total number of time target card shown on screen. Each card was displayed for 200 ms with an inter-stimulus interval of 800 ms. Subjects were asked to not do any body movements and eye movement during 800 ms inter-stimulus interval. 72% accuracy

was achieved using only single 800 ms ERP epoch for 25-subject identification from EEG biometrics. Authors concluded that identification accuracy can be improved to more than 96.7% by joint classification of multiple epochs.

One of the drawbacks of visual stimuli is that to trigger the VEP signal, external device is required, which makes system more complex compared to resting state and cognitive task.

2.3 Cognitive Activities

In these kinds of activities, subjects performed various tasks during signal acquisition such as imagery task or actual movement task. Imagery tasks were used by Marcel et al. [23] such as imagery left-hand movements, imagery right-hand movements, generation of words beginning with the same random letter, named as left, right, and word, respectively.

Palaniappan [24] used several imagined activities for data collection such as baseline activity (subjects just relax), math activity (subjects were given non-trivial multiplication problems and were asked to solve them without vocalizing and any other physical movement), geometric figure rotation activity (3D object was shown for 30 s and then removed then subjects were asked to visualize the object being rotated about axis when EEG were acquired), letter composing activity (subjects were asked to mentally compose a letter without vocalizing), visual counting activity (subjects were asked to imagine a blackboard and visualize numbers being written on board sequentially, with previous number being erased when next number was written).

Sun et al. [25] involved the task in which subjects had to imagine moving their index finger of any hand in reply to an extremely probable visual cue.

Hu [26] used BCI competition 2003 dataset. Sixty-four-channel EEG amplifier from Neuroscan was used to acquire data and sampling rate was 250 Hz. Subjects were asked to perform some tasks such as imagery left hand, right hand, foot or tongue movements according to a cue. Results show that when threshold 25% is taken, True acceptance rate (TAR) was 100% for k3b-T, k6b-R, k6b-F, 11b-T classifiers.

3 Preprocessing

When EEG signals are acquired, they are present in raw form which are usually noisy. So first, one needs to remove noise from them for further processing. Preprocessing of EEG signal is done to remove various artifacts from the raw signals.

EEG artifacts:

The undesirable potential that affect brain signals are called artifacts. These are generally originated from non-cerebral origin [27]. These come from physiological and non-physiological sources. Non-physiological sources are generated outside the

human body and artifacts can easily be eliminated by filtering, shielding, etc. Physiological artifacts are those which originate from different bodily activities such as impedance of electrodes can vary through skin response like sweating, etc.

- Human eye forms an electric dipole, when the eye moves or blinks, the electric field around the eye changes which produces an electric signal known as electro-oculogram (EOG). EOG is kind of physiological artifact which has high amplitude pattern in brain signal.
- Electromyogram (EMG) is another kind of physiological artifacts, which is usually caused by movement of head, body, jaw or tongue and causes large disturbances in brain signals.

Physiological artifacts such as EOG and EMG are more difficult to handle, than non-physiological artifacts. A review of different pre-processing techniques used for removal of these artifacts is given in this section.

Gui et al. [21] used ensemble averaging, which is average of multiple measurements. It is very efficient for noise reduction because square root of number of measurements reduces the standard deviation of noise after averaging. So, ensemble average of first 50 subjects' recordings was taken. After averaging, signal was much smoother than raw data. Then ensemble averaged signal passes through 60 Hz low pass filter to eliminate noise from large range of EEG data. Some authors [28], down-sample the signals by applying decimation factor; Rocca et al. [28] used this approach for preprocessing; sampling rate was 100 Hz and according to Nyquist theorem, its anti-aliasing and FIR filters were selected. Then bandpass filtering was applied to keep spectral information in band [0.5, 40] Hz, which contain useful frequency components during resting state condition. Resultant signals were segmented into M-overlapped frames, with length of each frame equal to 15 s and time interval of 1 s was used between successive frames. Rocca et al. [29] used the same approach of downsampling the signals. Acquired signals are α waves, originating from occipital lobe. During resting state, EEG waves consists of frequency elements less than 30 Hz. EEG waves have very small amplitude above 30 Hz, which was affected by noise like 50 Hz AC component. Decimation factor was applied to raw signals and anti-aliasing filter according to Nyquist theorem to retain spectral information existing in band [0.5, 30] Hz. Common average referencing (CAR) filtering can be applied to minimize artifacts concerned with improper reference choices and monopolar readings. This gives increased SNR.

Usually, major artifact in EEG signal is eye blinking; some authors pre-processed EEG signals to extract eye-blinking waveform from EEG signals. Eye blinking can be easily detected because it has largest amplitude, so we can extract it from its peaks. Some authors [30] used this method to extract eye-blinking waveform. Acquired EEG signal was first normalized to get mean equal to zero and max amplitude one. Then positive and negative peaks of eye blink were detected by applying threshold using MATLAB function "findpeaks".

Framing and bandpass filtering were also used for pre-processing stage. Authors in [31] used these steps for preprocessing of EEG recording. They segmented each EEG signal into frames and each frame having 1 s duration. Then filtering was done

on each frame to get different EEG bands such as $[\delta, \theta, \alpha, \beta, \gamma]$. Elliptic bandpass filter was used because it can get narrow transition width with small-order number. MATLAB function “`ellip`” was used to design elliptic filter and then used to filter each EEG frame having zero-phase using MATLAB function “`filtfilt`”.

As authors [32] acquired data using some portable EEG acquisition equipment, one of author [32] used Mindset headset to acquire EEG signals. This headset had inbuilt hardware filter which can filter out automatically 50 and 60 Hz noises from circuit. Also, it can detect muscular and ocular movements, using which EMG and EOG noises are easily eliminated. But, in this kind of system, there may be noise due to poor contact between electrode and scalp. Use of this headset cannot claim a good way to avoid such type of noises because of its randomness and irregularity. So, subjects had to relax and keep eyes closed.

Authors [33] also used bandpass filtering on raw data for the pre-processing stage. MATLAB function “`eegfilt`” was used which does not introduce any phase distortion. Hu [26] also used band pass filter for raw EEG data and the information present between 2 and 40 Hz was extracted.

Some of the authors [4] extracted particular band rhythm to process their EEG signal. Poulos et al. [4] extracted the alpha rhythm by spectrally analyzing the recorded signals using FT and retain the band between 7.5 and 12.5 Hz.

Yang et al. [34] used wavelet-based pre-processing technique, which involved two steps in preprocessing of raw EEG signals, one is segmentation and other is denoising. In wavelet-based denoising, three wavelet-based denoising methods were introduced, i.e., wavelet thresholding, multi-variate and multi-scale principle component analysis, and hybrid denoising method.

Palaniappan [24] used elliptic finite impulse response (FIR) high-pass filter [0.5 Hz] to reduce baseline noise. Elliptic filter was used due to its low order than other FIR filter like Butterworth. For no phase distortion, forward and reverse filtering was performed.

Zuquete et al. [19] considered artifacts produced by eyeblinking only, and by using amplitude threshold method and discard other VEP signals, the signals whose magnitude crossed $50 \mu\text{V}$ were assumed to be contaminated so they were discarded. Then resulting signals were filtered which were artifact-free VEP signals with 30–50 Hz passband, using tenth-order Butterworth digital filter. And by using forward and reverse filtering, the nonlinearity of filter was removed. Then resulting signal has zero-phase distortion and an amplitude multiplied by square of amplitude response of the filter. After filtering, first and last 20 samples were discarded because they do not represent a properly filtered signal.

In [15], Palaniappan and Ravi removed VEP signals with eye blinks artifact by detecting VEP signals having magnitude above $100 \mu\text{V}$. Threshold value $100 \mu\text{V}$ was used because blinking produces 100–200 μV potential which lasts for 250 ms. Then mean of the data was removed to set pre-stimulus baseline to zero. Then by using PCA, noise was removed from 61 channel VEP signal. Tenth-order forward and backward Butterworth digital filter was used to extract VEP in the 3 dB passband of 30–50 Hz, i.e., in gamma-band range. Zero-phase response was obtained by using forward and backward operations which can remove the nonlinear phase distortion

caused by butterworth filtering. Palaniappan and Mandic [17] detected EEG signals contaminated by eye blink artifact using $100 \mu\text{V}$ threshold. EEG signals were referenced to common average and gamma range was extended to 20–50 Hz, i.e., wider range. Then, EEG signals were filtered using elliptic filter because it needs lower order than Butterworth filter. Palaniappan and Mandic [16] used SD filter with 3 dB bandwidth over as wider bandwidth than previous one, i.e., 25–56 Hz. This filter consists of sum (low-pass) and difference (high-pass) filter. This filter has advantage over Butterworth and elliptic filter that the phase response was linear and the coefficients were integers. Also, symmetry (for low-pass) and anti-symmetry (high-pass) properties reduce the computational complexity by half. After SD filtering, they perform spatial averaging to reduce intraclass variance. In this, an average of filtered VEP signals was computed from all channels and used as a baseline measure.

4 Feature Extraction

After preprocessing of acquired EEG signals, next step is to extract their features. The selection of features is very important for the performance of EEG-based biometric system. Each section provides brief introduction of techniques used in respective literature reports.

4.1 Power Spectral Density (PSD)

PSD is a frequently used feature in EEG biometric [9, 23, 35]. PSD describes the signal power distribution over frequency. Unit of PSD is given by watts per hertz. Power spectral density features are calculated by computing fast Fourier transform (FFT) of time-domain signal or by taking autocorrelation function and then transforming it.

DFT is given by Eq. 1

$$X(f) = \sum_{i=1}^N x(i)w_N(i-1) \quad (1)$$

where

$$w_N = \exp(2\pi i)/N \quad (2)$$

is N th root of unity. PSD is given by:

$$S_X(f) = \frac{1}{N} \left(\sum_{i=1}^N |X(f)|^2 \right) \quad (3)$$

4.2 Autoregression Model (AR)

AR model was also very popular for feature extraction. AR model is a time-domain representation of the random process. In the autoregression model, we forecast the variable of interest using the past values of the variable.

$$X_t = c + \sum_{i=1}^p \varphi_i X_{t-i} + \varepsilon_t \quad (4)$$

where model coefficients = $(\varphi_1, \varphi_2, \dots, \varphi_p)$, c is constant, and ε_t = white noise.

The model given in Eq. 4 is known as the AR(p) model because this is an autoregressive model which has order p . The order of the autoregressive model is the number of immediately preceding values in the series that are used to forecast the value at the present time. For example:

$$X_t = c + \varphi_1 X_{t-1} + \varphi_2 X_{t-2} + \varepsilon_t \quad (5)$$

Equation 5 is called as AR (2) because values at time t is predicted from the values at time $t - 1$ and $t - 2$, i.e., previous two values. When lag operator B is introduced, then we can write Eq. 4 as Eq. 6:

$$X_t = c + \sum_{i=1}^p \varphi_i B^i X_{t-i} + \varepsilon_t \quad (6)$$

AR model coefficients can be used as features of the biometric system because they may reveal various intrinsic characteristics of EEG signals.

Rocca et al. [29] employed AR stochastic modeling, where AR reflection coefficients $(K_{i,m}^{ch}(Q))$ were estimated using Burg's method, where Q is order, and value of Q , determined using Akaike Information Criterion (AIC) which is given as Eq 7:

$$AIC(Q) = N_T \ln \sigma_Q^2 + 2Q \quad (7)$$

where N_T = sequence length, σ^2 = prediction error power. Values of Q from 8 to 12 were used, and the maximum value of Q , i.e., 12 has been selected for the AR model. The polynomial regression-based classification was used and recognition rates up to 98.73% were achieved.

4.3 Wavelet Transform (WT)

It is another useful feature extraction method for biometric systems [36]. Wavelet coefficients $WT_{\psi}\{x\}(a, b)$ can be used to derive wavelet-based features using Eq. 8:

$$WT_{\psi}\{x\}(a, b) = \langle x, \psi_{a,b} \rangle = \int_R x(t) \cdot \psi_{a,b}(t) dt \quad (8)$$

where $x(t)$ = time-domain signal, $\psi_{a,b}(t)$ = wavelet function.

Basically, a wavelet is a function $\psi \in L^2(R)$ with a zero average, i.e., $\int_{-\infty}^{+\infty} \psi(t) dt = 0$.

Gui et al. [21] also used WT to extract features from EEG signals and used wavelet packet decomposition (WPD). WPD is downsampling process from which time-frequency information of the signal is analyzed by passing the signal through multi-level filters. A four-level WPD was applied to calculate mean (μ_x), standard deviation (σ_x), entropy ($\varepsilon(x)$) and finally used these to form the feature vector. Classification rates achieved were up to 90%.

$$\mu_x = \frac{1}{N} \sum_{i=1}^N x_i \quad (9)$$

$$\sigma_x = \sqrt{\frac{1}{N} \sum_{i=1}^N (x_i - \mu_x)^2} \quad (10)$$

$$\varepsilon(x) = - \sum_t x^2(t) \log(x^2(t)) \quad (11)$$

4.4 Channel Spectral Powers and Interhemispheric Channel Spectral Power Differences

Channel spectral power as a feature extraction technique was used by Palaniappan [24] Channel spectral power was calculated by using the variance of filtered output and was given by:

$$P_{f_1, f_2} = \int_{f_1}^{f_2} S_X(f) df \quad (12)$$

where f_1, f_2 is a frequency band, $S_X(f)$ is power spectral density. Then, interhemispheric channel spectral power differences in each spectral band were calculated by:

$$P_{\text{difference}} = \frac{p_1 - p_2}{p_1 + p_2} \quad (13)$$

where p_1, p_2 is power in different channels in the same spectral band but in opposite hemispheres.

4.5 Energy Entropy (EE)

Hu [26] used energy entropy as one of feature extraction technique among many. Energy entropy was extracted from single channel, i.e., it is calculated for each channel without considering other ones. EE characterize single complexity with the change in time and many characteristics in the frequency domain.

$$E = \sum_{j=1}^m E_j \quad (14)$$

$$E_j = \sum_k |D_j(k)|^2 \quad (15)$$

D_j = spectrum on the j th frequency band, E_1, E_2, \dots, E_m represent energy distribution on m frequency bands. Let $P_j = E_j/E$, then $\sum P_j = 1$, the EE corresponding to:

$$W_e = - \sum_j P_j \log P_j \quad (16)$$

Then, multi-layer back propagation neural network was used as a classifier.

4.6 Phase Locking Value (PLV)

Hu [26] used PLV as one of the feature extraction technique. PLV is an example of two channel feature. To find the interaction between the EEG signal and having more direct interpretation between them, PLV was used. PLV is defined by considering the phase of two signals and given by

$$\text{PLV} = \left| \langle \exp(j\{\phi_i(t) - \phi_j(t)\}) \rangle \right| \quad (17)$$

where $\phi_i(t)$, $\phi_j(t)$ = instantaneous phase of electrode i and j at time t , and it was proved that phase value can be calculated by using either Hilbert transform or by convolving with a complex Gabor wavelet. Various other methods used in feature extraction [28, 33, 37] are given in Table 3.

5 Classification

After feature extraction, the next step is the classification of extracted features. We can define classification as a process in which the identity of the input vector is compared with feature vectors which are stored in the database. A brief review of some of the common classification techniques is provided in this section.

5.1 *k*-Nearest Neighbor Algorithm

k -NN is widely used in EEG pattern classification [16, 38] and it is one of the simplest algorithms. It is a non-parametric method. k -NN can be used for classification and regression. The basic principle for classification is that similarity among template features and test feature was obtained, the role of the test is to find the k -nearest-labeled samples in the training feature templates and then the decision is made using majority vote of its neighbors. If the value of k is 1, then it becomes the simplest nearest neighbor classifier. The k -NN classifier is sensitive to noisy data, hence, to remove this problem distance (d) weight is added in some k -NN classifiers.

5.2 *Elman Neural Network (ENN)*

Elman networks are artificial neural networks which are feed-forward networks with the addition of layer recurrent connections with tap delays. It is a three-layer network. Palaniappan and Mandic [17] used Elman neural network to classify EEG features which were extracted by Davies Bouldin Index (DBI). Three-layer ENN was chosen; the output layer has sigmoid activation function and the hidden layer has parabolic tangent activation function. For function activation task, ENN requires more hidden neurons than multi-layer perceptron (MLP). Using Nguyen-window algorithm, they initialize network weights and biases. And this initialization helps in faster training and more efficient use of available neurons. After some preliminary simulations, RB algorithm was used to train ENN. Maximum recognition rates up to $98.56 \pm 1.87\%$ were achieved.

Table 3 Comparison between various techniques used and their efficiency values

Author	Database	Subjects	Signal acquisition	Pre-processing techniques	Feature extraction techniques	Classification techniques	Efficiency
Poulos et al. [4]	Poulos DB	4	REC	BPF (1–30 Hz)	AR model	LVQ	72–84%
Poulos et al. [5]	Poulos DB	4	REC	Alpha rhythm isolation	PSD	LVQ	82–100%
Paranjape et al. [11]	Paranjape DB	40	REC, REO	ECG, EMG removal	AR model	Discriminant function analysis	83%
Su et al. [13]	Own DB recorded by HXD-1 dataset	40	REC	BPF (5–32) Hz	PSD + AR coefficients	LVQ, SVM, FDA with k-NN	k-NN + FDA (97.5%)
Rocca et al. [29]	Rocca DB	45	REC	Downsampling and CAR filtering	AR coefficients	Polynomial classification	98.73%
Rocca et al. [28]	Rocca DB	36	REC	Downsampling, BPF	BUMP modeling	LDA	89%
Dan et al. [32]	Own DB recorded by MindSet	13	REC	Muscular and ocular movement removal	Alpha wave extraction + AR	BP NN, SVM, LDA	87% (SVM)
Rocca et al. [40]	PhysioNet BCI	108	REC, REO	Down sampling, LPF (50 Hz)	PSD, spectral coherence connectivity	Mahalanobis distance	97.5% (EC) 96.26% (EO)
Fraschini et al. [33]	Physionet DB	109	REC, REO	BPF (0.5–50) Hz	PLI	Eigenvector centrality (EC)	99.5% (REO), 98.1% (REC)
Palaniappan and Ravi [15]	Palaniappan DB	20	Visual stimuli	PCA + Butterworth filter (30–50) Hz	PSD	SFA	95.75%

(continued)

Table 3 (continued)

Author	Database	Subjects	Signal acquisition	Pre-processing techniques	Feature extraction techniques	Classification techniques	Efficiency
Palaniappan et al. [16]	Palaniappan DB	10	Visual stimuli	SD filtering + spatial averaging	PSD using MUSIC algorithm	ENN, k-NN	98.12 ± 1.26
Palaniappan et al. [17]	Palaniappan DB	40	Visual stimuli	Elliptic filter	PSD and DBI to reduce the feature set	ENN	98.56 ± 1.87%
Zuquete et al. [19]	UCI KDD	70	Visual stimuli	tenth-order Butterworth filter	PSD	k-NN, SVDD	98.5% (SVDD)
Gui et al. [21]	Own DB using EASY CAP device	32	Visual stimuli	Ensemble averaging and LPF (60 Hz)	WPD	Feed-forward, multi-layer perception, BP NN	94.04%
Koike-akino et al. [22]	Own DB recorded by Emotiv EPOC	25	Mental task	BSS-CCA	PCA	SVM, QDA, NB, DT, k-NN, LR, DNN	96.7%
Marcel et al. [23]	Own DB recorded by Biosemi system	9	Cognitive activities	Surface Laplacian (SL)	PSD	GMM (Gaussian mixture model)/MAP	FRR- 96%
Sun [25]	NIPS 2001 BCI workshop DB	9	Cognitive activities	CAR, BPF (8–30) Hz, signal normalization	Common spatial patterns (CSP)	MTL NN	95.6%
Zahhad et al. [30]	Own DB using Neurosky Mindwave	25	Eye blinks	ICA and EMD (for EOG isolation)	Time delineation of eye blinking waveform	LDA	97.3%

(continued)

Table 3 (continued)

Author	Database	Subjects	Signal acquisition	Pre-processing techniques	Feature extraction techniques	Classification techniques	Efficiency
Yang and Deravi [34]	EMMI dataset	50	Cognitive activities	Wavelet-based noise removal and hybrid denoising	Wavelet packet decomposition (WPD)	Linear discriminant classifier (LDC)	95.5%
Safont et al. [9]	Own DB	50 + 20 intruders	REC	BPF (0.5–70) Hz, a narrow notch filter (50 Hz)	AR, FT, MI, cross-correlation, skewness, kurtosis, ICA, etc.	DA, TREE, COP, LDA, QDA, D-LDA	93.8%
Polous et al. [10]	Polous DB	4 + 75 intruders	Resting with eyes closed	Low-pass filter (1–30) Hz	AR parameters + bilinear model	LVQ	76–88%
Riera et al. [41]	FORENAP DB	51 + 36 intruders	REC	Passband filter, narrow notch filter (50 Hz)	AR, FT, MI, coherence, CC	DA	98.1%
Omerhodzic et al. [6]	Ralph DB	5	REC, REO	DWT with MRA	PSD	BP NN, FFNN	94%
Abdullah et al. [7]	Own DB using gMobilab + console	10	REC, cognitive activities	Elliptic LPF (45 Hz)	WPD	NN	81%
Palaniappan and Ravi [18]	Palaniappan DB	20	Visual stimuli	PCA	GBSP	SFA, LDA, k-NN	96.5%
Su et al. [8]	Own DB using HXD-1	40	REC	Notch filter	AR, PSD	k-NN + FDA	95.4%

5.3 *Linear Discriminant Analysis (LDA)*

LDA is one of the most widely used classification methods, which is developed by R. A. Fisher. Basically, it is used to separate two or more classes of objects or events. This algorithm is basically based on searching for a linear combination of variables that best separates two classes. LDA is used when the variance–covariance matrix does not depend on the population.

$$S = \frac{\sigma_{\text{inter}}^2}{\sigma_{\text{intra}}^2} \quad (18)$$

where S is the likelihood ratio.

LDA assumes the normal distribution of conditional probability density function with equal class covariance. Fisher’s LDA is a little bit different from conventional LDA, i.e., Fisher’s LDA does not assume normally distributed classes or equal class covariance. Along with PCA, LDA can also be used as a feature dimension reduction. LDA is a supervised algorithm, i.e., it takes the class label into consideration. It works on the basis of the centroid (or mean). Various authors [11, 28, 31] used LDA for classification are shown in Table 3.

5.4 *Support Vector Machine (SVM)*

It stands for a supervised learning model, which is used for analysis of data used for classification. SVM’s are based on decision planes (hyperplanes) which define decision boundaries. Decision plane separates objects belonging to different classes. Support vectors are that data points which are nearest to the hyperplane.

Ferreira et al. [20] used a multi-class support vector machine and in their work for classification of feature vector, two strategies were used, first was Support Vector Machine—One Against Other (SVM-OAO) and second was Support Vector Machine—One Against All. They tested both linear and nonlinear functions as SVM feature space mapping function and they chose radial bias function (RBF) for nonlinear case. Two training scenarios were considered: In the first one, the classifier was trained one by one with data set and experimental blocks and in the second scenario, the classifier was trained with data obtained from both experimental blocks and tested with unseen data from the same blocks.

5.5 *Principal Component Analysis (PCA)*

PCA can be used for the dimensionality diminution of the dataset which consists of many variables correlated with each other. PCA was invented by Karl Pearson

in 1901. The principal components are orthogonal because they are eigenvectors of the covariance matrix. If there are n observations with p variables then a number of distinct principal component is $\min(n - 1, p)$. PCA is an unsupervised learning algorithm, i.e., PCA ignores class labels that maximize the variance in a dataset, to find the directions. PCA works on the basis of variance.

Ferreira et al. [20] used PCA for enhancing the signal-to-noise ratio to escort the feature extraction step as PCA was designed to extract only principle components of normalized gamma-band spectral power which is having 95% of signal energy (we can call this as feature reduction). By using PCA processing, VEP power spectral density was reduced.

5.6 Learning Vector Quantizer (LVQ)

LVQ is basically a competitive layer which uses supervised learning. It may be defined as a process of classifying a pattern where each output unit represents a class. In it, the network is provided with training patterns with known classification and initial distribution of output class is also provided. LVQ will classify an input vector after completing the training process by assigning it to the same class as that of output.

Poulos et al. [10] used the LVQ neural network for the classification and the AR coefficient was used as a feature. LVQ is trained in two steps: In the first step, a standard clustering algorithm such as k-means or LBG algorithm was used to determine r -dimensional space of initial positions of class representatives. In the second step, class positions are iteratively updated to keep the minimum total classification error of the training set of vectors. For calculating distances, Euclidean distance was measured. An improved classification score via bilinear modeling was obtained.

5.7 BP Neural Network

It is a multi-layer feed-forward network trained according to the error backpropagation algorithm. It can be used to learn and store a lot of mapping relations of I/O model. BP NN used by various authors [6] in their research is given in Table 3.

5.8 Simplified Fuzzy ARTMAP (SFAM)

SFAM is growing neural network classifier, which performs incremental supervised learning. It is a simple and fast version of fuzzy ARTMAP, and SFAM has high-speed training ability than another neural network [39]. SFAM network is a combination of fuzzy ART and inter ART module [15].

Comparison between different signal acquisition, preprocessing, feature extraction, and classification technique along with their efficiencies obtained is shown in Table 3. It also shows different databases used by various authors and some of them are named after their author's name for easy understanding.

6 Conclusion

The paper provides an extensive literature survey on the electroencephalogram-based biometric systems and techniques used. Previous studies show that EEG signals have highly distinctive characteristics and stable across time, so they can be used as a biometric trait for an identification system. Different discriminative features and characteristics are detailed in Table 3. The whole paper was divided into four parts. In the first part, different signal acquisition techniques were discussed. Previous studies have shown that better results can be obtained using low-cost EEG sensors having a small number of electrodes, i.e., EEG biometric system can be built practically. Researchers used three different methods to acquire EEG signals for their study; the first one is resting state. Various authors acquire their signals when subjects were in a resting state either with eyes closed and eyes opened. The second was visual stimuli and third was cognitive activities in which subjects perform some imagery tasks. As data can easily be recorded in relaxed states, they can perform better in a practical scenario. In the second part, different pre-processing techniques were discussed, to filter raw EEG signals which include bandpass filtering, Butterworth filtering, elliptical filtering, etc. In the third part, feature extraction techniques were discussed, and it was found that PSD and AR parameters were commonly used for extracting features. Along with AR parameters, many different techniques were used to get better results. In the last part, many classification algorithms were discussed, such as k-NN, LDA, BP NN, LVQ, and SVM. PCA was also used as a dimensionality reduction technique. Nowadays's wavelets are more commonly used for feature extraction and classification purposes because their application gives better results.

References

1. Bao X, Wang J (2009) Method of individual identification based on electroencephalogram analysis. In: 2009 international conference on new trends in information and service science, pp 390–393. <https://doi.org/10.1109/NISS.2009.44>
2. Homan RW, Herman J, Purdy P (1987) Cerebral location of international 10–20 system electrode placement. *Electroencephalogr Clin Neurophysiol* 66:376–382. [https://doi.org/10.1016/0013-4694\(87\)90206-9](https://doi.org/10.1016/0013-4694(87)90206-9)
3. Maskeliunas R, Damasevicius R, Martisius I, Vasiljevas M (2016) Consumer grade EEG devices: are they usable for control tasks? *PeerJ* 4:e1746. <https://doi.org/10.7717/peerj.1746>
4. Poulos M, Rangoussi M, Chrissikopoulos V, Evangelou A (1999) Person identification based on parametric processing of the EEG. In: ICECS'99. Proceedings of ICECS '99. 6th IEEE

- international conference on electronics, circuits and systems, vol. 1, pp 283–286. <https://doi.org/10.1109/ICECS.1999.813403>
5. Poulos M, Rangoussi M, Alexandris N, Alezandris N (1999) Neural network based person identification using EEG. In: 1999 IEEE international conference on acoustics, speech, and signal processing. Proceedings, vol 2, pp 1117–1120
 6. Omerhodzic I, Avdakovic S, Nuhanovic A, Dizdarevic K (2010) Energy distribution of EEG signals: EEG signal wavelet-neural network classifier. *Neurocomputing* 2:210–215
 7. Abdullah MK, Subari KS, Leo J, Loong C, Ahmad NN (2010) Analysis of the EEG signal for a practical biometric system. *World Acad Sci Eng Technol* 4:1123–1127
 8. Su F, Xia L, Cai A, Ma J (2010) Evaluation of recording factors in EEG-based personal identification: a vital step in real implementations. In: 2010 IEEE international conference on systems, man and cybernetics, pp 3861–3866. <https://doi.org/10.1109/ICSMC.2010.5641768>
 9. Safont G, Salazar A, Soriano A, Vergara L (2012) Combination of multiple detectors for EEG based biometric identification/authentication. In: 2012 IEEE international caribbean conference on security technology (ICCST), pp 230–236. <https://doi.org/10.1109/CCST.2012.6393564>
 10. Poulos M, Rangoussi M, Evangelou A, Alexandris N (2002) Person identification from the EEG using nonlinear signal classification. *Methods Inf Med* 41:64–75
 11. Paranjape RB, Mahovsky J, Benedicenti L, Koles Z (2001) The electroencephalogram as a biometric. In: Canadian conference on electrical and computer engineering 2001. Conference proceedings, vol 2, pp 1363–1366. <https://doi.org/10.1109/CCECE.2001.933649>
 12. Parisa S, Mo B, Mohammad BS (2006) Person identification by using AR mode I for EEG signals. In: Proceedings of world academy of science, engineering and technology, vol 11, pp 281–285
 13. Su F, Xia L, Cai A, Wu Y, Ma J (2010) EEG-based personal identification: from proof-of-concept to a practical system. In: Proceedings—international conference on pattern recognition, pp 3728–3731. <https://doi.org/10.1109/ICPR.2010.908>
 14. Snodgrass JG, Vanderwart M (1980) A standardized set of 260 pictures: norms for name agreement, image agreement, familiarity, and visual complexity. *J Exp Psychol Hum Learn Mem* 6:174–215. <https://doi.org/10.1037/0278-7393.6.2.174>
 15. Palaniappan R, Ravi KVR (2003) A new method to identify individuals using signals from the brain. In: Fourth international conference on information, communications and signal processing, 2003 and the fourth Pacific Rim conference on multimedia. Proceedings of the 2003 joint, vol 3, pp 1442–1445. <https://doi.org/10.1109/ICICS.2003.1292704>
 16. Palaniappan R, Mandic DP, Member S (2007) Biometrics from brain electrical activity: a machine learning approach. *IEEE Trans Pattern Anal Mach Intell* 29:738–742
 17. Palaniappan R, Mandic DP (2007) EEG based biometric framework for automatic identity verification. *J VLSI Signal Process Syst Signal Image Video Technol* 49:243–250. <https://doi.org/10.1007/s11265-007-0078-1>
 18. Palaniappan R, Ravi KVR (2006) Improving visual evoked potential feature classification for person recognition using PCA and normalization. *Pattern Recognit Lett* 27:726–733. <https://doi.org/10.1016/j.patrec.2005.10.020>
 19. Zuquete A, Quintela B, Silva Cunha JP (2010) Biometric authentication using brain responses to visual stimuli. In: International conference on bio-inspired systems and signal processing, pp 103–112
 20. Ferreira A, Almeida C, Georgieva P, Tomé A, Silva F (2010) Advances in EEG-based biometry. In: Image analysis and recognition, pp 287–295
 21. Gui Q, Jin Z, Xu W (2015) Exploring EEG-based biometrics for user identification and authentication. In: 2014 IEEE signal processing in medicine and biology symposium (SPMB) 2014—proceedings. <https://doi.org/10.1109/SPMB.2014.7002950>
 22. Koike-akino T, Mahajan R, Marks TK, Wang Y, Watanabe S, Tuzel O, Orlik P (2016) High-accuracy user identification using EEG biometrics. In: 2016 38th annual international conference of the IEEE engineering in medicine and biology society (EMBC), pp 854–858
 23. Marcel S, Millan J del R (2005) Person authentication using brainwaves (EEG) and maximum a posteriori model adaptation. *IEEE Trans Pattern Anal Mach Intell* 24:1107–1146. <https://doi.org/10.1002/fut.20132>

24. Palaniappan R (2008) Two-stage biometric authentication method using thought activity brain waves. *Int J Neural Syst* 18:59–66. <https://doi.org/10.1142/S0129065708001373>
25. Sun SSS (2008) Multitask learning for EEG-based biometrics. In: 2008 19th international conference on pattern recognition, pp 1–4. <https://doi.org/10.1109/ICPR.2008.4761865>
26. Hu JF (2010) Biometric system based on EEG signals by feature combination. In: 2010 international conference on measuring technology and mechatronics automation, ICMTMA 2010, vol 1, pp 752–755. <https://doi.org/10.1109/ICMTMA.2010.27>
27. Fatourechi M, Bashashati A, Ward RK, Birch GE (2007) EMG and EOG artifacts in brain computer interface systems: a survey. *Clin Neurophysiol* 118:480–494. <https://doi.org/10.1016/j.clinph.2006.10.019>
28. La Rocca D, Campisi P, Sole-Casals J (2013) EEG based user recognition using BUMP modelling. In: 2013 international conference of the BIOSIG special interest group (BIOSIG), pp 1–12
29. La Rocca D, Campisi P, Scarano G (2012) EEG biometrics for individual recognition in resting state with closed eyes. In: Proceedings of the international conference of biometrics special interest group (BIOSIG), pp 1–12. https://doi.org/10.1007/978-3-662-44485-6_22
30. Abo-Zahhad M, Ahmed SM, Abbas SN (2015) A novel biometric approach for human identification and verification using eye blinking signal. *IEEE Signal Process Lett* 22:876–880. <https://doi.org/10.1109/LSP.2014.2374338>
31. Abo-Zahhad M, Ahmed SM, Abbas SN (2016) A new multi-level approach to EEG based human authentication using eye blinking. *Pattern Recognit Lett* 82:216–225. <https://doi.org/10.1016/j.patrec.2015.07.034>
32. Dan Z, Xifeng Z, Qiangang G (2013) An identification system based on portable EEG acquisition equipment. In: Proceedings—2013 third international conference on intelligent system design and engineering applications, ISDEA 2013, pp 281–284. <https://doi.org/10.1109/ISDEA.2012.70>
33. Fraschini M, Hillebrand A, Demuru M, Didaci L, Marcialis GL (2015) An EEG-based biometric system using eigenvector centrality in resting state brain networks. *IEEE Signal Process Lett* 22:666–670. <https://doi.org/10.1109/LSP.2014.2367091>
34. Yang S, Deravi F (2013) Wavelet-based EEG preprocessing for biometric applications. In: Proceedings—2013 fourth international conference on emerging security technologies, EST 2013, pp 43–46. <https://doi.org/10.1109/EST.2013.14>
35. Miyamoto C, Baba S, Nakanishi I (2008) Biometric person authentication using new spectral features of electroencephalogram (EEG). In: 2008 international symposium on intelligent signal processing and communications systems, pp 0–3. <https://doi.org/10.1109/ISPACS.2009.4806762>
36. Gupta CN, Khan YU, Palaniappan R, Sepulveda F (2009) Wavelet framework for improved target detection in oddball paradigms using P300 and gamma band analysis. *Soft Comput* 14:61–67
37. Nguyen P, Tran D, Huang X, Sharma D (2012) A proposed feature extraction method for EEG-based person identification. In: International conference on artificial intelligence
38. Yazdani A, Roodaki A, Rezatofighi SH, Misaghian K, Setarehdan SK (2008) Fisher linear discriminant based person identification using visual evoked potentials
39. Baghmisheh, Pavesic (2003) A fast simplified fuzzy ARTMAP network. *Neural Process Lett* 17:273–316
40. Rocca D La, Campisi P, Vegso B, Cserti P, Kozmann G, Babiloni F, De Vico Fallani F (2014) Human brain distinctiveness based on EEG spectral coherence connectivity. *IEEE Trans Biomed Eng* 61:2406–2412. <https://doi.org/10.1109/TBME.2014.2317881>
41. Riera A, Soria-Frisch A, Caparrini M, Grau C, Ruffini G (2008) Unobtrusive biometric system based on electroencephalogram analysis. *EURASIP J Adv Signal Process* 2008. <https://doi.org/10.1155/2008/143728>

Improved Neural Network-Based Plant Diseases Identification



Ginni Garg and Mantosh Biswas 

Abstract The agriculture sector is essential for every country because it provides a basic income to a large number of people and food as well, which is a fundamental requirement to survive on this planet. We see as time passes, significant changes come in the present era, which begins with Green Revolution. Due to improper knowledge of plant diseases, farmers use fertilizers in excess, which ultimately degrade the quality of food. Earlier farmers use experts to determine the type of plant disease, which was expensive and time consuming. In today's time, image processing is used to recognize and catalog plant diseases using the lesion region of plant leaf, and there are different modus-operandi for plant disease scent from leaf using neural networks (NN), support vector machine (SVM), and others. In this paper, we improve the architecture of the neural networking by working on ten different types of training algorithms and the proper choice of neurons in the concealed layer. Our proposed approach gives 98.30% accuracy on general plant leaf disease and 100% accuracy on specific plant leaf disease based on Bayesian regularization, automation of cluster, and without overfitting on considered plant diseases over various other implemented methods.

Keywords Plant diseases · Color transformation · Image segmentation · Feature extraction · Classification

1 Introduction

As far as India is concern, the agriculture sector has a significant contribution to the GDP of India. The agriculture sector employs a large number of people all across the world. For food, a person has to depend on agriculture products. As we see in

G. Garg (✉) · M. Biswas
Department of Computer Engineering, NIT Kurukshetra, Kurukshetra, India
e-mail: gargginni01@gmail.com

M. Biswas
e-mail: mantoshb@gmail.com

© Springer Nature Singapore Pte Ltd. 2021
G. S. Hura et al. (eds.), *Advances in Communication and Computational Technology*, Lecture Notes in Electrical Engineering 668,
https://doi.org/10.1007/978-981-15-5341-7_6

the past, to determine the type of plant diseases, farmers use the expert's people in the agriculture field, but that process is time consuming and not always give the correct result. Because it is always true in the majority of cases that a model gives correct results as compare to humans. As we see today, work is done in the area of the agriculture sector using image processing to improve the quality of products and help farmers to protect their crops from diseases, and it can extract relevant information from it. There are various methods for plant disease detection based on artificial neural network (ANN) [1–4], support vector machine (SVM) [5], k-nearest neighbors (KNN) [6], convolutional neural network (CNN) [7], fuzzy logic (FL) [8], and its combination. CNN-based plant disease detection gives good accuracy, but it needs a large amount of data for training, which increases computational cost. SVM-based plant disease detection is useful for both accurate separable and non-definite separable data but cannot return an anticipation credence value like logistic regression does. KNN-based plant disease detection is useful for inputs where the probability distribution is unknown, but it is sensitive to localized data and takes considerable long computational time due to lazy learning. Fuzzy logic-based plant disease detection is a heuristic modular way for defining any non-definite hegemony system and can attain a higher degree of cybernation but is not clearly understood and has no standard tuning and no stability criteria. Neural network (NN) is a supervised learning approach, and it recognizes the relationship among data by a process that behaves as the human brain operates. Neural network adjusts itself as input changes to produce the best result without the need to change the output criteria. Neural network contains layers having inter-connected neurons or perceptrons, and the output layer has to classify input features into various classes. ANN is a non-argument model, while most emblem methods are argument models that need a higher backcloth of emblem. In NN-based Bani-Ahmed et al., proposed plant disease detection method using color transformation scheme HIS and segmentation by K-mean with four clusters [1]. Other, Varthini et al., detected plant diseases using color transformation scheme HIS, threshold masking for green pixel of leaf image followed by segmentation of input image into patch size of $32 * 32$, and classification is completing by combination of the ANN and SVM [2]. Kamlu et al. proposed the spot and catalog of plant diseases using the threshold, k-means clustering, and ANN [3]. Moreover, Pradhan et al. review the paper based on major types of neural networks with hyperspectral data [9]. So, NN-based methods are resilient and can be accessible for both regression and catalog problems. It is good to miniature with no accurate data with a large number of inputs. Therefore, we proposed an improved NN-based plant disease identification approach, based on CIE LAB, k-means, elbow, and augmentation. The paper is sort as follows: The proposed approach for improved NN describes in Sects. 2 and 3, the results are discussing for the robustness of the proposed approach over the considered plant disease methods. Lastly, the paper cum in the conclusion section.

2 Proposed Method

Our proposed approach consists of various steps, firstly, we do image acquisition and color transformation by RGB to CIE LAB for making images device independent such that images captured with different color space like Standard-RGB and Adobe-RGB gives same results; secondly, segmentation is used to extract lesion region using k-means and elbow; thirdly, apply the augmentation in direction of 90° , 180° , and 270° to increase the dataset and avoid the over-fitting; fourthly extracted the feature using first-order and second-order statistics; fifthly prepared the training and testing data set; and finally, classify the plant diseases using improved NN. The details of the proposed steps (Fig. 1) for the identification of plant diseases are described below.

2.1 Image Acquisition and Color Transformation

Image acquisition is a process of collecting the required dataset to train the classifier. We have taken a total of 240 images of the widespread plant species and 516 images of the specific plant leaf species [10]. Image acquisition is made through free open source like plant village, Github, and Internet. Color transformation means transfiguration of the description of the color from one color leeway to another [11]. We need to do color transformation from RGB to LAB because RGB is device-dependent whereas $L^* a^* b$ color system is device independent, so that on transforming from s-RGB or Adobe-RGB to LAB produces the same set of three coordinates, so

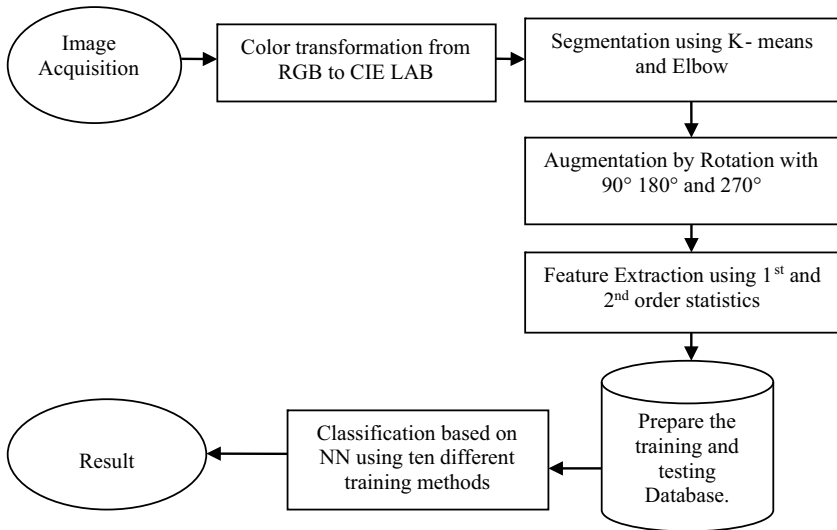


Fig. 1 Flow schema of the proposed modus-operandi for the identification of diseases

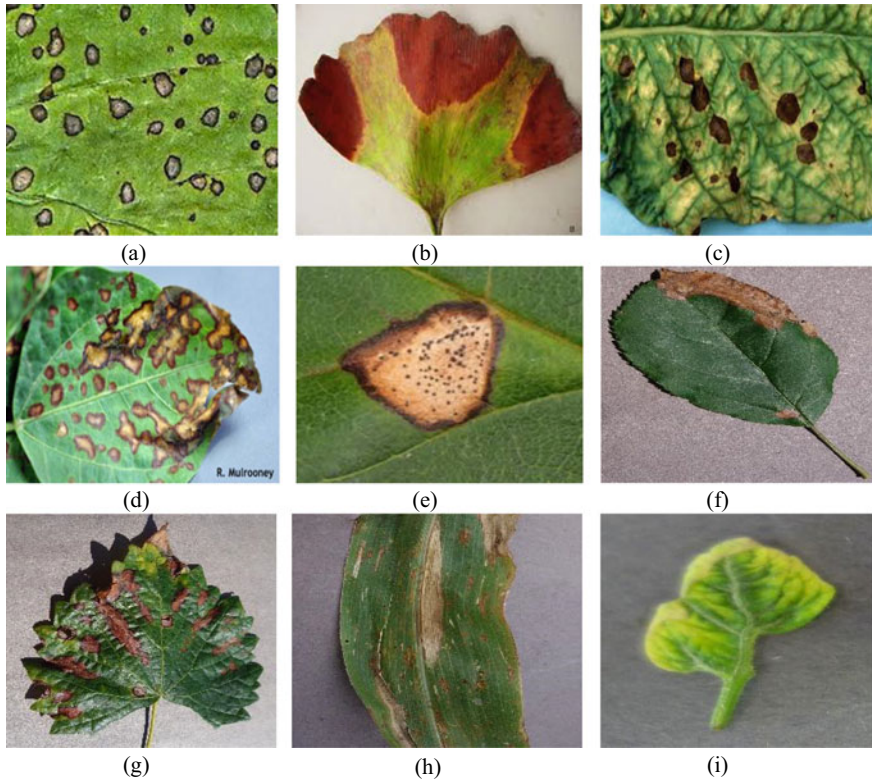


Fig. 2 Disease leaf. **a** Frog-leaf spot. **b** Early scorch. **c** Fungal disease. **d** Bacterial disease, and **e** Sunshine burn. **f** Apple rot. **g** Grape ESCA. **h** Maize blight and **i** Tomato Yellow_Virus

researcher working with s-RGB or Adobe-RGB compute same accuracy, i.e., independent of device used to capture the image of plant leaf. Moreover, the objective of the color leeway is to proficiency the enumeration of colors in some caliber way. CIE L^*a^*b color model perceives colors like human beings. This step is relevant in the feature extraction process because s-RGB and Adobe-RGB color space give different pixel values for an image, whereas LAB color space gives the same pixel values. Some of the disease leaf test images in s-RGB are as shown in Fig. 2.

2.2 Segmentation

Image septation in the catalog of an image into various categories. Proposed approach is to identify the affected areas under study. Many scientists have worked in the area of image segmentation using clustering, and one of modus-operandi is k-means clustering, which is used in our proposed approach aims at minimizing an objective

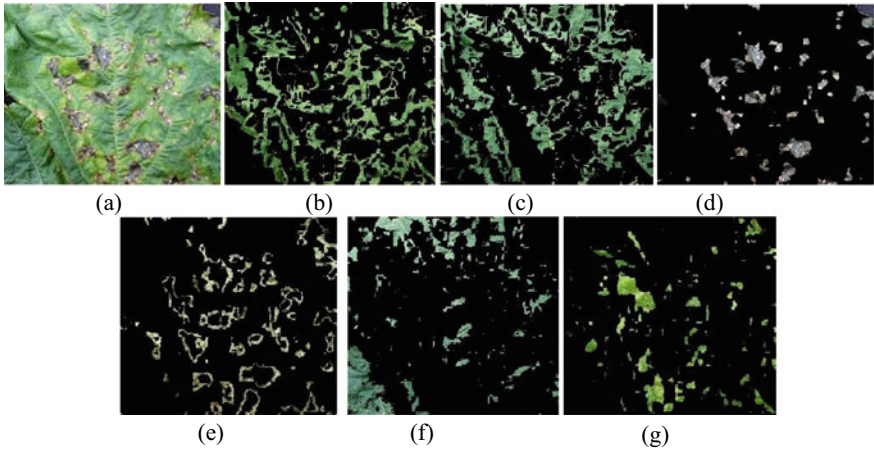


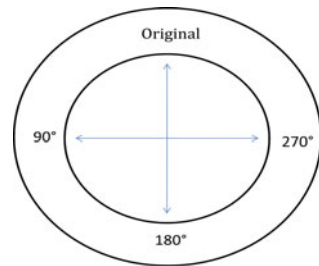
Fig. 3 Bacterial leaf disease. **a** Original. **b** Clutch-1. **c** Clutch-2. **d** Clutch-3. **e** Clutch-4. **f** Clutch-5. **g** Clutch-6

function [1, 3]. Moreover, we used Elbow for the automation of the clusters [12]. Figure 3 represents the clustering of the bacterial plant leaf using the k-means with Elbow, in which k-means produced six clusters for the input image.

2.3 Augmentation

Augmentation is an approach used to increase the dataset and overcoming the problem of overfitting [13]. This method is used for functional prediction of images when images are given with different orientation then orientation with which classifier is trained. In our proposed approach, we use rotated images by 90, 180, and 270° (Figs. 4 and 5).

Fig. 4 Augmentation approach by rotating 90°, 180°, 270°



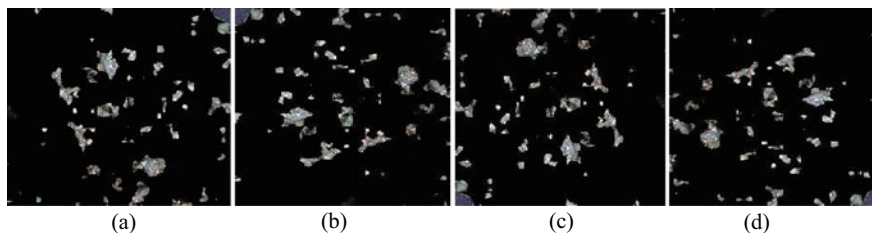


Fig. 5 Rotated lesion image. **a** Original. **b** 90°. **c** 180° and **d** 270°

2.4 Feature Extraction

Features are the measurable descriptors of an object, and it describes elementary characteristics such as shape, color, texture, or motion, among others, and used for classifying the type of plant diseases [14]. In our proposed work, we use first-order emblem to approximate properties of individual pixel values and second-order emblem for the spatial relationship between image pixels. We use first-order statistics for mean, kurtosis, standard deviation, variance and skewness, and second-statistics for contrast, correlation, energy, homogeneity, smoothness, IDM, RMS, and entropy (Table 1).

2.5 Training and Testing Set

The training set is used to fit the parameters of the miniature, whereas the testing set is used to deliver a fair estimation of a final miniature fit on the training dataset. In our proposed set includes a database of features and output classes used to train and test the classifier. We use improved NN of 13 features, and 5 output classes, representation as V and OC, respectively, describe below:

$$V = F_1, F_2, F_3, \dots, F_{13} \quad (1)$$

$$OC = C_1, C_2, C_3, \dots, C_5 \quad (2)$$

2.6 Classifier

Classification means to identify the type of category that a new observation belongs to the set of known categories. In our proposed approach, we used NN as classifier

Table 1 Represents the thirteen different features

Feature name	Formula
Contrast	$C = \sum_{x,y=1}^{A,B} x - y ^2 q(x, y)$; Here, $q(x, y)$ GLCM, x & y are row and column and A is total rows and B is total columns
Correlation	$\text{Corr} = \sum_{x,y=1}^{A,B} ((x - \mu)(y - \mu)q(x, y) / \sigma(x) * \sigma(y))$; Here, mean is μ and standard deviation is σ
Energy	$E = \sum_{x,y=1}^{A,B} q(x, y)^2$
Homogeneity	$H = \sum_{x,y=1}^{A,B} q(x, y) / (1 + x - y)$
Mean	$\mu = \frac{1}{AB} * \sum_{x=1}^A \sum_{y=1}^B q(x, y)$
Standard deviation	$\sigma = \sqrt{\frac{1}{AB} * \sum_{x=1}^A \sum_{y=1}^B (q(x, y - \mu))}$
Kurtosis	$K = \left\{ \frac{1}{AB} * \sum_{x=1}^A \sum_{y=1}^B ((q(x, y) - \mu) / \sigma) \wedge 4 \right\} - 3$
Skewness	$S = \frac{1}{AB} * \sum_{x=1}^A \sum_{y=1}^B ((q(x, y) - \mu) / \sigma)$
Variance	$\text{Var} = \frac{1}{AB} * \sum_{x=1}^A \sum_{y=1}^B (q(x, y) - \mu)$
Smoothness	$R = 1 - 1 / (1 + \sigma^2)$
IDM	$HH = \sum_{x,y=1}^{A,B} q(x, y) / (1 + x - y)$
RMS	$y = \sqrt[3]{\sum_{x,y=1}^{A,B} (q(x, y))^2 / A}$
Entropy	$h = - \sum_{x,y=1}^{A,B} q(x, y)(\log q(x, y))$

to identify the disease from leaf image and use various training algorithms in our improved NN is given below:

Bayesian Regularization Bayesian regularization is a mathematical procedure that converts a non-definite regression into a “well-posed” emblem problem in the way of a chine regression [13].

Levenberg–Marquard The LM fitting of a curve procedure is an amalgam of two diminution procedure: the Gauss–Newton procedure and the gradient descent procedure [15].

BFGS Quasi-Newton Quasi-Newton method is used to find the local minima or maxima as a substitute to the Newton method. Usually, it is used if the Jacobian or Hessian matrix is difficult to compute or is unavailable [16].

Resilient Back Propagation Resilient back propagation is a supervised learning method used in the feed-forward neural network [17].

Scaled Conjugate Gradient It is a training function used for the solution of the set of linear equations whose matrix is symmetric and positive definite [18].

Powell–Beale Restarts Conjugate Gradient The Beale–Powell restart method is used for large-scale depraved boost [19].

Conjugate Gradient with Fletcher–Powell The Davidon–Fletcher–Powell penalty function method is an approach that has been used successfully to solve constrained minimization problems. The method devised by combining an exterior penalty function with a performance function for solving constrained minimization problems [16].

Polak–Ribiere Conjugate Gradient It is a method based on the conjugate gradient used as a training function in the neural network [20].

One Step Secant This method lies in between conjugate gradient descent and the quasi-Newton method. This algorithm usually need less computation as compared to the BFGS algorithm [21].

Variable Learning Rate Back Propagation In reality, learning rate plays a significant role in the training algorithm such that proper choice of the learning rate is essential to have good accuracy such that the above method varies learning rate until one can get good accurate results [22].

3 Results

Simulation of our proposed approach and existing plant disease detection on [1–3] is performed on five general plant disease, namely Bacterial leaf spot, Early scorch, Frog-leaf spot, Fungal disease, and Sunburn disease (Fig. 1) and experiment is also extended on the specific plant diseases which include grape, tomato, apple, and maize (Fig. 2 and Table 5). Performance evaluation is done by accuracy (Tables 4 and 7), which is given by below Eq. (3), where TP is True Positive, TN is True Negative, FP is False Positive, and FN is False Negative.

$$\text{Accuracy} = (\text{TP} + \text{TN}) / (\text{TP} + \text{TN} + \text{FP} + \text{FN}) \quad (3)$$

In our approach, general plant species and specific plant leaf species are taken in ratio 7:3 for training and testing (Tables 2 and 5). In improved NN, we have given the input that consists of 13 features, Epoch is 1000, performance function is mean squared error (MSE), five output classes (general diseases), and activation function

Table 2 Represents the thirteen different features

Category	Training	Testing
Bacterial leaf spot	36	16
Early scorch	39	17
Frog eye spot	42	18
Fungal	36	16
Sunburn	14	6

Table 3 Represents the accuracy of thirteen different algorithms with neurons N : 5, 10, 15, 20

Training algorithm name	Number of neurons in only hidden layer (N)			
	$N = 5$	$N = 10$	$N = 15$	$N = 20$
Bayesian regularization	93.17	96.88	97.38	98.30
Levenberg–Marquardt	86.35	93.02	96.18	95.56
BFGS Quasi-Newton	47.85	55.83	64.31	53.97
Resilient back propagation	54.42	74.80	72.25	79.39
Scaled conjugate gradient	53.26	73.47	74.04	89.53
Conjugate gradient with Powell/Beale restarts	55.92	70.26	73.03	85.06
Fletcher–Powell conjugate gradient	53.38	64.39	67.37	76.76
Polak–Ribière conjugate gradient	55.55	69.83	79.55	89.08
One step secant	55.21	60.05	61.29	68.44
Variable learning rate back propagation	57.56	66.71	69.65	66.80

is sigmoidal in concealed layer and precarious in output layer. All the plant disease experimental computation is done in R2017b MATLAB toolbox with a personal computer of 4 GB memory, Window 10 64-bit operating system, and Intel (R) Core (TM) i3-6006U CPU @ 2.00 GHz.

Tables 2 and 5 are represented the general and specific, respectively, the dataset of the considered plant leaf for this experiment, which shown with the number of training and testing images.

Table 3 represents the computation used ten different training algorithms to train NN and different combinations of neurons used in the only concealed layer, i.e., 5–10–15–20. From this table, we found that Bayesian regularization gives excellent results over other training algorithms. All percentage is computed by taking an average of ten-fold observations of confusion matrix.

Table 4 represents the accuracy of the considered general plant disease detection method [1–3] and the proposed approach. From this table, it describes that the proposed improved NN gives the best accuracy results over [1–3].

Table 5 represents the dataset of the specific plant leaf for this experiment, which shown with the number of training and testing images.

Table 6 represents the results of accuracy for proposed improved NN using Bayesian regularization on the dataset shown in Table 5.

Table 7 represents the accuracy of the species considered for plant disease detection method [1, 3], and the proposed approach. From this table, it concludes that the proposed improved NN gives the best accuracy results over [1, 3].

Table 4 Comparison of results on considered dataset with proposed method and other results

[1]	[2]	[3]	Proposed with Bayesian regularization ($N = 20$)
93.05	87.52	88.67	98.30

Table 5 Comparison results on considered dataset with proposed method and other results

Plant species	Diseases category	Images training	Images testing
Grape	Black_rot	5	3
	Black_Measles (Esca)	34	14
Tomato	Bacterial Spot	17	7
	Early_blight	31	13
	Late_blight	25	11
	Septoria_spot	11	5
	Yellow_Curl_Virus	17	7
Apple	Cedar_Rust	81	35
	Black_Rot	76	32
Maize	Nothern_Blight	39	17
	Common_Rust	25	11

Table 6 Comparison results on considered dataset with specific plant diseases

Input feature	Training algorithm	Performance function	Epoch	Neurons	Output	Accuracy
13	Bayesian regularization	Mean square error	1000	1	2	100
				15	5	100
				1	2	100
				1	2	100
				<i>Total</i>		<i>100%</i>

Table 7 Results of accuracy for specific plant disease identification

[1]	[3]	Proposed with Bayesian regularization
90.58	72.33	100.00

4 Conclusion

In this paper, we proposed an improved NN-based plant disease identification. Our proposed approach includes automation for the clusters, proper identification of the lesion region, augmentation, and best training algorithm to train the neural network. Experimental results show that the choice of the training algorithm is vital to have good results of accuracy, and augmentation helps in increasing the dataset and overcoming the over-fitting problem. The overall proposed approach gives excellent accuracy of 98.30% on testing the widespread plant diseases and 100.0% on testing the specific plant diseases over a considered dataset. Further, accuracy can be improved for disease detection in plant leaf with the help of the fusion of various classifiers and integration of the fuzzy logic to the neural network.

References

1. Al Bashish D, Braik M, Bani-Ahmad S (2011) Detection and classification of leaf diseases using K-means based segmentation and neural networks based classification. *Inf Technol J* 10(2):267–275
2. Arivazhagan S, Shebiah RN, Ananthi S, Varthini SV (2013) Detection of unhealthy region of plant leaves and classification of plant leaf diseases using texture features. *Agric Eng Int CIGR J* 15(1):211–217
3. Tete TN, Kamlu S (2017) Detection of plant disease using threshold, k-mean cluster and ANN algorithm. In: 2nd international conference for convergence technology, pp 523–526
4. Ranjith, Anas S, Shelly M (2017) Cloud based automated irrigation and plant leaf disease detection system using an android application. In: International conference on electronics, communications and aerospace technology, pp 211–214 (2017)
5. Singh V, Misra AK (2017) Detection of plant leaf diseases using image segmentation and soft computing techniques. *Inf Process Agri* 4(1):41–49
6. Kaushal G, Bala R (2017) GLCM and KNN based algorithm for plant disease detection. *Int J Adv Res Electr Electron Instrum Eng* 6(7):5845–5852
7. Zhang X, Qiao Y (2018) Identification of maize leaf diseases using improved deep convolutional neural network. *IEEE Access* 6:30370–30377
8. VijayaLakshmi B, Mohan V (2016) Kernel-based PSO and FRVM: an automatic plant leaf type detection using texture, shape, and color features. *Comput Electron Agric* 125:99–112
9. Golhani K, Balasundram SK, Vadamalai G, Pradhan B (2018) A review of neural networks in plant disease detection using hyperspectral data. *Inf Process Agric* 5(3):354–371
10. https://github.com/salathegroup/plantvillage_deeplearning_paper_dataset/tree/master/raw/color
11. Nayyer R, Sharma B (2015) Use and analysis of color models in image processing. *Int J Adv Sci Res* 1(8):329–330
12. Kodinariya TM, Makwana PR (2013) Review on determining number of cluster in K-means clustering. *Int J* 1(6):90–95
13. Okut H (2016) Bayesian regularized neural networks for small n big p data. In: Artificial neural networks—models and applications, pp 1–22 (2016)
14. Al-Killdar S, George LE (2017) Texture recognition using color co-occurrence matrix features and neural network. *J Theor Appl Inf Technol* 95(21):5949–5961
15. Lourakis MIA (2005) A brief description of the Levenberg-Marquardt algorithm implemented by levmar. Technical report, Institute of Computer Science (2005)
16. Davidon WC (1991) Variable metric method for minimisation. *SIAM J Optim* 1(1):1–17
17. Igel C, Hüsken M (2001) Improving the R_{prop} learning algorithm. *Neurocomputing* 50:105–123
18. Hestenes MR, Stiefel E (1952) Methods of conjugate gradients for solving linear systems. *J Res Natl Bur Stan* 49(6):409–436
19. Dai Y, Yuan Y (1998) Convergence properties of Beale-Powell restart algorithm. *Sci China, Ser A Math* 41(11):1142–1150
20. Yuan G, Wei Z, Li G (2014) A modified Polak–Ribière–Polyak conjugate gradient algorithm for nonsmooth convex programs. *J Comput Appl Math* 255:86–96
21. Battiti R (1992) First and second order methods for learning: between steepest descent and Newton’s method. *Neural Comput* 4(2):141–166
22. Plagianakos VP, Sotiropoulos DG, Vrahatis MN (1998) Automatic adaptation of learning rate for backpropagation neural networks. University of Patras, Department of Mathematics, pp 337–341

Maximum Power Extraction Using Random Binary Searching Algorithm Under Non-uniform Insolation



Kusum Lata Agarwal  and Avdhesh Sharma 

Abstract Maximum power point tracker (MPPT) controls the DC/DC converter for extracting maximum power from solar photovoltaic (SPV) array connected with power generation system. MPPT operates at its maximum power point (MPP) (V_{mp} , I_{mp}) irrespective to load conditions and input weather conditions. Use of by-pass diodes in series-connected SPV modules under non-uniform insolation is a key cause for many power peaks in the power–voltage characteristics of SPV array. Henceforth the problem of MPPT under partial shading becomes a nonlinear optimization problem. A new quick and reliable MPPT technique is proposed in this paper to identify the global MPP under partial shadow conditions. The computation time and correctness in tracking global MPP are compared with standard soft computing techniques: modified binary (MB) search, differential evolution (DE) techniques, and particle swarm optimization (PSO). The results show correctness of the presented random binary search technique in tracking the global MPP in very less time than the conventional soft computing techniques. The technique is quick, simple, and oscillation-free for tracking global MPP in least iterations; hence, the computation (hardware) requirements are less than that using PSO and DE MPPT techniques.

Keywords Solar photovoltaic (SPV) array · Maximum power point tracking (MPPT) · Artificial intelligence (AI)-based techniques

1 Introduction

Partial shading of solar PV array is one of the key causes for decreased energy yield of many solar PV arrays. Use of by-pass diodes with series-connected modules may produce multiple power peaks in the power-voltage (P-V) characteristics under

K. L. Agarwal (✉)

Department of EE, JIET, Jodhpur, India

e-mail: kusum.agarwal@jietjodhpur.ac.in

A. Sharma

Department of EE, M.B.M. Engineering College, JNVU, Jodhpur, India

e-mail: avdheshmbm15@gmail.com

© Springer Nature Singapore Pte Ltd. 2021

G. S. Hura et al. (eds.), *Advances in Communication and Computational*

Technology, Lecture Notes in Electrical Engineering 668,

https://doi.org/10.1007/978-981-15-5341-7_7

non-uniform insolation. Load side voltage-to-current (V/I) ratio is decided by the load considerations; however, voltage-to-current (V/I) ratio for the solar PV array is governed by maximum power point of the solar array, as the input energy to the SPV array is free of cost. To match these divergent requirements, a DC/DC converter is interfaced between the solar PV array and the load. This situation is similar to a transformer used in the AC system to match the impedances for maximum power transfer from source to load. Here, the role of maximum power point tracker is to operate the DC/DC converter in such a way that the SPV array connected should operate at its maximum power point (V_{mp} , I_{mp}) irrespective of load conditions and input weather conditions.

Several MPPT schemes are available in the literature. A few popular schemes are short-circuit current (I_{sc}) method, open-circuit voltage (V_{oc}) method, perturb and observe (P and O) method, incremental conductance method, ripple correlation (RC) method [1–3]. The existing tracking techniques are efficient and well-proven under uniform solar insolation, where the P-V curve of the solar PV module exhibits only one peak for a given temperature and insolation. But non-uniform insolation (partial shading) results in a deformation of the overall power-voltage (P-V) curve, i.e., P-V curves repeatedly display many local maxima at dissimilar locations, which may exhibit in relatively odd ratios between global maximum power point (GMPP) voltage (V_{mp}) and open-circuit voltage (V_{oc}). These factors can put a substantial obstruction to the accurate operation of an MPPT technique.

Some of the research papers which present the solution methods to report this issue are Qiang Mei et al. [4] and Elgendy et al. [5] have introduced an innovative adjustable step-size incremental-resistance maximum power point algorithm, which inevitably regulates the step size to track the MPP of a PV array. Bader N. Alajmi et al. [6] have presented a modified fuzzy logic controller for maximum power point (MPP) tracking to increase photovoltaic (PV) system performance during partially shaded conditions. Koutroulis and Blaabjerg [7] have presented a technique to track the global MPP, which is based on controlling a DC/DC converter connected at the PV array output, such that it behaves as a constant input-power load. Ahmad Al Nabulsi and Rached Dhaouadi [8] have presented a digital control scheme for a standalone photovoltaic (PV) system using fuzzy logic and a twin maximum power point tracking (MPPT) controller. Xiao Li et al. [9] have presented the adaptive extreme seeking control (AESC) scheme to the PV MPPT problem. Peter and Agarwal [10] have determined the effect of the input resistance of a reconfigurable switched capacitor DC/DC converter-based MPPT of a photovoltaic system. Liu et al. [11], Ishaque et al. [12], and Azab [13] have presented a particle swarm optimization (PSO)-based MPPT algorithm for solar PV system (SPVS) operating under partial shadow condition. Latham et al. [14] presented the analysis and optimization of MPPT algorithms in the presence of noise. Hartmann LV [15] presented merging model-based and heuristic techniques for fast-tracking the maximum power point for SPV Systems. Kjer BS [16] presented hill climbing and incremental conductance method for tracking MPP. Young et al. [17] determined mismatching compensation in PV array under partially shaded conditions.

A brief comparison of seven dissimilar maximum power point tracking (MPPT) techniques is presented, with regards to the amount of power extracted, and their tracking precision is calculated [18]. An analog, BJT-tuned voltage reference MPPT method for photovoltaic (PV) modules is proposed by Al-soeidat [19]. An enhanced global MPPT (GMPPT) technique comprising of $0.8V_{OC}$ model and limited and adaptive scan approach is proposed by Başoğlu [20]. A hybrid GMPPT algorithm for constant voltage load applications using one current sensor was also suggested using hill climbing (SSHC) and artificial bee colony (ABC) algorithms to track the GMPP [21, 22]. A lot of research work pertaining to the MPPT of SPV array has been reported in the literature however very limited work has been presented about MPPT technique under non-uniform insolation, i.e., partial shading conditions. At the same time, MPPT execution time and precise tracking of global MPP play a key role in deciding the performance of the technique. A simple and reliable global MPPT technique is still required for quick tracking of MPP under uneven insolation conditions.

An effort has been made in this paper to develop a new quick and reliable global MPPT technique to track the MPP under partial shadow conditions over SPV array with the following main objectives:

1. To develop a new quick and reliable AI-based MPP technique to track GMPP under partial shadow conditions over SPV array.
2. To evaluate the performance of the projected technique with standard AI-based techniques, i.e., differential evolution, particle swarm optimization, and modified binary (MB) search.
3. To validate the results of MPPT techniques w.r.t. quickness (execution time) and correctness of estimation. The novelty of this proposed technique is minimum computation time along with minimum % average MPPT error.

The novelty of the proposed technique is minimum computation time to track maximum power point with minimum error in % average of MPP tracking. Uniqueness of the technique is the first-time linear search method which is applied for MPP tracking. The proposed technique requires minimum computation hardware hence sustainable and more energy will be harnessed through it. Innovation of technique is least MPPT error while solar power utilities and human society will be benefitted through the proposed technique. In future, MPPT power controller hardware for SPV plant may be developed using this technique.

Limitation of the present work is its direct application to DC/DC converter only and the output yield of DC/DC converter may be directly fed to the DC load. However, for transferring generated power to the AC loads or the electrical grid, the output of DC/DC converter should be fed via an inverter (voltage source converter), where the control takes place through modulation signal. With this application, MPPT systems will be applicable for simultaneous maximum power point tracking in hybrid AC and DC converters.

2 Maximum Power Extraction from SPV Array

The partial shade has more influence on series-connected SPV modules in comparison to parallel-connected modules. The multiple peaks on the P-V curve are mainly presented due to series connection in any arrangement of SPV array. The general I-V and P-V characteristics of series-connected solar PV array characteristics under unequal insolation condition are shown in Fig. 1 for different shadow patterns [17].

Inspection of Fig. 1a, b clearly indicates the following facts:

Current-voltage (I-V) curves Fig. 1a under unequal insolation (partial shadow) conditions have many steps, while the P-V curves Fig. 1b have several peaks. The highest number of peaks equals to the number of modules connected in series (N_s) in a string.

In accumulation to environmental conditions (insolation and temperature), the value of global maximum power (GMP) and the voltage at which it occurs are also dependent on solar array configuration [22]. In recent years, soft computing techniques have been used widely in the MPPT, especially under partial shading conditions, where there is a difficulty to track global MPP. Therefore, for an acceptable result, all ecological conditions (particularly instant weather changes and partial shadowing) must be taken into account in the design process of MPPT. Artificial intelligence (AI)-based techniques can generate suitable solutions for these conditions and AI-based MPPT algorithms are the most accurate and beneficial systems in terms of electrical effectiveness [23, 24]. For the implementation of AI techniques, firstly the problem needs to be formulated. MPPT under the partial shadow is typically a nonlinear problem having multiple peaks in its P-V characteristics.

2.1 Problem Formulation

A nonlinear optimization problem can be formulated in precise terms as given in Eq. (1)

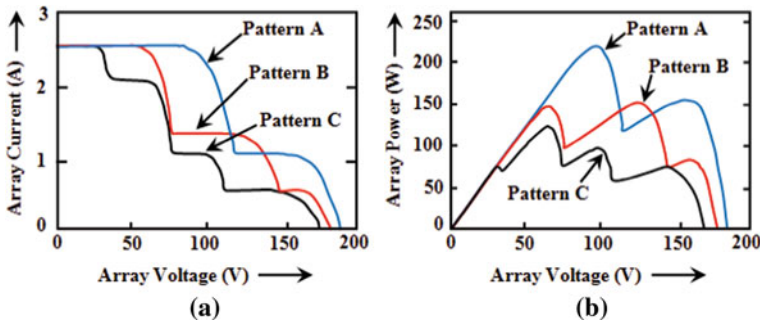


Fig. 1 Characteristics of solar PV array under three dissimilar shadow patterns A, B, and C

$$F(Y) = (y_1, y_2, \dots, y_n) \quad (1)$$

Such that $F(Y)$ is subjected to either minimization or maximization. Subject to the constraint and bounds are given by following Eq. (2).

$$\begin{aligned} g_j(Y) &\geq 0; \quad j = 1, 2, \dots, m \quad \text{and} \\ y_j^L &\leq y_j \leq y_j^U; \quad j = 1, 2, \dots, n \end{aligned} \quad (2)$$

where F is the objective function to be maximized or minimized, y_j 's are variables, g_j is constraint function, y_j^L and y_j^U are the minimum and maximum limits on the variables.

Following objective function may be considered for this problem:

$$F(Y) = \text{Maximization of SPV array power, } P_{pv}$$

The variable $y_j = \text{SPV array current } (I_{pv})$, and the constraint is $I_{pv\max} \geq I_{pv} \geq I_{pv\min}$. Here, $y_j^U = I_{pv\max}$.

3 Soft Computing Techniques for Maximum Power Extraction Under Partial Shadow

In this section, four different AI-based optimization techniques, viz. modified binary search [21], newly proposed random binary search, genetic algorithm (GA), particle swarm optimization (PSO), and differential evolution (DE) [11–13] techniques have been used to solve the above nonlinear optimization problem for tracking global maximum power point (GMPP). The performance of these techniques is compared w.r.t. its quickness and accurate tracking of GMPP.

3.1 Modified Binary Search Algorithm

The conventional binary search is a simple and very useful algorithm whereby many linear problems can be optimized using a linear algorithm to run in logarithmic time [25]. It locates an end value in a sorted array by sequentially removing half of the array from the search space on every iteration.

3.1.1 Algorithm

The different steps of algorithm are as follows

Step 1: Initialization of search space indexes:

Initialize minimum and maximum search index to lowest index (zero) and highest index ($N_s * V_{oc}$).

Step 2: Creation of search spaces

N_s search spaces are created (i.e., 0 to V_{oc} , V_{oc} to $2V_{oc}$, ... $(N_s - 1)V_{oc}$ to $N_s \cdot V_{oc}$) where N_s is no. of modules connected in series.

Step 3: Application of binary search to each of the search space created

Repeat while minimum \leq maximum

- (a) Compare item at the central index with that being hunted (value)
- (b) If item at middle equals value; return middle no.
- (c) If value comes before middle, then reset max to (middle - 1) If value comes after middle, reset min to middle + 1

Step 4: If min > max, value not found.

After 1st iteration, $M/2$ entries left i.e. ($M/2^1$)

After 2nd iteration, $M/4$ entries left ($M/2^2$)

After 3rd iteration, $M/8$ entries left ($M/2^3$)... Search terminates when items to search ($M/2^K$) \rightarrow 1

i.e., $M = 2^K$, $\log_2(M) = K$

where K is total no. of iterations required to complete the binary search.

The search is modified from the conventional binary search that piecewise search is carried out in N_s areas where N_s is no. of modules connected in series (i.e., 0 to V_{oc} , V_{oc} to $2V_{oc}$... $(N_s - 1)V_{oc}$ to $N_s \cdot V_{oc}$) and then maxima from each area has been identified and finally global maxima are tracked in case of partial shadow over SPV array (Fig. 2).

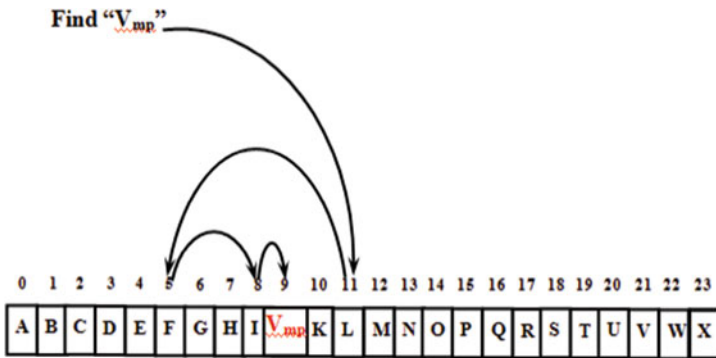


Fig. 2 Schematic diagram of conceptual binary search [25]

3.1.2 Limitation of Modified Binary Search

Modified binary search certainly seems quicker and more effective than a linear search. But the binary search has a drawback: it assumes the list in a sorted order and sometimes the algorithm may be struck into local maxima. As the power available at SPV array, under the partial shadow is not sorted linearly with respect to the operating voltage of array under partial shadow condition.

3.2 Proposed Random Binary Search Algorithm

Random binary search is an amendment to the established binary search algorithm in which it checks at every iteration, the occurrence of the entered element with the middle element of the given set of elements. Random binary search algorithm optimizes the nastiest case of the binary search algorithm by comparing the input element with the first and last element of randomly created search spaces. Inside the created search space, traditional binary search is applied whose steps are clearly mentioned in the previous Sect. 3.1.

For finding maximum power output from SPV array (P_{mp}), the following steps are to be followed in the proposed random binary search.

3.3 Algorithm

The different steps of the algorithm are as follows

Step 1: Initialization of search space limits

Minimum value of the search space is initialized by zero and maximum value is ($N_s * V_{oc}$).

Step 2: Choose no. of search spaces (K)

Search began by generating a K random numbers (r_1, r_2, \dots, r_K) between minimum and maximum value of search space.

Step 3: Creation of search spaces

K search spaces are created between ($0.9 * \text{random no. generated } (r_1, r_2, \dots, r_K)$) and ($1.1 * \text{random no. generated } (r_1, r_2, \dots, r_K)$).

Step 4: Application of binary search to each of the search space created

Traditional binary search is applied to each of K search spaces created in step 3. Here, K which is no. of maximas of each search space is determined by binary search.

Step 5: Identification of global maxima

The maximum of each search space is compared with other, to identify the global maxima in the power-voltage characteristic of SPV array under partial shaded conditions.

Step 6: Solution convergence

Steps 2, 3, and 4 are repeated until the difference of global maxima of two consecutive iterations falls below the tolerance value. This will indicate that the solution has converged.

The random binary search should be more reliable than modified binary search as the search spaces created are random in nature whereas search spaces were fixed in case of the modified binary search algorithm.

The computation time of random binary search depends upon no. of search spaces (K) and no. of iterations performed for solution convergence. If the value of K is more, fewer iterations would be required and more time will be consumed for the overall execution of the algorithm hence the computation time of random binary search may be more than modified binary search algorithm. The computation time may be reduced by decreasing the no. of search spaces (K) but this may increase the no. of iterations required for solution convergence (determination of global maxima on power-voltage characteristics of SPV array under partially shaded conditions). The performance of the proposed random binary search technique is compared with commonly used soft computing techniques, i.e., differential evolution (DE) and particle swarm optimization technique (PSO). For the algorithm of PSO and DE, one may read references [13, 26], respectively.

4 System Investigated

An array of [3 * 3] connected to a Cuk converter is investigated and a schematic connection diagram of the system with MPPT has been shown in Fig. 3 and its detailed specifications are mentioned in Table 2 of Appendix. Nine shadow patterns shown in Table 3 are considered as inputs to the SPV array. The individual element is simulated in MATLAB/Simulink and then the elements are interconnected in the manner shown in Fig. 3.

5 Analysis

The solar PV system shown in Fig. 3 with the specification mentioned in Table 1 is modeled in MATLAB/Simulink Version: 7.10.0.499 (R2010a) on Intel Core i5-based PC as the test platform. The various toolboxes such as Simpower systems, Simelectronics, control system, and Simscape are extensively used during the complete simulation of the SPV system.

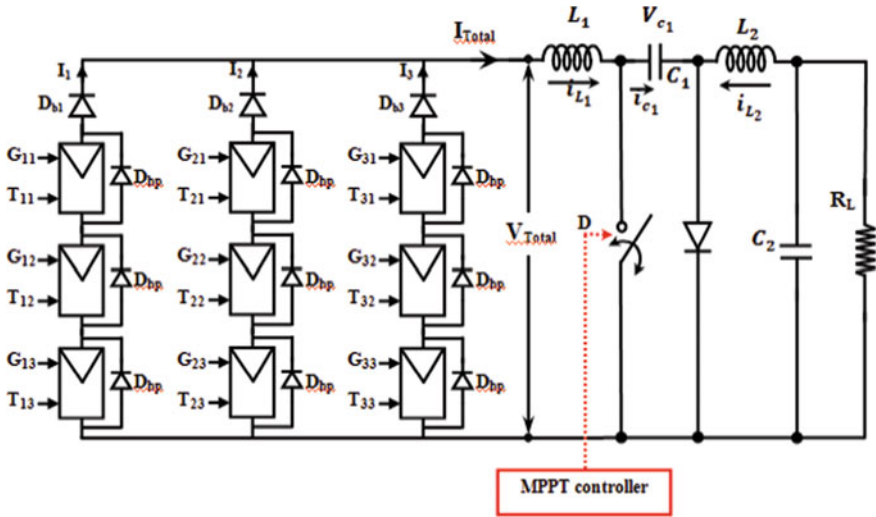


Fig. 3 Schematic connection diagram of system investigated

Table 1 Comparison of different MPPT regarding accuracy and computation time in tracking global MPP

MPPT technique	% Average MPPT error (%)	Computation time range (s)
Modified binary search (MB)	16.29	16.29–21.54
Random binary search (RB)	0.24	53.88–70.97
Particle swarm optimization (PSO)	0.57	141–210
Differential evolution (DE)	0.50	427–529

5.1 Reliability and Computation Time Analysis of Soft Computing MPPT Techniques

Reliability and computation time are two important performance parameters of MPPT techniques. Here, reliability indicates the closeness of tracked maximum power with the actual maximum power (P_{mp}) available at SPV array, whereas computation time shows the total time elapsed in tracking maximum power by MPPT algorithm (i.e., execution time of program). For an MPPT algorithm, it is desirable that its reliability should be high whereas the computation time should be low.

5.1.1 Modified Binary Search

As per the algorithm presented in Sect. 3.1, a MATLAB code has been developed and it is executed for the following parameter: No. of search spaces: $N_s =$ No. of SPV module connected in series $= N_s = 3$.

5.1.2 Random Binary Search

As per the algorithm presented in Sect. 3.2, a MATLAB program has been developed and it is executed for the following parameter: No. of search spaces: $K = 3$;

5.1.3 Differential Evolution (dE)

Population size (MP): 20, crossover rate constant (CR): 0.8, scale factor for mutation process (F) = 0.1, and maximum generations (G_{enmax}) = 50.

5.1.4 Particle Swarm Optimization (PSO)

Number of variable under optimization: 1, number of particles in search space: 20, acceleration constants: $c_1 = c_2 = 1.5$, limits of inertia weights $w_{\text{max}} = 0.9$, $w_{\text{min}} = 0.4$, and maximum iterations, $\text{Iter}_{\text{max}} = 50$.

5.2 Performance Analysis of AI-Based MPPT Technique

Performance comparison of soft computing MPPT techniques as applied to nine insolation patterns shown in Table 2 of Appendix is considered for SPV array of size [3 * 3]. Comparison is made on the basis of computation time and reliability in the tracking of GMPP under non-uniform insolation conditions. Performance of all four AI-based MPPT techniques is analyzed as follows:

5.2.1 Modified Binary (MB) Search MPPT Technique

The % MPPT error for different nine shadow patterns are shown in Fig. 4 and % average error is found as 6.29%, which is large and it is due to striking the algorithm at the local maxima on P-V curve under non-uniform insolation conditions. The largest error 16.29% found is at shadow pattern 1 and computation time found in the range of 16.29–21.54 s. The high % error in MPPT can be credited to linear nature of the MB search algorithm and lowest computation time can be accounted due to its simplicity.

Fig. 4 Percentage MPPT error for modified binary search algorithm

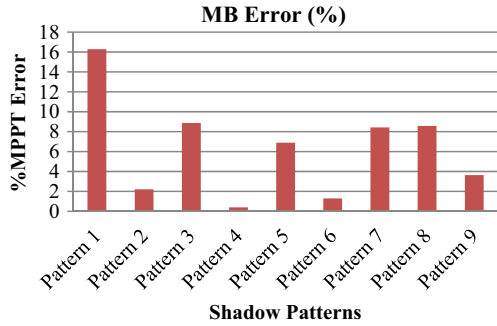
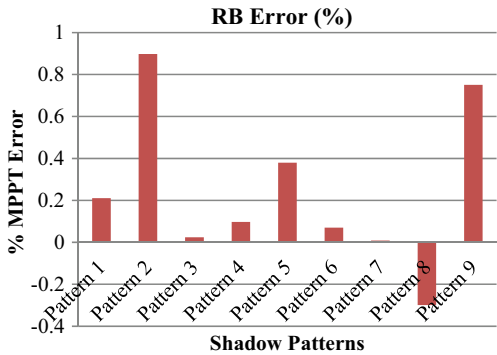


Fig. 5 Percentage MPPT error for random binary search algorithm



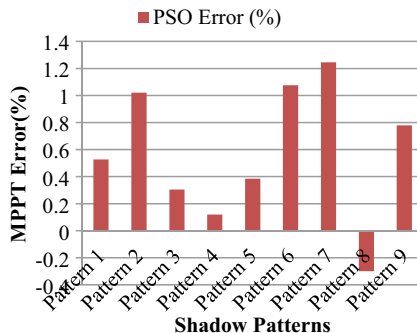
5.2.2 Random Binary (RB) Search MPPT Technique

The % MPPT error for different nine shadow patterns is shown in Fig. 5 and % average error is found as 0.24%, which is very small in comparison to the MB search algorithm. Largest error 0.9% found is at shadow pattern 2 and computation time found in the range of (53.88–70.97) s. Due to its heuristic nature, the % average error is found very less and the slight involvedness of algorithm leads to more computation time in comparison of MB search algorithm. The value of search spaces (K) is taken as three both in MB and RB search methods so that the results can be compared on akin basis.

5.2.3 Particle Swarm Optimization (PSO) Search MPPT Technique

The % MPPT error for different nine shadow patterns is shown in Fig. 6 and % average error is found as 0.57%, which is double in comparison to the RB search algorithm. Largest error 1.24% found is at shadow pattern 7 and computation time found in the range of 141–210 s, which is 2–3 times of the computation time of the

Fig. 6 Percentage MPPT error for particle swarm optimization (PSO) search algorithm

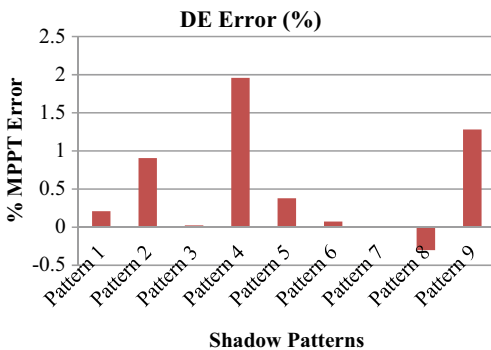


proposed RB search method. It is due to the involved nature of PSO algorithm in comparison of RB search algorithm.

5.2.4 Differential Evolution (dE) MPPT Technique

The % MPPT error for different nine shadow patterns is shown in Fig. 7 and % average error is found as 0.50%, which is slightly less in comparison to the PSO algorithm. Largest error 1.96% found is at shadow pattern 4 and computation time found in the range of 427–529 s which is 3–4 times of the computation time of PSO method. This shows the DE method of MPPT is most involved among the discussed four techniques but the accuracy of the technique is equally good as of RB and PSO methods. Initial population for both the algorithm (DE and PSO) is taken to be 20 so that the results can be compared on common grounds and maximum population is restricted to be 50 in DE algorithms. A sensible control of the two important parameters, viz. the scale factor F and the crossover rate CR can significantly modify the performance of DE. The value of CR normally ranges between 0.4 and 1 and its value is taken 0.8 and value of scaling factor for mutation is taken 0.1 for making faster convergence.

Fig. 7 Percentage MPPT error for differential evolution (DE) search algorithm



5.2.5 Comparative Analysis of AI-Based MPPT Techniques

As previously shown the % error in all four techniques separately in Figs. 4, 5, 6 and 7, a comparison chart of four different MPPT techniques with % error and computation time in tracking MPP is presented in Table 1 for ready reference. Examination of Figs. 8 and 9 clearly indicates that the computation time of modified binary search is lowest but it does not give accurate and reliable results. The results of the new proposed random binary search are tested and compared with conventional PSO and differential evolution soft computing techniques and it is found that computation time of random binary search is much less than these two techniques however reliability is equally good of DE and PSO techniques.

The computation time of search algorithm is directly related to the complexity of the algorithm and examination of Fig. 8 shows the %MPPT error and Fig. 9 shows

Fig. 8 Comparison chart of different MPPT regarding accuracy in tracking global MPP

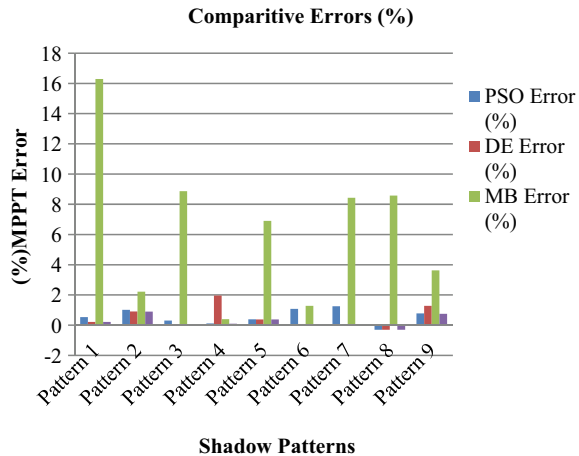
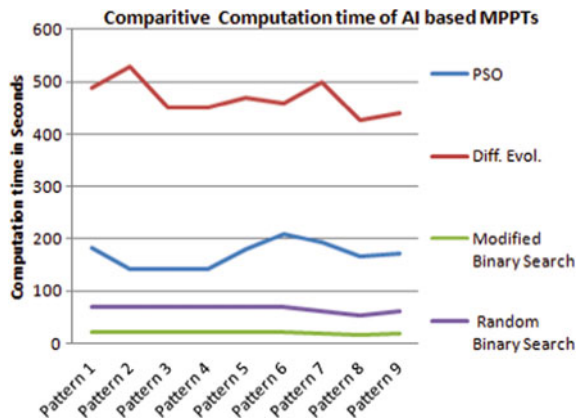


Fig. 9 Comparison chart of different MPPT regarding computation time



the computation time taken by all four AI-based MPPT techniques as applied to the nine shadow patterns.

Figure 9 clearly indicates that random binary search consumes much less computation time in comparison to PSO and differential evolution (DE) techniques. Hence, the random binary search is much simpler than PSO and DE techniques. The computation time is highest for DE-based MPPT and it is least for MB-based MPPT. Highest %MPPT error is observed for MB-based MPPT and least for proposed RB-based MPPT.

In the present work, these techniques are tested for a solar array of [3*3], practically size of the solar array is much larger than this, therefore, the complexity of algorithm and computation time become very important. During the time when the maximum power point is being tracked for the array, the maximum solar power is not fed to the grid, so fast-tracking of MPP plays an important role in deciding the performance of maximum power point tracking (MPPT) techniques. Therefore, it is revealed here that newly proposed random binary search is found best one among these four tested AI-based MPPT techniques under non-uniform as well as uniform insolation conditions on SPV array.

The output of DC/DC converter may be directly fed to the DC load but for transferring generated power to the AC loads or the electrical grid, the output of DC/DC converter must be fed via an inverter (voltage source converter), where the control takes place through control signal, i.e., modulation signal [10].

6 Conclusions

The significant contributions of the research work presented in this paper are:

- i. Four soft computation-based MPPT techniques have been tested for nine different solar insolation patterns over the SPV array and it is revealed that modified binary search method takes least computation time out of these four but the results of this technique are not found reliable, hence this technique is not capable to track the global MPP correctly.
- ii. Comparative studies with the results of random binary search, conventional PSO, and differential evolution techniques for actual values of maximum power show that results of all three techniques are equally accurate, i.e., all three techniques are capable of tracking GMPP under a partial shadow.
- iii. Investigations also show that the computation time of the random binary search technique is much less in comparison to other techniques. It indicates that a random binary search is much simpler than PSO and differential evolution techniques. Hence, the computation (hardware) requirement would be much less for random binary search than that for PSO and DE techniques.
- iv. Finally, investigations reveal that the newly proposed random binary search is superior to other three techniques, in terms of computation time, solution

quality, global exploration, and statistical soundness under non-uniform and uniform insolation conditions on SPV array.

Acknowledgement Authors are thankful to TEQIP-III at RTU-ATU for providing grant under the competitive research scheme (CRS) with project sanction id TEQIP-III/RTU(ATU)/CRS/2019-20/30.

Appendix

See Tables 2 and 3

Table 2 Specifications of system investigated

S. No.	Name of component	Particulars of subcomponent	Specifications
1	Solar array	No. of strings	3
		No. of modules connected in every string	3
		Module specifications	Module specifications at STC: V_{oc} : 21 V, I_{sc} : 2.55 A, V_{mp} : 16.8 V and I_{mp} : 2.2 A
		Model parameters	R_s : 3.407 Ω , R_p : 27.076 Ω , I_{sat} : $108 * 10^{-06}$ A, I_{ph} : 2.54 A, FF: 0.519
2	MPPT block	Algorithm used	Modified binary search, random binary search, differential evolution and particle swarm optimization
		Carrier signal	Sawtooth wave, frequency: 10 kHz, sample time(T_{s_power}): 10^{-6} s
3	DC/DC (C_{uk}) converter	Power electronic device	IGBT/diode
		Snubber capacitance	$1 * 10^5$
		Internal resistance (R_{on})	0 Ω
		Forward voltage of device and diode	0 V, 0 V
		Cuk converter components	$L_1 = 23$ mH, $L_2 = 44$ mH, $C_1 = 284.25$ μ F and $C_2 = 5$ μ F
4	Load	R_L (resistive load)	15 Ω and 25 Ω

Table 3 Various insolation patterns for SPV array of [3 * 3]

Shade pattern	Insolation pattern	V_{mp} (V)	I_{mp} (A)	P_{mp} (W)
1	$G_{11} = G_{12} = G_{13} = 0.9\text{Sun}$, $G_{21} = G_{22} = G_{23} = 0.7\text{Sun}$, $G_{31} = G_{32} = G_{33} = 0.4\text{Sun}$	39.42	3.91	154.21
2	$G_{11} = G_{21} = G_{31} = 1\text{Sun}$, $G_{12} = G_{22} = G_{32} = 0.8\text{Sun}$, $G_{13} = G_{23} = G_{33} = 0.5\text{Sun}$	24.58	6.14	151.01
3	$G_{11} = G_{12} = G_{13} = 1\text{Sun}$ $G_{21} = G_{23} = G_{31} = G_{32} = G_{33} = 1\text{Sun}$, $G_{22} = 0.5\text{Sun}$	28.69	7.49	215.13
4	$G_{11} = G_{12} = G_{13} = G_{21} = 1\text{Sun}$, $G_{22} = G_{23} = G_{31} = G_{32} = G_{33} = 0.5\text{Sun}$	28.52	5.70	162.58
5	$G_{11} = G_{12} = G_{13} = 1\text{Sun}$ $G_{21} = G_{22} = G_{23} = 1\text{Sun}$ $G_{31} = G_{32} = G_{33} = 0.4\text{Sun}$	38.24	5.41	206.93
6	$G_{11} = G_{12} = G_{13} = G_{21} = 1\text{Sun}$, $G_{22} = G_{23} = G_{31} = G_{32} = G_{33} = 0.5\text{Sun}$	37.18	4.19	156.09
7	$G_{11} = G_{12} = G_{13} = 0.4\text{Sun}$ $G_{21} = G_{22} = G_{23} = 0.6\text{Sun}$ $G_{31} = G_{32} = G_{33} = 0.8\text{Sun}$	34.1	4.55	155.38
8	$G_{11} = G_{12} = G_{13} = 1\text{Sun}$ $G_{21} = G_{22} = G_{23} = 0.8\text{Sun}$ $G_{31} = G_{32} = G_{33} = 0.5\text{Sun}$	36.74	5.85	215.13
9	$G_{11} = G_{12} = G_{13} = 0.5\text{Sun}$ $G_{21} = G_{22} = G_{23} = 0.5\text{Sun}$ $G_{31} = G_{32} = G_{33} = 0.8\text{Sun}$	37.45	3.19	119.60

References

1. Subudhi B, Pradhan R (2013) A comparative study on maximum power point tracking techniques for photovoltaic power systems. *IEEE Trans Sustain Energy* 4(1):89–98
2. Aureliano M, Galotto L, Poiltronieri L (2013) Evaluation of the main MPPT techniques for photovoltaic applications. *IEEE Trans Ind Electron* 60(3):1156–1167
3. ESRAM T, Chapman P (2007) Comparison of photovoltaic array maximum power point tracking techniques. *IEEE Trans Energy Convers* 22(2):439–449
4. Qiang M, Mingwei S, Liying L, Guerrero JM (2011) A novel improved variable step-size incremental-resistance MPPT method for PV systems. *IEEE Trans Ind Electron* 58(6):2427–2434
5. Elgendy MA, Bashar Z, Atkinson DJ (2013) Assessment of the incremental conductance maximum power point tracking algorithm. *IEEE Trans Sustain Energy* 4(1):108–117
6. Bader NA, Khaled HA, Finney SJ, Williams BW (2013) A maximum power point tracking technique for partially shaded photovoltaic systems in micro grids. *IEEE Trans Ind Electron* 60(4):1–4
7. Koutroulis E, Blaabjerg F (2012) A new technique for tracking the global maximum power point of PV arrays operating under partial-shading conditions. *IEEE J Photovolt* 2(2):642–649
8. Ahmad Al N, Rached D (2012) Efficiency optimization of a DSP-based standalone PV system using fuzzy logic and dual-MPPT control. *IEEE Trans Ind Inf* 8(3):573–580
9. Xiao L, Yaoyu L, John ES (2014) Maximum power point tracking for photovoltaic system using adaptive extreme seeking control. *IEEE Trans Control Syst Technol* 25(3):352–359

10. Peter PK, Agarwal V (2012) The input resistance of a reconfigurable switched capacitor DC–DC converter-based maximum power point tracker of a photovoltaic source. *IEEE Trans Power Electron* 27(12):574–581
11. Liu YH, Huang SC, Huang JW, Liang WC (2012) A particle swarm optimization -based maximum power point tracking algorithm for PV systems operating under partially shaded conditions. *IEEE Trans Energy Convers* 27(4):1027–1030
12. Ishaque K, Salam Z, Amjad M, Mekhilef S (2012) An improved particle swarm optimization (PSO)-based MPPT for PV with reduced steady-state oscillation. *IEEE Trans Power Electron* 27(8):3627–3634
13. Azab M (2012) Optimal power point tracking for stand-alone PV system using particle swarm optimization. *IEEE Trans Power Syst* 27(4):1978–1985
14. Latham AM, Pilawa RP, Odame K, Sullivan CR (2013) Analysis and optimization of maximum power point tracking algorithms in the presence of noise. *IEEE Trans Power Electron* 28(7):3479–3486
15. Hartmann LV (2013) Combining model-based and heuristic techniques for fast tracking the maximum-power point of photovoltaic systems. *IEEE Trans Power Electron* 28(6):2875–2881
16. Kjer BS (2012) Evaluation of the hill climbing and the incremental conductance, maximum power point trackers for photovoltaic power systems. *IEEE Trans Energy Convers* 27(4):316–324
17. Young HJ, Jung DY, Kim JG, Kim JH, Lee TW, Won CY (2011) A real maximum power point tracking method for mismatching compensation in PV array under partially shaded conditions. *IEEE Trans Power Electron* 26(4):1001–1007
18. Dhimish M (2019) Assessing MPPT techniques on hot-spotted and partially shaded photovoltaic modules: comprehensive review based on experimental data. *IEEE Trans Electron Devices* 66(3):1132–1144
19. Al-Soeidat M, Lu DD-C, Zhu J (2018) An analog BJT-tuned maximum power point tracking technique for PV systems. *IEEE Trans Circuits Syst II* 66:637–641
20. Başoğlu ME (2018) An improved 0.8VOC model based GMPPT technique for module level photovoltaic power optimizers. *IEEE Trans Ind Appl* 55:1913–1921
21. Saikrishna Goud J, Kalpana R, Singh B (2018) A hybrid global maximum power point tracking technique with fast convergence speed for partial shaded PV systems. *IEEE Trans Ind Appl* 54:5367–5376
22. Saikrishna Goud J, Kalpana R, Singh B, Kumar S (2018) Maximum power point tracking technique using artificial bee colony and hill climbing algorithms during mismatch insolation conditions on PV array. *IET Renew Power Gener* 12:1915–1922 ISSN 1752-1416
23. Lin WM, Hong CM, Chen CH (2011) Neural-network-based MPPT control of a stand-alone hybrid power generation system. *IEEE Trans Power Electron* 26(12):3571–3578
24. Shi Y, Eberhart RC (2001) Fuzzy adaptive particle swarm optimization. In: *Proceedings of the congress on evolutionary computation 2001*, Seoul, Korea. IEEE Service Center, pp 101–106
25. Thomas CH, Leiserson CE, Clifford S, Rivest RL (2009) *Introduction to algorithms*, 3rd edn. MIT Press and McGraw-Hill, Cambridge. ISBN 0-262-03384-4
26. Lata Agarwal K (2017) A performance maximization of small scale grid connected solar photovoltaic power plants. Ph.D. thesis, J.N.V.U., Jodhpur, Rajasthan, India

Prevention Against Internal Attack via Trust-Based Detection for Wireless Mesh Networks



Amit Kumar Roy  and Ajoy Kumar Khan 

Abstract Wireless mesh networks (WMNs) as compared to other conventional networks had emerged as the most popular choice in today's era due to its distributed nature. WMNs allow multi-hop communication with the capability of self-healing. Due to its distributed nature, internal attacks such as blackhole, wormhole, and DOS attack could be easily launched to degrade the overall performance of WMNs. The attack disrupts the normal operation of routing protocols and causes a large amount of packet drop between mesh entities. Therefore, to ensure secure routing, it is essential to compute the trustworthiness of each node and to detect the malicious nodes within the WMNs. In this paper, we had proposed a trust-based detection algorithm that ensures the detection of malicious nodes in WMNs. The experimental result of our proposed protocol ensures an efficient detection of the malicious node with a higher detection rate.

Keywords Security attacks · Trust model · Routing protocols

1 Introduction

Wireless mesh networks presently had become an appealing network as compared to other conventional networks due to its advanced technology. WMNs had embedded with advanced features which make it capable of self-organizing, self-configuring, and minimal upfront investment in deployment. The architecture of WMN divided into three tiers, the top-tier consists of gateway routers, the middle-tier is known as the backbone of WMNs consists of mesh routers (MRs), and the bottom-tier consists of mesh clients (MCs). Gateway routers are connected to the Internet through wired networks, the mesh routers (MRs) are connected to the gateway routers in multi-hop

A. K. Roy (✉) · A. K. Khan
Assam University, Silchar., Assam, India
e-mail: amitkroy12@gmail.com

A. K. Khan
e-mail: ajoyiitg@gmail.com

© Springer Nature Singapore Pte Ltd. 2021
G. S. Hura et al. (eds.), *Advances in Communication and Computational Technology*, Lecture Notes in Electrical Engineering 668,
https://doi.org/10.1007/978-981-15-5341-7_8

fashion [1]. Therefore, when a mesh client wants to get access to the Internet, it sends its request to MRs and then the MRs forward the request toward the gateway router in a multi-hop fashion. Therefore, cooperation and coordination among mesh routers (MRs) is an important factor for WMNs to influence its performance. The major functionality of mesh routers in a backbone is to offer secure network services to its clients [2, 3]. Therefore, a secure routing protocol for forwarding data packets toward the gateway is required for WMNs. At the backbone of WMNs, some of the mesh routers (MRs) deny to forward the data packets for other mesh routers (MRs) and behaves as a malicious node by violating the rules of routing protocols. This misbehavior act allows the malicious node to preserve their bandwidth and power by not utilizing them without forwarding the data packets for other nodes. Therefore, the selfish behavior of MRs degrades the overall performance of WMNs by dropping packets in a massive amount. Therefore, security is one of the major issues in WMNs. As the traffic of the end-user is forwarded in multi-hop fashion among MRs at the backbone, therefore, confidentiality and preservation of the user traffic is a major requirement. The nature of traffic transmission in a broadcast fashion through multi-hop communications among MRs leads to various security issues in WMNs. One of the important parts of WMNs is their routing services among MRs that are vulnerable to a number of threats from adversaries both internal and external to the network. A detailed survey of such routing attacks had made in [4]. Therefore, to enforce secure cooperation and coordination among nodes, various collaboration schemes had proposed in the literature [5] to detect the selfish nodes in the networks.

Several mechanisms had proposed that are based on frameworks to trust and believe the nodes in the networks and attempt to identify misbehaving nodes by suitable decision-making systems and then isolate or punish them [6]. In this paper, we had presented a detection algorithm that detects the malicious nodes in WMNs. Our proposed algorithm is mainly designed for the detection of malicious nodes that violets the rule of AODV routing protocols at the backbone of WMNs.

2 Related Works

Routing protocol plays an important role in forwarding packets between source and destination through relay nodes. Therefore, a massive research work had carried out in the past for implementing a secure routing protocols. As routing is one of the major functionalities of a network, an attacker could easily target the routing protocol to compromise the security of a network. Even though a lot of work had done in the past to overcome the security problems for routing protocols, but still the existing work suffers from certain security challenges as discussed in this section.

In 2008, Sen proposed an efficient algorithm for the detection of selfish packet dropping nodes in wireless mesh networks [7]. The algorithm is an extension work to [8] based on local observation of each node in the network. The algorithm involves the clustering technique which observed the nodes behavior locally within fixed a range or domain. The algorithm involves two nodes, monitor node and monitored

node where the monitor node observes the behavior of the monitored node locally by using a finite state machine. However, the algorithm suffers from computational overhead due to the clustering of WMNs. Moreover, the detection is based on local observation which is not efficient for large networks as WMNs. In 2002, Papadimitratos and Haas proposed a secure routing protocol for mobile ad hoc networks that secure the route discovery process against non-colluding Byzantine adversaries [9]. The protocol assures secure routing between the source node and the destination node. Without relying on any intermediate nodes the protocol provides end-to-end security association through the addition of extra fields in the routing protocol header that contains the query sequence number QSEC, query identifier number QID, and a 96 bit MAC field. The destination node responds to RREQ with an appropriate QSEC and QID to the source node. The source node validates the destination node by comparing the QSEC and QID in RREP send by the destination node. If the QSEC and QID of currently pending query matches with the QSEC and QID in RREP, then the source node accepts an RREQ. Vulnerabilities of SRP are identified in [10, 11] employing a formal verification approach. In 2017, Regan and Manickam proposed a security mechanism to resists the wormhole attack which forms a loophole tunnel and drops the packets later on. The mechanism was based on adaptive learning in collaboration with Blooms filter method. The mesh router acts as a cluster head identifies the malicious nodes forming the wormhole tunnel and later isolates them from the mesh network. As throughout the network the detection responsibility was on the cluster head, therefore, it puts an extra burden to the cluster head apart from its normal duties like simply forwarding the packets ahead toward the gateway router. Handling huge amount of traffic from mesh clients and verifying each packet for authentication at a time results in authentication delay [12]. In 2015, Subhash et al. proposed a mechanism for searching a valid neighbors among peer ones in a mesh network. The mechanism was carried out in two levels: firstly, a neighbor discovery process in which a ranking method with the value of at most 1 was considered and secondly, a link verification process where a check request message had considered for verifying the link between mesh entities [13]. Gao et al. in 2016 proposed a protocol for mutual authentication among mesh nodes. The authentication process was carried out by collaborating the identity-based group signature and Proxy group signature of mesh nodes [14]. Later, in 2017, Niizuma and Goto proposed an efficient authenticated path formation protocol to minimize the hardware deployment costs [15]. In their proposed work, the authentication took place between the users and APs by locally verifying the digital certificates as the authentication credentials. In 2015, Gaur and Pant proposed a trust computation metric based on nodes impulsive behavior to detect malicious nodes in ad hoc networks. The proposed protocol offers trustworthy communication in real-life applications such as healthcare through secure and trusted clustering to ensure security [16]. Later, in 2016, Singh et al. proposed a hybrid technique to ensure security against the wormhole attack (WRHT) [17]. The protocol is based on two schemes-watchdog and Delphi for dual detection of wormhole attacks. The WHRT makes the decision on two parameters—time delay probability and packet loss probability to establish a secure path between source and destination. Guo et al. in 2013 proposed a secure access control mechanism to ensure

guarding against internal attacks in distributed networks [18]. The protocol is based on a secure and efficient trust model using Bayesian theory and Diffie–Hellman key agreement protocol. The trust model detects the malicious nodes in the network by calculating the trust values of each individual node in the network to establish a secure route between the source node and the destination node. The protocol involves the clustering technique where each domain consists of a cluster head which calculates the trust values of nodes within each domain. Although the effectiveness of the low-energy adaptive clustering hierarchy (LEACH) routing protocol had demonstrated, security is one of its problems. Moreover, if the cluster head gets malicious the protocol fails to provide secure routing in distributed networks. Zhang et al. in 2013 proposed a virtual currency to simulate cooperation in self-organized mobile ad hoc networks based on a reward-based scheme [19]. To simulate the cooperative packets among each individual node in the wireless ad hoc network, the reward-based scheme uses virtual currency. This virtual currency is assumed as a credit provided to each node in the network based on their forwarding behavior. All nodes need to forward for others to earn credits for their own expenses. Also, reward-based scheme employee tamper-proof hardware technique that prevents illegal credit manipulation from adversaries. However, the proposed scheme suffers from inconsistency, where the nodes not having any packets to forward may not get a chance to earn any credits in the network, especially nodes at the edge of the WMN topology. Abdel-Azim et al. in 2018 proposed an intrusion detection system to ensure security against anomalies within the network [20]. The protocol is based on the fuzzy inference system (FIS) which is further optimized via an adaptive neuro-fuzzy inference system (ANFIS) using the genetic algorithm (GA) to detect the anomalies.

Although a variety of work had done in the past, related to secure routing in different types of networks, but still, they suffer from vulnerabilities and other issues as mentioned above. Moreover, some of the existing works are not suitable for WMNs due to their distributed environment. Therefore, in our proposed protocol, we had designed a detection algorithm to detect the malicious nodes in WMNs, which drops the packets which it requires to forward for other nodes. Through experimental result, our proposed protocol ensures an efficient detection of the malicious node with a higher detection capability.

3 Proposed Protocol

The proposed protocol is based on the detection of malicious nodes that drop packets of other nodes during multi-hop forwarding between source and destination. The proposed protocol allows the routing protocol to choose an alternate secure path toward the destination once the malicious nodes are detected between source and destination. Based on the trust values of each node, our proposed protocol detects the malicious nodes in WMNs. The trust value of each node depends on its current

behavior which the monitor node experiences from its neighboring nodes. We set a threshold value μ to 10% for the packet drop ratio. When a monitor node experiences its neighboring node dropping more than 10% of the packets, the trust value for this neighbor node is upgraded.

3.1 Trust Model of the Proposed Protocol

Starting phase: This phase assigns a default trust value to every node in a network which signifies that the monitoring node neither trusts nor distrusts its neighboring nodes.

Upgrading phase: This phase is used for upgrading the trust value based on the current behavior of the neighboring nodes. We use the following criteria to upgrade the trust value for the neighboring nodes. The upgraded trust value T_u is given as

$$T_u = \text{Packet Drop Ratio (DR)} \quad (1)$$

Database phase: This phase stores the trust information of each node and allows to extract information about stored trust values.

Monitor phase: This phase is used to adjust the trust values of neighboring nodes by fixing the threshold value between 0 and 1. We set the threshold value μ to 10% which equals to 0.5 between 0 and 1. If the drop rate of a neighboring node is higher than 10%, then the trust value of the neighbor node is decreased. If the drop rate of a neighboring node is lower than 10%, then the trust value of the neighbor node is increased.

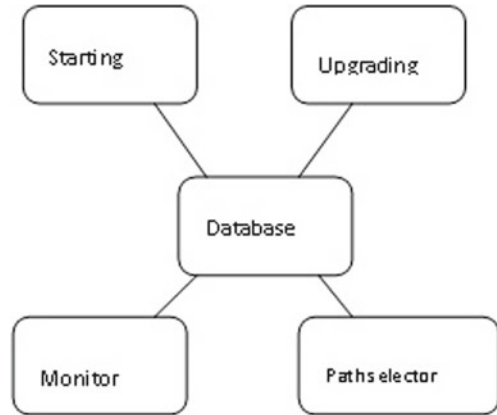
Path selector phase: This phase selects the path between two nodes with higher trust values. If the trust value between two nodes is less than the threshold value μ than that path is ignored and an alternate path is selected with trust value greater than the threshold value.

3.2 Trust-Based Detection Algorithm

1. Initially, the trust value is set to 0.5 for each node. At this point, the neighbor nodes could neither be trusted nor distrusts by the monitor node.
2. If the neighbor node had more than 10% of packet drops, then its trust value reduces starting from 0.5 toward 0 and then concludes as a malicious node.

$$0 \leq p < 0.5 \quad (2)$$

where p is a probability. Decrease of trust value from 0.5 toward 0, increases the chances of more packet drop beyond 10%.

Fig. 1 Trust model

3. If the neighbor node had less than 10% of packet drops, then its trust value increases starting from 0.5 toward 1 and then concludes as a non-malicious node.

$$0.5 < p \leq 1 \quad (3)$$

where p is a probability. The increase of trust value from 0.5 toward 1, increases the chances of less packet drop below 10% (Fig. 1).

4 Experimental Result

The proposed algorithm is simulated with NS3. The simulation results had analyzed with three performance metrics.

1. Packet delivery ratio (PDR): The ratio of the number of data packets sent by the source node and the number of packets received by the destination node in the next hop.

$$\text{PDR} = \left(\frac{R_x}{T_x} \right) \times 100 \quad (4)$$

where R_x is the total packets received and T_x is the total packet send.

2. Packet drop ratio (DR): If a sending node i sends “ x ” number of packets to a receiving node j and the receiving node j only forward “ y ” number of packets.

$$\text{DR} = \left(\frac{x - y}{x} \right) \times 100 \quad (5)$$

3. Detection rate: The detection of a malicious node in WMNs increases with the increase in packets drop ratio above 10% by the malicious node.

4.1 Performance Analysis

To evaluate the effectiveness of our proposed protocol, we consider 25 nodes (mesh routers MRs) in the presence of a malicious node and analysis the fluctuations in the packets drop of the flows. These fluctuations reflect the detection rate of a malicious node in wireless mesh networks (WMNs). We start a flow between MR 0 denoted as Sender1 and MR 24 denoted as Receiver in the presence of malicious nodes during the time period 10–100 s. MR 1 as a neighbor node to MR 0, it convinces the MR 0 that it had a shorter path toward the destination node MR 24; therefore, MR 0 forward the packets to MR 1. On receiving the packets, MR 1 drops all the packets which it requires to forward on behave of MR 0 at the time interval of 10–50 s (bad flow) shown in Fig. 2. At the same time period 10–50 s (good flow) shown in Fig. 2, the flow from MR 1 enjoys good packet delivery toward its destination node MR 24. Therefore, this misbehavior act of MR 1 in regards of packets send and packets drop, allows the MR 0 to conclude MR 1 as a malicious node. After detection of a malicious node, MR 0 purges their routing entry through MR 1 and re-route their traffic.

Table 1 shows two different flows performed by malicious node MR 1. Row one shows that MR 1 drops all the packets received from MR 0 at the time interval of 10–50 s. Row two shows that MR 1 forward all of its packets to the destination node MR 24 at the same time intervals of 10–50 s. In columns two and three, PDR and DR are the packet delivery ratio and packet drop ratio value for two different flows.

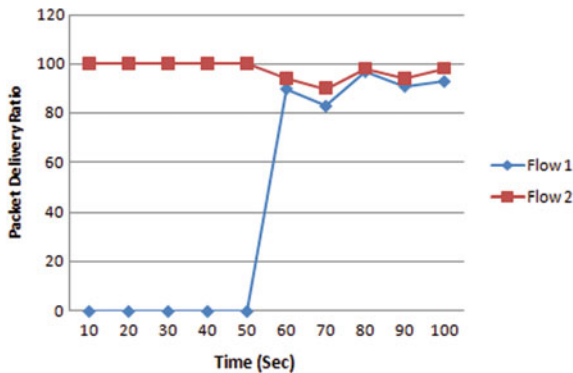


Fig. 2 Flow 1 (bad flow) versus flow 2 (good flow)

Table 1 Bad flow and good flow at same time intervals

Flows	PDR (%)	DR (%)	Time (s)
Flow 1 (bad flow)	0	100	10–50
Flow 2 (good flow)	100	0	10–50

5 Conclusion

In this paper, we had proposed an algorithm for the detection of malicious nodes that violets the normal operation of the AODV routing protocol. Our proposed protocol through simulation results shows that it efficiently detects the malicious nodes in WMNs. The experiment of the proposed protocol is done in network simulator. In the future, the work could be further extended to achieve a more reliable and efficient detection protocol for WMNs by embedding new ideas to the proposed protocol.

References

1. Akyildiz IF, Wang X (2005) A survey on wireless mesh networks. *IEEE Comm Mag* 9:S23–S30
2. Piechowiak M, Zwierzykowski P, Owczarek P, Wasowicz M (2016) Comparative analysis of routing protocols for wireless mesh networks. In: 10th international symposium on communication systems, networks and digital signal processing (CSNDSP). IEEE, Prague, Czech Republic, pp 1–5. <https://doi.org/10.1109/CSNDSP.2016.7573902>
3. Moudni H, Er-rouidi M, Mouncif H, El Hadadi B (2016) Secure routing protocols for mobile ad hoc networks. In: International conference on information technology for organizations development (IT4OD). IEEE, Fez, Moroccopp, pp 1–7. <https://doi.org/10.1109/IT4OD.2016.7479295>
4. Zhang W, Wang Z, Das SK, Hassan M (2008) Security issues in wireless mesh networks. Springer, Boston, MA, pp 309–330
5. Santhanam L, Xie B, Agrawal DP (2008) Selfishness in mesh networks: wired multihop MANETs. *IEEE Wireless Commun* 15:16–23
6. Altman Y, Keren AY, U.S. Patent No. 9,479,523, U.S. Patent and Trademark Office, Washington, DC
7. Sen J (2010) An efficient algorithm for detection of selfish packet dropping nodes in Wireless Mesh Networks. In: International conference on computer information systems and industrial management applications (CISIM). IEEE, Krakow, Poland, pp 283–288. <https://doi.org/10.1109/CISIM.2010.5643647>
8. Wang B, Soltani S, Shaprio JK, Tan PN, Mutka M (2008) Distributed detection of selfish routing in wireless mesh networks. Technical Report MSU-CSE-06-19, Department of Computer Science and Engineering, Michigan State University
9. Papadimitratos P, Haas ZJ (2002) Secure routing for mobile ad hoc networks. In: Communication networks and distributed systems modeling and simulation conference (No. CONF). SCS, San Antonio, TX, pp 1–13
10. Buttyan L, Thong TV (2010) Formal verification of secure ad-hoc network routing protocols using deductive model-checking. In: Proceedings of the wireless and mobile networking conference (WMNC). IEEE, Budapest, Hungary, pp 1–6. <https://doi.org/10.1109/WMNC.2010.5678752>
11. Pervaiz MO, Cardei M, Wu J (2005) Routing security in ad hoc wireless networks. Springer, Boston, MA, pp 117–142. <https://doi.org/10.1007/978-0-387-73821-5-6>
12. Regan R, Manickam JML (2017) Detecting and denying malicious behavior using adaptive learning based routing protocols in wireless mesh network. *Appl Math Inf Sci* 11:1155–1162
13. Subhash P, Ramachandram S (2015) Secure neighbour discovery in wireless mesh networks using connectivity information. In: International conference on advances in computing, communications and informatics (ICACCI). IEEE, Kochi, India, pp 2061–2066. <https://doi.org/10.1109/ICACCI.2015.7275920>

14. Gao T, Peng F, Guo N (2016) Anonymous authentication scheme based on identity-based proxy group signature for wireless mesh network. *EURASIP J Wirel Commun Netw*. <https://doi.org/10.1186/s13638-016-0685-2>
15. Niizuma T, Goto H (2017) Easy-to-deploy wireless mesh network system with user authentication and WLAN roaming features. *IEICE Trans Inf Syst* 100:511–519
16. Gaur MS, Pant B (2015) Trusted and secure clustering in mobile pervasive environment. *Human-centric computing and information sciences*. Springer, Berlin, Heidelberg. <https://doi.org/10.1186/s13673-015-0050-1>
17. Singh R, Singh J, Singh R (2016) WRHT: a hybrid technique for detection of wormhole attack in wireless sensor networks. *Mob Inf Syst*. <https://doi.org/10.1155/2016/8354930>
18. Guo J, Zhou X, Yuan J, Xu H (2013) Secure access control guarding against internal attacks in distributed networks. *Wirel Pers Commun* 68:1595–1609
19. Zhang Z, Long K, Wang J (2013) Self-organization paradigms and optimization approaches for cognitive radio technologies: a survey. *IEEE Wirel Commun* 20:36–42
20. Abdel-Azim M, Salah HED, Eissa ME (2018) IDS against black-hole attack for MANET. *IJ Netw Sec* 20:585–592

Sensor-Based Alarm System for Preventing Crop Vandalization by Birds in Agricultural Regions



Siddhanta Borah, Ankush Kumar Gaur, and J. Arul Valan

Abstract Farming is the most significant portion of Indian economy. It contributes 17–18% in India's gross domestic product (GDP) accordingly Indian economic survey of year 2018 and employs more than 50% of the workforce in India. This paper presented a microcontroller-based system to protect agriculture land from crop vandalization by designing a band-pass filter (BPF) with the help of a sound sensor. Presently most of our agriculturists follow traditional approaches to protect their agricultural area from birds attack. But these approaches are almost ineffective and time-consuming. This paper aims to solve the above-defined problem economically and effectively by delivering an automated surveillance system to our agriculturists. We examined this system in the campus of School of Agricultural Sciences & Rural Development Medziphema, Nagaland.

Keywords Band-pass filter (BPF) · Global system for mobile (GSM) · Relay · Sound sensor · Alarm

1 Introduction

The aim of this paper is to describe the automated surveillance system which targets to address the problem of crop vandalization by birds. It defines the difficulties that are handled by our agriculturists due to birds attack on their crop production area and plantations. And it also expresses the existing solutions and approaches that have been adopted to target this problem. The main objective of this paper is to

S. Borah · A. K. Gaur (✉) · J. A. Valan
National Institute of Technology, Nagaland, India
e-mail: ankushkumarddm@gmail.com

S. Borah
e-mail: borahsidd@gmail.com

J. A. Valan
e-mail: valanmspt@yahoo.co.in

give an effective solution to this problem so that the financial harms suffered by our agriculturists are reduced and they can get a decent crop yield.

Let see the images which show that how the sparrow birds attack paddy crops in Nagaland's agricultural area. The condition of crop before and after the attack is shown in Figs. 1 and 2. And some traditional ways that are used by that place farmers to handle this problem are shown in Figs. 3 and 4. Also, it is found that the methods which are used by the farmers are almost ineffective and that are not much enough to handle the problem.

Fig. 1 Birds attack on paddy crop



Fig. 2 Color of crop after attack



Fig. 3 Method-1 using polypropylene ribbon



Fig. 4 Method-2 using hanging empty pots in the air



To solve this problem, there is a demand of advanced system which could protect the crop field effectively from birds attack. Pooja et al. [9] have proposed a system in which passive infrared sensor (PIR) was used to detect intruder and radio frequency identification (RFID) was used to differentiate intruder and authorized person. They used a camera module with Raspberry Pi board for real-time monitoring of agriculture field.

Another system was proposed by Santhiya et al. [10] to protect agriculture land from animals. They used RFID technology to know the presence of animal in agriculture land. The RFID tag was inserted under an animal skin. RFID reader detects

the presence of animal when animals enter into the farm land and send the message to authorized person using GSM. They also used irritation noise speaker and fogging machine for automatic repellent of those animals. Giordano et al. [11] have demonstrated an Internet of things (IoT) application to monitor agriculture field using different sensors and actuators with the help of wireless sensor network technologies.

IoT technologies are used in agriculture land to monitor real-time data from anywhere at any time [12]. Different sensor nodes are used to collect information such as soil moisture, temperature, and weather condition. Using PIR sensor, RFID and IoT technologies can able to detect only the wild animals. Such systems are not efficient to prevent small bird (sparrow) attack in agriculture field. One of the major disadvantages of PIR sensor is that it can detect any movement. Some researchers also developed system based on combination of camera and PIR sensors. But such systems are not convenient to be used by our farmer from the cost point of view and also need prior training and knowledge to operate such system.

In this paper, we presented a cost-effective, ease of use, and ease of installation system for our farmer having capability to protect crop field effectively mainly from sparrow bird attack. To design the system, a sound sensor is used. The sound sensor output is the input of BPF circuit. The BPF is designed to detect only the sparrow bird voice frequency, and it will not detect other disturbances (sound) from surroundings. The presented system has a small microphone with an amplifier. The analog output of amplifier is filtered using band-pass filter (BPF) to detect the bird's voice frequency [1]. Two comparators are used at the output of band-pass filter (BPF) to get digital output when the desired frequency range is detected by microphone. The controller part mainly consists of W78E052D 8051 series microcontroller, GSM, four light-emitting diodes (LEDs) for indication and a 12 V relay to control an alarm system. The system is powered by 12 V lead-acid battery with a solar charging circuit. The presented system is superior than the other existing systems because it is less complex and needs less maintenance, low cost, and ease of installation process.

To reduce the cost of the system, a less expensive 8051 controller is used. The sound sensor used for this purpose covers a range up to 7 m in radius. The total cost involved to make the system is given in Table 1.

The presented hardware prototype is able to cover an area around ($A = \pi r^2 = 3.14 \times 7 \times 7 = 153.86$) 154 m². We can increase the range of the system by using high sensitivity and long-range sound sensor.

This paper will further put the discussion of the work in details regarding the architecture, methodology, result and analysis, and the conclusion of this project. Control system architecture for automated surveillance system used in this work is described below.

2 Control System Architecture

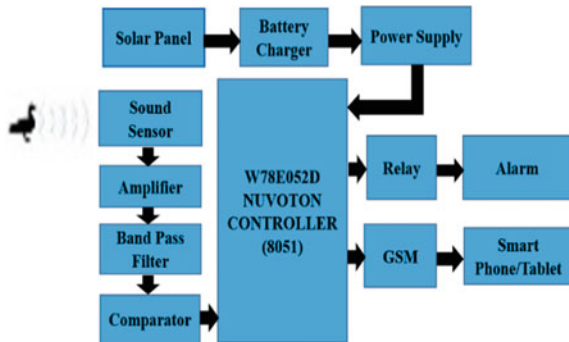
Overall control system is explained in this section. In Fig. 5, block diagram representation of the system is shown.

Table 1 List of hardware components

S. No	Description	Part number	Manufacturer	Cost/unit
1	Solar panel	12 V–10 W	Loom solar	750 ₹
2	Variable voltage regulator	LM317	Texas instrument	30 ₹
3	12 V lead–acid battery	12 V–5A	Amptek	650 ₹
4	Miscellaneous (diode, resistor, transistor, potentiometer, Zener diode, capacitor, oscillator, reset switch, LED, Veroboard, wires, etc.)			120 ₹
5	OPAMP	LM741	Texas instrument	30 × 4 = 120 ₹
6	Sound sensor	Waveshare 9534	Waveshare electronics	389 ₹
7	Microcontroller	W78E052D	Nuvoton	50 ₹
8	GSM	SIM900/800	Graylogix	750 ₹
9	Relay	12v, 1A	SONGLE	50 ₹
10	Alarm system	SLC-122	IOTA	290 ₹
			Total	3149 ₹

Note Parts are available from different online sources

Fig. 5 Block diagram of system



2.1 Electrical System Design

Electrical system part mainly consists of solar charger circuit. The solar charger circuit is designed to protect from overcurrent and overvoltage. High-efficient solar panel with antireflective tempered glass on the top used in this presented system is of capacity of 10 W, 12 V. Charging time to charge 12 V, 5 A battery is approximately 5–7 h. The solar panel is having maximum power voltage 17.83 V, maximum power current 0.57 A, open-circuit voltage 21.75 V, and short-circuit current 0.61 A.

A 12 V, 5 A lead–acid battery is used as a source of power supply of dimension $15.1 \times 6.6 \times 10$ cm. This battery has an excellent battery backup capability and compatible with solar charger circuit.

2.2 *Electronic System Design*

Electronic system part mainly comprises of two parts namely filter design and controller section. In filter design section, a BPF is designed to detect sparrow bird voice frequency which is within the range of 2–7 kHz. To design the filter circuit, LM741 OPAMP is used. To detect frequency of bird voice, a sound sensor module with amplifier is used. Sound sensor can able to detect frequency range of 50 Hz to 20 kHz, audio signal gain 200 dB, and with operating voltage 3.3–5.3 V.

The GSM module used here is SIM900A. The SIM900A GSM module works with dual band 900/1800 MHz. In this presented system, GSM is used to send real-time information to farmer from agriculture land [7, 8].

The 8051 series Nuvoton microcontroller W78E052D is used here as the main controller unit. The W78E052D controller is an 8-bit microcontroller having 8-Kbyte of flash EPROM, 256 byte of RAM and four 8-bit bidirectional input/output ports. Besides, it has three 16-bit timer/counter and in-built bootloader section to upload the hex file.

A 12 V, 1 A single-pole double-through (SPDT) relay is used along with 2N222A high current transistor to drive the alarm system. The detailed working of the circuit is explained in Sect. 3.

3 *Methodology and Hardware Design*

3.1 *Methodology*

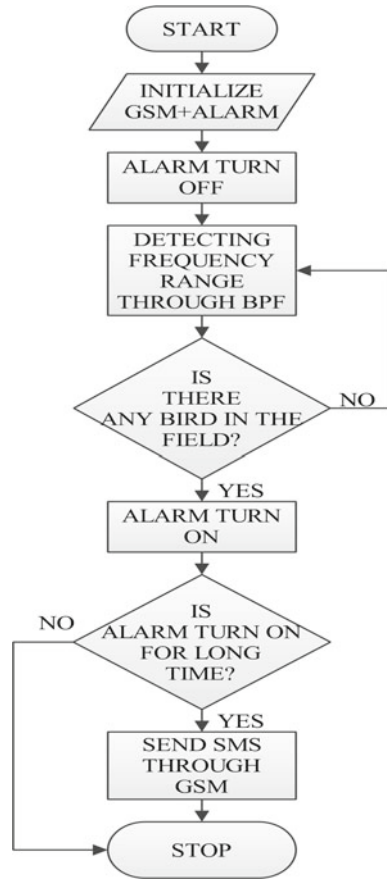
The flowchart of presented model is shown in Fig. 6.

Here, the BPF is designed to detect upper and lower cut-off frequency of bird voice [2]. The filter circuit is designed in such a way that the output will be high if the input frequency is within the range of sparrow bird voice frequency (2–7 kHz). To get high or low output at the end of BPF, two comparator circuits are used.

The low comparator output indicates there is no bird in the agriculture field. If sound sensor detects any frequency voice within the range 2–7 kHz, then output will be high and microcontroller (W78E052D) turns ON an alarm system through relay driver circuit otherwise alarm is turned OFF.

A GSM module is used to send real-time information to farmer. GSM will send message to farmer if alarm system is turned ON for a long time.

Fig. 6 Flowchart to understand how system works



3.2 Hardware Design

3.2.1 Solar Charger Circuit

Solar charger circuit is used to protect the battery from overcurrent and overvoltage. The solar charger circuit shown in Fig. 7 consists of adjustable voltage regulator IC LM317 [3]. The output voltage can be obtained using Eq. 1.

$$V_{out} = V_{R1} \times (1 + R_2/R_1) + I_{adj} \times R_2 \tag{1}$$

The I_{adj} is in the range of micro-ampere so it can be neglected. In the circuit, the 12 V Zener diode is used as voltage regulator to protect the battery from overvoltage [4].

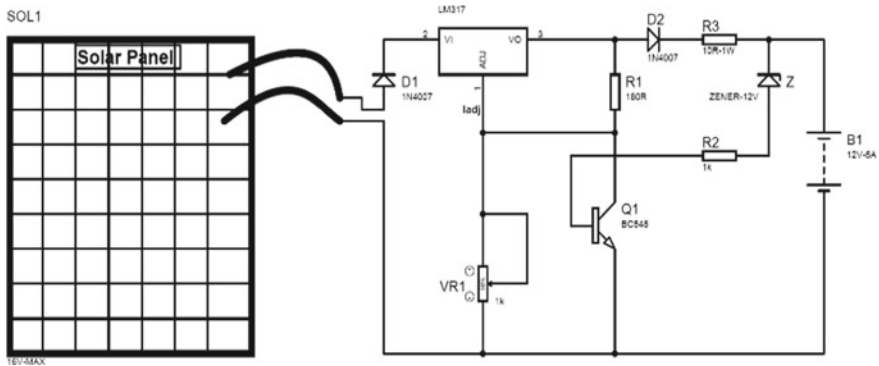


Fig. 7 Circuit diagram of solar charger circuit

3.2.2 Band-Pass Filter Design

The BPF used in this presented paper is designed to detect the voice signal having frequency range of 2–7 kHz. The second-order band-pass filter (BPF) is shown in Fig. 8.

The high-pass filter is used to set high cut-off frequency ($f_H = 2$ kHz), and low-pass filter is used to set low cut-off frequency ($f_L = 7$ kHz). This frequency cut-off can be achieved by using the following equations.

For high-pass filter (HPF),

$$C_1 = C_2 = 100 \text{ nF} \tag{2}$$

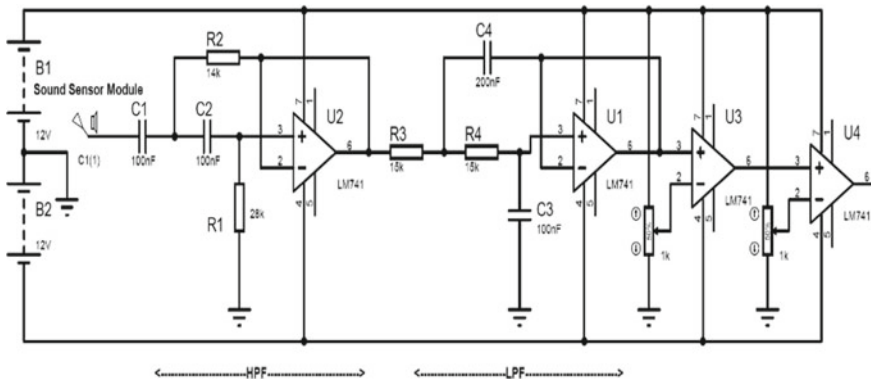


Fig. 8 Circuit diagram of band-pass filter

$$R_1 = \frac{1}{\sqrt{2\pi C_1 f_H}} \quad (3)$$

$$= \frac{1}{\sqrt{2 \times 3.14 \times 100 \times 10^{-9} \times 2 \times 10^3}} = 28 \text{ kHz}$$

$$R_2 = \frac{1}{2\sqrt{2\pi C_1 f_H}} \quad (4)$$

$$= \frac{1}{2\sqrt{2 \times 3.14 \times 100 \times 10^{-9} \times 2 \times 10^3}} = 14 \text{ kHz}$$

For low-pass filter (LPF),

$$C_3 = 100 \text{ nF}$$

$$C_4 = 2C_3 = 200 \text{ nF} \quad (5)$$

$$R_1 = R_2 = \frac{1}{\sqrt{2\pi C_3 f_L}} \quad (6)$$

$$R_1 = R_2 = \frac{1}{\sqrt{2 \times 3.14 \times 100 \times 10^{-9} \times 7 \times 10^3}} = 15 \text{ kHz}$$

$$B.W = f_L - f_H = (7 - 2) \text{ kHz} = 5 \text{ kHz} \quad (7)$$

To get digital output from BPF, two comparators are used. The output of the comparator is given to controller to drive relay and GSM module. The details of the working of controller part are explained below.

3.2.3 Controller Circuit

The 8051 series microcontroller W78E052D is used as a main controller unit [5]. The controller is interfaced with a relay circuit, LEDs and GSM module [7]. Detailed circuit diagram of controller part is shown in Fig. 9.

The reset circuitry for the controller is connected across pin 9. The external clock frequency of 11.0592 MHz crystal is used across pin 18 and 19 to run the of the programmable device (controller) [6].

The comparator output from BPF is connected to pin 1.1 (P1.1). When P1.1 is low that means, no voice of frequency 2–7 kHz is detected by the band-pass filter then pin 2.7 (P2.7) is low and if any voice is detected within the frequency range of 2–7 kHz then P1.1 is high and correspondingly P2.7 is high. P2.7 is connected to the base of a high current gain transistor 2N222A through a resistor. This transistor is used as a switch to drive the SPDT relay. When base of the transistor is high then current flows through relay coil and as a consequence com pin of relay is connected

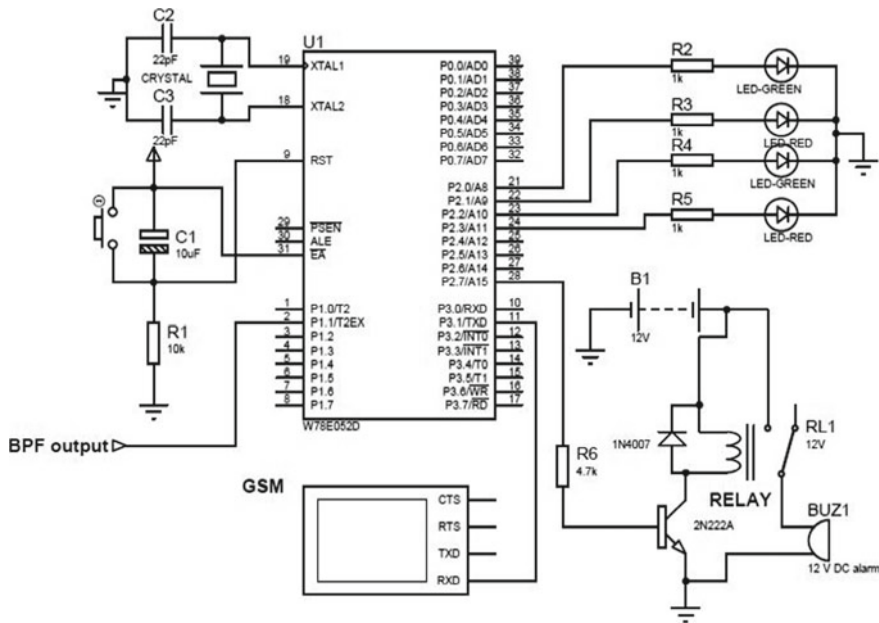


Fig. 9 Controller circuit

to N.O (normally open) pin and hence alarm system is turned ON. Across relay coil, a diode (1N4007) is used as freewheeling diode to protect from back electromotive force (emf).

In this circuit, 4 light-emitting diodes (LED) are used as an indicator. These LEDs will blink at an interval of 1 s when system is powered ON and blink very fast at an interval of 100 ms when system detects any bird voice around it.

Global system mobile (SIM900A-GSM) module is used here to send real-time information to farmer. GSM will send a message to famer if and only if alarm is turned ON for long duration.

4 Results and Discussion

The BPF design in this presented paper is to pass voice signal having frequency range of 2–7 kHz (Sparrow bird voice frequency). The output of BPF circuit is shown in details in Table 2.

In the above table, it is seen that when frequency of input voice signal is in between around 2–7 kHz then the gain of the BPF circuit is almost constant. Gain is deviated largely beyond the range of 2–7 kHz. That means BPF circuit to detect sparrow bird voice frequency is working nicely.

The input frequency (Hz) versus gain (dB) curve is shown in Fig. 10.

Table 2 Designed band-pass filter output

S. No.	Input voltage (V_i) (mV)	Input signal frequency (Hz)	Output voltage (V_o) (mV)	Gain (dB) $20\log_{10}(V_o/V_i)$
1	4000	200	10	-52.0412
2	4000	400	17	-47.432221
3	4000	600	27	-43.413925
4	4000	800	30	-42.498775
5	4000	1000	42	-39.576214
6	4000	1500	57	-36.923703
7	4000	2000	1525	-8.375803
8	4000	2200	2572	-3.8357805
9	4000	2400	3270	-1.7502448
10	4000	2600	3272	-1.7449339
11	4000	2700	3274	-1.7396263
12	4000	3000	3277	-1.731671
13	4000	3500	3277	-1.731671
14	4000	4000	3277	-1.731671
15	4000	4500	3277	-1.731671
16	4000	5000	3278	-1.7290208
17	4000	5500	3280	-1.723723
18	4000	6000	3282	-1.7184283
19	4000	6500	3283	-1.7157822
20	4000	6700	3285	-1.7104923
21	4000	6900	3287	-1.7052057
22	4000	7000	3290	-1.6972819
23	4000	7200	3292	-1.6920033
24	4000	7400	2778	-3.166555
25	4000	7700	2287	-4.8558765
26	4000	8000	2210	-5.1533544
27	4000	8500	1710	-7.3812776
28	4000	9000	110	-31.213346
29	4000	9500	27	-43.413925
30	4000	10,000	17	-47.432221

The device is successfully tested in campus of School of Agricultural Sciences and Rural Development Medziphema, Nagaland. The snapshots of the device from different angle is shown in Fig. 11. In Fig. 12, a screenshot of the message is shown when system is turned on for a long time.

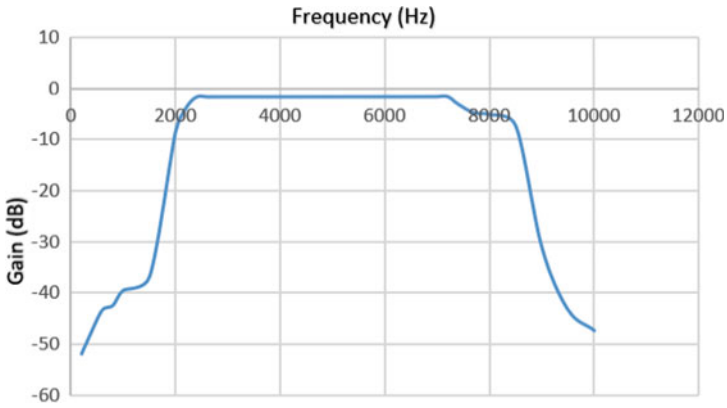


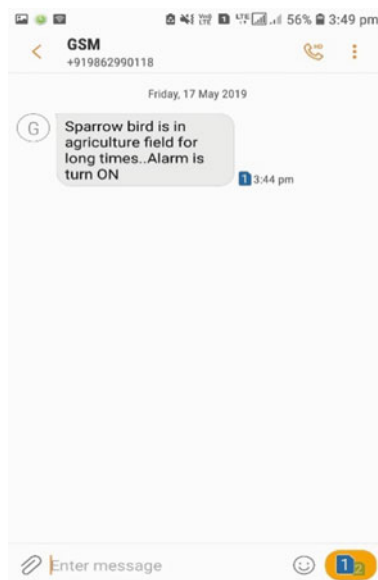
Fig. 10 Band-pass filter output curve-frequency versus gain



Fig. 11 Field testing of the device

5 Conclusion

Our main intention to develop this device is intensification of crop production in Nagaland, India, by giving solution to the problem of crop vandalism by sparrow birds in agricultural regions. Our automatic surveillance system will be very effective,

Fig. 12 GSM message

accurate, and adaptive with different agricultural regions of India. This device will not require any human intervention. It is an economical device to the agriculture and agriculturists. Device will monitor the activities in real time. It will not cause any harm to animals and humans. We hope our device will help agriculturists to solve the problem of crop vandalization by sparrow birds. We give our best efforts to achieve the solution of the above-stated problem so that the economic losses incurred by our farmers can be minimized and they can get a good crop yield.

Acknowledgements This research was supported by School of Agriculture Sciences and Rural Development (SASRD), Medziphema under Nagaland University and Special Manpower Development Program (SMDP) laboratory from National Institute of Technology Nagaland who provided insight and expertise that greatly assisted the research.

References

1. Jijesh JJ, Shivashankar Anush SK (2017) Design and development of band pass filter for X-Band RADAR receiver system. In: 2017 2nd IEEE international conference on recent trends in electronics information and communication technology (RTEICT), Bangalore, India, 19–20 May 2017
2. Barik BR, Keerthikiran V, Manmadha Rao G (2016) Designing of an ultra-high frequency-band pass filter using HFSS. *Open J Technol Eng Disciplines (OJTED)* 2(4):256–264
3. Osaretin CA, Edeko FO (2015) Design and implementation of a solar charge controller with variable output. *J Electr Electron Eng* 12(2). ISSN 1118-5058
4. Korenciak P, Fiedler P (2011) Charge controller for solar panel based charging of lead acid batteries. Department of Control and Instrumentation, Brno University of Technology, p 11

5. Sundar P, Mallikarjuna C, Suresh R (2017) Border security system with missile tracking. *Int J Sci Res Dev (IJSRD)* 5(3). ISSN 2321-0613
6. Mazidi MA, Mazidi JG, Rolin D, McKinlay The 8051 microcontroller and embedded systems using assembly and C, 2 edn. Pearson, London
7. Anand A, Parasar A, Prabhakar A (2017) GSM based agriculture monitoring system. *Int Res J Eng Technol (IRJET)* 4(03)
8. Liao Z, Dai S, Shen C (2012) Precision agriculture monitoring system based on wireless sensor networks. *Wireless Communications and Applications*. In: IET international conference on wireless communications and applications (ICWCA 2012), July 2013, Kuala Lumpur, Malaysia
9. Pooja G, Bagali MU, A smart farmland using Raspberry Pi crop vandalization prevention & intrusion detection system. *Int J Adv Res Innovative Ideas Educ* 1(5)
10. Santhiya S, Dhamodharan Y, Kavi Priya NE, Santhosh CS, Surekha M (2018) A smart farmland using Raspberry Pi crop prevention and animal intrusion detection system. *Int Res J Eng Technol (IRJET)* 05
11. Giordano S, Adami D, Vignoli F (2018) IoT solutions for crop protection against wild animal attacks. In: 2018 IEEE international conference on Environmental Engineering (EE), June 2018, Milan, Italy
12. Naveen Balaji G, Nandhini V, Mithra S, Priya N, Naveena R (2018) IOT based smart crop monitoring in farm land. *Imperial J Interdisciplinary Res (IJIR)* 4(1)

Pricing Mechanisms for Fair Bills and Profitable Revenue Share in Cloud Federation



Sameera Dhuria, Anu Gupta, and R. K. Singla

Abstract Cloud Federation is the coalition of multiple Cloud Providers (CPs) to surmount the constraint of finite physical resources of individual CPs. The collaboration enables them to share resources with each other at a certain price based on Federation Level Agreement (FLA). The pricing mechanism used for the resources requested by customer's acts as an important factor in the calculation of their bills and in the generation of revenues for CPs, in such an environment. Consequently, it performs a key role in the selection of a CP by customers and in incentivizing the CPs to remain in Federation. Considering this, the present paper aims to propose mechanisms of pricing to charge internal users and peer CPs. The proposed mechanisms are evaluated in a simulated environment. The simulation results illustrate that the proposed pricing mechanisms ensure fair bills for customers and profitable share of revenues for the collaborating CPs.

Keywords Cloud computing · Federation · Pricing mechanisms · Revenue · Bill

1 Introduction

Cloud computing technology represents a logically inexhaustible pool of ubiquitous infrastructure that can be accessed by different organizations and individuals from anywhere in the world through Internet [1]. The infrastructure is offered to customers in the form of Virtual Machines (VMs) by the Cloud Providers (CPs). Though customers are given an illusion of infinite resources, the market potential of CPs is hindered due to their finite and limited capacity. This reduces the number of service requests accepted and served by them. To offer Cloud services without any constraint on the number of accepted service requests, the CPs must be able to

S. Dhuria (✉)

Department of Computer Science, Sri Guru Granth Sahib World University, Fatehgarh Sahib, India
e-mail: sdhuria86@gmail.com

A. Gupta · R. K. Singla

Department of Computer Science and Applications, Panjab University, Chandigarh, India

© Springer Nature Singapore Pte Ltd. 2021

G. S. Hura et al. (eds.), *Advances in Communication and Computational Technology*, Lecture Notes in Electrical Engineering 668,
https://doi.org/10.1007/978-981-15-5341-7_10

133

scale up their resources [2]. This can be done by the interconnection of infrastructure of different CPs to form Cloud Federation so as to enable resource sharing among them [3]. Cloud Federation allows collaborating CPs to share and allocate resources requested by customers, consisting of internal users of a CP and peer CPs, based on the Federation policies that are described in a Federation Level Agreement (FLA) [4]. By collaborating in a Federation, CPs intend to earn profitable revenue either by renting their underutilized infrastructural resources or by outsourcing resources to peer CPs. Generally, when a collaborating CP receives resource request from internal users, it tries to serve the request locally. But in case of peak load, the resource constraint of local infrastructure is overcome through outsourcing of resources to other members of the Federation to fulfill user's request with a guaranteed Quality of Service (QoS).

Pricing is an important factor in such an environment to incentivize sharing of resources among CPs. Bills of customers and revenues of participating CPs are calculated based on the pricing mechanisms used. A user prefers to request resources from a CP that guarantees computation of fair bills based on the resource usage. Similarly, a CP outsources request to a peer CP if it is assured that the amount charged by outsourcing CP for the requested resources does not cause financial loss to it, and it is able to earn profitable revenue through outsourcing. An outsourcing CP also prefers to contribute resources for the service request of peer CP if the revenue obtained from leased resources is profitable. Such a scenario necessitates the selection and usage of an appropriate mechanism for pricing.

Selection of a suitable mechanism for resource pricing in Cloud Federation is a non-trivial and complex task and has been an area of focus of several studies [4–8]. Various pricing mechanisms have been proposed in the literature for single provider and Federated Cloud environment. But none of the existing studies has proposed pricing mechanisms to charge both internal users and peer CPs for the requested resources in a Federation of Clouds. The present work is focused on proposing pricing mechanisms for the on-demand VMs requested by internal users and peer CPs. Equations to calculate bills of customers and revenue earned by collaborating CPs are also formalized based on the proposed pricing mechanisms. The proposed mechanisms ensure the generation of fair bills for customers requesting resources and fair and profitable distribution of revenue for participating CPs. Usage of the proposed mechanisms shall persuade more customers to use the services of Clouds. It will also encourage resource contribution and participation of CPs in Federation. The paper is organized as follows: Related work is reviewed in Sect. 2. Section 3 discusses the issue of pricing in Federated Cloud scenario. Section 4 describes proposed pricing mechanisms and the equations to calculate bills and revenues based on the proposed mechanism. Evaluation of proposed mechanisms is presented in Sect. 5. Discussion is given in Sect. 6. Section 7 concludes the paper.

2 Related Work

The inability of CPs to handle the sudden spikes in resource demands of various users without compromising the QoS offered necessitates the creation of Federation of Clouds. Though a number of platforms have been proposed for Cloud Federation [9–11] with diverse motivations, various issues associated with it have yet not obtained substantial attention and need to be addressed. One of these issues is the pricing of resources that are offered to customers in this environment. Pricing is one of the most important metrics that motivate customers to use the services of a CP [12]. Numerous pricing mechanisms have been proposed in various studies [13–16]. But the existing literature on pricing in Cloud environment is largely inclined toward single provider Clouds that work alone without collaboration. Pricing problem in Cloud Federation is discussed in very few studies.

Jin and Tang [17] proposed pricing policies for a Cloud Federation scenario where one CP supplies resources and multiple CPs demand resources. The demanding CPs do not share their resource utility functions with the supplying CP due to privacy concerns. Therefore, a pricing scheme is proposed based on the predictions of the utility functions of the demanding CPs to maximize the social welfare and utilization of supplying CP's idle resources.

The broker defines a price for each VM type in the mechanism proposed by Hassan et al. [18]. The price is set strategically to encourage CPs to contribute resources to earn profit from Federation. The CPs cooperatively try to maximize the social welfare of the Federation by collectively deciding the amount of VM resources to supply based on the price of the broker. Double auction-based pricing mechanism has been used by Li et al. [7]. CPs acting as buyer and seller present buy-bid and sell bid. A broker in Cloud Federation collects entire buy and sell bids and executes a double auction to decide the set of successful buy and sell bids and their clearing prices. A strategy-proof dynamic pricing mechanism is proposed by Mihailescu and Teo [19]. It is suitable for requests of rational users containing multiple resource types. The proposed mechanism is incentive compatible and budget balanced. It is designed to cater to the requirements of large distributed systems.

Equations for revenue generation, resource utilization, and the calculation of cost incurred in the allocation of resources have been proposed by Goiri et al. [6]. These equations enable collaborating CPs to take decisions regarding resource outsourcing, insourcing, or shutting down of unused nodes in a Cloud Federation scenario. The limitation of their work is that the resource prices of all CPs are assumed to be the same, which is unrealistic in an actual Federation scenario. Peer CPs are charged by applying a factor α to the cost of VMs. The value of α is chosen in a random manner for various experiments. Similar kind of work has been performed by Toosi et al. [4] but with an option of termination of spot VMs to consider incoming on-demand VMs. The price of each CP for its contributed resources (VMs) is calculated dynamically based on the idling capacity of its data center. It results in lesser price for CPs having higher resource capacity. But at the same time, this approach may

also result in very high price for CPs having lower resource capacity. The adverse effect of this approach on bills of CPs and their revenue is overlooked.

Apart from these limitations, there are many other problems associated with the above-discussed approaches. In all the studies, mechanisms to charge only peer CPs are proposed. The mechanisms to charge internal users are not discussed. Moreover, proposed mechanisms are biased toward CPs. Main focus is on maximizing revenues of CPs without considering the benefits of customers. The present work intends to overcome these limitations. It proposes pricing mechanisms for both CPs and internal users. The aim is to ensure fair bills for all the entities requesting resources; along with fair and profitable share of revenue for all the participating CPs through the proposed mechanisms.

3 Pricing Issue in Cloud Federation

In a Federation scenario, when CPs receive service requests from customers for instantiation of VMs; resources are either allocated locally or are outsourced depending upon resource availability. The CP which originally receives resource requests from internal users is termed as host CP, and the CPs where requests are outsourced are called outsourcing CPs. To foster resource sharing in this environment and increase the utilization of idle resources, they must be allocated to customers at a suitable price. When resources are allocated locally, an appropriate pricing mechanism is required to charge only internal users. But when resources are outsourced, pricing mechanisms are required to charge both internal users and host CPs.

An outsourcing CP may charge host CP at the same or different price as compared to the price offered to internal users. Ideally, resources must be allocated to host CPs at a cheaper price. This ensures host CPs economic interest to participate in Federation by enabling it to earn profitable revenue from outsourced resources. On the contrary, if the expenditure to acquire outsourced resources is high, host CP may prefer to reject the request of its internal user instead of outsourcing resources. Alternatively, it may even charge its internal users at a higher price depending on the acquisition cost of resources from peer CPs. As a whole, pricing mechanism used to charge one entity affects the profitability of other, i.e., pricing mechanisms of both entities are correlated. Therefore, selection must be done in such a way so that any kind of financial loss to internal users or collaborating CP due to inflated bills can be avoided.

Broadly, customers may be charged using two pricing approaches: fixed and dynamic. Various fixed and dynamic pricing-based mechanisms are proposed in the literature. It is important to decide between these two approaches for resource pricing of both the entities: internal users and peer CPs. In fixed pricing approach, fixed prices are charged from customers irrespective of their characteristics and real-time market conditions [20]. A common example of this approach is ‘pay-per-use’ pricing, which is presently used by most of the commercial CPs. Using dynamic pricing, customers are charged at different prices based on various attributes like workload, Cloud market fluctuations, CP’s resource capacity [12]. Though dynamic

pricing reflects current market price of resources, it is difficult to be implemented in a multi-Cloud scenario. The unpredictability and uncertainty associated with values of different attributes of multiple CPs may cause the outsourced resources to be charged at a very high price, thus creating problem for both CPs and the end users. To address this problem, complex SLAs and FLAs need to be established that can define and fix the upper limits of resource prices under different situations. But as Cloud Federation is itself in early stages of development, defining and managing such complex rules for pricing in SLAs and FLAs are a difficult task. Apart from these limitations, reluctance of adoption of new pricing mechanisms by commercial CPs and lack of proper experimentation are some of the other factors due to which dynamic pricing has not yet been used at a large scale even by commercial single provider Clouds. Considering all these limitations, the present paper focuses on usage of fixed pricing-based approach to address the area of pricing in Cloud Federation.

4 Proposed Mechanisms for Pricing

Pricing mechanisms are proposed for internal users and peer CPs requesting resources in Cloud Federation keeping in view the interrelationship and dependency among them discussed in Sect. 3. The proposed mechanisms focus on the benefits of both entities. The motive is to increase user's satisfaction, CP's profit and resource contribution of CPs in Federation. This can be done through fair billing of both entities and ensuring profitable share of revenue to all the participating CPs. In this direction, equations to calculate bills and revenues using these mechanisms are also formalized. Various acronyms used in the equations are:

VM_{total}	Total number of VMs requested by internal users
VM_{own}	Number of VMs allocated from host CP's own resources
VM_{out}	Number of VMs outsourced to peer CP
VM_{ins}	Number of VMs insourced
t	Time for which VM is allocated
$Price_VM_{own}$	Price of VM per unit time offered by host CP
$Price_VM_{out}$	Price of VM per unit time of outsourcing CP
$Price_VM_{req}$	Price of VM per unit time of requesting CP
$Cost_{out}$	Amount paid for borrowing resources from insourcing CP
$Total_R_{out}$	Total revenue earned from outsourced resources
R_{total}	Revenue earned by a CP participating in Federation
R_{own}	Revenue earned from own resources allocated to internal users
R_{out}	Revenue earned from resources outsourced to peer CPs
R_{ins}	Revenue earned from resources leased to peer CPs

4.1 Internal Users

Internal users of CPs may be charged in the following ways:

Based on Price of Host CP (PHCP). In this mechanism, internal users are charged for all the requested VMs based on fixed uniform price of host CP which is offered to them at the time of service request, irrespective of the actual location of execution of requested VMs. Factors that affect users' bill in this mechanism are the number of VMs requested, price of host CP, and the time for which VMs execute. Thus, user's bills are calculated using the following equation:

$$\text{User Bills} = \text{Price_VM}_{\text{own}} * \text{VM}_{\text{total}} * t \quad (1)$$

Based on Price of Outsourcing CP (POCP) In this mechanism, internal users are charged for the requested service based on fixed prices of both host and outsourcing CPs, depending upon the location of execution of requested VMs. Factors that affect users' bill in this mechanism are the number of VMs requested, price of host CP, number of VMs outsourced, price of CP where VMs request is outsourced and the time for which VMs execute. Thus, user's bills are calculated using the following equation:

$$\text{User Bills} = ((\text{Price_VM}_{\text{own}} * \text{VM}_{\text{own}}) + (\text{Price_VM}_{\text{out}} * \text{VM}_{\text{out}})) * t \quad (2)$$

4.2 Peer CPs

Peer CPs are charged at a reduced price in comparison to the amount charged from internal users. For this, a *reduction factor* r ($0 < r < 1$) is used either with the price of host CP or outsourcing CP in the following ways:

Reduced Price of Host CP (RPHCP) In this mechanism, a reduction factor r is applied to the price of host CP. The host CP obtains resources from outsourcing CPs based on this reduced price. Factors that affect CP's bill and revenue in this mechanism are the price of host CP, number of VMs outsourced and the time for which VMs execute. Bills of peer CP for outsourced resources are calculated using the following equation:

$$\text{Peer CP Bills} = r * \text{Price_VM}_{\text{own}} * \text{VM}_{\text{out}} * t \quad (3)$$

Revenue (R_{total}) earned by a CP participating in Federation is the sum of revenue earned from its own resources allocated to internal users (R_{own}), resources outsourced to peer CPs (R_{out}), and resources leased to peer CPs (R_{ins}).

$$R_{\text{total}} = R_{\text{own}} + R_{\text{out}} + R_{\text{ins}} \quad (4)$$

This revenue is calculated as follows using proposed mechanism:

- Revenue from own resources (R_{own})

$$R_{\text{own}} = \text{Price_VM}_{\text{own}} * \text{VM}_{\text{own}} * t \quad (5)$$

- Revenue from outsourced resources (R_{out})

$$\text{Total_R}_{\text{out}} = \text{Price_VM}_{\text{own}} * \text{VM}_{\text{out}} * t \quad (6)$$

Host CP has to pay some amount to outsourcing CP to obtain resources from it, which is given by Eq. (3)

$$\text{i.e. Cost}_{\text{out}} = \text{Peer CP Bills}$$

Net revenue (R_{out}) is calculated by subtracting cost of obtaining outsourced resources from the total revenue generated from outsourced resources.

$$R_{\text{out}} = \text{Total_R}_{\text{out}} - \text{Cost}_{\text{out}} \quad (7)$$

- Revenue from insourced resources (R_{ins})

$$R_{\text{ins}} = r * \text{Price_VM}_{\text{req}} * \text{VM}_{\text{ins}} * t \quad (8)$$

Reduced price of Outsourcing CP (RPOCP) In this mechanism, a reduction factor r is applied to the price offered by outsourcing CP. Host CP is charged for outsourced resources based on this reduced price. Factors that affect CP's bills and revenues in this mechanism are the price of outsourcing CP, number of VMs outsourced and the time for which VMs execute. Bills of peer CP for outsourced resources are calculated using the following equation:

$$\text{Peer CP Bills} = r * \text{Price_VM}_{\text{out}} * \text{VM}_{\text{out}} * t \quad (9)$$

Revenue of a collaborating CP is calculated as follows using this mechanism:

- Revenue from own resources (R_{own}): It is calculated using Eq. (5).
- Revenue from Outsourced Resources: Total revenue earned from outsourced resources is calculated using Eq. (6).

Amount paid to outsourcing CP to obtain resources from it is same as given by Eq. (9)

$$\text{i.e. Cost}_{\text{out}} = \text{Peer CP Bills}$$

Net revenue earned is calculated using Eq. (7).

- Revenue from insourced resources

$$R_{\text{ins}} = r * \text{Price_VM}_{\text{own}} * \text{VM}_{\text{ins}} * t \quad (10)$$

5 Evaluation

The pricing mechanisms proposed in Sect. 4 are evaluated through experiments conducted using CloudSim simulation tool [21]. For this, a peer-to-peer simulated Cloud Federation is created in which Clouds commune directly with each other without the involvement of any mediator [22].

5.1 Simulation Settings

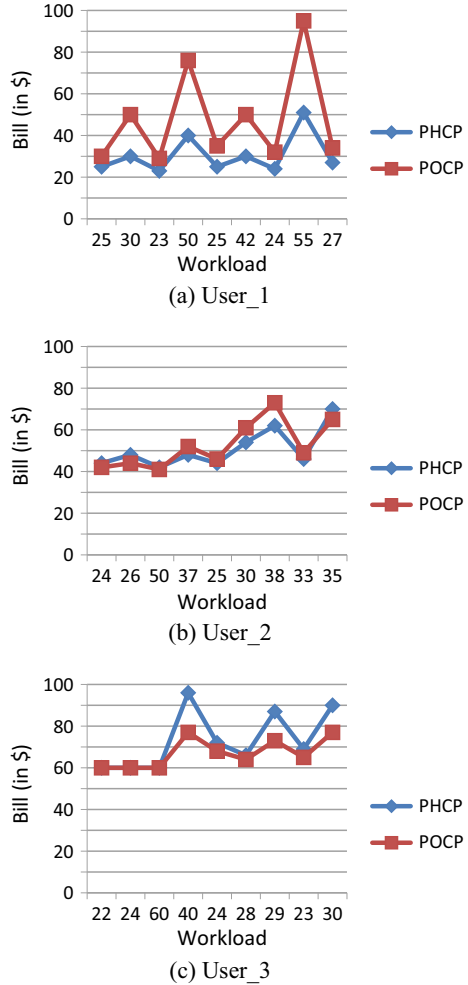
Federation scenario is created with the collaboration of three IaaS providers (CP_1, CP_2, and CP_3). Collaborating CPs receive service requests from own internal users (User_1, User_2, and User_3 are the internal users of CP_1, CP_2, and CP_3, respectively) and peer CPs. It is assumed that only 1 type of VM is offered by all CPs though different VM types may be used as an extension to this work. A 24 h long workload is generated. Prices of VMs offered by each CP are fixed to 1.0, 2.0, and 3.0 (\$/hour), respectively. Different resource prices have been used by CPs to study the impact of proposed mechanisms on bills and revenues when resources are outsourced.

The metrics considered for determining the effect of proposed mechanisms on CPs and customers are: Bills of internal users, Bills of host CPs, Revenues of host CPs, and Revenues of outsourcing CPs. The parameter used to study the behavior of pricing mechanisms proposed for internal users is ‘workload,’ while the parameters used to study the behavior of pricing mechanisms proposed for peer CPs are ‘workload’ and ‘reduction factor r .’ The proposed mechanisms differ in their way of calculation of bills and revenues based on whether the requested resources are allocated by local or remote CPs. Therefore, in various experiments, workload is varied to simulate the provisioning of requested VMs through resources of host and outsourcing CPs. As value of r determines the share of revenue of each CP obtained from outsourced resources. So, experiments are also conducted using different values of r varying from 0.1 to 1.0.

5.2 Results

Results of various experiments are shown in Figs. 1, 2, 3, 4, and 5. In Figs. 1, 3, 4, and 5, (a) represents the scenario when VMs are outsourced to CPs having higher

Fig. 1 User bills using PHCP and POCP mechanisms



price, (b) represents the scenario when some of the VMs are outsourced to CPs having higher price and others are outsourced to CPs having lower price, and (c) represents the scenario when VMs are outsourced to CPs having lower price. The entries corresponding to x-axis are different as the collaborating CPs receive different number of VM requests, i.e., their workload is different.

The first experiment is aimed at evaluating the impact of pricing mechanisms proposed for internal users on their bills. Bills of users are calculated using Eqs. 1 and 2 given in Sect. 4. It can be observed from Fig. 1a–c that in all the scenarios of outsourcing using PHCP mechanism, variation in the price of outsourcing CP does not adversely affect bills of users. As shown in Fig. 1a, even when the VMs are outsourced to a CP with higher price than that of host CP, fair bills are generated for internal users. On the contrary, in case of POCP mechanism, if the outsourcing CP has

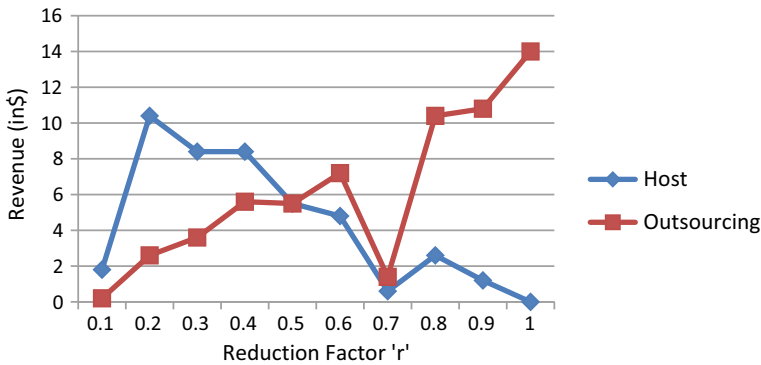


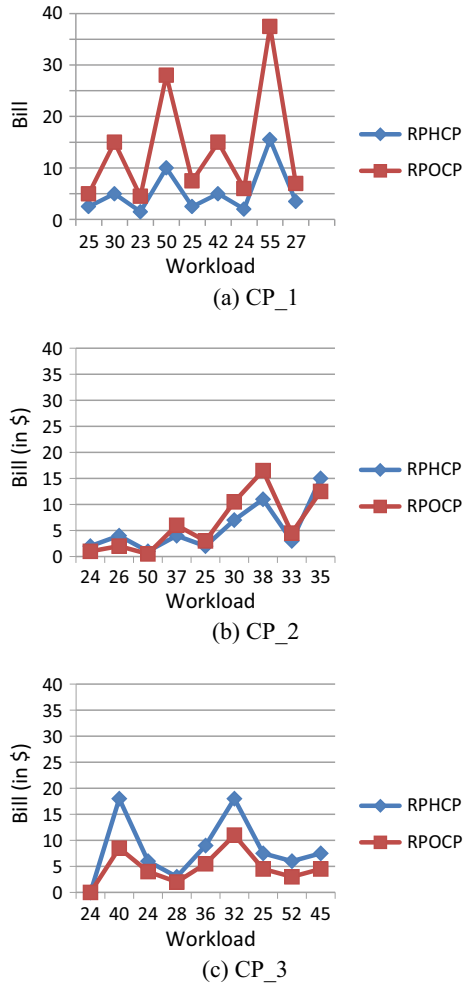
Fig. 2 Revenue of host and outsourcing CP with different values of r

higher price, unexpectedly high bills may be generated depending upon the number of VMs outsourced and the price of CP where they are outsourced as shown in Fig. 1a, b. *POCP* mechanism is appropriate for use only if the outsourcing CP is selected based on its price, i.e., CP with lesser price is selectively used for outsourcing. Such a scenario may help in avoiding financial loss to users, but at the same time it will prevent CPs having high prices from participating in Federation. Considering this, *PHCP* is found to be a suitable pricing mechanism to charge internal users.

The second experiment is aimed at selecting an appropriate value of r to be used for the pricing mechanisms proposed for peer CPs. It demonstrates and analyzes the effect of usage of different values of r on the revenues of host and outsourcing CPs. For this experiment, price of all CPs is assumed to be same (fixed to \$1.0/h) so that the results are generated based on the value of r only irrespective of the price of CPs. Value of r is varied from 0.1 to 1.0. For each value of r , various experiments are performed with different number of VMs contributed by outsourcing CPs. This is done to study the effect of increase or decrease of number of VMs on revenue (with same value of r). To present the results and analysis in a simplified manner, Fig. 2 shows the revenue obtained by a CP with each value of r in a single experiment. It is clear from the results that using value of 0.1 for r , outsourcing CP obtains very less revenue. As value of r is increased, the revenue share of outsourcing CP improves. But, for very high values of r (e.g., 0.9 or 1.0), the increase in revenue share of outsourcing CP causes loss to host CP. It earns less revenue despite being the original receiver of the resource request of users. Therefore, to generate genuine share of revenue for both host CP and outsourcing CP, the value of r should be neither very high nor very low. A fair revenue share for both is generated using $r = 0.5$. Though 0.5 is considered to be an ideal value to be used for r , its value can be varied from the range of 0.4–0.6 depending upon factors like QoS, resource availability of the outsourcing CP.

The third experiment evaluates the mechanisms proposed to charge peer CPs. Their impact on bills generated for host CP and revenues earned by host and

Fig. 3 Bills of host CPs using RPHCP and RPOCP mechanisms

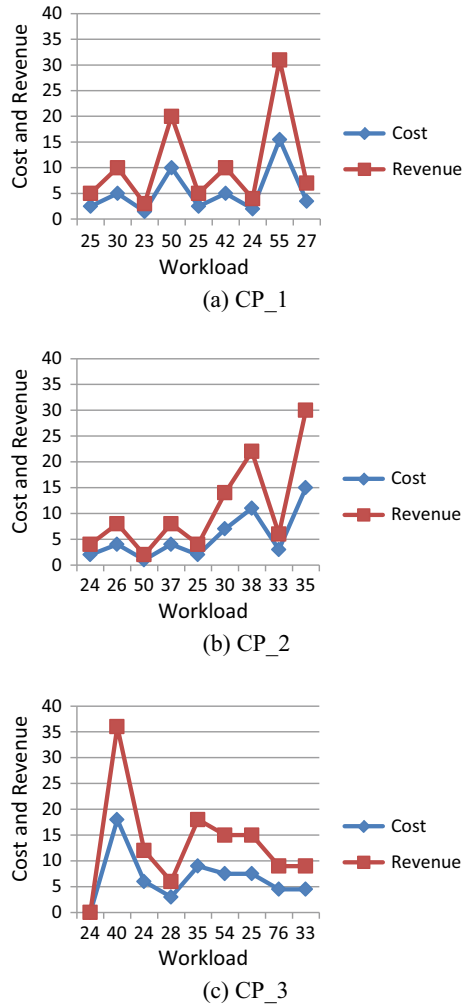


outsourcing CPs is analyzed. Experiments are performed by varying the workload and using 0.5 value for r .

Impact on bills of host CP: It can be observed from Fig. 3a–c that in all the scenarios of outsourcing, the bills generated for host CPs are genuine and predictable using RPHCP mechanism, i.e., fair bills are generated for host CPs irrespective of the price of CPs where VMs are outsourced. On the contrary, in RPOCP mechanism, if resources are outsourced to a CP with higher price, then despite using $r = 0.5$, host CP has to pay a high amount as bill as shown in Fig. 3a, b.

Impact on revenues of host and outsourcing CPs: The profitability of host CP is evaluated by comparing the cost of host CP to acquire resources from peer CPs and the revenue earned by it. It is observed from Fig. 4a–c that using RPHCP mechanism, the cost of host CP to acquire resources from peer CPs is lesser than the revenue

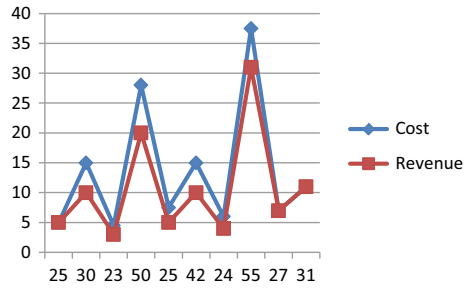
Fig. 4 Cost and revenue of host CP using RPHCP



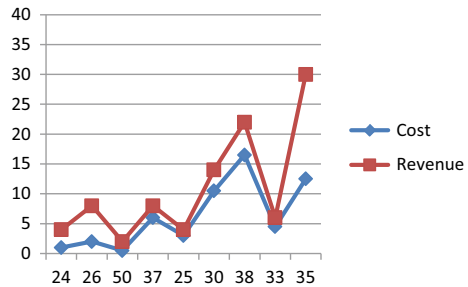
earned in all the scenarios of outsourcing. Therefore, a host CP always obtains a profitable share of revenue using RPHCP mechanism. The price of CPs where VMs are outsourced becomes inconsiderable. In all the scenarios, outsourcing CPs would also earn 50% of the total revenue earned from users for the VMs allocated to host CP as the price of reduction factor r is set to 0.5.

As shown in Fig. 5a, using *RPOCP* mechanism, when VMs are outsourced to a CP with higher price, then host CP pays a high amount to acquire resources. As the cost incurred is higher than the revenue earned, therefore, host CP does not obtain profitable revenue and thus suffers financial loss. It is observed from Fig. 5b that even when some of the VMs are outsourced to CPs with lower price while others are outsourced to CPs with higher price, the earned revenue may not ensure profit. Only

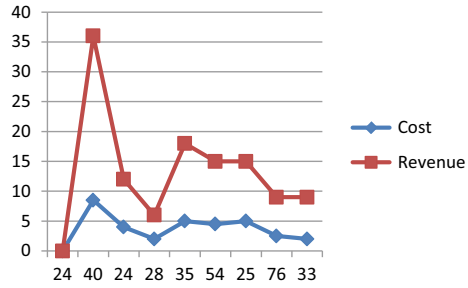
Fig. 5 Cost and revenue of host CP using RPOCP



(a) CP_1



(b) CP_2



(c) CP_3

when VMs are outsourced to CPs with cheaper price, profitable revenue is obtained, as shown in Fig. 5c. As a whole, *RPOCP* mechanism offers profitable revenue to host CP when price of outsourcing CP is less than or equal to the price of host CP. But outsourcing CP always obtains 50% of its own price for leased resources irrespective of the price of requesting CP.

Due to the benefits offered by *RPHCP* and limitations of *RPOCP*, *RPHCP* is found to be more suitable to be used for pricing of peer CPs requesting resources and revenue sharing of all collaborating CPs.

6 Discussion

Based upon the evaluation of various mechanisms in Sect. 5, ‘*Price of Host CP*’—and ‘*Reduced Price of Host CP*’—based mechanisms are found to be more suitable for user and CP pricing, respectively. These mechanisms offer many advantages. In *PHCP* mechanism, users know the values of all the attributes affecting their bills, i.e., host CP price, number of VMs requested, and time for which they execute. It helps users in predicting the tentative cost to acquire requested resources and enables them to select a CP based on the prices offered by it. It also offers transparency, prevents any unnecessary charges levied by CPs on users, and generates fair bills for them. This further attracts more customers to use the services of Cloud infrastructure.

RPHCP mechanism generates predictable and fair bills for host CP and profitable revenue for all the participating CPs. It guarantees cheaper price for outsourced resources. It is not biased toward host or outsourcing CP. It helps host CPs to outsource requests based on resource availability without any consideration of prices. The price to be paid for outsourced resources is predictable in this mechanism. Therefore, financial losses to host CP due to outsourcing are minimized. It further enables host CP to charge internal users in an impartial manner. As this method encourages outsourcing, therefore, host CP is able to accommodate more user requests which help in increasing its profit and building reputation. Outsourcing CP also finds it profitable to contribute its idle resources to Federation as it is assured that it will get at least 50% of the revenue of the VMs provided by it to host CP.

These mechanisms also overcome limitations of existing mechanisms. They are based on the fixed pricing approach. It helps in minimizing the increase in price due to various attributes related to dynamic pricing. This further prevents rejection of resource request, financial loss to CP, or any kind of wrong imposition of charges on customers by CPs. Pricing mechanisms are proposed considering different prices for participating CPs, to represent real Federation scenario. Rather than choosing random values of reduction factor to calculate bills and revenues, a suitable value is selected for it keeping in view of the benefits of users and CPs, which guarantees fair bills and profitable revenues. Apart from this, bill and revenue calculation are done on the basis of amount of work performed by each CP, i.e., on the basis of number of VMs contributed. All these factors assure that the selected pricing mechanisms are suitable to be used for the purpose of billing and revenue sharing.

7 Conclusion

In a Cloud Federation, resources are traded among various collaborating CPs through FLA. Pricing is considered to be an important factor in this environment to help users in selecting an appropriate CP for the fulfillment of their resource requirements. It is also a vital element in determining the benefit of CPs participating in Federation. Therefore, in the present work, pricing mechanisms are proposed for the resources

requested by internal users and peer CPs. For this, the relationship among pricing requirements of both entities is established. Based on it, pricing mechanisms are proposed with focus on minimal loss to internal users in terms of fairness in their bills, along with profitable and fair distribution of revenue among individual participating CPs. Experiments are conducted in a simulated Federation scenario to evaluate the proposed mechanisms. From the analysis of results of experiments, ‘*Price of Host CP*’—and ‘*Reduced Price of Host CP*’—based mechanisms are found to be suitable to charge internal users and peer CPs, respectively. These mechanisms attract more customers to use the services of Cloud. They also encourage the participation of CPs in Federation as collaborating CPs are able to completely keep their standalone revenue and obtain profitable share of revenue from the Federation.

References

1. Hilley D (2009) Cloud computing: a taxonomy of platform and infrastructure-level offerings. CERCS technical report, Georgia Institute of Technology
2. Toosi AN, Calheiros RN, Buyya R (2014) Interconnected cloud computing environments: challenges, taxonomy, and survey. *ACM Comput Surv* 47:1–47
3. Rochwerger B, Breitgand D, Levy E, Galis A, Nagin K, Llorente IM, Montero R, Wolfsthal Y, Elmroth E, Caceres J, Ben-Yehuda M (2009) The reservoir model and architecture for open federated cloud computing. *IBM J Res Dev* 53:535–545
4. Toosi AN, Calheiros RN, Thulasiram RK, Buyya R (2011) Resource provisioning policies to increase IaaS provider’s profit in a federated cloud environment. In: Proceedings of the international conference on high performance computing and communications, pp 279–287
5. Dhuria S, Gupta A, Singla RK (2017) Resource pricing in cloud federation: a review. *Int J Innov Adv Comput Sci* 6:1–5
6. Goiri I, Guitart J, Torres J (2010) Characterizing cloud federation for enhancing providers’ profit. In: Proceedings of the international conference on cloud computing, pp 123–130
7. Li H, Wu C, Li Z, Lau FC (2013) Profit-maximizing virtual machine trading in a federation of selfish clouds. In: Proceedings of the international conference on computer communications, pp 25–29
8. Rebai S, Hadji M, Zeglache D (2015) Improving profit through cloud federation. In: Proceedings of the annual conference on consumer communications and networking conference, pp 732–739
9. Buyya R, Ranjan R, Calheiros RN (2010) Intercloud: utility-oriented federation of cloud computing environments for scaling of application services. In: Proceedings of the international conference on algorithms and architectures for parallel processing, pp 13–31
10. Carlini E, Coppola M, Dazzi P, Ricci L, Righetti G (2011) Cloud federations in contrail. In: Proceedings of the European conference on parallel processing, pp 159–168
11. Ferrer AJ, Hernández F, Tordsson J, Elmroth E, Ali-Eldin A, Zsigri C, Sirvent R, Guitart J, Badia RM, Djemame K, Ziegler W (2012) OPTIMIS: a holistic approach to cloud service provisioning. *Future Gener Comput Syst* 28:66–77
12. Al-Roomi M, Al-Ebrahim S, Buqrais S, Ahmad I (2013) Cloud computing pricing models: a survey. *Int J Grid Distrib Comput* 6:93–106
13. Ma D, Huang J (2012) The pricing model of cloud computing services. In: Proceedings of the annual international conference on electronic commerce, pp 263–269
14. Ibrahim S, He B, Jin H (2011) Towards pay-as-you-consume cloud computing. In: Proceedings of the international conference on services computing, pp 370–377

15. Li H, Liu J, Tang G (2011) A pricing algorithm for cloud computing resources. In: Proceedings of the international conference on network computing and information security, pp 69–73
16. Xu H, Li B (2013) A study of pricing for cloud resources. *ACM SIGMETRICS Perform Eval Rev* 40:3–12
17. Jin L, Tang L (2016) Prediction-based pricing for request outsourcing in cloud federation. In: Proceedings of the international conference on wireless communications & signal processing, pp 1–5
18. Hassan MM, Abdullah-Al-Wadud M, Almogren A, Song B, Alamri A (2017) Energy-aware resource and revenue management in federated cloud: a game-theoretic approach. *IEEE Syst J* 11:951–961
19. Mihailescu M, Teo YM (2010) A distributed market framework for large-scale resource sharing. In: Proceedings of European conference on parallel processing, pp 418–430
20. Osterwalder A (2004) The business model ontology—a proposition in a design science approach. Doctoral thesis, University of Lausanne
21. Calheiros RN, Ranjan R, Beloglazov A, De Rose CA, Buyya R (2011) CloudSim: a toolkit for modeling and simulation of cloud computing environments and evaluation of resource provisioning algorithms. *Softw Pract Exp* 41(1):23–50
22. Grozev N, Buyya R (2014) Inter-Cloud architectures and application brokering: taxonomy and survey. *Softw Pract Exp* 44:369–390

Higher Order Squeezing in Pump Mode in Multi-wave Mixing Process



Priyanka and Savita Gill

Abstract Higher order squeezing and photon statistics in pump mode in five wave mixing process has been studied under short-time interaction in nonlinear medium. A comparison of squeezing in field amplitude and higher order amplitude has been investigated, and we have found that squeezing increases with higher order of field amplitude. Photon statistics has also been studied and found to be sub-Poissonian in nature. It is also observed that squeezing and photon statistics is directly related to number of photons present in the system prior to interaction in nonlinear medium.

Keywords Higher order squeezing · Quantum fluctuation · Nonlinear optics

1 Introduction

Coherent state of electromagnetic field is having equal uncertainty in both the quadrature components. Squeezed state of electromagnetic field is the minimum uncertainty state having less fluctuation in one quadrature component than the other quadrature. A review on squeezing was given by Dodonov [1] and Loudon et al. [2]. Squeezing has been based on theoretical investigation and experimental observation in nonlinear optical processes like harmonic generation [3, 4], multi-wave mixing [5–7], Raman and hyper-Raman [8, 9], nonlinear polarization rotation [10], and Faraday rotation of nonlinearity in atomic systems [11]. Mandal [12] and Hillery [13] have given the concept of amplitude squeezing in nonlinear medium. Non-classicality is directly related to higher order squeezing and antibunching [14, 15]. Higher order non-classicality was studied in codirectional nonlinear optical coupler [16] and Bose–Einstein condensation [17]. Higher order antibunching and the use of antibunching

Priyanka · S. Gill (✉)

Department of Applied Science, University Institute of Engineering and Technology, Kurukshetra University, Kurukshetra 136119, Haryana, India

e-mail: Savita2015@kuk.ac.in

Priyanka

e-mail: Chauhan7101@gmail.com

© Springer Nature Singapore Pte Ltd. 2021

G. S. Hura et al. (eds.), *Advances in Communication and Computational*

Technology, Lecture Notes in Electrical Engineering 668,

https://doi.org/10.1007/978-981-15-5341-7_11

in the detection of squeezing have also been reported [18–21]. Squeezing and antibunching of photons in parametric oscillator in Raman process have also been studied [22]. In this paper, we have studied higher order squeezing and antibunching in five-wave mixing process and found that squeezing can be tuned by varying the interaction time and number of photons prior to the interaction in nonlinear medium [23]. Squeezing of electromagnetic field has interesting applications in quantum information processing like cryptography [24], teleportation [25], dense coding [26], and quantum key distribution [27].

In the present work, higher order squeezing up to second order of field amplitude in pump mode in five-wave interaction process has been studied. In this paper, Sect. 2 gives the definition of higher order squeezing and sub-Poissonian photon statistics. In Sects. 3, 4, and 5, we derive an analytic expression of squeezing and photon statistics (antibunched light) along with the discussion of result. Finally, Sect. 6 is dedicated to conclusion.

2 Condition of Amplitude Squeezing and Sub-Poissonian Photon Statistics

Normal squeezing or the first-order squeezing is defined as [13].

$$X_1 = \frac{1}{2}(A + A^+) \text{ and } X_2 = \frac{1}{2i}(A - A^+) \quad (1)$$

where X_1 and X_2 are real and complex conjugate components of field amplitude, respectively.

where

$$\begin{aligned} A &= ae^{i\omega t} \\ A^+ &= a^+ e^{-i\omega t} \end{aligned} \quad (2)$$

Operator X_1 and X_2 obey commutation relation as

$$\begin{aligned} [X_1, X_2] &= (X_1 X_2 - X_2 X_1) \\ [X_1, X_2] &= \frac{1}{4i}(A^2 + A^\dagger A - AA^\dagger - A^{\dagger 2} - A^2 - AA^\dagger + A^\dagger A + A^{\dagger 2}) \\ [X_1, X_2] &= \frac{1}{2i}(A^\dagger A - AA^\dagger) \end{aligned}$$

After substituting value of $AA^\dagger = A^\dagger A + 1$ in above commutation expression, we get

$$[X_1, X_2] = \frac{i}{2} \quad (3)$$

The uncertainty in X_1 quadrature is

$$\begin{aligned} (\Delta X_1)^2 &= \langle \psi | X_1^2 | \psi \rangle - \langle \psi | X_1 | \psi \rangle^2 \\ &= \frac{1}{4} \langle \psi | \alpha^2 + a^{\dagger 2} + aa^\dagger + a^\dagger a | \psi \rangle - \frac{1}{4} \langle \psi | a + a^\dagger | \psi \rangle^2 \end{aligned}$$

where α is expectation value of operator A .

$$\begin{aligned} (\Delta X_1)^2 &= \frac{1}{4} (\alpha^2 + \alpha^{*2} + 2|\alpha|^2 + 1) - \frac{1}{4} (\alpha + \alpha^*)^2 \\ (\Delta X_1)^2 &= \frac{1}{4} (\alpha^2 + \alpha^{*2} + 2|\alpha|^2 + 1 - \alpha^2 - \alpha^{*2} - 2|\alpha|^2) \\ (\Delta X_i)^2 &= \frac{1}{4} \quad \text{for } i = 1 \text{ and } 2 \end{aligned} \quad (4)$$

The above relation holds for the coherent state.

Uncertainty criteria for squeezed light are given as

$$\Delta X_1 \Delta X_2 \geq \frac{1}{4} \quad (5)$$

X_i variable fulfill the condition of squeezing if

$$(\Delta X_i)^2 < \frac{1}{4} \quad (i = 1 \text{ or } 2) \quad (6)$$

Y_1 and Y_2 operators defining higher order squeezing as [13]

$$Y_1 = \frac{1}{2}(A^2 + A^{\dagger 2}) \quad \text{and} \quad Y_2 = \frac{1}{2i}(A^2 - A^{\dagger 2}) \quad (7)$$

Y_1 and Y_2 obey commutation relation

$$\begin{aligned} [Y_1, Y_2] &= (Y_1 Y_2 - Y_2 Y_1) \\ [Y_1, Y_2] &= \frac{1}{2i}(A^{\dagger 2} A^2 - A^2 A^{\dagger 2}) \end{aligned}$$

Substituting $A^2 A^{\dagger 2} = A^{\dagger 2} A^2 + 4A^\dagger A + 2$ in above commutation expression, we get $[Y_1, Y_2] = \frac{i}{2}[4A^\dagger A + 2]$

and

$$[Y_1, Y_2] = i(2N + 1) \quad \text{where } N = A^\dagger A \quad (8)$$

The uncertainty of Y_1 component is

$$(\Delta Y_1)^2 = \langle \psi | Y_1^2 | \psi \rangle - \langle \psi | Y_1 | \psi \rangle^2$$

$$(\Delta Y_1)^2 = \frac{1}{4} \langle \psi | A^4 + A^2 A^{\dagger 2} + A^{\dagger 2} A^2 + A^{\dagger 4} | \psi \rangle - \frac{1}{4} \langle \psi | A^2 + A^{\dagger 2} | \psi \rangle^2 \quad (9)$$

After substituting value of $A^2 A^{\dagger 2}$ and taking α as the expectation value of operator A in above Eq. (9), we get,

$$(\Delta Y_1)^2 = \frac{1}{4} (\alpha^4 + 2|\alpha|^4 + 4|\alpha|^2 + 2 + \alpha^{*4}) - \frac{1}{4} (\alpha^2 + \alpha^{*2})^2$$

$$(\Delta Y_i)^2 = N + \frac{1}{2} \quad \text{for } i = 1 \text{ and } 2$$

where $N = |\alpha|^2$ is photon's number present in coherent state.

The uncertainty criteria for squeezed state is given as

$$\Delta Y_1 \Delta Y_2 \geq \left\langle \left(N + \frac{1}{2} \right) \right\rangle \quad (10)$$

Higher order squeezing will exist if

$$(\Delta Y_i)^2 < \left\langle N + \frac{1}{2} \right\rangle \quad (11)$$

Condition of Photon Statistics

In sub-Poissonian photon statistics, deviation of photon number is less than the mean value of number of photons present in the system and can be defined as $[\Delta N(t)]^2 < \langle N(t) \rangle$.

where N is number of photons present in the system.

3 Squeezing in Multi-wave Mixing Process

3.1 Field Amplitude Squeezing

In five-wave mixing process, the interaction takes place in such a way that one photon of frequency ω_1 and two photons of frequency ω_2 each are absorbed and two photons of frequency ω_3 each are emitted, such that $\omega_1 + 2\omega_2 = 2\omega_3$.

Hamiltonian represents the total energy for the above process which is sum of kinetic energy, and potential energy of system and Hamiltonian for the above system is given as

$$H = \omega_1 a^\dagger a + \omega_2 b^\dagger b + \omega_3 c^\dagger c + g(ab^2 c^{\dagger 2} + a^\dagger b^{\dagger 2} c^2) \text{ taking } (\hbar = 1) \quad (12)$$

where g is coupling constant, $a^\dagger(a)$, $b^\dagger(b)$, $c^\dagger(c)$ are the creation(annihilation) operators, respectively. $A = a \exp i\omega_1 t$, $B = b \exp i\omega_2 t$, $C = c \exp i\omega_3 t$ are the slowly varying operators at frequencies ω_1 , ω_2 , and ω_3 .

Time evolution of operator in B mode is given by Heisenberg equation of motion as

$$\frac{dB}{dt} = \frac{\partial B}{\partial t} + i[H, B] \quad (13)$$

Commutation relation of H and B operators is given as $[H, B] = (HB - BH)$. Substituting H and B operator in the above expression, we get,

$$\begin{aligned} [H, B] &= (\omega_1 a^\dagger ab + \omega_2 b^\dagger bb + \omega_3 c^\dagger cb + gab^2 c^{\dagger 2} b + ga^\dagger b^{\dagger 2} c^2 b \\ &\quad - b\omega_1 a^\dagger a - b\omega_2 b^\dagger b - b\omega_3 c^\dagger c - bgab^2 c^{\dagger 2} \\ &\quad - bga^\dagger b^{\dagger 2} c^2) \exp(i\omega_2 t) = (\omega_2 b^\dagger bb - \omega_2 b^\dagger bb - \omega_2 b \\ &\quad + ga^\dagger b^{\dagger 2} bc^2 - ga^\dagger b^{\dagger 2} bc^2 - 2ga^\dagger b^\dagger c^2) \exp(i\omega_2 t) \\ [H, B] &= (-\omega_2 b - 2ga^\dagger b^\dagger c^2) \exp(i\omega_2 t) \end{aligned} \quad (14)$$

And

$$\frac{\partial B}{\partial t} = i\omega_2 b \exp(i\omega_2 t) \quad (15)$$

Substituting Eqs. (14) and (15) in Heisenberg equation of motion (13), we get

$$\begin{aligned} \dot{B} &= i\omega_2 b \exp(i\omega_2 t) - i\omega_2 b \exp(i\omega_2 t) - 2iga^\dagger b^\dagger c^2 \exp(i\omega_2 t) \\ \dot{B} &= -2iga^\dagger B^\dagger C^2 \end{aligned} \quad (16)$$

Similarly,

$$\begin{aligned} \frac{dA}{dt} &= \frac{\partial A}{\partial t} + i[H, A] \\ \dot{A} &= -igB^{\dagger 2} C^2 \end{aligned} \quad (17)$$

And

$$\frac{dC}{dt} = \frac{\partial C}{\partial t} + i[H, C]$$

$$\dot{C} = -2igAB^2C^\dagger \quad (18)$$

Now second derivative of B [from Eq. (16)] is

$$\begin{aligned} \frac{d^2B}{dt^2} &= -2ig[A^\dagger B^\dagger C^2 + A^\dagger \dot{B}^\dagger C^2 + A^\dagger B^\dagger \dot{C}C + A^\dagger B^\dagger C\dot{C}] \\ &= -2ig[(igB^2C^{\dagger 2})B^\dagger C^2 + A^\dagger(2igABC^{\dagger 2})C^2 \\ &\quad + A^\dagger B^\dagger(-2igAB^2C^\dagger)C + A^\dagger B^\dagger C(-2igAB^2C^\dagger)] \end{aligned}$$

So

$$\begin{aligned} \frac{d^2B}{dt^2} &= -2ig[igB^2B^\dagger C^{\dagger 2}C^2 + 2igA^\dagger ABC^{\dagger 2}C^2 \\ &\quad - 2igA^\dagger AB^\dagger B^2C^\dagger C - 2igA^\dagger AB^\dagger B^2CC^\dagger] \\ \frac{d^2B}{dt^2} &= 2g^2[-4A^\dagger AB^\dagger B^2C^\dagger C + B^\dagger B^2C^{\dagger 2}C^2 \\ &\quad + 2A^\dagger ABC^{\dagger 2}C^2 + 2BC^{\dagger 2}C^2 - 2A^\dagger AB^\dagger B^2] \end{aligned} \quad (19)$$

As interaction time is small during this process ($\approx 10^{-12}$ s), expanding $B(t)$ according to Taylor's expansion and taking terms up to second order in time g^2t^2 as,
 $B(t) = B(0) + \frac{t}{1!} \frac{dB(0)}{dt} + \frac{t^2}{2!} \frac{d^2B(0)}{dt^2}$.

Using Eqs. (16) and (19) in the above expression, we get

$$\begin{aligned} B(t) &= B - 2igtA^\dagger B^\dagger C^2 + g^2t^2(-4A^\dagger AB^\dagger B^2C^\dagger C + B^\dagger B^2C^{\dagger 2}C^2 \\ &\quad + 2A^\dagger ABC^{\dagger 2}C^2 + 2BC^{\dagger 2}C^2 - 2A^\dagger AB^\dagger B^2) \end{aligned} \quad (20)$$

And complex conjugate of $B(t)$ is

$$\begin{aligned} B^\dagger(t) &= B^\dagger + 2igtABC^{\dagger 2} + g^2t^2(-4A^\dagger AB^{\dagger 2}BC^\dagger C + B^{\dagger 2}BC^{\dagger 2}C^2 \\ &\quad + 2A^\dagger AB^\dagger C^{\dagger 2}C^2 + 2B^\dagger C^{\dagger 2}C^2 - 2A^\dagger AB^{\dagger 2}B) \end{aligned} \quad (21)$$

Field amplitude quadrature component is defined as

$$X(t) = \frac{1}{2}[B(t) + B^\dagger(t)] \quad (22)$$

To study the squeezing, initially we assume a quantum state which is the product of coherent state $|\alpha\rangle$ and $|\beta\rangle$ for pump mode A and B, respectively, and vacuum state $|0\rangle$ for mode C, i.e.,

$$|\psi\rangle = |\alpha\rangle_A |\beta\rangle_B |0\rangle_C \quad (23)$$

Substituting Eqs. (20), (21), and (23) in Eq. (22), we have

$$X(t) = \frac{1}{2}[B + B^\dagger - 2g^2t^2(A^\dagger AB^\dagger B^2 + A^\dagger AB^{\dagger 2}B)] \quad (24)$$

Expectation value of $X(t)$ is given as

$$\langle \psi | X(t) | \psi \rangle = \frac{1}{2}[\beta + \beta^* - 2g^2t^2(|\alpha|^2|\beta|^2\beta + |\alpha|^2|\beta|^2\beta^*)] \quad (25)$$

where α and β are the expectation value of operator A and B, respectively, with $A^\dagger A = |\alpha|^2$ and $B^\dagger B = |\beta|^2$.

Squaring of Eq. (25), we have

$$\langle \psi | X(t) | \psi \rangle^2 = \frac{1}{4}[\beta^2 + \beta^{*2} + 2|\beta|^2 - 2g^2t^2|\alpha|^2(2\beta^2|\beta|^2 + 2\beta^{*2}|\beta|^2 + 4|\beta|^4)] \quad (26)$$

Now

$$X^2(t) = X(t)X(t)$$

$$X^2(t) = \frac{1}{4}[B^2 + B^{\dagger 2} + 2B^\dagger B + 1 - 2g^2t^2(2A^\dagger AB^\dagger B^3 + 2A^\dagger AB^{\dagger 3}B + A^\dagger AB^2 + A^\dagger AB^{\dagger 2} + 4A^\dagger AB^{\dagger 2}B^2 + 4A^\dagger AB^\dagger B)] \quad (27)$$

And expectation value of $X^2(t)$ is given as

$$\langle \psi | X^2(t) | \psi \rangle = \frac{1}{4}[\beta^2 + \beta^{*2} + 2|\beta|^2 + 1 - 2g^2t^2|\alpha|^2(2\beta^2|\beta|^2 + 2\beta^{*2}|\beta|^2 + \beta^2 + \beta^{*2} + 4|\beta|^4 + 4|\beta|^2)] \quad (28)$$

Subtracting Eq. (26) from Eq. (28), we get

$$[\Delta X(t)]^2 = \langle \psi | X^2(t) | \psi \rangle - \langle \psi | X(t) | \psi \rangle^2 = \frac{1}{4}[1 - 2g^2t^2|\alpha|^2(\beta^2 + \beta^{*2} + 4|\beta|^2)] \quad (29)$$

So

$$[\Delta X(t)]^2 - \frac{1}{4} = -g^2t^2|\alpha|^2|\beta|^2(\cos 2\theta + 2) \quad (30)$$

where θ is phase angle of field amplitude with $\beta = |\beta| \exp(i\theta)$. The right-hand side of Eq. (30) is negative, which shows the existence of squeezing for all values of θ for which $\cos 2\theta > 0$ in pump mode. Squeezing will be maximum, when $\theta = 0$.

3.2 Higher Order Amplitude Squeezing

For higher order squeezing, quadrature component is defined as

$$Y(t) = \frac{1}{2}[B^2(t) + B^{\dagger 2}(t)] \quad (31)$$

Using Eqs. (20) and (23), we get

$$B^2(t) = [B^2 - 2g^2t^2(2A^\dagger AB^\dagger B^3 + A^\dagger AB^2)] \quad (32)$$

And complex conjugate of $B^2(t)$ is given as

$$B^{\dagger 2}(t) = [B^{\dagger 2} - 2g^2t^2(2A^\dagger AB^{\dagger 3}B + A^\dagger AB^{\dagger 2})] \quad (33)$$

Substituting $B^2(t)$ from Eq. (32) and $B^{\dagger 2}(t)$ from Eq. (33) in above $Y(t)$ expression (Eq. (31)), we get

$$Y(t) = \frac{1}{2}[B^2 + B^{\dagger 2} - 2g^2t^2(2A^\dagger AB^\dagger B^3 + A^\dagger AB^2 + 2A^\dagger AB^{\dagger 3}B + A^\dagger AB^{\dagger 2})] \quad (34)$$

Expectation value of $Y(t)$ is given as

$$\begin{aligned} \langle \psi | Y(t) | \psi \rangle &= \frac{1}{2}[\beta^2 + \beta^{*2} - 2g^2t^2(2|\alpha|^2|\beta|^2\beta^2 \\ &\quad + 2|\alpha|^2|\beta|^2\beta^{*2} + |\alpha|^2\beta^2 + |\alpha|^2\beta^{*2})] \end{aligned} \quad (35)$$

Squaring of Eq. (35), we get

$$\begin{aligned} \langle \psi | Y(t) | \psi \rangle^2 &= \frac{1}{4}[\beta^4 + \beta^{*4} + 2|\beta|^4 - 2g^2t^2|\alpha|^2(4\beta^4|\beta|^2 \\ &\quad + 4\beta^{*4}|\beta|^2 + 2\beta^4 + 2\beta^{*4} + 8|\beta|^6 + 4|\beta|^4)] \end{aligned} \quad (36)$$

And

$$Y^2(t) = Y(t)Y(t)$$

Substituting operator $Y(t)$ from Eq. (34) in the above relation, we get $Y^2(t)$ as

$$\begin{aligned} Y^2(t) &= \frac{1}{4}[B^4 + B^{\dagger 4} + 2B^{\dagger 2}B^2 + 4B^\dagger B + 2 - 2g^2t^2(4A^\dagger AB^\dagger B^5 \\ &\quad + 4A^\dagger AB^{\dagger 5}B + 6A^\dagger AB^4 + 6A^\dagger AB^{\dagger 4} + 8A^\dagger AB^{\dagger 3}B^3 \\ &\quad + 28A^\dagger AB^{\dagger 2}B^2 + 32A^\dagger AB^\dagger B + 4A^\dagger A)] \end{aligned} \quad (37)$$

Expectation value of $Y^2(t)$ is given as

$$\begin{aligned} \langle \psi | Y^2(t) | \psi \rangle &= \frac{1}{4} [\beta^4 + \beta^{*4} + 2|\beta|^4 + 4|\beta|^2 + 2 - 2g^2t^2|\alpha|^2(4\beta^4|\beta|^2 \\ &\quad + 4\beta^{*4}|\beta|^2 + 6\beta^4 + 6\beta^{*4} + 8|\beta|^6 + 28|\beta|^4 + 32|\beta|^2 + 4)] \end{aligned} \quad (38)$$

Subtracting Eq. (36) from Eq. (38), we get

$$\begin{aligned} [\Delta Y(t)]^2 &= \langle \psi | Y^2(t) | \psi \rangle - \langle \psi | Y(t) | \psi \rangle^2 \\ &= \frac{1}{4} [4|\beta|^2 + 2 - 2g^2t^2|\alpha|^2(4\beta^4 + 4\beta^{*4} + 24|\beta|^4 + 32|\beta|^2 + 4)] \end{aligned} \quad (39)$$

The photon number having frequency ω_2 in mode B is given as

$$N(t) = B^\dagger(t)B(t)$$

Using Eqs. (20), (21), and (23) in the above expression, we get

$$N(t) = B^\dagger B - 2g^2t^2(2A^\dagger AB^{\dagger 2}B^2) \quad (40)$$

And

$$N(t) + \frac{1}{2} = B^\dagger B + \frac{1}{2} - 2g^2t^2(2A^\dagger AB^{\dagger 2}B^2) \quad (41)$$

We can also write the above equation as

$$N(t) + \frac{1}{2} = \frac{1}{4} [4B^\dagger B + 2 - 8g^2t^2(2A^\dagger AB^{\dagger 2}B^2)]$$

Now expectation value of $\langle N(t) + \frac{1}{2} \rangle$ becomes

$$\left\langle N(t) + \frac{1}{2} \right\rangle = \frac{1}{4} [4|\beta|^2 + 2 - 8g^2t^2(2|\alpha|^2|\beta|^4)] \quad (42)$$

Subtracting Eq. (42) from Eq. (39), we obtain

$$\begin{aligned} [\Delta Y(t)]^2 - \left\langle N(t) + \frac{1}{2} \right\rangle &= \frac{1}{4} [4|\beta|^2 + 2 - 2g^2t^2|\alpha|^2(4\beta^4 + 4\beta^{*4} + 24|\beta|^4 \\ &\quad + 32|\beta|^2 + 4)] - \frac{1}{4} [4|\beta|^2 + 2 - 16g^2t^2|\alpha|^2|\beta|^4] \end{aligned}$$

and

$$[\Delta Y(t)]^2 - \left\langle N(t) + \frac{1}{2} \right\rangle = -2g^2t^2|\alpha|^2(2|\beta|^4 \cos 4\theta + 4|\beta|^4 + 8|\beta|^2 + 1)$$

Finally, we get

$$[\Delta Y(t)]^2 - \left\langle N(t) + \frac{1}{2} \right\rangle = -2g^2t^2|\alpha|^2[2|\beta|^4(\cos 4\theta + 2) + 8|\beta|^2 + 1] \quad (43)$$

Equation (43) fulfills the condition of higher order squeezing for which $\cos 4\theta > 0$. The squeezing can be tuned by varying the phase angle of field amplitude, interaction time, and number of photons prior to the interaction.

4 Photon Statistics

Condition of sub-Poissonian photon statistics is given as

$$[\Delta N_B(t)]^2 - \langle N_B(t) \rangle < 0 \quad (44)$$

where

$$[\Delta N_B(t)]^2 = \langle N_B^2(t) \rangle - \langle N_B(t) \rangle^2 \quad (45)$$

The expectation value of $N_B(t)$ from Eq. (40) is given as

$$\langle N_B(t) \rangle = |\beta|^2 - 4g^2t^2|\alpha|^2|\beta|^4 \quad (46)$$

After squaring of above equation, we get

$$\langle N_B(t) \rangle^2 = |\beta|^4 - 8g^2t^2(|\alpha|^2|\beta|^6) \quad (47)$$

As

$$N_B^2(t) = N_B(t)N_B(t)$$

Substituting N_B from Eq. (40) in above expression, we get $N_B^2(t)$ as $N_B^2(t) = B^{\dagger 2}B^2 + B^\dagger B - 8g^2t^2(A^\dagger AB^{\dagger 3}B^3 + 2A^\dagger AB^{\dagger 2}B^2)$

Expectation value of $N_B^2(t)$ is given as

$$\langle N_B^2(t) \rangle = |\beta|^4 + |\beta|^2 - 8g^2t^2(|\alpha|^2|\beta|^6 + 2|\alpha|^2|\beta|^4) \quad (48)$$

Substituting Eq. (47) and Eq. (48) in Eq. (45), we get

$$[\Delta N_B(t)]^2 = |\beta|^2 - 16g^2t^2(|\alpha|^2|\beta|^4) \quad (49)$$

Substituting Eqs. (46) and (49) in Eq. (44), we get

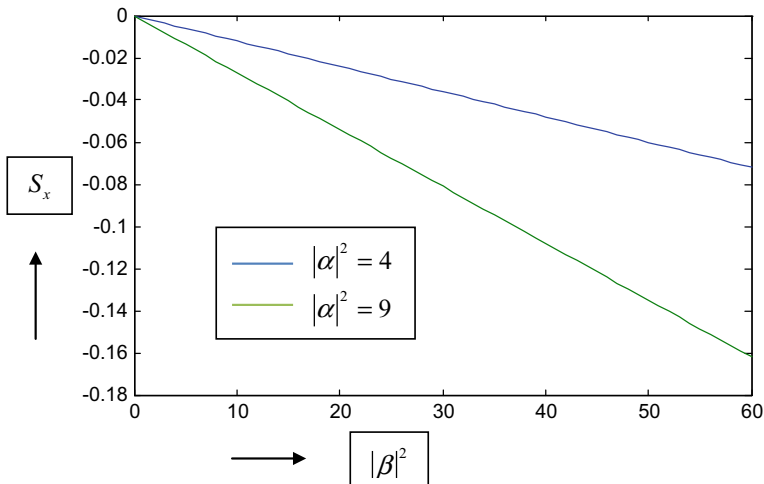


Fig. 1 Variation of field amplitude squeezing S_x with $|\beta|^2$ (taking $g^2t^2 = 10^{-4}$, $\theta = 0$ for maximum squeezing)

$$[\Delta N_B(t)]^2 - \langle N_B(t) \rangle = -12g^2t^2(|\alpha|^2|\beta|^4) \quad (50)$$

We are getting negative value which shows that photon statistics is sub-Poissonian or antibunched light.

5 Result

The presence of field amplitude squeezing and higher order amplitude squeezing in five-wave mixing process is shown in Eqs. (30) and (43), respectively. Figures 1 and 2 represent a graph between field amplitude squeezing say S_x and higher order squeezing say S_y with photon number in mode B, i.e., $|\beta|^2$, respectively. From Figs. 1 and 2, it is clear that for a fixed value of photons number in mode A, i.e., $|\alpha|^2$, squeezing increases nonlinearly with increase in photons number in mode B, i.e., $|\beta|^2$. Further, it is also shown that S_x and S_y increases with increase in photons number in coherent state A, i.e., $|\alpha|^2$. Thus, we can say that squeezing depends upon photon number in pump mode A and mode B.

6 Conclusion

The result shows the presence of higher order squeezing and sub-Poissonian photon statistics, i.e., antibunching of photon in pump mode in five-wave mixing process.

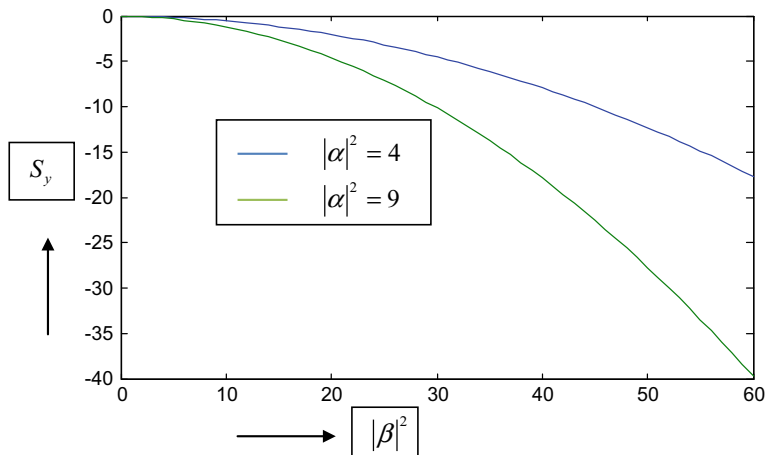


Fig. 2 Variation of higher order squeezing S_y with $|\beta|^2$ (taking $g^2t^2 = 10^{-4}$, $\theta = 0$ for maximum squeezing)

A comparison of Figs. 1 and 2 shows that squeezing increases with higher order of field amplitude. Further, squeezing and photon statistics is directly related to pump photons of optical field. Thus, we can conclude that the process of generation of higher order squeezing is more suitable for the generation of optimum squeezed light and antibunching of photons can be used as a single-photon source that is the primary requirement for quantum information processing [28].

References

1. Dodonov VV (2002) Nonclassical states in quantum optics: a ‘squeezed’ review of the first 75 years. *J Opt B: Quantum Semiclassical Opt* 4(1):R1–R33. <https://doi.org/10.1088/1464-4266/4/1/201>
2. Loudon R, Knight PL (2007) Squeezed light. *J Mod Opt* 34:709–759. <https://doi.org/10.1080/09500348714550721>
3. Gill S, Rani S, Singh N (2012) Higher order amplitude squeezing in fourth and fifth harmonic generation. *Indian J Phys* 86:371–375. <https://doi.org/10.1007/s12648-012-0060-z>
4. Pratap R, Giri DK, Prasad A (2014) Effects of squeezing and sub-poissonian of light in fourth harmonic generation up to first order Hamiltonian interaction. *Optik- Int J Light Electron Opt* 125(3):1065–1070. <https://doi.org/10.1016/j.ijleo.2-013.07.143>
5. Rani S, Lal J, Singh N (2012) Normal and higher order squeezing in eight wave mixing process. *Indian J Phys* 86(1):448–460. <https://doi.org/10.1007/s12648-012-0001-x>
6. Rani S, Lal J, Singh N (2011) Higher order amplitude squeezing in six wave mixing process. *Int J Opt.*: 9. <https://doi.org/10.1155/2011/629605>
7. Slusher RE, Hollberg LW, Yurke B, Mertz JC, Valley JF (1985) Observation of squeezed states generated by four-wave mixing in an optical cavity. *Phys Rev Lett* 55:2409–2412. <https://doi.org/10.1103/PhysRevLett.55.2409>

8. Giri DK, Gupta PS (2005) Higher order squeezing of the electromagnetic field in spontaneous and stimulated raman processes. *J Mod Opt* 52:1769–1781. <https://doi.org/10.1080/09500340500073065>
9. Kumar A, Gupta PS (1996) Higher order amplitude squeezing in hyper Raman scattering under short time approximation. *Quantum Semiclassical Opt: J Eur Opt Soc Part B* 8:1053–1060. <https://doi.org/10.1088/1355-5111/8/5/010>
10. Dong R, Heersink J, Corney JF, Drummond PD, Anderson UL, Leuchs G (2008) Raman induced limits to efficient squeezing in optical fibres. *Opt Lett* 33:116–118. <https://doi.org/10.1364/OL.33.000116>
11. Rebhi R, Anders K, Kaiser R, Lezama A (2015) Fluctuation properties of laser light after interaction with atomic system: comparison between two level and multi level atomic transition. *Phys Rev A* 92:033853–033861. <https://doi.org/10.1103/PhysRevA.92.033853>
12. Hong CK, Mandel L (1985) Higher order squeezing of a quantum field. *Phys Rev Lett* 54:323–325. <https://doi.org/10.1103/PhysRevLett.54.323>
13. Hillery M (1987) Amplitude- squared squeezing of the electromagnetic field. *Phys Rev A* 36:3796–3802. <https://doi.org/10.1103/PhysRevA.36.3796>
14. Gill S (2017) Non classical effects of light in higher order five wave mixing. *Int J Adv Sci Eng Technol* 5(3):16–20. IJASEAT-IRAJ-DOI-8716
15. Pathak A, Mandal S (2003) Photon-bunching, photon-antibunching and nonclassical photon statistics of coherent light coupled to a cubic nonlinear medium. *Mod Phys Lett B* 17(5–6):225–233. <https://doi.org/10.1142/S0217984903005123>
16. Thapliyal K, Pathak A, Sen B, Peřina J (2014) Higher-order nonclassicalities in a codirectional nonlinear optical coupler quantum entanglement, squeezing and antibunching. *Phys Rev A* 90:013808–013817. <https://doi.org/10.1103/PhysRevA.90.013808>
17. Giri, S. K., Sen, B., Raymond, O, Pathak, A.: Single-mode and intermodal higher order nonclassicalities in two-mode Bose- Einstein condensates. *Phys Rev A* 89:033628 (1–10) (2014). <https://doi.org/10.1103/physreva.89.033628>
18. Kim Y, Yoon TH (2002) Higher order sub-poissonian photon statistics of light. *Opt Commun* 212:107–114. [https://doi.org/10.1016/s00304018\(02\)01981-8](https://doi.org/10.1016/s00304018(02)01981-8)
19. Mishra DK (2010) Study of higher order non classical properties of squeezed kerr state. *Opt Commun* 283:3284–3290. <https://doi.org/10.1016/j.optcom.2010.04.007>
20. Perina J, Perinova V, Kodousek J (1984) On the relations of antibunching, sub-poissonian statistics and squeezing. *Opt Commun* 49:210–214. [https://doi.org/10.1016/003-4018\(84\)90266-9](https://doi.org/10.1016/003-4018(84)90266-9)
21. Prakash H, Mishra DK (2006) Higher order sub poissonian photon statistics and their use in detection of Hong and Mandel squeezing and amplitude squared squeezing. *J Phys B: At Mol Opt Phys* 39:2291–2297. <https://doi.org/10.1088/0953-4075/39/9/014>
22. Koashi M, Kono K, Hirano T (1993) Photon antibunching in pulsed squeezed light generated via parametric amplification. *Phys Rev Lett* 71(8):1164–1167. <https://doi.org/10.1103/physrevlett.71.1164>
23. Gill S, Sunil R, Nafe S (2012) Total minimum noise in wave mixing processes. *Int J Opt* 6:4. <https://doi.org/10.1155/2012/431826>
24. Thapliyal K, Pathak A (2015) Applications of quantum cryptographic switch: various tasks related to controlled quantum communication can be performed using Bell states and permutation of particles. *Quantum Inf Process* 14:2599–2616. <https://doi.org/10.1007/s11128-015-0987-z>
25. Thapliyal K, Verma A, Pathak A (2015) A general method for selecting quantum channel for bidirectional controlled state teleportation and other schemes of controlled quantum communication. *Quantum Inf Process* 14:4601–4614. <https://doi.org/10.1007/s11128-015-1124-8>
26. Hsu MTL, Delaubert V, Bowen WP, Fabre C, Bachor HA, Lam PK (2006) A quantum study of multibit phase coding for optical storage. *IEEE J Quantum Electron* 42:1001–1007. <https://doi.org/10.1109/JQE.2006.881634>

27. Shukla C, Pathak A (2014) Orthogonal state based deterministic secure communication without actual transmission of the message qubits. *Quantum Inf Process* 13:2099–2113. <https://doi.org/10.1007/s11128-014-0792-0>
28. Beveratos A, Brouri R, Gacoin T, Villing A, Poizat JP, Grangier P (2002) Single photon quantum cryptography. *Phys Rev Lett* 89:187901–187904. <https://doi.org/10.1103/PhysRevLett.89.187901>

Active Power Loss Diminution by Chaotic-Based Adaptive Butterfly Mating Optimization Algorithm



Kanagasabai Lenin

Abstract Real power loss minimization is the key objective of this work, and it has been attained by applying chaotic-based adaptive butterfly mating optimization algorithm (CABM). Butterfly mating limitations and scattering in the exploration area are articulated in the CABM algorithm. Butterfly positioned near to the border may get puzzled regarding the direction to the border since UV augments amid of an increase in distance. Through indistinguishable unchanging step, acceleration of butterflies is restricted in iterations. Chaotic-based adaptive butterfly mating optimization (CABM) algorithm's validity is verified by testing in IEEE 57 bus test system. Projected CABM algorithm reduced the power loss effectively.

Keywords Chaotic · Adaptive · Butterfly · Mating · Optimization · Reactive

1 Introduction

Active power loss is the key objective in this work. Different methods [1–6] solved the problem, and evolutionary algorithms [7–15] are utilized to solve the problem. This paper proposes chaotic-based adaptive butterfly mating optimization algorithm (CABM) to solve optimal reactive power problem. In butterfly mating optimization algorithm, both the male and female butterfly utilize ultraviolet (UV) for mating. UV value will be altered with reference to the adaptability and distance. Initially, there is lack of diversification and imbalance. Exploitation capability is determined by the mutual distances between the butterflies. In the projected chaotic-based adaptive butterfly mating optimization algorithm (CABM), it possesses chaotic dispersion. Adaptive movement has been incorporated in butterfly mating optimization algorithm. Proposed chaotic-based adaptive butterfly mating optimization algorithm (CABM) is evaluated in IEEE 57 test system. Projected algorithm has reduced active power loss effectively.

K. Lenin (✉)

Department of EEE, Prasad V. Potluri, Siddhartha Institute of Technology, Kanuru, Vijayawada
Andhra Pradesh, 520007, India
e-mail: gklenin@gmail.com

2 Problem Formulation

Active power loss is the key objective and defined by,

$$P_L = \sum_{k \in Nbr} g_k (V_i^2 + V_j^2 - 2V_i V_j \cos \theta_{ij}) \quad (1)$$

$$\text{Objective function} = \text{Power loss} + \text{weight } (\omega_v) \times \text{Deviation of Volatge} \quad (2)$$

$$\text{Deviation of volatge} = \sum_{i=1}^{Npq} |V_i - 1| \quad (3)$$

Equal and in equal constraints as follows

$$\text{Generation}(P_G) = \text{Demand}(P_D) + \text{Load}(P_L) \quad (4)$$

$$P_{g \text{ slack}}^{\min} \leq P_{g \text{ slack}} \leq P_{g \text{ slack}}^{\max} \quad (5)$$

$$Q_{gi}^{\min} \leq Q_{gi} \leq Q_{gi}^{\max}, \quad i \in N_g \quad (6)$$

$$V_i^{\min} \leq V_i \leq V_i^{\max}, \quad i \in N_B \quad (7)$$

$$T_i^{\min} \leq T_i \leq T_i^{\max}, \quad i \in N_T \quad (8)$$

$$Q_c^{\min} \leq Q_c \leq Q_c^{\max}, \quad i \in N_C \quad (9)$$

3 Chaotic-Based Adaptive Butterfly Mating Optimization Algorithm

Butterfly mating optimization algorithm has four stages [16]. Through ultraviolet reflectance, male butterfly mate with female butterfly, and ultraviolet value is rationalized by,

$$\begin{aligned} \text{Butterfly ultraviolet value } (\text{ultraviolet}_i(t)) = & \max\{0, \text{weight factor}(w_1) \times \text{ultraviolet}_i(t+1) \\ & + \text{weight factor}(w_2) \times f(t) \end{aligned} \quad (10)$$

Butterflies distance are defined by,

$$UV_{i \rightarrow j} = UV_i \times \frac{d_{ij}^{-1}}{\sum_k d_{ik}^{-1}} \quad (11)$$

Highest UV value of butterflies is taken as local mate and defined as

$$UV(i\text{th butterfly}) < UV(j\text{th butterfly}) \quad (12)$$

Movement of the butterfly is given by,

$$y_i(t+1) = y_i(t) + B_s * \left\{ \frac{y_{\text{local mate}}(t) - y_i(t)}{\|y_{\text{local mate}}(t) - y_i(t)\|} \right\} \quad (13)$$

In the proposed chaotic-based adaptive butterfly mating optimization algorithm (CABM), an adaptive approach is incorporated in the butterfly mating optimization algorithm.

$$\text{Initial sequence } \mu(t+1) = -4.559\mu(t)^2 - 0.559\mu(t) + 0.359 \quad (14)$$

$$\text{chaotic exploration sequence } X(t+1) = \frac{1}{\pi} \arcsin\left(\frac{57.0}{25.0}\mu(t+1) + \frac{7.0}{25.0}\right) \quad (15)$$

Adaptive movement mechanism is implemented, and then, modernization is done.

$$G_i(t+1) = G_i(t) + \omega(t) \cdot (P_{\text{local mate}}(t) - G_i(t)) \quad (16)$$

$$\begin{cases} \omega(t) = \exp\left(\frac{-\lambda(t)}{\lambda(t-1)+1}\right) \\ \lambda(t) = \frac{UV_i(t)}{UV_i(t-1)} \end{cases} \quad (17)$$

Chaotic-based adaptive butterfly mating optimization algorithm (CABM) procedure:

a. Candidate sequences are initialized: transformation of variables

$$b. \mu = \frac{50(X - X_{\min})}{57(X_{\max} - X_{\min})} - \frac{1}{2} \quad (18)$$

$$\bar{X} = \frac{X_{\min} + X_{\max}}{2 + X'(X_{\max} - X_{\min})} \quad (19)$$

c. With respect to fitness value, ultraviolet value is rationalized
 d. Calculate the scatter values and local mate chosen

Table 1 Constraints of control variables

Variables type	Minimum value (PU)	Maximum value (PU)
Voltage of generator	0.950	1.100
Value of tap in transformer	0.900	1.100
VAR source	0.000	0.200

Table 2 Reactive power generator minimum and maximum values

Variables	Q^{Min} (PU)	Q^{Max} (PU)
1	-140	200
2	-17	50
3	-10	60
6	-8	25
8	-140	200
9	-3	9
12	-150	155

- e. Renewal of key values with reference to the position of the local mate is done by Eqs. (16) and (17)
- f. Position of butterfly is computed, and redistribution is employed by using chaotic search.
- g. When maximum iteration is reached, stop the procedure or else replicate step (b) to step (e).

4 Simulation Study

In IEEE 57 bus system [17], proposed chaotic-based adaptive butterfly mating optimization algorithm (CABM) is validated. Table 1 gives variable limits. In Table 2, reactive power generators limits are given, and comparison results are given in Table 3. Figure 1 shows the comparison of real power loss, and Fig. 2 indicates the real power loss reduction in percentage.

5 Conclusion

Active power loss diminution has been attained by utilizing chaotic-based adaptive butterfly mating optimization algorithm (CABM). In proposed chaotic-based adaptive butterfly mating optimization algorithm (CABM), adaptive approach is incorporated successfully in basic butterfly mating optimization algorithm. UV based factor

Table 3 Simulation results of IEEE-57 system

Control variables	Base case	MPSO [18]	PSO [18]	CGA [18]	AGA [18]	CABM
Generator voltage –1	1.040	1.093	1.083	0.968	1.027	1.024
Generator voltage –2	1.010	1.086	1.071	1.049	1.011	1.017
Generator voltage –3	0.985	1.056	1.055	1.056	1.033	1.008
Generator voltage –6	0.980	1.038	1.036	0.987	1.001	1.014
Generator voltage –8	1.005	1.066	1.059	1.022	1.051	1.006
Generator voltage –9	0.980	1.054	1.048	0.991	1.051	1.012
Generator voltage 12	1.015	1.054	1.046	1.004	1.057	1.019
T_t 19	0.970	0.975	0.987	0.920	1.030	0.916
T_t 20	0.978	0.982	0.983	0.920	1.020	0.914
T_t 31	1.043	0.975	0.981	0.970	1.060	0.917
T_t 35	1.000	1.025	1.003	NR*	NR*	1.009
T_t 36	1.000	1.002	0.985	NR*	NR*	1.006
T_t 37	1.043	1.007	1.009	0.900	0.990	1.012
T_t 41	0.967	0.994	1.007	0.910	1.100	0.916
T_t 46	0.975	1.013	1.018	1.100	0.980	1.010
T_t 54	0.955	0.988	0.986	0.940	1.010	0.920
T_t 58	0.955	0.979	0.992	0.950	1.080	0.941
T_t 59	0.900	0.983	0.990	1.030	0.940	0.937
T_t 65	0.930	1.015	0.997	1.090	0.950	1.016
T_t 66	0.895	0.975	0.984	0.900	1.050	0.927
T_t 71	0.958	1.020	0.990	0.900	0.950	1.019
T_t 73	0.958	1.001	0.988	1.000	1.010	1.010
T_t 76	0.980	0.979	0.980	0.960	0.940	0.941
T_t 80	0.940	1.002	1.017	1.000	1.000	1.021
Q_C 18	0.1	0.179	0.131	0.084	0.016	0.145
Q_C 25	0.059	0.176	0.144	0.008	0.015	0.139
Q_C 53	0.063	0.141	0.162	0.053	0.038	0.119
P_G (MW)	1278.6	1274.4	1274.8	1276	1275	1272.63
Q_G (Mvar)	321.08	272.27	276.58	309.1	304.4	272.38
Reduction in P_{Loss} (%)	0	15.4	14.1	9.2	11.6	24.16
Total P_{Loss} (Mw)	27.8	23.51	23.86	25.24	24.56	21.082

NR* Not reported

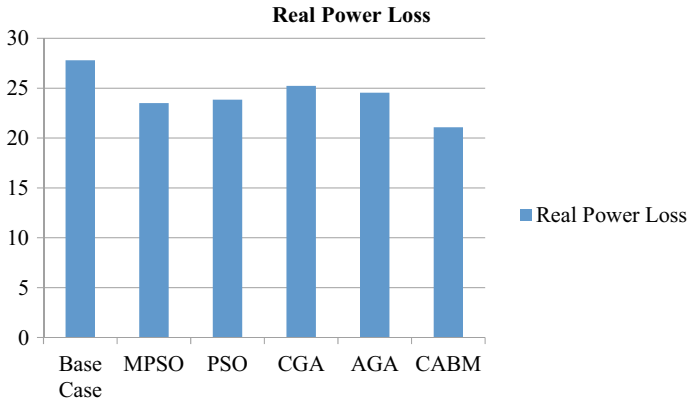


Fig. 1 Comparison of real power loss

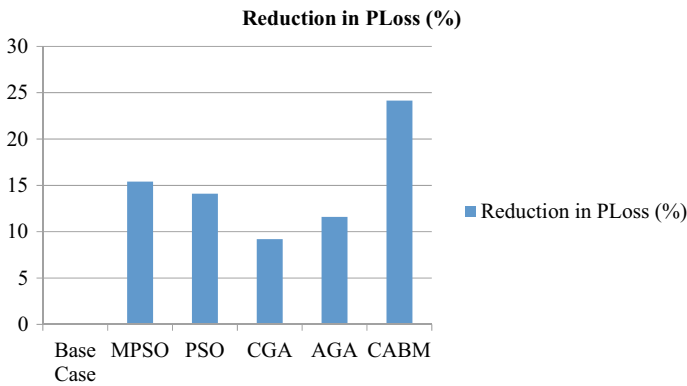


Fig. 2 Reduction of loss in percentage

is applied to the current variable, and through that, local mate exploration range is extended to other regions. In IEEE 57 bus test system, proposed chaotic-based adaptive butterfly mating optimization algorithm (CABM) is validated. Active power loss is attained, and there is enhancement in percentage of reduction in loss.

References

1. Lee K (1984) Fuel-cost minimisation for both real and reactive-power dispatches. Proc Gener Transm Distrib Conf 131(3):85–93
2. Deeb N (1998) An efficient technique for reactive power dispatch using a revised linear programming approach. Electr Power Syst Res 15(2):121–134

3. Bjelogrić M (1990) Application of Newton's optimal power flow in voltage/reactive power control. *IEEE Trans Power Syst* 5(4):1447–1454
4. Granville S (1994) Optimal reactive dispatch through interior point methods. *IEEE Trans Power Syst* 9(1):136–146
5. Grudin N (1998) Reactive power optimization using successive quadratic programming method. *IEEE Trans Power Syst* 13(4):1219–1225
6. Mei RNS (2017) Optimal reactive power dispatch solution by loss minimization using moth-flame optimization technique. *Appl Soft Comput* 59:210–222
7. Chen G (2017) Optimal reactive power dispatch by improved GSA-based algorithm with the novel strategies to handle constraints. *Appl Soft Comput* 50:58–70
8. Naderi E (2017) Novel fuzzy adaptive configuration of particle swarm optimization to solve large-scale optimal reactive power dispatch. *Appl Soft Comput* 53:441–456
9. Heidari A (2017) Gaussian bare-bones water cycle algorithm for optimal reactive power dispatch in electrical power systems. *Appl Soft Comput* 57:657–671
10. Morgan M (2016) Benchmark studies on optimal reactive power dispatch (ORPD) based multi-objective evolutionary programming (MOEP) using mutation based on adaptive mutation adapter (AMO) and polynomial mutation operator (PMO). *J Electr Syst* 12–1
11. Mei RNS (2016) Ant lion optimizer for optimal reactive power dispatch solution. *J Electr Syst* 68–74
12. Anbarasan, Optimal reactive power dispatch problem solved by symbiotic organism search algorithm. *Innov Power Adv Comput Technol* 1–8
13. Gagliano A (2017) Analysis of the performances of electric energy storage in residential applications. *Int J Heat Technol* 35(1):S41–S48
14. Caldera M (2018) Survey-based analysis of the electrical energy demand in Italian households. *Math Model Eng Probl* 5(3):217–224
15. Basu M (2016) Quasi-oppositional differential evolution for optimal reactive power dispatch. *Electr Power Energy Syst* 78:29–40
16. Wu H-N (2017) A novel binary butterfly mating optimization algorithm with sub array strategy for thinning of large antenna array. *Prog Electromagn Res M* 60:101–110
17. IEEE The IEEE-test systems <http://www.ee.washington.edu/trsearch/pstca/2019/01/21>
18. Hussain AN (2018) Modified particle swarm optimization for solution of reactive power dispatch. *Res J Appl Sci Eng Technol* 15(8):316–327

Mobile-Based Signature Database (MOBSIGN DB): A New Signature Database



Sudhir Rohilla, Anuj Sharma, and R. K. Singla

Abstract We have presented here an online signature database. The main issue in signature verification is to acquire the reliable signature database for checking the performance of the developed system. In this work, we have collected a signature database, mobile-based signature database (MOBSIGN DB). We have followed the same protocols as followed in SVC2004 signature database. We have collected dynamic as well as offline images of the signatures. The dynamic properties include xy coordinates and actual time taken for doing the signature (which was arbitrarily taken in SVC2004) for each data point of the captured signatures.

Keywords Online signature verification · Signature database · Mobile-based signature database · Online signature database

1 Introduction

It has been observed that research related to online signature verification continuously attracted many researchers in the past and nowadays as well. Various new features for representing the online signatures and the respective numerous techniques have been proposed for verification in the literature. Another important aspect of online signature verification is the database on which experimentation are conducted. It is always useful to compare the results of any verification methodology with the previous studies. But it is significant only if we consider a benchmark database. The work has been done in the past to establish a benchmark database. Some of these databases have been summarized in the next section which were collected using the

S. Rohilla

Department of Computer Science and Information Technology,
Central University of Haryana, Mahendergarh, Haryana, India

A. Sharma (✉) · R. K. Singla

Department of Computer Science and Applications, Panjab University, Chandigarh 160014, India

e-mail: anujs@pu.ac.in

URL: <https://sites.google.com/view/anujsharma/>

© Springer Nature Singapore Pte Ltd. 2021

G. S. Hura et al. (eds.), *Advances in Communication and Computational*

Technology, Lecture Notes in Electrical Engineering 668,

https://doi.org/10.1007/978-981-15-5341-7_13

pen tablets. In Sect. 3, we have presented an online signature database, mobile-based signature database (MOBSIGN DB), by using a mobile phone. The database follows the guidelines of SVC2004 (first signature verification competition held in 2004) signature database. In Sect. 4, the symbolic verification technique has been explained along with the features used. The results of online signature verification system using MOBSIGN DB have been reported in Sect. 5. In Sect. 6, the conclusion of the paper has been done along with some future directions and in the acknowledgements section, acknowledgement from the authors has been provided.

2 Benchmark Signature Databases

2.1 *MCYT Baseline Corpus*

One of the most popular signature database is MCYT baseline corpus developed by [5]. It was further divided into two parts: one is MCYT_fingerprint sub-corpus and another is MCYT_Signature sub-corpus. A graphic WACOM pen tablet is used to collect signature. The dynamic properties like xy coordinate points, pressure, azimuth, altitude angles, etc., are collected for online signature samples and the image of the signature is also stored for the purpose of offline signature verification, coordinates and in this signature database, signatures are collected from 330 users. Each user provided 25 genuine signature samples and 25 skilled forgery samples are collected from 5 subsequent users. In this way, there are total 8250 genuine signatures and the same number of forgery signature samples and 16,500 is the number of total signatures that are collected in this signature database.

2.2 *SVC2004 Signature Database*

Another popular signature database is SVC2004 signature database. [8] uses WACOM digitizing pen tablet to collect this signature database. In this signature database, there are two different datasets: TASK1 and TASK2. In each of the dataset, 100 users provide 20 genuine signature samples and 20 forgery signatures are collected from 5 different users. TASK1 contains only the coordinate point information whereas TASK2, in addition, contains pressure information also. After the competition, signatures from 40 users are provided to the research community as a sample of the signature database for each of the dataset.

2.3 *BIOMET Database*

In this signature database, Garcia-Salicetti et al. [2] have used WACOM pen tablet to collect signatures from 325 user in different sessions. 15 genuine signature samples for each writer and 17 forgery signature samples are collected in this signature database.

2.4 *Sabancı University SIGNature Database (SUSIG)*

SUSIG is another benchmark database in which two datasets are there: one is visual sub-corpus and another is blind sub-corpus [4]. The difference between two sub-corpus is that in visual sub-corpus, a person can see his/her signature while doing the signature on a screen mounted to the digitized pen tablet which is not the case with other sub-corpus. In visual sub-corpus, there are signatures from 100 writers and for each writer, there are 20 genuine signature samples with 10 forgery signature samples. In blind sub-corpus, 100 writers, different from the visual sub-corpus, provide 8 or 10 genuine signatures with 10 skilled forgery signature samples collected from one different writer.

2.5 *BiosecurID: A Multimodal Biometric Database*

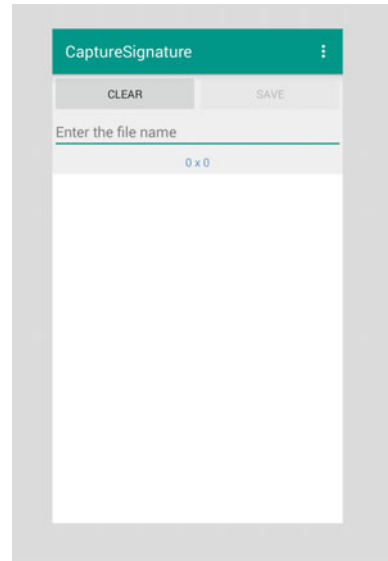
Another signature database has been developed in which signatures from 400 writers are collected [1]. Each writer has given 16 genuine signature samples with 12 forgery signature samples in four different sessions. In each session, level of forgery is increased by providing extra information in each of the subsequent session.

3 Mobile-Based Signature Database (MOBSIGN DB)

In this study, we have collected signatures from 75 users from the faculty, research scholar, and working staff in the university. We have followed the same protocols as followed in SVC2004 signature database. We have collected dynamic as well as offline images of the signatures. The dynamic properties include xy coordinates, actual time taken for doing the signature (which is arbitrarily taken in SVC2004), and the pressure information for each data point of the captured signatures. In this study, we have performed experiments by considering only the online properties of the signatures.

With advancement in technologies, the mobile phones are capable to provide the easy process to capture signatures. So, the device SAMSUNG GALAXY NOTE 11

Fig. 1 Interface of the application



(GT N7100) is used to capture signatures through mobile application. The device is equipped with a pen stylus which is quite useful in such an application. We have collected genuine signatures from 75 users. Each user has given 25 genuine signature samples. Thus, a total of 1875 genuine signatures have collected and the experiments are performed to check the random forgery for the MOBSIGN DB.

In Fig. 1, the interface of the Android-based application *CaptureSignature* has been shown. In this application, the region inside the outer gray area is the screenshot of the application. Writers can do the signature in the white region. “0 × 0” is the information of xy coordinates. The CLEAR button is used to erase the signature from the screen. SAVE button is used to store the image of the signature and the dynamic properties captured in a text file at the background with the name given by the writer as explained in Fig. 2. The few signature samples that are captured through the application are shown in Fig. 3. The online info for a signature is also shown for a signature in Fig. 4. In this figure, the first information is the touch event on the screen. It has multiple values of 0, 1, and 2 where 0 indicates a pen down, 1 indicates a pen-up event, and 2 indicates the continuation of the pen down event on the touch screen in a motion. The next data value, after the underscore, shows the time of the mobile internal clock. The next two data values are about the xy coordinates in the area of signature as indicated in Fig. 2 and the next two data values are about the xy coordinates in the whole touch screen of the device. The last information is about the pressure applied on each data point captured by the writer using stylus on the touch screen.



Fig. 2 Sample signature using application

A handwritten signature in cursive script, appearing to read "Srinivas", written in black ink on a white background.

(a) Writer 1

A handwritten signature in cursive script, appearing to read "Srinivas", written in black ink on a white background.

(b) Writer 2

A handwritten signature in cursive script, appearing to read "Srinivas", written in black ink on a white background.

(c) Writer 3

A handwritten signature in cursive script, appearing to read "Srinivas", written in black ink on a white background.

(d) Writer 4

A handwritten signature in cursive script, appearing to read "Srinivas", written in black ink on a white background.

(e) Writer 5

A handwritten signature in cursive script, appearing to read "Srinivas", written in black ink on a white background.

(f) Writer 6

Fig. 3 Images of sample signatures captured by the designed application

```

TouchEvent Time X-coordinate Y-coordinate rawX-coordinate
rawY-coordinate Pressure
1 1446620433671_42.181396_410.1206_42.181396_822.1206_0.5493646
2 1446620433673_42.181396_410.1206_42.181396_822.1206_0.5493646
2 1446620433688_38.744396_403.66278_38.744396_815.6628_0.5532747
2 1446620433705_44.681038_412.72455_44.681038_824.72455_
0.54447705
2 1446620433722_53.32562_434.07703_53.32562_846.077_0.55620724
2 1446620433740_69.26081_472.30304_69.26081_884.30304_0.5718475
2 1446620433757_80.09258_490.11414_80.09258_902.11414_0.53274685
2 1446620433774_92.174164_494.48877_92.174164_906.4888_
0.32942328
2 1446620433785_103.31839_486.8852_103.31839_898.8852_
9.775171E-4
1 1446620433786_103.31839_486.8852_103.31839_898.8852_
9.775171E-4
0 1446620433919_122.37813_321.3778_122.37813_733.3778_0.5073314
2 1446620433929_122.37813_321.58618_122.37813_733.5862_0.5073314
2 1446620433946_123.21134_326.8982_123.21134_738.8982_0.5073314
2 1446620433964_127.48156_342.8344_127.48156_754.8344_0.5278592
2 1446620433981_131.85593_356.5833_131.85593_768.5833_0.5356794
2 1446620433998_136.95935_371.7904_136.95935_783.7904_0.5043988
2 1446620434015_163.20555_444.38867_163.20555_856.3887_
0.062561095
2 1446620434026_162.8931_444.2845_162.8931_856.2845_9.775171E-4
1 1446620434027_162.8931_444.2845_162.8931_856.2845_9.775171E-4
0 1446620434151_81.3424_382.31036_81.3424_794.31036_0.42913002
2 1446620434153_81.3424_382.31036_81.3424_794.31036_0.42913002
2 1446620434171_66.34457_384.18524_66.34457_796.18524_0.4692082
2 1446620434188_28.849993_438.8683_28.849993_850.8683_0.49951124
2 1446620434205_59.470562_501.67566_59.470562_913.67566_
0.5483871
2 1446620434222_85.09186_517.19525_85.09186_929.19525_0.5904203

```

Fig. 4 Online raw information captured by the application

4 Features Set and Verification Technique:

We have used a feature set of 46 features taken from literature to represent the online signatures [7]. These features are derived from xy coordinates and time of each data point captured and are mentioned in Table 1. In these features, V is velocity, Acc_{tan} and Acc_{cent} is tangential and centripetal acceleration, Jerk, t is time instance with respect to start time of the signature and T is the time interval. There are two kinds of important dynamic features which are termed as directionChainCode, S_t , and dirChangeChainCode, C_m and considering K is the total number of data points, they have been defined as

$$S_t = \text{cardinality } \{\theta_k; (t-1) * \pi/4 < \theta_k <= t * \pi/4\} / k,$$

where $k = 1, 2, \dots, k$ and $t = 1, 2, \dots, 8$;

Table 1 Feature set used for representing online signatures

S. No.	Features	S. No.	Features
1	totalSignatureDuration	24	Jerk _{max}
2	totalPenDownTime, T_{pd}	25	$t(X_{min})/T_{pd}$
3	$T(V_x > 0)/T_{pd}$	26	$t(X_{max})/T_{pd}$
4	$T(V_x < 0)/T_{pd}$	27	$t(Y_{min})/T_{pd}$
5	$T(V_y > 0)/T_{pd}$	28	$t(Y_{max})/T_{pd}$
6	$T(V_y < 0)/T_{pd}$	29	rms(Acc _{tan})/Acc _{max}
7	$t(V_{x,min})/T_{pd}$	30	rms(Acc _{cent})/Acc _{max}
8	$t(V_{x,max})/T_{pd}$	31	$T((dx/dt)(dy/dt) > 0) /$ $T((dx/dt)(dy/dt) < 0)$
9	$t(V_{y,min})/T_{pd}$	32	$\Theta_{initial} = \tan^{-1}(V_y/V_x)$
10	$t(V_{y,max})/T_{pd}$	33	$\Theta_{lastPenUp}$
11	$t(V_{min})/T_{pd}$	34	$\Theta_{lastPenUp} - \Theta_{initial}$
12	$t(V_{max})/T_{pd}$	35	directionChainCode, S_1
13	$t(\text{Jerk}_{x,max})/T_{pd}$	36	directionChainCode, S_2
14	$t(\text{Jerk}_{x,min})/T_{pd}$	37	directionChainCode, S_3
15	$t(\text{Jerk}_{y,min})/T_{pd}$	38	directionChainCode, S_4
16	$t(\text{Jerk}_{y,max})/T_{pd}$	39	directionChainCode, S_5
17	$t(\text{Jerk}_{min})/T_{pd}$	40	directionChainCode, S_6
18	$t(\text{Jerk}_{max})/T_{pd}$	41	directionChainCode, S_7
19	Jerk _{x,min}	42	directionChainCode, S_8
20	Jerk _{x,max}	43	dirChangeChainCode, C_1
21	Jerk _{y,min}	44	dirChangeChainCode, C_2
22	Jerk _{y,max}	45	dirChangeChainCode, C_3
23	Jerk _{min}	46	dirChangeChainCode, C_4

$$C_m = \text{cardinality}\{\delta_k = \theta_k - \theta_{k-1}; (m-1) * \pi/2 < \delta_k \leq m * \pi/2\} / (k-1),$$

where $k = 2, \dots, k$ and $m = 1, 2, 3, 4$;

A verification technique based on the symbolic representation of online signatures has been followed in our work [3]. In this technique, an reference feature vector (RFV) is created to symbolize the signature vector which is describe below.

$$\text{RF}_j = \{[f_{j1}^-, f_{j1}^+], [f_{j2}^-, f_{j2}^+], \dots, [f_{jm}^-, f_{jm}^+]\}$$

where each interval is evaluated as $f_{jk} = \mu_{jk} \pm FLT(jk)$ where FLT is the feature-level threshold and μ_{jk} is the mean of the k th feature among “ m ” features for all the training signature samples of each j th user. The FLT is the function of the standard deviation of a particular feature in the training signature samples of a particular user. The k th feature of a testing signature is then compared to the interval-valued RFV of the claimed writer and contributed toward authentication count if it lies between

the interval otherwise added toward forgery. The total of such authentication count is equivalent to a matching score which decides that the test signature is genuine or forgery by using common threshold (CT).

To further enhance the results, we have applied the concept of sub-trajectories [6]. The sub-trajectories are formed by partitioning the signatures. This partitioning is done on the basis of equal number of data points captured in sequence. If there are total n data points in a signature and if it is divided into two halves, there will be $n = 2$ data points in each sub-trajectory. In this case, we have total two number of sub-trajectories and termed as sub-trajectory (ST) level-2. Similarly, if there are t sub-trajectories, it means signature is segmented into t parts with equal number of data points and again termed as sub-trajectory (ST) level- t .

5 Experimentation and Results

We have applied symbolic matching technique (as discussed in [7]) on MOBSIGN DB along with the sub-trajectories. These sub-trajectories are used to divide the signatures on the basis of equal number of data points captured as per the time sequence. We have used the same 46 features which is the optimal set of features as explained in their study. We have got the equal error rate (EER) of 1.018% using MOBSIGN DB for random forgery for sub-trajectory 3. The results are shown in Table 2 and optimum EER is shown in Fig. 5.

The implementation of sub-trajectories helps in reducing the EER to an optimal level as described in Table 2. This behavior is easily observed in the result table that the experiment without sub-trajectories ($ST = 1$) results into the EER of 2.525% and for the experiments with sub-trajectories ($ST = \{2, 3, 4, 5, 6, 7\}$), we have got the minimum EER of 1.018% for sub-trajectory level 3. In Table 3, these results are compared with the SVC2004 DB [8] as we have collected MOBSIGN DB on the same guidelines.

Table 2 The EER using MOBSIGN DB for random forgery

Sub-trajectory (ST) level	Min EER (%) for random forgery
ST-1	2.525
ST-2	1.533
ST-3	1.018
ST-4	1.216
ST-5	1.412
ST-6	1.793
ST-7	1.933

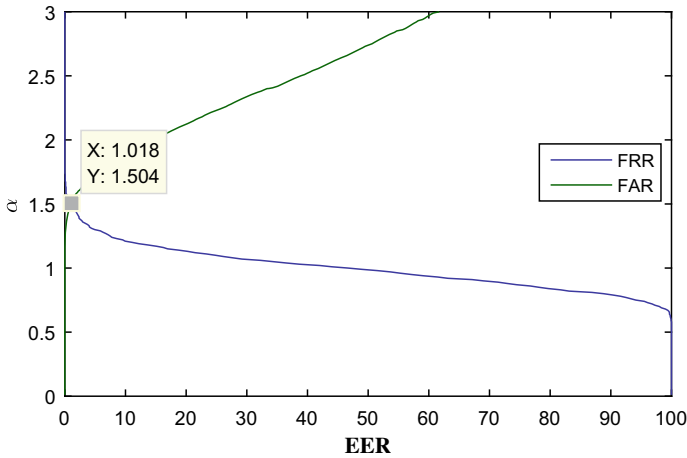


Fig. 5 Optimum EER using MOBSIGN DB for random forgery

Table 3 EER comparison with SVC2004 signature DB for random forgery

S. No.	Dataset	EER reported for random forgery (%)
1	SVC-2004 TASK1 (Team ID 6)	2.79
2	SVC-2004 TASK2 (Team ID 6)	2.51
3	MOBSIGN DB (without partitioning)	2.525
4	MOBSIGN DB (with partitioning)	1.018

6 Conclusion

We have presented here an online signature database: MOBSIGN DB. We have collected 25 signatures from each of the 75 writers and the EER reported is 1.018%. However, the main challenge in collecting the database is that people are reluctant in giving their original signatures. The other challenge is that if they agree to give signatures then they provide the secondary signature which they are not frequently used or make up a new signature which is not their behavioral signature. Apart from that, the challenge is to secure the signatures if we are going to use in a real scenario like an attendance system for the university staff.

Moreover, work is still on to expand this database and carry out the forgery signatures so that skilled forgery can also be introduced to check out the performance of the system.

Acknowledgements Authors acknowledge that the signatures used in building the mobile-based signature database (MOBSIGN DB) are collected only for the research purpose with the prior consent of the users. Also, the present study is included in the Ph.D. thesis of the principal author which was evaluated by the duly approved panel and the research committee of the Department of Computer Science and Applications, Panjab University, Chandigarh, India.

References

1. Fierrez J, Galbally J, Ortega-Garcia J, Freire MR, Alonso-Fernandez F, Ramos D, Toledano DT, Gonzalez-Rodriguez J, Siguenza JA, Garrido-Salas J, Anguiano E, de Rivera GG, Ribalda R, Faundez-Zanuy M, Ortega JA, Cardenoso-Payo V, Vitoria A, Vivaracho CE, Moro QI, Igarza JJ, Sanchez J, Hernaez I, Orrite-Uruñuela C, Martinez-Contreras F, Gracia-Roche JJ (2010) Biosecurid: a multimodal biometric database. *Pattern Anal Appl* 13(2):235–246
2. Garcia-Salicetti S, Beumier C, Chollet G, Dorizzi B, les Jardins JL, Lunter J, Ni Y, Petrovska-Delacrétaz D (2003) BIOMET: a multimodal person authentication database including face, voice, fingerprint, hand and signature modalities. Springer, Berlin, Heidelberg, pp 845–853
3. Guru DS, Prakash HN (2009) Online signature verification and recognition: an approach based on symbolic representation. *IEEE Trans Pattern Anal Mach Intell* 31(6):1059–1073
4. Kholmatov A, Yanikoglu B (2009) SUSIG: an on-line signature database, associated protocols and benchmark results. *Pattern Anal Appl* 12(3)
5. Ortega-Garcia J, Fierrez-Aguilar J, Simon D, Gonzalez J, Faundez-Zanuy M, Espinosa V, Satue A, Hernaez I, Igarza JJ, Vivaracho C, Escudero D, Moro QI (2003) Mcyt baseline corpus: a bimodal biometric database. *IEE Proc Vis Image Signal Process* 150(6):395–401
6. Rohilla S, Sharma A, Singla RK (2014) Online signature verification at sub-trajectory level. Springer, Cham, pp 369–374
7. Rohilla S, Sharma A, Singla RK (2017) Optimal feature set selection in online signature verification. *Int J Biometr* 9(4):1–25
8. Yeung DY, Chang H, Xiong Y, George S, Kashi R, Matsumoto T, Rigoll G (2004) SVC2004: first international signature verification competition. Springer, Berlin, Heidelberg, pp 16–22

Mining of Association Rules in R Using Apriori Algorithm



Anjali Mehta and Deepa Bura

Abstract Association rules are the strong rules which occur frequently in the dataset. Association Mining is the technique used to explore these rules with the help of various algorithms available in data mining. This paper discusses the use of apriori() to mine the strong rules which are helpful to find out the customer purchasing pattern and help to increase the sale. In this paper, R language is used and arules() package is used to mine the rules based on the value of support and confidence.

Keywords Association rules · Data mining · Apriori() · Support · Confidence

1 Introduction

Market Basket Analysis is a method that is based on the fact that if you are purchasing a product, you are more or less likely to buy or purchase another product. So the main purpose of Market Basket Analysis is to find out the purchasing pattern of customers for various objectives.

These are as follows:

1. To design the catalog.
2. To change the store layout by placing frequently purchasing items together.
3. To offer coupons on the products.
4. By providing a discount on the product to increase the sale.

Consider the following example:

The rule generated by calculating the value of support and confidence of all the above transactions is

{Diapers, Beer}

Diaper \geq Beer

In Fig. 1, when a person is buying a diaper, he is purchasing beer also. The above result does not make any sense but anyone can say that fathers who are young

A. Mehta (✉) · D. Bura

Manav Rachna International Institute of Research and Studies, Faridabad, India

e-mail: scorpiongirlanjali@gmail.com

© Springer Nature Singapore Pte Ltd. 2021

G. S. Hura et al. (eds.), *Advances in Communication and Computational*

Technology, Lecture Notes in Electrical Engineering 668,

https://doi.org/10.1007/978-981-15-5341-7_14

Fig. 1 Set of five transactions of five different customers

<i>TID</i>	Items
1	{Bread, Milk}
2	{Bread, Diapers, Beer, Eggs}
3	{Milk, Diapers, Beer, Cola}
4	{Bread, Milk, Diapers, Beer}
5	{Bread, Milk, Diapers, Cola}

are filling their supplies of beer for the weekend [1]. There are many other examples which are present in our daily life. Like Computer \geq Antivirus. This means if anyone is buying a computer then he is more likely to buy antivirus also.

The main purpose of the Market Basket Analysis is to increase the sale and profit by using the customer details which are available to the retail company already. In this paper, Sect. 2 tells us about the work that is related to our paper. Section 3 describes the used methodology in which the R language and apriori() algorithm is discussed. Section 4 is about experimental setup which gives the details about the rules generated according to the given value of support and confidence. The last Sect. 5 gives the conclusion of the paper.

2 Related Work

Data mining is very useful in generating rules which are useful in mostly each and every field like marketing, telecommunication, healthcare, etc. Various techniques are used to find out the most frequent items and to make these rules useful.

Agrawal and Srikant [2] in their paper fast algorithms to mine the association rules. In this paper, they explained how support and confidence help to generate rules. One can count all the items in the itemset and then generate the most frequent item but this process takes lots of time. Kaur and Kang [3] give details about Market Basket Analysis and it is used in various different fields like nuclear, educational, and marketing. The main purpose of Market basket analysis is to understand the nature of the customer and his buying pattern to increase the store sale and to increase the profit. Nengsih [4], in his paper, discussed the affinity analysis with the help of apriori and without the apriori algorithm. He concluded in his paper that both the methods mine the same rules but processes to generate the rules are different. M. Nidhi and D. Snehil use the online Instacart data in their paper to find out the most frequent item and use the apriori() algorithm with the help of the R language in his paper [5].

Berry and Linoff [6] main purpose is to discover the patterns by checking the associations between the transactional information of the store in their paper. People who buy bread can also purchase other products which are related to bread like jam, milk. So to increase the sale, the retailer can put up these things together to increase the sale and also to access them easily and quickly.

Agrawal and Srikant [7], in their paper, proposed apriori algorithm to explore the frequent items or patterns for association rules which are Boolean in nature. The authors also describe the method of mining rules in huge relational data which are quantitative in nature. Julander [8], a tool helps to analyze the customers in the percentage who are buying a certain item and also tells the percentage of the complete sale done by this item. By using this type of association share of the sale is calculated easily and one can know which item is the leading item. This is an important issue because if one knows about the leading product than he can place other products with the contact of leading products to increase the sale of other products also. Exploratory analysis is the other stream or field which works in the same way to generate association rules.

3 Used Methodology

3.1 Apriori()

In this paper, apriori() algorithm is used to mine strong rules which help us to develop the marketing strategy. These rules also give us misleading results if you are not careful with the data.

There are some measures which are used to find the strength of the rule. These are as follows:

1. Support
2. Confidence
3. Lift.

Let us discuss these terms one by one with the help of the following example:

Support

In a retail store, 500 customers visited in last one month from which 300 customers buy product X and 200 customers buy product Y and 150 customers buy product X and Y .

$$\begin{aligned} \text{Support } X &= \text{The number of transactions of } X / \text{Total number of transactions} \\ &= (300 * 100) / 500 = 60\% \end{aligned}$$

$$\begin{aligned} \text{Support } Y &= \text{The number of transactions of } Y / \text{Total number of transactions} \\ &= (200 * 100) / 500 = 40\% \end{aligned}$$

$$\begin{aligned} \text{Support } X \text{ and } Y &= \text{The number of transactions of } X \text{ and } Y / \text{Total number of transactions} \\ &= (150 * 100) / 500 = 30\% \end{aligned}$$

Confidence

$X \Rightarrow Y = \text{Number of transactions with both } X \text{ and } Y / \text{Total of } X.$

Now suppose 100 out of 300 customers who bought product X also bought product Y .

$$= (100 * 100)/300 = 33\%.$$

Lift

Higher the value of lift higher the chance of X and Y to be sold together.

$$\text{Lift}(X \Rightarrow Y) = (\text{confidence } X \Rightarrow Y) / \text{Support } Y.$$

If the value of lift is 1 then X and Y are independent of each other which means there is no frequent buying pattern between these products. If the value of lift is greater than 1 then X and Y are dependent on each other

which means there is a frequent buying pattern between these products or the value is less than 1 means X has a negative effect on Y .

3.2 R Language

R is a very useful language for enhanced analysis and also a graphical tool to create a visualization of different types like histograms, bar chart, etc. R language is used in this paper to mine the rules or to perform Market Basket Analysis by using `arules()` package. Michal Hahsler et al. maintains or develop very important and helpful packages in R to mine the association rules. These are `arules()`, `arulesViz()`. If you do not have these packages in your computer then install with the given instruction.

```
>install.packages("arules")
>install.packages("arulesViz").
```

`arules()` packages are packed with `apriori()` which is the simplest and most used algorithm to find and discover the association between different products.

4 Experimental Setup

The data analysis, in this paper, is based on groceries data that comes with `arules()` package. First of all `inspect()` function is used to see all transactions. It must be in transactions because association rule mining handled only transactions.

So from Fig. 2, one can see that it is transactional data set. In this language, the only transactional dataset is used. If anyone has any other type of dataset then he had to convert it into the transactional data set.

Fig. 2 Dataset groceries of `arules()` package

```
> data("Groceries")
> class(Groceries)
[1] "transactions"
attr(,"package")
[1] "arules"
```

```
> inspect(head(Groceries,3))
  items
[1] {citrus fruit,semi-finished bread,margarine,ready soups}
[2] {tropical fruit,yogurt,coffee}
[3] {whole milk}
>
```

Fig. 3 Shows the first three transactions

```
> grocery_rules <-apriori(Groceries, parameter = list( support = 0.01 , confidence = 0.
5))
Apriori

Parameter specification:
confidence minval smax arem aval originalSupport maxtime support minlen maxlen
target     ext
rules FALSE

Algorithmic control:
filter tree heap memopt load sort verbose
  0.1 TRUE TRUE  FALSE TRUE  2    TRUE

Absolute minimum support count: 98

set item appearances ...[0 item(s)] done [0.00s].
set transactions ...[169 item(s), 9835 transaction(s)] done [0.02s].
sorting and recoding items ... [88 item(s)] done [0.00s].
creating transaction tree ... done [0.00s].
checking subsets of size 1 2 3 4 done [0.02s].
writing ... [15 rule(s)] done [0.00s].
creating S4 object ... done [0.00s].
```

Fig. 4 Total number of rules generated

Figure 3 shows the three transactions from the start are the output from the above command. To see the most frequent item or rules in the dataset following command is used (Fig. 4).

So one can see that when the value of support is 0.01 and confidence is 0.5 then the total of 15 rules is generated (Fig. 5).

```
>frequentitems < eclat(Groceries, parameter = list(support = 0.07, maxlen =
15)).
```

With the help of R language, one can also plot the histogram of the items to see which product has a large number of sale. The following command is used to see the histogram (Fig. 6).

```
itemFrequencyPlot(Groceries, topN = 10, type = "absolute", main = "ItemFre-
quency").
```

This frequency plot shows 15 items and tells us that whole milk is liked by most people than any other item. Anyone can also find the rules which tell us which product is liked by the customer to increase the sale or profit in a retail store by keeping these things with each other.

If one wants to find out the strong rules, increase the value of confidence parameter.

If one wants to find out the longer rules then he had to increase the maxlen parameter because this parameter gives us the rules of more items.

```
> inspect(frequentitems)
  items                                     support  count
[1] {other vegetables,whole milk} 0.07483477 736
[2] {whole milk}                 0.25551601 2513
[3] {other vegetables}           0.19349263 1903
[4] {rolls/buns}                 0.18393493 1809
[5] {yogurt}                     0.13950178 1372
[6] {soda}                       0.17437722 1715
[7] {root vegetables}           0.10899847 1072
[8] {tropical fruit}            0.10493137 1032
[9] {bottled water}             0.11052364 1087
[10] {sausage}                   0.09395018  924
[11] {shopping bags}            0.09852567  969
[12] {citrus fruit}             0.08276563  814
[13] {pastry}                    0.08896797  875
[14] {pip fruit}                0.07564820  744
[15] {whipped/sour cream}       0.07168277  705
[16] {fruit/vegetable juice}    0.07229283  711
[17] {newspapers}               0.07981698  785
[18] {bottled beer}             0.08052872  792
[19] {canned beer}              0.07768175  764
```

Fig. 5 Shows the frequent items of $\text{maxlen} = 15$

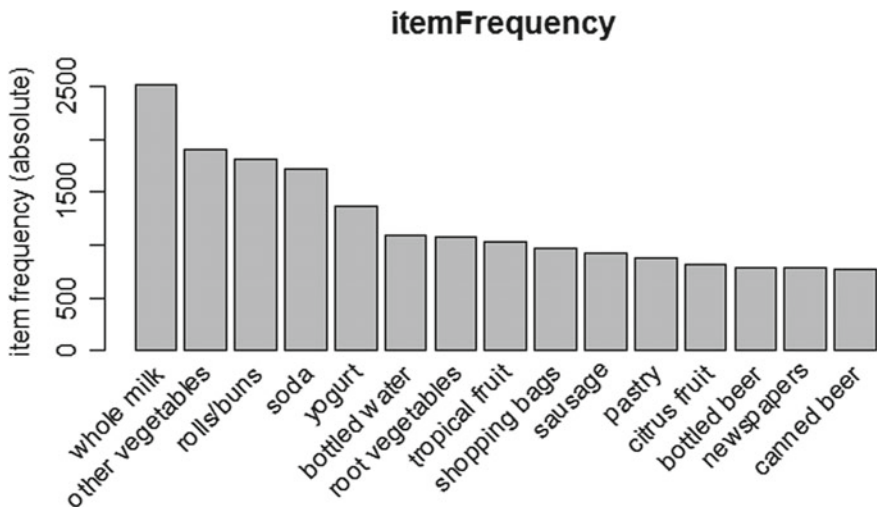


Fig. 6 Frequency plot for the used data set

```
> rules<-apriori(data= Groceries, parameter = list(supp=0.001,conf=0.08),appearance = list(
(default="lhs",rhs="whole milk"), control = list(verbose=F))
> rules_conf<-sort(rules,by="confidence",decreasing = TRUE)
> inspect(head(rules_conf))
  lhs                                     rhs      support
[1] {rice,sugar}                         => {whole milk} 0.001220132
[2] {canned fish,hygiene articles}       => {whole milk} 0.001118454
[3] {root vegetables,butter,rice}        => {whole milk} 0.001016777
[4] {root vegetables,whipped/sour cream,flour} => {whole milk} 0.001728521
[5] {butter,soft cheese,domestic eggs}    => {whole milk} 0.001016777
[6] {pip fruit,butter,hygiene articles}   => {whole milk} 0.001016777
  confidence lift      count
[1] 1          3.913649 12
[2] 1          3.913649 11
[3] 1          3.913649 10
[4] 1          3.913649 17
[5] 1          3.913649 10
[6] 1          3.913649 10
```

Fig. 7 Shows the items which are purchased before whole milk

```
> rules<-apriori(data= Groceries, parameter = list(support=0.001,conf=0.08),appearance
= list(lhs="whole milk", default="rhs"),control=list(verbose= F))
> rules_conf<-sort(rules,by=)
> rules_conf<-sort(rules,by="confidence",decreasing= TRUE)
> inspect(head(rules_conf))
  lhs      rhs      support confidence    lift count
[1] {whole milk} => {other vegetables} 0.07483477 0.2928770 1.513634 736
[2] {whole milk} => {rolls/buns} 0.05663447 0.2216474 1.205032 557
[3] {whole milk} => {yogurt} 0.05602440 0.2192598 1.571735 551
[4] {} => {other vegetables} 0.19349263 0.1934926 1.000000 1903
[5] {whole milk} => {root vegetables} 0.04890696 0.1914047 1.756031 481
[6] {} => {rolls/buns} 0.18393493 0.1839349 1.000000 1809
> |
```

Fig. 8 Shows the items which are purchased after whole milk

If one wants to eliminate shorter rules then he had to decrease the size of minlen parameter. If anyone wants to find out the rules belonged to a specific item then the following command is used.

Figure 7 tells us about the things which customers like to buy before the whole milk. Similarly, one can find out the items which customer buys after buying whole milk (Fig. 8).

By finding all the rules, the retailer can place these things together in the retail store to increase the sale.

5 Conclusion

There is a lot of competition in the market because lots of products are launching day by day. So there is a need to manage the people or customers for the long term. Association mining with the use of the simplest algorithm named apriori() is used to mine the rules about the products which are likely to purchase together by various customers. The study tells the behavior of various customers about the various products and items in a retail store. The software or R language which is

used in this paper is very useful to discover the rules with the help of apriori() to fulfill our objectives. A Retailer can use these rules to enhance the growth of their store and to increase the sale and profit of their products.

References

1. Affinity analysis (2018) Retrieved from http://en.wikipedia.org/wiki/Affinity_analysis
2. Agrawal R, Srikant R (1994) Fast algorithms for mining association rules. In: Proceedings of the 20th international conference on very large data bases, VLDB, vol 1215, pp 487–499
3. Kaur M, Kang S (2016) Market Basket Analysis: identify the changing trends of market data using association rule mining. *Procedia Comput Sci* 85:78–85
4. Nengsih W (2015) A comparative study on market basket analysis and apriori association technique. In: 2015 3rd international conference on information and communication technology (ICoICT), pp 461–464. IEEE
5. Kawale NM, Dahima S (2018) Market basket analysis using apriori algorithm in R language. *Int J Trend Sci Res Dev (IJTSRD)* 2(4). ISSN: 2456-6470
6. Berry MJ, Linoff GS (2004) *Data mining techniques for marketing, sales and customer relationship management*, 2nd edn. Hungry Minds, Chennai
7. Agrawal R, Srikant R (1994) Fast algorithm for mining association rules. In: Proceedings of the international conference on very large database, pp 487–499
8. Julander CR Basket analysis: a new way of analyzing scanner data. *Int J Retail and Distrib Manage* 20(7):10–18
9. Svetina M, Zupančič J (2005) How to increase sales in retail with market analysis. *Syst Integr* 418–428; Nicole R Title of paper with only first word capitalized. *J Name Stand Abbrev* in Press
10. Gupta S, Mamtara R (2014) A survey on association rule mining in market basket analysis. *Int J Inf Comput Technol* 4(4):409–414
11. Shmueli G, Bruce PC, Yahav I, Patel NR, Lichtendahl Jr KC (2017) *Data mining for business analytics: concepts, techniques, and applications in R*. Wiley, Hoboken
12. Ihaka R, Gentleman R (1996) R: a language for data analysis and graphics. *J Comput Graph Stat* 5(3):299–314
13. Team RC (2000) *R language definition*. R Foundation, Vienna, Austria
14. <https://www.datacamp.com/community/tutorials/market-basket-analysis-r>
15. <http://r-statistics.co/Association-Mining-With-R.html>
16. <http://www.salemmarafi.com/code/market-basket-analysis-with-r/>
17. <https://blog.exploratory.io/introduction-to-association-rules-market-basket-analysis-in-r-7a0dd900a3e0>
18. <https://towardsdatascience.com/association-rule-mining-in-r-ddf2d044ae50>
19. https://michael.hahsler.net/research/association_rules/
20. <https://www.rstudio.com/online-learning/>
21. <http://rststatistics.net/association-mining-with-r/>

Comprehensive and Comparative Analysis of Different Files Using CP-ABE



Sahil Jalwa, Vardaan Sharma, Abdur Rehman Siddiqi, Ishu Gupta, and Ashutosh Kumar Singh

Abstract In a business organization, the data needs to be shared among different personnel, therefore chances of fraud are more. In order to protect the organization's confidential and sensitive data among different levels of employees from theft or any other illegal activity that violates the company security policy, ABE known as Attribute-Based Encryption was introduced. ABE is a cryptographic parameter that plays a vital role in providing fine-grained access control of outsourcing data in data sharing system of the business organization but due to its non-efficiency and several other limitations, it was proved inefficient in outsourcing of data. However, Ciphertext Policy Attribute-Based Encryption (CP-ABE) was implemented to overcome the existing ABE issues and to protect the firm's confidential data from theft or leakage. CP-ABE defines an access policy that covers all the attributes within the system. In this scheme, the user's private key is associated with the set of attributes for encryption and decryption purposes. Our experimental simulations demonstrate the real encryption/decryption time over different types of files and their sizes and how they get affected after applying CP-ABE. The performance and security analysis stipulated that the used scheme is competent to securely manage the data in any organization.

Keywords Attribute-based encryption · Data sharing · CP-ABE · KP-ABE · Access policy · Access control · Public key cryptography · Data outsourcing

S. Jalwa (✉) · V. Sharma · A. R. Siddiqi · I. Gupta · A. K. Singh
Department of Computer Applications, National Institute of Technology, Kurukshetra, India
e-mail: sahiljalwa@gmail.com

V. Sharma
e-mail: vardaansharma096@gmail.com

A. R. Siddiqi
e-mail: abdur9808@gmail.com

I. Gupta
e-mail: ishugupta23@gmail.com

A. K. Singh
e-mail: ashutosh@nitkkr.ac.in

1 Introduction

Nowadays, in a paperless environment, use of computers to save important data has become a common scenario in every organization whether business, educational, or any other, field. All the data is stored in either database or cloud. As the number of users is increasing day by day along with the rapid increase in technology, there is need to improve the security feature of existing database models from any kind of malicious activity that tries to steal, leak or breach the information for any falsified means [1–4]. All the documents or files that have to be shared on business-wide servers need to be protected from any kind of activity that is forbidden by laws, and accessible to only authorized users of that company which further requires attributes of users to be matched with access policy attributes that were defined for that system or company. Access policy can be defined using any cryptographic parameter like KP-ABE, CP-ABE which requires attributes of users, existing model environment, or any other data object. Let us consider an example, if a business organization stores documents of every employee in a common data server, different employees of several departments can access any document. One way to solve this problem is encryption that stores and transmits information in encrypted form. Traditional techniques based on password or public key cryptography-based solutions require every user to have the same number of passwords or key pairs as many files user wants to retrieve. Also, there is a useful and secure cryptographic approach known as Attribute-Based Encryption (ABE) presented by Sahai and Waters [5] that helps us to achieve data access control for permitting different access rights to a group of users with different attributes. ABE defines access policies depending upon the credentials of the requestor, environment or the data object. Further, an alteration of ABE was introduced known as Cipher-text Policy Attribute-Based Encryption (CP-ABE) first presented by Bethencourt et al. [6] that imparts a better coherent access control procedure in comparison to traditional public key cryptographic encryption methodology. In order to decrypt the cipher-text and to administer it on the content CP-ABE grants encrypter to define a set of attributes over a universe of attributes that a decrypter needs to hold. Thus, different pieces of data as per the security policy are allowed to decrypt depending upon the set of attributes that the user holds. This will abolish the traditional mechanism of password-based cryptography techniques. But there is a major flaw that is of key revocation or update problem. Suppose some of the attributes associated with the user are changed, key update for each attribute is critically essential to make a system secure. As in ABE, the attributes are associated with a group of users or employees so the revocation will affect a group not a single person.

Furthermore, in this paper, we have discussed several cryptographic techniques like ABE, Traditional public key cryptography, and CP-ABE. Related work is summarized in Sect. 2. In Sect. 4, the problem related to a business organization is stated and the paper is concluded thereafter.

2 Related Work

Some of the techniques and approaches are pre-existed. In the Symmetric Key Cryptography-based cryptosystem Public Key Cryptography (PKC) private key is used to decrypt the cipher-text provides secure group communication that was first proposed by Rivest et al. [7]. But due to its complex public key infrastructure, it is proved inefficient. In 1984, Identity-Based Encryption proposed by Shamir [8] overcome PKC limitations. IBE majorly focuses on the user’s identity such as mail id or internet protocol address. However, the above two approaches in order to multi-cast the data, encryption is done using different public keys and this increases the computational overhead. In 2005 [9], Sahai et al. introduced the fuzzy identity-based encryption, in which only the person whose attributes satisfy the access policy can decrypt the message. Sahai further introduces ABE in two categories known as KP-ABE (key-policy ABE) and cipher-text policy ABE. In KP-ABE [10, 11], attributes outline the data in encrypted format and policies are assembled into users’ keys; while in CP-ABE, users’ credentials are described by the attributes, and an encrypter governs a policy that who can decrypt the data. From the above two approaches, CP-ABE is considered more suitable for the system of data sharing because it takes access to policy decisions in favor of data owners.

Implementation of Functional Encryption Library (the generalized term for ABE) proposed by Keisuke et al. [12]. They elaborate on the functionality of their tool by applying an access policy of an organization. Several other applications using ABE have been presented in the literature.

3 ABE

In Attribute-Based Encryption, there is a global public key (G) this key is the same for all the existing employees of an organization. And there is a private key (PR) of each employee which is unique for every employee and this PR is issued by an authority. Every employee encrypts the file using G and decrypts it by using their own private key that is related to their set of an attribute as shown in Table 1. Here in this scheme, another feature of attribute comes into play.

Table 1 List of attributes associated with employees

Name	E. Id.	Department	Designation	D.O.J	Salary
Emp1	193	-na-	CEO	02/02/14	2,00,000/-
Emp2	154	-na-	Managing director	11/11/13	1,00,000/-
Emp3	234	Sales	Sales manager	09/04/17	80,000/-
Emp4	654	Finance	Accountant	04/10/12	90,000/-
Emp5	678	Engineering	Engineer	05/12/12	65,000/-

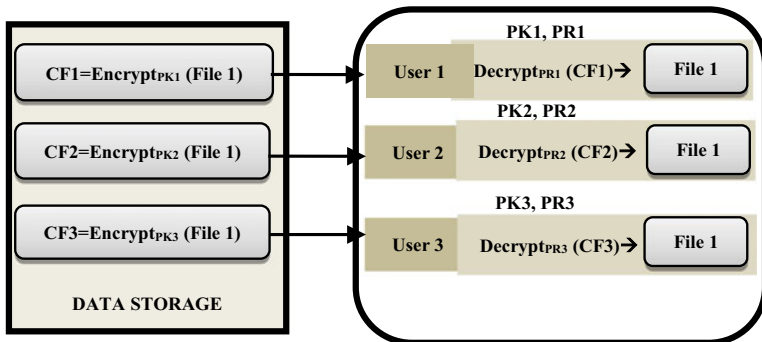


Fig. 1 Conventional public key cryptography system

In this paper, CP-ABE is the technique of encryption that is used to identify whether a user has a set of attributes like id, priority, etc. In the traditional system, there are mainly two keys that are the public key which is known to both sender and receiver and private key which is only known by the recipient of the message. Now suppose in a common scenario if two users Bob and Alice want to communicate by sending any secure messages to each other. Bob uses Alice’s public key to encrypt the message. Alice will then use his private key to decrypt it. This traditional scheme is shown in Fig. 1.

In a further enhancement, suppose in a business organization the CEO of the company wants that the data stored in central data storage should be ciphered in such a way that only a few of the employees (emp1, emp2, emp3) can access it. For this, the particular file of central data storage will be encrypted by using the public key of emp1, emp2 and emp3 (PK1, PK2, PK3, respectively) and then respective ciphered file CF1, CF2, CF3, will be generated, these ciphered or encrypted files can only be deciphered by corresponding employees private key (PR1, PR2, PR3).

Thus, in this way, if “n” employees are there in a company then for providing access control with the help of traditional method “n” different ciphered files and “2n” keys will be generated. But in a somewhat advanced version of this technique that is Attribute-Based Encryption, there will only be one ciphered file and “n + 1” keys will be generated. So both storage and time can be saved (Fig. 2).

4 Cipher-Text Policy Attribute-Based Encryption

It introduces the concept of an advanced version of ABE called CP-ABE [5] which is encryption based on attributes of cryptographic text criteria. In the CP-ABE schema, attribute policies are data-related and attributes are related to keys and only those keys that related attributes meet the data policy can decrypt data. It works opposite to KP-ABE. In CP-ABE, the encrypted text is related to access policy and each user’s

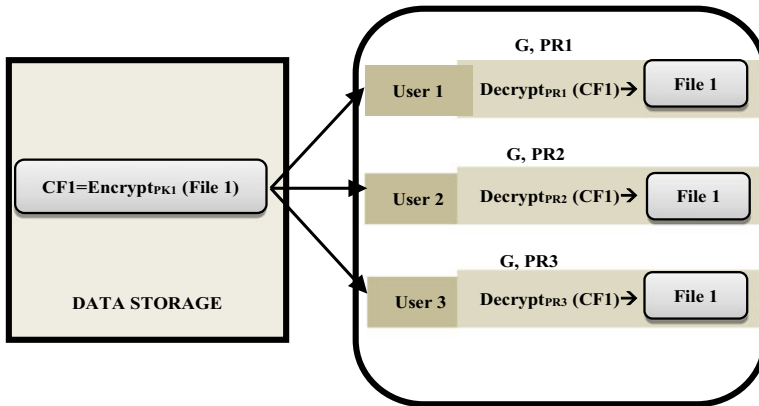


Fig. 2 Attribute-based encryption

secret key consists a bundle of attributes. In CP-ABE, each user is related to a set of attributes. The secret key is generated based on its attributes.

The CP-ABE scheme has four algorithms:

1. *Setup*

This main work of this procedure is to generate a global public key (G) and a master secret key (MK). These two generated keys are then used by the admin/boss for key generation (Key-Gen) of each user. G is known to every user and used in encryption and decryption of a particular file or data.

2. *Encrypt*

The main work of this algorithm is to generate an encrypted file “File1” according to the policy “D” using G and generating an enciphered file” E”. This file can be enciphered in such a way using access protocols such that only those users whose attributes are matching with the access policy. This policy can be defined with the help of operators like “<”, “>”, “<=”, “>=”, and “=”, particularly on the number based attributes such as salary, id, etc. After encryption a file “File1.*.cpabe” is created.

3. *Key-Gen*

The main work of this procedure is to generate a secret key for a particular user. It takes the G, MK and set of attributes A of a user as input. Administrator creates the private key (PR) for every single user/employee in the system.

4. *Decryption*

As the name suggests, the main work of this procedure is to produce a deciphered text. This procedure inputs PK (public key), E (Enc. File), and G (global_public_key). If the set of attributes that a particular user has is A, if A satisfies the access policy D, then file the “File1” is decrypted by PK and that file can be retrieved by the user.

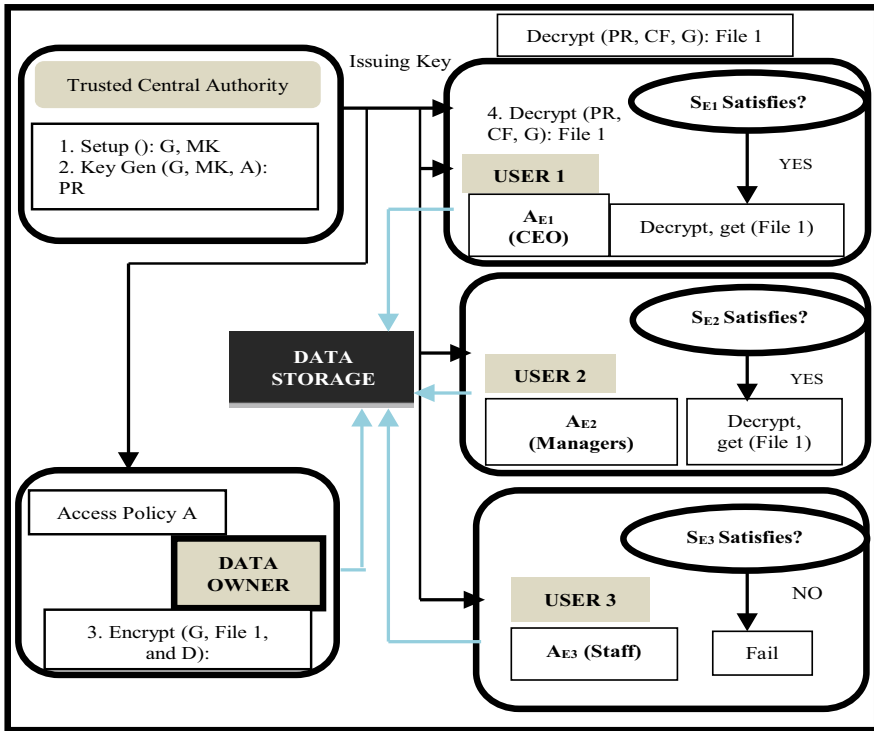


Fig. 3 CP-ABE

After decryption, the "File1.*.cpabe" got converted into "File1" that can be accessed normally (Fig. 3).

Problem Statement

The problem scenario we considered here is of a business organization, where all types of data are stored and reserved centrally at location "Data Here". All the employees of different departments can use this data. The role hierarchy of the employees in the business organization employees can be acknowledged in Table 1. Now suppose there is a file we call it to say, emp4_Salary_2019.doc is stored on the central location "Data Here". This file is basically the record of employee details. Here in the given below table D.O.J is the date of joining of the employee in the organization, Name, Employee Id, Department, Designation, and salary are some other information of the organizational employees. As records and data are stored on a server, it can be retrieved by an unauthorized person also. Password-based security mechanism is no longer efficient in modern-day technology. The employees as mentioned in Table 1 can access different types of data of the organization which is kept confidential for various reasons and organization policies and their terms and condition. There is a Cipher-text Policy Attribute-Based Encryption based solution for authorization and accessibility of sensitive, confidential, and private data. Each

Fig. 4 Setup and key generation time

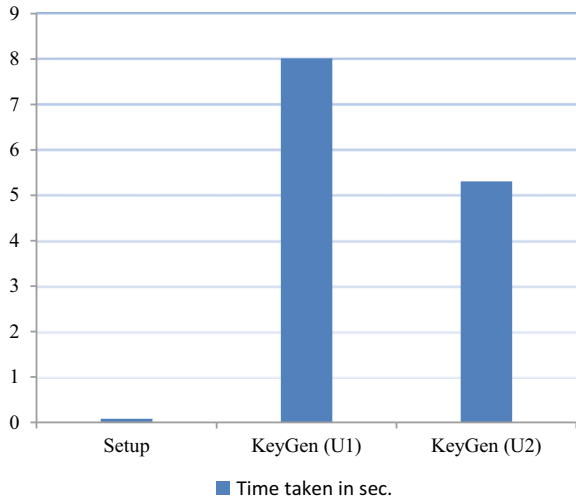
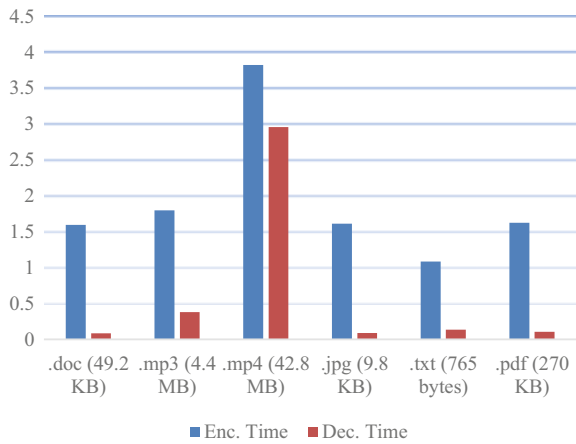


Fig. 5 Average encryption and decryption time in seconds



employee of the organization contains a different set of attributes and depending upon the type of access policy and employees attribute set, if their attributes satisfy the policies condition then they will be able to retrieve the data. These attributes values are used for the generation of private keys of each user.

Table 2 is a description of the environment in which the following implementation was performed. We evaluated the performance of predefined CP-ABE based model on various types of files which are generally required in every type of organization. All the experiment was conducted using the above Parameters and their corresponding results are shown in Figs. 6, 7, 8 and 9.

Table 2 Experimental Setup

Parameters	Specifications
CPU	Intel(R) core(TM) i5-5200U CPU @2.20 GHZ
RAM	8.00 GB
OS	Ubuntu 16.04
External library	GMP, PBC, OpenSSL
Language	C
Compiler	gcc

Fig. 6 Encryption and decryption time of .pdf file

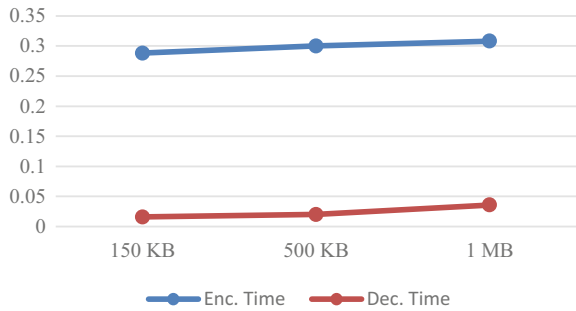


Fig. 7 Encryption and decryption time of .doc file

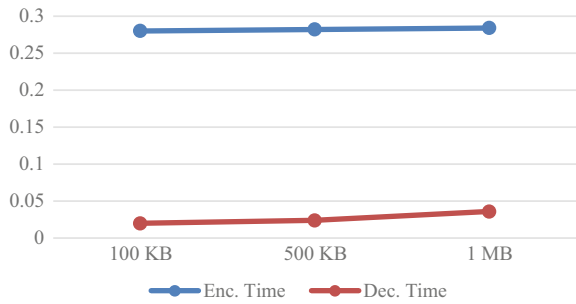


Fig. 8 Encryption and decryption time of .jpg file

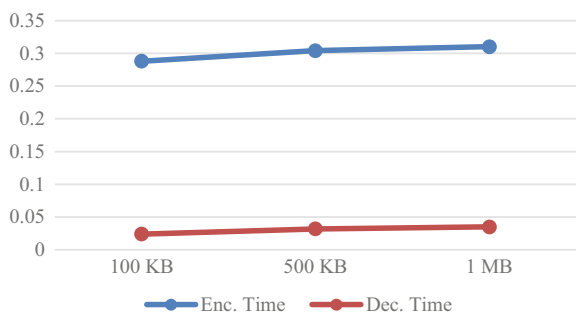
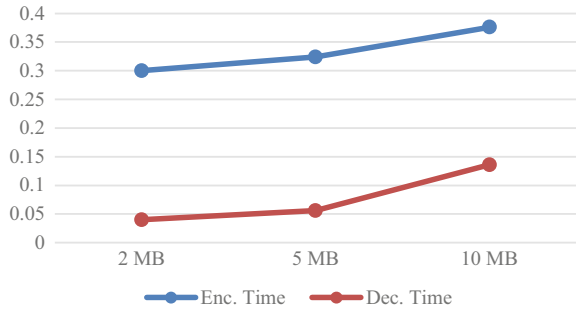


Fig. 9 Encryption and decryption time of .mp4 file



The graph drawn in Fig. 4 illustrates the setup time for the CP-ABE system and key generation time for the user1 (U1) and user2 (U2). The key generation time increases in a linear way as we increase the number of attributes.

Overall we can say that key generation time is dependent on a number of attributes.

Figure 5 shows the time taken in encryption and decryption for a different type of files which are used almost in every domain. Here we have taken files of different sizes and extensions like .doc, .mp3, .mp4, .jpg, etc. and encrypt it using CP-ABE methodology and calculate the average time for encryption and decryption. We also have seen that during encryption, the size of almost every file increases in kilobytes or megabytes after encryption and in some files; we observe that there is a very small increase in the size of file, i.e., in bytes. If we increase the size of a file then encryption time also increases and vice versa. Encryption time will also increase if we increase the number of attributes used in specifying access policy.

We also observed that the amount of time required in decryption is very much less than the amount of time required for encryption. However, decryption time depends on the particular access policy of cipher-text and number of attributes associated with private keys.

5 Conclusion

In this work, the CP-ABE toolkit was used which provides encrypted access control of data where private key of each user is clearly defined by a set of attributes and helps in determining which kind of users can decrypt what type of data by defining a specific access policy over these attributes. This system also helps in preventing the collusion attack where attacker can acquire more than one private keys, the secret key is developed by a secure two-party computation for each user. It also provides fine-grained access control of files among different levels in an organization and was found that it helps in enhancing the efficiency of cryptographic methodology in a data sharing system, as compared to traditional cryptographic techniques. In future, it would be interesting to consider, Attribute-Based Encryption system with multi-authority based setup to add, delete, or update the attributes.

References

1. Gupta I, Singh AK (2019) Dynamic threshold based information leaker identification scheme. *Inf Process Lett* 147:69–73
2. Gupta I, Singh N, Singh AK (2019) Layer-based privacy and security architecture for cloud data sharing. *J Commun Softw Syst (JCOMSS)* 15(2)
3. Gupta I, Singh AK (2018) A probabilistic approach for guilty agent detection using bigraph after distribution of sample data. *Procedia Comput Sci* 125:662–668
4. Gupta I, Singh AK (2017) A probability based model for data leakage detection using bigraph. In: 7th International Conference on Communication and Network Security (ICCNS-2017), Tokyo, Japan
5. Goyal V, Pandey O, Sahai A, Waters B (2006) Attribute-based encryption for fine-grained access control of encrypted data. In: Proceedings of the 13th ACM conference on Computer and communications security, pp 89–98. ACM
6. Bethencourt J, Sahai A, Waters B (2007) Ciphertext-policy attribute-based encryption. In: 2007 IEEE symposium on security and privacy (SP'07), IEEE
7. Chor B, Rivest RL (1988) A knapsack-type public key cryptosystem based on arithmetic in finite fields. *IEEE Trans Inf Theory* 34(5):901–909
8. Shamir A (1984) Identity-based cryptosystems and signature schemes. In: Workshop on the theory and application of cryptographic techniques. Springer, Berlin
9. Sahai A, Waters B (2005) Fuzzy identity-based encryption. In: Annual international conference on the theory and applications of cryptographic techniques. Springer, Heidelberg
10. Han F et al (2014) A general transformation from KP-ABE to searchable encryption. *Future Gener Comput Syst* 30:107–115
11. Liu P et al (2014) Efficient verifiable public key encryption with keyword search based on KP-ABE. In: 2014 ninth international conference on broadband and wireless computing, communication and applications, IEEE
12. Porwal S, Mittal S (2017) Implementation of ciphertext policy-attribute based encryption (CP-ABE) for fine grained access control of university data. In: 2017 tenth international conference on contemporary computing (IC3), IEEE

Efficient Data Cube Materialization



Raghu Prashant , Mann Suman , and Raghu Eashwaran 

Abstract In the field of business intelligence, we require the analysis of multidimensional data with the need for it being fast and interactive. Data warehousing and OLAP approaches have been developed for this purpose in which the data is viewed in the form of a multidimensional data cube which allows interactive analysis of the data in various levels of abstraction presented in a graphical manner. In data cube, there may arise a need to materialize a particular cuboid given that some other cuboid is presently materialized, in this paper, we propose an algorithm for cuboid materialization starting from a source cuboid to the target cuboid in an optimal way such that the intermediate cuboids consume less space and require lower time to generate by making sure those cuboids have the least number of rows compared to other valid cuboids available for selection, by sorting them based on the product of cardinalities of dimensions present in each cuboid.

Keywords Cuboid materialization · Lattice of cuboids · Data warehouse · OLAP · Data cube

1 Introduction

Think of a Data Warehouse as a central storage facility which collects information from many sources, manages it for efficient storage and retrieval, and delivers it to many audiences, usually to meet decision support and business intelligence requirements [1]. The basic principle of Data Warehousing is to provide statistics/data to the business users for well calculated and planned strategic decisions. The data stored is in the form of a multidimensional model. A Data Warehouse is basically of three main types:

R. Prashant (✉) · M. Suman · R. Eashwaran
Maharaja Surajmal Institute of Technology, GGSIPU, New Delhi 110059, India
e-mail: prashantraghu999@gmail.com

© Springer Nature Singapore Pte Ltd. 2021
G. S. Hura et al. (eds.), *Advances in Communication and Computational Technology*, Lecture Notes in Electrical Engineering 668,
https://doi.org/10.1007/978-981-15-5341-7_16

1. Operational Data Store Enterprise
2. Data Warehouse
3. Data Mart.

A Data Warehouse works as a primary repository where data from various origins materialize. Further data might be categorized into Structured, Semi-structured, and Unstructured data forms. In the past, the various organizations started using Data Warehousing, and over time they modified it and made it advanced and intricate.

The various general stages of the use of a Data Warehouse are as follows:

1. **Offline Operational database:** In this stage data is copied from OS to a different server so this way the operational server's performance is not affected as the processing would be done in the server which has the copied data.
2. **Offline Data Warehouse:** Data in the Data Warehouse is automatically updated and mapped to reach the objectives.
3. **Real-time Data Warehouse:** In this one, Data Warehouses are updated when there is a change in the database, like a transaction. These systems provide OLAP tools for interactive analysis of multidimensional data.

OLAP is the acronym for Online Analytical Processing. In OLAP, information is classified by dimensions. OLAP cubes are usually pre-compiled to improve query time in relational databases. One of the most coherent data structures is data cube, which is used to represent multidimensional aggregates in Data Warehouse systems.

A data cube refers to a 3D range of values that are used to view data from the multidimensional model in which the information is computed and stored. The data cube that is used is defined by two entities, Facts, and dimensions. Facts are used to analyze dimensions with their numerical values. Dimensions are the rules concerning which an organization stores its records.

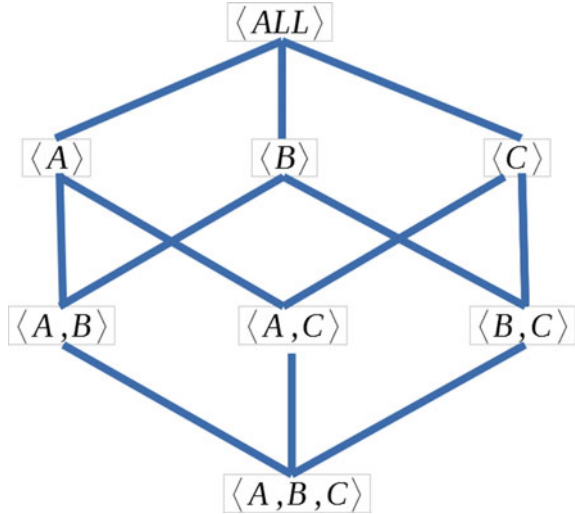
Data cubes are categorized into the following two categories:

1. Relational OLAP
2. Multidimensional data cube.

In Data Warehouse systems, query response time largely depends on the efficient computation of the data cube. However, creating a data cube is normally time and memory consuming. So, we normally materialize cuboids of a data cube. To do this, there are three possibilities:

1. *Materialize the whole Data Cube:* This is the best solution in terms of the query response time. However, computing every cuboid and storing them will take maximum space if the data cube is very large, which will affect indexing and the query response time.
2. *No Materialization:* In this one, Cuboids are computed as and when required. So, the query response time fully depends on the database which stores the raw data.
3. *Partial materialization:* This is the most feasible solution. In this approach, some cuboids or cells of a cuboid are pre-computed. However, the problem is how to

Fig. 1 A three-dimensional lattice of cuboids



select these cuboids and cells to be pre-computed. Generally, cuboids and cells which may help in computing other cells or cuboids, are pre-computed.

All the view materialization algorithms require to use some data structures to represent the data cube. One useful data structure is data cube lattice or lattice of cuboids.

In lattice of cuboids (Fig. 1), each cuboid represents a group-by and each level corresponds to different degrees of generalization containing a number of aggregate cells.

Rest of the paper is organized as follows: Sect. 2, discusses previous work done in related areas of study. Section 3, describes our approach to pathfinding. Section 4, provides proof by induction to our theorem based on which the algorithm is proposed. Section 5, presents the algorithm lowest first for cuboid materialization. Section 6, implements the algorithm to an example data cube and then verifies the resultant path. Section 7, presents the conclusion.

2 Related Work

There has been some synchronous work on the problem of computing and selection of data cube [2–7]. Shukla et al. [3] proposed a greedy algorithm which was a modified version of the Harinarayan et al. presented, which proposed a greedy algorithm that works on the lattice and picks the right views to materialize, subject to various constraints for the selection of data cube. This had an efficiency problem which was solved by Shukla et al. [8]. whose work proposed PBS (Pick by Size) that selects data cube according to the cube size. Gupta [9] proposed a polynomial-time

greedy heuristic framework that uses AND view (each view has a unique evaluation), OR view (any view may be computed from any of its related views), and AND-OR view graph. Shukla et al. [10] proposed three different algorithms, considering the view selection problem for multi-cube data models, SimpleLocal, SimpleGlobal, and Complex Global which picks aggregates for precomputation from multi-cube schemas. Sundararajan [11] proposed a simple MapReduce algorithm based on parallel computing which minimizes the number of copy-add operations, leverages locality of computation, and balances work evenly on machines.

A heuristic algorithm was proposed by Zhang et al. [6], for determining a set of materialized views based on the idea of reusing temporary results from the execution of global queries with the help of Multiple View Processing Plan (MVPP). For a special case of OR view graphs, Gupta et al. [12] designed an approximation greedy algorithm. To demonstrate that materialized views are practical and effective as compared to heuristic approaches Yang et al. [6] used genetic algorithm. Yang [13] proposed a greedy repaired genetic algorithm to select the set of materialized cubes and found that solution might greatly reduce the amount of query cost as well as the cube maintenance cost. Mami et al. [14] presented a constraint programming-based approach to address the view selection problem. A framework for materialized view selection was proposed by Aouiche et al. [15] that exploited a data mining technique (clustering), in determine clusters of similar queries. He also proposed a view merging algorithm that builds a greedy process and candidate for selecting a set of views to materialize. Mami [16] game surveys of the technique for selection of cube.

Deshpande [8, 17] proposed a sorting-based algorithm, for computing the cube that overlaps the computation of different group-by operations using the least possible memory for each computation of cube in the lattice of the cuboid. A Lvanova and Boris [18] designed a data cube based on the Object-oriented conceptual model. Sen [19, 20] proposed an algorithm for finding the optimal path in the lattice of the cuboid, which is based on two operations roll-up and drill-down for finding the optimized path to traverse between data cubes. Now the researchers are focusing on designing efficient algorithms for the complete cube.

3 Lowest First Approach

In lattice of cuboids, there may arise a situation where we require to materialize a particular cuboid given that only core cuboid is presently materialized. We propose an algorithm named lowest first, that does this by searching and materializing those intermediate cuboids that have the lowest number of rows present and hence low space and time complexities.

For example let us consider a lattice of cuboids having a total of four dimensions $\{A, B, C, D\}$ having values $A = 10, B = 20, C = 5, D = 15$. If we had to materialize cuboid $\langle A \rangle$ having cuboid $\langle A, B, C, D \rangle$ already materialized we have two ways to do this:

1. One is by starting from $\langle A, B, C, D \rangle$ to $\langle A, B, C \rangle$ and then to $\langle A, B \rangle$, and finally we reach $\langle A \rangle$.
2. Another path may be to start from $\langle A, B, C, D \rangle$ to $\langle A, C, D \rangle$ to $\langle A, D \rangle$ and finally to $\langle A \rangle$.

In total, we have ${}^3C_2 * {}^2C_1$ number of ways of doing so, which we might try all to compare and decide the most efficient path but our proposed algorithm finds the most efficient path by sorting and hashing the product of cardinalities of dimensions in each cuboid without the need to actually materialize intermediate cuboids and find the most efficient path.

First, we represent the cost of a path as a mathematical expression using which as a parameter we compare the efficiency of various paths and later optimize it. The expression involves the cardinalities of dimensions each intermediate cuboid has where cardinality of a dimension is the number of elements in the set containing all unique values a dimension has. For explanation, we use our previously described example of a data cube with four dimensions $\{A, B, C, D\}$ and we are required to find an efficient path starting from $\langle A, B, C, D \rangle$ to $\langle A \rangle$ by observation we may say that the path will involve two intermediate cuboids one having 3 dimensions and the other having 2 dimensions materializing both will result in our target cuboid, and both of these intermediate cuboids must contain all dimensions present in our target cuboid which is $\{A\}$ in our case.

$$a_1 a_2 a_3 + a_4 a_5 \quad (1)$$

is the expression for the cost where a_1, a_2, a_3 are the cardinalities of the dimensions present in intermediate cuboid having three dimensions and a_4, a_5 are the cardinalities of dimensions present in intermediate cuboid having two dimensions. We also know that a_4, a_5 must be present in a_1, a_2, a_3 so for simplicity we assume $a_1 = a_4$ and $a_2 = a_5$ so that our expression becomes

$$a_1 a_2 a_3 + a_1 a_2 \quad (2)$$

The target dimension $\{A\}$ must be present in both intermediate cuboids hence we assume a_1 to be A and take it common, so our expression further reduces to

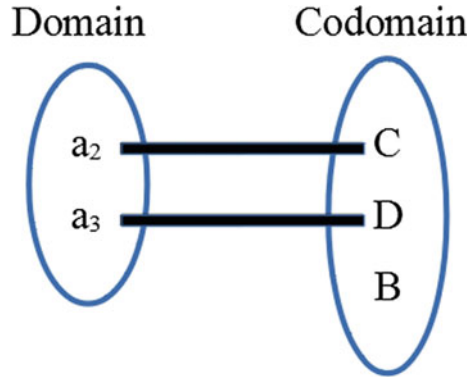
$$A(a_2 a_3 + a_2) \quad (3)$$

where $A = a_1$.

Now we need to find an optimal injection between the domain set $\{a_2, a_3\}$ containing elements present in our expression (3) to co-domain containing dimensions $\{B, C, D\}$ that are present in our source cuboid but absent in target cuboids we call this set difference set.

The way our algorithm finds this optimal injection is by performing the following operations.

Fig. 2 Optimal mapping for our example



Steps:

1. Sort the difference set based on cardinality of each dimension.
2. Map each element of domain set in order starting from a_1 to an to elements of difference set in sorted ascending order.

So the resultant mapping for our example data cube and particular pathfinding will look like (Fig. 2).

where the sorted difference set in ascending order is $\{C, D, B\}$ based on their values 5, 15, 20 respectively and the domain set is $\{a_2, a_3\}$ so our expression finally becomes

$$C * D + C \tag{4}$$

which means the optimal path from $\langle A, B, C, D \rangle$ to $\langle A \rangle$ is

$$\langle A, B, C, D \rangle \Rightarrow \langle A, C, D \rangle \Rightarrow \langle A, C \rangle \Rightarrow \langle A \rangle \tag{5}$$

and the intermediate cuboids are $\langle A, C, D \rangle$ and $\langle A, C \rangle$ which out of all other possibilities require the least space and time to materialize.

Now, we provide proof by induction to why the algorithm results in an optimal path.

4 Mathematical Proof

Theorem 1 *Minimum value of expression*

$$a_1 a_2 a_3 \dots a_n + a_1 a_2 a_3 \dots a_{n-1} + \dots + a_1 a_2 + a_1 \tag{6}$$

where $n \in W$ is obtained when the set containing all the variables present in the expression (6) in order starting from a_1 to a_n is mapped to a set containing m elements where $m \geq n$ and $m \in W$ in sorted ascending order.

Proof Let the co-domain to which we map be

$$\{A_1, A_2, A_3, \dots, A_m\} \quad (7)$$

and assume it is present in sorted ascending order so

$$A_1 \leq A_2 \leq A_3 \leq A_4 \leq \dots \leq A_m \quad (8)$$

Base Case $n = 1$

when $n = 1$ the domain becomes $\{a_1\}$ and the expression is reduced to a single term containing only a_1 now according to our theorem we map the variable a_1 to the first element of our sorted co-domain A_1 which is the minimum possible value of the expression a_1 as A_1 is the minimum value among all elements of set (7), hence base case is true.

Inductive assumption $n = k$

We suppose our theorem is true for $n = k$ which then implies for the expression

$$a_1 a_2 a_3 \dots a_k + a_1 a_2 a_3 \dots a_{k-1} + \dots + a_1 a_2 + a_1 \quad (9)$$

the optimal mapping that will result in minimum possible value is and the optimal value of expression for $n = k$ becomes

$$A_1 A_2 A_3 \dots A_k + A_1 A_2 A_3 \dots A_{k-1} + \dots + A_1 \quad (10)$$

For $n = k+1$ we need to show using Fig. 3 that the value of expression

$$a_1 a_2 a_3 \dots a_{k+1} + a_1 a_2 a_3 \dots a_k + \dots + a_1 a_2 + a_1 \quad (11)$$

is minimum when the mapping is as shown in

and to show this we split the expression (10) into two parts $\underbrace{A_1 A_2 A_3 \dots A_{k+1}}_{\text{Part1}} + \underbrace{A_1 A_2 A_3 \dots A_k + \dots + A_1 A_2 + A_1}_{\text{Part2}}$.

Part 2 of the expression is the same as (10) which by our inductive assumption for $n = k$ is minimum.

Now, we need to show whether part 1 is minimum possible which is true as to select $k + 1$ non-negative integers from a set such that their product is minimum is only possible when the lowest $k + 1$ terms are chosen and this is what we are doing by selecting $A_1, A_2, A_3, \dots, A_k$.

Hence for $n = k + 1$ our theorem holds true and (Fig. 4) is the optimal mapping of elements that proves our theorem to be true.

Fig. 3 Set mapping for inductive assumption

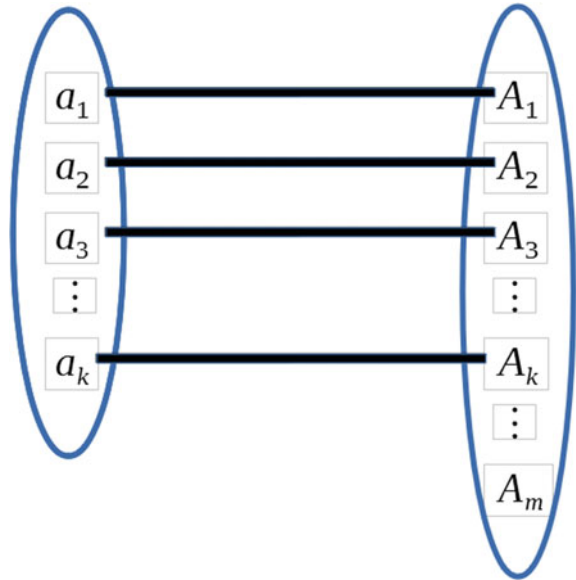
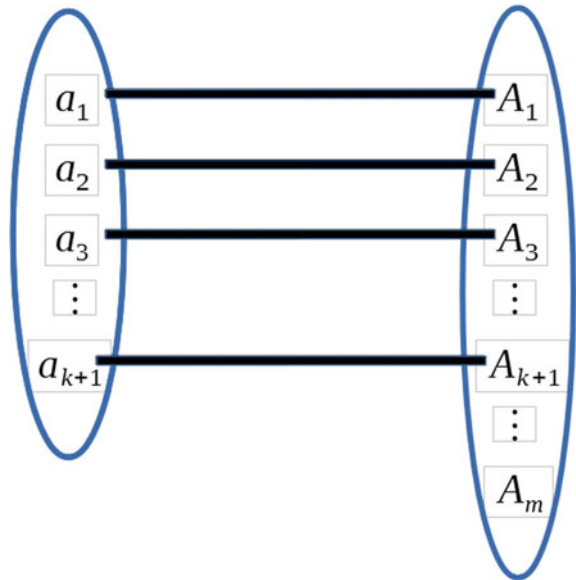


Fig. 4 Optimal mapping for $n = k + 1$



5 Proposed Algorithm

Now we describe the algorithm in a step by step way which may be replicated in any programming environment.

Preprocessing

Time complexity: $O(n\log(n))$

1. User input the values and names of all dimensions.
2. Check if they are valid.
3. Create an array named `sorted_dimensions` by sorting the dimensions given by the user based on the values of those dimensions in ascending order.

Query

Time complexity: $O(n)$

1. User input for the source and target cuboids.
2. Ensure the number of dimensions in source cuboid is greater than that in the target cuboid and if not then swap source cuboid with target cuboid.
3. Create a hash map for dimensions of source cuboid, Iterate over the array of dimensions of target cuboid and for each dimension check whether the hash map of source cuboid contains this dimensions if not then push it a new array named `difference_set` which after fully iterating over the target dimensions will contain dimensions that aren't present in source cuboid but present in target cuboid.
4. Create Hash map named `hash_diff_set` of the elements of `difference_set` to reduce access time complexity down to $O(l)$ from $O(n)$.
5. Iterate over the `sorted_attr` containing all the dimensions in sorted order by values, and for each element check if it exists in `hash_diff_set`, if present then pushes that dimension with its value to a new array named `sorted_diff_set` so that after iterating over `sorted_attr` we have `sorted_diff_set` containing dimensions that have the possibility to be present in intermediate cuboids for a given query in $O(n)$ time complexity.
6. Now the path from source cuboid to target cuboid is starting from Target cuboid and then to an intermediate cuboid containing dimensions of source cuboid and in addition the first dimension present in `sorted_diff_set` in its sorted ascending order, and from here to the next intermediate cuboid having dimensions of the present cuboid and in addition to this also the second dimension present in `sorted_diff_set` and continuing this procedure till we reach the Source cuboid.

6 Implementation of the Algorithm

Let us consider a lattice of cuboids of a data cube having a total of three dimensions namely Quarter, Brand and Region where cardinality of Quarter is 4 (Q_1, Q_2, Q_3, Q_4), cardinality of Brand is 2 (B_1, B_2) and cardinality of Region is 6 ($R_1, R_2, R_3,$

R_4, R_5, R_6) and the measure is Sales which is a number. We are required to find the optimal way of materializing cuboid $\langle Q \rangle$ starting from $\langle Q, B, R \rangle$.

Now, we use our algorithm to find what the optimal path is for the given data cube, source cuboid, and target cuboid.

Preprocessing We create an array named `sorted_dimensions` by sorting the dimensions $\{Q, B, R\}$ based on the values of those dimensions in ascending order and the result is `sorted_dimensions = [B, Q, R]` as values of $B = 2, Q = 4$ and $R = 6$.

Query: $\langle Q, B, R \rangle \Rightarrow \langle Q \rangle$

1. Source Cuboid = $\langle Q, B, R \rangle$
Target Cuboid $\Rightarrow \langle Q \rangle$
2. Ensure dimensions in target cuboid are strictly lower than that in source cuboid.
3. To create `difference_set` we first create a hash map of source dimensions and iterate over target cuboid checking whether this dimension exists in the hash map or not and if not present then push it to `difference_set`. So after doing this our `difference_set = [B, R]`.
4. Create a hash map of `difference_set`.
5. Iterate over `sorted_attr` created during preprocessing and for each dimension in it check whether it exists in the hash map of `difference_set` if present then push it to a new array `sorted_diff_set`. After doing this we'll have an array named `sorted_diff_set` which contains the elements of `difference_set` in sorted ascending order.
`sorted_diff_set = [B, R]`.
6. Our path now is starting from Target cuboid $\langle Q \rangle$ and to the intermediate cuboid having dimensions of target cuboid and the first dimension in `sorted_diff_set` i.e., $\{B\}$ and then the second dimension and so on.

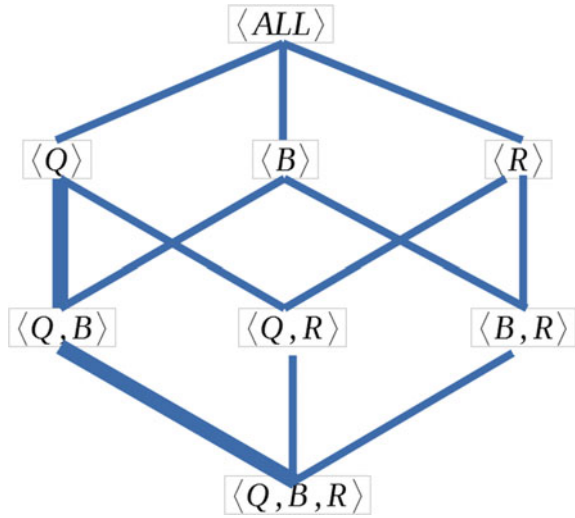
Hence, path given by algorithm $\langle Q \rangle \Rightarrow \langle Q, B \rangle \Rightarrow \langle Q, B, R \rangle$ is the optimal way to materialize cuboid $\langle Q \rangle$ starting from $\langle Q, B, R \rangle$.

Now we'll verify this result by comparing it with all other possibilities. All the paths we could've taken to materialize cuboid $\langle Q \rangle$ are

1. $\langle Q, B, R \rangle \Rightarrow \langle Q, R \rangle \Rightarrow \langle Q \rangle$, cost = sum of cost of materialization of intermediate cuboids i.e., cost ($\langle Q, R \rangle$) which is product of values of dimensions present in the cuboid = $4 * 6 = 24$.
2. $\langle Q, B, R \rangle \Rightarrow \langle Q, B \rangle \Rightarrow \langle Q \rangle$, cost = $4 * 2 = 8$ similar to how we calculate for the previous path.

Comparing the costs we see that path 2 is more efficient compared to path 1 and as we only have two paths in our example we can say path (2) is the most efficient way to materialize cuboid $\langle Q \rangle$ (Fig. 5).

Fig. 5 Lattice of cuboids for the example with three Dimensions $\{Q, B, R\}$ and optimal path highlighted from $\langle Q, B, R \rangle$ to $\langle Q \rangle$



7 Conclusion

In this paper, we have proposed an algorithm which has a preprocessing time complexity of $O(n \log(n))$ and query time complexity of $O(n)$ that finds the optimal path of materializing a cuboid starting from core cuboid in a lattice of cuboids or data cube and with the preprocessing it may extend its use case to massive pathfinding queries over the same Data Warehouse.

References

1. Mankad D, Dholakiya P (2013) The study on data warehouse design and usage. Int J Sci Res Publ
2. Li X, Han J, Gonzalez H (2004) High dimensional OLAP: a minimal cubing approach. In: Proceedings of the 2004 international conference very large databases (VLDB'04), Toronto Canada, pp 528–539
3. Harinarayan V, Ullman RA (1996) Implementing data cubes efficiently. In: ACM SIGMOD international conference on management of data, ACM Press, New York, pp 205–216
4. Stefanovic N, Han J, Koperski K (2000) Object-based selective materialization for efficient implementation of spatial data cubes. In: IEEE transaction on knowledge and data engineering, pp 938–958
5. Sanjay G, Alok C (1997) Parallel data cube construction for high performance online analytical processing. In: IEEE international conference, pp 10–14
6. Zhang C, Yang J (199) Genetic algorithm for materialized view selection in data warehouse environments. In: Proceedings of the international conference on data warehousing and knowledge discovery, vol 1676. LNCS, pp 116–125
7. Ivanova A, Rachev B (2004) Multidimensional models-constructing data cube. In: International conference on computer systems and technologies CompSysTech'2004

8. Shukla A, Deshpande PM, Naughton JF (1998) Materialized view selection for multidimensional datasets. In: Proceeding of the 24th international conference on very large databases, New York, pp 488–499
9. Gupta H (1997) selection of views to materialize in a data warehouse. ICDT, Delphi Greece
10. Shukla A, Deshpande PM, Naughton JF (2000) Materialized view selection for multi-cube data models. In: 7th international conference on extended database technology. Springer, Germany, pp 269–284
11. Sundarajan M, Yan Q (2017) Simple and efficient MapReduce algorithm for data cube materialization. Googleplex, Mountain View, CA
12. Gupta H, Mumick IS (1999) Selection of views to materialize under maintenance cost constraint. In: Proceedings of the 7th international conference on database theory (ICDT'99), Jerusalem, Israel, pp 453–470
13. Wen LY, Chung KI (2004) A genetic algorithm for OLAP data cubes. *Knowl Inf Syst* 6(1):83–102
14. Mami I, Coletta R, Bellahsene Z (2011) Modeling view selection as a constraint satisfaction problem. In: DEXA, pp 396–410
15. Aouiche K, Jouve P, Darmont J (2006) Clustering-based materialized view selection in data warehouses. In ADBIS'06, volume 4152 of LNCS, pp 81–95
16. Mami I, Bellahsene Z (2012) A survey of view selection method. *SIGMOD Rec* 41(1):20–30
17. Deshpande MP, Agarwal S, Naughton JF, Ramakrishnan R (1997) Computation of multidimensional aggregates. University of Wisconsin Madison, Technical Report
18. Antoaneta I, Boris R (2004) Multidimensional models constructing data cube. In: international conference on computer systems and technologies-CompSysTech'2004, vol 5, pp 1–7
19. Soumya S, Nabendu C (2011) Efficient traversal in data warehouse based on concept hierarchy using galois connections. In: Proceedings of the second international conference on emerging applications of information technology, pp 335–339
20. Soumya S, Nabendu C, Agostino C (2009) Optimal space and time complexity analysis on the lattice of cuboids using Galois connections for the data warehousing. In: Proceedings of the 2009, international conference on computer science and convergence information technology, pp 1271–1275

Ontology-Based Full-Text Searching Using Named Entity Recognition



Krishna Kumar, Md. Tanwir Uddin Haider, and Shamsh Sameed Ahsan

Abstract Travelling to different places depends on lots of factors such as hotels, restaurants, nearby hospitals, places to visit in cities, etc. All this information is available on different websites in an unstructured manner thus people do not get information as per their queries in organized format. People search for these factors on search engines which use keyword matching mechanism. Therefore, this paper presents full-text queries searching mechanism which gives precise results in a structured format. Here, our system scraps data from websites to collect information about cities, hotels and hospitals. Concepts of linked data using ontology are implied which has the capability to relate multiple sources of data available on different websites and infer new knowledge from it. Natural Language processing methods such as co-reference resolution is used, which forms a relationship between sentences scrapped from web, which helps to perform better search query without losing meaning of sentences during the processing. In our work, we have also used the Named entity recognition mechanism which applies tags on words with the real-world concepts that they represent. These tags are further utilized by Python library named RDFLib to match the tags which form a relationship between classes within ontology. This relationship between classes and tags are further used to insert and extract data from ontology.

Keywords Natural language processing · Ontology · Named entity recognition

K. Kumar (✉) · Md. T. U. Haider
National Institute of Technology Patna, Patna, India
e-mail: sahani.krisi@gmail.com

Md. T. U. Haider
e-mail: tanwir99@yahoo.com

S. S. Ahsan
Sikkim Manipal Institute of Technology, Majitar, Rangpo, Sikkim, India
e-mail: sameed18@gmail.com

1 Introduction

In modern days, travelling to different places depends upon lots of travelling factors such as best hotels, hospitals related to the user's health problem, places to visit such as museums, parks, best restaurants according to cuisines that user prefer, markets, gardens, water park, amusement parks, etc. This information is available on the web written and reviewed by experienced people. People search for these types of information on the web using search engines. The current available search engines are based on keyword matching. People have to search for all these questions separately. Current available recommendation systems are disjoint, they are either created for hospitals or restaurants or cities and so on. To provide a solution to these limitations researchers are utilizing the concept of linked data which has the capability to relate multiple sources of data available on different websites. To relate the data from multiple websites, Natural Language Processing (NLP) is used to mine full-text paragraph scrapped from the websites using co-reference resolution and named entity recognition (NER) methods. These concepts help to find out a relationship among the sentences and assign tags according to the meaning that the words represent. Since these tags are applied we need to match these tags to insert and extract data from ontology. Therefore, a Python library called RDFLib is used to work with RDF data. It is used to insert data in ontologies by matching NER tags which are predefined in the ontology. Ontologies provide a concept of linked data, due to interlinking of data in ontologies the computer becomes smart enough to understand these data and also has the potential to validate or infer new knowledge from these data [1].

In our research work, we are developing a system for full-text searching which provides the results according to the user's query related to their travelling priorities. These queries can be related to best restaurants in a city, places to shop, hotels considering user's budget, hospital-related to health problems, etc. or combination of these. The rest of the paper is described as follows. Section 2 explains about related works. Section 3 elaborates on the working of each module of our proposed system. Section 4 shows the results of user queries. Finally, Sect. 5 concludes our work along with future scopes.

2 Related Work

In this section, the literature to our work based on textual data, to develop an ontology-based full-text searching system have been summarized along with their applied methods, advantages and limitation. Bast et al. [2] in his proposed system shows that the search results are more accurate when the keywords are mentioned in the user queries are already present in the data extracted from the internet. Ittoo et al. [3] show the mechanism of their system which allows consumers to describe their priorities in text-based format, to capture consumer's preferences aiming to achieve more accurate recommendations. Ali et al. [4] show the advantage of using SVM in his system which

helps to identify the relevant information from things downloaded from the internet and then removes any data irrelevant to the system. Further merged ontology-based sentiment analysis is applied to get accurate results. Aloui and Touzi [5] shows an FCA (Formal Concept Analysis) based methodology for building ontologies from scratch then performing queries on them logically by combination of conceptual clustering and fuzzy logic. Collobert et al. [6] developed a unified neural network architecture and learning algorithm that is mainly used to perform NLP such as POS-tag, NER and semantic role labelling, etc.

3 Proposed Framework

Our key purpose of this research is to develop a generalized approach for model building to search user's textual questions while travelling and to give them more personalized results of cities, hotels and hospitals while travelling to any city as per their needs. Our approach makes use of Natural Language Processing techniques to understand user's questions and it is also used to extract and understand textual data available on the web about any cities, hotels and hospitals. In our NLP processing pipeline, we have added two modules. First module is co-reference resolution which forms a relationship between sentences which in turn helps to perform better search query without losing meaning of sentences during the NLP processing. Second module is Named entity recognition which applies tags on words with the real-world concepts that they represent. These tags are further used in the system to insert and extract data within ontology (Fig. 1).

3.1 *Web Scrapping*

We need to extract precise information from various websites it's always a difficult task to achieve. Our system uses distinct websites which has authentic details of the cities, hotels and hospitals. All relevant data related to classes of our ontology is scrapped from websites. These data include information regarding the cities such as hospitals in cities and their services, hotels and their features, shopping places, etc. The city details are scrapped from tripadvisor.in, hotel details are scrapped from oyo.rooms.com and hospital details are scrapped from practo.com.

3.2 *User Input Question (Query)*

It provides an interface to users where they can ask textual questions. Our system accepts full long paragraph based questions or just short questions related to city,

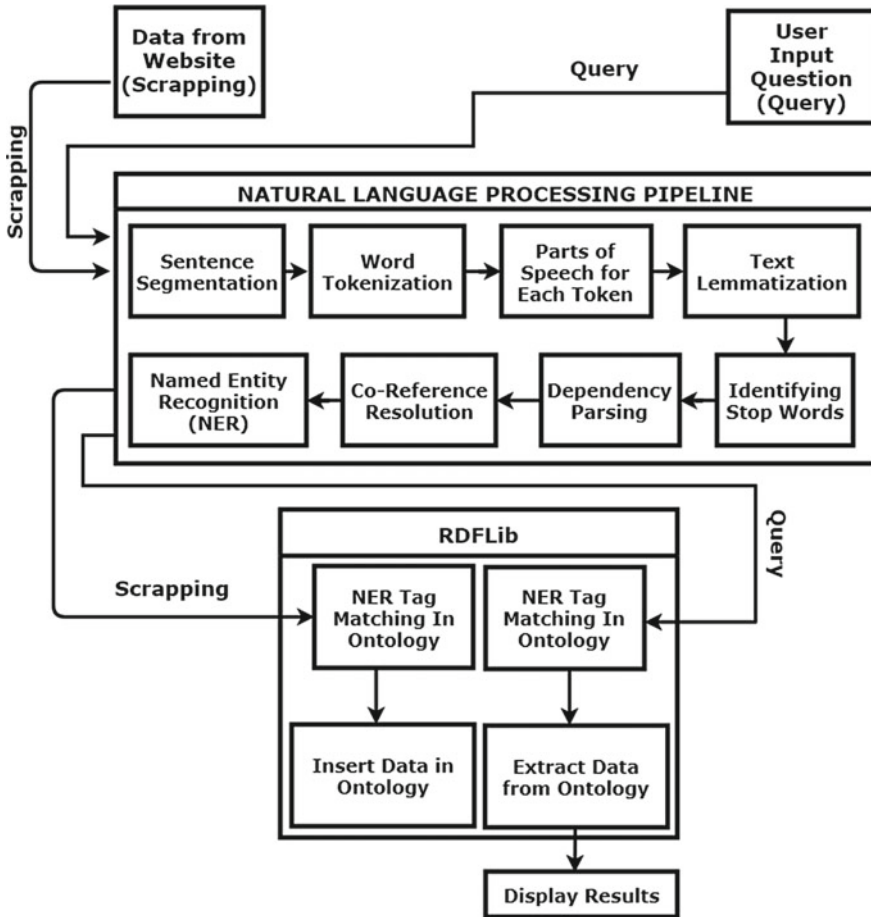


Fig. 1 Proposed framework of full-text searching

hotels and hospitals. Users have to enter their question in a textbox and click on ‘See Results’ to get the answers to their queries.

3.3 Natural Language Processing Pipeline

Textual data that we scrap from websites is not available in machine-understandable format and they do not convey any meaningful information so we need to pre-process the scrapped data using NLP pipeline. Here, sentences are broken into smaller pieces and then NLP is used to solve these individual small pieces. Then these NLP methods are combined together and result from first method becomes input to another method.

This helps us to determine the relationship between different sentences along with their meanings.

Sentence Segmentation It is used to break the text apart into separate sentences.

Word Tokenization Word tokenization means to break this sentence into separate words or tokens. We can process them one at a time. For demonstrating how this step works we'll select the first sentence from our document:

Delhi is capital of India.

The tokens generated for the above sentence are as follows:

“Delhi”, “is”, “capital”, “of”, “India”, “.”

Parts of Speech for Each Token In this process, we will take each token and find out its part of speech (POS) — whether it is a verb, a noun, an adjective and so on. We need to know the role of each particular word in the sentences which will help us to understand the context in which the sentence is written. A pre-trained POS classification model is used for each token to find out its POS. This is done by inputting each word (and some other words around it as extra context information) into a pre-trained POS model. To achieve this, we use ‘spaCy’ [7].

Text Lemmatization Lemmatization is the analysis of words with the aim to remove inflectional endings which return the base form or the dictionary form of a word.

Identifying Stop Words Stop words is commonly used word (such as ‘the’, ‘a’, ‘an’, ‘in’) in any sentence. When processing textual data, these words in the sentences create a lot of noise as these particular words are seen more often in the sentences.

Dependency Parsing It is the task of extracting a dependency parse of a sentence that represents its grammatical structure and defines the relationships between ‘head’ words and words, which modify those heads.

Co-Reference Resolution Now, we have a meaningful presentation of our sentence. We have understood the POS for every word, how these words are related to each other and which words are referring to real-world entities. However, English has plentiful pronouns — words like she, he and it. Since only one sentence at a time is processed, our NLP process doesn't know the meanings of these pronouns. To solve this problem, we use a model ‘NeuralCoref 4.0’ which is a co-reference algorithm [8]. This algorithm extracts a series of mentions (words which are related to real-world objects or things). For every mention, we calculate set of features. Then, an antecedent for each mention is recognized according to the set of features. Further, the algorithm takes a word and its relationship with several other words inside and around each mention, the average is calculated if required, add some simple features such as length of the mention, speaker information, location of the mentions to get a features presentation for each mention. Then we put these presentations into two neural nets. First neural net gives us a score of each pair of mentions and finds an antecedent,

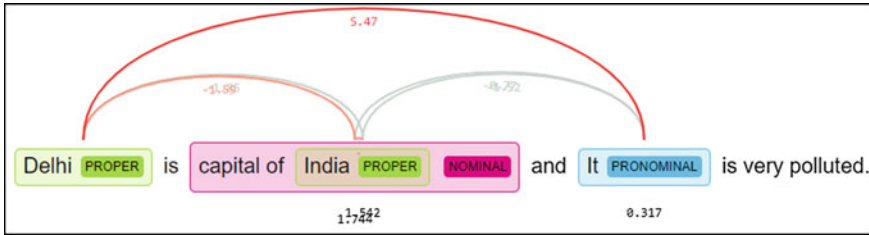


Fig. 2 Score of positive relationship between two sentences

while second neural net provides us with a mention which has no antecedent. A score is generated by neural net for each pair of mention. Further, these scores are compared to take the highest score and to find out whether a mention is having an antecedent. A non-probabilistic slack-rescaled max-margin objective is used to train this neural model. It means that this system can find a score for each pair of mentions and a score for each single mention but these scores are not related to probabilities, these are just scores in arbitrary units. The higher the score there is higher chance of the mention having an antecedent. Here, co-reference resolution is applied to the sample data which has been extracted from the web as shown below.

Delhi is Capital of India and it is very polluted.

If we pass this sentence in our NLP pipeline, we'll know that 'it' is very polluted. But it'll be more meaningful to find out that 'Delhi' is polluted (Fig. 2).

After using 'NeuralCoref' we are able to find out how pronouns are related in a sentence. We then replace the word 'It' with 'Delhi' which further helps us to create more meaningful sentences and get a deeper meaning of the sentences (Fig. 3).

Named Entity Recognition (NER) It is used to classify the named entities that is given in the sentence into predefined categories such as person's name, companies, places, organization, cities, dates, product terminologies, etc. It helps to answer many real-world questions. The job of the NER is to probe the given sentence and find out the name of persons, places, organizations, etc. which has been discussed in them and accordingly assign the tags. It helps to categorize the text in a well-defined hierarchy which enables smooth discovery of contents.

Some nouns in our sentences are real things of the world. For example, 'Ravi' represents a person, 'Patna', represents a city. 'Anisabad' represents an area and Hotel Patliputra represents a 'hotel'. A list of real-world places has to be created thus



Fig. 3 Replacement of words when a positive match score is present between sentences



Fig. 4 NER tags applied on the words

we have to find the real-world entities in the sentences. This same method is applied on other text scenarios to find out features of a city such as cleanliness, places to shop, parks, etc. The aim of NER is to detect and put these nouns referring to the real-world concepts that they show. Now, we have to extract ideas from the sentences and tag them. To achieve this, we use ‘spaCy’ [9]. We further trained this model to suit our needs so that it can recognize the names of areas in a city, names of parks, shopping places, names of hospitals, doctors, etc. Here, ‘spaCy’ consists of some predefined NER’s and few users defined NER’s which are trained for our work as shown below.

- FAC: It describes national highways, rivers, oceans, builds, etc.
- GPE: It describes cities, states and countries.
- LOC: It describes non GPE locations such as mountains, volcanoes, etc.
- HOTFEA: It describes about hotel amenities such as geyser, swimming pool, etc.

There are some more predefined NER tags such as EVENT, PERSON, MONEY, QUANTITY, LANGUAGE, TIME, DATE, etc.

We have taken a sample data to demonstrate the working of NER. As the sentences are passed through ‘spaCy’ the respective NER tags are recognized and they are applied on the respective words as shown in Fig. 4.

After processing, we finally know that Ravi is a person, Patna is a city which has tags such as PERSON and GPE. This forms the basis of our query creation for ontology searching. In the next sections, we describe how our ontologies are created and tagged with NER tags.

3.4 RDFLib

RDFLib is a pure Python package to work with RDF data. It is used to insert and extract data in ontologies by matching NER tags which are predefined in the ontology [10].

Ontology Creation and Searching In our proposed framework we have created an ontology that contains city as its main domain. The city domain consists of predefined classes and sub-classes such as hotels, hospitals, areas, museums, parks, restaurants, flights, markets, gardens, water park and amusement parks, nature parks, etc. as shown in OntoGraf Fig. 5. We have also elaborated one of the predefined class named Hotel along with their sub-classes which contains hotel names and features as shown in Fig. 6. The figure clearly shows ‘GPE’ and ‘HOTFEA’ tag which represents city

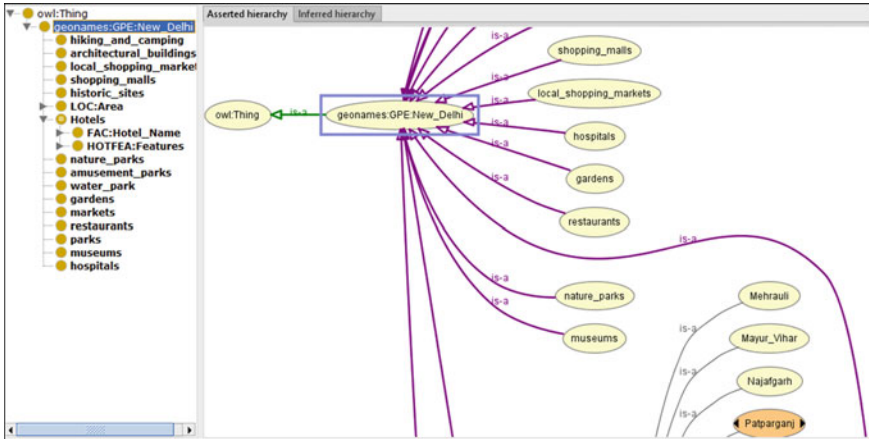


Fig. 5 OntoGraf showing different city features

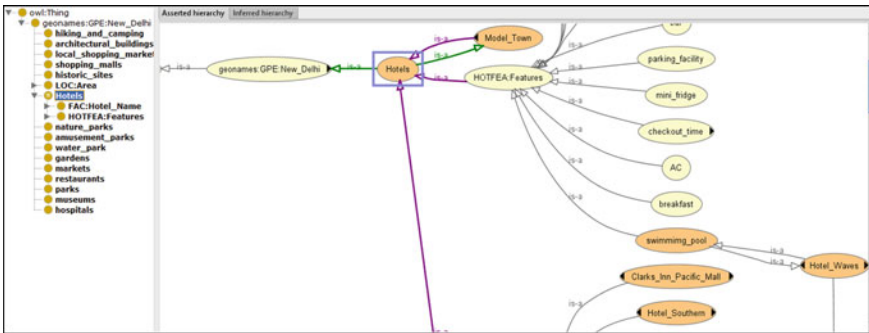


Fig. 6 OntoGraf showing different hotel features and NER HOTFEA tag which describes hotel features

and Hotel features, respectively.

We have tagged the classes and sub-classes of our ontology with the tags of NRE. We extract the sentences from the web and then analyze the text based on NLP pipelines as shown in all the steps above. Once we've recognized the entities and it's NER tags clearly we know where to insert this named entity in our ontology by matching the NER tags. To insert the data in our ontology we use Python library called RDFLib which has various methods and tools to operate on RDF data. At this stage, ontology has been created.

Now when the proposed system receives an input query from user, it pre-processes the query by applying various NLP techniques and applies NER tags on the words. Our system also has NER tags on ontologies. The system then matches the NER tags on ontologies with the help of RDFLib which has methods to import the ontology's

RDF file and then apply searching techniques on RDF data to get the most accurate results.

Each of these classes has their own properties and features used for knowledge creation and are also used to infer new knowledge from these relationships of linked data. The tagged NER queries which were obtained from user in the previous steps are then matched on the ontology. The ontologies are traversed and NER tags are matched to get the most meaningful answer to the user queries.

4 Results

In this section, the results of our proposed framework have been shown to demonstrate the working of some complex questions asked by the user. Also, the various steps of NLP pipeline applied on the query along with results of each processing step have been shown in Fig. 7. Suppose the first sample query entered in the system is as follows.

Book a Hotel in Delhi in Paharganj. It should have a swimming pool.

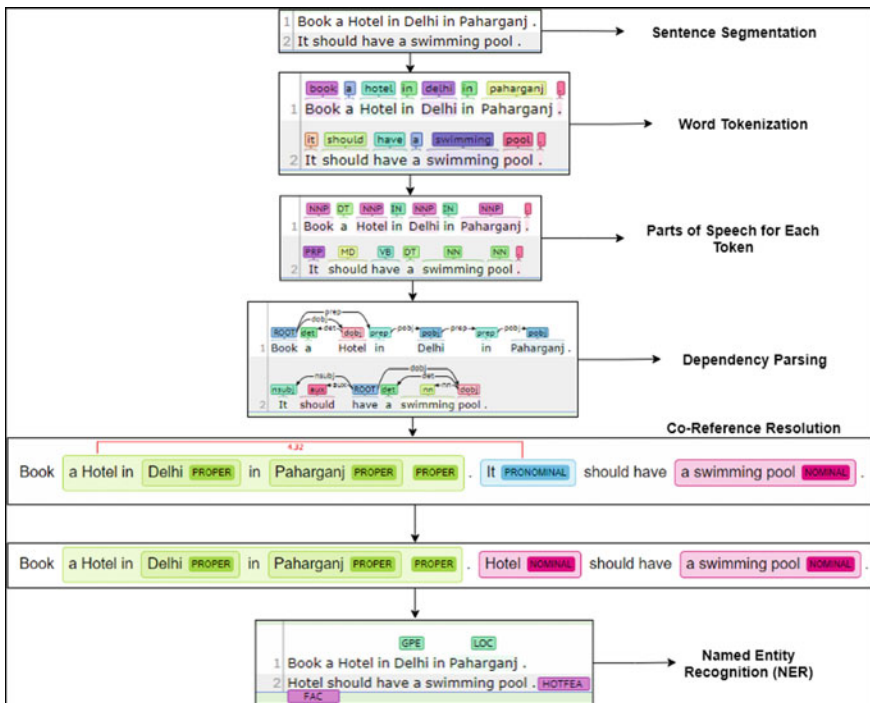


Fig. 7 Processing steps of a query in NLP pipeline

Figure 7 shows the results of NLP pipeline on the above-mentioned query. In the first step, sentence segmentation is performed to break down the sentence such that processing can be done more effectively as shown in Fig. 7 (sentence segmentation block). Further, second step is followed by performing word tokenization to find tokens of each sentence as shown in Fig. 7 (word tokenization block). Thereafter, in third step parts of speech such as nouns, pronouns are recognized which helps us to know the role of each particular word in the sentences that allow us to understand the context in which the sentence is written as shown in Fig. 7 (POS block). Next step perform lemmatization if required as per lemmas present in the text (In the above query lemmatization is not performed as no lemmas are present) followed by the identification of stop words but they are not removed since the removal of stop words will distort the meaning of sentences and affect the dependency parsing process, so we'll remove the stop words once NER tags are set on the words.

After this step dependency parsing is done which play a critical role in recognizing a sentence and assigning a syntactic structure to find out how words in the sentences relate to each other as shown in Fig. 7 (dependency parsing block). After identifying the dependencies between the words co-reference resolution is performed which helps to find expressions that refer to the same entity in a text. After using co-reference resolution we are able to find out how pronouns are related in a sentence. Further, these pronouns are replaced with their co-reference entity say 'It' with 'Hotel' as shown in Fig. 7 (co-reference resolution block) which further helps us to create more meaningful sentences and get a deeper meaning of the sentences.

Finally, NER with the key factor of relevant entities (tags) association overcome the limitations of existing model which arises during the searching mechanism. Since during processing we are extracting articles from web which comprises enormous data. Processing of any search query other than NER will maximize the execution time because it will search each and every word present in millions of articles. On the other hand, NER is run once on all the articles and probe the relevant entities (tags) associated, stores separately which speed up the search process considerably. Here, NER tags searching mechanism helps to match with only a small list of entities discussed in articles leading with faster search execution and ontology creation.

After the tags are found, the tags along with their context are sent ('Delhi' is context and 'GPE' is the tag as shown in Fig. 7 (NER block) to RDFLib which matches the data in the ontology's RDF file using tags. The system uses tags generated on the user input query and then matches those tags with the predefined tags on the system, once the tags are matched then it matches the context of the respective tag. Once the system finds out the results, it then displays the result as shown in Fig. 8.

Similarly, we have tested our system with another query that has hospital-related questions, its entire search process is performed in the same way as shown for the previous query. Its result along with the query is shown in Fig. 9. Our system is also able to recommend best places to stay near shopping areas, nearby amusement parks, or nearby hospitals if the traveller has health-related problems.



Fig. 8 User interface with query and results

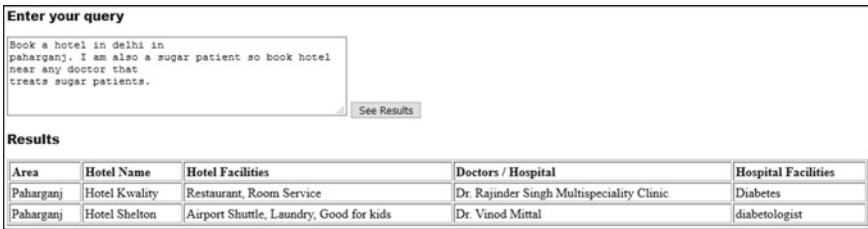


Fig. 9 User interface with query and results

5 Conclusion and Future Work

The results confirm the effectiveness of our proposed approach which has the potential to relate the meaning of multiple sentences available in a paragraph. The relationship between the multiple sentences helps the system to find out maximum relevant data which are co-related to each other in a particular context as per queries entered by the user. Our proposed system implies a number of Natural Language processing concepts which improves the system accuracy to understand the data scrapped from websites and it improves understanding of user questions. Here, we have added NLP methods named co-reference resolution and Named entity recognition in the NLP pipeline to improve the system’s capability to accurately identify the relationship between sentences and then map the words to real-world entities that they represent. In future work, we will enhance the accuracy of NER tags which are applied on the words. We will also focus on automatic classes detection and creation of ontologies when we scrap data from the websites, which will create a fully automated system.

References

1. W3C, OWL (2019) Web ontology language <http://www.w3.org/TR/owl-absyn/>. Last accessed 1 Apr 2019
2. Bast H, Bärle F, Buchhold B, Haussmann E (2012) A case for semantic full-text search. In: Proceedings of the 1st joint international workshop on entity-oriented and semantic search, p 4. ACM

3. Ittoo AR, Zhang Y, Jiao J (2006) A text mining-based recommendation system for customer decision making in online product customization. In: 2006 IEEE international conference on management of innovation and technology, vol 1, pp 473–477. IEEE
4. Ali F, Kwak D, Khan P, Ei-Sappagh SHA, Islam SR, Park D, Kwak KS (2017) Merged ontology and SVM-based information extraction and recommendation system for social robots. *IEEE Access* 5:12364–12379
5. Aloui A, Touzi AG (2015) A fuzzy ontology-based platform for flexible querying. *Int J Serv Sci Manage Eng Technol (IJSSMET)* 6(3):12–26
6. Collobert R, Weston J, Bottou L, Kavukcuoglu K, Kuksa P (2011) Natural language processing (almost) from scratch. *J Mach Learn Res* 12:2493–2537
7. spaCy Industrial-strength natural language processing in python, <https://spacy.io/>. Last accessed 28 Mar 2019
8. How to train a neural coreference model—Neuralcoref 2. <https://medium.com/huggingface/how-to-train-a-neural-coreference-model-neuralcoref-2-7bb30c1abdfc>. Last accessed 28 Mar 2019
9. Training spaCy’s Statistical Models (2019) spaCy usage documentation. <https://spacy.io/usage/training>. Last accessed 28 Mar 2019
10. W3C (2019) Resource description framework (RDF): concepts and abstract syntax. <http://www.w3.org/TR/rdf-concepts/>. Last accessed 28 Mar 2019

Recognition of Online Handwritten Gurmukhi Characters Through Neural Networks



Sukhdeep Singh and Anuj Sharma

Abstract This paper recognizes online handwritten Gurmukhi characters and words. The neural network-based recognition for online handwritten Gurmukhi characters and words has been observed first time in this study. In this work, a scheme is proposed to develop a feature vector and its use as an input to neural network recognition engine. A set of low-level, high-level, and Gabor features are extracted, and a feed-forward neural network is trained to recognize 40 classes of Gurmukhi characters. This work implements rearrangement of strokes stage after recognition and post-processing stages. The results have been achieved as 93.53% and 83.69% for 4511 Gurmukhi characters and 2576 Gurmukhi words, respectively.

Keywords Online handwriting · Gurmukhi · Neural network

1 Introduction

The advances in the research of handwriting recognition continuously motivate researchers to look forward in this area. Over four decades of research in this field, we have observed that usage and reliability of handwriting recognition-based devices have been increased in the recent past. These devices are not limited to the common international script as English but also use other popular scripts as Chinese, Japanese, Devanagari, and Arabic. The Indic scripts are very popular in respective geographic regions, and use of keyboard for such scripts has never gained an easy and popular way of interactive device. This happened mainly because of nature of scripts and its complexities. The existence of recognizer for online handwriting in Devanagari, Bangla, Gurmukhi, and other Indic scripts needs to give a natural mean

S. Singh (✉)
D.M. College, Moga, Punjab, India
e-mail: sukha13@gmail.com

A. Sharma
Department of Computer Science and Applications, Panjab University, Chandigarh 160014, India
e-mail: anuj@pu.ac.in

of exchanging information between computers and users, and it will result to a rise in the usage of tablet PCs and personal digital assistants in Indic scripts. The present study has been carried out using a popular script as Gurmukhi. The Punjabi language is one of the popular languages across the globe, and the rich Punjabi culture has always attracted other people to understand this language. This language is based on Gurmukhi script. The Gurmukhi characters with their class id's are shown in Fig. 1. Gurmukhi script follows the left-to-right writing direction and is written in top-down manner. Many Gurmukhi characters contain a horizontal line in the upper part. The headline connects the characters of the words. A Gurmukhi word is divided into three zones. These zones are called as: upper, middle, and lower zones. The region above the headline is the upper zone, where some vowels and other vowels sub-parts reside. The middle zone is the area which is below the headline that contains consonants and vowels sub-parts. The busiest zone is the middle zone. The area below the middle zone is the lower zone that contains certain half characters and vowels. Figure 2 shows these zones for a Gurmukhi word in Punjabi. The present study is focused to recognition of isolated handwritten characters presented in Fig. 1.

A script recognition review by Ghosh et al. discussed the nature of Gurmukhi script under tree of Brahmi script and its status among other Indic scripts. The study indicates many similarities among Indic scripts in the form of structural features [1]. The Gurmukhi script has many common properties to other Indic scripts such as Devanagari, Bangla, Tamil, and Telugu in vowels use, half and full characters, writing style

ੳ ¹	ਅ ²	ੲ ³	ਸ ⁴	ਹ ⁵	ਕ ⁶	ਖ ⁷	ਗ ⁸	ਘ ⁹	ਙ ¹⁰
ਛ ¹¹	ਜ ¹²	ਝ ¹³	ਵ ¹⁴	ਟ ¹⁵	ਠ ¹⁶	ਡ ¹⁷	ਦ ¹⁸	ਣ ¹⁹	ਤ ²⁰
ਥ ²¹	ਢ ²²	ਧ ²³	ਨ ²⁴	ਪ ²⁵	ਫ ²⁶	ਬ ²⁷	ਭ ²⁸	ਮ ²⁹	ਯ ³⁰
ਰ ³¹	ਲ ³²	ਵ ³³	ੜ ³⁴	ੳ ³⁵	ਸ਼ ³⁶	ਖ਼ ³⁷	ਗ਼ ³⁸	ਜ਼ ³⁹	ਲ਼ ⁴⁰

Fig. 1 Gurmukhi characters and their class id's

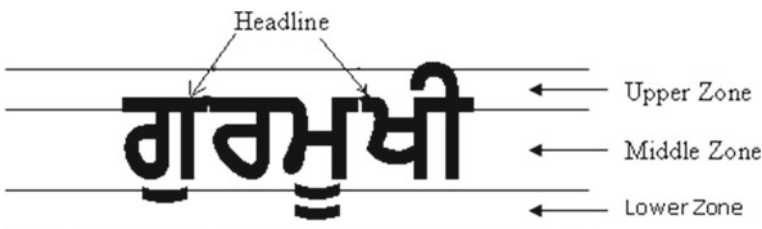


Fig. 2 Three zones in Gurmukhi word

and word formations. Therefore, we have presented here selected literature related to Gurmukhi script nature. The online handwriting research for Indic scripts has been done mainly in the last fifteen years, and we have discussed recent work in this section. The literature discussed in this section cannot be compared as the cited work includes different recognition methodologies, databases, and experimental environments. The early work for online handwritten Indic script Devanagari noticed in the year 2000 by Connell et al. They used hidden Markov model (HMM) to recognize Devanagari characters and achieved 86.5% as recognition rate [2]. In 2005, Joshi et al. reported recognition rate as 94.49%, where they used structural- and feature-based matching for Devanagari character recognition in a writer-dependent system [3]. A support vector machine (SVM)-based technique is used to construct stroke recognition engine in order to recognize Devanagari and Telugu characters where a character's representation is made as sequence of strokes whose features are classified and extracted [4]. In 2007, Bharath and Madhvanath recognized Tamil characters with accuracy of 97.76% for 1000 dictionary words using HMM [5]. Prasanth et al. used dynamic time warping methods for four features' set to recognize Telugu data set with 90.6% accuracy [6]. Bhattacharya et al. recognized Bangla words with an accuracy of 82.34% using analytic recognition approach [7]. Sharma et al. used elastic matching method to recognize Gurmukhi characters and reported 90.08% recognition rate in writer-independent system [8]. This study presents strokes recognition and evaluated characters based on recognized strokes. In 2009, Sharma et al. proposed rearrangement of strokes step after post-processing phase and achieved 81.02% recognition accuracy for 2576 Gurmukhi words [9]. Bharath and Madhvanath developed an HMM-based lexicon-driven and lexicon-free word recognizer for online handwritten Devanagari and Tamil words. They achieved 87.13% recognition rate for Devanagari words by combining lexicon-driven and lexicon-free word recognizer, and 91.8% for Tamil words using lexicon-driven recognizer [10]. Sundaram and Ramakrishnan developed an attention feedback segmentation-based approach for recognition of online handwritten Tamil words and attained word recognition rate as 64.9% [11]. In 2014, Kumar et al. proposed a SVM-based algorithm to recognize multi-stroke-based online handwritten Gurmukhi characters [12]. In 2016, Singh et al. developed a benchmarked Gurmukhi data set based on minimal set of words [13]. Recently, in 2019, Singh et al. [14] proposed a complete system for online handwritten Gurmukhi word recognition.

The established procedure that has been extensively used in literature, the same sequence of steps has been used in the present study [15]. A character is stored as a combination of one or more handwritten strokes in sequential order. The collected character is sent to preprocessing where character is transformed to standard size, interpolate missing points, smoothing of strokes, improving slant in character, and equidistant points in trajectories. The feature extraction includes computation of low-level and high-level features. After preprocessing and feature extraction, character is recognized using a recognition method as feed-forward neural network (NN) and post-processing is done to verify recognized character. NN models efforts to employ a few organizational principles like learning, adaptability, generalization, fault tolerance, distributed representation, and computation in a network of weighted directed

graphs where the nodes are artificial neurons and the directed edges denote the connections among neuron inputs and outputs. The main properties of NN are that they can learn complex nonlinear input–output relationships, employ sequential training procedures, and get used themselves to the data [16]. For the classification of patterns, the feed-forward networks are the most commonly used neural networks, which comprise multilayer perceptron and radial basis function networks. The neural networks have been used for handwriting recognition, and literature suggests a good scope of recognition accuracy using this recognition method [17, 18]. The present work has been done under motivation of previous work observed for online handwriting recognition in Indic scripts. It has been noticed that structural features of Indic scripts provide rich set of information in recognizing characters [10]. Also, strong mathematical nature of neural network recognition method explores the hidden nature of patterns [19]. The major characteristics of the present study are:

- The neural network-based recognition for online handwritten Gurmukhi characters has been observed first time in this study.
- A scheme is proposed to develop feature vector and its use as an input to neural network recognition engine.
- Two types of features are computed in the present study: low-level features and high-level features. In addition, chain code feature technique has also been applied.
- As Gurmukhi is not an isolated script, so the present study can also be extended for other Indic scripts as Devanagari and Bangla.
- The recognition task is performed with less time complexity.
- This work implements rearrangement of strokes stage after recognition and post-processing stages successfully.

The system development overview has been discussed in Sect.2. Section3 presents the preprocessing and feature computation techniques. The recognition for characters and post-processing stage has been explained in Sect.4. Sections5 and 6 present the results and summary of the present study.

2 Preprocessing and Feature Extraction

The present study includes size normalization, interpolation of missing points, centering, slant correction, smoothing, and resampling of points in preprocessing phase. Size normalization is referred to resize the input character to fixed size and centering fixes the position on axes that help in understanding the nature of characters graphically. Fast handwriting captures few points as compared to slow handwriting, and therefore, missing points can be interpolated in strokes trajectory. Smoothing is done to remove flickering in handwriting and slant correction correct the slants of strokes as it has been observed that most of the handwriting styles have left-side or right-side bends. Resampling of points equidistant the points inside strokes that help in recognition of strokes especially when points inside strokes are treated as variables. The

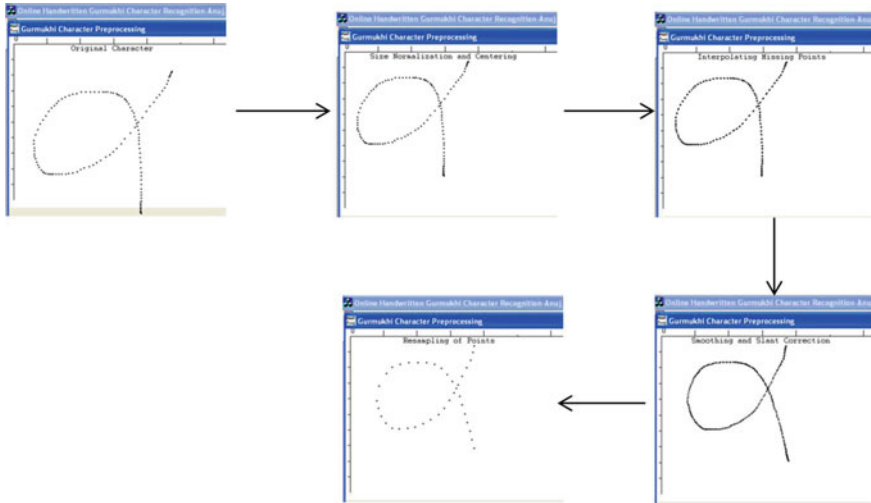


Fig. 3 Gurmukhi character ‘kakka’ (class id 6) during various stages of preprocessing

detailed study and their algorithms related to preprocessing in handwriting recognition are available in the literature [15, 20–23]. Figure 3 presents shapes of Gurmukhi character ‘kakka’ during these preprocessing stages in our system. The pseudocode to perform preprocessing stages has been explained in Algorithm 1.

Two types of features are computed in the present study: low-level features and high-level features. In addition, we have applied chain code features technique. The low-level features for strokes have been used as linearity, curliness, aspect ratio, and slope. The features as loops, headline, straight line, crossing of strokes, and dots are the high-level features. Low-level features are same as their names and mathematical meaning. In case of high-level features: Loops are referred to shapes that form bends and crosses itself in a stroke, crossings are the intersections of strokes, headline is referred to horizontal line present in joining of upper and middle zone, straight lines are strokes mostly with no curves and appear perpendicular to three zones in a word or character and dots are the small strokes usually isolated in a character or word. In Punjabi language, dot-like shape is called ‘bindi’. Figure 4 presents character ‘jhajja’ with high-level features. The computations of these low-level and high-level features have been explained by Sharma et al. for Gurmukhi characters which are available in the literature [23].

The low-level and high-level features are also used in post-processing stage to verify recognized stroke or character. We have used neural network as recognition method, the low-level, high-level, and chain code feature vectors are used to train network. The chain code has a linear structure, and it results from the quantization of the centers of an image array’s adjoining boundary elements [24]. In online handwriting recognition, the chain codes are the most commonly used structural representations. Chain code refers that a handwritten stroke is divided into segments,

Algorithm 1 Preprocessing steps

State: A character is group of M strokes and $M \geq 1$. The total number of points in a character are n and a point in a character is represented as P_i , $1 \leq i \leq n$. The L is the vector that include all points of a character in sequential order. The r is the ratio used to resize the character to fixed size and d is the distance to place character at fixed position.

Size normalization: $L \leftarrow L \times r$

Centering: $L \leftarrow L \pm d$

Interpolation: To interpolate points between P_i to P_{i+3} , a new point is P'_i and P_i to P_{i+3} must belong to single stroke in a character. The u and Δu are constants used with value between 0 and 1.

while $u \leq 1$ **do**

$$P'_i \leftarrow P_i \times (1-u)^3 + P_{i+1} \times 3 \times u \times (1-u)^2 + P_{i+2} \times 3 \times u^2 \times (1-u) + P_{i+3} \times u^3$$

$$u \leftarrow u + \Delta u$$

end while

Update L with new points.

Smoothing: To smooth the trajectory of a stroke inside a character, an angle α is calculated between points P_{i-2} to P_{i+2} in a stroke.

$$P'_i \leftarrow \frac{P_{i-2} + P_{i-1} + \alpha \times P_i + P_{i+1} + P_{i+2}}{2 \times 2 + \alpha}$$

Update L with new points.

Slant Correction: To perform slant correction of strokes inside a character, Yimei et al. 2000 technique has been used with 8 directions code as n_0 to n_7 . The slant of stroke is calculated as θ .

$$\theta \leftarrow \tan^{-1} \frac{(2 \times n_1 + 2 \times n_2 + n_3) - (n_5 + 2 \times n_6 + 2 \times n_7)}{(n_1 + 2 \times n_2 + 2 \times n_3) + 2 \times n_4 + (2 \times n_5 + 2 \times n_6 + n_7)}$$

if $(\theta > 45^\circ$ and $\theta < 90^\circ)$ OR $(\theta > 90^\circ$ and $\theta < 135^\circ)$ **then**

$$P'_{i_x} \leftarrow P_{i_x} + P_{i_y} \times \tan \theta$$

end if

Update L with new points.

Resampling of points: To resample the points, a filter is applied to place points at constant distance.

and these segments are coded. The structural approach is employed for recognition of online handwritten characters. Based on a structural approach, the existing study presented a real-time constraint-free system for recognition of handprinted characters. After preprocessing, the extraction of chain code is done for representation of the character. The classification is based on the use of a processor devoted for string comparison [25].

Let L_f be set of three feature vectors as L_{llf} , L_{hlf} , and L_{ccf} . The L_{llf} , L_{hlf} , and L_{ccf} present low-level, high-level, and chain code features vectors.

$$L_{\text{llf}} = \{\text{directions, positions, aspect ratio, width, height, length}\}$$

$$L_{\text{hlf}} = \{\text{loops, crossing, headline, straight line, dot}\}$$

To compute L_{ccf} from preprocessed character, the present study computes chain code for twelve different directions as shown in Fig. 5. In Fig. 5, every direction is of equal range. We have considered twelve directions in the range from 0 to 360°. The directions are named from numbers '1' to '12', and every direction has a range of 30° as shown in Fig. 5. It is important to note here that if the range other than 30° is considered, then the recognition accuracy does not improve. We have experimented with a range of 15°, 20°, and 45°. Figure 6 presents small line segments as chain

Fig. 4 High-level features in Gurmukhi character 'jajja' (class id 39)

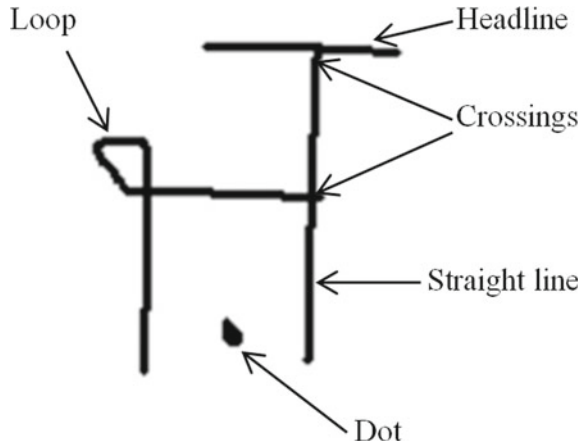
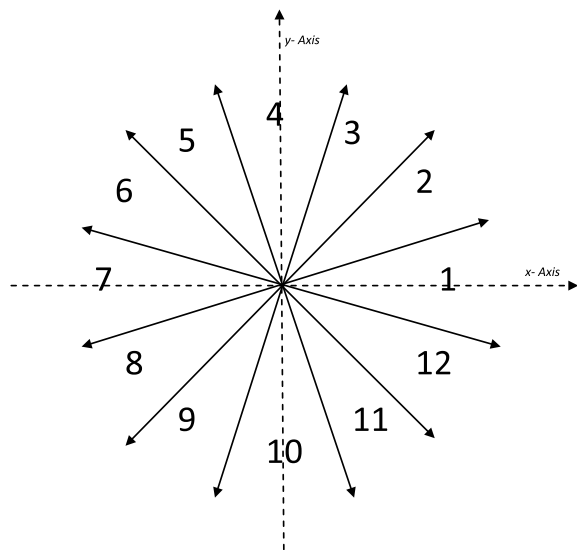


Fig. 5 Scope of twelve directions



code string for a handwritten stroke. The small line segments for Fig. 6 appear as {1, 12, 10, 9, 9, 8, 5, 3, 2, 1, 12, 12, 10, 9, 7, 4, 2, 2, 2}. The small line segments have been fixed to nineteen in present study, and joining of inter-stroke segments has been avoided inside a character. Therefore,

$$L_{ccf} = \{\text{nineteen small line segments}\} \text{ and}$$

$$L_f = \{L_{llf}, L_{hlf}, L_{ccf}\}.$$

The feature vector for a character 'kakka' presented in Fig. 3 is written as: $L_f = \{8.6, 0.6, 0.85, 4.5, 1, 0, 0, 0, 0, 10, 9, 9, 9, 8, 8, 7, 7, 6, 4, 3, 2, 1, 12, 12, 11, 11, 10,$

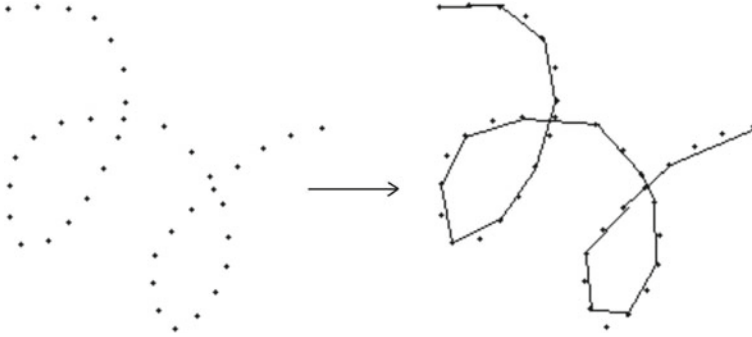


Fig. 6 Small line segments for points of a stroke

10}. In this feature vector, first four are L_{llf} as linearity, curliness, aspect ratio, and slope. The next five are L_{hlf} as loop, crossing, headline, straight line, and dot. The rest numerics are L_{ccf} .

3 Recognition and Post-processing

The steps carried out in recognition phase are listed as:

- (i) train network using extracted feature vectors as L_{llf} , L_{hlf} , and L_{ccf} .
- (ii) recognize character using trained network.
- (iii) post-processing steps to verify recognized character.

We have used feed-forward-based neural network in this study. A feed-forward network is organized in layers, where every layer has elements that get input from elements of preceding layers and send output to the succeeding layer. For N characters set, input neurons are p and the training of system is done to output neurons as required for characters. A set of n output symbols $\{a_1, a_2, \dots, a_n\}$ represent these output neurons. Forward and backward parameters' computation of back-propagation algorithm has been explained here. In forward computation:

$$v_j^{(l)}(n) = \sum_{i=0}^{m_0} w_{ji}^{(l)}(n) y_i^{(l-1)}(n);$$

$$y_j^{(l)} = \phi_j(v_j(n))$$

In backward computation:

$$\delta_j^{(l)}(n) = e_j^{(L)}(n) \phi'_j(v_j^L(n)), \text{ for neuron } j \text{ in output layer } L;$$

$$\delta_j^{(l)}(n) = \phi'_j(v_j^l(n)) \sum_k \delta_k^{(l+1)}(n) w_{kj}^{(l+1)}(n), \text{ for neuron } j \text{ in hidden layer } l;$$

Adjustment of the synaptic weights of network in layer l is:

$$w_{ji}^{(l)}(n+1) = w_{ji}^{(l)}(n) + \alpha[w_{ji}^{(l)}(n-1)] + \eta\delta_j^{(l)}(n)y_i^{(l-1)}(n)$$

In above equations, i , j , and k denote different neurons of network; n : n th training pattern in iteration n ; $e_j(n)$ is the error signal at output of neuron j for iteration n ; $y_j^{(n)}$ denotes the signal appearing at output of neuron j at iteration n ; $w_{ji}^{(n)}$ refers to synaptic weights connecting neuron i output to the input of neuron j at iteration n ; $v_j(n)$ represents the weighted sum of all synaptic weights of neuron j at iteration n ; $\phi_j(\cdot)$ is activation function explaining input–output functional association of nonlinearity linked with neuron j ; η denotes the learning rate parameter; m_l refers to the size of input layer and the size of number of nodes in layer l , and m_0 denotes size of input layer; L is the depth of network or last layer, and α is a positive number as momentum constant. The details of back-propagation algorithms are available in [19, 27].

The network has been trained for forty classes. Let C is group of all forty classes, and a character class is written as C_i , $1 \leq i \leq 40$. A character class C_i is trained with desired output as +1. The set of forty trained nets are referred as $\{N_1, N_2, \dots, N_{40}\}$. A character C_i from test database is recognized if $\max(N_i)$ is achieved, where $1 \leq i \leq 40$ and \max indicate maximum value after simulation among nets. Post-processing is applied after recognition process in order to refine the recognition results. In the present study, the post-processing includes verification of recognized character based on low-level and high-level features. An individual character's all possible outcomes are studied in terms of graph, and the character's best suitable nature is depicted. This includes processing of the output from shape recognition. For handwriting input, a single string of characters is yielded by some shape recognizers, while others yield a number of alternatives for each character, often with a measure of confidence for each alternative. In present study, post-processing uses verification for the presence of L_{llf} and L_{hlf} in recognized character of test database after recognition step. The presence of L_{llf} and L_{hlf} for forty classes have been observed manually and from experiments. The manual system includes verification from expert writers in Gurmukhi script and experiments include feature extraction algorithm results to match against manually verified features.

4 Results

The recognition system has been developed in MATLAB and C++. In order to check the stability of system, we have used our system with benchmarked database Unipen [26]. We have noted recognition rates for data '1a' (digits) as 90.76% using L_{llf} and L_{cef} only. The results indicate that present system is capable to recognize complex benchmarked data as Unipen. The network has been trained for all forty classes presented in Fig. 1. The database includes 10,337 handwritten characters. The training database for each class includes 66% of data of their respective classes and rest 33%

Table 1 Class id's and their respective recognition (rec.) rates

Class	Rec. rate (%)	Cass	Rec. rate (%)	Class	Rec. rate (%)	Class	Rec. rate (%)
1	98.43	11	95.02	21	96.62	31	96.43
2	97.73	12	96.17	22	96.14	32	98.04
3	93.05	13	95.11	23	98.95	33	97.19
4	93.46	14	95.91	24	97.42	34	96.01
5	98.98	15	99.22	25	96.26	35	95.25
6	96.46	16	95.55	26	95.97	36	94.05
7	97.52	17	95.76	27	97.19	37	95.80
8	98.43	18	96.68	28	96.01	38	98.58
9	99.14	19	93.87	29	97.79	39	97.19
10	96.29	20	96.42	30	96.20	40	95.63

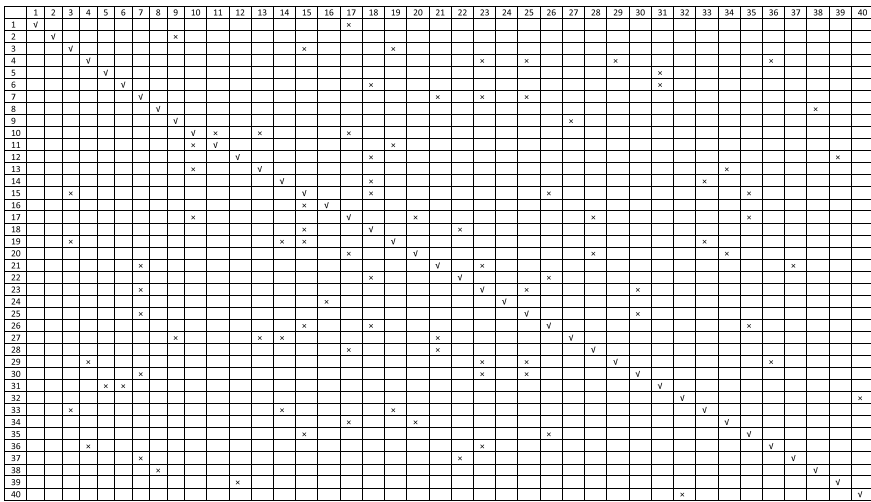


Fig. 7 Confusion matrix

of data refers to test database. The overall recognition accuracy has been achieved as 96.69% for test database includes 3515 characters. Table 1 presents recognition rate for individual classes. The recognition rate for each individual class is above 93%, and this recognition level is acceptable with respect to previous work in Indic scripts as discussed in Sect. 1. Figure 7 presents confusion matrix for forty classes from test database. The symbols '√' and '×' refer to right and wrong match for test classes. This also helps in the formation of groups where similarity of a character can be understood against other classes. Figure 7 presents eight groups where results show equal or more than three wrong matches and these groups are:

{4: 23, 25, 29, 36}, {10: 11, 13, 17}, {17: 10, 20, 28, 35}, {19: 3, 14, 15, 33}, {20: 17, 28, 34}, {21: 7, 23, 37}, {26: 15, 18, 35} and {30: 7, 23, 25}.

These groups indicate to improve post-processing stage where measures could be taken for classes that show multiple wrong matches. The characters with class id's 35–40 have higher error rate as these classes include 'bindi or dot' feature, and our data collection indicates that the stroke for bindi faces the challenge of collecting points as cursive writing does not attend very small strokes patiently.

5 Conclusion

Online handwriting recognition in Indic scripts offers many challenges, and the literature suggests for selection of suitable feature set improve recognition rate. We have found features as low-level, high-level, and Gabor features set. A feed-forward neural network has been used to recognize the Gurmukhi characters and words. The post-processing includes the formation of character based on recognized strokes and also uses rearrangement of strokes scheme which include rearranging the recognized strokes in original order and find suitable combination. The results indicate that word's recognition is more challenging and results motivate to extend this work by using large data sets for words. Also, post-processing stages should include more linguistics parts to fulfill the scope of a better recognition rate.

References

1. Ghosh D, Dube T, Shivaprasad PA (2010) Script recognition: a review. *IEEE Trans Pattern Anal Mach Intell* 32(12):2142–2161
2. Connell SD, Sinha RMK, Jain AK (2000) Recognition of unconstrained online Devanagari characters. In: *Proceedings of international conference on pattern recognition*, vol 2, pp 368–371
3. Joshi N, Sita G, Ramakrishnan AG, Deepu V, Madhvanath S (2005) Machine recognition of online handwritten Devanagari characters. In: *Proceedings of international conference of document analysis and recognition*, pp 1156–1160
4. Swethalakshmi H, Jayaraman A, Chakarvarthy VS, Sekhar CC (2006) Online handwritten character recognition of Devanagari and Telugu characters using support vector machines. In: *Proceedings of IWFHR*
5. Bharat A, Madhvanath S (2007) Hidden Markov models for online handwritten Tamil word recognition. In: *Proceedings of international conference on document analysis and recognition*, vol 1, pp 506–510
6. Prasanth L, Babu V, Sharma R, Rao GV, Mandalapu D (2007) Elastic matching of online handwritten Tamil and Telugu scripts using local features. In: *Proceedings of the ninth international conference on document analysis and recognition*, vol 2, pp 1028–1032
7. Bhattacharya U, Nigam A, Rawat YS, Purui SK (2008) An analytic scheme for online handwritten Bangla cursive word recognition. In: *Proceedings of ICFHR*, pp 320–325
8. Sharma A, Kumar R, Sharma RK (2008) Recognizing online handwritten Gurmukhi characters using elastic matching. In: *IEEE proceedings of international congress on image and signal processing*, vol 2, pp 391–396

9. Sharma A, Kumar R, Sharma RK (2009) Rearrangement of strokes in recognition of online handwritten Gurmukhi words. In: Proceedings of international conference on document analysis and recognition, pp 1241–1245
10. Bharath A, Madhvanath S (2012) HMM-based lexicon-driven and lexicon-free word recognition for online handwritten Indic scripts. *IEEE Trans Pattern Anal Mach Intell* 34(4):670–682
11. Sundaram S, Ramakrishnan AG (2012) Attention-feedback based robust segmentation of online handwritten isolated Tamil words. *Trans Asian Lang Inf Process*
12. Kumar R, Sharma RK, Sharma A (2014) Recognition of multi-stroke based online handwritten Gurmukhi Aksharas. *Proc Natl Acad Sci India Sect A: Phys Sci*
13. Singh S, Sharma A, Chhabra I (2016) Online handwritten Gurmukhi strokes dataset based on minimal set of words. *ACM Trans Asian Low-Resour Lang Inf Process* 16(1):1–20
14. Singh S, Sharma A (2019) Online handwritten Gurmukhi words recognition: an inclusive study. *ACM Trans Asian Low-Resour Lang Inf Process* 18(3):21:1–21:55
15. Jaeger S, Manke S, Reichert J, Waibel A (2001) Online handwriting recognition: the NPen++ recognizer. *Int J Doc Anal Recognit* 3(3):169–180
16. Jain AK, Duin RPW, Mao J (2000) Statistical pattern recognition: a review. *IEEE Trans Pattern Anal Mach Intell* 22(1):4–37
17. Bhowmik TK, Ghanty P, Roy A, Parui SK, SVM-based hierarchical architectures for handwritten Bangla character recognition. *Int J Doc Anal Recognit* 12:97–108
18. Govindaraju V, Setlur RS (2010) Guide to OCR for Indic scripts document recognition and retrieval. Springer, London
19. Haykin S (1999) Neural networks: a comprehensive foundation. Prentice Hall International Editions, Upper Saddle River
20. Beigi H (1996) Pre-processing and dynamics of online handwriting data, feature extraction and recognition. In: Proceedings of fifth IWFHR, pp 255–258
21. Govindaraju V, Srihari SN (1997) Paradigms in handwriting recognition. In: Proceedings of IEEE international conference on systems, man, and cybernetics, pp 1498–1503
22. Guerfali W, Plamondon R (1993) Normalizing and restoring online handwriting. *Pattern Recognit* 26:419
23. Sharma A, Sharma RK, Kumar R (2009) Online preprocessing of handwritten Gurmukhi strokes. *Int J Mach Graph Vis* 1:105–120
24. Lu CC, Dunham JG (1991) Highly efficient coding schemes for contour lines based on chain code representations. *IEEE Trans Commun* 39(10):1511–1514
25. Nouboud F, Plamondon R (1991) A structural approach to online character recognition: system design and applications. *Int J Pattern Recognit Artif Intell* 5(1):311–335
26. Guyon I, Schomaker L, Plamondon R, Liberman M, Janet S (1994) Unipen project of on-line data exchange and recognizer benchmarks. In: Proceedings of the 14th international conference on pattern recognition, pp 29–33
27. Kumpati NS, Parthasarthy K (1990) Identification and control of dynamical systems using neural networks. *IEEE Trans Neural Netw* 1(1):4–27

Optimizing Stream Data Classification Using Improved Hoeffding Bound



Arvind Pillania, Pardeep Singh, and Vrinda Gupta

Abstract Classification of online stream data is must for network analysis and providing Quality of Service (QoS). Stream data has properties which requires the algorithm to be incremental and should handle concept drift. Traffic classification is the prominent solution to handle bulk data streams to provide services like packet filtering, routing policies, traffic shaping, limiting traffic, etc. Many stream-based classification algorithms exists in literature to meet the requirements like scanning the data only once, any time analysis and fast response, and limited memory utilization. Further, more accurate, fast, and limited memory supporting algorithms and concepts are required to handle everyday increasing data over Internet. This research work proposes an improvement in accuracy of the classification performed using lesser number of training instances to decide a split during induction of the decision tree (Hoeffding tree). Jensens's inequality concept is used, and the Hoeffding bound reduces to minimize the bound for the bad events (i.e., it limits the margin of error of the algorithm). Number of examples reduced results in fast execution and decrease the memory used.

Keywords VFDT · Hoeffding bound · Jensen's inequality

1 Introduction

Network traffic classification is required for network management and maintaining Quality of Service. Analysis of huge data volume of dynamic data and continuous high arrival rate (i.e., stream data) is a complex task. Streaming data [10] is dynamic

A. Pillania (✉) · P. Singh · V. Gupta
National Institute of Technology Hamirpur, Hamirpur, HP 177005, India
e-mail: arvind.pillania@gmail.com

P. Singh
e-mail: pardeep@nith.ac.in

V. Gupta
e-mail: cs15mi512@nith.ac.in

© Springer Nature Singapore Pte Ltd. 2021
G. S. Hura et al. (eds.), *Advances in Communication and Computational Technology*, Lecture Notes in Electrical Engineering 668,
https://doi.org/10.1007/978-981-15-5341-7_19

and real-time online data, and main issues dealing with this data are to cope with the arrival rate of data and analyze dynamically. The prominent requirements are high computational and processing ability of the processor and the availability of the fast and efficient storage. Stream machine learning algorithms are available to handle different issues and requirements of stream data classification. The algorithms processing streams are unable to control the incoming sequence of the data stream, so an incremental approach [4] is used to handle the streams. Data over network is increasing rapidly which leads to approximation of the stream data, and the best possible accuracy is needed to be achieved with minimized amount of data. Several algorithms exist which are used for classification of streaming data. Classification is supervised machine learning, i.e., more powerful and mostly used technique for real world streaming applications. Techniques summarized in [1] have proposed methods like decision trees, Bayesian classification, k-nearest neighbor, support vector machines, and streaming random forest. Literature have many decision tree-based classifiers proposed for incremental approach which are: SLIQ [9] proposes a novel scalable algorithm for datasets on disk and gives accurate results in form of compact trees, tree generated from this algorithm is not dependent on the count of classes, attributes, and the number of samples. Rain forest [6] is designed for large datasets and defines a classifier that does not have any impact of data features on its scalability. BOAT [5] performs classification with only two scans of the datasets. A scalable and incremental approach works in dynamic environments and keeps on updating the generated decision tree. The above-mentioned are specifically for non-streaming approaches. Approach proposed in [8] finds out minimum count of the training samples required for selecting an attribute to be the split attribute. Incremental approaches based on ID3 were also the known algorithms out of the scope of the steaming classification. These above methods are incremental but does not include concept drift, which is a dominating aspect of the streaming data. Concept drift is changed in the accumulated features of the data over time, dominates the stream classification task, and is considered while classification.

Under the umbrella of stream data classification, the very first algorithm based on decision tree is very fast decision tree (VFDT) [2]. VFDT uses the Hoeffding bound [7], which says that fixing a maximum value for number of training samples provides the same decision tree for classification as the complete dataset provides.

This paper is divided in four sections, in first section, introduction to many decision tree-based algorithms is given. Section 2 provides a detailed introduction to the VFDT algorithm and Hoeffding bound. Section 3 proposed a method to decrease the number of training instances required to form a decision with some confidence and theoretically analyzed the values. Section 4 concludes the proposal and its expected result.

2 Background Information

VFDT handles stream data and generates a decision tree called Hoeffding tree, and its induction process is discussed next. Further, the Hoeffding bound and its improvement are helpful in explaining the reduction in the number of reduced input samples.

2.1 Hoeffding Tree Induction

VFDT generates Hoeffding tree (HT) as a decision-making tree for this model, and the process is called as Hoeffding tree induction. Algorithm gives a generic description of Hoeffding tree induction for learning. HT is initialized with a single node, and E is the training instance. With arrival of each training instance, the tree induction algorithm starts and sorts the instance as a leaf node l . The leaf is learning, so its sufficient statistics are updated in line 2. Number of instances (n_l) are incremented based on the instance E weight in line 3. A certain number of instances (n_{\min}) are selected for tree growing, and for growing data at leaf, nodes must belong to different class. Decision whether to grow the tree further or not is taken in line 4. Growing of tree infers the attempt to split the node, and for splitting algorithm, it iteratively performs for each attribute and evaluates information-theoretic criteria ($G_l(X_i)$) in line 5. The information-theoretic criteria is also calculated for no-split condition (X_ϕ) known to be pre-pruning. Two attributes are selected known as best (X_a) and second best (X_b) depending on the highest and second highest G_i values, respectively, given in lines 6 and 7, and then, the selected attribute is examined for the split based on the Hoeffding bound value (ϵ), for which inequality is given in line 9. In case of no-split (X_ϕ), algorithm uses τ for tie breaking to handle the case where the difference of information gain between X_a and X_b is very small ($\Delta \overline{G}_l < \epsilon < \tau$). In case of split node, leaf l is replaced with a split node, and it creates the corresponding leaves based on the best attribute (lines 10–13). The Hoeffding bound determines that the true mean of the variable is at least $\bar{r} - \epsilon$ with probability $1 - \delta$. In addition, ϵ is calculated with this following formula:

$$\epsilon = \sqrt{\frac{R^2 \ln 1/\delta}{2n}} \quad (1)$$

where r = real-valued random variable, with range R , n = number of independent observations have been made, and \bar{r} = mean value computed from n independent observations (Fig. 1).

Hoeffding bound is useful as it is independent of the probability distribution of the variable, but with different number of observations, δ attains certain values. As VFDT is for the streaming data, there is no termination condition, and tree may be growing infinitely, which in turn opposes the streaming algorithm requirement to deal with limited memory. To handle the infinite tree growing, a node limiting

Algorithm HoeffdingTreeInduction (E, HT)

Input: E is a training instance

Input: HT is the current state of the decision tree

- 1: Use HT to sort E into a leaf l
 - 2: Update sufficient statistic in l
 - 3: Increment the number of instances seen at l (which is n_l)
 - 4: **if** $n_l \bmod n_{min} = 0$ **and** not all instances seen at l belong to the same class **then**
 - 5: For each attribute, compute $G_l(X_i)$
 - 6: Find X_a , which is the attribute with highest G_l
 - 7: Find X_b , which is the attribute with second highest G_l
 - 8: Compute Hoeffding bound $\epsilon = \sqrt{\frac{R^2 \ln(1/\delta)}{2n}}$
 - 9: **if** $X_a \neq X_b$ **and** $(\bar{G}_l(X_a) - \bar{G}_l(X_b)) > \epsilon$ **or** $\epsilon < \tau$ **then**
 - 10: Replace l with a split-node on X_a
 - 11: **for all** branches of the split **do**
 - 12: Add a new leaf with derived sufficient statistic from the split node
 - 13: **end for**
 - 14: **end if**
 - 15: **end if**
-

Fig. 1 Hoeffding tree induction algorithm

technique is introduced which calculates promise for each leaf node l , defined as an expected upper bound of error reduction by keeping the leaf node alive. Nodes with low promise values are deactivated in case tree touches the memory limits. For each node, promise is evaluated although it is inactive node, to make them active if current active node is having lower promise value. One more technique is used for satisfying limited memory constraint attribute removal, which removes the attribute which does not look that much beneficial for splitting, and the corresponding sufficient statistics stored are deleted from memory.

2.2 Hoeffding Inequality

Hoeffding inequality evaluates a probabilistic upper bound on sum values of the independent random variable. Probability of deviation of evaluated mean of the random variable from the observed mean of the sample is bounded by an exponential value

depending on observed mean, confidence interval, and the sample size. Variation exists for the upper bound, one is when random variable values are only between 0 and 1, and two, when values of random variable is bounded in some different range other than [0, 1].

Theorem (Hoeffding Inequality): For independent random variables Z_1, Z_2, \dots, Z_n , for every Z_i $P(0 \leq Z_i \leq 1) = 1, i = 1, \dots, n$, it is defined as

$$P(\bar{Z} \geq \mu + \epsilon) \leq \left(\left(\frac{\mu}{\mu + \epsilon} \right)^{\mu + \epsilon} \left(\frac{1 - \mu}{1 - \mu - \epsilon} \right)^{1 - \mu - \epsilon} \right)^n \equiv B_H \tag{2}$$

where $\bar{Z} = \frac{1}{n} \sum_{i=1}^n Z_i, \mu = \frac{1}{n} \sum_{i=1}^n \mu_i$ and $\mu_i = E(Z_i)$, and $\alpha = 1 - \mu$, for $0 < \epsilon < \alpha$ this inequality is defined. Using concept of Markov's inequality and convexity of a function, the inequality is made more precise for $Z_i \in [0, 1]$ as shown,

$$P(\bar{Z} \geq \mu + \epsilon) \leq \exp(-2n\epsilon^2) \tag{3}$$

for $Z_i \in [a_i, b_i]$, the inequality becomes

$$P(\bar{Z} \geq \mu + \epsilon) \leq \exp \left(\frac{-2n^2\epsilon^2}{\sum_{i=1}^n (b_i - a_i)^2} \right) \tag{4}$$

and can be generalized as

$$P(\bar{Z} \geq \mu + \epsilon) \leq \exp \left(\frac{-2n\epsilon^2}{R^2} \right) \equiv B_H \tag{5}$$

where R is range of the random variable.

2.3 Improvisation of Hoeffding Bound

The bound B_H is improved by dividing the averages ($\mu_i s$) in two parts and applied Jensen's inequality [5] convex concept to support the smaller improved bound for the inequality, for complete proof refer [3]. Theorem: For independent random variables, Z_1, \dots, Z_n and assumed means such that $\mu_1 \leq \dots \leq \mu_n$. Let K be a number such that $K \in [1, n - 1]$ and divides $\mu_i s$ in two parts such that $\mu_{1,K} = \sum_{j=1}^K \frac{\mu_j}{K}$ and $\mu_{2,n-K} = \sum_{j=K+1}^n \frac{\mu_j}{n-K}$ are the means of two lists having smallest K means and largest $n - K$ means, respectively, for these the improved inequality using same notation which is defined as

$$P(\bar{Z} \geq \mu + \epsilon) \leq \exp(-n(\mu + \epsilon)s) * (1 - \mu_{1,K} + \mu_{1,K}e^s)^K * (1 - \mu_{2,n-K} + \mu_{2,n-K}e^s)^{n-K} \equiv B_N \tag{6}$$

We have used $K = \lfloor \frac{n}{2} \rfloor$ which gives results closer to the best.

3 Proposed Work and Discussion

A decision tree induction process can be improved in two ways, one is getting an improved and more accurate decision tree as output and other way followed by author is reducing the induction time of the decision tree. Proposal is focusing on decreasing the number of input samples required to make a decision on a particular node of a tree, and as a result, the output decision tree will be same as it was earlier but in less time and with less input data. In other words, proposal will provide same accuracy of the tree with less number of samples. Refinement in Hoeffding bound [3] is used by the author to reduce the number of samples required to provide the same confidence (accuracy) of the classification. This refinement of Hoeffding bound leads to reduction in memory required (an issue for streaming algorithms). In line 8 of the algorithm, we will evaluate the improved Hoeffding bound based on the refinement Eq. 7, and B_N will be the improved bound. The new ϵ value will be less as compared to the old ϵ , and in line 9, the condition will be satisfied with less input samples and leads to an early split at that node.

$$P(\bar{Z} \geq \mu + \epsilon) \leq w_L^{-n(\mu+\epsilon)} (1 - \mu_{1,L} + \mu_{1,L} w_L)^L (1 - \mu_{2,n-L} + \mu_{2,n-L} w_L)^{n-L} \equiv B_N \quad (7)$$

3.1 Evaluation and Analysis of Reduced N Using Bounds

Considering the inequality $P(\bar{Z} - \mu \geq \epsilon) \leq \exp\left(\frac{-2n\epsilon^2}{R^2}\right)$, this bounds the error with a margin δ and $1 - \delta$ as confidence interval. We can say $\delta \leq \exp\left(\frac{-2n\epsilon^2}{R^2}\right)$ (i.e., $\delta = \text{bound} \equiv B_H$ or B_N)

$$n \leq \frac{\ln(1/\delta)}{2\epsilon^2 R^2}, \quad (8)$$

From above equation, taking B_H as old bound with range R , we get new n value for the new range (i.e., N_{new}).

$$N_{\text{new}} \leq \frac{\ln(1/B_H)}{2\epsilon^2 R^2} \quad (9)$$

Similarly, N_{old} is the number of instances for the B_N with the new range IR .

$$N_{\text{old}} \leq \frac{\ln(1/B_N)}{2\epsilon^2 IR^2} \quad (10)$$

Both N_{new} and N_{old} are evaluated and compared with each other and also with the original N value.

The proposed work is to improve the Hoeffding bound shown in algorithm to implement it for the data stream classification algorithm VFDT. The modification is (dividing n number of examples of selected attribute randomly in L sets and evaluating the mean value for those L sets) which limits the error margin of the existing up to some extent. Analogical explanation of the bound refinement mathematically and in data stream environment. Initially, the independent and identical distributed random (IID) variables X_1, X_2, \dots, X_n are the samples entries of attributes in the data stream taken as input. In step 1, the sum S for each random variable is evaluated, and then, its mean value μ_i , expected value $E(S)$, and standard deviation σ^2 are evaluated, and sufficient statistics in stream environment are evaluated and updated for each attribute.

3.2 *N-Value and Comparison*

In this section, we are comparing the theoretically calculated new and old N -values. Comparing of the N values, N is the original number of instances for which both the bounds are calculated, N_{old} is the number of instances for the new bound but within the old range of the values, and N_{new} is the number of instances for the old bound with the new range. The interrelation of these three N values is $N_{new} < N < N_{old}$ always. The N -values are for a scenario, where mean (μ) of sample is kept 0.5 for the uniform distribution of the mean values (μ 's) of the random variable Z_i , such that $0 \leq Z_i \leq 1$ and the ϵ varies in between 0 and 1μ . Both tables give a comparative view of the all three N -values with different ϵ and μ combinations. Table 1 shows the new N -value N_{new} calculated using old bound B_H , and Table 2 shows the new N -value N_{old} calculated using old bound B_N .

4 Conclusion

Stream data classification requirement of fast execution with maintained accuracy is checked by the improved Hoeffding bound. Number of examples required by the stream classification algorithm is reduced by the newly calculated bound, and the new range of the random variable deals with it. Impact of improved Hoeffding bound is shown on the number of instances of random variable required when we divided the μ 's in two parts, only to get the reduced bound for the Hoeffding inequality by using convex function of Jensen's inequality. Reducing N_{min} can be analyzed in two ways, keeping the accuracy fixed, execution time will be reduced or keeping execution time fixed, accuracy will be increased, which is flexible to use for the learning algorithm. Here, we have only divided the μ 's in two part, but it can be divided in more groups to further limit the bound and N_{min} value which will be further reduced to make the learning algorithm faster. With further division, a trade-off needs to be maintained between the strictness of the bound and the complexity to handle multiple groups.

Table 1 Calculated values of N_{new} based on B_H and range R

N	μ	$K = \lfloor N/2 \rfloor$	ϵ	B_H	N_{new}
200	0.5	100	0.05	0.3672	151
200	0.5	100	0.1	0.0178	151
200	0.5	100	0.2	7.13×10^{-8}	153
200	0.5	100	0.4	1.07×10^{-32}	159
200	0.5	100	0.45	1.09×10^{-43}	162
400	0.5	200	0.05	0.1348	301
400	0.5	200	0.1	3.18×10^{-4}	302
400	0.5	200	0.2	5.08×10^{15}	305
600	0.5	300	0.05	0.0495	451
600	0.5	300	0.1	5.66×10^{-6}	452
600	0.5	300	0.2	3.62×10^{-22}	457
800	0.5	400	0.05	0.0181	601
800	0.5	400	0.1	1.0×10^{-7}	603
800	0.5	400	0.2	2.58×10^{-29}	609
1000	0.5	500	0.05	0.0069	751
1000	0.5	500	0.1	1.79×10^{-9}	753

Table 2 Calculated values of N_{old} based on B_N and range IR

N	μ	$K = \lfloor N/2 \rfloor$	ϵ	B_N	N_{old}
200	0.5	100	0.05	0.2633	267
200	0.5	100	0.1	0.0047	266
200	0.5	100	0.2	4.04×10^{-10}	263
200	0.5	100	0.4	4.75×10^{-41}	253
200	0.5	100	0.45	4.89×10^{-54}	249
400	0.5	200	0.05	0.0693	533
400	0.5	200	0.1	2.26×10^{-5}	532
400	0.5	200	0.2	1.63×10^{-19}	526
600	0.5	300	0.05	0.0183	800
600	0.5	300	0.1	1.07×10^{-7}	798
600	0.5	300	0.2	6.58×10^{-29}	789
800	0.5	400	0.05	0.0048	1066
800	0.5	400	0.1	5.09×10^{-10}	1063
800	0.5	400	0.2	2.66×10^{-38}	1052
1000	0.5	500	0.05	0.0013	1333
1000	0.5	500	0.1	2.41×10^{-12}	1329

References

1. Caruana R, Niculescu-Mizil A (2006) An empirical comparison of supervised learning algorithms. In: Proceedings of the 23rd international conference on machine learning, ICML '06. ACM, New York, NY, USA, pp 161–168
2. Domingos P, Hulten G (2000) Mining high-speed data streams. In: Proceedings of the sixth ACM SIGKDD international conference on knowledge discovery and data mining, KDD '00. ACM, New York, NY, USA, pp 71–80
3. From SG, Swift Andrew W (2013) A refinement of Hoeffding's inequality. *J Stat Comput Simul* 83(5):977–983
4. Gama João (2012) A survey on learning from data streams: current and future trends. *Prog Artif Intell* 1(1):45–55
5. Gehrke J, Ganti V, Ramakrishnan R, Loh W-Y (1999) Boat—optimistic decision tree construction. *SIGMOD Rec* 28(2):169–180
6. Gehrke J, Ramakrishnan R, Ganti V (2000) Rainforest—a framework for fast decision tree construction of large datasets. *Data Min Knowl Discov* 4(2):127–162
7. Hoeffding Wassily (1963) Probability inequalities for sums of bounded random variables. *J Am Stat Assoc* 58(301):13–30
8. Kalles D, Morris Tim (1996) Efficient incremental induction of decision trees. *Mach Learn* 24(3):231–242
9. Mehta M, Agrawal R, Rissanen J (1996) Sliq: a fast scalable classifier for data mining. In: Apers P, Bouzeghoub M, Gardarin G (eds) *Advances in database technology—EDBT '96*. Springer, Berlin, Heidelberg, pp 18–32
10. Toshniwal D (2013) Clustering techniques for streaming data—a survey. In: 2013 3rd IEEE international advance computing conference (IACC), pp 951–956

Outline of Lattice Structures: Morphology, Manufacturing, and Material Aspect



Sakshi Kokil Shah, Mohanish Shah, Anirban Sur, and Sanjay Darvekar

Abstract Additive manufacturing technologies possess the capability to produce products according to customer demands, which make these technologies as the best option for lightweight technology. Another advantage is the design complex intricate shapes can be easily manufactured by rapid prototyping technologies to include lattice structures in automobile applications like the body panels of the car, the engine's intercooler, or gas tank with the aim of weight and strength optimizations. There are various techniques available for manufacturing lattices. This paper presents an outline of lattice structure with respect to different morphologies, various manufacturing methods for it, and different materials available to produce lattice structures. It discusses how the variation of characteristics can improve the lattices' performance significantly, from a mechanical and application point of view. The characterization of lattice structures and the recent developments in finite element analysis models are studied. Many authors compared conventional techniques with additive manufacturing; it was found that manufacturing defects induced in Micro-Lattice Structure manufactured via additive manufacturing were less. With the help of additive manufacturing, complex morphologies can be easily developed by using CAD software.

S. K. Shah (✉)

Mechanical Engineering Department, TSSM'S BSCOER, Symbiosis Institute of Technology, Pune, Maharashtra, India
e-mail: kokilsakshi@gmail.com

M. Shah

Mechanical Engineering Department, MITAOE, Symbiosis Institute of Technology, Pune, Maharashtra, India
e-mail: monish2244@gmail.com

A. Sur

Mechanical Engineering Department, Symbiosis Institute of Technology, Pune, Maharashtra, India
e-mail: anirban.sur@sitpune.edu.in

S. Darvekar

Mechanical Engineering Department, Gayatri Pidya Parishad College of Engineering, Visakhapatnam, AP, India
e-mail: sanjay.kdarvekar@gmail.com

© Springer Nature Singapore Pte Ltd. 2021

G. S. Hura et al. (eds.), *Advances in Communication and Computational Technology*, Lecture Notes in Electrical Engineering 668,
https://doi.org/10.1007/978-981-15-5341-7_20

245

The simple, rapid, and scalable fabrication of MLS are achieved using additive manufacturing. This paper gives an overall idea about how research progressed by different researchers regarding lattices in terms of materials FE analysis and suggests future research directions required to improve their use in lightweight applications.

Keywords Lightweight technology · Additive manufacturing · Lattice structure · Morphology

1 Introduction

Lattice structures are the most popular materials because of their versatile applicability. The performance of these materials is exceptionally high when it comes to tensile, compressive, impact, and cyclic loading. They are claimed as one of the lightest material known. Cellular materials carry more functional characteristics than solid materials. The mechanical performance of cellular structure relies on factors like cell topology; geometric parameters, together with strut diameter and cell size; material and producing method characteristics; further structural boundary and loading conditions. Morphology alteration gives major change in mechanical properties of material. Hence it can be said that topology plays important role for different applications. The arrangement of strut and node forms topology. By changing the topology, relative density of lattice can be changed. So in lattice materials change in relative density can be achieved by altering the topology without changing the material [1]. Because of its excellent properties, it is used for battery electrodes, catalyst supports, and acoustic, vibration or shock energy damping. The stiffness, tensile, compressive strength, and fatigue response of various materials for MLS are verified by researchers. For an application that demands low weight, high-strength, and stiffness MLS is a perfect choice.

2 Theory

Small-scale cross-section might be a well-architected material that blends supportive mechanical properties of metals in with great geometrical directions giving bigger solidness, solidarity to-weight size connection, and shrewd vitality assimilation ability than various types of cell materials. Cell solids containing many thin cross-section individuals known as swagger and are sorted by a common structure. Cell material has more porosity than strong material. The obstruction of a cross-section material to applied power additionally relies upon its course of action of grids just as hubs and can be evaluated by the measure of strain vitality that is put away after the use of power a solitary part in a huge cross-section [2]. Metallic smaller scale grid is a metal created by a group of scientists from the University of California at Irvine, HRL Laboratories and the California Institute of Technology. Its

amazing attributes can discover applications in battery cathodes, impetus supports, and acoustic, vibration or stun vitality damping.

Small-scale grids are very lightweight and have high firmness, however, it likewise has high vitality assimilation and recuperation abilities. In light of the swaggers development isn't moderately dependant, the small-scale cross-section can support a lot of vitality without disappointment. This swagger adaptability likewise shows that the grid can be compacted to half of its size and it recaptures its unique shape. These properties settle on the small-scale cross-section a perfect decision for aviation applications like stun absorbance, where materials need to withstand huge effects and recoup to continue carrying out their responsibility. Precisely, these small-scale cross-sections are typically a sort of like elastomers and for all intents and purposes completely recuperate their structure after huge pressure. Mechanical properties of metallic cross-sections shift with:

- Constitution of the material used;
- Cell morphology;
- Making method.

These micro-lattice constructions have a variation of potential usefulness themselves—a soft polymer micro-lattice might be useful for building cozy but extremely defensive bike helmets, for example. It possesses extraordinary potential for use as thermal insulation; acoustic, vibration or shock dampening; energy retention and restoration; and electronic parts.

Normal applications of metal lattices are as follows:

- Lightweight basic concepts that can assimilate acoustic, stun, and vibration energy.
- Sandwich development of flying machine fuselages and wing structures (effective function/weight-efficiency proportion). In common, center topologies are showing extending and compression qualities without bending.
- Assurance framework for flight recorders: a micro-lattice layer secures the memory gadget against crash.
- Affect and impact safe structures.
- Biocompatible permeable structures.

Materials that recuperate rapidly after application of huge strains are utilized for storing energy, which counts in the enlargement of raw material after reversible inclusion of molecules in materials or adsorption, and for customized material demands to occupy less space deployable and then widen to original dimensions. As micro-lattice construction assimilate energy on contraction and regain, they are moreover used for auditive, impact, and vibration reduction.

3 Detailed Review of Literature

After taking a brief review of recent research regarding MLS, it was observed that the available literature can be classified into the following categories.

3.1 Literature Review Based on Structural Analysis

Patrick Köhnen et al. Considered mechanical properties and twisting conduct of hardened steel AISI 316L produced by SLM with f2ccz, tempered f2ccz, and empty round MLS. Ductile tests are completed to decide yield quality, elasticity, and lengthening of the mass and grid structure examples structure pressure strain chart. Stretch overwhelmed twisting of cross-section encourages better most extreme ductile and pressure quality just as higher flexible modulus and explicit vitality assimilation for f2ccz grid structures contrasted with empty circular cross-section structures [3] (Figs. 1 and 2).

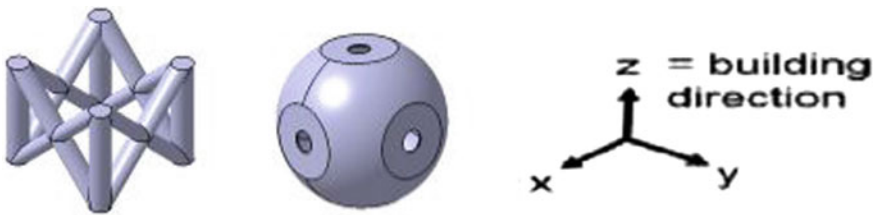


Fig. 1 Strut arrangement of f2ccz, and hollow spherical MLS [3]

Fig. 2 Comparison of stress–strain curve for f2ccz, f2ccz annealed, and hollow spherical, SLM produced bulk [3]

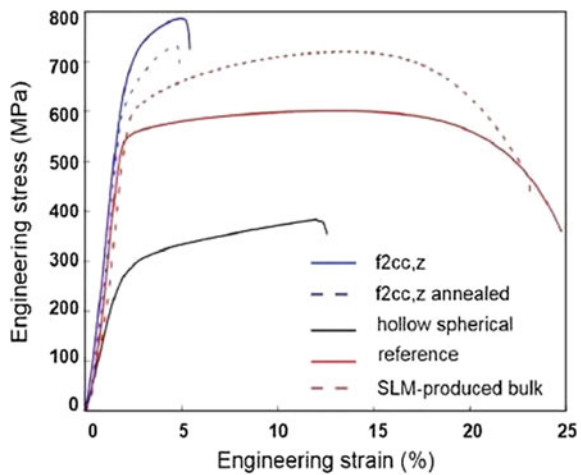
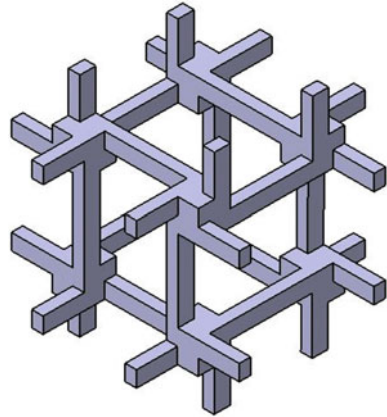


Fig. 3 Morphological structures [4]



P. Li et al. has explored the twisting procedure and stress/strain development of small-scale cross-section structures created by SLM systems of 316L steel utilizing FE model and approve it tentatively. FE model was produced utilizing ABAQUS with BCC morphology utilizing The FE model was coincided with tetrahedral components. Because of increment in plastic worry at the hub split inception happens. The creator detailed restriction of the 3D FE model maybe because of the admired barrel-shaped morphology of swaggers in the MLS which didn't consider the impact of unpleasant surface in real SLM examples [4] (Fig. 3).

Chang Quan Laia et al. have portrayed the mechanical properties and disfigurement of the stretch-commanded octet bracket configuration fabricated without anyone else waveguide spread procedure MLS under powerful stacking conditions, and discover their ease of use as meager and proficient effect safeguards. The disappointment of a grid layer was initiated by clasping for the stretch-commanded structure, and plastic yielding for the twisting ruled plans [5].

Francesco Rosa et al. checked the possibility of expanding damping limit MLS having BCC topology created by MLS. FEA model was set up with ABAQUS and to imitate the stacking condition, the bar was fixed toward one side, while the heap was applied on the opposite end. This conduct is watched on the grounds that inside contact wonders were dependent on abundance happening at shaft joints and in the longitudinal bars. The incredible favorable position of cross-section structures delivered by added substance fabricating over metallic froths is that grid geometry can be basically modified [6].

Wahyudin P. Syama et al. presents the plan, examination, and test confirmation of swagger-based cross-section structures to improve the mechanical vibration confinement properties of a machine outline. Creators performed structure and investigation of a few cross-sections utilizing limited component examination which was confirmed by test philosophy to account for the grids' normal recurrence and firmness (predominantly because of twisting) [7].

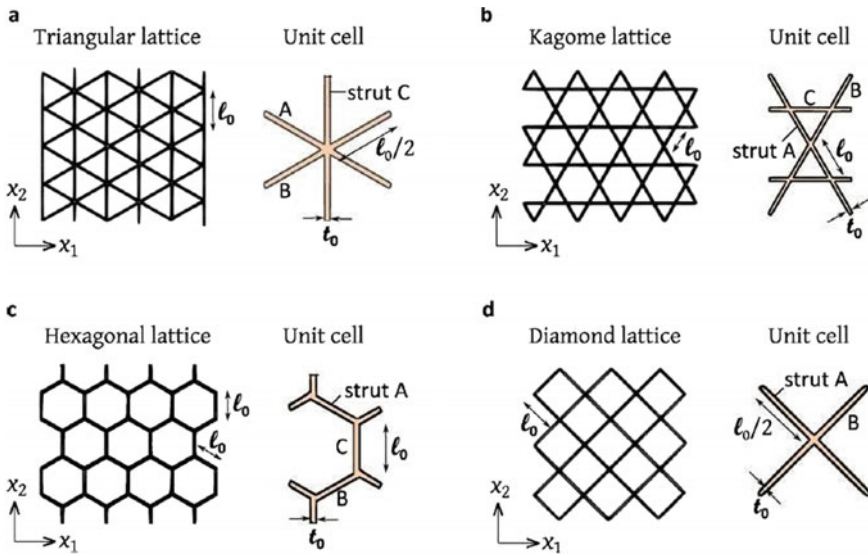


Fig. 4 Triangular, Kagome, hexagonal, and diamond topologies [8]

Xingchen Yan et al. Investigated the effects of pore size and porosity on both the mechanical and natural properties of SLM cross-area structure of Ti6Al4V having octahedral topology. Distinctive unit cells with different porosities (P), pore breadths (D_p), and swagger thicknesses (St) were arranged. Waiting pores found inside the swaggers are hurting to long stretch burden-bearing. It indicated post-drugs, for instance, HIP treatment is required. The effect of pore size doesn't seem, by all accounts, to be an important differentiation for the range that was mulled over [8] (Fig. 4).

H. C. Tankasala et al. centered to decide UTS and flexible modulus, study twisting component MLS made up of thermoplastic polyolefin with triangular, Kagome, hexagonal, and jewel topologies. For the LTS disappointment standard, we find that that the malleability of the Kagome cross-section, diminishes as for increment in level of flaws. For the ATS disappointment foundation, the hexagonal cross-section has the most noteworthy pliability autonomous of the degree of flaw [9].

X. Y. Chen and H. F. Tan determined the successful compressive firmness and quality under the activity of shear power and twisting minute, which has been approved by limited component reproductions and experiments. An octet cross-section with Polypropylene material is made utilizing SLM with differing relative densities from 10 to 30%. At low relative thickness, the swagger joint impact is the commanding element in solidness diagnostic deductions. Creator revealed relative thickness as well as curve and shear impact assumes a key job in grids, particularly with rising relative thickness [10].

Liang Dong et al. fabricated pyramidal grid with 316L tempered steel material (2 evaluations 17-7PH, SH 950 warmth treated) with unit cell measurements of 1 mm

or less and a swagger thickness beneath 100 μm from elite. This MLS created with metal powder bed based added substance producing techniques. At last, it is noticed that the assembling method investigated here can likewise be utilized to manufacture a polymer MLS [11].

The objective was to analyze and compare the fatigue response of AM (Direct metal laser sintering) MLS having BCC topology made up of Nickel-based IN718 and conventionally manufactured bar. From microstructure analysis, it was concluded that the surface finish of the strut node connections plays an important role in the crack initiation [12].

In this study, fatigue strength of multiple cellular structures, such as the re-entrant auxetic, the octet-truss, and the BCC lattice, were evaluated for their relative performance under the application of compression-compression cyclic loading manufactured by electron beam powder bed fusion (EB-PBF) made up of material Ti6Al4V. It was found that the effects of Poisson's ratio appear are insignificant while evaluating fatigue life while the combination of deformation mode or structural symmetry plays an important role. Hence auxetic showed homogeneous stress distribution. Octet-truss designs displayed higher fatigue life compared to the other structures [13].

Author focused on the fact that as the failure initiates at the node hence they investigated the effect of change in node geometry on the stiffness by analytical, experimental, and FEA model of topologies octahedron, octet, tetrakaidecahedron, and pyramidal lattices with node substructures with circle, square, and star. Micro-lattices were fabricated using Two-Photon Lithography (TPL) direct laser writing of PR-48 polymer resin material. Compressive tests were carried out to plot stress-strain curve and determination of elastic modulus [14].

Study aims to investigate the mechanical performance and ability to absorb energy with a different relative density polymeric octet-truss lattice structures under both static and cyclic compressive loading [15].

The present study focuses on quasi-static, dynamic, and impact loading on the performances of hollow tube MLS will be reported both experimentally and numerically. (Focused on vertical and inclined strut). To boost the energy absorption capacity, the amount of material being deformed has to be maximized. By improving thickness gradient and radius gradient energy absorption can be increased [16].

Strain concentration and geometrical irregularities are investigated experimentally and validated by FEA of BCC MLS made up of AlSi10Mg manufactured using Selective Laser Melting. A model based on an ideal geometry didn't give an idea of the real behavior of the printed lattice structure. Therefore, evaluation of the static and fatigue strength from a simplified geometry has to be modified in order to get accurate results [17].

3.2 Literature Based on Thermal Analysis

This paper deals with design of less weighted phase-change thermal regulator arrangement based on lattice cells created wholly with AlSi10Mg by direct laser sintering (aircraft application) with pyramid topology. The thermal regulator consists of lattice incorporates a 50% raise in thermal ability judged against created by a conventional method since raise in cubage [18].

This work focuses on the research of thermal expansion attributes of the anticipated lattice construction with twelve quarter-octahedral topologies. Author developed a mathematical model to calculate coefficient of thermal expansion depends on value of strain in MLS. The lattice construction anticipated here goes through negative or zero expansion in all three directions along the unit cell edge. The strains are directly proportional to the temperature alteration under the imperceptible strain guesses. The lattice construction displaces both mechanically and thermally. Author found essential to model the panels so that no thermo-mechanical failure occurs under thermo-mechanical forces [19].

3.3 Literature Based on Effect Manufacturing Process of MLS

In this examination, the pack cementation technique is used to change unadulterated Ni MLS, produced by methods for self-causing photopolymer waveguide prototyping, into oxidation-safe and γ' -strengthened Ni-based super-amalgams. This assessment shows another announcement based course for the formation of pitiful walled nickel-base super-compound little scale cross-segment structures that can't be taken care of by methods for other normal techniques. Alloying electrodeposited Ni MLS with Cr, Al, and Ti by and large improved their high-temperature quality, and the method can be progressed to achieve pieces and microstructures with the extent of mechanical and physical properties [20].

By utilizing SEM imaging, CT examining, and so forth the impact fabricating deserts prompted in Ni MLS with an empty octahedral topology on compressive quality is considered. Wellsprings of assembling blunder (1) because of unsteadiness in spread may cause non-roundabout poles of swagger, (2) Small misalignment in the UV beams bring about the thickening of the hubs, (3) The UV beams somewhat veer as they go through the shower bringing about an expansion in the measurement of the bars towards the base of the shower. This recommends by controlling the various parameters of assembling procedure of the cross-section and by diminishing the bar non-circularity we can get grids with best mechanical conduct [20].

Another proliferation model is proposed to diminish the computational expense and avoid poor work quality in emulating adaptable properties of Solid-Lattice cream structures (mix of cross-segment and solid structures) by Finite Element Analysis. In this strategy, the cross-area structure is concurred with Timoshenko bar segments

and the solid part is fit with 3D straight tetrahedral segments, the proposed FE model radically lessened the computational cost and improved the work quality appeared differently in relation to the regular FE model [21].

A numerical analysis of surface-based lattice structures with the objective of ease of fabrication using additive manufacturing. Mathematical model was developed to calculate iso-surface equation MLS, which will be utilized for FE model of MLS. In FE analysis, compressive loads are applied to determine elastic modulus in three directions. It was seen that elastic modulus depends on cell geometry [22].

To investigate the effectiveness of LMD of lattice with respect to SLM. Columnar and lattice samples were prepared on 3 mm thick substrate with the LMD system. Author successfully fabricated a columnar built-up process by stacking of spot welds using lattice structures [23].

To assess characteristics of SLM manufactured weld components. Tensile tests were carried out AISI 316L samples, by varying lase parameters like lase power and velocity different samples were prepared. Results showed that maximum UTS obtained for no HT SLM component than HT SLM component [24].

Proposed a geometric model for these beams that provides a compromise between shape flexibility and ease of computation. Mathematical model was prepared for analysis of Biquador beams, Biarc beams, Quintic beam. Its DOF is checked with respect to degree of computation. Author claimed to save computational time and cost of FEA of MLS. Due to the use of quador parameterization using lattice optimization, it provides the ability to reduce the width and mass of some beams indicating efficient use of lattice [25].

This paper demonstrated the printing and optimization of processing parameters of high-strength H13 stainless tool steel SLM. Numerical model was prepared for optimization of parameters like laser power, scanning speed. Numerical analysis found to be in agreement with microscopic analysis. This thermo-mechanical model can be explored in MLS for mechanical characterization [26].

4 Chronological Summary

The first time this MLS was invented in mid-2000 by a research team consisting of UC Irvine, HRL Laboratories, and Caltech. Up to 2016, only BCC topology was taken into consideration for the structural analysis. Researchers' approach was more focused on the study of strut-based failure analysis. Various types of loads such as quasi-static compression, tensile, fatigue, and impact loading are applied and its effect on failure analysis is investigated. Various mechanical properties like elastic modulus, yield strength, energy absorption capacity under dynamic loading are studied for MLS. Stress-strain response of MLS shows the crucial nature of MLS. Most of the authors reported that initiation of failure takes place at the nodal level. The role of relative density was found to be very important on mechanical properties of MLS. In 2017, more research were evolved regarding the study of various types of topologies under different loading conditions. Topologies like triangular Kagome,

diamond-shaped, octahedral, etc. were studied in detail. Effect of relative density on elastic modulus, effect of various alloying elements, their manufacturing as well as effectiveness from strength point view was investigated. More study of improvement of FE models and their verification with either experimental or analytical model was done. Effect of various defects generated due to manufacturing processes on the strength of MLS and its performance under various loading conditions is investigated. Broader aspect of failure analysis of strut, its stiffness, and energy absorption capacity for vibration isolation application is discussed. Topology optimization to achieve a more efficient FE model that can predict the efficient topology to sustain various types of loading is studied.

In the year 2018, lighter on the study of various topologies like ECC, VC, octahedral, octet, DOD, f2ccz, etc. was thrown. The response of stainless steel MLS under static, compressive, dynamic loading, use of alloying element its effect on strength, stiffness, and energy absorption capacity of MLS are explored. The more advancement in the development of FE analysis was the prime motive of many researchers. Use of new techniques like micro-CT scan techniques, improved analytical models to calculate stiffness, elastic modulus helped researcher to refine FE analysis. Various materials like durable resin, standard resin, alloying elements their effect on strength, and various mechanical properties are studied. The use of MLS can be for impact absorption, vibration isolation, battery electrodes are explored.

5 Results and Discussion

Many researchers have investigated the structural property of MLS by applying static, fatigue, and impact loading. With the application of tensile loading stress–strain curve plot can be obtained which ultimately gives rise to elastic modulus and yield strength. Compressive loadings are also applied with the help of experimental setup which helps the author to study the deformation mechanism of MLS determination of stiffness. Impact or dynamic force analysis gives an idea about energy absorption capacity and dynamic strength of MLS. During fatigue testing initiation of crack, crack propagation phenomenon, densification which leads to catastrophic failure can be studied in detail. To compare the above results, many authors also developed FEA model with the help of software like ABAQUS, etc. This software helps to calculate Von misses stresses, initiation of failure, and location of the start of failure. Some of the researchers have developed a whole new approach for solving response of MLS to a particular type of loadings like use developing new model of Topology Optimization which will be time as well as cost-saving numerical approach. Next chapter gives a more detailed idea about different trends in research regarding the study of MLS. Some of the researchers have also developed an analytical model to determine stiffness, stress, and strains in MLS.

References

1. Deshpande VS, Fleck NA, Ashby MF (2001) Effective properties of the octet-truss lattice material. *J Mech Phys Solids* 49(8):1747–1769
2. Lakso P et al (2016) Optimization and simulation of SLM process for high-density H13 tool steel parts
3. Koehnen P, Haase C, Buelmann J, Ziegler S, Schleifenbaum JH, Bleck W (2018) Mechanical properties and deformation behavior of additively manufactured lattice structures of stainless steel
4. Li P, Wang Z, Petrinic N, Siviour CR (2014) Deformation behavior of stainless steel MLS by selective laser melting
5. Lai CQ, Daraio C (2018) Highly porous MLS as ultrathin and efficient impact absorbers
6. Rosa F, Manzoni S, Casati R (2018) Damping behavior of 316L lattice structures produced by selective laser melting
7. Syam WP, Jianwei W, Zhao B, Maskery I, Elmadih W, Leach R (2018) Design and analysis of strut-based lattice structures for vibration isolation
8. Yan X, Li Q, Yin S, Chen Z, Jenkins R, Chen C, Wang J, Ma W, Bolot R, Lupoi R, Ren Z (2019) Mechanical and in vitro study of anisotropic Ti6Al4V lattice structure fabricated using selective laser melting
9. Tankasala HC, Deshpande VS, Fleck NA (2017) Tensile response of elastoplastic lattices at finite strain
10. Chen XY, Tan HF (2018) An effective length model for octet lattice
11. Dong L, King WP, Raleigh M, Wadley HN (2018) A microfabrication approach for making metallic mechanical meta-materials
12. Huynh L, Rotella J, Sangid MD (2016) Fatigue behavior of IN718 MLS produced via additive manufacturing
13. Wu Y, Yang L (2018) An investigation of the fatigue strength of multiple cellular structures fabricated by electron beam powder bed fusion additive manufacturing process
14. Liu Y, Schaedler TA, Xi C (2018) Impact of node geometry on the effective stiffness of non-slender three-dimensional truss lattice architectures
15. Portela CM, Greer JR, Kochmann DM (2019) Mechanical behavior of additively-manufactured polymeric octet-truss lattice structures under quasi-static and dynamic compressive loading
16. Liu Y, Schaedler TA, Jacobsen AJ, Chen X (2014) Quasi-static energy absorption of hollow MLS
17. Boniotti L, Beretta S, Foletti S, Patriarca L (2017) Strain concentration in BCC micro-lattices obtained by AM
18. Hao ZH, Zhang X, Huizhong ZE, Huning YA, Hongshuai LE, Xiao LI, Yaobing WA (2018) Lightweight structure of a phase-change thermal controller based on lattice cells manufactured by SLM
19. Jin Z-H (2017) A MSL material with negative or zero thermal expansion
20. Erdeniz D, Schaedler TA, Dunand DC (2017) Deposition-based synthesis of nickel-based super-alloy MLS
21. Maskery I, Area AO, Parry L, Wildman RD, Tucka CJ, Ashcroft IA (2018) Effective design and simulation of surface-based lattice structures featuring volume fraction and cell type grading
22. Salari-Sharif L, Godfrey SW, Tootkabonic M, Valdevita L (2018) The effect of manufacturing defects on compressive strength of ultralight hollow MLS: a data-driven study
23. Dong G, Tang Y, Zhao YF (2017) Simulation of elastic properties of solid-lattice hybrid structures fabricated by additive manufacturing
24. Sharma M, Dobbelsstein H, Thiele M, Ostendorf A (2018) Laser metal deposition of lattice structures by columnar built
25. Ascari A, Fortunato A, Liverani E, Gamberoni A, Tomesani L (2016) New possibilities in the fabrication of hybrid components with big dimensions utilizing SLM
26. Gupta A, Allen G, Rossignac J (2018) Quador: quadric-of-revolution beams for lattices

Image-Based Recommendation Engine Using VGG Model



Smrithi Vasudevan, Nishtha Chauhan, Vergin Sarobin, and S. Geetha

Abstract Image retrieval is broadly classified into two parts—Description-based image retrieval and content-based image retrieval. DBIR involves annotating the images and then using text retrieval techniques to retrieve them. This requires vast amount of labor and is expensive for large image databases. Semantic gap is another major issue in DBIR. Different people may perceive the contents of the image differently and hence annotate it differently, e.g., a bright shiny silver car for one person can be boring dull gray car for another. Thus, no objective keywords for search can be defined, whereas CBIR aims at indexing and retrieving images based on their visual contents like color, texture, and shape features. For a content-based image retrieval system, the performance is dependent on how the feature vector is represented and what similarity metrics is chosen. The disadvantage with visual content descriptor is that it is very domain specific, e.g., color correlogram and color histogram for color feature extraction, Tamura and GLCM for texture feature extraction, local binary pattern and HOG for face recognition, SIFT and SURF for object detection, etc. Hence, convolution neural network which is not domain specific would be a better approach.

Keywords Description-based image retrieval (DBIR) · Content-based image retrieval (CBIR) · Convolution neural network (CNN) · Visual geometry group (VGG)

1 Introduction

Image-based search and recommendation is of immense utility in the field of online shopping. The main motivation behind any recommendation is that people are likely to buy more if they find what they like. In simple words, recommendation engine helps the user in finding what he/she likes.

S. Vasudevan · N. Chauhan (✉) · V. Sarobin · S. Geetha
VIT University, Chennai, India
e-mail: nishtha.chauhan2016@vitstudent.ac.in

© Springer Nature Singapore Pte Ltd. 2021
G. S. Hura et al. (eds.), *Advances in Communication and Computational Technology*, Lecture Notes in Electrical Engineering 668,
https://doi.org/10.1007/978-981-15-5341-7_21

Many companies like Netflix, Google, Amazon, etc., have successfully implemented recommendation engines to increase revenue, customer satisfaction, and personalization.

Recommender systems provide recommendations about various products and services to their users while using other user's data. Their success is imperative for both users and the e-commerce sites utilizing such systems. Providing accurate and dependable recommendations increases user satisfaction that results in selling more products and services. Image-based recommender systems are receiving increasing attention in the recent years.

Product recommendation is a wide area especially in the case of online shopping. The products can vary from coffee mug to t-shirts, mobile covers, jewelry, books, shoes, furniture, laptops, and cosmetics. Therefore, conventional domain-specific CBIR techniques are not suitable. CNN which is being widely used for image classification and recognition can be also used for product recommendation.

In CBIR, a lot of time has to be spent for choosing the appropriate algorithm as per the domain for feature selection. In some cases, global features worked well, and in some cases, local features worked well. CNN does not require data preprocessing. Data preprocessing requires humans to come up with feature extractors, i.e., to do feature engineering.

On the contrary, CNN can be thought as an automatic feature extractor from the image. Through training, the network determines what features it finds important, to be able to categorize the images accurately. In CNN, the input image is convolved with a feature detector also called kernel or a filter. The filter is a window which is slid on the input image (see Fig. 1).

In a typical CNN model, each input image will pass through a series of convolution layers with filters layers and fully connected layers (FC). Finally, SoftMax function is used to classify an object with probabilistic values between 0 and 1.

For feature extraction of image, the last SoftMax layer is not required. Hence, the output of the last fully connect layer will act as feature vector. We have used VGG16 Model which is pretrained for ImageNet database.

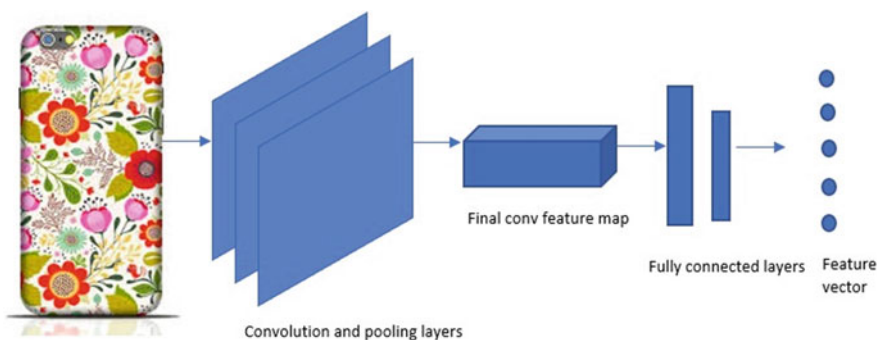


Fig. 1 CNN as feature extractor

2 Literature Survey

In paper [1], the effect of the depth of convolution neural network on its accuracy of image recognition has been studied. Paper [2] refers that one of the biggest problems in shifting from description- based image retrieval is that manual annotations of image are tedious. Also, there is a semantic gap between human perception of the query and the machines interpretation of query. Therefore, visual descriptors can be used for image matching, but it will not be able to capture intents and emotions.

Paper [3], paper [4], and paper [5] propose methods to improve image recommendations in sites like Instagram and Flickr. Paper [3] is inspired by Bayesian personalized ranking while paper [4] makes efficient use of tags and re-ranks them according to the image content to overcome semantic gap. Paper [6] describes about how to combine image-based and content-based filtering in a weighted mix to build a recommendation system. Each movie dataset has been used for performance evaluation. This new algorithm performs much better than the previous ones.

Paper [7] presents an idea of understanding human perception of visual relationship by recommending which clothes and accessories will match together. Paper [8] uses an algorithm for image recommendation that is based on ANNOVA cosine similarity. In paper [9], VisNet, a unified deep convolution neural network architecture, has been used for e-commerce recommendation. Paper [10] proposes a recommendation method exclusively for clothing using pretrained neural networks instead of SIFT or color histogram.

Paper [11] uses geotagged photo collection to suggest tourist destination to users based on input query image given by user and visual matching.

In paper [12], two neural networks have been used, one is for classification of images into one of the product categories, and the other is to compute the similarity score between pair of images. The metric used is Jaccard similarity. In our project, we have used a single neural network which is the VGG model. We have not used any separate network for classification. After extracting features from it, we have computed Manhattan distance between the two vectors because of its low computation complexity and displayed the top six results.

3 Proposed Model

3.1 VGG Model—Existing Model

VGG model is a type of convolution neural network. Input of the VGG model is 224×224 sized RGB image. The image is passed via a number of convolution layers having filter size of $3 * 3$. The stride is equal to 1 pixel. Five max-pooling layers carry out the spatial pooling. Max-pooling is performed over a 2×2 - pixel window, with stride 2. A stack of convolution neural networks is followed by three fully connected (FC) layers: the first two have 4096 channels each, the third performs 1000-way

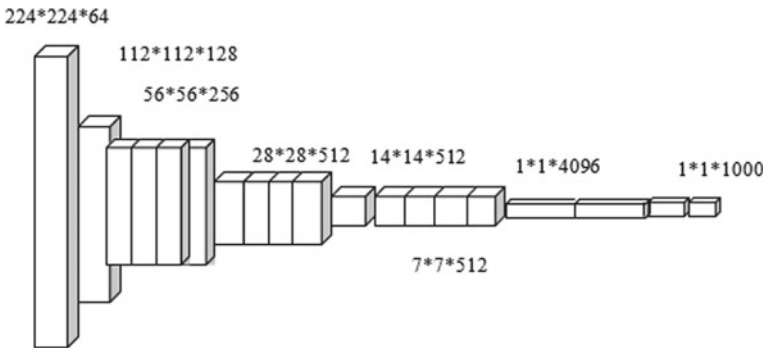


Fig. 2 Processing the input image using VGG model

ILSVRC classification and thus contains 1000 (see Fig. 2). The final layer is the SoftMax layer. All hidden layers are equipped with the rectification non-linearity.

3.2 Modifications to VGG Model—Model Proposed

The aim is to build an image-based product recommendation engine and not a classifier. Therefore, the output has not been passed through SoftMax layer. Training the image dataset through all 16 layer takes a lot of time and memory. For a recommendation engine, response time is the primary factor and is more important than precision, so the last two fully connected layers have been removed. Hence, the output of the block-5 pooling layer ($7 * 7 * 512$) acts as the feature vector.

4 Implementation

The dataset consists of a set of 60 images having a set of floral, plain, and striped mobile covers, t-shirts, skirts, shoes, spectacles along with coffee mug. The project was tested in Google Colab.

All images in the dataset are resized to $100 * 100 * 3$ instead of the standard $224 * 224 * 3$ input image size. Last two fully connected layers have been removed. Following is the architectural diagram of the model (see Fig. 3).

The calculations in the above figure can be explained using the equation:

$$\text{Output Parameters} = N * M * L + 1 * K \tag{1}$$

where $N * M$ is the filter size, L is the feature maps size, and K denotes the number of filters.

Layer (type)	Output Shape	Param #
input_92 (InputLayer)	(None, 100, 100, 3)	0
block1_conv1 (Conv2D)	(None, 100, 100, 64)	1792
block1_conv2 (Conv2D)	(None, 100, 100, 64)	36928
block1_pool (MaxPooling2D)	(None, 50, 50, 64)	0
block2_conv1 (Conv2D)	(None, 50, 50, 128)	73856
block2_conv2 (Conv2D)	(None, 50, 50, 128)	147584
block2_pool (MaxPooling2D)	(None, 25, 25, 128)	0
block3_conv1 (Conv2D)	(None, 25, 25, 256)	295168
block3_conv2 (Conv2D)	(None, 25, 25, 256)	590080
block3_conv3 (Conv2D)	(None, 25, 25, 256)	590080
block3_pool (MaxPooling2D)	(None, 12, 12, 256)	0
block4_conv1 (Conv2D)	(None, 12, 12, 512)	1180160
block4_conv2 (Conv2D)	(None, 12, 12, 512)	2359808
block4_conv3 (Conv2D)	(None, 12, 12, 512)	2359808
block4_pool (MaxPooling2D)	(None, 6, 6, 512)	0
block5_conv1 (Conv2D)	(None, 6, 6, 512)	2359808
block5_conv2 (Conv2D)	(None, 6, 6, 512)	2359808
block5_conv3 (Conv2D)	(None, 6, 6, 512)	2359808
block5_pool (MaxPooling2D)	(None, 3, 3, 512)	0
=====		
Total params: 14,714,688		
Trainable params: 14,714,688		
Non-trainable params: 0		

Fig. 3 Architecture diagram

For the first layer, the calculation is $(3 * 3 * 3 + 1 * 64)$. For the next layer, it is $(3 * 3 * 64 + 1 * 64)$.

The final output of the model is of size $1 * 2359808$. This feature vector is extracted for the query image as well as for all images in the dataset. Manhattan distance is computed between query feature vector and image feature vector. The top six recommendations are plotted in ascending order of the Manhattan distance. Manhattan distance has been chosen because of its low computational complexity.

5 Results

It has been observed that, VGG is capable of detecting patterns. When our query image is a plain mobile cover, the top five recommendations are also plain covers without design or strips; however, when the input is a mobile cover with floral design, then the output is a floral one (see Fig. 4).

Methodology—In all the results given below, the first image represents the query image (given by the user), and the rest of the images represent the results which are similar to that of the query image.

Result Five out of six results obtained for the plain mobile cover image are comparatively relatable, whereas the last result is somewhat different (Fig. 5).

Result Four out of six results obtained for the floral mobile cover image are comparatively relatable, whereas two results are somewhat different as they match only the color of the query image.

Fig. 4 Results for plain mobile cover

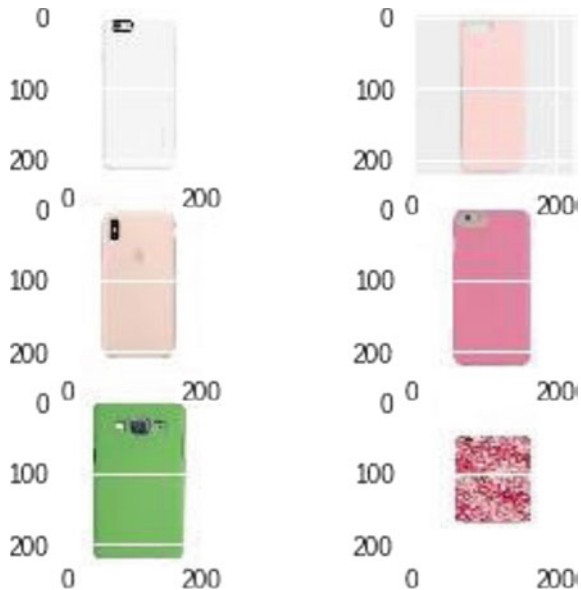


Fig. 5 Results when input image is a floral mobile cover



Table 1 Precision and recall results

	Recall	Precision
Figure 4	0.833	0.455
Figure 5	0.667	0.4

The precision and recall for the above figures can be calculated by—(see Table 1).

Precision and recall for Fig. 3, where input query is a plain mobile color, are 0.833 and 0.455, respectively. For Fig. 4, where input query is a floral mobile cover, the precision and recall are 0.667 and 0.4, respectively.

It is capable of color detection. It is also able to differentiate between a mobile cover and a t-shirt of almost the same design. If the query t-shirt contains a cartoon character, then the model recognizes it and tries to retrieve database images with the same cartoon character.

Result Top four out of six results obtained for the white colored shinchan t-shirt image are comparatively related, whereas the two results are somewhat different out of which one of the image matches with the white color of the query image (see Fig. 6).

Result Four out of six results obtained for the blue colored doremon t-shirt image are comparatively related, whereas two results are somewhat different out of which one image matches with the blue color of the query image (see Fig. 7).

It can differentiate between a coffee mug and a t-shirt of the same color and cartoon character.

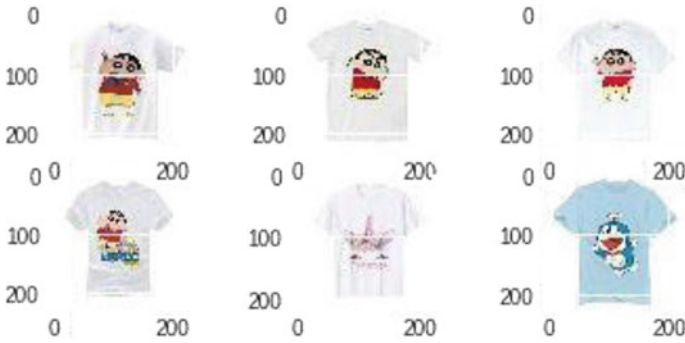


Fig. 6 Results for plain t-shirt

Fig. 7 Results for colored t-shirt



Result Top five out of six results obtained for the floral print coffee mug image are comparatively related, whereas the last result is somewhat different (see Fig. 8).

6 Conclusion

The result obtained justifies that the model is capable to be launched in the real-time scenario for image-based recommendation engine as it has high precision in terms of matching based on color, orientation, design, and product type.

Fig. 8 Results for coffee mug



References

1. Simonyan K, Zisserman A Very deep convolutional networks for large-scale image recognition. University of Oxford, Oxford
2. Zhang J, Yang Y, Tian Q, Zhuo L, Liu X (2016) Personalized social image recommendation method based on user-image-tag model. IEEE
3. Neural personalized ranking for image recommendation. Texas University (2018)
4. Image Based Fashion Product Recommendation with Deep Learning. University of Innsbruck, Austria (2018)
5. Just click: Personalized Image Recommendation via Exploratory Search From Large-Scale Flickr
6. Content Based Image Filtering for Recommendation. Springer, Sangji University Korea (2006)
7. Image Based Product Recommendation on Styles and Substitutes. University of Adelaide ACM digital library (2015)
8. Image recommendation based on ANOVA Cosine Similarity. University of Visvesvaraya College of Engineering, Bangalore University, Florida International University, USA, Indian Institute of Science, Bangalore, India (2016)
9. Deep Learning based Large Scale Visual Recommendation and Search for E-Commerce. Cornell University (2017)
10. Aesthetic-based clothing recommendation. Wenhui Yu Tsinghua University Beijing China
11. Cao L, Luo J, Gallagher A, Jin X, Han J, Huang TS A worldwide tourism recommendation system based on geotagged web photos. University of Illinois at Urbana-Champaign
12. Image-based Product Recommendation System using Convolution Neural Network. Stanford University (2015)

Stable Optimized Link Heuristic Using Cross-Layering for QoS of Secured HANETs



Anita Sethi, Sandip Vijay, and Vishal Gupta

Abstract Link availability, mobility, scalability, transmitting and receiving power, path loss model, signal quality and intelligent resource utilization heuristics are numerous factors for enhancing the network performance of HANETs. Quality of service and quality of experience can be improved with cross-layer, cross-domain and cross-network design which extracts the critical information from different platforms as required by dynamic behavior and heterogeneity of the network. Distance between the nodes, packet size, link availability, mobility model, and transmission range are simulation parameters which can degrade the heuristic performance of the network. In this paper, we worked on optimized link heuristic under heterogeneous network where handover plays an important role. We observed that in ad hoc network, the performance of optimized link heuristic is stable as compared to reactive protocols. 6LoWPAN with congestion control policy performs efficiently for IoT scalable architecture, and protocol stack handling is suitable for energy-efficient device.

Keywords PDR · Throughput · Goodput · Jitter · Delay · QoS

1 Introduction

Ad hoc network is a temporary network system having distributed nature formed by dynamic connection of nodes without any existing network infrastructure. Each node has peer to peer connectivity with functionality of data collection, processing, forwarding, and storage. For scenarios such as environment sensing, disaster rescue, and battlefield, it provides cost-effective solution while HANETs are autonomous and multi-hop networks provide the solution for quality of services [1]. Telecommunication network, wireless fidelity networks, smart ad hoc networks, wireless

A. Sethi (✉) · V. Gupta
ICFAI University, Dehradun, India
e-mail: seep4g@gmail.com

S. Vijay
Shivalik Engineering College, Dehradun, India

sensor networks, and VANETs are various types of HANETs which are accessible and interconnected through gateway nodes. With the advancement in IoTs, HANETs are rapidly growing with two types of nodes, regular node for sensing the data from surroundings and super node for collection of data and processing it, and connected with gateway to transfer the data in cloud environment [2].

Interoperability between standard and embedded devices using standard protocols is required for connectivity between all devices [IEEE802.15.4 and BT-LE], and access of Internet is essential foundation of IoT. Architecture of IoT uses 6LoWPAN protocol stack which is an adapter layer designed for devices with limitations of limited power source, small memory, low computational capability, and bandwidth availability. Enough address spaces and interconnectivity with other devices with auto network configuration with Internet accessibility are major features of designing 6LoWPAN. Several devices are connected as an entity to facilitate service with simple and easy discover, control, and maintenance process [3, 4]. It supports low computational complexity with tremendously low overhead in routing protocol, supporting multiple topologies for delay tolerant network. Frame size for data transmission should be small and single to minimize the overhead of reassembly and fragmentation. 6LoWPAN sensors are deployed in large numbers which requires small initial configuration and secured against physical as well as wireless attacks.

2 State of Art

Physical layer specifications like power control, data rate, modulation technique and frequency spectrum, and link layer specifications of error control and MAC for low-rate WPAN are defined in IEEE 802.15.4 Standard. Connectivity of the things or heterogeneous devices to Internet and E2E reliability and routing are the specifications of higher layer which are not in 802.15.4. Integration of low-complexity devices with IPv6 network under IEEE 802.15.4 protocol is specified in 6LoWPAN. Major challenge of 6LoWPAN is mismatch between packet size handling and routing tables format between IEEE 802.15.4 standard and IPv6 with granted E2E reliability. Development of new routing protocol for ROLL networks is the task of IETF ROLL Working group focused on efficiency not on QoS parameters. Ad hoc network is handled by ETSI m/c to m/c technical committee [5, 7]. In IoT architecture, heterogeneous devices are used with numerous network protocols for communication within the same machine to machine network which increases the burden on gateway. Numerous independent solutions are discussed by different authors for different functionalities of layer in the protocol stack which is presented in this section.

Modeling at the physical layer plays a significant role in performance evaluation of the network. Physical layer-driven technique for protocol design should never exploit the interrelation among higher layer and MAC functionality and on E2E communication performance. Spatial correlation-based collaborative MAC and energy-efficient

MAC exploit the spatial correlation in wireless sensor network and show the importance of MAC parameters in the performance of overall system and impact on other layers. Hierarchical, data-centric, and location-based are different approaches for routing. Communication overhead and energy saving are the objective of routing algorithm of author in [6, 8]. These heuristics are not suitable for IoT devices due to not consideration of physical layer parameters of the nodes putting direct impact on the performance of the network. Interaction with other layers is also not discussed. By using a classical approach, it is hard to develop “one-size-fits-all” solution to heterogeneous IoTs and network infrastructure.

Self-organization protocol is the key feature of the HANETs due to which communication capability is improved and easily maintained. In large-scale HANETs, route for transmission of information is easily maintained, and performance of network in terms of overhead and delays is improved. Maintenance of the network topology requires maximum of the communication cost between with limited data transfer bandwidth and energy consumption resources. Self-organizing framework proposed by Banerjee et al. reduces the path length using directional beam forming for creation of long-range shortcuts [9]. Distributed algorithm is for re-establishment of connectivity on link failure through the utilization of stem node specialized repairing unit. Dynamic routing functionality and self-positioning of stem node allow the damaged components to immediate repair of the original infrastructure in [10] Receiver-based MAC defines cooperative, passive acknowledgement, and distance-based geographic forwarder selection mechanism. Latency and energy consumption are analyzed and compared with 1-hopMAC, whereas at each hop, one receiver is defined.

Initially, randomly deployed smart nodes into an area are not self-organized. Self-organization to construct a topology by smart devices required self-organized lightweight protocols due to limited energy resource and computing capability [11]. Within certain deadline, all the smart devices must construct self-organizing topology. Scalability issue arises in massive IoT devices as more data is generated by the sensors and for maintenance no fixed topology is used in WSNs. In large-scale cyber-physical system, data collecting protocol should be dynamically adjustable according to change in topology. On wireless devices, dynamically mapping tasks model is introduced by Kim et al. [12] on which execution and assignment of resources to tasks that utilize the heterogeneity of the resources with taking care of energy constraints. 1-hop ad hoc grid heterogeneous environment maximizes the efficiency of limited resources of the system. For power-constrained resources, cost-effective routing protocols like m-limited forwarding protocol reduce the energy cost of disseminating information by limiting the number of nodes which retransmit packets. Advanced version of m-limited forwarding protocol is m-A4LP that utilizes the asymmetric links and performance with lower packet loss ratio than AODV in HANETs [13].

Accurate estimation of distance between vehicles without following any mobility model LDP [14] uses distribution of relative speed without considering the impact of traffic light, initial position of the vehicle, and turning direction of vehicles performance which is good as compared to other protocols. Accurate link duration can be

estimated by the latest ten relative speed samples in the simulation using exponential moving average method which filters the outliers. Anticipation of availability of future link between vehicles for effective and efficient prediction of neighbor node detection NPP [15] opt mobility prediction model which detect topology change and proper handling before degradation in network performance. As other vehicle enters in the range, capacity of neighborhood vehicle is predicted, and movement vectors of vehicles are estimated for future position. Periodic messages with information provide the benefit in prediction process which broadcasted further 1-hop neighbors.

Numerous parameters are defined in pattern of vehicle such as speed of the vehicle, driver's age, and distance between two consecutive vehicles to improve reactive routing using MADOV-P/PF [16]. Speed of vehicle is estimated within a time stamp, mobility pattern of the vehicle is inputted to the fuzzy module which generates connection failure, and congestion indicators are activated to prevent these failures. Proposed mechanism enhances the performance of network and prevents connection failure results minimization in congestion occurrences. Prediction holding time is defined for reliability in RB-MP [17] which is a broadcast routing heuristic to elect the most stable path using the estimated relative speed and inter-vehicle distance. Link connection between nodes i and j ($PTH_{i,j}$) is predicted within the time duration for which node j will remain in the transmission range of node i . Relative speed, communication range, and present coordinates of the nodes are used for calculating PTH. Relative speed, communication range, and present position are used for calculating PHT.

Link breakage problem reduction using possibility of observing local maxima results in improvement in the reliability of position-based routing in RIPR [18]. Road characteristics and number of 1-hop nodes are used to predict the position of relay nodes. Mobility prediction model predicts the velocity and direction of the moving node, which helps the sender to select a node that has highest relative velocity elected as relay vehicle. Link utility metric which reflects the impact of relative velocity and distance is used in the process of forwarding the message of EPBDF [19]. Optimization of packet routing with minimum number of hops utilization in highly dense area is the advantage of EPBDF heuristic.

3 Link Prediction Heuristic

With respect to time and space, link reliability replicates the degree of association stability between two mobile nodes with respect to each other. Beacon represents the significant existence of the nodes, and receiver increases the associativity value on receiving beacon signal. Problem of path stability and connection availability for communication purpose between source and destination while nodes are travelling along non-random pattern and prior knowledge of mobility model used for node movement are required to predict the path discontinuity. Route stability which is a subject to link failure due to node mobility is an important factor for performance of network. An active path duration at a given instance of time t is the time interval when

the communication route between source and destination node is established until one of the connections is unavailable along the route. Probability of path availability and path duration till time t is estimated under the model used for mobility of nodes. An expression for node distribution moving according to random direction or random way point model is derived which is inverted to obtain the temporal evolution and PDF under no deposition, given as initial condition. By using an exponential distributed function, in case of large hop-count limit, probability of path duration distribution is accurately defined due to route is adequately large, no matter which mobility model is assumed. From node density, map layout and other detailed parameters of the node are used to obtain empirically the parameters of exponential distribution. Connections along the path are in steady state and independent, and expected duration of the connection in the route using exponential distribution function is estimated.

4 Stable and Efficient Route and Maintenance

Objective of stable route is minimizing traffic latency and maximizing throughput, and during simulation, reliable source-destination connection is essential with prior knowledge of mobility model used by node, and probability model for prediction of the path availability in future helps in preparing a stable route. Path duration availability estimation can avoid service disruption due to unavailability of route which can be avoided by selecting an alternative path before the present one break which avoids waste of radio resources due to backup path pre-allocation. Using link dynamics, topology and connectivity of MANET are obtained, and fundamental network design issues are observed to determine the system capability for communication and reliability level. Performance of the network achieved by higher layer protocols depends on QoS metrics observed in the network layer. Duration and frequency of route disruption have a significant impact on TCP behavior like streaming and VOIP services.

5 Optimized Link State Heuristic

Path calculation between source and destination

1. Registration of all symmetric 1-hop neighbor to routing table.
2. For every symmetric 1-hop, add all 2-hop neighbor with condition not already available in the routing table and a symmetric connection to the neighbor.
3. For every entered node N with 2-hop count, add all entries from TC set where source in the TC entry $== N$, and destination should not be added in the routing table.
4. With hop-count $n + 1$, new flow ID is submitted.

- 5. Recurrence of the step 3 till the (RT) routing table is NULL after increment of value n.
- 6. MID set is checked for address aliases for all entries E in the routing table (RT). If address alias is already available, then added to the RT with hop-count set to Es hop-count.

6 Network Simulation

Optimized link heuristic performance is observed with different simulation attributes in NS3 simulator as well as in OMNET. In this simulation work OMNET is used presented in Fig. 1, scalability issue where number of nodes are equal to 200, and protocol used for traffic model is UDP. Constant position mobility model is used with RTS limit of 1500.

By varying the grid size, network performance e.g. throughput, jitter and packet delivery ratio of protocols are presented in the Figures 2-4. In case of routing protocol OL_{OF} traffic flows using UDP connection and traffic scheduling time (1, 1.5, 2s) in the simulation area of 500m data is transmitted from source (10.1.1) to destination (10.1.1.25) network performance is improved. Other simulation attributes are: packet size – 600, propagation model is Friis, constant speed mobility model, IEEE 802.11b model and at the transport layer connectionless services are used in the simulation scenario while measuring the network performance.

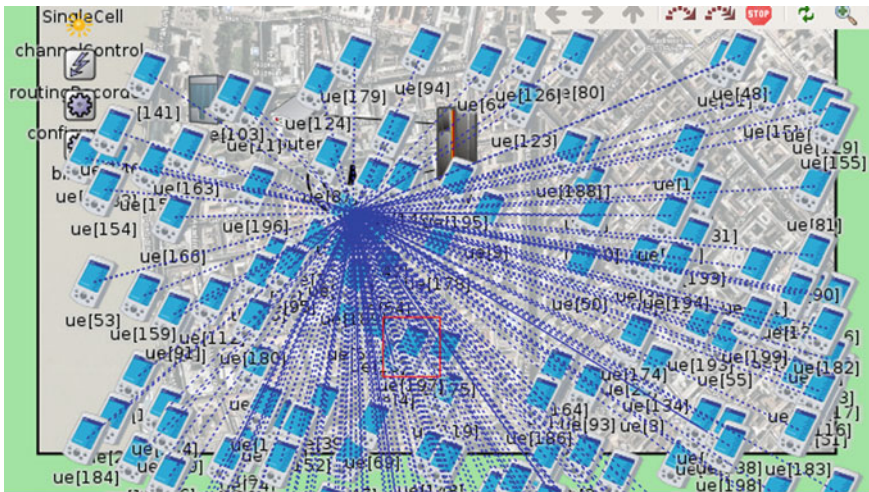


Fig. 1 Network simulation

7 Result Analysis

7.1 Delay

Real-time applications require UDP connection where delay is negligible. With increasing node density, UDP delay is so small as compared to TCP delay where traffic source has a great variation in delay graph. In higher denser environment, UDP and TCP work same as in delay context. Minimum mean delay of the network represents the efficient heuristic used on the network layer for routing and resource management technique used at transport layer. There are different heuristics which can improve the performance at different layers like intelligent queue technique which can be used for the improvement purpose. In NS3, we can use droptail and RED queue for buffer management at transport layer which can reduce the mean delay up to zero (Figs. 2 and 3).

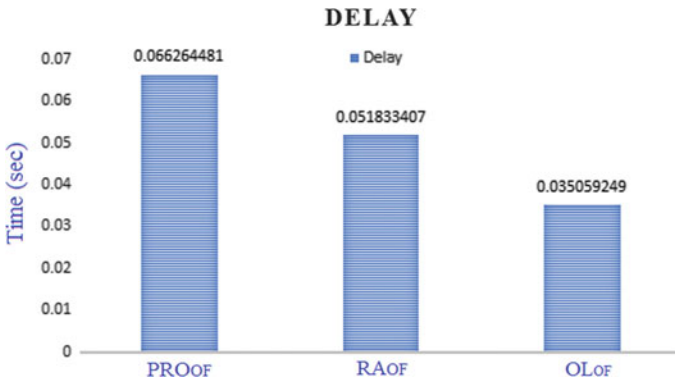


Fig. 2 Delay



Fig. 3 Jitter

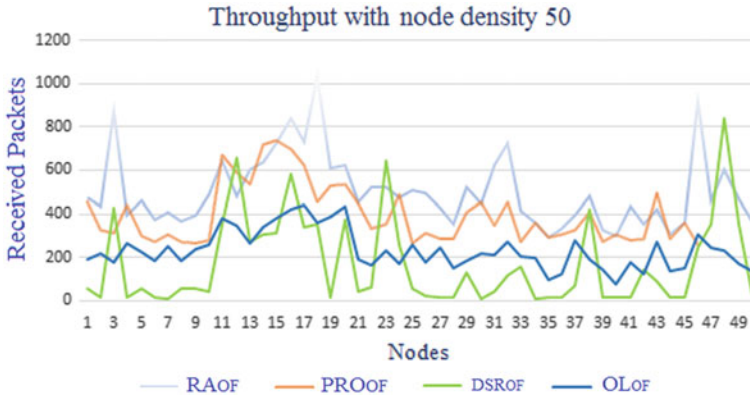


Fig. 4 Throughput

7.2 Throughput

Throughput is mostly influenced by node density in both cases of TCP and UDP traffic generation source. Denser environment can be easily handled by OLOF, and in UDP scenario, node density has very little impact on throughput and TCP traffic source connections. For lower node density, throughput remains relatively static. TCP results more throughput and goodput as compared to UDP due to default window size by varying data rate from 100 kbps to 1 Mbps (Fig. 4).

8 Conclusion

Network performance is measured by packet delivery ratio, throughput, goodput, lost packets, jitter, and delay. Mobility of a node, node density, speed, and MAC parameters has great impact on the routing protocol performance. Information of route is maintained in the routing table of the node which decreases the delay used in proactive routing protocols when compared with reactive routing protocols. Node density variation between 10 and 80 in a permanent topology of 500 * 500 meters with pause time variation of 0–50 s is represented by graph. OLOF performance is better in case of higher mobility scenario, and in dense area while small area DSDV provides effective results and with moderate traffic scenario, AODV is the best option. Grid topology boosts the performance of routing protocol. E2E delay is minimized with the help of optimized link heuristic. Based on the node density and transmission range, performance in terms of throughput and goodput of OLOF, PROOF, RAOF, and DSRof is represented in the graphs. E2E delay, jitter, throughput, and goodput of OLOF are better as compared to other heuristics under different attributes of network performance measurement.

References

1. Le T, Sinha P, Xuan D (2010) Turning heterogeneity into an advantage in wireless ad-hoc network routing. *Ad Hoc Netw* 8(1):108–118
2. Wang XB (2013) Heterogeneous architecture for ad hoc networks. *Adv Mater Res* 756:1059–1062
3. Boccardi F, Heath RW, Lozano A, Marzetta TL (2014) Five disruptive technology directions for 5G. *IEEE Commun Mag* 52(2):74–80
4. Palattella M et al (2016) Internet of things in the 5G Era: enablers, architecture and business models. *IEEE J Select Areas Commun* 34(3):1
5. Zhao M, Kumar A, Chong PHJ, Rongxing L (2017) A comprehensive study of RPL and P2P-RPL routing protocols: implementation, challenges and opportunities. *Peer-to-Peer Netw Appl* 5(10):1232–1256
6. Gohi A, Modi H, Patel SK (2013) 5G technology of mobile communication: a survey. In: *International conference on intelligent systems and signal processing*, pp 288–292
7. Fadlullah Z, Fouda M, Kato N, Takeuchi A, Iwasaki N, Nozaki Y (2011) Toward intelligent machine-to-machine communications in smart grid. *IEEE Commun Mag* 49(4):60–65
8. Vuran MC, Akyildiz IF (2010) Xlp: a cross-layer protocol for efficient communication in wireless sensor networks. *IEEE Trans Mob Comput* 9(11):1578–1591
9. Banerjee A, Agarwal R, Gauthier V, Yeo CK, Afifi H, Lee FB-S (2012) A self-organization framework for wireless ad hoc networks as small worlds. *Veh Technol IEEE Trans* 61(6):2659–2673
10. Trotta A, Di Felice M, Bedogni L, Bononi L (2013) Re-establishing network connectivity in post-disaster scenarios through mobile cognitive radio networks. In: *Ad Hoc networking workshop (MED-HOC-NET), 2013 12th annual mediterranean*. IEEE, pp 18–25.
11. Andrews JG, Buzzi S, Choi W, Hanly SV, Soong ACK, Zhang JC (2014) What will 5G be? *IEEE J Select Areas Commun* 32(6):1065–1082
12. Guo P, Wang J, Geng XH, Kim CS, Kim J-U (2014) A variable threshold-value authentication architecture for wireless mesh networks. *J Internet Technol* 15(6):929–935
13. Wang G, Turgut D, Bölöni L, Ji Y, Marinescu DC (2008) Improving routing performance through m-limited forwarding in power-constrained wireless ad hoc networks. *J Parall Distrib Comput* 68(4):501–514
14. Wang X, Wang C, Cui G, Yang Q (2015) Practical link duration prediction model in vehicular ad hoc networks. *Int J Distrib Sens Netw* (2):14
15. Rezende CG et al (2009) An efficient neighborhood prediction protocol to estimate link availability in VANETs. In: *Proceedings of the 7th ACM international symposium on mobility management and wireless access*. Tenerife, Canary Islands, Spain, pp 8390.
16. Chuang Y-T et al (2008) A mobility-aware link enhancement mechanism for vehicular Ad Hoc networks. *EURASIP J Wireless Commun Netw* 2008(1):1–10
17. Lai P et al (2009) A reliable broadcast routing scheme based on mobility prediction for VANET. In *Proc. IEEE intelligent vehicles symposium*, pp 1083–1087. Xi'an, China
18. Ryu M-W et al (2011) Position-based routing algorithm for improving reliability of inter-vehicle communication. *KSII Trans Internet Inf Syst* 5(8):1388–1403
19. Zhu W, Gao D, Foh CH (2015) An efficient prediction based data forwarding strategy in vehicular Ad Hoc network. *Int J Distrib Sens Netw ACM* 2015(1):1–11

Use of EEG as a Unique Human Biometric Trait for Authentication of an Individual



Bhawna Kaliraman, Priyanka Singh, and Manoj Duhan

Abstract With the advancement of biomedical technology, human brain signals are easy to measure and which are known as electroencephalogram (EEG) signals. These signals are used in different applications. One of the applications for brain waves is biometric authentication. For any signal to use as biometric parameter, it must possess some biometric characteristics such as universality, uniqueness, permanence, collectability, performance, acceptance, and circumvention. EEG has several characteristic to use as biometric parameter. This paper shows the uniqueness of EEG signal using some statistical parameters that support the uniqueness property of EEG.

Keywords Electroencephalogram (EEG) · Biometrics · Uniqueness · Root mean square (RMS) · Standard deviation (SD) · Spectral entropy (SEn)

1 Introduction

Electroencephalography (EEG) reads electrical activity on scalp generated by brain structures. EEG measures current flows produced by brain [1]. EEG is recorded non-invasively from the scalp. For acquiring brain signals, electrodes are positioned in standardized locations over scalp such as frontal, temporal, and parietal lobes.

A security system is used in almost all the fields for the protection purposes. So that, only authorized person can access certain resources or anything one may want to protect from unauthorized access. Authorized person who is allowed to access the

B. Kaliraman (✉) · P. Singh · M. Duhan

Department of Electronics and Communication Engineering, Deenbandhu Chhotu Ram Institute of Science and Technology, Murthal, Haryana 131039, India

e-mail: bhawna.kaliraman5@gmail.com

P. Singh

e-mail: priyankaiit@yahoo.co.in

M. Duhan

e-mail: duhan.manoj@gmail.com

© Springer Nature Singapore Pte Ltd. 2021

G. S. Hura et al. (eds.), *Advances in Communication and Computational Technology*, Lecture Notes in Electrical Engineering 668,
https://doi.org/10.1007/978-981-15-5341-7_23

277

protected application will be referred as a right person and the one who is not allowed is referred as wrong person. Every security system includes authentication process to identify authorized person. Various methods are used for authentication to access such type of systems, i.e., something only right person may know such as password, something only right person may have such as smart access card, and RFID tags, and something which is unique to right person, i.e., biometrics such as iris pattern, fingerprints, faceprint, and palmprint. Biometrics is the measure of biological or physiological characteristics used to identify a person. Biometrics provides better security among all the other methods because other methods such as passwords may be forgotten or smart access cards may be stolen. So, the importance of biometrics is increasing to avoid financial frauds and security threats. But, biometrics can also have spoofing attacks or can be forged, such as fingerprints that can be replaced by gummy finger, palmprints can be copied, and iris can be tricked by high resolution images. So, to provide more secure methods, researchers worked on EEG as a biometrics trait. Some advantages of EEG are: It is considered as robust biometric trait and difficult or impossible to forge. EEG has potential to be fraud resistant. Due to stress, brain print will change, so any unauthorized person cannot force the authorized person to provide them access to system. It is hard to duplicate another individual exact thought process. This paper focuses on proving the uniqueness of EEG, which is a major advantage of using EEG as a biometric trait.

Functional magnetic resonance imaging (fMRI) measures brain activity by tracking changes in blood flow. It can be used to recognize the individuals, but the cost and difficulty of using fMRI is much more. So, it is not practical to use it as everyday biometric authentication. Due to this reason, researches use EEG for the biometric authentication purposes, in which the data is collected from electrodes placed on scalp of subject. Earlier brain patterns are collected by placing gel-based electrodes on the scalp of user which will become cumbersome. But with advancement of technology, EEG recordings are taken from a device which looks like standard headphone, and no gel is needed in that device.

Any biometric system has several characteristics such as:

Universality: EEG is highly universal because each person's brain produces EEG signals.

Uniqueness: To use any signal as biometric parameter, signal should be sufficiently unique and should possess one or two traits which makes it individual. Due to which, biometric system distinguishes people.

Permanence: Biometric trait should possess permanence property, i.e., it should be stable over time. Since EEG is new area for biometric authentication, so research is going on EEG to prove its permanence.

Collectability: Biometric trait should be measured easily. With great advancement of technology, EEG signals can be acquired with portable headsets easily.

Performance: Any biometric system should have better recognition accuracy, speed, etc. EEG signal can be processed easily in short time because it is one-dimensional signal. Good recognition rates have been obtained in this field.

Circumvention: Any biometric system should be protected from fraudulent methods. EEG can be most trusted trait because it cannot be easily forged.

2 Literature Survey

Researchers used EEG as biometric trait for authentication purposes. To use EEG as biometric trait, first step is to preprocess the raw EEG signal to remove noise content from signal, in second step, features are extracted from preprocessed EEG signal, and then, classification is done in last step.

EEG signals of twins were studied by some authors [2]. They concluded that EEG at resting state for monozygotic twins is same, but EEG is not similar for dizygotic twins. Some authors [3] proved that EEG traits are highly heritable such as mean spectral power and frequency values of alpha and beta bands, and family members have more identical traits than other unrelated people. Napflin et al. [4] claimed that they found stability of EEG between different sessions which were recorded more than a year apart. Poulos et al. [5] used EEG features for person identification, in their work, FFT was used to extract features and neural network (LVQ) to classify them, and they claim correct classification score up to 80–100%. But only four subjects were considered to verify their work. At some other point of time, Poulos et al. [6] used AR parameters as features and LVQ as classifier, and they got correct classification score between 72 and 84%. Many researchers used AR model as feature extraction technique in their work. Paranjape et al. [7] achieved 83% classification score by using AR parameters for feature extraction and discriminant function analysis to classify them, and using this, they claim 83% classification score. Many of the authors [8] use PSD as features such as Palaniappan and Mandic [8] used MUSIC algorithm to extract power content for feature extraction, and for classification, they used k-NN using Manhattan distance and Elman neural network (ENN) and got 98.12 ± 1.26 (HU = 200) ENN classification accuracy.

3 Data Base for EEG Signals

The data acquired from all users are stored in database, and then, that data are used for further processing. Dataset provided by UCI KDD EEG database is used for present work, which uses 64 electrodes sampled at 256 Hz for 1 s. Data were collected from 122 subjects, and each having 120 trials where different stimuli were shown. Two groups of subjects were considered, one is control (i.e., subjects had no history of alcohol) and other is alcoholic. Visual stimulation technique is used to acquire data from subjects, and either single stimuli (S1) or two stimuli (S1 and S2) were shown to subjects. Each stimulus was taken from picture set given by Snodgrass and Vanderwart [9]. For this study, we considered data from 100 subjects (some are alcoholic and some are control) and one trial for each subject. Each trial consists of data from 64 channels and each channel having 256 samples.

4 Methodology

With advancement of signal processing, EEG has become a better option for authentication purposes. To prove the uniqueness of EEG signal, we considered some statistical parameters such as root mean square value, standard deviation, and entropy.

4.1 Root Mean Square (RMS) Value

Root mean square value is given by square root of mean square value, and mean is given by arithmetic average of a set of scores [10]. But, mean value does not tell anything about the signal's variability. While RMS value tells about the signal's variability and its average [11]. So, if RMS value of each channel comes out to be different, then we can say that each channel has unique value, which proves that signal is unique. RMS value tells about the size (strength) of the signal. RMS value is given by first calculating the square of signal, taking average of that squared value, and then, square root of this average is taken:

$$x(t)_{\text{rms}} = \left[\frac{1}{T} \sum_0^T x(t)^2 \right]^{1/2} \quad (1)$$

4.2 Standard Deviation (SD)

SD is the measure of variability of any set of numerical values about their arithmetic mean, which tells that each value has different position from mean or we can say that if standard deviation comes out to be different for each channel, then each channel has unique value, which proves that signal is unique. It is given by positive square root of variance and denoted by Greek letter sigma (σ). It measures the absolute variability of the distribution. Standard deviation is also known as root mean square deviation. It is given by Eq. (2):

$$\sigma = \sqrt{\sum \frac{(x_i - \bar{x})^2}{N}} \quad (2)$$

4.3 Entropy

Entropy measures the amount of information contained in generalized probability distribution, or it can be defined as measure of rate of information generation. So, entropy gives maximum information about signal. Due to this feature, we can use entropy as one parameter to prove distinctiveness of the signal, i.e., if each signal has unique entropy, then we can say that each signal has different information content present in it, which means each signal is unique. Here, we consider spectral entropy of EEG signal.

Spectral entropy gives the spectral regularity of the time series, and it is calculated using normalized Shannon entropy. Spectral entropy tells that how different the distribution of energy is. Power spectrum of the signal is used by spectral entropy for computing the regularity of time series. To calculate power spectral density, Fourier transform is used, which shows the distribution of power of signal according to the frequencies present in the signal [12]. Power level obtained after Fourier transform is denoted

by P_f , then normalization is done using Eq. (3):

$$P_f = \frac{P_f}{\sum P_f} \quad (3)$$

After calculating the normalized power, spectral entropy is calculated using Equation (4):

$$SE_n = \sum_f P_f \log(1/P_f) \quad (4)$$

In present work, spectral entropy for each channel for each user is calculated, which comes out to be different for each user. Hence, we can say that signal is unique.

As RMS, SD, entropy value for each user for a particular channel is obtained as different, it shows that each user has unique EEG signal.

4.4 Algorithm

Figure 1 shows the proposed algorithm which is used for proving the uniqueness of EEG signals.

- Step 1

The first step is to import the database into MATLAB. Further processing is done after loading data for all users. UCI KDD provides database into '.rd' files. So, first step is to load data from '.rd' files into MATLAB.

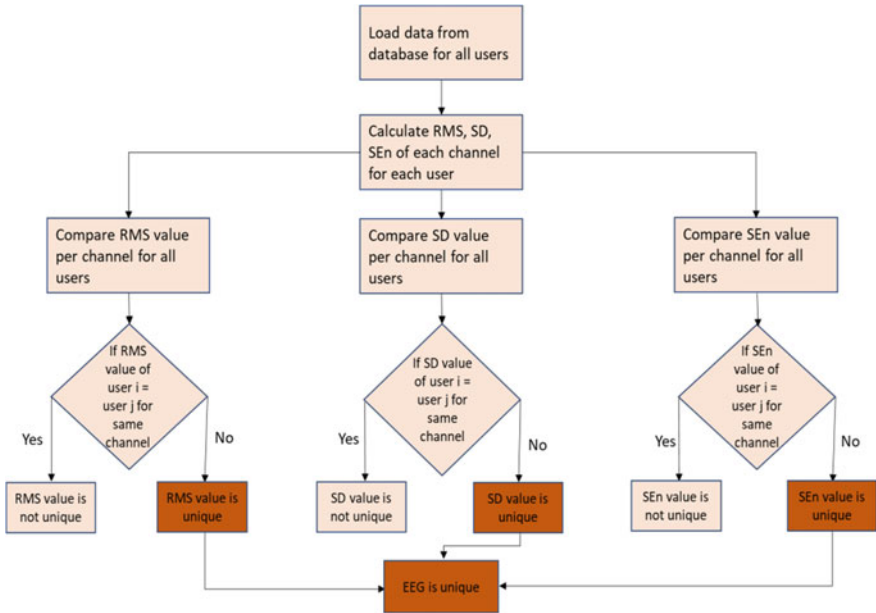


Fig. 1 Flowchart of the proposed algorithm used for proving uniqueness of EEG signal

- Step 2

After loading the data for all users, the next step is to calculate root mean square value (RMS), standard deviation (SD), and spectral entropy (SEn) for each channel per user. Here, database consists of 64 channels per user. So, for each 64 channel, RMS, SD, SEn values are calculated and put into different file which consist of RMS, SD, SEn value of all 64 channels for each user.

- Step 3

Now, compare RMS value of each user per channel, i.e., firstly compare RMS value for first channel for each user. If any two users have same RMS value for that particular channel, then we can say that RMS value is not unique, and otherwise, if RMS value of that particular channel is not same for any user, then our RMS value is unique for each user. Similarly, compare RMS value for every channel.

Secondly, compare SD value of each channel for all users and using same process check whether it is unique or not. Finally, compare spectral entropy values of each channel for all users and found whether they are unique or not.

- Step 4

This is final decision step; in this step, we decide whether EEG of person is unique or not. If our RMS, Sd, and SEn values come out to be unique in the previous step

for each channel for all users, then we can conclude that EEG of a person is unique, because the above parameters give more information about the signal, and if each of the details for the user found as unique value, then we can say that each user has unique EEG pattern.

5 Results and Discussion

This paper focuses on statistical parameters of the signal such as root mean square value (RMS), standard deviation (SD), spectral entropy (SEn), all of which gives information about the signal, i.e., its variability, average, information content, etc.

We have calculated RMS value, standard deviation values and spectral entropy values for all users and all channels and found them to be unique. It is very difficult to visualize values for all 64 channels for 100 users with bare eyes in single plot. So, for better understanding, we have selected randomly five users and ten channels. Figures 2, 3, and 4 show the RMS, standard deviation, and spectral entropy values of five random users on ten randomly selected channels.

To prove uniqueness, we extract RMS value per channel for first user because each channel has 256 samples, which means that we got 64 RMS values for user 1, i.e., 1 RMS value for each channel, then for all other users, RMS value per channel is calculated. After calculating RMS value for all users, these values are stored in separate file. Now, RMS value of first channel is compared for all users, and we found

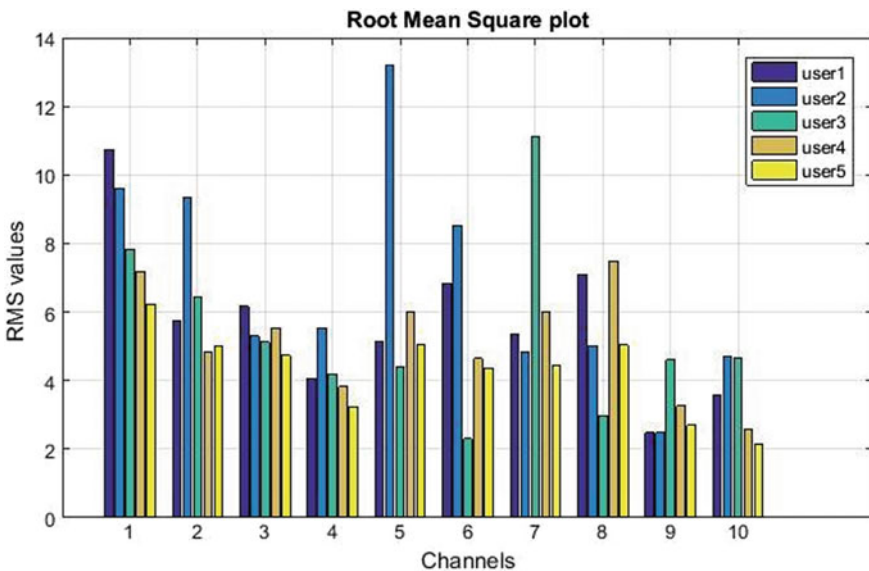


Fig. 2 Root mean square value plot for proving uniqueness property of EEG signal

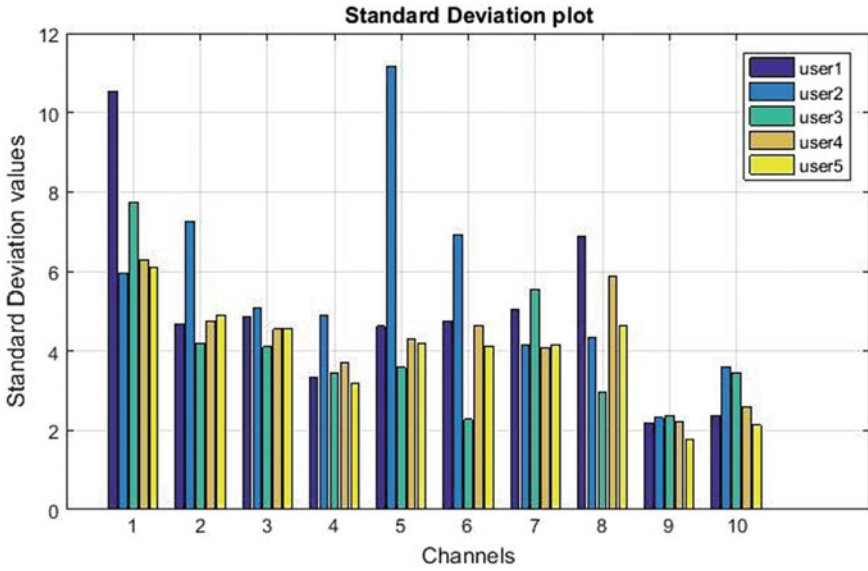


Fig. 3 Standard deviation values plot for proving uniqueness of EEG signals

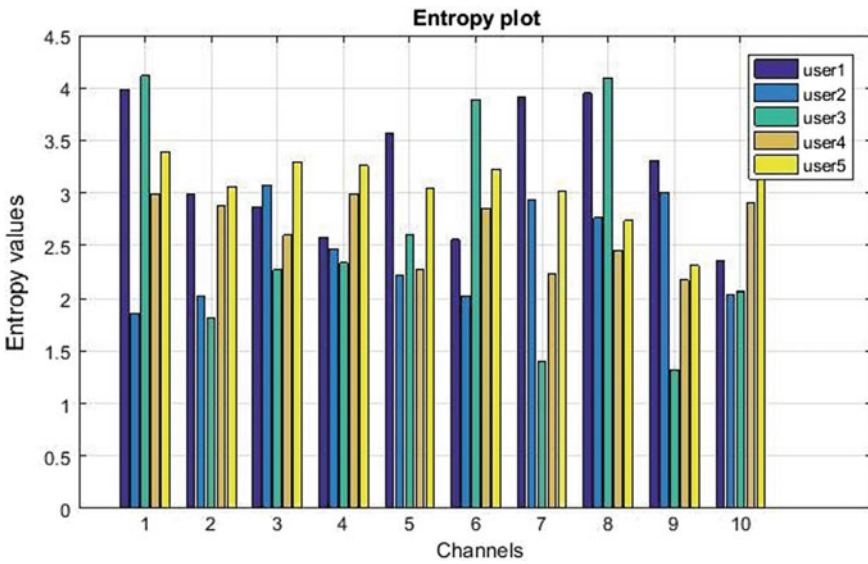


Fig. 4 Entropy values plot for proving uniqueness of EEG signals

that it comes out to be different for all users. And, the results satisfy the uniqueness property. Figure 2 shows the RMS value of ten channels for five users, which shows that at each channel, every person has different RMS value.

But one parameter is not sure and sufficient condition. To consolidate upon this result, a greater number of parameters like standard deviation and spectral entropy were also calculated in next section and tried to authenticate the existing results in Fig. 2.

The standard deviation values are computed for 256 samples of each channel for all users. These SD values for each user are then stored in separate file. Now, for each channel, SD value of all users is compared. And it is found that these values are different for each user for every particular channel. So, uniqueness property is satisfied. Figure 3 shows the plot for standard deviation value for ten random channels of randomly selected five users. As both RMS value and SD prove the uniqueness of EEG signal, we consider one more parameter, i.e., spectral entropy to prove its uniqueness.

Similarly, spectral entropy of each 64 channel for all 100 users is calculated. Then, all these 100×64 values are stored in file. Then, we compare SEN value of all 100 users for each channel. And, we found them different for all users, which prove that these are unique for each user. Figure 4 shows the plot for spectral entropy values of ten random channels for five randomly selected users. After computing all three statistical parameters, i.e., RMS, Sd, SEN and finding each of them as unique for each user, we can conclude that each user has different EEG pattern, which proves that we can use EEG for authentication purposes because it shows uniqueness property.

6 Conclusion and Future Scope

Previous studies show that there is possibility of using EEG as biometric trait for authentication purposes. This work proves the distinctiveness property of EEG signal to use it as biometric trait, using some statistical parameters such as root mean square value, standard deviation, and spectral entropy for authentication purposes. From previous studies, it was clear that EEG signals possess most of the characteristics used by any biometric system. The above study proves that no two individual has same EEG, i.e., EEG signal of every individual is unique which is shown by different statistical plots in the paper.

In this paper, uniqueness of EEG signal is proved, which is one of the characteristics for biometric system. There are some more open issues which are still to be addressed such as permanence of EEG, i.e., repeatability. In literature survey, it is not clear that EEG signals can vary with age or not. Also, there is one other issue which needs to be explored is mental disorder, i.e., most of the methods used for EEG as biometric trait based on data acquired from healthy individuals. Mental disorders can affect the performance of biometric system. So, these are some issues which need to be addressed for future prospects.

References

1. Teplan M (2002) Fundamentals of EEG measurement. *Meas Sci Rev* 2:1–11. <https://doi.org/10.1021/pr0703501>
2. Davis H, Davis P (2015) Action potentials of the brain: in normal persons and in normal states of cerebral activity. *Arch Neurol psychiatry* 36(6):1214–1224
3. Vogel F (2000) Genetics and the electroencephalogram
4. Näpflin M, Wildi M, Sarnthein J (2007) Test-retest reliability of resting EEG spectra validates a statistical signature of persons. *Clin Neurophysiol* 118:2519–2524. <https://doi.org/10.1016/j.clinph.2007.07.022>
5. Poulos M, Rangoussi M, Alexandris N, Alezandris N (1999) Neural network based person identification using EEG. *Proc Int Conf Acoust Speech Signal Process* 2:1117–1120
6. Poulos M, Rangoussi M, Chrissikopoulos V, Evangelou A (1999) Person identification based on parametric processing of the EEG. In: *Proceedings of ICECS '99. 6th IEEE international conference on electronics, circuits and systems, vol 1*, pp 283–286. <https://doi.org/10.1109/ICECS.1999.813403>
7. Paranjape RB, Mahovsky J, Benedicenti L, Koles Z (2001) The electroencephalogram as a biometric. *Can Conf Electr Comput Eng* 2:1363–1366. <https://doi.org/10.1109/CCECE.2001.933649>
8. Palaniappan R, Mandic DP, Member S (2007) Biometrics from brain electrical activity: a machine learning approach. *IEEE Trans Pattern Anal Mach Intell* 29:738–742
9. Snodgrass JG, Vanderwart M (1980) A standardized set of 260 pictures: Norms for name agreement, image agreement, familiarity, and visual complexity. *J Exp Psychol Hum Learn Mem* 6:174–215. <https://doi.org/10.1037/0278-7393.6.2.174>
10. Frederick C (2013) Statistical parameters. *Stat A Gen Introd* 80–102. <https://doi.org/10.1109/MILCOM.1999.822672>
11. Semmlow J (2005) *Circuits, signals, and systems for bioengineers*. Elsevier, Amsterdam
12. Mu Z, Hu J, Min J, Yin J (2017) Comparison of different entropies as features for person authentication based on EEG signals. *IET Biometrics* 6:409–417. <https://doi.org/10.1049/iet-bmt.2016.0144>

Performance of Feature Extracted on Leaf Images by Discriminant Analysis on Various Classifiers



Anjali Pathak, Bhawna Vohra, and Kapil Gupta

Abstract According to IUCN's global analysis of extinction risk for plant species, there is a true extent of threat to 380,000 plant species worldwide (Amlekar et al. in *IBMRD J Manage Res* 3:224–232, [1]). For future concerns, it is important to spread more awareness about conservation of plants. Thus, to save plants, it is first important to identify them. It is important to identify plants in that case. This shows that recognition and classification of plant leaves have become an essential field of research. Plants can be classified on various bases like flowers or on cellular structures, but these can be done only by botanists. Thus, as plant leaves are easily available, they can be taken as the desired option for classification. Now, to classify a leaf image into a particular class of species, it is necessary to select those features which differentiate the classes as much as possible. To select these features, discriminant analysis is done (Wu et al. in *IEEE*, pp 11–16, [2]). This paper focuses on two discriminant analysis approaches—linear and quadratic discriminant analysis to reduce the number of features in plant leaf images, and then, various classifiers including SVM (SVC), KNN and logistic regression [21] are used to classify a particular image into a particular class of plant species. The other two phases include feature extraction and classification (Rahmani et al. in *Int J Organ Collective Intell (IJOICI)* 6:15–28, [3]). All the experiments are conducted on Flavia dataset, and the highest accuracy of 87% is obtained on KNN classifier using quadratic discriminant analysis. The takeaway of our experiment is that QDA performed better as compared to LDA in case classes that have different variances.

Keywords Plant leaf classification · KNN classifier · Logistic regression classifier · SVM (SVC) · LDA · QDA

A. Pathak (✉) · B. Vohra · K. Gupta
Department of Computer Applications, National Institute of Technology, Kurukshetra, India
e-mail: anjali_51710058@nitkkr.ac.in

B. Vohra
e-mail: vohrab1896@gmail.com

K. Gupta
e-mail: kapil@nitkkr.ac.in

1 Introduction

Plants are a crucial part of our environment. Their existence maintains the ecological balance on earth. However, according to IUCN's global analysis of extinction risk for plant species, there is a true extent of threat to 380,000 plant species worldwide [4]. To protect plants and store various plant leaf species, a plant leaf database is important [5]. In order to handle that, database various classification methods are needed. Plants can be classified on the basis of their cellular structures, but these kinds of analysis can only be done by botanists and experienced taxonomists. As classifying on the basis of their physical appearance is a feasible task, leaves can be taken into consideration. This can help in determining the medicinal properties and use them as alternative energy source. So, out of many methods to recognize a plant, we are focusing our paper on leaf recognition. Leaf recognition is important to classify plants, and this task is challenging when done by computers. Extraction of leaf features is an important step in recognition process. Many researchers have been using various options to classify leaf images like K-nearest neighbour (KNN), logistic regression or artificial neural network or probabilistic neural network [6]. In this paper, our focus is on comparing performance of three classifiers namely—KNN, logistic regression and SVM (SVC). But, before that, we have done feature extraction to obtain those features which play a major role to differentiate leaves [4]. The major part of our work is comparing performance of different classifiers after using either LDA or quadratic LDA as a feature extraction method.

1.1 Linear and Quadratic Discriminant Analysis

In a classification problem, whenever we have more than two classes, then linear discriminant analysis and quadratic discriminant analysis (QDA) come into play [7].

Discriminant analysis models Gaussian distribution of data in each class. After this, Bayes theorem is used to find the correct class for a particular data point [8].

Below-mentioned work is cited from [9–11]. Let us suppose $D: \{(x^{(i)}, y^{(i)}), \dots\}$
 $y \in \{0, 1, \dots\}$ (classes)

and X is a leaf image which we want to classify. We will refer to this X leaf image as a data point below. Using conditional probability, probability of a data point to lie in a class i is

$$P(X|y = i)P(y = i)$$

So, the ratio of probability of a data point X to lie in class 0 to its probability to lie in class 1 is

$$\log\left(\frac{P(X|y = 0)P(y = 0)}{P(X|y = 1)P(y = 1)}\right) \quad (1)$$

So, in a multi-class dataset, the above ratio is calculated for every pair of class. As the data belongs to Gaussian distribution, the PDF becomes

$$P(X | y = i) = N(\mu_i, \Sigma)$$

Every leaf image is a data point X , and as every X has more than 1 features, and thus, it is a multivariate normal distribution.

This gives PDF of joint distribution as

$$P(X|y = i) = N(\mu_i, \Sigma) = \frac{1}{(2 \times \pi)^m \times |\Sigma|} \times e^{-\frac{2}{2} \times (X - \mu_i)^T \times \Sigma^{-1} \times (X - \mu_i)} \tag{2}$$

where m is the size of X

$|\Sigma|$ is variance

μ_i is mean of i th class.

Taking log on both sides of Eq. (2),

$$\begin{aligned} \log(P(X|y = i)) &= -\frac{1}{2} \times (X - \mu_i)^T \times \Sigma^{-1} \times (X - \mu_i) \\ &\quad - \frac{m}{2} \times \log(2 \times \pi) - \frac{1}{2} \log(|\Sigma|) \end{aligned}$$

The prior probabilities are

$$\begin{aligned} P(y = i) &= q_i \\ P(y = j) &= q_j \\ P(y = i|X) &= \frac{P(X|y = i)P(y = i)}{P(X)} \end{aligned}$$

Putting these values in Eq. (1),

The ratio of probability of data point X to lie in class i to the probability of data point X to lie in class j is

$$w^T X + w_0$$

This is a linear equation representing a straight line given that variances of both classes are equal. In case the variances of both classes are different, QDA is used.

PDF in this case becomes

$$\begin{aligned} \log(P(X|y = i)) &= -\frac{1}{2} \times (X - \mu_i)^T \times \Sigma_1^{-1} \times (X - \mu_i) \\ &\quad - \frac{m}{2} \times \log(2 \times \pi) - \frac{1}{2} \log(|\Sigma_1|) \end{aligned}$$

Thus, in this case, the ratio of probability of data point X to lie in class i to the probability of data point X to lie in class j is

$$X^T W_2 X - W_1^T X + W_0$$

where W_2 is a matrix, W_1^T is a vector and W_0 is a constant. This gives a quadratic equation for QDA.

The paper is organized in the following format: Sect. 2 states related works, Sect. 3 shows experiment and result analysis which is divided into subsections. The first subsection in Sect. 3 gives a description of the dataset. The second subsection gives the idea about the representation of samples, and the last subsection explains the classification methods along with the evaluation metrics.

2 Related Work

Various other researchers have done some significant amount of work. Stephen Gang Wu and few others employed probabilistic neural network (PNN) to recognize and classify images. PNN was trained by 1800 leaves to classify 32 plant types, and they obtained 90% accuracy [12]. Manisha Amlekar focused on artificial neural network in her paper [1]. Mohamed Elhadi Rahmani, in his paper, proposed a contrast of plant leaf classification using various approaches including naive Bayes and KNN [4]. Miao et al. worked on classifying roses [13]. Gu et al. used skeleton segmentation to recognize leaf. Du et al. and Wang et al. both proposed similar work on moving media centre hypersphere classifier [14]. Ye et al. did a comparison of similarities between plant features during classification [13]. While the above-mentioned researchers focused on PNN or ANN and various other techniques, our experiment aims to explore the performance of linear and quadratic LDA with various classifiers.

3 Experiment Study

3.1 Dataset [2]

We have performed the experiments on the Flavia dataset. This dataset consists of 33 classes out of which the 13th class is missing. Each class majorly denotes the type of plant the leaf image belongs to or in other words each class represents the plant species of the particular leaf image. There are on an average 60 leaf images in each class (Fig. 1).

Fig. 1 Different types of leaf images present in the FLAVIA dataset



3.2 Representation of Samples

In our experiment, we have initially converted the leaf images to gray scale images. Later, we have resized the images to a 60×80 size. Hence, each image corresponds to 4800 pixel intensities, i.e., 4800 features per image. Now, in each image matrix, one more column is appended in the end which represents the class number which that particular leaf image belongs to. In this way, there are 4801 features per image. Now, after completing these required measures, we have normalized the pixel intensities using the StandardScalar function. The StandardScalar function is used to standardize the features by removing the mean and scaling to unit variance. After normalization, we have applied our algorithm on the dataset.

3.3 Classification and Evaluation

Initially, we applied linear discriminant analysis algorithm on our dataset. LDA is used to transmute the features to a lesser dimensional space by increasing the ratio of the variance (between-class) to the variance (within-class) and finding out the eigen vectors that form the new axes, and their corresponding eigen values provide insight about the informativeness of the new axes of the lower dimensional feature space. The new lower dimensional space excludes the redundant or less informative features thereby reducing the dimensionality of the dataset and projecting the data on the new axes which maximizes the separability between the various classes in the

dataset. In our experiment while applying the LDA algorithm, we have taken the test size to be 60% because test size below 60% was giving extremely poor accuracy. The number of components that we have used in LDA is 25 since the accuracy estimate was best at this number. Making the number of components less than or greater to 25 was more or less decreasing the accuracy of the dataset. After applying LDA, we observed the accuracy of the dataset using three classifiers which were further used to classify the data and predict the results on the test data. The three classifiers are as follows:

The first classifier that we have used is the **K-nearest neighbour classifier** [6]. The KNN algorithm is a lazy algorithm, and therefore, we do not learn the model during training. Hence, in other words, we are just saving the examples in the training phase. So, when the algorithm gets the test instance, it uses the stored instance in memory in order to find the possible output. At the test time, what we do is we get a test instance and find k training examples. Now, suppose for the test instance, we are given only the 'x' value, and we have to predict the corresponding 'y' value. In our case, 'x' represents the leaf image, and 'y' value represents the plant type that particular leaf image belongs to. In our experiment, we found the best results when the number of neighbours were considered to be 1. LDA along with the KNN classifier resulted in 75.07% accuracy on the Flavia dataset.

The second classifier that we have used is the **SVC (support vector classification)** classifier [6] that is provided by the support vector machines (SVM) which are a set of supervised learning methods used for classification, outlier detection, etc. This classifier finds the optimal hyperplane that further helps in classifying the new data points. When we apply LDA along with this classifier on the dataset, then it resulted in 67.987% accuracy.

The last classifier that we used is the **logistic regression classifier** [6]. This classifier uses the logistic function to predict the classes that the leaf image belongs to. With this classifier, we received a 68.613% accuracy. Clearly, we can observe that out of these three classifiers, the KNN classifiers with one nearest neighbour gave the maximum accuracy of 75.07%.

One thing to **note** here is that when we were applying the LDA, we calculated the mean vectors for the classes, and later, we calculated the covariance matrices of the classes. We then reduced the covariance matrix to row-echelon form, and then, we observed that in few classes's covariance matrix, the rows were linearly dependent on each other. The linear dependency in the rows indicated that there were many images that were of similar pixel intensities or in other words, the features were redundant. Due to this redundancy, the overall accuracy of the dataset was decreasing. The above accuracy values have been computed by omitting those classes. The classes that have been omitted namely correspond to class numbers 2, 24, 27 and 30. After omitting these classes, the accuracy of the dataset drastically increased. The common names of these classes are as follows: Chinese horse chestnut, glossy privet, ford woodlotus and southern magnolia. As we can see that even after omission of classes from the dataset, the maximum accuracy value that we got with LDA is 75.07% which is poor as compared to the desirable accuracy in the Flavia dataset. For this reason, we applied the quadratic discriminant analysis algorithm in the dataset. Now, the

linear discriminant analysis algorithm assumes that the covariance matrices of all the classes are homogeneous in nature. We have considered a total of 28 classes in our dataset, and hence, this assumption can affect the accuracy of our dataset. Since we were getting a maximum accuracy of 75.07% on our dataset, and hence, we applied QDA algorithm on our dataset. QDA does not assume the homogeneity of the covariance matrices rather it allows heterogeneity of the matrices in different classes. Therefore, after applying QDA on our dataset, we noticed that the accuracy of our dataset drastically increased. We applied QDA with 24% test size as this test size measure was giving us the best accuracy. With KNN classifier with one nearest neighbour, we got an accuracy of 87.23%. The results with SVC classifier were also equally promising and SVC classifier resulted in an accuracy of 84.37%. The logistic regression classifier resulted in an accuracy of 69.270% which clearly indicated that this classifier gave poor results in both LDA and QDA algorithms on the Flavia dataset. With these accuracy values, we came to the conclusion that the KNN classifier is performing better than the other two classifiers. We also tried various other classifiers including decision tree classifier, etc., but even then KNN was giving the best accuracy.

3.4 Calculated Measures for Evaluation [6] Confusion Matrix

Confusion matrix is a table which shows how a classifier performs on every test data. Rows are denoted by actual values and columns are denoted by the predicted values. It is used to measure precision, recall and accuracy of the classifier. Every cell in confusion matrix denotes the number of data values where it was actually the row class and predicted the column class.

Accuracy

In a multi-class approach, accuracy is calculated by adding numbers along the diagonal of confusion matrix. In a 2 class approach, it can be defined by sum of True Positives and True Negatives by the total numbers of predictions. Accuracy shows the number of data values which are predicted under a class under which it actually belongs.

Precision

Precision denotes how much correct is our prediction. It answers the question that when it predicts yes and then how often does it predict correct data. Precision shows the ratio of correctly identified data under a particular class among the data which is predicted under that class.

$$\text{Precision} = \frac{\text{TP}}{\text{TP} + \text{FP}}$$

Here, TP is True Positives, and FP is False Positives.

Recall

Recall is the ability of a classifier to find all positive instances. It calculates the number of times when the data is actually yes and then how often does the classifier predicts the output as yes. It is also known as sensitivity of the classifier. Recall computes that the number of values which belongs to a particular class is also predicted as that class only.

$$\text{Recall} = \frac{\text{TP}}{\text{TP} + \text{FN}}$$

Here, TP is True Positives, and FN is False Negatives

F1 score

F1 score measures the trade-off between recall and precision. It is defined as

$$\text{F1-score} = \frac{2 \times \text{precision} \times \text{recall}}{\text{precision} + \text{recall}}$$

This metric tells about the number of actual occurrences of a class in a dataset.

Average Precision

The average precision summarizes the plot as the weighted mean of precisions. Here, the increase in recall from previous threshold is taken as the weight. This measure just describes the discriminative power of the classifier independent of class distribution.

$$\text{AP} = \sum n (R_n - R_{n-1}) P_n$$

where R_n is the recall in n th threshold and P_n is the precision in n th threshold.

4 Result Analysis

4.1 Results with LDA

Test Size: 60%

No. of components: 25

KNN Classifier (No. of neighbours = 1)

Accuracy: 75.07820646506778.

Accuracy indicates that on an average, 75% of leaf images were accurately classified to their corresponding plant (Fig. 2).

Classification Report (LDA-KNN)

Class	Precision	Recall	F1-score	Support
1	0.70	0.41	0.52	34
3	0.61	0.64	0.62	44
4	0.76	0.82	0.79	39
5	0.80	0.88	0.84	41
6	0.83	0.71	0.77	35
7	0.77	0.71	0.74	34
8	0.78	1.00	0.87	31
9	0.52	0.42	0.46	36
10	0.68	0.74	0.70	34
11	0.54	0.38	0.45	34
12	0.91	0.77	0.83	39
14	0.62	0.81	0.70	32
15	0.79	0.79	0.79	39
16	0.95	0.95	0.95	40
17	0.72	1.00	0.84	28
18	0.94	1.00	0.97	46
19	0.82	0.93	0.87	40
20	0.82	0.84	0.83	37
21	0.97	0.80	0.88	40
22	0.68	0.87	0.76	31
23	0.77	0.51	0.62	39
25	0.67	0.65	0.66	37
26	0.45	0.63	0.53	30
28	0.75	0.80	0.77	30
29	0.71	0.63	0.67	27
31	0.77	0.75	0.76	32
32	0.88	0.77	0.82	30

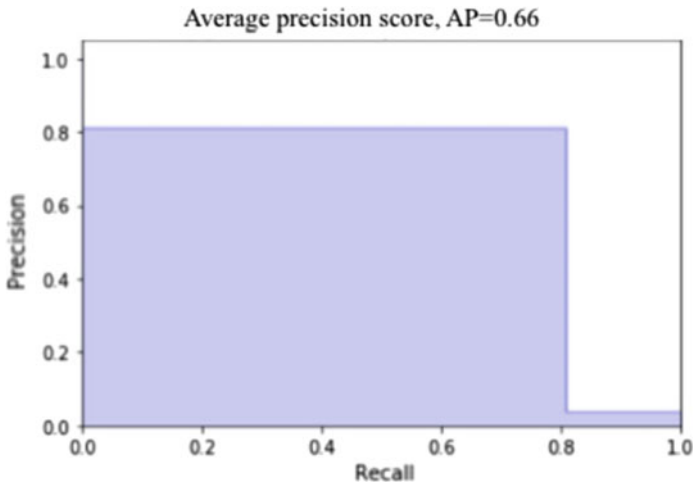


Fig. 2 Classification report and precision–recall graph of LDA in case of KNN classifier

The area under the curve is 0.66 which indicates that the probability that KNN classifier will rank a randomly chosen leaf image instance to its positive (correct) class than assigning the randomly chosen leaf image to its negative class is 0.66.

SVC Classifier

Accuracy: 67.98748696558916

This metric indicates that on an average, 67% of leaf images were accurately classified to their corresponding plant type (Fig. 3).

The area under the curve is 0.04 which indicates that the probability that this classifier will rank a randomly chosen leaf image instance to its positive (correct) class than assigning the randomly chosen leaf image to its negative class is 0.04. This shows a poor discriminative power of SVC classifier, but this classifier classifies 67% of leaf images accurately.

Logistic Regression

Accuracy: 68.61313868613139.

This metric indicates that on an average, 68% of leaf images were accurately classified to their corresponding plant type (Fig. 4).

The area under the curve is 0.72 which indicates that the probability that this classifier will rank a randomly chosen leaf image instance to its positive (correct) class than assigning the randomly chosen leaf image to its negative class is 0.72. Although it seems that the discriminative power of this classifier is more, but it actually only classifies 68% of the leaf images accurately. Hence, it does not do complete justice to its discriminative power which is independent of the class distribution.

4.2 Results with QDA

Test Size: 24%

KNN Classifier (No. of neighbours = 1)

Accuracy: 87.23958333333334

This metric indicates that on an average 87% of leaf images were accurately classified to their corresponding plant type.

This is a good accuracy (Fig. 5).

The area under the curve is 0.72 which indicates that the probability that KNN classifier will rank a randomly chosen leaf image instance to its positive (correct) class than assigning the randomly chosen leaf image to its negative class is 0.72. It seems that the discriminative power of this classifier is more, and in the similar way,

Classification Report (LDA-SVC)

Class	Precision	Recall	F1-score	Support
1	0.88	0.41	0.56	34
3	0.61	0.61	0.61	44
4	0.81	0.87	0.84	39
5	0.81	0.85	0.83	41
6	1.00	0.43	0.60	35
7	0.78	0.82	0.80	34
8	0.83	0.97	0.90	31
9	0.58	0.39	0.47	36
10	0.21	0.94	0.34	34
11	0.68	0.38	0.49	34
12	0.90	0.49	0.63	39
14	0.52	0.81	0.63	32
15	0.88	0.72	0.79	39
16	1.00	0.47	0.64	40
17	0.72	0.75	0.74	28
18	0.85	0.96	0.90	46
19	0.97	0.85	0.91	40
20	0.66	0.95	0.78	37
21	0.97	0.80	0.88	40
22	0.67	0.77	0.72	31
23	0.78	0.54	0.64	39
25	0.69	0.59	0.64	37
26	0.52	0.47	0.49	30
28	0.95	0.70	0.81	30
29	0.70	0.26	0.38	27
31	0.84	0.66	0.74	32
32	0.88	0.73	0.80	30

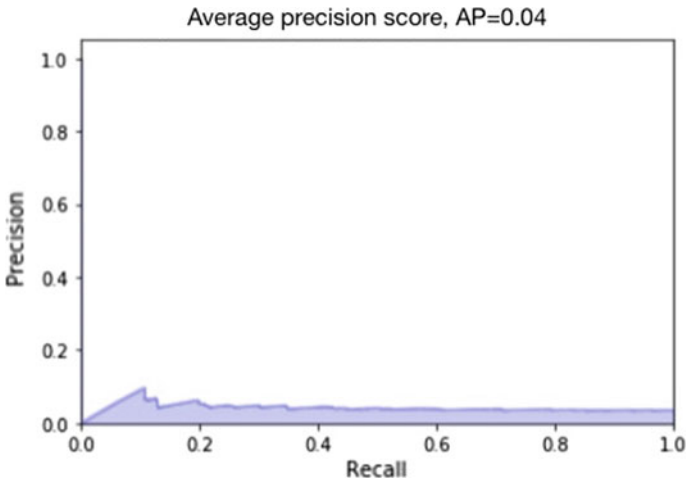


Fig. 3 Classification report and precision–recall graph of LDA in case of SVC classifier

Classification Report(LDA-LogisticRegression)

Class	Precision	Recall	F1-score	Support
1	0.76	0.38	0.51	34
3	0.60	0.55	0.57	44
4	0.71	0.74	0.72	39
5	0.66	0.85	0.74	41
6	1.00	0.51	0.82	35
7	0.74	0.74	0.38	34
8	0.71	0.97	0.62	31
9	0.43	0.33	0.39	36
10	0.49	0.85	0.83	34
11	0.50	0.32	0.50	34
12	0.94	0.74	0.77	39
14	0.50	0.50	0.94	32
15	0.74	0.79	0.73	39
16	0.93	0.95	0.81	40
17	0.59	0.96	0.76	28
18	0.75	0.87	0.78	46
19	0.73	0.80	0.88	40
20	0.68	0.92	0.67	37
21	0.94	0.82	0.55	40
22	0.57	0.81	0.42	31
23	0.74	0.44	0.55	39
25	0.47	0.38	0.42	37
26	0.61	0.57	0.59	30
28	0.77	0.80	0.79	30
29	0.70	0.52	0.60	27
31	0.69	0.69	0.69	32
32	0.83	0.63	0.72	30

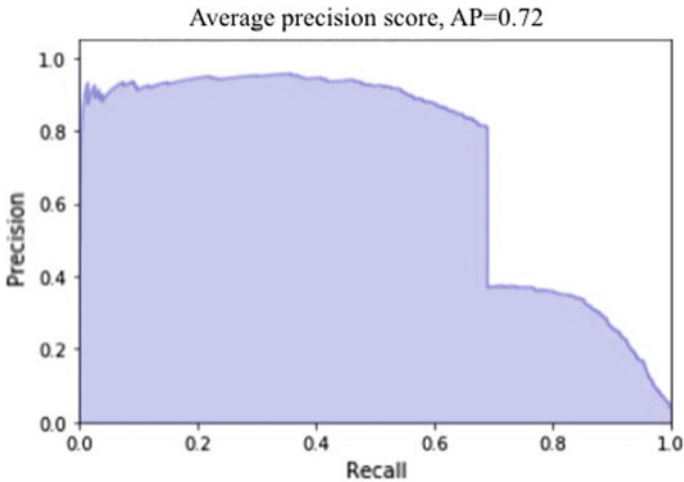


Fig. 4 Classification report and precision–recall graph in case of logistic regression

Classification Report(QDA-KNN)

Class	Precision	Recall	F1-score	Support
1	1.00	0.64	0.78	11
3	0.85	0.89	0.87	19
4	0.88	1.00	0.93	14
5	0.88	0.78	0.82	18
6	1.00	0.76	0.87	17
7	0.83	1.00	0.91	10
8	0.89	1.00	0.94	17
9	1.00	0.86	0.92	7
10	0.65	0.93	0.76	14
11	0.53	0.73	0.62	11
12	1.00	0.78	0.88	23
14	0.64	0.64	0.64	14
15	0.71	0.91	0.80	11
16	1.00	0.93	0.96	14
17	0.83	0.83	0.83	12
18	1.00	1.00	1.00	14
19	1.00	0.95	0.97	20
20	0.88	0.94	0.91	16
21	1.00	1.00	1.00	11
22	0.93	1.00	0.96	13
23	0.75	0.75	0.75	16
25	0.93	0.88	0.90	16
26	0.73	0.89	0.80	9
28	1.00	1.00	1.00	11
29	0.89	0.67	0.76	12
31	1.00	0.80	0.89	15
32	0.95	1.00	0.97	19

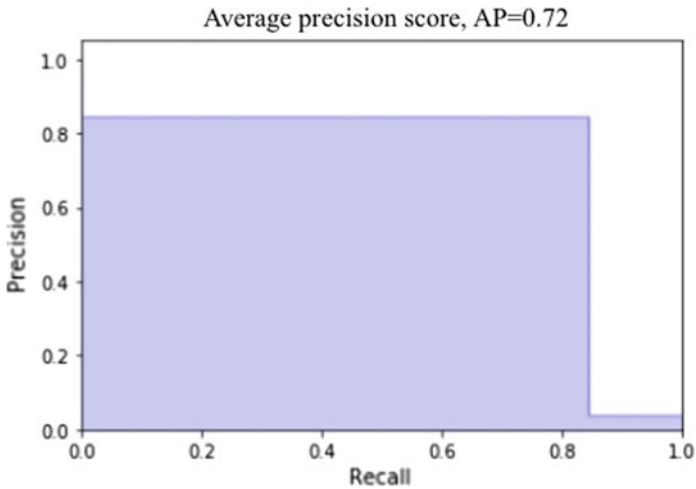


Fig. 5 Classification report and precision–recall graph of QDA in case of KNN classifier

it also classifies 87% of the leaf images accurately. Hence, this classifier along with QDA delivers a good performance on the Flavia dataset.

SVC Classifier

Accuracy: 84.375

This metric indicates that on an average, 84% of leaf images were accurately classified to their corresponding plant type.

This is a fairly acceptable accuracy (Fig. 6).

The area under the curve is 0.05 which indicates that the probability that this classifier will rank a randomly chosen leaf image instance to its positive (correct) class than assigning the randomly chosen leaf image to its negative class is 0.05. This shows a very poor discriminative power of SVC classifier, but on contrary, this classifier classifies 84% of leaf images accurately.

Logistic Regression Accuracy: 69.27083333333334

This metric indicates that on an average, 69% of leaf images were accurately classified to their corresponding plant type (Fig. 7).

The area under the curve is 0.76 which indicates that the probability that this classifier will rank a randomly chosen leaf image instance to its positive (correct) class than assigning the randomly chosen leaf image to its negative class is 0.76. Although it seems that the discriminative power of this classifier is more, but it actually only classifies 69% of the leaf images accurately. Hence, it does not do complete justice to its discriminative power which is independent of the class distribution.

5 Conclusion

In this paper, we have worked on the Flavia dataset which is a plant leaf species dataset. We have applied LDA and QDA algorithms on the dataset to reduce the number of features in the leaf images, and later, we have used classifiers, namely KNN, SVC and logistic regression which classified the leaf images to their accurate plant species classes. After running the algorithms, we found out that KNN classifier with number of neighbours equating to one gave maximum accuracy in the case of both LDA and QDA algorithms. In our result analysis, one thing that we also noticed was that the rows of the covariance matrix of some of the plant species classes were linearly dependent on each other. The linear dependency in the rows indicated that there were many images that were of similar pixel intensities or in other words, the features of those leaf images were redundant. Due to this redundancy, the overall accuracy of the dataset was decreasing. Hence, we eliminated those classes from our dataset which were giving us similar covariance matrices. In our experiment, we have also shown all the other evaluation metrics including precision, recall, f1-score, precision–recall graph, support, etc., with every classifier in the case of both LDA and QDA. The best accuracy that we got from LDA (with test size 60%) was 75.07%.

Classification Report(QDA-KNN)-1

Class	Precision	Recall	F1-score	Support
1	1.00	0.64	0.78	11
3	0.85	0.89	0.87	19
4	0.88	1.00	0.93	14
5	0.88	0.78	0.82	18
6	1.00	0.76	0.87	17
7	0.83	1.00	0.91	10
8	0.89	1.00	0.94	17
9	1.00	0.86	0.92	7
10	0.65	0.93	0.76	14
11	0.53	0.73	0.62	11
12	1.00	0.78	0.88	23
14	0.64	0.64	0.64	14
15	0.71	0.91	0.80	11
16	1.00	0.93	0.96	14
17	0.83	0.83	0.83	12
18	1.00	1.00	1.00	14
19	1.00	0.95	0.97	20
20	0.88	0.94	0.91	16
21	1.00	1.00	1.00	11
22	0.93	1.00	0.96	13
23	0.75	0.75	0.75	16
25	0.93	0.88	0.90	16
26	0.73	0.89	0.80	9
28	1.00	1.00	1.00	11
29	0.89	0.67	0.76	12
31	1.00	0.80	0.89	15
32	0.95	1.00	0.97	19

Average precision score, AP=0.05

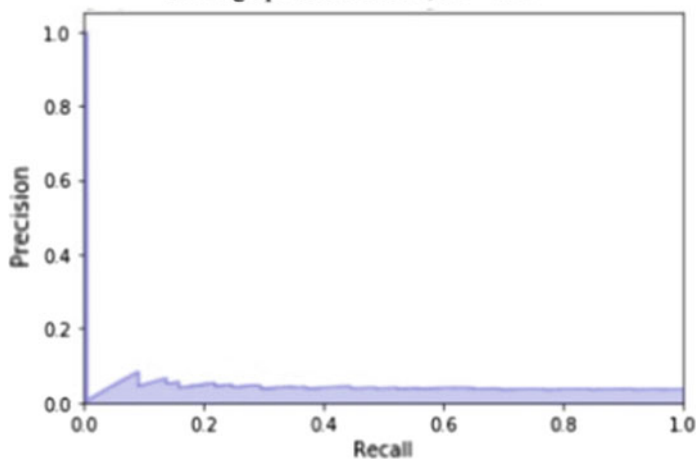


Fig. 6 Classification report and precision–recall graph in case of QDA using SVC classifier

Classification Report(QDALogisticRegression)

Class	Precision	Recall	F1-score	Support
1	0.83	0.45	0.59	11
3	0.58	0.37	0.45	19
4	0.71	0.86	0.77	14
5	0.59	0.72	0.65	18
6	0.92	0.65	0.76	17
7	0.67	1.00	0.80	10
8	0.89	1.00	0.94	17
9	0.12	0.14	0.13	7
10	0.50	0.79	0.61	14
11	0.56	0.45	0.50	11
12	0.88	0.61	0.72	23
14	0.77	0.71	0.74	14
15	0.67	0.73	0.70	11
16	0.76	0.93	0.84	14
17	0.82	0.75	0.78	12
18	0.67	0.86	0.75	14
19	0.73	0.80	0.76	20
20	0.65	0.94	0.77	16
21	0.71	0.91	0.80	11
22	0.71	0.77	0.74	13
23	0.62	0.50	0.55	16
25	0.53	0.50	0.52	16
26	0.60	0.33	0.43	9
28	0.67	0.91	0.77	11
29	0.86	0.50	0.63	12
31	0.67	0.67	0.67	15
32	1.00	0.63	0.77	19

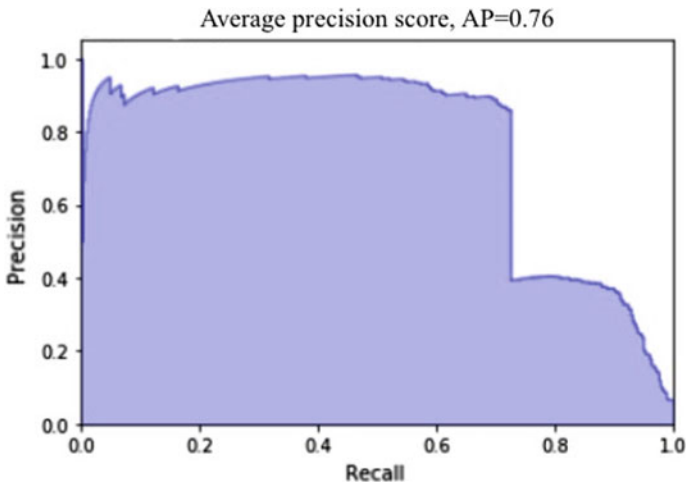


Fig. 7 Classification report and precision–recall graph of QDA in case of logistic regression

One drawback of LDA algorithm is that it assumes that the covariance matrices of all the classes are same or in other words, they are homogeneous in nature, whereas this limitation is not there in the QDA algorithm. Hence, QDA with test size 24% resulted in a better accuracy with the classifiers. Therefore, the takeaway of our experiment is that QDA performed better than LDA on the Flavia dataset giving us an accuracy of 87.23% with the KNN classifier (considering the number of neighbours to be equal to 1).

References

1. Amlekar M, Manza RR, Yannawar P, Gaikwad AT (2014) Leaf features based plant classification using artificial neural network. *IBMRD J Manage Res* 3(1):224–232
2. Wu SG, Bao FS, Xu EY, Wang YX, Chang YF, Xiang QL (2007) A leaf recognition algorithm for plant classification using probabilistic neural network. In: 2007 IEEE international symposium on signal processing and information technology. IEEE, pp 11–16
3. Rahmani ME, Bouarara HA, Amine A, Hamou RM, Menad H (2016) New supervised approach for plant leaves classification using artificial social bees. *Int J Organ Collective Intell (IJOCI)* 6(1):15–28
4. New study shows over one fifth of the world's plants are under threat of extinction (2010) Retrieved from <http://www.iucn.org>
5. Quadratic Discriminant Analysis (n.d.). Retrieved from <https://newonlinecourses.science.psu.edu/stat505/node/97/>
6. Statistical Learning—Discriminant Analysis (n.d.) Retrieved from https://gerardnico.com/data_mining/discriminant_analysis
7. Raschka S (2014) Linear discriminant analysis—bit by bit. Retrieved from https://sebastianraschka.com/Articles/2014_python_lda.html
8. Sklearn neighbours Kneighbours Classifiers (n.d.) Retrieved from <https://scikit-learn.org/stable/modules/generated/sklearn.neighbors.KNeighborsClassifier.html>
9. Du J, Huang D, Wang X, Gu X (2005) Shape recognition based on radial basis probabilistic neural network and application to plant species identification. In: International symposium on neural networks. Springer, Berlin, pp 281–285
10. Dimensionality Reduction (n.d.) Retrieved from https://en.wikipedia.org/wiki/Dimensionality_reduction
11. Training Models (n.d.) Retrieved from <https://www.oreilly.com/library/view/hands-on-machine-learning/9781491962282/ch04.html>
12. Metre V, Ghorpade J (2013) An overview of the research on texture based plant leaf classification. Preprint at [arXiv:1306.4345](https://arxiv.org/abs/1306.4345)
13. Zhenjiang M, Gandelin MH, Baozong Y (2006) An OOPR-based rose variety recognition system. *Eng Appl Artif Intell* 19(1):79–101
14. Chaki J, Parekh R (2011) Plant leaf recognition using shape based features and neural network classifiers. *Int J Adv Comput Sci Appl* 2(10)
15. Gu X, Du JX, Wang XF (2005) Leaf recognition based on the combination of wavelet transform and gaussian interpolation. In: International conference on intelligent computing. Springer, Berlin, pp 253–262
16. Ye Y, Chen C, Li CT, Fu H, Chi Z (2004) A computerized plant species recognition system. In: Proceedings of 2004 international symposium on intelligent multimedia, video and speech processing, 2004. IEEE, pp 723–726
17. Linear and Quadratic Discriminant Analysis (n.d.) Retrieved from http://uc-r.github.io/discriminant_analysis

18. Linear and Quadratic Discriminant Analysis (n.d.) Retrieved from <http://mlweb.loria.fr/book/en/lda.html>
19. Hackeling G (2017) Mastering machine learning with scikit-learn. Packt, Birmingham

Graph Isomorphism Using Locality Sensitive Hashing



R. Vinit Kaushik  and Kadiresan Nalinadevi 

Abstract Isomorphism has been a long-standing research problem, an instance of which is to determine if two graphs are structurally the same. Verification of isomorphism gets computationally intensive for huge graphs with nodes in the order of millions. The computational complexity is high because the current forms of graph representations require complex data structures for processing. This paper presents an experimental proof of an expedient means to detect isomorphism, using Locality Sensitive Hashing (LSH). LSH was originally designed to find similar document pairs, within massive datasets, in polynomial time. The graphs are modeled as simple bag-of-words documents, using the proposed *Node-Neighbor-Degree* sequence approach. For huge graphs, this representation facilitates in-memory computation. This approach was validated on graphs, with nodes in the order of thousands. The proffered method was found to be significantly faster than conventional graphic tools.

Keywords Graph isomorphism problem · Linear time complexity · Locality · Sensitive hashing · Massive datasets · Hashing

1 Introduction

The mathematical definition of isomorphism is a one-to-one correspondence between two mathematical sets. Graph isomorphism (GI) problem basically involves computational determination of whether two finite graphs have a one-to-one correspondence with respect to the vertices and edges of the graphs. Solvability of the GI problem in polynomial time has been an active research topic, due to inadequate evidence that the problem is NP-complete. Therefore, it is widely known to belong to the

R. V. Kaushik (✉) · K. Nalinadevi
Department of Computer Science and Engineering, Amrita School of Engineering, Amrita
Vishwa Vidyapeetham, Coimbatore, India
e-mail: vinitkaushik24@gmail.com

K. Nalinadevi
e-mail: k_nalinadevi@cb.amrita.edu

© Springer Nature Singapore Pte Ltd. 2021
G. S. Hura et al. (eds.), *Advances in Communication and Computational
Technology*, Lecture Notes in Electrical Engineering 668,
https://doi.org/10.1007/978-981-15-5341-7_25

NP-intermediate class of complexity. This arises due to the fact that isomorphism for many special classes of graphs, can indeed be solved in polynomial time [1].

There are several applications of the GI Problem [2] in the field of mathematical chemistry, where GI is used to categorize chemicals based on their chemical structure. In organic mathematical chemistry, isomorphism is used to generate molecular graphs, and also for computer synthesis. GI plays a significant role in electronic design automation, which is the basis of the layout versus schematic step of circuit design [3], here it is used to verify whether the electric circuit represented by a circuit schematic and a given integrated circuit layout is the same. Graph theory such as GI are also used for robot traversal in a network [4]. GI can also be used to show that two languages are equal in the field of automata theory. Some of the other applications like checking for similarity in fingerprints, facial, and retina scanners in the field of security.

An emerging field of GI applications is in the area of Zero-Knowledge Proofs. Zero-Knowledge Proofs, a concept under cryptography, serves as a form of authentication in cryptocurrency. zk-SNARKS (Zero-Knowledge Succinct Non-Interactive Argument of Knowledge), a variant of Zero-Knowledge Proofs, is being used in ZCash, a cryptocurrency similar to Bitcoin. Zero-Knowledge Proof requires computationally intensive problems to be effective. Large isomorphic graph pairs would be excellent candidates to implement the same [5].

There are various solvers of isomorphism, the algorithms that currently in use are nuances of one core idea of tree construction [6]. To solve the same problem, this paper proposes the implementation of an information retrieval algorithm called “Locality Sensitive Hashing” (LSH) [7] for solving GI problems. The LSH algorithm is traditionally used to find similar document pairs in datasets of huge size, (order of a million documents) in polynomial time. LSH has been used in several other applications such as Traffic Density Analysis [8]. This paper proffers a novel idea to model a graph as documents of *Node-Neighbor-Degree* sequence and compute the graph’s signature with a polynomial time complexity. Generally, documents are articles (bag-of-words document). The graph is represented as bag-of-words which can be used for shingling. The representation is such that two graphs having the same structure will have the same document form of representation. LSH is then applied over these documents, identified as a candidate pair of being similar, ensue in a pair of isomorphic graphs. The rest of this paper is organized as follows. Section 2 presents an overview of the past research in the GI context, the tools used in solving the isomorphism, and LSH literature. Section 3, describes an architecture of the proposed approach, LSH modeling using *Node-Neighbor-Degree* sequence and algorithmic complexity. Section 4, describes the dataset used to conduct the experiment. Section 5, provides the performance analysis and application of the result in graph problems. Finally, Sect. 6 provides a conclusion and future work.

2 Related Work Resume

2.1 Literature of Graph Isomorphism

Algorithms that practically solve the isomorphism problem belong to two main categories. The first is a direct approach, where they compare graphs based on some invariants, and apply a classical depth-first search algorithm, to traverse the graph and a backtracking algorithm, to find the similarity in traversal. This generally involves the construction of trees, where each node represents a combination of the traversal of nodes. The leaves and nodes are pruned later based on certain optimizations [6].

The second approach used a canonical labeling algorithm. This is an algorithm where a function returns a “certificate” of a given input graph. This “certificate” is a form—labeling of the vertices such that, two graphs that are isomorphic will have the same labeling, hence the same “certificate”. These vertex labeling routines have a polynomial complexity of solving the isomorphism problem, but they do not work with all types of graphs, therefore these algorithms are incomplete [9].

Two practical approaches, used by a number of tools such as nauty, bliss, traces [6] identify the graph invariants such as graph automorphisms, and searches through them to find isomorphism.

A mathematical approach considers the idea that if two graphs are isomorphic, then their adjacency matrices should also be the same. This method involves transformation of the adjacency matrix, using another permutation matrix, such that the transformation will result in the adjacency matrix of the other isomorphic graph [10].

The method proposed, in this paper, used belongs to the second category. It is a form of canonical vertex labeling, but rather than assigning labels from $(1, n)$, the proposed algorithm assigns them with strings. These strings, generated using the degrees of vertices, are such that they are the same value for the same vertex, in the graph’s isomorphic graph.

2.2 Locality Sensitive Hashing

Three fundamental steps are performed in sequence, to find the similarity among documents: shingling, minhashing, and Locality Sensitive Hashing [7].

Shingling In this step, every “ n ” consecutive words in a document are combined to generate a shingle (n -gram). Collections of such shingles represent a specific document. These shingles are then hashed, using a hashing function, and the derived hash-code is a smaller signature of the document [7].

Minhashing When all the shingles for a document have been obtained, a shingle-document matrix is generated. This matrix is usually very large and sparse. In order to obtain a representation of the document that can be accommodated in memory, the matrix is hashed, with a different permutation of a document’s indices. For each

permutation, the least value of the document index containing the shingle is considered. This generates Minhash signature for documents in such a way that the fraction of similarity in Minhash signatures is approximately equal to the actual similarity of the documents [7].

Locality Sensitive Hashing Once the Minhash signatures are obtained, a Minhash-document matrix is generated. In the LSH step, the matrix rows are split into bands. Each band contains a set of rows. The Minhash signatures, in these rows, are then compared, by hashing each band with a random hash function. The column in a band, which hash to the same hash-code or “bucket”, will be two documents that are candidate pairs of being similar [7]. The distance measure used to compute the similarity of candidate isomorphic pair is Jaccard similarity as in [7].

3 Proposed Architecture

This section discusses the approach followed to model the graph as a bag-of-words document. The application of the LSH algorithm over this document finds similar graphs (Fig. 1).

First, synthetic graphs (random-graphs) are generated using the *graph-tool* and hash functions are used to generate the isomorphic pairs. These graphs are further modeled to bag-of-words format [7], which serves as input to the LSH.

Consider a graph, $G = \langle V, E \rangle$ where $V = \{v_1, v_2, \dots, v_m\}$ representing m nodes and $E = \{e_1, e_2, \dots, e_n\}$ representing n edges; various representations of the graph was considered as bag-of-words, such that the shingled documents are similar. Below are the various tested representations of the graph.

3.1 Adjacency Matrix Form

For this representation, the adjacency matrix $A_{n,n} = |V| \times |V|$ was converted to a set of words. Here each adjacency array, $A[i]$, where i is $(1, n)$ is taken as a word. The objective is to compare the adjacency matrices as zeros and ones, and the graph signatures of two isomorphic graphs will contain an equal number of ones and zeros. This representation failed because a simple renaming, or another graph with the same number of vertices and edges would have the same bag-of-words document.

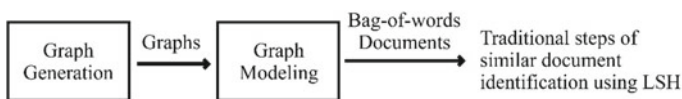


Fig. 1 Program architecture diagram

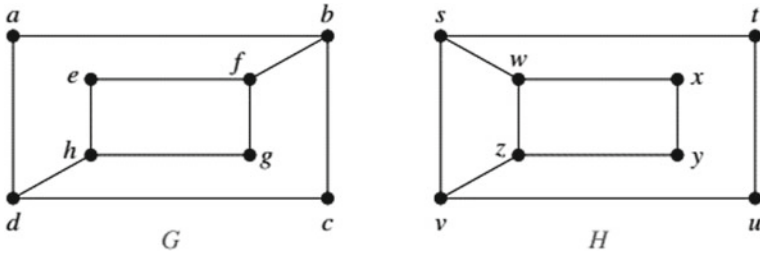


Fig. 2 Non-isomorphic graphs with same degree sequence

3.2 Degree Sequence Form

Degree sequence of a graph is the degrees of every vertex of the graph, written in ascending order. This method again failed as the graph signature was not unique. Two graphs that are not isomorphic, but have equal number of vertices, with same degree, also have same graph signatures. An instance is shown in Fig. 2; both the graphs, G and H, have equal number of vertices with same degree.

The signatures generated for G was (2, 2, 2, 2, 3, 3) and for H was (2, 2, 2, 2, 3, 3). Though the computed graph signatures are similar, the graphs are not isomorphic, hence this approach had to be discarded.

3.3 Novel Approach of Node-Neighbor-Degree Sequence

This representation efficiently generated graph signatures that captured the essence of a graph’s structure and adjacency. Two graphs with the same structure have the same graph signature, irrespective of the labeling of the graph vertices.

As mentioned before, the proposed approach is nuance of the degree sequence, but the degree sequence is computed and stored for every vertex, rather than the entire graph as a whole. This degree sequence is called the **Node-Neighbor-Degree** sequence.

In graph G, every vertex in v_i has a degree $d(v_i)$, which is equal to the number of vertices it is connected to. The approach considers only undirected graphs, and it generates the degree sequence, at every vertex. The bag-of-words form of the graph contains “n” number of words, each corresponding to a vertex.

Consider $neighbor(v_i) = U = \{u_1, u_2, \dots, u_{d(v_i)}\}$, the word is the ascending order degree sequence of the vertices in U. This sequence is specific to each vertex; hence, each vertex is now given its neighbor’s degree sequence as a label, it is a form of canonical labeling. An instance is shown in Fig. 3.

As shown, the node’s neighbor’s degree sequence is listed for each node. These sequences are then added as individual strings to the document, forming the required bag-of-words. This document is then input to Locality Sensitive Hashing (LSH).

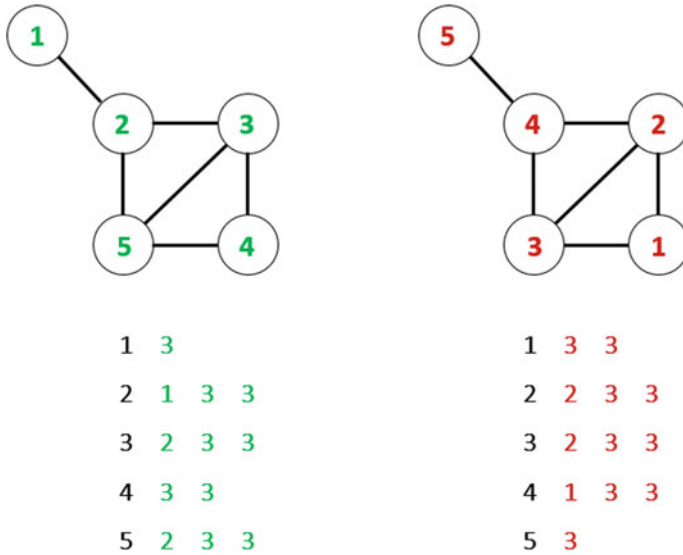


Fig. 3 Neighbor's degree sequence

3.4 Complexity of the Algorithm

The objective of this paper is to model the graph and compute the graph signature with a complexity of $O(n)$. Achieving this would theoretically solve the graph isomorphism problem in $O(n)$ time complexity, as this would be an input to the LSH algorithm, whose run time is also $O(n)$.

The current flow of the program traverses the graph (using breadth-first search traversal) twice to generate the graph signatures. The BFS (breadth-first search) traversal has a known complexity of $O(V + E)$, where V is the number of vertices and E is the number of edges.

Including the LSH algorithm complexity and computing the effective complexity of modeling graphs to obtain graph similarity, the overall complexity is $O(V + E) + O(V + E) + O(n) \equiv O(n)$

4 Experimental Setup

4.1 Dataset Description

The dataset was generated using the Python *graph_tool* [11]. Dataset of 20 graphs was generated, named graph k , where k is (1, 20). Each graph comprised of 300 vertices and 37,489 edges.

Three isomorphic pairs of graphs have been randomly inserted in the dataset, namely (graph 6, graph 14), (graph 7, graph 17) and (graph 11, graph 19). Each of these isomorphic graph pairs were non-isomorphic with the remaining 18 graphs. The 14 non-isomorphic graphs are non-isomorphic to one-another as well.

The ground truth of the dataset generated was verified using the *isomorphism()* API (Application Program Interface) supported in the *graph_tool*. All the combinations (${}^{20}C_2$) of graphs were checked, which was a total of 190 comparisons.

4.2 Finding Similarity Between Documents

The construction of shingle is discussed for a smaller graph. The sample isomorphic graph generated by the *graph_tool* of 6 nodes is shown in Fig. 4.

Shingling of Graphs The bag-of-words of each of the graph in the dataset is shingled as a 1 g shingle. Figure 5 shows shingle instance of a 6 node isomorphic graph pair.

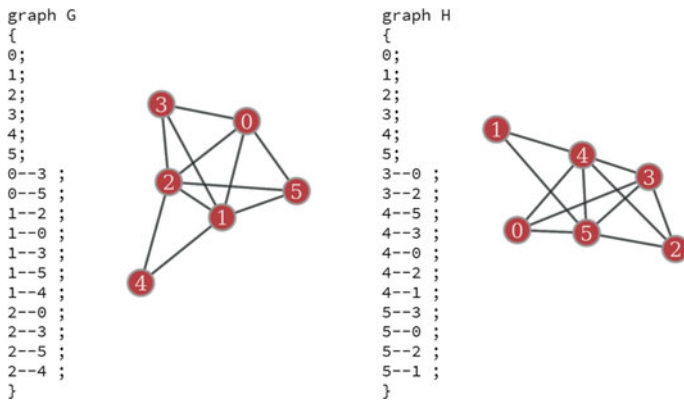


Fig. 4 Nodes and edges representation as obtained from graph_tool

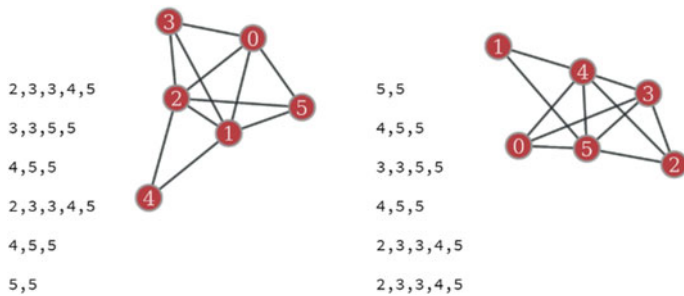


Fig. 5 Obtained the bag-of-words format by traversing the graph input twice

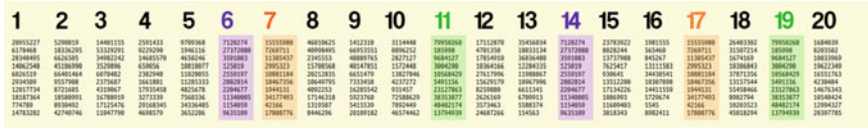


Fig. 6 The 20 * 10 Minhash Signature matrix of 20 graphs, highlighted columns are similar isomorphic graphs

It can be observed that both the graphs have same set of shingles but in different orders.

The obtained shingles were mapped to 32-bit shingles, using Python. These shingle IDs were next used to obtain the Minhash signature matrix of the document. Similar procedure was used for shingling the 20 graphs in the dataset.

Minhashing The obtained shingles IDs are then permuted, using random hash values. For each permutation, the least value of the document index containing the shingle ID is added to the signature matrix of the document. At this stage, each column in the matrix represents a set of a document. Similar documents will have similar column values. The Minhash matrix of the 20 graphs is shown in Fig. 6.

Locality Sensitive Hashing The LSH algorithm suggests to set the length of Minhash “k” to 100, for 1 million documents [7]. For this experiment, the length of the Minhash signature was set to 10. Minhash-Document matrix was of the order 20 * 10. The bands were set to two (b = 2), with each band having 5 rows (r = 5). The threshold of similarity is given as (1/b)^(1/r) [7]. Hence this set the threshold of similarity to 87.055% and higher. This threshold was the maximum that was possible with 20 * 10 Minhash matrix.

This ensured that only the isomorphic pairs were detected as candidate pairs because isomorphic pairs have a similarity of 100%. Figure 7 shows the candidate pairs in the buckets are the same isomorphic graph pairs inserted in the dataset. Each band was hashed with a random vector of row number of dimensions, and the hash-code was the cosine angle made against the column values of the band.

4.3 Finding the Bijection

Given a graph G, and its isomorphic pair H, the vertices of G can be mapped one-to-one to the vertices of H, by considering each vertex’s Node-Nearbor-Degree sequence as a document. Hence, similar documents will imply the mapping of the respective vertices.

The Node-Nearbor-Degree sequence is unique for nodes of a non-symmetric graph. This was tested on 50, 100, 300, 500, 1000, and 2000 node graphs. It was observed that with the increase in connectivity of the graph, the number of unique

```
Bucket 1 : [9]
Bucket 2 : [4]
Bucket 3 : [13]
Bucket 4 : [6, 14] < Duplicate Detected!

Bucket 5 : [18]
Bucket 6 : [8]
Bucket 7 : [16]
Bucket 8 : [1]
Bucket 9 : [3]
Bucket 10 : [13]
Bucket 11 : [16]
Bucket 12 : [8]
Bucket 13 : [4]
Bucket 14 : [5]
Bucket 15 : [2]
Bucket 16 : [18]
Bucket 17 : [2]
Bucket 18 : [1]
Bucket 19 : [15]
Bucket 20 : [20]
Bucket 21 : [20]
Bucket 22 : [12]
Bucket 23 : [6, 14] < Duplicate Detected!

Bucket 24 : [11, 19] < Duplicate Detected!
Bucket 25 : [11, 19] < Duplicate Detected!

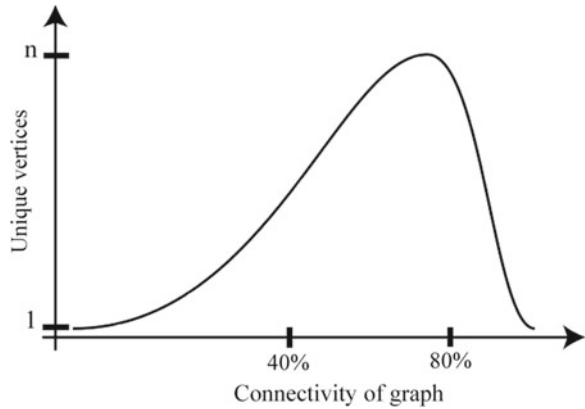
Bucket 26 : [3]
Bucket 27 : [7, 17] < Duplicate Detected!

Bucket 28 : [10]
Bucket 29 : [10]
Bucket 30 : [7, 17] < Duplicate Detected!

Bucket 31 : [9]
Bucket 32 : [5]
Bucket 33 : [12]
Bucket 34 : [15]
True positives: 3 / 3
False positives: 0
```

Fig. 7 The candidate pairs detected inside LSH buckets

Fig. 8 Variation of the number of unique nodes for randomly generated 50, 100, 300, 500, 1000 and 2000 vertex graphs



nodes in a graph follows a curve similar to a normal distribution curve. Figure 8 shows the connectivity plotted against the number of unique nodes in a graph.

4.4 Results Analysis

The time taken, to obtain the three isomorphic pairs from the dataset of 20 graphs, using LSH, was 0.08711 s which is roughly 25 times faster compared to the *graph_tool isomorphism()* API which took 2.23560 s to obtain the same result.

5 Conclusion and Future Work

The presented approach with Node-Neighbor-Degree sequence representation of the graph as bag-or-words document, ensures that two isomorphic graphs will always have the same graph signature. The graph signatures are ideal inputs for the LSH algorithm, which further computes the similarity of documents, and a candidate pair identified by LSH, shall be the documents of two isomorphic graphs. The modeling of the graph can be achieved using only traversal algorithms, hence achieving the computation in $O(n)$ time.

Anomalies exist for bijection computation of two isomorphic graphs, which are highly symmetric. These anomaly identifications may be done by applying set theory concepts to automorphic graphs generated by the model. Another possibility would be to relabel the invariant vertices in the graph signatures and then traverse the graph again. This program can be tested against some of the toughest graphs such as the Hadamard matrix, Incidence graph of projective plane, and Latin squares [6].

References

1. Babai L (2015) Graph isomorphism in quasipolynomial time. [arXiv:1512.03547v1](https://arxiv.org/abs/1512.03547v1)
2. Rachna S, Vinod MV (2017) A comparative study of graph isomorphism applications. *Int J Comput Appl* 162(7):34–37
3. <https://www.emathzone.com/tutorials/group-theory/properties-of-isomorphism.html>. Accessed 10 Nov 2018
4. Manjusha R, Sunny KA (2015) Metric dimension and uncertainty of traversing robots in a network. *Int J Appl Graph Theor Wirel Ad hoc Netw Sens Netw (GRAPH-HOC)* 7(2/3)
5. Daniel N, Pascal S (2017) Benchmark graphs for practical graph isomorphism. [arXiv:1705.03686](https://arxiv.org/abs/1705.03686)
6. Brendan DM, Adolfo P (2013) Practical graph isomorphism II. [arXiv:1301.1493v1](https://arxiv.org/abs/1301.1493v1)
7. Jure L, Anand R, Jeffrey DU (2011) Mining of massive datasets. Cambridge University Press, New York
8. Sowmya K, Kumar PN (2018) Traffic density analysis employing locality sensitive hashing on GPS data and image processing techniques. *Lecture notes in computational vision and biomechanics*, vol 28, pp 959–971
9. Aimin H, Qingqi Z, Yurou C (2014) A practical graph isomorphism algorithm with vertex canonical labeling
10. Dan R, Ron K, Alfred MB (2012) Graph isomorphisms and automorphisms via spectral signatures. *IEEE Trans Pattern Anal Mach Intell*
11. <https://graph-tool.skewed.de>. Accessed 20 Aug 2019

Comparative Analysis of Image Segmentation Techniques



Snehil Saxena, Sidharth Jain, Saurabh Tripathi, and Kapil Gupta

Abstract Image segmentation is a prominent task done in computer vision. Image thresholding is one such technique in image segmentation. Thresholding is a method of categorizing image intensities into two classes and on the basis of that yielding an image which is a binary image, and ideally also has all the fine details of region of interest which an image should have for analysis. Image thresholding is widely used as it reduces the computational cost of processing the image and makes processing feasible in real-world applications like medical imaging, object detection, recognition task, character recognition, etc. This paper dwells into the depth of thresholding techniques to know which technique can perform better on all kinds of images so as to extract region of interest. We found out that not every technique is good for all cases, Otsu's global thresholding is a promising and faster way to segment and generate a binary image, but works well with images having negligible noise and region of interest already being very much clear in the original image, whereas applying methods like Otsu's thresholding on sliced blocks of images and then merging them or applying moving averages (sliding windows) on images having noise which is distributed in a specific region of image, moving averages gave result better on images which have distributed gradient noise. Whereas the hybrid technique used are a combination of global and local thresholding.

Keywords Segmentation · Thresholding · Otsu's · Niblack's · Sauvola's · Image processing

S. Saxena · S. Jain (✉) · S. Tripathi · K. Gupta
Department of Computer Applications, National Institute of Technology, Kurukshetra, India
e-mail: sidharthjain97@gmail.com

S. Saxena
e-mail: saxenasnehil@gmail.com

S. Tripathi
e-mail: srhtrip@gmail.com

K. Gupta
e-mail: kapil@nitkkr.ac.in

1 Introduction

A digital image is fundamentally a two-dimensional function of spatial coordinates. Let $f(x, y)$ represents the image (Gonzalez & Woods, Digital image processing: Pearson 3rd edition: [1]). The amplitude of the f at a given set of coordinates (x, y) gives a positive scalar quantity which specifies the intensity value of the image. The function can be expressed as the product of:

$$f(x, y) = i(x, y) \times r(x, y)$$

where $i(x, y)$ is the amount of illumination incident on the scene,
 $r(x, y)$ is the amount of illumination reflected by the objects.

Digital image processing is an area where with the use of computer algorithms we can process digital images. The main objective of image processing is to extract useful information from images. It also gives several advantages over analog image processing. And segmentation is the first essential step of digital image processing [2]. Image segmentation can be defined as the process of partitioning an image into similar groups such that each group or region is more similar but when two or more groups taken into account, they are heterogeneous [3]. There are various applications of image segmentation. For example, object detection deals with identifying instances of semantic objects of various classes (such as buses, skyscrapers, living beings) in digital images. It is majorly used in computer vision tasks such as face recognition, object detection. It is also used in tracking objects, for example, tracking a ball during a football match, tracking movement of bat in cricket, tracking a movement of a person in a video. There are many techniques developed for image segmentation still there is no single technique which is considered as good for all type of images [3]. Since algorithms are developed based on the distribution of the image's intensity value, therefore, algorithms developed for a class of images cannot give good results for another class of images. Segmentation also depends on many other features that the image accommodates [4]. The efficiency of the segmentation process is its speed, good shape matching and better shape connectivity with its segmenting result [5].

2 Related Work

Some other researchers have done some significant amount of work.

R. Yogamangalam, B. Karthikeyan focused on segmentation techniques like thresholding, Model-based, Edge detection, Clustering, and also Markov Random Field for noise cancellation in images. Salem Saleh Al-amri, N. V. Kalyankar, and Khamitkar S. D employed segmentation image techniques by using five threshold methods as mean method, P-tile method, Histogram Dependent Technique (HDT), Edge Maximization Technique (EMT), and visual technique. M. Khan, Ravi. S adopted intensity-based segmentation, Discontinuity based methods like First-order

derivative operators namely Robert's operator, Prewitt's operator, Sobel's Operator, and Second-Order Derivative operators, namely Laplacian of Gaussian Operator, Canny Edge Operator and REGION BASED SEGMENTATION. Tien-Ying Kuo, Yun-Yang Lai, Yi-Chung Lo performed Otsu's, Niblack's, and Sauvola's which effectively considering the image characteristics to give better results as compared to employing the techniques separately. While the above-mentioned researchers focused on various other techniques, our experiment aims to explore the performance of Otsu's thresholding on both global and local levels and using it with Niblack's and Sauvola's method, thus checking the performance of hybrid technique as well.

3 Literature Review

3.1 Global Thresholding

It can be applied to the images when the intensity distribution of the foreground objects and background objects are quite distinct [6]. In this, a single value is chosen to binarize the image. The intensity value of the pixels which are greater than the computed threshold value is considered as foreground whereas the pixels value which are less are considered as background. So, calculating a single value can be done in various ways. One of the easiest ways is to use each value between 0 and 255 as a threshold value and check and compare the result to get the best-suited value but it requires lots of computations [7].

K-Means Clustering

K-Means clustering algorithm is an unsupervised learning algorithm in which we are given some data sets of items with some features of it. The main focus is to categorize these data points of the data sets into groups. To know which data item, lie in which group, we make use of homogeneity and this homogeneity is achieved through Euclidean distance.

Otsu's Method

In computer vision and image processing, Otsu's method, is used to automatically carry out image thresholding or the conversion to a binary image from grey-level image. The algorithm presumes that the image consists of two classes of pixels following bimodal histogram (pixels which consist region of interest and background pixels), it then evaluates the optimum threshold separating the two classes to maximize between-class variance. This method involves iterating through all the possible threshold values and calculate the measure of spread for the pixels which is in the foreground as well as in the background. The main motive is to find out the threshold value for which the sum of pixels which is our region of interest and background pixels spread is minimum.

The crux of the algorithm is that an optimum threshold will give well-separated classes or conversely well-thresholded classes will give maximum separation based

on intensity values hence yielding a well-thresholded image. Otsu's thresholding algorithm performs computations on intensity histogram, hence space complexity of storing image information is rather less, not more than 255 memory blocks for storing histogram of intensity for a grey-level image of size $M \times N$, further this histogram is normalized. Now, for a selected threshold histogram is divided into two classes C_1 and C_2 , respectively, where class C_1 consists of intensities in range $[0, t]$ and C_2 in the range $[t + 1, L - 1]$. We need to find such a value of threshold t for which there is maximum between-class variance, which ensures maximum distinction between two classes, hence a well-thresholded binary image is gained as output. Between-class variance is given in terms of class means and class probabilities.

$$\sigma_B^2(t) = P_1(t)(\mu_1(t) - \mu_G)^2 + P_2(t)(\mu_2(t) - \mu_G)^2$$

$$\sigma_B^2(t) = P_1(t)P_2(t)[\mu_1(t) - \mu_2(t)]^2$$

where probability $P_1(t)$ is the probability of a pixel being assigned to class C_1 , this probability is nothing but a cumulative sum of normalized histogram frequencies, which can also be viewed as probability of occurrence of class C_1 . Similarly, probability of occurrence of class C_2 is $P_2(t)$. While $\mu_1(t)$ and $\mu_2(t)$ are mean intensity values of assigned class C_1 and C_2 respectively and μ_G being average intensity of the entire image. We can easily verify the preceding results:

$$P_1\mu_1 + P_2\mu_2 = \mu_G$$

$$P_1 + P_2 = 1$$

The between-class variance can be calculated iteratively by computing class means and probabilities in every iteration. This leads to build an effective and efficient algorithm for Otsu's method of thresholding.

Algorithm

1. Compute normalized histogram for each intensity level which gives probability P_i for each intensity level.
2. Initialize class means and probabilities as $\mu_i(0), P_i(0)$
3. Iterate through all threshold values from $t = 1$ to L
 - a. Update with new values of μ_i and P_i
 - b. Calculate between-class variance $\sigma_B^2(t)$
4. Find the maximum of $\sigma_B^2(t)$ to get the desired threshold value t .

3.2 Local Thresholding

Most of the time, a single threshold value is not sufficient for binarizing the image. Due to shadows or uneven illumination, binarizing the image using a single threshold does not produce desired results thus multiple thresholds are determined [6]. So, the

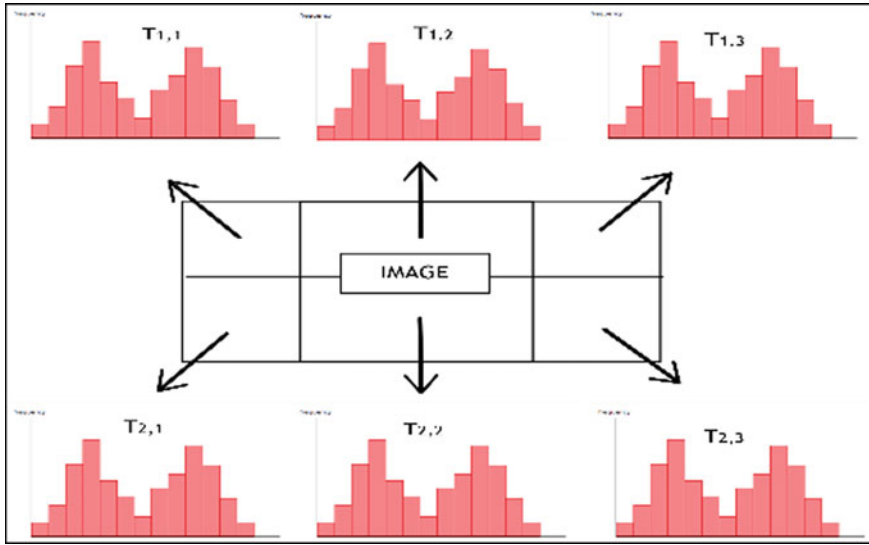


Fig. 1 Histograms generated from different regions

image is sub-divided into blocks or windows and then threshold is computed for each block and applied on the pixel value of the block [8]. Local thresholding methods do more computations than the global threshold. As we can see in Fig. 1. Bhargavi and Jyothi [6], the threshold depends on some local properties of the image as well as a pixel value.

Image Partitioning

Images normally have non-uniform illumination hence applying global thresholding does not provide the desired result. One simple idea is to divide images into small non-overlapping rectangular blocks and applying Otsu's thresholding on each of them. The size of the rectangle is kept relatively small compared to the size of the image, so that we may get blocks with approximately uniform illumination. This idea helps in generating better binary images with utmost clarity of objects as well as negligible noise, which otherwise would be present in the image in case of global Otsu's thresholding.

Moving Averages

Usually, images require to be thresholded locally, as an image has different thresholding value in different regions this can be easily done using a moving average or sliding windows, where we slide a smaller window across the image applying Otsu's thresholding in that small region and hence achieving local threshold for every sub-image or window within that image and in the end yielding a well-thresholded image,

which will not be the case when global Otsu's thresholding is applied. This type of thresholding is very useful in processing images of documents where there can be varying illumination.

3.3 Hybrid Thresholding

Hybrid thresholding takes advantage of both local thresholding and global thresholding [9]. So, basically, a combination of both local thresholding technique and global thresholding technique is used. There a global threshold value is determined and a local threshold of the blocks or windows are determined, and accordingly one of these threshold values is used on the target pixel [7].

Local and Global

In this method, we used global and local thresholding to partition the image into various segments. We can define global and local thresholds to convert the grayscale image into binary image. Global threshold is computed by Otsu's method in which threshold is determined by maximizing the between-class variable. Local threshold is computed by two methods which are described below and calculates the threshold using the mean and standard deviation. A sliding window is created in which our target pixel p is at the Centre. Size of the window is determined in such a way that it preserves the local details as well as reduces the noise. We calculate a S value that is picked from the pixels of the window such that it is greater than 0 and less than the global threshold. After computing these values, we can finally determine one of the binary values for that target pixel by the following way:

$$g(p) = \begin{cases} 1, & i(p) > \text{global threshold} \\ \text{local threshold, } & \text{global thresholding} \geq i(p) > S \\ 0, & i(p) \leq S \end{cases}$$

Chou et al. [10].

where $i(p)$ = intensity of grayscale pixel,

$g(p)$ = calculated target pixel intensity.

Local threshold using Niblack's method:

$$\text{local}_{\text{threshold}} = \left\{ \text{mean}_{\text{local}} - \frac{\text{SD}}{\text{global}_{\text{threshold}}} \right.$$

Niblack et al. [11].

Local threshold using Sauvola's method:

$$\text{local}_{\text{threshold}} = \{\text{mean}_{\text{local}} * 1 + k \left[\frac{\text{SD}}{\text{global}_{\text{threshold}}} - 1 \right]\}$$

Sauvola and Pietikäinen [12].

Region Growing

Region growing method gives good output compared to its other fellow parts. It is basically extracting a region from the image using some pre-defined procedure. The simplest procedure is to compare the seed valued pixel to its neighbors to check the homogeneity criteria allotted to the class to which its neighbor belongs.

Region Split and Merge

This is a two-step process, i.e., top-down and bottom-up. In top-down image is split into homogenous quadrant region. In this, we successively subdivide image into quadrant and stops when all regions become homogenous and obtain quadtree structure. In bottom-up, we merge each adjacent region on the basis of homogeneity and keeps on merging them until no further merging is possible.

4 Experimental Setup

4.1 Dataset

Images that we have tried to use are a combination of standard images as well as few images of our choices, which we thought would be beneficial in comparative analysis and the standard images will help the reader make comparisons with other works done on the same standard images on this field. Following are the information of images used:

Figure 2 has five original images which have been used by us; image a. is a standard image used in various image processing algorithm which is owned by MIT and is free to use. This image is originally of size 256×256 . Image b. is a standard image used by various researchers since 1973, it is an image of the Swedish model Lena Söderberg. Image c. is another standard image that has been used in various books as well as journals. Image d. is also a standard image that we picked from the paper titled—*Adaptive Thresholding Using the Integral Image by Derek Bradley and Gerhard Roth*. Image e. is an image selected from internet for comparative analysis.

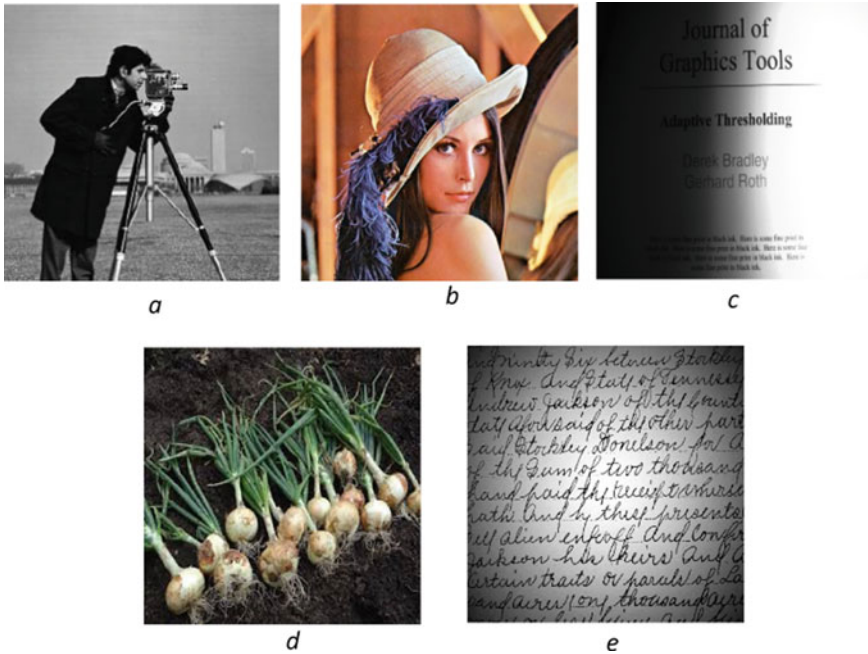


Fig. 2 Sample dataset

4.2 Representation of Samples

In our experiment, we have first converted the images into grayscale image. Afterwards, we have scaled all images to the same dimension of 400×400 . Hence making the processing of each image easier without worrying about varying size. Thereafter, we have generated image histograms and then normalized them for processing. Then, we have applied our algorithms on these generated normalized histograms to yield our results.

4.3 Experiment Conducted

We used five techniques in our experiment for comparison which are varying versions of Otsu's thresholding out of which two are global thresholding, two of them are local thresholding, and last one is hybrid technique, which are namely—Otsu's thresholding, OpenCV's version of implementation of Otsu's thresholding (which has been used to compare the results of our implementation of Otsu's thresholding), Otsu's thresholding applied on rectangular blocks (image partitioning), Otsu's thresholding applied on sliding windows (moving averages), and Otsu's thresholding applied along

with Niblack’s and Sauvola’s methods which is a hybrid technique. These techniques were implemented in python and above-mentioned dataset was processed on them to yield a thresholded image.

5 Comparative Analysis

5.1 OpenCV’s Otsu’s Thresholding

In Fig. 3, we can clearly see that Cameraman.tif (image a. hereafter) has been thresholded nicely with most of the details from original image preserved, same is the case with Lenna.png (image b. hereafter) and Onion.jpg (image d. hereafter), while in case of remaining two images which are journal.jpg (image c. hereafter) and text.png (image e. hereafter) have clearly lost a lot of textual information due to non-uniform illumination in background.

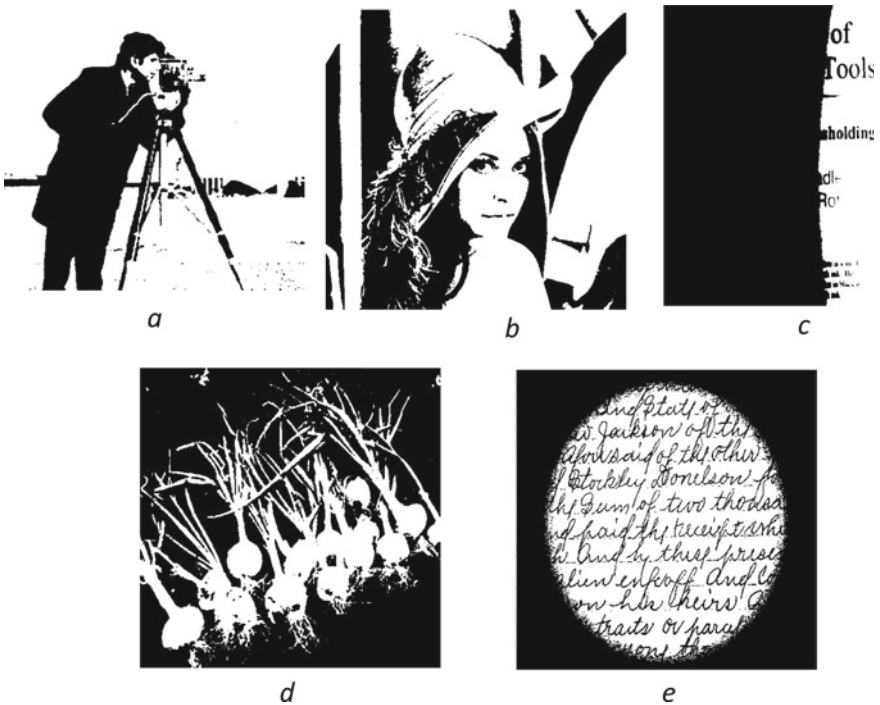


Fig. 3 Results generated from Otsu’s thresholding (OpenCV’s function)

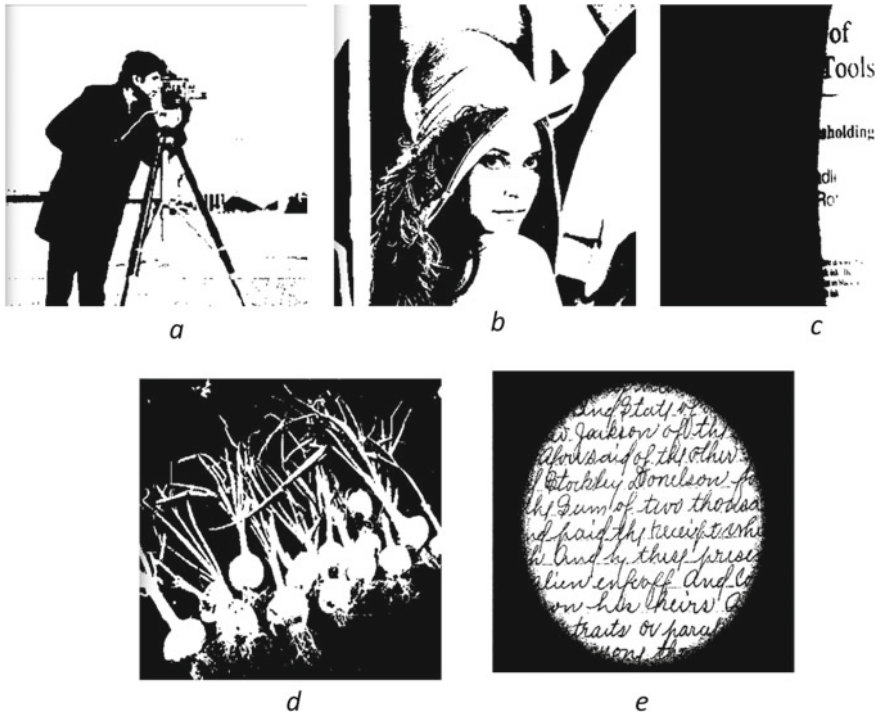


Fig. 4 Results generated from Otsu’s thresholding (manual coded)

5.2 Otsu’s Thresholding Our Implementation

When we applied our method of Otsu’s thresholding, we saw that results were very much similar to that of openCV’s implementation which is clear from Fig. 4, which is obvious since both techniques work on the same concept. Hence, we conclude that both techniques cannot yield better results for images that have non-uniform background illumination or in general background noise.

5.3 Image Partitioning

When applying Otsu’s thresholding on image partitioning or rectangular blocks we saw due to local thresholding some of the background details were retained which decreased the quality of thresholded image which can be seen in Fig. 5, which was not the objective, as we wanted to separate background and foreground pixels, and neither it solved the non-uniform illumination background detail retained in image c. and image d. This technique though definitely helped increase the details of facial features of image b., which is a positive. This technique was found to be effective

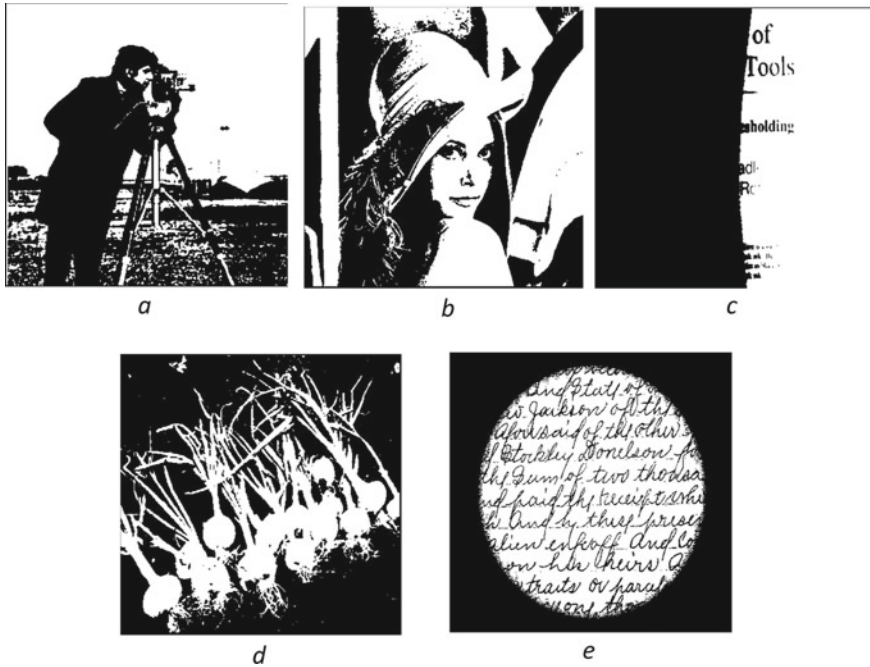


Fig. 5 Results generated after applying image partitioning approach

to reduce noise to some extent in image and generate clear features for region of interest but definitely added some background features in the foreground.

5.4 Moving Averages

Moving averages or sliding window showed drastically improved results for document images, which are image c. and image e., both images have background noise in the form of non-uniform illumination. Almost entire-textual information was retained for image e., and most of it was also retained for image c. with minimal background noise. Hence, moving average proved to be very good for document type images that have non-uniform illumination or gradient noise in the background, which can be there in the image due to lighting conditions or because of camera flash while taking the picture. While there were really good results for image c. and e., rest of the images when thresholded were distorted with intertwined background and foreground pixels, and these are those images which were yielding better results on global thresholding techniques, hence moving averages are not good for them (Fig. 6).

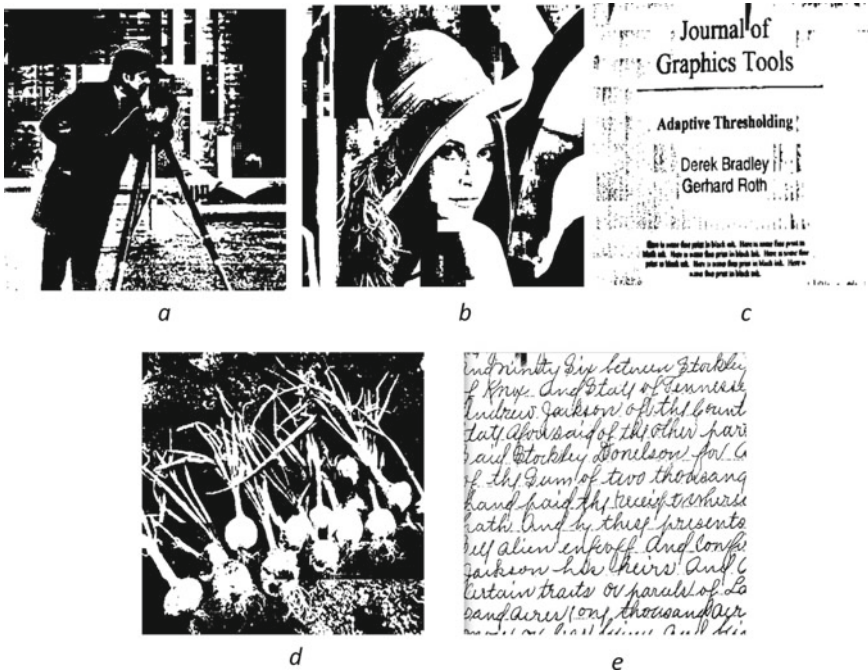


Fig. 6 Results generated after applying moving averages approach

5.5 Hybrid Using Otsu's and Niblack's Method

As seen in the results there is a lot of noise preserved in the images, i.e., because the neighbors are considered while finding the threshold. In image b, still the results are better and showing the object features. While in image c and image e, characters are readable but due to the non-uniform distribution of noise, noise is still present in the results. In image d, our object under consideration can be seen but with that its neighborhood noise is making the results blurry (Fig. 7).

5.6 Hybrid Using Otsu's and Sauvola's Method

In image a, up to some extent the object under consideration is visible but not much clear. The results of image b are better and preserving most of the foreground pixels. Image c and image d are not showing any good results, local consideration taken in the technique has decreased the quality and nothing is clearly visible. The result of image c is good but again with lots of background noise, foreground pixels are not clearly visible (Fig. 8).

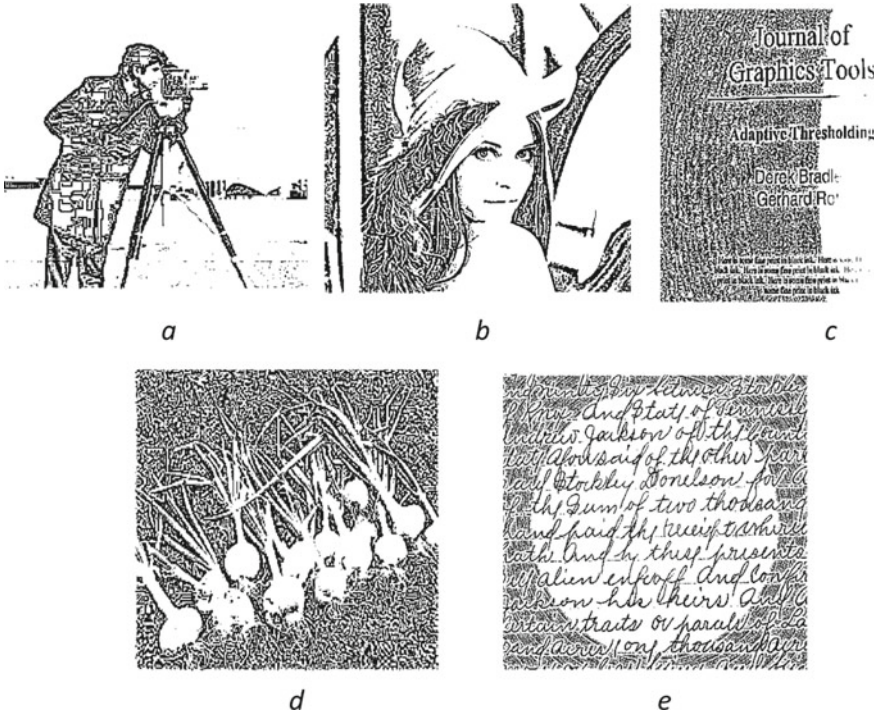


Fig. 7 Results generated from hybrid thresholding (Otsu's and Niblack's method)

6 Conclusion

This paper indulges in the depth of thresholding techniques to know which technique can perform better on all kinds of images so as to extract region of interest. We found out that not every technique is good for all cases, Otsu's global thresholding is a promising and faster way to segment and generate a binary image, but works well with images having negligible noise and region of interest already being very much clear in original image, whereas applying methods like Otsu's thresholding on sliced blocks of images and then merging them or applying moving averages (sliding windows) on images having noise which is distributed in a specific region of image, moving averages gave result better on images which have distributed gradient noise. Whereas the hybrid technique used are a combination of global and local thresholding.

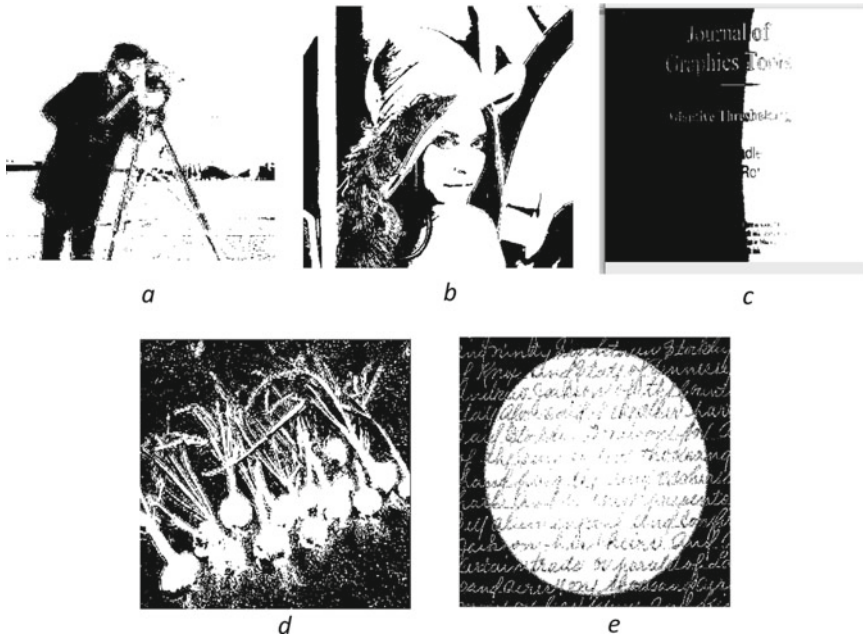


Fig. 8 Results generated from hybrid thresholding (Otsu's and Sauvola's method)

References

1. Gonzalez RC, Woods RE, Eddins SL (2018) Digital image processing, 3rd edn. Pearson, London
2. Khan AM, Ravi S (2013) Image segmentation methods: a comparative study
3. Pal NR, Pal SK (1993) A review on image segmentation techniques. *Pattern Recogn* 26(9):1277–1294
4. Yogamangalam R, Karthikeyan B (2013) Segmentation techniques comparison in image processing. *Int. J Eng Sci Technol* 5(1):307–313
5. Gurusamy V, Kannan S, Nalini G (2013) Review on image segmentation techniques. *J Pharm Res* 20125:4548–4553
6. Bhargavi K, Jyothi S (2014) A survey on threshold based segmentation technique in image processing. *Int J Innovative Res Dev* 3(12):234–239
7. Kumar N (2018) Thresholding in salient object detection: a survey. *Multimedia Tools Appl* 77(15):19139–19170
8. Chang KY, Liu TL, Chen HT, Lai SH (2011) Fusing generic objectness and visual saliency for salient object detection. In: 2011 international conference on computer vision. IEEE, pp 914–921
9. Kuo TY, Lai YY, Lo YC (2010) A novel image binarization method using hybrid thresholding. In: 2010 IEEE international conference on multimedia and expo. IEEE, pp 608–612
10. Chou CH, Huang CC, Lin WH, Chang F (2005). Learning to binarize document images using a decision cascade. In: IEEE international conference on image processing 2005, vol 2. IEEE, pp II–518
11. Niblack W (1986) An introduction to digital image processing, vol 34. Prentice-Hall, Englewood Cliffs

12. Sauvola J, Pietikäinen M (2000) Adaptive document image binarization. *Pattern Recogn* 33(2):225–236

Levels and Classification Techniques for Sentiment Analysis: A Review



Devendra Sharma and Anoj Kumar

Abstract Sentimental Analysis (SA) is a process by which one can examine the feelings towards services, products, movies with the help of reviews. SA is a computing treatment of feeling, opinion, and subjectivity of contents. In this survey paper, we explain the overview of the sentiment analysis. For finding the sentiment analysis of reviews, different types of levels and classification of text data are explained. Three types of levels are explained and for classification two approaches machine learning approach and lexicon-based approach are explained. Some latest articles are used to show the accuracy of the classifiers.

Keywords Sentiment analysis · Analysis levels · Machine learning · Lexicon

1 Introduction

In the world of the Internet, there are many number of sites such as social sites, e-commerce sites, blogs, etc. that are available where the users give their own opinion about the services of sites. A simple example of sentiment analysis is when we are want to buy any product online from e-commerce sites (Amazon, Flipkart, Snap deal, etc.) then first we see the users review which is given in stars or points or emoji impression or read the few comments about that product, after that we take decision to buy or not buy that product. So sentiment analysis helps us to make a decision-making process. E-commerce sites are leads to transform, extract, load, and analyze a very huge amount of data. Sentiment analysis is one of the important aspects of data mining, where important data can be analyzed based on the negative or the positive sense of the collected data. The feedback of the people may be positive or negative which plays a major role in the development as well as improvement in upcoming

D. Sharma (✉)

Computer Science and Engineering, MNNIT Allahabad, Prayagraj, Uttar Pradesh, India
e-mail: dsmnnit@gmail.com

A. Kumar

MNNIT Allahabad, Prayagraj, Uttar Pradesh, India
e-mail: anojk@mnnit.ac.in

© Springer Nature Singapore Pte Ltd. 2021

G. S. Hura et al. (eds.), *Advances in Communication and Computational Technology*, Lecture Notes in Electrical Engineering 668,
https://doi.org/10.1007/978-981-15-5341-7_27

333

applications. It is an emerging area to collect subjective information from source material by applying Linguistics and text analytics, Natural Language Processing, Computational and categorized the polarity of the sentiment or opinion. Sentiment analysis is performed on various kinds of datasets such as movie reviews, hotel services feedback, online services feedback, etc. Sentiment analysis is measured by the identification and classification of feedback on various social sites.

In this paper, in Sect. 2, we describe the different types of levels of sentiment analysis. In Sect. 3 we describe the classification techniques for classification of the review data. Section 4 shows the previous some result using these classification techniques. At the end, conclusion is presented.

2 Levels of Classification

There are three types of classification explain as follows:

2.1 Document Level Classification

In this level sentiment analysis whole document is give the result as a document is a positive or negative opinion. The whole document is supposed as the basic data unit [1]. For this level there are two approaches supervised learning and unsupervised learning. In supervised learning, there are a finite set of classes in which a document is classified for each class. In unsupervised learning, document determine the semantic orientation of specific phrases [2].

2.2 Sentence Level Classification

This level is used to find that each sentence give a positive or negative opinion for reviews. It is performed based on two tasks that are objective and subjective. Subjective classification makes a differentiation between subjective and objective sentences. Objective words gives the true information about sentences. Subjective sentences are more thoughtful by which improves the accuracy of sentiment analysis [2].

2.3 Aspect or Entity or Feature Level Classification

People are more interested in specific aspects (for example, ambiance or services of a hotel) than the whole operations. The prices, size, battery, model of mobile phones all

are aspects. Aspect-level sentiment analysis could help users effectively navigate into detailed information of their interesting aspects. For performing this level sentiment analysis need to find out the major aspects of entities in a specific domain (e.g., hotel) [3]. This sentiment analysis yields very fine-grained sentiment information by which it develops applications in various areas. There are three processing steps identification, classification, and aggregation [4].

3 Classification Techniques

Mainly classification techniques are categorized into two parts namely machine learning based approach and lexicon-based approach. Both classifications are explained as follows:

3.1 Machine Learning Approach

It is area of computer science that develops learnable machines which predict the datasets without external programmed [5]. In machine learning there are two types of classification: supervised and unsupervised. In supervised classification, the classifier is first trained (learned) based on the labeled datasets. After training completed the test dataset is used for classification to obtain the class label of test dataset. Here different supervised machine learning classifiers are discussed as follows.

3.1.1 Naïve Bayes (NB)

The Naïve Bayes classifier is a probabilistic approach that classifies the input data in different classes. This algorithm is commonly used for text classification. It has low computational cost and gives high accuracy. It takes every word from the training data sets and evaluates the probability of it being in each class [6]. This classifier is first trained by training data set. Now classifier is ready to classify the new (test) data sets. The working process of this classification is explained as follows:

Let there be a set of training data T , in which each instance is represented by m independent attributes (Z is a set of attributes) which are represented by $\langle z_1, z_2, z_3, \dots, z_m \rangle$. Suppose that there are n classes C_1, C_2, \dots, C_n . It assigns to this instance probabilities. $P(C_n|z_1, z_2, z_3, \dots, z_m)$ for each of n classes C_n [7]. For a single attribute:

$$P(C_n|Z) = \frac{p(C_n)p(Z|C_n)}{p(Z)} \quad (1)$$

3.1.2 Support Vector Machine (SVM)

It is a classification technique that is used for both non-linear and linear data. When data is linearly separable then SVM searches for linear optimal separable hyperplane that is a boundary of decision that separates data from one class to another class. A separating decision boundary can be written as:

$$W.X + b = 0 \quad (2)$$

Where W is weight vector, i.e., $W = w_1, w_2, w_3, \dots, w_n$. X is a training tuple, b is a scalar [6]. It is a non-probabilistic classifier technique. It looks for a hyperplane with the maximum margin between the negative and positive data of the training sets. It is based on the concept of the decision planes which define decision boundaries. Decision plane is that form a separation plane between a set of objects, which belongs to dissimilar classes. Decision planes are generally a line or a curve [7]. It is a supervised learning model for classification, outlier detection, and regression. The main advantage of SVM is effectiveness in high dimensional data spaces and it is memory efficient. It performs well on the majority data but not well perform on minor data [8]. Disadvantage of SVM is that if the number of attributes is much higher than the number of samples, then it gives poor performance. SVM is a vector space model based classification technique. Before the classification of text document should be transformed to attribute multidimensional vectors [9].

3.1.3 Decision Tree (DT)

It is a classification technique. The learning approach of decision tree is based on the divide and conquer technique. Decision tree have structure like a tree. General tree have nodes and edges, decision tree also has nodes and edges. Nodes are used for testing a particular feature. Nodes are divided into three category root node, internal node, and leaf node. In decision tree, these three nodes have their own meaning. The meaning of edges and each node are shown as:

Root node—It is selected as an attribute that data efficiently.

Internal node—The test on attribute is represented by this node.

Leaf node—It is used to represent the class label. It is also called terminal node.

Edges—The outcomes (conjunctions of attributes that lead to leaf node) of the test is represented by each edges of the decision tree.

Class prediction is held by a path that is traced from root to a leaf node. Decision tree is built with the help of training test. The tuples with unknown class are classified with the help of this tree [10]. In Fig. 1 here two classes are unfit and fit which assigns to a person according to age.

Decision tree algorithm has three major steps:

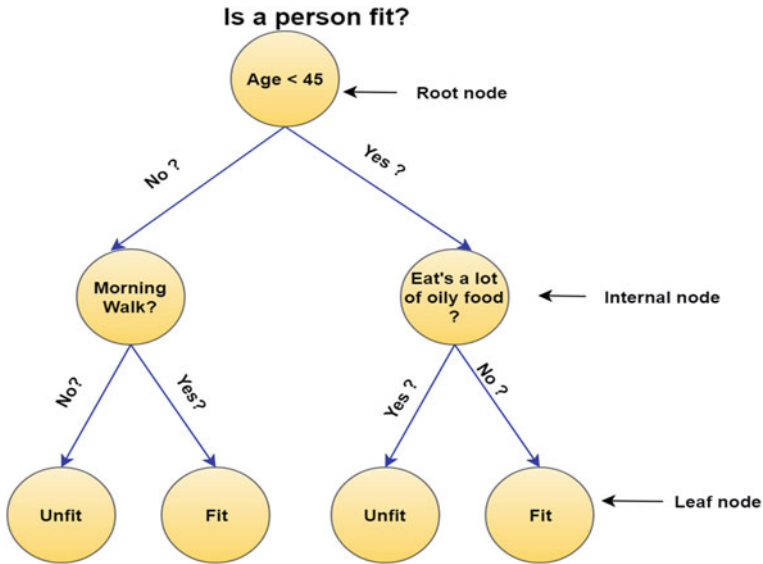


Fig. 1 Decision tree showing whether a person is fit or unfit depending on age

1. For an available dataset D , choose the features as target class for divide tuples in partitions.
2. Define a dividing norm for generate a partition in which every tuples be parts of a single class. Select the best partitions to create a node.
3. Recursively repeat above two steps until the complete tree is grown [11].

Some decision tree algorithms are CHID, CART, ID3, C4.5, and Hunt’s algorithms [12].

3.1.4 K-Nearest Neighbor (KNN)

It is a non-parameter algorithm. It is a supervised predictable classification model. KNN classification rules are generated from the training dataset themselves without the help of additional datasets [13]. In the nearest neighbor the technique of classification of an unknown data example is achieved by analyzing classes of its nearest neighbors. KNN algorithm uses the technique of nearest neighbor for classifying the datasets. In KNN only a fixed number of nearest neighbors are granted for classification of unknown datasets [14]. This fixed number is known as k which is a positive integer. If $k = 1$ it means unknown data is classified as training data which is most nearest to it. KNN is also known as a lazy learner algorithm. It is applicable in a number of different areas like text categorization, pattern recognition, agriculture, and finance. It has a very easy implementation and gives a good result. It does not have a learning phase. The training tuples are viewed as a set of data points in

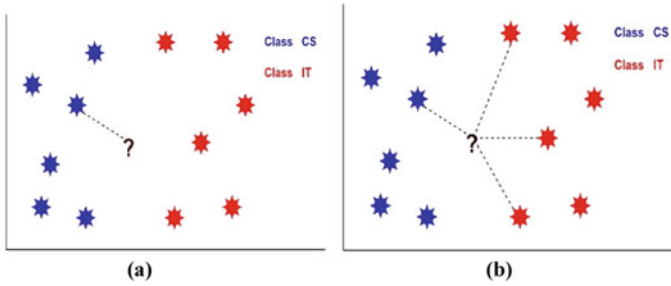


Fig. 2 **a** The 1-NN decision rule: the point? is assigned to the class CS; **b** the KNN decision rule: with $k = 4$ the point? is assigned to the class IT

m -dimensional space, m is the number of attributes describing datasets. When an unknown example comes for classification, then discover k most nearest data points to it in m -dimensional space.

In Fig. 2a, an unknown example is classified by only one known example. In Fig. 2b more than one known example is used, $k = 4$ so closest four examples are considered for classifying unknown one. Three belong to the same class and only one belongs to another class [15]. To determine the k -nearest data points to unknown example, for these different kinds of distance measuring metrics [16, 17] are used which are given as follows:

The Euclidean distance between two examples P and Q is

$$\sqrt{\sum_{1 \leq i \leq n} (p_i - q_i)^2} \tag{3}$$

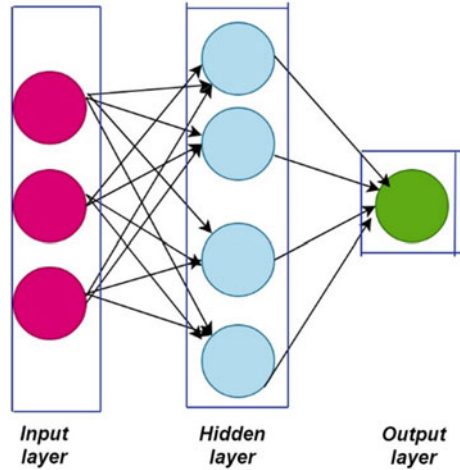
Manhattan distance between two examples P and Q is:

$$\sum_{1 \leq i \leq n} |p_i - q_i| \tag{4}$$

3.1.5 Neural Network (NN)

The recent research in neural classification has a network of neurons, make an alternative to different conventional classification models. Working process of neural network based on the human brain’s neural network. It is a circuit or network of neurons. The connections of the neurons are done by weights. Input layer takes input and hidden layer done processing on input and produces output in the output layer. Neurons are shown by circle and arrow (connections) represents the weights. All inputs are modified by weight and summed. The amplitude of the outputs is controlled by the activation function. A neural network in the case of artificial neurons called an

Fig. 3 Structure of neural network



artificial neural network (ANN). An ANN is a device with a large number of inputs and a single output (Fig. 3).

It is data-driven self-adaptive methods. It is a global functional approximator in a network which can approximate any functions with arbitrary accuracy [18]. In these different models are available for classification such as recurrent neural network and conventional neural network etc. [19].

3.1.6 Random Forest (RF)

When random forest is used for classification then there many numbers of tree classifiers are produced. In this classification process certain classes are voted by these trees. In this classification method, all tree classifiers are randomly given the vote to classes by which classification is done [20]. It is an ensemble learning method. It is storing the trees which are used for classification. Random forest classifier is defined as comprised of structured tree classifier $\{h(y, j), j = 1, \dots\}$, where $\{j\}$ is independently identically distributed random vectors, and each tree casts a united vote for famous class at input y [21]. Classification is performed with less numbers of trees. Automatic classification is done with the help of an improved random forest classifier. Dynamically change the number of trees of this improved classifier which produce optimized performance [22].

3.2 Lexicon-Based Approach

In this approach, phrases are classified as negative or positive by reading those phrases and computer their polarity using different kinds of dictionaries. Positive or negative

sense of the phrase is called semantic orientation. Using semantics words the accuracy of classification is improved. In this approach assign a positive value (+) to phrase or words which have positive sense and a negative value (−) to negative words or phrases. Phrase or word having no meaning that is called neutral and assign zero value (0). This approach is classified into two approaches:

3.2.1 Manual Approach

It is a time taken an approach to make a dictionary. So it is combined with one of the two following approaches [5].

3.2.2 Dictionary-Based Approach

In this approach, manually build a dictionary of semantic words with its known polarity value. After built, it executes a program that collects antonyms and synonyms by this dictionary. This is a recursive process in which new words can be found [5].

In this approach, two freely available dictionaries, WordNet, and its improved version SentiWordNet are used [23].

3.2.3 Corpus-Based Approach

In this identifies opinion words by considering word list. Lexicon is built for a specific domain. This method is used to build semantic lexicons automatically [24] (Tables 1 and 2).

Table 1 Comparison between machine learning approach and lexicon approach [23]

Basis	Machine learning	Lexicon-based
Domain	Dependent	Independent
Classification	Supervised	Unsupervised
Prior training	Yes	No
Adaptive learning	Yes	No
Speed	Slow	Fast
Accuracy	Higher	Lower

Table 2 Applications of sentiment analysis

Domain	Description
Purchasing stock or services	Customers can easily check and reviews of any stock or services and easily compare their brands
Marketing research	The mentality of customers about services or items or the latest government policy can be evaluated
Recommendation systems	According to interests and preferences, the system can forecast which product should be suggested and which one should not be suggested
Detection of flame	By this detect insolent arrogant, abusive, overheated words used in Facebook, Twitter, Instagram or blogs on the internet
Quality improvement in product	Manufacturers can gather the customer opinion whether agreeable or not with products, and then they improve the quality of their products

4 Accuracy Measures of Classifiers

The performance SA is evaluated by helped of a confusion matrix which is created when an algorithm is implemented on datasets. Different types of performance measures are used that are Recall, Precision, Accuracy, and F-measure.

	Correct Labels	
	Positive	Negative
Positive	True positive	False positive
Negative	False negative	True negative

Accuracy = It is a performance evaluation metric and it is evaluated by the number of correctly predicted reviews divided by the total number of reviews present in the corpus.

Formula is:

$$Accuracy = \frac{TN + TP}{TN + TP + FP + FN}$$

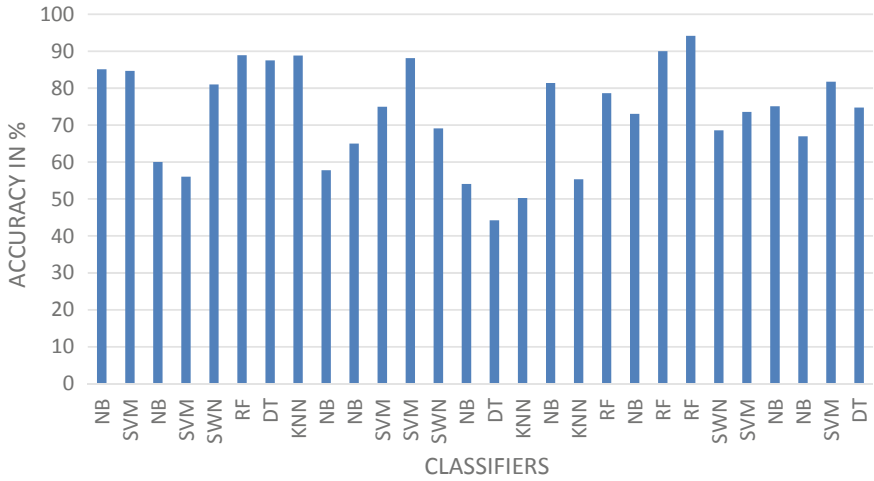


Fig. 4 Comparison of accuracy of existing techniques

Figure 4 display graphical view of the accuracy comparison of existed techniques which is already shown in Table 3.

5 Conclusion

This survey paper represents an overview of recent works in SA. A large number of published and cited articles are used for writing this survey paper. Three types of levels are explained. For classification supervised machine learning algorithms and lexicon-based approaches are used. Accuracy with respected classifiers is shown in some recent previous articles. In different areas applications are explained. Mostly review data sets are about movies from different online sites like IMDb, Online newspapers, and Rotten Tomatoes. Product review is taken from e-commerce sites and different laptop companies. SA process needs some enhancements and it interested area in computer science.

Table 3 Accuracy measurement by different classifiers

Year	Data and reference	Classifier	Accuracy (%)
2015	Movie review [25]	NB	85.10
		SVM	84.70
	Lankadeepa newspaper [7]	NB	60
		SVM	56
2016	Movie review [26]	SWN	81
	Movie review [27]	RF	88.95
		DT	87.53
		KNN	88.86
		NB	54.77
	Twitter review of movie [20]	NB	65
		SVM	75
Review of laptop companies and e-commerce sites [28]	SVM	88.13	
Movie review [29]	SWN	69.1	
2017	Movie review [30]	NB	54.10
		DT	44.26
		KNN	50.28
	Movie review [31]	NB	81.4
		KNN	55.30
		RF	78.65
	Movie review [32]	NB	73.04
	Movie Review [33]	RF	90
Movie review [34]	RF	94.14	
Movie review [35]	SWN	68.6	
	SVM	73.6	
	NB	75.1	
Product review [36]	NB	66.95	
	SVM	81.77	
	DT	74.75	

References

1. Alessia D, Ferri F, Grifoni P, Guzzo T (2015) Approaches, tools and applications for sentiment analysis implementation. *Int J Comput Appl* 125(3)
2. Kaur R, Verma P (2017) Sentiment analysis of movie reviews: a study of machine learning algorithms with various feature selection methods. *ICSE* 5(9):113–121. E-ISSN: 2347-2693
3. Dhande LL, Patnaik GK (2014) Analyzing sentiment of movie review data using Naive Bayes neural classifier. *IJETTCS* 3(4):313–320
4. Schouten K, Frasinca F (2016) Survey on aspect-level sentiment analysis. *IEEE Trans Knowl Data Eng* 28(3):813–830
5. Mumtaz D, Ahuja B (2016) A lexical approach for opinion mining in twitter. *Int J Educ Manage Eng* 6(4):20
6. Fang X, Zhan J (2015) Sentiment analysis using product review data. *J Big Data* 2(1):5
7. Medagoda N, Shanmuganathan S, Whalley J (2015) Sentiment lexicon construction using SentiWordNet 3.0. In: 2015 11th ICNC, pp 802–807
8. Wijesinghe A (2015) Sentiment analysis on movie reviews

9. Khobragade P, Jethani V (2017) Sentiment analysis of movie reviews. *Int J Adv Res Comput Sci* 8(5)
10. Sharma H, Kumar S (2016) A survey on decision tree algorithms of classification in data mining. *IJSR* 5(4):2094–2097
11. Kaur S, Kaur H (2017) Review of decision tree data mining algorithms: CART and C4. 5. *Int J Adv Res Comput Sci* 8(4)
12. Brijain M, Patel R, Kushik M, Rana K (2014) A survey on decision tree algorithm for classification. *IJEDR* 2(1)
13. Yong Z, Youwen L, Shixiong X (2009) An improved KNN text classification algorithm based on clustering. *J Comput* 4(3):230–237
14. Serrano-Guerrero J, Olivás JA, Romero FP, Herrera-Viedma E (2015) Sentiment analysis: a review and comparative analysis of web services. *Inf Sci* 311:18–38
15. Imandoust SB, Bolandraftar M (2013) Application of k-nearest neighbor (KNN) approach for predicting economic events: theoretical background. *Int J Eng Res Appl* 3(5):605–610
16. Lamba A, Kumar D (2016) Survey on KNN and its variants. *IJARCC* 5(5)
17. Dey L, Chakraborty S, Biswas A, Bose B, Tiwari S (2016) Sentiment analysis of review datasets using naïve bays and k-NN classifier. Preprint at [arXiv:1610.09982](https://arxiv.org/abs/1610.09982)
18. Zhang GP (2000) Neural networks for classification: a survey. *IEEE Trans Syst Man Cybern Part C (Appl Rev)* 30(4):451–462
19. Stojanovski D, Strezoski G, Madjarov G, Dimitrovski I, Chorbev I (2018) Deep neural network architecture for sentiment analysis and emotion identification of twitter messages. *Multimedia Tools Appl* 77(24):32213–32242
20. Deshwal A, Sharma SK (2016) Twitter sentiment analysis using various classification algorithms. In: 2016 5th international conference on reliability, infocom technologies and optimization (Trends and Future Directions) (ICRITO), pp 251–257
21. Ahmad M, Aftab S, Muhammad SS, Ahmad S (2017) Machine learning techniques for sentiment analysis: a review. *Int J Multidiscip Sci Eng* 8(3):27–32
22. Paul A, Mukherjee DP, Das P, Gangopadhyay A, Chinthra AR, Kundu S (2018) Improved random forest for classification. *IEEE Trans Image Process* 27(8):4012–4024
23. Vaghela VB, Jadav BM, Scholar ME (2016) Analysis of various sentiment classification techniques. *Int J Comput Appl* 140(3):0975–8887
24. Mumtaz D, Ahuja B (2016) Sentiment analysis of movie review data using sentimentlexicon algorithm. In: 2016 2nd international conference on applied and theoretical computing and communication technology (iCATccT), IEEE, pp 592–597
25. Shaziya H, Kavitha G, Zaheer R (2015) Text categorization of movie reviews for sentiment analysis. *Int J Innovative Res Sci Eng Technol* 4:11255–11262
26. Sharma P, Mishra N (2016) Feature level sentiment analysis on movie reviews. In: 2016 2nd international conference on next generation computing technologies (NGCT), IEEE, pp 306–311
27. Sahu TP, Ahuja S (2016) Sentiment analysis of movie reviews: a study on feature selection and classification algorithms. In: 2016 international conference on microelectronics computing and communications (MicroCom), IEEE, pp 1–6
28. Devi DN, Kumar CK, Prasad S (2016) A feature based approach for sentiment analysis by using support vector machine. In: 2016 IEEE 6th international conference on advanced computing (IACC), IEEE, pp 3–8
29. Tomar DS, Sharma P (2016) A text polarity analysis using sentiWordNet based an algorithm. (IJCSIT) *Int J Comput Sci Inf Technol* 7(1):190–193
30. Singh V, Saxena P, Singh S, Rajendran S (2017) Opinion mining and analysis of movie reviews. *Indian J Sci Technol* 10(19):1–6
31. Baid P, Gupta A, Chaplot N (2017) Sentiment analysis of movie reviews using machine learning techniques. *Int J Comput Appl* 179(7):0975–8887
32. Naiknaware BR, Kawathekar S, Deshmukh SN (2017) Sentiment analysis of movie ratings system. *IOSR J Comput Eng (IOSR-JCE)* 43–47

33. Wankhede R, Thakare AN (2017) Design approach for accuracy in movies reviews using sentimentanalysis. In: 2017 international conference of electronics, communication and aerospace technology (ICECA), pp. 6–11
34. Wankhede R, Thakare AN (2017) To improve accuracy in movies reviews using sentiment analysis. IOSR J Comput Eng (IOSR-JCE) 19(4):80–89
35. Garje AR, Kale KV (2017) Sentiment polarity with sentiwordnet and machine learning classifiers. Int J Adv Res Comput Sci 8(9)
36. Singla Z, Randhawa S, Jain S (2017) Sentiment analysis of customer product reviews using machinelearning. In: 2017 international conference on intelligent computing and control (I2C2), pp 1–5

Breast Cancer Recurrence Prediction in Biopsy Using Machine Learning Framework



Akriti Sharma, Nishtha Hooda, and Nidhi Rani Gupta

Abstract There are numerous toxic and lethal substances that are available in the environment due to the rapid industrial growth and excessive application of pesticides. These substances get into the human food chain majorly through air, water, and soil. This paper presents a case study investigating the organochlorine pesticide levels in women experiencing the malignant and benign growth of breast cancer disease in order to evaluate the exposure against the chemicals and its association with the risk of breast cancer among women. After obtaining the blood and adipose tissue samples, levels of 51 chemicals including DDT, its metabolites, and isomers of HCH among 50 women each with the malignant and benign growth of breast cancer disease are measured. The levels of the chemicals in women with malignant growth of breast cancer are compared with benign cases and a prediction model is built using popular ensemble machine learning framework. The proposed framework is an optimized version of Random Forest algorithm in which feature selection is implemented and the process is incorporated with the preprocessing filters. The proposed framework for breast cancer prediction successfully achieved a prediction accuracy of 90.47%, which is found to be better than the standard classifiers like SVM, neural network, etc.

Keywords Breast cancer · DDT · Pesticides · Prediction · Machine learning · Ensemble

A. Sharma (✉) · N. Hooda
Chandigarh University, Gharuan, Mohali, Punjab 140413, India
e-mail: Akriti.7799@gmail.com

N. R. Gupta
Multani Mal Modi College, Patiala, Punjab 147001, India

© Springer Nature Singapore Pte Ltd. 2021
G. S. Hura et al. (eds.), *Advances in Communication and Computational Technology*, Lecture Notes in Electrical Engineering 668,
https://doi.org/10.1007/978-981-15-5341-7_28

347

1 Introduction

Cancer today is liable for one out of three premature deaths which are occurred due to non-communicable diseases across the world and the count of cancer diagnosis is projected to ascend annually [1]. Among different types of cancer, lung cancer is the most prominent and the major reason of mortality due to cancer among males. Most commonly identified cancer in females appears to be breast cancer and dominates as a reason of female mortality due to any type of cancer. Across the world, nearly about 2.1 million breast cancer cases in females are reported in 2018 representing one out of four cancer diseases in women [2].

Occurrence of the breast cancer is suspected due to certain factors like reproductive, genetic, lifestyle, and environmental. Out of these, environmental factor plays an important role [3] to the extent that it is presumed that numerous environmental factors are responsible in developing this disease. Persistent contact to the pollutants in the environment notably the ones having the estrogenic impact may worsen the situation especially in the tumors related to the hormones such as breast tumours that eventually lead to cancer. Among variety of environmental pollutants, organochlorines (OCs) are among the most common pollutants linked to the various health-related issues including cancer [4]. Among the endocrine disruptors, organochlorine pesticides alter the normal estrogen–progesterone equity and may show a significant part in breast cancer risk [5]. Several lines of investigation support that the getting exposed to dichlorodiphenyltrichloroethane all through fetal life is closely linked with the high risk of malignant growth of the disease [6]. Other evidences suggest that environmentally induced risk factors linked with the high risk of malignant growth are more prominent while the sufferer is in the direct contact to pesticide agents for a prolonged duration, e.g., dichlorodiphenyldichloroethylene (DDE) and dichlorodiphenyltrichloroethane (DDT), cadmium, and high exposure to emissions from transportation especially at the stage of menarche for premenopausal women [7]. Studies have reported that there is the presumed positive link between DDE (main metabolite of DDT) and the breast cancer [8]. Studies highlight the close link between high serum count for p, p'-DDE, β -HCH, and heptachlor with an elevated breast cancer risk [9].

Various types of the cancer including breast cancer are treatable whenever identified at beginning stage. There are several features of a cancerous cell that can be analyzed to get an assessment of the risk of the disease. ML can be introduced for early prediction of breast cancer, taking into account the characteristics of the patients and life style measures. Cruz et al. conducted a comprehensive survey of the various types of machine learning methods in use, the data types being integrated, and the performance of these approaches in cancer prognosis and prediction. Among the studies that have been better validated and designed, it is apparent that ML can be used to increase the effectiveness of predicting cancer recurrence significantly (15–25%), mortality and susceptibility. It is also noticeable at a more primitive level that machine learning also significantly improves our basic understanding of the progression and development of cancer [10]. Kourou et al. discussed

machine learning concepts while detailing their application in prediction or prognosis of cancer. Most of the studies proposed over the past few years focus on developing prediction models utilizing supervised machine learning techniques and classification algorithms for predicting valid disease outcomes. From the observation of their findings, it is clear that the integration of heterogeneous multidimensional data, combined with the application of various methods for the selection of features and classification, can provide promising inference tools in the field of cancer [11]. Montazeri et al. proposed a rule-based classification method for predicting various types of breast cancer survival using ML techniques. This study shows that the Trees Random Forest (TRF) model was the best model having the highest accuracy level, which is a rule-based classification model [12].

In this study, machine learning models are trained with datasets containing different features of the patient so as to predict breast cancer possibilities. Accuracy of 90.47% achieved in the proposed model. The proposed model can be helpful to cure the disease before it enters the advanced stage and chances of cure gets weaker. After data processing, ML algorithms are trained in this work to test the classification performance.

The remaining part of the paper is outlined as follows: Section 2 outlines the experimental investigation which comprises of brief explanation of sample analysis and tool utilized in the proposed framework. Section 3 demonstrates prediction framework with its detailed description. Section 4 discusses the experimental result and performance matrix. Section 5 concludes the work while addressing further research issues.

2 Experimental Investigation

This segment explains the experimental setting, the dataset consisting of sample analysis, and the tool used in the proposed framework for risk prediction.

2.1 Dataset

The research presented in the paper is carried out at the Malwa region of Punjab state of India significantly known for the production of food grains, cotton farming, and furthermore for the highest cancer cases recorded. To examine the possibility of breast cancer against the exposure to these chemicals, 100 different samples of adipose tissue and blood are obtained from the women of Malwa belt Punjab (consisting 11 districts) each with malignant and benign growth of breast cancer disease.

2.2 Experiment Setting

The results are empirically evaluated over the dataset with Weka 3.6.9, a data mining tool in order to classify the data through various algorithms. Several model building approaches are implemented, evaluated, and analyzed using the tool with the specific optimizing the classifiers predictive accuracy.

3 Prediction Framework

Machine learning, an artificial intelligence subdivision, uses the variety of optimization, statistical, and probabilistic techniques which allows machines (or computational systems) to pick up from the past instances and to observe the patterns which are hard-to-discern from the large, complex, and noisy datasets [10]. ML centers on ingenious techniques for processing massive complicated information at reduced cost. Designing a computing machine configured to divide object predictions on the basis of the available dataset and samples is the main goal for performing the experimentation in machine learning. Figure 1 shows the abstract view of the proposed framework. The result of the proposed model allows predicting the risk of breast cancer with high accuracy. Biopsy samples are analyzed in the proposed framework to obtain the information on the various risk factors. The prediction model is then

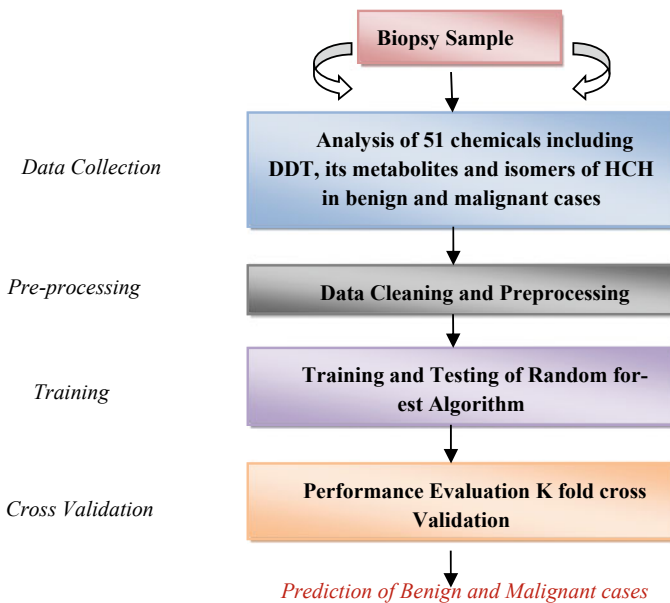


Fig. 1 Proposed framework

trained applying different classifiers for ML to generate an efficient result that allows predicting the risk of the disease mentioned.

3.1 *Machine Learning Models*

Following are a few machine learning models that exhibit their own benefits and shortcomings. The proposed framework is an attempt to develop an ensemble solution exploiting the merits of following existing models.

- i. **Random Forest:** RF is the set of tree predictors where every tree focuses on the values of a random vector which independently sampled with the similar allocation for all kind of trees in the forest. The generalization fault of a forest of tree classifiers is based on the vigor of the respective trees in the forest and their correlation. Adopting a random selection of attributes to divide every node yields failure rates that are more robust in terms of noise than AdaBoost [13].
- ii. **Neural Network:** Artificial Neural network is a synchronized set of nodes that is similar to a massive brain neuron network. It is used to control binary classifiers learning, which can determine whether an input belongs to a particular class [14]. The neural network categorization models had the multitude output nodes proportional to the number of classes, where the predicted class is the largest response from the output [15].
- iii. **Support Vector Machine:** SVMs utilize a linear model to incorporate nonlinear class boundaries into a high-dimensional feature space via some nonlinear mapping input vectors [16]. This model represents examples as points in space, plotted in space, plotted to create distinct categories, or separated by a clear gap. New samples are then plotted into the similar space and then projected to correspond to a class based upon the side of the space where it fall [17].
- iv. **AdaBoost:** AdaBoost is a strong technique proposed originally for pattern detection. AdaBoost's geometric interpretation is that it discovers an accurate ruler of classification, a powerful learning algorithm, combined with many other weak learning algorithms [18]. Statistics aggregated at every stage of the AdaBoost algorithm where each sample that is to be trained is supplied to the tree and an efficient ensemble classifier is developed [19].
- v. **Bayes Net:** This is a technique that symbolizes the joint probability spread of a random variables set taking advantage of the conditional independence relationships between variables, almost always significantly lowering the count of parameters required to show the full joint probability distribution. Bayes nets also provide a robust and natural approach of representing the dependencies that occur [20]. Bayesian network is represented by the directed acyclic graphs where nodes describe the variables in the Bayes net perception. Each individual node pertains to a probability function which takes as input and passes the variable's probability distribution presented by the node [21].

- vi. **Decision Tree:** Decision tree approach is a widely applied data mining technique for building multiple covariate-based classification systems or for establishing target variable prediction algorithm. This technique categorizes a population into branchlike segments that build an inverted tree with an internal nodes, root node, and leaf nodes. It is a non-parametric algorithm. The algorithm can effectively deal with complicated, large datasets without imposing a complex parametric structure [22].

3.2 Proposed Framework

In the proposed machine learning framework as delineated in Fig. 1, biopsy samples are taken and information is extracted in the form of 51 different chemicals like DDT and its metabolites. These 51 features are supplied into the proposed framework and training of the sample is done using Random Forest algorithm which is presented in Algorithm 1.

Algorithm 1 Random Forest Algorithm

Comment: {Let the total number of input variables are represented by F that is to be used for growing ensemble of trees using boot strapped samples of training data set.}

- Select m variables randomly from F input variables to find the decision at anode of the tree.
- From the training set, select a bootstrap sample for the tree by selecting n times with replacement from all N available training cases.

The rest of the cases are used to measure the error of the tree by predicting their classes.

- Depending on these m variables, evaluate the best split in the training set.
- Each tree is not pruned and is fully grown.
- A new sample will be moved down the tree for prediction. The label of the training sample is assigned in the terminal node in which it ends.
- Repeat actions 1–5 over all the considered trees in the ensemble.
- Calculate the average vote of all trees considered as Random Forest prediction.

While processing the information, missing values are identified in the dataset and are supplanted with the suitable values by selecting replace missing values filter of the simulation tool. In the proposed system, the input is the set of all the chosen features while the output of the system is to obtain a value 1 or 0 indicating the presence or absence of the breast cancer in sufferers. Classifier analyzes the selected samples without actually addressing their classes. K-fold cross validation method is used during experiments, where value of K is specified to 10. First, dataset is split into ten equivalent size subsamples. Then, best ML algorithms are chosen being base classifier in order to instruct the nine subsamples and testing the one sample which is left. The operation is replicated ten times for $K = 1, 2, 3, \dots, 10$ to evaluate the

robustness of the designed prediction framework. To assess the proposed framework's performance, different discrete parameters are used such as FP rate, precision, TP rate, recall, F-measure, and ROC area. Confusion matrix is also obtained for the classifier.

Random Forest is an ensemble machine learning algorithm with an efficient prediction performance and hence is implemented for building the proposed prediction framework. After the preprocessing stage which involves removal of the missing value and cleaning of the data, best features are selected to train the algorithm. Proposed framework performance is calculated using various performance parameters of confusion matrix like accuracy, sensitivity, F-score and comes out to be outstanding with 90.47% measured accuracy.

4 Results and Discussion

This section discusses the results and performance evaluation of the model building using K -fold cross validation. Confusion matrix based on various parameters and performance matrix is also presented to support the claim of the achieved accuracy of the proposed framework.

4.1 Performance Evaluation

The proposed framework is well examined with the distinct parameters of the confusion matrix shown in Table 1 while Table 2 presents various performance metrics formulas derived using Table 1.

Table 1 Confusion matrix

	Predicted condition	Positive (cancerous)	Negative (non-cancerous)
True reference	Positive (cancerous)	True positive L	False negative M
	Negative (non-cancerous)	True positive L	False negative M

Table 2 Performance metrics formulas derived using Table 1

Performance metrics	Formula Used
Sensitivity	$L/(L + N)$
Specificity	$M/(O + M)$
Accuracy	$(L + M)/(L + N + O + M)$
F-score	$(2 - L)/(2 - L) + (O + N)$
MCC	$(L - M) - (O - N)/\text{SQRT}((L + O) + (L + N) + (M + O) + (M + N))$

Table 3 Performance of Random Forest

Performance parameters	Result
Accuracy (%)	90.47
TP rate	0.88
FP rate	0.12
Precision	0.9
Recall	0.88
F-measure	0.88
ROC area	0.94

4.2 Experimental Results

The empirical evaluation is performed with different machine learning algorithm like SVM, neural network, Bayes net, decision tree, and AdaBoost. It is observed that in terms of performance, Random Forest model is more efficient than the other machine learning models. The various performance matrixes with their formula are presented in Table 3.

90.47% accuracy by an error rate of 10% is achieved with the Random Forest classifier model of ML. The prediction model proposed in the work allows to predict breast cancer risk using Random Forest algorithm having FP rate, precision, TP rate, F-measure, ROC area, and recall with the measure of 0.12, 0.90, 0.88, 0.88, 0.94, and 0.88, respectively. Upon comparison with other existing classifiers, it is analyzed that the proposed model achieves much better outcomes with regard to high predictability. The proposed model, however, is unable to attain the highest AUC, although it has managed to achieve 0.96 AUC which is much better than other existing classifiers. Table 4 presents the comparison with other existing classifiers.

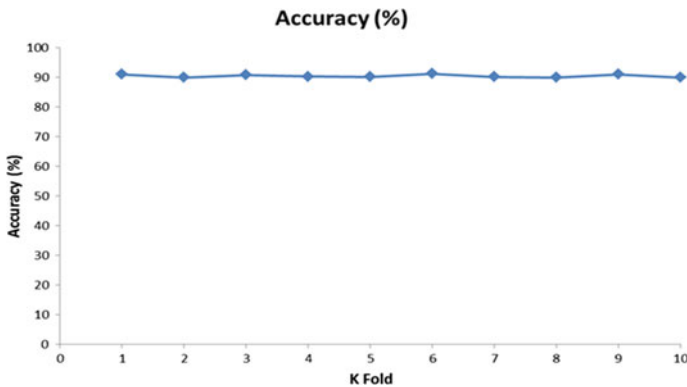
To validate the Random Forest performance and to check the stability in the performance, K-fold validation technique is implemented for ten iterations and the quality of the proposed framework is noted to be robust. The stability of the performance matrix like accuracy and AUC is presented in Fig. 2 and Fig. 3, respectively. Figure 2 presents the accuracy using K-fold validation while Fig. 3 represents the area under the curve using K-fold validation method. The graph in Fig. 2 shows the accuracy and Fig. 3 shows that the Random Forest is quite robust in performance and can be selected to predict the breast cancer in the proposed prediction system.

5 Conclusion

This paper showcases a case study where machine learning algorithm is trained for proficiently predicting the breast cancer disease from medical records of patients. Data is extracted out from the biopsy sample of patients in order to train the model. The proposed framework succeeded in achieving 90.47% prediction accuracy

Table 4 Comparison with other existing classifiers

Performance parameters	TP rate	FP rate	Precision	Recall	F-measure	ROC area	Accuracy
Random forest	0.88	0.12	0.9	0.88	0.88	0.94	90.47
Naïve Bayes	0.67	0.33	0.74	0.67	0.644	0.713	67
BayesNet	0.72	0.28	0.762	0.72	0.708	0.71	72
Logistic	0.61	0.39	0.618	0.61	0.603	0.619	61
Voted perceptron	0.62	0.38	0.62	0.62	0.62	0.635	62
AdaBoost M1	0.68	0.32	0.68	0.68	0.68	0.733	68
Bagging	0.66	0.34	0.661	0.66	0.659	0.623	66
SVM	0.68	0.32	0.701	0.68	0.672	0.68	68
J48	0.63	0.37	0.787	0.63	0.571	0.589	63
Decision stump	0.57	0.43	0.589	0.57	0.546	0.608	57
Decision table	0.61	0.39	0.64	0.61	0.588	0.622	61

**Fig. 2** K-fold cross validation results of accuracy

using optimized ensemble version incorporated with feature selection. The proposed prediction model is helpful in predicting the risk of breast cancer using Random Forest algorithm with an efficacious performance of different parameters namely; TP rate, precision, FP rate, recall, ROC area, F-measure, with the measure of 0.88, 0.90, 0.12, 0.88, 0.94, and 0.88, respectively. The proposed method is efficient, accurate, and faster method having a wide scope in medical assistance which contributes to the early detection of the disease saving many lives. Collection of more detailed data and processing using big data Hadoop framework holds a promising scope as a future work of the case study presented in the paper.

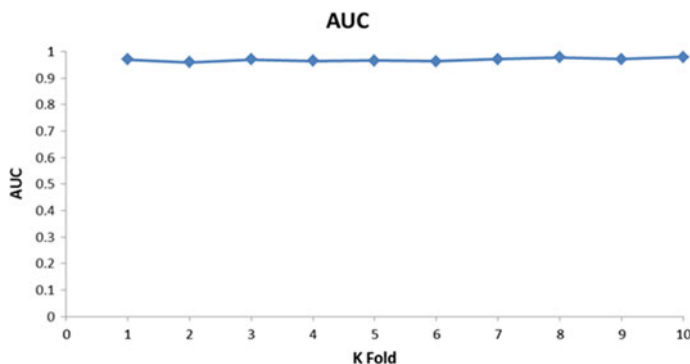


Fig. 3 K-fold cross validation results of accuracy

References

1. Bray F (2016) The evolving scale and profile of cancer worldwide: much ado about everything. *Cancer Epidemiol Prev Biomarkers* 25(1):3–5
2. Bray F, Ferlay J, Soerjomataram I, Siegel RL, Torre LA, Jemal A (2018) Global cancer statistics 2018: GLOBOCAN estimates of incidence and mortality worldwide for 36 cancers in 185 countries. *CA Cancer J Clin* 68(6):394–424
3. Patrono C, Sterpone S, Testa A, Cozzi R (2014) Polymorphisms in base excision repair genes: breast cancer risk and individual radiosensitivity. *World J Clin Oncol* 5(5):874
4. Eldakroory SA, Morsi DE, Abdel-Rahman RH, Roshdy S, Gouida MS, Khashaba EO (2017) Correlation between toxic organochlorine pesticides and breast cancer. *Hum Exp Toxicol* 36(12):1326–1334
5. Yang JZ, Wang ZX, Ma LH, Shen XB, Sun Y, Hu DW, Sun LX (2015) The organochlorine pesticides residues in the invasive ductal breast cancer patients. *Environ Toxicol Pharmacol* 40(3):698–703
6. Soto AM, Sonnenschein C (2015) Endocrine disruptors: DDT, endocrine disruption and breast cancer. *Nat Rev Endocrinol* 11(9):507
7. Sauter ER, Daly MB (eds) (2010) *Breast cancer risk reduction and early detection*. Springer, Berlin
8. Wolff MS, Toniolo PG, Lee EW, Rivera M, Dubin N (1993) Blood levels of organochlorine residues and risk of breast cancer. *JNCI J Natl Cancer Inst* 85(8):648–652
9. Arrebola JP, Belhassen H, Artacho-Cordón F et al (2015) Risk of female breast cancer and serum concentrations of organochlorine pesticides and polychlorinated biphenyls: a case–control study in Tunisia. *Sci Total Environ* 520:106–113
10. Cruz JA, Wishart DS (2006) Applications of machine learning in cancer prediction and prognosis. *Cancer Inform* 2:117693510600200030
11. Kourou K, Exarchos TP, Exarchos KP, Karamouzis MV, Fotiadis DI (2015) Machine learning applications in cancer prognosis and prediction. *Comput Struct Biotechnol J* 13:8–17
12. Montazeri M, Montazeri M, Montazeri M, Beigzadeh A (2016) Machine learning models in breast cancer survival prediction. *Technol Health Care* 24(1):31–42
13. Breiman L (2001) Random forests. *Mach Learn* 45(1):5–32
14. Freund Y, Schapire RE (1999) Large margin classification using the perceptron algorithm. *Mach Learn* 37(3):277–296
15. Lazarevic A, Obradovic Z (2001) Effective pruning of neural network classifier ensembles. In: *Proceedings on IJCNN'01 international joint conference on neural networks* (Cat. No. 01CH37222), vol 2, pp 796–801. IEEE

16. Min JH, Lee YC (2005) Bankruptcy prediction using support vector machine with optimal choice of kernel function parameters. *Expert Syst Appl* 28(4):603–614
17. Cortes C, Vapnik V (1995) Support-vector networks. *Mach Learn* 20(3):273–297. <https://doi.org/10.1007/bf00994018>
18. Freund Y, Schapire RJ (1997) *Comput Syst Sci* 55:119–139
19. Kégl B (2013) The return of AdaBoost. MH: multi-class Hamming trees. [arXiv:1312.6086](https://arxiv.org/abs/1312.6086)
20. Bockhorst J, Craven M, Page D, Shavlik J, Glasner J (2003) A Bayesian network approach to operon prediction. *Bioinformatics* 19(10):1227–1235
21. Pearl J (2000) *Causality: models, reasoning, and inference*. Cambridge University Press, Cambridge. ISBN: 0-521-77362-8. OCLC: 42291253
22. Song YY, Ying LU (2015) *Decision tree methods: applications for classification and prediction*. *Shanghai Arch Psychiatry* 27(2):130

Realization of Grounded Inductance Circuit Using Bulk-Driven Current Conveyors



Anu Tonk and Neelofer Afzal

Abstract The paper presents the realization of a lossless grounded inductance circuit that is capable of low-voltage (LV) operations. This has been possible by incorporating an important non-conventional circuit design technique known as bulk-driven (BD) for implementing a second-generation current conveyor (CCII) cell. The bulk-driven second-generation current conveyor (BDCCII) nearly allows rail-to-rail input-output operations while operating at supply voltage levels as low as ± 0.5 V. Further three voltage-mode filter configurations namely: a second-order band-pass (BP), band-elimination (BE) and high-pass (HP) have been implemented to verify the workability of the simulated high-valued inductance. These filters have been specifically designed for applications which involve extremely low-frequency operation like biosensors, bio-signal processing, etc. PSPICE simulations have been performed using 0.18 μm CMOS standard technology and obtained results confirm the theoretical analysis.

Keywords BDCCII · GIS · LV · Biquad · Q-factor · Bio-signal processing

1 Introduction

Low-voltage (LV) approach [1–3] to analog circuit design continues to gain special attention in the last few decades. Tremendous efforts are being put towards developing variants of analog modules that can meet the expanding demands for LV battery operated and small-sized portable electronic modules. Most importantly, constraints on reducing threshold voltage (V_T) [4, 5] pose a serious difficulty while continuously scaling devices for miniaturization. One of the most promising solutions—Bulk-Driven (BD) technique can help an engineer to efficiently accomplish his target of designing an integrated circuit (IC) with utmost low supply voltage requirements. In

A. Tonk (✉) · N. Afzal
Department of ECE, Jamia Millia Islamia, New Delhi 110025, India
e-mail: tonkanu.saroaha@gmail.com

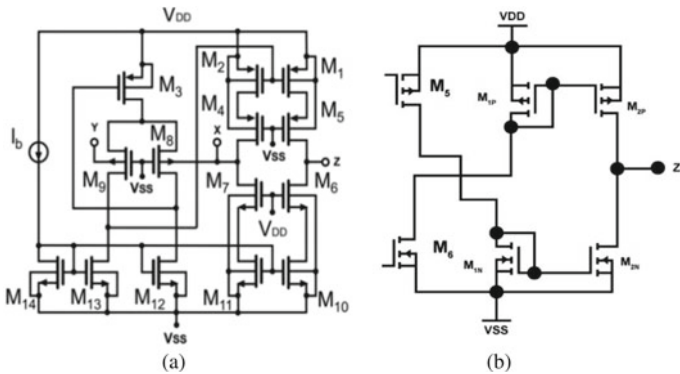


Fig. 1 a BDCCII+ schematic [10]. b Transistor set for BDCCII– realization

lieu of this present scenario, it is seen that LV concepts are also being extensively explored in the field of current conveyors [6–11]. Synthetic grounded inductance simulators (GIS) using different active blocks have been detailed in the past [12–38]. It is already difficult to implement an inductor in integrated circuits, and to the best knowledge and belief of the authors, none of them is capable of operating with such low supply levels. Thus, in accordance with the state of art, authors have decided to implement a ± 0.5 V grounded inductance (GI) with bulk-driven second-generation current conveyors (BDCCII). The paper is organized in four main sections. In Sect. 2, transistor-level design of a BDCCII—plus-type (Fig. 1a) and minus-type (Fig. 1b)—has been given to briefly demonstrate its characteristic properties. This is followed by a discussion on the proposed GIS circuit. To confirm the performance of suggested GIS topology, three single-input single-output (SISO) biquad filters: band-pass (BP), band-elimination (BE) and high-pass (HP) have been presented along-with their non-ideal and sensitivity analysis in Sect. 4. However, a lot many other applications, such as oscillators and resonators etc., can be further realized with the GIS. Frequency- and time-domain results have been given to illustrate the performance of all presented circuits. The main features of the proposed GIS and those in [12–36] are summarized in Table 3. PSPICE simulations have been performed with TSMC 0.18 μm standard technology and the evaluations verify the potential of proposed circuits. This study extrapolates further possibilities for designing BDCCII based LV circuits.

2 Bulk-Driven CCII

Second-generation current conveyor (CCII) is the most versatile active building block available for realizing various analog signal processing circuits. Port relations of a plus-type BDCCII (BDCCII+) are given in form of a matrix below. Use of plus-type CC is more attractive than minus-type because of its simplicity. For BDCCII, $-I_z = -I_x$.

$$\begin{bmatrix} V_X \\ I_Z \\ I_Y \end{bmatrix} = \begin{bmatrix} 0 & 0 & 1 \\ 1 & 0 & 0 \\ 0 & 0 & 0 \end{bmatrix} \begin{bmatrix} I_X \\ I_Z \\ V_Y \end{bmatrix}$$

BDCCII (Fig. 1) has 14 transistors in plus-type and 18 transistors in its minus-type structure. These implementations allow almost rail-to-rail swing capability at all the ports. The bulk terminals of transistors M_8 and M_9 are supplied with input signals X and Y which enable operations under LV input supply. Bulk of other PMOS/NMOS is connected to positive/negative supply voltages. An appropriate DC bias (V_{SS}) is also supplied to the gate terminals of M_8 - M_9 and M_4 - M_5 , apposite to create a conduction channel inversion layer. This is because V_T requirements are reduced or completely eliminated in BDMOS transistors [39]. Transistor M_1 - M_2 , M_4 - M_5 and M_6 - M_7 are used to transfer X terminal current to $Z+$. Another set of transistors M_{1P} - M_{2P} and M_{1N} - M_{2N} completes the inverting current tracking from port X to $Z-$. Voltage tracking from Y to X terminal is achieved by M_8 - M_9 and M_3 . Current copying (from X to $Z+/Z-$ terminal) and voltage following (from Y to X terminal) actions of BDCCII+ & BDCCII- are shown by Figs. 2 and 3 respectively.

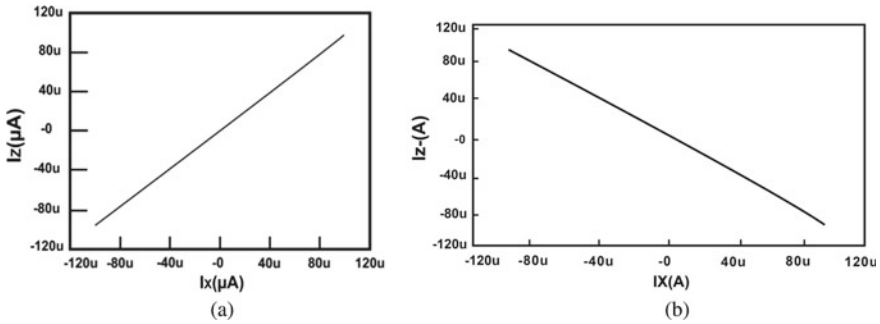


Fig. 2 DC current transfer from terminal X to a $Z+$, b $Z-$

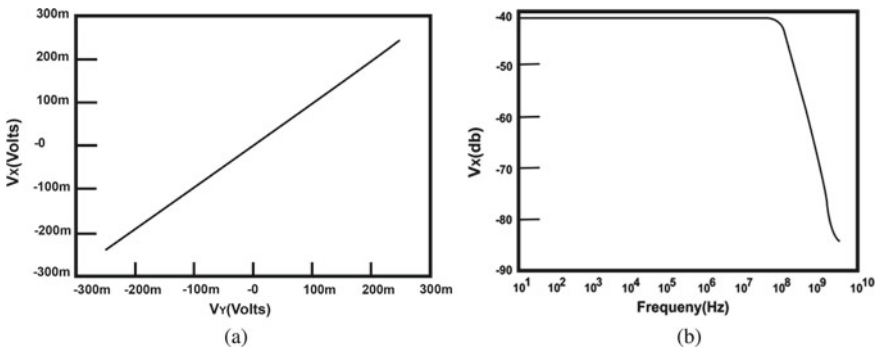


Fig. 3 a DC voltage transfer from port Y to X . b AC voltage response at port X

Table 1 Measured performance characteristics

Characteristics	Simulated results
Biasing current (I_b)	28 μ A
Transistor count	14 ⁺ , 18 ⁻
Linear voltage range	-250–250 mV
Linear current range	-100–100 μ A
-3 dB bandwidth (I_{Z+}/I_X)	72 MHz
-3 dB bandwidth (I_{Z-}/I_X)	66 MHz
-3 dB bandwidth (V_X/V_Y)	114 MHz

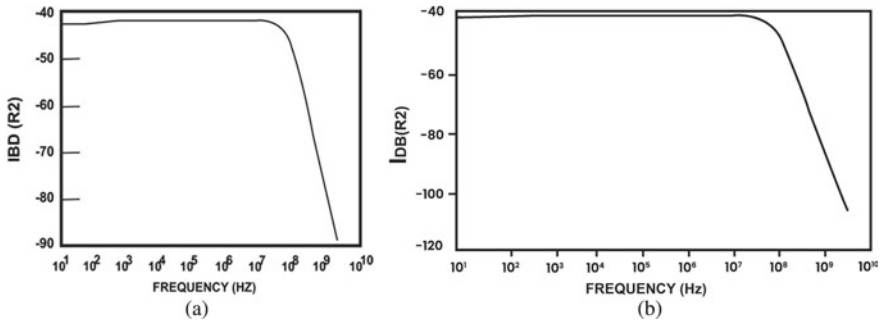


Fig. 4 AC current response at port **a** Z+ **b** Z-

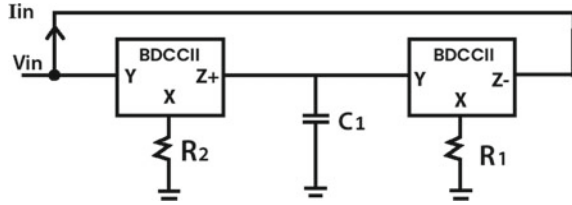
-3 dB current bandwidth for BDCCII+ at Z+ terminal is 72 MHz, and -3 dB current bandwidth for BDCCII- at Z- terminal is 66 MHz. 114 MHz is the -3 dB voltage bandwidth at port X. This bandwidth response obtained is much greater as compared to the other available LV CC cells [6–8]. This circuit is not only better in terms of high current and voltage bandwidth but it also provides decent power consumption in a minimal transistor structure. Table 1 illustrates the simulated parameters of BDCCIIs. Figures 2, 3 and 4 present simulated current and voltage response of the current conveyors.

3 BDCCII Based GIS

Grounded inductance realization discussed in this paper is a modification to the well-known inductance simulation circuit proposed by Sedra and Smith [40]. It employs two BDCCIIs with minimal number of active and passive elements. Routine analysis of the proposed GIS (Fig. 5) yields that

$$Z_{in}(s) = \frac{V_{in}}{I_{in}} = sC_1 R_1 R_2 \tag{1}$$

Fig. 5 BDCCII based grounded inductance simulator



From Eq. (1) the equivalent value of simulated grounded inductance (L_{eq}) obtained is:

$$L_{eq} = C_1 R_1 R_2 \tag{2}$$

Considering both BDCCII to be ideal and $R_1 = R_2 = R$, the input impedance Z_{in} can be rewritten as:

$$Z_{in}(s) = s C_1 R^2 \tag{3}$$

Thus, equivalent value of grounded inductance becomes cR^2 . From (2) it should be noted that the simulated GIS can be tuned using grounded resistances R_1 and R_2 . Now, taking the non-ideal effects associated with BDCCII into account characteristic matrices for BDCCII+ and BDCCII- can be redefined as follows:

$$\begin{bmatrix} V_X \\ I_Z \\ I_Y \end{bmatrix} = \begin{bmatrix} 0 & 0 & \beta_1 \\ \alpha_1 & 0 & 0 \\ 0 & 0 & 0 \end{bmatrix} \begin{bmatrix} I_X \\ I_Z \\ V_Y \end{bmatrix} \quad \begin{bmatrix} V_X \\ I_Z \\ I_Y \end{bmatrix} = \begin{bmatrix} 0 & 0 & \beta_2 \\ \alpha_2 & 0 & 0 \\ 0 & 0 & 0 \end{bmatrix} \begin{bmatrix} I_X \\ I_Z \\ V_Y \end{bmatrix}$$

where α_i and β_i are frequency-dependent current and voltage gains. α_1 and α_2 are the transfer gains from terminal I_{X1} to I_{Z+} and I_{X2} to I_{Z-} , respectively. β_1 and β_2 are the transfer gains from V_{Y1} to V_{X1} and V_{Y2} to V_{X2} , respectively. Using these matrices, the non-ideal input impedance can be expressed as:

$$Z_{in}(s) = s(C_1 R_1 R_2 / \alpha_1 \alpha_2 \beta_1 \beta_2); L_{eq1} = C_1 R_1 R_2 / \alpha_1 \alpha_2 \beta_1 \beta_2 \tag{4}$$

Consequently, equivalent GIS value becomes equal to $C_1 R_1 R_2 / \alpha_1 \alpha_2 \beta_1 \beta_2$. Various active and passive sensitivities of GIS can be expressed as given in Eq. (5) which shows that the sensitivity figures are within reasonable limits.

$$S_{R_1, R_2, C_1}^{L_{eq}} = 1 = -S_{\alpha_1, \alpha_2 \beta_1, \beta_2}^{L_{eq}} \tag{5}$$

Equivalent impedance, $Z_{in}(s)$, under the influence of parasitic components can be approximated [15] as given in Eq. (5). Here, R_{xp} and R_{xn} are low-valued series resistance at port X of the BDCCII.

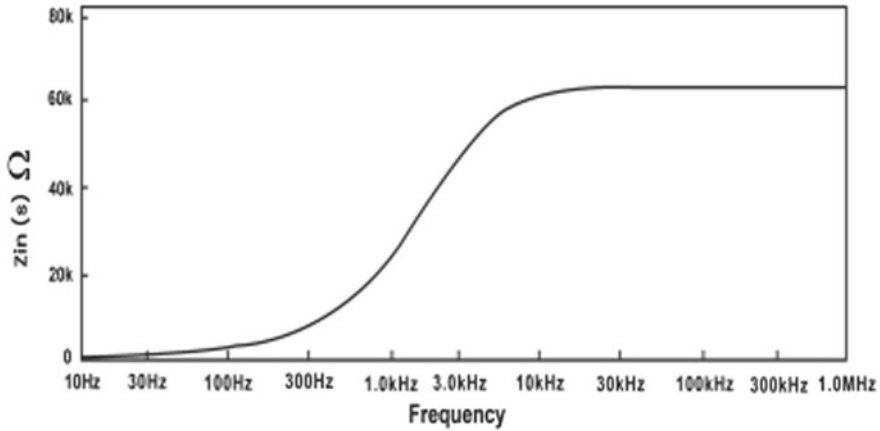


Fig. 6 Frequency response of Z_{in} for simulated GIS

$$Z_{in}(s) = sC_1(R_1 + R_{xn})(R_2 + R_{xp}) \quad (6)$$

Figure 6 presents the curve obtained for simulated input impedance $Z_{in}(s)$. A bias current (I_b) of $21 \mu\text{A}$ and voltages of $\pm 0.5 \text{ V}$ were supplied. Resistor values (R_1 and R_2) were set equal to $2 \text{ k}\Omega$ while capacitor value (C_1) was set as $1 \mu\text{F}$. At a frequency of 1 kHz , simulated impedance is $23.75 \text{ k}\Omega$ while its theoretical value is $25.12 \text{ k}\Omega$. The simulated inductance (L_{eq}) value is 3.75 H whereas its theoretical value is 4 H . The proposed circuit is not only able to realize a high-valued inductance but it can also be seen that it has excellent performance over wide range of extremely low frequencies. Low-frequency performance improvement is an important topic because the spectrum of audio signals, e.g. speech and music, extends from approximately 20 Hz to 20 kHz [41].

4 Verification of Workability of GIS

Workability of proposed grounded inductance circuit has been confirmed by realizing a second-order BPF, BEF and HPF filter configuration. Routine analysis of the schematic for BPF realization, see Fig. 7a, using the new GIS results in the following expression for its transfer function:

$$\frac{V_{bp}}{V_i} = \frac{s/RC}{s^2 + s/RC + 1/LC} \quad (7)$$

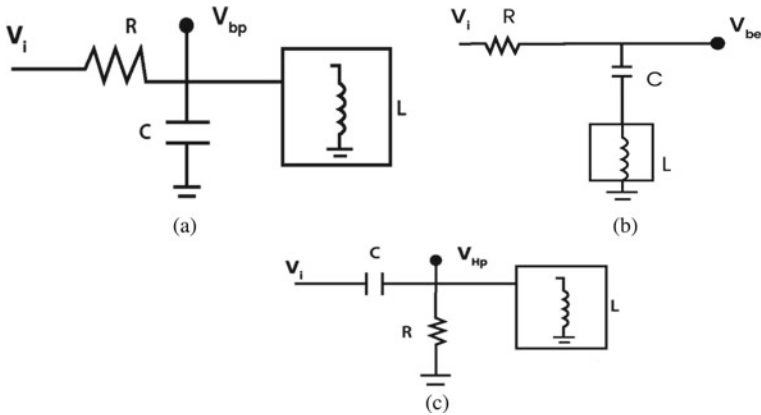


Fig. 7 Second-order filter structure **a** BP, **b** BE, **c** HP

Similarly, the active realization of BEF using the proposed GIS has been shown in Fig. 7b whose transfer function is given by Eq. (7):

$$\frac{V_{be}}{V_i} = \frac{s^2 + 1/LC}{s^2 + sR/L + 1/LC} \tag{8}$$

Transfer function of the filter realized by configuration given in Fig. 7c is given by:

$$\frac{V_{hp}}{V_i} = \frac{s^2}{s^2 + s/RC + 1/LC} \tag{9}$$

From Eqs. (6–8), angular resonance frequency ω_o is given by $\frac{1}{\sqrt{LC}}$. Further, taking the value of $L = L_{eq}$

$$\omega_o = \frac{1}{\sqrt{L_{eq}C}} \tag{10}$$

L_{eq} can be further substituted from Eq. (2). The value of other important parameters, i.e. quality factor can be expressed as follows for the three filter configurations:

$$Q_{bp} = Q_{hp} = \frac{R}{\sqrt{L_{eq}}}; Q_{be} = \frac{1}{R} \sqrt{\frac{L_{eq}}{C}} \tag{11}$$

It can be noted from Eqs. (10)–(11) that ω_o and Q can be tuned independently through R_1 (or R_2) and R , respectively. It is also apparent that Q can be made greater than unity by proper selection of passive element values. Using the characteristic

matrices rewritten for BDCCII+ and BDCCII– in Sect. 2, the non-ideal voltage transfer functions for BP, BE and HP configurations becomes:

$$\frac{V_{bp}}{V_i} = \frac{s/RC}{s^2 + s/RC + 1/L_{eq1}C} \quad (12)$$

$$\frac{V_{be}}{V_i} = \frac{s^2 + 1/L_{eq1}C}{s^2 + sR/L_{eq1} + 1/L_{eq1}C} \quad (13)$$

$$\frac{V_{hp}}{V_i} = \frac{s^2}{s^2 + s/RC + 1/L_{eq1}C} \quad (14)$$

Value of L_{eq1} can be now substituted from Eq. (4). Resonance angular frequency (ω_o) and quality factor (Q) values become:

$$\omega_o = \frac{1}{\sqrt{L_{eq1}C}}; Q_{bp} = Q_{hp} = \frac{R}{\sqrt{L_{eq1}}}; Q_{be} = \frac{1}{R} \sqrt{\frac{L_{eq1}}{C}} \quad (15)$$

The absolute ω_o and Q active and passive sensitivities have been calculated as follows, all of which are less than or equal to unity.

$$S_{R_1, R_2, C_1, C}^{\omega_o} = -S_{\alpha_1, \alpha_2, \beta_1, \beta_2}^{\omega_o} = \frac{1}{2}; S_R^{Q_{be}} = S_R^{Q_{hp}} = -S_R^{Q_{be}} = 1; S_C^{Q_{be}} = -1 \frac{1}{2} \quad (16)$$

$$S_{R_1, R_2, C_1, C}^{Q_{hp}} = S_{R_1, R_2, C_1, C}^{Q_{bp}} = -\frac{1}{2}; S_{\alpha_1, \alpha_2, \beta_1, \beta_2}^{Q_{hp}} = S_{\alpha_1, \alpha_2, \beta_1, \beta_2}^{Q_{bp}} = \frac{1}{2} \quad (17)$$

$$S_{R_1, R_2, C_1, C}^{Q_{be}} = -S_{\alpha_1, \alpha_2, \beta_1, \beta_2}^{Q_{be}} = \frac{1}{2} \quad (18)$$

5 Filter Simulation Results

PSPICE (version 9.1) simulations have been carried out to verify the given mathematical analysis. Behaviour and performance analysis of the BDCCIIs has already been discussed at the beginning of Sect. 2. Filter configurations given in this paper have been specifically demonstrated to operate at a very low-frequency, sub-Hertz range, typically required for biomedical signals. Analog designs for bio-signal processing systems may require large passive component values, often not permissible by contemporary technology. So we have extended the use of bulk-driven technique

Table 2 Transistor sizing

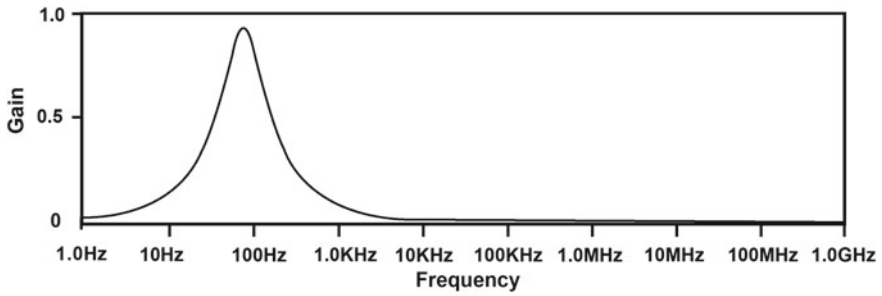
Transistor	W (μm)	L (μm)
M_1, M_2	100	0.3
M_3	18	0.3
M_4, M_5	100	2
M_6, M_7	50	2
M_8, M_9	10	0.3
M_{10}, M_{11}	40	0.3
M_{12}, M_{13}, M_{14}	4	0.3
M_{1P}, M_{2P}	100	0.5
M_{1N}, M_{2N}	50	0.5

to implement second-generation current conveyor in order to realize a high-valued grounded inductance, simulations refer to in Sect. 3. The common bio-potential signals namely electrocardiogram (ECG), electroencephalogram (EEG) and electromyogram (EMG) have very low amplitudes ($10 \mu\text{V}$ – 100mV) and are located in a very low-frequency band (0.5Hz – 1kHz). Interestingly, the only current conveyor GIS-based filters with such low-frequency performance that can be cited in this context is [15]. The following values of the passive components were used for the grounded inductor circuit (Fig. 5) $C_1 = 1 \mu\text{F}$, $R_1 = 2 \text{k}\Omega$, $R_2 = 2 \text{k}\Omega$ and for Figs. 7a–c $R = 2 \text{k}\Omega$, $C = 1 \mu\text{F}$. The bulk-driven current conveyors were biased at $\pm 0.5 \text{V}$ DC power supplies with $I_B = 21 \mu\text{A}$ where I_B is the biasing current, for both current conveyors. The dimensions of MOSFETs of the filter are summarized in Table 2. All circuits enjoy independent tuning of the filter parameters, ω_o and Q . Keeping the component values as given above, f_o has been set to 77Hz and quality factor (Q_{bp} , Q_{be} and Q_{hp}) is set to be unity, in all three cases. We present the results of simulated filter responses in Figs. 8, 9 and 10. Figures 11a, b demonstrates the Q -tuning of BP and BE filter with resistance R .

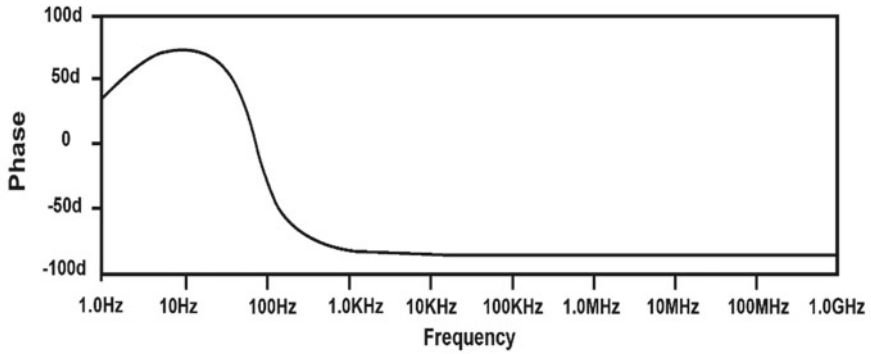
Resistor R , inferred according to Eq. (15), can be used for the fine-tuning of Q value. For example, Q_{bp} can be tuned to 1, 2, 3, 4, 5 and 6 by varying R as 2 k, 4 k, 6 k, 8 k, 10 k and 12 k, respectively. Conversely, Q_{be} can be tuned to 1, 2, 4, 5 and 10 by varying R 2 k, 1 k, 0.5 k, 0.4 k and 0.2 k, respectively.

6 Conclusion

Active realization of grounded/floating passive impedances has always been a popular objective of research in analog circuit design. The use of bulk-driven techniques for implementing basic CC cells can be found in open literature but its versatility in designing analog signal processing and integrated circuits is less known. Authors have filled this void by introducing a BDCCII based grounded inductor

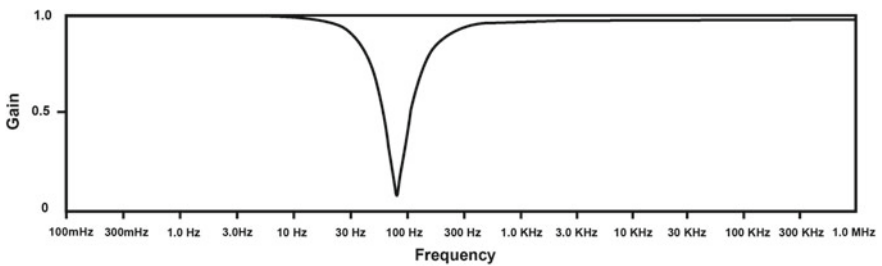


(a)

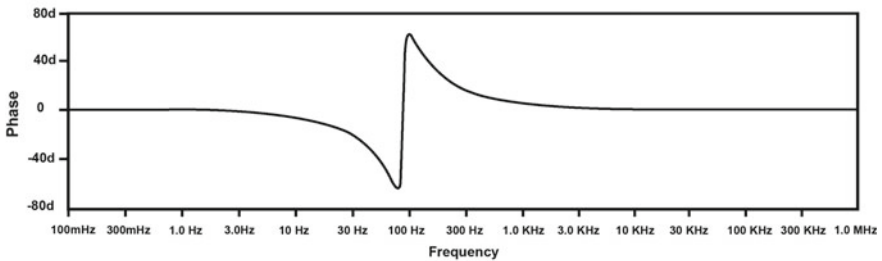


(b)

Fig. 8 BPF response using proposed GIS a Frequency, b phase



(a)



(b)

Fig. 9 BEF response using proposed GIS a Frequency, b phase

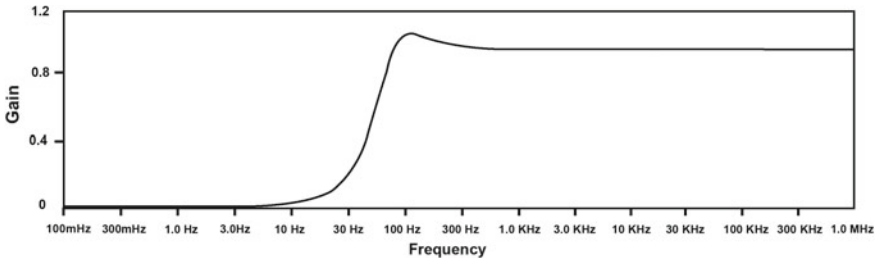


Fig. 10 Frequency response of HPF using proposed GIS

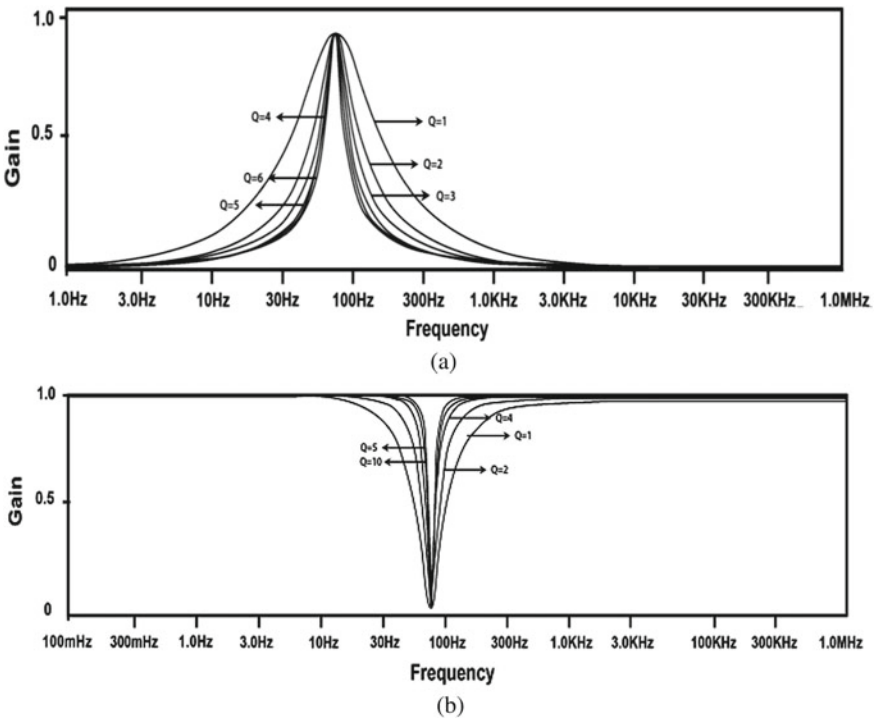


Fig. 11 Q-factor tuning of a BPF, b BEF

and adding three single-input single-output filters to the existing repertoire of the bulk-driven analog signal processing applications.

Acknowledgements The authors would like to thank the Department of Electronics, F/o Engineering & Technology, JMI, New Delhi and UGC for providing valuable support in the form of the NET-JRF grant.

Table 3 Feature comparison with previous circuits (since 2000)

Reference No.	Technology and voltage supply	Active element used	No. of resistors used	No. of capacitor used	Matching conditions required	LV operable
[12]	OTA + AD844; ± 1 V	2VD-DIBA	-	1 G	No	No
[13]	AD844; ± 12 V	3CCII+	2 G	1 G	Yes	No
[14]	AD844; ± 12 V	2CCII+ (Fig. 1)	3 G	1 F	Yes	No
[15]	0.35 μ m; ± 1.5 V	3CCII+ (Fig. 4)	2 G, 1 F	1 G	Yes	No
[16]	0.35 μ m; ± 2.5 V	1MICCII-	1 G, 1 F	1 F	Yes	No
[17]	~	2CCII+ (Fig. 1)	2 G	1 G	No	No
[18]	0.13 μ m; ± 1 V	3CCII+ (Fig. 7)	2 G, 1 F	1 G	Yes	No
[19]	AD844; ± 5 V	3CFAO	2 G, 1 F	1 G	No	No
[20]	0.35 μ m; ± 1.5 V	IDXCII (Fig. 2b)	1 G, 1 F	1 F	Yes	No
[21]	0.35 μ m; ± 1.65 V	IDXCII (Fig. 3b)	2 G	1 F	Yes	No
[22]	0.35 μ m; ± 2.5 V	IDXCII (Fig. 2a)	1 G, 1 F	1 F	Yes	No
[23]	BJT; ± 2.5 V	IDCII	1 G, 1 F	1 G	Yes	No
[24]	AD844; ± 12 V	ICDBA	2 F	1 G	Yes	No
[25]	0.35 μ m; ± 1.5 V	1ZC-CCCITA	0	1 G	No	No
[26]	0.5 μ m; ± 1.5 V	1OTRA	2 F	0	Yes	No
[27]	2OPA860; ± 5 V	1VDBA	1 F	1 F	No	No
[28]	0.35 μ m; ± 1.5 V	MDO-DDCC (Fig. 5)	1 G, 1 F	1 G	Yes	No
[29]	0.5 μ m/AD844; $\pm 1.5/5$ V	1OTRA	3 F	2 F	Yes	No
[30]	0.35 μ m; ± 2 V	1VD-DIBA	1 F	1 G	No	No

(continued)

Table 3 (continued)

Reference No.	Technology and voltage supply	Active element used	No. of resistors used	No. of capacitor used	Matching conditions required	LV operable
[31]	0.18 μm ; $\pm 0.9\text{ V}$	1VDTA	0	1 G	No	No
[32]	0.35 μm ; $\pm 1.5\text{ V}$	ICCCCTA	0	1 G	No	No
[33]	ALA400 + 0.35 μm ; $\pm 1.5\text{ V}$	2CC-CFA	0	1 G	No	No
[34]	0.5 μm ; $\pm 2\text{ V}$	ICCFTA	0	1 G	No	No
[35]	Discrete; $\pm 15\text{ V}$	ICFOA	1 G, 1 F	1 F	Yes	No
[36]	0.13 μm ; $\pm 0.75\text{ V}$	ICFOA -	1 G, 1 F	1 F	Yes	No
This work	0.18 μm ; $\pm 0.5\text{ V}$	1BDCCII+, 1BDCCII-	2 G	1 G	No	Yes

* Acronyms *F* floating; *G* grounded

References

1. Yan S, Sanchez-Sinencio E (2000) Low voltage analog circuit design techniques: a tutorial. *IEICE Trans Fundam Electron Commun Comput Sci* 83(2):179–196
2. Rajput SS, Jamuar SS (2002) Low voltage analog circuit design techniques. *IEEE Circ Syst Mag* 2(1):24–42
3. Khateb F, Dabbous SBA, Vlassis S (2013) A survey of non-conventional techniques for low-voltage low-power analog circuit design. *Radioengineering* 22(2):415–427
4. Tonk A, Goyal S (2015) A literature review on leakage and power reduction techniques in CMOS VLSI design. *Int J Adv Res Comput Comun Eng* 3(2):554–558
5. Tonk A (2016) Short channel effects in conventional MOSFETs and their suppression. *Int J Eng Res Gen Sci* 4(3):738–743
6. Khateb F, Khatib N (2011) New bulk-driven class AB CCII. *IEEE Int Conf Radioelektronika* 1–4
7. Khateb F, Birolek D, Novacek K (2006) On the design of low voltage low-power bulk-driven CMOS current conveyors. *Int Spring Semin Electron Technol* 318–21
8. Khateb F, Khatib N, Kubánek D (2011) Novel low-voltage low-power high-precision CCII± based on bulk-driven folded cascode OTA. *Microelectron J* 42(5):622–631
9. Rana C, Afzal N, Prasad D (2018) Low-voltage low-power FGMOS-based current conveyor III. *Advances in power systems and energy management*. Springer, Singapore, pp 673–81
10. Tonk A, Afzal N (2018) Bulk driven second generation current conveyor based all-pass section for low voltage operation. In *IEEE international conference on computing, power and communication technologies*, pp 946–949
11. Tonk A, Afzal N (2018) Ultra-low voltage operable bulk-driven second generation current conveyor based filters with single-input and single-output. *J Eng Sci Technol* 14(1):216–226
12. Prasad D, Bhaskar DR, Pushkar KL (2011) Realization of new electronically controllable grounded and floating simulated inductance circuits using voltage differencing differential input buffered amplifiers. *Act Passiv Electron Compon*
13. Çiçekoğlu O, Toker A, Kuntman H (2001) Universal immittance function simulators using current conveyors. *Comput Electr Eng* 27(3):227–238
14. Yuce E, Cicekoglu O (2006) The effects of non-idealities and current limitations on the simulated inductances employing current conveyors. *Analog Integr Circ Sig Process* 46(2):103–110
15. Yuce E (2008) Grounded inductor simulators with improved low-frequency performances. *IEEE Trans Instrum Meas* 57(5):1079–1084
16. Yuce E, Minaei S, Cicekoglu O (2005) A novel grounded inductor realization using a minimum number of active and passive components. *ETRI J* 27(4):427–432
17. Ferri G, Guerrini NC, Romanato R, Scotti G, Trifiletti A (2007) CCII-based high-valued inductance simulators with minimum number of active elements. In: *IEEE European conference on circuit theory and design*, pp 440–43
18. Alpaslan H, Yuce E (2011) Bandwidth expansion methods of inductance simulator circuits and voltage-mode biquads. *J Circ Syst Comput* 20(03):557–572
19. Yuce E, Minaei S (2009) On the realization of simulated inductors with reduced parasitic impedance effects. *Circ Syst Sig Process* 28(3):451
20. Kaçar F, Yeşil A (2010) Novel grounded parallel inductance simulators realization using a minimum number of active and passive components. *Microelectron J* 41(10):632–638
21. Myderrizi I, Minaei S, Yuce E (2011) DXCCII-based grounded inductance simulators and filter applications. *Microelectron J* 42(9):1074–1081
22. Metin B (2011) Supplementary inductance simulator topologies employing single DXCCII. *Radioengineering* 20(3):614–618
23. Metin B (2012) Canonical inductor simulators with grounded capacitors using DCCII. *Int J Electron* 99(7):1027–1035
24. Pathak JK, Singh AK, Senani R (2016) New canonic lossy inductor using a single CDBA and its application. *Int J Electron* 103(1):1–3

25. Herencsar N, Lahiri A, Koton J, Vrba K, Metin B (2012) Realization of resistorless lossless positive and negative grounded inductor simulators using single ZC-CCCITA. *Radioengineering* 21(1)
26. Senani R, Singh AK, Gupta A, Bhaskar DR (2016) Simple simulated inductor, low-pass/band-pass filter and sinusoidal oscillator using OTRA. *Circ Syst* 7(03):83
27. Yeşil A, Kaçar F, Gürkan K (2014) Lossless grounded inductance simulator employing single VDBA and its experimental band-pass filter application. *AEU Int J Electron Commun* 68(2):143–150
28. Ibrahim MA, Minaei S, Yüce E, Herencsar N, Koton J (2012) Lossy/lossless floating/grounded inductance simulation using one DDCC. *Radioengineering* 21:3–10
29. Pandey R, Pandey N, Paul SK, Singh A, Sriram B, Trivedi K (2014) Novel grounded inductance simulator using single OTRA. *Int J Circ Theo Appl* 42(10):1069–1079
30. Bhaskar DR, Prasad D, Pushkar KL (2013) Electronically-controllable grounded-capacitor-based grounded and floating inductance simulated circuits using VD-DIBAs. *Circ Syst* 4(5)
31. Prasad D, Bhaskar DR (2012) Grounded and floating inductance simulation circuits using VDTAs. *Circ Syst* 3(04):342
32. Siripruchyanun M, Silapan P, Jaikla W (2009) Realization of CMOS current controlled current conveyor transconductance amplifier (CCCCTA) and its applications. *J Act Passiv Electron Devices* 4(1–2):35–53
33. Siripruchyanun M, Chanapromma C, Silapan P, Jaikla W (2008) BiCMOS current-controlled current feedback amplifier (CC-CFA) and its applications. *WSEAS Trans Electron* 5(6):203–219
34. Siriphot D, Maneewan S, Jaikla W (2013) Single active element based electronically controllable grounded inductance simulator. In *IEEE Biomedical Engineering International Conference*, pp 1–4
35. Yuce E (2009) Novel lossless and lossy grounded inductor simulators consisting of a canonical number of components. *Analog Integr Circ Sig Process* 59(1):77–82
36. Alpaslan H, Yuce E (2015) Inverting CFOA based lossless and lossy grounded inductor simulators. *Circuits Syst Signal Process* 34(10):3081–3100
37. Kaçar F, Yeşil A, Minaei S, Kuntman H (2014) Positive/negative lossy/lossless grounded inductance simulators employing single VDCC and only two passive elements. *AEU Int J Electron Commun* 68(1):73–78
38. Mohammad F, Sampe J, Shireen S, Ali SH (2017) Minimum passive components based lossy and lossless inductor simulators employing a new active block. *AEU Int J Electron Commun* 82:226–240
39. Bano S, Narejo GB, Ali Shah SM (2018) Power efficient fully differential bulk driven OTA for portable biomedical application. *Electronics* 7(3):41
40. Sedra AS, Smith KC (1970) A second-generation current conveyor and its applications. *IEEE Trans Circ Theor* 17(1):132–134
41. Sedra AS, Smith KC (1998) *Microelectronic Circuits*, 4th edn. Oxford University Press, London

Neural Network Ensemble-Based Prediction System for Chemotherapy Pathological Response: A Case Study



Raghvi Bhardwaj and Nishtha Hooda

Abstract During the diagnosis of breast cancer, neoadjuvant chemotherapy is supplied intravenously. Physicians recommend chemotherapy before surgery to reduce the invasive tumor's large size. This research work suggests a model for Neural Network Ensemble Machine Learning, Implementation of a series of machine learning algorithms to create an enhanced and efficient predictable solution patients 'maximum pathological response after Neoadjuvant Chemotherapy. The quality of the neural network ensemble framework for machine learning is measured using multicriteria technique of decision making known as simple weighted additive (WSAW). The performance score for WSAW is calculated by taking into account ten measurements, namely accuracy, mean absolute error, root mean square error, TP rate, FP rate, accuracy, recall, F-measure, MCC, and ROC. The results are verified using the technique of cross-validation K-fold to achieve 97.20% accuracy. The findings are quite positive when the execution of the proposed system is coupled with the output of state-of-the-art classifiers, for example, Bayes Net, Naïve Bayes, logistic, multilayer perceptron, SMO, voted perceptron, etc. With the increasing trend of artificial intelligence applications in cancer research, machine learning has a great future in forecasting and decision making.

Keywords Machine learning · Neural network · Prediction · Neoadjuvant chemotherapy · Breast cancer · Pathological response

1 Introduction

The most common form of cancer found in women around the world is breast cancer. In India, breast cancer accounts for 23% of all female cancers. Breast cancer is

R. Bhardwaj · N. Hooda (✉)
Department of Computer Science and Engineering, Chandigarh University, Mohali, Punjab, India
e-mail: 27nishtha@gmail.com

R. Bhardwaj
e-mail: raghvibhardwaj@gmail.com

caused by breast lumps [1]. In young women, lumps are very widespread as they pass through puberty and even as they enter their 80s, they occur in women. This becomes more worried about breast lumps in women after menopause because they have no hormonal changes that would normally trigger benevolent lumps, but in growing women, most of these lumps are benevolent because there are very common lumps called fibroadenomas that occur in young women in their early 20s [2].

A proper diagnosis of breast cancer should be made on time without spreading to the underlying breast tissues in an invasive manner. Neoadjuvant chemotherapy is therefore administered to the sufferer. The majority of the time, patients receive chemotherapy for early-stage breast cancer if they need it after surgery [2, 3]. The breast cancer stage is the main aspect. There is not so much risk that breast cancer will be replicated in the early stages, so it has a more favorable prognosis. Later detected breast cancer has a higher risk of repetition, so it has a less positive outlook [3].

Different machine learning algorithms were trained in this research work after preprocessing the data to test classification efficiency. Also compared to classifiers like SVM, Naïve Bayes, Bayes Net, etc. is the most prominent classification execution. Rather than focusing solely on the reliability of the prospective system, ten assessment metrics are measured and detailed quality rating is assessed using K-fold cross-validation technique. The ten assessment metrics are used to measure the SAW quality score, namely accuracy, mean absolute error, root mean square error, TP rate, FP rate, precision, recall, F-measure, MCC, and ROC.

This paper is summarized as follows: Sect. 2 includes a short description of the approaches used in the existing classification system. Section 3 consists of the data analysis, observational setup, and details of the data. Section 4 is a description of the effects of the experiment and the differentiation of output. Finally, the conclusion is discussed in Sect. 5.

2 Review

Researchers compared the efficiency and efficacy of different stratagems linked to precision, accuracy, tolerance, and specificity in order to discover the highest accuracy of categorization [4]. In this paper, machine learning mpMRI enables the initial assumption of PCR to NAC and thus can provide profitable knowledge of predictions to accompany medication settlements [5]. In radiation oncology, an excellent pattern of big data analytics and machine learning will create optimistically elevated property verification. Reducing the value of computer power, rationalizing EHR and strategies in algorithms of artificial intelligence will reflex changes in this field [6]. This work is also primarily due to the equation of four different methods of ML. The acquired reliability rate cannot, therefore, be presumed to be enormous. This analysis has investigated the useful identification of certain data in breast cancer with ML techniques [7].

In this paper, five DNA viruses were investigated by researchers, i.e., breast cancer impacts HSV-1, EBV, CMV, HPV, and HHV-8 through the use of SVMs. The results revealed a better presentation of the SVM build model when breast cancer is identified according to their dataset [8]. In this research, the researchers focused primarily on the ensemble algorithms. Generally, an ensemble classifier carefully constructed provides more precision and solidity classification and forecast than a single algorithm can achieve [9]. Researcher examined the machine learning ideas though they describe their own prosecution in the prediction/prognosis of cancer. Most of the studies were in depth in previous years and focused on predictive model development using supervised machine learning techniques and predictive classification algorithms to predict the results of authentic diseases [10].

Researchers have studied that patients with full pathological response after neoadjuvant chemotherapy have significant particular survival improvements and extensive survival [11]. Researchers have expanded different support systems for medical decision making to analyze data on expression of genes that can strengthen the prognosis of cancer patient survival and patients [12]. Researcher suggested an outstanding SVM constructed weighted AUC ensemble learning system for breast cancer research. Five programs for fusion are designed specifically to combine the views of different basic models to distinguish between the scheduled WAUCE model, the one which shows that the WAUCE model can significantly increase the execution of cancer diagnosis [13].

3 Methods

This section is a summary of machine learning classifiers, their advantages and presents the detailed view of the proposed neural network ensemble machine learning framework.

Some advantages of machine learning classifiers are given below:

- (i) Machine learning can easily recognize trends and patterns.
- (ii) No human intercession is needed in machine learning.
- (iii) Machine learning algorithms are virtuous at handling multivariety data.
- (iv) Machine learning algorithms keep improving in efficiency and precision with experience.

Machine Learning Classifiers:

Bayes Net: This classifier is directed acyclic graphs (DAG), the nodes of which are parameters in the section sense of the Bayes Net. That network refers to a possible feature that takes as an insight some certain set of morals for the defined node variables and gives up the node variable grouping possibility [14].

Naïve Bayes: Such classification systems are infinitely scalable, allowing a variety of amount of variables specifications in the learning process [15].

Logistic: It is usually the structure in depth and performance of a complicated action. This is the mainframe of the stream of items between the point of origin and the point of use [16].

Multilayer perceptron neural network: This is a neural artificial network class feedforward. A minimum of three levels of nodes was incorporated into a multilayer perceptron: a layer of input, a hidden layer as well as an output layer [17].

Support vector machine or SMO: It is a representation of examples as space points, separated by a clear gap, plotted to establish distinct categories. Then, virtual instruments are shown in the new region and same area predicted to belong to a category on the basis of space side that they fall [18].

Voted perceptron neural network: It is a neuronal net or orbit, or an artificial neural network in other words, gathered from artificial impulses or crossings of the nerve [19].

3.1 Proposed Framework

In this study, the model for neural network ensemble machine learning was designed to implement an improved version of the breast cancer machine learning computer algorithm for pathological complete response prediction only after neoadjuvant chemotherapy as illustrated throughout Fig. 1.

The abstract view of neural network ensemble machine learning framework is presented in Fig. 1. This whole framework is split into three layers as explained below:

- (i) Layer 1: Chemotherapy uses drugs that include anthracycline and taxane for cancer which prevents the growth of cancer cells.
- (ii) Layer 2: In this, the neural network ensemble machine learning framework for pathological complete response (PCR) prediction is implemented.
- (iii) Layer 3: Post-operative and follow-up treatment are conducted in layer 3.

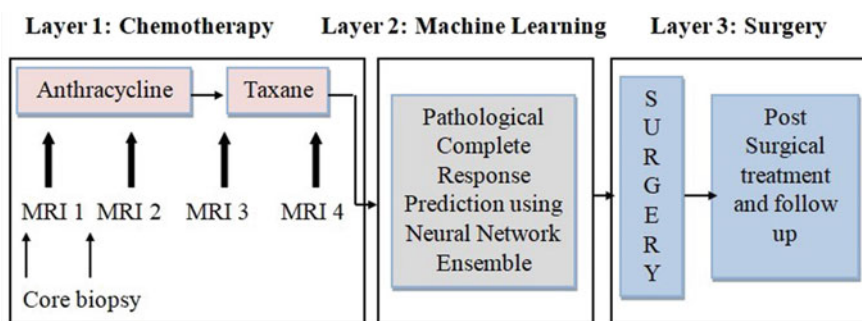


Fig. 1 Abstract view of neural network ensemble machine learning framework

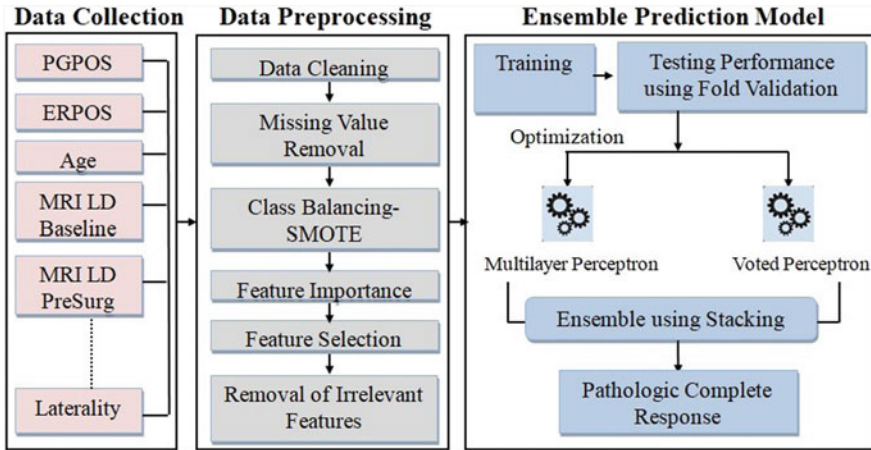


Fig. 2 Detailed view of neural network ensemble machine learning framework

Figure 2 presents a detailed perspective of the model for the neural network ensemble. As explained below, the whole framework is split into three sections:

- (i) **Data collection:** The dataset I-SPY-1-TRIAL consists of 222 breast cancer diagnosed cases for which information was extracted from the documentation on cancer scanning and the UCSF plan of the analysis on breast imaging. In this data, information on various variables such as PGPOS, MRI LD PreSurg, ERPOS, MRI LD PreSurg, age, MRI LD baseline, and laterality is collected and computed in an estimated system. These variables then allow the end results to be analyzed.
- (ii) **Data preprocessing:** It is an important step in projects related to machine learning. Data collected from the dataset are cleared in this chapter. This means the recognition process and enhancing inappropriate registry or server information by data cleaning. After the data cleaning process, missing values are deleted from the dataset. It is necessary to conceptualize the missing values in order to track the data successfully. The elimination of missing values causes the data set to be unbalanced, thus the balancing of the unstable dataset is performed after the missing value removal stage using synthetic minority over-sampling technique (SMOTE) to create synthetic instances to keep the balance in the dataset. After this mechanism, various important characteristics will be determined and the remaining irrelevant characteristics will be eliminated.
- (iii) **Prediction model:** Nine various forms of classification models have been used: Bayes Net, Naïve Bayes, logistic, multilayer perceptron neural network, SMO, voted perceptron neural network, etc. Training and evaluation were carried out by these designs. Different classification models of machine learning are trained to test classification efficiency. Testing is carried out using K-fold cross-verification scheme and findings are shown. Through optimizing, two ensemble classification models, namely multilayer perceptron, voted perceptron, etc., are

Table 1 Variable description

PGPOS	Progesterone receptor status, pre-treatment
ERPOS	Estrogen receptor status, pre-treatment
AGE	Patient age
MRI LD baseline	Massive tumor extent at baseline evaluated by MRI
MRI LD PreSurg	Massive tumor extent before surgery estimated by MRI
Laterality	Breast with major or single tumor

just used to measure different performance measures such as accuracy, TP level, FP rate, and ROC. Such classifiers have successfully achieved adequate results. By using the stacking, we assembled the two classifiers and obtained a 97.20% accuracy.

4 Experimental Investigation

This segment explains the framework's dataset and observational settings.

4.1 Dataset

Data from 222 patients diagnosed for breast cancer are extracted from the UCSF research plan with the ACRIN, CALGB, I-SPY TRIAL, and TCIA alliances. Table 1 shows the description of each variable and also the specified class.

4.2 Experimental Setting

The various template design techniques are incorporated in the R language using Rattle. The primary goal is to calculate the accuracy of this classifier's prediction. Numerous discrete parameters are used to test the quality of the designed model: accuracy, mean absolute error, accuracy, recall, root mean squared error, F-measure, MCC, ROC area, PRC area, TP rate, FP rate, etc.

Table 2 Confusion matrix

Predicted condition	True reference	
	Positive response	Negative response
Positive response	True positive X	False positive Z
Negative response	False negative Q	True negative Y

Table 3 Performance metrics

Precision	TP/predicted yes
F-score	$2 * (\text{precision} * \text{recall} / (\text{precision} + \text{recall}))$
TP rate	TP/FN + TP
FP rate	FP/TP + FP
Accuracy	TP + TN / (TP + FN + FP)

5 Results and Discussions

This whole paragraph sums up the performance testing and analyzed research findings of the proposed model using K-fold cross-verification approach.

5.1 Performance Evaluation

As shown in Tables 2 and 3, the proposed model is checked with definite uncertainty matrix parameters and Table 4 shows the research findings. The ten measurements of the evaluation are used to calculate the performance score, namely accuracy, mean absolute error, root mean square error, TP rate, FP rate, precision, recall, F-measure, MCC, and ROC. In estimation along with neoadjuvant survivability breast

Table 4 Experimental results

Classifiers	Acc%	MAE	RMSE	TPR	FPR	Precision	Recall	F-M	MCC	ROC
Bayes Net	94	0.05	0.15	0.97	0.05	0.97	0.97	0.97	0.93	0.96
Naïve Bayes	93	0.03	0.13	0.96	0.03	0.96	0.96	0.96	0.95	0.97
Logistic	90	0.07	0.25	0.93	0.11	0.93	0.93	0.93	0.81	0.89
Multilayer perceptron	94	0.04	0.17	0.96	0.04	0.96	0.96	0.96	0.91	0.97
SMO	95	0.02	0.16	0.97	0.03	0.97	0.97	0.97	0.93	0.94
Voted perceptron	71	0.26	0.51	0.73	0.73	0.53	0.73	0.51	0.50	0.51
NN ensemble	98	0.02	0.10	0.98	0.01	0.98	0.98	0.97	0.96	0.99

cancer chemotherapy with machine learning system, the false positive frequency is more costly in addition to other parameters such as false negative and true negative. Therefore, true positive rate and false negative rate analytics are assigned a double weight. In addition to true positive rate, false negative rate, prediction, it also grants precision with dual weighting. In machine learning, if the data has imbalanced class samples during machine learning classification training, then correctness is deemed to be perplexing. In certain instances, the region below the quality of the ROC shows us the classifier’s precise output. A binary weight is therefore allocated to the performance parameter of the AUC. WSAW’s detailed quality score helps to find the best prediction model, taking into account all ten assessment indicators, doubling precision, AUC, TP frequency, and FP rate.

In Fig. 3, the performance comparison of the neural network ensemble machine learning system is presented graphically using accuracy, true positive rate, false positive rate, and ROC curve with generic classifiers such as Bayes framework, Naïve Bayes, logistic, multilayer perceptron, SMO, and voted perceptron. It can be found that the reliability of the machine learning system for neural network ensemble is the maximum. Voted perceptron is less than 70% accurate and multilayer perceptron is 94% accurate. It may be true that the ensemble clustering algorithm results are better than most of conventional machine learning techniques, because classifiers achieve better results at true positive rate and false positive rate.

The K-fold cross-validation research technique test findings are displayed in Fig. 4 using accuracy, TP rate, FP rate, and ROC. The figure shows the consistency of the

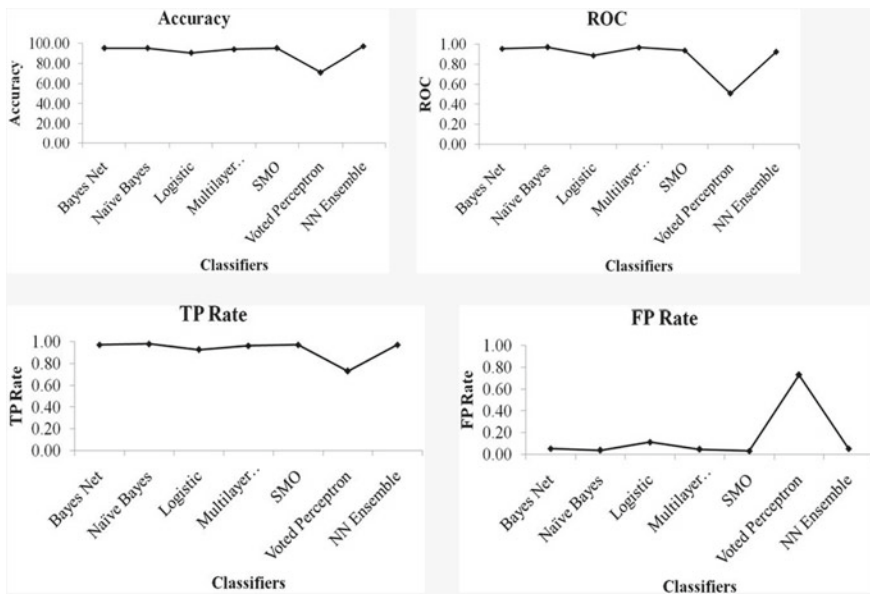


Fig. 3 Result comparison of neural network ensemble traditional ML framework classifiers using accuracy, ROC, TP rate, and FP rate

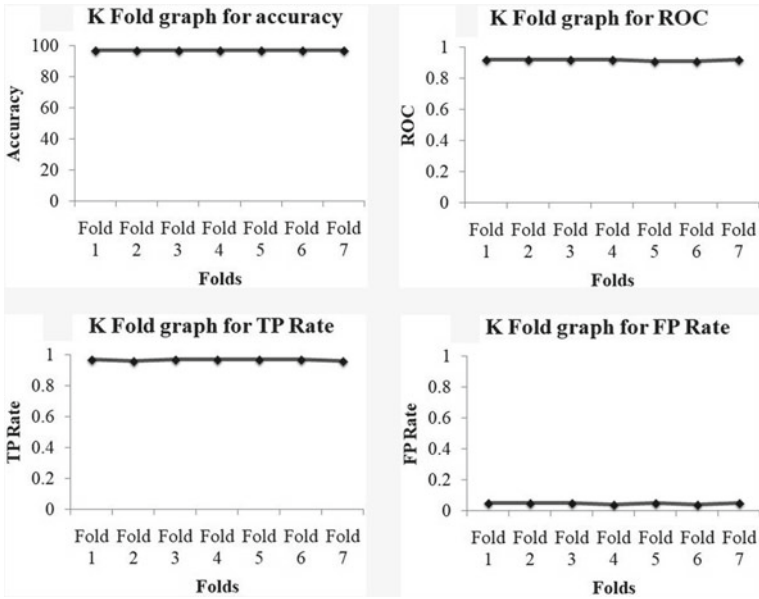


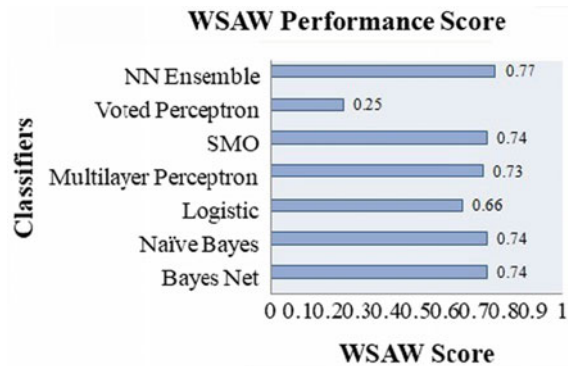
Fig. 4 K-fold cross-verification testing experimental results using accuracy, ROC, TP rate, and FP rate

different machine learning metrics of the neural network ensemble. It can be easily observed that in all ten iterations (folds) the propound framework is immensely stable. Finally, instead of focusing solely on the reliability of the suggested system, systematic quality analysis is carried out using a weighted SAW technique for multicriteria decision making. Due to their severity, the FP rate and AUC values are doubled. Pathological response prediction is a key decision and also the reason for reducing false positive’s predictions. In addition, the AUC value is taken into account by using the plot of true positive versus false positive versus AUC value helps to cater for the best prediction algorithm when the data is imbalanced. Figure 5 compares the WSAW performance score of the proposed framework (assessed using 10 machine learning key measures) using nine optimal classifiers for machine learning. The graph shows that the neural network ensemble’s comprehensive performance score is high-ranking. This can, therefore, be used to enforce the pathological complete response Web application.

6 Conclusion

Efficient ensemble machine learning based on the name neural network ensemble is proposed in this study to forecast the comprehensive pathological response on account of neoadjuvant chemotherapy. Experimentation is carried out for this

Fig. 5 SAW performance graph



ensemble building for various combinations of neural network-work machine learning classifiers, and a final ensemble model is built for prediction after thousands of iterations. Unlike traditional methods, the proposed framework for the neural network ensemble with a full weighted SAW decision-making method is tested. The planned implementation performs other state-of-the-art optimization algorithms by showing an accuracy of 97.20%, TP rate, FP rate, ROC, 0.97, 0.05, 0.92, respectively. In this context, the NN ensemble's WSAW score is the highest, i.e., 0.77, which shows that the two machine learning classifiers ensemble delivers more accurate results than the basic machine learning classifiers. The proposed plan serves as a diagnostic network of support for pre-operative health professionals/physicists to identify the complete pathological reaction of the sufferer at the preliminary level of cancer. A Web service for the neural network ensemble framework is planned for the future at the top of the Hadoop framework to process more patient data.

References

1. Asano Y et al (2017) Prediction of survival after neoadjuvant chemotherapy for breast cancer by evaluation of tumor infiltrating lymphocytes and residual cancer burden. *BMC Cancer* 17(1):88
2. Borchert et al (1997) Elevated levels of prostate-specific anti- gen in serum of women with fibroadenomas and breast cysts. *J Natl Cancer Inst* 89(8):587–588
3. Haffty B et al (2011) Meta-analysis confirms achieving pathological complete response after neoadjuvant chemotherapy predicts favourable prognosis for breast cancer patients. *Eur J Cancer* 47(14):2084–2090
4. Asri H et al (2016) Using machine learning algorithms for breast cancer risk prediction and diagnosis. *Procedia Comput Sci* 83:1064–1069
5. Tahmassebi A et al (2019) Impact of machine learning with multiparametric magnetic resonance imaging of the breast for early prediction of response to neoadjuvant chemotherapy and survival outcomes in breast cancer patients. *Invest Radiol* 54(2):110–117
6. Bibault JE et al (2016) Big data and machine learning in radiation oncology: state of the art and future prospects. *Cancer Lett* 382(1):110–117
7. Aslan MF et al (2018) Breast cancer diagnosis by different machine learning methods using blood analysis data. *Int J Intell Syst Appl Eng* 6(4):289–293

8. Huang CL et al (2008) Prediction model building and feature selection with support vector machines in breast cancer diagnosis. *Expert Syst Appl* 34(1):578–587
9. Yang P et al (2010) A review of ensemble methods in bioinformatics. *Curr Bioinform* 5(4):296–308
10. Kourou K et al (2015) Machine learning applications in cancer prognosis and prediction. *Comput Struct Biotechnol J* 13:8–17
11. Cain EH et al (2019) Multivariate machine learning models for prediction of pathologic response to neoadjuvant therapy in breast cancer using MRI features: a study using an independent validation set. *Breast Cancer Res Treat* 173(2):455–463
12. Bashiri A et al (2017) Improving the prediction of survival in cancer patients by using machine learning techniques: Experience of gene expression data: A narrative review. *Iran J Publ Health* 46(2):165
13. Wang H et al (2018) A support vector machine-based ensemble algorithm for breast cancer diagnosis. *Eur J Oper Res* 267(2):687–699
14. Pearl J (2000) *Causality: Models, reasoning, and inference*. Cambridge University Press. ISBN 0-521-77362-8. OCLC 42291253
15. McCallum A et al (1998, July) A comparison of event models for naive bayes text classification. In: *AAAI-98 workshop on learning for text categorization*, vol 752, No. 1, pp. 41–48
16. Syarif A et al (2002) Study on multi-stage logistic chain network: a spanning tree based genetic algorithm approach. *Comput Ind Eng* 43(1–2):299–314
17. Orhan U et al (2011) EEG signals classification using the K-means clustering and a multilayer perceptron neural network model. *Expert Syst Appl* 38(10):13475–13481
18. Cortes C et al (1995) Support-vector networks. *Mach Learn* 20(3):273–297. <https://doi.org/10.1007/BF00994018>
19. Huang YM et al (2006) Evaluation of neural networks and data mining methods on a credit assessment task for class imbalance problem. *Nonlinear Anal Real World Appl* 7(4):720–747

Outage and ABER Analysis for L-MRC on OWDP Fading Channels



Suparna Goswami, Laishram Mona Devi, and Aheibam Dinamani Singh

Abstract The performance measure of M -ary phase shift keying and M -ary frequency shift keying for maximal ratio combiner (MRC) is numerically investigated on the channel with one-wave-diffused-power (OWDP) fading. The numerical evaluation of the performance parameters is done by the probability density function (pdf) based method. The pdf of the MRC receiver is evaluated using the characteristic function. The outcomes obtained are plotted to observe the effect of OWDP fading parameter K and MRC diversity with L branch. The outcomes are simulated by Monte Carlo simulation.

Keywords MFSK · MPSK · MRC · pdf · OWDP

1 Introduction

The quality of the wireless channels is degrading due to fading. In the literature, fading channels are modeled using various distributions. The methods of diversity are employed to eliminate the consequence of the fading. In this technique, various versions of the signal transmitted are combined at the diversity receiver to have a better overall signal-to-noise ratio (SNR). So, at the receiver, a diversity method named as maximal ratio combiner (MRC) is employed. In this combining system, the received signals are co-phased and weighted to produce the improved SNR. This combining system gives an ideal performance [1] than other combiner methods. In [2], the model of two-wave diffused-power (TWDP) fading channels is developed by dual specular multi-path wave along with diffusely propagation waves. The authors

S. Goswami (✉) · L. M. Devi · A. D. Singh
Department of ECE, NERIST, Nirjuli, Arunachal Pradesh, India
e-mail: suparnanerist@gmail.com

L. M. Devi
e-mail: monalaishram16@gmail.com

A. D. Singh
e-mail: ads@nerist.ac.in

also analyzed this model in the operation of a narrow-band receiver. In [3], the pre-detection of the MRC technique was used to analyze the system upon two-wave diffused-power (TWDP) channels. The cumulative distribution function (cdf) is applied to investigate the average bit error rate (ABER) of quadrature amplitude modulation (QAM) for TWDP in [4]. The performance parameter was evaluated for multiple branches of SC receivers on κ - μ and η - μ fading in [5]. The symbol error probability (SEP) using moment generating function (mgf) approach for M -ary rectangular QAM for TWDP model was presented in [6]. The analysis of SC upon TWDP channel was given in [7]. The evaluation of adaption schemes for MRC diversity on TWDP was given in [8]. Moreover, the capacity study of dual-MRC on non-identical TWDP was derived in [9]. Adaptive transmission methods over dual branch MRC diversity system of TWDP for channels capacity were derived in [10]. The study on the comparison of SC, MRC, and equal gain combining (EGC) was done in [11]. The analysis for dual-MRC scheme employing pdf method for non-identical TWDP model was presented in [12]. In [13], the outage probability and average symbol error rate (ASER) for TWDP fading were investigated. For coherent and non-coherent modulation, closed-form analytical equation for cdf, mgf, average channels capacity, and average SEP were evaluated in [14].

In literature views, performance and capacity evaluation in the field of MRC scheme has been studied on plenty of fading channels. But the work on the performance evaluation of MRC scheme on one-wave-diffused-power (OWDP) fading channel is not available yet.

The OWDP channel is discussed in Sect. 2. The expression for SNR pdf of MRC is expressed in Sect. 3. In Sect. 4, the expression for outage probability and ABER is present. In Sect. 5, the discussion of the output obtained is given. Lastly, in Sect. 6, the conclusion is given.

2 OWDP Fading Channels

The OWDP has one specular component and many diffused components. The one wave has one amplitude wave which is constant. According to the sensor in the wireless network, the OWDP fading channel is more efficient because this fading channel is ascending within a cavity. For analysis, this fading channel is supposed to have a flat and a slow fading. The envelope pdf of the OWDP channel is [2]

$$P_R(r) = \sum_{i=1}^N a_i \frac{r}{\sigma^2} e^{-\left\{ \frac{r^2 + 2\sigma^2 K}{2\sigma^2} \right\}} I_0 \left(\frac{r}{\sigma^2} \sqrt{2\sigma^2 K} \right), \quad (1)$$

where N represents order approximation; a_i represents the coefficient; r represents fading amplitude; σ^2 represents variance; K represents specular power upon diffused power; and $I_0(\cdot)$ represents the Bessel function of first kind with order zero. The pdf expression of output SNR for OWDP fading channel is derived by

performing square and random variable transformation. Therefore, after performing square transformation in Eq. (1), the expression can be written as

$$f_r(r) = \sum_{i=1}^N \frac{a_i}{2\sigma^2} \left[e^{-\left\{ \frac{s}{2\sigma^2} + K \right\}} I_0 \left(\frac{1}{\sigma} \sqrt{2Ks} \right) \right]. \tag{2}$$

Now, in Eq. (2), the random variable transformation is being performed. The expression is obtained as

$$f_\gamma(\gamma) = \sum_{i=1}^N \frac{N_o}{E_b} \frac{a_i}{2\sigma^2} \left[e^{-\left\{ \frac{N_o \gamma}{E_b} + K \right\}} I_0 \left(\frac{1}{\sigma} \sqrt{2K \frac{N_o}{E_b} \gamma} \right) \right]. \tag{3}$$

Simplifying Eq. (3), the SNR pdf of OWDP fading is obtained as

$$f_\gamma(\gamma) = \beta \sum_{i=1}^N a_i e^{-l(\beta\gamma+K)} I_0(2\sqrt{K\beta\gamma}), \tag{4}$$

where $\beta = \frac{1+K}{\bar{\gamma}}$.

3 SNR Pdf of Maximal Ratio Combiner

The SNR of the MRC receiver is expressed in [1] as

$$\gamma_{MRC} = \sum_{l=1}^N \gamma_l = \frac{E_b}{N_0} (r_1^2 + r_2^2 + \dots + r_L^2), \tag{5}$$

where E_b is termed as the energy per bit. $\gamma_1 = \frac{E_b}{N_0} r_1^2$, $\gamma_2 = \frac{E_b}{N_0} r_2^2$, and $\gamma_L = \frac{E_b}{N_0} r_L^2$ are the 1st, 2nd, and L th receiving branch SNRs, respectively. The average SNRs for γ_1 , γ_2 , and γ_L is $\bar{\gamma}_1$, $\bar{\gamma}_2$, and $\bar{\gamma}_L$, respectively. Considering the average SNR is equal in all branches of MRC receiver, it is assumed that $\bar{\gamma}_1 = \bar{\gamma}_2 = \bar{\gamma}_L = \bar{\gamma}$. The SNR pdf of each branch of the receiver is expressed as

$$f_{\gamma_l}(\gamma_l) = \beta \sum_{i=1}^N a_i e^{-l(\beta\gamma_l+K)} I_0(2\sqrt{K\beta\gamma_l}), \tag{6}$$

where the SNR of the l th branch is termed as γ_l .

By using the characteristic function (CF) method, the SNR output pdf for MRC receiver is found. The formula used for deriving the CF SNR expression is given in [14] as

$$\phi_{\gamma_l}(j\omega) = \int_0^\infty f_{\gamma_l}(\gamma_l) e^{-j\omega\gamma_l} d\gamma_l. \tag{7}$$

After substituting Eq. (6) in Eq. (7), the resulting expression for CF is obtained as

$$\phi_{\gamma}(j\omega_l) = \beta \sum_{i=1}^N a_i e^{-K} \frac{1}{(\eta + j\omega_l)} e^{\frac{4K\beta}{2(\beta+j\omega_l)}}. \tag{8}$$

From the above expression, the CF of the joint pdf is obtained as

$$\phi_{\gamma_1 \dots \gamma_L}(j\omega_1, \dots, j\omega_L) = \prod_{t=1}^L \left\{ \beta \sum_{i=1}^N a_i e^{-K} \frac{1}{(\beta + j\omega_t)} e^{\frac{K\beta}{(\beta+j\omega_t)}} \right\}. \tag{9}$$

Further simplifying Eq. (9) by considering $\omega_1 = \omega_2 \dots = \omega_L = \omega$, the expression is obtained as

$$\phi_{\gamma_{MRC}}(j\omega) = (\beta)^L \sum_{i_1=1}^N \dots \sum_{i_M=1}^N \left\{ \prod_{t=1}^L a_{i_t} \right\} \frac{e^{-LK} e^{\frac{LK\beta}{(\beta+j\omega)}}}{(\beta + j\omega)^L}. \tag{10}$$

Also, the exponential term in Eq. (10) can be obtained in terms of infinite series. Hence, the expression is written as

$$\phi_{\gamma_{MRC}}(j\omega) = (\beta)^L \sum_{i_1=1}^N \dots \sum_{i_L=1}^N \sum_{s=0}^\infty \left\{ \prod_{t=1}^L a_{i_t} \right\} \frac{e^{-LK} (LK\beta)^s}{s!(\beta + j\omega)^{L+s}}. \tag{11}$$

The summation of the SNR pdf is calculated by the inverse Fourier transform of joint CF as [14]

$$f_{\gamma_{MRC}}(\gamma) = \frac{1}{2\pi} \int_{-\infty}^\infty \phi_{\gamma_{MRC}}(j\omega) e^{j\omega\gamma} d\omega. \tag{12}$$

After substituting the expression from Eq. (11) in Eq. (12), the resulting expression for the SNR pdf is obtained as

$$f_{\gamma_{MRC}}(\gamma) = (\beta)^L \sum_{i_1=1}^N \dots \sum_{i_L=1}^N \sum_{s=0}^\infty \left\{ \prod_{t=1}^L a_{i_t} \right\} \frac{e^{-LK} (\beta LK)^s}{s! 2\pi} \int_{-\infty}^\infty \frac{e^{j\omega\gamma}}{(\beta + j\omega)^{L+s}} d\omega. \tag{13}$$

The integral is solved by using [15, (3.382.6)]. The equation for SNR pdf of MRC receiver is obtained as

$$f_{\gamma_{\text{MRC}}}(\gamma_{\text{MRC}}) = (\beta)^L \sum_{i_1=1}^N \dots \sum_{i_L=1}^N \left\{ \prod_{t=1}^L a_{i_t} \right\} \frac{e^{-LK}}{\Gamma(L)} {}_0F_1(; L; \gamma_{\text{MRC}} L K \beta) \gamma_{\text{MRC}}^{L-1} e^{-\beta \gamma_{\text{MRC}}}, \tag{14}$$

where ${}_0F_1(\cdot)$ is the hypergeometric function.

The hypergeometric function in the above equation can be represented in terms of infinite series. The resulting expression derived for SNR pdf is given as

$$f_{\gamma_{\text{MRC}}}(\gamma) = (\beta)^L \sum_{i_1=1}^N \dots \sum_{i_L=1}^N \left\{ \prod_{t=1}^L a_{i_t} \right\} \times \sum_{s=0}^{\infty} (\beta L K)^s \frac{e^{-LK} e^{-\beta \gamma}}{s!(L)_s \Gamma(L)} \gamma^{L+s-1}, \tag{15}$$

where L indicates diversity branches. $(L)_s$ is the Pochhammer symbol.

4 Analysis of MRC Scheme

The outage and average bit error rate of L -MRC are analyzed in this section.

4.1 Outage Probability

The outage in a communication system occurs when the SNR reduces below some threshold (γ_{th}). The outage probability (P_{out}) is the probability of occurrence of outage. To evaluate the expression for P_{out} , the cdf of SNR output must be known first. The cdf expression is obtained as

$$F_{\gamma_{\text{MRC}}}(\gamma) = (\beta)^L \sum_{i_1=1}^N \dots \sum_{i_L=1}^N \sum_{s=0}^{\infty} \frac{\left\{ \prod_{t=1}^L a_{i_t} \right\} e^{-LK} (\beta L K)^s}{s!(L)_s \Gamma(L)} \times \int_0^{\gamma_{\text{MRC}}} \gamma^{L+s-1} e^{-\beta \gamma} d\gamma. \tag{16}$$

The expression for outage is found by putting γ_{MRC} as γ_{th} . Thus, the resulting expression for outage is obtained as

$$\begin{aligned}
 P_{\text{out}}(\gamma_{\text{th}}) &= (\beta)^L \sum_{i_1=1}^N \dots \sum_{i_L=1}^N \sum_{s=0}^{\infty} \frac{\left\{ \prod_{t=1}^L a_{i_t} \right\} e^{-LK} (\beta LK)^s}{s!(L)_s \Gamma(L)} \\
 &\quad \times \int_0^{\gamma_{\text{th}}} \gamma^{L+s-1} e^{-\beta\gamma} d\gamma.
 \end{aligned} \tag{17}$$

The integral in (9) is solved by means of [15, (3.381.1)] and obtained P_{out} as

$$\begin{aligned}
 P_{\text{out}}(\gamma_{\text{th}}) &= \sum_{i_1=1}^N \dots \sum_{i_L=1}^N \sum_{s=0}^{\infty} \left\{ \prod_{t=1}^L a_{i_t} \right\} e^{-LK} \\
 &\quad (KL)^s \frac{g(L+s, \beta\gamma_{\text{th}})}{s!(L)_s \Gamma(L)},
 \end{aligned} \tag{18}$$

where lower incomplete gamma function is represented by $g(\cdot)$.

4.2 Average Bit Error Rate

The average of conditional BER ($p_e(\varepsilon/\gamma)$) over pdf of receiver SNR output is ABER. The ABER is found as

$$P_E = \int_0^{\infty} p_e(\varepsilon/\gamma) f_{\gamma_{\text{MRC}}}(\gamma) d\gamma, \tag{19}$$

4.2.1 Coherent Modulation

The coherent modulation is evaluated by using $p_e(\varepsilon/\gamma) = aQ(\sqrt{\gamma b})$ where the value of a and b are mentioned in [13]. Putting $p_e(\varepsilon/\gamma)$ and $f_{\gamma_{\text{MRC}}}(\gamma)$ from (8) in (11), the ABER of coherent modulation is evaluated as

$$\begin{aligned}
 P_{e,\text{coh}}(\bar{\gamma}) &= (\beta)^L \sum_{i_1=1}^N \dots \sum_{i_L=1}^N \sum_{s=0}^{\infty} \frac{\left\{ \prod_{t=1}^L a_{i_t} \right\} a e^{-LK} (\beta LK)^s}{s!(L)_s \Gamma(L)} \\
 &\quad \times \int_0^{\infty} Q(\sqrt{\gamma b}) e^{-\beta\gamma} \gamma^{L+s-1} d\gamma.
 \end{aligned} \tag{20}$$

The expression is finally found as

$$\begin{aligned}
 P_{e,\text{coh}}(\bar{\gamma}) &= \frac{1}{\sqrt{\pi}} \sum_{i_1=1}^N \dots \sum_{i_L=1}^N \sum_{s=0}^{\infty} \left\{ \prod_{t=1}^L a_{i_t} \right\} \\
 &\quad \frac{a\sqrt{b}e^{-LK}(LK)^s \Gamma(L+s+\frac{1}{2})}{\Gamma(L)s!(L)_s(L+s)(b+2\beta)^{L+s+\frac{1}{2}}} \\
 &\quad \beta^{L+s} \times {}_2F_1\left(1, L+s+\frac{1}{2}; L+s+1; \frac{2\beta}{b+2\beta}\right), \tag{21}
 \end{aligned}$$

where the integral in (12) is solved by using [15, (6.455.1)]. The Q-function is written as $Q = \frac{a}{2\sqrt{\pi}} \Gamma\left(\frac{1}{2}, \frac{b}{2}\gamma\right)$. ${}_2F_1(\cdot)$ is the hypergeometric function.

4.2.2 Non-coherent Modulation

The non-coherent modulation is evaluated by using $p_e(\varepsilon/\gamma) = e^{-b\gamma}a$, where the parameters of a and b are mentioned in [13]. Putting $p_e(\varepsilon/\gamma)$ and $f_{\gamma\text{MRC}}(\gamma)$ from (8) in (11), the ABER of non-coherent modulation is evaluated as

$$\begin{aligned}
 P_{e,\text{non}}(\bar{\gamma}) &= (\beta)^L \sum_{i_1=1}^N \dots \sum_{i_L=1}^N \frac{\left\{ \prod_{t=1}^L a_{i_t} \right\} a e^{-LK}}{\Gamma(L)} \\
 &\quad \times \int_0^{\infty} \gamma^{L-1} e_0^{-(\beta+b)\gamma} F_1(; L; (LK)\beta\gamma) d\gamma. \tag{22}
 \end{aligned}$$

Further, the integral in (14) is solved by using [15, (7.525.1)]. The final expression after simplification of ABER of non-coherent modulation is

$$P_{e,\text{non}}(\bar{\gamma}) = (\beta)^L \sum_{i_1=1}^N \dots \sum_{i_L=1}^N \left\{ \prod_{t=1}^L a_{i_t} \right\} \frac{a e^{-LK}}{(\beta+b)^L} e^{\frac{LK\beta}{\beta+b}}. \tag{23}$$

5 Numerical Outcomes and Discussions

From Fig. 1, the system performance enhances with greater diversity branch. The reason is that the fading channels will have a deep fade when the total probability decreases. Also, the system’s performance boosted when K value increases. This means that greater K value gives more power of specular signals; therefore, it enhances the channel. In Fig. 2, the graph is obtained for M -ary phase shift keying (MPSK) coherent modulation scheme for a constant K value. The system performance is better in BPSK coherent modulation scheme. It is concluded that the system

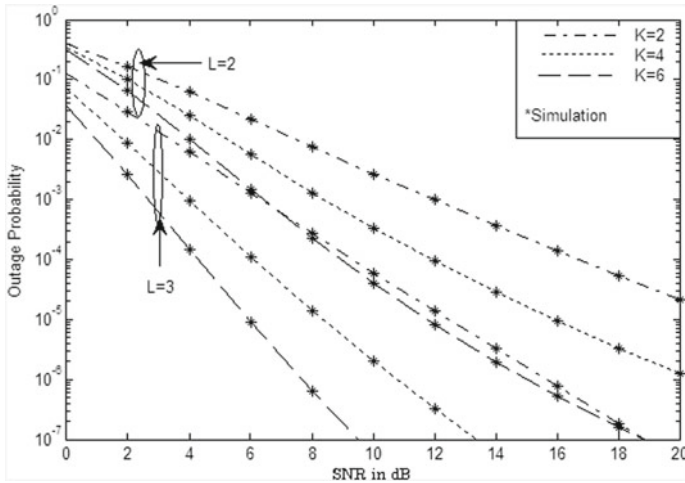


Fig. 1 Outage probability of L -MRC scheme

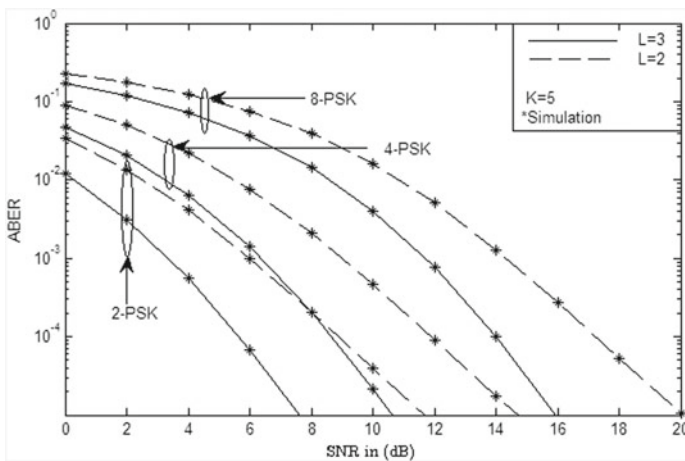


Fig. 2 ABER for coherent modulation of L -MRC scheme

performance is worst in 8-PSK coherent modulation scheme. The reason behind is, in BPSK, the space between the message points has a larger gap. Therefore, the probability to take a wrong decision for a particular symbol is less. For 8-PSK, the message points are close enough. That is why the probability to take a wrong decision for a particular symbol is more. The bit rate is higher for the higher-order modulation. Therefore, the fade occurred in some duration causes more error in numbers of bits for higher-order modulation. Figure 3 shows the curve for M -ary frequency shift keying (MFSK) non-coherent modulation scheme at a constant K . From this graph, a similar observation is observed as the plot as coherent modulation. The ABER

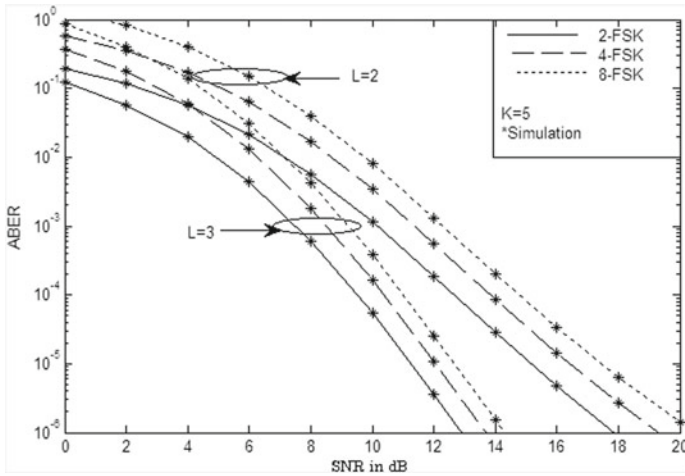


Fig. 3 ABER for non-coherent modulation of L -MRC scheme

system’s performance improves for binary frequency shift keying (BFSK) modulation scheme. The system performance degrades in 8-FSK modulation scheme. The reason is stated above.

6 Conclusions

The mathematical equation for P_{out} and ABER of L -MRC scheme has been evaluated. To get the pdf of the SNR with MRC system on OWDP channel, the pdf method and CF have been used. The results are then plotted and are verified. The obtained outcomes are found to be correct.

References

1. Simon MK, Alouini M-S (2000) Digital communications over fading channels: A unified approach to performance analysis. Wiley, New York
2. Durgin GD, Rappaport TS, de Wolf DA (2002 January) New analytical models and probability density functions for fading in wireless communication. IEEE Trans Commun 50(6):1005–1015
3. Oh SH, Li KH, Lee WS (2007, August) Performance of BPSK pre-detection MRC systems over two-wave with diffuse power fading channels. IEEE Trans Wireless Commun 6(8):2772–2775
4. Suraweera HA, Lee WS, Oh SH (2008, February) Performance analysis of QAM in a two-wave with diffuse power fading environment. IEEE Commun Lett 12(2):109–111
5. Subadar R, Reddy TSB, Sahu PR (2010) Performance of an L-SC receiver over kappa-mu and eta-mu fading channels. 2010 IEEE International Conference on Communications. Cape Town, pp 1–5, <https://doi.org/10.1109/ICC.2010.5502444>

6. Lu Y, Yang N (2011, January) Symbol error probability of QAM with MRC diversity in two-wave with diffuse power fading channels. *IEEE Commun Lett* 15(1):10–12
7. Subadar R, Singh AD (2013, June) Performance of SC receiver over TWDP fading channels. *IEEE Wirel Commun Lett* 2(3):267–270
8. Aldalgamouni T, Magableh AM, Al-hubaishi A (2013, February) Performance of selected diversity Techniques over the α - μ fading channels. 12(2). E-ISSN:2224-2864
9. Singh AD, Subadar R (2015) Capacity analysis of MRC receiver with adaptive transmitters over TWDP fading channels. In: International symposium on advanced computing and communication (ISACC)
10. Singh AD, Subadar R (2015) Capacity of dual MRC receiver with adaptive transmitters over non-identical TWDP fading channels. In: International conference on advances in computer engineering and applications (ICACEA). IMS Engineering College, Ghaziabad, India
11. Singh AD, Loyalkpa Meitei N (2015) Performance comparison of diversity receivers over TWDP fading channels. In: International conference on advances in computer engineering and applications (ICACEA). IMS Engineering College, Ghaziabad, India
12. Singh AD, Goswami S (2015) Performance of digital modulations over TWDP fading channel. In: IEEE-international conference on electronic design, computer networks and automated verification (EDCAV), pp 135–138
13. Badarneh OS, Aloqlah MS (2016, October) Performance analysis of digital communication system Over α - η - μ fading channels. *IEEE Trans Veh Technol* 65(10)
14. Singh AD, Subadar R (2015) Performance of dual MRC receiver over non-identical TWDP fading channels. In: International conference on advances in computer engineering and applications (ICACEA) IMS Engineering College, Ghaziabad, India
15. Gradshteyn IS, Ryzhik IM (2007) Table of integrals, series, and products, 7th edn. ISBN-13: 978-0-12-373637-6, ISBN-10: 0-12-373637-4

Performance Evaluation of Incremental PCA and Its Variants in Face Recognition



Nitin Kumar and Suresh Madhavan

Abstract Face recognition is a challenging research problem with several critical applications. Incremental Learning is an approach which does not require all the training samples beforehand for model development. In this direction, a popular approach called incremental principal component analysis (IPCA) was suggested by Chandrashekara et al. Later, several variants of IPCA were suggested by various researchers from time to time. However, it is not clear which of these methods are better for face recognition. To determine this, in this paper, we have performed extensive experiments on two publicly available face datasets, i.e. AR and ORL. The performance of the methods is determined in terms of average classification accuracy and average training time. IPCA and its 11 variants as suggested in the literature are considered for comparison. It has been found that there is no clear winner among the compared methods. However, the performance of MCT-based incremental two-dimensional two-directional PCA (MI(2D)²PCA), incremental indefinite kernel PCA (IIKPCA), incremental two-dimensional kernel PCA (I2DKPCA), and incremental two-dimensional PCA (I2DPCA) methods is comparable and better than rest of the methods.

Keywords Incremental learning · Incremental principal component analysis · Performance evaluation

1 Introduction

Face recognition [1] is an important research domain having applications in several critical areas such as government ID cards, personal login, application security, Internet security, video surveillance, video games, virtual reality, and human–computer interactions. Most of the approaches in the literature require that all the training

N. Kumar (✉) · S. Madhavan
Department of Computer Science and Engineering,
National Institute of Technology Uttarakhand, Srinagar, Uttarakhand, India
e-mail: nitin@nituk.ac.in

© Springer Nature Singapore Pte Ltd. 2021
G. S. Hura et al. (eds.), *Advances in Communication and Computational Technology*, Lecture Notes in Electrical Engineering 668,
https://doi.org/10.1007/978-981-15-5341-7_32

397

samples must be available in advance for training. However, this constraint may not be satisfied always, and therefore, several methods have been suggested in the literature which can incorporate new training samples on the fly and do not require model development from scratch. These methods are usually called incremental learning methods.

Over the past decade or so, incremental learning [2–5] has drawn the attention of the research community due to its advantages. Data is generally dynamic in nature in most real-world situations and changes from time to time rapidly or gradually. Due to this dynamic nature of data, machine learning models are required to be frequently updated with respect to the new incoming data. Recompiling such a model is disadvantageous in terms of both space and time complexity as previous data needs to be stored and processed for every training iteration. This is a critical problem and is alleviated by incremental learning methods by incorporating the information from the new samples to already existing model. Thus, space and time complexity is greatly reduced. Furthermore, privacy and security issues are another concern in the machine learning algorithms. Data can be distributed in various geographically apart locations for security reasons. Development of a model on such scattered data is also solved by incremental learning where small models corresponding to each of the locations can be merged to form a single model. As an additional advantage, experimentation reveals that incremental learning algorithms offer way faster model generation than batch algorithms over large datasets by splitting them into batches and feeding to the Incremental Learning model.

1.1 Motivation

Eigenspace update algorithm proposed by Chandrasekaran et al. [6] is among the earliest proposed incremental principal component analysis (IPCA) method. Afterwards, there are several variations of IPCA (as described in Sect. 3) which were suggested by various researchers from time to time. However, it is not clear which of these methods (i.e. IPCA and its variants) are efficient with higher classification accuracy. Hence, there is a need to investigate which method among IPCA and its variants is best-suited for face recognition. In this paper, we have investigated the performance of IPCA and its 11 variants and performed experiments on two publicly available face datasets, viz. AR [7] and ORL [8].

The rest of the paper is organized as follows: Sect. 2 provides a brief description of incremental principal component analysis (IPCA) method while Sect. 3 provides a brief overview of the IPCA variants. Experimental setup and results are given in Sect. 4 while concluding remarks are given in Sect. 5 in the end.

2 Incremental Principal Component Analysis

Principal component analysis (PCA) [9] is an unsupervised method in which the main aim is to find those directions in which the spread in the data is maximum. Let $\mathbf{X} \in \mathbb{R}^{d \times N}$ be the matrix where each column is a d -dimensional feature vector and N is the total number of samples. Let \mathbf{S} represents the scatter matrix which is defined as follows:

$$\mathbf{S} = (\mathbf{X} - \mathbf{m})(\mathbf{X} - \mathbf{m})^T \quad (1)$$

where \mathbf{m} is the mean feature vector. The objective in PCA is given as follows:

$$J(\mathbf{W}) = \arg \max_{\mathbf{W}} |\mathbf{WSW}^T| \quad (2)$$

The above mathematical formulation is for batch PCA, i.e. when all the samples are available beforehand. Now, suppose due to some new samples, \mathbf{X} is updated as \mathbf{X}' and mean \mathbf{m} is updated as \mathbf{m}' . Now, new scatter matrix \mathbf{S}' can be represented as:

$$\mathbf{S}' = \mathbf{S} + \delta\mathbf{S} \quad (3)$$

Hence, instead of computing the scatter matrix from scratch, the existing scatter matrix is used and the small change, i.e. $\delta\mathbf{S}$ is incorporated into \mathbf{S} . The details can be found in the research work on incremental principal component analysis (IPCA) by Chandrasekaran et al. [6]. IPCA aims to generate incremental subspaces by using algorithms to update central tendencies along with covariance matrix IPCA achieves a better performance than PCA in terms of time complexity.

3 Incremental Principal Component Analysis Variants

Incremental learning methods have been widely used to solve the face recognition problem. Various incremental PCA variants have been suggested for face recognition in the literature. Here, we provide a brief overview of IPCA variants suggested from 2003 to 2016:

Liu et al. [2] have proposed an Incremental PCA that uses a decay parameter to update the eigenspace. This decay parameter controls the effect of updation of new data as well as the utilization of previous data. The authors have further specified that the decay parameter can be set specific to the dynamic nature of the data. If the data is highly dynamic, meaning changes frequently, the decay parameter is set sufficiently low and vice-versa. This allows the updated model to solve the plasticity–stability problem efficiently as per the data requirements. The disadvantage of this method is that the chunk updation has not been proposed which can result in increased computational requirements.

Ozawa et al. [3] have suggested a fast Incremental PCA which employs an updated accumulation ratio to check whether the model needs to be updated or not. The eigenspace model is updated by using a thresholding criteria over this accumulation ratio and residual vector. The main advantage of this method is computationally efficiency. The disadvantage lies in that it involves several approximations that may not improve the classification accuracy.

Oyama et al. [4] have presented an incremental version of simple PCA. In this method, a randomly initialized vector is used as eigenvector and is recursively optimized using a threshold function and an output function. This is computed using the previous iteration vector and the input data. This process is repeated until the eigenvector converges, and a sufficient approximation to the principal component vector is achieved. The disadvantage is that the algorithm is an approximation and may not always converge as an optimal vector.

A two-dimensional incremental reduction PCA has been proposed by Mutelo et al. [5] in which firstly row-wise and column-wise structural information is extracted. Then, the corresponding covariance matrices are generated which are subsequently used to form the eigenvectors for transforming the data to lower dimensions. This method is computationally more efficient than regular incremental PCA as the covariance matrices are decomposed over row and column dimensions.

Another incremental variant of PCA has been suggested by Ren and Dai [10] in which principal components are extracted in row and column directions. Subspacing is made compact using SVD decomposition whose singular values are extracted in row-wise and column-wise direction as shown in Fig. 1. This method is called **incremental bidirectional PCA** and significantly reduces computational complexity. This is due to the fact that the whole matrix is not updated at once and hence not used for eigendecomposition. Authors have further proposed an alternative QR decomposition over the SVD matrices that efficiently reduces the computational complexity of eigendecomposition.

An efficient incremental two-dimensional PCA has been proposed by Shi [11] in which a popular approach called candid covariance-free IPCA (CCIPCA) [12] has been utilized for the updating two-dimensional PCA. This method has several advantages and provides a huge improvement in the computational complexity as the update algorithms are covariance-free and do not require frequent eigendecomposition.

Choi et al. [13] have proposed an incremental two-dimensional two-directional PCA (I(2D)²PCA) where a two-dimensional PCA technique is employed. Here, either row-wise or column-wise structural information of the data is computed and applied over both row and column directions. The two-dimensional PCA computes eigenvector matrix by eigen of the covariance matrix along either of the row or column direction. Upon incrementally updating this row and column covariance matrices, the authors have proposed to achieve greater accuracy with relatively lower computational complexity.

Duan and Chen [14] have suggested an incremental variant of PCA in which a batch update algorithm is proposed using exact mean update to improve approximations and thereby accuracies. The authors have proposed a novel algorithm that

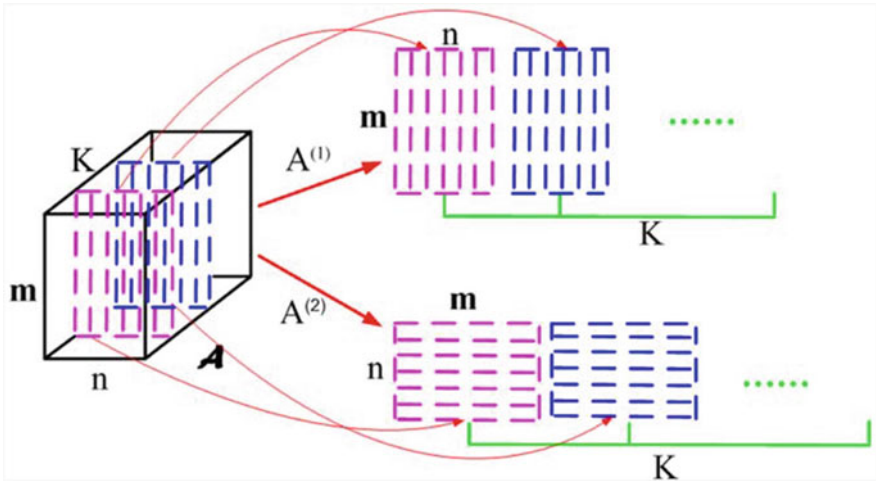


Fig. 1 Bidirectional principal component analysis by Ren and Dai [10]

supports the decay of previous data or regulates the effect of incoming data along with maintaining exact mean and covariance matrix computations. This method is more efficient and accurate and is relatively possesses less computationally complexity.

Kim and Park [15] have proposed an **Incremental two-dimensional two-directional PCA** ($I(2D)^2PCA$) along with an efficient preprocessing technique called modified census transformation (MCT). MCT is used to binarize the image based on the comparison of intensities of a neighbourhood of pixels with the average intensity of the neighbourhood pixels. This efficiently overcomes several face variation challenges, especially illumination variation as depicted in Fig. 2. Further, this MCT domain image is used for eigenspace generation using the popular IPCA-variant incremental two-dimensional two-directional PCA.

Incremental indefinite kernel PCA has been proposed by Liwicki et al. [16] in which the data is projected onto Krien space where every point is symmetric in

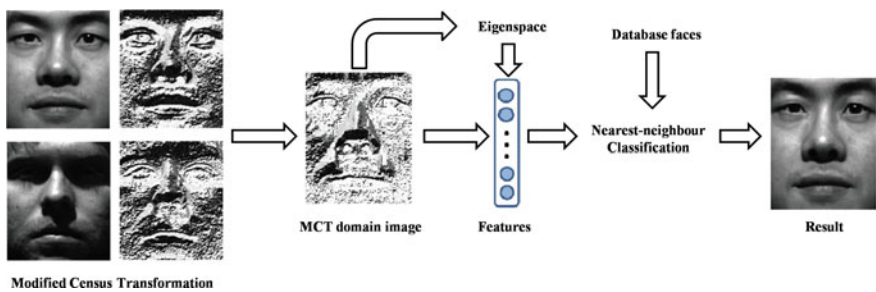


Fig. 2 Modified census transformation-based $I(2D)^2PCA$ by Kim and Park [15]

nature. Every Krein space is associated with a Hilbert space which satisfies a fundamental symmetry where every data matrix shall be equal to both its inverse and transpose. This property is highly advantageous and causes reduction in computational complexity. The authors have proposed a gradient-based incremental kernel PCA that can be easily updated in the gradient-based Krein subspace. This method has several advantages over other popular approaches in reducing the space and time complexity while achieving sufficiently high accuracy.

Incremental two-dimensional kernel PCA (I2DKPCA) has been suggested by Choi et al. [17] in which incoming data are incrementally updated into the trained model by axis rotation of the generated subspace. This is achieved by checking the linear dependencies of the incoming data and computing coefficient vectors and rotation matrices. This method possesses higher accuracy as the feature extraction is nonlinear in nature and can reach sufficient approximation in the updated subspaces in comparison with several other popular methods.

Incremental two-dimensional PCA (I2DPCA) has been given by Nakouri and Limam [18] in which two-dimensional images are conveniently used to generate two different covariance matrices over rows and columns of the images. The authors have further proposed an efficient QR-based decomposition for the updation algorithms which have low computational complexity. The authors have further proposed and utilized a matrix approximation technique called generalized low-rank approximation of matrices (GLRAM) which maintains the integrity of reconstructed images while sufficiently approximates the matrices to improve computational complexities.

4 Experimental Setup and Results

To compare the performance of IPCA and its variants, we have performed experiments on two publicly available face datasets viz. AR [7] and ORL [8]. A summary of both these datasets is given in Table 1.

For the performance evaluation of the IPCA variants, K -fold cross-validation is employed with various K values and varying the number of principal components. In K -fold cross-validation, the data is divided into K different blocks randomly and $(K - 1)$ blocks are used for training while the final block is used for testing. This

Table 1 Summary of the datasets used in experiments

Dataset	# of images	# of identities	Image size	Face variations
AR [7]	4000	126	768×576	Occlusion, illumination, expression
ORL [8]	400	40	92×112	Occlusion, illumination, expression



Fig. 3 Samples images from publicly available face datasets **a** AR [7], **b** ORL/Olivetti Faces/AT&T [8]

process is repeated K times by changing the testing block from 1 to K and then average performance is determined. By using different values of K , different proportions of training and testing data are generated. For the purpose of evaluation, four different K values have been chosen, viz. $K = 2, 3, 4, 5$ each resulting in different proportions of training and testing data, i.e. 50%, 66.67%, 75% and 80%, respectively. With these different K values, we have tested the IPCA variants over two publicly available face datasets, i.e. AR [7] and ORL/ATT [8]. These datasets are among the most commonly used datasets to test face recognition and are versatile, offering various face variations such as partial occlusions, illumination variations and expression variations. Figure 3 shows some sample images from the AR and ORL face datasets of one person.

Further to generalize the evaluation, the number of principal components is varied from 1 to 30 which limits the number of dimensions in the reduced subspace. All the experiments are repeated 20 times to obtain average classification accuracy. Figure 4 summarizes the results of K -fold cross-validation along with varying number of principal components. As evident from the results, the number of principal components directly affects the accuracy in every dataset and for every variant of IPCA. As the number of principal component increase, the accuracy increases steadily to a maximal value at 30 principal components. Thus, it can be generalized that the number of principal components can be chosen at a maximal value where the computational complexity is sufficiently low and the accuracy is steadily high. Furthermore, among the several variations of K value, all variants have consistently depicted higher accuracies at $K = 5$, meaning a 80% split of the training and testing data has consistently resulted in higher accuracy than other proportions.

At various K values of K -fold cross-validation and over different face datasets, some different IPCA variants have shown higher classification accuracy than the rest. At $K = 2$ over both AR and ORL face dataset, $I(2D)KPCA$ by Choi et al. [17] has shown significantly better performance over most of the values of the number of principal components. At $K = 3$, over AR dataset, MCT-based $I(2D)^2PCA$ by Kim

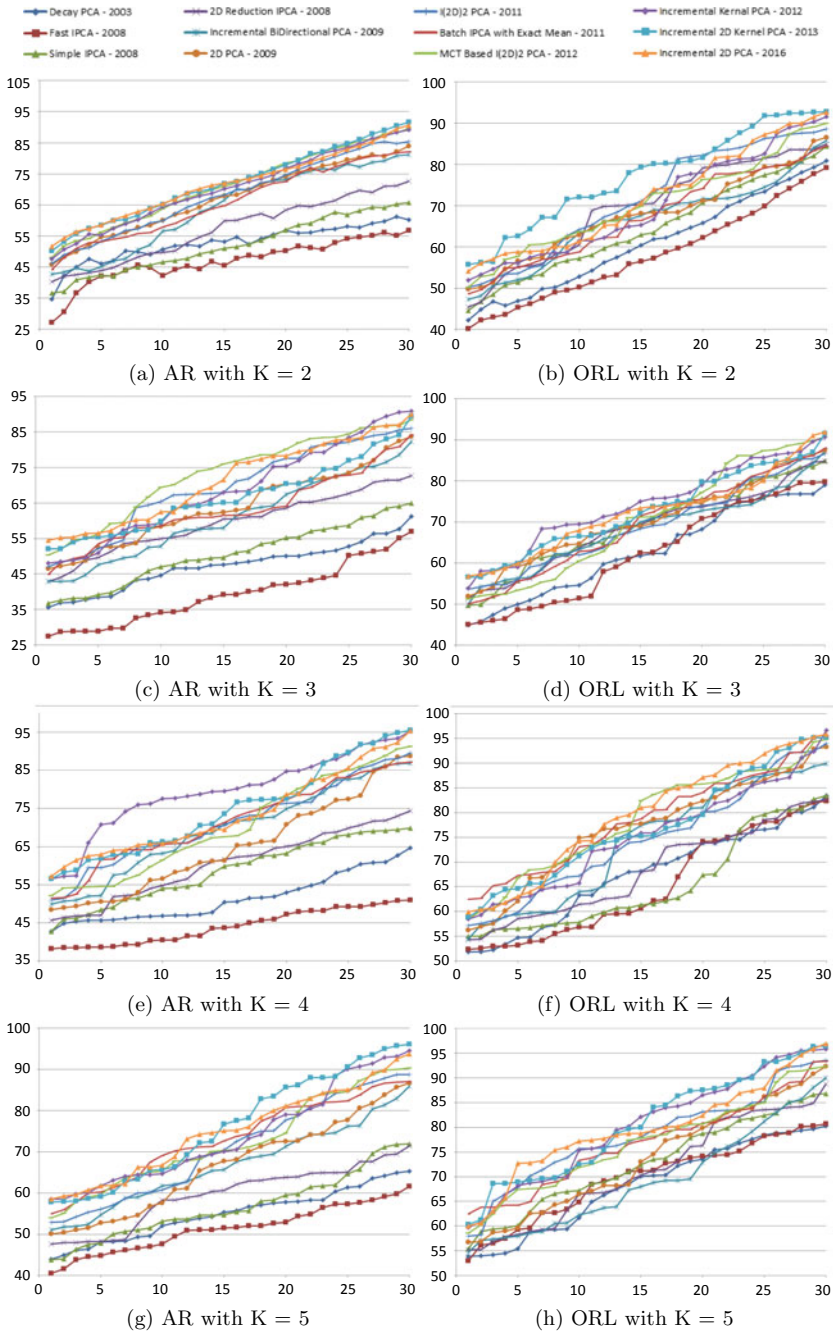


Fig. 4 Results of K -fold validation with various K values (2, 3, 4, 5) and number of principal components limitation (1–30)

and Park [15] has shown higher accuracy and over ORL dataset, IKPCA by Liwicki et al. [16] has shown better performance.

IKPCA by Liwicki et al. [16] has again shown higher accuracy than the remaining variants at $K = 4$ and over AR dataset. I(2D)PCA by Nakouri and Limam [18] has been, at average, better than the rest at $K = 4$ and over ORL dataset. AR dataset at $K = 5$ has marked more than one variants of IPCA, but especially I(2D)KPCA by Choi et al. [17] has shown a slight advantage over the rest while ORL dataset at $K = 5$ has shown both I(2D)KPCA by Choi et al. [17] and I(2D)PCA by Nakouri and Limam [18] having better results at different values of the number of principal components.

Furthermore, from Table 2, we can observe that the training time is less when the K values of K -fold cross-validation is smaller. This is a direct influence of the amount of training data used, since higher K value corresponds to higher proportion of training data, the training time is larger. It is also observed that IPCA variants such as batch incremental PCA, incremental indefinite kernel PCA, incremental two-dimensional kernel PCA and incremental two-dimensional PCA have been among the fastest IPCA variants with relatively low computational complexity in comparison with the rest of the variants. These methods require less training time in all different K values of K -fold cross-validation and over both the face datasets, and it is worth noting that all of these methods have batch increment algorithms where bulk data can be updated into a existing model which drastically reduces the training time.

Table 2 Training time (ms) of IPCA variants per image

Dataset method	AR				ORL			
	$K = 2$	$K = 3$	$K = 4$	$K = 5$	$K = 2$	$K = 3$	$K = 4$	$K = 5$
D-IPCA	44.06	33.74	33.09	32.14	391.80	334.76	312.23	305.78
F-IPCA	43.66	33.35	32.92	32.03	384.60	333.78	305.9	304.69
S-IPCA	43.45	32.58	32.75	31.40	384.45	333.22	299.50	298.91
2D IPCA	41.63	31.08	31.68	30.10	379.95	315.86	285.00	294.16
B-IPCA	42.21	31.59	32.01	30.53	381.10	321.37	285.03	294.38
I(2D)PCA	40.60	30.45	30.06	29.84	369.10	302.81	281.53	287.94
I(2D)2 PCA	40.87	30.93	30.87	30.09	371.00	303.56	283.17	290.53
Ba-IPCA	37.82	28.87	28.82	27.93	361.15	296.36	276.67	272.88
M-I(2D)2 PCA	39.26	30.21	29.03	29.34	362.15	298.16	278.80	275.91
IKPCA	37.16	28.85	28.78	27.36	353.60	291.75	258.07	264.41
I(2D)KPCA	37.05	28.73	27.64	27.30	345.60	271.08	257.43	264.06
I(2D)PCA	35.26	28.40	26.71	26.69	330.15	263.81	251.17	257.78

5 Conclusion

In this paper, we have compared the performance of incremental PCA and its 11 variants suggested in the literature for face recognition. These variants are implemented and are tested under similar conditions and criteria, and the results of the experimentation have been presented. MCT-based incremental two-dimensional two-directional PCA by Kim and Park [15], incremental indefinite kernel PCA by Liwicki et al. [16], incremental two-dimensional kernel PCA by Choi et al. [17] and Incremental Two-Dimensional PCA by Nakouri and Limam [18] have been among the most consistent variants that have reported the highest accuracy among the several chosen IPCA variants. These methods have shown computational as well as accuracy advantages that make these methods a better option in terms of performance when compared to other variants.

Further, Incremental PCA with exact mean by Duan and Chen [14], incremental indefinite kernel PCA by Liwicki et al. [16], incremental two-dimensional kernel PCA by Choi et al. [17] and incremental two-dimensional PCA by Nakouri and Limam [18] have been among the methods which require less training time in comparison to other IPCA variants.

References

1. Zhao W, Chellappa R, Phillips PJ, Rosenfeld A (2003) Face recognition: a literature survey. *ACM Comput Surv* 35(4):399–458
2. Liu X, Chen T, Thornton SM (2003) Eigenspace updating for non-stationary process and its application to face recognition. *Pattern Recognit* 36(9):1945–1959
3. Ozawa S, Pang S, Kasabov N (2008) Adaptive face recognition system using fast incremental principal component analysis. In: Ishikawa M, Doya K, Miyamoto H, Yamakawa T (eds) *Neural information processing*. Springer, Berlin, Heidelberg, pp 396–405
4. Oyama T, Karungaru S, Tsuge S, Mitsukura Y, Fukumi M (2008) Incremental learning method of simple-PCA. In: Lovrek I, Howlett RJ, Jain LC (eds) *Knowledge-based intelligent information and engineering systems*. Springer, Berlin, Heidelberg, pp 403–410
5. Mutelo RM, Dlay SS, Woo WL (2008) Two dimensional incremental reduction PCA: a novel appearance based technique for image representation and recognition. In: 5th international conference on visual information engineering (VIE 2008), pp 588–593
6. Chandrasekaran S, Manjunath BS, Wang YF, Winkeler J, Zhang H (1997) An eigenspace update algorithm for image analysis. *Graph Models Image Process* 59(5):321–332
7. Martinez AM, Benavente R (1998) CVC technical report# 24, The AR Face Database
8. ORL/Olivetti Faces/AT&T face dataset. <https://www.cl.cam.ac.uk/research/dtg/attarchive/facedatabase.html>. Accessed 29 Jan 2019
9. Turk M, Pentland A (1991) Eigenfaces for recognition. *J Cogn Neurosci* 3(1):71–86
10. Ren CX, Dai DQ (2010) Incremental learning of bidirectional principal components for face recognition. *Pattern Recognit* 43(1):318–330
11. Shi W (2009) Efficient two dimensional principal component analysis for online learning. In: 2009 Asia-Pacific conference on computational intelligence and industrial applications (PACIIA), vol 2, pp 250–253
12. Weng J, Zhang Y, Hwang W (2003) Candid covariance-free incremental principal component analysis. *IEEE Trans Pattern Anal Mach Intell* 25(8):1034–1040

13. Choi Y, Tokumoto T, Lee M, Ozawa S (2011) Incremental two-dimensional two-directional principal component analysis ($I(2D)^2PCA$) for face recognition. In: Proceedings of the 2011 IEEE international conference on acoustics, speech and signal processing (ICASSP), pp 1493–1496
14. Duan G, Chen Y (2011) Batch-incremental principal component analysis with exact mean update. In: 18th IEEE international conference on image processing, pp 1397–1400
15. Kim B, Park H (2012) Efficient face recognition based on MCT and $I(2D)^2PCA$. In: IEEE international conference on systems, man, and cybernetics (SMC), pp 2585–2590
16. Liwicki S, Zafeiriou S, Tzimiropoulos G, Pantic M (2012) Efficient online subspace learning with an indefinite kernel for visual tracking and recognition. *IEEE Trans Neural Netw Learn Syst* 23(10):1624–1636
17. Choi Y, Ozawa S, Lee M (2014) Incremental two-dimensional kernel principal component analysis. *Neurocomputing* 134:280–288
18. Nakouri H, Limam M (2016) An incremental two-dimensional principal component analysis for image compression and recognition. In: 12th international conference on signal-image technology internet-based systems (SITIS), pp 725–731

3-Axis Robot Arm Using Micro-Stepping with Closed-Loop Control



G. A. Rathy, P. Sivasankar, Aravind Balaji, and K. Gunasekaran

Abstract Robot arm is one of the most buzzing words in industrial automation. The challenge of designing a robot arm is anticipating and controlling its system dynamics. This paper focuses on developing of robot arm with 3 degrees of freedom (DoF) with high speed and precision. The position of the robotic arm is determined from the accelerometer using closed-loop feedback system. The stepper motor in the arm of the robot decides the direction; the desired movements will be controlled by PWM pulses through the controller, as per the requirement of the user. A4988 stepper motor driver is used instead of rotary encoder to control the movements of robotic arm by stepper motor. The step angle of the arm is controlled by micro-stepping using 200 steps to 3200 steps resolution which provides a smooth movement and precision degree of accuracy. A graphical user interface is designed using LabVIEW to display and control the position of arm. Finally, 3-axis robot arm with micro-stepping is developed by integrating the electronic circuitry and mechanical parts.

Keywords Accelerometer · LabVIEW · Micro-stepping · Stepper motor · PWM

1 Introduction

The use of robots in industries is proliferating due to the necessity of automation, reducing worker fatigue and faster productivity. Robots applications are primarily in material handling, operations, assembly, and inspection. Apart from industries, robots are also deployed in home sector, health care, service sector, agriculture and farms, research and exploration. Robotic arms play an important role in all these applications

G. A. Rathy · P. Sivasankar (✉) · K. Gunasekaran
NITTTR, Chennai, India
e-mail: siva_sankar123p@yahoo.com

G. A. Rathy
e-mail: rathysanju@gmail.com

A. Balaji
HIET, Chennai, India

[1, 2]. The three axes robotic arms are normally designed with either servo or dc motors to achieve more accurate positioning and smooth movement. Though servo and dc motors are trying to achieve more accurate positioning and smooth movement, they are lagging to achieve a high torque. Hence, this paper proposes to design a 3-axis robot using stepper motor with micro-stepping and closed-loop control to achieve precise positioning, smooth movement, and high torque. Micro-stepping is an approach of directing stepper motors, typically used to get good resolution or even motion at minimal speed. The angle of degree of the arm is read from the accelerometer and is compared with the lookup table. The arm angle is controlled by giving the required input through the LabVIEW front panel. The required position of the arm is achieved by calculating the position, forward and backward movement of the arm using LabVIEW block diagram. Accordingly, the PWM is adjusted to control the stepper motor in the required direction. Literature survey is discussed in Sect. 2, design of the proposed work is in Sect. 3, and implementation and conclusion will be discussed in Sects. 4 and 5.

2 Review of Literature

Palok et al. [3] developed a 3 axes pneumatic robot arm using double acting pneumatic actuators controlled by 5/3 proportional valves. OMRON PLC and Arduino microcontrollers are used for control purpose. Open-loop control system is derived through PLC to achieve sequential tasks in material handling whereas closed-loop control system is derived through Arduino to improve control system using feedback from MPU-6050 (MEMS accelerometer and MEMS gyroscope) sensor [3, 4].

Niranjan and et al. [5] designed a robotic arm which is controlled using flex sensor, Arduino Uno, RF module (Wi-Fi module), and servo motor. Flex sensor will send the values to the controller to run the system. The acquired values are analyzed to control the arm and the fingers how much they have to move and grab materials. This task is carried out with the help of five servo motors and the controller [6].

Abhishek [7] designed a 6-axis robotic arm consisting of manipulators to do perform pitching, rolling, and yawing. V-Rep software is used to develop robotic arm using simulation and calculating the Torque [5, 7].

Chen and Chen [8] proposed remote controlled 6-axis robotic arm to read barcodes and handle products. The control is achieved using Raspberry Pi with onboard Wi-Fi. Robotic arm is monitored through Wi-Fi by the designed mobile app. [9].

From the literature, it is observed that the control of robot arm is achieved using PLC, Arduino Raspberry Pi, etc. But none of the paper is considering the control of precise positioning, smooth movement, and high torque of the robotic arm. Some literature uses servo or dc motor for precise positioning and smooth movement without considering high torque. Similarly, some of the literature suggested to design the arm for high torque using stepper motor with rotary encoder without micro-stepping. Hence, precise positioning, smooth movement could not be achieved through earlier designs. In this paper, it is proposed to design 3-axis robot arm

using micro-stepping with closed-loop control to achieve precise positioning, smooth movement, and high torque.

The novelty of the paper is to achieve high precision by reading the angle of the arm from the accelerometer by comparing the lookup table values and smooth movement and high torque are achieved by stepper motor with stepper motor driver using micro-stepping through PWM control. LabVIEW and Arduino are used to generate the PWM to achieve the objective. The following section will elaborate the design of the proposed work.

3 Designing of the Proposed 3-Axis Robot Arm with Micro-Stepping

This work is aimed to design a 3-axis robot using stepper motor with micro-stepping and closed-loop control to achieve precise positioning, smooth movement, and high torque. The proposed design will use accelerometer to acquire the present position of robot arm; rotary ball bearing potentiometer, Arduino, and LabVIEW are used to generate the required PWM to control robotic arm and shoulder; stepper motor driver circuit A4988 will produce the required current in the closed loop to control the three stepper motors of the 3-axis robot arm. Stepper motor with micro-stepping in the closed-loop control will achieve the objectives such as precise positioning, smooth movement, and high torque. The following figure Fig. 1 illustrates the block

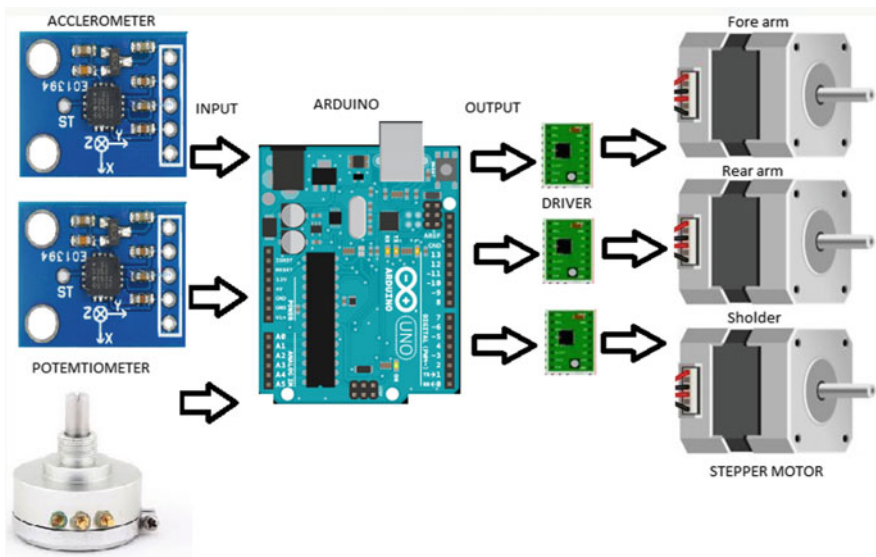


Fig. 1 Block schematic of the 3 axes robot arm

schematic of the design. The details and description of the blocks will be briefed in the following subsections.

3.1 Accelerometer

The 3-axis acceleration is estimated using ADXL335. The acceleration measurement range is within ± 3 g in the *x-axis*, *y-axis*, and *z-axis*. The measured acceleration is converted into the respective analog voltages as output signals by the module. The angle of inclination is derived from the acquired *X*, *Y*, *Z*'s value. Also, the roll, pitch, and yaw angles are estimated using *X-axis*, *Y-axis*, and *Z-axis*. Initially, g unit is obtained from the 10-bit ADC. 9.8 m/s^2 is the acceleration equivalent of 1 g on the Earth. 1/6th of the said value is on the moon and 1/3rd is on mars. Tilt-sensing applications, motion, and vibration due to dynamic acceleration are obtained from accelerometer.

Maximum voltage level at 0 g is 1.65 V and sensitivity scale factor of 330 mV/g is estimated as per ADXL335 datasheet. Acceleration output is given in Eq. (1)

$$A_{\text{out}} = \frac{\frac{\text{ADC value} * V_{\text{ref}}}{1024} - \text{Voltage Level at 0 g}}{\text{Sensitivity Scale Factor}} \quad (1)$$

X-axis, *Y-axis*, and *Z-axis* g unit acceleration values are given in Eqs. (2a), (2b), and (2c)

$$A_{x_{\text{out}}} = (((\text{ADC value of } X \text{ axis} * V_{\text{ref}})/1024) - 1.65)/0.33 \quad (2a)$$

$$A_{y_{\text{out}}} = (((\text{ADC value of } Y \text{ axis} * V_{\text{ref}})/1024) - 1.65)/0.33 \quad (2b)$$

$$A_{z_{\text{out}}} = (((\text{ADC value of } Z \text{ axis} * V_{\text{ref}})/1024) - 1.65)/0.33 \quad (2c)$$

Based on the *X-axis*, *Y-axis*, and *Z-axis* values, the inclination of the robot arm is estimated. The details of the angle of inclination estimation are as follows.

3.1.1 Inclination Angle

Inclination angle is defined as the tilting level of the device from its surface plane. Inclination angle is illustrated in Fig. 2.

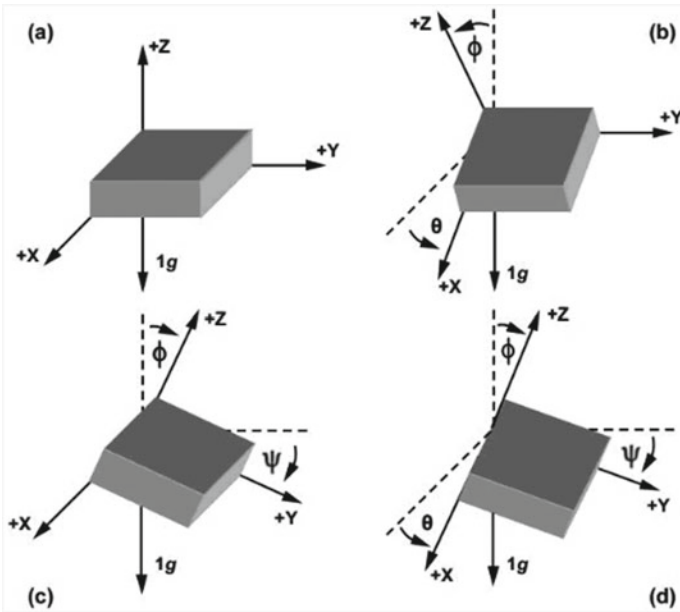


Fig. 2 Inclusion angle

Let θ as the angle between the horizon and the x -axis of the accelerometer, ψ as the angle between the horizon and the y -axis of the accelerometer, and ϕ as the angle between the gravity vector and the z -axis. The inclination angle of X -axis, Y -axis, and Z -axis is estimated from its reference. This is calculated using Eqs. (3), (4), and (5).

$$\theta(\text{theta}) = \text{atan}\left(\frac{Ax_{out}}{\sqrt{Ay_{out}^2 + Az_{out}^2}}\right) \tag{3}$$

$$\psi(\text{psi}) = \text{atan}\left(\frac{Ay_{out}}{\sqrt{Ax_{out}^2 + Az_{out}^2}}\right) \tag{4}$$

$$\phi(\text{phi}) = \text{atan}\left(\frac{\sqrt{Ax_{out}^2 + Ay_{out}^2}}{Az_{out}}\right) \tag{5}$$

The angular movement of the arms is sensed using two accelerometers whose analog voltage varies along with the arm movement. The respective values are converted to angular degree by mapping with efficient lookup table values. The mapping of the lookup table with angular degree will estimate the precise positioning effectively.

3.2 Precision Potentiometer

Rotary movement of the robot is feedback from the rotary ball bearing potentiometer to read the present position of the robot arm. Metal ball bearing is used for rotation of the potentiometer to provide exact analog value. The acquired precise analog value is to be scaled to the angle of degree of the robot arm.

3.3 Arduino Controller

Controlling application is achieved with the help of low-cost Arduino controller. The generated PWM outputs of the Arduino Uno controller are taken from the digital I/O pins 3, 5, 6, 9, 10, and 11. The duty cycle of a PWM pulse train is set at 500 Hz using the analog write function. The forearm and rear arm and shoulder are controlled by the stepper motor using the PWM generation from the Arduino. The feedback regarding the current position of the arm is given from the accelerometer and the potentiometer. The forearm and rear arm movement are sensed by the accelerometer, and the shoulder movement is sensed by the potentiometer which is given as input to the Arduino and the analog value is converted to bits. Depending upon the bit value, the desired angle is determined by lookup table which is stored in the EEPROM of the Arduino and the present value is displayed in the graphical user interface (LabVIEW) using serial protocol.

3.4 GUI Using LabVIEW

The graphical user interface is developed using LabVIEW and data transfer between LabVIEW and Arduino is done using serial communication [10]. The destination angle can also be set using GUI such that the arm moves to the desired position. Figure 3a, b presents the 3-axis robot front panel design and control programming using LabVIEW.

The front panel design contains string control to get the angular position from the user to control the movement of robot arm. A Boolean pushbutton called “send button” will have a control on string control to feed the controlling input to the block diagram to process the acquired input. Present position of the robot arm is collected and displayed through COM port and current angular position string indicator.

From the block diagram, the controlling decision action will be carried out using selector switch LabVIEW operator. Sensor values will be acquired continuously with the interval of 50 ms. The commands for all the three arms are send serially and the differentiation between each command is defined using the special character. These are sent along with the commands such that each stepper motor driver gets the command.

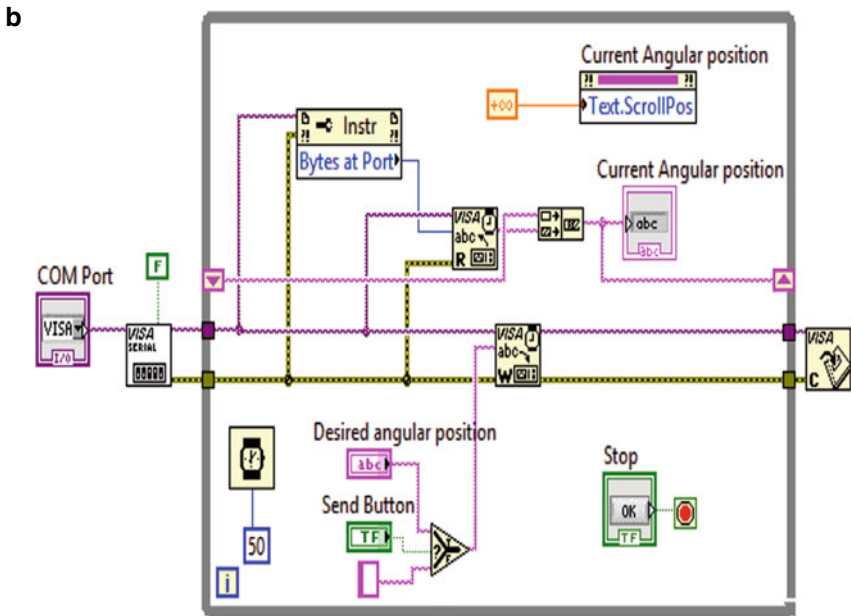
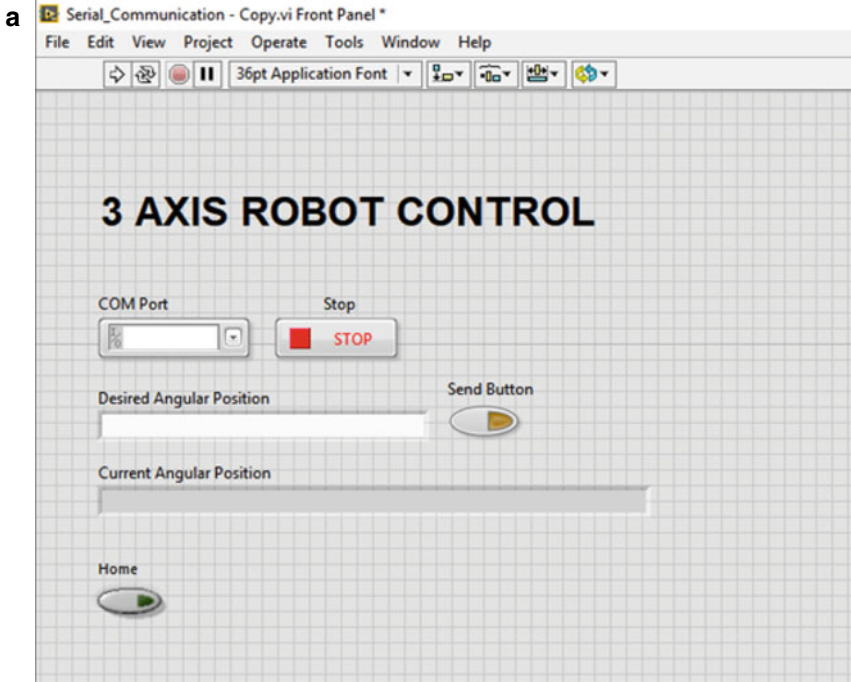


Fig. 3 a LabVIEW front panel control design. b LabVIEW block diagram control programming

3.5 Stepper Motor and Micro-Stepping

The most important quality that a pick and place robot should have is the precise angle of rotation with higher torque which makes stepper motor the best choice for higher torque applications. The movement of stepper motors will be defined in terms of discrete steps or revolution fraction [11]. For example, for every full revolution of the stepper motor with 1.8° step angle, it will make 200 steps ($360/1.8$). This 1.8° step will give imperfect smooth in the rotation of the motor which will cause slow rotation. The relatively large step size results in lack of smoothness at slow speeds. A way to improve the smoothness is to reduce the size of the motor step. Hence, the need of micro-stepping arises. Micro-stepping controls the stepper motor by producing higher resolution or smoother motion at low speeds. But providing smaller degree of movement such as micro-stepping is quite difficult in normal stepper motor. In this 3-axis robot, micro-stepping is achieved by using step stick driver which provides up to 3200 steps making resolution of 0.11 degree per rotation. To get smooth motor's rotation, especially at slow speeds, the step stick driver splits each full step into smaller steps. For example, to achieve a step angle of 0.007° , a 1.8 -degree step can be divided up to 256 times, ($1.8/256$), or 51,200 micro-steps per revolution [12]. The current to the motor winding is controlled by pulse-width modulated (PWM) voltage to achieve micro-stepping.

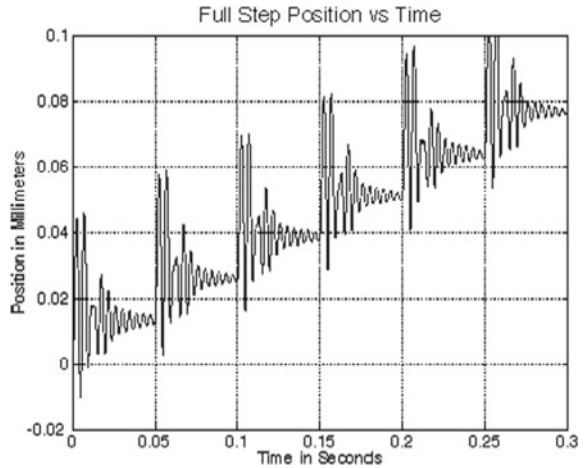
The driver is controlled by PWM generated using Arduino and the direction is also controlled by Arduino. The controls are given through serial protocol by which the present coordinates are read using accelerometer and servo potentiometer. The output analog voltage depending upon each angle of movement of the arms is noted as lookup table and depending upon the difference between the present and the destination coordinates, the PWM is incremented or decremented with reference to the lookup table [1].

The two voltages sine waves sent to the motor windings are 90° out of phase. If current increases in one winding, the same will decrease in the other winding. Due to this gradual transfer of current, smoother motion and more consistent torque are produced. Figure 4 shows the graph of full steps versus time.

3.6 A4988 Stepper Motor Driver

The required supply voltage of 3–5.5 V for the driver is connected across the VDD and GND pins and a supply voltage of 8–35 V for motor is connected across VMOT and GND. The appropriate decoupling capacitors are used to deliver the expected currents (up to 4 amp peak for the motor supply). A4988 will drive four-wire, six-wire, and eight-wire stepper motors. A typical step size of 1.8° or 200 steps per revolution stepper motors is used to attain full steps. A4988 micro-stepping driver allows higher resolutions by permitting intermediate step locations. These are attained by stimulating the coils in-between current levels. Four different current levels will support

Fig. 4 Graph of full-step position versus time



to drive a motor in quarter-step mode of 200-step-per-revolution or 800 micro-steps per revolution. Selection from the five-step resolutions is enabled from the resolution (step size) selector inputs such as MS1, MS2, and MS3. 100 k Ω pull-down resistors and 50 k Ω pull-down resistor are the internal resistance values of MS1 & MS3 and MS2. Hence, leaving these three micro-step selection pins disconnected will cause full-step mode. The current limit should be set low for the micro-step modes to function perfectly. This, in turn, makes the current limiting gets engaged. Else, the in-between current levels will not be maintained perfectly which will cause skipping of micro-steps [13].

STEP input of each pulse will produce one micro-step of the stepper motor in the direction selected by the DIR pin. The STEP and DIR pins are not pulled to any specific voltage internally, so these pins should not be left floating in the application. If the stepper motor is rotating in a single direction, DIR is directly connected to VCC or GND. Three different inputs of the chip are used in controlling its various power states like RST, SLP, and EN. If the RST pin is floating; then the pin is connected to the neighbor SLP pin on the PCB to make it high and activate the board. Active current limiting is supported by the A4988; to set the current limit, the trimmer potentiometer is used on the board. Keeping the driver into full-step mode is one of the ways to set the current limit. Current passing through a single motor coil is to be measured while adjusting the current limit potentiometer. This should be carried out with the motor holding a fixed position [14].

4 Implementation of the Proposed Work

Initially, the current position of the arms is noted from the accelerometer and the potentiometer serially and the values have been compared with the lookup table

stored in the EEPROM and the angle of each is determined. The desired value is sent through LabVIEW which is compared with the current value, if the current value is greater than the desired value, the PWM pulse is been decremented such as no. of pulse count which is been stored is been decremented till it reaches the desired value. Pulse count is initially determined as zero from the initial power-up of the robot from which it is incremented or decremented depending upon the current position similarly if the current value is less than the desired value, the PWM pulse is been incremented till it is equal to the desired value. Once the current value reaches the desired value, the PWM pulse is been latched. The PWM pulse is been counted using counter initially and depending upon the current value, the counter value is been incremented or decremented using which the arms are been moved. The PWM is varied depending upon the pattern at which the driver is been set. The steps involved in the working of 3-axis robot and its PWM control are illustrated in Fig. 5.

In general, the 3-axis robot arms are designed with servo or dc motors to achieve more accurate positioning and smooth movement. But servo and dc motors are lagging to achieve a high torque. Hence, designing of a 3-axis robot to achieve precise positioning, smooth movement and high torque is important. In this work, stepper motor with A4988 driver is used to achieve high torque by applying the principle of micro-stepping. Micro-stepping is an approach of directing stepper motors, used to get good resolution or even motion at minimal speed. Accelerometer sensor will continuously monitor the position of the robot arm and provide necessary inputs to adjust the movement of robot arm. The angle of degree of the arm is read from the accelerometer and is compared with the lookup table. The forearm movement and rear arm movement are sensed by the accelerometer, and the shoulder movement is sensed by the potentiometer which is given as input to the Arduino and the analog value is converted to bits. Depending upon the bit value, the desired angle is determined by lookup table which is stored in the EEPROM of the Arduino and the present value is displayed in the graphical user interface (LabVIEW) using serial protocol. The lookup table will decide and adjust the robot arm position from the acquired accelerometer values by mapping. The arm angle is controlled by giving the required input through the LabVIEW front panel. The required position of the arm is achieved by calculating the position, forward and backward movement of the arm using LabVIEW block diagram. Accordingly, the PWM is adjusted to control the stepper motor in the required direction.

5 Experimental Setup

Robot arms are playing a vital role in industrial automation, particularly for pick and place operations and applications. Hence, the work proposes to develop robot arm with 3 degrees of freedom (DoF) with high speed and precision. In the work, experimental setup is developed with the 3-axis robot, stepper motor with driver for micro-stepping, potentiometer, Arduino Uno, and LabVIEW software. Experimental setup has been fabricated with aluminum alloy, and nema stepper motor with 1:10

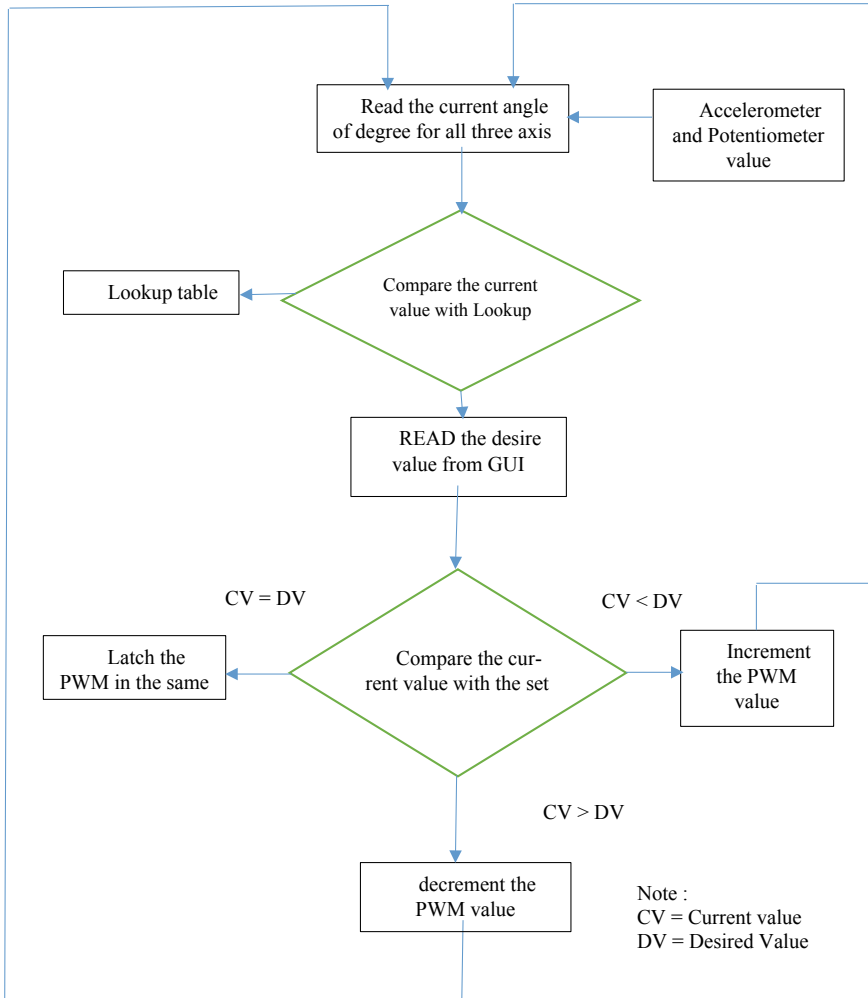
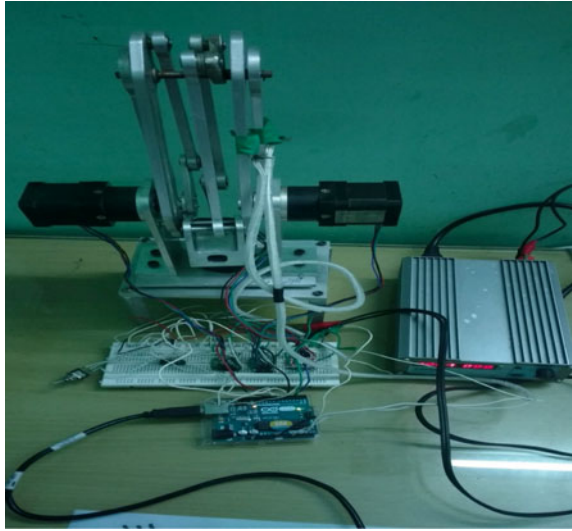


Fig. 5 Flowchart of the proposed work

ratio gear has been used to reduce the set for smoothness and précised angular movement. The power supply to the motor is provided with external DC source with current limitation of 1A. The payload up to 1 kg can be driven by each stepper motor. The current status is sent serially using Arduino and is displayed in the LabVIEW front panel. Figure 6 shows experimental setup of the proposed work.

Fig. 6 Experimental setup of the proposed work



6 Conclusion

A 3-axis robot using stepper motor with micro-stepping and closed-loop control is designed and implemented to achieve precise positioning, smooth movement, and high torque. Control input was given through the LabVIEW software to fix the robot arm at the required position. The current position of the robot arm is acquired through the accelerometer by mapping with the lookup table to achieve precise positioning. Interfacing Arduino with LabVIEW provides PWM pulses according to the controlled input fed through the front end. The smooth movement and high torque are achieved with the help of stepper motor using micro-stepping. The usage of stepper motor driver replaces the existing conventional rotary encoder whose cost is more than the stepper motor driver. The adjustment of the arm positioning is carried out through the closed-loop control. The work can be extended for higher axis robot arm design.

References

1. Gorez R, Shea JO (1990) Robots positioning control revisited. *J Intell Robot Syst* 3(3):213–231
2. Siciliano B, Khatib O (2016) Springer handbook of robotics. Springer, Berlin, Heidelberg
3. Palok B, Shanmugam SA (2016) Design and development of a 3 axes pneumatic robotic arm. *Int J Adv Res Electr Electron Instrum Eng* 5(9):1–8
4. Tarn TJ, Bejczy AK, Isidori A, Chen Y (2007) Nonlinear feedback in robot arm control. In: 23rd IEEE conference on decision and control
5. Niranjan L et al (2018) Design and implementation of robotic arm using proteus design tool and arduino-uno. *Indian J Sci Res* 17(2):126–131
6. Spang MW, Fujita M (2011) Control in robotics. *Impact Control Technol Overview*

7. Abhishek B (2018) Design of 6-axis robotic arm. *Int J Adv Res Ideas Innovations Technol* 4(4):631–636
8. Chen Z-Y, Chen C-T (2018) A remote controlled robotic arm that reads barcodes and handles products. *Inventions* 3(1):17
9. SGS Thomson Microelectronics (2012) Stepper motor driving, Application note
10. Ganesan A, Nhizanth R, Kamban S, Gopalakrishnan R (2015) Stepper motor control using LabVIEW and NI-myRIO. *Int J Sci Res Dev* 2(12):478–482
11. Acarnley PP (1982) *Stepping motors: a guide to modern theory and practice*. Peter Peregrinus Ltd
12. Baluta G (1988) Microstepping mode for stepper motor control. *IEEE Int Symp Signals Circ Syst* (2):1–4
13. Ortega R, Spong MW (1989) Adaptive control of robot manipulators: a tutorial. *Automatica* 25(6):877–888
14. Jones DW (2001) *Handbook of small electric motors*. McGraw-Hill

False-Positive-Free and Geometric Robust Digital Image Watermarking Method Based on IWT-DCT-SVD



Priyanka Singh, Ashok Kumar Pradhan, and Subhash Chandra

Abstract This paper presents a new hybrid image watermarking method based on IWT, DCT, and SVD domains, to solve the problem of false-positive detection and scale down the impact of geometric attacks. Properties of IWT, DCT, and SVD enable in achieving higher imperceptibility and robustness. However, SVD-based watermarking method suffers from a major flaw of false-positive detection. Principal component of watermark is embedding in the cover image to overcome this problem. Attacker cannot extract watermark without the key (eigenvector) of the embedded watermark. To recover geometrical attacks, we use a synchronization technique based on corner detection of the image. Computer simulations show that the novel method has improved performance. A comparison with well-known schemes has been performed to show the leverage of the proposed method.

Keywords IWT · DCT · Image watermarking · Robustness · SVD

1 Introduction

Rapid growth of Internet and digital technology provides advantage of easy sharing, editing, and copying of images without quality degradation. But, these advantages give rise to the problem of security infringement or processing of images [1, 2]. Digital image watermarking [3, 4] has come up as a way out to protect ownership rights against unauthorized copying and redistribution of images. It is a potential

P. Singh (✉) · A. K. Pradhan

Department of Computer Science and Engineering, SRM University—AP, Amaravati, India
e-mail: priyankasingh401@gmail.com

A. K. Pradhan

e-mail: ashokkumar.p@srmmap.edu.in

S. Chandra

Department of Computer Science and Engineering, National Institute of Technology,
Jamshedpur 831014, India
e-mail: subhashchandra.cse@nitjsr.ac.in

© Springer Nature Singapore Pte Ltd. 2021

G. S. Hura et al. (eds.), *Advances in Communication and Computational Technology*, Lecture Notes in Electrical Engineering 668,
https://doi.org/10.1007/978-981-15-5341-7_34

solution for copyright management, tamper detection, content authentication, and protection of images [5–7]. Spatial techniques are fragile which provides the advantage that the distorted area can be located [8] and we can recreate the host image from the distorted one [9]. Comparatively, transform domain techniques are more robust [10–12]. Each transform represents the image in different ways and has its own characteristics. A transform may be sturdy against a certain set of attacks but may not sustain another set of attacks. Therefore, combinations of transforms are used to improve the performance. Improving imperceptibility and robustness is the core motivation for our proposed work.

In recent years, a number of hybrid image watermarking techniques have been proposed. These schemes implement two or more transforms to achieve higher imperceptibility and robustness. SVD transform is popularly used in devising hybrid techniques. They have good stability and are robust against geometrical and signal processing attacks. It yields high imperceptibility and robustness but leads to false-positive problem (FPP) where a counterfeit watermark can be detected. Example of such schemes includes [13–16]. Loukhaoukha et al. [17] applied hash function on U and V matrices to overcome FPP. Signature-based authentication for SVD-factorized matrices prior to the extraction was suggested by Makbol and Khoo [18] and Ansari et al. [1]. Makbool and Khoo [18] embedded a digital signature in the watermarked image to authenticate the user-supplied singular matrices. Special key and SHA-1 algorithm are used to generate the digital signature. But, there is error in the signature matching scheme [1]. This problem was overcome by the scheme proposed by Ansari et al. [1]. Jain et al. [19] proposed to embed the principal component of the watermark into the host image to solve false-positive detection. Another most challenging task in developing a new watermarking scheme is to ensure watermark robustness as different geometric attacks and signal processing transformations defaces the synchronization of watermark resulting in serious problems especially in blind extraction. Moreover, the later scheme can be further improved by replacing DWT with IWT in order to overcome rounding off errors in inverse transform, thus ensuring proper reconstruction.

2 The Proposed Scheme

The proposed IWT-DCT-SVD-based watermarking scheme is presented in this section. The scheme is described in three parts: watermark embedding, watermark extraction, and the process of correcting geometric attack process. Figures 6 and 7 show the block diagram of watermark embedding and watermark extraction scheme, respectively.

2.1 Watermark Embedding Process

See Algorithm 1 and Fig. 1.

Algorithm 1 Watermark Embedding

Require: Cover Image, Watermark

Ensure: Watermarked Image

```

1: BlockSize  $\leftarrow$  8
2: NumberOfBlocks  $\leftarrow$   $(M/2) \times (N/2) / (\text{BlockSize})^2$ 
3: I  $\leftarrow$  read the cover image
4: W  $\leftarrow$  read the watermark image
5: [CA; CH; CV; HH]  $\leftarrow$  IWT(I)
6: for sub-band  $\leftarrow$  CH,CV do
7:   kk  $\leftarrow$  0
8:   for i=1:(256/BlockSize) do
9:     for j=1:(256/BlockSize) do
10:      Block(:, :, kk+j)=sub-band((BlockSize*(i-1)+1:BlockSize*(i-1)+BlockSize),(BlockSize*(j-1)+1:BlockSize*(j-1)+BlockSize))
11:    end for
12:    kk=kk+(256/bs)
13:  end for
14:  for i  $\leftarrow$  1 :NumberOfBlocks do
15:    Block(:, :, i)  $\leftarrow$  DCT(Block(:, :, i))
16:  end for
17:  for i  $\leftarrow$  1:M/16 do
18:    for i  $\leftarrow$  1:N/16 do
19:      A(i,j)  $\leftarrow$  Block(5,3,i)
20:    end for
21:    W  $\leftarrow$  arnold(W)
22:    [UA SA VA]  $\leftarrow$  SVD(A)
23:    [Uw Sw Vw]  $\leftarrow$  SVD(W)
24:    S  $\leftarrow$  SA +  $\alpha$ UwSw
25:    Aw  $\leftarrow$  UASAVA
26:    for i  $\leftarrow$  1:M/16 do
27:      for i  $\leftarrow$  1:N/16 do
28:        Block(5,3,i)  $\leftarrow$  Aw(i,j)
29:      end for
30:    end for
31:  end for
32:  for i  $\leftarrow$  1 :NumberOfBlocks do
33:    Block(:, :, i)  $\leftarrow$  iDCT(Block(:, :, i))
34:  end for
35:  counter  $\leftarrow$  0
36:  for i=1:8:256 do
37:    for j=1:8:256 do
38:      modified-CH(i:i+7,j:j+7)  $\leftarrow$  Block(:, :, c)
39:      counter  $\leftarrow$  counter +1;
40:    end for
41:  end for
42: WImage  $\leftarrow$  inverseIWT(CA;modified-CH;CV;HH)

```

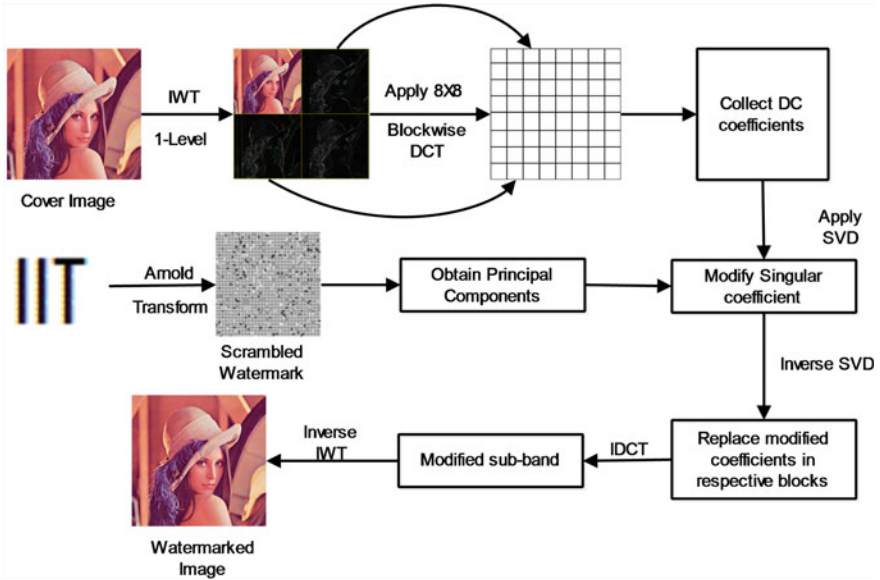


Fig. 1 Proposed watermark embedding scheme

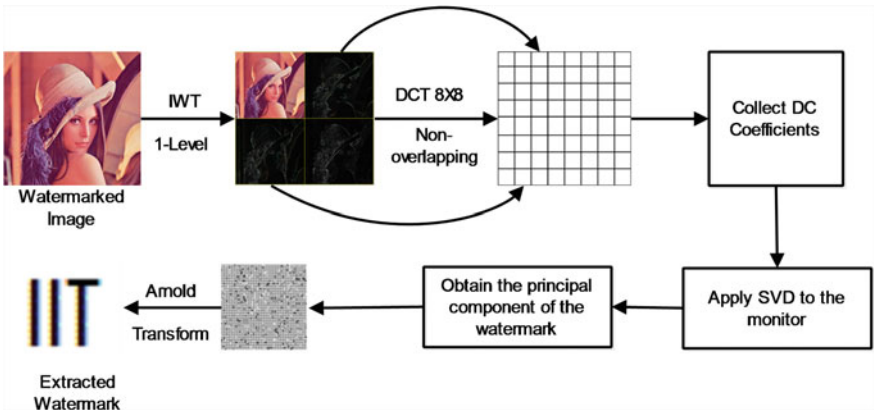


Fig. 2 Proposed watermark extraction scheme

2.2 Watermark Extraction Process

See Algorithm 2 and Fig. 2.

Algorithm 2 Watermark Extraction

Require: Watermarked Image(possibly distorted), V_w, S
Ensure: Extracted Watermark Image

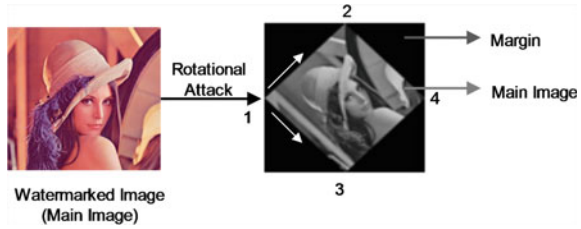
- 1: BlockSize $\leftarrow 8$
- 2: NumberOfBlocks $\leftarrow (M/2) \times (N/2) / (\text{BlockSize})^2$
- 3: $I_M \leftarrow$ read the watermarked image
- 4: $I_M^* \leftarrow$ geometricCorrection(I_M)
- 5: $[CA; CH; CV; HH] \leftarrow$ IWT(I_M^*)
- 6: **for** sub-band $\leftarrow CH, CV$ **do**
- 7: kk $\leftarrow 0$
- 8: **for** i=1:(256/BlockSize) **do**
- 9: **for** j=1:(256/BlockSize) **do**
- 10: Block(:, :, kk+j) = sub-band((BlockSize*(i-1)+1:BlockSize*(i-1)+BlockSize), (BlockSize*(j-1)+1:BlockSize*(j-1)+BlockSize))
- 11: **end for**
- 12: kk = kk + (256/bs)
- 12: **end for**
- 13: **for** i $\leftarrow 1$:NumberOfBlocks **do**
- 14: Block(:, :, i) \leftarrow DCT(Block(:, :, i))
- 15: **end for**
- 16: **for** i $\leftarrow 1$:M/16 **do**
- 17: **for** i $\leftarrow 1$:N/16 **do**
- 18: $A_M^*(i, j) \leftarrow$ Block(5,3,i)
- 19: **end for**
- 20: **end for**
- 21: $[U^* S^* V^*] \leftarrow$ SVD(A_M^*)
- 22: watermark $\leftarrow ((S - S^*) V_w^T) / \alpha$
- 23: watermark \leftarrow inverse-arnold(watermark)
- 24: **end for**

2.3 Geometric Distortion Correction Process

Geometric attacks generate a margin around the “main image” (desired image) [20]. The resulting image is referred as “entire image” having main image and the margin. Margin generates borderlines and corners of the main region. Using this very fact, we develop a technique to correct geometric distortions. Image is reconstructed by locating corners of the main image region. Detailed steps are as follows:

1. Corners are detected with the help of margin, so the presence of margin is necessary. But margin is not necessarily present in all case as in the case of unattacked watermarked images. To ensure the presence of margin in all cases, we add a margin to the main image.
2. Borderline of the main region is detected by applying Canny edge detector. To make the borderline appear clearer, closing operation is applied.
3. Margin added in step 1 is discarded, and narrow broken edges are joined by applying morphological closing operation, to get clear boundary.
4. Image is divided horizontally and vertically into four equal square segments. Corner of the main region is detected in each segment.

Fig. 3 Margin around main image after rotational attack and the four corners of main image



5. Image is reconstructed using the pixels in the region enclosed within corners shown in Fig. 3. Pixels located on the horizontal line between corners 1 and 2 are taken as first row of new reconstructed image matrix. Then, we move toward corner 3 from corner 1 and similarly toward corner 4 from corner 2 and store the pixel values from first and last point of each horizontal line in new matrix. Discrete points (D) can be calculated by Eq. 1:

$$D = \sqrt{((a_2 - a_1)^2 + (b_2 - b_1)^2)} + 1 \tag{1}$$

where (a_1, b_1) , and (a_2, b_2) are coordinates of the starting and last point of the line. Length of line is given by $D - 1$ in terms of pixel. We use Eq. 5 to calculate point coordinates located on the line, where $i = 1, 2, 3, \dots, D$ and $\text{round}(\cdot)$ rounds off to the nearest integer. (x_i, y_i) is the coordinate of the i th point. Proposed technique restored the synchronization destroyed by the translation, rotation, and affine transformation.

3 Experimental Results

Simulation was conducted to evaluate performance of the proposed scheme. For evaluation, grayscale cover images and watermark of sizes 512×512 and 32×32 were taken, respectively, as shown in Fig. 4. 8×8 image block size is used in embedding. The visual quality and robustness of the watermarked image are objectively measured in terms of PSNR and normalized correlation (NC). Scaling factor (α) = 0.05.

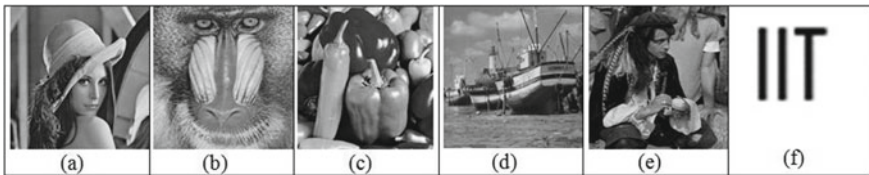


Fig. 4 Original standard test images a–e (Lena, mandrill, pepper, boat, man), f original watermark

Table 1 PSNR of proposed scheme on test images (using grayscale watermark)

Test image	PSNR (dB) IWT-DCT-SVD	PSNR (dB) DWT-DCT-SVD
Lena	47.5923	45.9763
Mandrill	47.8976	45.8756
Pepper	47.7960	45.7996
Boat	48.6159	46.1895
Man	48.4911	46.9814

**Fig. 5** **a** Original host Lena, **b** watermarked image (PSNR = 47.5923 dB), **c** watermark, **d** extracted watermark from unattacked watermarked image (NC = 0.9981)

3.1 Imperceptibility Test

It is observed from Table 1 that the average PSNR is more than the threshold value in all test cases. Watermarked Lena image shown in Fig. 5 has PSNR = 47.5923 dB. We have also tested our scheme by replacing IWT with DWT and compared the results in Table 1. Comparison justifies the implementation of IWT for improved imperceptibility.

3.2 Robustness Test

To exhibit the robustness of the proposed scheme, watermarked images were subjected to various geometric and non-geometric attacks and the corresponding extracted watermark is shown in Fig. 6. Table 2 shows the NC values under different attacks from different host images.

3.2.1 Noise Addition

Generally, noise addition in watermarked images degrades the quality of extracted watermark. We have tested our proposed scheme with different densities and magnitude as shown in Table 3. Proposed scheme shows resistance against noise attacks.














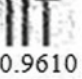
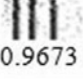




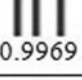
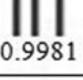

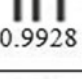
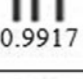
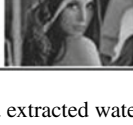
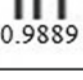
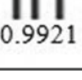
Attacks	Attacked Watermarked image	Extracted watermark and NC value	
		LH	HL
Salt & pepper (0.002)		 0.9841	 0.9826
Median Filter (3×3)		 0.9871	 0.9818
Rotation (45°)		 0.9773	 0.9665
Speckle (0.001)		 0.9842	 0.9865
Gaussian noise (M=0, var=0.005)		 0.9610	 0.9673
Gamma correction		 0.9861	 0.9903
Flip horizontally		 0.9969	 0.9981
Flip vertically		 0.9928	 0.9917
JPEG compression (Q=50)		 0.9889	 0.9921

Fig. 6 Watermarked image (Lena) and extracted watermark (NC values) under various attacks

Table 2 NC of extracted watermark from different images under attack

Attacks	Lena	Mandrill	Pepper	Boat	Man
Salt and pepper (0.001)	0.9462	0.9876	0.9627	0.9538	0.9802
Speckle noise (0.001)	0.9841	0.9901	0.9739	0.9533	0.9853
Median filter (3 × 3)	0.9657	0.9381	0.7919	0.9804	0.8094
Gaussian noise (0.001)	0.7649	0.9707	0.8090	0.7900	0.8867
Flip horizontally	0.9969	0.9663	0.9967	0.9958	0.9909
Flip vertically	0.9928	0.9359	0.9918	0.9979	0.9884

Table 3 NC of extracted watermark (from Lena image) under noise attacks

Attacks	Intensity	LH	HL
Salt and pepper noise	0.01	0.9710	0.9794
	0.001	0.9950	0.9770
	0.005	0.9810	0.9286
Speckle noise	0.01	0.9720	0.9656
	0.001	0.9841	0.9890
	0.005	0.9800	0.9863
Gaussian noise	0.01	0.9360	0.9498
	0.001	0.9820	0.9874
	0.005	0.9610	0.9622

Table 4 NC of extracted watermark (from Lena image) under filtering attack

Attacks	Size	LH	HL
Average filter	2×2	0.9323	0.9733
	3 × 3	0.9817	0.9932
	5 × 5	0.9733	0.9770
Median filter	2 × 2	0.9071	0.9635
	3 × 3	0.9851	0.9816
	5 × 5	0.9537	0.9618

3.2.2 Filtering

Filtering is the common image manipulation. Average and median filters were applied with different sizes. Table 4 shows the NC values under filtering attacks of different sizes.

3.2.3 JPEG Compression

JPEG compression is the most typical and significant non-geometric attack. Watermarked image is tested at different compression rates. Table 5 shows NC values under JPEG compression attack.

3.2.4 Rotation

Table 6 shows that our scheme is robust against rotational attack at various angles. Wavelet transforms are not rotational invariant. We recover the image from rotational attacks and thus can extract the watermark from large rotations.

3.3 False-Positive Detection Test

Watermark extraction without knowing the original left singular vector is not possible. Hence, no reference image can be extracted from any arbitrary image using our scheme as shown in Fig. 7 (Table 7).

Table 5 NC of extracted watermark (from Lena image) under JPEG compression

Attack	LH	HL
JPEG ($Q = 20$)	0.9874	0.9902
JPEG ($Q = 50$)	0.9889	0.9921
JPEG ($Q = 70$)	0.9916	0.9937

Table 6 NC of extracted watermark (from Lena image) under rotation attacks at various angles

Attack	LH	HL
Rotation 30°	0.9864	0.9823
Rotation 45°	0.9846	0.9885
Rotation 70°	0.9872	0.9794
Rotation 80°	0.9872	0.9829

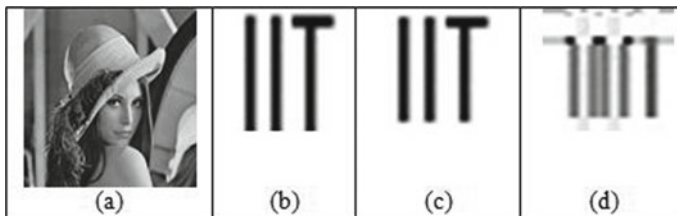


Fig. 7 a Watermarked image, b original watermark, c authentic watermark extracted using V1, d distorted watermark extracted using V2

Table 7 Imperceptibility comparison

Images	Proposed scheme	Fazil and Moeini [20]
Lena	58.457	57.090
Mandril	57.092	56.061
Pepper	57.588	56.848
Airplane	58.452	56.417

Table 8 NC of the proposed scheme and Fazil and Moeini's scheme [20]

Attacks	Proposed scheme	Fazil and Moeini's scheme [20]
Translation (35, 25)	0.991	0.987
Scaling (1.5)	0.993	0.986
Rotation (45°)	0.984	0.977
Cropping	0.916	1
JPEG ($Q = 20$)	0.987	0.984
Gaussian noise (0.003)	0.994	0.992
Salt and pepper (0.005)	0.981	0.996
Median filter (3, 3)	0.988	0.982
Average filter (3, 3)	0.987	0.981
Gaussian filter (3, 3)	0.964	0.984

Table 9 Feature comparison of proposed scheme and Fazil and Moeini's scheme

Description	Proposed scheme	Fazil and Moeini's scheme [20]
Domain used	IWT-DCT-SVD	DWT-DCT-SVD
Embedding sub-band	LH, HL	LH, HL
Size of host	512 × 512	512 × 512
Type of host	Gray scale	Gray scale
Size of watermark	32 × 32	32 × 32
False-positive error	No	Yes

Table 8 compares the robustness of proposed scheme and Fazil and Moeini's scheme [20] in terms of NC. In most of the attacks, our scheme surpasses Fazil and Moeini's scheme [20]. Table 9 shows that our scheme is free from FPP whereas Fazil and Moeini's scheme [20] lacks in this respect. Hence, our scheme is superior to Fazil and Moeini's scheme [20].

4 Conclusion

Genuine watermark can be obtained only if the eigenvector from the original watermark is provided. In this way, our scheme solves the false positive. Geometric attacks especially rotation attack break the synchronization of spatial relation between watermarked and original images. We recover from geometric attacks by reviving the synchronization. For this, we use corner detection of the desired image and thus recover the image. Simulation results evidence that the proposed scheme is robust, especially against geometrical attacks, and at the same time achieves good imperceptibility. Performance comparison of our scheme with Fazil and Moeini's scheme [20] shows that it outperforms the scheme.

References

1. Ansari IA, Pant M, Ahn CW (2016) Robust and false positive free watermarking in IWT domain using SVD and ABC. *Eng Appl Artif Intell* 49:114–125
2. Verma VS, Jha RK, Ojha A (2015) Significant region based robust watermarking scheme in lifting wavelet transform domain. *Expert Syst Appl* 42(21):8184–8197
3. Cox IJ, Miller ML, Bloom JA, Honsinger C (2002) *Digital watermarking*, vol 1558607145. Springer, Berlin
4. Van Schyndel RG, Tirkel AZ, Osborne CF (1994) A digital watermark. In: *IEEE international conference on image processing*, 1994. Proceedings. ICIP-94, vol 2. IEEE, pp 86–90
5. Feng J-B, Lin I-C, Tsai C-S, Chu Y-P (2006) Reversible watermarking: current status and key issues. *IJ Netw Secur* 2(3):161–170
6. Zheng D, Liu Y, Zhao J, El Saddik A (2007) A survey of RST invariant image watermarking algorithms. *ACM Comput Surv (CSUR)* 39(2):5
7. Potdar VM, Han S, Chang E (2005) A survey of digital image watermarking techniques. In: *2005 3rd IEEE international conference on industrial informatics*, 2005. INDIN'05. IEEE, pp 709–716
8. Rawat S, Raman B (2011) A chaotic system based fragile watermarking scheme for image tamper detection. *AEU—Int J Electron Commun* 65(10):840–847
9. Ansari IA, Pant M, Ahn CW (2015) SVD based fragile watermarking scheme for tamper localization and self-recovery. *Int J Mach Learn Cybern* 1–15
10. Mahmoud KW, Datta S, Flint JA (2005) Frequency domain watermarking: an overview. *Int Arab J Inf Technol* 2(1):33–47
11. Kundur D, Hatzinakos D (2004) Toward robust logo watermarking using multiresolution image fusion principles. *IEEE Trans Multim* 6(1):185–198
12. Meerwald P, Uhl A (2001) Survey of wavelet-domain watermarking algorithms. In: *Photonics west 2001-electronic imaging*. International Society for Optics and Photonics, pp 505–516
13. Liu R, Tan T (2002) An SVD-based watermarking scheme for protecting rightful ownership. *IEEE Trans Multim* 4(1):121–128
14. Bhatnagar G, Jonathan Wu QM, Raman B (2013) A new aspect in robust digital watermarking. *Multim Tools Appl* 66(2):179–200
15. Patra JC, Soh W, Ang EL, Meher PK (2006) An improved SVD-based watermarking technique for image and document authentication. In: *IEEE Asia Pacific conference on circuits and systems*, 2006. APCCAS 2006. IEEE, pp 1984–1987
16. Ganic E, Zubair N, Eskicioglu AM (2003) An optimal watermarking scheme based on singular value decomposition. In: *Proceedings of the IASTED international conference on communication, network, and information security*, vol 85

17. Loukhaoukha K, Chouinard J-Y, Taieb MH (2011) Optimal image watermarking algorithm based on LWT-SVD via multi-objective ant colony optimization. *J Inf Hiding Multim Signal Process* 2(4):303–319
18. Makbol NM, Khoo BE (2014) A new robust and secure digital image watermarking scheme based on the integer wavelet transform and singular value decomposition. *Digit Signal Process* 33:134–147
19. Jain C, Arora S, Panigrahi PK (2008) A reliable SVD based watermarking scheme. [arXiv:0808.0309](https://arxiv.org/abs/0808.0309)
20. Fazli S, Moeini M (2016) A robust image watermarking method based on DWT, DCT, and SVD using a new technique for correction of main geometric attacks. *Optik* 127(2):964–972

Fair Fit—A Load Balance Aware VM Placement Algorithm in Cloud Data Centers



Bhavesh N. Gohil, Sachin Gamit, and Dhiren R. Patel

Abstract Cloud computing is a kind of large-scale distributed computing. It has recently emerged as a new technology for providing services over the Internet. It has gained a lot of attention in individual, industry, and academia. Cloud computing dynamically allocates virtual resources as per the demands of users. The rapid increase of data computation and storage in cloud results in uneven distribution of workload on its heterogeneous resources, which may violate SLAs and degrades system performance. Distributing balanced workload over the available hosts is a key challenge in cloud computing environment. VM placement is the process by which it selects the most suitable physical machine (PM) in cloud data centers to deploy newly created virtual machine (VM) during runtime. In this paper, we study VM placement problem with the goal of balanced resource utilization in cloud data centers. Several algorithms have been proposed to find a solution to this problem. Most of the existing algorithms balance the cloud resources based on its utilization which results in unbalanced and inefficient cloud resource utilization. We propose an algorithm, which minimizes the imbalance of resource usage across multiple dimensions, reduces resource leak and wastage, and maximizes the resource utilization. Our algorithm finds a suitable host for incoming VM from categorized host list based on remaining resources using cosine similarity measure. Simulation results show major improvements over the existing algorithms like Binary Search Tree-based Worst Fit and Best Fit, Round Robin, and default Worst Fit.

Keywords Balanced resource utilization · Cloud computing · Cosine similarity · Load imbalance · Resource leak · VM placement

B. N. Gohil (✉) · S. Gamit
S.V. National Institute of Technology, Surat, Gujarat 395007, India
e-mail: bng@coed.svnit.ac.in

S. Gamit
e-mail: sachin1992d@gmail.com

D. R. Patel
VJTI, Mumbai, India
e-mail: dhiren@coed.svnit.ac.in

1 Introduction

Since last many years, cloud computing has become a popular computing platform because of the benefits it offers. It is based on virtualization technology and provides maximum usage of underlying resources. The cloud resources can be accessed at any time and from anywhere by the users. With the increasing number of users and requests of different sizes, many issues required to be addressed for efficient cloud management. One of the most important issues is VM placement, which is to select a suitable PM to deploy incoming VM.

The VM placement is an N-dimensional bin packing NP-hard problem. PM is known as fully loaded if any type of resource is used up to its threshold mark, which does not allow to accommodate additional VMs. Resource leak is an undesired problem where some type of resource is mostly consumed while other types of resource are still available. The available resource is called 'wasted resource' because the PM is declared as fully loaded due to its exhausted resource.

In this paper, we consider the VM placement problem from the perspective of load balancing in the cloud. The key contributions of our work are summarized as follows:

- (1) We address the load balance aware virtual machine placement problem in clouds.
- (2) We present a novel approach to reduce the imbalance of cloud load to improve resource utilization.
- (3) We propose an algorithm with the principle of balancing a load of multiple resources in the cluster of heterogeneous PMs.

The remainder of this paper is structured as follows: Related work of load balance aware VM placement mechanisms in the cloud is outlined in Sect. 2. The details of the proposed load balancing algorithm are discussed in Sect. 3. Simulation results with comparative analysis are explained in Sect. 4. Concluding notes with the future scope are mentioned in Sect. 5.

2 Related Work

In this section, we present relevant heuristic algorithms proposed in the literature for load balance aware VM placement in the cloud.

Tian et al. [1] introduced a novel dynamic and integrated resource scheduling algorithm (DAIRS) for cloud data centers. DAIRS integrates CPU, memory, network bandwidth resources for both VMs and PMs instead of considering only CPU resource in traditional algorithms. They developed an integrated measurement to calculate the total imbalance level for the entire data center and the average imbalance level for each server.

Li et al. [2] proposed a load balancing algorithm to avoid the problem of resource leak and guarantees high resource utilization. PMs are divided into four different

categories while handling VMs request, i.e., resource limited, fully loaded, resource leak, and standby. If the remaining resource of PM is insufficient to host newly created VM with its resource requirements, such PM is labeled as resource limited PM. If PM becomes fully loaded after hosting VM requirements, it is labeled as fully loaded PM. If resource utilization of PM is abnormal which may results in resource leak if it hosts newly created VM, such PM is labeled as resource leak PM and PM is labeled as standby PM, if its resource usage remains regular even after hosting newly created VM. With this VM scheduling, they could minimize the number of running PMs compared to greedy approach.

Huang et al. [3] proposed a novel VM placement algorithm, which balances the utilization of multidimensional resources, reduces the number of PMs and thus lower the consumption of energy. They introduced a multidimensional space partition model to represent the current utilization of resources of each PM. They divide the whole space into three domains (acceptance domain, forbidden domain, and safety domain) and each dimension of space represents a one-dimensional resource.

Tian et al. [4] introduced a dynamic scheduling algorithm named Lowest Integrated load First (LIF) to allocate and migrate multitype VMs on PMs with multidimensional resources like CPU, memory, network bandwidth, etc. and thus optimize the total imbalance of load. They developed various performance metrics like average CPU utilization, average utilization of all CPUs, data center wide integrated (CPU, RAM, and network bandwidth) imbalance value, imbalance value of all CPUs, RAMs, network bandwidths individually and together, average imbalance value of all PMs, average imbalance value of entire data center, and makespan of cloud data center.

Hieu et al. [5] proposed Max-BRU algorithm, which optimizes the utilization of resources and balances the use of multidimensional resources. Their algorithm uses d th dimensional resource utilization ratio and resource balance ratio as allocation metrics to select PMs for VMs. Use of combined metrics utilizes resources efficiently and hence increases the utilization of resources, minimizes the number of running PMs, and increases their profit.

Rathor et al. [6] proposed two dynamic virtual machine scheduling techniques, i.e., Best Fit and Worst Fit. It outperformed vector based algorithm [7] in terms of response time and balanced utilization of resources. To calculate the load of PM, an average remaining capacity is used. All the hosts are classified according to their availability of resources. If there are N different types of resources, hosts can be divided into $N!$ lists. They also proposed a Binary Search Tree-based Best Fit and Worst Fit techniques to place VM to PM and effectively reduced the total number of PMs.

Fang et al. [8] proposed multiobjective ant colony optimization algorithm to solve the virtual machine placement problem, which balances the load among physical machines and the internal load of physical machine simultaneously.

Xu et al. [9] proposed multidimensional resource load balancing of all the physical machines in the cloud computing platform to maximize the utilization of resources.

They customized the ant colony optimization in the context of virtual machine allocation and introduce an improved physical machine selection strategy to the basic ant colony optimization in order to prevent the premature convergence or falling into the local optima.

2.1 Open Issues and Challenges

In [1, 3–5, 7–9] algorithms shown in Table 1, the load on PM is measured using resource utilization. But in a real cloud environment, resources of PMs can be of different specifications and capacities. So here, a load of PM is measured based on the remaining capacity of resources.

In [2, 3, 6], PMs are labeled in different groups based on available resources. By which VMs request can be directed to an appropriate group which in turn reduces resource leak, number of required PMs.

In [2], resource leak or load imbalance is calculated by considering all the PMs are of the same capacity. But in a real cloud environment, it may have PMs of different capacities and sizes.

PMs in [3] are categorized based on the utilization of hosts instead of resources types, which may create the problem of resource leak.

Due to heterogeneous resources of VM and PM, VM may not find its place in the chosen PM list [6]. Also, authors have not mentioned about the creation of VM lists and objective function to measure the imbalance of load, which are required to be addressed for any VM placement problem.

In [7], the authors proposed a novel vector-based approach to remove anomalies in existing approaches. This approach is not appropriate when there comes an equal demand for different resources of VM.

Table 1 Comparison of load balance aware VM placement algorithms

Techniques	Load measurement technique	Scheduling objective
DAIRS [1]	Based on the utilization of resources	Min (imbalance level of data center)
Li et al. [2]	Based on resource availability	Min (number of PMs to host VMs)
Huang et al. [3]	Based on the utilization of resources	Min (number of PMs to reduce energy consumption)
LIF [4]	Based on the utilization of resources	Min (total imbalance value of all clusters)
Max-BRU [5]	Based on the utilization of resources	Min (number of active PMs)
Rathor et al. [6]	Based on resource availability	Min (imbalance level of the host)
Vector Dot [7]	Based on the utilization of resources	Min (total imbalance of the system)
Fang et al. [8]	Based on the utilization of resources	Min (outer and internal load balancing degree)
Xu et al. [9]	Based on the utilization of resources	Min (global load imbalance degree)

3 Proposed Algorithm

During VM placement, it is possible to have resource leak in the cloud along with overutilization and underutilization of resources. To overcome such issues, Fair Fit, a load balance aware VM placement algorithm is proposed for cloud computing environment.

The proposed algorithm basically contains the simple algorithms like. (i) Hosts/VMs categorization in which we categorize the hosts based on the availability of resources and VMs are categorized based on resource demands. (ii) The cosine similarity has been used for subjecting multidimensional resource utilization. (iii) For finding out the best possible host, both categorization algorithm and cosine algorithm are used.

In proposed algorithm for finding out the best host for placing incoming VM basic steps are (i) categorize the hosts and then categorize the VM, (ii) find out the best possible host from the categorized list using cosine similarity between host and VM.

For measuring the imbalance of data center, we use standard deviation [10] to figure out resource utilization across the data center in which we calculate the average of multidimensional resources standard deviation of utilized host. We find the standard deviation of various dimensions like remaining CPUs, remaining network bandwidth, and remaining memory and then take an average of them. This measurement gives an imbalance of data center. Lesser the value of imbalance better the utilization of hosts across the data center.

3.1 Measurement of Load Imbalance

Consider M as the number of virtual machines (VMs) with resource requirements RR_{VM} (CPU, memory, NW bandwidth, storage), which are to be positioned on N number of PMs with resource capacity R_{CPM} (CPU, memory, NW bandwidth) and scattered in total C number of clusters. Also, consider $PM_1, PM_2, PM_3 \dots PM_n$ as members of PM in the cluster of cloud, where n is the total number of PMs. Any PM can be identified as PM_i , where i represents the PM number with range $1 \leq i \leq n$.

Likewise, the set of VMs on PM_i is $VM_{i1}, VM_{i2} \dots VM_{im}$ where m is the number of VMs on PM_i . If we place any VM to any PM, a load of the CPU, memory, NW bandwidth has to be calculated individually. The CPU, memory, NW bandwidth utilization of the PM_i during time 'td' is denoted as below:

$$PM_i(R_k, td) = \sum_{j=1}^m VM_{ij}(R_k, td) \quad (1)$$

Here, PM_i indicates the i th physical machine of cluster C , VM_{ij} indicates the j th VM of PM_i , R_k denotes the utilization of system resource k , where $k =$ CPU, RAM, NW bandwidth, etc. of VMs in PM_i . Hence, the average weighted workload of cluster C during time 'td' can be calculated as below:

$$PMCC(AWL, td) = \sum_{j = 1 \text{ to } n} PMi(AWL, td) \tag{2}$$

where PMCC denotes the Cth cluster of the cloud, AWL denotes the average weighted load of cluster during time ‘td’ and PMi denotes the ith PM of cluster C. Also, a load of all VMs of any PM should be less than the capacity of PM at any point in time.

When there are n physical machines in cluster C of cloud with m number of VMs in each machine, we can calculate remaining resource capacity as below:

$$PMi(RemRk, td) = PMi(TotRk, td) - \sum_{j = 1 \text{ to } m} VMij(ReqRk, td) \tag{3}$$

where PMi (RemRk, td) represents the remaining capacity of resource Rk of the ith physical machine (PM) during time ‘td’, respectively. TotRk represents the total capacity of resource Rk of ith PM, respectively. VMij (ReqRk, td) represents the requested resource Rk of jth virtual machine (VM) of ith PM during time ‘td’.

$$PMCC \mu RemRk = \sum_{x = 1 \text{ to } n} (PMi RemRk)/n \tag{4}$$

where PMCC μ RemRk denotes the mean value of the remaining resource Rk of physical cluster C.

To calculate the imbalance of load (IoL) of a cloud cluster, following objective function is used. By having IoL, the load differences of PMs with its mean are identified. This makes it easy to identify the type and size of VMs to be moved/migrated to achieve load balancing and maintaining service-level agreement (SLA) standards.

$$IoL_{minimize} = \min \left(\begin{array}{l} \sqrt{\sum_{i=1}^n \frac{1}{n} (PMiRemCPU - PMC_C \mu RemCPU)^2} \\ + \sqrt{\sum_{i=1}^n \frac{1}{n} (PMiRemRAM - PMC_C \mu RemRAM)^2} \\ + \sqrt{\sum_{i=1}^n \frac{1}{n} (PMiRemNWB - PMC_C \mu RemNWB)^2} \end{array} \right) \tag{5}$$

Here, the entire physical cluster is considered to calculate the workload instead of the only number of VMs in PM.

3.2 Hosts and VM Categorization

Initially, hosts are categorized based on their available resources. If hosts are having m types of different resources, it can be divided into m! lists. For example, if there

exist three types of resources in hosts, i.e., CPU (C), memory (M) and network bandwidth (N), hosts are divided into six different lists [6].

First host list will contain hosts which are having resource availability in order of $C \geq N \geq M$, second will have $C \geq M \geq N$, third will have $M \geq N \geq C$, fourth will have $M \geq C \geq N$, fifth will have $N \geq C \geq M$, and sixth will have $N \geq M \geq C$. Here, list $C \geq M \geq N$ contains hosts which are having CPU availability greater than or equal to memory availability and memory availability greater than or equal to network bandwidth.

Algorithm 1: Hosts_Categorization

Input: Hosts

Output: Categorized HostLists

1. Get HostLists from data center broker (If type of resources = 3, then number of host lists = 6)
2. **for** each host in data center
3. **If** available resources of host are in order of $C \geq N \geq M$ then
4. add it to the HostList of $C \geq N \geq M$.
5. **Else** check for others ($C \geq M \geq N$, $M \geq N \geq C$, $M \geq C \geq N$, $N \geq M \geq C$, $N \geq C \geq M$)
6. **End If**
7. **End for**

Algorithm 2: VM_Categorization

Input: VM

Output: Appropriate_HostList (For VM)

1. Get HostLists from data center broker (If the type of resources = 3, then the number of host lists = 6)
2. Calculate the requirement of different resources of VM with reference to any of the host's resources.
3. **If** the requested resources of VM are in order of $C \geq N \geq M$ then
4. return (CNM)
5. **Else** check for others ($C \geq M \geq N$, $M \geq N \geq C$, $M \geq C \geq N$, $N \geq M \geq C$, $N \geq C \geq M$)
6. **End If**

3.3 Cosine Similarity

Cosine similarity gives the measure of the angle between two vectors. If the angle between two vectors is small, then they are said to possess a similar alignment. The cosine of two vectors lies between -1 and 1 . If the vectors point in the same direction,

the cosine between them is 1 and the value decreases and falls to -1 with an increase in the angle between them.

Using the Euclidean dot product, the cosine of two vectors is defined as

$$a \cdot b = \|a\| \|b\| \cos \theta$$

And the similarity is shown as follows

$$\text{Similarity} = \frac{A \cdot B}{\|A\| \|B\|} = \frac{\sum_{i=1}^n A_i \times B_i}{\sqrt{\sum_{i=1}^n (A_i)^2} \times \sqrt{\sum_{i=1}^n (B_i)^2}}$$

Here, this similarity model is used which tries to allocate the incoming VM request on to a physical machine based on the similarity measure between the resource requirement of incoming VM and resource availability of physical machine.

Here, we calculate cosine similarity between the resource requirement of incoming VM (VM_{req}) and available resources of PM (PM_{free})

$$\text{Similarity} = \frac{VM_{req} \cdot PM_{free}}{\|VM_{req}\| \|PM_{free}\|}$$

Here, a running physical machine is selected which gives the maximum cosine similarity measure with the incoming VM. The maximum cosine similarity value implies that the incoming VM's resource requirements are most compatible with the free resources of the physical machine. The similarity value lies between 0 and 1.

Algorithm 3: COSINE_SIMILARITY (Host, VM)

Input: Host, VM (To be placed)

Output: Similarity Measure

1. Create vector of available resources of host \vec{Host}
2. Create vector of requested resources of VM \vec{VM}
3. Find Cosine Similarity

$$\text{Cosine Similarity} = \frac{\vec{Host} \cdot \vec{VM}}{\|\vec{Host}\| \|\vec{VM}\|}$$

4. Return cosine similarity

3.4 VM Placement

In this section, a novel VM placement algorithm is proposed which effectively utilizes the cloud resources in a balanced manner. There exist various VM placement algorithms to achieve a different kind of features in the cloud. Here, the cosine similarity-based model has been used to achieve load balanced aware VM placement.

For every incoming VM, Host_Categorization algorithm is called first to get updated hosts list based on available resources. Then after, VM_Categorization is being called to find out appropriate HostList for VM requirements. If VM requirements are in order of $C \geq N \geq M$, i.e., CPU intensive, CNM is chosen as Appropriate_HostList for VM placement.

Then it comes to choose Appropriate_Host from Appropriate_HostList. For that, cosine similarity between all hosts with available resources from Appropriate_HostList and VM with requested resources is measured to finally chose the host with the highest similarity value.

In case Appropriate_HostList is empty, we go for other host lists of cloud data center to choose an appropriate host with highest cosine similarity measure.

Algorithm 4. Fair Fit algorithm

Input: Appropriate_HostList, VM

Output: Appropriate_Host

1. **If** (!Appropriate_HostList.isEmpty)
2. **If** (Appropriate_HostList.size() == 1
3. Appropriate_Host = Appropriate_HostList[0]
4. **Else**
5. **For** each Host from HostList
6. COSINE_SIMILARITY (Host, VM)
7. Save Host with highest cosine similarity (except Hosts with cosine similarity = 1)
8. **End For**
9. Appropriate_Host = Host with highest cosine similarity (except Hosts with cosine similarity = 1)
10. **Else**
11. **For** each Host in the data center
12. COSINE_SIMILARITY (Host, VM)
13. Save Host with highest cosine similarity (except Hosts with cosine similarity = 1)
14. **End For**
15. Appropriate_Host = Host with highest cosine similarity (except Hosts with cosine similarity = 1)
16. **End If**
17. return (Appropriate_Host)

4 Simulation Results and Comparison

The proposed algorithms are simulated on CloudSim [11], which provides a simulation environment for cloud applications. Proposed Fair Fit policy is compared with algorithms BST Best Fit [6], BST Worst Fit [6], Round Robin, and default policy of CloudSim, i.e., Worst Fit. Simulation results are carried out in the cloud of heterogeneous hosts of configuration presented in Table 2. Moreover, VMs are also created of a random configuration of resources presented in Table 3.

4.1 Simulation Results

Figure 1 shows the hosts utilization in terms of number of VMs per hosts for Round Robin, BST Best Fit, BST Worst Fit, Worst Fit, and Fair Fit. The more number of VMs per hosts indicates better resource utilization of hosts. Our proposed Fair Fit algorithm outperformed existing ones for heterogeneous hosts and VMs. Results also indicate that relatively a less number of hosts are required for Fair Fit algorithm to accommodate a certain number of VMs compared to others. Hence, in case of Fair Fit, unutilized hosts can be turned OFF, which in turns support server consolidation and reduce resource leak.

Figure 2 represents the imbalance measurement (Eq. 5) of the cloud data center against various hosts for BST Best Fit, BST Worst Fit, and Fair Fit algorithms. The lower value of load imbalance indicates a more balanced data center. Our proposed Fair Fit algorithm outperformed existing ones against different numbers of heterogeneous hosts for 1000 heterogeneous VMs and Cloudlets.

Figure 3 represents the imbalance measurement of the cloud data center against VMs for BST Best Fit, BST Worst Fit, and Fair Fit algorithms. Our proposed Fair Fit

Table 2 Specification of heterogeneous hosts

Resource	Capacity
RAM	1/2/4 GB
Network bandwidth	10 Gbps
MIPS	500/1000/1500
PES	1/2/4

Table 3 Specification of heterogeneous VMs

Resource	Capacity
RAM	512 MB/1 GB/1.5 GB
Network bandwidth	1.5/3/4.5 Gbps
MIPS	250/500/750
PES	1

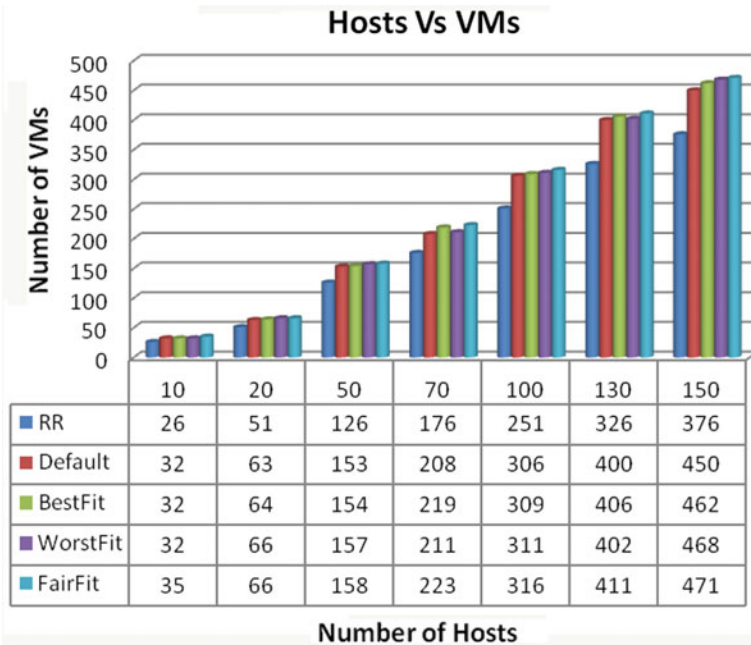


Fig. 1 Hosts utilization

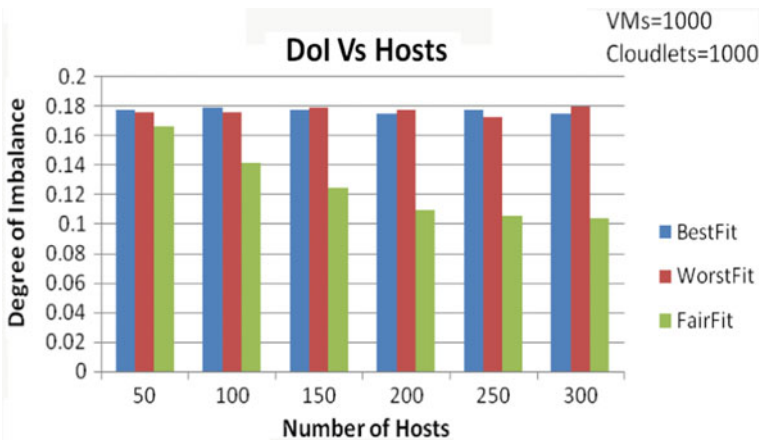


Fig. 2 Number of hosts versus degree of imbalance

algorithm outperformed existing ones against different numbers of heterogeneous VMs for 100 and 1000 heterogeneous hosts and Cloudlets, respectively.

Figure 4 represents the imbalance measurement of the cloud data center against Cloudlets for BST Best Fit, BST Worst Fit, and Fair Fit algorithms. Our proposed Fair

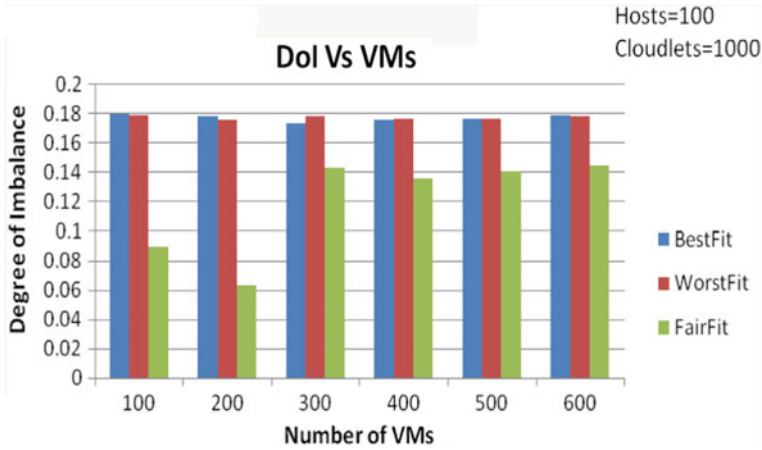


Fig. 3 Number of VMs versus degree of imbalance

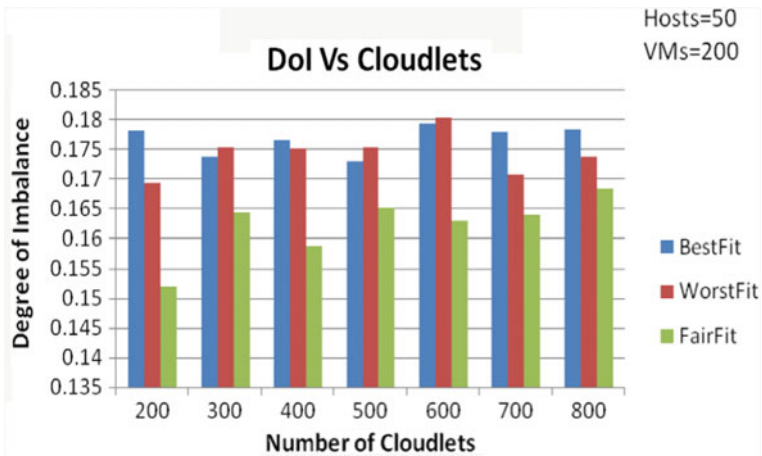


Fig. 4 Number of Cloudlets versus degree of imbalance

Fit algorithm outperformed existing ones against different numbers of heterogeneous Cloudlets for 50 and 200 heterogeneous Hosts and VMs respectively.

Figure 5 represents the number of overutilized hosts in the cloud data center against hosts for BST Best Fit, BST Worst Fit, and Fair Fit algorithms. Our proposed Fair Fit algorithm outperformed existing ones against different numbers of heterogeneous hosts for 700 and 1000 heterogeneous VMs and Cloudlets, respectively.

Figure 6 represents the number of overutilized hosts in the cloud data center against VMs for BST Best Fit, BST Worst Fit, and Fair Fit algorithms. Our proposed Fair Fit algorithm outperformed existing ones against different numbers of heterogeneous VMs for 100 and 1000 heterogeneous hosts and Cloudlets, respectively.

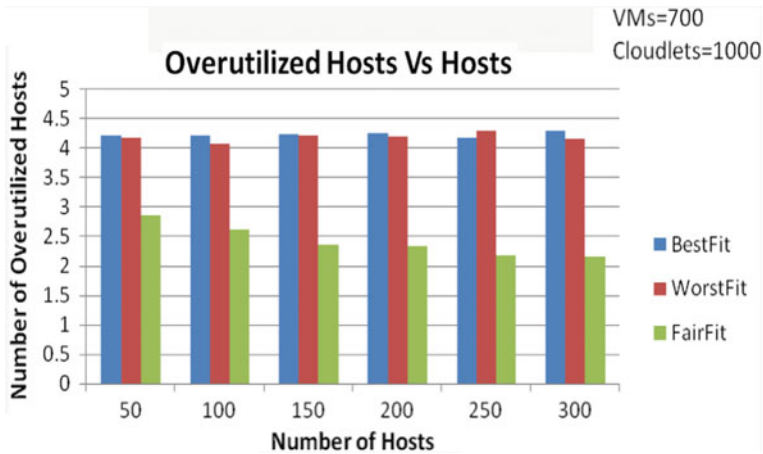


Fig. 5 Number of hosts versus overutilized hosts

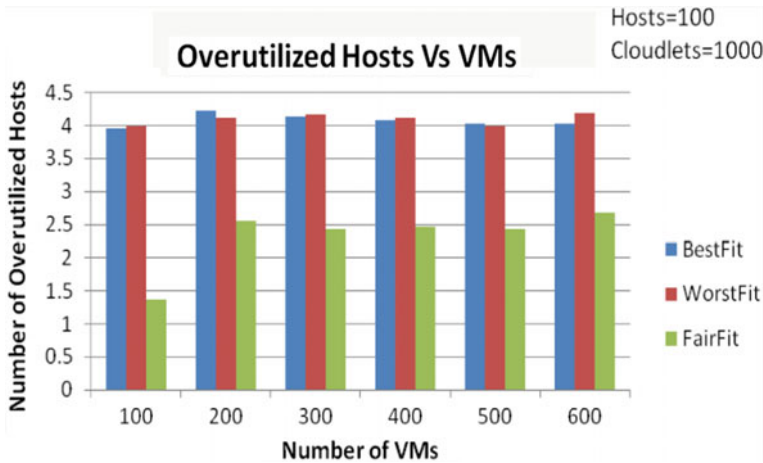


Fig. 6 Number of VMs versus overutilized hosts

Figure 7 represents the number of overutilized hosts in the cloud data center against Cloudlets for BST Best Fit, BST Worst Fit, and Fair Fit algorithms. Our proposed Fair Fit algorithm outperformed existing ones against different numbers of heterogeneous Cloudlets for 100 heterogeneous hosts and VMs.

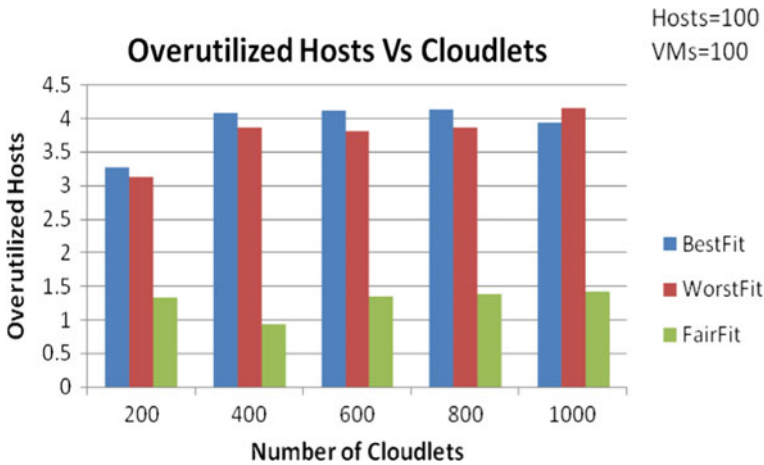


Fig. 7 Number of Cloudlets versus overutilized hosts

4.2 Contributions of Proposed Work

The proposed Fair Fit algorithm removes the flaws present in BST Best [6] and Worst Fit [6] approaches and gives a new approach to improve resource utilization and imbalance of cloud load.

BST Best and Worst Fit approaches have following flows which are removed in the proposed algorithm.

- A new host is powered ON if the suitable host is not found for the incoming VM from the chosen host list. Instead of starting new host, the nearly suitable host may be selected to place VM to achieve server consolidation and avoid underutilization of the data center.
- Hosts are categorized into six different lists and arranged in ascending and descending order for BST Best and Worst Fit, respectively. Binary Search Algorithm is mainly used to find a suitable host which can accommodate incoming VM with its requested resources. Sorting of hosts in the list is based on one type of resource, i.e., CPU, memory, network bandwidth, etc. Hence, the case may be possible where other types of resources are not in order of their sizes or capacities which in turns select the inappropriate host in a host list.

5 Conclusion

This paper presents the importance of load balance aware VM placement in the cloud. The proposed Fair Fit algorithm is cost saving and beneficial for cloud users and providers. The simulation results show that the Fair Fit algorithm provides better

improvements in resource utilization, resource leak, imbalance of cloud load, under and over utilization of hosts, etc. with other existing algorithms.

Hosts categorization helps to find out the cluster of hosts for hosting incoming VM in the best possible host using cosine similarity measure. Imbalance of average remaining load calculation is based on standard deviation calculation of cloud which provides a better understanding of performance for various algorithms. Simulation results of our proposed work outperformed default Worst Fit, BST Worst Fit, BST Best Fit, and Round Robin algorithms.

Our work can be further improved using efficient live VM migration and host load prediction methods.

References

1. Tian W, Zhao Y, Zhong Y, Xu M, Jing C (2011) A dynamic and integrated load balancing scheduling algorithm for cloud datacenters. In: 2011 IEEE international conference on cloud computing and intelligence systems (CCIS), pp 311–315
2. Li X, Qian Z, Chi R, Zhang B, Lu S (2012) Balancing resource utilization for continuous virtual machine requests in clouds. In: 2012 sixth international conference on innovative mobile and internet services in ubiquitous computing (IMIS), pp 266–273
3. Huang W, Li X, Qian Z (2013) An energy-efficient virtual machine placement algorithm with balanced resource utilization. In: 2013 seventh international conference on innovative mobile and internet services in ubiquitous computing (IMIS), pp. 313–319
4. Tian W, Liu X, Jin C, Zhong Y (2013) Lif: a dynamic scheduling algorithm for cloud data centers considering multi-dimensional resources. *J Inf Comput Sci* 10(12):3925–3937
5. Hieu NT, Di Francesco M, Jaaski AY (2014) A virtual machine placement algorithm for balanced resource utilization in cloud data centers. In: IEEE 7th international conference on cloud computing (CLOUD), pp 474–481
6. Rathor VS, Pateriya R, Gupta RK (2015) An efficient virtual machine scheduling technique in cloud computing environment. *Int J Mod Educ Comput Sci* 7(3):39
7. Mishra M, Sahoo A (2011) On theory of VM placement: anomalies in existing methodologies and their mitigation using a novel vector based approach. In: International conference on cloud computing (CLOUD), IEEE, Washington
8. Fang F, Qu B-B (2017) Multi-objective virtual machine placement for load balancing. In: 2017 international conference on information science and technology (IST 2017), ITM web of conferences, vol 11, Wuhan, Hubei, China
9. Xu P, He G, Zhang Z (2018) An efficient load balancing algorithm for virtual machine allocation based on ant colony optimization. *Int J Distrib Sens Netw* 14(12)
10. Thiruvenkadam T, Kamalakkannan P (2015) Energy efficient multi dimensional host load aware algorithm for virtual machine placement and optimization in cloud environment. *Indian J Sci Technol* 8(17)
11. Calheiros RN, Ranjan R, Rose C, Buyya R (2009) CloudSim: A Novel framework for modeling and simulation of cloud computing infrastructure and services. Technical report of GRIDS laboratory, The University of Melbourne, Australia

Computationally Efficient and Secure Session Key Agreement Techniques for Vehicular Cloud Computing



Saurabh Rana, Dheerendra Mishra, and Saurabh Gupta

Abstract Vehicular cloud computing (VCC) has emerged as a new technology to present better and uninterrupted information to traffic management and road safety. However, the exchange of information among all different vehicles, device and roadside infrastructure over the public network presents a favorable scenario to the adversary to perform active and passive attacks. Therefore, there is an organizing demand for an efficient and secure architecture of the secure exchange of information in VCC. In this direction, one of the big challenges is to mutually authenticate the legitimate sources of the information provider and receiver, and then to manage secure session among them. To ensure secure and authorized communication in VCC, this paper discusses the construction of the authenticated session key agreement protocol for VCC. The proposed framework also maintains the anonymity of participating vehicles. The proposed protocol requires fewer computations from the user side as compare to the cloud server and roadside infrastructures. Moreover, the proposed scheme is theoretically proved secure in the random oracle model. Proposed scheme's performance analysis and comparison with related results on security and performance attributes keep it ahead.

Keywords Vehicular cloud computing · Session key · Security · Anonymity

S. Rana · D. Mishra (✉) · S. Gupta
Department of Mathematics, The LNM Institute of Information Technology, Jaipur, India
e-mail: dheerendra.mishra@lnmiit.ac.in

S. Rana
e-mail: saurabhrana.y16@lnmiit.ac.in

S. Gupta
e-mail: 16ucs170@lnmiit.ac.in

© Springer Nature Singapore Pte Ltd. 2021
G. S. Hura et al. (eds.), *Advances in Communication and Computational Technology*, Lecture Notes in Electrical Engineering 668,
https://doi.org/10.1007/978-981-15-5341-7_36

1 Introduction

Vehicular cloud computing (VCC) is a rising and promising new technique integrating cloud computing with the vehicular ad-hoc network (VANET) to support an intelligent transport system. It is ameliorating transportation safety and also fulfilling the administration requests through message broadcasting. VCC consists of roadside infrastructures like roadside units(RSUs), onboard units (OBUs) [1]. There are mainly three different types of vehicular networks such as vehicle to vehicle, vehicle to infrastructure and vehicle to sensors. In-vehicle to vehicle communication, any two vehicles interact with each other by utilizing all onboard units and in the vehicle to infrastructure, vehicles communicate with roadside units. In-vehicle to sensors communication, vehicles directly interact with any sensing devices [2]. The new resource management has been proposed to provide maximum overall computation and communication efficiency. The wide application of VCC depends on secure and efficient message sharing, which is decisive in many situations. VCC can be applied to all type of automobiles by utilizing the remote system for controlling transport and traffic.

VCC works on a principle in which portable hub allows to interface with different automobiles in the system. VCC does not have the ability to break down and gathered worldwide data. In many cases, VCCs are appropriate for transient applications for little scale administrations, or crash avoidance administrations. Since, a few years ago, a system pulled in consideration of numerous scientist to improve the traffic screen, street security, and signs with proper clarity [8]. The VCC basic structure has been demonstrated in Fig. 1. As of now, different techniques are invoked to find difficulties in vehicular systems. Many researchers believe that VCC will be adopted

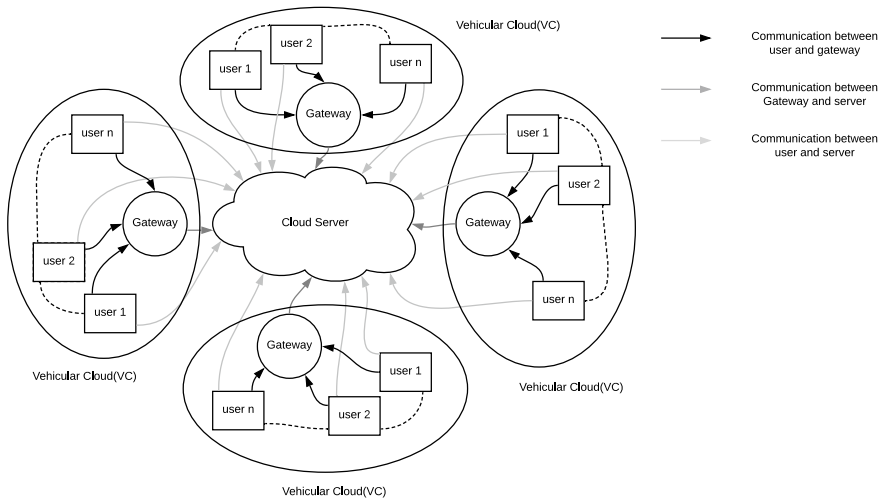


Fig. 1 Architecture of VCC

with portability requirements, influenced by the number of associated vehicles and other factors, for example, congested roads, tall structures, and terrible driver practices, which effects on its execution and use [10]. VCC does not have any limit to take care of worldwide data. Automobiles basically rely upon to convey information for all corresponding frameworks, onboard units, information gathering units and all sensor devices on vehicles. VCC security administration has become a huge region by some hardware and software applications, for example, traffic security administration to remove the congestion and information gathering institution. Authentication and session key agreement play an important role in the enhancement of security and authentication of resources [5, 13].

2 Related Work

Nicola et al. [19] proposed an unadulterated cloud-shaped protocol for vehicles. It was another worldview sensor as a service(SaaS) for sensor automobile. At correspondence stages, it makes vehicles accessible to outsider automobile checking applications with involving some sensors and gadgets. That kind of cloud computing assets called sensor service. The suggested idea came up short on the utilization of the conventional cloud to improve the processing limit generally mentioned by vehicles. Rangarajan et al. [15] managed the cloud security for vehicular systems. And they also suggested another protected prerequisite model called vehicle-to-cloud (V2C) model. V2C was made for provisioning foundation, which joins two different dimensions such as client and framework supplier. To improve protection and security for suggested framework, developers incorporated three types of security as a validation phase, an access control arrangements phase, and a confirmation phase. The verification phase oversees personalities and verifies an appropriator in V2C. To manage the problems of making dodge hindrances in vehicles, a cloud framework for self-ruling driving was proposed by Kumar et al. [8]. This framework gave an idea to empower the server and it gathered data from independent vehicle sensors. Which made roadside units to automobiles enable to maintain a strategic distance from hindrances. From this, those walking people and vehicles which cannot be straightforwardly identified by vehicular sensors, thus, common vehicular and people could be benefited. This framework compared with two different servers, namely, a solicitation server and an organizer server. The first problem demands that computerized data to the vehicle in which walking people or with different vehicles onto the street. The second considers total sensible data acquired from different independent vehicles and RSUs to recognize obstructions.

Lin et al. [9] proposed an issue of consistent access to the Internet by utilizing VCC. They suggested a cloud-bolstered entryway display which called Gateway as a Service (GaaS), so as to have a proficient gateway and improved the utilization of the internet for experiencing vehicular systems. The suggested framework comprises of four segments: door, customer vehicle, emergency responders vehicle, and cloud server. The movable vehicle required to get a piece of access information to the

Internet and solicitations GaaS. In Olariu et al. [14] proposed previous idea with some improvisations called vehicular cloud which was capable of utilizing unutilized vehicular assets for framing a cloud by accumulating vehicular figuring assets. This technique was significant because due to this suggestion, the framework did not exploit the regular cloud and just founded on the automobile assets. Interestingly, Vehicular cloud assets generally are exchanged, and regularly required for approval of a vehicle's proprietor. It would be missed if automobiles are in a constant state (e.g., vehicles in a parking garage). Mershad and Artail suggested an issue of empowering automobiles in a network called VCC to find their required administrations from versatile servers which remains on the same place [12]. The proposed framework called CROWN framework, which relies upon some infrastructure like RSUs that go above as cloud registration. They gave protocol to make RSUs accessible to allow vehicles to find their own vehicular cloud by collected information by the RSUs and take the benefits inside the zone secured. Besides from the RSU infrastructure, CROWN framework did not view the installed PC as a vehicular cloud computing element which can be accessible by users. Doshi et al. [6] proposed a password based authentication protocol. But, this scheme was not able to provide the security proof in proper mathematical way and also not resist against many security threats. Azees et al. [3] proposed an efficient anonymous authentication protocol for VANETs. They claimed that mostly existing schemes suffer from high computation cost. But, the proposed scheme also used the very high computation operations such as bilinear pairing, elliptic curve, exponent modulo. So, the proposed scheme cannot preserve the high efficiency in term of computation cost.

Islam et al. [7] proposed a password-based authentication and key management protocol for VANETs. They claimed that the proposed protocol provides the join, remove user, password update facilities efficiently. However, the password-based protocol cannot resist against stolen or forgotten password attacks. Ahmed et al. [2] proposed VCC technology which provides services to vehicles and capable of managing road traffic efficiently by using the vehicular sources (such as internet) to make decisions and for storage. But with not proper security handles, safety and trust. This work was for road safety management, message sharing services by introducing VCC. Maitra et al. [11] introduced a secure authentication protocol. But, it's protocol does not much computationally efficient. We proposed a framework in which protocols compute efficiently with less costs and with less communication overhead and give real life scenarios with mathematical proofs and assumptions of security model.

Contribution: Firstly, we discuss a taxonomy of existing research with a major focus on authenticated key management in VCC. The existing frameworks are either have higher computation overhead or do not attain desirable security attributes. To address the existing gap identify based on the existing literature, we design a session key management protocol with the following merits:

- Proposed framework ensure mutual authentication before session key adoption.
- Formal proof of security is given in random oracle model.
- Security analysis indicates that proposed scheme attains desirable security attribute.

- It is also found that proposed scheme is computationally efficient.
- Comparative study of the proposed scheme with existing protocols is presented on desirable security and performance attributes.

3 Preliminaries

In this section, we briefly gives the description of required preliminaries. Table 1, demonstrates the notations and symbol, which are used in throughout the paper.

3.1 Fuzzy Extractor

Fuzzy extractor is usually adopted in key authentication to control noisy biometric imprint. It produces a string which is in the form of fixed binary length. Extractor extract public information from imprint biometric template ω . It covers the original key which is biometric with malicious key using string of binary length. It is represented by $Gen(\cdot)$ and $Rep(\cdot)$ [11]. It has the following functionalities:

- $Gen(\omega) = (R, a)$, With the help of a string a which is uniform and random string works as a output, algorithm uses a biometric imprint ω as input. If he information changes then even R will be same with a .

Table 1 Notations used in the scheme

Notation	Description
U_i	User- i
S_j	Server- j
N_j	Vehicular node
\mathfrak{R}	Adversary
VCC	Vehicular cloud computing
VC_i	Vehicular cloud memory
ID_{U_i}	Identity of U_i
ID_N	Vehicular node identity
N_j	Vehicular node
PW_i	Password of U_i
s	Secret value of S_j
$h(\cdot)$	A collision resistant hash function
$Gen(\cdot)$	Fuzzy extractor
\oplus	Bitwise XOR
\parallel	String concatenation

- $\text{Rep}(\omega', a) = R$, It covers the original key which is biometric with malicious key ω' using string of binary length a and produces a new template ω . To produce the same R with a , the distance between ω and ω' have to give threshold verification.

3.2 Cryptographic One-Way Hash Function

One way hash function is mapping in which some random length string maps to some fixed length string but it is not invertible. It can be represented as $h: P \rightarrow Q$, where $P = (0, 1)^*$ and $Q = (0, 1)^n$. Here random length binary string is P and Q is fixed length binary string. Hash function used in many applications like digital signature, key agreement and authentication and many more cryptographic applications [11]. It has the following properties:

1. Preimage resistant: It is hard to find $x \in P$ if $y \in Q$ is given, where $h(x) = y$.
2. Second preimage resistant: It is hard to find $x^* \in P$ s.t., $h(x) = h(x^*)$ if x is given and $x \neq x^*$.
3. Collision resistant: It is hard to find a $(x, x^*) \in P \times P$ s.t. $h(x) = h(x^*)$, where $x \neq x^*$.
4. Indistinguishable: For any input x , hashed value will be $y = h(x)$, which is indistinguishable form uniform binary string in interval $(0, 2^n)$, where n is the output of hash.

4 Proposed Secure Session Key Management Mechanism for VCC

In this section, we present authenticate key establishment mechanism for VCC environment. It adopts password based mutual authentic mechanism and session key agreement. The proposed scheme enhance the computational efficiency and improves the security of existing framework for VCC. It has following two phases:

- Registration phase
- Session key establishment phase.

4.1 Registration Phase

Initially, U_i and N_j will be to register in conventional clouds S_j . U_i will have to register with S_j , then vehicular N_j will be register for further authentication by his personal unique identity.

4.1.1 User Registration

Each U_i registers in cloud server with our credentials in which, U_i securely used these at time of authentication. Following steps are taken by U_i and S_j through secure channel to complete the registration. U_i registration phase briefly demonstrated in Fig. 2.

- Step 1:** Each U_i registers in conventional cloud to obtain an identity based public and private authentication. U_i gives the identity ID_{U_i} and password PW_{U_i} and then imprints ω . Then fuzzy extractor used to generate values $Gen(\omega) = (R, \alpha)$ where R is a uniformly random value and a is a helper string. U_i chooses a random number $r_1 \in Z_p^*$. Then, U_i computes $G_1 = h(PW_{U_i} || r_1)$, $G_2 = H(ID_{U_i} || \alpha)$ and sends G_1 and G_2 to the S_j via secure channel.
- Step 2:** After receiving the request, S_j select secret parameter S and determine $G_3 = h(G_2 || S)$, $G_4 = h(G_1 || s)$, where s is secret key of server S_j . Further computes, $G_5 = G_3 \oplus G_4$. S_j sends G_5 , S to U_i through secure channel.
- Step 3:** After receiving G_5 , S , U_i computes G_6 by computing $G_6 = h(ID_{U_i} || PW_{U_i} || G_4 || G_5)$ and store r_1 , S , G_5 in memory smart device.

4.1.2 Vehicular Node Registration

In this phase, Gateway register in cloud server for further process provides the information to user which is used for sharing the message between user and server by vehicular nodes. The node registration phase demonstrated in Fig. 3. Nodes N_j registers itself in server in steps listed below:

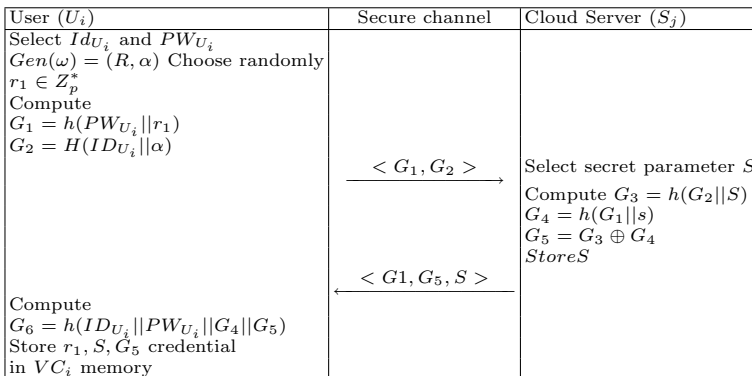


Fig. 2 Illustration of user’s registration mechanism with server

Vehicular node (N_j)	Secure channel	Cloud Server (S_j)
Generate random nonce r_2 Compute $G_7 = h(r_2 ID_N)$		
	$\xrightarrow{\langle ID_N, G_7 \rangle}$	Compute $G_{10} = h(ID_N s)$ $G_{11} = G_{10} \oplus G_7$
Compute $G_{12} = h(G_{10} r_2 ID_N)$ Store r_2, G_{11}	$\xleftarrow{\langle G_{10}, G_{11} \rangle}$	

Fig. 3 Illustration of registration of IoT node with gateway of server node

- Step 1:** Now each gateway N_j must have to register in S_j . Then, N_j computes random nonce r_2 and computes $G_7 = h(r_2 || ID_N)$. N_j sends ID_N, G_7 to S_j through secure channel.
- Step 2:** After receiving the request, S_j computes $G_{10} = h(ID_N || s)$, $G_{11} = G_{10} \oplus G_7$, sends back to node G_{10}, G_{11} through secure channel.
- Step 3:** After receiving the request by node side computes $G_{12} = h(r_2 || ID_N || G_{10})$ and store r_2, G_{11} in memory.

4.2 Session Key Establishment Phase

After completing the registration phase U_i and N_j . They must have to authenticate to the S_j . This whole process of session key establishment phase demonstrated in Fig. 4. To provides the real access time and essential information, U_i computes the operations and share some credentials which is verified by S_j and N_j in some steps listed below:

- Step 1:** Initially U_i gives the input as ID_{U_i}, PW_{U_i} and ω . Then apply the fuzzy extractor and determine $G(\omega) = (R, \alpha)$. Select a random number r_1 and compute $G_2 = h(ID_{U_i} || \alpha)$, $G_3 = h(G_2 || S)$ and $G_4 = G_5 \oplus G_3$ and verifies $G_6 = ?h(ID_{U_i} || PW_{U_i} || G_3 || G_4)$. If it holds successfully then login success.
- Step 2:** After the success of login phase, generate a random number r_3 and further computes $G_{13} = r_3 \oplus h(G_3 || G_4 || T_i)$, where T_i is a fresh time stamp, $G_{14} = h(r_3 || G_3 || G_5 || T_i)$. Then choose a nearest node to connect with them and sends $M_1 = (G_5, G_1, G_{13}, G_{14}, T_i)$ to the node server via public channel.
- Step 3:** After receiving the request from user side, firstly it verifies $|T_i - T_i'| < \Delta T$. N_j , Generates T_j time stamp. N_j computes $G_{15} = G_7 \oplus r_4$, $G_{16} = h(G_{15} || r_4 || T_j)$ and $G_{17} = h(G_{16} || G_{13} || T_i || T_j)$. N_j sends $M_2 = \{G_{16}, G_{17}, G_{15}, G_1, G_5, G_{11}, G_{13}, G_{14}, ID_N, T_i, T_j\}$ to S_j .

User U_i	Vehicular node N_j	Cloud server S_j
ID_{V_i} and PW_{V_i} $G(\omega) = (R, \alpha)$, imprints ω Compute $G_2 = h(ID_{V_i} \alpha)$ $G_3 = h(G_2 S)$ $G_4 = G_5 \oplus G_3$ $G_6 = ?h(ID_{V_i} PW_{V_i} G_3 G_4)$ If verification hold Selects $r_3 \leftarrow Z_q^*$ Generates a time stamp T_i Compute $G_{13} = r_3 \oplus h(G_3 G_4 T_i)$ $G_{14} = h(r_3 G_3 G_5 T_i)$ $M_1 = \{G_5, G_4, G_{13}, G_{14}, T_i\}$ \rightarrow	Verify $ T_i - T_i' < \Delta T$ Select $r_4 \leftarrow Z_p^*$ Generates T_j time stamp $G_{15} = G_7 \oplus r_4$ $G_{16} = h(G_{15} r_4 T_j)$ $G_{17} = h(G_{16} G_{13} T_i T_j)$ $M_2 = \{G_{16}, G_{17}, G_{15}, G_1, G_5, G_{11}, G_{13}, G_{14}, ID_N, T_i, T_j\}$ \rightarrow	$T_j' - T_j \leq \Delta T$ Computes $G_4^* = h(G_1 s)$ $G_3^* = G_4^* \oplus G_5$ $r_3^* = G_{13} \oplus h(G_5^* G_4^* T_i)$ Check's $G_{14}^* = h(r_3^* G_5^* G_5 T_i)$ $G_{14}^* = ?G_{14}$ If hold's Compute $G_{10}^* = h(ID_N s)$ $G_7^* = G_{11} \oplus G_{10}^*$ $r_4^* = G_{15} \oplus G_7^*$ $G_{16}^* = h(G_{15} r_4^* T_j)$ Checks $G_{17} = ?G_{17}^*$ If hold's then further compute Choose $r_5 \leftarrow Z_p^*$ Select time stamp T_k Generates $SK = h(r_3 r_4 r_5)$ $V = r_5 \oplus h(r_3 G_4 T_k)$ $W = r_5 \oplus h(G_{10} r_4 T_k)$ $G_{18} = SK \oplus h(r_5 G_7 T_k)$ $G_{19} = SK \oplus h(r_5 G_3 T_k)$ $G_{20} = h(r_5 SK G_{18} G_{19} V W T_k)$ $M_3 = \{G_{19}, G_{20}, G_{18}, V, W, T_k\}$ \leftarrow
$ T_i - T_i' \leq \Delta T$ Computes $G_3 = h(G_2 S)$ $G_4^* = G_5 \oplus G_3$ $r_5^* = V \oplus h(r_3 G_4 T_k)$ $SK^* = G_{19} \oplus h(r_5^* G_3 T_k)$ $G_{20}^* = h(r_5^* SK^* G_{18} G_{19} V W T_k)$ $G_{21} = h(SK G_{19} V G_{20}^* T_i)$ $G_{21}^* = ?G_{21}$ if holds Store corresponding SK	$T_k - T_k' \leq \Delta T$ Computes $G_{10} = G_7 \oplus G_{11}$ $r_5^* = W \oplus h(G_{10} r_4 T_k)$ $SK = G_{18} \oplus h(r_5^* G_7 T_k)$ If holds, Computes $G_{20}^* = h(r_5^* SK^* G_{18} G_{19} V W)$ $G_{20} = ?G_{20}^*$ Generate T_i as fresh time stamp $G_{21} = h(SK G_{19} V G_{20} T_i)$ $M_4 = \{G_{21}, G_{19}, G_{20}, V, T_k, T_i\}$ \leftarrow	

Fig. 4 Illustration of session key establishment phase

- Step 4:** After receiving the request, S_j first verifies $|T_j - T_j'| \leq \Delta T$. If time threshold value satisfies then S_j computes $G_4^* = h(G_1||s)$, $G_3^* = G_4^* \oplus G_5$, $r_3^* = G_{13} \oplus h(G_3^*||G_4^*||T_i)$. Check's $G_{14}^* = h(r_3||G_3^*||G_5||T_i)$, $G_{14}^* = ?G_{14}$. If hold's Compute $G_{10}^* = h(\text{ID}_N||s)$, $G_7^* = G_{11} \oplus G_{10}^*$, $r_4^* = G_{15} \oplus G_7^*$ and $G_{16}^* = h(G_{15}||r_4||T_j)$ verifies $G_{17} = ?G_{17}^*$. If hold's then further compute and choose random number $r_5 \leftarrow Z_p^*$. Then select time stamp T_k . Generates the session key $\text{SK} = h(r_3||r_4||r_5)$, $V = r_5 \oplus h(r_3||G_4||T_k)$, $W = r_5 \oplus h(G_{10}||r_4||T_k)$, $G_{18} = \text{SK} \oplus h(r_3||G_7||T_k)$, $G_{19} = \text{SK} \oplus h(r_5||G_3||T_k)$, and $G_{20} = h(r_5||\text{SK}||G_{18}||G_{19}||V||W||T_k)$. Finally, S_j sends back $M_3 = \{G_{19}, G_{20}, G_{18}, V, W, T_k\}$ to N_j via public channel.
- Step 5:** After receiving $G_{19}, G_{20}, G_{18}, V, W, T_k$ from S_j . N_j checkers $|T_k - T_k'| \leq \Delta T$ and computes $G_{10} = G_7 \oplus G_{11}$, $r_5^* = W \oplus h(G_{10}||r_4||T_k)$ $\text{SK} = G_{18} \oplus h(r_5^* ||G_7||T_k)$. If holds, Computes $G_{20}^* = h(r_5^*||\text{SK} * ||G_{18}||G_{19}||V||W)$ $G_{20} = ?G_{20}^*$. Generate T_l as fresh time stamp $G_{21} = h(\text{SK}||G_{19}||V||G_{20}||T_l)$. N_j sends back $M_4 = \{G_{21}, G_{19}, G_{20}, V, T_k, T_l\}$ via public channel.
- Step 6:** After receiving the request, U_i verifies $|T_l - T_l'| \leq \Delta T$. U_i computes $G_3 = h(G_2||s)$, $G_4^* = G_5 \oplus G_3$, $r_5^* = V \oplus h(r_3||G_4||T_k)$, $\text{SK}^* = G_{19} \oplus h(r_5^*||G_3||T_k)$, $G_{20}^* = h(r_5^*||\text{SK}^* ||G_{18}||G_{19}||V||W||T_k)$, and checks either its holds or not. If holds correctly, then U_i computes $G_{21} = h(\text{SK}||G_{19}||V||G_{20}^*||T_l)$, $G_{21}^* = ?G_{21}$ if holds, store corresponding SK.

5 Security Proof

In this phase, Initially introduce the security model \mathcal{P} and then establishes the proposed protocol under random oracle model (ROM).

Collision resistance attack (CRA) algorithm If any \mathfrak{R} finding a collision for a one way hash function $h(\cdot)$, we have

$$\text{Adv}_{\mathfrak{R}} = \Pr[(x, x') \stackrel{R}{\leftarrow} \text{Ad} : x \neq x' \text{ and } h(x) = h(x')]$$

where probability of this event is $\Pr[E]$, and (x, x') is randomly selected by \mathfrak{R} and $h(\cdot)$ is secure if $\text{Adv}_{\mathfrak{R}} \leq \epsilon$, where ϵ is arbitrary small number $\epsilon > 0$.

Theorem 1 *In the random oracle model, if \mathfrak{S}_{Ad} has negligible advantage ϵ against CRA algorithm, then our proposed protocol P_s with stand against man in the middle (MIM) attack.*

Proof

- U_i gives the input as identity ID_{U_i} , password PW_{U_i} , and biometric ω in his device. Then they use fuzzy extractor $G(\omega) = (R, \alpha)$. Then U_i computes $G_2 = h(\text{ID}_{U_i}||\alpha)$, $G_3 = h(G_2||s)$, and $G_4 = G_5 \oplus G_3$. Then it verifies $G_6 =$

- $?h(\text{ID}_{U_i}||\text{PWD}_{U_i}||G_3||G_4)$. If this holds then generates r_3 as random number from Z_p^* . U_i computes $G_{13} = r_3 \oplus (G_3||G_4||T_i)$, $G_{14} = h(r_3||G_3||G_5||T_i)$ and sends $\langle G_1, G_5, G_{13}, G_{14}, T_i \rangle$ to the N_j via insecure channel.
- If any \mathfrak{S}_{Ad} have capability to impressions communication between U_i and N_j . It's try to transmit either G_1 or G_5 . \mathfrak{S}_{Ad} needs to generates random number r_1' and try to generates G_1^* , and G_5^* . But, without knowing the PW_{U_i} , and ID_{U_i} , it is not practical to retrieve G_1^* , and G_5^* . In the similar manner, G_{13}^* , G_{14}^* can not be trivial to getback without knowing actual G_3 , and G_4 .
 - Upon receiving $\langle G_1, G_5, G_{13}, G_{14}, T_i \rangle$, the N_j verifies verifies time stamp, N_j generates a fresh random number r_4 , and computes $G_{15} = G_7 \oplus r_4$, $G_{16} = h(G_{15}||r_4||T_j)$ and $G_{17} = h(G_{16}||G_{13}||T_i||T_j)$, and sends back $\langle M_2 \rangle$ to the S_j via insecure channel.
 - If an \mathfrak{S}_{Ad} try to impersonate G_{15}^* , it generates random number r_4^* . But, \mathfrak{S}_{Ad} not able to generate G_7^* . Because it is protected by secret key of S_j . So without knowing G_7 , \mathfrak{S}_{Ad} could not generates G_{15}^* and G_{16}^* . So any type impersonation is not possible.
 - Upon receiving the M_2 from N_j , S_j computes the session key SK. By generating the random number r_5 . It's computes $\text{SK} = h(r_3||r_4||r_5)$ and protect the SK by computing $G_{18} = \text{SK} \oplus h(r_5||G_7||T_k)$, where T_k is the time stamp of S_j . Further, S_j computes $G_{19} = \text{SK} \oplus h(r_5||G_3||T_k)$, $V = r_5 \oplus h(r_3||G_4||T_k)$, $W = r_5 \oplus h(G_{10}||r_4||T_k)$. $G_{20} = h(r_5||\text{SK}||G_{18}||G_{19}||V||W||T_k)$.
 - If \mathfrak{S}_{Ad} intended to impersonate the message M_3 . Then it generates another random number r_5^* . After generating the random number, \mathfrak{S}_{Ad} computes V^* , W^* . But the \mathfrak{S}_{Ad} do not have any information about the G_4 , G_{10} respectively and another random number r_3' , r_4' . These credential are protected by the secret parameter of respected authority. There are no way to extract hidden parameter. \mathfrak{S}_{Ad} have a negligible advantage to get them back. No impersonation possible. S_j sends back to the N_j $M_3 = \{G_{19}, G_{20}, G_{18}, V, W, T_k\}$ to N_j via insecure channel.
 - Upon receiving the $G_{19}, G_{20}, G_{18}, V, W, T_k$ parameters. N_j verifies the session key the sends to U_i with additional parameter G_{21} . If any active \mathfrak{S}_{Ad} came in the middle and extract all the information from the insecure channel. It can not get the $r_5^* = V \oplus h(r_3||G_4||T_k)$, $r_5^* = W \oplus h(G_{10}||r_4||T_k)$ because it will be protected by G_4, r_3 , and G_{10}, r_4 which is not practical. If \mathfrak{S}_{Ad} going to retrieve the $\text{SK}^* = G_{18} \oplus h(r_5||G_7||T_k)$, $\text{SK}^* = G_{19} \oplus h(r_5||G_3||T_k)$. From here, \mathfrak{S}_{Ad} get nothing without knowing r_5, G_3, G_7 . Thus we claim that \mathfrak{S}_{Ad} has negligible advantage to break the proposed scheme in polynomial time.
 - If \mathfrak{S}_{Ad} guesses to be a U_i^{th} to rip off the information form the S_j , it must grant for approach the biometric trait and personal information of U_i . Then, \mathfrak{S}_{Ad} must purchase a permit form the central authority. So there are no such \mathfrak{S}_{Ad} exist, who impersonate a Vehicular system with some particular information. In that manner, the proposed scheme is secure against any \mathfrak{S}_{Ad} with MIM.

Security analysis Security performance of MIM attack as below.

- If the \mathfrak{S}_{Ad} attacks the model in a initialization phase. \mathfrak{S}_{Ad} guess the correct ID_{U_i} and password PW_{U_i} compiled with d and w bit length respectively.

- Then probability of right guessing of ID_{U_i} and PW_{U_i} $\Pr[R_r(ID_{U_i}, PW_{U_i})] = \frac{1}{2^{6d+w}}$ approximately [13]. In our scheme private key of S_j is based on hardness of CRA problem.
- To reconstruct SK \mathfrak{S}_{Ad} requires G_7, G_4 , for SK we must know about r_5 and secret key of S_j . For G_7, G_4 we must requires the identity of U_i and N_j . Then probability

$$\Pr[\mathfrak{S}_{Ad_{succ}}] = \frac{1}{2^{6d+w} + 256} \leq \text{neg}(n)$$

which is actually very negligible. Further, we can claim that proposed protocol is secure against any kind impersonation.

6 Performance Analysis

In this section, we perform a complete performance analysis considering the computation time and communication time for various authentication schemes Hang et al. [18], Tsai et al. [17], Doshi et al. [6], Maitra et al. [11]. The symbols used for comparison are: T_h for hash function, T_e for elliptic curve operation, T_{fe} fuzzy extractor computation. The values for all these operations for comparison are taken from [4, 16, 17]. It is observed that T_h is a very light weight operation as compared to other operations such as T_{fe}, T_e , etc.

The approximate time for computation of the SHA-1 is $T_h \approx 0.00032$ s, $T_{fe} \approx 0.0171$, and $T_e \approx 0.0171$. Using the above mentioned data, it is observed that Tsai et al. [17] has the higher computational costs comparison with other schemes. The total performs operations compute $5T_h + T_e + 5T_h + 3T_e$. Then computes communication cost $10 \times 0.00032 + 4 \times 0.0171 \approx 0.0716$. Similarly, we computes with the other existing scheme and demonstrated the efficiency of proposed scheme in Fig. 5.

To evaluating the communication overhead in communication between the involved parties, we demonstrate various scheme and examine them on behalf of bit length in time of communication. In this process, we chooses accepted a compatible hash function which gives 160-bit of hash output. And timestamp will be 32-bit with 160-bit of elliptic curve output. Overhead in proposed scheme will be computed as $(160 + 160 + 160 + 32)$ bit = 512 bit where three 160 bit shows the hash function costs and 32 bit shows the timestamp which is sending from user to server and server sends backs to user overhead is (15×160) bit = 2400 bit where three 160 bit shows the hash functions costs and last 160 bit shows by sending five timestamp costs $(10 \times 32 = 320)$. Total communications overhead between user and server will be computed as $2400 + 320 + 32 = 2752$. The communication over head of proposed model is much higher than some of existing scheme but on the security prospective proposed scheme is much efficient and secure under the VCC architecture. The comparative demonstration of communication overhead is given in Fig. 6 and total computation cost of related schemes is given in Table 2.

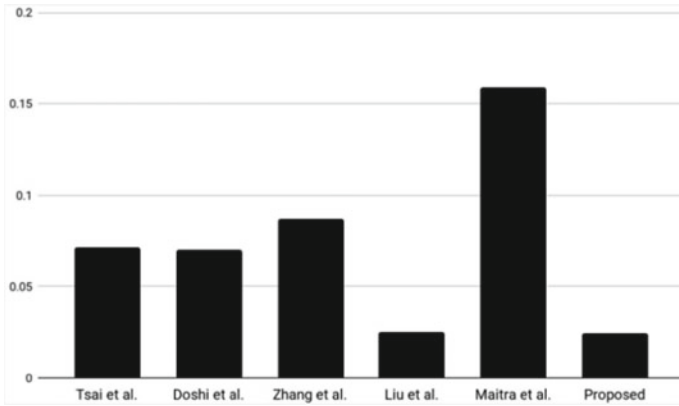


Fig. 5 Comparison of computational costs

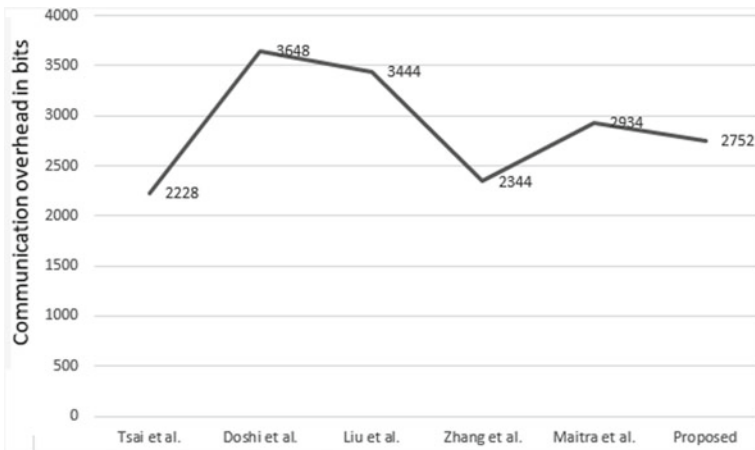


Fig. 6 Comparison of total communications overhead

Table 2 Computational overhead of related schemes

Schemes	User side	Server side	Total computation cost
Tsai et al.'s [17]	$5T_h + T_e$	$5T_h + 3T_e$	0.0716
Doshi et al.'s [6]	$2T_e + 3T_h$	$2T_e + 3T_h$	0.07032
Zhang et al.'s [18]	$2T_h + 1T_e + T_{fe}$	$2T_h + 2T_e$	0.08742
Liu et al.'s [10]	$13T_h + T_{fe}$	$13T_h$	0.02542
Maitra et al.'s [11]	$9T_h + 5T_e + T_{fe}$	$6T_h + 3T_e$	0.1587
Proposed	$10T_h + T_{fe}$	$12T_h$	0.02414

7 Conclusion

This paper has presents a brief overview of the VCC environment and recent development. The basic idea of VCC is to utilized cloud resources properly and securely in vehicular communication by offering access to cloud resources to different vehicles and users. With an increasing number of vehicular edges, VCC brought better opportunities, but increase security threat. To meet the requirement of VCC architecture, we have designed a new security framework for VCC to ensure secure and efficient communication. The proposed scheme supports securely information exchange among vehicles and any infrastructures, and cloud infrastructure. It ensures mutual authentication and secure session establishment among user and node and server. Moreover, we have enhanced the computational efficiency to make it applicable to real-life scenarios.

Acknowledgements This work is supported by Science and Engineering Research Board under File No.: ECR/2015/000243.

References

1. Abid H, Phuong LTT, Wang J, Lee S, Qaisar S (2011) V-cloud: vehicular cyber-physical systems and cloud computing. In: Proceedings of the 4th international symposium on applied sciences in biomedical and communication technologies. ACM, p 165
2. Ahmed ZE, Saeed RA, Mukherjee A (2019) Challenges and opportunities in vehicular cloud computing. In: Cloud security: concepts, methodologies, tools, and applications. IGI Global, pp 2168–2185
3. Azees M, Vijayakumar P, Deboarh LJ (2017) EAAP: efficient anonymous authentication with conditional privacy-preserving scheme for vehicular ad hoc networks. *IEEE Trans Intell Transp Syst* 18(9):2467–2476
4. Chatterjee S, Roy S, Das AK, Chattopadhyay S, Kumar N, Vasilakos AV (2018) Secure biometric-based authentication scheme using Chebyshev chaotic map for multi-server environment. *IEEE Trans Depend Secur Comput* 15(5):824–839
5. Chaturvedi A, Mishra D, Jangirala S, Mukhopadhyay S (2017) A privacy preserving biometric-based three-factor remote user authenticated key agreement scheme. *J Inf Secur Appl* 32:15–26
6. Doshi N, Kumari S, Mishra D, Li X, Choo KKR, Sangaiah AK (2017) A password based authentication scheme for wireless multimedia systems. *Multim Tools Appl* 76(24):25893–25918
7. Islam SH, Obaidat MS, Vijayakumar P, Abdulhay E, Li F, Reddy MKC (2018) A robust and efficient password-based conditional privacy preserving authentication and group—key agreement protocol for VANETS. *Future Gen Comput Syst* 84:216–227
8. Kumar S, Gollakota S, Katabi D (2012) A cloud-assisted design for autonomous driving. In: Proceedings of the first edition of the MCC workshop on mobile cloud computing. ACM, pp 41–46
9. Lin YW, Shen JM, Weng HC (2013) Cloud-supported seamless internet access in intelligent transportation systems. *Wirel Pers Commun* 72(4):2081–2106
10. Liu X, Zhang R (2018) A robust authentication scheme with continuously updated information for vehicular sensor networks. *IEEE Access* 6:70473–70486
11. Maitra T, Giri D, Mohapatra RN (2019) SAS-SIP: a secure authentication scheme based on ECC and a fuzzy extractor for session initiation protocol. *Cryptologia* 43:212–232

12. Mershad K, Artail H (2013) Finding a star in a vehicular cloud. *IEEE Intell Transp Syst Mag* 5(2):55–68
13. Mishra D, Das AK, Chaturvedi A, Mukhopadhyay S (2015) A secure password-based authentication and key agreement scheme using smart cards. *J Inf Secur Appl* 23:28–43
14. Olariu S, Hristov T, Yan G (2013) The next paradigm shift: from vehicular networks to vehicular clouds. *Mobile ad hoc networking: cutting edge directions*, vol 56, no 6, pp 645–700
15. Rangarajan S, Verma M, Kannan A, Sharma A, Schoen I (2012) V2C: a secure vehicle to cloud framework for virtualized and on-demand service provisioning. In: *Proceedings of the international conference on advances in computing, communications and informatics*. ACM, pp 148–154
16. Srinivas J, Das AK, Kumar N, Rodrigues J (2018) Cloud centric authentication for wearable healthcare monitoring system. *IEEE Trans Depend Secur Comput*
17. Tsai JL, Lo NW (2016) Secure anonymous key distribution scheme for smart grid. *IEEE Trans Smart Grid* 7(2):906–914
18. Zhang M, Dai Q, Zheng H, Chen M, Dai L (2018) Novel MOF-derived Co@ N-C bifunctional catalysts for highly efficient Zn-air batteries and water splitting. *Adv Mater* 30(10):1705431
19. Zingirian N, Valenti C (2012) Sensor clouds for intelligent truck monitoring. In: *2012 IEEE intelligent vehicles symposium*. IEEE, pp 999–1004

Recent Trends in Image Processing Using Granular Computing



Shankar Shambhu  and Deepika Koundal 

Abstract The purpose of this paper is to describe recent trends in image using granular computing. Granular computing is used to solve any type of problem with the help of granules. Granules are the key of granular computing. This paper presents granular computing view to solve problem of image processing. Hence, it discusses about different parameters of granular computing, role of granular computing in image processing, different techniques of image processing and how granular computing helps to solve image processing problems, granular computing achievements, literature survey of granular computing and image processing techniques, how granular computing is better than other image processing techniques, and at last discusses about problem or challenges in granular computing and image processing.

Keywords Image processing · Granular · Computing

1 Introduction

Image processing is used to enhance the quality and extract any type of information from an image [1]. In image processing, there are many different techniques to solve these problems. Granular computing is an emerging field to solve multidisciplinary problems [2]. Granular computing provides conceptual theories, techniques, tools, and models to solve any problem. In granular computing, granules are used to solve problems. In this technique, granule is a method of granular computing in image processing that divides an universe into different parts and organization is a

S. Shambhu (✉)

Chitkara University School of Computer Applications, Chitkara University, Himachal Pradesh, India

e-mail: shankar.shambhu@chitkarauniversity.edu.in

D. Koundal

Chitkara University School of Engineering and Technology, Chitkara University, Himachal Pradesh, India

e-mail: deepika.koundal@chitkarauniversity.edu.in

© Springer Nature Singapore Pte Ltd. 2021

G. S. Hura et al. (eds.), *Advances in Communication and Computational Technology*, Lecture Notes in Electrical Engineering 668, https://doi.org/10.1007/978-981-15-5341-7_37

469

method that performs action between two granules and integrates them in an universe [3]. Granular computing techniques are very helpful in image processing to solve problems.

2 Overview of Granular Computing

Granular computing (GrC) is a dynamic emerging field that provides conceptual theories, techniques, tools, and models for solving problems [2]. Granule is a basic element of GrC to solve complex problems. Common properties of patterns and objects in data, i.e., equality, proximity, similarity, indiscernibility, reflexivity, etc. are used to construct granules [4]. Granules construction is very important process; because granular computing-based model success is totally depend on shape and size of granules. Instead of size and shape of granules, granules inter- and intra-association play very important role.

2.1 Granules

Granule is like an object, cluster, subset, or class in a universe in granular computing [5]. In other words, granules can be considered as a combination of different elements taken from the universe according to their similarities and property.

Every granule plays a very important role to solve specific problem on the basis of granularity level, size, and shape of granule. Each granule and its granularity level characterize the system in different way. For example, at first level of granularity, a colored image can be categorized with three granules or standard colors green, blue, and red. This is the broader level of image information categorized. At this level, image regions may be reddish, bluish, or greenery. When moves to next level of granularity with respect to these three colors or granules, then each granule can be separated into several divisions. And, every granule division can be recognized as an object in a particular color.

2.2 Granulation

Granulation is a natural aspect of human philosophy and reasoning system performed in daily life. It is the method of developing the biggest cluster (object) into smaller and smaller cluster into biggest on the basis of problem. Granulation means breakdown of an object into different parts. In opposite, organization is grouping of different parts of an object into whole. As per these concepts, GrC has two central operations, granulations, and organization. Granulation implemented on the whole problem space and at this stage problem is divided into different subspaces or granules, and it constructs

similar property granules. On the other hand, the organization puts every granule together to create blocks and to construct granules at predictable levels.

2.3 Granular Relationships

Granular relationship between granules is a very important factor in granulation development. Relationship of granular is divided into two parts; inter-relations relationship and intra-relation relationship [6]. The former is collecting small granules together to develop a bigger granule on the basis of common properties, i.e., equality, proximity, similarity, indiscernibility, reflexivity, etc. Granulation of a bigger granule into smaller granule and the communications among different components of a granule is the main objective of granular relationships.

2.4 Computation with Granules

In GrC process, computation with granules is the last phase. Computing with different methods with different types of granules and their relationship and importance is the origin for the computation process. These computation methods are known as computation within granules and computation among granules. In computation within granules, finds the different properties of granules. It includes different rules for classification that differentiate the objects of classes. Computation among granules generally work on the inter-relations among granules, for transfer a granule to different granule, grouping granules and partitioning granules.

2.5 Applications of Granular Computing

GrC is an extended version of data mining and it is use in multiple fields to solve problems. There is a huge potential of GrC applications in knowledge discovery and patter detections; machine learning; behavioral detection; information retrieval from different types of images and data; human to computer interaction; medical informatics; segmentation of an image; classification of an image, and much more [7]. These are the some important applications area of GrC. In image processing, GrC plays a very important role for image preprocessing, segmentation, classification, fusion, and registration. Researchers developed many algorithms in last three to four decades.

3 Granular Computing in Imaging

In the field of image processing, GrC plays a very important role. In last three to four decades, multiple techniques have been developed by researchers in image processing using granular computing. Researchers applied different algorithms using granular computing for image preprocessing, segmentation, classification, fusion, and registration.

GrC is a conversion technique between universe and granule or parts and it is mostly used in recognition of patterns, prediction in image processing. According to Zadeh, “granulation, organization and causation are the three basic concepts human cognition process” [8]. Granules is a method of GrC in image processing that divides an universe into different parts and organization is a method that performs action between two granules and integrate them in an universe. Effects and causes that are involved in organization are causation. In image processing, integration of different granules clusters and operations between them and measure between them are most important research in GrC.

3.1 Introduction to Image Processing

To extract any important information and enhanced the quality of an image and to perform the different operation on an image for some reasons or results is called image processing. These different operations of image processing applied on raw images those are coming from multiple sources like satellites, digital cameras, aircrafts, sensors, medical image capturing devices and more different applications and devices. Image processing is like a signal processing. In this image is an input and output is features/characteristics connected with that image. Currently, image processing is speedily rising technology. Different techniques have introduced by many researchers during last three to four decades in the field of image processing. Maximum techniques of image processing are developed by researcher for enhancement and segmentation of images received by different sources. Various application areas of image processing are medical imaging, forensic studies, film industry, remote sensing, document processing, textiles, military, graphic arts, etc.

In image processing, analogue and digital image processing are the two methods that are used for image processing [9]. Analogue method is applied on images available in the form of hard copy. Digital methods help in apply different operations by using computers on the images acquire by cameras and other devices.

Basic steps of image processing are importing image, analyzing or manipulating image and output [9]. In first step, researchers import the image using different image acquisition applications and tools. After successfully importing of image, researcher applied different methods or algorithms on that image to analyze and manipulate that image. And at last step, researcher gets output in form of results that may be modified image or statistics based on image study.

3.2 Image Processing Techniques

A digital image is a two-dimensional array that is arranged in multiple rows and columns [1]. In this two-dimensional array, each pixel has a function $F(x, y)$, where x, y represent a spatial coordinate of an image and F represents pair of (x, y) image coordinates. It is the intensity of a particular point of an image. An image is a group of fixed number or pixels and each pixel has particular location and particular value in two dimensional array of image. This pixel value depends on type of image. If an image type is binary, then in two-dimensional array of that image, only two types of pixel values 0 or 1 will exist. As same if an image type is 8-bit color format, then the range of two-dimensional array pixels value varies from 0 to 255 and here 0 pixel value means black and 255 means white and pixel value 127 stands for gray color. So any type of image is a two-dimensional array on which different image processing techniques are applied. Those techniques are as follows.

3.2.1 Preprocessing

Image preprocessing is a technique that removes errors associated to geometry and pixels values of images those are recorded by different sources [10]. To remove these types of errors in images, researchers used different types of statistical or definite mathematical models. Image enhancement and denoising are two main subparts of image preprocessing. Through image enhancement techniques, raw images can be adjusted into digital images so that output images more appropriate for image analysis or display. To improve the visual impact of an image, researchers modify the brightness values of pixels using different image enhancement algorithms or techniques like contrast stretching, histogram modification, noise filtering, etc. Using these techniques of image enhancement, an image can be converted into improved visual appearance image which is best fit for interpretations. Many times images received from different resources like medical images, satellite images, digital camera images, scanned image have many problems like poor brightness and contrast. Reason of these problems in images is lighting conditions and imaging system while taking images. Different types of noise are found in an image and to remove that noise, image sharpening, edge enhancement, magnifying, contrast enhancement, noise filtering techniques are used. These techniques are very helpful of researchers in image analysis, feature extraction from an image and to display image.

3.2.2 Segmentation

Image segmentation is a very important and mostly used technique of image processing. Image segmentation is used to identify a particular object from an image it may be gray scale or colored image [11]. Object or area that needs to extract from the image is called region of interest (ROI) or object of interest. Motive to apply

segmentation on an image is visualize an object more clear and makes it meaningful for analyze. It is a process in which a digital image is divided into different subgroup of pixels (segments) of same properties [12]. The level of creating of these subgroups depends on problem to solve. When region of interest from an image isolated, then segmentation should stop. For example, from a medical image, to find a tumor, measuring tumor size or volume of tumor, segmentation techniques are used. Different segmentation techniques that are used by researcher are threshold method, region-based method, clustering-based method, watershed-based method, edge-based method, ANN-based and PDE-based methods.

3.2.3 Classification

Image classification is a technique that is widely used in image processing for labeling of group of similar pixels on the basis of gray value to extract information from images [13]. If a pixel satisfies all the rules that are defined to fit in a class, then that pixel is assigned to a particular class. Type of classes can be unknown or known [14]. Known classes are those classes in which researcher can differentiate the classes on the basis of training of data; otherwise, they are classes of unknown type. Depending upon the prior knowledge of classes classification techniques are subdivided into two categories, supervised classification and unsupervised classification. Different supervised classification techniques that are used by researchers are K-Nearest Neighbor (KNN), Support Vector Machine (SVM), Decision Trees, Artificial Neural Network (ANN), Naïve Bayes, Linear Regression, and unsupervised classification techniques are K-Means clustering and Association Rules.

3.2.4 Image Fusion

A main feature that is very important in an image is focus. Sharp images are better than blurry images because sharp images provide all important information of an image. Many times, it is very difficult to obtain sharp or focused images and received blurred images of same scene due to several reasons. So, to solve this problem, various image fusion techniques are used by researchers.

Image fusion is a technique of image processing in which extracts the important data from the different images of same scene and converted them into single image [15]. Single image which is received after applying image fusion technique is very informative as compared to any other single image of same scene. Received single image consists of all important information. Researcher motive for using image fusion technique is build appropriate images that are easily understandable by a human being or machine perception. Image fusion is a very important technique that is widely used in different areas like remote sensing, medical imaging astronomy, etc. Different image fusion techniques that are used by the researchers are principal component analysis (PCA), high pass filtering technique, independent component

analysis (ICA), IHS transform-based image fusion, discrete cosine transform (DCT), and wavelet transform image fusion.

3.2.5 Image Registration

Image registration is an image processing technique that is used to align different scenes images into a one integrated image with reference to a single image [16]. This technique of image processing helps researcher to solve many problems of images like skew, scale, and rotation that are very commonly found in overlaying images. This technique is mostly used in satellite and medical images to align different images taken from different angles into single image. Different image registration techniques that are used by the researchers are FFT-based image registration technique, correlating and sequential technique, contour-based image registration technique, wavelet-based technique, Harris–PCNN-based approach, Harris–Moment-based approach, etc.

4 Granular Computing Achievements

In last two decades, researchers done many experiments on granular computing techniques and achieved their goals. Wieclawek et al. [10] developed a nonlinear granular filtering technique to remove the noise from ultrasound medical images of breast. This granular computing filtering method achieved better results as compared to other commonly used approaches and improve quality of ultrasound medical images. Liu et al. [18] developed a granular computing based clustering algorithm for segmentation of color images and researchers achieved good results. Developed algorithm is fast as compared to FCM and K-means algorithms of segmentation. Wang et al. [19] developed a granular computing-based algorithm for segmentation of gray multi-texture CT medical images. Developed algorithm by researchers achieved good results on low contrast CT images. Instead of these achievements, granular computing achieved many more achievements in the field of image processing.

5 Literature Review

Wojciech et al. [10] developed a granular filtering technique (nonlinear) to remove noise from medical images. Researchers used ultra sound images of breast in which 2496 frames and 15 CT studies with 3396 slices are included in dataset. This technique improves the quality of ultra sound images that is very useful in spatial filtering but granular filter frequency domain has yet to be explored. Performance metrics used to evaluate technique are MSE, NMSE, PSNR, MAE, SNR, RMS, SSIM, and edge preservation indexes.

Juszczyk et al. [12] developed an image segmentation technique for automatically extraction anatomical organ specific area. Researchers used 80 CT abdominal examinations and DICOM images to test technique. This technique automatically extract the initial region gives good result as compared to manual extraction on the initial region of anatomical structures but specificity of the information granules for spleen and kidneys needs to be increase. Performance metrics that is used to evaluate result is SPEC.

Lalaoui et al. [17] developed a region-based MEM algorithm for segmentation of a region of image. Researchers used IBSR image segmentation database which include total 100 MRI images 50 real and 50 synthetic. Modified MEM methods give good results by applying on real and synthetic images as compared to other methods. This method minimizes the number of iterations and execution time but purposed algorithm by researchers is not tested on color images in RGB and YUV spaces as well as on videos. Need to be explored in this. SSIM, VIP, Martin, Inter Intra performance metrics are used to evaluate results.

Hongbing Lie et al. [18] used a granular computing clustering algorithm for segmentation of color images. As per experiment results, proposed algorithm is fast as compared with FCM and K-means segmentation algorithms. It gives good result from the aspects of RI, GCE, and VI.

Wang et al. [19] proposed a granular computing-based algorithm for segmentation of medical image. Images used for segmentation are gray multi-texture CT images. Researchers first perform rough segmentation and then perform lower-level analysis and pattern recognition, etc. Given result of proposed algorithm on low contrast CT images is good.

Golestani et al. [20] applied three image segmentation algorithms FCM, K-means and region-based level set on 30 breast thermal images. Given results explain the excellent performance of improved level set algorithm in efficiency, robustness, and accuracy.

Sandhya et al. [21] purposed a modified K-means algorithm for segmentation of mammogram images. Researchers extracted 14 Haralick features from images with the help of gray -level co-occurrence matrix. MSE and RMSE measures are used to evaluate the performance of modified K-means segmentation algorithm and compare evaluated results with FCM and K-means algorithm. Purposed modified K-means segmentation algorithm gives better results as compared to K-means and FCM algorithm.

Rizzi et al. in [22] develops a classification technique using granular computing approach to solve wide set of instance images problem of classification in F-classification problem on structured data. F is a large group of images in which many objects have same features. Number of classification functions that are used in this technique is equal to the number of number of rules defined for label images. This technique taking around 3 h to train the model it can be decrease by more efficient search.

Bianchi et al. [23] developed a fully automated classification system using graph mining technique based on identification of frequent subgraph and applied this system on images. During training, relevant features are automatically identified.

Stathakis et al. in [24] develop a technique to classify satellite images using granular neural network (GNN) implemented in the NEFCLASS-J software to classify spectral and non-spectral information into land cover classes. Implemented technique by researchers gave 1% less accuracy as compared to neural network classifier. But GNN processing is done on a conceptual rather than numerical level; this is the actual benefit of GNN.

6 Granular Computing Versus Other Image Processing Methods

Granular computing is an intra-disciplinary and developing technique. In recent years, it gives good and fast results in the field of image processing as compared to other image processing techniques. Lie et al. in [18] proved that developed granular computing clustering algorithm is fast as compared to FCM and K-means segmentation algorithms. Some other researchers in [10, 12, 19, 21, 23] proved that granular computing-based image processing techniques give better results as compared to other image processing techniques.

7 Challenges and Issues in GrC and Image Processing

Many aspects of human day-to-day life are affected by images. Because presence of images plays a very important role in every field like medical, geographical, security related, remote sensing, scientific imaging, or much more. For example, medical images are used to detect human diseases. In same way, images are used in every field. In every area, when a raw image is received from any source, then a researcher needs to apply some technical operations on that image. Those operations are image acquisition, enhancement, restoration, segmentation, classification, fusion, registration, etc. To perform different operation of image processing fuzzy sets, neural networks, rough sets, filtering techniques, region-based modified methods of granular computing are found successful to perform image processing operations. Research challenges in image processing and granular computing come from different aspects. Main challenge that comes is that data set of images takes large amount of space and it takes large training time and required high configuration computer systems. Other than this another challenge is sometimes images that received are partially images and to work on partially images is very difficult task. As already knows GrC is used to extract information from an image, an image is subdivided into multiple granules and after that integrates those granules on the basis of their similarities and properties. Performing this task on different images is very challenging for a researcher. Rather than this applying GrC on moving clips instead of still images is very challenging.

8 Conclusion

We present here recent trends of granular computing in image. GrC is a multidisciplinary field. It provides conceptual theories, techniques, tools, and models for solving problems. Using this, we can find solution of any type of problem as well as image processing problems. We can solve those using granular computing techniques. Here, we discuss about granular computing subparameters, how granular computing works in imaging and challenges and issues in granular computing. After discussion about all, we can conclude that granular computing and its different techniques play a very important role in image processing to solve image problems. It has some problem also but these problems can be solved in future.

References

1. Olsson S (2017) FLIR Systems AB. Image processing method for detail enhancement and noise reduction. U.S. Patent Application 15/457,783
2. Yao Y (2006, April) Granular computing for data mining. In: Data mining, intrusion detection, information assurance, and data networks security 2006. International society for optics and photonics, vol 6241, p 624105
3. Yao Y, Deng X (2013) A granular computing paradigm for concept learning. In: Emerging paradigms in machine learning. Springer, Berlin, Heidelberg, pp. 307–326
4. Ganivada A, Sankar Ray S, Pal SK (2017) Fuzzy rough granular neural networks for pattern analysis. In: PATTERN recognition and big data, pp. 487–511
5. Singh GK, Minz S (2007) Granulation using clustering and rough set theory & its tree representation. The School of Computer & System Sciences of Jawahrlal Nehru University, World Academy of Science, Engineering and Technology, vol 25
6. YaoJ (2005, July). Information granulation and granular relationships. In: 2005 IEEE international conference on granular computing, vol 1, pp 326–329. IEEE
7. Sikder IU (2017) Application of granular computing paradigm in knowledge induction. World Acad Sci Eng Technol Int J Comput Electr Autom Control Info Eng 11(10):1091–1094
8. Zadeh LA (1997) Toward a theory of fuzzy information granulation and its centrality in human reasoning and fuzzy logic. Fuzzy Sets Syst 90(2):111–127
9. Rao RM, Arora MK (2004) Overview of image processing. In Advanced image processing techniques for remotely sensed hyperspectral data. Springer, Berlin, Heidelberg, pp 51–85
10. Wieclawek W, Pietka E (2019) Granular filter in medical image noise suppression and edge preservation. Biocybernetics Biomed Eng 39(1):1–16
11. Kaur D, Kaur Y (2014) Various image segmentation techniques: a review. Int J Comput Sci Mobile Comput 3(5):809–814
12. Juszczyk J, Pietka E, Pyciński B (2015) Granular computing in model based abdominal organs detection. Comput Med Imaging Graph 46:121–130
13. Abburu S, Golla SB (2015) Satellite image classification methods and techniques: a review. Int J Comput Appl 119(8)
14. Soofi AA, Awan A (2017) Classification techniques in machine learning: applications and issues. J Basic Appl Sci 13:459–465
15. Suthakar JR, Esther JM, Annapoorani D, Richard F, Samuel S (2014) Study of image fusion-techniques method and applications. Int J Comput Sci Mobile Comput (IJCSMC) 3(11):469–476
16. Nag S (2017) Image registration techniques: a survey. arXiv preprint [arXiv:1712.07540](https://arxiv.org/abs/1712.07540)

17. Yanowitz SD, Bruckstein AM (1989) A new method for image segmentation. *Comput Vis Graph Image Process* 46(1):82–95
18. Liu H, Li L, Wu CA (2014) Color image segmentation algorithms based on granular computing clustering. *Int J Signal Process Image Process Pattern Recogn* 7(1):155–168
19. Wang F, Ruan JJ, Xie G (2012) Medical image segmentation algorithm based on granular computing. In: *Advanced materials research*. Trans Tech Publications, vol. 532, pp 1578–1582
20. Golestani N, EtehadTavakol M, Ng EYK (2014) Level set method for segmentation of infrared breast thermograms. *EXCLI journal* 13:241
21. Sandhya G, Vasumathi D, Raju GT (2015) Mammogram image segmentation quality enhancement using clustering techniques. *Am J Eng Res* 4(4)
22. Rizzi A, Vescovo G (2006, September) Automatic image classification by a granular computing approach. In: *2006 16th IEEE signal processing society workshop on machine learning for signal processing*, pp 33–38. IEEE
23. Bianchi FM, Scardapane S, Rizzi A, Uncini A, Sadeghian A (2016) Granular computing techniques for classification and semantic characterization of structured data. *Cogn Comput* 8(3):442–461
24. Stathakis D, Vasilakos A (2006) Satellite image classification using granular neural networks. *Int J Remote Sens* 27(18):3991–4003

Enveloped Inverted Tree Recursive Hashing: An Efficient Transformation for Parallel Hashing



Neha Kishore and Priya Raina

Abstract Security and performance are two of the most important concerns for cryptographic hashing algorithms, presenting a compelling challenge, since there seems to be a trade-off between achieving high speed on one hand and robust security on the other. However, with the advances in computer architecture and semiconductor technology, it is possible to achieve both by adopting parallelism. This paper presents a novel transformation based on the recursive tree hashing to parallelize and speed up typical hashing algorithms. The proposed transformation, called Enveloped Inverted Tree Recursive Hashing (EITRH), has three steps: “message expansion,” “parallel reduction,” and “hash value generation.” It improves upon the accuracy and the speed of hash code generation. Also proposed are some algorithms using the EITRH transformation for high-speed hashing on multiple cores. The security analysis of EITRH framework demonstrates its multi-property preservation capabilities. Discussion of EITRH w.r.t. performance benchmarks suggests its potential to achieve high speed in practical implementation.

Keywords Cryptography · Parallel hashing · Tree hashing · Multi-property preservation

1 Introduction

Cryptographic hash functions (CHFs) [1] are a relatively recent addition to the cryptographic toolbox. They are used in various application areas where the integrity of data, the authenticity of the source, and the non-repudiation of delivery are impor-

This work is supported by the Science and Engineering Research Board, Department of Science and Technology under Young Scientist Scheme [YSS/2015/001573].

N. Kishore (✉) · P. Raina
Chitkara University School of Engineering and Technology,
Chitkara University, Baddi, Himachal Pradesh, India
e-mail: neha.kishore@chitkarauniversity.edu.in

P. Raina
e-mail: priya.raina@chitkarauniversity.edu.in

© Springer Nature Singapore Pte Ltd. 2021
G. S. Hura et al. (eds.), *Advances in Communication and Computational Technology*, Lecture Notes in Electrical Engineering 668,
https://doi.org/10.1007/978-981-15-5341-7_38

tant, including digital forensics, digital signatures, communication protocols like SSL, crypto-currency, etc. They are critical for all cloud computing services which require ensuring the integrity and correctness of the transmitted data, e.g. validation of downloaded files. Security is considered to be the most critical aspect of all cryptographic primitives and CHF's are no different. For a majority of the popular CHF's like the SHA-x family [2], the idea of security is based on computational complexity. This has adverse implications for performance, as the sequential nature of signature calculations in most algorithms leads to unwanted delays. Due to their sequential nature, the software performance of many hash functions on modern architectures, while decent in terms of speed and the no. of cycles used, is not optimal, resulting in wasted CPU cycles. The volume of data, easily running into terabytes, further deteriorates the performance as the compute-intensive nature of these algorithms makes the calculation of hash code for large files cumbersome and time-consuming. In 2007, National Institute Standards and Technology (NIST) made an announcement calling for suitable hash functions as candidates for the next standard SHA-3 [3], even though SHA-2 was still secure—because of the growing sophistication of attacks since Wang et al. [4], resulting in reduced lifespan for hash functions. The SHA-3 competition introduced parallelizability for increased performance as a desirable feature for the new hash function, suggesting that hashing algorithms need to be fast and efficient, as much as they need to be secure. However, it is remarkable that the focus was on parallelizable rather than parallel CHF's, implying that the design approach continued to remain sequential. It is suggested that a parallel and distributed approach toward CHF's would not only improve performance, but also enhance the security of CHF's. This paper presents a new parallel framework for CHF's to deal with the problem of long computations by lowering the computational complexity through the use of parallel implementation on multi-core processors.

The paper is organized as follows: Sect. 2 provides a brief introduction to the CHF's, followed by a detailed description of the proposed framework in Sect. 3. Section 4 presents the security analysis of the framework giving arguments in support of pre-image resistance, weak collision resistance, collision resistance, non-correlation resistance, parallel pre-image resistance, and pseudorandom oracle preservation properties. Section 5 discusses briefly the various performance benchmarks for evaluation of the framework. The conclusions along with the scope for future research work are given in Sect. 6.

2 Previous Work

A comprehensive study of the literature suggests that prior to the SHA-3 competition, parallelization of CHF's was not on the agenda of many researchers [5]. The evolution of parallel CHF's should thus be viewed in the light of SHA-3 competition, dividing the timeline into three phases, namely pre-SHA3, the years of the competition itself, and post-SHA3. In the initial stage, the efforts were concentrated toward software performance analysis of existing CHF's on the newly arrived Pen-

tium processors [6–8]. The focus was largely on fine-grained parallelism. Hardware parallelism with FPGAs and ASICs was also prevalent and discussed in a few of the papers [9–11]. The arrival of GPUs in 2006 was a real game-changer for parallel CHF's as demonstrated by [12, 13]. The SHA-3 competition established parallelism/parallelizability of algorithm designs as a criterion for evaluation leading to the emergence of several promising designs like BLAKE [14], GRΦSTL [15], MD6 message-digest algorithm [16], skein [17, 18], Keccak [19], etc. These were subject to rigorous tests and analyses and eventually in the year 2013, Keccak was declared the winner of the SHA-3 competition because of its novel sponge construction [20]. The post-SHA-3 era saw the emergence of improved versions for SHA-3 candidates like BLAKE-2 [21], SHAKE [22], ParallelHash [23], etc. Some of the work was done in the domain of lightweight hash functions for resource-constrained environments [24–27]. Presently, efforts are being made toward standardization of tree modes for hash functions in order to achieve medium to coarse-grained parallelism [28–30]. The efforts in the three phases should be seen in the continuation of one other. The three-stage classification does not imply obsolescence of the techniques in the previous stage(s), and it merely signifies a change in approach toward parallel CHF's.

In 2014, Kishore and Kapoor [31] proposed ITRH transformation for a faster, more secure CHF, based on recursive tree hashing and presented its framework as well as detailed analysis. An algorithm RSHA-1 was proposed too. Speedup upto $3.5\times$ was observed when large files were hashed using the proposed framework. Additionally, linear speedup proportional to the no. of processing elements was observed. However, at the time of security analysis, it was observed that the proposed transformation was vulnerable to certain attacks, a side-effect of removal of chain dependencies of the underlying function.

In order to overcome these deficiencies, this paper proposes an improved parallel transformation, Enveloped Inverted Tree Recursive Hashing (EITRH), which comes with an enhanced security level. The design is modeled on the lines of ITRH, but uses enveloping [32] as an additional measure for security.

3 The EITRH Transformation

Definition 1 Let a set of bit strings be denoted as $\{0, 1\}^*$, a message $M \in \{0, 1\}^*$, and k be the no. of blocks of size l , then keyless EITRH ($H: \{0, 1\}^* \rightarrow \{0, 1\}^n$) accepts a message $M \in \mathcal{M}$ and maps it to a unique n -bit digest as follows:

$$h(i) = \begin{cases} h(M_i, H_0), & 0 < i \leq k - 1 \\ h(M_i, H_{00}), & i = k \end{cases}$$

and

$$H_i = h_1 \parallel h_2 \dots \parallel h_k, M \rightarrow H_i \text{ until } H_i \rightarrow \{0, 1\}^n$$

Definition 2 Let a set of bit strings be denoted as $\{0, 1\}^*$, a message $M \in \{0, 1\}^*$, and k be the no. of blocks of size l , then a keyed EITRH ($H_k: \{0, 1\}^{\mathcal{K}} \times \{0, 1\}^* \rightarrow \{0, 1\}^n$) accepts a message $M \in \mathcal{M}$ along with a fixed-length key $\mathcal{K} \in \mathcal{M}$ and maps it to a unique n -bit digest as follows:

$$h(i) = \begin{cases} h(M_i, H_0), & 0 < i \leq k - 1 \\ h(M_i, H_{\mathcal{K}}), & i = k \end{cases}$$

and

$$H_i = h_1 \parallel h_2 \dots \parallel h_{k-1} \parallel h_k, M \rightarrow H_i \text{ until } H_i \rightarrow \{0, 1\}^n$$

Definitions 1 and 2 formally describe the keyless EITRH and keyed EITRH, respectively [33]. The sub-sections of this section further explain the structure and properties of the framework.

3.1 Describing the Framework

As depicted in Fig. 1, EITRH has an inverted tree structure. The transformation comprises of three recursive steps: “message expansion,” “parallel reduction,” and “hash value generation.” The process terminates when the size h_n (of the final hash value) is reached, where h_n depends upon the EITRH variant being used.

Step 1: “Message Expansion” It is performed at every level of the inverted tree of height h_i (determined by the file size and EITRH variant being used). This step is necessary for improving the sensitivity of the hashing process. The message M_i at level h_i ($0 < i < h_i$) is divided into k blocks of size l (determined by the variant used), where $k = (|M| \bmod l) + 1$. Padding is applied to the k th (last) block by appending a string of 10^* followed by the length of M_i at the end. The no. of 0s is adjusted to make the padded block-length a multiple of l .

$$M_i = M_i \parallel 10 \dots 0 \parallel |M_i| \quad \text{for each level } h_i.$$

Parallelism is achieved by executing each block on a multi-core processor. For enveloping, two distinct initial vectors of size h_n are used: $IV_1(H_0)$ for $k - 1$ blocks and $IV_2(H_{00})$ for the k th block.

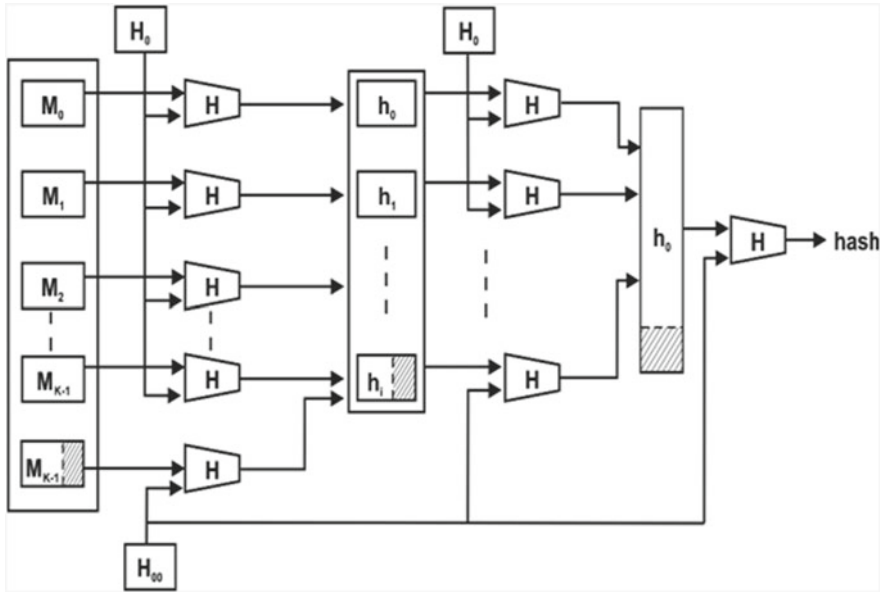


Fig. 1 Enveloped Inverted Tree Recursive Hashing (EITRH) framework

Step 2: “Parallel Reduction” For each block reduction is done in a parallel mode, using nonlinear compression function ($f()$) and set of IVs ((H_0) for $k - 1$ blocks and $IV_2(H_{00})$ for the k th block). Once the hash values are computed for each of the blocks, they become internal state hashes for the next level. These values are concatenated to generate H_i , which acts as the message M for the next level of the tree. Thus, a h_n -bit collective hash H_i is obtained by recursive application of steps 1 and 2.

$$h(i) = \begin{cases} h(M_i, H_0), & 0 < i \leq k - 1 \\ h(M_i, H_{00}), & i = k \end{cases}$$

This step is uniform for each block of M_i and is performed independently, since there is no chaining input from the previous blocks.

Step 3: “Hash Generation” Once all the blocks of level $h_t - 1$ have been processed using the steps 1 and 2, the final digest is generated by $h = H(M_{h_t-1}, H_{00})$.

Algorithm 1 presents the pseudocode for the EITRH domain extender in a data parallel model.

Algorithm 1

```

Procedure: Domain Extender
Model: Data Parallel Model with  $P$  processors
Input: Message  $M$ ,  $n$ ,  $IV_1$ ,  $IV_2$ 
Output: Hash Code
Given: Compression function  $f : \{0, 1\}^{l+n} \times \{0, 1\}^n \rightarrow \{0, 1\}^n$ ;
           $n$ -bit constant  $IV$ 
Declare:    $Number\_of\_Cores, Block\_Size, K$ 
              Set  $Number\_of\_Cores := P$ 
              Break  $M$  into  $l$ -bit blocks  $M_1, \dots, M_k$ , padding if
              necessary;
              Let  $M_{k+1}$  be encoding of  $|M|$ ;
              Declare  $No\_of\_Iterations := \frac{K}{Block\_Size}$ 
              Set  $H_0 := IV_1, H_{00} := IV_2$ ;
ParBegin
    For ALL  $i : [1, k + 1]$  in ASYNC
      If ( $i == k + 1$ )
        Set  $H_i := f(H_{00}, M_i)$ ;
      else
        Set  $H_i := f(H_0, M_i)$ ;
      end if
    End For
    Append  $H_i (1 < i < k + 1)$  to form  $H$  such that
     $H := H_1 || H_2 || \dots || H_{k+1}$ 
Parent
  if  $|H| > n$ 
     $DomainExtender(message H, n)$ 
  return  $H$ 

```

3.2 Properties

As described in Sect. 2, EITRH is an improved construction designed to overcome the security flaws in ITRH construction. Like ITRH, it is a recursion-based construction. Passing $IV_2(H_0)$ to each block separately removed data dependencies, making parallel reduction possible for both the constructions. However, unlike its predecessor, EITRH is an enveloped construction. It uses an additional input $IV_2(H_{00})$ for hashing the last block at each level of the tree. Enveloping the last block in this manner improved the security level of the transformation, improving non-correlation, making it resistant against multi-collision attacks and partial pre-image attacks, in addition to the generic attacks. Also, due to IV_2 , it is possible to use EITRH as both a keyless as well as a keyed construction; if H_{00} in Definition 1 is replaced with a

Table 1 CHF's based on EITRH

Reference	After EITRH	Digest size
SHA-1	RSHA-1	160
SHA-224	RSHA-224	224
SHA-256	RSHA-256	256
SHA-384	RSHA-384	384
SHA-512	RSHA-512	512

fixed-length key \mathcal{K} , as defined in Definition 2. In this manner, a keyless hash function is transformed into a keyed variant simply by replacing IV_2 in the compression function with \mathcal{K} , without the necessity of separate provision for handling the key.

3.3 EITRH Variants

Table 1 indicates the CHF variants using EITRH construction and their internal state sizes. The proposed variants are derived from the SHA family where application of EITRH is done for enhancing security and parallelization. RSHA-1 [31], like SHA-1, gives a digest of 160 bits. Similarly, the digest size in RSHA-224, RSHA-256, RSHA-384, and RSHA-512 correspond to those in the SHA-2 standard.

This paper presents the analysis of EITRH based on the experiments done using RSHA-1. The outcomes can be extended to other variants as well.

4 Security Analysis of EITRH

The EITRH transformation is designed to be a *multi-property preserving domain extension transformation* which can preserve multiple properties in addition to the ideal properties, viz. pre-image resistance (PIR), weak collision resistance (WCR), and collision resistance (CR). The sub-sections of this section provide the security analysis of the proposed framework.

4.1 Pre-image Resistance (PIR)

The pre-image resistant property refers to the one-wayness of the hash functions, which means that inverting the hash value in order to retrieve the original message should be computationally infeasible. The property of PIR is strongly preserved in EITRH as compared to MD construction because of its recursive nature. The fact

that the final digest itself is a hash of hashes makes the use of backtracking to deduce the input message computationally difficult.

4.2 Weak Collision Resistance (WCR)

Weak collision resistance, also called second pre-image resistance, is the property which ensures that given a message M , it is difficult for the adversary (A) to find M'' which generates an identical hash. Due to this property, attacks involving falsification of the message may be thwarted by using encrypted hash. For a n -bit digest, the effort required to find a second pre-image is proportional to 2^n . In Sect. 4.4, it will be proved that EITRH transformation supports the “avalanche effect.” Therefore, for any message, it would be computationally infeasible for an adversary to find another distinct message mapping to the same hash value, as the level of effort required for this type of attack is 2^n . As n increases, the level of effort increases exponentially.

4.3 Collision Resistance (CR)

Strong collision resistance property implies that it should be computationally difficult for A to find two distinct messages M and M'' such that $H(M) = H(M'')$. For a n -bit digest, attacking CR requires an effort of $2^{\frac{n}{2}}$, much less than pre-image and second pre-image attacks, on account of the birthday paradox. Consider two inputs M and M'' (where $M \neq M''$) of the same size, differing by Δ . Let the difference be in only half of the input blocks. *Partial collision* may happen, effecting the intermediate hashes and/or input to the next stage. Due to recursion, a collision in one half of the intermediate hashes ensures that the other half differs by Δ . Further, the colliding values become input for the nonlinear compression function $f()$ in the next stage, which uses sub-key values that are distinct from those used in the previous stages. As a result, in the succeeding stages, the internal collision is unlikely to persist.

4.4 Non-correlation Resistance (Confusion and Diffusion Analysis)

The avalanche effect for CHFs, as in encryption, requires a complex correlation between the input and hash value bits, such that a change in the former should cause a drastic change in at least half of the output bits.

EITRH demonstrated the avalanche effect when it was subjected to tests for confusion and diffusion on a simulator. A random text file from t5-corporus was used for this purpose; its hash was calculated using EITRH variant (RSHA-1). A random bit

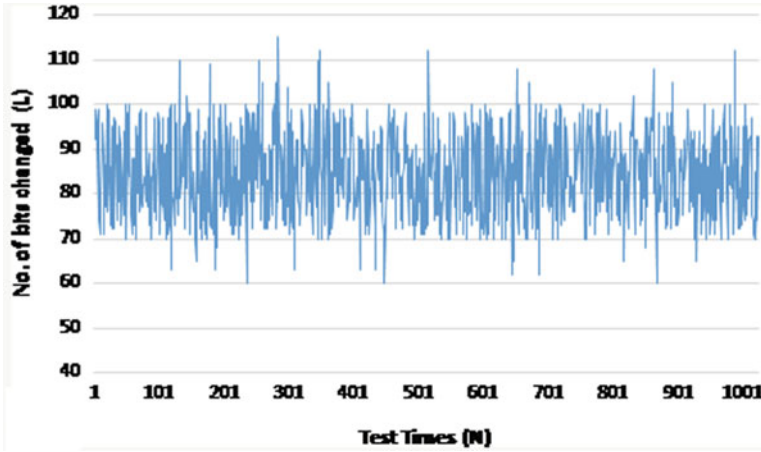


Fig. 2 Testing EITRH for confusion and diffusion properties by measuring the distribution of changed bits L_i in a simulation. The algorithm used is RSHA-1 with digest size of 160 bit. values of L_i suggest a change in more than 50% of the output bits with every single-bit change in the input file

in the original input file was toggled and hash was re-calculated. The two hash values were XORed and the no. of set bits were counted, giving the no. of bits that had changed. The test was repeated N times on the algorithm (where $N = 128, 256, 512$ or 1024) and the results shown in Fig. 2 were plotted after the following calculations.

$$\text{Minimum no. of bits changed: } L_{\min} = \min(\{L_i\}_i^N) \quad (1)$$

$$\text{Maximum no. of bits changed: } L_{\max} = \max(\{L_i\}_i^N) \quad (2)$$

$$\text{Mean no. of bits changed: } \bar{L} = \frac{1}{N} \sum_{i=1}^N L_i \quad (3)$$

$$\text{Mean Changed Probability: } \text{Pr} = \frac{\bar{L}}{\text{Hash Size}} \times 100\% \quad (4)$$

$$\text{Standard Deviation of bits changed: } \sigma_L = \sqrt{\frac{1}{N-1} \sum_{i=1}^N (L_i - \bar{L})^2} \quad (5)$$

$$\text{Standard Deviation: } \sigma_{\text{Pr}} = \sqrt{\frac{1}{N-1} \sum_{i=1}^N \left(\frac{L_i}{\text{Hash Size}} - \text{Pr} \right)^2 \times 100\%} \quad (6)$$

Table 2 Statistics of no. of changed bit L_i

Statistics	No. of times test taken (N)				Mean
	128	256	512	1024	
L_i	82.85156	84.60938	83.64453	84.66504	83.94263
Pr (%)	51.78223	52.88086	52.27783	52.91565	52.46414
σ_L	9.714094	9.934479	9.906738	9.662542	9.804463
σ_{Pr} (%)	6.071309	6.209049	6.191711	6.039089	6.127789
L_{min}	63	58	60	61	60.5
L_{min}	100	98	103	115	104

Here, N is the total no. of statistics, L_i is the no. of bits changed in the i th test, and σ_{Pr} , σ_L indicate the stability of confusion and diffusion.

Table 2 records the statistics L_{min} , L_{max} , L_i , Pr, σ_L , σ_{Pr} calculated using Eqs. (1)–(6), respectively. The table also shows the mean values for these statistics. It can be noted that mean values of L_i and Pr for EITRH-based RSHA-1 are 83.94 and 52.46%, respectively. These are close to the benchmark values for the standard 160-bit CHF SHA-1, i.e., 64 bits and 50%. σ_L and σ_{Pr} indicate the stable capability of confusion and diffusion of the algorithm. The results show that the proposed algorithm is resistant to statistical attacks.

4.5 Partial Pre-image Resistance (PPR)

Partial pre-image resistance or local one-wayness is the computational difficulty in retrieving the message partially, given that A knows a part of the message. The EITRH transformation preserves PPR property. Since the final digest is a hash of hashes, it is difficult for A to recover the message even partially. The no. of intermediate hashes at each level is n and thus, can never lead to discovery of the original message even partially.

4.6 Pseudorandom Oracle Preservation (PRO-Pr)

EITRH transformation is an inverted tree hash that is inspired by EMD transformation. EITRH, like EMD, uses two distinct initial vectors (IV). The second IV is used as an input while hashing the last block of each level. This leads to a high probability of the random oracle behaving independently at the last application. Since EMD is proven to be PRO-Pr [32], EITRH using the same principle is PRO-Pr.

5 Performance Evaluation

The sub-sections of this section present an evaluation of EITRH variants based on the performance metrics for a parallel program, namely *complexity*, *speedup*, *efficiency*, *cost optimality* and *iso-efficiency*, using some analytical tools [31].

5.1 Algorithm Complexity

For calculating the algorithmic complexity of EITRH, the following assumptions were made.

Suppose the complexity of calculating the hash value $H(M(i))$ for each message block $M(i)$ is $\text{Cmplx}(H(M(i)))$, and the no. of original blocks is b , then the computational complexity for standard CHF model can be given by Eq. (7).

$$b \cdot \text{Cmplx}(H(M(i))) \quad (7)$$

The first phase of EITRH on p processors, where $p \geq 1$ has the complexity,

$$\frac{b}{p} \cdot \text{Cmplx}(H(M(i))) \quad (8)$$

For the parallel reduction phase of EITRH, the no. of message blocks determines the no. of times $H(M(i))$ is called. After the first reduction, the remaining length of the message is $\frac{x}{y}$ of the length of the last message where x is the size of hash to be generated and y is the block size. x and y depend upon the variant of EITRH. Therefore, to achieve the x -bit hash value, $\lceil \log_{\frac{x}{y}} b \rceil$ recursive reductions are required and the no. of times it will be called, n_{call} , is calculated as follows:

$$\begin{aligned} n_{\text{call}} &= \left\lceil \left(\frac{x}{y}\right)^1 \cdot \frac{b}{p} \right\rceil + \left\lceil \left(\frac{x}{y}\right)^2 \cdot \frac{b}{p} \right\rceil \cdots + \left\lceil \left(\frac{x}{y}\right)^z \cdot \frac{b}{p} \right\rceil \\ &= \sum_{i=1}^z \left\lceil \left(\frac{x}{y}\right)^i \cdot \frac{b}{p} \right\rceil \end{aligned} \quad (9)$$

where

$$z = \lceil \log_{\frac{x}{y}} b \rceil, \quad \frac{x}{y} = \frac{\text{Hash Size}}{\text{Block Size}}$$

Now, the complexity for the complete reduction process is given by:

$$O(\text{rdc}) = n_{\text{call}} \cdot \text{Cmplx}(H(M(i))) \quad (10)$$

From Eqs. (8) and (10), the overall computational complexity $f(\text{rdc})$ of EITRH transformation is given as:

$$\begin{aligned}
 f(\text{rdc}) &= \frac{b}{p} \cdot \text{Cmplx}(H(M(i))) + n_{\text{call}} \cdot \text{Cmplx}(H(M(i))) \\
 &= \left(\frac{b}{p} + n_{\text{call}} \right) \cdot \text{Cmplx}(H(M(i)))
 \end{aligned}
 \tag{11}$$

Therefore, from Eqs. (7) and (11), it may be concluded that even though the no. of calculations required in EITRH transformation is more computations than that in the Merkle-Damgård (MD) construction, in terms of computational complexity EITRH is at par with MD construction.

5.2 Speedup

Suppose that the reference CHF model (SHA-1 in this case) is able to hash a message block $M(i)$ in the time $T(M(i))$, measured as the no. of elementary steps in the computation (provided each step is completed in constant time).

Thus, for b message blocks, time = $b \cdot T(M(i))$

Therefore, the sequential time can be given as:

$$T_s = b \cdot T(M(i)) = \Theta(b) \tag{12}$$

From Fig. 1, we know that the process of calculating hash using EITRH involves producing the intermediate hash of sub-blocks, concatenating these hashes and using recursion to determine the final hash value. The computation of the time complexity of EITRH on p processors, where $p \geq 1$ is done as follows:

Let $T(M(i))$ be the time required to hash i th block.

Let t_c be the constant time required for concatenating the intermediate hashes.

From Eq. (9), the no. of recursive calls (n_{call}) is calculated as:

$$\begin{aligned}
 n_{\text{call}} &= \left\lceil \left(\frac{x}{y} \right)^1 \cdot \frac{b}{p} \right\rceil + \left\lceil \left(\frac{x}{y} \right)^2 \cdot \frac{b}{p} \right\rceil \cdots + \left\lceil \left(\frac{x}{y} \right)^z \cdot \frac{b}{p} \right\rceil \\
 &= \sum_{i=1}^z \left\lceil \left(\frac{x}{y} \right)^i \cdot \frac{b}{p} \right\rceil
 \end{aligned}$$

where

$$z = \lceil \log_{\frac{x}{y}} b \rceil \quad \frac{x}{y} = \frac{\text{Hash Size}}{\text{Block Size}}$$

Time taken for reduction and recursive calls = $n_{\text{call}} \cdot T(M(i))$.

So, parallel time is given by:

$$\begin{aligned} T_p &= \frac{b}{p} \cdot T(M(i)) + n_{\text{call}} \cdot T(M(i)) + t_c \\ &= T(M(i)) \cdot \left(\frac{b}{p} + n_{\text{call}} \right) = \Theta\left(\frac{b}{p} + n_{\text{call}} \right) \end{aligned} \quad (13)$$

Based on the above results, total parallel overhead is given by:

$$T_o = p \cdot T_p - T_s \quad (14)$$

$$\begin{aligned} &= p \cdot T(M(i)) \cdot \left(\frac{b}{p} + n_{\text{call}} \right) - b \cdot T(M(i)) \\ &= p \cdot n_{\text{call}} \cdot T(M(i)) = \Theta(p \cdot n_{\text{call}}) \end{aligned} \quad (15)$$

Now, from Eqs. (12) and (13), speedup can be given as:

$$\begin{aligned} S(b) &= \frac{T_s}{T_p} = \frac{b}{\left(\frac{b}{p} + n_{\text{call}} \right)} = \frac{b}{b \cdot \left(\frac{1}{p} + \frac{n_{\text{call}}}{b} \right)} \\ &= \frac{1}{\left(\frac{1}{p} + \frac{n_{\text{call}}}{b} \right)} = \Theta\left(\frac{p}{1 + \frac{p}{b} \cdot n_{\text{call}}} \right) \end{aligned} \quad (16)$$

The speedup $S(b)$ (from Eq. (16)) is a function of both problem size b and the no. of processing cores p . The growth of $S(b)$ is sub-linear, with respect to b . Therefore, if b is increased, keeping p fixed, there is no significant increase in speedup, as observed in Fig. 3. However, there is a proportional increase in speedup, if both b and p are increased, as shown in Fig. 4.

5.3 Efficiency

Efficiency is an indicator of resource utilization. It is measured as the fraction of time for which the processor is usefully employed. Its value ($E(b)$) lies in the range $\frac{1}{b} \leq E(b) \leq 1$. The efficiency of the EITRH variant on p processors can be calculated as:

$$E(b) = \frac{\text{Speedup}}{\text{No. of processors}} = \frac{T_s}{p \cdot T_p}$$

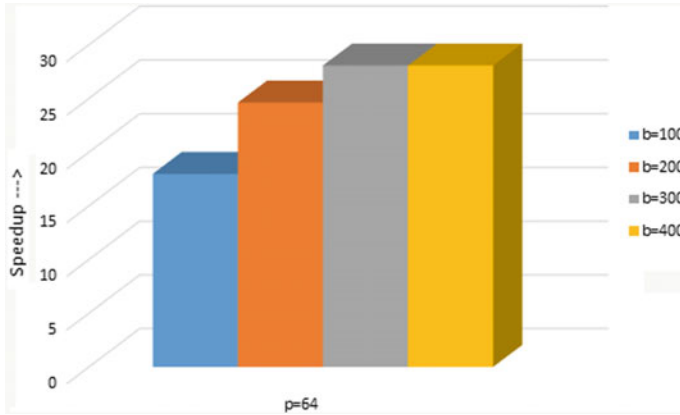


Fig. 3 Speedup versus file size (b): simulation results showing that speedup is almost constant (around 26) if b is increased, but the no. of cores (p) is kept fixed

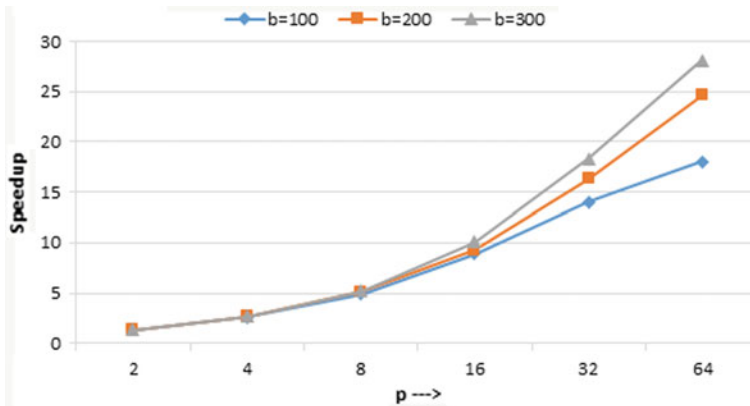


Fig. 4 Speedup versus the no. of processing elements (p) and problem size (b): simulation results showing that speedup increases if both b and the no. of p are increased proportionally

$E(b)$ can be expressed in terms of parallel overhead, as done in Eqs. (14) and (15):

$$E(b) = \frac{1}{1 + \frac{T_o}{T_s}} \quad \therefore \quad E(b) = \Theta\left(\frac{1}{1 + \frac{p \cdot n_{call}}{b}}\right) \tag{17}$$

Generally, $b \gg p$, so $\frac{p \cdot n_{call}}{b}$ and efficiency cannot be 1, due to the parallel overhead. From Eq. (17), it is evident that, unlike speedup, efficiency increases if the problem size is increased while keeping the no. of processing elements fixed. However, due to Amdahl’s law, the speedup tends to saturate and correspondingly the efficiency drops with the increase in p in the results shown in Figs. 4 and 5.

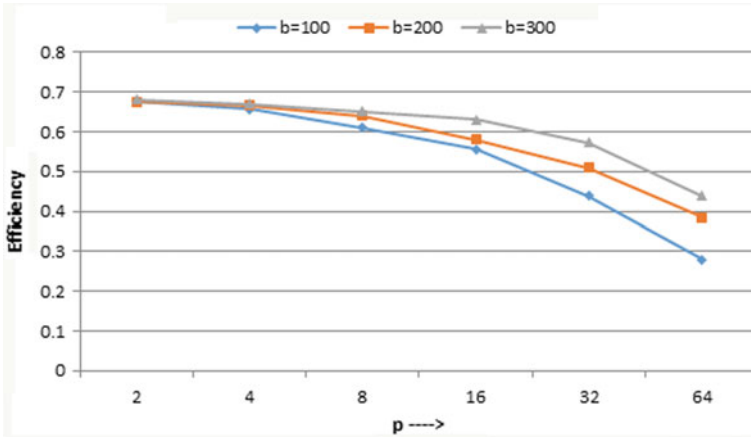


Fig. 5 Efficiency versus no. of processors (p) and problem size (b): simulation results showing that efficiency improves if b is increased by keeping p constant. The efficiency drops with increase in p

5.4 Cost Optimality

In parallel systems, cost optimality means that the cost of solving a problem, as a function of input size, has the same asymptotic growth as the fastest known sequential algorithm on a single core [34]. The cost of using EITRH framework for computing hash value is:

$$\begin{aligned}
 T_{\text{cost}} &= p \cdot T_p \\
 &= p \cdot \left(\frac{b}{p} + n_{\text{call}} \right) \\
 &= \Theta(b + p \cdot n_{\text{call}})
 \end{aligned} \tag{18}$$

From Eq. (18), it may be concluded that as long as the input size $b = \Omega(p \cdot n_{\text{call}})$, EITRH is cost optimal as the cost is $\Theta(b)$, which is the same as the cost for sequential algorithm (see Eq. (12)).

5.5 Minimum Execution Time

For a problem of a fixed size, increasing the no. of processing cores does not always lead to improvement in execution time of the program. Initially, it decreases asymptotically, till it reaches a minimum value. After achieving the minima, any further

increase in p leads to an increase in run-time. Therefore, the minimum parallel execution time T_p^{\min} , given by Eq. (19), can be calculated as follows:

$$\begin{aligned} \frac{d}{dp}T_p &= 0 \\ \frac{d}{dp}T_p &= \frac{d}{dp}\left(\frac{b}{p} + n_{\text{call}}\right) = \frac{b}{p^2}(-c) \end{aligned}$$

where c is constant.

$$\therefore b = p^2 \implies p = \sqrt{b}$$

Substituting $p = \sqrt{b}$ in Eq. (13), we get

$$T_p^{\min} = 2\sqrt{b} \tag{19}$$

5.6 Scalability

Scalability is defined as the ability of a parallel system to maintain its efficiency at a constant level, even as the size of the system is expanded by increasing, both, the problem size as well as the no. of processing elements. It is measured using an iso-efficiency function [34], defined as follows:

$$\text{Problem size } (W) = \frac{E}{1-E} \cdot T_o(T_s, p)$$

From Eq. (14), the parallel overhead function of EITRH is approximately $p \cdot n_{\text{call}}$. Therefore,

$$W = \frac{E}{1-E} \cdot p \cdot n_{\text{call}} \tag{20}$$

Using the asymptotic notation, the iso-efficiency for EITRH framework is $\Theta(p \cdot n_{\text{call}})$. This suggests that, if the no. of processors/cores is increased by a factor of $\frac{p'}{p}$ (p' being the increased no. of processors), then in order to achieve a gain in the speedup by the same factor, the problem size (b) should be correspondingly increased by a factor of $\frac{p' \cdot n'_{\text{call}}}{p \cdot n_{\text{call}}}$.

The discussion presented in this section evaluated the EITRH framework with respect to various metrics for parallel programs. The results suggest that EITRH framework is at par with its sequential counterparts in terms of scalability, efficiency as well as optimality with respect to costs.

6 Conclusion and Future Work

In this paper, a fast parallel recursive tree-based transformation, called EITRH, was proposed. It can be used to design parallel algorithms from their sequential counterparts. The proposed transformation combines the use of tree hashing and EMD construction. It has three recursive steps, viz. “message expansion,” “parallel reduction,” and “hash value generation.” The envelope of the transform, provided by the use of the second vector (IV_2), makes it suitable for both keyed and keyless CHF. Further, this paper proved that EITRH satisfies all the essential security properties for hash functions, namely PIR, WCR, CR, avalanche effect, PPR, and PRO-Pr, as discussed in the previous sections. This suggests that EITRH is a secure and flexible hash transformation that is multi-property preserving. Performance evaluation of the framework indicates its scalability for hashing long messages, implying potential application in digital forensics and parallelization of digital signatures. In the future, the theoretical results presented in this paper shall be confirmed by practical implementation of CHF based on EITRH transformation.

References

1. Stallings W (2006) *Cryptography and network security—principles and practice*, 4th edn. Prentice Hall, Upper Saddle River, NJ
2. National Institute of Standards and Technology (2015) FIPS PUB 180-4. Secure hash standard. Technical report
3. Kayser RF (2007) Announcing request for candidate algorithm nominations for a new cryptographic hash algorithm (SHA-3) family. Fed Reg 72(FR 62212):62212–62220
4. Wang X, Yin YL, Yu H (2005) Finding collisions in the full SHA-1. In: Shoup V (ed) *Advances in cryptology—CRYPTO 2005: 25th annual international cryptology conference*, Santa Barbara, CA, USA, 14–18 Aug 2005. Proceedings. Lecture notes in computer science, vol 3621. Springer, pp 17–36
5. Kishore N, Raina P (2019) Parallel cryptographic hashing: developments in the last 25 years. *Cryptologia* 43(6):504–535
6. Bosselaers A, Govaerts R, Vandewalle J (1996) Fast hashing on the Pentium. In: Koblitz N (ed) *Advances in cryptology—CRYPTO '96*, 16th annual international cryptology conference, Santa Barbara, CA, USA, 18–22 Aug 1996, proceedings. Lecture notes in computer science, vol 1109. Springer, pp 298–312
7. Bosselaers A, Govaerts R, Vandewalle J (1997) SHA: a design for parallel architectures? In: Fumy W (ed) *Advances in cryptology—EUROCRYPT '97*, international conference on the theory and application of cryptographic techniques, Konstanz, Germany, 11–15 May 1997, proceeding. Lecture notes in computer science, vol 1233. Springer, pp 348–362
8. Nakajima J, Matsui M (2002) Performance analysis and parallel implementation of dedicated hash functions. In: Knudsen LR (ed) *Advances in cryptology—EUROCRYPT 2002*, international conference on the theory and applications of cryptographic techniques, Amsterdam, The Netherlands, 28 Apr to 2 May 2002, proceedings. Lecture notes in computer science, vol 2332. Springer, pp 165–180
9. Khalil M, Nazrin M, Hau Y (2008) Implementation of SHA-2 hash function for a digital signature system-on-chip in FPGA. In: *International conference on electronic design, 2008. ICED 2008*. IEEE, pp 1–6

10. Li H, Miao C (2006) Hardware implementation of hash function SHA-512. In: First international conference on innovative computing, information and control (ICICIC 2006), Beijing, China, 30 Aug to 1 Sept 2006. IEEE Computer Society, pp 38–42
11. McEvoy RP, Crowe FM, Murphy CC, Marnane WP (2006) Optimisation of the SHA-2 family of hash functions on FPGAS. In: 2006 IEEE Computer Society annual symposium on VLSI (ISVLSI 2006), Karlsruhe, Germany, 2–3 Mar 2006. IEEE Computer Society, pp 317–322
12. Changxin L, Hongwei W, Shifeng C, Xiaochao L, Donghui G (2009) Efficient implementation for MD5-RC4 encryption using GPU with CUDA BT. In: 2009 3rd international conference on anti-counterfeiting, security, and identification in communication, ASID 2009, 20–22 Aug 2009. IEEE
13. Hu G, Ma J, Huang B (2009) High throughput implementation of MD5 algorithm on GPU. In: Proceedings of the 4th international conference on ubiquitous information technologies & applications, 2009. ICUT'09. IEEE, pp 1–5
14. Aumasson JP, Henzen L, Meier W, Phan RCW (2008) SHA-3 proposal Blake. Submission to NIST
15. Gauravaram P, Knudsen LR, Matusiewicz K, Mendel F, Rechberger C, Schläpfer M, Thomsen SS (2009) Grøstl—a SHA-3 candidate. In: Handschuh H, Lucks S, Preneel B, Rogaway P (eds) Symmetric cryptography, 11–16 Jan 2009. Dagstuhl seminar proceedings, vol 09031. Schloss Dagstuhl—Leibniz-Zentrum für Informatik, Germany
16. Rivest RL, Agre B, Bailey DV, Crutchfield C, Dodis Y, Fleming KE, Khan A, Krishnamurthy J, Lin Y, Reyzin L et al (2008) The MD6 hash function—a proposal to NIST for SHA-3. Submission to NIST
17. Atighehchi K, Enache A, Muntean T, Risterucci G (2010) An efficient parallel algorithm for skein hash functions. Cryptology ePrint Archive, Report 2010/432
18. Ferguson N, Lucks S, Schneier B, Whiting D, Bellare M, Kohno T, Callas J, Walker J (2010) The skein hash function family. Submission to NIST (round 3)
19. Bertoni G, Daemen J, Peeters M, Assche GV (2013) Keccak. In: Johansson T, Nguyen PQ (eds) Advances in cryptology—EUROCRYPT 2013, 32nd annual international conference on the theory and applications of cryptographic techniques, Athens, Greece, 26–30 May 2013. Proceedings. Lecture notes in computer science, vol 7881. Springer, pp 313–314
20. NIST selects winner of secure hash algorithm (SHA-3) competition. <https://www.nist.gov/news-events/news/2012/10/nist-selects-winner-secure-hash-algorithm-sha-3-competition>
21. Aumasson JP, Neves S, Wilcox-O’Hearn Z, Winnerlein C (2013) BLAKE2: simpler, smaller, fast as MD5. In: Jacobson MJ, Locasto ME, Mohassel P, Safavi-Naini R (eds) Applied cryptography and network security—11th international conference, ACNS 2013, Banff, AB, Canada, 25–28 Jun 2013. Proceedings. Lecture notes in computer science, vol 7954. Springer, pp 119–135
22. Dworkin MJ (2015) FIPS PUB 202- SHA-3 standard: permutation-based hash and extendable-output functions. Technical report, National Institute of Standards and Technology
23. Kelsey J (2016) SHA-3 derived functions: SHAKE, KMAC, TupleHash, and ParallelHash. Technical report, National Institute of Standards and Technology. NIST Special Publication
24. Aumasson JP, Henzen L, Meier W, Naya-Plasencia M (2013) Quark: a lightweight hash. J Cryptol 26(2):313–339
25. Bogdanov A, Knezevic M, Leander G, Toz D, Varici K, Verbauwhede I (2011) SPONGENT: a lightweight hash function. In: Preneel B, Takagi T (eds) Cryptographic hardware and embedded systems—CHES 2011—13th international workshop, Nara, Japan, 28 Sept to 1 Oct 2011. Proceedings. Lecture notes in computer science, vol 6917. Springer, pp 312–325
26. Cabral R, López J (2016) Fast software implementation of quark on a 32-bit architecture. In: Lightweight cryptography for security and privacy: 4th international workshop, LightSec 2015, Bochum, Germany, 10–11 Sept 2015. Revised selected papers, pp 115–130
27. Guo J, Peyrin T, Poschmann A (2011) The PHOTON family of lightweight hash functions. In: Rogaway P (ed) Advances in cryptology—CRYPTO 2011—31st annual cryptology conference, Santa Barbara, CA, USA, 14–18 Aug 2011. Proceedings. Lecture notes in computer science, vol 6841. Springer, pp 222–239

28. Atighehchi K (2016) Note on optimal trees for parallel hash functions. CoRR abs/1604.04206
29. Atighehchi K, Bonnacaze A (2016) Asymptotic analysis of plausible tree hash modes for SHA-3. Cryptology ePrint Archive, Report 2016/658
30. Bertoni G, Daemen J, Peeters M, Assche GV (2014) Sakura: a flexible coding for tree hashing. In: Boureanu I, Owesarski P, Vaudenay S (eds) Applied cryptography and network security—12th international conference, ACNS 2014, Lausanne, Switzerland, 10–13 Jun 2014. Proceedings. Lecture notes in computer science, vol 8479. Springer, pp 217–234
31. Kishore N, Kapoor B (2014) An efficient parallel algorithm for hash computation in security and forensics applications. In: Souvenir of the 2014 IEEE international advance computing conference, IACC 2014, pp 873–877
32. Bellare M, Ristenpart T (2006) Multi-property-preserving hash domain extension and the EMD transform. In: Lai X, Chen K (eds) Advances in cryptology—ASIACRYPT 2006, 12th international conference on the theory and application of cryptology and information security, Shanghai, China, 3–7 Dec 2006. Proceedings. Lecture notes in computer science, vol 4284. Springer, pp 299–314
33. Kishore N (2014) Parallel hashing algorithms for security and Forensic Applications. PhD thesis, Chitkara University School of Engineering and Technology, Chitkara University, Himachal Pradesh, India. <http://shodhganga.inflibnet.ac.in/handle/10603/46759>
34. Kumar V, Grama A, Gupta A, Karypis G (1994) Introduction to parallel computing. Benjamin/Cummings, Redwood City, CA

The Techniques of Vedic Mathematics for ECC Over Weierstrass Elliptic Curve

$$Y^2 = X^3 + Ax + B$$


Ankur Kumar, Pratik Gupta, and Manoj Kumar

Abstract An analysis is presented to the study, the proficient implementation of ancient mathematics formulae for multiplications and squares in the cryptographic system. In this approach, we have used ancient mathematics techniques and algorithms in the different projective coordinates system (Jacobian, Chudnovsky-Jacobian, Modified Jacobian coordinates system) to get minimum steps in the calculation of addition algorithm, doubling algorithm and for improving the speed of processing time in the operations of ECC (points addition, points doubling). The coding and synthesis are done in MATLAB for 16-bit digit multiplications and squares. The results proved that the Vedic mathematics-based scheme shows better performance compared to the conventional method and total delay in computation is reduced by Vedic mathematics Sutras (Urdhva-tiryagbhyam, Dvandva-yoga). The results of some AVIM techniques over ECC were obtained and discussed in the form of tables and graphs.

Keywords Cryptography · Elliptic curve · Jacobian coordinates · Chudnovsky-Jacobian · Modified Jacobian · Urdhva Tiryabhyam · Dvandva-yoga · Encryption · Decryption · Point doubling · Point addition

A. Kumar (✉) · M. Kumar
Gurukul Kangri University, Haridwar 249404, India
e-mail: ankurgkv99@gmail.com

M. Kumar
e-mail: sdmkg1@gmail.com

P. Gupta
The LNMIIT, Jaipur 302021, India
e-mail: pratikgupta1810@gmail.com

1 Introduction

In the field of cryptography, elliptic curves are studied for more than three decades. It is well known that the cryptosystem based on elliptic curves provides equal security even using smaller key size as compared to conventional cryptosystem like RSA, ElGamal, AES, etc.

Furthermore, they use lower power consumption and less memory resulting in a faster speed of executions. For cryptography purpose, elliptic curves were independently proposed by Miller and Koblitz [7]. Elliptic curves are comprehensively described by Weierstrass equation as [5]

$$E(x, y) : y^2 + \alpha_1xy + \alpha_3y = x^3 + \alpha_2x^2 + \alpha_4x + \alpha_5 \quad (1)$$

where $\alpha_1, \alpha_2, \alpha_3, \alpha_4, \alpha_5$ are the finite field and E (discriminates) are given below:

$$\Delta_1 = D_2D_8 - 8D_4 - 27D_6 + 9D_2D_4D_6$$

$$D_2 = \alpha_1 + 4\alpha_2$$

$$D_4 = 2\alpha_4 + \alpha_1\alpha_3$$

$$D_6 = \alpha_3 + 4\alpha_5$$

$$D_8 = \alpha_1\alpha_6 + 4\alpha_2\alpha_5 - \alpha_1\alpha_3\alpha_4 + \alpha_2\alpha_3 - \alpha_4$$

To simplified forms of Weierstrass Eq. (1) which are commonly used for cryptography purpose are given below [5]

$$y^2 = x^3 + ax + b, \quad (2)$$

$$y^2 + xy = x^3 + ax^2 + b \quad (3)$$

The curve (2) is implemented over the field of prime numbers for software applications, whereas curve (3) is implemented over the binary field for hardware applications. The points on elliptic curves are represented by the pairs (x, y) satisfying the elliptic curve Eq. (2).

In fact, the set

$$E = \{(x, y) : y^2 = x^3 + ax + b \pmod{p}\} \quad (4)$$

Represented all the points on an (EC) elliptic curve for a particular value of real numbers a, b and a particular value of a prime number p . The above representation (x, y) of the points on EC is generally termed as the affine coordinate system. Since the algebraic equation for the addition of points (discussed in next session) on elliptic curve consists inverse operation that is very expensive in term of computation time and memory; therefore, there became a need of another alternating coordinate system

which is substantially cheaper than the affine coordinate system. A most useful alternate operation for the (ACS) affine coordinate system is the (PCS) projective coordinate system [5].

Since modern technology growing from complexity toward efficiency, therefore, there is always a need for some efficient methods or techniques that make the existing devices easier and faster. As we mentioned in the previous paragraph that the advantages of ECC over conventional cryptosystem like RSA, including power consumption, higher speed, and smaller certificates that are specifically so useful for many applications of non-wireless or wireless connections.

The larger time-consuming arithmetic operations (point doubling and point addition) in ECC as exponentiation operations like multiplications, cubes, and squares take place in these operations.

This approach expresses proficient algorithms for cryptographic operations (point addition and points doubling) using algorithms for computation of multiplications, cubes, and squares of numbers from AIVM techniques of many operations. Generally, in cryptosystems, the algorithm of points doubling and points addition contains the number of cubes, squares, and multiplications. So for all these calculations, the computational time is too high; to resolve this problem, we have used Vedic mathematics techniques to reduce the computational time. With the help of Vedic mathematics techniques, we can increase the processing speed of operations (encryption and decryption) in ECC.

In the core work, we shall discuss ECC over the Jacobian projective coordinate system and we have used some Ancient Indian Vedic Mathematics techniques (AIVM) for reducing the steps in calculation and execution time of ECC operations. In conduct, ECC operations are found to be very complex and the most time-consuming operations [5].

In the current approach, we have used two techniques of AIVM (Urdhva-tiryagbhyam and Dvandra-yoga) to speed up the above-mentioned complex computations occurring in the projective coordinate system and Jacobian elliptic curve cryptography (JECC). Our result shows that JECC-based schemes give better performance compared to the conventional methods.

The selected projective coordinates system's algorithms were tested and coded by MATLAB tool. The objective of this approach is to reduce the computational and processing time of cryptographic operations using Ancient Indian Vedic Mathematics (AIVM) techniques. This approach increases the algorithms processing speed, decreases the area of chip circuits, achieves better efficiency in storage space, processing power, power consumption or bandwidth and the average of reducing time is 70% (appx.) less than conventional methods.

2 Literature Survey

In the last three decade Ancient Indian Vedic Mathematics (AIVM) branch of mathematics. These Sutras using so much in research across the world; it has a different

computational technique in the comparison of other computational techniques for solving any problem in mathematics. The AIVM techniques are used so well in the doubling and addition algorithm of JECC. A. Nanda and S. Behera well explained the AIVM techniques name is Urdhva Tiryakbhyam with the 8×8 bit Vedic Binary Multiplier and Dvandva-yoga for square any n digit number in 2014 [8]. These AIVM techniques are so useful in the doubling and addition as well as in the blocks of encryption and decryption of ECC.

In 2015, Ruchi Anchaliya and G.N Chiranjeevi proposed Dvandva-yoga Sutra for squaring of a number, Urdhva Tiryakbhyam Sutra for multiplication, Dhvajanka Sutra used for division [2]. This paper shows implementation in ECC by using Vedic multiplication of n digits number and squaring of a number in the algorithms of doubling and addition. This paper concludes that AIVM technique gives impressive output in the minimization of memory and time in the ECC operations and it helps to get speed in running time as compared to the implementation of conventional multiplication techniques. In 2017, K. N. Palata et. al. have described the implementation of encryption and decryption algorithms with the help of AIVM algorithms to improve performance of doubling of the points and addition of the points in ECC [9].

T. Abdurahmonov et al. described the elliptic curve exponentiation include in coordinate systems of ECC that coordinate systems will be implemented in the global smart card like digital signature and encryption in 2013 [1]. ECC has these kinds of the coordinate system (Modified Jacobian, Jacobian, Jacobian-Chudnovsky and Affine coordinate systems); they consist of a pair of points (point doubling, point addition). It has been observed that ECC and AIVM techniques are giving better result in running time, cost, and power than RSA and ElGamal cryptography. A cryptographic system is maximally applied in security and networking areas because ECC having small key size. It is using in many low storage memory devices. In the current decade, ECC is using because it gives reliability and security in the banking sector it makes more secure smart cards for credit and debit, also electronic tickets and personal registration cards identification documents. In the above references paper by the using of AIVM techniques and ECC's small key size, we get the best output in faster execution time in this cryptographic system [4–6, 10, 12].

3 Background of Elliptic Curve Cryptography

3.1 Encryption System [3, 11]

A cryptographic system or encryption system can be characterized by the tuple $(C, P, K, E, \text{ and } D)$ with these five axioms.

- The elements of the set K (Keyspace) are termed as Keys.
- The set $E = \{E_k : k \in K\}$ has functions $E_k : P \rightarrow C$ and all the members of E is termed as encryption functions.

- The members of the set C (Ciphertext space) are termed as Ciphertext.
- The members of the set P (Plaintext space) are termed as Plaintext.
- The set $D = \{D_k : k \in K\}$ has functions $D_k : C \rightarrow P$ and all the members of D is termed as decryption functions. For each, $e \in K$, there is $d \in K$, such that $D_d(E_e(p)) = p$ for all $p \in P$.

3.2 Properties of Elliptic Curve

See Figs. 1 and 2.

- $P + O = O + P$ (Property of additive identity) where $P \in E(F_p)$
- $(x, y) + (x, -y) = O$ (Property of additive inverse) where $(x, y) \in E(F_p)$

Fig. 1 $(P + Q)$ point addition

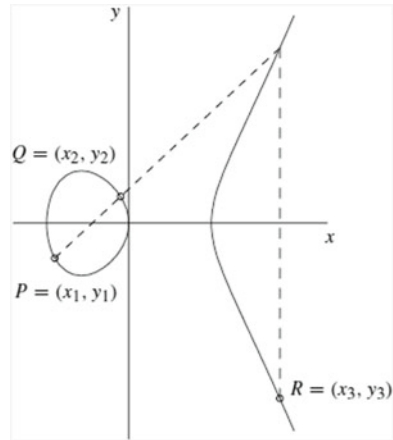
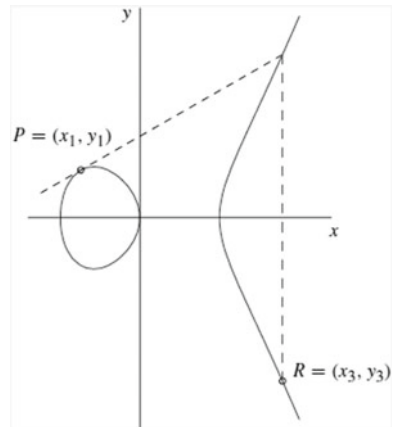


Fig. 2 $(2P = R)$ point doubling



- For Addition, $P(x_1, y_1) + Q(x_2, y_2) = R(x_3, y_3)$ where

$$\begin{aligned} \text{value of } x_3 &= (\lambda^2 - x_1 - x_2), \\ \text{value of } y_3 &= (\lambda(x_1 - x_3) - y_1), \\ \text{and value of } \lambda &= (y_2 - y_1)/(x_2 - x_1) \end{aligned}$$

- For doubling,

$$\begin{aligned} P(x_1y_1) + P(x_1y_1) &= 2P(x_1y_1) \\ &= R(x_3y_3) \end{aligned}$$

where

$$\begin{aligned} \text{value of } x_3 &= (\lambda^2 - 2x), \\ \text{value of } y_3 &= (\lambda(x - x_1) - y), \\ \text{value of and } \lambda &= (3x^2 + a)/2y. \end{aligned}$$

4 Ancient Indian Vedic Mathematics (AIVM)

In this part of AIVM, we will deliberate about some useful and efficient techniques (Dvandva-yoga and Urdhva-tiryagbhyam) of Ancient Indian Vedic Mathematics which will be used in a later section to improve the performance of cryptographic operations [13].

4.1 Urdhva-tiryagbhyam

Urdhva-tiryagbhyam has expressed as “urdhva” means “vertically” and tiragbhyam means “crosswise”. The steps and examples of Urdhava-tiryagbhyam technique are shown below [13] (Fig. 3).

Example 1 Evaluate the multiplication of 5498×2314 by Urdhva-tiragbhyam

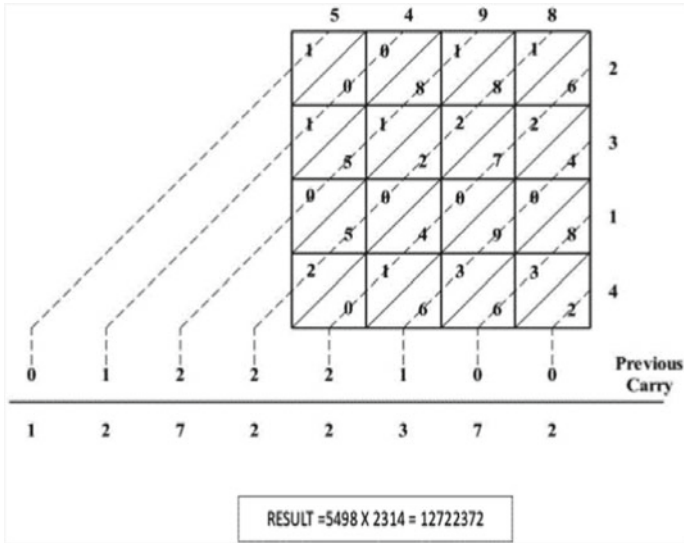


Fig. 3 Multiplication of 5498 × 2314 by Urdhva-tiragbhyam technique

4.2 Dvandva-yoga Sutra

This is also an ancient technique of mathematics for squaring a digit and its results give the best output in all branches of mathematics. This sutra is used to get square of any binary or decimal number [13].

Example 2 Evaluate the square of the number 234 by Dvandva-yoga technique.

$D_y(4)$	$D_y(34)$	$D_y(234)$	$D_y(23)$	$D_y(2)$
4^2	$2(3 \times 4)$	$2(2 \times 4) + 3^2$	$2(2 \times 3)$	2^2
16	24	25	12	4
4	12	25	24	16
$4+1$	$2+2$	$5+2$	$4+1$	6
5	4	7	5	6
Answer is 54756.				

5 Elliptic Curve Cryptosystem Using Urdhva-triyabhyam and Dvanda-yoga Technique and Algorithm

This section describes a few imperative calculations of ECC (Elliptic Curve Cryptography) using some effective algorithm and techniques of Ancient Mathematics.

Over a field F_p having finite elements, the term $E(F_p)$ elliptic curve is explained by

$E = \{(x \text{ and } y) : (y^2 = x^3 + ax + b) \bmod p \text{ and } 4a^3 + 27b^2 \neq 0\} \cup \{O\}$ In this cryptosystem's calculation, Urdhva-tiryagbhyam and Dvanda-yoga technique can be applied in λ^2 and $\lambda(x_1 - x_3)$.

For the addition of two points (P, Q) on the elliptic curve and doubling of a point (P) explain by:

if value of $P = (x_1, y_1)$

and value of $Q = (x_2, y_2)$

Case 1 $P \neq Q$, then $R(x_3, y_3) = P(x_1, y_1) + Q(x_2, y_2)$

where

$$x_3 = \lambda^2 - x_1 - x_2,$$

$$y_3 = \lambda(x_1 - x_3) - y_1$$

$$\text{and } \lambda = \frac{(y_2 - y_1)}{(x_2 - x_1)}$$

Doubling of a point can be explained as:

If $P = Q$ then the doubling of a point $P = (x, y)$ is

$$R(x_3, y_3) = P(x_1, y_1) + P(x_1, y_1)$$

where

$$x_3 = \lambda^2 - 2x,$$

$$y_3 = \lambda(x - x_1) - y,$$

$$\text{and } \lambda = \frac{(3x^2 + a)}{2y}$$

By the using of Urdhva-tiryagbhyam and Dvanda-yoga technique, we can get the values of the terms λ^2 , $\lambda(x - x_1)$ and $3x^2$.

6 Background of Coordinate System for ECC [5]

The elliptic curve (EC) contains a pair of coordinate systems first is affine and other is projective. For inversion, the affine coordinate system has needed the inversion at the time of doubling and addition of the points, which are so expensive in terms of time, area and speed. We have used the projective plane or coordinate system to remove very demanding operating inversion operation [14, 15]. For better performance in cryptosystem we can be applied Standard projective coordinates, Jacobean projective coordinates, Chudnovsky coordinates all these various coordinate systems in cryptography.

The affine plane $A_F^2 = \{(x, y) \in F \times F\}$ for coordinates (x, y) is mapped to the projective plan $P_F^3 = (X, Y, Z)$ these coordinates belongs to $F \times F \times F$.

The coordinates (x, y) of the affine plane $A_F^2 = \{(x, y) \in F \times F\}$ are mapped to the coordinates (X, Y, Z) of the projective plane $P_F^3 = \{(X, Y, Z) \in F \times F \times F\}$ with this rule [13]: $(X, Y, Z) = (x \cdot Z^c, y \cdot Z^d, 1)$ or $X = x \cdot Z^c, Y = y \cdot Z^d$.

$A_F^2 = \{(x, y) \in F \times F\}$ (The Affine plane) with (x, y) coordinate which is mapped to the $P_F^3 = (X, Y, Z)$ (The projective plan) with (X, Y, Z) coordinate. The mapping will be explained by [5]:

$$P_F^3 = \{(X, Y, Z) \in F \times F \times F\}$$

$$(X, Y, Z) = (x \cdot Z^c, y \cdot Z^d, 1) \text{ or } x = X/Z^c \text{ and } y = Y/Z^d$$

6.1 The Jacobian Coordinate System (JCS)

If we take the values of $c = 2$, and $d = 3$ respectively then we get the Jacobian projective coordinate system.

For the JCS the elliptic curve (EC) E can be express as:

$$E : Y^2 = X^3 + aXZ^4 + bZ^6.$$

Addition of points: If we have the value of point $P_1 = (X_1, Y_1, Z_1)$ and point $P_2 = (X_2, Y_2, Z_2)$ which are distinct on the projective plane. Then the point $P_3 (X_3, Y_3, Z_3)$ is termed addition of points.

$$P_3 = P_1 + P_2 = (X_3, Y_3, Z_3)$$

where

$$X_3 = (Y_2Z_1^3 - Y_1Z_2^3)^2 - (X_2Z_1^2 - X_1Z_2^2)^2(X_1Z_2^2 + X_2Z_1^2)$$

$$Y_3 = (X_2Z_1^2 - X_1Z_2^2)^2(Y_2Z_1^3 - Y_1Z_2^3)(2X_1Z_2^2 + X_2Z_1^2)$$

$$- Y_1 Z_2^3 (X_2 Z_1^2 - X_1 Z_2^2)^3 - (Y_2 Z_1^3 - Y_1 Z_2^3)^3$$

$$\text{and } Z_3 = (X_2 Z_1^2 - X_1 Z_2^2) Z_2 Z_1$$

Doubling of Point: If we have the value of point $P_1 = (X_1, Y_1, Z_1)$ and point $P_1 = (X_1, Y_1, Z_1)$ which are same on the projective plane. Then the point $P_3(X_3, Y_3, Z_3) = P_1 + P_1 = 2P_1$ is termed as point doubling.

$$X_3 = (3X_1^2 + aZ_1^4)^2 - 8X_1Y_1^2$$

$$Y_3 = 12X_1Y_1^2(3X_1^2 + aZ_1^4) - (3X_1^2 + aZ_1^4)^3 - 8Y_1^4 \text{ and}$$

$$Z_3 = 2Z_1Y_1$$

6.2 Algorithm for Jacobian Projective Plane Using Urdhva and Dvanda Technique

Addition of two points: Let $P_1 = (X_1, Y_1, Z_1)$ and $P_2 = (X_2, Y_2, Z_2)$, we can apply the following calculation to get $P_3(X_3, Y_3, Z_3)(P_3 = 2P_1)$.

Algorithm

Input: Value of P_1 point = (X_1, Y_1, Z_1) , and $P_2 = (X_2, Y_2, Z_2)$

Output: Value of P_3 point = $(X_3, Y_3, Z_3) = P_1 + P_2$. $A = Z_1^2$

2. $B = Z_1 \cdot A$

3. $C = Y_2 \cdot B$

4. $D = Z_2^2$

5. $E = Z_2 \cdot D$

6. $F = Y_1 \cdot E$

7. $G = C - F$

8. $H = X_1 \cdot D$

9. $I = X_2 \cdot A$

10. $J = I + H$

11. $K = I - H$

12. $L = 2H + I$

13. $X_3 = G^2 - J \cdot K^2$

14. $Y_3 = K^2 \cdot (G \cdot L - F \cdot K) - G^3$

15. $Z_3 = Z_1 \cdot Z_2 \cdot K$

16. **Return** $(X_3 : Y_3 : Z_3)$.

In this algorithm, we can get the value of

$$P_3 = (X_3, Y_3, Z_3) = P_1 + P_2$$

where

$$X_3 = G^2 - J \cdot K^2, Y_3 = K^2 \cdot (G \cdot L - F \cdot K) - G^3, \text{ and } Z_3 = Z_1 \cdot Z_2 \cdot K$$

using Urdhva-tiryagbhyam technique for multiplying and Dvandwa-yoga technique for squaring.

Doubling of a point: Let a point $P_1 = (X_1, Y_1, Z_1)$ we use the following calculation to get

$$P_3(X_3, Y_3, Z_3) = 2P_1(X_1, Y_1, Z_1)$$

Algorithm

Input : Value of P_1 point = (X_1, Y_1, Z_1) , and 'a'

Output : Value of P_3 point = $(X_3, Y_3, Z_3) = 2P_1$

1. $A = Y_1^2$
2. $B = 4X_1 \cdot A$
3. $C = 8A^2$
4. $D = 3X_1^2 + a \cdot Z_1^4$
5. $X_3 = D^2 - 2B$
6. $Y_3 = D \cdot (3B - D^2) - C$
7. $Z_3 = 2Y_1 \cdot Z_1$
8. Return $(X : Y_3 : Z_3)$

In this algorithm, we can get the value of

$$P_3 = (X_3, Y_3, Z_3) = 2P_1$$

where

$$X_3 = D^2 - 2B, Y_3 = D \cdot (3B - D^2) - C, Z_3 = 2Y_1 \cdot Z_1$$

using Urdhva-tiryagbhyam technique for multiplying and Dvandwa-yoga technique for squaring.

6.3 The Chudnovsky-Jacobian Coordinate System

The Chudnovsky-Jacobian coordinate systems are based on Jacobian coordinates system it is formula is the same for these coordinate systems. In the Jacobian coordinate system, we observed that doubling is faster because the number of square and multiplication operations is less than the Chudnovsky-Jacobian coordinate systems and its addition is slower because the number of operations is one or more extra. For improving and fast result in the addition we fixed a Jacobian point Z_1^3 in P_1 without any loss in the elliptic curve. In its addition of two-point, we reduced one square and one multiplication which makes an addition faster than Jacobian coordinate system and doubling of a point one multiplication operation increased which is described in results analysis Tables 1 and 2.

Addition of two points: The point Value of

$$P_1 = (X_1, Y_1, Z_1, Z_1^2, Z_1^3) \text{ and } P_2 = (X_2, Y_2, Z_2, Z_2^2, Z_2^3)$$

Then the sum of these values is $P_1 + P_2 = P_3 = (X_3, Y_3, Z_3, Z_3^2, Z_3^3)$.

The Chudnovsky-Jacobian coordinate system coordinates' addition of two points is the same as Jacobian coordinate system's addition of two points where $X_3 = G^2 - J \cdot K^2$, $Y_3 = K^2 \cdot (G \cdot L - F \cdot K) - G^3$, and $Z_3 = Z_1 \cdot Z_2 \cdot K$ but these $Z_3^2 = Z_3^2$, $Z_3^3 = Z_3^3$ equations are different. Therefore, these B, C, E, F, G , and K remain the same as Jacobian coordinate systems.

The point doubling of a point $P_1 = (X_1, Y_1, Z_1, Z_1^2, Z_1^3)$, is

$$P_3 = P_1 + P_1 = 2P_1 = (X_3, Y_3, Z_3, Z_3^2, Z_3^3).$$

Table 1 No. of operation required for point addition and point doubling in projective coordinate system of JECC with the conventional method

Point coordinate	The points addition						The points doubling					
	Mult.	Squ.	Cub.	P4	P5	Tot.	Mult.	Squ.	Cub.	P4	P5	Tot.
Jacobian	25	15	9	0	0	49	4	6	1	4	0	15
Chudnovsky-Jacobian	24	14	9	0	0	47	5	6	1	4	0	16
Modified Jacobian	26	16	9	0	0	51	4	5	1	4	0	14

Table 2 Number of operation required in projective coordinate system of JECC with the algorithm of AIVM

Point coordinate system	The POINTS addition						The points doubling					
	Mult.	Squ.	Cub.	P4	P5	Tot.	Mult.	Squ.	Cub.	P4	P5	Tot.
Jacobian	12	4	1	0	0	17	3	4	0	1	0	08
Chudnovsky-Jacobian	11	3	1	0	0	15	4	4	0	1	0	09
Modified Jacobian	13	6	1	0	0	20	3	3	0	1	0	07

Doubling of a point: The Chudnovsky-Jacobian coordinate systems's doubling of a point same as the Jacobian coordinate system's doubling of a point

$$\begin{aligned} \text{value of } X_3 &= D^2 - 2B, \\ \text{value of } Y_3 &= D \cdot (B - X_3) - C, \\ \text{and value of } Z_3 &= 2Y_1 \cdot Z_1 \end{aligned}$$

but these two equations $Z_3^2 = Z_3^2$, $Z_3^3 = Z_3^3$ are different from the Jacobian coordinate system. Therefore, these B , C , E , F , G , and K remain the same as Jacobian coordinate systems.

6.4 Modified Jacobian Coordinate System

The Modified Jacobian coordinate systems are based on Jacobian coordinates system; it is used to get more speed in doublings comparatively Jacobian projective and Chudnovsky-Jacobian projective system. For addition p and Q , the formula is the same as Jacobian coordinate systems but in the doubling of a point, it has little bit different formula. In Modified Jacobian coordinate system, we observed that doubling is faster because the number of all operation is extra than the Jacobian and Chudnovsky-Jacobian coordinate systems and addition is slowest. For improving and fast result in the doubling, we fixed a Jacobian point aZ_1^3 in P_1 without any loss in the elliptic curve. In the doubling, we reduced two square and one multiplication operations which make a doubling faster than Jacobian coordinate, Chudnovsky-Jacobian coordinate systems which are described in the analyses of the results Tables 1 and 2.

Addition of two points: The value of the point $P_1 = (X_1, Y_1, Z_1, aZ_1^4)$ and $P_2 = (X_2, Y_2, Z_2, aZ_2^4)$ then the addition is $P_3 = P_1 + P_2 = (X_3, Y_3, Z_3, aZ_3^4)$.

The addition of two points in Modified Jacobian coordinates systems in addition of two points is the same as the Jacobian coordinate system's addition of two points, where $X_3 = G^2 - J \cdot K^2$, $Y_3 = K^2 \cdot (G \cdot L - F \cdot K) - G^3$, and $Z_3 = Z_1 \cdot Z_2 \cdot K$ but this one $aZ_3^4 = aZ_3^4$ equation is different. Therefore, these B , C , E , F , G , and K remain the same as Jacobian coordinate systems.

Doubling of a point: The doubling of a point $P_1 = (X_1, Y_1, Z_1, aZ_1^4)$ is

$$P_3 = P_1 + P_1 = 2P_1 = (X_3, Y_3, Z_3, aZ_3^4).$$

The Modified Jacobian coordinates' doubling where

$$\begin{aligned} \text{value of } X_3 &= D^2 - 2B, \\ \text{value of } Y_3 &= D \cdot (B - X_3) - C, \\ \text{and value of } Z_3 &= 2Y_1 \cdot Z_1 \end{aligned}$$

Table 3 Synthesis results for cryptographic operations

16 bits running time	Running time processed using conventional methods	Running time processed using Vedic mathematics sutras	Average of reducing time
Point addition	0.010880 (s) app.	0.0020300 (s) app.	80.00% (app.)
Point doubling	0.011010 (s) app.	0.0024800 (s) app.	75.00% (app.)

Table 4 Synthesis results for cryptographic operations

8 bits running time	Running time processed using conventional methods	Running time processed using Vedic mathematics sutras	Average of reducing time (%)
Point addition	0.01109 app. (s)	0.0025012 app. (s)	77.2803
Point doubling	0.01048 app. (s)	0.0030219 app. (s)	71.1643

but these equations $aZ_3^4 = 2C(aZ_1^4)$ are different from the Jacobian coordinate system. Therefore, these $B, C, E, F, G,$ and K remain the same as Jacobian coordinate systems.

7 Results Analysis and Comparison

The comparison is between ECC and VECC which are containing multiplications, square, cube and fourth power in cryptographic operations (like as point doubling and addition). Tables 1 and 2 showing the comparison of all arithmetic operations and Table 2 shows the minimum number of arithmetic operations comparatively Table 2 of Jacobian Elliptic Curve Cryptography (JECC) based on AVIM algorithms. In Table 3, we observed that running time process using Vedic mathematics takes 70% (app.) less time than running time process using conventional methods for four bits, eight bits, and sixteen bits (Table 4).

8 Conclusion

The speed of cryptographic operations such as encryption, decryption, point addition and doubling is found to be quicker in term of running time. The work well displays the enhanced performance of AIVM-based ECC, in the term of the small size of the key, minimum time to develop the key and the full time which is required in processing. To be achieved better efficiency in storage space, processing power, power consumption or bandwidth are studied in the large scale.

Various Ancient Indian Vedic Mathematics sutras discussed above have been implemented in MATLAB and are synthesized and simulated using MATLAB. The

code is written for the square of the 16-bit and 8-bit binary number, multiplication of the 16-bit and 8-bit binary numbers. For cryptographic operations using Vedic mathematics, the average of reducing time is 70% (appx.) less than conventional methods.

References

1. Abdurahmonov T, Yeoh T, Hussain HM (2013) A proposed implementation of elliptic curve exponentiation over prime field in the global smart cards. *Int J Inf Electron Eng* 3(1)
2. Anchaliya R, Chiranjeevi NG, Kulkarni S (2015) Efficient computing techniques using Vedic mathematics sutras. *Int J Innov Res Electr Electron Instrum Control Eng* 3(5):24–27
3. Diffie W, Hellman M (1976) New directions in cryptography. *IEEE Trans Inf Theor* 22(6):644–654
4. Gutub AAA (2010) Remodeling of elliptic curve cryptography scalar multiplication architecture using parallel Jacobian coordinate system. *Int J Comput Sci Secur* 4(4):409–425
5. Hankerson D, Menezes JA, Vanstone S (2004) *Guide to elliptic curve cryptography*. Springer, Germany
6. Kan he A, Das SK, Singh AK (2012) Design and implementation of low power multiplier using Vedic multiplication technique. *Int J Comput Sci Commun* 3(1):131–132
7. Koblitz (1987) Elliptic curve cryptosystem. *J Math Comput* 48(177):203–209
8. Nanda A, Behera S (2014) Design and implementation of Urdhva-Tiryakbhyam based fast 8.8 Vedic binary multiplier. *Int J Eng Res Technol* 3(3):1856–1859
9. Palata KN, Nadar VK, Jethawa JS, Surwadkar TJ, Deshmukh RS (2017) Implementation of an efficient multiplier based on Vedic mathematics. *Int Res J Eng Technol* 4(4):494–497
10. Pawar A, Sahu AK, Sinha GR (2014) Implementation of high-speed Vedic multiplier. *Int J Innov Res Adv Eng* 1(10):396–401
11. Stallings W (2003) *Cryptography and network security: principals and practices*. Prentice Hall, India
12. Thapliyal H, Arbania HR (2004) A time-area-power efficient multiplier and square architecture based on ancient Indian Vedic mathematics. In: *Proceedings of the 2004 international conference on VLSI (VLSI'04)*, Las Vegas, Nevada, pp 434–439
13. Tirthaji JSSBK (1986) *Vedic mathematics or sixteen simple sutras from Vedas*. Motilal Bhandaridas Varanasi India

EEHCR: Energy-Efficient Hierarchical Cluster-Based Routing Protocol for Wireless Sensor Networks



Sakshiwala and M. P. Singh

Abstract This paper proposes a new energy-efficient hierarchical cluster-based routing protocol (EEHCR). It assures for inter-cluster communication between cluster head to cluster head toward the base station irrespective of the deployment strategy. The proposed protocol works in two phases, namely cluster-formation phase and hierarchy-formation phase. Intra-cluster communication may take place between either member to cluster head directly or member to cluster head indirectly, through proxy cluster head. Depending on the deployment of sensor nodes, inter-cluster communications between clusters may take place in either of four ways: (i) cluster head to cluster head or (ii) cluster head to a member or (iii) member to cluster head or (iv) member to member, during the formation of hierarchy. The proposed protocol provides a solution for all four cases of inter-cluster communication in order to implement the proposed network model. The EEHCR is implemented in OMNeT++ network simulator. The result is compared with TL-LEACH and MR-LEACH hierarchical routing protocols. Simulation results demonstrate that the proposed protocol is effective in prolonging the network lifetime.

Keywords WSN · Clustering · Hierarchy · Routing · Network connectivity

1 Introduction

Wireless sensor network (WSN) consists of resource constraint tiny sensor nodes (SNs) [1, 2]. In most of the scenarios, SNs are deployed in the hostile and unreachable area for human beings in order to minutely observe various phenomenon and activities of the environment [2]. It has diverse applications in various fields ranging from small to a large area or sparse to dense deployment or dynamic and static deployment [3].

Sakshiwala (✉) · M. P. Singh
National Institute of Technology, Ashok Rajpath, Mahendru, Patna, Bihar 800005, India
e-mail: sakshi37sonal@gmail.com

M. P. Singh
e-mail: mpps@nitp.ac.in

For longer network lifetime, there is a need to save the battery power of SNs irrespective of deployment strategy [4]. There are many routing protocols based on clustering which claim for energy efficiency to maximize network lifetime [5]. In clustering, WSN is logically divided into groups known as clusters. Each cluster consists of one cluster head (CH) and one or more member nodes (MNs). Election of CHs may be decided by MNs in collaboration (communication) or by doing computations [6]. The computation may save energy in comparison to communications [6].

A CH may save energy either by data aggregation to avoid redundant data transmission and reduce congestion [7] or by reducing delay latency in the packet transmission or by load balancing [8]. Hence, clustering in WSN is still the topic of research in WSN [9].

This paper presents a hierarchical clustering multi-hop communication approach which tries to (i) cover the target area by means of connectivity of clusters by inter-cluster and intra-cluster communications in the WSN (ii) prolong the network lifetime.

The organization of this paper is as follows: Section 2 presents the related work. Section 3 presents the proposed problem and solution. Section 4 analyses the simulation results. Section 5 concludes the paper.

2 Related Work

This section presents related work on cluster-based routing protocols in WSN.

LEACH [10] declares CH based on the threshold value. CH election may have high message overhead which may consume extra energy. In LEACH, CHs may consume more energy compared to the other nodes of the cluster as CHs do single-hop communication with the base station (BS).

TL-LEACH [11] is similar to LEACH with the two-level hierarchy of CHs. The nodes send their data toward BS through secondary CHs and then primary CHs. The two-hop communication in TL-LEACH effectively reduces the total energy usage. A secondary CH has to be in transmission range to a primary CH and a primary CH has to be in communication range to the BS. Then, it assures for successful delivery of data to the BS.

LEACH-C [12] is a centralized clustering algorithm where each node sends information about its location and residual energy to sink. For this, it needs GPS or other tracking methods.

HEED [13] forms clusters and CHs based on two parameters, namely residual energy and cluster density. HEED may take several iterations to form clusters which increase the number of packets exchanged. EG LEACH [8] is the same as LEACH which uses improved threshold condition to consider residual energy into account. It ensures proper selection of CHs in every round.

TEEN [14] is a hierarchical clustering reactive protocol which is based on LEACH protocol for CH selection and cluster formation. APTEEN [15] is the advancement

of TEEN protocol; BS forms the cluster which exists for an interval called cluster period. BS has the power to transmit directly to all the nodes in the network.

EECS [16] uses hop communication between CH and BS which may result in longer delay ratio. In UCBR [17], BS through informer nodes knows the location and initial energy of all SNs based on which it decides the radius and CH sequence table for every cluster. A node determines its CH on the basis of received signal strength of advertisement message from CHs. CHs use location-based multi-hop communication to forward data to BS.

In PEGASIS [18], all nodes form a single-chain structure where a single node takes a turn to transmit data to the BS. Data from nodes is to be transmitted to the nearest neighbor node saving larger transmission energy cost. Load on the cluster member which is closer to CH increases due to the chain. CCS [19] is a modification of PEGASIS protocol where the whole network is divided into co-centric circular tracks called clusters. The members of a cluster form a single-chain structure choosing one of them as the head node. BS forms level-wise hierarchy. Data redundancy exists in CCS because data from a node which is far away from its CH has to travel a large distance in order to reach its CH.

TSC [20] is a hierarchical clustering based on the concept of tracks and sectors. It breaks long chain formed in a single track of CCS into sectors, where each sector now represents clusters that are a level may have more than one clusters. In [21], the chain of PEGASIS protocol is logically divided into a layered transmission node tree.

Authors [22] summarize different routing protocols based on clustering of WSNs during the year 2000 to 2016. Authors [7] present existing hierarchical-based routing protocols during the year 2000 to 2004. It concludes that the hierarchical routing helps in declining the number of redundant messages transmitted to the BS.

Clustering hierarchy protocol based on PSO algorithm [23] is a centralized approach in which BS uses location, residual energy, relay nodes to form clusters and CHs. To reduce the transmission energy cost of CHs, relay nodes are used. CHs send their data to relay nodes which forwards data to BS.

EECP-EI [24] is a multi-level protocol. Selection of CHs and formation of clusters are based on the energy of sensor nodes. The minimum transmission range is set for all nodes in order to form a hierarchy. The CHs are supposed to lie at a minimum distance of ten meters from destination CH.

Authors [25] present a review on recent clustering solution based on machine learning techniques. Concepts like fuzzy logic, swarm intelligence, etc., are used to form clusters. In some of these protocols like ABC-SD, PSO-ECHS, PSO-C, etc., BS use location information of nodes in order to form clusters.

The above protocols do not guarantee connectivity among CHs as there may be a possibility of selection of CHs which may not be in the direct communication range of any other CH in the network. This may happen when the cluster formation is not centralized. In such a case, the formation of the hierarchy is not possible. This paper proposes a solution to establish intra-cluster and inter-cluster communications in the hierarchy.

3 Proposed Problem and Solution

3.1 Proposed Problem

Single-hop communication between CHs and BS is suitable in small-target areas. In large-target areas, BS may use location data of SNs to build hierarchy among CHs. It may not be possible to form hierarchy among CHs when clusters are formed independently or clusters are formed based on local information. Some routing protocols form a multi-hop communication hierarchy from BS, but they fail to describe how the hierarchy will be formed when a CH is not in direct communication range of any other CH in the network. This situation may result in the non-transmission of data toward BS. This paper proposes an algorithm to solve these issues unless a hole is present in the network during deployment itself.

3.2 Network Model

Figure 1 presents the network model of the proposed algorithm. The network model is based on multi-hop hierarchical clustering approach. Communication between the CHs to the BS can be in single or multiple hops. Member nodes communicate to their CH directly or by way of proxy CH.

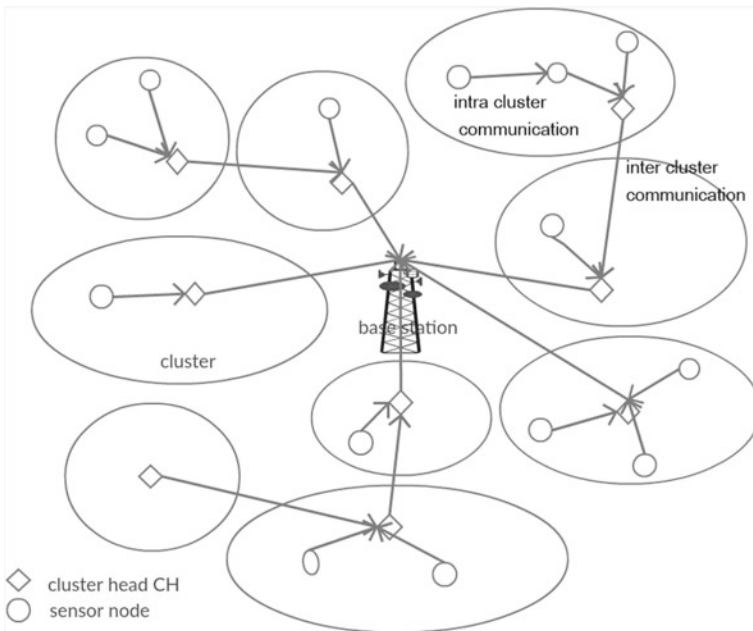


Fig. 1 Proposed network model

3.3 Assumptions

- (i) SNs are static.
- (ii) Every SN has a unique ID.
- (iii) Single BS is inside the network.

3.4 Proposed Algorithm

1. Cluster-formation phase (modified version [6])
2. Hierarchy-formation phase
 - (a) Case 1: Hierarchy formation between CHs if they are in communication range of each other.
 - (b) Case 2: Hierarchy formation between CH (already joined in the hierarchy) and a MN of another cluster whose CH is not in communication range to any already joined CH in the hierarchy.
 - (c) Case 3: Hierarchy formation between a MN (whose CH has already joined hierarchy) and CH which has not joined hierarchy.
 - (d) Case 4: Hierarchy formation between a MN (whose CH has already joined hierarchy) and a MN whose CH has not joined hierarchy.
3. If a cluster is not able to join the hierarchy by above four cases of hierarchy formation, then it is a hole in the network.
4. The algorithm terminates, after all, CHs have either joined hierarchy or is declared as a hole.

3.5 Explanation of the Proposed Algorithm

Cluster-Formation Phase The proposed algorithm chooses CH based on computation [6]. Figure 2 describes the cluster-formation phase of the proposed algorithm. Every node randomly takes a value 0 or 1 for variable p . If $p = 0$, then the node generates a random value x .

Now *holdback* value will be x th random value. *holdback* value restricts SN to either declare or not to declare itself as CH. If $p = 1$, then that particular node will generate *holdback* value only once. This may decrease the probability of generating the same *holdback* value for neighboring nodes.

Initially, every node has a cluster identity (CID) which is initialized as NULL. If *holdback* = 0, then node declares itself as CH and broadcasts the clustering message *CLUSTER* (CID, noh) where $noh = 1$ is the hop count. Upon receiving this message, nodes check their CID value. If $CID = NULL$, then $CID = cid$ to join the respective cluster. The *holdback* value decreases after every time ' t ' until the node joins a cluster or declares itself as CH. After the cluster-formation phase, the entire network gets divided into a group of clusters.

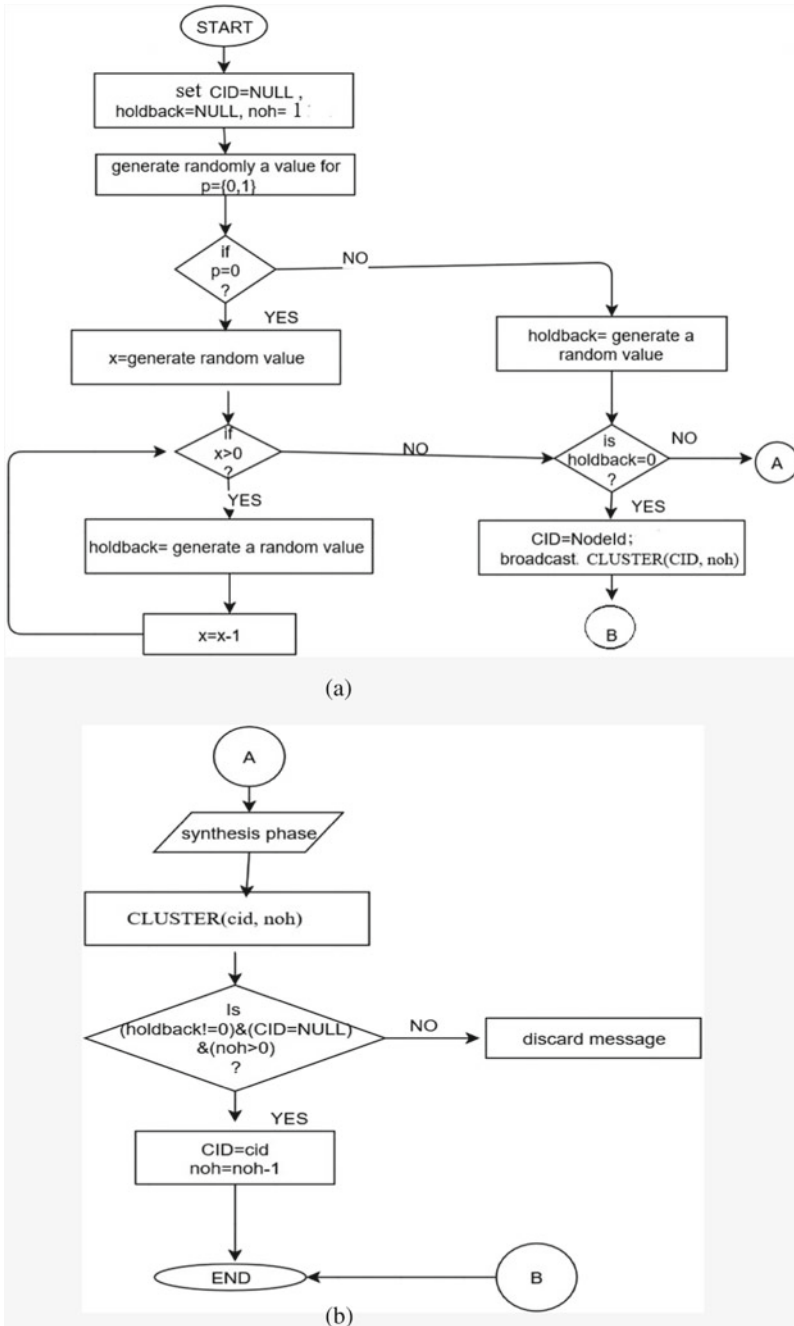


Fig. 2 Cluster-formation phase **a** initialization **b** synthesis phase

Hierarchy-Formation Phase. In this phase, BS starts the formation of hierarchy among CHs. This assures for intercommunication between two clusters. This phase may use the following cases: (i) Case 1: CH to CH (ii) Case 2: CH to Member (M) (iii) Case 3: Member to CH (iv) Case 4: Member to Member. Figure 3 describes the hierarchy-formation phase of the algorithm.

Case 1 CH1 to CH2 (CH-CH). In CH1 to CH2, the cluster heads of two different clusters can directly communicate with each other. They join the partial hierarchy tree as shown in Fig. 4. After joining the hierarchy, the respective CHs inform their

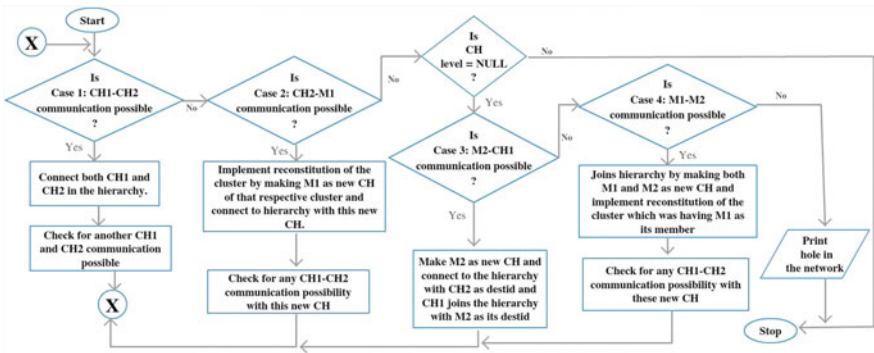


Fig. 3 Hierarchy-formation phase

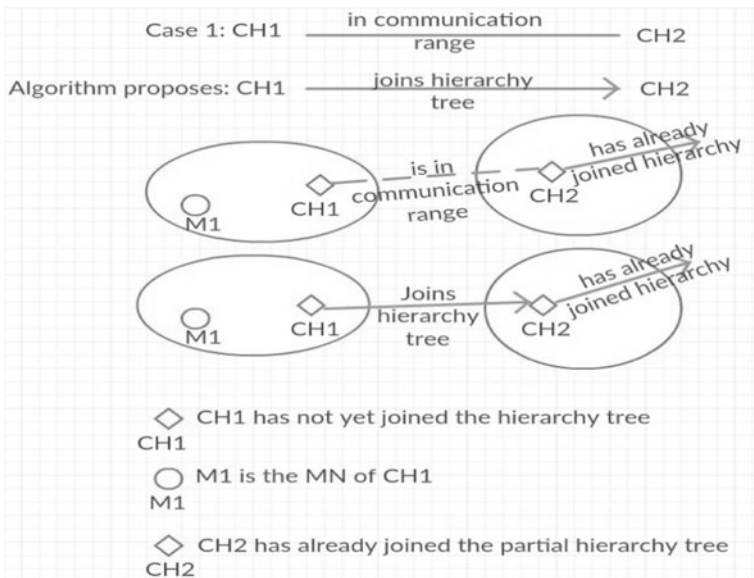


Fig. 4 Case 1: CH-CH communication possibility in hierarchy formation

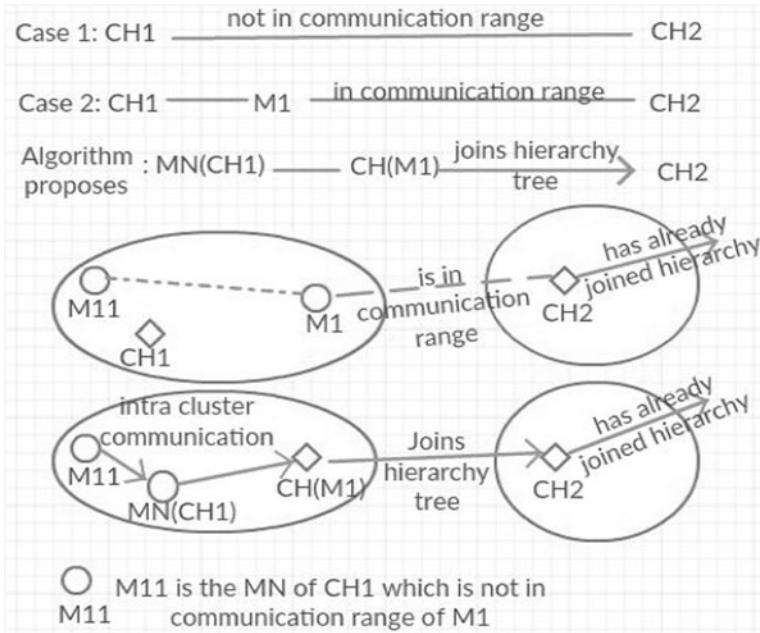


Fig. 5 Case 2: CH-M communication possibility in hierarchy formation

members that it has joined the hierarchy. And then, CHs broadcast messages to search for another CHs who has not yet joined the hierarchy.

Case 2 CH2 to M1 (CH-M). CHs after joining the hierarchy check for Case 2 possibility. There may be a case where some CHs are not in communication range to any of the CHs that has already joined the partial hierarchy tree. But some members of such clusters are reachable by a CH that has joined the partial hierarchy tree. Figure 5 shows Case 2 where the proposed protocol implements reconstitution of that cluster by electing the reachable member (M1) as new CH of that cluster. MNs join their new CH and old CH becomes a member of new CH. Here, there may be a possibility of intra-cluster communication through M11 to old CH (named as Proxy CH) to new CH.

Case 3 M2 to CH1 (M-CH). A CH may not be able to join the partial hierarchy tree by Case 1 and Case 2. Figure 6 shows Case 3 communication possibility. The unjoined CH searches for a MN whose CH has joined the partial hierarchy tree. It chooses any one such member (say, M2). M2 becomes CH and joins the partial hierarchy tree through CH2. CH1 joins the partial hierarchy tree through M2.

Case 4 M1 to M2 (M-M). If the above three cases (Case 1, Case 2, and Case 3) are not possible between two clusters, then Case 4 communication may be possible. Figure 7 describes Case 4. The unjoined CHs (say, CH1) chooses any one of its MN

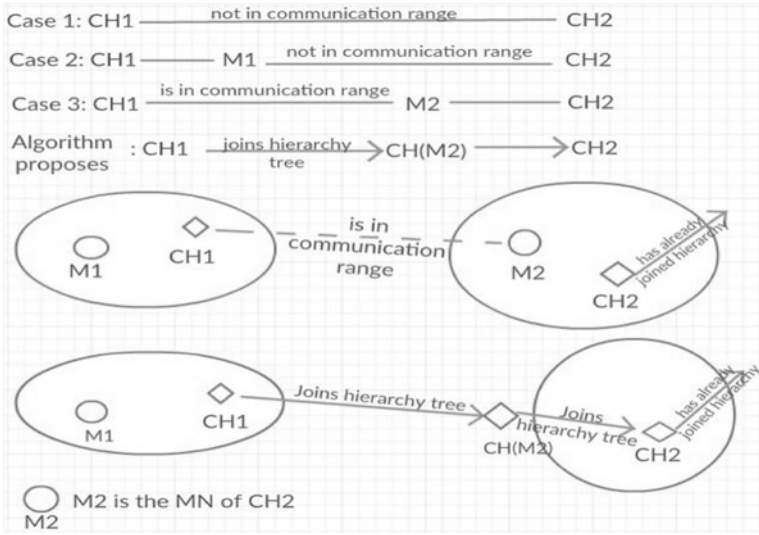


Fig. 6 Case 3: $M-CH$ communication possibility in hierarchy formation

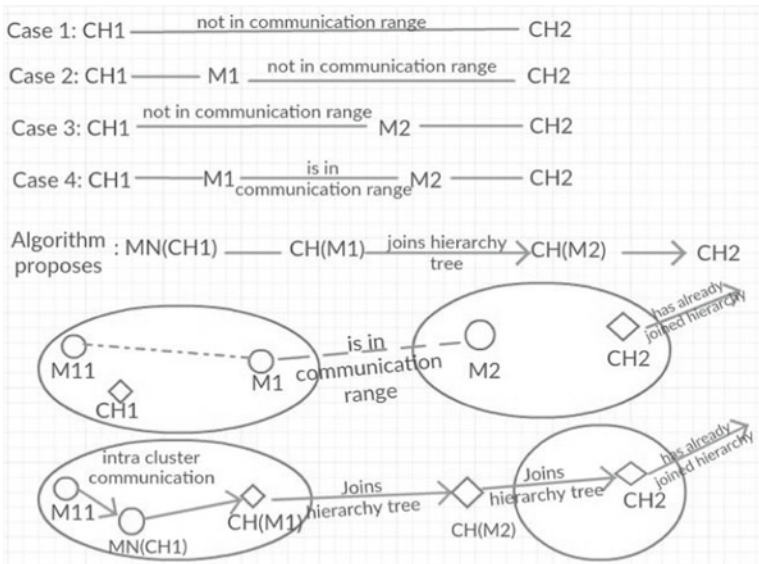


Fig. 7 Case 4: $M-M$ communication possibility in hierarchy formation

(M1) that is in communication range to a MN (M2) belonging to already joined CH in the partial hierarchy tree. M2 becomes CH. M1 becomes new CH, CH1 becomes MN of M1, and MNs join their new CH. Intra-cluster communication may be possible. Both members M1 and M2 join the hierarchy tree through CH2.

In the end, the proposed algorithm synthesizes the hierarchy of clusters. If not, there is a chance of hole in the network. The proposed algorithm detects the hole in the network; if any, but, does not provide solution to remove the holes.

4 Implementation and Result Analysis

The proposed algorithm (EEHCR), TL-LEACH [11], and MR-LEACH [26] are simulated in OMNeT++ network simulator and results have been captured. The nodes are deployed randomly in the target area. Table 1 lists parameters used for setting up the simulation environment:

Figure 8 shows that on increasing the number of SNs, there is a greater number of Case 1: *CH-CH* and probability of other three cases (Case 2: *CH-M*, Case 3: *M-CH* and Case 4: *M-M*) of the proposed algorithm decreases. This will reduce the number of communications for synthesizing hierarchy, resulting in saving of battery power.

Figure 9 shows the total number of CHs formed in three different protocols, TL-LEACH, MR-LEACH, and the proposed algorithm. It also shows how many CHs have not joined in the hierarchy tree formed by the above protocols. Here, communication range of sensor nodes is considered the same for all the three protocols.

Table 1 Assumed parameters of the simulation

Parameter	Value
Simulation area	$200 \times 200 \text{ m}^2$
Base station location	(50,175)
Total number of nodes (\$N\$)	Varies 20–300
Holdback value range	0–20
The initial energy of sensor node	2 Joules (J) considered for TL-LEACH [11] and proposed algorithm 0.003 J considered for MR-LEACH [26] and proposed algorithm
Data packet size	200 bits
Transceiver electronics	50 nJ/bit
Transmit amplifier	5 nJ/bit/m ² considered for TL-LEACH [11] and proposed algorithm 100 pJ/bit/m ² considered for MR-LEACH [26] and proposed algorithm

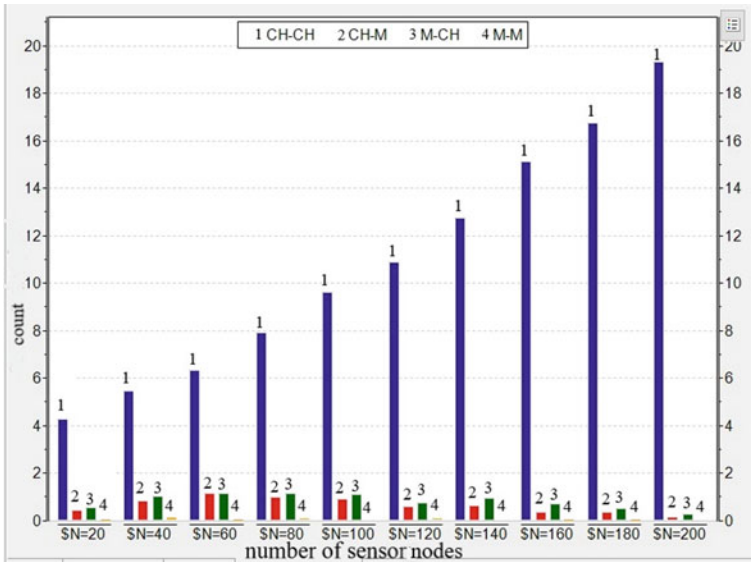


Fig. 8 Count of all four cases of communication possibility in hierarchy-formation phase

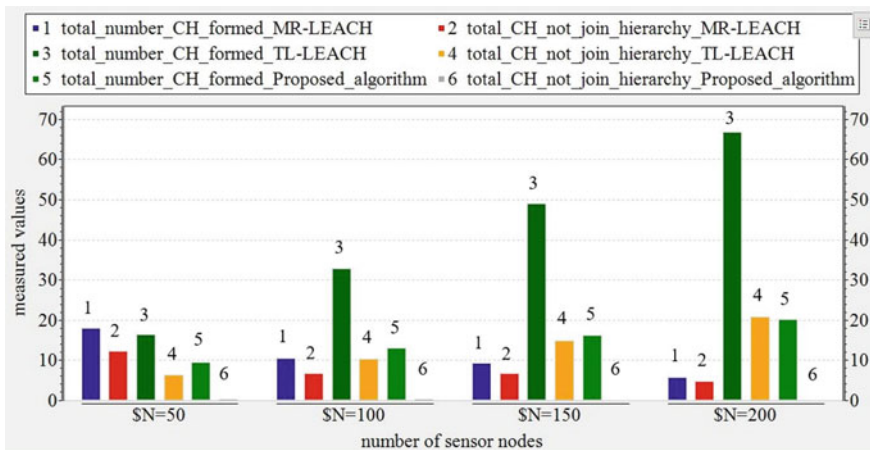
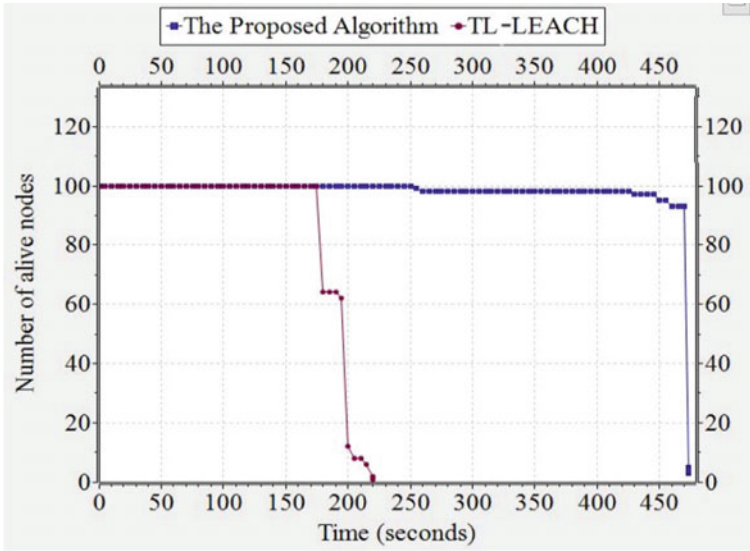


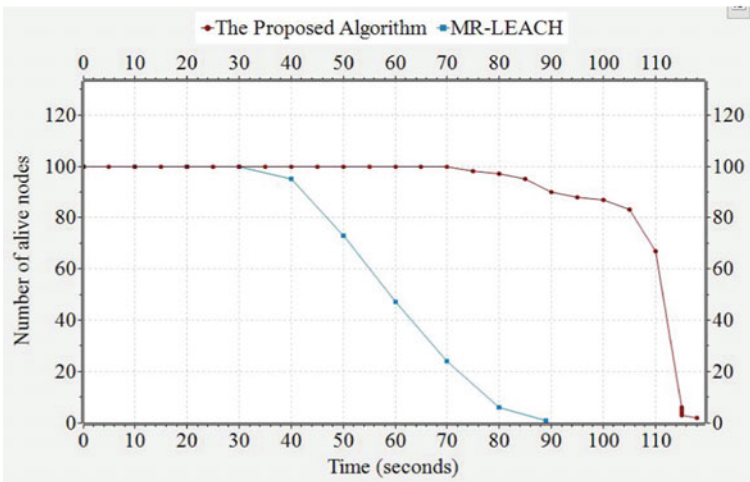
Fig. 9 Comparison of network connectivity among protocols

The result shows that the proposed algorithm performs better than TL-LEACH and MR-LEACH protocol. The proposed algorithm can connect 99.9% of formed CHs of the network in the hierarchy tree.

Figure 10a shows that in the TL-LEACH, all nodes are dead by 220 s whereas in the proposed algorithm, nodes are alive up to 475 s. Figure 10b shows that in the



(a)



(b)

Fig. 10 Alive nodes with time. **a** TL-LEACH and the proposed algorithm **b** MR-LEACH and the proposed algorithm

MR-LEACH, all nodes are dead by 90 s whereas in the proposed algorithm, nodes are dead by 118 s. The proposed algorithm performs better than the TL-LEACH and MR-LEACH.

Figure 11 illustrates the performance of the proposed algorithm with respect to number of messages received at BS in comparison to TL-LEACH and MR-LEACH. Figure 11a shows that 330 more number of messages are able to reach the BS in the proposed algorithm compared to TL-LEACH while compared to MR-LEACH in Fig. 11b, six more number of messages are received at the BS in the proposed algorithm. The proposed algorithm performs better than TL-LEACH and MR-LEACH.

Figure 12 shows the network lifetime of the proposed algorithm, TL-LEACH, and MR-LEACH. This paper considers a network is alive until first CH is dead for simulation purpose because when a CH node dies, messages to this node could not be forwarded toward BS. A particular area of the network could not be communicated now. But in case of a non-CH node dies in the current round, neighboring SNs to this node could still sense the area. The proposed algorithm performs better than TL-LEACH and MR-LEACH.

5 Conclusion

This paper proposed the EEHCR protocol for WSN. It is implemented in OMNeT++ simulator and is compared with two cluster-based hierarchical routing protocols, TL-LEACH and MR-LEACH. The proposed algorithm achieves better connectivity between clusters and shows an increase in network lifetime. A higher number of messages are successfully able to reach the BS in the proposed algorithm compared to TL-LEACH and MR-LEACH. The proposed algorithm performs best when all the CHs join the hierarchy tree by Case 1: CH-CH because, then, new CH is not needed. Simulation results show that the proposed protocol outperforms other comparative clustering protocols.

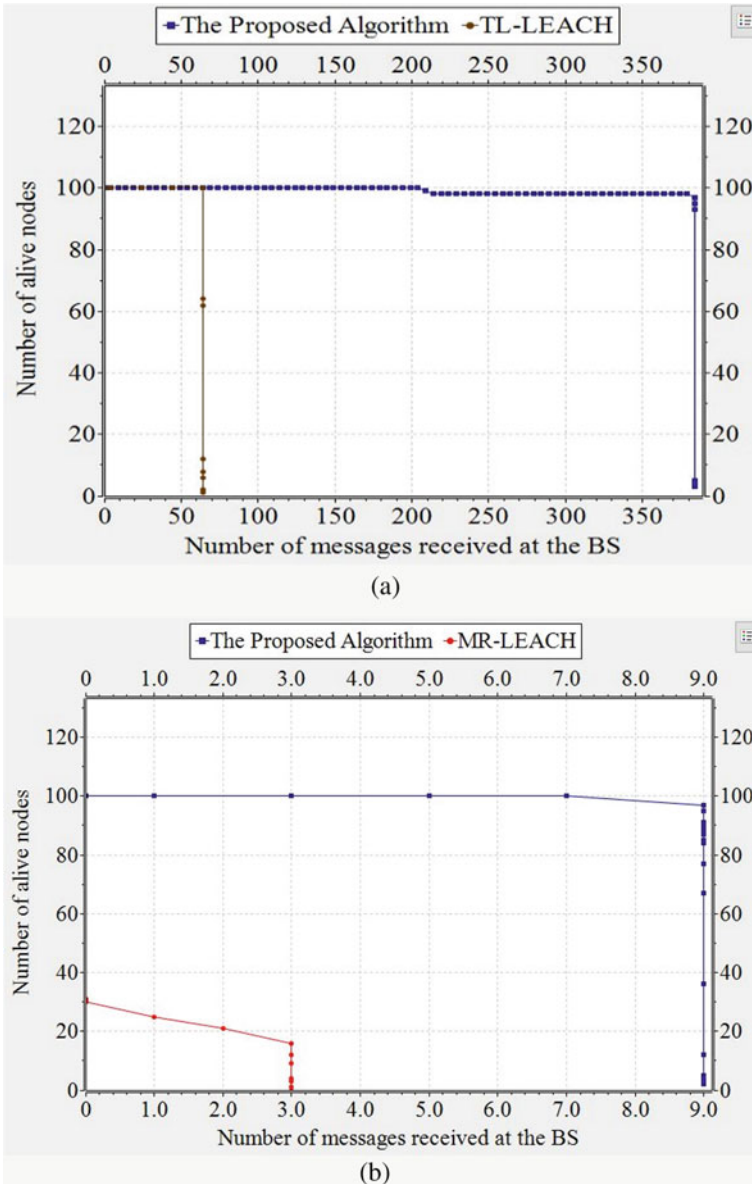


Fig. 11 A number of nodes alive to messages received at BS **a** TL-LEACH and the proposed algorithm **b** MR-LEACH and the proposed algorithm

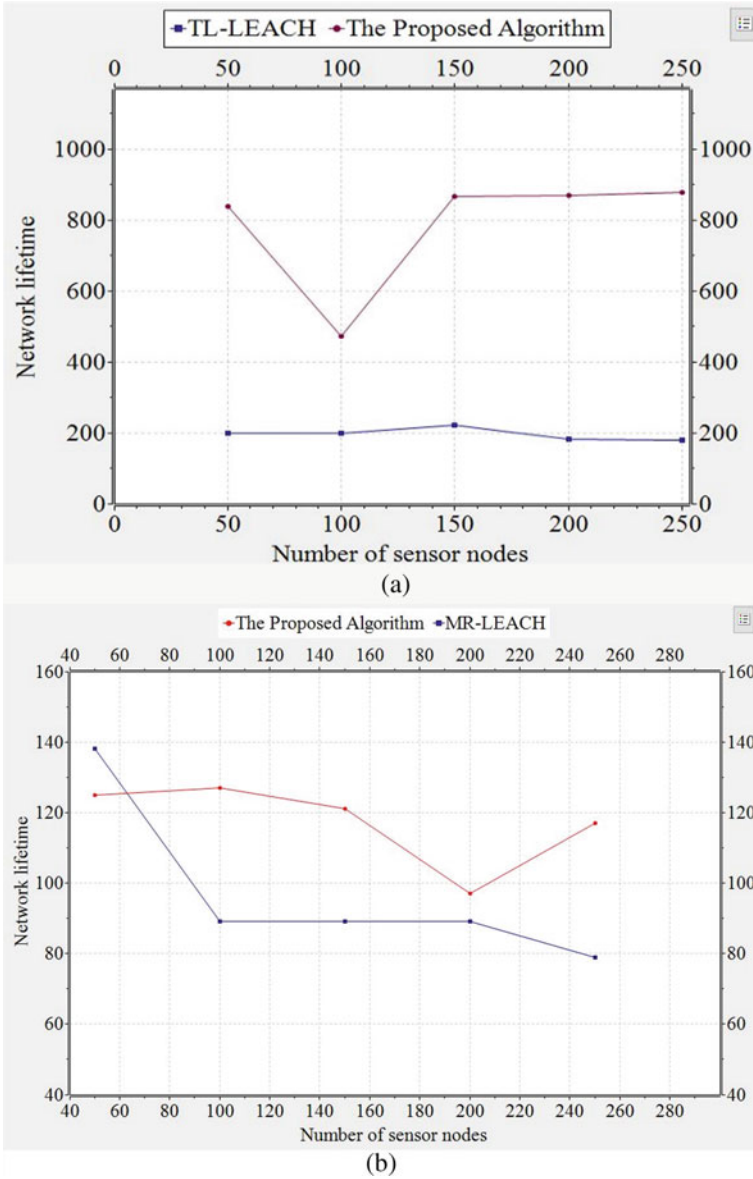


Fig. 12 Network lifetime in high-density nodes **a** TL-LEACH and the proposed algorithm **b** MR-LEACH and the proposed algorithm

References

1. Alkhatib AAA, Baicher GS (2012) Wireless sensor network architecture. In: 2012 International conference on computer networks and communication systems (CNCs 2012)
2. Akyildiz IF, Su W, Sankarasubramanian Y, Cayirci E (2002) A survey on sensor networks. *IEEE Commun Mag* 40(8):102–114. <https://doi.org/10.1109/mcom.2002.1024422>
3. Sundararaman B, Buy U, Kshemkalyani AD (2005) Clock synchronization for wireless sensor networks: a survey. *Ad Hoc Netw* 3(3):281–323. <https://doi.org/10.1016/j.adhoc.2005.01.002>
4. Swati AJ, Priyanka R (2010) Wireless sensor network (WSN): architectural design issues and challenges. *Int J Comput Sci Eng* 2(9):3089–3094
5. Narmadha C, Marichamy P, Narayanan A (2018) A survey on hierarchical-based routing protocols for wireless sensor networks. *Int J Pure Appl Math* 119(16):3663–3676
6. Singh M, Gore M (2005) A new energy-efficient clustering protocol for wireless sensor networks. In: 2005 International conference on intelligent sensors, sensor networks and information processing, pp 25–30. IEEE. <https://doi.org/10.1109/issnip.2005.1595551>
7. Goyal P, Singh U (2016) Hierarchical based routing protocol in WSN. *Int J Comput Appl* 16–21
8. Ngangbam R, Hossain A, Shukla A (2018) An improved clustering based hierarchical protocol for extending wireless sensor network lifetime–EG LEACH. In: 2018 IEEE international conference on system, computation, automation, and networking (ICSCA), pp 1–5. IEEE. <https://doi.org/10.1109/icscan.2018.8541241>
9. Xu D, Gao J (2011) Comparison study to hierarchical routing protocols in wireless sensor networks. *Procedia Environ Sci* 10:595–600. <https://doi.org/10.1016/j.proenv.2011.09.096>
10. Heinzelman WR, Chandrakasan A, Balakrishnan H (2000) Energy-efficient communication protocol for wireless microsensor networks. In: Proceedings of the 33rd annual Hawaii international conference on system sciences, 10 pp. IEEE. <https://doi.org/10.1109/hicss.2000.926982>
11. Loscri V, Morabito G, Marano S (2005) A two-level hierarchy for low-energy adaptive clustering hierarchy (TL-LEACH). In: IEEE vehicular technology conference, vol 62, p 1809. IEEE 1999. <https://doi.org/10.1109/vetecf.2005.1558418>
12. Heinzelman WB, Chandrakasan AP, Balakrishnan H (2002) An application-specific protocol architecture for wireless microsensor networks. *IEEE Trans Wirel Commun* 1(4):660–670. <https://doi.org/10.1109/twc.2002.804190>
13. Younis O, Fahmy S (2004) HEED: a hybrid energy-efficient distributed clustering approach for ad hoc sensor networks. *IEEE Trans Mob Comput* 4:366–379. <https://doi.org/10.1109/tmc.2004.41>
14. Manjeshwar A, Agrawal DP (2001) TEEN: a routing protocol for enhanced efficiency in wireless sensor networks. In: *ipdps*, vol 1, p 189. <https://doi.org/10.1109/ipdps.2001.925197>
15. Manjeshwar A, Agrawal DP (2002) APTEEN: a hybrid protocol for efficient routing and comprehensive information retrieval in wireless sensor networks. In: *ipdps*, p 0195b. Citeseer. <https://doi.org/10.1109/ipdps.2002.1016600>
16. Ye M, Li C, Chen G, Wu J (2005) EECS: an energy efficient clustering scheme in wireless sensor networks. In: PCCC 2005. 24th IEEE international performance, computing, and communications conference, pp 535–540. IEEE. <https://doi.org/10.1109/pccc.2005.1460630>
17. Chen G, Li C, Ye M, Wu J (2009) An unequal cluster-based routing protocol in wireless sensor networks. *Wirel Netw* 15(2):193–207. <https://doi.org/10.1007/s11276-007-0035-8>
18. Lindsey S, Raghavendra CS (2002) PEGASIS: power-efficient gathering in sensor information systems. In: Proceedings, IEEE aerospace conference, vol 3, pp 3–3. IEEE. <https://doi.org/10.1109/aero.2002.1035242>
19. Jung SM, Han YJ, Chung TM (2007) The concentric clustering scheme for efficient energy consumption in the PEGASIS. In: The 9th international conference on advanced communication technology, vol 1, pp 260–265. IEEE. <https://doi.org/10.1109/icact.2007.358351>

20. Gautam N, Lee WI, Pyun JY (2009) Track-sector clustering for energy efficient routing in wireless sensor networks. In: 2009 ninth IEEE international conference on computer and information technology, vol 2, pp 116–121. IEEE (2009). <https://doi.org/10.1109/cit.2009.130>
21. Lindsey S, Raghavendra CS, Sivalingam K (2001) Data gathering in sensor networks using the energy delay metric. In: Proceedings of the IPDPS workshop on issues in wireless networks and mobile computing, vol 10. Citeseer. <https://doi.org/10.1109/ipdps.2001.925196>
22. Zeb A, Islam AM, Zareei M, Al Mamoon I, Mansoor N, Baharun S, Katayama Y, Komaki S (2016) Clustering analysis in wireless sensor networks: the ambit of performance metrics and schemes taxonomy. *Int J Distrib Sens Netw* 12(7):4979142. <https://doi.org/10.1177/155014774979142>
23. Zhou Y, Wang N, Xiang W (2017) Clustering hierarchy protocol in wireless sensor networks using an improved PSO algorithm. *IEEE Access* 5:2241–2253. <https://doi.org/10.1109/ACCESS.2016.2633826>
24. Khan MA, Qureshi MA, Raza I, Hussain SA (2019) EECP-EI: energy-efficient clustering protocol based on energy intervals for wireless sensor networks. In Proceedings of the international conference on information and communication technology, pp 113–119. ACM. <https://doi.org/10.1145/3321289.3321316>
25. Wohwe Sambo D, Yenke BO, Förster A, Dayang P (2019) Optimized clustering algorithms for large wireless sensor networks: a review. *Sensors* 19(2):322. <https://doi.org/10.3390/s19020322>
26. Farooq MO, Dogar AB, Shah GA (2010) MR-LEACH: multi-hop routing with low energy adaptive clustering hierarchy. In: 2010 fourth international conference on sensor technologies and applications, pp 262–268. IEEE. <https://doi.org/10.1109/sensorcomm.2010.48>

Current-Controlled Chaotic Chua's Circuit Using CCCII



Manoj Joshi  and Ashish Ranjan 

Abstract A simple electronically tunable current-controlled chaotic Chua's circuit using second-generation current-controlled current conveyor (CCCII) with 0.25 μm CMOS technology is presented. An electronically control behavior of nonlinear resistance (NR) produces significant change in voltage–current characteristics due to the bias current present in CCCII. The nature of the chaotic circuit in terms of different attractor can be achieved by controlling the variable resistor. The phase portraits of the proposed design are well simulated in PSPICE. The proposed circuit has several advantages viz. uses minimum number of passive components, low frequency operation, and tunable chaotic nature. Finally, a comparative study in terms of physical parameter is tabulated in this scientific literature.

Keywords Nonlinear dynamics · Current-controlled current conveyor (CCCII) · Chaotic system · Negative resistance · Chua's circuit · Double scroll attractor

1 Introduction

The chaotic system provides a new horizon in the world of chaos theory that facilitates security applications like secured communication system, data encryption, adaptive control, cryptography [1], etc. These systems are generalized in terms of their orientation and classification based on ordinary differential equations (ODEs), namely Lorenz system [2], Rosler system [3], 2D oscillators [4], Chua's circuit [5–18], Wien Bridge chaotic oscillator [19], Duffing oscillators [20, 21], Chaotic Jerk oscillator [22, 23], and few more. They have given a challenging ambience for the researcher to design a high-performance dynamical system over the past few decades with low power dissipation, bandwidth, chip area, and simple design.

M. Joshi (✉) · A. Ranjan
Department of Electronics and Communication Engineering, National Institute of Technology
Manipur, Imphal 795001, India
e-mail: Manojjoshi1506@gmail.com

A. Ranjan
e-mail: ashish.ism@rediffmail.com

© Springer Nature Singapore Pte Ltd. 2021
G. S. Hura et al. (eds.), *Advances in Communication and Computational Technology*, Lecture Notes in Electrical Engineering 668,
https://doi.org/10.1007/978-981-15-5341-7_41

Over the past few decades, various implementations of chaotic systems are available in the literature using voltage-mode [4–8] and current-mode building blocks [9–17, 23–25]. In addition, the introduction of an advanced current-mode analog building block in chaotic circuits facilitates wide dynamic range, low power design, and many more [9–17, 23–25] in comparison with op-amp-based circuitry [4–8]. In recent time, considerable amount of conventional analog and digital signal processing circuits are available but the unpredictable nature of chaotic waveform dominates the chaos-based application in VLSI integration. An advance signal processing units by utilizing the current-mode technique provides high performance analog circuit design in comparison to voltage-mode technique.

The subsequent implementation of the basic chaotic system comes with extended Chua's circuit using different kinds of active block like current feedback operational amplifier (CFOA) [9, 10], CCII [13], OTRA [16], and DVCCTA [17]. Recently, some other chaotic circuit is also implemented by using advanced active block like an advanced implementation of Sprott's CFOA based oscillator [23], a chaotic system realization using OTRA [24], and its extended implementation as hyperchaotic system by using single external capacitor, a simple chaotic and hyperchaotic circuit using CFOA [25] and multi-scroll 2D chaotic oscillator using DVCC [26].

However, those implementations have an absence of electronic tenability and utilized the more number of components (both active and passive). These problems are effectively minimized in second-generation current-controlled current conveyor (CCCII) [27] structure. This electrically bias current-based controllable CCCII allows the design of numerous applications, like a filter [28, 29], oscillator [30], Schmitt trigger [31], and many others.

In this research article, an implementation of chaotic oscillator current-controlled current conveyor (CCCII) is presented with a current-controlled negative resistance (NR). The proposed design requires six passive components and its behaviors depending on the bias current of CCCII. It gives ultra-low frequency of oscillation. The performance characteristics of the proposed design are evaluated by using circuit simulator PSPICE and end with the comparative study.

2 Circuit Description

The modified version of the CCII is CCCII [27] which can provide electronic control in various circuit parameters. The circuit symbol and CMOS-based internal structure of the CCCII [32] are shown in Fig. 1. Its port relationships are given by the following equation:

$$I_Y = 0, V_X = V_Y + I_X R_x \text{ and } I_Z = I_X \quad (1)$$

where R_x is the intrinsic resistance developed at port X and electronically control by I_0 as:

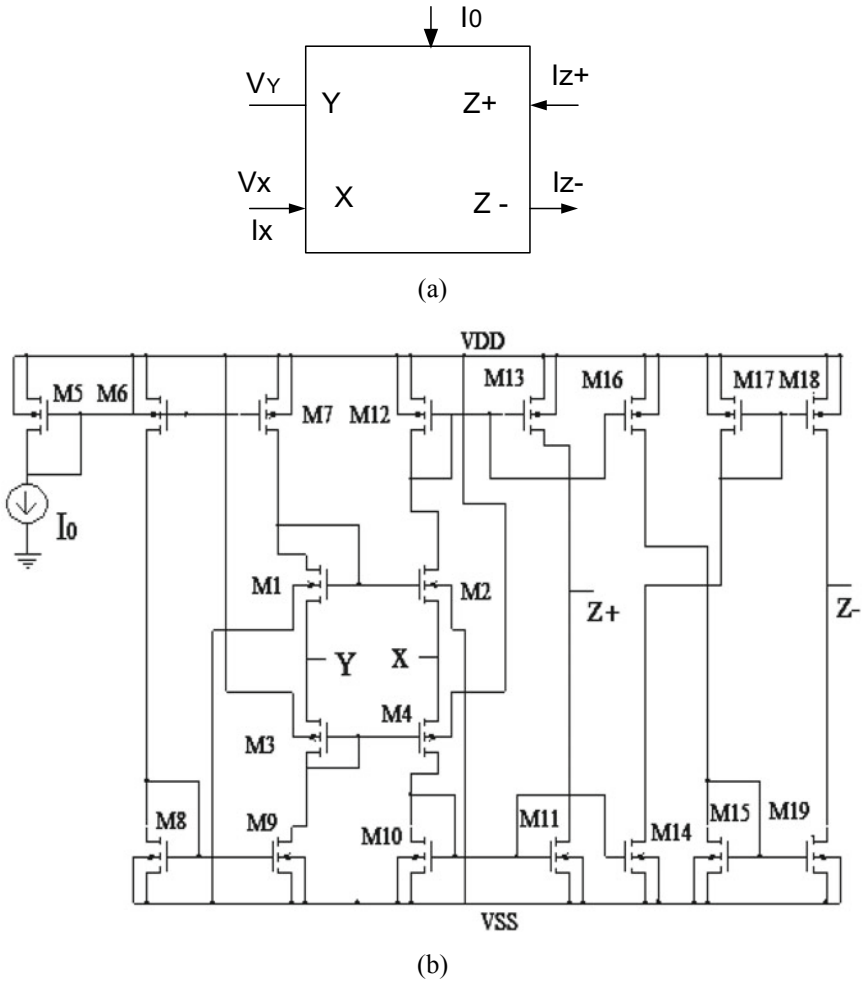


Fig. 1 **a** symbol **b** internal constituent

$$R_x = \frac{1}{g_{m2} + g_{m4}} \text{ and } g_{mi} = \sqrt{2\beta I_{0i}} \tag{2}$$

The basic for the design of Chua's circuit uses a negative resistance (NR) where the voltage-current ($V-I$) ratio exhibits a nonlinear piecewise segment. The proposed NR using two resistors and two CCCII as an active block are shown in Fig. 2.

Here, V_{in} and I_{in} represent input voltage and current. The value of nonlinear slope and the breakpoint is also electronically adjusting by I_0 . The circuit operation for NR1 exhibits the following slope:

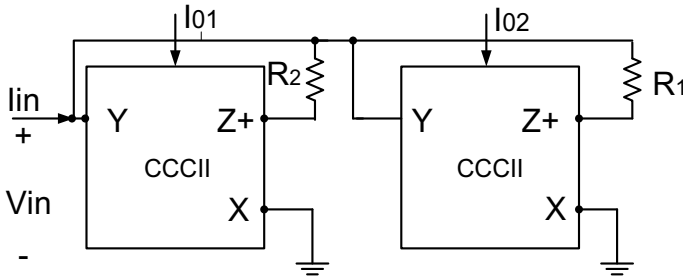


Fig. 2 Negative resistances (NR) using CCCII

$$m_{1i} = -\frac{I_{in}}{V_{in}} = -\frac{1}{R_x} \text{ and } m_{0i} = -\frac{I_{in}}{V_{in}} = -\frac{1}{R_i} \tag{3}$$

and the breakpoint for NR1 is defined by:

$$V_{B_{p_{i\pm}}} = \left(\frac{R_x}{R_x + R_i} \right) \tag{4}$$

where $i = 1,2$ represent for NR_1 and NR_2 , respectively. The voltage–current ($V-I$) characteristic of the nonlinear resistance NR_1 with different bias current I_0 is shown in Fig. 3a. To obtain the m_0 and m_1 , we have used the mathematical expression as given in [16, 17] as: $m_0 = m_{11} + m_{02}$ and $m_1 = m_{12} + m_{02}$. The nonlinear voltage–current ($V-I$) characteristic of the nonlinear resistance NR can be written as [5–11].

$$I_{in} = m_0 V_{IN} + \frac{1}{2}(m_1 - m_0)[|V_{IN} + B_p| - |V_{IN} - B_p|] \tag{5}$$

For absolute values of voltage less than breakpoint $|B_{p1}|$, the $V-I$ characteristic shows a linear segment with negative slope m_0 . Although, the absolute voltage in between $|B_{p1}|$ and $|B_{p2}|$ allows two linear segments of negative slope m_1 beside the slope m_0 . The PWL behavior is valid in the range between (B_{p1}, B_{p2}) in which the NR is worked as piecewise negative resistance. For voltages outside this range (greater than $|B_{p2}|$) shows the V/I ratio increases monotonically. Figure 3b shows the nonlinear five-segment $V_{in}-I_{in}$ characteristic of the negative resistance, where $m_0 = -0.46$ ms, $m_1 = -0.74$ ms are sloped in the inner and outer regions for bias current value ($I_{01} = 0.6 \mu\text{A}$, $I_{02} = 0.8 \mu\text{A}$) with the resistor value ($R_1 = 200 \Omega$, $R_2 = 22 \text{ k}\Omega$).

The next step for the design of Chua’s circuit has a traditional Chua’s circuit reported as [15–17]. Figure 4 signifies proposed CCCII-based chaotic circuit with the nonlinear element (NR) and active inductor (L_{eq}).

The routine analysis provides an expression for the inductance as $L_{eq} = sC_3R_x^2$. It reveals that the value of L_{eq} can be easily varied by changing the value of bias current (I_0) of CCCII. The inductance value ($L = 1\text{mH}$) is determined by putting passive component value $C_3 = 1 \text{ nF}$ and $R_x = 1 \text{ k}\Omega$ for $I_0 = 1\mu\text{A}$.

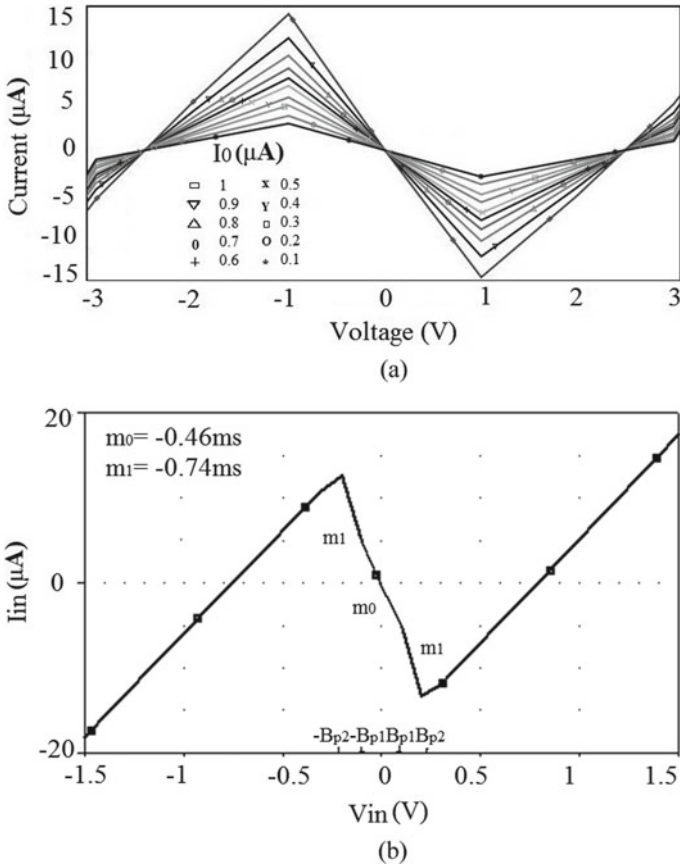


Fig. 3 a Voltage–Current ($V-I$) characteristic of the nonlinear resistance NR_1 with different bias current I_0 b 5-segment $V_{in}-I_{in}$ characteristic (for $I_{01} = 0.6 \mu A$, $I_{02} = 0.81 \mu A$, $R_1 = 200 \Omega$, $R_2 = 22 k\Omega$)

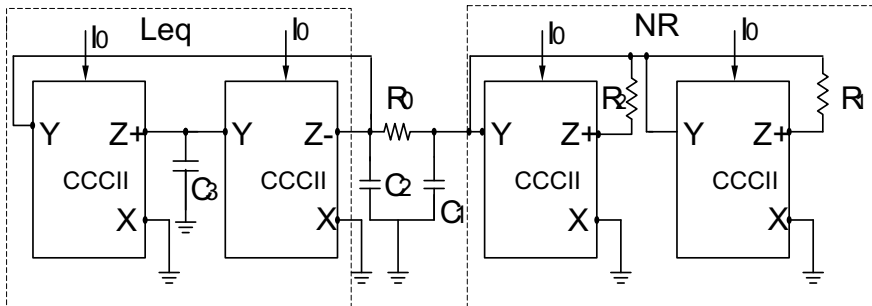


Fig. 4 Proposed current mode Chua's circuit using CCCII

To obtain the state equations, we may apply Kirchoff's law to the nodes above C_1 and C_2 and the loop containing L and C_1 . Thus, the proposed state equations are written as:

$$\begin{aligned} C_1(dV_{C_1}/dt) &= (V_{C_2} - V_{C_1})/R_0 - I_{in} \\ C_2(dV_{C_2}/dt) &= (V_{C_1} - V_{C_2})/R_0 + I_L \\ L(dI_L/dt) &= -V_{C_2} + I_L r_0 \end{aligned} \quad (6)$$

where I_L represent current through the inductance L , r_0 is a small parasitic resistance added in series to account for the internal resistance of a physical inductor. It reduces the effect of parasitic resistance. The above Eq. (6) may also be modified to dimension-less equation as:

$$\begin{aligned} \dot{x} &= \alpha(y - x - f(x)) \\ \dot{y} &= x - y + z \\ \dot{z} &= -\beta y + \gamma z \end{aligned} \quad (7)$$

Here, the symbol (\cdot) denotes differentiation of respective state variable with respect time t , the scaled time (τ) , and $(\alpha, \beta$ and $\gamma)$ are dimension-less parameters of state equation calculated by the mathematical relation $\tau = t/R_0 C_2$, $\alpha = C_2/C_1$, $\beta = R_0^2 C_2/L$, $\gamma = C_2 R_0 r_0/L$, respectively. The dimension-less variables and the parameters are defined by:

$$\dot{x} = (dV_{C_1}/dt), \dot{y} = (dV_{C_2}/dt), \dot{z} = (dR_0 I_L/dt) \quad (8)$$

The initial parameters (x_0, y_0, z_0) are assigned as three minimum random values to system working as an ideal solution for numerical analysis and given as:

$$x = V_{C_1}/B_p, y = V_{C_2}/B_p, \text{ and } z = I_L R_0/B_p \quad (9)$$

The Chua's circuit with current-controlled nonlinear negative resistance (NR) is very useful to reduce the number of resistors. The RLC parameters for the proposed design are determined as $C_1 = 10$ nF, $C_2 = 100$ nF, $R_0 = 1.79$ k Ω , $L = 1$ mH, and slope $m_0 = -0.467$ ms, $m_1 = -0.74$ ms for parameter values $\alpha = 10$, $\beta = 330$, and $\gamma = 1.8$.

3 Simulation Results

To validate the proposed Chua's model, a simulation setup by using PSPICE is elaborated. An active block CCCII is integrated with 0.25 μ m CMOS technology [33].

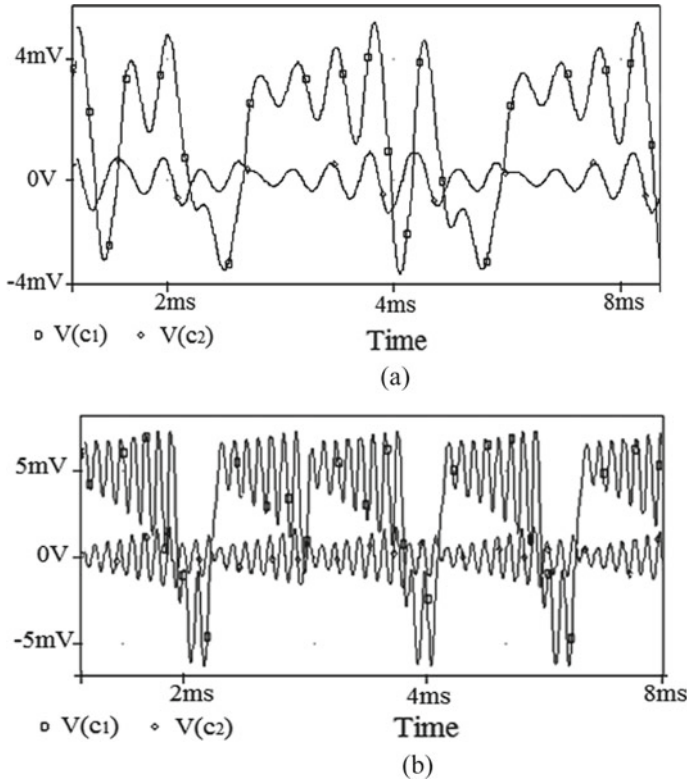
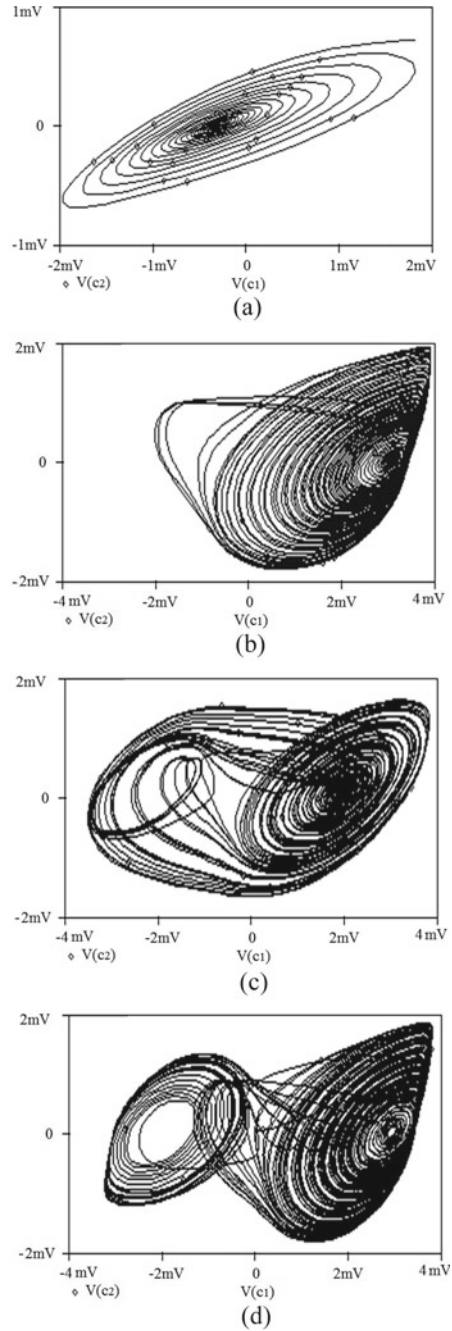


Fig. 5 Chaotic voltage waveform V_{C_1} and V_{C_2} verses time **a** $R_0=1.65\text{ k}\Omega$; **b** $R_0=1.88\text{ k}\Omega$

Figure 5 shows the chaotic voltage waveform V_{C_2} and V_{C_1} with respect to time for different values of R_0 ($1.65\text{ k}\Omega$ and $1.88\text{ k}\Omega$) with bias current (I_0) as ($0.5\ \mu\text{A}$ & $0.7\ \mu\text{A}$) and ($0.4\ \mu\text{A}$ & $0.8\ \mu\text{A}$), respectively, for NR1 and NR2. The other fingerprint of Chua's circuit is phase portraits. Figure 6 shows different phase portraits, i.e., V_{C_2} verses V_{C_1} plot for the different values of R_0 from 1.44 to $1.95\text{ k}\Omega$. That results show different chaotic nature with a variable resistor (R_0). Also, the Fourier analysis is shown in Fig. 7 with $R_0=1.78\text{ k}\Omega$, $L=1\text{ mH}$, $C_1=10\text{ pF}$, $C_2=100\text{ pF}$ for frequency 13.04 kHz , and measured peak-peak voltage $V_{C_1}=7.8\text{ mV}$, $V_{C_2}=1.86\text{ mV}$. Here, the frequency of oscillation obtained from proposed current-controlled chaotic system is 13.04 kHz , which is may be useful for secure communication.

Finally, a brief comparative study of the chaotic circuit is investigated in Table 1 in terms of component, technology used, and power. It reveals that the proposed circuit uses an active inductor as that of implementations in [9–13, 16, 17]. Also, observed that in comparison to literature, the proposed circuit uses a minimum number of components and low power dissipation. Implementations in [5–7] and [16, 17] use less active building block, but in [5–7], the inductor is a passive one. In addition, the

Fig. 6 Computer simulation: Chaotic nature (V_{C_1} vs. V_{C_2}) **a** $R_0 = 1.44 \text{ k}\Omega$; **b** $R_0 = 1.75 \text{ k}\Omega$; **c** $R_0 = 1.945 \text{ k}\Omega$; **d** $R_0 = 1.95 \text{ k}\Omega$



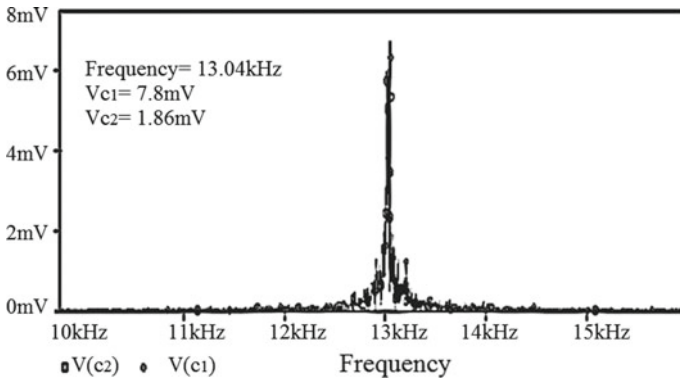


Fig. 7 Fourier analysis of current-controlled Chua's circuit

Table 1 Comparative study of the different chaotic circuit

Ref.	Active block	CMOS technology	Power dissipation	Nonlinear resistance	Active inductor	Total components
[5]	Op-Amp	–	120 mW	7 R	No	11
[6]	OTA	0.5 μm	–	2 OTA	No	4
[7]	Op-Amp	–	–	6 R	No	9
[9]	CFOA	–	270 mW	4 R	2 R, 1C	10
[10]	Op-Amp	–	–	CFO 4 R	RC network	13
[11]	Op-Amp	–	305 mW	6 R	4 R, 1C	14
[13]	CCII	0.5 μm	–	4 R	2 R, 1C	10
[14]	CFOA	–	–	6 R, 2C	No	12
[15]	CFOA	–	250 mW	4 R	2 R, 1C	11
[16]	OTRA	0.5 μm	56.3 mW	6R	3 R, 2C	14
[17]	DVCCTA	0.25 μm	17.5 mW	4 R	1 R, 1C	9
[24]	OTRA	0.25 μm	23 mW	2 diode	No	6
Proposed	CCCII	0.25 μm	19 mW	2R	1C	6

C = Capacitor, R = Resistor

nonlinear resistance circuit uses a minimum number of passive components in the count, only [6] uses two OTA block.

4 Conclusion

A simple and robust current-controlled chaotic Chua's circuit is designed by using CCCII with standard passive components. The workability of the proposed design is justified through the PSPICE simulation. A number of bifurcation sequences along with its voltage-current characteristics for different bias current are well observed. The proposed circuit offers (i) simple and versatile design, (ii) advance CMOS based CCCII design for Chua's Circuit (iii) uses minimum number of components, (iv) low frequency operation, and (v) low power dissipation.

References

1. Vaidyanathan S, Volos C (2016) *Advances and applications in Chaotic systems*. Springer International Publishing Switzerland (2016)
2. Lorenz EN (1963) Deterministic non-periodic flow. *J Atmos Sci* 20:130–141
3. Rossler OE (1976) An equation for continuous chaos. *Phy Lett* 57A(5):130–141
4. Tamasevicius A et al (2001) Two-stage chaotic Colpitts oscillator. *Electron Lett* 37(9):549–551
5. Matsumoto T, Chua LO, Komuro M (1986) The double scroll bifurcations. *Int J Circ Theory Appl* 14(2):117–146
6. Cruz JM, Chua LO (1992) A CMOS IC nonlinear resistor for Chua's circuit. *IEEE Trans Circ Syst I Fundam Theor Appl* 39(12):985–995
7. Kennedy M (1992) Robust Op-Amp realization of Chua's circuit. *Frequenz* 46(10):66–80
8. Kapitaniak T, Chua LO, Zhang GQ (1994) Experimental hyperchaos in coupled chuas circuits. *IEEE Tran Circ Syst* 41:499–503
9. Senani R, Gupta SS (1998) Implementation of Chua's chaotic circuit using current feedback op-amps. *Electron Lett* 34(9):829–830
10. Elwakil AS, Kennedy MP (2000) Improved implementation of Chua's chaotic oscillator using current feedback op amp. *IEEE Trans Circ Syst I Fundam Theor Appl* 47:76–79
11. Torres LAB, Aguirre LA (2000) Inductorless Chua' circuit. *Electron Lett* 36(23):1915–1916
12. Recai K (2003) A comparative study on realization of Chua's circuit: hybrid realizations of Chua's circuit combining the circuit topologies proposed for Chua's diode and inductor elements. *Int J Bifurcat Chaos* 13(06):1475–1493
13. Gaurav G (2006) An improved Chua's circuit and its use in hyperchaotic circuit. *Anal Integr Circ Sig Process* 46(2):173–178
14. Tlelo-Cuautle EA, Gaona-Hernández J (2006) Implementation of a chaotic oscillator by designing Chua's diode with CMOS CFOAs. *Analog Integr Circ Sig Process* 48(2):159–162
15. Jothimurugan R et al (2014) Improved realization of canonical Chua's circuit with synthetic inductor using current feedback operational amplifiers. *Int J Electron Commun (AEÜ)* 68:413–421
16. Kushwaha AK, Paul SK (2016) Chua's oscillator using operational transresistance amplifier. *Rev Roum des Sci Tech-Serie Electrotechnique et Energetique* 61(3):299–303
17. Kushwaha AK, Paul SK (2016) Inductorless realization of Chua's oscillator using DVCCTA. *Analog Integr Circ Sig Process* 8(1):137–150
18. Recai K, Yildirim F (2008) A survey of Wien bridge-based chaotic oscillators: design and experimental issues. *Chaos Solitons Fractals* 38:1394–1410
19. Tamasevicius A, Lindberg E, Kirvaitis R (2009) Autonomous Duffing-Holmes type Chaotic oscillator. *Elektron ir Elektrotechnika* 5:43–46
20. Tamasevicius A et al (2009) Autonomous Duffing-Holmes type chaotic oscillator. *Electron Electr Eng* 5(93):43–46

21. Piper JR, Sprott JC (2010) Simple autonomous chaotic circuits. *IEEE Trans Circ Syst II Express Briefs* 57:730–734
22. Sprott JC (2011) New chaotic jerk circuit. *IEEE Trans Circ Syst II Express Briefs* 58(4):240–243
23. Srisuchinwong B, Liou CH (2007) Improved implementation of Sprott's chaotic oscillators based on current-feedback Op Amps. In: *Proceedings of the Electrical Engineering./Electronics. Computer, telecommunications and information technology (ECTI-CON 2007)*, pp 38–40. ECTI-CON 2007
24. Joshi M, Ranjan A (2019) An autonomous chaotic and hyperchaotic oscillator using OTRA. *Analog Integr Circ Signal Process* 101:401–413
25. Joshi M, Ranjan A (2019) New simple chaotic and hyperchaotic system with an unstable node. *AEU Int J Electron Commun* 108:1–9
26. Joshi M, Ranjan A (2019) Realization of novel multi-scroll 2D chaotic oscillator using DVCC. In: Mishra S, Sood Y, Tomar A (eds) *Applications of computing, automation and wireless systems in electrical engineering*, vol 553. *Lecture notes in electrical engineering*. Springer, Singapore, pp 1093–1101
27. Fabre A, Saaid O, Wiest F, Baucheron C (1996) High frequency applications based on a new current controlled conveyor. *IEEE Trans Circ Syst I* 43(2):82–90
28. Ranjan A, Paul SK (2011) Nth order voltage mode active-C filter employing current controlled current conveyor. *Circ Syst* 2(2):85–90
29. Pandey N, Paul SK, Jain SB (2009) A new electronically tunable current mode universal filter using MO-CCCII. *Analog Integr Circ Signal Process* 58(2):171–178
30. Pandey N, Paul SK (2008) A novel electronically tunable sinusoidal oscillator based on CCCII (-IR). *J Active Passive Electron Devices* 3(2):135–141
31. Faseehuddin M, Sampe J, Islam S (2016) Schmitt Trigger based on dual output current controlled current conveyor in 16 nm CMOS technology for digital applications. In: *Proceedings of IEEE-ICSE 2016*, Kuala Lumpur, Malaysia
32. Joshi M, Ranjan A (2017) Realization of Colpitts oscillator using second generation current controlled current conveyor. In: *Proceedings of the second international conference on research in intelligent and computing in engineering*, vol 10, pp 49–52
33. Agrawal D, Maheshwari S (2017) Current mode filters with reduced complexity using a single EX-CCCII. *Int J Electron Commun* 1–19

Phishing URL Detection Using Machine Learning



Preeti, Rainu Nandal, and Kamaldeep Joshi

Abstract Phishing attack is used to obtain the information like username, password, bank account details, and credit card details. It is a most popular cybercrime today. Phishing attacks also affect the online payment sector financial institution, file hosting or cloud storage, and many others. Phishing attack always targets to these Web sites which are related to the online payment sector and Web mail. Many techniques are used to prevent the phishing attack like blacklist, Heuristic, visual similarity, and machine learning. Blacklist technique is most commonly used because it is easy to implement, but this technique cannot detect a new phishing attack. So, now, machine learning is most efficient technique to detect the phishing attack and this technique is able to detect all drawback of other phishing detect techniques. So this research work is completely based on machine learning algorithms which are logistic regression, decision tree, random forest, and SVM to detect phishing Web site. In this research work, select the best model on the basis of six analysis factors.

Keywords Phishing detection · Feature extraction · Phishing Web site · Phishing attack · Logistic regression · Decision tree · Random forest classifier and support vector machine

1 Introduction

Nowadays, many people use the Internet for the purpose of online shopping, online bill payment, online mobile recharge, and banking transaction. There are many cybercrimes which happened on the Internet like spam, fraud, cyber terrorism,

Preeti (✉) · R. Nandal · K. Joshi
UIET, MDU, Rohtak, India
e-mail: Miskhokhar121@gmail.com

R. Nandal
e-mail: rainu_nandal@yahoo.com

K. Joshi
e-mail: kamalmintwal@gmail.com

and phishing. Phishing is a cybercrime which is performed to obtain important information of the user. A Fisher designs Web site which looks same as any legitimate site and spoof user for obtaining private information of users such as username, password, and banking details for miscellaneous reasons. This table shows the APEG RPORT base on phishing Web site detection.

Report	Year	Phish detected
APEG 3Q [1]	2017	190,942
APEG 2Q [1]	2018	233,040
APEG1Q [2]	2018	263,538

So, according to the APEG reports, phishingWweb site detection is increasing day by day.

2 Background Theory

Phishing is used to obtain sensitive information such as user names, pass words and credit card details, often for malicious reasons, by disguising as a trustworthy entity in an electronic communication [2]. Phishing attacks can be implemented in various forms like e-mail phishing, Web site phishing, spear phishing, Whaling, Tab is napping, Evil twin phishing. Avoiding this phishing attack has many technologies like Blacklist, heuristic, visual similarity, machine learning, which are described below:

2.1 Blacklist Method

In this technology, phishing URL is stored in the database. So at the base of database, detect phishing URL and give warning; otherwise, it is called legitimate sites. So this technique is easy to implement because using only malicious ULR can detect phishing Web site. But this technique is not able to detect a new phishing attack, because to implement this technique with 90% efficient, we need to change the dataset time to time.

2.2 Heuristic Based Method

This is extended version of Blacklist technology. It is able to detect new phishing site. It is used for feature extraction to detect the phishing Web sites. This technique

cannot detect all new attacks and easiest to bypass once attacker know algorithm or features used. In addition, this has poor detection because site may or may not have common features.

2.3 Visual Similarity

This technique is used to extract image from legitimate site. But limitation of this is an image comparison takes more time as well as more space to store images. It produces a high false negative rate and fails to detect when the visual appearance slightly changes.

3 Machine Learning

This approach works efficiently in large dataset. This also removes drawback of existing approaches and able to detect zero-day attack. Machine learning used classification algorithm and achieved accuracy more than 99%. The performance of machine learning algorithm depends upon the size of training data as well as test data. The limitation of this is it fails to detect when attacker use compromised domain for hosting their site. Most research has worked on improving accuracy of phishing Web site detection using different classifiers. Various classifiers used are KNN, SVM, decision tree, ANN, Naïve Bays, PART, ELM, and random forest. Among all of this, tree-based classifiers and SVM are best as increase dataset as per in this research work. Therefore, the proposed approach will be on phishing Web site detection using tree-based classifiers. Various performance measures used for analysis of best algorithm are F-measure, precision, recall, accuracy, AUC, ROC curve, etc., and have 16 analysis factors for analysis the performance of machine learning model. Among of 16 analysis factors select only 6 factories which are mean absolute error, root mean square error, sensitivity, training time, Cohen_Kappa_Score, Roc_auc_score. Then, on the basis of these factors, select the best model to solve the problem of malicious URL detection (Fig. 1).

4 Classification Techniques

4.1 Logistic Regression

It is most popular classification machine learning algorithm. The logistic regression algorithm also uses linear equations for prediction. The predicted value exits between positive to negative infinities. It is predicted 0 for bad URL and 1 for good URL. But

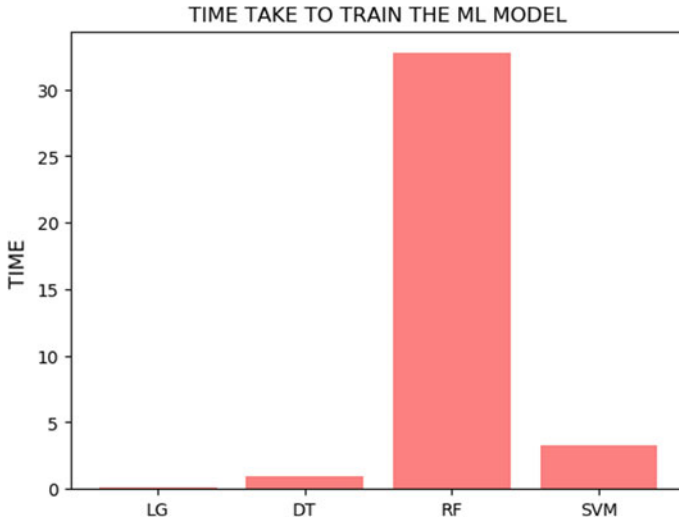


Fig. 1 How many second take to train the models (LR, DT, RF, and SVM) to solve the problem of phishing Web site detection

according to this research work, the performance of the logistic regression algorithm depends upon the training data set. If the training data set is small or large, then prediction becomes wrong. If the training data set is medium, the prediction becomes right. Accuracy of this algorithm is 93%.

4.2 Decision Tree

The decision tree is supervised machine learning algorithm and used in solving the classification as well as regression problem. It uses a tree structure to represent the number of decision and selects the best decision on the basis of entropy and information gain. In this research work used Python to implement the decision tree. For import decision tree used from sklearn_tree import Decision Tree Classifier. It is a most popular algorithm to solve phishing URL detection problem. On the basic of 6 analysis factors, we can say it is the best algorithm to solve this problem.

4.3 Random Forest

Random forest (RF) is a more powerful full machine learning algorithm for classification. This model builds multiple decision tree and merges them together to get a more accurate and stable prediction. This model gives more accuracy. But the

performance of this method will be decreased when we take more training data set. So we cannot say this model is well suited to solve the problem of phishing Web site detection.

4.4 Support Vector Machine

This model is developed by Vladimir in 1963. SVM is the supervised machine learning algorithm, and it is used for classification as well as regression problem. It is also called support vector network and non-probabilistic, binary linear classification. SVM is used to sort the data and perform grouping according to pattern. For classification, it is used hyper planes. It required labeled data to be trained. According to this research work, the working of SVM is good, but not for all analysis factors. On the basis of 16 analysis factors, we can say it is better then logistic regression and random forest model.

5 Literature Survey

Rao and Pais [3]: It proposed a novel classification approach that uses heuristic-based feature extraction approach. For feature extraction, use third-party-based features, hyperlink-based features, obfuscation features. This proposed technique gives 99.55% accuracy. The drawback of this is that as this model uses third-party features, classification of Web sites depends on speed of third-party services.

Liu and Lang[4]: For developing the classification model, combine the statistical tool with a machine learning algorithm. This algorithm gives 99.7% efficiency.

Gautam et al. [5]: In this paper used association data mining approach to develop the model. It Is based on a classification technique for phishing Web sites. This technology gets 92.67% accuracy by extracting 16 features. But it is not up to mark so proposed algorithm can be enhanced for efficient detection rate.

Pujara andChaudhari [6]: In this paper, performed a detailed literature survey about phishing Web site detection. It describes various techniques to solve this problem like heuristic-based method, visual similarity, blacklist method, machine learning. According to this research paper, we can say that tree-based classifiers in machine learning approach is best suitable than another.

Mohammad et al. [7]: The proposed model that automatically extracts important features for phishing Web site detection without requiring any human intervention. The author has concluded in this paper that the process of extracting feature by their tool is much faster and reliable than any manual extraction.

Ahmad et al. [8]: In proposed model, use three new features for increase the accuracy rate of phishing Web site detection. In this research paper use both common and new features to detect that particular Web site either phishing or not. At the end,

author has concluded this work can be enhanced by using this novel feature with decision tree machine learning classifiers.

Sampat et al. [9]: In this research paper, proposed work completely depends upon the machine learning algorithm with a wrapper feature selection method. This model has given 98% accuracy. But have some drawback like wrapper feature selection method take more space and more time. So we cannot say that this technology is best to solve the problem of phishing Web site detection.

Ali [10]: Proposed work based on novel classification model. The proposed classification model builds on sophisticated machine learning methods that not only take care about the syntactical nature of the URL but also the semantic and lexical meaning of these dynamically changing URLs (Table 1).

6 Exprement Result

6.1 Dataset

Dataset has 12532 URL and feature set. For each model contains 10024 training data as well as 2507 test data. Feature set A contains binary values either 0 for bad or 1 for good Web sites. Feature set B contains label either good or bad depending upon the URL. For example

```
In [4]: urls_data.head(10)
Out[4]:
```

	uri	label	Rating Factors
0	daryofagameaddict.com	bad	0
1	google.com/search?q=haristech	good	1
2	google.com/search=faizanahmad	good	1
3	pakistanfacebookforever.com/getpassword.php	good	1
4	www.radsport-vogel.de/wp-admin/includes/bugfix	bad	0
5	shranhel.without-transfer.ru/methotaxe	bad	0
6	www.itidea.it/centroestetico/sothy/rimf/_notes/...	bad	0
7	www.buyfakebillsonline.blogspot.com	bad	0
8	www.unitedairlineslogistics.com	bad	0
9	www.stonehousedelivery.com	bad	0

This dataset contains both types of URL, either good or bad. Rating factors are used to calculate some analysis factor. On the basis of these factors we can analysis the performance of LR, DT, RF, and SVM to solve the problem of phishing Web site detection.

7 Method Comparison

To analysis the performance of machine learning models, we use different metrics like confusion metrics, performance evolution metrics, and use 16 another analysis factors for analyzing the performance of logistic regression, decision tree, random forest classifier, and support vector machine. Shown in Table 2.

Table 1 Final result of literature survey

Author	Findings/methodology	Research gap
Naveen et al. [11]	In this paper, develop the hybrid model for classification of phishing Web site. To develop this model, use 3 classification model, then select the best one on the basis of accuracy	They achieved 97.75% accuracy on testing dataset. There is a limitation of this model that it requires more time to build hybrid model
Tahir et al. [12]	It developed the open-source framework which is called Fresh-Phish using a machine learning classification algorithm	This framework gives more accuracy, but take more time to train the model
Shirazi et al. [13]	In this paper, proposed the model using decision tree. This model detects the phishing attack only from the client site	This model achieved 99.09% efficiency. It can detect Web page written in HTML. No n-HTML Web page
Jain and Gupta [14]	In this model, proposed the model using data mining and machine learning algorithm. In this model used the dataset of phishing Web sites	In this paper, Web-mining, classification is used
Sananse and Sarode [15]	In this paper, developed safer framework for detecting phishing Web site. To develop the model, use machine classification algorithm	Give only 96% efficiency
Mustafa and Nazife [16]	In this paper, the author has implemented two algorithms Adaline and Backpropion along with SVM for getting good detection rate and classification purpose	Give 99% efficiency
Singh et al. [17]	In this paper, developed the model base of tree-based classifier is best and gives better accuracy for phishing URL detection	In this paper used lexical features, URL-based feature, network-based features, and domain-based feature
Pradeepthi and Kannan [18]	In the proposed method, author used six heuristics that are subdomain, path, domain, page rank, and Alexa rank, primary domain, Alexa reputation whose weight and values are evaluated	This approach gives 97% accuracy but still improvement can be done by enhancing more heuristics
Nguyen et al. [19]	It is proposed three new features to increase the accuracy of phishing Web sites detection	At the end author has concluded this work can be enhanced by using this novel feature with decision tree machine learning classifiers

(continued)

Table 1 (continued)

Author	Findings/methodology	Research gap
Abunadi et al. [21]	It proposed the model which automatically extracts important features for phishing Web site detection without requiring any human intervention	In this paper the Author concluding the process of extracting feature by their tool is much faster and reliable than any manual extraction
Shirazi et al. [13]	In this paper, proposed the model using decision tree. This model detects the phishing attack only from the client site	This model achieved 99.09% efficiency. It can detect Web page written in HTML. No n-HTML Web page
Jain and Gupta [14]	In this model, proposed the model using data mining and machine learning algorithm. In this model used the dataset of phishing Web sites	In this paper, Web-mining, classification is used
Sananse and Sarode [15]	In this paper, developed safer framework for detecting phishing Web site. To develop the model, use machine classification algorithm	Give only 96% efficiency
Mustafa and Nazife [16]	In this paper, the author has implemented two algorithms Adaline and Backpropion along with SVM for getting good detection rate and classification purpose	Give 99% efficiency
Singh et al. [17]	In this paper, developed the model base of tree-based classifier are best and gives better accuracy for phishing URL detection	In This paper used lexical features, URL-based feature, network-based features, and domain-based feature
Pradeepthi and Kannan [18]	In the proposed method, author used six heuristics that are sub domain, path, domain, page rank, and Alexa rank, primary domain, Alexa reputation whose weight and values are evaluated	This approach gives 97% accuracy but still improvement can be done by enhancing more heuristics
Nguyen et al. [19]	It is proposed three new features to increase the accuracy of phishing Web sites detection	At the end, author has concluded this work can be enhanced by using this novel feature with decision tree machine learning classifiers
Abunadi et al. [20]	It proposed the model which automatically extracts important features for phishing Web site detection without requiring any human intervention	In this paper, the author concluding the process of extracting feature by their tool is much faster and reliable than any manual extraction

Table 2 Comparison between logistic regression, decision tree, random forest, and support vector machine on the basis of 16 analysis factor

Analysis factor	Logistic regression model	Decision tree model	Random forest classifier model	Support vector machine model
Accuracy	0.9341842840047866	0.963302752293578	0.9533306741124851	0.9617072197846032
Mean absolute error	0.06581571599521341	0.0366972477064220	0.04547267650578381	0.038292780215396886
Root mean squared error	0.2565457386027166	0.19156525704423027	0.04547267650578381	0.19568541135045525
Logloss results.mean()	-0.17131802244213779	-1.3162299148057657	-0.21246194115588576	-0.312466745897645879
results.std()	0.0051673255915062905	0.14675956160747217	0.07272056941658407	0.0827245342876
Sensitivity	0.4245614035087719	0.8160919540229885	0.602112676056338	0.6529850746268657
Training time	0.08412027200029115	0.939159256999119	32.72516879699833	3.2713975879996724
brier_score_loss	0.06581571599521341	0.03669724770642202	0.0314567823234	0.038292780215396886
jaccard_similarity_score	0.9341842840047866	0.963302752293578	0.9545273234942162	0.9617072197846032
cohen_kappa_score	0.5649441685974786	0.8019325496877555	0.7266388393642826	0.7646732126479152
roc_auc_score	0.7120556792521358	0.8982507855600249	0.8008314167506161	0.82582225953750675
hamming_loss	0.06581571599521341	0.03669724770642202	0.04547267650578381	0.038292780215396886
Precision	0.9918032786885246	0.8287937743190662	0.9941860465116279	0.9831460674157303
False positive rate	0.00045004500450045	0.019590382902938557	0.000449842555105713	0.0013398838767306833
Specificity	0.9995499549954996	0.9804096170970614	0.9995501574448943	0.9986601161232693
AUC: results.Mean ()	0.9773742457565966	0.888565050625371	0.976260534655243	0.9898137446908531
results.std ()	0.003831903513936734	0.02665332039177378	0.00846531962124643	0.004661992243580998

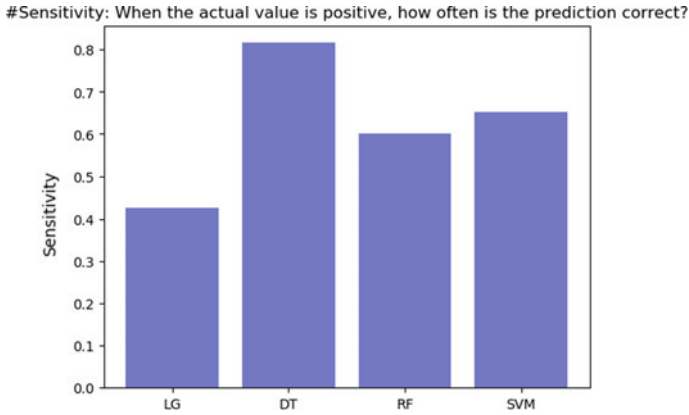


Fig. 2 Result after analyze sensitivity performance analysis factor

Among 16 analysis factors, select only 6 factors. On the basic of these factors, select the best model to solve the problem of phishing Web site detection, which are mean absolute error, root mean squared error, sensitivity, training time, cohen_kappa_score, roc_auc_score and Show the comparison with the help of final implementation.

Training time: How much time taken to train the machine learning model. LG take less time, but it gives wrong prediction. DT gives more accurate results as compared to RF and SVM (Fig. 2).

After analysis, sensitivity factor can say that DT is better than LR, RF, and SVM. $Sensitivity = \frac{True\ Positives}{True\ Positives + False\ Negatives}$ (Fig. 3).

Mean absolute error is the average of the difference between the original values and the predicted values. It gives us the measure of how far the predictions were from the actual output. MSE takes the average of the square of the difference between the original values and the predicted values. So, on the basis of this analysis factors, we can say decision tree is better then other (Fig. 4).

It's usefulness as a metric of comparison between observed and expected accuracy. So the performance of the DT is better than other (Fig. 5).

A useful tool when predicting the probability of a binary outcome is the receiver operating characteristic curve or ROC curve. After analyzed, this factor can say decision tree is the best model to solve the problem of phishing Web site detection.

“So on the basis of sex analysis factors can say Decision tree is the best model to solve the problem of phishing web site detection.” To implement this research work used Python language. In which these are standard library has been used.

- “Python
- Pandas library Numpy library
- `from sklearn.linear_model import LogisticRegression from sklearn.tree import DecisionTreeClassifier`

SHOW THE RESULT OF Root MEAN ABSOLUTE ERROR AND ROOT MEAN SQUARED ERROR

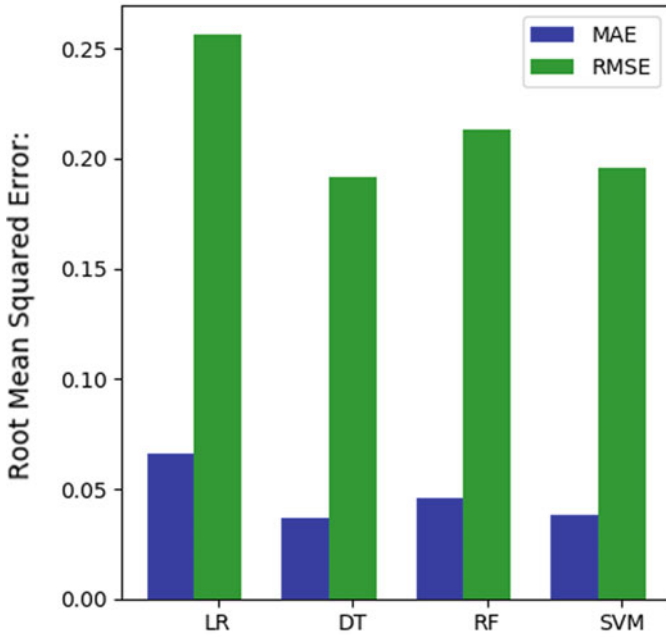


Fig. 3 Result after analyzed RMSE (root mean squared error)

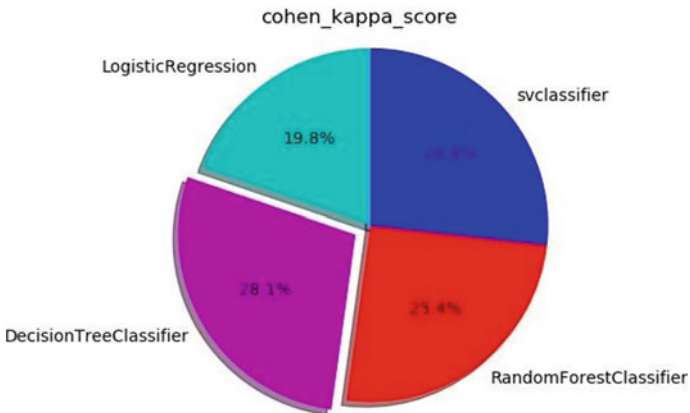


Fig. 4 Result after analysis Cohen_kappa_score performance analysis factor

Receiver Operating Characteristic (ROC) metric to evaluate classifier output quality.

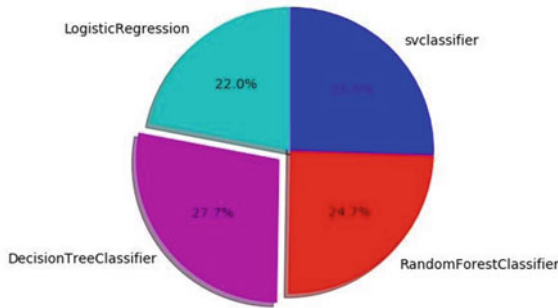


Fig. 5 Result after analysis ROC factor

- from sklearn.ensemble import RandomForestClassifier from sklearn.svm import SVC
- from sklearn.feature_extraction.text import CountVectorizer from sklearn.feature_extraction.text import TfidfVectorizer from sklearn.model_selection import train_test_split
- from sklearn.metrics import classification_report, confusion_matrix from sklearn.metrics import accuracy_score”

Pandas library: It is used for data analysis. It represents dataset in the form of data frame after then performed various operations.

Numpy library: It is used for mathematical analysis. It provides various mathematics functions which can be directly applied to the dataset.

From skyline.Linear: It provides various machine learning models. Each machine learning algorithm can be imported directly using this library.

CountVectorizer and TfidfVectorizer: It is used to convert the data frame in the form of numeric values. These numeric values used to train the machine learning algorithms.

Confusion matrix: using this matrix, we can calculate accurately: Precision, Recall, F-measure.

```

jupyter decision tree final Last Checkpoint: 03/31/2019 (autosaved)
File Edit View Insert Cell Kernel Widgets Help
Python 3

In [35]: from sklearn.metrics import classification_report, confusion_matrix
print(confusion_matrix(y_test, y_pred))
print(classification_report(y_test, y_pred))
[[2292  44]
 [ 49 213]]
          precision    recall  f1-score   support

 0       0.98      0.98      0.98      2346
 1       0.83      0.82      0.82       261

 micro avg       0.90      0.90      0.90      2607
 macro avg       0.90      0.90      0.90      2607
 weighted avg       0.90      0.90      0.90      2607

In [36]: # Accuracy of Our Model
print("Accuracy: ",logit_score(X_test, y_test))
Accuracy: 0.9538275209578

In [37]: print("Mean Absolute Error:", metrics.mean_absolute_error(y_test, y_pred))
print("Mean Squared Error:", metrics.mean_squared_error(y_test, y_pred))
print("Root Mean Squared Error:", np.sqrt(metrics.mean_squared_error(y_test, y_pred)))
Mean Absolute Error: 0.02669724770642292
Mean Squared Error: 0.02669724770642292
Root Mean Squared Error: 0.163402766423827

```

By using these analysis factors can analysis the performance of classification models.

Conclusion: Phishing attack is used to obtain the private information of the user for malicious purpose. To prevent this attack, many techniques used. But each technique has some drawback. Machine learning is most popular technique to solve this problem. In this research work, select four models to solve this problem. Which are LR, DT, RF, and SV. On the basis of this research work, the performance of logistic regression depends upon the URL dataset. If we take 1200 URL, then LR gives a more accurate prediction, but in other case, if we take 12000 URL than LR give wrong prediction. So the performance of LR depends upon the size of training data set. We cannot say that this model is good to solve the problem to phishing Web site detection. Among in these three models DT, RF and SVM give more accurate results as compare to LG. According to this research work, on the basis of six analysis factor like mean absolute error, root mean squared error, sensitivity, training, time, cohen_kappa_score, roc_auc_score can say that the decision tree is the best model to solve the problem of phishing Web site detection. In future research, we will use deep learning algorithm and combine this problem with anomaly detection.

References

1. APWG Report 1. http://docs.apwg.org/reports/apwg_trends_report_q2_2018.pdf
2. Phishing definition. <https://en.wikipedia.org/wiki/Phishing>
3. Rao RS, Pais AR (2018) Detection of phishing websites using an efficient feature-based machine learning framework. Springer
4. Liu C, Lang B (2018) Finding effective classifier for malicious URL detection. ACM, VNO-5
5. Gautam S, Rani K, Joshi B (2018) Detecting phishing websites using rule-based classification algorithm: a comparison. Springer
6. Pujara P, Chaudhari MB (2018) Phishing website detection using machine learning: a review. In: 2018 IJSRCSEIT, vol 3, issue no 7. ISSN 2456-3307
7. Mohammad RM, Thabtah F, McCluskey L (2012) An assessment of features related to phishing websites using an automated technique. In: International conference for internet technology and secured transactions (ICITS). IEEE
8. Abunadi A, Akanbi O, Zainal A (2013) Feature extraction process: a phishing detection approach. IEEE
9. Sampat H, Saharkar M, Pandey A, Lopes H (2018) Detection of phishing website using machine learning. Int Res J Eng Technol (IRJET) 5(3). E-ISSN 2395-0056. P-ISSN 2395-0072. www.irjet.net
10. Ali W (2017) Phishing website detection based on supervised machine learning with wrapper features selection. IJACSA 8
11. Naveen INVD, Manamohana K, Verma R (2019) Detection of malicious URLs using machine learning techniques. IJITEE 8. ISSN 2278-3075
12. Tahir MAUH, Asghar S, Zafar A, Gillani S (2016) A hybrid MAUH model to detect phishing-sites using supervised learning algorithms. In: International conference on computational science and computational intelligence. IEEE
13. Shirazi H, Haefner K, Ray I (2017) Fresh-phish: a framework for auto-detection of phishing websites. In: International conference on information reuse and integration (IRI), IEEE
14. Jain AK, Gupta BB (2017) Towards detection of phishing websites on client-side using machine learning based approach. IEEE

15. Sananse BE, Sarode TK (2015) Phishing URL detection: a machine learning and web mining-based approach. In: *Int J Comput Appl*
16. Mustafa AYDIN, Nazife BAYKAL (2015) Feature extraction and classification phishing websites based on URL. *IEEE*
17. Singh P, Maravi YP, Sharma S (2015) Phishing websites detection through supervised learning networks. *IEEE*
18. Pradeepthi. KV, Kannan A (2014) Performance study of classification techniques for phishing URL detection. In: 2014 (ICoAC) *IEEE*, vol 2
19. Nguyen LAT, To BL, Nguyen HK, Nguyen, MH (2013) Detecting phishing web sites: a heuristic URL-based approach. In: The 2013 international conference on advanced technologies for communications (ATC'13)
20. Abunadi A, Zainal A, Akanb O (2013) Feature extraction process: a phishing detection approach. *IEEE*
21. Mohammad RM, Thabtah F, McCluskey L (2012) An assessment of features related to phishing websites using an automated technique. In: The 7th international conference for internet technology and secured transactions, *IEEE*

Sybil-Free Hybrid Localization Scheme in Wireless Sensor Networks



Narendra Dodwaria and Naveen Chauhan

Abstract Applications of wireless sensor networks such as target tracking, estimating the location of the fire in forests, tracking the enemy tanks in the battlefield and geographical routing require the location of sensor nodes. There are various existing range-free localization approaches to localize the sensor nodes like APIT, DV-hop, centroid method, etc. But because of the wireless transmission medium of sensor networks, security threats like Sybil attack, wormhole attack, selective forwarding, sinkhole attack, etc., could happen more easily. Sybil attack is the most common and vital security threat in WSN. Sybil attack-affected node can have multiple identities which can affect the localization process and increase localization error. Recently, Sybil-free localization scheme SF-APIT has been proposed to detect Sybil attack but because of the exclusion of suspected nodes in the localization process, the number of blind nodes or unresolved sensor nodes is increased significantly. In this paper, we have proposed a novel lightweight secure hybrid localization scheme against Sybil attack, named Sybil-Free Hybrid Localization Scheme (SFHL), to address Sybil attack more efficiently and to localize blind or ghost nodes using a hybrid approach. Firstly, the Sybil attack is detected while using the APIT localization scheme, and then, Sybil nodes and blind nodes are identified. At last, unresolved nodes are localized using a hybrid localization scheme. Simulation results depict that SFHL performed better than existing localization approaches in the presence of Sybil attack, in terms of minimizing the number of blind nodes and localization error.

Keywords Sybil attack · Range free · Localization · Wireless sensor network · Security

N. Dodwaria (✉) · N. Chauhan
National Institute of Technology, Hamirpur, HP, India
e-mail: narendra.dodwaria@gmail.com

N. Chauhan
e-mail: naveen@nith.ac.in

© Springer Nature Singapore Pte Ltd. 2021
G. S. Hura et al. (eds.), *Advances in Communication and Computational Technology*, Lecture Notes in Electrical Engineering 668,
https://doi.org/10.1007/978-981-15-5341-7_43

561

1 Introduction

Nowadays, application of wireless sensor networks is rapidly increasing because WSNs are capable of dealing with challenging problems. A wireless sensor network is a collection of a huge number of inexpensive and networked sensor nodes. These sensor nodes can do limited tasks and have limited resources [1]. These sensor nodes gather information from selective sensor nodes and forward toward the sink node as per the requirement. Many applications of WSN like environment monitoring, target tracking, determining the location of the fire in the forest, the location of enemy tanks in the battlefield, geographical routing, military operations, etc., require the location information of the sensor nodes, otherwise the information is meaningless [1–3].

Localization is the process to localize unknown sensor nodes. One straightforward solution of the localization problem is that equip each sensor node with GPS technology but in real-life applications, there are thousands of sensor nodes and enabling them with GPS is very costly and infeasible. The second solution is that some of the sensor nodes are localized with the help of either GPS or manually; these are identified as anchor or beacon nodes [1, 4]. Anchor nodes are capable of doing heavy computation and have more storage than normal sensor nodes. Several localization schemes have been proposed like APIT, DV-hop, MDS, SeRLoc, and HiRLoc. Localization approaches can be grouped into two kinds, range free and range based. Range-free schemes like APIT, DV-hop do not need any extra hardware, and these are straightforward to understand and implement, whereas range-based localization schemes need extra directional antennas to localize unknown nodes. Wireless sensor networks have wireless communication medium because of that security threats are higher in WSNs than wired networks [1]. Security attacks like Sybil attack, wormhole attacks, sinkhole attack, blackhole attack, selective, and jamming attacks are the most common security threats in wireless sensor network [2]. These security threats can affect the localization process which decreases the localization accuracy. Sybil attack is one of the most challenging attacks in which normal anchor nodes can be compromised and can forge multiple identities with different locations which can affect the localization badly [3, 5, 6]. One standard solution is the encryption with larger size key, but it requires more computational operations; sensor nodes have limited power and computational resources so that it is not a feasible solution [7].

Recently, several Sybil-free localization approaches have been proposed that have better accuracy like improved APIT, SF-APIT, etc. With SF-APIT, localization accuracy was improved, but the number of unknown nodes or blind nodes had increased than compared to standard APIT localization scheme [3]. In this paper, we have proposed a novel lightweight secure hybrid localization scheme against Sybil attack that detects and excludes Sybil nodes from the network and increases the localization accuracy in more than 70% experiments than compared to SF-APIT and standard APIT localization scheme [2, 3]. Apart from that, the number of blind nodes is narrowed down to zero which is very important in location-aware applications and by minimizing localization error harmful disasters can be detected correctly so that can be handled properly. Proposed secure hybrid localization scheme—SFHL—uses

standard APIT to localize normal nodes, and then based on received signal strength (RSS), Sybil attack is detected and resolved. Further to localize remaining unresolved sensor nodes DV-hop algorithm is used which is based on the connectivity and hop distance of the network rather than on PIT test [2–4]. In this way, localization accuracy is increased, and Sybil and unresolved nodes are handled properly which is the significant improvement in the localization process in WSNs. Simulation results depict that the proposed localization scheme performs better than existing approaches like APIT or DV-hop.

The rest of the paper is arranged as follows. In Sect. 2, the existing and related work in secure localization is discussed. In Sect. 3, existing standard APIT and DV-hop algorithms are included. Further, the influence of the Sybil attack on the APIT approach is also discussed. Section 4 elaborates on the network and Sybil attacks model used in this paper. In Sect. 5, the proposed SFHL approach is given in detail. Section 6 includes a time complexity analysis. In Sect. 7, simulation results are exhibited with the help of plotted graphs. In Sect. 8, the paper is concluded, and research directions are provided for future research.

2 Related Work

Recently, several secure localization methods have been proposed. Lazos et al. [8–10] proposed a robust location system (ROPE) in which a nanosecond precision counter is required to check the sensors before the information gathering. But nanosecond precision counter is infeasible at low cost in wireless sensor networks. Shin and Park also proposed a secure location scheme which requires extra hardware and uses signal strength, but it can only defend against simple attacks in which attacker tries to alter the location of random sensor nodes. Further, Capkun et al. [11] and Rasmussen et al. introduced a localization approach utilizing covert base stations (CBS) and the mobile base station (MBS) which can defend against normal security attacks. In covert base station, distances between nodes have been calculated by using nodes recorded location information; then, it was compared with the actual location of CBS, and if it exceeds a defined threshold, then such nodes marked as compromised nodes. A secure location approach was proposed by Perazzo et al. which uses multilateration method to localize sensor nodes by using the overlapped areas by anchor nodes; further, fixed anchor nodes can be replaced with single mobile node [11] that is cheaper than previous localization scheme.

A variety of secure localization schemes were proposed specifically to address the Sybil attack. Paper [8] proposed a secure localization system that uses bidirectional antennas to transmit the exact location of the locators. These locators transmit their location information to unknown nodes; then, the approximate location is determined by using transmitted beacon information. Since this approach requires costly antennas so that it is infeasible for a low-cost WSN [12]. The overlapped antenna sector is measured by employing a majority vote scheme. In the last step, COG of the overlapped area is computed to localize unknown nodes. However, SeRLoc [8] and

HiRLoc [9] were proposed to secure the localization process, but SeRLoc requires extra bidirectional antennas and HiRLoc provides additional capability to change the orientation of locators antennas; but again these approaches also require costly hardware resources which is infeasible for low-cost WSNs. Further, some range-based secure localization approaches were proposed which were using the feature of communication like RSSI-based [13], TDOA (time difference of arrival) [14], AOA (angle of arrival), etc. In RSSI-based method, received signal strength was shared between unknown nodes which are used to calculate the ratio of received signal strength to detect the Sybil nodes [3, 6, 15]. In TDOA-based method, time difference of arrival was monitored to calculate the exact location of unknown nodes apart from that angle-of-arrival method was also proposed to estimate the location of unknown nodes securely. But these range-based localization schemes needed additional costly hardware which made them infeasible for low-cost WSNs.

Recently, range-free secure localization schemes have been suggested that it does not require any additional costly hardware and these are easy to understand and implement. APIT is one of the range-free localization approaches which uses approximate point-in-triangle test to check whether an unknown node is inside or outside of the triangle of anchor nodes; then, the location of unknown nodes is calculated by estimating the center of gravity of overlapped areas. Further, DV-hop algorithm was proposed which based on connectivity or topology of the network, and it uses hop count to estimate the approximate location of unknown sensor nodes [2]. However, the localization accuracy of the range-free scheme is less than range based but range free does not need any costly hardware, so that they are feasible for low-cost WSNs. Recently, SF-APIT was proposed that defend against Sybil attack, but it increases the number of blind nodes which is not a good solution for the location-aware applications [3]. To address the problem of localization accuracy improvement and to localize unresolved or blind nodes we have proposed a secure hybrid localization system that performs better than existing ones.

3 Problem Statement

In this division, we have discussed the standard APIT and DV-hop localization schemes. Also, the vulnerability of these schemes to security attacks like Sybil and wormhole has described. It also includes the influence of Sybil attacks on localization accuracy and the number of unresolved nodes.

3.1 *Basic APIT Localization Scheme*

Initially, the approximate point-in-triangle localization approach was introduced by He et al. [16] in 2003. The basic APIT scheme is a lightweight and distributed localization approach. APIT localization scheme is easy to understand and implement,

and it also costs too little because it needs only RSS (Received Signal Strength) values from anchor nodes to localize the unknown nodes. Later on, many revised versions of the APIT had been proposed [5, 6, 15].

The basic APIT scheme includes four major steps. The first step includes the beacon exchange. All anchor nodes disseminate their beacon message to neighbor sensor nodes [1]. This beacon information includes the ID and location of anchor nodes. After receiving these beacons, each sensor node builds its neighbor list according to the received beacon information. At last, after building individual neighbor lists, each unknown nodes broadcast their neighbor list and all these neighbor lists are merged into a single list and stored at each sensor node [3].

The second step makes use of the point-in-triangle test to check if an unknown sensor node lies inside the triangle of selected anchor nodes or lies outside of the triangle. In Fig. 1, *M* is an unknown sensor node to be localized. Based on below-mentioned two conditions, it is decided whether node *M* lies inside or outside of selected triangle ΔPQR . Node *M* lies inside ΔPQR if node *M* moves toward closer or further from any selective anchor nodes. In most of the applications of WSN, sensor nodes are static nodes which means it is not feasible to apply the PPIT test so that approximate point in the triangle is applied in which neighbor nodes of unknown node *M* are monitored to infer the sensor nodes *M* as shown in Fig. 2.

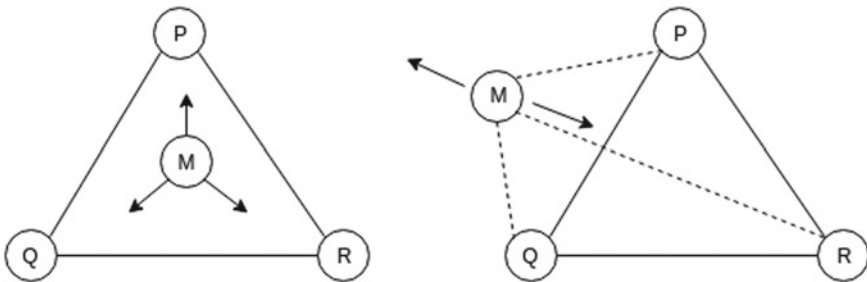


Fig. 1 An inside and outside scenario of perfect PIT test

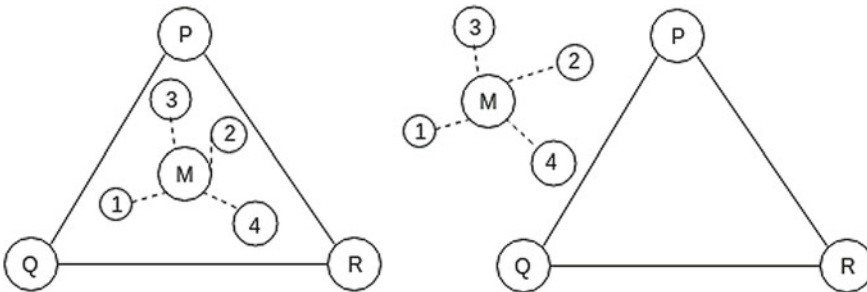
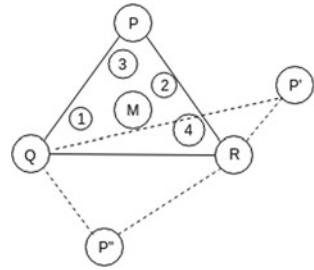


Fig. 2 An inside and outside scenario of approximation PIT test

Fig. 3 Illustration of Sybil attack



The third step includes the APIT aggregation step in which all the results of PIT testing are combined to find the maximum overlying region [5].

At last, the center of gravity of the maximum overlain region is measured to determine the location of sensor nodes with an unknown location (Fig. 3).

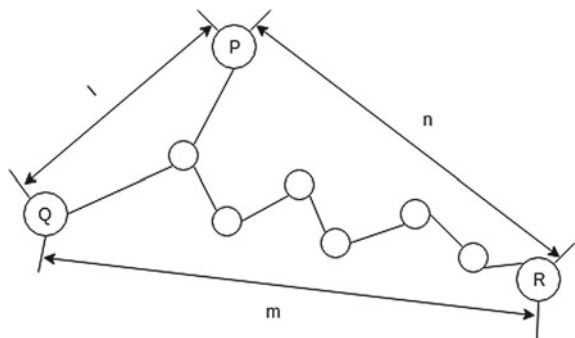
3.2 Basic DV-hop Localization Scheme

DV-hop is a localization scheme that is used to localize the unknown sensor nodes by using connectivity and topology of the wireless sensor network [2] as mentioned in Fig. 4. It uses distance vector routing to build the neighbor node relationship list (NNRL). DV-hop includes three major steps.

In the first step, the least hop counts between unknown nodes and anchor nodes are calculated. Each anchor node broadcasts an information packet which carries the ID of the anchor node and its location with the hop count field [2]. The structure of the broadcasting data packet is $(ID, x_i, y_i, hops)$. When an unknown node receives a data packet, it increases the hop counts by 1 and stores the least hop counts [17, 18].

In the second step, after obtaining the location and hop information from all other beacon nodes, average hop distance is computed from each beacon node [2]. The average hop distance is estimated as

Fig. 4 Illustration of DV-hop localization scheme



$$d_p = \frac{\sum_{p \neq q} \sqrt{((x_p - x_q)^2 + (y_p - y_q)^2)}}{\sum_{p \neq q} h_{pq}} \quad (1)$$

where (x_p, y_p) and (x_q, y_q) are the position of anchor nodes X_p and X_q . h_{pq} is the number of hops between the nearest anchor node, and d is the average hop distance.

In the last step of DV-hop algorithm, coordinates of unknown nodes are estimated, if average hop distance of minimum three different anchor nodes has been estimated, using trilateral or three-side measuring method [19].

3.3 Impact of Sybil Attack on APIT and DV-hop

In the APIT localization scheme, Sybil attack is the most common security threat. It is relatively easy to happen Sybil attack and difficult to resolve. In a Sybil attack, if the anchor node is compromised it can forge multiple identities with different location information but in reality, it is only one sensor node at one physical location. Such Sybil nodes can affect the localization process badly. So that in the presence of Sybil attack, localization of unknown nodes cannot be done precisely.

For example in Fig. 3, P , Q , and R are three anchor nodes and M is a unknown node with the neighbor nodes 1, 2, 3, and 4. If anchor node P is compromised as a malicious node, it can have two identities as shown in Fig. 6, P' and P'' with location coordinates (X'_p, Y'_p) and (X''_p, Y''_p) . If the P' and P'' are considered while localizing, then M lies outside of the $\Delta P'QR$ and $\Delta P''QR$ but inside the ΔPQR so the location will not be the correct one. So that Sybil nodes must be detected and excluded from the localization process [3, 14]. However, after removing the Sybil nodes, the number of the triangle will be reduced that leads to an increase in the number of the blind nodes, and fewer unknown nodes will be localized, but localization accuracy will increase [4]. To maintain the same accuracy while addressing blind node, we have proposed a secure hybrid localization scheme (SFHL) that also localizes blind nodes and detects and excludes suspected Sybil nodes simultaneously. By simulation results, it is concluded that the proposed algorithm performed better than existing ones—SF-APIT and basic APIT.

4 System Model

System models used in the proposed approach are described. The network model and the Sybil attack model are two system models included in this section.

4.1 Network Model

In the proposed localization scheme (SFHL), sensor nodes are deployed in two ways—first one is a random distribution of sensor nodes in a given square shape area, and the second one is the regular distribution of sensor nodes in which sensor nodes are placed on cross points of the square grids [1, 2]. These sensor nodes are considered as static. Some anchor nodes are enabled with GPS to localize anchor nodes. These nodes have a higher communication range, a high computational unit, and large storage than compare to normal sensor nodes [7]. All the sensor nodes lie inside the range of anchor nodes that can receive a broadcasted message by anchor nodes [3]. The ratio of anchor nodes to the total number of sensor nodes is varied from 0.1 to 0.4 in the proposed hybrid localization scheme.

4.2 Sybil Attack Model

One or multiple anchor nodes can be compromised by the attacker to affect the localization process. Sybil nodes are physically at one place but can generate multiple Sybil nodes with different identities and locations; in such cases, the location of unknown nodes cannot be estimated precisely [13]. For example, in Fig. 3 anchor node P generates two other Sybil nodes P' and P'' which are having different identities and locations, but physically there is only one node P . Such location of unknown node M will not be calculated correctly, and to detect such type of nodes, RSS value of these nodes can be used because RSS value depends on physical distance of the node. Sybil attacks can take place in two ways [3, 4]. In the first type, the number of Sybil node is one at a time, it could be with a different location at a different time, and in the second type, there could be multiple Sybil nodes simultaneously as shown in Fig. 3. In this paper, multiple Sybil nodes at the same time model are used.

5 Sybil-Free Hybrid Localization Scheme (SFHL)

In this section, the proposed secure localization scheme, called Sybil-Free Hybrid Localization Scheme (SFHL), is illustrated. SFHL can localize sensor nodes with an unknown location, even in the presence of Sybil attack and also localize blind or unresolved node which is not possible in existing basic APIT and SF-APIT localization scheme [3, 17]. The goal of this paper is to decrease the localization error of basic APIT in the presence of the Sybil attack and to localize blind or unresolved sensor nodes. The suggested algorithm works way better than the existing one in terms of localization error minimization and the number of nodes localized (Table 1).

Table 1 Special symbols used in SFHL scheme

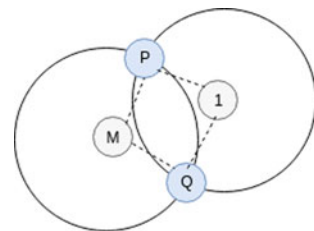
Symbol	Meaning
$\{N_a\}$	Set of the anchor nodes
$\{N_s\}$	Set of the sensor nodes with unknown location
L_h	The h th anchor node
$R_M^{L_h}$	RSS reading of unknown node M from L_h
$R_t^{L_h}$	RSS reading of unknown node t from L_h
S_{L_h, L_k}	The suspect counter of the pair of L_h and L_k

5.1 Sybil-Free APIT Detection Scheme

In Sect. 3.1, the major steps of the APIT are explained. Standard APIT includes four major steps: Beacon information exchange, point-in-triangle (PIT) testing, APIT aggregation, and center of gravity calculation of maximum overlapped area. Sybil nodes are detected in the PIT phase in the proposed approach [3, 4]. In the PIT phase after selecting the pair of three anchor nodes, each pair of two anchors from these three anchor nodes is considered one by one if any pair satisfies condition of Eq. (1), where RSS_{ji} and RSS_{ki} are the RSS readings at i th unknown sensor node obtained from the k th and j th sensor nodes ($k \neq j$), will be suspected [20]. If the difference of RSS value of the received signal at an unknown sensor node from two anchor nodes is less than τ , then its count of the suspect will be increased by 1. If a pair has suspected count more than three, then both the anchor nodes will be marked as Sybil nodes and excluded from further localization process [20]. We have considered suspect counter at least 3 to mark as Sybil node because two unknown nodes are not sufficient, as mentioned in Fig. 5, to identify a Sybil node [3, 21].

For example in Fig. 5 Eq. (1) at unknown nodes M and 1 , having the value of $S = 1$ for pair of anchor nodes P, Q but sensor node P and Q are not Sybil nodes. After the detection of the Sybil nodes, the suspected node will be removed from the network after that unknown sensor nodes will be localized. Since the removal of Sybil nodes, a number of a triangle of anchor nodes will be decreased so that the number of blind nodes may increase [16]. Further, DV-hop algorithm is applied to localize blind node because DV-hop is based on the topology and connectivity of

Fig. 5 An example of wrong judging



the network rather than the PIT test [2]. Such that the accuracy of localization in the presence of Sybil attack will be increased, and blind nodes will also be localized efficiently.

$$S = \begin{cases} 1, & \text{if } |\text{RSS}_{ji} - \text{RSS}_{ki}| \leq \tau \\ 0, & \text{else} \end{cases} \tag{2}$$

$$f(s) = \sum_{p=1}^p S_p \tag{3}$$

$$S = \begin{cases} \text{sybil nodes,} & \text{if } |f(S)| \geq 3 \\ \text{legitimate nodes,} & \text{else} \end{cases} \tag{4}$$

5.2 Steps in SFHL Detection Scheme

In this section, the major steps included in the proposed approach are explained with the help of Fig. 3. SFHL consists of six phases which are as follows:

- **Phase 1:** In this phase beacon message “Hello” with the anchor node ID and location (id, X_i, Y_i) are broadcasted within anchor nodes communication range [20]. After receiving these data packets, each sensor node builds a neighbor anchor node table with fields ID of beacon node, Position, and RSS reading as mentioned in Fig. 3, nodes 1 and M builds Tables 2 and 3.
- **Phase 2:** All individual neighbor anchor tables are shared to build a common table like Table 3, which includes information about all anchor nodes.

Table 2 Table of received beacons by node M

ID	Location	RSS
P	loc_P	R_M^P
Q	loc_Q	R_M^Q
R	loc_R	R_M^R
P'	$\text{loc}_{P'}$	$R_M^{P'}$

Table 3 Combined table of sensor nodes $M, 1, 2$ and 3

ID	Location	RSS $_M$	RSS $_1$	RSS $_2$	RSS $_3$
P	loc_P	R_M^P	R_1^P	R_2^P	R_3^P
Q	loc_Q	R_M^Q	R_1^Q	R_2^Q	R_3^Q
R	loc_R	R_M^R	R_1^R	R_2^R	R_3^R
P'	$\text{loc}_{P'}$	$R_M^{P'}$	$R_1^{P'}$	$R_2^{P'}$	$R_3^{P'}$

- **Phase 3:** SFHL selects three nodes from Table 3 to make a triangle, for example, ΔPQR ; then, possible pairs of selected beacon nodes like (P, Q) , (Q, R) and (P, R) operate on each column of Table 3 to identify the Sybil nodes by applying Eq. (2). If any pair of beacon nodes having $S = 1$, then this pair is suspected and suspect counter increased by one [3]. Each unknown sensor nodes are determined whether it is outside or inside of the triangle based on RSS value in Table 3.
- **Phase 4:** Phase 3 executed repeatedly until every plausible combination of beacon nodes in Table 3 is finished.
- **Phase 5:** Once every iteration executed completely, the maximum overlapped region is calculated, and the center of gravity is determined for the overlapped region to find the position of the unknown nodes [16].
- **Phase 6:** If the number of unresolved sensor nodes is nonzero, then further basic DV-hop approach is applied on blind nodes only in such a way that all the blind nodes will also be localized without affecting the complexity of the localization scheme. It gives the performance results lies between the SF-APIT and APIT, but it also minimizes the number of blind nodes that is most important for location-aware applications.

Figure 6 is the flowchart of the purposed hybrid approach. As shown in the figure, if an unknown node lies inside any triangle of anchor nodes, SF-APIT will be applied to it; otherwise, at last, DV-hop will be applied on all remaining unknown nodes that will minimize the number of blind nodes and manage the decent localization accuracy.

Algorithm 1 consists of the pseudocode of SFHL.

5.3 Calculating Error Range Threshold of RSS Values

Error range threshold of RSS values is needed while determining suspected nodes for Sybil attack [14]. It is represented by ‘ τ ’. Since RSS readings from the same physical location cannot be the same because of random noises, multiple path effects, and biased environment, we need to determine an error range threshold of RSS values [3, 10]. This can be calculated with the help of Eqs. (5)–(7). Firstly, broadcast hello message to its neighbor nodes; then, calculate d_{ji}^{rss} by using equation (5). After that calculate the actual distance by using location coordinates of anchor nodes using Eq. (6) and estimate ϵ using Eq. (7) and get the value of τ by using $\tau = \epsilon + e$, where e is a fluctuation value.

$$RSS_{ji} = -10n \log(d_{ji}^{rss}) + K \tag{5}$$

$$d_{ji}^{real} = \sqrt{((x_j - x_i)^2 - (y_j - y_i)^2)} \tag{6}$$

$$\epsilon = \frac{\sum_{i=1}^{N-1} \sum_{j<i}^N |d_{ji}^{real} - d_{ji}^{rss}|}{C_N^2} \tag{7}$$

Algorithm 1 Proposed SFH Localization

```

1: Input :  $\{N_s\}, \{N_a\}$  .
2: for Every beacon node in  $\{N_a\}$  do
3:   Disseminate 'Hello' packet with beacon information.
4: end for
5: for Every unknown node in  $\{N_s\}$  do
6:   Create the obtained neighbor beacon nodes table.
7: end for
8: for Every unknown sensor in  $\{N_s\}$  do
9:   Build a combined list, named MAL, using the received anchor lists.
10: end for
11: for Every triangle  $T_i \in \binom{N}{3}$  of the beacon nodes do
12:   for Every pair beacon nodes in  $T_i$  from distinct columns of MAL do
13:     if  $S_{L_h, L_k} \leq 2$  then
14:       if  $|(R_i^{L_h} - R_i^{L_k})| < \tau$  then
15:         Increment suspect coefficient  $S_{L_h, L_k}++$ .
16:       end if
17:     end if
18:   end for
19:   if  $S_{L_h, L_k} \geq 3$  then
20:     Both  $L_h$  and  $L_k$  detected as sybil nodes.
21:     Remove them from connectivity and broadcast.
22:     Continue.
23:   end if
24:   if  $APIT(T_i) == Out$  then
25:     Add  $T_i$  as negative triangle,  $AddNegativeTriangle(T_i, -1)$ .
26:   end if
27:   if  $APIT(T_i) == Out$  then
28:     Add  $T_i$  as positive triangle,  $AddPositiveTriangle(T_i, 1)$ .
29:   end if
30: end for
31: Find the maximum overlapped area.
32: Find the location,  $(x_i, y_i)$ , of the unknown node by employing the Center of Gravity(COG) method.
33: if Number of blind nodes  $> 0$  then
34:   Apply shortest path algorithm to find nearest anchor node to blind nodes.
35:   Determine avg. hop distance for each anchor node.
36:   for Each blind node  $B_i$  do
37:     Find location  $(x_{B_i}, y_{B_i})$  of  $B_i$  using three side measuring method.
38:   end for
39: end if
40: Output: Estimated location of sensor nodes,  $(x, y)$ .

```

6 Complexity Analysis

In this section, storage and computational cost are analyzed and compared to the localization scheme APIT. The set of sensor nodes and anchor nodes is represented by N_s and N_a . In the proposed localization scheme SFHL, only RSS value is used in the PIT testing phase to detect suspected nodes so that additional storage and communication cost are negligible.

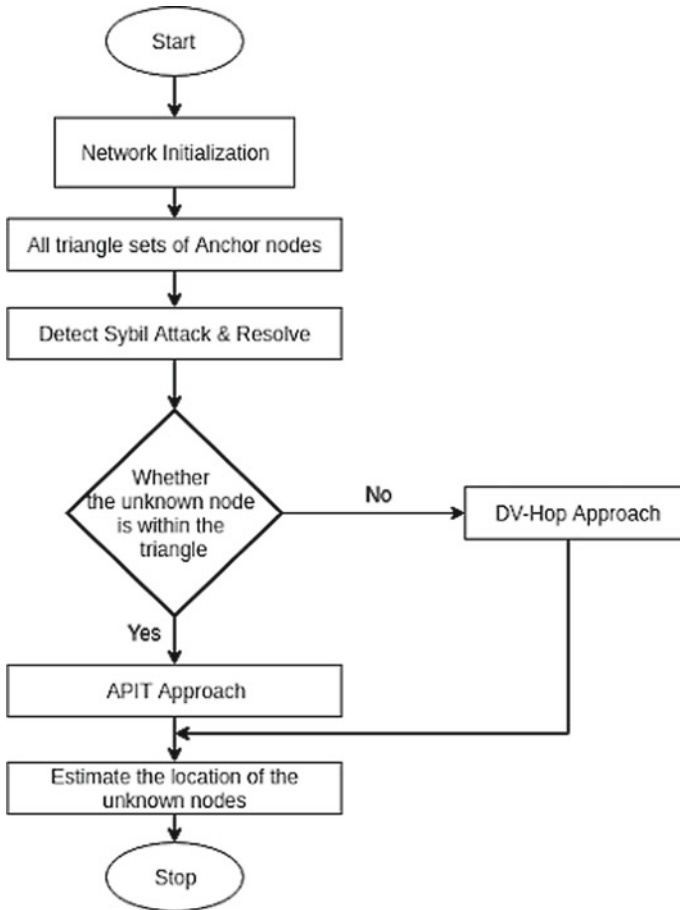


Fig. 6 Flowchart of SFHL

6.1 Computational Cost

The computational cost of the proposed approach can be analyzed with the help of Sect. 5.3 in which major steps of SFHL are included. As we see that upper bound of computational cost is in phase 3 because of selecting possible triangle of anchor nodes than further considering possible pair of two anchor nodes from chosen triangle, approximately $C_3^K \times C_2^3$, where C_3^K is required to select three anchor nodes from K neighbor anchor nodes; then, further C_2^3 is needed to choose two out of three anchor nodes. But since this is already included in the APIT algorithm, there is no additional cost in this PIT phase of the proposed algorithm but in phase 6, DV-hop is applied on only blind nodes so that it will increase the computational cost slightly [3, 22].

6.2 Storage Requirement

Storage cost of proposed algorithm (SFHL) is slightly high than existing basic APIT approach because we need to store flag for suspected nodes, and in addition, we also require shortest paths between sensor nodes to implement DV-hop, to store these we need a 2D vector additionally that will require little more storage than existing localization scheme. Since Sybil-free APIT only needed 4 KB of RAM and 512 kB of flash memory [6] for one sensor node and it will approximately the same for SFHL also, the storage requirement is very less for SFHL [3].

7 Simulation Results

The simulation of the proposed approach, SFHL, is performed in MATLAB R2018a. The simulation area is considered of 500 m \times 500 m, and the communication range of the beacon node and unknown nodes is varied from 100 to 200 m. The proportion of beacon nodes to the total number of sensor nodes is varied from 0.1 to 0.3, but in most of the experiments, it is considered 0.2. Sybil attack simulated by generating two Sybil nodes by an anchor node with different ID and locations but having RSS value difference less than defined threshold τ [22]. Results of simulation are obtained by running the proposed approach SFHL around 30–40 times with the different number of sensors and Sybil nodes. Simulation is performed on an HP Pavilion G series laptop with 2 GB RAM and AMD A4 graphics.

7.1 Performance Evaluation of Simulations

The simulation results evaluated based on average localization estimated error (LEE) (Eq. 8) and detection rate (Eq. 9) which helps to study the number of blind nodes after the completion of the SFHL [3]. The detection rate in existing Sybil-free APIT is around 90% with around 100 sensor nodes, and in the proposed approach, SFHL it is improved up to 95%. Above matrices can be determined as follows:

$$\text{Detection rate} = \frac{|\text{No. of identified sybil nodes}|}{|\text{Total no. of sybil nodes}|} \times 100\% \quad (8)$$

$$\text{LEE} = \frac{\sqrt{((x - x_i)^2 - (y - y_i)^2)}}{R} \quad (9)$$

7.2 Results and Analysis

The simulation results are analyzed, and comparison graphs were plotted. Further, simulation is performed with different parameters to analyze the influence of the Sybil nodes and the performance of the proposed approach.

Figure 7 shows the random node deployment in the squared area. In square regular deployment, sensor nodes are placed on cross points of the grid but in real-life application like in military operation, square regular deployment is not feasible so that in most of simulation experiment, square random deployment is used.

1. **Illustration of Localization Process of SFHL:** Fig. 8 illustrates the localization process of SFHL. Sensor nodes are disposed of randomly in the 500 m × 500 m area. The total number of sensor nodes and beacon nodes is considered 100 and 30. The position of unknown nodes is determined using SFHL and represented by blue circles, and localization errors are represented by plotting lines between the actual and estimated location of sensor nodes. Anchor nodes are represented by red stars.
2. **Comparison of No. of Blind Nodes:** In Figs. 9 and 10, the number of blind nodes is compared with different localization schemes. Blind nodes are depicted by the black-colored small circle, and Sybil nodes are denoted by using red-colored cross symbols. From Fig. 9, it is clear to see that the number of blind nodes is approximately zero using SFHL and higher using APIT and SF-APIT.
3. **Localization Error Versus No. of Sensor Nodes:** Fig. 11 describes the comparative analysis of estimated localization error with the varying number of sensor nodes. The number of sensor nodes varies from 20 to 150, and localization error is estimated with three different approaches APIT, SF-APIT, and SFHL. The

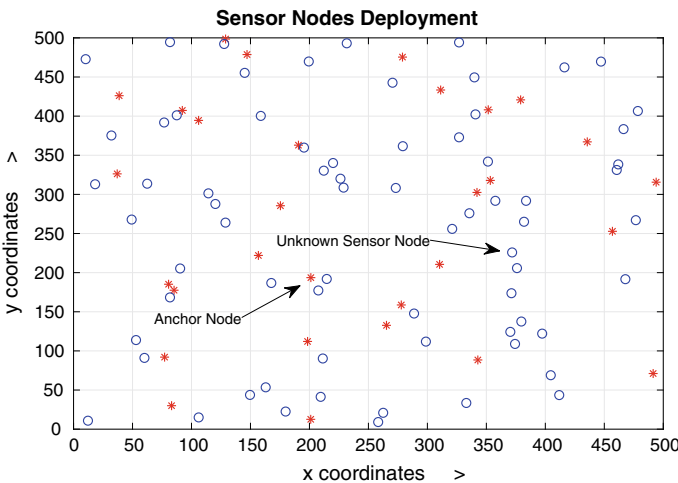


Fig. 7 Sensor nodes deployment

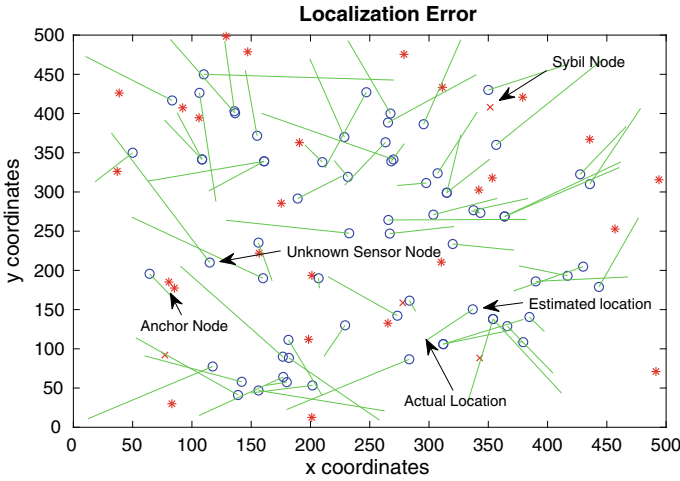


Fig. 8 Illustration of localization error after SFHL

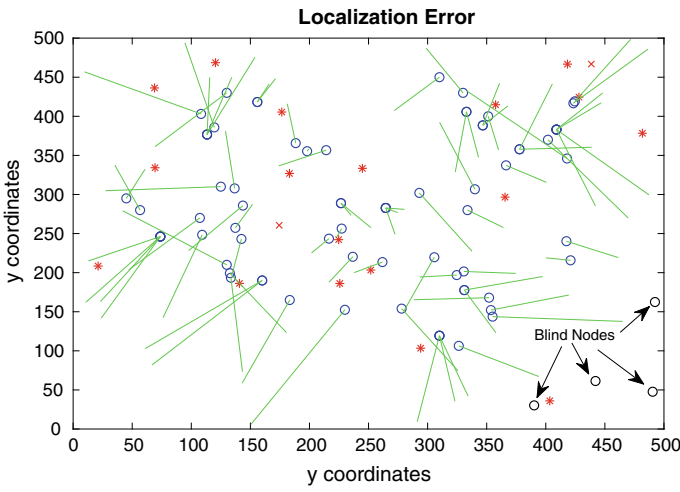


Fig. 9 Blind nodes depiction before SFHL

average localization error using the APIT approach, SF-APIT, and SFHL are 0.38, 0.35, and 0.36, respectively. In the proposed approach, SFHL, to localize blind nodes, hybrid approach is used because of that localization error increased than compared to SF-APIT but less than the basic APIT localization approach.

4. **Localization Error Versus Communication Range:** In Fig. 12, the communication range of anchor nodes is varied from 50 to 200m and localization error is estimated with different localization schemes and compared to plot analysis graph. The estimated localization error is higher with a large communication

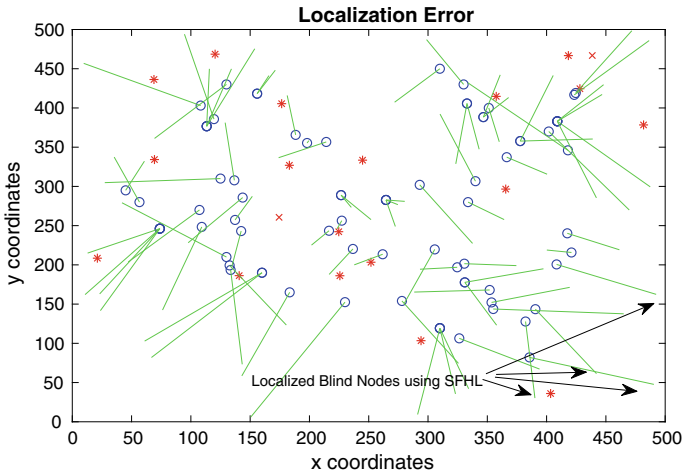


Fig. 10 Blind nodes depiction after applying SFHL

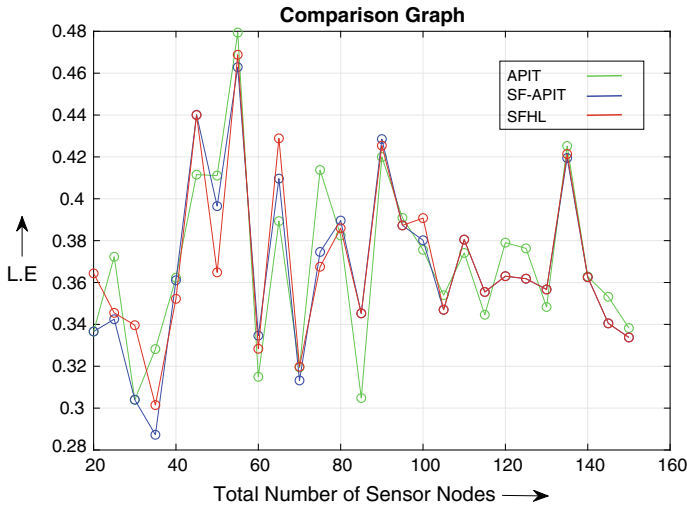


Fig. 11 Localization error variation with the total no. of sensor nodes

range. But with a low communication, range number of blind nodes would be higher so that the communication range should not be too small and large.

5. **Detection Rate Versus No. of Sybil Nodes:** Fig. 13 represents the comparison between the count of Sybil nodes that are identified versus the total number of Sybil nodes in WSNs. The number of Sybil nodes is varied from 2 to 16. The number of beacon nodes is considered from 10 to 30. From the plotted graph, it is easy to conclude that with more anchors and Sybil nodes, detection rate is more than 90%. Because a higher number of beacon nodes lead to a more number of

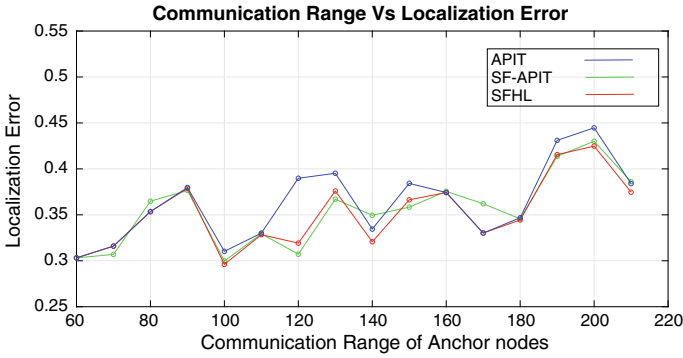


Fig. 12 Localization error variation with communication range of beacon nodes

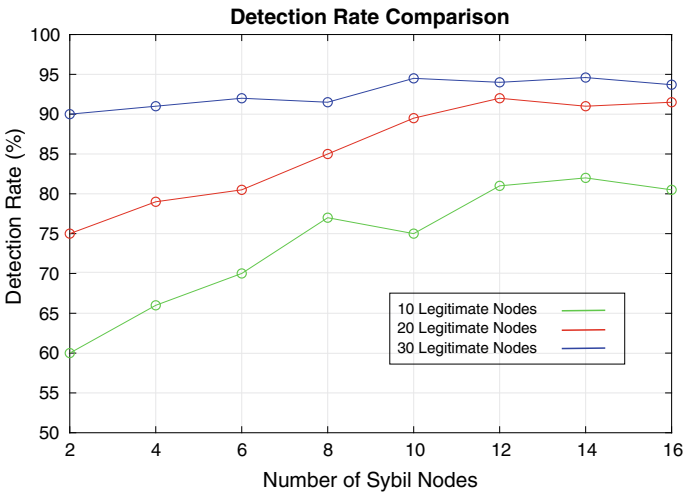


Fig. 13 Depiction of detection rate with varying number of sybil nodes

triangles of beacon nodes which affect the Sybil nodes detection step of SFHL and with the low number of beacons, the detection rate will also be lesser.

6. **Localization Error Versus No. of Beacon Nodes:** In Fig. 14, the estimated localization error is monitored with a varied number of beacon nodes. The number of beacon nodes is changed from 10 to 30. From Fig. 14, it is clear to see that with more no. of beacon nodes, avg. localization error of proposed localization scheme SFHL is approximately 0.37 which is higher than SF-APIT but better than APIT. Thus, proposed approach SFHL performed better than existing localization schemes in terms of minimizing the number of blind nodes and localization error.

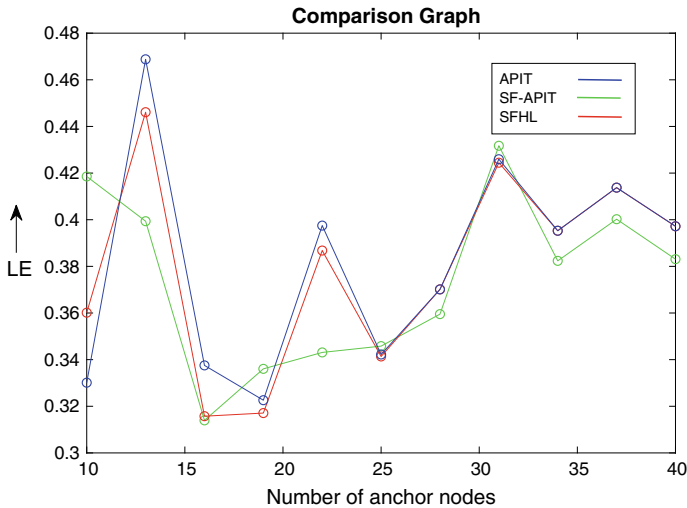


Fig. 14 Comparison of localization error with changing no. of beacon nodes

8 Conclusion and Future Scope

Wireless sensor networks are vital to a variety of security threats because of its wireless communication medium. Sybil attack has a significant effect on the localization schemes like APIT and DV-hop, etc. Since many applications of WSNs are critically depended on the location of sensor nodes, Sybil attacks should be resolved. In this paper, we have proposed a lightweight and less complex secure hybrid localization which is easy to understand and implement. From the simulation results, it is concluded that the suggested approach, SFHL, performs beneficial than the APIT approach. SFHL detects the Sybil attack and removes suspected node apart from that it also localizes the remaining unresolved sensor nodes or blind nodes. SFHL efficiently detects the Sybil attack and localizes all legitimate sensor nodes which is a significant improvement in the localization. In future research, the proposed algorithm can be extended to detect and resolve multiple security attacks and should be tested in real WSN environment.

References

1. Jiang J, Han G, Zhu C, Dong Y, Zhang N (2011) Secure localization in wireless sensor networks: a survey. *J Commun* 6(6):460–470. <https://doi.org/10.4304/jcm.6.6.460-470>
2. Li J, Wang D, Wang Y (2018) Security DV-hop localisation algorithm against wormhole attack in wireless sensor network. *IET Wirel Sensor Syst* 8(2):68–75. <https://doi.org/10.1049/iet-wss.2017.0075>

3. Yuan Y, Huo L, Wang Z, Hogrefe D (2018) Secure APIT localization scheme against Sybil attacks in distributed wireless sensor networks. *IEEE Access* 6:27629–27636. <https://doi.org/10.1109/ACCESS.2018.2836898>
4. Atul G, Dhonde SB (2016) A survey on security attacks in wireless sensor networks. In: *International conference on computing for sustainable global development (INDIACom)*
5. Zeng J, Wang Hong XII (2009) Improvement on APIT localization algorithms for wireless sensor networks. In: *International conference on networks security, wireless communications and trusted computing, Wuhan*, pp 719–723. <https://doi.org/10.1109/NSWCTC.2009.370>
6. Tan H, Feng L (2012) Research and implementation of APIT positioning algorithm WSN. In: *9th international conference on fuzzy systems and knowledge discovery, Sichuan*, pp 2214–2215. <https://doi.org/10.1109/FSKD.2012.6234209>
7. Chen X, Makki K, Yen K, Pissinou N (2009) Sensor network security: a survey. *IEEE Commun Surv Tutor* 11(2):52–73
8. Lazos L, Poovendran R (2004) SeRLoc: secure range independent localization for wireless sensor networks. In: *Proceedings of the 3rd ACM workshop on wireless security (WiSe '04)*. ACM, New York, pp 21–30. <https://doi.org/10.1145/1023646.1023650>
9. Lazos L, Poovendran R (2006) HiRLoc: high-resolution robust localization for wireless sensor networks. *IEEE J Sel Areas Commun* 24(2):233–246. <https://doi.org/10.1109/JSAC.2005.861381> Feb
10. Lazos L, Poovendran R, Capkun S (2005) ROPE: robust position estimation in wireless sensor networks. In: *Fourth international symposium on information processing in sensor networks, Boise*, pp 324–331. <https://doi.org/10.1109/IPSNS.2005.1440942>
11. Capkun S, Cagalj M, Srivastava M (2006) Secure localization with hidden and mobile base stations. In: *IEEE INFOCOM, 25th IEEE international conference on computer communications, Barcelona*, pp 1–10. <https://doi.org/10.1109/INFOCOM.2006.302>
12. Li S, Wang X, Zhao S, Wang J, Li L (2014) Local semidefinite programming-based node localization system for wireless sensor network applications. *IEEE Syst J* 8(3):879–888. <https://doi.org/10.1109/JSYST.2013.2260625> Sept
13. Demirbas M, Song Y (2006) An RSSI-based scheme for Sybil attack detection in wireless sensor networks. In: *Proceedings of the 2006 international symposium on on world of wireless, mobile and multimedia networks (WOWMOM '06)*. IEEE Computer Society, Washington, pp 564–570. <https://doi.org/10.1109/WOWMOM.2006.27>
14. Wen M, Li H, Zheng Y et al (2008) TDOA-based Sybil attack detection scheme for wireless sensor networks. *J Shanghai Univ (Engl Ed)* 12(2):66–70. <https://doi.org/10.1007/s11741-008-0113-2>
15. Jaya, Payal A (2018) Analysis and implementation of APIT localization algorithm for wireless sensor network. In: *3rd international conference on computer and communication systems (ICCCS), Nagoya*, pp 310–313. <https://doi.org/10.1109/CCOMS.2018.8463241>
16. Wang Jz, Jin H (2009) Improvement on APIT localization algorithms for wireless sensor networks. In: *International conference on networks security, wireless communications and trusted computing, Wuhan*, pp 719–723. <https://doi.org/10.1109/NSWCTC.2009.370>
17. Liu C, Liu S, Zhang W et al (2016) The Performance evaluation of hybrid localization algorithm in wireless sensor networks. *Mobile Netw Appl* 21:994. <https://doi.org/10.1007/s11036-016-0737-1>
18. Wu J, Chen H, Lou W, Wang Z, Wang Z (2010) Label-based DV-HOP localization against wormhole attacks in wireless sensor networks. In: *Proceedings of the 5th IEEE international conference on networking, architecture, and storage, Macau*, pp 79–88. <https://doi.org/10.1109/NAS.2010.41>
19. Guo Z, Min L, Li H, Wu W (2013) Improved DV-Hop localization algorithm based on RSSI value and hop correction. In: Wang R, Xiao F (eds) *Advances in wireless sensor networks*. CWSN 2012. Communications in computer and information science, vol 334. Springer, Berlin, Heidelberg
20. Cheng W, Li J, Li H (2012) An improved APIT location algorithm for wireless sensor networks. In: Xie A, Huang X (eds) *Advances in electrical engineering and automation*. Advances in

- intelligent and soft computing, vol 139. Springer, Berlin, Heidelberg. https://doi.org/10.1007/978-3-642-27951-5_17
21. Lu D, Shi-qi L (2014) An improved localization algorithm of APIT in wireless sensor network. *J Harbin Univ Sci Technol* 19(4):94–99
 22. Kumar P, Reddy L, Varma S (2009) Distance measurement and error estimation scheme for RSSI based localization in wireless sensor networks. In: Fifth international conference on wireless communication and sensor networks (WCSN), Allahabad, pp 1–4. <https://doi.org/10.1109/WCSN.2009.5434802>
 23. Lin Z, Houwang Z (2015) DV-HOP based node localization algorithm in wireless sensor network. *Comput Ap Softw* 32(11):92–96
 24. Man DP, Qin GD, Yang W, Xuan SC (2014) Improved DV-HOP algorithm for enhancing localization accuracy in WSN. *Appl Mech Mater* 543–547:3256–3259
 25. Bochem A, Yuan Y, Hogrefe D (2016) Tri-MCL: synergistic localization for mobile ad-hoc and wireless sensor networks. In: IEEE 41st conference on local computer networks (LCN), Dubai, pp 333–338. <https://doi.org/10.1109/LCN.2016.61>
 26. Elnahrawy E, Li X, Martin RP (2004) The limits of localization using signal strength: a comparative study. In: 1st annual IEEE communications society conference on sensor and ad hoc communications and networks. IEEE SECON 2004, Santa Clara, pp 406–414. <https://doi.org/10.1109/SAHCN.2004.1381942>
 27. He T, Huang C, Blum BM, Stankovic JA, Abdelzaher T (2003) Range-free localization schemes for large scale sensor networks. In: Proceedings of the 9th annual international conference on mobile computing and networking (MobiCom '03). ACM, New York, pp 81–95. <https://doi.org/10.1145/938985.938995>
 28. Zhang Y, Fan KF, Zhang SB, Mo W (2010) AOA based trust evaluation scheme for Sybil attack detection in WSN. *Appl Res Comput* 27(2):1847–1849
 29. Liu J, Wang Z, Yao M et al (2016) VN-APIT: virtual nodes-based range-free APIT localization scheme for WSN. *Wirel Netw* 22:867. <https://doi.org/10.1007/s11276-015-1007-z>

Hybrid-RPL: A Step Toward Ensuring Scalable Routing in Internet of Things



K. V. Amal , J. Jaisooraj , Priya Chandran , and S. D. Madhu Kumar 

Abstract The complete realization of Internet of Things (IoT) paradigm comes with its own share of challenges. Scalability, which is one among these challenges, can be addressed through efficient routing protocols developed for low power and lossy networks (LLNs). The paper proposes an LLN routing protocol, hybrid-RPL (H-RPL), which allows the nodes to efficiently and adaptively switch\storing and non-storing modes of operation. H-RPL takes into account the network resources like node memory and node battery while performing the switch operations. Also, the proposed routing protocol performs the dual role of reducing traffic surrounding the root node, as well as preventing the routing table overflow. H-RPL has been simulated and tested, and the results show considerable improvements compared to the storing and non-storing modes of traditional RPL.

Keywords Internet of things · Low power and lossy networks · RPL · Scalability

1 Introduction

Internet of Things (IoT) has become a reality. With that, more and more ‘things’ have found their place in the global Internet platform. A constructive fusion of various computing and communication technologies can rightly be termed as the backbone of such a compelling paradigm. Considering the enormous possibilities associated with such a paradigm, the current surge in the development of various socially relevant applications (on the top of IoT paradigm) seems justifiable. Such a path-breaking consequent undoubtedly requires a combination of more than one antecedents. Seamless connectivity among the ‘things’ is one such antecedent and in all probability, the most important too.

It is quite obvious that networking protocols play an important role in ensuring such a persistent connectivity among ‘things’/sensors. *Low power and lossy networks*

K. V. Amal · J. Jaisooraj (✉) · P. Chandran · S. D. Madhu Kumar
Computer Science and Engineering Department, National Institute of Technology Calicut,
Kozhikode, Kerala 673601, India
e-mail: jaisooraj11@gmail.com

(LLNs) can quite correctly be addressed as an enabling technology for the realization of IoT paradigm. If we are to define LLNs using a single feature, it will be the resource-constrained nature of LLN nodes. LLNs consist of a significant portion of constrained nodes, thereby making it a resource-constrained network [1]. As a consequence, low throughput, high packet loss (and thereby low packet delivery ratio), and increased delay characterize low power and lossy networks (LLNs). LLNs being such an important enabling technology, seamless connectivity among ‘things’ weighs heavily on LLN routing protocols.

Routing in LLNs has always attracted an active attention of the researchers, ever since the inception of *routing protocol for LLNs (RPL)* by the *Internet Engineering Task Force (IETF)* in 2012 [2]. Subsequent years saw a lot of works being taken up in this area, so as to improve the efficiency of core RPL protocol (both in static as well as mobile versions of LLNs). In addition to RPL, which is a proactive routing protocol, works have also been undertaken by the IETF as well as other eminent researchers to develop on-demand as well as opportunistic LLN routing protocols. A brief analysis on such existing LLN routing protocols will be discussed in Sect. 2. Here, we have developed an enhanced version of RPL known as the *hybrid-RPL (H-RPL)*.

To be more specific, H-RPL has been designed and developed as a step to address the scalability issues put forward by the IoT paradigm. We claim this by completely acknowledging the fact that solutions from different viewpoints are required to completely answer the scalability challenges. Here, we propose a solution concentrating on the two modes of operation allowed in RPL, i.e., the non-storing and storing modes of operation. Non-storing mode requires only the root node to store the routing information about the entire network. In contrast, storing mode requires each and every node to store the routing information. Both these modes have their own share of advantages and disadvantages. While the non-storing mode of operation has an advantage that it allows the resource-constrained LLN nodes to be free from storing the routing information, it is also exposed to the concern of an increased traffic surrounding the root node. It is highly inefficient considering the fact that, even if the source and destination are in the same network, the network traffic will have to pass through the root. On the other hand, storing mode of operation tackles the risk of an increased traffic surrounding the root by compromising the memory capacity of nodes. Unlike the most common versions of RPL, where all the nodes are either storing or non-storing, H-RPL allows the nodes to switch between these two modes depending on the network conditions. By an efficient and adaptive mixing of these two modes of operation, it bypasses the risk of an increased traffic surrounding the root as the network size increases. The periodic switching allows this to be done without overly exhausting the node memory. Further, H-RPL is interoperable with the nodes running on standard RPL, i.e., backward compatibility is ensured.

The paper is structured as follows: Sect. 2 explains the state-of-the-art routing in LLNs, Sect. 3 discusses the proposed routing protocol, H-RPL, Sect. 4 provides the performance analysis of H-RPL, and Sect. 5 concludes the paper.

2 Related Work

Routing in low power and lossy networks (LLNs) puts forward a lot of challenges, be it either scalability, mobility, resource management, or interoperability. Being an IoT enabling technology, LLN has received considerable attention of the researchers. A working group named *Routing over Low Power and Lossy Networks (ROLL)* has been created by the IETF, with a specific objective of developing efficient LLN routing protocols. This section provides a brief review regarding the most important works in the area of LLN routing.

Routing protocol for LLNs (RPL), developed by the IETF in 2012, is quite often referred to as the de facto IoT routing protocol [2]. RPL, being a proactive routing protocol, operates by constructing a *Destination Oriented Directed Acyclic Graph (DODAG)* pointing toward the root. The root node could either be a gateway or a node connected to the gateway. In either case, the root node has a consistent power supply. Further, RPL maintains the topology through periodic transmission of control messages, governed by a trickle timer. *DODAG Information Object (DIO)* aids in the initial construction of the topology as well in the periodic maintenance, *DODAG Information Solicitation (DIS)* helps the new/disconnected nodes to get attached/reattached to the topology, and *Destination Advertisement Object (DAO)* expresses the willingness of a node to act as destination. Even though on-demand [3] and opportunistic [4, 5] routing protocols have been developed for LLNs, we focus on the important variants of RPL in this paper.

RPL was designed primarily for static networks. But, with advancements like *Industrial IoT (IIoT)*, mobility and scalability have become quintessential in the design of LLN routing protocols. Hence, a lot of developments have been incorporated over the core RPL protocol in order to make it more efficient. Now, let us categorize the most important RPL variants into two—those focusing on mobility, and those focusing on mixing of the two modes of operation (i.e., storing and non-storing modes). Coming to the first category, [6–9] focus on incorporating mobility into RPL. Fotouhi et al. [6] successfully employ the concept of smart hop, which allows the mobile nodes to switch their parents as per the topology changes. The authors in [7] attempt to develop an enhanced version of the RPL by setting up multiple paths to the destination and then distributing the traffic uniformly among them. Sanshi et al. [8] and [9] put forward the usage of different routing metrics for static and mobile nodes, in order to make the protocol more efficient. Coming to the second category of protocols, there are interesting attempts to mix both storing and non-storing nodes in a single network [10–12]. However, these solutions incur additional overhead to the entire process. The solutions proposed in [10] and [11] involve a combination of source routing as well as hop-by-hop routing, thereby increasing the complexity. On the other hand, solution proposed in [12] requires a parent node to store the operating modes of nodes present in its sub-DODAG. Also, these proposed solutions do not allow a node to switch its mode of operation from storing to non-storing and vice versa. However, Kunal Vyas et al. in [13] do propose a solution

which allows the switching of modes. But, it does not consider highly significant networking resources like battery capacity, while performing a switch.

Hybrid-RPL (H-RPL), which we propose in this paper, falls into the second category mentioned above. Even though similar to [13], H-RPL considers the residual battery capacity of nodes while performing the switch. It efficiently allows the individual nodes to switch between storing and non-storing modes of operation, by considering vital network resources like memory capacity of a node and the energy consumed by it. Such a measure prevents the obvious performance degradation as the network size increases. In more technical terms, we can say that it enhances the scalability of LLNs with respect to routing. A detailed account of the proposed routing protocol has been provided in Sect. 3.

3 Hybrid-RPL

This section discusses in detail the proposed routing protocol, hybrid-RPL (H-RPL). As already mentioned in Sect. 1 and Sect. 2, H-RPL allows the nodes in an LLN to switch between storing and non-storing modes of operation, where the nodes are static in nature. Such a decision to switch between these two modes is taken based on the routing table overflow and residual battery of the node. H-RPL operates in two phases: DODAG construction phase (Algorithm 1) and routing phase (Algorithm 2). Each of the above two phases is explained in the following subsections.

3.1 *DODAG Construction and Maintenance*

Destination-Oriented Directed Acyclic Graph (DODAG) construction is similar to the procedure followed in the storing mode of standard routing protocol for LLNs (RPL). To start with, all the nodes in the network are assumed to follow the storing mode of operation, i.e., each and every node should store the routing information regarding its sub-DODAG. Contrary to standard RPL, there is a significant difference in the DODAG maintenance phase of H-RPL. H-RPL allows the individual nodes in LLN to switch from storing to non-storing mode.

As already mentioned in Sect. 1, a node operating in storing mode requires to store the routing information of its sub-DODAG, whereas a node operating in non-storing mode does not store any routing information. A non-storing node simply forwards the packet to its parent node, until it reaches the root node. Hence, it is quite obvious to interpret an increased traffic surrounding the root node, if there is an increased number of non-storing node in the network. Storing nodes, on the other hand, possess the risk of both routing table overflow (memory) as well as battery depletion. Hence, H-RPL takes into account both these parameters (i.e., memory and residual battery of nodes) while performing the switch operation. In H-RPL, a node changes its mode from storing to non-storing owing to either a routing table overflow or the residual

battery going below a threshold. This is unlike [13], where the residual battery is not considered. The switching from storing to non-storing mode is marked by the flushing of routing table of that node. If a node is operating in the storing mode, it adds the corresponding routing table entry on receiving a DAO message. On the other hand, if it is operating in non-storing mode, the DAO message will be forwarded to its preferred parent, without adding a new routing information in its table. Such an adaptive switching of modes ensures that the count of non-storing nodes does not cross a limit at any instant in the network.

Algorithm 1: DODAG Maintenance

Input: DAO messages from child nodes

Output: Mode = Storing/ Non-storing

(Runs on all nodes except the root)

Begin

if (mode=="Storing") **then**

if (is_present (entry)!=TRUE) **then**

 Add (entry) // Add the corresponding routing entry

if (overflow (table) == TRUE **OR** residual_battery < threshold) **then**

 mode = "Non-storing"

 Delete (entries) // Delete all routing entries

End if

End if

else

 Forward (preferred_parent)

End

3.2 Routing Procedure

A node operating in the non-storing mode does not store any routing entries. Consequently, such a node always forwards the received data packet to its preferred parent. In contrast, a storing node, on receiving a data packet, checks whether it has a routing table entry pointing toward the intended destination. If so, it will forward the packet to the next hop in that route. Else, the packet will be forwarded to its preferred parent, which in turn does the same operation. In either case, if all the en-route nodes fail to find a path to the destination, the data packet will eventually reach the root. The root will surely contain routing information of the entire network, and thus, the data packet will be forwarded to the destination. Thus, in H-RPL, a packet passes through the root if either all the intermediate nodes are non-storing or if none of the intermediate storing nodes have a path toward the destination [13]. As per our simulation

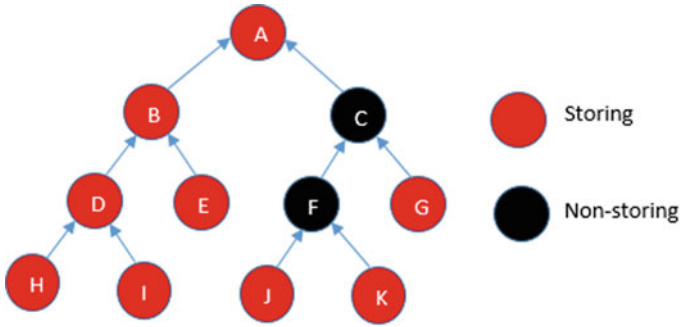


Fig. 1 H-RPL topology

Table 1 Routing entries

Node	Parent	Routing entry (destination, parent)
A	Nil	(B, A), (C, A), (D, B), (E, B), (F, C), (G, C), (H, D), (I, D), (J, F), (K, F)
B	A	(D, B), (E, B), (H, D), (I, D)
D	B	(H, D), (I, D)
C, F	A, C	Nil (non-storing)
E, G, H, I, J, K	B, C, D, D, F, F	Nil (leaf nodes)

results, such a probability is very less. Hence, there is a reduced traffic surrounding the root, and there is an increase in packet delivery ratio. Figure 1 shows an instance of the H-RPL topology consisting of both storing and non-storing nodes. Table 1 shows the corresponding routing entries of each node in that topology.

For instance, suppose node H wants to send a packet to node E. On receiving the packet from H, node D checks whether it has a routing entry so as to reach E. Since D does not have a route to E, the data packet is forwarded to its preferred parent, B. B consists of a routing entry to E, and hence, the packet will be directly forwarded to E, without going to A, i.e., root. A data packet will have to traverse the root only in worst cases. Even as the network scales up in size, occurrence of such instances will be less. This has been justified using the results we have obtained and is discussed in Sect. 4.

Algorithm 2: Routing

Input: Data packet**Output:** Forwards the packet*(Runs on all nodes)***Begin****if** (mode == “Storing”) **then** **if** (is_reachable (destination) == TRUE) **then**

Forward (next_hop) // if path to the destination is available

else

Forward (preferred_parent) // if path to the destination is not available

else

Forward (preferred_parent) // if non-storing mode

End

3.3 Interoperability with RPL

It is always desirable for a routing protocol to be compatible with the previous versions. The case of H-RPL is also not different. H-RPL can interoperate with nodes running on standard RPL. H-RPL does not make any alteration on various control messages used in RPL, be it DIS, DIO, or DAO. Mode switching performed in H-RPL is solely based on the characteristics of individual nodes. Hence, even if a node running on RPL does not have the ability to switch between modes, it can operate in its own inherent mode (be it either storing or non-storing) along with other H-RPL nodes.

4 Performance Analysis

This section provides a detailed account on the performance analysis of H-RPL. A series of simulations were conducted using Cooja simulator within the Contiki operating system. Various parameters used for the simulations, along with their values, are summarized in Table 2.

4.1 Observations

The proposed routing protocol, H-RPL, has been simulated and tested against standard performance metrics. Comparisons were made with standard RPL operating in storing and non-storing modes separately. Simulation results have shown better results for H-RPL in packet delivery ratio, packet loss, and end-to-end delay. Such an

Table 2 Simulation environment

Parameters	Value
Area	2500 m ²
Number of nodes	10, 20, 30, ..., 900
Objective function	ETX
Transmission range	50 m
Network protocol	RPL
Transmission mode	Storing, non-storing, mixed
Topology	Random
Radio medium	Unit disk graph (UDG)
Contiki mote type	Tmote Sky, Wismote, z1
Mote startup delay	1000 ms

enhancement in performance of H-RPL has been obtained by maintaining comparable levels of convergence time and average power consumption of nodes with standard RPL. The details of these observations have been given below:

- Packet Delivery Ratio**—It finds its definition as the ratio of total number of packets received correctly at the destination, over the total number of packets sent. As shown in Fig. 2, H-RPL shows a considerable increase in packet delivery ratio, as compared to standard RPL. Even if the network size scales up to 900, H-RPL quite decisively outperforms RPL in terms of packet delivery ratio.

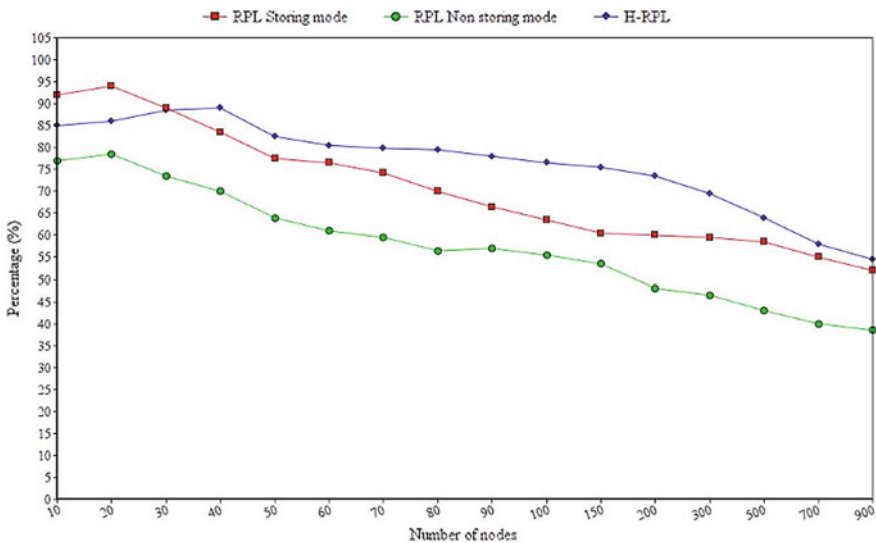


Fig. 2 Packet delivery ratio versus number of nodes

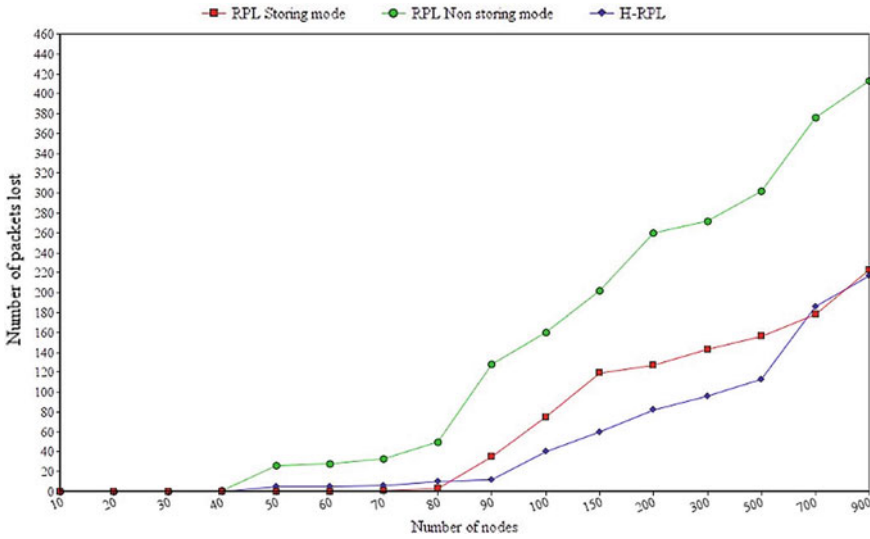


Fig. 3 Packets lost versus number of nodes

- Packet Loss**—It signifies the total number of packets that fail to reach the intended destination over a given period of time. In order to measure the packet loss for RPL–storing, RPL–non-storing, and H-RPL, we have performed the simulation for 20 min. The values captured for packet loss, using *Wireshark network analyzer*, in each of the three cases are plotted as a graph in Fig. 3. The reduction in number of packets lost for H-RPL can be attributed to a less traffic surrounding the root node, as well as the periodic mode switching.
- End-to-end Delay**—This is termed as the total time elapsed between sending and receiving of a data packet. Figure 4 shows the graphical representation of results which we have obtained while calculating end-to-end delay. As it can be inferred from the graph, H-RPL outperforms the other two as the size of network increases. In all other cases, the value remains comparable without any degradation.
- Convergence Time**—In simple terms, convergence time can be defined as the time taken for setting up the DODAG topology. More technically, it is the time elapsed between the first DIO sent by the root and the last node joining the topology [13]. In spite of the additional functionality of mode switching, the convergence time of H-RPL remains almost similar compared to the other two RPL versions (Fig. 5).
- Average Power Consumption**—Since the nodes in storing mode have to handle routing functionalities, the average power consumption of individual nodes will be higher when compared to the nodes in non-storing mode. As depicted in Fig. 6, the average power consumption of nodes in H-RPL is less compared to storing mode and comparable with non-storing mode.
- Mode switching**—Fig. 7 shows the number of nodes which got switched from storing to non-storing mode of operation. We can see that there are more number of

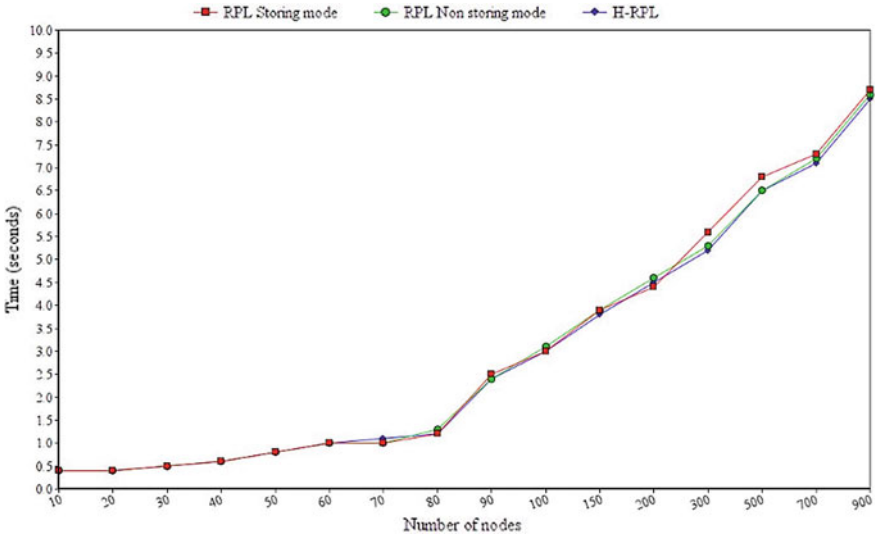


Fig. 4 End-to-end delay versus number of nodes

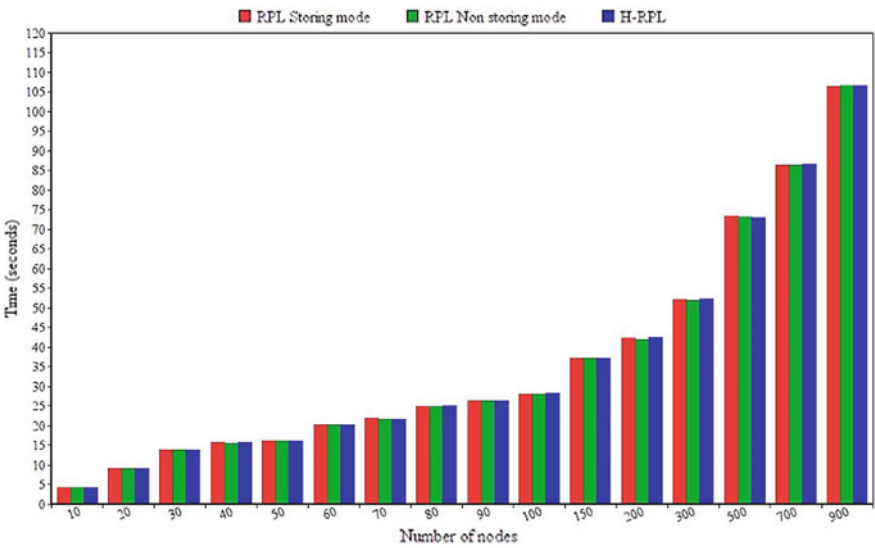


Fig. 5 Convergence time versus number of nodes

switches as the network grows in size. But still, the storing nodes constitute a huge majority of the entire network, thereby ensuring a reduced traffic surrounding the root.

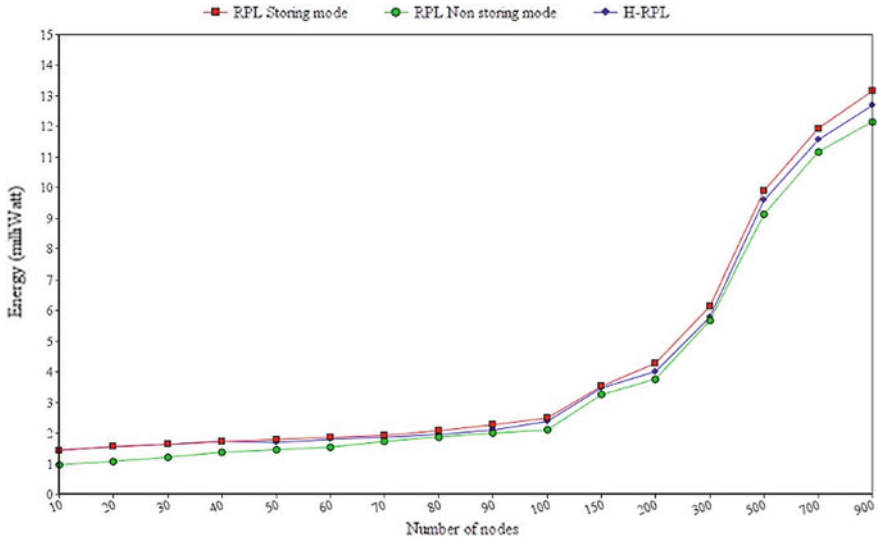


Fig. 6 Energy consumed versus number of nodes

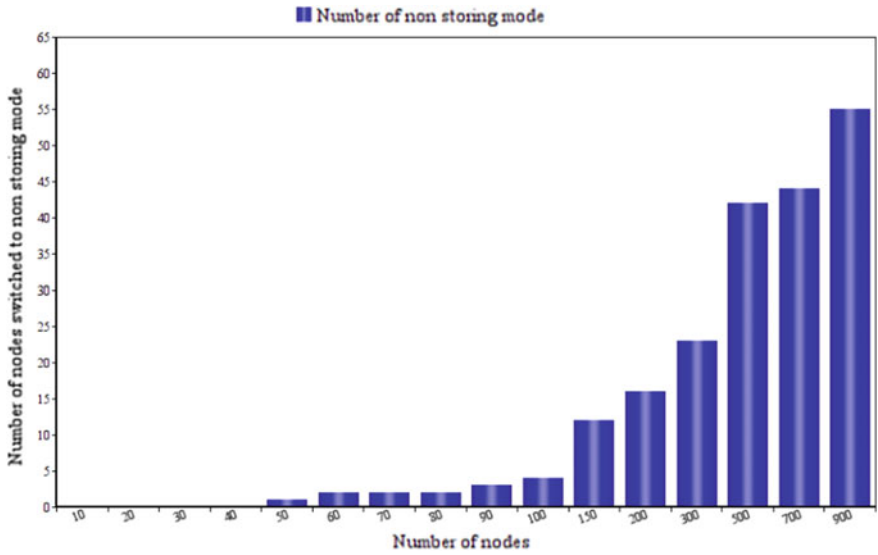


Fig. 7 Number of nodes switched to non-storing mode

In the above depicted evaluations, we have not included network lifetime and control overhead. Network lifetime is termed as the time at which the first node dies out of battery. Since we are immediately switching to non-storing mode on an event of either routing table overflow or battery drain out, no node has died out of battery in our simulation which extends up to 900 nodes. Also, the additional operation of mode switching in H-RPL does not require any control messages. As a result, additional control overhead is not incurred in H-RPL as compared to the storing and non-storing modes of RPL. In all other cases, H-RPL outperforms the other two in a large-sized network. Hence, it is safe to assume that as the network scales up in size, H-RPL performs better. Therefore, even though there are other issues to be tackled, we can say this as a step to improve the scalability of routing in Internet of Things (IoT).

5 Conclusion

In this paper, we have proposed a novel low power and lossy network (LLN) routing protocol, hybrid-RPL (H-RPL). H-RPL has been designed so as to allow the individual nodes in a network to switch between storing and non-storing modes of operation. The protocol facilitates switching of modes from storing to non-storing on the basis of vital network resources like memory and residual battery capacity of a node. Such a periodic switching ensures that the number of non-storing nodes does not go beyond a limit, thereby mitigating the risk of an increased traffic surrounding the root. Also, the protocol ensures, through a check on routing table overflow, that the resource-constrained nodes do not overly exhaust their memory. The paper also provides sufficient simulation results, which indicate that the proposed routing protocol is scalable. As part of the future work, H-RPL can be extended so as to operate with mobile nodes.

References

1. Bormann C et al (2014) Terminology for constrained-node networks. IETF RFC 7228
2. Winter T et al (2012) RPL: IPv6 routing protocol for low-power and lossy networks. In: IETF RFC 6550
3. Clausen T et al (2013) The lightweight on-demand ad hoc distance-vector routing protocol—next generation (LOADng). Internet Draft
4. Gormus S, Fan Z, Bocus Z, Kulkarni P (2011) Opportunistic communications to improve reliability of AMI mesh networks. In: 2nd IEEE PES international conference and exhibition on innovative smart grid technologies, IEEE
5. Gormus S, Tosato F, Fan Z, Bocus Z, Kulkarni P (2011) Opportunistic RPL for reliable AMI mesh networks. *Wireless networks*. Springer, Berlin
6. Fotouhi H, Moreira D, Alves M (2015) mRPL: boosting mobility in the Internet of Things. *Ad hoc networks*. Elsevier, Amsterdam, pp 17–35

7. Iova O, Theoleyre F, Noel T (2015) Using multiparent routing in RPL to increase the stability and the lifetime of the network. *Ad hoc networks*, Elsevier, Amsterdam, pp 45–62
8. Sanshi S, Jaidhar CD (2017) Enhanced mobility aware routing protocol for low power and lossy networks. *Wireless networks*, Springer, Berlin
9. Sanshi S, Jaidhar CD (2018) Enhanced mobility routing protocol for wireless sensor network. *Wireless networks*. Springer, Berlin
10. Ko J, Jeong J, Park J, Jun JA, Gnawali O, Paek J (2015) DualMOP-RPL: supporting multiple modes of downward routing in single RPL networks. *ACM Trans Sens Netw (TOSN)* 11(2):39:1–39:20
11. Guo J, Orlik P, Parsons K, Ishibashi K, Takita D (2015) Resource aware routing protocol in heterogeneous wireless machine-to-machine networks. In: *IEEE global communications conference (GLOBECOM)*, pp 1–6
12. Ko J (2014) RPL routing pathology in a network with a mix of nodes operating in storing and non-storing modes. Draft RFC
13. Vyas K, Sengupta J, Bit SD (2018) ARPL: supporting adaptive mixing of RPL modes to overcome memory overflow. In: *IEEE iSES*, 2018

Linear Interpolation-Based Fuzzy Clustering Approach for Missing Data Handling



Sonia Goel and Meena Tushir

Abstract Clustering of incomplete data set containing missing values is a common problem in the literature. Methods to handle this problem have vast variations, including several imputation as well as non-imputation techniques for clustering. In this work, we have described the analysis of different approaches explored for handling missing data in clustering. The aim of this paper is to compare several FCM clustering approaches based on imputation and non-imputation strategies. Experimental results on one artificial and four real-world data sets from UCI repository show that linear interpolation-based FCM clustering approach performs significantly better than other techniques for these data sets.

Keywords FCM clustering · Missing data · Imputation · Non-imputation · Incomplete data sets · Interpolation

1 Introduction

Fuzzy c-means clustering is a most commonly used clustering technique to partition a data into different clusters based on some similarity metric [1]. One of the major restrictions of this clustering is that it cannot be applicable on data with missing attributes. However, in many research domains such as data mining, environmental research and medical sciences [2–6], the data sets with missing features are common problems. The cause for missing attributes may be numerous; inaccuracy in data attainment, machine malfunctioning and human error in tabulating the data. Hence, incomplete data is a very common problem in many research areas. Two techniques

S. Goel (✉) · M. Tushir
Department of Electrical and Electronics Engineering, Maharaja Surajmal Institute of Technology, GGSIPU, New Delhi, Delhi 110058, India
e-mail: soniagoel@msit.in

M. Tushir
e-mail: meenatushir@yahoo.com

© Springer Nature Singapore Pte Ltd. 2021
G. S. Hura et al. (eds.), *Advances in Communication and Computational Technology*, Lecture Notes in Electrical Engineering 668,
https://doi.org/10.1007/978-981-15-5341-7_45

have been explored in the literature for incomplete data handling in cluster analysis: (1) imputation based preprocessing of data and then application of clustering approach (2) handling incomplete data in clustering process itself.

Various approaches are explored for imputation of missing attributes where missing values are replaced by some imputed value [7, 8]. After the imputation, standard clustering algorithm may be used. Hathway and Bezdek [9] presented different approaches for clustering of incomplete data. Several researches explored different clustering approaches in which the missing features are treated throughout clustering. Himmalspach and Conrad [10] proposed fuzzy clustering for incomplete data considering dispersion of clusters. Jinhua et al. [11] presented robust fuzzy c-mean clustering in which incomplete features are filled by intervals using k-nearest neighbor method. Gautam and Ravi [12] explore hybrid data imputation method using particle swarm optimization and neural network. Zhunga et al. [13] presented adaptive imputation of missing values using self-organizing map and k-nearest neighbor techniques. Loai and Iian [14] explored a mean shift clustering algorithm in which a weighted distance function is used to analyze missing features. Heiko et al. [15] extended Geth and Geva algorithm in which class-specific probability for handling missing data is explored

In this work, we examine the effect of various imputation as well as non-imputation approaches for incomplete data handling in clustering. Section 2 presents the proposed interpolation-based FCM clustering of incomplete data. Section 3 reports the results of the proposed work on artificial and real data sets. Conclusion is drawn in Sect. 4.

2 Proposed Interpolation Based FCM Clustering

Various techniques are explored in statistics for the analysis of incomplete data [7, 8]. The simplest approach is removal strategy that deletes the missing data and then considers the remaining complete data for analysis. Another commonly used approach is imputation, which replaces a missing attribute by an “*imputed*” value. Imputation-based approaches are broadly categorized as: single imputation and multiple imputations. Single imputation techniques involve imputation of missing features by a specific value calculated using mean, median and nearest neighbor approaches, whereas multiple imputation approach assigns several imputed values to missing features. Hathway and Bezdek [9] explored non-imputation-based clustering techniques in which missing data points are analyzed in clustering itself. Whole data strategy (WDS), a technique based on list-wise removal approach, first deletes all the data points with missing attributes, and then, conventional FCM is applied on remaining data points. Partial distance strategy (PDS) is based on distance calculation method suggested by Dixon [16], in which missing attributes are ignored while calculating distance between data points and cluster centers. In optimal control strategy (OCS), missing attributes are estimated as special variables during clustering process

in an iterative manner, whereas nearest prototype strategy (NPS) assigns specific values to missing features by nearest prototype.

The fuzzy c-means algorithm minimizes the objective function, which is defined as:

$$Z(U, C) = \sum_{i=1}^n \sum_{j=1}^s u_{ij}^m \|y_j - c_i\|^2 \tag{1}$$

where $Y = \{y_1, y_2, \dots, y_s\}$ is sample data set and $c = \{c_1, c_2, \dots, c_n\}$ describe fuzzy clusters. u_{ij} is the fuzzy partition matrix.

$$u_{ij} \in [0, 1], \sum_{i=1}^n u_{ij} = 1 \text{ for } j = \{1, 2, \dots, s\}$$

Fuzzy partition matrix is updated as follows:

$$u_{ij} = \left[\sum_{i=1}^n \left(\frac{y_s - c_n}{y_s - c_i} \right)^{\frac{2}{m-1}} \right]^{-1} \tag{2}$$

Finally, cluster centers are updated as follows:

$$c_n = \frac{\sum_{j=1}^s (u_{ij})^m Y_s}{\sum_{j=1}^s (u_{ij})^m} \tag{3}$$

We have considered linear interpolation imputation technique that assumes the non-missing attribute and missing variable which are linearly related as shown in Fig. 1. If x_1, x_2 and x_3 represents three data points where point x_2 contains missing feature, $(x_{11}, x_{12}), (x_{21}, x_{22})$ and (x_{31}, x_{32}) are the coordinates of points x_1, x_2 and x_3 , respectively. Missing value x_{22} at x_{21} for x_2 observation is calculated as:

$$x_{22} = x_{12} + \frac{(x_{32} - x_{12})}{(x_{31} - x_{11})} (x_{21} - x_{11}) \tag{4}$$

The proposed work can be formulated as:

- Step 1: Input number of clusters n, fuzzification constant m.
- Step 2: Set the iteration count = 1 and the initialize cluster center c_n^0 .
- Step 3: Replace incomplete data points with imputed values as calculated by linear interpolation Imp method in Eq. (4)

Repeat

- Step 4: Update u_{ij} using Eq. (2)
- Step 5: Update c_n using Eq. (3)
- Until the given stopping criterion, i.e., $\square = 0.0001$, is satisfied

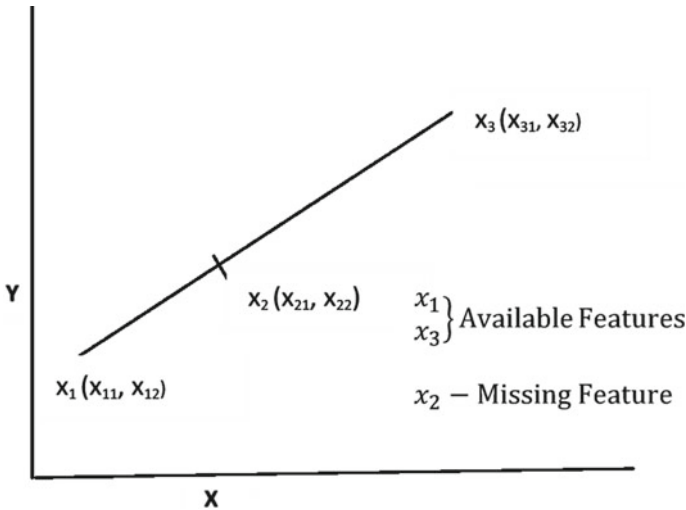


Fig. 1 Linear relationship between available features and missing feature

3 Numerical Analysis

We now present the comparison of our proposed work with several other approaches used for clustering involving incomplete data on different data sets. We have considered Iris, Glass and Wine data sets [17] that are real data sets without any missing features. Iris data set comprises three groups with 150 samples, and each sample has four distinct features. Glass data set contains 214 samples, nine features and two clusters. Wine data set with 178 data points and 13 features illustrates three different varieties of wine, whereas Stone flake data set [17] with missing values naturally present in data itself consists of 79 objects, eight features and three classes.

An artificial data, namely NC200C2, is generated to validate the proposed work. This 2-D complete data set consists of two clusters with equal data points having mean (m_1, m_2) and covariance vectors (σ_1, σ_2) as $m_1 = \begin{bmatrix} -50 \\ -50 \end{bmatrix}$, $m_2 = \begin{bmatrix} 50 \\ 50 \end{bmatrix}$

$\sigma_1 = \sigma_2 = \begin{bmatrix} 3600 & 0 \\ 0 & 3600 \end{bmatrix}$ is altered by randomly removing some of the features resulting in incomplete data. The missing features may be from any attribute, and one feature of every attribute must be present.

3.1 Results and Discussion

We have checked the performance of the proposed algorithm with different missing ratios varying from 10 to 30% with step size of 10% using three different evaluation

indices, namely misclassification error (Mis), cluster prototype error and random index. Misclassification error is an evaluation index used to determine clustering accuracy considering ratio of clusters assigned to correct class. Random index (RI) is considered to check the dissimilarity between clustering algorithms. Cluster prototype error (Err) is the difference between known cluster center and cluster centers calculated by a specific algorithm. We have reiterated 10 trials on similar set of data for all the algorithms to analyze and compare the proposed algorithm properly. For all clustering approaches using single imputation (SI), we first filled the missing values by mean imputation (mean), nearest neighbor (NN) approach, regression (REG) technique and expectation maximization (EM) algorithm. Standard fuzzy c-means clustering algorithm is then implemented. Multiple imputation technique (MI_Fuzzy) involved 10 different tests of imputation process for assigning values to missing data. Each test consists of five different measurements of imputed values for each missing attribute. Missing attribute is then filled by average of all sets, and then, conventional fuzzy clustering algorithm is incorporated. Cluster centers of all real data sets are initialized using standard FCM clustering algorithm when applied on whole data sets, whereas mean vector used to generate artificial data set is considered as cluster center.

Table 1 presents the performance of all algorithms on real complete data sets considering missing ratio of 10%. It is noticed that the proposed LIFCM clustering algorithm gives least number of misclassifications and highest value for RI, which proves the efficiency of the proposed algorithm. No clustering algorithm is said to be best in terms of cluster prototype error as cluster center is calculated using standard clustering algorithms when applied on whole data set. Next, the proposed algorithm is applied on artificial data, and results in Table 2 show that the proposed algorithm is giving best results for all evaluation indices. Even cluster prototype error is least because for artificial data set, actual cluster center is known. To check the validity

Table 1 Experimental results on real complete data sets with missing rate of 10%

Algorithm	Real complete data sets								
	IRIS data set			Glass data set			Wine data set		
	MIS	ERR	RI	MIS	ERR	RI	MIS	ERR	RI
Mean	16.6	0.006	0.705	26.6	0.225	0.522	11.2	0.402	0.815
NN	14	0.001	0.757	18.2	0.109	0.667	6.8	0.049	0.885
EM	16.75	0.001	0.712	22	0.046	0.601	10	0.038	0.833
REG	17.5	0.001	0.701	24.4	0.064	0.564	10.8	0.076	0.823
MI Fuzzy	17	0.006	0.701	51	5.241	0.053	15.8	0.637	0.745
WDS	16	0.001	0.723	24.2	0.403	0.565	11.3	0.501	0.811
PDS	18	0.0001	0.696	21.8	0.143	0.606	10	0.075	0.835
OCS	17	0.001	0.684	22	0.148	0.602	10	0.667	0.833
NPS	17	0.0001	0.709	21.2	0.059	0.616	10.4	0.039	0.827
LI FCM	13.4	0.002	0.766	17.8	0.13	0.674	5.7	0.049	0.903

Table 2 Experimental results on real incomplete data set and artificial data set with missing rate of 10%

Algorithm	Stone flake data set (real incomplete data Set)			Artificial data set		
	MIS	ERR	RI	MIS	ERR	RI
Mean	17	N/A	0.464	26.8	161.25	0.537
NN	18		0.421	23.2	143.22	0.59
EM	17		0.437	28.2	144.6	0.517
REG	17		0.464	28.8	147.41	0.509
MI Fuzzy	17		0.435	31.8	192.2	0.464
WDS	18		0.425	26	136.04	0.548
PDS	18		0.421	26.2	187.48	0.546
OCS	17		0.458	26.4	186.65	0.543
NPS	17		0.437	26.6	189.27	0.54
LI FCM	16		0.467	16	76.731	0.649

of the proposed algorithm, all algorithms are applied on Stone flake data set which naturally contains 10 missing features. Table 2 represents the numerical values in terms of all performance indices, which indicate the robustness of LIFCM.

Now, the proposed algorithm is compared with all the other algorithms in terms of misclassification error on real complete data sets and artificially generated data considering all missing ratios. Experimental results in Fig. 2 show that the proposed algorithm gives least number of misclassifications with all the data sets.

4 Conclusion

In this paper, we have explored various imputation and non-imputation methods for incomplete data handling in clustering. For all imputation methods, conventional fuzzy c-means clustering is used for clustering of incomplete data. The missing values are introduced by removing certain features, and three different missing rates are used for analysis. We have compared the results on one artificial and four real data sets and found that linear interpolation-based fuzzy c-means clustering gives the best results among all the tested algorithms.

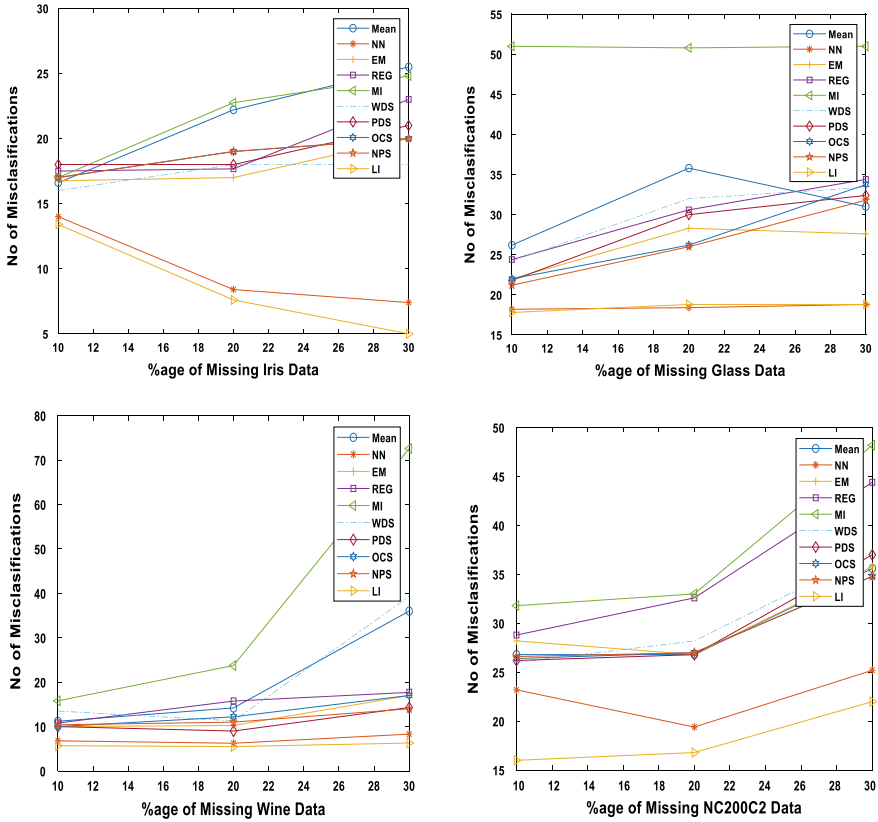


Fig. 2 Number of misclassifications with percentage increases in missing ratio on different data sets

References

1. Bezdek JC (1981) Pattern recognition with fuzzy objective function algorithms: advanced applications in pattern recognition
2. Noor NM, Al Bakri Abdullah, MM, Yahaya, AS, Ramli NA (2015) Comparison of linear interpolation method and mean method to replace the missing values in environmental data set. In: Materials science forum. Trans Tech Publications, vol 803, pp 278–281
3. Zainuri NA, Jemain AA, Muda N (2015) A comparison of various imputation methods for missing values in air quality data. Sains Malaysiana 44(3):449–456
4. Li P, Chen Z, Hu Y, Leng Y, Li Q (2017) A weighted fuzzy c-means clustering algorithm for incomplete big sensor data. China conference on wireless sensor networks. Springer, Singapore, pp 55–63
5. Morisot A, Bessaoud F, Landais P, Rébillard X, Trétarre B, Daurès JP (2015) Prostate cancer: net survival and cause-specific survival rates after multiple imputation. BMC Med Res Methodol 15(1):54
6. Sullivan TR, Lee KJ, Ryan P, Salter AB (2017) Multiple imputation for handling missing outcome data when estimating the relative risk. BMC Med Res Methodol 17(1):134

7. Schmitt P, Mandel J, Guedj M (2015) A comparison of six methods for missing data imputation. *J Biometrics Biostatistics* 6(1):1
8. Peeters M, Zondervan-Zwijnenburg M, Vink G, Van de Schoot R (2015) How to handle missing data: a comparison of different approaches. *Eur J Dev Psychol* 12(4):377–394
9. Hathaway RJ, Bezdek JC (2001) Fuzzy c-means clustering of incomplete data. *IEEE Trans Syst Man Cybern Part B (Cybernetics)* 31(5):735–744
10. Himmelspach L, Conrad S (2010) Fuzzy clustering of incomplete data based on cluster dispersion. *International conference on information processing and management of uncertainty in knowledge-based systems*. Springer, Berlin, Heidelberg, pp 59–68
11. Jinhua L, Song S, Zhang Y, Kang L (2017) A robust fuzzy c-means clustering algorithm for incomplete data. *Intelligent computing, networked control, and their engineering applications*. Springer, Singapore, pp 3–12
12. Gautam C, Ravi V (2015) Data imputation via evolutionary computation, clustering and a neural network. *Neurocomputing* 156:134–142
13. Zhunga L, Pan Q, Dezert J, Martin A (2016) Adaptive imputation of missing values for incomplete pattern classification. *Pattern Recogn* 52:85–95
14. AbdAllah L, Shimshoni I (2014) Mean shift clustering algorithm for data with missing values. *International conference on data warehousing and knowledge discovery*. Springer, Cham, pp 426–438
15. Heiko T, Döring C, Rudolf K (2004) Different approaches to fuzzy clustering of incomplete datasets. *Int J Approximate Reasoning* 35(3):239–249
16. Dixon JK (1979) Pattern recognition with partly missing data. *IEEE Trans Syst Man Cybern* 9(10):617–621
17. Bache K, Lichman M (2013) UCI machine learning repository. <http://archive.ics.uci.edu/ml>. University of California. School of information and computer science, Irvine, CA, vol 28

Dynamic Web View Materialization



Akshay Kumar and T. V. Vijay Kumar

Abstract Dynamic Web applications, such as e-commerce Web application, extensively use databases as backend servers. These Web applications are highly dependent on the efficiency with which the Web databases can be accessed. A dynamic Web page consists of many small fragments of scripting languages, called Web views, which may require access to data in disparate databases. These Web views when materialized can enhance the efficiency of database access. An e-commerce Web application has large number of users involved in various personalized interactive activities. These generate a stream of Web page accesses and modification requests that necessitate taking dynamic decisions for selecting Web views for materialization, which minimize the average access time of Web views. In this paper, a Web view selection algorithm (WVSA) that selects Web views for materialization is proposed. Experimental results suggest that materializing Web views using WVSA increases the efficiency of Web view accesses.

Keywords View materialization · Web views · Big Data

1 Introduction

Database systems constitute a vast organized reservoir of integrated and shared data of an organization that caters to a number of applications. Database technologies have shown remarkable enhancements since the inception of the relational model [4]. The advancements of database technologies resulted in the deployment of database systems in organizations that result in an increase in the volume of structured data. Though database systems supported transaction processing, they were not capable of

A. Kumar (✉)

School of Computer and Information Sciences, Indira Gandhi National Open University,
New Delhi, Delhi 110068, India
e-mail: akshay@ignou.ac.in

A. Kumar · T. V. Vijay Kumar

School of Computer and Systems Sciences, Jawaharlal Nehru University,
New Delhi, Delhi 110067, India

© Springer Nature Singapore Pte Ltd. 2021

G. S. Hura et al. (eds.), *Advances in Communication and Computational Technology*, Lecture Notes in Electrical Engineering 668,
https://doi.org/10.1007/978-981-15-5341-7_46

605

supporting analytical processing, due to unavailability of historical and time variant data required for decision making. In order to support analytical queries, a central repository, such as data warehouse, was created [23]. A data warehouse contains subject-specific, integrated, non-volatile, and time variant data needed for providing answers to analytical queries in order to facilitate decision making [9].

In addition to rise in the volume of structured data, emergence of Web 2.0 technologies resulted in the development of applications like social networking, healthcare management, online education, scientific measurements, meteorological modeling, sensor networks, e-commerce, etc. These applications generated large volume of heterogeneous streaming data having low trustworthiness or veracity [6, 10, 19], which is a key characteristic of Big Data [10]. What makes data big, is not just the volume of data but its dynamic nature and heterogeneity. Thus, Big Data poses many challenges during the entire life cycle of analytics, viz acquiring raw data from dynamic or continuous data streams, cleaning, aggregating, processing, and storing the required data in a structured format; data integration from heterogeneous sources; transforming data for analytics, and the designing of models for data analytics [10].

With the introduction of Web 2.0 and Web 3.0 technologies, importance of databases, as backend to Web sites and Web applications, has grown multifold. An interactive Web application, such as B2C e-commerce application, irrespective of technology, involves large number of transactions and interactions among application users. Since e-commerce applications have a large number of users, it results in large number of access, insert, and update requests to the database servers. Accordingly, such applications can be categorized in the domain of Big Data [10]. These applications, being dynamic in nature, require efficient access to such data. View materialization provides an alternate way to provide such efficient access to data.

View materialization has been studied in the context of databases and data warehouses. Database views provide a window to data which facilitates logical data independence, security, and privacy of data. View materialization concerns the storing of data corresponding to a view, with the aim of reducing the response time for analytical queries [20]. All views cannot be materialized due to storage space constraints, and optimal view selection is a NP-hard problem [3, 8]. Alternatively, an appropriate subset of views needs to be materialized that improves the response time for analytical queries. This is referred to as the view selection problem [3]. View selection problem has been defined for a specific query workload with the aim to minimize the cost of query processing under the constraints of handling view updates and optimum resource utilization [3, 17].

View selection in the context of databases and data warehouse is a widely researched problem [8, 11, 21, 22]. However, limited research has gone into the selection of views for materialization in the context of the dynamic Web applications. The first attempt in the related context is given in [1], where the need to move database research to address the issues relating to online database systems were discussed. [1] suggested the creation of newer database models, as large volumes of unstructured data are available on the WWW, exploring possibilities of direct data capture and storage and performing analysis on such data to create summary reports and presentations using advanced techniques and technologies. The challenge still

lies in providing efficient access to data on the Web. This data, which is voluminous, heterogeneous, dynamic, and has a certain level of trust associated with it, is complex and Big in nature.

This paper focuses on the issue of selection of Web views for materialization that can improve the efficiency of accessing such data on the Web. The paper is organized as follows: Sect. 2 discusses Web view materialization followed by Web access architecture used for it in Sect. 3. In Sect. 4, Web view selection for materialization is discussed. Experimental results are discussed in Sect. 5. Section 6 is the conclusion.

2 Web View Materialization

Dynamic Web applications, in general, use database servers as the backend to Web servers. A dynamic Web page consists of several components. Each of these components may require database access from different relations or different databases. Therefore, a single Web page generation of a database-driven Web application may require several database accesses from different database servers [15]. For example, an e-commerce Web application may involve database accesses for components like login of users, display of product features, search of specific items, information on previous purchases, review of items, related advertisements, etc. These interactive components may be a part of the same Web page or of different Web pages. For example, the home page of a user may consist of components such as the last searched product, the last purchased product information, related advertisements, and a review of items. Thus, dynamic Web applications require efficient models for faster data access from databases that serve as a backend to the Web sites. In this context, [12] proposed the concept of Web views. A Web view is defined in [12] and [14] as a fragment of a Web page that may be created by the data retrieved from a Web database query. A Web view is directly created through database accesses or can also be created from another Web view. Further, a Web view can be part of several Web pages and a Web page may comprise of many Web views. In [18], materialization of Web pages of an e-commerce application using measures like quality of response time and quality of data have been discussed. [7] highlighted the interdependence and reuse of Web page fragments, referred to as Web views in [14], and addressed the problem of view materialization by proposing an algorithm that can adapt to the system load and the interdependencies among the data usage. [13] used two parameters, viz quality of data and response time, and highlighted how updates can be propagated to Web views, so that a high level of quality of data is maintained.

Ceri et al. [2] discusses issues relating to data-intensive Web page design, wherein it mentions that a data-intensive Web site must support a data model, a hypertext model, and a content management model. The Data model describes the structure of data and identifies data requirements and the functional association of data elements. Further, [2] also defines the concept of a data access unit that can be identified by metadata such as name, source, selection condition and global parameters that can contextualize database access. A Web page display requires evaluation of all the

units of that page under the constraint of input parameters identified by the Web link through which it is accessed. Thus, the data access units as described by [2] can be compared to Web view access as defined in [14].

Materializing a Web view is a much more complex problem than materializing views over structured data, since the Web comprise of semi-structured and unstructured data that has Big Data characteristics, as discussed earlier, and this can misguide the analysis. This makes selecting Web views a complex problem. Further, this complexity increases, since the queries of a Web view can be personalized and a Web view access for the same web page may involve additional parameters. The parameterized query requires query modification using attributes that may not be part of the query but are required for personalization. For example, on an e-commerce Web site, the list of recommended items for a customer would be created on using the credit rating, which is not a part of the query. Such queries would require the values of additional attributes for query evaluation. This increases the number of views to be materialized, resulting in an increased complexity of materialized view selection.

A Web application, which uses Web views, should follow an access mechanism of data, such that a request to a Web page can be answered in the most efficient manner. In this regard, a Web access architecture for accessing relations and Web views is discussed next.

3 Web Access Architecture

A Web application has a definitive architecture, which can mostly be characterized as three-tier or multi-tier architecture, and in some applications, as model-view-controller (*MVC*) architecture [16]. With the advancement of mobile technologies and cloud computing, newer architecture models have emerged. [5] presents a survey of the mobile cloud computing architectures. The mobile devices are part of the client-side, whereas cloud computing becomes the infrastructure for the server-side applications. Thus, irrespective of the architecture, a data-intensive Web application requires an interaction with the database server through the Web server.

A database access operation can be a relational operation, which involves relational operators such as *selection*, *projection*, *join*, while parameters are required for creating query conditions. A database query evaluation uses a query optimization model, which develops an optimal query evaluation plan, based on database statistics and indexes. In order to further optimize the data access time, materialized views can be used for a given query workload [21]. The proposed Web access architecture (Fig. 1) suggests that any database access query either can be answered by a materialized view or by a query cache or both. In case if the query cannot be answered using these, the query would need to be processed directly against the database.

After a query has been answered, the resultant data is transformed to Web views by using a scripting language. These Web views can be stored either in the application servers or the Web servers, along with the necessary metadata related to the query definition of the Web view. A Web page access is directed to its constituent Web

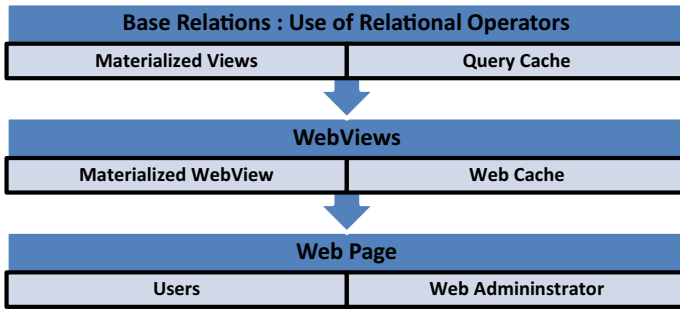


Fig. 1 Web data access process

views. If a Web view is materialized or is available in Web cache, it can be accessed directly; else, the Web view is computed from the database and the processed data stored in the Web cache [14]. Materialized Web views and Web caches can be stored on any of the servers, viz the web server, the application server, or the database server [15]. Therefore, the architecture may have a separate Web cache and a query cache. A large Web application can have access to many database servers, application servers, and Web servers, which would further enhance its complexity. Figure 1 illustrates the Web data access process for Web view materialization.

In order to ensure consistent data in materialized views and Web views, all the updates to databases must be propagated to materialized views and materialized Web views. [15] has defined these data consistency models under constant updates. This paper uses the data consistency model that **invalidates** all the materialized views and materialized Web views while updating a database. An algorithm for selection of Web views for materialization is discussed next.

4 Materialized Web View Selection

A data-intensive web application contains a large number of users generating large numbers of access and update requests. These requests are answered using materialized Web views or database relations. As Web views can be personalized, the number of Web views is larger than the number of views over relations. Therefore, the problem of materialized Web view selection is a complex problem, similar to the materialized view selection problem, which is NP-hard [3, 8]. In addition, materialized Web views selection has to be dynamic to handle a large number of user requests. The selection of Web views for materialization may require parameters like ratio of size of Web view to the total size of Web views, update operations on data, expected number of queries that can be answered using the selected Web views, and the quality of data, with the aim to minimize the access time. The following Web view selection algorithm (WVSA) is proposed to dynamically select Web views for materialization.

Input:

M_{WPV} : Web page to Web view mapping,
 M_{WVR} : Web view to relation mapping,
 AS_{WP} : Web page access sequence (with timestamp; Zipf distribution),
 U_R : Relational updates (with timestamp; uniform distribution),
 SR_{WV} : Size ratio of size of Web view to total Web view size

Output:

L_{MV} : List of materialized views and
 AT_{Avg} : Average access time for every Web view

Procedure:

Initialization:

Initialize:

$AT_R = 100$ // Time to access a relation (milliseconds (assumed)),
 $AT_{M WV} = 10$ // Time to access a materialized Web View (milliseconds)
 $AT_{WC} = 10$ // Time to access a Web Cache (milliseconds)
 $AF_{WV} = 0$ // frequency of access of each web view

Method:

For each Access and Update in the sequence of timestamp in AS_{WP} and U_R

if Web page Access:

Use M_{WPV} to determine list of Web Views being accessed (V_p)

for each element WV in the list (V_p)

Increment $AF_{WV}(WV)$

re-calculate $AT_{Avg}(WV)$

if (status (WV) = Non-Materialized

status (WV) = Web-Cache; $AT_{WV} = AT_{WC}$;

if (status (WV) = Web-Cache No change in status (WV))

for each element WNA NOT in (V_p)

if (status(WNA)= Web-Cache) then status(WNA)= Non-Materialized

$AT_{WNA} = AT_R$

if Relation R_i updates in U_R :

for every WA in (M_{WVR}) of R_i

if status(WA) = Materialized or Web-Cache

status(WA)=Non-Materialized

$AT_{WA} = AT_R$

Dynamic Materialization:

After every access operation:

for each web view WV

if status = Materialized or Web-Cache, put web view in List (LM)

Sort LM in order of AT_{Avg} // changes due to Access and update

For every WV in LM in order of AT_{Avg}

if ((incremental sum of SR_{WV} for WV) < Available Size for materialization)

Status(WV)= Materialized

$AT_{WA} = AT_{MWV}$

Terminate once the condition is fulfilled or complete list is checked

return LMV and AT_{Avg} : for every Web page Access.

The algorithm $WVSA$, which is based on the greedy approach, assumes that any update to a database is communicated to the views, in order to ensure consistency among the Web views and the database. Input to the proposed algorithm are Web page to Web view mapping (M_{WPV}), Web view to database relation mapping (M_{WVR}), the sequence of Web page access operation in the order of the timestamp of the access operation (AS_{WP}), update operation on the relations in the order of the timestamp (U_R), and the ratio of size of the Web view to the total size of Web views (SR_{WV}). The update operations have uniform distribution over the relations, whereas access operations have Zipf distribution over the Web pages [14]. In addition, variables like the time to access a relation (AT_R), the time to access a materialized Web view (AT_{MWV}), and time to access Web cache (AT_{WC}) are kept similar as in [14]. The output of the algorithm are the two lists namely the list of materialized views (LMV) and the average access time of each Web view (AT_{Avg}). Both these lists are updated after each access operation. $WVSA$ dynamically updates the average access time (AT_{Avg}) in accordance with the changing trends in accesses and updates.

A dynamic decision is taken to identify the possible cluster of Web views for materialization. Every Web page access operation requires the computation of Web views using M_{WPV} . All these Web views are required to be computed either using the materialized Web view or the Web cache or directly from the database. Therefore, $WVSA$ defines three states for every Web view namely Non-materialized Web view, web-cached Web view, and a materialized Web view. These states are related to AT_R , AT_{WC} , AT_{MWV} , respectively. $WVSA$ computes the frequency of access (AF_{WV}) and average access time (AT_{Avg}) for each Web view after accessing each Web page. The state of a Web view can be changed in three situations—first, when a Web page is accessed, where those Web views in Web cache, which are not accessed become non-materialized; second, when a relation is updated, where all the materialized and cached Web views are non-materialized; and third, when materialization is performed, where a materialized view is selected using the materialized views and Web-cached views. The decision to select a Web view depends on its average access time (AT_{Avg}) and the size of the Web views (SR_{WV}). A list of candidate Web views sorted in increasing order of average access time (AT_{Avg}) is created. Web views are

selected for materialization from this sorted list of candidate Web views. These Web views should conform with the storage space constraint.

5 Experimental Results

The proposed algorithm *WVSA* is implemented using *GNU Octave 4.4.1* on an Intel dual core *I5, 2.5 GHz*, 64 bit processor having *6 GB RAM*. *WVSA* uses a random framework of 30 Web pages sharing 12 Web views, which are derived from five relations. Every Web page consists of 1–5 Web views, selected randomly for experiment, having an overall average of 2.5 Web views per Web page. Similarly, each relation is part of about 3–4 Web views. This experiment studies the selection of Web views for 1001 Web page accesses and 300 relational updates over a time frame of 15,000 ms. The distribution of Web page accesses have been selected using *Zipf* distribution, and the distribution of relation updates follows the uniform distribution, as suggested in [14]. This experiment uses similar values of the basic parameters like number of Web views, number of relations, number of Web pages, and access time of objects, as used in [14]. However, this experiment uses a different structure of Web pages and Web views from the ones used in [14]. Figure 2 shows Web page accesses with respect to time, and Fig. 3 shows the relation updates with respect to time. In Fig. 2, the y-axis shows the Web page that is being accessed, with each Web page being recognized by its number. Thus, each number 1, 2, 3 ...30 represents an individual Web page. The y-axis in Fig. 3 represents a relation that is being updated. Thus, Figs. 2 and 3 show the sequence of Web pages that are being accessed, and the relations that are being updated, respectively.

The distribution of access operations and update operations can also be visualized in Figs. 2 and 3. It can be noted from Fig. 2 that all the Web pages are not accessed

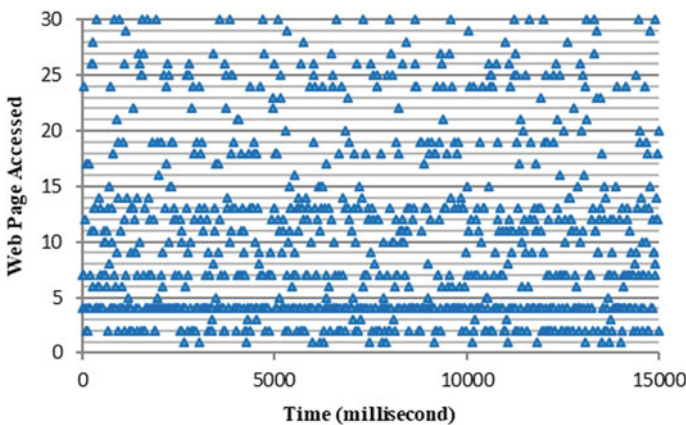


Fig. 2 Web page access versus time chart

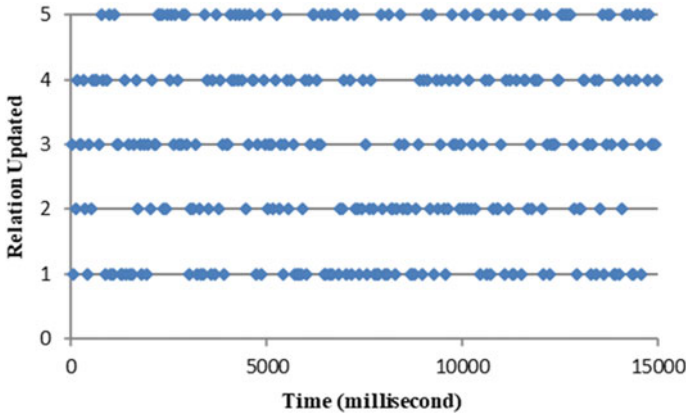


Fig. 3 Relation update versus time chart

with the same frequency, since some pages have very high frequency of access while others have lower frequency of access. This is due to *Zipf* distribution. However, in Fig. 3, the accesses to relations for updates are relatively uniform. The algorithm *WVSA* was run on the same data under two situations—first using only Web-cached Web views, without view materialization; and second using both materialized Web views and Web-cached Web views. The results after completion of all the access and update operations are given in Table 1.

Table 1 Average access time using only Web-cached Web views and materialized Web views with Web-cached Web views

WebView #	Only Web-cached Web views	Materialized Web view with Web-cached Web views	Change in percentage
V1	70.29	35.12	-35.17
V2	63.04	63.04	0.00
V3	93.68	92.89	-0.79
V4	87.07	73.67	-13.40
V5	90.71	86.43	-4.29
V6	87.26	83.02	-4.25
V7	89.41	86.39	-3.03
V8	90.66	90.66	0.00
V9	93.57	93.57	0.00
V10	96.40	96.40	0.00
V11	88.06	83.47	-4.59
V12	85.90	41.57	-44.33
Overall	80.06	67.66	-12.40

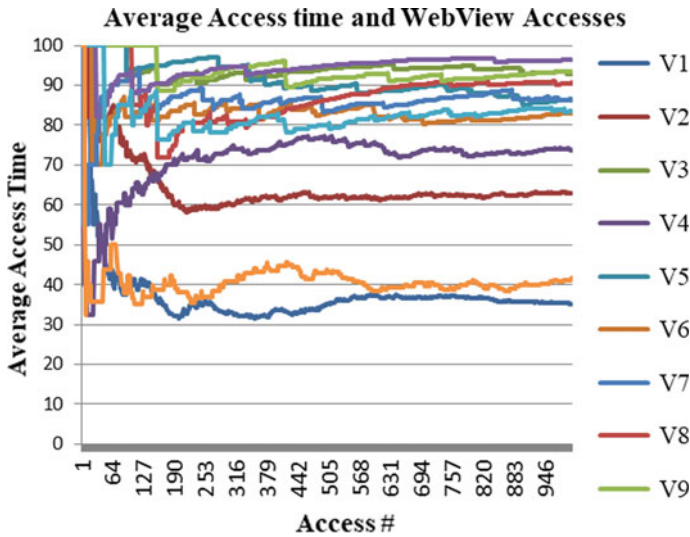


Fig. 4 Average access time output by WWSA

Table 1 clearly shows that there is an overall change of 12.4% when both materialized Web views and Web-cached Web views are used. This change is most significant for Web view *V1* and Web view *V12*, though the most accessed Web view was Web view *V2* followed by Web view *V1*. Web view *V12* has comparatively less number of accesses than Web view *V1* and Web view *V2*. Thus, it is not just the number of accesses, but other factors like size and updates on data also affect the optimization of the average access time. Further, it was noted that the Web views, already available in the Web cache, show less than 5% change in access time.

Figure 4 shows the graph of average access times of each Web view, as produced by WWSA, with respect to Web page accesses. The graph shows that there is a major reduction in the average access time for two Web views *V1* and *V12*. This was not the case (see Table 1) when only Web cache was used. Thus, the reduction in the average access time is due to Web view materialization. Figure 4 also illustrates the clustering of Web views into two basic categories—Web views with major average access time improvement, and Web views with minor improvements in access time. It also shows that the Web view *V1* has the lowest average access time, which remains below 40 ms after accessing about 150 Web pages. Similarly, Web view *V12* has an average access time around 40 ms. Thus, these two Web views *V1* and *V12* are selected for materialization. Further, the average access time for most of the Web views after some iterations becomes almost linear, and therefore, the average access time can be reset periodically, so that all Web view get a chance for materialization for a long Web access sequence.

Even though WWSA performs dynamic Web view materialization, yet it has reasonable space and time complexity. For a Web application having W Web pages, WV Web views, and R relations, since $W > WV \gg R$, the space complexity will be mainly

determined by M_{WPV} , as it is the largest matrix of size $W \times WV$. All other input and output variables are either linear in size or are much smaller than M_{WPV} . It may be noted that the size of variables AS_{WP} and U_R can be changed in accordance with the available space, as they represent a stream of input, for which the window size can vary without compromising the efficiency of the algorithm. This is due to the fact that the decision for materialization is taken dynamically after each Web access. The space complexity of $WVSA$ can be reduced further as M_{WPV} is a sparse matrix.

Time complexity of $WVSA$ for every Web page access is dependent on M_{WPV} , which will be restricted to a single row corresponding to the accessed Web page, and the number of Web views (N_{WV}) in an accessed Web page, which are significantly less than the total number of Web views (WV). The algorithm requires sorting on the average access time for N_{WV} Web views. Thus, the time complexity of the algorithm is low for every Web page access. These operations can be performed as a part of a metadata collection process for every Web page access.

6 Conclusion

Data-intensive Web sites, which are highly dependent on databases, seek reduction in the average Web access time. One way to reduce this Web access time is by materializing Web views. This paper proposes an algorithm $WVSA$ that dynamically select Web views for materialization that aims to minimize the average access time for a given workload of Web page accesses. In general, large Web applications, which use the database as backend, require a number of database servers. The $WVSA$ algorithm can be used independently on each Web server by selecting Web views, based on the query workload of each server. Further, to ensure dynamic selection of Web views for materialization, periodically, the average access time for every Web view can be reset to maximum. The time complexity of $WVSA$ for every web access is dependent on the number of Web views in a Web page, which are significantly less than the total number of web pages. Thus, materializing selected Web views using $WVSA$ reduces the Web access time resulting in efficient decision making.

References

1. Bernstein P, Jagadish HV, Lesk M, Maier D, Naughton J, Pirahesh H, Hellerstein J (1998) The Asilomar report on database research. *ACM SIGMOD Rec* 27(4):74–80
2. Ceri S, Fraternali P, Bongio A, Brambilla M, Comai S, Matera M (2003) Designing data intensive web application. Morgan Kaufmann Publisher, Elsevier
3. Chirkova R, Halevy AY, Suciu D (2001) A formal perspective on the view selection problem. In: Proceedings of the 27th VLDB conference, Roma, Italy
4. Codd EF (1970) Relational model of data for large shared data banks. *Commun ACM* 13(6):377–387
5. Dinh HT, Lee C, Niyato D, Wang P (2013) A survey of mobile cloud computing: architecture, applications, and approaches. *Wirel Commun Mobile Comput* 13:1587–1611

6. Grover V, Chiang RHL, Liang T, Zhang D (2018) Creating strategic business value from big data analytics: a research framework. *J Manag Inf Syst* 35(2):388–423
7. Guirguis S, Sharaf MA, Chrysanthis PK, Labrinidis, A, Pruhs K (2009) Adaptive scheduling of web transactions. In: IEEE international conference on data engineering
8. Harinarayan V, Rajaraman A, Ullman J (1996) Implementing data cubes efficiently. *ACM SIGMOID*, Canada, pp 205–216
9. Inmon WH (2002) *Building the data warehouse*, 3rd edn. Wiley
10. Kumar A, Vijay Kumar TV (2016) Big data and analytics: issues, challenges, and opportunities. *Int J Data Sci* 1(2)
11. Kumar S, Vijay Kumar TV (2018) A novel quantum inspired evolutionary view selection algorithm. *J Sadhana, Springer Indian Acad Sci* 43(10) (Article 166)
12. Labrinidis A, Roussopoulos N (2000, May) WebView materialization. *ACM SIGMOD Record* 29(2):367–378
13. Labrinidis A, Roussopoulos N (2001, September) Update propagation strategies for improving the quality of data on the web. In: Proceedings of the 27th VLDB conference, Rome, Italy
14. Labrinidis A, Roussopoulos N (2002) Online view selection for the web, UM Computer Science Department; CS-TR-4343. Accessed from <https://drum.lib.umd.edu/bitstream/handle/1903/1187/CS-TR-4343.pdf?sequence=2&isAllowed=y>
15. Labrinidis A, Luo Q, Xu J, Xue W (2009) Caching and materialization for web databases. *Found Trends Databases* 2(3):169–266
16. Leff A, Rayfield JT (2001) Web-application development using the Model/View/Controller design pattern. In: Proceedings fifth IEEE international enterprise distributed object computing conference, Seattle, WA, USA, pp 118–127
17. Mami I, Bellahsene Z (2012, March) A survey of view selection methods. *SIGMOD Rec* 41(1)
18. Papastavrou S, Chrysanthis, PK, Samaras G (2013) Performance vs. freshness in web database applications. *WWW Springer Science*
19. Raghupathi W, Raghupathi V (2014) Big data analytics in healthcare: promise and potential. *Health Inf Sci Syst* 2(1)
20. Roussopoulos N (1998) Materialized views and data warehouses. *SIGMOD Rec*
21. Vijay Kumar TV, Mohammad H (2010) Materialized views selection for answering queries. In: *ICDEM 2010: data engineering and management*, pp 44–51
22. Vijay Kumar TV, Arun B (2017) Materialized view selection using HBMO. *Int J Syst Assurance Eng Manag* 8(1):379–392
23. Widom J (1995, November) Research problems in data warehousing. In: Proceedings of 4th International conference on information and knowledge management (CIKM), pp 25–30

A Multi-Hop Bit-Map-Assisted Energy-Efficient MAC Protocol for Wireless Sensor Networks



Kumar Debasis, M. P. Singh, and Rajat Gupta

Abstract The proposed model is a cluster-based multi-hop routing protocol which employs a time-division multiple access (TDMA)-based medium access method. The model employs a centralized cluster head (CH) selection scheme in which the base station (BS) appoints the node with the highest residual energy (RE) as the CH in each cluster. A centralized CH selection scheme ensures that all the CHs are evenly distributed in the network. The BS also sets up multi-hop paths to communicate with the CHs. This ensures that none of the CHs make long-range transmissions to communicate with the BS. If a non-cluster-head (non-CH) node wants to claim one or more data slots in a frame, it sends a control message to its CH in the allocated control slot. However, the node has to turn its radio ON from the beginning of the control period. This is so because before claiming any data slot(s), it should know which data slots have already been claimed. The experimental results show that the proposed model saves a considerable amount of energy in sensor nodes.

Keywords Data slot · Control slot · Energy · Radio · Communication

1 Introduction

A wireless sensor network (WSN) is a network of small autonomous devices that coordinate with each other to send the sensed data to the BS [1, 2]. Some applications require the sensor nodes to operate for a very long duration, for example, a couple of months/years. Nonetheless, these devices may be equipped with low capacity

K. Debasis (✉) · M. P. Singh · R. Gupta
National Institute of Technology Patna, Patna, Bihar 800005, India
e-mail: debasis.cse14@nitp.ac.in

M. P. Singh
e-mail: mpps@nitp.ac.in

R. Gupta
e-mail: rajat160454@nitp.ac.in

batteries. Moreover, it may not be feasible to recharge or replace the batteries of these devices once they have been deployed. Both these issues signify the importance of energy conservation in sensor nodes.

Usually, the radio/transceiver of a sensor node consumes the maximum amount of energy in the lifetime of the node. It has been found that the radio drains a considerable amount of energy even when it is idle (neither transmitting nor receiving) [3]. Therefore, most of the medium access control (MAC) protocols turn OFF the radio when it is not working. In TDMA based MAC protocols, each node is allotted one or more slots in a time frame during which it may send/receive data. At all other times, a sensor node keeps its radio OFF. This helps in minimizing overhearing, idle listening, and collision.

Clustering is also an energy conservation technique in which sensor nodes are grouped into separate clusters. In each cluster, one node is appointed as the CH [4]. The function of a CH is to collect data from its member nodes and forward the aggregate data toward the BS. Clustering ensures that all the non-CH nodes are involved in short-range communications only.

This paper proposes a cluster-based multi-hop routing protocol named multi-hop bit-map-assisted energy-efficient MAC (MBEE-MAC) which employs a TDMA channel access scheme. MBEE-MAC assumes that the deployment area is composed of n equal-sized grids. Sensor nodes lying within a grid are considered to be the part of the same cluster. The BS appoints the node with the highest RE as the CH in each cluster. The BS also sets up multi-hop paths to communicate with the CHs. MBEE-MAC employs a centralized CH selection scheme which results in uniform distribution of CHs in the network. An efficient CH rotation scheme (based on the RE of nodes in a cluster) ensures even distribution of load among the nodes in the network.

The rest of the paper has the following structure. Section 2 describes some existing MAC protocols. Section 3 describes the proposed model in detail. Section 4 presents the simulation results. Section 5 concludes the paper.

2 Related Work

BMA-MAC [5] divides a round into a *set-up phase* and a *steady-state phase*. In the set-up phase, sensor nodes are grouped into separate clusters as in LEACH [6]. The steady-state phase is composed of k equal-sized sessions/frames. Each frame is divided into three parts—(i) contention period, (ii) data transmission period, and (iii) idle period. The contention period comprises small time slots called control slots. A CH allocates one control slot to each of its member nodes. A source node (node that has data) sends a control message to its CH in the allocated control slot. It stays idle during the other control slots. A non-source node is idle for the complete duration of the contention period. Each CH broadcasts a transmission schedule in its cluster on the basis of the control messages received. Each source node is allocated one data slot. A source node's radio is ON only during the allotted data slot (to

transmit the data). A non-source node's radio is OFF for the complete duration of the data transmission period. When a CH receives data from all the source nodes, it computes the aggregate and sends it to the BS. One of the drawbacks of BMA-MAC is that sensor nodes lose a considerable amount of energy in idle listening during the contention period.

In BMA-RR [7], a source node may claim multiple data slots. After receiving control messages from all the source nodes, a CH broadcasts a transmission schedule in its cluster. A one-bit S/R flag informs each source node whether it should go into the sending mode or the receiving mode during the allocated slots. Data slots are allotted on the basis of the round-robin algorithm. Each source node's radio is ON during the allocated data slot(s) to perform the assigned task (send or receive data). If a source node has data for a member node, then the data is sent to the CH in the current session, and to the destination in the next session. In BMA-RR, a node with multiple data slots has to toggle its radio between ON and OFF numerous times within a frame duration.

In BS-MAC [8], each CH broadcasts a CS_ALLOC (control slot allocation) message at the end of the set-up phase. The purpose of this announcement is to assign one control slot to each member node. The message contains a unique one-byte address each for the CH and its members. These short addresses are used by the CH and its member nodes to exchange messages. The steady-state phase starts with a control period that consists of control slots. Each source node sends a data request in the allocated control slot. In the announcement period that follows, each source node's radio is ON to check if the CH has allocated any data slot(s) to it. A source node may be allotted one or more data slots to transmit/receive data to/from the CH. Such a node wakes up in its allotted slot(s) to perform the assigned task. If the number of slots needed is more than that is available, then some of the nodes are not allotted data slots in the current frame. In BS-MAC, data slots are allocated on the basis of the shortest job first (SJF) algorithm. In other words, nodes that require less data slots are given preference over the nodes that require more data slots. A node can also send data to another member via the CH. One of the drawbacks of BS-MAC is that it uses shorter data slots which may lead to frequent reservation and scheduling.

BEST-MAC [9] is a modification of BS-MAC in which a contention access period (CAP) is introduced after the control period. During the CAP, non-CH nodes that could not join the network send join-request messages to their selected CHs. A CH acknowledges the receipt of all these messages. However, it does not allocate control slots to such nodes instantly. They are allocated control slots in the announcement period (when data slots are allocated to existing member nodes). Data slots are allocated on the basis of the *knapsack optimization algorithm* in which the optimal solution is the maximum number of nodes with the maximum slot utilization. BEST-MAC also uses shorter time slots which may lead to frequent reservation and scheduling. The CAP may lead to idle listening in CHs after a few sessions. This is so because all the left-out nodes may have joined the network by then.

In LDC-MAC [10], each CH broadcasts a transmission schedule at the end of the set-up phase. Each member node is allotted one control slot and one data slot. A

source node transmits a control message and a data message in the allocated control slot and data slot, respectively. A non-source node's radio is OFF for the entire frame duration. A CH can identify the source nodes from the control messages received. It stays awake during the corresponding data slots to receive data from the source nodes. In LDC-MAC, a CH may have to toggle its radio between ON and OFF numerous times within a frame duration. Moreover, if a member node does not use its data slot, it is wasted.

BEE-MAC [11] is a modification of LDC-MAC in which a member node may claim multiple data slots. A source node turns its radio ON from the beginning of the control period. The purpose is to know how many data slots have already been claimed. This information is used to successfully claim one or more subsequent data slots in the current frame. In BEE-MAC, the radio of a CH is continuously ON for the period during which it is receiving data from source nodes. All the unused slots appear together toward the end of a frame. During this period, each node keeps its radio OFF to save energy. The downside of this protocol is that a source node may lose a significant amount of energy in idle listening and receiving control messages from other source nodes in its cluster.

The proposed model is a modification of BEE-MAC in which CHs are appointed by the BS. This ensures that all the CHs are evenly distributed in the network. The BS also sets up multi-hop paths to communicate with the CHs. This ensures that none of the CHs makes long-range transmissions to communicate with the BS. In the next section, the proposed model is discussed in detail.

3 Proposed Model

The proposed model assumes that the deployment area is composed of n equal-sized grids. Sensor nodes lying within a grid are considered to be the part of the same cluster. All the sensor nodes are homogenous, stationary, and fitted with GPS devices that can be used to know their locations. Each node can transmit to the BS directly. All the nodes are time synchronized. This can be achieved by having the BS broadcast periodic synchronization pulses.

The proposed model divides a round into two phases: (i) set-up phase and (ii) steady-state phase. In the first phase, the BS appoints CHs and sets up multi-hop paths to communicate with them. In the second phase, each CH collects data from the source nodes and forwards it toward the BS.

3.1 Set-up Phase

After deployment, each sensor node transmits a HELLO message to the BS. This message contains information in the following format—(SN_{id} , SN_{loc} , SN_{re}). Here, SN_{id} represents the sensor node ID, SN_{loc} represents its location, and SN_{re} represents

its RE. When the BS receives HELLO messages from all the sensor nodes, it chooses the node with the highest RE as the CH in each cluster. If two or more nodes fulfill this criterion, any node can be elected CH randomly. A node whose SN_{re} is below a predefined threshold is not considered in the CH election process.

After CH election, BS broadcasts a duty allocation (DUTY) message that contains information tuples in the following format— $(SN_{id}, CH_{id}, SN_{loc})$. Here, CH_{id} represents the ID of the node's CH. If the CH_{id} matches the SN_{id} , then the node is a CH itself. The location information of a node can be used to adjust the transmission power of the source while communicating with the node. Figure 1 shows a network which consists of nine clusters. Each cluster is composed of four/five sensor nodes. The clusters are numbered from left to right and top to bottom. This means that the grid in the first row and first column represents the first cluster, the grid in the first row and second column represents the second cluster, and so on.

In Fig. 1, nodes numbered 1–5 belong to the first cluster. Suppose, BS decides to appoint node 4 (node 4 has the highest SN_{re}) as the CH of this cluster. The DUTY message should contain the information tuples $(4, 4, 4_{loc})$ and $(2, 4, 2_{loc})$ among others. Node 4 learns from the first tuple that it is a CH itself. It learns from the second tuple that node 2 is a member node and the location of node 2 is 2_{loc} . Node 4 records the information of node 2 in a table maintained for its member nodes. Node 2 learns from the second tuple that node 4 is its CH. It learns from the first tuple that the location of node 4 is 4_{loc} . Node 2 records the information of node 4 in a table maintained for its CH. In this way, each CH records the information of its member nodes, and each non-CH node records the information of its CH.

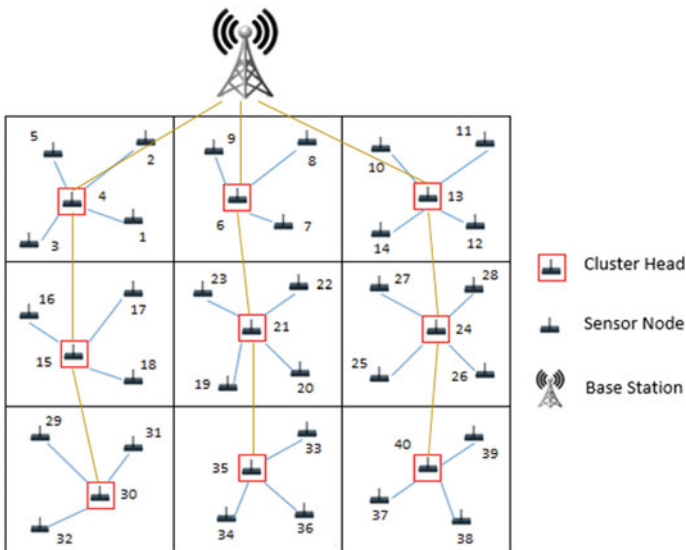


Fig. 1 Network connectivity after the establishment of multi-hop paths

After a timeout period, BS broadcasts a schedule for the inter-cluster communication (SCH_{bs}) in the network. This message contains information about the locations and sizes of control slots as well as data slots within a frame. The message also contains information tuples in the following format— $(SN_{id}, UCH_{id}, DS_{num}, UCH_{loc})$. Here, SN_{id} represents the ID of a CH, UCH_{id} represents the ID of the upstream CH, DS_{num} represents the slot in which the CH can communicate with its upstream CH, and UCH_{loc} represents the location of the upstream CH. In Fig. 1, node 15 is the upstream CH of node 30, node 4 is the upstream CH of node 15, and node 0 (BS) is the upstream CH of node 4. The schedule message (SCH_{bs}) should contain the information tuple $(30, 15, 9, 15_{loc})$ among others. Node 30 learns from this tuple that node 15 is the upstream CH, the slot allocated for communicating with node 15 is slot 9, and the location of node 15 is 15_{loc} . Node 30 records all this information in a separate table maintained for the upstream CH. In this way, each CH retrieves the necessary information from the corresponding tuple.

After receiving the SCH_{bs} message, each CH broadcasts a schedule for the intra-cluster communication (SCH_{ch}) in its cluster. This message contains information tuples in the following format— (SN_{id}, CS_{num}) . Here, CS_{num} represents the control slot that is allocated to the member node. The SCH_{ch} message from node 4 should contain the information tuple $(1, 1)$ among others. Node 1 learns from this tuple that it has been allocated slot 1 to send its control message. In this way, each member node learns about the allocated control slot from the corresponding tuple.

A frame consists of two parts: (i) *intra-cluster communication period* (for communication between a CH and its members) and (ii) *inter-cluster communication period* (for communication in between CHs). The intra-cluster communication period is a combination of control slots and data slots. The inter-cluster communication period is a combination of data slots only. The number of control slots in the intra-cluster communication period is same as the maximum number of non-CH nodes in any cluster. For the network shown in Fig. 1, the number of control slots in the intra-cluster communication period is four. The number of data slots in the intra-cluster communication period is m times the number of control slots. Here, m is the maximum number of data slots that a source node can claim. If $m = 1$, then the number of data slots in the intra-cluster communication period is also four. The number of data slots in the inter-cluster communication period depends on two factors: (i) number of communications needed for the data originating at the farthest CH to reach the BS and (ii) number of CHs that are directly communicating with the BS. For the network shown in Fig. 1, the inter-cluster communication period should contain five data slots. In Fig. 2, the first row shows the slots used for intra-cluster as well as inter-cluster communications in the seventh cluster. The second row shows the slots used for intra-cluster as well as inter-cluster communications in the fourth cluster. The third row shows the slots used for intra-cluster as well as inter-cluster communications in the first cluster.

In Fig. 2, the first three slots of the first row represent the control slots that node 30 has allocated to member nodes 29, 31, and 32, respectively. The fourth slot (gray-shaded) is an unused control slot. The ninth slot is allocated for communication between node 30 and node 15. The tenth slot is allocated for communication between

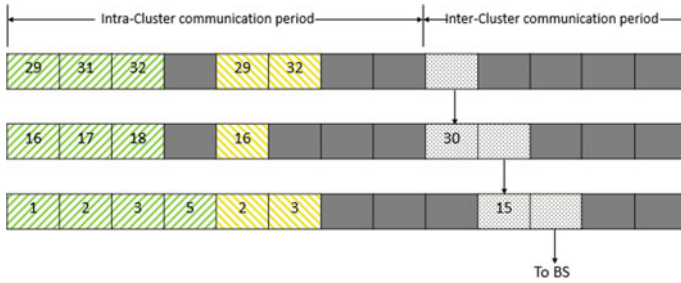


Fig. 2 Intra-cluster and inter-cluster communications in a frame

node 15 and node 4. The eleventh slot is allocated for communication between node 4 and the BS. The twelfth and thirteenth slots are allocated to node 6 and node 13, respectively, to communicate with the BS. As Fig. 2 shows the slot allocations in the clusters of the first column only, the twelfth and thirteenth slots are shown as unused slots.

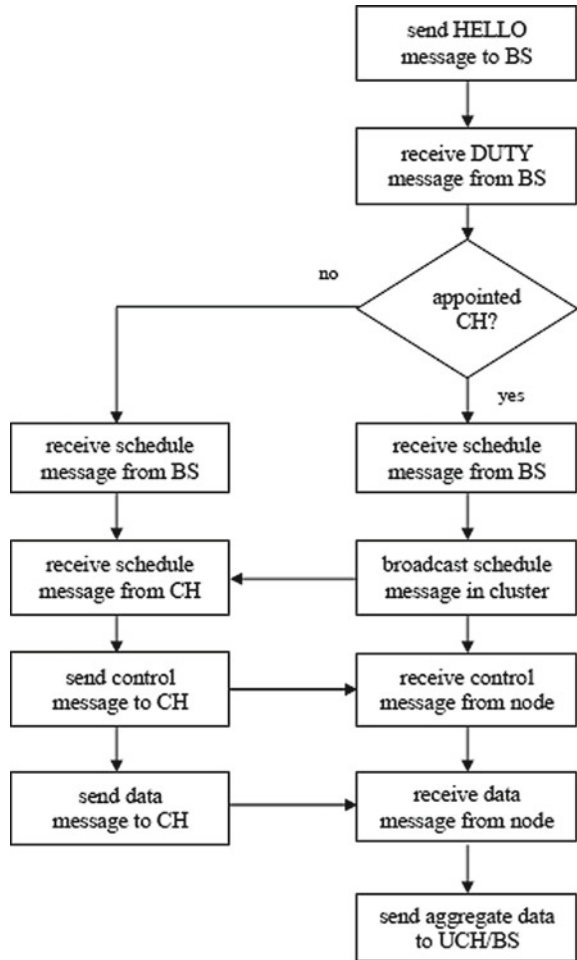
3.2 Steady-State Phase

This phase consists of k frames of equal size. If a member node wants to claim one or more data slots in a frame, it sends a control message to its CH in the allocated control slot. However, the node has to turn its radio ON from the beginning of the control period. This is so because before claiming any data slot(s), it should know which data slots have already been claimed. Figure 3 shows the working of MBEE-MAC protocol through a flowchart.

The control message has the following format— (SN_{id}, DS_{num}) . Here, DS_{num} represents the last data slot that a source node claims (among all the data slots claimed). After sending the control message, the node turns its radio OFF. It turns the radio ON in its data slot(s) to send data to the CH. After collecting data from all the source nodes, the CH calculates the aggregate and sends the aggregate data to the upstream CH/BS. A new round begins after k frames in which each node sends a HELLO message, and the whole process is repeated.

As shown in Fig. 2, node 4 has allocated slot 1, slot 2, slot 3, and slot 4 to node 1, node 2, node 3, and node 5, respectively. Node 2 and node 3 want to claim data slots. So, they keep their radios ON from the beginning of the control period. Node 1 does not claim slot 5 (first data slot in the intra-cluster communication period). Hence, node 2 claims this slot. It sends a control message which is (2, 5). Node 3 receives this message. It claims slot 6 (second data slot in the intra-cluster communication period). Node 4 keeps its radio ON in slot 5 and slot 6 to receive data from node 2 and node 3, respectively. Each node (including the CH) keeps its radio OFF in slot 7, slot 8, and slot 9. Node 4 turns its radio ON in slot 10 to receive data from node 15. Node 4 sends the aggregate data to the BS in slot 11.

Fig. 3 Working of MBEE-MAC protocol



4 Results and Analysis

The simulation results of MBEE-MAC are compared with the simulation results of BEE-MAC and BMA-MAC. All the protocols are simulated using the Python programming language. In all the simulations, the first-order radio model [6] is used to calculate the energy consumption in sensor nodes. Table 1 shows the parameters that are used in the simulations.

For the first simulation, a $50 \times 50 \text{ m}^2$ area is considered, and the total number of nodes in the deployment area is 100. The percentage of CHs (P) that is desired is 25%. The BS is located outside the deployment area, but very close to it. Figure 4 shows the graph that is generated after the first simulation. Table 2 shows when the

Table 1 Simulation parameters

Parameter	Value
Deployment area size (A)	$50 \times 50 \text{ m}^2, 100 \times 100 \text{ m}^2$
Sensor node's initial energy	5 J
E_{elec} (energy spent in running the transmitter or receiver circuitry)	50 nJ/bit
E_{idle} (energy spent in idle mode)	40 nJ/bit
ϵ_{amp} (energy spent in running the transmit amplifier)	100 pJ/bit/m ²
Data/schedule message size	250 Bytes
Control message size	20 Bytes
Number of frames in a round	20
Number of nodes (N)	100, 200

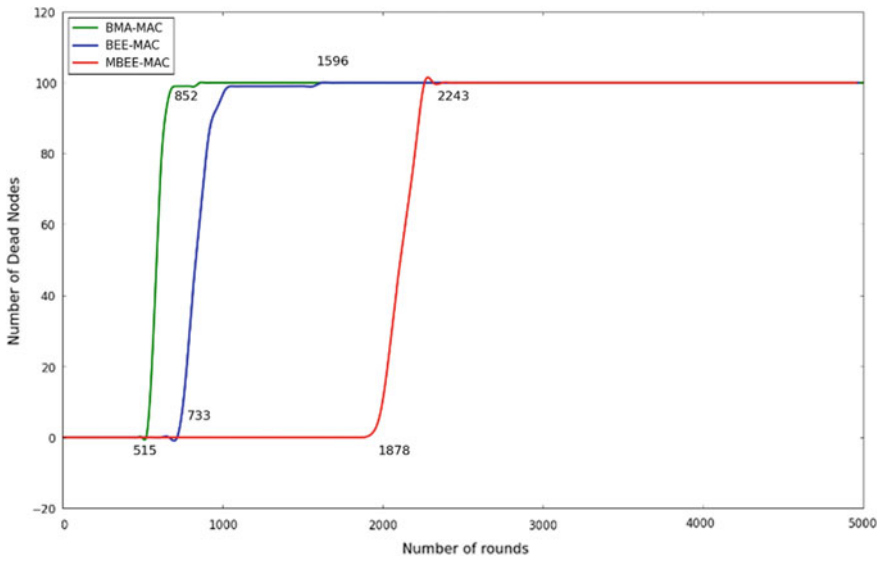


Fig. 4 First simulation: $N = 100$ nodes, $A = 50 \times 50 \text{ m}^2$, and $P = 25\%$

Table 2 First simulation: results in terms of RF and RL

Protocol	RF	RL
BMA-MAC	515	852
BEE-MAC	733	1596
MBEE-MAC	1878	2243

first node and the last node of each protocol dies in the first simulation. RF represents the round in which the first node dies, and RL represents the round in which the last node dies.

For the second simulation, a $100 \times 100 \text{ m}^2$ area is considered, and the total number of nodes in the deployment area is 100. The desired percentage of CHs is set to 25%. Figure 5 shows the graph that is generated after the second simulation. Table 3 shows when the first node and the last node of each protocol dies in the second simulation.

The RF value for a protocol is assumed to be the network lifetime in the protocol. Hence, the percentage increase/decrease in the network lifetime can be calculated by comparing the RF value for MBEE-MAC with the RF values for BMA-MAC and BEE-MAC. It is observed that MBEE-MAC increases the network lifetime by 156% compared with BEE-MAC and 265% compared with BMA-MAC in the first simulation. In the second simulation, MBEE-MAC increases the network lifetime by 105% compared with BEE-MAC and 172% compared with BMA-MAC. MBEE-MAC performs relatively better when 100 nodes are placed in a $50 \times 50 \text{ m}^2$ area than when they are placed in a $100 \times 100 \text{ m}^2$ area.

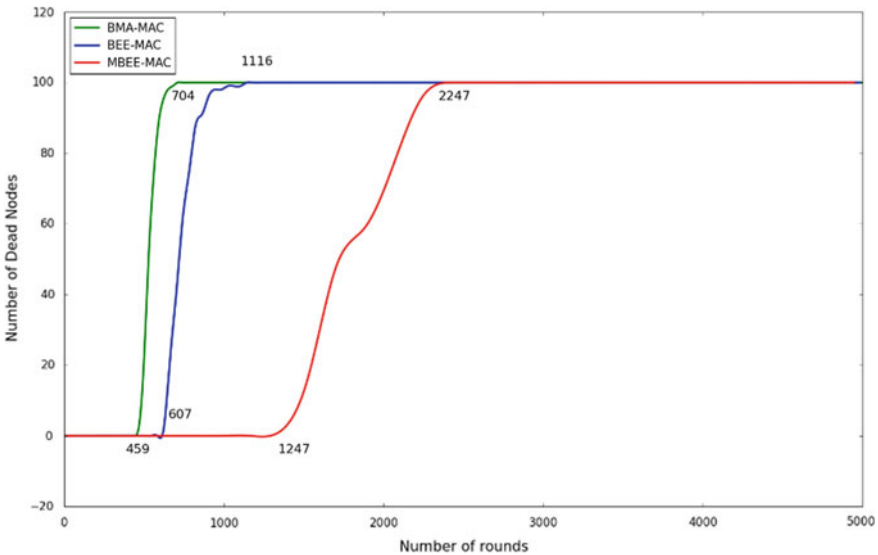


Fig. 5 Second simulation: $N = 100$ nodes, $A = 100 \times 100 \text{ m}^2$, and $P = 25\%$

Table 3 Second simulation: results in terms of RF and RL

Protocol	RF	RL
BMA-MAC	459	704
BEE-MAC	607	1116
MBEE-MAC	1247	2247

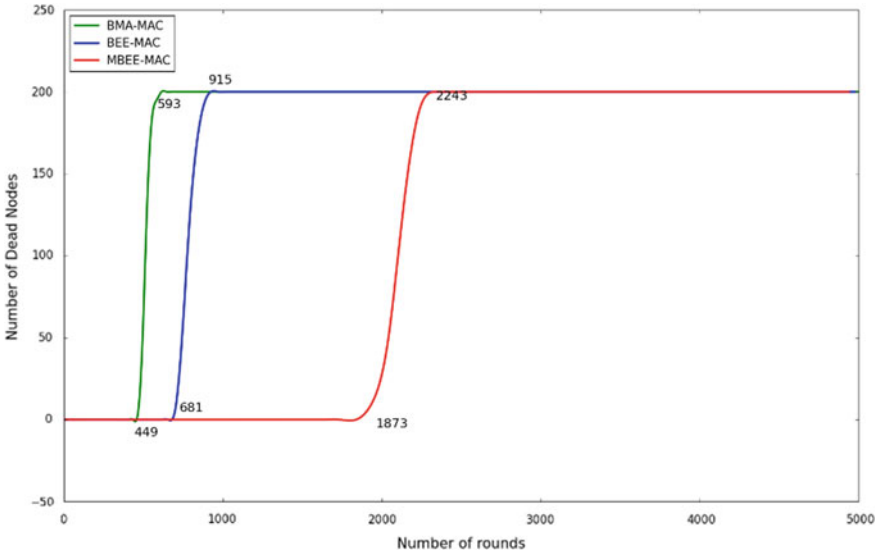


Fig. 6 Third simulation: $N = 200$ nodes, $A = 50 \times 50 \text{ m}^2$, and $P = 12.5\%$

Table 4 Third simulation: results in terms of RF and RL

Protocol	RF	RL
BMA-MAC	449	593
BEE-MAC	681	915
MBEE-MAC	1873	2243

For the third simulation, a $50 \times 50 \text{ m}^2$ area is considered, and the total number of nodes in the deployment area is 200. The percentage of CHs that is desired is 12.5%. Figure 6 shows the graph that is generated after the third simulation. Table 4 shows when the first node and the last node of each protocol dies in the third simulation.

For the fourth simulation, a $100 \times 100 \text{ m}^2$ area is considered, and the total number of nodes in the deployment area is 200. The percentage of CHs that is desired is 12.5%. Figure 7 shows the graph that is generated after the fourth simulation. Table 5 shows when the first node and the last node of each protocol dies in the fourth simulation.

It is observed that MBEE-MAC increases the network lifetime by 175% compared with BEE-MAC and 317% compared with BMA-MAC in the third simulation. In the fourth simulation, MBEE-MAC increases the network lifetime by 97% compared with BEE-MAC and 181% compared with BMA-MAC. MBEE-MAC performs relatively better when 200 nodes are placed in a $50 \times 50 \text{ m}^2$ area than when they are placed in a $100 \times 100 \text{ m}^2$ area.

For the fifth simulation, a $100 \times 100 \text{ m}^2$ area is considered, and the total number of nodes in the deployment area is 100. The number of CHs (C) is fixed at 16. Figure 8 shows the graph that is generated after the fifth simulation. Table 6 shows when the first node and the last node of each protocol dies in the fifth simulation.

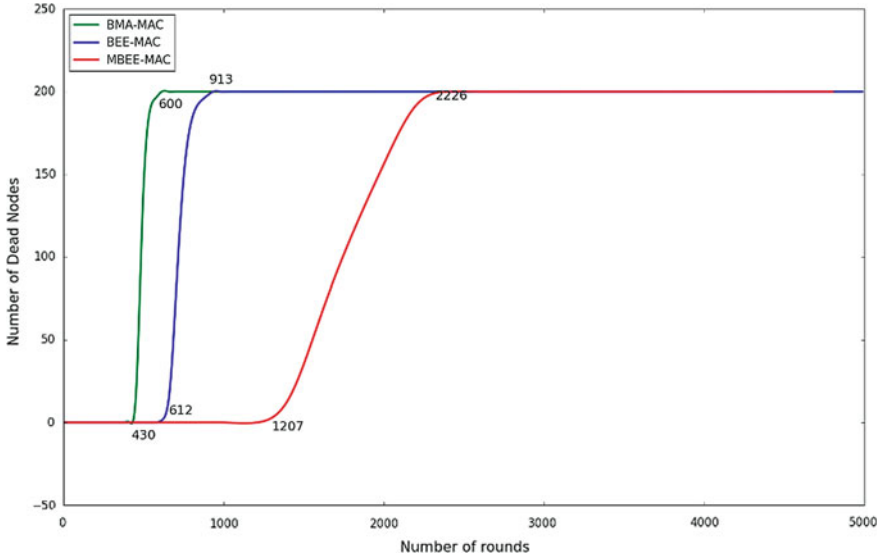


Fig. 7 Fourth simulation: $N = 200$ nodes, $A = 100 \times 100 \text{ m}^2$, and $P = 12.5\%$

Table 5 Fourth simulation: results in terms of RF and RL

Protocol	RF	RL
BMA-MAC	430	600
BEE-MAC	612	913
MBEE-MAC	1207	2226

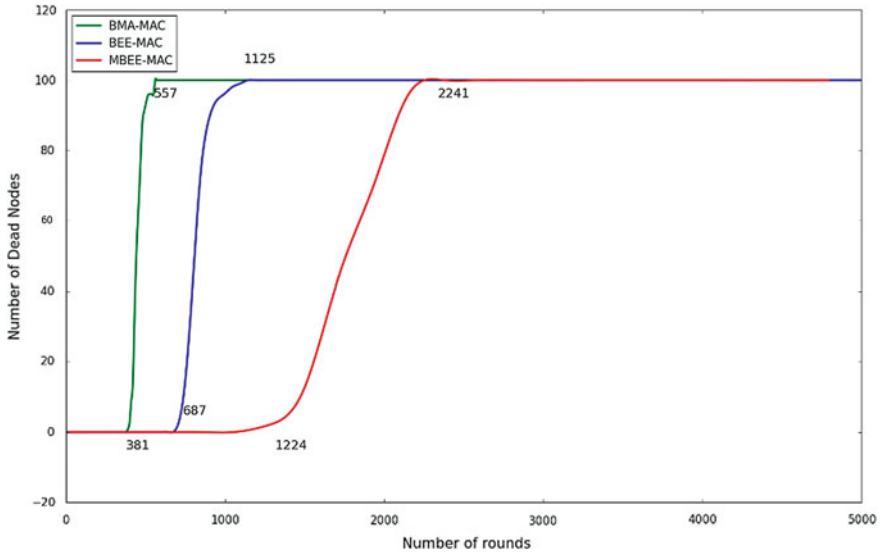


Fig. 8 Fifth simulation: $N = 100$ nodes, $A = 100 \times 100 \text{ m}^2$, and $C = 16$ CHs

Table 6 Fifth simulation: results in terms of RF and RL

Protocol	RF	RL
BMA-MAC	381	557
BEE-MAC	687	1125
MBEE-MAC	1224	2241

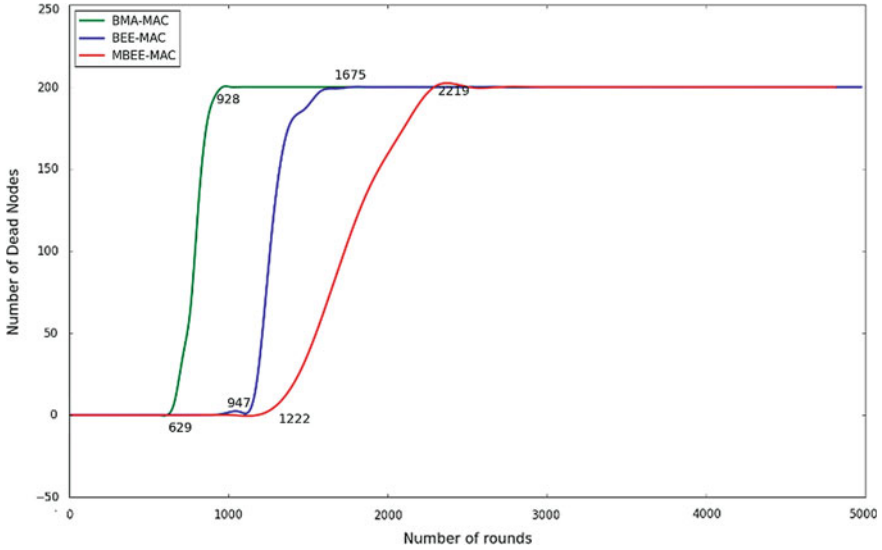


Fig. 9 Sixth Simulation: $N = 200$ nodes, $A = 100 \times 100 \text{ m}^2$, and $C = 16$ CHs

For the sixth simulation, a $100 \times 100 \text{ m}^2$ area is considered, and the total number of nodes in the deployment area is 200. The number of CHs is fixed at 16. Figure 9 shows the graph that is generated after the sixth simulation. Table 7 shows when the first node and the last node of each protocol dies in the sixth simulation.

It is observed that MBEE-MAC increases the network lifetime by 78% compared with BEE-MAC and 221% compared with BMA-MAC in the fifth simulation. In the sixth simulation, MBEE-MAC increases the network lifetime by 29% compared with BEE-MAC and 94% compared with BMA-MAC. MBEE-MAC performs relatively

Table 7 Sixth simulation: results in terms of RF and RL

Protocol	RF	RL
BMA-MAC	629	928
BEE-MAC	947	1675
MBEE-MAC	1222	2219

better when the total number of nodes is 100 than when it is 200 (keeping the number of CHs fixed at 16).

5 Conclusion

MBEE-MAC has a centralized approach toward CH election unlike BMA-MAC and BEE-MAC. In MBEE-MAC, the BS is responsible for electing CHs in the network. This ensures that the CHs are evenly distributed in the network. MBEE-MAC establishes multi-hop paths between CHs and the BS. This eliminates the requirement of long-range communications that are inevitable in BMA-MAC and BEE-MAC. Each CH communicates with its upstream CH that lies above it in the same column. This prevents any CH from being overloaded with traffic coming from multiple CHs belonging to the lower layers. The simulation results show that MBEE-MAC saves more energy in comparison with BMA-MAC and BEE-MAC.

Acknowledgements The authors would like to acknowledge the Ministry of Electronics and Information Technology (MeitY) of the Government of India for supporting this research work through the Visvesvaraya Ph.D. Scheme for Electronics and IT.

References

1. Yick J, Mukherjee B, Ghosal D (2008) Wireless sensor network survey. *Comput Netw* 52(12):2292–2330
2. Akyildiz IF, Su W, Sankarasubramaniam Y, Cayirci E (2002) A survey on sensor networks. *IEEE Commun Mag* 40(8):102–114
3. Khan JA, Qureshi HK, Iqbal A (2015) Energy management in wireless sensor networks: a survey. *Comput Electr Eng* 41:159–176
4. Anastasi G, Conti M, Di Francesco M, Passarella A (2009) Energy conservation in wireless sensor networks: a survey. *Ad hoc Netw* 7(3):537–568
5. Li J, Lazarou GY (2004) A bit-map-assisted energy-efficient MAC scheme for wireless sensor networks. In: *Proceedings of the 3rd international symposium on Information processing in sensor networks*, pp 55–60. ACM
6. Heinzelman WR, Chandrakasan A, Balakrishnan H (2000) Energy-efficient communication protocol for wireless microsensor networks. In: *Proceedings of the 33rd annual Hawaii international conference on system sciences*, 10 pp. IEEE
7. Hsu T-H, Yen P-Y (2011) Adaptive time division multiple access-based medium access control protocol for energy conserving and data transmission in wireless sensor networks. *IET Commun* 5(18):2662–2672
8. Alvi AN, Bouk SH, Ahmed SH, Yaqub MA, Javaid N, Kim D (2015) Enhanced TDMA based MAC protocol for adaptive data control in wireless sensor networks. *J Commun Netw* 17(3):247–255
9. Alvi AN, Bouk SH, Ahmed SH, Yaqub MA, Sarkar M, Song H (2016) BEST-MAC: Bitmap-assisted efficient and scalable TDMA-based WSN MAC protocol for smart cities. *IEEE Access* 4:312–322

10. Debasis K, Singh MP (2016) A low duty cycle MAC protocol for energy conservation in wireless sensor networks. *Int J Control Theor Appl* 9(41):991–995
11. Debasis K, Singh MP (2018) Bit-map-assisted energy-efficient mac protocol for wireless sensor networks. *Int J Adv Sci Technol* 119:111–122

PID Control of a Quadrotor



Ritika Thusoo , Sheilza Jain, and Sakshi Bangia

Abstract A Quadrotor comes under the rotor-type category of Unmanned Aerial Systems (UAS) which has four rotors. They are non-linear multivariable system that is highly underactuated. The Quadrotors have the capability to hover at one place during their flight and to take-off and land at any place vertically with the help of the vertical thrust produced by four rotors. They do not require a track to lift-off and land like fixed-wing UASs. They have three rotational motions, i.e. roll, pitch and yaw. These are obtained by changing the speed of the rotors. The model of a Quadrotor is simulated using MATLAB and Simulink and a PID control action is used to sustain its roll, pitch, yaw and altitude.

Keywords Quadrotor · UAS · VTOL

1 Introduction

Unmanned Aerial Systems (UAS) [1] can be categorized as rotor-type, heavier-than-air and lighter-than-air vehicles [2]. A Quadrotors is a rotor-type Unmanned Aerial Vehicle which has four rotors [3]. It can be used in areas where there is a risk to human life or in areas where mobility is very low [4]. The increase in the popularity of the Quadrotors is due to the progress in the motor and sensor technology, computation systems and communication systems. This has led to a decrease in the manufacturing costs of UAVs such as Quadrotors [5]. The availability of new microcontrollers like BeagleBone [6], Arduino [7], Raspberry Pi [8] and Texas Instrument's CC3200 [9] give Quadrotors a chance to be smaller in size with higher

R. Thusoo (✉) · S. Jain · S. Bangia
JC Bose University, YMCA, Faridabad, India
e-mail: ritikathusoo@gmail.com

S. Jain
e-mail: sheilzajain@gmail.com

S. Bangia
e-mail: sakshibangia@gmail.com

performance capability than the existing systems [10]. This makes Quadrotors very famous among the researchers and they are being studied at various universities and organizations. The applications of Quadrotors include inspection of agricultural fields [11], search and rescue operations [12], remote sensing and geographical mapping [13], recreational photography and drone racing [14]. Some companies are even trying to build UAVs that can deliver products to their customers like Amazon Prime Air [15].

Multicopters such as a Quadrotor have four rotors [16]. The voltages of these rotors act as the control variables. There are six motions of a Quadrotor which comprises of three rotational motions and three translational motions [17]. The rotational motion includes roll motion, pitch motion and yaw motion. The translational motion includes motion along the x-direction, motion along the y-direction and motion along the z-direction. This makes the Quadrotor system an underactuated multivariable system [18]. They have the capability to hover in one place, and they can vertically take-off and land without any runway [19]. Different mathematical techniques have been used over the years to model the Quadrotor. Force moment approach [20] was used to design an algorithm that could control the attitude as well as the altitude of the Quadrotor system. A non-linear algorithm [21] was also developed which was based on the backstepping methodology [22] and adaptation schemes [21]. An intelligent fuzzy controller was designed using force moment approach [23] and the simulation results obtained were quite promising. However, the control technique had to compromise with the exactness and speed of the system response. A Quadrotor system was designed to manage roll angle, pitch angle and yaw angle employing a stability enhancement system [24]. A unique contact force control approach was used to design a Quadrotor to collaborate with the surroundings in a strained space [25]. A definite trajectory tracking control for a Quadrotor using sliding mode control technique was designed [26]. The model was assumed to be in the vicinity of extraneous disturbance and model framework ambiguity. The simulation outputs indicate the expertise of the system. LQR technique was tested on a micro Quadrotor [27] and various simulations performed on the OS4 bench, validated the results.

This paper uses voltage-based approach to model a Quadrotor. The voltage-based approach uses Newton–Euler equations. The input voltages supplied to the quadrotor's rotors act as the control variable whereas the altitude and attitude are to be controlled. Proportional-Integral-Derivative (PID) [28] controller is used to stabilize the attitude, i.e. roll (ϕ), pitch (θ), yaw (ψ) angles and altitude (force along z-axis). The outline of the paper is as follows: The modelling of a Quadrotor is presented in Sect. 2. The Control of the Quadrotor is given in Sect. 3. The results and discussion are presented in Sect. 4 and the conclusion and future scope are given in Sect. 5.

2 Modelling of Quadrotor

A Quadrotor is a non-linear, strongly coupled [18], underactuated [29], multivariable [30] and unstable system [31]. These characteristics of the Quadrotors are evident because of their six Degrees of Freedom (DoF) [32] and the fact that there are only four actuators [18], i.e. the four rotor voltages to control them.

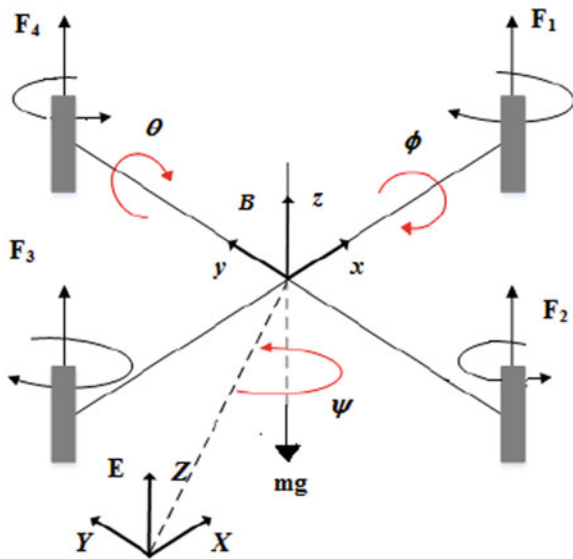
The Quadrotor structure has four rotors that are affixed at the ends of the arms of a balanced frame [33]. The quadrotor’s rotors can be divided into two pairs: motor R1 and R3 and motor R2 and R4 as shown in Fig. 1. The rotors (R1, R3) have clockwise rotation and rotors (R2, R4) have anti-clockwise rotation. The domineering forces and moments delegating on the Quadrotor are produced by rotors that are run by motors, for example, a Brushless DC (BLDC) motor [18]. The thrust force generated by rotor R1, R2, R3 and R4 can be denoted by F_1, F_2, F_3 and F_4 , respectively, as shown in Fig. 1.

There are two coordinate systems that are used to design a Quadrotor system, as shown in Fig. 1. The first frame is the earth’s inertial frame [34] or E-frame. The other frame is imagined to be affixed to the body of the Quadrotor and is known as B-frame [35].

There are four elemental movements of a Quadrotor: roll, pitch, yaw and force along z-axis, i.e. altitude of the Quadrotor [36]. In Fig. 1, roll angle is denoted by ϕ (phi) angle in x-direction [22]; pitch angle is denoted by θ (theta) angle in y-direction and yaw angle is denoted by ψ (psi) angle in z-direction.

Quadrotor configurations can be classified as plus and cross-configuration [18]. These configurations are based on the location of the rotors in a Quadrotor frame [37]. Cross-configuration of a Quadrotor is shown in Fig. 1, with respect to inertial and

Fig. 1 Quadrotor structure with earth and body-fixed frames [53]



body-fixed frame. The plus configuration schematic is shown in Fig. 2 whereas Fig. 3 shows the cross-configuration schematic for a Quadrotor. The cross-configuration is preferred because the speed of all four rotors is varied whereas in plus configuration only two rotor speeds are varied to obtain the rotational and translational motion. This ensures that the quadrotor’s engine does not saturate, and thus ensures the Quadrotor’s safety [38].

The equations of motion for a Quadrotor are derived from the force moment balance equations and can be represented by Eq. (1) [39]:

$$\theta'' I_{xx} = (-F_1 - F_2 + F_3 + F_4)d$$

$$\varphi'' I_{yy} = (-F_1 + F_2 + F_3 - F_4)d$$

Fig. 2 Plus configuration [54]

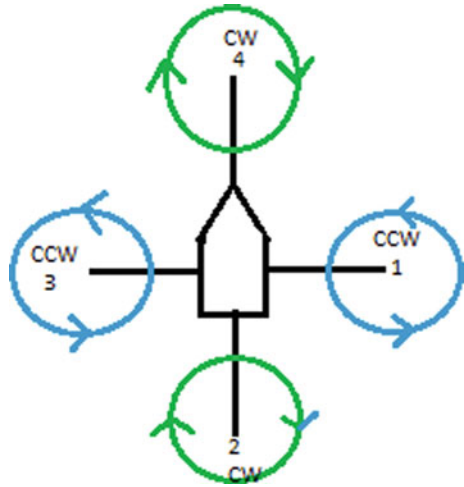
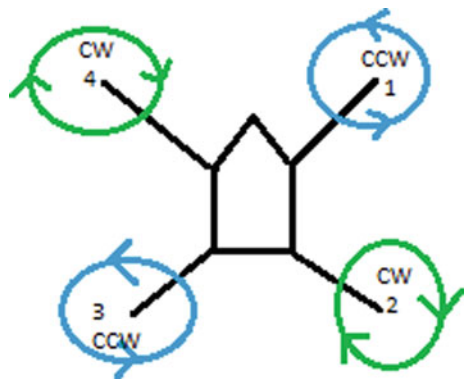


Fig. 3 Cross-configuration [54]



$$\begin{aligned}
 \psi'' I_{zz} &= (\tau_{m1} - \tau_{m2} + \tau_{m3} - \tau_{m4})d \\
 x'' &= \frac{1}{m} \sum_1^4 F_i [\sin \varphi \sin \psi + \cos \varphi \cos \psi \sin \theta] \\
 y'' &= \frac{1}{m} \sum_1^4 F_i [\sin \psi \sin \theta \cos \varphi - \cos \psi \sin \varphi] \\
 z'' &= \frac{1}{m} \sum_1^4 F_i [\cos \varphi \cos \theta] - g
 \end{aligned} \tag{1}$$

where the thrust force caused by motor $i = 1, 2, 3, 4$ is F_i , d represents the Quadrotor-arm length [40], τ_{mi} denoted the torque generated across all four motors, I_i 's are the moments of inertia and m the mass of the Quadrotor [39].

Equation (1) can be modified to obtain the respective equations for roll motion, pitch motion, yaw motion and equations for forces in x -direction, y -direction and z -direction.

2.1 Roll

The roll motion or roll angle is obtained with respect to the x -axis. It occurs due to the difference between the voltages of rotors R2 and R4 that move in a clockwise direction. The differential equation for roll angle can be defined as [39]:

$$\varphi'' = \frac{1}{I_{yy}} \left[\left(2\rho A d \left[\frac{\eta f K_t}{K_a} \right]^2 (V_2^2 - V_4^2) \right) \right] \tag{2}$$

where ρ is the air density, voltage of the rotors is denoted by V , rotor efficiency is η , f is the figure of merit [33], rotor's torque constant is denoted by K_a .

2.2 Pitch

The pitch angle is obtained with respect to the y -direction and is caused due to the rotation of rotors R1 and R3 in the anti-clockwise direction [41]. The voltage of rotor R3 is greater than the voltage of rotor R1 which indicates the speed of the rotor R3 is greater than that of rotor R1. This creates a pitch moment and it can be defined as [39]:

$$\theta'' = \frac{1}{I_{xx}} \left[\left(2\rho A d \left[\frac{\eta f K_t}{K_a} \right]^2 (V_3^2 - V_1^2) \right) \right] \tag{3}$$

where ρ is the air density, voltage of the rotors is denoted by V , rotor efficiency is η , K_a is the rotor's torque constant.

2.3 Yaw

The yaw angle is obtained with respect to the z -direction and is produced due to the torque inequality between the torque generated by the clockwise rotors and anti-clockwise moving rotors [42]. The differential equation for yaw can be defined as [39]:

$$\psi'' = \frac{J}{I_{zz}} (\Omega'_1 + \Omega'_3 - \Omega'_2 - \Omega'_4) + D(\Omega_1^2 + \Omega_3^2 - \Omega_2^2 - \Omega_4^2) \tag{4}$$

where Ω is the speed of the propeller.

2.4 Differential Equation for Force Along z-Direction

The force along the z -axis can be given by Eq. (5) which is the result of the net forces that occur due to the rotor R1, R2, R3 and R4 [39]:

$$z'' = \frac{2\rho A}{m} \left[\left[\frac{\eta f K_t}{K_a} \right]^2 (V_1^2 + V_2^2 + V_3^2 + V_4^2) \right] (\cos \theta \cos \varphi) - g \tag{5}$$

where V is the voltage of the rotors, ρ is the air density, η is rotor efficiency, f is propeller's figure of merit, K_a is the rotor's torque constant and g is acceleration due to gravity.

2.5 Differential Equation for Force Along x-Direction

The forces that operate along the x -direction is given in Eq. (6) and this occurs due to the actuator action [39]:

$$x'' = \frac{2\rho A}{m} \left[\left[\frac{\eta f K_t}{K_a} \right]^2 (V_1^2 + V_2^2 + V_3^2 + V_4^2) \right] (s\varphi s\psi + c\psi c\varphi s\theta) \tag{6}$$

where ρ is the air density, voltage of the rotors is denoted by V , rotor efficiency is η , f is the figure of merit, K_a is the rotor's torque constant and c stands for cosine and s stands for sine angle.

2.6 Differential Equation for Force Along y-Direction

The forces that operate along the y-direction is given in Eq. (7) and this occurs due to the actuator action [39]:

$$y'' = \frac{2\rho A}{m} \left[\left[\frac{\eta f K_t}{K_a} \right]^2 (V_1^2 + V_2^2 + V_3^2 + V_4^2) \right] (\sin \psi \sin \theta \cos \varphi - \cos \psi \sin \varphi) \tag{7}$$

where ρ is the air density, voltage of the rotors is denoted by V , rotor efficiency is η , f is figure of merit, K_a is the rotor's torque constant.

2.7 Model of the Quadrotor System

In Fig. 4, the model of the Quadrotor system is shown. The Phi_d represents the desired roll or phi angle, Theta_d denotes the desired theta angle or the desired pitch angle, Psi_d denotes the desired psi or yaw angle and the desired Z motion, i.e. altitude is denoted by Z_d . A proportional-differential-integrator (PID) controller [43] is employed to manipulate the roll, pitch, yaw angles and the altitude of the system.

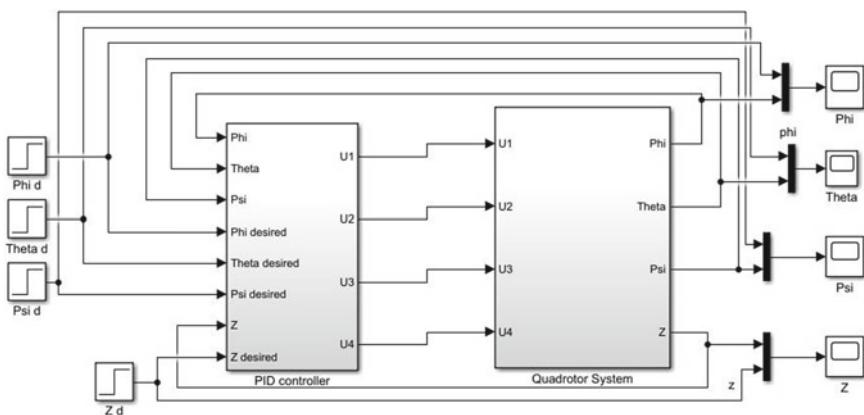


Fig. 4 The model of Quadrotor system developed using Simulink

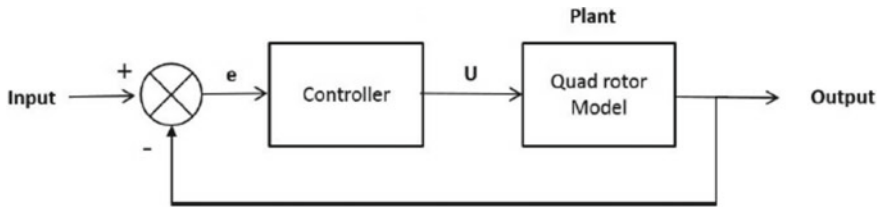


Fig. 5 Schematic diagram of a closed-loop control system

3 Control of the Quadrotor

A closed-loop control compensates for any changes in the input with the help of a feedback controller. The schematic diagram of a closed-loop control system is displayed in Fig. 5. A Proportional-Integral-Derivative (PID) [43, 44] control action is used to control roll (phi), pitch (theta) and yaw (psi) angles and altitude (force along z-axis) of the Quadrotor.

The control function for the closed-loop system is given by Eq. (8):

$$u(t) = G_p e(t) + G_i \int_0^t e(t) dt + G_d \frac{de(t)}{dt} \quad (8)$$

where G_p , G_i and G_d are the proportional, integral and differential gain of the controller [44].

A PID Tuner that is a part of the Simulink Control Design product is used to tune the PID controller for phi, theta, psi and altitude. The PID Tuner computes a linearized approximation of the model. In this model, PID controller is used separately for phi, theta and psi and the altitude. All the PID controllers are tuned using this PID Tuner. This uses a propriety algorithm developed by MATLAB. The robustness and response time of the system can be adjusted by using this PID Tuner [45].

4 Results and Discussion

The Quadrotor model denoted by Eqs. (2), (3), (4), (5), (6) and (7) is simulated using MATLAB and Simulink. A Proportional-Integral-Derivative (PID) controller [44] is employed to control the roll (phi) angle, pitch (theta) angle, yaw (psi) angle and altitude (force along z-axis) of the Quadrotor. A step input is given to test the designed model. The results obtained are shown in Figs. 6, 7, 8 and 9.

Figure 6 shows the response for the roll (phi) angle to the step input change when a PID control action is used to stabilize the roll angle. The response has little undershoot but it becomes stable after 5 s. However, there is a little offset in the output.

Fig. 6 Response of Roll angle (ϕ) versus time

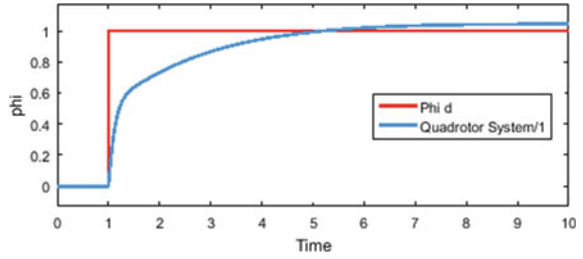


Fig. 7 Response of Yaw angle (ψ) output versus time

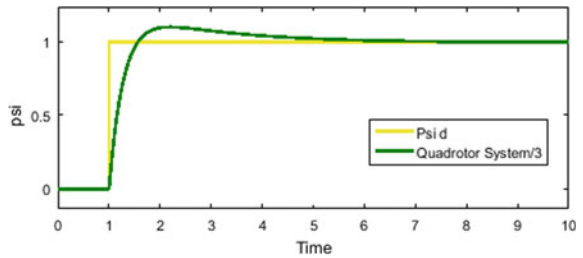


Fig. 8 Response of Theta angle (pitch) output versus time

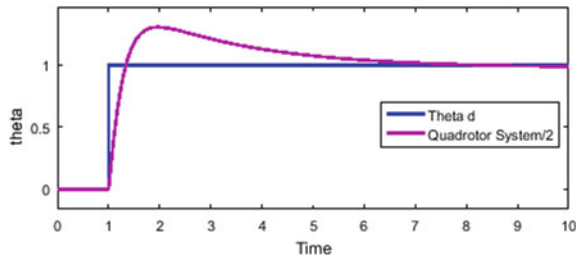


Fig. 9 Response of force along z-axis output versus time

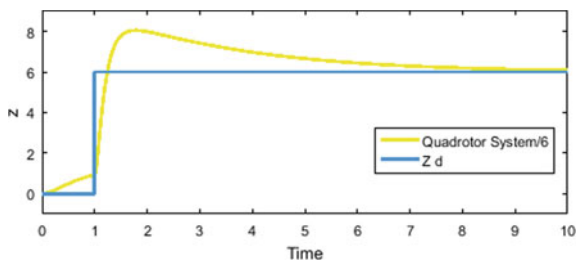


Figure 7 shows the response for the yaw (ψ) angle when a PID controller is used to compensate for the change in the input. The output shows a little overshoot and becomes stable after 5 s. The offset is zero.

Figure 8 shows the pitch (θ) angle response. The output has an overshoot at the beginning. The settling time is 6 s whereas the offset is zero.

Table 1 PID controller gains

	Phi angle (Roll)	Theta angle (Pitch)	Psi angle (Yaw)	Force along z-axis
G_p	0.017733	0.03143	0.013693	5.6074
G_i	0.0012492	0.003984	0.0004754	1.44260
G_d	0.034088	0.05383	0.032586	5.35209

Figure 9 shows the response of the force along z-axis. The output becomes stable at 8 s and there is no offset from the setpoint input given.

The PID controller parameters for the control of roll (phi) angle, pitch (theta) angle, yaw (psi) angle and force along z-axis are summarized in Table 1.

5 Conclusion and Future Scope

The quadrotor modelling is done using voltage-based approach. The model is simulated using Simulink and PID control action is applied to stabilize the roll(phi) angle, pitch(theta) angle, yaw(psi) angle and altitude (force along z-axis) of the quadrotor. The responses are obtained for a step input and are quite satisfactory. However, other control techniques would be implemented in the future like integral backstepping [46], fuzzy control to the quadrotor. Optimization of the controller action would be the future scope of this paper [47–50]. Model-based control techniques like model reference adaptive control (MRAC) [51] and Internal Model Control (IMC) [52] would also be implemented in the future.

References

1. Colomina I, Molina P (2014) Unmanned aerial systems for photogrammetry and remote sensing: a review. *ISPRS Journal of photogrammetry and remote sensing* 92:79–97
2. Valavanis KP (2007) *Advances in unmanned aerial vehicles: state of the art and the road to autonomy*. Springer Science & Business Media
3. Li Y, Song S (2012) A survey of control algorithms for quadrotor unmanned helicopter. In: 2012 IEEE 5th international conference on advanced computational intelligence, ICACI 2012, pp 365–369
4. Joyo MK, Ahmed SF, Hazry D, Tanveer MH, Warsi FA (2013) Position controller design for quad-rotor under perturbed condition. *Wulfenia* 20:178–189
5. Cooper AJ, Redman CA, Stoneham DM, Gonzalez LF, Etse VK (2015) A dynamic navigation model for unmanned aircraft systems and an application to autonomous front-on environmental sensing and photography using low-cost sensor systems. *Sensors (Switzerland)* 15:21537–21553
6. Guevara K, Rodriguez M, Gallo N, Velasco G, Vasudeva K, Guvenc I (2015) UAV-based GSM network for public safety communications. In: *Conference proceedings of IEEE SOUTHEASTCON*. Institute of Electrical and Electronics Engineers Inc.

7. Elsamanty M, Khalifa A, Fanni M, Ramadan A, Abo-Ismael A (2013) Methodology for identifying quadrotor parameters, attitude estimation and control. In: 2013 IEEE/ASME international conference on advanced intelligent mechatronics: mechatronics for human wellbeing, AIM 2013, pp 1343–1348
8. Bhatkhande P, Havens TC (2014) Real time fuzzy controller for quadrotor stability control. In: IEEE international conference on fuzzy systems. Institute of Electrical and Electronics Engineers Inc., pp 913–919
9. Kent S, Weideman R, Kimball N (2018) Dynamic video streaming for nano quadcopters. *Comput Eng*
10. Zulu A, John S (2014) A review of control algorithms for autonomous quadrotors. *Open J Appl Sci* 04:547–556
11. Zhao J, Li Y, Hu D, Pei Z (2016) Design on altitude control system of quad rotor based on laser radar. In: AUS 2016—2016 IEEE/CSAA international conference on aircraft utility systems. Institute of Electrical and Electronics Engineers Inc., pp 105–109
12. Cacace J, Finzi A, Lippiello V, Furci M, Mimmo N, Marconi L (2016) A control architecture for multiple drones operated via multimodal interaction in search & rescue mission. In: SSRR 2016—international symposium on safety, security and rescue robotics. Institute of Electrical and Electronics Engineers Inc., pp 233–239
13. Janusz W, Niezabitowski M, Orwat J, Sikora P (2016) The concept of combined measurements of the Gliwice radio tower deflection in relation to the speed and direction of the wind with use of quadrotor. In: Proceedings of the 2016 17th international carpathian control conference, ICC 2016. Institute of Electrical and Electronics Engineers Inc., pp 280–285
14. Sun J, Li B, Jiang Y, Wen CY (2016) A camera-based target detection and positioning UAV system for search and rescue (SAR) purposes. *Sensors (Switzerland)* 16
15. Motlagh NH, Baggaa M, Taleb T (2017) UAV-Based IoT platform: a crowd surveillance use case. *IEEE Commun Mag* 55:128–134
16. Elfeky M, Elshafei M, Saif AWA, Al-Malki MF (2016) Modeling and simulation of quadrotor UAV with tilting rotors. *Int J Control Autom Syst* 14:1047–1055
17. Liu H, Xi J, Zhong Y (2014) Robust motion control of quadrotors. *J Franklin Institute* 351(12):5494–5510
18. Zhang X, Li X, Wang K, Lu Y (2014) A survey of modelling and identification of quadrotor robot. *Abstract and Applied Analysis (Vol. 2014)*
19. Intwala A (2015) A review on vertical take off and landing (VTOL) vehicles. *Innov Res Adv Eng* 2:186–191
20. Khalil W (2011) Dynamic modeling of robots using newton-euler formulation. In: *Lecture notes in electrical engineering*. Springer, Berlin, Heidelberg, pp 3–20
21. Al-Younes YM, Al-Jarrah MA, Jhemi AA (2010) Linear vs. nonlinear control techniques for a quadrotor vehicle. In: 7th International Symposium on Mechatronics and its Applications, Sharjah, pp 1–10
22. Madan T, Benallegue A (2006) Backstepping control for a quadrotor helicopter. In: IEEE international conference on intelligent robots and systems. IEEE, pp 3255–3260
23. Santos M, López V, Morata F (2010) Intelligent fuzzy controller of a quadrotor. In: Proceedings of 2010 IEEE International conference on intelligent systems and knowledge engineering, ISKE 2010. pp 141–146
24. Kim GB, Nguyen TK, Budiyo A, Park JK, Yoon KJ, Shin J (2013) Design and development of a class of rotorcraft-based UAV. *Int J Adv Robot Syst* 10
25. Jung S (2012) A position-based force control approach to a quad-rotor system. In: 2012 9th international conference on ubiquitous robots and ambient intelligence. URAI 2012. 373–377 (2012)
26. Fan Y, Cao Y, Zhao Y (2017) Sliding mode control for nonlinear trajectory tracking of a Quadrotor. In: 2017 36th Chinese Control Conference (CCC), Dalian, pp 6676–6680
27. Bouabdallah S, Noth A, Siegwart R (2004) PID vs LQ control techniques applied to an indoor micro quadrotor. In: 2004 IEEE/RSJ international conference on intelligent robots and systems (IEEE Cat. No.04CH37566). vol 3, pp 2451–2456

28. Khatoun S, Shahid M, Ibraheem, Chaudhary H (2014) Dynamic modeling and stabilization of quadrotor using PID controller. In: 2014 International Conference on Advances in Computing, Communications and Informatics (ICACCI), New Delhi, pp 746–750
29. Mian AA, Daobo W (2008) Nonlinear flight control strategy for an underactuated quadrotor aerial robot. In: Proceedings of 2008 IEEE international conference on networking, sensing and control, ICNSC, pp 938–942. IEEE
30. Yali Y, SunFeng, Yuanxi W (2012) Controller design of quadrotor aerial robot. Phys Procedia (33):1254–1260, ISSN 1875–3892. <https://doi.org/10.1016/j.phpro.2012.05.207>
31. Babaei R, Ehyaei AF (2015) Robust backstepping control of a quadrotor uav using extended kalman bucy filter. International Journal of Mechatronics, Electrical and Computer Technology (IJMEC) 5(16):2276–2291
32. Yu Y, Ding X (2012) A quadrotor test bench for six degree of freedom flight. J Intell Robot Syst Theor Appl
33. Martinez V (2007) Modelling of the flight dynamics of a quadrotor helicopter. A M.Sc. Thesis Cranfield University, pp 1–289
34. Bouallègue S, Fessi R (2018) Modelling and hardware co-simulation of a Quadrotor unmanned aerial vehicle. Int J Simul Process Model 13:3
35. Tewari A (2011) Advanced control of aircraft, spacecraft and rockets. Wiley (BBS.pdf)
36. Fadholi MI, Sasongko PS (2019) Autonomous pole balancing design in quadcopter using behaviour-based intelligent fuzzy control. In: 2018 2nd international conference on informatics and computational sciences. ICICoS 2018, pp 208–213
37. Zhang X, Li X, Wang K, Lu Y (2014) A survey of modelling and identification of quadrotor robot. <http://www.hindawi.com/journals/aaa/2014/320526/>
38. Orsag M, Bog S (2012) Influence of forward and descent flight on quadrotor dynamics. In: Recent advances in aircraft technology. <https://doi.org/10.5772/37438>
39. Hong M, Bousbaine A, Wu MH, Poyi GT (2016) Modelling and simulation of a quad-rotor helicopter
40. Chovancová A, Fico T, Chovanec E, Hubinský P (2014) Mathematical modelling and parameter identification of quadrotor (a survey). Procedia Eng 96:172–181
41. Lukmana MA, Nurhadi H (2015) Preliminary study on Unmanned Aerial Vehicle (UAV) Quadcopter using PID controller. In: 2015 International Conference on Advanced Mechatronics, Intelligent Manufacture, and Industrial Automation (ICAMIMIA), Surabaya, pp 34–37
42. Jithu G, Jayasree PR (2016) Quadrotor modelling and control. Int. Conf. Electr. Electron. Optim. Tech. ICEEOT 2016. 1167–1172 (2016)
43. Rathore NS, Singha VP (2018) Design of optimal PID controller for the reverse osmosis using teacher-learner-based-optimization. Membr Water Treat 9:129–136
44. Ang KH, Chong G, Li Y (2005) PID control system analysis, design, and technology. IEEE Trans Control Syst Technol 13:559–576
45. Open PID Tuner for PID tuning—MATLAB, <https://in.mathworks.com/help/slcontrol/ug/designing-controllers-with-the-pid-tuner.html>. Last accessed 2019/10/07
46. Fang, Z. Gao W (2011) Adaptive integral backstepping control of a micro-quadrotor. In: 2011 2nd International conference on intelligent control and information processing, pp 910–915. IEEE
47. Rathore NS, Singh VP, Kumar B (2018) Controller design for Doha water treatment plant using grey wolf optimization. J Intell Fuzzy Syst 35:5329–5336
48. Singh SP, Singh V, Singh VP (2019) Analytic hierarchy process based approximation of high-order continuous systems using TLBO algorithm. Int J Dyn Control 7:53–60
49. Singh SP, Prakash T, Singh VP (2019) Coordinated tuning of controller-parameters using symbiotic organisms search algorithm for frequency regulation of multi-area wind integrated power system. Eng Sci Technol Int J
50. Rathore NS, Singh VP, Phuc BDH (2019) A modified controller design based on symbiotic organisms search optimization for desalination system. J Water Supply Res Technol 68:337–345

51. Kreisselmeier G, Anderson B (1986) Robust model reference adaptive control. *IEEE Trans Automat Contr* 31:127–133
52. Rivera DE, Morarl M, Skogestad S (1986) Internal model control: pid controller design. *Ind Eng Chem Process Des Dev* 25:252–265
53. Ghamry KA, Zhang Y (2015) Formation control of multiple quadrotors based on leader-follower method. In: 2015 International conference on unmanned aircraft systems, ICUAS 2015, pp 1037–1042. IEEE
54. Vargas AM, Gómez GR, Carranza JM (2017) Quadrotor flight in constrained indoor environments

Levy Flight-Based White Wolf Algorithm for Solving Optimal Reactive Power Problem



Kanagasabai Lenin

Abstract In this work, reactive power problem is solved by levy flight-based white wolf (LFW) algorithm. White wolf actions such as hunting, encircling the prey are imitated to design the algorithm. Mainly population of white wolf will be in stagnation mode in leader wolves. In the projected algorithm, levy flight has been applied in the white wolf algorithm to improve the global search very effectively. Predominantly stagnation of leader white wolf will be evaded, and candidate solution will be enhanced during all phases of the search system. In standard IEEE 14, 30 bus test system levy flight-based white wolf (LFW) algorithm is evaluated. LFW approach reduced the loss efficiently.

Keywords Optimal reactive power · Transmission loss · Levy flight-based white wolf algorithm

1 Introduction

Power loss minimization is the main objective of this work. Optimal reactive power problem is solved by applying numerous techniques [1–6], and many evolutionary computation approaches [7–16] are utilized for minimization of power loss. In this work, levy flight-based white wolf (LFW) algorithm is proposed. Deeds of white wolf are imitated to formulate the algorithm. Population of white wolf is inclined to stagnation, and problem of immature convergence will occur. In the projected algorithm, levy flight has been applied in the white wolf algorithm such that global searching can be done more efficiently. Candidate solution is improved in all phases of the exploration procedure. Alpha, beta, and delta states are projected in levy flight-based white wolf (LFW) algorithm to modernize the ability of hunting procedure. In

K. Lenin (✉)

Department of EEE, Prasad V. Potluri, Siddhartha Institute of Technology, Kanuru, Vijayawada, Andhra Pradesh 520007, India
e-mail: gklenin@gmail.com

standard IEEE 14, 30, bus test system proposed levy flight-based white wolf (LFW) algorithm is evaluated. Simulation study shows that the projected algorithm reduced the power loss efficiently.

2 Problem Formulation

Active power loss is the key objective and defined by,

$$P_L = \sum_{k \in Nbr} g_k (V_i^2 + V_j^2 - 2V_i V_j \cos \theta_{ij}) \quad (1)$$

$$\text{Objective function} = \text{Power loss} + \text{weight}(\omega_v) \times \text{Deviation of Volatge} \quad (2)$$

$$\text{Deviation of volatge} = \sum_{i=1}^{Npq} |V_i - 1| \quad (3)$$

Equal and inequal constraints are as follows:

$$\text{Generation } (P_G) = \text{Demand } (P_D) + \text{Load } (P_L) \quad (4)$$

$$P_{g \text{ slack}}^{\text{minimum}} \leq P_{g \text{ slack}} \leq P_{g \text{ slack}}^{\text{maximum}} \quad (5)$$

$$Q_{gi}^{\text{minimum}} \leq Q_{gi} \leq Q_{gi}^{\text{maximum}}, i \in N_g \quad (6)$$

$$V_i^{\text{minimum}} \leq V_i \leq V_i^{\text{maximum}}, i \in N_B \quad (7)$$

$$T_i^{\text{min}} \leq T_i \leq T_i^{\text{max}}, i \in N_T \quad (8)$$

$$Q_c^{\text{min}} \leq Q_c \leq Q_c^{\text{max}}, i \in N_C \quad (9)$$

3 Levy Flight-Based White Wolf Algorithm

In the proposed levy flight-based white wolf (LFW) algorithm, deeds of the white wolf are emulated to design the algorithm. In white wolf algorithm, the motion of wolf during hunting and encircling is described by,

$$\bar{U} = |\overrightarrow{IR}_p(t.) - \bar{R}(t.)| \tag{10}$$

$$\bar{R}(t + 1) = \bar{R}_p(t) - \bar{M} \cdot U \tag{11}$$

$$\bar{M} = 2m \cdot r_1 - m \tag{12}$$

$$\bar{I} = 2 \cdot r_2 \tag{13}$$

$$m = 2 - 2t./t.\max \tag{14}$$

The state of wolves is adjusted by,

$$\bar{U}_\alpha = |\bar{I}_1, \bar{R}_\alpha - \bar{R}| \tag{15}$$

$$\bar{U}_\beta = |\bar{I}_2, \bar{R}_\beta - \bar{R}| \tag{16}$$

$$\bar{U}_\gamma = |\bar{I}_3, \bar{R}_\delta - \bar{R}| \tag{17}$$

$$\bar{R}_1 = \bar{R}_\alpha - \bar{M}_1 \cdot (\bar{U}_\alpha) \tag{18}$$

$$\bar{R}_2 = \bar{R} - \bar{M}_2 \cdot (\bar{U}_\beta) \tag{19}$$

$$\bar{R}_3 = \bar{R}_\delta - \bar{M}_3 \cdot (\bar{U}_\delta) \tag{20}$$

$$\bar{R}(t. + 1) = 0.33(\bar{R}_1 + \bar{R}_2 + \bar{R}_3) \tag{21}$$

Alpha, beta, and delta states projected levy flight-based white wolf (LFW) algorithm modernize its ability of hunting. The position of the wolf can be described by,

$$\bar{R}(t) = 0.5 \times (\bar{R}_\alpha - \bar{M}_1 \bar{U}_\alpha + \bar{R}_\beta - \bar{M}_2 \bar{U}_\beta) \tag{22}$$

Levy distribution [17];

$$L(s, \gamma, \mu) = \begin{cases} \sqrt{\frac{\gamma}{2\pi}} & \exp\left[-\frac{\gamma}{2(s - \mu)}\right] \frac{1}{(s - \mu)^{3/2}} \text{ if } 0 < \mu < s < \infty \\ 0 & \text{if } s \leq 0 \end{cases} \tag{23}$$

$$F(k) = \exp[-\alpha |k|^\beta], 0 < \beta \leq 2, \tag{24}$$

$$R^{t+1} = R^t + \alpha \oplus \text{Levy}(\beta) \tag{25}$$

$$R^{t+1} = R^t + \text{random}(\text{size}(D)) \oplus \text{Levy}(\beta) \tag{26}$$

$$\vec{R}_{\text{new}}(t) = \begin{cases} 0.5 \times (\vec{R}_\alpha - \vec{A}_1 \vec{D}_\alpha + \vec{R}_\beta - \vec{M}_2 \vec{U}_\beta) + \alpha \\ \oplus \text{Levy}(\beta) \quad |M| > 0.5 \\ \vec{R}(t) = 0.5 \times (\vec{R}_\alpha - \vec{R}_1 \vec{U}_\alpha + \vec{R}_\beta - \vec{M}_2 \vec{U}_\beta) \\ |M| < 0.5 \end{cases} \tag{27}$$

$$\vec{R}_{\text{new}}(t) = 0.5 \times (\vec{R}_\alpha - \vec{M}_1 \vec{U}_\alpha + \vec{R}_\beta - \vec{M}_2 \vec{U}_\beta) + \text{random}(\text{size}(U)) \oplus \text{Levy}(\beta) \tag{28}$$

$$\vec{R}^{t+1} = \vec{R}^t + \text{random}(\text{size}(D)) \oplus \text{Levy}(\beta) \sim 0.010 \frac{u}{|v|^{1/\beta}} (\vec{R}(t) - \vec{R}^\alpha(t)) \tag{29}$$

$$u \sim N(0, \sigma_u^2) \quad v \sim N(0, \sigma_v^2) \tag{30}$$

$$\sigma_u = \left\{ \frac{\Gamma(1 + \beta) \sin(\pi \beta / 2)}{\Gamma[(1 + \beta) / 2] \beta 2^{(\beta - 1) / 2}} \right\}^{1/\beta}, \sigma_v = 1 \tag{31}$$

The worst positions will be disregarded by, otherwise

$$\vec{R}(t + 1) = \begin{cases} \vec{R}(t) & f(\vec{R}_{\text{new}}(t)) > f \vec{R}(t) \text{ and } r_{\text{new}} < P \\ \vec{R}_{\text{new}}(t) & \text{otherwise} \end{cases} \tag{32}$$

- (a) Define the preliminary swarm size
- (b) Capriciously engender the preliminary population of wolves
- (c) “a”, “p”, “A”, “C” values are initialized
- (d) Fitness of each white wolf will be computed
- (e) “X_α” is chosen as most excellent white wolf
- (f) “X_β” is chosen as second to the most excellent white wolf
- (g) While (t < T)
- (h) For each wolf
- (i) modernize the position of existing white wolves by Eqs. 27 and 28
- (k) End for
- (l) “a”, “p”, “A”, “C” values are modernized
- (m) fitness of white wolves are computed

Table 1 Control variables limits

	Minimum (PU)	Maximum (PU)
Generator voltage	0.950	1.100
Transformer tap	0.900	1.100
VAR source	0.000	0.200

Table 2 Reactive power generators limits

Variables	Q Minimum (PU)	Q Maximum (PU)
1	0	10
2	-40	50
3	0	40
6	-6	24
8	-6	24

- (n) “ X_α ” and “ X_β ” are modernized
- (o) iteration = iteration + 1
- (p) End while
- (q) Revert to “ X_α ”

4 Simulation Results

Levy flight-based white wolf (LFW) algorithm is tested in IEEE 14 bus system [18]. Table 1 shows control variable limits, and Table 2 provides limits of reactive power generators. Table 3 shows the comparison results.

Then, the proposed levy flight-based white wolf (LFW) algorithm tested in IEEE 30 bus system. Table 4 and Table 5 give control variable limits and limits of reactive power generators. In Table 6, power loss comparisons have been given.

5 Conclusion

In this paper, levy flight-based white wolf (LFW) algorithm solved the optimal reactive power problem effectively. Population of white wolf is in stagnation mode in leader wolves. Consequently, problem of immature convergence will occur and is unable to perform flawless changeover from exploration to exploitation phase. Updates of hunters are based on the state of alpha, beta, and delta in projected levy flight-based white wolf (LFW) algorithm. The proposed levy flight-based white wolf (LFW) algorithm is tested IEEE 14, 30 bus systems. Power loss is reduced efficiently. Mainly percentage of power loss reduction has been improved.

Table 3 Simulation results of IEEE—14 system

Control variables	Base case	MPSO [19]	PSO [19]	EP [19]	SARGA [19]	LFW
Generator voltage-1	1.060	1.100	1.100	NR*	NR*	1.024
Generator voltage-2	1.045	1.085	1.086	1.029	1.060	1.029
Generator voltage-3	1.010	1.055	1.056	1.016	1.036	1.027
Generator voltage-6	1.070	1.069	1.067	1.097	1.099	1.020
Generator voltage-8	1.090	1.074	1.060	1.053	1.078	1.031
Tap 8	0.978	1.018	1.019	1.04	0.95	0.948
Tap 9	0.969	0.975	0.988	0.94	0.95	0.939
Tap10	0.932	1.024	1.008	1.03	0.96	0.937
QC – 9	0.19	14.64	0.185	0.18	0.06	0.136
PG	272.39	271.32	271.32	NR*	NR*	271.87
QG (Mvar)	82.44	75.79	76.79	NR*	NR*	75.92
Reduction in PLoss (%)	0	9.2	9.1	1.5	2.5	25.85
Total PLoss (Mw)	13.550	12.293	12.315	13.346	13.216	10.046

NR* Not reported

Table 4 Control variables

Variables	Minimum (PU)	Maximum (PU)
Generator voltage	0.950	1.100
Transformer tap	0.900	1.100
VAR source	0.000	0.200

Table 5 Constraints of reactive power generators

Variables	Q Minimum (PU)	Q Maximum (PU)
1	0	10
2	−40	50
5	−40	40
8	−10	40
11	−6	24
13	−6	24

Table 6 Simulation results of IEEE—30 system

Control variables	Values of base case	MPSO [19]	PSO [19]	EP [19]	SARGA [19]	LFW
Generator voltage-1	1.06	1.101	1.100	NR*	NR*	1.026
Generator voltage-2	1.045	1.086	1.072	1.097	1.094	1.031
Generator voltage-5	1.010	1.047	1.038	1.049	1.053	1.027
Generator voltage-8	1.010	1.057	1.048	1.033	1.059	1.042
Generator voltage-12	1.082	1.048	1.058	1.092	1.099	1.047
Generator voltage-13	1.071	1.068	1.080	1.091	1.099	1.036
Tap11	0.978	0.983	0.987	1.01	0.99	0.948
Tap12	0.969	1.023	1.015	1.03	1.03	0.939
Tap15	0.932	1.020	1.020	1.07	0.98	0.931
Tap36	0.968	0.988	1.012	0.99	0.96	0.940
QC10	0.19	0.077	0.077	0.19	0.19	0.090
QC24	0.043	0.119	0.12	0.04	0.04	0.124
PG (MW)	300.9	299.54	299.54	NR*	NR*	297.72
QG (Mvar)	133.9	130.83	130.94	NR*	NR*	131.48
Reduction in PLoss (%)	0	8.4	7.4	6.6	8.3	20.06
Total PLoss (Megawatts)	17.55	16.07	16.25	16.38	16.09	14.029

NR* indicates Not Reported

References

1. Lee K (1984) Fuel-cost minimisation for both real and reactive-power dispatches. In: Proceedings of generation, transmission and distribution conference, vol 131, issue no 3, pp 85–93
2. Deeb N (1998) An efficient technique for reactive power dispatch using a revised linear programming approach. *Electr Power Syst Res* 15(2):121–134
3. Bjelogrić M (1990) Application of Newton’s optimal power flow in voltage/reactive power control. *IEEE Trans Power Syst* 5(4):1447–1454
4. Granville S (1994) Optimal reactive dispatch through interior point methods. *IEEE Trans Power Syst* 9(1):136–146
5. Grudin N (1998) Reactive power optimization using successive quadratic programming method. *IEEE Trans Power Syst* 13(4):1219–1225
6. Ng Shin Mei R (2017) Optimal reactive power dispatch solution by loss minimization using moth-flame optimization technique. *Appl Soft Comput* 59:210–222
7. Chen G (2017) Optimal reactive power dispatch by improved GSA-based algorithm with the novel strategies to handle constraints. *Appl Soft Comput* 50:58–70

8. Naderi E (2017) Novel fuzzy adaptive configuration of particle swarm optimization to solve large-scale optimal reactive power dispatch. *Appl Soft Comput* 53:441–456
9. Heidari A (2017) Gaussian bare-bones water cycle algorithm for optimal reactive power dispatch in electrical power systems. *Appl Soft Comput* 57:657–671
10. Morgan M (2016) Benchmark studies on optimal reactive power dispatch (ORPD) based multi-objective evolutionary programming (MOEP) using mutation based on adaptive mutation adapter (AMO) and polynomial mutation operator (PMO). *J Electr Syst* 12(1)
11. Mei RNS (2016) Ant lion optimizer for optimal reactive power dispatch solution. *J Electr Syst* 68–74
12. Anbarasan P (2017) Optimal reactive power dispatch problem solved by symbiotic organism search algorithm. *Inno Power Adv Comput Technol* 1–8
13. Gagliano A (2017) Analysis of the performances of electric energy storage in residential applications. *Int J Heat Technol* 35(Special Issue 1):S41–S48
14. Caldera M (2018) Survey-based analysis of the electrical energy demand in Italian households. *Math Model Eng Prob* 5(3):217–224
15. Basu M (2016) Quasi-oppositional differential evolution for optimal reactive power dispatch. *Electr Power Energy Syst* 78:29–40
16. Wang G-G (2016) Moth search algorithm: a bio-inspired metaheuristic algorithm for global optimization problems. *Memetic Comput* 1–14
17. Li L (2017) Modified discrete grey wolf optimizer algorithm for multilevel image thresholding. *Comput Intell Neurosci* 2017 (Article ID 3295769)
18. IEEE The IEEE-test systems. <http://www.ee.washington.edu/trsearch/pstca/2019/01/21>
19. Ali Nasser Hussain (2018) Modified particle swarm optimization for solution of reactive power dispatch. *Res J Appl Sci Eng Technol* 15(8):316–327

Performance of MIMO System—A Review



Sweta Sanwal, Aman Kumar, Md. Arib Faisal,
and Mohammad Irfanul Hassan

Abstract The present communication system demands high data rate, spectral efficiency, and reliability. By employing numerous antennas in transmitter and receiver sides of a wireless channel, the spatial multiplexing or diversity gains can be explored. The modern communication network can be designed to attain a high data rate, enhanced link reliability, and improved range. MIMO technique can increase spectral efficiency without using extra bandwidth. This paper reviews recently published results on MIMO—Multiple Input Multiple Output. This paper describes the BER performance using Alamouti Space-Time Block Code and Average Channel Capacity has been discussed for different antenna system, i.e., SISO—Single Input Single Output, SIMO—Single Input Multiple Output, MISO—Multiple Input Single Output, and MIMO—Multiple Input Multiple Output systems under Rayleigh and Rician fading conditions. The simulated BER of MIMO has been compared with its theoretical result and with all other antenna configuration systems. Finally, the Average Channel Capacity for all the systems is analyzed and simulated under both Rayleigh and Rician Fading Channels.

Keywords Alamouti scheme · BER · Rayleigh channel · Rician channel · Space-time block coding · Space-time coding · Space-time trellis coding · Multiple input multiple output · Multiple input single output · Single input multiple output · Single input single output

S. Sanwal · A. Kumar · Md. Arib Faisal · M. I. Hassan (✉)
Department of Electronics and Communication Engineering, Graphic Era (Deemed to be University), Dehradun, Uttarakhand 248002, India
e-mail: irfu_hasan@rediffmail.com

S. Sanwal
e-mail: sawalsweety98@gmail.com

A. Kumar
e-mail: amankumar.8651@gmail.com

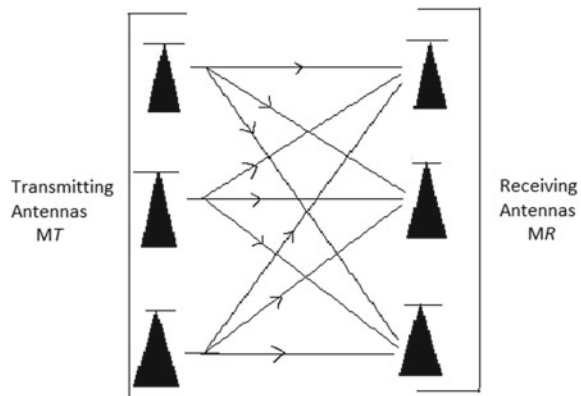
Md. Arib Faisal
e-mail: arib.faisal@gmail.com

1 Introduction

The rapid growth of the next-generation of wireless mobile communication systems demands high-speed facilities by a large number of potential users [1]. Because of three particular limitations of wireless mobile communication systems, such as compounded and bleak channels, deficient usable radio spectrum, and limitation of the power and size of hand-held terminals [2], makes a challenging issue to fulfill the demand of high-speed facility. Therefore, to reduce those constraints [2], efficient spectral, and power fading alleviation techniques are required. MIMO antenna techniques provide the required spectral efficiency and communication reliability [3]. However, the MIMO system implementation increased the cost and hardware requirements [4]. To solve the implementation complexity of MIMO antenna system with retaining all its benefits, there are practical and effective antenna techniques used called antenna selection (AS) approach [3, 4]. The basic concept of AS is to choose an optimal set of well-organized transmit and/or receive antennas [5]. This is accomplished by using channel state information (CSI) feedback which maximizes spectral efficiency and improves the error performance in wireless mobile system networks [5]. By utilizing a number of antennas at both the transmitter and receiver ends of wireless mobile channels is to explore and analyses the spatial multiplexing or diversity gain, today mobile communication system can be designed to attain a high data rate, improved channel reliability, and range [6]. One important feature of MIMO technique is to provide increased spectral efficiency without using extra bandwidth. In fact, MIMO technique is compulsory by many wireless communication standards like IEEE 802.11n (WLAN), 802.16e (WiMAX), LTE (cellular), and other emerging applications [4].

In Fig. 1, MIMO system is shown with M_T transmitting antennas and M_R receiving antennas. After applying appropriate operation on the transmitter side, the input data is sent by using M_T antennas. The applied operation may include channel coding, modulation, space-time-encoding, spatial mapping [3]. Wireless mobile channel is used by each antenna to sends a signal. All antennas at left-hand side of Fig. 1 used

Fig. 1 A typical MIMO antenna configuration



as an entire transmitter. The radiated signals are shown by the column vector (x) that has $M_T \times 1$ dimensions. These radiated are collected by signals, M_R receiving antennas after passing through the wireless mobile channels [6].

The remainder of this paper is organized as follows. In Sect. 1.1, MIMO system is discussed. In Sect. 1.2, a different antenna configuration is defined. In Sect. 1.3, STC in MIMO system is defined. Whereas in Sect. 1.4, Alamouti Scheme for 2×1 MISO system, 2×2 MIMO system, BER performance, and Channel Capacity are derived and analyzed. Finally, the result analysis has been carried out and the conclusion has been drawn.

1.1 MIMO System Model

A typical MIMO configuration is shown below in Fig. 2. MIMO configuration is represented in space domain [6]. Let us suppose that a MIMO communication system has N_t transmit antennas and N_r receive antennas. This results in $N_t \times N_r$ different channels in between transmitter in receiver. A wireless channel in multipath environment may correspond to a complex Gaussian random variable. The MIMO system channel between N_t transmit and N_r receive antennas can be depicted as a $N_r \times N_t$ complex Gaussian random matrix, indicated by H [5]. A complete understanding of MIMO system channel model is essential to appropriately design and estimate the working of a wireless communication system using MIMO. Practically the MIMO channels are triply selective, i.e., a MIMO channel may exhibit fading across space, time, and frequency [7].

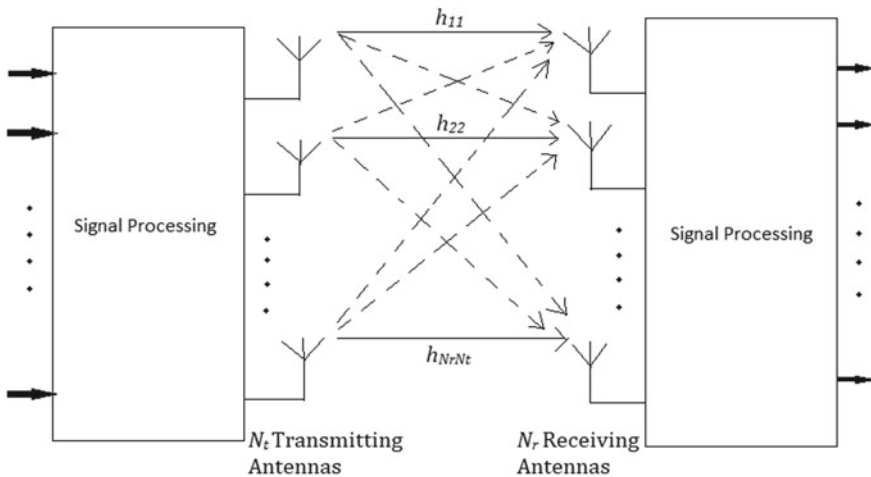


Fig. 2 A typical MIMO configuration

The input and output relation of a MIMO structure, assuming a time-invariant channel can be represented in vector notation as:

$$y = Hx + n \tag{1}$$

Here x is $(N_t \times 1)$ transmit vector, y is $(N_r \times 1)$ receiving vector, H is $(N_r \times N_t)$ channel gain matrix, and $n(N_r \times 1)$ is called Additive White Gaussian Noise (AWGN) vector. Assuming frequency flat fading (which implies that the MIMO channel is static and deterministic for the given time interval), a MIMO channel gain matrix for N_t transmit and N_r receive antennas could be represented as [6]:

$$H = \begin{matrix} \begin{bmatrix} h_{11} & \cdots & h_{1N_t} \\ \vdots & \ddots & \vdots \\ h_{N_r,1} & \cdots & h_{N_r,N_t} \end{bmatrix} \\ N_t \text{ transmit antennas} \end{matrix} \begin{matrix} N_r \text{ receive antennas} \\ \tag{2} \end{matrix}$$

Generally, a single element of $(N_r \times N_t)$ channel matrix is represented by h_{ij} ($i = 1, 2 \dots N_r$ and $j = 1, 2 \dots N_t$) which represents a complex channel gain between the j th sending and i th collecting antenna. The channel gains of $N_r \times N_t$ elements in MIMO channel matrix H are the function of characteristics of the propagation environment and antenna spacing in the transmitter and receiver (i.e., array characteristics) [5].

Let us say all the transmitter has an average power constraint P , overall the transmit antennas, and noise power is supposed unity (making power equivalent to SNR). After passing via the MIMO channel, at each receiver antenna, the signal that is received is a superposition of the N_t received signals (product of transmitted signals and channel gain coefficients), in addition to noise introduced in the channel. Then the received signal at antenna i can be written as [5]:

$$y_i = \sum_{j=1}^{N_t} h_{ij}x_j + n_i \quad i = 1, 2, \dots, N_r \text{ and } j = 1, 2, \dots, N_t \tag{3}$$

The term n_i denotes the additive complex channel noise added by the channel. Following the discrete-time model, it can be illustrated in matrix notation as:

$$\begin{bmatrix} y_1 \\ \vdots \\ y_{N_r} \end{bmatrix} = \begin{bmatrix} h_{11} & \cdots & h_{1N_t} \\ \vdots & \ddots & \vdots \\ h_{N_r,1} & \cdots & h_{N_r,N_t} \end{bmatrix} \begin{bmatrix} x_1 \\ \vdots \\ x_{N_t} \end{bmatrix} + \begin{bmatrix} n_1 \\ \vdots \\ n_{N_r} \end{bmatrix} \tag{4}$$

The above matrix can be written in vector notation as Eq. (1).

After reception, the signal is decoded to estimate the sent data. Generally, the maximum likelihood (ML) decoding algorithm is applied, which uses a decision

metric that is based on the squared Euclidean distance between the received sequence and the actual sequence. It selects a code with a minimum value of the metric to determine the transmitted data. This concept is discussed previously in the paper of Sivash M. Alamouti [8].

1.2 Different Antenna Configurations

There are various antenna layouts can be applied to define space-time systems. Traditionally, a transmitter and a receiver have a sole antenna (i.e., $N_t = N_r = 1$), recognized as Single Input Single Output (SISO) system [6]. Another system, known as Single-Input-Multiple-Outputs (SIMO) has a sole antenna at the transmitter ($N_t = 1$) and N_r , a number of antennas at the receiver [6]. In the Multiple Input Single Output (MISO) system, the transmitter has N_t antennas, and receiver have a sole antenna ($N_r = 1$). On the other hand, MIMO uses multiple antennas at both ends [6]. Figure 3 shows four different antenna configurations. SISO is severely affected by multipath propagation, which increases error probability [6]. SIMO enables receiver diversity, where a suitable combining technique is used at the receiver to combat signal fading [6]. Use of combining technique requires the concept of the Channel State Information (CSI) at the receiver. MISO enables beamforming, which aims to focus transmission powers from different antennas in the desired direction [6]. Beamforming requires knowledge of the CSI at the transmitter [6].

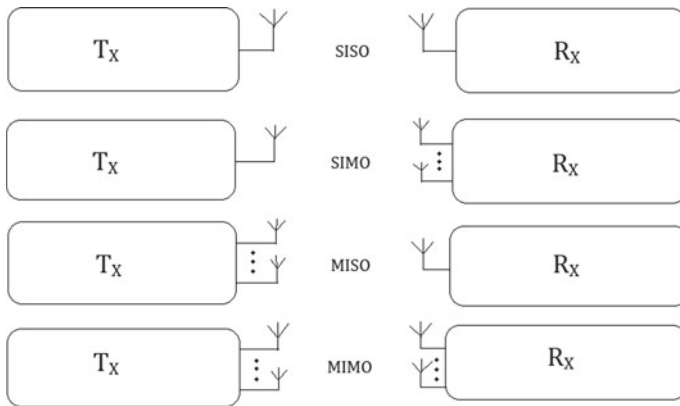


Fig. 3 Different antenna configuration

1.3 Space-Time Coding (STC) in MIMO

MIMO system offers a much higher capacity than a conventional system. The capacity increase in MIMO is obtained by appropriate coding in space and time domain before transmission, called time coding (STC) [9]. In STC, at first, the input data stream (i.e., source data bits and error correction bits) is split into a number of sub-streams, and then each sub-stream is mapped onto a sender antenna [6, 9]. In this way, a signal is encoded in space and time.

In STC, at each instant, a block of m data bits are given into the space-time encoder. The m data bits make a set of $M = 2^m$ symbols [9]. The space-time encoder maps these symbols on N_t transmitting antennas. Say the symbol in each antenna is denoted by as x_j , where $j = 1, 2, \dots, N_t$ then the transmission code vector is $x = [x_1, x_2, \dots, x_{N_t}]$. A serial to parallel converter, i.e., Multiplexer converts the incoming data stream to $N_t \times 1$ column vector, to be transmitted simultaneously by N_t transmit antennas [9]. These parallel data streams pass through the MIMO channel matrix, where each individual channel may have an independent channel gain coefficient [9].

In STC, the code matrix is designed such that the rows and columns are orthogonal to each other [9]. This yields that the inner product of each row with any other row results to zero, and therefore the rows of the matrix are independent eigenvalues, helping to realize full transmit diversity [9]. Full transmit diversity implies that each transmit antenna contributes to one row in the matrix (this is called full rank matrix) [10]. The orthogonality enables the decoupling of the various signals transmitted from different antennas at the receiver [10, 11]. This permit using simple ML-based decoding, using linear processing at the receiver, which simplifies the reception process [10, 11].

CSI is not required by STC at the transmitter, thus simplifies the transmission process. STC can be easily combined with channel coding, offering coding gain furthermore spatial diversity gain [9]. STC facilitates MIMO to realize significant improvements in error rate performance (Compared to SISO), and therefore enables to minimize outage probability (or equivalently maximize outage capacity) [9]. As a result, in a few years only, STC has progressed from invention to adoption in major wireless standards [9]. Figure 4 shows a MIMO communication system where STC is used as a part of it [9].



Fig. 4 STC in MIMO

1.4 STC and Pre-coding

STC and pre-coding are two different encoding concepts in MIMO. STC assumes no knowledge of CSI at the transmitter; on the other hand, pre-coding essentially needs knowledge of CSI at the transmitter side [6]. In fact, knowledge about CSI at the transmitter antenna makes a significant difference in system performance, by enabling the transmitter to adapt appropriately the power and rate of data in accordance with channel states [9, 10]. This concept is used in pre-coding [9, 10]. However, STC simplifies implementation by avoiding the need for CSI [9, 10]. The STC is an open-loop approach, whereas pre-coding is a closed-loop approach [9, 10].

Pre-coding is different from beamforming also; however, both require knowledge of CSI at the transmitter [10]. Beamforming offers a well-defined directional beam pattern, which maximizes the received signal power [10]. However, just as multiple antennas are present at the receiver, the received signal power cannot be maximized by beamforming at all the receiver antennas simultaneously [10]. Then pre-coding is required. Pre-coding can be combined along with spatial multiplexing to increase the rate of data performance [11]. It can be mixed with spatial diversity to enhance the reliability of decoding [11]. Pre-coding has been successfully implemented in the IEEE 802.16e standard for broadband WMAN networks [11].

1.5 Spatial Multiplexing and Spatial Diversity

STC uses two different approaches to improve MIMO system performance, which are the spatial multiplexing (SM) and spatial diversity (SD) [5]. SM aims to enhance transmission data rate (in fact, spectral efficiency) and SD aims to enhance transmission reliability [5]. These are two important motivations for using MIMO [5].

1.5.1 Spatial Multiplexing (SM)

Intuitively, if a receiver can differentiate between two streams (using STC), then it can also differentiate between two streams carrying different data [6]. In SM, various data signals are sent over N_t transmitting antennas [6]. It may correspond to a situation, where a high rate of data stream is bifurcated into several lower rate of data streams, and then are sent parallelly through different antennas [6]. At the receiver, these parallel streams are combined to acquire the indigenous rate of data [6]. Therefore, it makes it possible to realize a high data rate performance [8]. The SM gain obtained, simply indicates the increased data rate over the entire given bandwidth (i.e., the upgraded spectral efficiency) and is represented as a function of

SNR (at a specified BER) [8]. The maximum SM gain (r_{\max}) is represented as a ratio between the spectral efficiency (S) at given SNR to the logarithmic value of SNR when the SNR is assumed to be asymptotically high, as given below [8]:

$$r_{\max} = \lim_{\text{SNR} \rightarrow \infty} \frac{S(\text{SNR})}{\log_2 \text{SNR}} \quad (5)$$

It is essential that to reliably separate the streams of data received, the number of collecting antennas must be at least same as the number of transmitting antennas ($N_r \geq N_t$) [6]. SM is considered to be a powerful technique to enhance Channel Capacity in high SNR conditions [6]. It can be utilized to offer a high rate of data to the users near the base station (where SNR is high). SM could be utilized with or without CSI at the transmitter [6].

1.5.2 Spatial Diversity (SD)

SD does not aim to enhance data rate; rather it aims to enhance the reliability of communication made across the fading channel [10]. In SD, a stream of data is sent through all the transmitter antennas [10]. This contrasts with SM, where different data streams are sent through different antennas [10]. SD employs orthogonal or near orthogonal coding using STC [10]. At the receiver end, duplicate of the same stream of data are collected and mixed to yield improved SNR [10]. This improves reliability and the gain so realized is called SD gain [10]. The negative of the maximum SD gain ($-d_{\max}$) is a ratio of the log of the probability of error (P_e at a given SNR) to the log of SNR when the SNR is assumed to be asymptotically high, as given below [10]:

$$-d_{\max} = \lim_{\text{SNR} \rightarrow \infty} \frac{\log P_e(\text{SNR})}{\log \text{SNR}} \quad (6)$$

In the above expression, the log can be of any base (since it cancels out as the ratio of the two logs having the same base). SD is used when CSI is not present at the transmitter.

1.6 STTC and STBC

STC (Space-Time Coding) can be classified into two parts which depend on the way of transmission of signal in the wireless channel [6]:

- STTC (Space-Time Trellis Coding)
- STBC (Space-Time Block Coding).

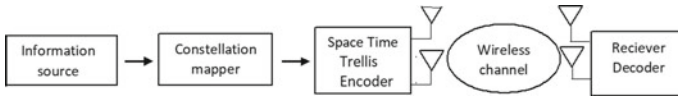


Fig. 5 STTC in MIMO

1.6.1 STTC

It is an extended version of conventional Trellis codes to MIMO systems [11]. In STTC, the symbols are transmitted serially, encoding is done in the transmitter end and the processing of signal is done in the receiver end [11]. Significant diversity and coding gains over fading channels are realized by STTC [11]. The delay diversity can be considered as a simple form of STTC because in delay diversity same code is transmitted from N_t transmit antennas and viewed as $1/N_t$ repetition code [11]. To combat fading, error control coding, and diversity scheme (joint design of modulation scheme) are performed in STTC to outline an effective signaling scheme [11]. ML sequence estimation is used by STTC via the Viterbi algorithm for decoding at the receiver end. Figure 5 shows STTC in MIMO [11].

1.6.2 STBC

It transmits data in blocks and involves three design parameters [6]:

- N_t (number of transmitter antennas which defines the transmission matrix size).
- K (number of transmitted symbols per time slot).
- T (number of time slots used to transmit one block of data or encoded symbols).

In STBC, blocks are nothing but the divided data streams [10]. A block is transmitted over T time slots in STBC [10]. During each and every time slot K symbols are encoded and then transmitted parallelly using N_t transmitters which develops a transmission matrix S of size $N_t \times T$ as [10]:

$$\begin{bmatrix} s_{11} & \cdots & s_{1N_t} \\ \vdots & \ddots & \vdots \\ s_{T1} & \cdots & s_{TN_t} \end{bmatrix}$$

Here s_{ij} is encoded symbol which is sent in time slot “ i ” from “ j ” transmitter antenna where $i = 1, 2, 3, \dots, T$ and $j = 1, 2, \dots, N_t$ [10]. STBC assumes N_r receiver antennas and can be designed to exploit full diversity order ($N_r \times N_t$), but it is not designed for full diversity order, rather be able to reduce fading effectively it is designed for a sufficiently high diversity order [10, 11]. Channel State Information (CSI) is not required at transmitter [10].

STBC could use a square transmission matrix (complex orthogonal design) which satisfies the conditions of orthogonality both in time and space [10]. It can also

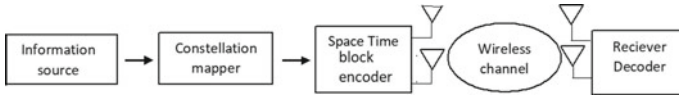


Fig. 6 STBC in MIMO

use non-orthogonal design which has a non-square transmission matrix that satisfies orthogonality only in time, not in space [10]. Using simple linear processing symbols can be detected at the receiver in STBC [6]. In STBC same data is transmitted through different antennas so it can be viewed as repetition code over space and time. Figure 6 shows STBC in MIMO [6].

1.6.3 Comparison Between STBC and STTC

STTC offers both diversity as well as coding gain whereas STBC provides only diversity gain [6]. STBC gives a lower performance as compared to STTC [6]. STBC is less complex in implementing [6]. STBC requires simple decoding at the receiver end to retrieve data whereas STTC requires complex decoding techniques to retrieve data at the receiver end [6].

1.7 Alamouti Scheme

The Alamouti scheme provides a simple transmit diversity technique that uses space-time coding [8]. Two transmit antennas and a single receiver antenna are used to achieve transmit diversity when CSI is not available at the transmitter [8]. This is the simplest form of STBC. Complex orthogonality is satisfied with a square transmission matrix in the space domain as well as time domain [8]. Alamouti STBC gives STBC with rate one and offers full diversity gain without compromising with data rate performance. The Alamouti code matrix is [8]:

$$S = \begin{bmatrix} s_1 & s_2 \\ -s_2^* & s_1^* \end{bmatrix} \begin{matrix} \text{space} \rightarrow \\ \text{Time} \downarrow \end{matrix} \tag{7}$$

S is a complex orthogonal matrix known as transmission matrix, where $*$ denotes complex conjugate [8]. There are two-time slots used to send two symbols s_1 and s_2 using two antennas [8]. Since, there are two-time slots that are needed for sending two symbols, using two antennas, thus $k = 2$ and $T = 2$. Hence, the code rate is 1. It is supposed that the gain of channel remains unchanged over the same time interval [8].

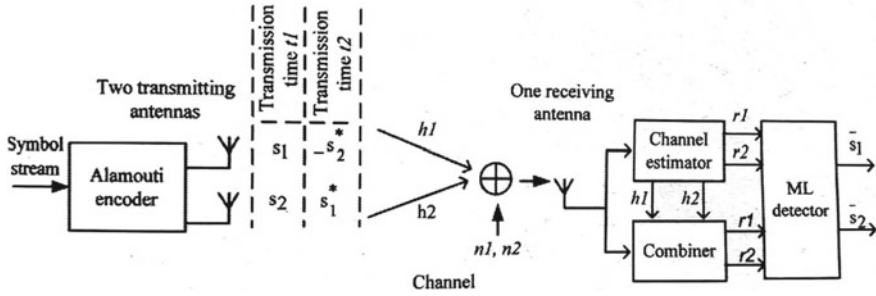


Fig. 7 An illustration of the Alamouti scheme

In code matrix, row at the first represents the first transmission period, where s_1 is sent by first antenna and s_2 is sent by second antenna [8]. Row at the second represents second transmission period, where $-s_2^*$ is sent by first antenna and the s_1^* is sent by second antenna. This implies that the transmission takes place in space (using two antennas) as well as time (at two-time instant) [8]. The information sequence received by first antenna is $[s_1, -s_2^*]$ and by second antenna is $[s_2, s_1^*]$ [8]. This satisfies the condition of orthogonality, both in space and time domain [8, 12]. It is inferred that the two completely orthogonal streams are collected by the receiver [12], giving transmit diversity of two. The approach used in the Alamouti scheme is shown in Fig. 7.

Let us assume, $h_1(t)$ and $h_2(t)$ represents the fading coefficients, respectively from antenna 1 and antenna 2. It is supposed that the fading coefficients are constant during the symbol interval, then [12]:

$$h_1(t) = h_1(t + T) = h_1 = |h_1|e^{j\theta_1} \tag{8}$$

And

$$h_2(t) = h_2(t + T) = h_2 = |h_2|e^{j\theta_2} \tag{9}$$

Here, T denotes the symbol duration, amplitude gains, and phase shifts, respectively, are $|h_i|$ and θ_i (for $i = 1, 2$). During the first and the second symbol periods the received signals are r_1 and r_2 after passing through the channel that can be expressed as [12]:

$$r_1 = h_1s_1 + h_2s_2 + n_1 \tag{10}$$

$$r_2 = -h_1s_2^* + h_2s_1^* + n_2 \tag{11}$$

where n_1 and n_2 are independent complex variable AWGN samples having zero mean and unit variance that are being added to the transmitted signal during the interval of transmission [12]. Euclidian distance between the received symbol and the possible

transmitted symbol are estimated after which the received signals are passed through the ML detector [12]. The decision rule is used to identify the symbol which is detected is the symbol which has the minimum Euclidian distance is identified as the transmitted symbol [12].

1.8 Alamouti STBC (2 × 1 System Model)

A simple method for achieving spatial diversity with two transmit antennas which are described as A simple transmit diversity presented in the paper of Alamouti [7] and in [13]. For the channel model, refer to Sect. 1.4. The channel gain matrix is shown in Table 1. And the antenna configuration is shown in Fig. 8.

1.8.1 Alamouti STBC Receiver

The signal received in the first time slot is:

$$y_1 = h_1x_1 + h_2x_2 + n_1 = [h_1 \ h_2] \begin{bmatrix} x_1 \\ x_2 \end{bmatrix} + n_1 \tag{12}$$

The signal received in the second time slot is:

$$y_2 = -h_1x_2^* + h_2x_1^* + n_2 = [h_1 \ h_2] \begin{bmatrix} -x_2^* \\ x_1^* \end{bmatrix} + n_2 \tag{13}$$

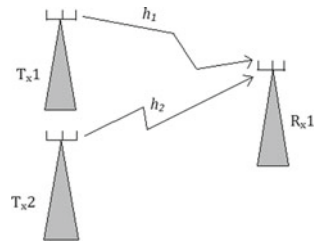
where:

1. y_1, y_2 is the symbol received, respectively, in the first and second time slot.

Table 1 2 × 1 Alamouti channel model

	Time t	Time $t + T$
Antenna 1	x_1	$-x_2^*$
Antenna 2	x_2	x_1^*

Fig. 8 2 × 1 Alamouti STBC



2. h_1, h_2 is the gain of channel by first and second transmitting antennas.
3. x_1, x_2 are the transmitted symbols.
4. n_1, n_2 is the noise in 1st and 2nd-time slots, noise terms are identically and identically distributed.

$$E \left\{ \begin{bmatrix} n_1 \\ n_2^* \end{bmatrix} \begin{bmatrix} n_1^* & n_2 \end{bmatrix} \right\} = \begin{bmatrix} |n_1|^2 & 0 \\ 0 & |n_2|^2 \end{bmatrix} \tag{14}$$

Equation 15 can be depicted in matrix as:

$$\begin{bmatrix} y_1 \\ y_2^* \end{bmatrix} = \begin{bmatrix} h_1 & h_2 \\ h_2^* & -h_1^* \end{bmatrix} \begin{bmatrix} x_1 \\ x_2 \end{bmatrix} + \begin{bmatrix} n_1 \\ n_2^* \end{bmatrix} \tag{15}$$

where, $H = \begin{bmatrix} h_1 & h_2 \\ h_2^* & -h_1^* \end{bmatrix}$, then we want to solve for $\begin{bmatrix} x_1 \\ x_2 \end{bmatrix}$, for this the inverse of H would be found.

And the pseudo-inverse for a $m \times n$ matrix is:

$$H^+ = (H^H H)^{-1} H^H \tag{16}$$

$$(H^H H) = \begin{bmatrix} h_1^* & h_2 \\ h_2^* & -h_1 \end{bmatrix} \begin{bmatrix} h_1 & h_2 \\ h_2^* & -h_1^* \end{bmatrix} = \begin{bmatrix} |h_1|^2 + |h_2|^2 & 0 \\ 0 & |h_1|^2 + |h_2|^2 \end{bmatrix} \tag{17}$$

Since, inverse of a diagonal matrix (Eq. 17) is just the inverse of diagonal elements that is:

$$(H^H H)^{-1} = \begin{bmatrix} \frac{1}{|h_1|^2 + |h_2|^2} & 0 \\ 0 & \frac{1}{|h_1|^2 + |h_2|^2} \end{bmatrix} \tag{18}$$

Approximately, the transmitted symbol is:

$$\begin{aligned} \begin{bmatrix} x_1 \\ x_2 \end{bmatrix} &= (H^H H)^{-1} H^H \begin{bmatrix} y_1 \\ y_2^* \end{bmatrix} \\ &= (H^H H)^{-1} H^H \left(H \begin{bmatrix} x_1 \\ x_2 \end{bmatrix} + \begin{bmatrix} n_1 \\ n_2^* \end{bmatrix} \right) \\ &= \begin{bmatrix} x_1 \\ x_2 \end{bmatrix} + (H^H H)^{-1} H^H \begin{bmatrix} n_1 \\ n_2^* \end{bmatrix} \end{aligned} \tag{19}$$

1.9 Alamouti STBC (2 × 2 System Model)

By getting some motivation from Alamouti 2 × 1 channel model, our further work is on 2 × 2 (a simple transmit and receiver diversity) which provides spatial diversity and less BER [14, 15]. For the channel model, refer to Sect. 1.4. The channel gain matrix is same as the 2 × 1 model and is shown in Table 1. And the antenna configuration is shown in Fig. 9.

1.9.1 Receiver in Alamouti 2 × 2

The signal received in the first time slot,

$$\begin{bmatrix} y_{11} \\ y_{12} \end{bmatrix} = \begin{bmatrix} h_{11} & h_{12} \\ h_{21} & h_{22} \end{bmatrix} \begin{bmatrix} x_1 \\ x_2 \end{bmatrix} + \begin{bmatrix} n_{11} \\ n_{12} \end{bmatrix} \tag{20}$$

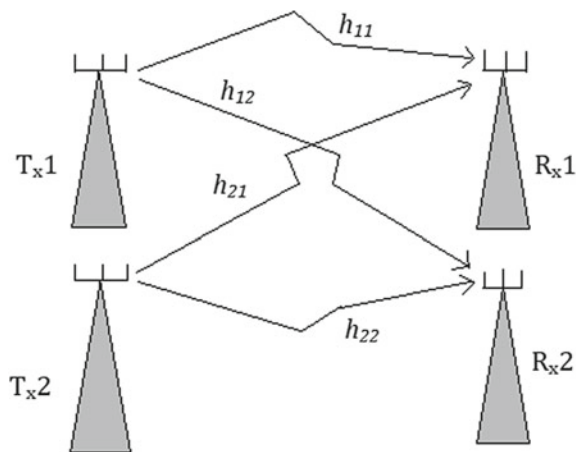
The signal received in the second time slot,

$$\begin{bmatrix} y_{21} \\ y_{22} \end{bmatrix} = \begin{bmatrix} h_{11} & h_{12} \\ h_{21} & h_{22} \end{bmatrix} \begin{bmatrix} -x_2^* \\ x_1^* \end{bmatrix} + \begin{bmatrix} n_{21} \\ n_{22} \end{bmatrix} \tag{21}$$

where

y_{ij} = received signal in i th time slot by j th antennas
 x_1, x_2 = modulated symbols
 h_{ij} = channel gain
 n_{ij} = AWGN noise during i th time slot.

Fig. 9 Alamouti 2 × 2 STBC



$$H = \begin{bmatrix} h_{11} & h_{12} \\ h_{21} & h_{22} \\ h_{12}^* & -h_{11}^* \\ h_{22}^* & -h_{21}^* \end{bmatrix}$$

Then, we want to solve for $\begin{bmatrix} x_1 \\ x_2 \end{bmatrix}$, for this, we would have to get H inverse. It is known that the pseudo-inverse for a $m \times n$ matrix is:

$$H^+ = (H^H H)^{-1} H^H \tag{22}$$

$$(H^H H) = \begin{bmatrix} |h_{11}|^2 + |h_{21}|^2 + |h_{12}|^2 + |h_{22}|^2 & 0 \\ 0 & |h_{11}|^2 + |h_{21}|^2 + |h_{12}|^2 + |h_{22}|^2 \end{bmatrix} \tag{23}$$

Since, inverse of a diagonal matrix (Eq. 23) is just the inverse of diagonal elements that is:

$$(H^H H)^{-1} = \begin{bmatrix} \frac{1}{|h_{11}|^2 + |h_{21}|^2 + |h_{12}|^2 + |h_{22}|^2} & 0 \\ 0 & \frac{1}{|h_{11}|^2 + |h_{21}|^2 + |h_{12}|^2 + |h_{22}|^2} \end{bmatrix} \tag{24}$$

Approximately, the transmitted symbol is:

$$\begin{bmatrix} x_1 \\ x_2 \end{bmatrix} = (H^H H)^{-1} H^H \begin{bmatrix} y_{11} \\ y_{12} \\ y_{21}^* \\ y_{22}^* \end{bmatrix} \tag{25}$$

1.10 BER Calculation

In this paper, simulation of BER performance of MISO (2×1 Model) and MIMO (2×2 Model) has been brought for BPSK modulation under Rayleigh as well as Rician channel.

The theoretical BER of MRC system [15, 16] is given below:

$$P_{e,MRC} = p_{MRC}^2 [1 + 2(1 - p_{MRC})] \tag{26}$$

where,

$$P_{\text{MRC}} = \frac{1}{2} - \frac{1}{2} \left(1 + \frac{1}{E_b/N_0} \right)^{-1/2} \quad (27)$$

And BER for STBC case, i.e., two transmitters with two receivers or one receiver is given below:

$$P_{e,\text{STBC}} = p_{\text{STBC}}^2 [1 + 2(1 - p_{\text{STBC}})] \quad (28)$$

where,

$$P_{\text{MRC}} = \frac{1}{2} - \frac{1}{2} \left(1 + \frac{1}{E_b/N_0} \right)^{-1/2} \quad (29)$$

1.11 Channel Capacity Calculation

1.11.1 SISO Channel Capacity

The SISO system has gain of channel h , therefore, signal to noise ratio at the receiving antenna, then without knowing the CSI the capacity is [17]:

$$C = \log_2(1 + \text{SNR}|h|^2) \text{ Bits} \quad (30)$$

And the theoretical capacity of this system will be:

$$C_{\text{Theoretical}} = \log_2(1 + \text{SNR} \cdot E(|h|^2)) \quad (31)$$

Or $E(|h|^2) = 1$

Thus:

$$C_{\text{Theoretical}} = \log_2(1 + \text{SNR}) \quad (32)$$

1.11.2 SIMO Channel Capacity

SIMO system has a transmitting antenna and M receiving antenna. the complex gain between the transmit antenna is h_i and the i th receiver, then the Channel Capacity of the system is [17]:

$$C = \log_2 \left(1 + \text{SNR} \cdot \sum_{i=1}^M |h|^2 \right) \quad (33)$$

And $\sum_{i=1}^M |h|^2 = M^2$, its Shannon capacity is given by:

$$C_{\text{Theoretical}} = \log_2(1 + \text{SNR} \cdot M^2) \quad (34)$$

1.11.3 MISO Channel Capacity

Channel Capacity of MISO system having M_T transmitting antenna and a receiver antenna is given by:

$$C = \log_2(1 + \text{SNR}|h|^2/M_T) \quad (35)$$

1.11.4 MIMO Channel Capacity

In the MIMO system, multiple transmitting and receiving antennae are used. N transmitting and M receiving antennas are connected using a wireless link called MIMO channel. It contains $N \times M$ MIMO channel coefficients. For MIMO system matrix is H (refer Eqs. (4) and (5)) [17].

Where the complex gain of channel is h_{ij} between the j th transmitting antenna and i th receiving antenna:

$$C = \log_2 \left(\det \left[I_M + \frac{\text{SNR}}{N} \mathbf{H}\mathbf{H}^H \right] \right) \quad (36)$$

where “det” is determinant, I_M depicts $N \times M$ identity matrix and H^H is transposed conjugate of a matrix [17].

2 Numerical and Result Analysis

In this part, we have discussed the simulation result for BER performance of 2×1 Alamouti scheme model with the theoretical 2×1 Alamouti model, 1×1 model (with no diversity) and 1×2 theoretical MRC system under Rayleigh as well as Rician Fading Channels. Then, the simulation result for BER performance of 2×2 system model with the theoretical 2×1 Alamouti model, 1×1 model (with no diversity) and 1×2 theoretical MRC system under Rayleigh as well as

Rician Fading Channels. This simulation is being done in MATLAB using a digital modulation scheme called as BPSK (Binary Phase Shift Keying) with Zero Forcing (ZF) Equalizer using MATLAB. The values of BER as a function of E_b/N_0 (dB) has been found for all other antenna configuration models and compared with each other under Rayleigh as well as Rician Fading Channels.

Finally, the Channel Capacity of all antenna configuration systems (SISO, SIMO, MISO, MIMO) has been determined. The Average Channel Capacity per unit Bandwidth values as a function of SNR—Signal to Noise Ratio in dB scale has been determined and compared under Rayleigh as well as Rician Fading Channels.

In Figs. 10 and 11, we have simulated the BER curve for 2×1 system model, and the rest curves were plotted using the theoretical values of BER. 1×2 MRC system has the very lowest BER with respect to other system models. Alamouti 2×1 model has a slightly higher BER than of 1×2 MRC system. 1×1 system model with no diversity has very poor BER performance. It can be found that BER of simulated Alamouti 2×1 model is better at higher average SNR (dB) in Rician condition than in Rayleigh condition.

In Figs. 12 and 13, we have simulated the BER curve for the 2×2 system model and the rest curves were plotted using the theoretical values of BER, where the ratio of bit energy to the noise power density is called as E_b/N_0 . We can see that the 2×2 system model has the best BER performance than the other model. 1×2 MRC system has lower BER performance than that of the 2×2 model. 2×1 Alamouti scheme has lower BER performance than that of 1×2 MRC system. Finally, the 1×1 system has the poorest BER performance.

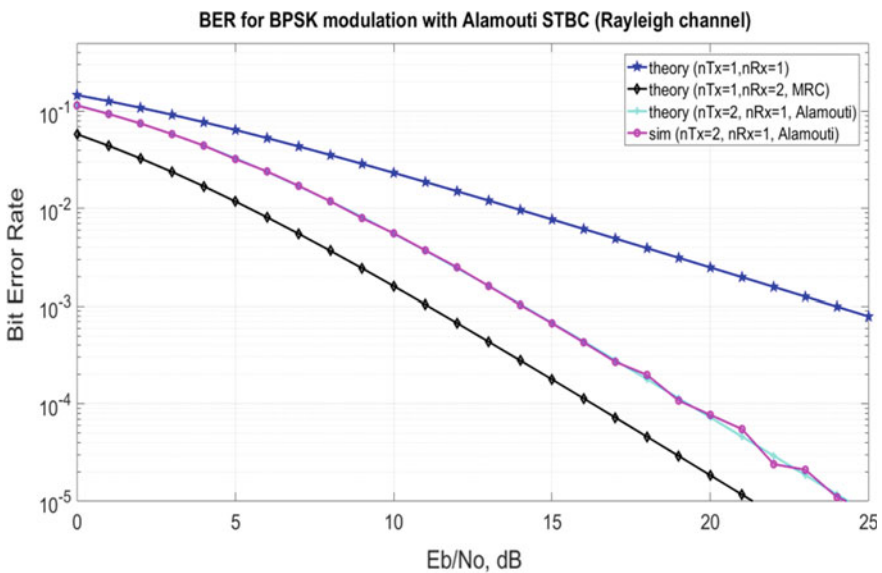


Fig. 10 Bit error rate versus E_b/N_0 (dB) curve for simulation of 2×1 Alamouti Scheme under Rayleigh condition

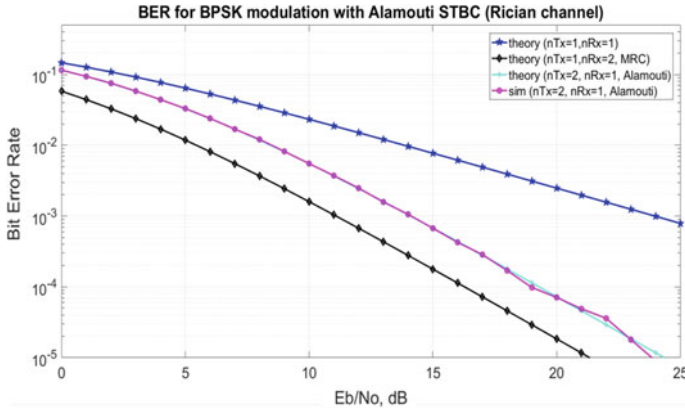


Fig. 11 Bit error rate versus E_b/N_0 (dB) curve for simulation of 2×1 Alamouti scheme under Rician condition

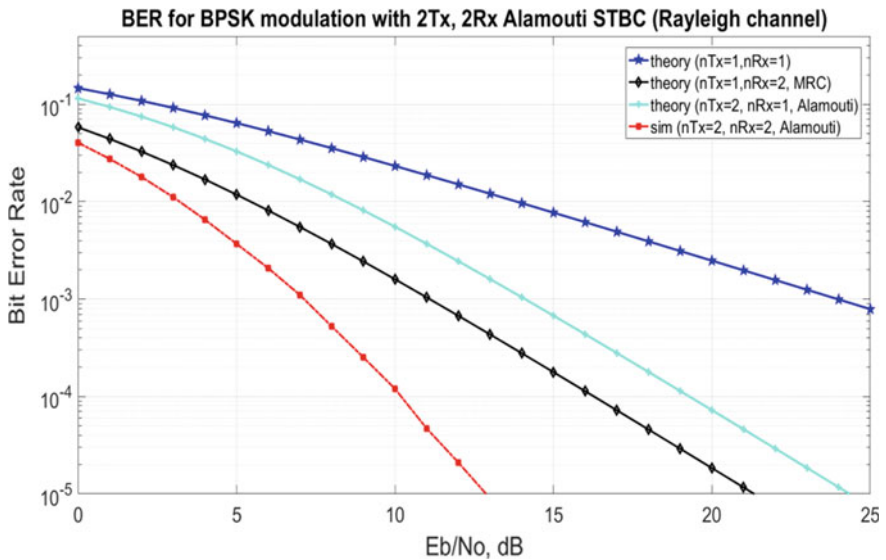


Fig. 12 Bit error rate versus E_b/N_0 (dB) curve for simulation of 2×2 system model under Rayleigh condition

In Figs. 14 and 15, for various antenna configuration, i.e., SISO—one transmitter one receiver, SIMO—one transmitter and two receivers, MISO—two transmitters and one receiver and MIMO—two transmitters and two receivers, Average Channel Capacity per unit Bandwidth as a function of SNR is plotted under Rayleigh as well Rician condition. It can be found that the 2×2 system, i.e., MIMO has the highest capacity and 1×1 SISO has lowest Channel Capacity in both fading conditions. 1×2 SIMO system has better capacity than the 2×1 system, i.e., MISO.

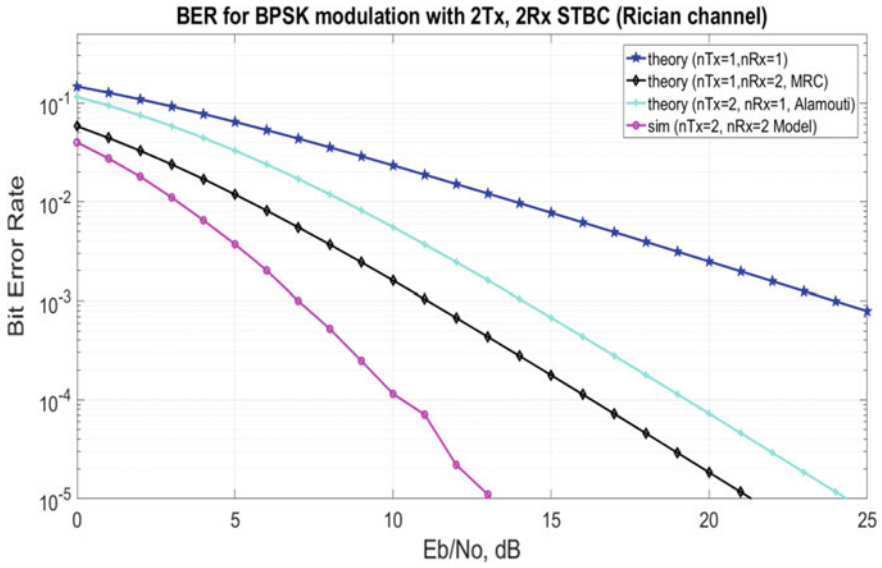


Fig. 13 Bit error rate versus Eb/No (dB) curve for simulation of 2×2 system model under Rician condition

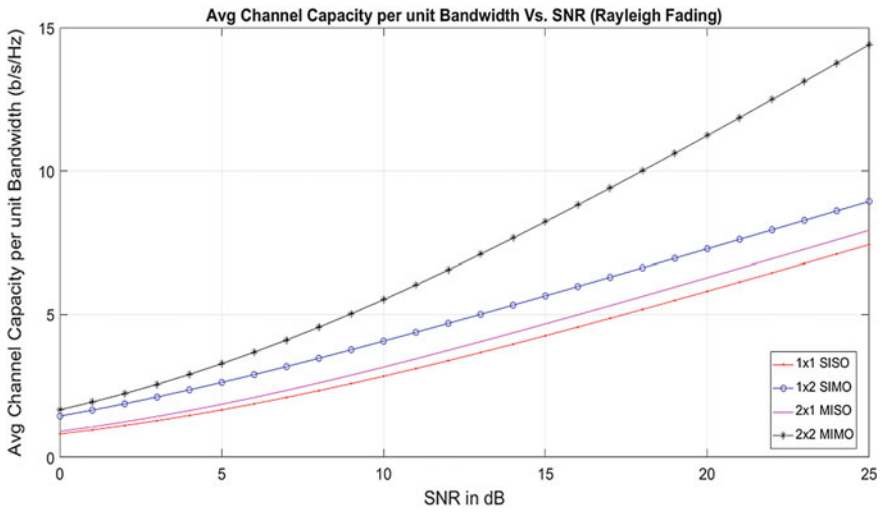


Fig. 14 Channel capacity curve for SISO, SIMO, MISO and MIMO system under Rayleigh fading

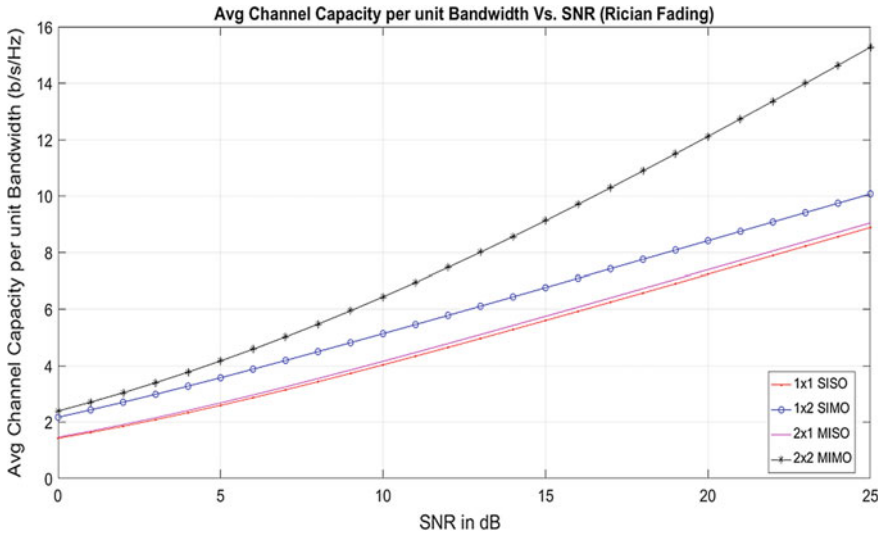


Fig. 15 Channel capacity curve for SISO, SIMO, MISO and MIMO system under Rician fading

As expected capacity in Rician fading condition is found to be better than Rayleigh fading condition as Rician has one line of sight signal. In Fig. 15, the plot is plotted for $k = 5$, where, k is Rician Factor which is defined by the ratio of the power of LOS components to the power of NLOS components.

On comparing Figs. 13 and 14, It was found that Average Channel Capacity per unit Bandwidth of 2×2 system, i.e., MIMO is 14.46 bits/s/hz and 15.39 bits/s/hz under Rayleigh and Rician fading respectively.

3 Conclusions

Through the BER performance of different antenna configuration systems, we found that the BER performance 1×1 system is worst. 1×2 theoretical MRC system has better BER performance than 2×1 system (Both simulated and theoretical) and 1×1 system in Rayleigh fading. At the same moment, in Rician fading all antenna configuration system has better performance than in Rayleigh fading condition. And when we move towards more antenna in the transmitter and receiver side, i.e., 2×2 MIMO system, it has better BER performance in comparison to 1×2 theoretical MRC system.

In terms of Channel Capacity, it increases if we increase the number of transmitting and receiving antenna. Thus, 2×2 MIMO has the best Channel Capacity. It can also be found that the Channel Capacity is more in Rician fading condition than Rayleigh fading condition.

References

1. Simon MK, Alouini MS (2002) Digital communication over fading channels—a unified approach to performance analysis, 1st edn. Wiley, USA
2. Molisch AF (2001) Wideband wireless digital communications. Pearson Education Inc (2001)
3. Goldsmith A (2005) Wireless communications. Cambridge University Press
4. Dalal U (2011) Wireless communications. Oxford University Press
5. Biglieri E, Calderbank R, Constantinides A, Goldsmith A, Paulraj A, Poor HV (2007) MIMO wireless communications. Cambridge University Press
6. Kumar S (2015) Wireless communication—the fundamental and advanced concepts. River Publishers, Denmark
7. Tarokh V (ed) (2009) New directions in wireless Communication research. Springer, Berlin
8. Alamouti SM (1998) A simple transmit diversity technique for wireless communications. *IEEE J Sel Areas Commun* 16(8)
9. Jankikaran M (2004) Space-time codes and MIMO systems. Artech House Inc, Boston, London (2004)
10. Luo T, Teng Y, Tong X-j, Yue G-x (2004) Space-time block codes design in OFDM system. *J Beijing Univ Posts Telecommun* 27
11. Tarokh V, Jafarkhani H, Calderbank AR (1999) Space-time block coding for wireless communications: performance results. *IEEE J Sel Areas Commun* 17(3)
12. Jiang M, Hanzo L (2007) Multiuser MIMO-OFDM for next-generation wireless systems. In: *Proceeding of the IEEE*, vol 95, issue no 7. IEEE
13. Lalitha Kumari D, Giri Prasad MN (2017) A review paper on performance analysis of MIMO based OFDMA system under fading channel. *Int J Electr Commun Eng Technol (IJECET)* 8(1):32–42
14. Bhagya R, Ananth AG (2012) Study of transmission characteristics of 2×2 MIMO system for OFDM multiplexing and Bpsk modulation with ZF equalizer and MMSE receivers. *Int J Soft Comput Eng (IJSCE)* 2(3)
15. Mindaudu AS, Miyim AM (2012) In: BER performance of MPSK and MQAM in 2X2 Alamouti MIMO systems. *Int J Inf Sci Tech (IJIST)* 1&2(5)
16. Gupta S, Bhardwaj L, Anand A, Rajpoot AS (2016) Comparison of BER performance & capacity analysis of MIMO system with STBC & MRC to improve link performance in fading environment. *Int J Sci Eng Appl Sci (IJSEAS)* 2(5)
17. Ghayoula E, Bouallegue A, Ghayoula R, Chouinard J-Y (2014) Capacity and performance of MIMO systems for wireless communications. *J Eng Sci Technol Rev* (3)

Incremental Weighted Linear Discriminant Analysis for Face Recognition



Nitin Kumar and Suresh Madhavan

Abstract Face recognition has been a popular research area with several real-world applications. Linear discriminant analysis (LDA) is a well-known method for face recognition in literature. However, one of the requirements of LDA is the availability of all data samples available before training. In this paper, we have proposed a novel variant of LDA method based on incremental learning and is called incremental weighted linear discriminant analysis (IWLDA). In IWLDA, a weighted pairwise Fischer criterion is suggested to efficiently separate all class data homogeneously in the transformed subspace. IWLDA is developed in such a manner that the distance between nearby classes is increased and simultaneously the distance between farther classes is reduced and the overall distance is preserved. This results in improved classification accuracy. Experimental results on 5 publicly available datasets, viz. AR, CACD, YaleB, FERET, and ORL show that the proposed method outperforms the popular methods, i.e., principal component analysis (PCA), LDA, incremental principal component analysis (IPCA), and incremental linear discriminant analysis (ILDA) on all the datasets in terms of K -fold ($K = 2, 3, 4, 5$) cross-validation. Further, it is also found that the training time of IWLDA is better than the batch methods, i.e., PCA and LDA.

Keywords Fisher criterion · Pairwise · Datasets · Training time

1 Introduction

Human face has been the primary identity of a human and has been used as one of the important aspects of recognition in human–machine interactions. Face recognition is a research area where the identity of an individual is established using digital face images of people. It has played a critical role in several industrial applications [1] such

N. Kumar (✉) · S. Madhavan
Department of Computer Science and Engineering,
National Institute of Technology, Srinagar, Uttarakhand, India
e-mail: nitin@nituk.ac.in

© Springer Nature Singapore Pte Ltd. 2021
G. S. Hura et al. (eds.), *Advances in Communication and Computational Technology*, Lecture Notes in Electrical Engineering 668,
https://doi.org/10.1007/978-981-15-5341-7_51

677

as personal security, mobile security, government ID verification, and video games. With the advent of machine learning, face recognition has quickly adapted the methods available in literature. However, there are some challenges in face recognition such as illumination, expression, and pose changes that can affect the accuracy of these methods. One interesting aspect is that model development may not be possible if we do not have all the data available with us beforehand.

Incremental learning [2] methods have been suggested to address the problem of non-availability of all the data samples beforehand. In incremental learning, model is developed with initial training data and then can be further updated with incoming data as and when necessary using updating algorithms as specified in the literature. Over the past few decades, incremental learning methods have made significant improvements in performance. Additionally, these methods offer various advantages in terms of privacy and security. Data from various geographic locations can be updated into the model thereby maintaining data privacy and security by sending only the model parameters instead of the real data. A comprehensive survey of incremental methods in face recognition has been given by Madhavan and Kumar [3].

1.1 Motivation

Supervised learning approach has been among the most popular approaches for better performances in classification-related applications such as face recognition. Pang et al. [4] had proposed incremental linear discriminant analysis (ILDA) which was one of the earliest incremental supervised algorithms. Subsequently, several other approaches have been proposed in literature to improve the performance of ILDA such as a generalized singular value decomposition (SVD)-based incremental LDA by Zhao and Yuen [5], Wang et al. [6] who have given incremental two-dimensional LDA, a fast updation algorithm for incremental LDA by James and Annadurai [7], to name a few.

Weighted linear discriminant analysis (WLDA) is suggested by Chen et al. [8] and improves the classification accuracy of LDA. An incremental version of WLDA can be much more efficient in terms of space and time complexity and can achieve better classification accuracy. A variant of WLDA is proposed by Liang et al. [9] which uses weighted pairwise Fischer criterion to improve the performance of LDA. In this paper, we propose a novel method which combines the advantages of incremental learning and weighted linear discriminant analysis suggested by Liang et al. [9].

The rest of the paper is organized as: Sect. 2 describes the related work in literature while Sect. 3 describes the proposed method. Experimental setup and results along with discussion are given in Sect. 4. Lastly, conclusion and future work are given in Sect. 5.

2 Related Work

2.1 Incremental Linear Discriminant Analysis (ILDA)

Pang et al. [4] have proposed an incremental linear discriminant analysis based on other incremental algorithms in literature which is among the earliest variant of incremental LDA. The authors have proposed update algorithms to central tendencies and scatter matrices, and eigendecomposition of the updated scatter matrices formulae gives the updated subspace. The updation formulae of mean and scatter matrices, as specified by the authors, are given below [4].

Mean updation:

$$\bar{x}' = \frac{(N\bar{x} + \mathbf{y})}{N + 1} \tag{1}$$

where \bar{x}' is updated mean, \bar{x} is previous mean, N is the total number of samples, and \mathbf{y} is the new sample.

Between-class scatter matrix updation [4]:

$$\begin{aligned} \mathbf{S}'_b &= \sum_{c=1}^M n_c (\bar{\mathbf{x}}_c - \bar{\mathbf{x}}') (\bar{\mathbf{x}}_c - \bar{\mathbf{x}}')^T + (\mathbf{y} - \bar{\mathbf{x}}') (\mathbf{y} - \bar{\mathbf{x}}')^T \\ &= \sum_{c=1}^{M+1} n'_c (\bar{\mathbf{x}}_c - \bar{\mathbf{x}}') (\bar{\mathbf{x}}_c - \bar{\mathbf{x}}')^T \end{aligned} \tag{2}$$

where M is the previous total number of classes, n_c is the previous total number of samples in class c , n'_c represents the updated number of samples in class c , and $\bar{\mathbf{x}}_c$ is the sample mean.

Within-class scatter matrix updation [4]:

$$\mathbf{S}'_w = \sum_{c=1, c \neq k} \Sigma_c + \Sigma'_k \tag{3}$$

$$\Sigma'_k = \Sigma_k + \frac{n_k}{n_k + 1} (\mathbf{y} - \bar{\mathbf{x}}_k) (\mathbf{y} - \bar{\mathbf{x}}_k)^T \tag{4}$$

where Σ_c is the within-class scatter matrix of class c , k is the class with the new sample, Σ'_k represents the updated within-class scatter matrix of class k , n_k denotes the total number of samples in class k , $\bar{\mathbf{x}}_k$ is the prior mean of class k , and \mathbf{y} is the new sample.

Further, an LDA criterion [4] is used to obtain the subspace vectors which is given below:

$$J(\mathbf{W}) = \frac{\mathbf{W}^T \mathbf{S}'_b \mathbf{W}}{\mathbf{W}^T \mathbf{S}'_w \mathbf{W}} \tag{5}$$

Using these formulae, the authors have proposed to update the scatter matrices and the LDA criteria are reduced to an eigendecomposition of $\mathbf{S}'_w^{-1}\mathbf{S}'_b$ matrix gives the eigenvectors that are the updated subspace vectors. This effectively utilizes the incoming sample to update the model without a knowledge of prior data but only model parameters such as number of samples, number of samples per class, sample mean, class means, between-class, and within-class scatter matrices.

2.2 Weighted Linear Discriminant Analysis

Liang et al. [9] proposed a variant of weighted linear discriminant analysis (WLDA) called uncorrelated linear discriminant analysis which is based on weighted pairwise Fischer criterion. In this variant, LDA is performed by improving the worst case class separation using a weighted pairwise Fischer criterion, proportional to the mean distances between class samples, to compute the between-class scatter matrix. This effectively improves the distance between classes with low class mean distances and hence separates them in a much better way in the subspace to improve the classification accuracy. The weighted pairwise Fischer criterion for the weighted between class scatter matrix ($\hat{\mathbf{S}}_b$), as proposed by the authors, is specified in equation below [9]:

$$\hat{\mathbf{S}}_b = \sum_{i=1}^{M-1} \sum_{j=i+1}^M p_i p_j w(d_{ij}) (\bar{\mathbf{x}}_i - \bar{\mathbf{x}}_j)(\bar{\mathbf{x}}_i - \bar{\mathbf{x}}_j)^T \tag{6}$$

where M is the total number of classes, p_c is the prior probability of class c in general, $\bar{\mathbf{x}}_c$ denotes the mean of class c in general, $w(d_{ij})$ is the Fischer criterion, and d_{ij} is the distance between the means of class i and class j .

Fisher criterion $w(d_{ij})$ [9] is computed as given in the equations below:

$$w(d_{ij}) = \frac{1}{2d_{ij}^2} \operatorname{erf}\left(\frac{d_{ij}}{2\sqrt{2}}\right) \tag{7}$$

where $\operatorname{erf}()$ represents the Gaussian error function and is computed as:

$$\operatorname{erf}(x) = \frac{2}{\sqrt{\pi}} \int_0^x e^{-t^2} dt \tag{8}$$

The mean distance d_{ij} in the computation of the Fischer criterion according to the equation below [9]:

$$d_{ij} = \sqrt{(\bar{\mathbf{x}}_i - \bar{\mathbf{x}}_j)^T \mathbf{S}_w^{-1} (\bar{\mathbf{x}}_i - \bar{\mathbf{x}}_j)} \tag{9}$$

The resulting Fischer criterion $w(d_{ij})$, is referred to as weighted pairwise Fischer criterion. This criterion efficiently handles the weights of various classes based on

their class mean differences and the within-class scatter matrix. It can be observed that this criterion is almost inversely proportional to the square of mean distances of the two classes. If any two classes have low mean distances, their subsequent Fischer criterion is a very high value while if the mean distances are high the Fischer criterion shall be relatively low. This efficiently preserves the mean distances of the classes.

The proposed model, incremental weighted linear discriminant analysis, is based on this weighted pairwise Fischer criterion and is aimed to improve the accuracy over LDA, ILDA, and other popular algorithms for face recognition.

3 Incremental Weighted Linear Discriminant Analysis

The primary disadvantage in LDA and its several variants are that the subspace aims to directly separate the samples of different classes while bringing the samples of same classes closer. The disadvantage of this approach is that the classes with insignificant separation or with low class mean difference are not well-separated. This leads to a drop in classification accuracy as the samples of these classes can be misclassified in either of the classes. To overcome this, weights are introduced to the between-class scatter matrix as specified in the weighted pairwise Fischer criterion in the previous section. The incremental version of WLDA (IWLDA) proposed is as follows:

If $\mathbf{x}_1, \mathbf{x}_2, \dots, \mathbf{x}_N$ are N training samples, then their mean is computed as:

$$\bar{\mathbf{x}} = \frac{\sum_{i=1}^N \mathbf{x}_i}{N} \tag{10}$$

where $\bar{\mathbf{x}}$ is the mean of the samples.

Mean can be updated with incoming sample \mathbf{y} as:

$$\bar{\mathbf{x}}' = \frac{(N\bar{\mathbf{x}} + \mathbf{y})}{N + 1} \tag{11}$$

where $\bar{\mathbf{x}}'$ is the updated mean of the samples.

The within-class scatter matrix is updated before the between-class scatter matrix and its formulation is as specified below:

$$\mathbf{S}'_w = \sum_{c=1, c \neq k} \Sigma_c + \Sigma'_k \tag{12}$$

$$\Sigma'_k = \Sigma_k + \frac{n_k}{n_k + 1} (\mathbf{y} - \bar{\mathbf{x}}_k)(\mathbf{y} - \bar{\mathbf{x}}_k)^T \tag{13}$$

Using the updated within-class scatter matrix, the weighted pairwise Fischer criterion is updated for every possible class combinations. This updated Fischer criterion

is then used to compute the updated weighted between-class scatter matrix. The formulae for the updated weighted pairwise Fischer criterion and the updated weighted between-class scatter matrix are as follows:

$$d_{ij} = \sqrt{(\bar{\mathbf{x}}_i - \bar{\mathbf{x}}_j)^T \mathbf{S}'_w^{-1} (\bar{\mathbf{x}}_i - \bar{\mathbf{x}}_j)} \quad (14)$$

$$\hat{\mathbf{S}}'_b = \sum_{i=1}^{M-1} \sum_{j=i+1}^M p_i p_j w(d_{ij}) (\bar{\mathbf{x}}'_i - \bar{\mathbf{x}}'_j) (\bar{\mathbf{x}}'_i - \bar{\mathbf{x}}'_j)^T \quad (15)$$

$$w(d_{ij}) = \frac{1}{2d_{ij}^2} \operatorname{erf} \left(\frac{d_{ij}}{2\sqrt{2}} \right) \quad (16)$$

Thus, the proposed criterion of IWLDA is given by:

$$J(\mathbf{W}') = \frac{\mathbf{W}'^T \hat{\mathbf{S}}'_b \mathbf{W}'}{\mathbf{W}'^T \mathbf{S}'_w \mathbf{W}'} \quad (17)$$

At every iteration, when a new sample arrives, the mean is initially updated using Eq. 11, following which the within-class scatter matrix is updated as specified in Eq. 12. Further, the weighted pairwise Fischer criterion is updated as given in Eq. 14 and is used to update the between-class scatter matrix of Eq. 15. The new updated subspace is obtained from the LDA criterion in Eq. 17 which can further be reduced to the eigendecomposition of the updated within-class and between-class scatter matrices ($\mathbf{S}'_w^{-1} \hat{\mathbf{S}}'_b$).

3.1 Classification

Once the transformation matrix (\mathbf{W}') is generated, all the training samples are projected onto the subspace. Similarly, the probe image is also transformed using (\mathbf{W}'). Afterward, the nearest samples to the probe are found using K -nearest neighbor in which K neighbors that are closest to the data sample are chosen in the subspace. The class label that is most common, i.e., with maximum occurrence, among these K neighbors is chosen as the class label for the probe. For our experimentation, we have used $K = 5$ in K -nearest neighbor classifier with Euclidean distance metric.

4 Experimental Setup and Results

To compare the performance of the proposed method IWLDA, we have performed experiments on five publicly available face datasets, viz. AR [10], CACD [11], Yale B [12], FERET [13], and ORL [14]. A summary of these datasets are given in Table 1. Sample images from these datasets are given in Fig. 1 for reference.

Table 1 Summary of the datasets used in experiments

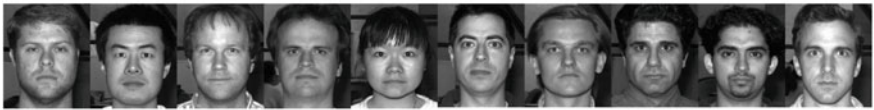
Dataset	# of images	# of identities	Image size	Face variations
AR [10]	4000	126	768 × 576	Occlusion, illumination, expression
CACD [11]	163,446	2000	250 × 250	Occlusion, illumination, expression, pose, unconstrained background
Yale B [12]	5760	10	640 × 480	Illumination, pose
FERET [13]	14,126	1199	N/A	Illumination, expression, pose
ORL [14]	400	40	92 × 112	Occlusion, illumination, expression



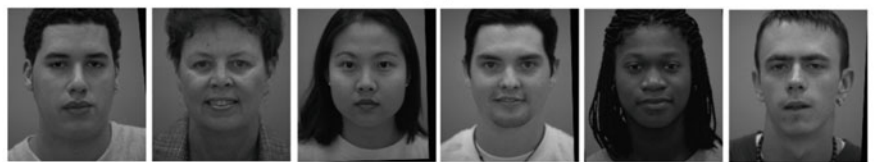
(a)



(b)



(c)



(d)



(e)

Fig. 1 Samples images from publicly available face datasets **a** AR [10], **b** CACD [11], **c** Yale B [12], **d** FERET [13], and **e** ORL [14]

For the performance evaluation of the proposed IWLDA, a K -fold cross-validation technique has been employed. In K -fold cross-validation, the data is randomly split into K different blocks in which $K - 1$ blocks are used for training the model while the final block is reserved for testing the classification accuracy of the model trained. For the K -fold cross-validation, we have chosen several K values: 2, 3, 4, 5, which splits the training and testing data in different proportions for an effective testing. To avail incrementation, the first two samples of the training data are used to generate the model while the rest of the training data are fed into the model one after another. As every sample arrives, the model is updated using the proposed method IWLDA. This experimentation is performed with random splits over 40 times for each K -value and the average classification accuracy is noted down.

Further other popular methods such as PCA as given in [15], LDA specified in [16], IPCA mentioned in [17] and ILDA proposed by Pang et al. [4] were implemented and evaluated over the same datasets. The PCA, LDA, and IPCA are from the standard library for Python, sklearn [18]. The non-incremental versions, PCA and LDA, were evaluated by utilizing the entire training data for the training while the incremental versions, IPCA and ILDA, were evaluated in a similar fashion to that of IWLDA, i.e., the first two samples in training data are used to generate a model while the rest of the samples in training data are used to incrementally update the model. The experimentation is similarly repeated over 40 times with different K values (2, 3, 4, 5) and the average classification accuracy is noted. Figure 2 summarizes the results of the proposed method over popular methods for the face recognition by plotting the average classification accuracy over various K values chosen.

In every dataset and at every K value chosen, the proposed IWLDA has shown significant improvement in average classification accuracy over the popular methods of face recognition, viz. PCA [15], LDA [16], IPCA [17], and ILDA [4]. The classification accuracy over ORL dataset of the proposed model has reached a 90% maximal value while the rest of the datasets have registered relatively lesser accuracy. This can be inferred from the lesser face variation and lesser number of images available in the ORL dataset in comparison with the remaining dataset as can be deduced from Table 1. It can be further noted that among the remaining methods, other than the proposed method, the incremental methods (IPCA, ILDA) have been dominant in performance over the batch methods (PCA, LDA). Furthermore, in datasets with very high number of images and identities (CACD [11]), IPCA has shown better performance than ILDA which can be attributed to efficient subsampling of large volume of data, while ILDA has shown significantly better performance in the remaining datasets (AR [10], Yale B [12], FERET [13], and ORL [14]).

Further, from Table 2, it can also be concluded that the incremental methods require less training time than the batch methods, although the proposed IWLDA shows a slightly higher time complexity which is a mild trade-off for better classification accuracy. To summarize, incremental variants have shown better performance in face recognition than batch counterparts and the proposed method IWLDA, have been dominant in classification accuracy, and have less training time than the batch methods on all 5 datasets.

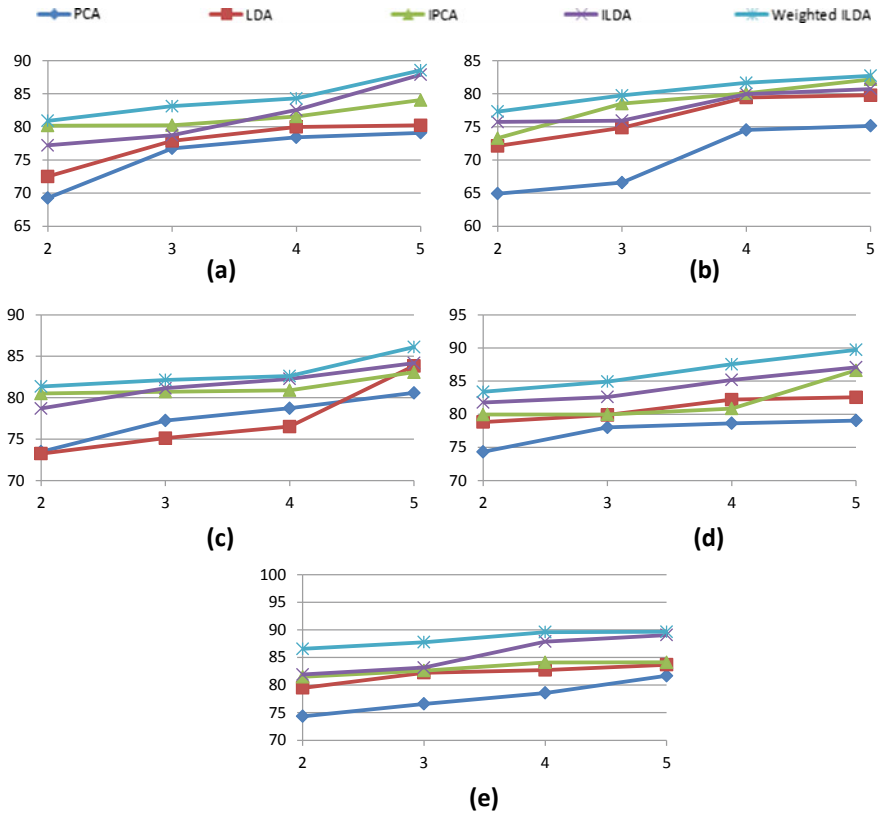


Fig. 2 Results of the proposed method (IWLDA) in comparison to popular methods (PCA, LDA, IPCA, ILDA) plotted with average classification accuracy over various K values chosen (2, 3, 4, 5)

Table 2 Time taken per image for each dataset for the methods (in ms)

K values	Datasets	PCA	LDA	IPCA	ILDA	IWLDA
$K = 2$	AR	20.84	20.3	18.72	18.8	19.97
	CACD	2.99	2.77	2.62	2.65	2.68
	Yale B	15.09	14.15	12.85	13.07	13.96
	FERET	2.95	2.86	2.75	2.77	2.8
	ORL	0.48	0.48	0.43	0.43	0.45
$K = 3$	AR	20.9	20.57	19.66	19.87	20.23
	CACD	3.16	3.06	2.85	2.86	3.03
	Yale B	15.22	14.76	13.82	14.21	14.58
	FERET	3.08	3.01	2.78	2.87	2.9
	ORL	0.48	0.48	0.43	0.45	0.48

(continued)

Table 2 (continued)

K values	Datasets	PCA	LDA	IPCA	ILDA	IWLDA
$K = 4$	AR	22.73	21.66	20.91	21.16	21.34
	CACD	3.18	3.03	2.86	2.98	2.98
	Yale B	15.78	14.72	13.82	13.83	14.39
	FERET	3.13	3.09	2.9	2.96	2.99
	ORL	0.5	0.48	0.45	0.45	0.45
$K = 5$	AR	23.43	22.26	20.86	21.09	21.74
	CACD	3.24	3.09	2.87	3.01	3.09
	Yale B	15.48	14.9	14.08	14.3	14.43
	FERET	3.28	3.15	2.92	3	3.14
	ORL	0.5	0.48	0.45	0.45	0.45

5 Conclusion and Future Work

In this paper, we have presented a novel incremental version of weighted linear discriminant analysis called IWLDA using weighted pairwise Fischer criterion. The proposed method possess the advantages of incremental learning as well as performance of weighted linear discriminant analysis. The proposed method performs better than popular methods in literature such as PCA, LDA, IPCA, and ILDA. To support our claim, we have performed experiments on five publicly available datasets, i.e., AR, ORL, CACD, YaleB, and FERET which include small, medium, and large datasets. The performance of the methods is determined in terms of average classification accuracy and time taken per image of each dataset. The experimental results have clearly shown a dominance of the proposed method over aforementioned techniques in terms of both average classification accuracy and time complexity, despite a minor trade-off for time complexity.

References

1. Zhao W, Chellappa R, Phillips PJ, Rosenfeld A (2003) Face recognition: a literature survey. *ACM Comput Surv (CSUR)* 35(4):399–458
2. Huang W, Lee B-H, Li L, Leman K (2003) Face recognition by incremental learning. In: *IEEE international conference on systems, man and cybernetics*, vol 5, pp 4718–4723
3. Madhava S, Kumar N (2019) Incremental methods in face recognition: a survey. *Artificial Intelligence Review*. <https://doi.org/10.1007/s10462-019-09734-3>
4. Pang S, Ozawa S, Kasabov N (2005) Incremental linear discriminant analysis for classification of data streams. *IEEE Trans Syst Man Cybern Part B Cybern* 35(5):905–914
5. Zhao H, Yuen PC (2008) Incremental linear discriminant analysis for face recognition. *IEEE Trans Syst Man Cybern Part B Cybern* 38(1):210–221
6. Wang JG, Sung E, Yau WY (2010) Incremental two-dimensional linear discriminant analysis with applications to face recognition. *J Netw Comput Appl* 33(3):314–322

7. James EAK, Annadurai S (2009) Implementation of incremental linear discriminant analysis using singular value decomposition for face recognition. In: First IEEE international conference on advanced computing. IEEE, pp 172–175
8. Chen F, An S, Liu W (2008) A new face recognition approach to boosting the worst-case performance. In: Pacific-Rim conference on multimedia. Springer, Berlin, Heidelberg, pp 927–930
9. Liang Y, Li C, Gong W, Pan Y (2007) Uncorrelated linear discriminant analysis based on weighted pairwise Fisher criterion. *Pattern Recogn* 40(12):3606–3615
10. Martinez AM, Benavente R (1998) CVC technical report# 24, The AR Face Database
11. Chen BC, Chen CS, Hsu WH (2014) Cross-age reference coding for age-invariant face recognition and retrieval. In: European conference on computer vision (CACD dataset). Springer, pp 768–783
12. Belhumeur PN, Hespanha J, Kriegman DJ (1997) Eigenfaces vs. fisherfaces: recognition using class specific linear projection. *IEEE Trans Pattern Anal Mach Intell* 19(7):711–720
13. Feret face dataset. <https://www.nist.gov/programs-projects/face-recognition-technology-feret>. Accessed 29 Jan 2019
14. ORL/Olivetti Faces/AT&T face dataset. <https://www.cl.cam.ac.uk/research/dtg/attarchive/facedatabase.html>. Accessed 29 Jan 2019
15. Tipping ME, Bishop CM (1999) Probabilistic principal component analysis. *J R Stat Soc: Ser B Stat Methodol* 61(3):611–622
16. Hastie T, Tibshirani R, Friedman J (2008) The elements of statistical learning section, vol 4, no 3, pp 106–119
17. Ross D, Lim J, Lin R, Yang M (2008) Incremental learning for robust visual tracking. *Int J Comput Vis* 77(1–3):125–141
18. Scikit Learn Python library. <https://scikit-learn.org>. Accessed 01 May 2019

Capacity Using *L*-Branch Channel MRC System Over Weibull Fading Channels—A Review



Adarsh Joshi, Aditya Narayan, Mohammad Irfanul Hasan, and Shalini Singh

Abstract Weibull distribution is a befitting prototype for explaining fading channels that consist of multipath environment in radio propagation surrounding it in indoor or outdoor. This work shows a review on the expression of channel capacity with *L*-branch maximal ratio combining system and over uncorrelated Weibull fading channel using optimum rate adaptation with constant transmit power scheme. An expression for the probability of outage has been also deduced in this paper. In this paper, an expression for a relation between the fading parameter of Rayleigh fading and Weibull fading has been also established.

Keywords Channel capacity · Dual-branch · Fading parameters · MRC · Optimal rate adaptation with constant transmit power

1 Introduction

In today's scenario, the requirement for the wireless communication assistance like the high speed of data transmission and VoLTE, etc., is expanding rapidly [1]. These facilities require a high data transfer rate with stable transmission, which is a difficult undertaking as the wireless setup works over mediums having multiple replicas of the message. Channel capacity is crucial in creating a wireless transmission setup as it indicates the best attainable data transfer rate [1]. The channel capacity, in general, is also called average channel capacity as it is attained by averaging the Shannon

A. Joshi · A. Narayan · M. I. Hasan (✉) · S. Singh
Graphic Era Deemed to be University, Dehradun, Uttarakhand 248002, India
e-mail: irfu_hasan@rediffmail.com

A. Joshi
e-mail: dhruvj414@gmail.com

A. Narayan
e-mail: adityanarayan1396@gmail.com

S. Singh
e-mail: shalini111.raj@gmail.com

capacity of an additive white Gaussian noise (AWGN) medium [1, 2]. The capacity of a band-limited AWGN medium which is an anti-fading medium is known as Shannon capacity and is expressed as [1, 2].

$$C = B \times \log_2(1 + \gamma) \quad (1)$$

where γ is the instantaneous accepted SNR and the bandwidth of the channel is denoted by B expressed in Hz.

Shannon capacity of an AWGN medium denotes an upper bound for transmitting message stably [1, 2]. The channel capacity of an AWGN medium is certainly higher in respect of the fading environment [1–3]. Enhancement in the channel capacity can be attained just by incrementing the transmission power of signal in order to minimize the enactment of fading, and still, it leads in an increment in the interference level [1–3]. Approaches like adaptive transmission scheme or combining scheme are other approaches used in fading environment to enhance the capacity without incrementing the transmit power and bandwidth [1–3].

1.1 Diversity Combining Techniques

Diversity combining approach is used in fading medium to enhance the system performance with minimizing the problems of fading [1]. It contains multiple copies of message bearing signal over multiple branches, and then, those branches are combined in order to attain an increment in the general instantaneous or mean received SNR [1–3]. For attaining the benefit of diversity scheme, it is required to bind the independently faded signals that were accepted from the diversity divisions. Subsequent are some best combining methods [1–3].

- (i) Selection combining
- (ii) Equal gain combining
- (iii) Maximal ratio combining.

(i) Selection Combining (SC)

The diversity branch with the biggest instantaneous SNR relatively to the rest of the branch is picked up in SC [1]. The fundamental phenomenon of SC is to choose the replica having the biggest SNR among all signals at the receiver's section [1, 2]. To check all the diversity branches and select the best one, i.e., the one which has highest spontaneous SNR, the conventional process of selection combining approach is detected [1–3]. Therefore, SC is not a combining approach but a kind of selection approach from the different accepted signals [1–3]. But, determining SNR value is quite difficult as the selection has to be achieved in an extremely diminutive time [1, 4]. But when mean power of the noise is the same for every branch, picking the branch with the biggest SNR is similar to pick the branch with paramount received

power [1, 4]. Because of this, it is practical to select the branch which is having the highest SNR [1, 4].

(ii) **Maximal Ratio Combining (MRC)**

In the case of the MRC, replicas are firstly co-phased, then separately weighted, and finally aggregated. For maximizing the aggregate SNR, the weights are selected proportionally to the solitary signal level [1, 4]. The weighting employed to the branches must be equivocal with respect of the SNR. The MRC is identified as the optimum diversity techniques to mitigate faded signal issues [1, 4, 5].

But, the disadvantage of MRC lies in its complexity, since it consists of knowledge of all branch factors like fading amplitude levels, phase shift, and delay factor [1, 4, 5].

(iii) **Equal Gain Combining (EGC)**

EGC is a special analogous to MRC, but the fact is that here every branch weights are made unity or equal; however, the signals from every branch are co-phased prior to aggregation [1, 5, 6]. The increase in level of performance is little deprived in this in comparison with MRC as there is a chance of joining the signal of low strength and high strength in terms of noise and interference levels [1, 4, 6]. But, EGC is less difficult to perform in comparison with MRC as there is no need to calculate fading amplitudes [1, 4, 6].

1.2 Adaptive Transmission Schemes

Adaptive transmissions are of four types [1, 2, 4, 6].

- (a) Optimal rate adaptation with constant transmission power (ORA)
- (b) Optimal power and rate adaptation
- (c) Channel inversion with fixed rate
- (d) Truncated channel inversion with fixed rate.

Here, we have focused on optimal rate adaptation with constant transmit power method.

(a) Optimal rate adaptation with constant transmission power (ORA): In this approach, the transmitter power is being unchanged, but the data rate is adapted by the transmitter in accordance to the fading conditions of the medium [2, 3, 6]. The capacity is obtained by averaging the Shannon capacity of an AWGN channel [2, 3, 6].

$$\langle c \rangle_{ORA} = B \int_0^{\infty} \log_2(1 + \gamma) p_{\gamma}(\gamma) d\gamma$$

where the probability density function (PDF) of the instantaneous is received.

SNR (γ) [1, 2] is denoted as $p_\gamma(\gamma)$.

1.3 Rayleigh Fading Model

Rayleigh fading distribution is characterized by the absence of the line-of-sight (LOS) component at the receiver [1, 2]. During the multipath propagation of the signal, no line-of-sight path is there in between of the transmitter and the receiver, only the reflected, diffracted, and scattered multipath components are present [1]. The line-of-sight path is defined as the candid path by the transmitter to the receiver which is not reflected, diffracted, or scattered [1–3]. In Rayleigh fading, there is a possibility in which the signal may go in deep fade [3, 4].

PDF under no diversity is as given in [2]:

$$P_\gamma(\gamma) = \frac{e^{-\frac{\gamma}{\gamma'}}}{\gamma'} \quad \gamma \geq 0 \quad (2)$$

where γ is alias for spontaneously received SNR and γ' is the alias for average received SNR.

PDF under MRC diversity is as given in [1, 2]:

$$P_\gamma^{\text{MRC}}(\gamma) = \frac{\gamma^{L-1} e^{-\frac{\gamma}{\gamma'}}}{(L-1)! (\gamma')^L} \quad (3)$$

where γ is the alias for spontaneously received SNR, L indicates the count of diversity branches, and γ' indicates the average received SNR.

1.3.1 Channel Capacity with no Diversity

By using optimum data rate adaptation with constant transmit power, the channel capacity (in bps) is stated by [1, 2]

$$\langle C \rangle_{\text{ORA}} = B \int_0^\infty \log_2(1 + \gamma) \frac{e^{-\frac{\gamma}{\gamma'}}}{\gamma'} d\gamma \quad (4)$$

where B denotes the bandwidth of the channel and γ denotes the instantaneous received SNR.

Now after putting Eq. 2 in Eq. 4, we get [2]

$$\langle C \rangle_{\text{ORA}} = B \int_0^{\infty} \log_2(1 + \gamma) \frac{e^{-\frac{\gamma}{\gamma'}}}{\gamma'} d\gamma$$

where γ denotes the spontaneously received SNR, γ' denotes the mean received SNR, and channel bandwidth is indicated by B [1, 2].

After rearranging the equation above, we get [2]

$$\langle C \rangle_{\text{ORA}} = \frac{B \log_2 e \int_0^{\infty} \ln(1 + \gamma) e^{-\frac{\gamma}{\gamma'}} d\gamma}{\gamma'}$$

The integral of the above equation is evaluated using partial integration given as [2]

$$\int_0^{\infty} u dv = \lim(uv) - \lim(uv) - \int_0^{\infty} v du$$

Now first, let

$$u = \ln(1 + \gamma)$$

Thus

$$du = \frac{d\gamma}{1 + \gamma}$$

And let

$$dv = e^{-\frac{\gamma}{\gamma'}}$$

Thus, we get

$$\begin{aligned} v &= \int e^{-\gamma/\gamma'} / \gamma' d\gamma \\ &= \frac{e^{-\gamma/\gamma'}}{-\frac{1}{\gamma'}} \end{aligned}$$

Substituting the above equation in the partial integration above, we see that the first the term goes to zero; hence, result becomes as in [2]

$$\frac{\langle C \rangle_{\text{ORA}}}{B} = \log_2 e \int_0^\infty \frac{e^{-\gamma/\gamma'}}{1 + \gamma} d\gamma$$

The integral in the above equation can be stated as a closed form expression with the help of [2, 4] as:

$$= e^{1/\gamma'} \Gamma\left(0, \frac{1}{\gamma'}\right) \times \log_2 e$$

Here, $\Gamma(\cdot)$ is the complementary gamma function which is defined in [1, 2]. We know from [2]:

$$\Gamma\left(0, \frac{1}{\gamma'}\right) = E_1\left(\frac{1}{\gamma'}\right)$$

where $E_1(\cdot)$ is exponential integral explained in [2].

$$\frac{\langle C \rangle_{\text{ORA}}}{B} = e^{1/\gamma'} E_1\left(\frac{1}{\gamma'}\right) \log_2 e \tag{5}$$

1.3.2 Channel Capacity with Diversity

By using optimum data transfer rate adaptation with stable transmission power, medium capacity (in bps) is stated as [1, 2]

$$\langle c \rangle_{\text{ORA}} = B \int_0^\infty \log_2(1 + \gamma) p_\gamma(\gamma) d\gamma \tag{6}$$

where the channel bandwidth and the spontaneous received SNR are denoted by B and γ , respectively.

Now putting Eq. 3 in Eq. 6, we get [2]:

$$\langle C \rangle_{\text{ORA}} = B \int_0^\infty \log_2(1 + \gamma) \frac{\gamma^{L-1} e^{-\gamma/\gamma'}}{(L - 1)! (\gamma')^L} d\gamma$$

where L denotes the count for number of diversity branches and γ' indicates the average received.

In SNR, γ is the spontaneously received SNR, and B indicates the medium bandwidth [1, 2].

After rearranging the equation above equation, we get [2]

$$\langle C \rangle_{\text{ORA}} = \frac{B \log_2 e}{(L - 1)!} \times \left(\frac{1}{\gamma'} \right)^L \int_0^\infty \text{In}(1 + \gamma) \gamma^{L-1} e^{-\gamma/\gamma'} d\gamma$$

The integral in the above equation is evaluated using partial integration given as [2]

$$\int_0^\infty u dv = \lim(uv) - \lim(uv) - \int_0^\infty v du$$

Now first, let

$$u = \text{In}(1 + \gamma)$$

Thus

$$du = \frac{d\gamma}{1 + \gamma}$$

And let

$$dv = \gamma^{L-1} e^{-\gamma/\gamma'}$$

Thus, we get [2]:

$$v = \int \gamma^{L-1} e^{-\gamma/\gamma'} d\gamma$$

After performing successive integration on the above equation of dv, we get [2, 9]

$$v = e^{-\gamma/\gamma'} \left(\sum_{k=0}^{L-1} \frac{(-1)^k k! \binom{L-1}{K}}{\left(\frac{-1}{\gamma'}\right)^{k+1}} \times \gamma^{L-1-k} \right)$$

After rearranging the terms given in the equation above, we get [2]

$$v = - \sum_{K=0}^{L-1} e^{-\gamma/\gamma'} \frac{(L - 1)! \gamma^{L-1-K}}{(L - 1 - K)! \left(\frac{-1}{\gamma'}\right)^{K+1}}$$

Hence, we get [2]:

$$I_L\left(\frac{1}{\gamma'}\right) = \sum_{K=0}^{L-1} \frac{(L-1)!}{(L-1-K)! \left(\frac{1}{\gamma'}\right)^{K+1}} \int_0^\infty \frac{\gamma^{L-1-K} e^{-\gamma/\gamma'}}{1+\gamma} d\gamma$$

The integral in the above equation can be modified as a closed form using [2, 9] as

$$\begin{aligned} \int_0^\infty \frac{e^{-\gamma/\gamma'} \gamma^{L-K-1} d\gamma}{1+\gamma} &= (1)^{L-K-1} \times e^{1/\gamma' \Gamma(L-K) \times \Gamma(1-L+K, \frac{1}{\gamma'})} \\ &= e^{1/\gamma' (L-K-1)! \Gamma\left(1-L+K, \frac{1}{\gamma'}\right)} \end{aligned}$$

After solving the above equation, the result we get is [2]

$$\begin{aligned} \int_0^\infty \frac{e^{-\gamma/\gamma'} \gamma^{L-K-1} d\gamma}{1+\gamma} &= (1)^{L-K-1} \times e^{1/\gamma' \Gamma(L-K) \times \Gamma(1-L+K, \frac{1}{\gamma'})} \\ &= e^{1/\gamma' (L-K-1)! \Gamma\left(1-L+K, \frac{1}{\gamma'}\right)} \end{aligned}$$

Here, let $z = L - k - 1$

As $k = 0$, $z = (L - 1)$

And $k = L - 1$, $z = L - L + 1 - 1 = 0$

Thus, we get:

$$\frac{\langle C \rangle \text{MRC}_{\text{,ORA}}}{B} = (\log_2 e) e^{1/\gamma'} \sum_{z=0}^{L-1} \frac{\Gamma\left(-z, \frac{1}{\gamma'}\right)}{(\gamma')^z}$$

The final equation for medium capacity per unit bandwidth for ORA in the scenario of MRC diversity using [2, 8]:

$$\frac{\langle C \rangle \text{MRC}_{\text{,ORA}}}{B} = (\log_2 e) \sum_{z=0}^{L-1} \frac{(-1)^z}{z!} \left(\frac{1}{\gamma'}\right)^z \times \left(e^{1/\gamma'} E_1\left(\frac{1}{\gamma'}\right) - \sum_{y=0}^{z-1} \frac{(-1)^y y!}{\left(\frac{1}{\gamma'}\right)^{y+1}} \right)$$

1.4 Weibull Fading Model

The Weibull distribution is a general model for explaining multipath fading mediums in both outdoor and indoor radio mode surroundings [2, 7, 8]. Weibull-type distribution is helpful for modeling multiple path faded signal amplitude [2, 7, 8]. The Weibull-type distribution is a generalized model, i.e., for the different results of shape parameter (β), it reduces into different other distributions. Let us assume that when $\beta = 1$, it converges to exponential distribution, for $\beta = 2$, its distribution type becomes Rayleigh, and for $\beta = 2.5$, it becomes lognormal distribution [2, 7, 8].

The PDF under no diversity is as given in [2, 7, 8]:

$$P_{\gamma}(\gamma) = \frac{\beta}{2a\gamma'} \left(\frac{\gamma}{a\gamma'} \right)^{\beta-2/2} e^{-(\gamma/a\gamma')^{\beta/2}} \quad (7)$$

where γ denotes the spontaneous SNR at the receiver end, β denotes the shape parameter in case of Weibull fading, and γ' denotes the overall SNR at the receiver end.

PDF under MRC diversity scheme is as given in [2, 7, 8]:

$$P_{\gamma}^{\text{MRC}}(\gamma) = \frac{\beta \gamma^{\frac{L\beta}{2}-1}}{2\Gamma(L)(\mathcal{E}\gamma)^{\frac{L\beta}{2}}} e^{-\left(\frac{\gamma}{\mathcal{E}\gamma'}\right)^{\frac{\beta}{2}}} \quad (8)$$

where Weibull power factor is given as [7, 8]

$$\mathcal{E} = \frac{\Gamma(L)}{\Gamma\left(L + 2/\beta\right)}$$

Here, L denotes the count for diversity branches, β indicates the shape parameter for Weibull fading, γ denotes the spontaneously received SNR at the receiver end, and γ' is the mean received SNR [7, 8].

1.4.1 Mapping the Weibull Fading and Nakagami- m Parameter

Using reference [2, 7], we know that the fading amount (AF):

$$\text{AF} = \frac{\text{var}(R^2)}{(E\{R^2\})^2} = \frac{E\{R^2\} - (E\{R^2\})^2}{(E\{R^2\})^2}$$

where AF is the fading amount [2, 7].

$$\frac{\Gamma\left(1 + \frac{4}{\beta}\right) - \Gamma^2\left(1 + \frac{2}{\beta}\right)}{\Gamma\left(1 + \frac{2}{\beta}\right)} = \frac{\Gamma\left(1 + \frac{4}{\beta}\right)}{\Gamma^2\left(1 + \frac{2}{\beta}\right)} - 1$$

Here, $AF = 1/m$ and putting $m = 2$, we calculate the value of $\beta = 2.85$ which is one of the case of the Rician fading.

where m denotes the fading parameter for Nakagami- m and β denotes the Weibull fading parameter [2, 8].

1.4.2 Channel Capacity with no Diversity

By using optimum rate adaptation keeping the stable transmission power, the medium capacity (in bps) is denoted as [1, 2, 7]:

$$\langle c \rangle_{\text{ORA}} = B \int_0^{\infty} \log_2(1 + \gamma) p_{\gamma}(\gamma) d\gamma \tag{9}$$

where channel bandwidth is denoted by B and γ is the spontaneous SNR at the receiver end.

Now after putting Eq. 7 in Eq. 9, we get [7, 8]

$$\langle C \rangle_{\text{ORA}} = \frac{\beta B \log_2 e}{2a\gamma'} \int_0^{\infty} \left(\frac{\gamma}{a\gamma'}\right)^{(\beta/2)-1} e^{-(\gamma/a\gamma')\beta/2} \ln(1 + \gamma) d\gamma$$

where channel bandwidth is denoted by B , γ is the spontaneous SNR at the receiver end, and γ' denotes mean received SNR and is the Weibull power factor which is given as [7]

$$a = \frac{1}{\Gamma\left(1 + \frac{2}{\beta}\right)}$$

Here, let us take the following assumptions:

Thus

$$t = (\gamma/a\gamma')$$

$$\gamma = a\gamma't$$

After performing the substitution in Eq. (10), we get [7, 8]

$$\frac{\langle C \rangle_{\text{ORA}}}{B} = \frac{\beta}{2} (\log_2 e) \int_0^\infty \ln(1 + a\gamma't) t^{(\beta/2)-1} e^{(-\beta/2)t} dt$$

The integral in the above equation is evaluated using partial integration given as [2, 7, 8]:

$$\int_0^\infty u dv = \lim_{\gamma \rightarrow 0} (uv) - \lim_{\gamma \rightarrow \infty} (uv) - \int_0^\infty v du$$

Now first, let

$$u = \ln(1 + a\gamma't)$$

Thus,

$$du = \frac{1}{1 + a\gamma't} \times a\gamma' dt$$

Further, let

$$dv = t^{(\beta/2)-1} e^{-t\beta/2} dt$$

Therefore, after integrating the equation above by using [7–9], we get

$$v = \frac{e^{-t\beta/2}}{-\beta/2}$$

Substituting the above assumptions in Eq. (11), we see that the first term goes to zero; hence, the result using [3] is finally written in the closed form expression as [7, 8]

$$\int_0^\infty \frac{e^{-t\beta/2}}{\left(\frac{1}{a\gamma'} + t\right)} dt = \Gamma(1) e^{1/a\gamma'} \Gamma\left(0, \frac{1}{a\gamma'}\right) \log_2 e$$

Here, $\Gamma(\dots)$ is the complementary function of type gamma explained by [2, 7]. We know from [2, 7]:

$$\Gamma\left(0, \frac{1}{a\gamma'}\right) = E_1\left(\frac{1}{a\gamma'}\right)$$

where $E_1(\dots)$ is exponential integral explained in [2, 7].

Therefore, the final equation for channel capacity under no diversity is [2, 7, 8]

$$\frac{\langle C \rangle_{\text{ORA}}}{B} = (\log_2 e) e^{1/a\gamma'} E_1\left(\frac{1}{a\gamma'}\right)$$

1.4.3 Channel Capacity with Diversity

By using optimum rate adaptation having stable transmission power, the medium capacity (in bps) is stated in the form [1, 2, 7]:

$$\langle c \rangle_{\text{ORA}} = B \int_0^\infty \log_2(1 + \gamma) P_\gamma(\gamma) d\gamma \tag{10}$$

Here, B denotes the bandwidth associated with the channel, and γ is the spontaneous SNR at the receiver end.

Now after putting (10) in (7), we get as in [7]

$$\frac{\langle C \rangle_{\text{ORA}}}{B} = \frac{\beta}{2\Gamma(L)(\Xi\gamma')^{L\beta} \ln 2} \int_0^\infty \gamma^{L\beta/2} \ln(1 + \gamma) e^{-(\gamma/\Xi\gamma')^{\beta/2}} d\gamma$$

Here, L indicates the count of diversity branches and γ denotes the spontaneously received signal-to-noise ratio, β denotes shape parameter for Weibull fading, and γ' is the mean received SNR. By changing the logarithmic and exponential integrands in terms of the Meijer's G-functions [9, 10] and using [7, 8], integral in above equation becomes as Fox-H function [9, 10]:

$$\frac{\langle C \rangle_{\text{ORA}}}{B} = \frac{\beta}{2\Gamma(L)(\Xi\gamma')^{\frac{L\beta}{2}} \ln 2} H_{2.3}^{3.1} \left(\begin{matrix} (\Xi\gamma')^{-\beta/2} |(-L\beta/2, \beta/2)|, (1 - L\beta/2, \beta/2) \\ (0, 1), (-L\beta/2, \beta/2), (-L\beta/2, \beta/2) \end{matrix} \right)$$

1.4.4 Outage Probability for Weibull Fading Model

Outage probability is given as [2, 3]

$$P_{\text{out}} = \int_0^{\gamma^{\text{th}}} P_\gamma(\gamma) d\gamma \tag{11}$$

where γ is the spontaneously received SNR.

Now putting Eq. 11 in Eq. 7, we get outage probability [2, 3]

$$P_{\text{out}} = \int_0^{\gamma^{\text{th}}} \int p_{\gamma}(\gamma) d\gamma = \int_0^{\gamma^{\text{th}}} \frac{\beta}{2a\gamma'} \left(\frac{\gamma}{a\gamma'} \right)^{\beta-2/2} e^{-\left(\frac{\gamma}{a\gamma'}\right)^{\beta/2}} \beta/2 d\gamma$$

where γ' and γ denotes the mean received SNR and spontaneous SNR at receiver end.

Now first, let [7, 8]

$$t = \left(\frac{\gamma}{a\gamma'} \right)^{\beta/2}$$

Thus,

$$t^{2/\beta} = \left(\frac{\gamma}{a\gamma'} \right)$$

Therefore,

$$\gamma = a\gamma' t^{2/\beta}$$

$$d\gamma = a\gamma' \times (2/\beta) \times (t)^{(2/\beta)-1} dt$$

Now when $\gamma = 0$, then $a\gamma' t^{2/\beta} = 0$, i.e., $t = 0$

And when $\gamma = \gamma^{\text{th}}$, then $t = (\gamma^{\text{th}}/a\gamma')^{\beta/2}$

After performing the substitution in Eq. (12), we get [3, 7, 8]

$$\int_0^{(\gamma^{\text{th}}/a\gamma')^{\beta/2}} \frac{\beta}{2a\gamma'} (t)^{\frac{2}{\beta}-1} e^{-1} a\gamma' \frac{2}{\beta} (t)^{\frac{2}{\beta}-1} dt$$

After rearranging the equation above, we get [3, 7, 8]

$$\int_0^{(\gamma^{\text{th}}/a\gamma')^{\beta/2}} e^{-t} dt \tag{12}$$

On solving integral in the above equation, we get [3, 7, 8]

$$= 1 - e^{-(\gamma^{\text{th}}/a\gamma')^{\beta/2}}$$

Therefore, the final equation for outage probability is [3, 7, 8]

$$= 1 - e^{-(\gamma_{th}/a\gamma')^{\beta/2}}$$

1.4.5 Numerical and Result Analysis

The segment expresses the calculation part associated for finding the mean channel capacity per unit bandwidth. Here, it uses only dual-branch MRC and without diversity case working for uncorrelated Weibull and Rayleigh fading channel. The work has been presented and analyzed. In this section, we have also presented and analyzed mapping between fading parameter, m , and Weibull fading parameter, β , and outage probability is also presented and analyzed.

In Fig. 1, the overall channel capacity per unit bandwidth beneath ORA method is drawn as an expression of the overall accepted SNR per division. As predicted, by incrementing SNR under the case of without diversity, channel capacity per unit bandwidth enhances.

In Fig. 2, the channel capacity per unit bandwidth beneath ORA method is drawn as an expression of the overall accepted SNR per branch. As predicted, by incrementing γ with MRC, channel capacity by unit bandwidth enhances.

In Fig. 3, relation between the fading parameter, m , and Weibull parameter, β , is

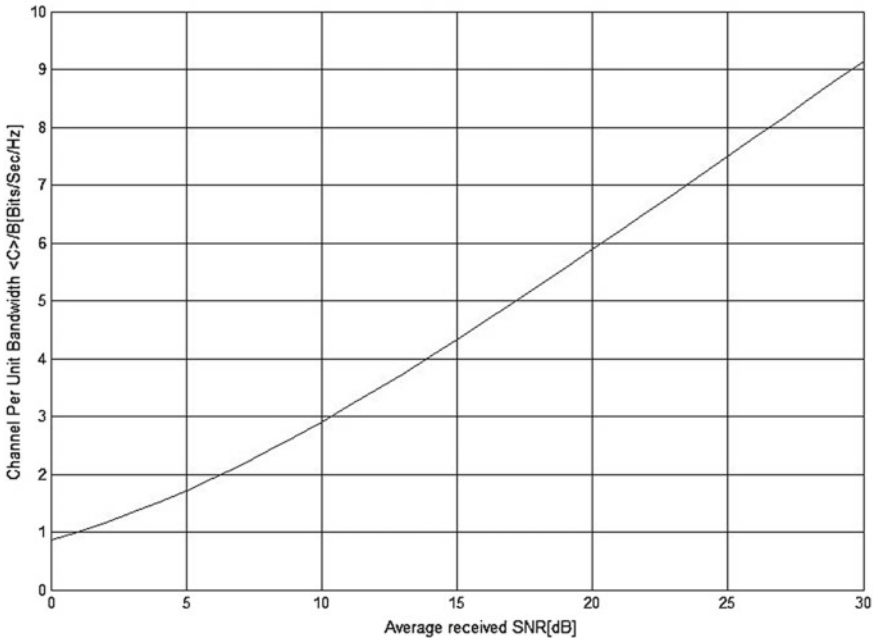


Fig. 1 Channel capacity by unit bandwidth versus overall SNR at the receiver under ORA without diversity for Rayleigh fading channel

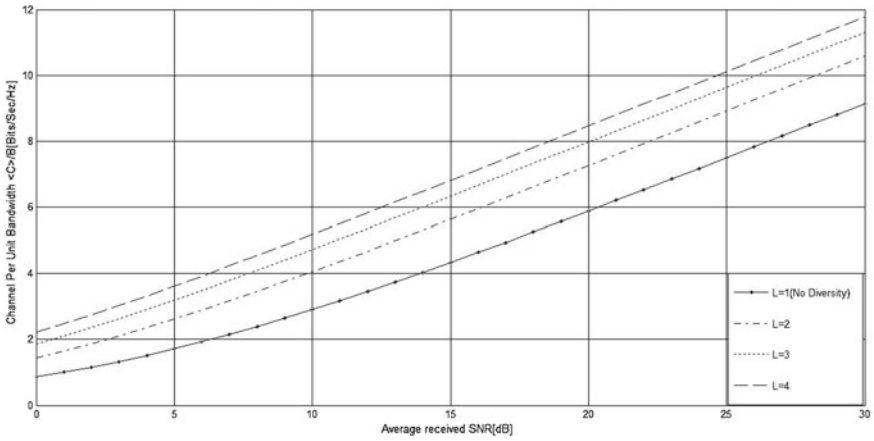


Fig. 2 Channel capacity by unit bandwidth versus mean overall SNR under ORA with MRC diversity for Rayleigh fading channel

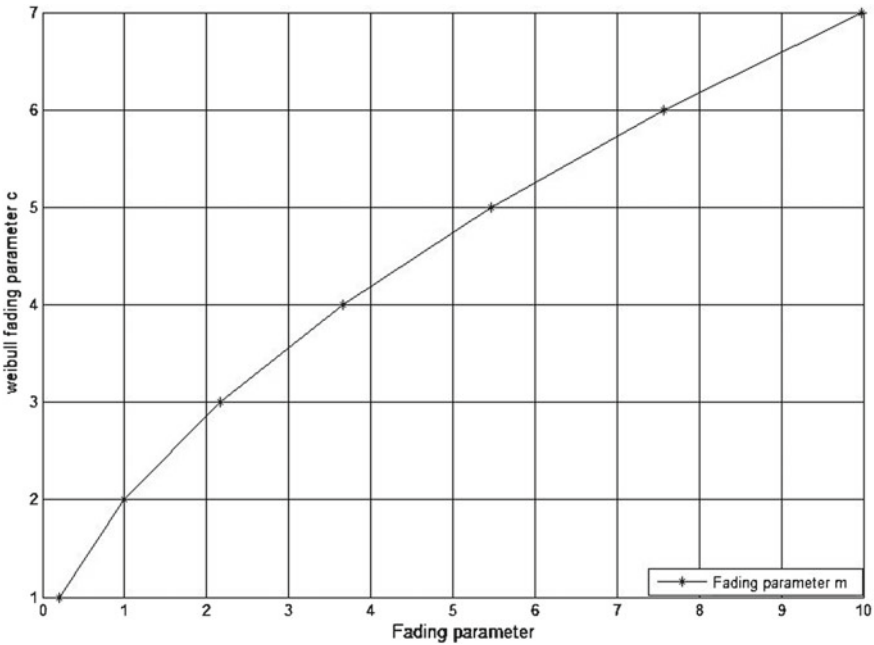


Fig. 3 Mapping between fading parameter, m , and Weibull fading parameter β

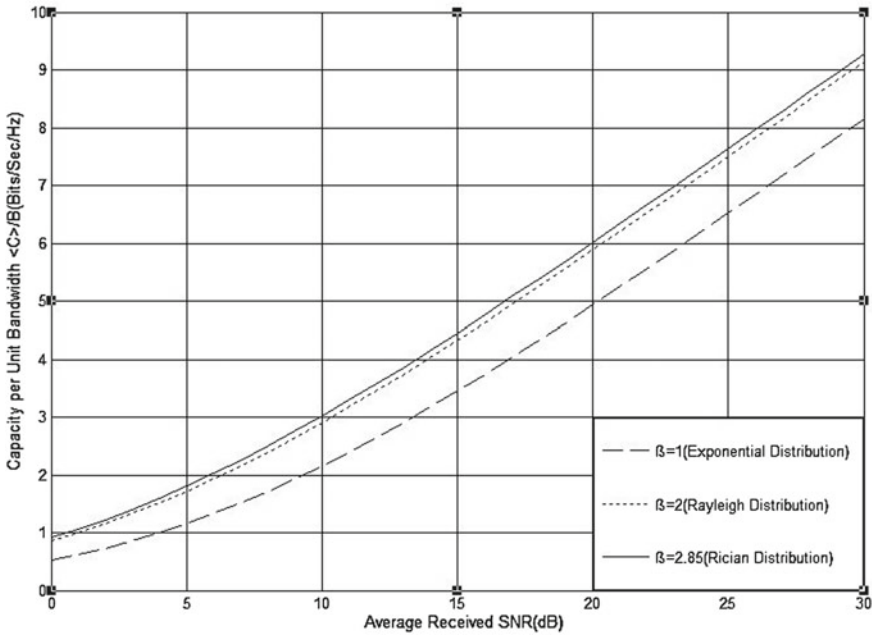


Fig. 4 Channel capacity per unit bandwidth versus overall received SNR under ORA without diversity for Weibull fading channel

plotted, and here, if fading parameter value, $m = 2$, then we get the value of one of the Rician fading under Weibull distribution, i.e., $\beta = 2.85$.

In Fig. 4, the channel capacity by unit bandwidth beneath ORA method with no diversity is plotted as a function of the overall accepted SNR per branch. We predicted that by increasing γ , the overall medium capacity unit bandwidth enhances.

In Fig. 5, the overall medium capacity by unit bandwidth beneath ORA method with MRC diversity is drawn as a function of the overall accepted SNR per branch. As predicted, by incrementing γ , the channel capacity by unit bandwidth enhances. For lower value of γ , and the curve at $L = 2$ and $L = 3$ overlap for comparable values of fading parameter, this shows that for worst channel scenario incrementing the number of branches only incrementing the complexity, so instead of this, we can increase the value of fading parameter.

In Fig. 6, the probability of outage is drawn versus threshold SNR. As expected, by incrementing threshold SNR, the probability of outage decreases. It has been also seen that outage probability decreases as we move from Rayleigh to Rician fading channel.

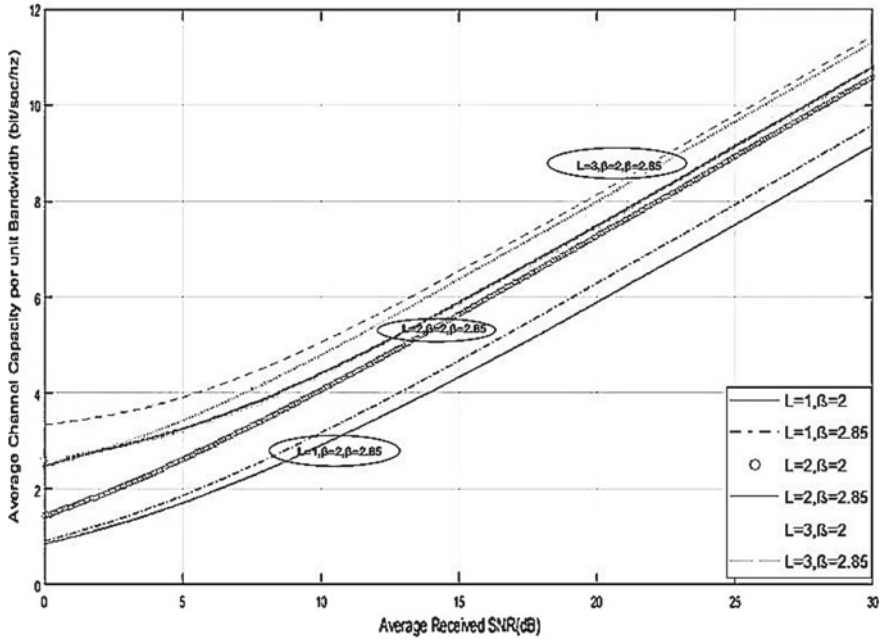


Fig. 5 Channel capacity by unit bandwidth versus overall received SNR's under ORA with MRC diversity for fading channel of type Weibull

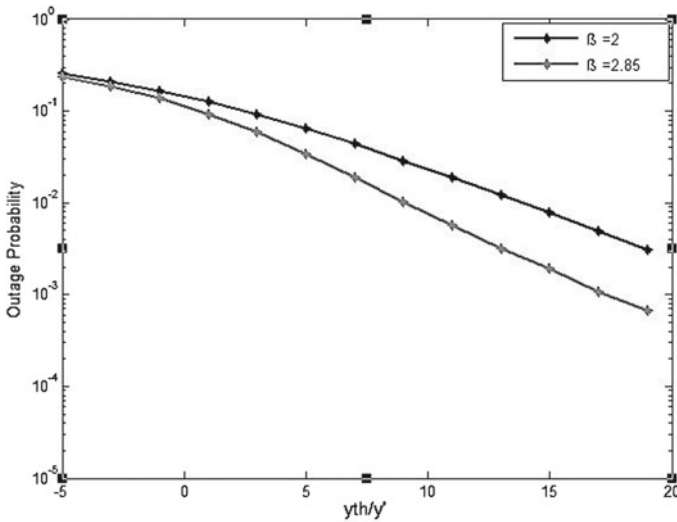


Fig. 6 Probability of outage versus threshold SNR for Weibull-type faded channel

2 Conclusion

This review paper derives and analyzes the channel capacity expression over uncorrelated Weibull fading channel under ORA scheme with balanced average received SNR of dual-branch MRC system. Through numerical calculations, it has been found that the channel capacity enhances by incrementing mean SNR and/or by employing MRC diversity. In this review paper, the relation between the Rayleigh fading parameter, m , and Weibull fading parameter, β , has been plotted through which we got to know that for $m = 2$ the Weibull parameter $\beta = 2.85$ which is the value for Rician fading channel. This review paper also observed that channel capacity for $\beta = 2$ is same as that of Rayleigh fading channel, and at $\beta = 2.85$, the channel capacity is same as Rician fading channel. It has been observed that at a low value of mean received SNR, the channel capacity overlaps different for the different number of branch. It has been also observed that by increasing threshold SNR, the probability of outage decreases. It has been also observed that outage probability decreases as we move from Rayleigh to Rician fading channel.

References

1. Sanjay K (2016) *Wireless communication the fundamental concept*. River Publication
2. Simon MK, Alouini MS (2005) *Digital communication over fading channels*. Wiley
3. Alouini MS, Goldsmith AJ (1999) Capacity of Rayleigh fading channels under different adaptive transmission and diversity-combining techniques. *IEEE Trans Veh Technol* 48:1165–1181
4. Hasan MI, Kumar S (2015) Average channel capacity of correlated dual-branch maximal ratio combining under worst case of fading scenario. *Wirel Personal Commun* 83(4):2623–2646
5. Hasan MI, Kumar S (2014) Channel capacity of dual-branch maximal ratio combining under worst case of fading scenario. *WSEAS Trans Commun* 13:162–170
6. Hasan MI, Kumar S (2015) Average channel capacity evaluation for selection combining diversity schemes over Nakagami0.5 fading channels. *Int J Commun Netw Inf Sec (IJCNIS)* 7(2):69–79
7. Stefanović M, Anastasov J, Panić S, Spalević P, Dolićanin Ć (2012) Channel capacity analysis under various adaptation policies and diversity techniques over fading channels. *Wirel Commun Netw Recent Adv In: Dr. Eksim A (ed)*. ISBN 978-953-51-0189-5 (InTech)
8. Cheng J, Tellambura C, Beaulieu NC (2003) Performance analysis of digital modulations on Weibull fading channels. *IEEE Trans Wirel Commun* 1:236–240. <https://doi.org/10.1109/vetecf.2003.128501>
9. Gradshteyn IS, Ryzhik IM (1994) *Table of integrals, series and products*, 5th edn. Academic Press, San Diego, CA
10. Wolfram (2015) The Wolfram function site (2015), Internet (online)

Classification of Static Signature Based on Distance Measure Using Feature Selection



Subhash Chandra  and Priyanka

Abstract In this paper, eigenvector-based moments are proposed for offline signature validation. Here, principal component analysis (PCA) and linear discriminant analysis (LDA) techniques are used for dimension reduction and generated eigenvector which is calculated using Euclidean distance. It measured the distance between two vectors having an equal size in 2-D space. A newly suggested approach to generate the eigenvector from training and testing samples of signatures, which is calculated through Euclidean distance as a classifier. In which, it has shown high verification accuracy of 91.07% on the MCYT-75 corpus and GPDS synthetic signature database.

Keywords Biometric · Signature · Linear discriminant analysis · Principal component analysis · Euclidean distance

1 Introduction

Biometric traits have become well established in commerce and forensics. Biometrics such as fingerprint, face, voice, iris are the major challenges to researcher in last decades [1–3]. In the field of security at the airport and financial transaction, biometric techniques are used immensely for authentication purposes [4, 5]. Handwritten signature is behavioral biometric technique which means for personal authentication. In signature verification, it is to know whether the test signature is belonging

S. Chandra (✉)

Department of Computer Science and Engineering,
National Institute of Technology, Jamshedpur 831014, India
e-mail: subhashchandra.cse@nitjsr.ac.in

Priyanka

Department of Computer Science and Engineering,
SRM University, Amaravati, Andhra Pradesh, India
e-mail: priyankasingh401@gmail.com

to individual or someone else. It is used in the field of bank cheque authentication, certificates, credit card validation, etc.

Signature classification is categorized into two types, namely online and offline signature [4, 6, 7]. In an offline signature verification technique, signature is signed on a paper and we use a scanner or camera for the acquisition of the signature image. Verification is usually done on the local, geometrical, global, or statistical features which are extracted from the signature [8, 9]. In case of online signature verification, the dynamic feature of signature images is extracted using digitizing tablet [10]. In which, signature is done on a digitizer pad and captured dynamic feature like speed, velocity, and pressure. Due to the different types of data involved, online and offline methods differ a lot. In case of online method, data analysis is performed on 1-D [5, 11] while offline data analysis is performed on 2-D [12, 13].

Variation occurred in signature images are inter- and intra-class variation. Inter-class variation occurred due to the forged signatures from a different writer being claimed to be genuine while intra-class variation occurred when a person may not always oppose his signature exactly the same. Here, inter- and intra-class variations are considered during the verification stage of signature. The efficiency of signature recognition is measured in terms of two error rates, i.e., false acceptance rate (FAR) and false rejection rate (FRR) [14, 15]. Random, simple, and skilled forgeries are found in validation of signature [16]. A random forgery is signed randomly, without having any information about the pattern of signature. However, in simple forgery, individuals know the pattern of the signature but not well-practiced. While in skilled forgeries, individuals know the pattern of the signature and are well-practiced.

This paper is organized as follows: Sect. 2 deals with preprocessing, feature extraction, and classifiers are explained. Section 3 focuses on the experiment demonstrated on distance measure approach. Section 4 concludes the paper.

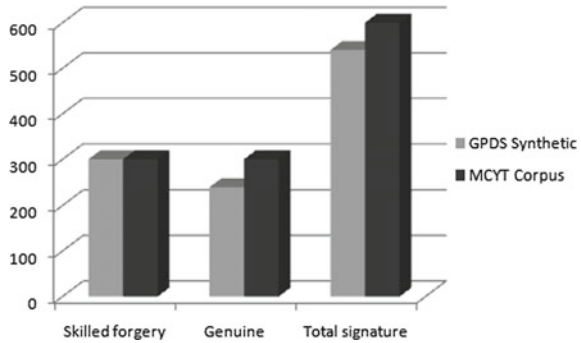
2 Methodology

In this section, four stages are discussed, namely signature database, signature database, feature extraction, and classification. The detail description is discussed separately:

2.1 *Signature Dataset*

Here, two databases MCVT and GPDS are used for experimental purposes. These are scanned at 600 dpi [17]. In the MCVT database, all individuals put their signature having a similar pen and surface. However, in the GPDS dataset, all individuals put their signature having different pen and surface. Figure 1 shows dataset of genuine and forgery signature.

Fig. 1 Signature used in MCYT and GPDS dataset



2.2 Signature Preprocessing

Preprocessing is the stage in which quality of signature is enhanced as signature contain noise [18]. To enhance the quality of signature, we perform signature binarization, cropping, and normalization [19, 20]. Figure 2a is the original signature before preprocessing.

2.2.1 Signature Binarization

OTSU method is used for signature binarization and removes noise in the boundary region of the image. Figure 2b shows the binary image of the original signature.

2.2.2 Cropped Signature

After binarization of the image, traverse the signature image in all four directions to fetch 0 of value pixel. After fetching pixel having 0, the area enclosed by it is the bounded region of cropped signature. Figure 2c shows the portion of cropped signature.

2.2.3 Normalization

The cropped signatures are normalized. X and Y are new value corresponding to X_i and Y_i . Figure 2d shows the normalized image of the cropped signature.

$$X = \frac{(X_i - X_{\min})}{(X_{\max} - X_{\min})} \times \text{length} \tag{1}$$

$$Y = \frac{(Y_i - Y_{\min})}{(Y_{\max} - Y_{\min})} \times \text{height} \tag{2}$$

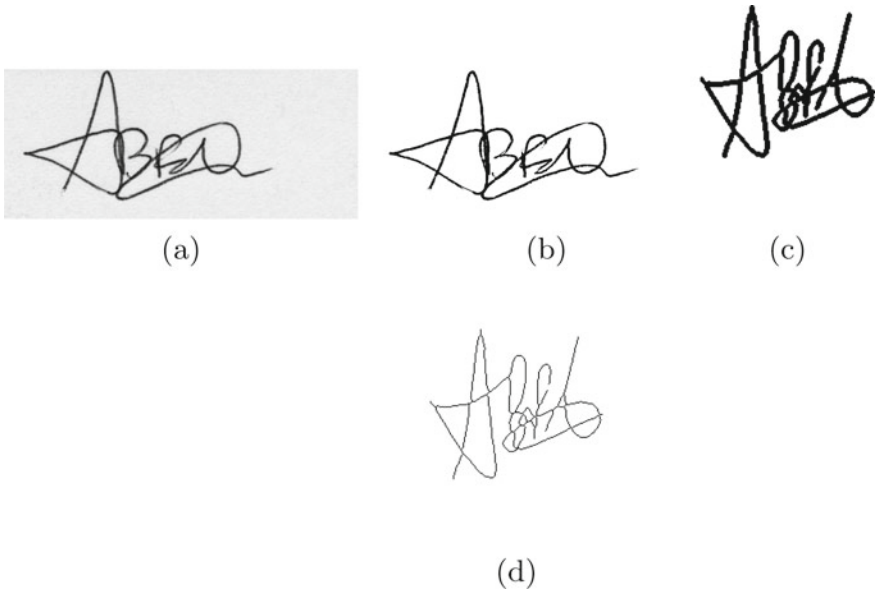


Fig. 2 Binarized signature images

2.3 Feature Extraction

Feature extraction is done in two ways, viz. PCA and LDA [21, 22]. Each of these is explained in detail given below.

2.3.1 PCA Algorithm

It is used to analyze data of high dimension by reducing the size without any loss of information [23–25].

- 1: Input the dataset
- 2: Mean value is subtracted from original data

$$\mu_x = \frac{(x_1 + x_2 + x_3 + \dots + x_n)}{n} \quad (3)$$

$$\mu_y = \frac{(y_1 + y_2 + y_3 + \dots + y_n)}{n} \quad (4)$$

- 3: Find covariance matrix

$$Cov(x, y) = \frac{\sum_{i=1}^n (x_i - \mu_x)(y_i - \mu_y)}{n - 1} \quad (5)$$

$$C^{n \times n} = cov(dim_i, dim_j) \tag{6}$$

The covariance matrix C of the $n \times n$ matrix is

$$\begin{pmatrix} cov(x_1, y_1) & cov(x_1, y_2) & cov(x_1, y_3) & \dots & cov(x_1, y_n) \\ cov(x_2, y_1) & cov(x_2, y_2) & cov(x_2, y_3) & \dots & cov(x_2, y_n) \\ cov(x_3, y_1) & cov(x_3, y_2) & cov(x_3, y_3) & \dots & cov(x_3, y_n) \\ \vdots & \vdots & \vdots & \ddots & \vdots \\ cov(x_n, y_1) & cov(x_n, y_2) & cov(x_n, y_3) & \dots & cov(x_n, y_n) \end{pmatrix}$$

Since $cov(x_1, y_2) = cov(x_2, y_1)$, the matrix is symmetrical about the main diagonal.

4: From covariance matrix finds eigenvectors and eigenvalues

5: With different components, form feature vector

$$FeatureVector = (eig1 eig2 eig3 \dots eig_n) \tag{7}$$

6: Form new dataset

$$FinalData = (RowFeatureVector) \times (RawDataAdjust) \tag{8}$$

7: Get back old dataset

$$RawDataAdjust = (RowFeatureVector)^{-1} \times (FinalData) \tag{9}$$

$$RawDataAdjust = (RowFeatureVector)^T \times (FinalData) \tag{10}$$

$$RawOriginalData = (RowFeatureVector)^T \times (FinalData) + (originalMean) \tag{11}$$

2.3.2 LDA Algorithm

Used for dimensionality reduction and preserve the information. The predicted y obtained by:

$$y = W^T X \tag{12}$$

where $X = \begin{pmatrix} x_1 \\ x_2 \\ x_3 \\ \vdots \\ \vdots \\ x_n \end{pmatrix}$ and $W = \begin{pmatrix} w_1 \\ w_2 \\ w_3 \\ \vdots \\ \vdots \\ w_n \end{pmatrix}$

Mean vector of each class in x and y feature space is

$$\mu_i = \frac{1}{n_i} \sum_{x \in W_i} x \quad (13)$$

$$\mu_i = \frac{1}{n_i} \sum_{y \in W_i} y = \frac{1}{N_i} = \sum_{x \in W_i} W^T x = W^T \mu_i \quad (14)$$

$$J(W) = \mu_1 - \mu_2 = W^T (\mu_1 - \mu_2) \quad (15)$$

$$S_i^2 = \sum_{y \in W_i} (y - \mu_i)^2 \quad (16)$$

$$J(W) = \frac{(\mu_1 - \mu_2)^2}{S_1^2 + S_2^2} \quad (17)$$

$$S_i = \sum_{x \in w_i} (X - \mu_i)(X - \mu_i)^T \quad (18)$$

$$S_1 + S_2 = S_W \quad (19)$$

$$S_i^2 = \sum_{y \in W_i} (Y - \mu_i)^2 = \sum_{x \in W_i} (W^T - W^T \mu_i)^2 = \sum_{x \in W_i} (W^T X - W^T \mu_i)^2 = W^T S_i W \quad (20)$$

$$S_1^2 + S_2^2 = W^T S_W W \quad (21)$$

The original feature space which is shown in Fig. 3.

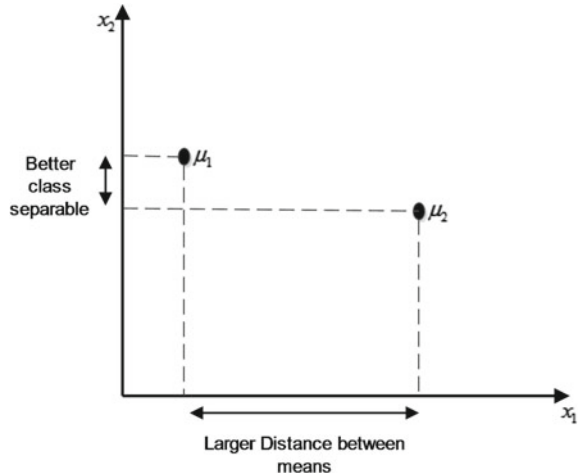
$$(\mu_1 - \mu_2)^2 = (W^T \mu_1 - W^T \mu_2)^2 = W^T (\mu_1 - \mu_2)(\mu_1 - \mu_2)^T W = W^T S_B W \quad (22)$$

$$J(W) = \frac{W^T S_B W}{W^T S_W W} \quad (23)$$

2.4 Verification

In this section, Euclidean distance is used to measure distance between two vectors in 2-D space. Here, F_{train} is the feature vector of train data and F_{test} is the feature vector

Fig. 3 Distance between projected mean



of test data [26, 27]. The distance between F_{train} and F_{test1} is obtained by Euclidean distance d .

$$d = \sqrt{(F_{train} + F_{test})} \tag{24}$$

3 Results and Discussion

3.1 Performance Measure

FAR and FRR are used for performance measure. They are defined in the following terms

$$FRR = \frac{\text{No. of genuine signature rejected}}{\text{No. of genuine signature tested}} \times 100 \tag{25}$$

$$FAR = \frac{\text{No. of forgeries signature accepted}}{\text{No. of forgery signature tested}} \times 100 \tag{26}$$

$$\text{Accuracy} = \frac{(100 - FRR) + (100 - FAR)}{2} \tag{27}$$

3.2 Experimental Results

In this segment, features are extracted through PCA and LDA.

Table 1 represents acceptance and rejection on different samples of static signatures using PCA on MCYT Corpus dataset. The FAR and FRR are 18.25 and 18.76

Table 1 Results using PCA on MCYT Corpus dataset

No. of users	Skilled forgery	Genuine	FAR	FRR
5	75	75	10.28	20.11
10	150	150	19.04	19.59
15	225	225	18.91	19.04
20	300	300	18.25	18.76

Table 2 Results using PCA on GPDS synthetic dataset

No. of users	Skilled forgery	Genuine	FAR	FRR
3	90	72	21.74	20.14
6	180	144	21.06	19.84
10	300	240	19.95	19.61

Table 3 Results using LDA on MCYT Corpus dataset

No. of users	Skilled forgery	Genuine	FAR	FRR
5	75	75	18.81	20.54
10	150	150	18.04	19.86
15	225	225	17.62	19.94
20	300	300	16.54	18.82

on the sample of 20 users, respectively. Here, experimentation is performed on 300 signature each for genuine and forged signatures. However, in Table 2 gives the performance of rejection and acceptance on different samples of signatures using PCA on GPDS synthetic dataset. The FAR and FRR are 19.95 and 19.61 on the sample of 10 users, respectively. Here, experimentation is done on 240 genuine and 300 forged signature.

Table 3 shows the overall acceptance and rejection on different samples of signatures using LDA on MCYT Corpus dataset. The FAR and FRR are 16.54 and 18.82 on the sample of 20 users, respectively, which is better than the experiment demonstrated on PCA. Here, experimentation is performed on 300 signature each for genuine and forged signatures. However, in Table 4 gives the performance of rejection and acceptance on different samples of signatures using LDA on GPDS synthetic dataset. The FAR and FRR are 18.24 and 17.07 on the sample of 10 users, respectively, which is better than the experiment demonstrated on PCA. Here, experimentation is done on 240 genuine and 300 forged signature.

Table 5 shows the performance of overall acceptance and rejection on different samples of signature using PCA + LDA on MCYT Corpus dataset. The FAR and FRR are 8.54 and 8.02 on the sample of 20 users, respectively, which is better than the

Table 4 Results using LDA on GPDS synthetic dataset

No. of users	Skilled forgery	Genuine	FAR	FRR
3	90	72	21.11	18.66
6	180	144	19.66	17.14
10	300	240	18.24	17.07

Table 5 Results using PCA +LDA on MCYT Corpus dataset

No. of users	Skilled forgery	Genuine	FAR	FRR
5	75	75	11.07	10.66
10	150	150	9.86	9.81
15	225	225	9.14	8.11
20	300	300	8.54	8.02

Table 6 Results using PCA +LDA on GPDS synthetic dataset

No. of users	Skilled forgery	Genuine	FAR	FRR
3	90	72	11.04	9.19
6	180	144	10.91	9.46
10	300	240	9.11	7.86

experiment demonstrated on PCA and LDA independently. Here, experimentation is performed on 300 signature each for genuine and forged signatures. However, in Table 6 gives the performance of rejection and acceptance on different samples of signatures using PCA + LDA on GPDS synthetic dataset. The FAR and FRR are 9.11 and 7.86 on the sample of 10 users, respectively, which is better than the experiment demonstrated on PCA and LDA independently. Here, experimentation is done on 240 genuine and 300 forged signature.

Table 7 shows extracted feature compared with the existing technique (grid, morphology, and local interest point).

4 Conclusion

In this paper, a novel approach based on distance measure using feature selection is proposed for static signature validation. The feature extraction of signature is performed by PCA and LDA on MCYT-75 and GPDS offline signature subcorpus dataset. Our experimentation is performed using distance measure approach. PCA + LDA results FAR and FRR of 8.54 and 8.02 on MCYT Corpus dataset which gives a far better result than the experiment performed independently. The combination of PCA and LDA on GPDS dataset gives FAR and FRR of 9.11 and 7.66, respectively,

Table 7 Proposed technique compared with the previous method

Method	Performance
Local interest point [23]	Results 16.40% rejection rate of genuine
Morphology-based [26]	FRR of 12.39% is achieved through morphology-based feature extraction
Proposed scheme (PCA and LDA parametric features)	FAR and FRR are 8.54 and 8.02 on the sample of 20 users, respectively, using PCA +LDA on MCYT Corpus dataset. However, overall acceptance and rejection on different samples of signatures using PCA +LDA on GPDS synthetic dataset are 9.11 and 7.86 on the sample of 10 users, respectively, which is better than the experiment demonstrated on PCA and LDA independently

which is a far better result than the experiment performed independently. Here, comparison between different number of users is performed by PCA and LDA using distance measure.

References

1. Shukla A, Dhar J, Prakash C, Sharma D, Anand RK, Sharma S (2009) Intelligent Systems. IEEE, pp 267–272 (2009)
2. Fang-jun L, Lan L (2011) Biomedical engineering and informatics. IEEE, pp 757–761
3. Coetzer J, Herbst BM (2004) Offline signature verification using the discrete radon transform and a hidden Markov model. EURASIP J Adv Sign Process 2004:1–13
4. Kolhe SR, Patil PM (2009) Dynamic time warping based static hand printed signature verification. J Pattern Recogn Res 1:52–65
5. Ferrer MA, Diaz-Cabrera M, Morales A (2003) Synthetic off-line signature image generation. IEEE, pp 1–7
6. Impedovo D, Giuseppe P (2008) Automatic signature verification: the state of the art. IEEE Trans Syst Man Cybern Part C Appl Rev 38:609–635
7. Abuhaiba ISI (2007) Offline signature verification using graph matching. Turk J Electr Eng Comput Sci 15:89–104
8. Ahmed H, Shukla S (2012) Global features based static signature verification system using DTW. Int J Syst Algorithms Appl 2(4):13
9. Batista L, Granger E, Robert Sabourin (2012) Dynamic selection of generative-discriminative ensembles for off-line signature verification. Pattern Recogn 45:1326–1340
10. Khuwaja GA, Laghari MS (2011) Offline handwritten signature recognition. World Acad Sci Eng Technol 59:1300–1303
11. Cpałka K, Zalasieński M, Rutkowski L (2016) A new algorithm for identity verification based on the analysis of a handwritten dynamic signature. Appl Soft Comput 43:47–56
12. Le H-H, Nang-Toan Do (2015) Offline handwritten signature verification using local and global features. Ann Math Artif Intell 75:231–247
13. Mahmoud SA, Ahmad I, Al-Khatib WG, Alshayeb M, Parvez MT, Märgner V, Fink GA (2014) KHATT: an open Arabic offline handwritten text database. Pattern Recogn 47(3):1096–112

14. Ruiz-del-Solar J, Devia C, Loncomilla P, Concha F (2008) Progress in pattern recognition, image analysis and applications. Springer, Berlin, pp 22–29
15. Bertolini D, Oliveira LS, Justino E, Sabourin R (2010) Reducing forgeries in writer-independent off-line signature verification through ensemble of classifiers. *Pattern Recogn* 43:387–396
16. Halder C, Obaidullah SM, Roy K (2016) Offline writer identification and verification—a state-of-the-art. In: *Information systems design and intelligent applications*, pp 153–163
17. Ortega-Garcia J, Fierrez-Aguilar J, Simon D, Gonzalez J, Faundez-Zanuy M, Espinosa V, Satue A, Hernaez I, Igarza J-J, Vivaracho C (2003) MCYT baseline corpus: a bimodal biometric database. *IET*, pp 395–401
18. Ammar M, Yoshida Y, Teruo Fukumura (1988) Off-line preprocessing and verification of signatures. *Int J Pattern Recogn Artif Intell* 2:589–602
19. Qiao Y, Wang X, Xu C (2011) Information and automation. *IEEE*, pp 333–338
20. Zalasiński M, Cpałka K (2013) Artificial intelligence and soft computing. Springer, pp 493–502
21. Fang-jun L, Lan L (2011) Fusing multi-biometrics authorization with PCA. In: *Biomedical engineering and informatics*, pp 757–761
22. Sushma Jaiswal (2011) Morphological method, pca and lda with neural networks-face recognition. *J Glob Res Comput Sci* 2:35–38
23. Ruiz-Del-Solar J, Devia C, Loncomilla P, Concha F (2008) Offline signature verification using local interest points and descriptors. *Iberoamerican congress on pattern recognition*, pp 22–29
24. Ghosh A, Barman S (2016) Application of Euclidean distance measurement and principal component analysis for gene identification. *Gene* 583:112–120
25. Jolliffe IT, Cadima J (2016) Principal component analysis: a review and recent developments. *Phil Trans R Soc A* 374:20150202
26. Kumar R, Kundu L, Chanda B, Sharma JD (2010) A writer-independent off-line signature verification system based on signature morphology. In: *Proceedings of the first international conference on intelligent interactive technologies and multimedia*, pp 261–265
27. Kumar R, Sharma JD, Chanda B (2012) Writer-independent off-line signature verification using surroundedness feature. *Pattern Recogn Lett* 33(3):301–308
28. Prakash HN, Guru DS (2010) Offline signature verification: an approach based on score level fusion. *Int J Comput Appl Gene* 583:0975–8887
29. Zalasiński M, Cpałka K, Hayashi Y (2015) New fast algorithm for the dynamic signature verification using global features values. In: *Artificial intelligence and soft computing*, pp 175–188

Computational Technique for Fractional Model of Electrical Circuits



Amit Prakash and Vijay Verma

Abstract In this chapter, we have tried to compose a user-friendly method primarily for expansion of q -homotopy analysis method (q -HAM) among Laplace transform (LT), especially q -homotopy analysis transform method (q -HATM) to resolve fractional model of electrical circuits in equation with Caputo sense. Thereafter, the analytical solution of fractional model of electrical circuits is compared with the exact solution. The results attained by q -HATM may be hypothesized as a different and effective method for solving fractional model. Two test examples demonstrate the correctness as well as effectiveness of the present technique.

Keywords Caputo fractional derivative · Fractional electrical circuits · q -HATM

1 Introduction

Fractional calculus (FC) [1–6] is a field of empirical mathematics was introduced by Guillaume de l’Hopital as the conventional calculus around 300 years ago. The curiosity of FC is to examine that fractional derivative is not a local property. Through this appraisal, the history and non-local appropriated influence interpret the FC to the reality of the universe which is superior as well as charming. Consequently, it would build FC as a well-liked subject in science and technology. In current year, fractional differential equation has been promoted in varied areas of engineering and technology such as diffusion equation, biology, control theory viscoelasticity, biomedical engineering and finance and many others physical processes.

Many authors have described various techniques to reach the objective of most correct solution [7–19], and recently Singh et al. have suggested HPSTM [20] also.

A. Prakash

Department of Mathematics, National Institute of Technology, Kurukshetra, Haryana 136119, India

e-mail: amitmath@nitkr.ac.in; amitmath0185@gmail.com

V. Verma (✉)

Department of Mathematics, Pt. C. L. S. Govt. (PG) College, Karnal, Haryana, India

e-mail: vijay_mtech21@rediffmail.com

© Springer Nature Singapore Pte Ltd. 2021

G. S. Hura et al. (eds.), *Advances in Communication and Computational*

Technology, Lecture Notes in Electrical Engineering 668,

https://doi.org/10.1007/978-981-15-5341-7_54

Here, we are analysing the two basic models, inductor–capacitor circuit (LC circuit) and resistor–capacitor circuit (RC circuit) model of electrical circuits which contain resistors, capacitors, inductors with the aids of efficient numerical technique q -HATM and two basic model of electrical circuits which are given as:

$$I''(t) + \frac{1}{LC}I(t) = 0 \quad (1)$$

$$CV'(t) + \frac{1}{R}V(t) = 0 \quad (2)$$

where $I(t)$, L , C , R and V represent the current at time t , and inductance, capacitance, resistance, and voltage across the circuit, respectively.

Now, fractional model of electrical circuits which represent inductor–capacitor circuit (LC circuit) and resistor–capacitor circuit (RC circuit) are given as:

$$I_t^{2\alpha}(t) + \frac{1}{LC}I(t) = 0, \quad t > 0, 0 < \alpha \leq 1 \quad (3)$$

$$V_t^\alpha(t) + \frac{1}{RC}V(t) = 0, \quad t > 0, 0 < \alpha \leq 1 \quad (4)$$

Recently, A. Atangana et al. found numeric results of RLC model [21]. A. Ahmed et al. studied the fractional electric circuit model [22], W. K. Zahra et al. found numeric results of RC, RL, and RLC model by Laplace transform method [23], and F. Gomez et al. studied the fractional RLC model [24], for more analysis of fractional electric circuit which refers to Kaczorek [25]. H. Ertik et al. experimentally studied the behaviour of capacitor in RC electric circuit model [26], A. M. A. El-Sayed et al. found numeric results of RLC circuit model [27], and Tadeusz Kazorekv found numeric result of electric circuit RC and RL model [28].

Quite differently, here we have used q -HATM to find the approximate result of fractional electrical circuit model. The q -HATM is a amalgamation of dual efficient methods of q -HAM and LT. Also, q -HATM is an modification of the insert parameter $q \in [0, 1]$, studied by Liao also in HAM [29–31] to $q \in [0, \frac{1}{n}]$, which provide result like a convergent series.

The framework of this chapter has been outlined as follows: Introductory part explained in section first, the key classification of fractional calculus is explained in Sect. 2, solution process of proposed q -homotopy analysis transform method is explained in Sect. 3, the proposed method q -HATM examined by two test examples of fractional model of electrical circuits equation is in Sect. 4, and in Sect. 5 outcome of the effort is drawn.

2 Preliminaries

The present section explains the key definitions of FC used to discuss the suggested numerical technique.

Definition 2.1. Let $g(t), g \in C_{-1}^n, n \in N, n > 0$, be a given function, then fractional derivative of $g(t)$ in Caputo sense is explained as follows

$$D^\alpha g(t) = I^{n-\alpha} D^n g(t) = \frac{1}{\Gamma(n-\alpha)} \int_0^t (t-x)^{n-\alpha-1} g^n(x) dx,$$

where $n - 1 < \alpha \leq n$,
having properties

- (1) $D^\alpha I^\alpha g(t) = g(t)$,
- (2) $I^\alpha D^\alpha g(t) = g(t) - \sum_{k=0}^{n-1} g^{(k)}(0^+) \frac{t^k}{\Gamma(k+1)}, n > 0$.

Definition 2.2. We can explain the Laplace transform (LT) of a given function $g(t)$ as

$$L[g(t)] = g(s) = \int_0^\infty e^{-st} g(t) dt.$$

Definition 2.3. We can explain LT of the fractional derivative in Caputo sense as follows

$$L[D_t^\beta g(t)] = s^\beta g(s) - \sum_{k=0}^{n-1} s^{(\beta-k-1)} g^{(k)}(0), n - 1 < \beta \leq n.$$

3 Key Objective of q -Homotopy Analysis Transform Method

Here, we analyse a nonlinear fractional-order basic PDE of the form:

$$D_t^\alpha v(x, t) + Rv(x, t) + Nv(x, t) = g(x, t), n - 1 < \alpha \leq n, \tag{5}$$

where $D_t^\alpha v(x, t)$, R , N and $g(x, t)$ represent the fractional derivative in Caputo sense, linear differential operator, nonlinear differential operator, and source term of the function $v(x, t)$, respectively. After, operating the LT operator on Eq. (5), we obtain

$$L[D_t^\alpha v(x, t)] + L[Rv(x, t)] + L[Nv(x, t)] = L[g(x, t)].$$

After, applying the LT differentiation property, it gives

$$s^\alpha L[v] - \sum_{k=0}^{n-1} s^{\alpha-k-1} v^{(k)}(x, 0) + L[Rv] + L[Nv] = L[g(x, t)].$$

After, simplifying the earlier equation, we get

$$L[v] - \frac{1}{s^\alpha} \sum_{k=0}^{n-1} s^{\alpha-k-1} v^{(k)}(x, 0) + \frac{1}{s^\alpha} (L[Rv] + L[Nv] - L[g(x, t)]) = 0.$$

Now, nonlinear differential operator is explained as

$$N[\varphi(x, t; \tau)] = L[\varphi(x, t, \tau)] - \frac{1}{s^\alpha} \sum_{k=0}^{n-1} s^{\alpha-k-1} \varphi^{(k)}(x, t, \tau)(0^+) + \frac{1}{s^\alpha} (L[R\varphi(x, t, \tau)] + L[N\varphi(x, t, \tau)] - L[g(x, t)]),$$

where parameter $\tau \in [0, \frac{1}{n}]$ and $\varphi(x, t, \tau)$ represent the real functions depend on the parameter x, t and τ . Next formulate a homotopy as follows:

$$(1 - n\tau)L[\varphi(x, t; \tau) - v_0(x, t)] = h\tau H(x, t)N[\varphi(x, t; \tau)], \tag{6}$$

where $n \geq 1, \tau \in [0, \frac{1}{n}]$ denote the insert parameter, $L, H(x, t)$ and $h \neq 0$ represent the Laplace transform, and a nonzero auxiliary function and an auxiliary parameter, respectively. $v_0(x, t)$ is an initial approximation of $v(x, t)$ and $\varphi(x, t; \tau)$ is an unspecified function. Clearly, when the insert parameter $\tau = 0$ and $\tau = \frac{1}{n}$, it carries the solution $\varphi(x, t; 0) = v_0(x, t)$ and $\varphi(x, t; \frac{1}{n}) = v(x, t)$ respectively. Hence, as τ rises from 0 to 1, the result $\varphi(x, t; \tau)$ extend from initial approximation $v_0(x, t)$ to the result $v(x, t)$, extend from the function $\varphi(x, t; \tau)$ we attain

$$\varphi(x, t; \tau) = v_0(x, t) + \sum_{m=1}^{\infty} v_m(x, t)\tau^m, \tag{7}$$

where $v_m(x, t) = \frac{1}{m!} \frac{\partial^m \varphi(x, t; \tau)}{\partial \tau^m}$.

After suitable choice of the preliminary guess, auxiliary function H, auxiliary parameter $n; h$, and auxiliary linear operator, the series (7) converges at $\tau = \frac{1}{n}$ and then we have solution of the form

$$v(x, t) = v_0(x, t) + \sum_{m=1}^{\infty} v_m(x, t) \left(\frac{1}{n}\right)^m.$$

After applying, definition to Eq. (6), vectors can be defined in the following pattern $\vec{v}_m = \{v_0(x, t), v_1(x, t), \dots, v_m(x, t)\}$. Later, zeroth-order deformation of Eq. (5) differentiating m -times with respect to τ ; we acquire m th-order deformation equation as follows:

$$L[v_m(x, t) - k_m v_m(x, t)] = hH(x, t)R_m(\vec{v}_{m-1}).$$

Lastly, when we operate the inverse Laplace transform, we attain

$$v_m(x, t) = k_m v_m(x, t) + hL^{-1}[H(x, t)R_m(v_{m-1})],$$

where $k_m = \begin{cases} 0, & m \leq 1 \\ n, & m > 1 \end{cases}$.

4 Numerical Examples

In present segment, we implemented the present scheme q -HATM on two examples of electrical circuit.

Example 1 Consider the fractional model of LC circuit which contains only charge capacitor, inductor, and differential equation which illustrate the LC circuit are as follows:

$$I_t^{2\alpha} + \frac{1}{LC}I(t) = 0, t > 0, 0 < \alpha \leq 1, \tag{8}$$

with

$$I(0) = I_0 \text{ and } \frac{1}{LC} = \omega_0^2 \tag{9}$$

The exact solution of fractional model of LC circuit (8), when $\alpha = 1$ and subject to the initial condition (9) is given as: $I(t) = I_0 \cos(\omega_0 t)$. We use Caputo fractional derivative to analyse the fractional model of LC circuit.

After applying the suggested technique q -HATM to fractional model of LC circuit, we attain the following successive approximations

$$I_0 = I(0)$$

$$I_1 = h\omega_0^2 I_0 \frac{t^{2\alpha}}{\Gamma(2\alpha + 1)},$$

$$\begin{aligned}
 I_2 &= h^2 \omega_0^4 I_0 \frac{t^{4\alpha}}{\Gamma(4\alpha + 1)} + h(n + h) \omega_0^2 I_0 \frac{t^{2\alpha}}{\Gamma(2\alpha + 1)}, \\
 I_3 &= h^3 \omega_0^6 I_0 \frac{t^{6\alpha}}{\Gamma(6\alpha + 1)} + 2h^2(n + h) \omega_0^4 I_0 \frac{t^{4\alpha}}{\Gamma(4\alpha + 1)} \\
 &\quad + h(n + h)^2 \omega_0^2 I_0 \frac{t^{2\alpha}}{\Gamma(2\alpha + 1)}, \\
 I_4 &= h^4 \omega_0^8 I_0 \frac{t^{8\alpha}}{\Gamma(8\alpha + 1)} + 3h^3(n + h) \omega_0^6 I_0 \frac{t^{6\alpha}}{\Gamma(6\alpha + 1)} \\
 &\quad + 3h^2(n + h)^2 \omega_0^4 I_0 \frac{t^{4\alpha}}{\Gamma(4\alpha + 1)} \\
 &\quad + h(n + h)^3 \omega_0^2 I_0 \frac{t^{2\alpha}}{\Gamma(2\alpha + 1)},
 \end{aligned}$$

Figures 1 and 2 represent the h -curve for distinct value of $\alpha = 0.8, 0.9, 1$ and $n = 1, 2, 3$ for Example 1, respectively, and horizontal straight line in Figs. 1 and 2 represent the range of convergence. It is observed from Figs. 1 and 2 that the range of convergence grows with rise of the value of α and n . Fig. 3 presents the asymptotic n -curve for distinct values of $\alpha = 0.8, 0.9, 1$, and Fig. 4 represents the q -HATM results for distinct values of $\alpha = 0.8, 0.9, 1$, and results acquired by q -HATM are nearly similar to exact solution. Presently, fourth-order approximation is worn to

Fig. 1 q -HATM sol. h -curve for distinct values of α at $t = 0.2, I_0 = 0.01, L = 1, C = 1$ and $n = 1$, for Example 1

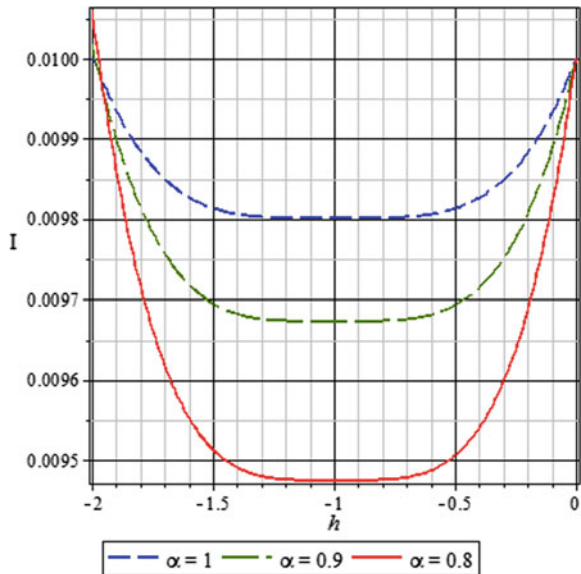


Fig. 2 q -HATM sol. h -curve for distinct values of n at $t = 0.2, I_0 = 0.01, L = 1, C = 1$ and $\alpha = 1$, for Example 1

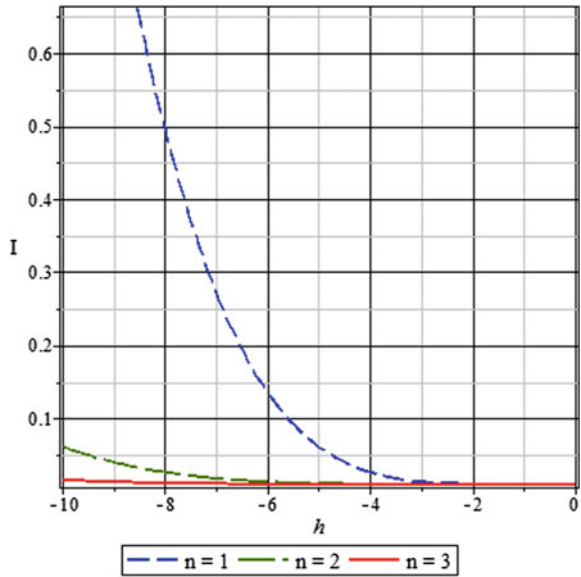
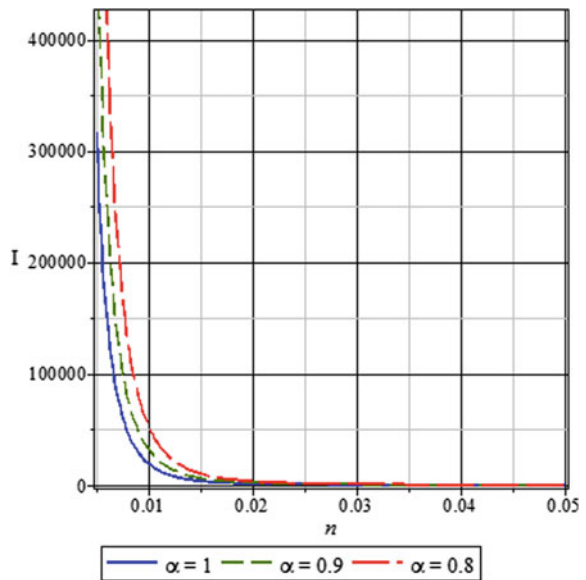
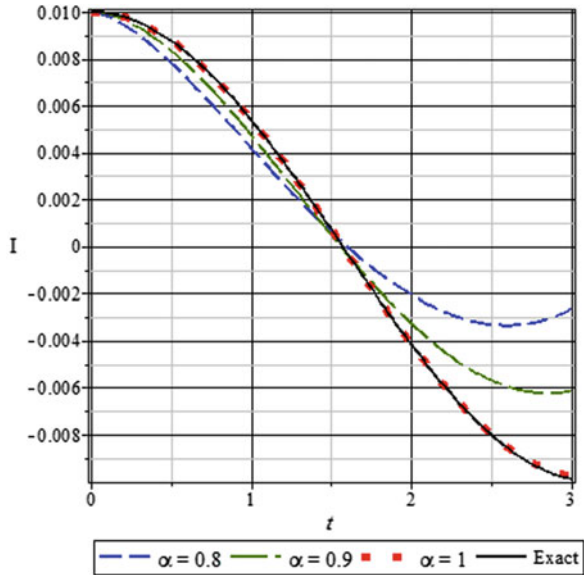


Fig. 3 q -HATM sol. n -curve for distinct values of α at $t = 0.2, I_0 = 0.01, L = 1, C = 1$ and $h = -1$, for Example 1



depict Figs. 1, 2, 3 and 4. Numerical solution and structured of q -HATM can be magnified by evaluating higher-order approximations.

Fig. 4 q -HATM sol. t -curve for distinct values of α at $I_0 = 0.01, L = 1, C = 1, h = -1$ and $n = 1$, for Example 1



Example 2 Consider the fractional model of RC circuit which contains only charge capacitor, resistor and differential equation which illustrate the RC circuit are as follows:

$$V_t^\alpha + \frac{1}{RC}V(t) = 0, t > 0, 0 < \alpha \leq 1, \tag{10}$$

with

$$V(0) = V_0 \tag{11}$$

The exact solution of fractional model of RC circuit (10), when $\alpha = 1$ and subject to the initial condition (11) is given as: $V(t) = V_0e^{-\frac{t}{RC}}$. We use Caputo fractional derivative to analyse the fractional model of RC circuit.

After, applying the suggested technique q -HATM to fractional model of RC circuit, we attain the following successive approximations

$$V_0 = V_0$$

$$V_1 = h \frac{V_0}{RC} \frac{t^\alpha}{\Gamma(\alpha + 1)},$$

$$V_2 = h^2 \frac{V_0}{(RC)^2} \frac{t^{2\alpha}}{\Gamma(2\alpha + 1)} + h(n + h) \frac{V_0}{RC} \frac{t^\alpha}{\Gamma(\alpha + 1)},$$

$$\begin{aligned}
 V_3 &= h^3 \frac{V_0}{(RC)^3} \frac{t^{3\alpha}}{\Gamma(3\alpha + 1)} + 2h^2(n + h) \frac{V_0}{(RC)^2} \frac{t^{2\alpha}}{\Gamma(2\alpha + 1)} \\
 &\quad + h(n + h)^2 \frac{V_0}{RC} \frac{t^\alpha}{\Gamma(\alpha + 1)}, \\
 V_4 &= h^4 \frac{V_0}{(RC)^4} \frac{t^{4\alpha}}{\Gamma(4\alpha + 1)} + 3h^3(n + h) \frac{V_0}{(RC)^3} \frac{t^{3\alpha}}{\Gamma(3\alpha + 1)} \\
 &\quad + 3h^2(n + h)^2 \frac{V_0}{(RC)^2} \frac{t^{2\alpha}}{\Gamma(2\alpha + 1)} \\
 &\quad + h(n + h)^3 \frac{V_0}{RC} \frac{t^\alpha}{\Gamma(\alpha + 1)},
 \end{aligned}$$

Figures 5 and 6 represent the h -curve for distinct value of $\alpha = 0.8, 0.9, 1$ and $n = 1, 2, 3$ for Example 2, respectively, and horizontal straight line in Figs. 5 and 6 present the range of convergence. It is observed from Figs. 5 and 6 that the range of convergence grows with rise in the value of α and n . Figure 7 presents the asymptotic n -curve for distinct values of $\alpha = 0.8, 0.9, 1$, and Fig. 8 represents the q -HATM results for distinct values of $\alpha = 0.8, 0.9, 1$, and results acquired by q -HATM are nearly similar to exact solution. Presently, fourth-order approximation is worn to depict Figs. 5, 6, 7, and 8. Numerical solution and structure of q -HATM can be magnified by evaluating higher-order approximations

Fig. 5 q -HATM sol. h -curve for distinct values of α at $t = 0.2, C = 1, R = 10, V_0 = 20$ and $n = 1$, for Example 2

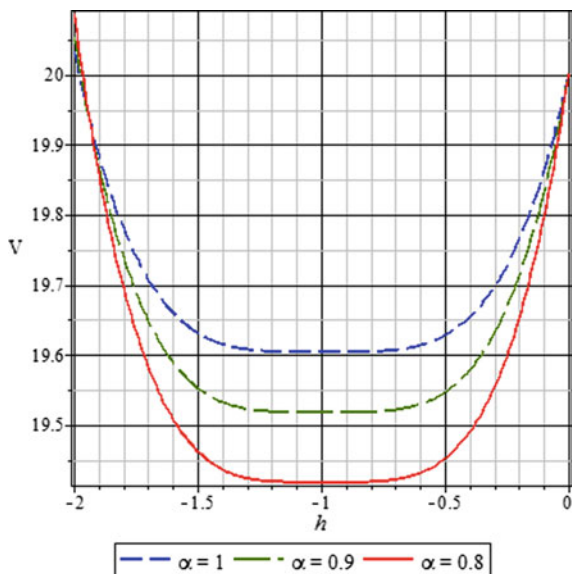


Fig. 6 q -HATM sol. h -curve for distinct values of n at $t = 0.2, C = 1, R = 10, V_0 = 20$ and $\alpha = 1$, for Example 2

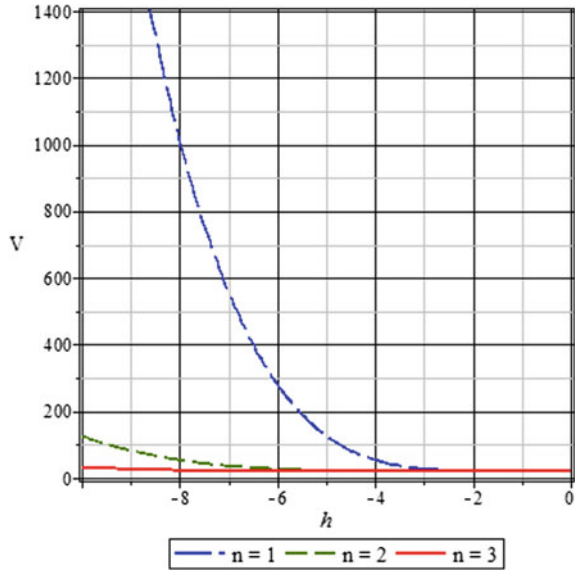
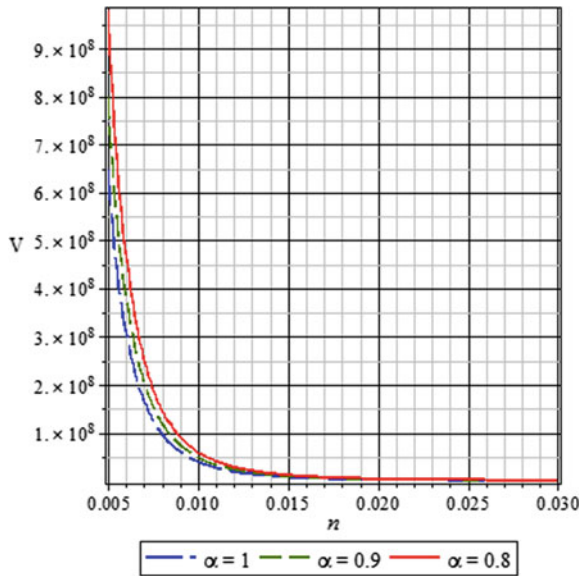


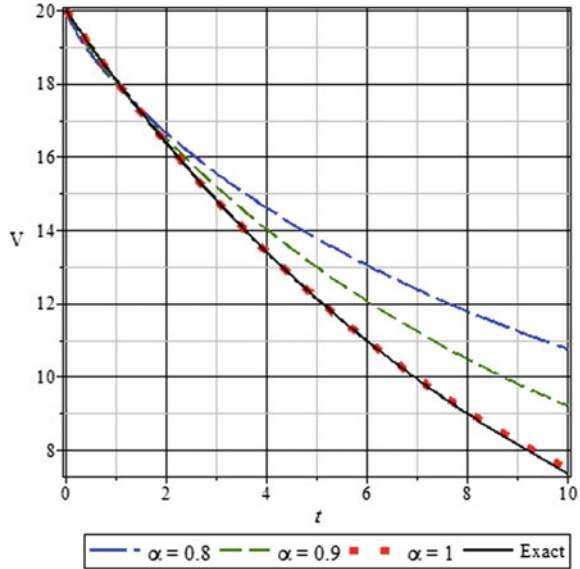
Fig. 7 q -HATM sol. n -curve for distinct values of α at $t = 0.2, C = 1, R = 10, V_0 = 20$ and $h = -1$, for Example 2



5 Conclusions

In the existing effort, analytical result of fractional model of electrical circuits is attained with the aids of effective technique called q -HATM. The represented figure

Fig. 8 q -HATM sol. t -curve for distinct values of α at $h = -1, C = 1, R = 10, V_0 = 20$ and $n = 1$, for Example 2



and analytical solution depict the validity as well as accuracy of the proposed techniques q -HATM, and solution is converged towards the exact solution very rapidly which has been demonstrated numerically. We perceived the wonderful coincidence among q -HATM and the exact solution. Moreover, efficient techniques of q -HATM can be further tested to construct the exact result of nonlinear fractional model.

References

1. Oldham KB, Spanier J (1974) The fractional calculus. Academic Press, New York
2. Podlubny I (1999) Fractional differential equation. Academic, New York
3. Raberto M, Scalas E, Mainardi F (2002) Waiting times and returns in high frequency financial data an empirical study. Physica A 314:749–755
4. Magin RL (2006) Fractional calculus in bioengineering. Begell House Publishers
5. Ray SS, Bera RK (2005) Analytical solution of Bagley-Torvik equation by Adomian decomposition method. Appl Math Comput 168(1):398–410
6. Momani S, Odibat Z (2007) Numerical approach to differential equations of fractional orders. J Comput Appl Math 207(1):96–110
7. Odibat Z, Momani S (2008) Numerical methods for nonlinear partial differential equations of fractional order. Appl Math Model 32:28–29
8. Meerschaert M, Tadjeran C (2006) Finite difference approximations for two sided space fractional partial differential equations. Appl Numer Math 56:80–90
9. Odibat Z, Momani S, Erturk VS (2008) Generalized differential transform method: application to differential equations of fractional order. Appl Math Comput 197:467–477
10. Jiang Y, Ma J (2011) Higher order finite element methods for time-fractional partial differential equations. J Comput Appl Math 235(11):3285–3290
11. Arikoglu A, Ozkol I (2007) Solution of a fractional differential equations by using differential transform method. Chaos Solitons Fract 34:1473–1481

12. Zhang X (2014) Homotopy perturbation method for two dimensional time-fractional wave equation. *Appl Math Model* 38:5545–5552
13. Prakash A (2016) Analytical method for space-fractional telegraph equation by homotopy perturbation transform method. *Nonlinear Engineering* 5(2):123–128
14. Dhaigude CD, Nikam VR (2012) Solution of fractional partial differential equations using iterative method. *Fract Calc Appl Anal* 15(4):684–699
15. Safari M, Ganji DD, Moslemi M (2009) Application of He's Variational iteration method and Adomain decomposition method to the fractional KdV-Burger-Kuramoto equation. *Comput Appl* 58:2091–2097
16. Liao S (2004) On the homotopy analysis method for nonlinear problem. *Appl Math Comput* 147:499–513
17. Jiware R, Pandit S, Mittal RC (2012) Numerical solution of two dimensional Sine-Gordon Solitons by differential quadrature method. *Comput Phys Commun* 183:600–616
18. Singh J, Kumar D (2011) Homotopy perturbation Sumudu transform method for nonlinear equation. *Adv Appl Mech* 14:165–175
19. He JH (1999) Homotopy perturbation technique. *Comput Method Appl Mech Eng* 178:257–262
20. He JH (2003) Homotopy perturbation method: a new nonlinear analytical technique. *Appl Math Comput* 135:73–79
21. Atangana A, Nieto JJ (2015) Numerical solution for the model of RLC circuit via the fractional derivative without singular kernel. *Adv Mech Eng* 7(10):1–7. <https://doi.org/10.1177/1687814015613758>
22. Alsaedi A, Nieto JJ, Venkatesh V (2015) Fractional electrical circuits. *Adv Mech Eng* 7(12):1–7
23. Zahra WK, Hikal MM, Bahnasy TA (2017) Solutions of fractional order electrical circuits via Laplace transform and nonstandard finite difference method. *J Egypt Math Soci* 25:252–261
24. Gómez-Aguilar JF, Yépez-Martínez H, Escobar-Jiménez RF, Astorga-Zaragoza CM, Reyes J (2016) Analytical and numerical solutions of electrical circuits described by fractional derivatives. *Appl Math Model* 40:9079–9094
25. Kaczorek T (2011) Positive electrical circuits and their reachability. *Arch Elect Eng* 60:283–301
26. Ertik H, Calik AE, Sirin H, Sen M, Oder B (2015) investigation of electrical RC circuit with in framework of FC. *Rev Mex Fisica* 61:58–63
27. Ei-Sayad AMA, Nour HM, Raslanand WE, Ei-Shazly ES (2012) Fractional parallel RLC circuit. *Alex J Math* 3(1)
28. Kaczorek T (2011) Singular fractional linear system and electrical circuit. *Int J Appl Math Comput Sci* 21(2):379–384
29. Liao SJ (1992) The proposed homotopy analysis technique for the solution of nonlinear problems. Ph.D. Thesis, Shanghai Jiao Tong University
30. Liao SJ (1997) Homotopy analysis method a new analytical technique for nonlinear problems. *Commun Nonlinear Sci Numer Simul* 2:95–100
31. Liao SJ (2003) Beyond perturbation: introduction to the Homotopy analysis method. Chapman and Hall/CRC Press, Boca Raton

Steganographic Method Based on Interpolation and Cyclic LSB Substitution of Digital Images



Jyoti Pandey, Kamaldeep Joshi, Mangal Sain, Gurdiyali Singh,
and Mohit Jangra

Abstract In the era of the Internet, many files (text, image, audio, and video) are shared through the Internet. Security is the main issue, during sharing information. To resolve the security problem, two techniques are used to make our information secure, i.e., cryptography and steganography. Cryptography is used for encryption but does not hide the information. So, it is not too much secure. The emerging Internet technology has led to the need for a high level of security which is provided by steganography. Steganography is used to hide the existence of a secret message. As a result, unauthorized users cannot access secret information in different multimedia files. This paper gives a brief overview of steganography, type of steganography, insertion technique used in image steganography search such as LSB, GLM, parity checking, and interpolation. It also includes the application and a set of parameters to test the imperceptibility of an algorithm. In image steganography, the cover medium used for hiding data is an image. The most common technique for image steganography involves the least significant bits (LSBs) of image pixels which are altered with the bits of secret message. There are a lot of limitations in the LSB techniques, due to which many new image steganography techniques are developed. The cyclic LSB technique is such a technique. In this paper, an altered version of the cyclic LSB technique is presented. The advantage of this method is that RGB channels of the image are rotated into the cycle, i.e., red channel is used for hiding

J. Pandey (✉) · K. Joshi · M. Jangra
Department of Computer Science, Maharshi Dayanand University, Rohtak, India
e-mail: jyotipandey2004@gmail.com

K. Joshi
e-mail: kalamintwal@gmail.com

M. Jangra
e-mail: itsmohitj@gmail.com

M. Sain
Department of Electronics and Communication Engineering, MSIET, Kalanaur, India
e-mail: vijmangal@yahoo.com

G. Singh
Department of Electrical Engineering, Maharshi Dayanand University, Rohtak, India

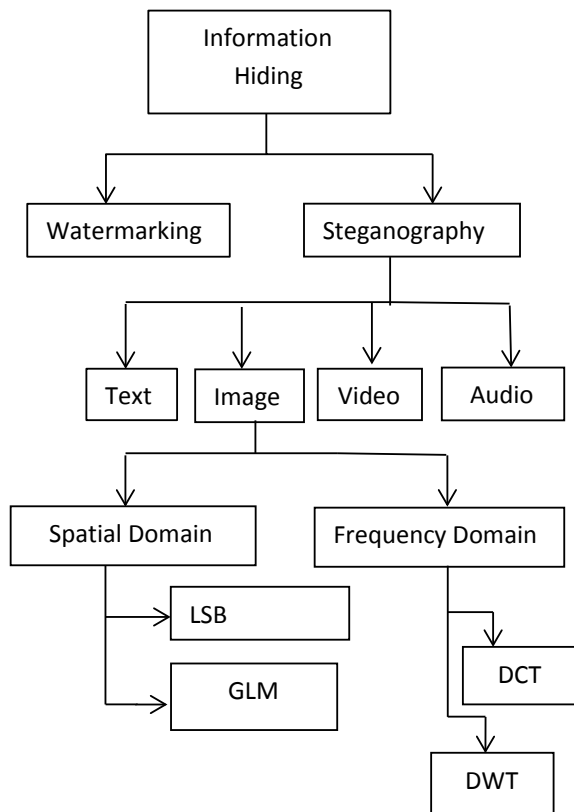
first bit, the green channel is used for hiding the second bit, the blue channel is used for hiding third bits, and then this cycle is repeated. In this method, no separate key is used for encryption and decryption, thus avoiding any overhead of managing key. This technique provides enhanced capacity and security over any other image steganography techniques.

Keywords Steganography · Type of steganography LSB · GSM · Interpolation · Cyclic LSB algorithm · Information security · Histograms · PSNR · MSE

1 Introduction

Steganography is the art that hides the secret data in a suitable multimedia carrier. Cryptography only encrypts the data, but steganography also hides the existence of secure data. The chances of the attack are less in steganography as compared to cryptography because steganography is used to hide the data into the multimedia files [1] (Figs. 1 and 2).

Fig. 1 Information hiding



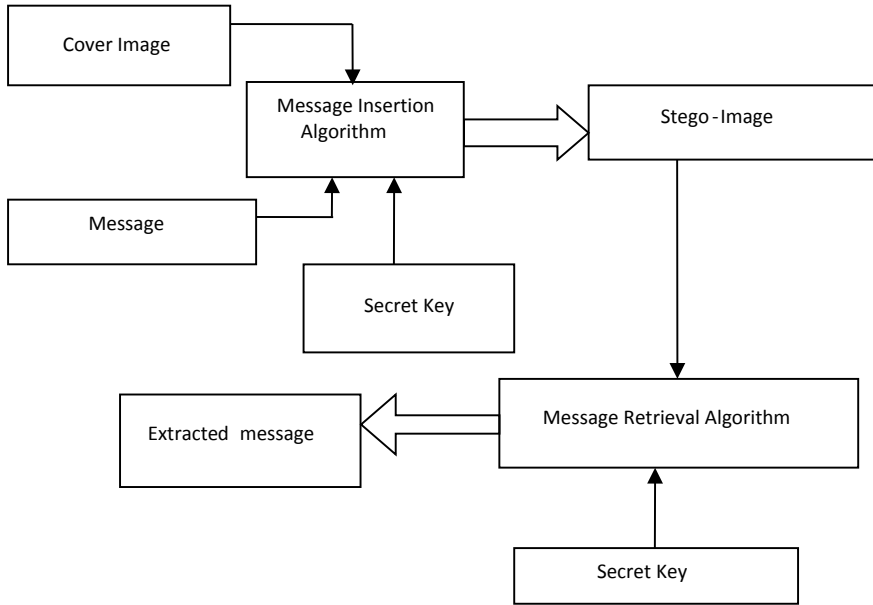


Fig. 2 Block diagram of a steganography system

Some important terms used in steganography are:

Cover image—The image used for hiding the information.

Stego image—The image obtained after hiding the secret message into the image using steganography.

Message—By using the cover image, hide the secret message.

Key—It is used for hiding and extracting hidden data.

In the insertion process, first, select a cover file that contains the cover image. In this file, hiding data use a secret key which is only known to the sender and the receiver. In the retrieval process, using the stage image as an input and the same secret key this is used to hide the message and message retrieval algorithm [2].

2 Types of Steganography

2.1 Text Steganography

Text steganography is a subpart of steganography that hides the message behind other cover text files. In this technique, the first position of the words is changed and then formatting is done in order to conceal the data into the file.

2.2 *Audio Steganography*

Audio steganography is used to transmit hidden information by modifying an audio signal which cannot be audible to the human. Different techniques are used for this purpose like echo hiding, tone insertion phase coding, etc.

2.3 *Video Steganography*

In this technique, the different types of data can be hidden because it has a complex structure and high capacity of frames. In videos, more amounts of data can be hidden as compared to image files.

3 **Kinds of Steganography**

3.1 *Spatial Domain Steganography*

In this technique, secret message is embedded by direct manipulation in the intensity of pixels of an image in which some pixel values of the image are changed directly during hiding data using logarithmic transform, power-law transforms, and histogram equalization [3].

3.2 *Transform Domain*

In this technique, instead of changing the image itself, orthogonal transform on the image is performed. This steganography technique is appropriate for images which are needed to be processed according to their frequency [3].

The principle involved in this transform domain is:

- i. Enhancing the image using the computation of a 2D DFT.
- ii. Then, the transform coefficient is changed by operator M .
- iii. Finally, the inverse of the transform is performed.

3.3 *Discrete Cosine Transformations*

DCT method is used to hide the message in which the original image is divided into $8 * 8$ blocks of pixels. The result of this is 64 DCT coefficients of each sub-block, in which the image has three frequency domains low, medium, and high frequency.

If any change occurs in a single coefficient, then it can affect all the 64 blocks of pixels. It is used for image compression [4].

3.4 Discrete Wavelet Transform

DWT used wavelet function, and it has its own space–frequency property. It provides spatial and frequency spread of watermark in the cover image and divides the signal into two frequency domains: One is high frequency, and another is low frequency. The first part which is high contains a component, and the second part is again divided into the low and high parts. In high part, frequency change in edges is invisible to the human. It performs DWT in two directions: First is vertical direction, and the second is horizontal direction [5]. To perform the second-level decomposition, it divides the frequency into four sub-bands, in which LL1 band is divided into four sub-bands: LL11, LH11, HL11, and HH11 (Fig. 3).

4 Digital Era of Steganography

Steganography can be applied by simply using the command in the Windows Command Prompt. In a carrier, this image is needed in order to hide the message. The message is stored in a text file. Stego image can be generated using this command:

C:>cvr.jpg/k+msg. text/kstg.jpg. This code will generate a stage image that will append the secret data from the text file into the cover file [6].

When this stego file is opened in any photograph editing application, it just displays the picture so that no one can retrieve the secret data. As shown in Fig. 4, data can be retrieved by opening the stego file in notepad.

Fig. 3 a One-level decomposition. b Two-level decomposition

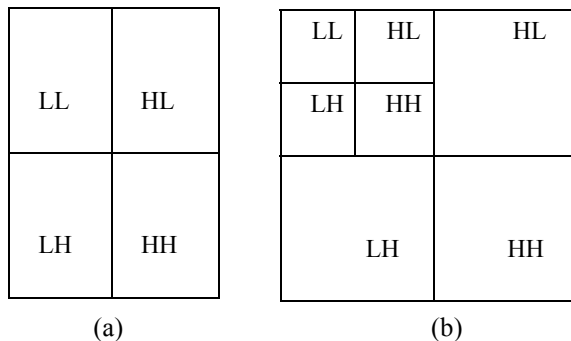




Fig. 4 Stego file when opened in notepad

5 Literature Survey

N. F. Johnson, Z. Duric, and S. Jajodia introduced the first method which is least significant bit (LSB) method. According to this method, the least significant bits of the cover image would be used to hide the secret message for security intent. The last bit of every data value is changed according to the message bit, which is to be hidden [7].

Shilpa Gupta, Neha Aggarwal, and Geeta Gujral proposed an appreciated least significant bit (LSB) method which gives extra features as compared to the existing LSB method. Here, data will be stored in the blue channel of the cover image since it can only be stored in the one-color channel [8].

Abikoye Oluwakemi, C. Adewole Kayode, and S. Oladipupo Ayotunde introduced a new method for security objectives. In this, a data hiding system based on audio steganography and cryptography is used to protect data and transfer between the source and the destination [9].

Ki-Hyun Jung suggests a method that uses two techniques: interpolation and LSB. Interposition is used before hiding, and LSB is used to expanding the secret data. Firstly, the input image is scaled down and interposition pixels are generated; then, hide the data in these interposition pixels and send this to the receiver.

Mamta Juneja and Parvinder Singh Sandhu introduced improved LSB-based steganography techniques for the color image in the structural domain. Using a hybrid feature detection technique, a new method was devised in the RGB color images for information security. The approach achieved improved gradually and capacity than the many existing techniques [10].

6 Different Methods of Image Steganography

In image steganography, a lot of techniques have been formulated for hiding data in them; some of them are:

6.1 Least Significant Bit Method

In this technology, the LSB values of the pixels of the cover image are used to inhibit the information. In this, the last bit of data value is replaced by the message bit, which can inhibit all the information of the message which needs to be hidden in the cover medium.

Let us just take an example: Suppose you have to hide the alphabet “w” in the image, value of the pixel (0–255) is given. First, convert them in binary form. Suppose the values of pixels are the following [11]

150 – 10010110 160 – 10100000
 170 – 10101010 180 – 10110100
 200 – 11001000 230 – 11100110
 240 – 11110000 250 – 11111010

ASCII value of “w” = 119 and in binary = 01110111. Now, check the last pixel value; if it is the same as message bit, then there is no need to change the value. If not, then try to convert it in message bit by adding or subtracting “1” and send it to the receiver. After applying the algorithm, pixel values become:

150 → 10001100. No need to change the value of a pixel as the last bit of the pixel is the same as the message bit.

160 → 10100001 → by add 1
 170 → 10101011 → by add 1
 180 → 10110101 → by add 1

The remaining values are

11001000 111000111 11110001 11111011

At the receiver end or retrieval of the message, it checks the last pixel value of the image. This is simply the retrieval algorithm. The receiver gets 01110111 when he extracts the last bit from each pixel.

Advantages:

- It is more effective and efficient.
- It provides less distortion after the embedding process.
- In the original image, it is hard to detect the alterations.

Disadvantages:

- When a translation or rotation is applied to image, then the message cannot be recovered.
- In the original images not vulnerable to different attacks, it causes any distortion.

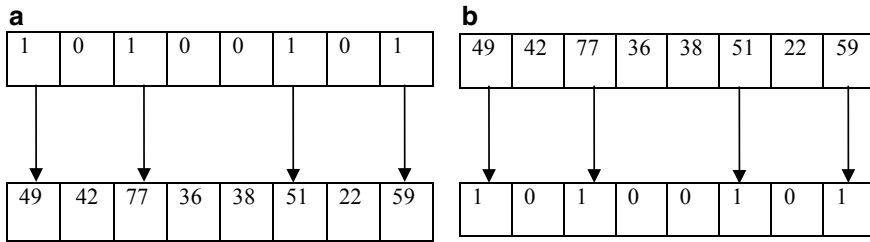


Fig. 5 **a** Embedding of data in GLM. **b** Retrieval of data in GLM

6.2 Gray-Level Modification (GLM) Method

In this method of the gray images, first, the gray-level value of the selected pixels is checked. After this, it is compared to the byte stream. If the pixel value is odd, then convert it into even by changing its value by one unit. If the pixel value is even, then there is no need to change the value. For example, if bitstream has eight elements, then only eight pixels are needed to hide the data [12].

If a bitstream is 10100101, then the pixel value will be decremented since the first element of this bitstream is even (Fig. 5).

Algorithm for embedding data in GLM

1. Using a function $f(x, y)$ selects the pixel.
2. If the value of the pixel is odd, then decrement by one and make it even.
3. If the value is 0, then we do not need to change.
4. If the value is 1, the pixel value is decremented by 1.
5. According to the value of the pixel, both 1 and 0 can be represented.

Algorithm for retrieval of data in GLM

1. Apply the secret function of the stego image to identify the pixels in which the message is hidden.
2. The receiver knows that even the value of the gray-level pixel represents 0 while 1 is represented by odd values.
3. Then, the receiver will select the pixel and map the binary data with it.
4. Collect this binary data to generate a secret.

Advantages:

- In this method, chances of insertion in a message can be done easily.
- Here, the chances of attacks are less.

Disadvantages:

- It is vulnerable in steganalysis technique.

Here, if the image is distorted, message cannot be extracted.

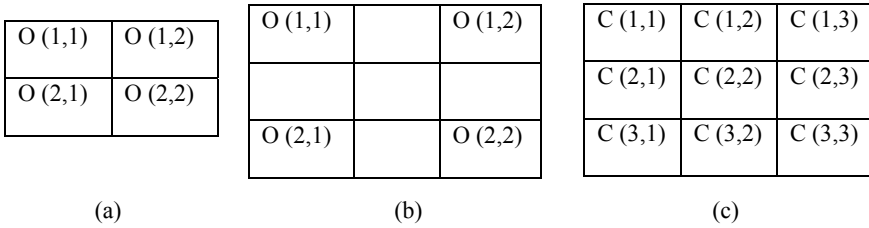


Fig. 6 **a** Original image, **b** the original image after upsampling, **c** the cover image after generating interpolated pixels

7 Interpolation

Interpolation techniques are divided into two categories: One is deterministic interpolation technique, and the second is statistical interpolation technique. Image interpolation is used to convert high-resolution images using a low-resolution image [13].

Jung and Yoo proposed a new method which uses the two adjacent know pixels to find out a value between these two pixels; the newly generated pixel is known as an interpolated pixel. These interpolated pixels are now used to hide the secret message. Here, secret message A is enclosed inside a cover image D. The cover image is generated from the original image by using the nearest mean interpolation (NMI) method. If the size of a cover image is an $M \times N$ pixel, then after the scaling-up process, the scaled-up image is of size $(2M - 1) \times (2N - 1)$ pixels (Fig. 6).

Advantages:

- The chance of insertion of hiding a message is increased.
- Here in steganalysis, new interpolated pixel is used for data hiding instead of old pixels that is why it is difficult in interpolation.

Disadvantages:

- Different attacks cause some distortion in the original image that is not vulnerable.
- If the image is distorted, message cannot be recovered.

8 The Proposed Method

The original quality of the cover image is retained in LSB-based techniques. The quality of the stego image is nearly equal to the cover image. But information hiding using LSB can be easily detected by attackers because these techniques are simple and straightforward. In order to increase the security of the secret message, it has to be scattered into the whole cover image. Therefore, a new LSB technique was developed which allows data dispersion in the whole image [14].

This method is called cyclic because RGB channels are rotated into the cycle, i.e., red channel is used for hiding first bit, the green channel is used for hiding the second bit, the blue channel is used for hiding the third bit, and then this cycle is rotated.

An algorithm for hiding the data:

1. Select the cover image as well as a secret message.
2. Then, the conversion of this secret message is to be done in a 1D array.
3. From the cover image, separate different planes into red, green, and blue channels.
4. Create a flag named Channel Flag which will be used for determining which channel will be used for information hiding. Initialize Channel Flag with value 1.
5. Check the value of Channel Flag.
 - 5.1 If Channel Flag==1, red channel will be used for embedding the secret message.
 - 5.2 If Channel Flag==2, the green channel will be used for embedding the secret message.
 - 5.3 If Channel Flag==3, the blue channel will be used for embedding the secret message.
6. Increase the value of Channel Flag in 1.
7. If the value of Channel Flag is 3, then set Channel Flag=1.
8. Repeat steps 5–7 until the complete secret message is embedded into the cover image.
9. Combine all the channels to form the stego image.

An algorithm for extracting the hidden data:

1. Select the stego image.
2. From the cover image, separate different planes into red, green, and blue channels.
4. Initialize Channel Flag with value 1.
5. Check the value of Channel Flag.
 - 5.1 If Channel Flag==1, extract the secret information from the red channel.
 - 5.2 If Channel Flag==2, extract the secret information from the green channel.
 - 5.3 If Channel Flag==3, extract the secret information from the blue channel.
6. Increase the value of Channel Flag in 1.
7. If the value of Channel Flag is 3, then set Channel Flag=1.
8. Repeat steps 5–7 until all information is extracted from the stego image.
9. Combine all the extracted bits to form the secret message.

9 Result Analysis

In the cyclic LSB technique, security and capacity are of utmost importance. In security, it is assumed that the steganography system cannot be broken easily.

When analyzing security, the original image is compared with the stego image. This comparison is done based on the histogram of the images. In a steganography technique, the level of the security depends on how much the cover medium is different from the stego medium after the message has been embedded in it. If the stego image is very much different than that of the original image, then the technique is not secure. The histogram of the images can easily tell the difference between both the images. For a better steganography system, this change should be least or minimal as possible. The stego image should not be so visually different that it can be identified easily. The histogram of various channels of the original and stego images is shown in the figure. The histograms of the respective channels have minimal differences indicating the better steganography system.

Figure 7a, b shows the cover image of Lena with its stego image.

Figure 8a, b shows the cover image of peppers with its stego image.

Figure 9a, b shows the cover image of pink flower with its stego image.



Fig. 7 a Original Lena image. b Stego Lena image



Fig. 8 a Original peppers image. b Stego peppers image

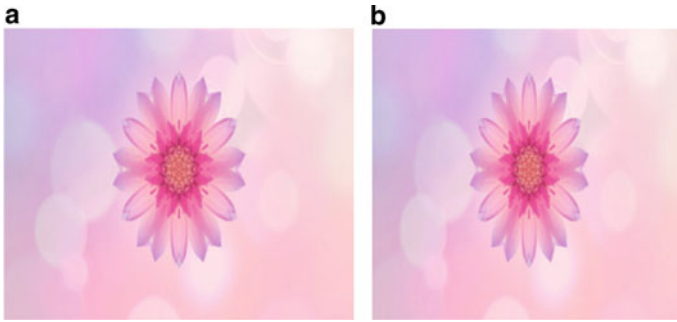


Fig. 9 a Original pink flower. b Stego pink flower image

Table 1 Comparison between proposed work and existing methods

Technique	Image	Image size	PSNR
LSB	Lena	512 * 512	53.6442
LSB	Baboon	512 * 512	53.3499
Chaotic approach	Lena	512 * 512	38.6432
Chaotic approach	Baboon	512 * 512	34.1444
Braille method	Lena	512 * 512	60.415
Braille method	Baboon	512 * 512	58.456
Proposed method	Lena	512 * 512	62.2488
Proposed method	Baboon	512 * 512	61.1474

Evolution Result

As compared to various steganography techniques like LSB, the cyclic LSB technique has a higher capacity. This capacity can be increased by changing the number of bits. But if the same numbers of bits are hidden and then this technique is compared with other techniques, then the cyclic LSB technique is more secure too, mainly because it is a keyless technique, i.e., no key is required. Therefore, there is no fear of detection of key midway by third-party users. Compared to traditional steganography techniques, the cyclic LSB technique is much faster and secure having much more capacity than those techniques (Tables 1 and 2).

10 Conclusion and Future Work

This technique uses RGB channels that are rotated into the cycle, i.e., the first bit of secret message is hidden into the red channel of first pixel, second is hidden in the green channel of the next bit, third bit is hidden into the blue channel of next pixel, and then this cycle is repeated. At the receiver’s end, the reverse process is used to

Table 2 Comparison between different sizes of images using proposed work methods

Image	Image size	PSNR
Beans	256 * 256	58.4521
Trees	256 * 256	55.4215
House	256 * 256	50.4012
Ca2	320 * 432	61.5059
Peppers	512 * 512	60.4512
Ice age	444 * 300	64.5547
Penguins	768 * 1024	73.0843
Building	1024 * 1024	72.4514
Flower	1920 * 1080	71.9901
Sound waves	2560 * 1440	72.4221
Average of 100 images		62.4512

decrypt the media and to obtain the secret message. After that, the PSNR and MSE values are calculated based on different sizes of data in an image.

Cyclic LSB is still a new technique as compared to other image steganography techniques. But still, it provides better security and capacity than other techniques. By controlling the secret message length, its security may be further improved. The biggest advantage of this technique is its keyless feature as there is no key needed for encryption and decryption. So, there is no need for transferring key over a secure channel. Also, this technique tries to take less amount of time in data embedding as compared to other techniques making it faster than other techniques.

References

1. Silman J (2001) Steganography and steganalysis: an overview. SANS Institute
2. Jamil T (1999) Steganography: the art of hiding information is plain sight. IEEE Potentials 18:01
3. Kumar A, Pooja KM (2010) Steganography—a data hiding technique. Int J Comput Appl 9(7) (0975–8887)
4. Singh R, Chawla G (2014) A review on image steganography. Int J Adv Res Comput Sci Softw Eng 4(5)
5. Poornima R, Iswarya RJ (2013) An overview of digital image steganography. Int J Comput Sci Eng Surv (IJCSSES) 4(1)
6. Garg M, Gurudev Jangra AP (2014) An overview of different type of data hiding scheme in image using steganographic techniques. Int J Adv Res Comput Sci Softw Eng 4(1). ISSN: 2277 128X
7. Johnson NF, Duric Z, Jajodia S (2001) Information hiding: steganography and watermarking-attacks and countermeasures. Kluwer, Norwell, MA
8. Gupta S, Gujral G, Aggarwal N (2012) Enhanced least significant bit algorithm for image steganography. Int J Comput Eng Manage 15(4). ISSN (Online): 2230-7893
9. Gutub A (2010) Pixel indicator technique for RGB image steganography. J Emerg Technol Web Intell 3(2)

10. Bailey K, Curran K (2006) An evaluation of image based steganography methods. *J Multimedia Tools Appl* 30(1)
11. Joshi K, Yadav R, Chawla G (2017) An enhanced method for data hiding using 2-bit xor in image steganography. *Int J Eng Technol* 8(6)
12. Joshi K, Yadav R, Allwadhi S (2016) PSNR and MSE based investigation of LSB. In: *The proceeding of computational techniques in information and communication technologies (ICCTICT)*, vol 2, issue 10
13. Sharma K, Joshi K (2017) A novel approach of data hiding technique using interpolation and Braille method. *Int J Eng Technol (IJET)* 9(3)
14. Joshi K, Yadav R (2015) A new LSB-S image steganography method blend with cryptography for secret communication. In: *The proceeding of image information processing (ICIIP)*

Ensuring Food Safety Through Blockchain



Ashish Singh, Vineet Kumar, Alok Kumar Ravi, and Kakali Chatterjee

Abstract Food safety is a most highlighted area in today's fast-food world as many health problems such as diarrhea, vomiting, typhoid, and food poisoning can be happened by consuming those contaminated packed foods. Hence, every possible detail of a packed food item must be placed in a supply chain management (SCM) to trace the path of the food item before delivery. Blockchain technology can be used to track the records of the journey of a packed food item from the manufactured time to the delivery time of the packet. In this paper, we have proposed a model based on blockchain technology (BT) to trace food items through various stages of supply chain management. Security analysis discussed in the paper proved that this chain will achieve the desired level of security in this area.

Keywords Blockchain · Food traceability · Hashing · Food safety

1 Introduction

With the rise in global markets, there is a need to build trust among the food producer and the consumers in the food supply chain (FSC) because nowadays food is originated from one part of the globe and it is consumed in another part of the globe. A FSC refers to the system through which all the records of the journey of food items from the day of its origin are being listed. The processes include in this journey are

A. Singh (✉) · V. Kumar · A. Kumar Ravi · K. Chatterjee
Department of Computer Science and Engineering,
National Institute of Technology Patna, Patna, Bihar 800005, India
e-mail: ashish.cse15@nitp.ac.in

V. Kumar
e-mail: vinetchoudhary@gmail.com

A. Kumar Ravi
e-mail: alokravi63@gmail.com

K. Chatterjee
e-mail: kakali@nitp.ac.in

© Springer Nature Singapore Pte Ltd. 2021
G. S. Hura et al. (eds.), *Advances in Communication and Computational Technology*, Lecture Notes in Electrical Engineering 668,
https://doi.org/10.1007/978-981-15-5341-7_56

production, processing, distribution, and consumption. The FSC binds three primary industries: agriculture, food processing, and distribution industries. Traceability or the ability to track the food product and many details about the processes through all stages of the supply chain is now more in demand among the consumer. Many consumers now want to know from where the food item is originated, and what alterations the item has gone throughout the journey of the item. This can be possible by introducing a higher level of transparency in the FSC which exposes all stages in the supply chain management and various processes that their food has been followed. In order to improve food safety with brand dignity and increase customer retention, it is necessary to share product data at each stage of the FSC [1, 2]. Also, it has to ensure that there is no possibility of data modification or alteration in the FSC. In this case, blockchain is the most suitable solution to build a secure supply chain. It will keep a record of all the details which will bring transparency and aid in customer's trust to improved food quality and security.

In this paper, our contribution is as follows:

- We have proposed a food traceability system which traces the food material at every stage in the supply chain.
- The concept of food traceability is developed by using blockchain technology.
- The security analysis part of the work demonstrated that the model is secured and transparent.

This paper is structured as follows: In Sect. 2, we have discussed the background and existing literature work. In Sect. 3, we demonstrate our proposed architecture of food blockchain. In Sect. 4, we have briefly explained the implementation of our blockchain. In Sect. 5, the security analysis of the system is discussed. Finally, in Sect. 6, we have concluded the work.

2 Background and Related Works

2.1 Blockchain Technology

Satoshi Nakamoto was the first to introduce the blockchain technology [3]. Firstly, it was implemented on a peer-to-peer payment system without a centralized authority. It is an ordered data structure that includes a block-shaped growing list of records (transaction). Each block is connected to the prior block to preserve the chain structure [4]. The entire chain structure is secured using the cryptographic algorithm, encryption technique, and hash algorithm. The first block of the chain (genesis block) is the basis of the blockchain. The SHA-256 hash algorithm will take any size of plaintext as an input and produce a hashed output which is 256-byte binary value. Each block header includes the prior block's hash data, Merkle root hash, and signature. The complete structure of the blockchain is shown in Fig. 1.

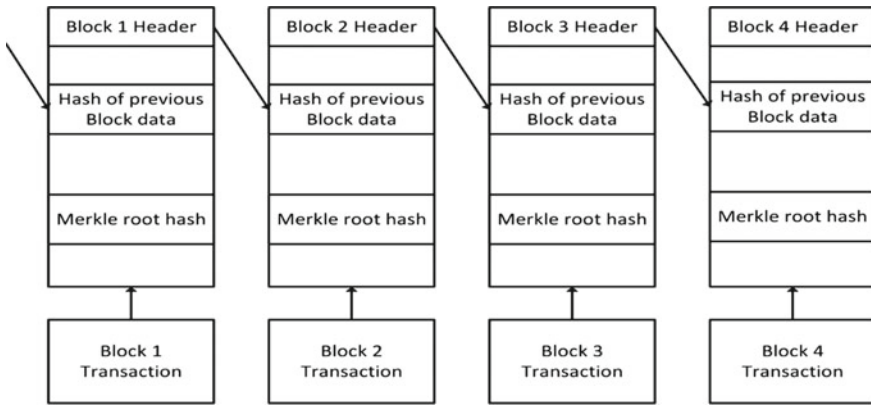


Fig. 1: Blockchain structure [5]

2.1.1 Features of Blockchain

- **Cannot be corrupted**—In the network, every node has a digital copy of complete data. Each node validates it to add a transaction, and if the majority believes it is valid, then it is added to the ledger. This makes it hard to corrupt, and data is transparent to the whole network.
- **Decentralized technology**—The nature of the blockchain network is decentralized. It does not have any ruling authority or individual that manages the network. For decentralization, the network is maintained by a group of nodes.
- **Improved security**—The need of a central authority is eliminated by this technology. Thus, no single authority can tamper the block and cryptographic technique ensures another layer of security.
- **Distributed ledgers**—All other users in the system maintain the ledger in the network. To guarantee a better result, this ledger distributes the computing energy throughout the other devices.
- **Consensus** There is consensus algorithm which enables all of them to agree on a state.
- **Faster settlement**—Compared to conventional banking system, blockchain provides quicker resolution.

2.2 Related Works

The conventional food chain is not sufficient enough to take care of food safety and win the trust of its consumers due to expensive and less decentralized private blockchain processes. Most of the supply chain systems are inefficient due to the

present of several problems such as food fraud, foodborne illness, illegal production, and food recalls. We have explained several earlier works in this section that are used to fix the issues mentioned.

Lin et al. [6] proposed a food chain traceability model which uses blockchain and Internet of things (IoT) technologies. IoT devices are used to overcome the manual process. The low-power wide-area network (LPWAN) IoT model uses a trusted blockchain validation and tamperproof mechanism to make IoT-based smart agriculture system.

Tian [7] proposed an agri-FSC traceability model which uses the concept of RFID and BT. This model reduces the losses during the logistics process as well as enhance food safety and quality of the agriculture system.

Tse et al. [8] discussed an idea of FSC management using BT. The presented blockchain application, authentication model for supply chain management, and the aspect of information security are to provide a direction to develop a new application for the safety of food.

Lin et al. [9] developed a prototype for the tracing of food safety. This prototype composed of blockchain and EPC Information Services (EPCIS). On-chain and off-chain architecture for information leadership are designed to remove the problem of information explosion. Tampering data and sensitive information disclosure issues are solved during communication using a smart contract at the enterprise level that can ensure the tamperproof feature of sensitive information.

Kamilaris [10] discussed several challenges, social impact, and issues present in the management of the FSC. They also present an overview of existing BT present in the FSC. The provided directions, ongoing projects, research, and initiatives are beneficial for further research in this area.

In [11], Walmart discussed their projects and investment plan which is established in 2016 to provide food security and maintain transparency in the FSC. They used IBMs BT which is based on Hyperledger Fabric for reducing the tracking time of mango origin from seven days to 2.2 s.

In [12] present an AgriBlockIoT model which is based on a combination of the BT and IoT devices. This decentralized traceability technique provides an ideal solution to trace the food from origin to customer end. Ethereum and Hyperledger Sawtooth blockchain are used to design the food traceability model.

Feng [13] proposed a FSC traceability model for real-time analysis and monitoring of the food. The model uses the BT and hazard analysis and critical control points (HACCP) approach to achieve transparency, openness, trust, and food safety. BigchainDB approach is proposed for removing the problem present in the decentralized systems.

Saberi et al. [14] categorized the barrier of adoption of BT and discussed each category in details. They also present blockchain future, smart contracts [15, 16], and management of the supply chain to enhance the system tracing ability.

3 Proposed Architecture of Food Chain

In this section, we have discussed our proposed food chain in Fig. 2 which is based on BT. This is a permissionless blockchain network where the users do not have place their trust in a third party to use blockchain.

Stakeholders have to connect to the network by using their public and private key pair when they are going to upload their product information. The products will be given a unique identity at provenance, and it will remain the same throughout the supply chain. It is used to track the food item in the blockchain. Others details of sender and receiver can also be attached along with product ID. On receiving the product the customer can see the complete history of the product with the help of the unique id of the product. Algorithm [1] is used for tracking of the food items at various stage of the supply chain.

Algorithm 1 Food traceability system

```
1: procedure INPUT:(Product)
2:   if product ID == Used product ID then
3:     Scan product ID.
4:   else
5:     Generate product ID
6:   endif
7:   Enter details and sign it with public and private key pair.
8:   if Details are valid then
9:     Update blockchain
10:  else
11:    Blockchain not updated
12:  endif
```

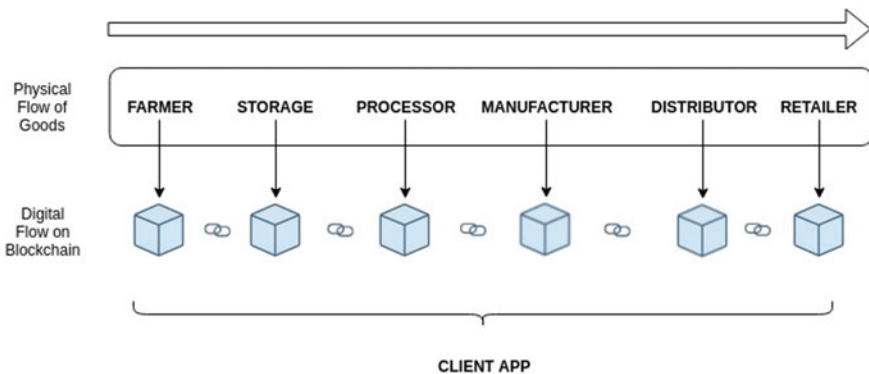


Fig. 2: Proposed food chain for food traceability

4 Implementation of Blockchain Operations

In the proposed food chain, we have performed six different operations for different activities for traceability of the food items. All the transactions are done using two methods “GET” and “POST”.

We have implemented all the above operations in python using various libraries like urlparse, datetime, hashlib, json. We have used flask Web Server Gateway Interface (WSGI) micro-web framework using the python library flask. Our transaction details fetched through the POST method on the web server are in the form of JavaScript Object Notation (JSON), and requests made through GET are also sent in JSON format. After using these operations, the created blockchain structure is shown in Fig. 3. In this, blockchain is 0.5 MB which contains index number, timestamp, proof of work, previous hash, and Merkle root with transaction details. These transactions are securely signed by RSA-based signature algorithm. Secure Hash Algorithm (SHA) 256 is used to generate the hash of the previous block which is stored in the next block.

The operation details are given below.

- **Operation 1. Mine Block**—It is used to make and add the next block to the blockchain. The block which remains in the meme pool is linked with the previous block, generate its hash, creates Merkle root, and proof of work. This can be demonstrated by Code 1. On a GET call, it returns a json object with message, index, proof, Merkle root, timestamp, previous hash, and transaction details. While mining the block, the task of miners is to find out the nonce which is supported by proof of work. Miner’s objective is to the generated hash value which has a certain number of hash values at the beginning.

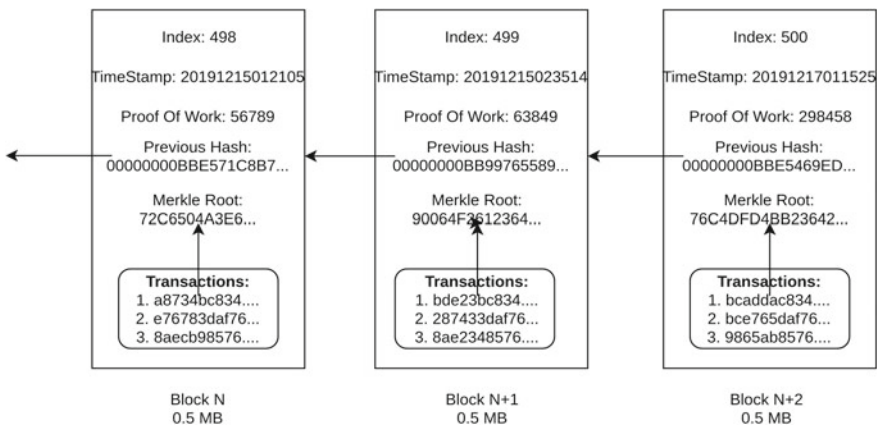


Fig. 3: Created block structure

```

1 # Mining a Blockchain
2 @app.route('/mine_block', methods= ['GET'])
3 def mine_block():
4     previous_block= blockchain.get_previous_block()
5     new_proof= blockchain.proof_of_work(previous_block['
        proof'])
6     previous_hash= blockchain.hash(previous_block)
7     #blockchain.add_transaction(sender= 'reward',
            receiver='Satoshi', amount=1000)
8     block= blockchain.create_block(new_proof,
            previous_hash)
9     responce= {'message': 'Congratulations, you just
            mined a block!'
10     'index': block['index'],
11     'proof': block['proof'],
12     'merkle_root': block['merkle_root'],
13     'timestamp': block['timestamp'],
14     'previous_hash': block['previous_hash'],
15     'transactions': block['transactions']}
16     return jsonify(response), 200

```

Code 1: Mine Block

- **Operation 2. Get Chain**—This operation returns the complete blockchain. All the saved data on the blockchain are used for checking details of the product and analysis of the data. On the user side, this data can be used for different purpose according to user needs. This operation is shown in Code 2.

```

1 # Getting the full Blockchain
2 @app.route('/get_chain', methods= ['GET'])
3 def get_chain():
4     response= {'chain':blockchain.chain,
5     'length': len(blockchain.chain)}
6     return jsonify(response ), 200

```

Code 2: Get Chain

- **Operation 3. Add Transaction**—This method is called when the stakeholder or anyone wants to upload data block in the blockchain. It requires the user to send sender id, receiver id, and product id. The transaction is added to meme pool if it is signed correctly and the product is newly generated. A transaction is verified based on a signature. The transaction operation is shown in Code 3.

```

1 @app.route('/add_transaction', methods = ['POST'])
2 def add_transaction():
3     json= request.get_json()
4     tranasaction_keys= ['sender', 'receiver', 'pid']
5     if not all(key in json for key in tranasaction_keys)
6         :
7     return 'some elements are missing', 400
8     index_block= blockchain.add_transaction(json['sender
        '],json['receiver'], json['pid'])
9     responce={'message': 'This transaction will be added
        to block %s' % index_block}

```



```
9 return jsonify(response), 200
```

Code 3: Add Transaction

- **Operation 4. Add Nodes**—When a new node arrives, the information is sent to all nodes. The other nodes will decide whether it becomes a part of the food chain in the blockchain network or not. It is given all necessary updates of blockchain and helps to make the system secure by providing updates. A node is going to receive an update only if its chain is shorter than the node, it is comparing with. This can be shown in Code 4.

```
1 @app.route('/add_nodes', methods = ['POST'])
2 def add_nodes ():
3     json= request.get_json()
4     nodes= json.get ('nodes')
5     if nodes is None:
6         return "No node", 400
7     for node in nodes:
8         blockchain.add_node (node)
9     response= {'message': 'all nodes added to main chain
10              ', 'total nodes': list (blockchain.nodes)}
11 return jsonify (response), 200
```

Code 4: Add node

- **Operation 5. Update Chain**—This operation is used for updating the chain and adding transactions. In the case of multiple different blockchains, the one with the highest number of blocks will be accepted. A chain will be updated with newer chain only if the arriving chain is valid, i.e., have all the previous hashes linked correctly, transactions signed, and necessary proof of work done. The updation of blockchain is shown in Code 5.

```
1 @app.route('/update_chain', methods=['GET'])
2 def update_chain():
3     is_chain_replaced= blockchain.update_chain()
4     if is_chain_replaced:
5         response= {'message': 'the chain is updated', '
6                   new_chain': blockchain.chain}
7     else:
8         response= {'message': 'No change',
9                   'chain': blockchain.chain}
9     return jsonify (response), 200
```

Code 5: Update Chain

- **Operation 6. Check Validity**—Checks that contain of each transaction in the blockchain is valid or invalid. A chain is valid if it has all the previous hashes linked accordingly, transactions signed with correct Merkle root and proof of work done and the timestamp is the correct order. The validity of the blockchain is demonstrated in Code 6.

```
1     # Checking the Blockchain validity
2 @app.route('/is_valid', methods= ['GET'])
```

```
3 def is_valid() :
4 is_valid= blockchain.is_chain_valid(blockchain.chain
   )
5 if is_valid:
6 response= {'message': 'All good. The block chain
   is valid.'}
7 else:
8 response= {'message': 'Error: Blockchain Not Valid'}
9 return jsonify(response),200
```

Code 6: Check Validity

5 Security Analysis

In this section, we have analyzed our proposed food traceability model which uses the concept of blockchain. We have considered the following security point during the development of the model.

5.1 Data Tampering

Data tampering is extremely difficult as the underlying technology of our system is blockchain-based which makes many copies of the whole blockchain among the nodes of the network. So, for tampering a block, there is a need to tamper all the copies of blockchain. It is impossible to tamper all the copies at a time because it is distributed among different nodes. Data of the blockchain is secured using public-key cryptography and hash code which uniquely identifies the block data.

5.2 Secure Transactions

All the transactions are secured with RSA public-key cryptography-based. In this transaction, the signature has the private key of that public address which will be verified by matching against the public-key counterpart.

5.3 Unauthorized Access

Most of the time permissionless blockchain suffered from this type of attack. This type of permissionless system can cause an attacker to access or modify a function. In

this food chain, all transactions are verified using his public key. Only the person with the product can insert information regarding that product ID. Once the information is added and verified, it will be placed in a blockchain which remains unchanged.

5.4 Blockchain Structure Attack

One of this types of attack is blockchain forks. This forks can be created unintentionally through protocol vulnerabilities or malicious content implemented by “Sybil nodes”. This creates conflict in validation rules. In this food chain, we have used proof of work as a consensus mechanism to handle this type of attack.

5.5 Duplication and Forgery

We make a unique product ID before entering it into the system. This unique identification gives the guarantee that no one can create a duplicate product ID. The blockchain includes the earlier block hash, signature, and root hash Merkle. The signature is used to demonstrate the transaction data authenticity and integrity. The prior block’s hash is used to keep the blockchain data integrity. The Merkle root hash informs the voting information root (origin). This proposed approach ensures no can perform duplicity and forgery into the system.

6 Conclusion

We have introduced a blockchain-based traceability model for the FSC to improve food quality and safety. The used BT provides tamperproof, more authentic, and secure supply chain management. In this model, all food information is stored in a blockchain. This blockchain can be accessed by anyone and fetch product details and get assured of the quality of their food.

References

1. Hackius N, Petersen M (2017) Blockchain in logistics and supply chain: trick or treat? In: Proceedings of the Hamburg international conference of logistics (HICL). epubli, pp 3–18
2. Mena C, Stevens G (2010) delivering performance in food supply chains: an introduction. In: Mena C, Stevens G (eds) Delivering performance in food supply chains. Woodhead Publishing Series in Food Science, Technology and Nutrition, Woodhead Publishing, pp 1–15
3. Nakamoto S et al (2008) Bitcoin: a peer-to-peer electronic cash system

4. Singh A, Chatterjee K (2018) Secevs: secure electronic voting system using blockchain technology. In: 2018 International conference on computing, power and communication technologies (GUCON). IEEE, pp 863–867
5. Hanifatunnisa R, Rahardjo B (2017) Blockchain based e-voting recording system design. In: 2017 11th International conference on telecommunication systems services and applications (TSSA). IEEE, pp 1–6
6. Lin J, Shen Z, Zhang A, Chai Y (2018) Blockchain and IoT based food traceability for smart agriculture. In: Proceedings of the 3rd international conference on crowd science and engineering, ICCSE'18. New York, NY, USA. ACM, pp 3:1–3:6
7. Feng T (2016) An agri-food supply chain traceability system for china based on rfid amp; blockchain technology. In: 2016 13th International conference on service systems and service management (ICSSSM), pp 1–6
8. Tse D, Zhang B, Yang Y, Cheng C, Mu H (2017) Blockchain application in food supply information security. In: 2017 IEEE international conference on industrial engineering and engineering management (IEEM), pp 1357–1361
9. Lin Q, Wang H, Pei X, Wang J (2019) Food safety traceability system based on blockchain and epcis. *IEEE Access* 7:20698–20707
10. Kamilaris A, Prenafeta Bold F, Fonts A (2018) The rise of the blockchain technology in agriculture and food supply chain
11. Kamath Reshma (2018) Food traceability on blockchain: Walmarts pork and mango pilots with ibm. *The JBBA* 1(1):47–53
12. Caro MP, Ali MS, Vecchio M, Giaffreda R (2018) Blockchain-based traceability in agri-food supply chain management: a practical implementation. In: 2018 IoT vertical and topical summit on agriculture—Tuscany (IOT Tuscany), pp 1–4
13. Feng T (2017) A supply chain traceability system for food safety based on haccp, blockchain amp; internet of things. In: 2017 International conference on service systems and service management, pp 1–6
14. Saberi S, Kouhizadeh M, Sarkis J, Shen Lejia (2019) Blockchain technology and its relationships to sustainable supply chain management. *Int J Prod Res* 57(7):2117–2135
15. Sadiku MNO, Eze K, Musa SM (2018) Smart contracts: a primer
16. Rosic A (2017) Smart contracts: the blockchain technology that will replace lawyers. Retrieved from Blockgeeks: <https://blockgeeks.com/guides/smart-contracts>

Design of Observer-Controller Digital Phase-Locked Loop Using Kalman Filter



Rachana Arya, B. K. Singh, and Lalit Garia

Abstract Digital PLL is a fundamental construction block for Bluetooth Low Energy (BLE) systems and several other wireless technologies like applications of Internet of Things (IoT), clock generation, recovery, and reconstruction of data. It is also used for ultra-low power operations and numerous digital signal processing techniques. The proposed Digital PLL is based on the loop filter that is observer-controlled, which helps to filter out entire additive noise and the output is improved in the terms of phase noise and transient time response. The main drawback of the previous PLLs is current transceiver noise that modifies the overall phase noise output of the system is overcome by the new technique known as oscillator pulling technique. Here the output can be separated out without modifying the general performance of phase noise. The observer filter is fundamentally a second-order time-varying system having fundamental gain value. The proposed Digital PLL has been simulated using 0.35 μm CMOS technology. The proposed DPLL is having lesser phase jitter, high operating frequency, and less complexity of the circuit. The designed digital phase-locked loop is 1.5–3 times faster than that of the conventional one.

Keywords Digital phase-locked loop (DPLL) · Phase detector · Kalman filter (KF) · VCO

1 Introduction

In present day digital systems utilize clocks, designed for sequencing the different operations among different internal functional units. The data rate and reference clock frequencies of the system continuously increasing by degrees. PLLs are extensively used toward the production of well-timed clock generation for present day's digital systems. A closed-loop system is applied on the phase-locked loop to lock the output and the reference input signal. The basic building blocks are phase-frequency detector

R. Arya (✉) · B. K. Singh · L. Garia
Department of Electronics and Communication Engineering, B.T.K.I.T., Dwarahat, India
e-mail: rachna009@gmail.com

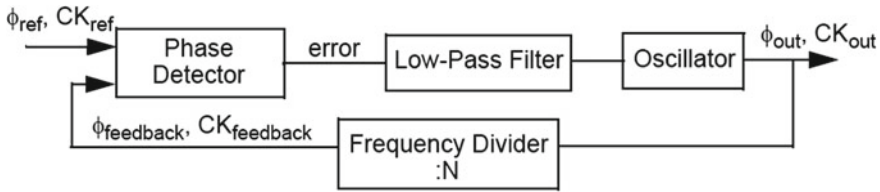


Fig. 1 Block diagram of basic PLL

or phase detector, frequency divider, low-pass filter, and a voltage-controlled oscillator (VCO). The fundamental diagram of phase-locked loop is presented by Fig. 1. The phase-frequency detector or phase detector acts as an error amplifier to minimize the phase difference between output signal $y(t)$ to input signal $x(t)$. The feedback path will be locked if phase and frequency of output and those of input signals are the same [1, 2].

By the PLL circuit, the first essential block is a charge pump circuit that is used to mix the output of the phase-frequency detector and provide solo output. Depending upon the phase and frequency variations, two output signals are generated as “UP” and “DOWN” signals. The output of phase detector is an error signal, i.e., filtered by low-pass filter. The filter blocks the high-frequency component and passes the low-frequency component (control signal) to the Voltage-controlled oscillator [3–5]. Based on the produced DC Voltage signal the voltage-controlled signal is generated. If the output signal is high denotes as “UP” signal, the corresponding voltage of low-pass filter increase to raise the oscillator output signal. On the opposite, if a low signal is generated, the resultant output is feedback to phase-frequency detector to calculate the difference in phase moreover after that circuit generates a closed-loop frequency control system [6, 7].

VCOs can be classified as linear VCO and relaxation type VCO. Linear VCO uses LC tank circuit to produce sinusoidal oscillations. Fast-locking phase lock loop response of two major stages; a coarse alteration stage considers as fast changes in output frequencies, followed by a fine-tuning stage for flat transitions. Universal Challenges of fast-locking PLLs are as follows:

- I. Reducing the lock in time measured by the number of clock cycles
- II. Minimizing frequency overshoot
- III. Reducing jitter or phase noise
- IV. Improvement in system stability.

2 System Description

The Digital PLL consists of subsequent subsystems as below:

- I. Input sub-system
- II. Phase and frequency detector

- III. Digital-controlled oscillator
- IV. Observer sub-system
- V. Controller sub-system
- VI. Noise modelling.

In All-Digital PLL (ADPLL), the designing of an input sub-system is dependent on the nature of the phase detector. For the simulation of ADPLL, J-K edge-triggered type phase detector is used. This phase detector converts the input sinusoidal signal to the digital signal [4]. Initially, the input signal is passed through zero-crossing detectors, which provide the output signal high to input signal that is greater than or equal to zero [8, 9]. When input signal is less than zero it provides zero output. With the help of a comparator circuit, the reference level of the output signal is calculated. The feature of the comparator is given by the following Eq. (1):

$$Y = f(x) = \begin{cases} 0, & x < 0 \\ 1, & x \geq 0 \end{cases} \quad (1)$$

The comparator's output is applied to the mono-shot pulse generator circuit. This will generate a small amplitude pulse for the second level circuit. The low to high transition of the signal or vice versa specify the reference level as zero point [3]. By this technique, the time period of output pulse increases by one-tenth of mono pulse input.

Digitally controlled oscillator (DCO) is thus recognized as frequency synthesizers; used to generate frequencies that are compounded of reference frequency. Therefore, it is also recognized as an integer N-frequency synthesizer and is used in FM and PM detector. Observer DCO is mostly used to obtain an approximation state of the system. When the observer observes all the output states it is acknowledged as a full state observer. Now for PLL design, the essential states are phase and frequency difference. An additional state (quantization noise) is also considered for the designing of DPLL, since quantization noise remain present in the system. The incremental value of phase angle is given by the following equation [10, 11]:

$$\Delta\theta_{n+1} = \theta_{n+1} - \theta_n + 2\pi \left(\frac{f_{des} - f_{ex}}{f_r} \right) - n_n - q_n \quad (2)$$

where θ_n denotes the phase of n signal

- f_{des} is the preferred frequency
- f_{ex} is the excess frequency of DCO
- f_r is the reference (clock)frequency
- n_n represents the band limited noise
- q_n is the quantization noise presented in the system,

Equation (2) can be rewritten as follows:

$$\Delta\theta_{n+1} = \Delta\theta_n + 2\pi(\Delta f_n) - n_n - q_n \quad (3)$$

By this observer circuit, nullify the phase error and frequency error; hence Eq. (3) can be rearranged as Eq. (4):

$$\Delta\theta_{n+1} = \Delta\theta_n + 2\pi(\Delta f_n) - n_n - q_n + u_n(0) \quad (4)$$

The equation of incremental changes in frequency is given as:

$$\Delta f_{n+1} = \Delta f_n + u_n(1) \quad (5)$$

where $u_n(0)$ and $u_n(1)$ are control signals for stages first and second. The controller sub-system enforces the entire system to obtain the frequency and phase error toward zero. By altering the maximum counted value of DCO, its frequency and phase are changed [3, 12]. According to the observer's input, the bidirectional UP/DOWN counter is used.

3 Methodology of Proposed Work

The digital low-pass filter converts a continuous-time response into discrete-time signal at the sampling rate of reference clock frequency. With the use of digital controlled oscillator (DCO), time to digital convertor (TDC) and digital loop filter can simply control all the parameters into ADPLL. The output angular frequency (ω_2) of the PLL system can be determined through the LPF output described as per equation below:

$$\omega_2 = \omega_0 + k * u_f(t) \quad (6)$$

where ω_0 is the center angular frequency and k is the voltage gain of VCO stage. The phase detector (PD) compares the phase of input and output signal. The output of phase detector which is generally the error voltage is given by the following equation:

$$u_p(t) = k_d * \theta_e \quad (7)$$

where k_d is the gain of the phase detector and θ_e is the phase error of both input and output signal. The output signal is having both dc and ac components. These components are not desirable hence it is eliminated using low-pass filter, i.e., basically a 1st order low-pass filter [5, 13]. The VCO generates an average frequency signal with zero phase error. At the same time, output frequency has to match the reference frequency so the oscillator frequency is increased and decreased as per the prerequisite of output frequency. If the error voltage is zero or input and output voltage are at the same phase the PLL is said to be locked. Let $u(t)$ be the input signal so

$$u(t) = u * \sin(\omega t + \theta) \quad (8)$$

where f is input frequency and θ is input phase and $Y(t)$ is the oscillator's output signal.

$$Y(t) = v * u * \sin(\omega t + \theta) * \left[\frac{4}{\pi} \cos(\hat{\omega}t + \varphi) + \frac{4}{3\pi} \cos(3\omega t + \varphi) + \frac{4}{5\pi} \cos(5\omega t + \varphi) \dots \right] \quad (9)$$

By the Eq. (9), the terms are ac components having higher frequencies, i.e., multiples of the input frequency. As these frequencies are redundant signal so they are to be filtered out by the loop filter [14, 15]. The vital characteristic of PLL is to suppress the noise signal presented in the input signal. The average phase of the input signal is considered by the VCO moderately than allowing for the current phase of the signal. As a result, PLL circuit can follow the input signal with noise as well.

The designing of analog PLL is suffering from higher phase noise due to quantization error so it is not suited for frequency synthesizer application. In the designing of the observer control approach, the consequence of the oscillator pulling technique is effectively removed. The observer is fundamentally a second-order loop filter through time-varying proportional and integral gain values [16]. Based on the affirm values of the second-order loop filter, the controller uses integrators and delay elements to generate the digital controlled input.

4 Kalman Filter

Kalman filter is state estimators model that works on the plant to measure the noise covariance facts. A Kalman filter is positioned in frontage of the PLL, in order to make sure that the input of the PLL at all times matches an ideal sinusoidal waveform as intimately as possible. When the input voltage is highly distorted (by the presence of harmonics) then also it provides an ideal waveform. This technique ensures quick and small distortion of the PLL operation. The design and simulation of both the PLL and the Kalman filter are described in detail and demonstrated by simulation under various voltage conditions [17, 18]. Exclusively, lying on the time-domain form of the plant by Eqs. (6) and (7), the optimal control signal is analytically derived. For computational steps, this Kalman filters provide an estimate of the present state variables with their uncertain variables. After the estimation, the result of the measured data (essentially some amount of error and random noise) is observed. Naturally, the Kalman filter is used to execute a single step calculation for the TDC output hence the output of DCO is simplified on the current predicted error signals. The optimization of the problem is solved by using MATLAB. The algorithm for this problem is recursive so it can be executed in real-time. The Kalman filter model

assumes states at time (t) change from the past state at time ($t - 1$) [1, 6]. Typically, output signals (i.e., to be measured) and the control procedures are noisy, so, a better model of a particular dynamical structure be supposed to an explanation for both these factors. As per a linear stochastic difference equation is following (8):

$$x_t = F_t x_{t-1} + B_t u_t + w_t \quad (8)$$

where

x_t = state vector enclosed designed for methods (e.g., location, speed, heading) at time t

u_t = vector enclosed for organizing input (like routing angle, garrote surroundings, brake power)

F_t = state transition matrix to relate the consequence of every position parameters at time ($t - 1$) to the structure condition next to time (t) as well as speed on time ($t - 1$)

B_t = control key matrix which relate the consequence of every controlled i/p parameter in the vector u_t (e.g. the outcome of the garrote set lying on the speed of system and location)

w_t = vector contain the procedure noise in stipulations of all factors inside the position vector.

Procedure disturbances are understood to be drained at starting a null mean multivariate regular distribution by covariance. Consider MATLAB programming tool for the all-digital PLL. During the simulation process, the gain of the open system fixed as a result the damping ratio is observed as 0.7 and the phase margin is observed as 45. While shaping the steady-state jitter, the conventional filters bandwidth is reduced until the jitter is low and responds vice versa. The Digital-Controlled Oscillator, TDC, and LPF are simulated in distinct time with the reference clock frequency or input frequency.

5 Results and Discussion

The output of the projected observer-controlled Kalman loop filter is compared with the predictable low-pass filter output. During the simulation, it is observed that gain of the predictable loop filter is laid down. The value of the damping ratio is observed as 0.7 and the loop filter margin for phase is observed as 45 that is projected by Fig. 2.

The output graph is plotted in Fig. 2 is in between amplitude and time. It shows the performance of digital phase-locked loop output, showing that the output is locking at a very small time interval. Jitter has also on the minimum value as per the output graph. The frequency of oscillation is about 100 Hz. As per Fig. 3, the VCO output is locked at 20 Hz frequency with less noise. By the help of Fig. 4, output simulation (same observer gain) of highly noisy output (position) is shown. By the help of the simulation results the output noise significantly affects the state estimation

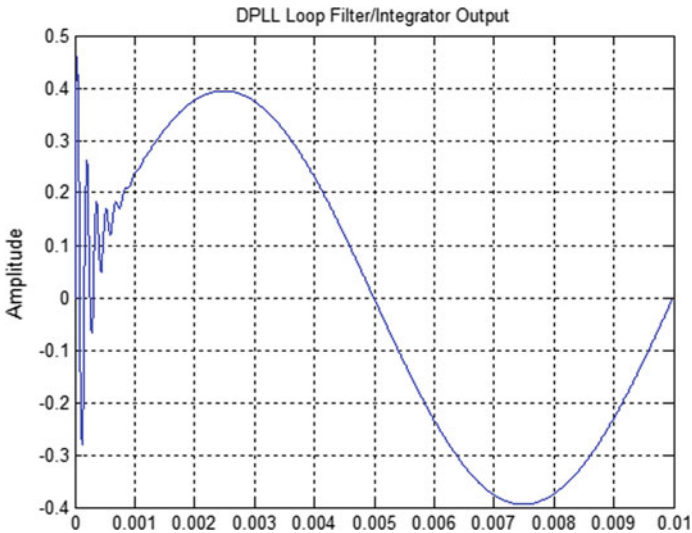


Fig. 2 Output graph of loop filter

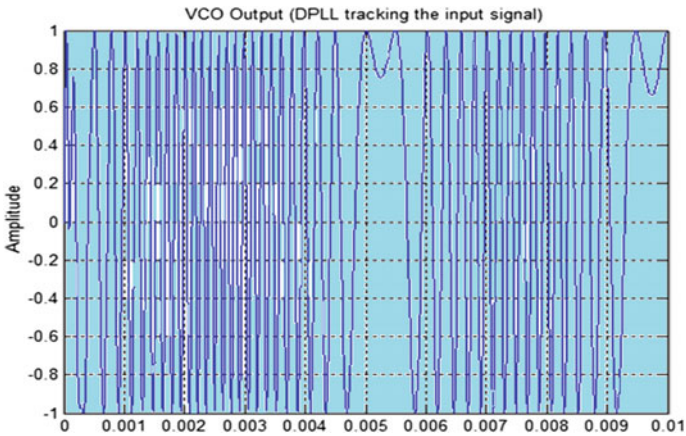


Fig. 3 Output of VCO that is tracking the input signal

performance. Next Fig. 5 shows the spectrum of phase noise of predictable filter with injection pulling method that shows some glitches at the same time interval of the PLL.

Figure 6 is presenting a comparison graph between DPLL and Observer-Controller DPLL. The dissimilarity of the two methods is in the performance of the phase noise. Both approaches become further distinct when the DCO flicker noise is huge as to the TDC noise.

Fig. 4 PD output, i.e., constant after a significant point

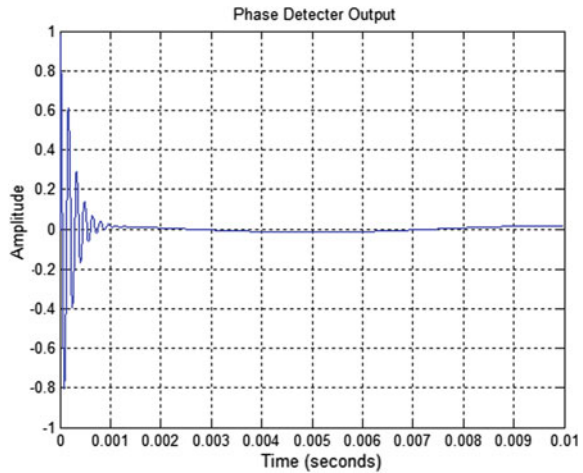
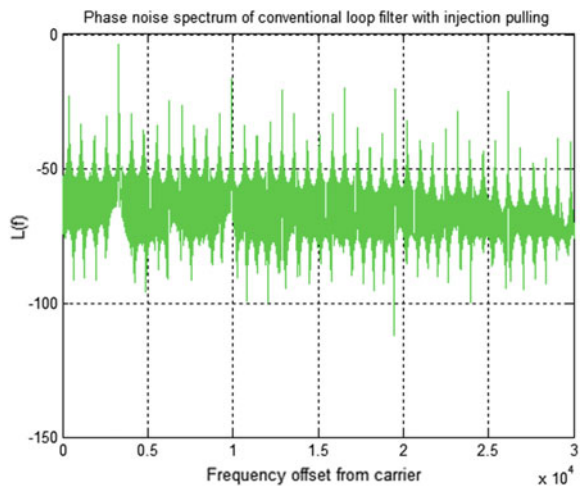


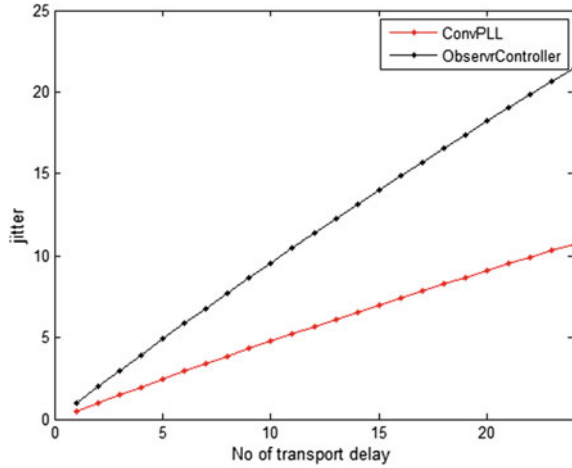
Fig. 5 Spectrum of phase noise of observer controller loop filter



6 Conclusion

In this paper, the simulation of the proposed scheme describes the different techniques of Dpll. On account of simulated outcomes it is observed that by increasing the transistor speed, Digital PLL performs better in terms of noise and jitter. By the observation, this projected observer-controller low-pass filter is moderately superior in complexity and improvement in phase noise, transitory response as well as strength in the direction of oscillator pulling technique. The related equations are specifically used as the designing parameters for the Kalman filter and the proposed PLL. As a result, a precise and speedy assessment for the output frequency is achieved. It can

Fig. 6 The comparison of the conventional DPLL and Observer-Controller DPLL



be intended for space communication synchronization techniques, coherent demodulation, and threshold extension and symbol, and bit synchronization. Also in radio transmitter circuits, PLL can be used to combine original frequencies that are manifold of the reference frequency, by means of a similar constancy as original frequency. In addition, it is also helpful for the renewal of clock time period in sequence from the data stream.

References

1. Staszewski BR, Balsara P (2006) All-digital frequency synthesizer in deep submicron CMOS. Wiley, New York
2. Kelkar R, Novof II (1997) Frequency lock indicator circuit with frequency only detection. U.S. Patent 5 656 977 (Aug)
3. Babu A, Daya B et al (2012) All digital phase locked loop design and implementation. IEEE J Solid State Circuits 39(5)
4. Chiou TY, Gebre-Egziabher D et al (2007) Model analysis on the performance for an inertial aided FLL-assisted PLL carrier tracking loop in the presence of ionospheric scintillation. In: Proceedings of the 2007 National Technical meeting of The Institute of Navigation, San Diego, CA, pp 1276–1295
5. Wolaver DH (1991) Phase locked loop circuit design. Prentice Hall Publication
6. Namgoong W (2010) Observer controller dpll. IEEE Trans Circuits Syst 57(3):631–641
7. Best RE (2003) Phase locked loops design, simulation and applications, 5th edn. McGraw-Hill Publication
8. Shahruz SM (2001) Novel phase-locked loops with enhanced locking capabilities. J Sound Vib 241(3):513–523
9. Woo Y et al (2002) Phase-locked loop with dual phase frequency detectors for high-frequency operation and fast acquisition. Microelectron J 33(3):245–252
10. Loveless T, Massengill L et al (2006) A hardened-by-design technique for RF digital phase-locked loops. IEEE Trans Nucl Sci 53(6):3432–3438
11. Li SJ, Hsieh HH (2009) A 10 GHz phase-locked loop with a compact low-pass filter in 0.18 μm CMOS technology. IEEE Microwave Wirel Compon Lett 19(10):659–661

12. Mansuri M, Liu D, Yang CK (2002) Fast frequency acquisition phase frequency detector for G samples/s phase locked loops. *IEEE J Solid State Circuit* 37(10)
13. Razavi B (2002) *Design of analog CMOS integrated circuits*. Tata McGraw Hill Edition
14. Baker RJ, Li HW, Boyce DE (2002) *CMOS circuit design, layout, and simulation*. IEEE Press Series on Microelectronic Systems
15. Kang SM, Leblebici Y (2003) *CMOS digital integrated circuits: analysis and design*, 3rd edn. McGraw-Hill Publication
16. Sun Q et al (2010) A fully integrated CMOS voltage regulator for supply-noise-insensitive charge pump PLL design. *Microelectron J* 41(4):240–246
17. Janardhan H, Wagdy MF (2006) Design of a 1 GHz digital PLL using 0.18 μm CMOS technology. In: *IEEE Proceedings of the third international conference on information technology*
18. Arakali A, Gondi S, Hanumolu PK (2010) Analysis and design techniques for supply-noise mitigation in phase-locked loops. *IEEE Trans Circuits Syst I: Regul Pap* 57(11)

Supervised Machine Learning Algorithms for Fake News Detection



Ankit Kesarwani, Sudakar Singh Chauhan, Anil Ramachandra Nair, and Gaurav Verma

Abstract In our modern era where the Internet is ubiquitous, everyone consumes various informations from the online resources. Along with the use of a huge amount of social media, news spread rapidly among the millions of users within a short interval of time. However, the quality of news on social media is lower than the traditional news outlets; the main reason behind that is the large amount of fake news. So in this paper, we have explored the application of machine learning techniques to identify the fake news. We have developed two models with the help of support vector machine, random forest, logistic regression, naive Bayes, and k-nearest neighbor machine learning algorithms, and this method is compared in terms of accuracy. A model focuses on identifying the fake news, based on multiple news articles (headline) and Facebook post data which gather informations about user social engagement. We achieved maximum classification accuracy of 98.25% (logistic regression) for a dataset A and 81.40% (KNN) accuracy for a dataset B.

Keywords Fake news · Classification · User profile

A. Kesarwani (✉)

School of VLSI and Embedded Systems Design, National Institute of Technology Kurukshetra, Kurukshetra, Haryana 136119, India

e-mail: ankit981143@gmail.com

S. S. Chauhan · G. Verma

Department of Electronics and Communication, National Institute of Technology Kurukshetra, Kurukshetra, Haryana 136119, India

e-mail: sudakar@nitkkr.ac.in

G. Verma

e-mail: gaurav@nitkkr.ac.in

A. R. Nair

R&D Divisions, Toshiba Software (India) Pvt. Ltd., Bangalore, India

e-mail: anil.nair@toshiba-tsip.com

© Springer Nature Singapore Pte Ltd. 2021

G. S. Hura et al. (eds.), *Advances in Communication and Computational*

Technology, Lecture Notes in Electrical Engineering 668,

https://doi.org/10.1007/978-981-15-5341-7_58

1 Introduction

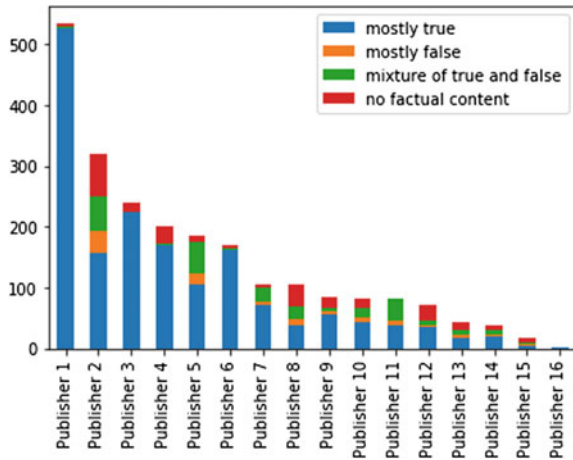
Fake news refers to the fictitious article/media that are deliberately circulated on the Internet with the aim of deceiving the readers. There are a lot of things you read online especially from the social media it can be true or fake. “Fake news is news, article, or hoaxes that is factually incorrect and is delivering to misinform or deceive readers.” One of the strongest evidences of the fake News came up during the time of demonetization. The concept of fitting a GPS chip on the 2000 rupees notes made a big news until the RBI clarified officially that no such advance features used in new currency of India. Reason behind spreading fake news on social media is that most of the people spent their time online and gather information. In a survey, the Pew Research Centre announced [1] that 62% US adults collected the information through social media in 2016 while in 2012, it was only 49%. But the content of news on social media is lower than other traditional sources.

Fake news was not a technical word in the past few years, but in present, we give it more importance. Fake news is intentionally spread to change the mentality of human beings. Identification of fake news can be challenging because it is written intentionally to mislead peoples and distort the truthfulness of information. In the previous work, many authors solve this problem in different ways. They have mainly focused on news contents and social contexts linguistic features [1] capture the total word, character per word, frequency of words, and frequency of function words and phrases. Visual features extract from videos and images to classify the different characteristics of news.

Open your eyes and see around, and you will find many applications which are based on the machine learning like face detection in Facebook or getting a recommendation for a similar product from the Amazon. Now we are applying these techniques to find out a fake news or a real news, fake news detection is a classification problem. Classification is the technique of dividing the datasets into different categories or groups on the basis of learning behavior. How the receive mail is classified the as spam or not, this is nothing but classification. In this study, we have chosen five machine learning algorithms: k-nearest neighbor (KNN), support vector machine (SVM), random forest, logistic regression, and naive Bayes, and compare them in terms of accuracy.

2 About Dataset

In this research work, we have taken two datasets. First one (Dataset A) is taken from Kaggle’s [2] which is based on the new content (sports news article). This dataset is consisting 4000 news articles out of which 2137 are fake news and 1872 are real news. News contents have been taken from the different sources like CNN, NYTimes, Activist Post, and Daily Buzz Live among many. Datasets contain information about the news article taken from which Web site, what are the headlines of news article

Fig. 1 Publisher post counts

and body text where they elaborate the news story. Data points with class label of one are considered as true news, and the data points belonging to zero are labeled as fake news.

The second dataset (dataset B) is taken from BuzzFeed news organization. This dataset gathers information about the user social engagement which was taken from Facebook API.

On social media, people express their emotions or opinions on the basis of news content. This dataset collects all such types of thing which is based on the user social engagement like number of likes in post, number of comments in post, number of time people shared the post. Total number of post in this datasets is 2200 in which is the 1669 number of the post that are mostly true, 104 is the number of the post are mostly false, 245 is the number of the post are mixture of true and false, and 264 is the number of the post is no factual content. After collecting the data, we explore the analysis of our dataset more deeply as shown in Fig. 1.

Total number of news publisher is 16 who have published the news articles. We look at the mechanism for share count, reaction count, and comment count. Most of the time, publisher 1 and publisher 6 mostly time publish true information compared to another publisher. When publisher 2 (“1.25E+15”) published true news, reaction count and share count are very less and if they publish fake news, number of share count and reaction count increase as shown in Figs. 2 and 3.

2.1 Features Extraction and Features Selection

Detection of fake news in traditional news media is mainly dependent on the news content, while in social media it depends on user social engagement. The first dataset is based on linguistic approaches that gather information about the news stories. For

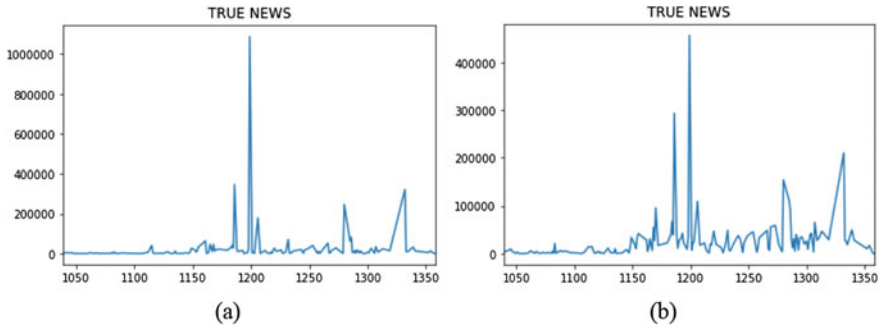


Fig. 2 True news; a share count, b reaction count

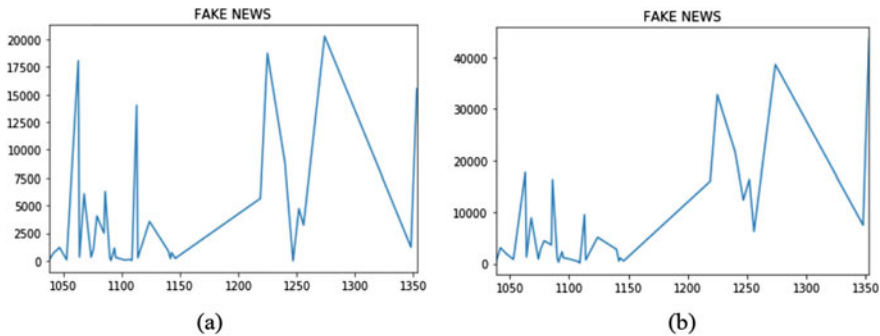


Fig. 3 Fake news; a share count, b reaction count

text data, some special preparation is required before training our model. It is the most common task in machine learning. So, we are using TF-IDF to convert unstructured text to use full features. The term frequency–inverse document frequency (TF-IDF) is a well-known technology to evaluate how important a word in a document. It is very interesting thing to convert string data into sparse features. The TF-IDF is a numerical measure that tells about the importance of the word with respect to the text body. It measures the weight that how often the word appears in a document, over how often it appears in everywhere. If TF-IDF value of the article is very low, then we give less importance to article and vice versa. A word which rarely comes in the document has a higher TF-IDF value. Spares matrix was generated with the help of tokenized data than this feature is used in the prediction problem.

Second datasets are based on the user social engagement. User profile is categorized in two ways: one is explicit and other is implicit features [3]. Explicit features are based on the user social activity. If user shares more number of true news compared to other user, then degree of trust is high for that user and if user shares more number of fake news than they have higher trust degree. We explore different implicit features: gender, age, and personality. This data contains different features out of which are

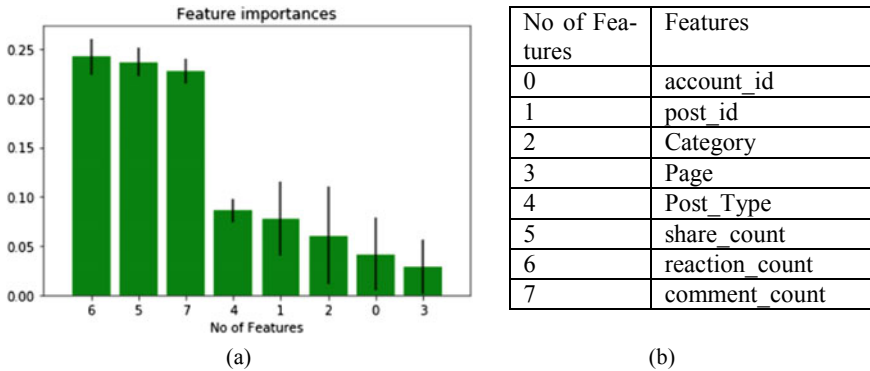


Fig. 4 Data B; a features importance, b features

important for classification can be found with the help of forests of trees which are shown in Fig. 4.

The green bar shows the features importance of the dataset. This plot shows that five features are informative, while the remaining are not.

3 Models

3.1 K-Nearest Neighbor

K-nearest neighbor is the instance-based learning or lazy learning which is used for classification and regression problem. It is based on the supervised machine learning algorithm which is mostly used for the classification problems. Why this is called lazy because when we get the training example, they do not process them or learn a model; instead we just store the data and when we need to classify the instance; at that time, we perform some mathematical calculation. In k-nearest neighbor, K is the number of nearest neighbors which are voting class of new data or testing data [4]. See Fig. 5, suppose this is an instance space and we have different points (x, y values) in each instance space; when a new instance arrives, they classify the new data on the basis of most similarity to the nearest neighbor.

Let us assume that $K = 3$, it means that we are choosing three points which have the minimum distance from the new data or new instance, and if $K = 6$, we are looking for six points which have the minimum distance from the new instances. When we are building k-nearest neighbor model, so to choose the value of “K”, we perform cross-validation technique to test the several value ok K and in order to determine the optimal value of “K”. K-nearest neighbor algorithm used Euclidean distance to find out the nearest neighbor.



Fig. 5 a 3-NN decision rule, b 6-NN decision rule news

$$d(q, p) = \sqrt{\sum_{i=1}^n (q_i - p_i)^2}$$

where $d(q, p)$ is the distance between training object and testing object.

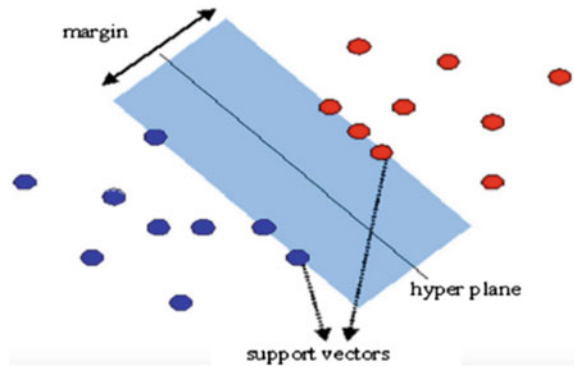
3.2 Logistic Regression

Logistic regression is one of the algorithms used for binary classification. Logistic regression is the proper regression analyses to conduct when the dependent variable is categorical. It is used to explain the relationship between one dependent binary variable and one or more nominal, interval or ratio-level independent variables.

3.3 Support Vector Machine

Support vector machine is a supervised learning algorithm that takes data and sorts it into one of the two classes. This is used for both classification and regression problem. Support vector machine is one of the most accurate classifiers, the reason behind that it has good mathematical intuition, and we can easily handle certain situations where nonlinearity happens with the help of different kernel functions. The objective of the support vector machine algorithm is to discover the hyperplane in N-dimension space that classifies all training vectors in two classes. To distinguish two or more classes of data points, there are numerous hyperplanes that can be used. So, we find the extreme edge hyperplane which has the maximum margin (the maximum distance between the training vectors of both the classes) as shown in Fig. 6. The advantage of the SVM model is to prevent overfitting, and we can easily handle large number of features without a lot of calculations.

Fig. 6 Support vector machine



3.4 Random Forest

Random forest is a technique that depends on the multiple decision trees, and the decision of the majority of the tree is chosen by the random forest. In other word, random forest is a method where we build multiple decision trees and merge them together to get more accurate prediction. A decision tree is a graphical representation of all the possible solutions. In real-life scenario, most of them used it; for example, when you dial a toll-free number of any organization, it redirects to intelligent computer assistance, where we ask some question like press 1 for English or press 2 for Hindi and press 4 for this and so on, now when you select 2, and now again it redirects to certain sets of the question so this keep repeating until you not get the right person. All these things are done with the help of decision tree algorithm.

3.5 Naive Bayes

Naive Bayes classifier works on the principle of conditional probability as given by Bayes' theorem. Bayes' theorem finds the conditional probability of event A given the probability another event B has already occurred:

$$P(A|B) = \frac{P(B|A)P(A)}{P(B)}$$

where $P(A|B)$ is the probability of given A given B , $P(B|A)$ is the probability of given B given A , $P(A)$ is the probability of A occurring, and $P(B)$ is the probability of B occurring.

Naive Bayes algorithm is primarily used for text classification. A few examples are spam filtering and sentimental analysis.

4 Implementation Details

In this research work, we have two types of datasets, so we have built two models. First model, this is based on the linguistic approach. A machine learning model can be a mathematical representation of real-world process. To generate a machine learning model, we need to provide training data to a machine learning algorithm to learn from it. Data are split into training and testing datasets in the ratio of 80–20. Model learns only numerical data so we have extracted meaningful features with the help of TF-IDF. The TF-IDF is a numerical measure that tells about the importance of the word with respect to the text body and generates a sparse matrix with the help of tokenized data, and then these features have been used in prediction problems. After the learning period of model, we have tested the performance of the model and compared them to find out which one is best (Fig. 7).

Second model, in this experiment BuzzFeed organization dataset is used that gathered the information about user’s social engagement. First steps are loading the information, and after that, it performs feature selection and preprocessing. Before splitting datasets into training and testing, we perform normalization and transformation of data into standard dataset then after dataset was split into 80 splits of training and 20 splits of testing sets. Algorithms have been run 15 times with different training and testing datasets and prediction accuracy obtained from these runs (Fig. 8).

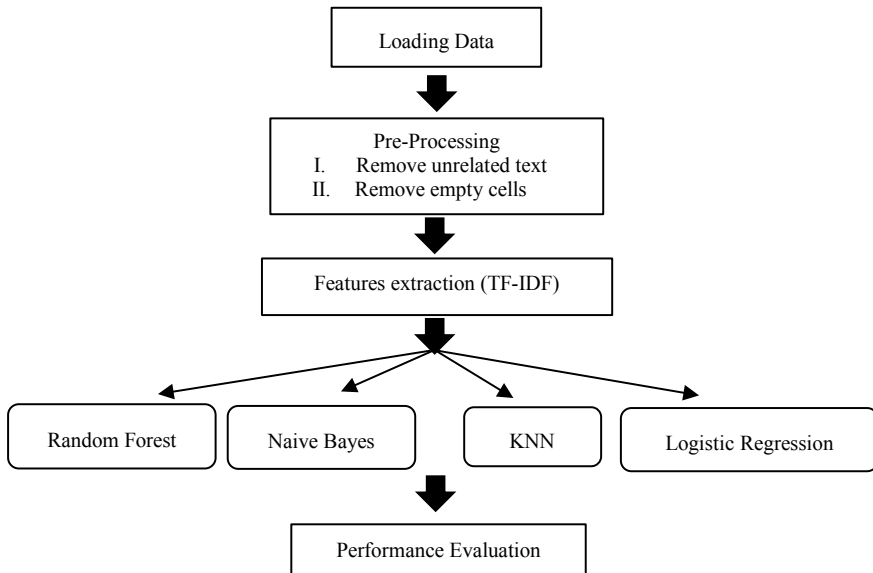


Fig. 7 Procedure of building model one

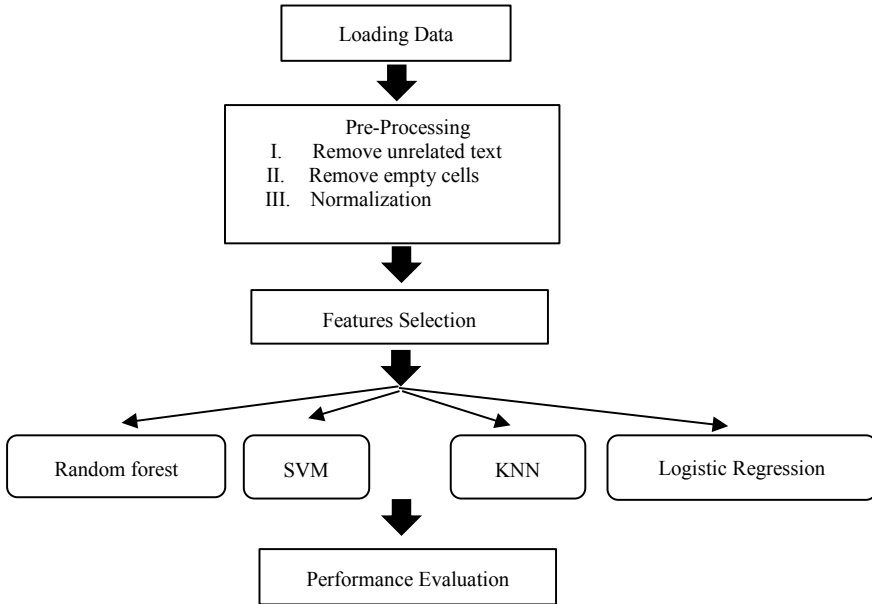


Fig. 8 Procedure of building model two

5 Result

In this section, we have discussed the performance metrics and classification result.

- We compared our models using confusion matrices. A confusion matrix showed the number of misclassification and correct classification made by the model. The result observed in terms of confusion metrics is shown in Fig. 9.
- Figure 9 shows that out of 1203 news articles, 1179 news articles are classified correctly while 24 are misclassified in model, while in model two out of 457 news article, 372 news articles are classified correctly and 85 are misclassified.
- In this research work, we have compared logistic regression, support vector machine, random forest, naive Bayes, and k-nearest neighbor classification model. In a dataset A, logistic regression and naive Bayes performed well on this dataset and we achieved maximum classification accuracy is 98.25% in logistic regression. For this dataset, we have not considered SVM because it is not performing well (53% accuracy). For a dataset B, support vector machine and KNN well performed and maximum accuracy achieved by k-nearest neighbor model, i.e., 81.40%. The average accuracy, average precision, average recall, and F1-score of each model are shown in Tables 1 and 2.
- In dataset A, though the average accuracy of logistic regression is higher than naive Bayes, support vector machine, and random forest, random forest did not

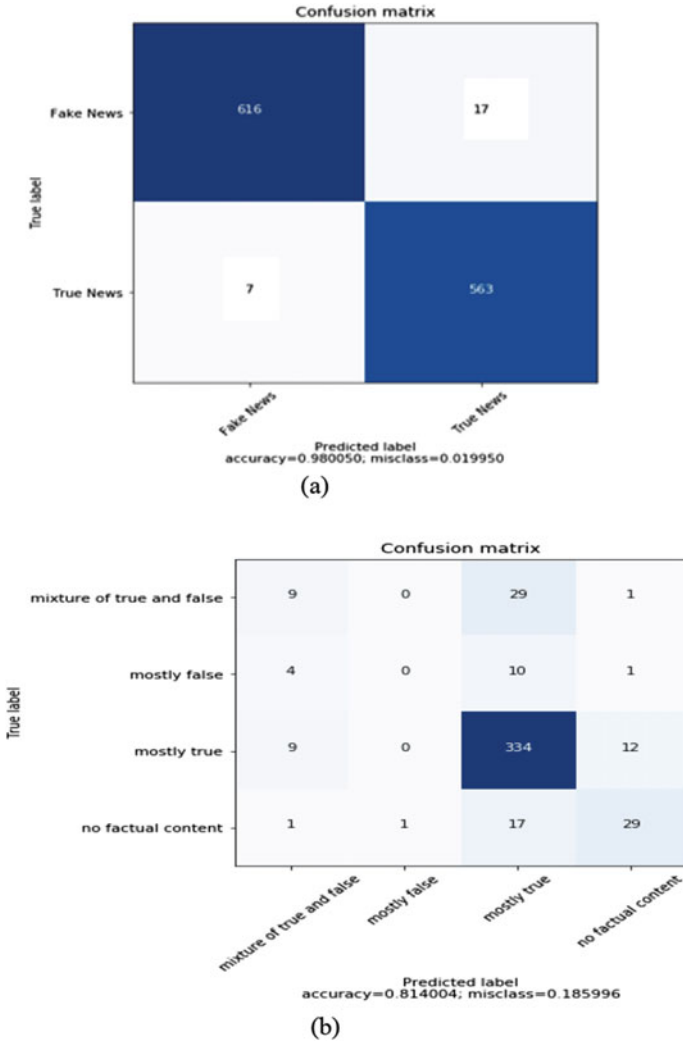


Fig. 9 Confusion matrices; a Dataset A, b Dataset B

Table 1 Performance of model one on test set

Algorithms	Accuracy	Precision	Recall	F1-score
Naive Bayes	94.14	0.94	0.95	0.94
KNN	92.04	0.92	0.93	0.92
Random forest	77.67	0.83	0.77	0.76
Logistic regression	97.93	0.97	0.98	0.97

Table 2 Performance of model two on test set

Algorithms	Accuracy	Precision	Recall	F1-score
KNN	76.13	0.70	0.76	0.72
SVM	76.19	0.64	0.76	0.70
Random forest	75.05	0.63	0.75	0.67
Logistic regression	73.56	0.61	0.73	0.64

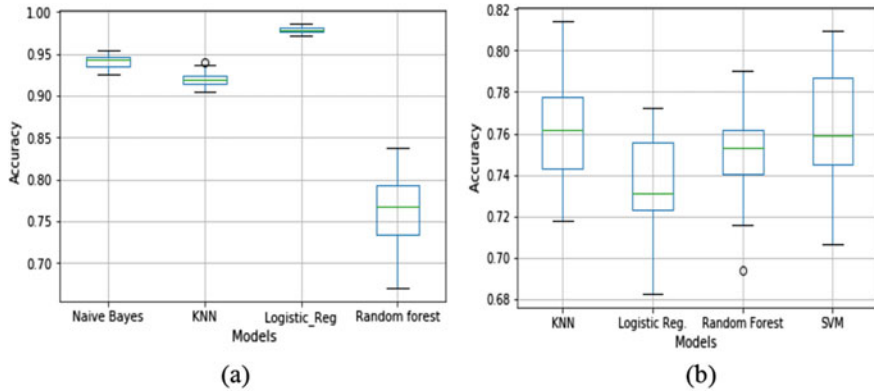


Fig. 10 Box plot for accuracy comparison of the models; **a** Dataset A, **b** Dataset B

perform well. In a dataset B, support vector machine and k-nearest neighbor both performed well (see Fig. 10).

6 Conclusion and Future Work

Nowadays, fake news on social media is a very interesting problem. We have proposed different classification methods to detect fake news on the basis of content of news (headline) and user’s engagement on social media. In a dataset A, logistic regression performs better than the support vector machine, naive Bayes, and random forest. In a dataset B, support vector machine performs better than k-nearest neighbor, logistic regression, and random forest. In the future, it would be interesting to modify the model based on add features and data points or built a well-performed classifier using bootstrapping. We also understand the other users’ profile features which can be used for fake news detection.

References

1. Shu K, Sliva A, Wang S, Tang J, Liu H (2017) Fake news detection on social media: a data mining perspective. *Newsletter ACM New York*
2. Datasets A, Kaggle. <https://www.kaggle.com/jruvika/fake-news-detection/activity>
3. Yumeng Q, Wurzer D, Cunchen T (2017) Predicting future rumours. *Chin J Electron*
4. Okfalisa M, Gazalba I, Gayatri N, Reza I (2017) Comparative analysis of K-Nearest Neighbor and modified K-Nearest Neighbor algorithm for data classification. In: 2nd international conferences on information technology, information systems and electrical engineering (ICITISEE) (2017)
5. Granik M, Mesyura V (2017) Fake news detection using Naive Bayes classifier. In: IEEE first Ukraine conference on electrical and computer engineering (UKRCON)
6. Tacchini E, Ballarin G, Veova MLD, Moret S, Alfaro L (2017) Some Likeit Hoax: automated fake news detection in social network
7. Wikipedia—K-Nearest Neighbors Algorithm, from www.wikipedia.org
8. Golbeck J, Mauriello M, Auxier B, Bhanushali KH (2018) Fake news vs. satire: a dataset and analysis. *Web science* (2018)
9. Imandoust SB, Bolandraftar M (2013) Application of K-Nearest Neighbor (KNN) approach for predicting economic event: theoretical background. *Int J Eng Res Appl*
10. Zhang Q, Zhang S, Dong J, Xiong J, Cheng X (2015) Automatic detection of rumor on social media. Springer, *Natural Language Processing and Chinese Computing*
11. Aldwairi M, Alwahedi A (2018) Detecting fake news in social media networks. In: The 9th international conference on emerging ubiquitous systems and pervasive networks (EUSPN)
12. Jin Z, Cao J, Zhang Y, Zhou J, Tian Q (2017) Novel visual and statistical image features for microblogs news verification. *IEEE Trans Multimedia*
13. Wikipedia—Fake news websites, from www.wikipedia.org
14. Biyani P, Tsioutsoulis K, Blackmer J (2016) 8 amazing secrets for getting more clicks: detecting Clickbaits in news streams using article informality. In: Thirtieth AAAI conference on artificial intelligence (AAAI-16) (2016)
15. Shu K, Wang S, Liu H (2019) Understanding user profiles on social media for fake news detection. *IEEE MIPR*
16. Conroy NJ, Rubin VL, Chen Y (2015) Automatic deception detection: method for finding fake news. *ASIST*
17. Gupta S, Thirukovalluru R, Sinha M, Mannarswamy S (2018) A community infused matrix-tensor coupled factorization based method for fake news detection. In: IEEE/ACM international conference on advances in social network analysis and mining (ASONAM) (2018)
18. Rubin VL, Conroy NJ, Chen Y, Cornwell S (2016) Fake news or truth? Using satirical cues to detection potentially misleading news. In: *Proceeding of NAACL-HLT*
19. Brewer PR, Young DG, Morreale M (2013) The impact of real news about “fake news”: intertextual processes and political satire. *Int J Public Opin Res*
20. Wang WY (2016) “Liar, liar pants on fire”: a new benchmark dataset for fake news detection

Vehicle Tracking System Using GPS and GSM



Shreya Verma, Abhay Singh Jamwal, Surabhi Chauhan,
and Sribidhya Mohanty

Abstract The vehicle tracking system is a modern security and armada handling method. This module is an example of an embedded system that can be used by vehicles to track and know the position is known by global positioning system and global system in particular vehicle. The proposed system is embedded in the car that provides exact real-time location and position. Whenever there occurs any vehicle problem like robbery, accident, fire alarm, etc., in view of these issues, a message will be delivered from the vehicle about its position in view of latitude and longitude to the expected receiver who is asked for help. A program is coded to get the proper position of the vehicle which is on move or steady. In order to identify the location of the vehicle that includes Latitude and Longitude position and also receive continuous data from the two effective systems used which is a GSM and a GPS Modem identifying the position.

Keywords GPS · GSM · Embedded system · Real-time tracking system

1 Introduction

This smart world needs new, cost-effective, and advanced technologies to work and have a comfortable leaving. This vehicle tracking is one of those technologies which is used to design a cost-effective module for tracking a vehicle such as truck or bus in our day-to-day life. The safety and security is also a prime concern in today's life.

S. Verma · A. S. Jamwal · S. Chauhan · S. Mohanty (✉)
Graphic Era (Deemed to be) University, Dehradun, India
e-mail: vidhya.mohanty@gmail.com

S. Verma
e-mail: shreya8256@gmail.com

A. S. Jamwal
e-mail: abhayjamwal04@gmail.com

S. Chauhan
e-mail: chauhansurabhi04@gmail.com

By finding the real-time location a person, we can plan a to-do list to decrease the traveling time and distance covered. With the help of this, any individual can plan a program which takes less time and managed plan. The proposed research paper deals with an efficient vehicle tracking system using the core communication technologies like for position finding—global positioning system [1, 2], for data transmission—General Packet Radio System [3], and for display of location—Google Maps-related software. The proposed setup can be used for an effective intelligent transportation system [4]. This designed vehicle tracking system can behave as a life-saving device in case of any emergency condition where it can provide quick and automatic report of the vehicle which needs to be rescued or needs help to the concerned person not only in this mentioned matter, but if the vehicle is lost or stolen, the position can also be detected and intimated. The technology defined in this process is highly helpful to track, secure, and plan the traffic and your destination goal by just your finger tip. The technological development made here helps the management of traffic and security of the vehicles in all aspects.

The proposed system provides a tracking module used in real time with the implementation of GSM and GPS. In order to identify the exact location of the device, GPS module is used which transmits the information of location time to time to a server. The server here can be a personal computer or laptop which needs to have a server program or Web server program to get the location data which can be converted to the pattern which can be displayed over Google Maps. The module used to be kept in vehicle for tracking that is the vehicle unit; this unit involves the hardware like the Arduino, GPS, and GSM modem. This module mostly has a GPS modem that involves a GPS antenna to receive the signal from satellite. The GPS modem provided converts the data received and sends via SMS. The position and the coordinates can be visualized using Google Maps with proper database and software that gives the location of coordinates of each position in search and then stored in expected database. However, to get the present location of the concerned automobile it has travelled, the user has to connect it to the Web server.

We reviewed the technology in Sect. 2. Section 3 deals with the architecture of the system and its realization with the GPS system. Section 4 here deals with the prototype of the system used and images related to our proposed work. The conclusion deals with our work and its future implementation which is given in Sect. 5.

2 Background

2.1 GPS System

Global positioning system is an effective satellite-related system which has 24 satellites of the USA; it was mostly designed for military applications and later implemented for general application. The prescribed satellites time to time provide short-pulse radio signals to GPS receiver. This GPS module is used to measure the distance

Fig. 1 GPS module

and calculate two-dimensional position (latitude and longitude) which needs two satellite and for three-dimensional position at least four satellites. After the location is calculated, the average speed and the expected direction of the moving vehicle are calculated.

This module is used for tracking the position of the means of transportation. A GPS satellite helps in getting the geographical location by receiving information. Figure 1 shows the GPS module.

2.2 *GSM Module*

The proposed vehicle tracking system needs a GSM modem which requires a SIM card and a mobile phone. GSM modem is used to provide Internet connection and also used for transmitting and receiving SMS and MMS; for these purposes, the GSM modem is connected to a computer.

Our proposed GSM module is SIM900A Mini (Fig. 2).

2.3 *Arduino Uno*

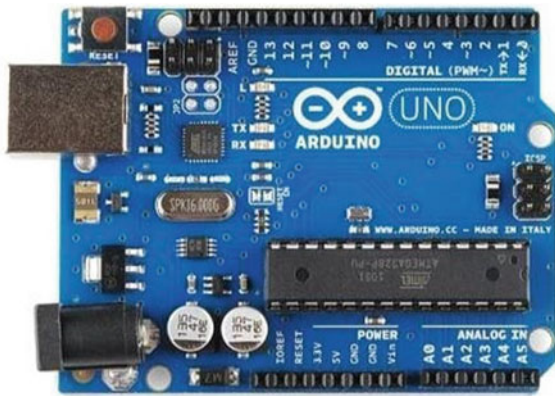
For the programming of the module, Arduino Uno was considered. It is microcontroller board on the ATmega328P. Arduino Uno is self-defined board designed for training and development for the projects; it has mostly all the hardware and software details needed by microcontroller. The features of ATmega328 memory are 32, 2 KB of SRAM, and 1 KB of EEPROM. This Arduino Uno board has 20 digital input/output pins, a USB connector, a power jack, an in-circuit system programming header, and a reset button. The connection here is very simple and can be done with computer through a USB.

The power supply of the board can be given by a USB connector from the computer, a DC power jack, or the V_{in} pin present onboard. The supply voltage can be 5 V or 3.3 V pins, and the maximum current drawn is 50 mA [4] (Fig. 3).

Fig. 2 GSM module



Fig. 3 Arduino Uno



3 Proposed System and Design

The proposed vehicle tracking system is an cost-effective, smart, and less expensive tracking technology. This model deals with the flow of taking input from GPS and delivering it to GSM module of the expected mobile or laptop which is used for mobile linkage. For the security of the system, the module uses a global positioning system, which locates the vehicle that is to be traced and uses the satellite to transmit the coordinates of the vehicle to the monitoring system. At the monitoring system, many number of software are needed to locate the vehicle in the specified map.

Therefore, by the above-mentioned way, the owners of the vehicle are able to locate their respective vehicle. This vehicle tracking system is efficient as it uses the real-time tracking facility.

In this proposed design, we are designing an embedded system that implements tracking and locating a vehicle by the use of global positioning system and global system for mobile communication. The system continuously monitors a moving vehicle and time to time reports its status. In order to do this application, the microcontroller is serially interfaced with the GSM modem and GPS receiver. The GSM modem is needed to identify the latitude and longitude of specific vehicle, and GPS modem periodically delivers the data which involves the latitude and longitude giving the location of the vehicle. This GPS modem provides the output of many parameters, and LCD is used for display. Obtained data is transferred to the mobile which is at a distance from the vehicle. A memory is needed for the data received by the receiver at the GPS; the memory used can be EEPROM.

To visualize the position information of the tracking vehicle, LCD is interfaced with the microcontroller, and along with LCD, the other interfacing modules mentioned are GSM modem and GPS receiver. Whenever request is generated by the user to the mentioned number in modem, the system defined will send an answer to that mobile telling the location of the vehicle in terms of its latitude and longitude. The proposed vehicle tracking system has a program to get the exact position of the vehicle along with its navigating track detail of the moving vehicle on Google Maps.

3.1 Working

The proposed model consists of microcontroller interfaced with GPS receiver and GSM module. Whole system is fixed inside a vehicle with a power source. This GPS system is used to gather exact longitudinal and latitude values representation of the position of the vehicle and send to microcontroller which will further send this data with the use of GSM modem.

By chance if the vehicle leaves the destination, then the record of the person can be maintained by the other users like his friends, or boss who can send command to the registered SIM card and the data will be received. The process of SMS is that the SMS is sent and would come by service provider of GSM, and then, it would arrive at the vehicle, which is on the move, due to the GSM device installed over the vehicle. The microcontroller will get the SMS from the GSM modem. The data received will be checked, compared, and verified with the command sent, and if it matches all the data, the information will be sent to the user.

For receiving the data, the system needs the GSM as a receiver in the vehicle that achieves these data and gives PC serially. The security of the device is maintained by the password; i.e., only the person who is familiar with password will only be able to use it. For any emergency condition, the device will automatically send an alert to registered number.

4 System Prototype

Prototype of the design in Sect. 3 is implemented. Vehicle tracking prototype is shown in Fig. 4. GPS tracking which deals with the tracking history is shown in Fig. 5. Example of one GPS tracking modules via Google Maps is represented in Fig. 6 [5, 6].

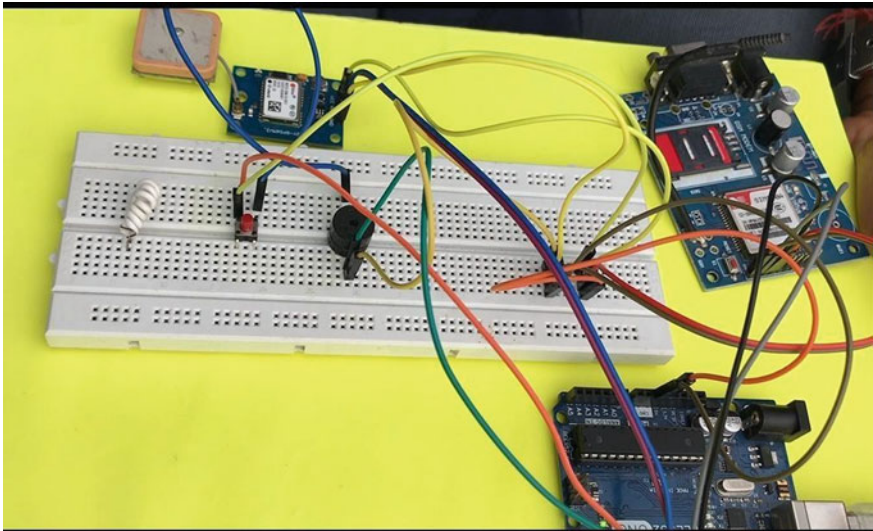


Fig. 4 Vehicle tracking prototype system

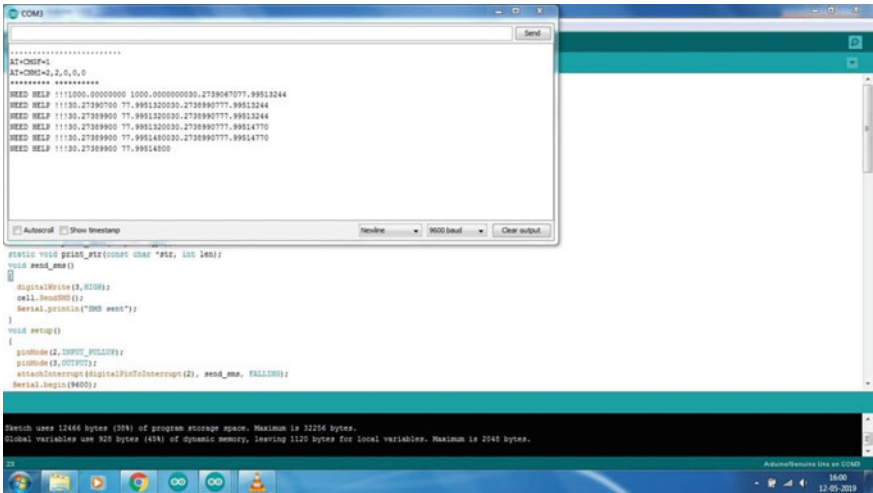


Fig. 5 GPS tracking modules

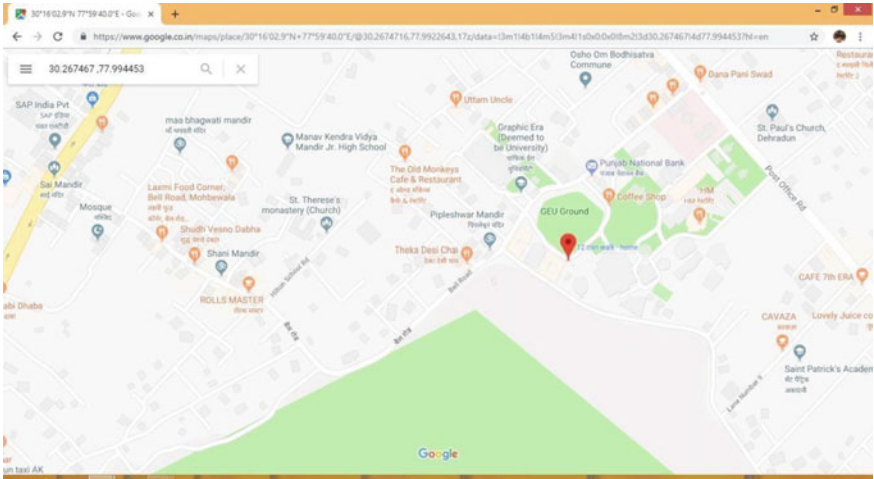


Fig. 6 Example of one GPS tracking modules via Google Maps

5 Conclusion and Future Implementation

The proposed paper deals with a prototype having a product-based hardware and open software for a feasible source vehicle tracking system. Vehicle tracking system has shown the proper compatibility of using it for complicated environment of traffic. This prototype has an important application in lost vehicle tracking. In future, we expect to add more precise and effective sensors in the vehicle. For effective tracking management, the sensors in the vehicle report the status detail to the expected server used for handling the information and in effective tracking. This proposed model can also be useful to keep safety of the women by tracking it into their vehicles and to enhance their safety. By connecting piezoelectric sensors, we can predict the pressure level of the vehicle along with tracking. Vehicle tracking systems are mostly implemented in armada operators to deal with armada management parameters which include operations like routing, onboard information, and security. Other uses may be checking the driver behavior by the boss and parents of minor driver [7].

References

1. Kaplan ED (1996) Understanding GPS: principles and applications. Artech House Publishers. ISBN 0890067937
2. Maurya K, Singh M, Jain N (2012) Real time vehicle tracking system using GSM and GPS technology—an anti-theft tracking system. Int J Electron Comput Sci Eng. ISSN- 2277-1956
3. Bates RJ (2001) GPRS: general packet radio service, 1st edn. McGraw-Hill Professional. ISBN 0071381880

4. McDonald M, Keller H, Klijnhout J, Mauro V (2006) Intelligent transport systems in Europe: opportunities for future research. World Scientific Publishing Company. ISBN 981270082X
5. Google, Inc., Google Earth software. <http://earth.google.com/>
6. Google, Inc. Keyhole markup language documentation introduction. <http://code.google.com/apis/kml/documentation/>
7. Goel A, Gruhn V (2006) Fleet monitoring system for advanced tracking of commercial vehicles. In: Proceedings of the 2006 IEEE international conference on systems, man, and cybernetics (SMC 2006)

Multi-factor Authentication Scheme Using Mobile App and Camera



Sajal Jindal and Manoj Misra

Abstract Phishing attacks are one of the most serious threats faced by the users on the internet the attackers try to steal sensitive information such as login details, credit card details, etc. by deceiving the users to enter sensitive information on the phishing websites and thus leading to huge financial losses. Many schemes have been proposed to detect phishing attacks but the amount of such attacks has not decreased. New attacks like Active Man-In-The-Middle (MITM) phishing attacks have emerged which include Real-Time Man-In-The-Middle (RT MITM) and Controlled Relay Man-In-The-Middle (CR MITM) phishing attacks. These attacks allow the attackers to obtain the users' account details and relay them in real-time. Similarly, the attacker can lure the user to enter details on a spoofed app and thus gain access to the user's account. The existing popular authentication schemes fail to address these attacks. In this paper, we propose a novel user authentication scheme that enables the user to log into his/her account without memorizing any password or any other authentication token. In the proposed scheme, the user has to scan a dynamically generated QR-code using the smartphone app and then verify the image, captured by the webcam and sent it on the smartphone via push notification. Thus, the complete authentication procedure requires minimal user involvement and implements automatically. We have implemented and evaluated the proposed scheme in terms of usability, deployability, and security parameters and the results depict that the proposed authentication scheme performs well and can be used as a secure user authentication scheme.

Keywords Phishing · RT MITM · CR MITM · Malicious browser extension · QR-code · Multi-factor authentication

S. Jindal (✉) · M. Misra
Department of Computer Science and Engineering, Indian Institute of Technology Roorkee,
Roorkee, Uttarakhand, India
e-mail: sjindal@cs.iitr.ac.in

M. Misra
e-mail: manojfec@iitr.ac.in

© Springer Nature Singapore Pte Ltd. 2021
G. S. Hura et al. (eds.), *Advances in Communication and Computational Technology*, Lecture Notes in Electrical Engineering 668,
https://doi.org/10.1007/978-981-15-5341-7_60

787

1 Introduction

1.1 Phishing

Phishing is a deception technique that is used to steal users' credentials with the goal of obtaining their personal information [1]. Phishing is an attack scenario in which the attackers known as the phishers masquerade as authentic websites and somehow lure the users into entering their credentials. The URL link of the phishing website is generally spread by spreading email in bulk or other communication medium. Naive users, who still don't verify the domain names or other technical information tend to follow the instructions mentioned on the phishing website or email. In this way, the users generally reveal their credentials which are used by phishers for various malicious purposes such as identity theft, online credit card, and banking frauds, etc. [2–6]. For redirecting users to the phishing website, the attackers can use one of the following techniques—email spoofing, deceptive links, malicious browser extensions, etc. There are various kinds of attacks that are used by the attackers to access the users' account, such as—RT MITM, CR MITM, malicious browser extension based phishing attacks.

After the first official cyber threat was recorded in 1996, many anti-phishing organizations such as APWG, RSA [7], Phishtank, etc. have not only recorded numerous phishing attacks but also analyzed them. According to the APWG phishing trends report [8], the number of phishing websites recorded in the 4th quarter of 2018 was 138,328 which is not a significant decrease from the previous quarter. Thus, we can see that even after the proposal of various phishing detection and prevention schemes, the number of phishing websites and the number of phishing emails do not decrease drastically. Table 1 shows the phishing attack trends as per APWG report [8, 9] from H1 2017 to Q4 2018. The parameters considered by the reports for recording

Table 1 Current phishing attack trends [8, 9]

Parameter	4Q2018	3Q2018	2Q2018	1Q2018	4Q2017	3Q2017	1H2017
Number of unique phishing websites detected	138,328	151,014	233,040	263,538	180,757	190,942	291,096
Number of unique phishing email reports received by APWG from consumers	239,910	270,557	264,483	262,704	233,613	296,208	592,335
Number of brands targeted by phishing campaigns	836	777	786	746	939	915	2660
Most Targeted Industry Sectors (Payment) (%)	33.0	38.2	36	39.4	42	41.99	45

and analyzing the attack trends are number of unique phishing websites detected, number of unique phishing websites reported, and number of brands targeted. The most targeted industry sector by the attackers have been payment with 33% in 4th quarter of 2018 followed by webmail or software as a service (SaaS) with 20% in 4th quarter of 2018.

1.2 Motivation and Contribution

There have been continuous efforts in the past by the researchers to provide an authentication scheme that is secure as well as usable. Multi-factor authentication schemes were proposed because single-factor authentication schemes were incompetent in handling traditional phishing attacks. Multi-factor authentication schemes such as OTP-based, QR-code, push login and graphical password-based authentication schemes are not secure against advanced phishing attacks including RT MITM (Real-Time Man-In-The-Middle) phishing attack and CR MITM (Controlled Relay Man-In-The-Middle) phishing attack. The phisher gets access to the user's account in OTP as well as QR-code based authentication scheme by relaying the information in real-time. The attacker can compromise CAPTCHA-based graphical password-based schemes either by monitoring the user's desktop screen or by relaying the desktop terminal over the user's terminal. Since biometric-based authentication scheme does not offer 100% accuracy and requires external hardware, hence it is not user-friendly. Moreover, biometrics such as fingerprints, facial recognition, etc. are prone to spoofing by the attacker.

This paper proposes a novel secure user authentication scheme that makes use of the user's smartphone and the desktop's webcam. The scheme requires the user to scan the QR-code displayed on the browser using the smartphone app which stores a secret key for that particular user in secure storage. The webcam then captures the user's image, adds a random text at a random position in the image, and sends it to the user via push notification for verification. Once the user verifies the authenticity of the image, the user gets access to the account. Thus, the scheme proposed in this paper requires minimal user involvement as there is no need for the user to remember any username or password. Since the user does not enter any information, there are less chances for the attacker to retrieve any user information using the phishing website.

1.3 Paper Organization

Section 1 gives a brief introduction to phishing and its effect in various industry sectors. Section 2 gives a brief description of various multi-factor authentication schemes, their advantages, and the research gaps present in them. In Sect. 3, a detailed

design of the registration and the login phase have been explained. Section 4 is dedicated to the testing and performance evaluation of the proposed user authentication scheme. Section 5 concludes our work and describes how it can be taken forward.

2 Related Work

There are various web authentication schemes available using which the user can login to the website. The simplest authentication scheme is by providing a username and password. The existing authentication schemes can be categorized as:

1. **Authentication using OTP/PIN:** The OTP-based schemes such as Google 2-step [10] requires the user to first enter his/her username and password. The server then generates and sends an OTP (one-time-password) to the user's registered phone via SMS. If the credentials and the OTP are entered correctly by the user, then the user will be logged into the website. Other OTP/PIN-based two-factor authentication scheme is SAASPASS [11] in which the SAASPASS application is installed by the user on his/her smartphone which is linked to the user's personal web account. At the time of login, SAASPASS generates and sends a 6-character PIN to the server as well as the user. This 6-character PIN is updated and sent every 30 s. Both the above-mentioned schemes are vulnerable to MITM phishing attacks as the attacker can get the OTP/PIN with the help of a phishing website or through a malicious browser extension.
2. **Authentication using QR-code:** Xie et al. [12] proposed a QR-code based authentication scheme in which, the user first gives the username and password to the web-browser. The server validates the user's credentials and renders a barcode on the desktop screen which is scanned by the users using a mobile app and a vouch request is generated in the form of a barcode which is scanned by the PC webcam. This authentication scheme claims to be secure against MITM phishing attack and Diffie–Hellman algorithm is used for securing the communication channel between the browser and the server. Kim et al. [13] also proposed a QR-code based authentication scheme in which the IP address of the smartphone was used to verify that the user and PC are in proximity. In Mukhopadhyay et al.'s [14] scheme, a third-party verifier is used for checking the user's credentials and after verification, sends a challenge in the form of a QR-code to the user. The user, in turn, scans the QR-code using the mobile app and sends back an encrypted response to the third-party verifier. In Dodson et al.'s [15] scheme, the server sends a QR-code consisting of a server challenges to the user. The user then scans the QR-code using his/her smartphone and a challenge response is sent to the server. Once the server verifies the challenge response, the user can access his/her account. This scheme has also been proposed by Dodson et al. in the work [16] for secure payment through a credit card where the user scans the QR-code and gets authenticated. The disadvantage of this scheme is that the

phisher can easily relay the QR-code displayed on the webpage to the phishing webpage and thus luring the user to scan the phished QR-code.

The QR-code scheme proposed by Bakdi [17] requires the user to scan the QR-code displayed on the desktop's screen which contains the server's address URL and then the mobile terminal authenticates the user by extracting the password from the web server and transmitting the same to the authentication server. The authentication is done on the basis of asymmetric key cryptography. A similar QR-code authentication scheme has been proposed in Venkat et al.'s [18] scheme where the webpage contains a QR-code and an animated security image. The user scans the QR-code using the mobile camera and with the information extracted from the QR-code, the user gets identified and then the same security image is sent to the mobile device for verification. Both the above-mentioned schemes are vulnerable to RT MITM and CR MITM attack as the QR-code and any image that is displayed on the screen can be easily spoofed, relayed in real-time on the phishing website. The QR-code scheme proposed by Nunn et al. [19] requires the user to enter the login credentials on the webpage which are transmitted to the web server and then a QR-code is displayed on the webpage. The user scans this code and gets authenticated as the information from the mobile goes directly to the server. This scheme is also vulnerable to RT MITM and CR MITM phishing attacks as the QR-code can be easily phished. Moreover, this scheme also requires login credentials on the webpage due to which it is also vulnerable to malicious browser extension based attacks.

3. **Authentication using CAPTCHA:** In Leung et al.'s [20] scheme, the concept of flash-based OTP CAPTCHA was proposed to provide security against the MITM and malicious browser extension based attacks in which the user's screen is captured by the attacker to steal credentials. The user enters the username and mouse click coordinates of the OTP CAPTCHA which consists of moving letters and numbers. The user's mouse click coordinates on the OTP plugin and the click timestamp is also taken as an input. Zhu et al. [21] proposed a scheme in which CAPTCHA was used as graphical password. The user enters the password by clicking characters in the CAPTCHA and the click coordinates are used by the server for verification. Both the above-mentioned authentication schemes are not secure as Leung et al.'s [20] scheme is vulnerable to CR MITM attack and Zhu et al.'s scheme [21] can be compromised using MITM and screen logging attacks.
4. **Authentication using push notification:** Push notification based login schemes are provided by Yahoo mail [22, 23], in which the user enters his/her username on the website. The server verifies the user's credentials and sends a push notification message to the registered mobile app. The user gets access once he/she verifies the push notification message received on the mobile app. The push notification based login schemes are also provided by Google. The push notification based authentication schemes cannot withstand MITM attacks.
5. **Authentication using password managers:** Password managers [24] helps the user by storing their credentials for different websites and they automatically fill these credentials when the user logs into that website. Most of the password

managers store the user credentials in browser storage. Ross et al. [25] proposed a similar scheme in which, the browser extension is used to modify the password entered by the user with the help of the SALT stored at the client machine and the domain information of the website. Though the attacker won't gain anything even if the credentials are entered by the user on the phishing website, yet this scheme is not secure against malware attacks as well as it is client dependent because the SALT is stored in plain-text on the client machines.

6. **Authentication using hardware token:** This category of authentication scheme requires the user to carry a special hardware token such as security keys, USB, smart cards, etc. for authentication. These hardware tokens may store some passwords which are communicated during the authentication process. Tricipher scheme [26] uses multipart credentials where one part remains with the user and the other part of the credentials is stored in a secure appliance kept in the enterprise data center. A secret key is also stored in the user's device which is also known to the server. The username and password entered by the user are encrypted using this secret key. The secure appliance encrypts the user's credentials using the credentials stored on it, which is then sent to the server, and thus the authentication process is completed. Other hardware token based authentication schemes are RSA SecurID which updates the authentication code every 60 s as well as U2F security keys such as Yubikey [27] which follows the U2F protocol for user verification. In RSA SecurID [28], an authentication code is usually generated every 60 s using the clock and random seed which is provided to the token by the RSA server at the time of purchase of the device. The server computes the authentication code using the seed stored in its database for the token and the clock and verifies it with the code given during the login process.

3 Proposed Scheme

The proposed multi-factor authentication scheme uses a trusted mobile application and a webcam on the client's machine (desktop/laptop). Whenever the user wants to access his/her account on the website, then a QR-code will be displayed on the webpage by the server. This authentication protocol assumes that the mobile application in the user's phone is trusted. The user scans the QR-code displayed on the webpage using the mobile application. The application then sends the user's data along with the session token obtained from the QR-code to the server. The server then gives a prompt on the client's machine to access the webcam and takes a picture using the webcam. This picture is then sent by the server to the mobile application using push notification. The user will then approve or reject the authenticity of the received picture. On approving the picture, the user will get authenticated. Thus, the server authentication is done with the help of the picture taken on the legitimate user's client machine because only the legitimate website can take user's picture using webcam and send the same picture to the user's mobile phone.

3.1 Assumptions

1. PC is assumed to have a webcam that is cheap and easily available.
2. It is assumed that the user uses the authentic Android App during the registration and like many other schemes, the new user registration is free from attacks.
3. The proposed scheme assumes that the data transfer between the client and the server happens over HTTPS and is secure from network sniffing and can be used to exchange secret keys.
4. Authentic website servers and the information stored in their databases are assumed to be secure.

3.2 Threat Model

1. Phishing, MITM Phishing: The attacker can lure the user by directing him/her to the phishing website and then obtain personal information. The attacker can either relay this information in real-time (RT MITM) or can install remote desktop capturing or relay modules on the user's terminal (CR MITM) to steal credentials.
2. Malicious browser extension based phishing attacks: The attacker can steal user's credentials by making the user install a malicious browser extension, asking for permissions to carry out some cautious activity in the background while providing functionality in the foreground. The malicious browser extensions can perform keylogging, screen logging, or password sniffing in the background.
3. App spoofing: The attacker can build a spoofed Android App which looks similar to the authentic app required for login. The attacker can then install this spoofed app on the user's PC and lure the user into entering his/her credentials over this app

3.3 Registration

The user registration involves the registration of the user on the mobile app. Thus, the two entities that are involved in the registration phase are—the mobile app and the web server. The user registration is done on the mobile app which will store the details of the user to be used at the time of login. The user registration in the proposed authentication protocol has been shown in Fig. 1. The steps for registering the user are as follows:

1. The user will first enter relevant details in the mobile app such as username (UID), password (PWD), email address (Email-ID), phone number, etc.
2. The details given by the user are then sent to the web server over the HTTPS session. The web server generates an OTP (one-time-password) and sends the generated OTP to the phone number given by the user.

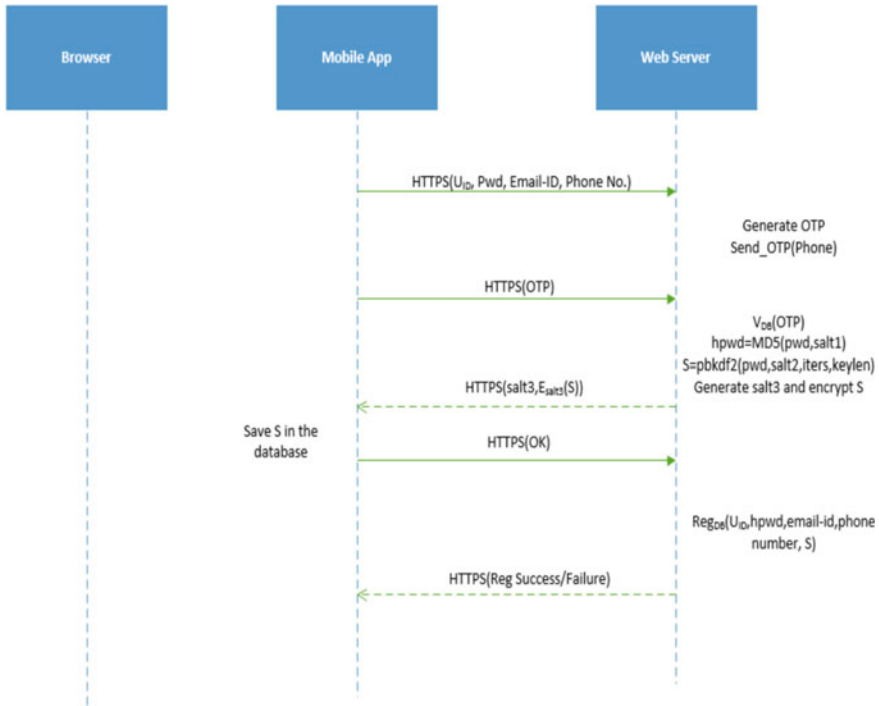


Fig. 1 Registration message exchange

3. The user then enters the OTP received on his phone which the web server verifies.
4. The web server then generates a hashed password (hpwd) from the password (pwd) entered by the user in step (a) and a random salt (salt1).
5. The web server also generates a secret S using password-based key derivation function 2 (PBKDF2). The parameters that are used in the PBKDF2 function are the password (pwd), a random salt (salt2), iterations (itiers) and key length (keylen).
6. The web server then generates another random salt (salt3) which is used for encrypting the secret (S) generated in the above step.
7. After the user presses the OK button on the mobile screen, a confirmation message is sent to the web server over HTTPS session and all the user details along with the shared secret (S) is stored in the web server as well as the mobile database which is secured by the Android Keystore API.
8. The web server finally sends a message acknowledging the successful registration of the user.

3.4 Login

The proposed authentication protocol makes use of three entities for logging the user into the website. The entities used are—the mobile app, browser, and web server. The user will also need a webcam for logging into the system. To login to the website account, the user must be logged into the mobile app of the website. The reason is that the push notification is sent to the app on which the user is logged in. For logging into the mobile app, the user enters the user-id (UID) and password (pwd), which is sent to the web server for verification. Since most of the users do not logout from their account, the chances of re-login to the mobile app is less. The login procedure is as follows:

1. The user first opens the login webpage on the browser.
2. The website login page displays a QR-code which contains a session token generated by the web server.
3. The user scans the QR-code rendered by the website using his mobile's camera.
4. After the QR-code is received by the mobile app, the session token is retrieved from the QR-code. Now a secret (S') is generated by using SHA-256. The parameters used are the secret (S) stored in the Android Keystore API, user-id (UID), and the timestamp (TS).
5. The mobile app also generates request data (RD) which consists of user-id (UID), timestamp (TS), and session token obtained from the QR-code. The request data is then encrypted to form ERD using the secret (S') calculated in step (d) and sent to the web server along with user-id (UID), timestamp (TS) over HTTPS session.
6. The web server also generates a secret (S'') similar to that in step (d) using the secret (S) stored in the server's database and received user-id (UID) and timestamp (TS).
7. The encrypted request data (ERD) is then decrypted using the secret (S'') generated in step (f). The web server then verifies the user-id (UID), session token and the timestamp (TS) obtained from the decrypted request data (RD).
8. A pop-up window then comes up on the browser asking permission to access the client's machine webcam. The user must allow access so as to login to the website.
9. A pop-up window then comes up on the browser asking permission to access the client's machine webcam. The user must allow access so as to login to the website.
10. The webcam then takes a picture of the user, adds a random text at a random position over the image taken, and sends it to the web server, which in forwards this picture to the user's mobile app via push notification.
11. The smartphone app shows the image received via push notification to the user asking for login approval.
12. At this step, the user will verify the image received and will approve login attempt if and only if the login attempt is done by the user himself/herself as well as the image received is authentic.

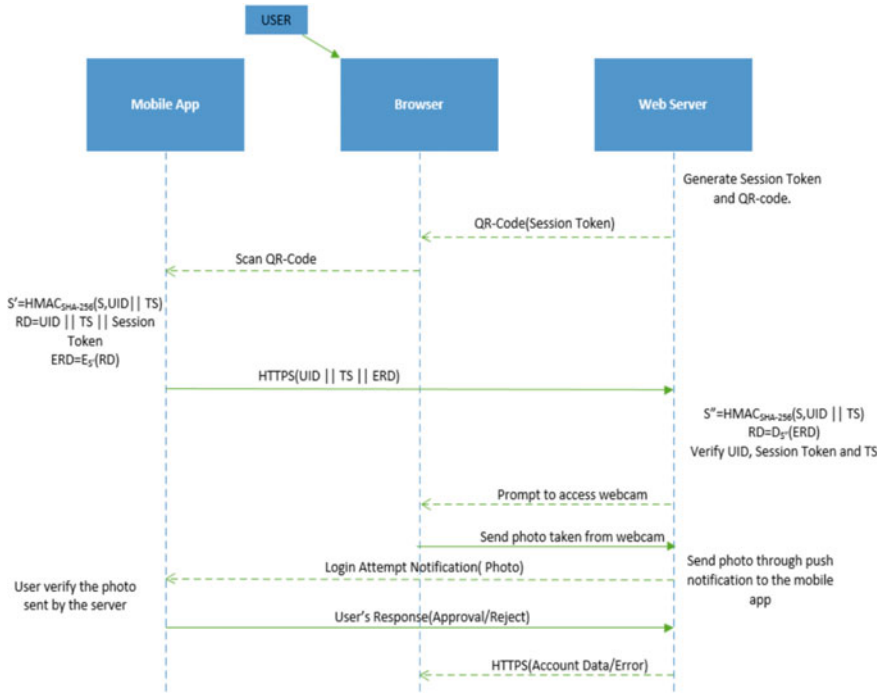


Fig. 2 Login message exchange

- The mobile app sends the user’s response (Approval/Reject) to the web server and based on the response, the web server shows user his/her account or displays login error.

The login session is alive for a particular time period, after which the session will expire and the web server will redirect the user back to the home page displaying a new QR-code and thus preventing the attacker from using the picture taken by the webcam in the later stage for authentication (Fig. 2).

3.5 Recovery

The user can recover his/her account in case the mobile phone is lost or stolen. The user can request the same by using the registered email address. Once the server receives the request for recovery, a link will be shared with the user via the registered email address, where the user will be asked for the password. Once the password is verified, then the previous secret key which was stored in the Android Keystore API, will be replaced with a newly generated secret key which will be automatically sent to the user’s new smartphone, where it will be stored in the Android Keystore API.

4 Testing and Evaluation

4.1 Test Setup

1. A OnePlus 5T smartphone with Qualcomm Snapdragon 835 MSM8998 Chipset, Octa core CPU (Four 2.35 GHz Kryo 280 Performance cores and four 1.90 GHz Kryo 280 Efficiency cores), 6 GB RAM and Android Pie operating system having OxygenOS version 9.0.4.
2. The desktop used for web login phase, i.e., client machine was a PC running Windows 7 Ultimate 64-bit operating system with Mozilla Firefox (Version 66.0.2), a webcam and an Intel® Core™ i5-3230 M CPU @ 2.60 GHz with 8 GB of RAM.
3. The website for testing the registration and login phase was hosted on a desktop running Windows 10 64-bit operating system on an Intel® Core™ i7-3770 CPU @ 3.40 GHz with 8 GB of RAM.
4. The website was written in JAVA and was hosted on Apache Tomcat 8.5.39 server.
5. MySQL server version 8.0.13 has been used for storing the user's information on the server side.

4.2 Timing and Resource Analysis

The time required for user registration ($T_{\text{Registration}}$) can be expressed using the following expression:

$$T_{\text{Registration}} = T_{\text{OTP}} + T_{\text{MD5}} + T_K + T_E + T_{\text{DB}}$$

where, T_K = Time taken to generate 256-bit AES key using PBKDF2, T_E = Time taken for 256-bit AES encryption, T_{DB} = Time taken to store registration metadata securely in the app database using Android Keystore API, T_{OTP} = Time taken to send the OTP from the server and receive the OTP on the user's phone, and T_{MD5} = Time taken to generate hash password from the password entered by the user.

The average time for the registration phase comes out to be 13.885 s if the phone is connected via Wi-Fi whereas it takes 14.704 s if it is connected over 4G network.

Similarly, the time required by the user for logging (T_{Login}) into the website using the proposed authentication protocol will be:

$$T_{\text{Login}} = T_{\text{FQR}} + T_{\text{SQR}} + T_E + T_D + T_{\text{CAM}} + T_{\text{PN}} + T_F$$

where, T_{FQR} = Time taken to fetch the metadata from the server and display the QR-code on the webpage, T_{SQR} = Time taken to scan the QR-code by the user's mobile camera, T_E = Time taken for 256-bit AES encryption, T_D = Time taken for

256-bit AES decryption, T_{CAM} = Time taken to capture the photo from the webcam, T_{PN} = Time taken for sending and verifying photo via push notification, and T_F = Time taken to fetch the user's account after submitting the login details.

On average, a user takes 4.744 s to login over a website using the proposed scheme when the smartphone is connected via Wi-Fi whereas it takes 5.222 s when the smartphone is on a 4G network.

The resources utilized by the Android App of the proposed scheme is determined by using the profiling tool of Android Studio. The recorded values of the minimum and maximum CPU utilization in the registration and login phase are 1.2–19.8% and 1.4–27.3%, respectively. The average memory used by the Android App for the proposed scheme is 46 MB. From the statistics recorded, it can be concluded that the CPU and Memory utilization for the proposed scheme is low enough and therefore, the proposed scheme can be utilized for logging into websites.

4.3 Comparison on the Basis of Usability

The proposed scheme has been compared with the various existing schemes based on usability. The usability of an authentication scheme considers the number of tokens required by the authentication scheme and the number of authentication tokens that the user has to remember. This comparison also takes any additional software or hardware needs into consideration. Smartphone is required by most of the existing schemes as it is carried by all the internet users. Some of the existing schemes require a particular module or driver to be installed on the client machine, hardware token or trusted third-party, etc. The proposed scheme requires PC camera which is easily available in all the desktops, especially laptops. Also, the proposed scheme does not require the user to remember any authentication token and thus, it is more user-friendly as compared to other authentication schemes. The comparison based on usability also considers the need for the internet on the phone as one of the factors for measuring usability in different authentication schemes for understanding the cost incurred when using the scheme. The proposed scheme requires the internet on the phone, which has become synonymous with smartphones. Table 2 describes the comparative analysis based on usability.

4.4 Comparison on the Basis of Security

This section compares the proposed scheme with the existing schemes based on the security they provide against the attacks described in Sect. 3.2.

1. RT MITM and CR MITM phishing attacks:

- a. U-PWD [30, 31] and OTP/PIN-based authentication schemes such as Google 2-step [10] and SAASPASS [11] are vulnerable to RT MITM as well as CR

Table 2 Comparison in terms of number of tokens used and their security

S. No.	Scheme	Tokens used by the scheme	Tokens to be remembered by the users	Additional needs	The need for Internet on the phone
1	Google 2 Step [10]	3-U, PWD, OTP on SP	2-U, PWD	Cellphone	N
2	SAASPASS [11]	3-U, PWD, OTP on App	2-U, PWD	Smartphone	Y
3	Xie et al. [23]	4-U, PWD, DH Public (g, p), Private Up	2-U, PWD	PC Cam, Smartphone	N
4	Kim et al. [13]	4-U, PWD, Session ID, Secret Key	2-U, PWD	Smartphone with GPS	Y
5	Mukhopadhyay et al. [14]	3-U, PWD, Secret Key in SP	2-U, PWD	Smartphone, TTP	Y
6	Dodson et al. [15]	4-U, PWD, Secret Key, QR-Code	0-NIL (QR-Code Scan)	Smartphone	Y
7	Leung et al. [20]	4-U, PWD, Secret Key, OTP CAPTCHA	2-U, PWD	NIL	NA

(continued)

Table 2 (continued)

S. No.	Scheme	Tokens used by the scheme	Tokens to be remembered by the users	Additional needs	The need for Internet on the phone
8	Zhu et al. [29]	3-U, SALT, PWD, CAPTCHA	2-U, PWD	NIL	NA
9	Tricipher [26]	4-U, PWD, TPM Secret Key, TACS credential	2-U, PWD	CAPIDriver, Separate Hardware, TPM	N
10	RSA SecurID HW Token [28]	4-U, PWD, HW token information, PIN	2-U, PWD	Separate Hardware	NA
11	Yubikey U2F [21]	5-KPUJB, KPRIV, Counter, U, PWD	2-U, PWD	Separate Hardware	NA
12	Push Login [22, 27]	3-U, PWD, SP	1-U	Smartphone	Y
13	Password Managers [24, 25]	3-U, PWD, the master key of the password manager	Master PWD	NIL	NA
14	U-PWD [30, 31]	2-U, PWD	2-U, PWD	NIL	NA
15	Proposed Scheme	3-U, Secret key stored on SP; photo taken by PC Cam	0-NIL (QR-Code Scan)	Smartphone, PC Cam	Y

MITM phishing attacks. The attacker can easily obtain the user credentials with the help of the phishing website. The attacker can deceive the user by showing him/her an exact copy of the authentic website and relay the credentials entered by the user on the phishing website in real-time to the authentic website. The attacker can also launch CR MITM phishing attack on the OTP/PIN-based scheme, simply by relaying his/her remote desktop over the client's terminal and the user is lured to enter the credentials, which is actually entered on the attacker's remote desktop.

- b. QR-code based schemes also fail to stand against RT MITM and CR MITM attacks. The scheme proposed by Xie et al. [23] can be attacked using a spoofed malicious browser extension. The attacker can install a spoofed malicious browser extension on the user's PC. In this way, the attacker will obtain the credentials, which the attacker will relay to the CamAuth extension. The CamAuth extension will send the user information to the server and will also initiate Diffie–Hellman exchange. The server verifies the credentials and in this way, user's account will be sent by the server to the attacker's browser. However, Xie et al.'s scheme [23] is secure against CR MITM attack because the attacker cannot access the user's PC cam. Similarly, the QR-code based scheme proposed by Kim et al. [13] is also not secure against RT MITM and CR MITM attack. The reason is that the IP address present in the QR-code can be spoofed and a login request can be sent by the attacker to the server. The scheme proposed by Mukhopadhyay et al. [14] is also vulnerable to these attacks because the credentials entered by the user can be easily obtained by the attacker using the phishing website and the QR-code can be relayed to the phishing website. Thus, the login process gets completed and the attacker gets access to the user's account. In the same way, Dodson et al.'s scheme [15] is also vulnerable to RT MITM as well as CR MITM attack because the attacker relays the QR-code to the phishing website, which is scanned by the user's smartphone.
- c. Hardware token based schemes such as Tricipher [26] and Yubikey using U2F [27] are secure against RT MITM and CR MITM phishing attacks due to the use of multipart credentials. However, RSA SecurID soft token/hardware token [28] are not safe from these attacks as the attacker can obtain the RSA passcode via the phishing website.
- d. Graphical password-based authentication scheme proposed by Leung et al. [20] is secure against RT MITM attack because relaying the user mouse click coordinates on moving CAPTCHA is quite difficult and there might be a difference in screen resolution of the attacker's desktop and user's desktop. However, this scheme is not safe from CR MITM attack. Zhu et al.'s scheme [21] is not safe from RT MITM as well as CR MITM attack because the attacker can record and map the user's click coordinates on the CaRP displayed on the authentic website.
- e. Push notification login based schemes [22, 23] are vulnerable to RT MITM and CR MITM attack because the attacker can relay the credentials entered

by the user and the user will then approve the push notification received on the smartphone app.

- f. Password managers [24, 25] are secure against RT MITM and CR MITM attacks as the user's credentials are automatically sent by the password managers and the user is not required to enter them. However, if wrong credentials are entered by the attacker, then it will prompt the user for re-entering the username and password, thus leading to RT MITM and CR MITM attack.
 - g. The proposed scheme safeguards the user from RT MITM phishing attack because even after relaying the QR-code, the attacker cannot send the user's photo taken from the user's webcam to the server. The reason is that the photo has to be taken by the attacker's webcam. Moreover, after the user scans the QR-code from the smartphone app, the attacker's webcam will immediately click the attacker's photo using his/her webcam and send that photo to the user via push notification, thus alerting the user. The proposed scheme is also safe from CR MITM phishing attack as the attacker cannot access the user's webcam.
2. **Malicious browser extension based phishing attacks:** The malicious browser extension based phishing attack includes keylogging, screen logging, and password sniffing. The attacker can break Google 2-step [10], U-PWD [31], SAAS-PASS [11], RSA SecurID software/hardware [28] token using keylogging and password sniffing because, in the above-mentioned schemes, all the credentials are entered on the website and thus the attacker can sniff them via the malicious browser extension. The attacker can also break the password managers by installing a malicious browser extension on the client's terminal which can sniff the password before it is sent to the server. Xie et al.'s scheme [12] is safe from keylogging and password sniffing because the malicious browser extension cannot access the information entered by the user on the CamAuth extension due to the same-origin policy. However, the attacker can access the QR-code using the screen logging but won't be able to break the complete authentication. Kim et al. [13] and Dodson et al. [15] safeguard the users from these attacks as it does not require the user to enter any credential. Leung et al.'s CAPTCHA-based scheme [20] is safe from keylogging and password sniffing because flash-based moving OTP CAPTCHA is used. On the other hand, the attacker can break Zhu et al.'s scheme [21] and obtain the user input via screen logging. Since Zhu et al. [21], Tricipher [26], Mukhopadhyay et al. [14] and push login based schemes [22, 23] either use trusted device or second authentication factor, therefore the attacker can only obtain the user's authentication token or identification but cannot compromise these schemes. The proposed scheme is safe from these attacks because the user does not need to enter any credentials and thus the malicious browser extensions won't be able to sniff any information.
 3. **App spoofing:** The attacker can install spoofed mobile app or extension on user's smartphone or desktop, so as to obtain user's information. Xie et al. [12], Google 2-step [10], SAASPASS [11], U-PWD, Kim et al. [13] and push login based

schemes [22, 23] are vulnerable to this attack as the spoofed app can be installed on the user's device and the credentials entered by the user are stored in the spoofed app, which is received by the attacker. Zhu et al. scheme [21] is secure against this attack as it does not use any app or extension. Mukhopadhyay et al. [14], Tricipher [26], and Dodson et al. [15] are safe from this attack as these schemes have at least one part of the authentication token stored in the user's device and not entered in the app. The proposed scheme is also secure against app spoofing because the secret key (S) is stored in the app encrypted by Android Keystore API [32], which will not be available in the spoofed app. The comparison of the proposed scheme with other existing schemes based on security has been summarized in Table 3.

4.5 User Survey

A user survey was conducted in order to understand the user's opinion about different authentication schemes that they use for login over websites on desktop. The participants were selected from different backgrounds, age group, and computer proficiency. A total of 20 people from different age groups having different computer proficiency participated in the survey. A detailed introduction was given for the following seven authentication schemes: (1) U-PWD, (2) U-PWD and OTP, (3) QR-code based, (4) Graphical PWD based, (5) Hardware token based, (6) Push notification based login scheme, and (7) Proposed Scheme. Figure 3 shows the percentages of the participants on the basis of their age and computer proficiency, respectively.

It should be noted that there was not much participation from people having age above 40 and thus the survey does not completely reflect the opinion of a majority of elderly aged people. Most of the people that participated in the survey are probable users of the scheme and thus the opinion of the people who do not use computer frequently will be done in the future. All the participants were given a brief introduction about all the seven schemes and then the following questions were asked, out of which question (b), (c) and (d) allowed the users to select more than one authentication scheme:

1. Rate individual schemes from 1 to 5 (5—Very Easy, 1—Not Easy) with respect to “Easy to Learn and Use” in your daily life.
2. Mention the schemes that the user considers to be secure against known attacks.
3. Mention the schemes that the user will prefer to login over a website containing data of high importance such as banks, etc.
4. Mention the schemes that the user thinks maintain a balance between “Easy to learn & use” and “Security” and should be standardized by companies.

Figure 4a shows the result for question 1, in which each authentication scheme has an overall score on a scale of 100. From Fig. 4a shown, it can be concluded that the users find U-PWD scheme easiest to learn and use. The proposed scheme comes in third position after OTP-based schemes. It can also be observed that the hardware

Table 3 Comparison in terms of security against known threats

S. No.	Scheme	RT MITM	CR MITM	Key logging	Screen logging	Password Sniffing	App Spoofing	Secure count
1	Google 2 step	✗	✗	✗	○	✗	✗	0
2	SAA SPASS	✗	✗	✗	○	✗	✗	0
3	Xie et al.	✗	✓	✓	○	✓	✗	3
4	Kim et al.	✗	✗	✓	✓	✓	✗	3
5	Mukhopadhyay et al.	✗	✗	○	○	○	✓	1
6	Dodson et al.	✗	✗	✓	✓	✓	✓	4
7	Leung et al.	✓	✗	✓	○	✓	○	3
8	Zhu et al.	✗	✗	○	✗	○	✓	1
9	Tricipher	✓	✓	○	○	○	✓	3
10	RSA SecurID HW token	✗	✗	✗	○	✗	✗	0
11	Yubikey U2F	✓	✓	✓	○	○	✓	4
12	Push login	✗	✗	○	○	○	✗	0
13	Password Managers	✓	✓	✓	○	✓	✓	3
14	U-PWD	✗	✗	✗	○	✗	✗	0
15	Proposed scheme	✓	✓	✓	✓	✓	✓	6

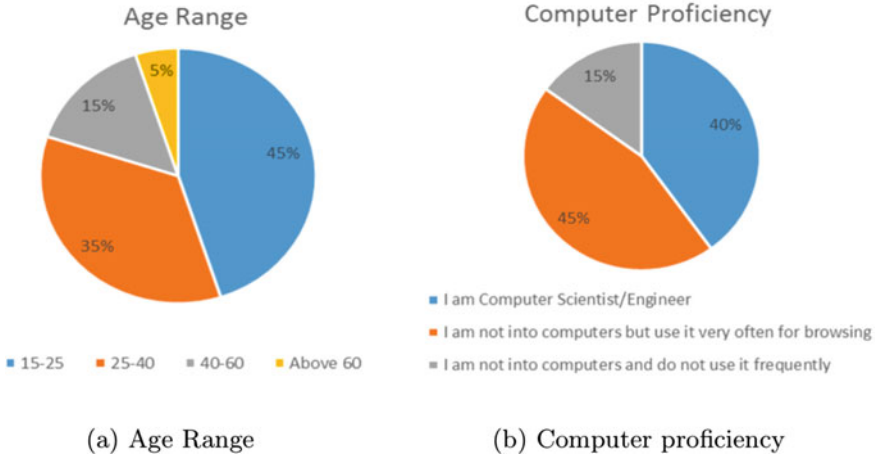


Fig. 3 Surveyed participants information

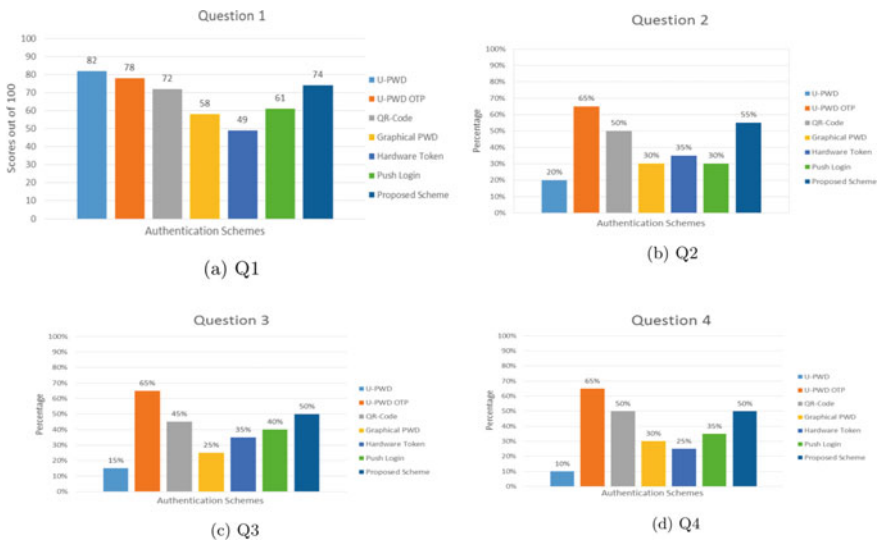


Fig. 4 User survey statistics

token based schemes have the least score as the users have to carry an additional token for the purpose of authentication.

For the second question, the proposed scheme scored 55% which is more than most of the schemes taken for comparison. The proposed scheme was voted second out of all the schemes in second question which shows the users' confidence in the proposed protocol. The graph in Fig. 4b also shows that the users were confident

the most about OTP-based authentication scheme whereas they were least confident about the U-PWD authentication scheme.

The graph in Fig. 4c shows the result for the third question, in which the users were asked to choose the schemes that should be used to secure the data in banks or financial accounts. The graph shows that according to the users, the proposed authentication protocol can be used in banks to secure the data. The users prefer the proposed authentication protocol more than other schemes. OTP-based authentication schemes were voted the most as it was chosen by 65% of the total participants. The proposed scheme, on the other hand, was chosen by 50% of the participants. The graphical password-based scheme and the push login based scheme received almost equivalent votes and the basic U-PWD scheme received the least votes as it is not much secure

The result for the 4th question can be seen in Fig. 4d. The graph clearly shows that 65% of the users thought that U-PWD with OTP offers a great balance between usability and security. It can also be seen that the proposed authentication scheme and QR-code based scheme received an equal amount of votes, i.e., 50% and after the OTP-based scheme, the proposed scheme is considered to have a balance between usability and security and thus the proposed scheme can be used for login over different websites.

After the survey, we also interacted with the participants and we concluded that since the participants have not used the proposed scheme, they were not sure about selecting it in the first question. Also, most of the participants were not aware of the security vulnerabilities in the authentication schemes that were safe according to them. The survey respondents were unaware of the phishing attacks that can be easily launched on the OTP-based authentication scheme. They had the perception that OTP provides security from all the attacks. From the above user survey, we can conclude that the proposed scheme provides usability and security as compared to hardware token based schemes, push login, QR-code-based schemes, etc. The above-mentioned survey can be found at https://docs.google.com/forms/d/1YBF1wPk4TrxMWyncjRWqFxSwxN_FAFV0XwVuxQ5e_Io/ and the responses can be found at <https://docs.google.com/spreadsheets/d/1oeXQk87j00o4jAgPCOm5GD52U69SNA5VfmJDVwYX2Zo/edit?usp=sharing>.

4.6 Comparison Using Bonneau et al. Framework [31]

Bonneau et al. [31] proposed a usability-deployability-security evaluation framework using which an authentication scheme can be evaluated. The framework evaluates the user authentication protocol using 25 parameters comprising of 8 usability, 6 deployability, and 11 security parameters. This section compares the proposed scheme with the existing authentication using the Bonneau et al. framework [31]. This section also gives a brief description of various parameters of Bonneau et al. framework and which schemes offer the benefit for that particular framework parameter. Table 4 summarizes the evaluation of the proposed scheme and the existing authentication schemes.

Table 4 Comparison with existing schemes using Bonneau et al.'s framework

	[10]	[11]	[23]	[13]	[14]	[15]	[20]	[29]	[26]	[28]	[21]	[27]	[24, 25]	U-PWD	Proposed Scheme
1 Mem. wise effortless	✗	✗	✗	○	✗	✓	✗	✗	✗	✗	✗	○	○	✗	✓
2 Scalability for users	✗	✗	✗	✗	✓	○	○	○	✗	✗	✗	✓	✓	✗	○
3 Nothing to carry	○	○	○	○	○	○	✓	✓	✗	✗	✗	○	✓	✓	○
4 Physically effortless	✗	✗	✗	✗	✓	○	✗	✗	✗	✗	✗	○	✓	○	✓
5 Easy to learn	✓	✓	○	✓	✓	○	○	○	✓	✓	✓	✓	✓	✓	✓
6 Efficient to use	○	○	✗	○	✓	○	✗	✗	✓	✓	✓	✓	✓	✓	✓
7 Infrequent errors	○	✓	✗	✗	○	○	✗	○	✓	✓	✓	✓	✓	✓	✓
8 Easy recovery from loss	○	○	○	○	○	○	✓	✓	○	○	○	○	○	○	○
9 Accessible	○	○	✗	✗	✗	✗	✗	✗	✓	✗	✓	○	✓	✓	✗
10 Negligible cost/user	✗	○	○	○	○	○	✗	✓	✓	✗	✗	○	✓	✓	✓
11 Server compatible	✗	✗	✗	✗	✗	✗	✗	✗	✗	✗	✗	✗	✓	✓	✗
12 Browser compatible	✓	✓	○	○	○	○	○	○	✓	✓	○	✓	✓	✓	✓
13 Mature	✓	✓	✗	✗	○	○	✗	✗	○	✓	✓	✓	✓	✓	○

(continued)

Table 4 (continued)

	[10]	[11]	[23]	[13]	[14]	[15]	[20]	[29]	[26]	[28]	[21]	[27]	[24, 25]	U-PWD	Proposed Scheme
14 Non-Proprietary	✗	○	✓	✓	✓	✓	✓	✓	✗	✗	✗	○	✓	✓	✓
15 Res. to physical observation	○	○	✓	✓	✓	✓	○	○	○	✓	✓	○	○	✗	✓
16 Res. to target impersonation	✓	✓	✓	✓	✓	✓	✓	✓	✓	✓	✓	✓	✗	✗	✓
17 Res. to throttled guessing	✓	✓	✓	✓	✓	✓	✓	✓	✓	✓	✓	✓	✗	✗	✓
18 Res. to unthrottled guessing	✓	✓	✓	✓	✓	✓	✓	✓	✓	✓	✓	✓	✗	✗	✓
19 Res. to internal observation	✗	✗	✗	○	✗	✗	○	○	✗	✗	○	○	✗	✗	○
20 Res. to leak from other verifiers	✓	○	✓	✓	○	✓	✓	✓	○	○	○	✓	○	✗	✓
21 Res. to Phishing	✗	✗	✗	✗	✗	✗	✗	✗	✓	✗	✓	✓	✓	✗	✓
22 Res. to Theft	✓	✓	✓	✓	✓	✗	✓	✓	✓	✓	✓	✓	✗	○	○
23 No Trusted Third-Party	✓	✓	✓	✓	✗	✓	✓	✓	✗	✗	✗	✓	✗	✓	✓
24 Requiring explicit consent	✓	✓	✓	✓	✓	✓	✓	✓	✓	✓	✓	✓	✓	✗	✓
25 Unlinkable	✓	✓	✓	○	✓	✓	✓	✓	✓	✓	✓	✓	✓	✓	✓
Benefit Offered Count	11	10	10	10	9	14	11	12	13	12	13	14	14	13	17

Note ✓: Offer the benefit, ✗: Benefit is not offered, ○: Partially offers the benefit, Benefit offered count: Number of benefits completely offered by the given scheme

1. **Memory wise effortless:** The proposed scheme does not require the user to memorize any token for login and therefore it completely offers this benefit.
2. **Scalable for users:** The proposed scheme partially offers this benefit because the user does not have to remember any token or credential. The user has to scan the QR-code and verify the image sent via push notification.
3. **Nothing and quasi-nothing to carry:** Nowadays, since mostly all the users carry a smartphone, therefore carrying a smartphone is considered as quasi-nothing to carry. Since almost all the users have desktops with built-in webcams, therefore the proposed scheme partially offers this benefit.
4. **Physically effortless:** The proposed scheme completely offers this benefit because the user does not have to enter any username and password. Moreover, the proposed scheme requires to just click once to verify the image sent via push notification, thus making it physically effortless.
5. **Easy to learn:** The proposed scheme requires the user to only scan a QR-code and verify the image that he/she receives on the smartphone which makes it easy to use.
6. **Efficient to use:** The proposed scheme does not require the user to enter any credentials and only requires 1 QR-code scan and the complete authentication process takes an average time of 4.74 s which is less than many OTP/PIN, CAPTCHA, QR-code and hardware token based schemes. Thus, the proposed authentication protocol completely offers this benefit.
7. **Infrequent error:** The proposed scheme involves only one QR-code scan containing the session token in which errors are very infrequent, and thus the proposed scheme completely offers this benefit.
8. **Easy Recovery:** Most of the authentication schemes offer this benefit either partially or completely. If the user forgets the credentials or any token is lost and the user account is recovered easily, then the scheme offers this benefit. However, some schemes which involve a mobile phone or any external device may require some additional steps for user verification and registering the device again. Due to this reason, the proposed scheme partially offers this benefit.
9. **Accessible:** If an authentication scheme can be accessed by all the users including those having some physical condition or disability, then the scheme offers this benefit. Also, if the scheme requires the user to have some technical knowledge particular to that scheme, then it cannot be considered as accessible. CAPTCHA-based scheme is not accessible because the users having visual impairment cannot use a scheme that involves graphical passwords. Similarly, QR-code-based schemes are also not accessible as scanning a QR-code requires visual interaction and therefore, the proposed scheme is not accessible.
10. **Negligible cost per user:** OTP/PIN or an external hardware token adds a certain amount of cost to an authentication scheme, and thus these schemes do not offer this benefit. However, the need for the internet in a smartphone does not add any cost per user because the internet has now become synonymous with smartphones. This is why the proposed scheme completely offers this benefit.
11. **Server compatible:** Most of the schemes are not server compatible as they enhance the security of the scheme by additional implementation on the server

side. U-PWD and the password managers are server compatible as they do not require any separate implementation on the server side.

12. **Browser compatible:** Since the proposed scheme does not have any client or browser side requirement, therefore it is browser compatible.
13. **Mature:** A scheme is considered mature if it is rigorously tested and has been deployed for people. Quasi-mature is granted to those schemes which have only slight variations from the existing authentication schemes. The proposed scheme has slight variations which can be easily put to use and thus it partially offers this benefit.
14. **Non-proprietary:** If a scheme can be used without any explicit consent from the author of that scheme, then the scheme is considered as non-proprietary. The proposed scheme can be used by any person without any approval, and thus it is non-proprietary.
15. **Resilient to physical observation:** The proposed scheme is secure against this attack as the user does not enter any login details while authenticating into the website. The attacker won't get any login details by physically observing the user. Moreover, the secret key is stored in the Android Keystore API [32] which is not visible and thus, the attacker won't be able to login to the website by physical observation.
16. **Resilient to Target impersonation:** The proposed scheme, OTP/PIN-based schemes, QR-code, CAPTCHA, and hardware token based schemes are resilient to target impersonation because some credential/token or secret key is not available with the attacker and thus, the attacker is not able to break these authentication schemes by impersonating the target.
17. **Resilient to Throttled guessing:** The proposed scheme along with other schemes taken into comparison is resilient to throttled guessing because all these schemes have some token that the attacker cannot know just by mere guessing.
18. **Resilient to Unthrottled guessing:** In unthrottled guessing, the verifier does not put any limit on the number of guesses. However, the number of guesses is limited by the computing resources available to the attacker. Just like the throttled guessing, the basic U-PWD and password managers are not resilient to unthrottled guessing whereas all other schemes completely offer this benefit because they are safe from this attack.
19. **Resilient to Internal observation:** Most of the authentication schemes are still vulnerable to the internal observation in which the attacker obtains the user's credentials by using tools like keylogging or by using malicious browser extensions. Since the proposed scheme stores the secret key in the smartphone which is encrypted by Android Keystore API, therefore the attacker is not able to obtain all the tokens, the proposed scheme is Quasi-Resilient-to-Internal-Observation.
20. **Resilient to leaks from other verifiers:** The schemes which involve third-party for verification or other purposes are not resilient to leaks from other verifiers. Since the proposed scheme does not have any third-party verifier, therefore it secures against this attack.

21. **Resilient to Phishing:** If a scheme is safe from RT MITM, CR MITM, and traditional phishing attacks, then it is resilient to phishing. The proposed scheme is resilient to phishing because even after relaying the QR-code to the phishing website which is opened by the user, the attacker cannot access the user's webcam due to which image will be taken by the attacker's webcam and not that of the user.
22. **Resilient to theft:** If the smartphone is stolen by the attacker, then it can be used for logging into the website. However, the smartphones are password or pin protected which makes it difficult for the attacker to access the smartphone app. Moreover, the attacker would still not be able to access the secret key as it stored securely using Android Keystore API [32]. Also, the user will notify the verifier about the stolen device via email which will lead to blocking of the account and the secret key stored in the device would be expired and the user will be asked to register again. Thus, the proposed scheme is Quasi-Resilient-to-theft.
23. **No trusted third-party:** The schemes having trusted third-party for verification or storing the credentials do not offer this benefit.
24. **Explicit consent:** The schemes which require explicit consent from the user before logging into the account are resilient to explicit consent. Except password managers, all other authentication schemes need consent from the user explicitly.
25. **Unlinkable:** If the attacker can determine that the same user is trying to login to different websites, then the scheme is linkable. Most of the schemes are unlinkable except Kim et al. because IP address is used as a token in the scheme proposed by Kim et al. [13]. When the user will login to different websites using the scheme proposed by Kim et al. [13], then it can be determined from the IP address that the same user is accessing accounts on different websites. The proposed scheme offers this benefit completely as there is no such token used in the authentication scheme which can be used for linking. Table 4 shows the comparison of the authentication schemes based on Bonneau et al. framework [31]. From the table, it can be observed that the proposed scheme obtained a count of 17 out of 25 which is more than all other schemes. Thus, it can be concluded that the proposed scheme performs better than other schemes in terms of usability, security, and deployability.

5 Conclusions and Future Work

In this paper, a novel authentication scheme has been proposed which is able to handle traditional as well as advanced phishing attacks. Not only the proposed authentication protocol is able to handle RT MITM and CR MITM attacks, but it also safeguards the user from malicious browser extensions and app spoofing. Additionally, the proposed scheme does not require the users to remember any token or credential, as they just have to scan the QR-code and verify the image taken from the webcam. This makes

the proposed scheme more user-friendly as compared to other existing authentication schemes.

Currently, the proposed scheme requires the websites to use HTTPS for all communication and thus the proposed protocol can be implemented for secure cookie management so that it will not be vulnerable to session hijacking. More extensive user testing of the proposed scheme can be done in the future to determine usability parameters such as learning-curve and scalability to see how the proposed scheme will handle simultaneous requests.

References

1. Lastdrager E (2014) Achieving a consensual definition of phishing based on systematic review of the literature. *Crime Sci* 3:9
2. Abdelhamid N (2007) Multi-label rules for phishing classification. *Appl Comput Inform* 11:29–46
3. Banday MT, Qadri JA (2011) Phishing—a growing threat to e-commerce. arXiv preprint arXiv: 1112.5732
4. Badra M, El-Sawda S, Hajjeh I (2007) Phishing attacks and solutions. In: Proceedings of the 3rd international conference on mobile multimedia communications, p 42
5. Mohammad RM, Thabtah FT, McCluskey L (2015) Tutorial and critical analysis of phishing websites methods. *Comput Sci Rev* 17:1–24
6. Jagatic TN, Johnson NA, Jakobsson M, Menczer F (2007) Social phishing. *Commun ACM* 50:94–100
7. EMC (2019) RSA monthly fraud report dec 2018 @ ONLINE (Feb). <https://www.rsa.com/content/dam/premium/en/e-book/rsa-fraud-report-q4-2018.pdf>
8. (APWG), A.P.W.G.: Phishing activity trends report 2018 @ONLINE. <https://www.antiphishing.org/resources/apwg-reports/>
9. (APWG), A.P.W.G.: Phishing activity trends report 2017 @ONLINE. <https://www.antiphishing.org/resources/apwg-reports/>
10. Google (2015) Stronger security for your Google account @ ONLINE (Oct). <https://www.google.com/landing/2step>
11. SAASPASS (2019) Multifactor authentication @ ONLINE (Jan). <https://saaspass.com/>
12. Varshney G, Misra M, Atrey P (2018) Secure authentication scheme to thwart RT MITM, CR MITM and malicious browser extension based phishing attacks. *J Inf Secur Appl* 42:1–17. <https://doi.org/10.1016/j.jisa.2018.07.001>, <http://www.sciencedirect.com/science/article/pii/S2214212618300140>
13. Kim SH, Choi D, Jin SH, Lee SH (2013) Geo-location based qr-code authentication scheme to defeat active real-time phishing attack. In: Proceedings of the 2013 ACM workshop on digital identity management. ACM, pp 51–62
14. Mukhopadhyay S, Argles D (2011) Ananti-phishing mechanism for single sign-on based on qr-code. In: 2011 international conference on information society (i-Society). IEEE, pp 505–508
15. Dodson B, Sengupta D, Boneh D, Lam MS (2010) Secure, consumer-friendly web authentication and payments with a phone. In: International conference on mobile computing, applications, and services. Springer, pp 17–38
16. Dodson B, Boneh D, Lam MSL (2012) Method and system for making digital payments. <https://patents.google.com/patent/US20130185210A1/en>
17. Bakdi I (2013) Method, devices, and system for authentication with respect to a server. <https://patents.google.com/patent/EP3053317A1/en>

18. Venkat R, Qiao Y, Vazquez H (2013) Sight codes for website authentication. <https://patents.google.com/patent/US9887992B1/en>
19. Nunn JW, Mathews C (2014) System and method for authenticating a computer session on a mobile device using a two dimensional barcode. <https://patents.google.com/patent/US9203824>
20. Leung CM (2009) Depress phishing by captcha with OTP. In: 2009 3rd international conference on anti-counterfeiting, security, and identification in communication. IEEE, pp 187–192
21. Yubico (2019) Your key to a safer internet @ ONLINE (Jan). <https://www.yubico.com/>
22. Varshney G, Misra M (2017) Push notification based login using BLE devices. In: 2017 2nd international conferences on information technology, information systems and electrical engineering (ICITISEE), pp 479–484 (Nov). <https://doi.org/10.1109/ICITISEE.2017.8285554>
23. Xie M, Li Y, Yoshigoe K, Seker R, Bian J (2015) Camauth: Securing web authentication with camera. In: 2015 IEEE 16th international symposium on high assurance systems engineering. IEEE, pp. 232–239
24. Lastpass (2019) Lastpass remembers all your passwords, so you don't have to @ONLINE (Jan). <https://www.lastpass.com/>
25. Ross B, Jackson C, Miyake N, Boneh D, Mitchell JC (2005) Stronger password authentication using browser extensions. In: Usenix security, Baltimore, MD, USA, pp 17–32
26. Tricipher (2019) White paper preventing man in the middle phishing attacks with multi-factor authentication @ONLINE (Jan). <https://www.globaltrustit/documents/press/phishing/PhishingSolutionWhitepaper.pdf>
27. Yahoo (2016) Yahoo sign in @ ONLINE. <https://login.yahoo.com/>
28. Beal V (2019) RSA secure id @ ONLINE (Jan 2019). https://www.webopedia.com/TERM/R/rsa_secure_id.html/
29. Zhu BB, Yan J, Bao G, Yang M, Xu N (2014) Captcha as graphical passwords A new security primitive based on hard AI problems. IEEE Trans Inf Foren Secur 9(6):891–904
30. Bonneau J, Preibusch SR (2010) The password thicket: technical and market failures in human authentication on the web. In: WEIS, pp 1–48
31. Bonneau J, Herley C, Van Oorschot PC, Stajano F (2012) The quest to replace passwords: a framework for comparative evaluation of web authentication schemes. In: 2012 IEEE symposium on security and privacy. IEEE, pp 553–567
32. Android Developers (2016) Android keystore system @ ONLINE (Mar). <http://developer.android.com/training/articles/keystore.html>

Speech Emotion Recognition: A Review



Anuja Thakur and Sanjeev Dhull

Abstract Research-oriented work in speech recognition has garnered a lot of interest since last two decades. Emotions derived from speech have drawn considerable interest of researchers especially for analysis of human behavior. Emotions from a speech are extracted and identified by classifiers and systems being developed and improved over a period of time. This paper attempts to discuss the process of speech emotion recognition, different methods of pre-processing techniques, feature extraction methods, and classifiers used for speech emotion recognition.

Keywords Pre-processing techniques · Feature extraction · Classifier · Speech emotion recognition

1 Introduction

One of the primary reasons that human civilization thrived and developed over generations and centuries was their ability to communicate with each other effectively. Development of languages coincided with development of civilizations. In terms of effectiveness, verbal form of conversation is far more effective than its written form. The human vocal tract can produce variations and intonations in voice, thereby giving us the ability to express our emotions, anger, disgust, happiness, etc. Speech emotion recognition is aimed at developing techniques to enhance man–machine interaction. These systems can be improved with better understanding of emotions behind speaker’s voice.

The emotions can also be recognized by image and text but speech is most effective way of recognizing emotions. Emotions represent the nonverbal means of communication. The intention of the speaker is to convey through emotions. Our uttered

A. Thakur (✉) · S. Dhull
Guru Jambheshwar University of Science and Technology, Hisar, India
e-mail: anuja879@gmail.com

S. Dhull
e-mail: sanjeevdhull2011@yahoo.co.in

© Springer Nature Singapore Pte Ltd. 2021
G. S. Hura et al. (eds.), *Advances in Communication and Computational Technology*, Lecture Notes in Electrical Engineering 668,
https://doi.org/10.1007/978-981-15-5341-7_61

speech is the outcome of deliberations caused by our mental and psychological state which is directly influenced by our emotions. A lot of research has already taken place to detect emotions from speech and the scope of work present has drawn many researchers in this field [1, 2].

There are various applications of speech emotion recognition (i) Human-machine interaction [3, 4]. (ii) Important tool for automatic translation system [5]. (iii) Automatic safety-emotion capture on the basis of voice inputs of driver can be feeded to car's operating system to identify driver's current mental state issue requisite alerts [6]. (iv) Diagnostic tool for therapists/psychiatrists to treat psychological disorders [7, 8]. (v) Call centers employs emotion categorization to prioritize angry calls [9, 10]. (vi) Critical application of speech detection and emotion recognition can be in the field of law enforcement, intelligence gathering, and psycho analysis of detainees. The captured speech data of a suspect, informant, and approver can be analyzed to ascertain genuineness of information or validity of the statement [11]. (vii) To recognize frustrated or annoyed customers, ticket reservation systems make use of emotion detection system and take action accordingly [12].

The paper discusses the different steps for emotion recognition from speech. Section 2 describes the various speech emotion databases. Section 3 describes speech emotion recognition review in detail, pre-processing techniques, speech features extraction techniques, classifier techniques, and Sect. 4 describes final conclusion.

2 Emotion Speech Databases

Primarily, three different classifications of databases have been studied in literature for the purpose of speech emotion recognition. These are acted, naturalistic, and induced. For evenly distribution of class of emotions, a large number of speakers are included in the database evenly represented on the basis of gender, age groups, accents, and even recording quality [13]. For the speech emotion recognition system to produce optimum results, we need to have most natural database which holds identical real-world emotions.

Languages used for databases

(i) German

Berlin database of emotional speech is most commonly used database and has about 500 utterances used in [14–16] whose complete explanation is given in [17]. 'Vera-Am Mittag' database used recordings taken from TV talk show [14]. FAU AIBO emotion corpus used children's interaction with Sony's AIBO robot and consisted emotions like surprise, joy, anger, irritation, and boredom [18].

(ii) English

Databases in English are used by various researchers. One of the databases was formed by taking telephone recordings from travel agencies in the Darpa Communicator Project [12]. In this project, deviation from archetypal emotions are sought and

explored. In Neiberg, [19] ISL meeting corpus database obtained as set of recordings of meetings with average duration of 35 min. In Lee [20], data set gathered from conversation of callers with machine agent from a call center. Here, classification is limited to negative and nonnegative due to limited scope of available data.

(iii) Indian

Not much work done in Indian languages. There are 22 official languages in India with over 720 dialects which can be useful in development of an effective and versatile speech emotion recognition system with ability to recognise emotions on varied speeches and languages. Attempts have been made to use Hindi and its various dialects for dialect recognition as well as emotion recognition [21]. The database of Assamese, Dimasa, Bodo, Karbi, and Mishing all native of Assam have also been created [22].

3 Speech Emotion Recognition System (SER)

Speech emotion-recognition system consists of mainly three steps, pre-processing, feature extraction, and classification. The aim of emotion identification through speech is to classify the input speech into different emotion categories like fear, disgust, happiness, neutral, anger, sadness, etc. [23] (Fig. 1).

3.1 Preprocessing

Signal preprocessing means using several speech enhancement techniques for noise elimination. The existence of noise in speech signal is a major problem. It degrades the quality of signal, intelligibility, and hence affects the results. With the presence of noise, speech characteristics changes and causes variation between training and testing data, hence accuracy of the system gets affected. It becomes imperative to build up a digital-signal-processing method to clean the recorded signal before it is stored, transmitted, or played out and this is done by speech enhancement or noise reduction [24]. There are different types of noises which corrupt the speech signal in different ways. Some categories of noise are:

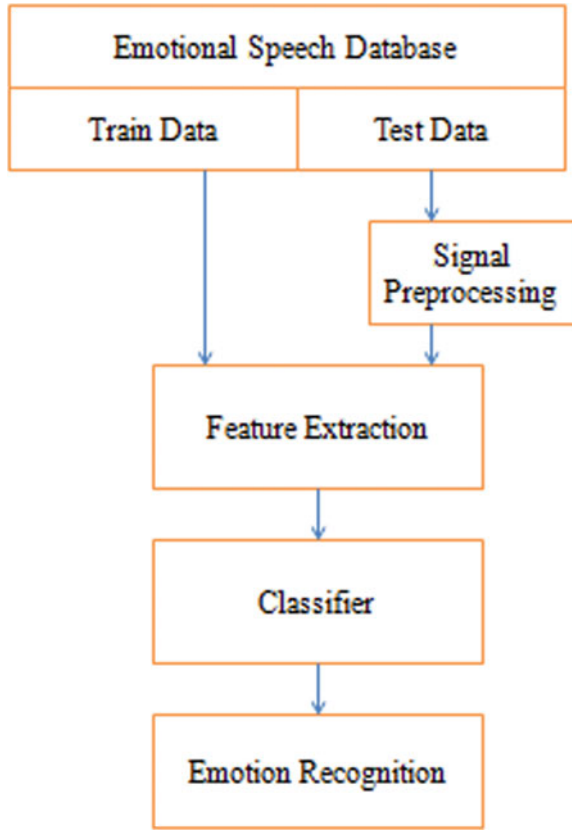
Additive noise—Source of additive noise come from natural sound source as well as artificially introduced.

Echo—Due to presence of echo, conversion will become very difficult. Coupling between microphones and loudspeakers results echo.

Reverberation—Multipath propagation results in reverberation. Due to reverberation spectral-distortion occurs which vitiates speech intelligibility.

Interference—The source of interference is simultaneous sound sources. In a multi-speaker setup like teleconference, group discussion, argument, etc., where

Fig. 1 Speech emotion recognition



source of input comes from multiple sources each source is creating interference for the other.

There are different pre-processing algorithms for noise elimination from speech signal.

Spectral subtraction method

Spectral subtraction algorithm is one of the oldest algorithms proposed for noise removal. It requires only an approximation of noise spectrum. The spectral subtraction is based on the principle of subtracting magnitude spectrum of noise from noisy speech signal. One of the shortcomings of the method is retention of small amount of speech information on too much subtraction and on the other hand, retaining lot of interfering noise if too less is subtracted. To evade any speech corruption, subtraction method need to be performed very selectively. Spectral subtraction is one of the commonly used algorithms. This is one of the simplest methods for speech enhancement but noise must be stationary throughout the signal and noise samples are required before starting the process to learn its frequency behavior [25].

Wiener filter

Wiener filters produce an approximation of a required signal by minimizing the mean square error between required and estimated signal [26]. Wiener filter approaches the problem by estimating the signal as linear sum of previous observed samples. To obtain the coefficients, we need prior information of the joint spectral density of the actual signal and the noisy signal, and finally, an estimate of noise power spectral density.

Subspace method

Subspace analysis uses an autocorrelation domain where the speech and noise components can be assumed to be orthogonal by which their contributions in the signal can be separated. Subspace filtering methods are based on the orthogonal decomposition into signal subspace and noise subspace. The decomposition is possible based on the estimate of the noise correlation matrix [27].

Adaptive noise cancellation (ANC)

The adaptive filters have the characteristics of self-optimization. ANC is mostly used to resolve two microphone problems. Speech and noise signal are measured together on one microphone and noise signal alone is measured on the other microphone. The algorithm removes the noise by optimising filter coefficients. Steepest descent algorithm and least mean square (lms) algorithm are adaptive algorithms which require no previous information of the statistics of noise [28].

3.2 Feature Extraction

Emotions in general are identified through their distinct features like pitch of voice, volume intonation, etc. Similarly, when features are extracted from speech signal, the entwined emotions are identified and distinguished. Categorization of features is broadly done in prosodic, spectral, and combination of both prosodic and spectral features.

Prosodic features

Prosody mostly indicates the emotional condition of speaker [29, 30]. Prosodic features do not include smaller elements like syllables or words rather they are concerned upon rhythm, spectral tilt, and stress of the intonated speech. Prosody reflects: emotional state of a speaker, features of the utterance, ironic or sarcastic, emphasis, contrast, and focus. Prosodic features include stress, spectral tilt, intonation, volume, pitch, energy, duration, etc. [31]. Prosodic feature are also known as suprasegmental features. Prosodic features are extracted at word, utterance, sentence, and syllable level. These features are difficult to extract at frame level [32]. Table 1 gives reference of these features.

Table 1 Characteristics of prosodic feature

Feature extracted	Pitch	Intonation	Volume
Characteristics	<ul style="list-style-type: none"> • The degree of highness or lowerness of a tone • Also known as fundamental frequency. Pitch varies according to on air pressure at sub-glottal and tension of vocal chords. Therefore pitch carries emotion specific information 	Variation of spoken pitch, used to express emotion and for emphasizing something	Volume usually show emotions such as fear or anger, It also indicate stress when slight increase in loudness is present

Spectral features

The human vocal tract has unique shape for different emotions and spectral analysis helps in estimation of shape of vocal tract. Spectral features are important for categorizing emotions [33, 34]. Spectral features are also known as vocal tract features. To obtain spectral feature, the signal is divided into short segments called frames within the range of 10–30 ms. Within these frames, the speech signal is considered as stationary. To smoothen the signal window function is applied. Size of frame is selected which depends upon the sampling frequency. Feature extracted from frames are known as spectral features. Several popularly extracted spectral-features include Log-Frequency-Power-Coefficients (LFPC) [35], Mel-Frequency-Cepstral Coefficients (MFCC) [36, 37], Linear-Prediction-Cepstral-Coefficients (LPCC) [38], Zero-Crossing-Rate (ZCR), jitter, shimmer [39, 40], etc. The study of various spectral features is mentioned in Table 2 [41].

Table 2 Analysis of spectral features

Feature Extraction	Strengths	Weakness
LPCC	Represents the speech phonetic content and most popular feature	For different emotions like anger and sadness overlapping of coefficient value is observed
MFCC	Widely used feature, includes delta, double delta values which increase the accuracy of recognition	No robustness to noise
Jitter, Shimmer	By Combining jitter, shimmer with other spectral features, resulting better classification accuracy	Emotions like disgust and anger be likely to illustrate similar jitter and shimmer values
ZCR	Simple calculation, time domain feature	ZCR values have tendency to vary it depends on quantity of noise present

Combination of both prosodic and spectral features

The temporal-information is not there with the features like MFCCs and PLP values. While recognizing emotions, the temporal-information is very helpful [42]. On this basis, temporal information is estimated by introducing modulation spectral features (MSF) in speech signal which ultimately helps to determine the emotion [43]. The prosodic and spectral features are combined to get better efficiency while identifying emotions [44, 45].

3.3 Classifier

There is always possibility of multiple emotions or reactions for a similar instance. The role of classifier is to interpret multiplicity of emotions. Different classification techniques for recognizing emotions are artificial neural network, k-nearest neighbor, Naive Bayes, decision tree, support vector machine, hidden Markov model, and Gaussian mixture model.

Artificial Neural Network (ANN)

Artificial neural networks are mathematical models based on working of nervous system that try to replicate decision making process similar to human behavior. These techniques are gaining ground and acceptability in everyday business applications. Neural networks are less dependent on explicit coding instead they are used to learn pattern and relationship in data. Mathematical formulations derived for mimicking the nervous system are derived after careful examination of human behavior. Biological neurons are complex with limited understanding, resulting in development of several architectures in the past. An artificial neural network consists of a number of artificial neurons wherein each neuron acts as a basic computational unit replicating an idle neuron. Neural networks applications try mimic human ability to adapt as per given situation and conditions by learning from events occurred in past and their applications to future tasks [1].

K-Nearest Neighbor (KNN)

It is a simple and easy method of machine learning algorithm. It is an instance-based learning method working on the principle of similar samples lying in close vicinity [46]. Due to this approach, instance-based learning methods are also known as lazy learners as they store all the sample data. Work upon a new classifier is done only when a new sample arrives for classification. One of the pros of these algorithms is less computation time during training phase as they work on already stored samples [47]. On the other hand, more computation time is required during classification of new unlabelled sample. Since neighbor classifiers work on the principle of similar samples, their learning is based on resemblance of test sample with training samples. For example, a data sample A to be classified is searched among its nearest k-neighbors and is assigned the class label of the majority of its K neighbors. In this classification process, choice of K neighbors is important. The choice and size of k

affect the performance of the classifier algorithm [48]. Too small the value of K may result in over fitting and noise in data set cannot factor in. Too large value of K may result in wrong classification as some of the data sets in nearest neighbors may be located too far in the neighborhood. K-NN works on fundamental principle of data being connected in feature space. Tarunika et al. [49] applied two machine learning algorithms which included deep neural network (DNN) and k-nearest neighbor (k-NN) for emotion recognition in speech especially scary condition of mind. The application of the system primarily addresses the healthcare units.

Naive Bayes

A statistical model-based classifier [50]. It works on the assumption that all variables in a data set contribute toward classification and all are mutually correlated. This assumption is called class conditional independence [51]. Because of the kind of assumption, it works upon, it is called Naive or also known as simple Bayes and independence Bayes. This method of classification when provided with class variable does not require any class feature or attribute for classification. This classification technique is based on Bayesian theorem. It is used when the inputs dimensionality is high. The Bayesian classification is based on Bayes theorem.

Decision Tree

A decision tree is structure of problems and their possible solutions. Like a tree, the structure comprises of root which is essentially a problem/objective, branches or internal nodes which represent the result of test condition on leaf node or terminal node which is assigned with a class label. Approach of decision tree is to divide the problem in subsets and conquer. Each direction or path in a decision tree represents a decision rule. Classification technique of decision tree follows top-to-bottom approach and is performed in two phases [52].

- (1) Tree-building phase—Formation of branches till the time all data sets are aligned to the same class label. The data set is traversed repeatedly therefore making the whole process computationally intensive.
- (2) Tree-pruning phase—To improve the estimation of results and achieving maximum accuracy in classification over fitting problem and data sets repetition is to be minimized.

Figure 2 explains a weather forecast model which helps to arrive at a decision whether mountaineering expedition can be undertaken or not. Each and every set of climatic condition is accompanied by possibilities of their level of occurrence which is most likely to influence the decision [53].

Support Vector Machine (SVM)

There is another technique which uses state-of-the-art machine learning technique named support vector machine (SVM). It works on the rule of margin calculation which draws margins among the classes. The classification errors are minimized as drawn margins maximize the distance between the margin and the classes. Yang et al. [54] presented a SVM and a thresholding fusion mechanism for speech

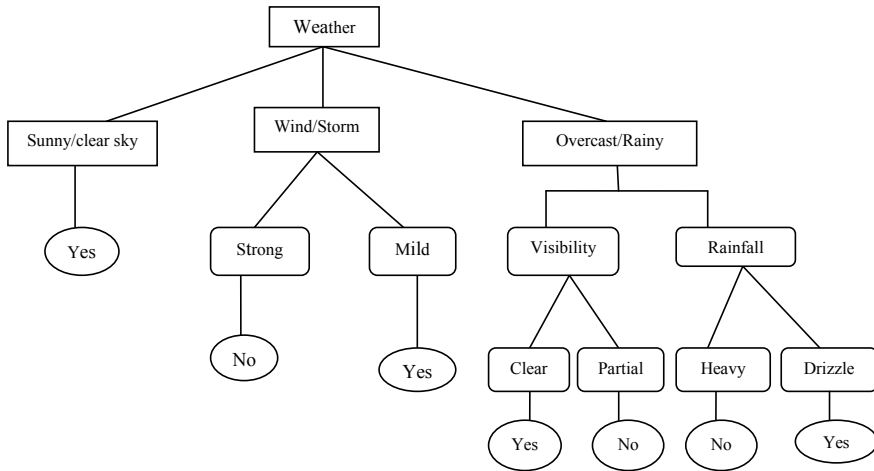


Fig. 2 Decision tree example for a mountaineering team

emotion recognition. The result shows the emotion classification accuracy is affectively increasing by using threshold fusion mechanism. Average emotion recognition rate achieved is 82.8% by using genetic algorithm and SVM as classifier.

Hidden Markov Model (HMM)

This model is a dominant statistical model and considered as a finite state machine.

It illustrates observed data samples in discrete or continuously distributed time series. Hidden Markov model uses a nondeterministic method to generate output observation symbols for given state. HMM is a stochastic technique developed by two interrelated procedures: Markov chain and a set of random functions. In Markov chain, the number of states is fixed and the transitions among these states depend on calculation of transition probabilities [55]. Nwe et al. used HMM as the classifier and concluded that HMM with four states delivered the excellent optimal performance with average rate of 78 and 96% in best situation [35].

Other classifier techniques are K fuzzy means [56] and brain emotional learning optimized model (BEL) [57] that merge the adaptive neuro-fuzzy inference system (ANFIS) and multilayer perceptron (MLP) for emotion speech recognition (Table 3).

4 Conclusion

Emotion recognition in speech has been studied extensively. Current study is based on a number of research papers that have elaborated their work on the basis of database, feature extraction, and classifiers for emotion recognition using speech. Bulk of the research work has been observed in extraction of features and selection of best features to improve accuracy in performed result. Research on available data

Table 3 Comparison of different classifier

Classifier	Feature category	Emotions	Accuracy obtained	References
AANN, SVM	Excitation source and spectral	Anger, disgust, fear, happy, neutral, sadness	up to 84%	Koolagudi and Rao [2]
SVM	Both spectral and prosodic	Anger, Bored, disgust, fear, happy, neutral and sad	89.80%	Seehapoch and Wongthanavasu [16]
HMM	Spectral	Joy, surprise, disgust, anger, fear, Sadness	Average 78%	Nwe et al. [35]
Naïve Bayes	Both spectral and prosodic	Anger, joy, sadness, fear, disgust, boredom, neutral	77.4% for reduced set as against	Vogt and André [37]
GMM, SVM	Both spectral and prosodic	Anger, happy, surprise, neutral and sad	88.35%	Zhou et al. [45]
Fuzzy k means	Both spectral and prosodic	Anger, sadness, astonish, fear, happiness, neutral	65.16%	Mohanty and Swain [56]

shows that to improve performance, identification of correct emotions is important, where the role of classifiers comes into play. Choice and selection of classifiers are a challenging task and results vary, hence there is no clear outcome which one is better. To improve further, recent studies have shifted focus toward neural networks, hybrid classifiers, and fusion methods. As these new protocols are evolving and developing with enhanced learning, there is enough scope for further research to improve these designs with aim on accuracy, specificity, and reproducibility.

References

1. Ayadi ME, Kamel MS, Karray F (2011) Survey on speech emotion recognition: features, classification schemes, and databases. *Pattern Recogn* 44:572–587
2. Koolagudi SG, Rao KS (2012) Emotion recognition from speech: a review. *Int J Speech Technol* 15(2):99–117
3. Huahu X, Jue G, Jian Y (2010) Application of speech emotion recognition in intelligent household robot. In: *Proceedings of international conference on artificial intelligence and computational intelligence*, vol 1, pp 537–541
4. Schuller B, Rigoll G, Lang M (2004) Speech emotion recognition combining acoustic features and linguistic information in a hybrid support vector machine-belief network architecture. In: *Proceedings of IEEE international conference acoustics, speech, and signal processing*, pp 577–580
5. Bao H, Xu M, Zheng TF (2007) Emotion attribute projection for speaker recognition on emotional speech. In: *INTERSPEECH*, pp 758–761

6. Al Machot F, Mosa AH, Dabbour K, Fasih A, Schwarzlmüller C, Ali M et al (2011) A novel real-time emotion detection system from audio streams based on Bayesian Quadratic Discriminate Classifier for ADAS. In: Proceedings of joint 3rd international work nonlinear dynamic synchronization. INDS '11 16th international symposium theoretical electrical engineering ISTET '11, pp 47–51
7. Tacconi D, Mayora O, Lukowicz P, Arnrich B, Setz C, Tröster G, Haring C (2008) Activity and emotion recognition to support early diagnosis of psychiatric diseases. In: Proceedings of 2nd international conference on pervasive computing technologies for healthcare '08, Tampere, Finland, pp 100–102
8. Cowie R, Douglas-Cowie E, Savvidou S, McMahon E, Sawey M, Schroder M (2000) FEEL-TRACE: an instrument for recording perceived emotion in real time. In Proceedings of ISCA speech and emotion workshop, pp 19–24
9. Gupta P, Rajput N (2007) Two-stream emotion recognition for call center monitoring. In: INTERSPEECH, pp 2241–2244
10. Lee C, Narayanan S (2005) Toward detecting emotions in spoken dialogs. *IEEE Trans Speech Audio Process* 13(2):293–303
11. Sanaullah M, Gopalan K (2013) Distinguishing deceptive speech from truthful speech using MFCC. In: Proceedings of the 7th international conference on circuits, systems and signals. WSEAS, pp 167–171
12. Ang J, Dhillon R, Krupski A, Shriberg E, Stolcke A (2002) Prosody-based automatic detection of annoyance and frustration in human–computer dialog. In: Proceedings of international conference on spoken language processing (ICSLP '02), vol 3, pp 2037–2040
13. Batliner A, Schuller B, Seppi D, Steidl S, Devillers L, Vidrascu L, Vogt T, Aharonson V, Amir N (2011) The automatic recognition of emotions in speech. *Emot Oriented Syst* 2:71–99
14. Schuller B, Zhang Z, Wenginger F, Rigoll G (2011) Using multiple databases for training emotion recognition: to unite or to vote? In: International Science Congress Association, pp 1553–1556
15. Pan Y, Shen P, Shen L (2012) Speech emotion recognition using support vector machine. *Int J Smart Home* 6(2):101–108
16. Seehapoch T, Wongthanavasu S (2013) Speech emotion recognition using support vector machines. In: 2013 5th international conference on knowledge and smart technology, Piscataway. IEEE, pp 86–91
17. Burkhardt F, Paeschke A, Rolfes M, Sendmeier W, Weiss B (2005) A database of German emotional speech. In: Proceedings of INTERSPEECH, pp 1517–1520
18. Schuller B, Steidl S, Batliner A (2009) The INTERSPEECH 2009 emotion challenge. In: Proceedings of INTERSPEECH, pp 312–315
19. Neiberg D, Elenius K, Karlsson I, Laskowski K (2006) Emotion recognition in spontaneous speech. In: Proceedings of FONETIK, pp 101–104
20. Lee CM, Narayanan S, Pieraccini R (2001) Recognition of negative emotion in the human speech signals. In: IEEE workshop on automatic speech and understanding, pp 240–243
21. Rao KS, Koolagudi SG (2011) Identification of Hindi dialects and emotions using spectral and prosodic features of speech. *Syst Cybern Inform* 9(4):24–33. ISSN: 1690-4524
22. Kandali AB, Routray A, Basu TK (2009) Vocal emotion recognition in five native languages of assam using new wavelet features. *Int J Speech Technol* 12:1–13
23. Swain M, Routray A, Kabisatpathy P (2018) Databases, features and classifiers for speech emotion recognition: a review. *Int J Speech Technol* 21(1):93–120
24. Li J, Deng L, Gong Y, Haeb-Umbach R (2014) An overview of noise-robust automatic speech recognition. *IEEE/ACM Trans Audio Speech Lang Process* 22(4):745–777
25. Boll SF (1979) Suppression of acoustic noise in speech using spectral subtraction. *IEEE Trans Acoust Speech Sig Process* 27(2):113–120
26. El-Fattah MAA, Dessouky MI, Abbas AM, Diab SM, El-Sayed M, El-Rabaie WA-N, Alshebeili SA, El-samie FEA (2013) Speech enhancement with an adaptive Wiener filter. *Int J Speech Technol* 1–12
27. Hermus K, Wambacq P, Van Hamme H (2007) A review of signal subspace speech enhancement and its application to noise robust speech recognition. *EURASIP J Appl Sig Process* 1:195–209

28. Sayed A, Hadei M (2010) A family of adaptive filter algorithms in noise cancellation for speech enhancement. *Int J Comput Electr Eng* 2(2):1793–1816
29. Chen C, You M, Song M, Bu J, Liu J (2006) An enhanced speech emotion recognition system based on discourse information. In: *Computational Science–ICCS*. Springer, New York, pp 449–456
30. Ortony A, Clore GL, Collins A (1990) *The cognitive structure of emotions*. Cambridge University Press, Cambridge
31. Rao KS, Yegnanarayana B (2006) Prosody modification using instants of significant excitation. *IEEE Trans Audio Speech Lang Process* 14:972–980
32. Rao KS, Koolagudi SG (2012) *Emotion recognition using speech features*. Springer Science & Business Media, New York
33. Bitouk D, Verma R, Nenkova A (2010) Class-level spectral features for emotion recognition. *Speech Commun* 52:613–625
34. Rao KS, Koolagudi SG, Vempada RR (2013) Emotion recognition from speech using global and local prosodic features. *Int J Speech Technol* 16(2):143–160
35. Nwe TL, Foo SW, Silva LCD (2003) Speech emotion recognition using hidden Markov models. *Speech Commun* 41:603–623
36. Chapaneri SV (2012) Spoken digits recognition using weighted MFCC and improved features for dynamic time warping. *Int J Comput Appl* 40(3):6–12
37. Vogt T, André E (2005) Comparing feature sets for acted and spontaneous speech in view of automatic emotion recognition. In: *Proceedings IEEE international conference on multimedia and expo*, pp 474–477
38. Xu M, Maddage NC, Xu C, Kankanhalli M, Tian Q (2003) Creating audio keywords for event detection in soccer video. In: *Proceedings IEEE international conference on multimedia and expo*, vol 2, pp 281–284
39. Drioli C, Tisato G, Cosi P, Tesser F (2003) Emotions and voice quality: experiments with sinusoidal modeling, pp 127–132
40. Patel S, Scherer KR, Bjorkner E, Sundberg J (2011) Mapping emotions into acoustic space: the role of voice production. *Biol Psychol* 93–98
41. Chandrasekar P, Chapaneri S, Jayaswal D (2014) Automatic speech emotion recognition: a survey. In: *International conference on circuits, systems, communication and information technology applications*, pp 341–346
42. Wu S, Falk TH, Chan WY (2011) Automatic speech emotion recognition using modulation spectral features. *Speech Commun* 53(5):768–785
43. Razak A, Komiya R, Abidin M (2005) Comparison between fuzzy and nn method for speech emotion recognition. In: *Proceedings of 3rd international conference on information technology and applications ICITA*, vol 1, pp 297–302
44. Nicholson J, Takahashi K, Nakatsu R (2000) Emotion recognition in speech using neural networks. *Neural Comput Appl* 11:290–296
45. Zhou Y, Sun Y, Zhang J, Yan Y (2009) Speech emotion recognition using both spectral and prosodic features. In: *International conference on information engineering and computer science, ICIECS, Wuhan*. IEEE Press, New York, pp 1–4
46. Cover TM, Hart PE (1967) Nearest neighbor pattern classification. *Inst Electr Electron Eng Trans Inf Theory* 13:21–27
47. Kotsiantis SB (2007) Supervised machine learning: a review of classification techniques. *Informatica* 31:249–268
48. Bhavsar H, Ganatra A (2012) A comparative study of training algorithms for supervised machine learning. *Int J Soft Comput Eng (IJSCE)* 2(4):2231–2307
49. Tarunika K, Pradeeba RB, Aruna P (2018) Applying machine learning techniques for speech emotion recognition. In: *9th ICCCNT*
50. Duda R, Hart P (1973) *Pattern classification and scene analysis*. Wiley, New York
51. Friedman N, Geiger D, Goldszmidt M (1997) Bayesian network classifiers. *Mach Learn* 29:131–163

52. Anyanwu M, Shiva S (2009) Comparative analysis of serial decision tree classification algorithms. *Int J Comput Sci Secur* 3(3):230–240
53. Jadhav SD, Channe HP (2013) Comparative study of K-NN, naive Bayes and decision tree classification techniques. *Int J Sci Res (IJSR)* 5(1):1842–1845
54. Yang N, Yuan J, Zhou Y, Demirkol I, Duan Z, Heinzelman W, Sturge-Apple M (2017) Enhanced multiclass SVM with thresholding fusion for speech-based emotion classification. *Int J Speech Technol* 20(1):27–41
55. Londhe ND, Ahirwal MK, Lodha P (2016) Machine learning paradigms for speech recognition of an Indian dialect. In: *International conference on communication and signal processing*, pp 780–786
56. Mohanty S, Swain BK (2010) Emotion recognition using fuzzy K-means from Oriya speech, vol 1, pp 188–192
57. Motamed S, Setayeshi S, Rabiee A (2017) Speech emotion recognition based on a modified brain emotional learning model. *Biol Inspired Cogn Archit* 19:32–38

CDMA-Based Security Against Wormhole Attack in Underwater Wireless Sensor Networks



Nitin Goyal, Jasminder Kaur Sandhu, and Luxmi Verma

Abstract The sensors are positioned below the water to monitor the underwater environment in an Underwater Wireless Sensor Network. This network is vulnerable to antagonistic environmental conditions and is more prone to attacks. Since the underwater environment begets a fluctuating nature in reference to temperature, speed, it is necessary to make the network reliable to numerous deviations. This paper suggests a detection and prevention technique for wormhole attack in Underwater Wireless Sensor Networks. Using the suggested technique, unwanted packets can be avoided at the destination node, hence decreasing the overall traffic on the network. This scenario does not consider the number of packets and also sustains against the wormhole attack. This lead to a considerable decrease in the accumulation of extra hardware at nodes. The counter function uses an easy algorithm. Therefore, to ensure the efficient functioning of the network, the error is adaptively controlled. The proposed method also improves the energy-efficiency as compared to the existing techniques.

Keywords Underwater Wireless Sensor Networks · Reliability · Cluster-based · Security · Wormhole attack

1 Introduction

As it is a well-known fact, 70% of the surface of Earth is blanketed with water. This fact paves a way for futuristic exploration in the underwater domain [1–3]. The disasters (natural and man-made) occurred in the span of the previous few years inculcated an interest in the successful monitoring of environments underwater for methodical, ecological, profitable, safety, security, and army needs [4, 5]. Monitoring of sea flows and winds, improved climate forecasting, the detection of environmental change, predicting the influence of human movements on maritime environments, biotic monitoring such as tracking the miniaturized-scale

N. Goyal · J. K. Sandhu (✉) · L. Verma
Chitkara University Institute of Engineering and Technology, Chitkara University, Punjab, India
e-mail: jasminder.sandhu@chitkara.edu.in

© Springer Nature Singapore Pte Ltd. 2021
G. S. Hura et al. (eds.), *Advances in Communication and Computational Technology*, Lecture Notes in Electrical Engineering 668,
https://doi.org/10.1007/978-981-15-5341-7_62

individuals, fishes which are popularly known as micro-organisms, is another application area. The interconnection of underwater vehicles and sensor nodes is useful in performing succinct, supportive, adaptable, and challenging monitoring of coastal aquatic conditions [6–8].

Underwater Wireless Sensor Network (UWSN) is the empowering innovation for ocean applications that can perform contamination observing (nuclear, chemical, and biological), distinguish underwater oil-fields or repositories, decide traversal pathway for the underwater routes, and aid examination of profitable minerals, planning versatile detection of the concoction spills or natural wonders and equipment checking [9–11]. The self-reconfigurable UWSN endures a larger number of shortcomings than the currently existing arrangement. The seismic movements at distant geographical areas can be measured using the sensors. They provide alerts in case of tidal waves at beach front region and concentrate the impacts of tremors also known as seaquakes; and the submarines. Varied sensors are utilized for differentiating risks at the seashore, find hazardous shakes or shores in the waters near the shoreline, securing locations, plummeted sink, and carry out the reporting of the depth of water. The main area of interest can be monitored with the help of the Autonomous Underwater Vehicles (AUVs) and static sensor nodes deployed underwater [12, 13].

UWSN comprises of multiple Underwater Local Area Networks (UW-LANs, otherwise called cells or clusters). Every sensor is associated with the base station or the sink node inside a cluster. The sensor nodes communicate hop by hop. These nodes can be attached to underwater sink nodes with the help of direct linkage. The collected information at the sink node or the base station is sent to a terrestrial station with the help of vertical interconnections. The terrestrial station is furnished with underwater transceivers fit for taking care of various parallel interchanges with the conveyed UW-Sinks [14, 15]. A portion of the structures supporting underwater sensor systems is static 2-dimensional and 3-dimensional Underwater Acoustic Sensor Networks (UW-ASNs). Static 2-dimensional UW-ASNs are established with the help of sensor hubs tied at the base of the ocean. Static 3-dimensional UW-ASNs incorporate systems comprising of multiple sensor nodes which are utilized in case of exploration applications or observation for sea wonders (water streams, sea biogeochemical forms, and contamination). 3-dimensional systems of AUVs incorporate static parts made with the help of moored sensor nodes and versatile bits comprised via autonomous vehicles [16–18].

2 Related Work

The genuine difficulties become an integral factor during the deployment phase when recovering and utilization of sensors is a mandate. The manual collection of data utilizing the sensors lead to mistakes and unnecessary delay. The spatial degree for information gathering with every sensor is restricted because every sensor is unfit to implement tasks that require collaboration, for example, following relative moment and finding the event changes. UWSNs can be affected due to various attacks and

thus results in reduced energy efficiency. To deal with such attacks on the network, the existing work is discussed as follows.

Wang et al. [1] discussed the discovery of a wormhole attack. The sensor nodes utilize a mutual acoustic channel to traverse data in underwater environments. Now, intruder nodes basically listen in a group, burrow them to another location, and retransmit them. It produces a bogus situation where the first sender is somewhere near the neighborhood of the remote area. Authors suggest a technique, Dis-VoW. Based on the distances measured, each sensor rebuilds the local network topology. Dis-VoW identifies wormhole attacks by envisioning the alterations in edge lengths and angles between other nearby sensor nodes. A standardized variable wormhole pointer is characterized on the basis of distinguished counterfeit neighbor associations. The Dis-VoW technique senses the maximum number of counterfeit neighboring nodes and does not introduce the false alarms, in spite of the presence of multiple wormhole attacks. The Dis-VoW technique reproduces the entire network scenario and recognizes the presence of a geographically distributed network. This technique will result in a limited calculation and lesser overhead for the storage of data at the sensor nodes. This exploration prompts an increasingly precise, strong, and productive answer for safeguard against wormhole assaults in the event that it will be connected to the 3D condition.

The comprehensive technique has some primary standards such as, in a prescribed system; security is mandatory for each layer in the protocol stack, expense while guaranteeing the security ought not to outperform security survey at a particular instance of time. A solitary security answer for every layer is not a proficient arrangement rather utilizing a complete methodology could be the best choice. On the other hand, in the absence of physical security guaranteed for sensor nodes, various efforts for achieving a secure network will most likely display a degradation phase. In the event that a portion of the sensors in the system is under attack, because of request or caught by an intruder, the security efforts created to work in a dispersed way. Pathan et al. [6] proposed a method wherein security is not considered for the majority layers, for example; if a sensor node is somehow caught or jammed within the physical layer, entire network security is hampered regardless of the fact that there are well-established methods for achieving security at various layers.

A comprehensive methodology proposed by Palacios [8] considers the improvement in the performance parameter of wireless sensor networks in terms of security, life span, and availability in varied environmental conditions. The comprehensive security-related methodology considers including every layer, thereby guaranteeing the overall system security. The creation of various security layers in comprehensive methodology enhances the protection of the entire network.

Kim et al. [10] recommend a multi-query result combining schematic answers for issues in underwater data transmittal. The suggested structure is a system for giving information on-request from UWSN to different clients maintaining energy-efficiency. This strategy does not necessitate the ability of processing more prominent traditional pervasive sensor hubs. The suggested models for query processing are straightforward which does not store the past information, in this way expending the memory constraint. The condition of the query combining the QRP process is

additionally progression of sensibly strenuous logic-related procedures and requests the microprocessors which possess the consistent capability and hence form the management procedure for query processing. The present technology is excessively powerless against submerged conditions for pragmatic time synchronization to occur. The present technological advances are quite susceptible to the underwater environments for synchronization of a particular time of event occurrence. Constructing a technique for allocating queries or queries set effectively to targeted nodes also suggestively improve the recital of the framework.

3 Problem Identification

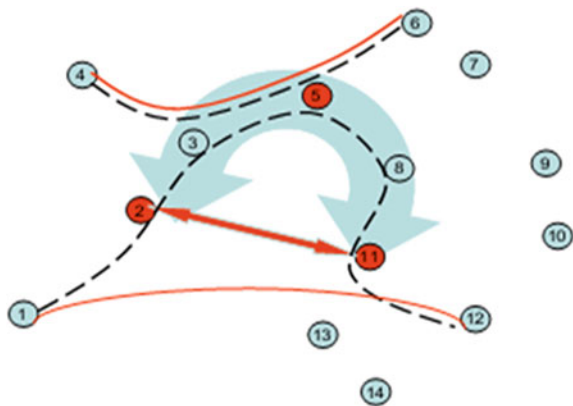
The problem of wormhole attack occurrence in underwater systems can be better understood with the help of Fig. 1. The route attracted by the wormhole contains various advertised routes (shown in solid lines) and actual routes (shown in dotted lines). The following figure shows that the advertised routes are comparatively ample short as compared to the actual routes crossing wormhole intruder deployed at the tunnel passageway. Let us take into consideration the path between node 1 and node 12 in Fig. 1. The path using the advertised channel passes through the nodes 2 and 11, whereas the actual channel traversed by packets passes through nodes 1 and 12 and nodes 2, 3, 5, 8, and 11. Also, the advertised path and the actual path passing through node 4 and 6 are kept the same but interfere with the wormhole tunnel.

Assumptions

For eliminating unsolicited data packets using CDMA technology, we have the following assumptions:

1. The nodes are assigned a unique code and communicate with each other using CDMA technology.

Fig. 1 Network topology created by wormhole attack using nodes 2, 5, and 11



2. The various communicating nodes deployed in a cluster must have the authentication of fetching information at some particular count of nodes and will not be modified automatically.
3. Also, the pre-determined index table is contained at the destination node that will be determined at the time of network initialization.

4 Proposed Solution

Some modification in modulation techniques leads to a reduction in the probability of wormhole attack, as mentioned below in the following steps:

1. We have used CDMA techniques for the modulation of the signal.
2. In each data packet, there will be an ID number of the sender node. The receiver node has the authentication of accepting the packets only from those nodes which contain data without much degradation.
3. The data packet format is described in Fig. 2. Each data packet should carry a count function. The count function changes its value after passing through a node. Using this technique, it becomes easy to know the numbers of nodes traversed and the amount of data being processed.
4. We will introduce a pre-determined index for the count values at the receivers so that the receiver can easily identify the sender by using an index table. Each time when a data packet reaches the receiver node, first it has to check the index table.
5. To make energy-efficient and to recognize intruder easily, we introduced the different values of battery with different transmission power in each node.

Example To better understand the concept, kindly refer to Fig. 1. Considering the scenario, the data packets traverse from node 1 to 12. For this, the packets must then pass through nodes 2, 3, and 4, 5, 11. In this scenario, the packets traverse through nodes 2 and 11. With the help of CDMA technology, different nodes will be assigned different IDs, e.g., the ID of node 1 is 119, node 2 is 121, node 3 is 100, node 5 is 110, node 8 is 112, node 11 is 115 and node 12 is 100. We have used a function known as count at node 1. The count function is initialized to zero (0) in this scenario. Whenever, the packets pass through a node, this function adds 1 to the count (to add more security, further complex numbers can be added). The pre-determined index table stored at node 12. Table 1 gives a summary.

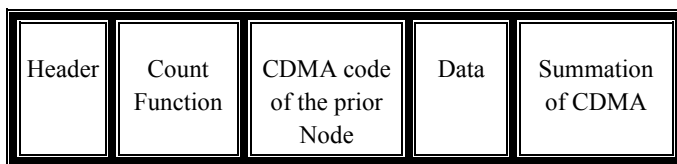


Fig. 2 Data packet structure

Table 1 Example summary of data received at Node 12

Counter function (value of c)	Sender node	Summation of CDMA code
4	2	658
5	1	777

When node 12 receives the packet forwarded through node 1, and the value of counter function tends to be 4, the added-up value of CDMA be 777, the node 12 packet will be acknowledged. Whereas, when a packet traverses only by nodes 2 and 11, the value perceived by the counter function is 2 and the added-up value of CDMA code is 355. Verifying from the table, node 12 deprived of the index match finally rejects the packet. The intruder wormhole will be diagnosed at node 12 without forwarding to node 11. It further stops the processing of data.

5 Conclusion

This paper proposes a wormhole detection and prevention method for the Underwater Wireless Sensor Network. Using the above-described methodology, the unwanted packets are easily avoided at the destination node. Hence, it causes traffic in the network to get decreased considerably. This technique will prevent a large number of wormhole attacks as the total number of packets is not considered. Also, the requirement of hardware addition at various nodes is eliminated. A less complex algorithm is used by the counter function. Thus, the proposed technique adaptively controls the error occurrence probability to guarantee the efficient functioning of the operation of the network.

References

1. Wang W, Kong J, Bhargava B, Gerla M (2008) Visualisation of wormholes in underwater sensor networks: a distributed approach. *Int J Secure Netw* 3(1):10–23
2. Kumar R (2014) A survey on data aggregation and clustering schemes in underwater sensor networks. *Int J Grid Distrib Comput* 7(6):29–52
3. Kumar M, Goyal N (2014) Reviewing underwater acoustic wireless sensing networks. *Int J Comput Sci Technol* 5(2):95–98
4. Goyal N, Dave M, Verma AK (2017) Data aggregation in underwater wireless sensor network: recent approaches and issues. *J King Saud Univ Comput Inf Sci*
5. Sandhu JK, Verma AK, Rana PS (2019) Enhancing the dependability of wireless sensor networks under flooding attack: a machine learning perspective. *Int J Ad Hoc Ubiquit Comput*
6. Pathan ASK, Lee HW, Hong CS (2006) Security in wireless sensor networks: issues and challenges. In: 8th international conference advanced communication technology, vol 2. IEEE, p 6
7. Burrowes G, Khan JY (2011) Short-range underwater acoustic communication networks. In: Autonomous underwater vehicles. IntechOpen

8. Palacios Trujillo R (2010) Interference cancellation and network coding for underwater communication systems. Master's thesis, Universitat Politècnica de Catalunya
9. Sandhu JK, Verma AK, Rana PS (2018) A novel framework for reliable network prediction of small scale wireless sensor networks (SSWSNs). *Fundam Inf* 160(3):303–341
10. Kim Y, Park SH (2011) A query result merging scheme for providing energy efficiency in underwater sensor networks. *Sensors* 11(12):11833–11855
11. Cui JH, Kong J, Gerla M, Zhou S (2006) The challenges of building scalable mobile underwater wireless sensor networks for aquatic applications. *IEEE Netw* 20(3):12
12. Akyildiz IF, Pompili D, Melodia T (2005) Underwater acoustic sensor networks: research challenges. *Ad Hoc Netw* 3(3):257–279
13. Goyal N, Dave M, Verma AK (2019) Protocol stack of underwater wireless sensor network: classical approaches and new trends. *Wirel Pers Commun* 104(3):995–1022
14. Juneja D, Arora N (2010) An ant based framework for preventing DDoS Attack in wireless sensor networks. arXiv preprint [arXiv:1007.0413](https://arxiv.org/abs/1007.0413)
15. Goyal N, Dave M, Verma AK (2018) Adaptive error control technique for cluster-based underwater wireless sensor networks. In: *International conference on wireless intelligent and distributed environment for communication*. Springer, Cham, pp 269–280
16. Goyal N, Dave M, Verma AK (2018) A novel fault detection and recovery technique for cluster-based underwater wireless sensor networks. *Int J Commun Syst* 31(4):e3485
17. Goyal N, Dave M, Verma AK (2017) Improved data aggregation for cluster based underwater wireless sensor networks. *Proc Natl Acad Sci India Sect A Phys Sci* 87(2):235–245
18. Xiao L, Zhu Y (2012) Modeling the wormhole attack in underwater sensor network. In: *2012 8th international conference on wireless communications, networking and mobile computing*. IEEE, pp 1–4. LNCS Homepage <http://www.springer.com/lncs>. Last accessed 21 Nov 2016

Sensing Performance of Ionic Polymer Metal Nanocomposite Sensors with Pressure and Metal Electrolytes for Energy Harvesting Applications



Priya Khanduri, Alankrita Joshi, Lokesh Singh Panwar, Anant Goyal, and Varij Panwar

Abstract Flexible ionic polymer metal composite sensors are desired for detecting pulse rate of the human body and underwater energy harvesting application as compared to the brittle inorganic piezoelectric material. The present research reports the sensing performance of ionic polymer metal nanocomposite (IPMNC) using Platinum (Pt) coated polyvinylidene fluoride (PVDF) (PVDF)/polyvinyl pyrrolidone (PVP)/polystyrene sulfonic acid (PSSA) ionic membrane. The Pt electrode was attached on PVDF/PVP/PSSA ionic membrane using electroless deposition method. The simple solvent casting method was used to fabricate the PVDF/PVP/PSSA ionic membrane. The PVDF/PVP/PSSA based IPMNC generated a sensing voltage of 0.65 V with an application of 0.6 N force. Our IPMNC sensor produces sensing signals with different metal electrolytes and produced highest sensing signal of 0.56 V with immersing the IPMNC sample in 1.5 N NaCl. The data was obtained using data acquisition system (DAS) consists of IPMNC sample on PCB that was connected amplifier, analog to digital convertor, and an Arduino Uno board. The DAS was connected to computer for obtaining data. Our proposed IPMNC sensor can be applicable to the pressure sensor and wearable technology for generation of energy. Our IPMNC can also be useful for detecting metal ions in water and generation of electricity from water medium.

Keywords IPMC · WUP · DAS · IEC · PSSA · PVDF · PVP · PCB

1 Introduction

The ionic polymer metal nanocomposites (IPMNCs) belong to the ionic electroactive polymers which comprise of conducting polymers and ionic gel. The IPMNC is developed using metal nanoparticles (Nps) deposition on the ionic polymer membrane.

P. Khanduri · A. Joshi · L. S. Panwar · A. Goyal · V. Panwar (✉)
Polymer Sensors and Actuator Laboratory, Department of Electronics and Communication Engineering, Graphic Era (Deemed to be University), Dehradun 248002, India
e-mail: varijpanwarcertain@gmail.com; varijpanwar@geu.ac.in

The IPMNC can be utilized for sensor and actuator applications due to the generation of sensing signals with mild force and actuation displacement with electric field, respectively. Due to the application of the pressure on IPMNC, free cations and anions are migrated towards the electrodes that generate the polarization of voltage near the electrode and create the sensing signals. Previously, various researchers utilized IPMCs for sensing and energy harvesting applications [1–7]. Bahramzadeh et al. [3] performed sensing signals of IPMNC sensors with various deflections such as sinusoidal and square wave deflection to monitor response bending to monitor of bridges, twisting measurement of any structure for injuries, and shape monitoring. Shahinpoor et al. [4] presented a theoretical model of IPMC as sensors and actuators and relate them for experimental results of the IPMNC. Tiwari et al. [5] proposed IPMC for energy harvester applications in lower frequency regions (≤ 50 Hz). Cha et al. [6] analyzed underwater energy harvesting from the annular form of Nafion based ionic polymer metal composite (IPMC) using bending vibrations. Cellini et al. [7] analyzed ionic polymer metal composites (IPMCs) for energy harvesting applications from flowing liquid. Previously, various researchers utilized PMNCs as actuators due to the large displacement at very low voltage due to the expansion and contraction phenomenon [8–16].

The sensing mechanism of IPMNC is realized on water uptake (WUP), ion exchange capacity (IEC), and ionic conductivity. A large value of WUP is needed for IPMNC, due to the movement of hydrated molecules in coordination with the cations, under the application of force and flow of electrolytes. Further, the high value of the ionic membrane's WUP helps to improve the conductivity of proton along with the membrane's dielectric constant. Because of the high value of IEC, Platinum (Pt) nanoparticles (NP) are embedded within the membrane's pores by the process of electroless plating. It can also reduce the membrane's resistance, and increases the membrane's capacitance and the electric current of IPMNC. A high value of ionic conductivity is required to generate fast movement of charge ions that enhanced the sensing electric current of the IPMNC under the application of force and electric current [1, 2]. In this research, we have utilized IPMNC using PVDF/PVP/PSSA in 25/15/60 blending ratio as it showed the highest IEC and proton conductivity. Figure 1 shows the chemical structure of PVDF, PVP, and PSSA polymers. Figure 2 shows the sensing mechanism of our proposed IPMNC

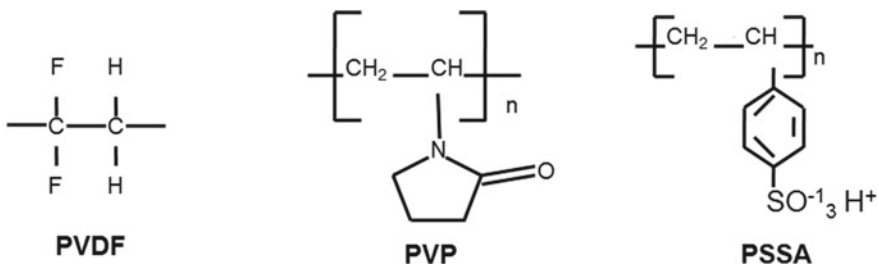


Fig. 1 Chemical structure of PVDF, PVP, and PSSA

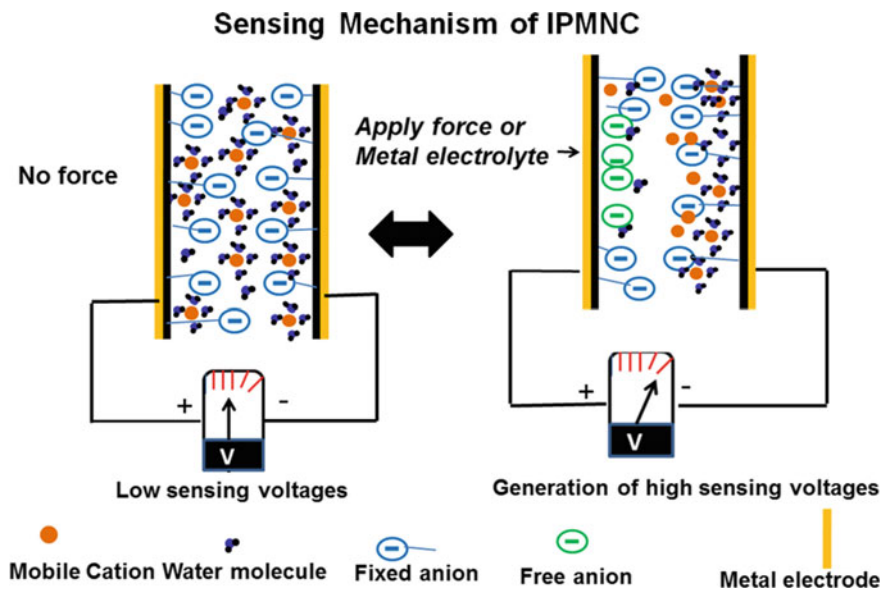


Fig. 2 Schematic diagram of sensing mechanism of IPMNC sensor

with the application of mechanical force and metal electrolytes. With the application of mechanical force and metal electrolyte, the free metal cations ions and anions were generated at anode and cathode side, respectively, that generate the sensing signals.

2 Experimental Work

2.1 Material

PVDF, PVP, and PSSA, Dimethylformamide (DMF), Platinum (Pt) powder was purchased from Aldrich.

2.2 Membrane Fabrication

To fabricate the ionic membrane, various compositions of PVDF, PVP, and PSSA were mixed in DMF with 10 wt% solution. After mixing the solution using a magnetic stirrer, the blending solution was cast on a glass petri disc and kept at hot plate for drying the DMF solvent. After drying the solution, ionic membrane was carefully

strip-off from the glass disc after immersing the solution in distilled water (D.I). The membrane was kept in D. I. water for further use.

2.3 Pt Electrode Fabrication

The Pt electrode was fabricated on the ionic membrane using electroless deposition Method as described earlier (1–5).

2.4 Characterization

Ionic polymer membranes were characterized the water uptake, ion exchange capacity, and ionic conductivity.

Water uptake (WUP) of ionic polymer membrane was determined by the following Eq. (1):

$$\text{WUP} = (W_w - W_d) / W_d \quad (1)$$

where W_w shows mass of hydrated sample and W_d shows the mass of dehydrated membranes, respectively.

For the calculation of IEC, the titration process was used. The acidic (H^+) sample was dipped in 1 M NaCl to convert in sodium (Na^+) ion. The H^+ ions in the solution were treated with 0.1 M NaOH solution. The IEC was calculated using Eq. (2):

$$\text{IEC (mequiv/g)} = \frac{\text{Consumed NaOH (ml)} \times \text{molarity of NaOH}}{\text{Weight of the membrane}} \quad (2)$$

Ionic conductivity (S/cm) was obtained using Eq. (3) as follows:

$$\sigma = \frac{L}{R \times A} \quad (3)$$

where σ is the ionic conductivity, L is thickness of the ionic membrane, R is the resistance of ionic membrane using impedance analyzer, and A is the surface area of the membrane.

The scanning electron microscopy (SEM) images of the dry ionic membrane and based IPMNC were carried out using Hitachi S-4700 SEM instrument.

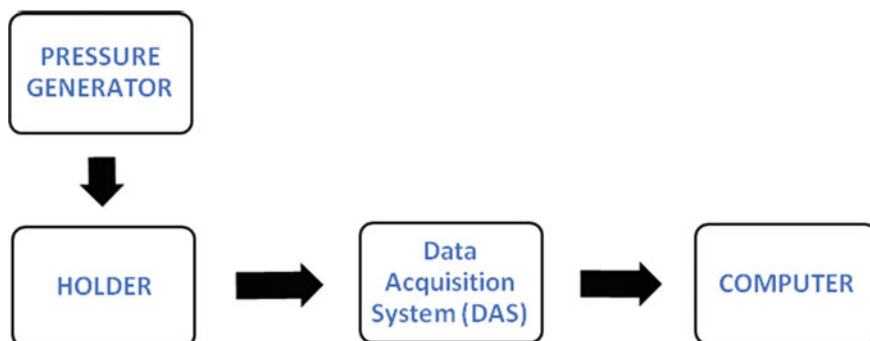


Fig. 3 Schematic diagram for assembly for sensing signals of IPMNC

2.5 Measurement

Figure 3 shows a schematic diagram of a measurement system which includes the pressure sensor, holder, DAS, and computer system. Pressure generator generates pressure on IPMNC sample required to get an induced voltage across the IPMNC membrane's thickness. Holder is made from ceramic plate embedded with a soft holder holding dual PCB inside which the IPMC membrane is placed. Data Acquisition System (DAS) is a block which further consists of an amplifier, analog to digital convertor, and an Arduino Uno board for signal conditioning. A computer system with Intel inside™ CORE™ i3 processor of 3.2 GHz clock frequency with 4 GB of memory is used to store the data acquired for further processing. Figure 4 shows the digital image of the assembly onboard for obtaining data. This figure shows the sample holder, DAS, microcontroller on PCB.

3 Result and Discussion

3.1 Electrochemical Properties

The sensing performance of ionic membrane depends on the electrochemical properties such as WUP, IEC, and ionic conductivity. Table 1 shows the WUP, IEC, and ionic conductivity of PVDF/PVP/PSSA ionic membrane. The WUP of ionic membrane is required for the ions movement and enhances the conduction that improves the sensing signals with the application of mechanical force and metal electrolytes. IEC of the ionic membrane is important for exchanging ions with other metal ions and developing electrode on ionic membrane. The significance of ionic conductivity is to provide fast moment of free ions in the backbone of the ionic membrane.

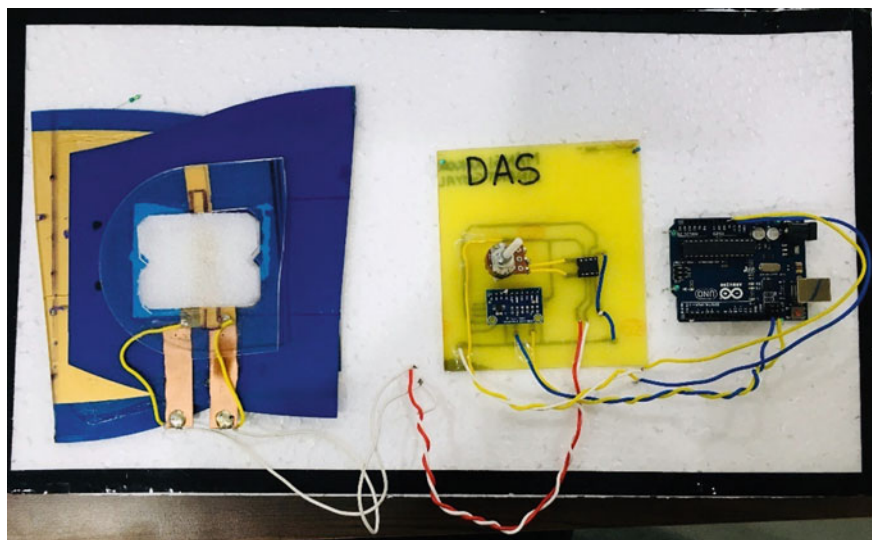


Fig. 4 Assembly on board

Table 1 Electrochemical properties

Membrane	WUP	IEC (meq/g)	Ion conductivity (S/cm)
PVDF/PVP/PSSA 25/15/60	0.53	2.51	0.12
PVDF/PVP/PSSA 30/15/55	0.49	2.35	0.094

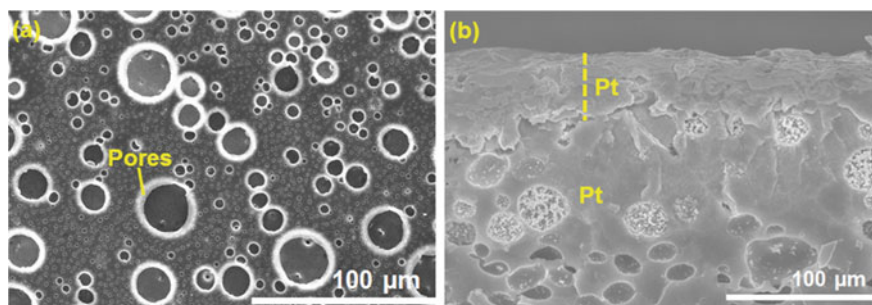


Fig. 5 **a** SEM analysis of PVDF/PVP/PSSA ionic membrane. **b** Pt coated PVDF/PVP/PSSA IPMNC

3.2 SEM Analysis

Figure 5a shows the scanning electron microscope (SEM) of ionic membrane. This figure shows the pores structure of the ionic membrane which absorbs the water and improves the proton conduction. Figure 5b shows the SEM image of the Pt coated IPMNC. This shows the Pt coated on ionic membrane and Pt nanoparticles were penetrated inside the pores of the membranes.

3.3 Sensing Performance

Figure 6 shows the sensing voltage of IPMNC with mechanical force. We have investigated that a sensing signal of 592 V was achieved after the applied mechanical force of 0.6 N. In addition, we found that IPMNC sensor shows sensing signals without mechanical force, it may be due to the free charge ions available inside the IPMNC. The sensing phenomenon of IPMNC with mechanical force can analyzed for energy harvesting application, bandage sensor for biomedical application for detecting heartbeats of human body.

Figure 7 shows the sensing signals of IPMNC as a function of time with pouring of 1.5 N sodium chloride (NaCl) and lithium chloride (LiCl) solution. IPMNC shows higher value of sensing signals (501 mV) with NaCl solution as compared to the LiCl solution (sensing voltage of 297 mV). The sensing behavior of IPMNC with metal electrolytes can be applied for toxic metal ion detection in water environment conditions.

Fig. 6 Sensing voltage of IPMNC with time with the application of force

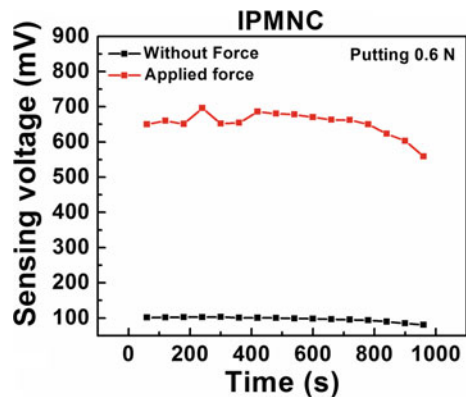
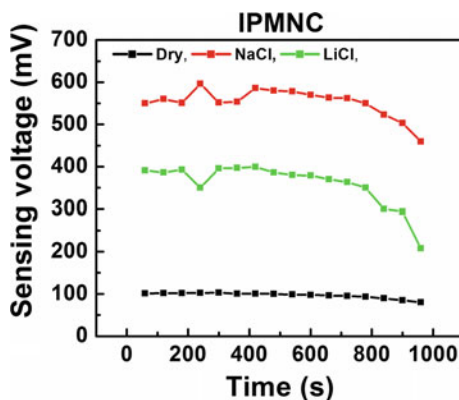


Fig. 7 Sensing voltage of IPMNC with time with the application of electrolyte



4 Conclusion and Future Work

In summary, the sensing mechanism PVDF/PVP/PSSA based IPMNC sensor was examined with the application of mechanical force and metal electrolytes. The based IPMNC generate high sensing signals (550 mN) with the application of the mild force of 0.6 mN, due to a large number of free cations in PVDF/PVP/PSSA based IPMNC. The generation of sensing signals with mild force can be useful to check the heart-beats of human body during walking, for energy harvesting application, and bandage sensors for biomedical application. IPMNC sensor shows high sensing signals of 501 mV with NaCl. The sensing phenomenon of IPMNC with metal electrolytes can be applied for toxic metal ion detection in water environment conditions.

Acknowledgements This work was accomplished by the financial support of the SERB, India (File No.-ECR/2016/001113).

References

1. Panwar V, Gopinathan A (2018) Enhanced sensing performance of carboxyl graphene–ionic liquid attached ionic polymer–metal nanocomposite based polymer strain sensors. *J Mater Chem C* 6:8395–8404
2. Panwar V, Gopinathan A (2019) An ionic polymer–metal nanocomposite sensor using the direct attachment of an acidic ionic liquid in a polymer blend. *J Mater Chem C* 7:9389–9397
3. Bahramzadeh Y, Shahinpoor M (2011) Dynamic curvature sensing employing ionic–polymer–metal composite sensors. *Smart Mater Struct* 20:7
4. Shahinpoor M, Kim KJ (2004) Ionic polymer–metal composites: III. Modeling and simulation as biomimetic sensors, actuators, transducers, and artificial muscles. *Smart Mater Struct* 13:1362–1388
5. Tiwari R, Kim KJ (2012) IPMC as a mechanoelectric energy harvester: tailored properties. *Smart Mater Struct* 22
6. Cha Y, Dolhamidi S, Porfiri M (2015) Energy harvesting from underwater vibration of an annular ionic polymer metal composite. *Meccanica* 50(11):2675–2690

7. Cellini F, Pounds J, Peterson SD, Porfiri M (2014) Underwater energy harvesting from a turbine hosting ionic polymer metal composites. *Smart Mater Struct* 23:10
8. Shahinpoor M, Kim KJ (2005) Ionic polymer–metal composites. *Smart Mater Struct* 10:197–214
9. Jeon JH, Kang SP, Lee S, Oh IK (2009) Novel biomimetic actuator based on SPEEK and PVDF. *Sens Actuators B Chem* 143(1):357–364
10. Feng GH, Chen RH (2008) Fabrication and characterization of arbitrary shaped IPMC transducers for accurately controlled biomedical applications. *Sens Actuators B Chem* 143(1):34–40
11. Panwar V, Lee C, Ko SY, Park JO, Park S (2012) Dynamic mechanical, electrical, and actuation properties of ionic polymer metal composites using PVDF/PVP/PSSA blend membranes. *Mater Chem Phys* 135(2–3):928–937
12. Panwar V, Cha K, Park JO, Park S (2012) High actuation response of PVDF/PVP/PSSA based ionic polymer metal composites actuator. *Sens Actuators B Chem* 161(1):460–470
13. Panwar V, Kang BS, Park JO, Park SH (2011) New ionic polymer–metal composite actuators based on PVDF/PSSA/PVP polymer blend membrane. *Polym Eng Sci* 51:1730–1741
14. Panwar V, Jeon JH, Gopinathan A, Lee HJ, Oh II-K, Jo JY (2015) Low voltage actuator using ionic polymer metal nanocomposites based on a miscible polymer blend. *J Mater Chem A* 3:19718–19727
15. Kukreti K, Panwar V (2018) Improve energy harvesting from low frequency vibrations. *Int J Manage Technol Eng* 2:112–115
16. Jeon JH, Cheedarala RK, Kee CD, Oh II-K (2013) Dry-type artificial muscles based on pendent sulfonated chitosan and functionalized graphene oxide for greatly enhanced ionic interactions and mechanical stiffness. *Adv Funct Mater* 23(48):1–11

Privacy Preserving on Searchable Encrypted Data in Cloud



Deepak Sharma and Avtar Singh

Abstract Cloud computing is the latest paradigm which offers different cloud services by rearranging of resources and provides them on the bases of user's demand. Users are using cheaper data storage and computation offered in the cloud environment, and they are also facing many problems about reliability, privacy-preserving, and optimized searching of their outsourced data. Proposed scheme "Privacy-preserving keyword search" allows users to encrypt their stored data while preserving some search capabilities and also seek few efforts to consider the reliability of the searchable encrypted data outsourced to the clouds. Client-side encryption and server-side searching of encrypted data without decryption in server-side enable more efficient and eliminate privacy issues between client and server.

Keywords Privacy-preserving keyword search · Optimized searching · Secret sharing · Reliability · Cloud computing

1 Introduction

Cloud computing is the latest paradigm which plays a significant role in the IT industry and the government sector. It provides various computing services over the Internet on the basis of pay-per-use, e.g., storage, server, services, etc. Cloud computing helps users to access database resources via the Internet from anywhere. Confidentiality of data can be maintained by storing the encrypted form of data. Cloud data security and efficient searching are becoming more important for the future development of cloud computing technology in government, industry, and business sectors. The cloud storage [1] offers plenty of new opportunities to cloud consumers. Cloud consumer enjoys powerful computation and storage capabilities

D. Sharma (✉) · A. Singh
National Institute of Technology Jalandhar, Jalandhar 144011, India
e-mail: deepaksharma.51000@gmail.com

A. Singh
e-mail: avtarz@gmail.com

offered by clouds and consumers also suffer from more complicated issues related to reliability, privacy-preserving and complex analysis problems of their cloud data, so it is difficult to obtain full reliability guarantee on the CSP.

In cloud storage, confidentiality of data can be maintained by storing the encrypted form of the data in the cloud. Encryption on data assures security but imposes issues in case of performing any operations on such data. These security issues lead to direct exposure of sensitive data to the adversary. Each time when it is necessary to apply any operations on cloud data, then decryption of encrypted data is required. Hence, it is required to apply operations directly on to encrypted data. But it is not practically operational on encrypted data [2]. By applying operations to partially encrypted data, make things practically operational.

For making accurate and optimized searching, there are comparison and partition base searching and sorting techniques. Efficiency is one of the most important challenges in the cloud domain. Storage as a service efficiency is an important factor occur when to encrypt/decrypt the files and searches that files in the server side. Similarly, the privacy of data also plays a vital role in cloud computing. Server-side operations are most vulnerable to risk. There are so many trust issues between cloud service providers and the client in the cloud. Executing most of the operations in client-side helps to make data more secure and also avoid trust issues between the server and the client. Client-side encryption and decryption provide transfer security and data storage security in server. But clients are not rich with resources and not faster enough to execute large data at a faster rate. It is very important to do things efficiently on client-side. Searching time depends on how the data is stored in server-side and encryption/decryption time depends on how fast the cryptographic algorithm. The suggestion is to use searchable encryption to execute a keyword-based search directly on encrypted data to reduce the costly operation in cloud computing and efficient searching algorithm for optimized performance and QoS.

As shown in Fig. 1, data owner stores their encrypted data to Cloud to achieve data protection but it is not a cost-efficient approach. Above approach has the main purpose to achieve efficient and time-saving encryption/decryption for privacy protection of

Fig. 1 Cloud architecture



sensitive data from a third party (CSPs) in the user side. Achieve efficient retrieval of documents containing the queried keyword in increasing network traffic with the help of index which is constructed and encrypted to search directly on encrypted formats and learn nothing from the encrypted index and encrypted documents.

The overall paper is organized as follows: Sect. 2 describes the recent study which shows what is already done in privacy protection and searching of data and how the motivations are arising about security, privacy protection, and performance efficiency. Section 3 shows the modified AES algorithm. Section 4 shows some approaches which are used to solve the research objective, and Sect. 5 shows the implementation and result analysis.

2 Recent Study

The cloud infrastructure is owned by single CSP or multiple-CSPs and provides different on-demand services like resource allocation, memory, storage, computation, etc. In cloud computing, availability of data gives rise to the vulnerabilities and unauthorized breaches to use sensitive data in cloud storage. Data security and privacy protection are one of the main factors of the user's concerns about cloud technology. There are different approaches that make use of encryption techniques to achieve privacy in the cloud. The encryption system not only preserves the privacy of the file but also provides keyword search over encrypted data and high performance. Initially how to do keyword search over encrypted file effectively was arise in Song et al. [3]. Since then there are lots of work conducted in this field. In 2004, Bonech et al. [4] proposed public-key encryption with keyword searching (PEKS), which enables a way of checking the keywords in an email without learning any information about the email and keywords.

In 2009, Liu et al. [5] allow users to efficiently access files containing certain keywords in a cloud anytime and propose a scheme efficient privacy-preserving keyword searching (EPPKS) in the cloud which improves the performance of previous one. But in 2012, Liu et al. [6] propose a scheme of secure privacy-preserving keyword searching (SPKS) which allows the CSP to participate in the decipherment, so users pay less computation overhead for decryption. But that arises the security concern related to exposé of sensitive data to un-trusted CSPs.

Wang et al. [7] provide a solution for supporting efficient ranked-based keyword search for achieving efficient utilization of cloud-stored encrypted data. The proposed scheme provides a security guarantee and efficiency of the solution. Sajid et al. [8] propose a scheme where fast, efficient ranked based searching over data without decryption overhead, which minimize the searching time. But they are not talking about minimizing the encryption and decryption time at the user side. In cloud environment, most users are not capable to encrypt/decrypt the large size data in faster speed which is the biggest problem in those scenarios. To solving that problem, proposed scheme should need less computation power and less time overhead to make thing simple and compatible.

Related work on searchable encryption focus on Boolean keyword search and single keyword search, and rarely sort the result. Cao et al. [9] propose a solution which solves the problem of privacy-preserving multi-keyword ranked search over encrypted data (MRSE).

Efficient similarity searching over encrypted data scheme shows how they create trapdoor to search user query over a highly secure data index list. They will use locality-sensitive hashing (LSH) for fast nearest neighbor search in high-dimensional spaces. LSH hashes input items so that similar items map to the same bucket metric with high probability.

3 Modified AES Algorithm

First of all, the privacy of data is archived by some encryption algorithms which provide confidentiality and consume lesser time. AES is a cryptographic algorithm which provides high security in lesser time. But to seduce time furthermore, our security parameter is also going downward. By stabilizing the security but continues reduction in time gives efficiency in cloud computing when try to encrypt and decrypt data in the user side. So, the proposed algorithm makes existing AES more secure and less time-consuming. Figure 2 shows the modified AES encryption, and Fig. 2 shows the modified AES decryption. These figures show different modifications made inside the basic AES algorithms. Modifications inside AES algorithm are briefly decied.

3.1 *Cyclic Encryption*

Cyclic encryption performs different operations over data to provide diffusion and confusion, and S-box is fundamental component used in symmetric key cryptography. Generally, it takes m bits as input and generates n bits as output. This is sometimes often called $m * n$ S-box. Key adding is also a main component in diffusion. Here, key is XOR with data linearly and all the process of cyclic encryption is given in this algorithm. In cyclic encryption, three functions are evoked in sequence: S-box, cyclic key addition, and linear XORing. S-box is the common permutation function using S-box/inverse S-box table [10]. Linear XOR is used to mix the data value and form new result. In XOR, firstly initialize the initialization vector IV. This vector IV is XOR with first byte of data and the outcome is then XOR with next byte and procedure stays proceeded as far as possible.

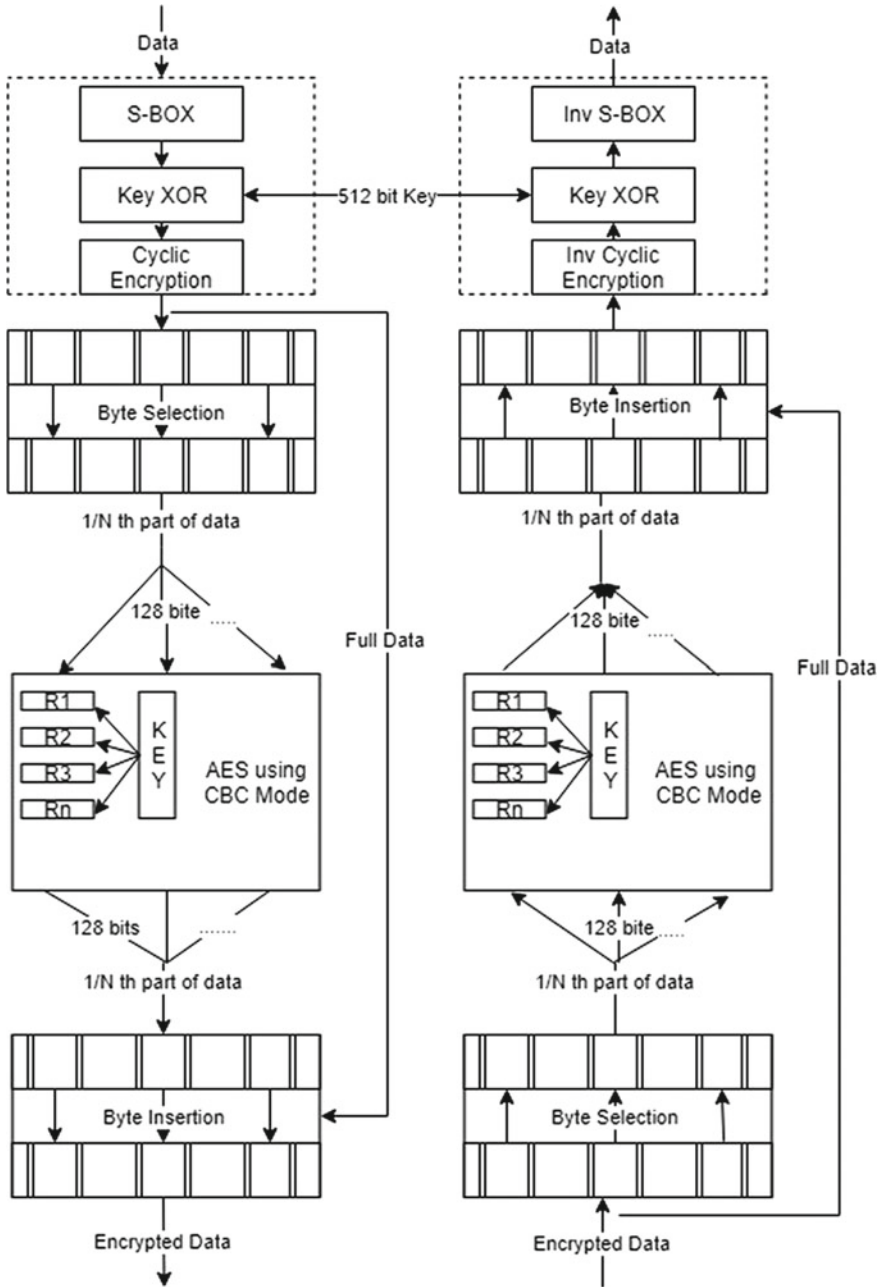


Fig. 2 Encryption process and decryption process

Algorithm: Cyclic Encryption

Require: Key← secret key 256 bits D: Data items**Cyclic Encryption:**

1. S-box of data
2. Cyclic Key adding
3. Linear XORing

Cyclic Key adding

1. **for all** $D_{t_i} \rightarrow D$ **do**
2. $D_{t_i} \leftarrow D_{t_i} \oplus key_j$
3. **end for**

Linear XOR

1. **for all** $D_{t_i} \rightarrow D$ **do**
 2. $IV \leftarrow D_{t_i} \oplus IV$
 3. $D_{t_i} \leftarrow IV$
 4. **end for**
-

3.2 Inverse Cyclic Encryption

Inverse cyclic encryption performs some inverse operation of cyclic encryption and same operations. Inverse S-box is fundamental component used in symmetric key cryptography. In key adding, key is XOR with data linearly.

Algorithm: Inverse Cyclic Encryption

Require: Key← secret key 256 bits D: Data items**Inverse Cyclic Encryption:**

1. Inverse Linear XORing
2. Cyclic Key adding
3. Inverse S-box of data

Cyclic Key adding

1. **for all** $D_{t_i} \rightarrow D$ **do**
2. $D_{t_i} \leftarrow D_{t_i} \oplus key_j$
3. **end for**

Inverse Linear XOR

1. **for all** $D_{t_i} \rightarrow D$ **do**
 2. $Temporary_j \leftarrow D_{t_i} \oplus IV$
 3. $IV \leftarrow D_{t_i}$
 4. $D_{t_i} \leftarrow Temporary_j$
 5. **end for**
-

In inverse linear XOR, initialize vector IV is XOR with first byte of data and the outcome is stored. But previous dt_i XOR with next byte and procedure stays proceeded as far as possible.

3.3 Byte Abstraction

It is not possible to predict the user data size. It may vary from small to large. To encrypt a large file encryption, algorithm takes a larger amount of time. Encryption algorithm is not applied over the whole data. So only $1/N$ th part is encrypted that is discussed further.

3.4 AES Implementation

It is a symmetric encryption calculation and utilizes substitution and stage approach. Key sizes of 256 bits AES encryption take 14 rounds separately. All rounds preparing is same with the exception of the last round.

3.5 Byte Embedding

In this Nth part that is encrypted is placed on its original place of data. Modified AES algorithm is useful in achieving the proposed scheme goals. This provides optimized encryption/decryption and maintains the security level as well. As shown in Figs. 2, extra function is added in front of encryption of AES and backside of decryption of AES. These two addition functions add extra security factor to algorithm but increase time consumption also but after applying N factor, that addition functions provide nearly same security with lesser time consumption. That N factor is described in Sect. 3.

4 Approach

To provide the privacy-preserving and optimized searching, use reliable cloud storage and privacy-preserving keyword search scheme in a cloud environment. Use of searchable encryption is to execute keyword-based search directly on encrypted data and to reduce the costly operation in cloud computing. Generation of an index which embedded the file features and keywords is used for keyword search. The server performs the searching of keywords on the index without learning anything about the data.

4.1 Data Encryption/Decryption

Data is unstructured, and the service provider does not know about the properties of data. Service provider gets the data in encrypted form. The client provides the data items D and encrypts the data items say D by using key to form the encrypted collection. From encryption, AES 512-bit keys are used for storing data in a cloud server. Generally, AES has various key sizes (128, 192, and 256) for encryption. But 512-bit key size AES is more secure and reliable as compared to rest. Similarly, AES-512 has mostly 22 numbers of rounds for encryption, which is mapped with key size.

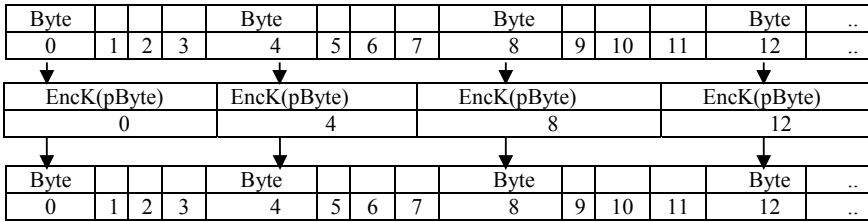


Fig. 3 An example for encryption of files $N = 4$

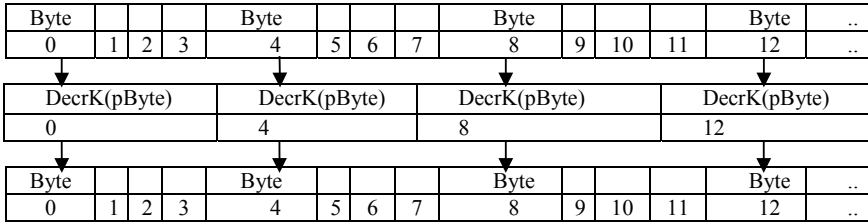


Fig. 4 An example for decryption of files $N = 4$

User data sizes are not predictable, which are either larger or small. If AES-512 encryption is applied over large size data, it will take a lot of time to implement. So, encrypting whole data is not a good choice. Encryption applies over one/ N th part of a file only and embeds that one/ N th part into that particular file. Using that way hiding of sensitive data from unauthorized people and secure the file from tempering.

For data encryption files are in a byte array format and took every N th byte (mean index multiple of N) from the byte array and encrypt that streamed byte array. This process is part of byte abstraction in Fig. 2 and in byte embedding encrypted bytes array again rearranges to their actual position from where they are extracted. Like the above example, Fig. 3 shows how bytes are abstracted, which are multiple of N and encrypt them sequentially and place encrypted byte again to their original position using byte embedding. After that whole encrypted files are stored along with their encrypted index. Similarly, decryption of file is carried out when server retrieves the file which is searched using appropriate query keyword. In decryption of file, firstly byte abstraction and decrypt them sequentially and place encrypted byte again to their original position using byte embedding shown in Fig. 4.

4.2 Feature Extraction

In feature extraction, frequent keywords are extracted from file data item $D_{item}(D_i, \dots, D_n)$ which contains their features $f(f_i, \dots, f_n)$ (keywords or sensitive data). Feature extraction maps D_i to f_i . For feature extraction, there is a different algorithm which is optimized and reliable for extraction.

4.3 Index Construction

Construction of hash function $H(h_1, h_n)$ is according to the requirement of our application. Mapping each feature f_i to hash function g_i . Like $g_i(f_i)$ be the output by applying hash function g_i over feature f_i . Then, $g_i(f_i)$ is one bucket identifier of the data item index and the data items that contain characteristic are the member of it. Content is simply a bit matrix of size L where L is the total number of data file stored on the server. Each data item has assigned an identifier from 1 to L . As always storing of data index in matrix form is not space-efficient but it required lesser time to search the index in matrix. So, storing data index in matrix format is efficient and simple. Hashing and matrix construction are given in build index algorithm.

4.4 Index Encryption

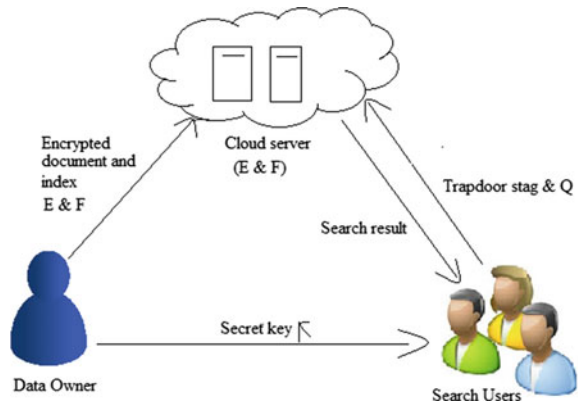
After index construction, secure index by applying encryption on bit matrix identifiers and contents. Only users should able to encrypt that bit identifiers during the query process. Data owner will not share that secret key with other entrusted person. Otherwise, the adversary could apply that encryption and find out any index of file easily. Similarly, the whole bit matrix of indexes is encrypted to hide the leakage of important information.

There is the algorithm which is used to build index using secret keys (Key_{id} , $Key_{payload}$), and $EncKey_{id}$, $EncKey_{payload}$ be an encryption technique like AES-512 in CTC mode. D_{item} denotes data items, Max: maximum possible number of features, F_i denotes extracted feature of data items, $h_i(f_{ij})$ denotes hashing implemented over feature f_i , M_k denotes matrix identifier, and V_{Mk} is the bit of matrix. After encryption, fake records are added into the index to hide the actual number of features.

Algorithm: Buid Index

- Require:** D_{item} : data items, h : hash functions, Max: maximum possible number of features
1. $Key_{id} \leftarrow$ Key generation, $Key_{payload} \leftarrow$ Key generation
 2. **for all** $D_i \rightarrow D_{item}$ **do**
 3. $F_i \leftarrow$ extract characteristic of D_i
 4. **for all** $f_{ij} \rightarrow F_i$ **do**
 5. $F_{ij} \leftarrow$ apply hash function on f_{ij}
 6. **if** $h(f_{ij}) \neq$ bucket identifier list **then**
 7. add $h(f_{ij})$ to the bucket identifier list
 8. **end if**
 9. $V_{h(f_{ij})[id(D_i)]} \leftarrow 1$
 10. **end for**
 11. **end for**
 12. **for all** $M_k \rightarrow$ bucket identifier list **do**
 13. $V_{Mk} \leftarrow$ retrieve payload of M_k
 14. $\pi_{Mk} \leftarrow EncKey_{id}(M_k)$, $\sigma V_{Mk} \leftarrow EncKey_{payload}(V_{Mk})$
 15. add $(\pi_{Mk}, \sigma V_{Mk})$ to I
 16. **end for**
 17. **return** I
-

Fig. 5 Condition trapdoor security for partial encrypted patterns



4.5 Trapdoor Construction

Initially it applies a hash function over feature f_i to construct the plain query $(h_i(f_i))$, and then applies $EncKey_{id}(h_i(f_i))$ on each component of the plain query. Once the trapdoor T_f is constructed, it is sent to the server. Figure 5 shows that data owner stores encrypted data and index in the cloud server, and a different user can search their query and retrieve result using the secret key, which is shared by the data owner.

4.6 Keyword Search

As shown in the algorithm search keyword, where client generates the trapdoor using LSH algorithm and sends query trapdoor to server. Server gets the trapdoor T_f from user and performs an operation for each “Query Trapdoor” on the index, and sends back the result which contains the encrypted bit vector.

Algorithm: Search Keyword

- CLIENT:**
Require: h : hash functions, Max : maximum possible number of features
1. $Key_{id} \leftarrow$ secret key, f : characteristics to search
 2. **for all** $f_i \rightarrow f_{do}$
 3. $F_{di} \leftarrow EncKey_{id}(h(f_i))$
 4. **end for**
 5. Trapdoor $T_f \leftarrow (f_1, \dots, f_{dn})$
 6. Send T_f to Server
- SERVER**
Require: I : index, T_f : Trapdoor
7. **for all** $f_{di} \rightarrow T_f$ **do**
 8. **If** $(f_{di}, V_{Mk}) \rightarrow I$ **then**
 9. Send V_{Mk} to Client
 10. **end if**
 11. **end for**
-

Table 1 Tools and platform used

IDE	Net beans
Programming language	Java 1.8
Operating system	Windows 10 Pro 64-bit
Analytical tool	SigmaPlot
Processor	Intel Core I7 3rd Gen, 2.4 Ghz
RAM	4.00 GB, 1600 MHz
Graphics	1.00 GB, Nvidia Geforce 650 M

Both the owners’ cloud data and data index contain important information and required protection against adversary. So, system should fulfill this security requirement:

- **Data privacy:** Secret key is required to breach the security of cloud data. Including cloud server, no one can able to learn any about private data and index data.
- **Search privacy:** Most important requirement of users is to protect the searching criteria they are using on data. These searchable criteria are not reducible from trapdoor query and data/index sent by user.

5 Implementation and Result Analysis

Proposed scheme takes place in two stages. In the first stage, storage of data in cloud takes place by encryption and indexing of files. Then, encrypted file along with encrypted index (which is constructed by feature extraction from data items D_i) is sent to cloud. In the second stage, retrieval of files is done by keyword searching (take place in cloud side).

5.1 Simulation Settings

See Table 1.

5.2 Throughput Analysis

Performance is evaluated over different sizes of data with different key sizes. Simulation result shows encryption/decryption time against file size and encryption parameter N .

Different sizes of data demonstration of results in graphical form are shown in Figs. 6 and 7. A graph of encryption and decryption with respect to changing value of $N = \{4, 8, 16, \dots, n\}$. Figures analyze that if larger size N is taken then

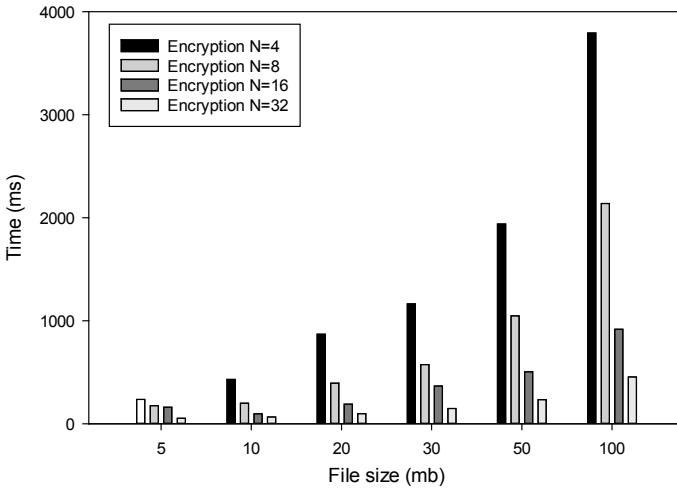


Fig. 6 Encryption (Data_{byte}/Time_{millisec})

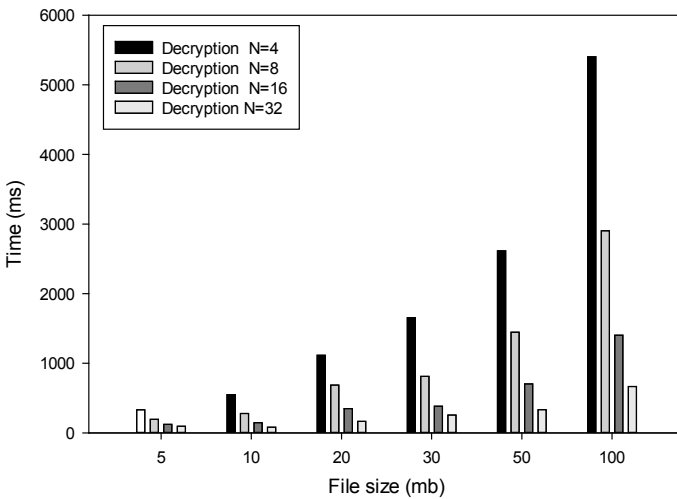


Fig. 7 Decryption (Data_{byte}/Time_{millisec})

encryption time for $N = \{4, 8, 16, 32\}$ are decreasing (N value used in selection of byte for encryption/decryption).

Figure 8 shows the throughput (Data_b/Time_{millisec}) and shows how much data in byte form is encrypted or decrypted in one millisecond. This also shows as the increase in $N = \{4, 8, 16, 32, \dots, n\}$ the throughput of encryption increases.

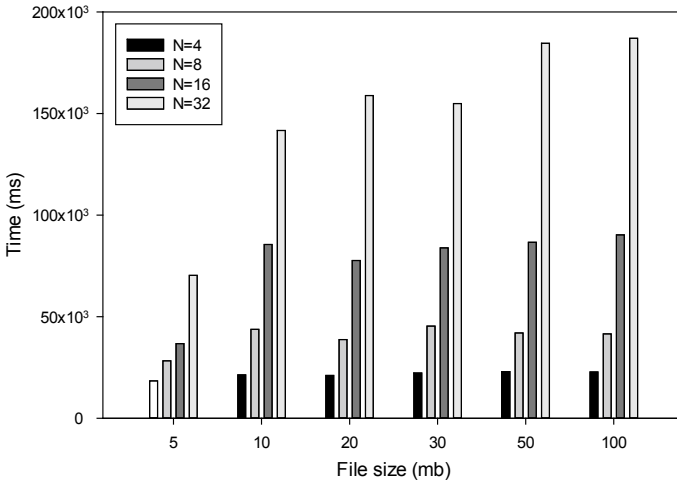


Fig. 8 Throughput ($\text{Data}_{\text{byte}}/\text{Time}_{\text{millisec}}$)

5.3 Storage and Retrieval of Data from Cloud

Experiment 1–10 mb of data is taken for comparison of data upload and download time of proposed scheme and client-side deduplication scheme (CSDS) [11] with respect to average time (ms). Figure 9 shows that the proposed scheme consumes less time in both upload and download of files.

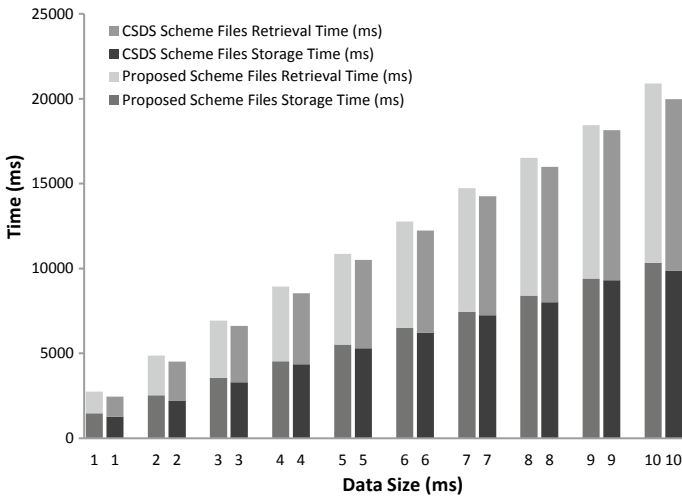


Fig. 9 Files storage time and retrieval time (Data mb/Time ms)

Figure 10 shows encryption time and index construction time with respect to N value. N value is the value which shows amount of data is encrypted. Figure 10 shows decryption time and searching time with respect to N value. As shown in Figs. 10 and 11, encryption times are more as compared to decryption time. Index construction time and searching time are linear as compared to encryption/decryption time. Here, encryption and decryption take place in user's side which are not capable

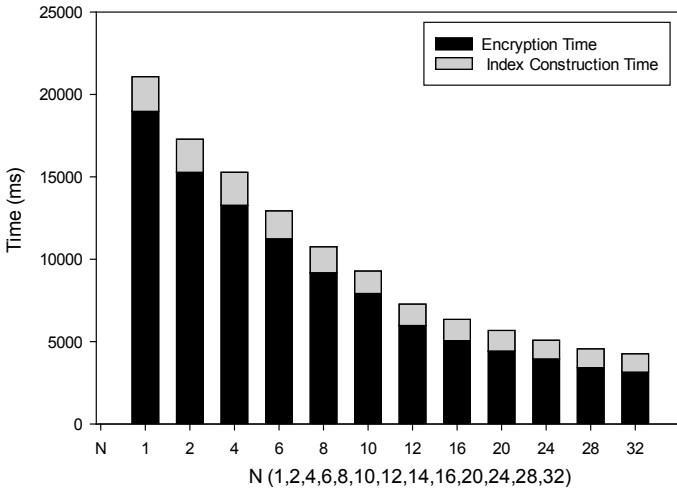


Fig. 10 Storage of file

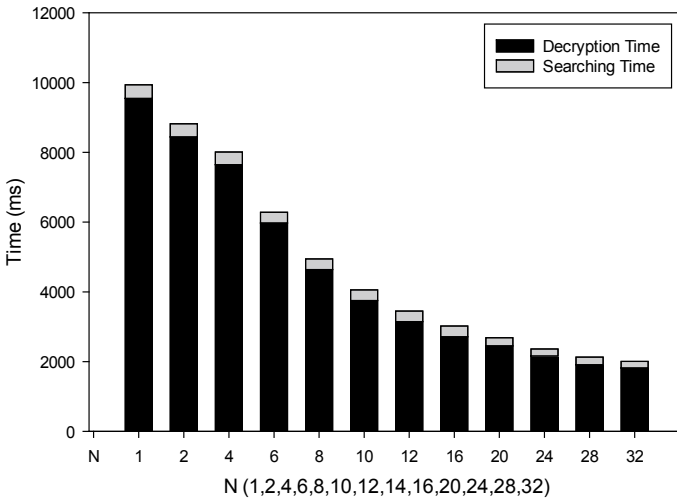


Fig. 11 Retrieval of file

Table 2 Algorithms with avalanche effect (%)

<i>N</i>	Avalanche effect of basic AES (%)	Avalanche effect of propose AES (%)	Proposed AES avalanche effect (%) rate of change
1	46.88	56.01000	0
2	24.431	51.99631	7.1433
4	12.190	46.99631	9.6160
6	6.700	41.03711	12.680
8	7.259	37.93308	7.5639
10	7.994	35.06430	7.5628
12	7.590	31.96428	8.8409
16	7.035	30.96428	3.1284
20	6.812	30.56428	1.2918
24	7.37	30.26428	0.9815
28	5.69	30.06428	0.6608
32	7.705	30.00010	0.2136

of encrypting/decrypting large size data and also have low hardware configurations. Parameter *n* trying to make possible to execute large data with low hardware configurations.

Avalanche effect shows the property of security which is crucial for block cipher. Avalanche effect measures the change of one bit in plaintext and leads to how much change in ciphertext. That is totally depending on amount of confusion and diffusion in cryptographic algorithm.

Original AES [12] has lesser avalanche effect as compared to the proposed avalanche effect when value of *N* is 1. As decreasing of *N* value propose AES have high avalanche effect then original AES (shown in Table 2).

Figure 11 shows percentage value of avalanche effect with respect to *N* value and Fig. 12 is the graph which shows us the change of values of Figs. 9 and 11 with respect to *N*. As shown in Fig. 12, avalanche effect is not changed as much as compared to encryption time. Purpose of the proposed scheme is to lower the encryption/decryption overhead on user side but not compromising the security. Above graph shows that purpose of the proposed scheme is fulfilled in some extend (Fig. 13).

6 Conclusion

Cloud storage as a service is one of the main services provided by cloud. Proposed scheme maintains the confidentiality of sensitive data and minimizes the time consumption in encryption/decryption and enables direct searching over encrypted data without compromising much privacy guarantee of sensitive data. Matrix-based index construction and comparison-based searching obtain better efficiency

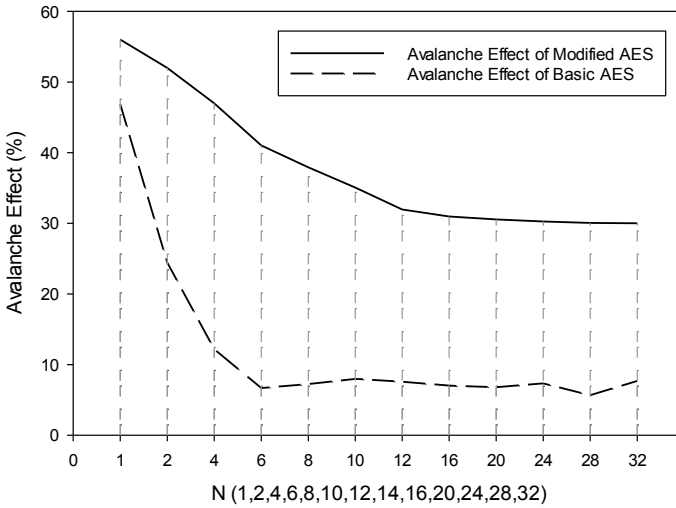


Fig. 12 Avalanche effect of data [(%)/N (1, 2, 4, 6, 8, 10, 12, 16, 20, 24, 28, 32)]

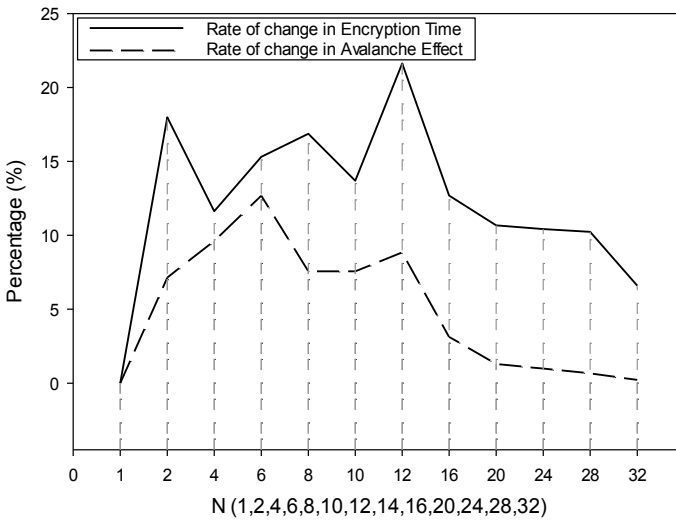


Fig. 13 Rate of change in encryption time with respect to change in avalanche effect

in searching. There are still many challenges in the proposed scheme like there is future work on dynamic deletion/insertion of files and large-sized data. There are many security challenges in a multi-user scheme. Firstly, all the users share secret key for indexing and trapdoor generation. In this scenario, user revocation is the big challenge. In the future work, improvement is required in the proposed scheme to handle these challenges.

References

1. Li J, Lin D, Squicciarini AC, Li J, Jia C (2017) Towards privacy-preserving storage and retrieval. *IEEE Trans Cloud Comput* 5(3):499–509
2. Chatterjee A, Sengupta I (2015) Searching and sorting of fully homomorphic encrypted data on cloud. In: *IACR cryptology ePrint archive*. IACR, p 981
3. Song DX, Wagner D, Perrig A (2000) Practical techniques for searches on encrypted data. In: *IEEE symposium on security and privacy*. S&P. IEEE, pp 44–55
4. Boneh D, Di Crescenzo G, Ostrovsky R, Persiano G (2004) Public key encryption with keyword search. In: *International conference on the theory and applications of cryptographic techniques*. Springer, pp 506–522
5. Liu Q, Wang G, Wu J (2009) An efficient privacy preserving keyword search scheme in cloud computing. In: *International conference on IEEE computational science and engineering, 2009. CSE'09*. IEEE, pp 715–720
6. Liu Q, Wang G, Wu J (2012) Secure and privacy preserving keyword searching for cloud storage services. *J Netw Comput Appl* 35(3):927–933
7. Wang C, Cao N, Ren K, Lou W (2012) Enabling secure and efficient ranked keyword search over outsourced cloud data. *IEEE Trans Parallel Distrib Syst* 23(8):1467–1479
8. Khan MS, Wang C, Kulsoom A, Ullah Z (2013) Searching encrypted data on cloud. *Int J Comput Sci Issues IJCSI* 10(6):230
9. Cao N, Wang C, Li M, Ren K, Lou W (2013) Privacy-preserving multi-keyword ranked search over encrypted cloud data. *IEEE Trans Parallel Distrib Syst* 222–233
10. https://en.wikipedia.org/wiki/Rijndael_S-box
11. Kaaniche N, Laurent M (2014) A secure client side deduplication scheme in cloud storage environments. In: *2th international conference on new technologies, mobility and security (NTMS)*. IEEE, pp 1–7
12. Sriperumbudur Tamil Nadu (2018) A block cipher algorithm to enhance the avalanche effect using dynamic key-dependent S-box and genetic operations. *Int J Pure Appl Math* 119(10):399–418
13. Kartheeban K, Durai Murugan A (2017) Privacy preserving data storage technique in cloud computing. In: *IEEE international conference on intelligent techniques in control, optimization and signal processing (INCOS)*. IEEE, pp 1–6
14. Al-Mamun A, Rahman S, Ahmed Shaon T, Hossain M (2017) Security analysis of AES and enhancing its security by modifying S-box with an additional byte. *Int J Comput Netw Commun IJCNC* 9(2)
15. Shankarwar MU, Pawar AV (2015) Security and privacy in cloud computing: a survey. In: *Proceedings of the 3rd international conference on frontiers of intelligent computing theory and applications (FICTA)*. Springer, pp. 1–11
16. Li J, Lin D, Squicciarini A, Jia C (2015) STRE: privacy-preserving storage and retrieval over multiple clouds. In: *International conference on security and privacy in communication networks*, pp 36–44
17. Kamara S, Papamanthou C, Roeder T (2012) Dynamic searchable symmetric encryption. In: *Proceedings of the 2012 ACM conference on computer and communications security*. ACM, pp 965–976
18. Kuzu M, Islam MS, Kantarcioglu M (2012) Efficient similarity search over encrypted data. In: *IEEE 28th international conference on data engineering*. IEEE, pp 1156–1167
19. Ananthi S, Sadish Sendil M, Karthik S (2011) Privacy preserving keyword search over encrypted cloud data. In: *International conference on advances in computing and communications*. Springer, pp 480–487
20. Owens D (2010) Securing elasticity in the cloud. *Commun ACM* 53(6):46–51
21. Chang Y-C, Mitzenmacher M (2005) Privacy preserving keyword searches on remote encrypted data. In: *International conference on applied cryptography and network security*. Springer, pp 442–455

Adaptive Approximate Community Detection Algorithm for Bubble Rap Routing Protocol



Sweta Jain, Neerali Chauhan, and Pruthviraj Choudhari

Abstract A social graph is a network that shows the representation of how the nodes are connected. The classification of the network is done into different communities for data transmission. In the Bubble Rap routing protocol, the local and global centrality of a node is considered for message transmission. The global centrality tells how much the node is important in the entire network while the local centrality tells how much a node is important in its community. In Bubble Rap routing algorithm communities are formed with the help of K-Clique algorithm. The K-Clique algorithm is mainly designed for binary static graphs whereas Delay-Tolerant Network is highly dynamic in nature as the connections among the nodes keep on changing with time. In an Adaptive Approximate community detection algorithm, the information of the current network and previous community structure is followed to deduce the current structure of the community for the network. The community is decided using node degree and a frequency-duration utility. In this paper, we have implemented the algorithm for bubble rap protocol, and depending on the results of simulation it can be seen that performance-wise this algorithm is a better than clique community detection algorithm.

Keywords Community detection · Bubble rap algorithm · Delivery ratio · K-clique algorithm

1 Introduction

A Delay-Tolerant Network (DTN) is a general-purpose overlay network operating in addition to various regional networks, including the Internet [1]. The end-to-end path is usually not available as the node connectivity is dynamic and sparse network density in DTNs [2]. Nodes can only transfer data with each other when they are within each other's transmission range. In DTN, nodes adopt store carry

S. Jain · N. Chauhan · P. Choudhari (✉)

Department of Computer Science and Engineering, Maulana Azad National Institute of Technology, Bhopal, India

e-mail: pruthviraj5696@gmail.com

© Springer Nature Singapore Pte Ltd. 2021

G. S. Hura et al. (eds.), *Advances in Communication and Computational*

Technology, Lecture Notes in Electrical Engineering 668,

https://doi.org/10.1007/978-981-15-5341-7_65

and forward routing mechanism whereby nodes store a copy of the message in their buffer and on meeting new nodes, forwards it to them. Some routing protocols do this forwarding blindly like epidemic routing [3] while other routing protocols use selective forwarding by sending messages to nodes more likely to meet the destination of the message [3]. Certain routing protocols utilize social properties of nodes such as their community labels, their popularity in the community, etc. to take this forwarding decision [4]. In online social networks [5], a community represents a collection of users who have either common interests such as music or who speak common language or belong to a common locality. Community detection basically involves dividing network nodes into community structures based on their characteristics. Many network-based problems such as message forwarding strategies or routing techniques can be designed by utilizing the community structure of nodes and their social characteristics [6]. Bubble Rap is a popular routing protocol in the category of social-based routing protocols, designed specifically for DTNs. It uses both node community structure and node centrality concept to take message forwarding decisions. However, bubble rap uses K-Clique algorithm for community detection that is suitable for binary static graphs. Also, K-Clique is unable to find overlapping communities in the network [1, 7, 8]. The networks where node membership in a particular community changes over time are called as dynamic networks. Delay-Tolerant Networks is also a highly dynamic network where network topology changes very frequently with time. Although the community detection problem has been extensively explored in the context of static networks, it has not received much attention for dynamic networks [9]. In such kind of dynamic networks, it is required to find community structure which is adaptive with each network snapshot, and this problem is known as Adaptive Community Detection Problem. This means that the change in the community structure at any time t is determined by the community structure at the previous time shot $t - 1$, rather than recalculating the community structure from scratch [10, 11]. In the current work, we have adopted a dynamic community detection algorithm in Bubble Rap routing protocol to overcome the shortcomings of the static community detection algorithm.

Section 2 emphasizes on the literature review and work related to community detection algorithms. Various fundamental terminologies related to the community detection algorithm are also explained in this section. Section 3 presents the adaptive algorithm used for the determination of community structures in dynamic networks. Section 4 presents the simulation results based on different scenarios and also evaluates their respective performances.

2 Related Work

Hui and Crowcroft proposed a routing strategy for Pocket Switched Networks (PSNs) known as label routing that utilizes the community labels of nodes to select the next message forwarder [12]. Each node has an associated label that informs the

other nodes about its association with a group or community. The message is either transmitted directly to the destination node or to a node with a label similar to the destination. Since there is a possibility that nodes from the same community will meet more consistently, they are more suitable forwarders for messages intended for community nodes.

In [4], Hui et al. proposed another very popular social-based routing protocol called Bubble Rap routing protocol which uses both community structure of network nodes and their centrality value to make a routing decision. In the first phase, nodes transmit messages to nodes having high centrality value in the global community, and in the second phase once the message is reached at the destination community then nodes forward messages to nodes having high centrality value in the local community [13].

SimBet [7, 8] routing protocol proposed by Daly and Haahr uses a new utility metric that combines two-node social characteristics namely similarity and betweenness centrality of a node to select the most appropriate node forwarder. In SimBet routing scheme, the node having high SimBet utility receives the forwarded packet. Similarity occurs when two nodes fall in the same equivalence class. Betweenness is a measure of centrality based on shortest paths.

In Friendship Based routing [14] Bulut et al. have used another metric based on the past encounters of a node with other nodes which measure diverse parts of friendship. Utilizing the presented metric, every node characterizes the arrangement of nodes as its friends which has direct or indirect companionship with itself. The present metrics only consider some of these highlights. Social Pressure Metric (SPM) [14] is the metric of a social weight that depends on the friendship of the nodes and is evaluated based on features like longevity frequency and regularity.

Depending on its social characteristics in SOSIM [15] routing protocol each node has a vector. The name of vectors is the same as the label of node. Consider the social features city and language as a node P having vector $\{p_1, p_2, p_3, \dots, p_m\}$ and a node Q having vector $\{q_1, q_2, q_3, \dots, q_m\}$, respectively. A metric $S(P, Q)$ is generated to figure out a social similarity between two nodes P and Q .

A transformation mechanism that applies decay operation as well as convolution on utility calculation and can dispense the reason for dead ends and blind spots [16, 17] is presented by SMART protocol. Based on the observations of the locality property of mobile nodes it can be noted that the movements of the nodes are mostly confined in a neighbourhood except there is a movement of some nodes remotely. In light of the movement territory, a disseminated community dividing strategy is applied, which can adjust to the dynamic DTN conditions. It isolates a DTN into a few communities and exploits distinctive parameters for information directing, should the source and destination be the similar community? Inspired by particle physics general laws, a new social metric to measure a node's social capacity to relay messages to other nodes is presented in SEBAR routing protocol [18]. Generation of Social energy is done by node encounters and is shared by an encounter group of nodes. There will be more social energy for the nodes with more encounters. The community containing a large number of encounters among its nodes or with nodes outside the community will have higher social energy. Social energy of a

certain amount is created when two mobile nodes meet each other, a collision occurs between them. The energy which is generated is evenly distributed to these two nodes. The contribution to its community part of this generated energy is done by each node and the remaining part of the energy is also held.

In [19], ANBR uses the concept of articulation points to spread the messages in the network. The message is directly transmitted to the destination node if it is present in that node's neighbouring vector, otherwise, the message is sent to every articulation node which is directly connected. Similar to the source node, these articulation nodes will transmit the message.

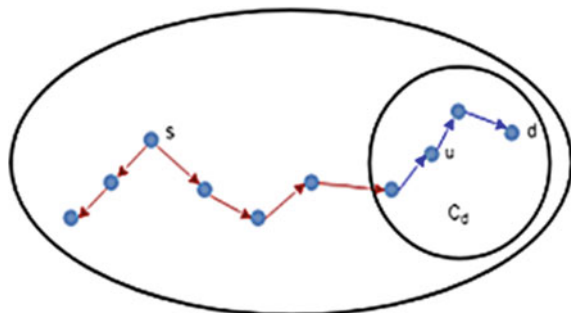
Li et al. in [20] have considered both node contact frequency and contact duration to design a utility metric for making forwarding decisions.

Bubble Rap routing Protocol:

Hui et al. [4] proposed Bubble Rap routing protocol which works in two phases. Messages are sent to the nodes having high global centrality value in bubble-up phase. Global centrality is used until the message reaches a node belonging to the destination community. Once the message reaches the destination community, the second phase of bubble rap starts where the messages are then forwarded based on the node's local centrality value until the destination receives the message. The first phase of bubble up is represented using red arrows and the second phase is shown using blue arrows in Fig. 1. The Bubble Rap Algorithm uses K-Clique community detection algorithm. A K-Clique community is defined as the union of every K-Clique which can be reached by a series of adjoining k-cliques, where if the two cliques share $k - 1$ node they are said to be adjacent. The K-Clique community detection algorithm was designed for binary static graphs whereas Delay-Tolerant Network is a dynamic network, i.e. the connections among the nodes keep on changing with time [21]. In [9] a dynamic community detection algorithm for a scale-free network is proposed. The entire algorithm is divided into four functions.

A-Base: This function finds $G(0)$'s community structure through network labelling nodes. Nodes are sorted in increasing order of degree and then select one of their neighbours to follow each unlabelled and low-degree node.

Fig. 1 Bubble up phases



A-Adaptive: Depending on $G(t)$ and $C(t - 1)$, it finds the structure of community at time t . It also corrects any possible mislabelling resulting from changes in degree. Two cases of mislabeling may occur.

- (1) Low-degree nodes resulting from the removal of edges are unlabelled.
- (2) Nodes above the threshold are labelled as followers resulting from the addition of new edges or nodes.

Follow-Neighbor: This algorithm finds a neighbour j in order to be able to follow a given node j . If all of i 's neighbours are followers, the first UNFOLLOW algorithm will be used to unlabelled or label neighbours j with leaders.

Unfollow: It is invoked when a node has to be stopped from following its current leader j .

In [22], a rapid community detection algorithm is proposed in temporary networks. This method builds a small network for each time step by taking advantage of structures of the community at the earlier stage and then detecting communities in new networks.

Blondel Algorithm

1. Initially, each node in the network in itself forms a community.
2. A node i is placed in the community of its neighbour node j and the modularity gain of the community is calculated.
4. Finally, node i is placed in the community of node j that results in the largest increase in modularity gain.
5. Each community now represents a node in the social graph of the network, while the sum of the edge weights between the original nodes in the two communities denotes the edge weights between new nodes.

Dynamic Community Detection Algorithm:

1. The initial network community structure G_t at time $t = 1$ is determined using Blondel's algorithm.
2. At time $t = 2, 3, \dots, T$, the new community structure is G_{new} is determined based on the community information at time $t - 1$ G_{t-1} .
3. Detecting communities in G_{new} by using Blondel Algorithm.

3 Proposed Algorithm

3.1 Algorithm Description

This section presents the adaptive algorithm for detection of community structures in dynamic networks. The algorithm uses two arrays namely *label* and *follows* to keep track of the status of each node and its leader in the community structure,

respectively. Each node i in the network is either unlabelled or labelled as leader or follower. If a node i is labelled as a follower then $\text{follow}[i]$ stores the name of the leader j which i follows. If a node i is labelled as leader then $\text{follow}[i] = i$; if a node i is unlabelled then $\text{follow}[i] = \text{null}$.

After the execution of the algorithm following properties hold:

- (1) All the nodes having a degree greater than the degree threshold are defined as leaders.
- (2) Nodes having low-degree are labelled as followers.
- (3) Each follower has exactly one leader and each leader has at least one follower.

Followers always follow nodes labelled as a leader; they do not follow any unlabelled nodes or other nodes labelled as followers. This algorithm finds $G^{(0)}$'s community structure through network labelling nodes. Initially, nodes are sorted in increasing order of their degree values and then as per the FOLLOW-NEIGHBOR algorithm each unlabelled node having degree less than a certain threshold is assigned label $[i] = \text{follower}$ and its $\text{follow}[i]$ value is set appropriately.

If nodes have a high rate of mobility, the communication time between two nodes during one contact is short. Then, the link between two nodes is likely to break during the process of transmitting messages, leading to failures in transmitting messages. The high communication capacity is not guaranteed by contact frequency utility. Hence, we propose to use a new utility metric that uses both contact frequency as well as contact duration between nodes.

For every pair of nodes, the frequency-duration utility value is calculated using the formula:

$$\begin{aligned} \text{ContactUtilmax}(\text{DirectUtil}, \text{IndirectUtil}) \\ \text{FreqDuraUtil} = \log(\text{ContactUtil}) + \text{FreqUtil} \end{aligned}$$

Follow Algorithm The algorithm determines a neighbour j based on the given node i such that i can follow j . If a follower is connected to two or more leaders than it will check the FreqDura utility value of the leaders, Node i will follow the leader that has the highest utility value. If a node i have only followers as neighbours then, the leaders for the neighbour nodes are re-evaluated.

In the current work, the algorithm [11] has been modified by including an additional utility which is used for the decision-based association of nodes to an appropriate community so that its membership in the community remain stable.

3.2 Pseudocode

Algorithm—Pseudocode

- (1) Initialize $\text{label}[i] = \varphi$, $\text{follow}[i] = \varphi$ for all nodes $1, 2, \dots, n$

(2) Sort all nodes in increasing order of degree value.

(3) **for each** vertex i with $d_i > d_0$ **do**

if $\text{label}[i] == \varphi$ **then**

$\text{label}[i] = \text{leader}$

(4) **for each** vertex j with $d_j \leq d_0$ and $d_j > 0$

FOLLOW-NEIGHBOR(j)

(5) **return** $C^{(0)} = \langle \text{follow} \rangle$

(6) **for each** edge $\langle u, v \rangle \in \Delta G(t)$ **do**

Update degrees of nodes u and v and Calculate frequency-duration utility

(7) **for each** vertex i appearing in $G(t)$ **do**

if $d_i \leq d_0$ & $(\text{label}[i] == \varphi)$ **then**

UNFOLLOW(i)

(8) **else if** $((d_i > d_0)$ and $(\text{label}[i] == \text{follower}))$ **then** UNFOLLOW(i)

(9) **return** $C^{(t)} = \langle \text{follow} \rangle$

FOLLOW-NEIGHBOR(i)

(1) $\text{label}[i] = \text{follower}$

(2) **if** $\exists j \in N(i): \text{label}[j] == \text{leader}$, **then**

$\text{follow}(i) = j$

break;

(3) **if** $\exists j \in N(i): \text{label}[j] == \text{leader}$, **then**

(4) **if** $(\text{FreqDura_Util}(i, k) > \text{FreqDura_Util}(i,))$

$\text{follow}[i] = k$

(5) **else**

continue;

(6) **if** all nodes j in $N(i): \text{label}[j] == \text{follower}$, **then**

if $(\text{FreqDura_Util}(i, j) > \text{FreqDura_Util}(\text{follow}[j], j))$

then

$\text{follow}[j] = i$

else

continue;

4 Simulations

In this section, we present the simulation results of the Adaptive-Bubble Rap algorithm and compare its performance with a baseline Bubble Rap Algorithm that uses a K-Clique algorithm for community detection. The results have been evaluated under three different simulation scenarios one is heterogeneous scenario consisting of nodes following different mobility model and in other scenario nodes follow Working Day Movement Model and in the third scenario, the link between nodes goes up and down according to real mobility tracer generated from INFOCOM05 scenario [3]. The performance of the modified and existing Bubble Rap routing protocol has been compared in three parameters namely delivery probability, latency, and overhead ratio.

4.1 Performance Parameters

Metrics selected for performance study are as follows:

Average Latency (ALat), Delivery Ratio (DR), and Overhead Ratio (OR). While delivery probability and average latency metrics help us to evaluate the effectiveness of routing protocol in the delivery of messages to their destinations, the overhead ratio signifies the resource consumption of the protocol.

Higher overhead ratio signifies that the protocol is less resource friendly. On the other hand, a high value of Delivery Ratio signifies the capability of the protocol to deliver more messages to their destinations. It is desired to design a protocol having high DR value with low values for OR and ALat.

Delivery Ratio (DR): is computed as the ratio of a number of messages which are timely delivered (N_{delv}) to their destination to the total number of messages generated in the network ($N_{\text{generated}}$) [23].

$$\text{DR} = \frac{N_{\text{delv}}}{N_{\text{generated}}}$$

Average Latency (ALat): is computed as the average of the time, taken between a message is generated and is delivered to its destination, for all the delivered messages [24].

$$\text{ALat} = \text{Average}(\forall_{\text{delivered}}(T_{\text{delv}} - T_{\text{create}}))$$

where

T_{delv} —time of message delivery

T_{create} —time of message creation

delivered—list of messages that are delivered.

Overhead Ratio (OR): is computed as the ratio of the total number of extra messages relayed ($N_{rel} - N_{delv}$) to the total number of delivered messages (N_{delv}) [25].

$$\frac{N_{rel} - N_{delv}}{N_{delv}}$$

4.2 Result Analysis

4.2.1 Delivery Ratio

Figures 2, 3, and 4 show the effect of varying TTL on the Delivery Ratio (DR) of the proposed Adaptive-Bubble Rap and Bubble Rap routing protocols in a heterogeneous scenario, working day model scenario and Infocom05 scenario, respectively. Figure 2 clearly shows that Adaptive-Bubble Rap achieves a higher Delivery Ratio in comparison to the Bubble Rap routing protocol. Bubble Rap routing protocol observes a decline in the DR with the increase in message TTL, as the K-Clique algorithm used in bubble rap is unable to identify overlapping communities in the network due to which the message keeps on forwarding to other nodes in the network and it

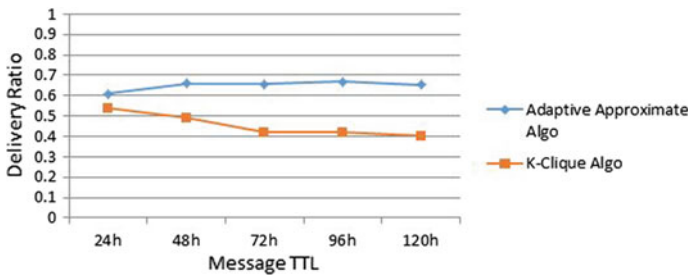


Fig. 2 Delivery ratio in heterogeneous scenario

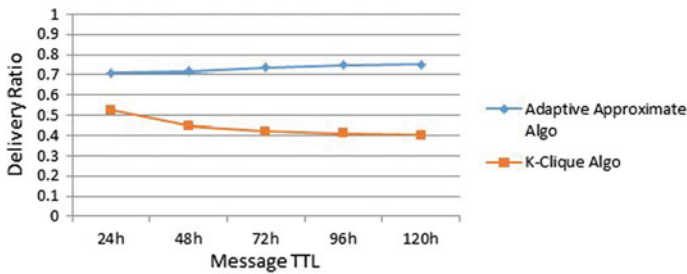


Fig. 3 Delivery ratio in WDM scenario

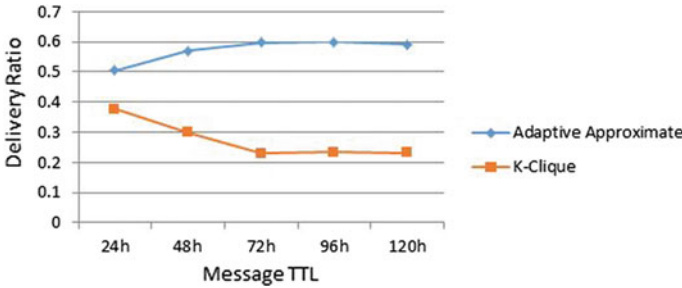


Fig. 4 Delivery ratio in the scenario of INFOCOM05

may happen that the message expires. On the other hand, in Adaptive-Bubble Rap protocol, communities are formed based on node’s degree and the contact frequency utility between the nodes, i.e. the nodes which are closely and regularly connected lie in the same community, resulting in a better community structure.

Hence, more messages reach their destinations in a lesser number of hops and faster. The Adaptive-Bubble Rap routing protocol also shows better performance in the WDM scenario and in real mobility trace scenario compared to traditional bubble rap, as apparent from Figs. 3 and 4, respectively, for the reasons mentioned.

4.2.2 Overhead Ratio

In Adaptive-Bubble Rap routing protocol, the community is formed on the basis of node’s degree and contact history-based utility.

Hence, the nodes in a particular community have very strong social ties with other members. The use of Adaptive Approximate Algorithm for community detection and the use of contact history-based social metric for community formation results in better social ties which help the messages to reach their destination in an easy way rather than being relayed to a large number of nodes. Figures 5, 6, and 7 show the simulation results for overhead ratio in heterogeneous, working day model and Infocom05 scenarios, respectively, of the proposed Adaptive-Bubble Rap and

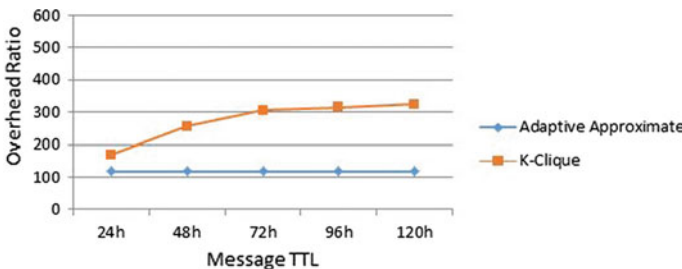


Fig. 5 Overhead ratio in heterogeneous scenario

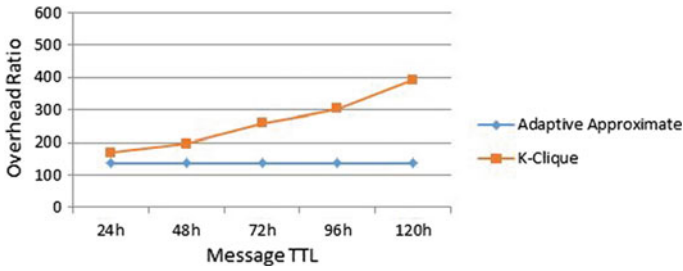


Fig. 6 Overhead ratio in WDM scenario

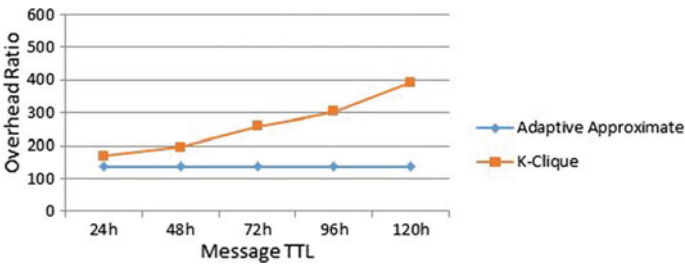


Fig. 7 Overhead ratio in INFOCOM05 scenario

Bubble Rap routing protocol. It can be observed that the overhead ratio remains almost constant for Adaptive-Bubble Rap routing protocol for various message TTL values.

4.2.3 Average Latency

Figures 8, 9, and 10 show the performance of both Adaptive-Bubble Rap and baseline Bubble Rap routing protocols in terms of average latency metric with varying

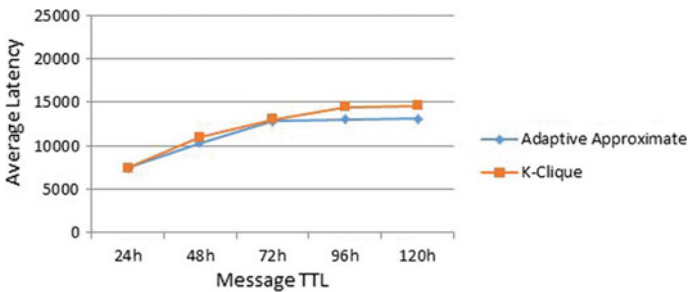


Fig. 8 Average latency in heterogeneous scenario

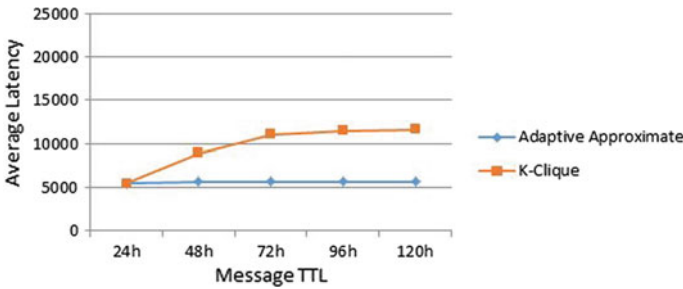


Fig. 9 Average latency in WDM scenario

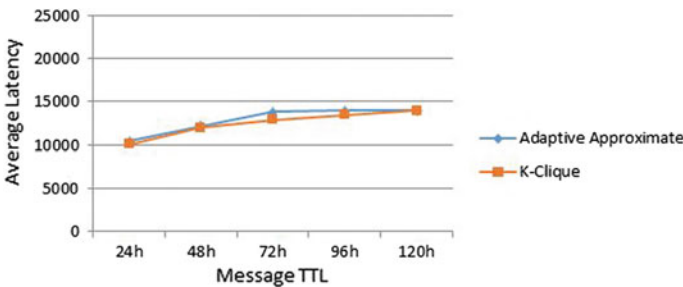


Fig. 10 Average latency in INFOCOM05 scenario

message TTL different network scenarios. Average latency basically gives an estimate of how fast delivered messages reach their destinations. As compared to bubble rap, the Adaptive-Bubble Rap observes a lower value of average latency in both heterogeneous scenarios and WDM scenarios.

It proves that the community structure formed in a proposed Adaptive-Bubble Rap routing protocol is much better and helps messages reach their destination faster due to the selection of better relay. However, it is observed that the average latency increases with an increase in message TTL for Bubble Rap routing protocol because it lacks the ability to discover strong social ties among nodes.

5 Conclusion

Bubble Rap routing Protocol uses K-Clique community detection algorithm which was designed for a static binary graph. DTN is a dynamic graph in which the connections between nodes keep changing. In this paper, we have introduced an Adaptive Approximate Algorithm to detect communities in a network for Bubble Rap routing. This algorithm detects community using the information of the current network and the previous network structure of the community. For the more cohesive structure

of the community, the frequency-duration utility value is used. From the simulation results, we conclude that our applied Adaptive Approximate bubble rap has the performance which is better as compared to the traditional Bubble Rap Algorithm.

References

1. Zhu Y, Xu B, Shi X, Wang Y (2013) A survey of social-based routing in delay tolerant networks: positive and negative social effects. *IEEE Commun Surv Tutor* 15(1)
2. Wei K, Liang X, Xu K (2014) A survey of social-aware routing protocols in delay tolerant networks: applications, taxonomy and design-related issues. *IEEE Commun Surv Tutor* 16(1)
3. Jain S, Chawla M (2014) Evaluation of spray based routing approaches in delay tolerant networks. *J Commun Softw Syst*
4. Hui P, Crowcroft J, Yonek E (2008) Bubble rap: social-based forwarding in delay tolerant networks. In: *Proceedings of 9th ACM international symposium on Mobile Ad Hoc networking and computing (MobiHoc), May 2008*
5. Zhao L, Li F, Zhang C, Wang Y (2012) Routing with multi-level social groups in mobile opportunistic networks. In: *IEEE global communications conference—wireless networking symposium*
6. Thakur GS, Helmy A, Hsu WJ (2010) Similarity analysis and modeling in mobile societies: the missing link. In: *Proceedings of 5th ACM workshop on challenged networks*
7. Daly EM, Haahr M (2007) Social network analysis for routing in disconnected delay-tolerant manets. In: *Proceedings of 8th ACM international symposium on Mobile Ad hoc networking and computing*
8. Patel CM, Gondaliya N (2015) Enhancement of social based routing protocol in delay tolerant networks. *Int J Comput Appl* 122(4)
9. Dinh TN, Nguyen NP, Thai MT (2013) An adaptive approximation algorithm for community detection in dynamic scale-free networks. In: *2013 proceedings IEEE INFOCOM, Apr 2013*, pp 55–59
10. Xu K, Zou K, Huang Y, Yu X, Zhang X (2106) Mining community and inferring friendship in mobile social networks. *Neurocomputing* 174
11. Wang C, Tang W, Sun B, Fang J, Wang Y (2015) Review on community detection algorithms in social networks. In: *International conference on progress in informatics and computing (PIC)*
12. Hui P, Crowcroft J (2007) How small labels create big improvements. In: *International workshop on intermittently connected Mobile Ad hoc networks in conjunction with IEEE PerCom, 19–23 Mar 2007*
13. Jain S, Yadav P (2018) Chapter 5: Controlled replication based bubble rap routing algorithm in delay tolerant network. Springer Nature
14. Bulut E, Szymanski BK (2010) Friendship based routing in delay tolerant mobile social networks. In: *Proceedings of IEEE global telecommunications conference (GLOBECOM), Dec 2010*
15. Rothfus D, Dunning C, Chen X (2013) Social-Similarity-based routing algorithm in delay tolerant networks. In: *IEEE international conference on communications (ICC)*
16. Zhu K, Li W, Fu X (2014) SMART: a social- and mobile-aware routing strategy for disruption-tolerant networks. *IEEE Trans Veh Technol* 63(7)
17. Chen K, Shen H (2014) SMART: utilizing distributed social map for lightweight routing in delay-tolerant networks. *IEEE/ACM Trans Netw* 22(5)
18. Li F, Jiang H, Wang Y, Li X, Wang M, Abdeldjalil T (2017) SEBAR: social energy based routing scheme for mobile social delay tolerant networks. *IEEE Trans Veh Technol* 66(8)
19. Ding L, Gu B, Hong X, Dixon B (2009) Articulation node based routing in delay tolerant networks. In: *IEEE international conference on pervasive computing and communications*

20. Li Z, Shen H (2013) SEDUM: exploiting social networks in utility-based distributed outing for DTNs. *IEEE Trans Comput* 62(1)
21. Palla G, Derenyi I, Farkas I, Vicsek T (2005) Uncovering the overlapping community structure of complex networks in nature and society. *Nature* 435(7043):814
22. He J, Chen D (2015) A fast algorithm for community detection in a temporal network. *Phys A Stat Mech Appl* 429:87–94
23. research.ijca.online.org
24. Gao Z, Zhou W, Wang Y (2016) Exploiting social relationship for secure routing in mobile social networks. In: MILCOM 2016—2016 IEEE military communications conference
25. onlinelibrary.wiley.com

Automatic Control of Electrical Loads Based on the Atmospheric Conditions



T. Ramachandran, Sanjiv Kumar, and Savita

Abstract In today's technical era, automation is the most important sector where unbelievable progress and growth is shown in all over the world. In all field including home, industry, domestics, agriculture, transport, etc., the automation is reducing the physical work of human being and also it reduces the error in executing the work/operation. This paper presents the automatic control of electrical loads based on the atmospheric condition where the load is located (smart home/office/conference room). The controlling of the electrical loads will be wireless, and microcontroller-based control methodology is adopted. In addition to the control of the loads, the surrounding atmospheric conditions will be monitored with the help of sensing devices which will be used as feed for controlling the devices. And based on the response obtained from the sensing devices, the microcontroller-based kit will send command to the electrical appliances concern so that operation of which will be controlled. Two-way supply will be given to the load that one from conventional (EB) and the other from solar system. The supply will be connected based on the availability of the source.

Keywords GSM technology · Temperature sensor · Smoke sensor · Light sensor · Microcontroller · Bidirectional input

T. Ramachandran (✉) · S. Kumar
Department of Electrical & Electronics Engineering, Subharti Institute of Technology and Engineering, Swami Vivekanand Subharti University, Meerut, UP 250005, India
e-mail: ramspowerthangamugam@gmail.com

Savita
Kanya Gurukula Campus, Dehradun, Uttarakhand 248001, India

© Springer Nature Singapore Pte Ltd. 2021
G. S. Hura et al. (eds.), *Advances in Communication and Computational Technology*, Lecture Notes in Electrical Engineering 668,
https://doi.org/10.1007/978-981-15-5341-7_66

1 Introduction

1.1 Introduction to Automation Technology

In the today's technological era, the automation is of the fast-growing field where the automation takes place almost in all sectors which include home automation as well. According to the field of the nature of the industry/home, it may go for process automation and or product manufacturing automation. The automation implemented in the industry also reflects in home/office appliance automation because many appliances are also used in home/office which can be controlled automatically. At the present technological era, more than 80% of the homes have more than one electrical and or electronic appliance. These appliances are controlled manually at present on need base. But now there are much technology controls, or the electrical and electronic appliances are operated in home/office for effective and efficient utilization [1]. The main purpose of the automation is to use the appliance in an efficient and effective manner. The automation at home will save the energy and money as it will work in efficient manner with zero time delay.

The product which will be made with this technology can help the human beings to have effect control of their home appliances for energy saving and money saving. This paper presents the control of appliance used in home/office with the help of RF technology. There are four appliances taken in this paper to monitor, control, ON, and OFF as and when required. This proposed module includes GSM module, wireless transmitter and receiver, and microprocessor and main circuit hardware. Wireless Based Device Control.

1.2 GSM Technology-Based Device Control

The GSM system has been widely used in the wireless communication field with the different operating frequencies (850, 900, 1800, and 1900 MHz) for the purpose of mobile phone voice and data communication service. The GSM system is a digital system, and it uses the concept of time division multiple access (TDMA) technique, which works on the principle that the different time slot is provided for each users, but the operating frequency remains same (Fig. 1).

In this paper, the GSM technology has been used to send and receive SMS through the registered mobile phone based on the operating condition of the electrical appliances placed in home/office/conference hall. The operating conditions of the electrical/electronic appliances have to be changed in accordance with the condition of the atmosphere. If there is any change in the atmosphere condition in the place where the electrical appliance has been located, the corresponding sensor will provide the information to the controller, and according to that, the control action will be taken by the controller. The same will be sending as SMS to the registered GSM-based mobile phone sim.

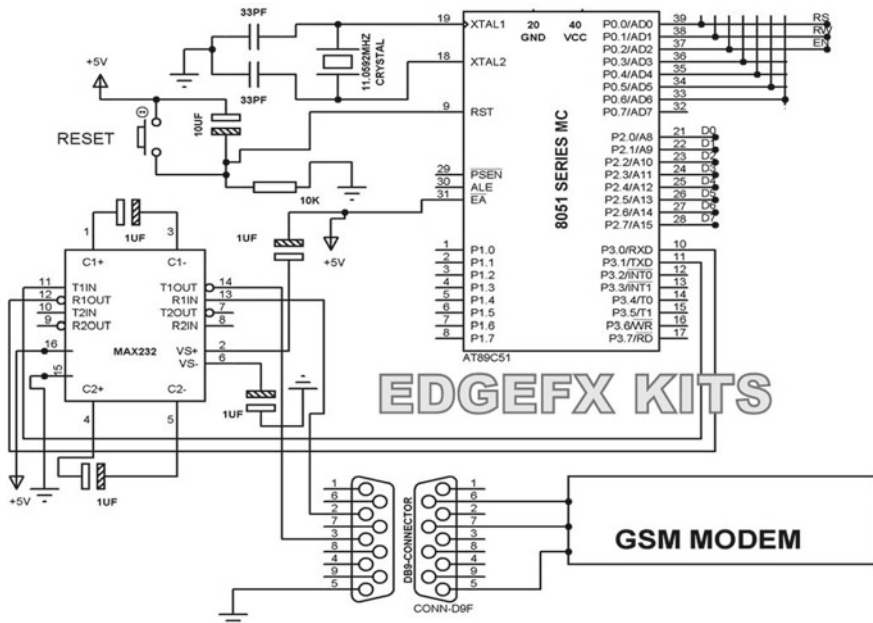


Fig. 1 Test circuit GSM technology

1.3 Temperature Measurement by Temperature Sensor

The regulation of the fan and need of the cooling in AC will be monitored and controlled based on the temperature in the specified area. For this purpose, the temperature is continually monitored. Figure 2 represents the test circuit for the purpose of

Fig. 2 Test circuit of temperature sensor



temperature measurement. The module used here is of thermometric ZTP 188MA thermopile IR sensor. The output of the sensor is very high, and there is no need of any recalibration.. The output of the sensor would be temperature-compensated 8 line arrays. Number of wires needed for this sensor is 4:2 for output, 1 for power supply, and 1 for ground. The calibration of the device has been done with high accuracy.

1.4 Smoke Detector and Its Operation

The smoke detector sensor shown in Fig. 3 is been used in the project in order to switch off the all electrical load so that any further fire hazard does not take place. In this system, if any smoke is detected, then the smoke detector circuit will detect it, and based on the finding, the alarm will be given in addition to the switch off of the all loads. In addition to this, the information will also be sent to the registered mobile number so that further action in this can be taken. There are different types of smoke sensors like optical smoke detector, ionization smoke detectors, etc., which are used in finding and detecting the fire incidence. In this paper, the ionization smoke detectors have been used for the purpose of fire detection, and circuit arrangement of the same has been shown below. In comparison with the photoelectric alarm, the ionization-type smoke sensors are most suitable and provide better response to the flaming fires. However, the ionization-type alarms are not providing faster response to the smoldering fire. The cost need to provide safety against fire is concern is high if the fire alarm is not provided.

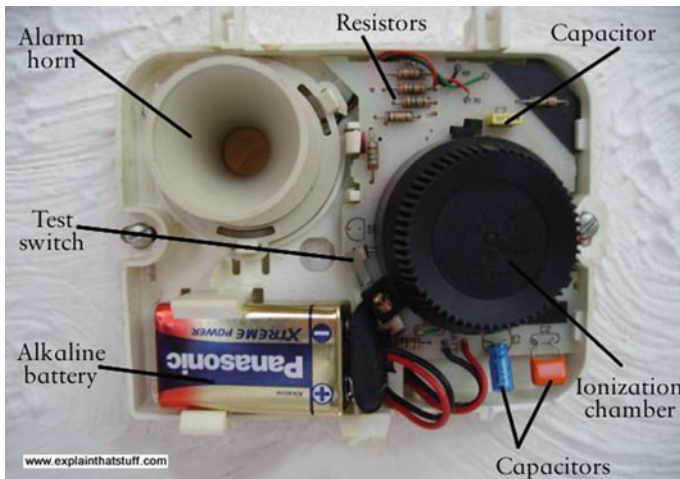


Fig. 3 Smoke sensor circuit

Ionization chamber is placed inside the detector. This is open to the air filled with ions which, in this case, are atoms that have lost electrons to make positively charged nuclei. Chemical element called small piece is kept inside the chamber, and it is named as americium. Radioactive particles come out from americium, which in turn enter into the detection chamber. Now, positively and negatively charged ions are formed in the detection chamber. The ions and electrons move in the opposite; it means that a current flow takes place among the electrodes, and hence, the alarm remains silent. Smoke particles will be detected in the detector if the fire accident took place and the smoke particles start to clog up the ionization chamber. As a result of this, the electric current flow has been got off. Now, the alarm circuit is activated and it sounds the alarm. After the clearing of the fire, the detection chamber will be cleared and the alarm circuit comes to the initial position; thus, the alarm stops the sounds. In this way, the smoke detector functions and provides safety to the human being inside the home/office/conference hall.

1.5 Light Sensor for Brightness Control

This project provides options for the automatic adjustment of the light intensity according to the need of the brightness on that particular place. This can be achieved if the light intensity of the place is continually monitored. For this purpose, the light sensor device has been used. By providing proper window arrangement during the construction of home/office/conference hall, the need of ON of electrical light would be avoided if the sun light is available during the day time. Varieties of light illumination control sensors are available in the market which would sense the illumination of the light, and accordingly, it sends the signal to control device for the proper control of the light illumination. There are many light sensors like photocell/photoresistor which works on the principle that its resistance would be affected according to the light intensity falling on them. This change in resistance will provide corresponding electrical signal in the form of voltage/current which would be used as control signal for the illumination control of the light illumination. The light sensor is shown in Fig. 4

Digital cameras and night vision devices use the charged coupled device (CCD) as the light sensing device. The automatic control of brightness of different display systems is widely using the ambient light sensors as sensing device. These sensors will detect the light intensity in the room/hall and send the input signal to the controller for the purpose of controlling the brightness of the illumination device. Microcontroller will take action accordingly.

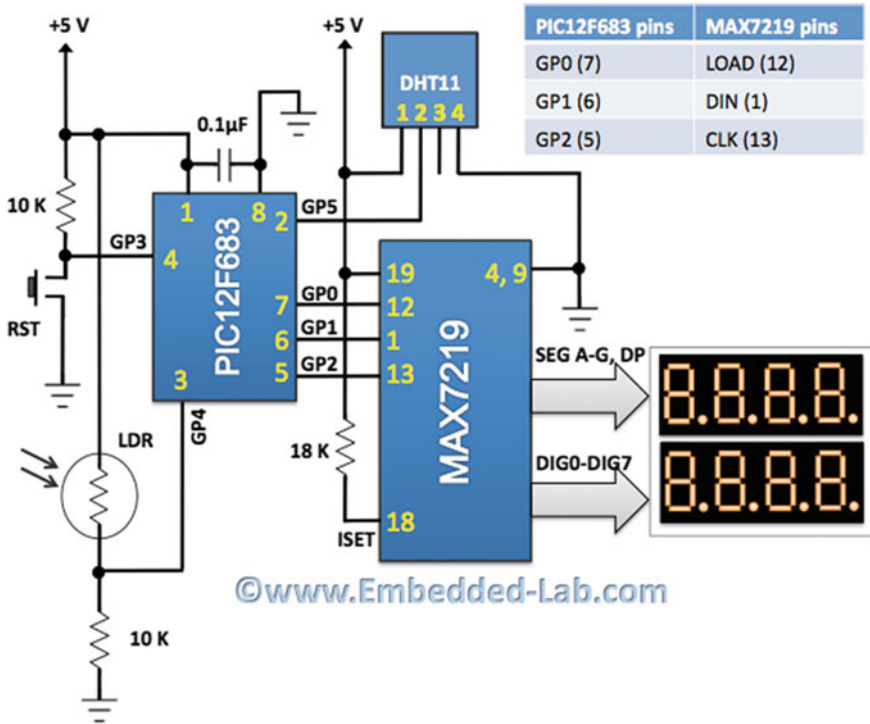


Fig. 4 Schematic diagram of the light sensor

2 Proposed Wireless-Based Automation System

2.1 Circuit Description and Working

This paper designed an automation systems with GSM technology and controller, in which different electrical and electronics appliances located in home/office/conference hall are operated and controlled using microcontroller as control device [2]. It is GSM-based technology, and hence, the working of the proposed system starts with the turn ON of the GSM module transmission and receiving systems. The schematic figure is shown in Fig. 5. The main purpose of doing this is to avoid the junk data or clearing of junk data. After the successful pairing of the transmitter and receiver modules of the GSM technology, the display system attached with this proposed system will glow as an indicator. At this moment onwards, the detector output pin would indicate it is in a high logic till any button of the transmitter is pressed.

Now, turn ON of the microcontroller the OFF of the all loads as it receive logic high signal from the receiver. The LED display system will indicate the current status of the condition of the all the loads. The microcontroller will turn ON/OFF of the

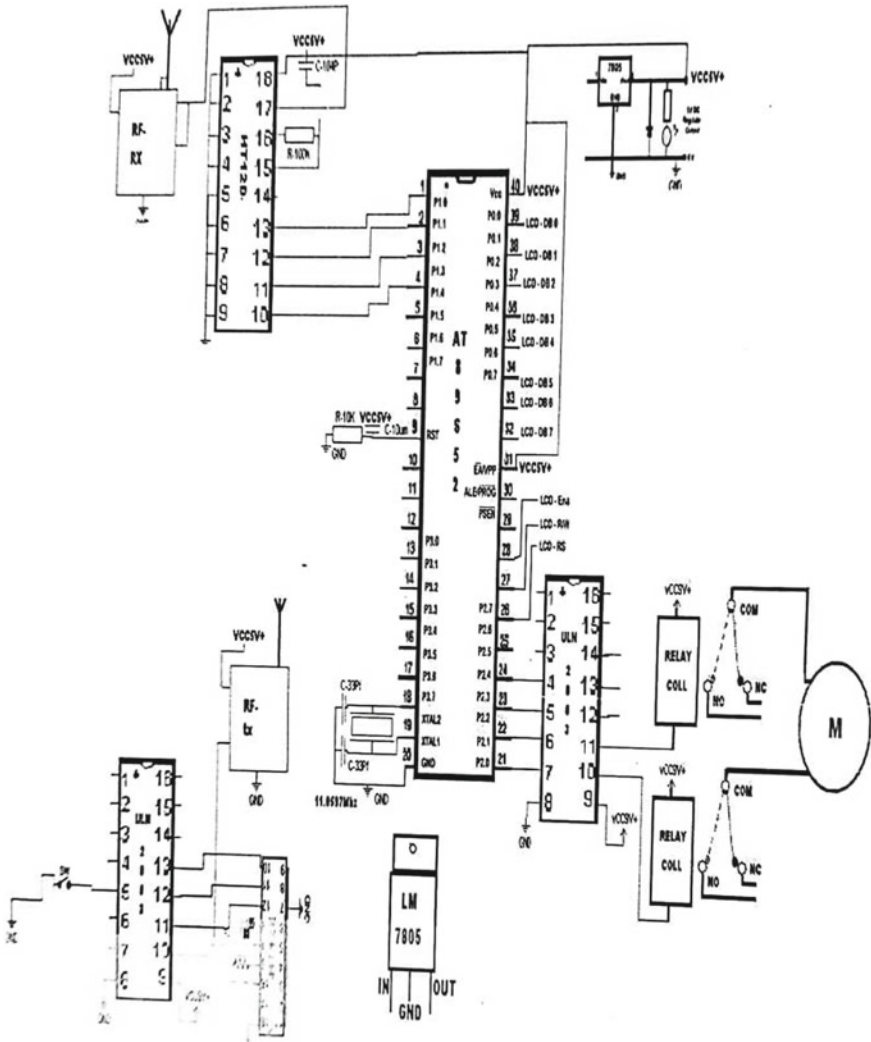


Fig. 5 Schematic diagram of the proposed method

corresponding electrical/electronic appliances if the corresponding button is pressed in the transmitter. In addition to just ON/OFF of the loads/devices, the operating conditions also changed with the help of the input signal coming from the corresponding sensors like temperature sensor, illumination sensor, fire indicating sensor, etc. If the same button is pressed once again, the microcontroller will turn OFF the load.

The microcontroller used here is of 8051 family, and its block diagram along with the basic architecture of the same is shown in Fig. 6. The Atmel AT89C51 made as a

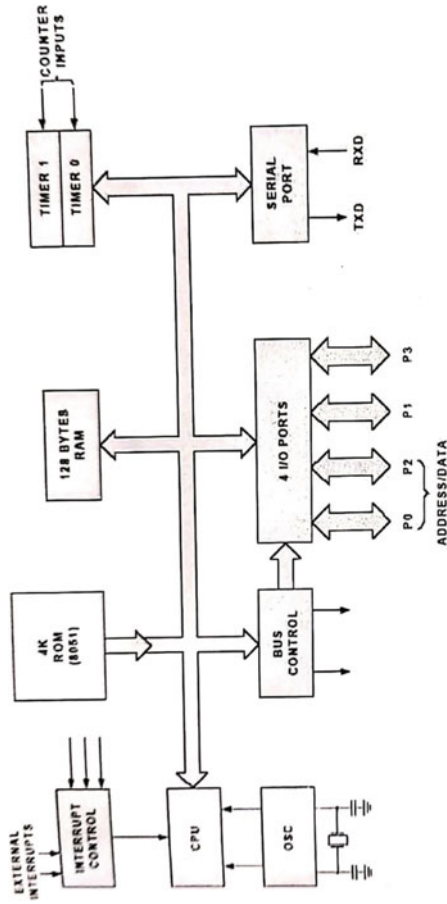


Fig. 6 Microcontroller AT89C51

powerful microcontroller in order to provide a high-quality cost-effective solution in controlling the electrical and electronics appliance controlled based on the embedded system, by combining a versatile 8-bit CPU flash on a monolithic chip. By doing this, the AT89C51 has been enhanced to provide the standard features of the controller.

2.2 *Microcontroller AT89C51*

In addition, the design of the AT89C51 is done with logic operation to save the power [3]. The function of the CPU will be stopped during the ideal mode while allowing the other devices like RAM, timer/counters, serial ports, and there will be an interrupt in continuous function. RAM counts are saved, but the other functions are stopped till the next hardware reset command comes, during the power down mode.

2.3 *Programming Algorithm*

The address mode, data, and control signals of the AT89C51 have to be set in accordance with the flash programming mode and the proposed project circuit diagram. The steps which will be followed in the programming are as below [4].

1. The input data of the program will be given in the desired memory location on the address line.
2. The input data lines will be given with corresponding data byte.
3. Control signal of the correct combination must be activated according to the circuit diagram working.
4. To make a high-voltage programming mode, set the EA/VPP to 12 V.
5. The ALE/PROG will be given pulse to program the controller. The cycle of byte-write is auto-timed and generally does not take time more than 1.5 ms. The steps are repeated from 1 to 5 until the objective is reached.
 - a. Data Polling and Ready/Busy: The AT89C51 features data polling to indicate the end of a write cycle. During a write cycle, an attempted read of the last byte written will result in the complement of the written datum on PO.7. Completion of cycle will evaluate the actual data and initiate the new cycle. Data polling will take place at any instant, and write cycle will be initiated. The READY & BUSY output signal will monitor the progress of byte programming. P3.4 set as low, whereas ALE set as high is a busy indication during programming, and it would be vice versa once programming is done as the ready indication.
 - b. Program Verify and Chip Erase: If lock bits LB1 and LB2 have not been programmed, the programmed code data can be read back via the address and data lines for verification [5]. The lock bits cannot be verified directly.

Verification of the lock bits is achieved by observing that their features are enabled.

With the creation of better and actual proper control signals, and by setting the ALE/PROG as low for 10 ms, the flash array is electrically erased. The code array is written with all “1”s. Before reprogramming the code memory the controller the chip erase instruction must be operate [6].

- c. Reading the Signature Bytes and Programming Interface: The signature bytes are read by the same procedure as a normal verification of locations 030H, 031H, and 032H, except that P3.6 and P3.7 must be pulled to logic low.
- d. With the generation of proper control signal combination, the each and every byte of the flash array may be written and erased. The cycle of write operation is auto-timed, and once it starts, it will automatically time itself to completion [7]. Major programming details can be collected from the local supplier.

3 Proposed Wireless-Based Automation System

3.1 Hardware of the Proposed Method

The hardware is shown in Fig. 7, and the same has two modules, namely one is the main module and the other one is the remote module.

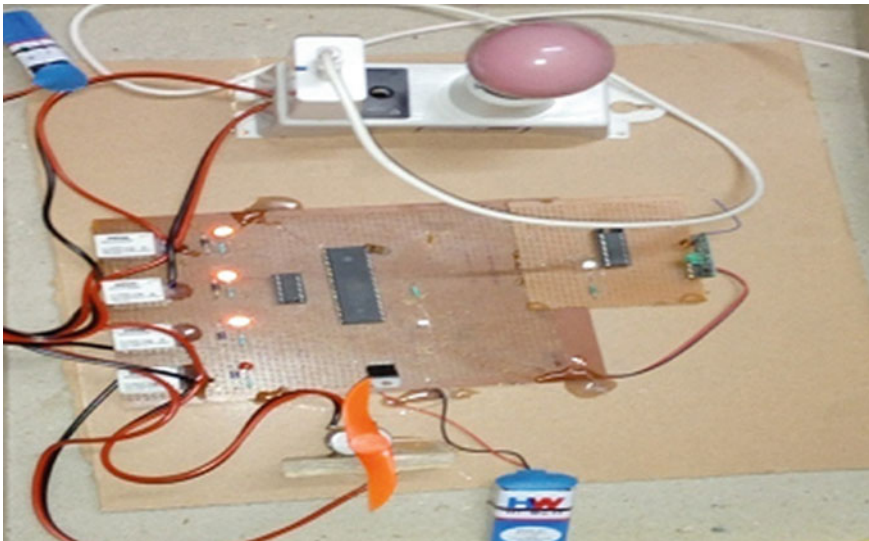


Fig. 7 Hardware image of the proposed method

4 Conclusion

GSM-based device control technology has been used in this paper to control and automatic operation of the home/office appliances. There are four home appliances (motor, mobile charging, bulb, and blank supply) which have been controlled using the proposed GSM-based device control technology module. Microcontroller AT89C51 is used as part of programming and controlling device. The controlling of the electrical loads was by wireless, and microcontroller-based control methodology is adopted. In addition to the control of the loads, the surrounding atmospheric condition was monitored with the help of sensing devices which was used as feedback information for controlling the devices. And based on the response obtained from the sensing devices, the microcontroller-based kit sends command to the electrical appliance concern so that operation of which would be controlled. Two-way supply was given to the load that one from conventional (EB) and the other from solar system. The supply was connected to the load based on the availability of the source.

References

1. Chandramohan J, Nagarajan R, Sathesh Kumar K, Ajithkumar N, Gopinath PA, Ranjithkumar S (2017) Intelligent smart home automation and security system using Arduino and Wi-fi. *Int J Eng Comput Sci* 6(3)
2. Abdullah R, Rizman ZI, Dzulkefli NNSN, Ismail SI, Shafie R, Jusoh MH (2016) Design an automatic temperature control system for smart TudungSaji using Arduino microcontroller. *ARPN J Eng Appl Sci* 11(16):2016
3. Jebelli A, Yagoub MC (2015) Development of sensors and microcontrollers for small temperature controller systems. *J Autom Control Eng* 3(4):322–328
4. Mowad MAE-L, Fathy A, Hafez A (2014) Smart home automated control system using android application and microcontroller. *Int J Sci Eng Res* 5(5):935–939
5. Lin H-T (2013) Implementing smart homes with open source solutions. *Int J Smart Home* 7(4):289–295
6. Chauhan JS, Semwal S (2013) Microcontroller based speed control of DC geared motor through RS-232 interface with PC. *Int J Eng Res Appl* 3(1):778–783
7. Gowthami T, Macriga A (2013) Smart home monitoring and controlling system using android phone. *Int J Emerg Technol Adv Eng* 3(11)

A Comprehensive Study on Vehicular Ad Hoc Networks: Architecture, Security and Privacy Challenges, and Future Trends



Upendra Singh

Abstract The vehicular ad hoc network (VANET) is an interesting research area in the domain of mobile ad hoc networks (MANET). The VANET is a subform of MANET which composed of several vehicles, wireless gadgets, and roadside base stations. Through a wireless strategy, they interact with each other to create a smart and secure transport system. Due to high mobility, dynamic topology, and no power constraints, VANET is much attracted to both researcher and business persons. Regardless of its facilities and advantages, it suffers from many security and privacy issues which needed more focused on. In this paper, we have discussed security and privacy aspect of VANET. In this paper, VANET architecture, VANET models, security and privacy requirements, application of VANET, and other aspects are investigated. Additionally, we also provide some open issues and future trends, which still create a barrier for the wide adoption of VANET. The given security and privacy challenges and solutions will provide directions to researchers for designing a more secure and reliable VANET system.

Keywords Vehicular ad hoc networks (VANET) · VANET architecture · VANET characteristic and applications · Security requirements · Security and privacy issues

1 Introduction

Nowadays, due to the development of the vehicle industry and wireless communication technology, VANET becomes new interesting and promising research area. It is a self-organized and distributed networks deployed for communication between vehicle-to-vehicle or vehicle-to-roadside base stations. It is a specialized form of MANET which consists of several autonomous mobile nodes. For the communication between mobile nodes, all the nodes are connected through a wireless system

U. Singh (✉)

Department of Computer Science and Engineering,
National Institute of Technology Patna, Patna, Bihar 800005, India
e-mail: upendra.singh@nitp.ac.in

© Springer Nature Singapore Pte Ltd. 2021

G. S. Hura et al. (eds.), *Advances in Communication and Computational Technology*, Lecture Notes in Electrical Engineering 668,
https://doi.org/10.1007/978-981-15-5341-7_67

891

and arranged in random order. The capabilities of wireless networks and vehicle nodes build a robust system for data exchange and efficient network administrations. The communications and data exchange between nodes can be done using different tools such as Bluetooth, Wi-Fi IEEE 802.11 b/g, intelligent routing algorithm (IRA), and WiMAX IEEE 802.10 [1]. VANET builds an ad hoc network to pass the safety-related information, traffic management, real-time vehicle monitoring, navigation, and other traveling information which could affect human life. The main application of VANET is to provide critical medical services where no infrastructure is available to pass the information for saving of human lives. There are lots of facilities and services that are available to make human life easier and comfortable.

Due to its characteristics, it differs from other networks. However, along with its personal and featured services, new emerging security challenges also comes. The vehicles in the VANET are limited to dynamic road topology while traveling. If the vehicle is not connected as well as roadside stations, no information is available to predict the future position of the vehicle. Also, it needed computing, communication, sensing, and continuous power transmission capabilities to support system functionalities. Most of the ad hoc protocols do not support all the security requirements for large-scale and high-mobility VANET. In safety-critical infrastructure, the low-security level becomes more vulnerable and attract to the attacker for frequent attacks. Without prior knowledge of the vehicles, the management of VANET is another significant issue. For the protection of VANET from attacks, misuse, and threats, some standard security protocols are needed. In the VANET mainly, two entities are involved, a vehicle which are moving nodes and access point which are roadside fixed point connected through the Internet.

From the above discussion, we have found several design and security challenges of VANET. Lots of articles [2–8] are presented to solve these issues and provide a reliable and secure routing protocols. For instance, in [9, 10], author presents secure routing issues in VANET. They also compare the performance of the routing protocols. Hernández et al. [11] proposed routing protocol for traffic management. This concept is based on autonomous agent architecture, which provides a decision support system for real-time traffic management using knowledge-based similarity approach. Torrent-Moreno et al. [12] proposed a method to improve the reception rate and measure the probability of successful reception. They provide high priority access in emergency cases. Sung et al. [13] develop an authentication technique to preserve the privacy of the VANET. The vehicles communicate with each other as well as roadside stations so that a mutual authentication protocol and traceability system is developed. In [14], several models to save energy consumption in the multi-hop machine-to-machine communication were discussed. They provide an overall look on shortest-path-based energy-efficient routing algorithms for VANET. In [15], author developed an efficient communication channel for real-world highway in VANET environment. The obstacle-based channel model is used to make a realistic and sophisticated model. In [16], authors proposed energy-aware quality of service (QoS) model. The queuing model and routing algorithm is used to provide real-time data transmission path at a low cost. In [17], authors proposed a security algorithm to ensure on-time delivery of packets without loss. The new safety routing

technique named as VANSec resists different types of threats and attacks to secure the VANET nodes. This approach is based on the trust degree of the communication nodes. The authentication of new vehicle node who wants to join the network is an important security challenge. Each node carefully permitted to enter a new strange node in the large vehicle network. View of this security challenge, the authors [18] proposed a secure authentication method which is based on the trust degree of the joining node. The trust computation is based on the direct and indirect behavior of the node. The indirect behavior of the node is computed based on the recommendation approach. In [19], authors address the conditional privacy-preserving authentication security issues present in the vehicle devices. To solve this problem, they proposed the identity-based cryptography framework as an authentication solution. They also achieved non-frameability and improved version of an authentication mechanism which is distributed to every roadside units. In [20], authors address different V2V routing architecture which is used in the intelligent transportation system without interference of roadside units. They implemented all the routing protocols on Opnet simulator to know the best routing algorithm. After that, they demonstrated that the proposed routing algorithm without roadside units performed well manner which improves the security model. In [21], authors solve the security problem arises due to rogue node present in the VANET. They proposed identity-based cryptography which manages the digital identity of the vehicle as well as users in the network. The authentication is done separately by using two authority centers and communicate securely via the proposed method. In [22], authors solve the security problem arises due to Sybil attacks. They proposed a Sybil attack detection method based on the signal strength variation received by the other node. The localization of other communicating nodes is used for the authentication purpose. In [23], authors address spoofing and forgery attacks. They introduce key insulation in the proposed method. Vehicles could update their secret keys periodically with the help of a device named as helper device. The forward and backward secrecy was accomplished in this manner. Furthermore, to enhance efficiency, elliptic curve activities were incorporated. Random oracle model is used to show the safety of the proposed system. In [24], authors proposed a technique for the authentication of safety and non-safety messages. The main objective of this information sharing is to reduce road accidents by alerting the driver to unexpected hazards. The proposed method used social networks to create an active topology from all possible users in the profile of the sender, who are active at a specific point in time. Message authentication is achieved by providing a profile of the user and quick response code (QR code) technique. This proposed architecture is used from the car dashboard.

The main contribution of this survey paper is summarized as follows:

- This comprehensive study considered all the aspect of VANET such as architecture, applications, characteristics, security requirements, and attacks.
- VANET architecture with different topologies is considered for the evaluation purpose.
- The security and privacy challenges of VANET are analyzed to provide an efficient and reliable communication network.

- The given direction and future trends will help to model a secure and trustworthy system.

The rest of the paper is summarized as follows: In Sect. 2, the architecture of VANET is discussed. In Sect. 3, we have listed out application and characteristic of VANET. The security and privacy requirements of VANET are discussed in Sect. 4. Possible security attacks are listed out in Sect. 5. After that, we have analyzed the security and privacy issues of VANET in Sect. 6. In Sect. 7, we have summarized the analysis of the work. The open issues and challenges present in Sect. 8. At last, the conclusion is discussed in Sect. 9.

2 Architecture of VANET

In this section, we have discussed the architecture of VANET. In real-time scenario, VANET has no fixed architecture or topology that must be followed by VANET. A simple VANET architecture is presented in Fig. 1. In general, VANET architecture must contain three main components:

1. *Mobile component*: This component consists of two different types of nodes. First one is the vehicle node such as car and bus, and another is a mobile node such as navigation device or smartphones.
2. *Infrastructure component*: The roadside infrastructure and central infrastructure are considered as an infrastructure component. The roadside infrastructure consists of roadside units such as traffic lights, and central infrastructure consists of traffic and vehicles management center.
3. *Communication channel*: Radio waves frequency are higher than infrared light so that it can be used for the communication in VANET. The CAR-2-X communication system is also used in VANET.

Communication model in VANET: The communication model in VANET is categorized as follows [26]:

- In *vehicle communication model*, each component of the vehicle communication with each other to know the performance of the vehicle such as speed, vehicle parts conditions, alert message generator, driver conditions, and its behavior.
- In *vehicle-to-vehicle communication* system, two different vehicles communicate with each other to data exchange for safety and assistance purpose.
- In *vehicle-to-road infrastructure* communication is used for real-time traffic monitoring and weather updates, which is sent to the vehicle drivers.
- In *vehicle-to-base station communication* is used to know more information or history of the road traffic and active driver tracking.

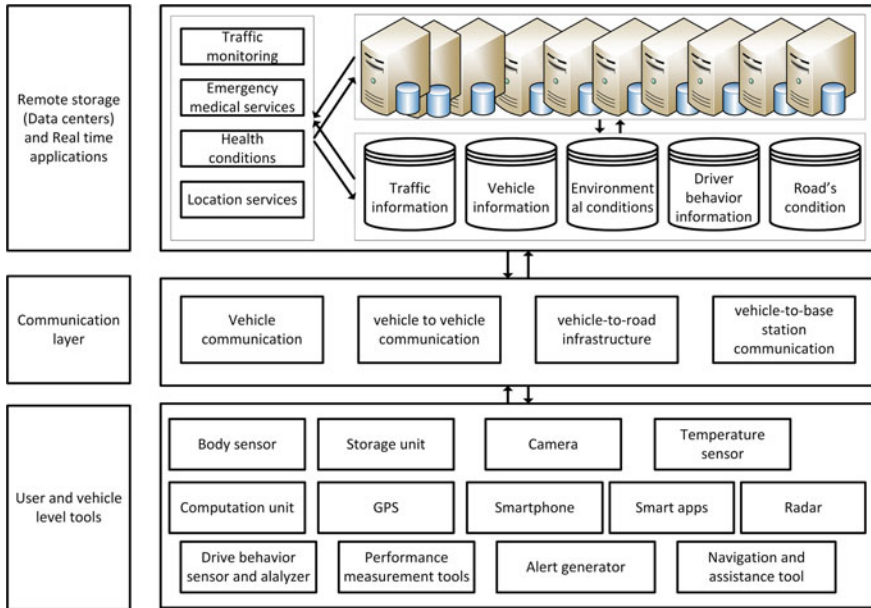


Fig. 1 VANET architecture [25]

3 Application and Characteristic of VANET

The VANET has many application in today’s world which fulfill user requirements [27, 28]. VANET supports a wide range of applications which can be changed according to user needs. Some of the main application of VANET is listed as [28–30]:

- VANET is used to increase traffic safety while driving by giving an alert message to the driver in advance.
- It can be used to reduce the traveling cost and traffic congestion.
- VANET environment provides a comfort and quality travel experience.
- It supports medical emergency cases by sending an emergency alert message to the responsible person for saving of human life.
- It can be used for management of traffic light during the traffic density increase or decrease.
- It is also used to manage parking facilities in a shopping mall or airport.
- It can be used to make high occupied vehicle lanes in a self-organized manner.
- It is also used to manage and store the parking schedule data.

The following characteristic and features are supported by VANET [31, 32]:

- The VANET nodes are moved at a very high speed. So, high-mobility feature can lead to many other issues.

- The high-mobility feature rapidly changes vehicle positions. So, VANET environment includes dynamic network topologies.
- To support all the functionalities, there is no power and storage constraints.
- It provides on-demand applications and services in a virtualized and elastic manner.
- The VANET size is potentially large and worldwide implemented. So, the VANET size is unbounded.
- The timely delivered is an important feature in VANET. When the information is available, it is delivered within a given time.
- The dynamic nature of the network and the generated information are also frequently changed.
- All the communication is done through wireless.
- The density of the network depends on the traffic density and number of the vehicle.
- The computation and sensing capability are very high.

4 Security and Privacy Requirements of VANET

In the VANET architecture, each component, especially vehicle nodes, is connected through a wireless system. Also, the data are stored in a remote location and accessed through the Internet. It must be ensured that all the components know the security and privacy aspect to make a more robust and efficient system. There are several features available in the VANET. But, the dynamic nature of the VANET does not fulfill all the security and privacy requirements. It should be required to analyze all the security and privacy services and goals to design any robust system, i.e., we have listed out some security and privacy requirement of VANET, which is essential for developing the system.

- In VANET, authentication is one of the basic security requirements. Before entering into the network, the entry point identity checking is necessary. The authentication mechanism fulfills these needs.
- The message integrity must be ensured and cannot be modified by an unauthorized entity.
- The data confidentiality ensured the data could not disclose in front of any unauthorized entity.
- The availability of the data improves the adaptability of the VANET.
- The VANET information such as user identity or location of the device should be preserved.
- Non-repudiation ensured the sender and vehicle identity and approved the message source.
- Access control must be needed to restrict the user access privileges.
- To preserve vehicle privacy, non-traceability and anonymity are also required.
- During the communication, mutual authentication is needed to ensure the security of the communication link.

- The device and alert message generator should be flexible for emergency medical cases.
- The message and nodes (vehicles) authentication improved network security.
- A share session key must be established for secure data exchange.
- Freshness of the data improves the system reliability and service experience.
- The VANET must support all the secure routing protocols and follows all the security standards [33].

5 Security Attacks in VANET

In the VANET architecture, each component is connected through wireless and accessed by the remote location. Due to this, the security of the system may hamper by an attacker. This section listed out most of the security attacks which is performed by an attacker for compromising the security of the system [34, 35].

1. *Denial of Service*: The attacker sends a large number of false request to make the service shut down or unavailable.
2. *Data spoofing*: An attacker gets the useful information about the vehicle/driver such as the location of vehicle or user identity to gain access in the network.
3. *Vehicle data modification*: An attacker somehow enters into the network and tempers the sensor information, modifies the vehicle location, hampers the security services, or appends some bogus information into the networks.
4. *Masquerading*: An attacker somehow gets the credentials of a valid user or using the false identities he may access all the privileges of an authorized user.
5. *Wormhole*: An attacker creates a tunneling packets to control at least two vehicle nodes from each other by sending correctly signed packets to the destination.
6. *Information leakage*: An attacker gets sensitive information about the user and vehicles such as user credentials, vehicle locations, financial conditions, etc. This information is opened in front of some unauthorized user to perform the attack.
7. *Sybil attack*: An attacker shows multiple identities at the same time to gain access. For instance, an attacker sends traffic jam message to different users using different identities.
8. *Bush telegraph*: Insertion of bogus packets into the network is considered bush telegraph attack. In this attack, the attacker considers a multi-hop wireless network. The attacker inserts small bogus packets at the source hop and in each hop the size of the bogus packet, and at the last hop, the error may be large. It means the insertion of a small bogus packet creates great serious harm in the network.

6 Security and Privacy Issues

VANET facilities provide a network topology in which different application is implemented to provide the service. All the devices and components are communicated with each other and followed several security standards such as IEEE Std 1609.2-2016, WAVE Internal Security Services, and Certificate Revocation List (CRL) Verification Entity (CRLVE), and Peer-to-Peer Certificate Distribution (P2PCD) Entity (P2PCDE). But, due to location difference and high mobility, such security standard contains some security and privacy flaws. In this section, we have summarized the following security and privacy flaws [36–42]:

1. *Authentication* of the user and devices (vehicles) is compulsory to make the system reliable and secure [43]. The VANET environment is open and highly dynamic. After a certain time, the network density and location of the device may be changed. So, a secure and strong authentication mechanism must be implemented. Author [44] proposed anonymous authentication model for VANET, which is based on the probabilistic approach. Due to weak authentication, the user credentials and access privileges may be explored. All the communication is done with the help of the application interface, so the application-authenticity is also required.
2. *Security of the location information* is another issue in VANET environments. All the connection and communication depend on the location of the vehicles. Most of the application uses the location information to send emergency alert message, traffic support, driving assistance, etc. In general, three models are used to validate and provide integrity of the location information [25].
3. In VANET, the vehicles are communicated with each other as well as roadside infrastructure. The security of the communication channel is an important security issue because a safe and secure communication maintain the privacy of the entities as well as provide faster services. The signals jamming, send forgery messages, dropping or modify message are some issues in this category. ElGamal signature scheme, digital signature, shared session key, and mutual authentication are some security solutions which provide secure communication.
4. Vehicular infrastructure is another security issues because VANET does not follow a fixed topology. Each time new vehicles are registered into the VANET. So, there is a need for robust key management in which each registered vehicle are assigned security key for the communication. This scheme follows three steps: key generation by a certificate authority, key verification, and key revocation.
5. The VANET consists of different heterogeneity environment which includes different devices, GPS, wireless transceiver, onboard devices, radars, etc. These devices are worked on a different platform and used different security protocols. Also, for communication, they follow different communication protocols and have different working speed. Due to these reasons, the security may be hamper because implemented security solution is differed and does not follow a standard security solution.

6. The security of the data is also an important issue. The data are stored in a centralized server for future analysis purpose. These stored data contain some sensitive information. So, for the security purpose, it must be required all the stored data are encrypted with secure private keys and only accessed by an authenticated user. If the stored data are modified or leak, then it is vulnerable to the system.
7. An access control mechanism is required to restrict the access on the resources in the VANET. The authentication process checks the entity is valid or not. But, after the authentication, access control defines the level of access, quantity of accessed data, etc., based on the vehicle condition, roles, and capabilities.
8. Trust management between all the communicating entities is essential. Without trust, communication is not possible. This can be achieved by using different metric such as QoS, secure, and user-friendly infrastructure.
9. Secure and energy-efficient routing protocols are another security issue. Lots of articles are present to solve this issue.

7 Analysis of the Literature Work

We have analyzed several works which are proposed for providing the security in VANET. All the works are summarized in Table 1.

8 Open Issues and Challenges

In the above sections, we have discussed lots of security and privacy challenges. Several works have been done to provide a secure VANET environment. However, we have found several challenges which still exist and remain unsolved. Such open issues and challenges are:

- In VANET, all the nodes are connected through wireless technology. So, the disconnection between the vehicles is a challenging issue.
- The VANET architecture consists of several small and large devices which have different security and working protocols and platforms. For each device, the challenge is to define security and working platform.
- Several secure routing protocols have been proposed for secure routing. But, this issue still presents in VANET. A routing protocol that follows all the security standards is still not available in the VANET architecture.
- To improve the adaptability of the VANET, the system must be flexible and robust. The safety alert message will reach in minimum time with low energy.
- The performance of the behavior analysis can be improved for safety and assistance purpose.
- The user-friendly application and its security are vulnerable from several threats.
- Efficient and low-cost routing protocols are required in the future.

Table 1 A summary of the related works

Paper	Year	Topic discussed	Purpose	Proposed approach
[8]	2007	System model, attacks, and some security aspect	Provide security to VANET	Public key infrastructure based authentication mechanism
[5]	2008	Routing protocols	Efficient routing protocols for rural area	Epidemic routing and border node-based routing
[13]	2008	Authentication and security requirements	Proposed audit-able and privacy-Preserving authentication protocol	Mutual authentication and message authentication code
[45]	2011	Access approaches	Improved the channel access	Changed MAC layer formation, dynamically self adaptive based omn context
[46]	2011	Security architecture and key management	Secure communication	PKI and pre-group approach
[3]	2012	Routing protocols	Scalability in routing	Hybrid location based
[47]	2012	System model and channel allocation procedure	Save the energy while allocation of channel	Learning automata (LACAV)
[48]	2014	Key management and cryptographic approach	Key management for group communication	Dynamic secret sharing (EDKM-DSS)
[49]	2016	Access control	Self schedule access control	Time division multiple access and frequency division multiple access approach with cognitive radio techniques
[50]	2017	Trust management	Secure information exchange with trust	Neighbor communication based
[6]	2018	Routing protocols	Secure and reliable routing protocol	Virtual backbone based
[7]	2019	Routing protocols	Management of traffic network	Greedy routing protocol

- The security aspects, such as privacy of the location, data, and entity verification, attack resistant mechanism, are some of the key points for future research.

9 Conclusion

The VANET is a new promising technology composed of many technologies such as wireless technology, vehicle technology, and ubiquitous sensing devices. It provides several features and applications with the help of the Internet, storage, virtualization,

and computing power. But, due to the dynamic and open nature of the network, the model has many security and privacy challenges.

In this paper, we have discussed VANET architecture, security attacks, and security and privacy requirements. After that, we have analyzed security and privacy issues such as authentication, trust, secure communication, and location privacy. After the analysis, we have found some security challenges, which is still unsolved. The reviewed and highlighted research challenges will be helpful for further research.

References

1. Pathan ASK (2016) Security of self-organizing networks: MANET, WSN, WMN, VANET. CRC Press, London
2. Minhas UF, Zhang J, Tran T, Cohen R (2010) Intelligent agents in mobile vehicular ad-hoc networks: leveraging trust modeling based on direct experience with incentives for honesty. In: 2010 IEEE/WIC/ACM international conference on web intelligence and intelligent agent technology, vol 2, pp 243–247
3. Al-Rabayah M, Malaney R (2012) A new scalable hybrid routing protocol for vanets. *IEEE Trans Veh Technol* 61(6):2625–2635
4. Rawashdeh ZY, Mahmud SM (2012) A novel algorithm to form stable clusters in vehicular ad hoc networks on highways. *EURASIP J Wirel Commun Network* 2012(1):15
5. Zhang M, Wolff RS (2008) Routing protocols for vehicular ad hoc networks in rural areas. *IEEE Commun Mag* 46(11):126–131
6. Ji X, Yu H, Fan G, Fu W (2018) A reliable and efficient routing protocol based on virtual backbone in vehicular ad hoc networks. *IEICE Trans Commun*, p 2017EBP3343
7. Vinnarasi FS, Chandrasekar A (2019) VANET routing protocol with traffic aware approach. *Int J Adv Intell Paradigms* 12(1–2):3–13
8. Raya M, Hubaux Jean-Pierre (2007) Securing vehicular ad hoc networks. *J Comput Secur* 15(1):39–68
9. Li F, Wang Y (2007) Routing in vehicular ad hoc networks: a survey. *IEEE Veh Technol Mag* 2(2):12–22
10. Bilal SM, Bernardos CJ, Guerrero C (2013) Position-based routing in vehicular networks: a survey. *J Netw Comput Appl* 36(2):685–97
11. Hernández JZ, Ossowski S, Garcia-Serrano A (2002) Multiagent architectures for intelligent traffic management systems. *Transp Res Part C Emerg Technol* 10(5–6):473–506
12. Torrent-Moreno M, Jiang D, Hartenstein H (2004) Broadcast reception rates and effects of priority access in 802.11-based vehicular ad-hoc networks. In: Proceedings of the 1st ACM international workshop on vehicular ad hoc networks. ACM, pp 10–18
13. Kim SH, Kim BH, Kim YK, Lee DH (2008) Auditable and privacy-preserving authentication in vehicular networks. In: Proceedings—The 2nd international conference on mobile ubiquitous computing, systems, services and technologies, UBICOMM 2008, pp 19–24
14. Tekbiyik N, Uysal-Biyikoglu E (2011) Energy efficient wireless unicast routing alternatives for machine-to-machine networks. *J Netw Comput Appl* 34(5):1587–1614. Dependable Multimedia Communications: Systems, Services, and Applications
15. Akhtar N, Ergen SC, Ozkasap O (2015) Vehicle mobility and communication channel models for realistic and efficient highway vanet simulation. *IEEE Trans Veh Technol* 64(1):248–262
16. Akkaya K, Younis M (2003) An energy-aware QoS routing protocol for wireless sensor networks. In: 23rd International conference on distributed computing systems workshops, 2003. Proceedings. IEEE, pp 710–715
17. Ahmed S, Rehman MU, Ishtiaq A, Khan S, Ali A, Begum S (2018) VANSec: Attack-resistant VANET security algorithm in terms of trust computation error and normalized routing overhead. *J Sens* 2018

18. Zhou A, Li J, Sun Q, Fan C, Lei T, Yang Fangchun (2015) A security authentication method based on trust evaluation in vanets. *EURASIP J Wirel Commun Netw* 2015(1):59
19. Wang B, Wang Y, Chen R (2019) A practical authentication framework for vanets. *Secur Commun Netw* 2019
20. Yasser A, Zorkany M, Abdel Kader N (2017) VANET routing protocol for V2V implementation: a suitable solution for developing countries. *Cogent Eng* 4(1):1362802
21. Zaidi, S (2016) Detecting rogue nodes in vehicular ad-hoc networks (DETER). Ph.D. thesis, City, University of London
22. Bouassida MS, Guette G, Shawky M, Ducourthial B (2009) Sybil nodes detection based on received signal strength variations within VANET. *IJ Netw Secur* 9(1):22–33
23. Zhou Y, Liu S, Xiao M, Deng S, Wang X (2018) An efficient V2I authentication scheme for VANETs. *Mob Inf Syst* 2018
24. Paranjothi A, Khan MS, Nijim M, Chaloo R (2016) Mavanet: message authentication in vanet using social networks. In: 2016 IEEE 7th annual ubiquitous computing, electronics mobile communication conference (UEMCON), pp 1–8
25. Whaiduzzaman Md, Sookhak M, Gani A, Buyya Rajkumar (2014) A survey on vehicular cloud computing. *J Netw Comput Appl* 40:325–344
26. Liang W, Li Z, Zhang H, Wang S, Bie R (2015) Vehicular ad hoc networks: architectures, research issues, methodologies, challenges, and trends. *Int J Distrib Sens Netw* 11(8):745303
27. Sharma MK, Kaur A (2015) A survey on vehicular cloud computing and its security. In: 2015 1st International conference on next generation computing technologies (NGCT), pp 67–71
28. ur Rehman S, Khan MA, Zia TA, Zheng L (2013) Vehicular ad-hoc networks (VANETs)-an overview and challenges. *J Wirel Networking Commun* 3(3):29–38
29. Hartenstein H, Laberteaux K (2010) VANET: vehicular applications and inter-networking technologies, vol 1. Wiley Online Library
30. Hartenstein H, Laberteaux LP (2008) A tutorial survey on vehicular ad hoc networks. *IEEE Commun Mag* 46(6):164–171
31. Divya Chadha and Reena (2015) Vehicular ad hoc network (vanets): a review. *Int J Innov Res Comput Commun Eng* 3(3):2339–2346
32. Al-Sultan S, Al-Doori MM, Al-Bayatti AH, Zedan H (2014) A comprehensive survey on vehicular ad hoc network. *J Netw Comput Appl* 37:380–392
33. Sharaf BT, Alsaqour RA, Ismail M (2014) Vehicular communication ad hoc routing protocols: a survey. *J Netw Comput Appl* 40:363–396
34. Hoa La Vinh and Ana Rosa Cavalli (2014) Security attacks and solutions in vehicular ad hoc networks: a survey. *Int J AdHoc Networking Syst (IJANS)* 4(2):1–20
35. Martinez FJ, Toh CK, Cano JC, Calafate CT, Manzoni P (2011) A survey and comparative study of simulators for vehicular ad hoc networks (VANETs). *Wirel Commun Mob Comput* 11(7):813–828
36. Mokhtar B, Azab M (2015) Survey on security issues in vehicular ad hoc networks. *Alexandria Eng J* 54(4):1115–1126
37. Azees M, Vijayakumar P, Deborah LJ (2016) Comprehensive survey on security services in vehicular ad-hoc networks. *IET Intell Transp Syst* 10(6):379–88
38. Samara G, Al-Raba'nah Y (2017) Security issues in vehicular ad hoc networks (vanet): a survey. arXiv preprint [arXiv:1712.04263](https://arxiv.org/abs/1712.04263)
39. Chaubey NK (2016) Security analysis of vehicular ad hoc networks (vanets): a comprehensive study. *Int J Secur Appl* 10(5):261–274
40. Rasheed A, Gillani S, Ajmal S, Qayyum A (2017) Vehicular ad hoc network (VANET): a survey, challenges, and applications. In: *Vehicular ad-hoc networks for smart cities*. Springer, Singapore, pp 39–51
41. Kelarestaghi KB, Foruhandeh M, Heaslip K, Gerdes R (2019) Survey on vehicular ad hoc networks and its access technologies security vulnerabilities and countermeasures. arXiv preprint [arXiv:1903.01541](https://arxiv.org/abs/1903.01541)
42. Arif M, Ahmad S (2018) Security issues in vehicular ad hoc network: a critical survey. In: *Intelligent communication, control and devices*. Springer, Singapore, pp 527–536

43. Ali I, Hassan A, Li F (2019) Authentication and privacy schemes for vehicular ad hoc networks (VANETs): a survey. *Veh Commun* 16:45–61
44. Xi Y, Sha K-W, Shi W-S, Schwiebert L, Zhang T (2008) Probabilistic adaptive anonymous authentication in vehicular networks. *J Comput Sci Technol* 23(6):916–928
45. de Souza AB, Barros AL, Vieira AS, Roberto FM, Júnior, JC (2011) An adaptive mechanism for access control in vanets. In: *Proceedings of the 10th international conference on networks*. Mongol City, California, USA: ICN, pp 183–188
46. Busanelli S, Ferrari G, Veltri L (2011) Short-lived key management for secure communications in vanets. In: *2011 11th International conference on ITS telecommunications*, pp 613–618
47. Misra S, Krishna PV, Saritha V (2012) LACAV: an energy-efficient channel assignment mechanism for vehicular ad hoc networks. *J Supercomput* 62(3):1241–1262
48. Duan G, Xiao Y, Ju R, Song H (2014) A novel key management scheme in vanets. In: Sun X-h, Qu W, Stojmenovic I, Zhou W, Li Z, Guo H, Min G, Yang T, Wu Y, Liu L (eds) *Algorithms and architectures for parallel processing*. Springer International Publishing, Cham, pp 587–595
49. Jothy MKA, Murugesan D (2016) An enhanced self-scheduled access control in vehicular ad hoc networks (vanet). In: *2016 International conference on information communication and embedded systems (ICICES)*, pp 1–5
50. Tangade S, Manvi SS (2017) Trust management scheme in vanet: neighbour communication based approach. In: *2017 International conference on smart technologies for smart nation (SmartTechCon)*, pp 741–744

Performance Analysis of Hybrid Diversity Combiner Over Nakagami- m Fading Channels—A Review



Prabhat Kumar, Karan Arora, Mohammad Irfanul Hasan,
and Shalini Singh

Abstract Various papers on the analysis of hybrid diversity combiner are available to improve the mean output SNR at receiver end. In this paper, we will provide the review on performance of hybrid diversity combiner over Nakagami- m fading channels. This paper also reviews a mathematical expression for analyzing mean SNR gain and outage probability of hybrid diversity combiner.

Keywords Maximal ratio combining · Mean output SNR · Moment generating function · Outage probability · Selection combining

1 Introduction

Need for the wireless communication utilities, such as wireless mobile phones, Internet satellite television, etc., is growing rapidly. These services require tremendous data rate with reliable communication, which is a difficult task as the wireless system works over fading channels [1]. Due to fading, the signal strength decreases as signal travel over a long distance. Therefore, the availability of multipath is necessary, because we create multipath so that if one path experience more fading, then another path has less [2]. In multipath transmission, we transmit an identical signal through the different paths so that if one signal goes under more fade, then others have less [2]. Therefore, multiple paths at the receiver end, which is required to combine. Thus, there are different basic combining techniques available in literature

P. Kumar · K. Arora · M. Irfanul Hasan (✉) · S. Singh
Graphic Era Deemed to be University, Dehradun, Uttarakhand 248001, India
e-mail: irfu_hasan@rediffmail.com

P. Kumar
e-mail: prabhat.singh531@gmail.com

K. Arora
e-mail: karanarora.ind@gmail.com

S. Singh
e-mail: shalini111.raj@gmail.com

like selection combining (SC), maximal ratio combining (MRC), and equal gain combining (EGC) [2]. The main idea behind receiver diversity is that by receiving several uncorrelated classes of transmitted signals so that at any one time all class would be suffering from more fading is very small and thus SNR at receiver would be enough for detection with a low probability of error [3].

Tremendous works have been done on the analysis of hybrid diversity combiner over Nakagami- m fading channels [4–6]. The paper presents related work done in this field. We will summarize some related work in this paper.

The pre-detection and post-detection combining techniques of selection diversity having multiple antennas for millimeter wave communication have been proposed in [7]. Analysis of a coherent receiver with hybrid diversity (SC/MRC) over the Nakagami- m channel is given by in [8]. This paper compares the performance of SC, MRC, SC/MRC for different value amounts of fading m is done by [8]. Closed form expressions are derived to analyze the performance of MRC having L number of correlated branches in Nakagami- m fading [9]. The expressions for the capacity of Nakagami- m fading channel with diversity is provided by [10]. The author in [5] discussed an MGF-based analysis of hybrid combiner over Rayleigh fading channels. The expression for mean SNR and the outage probability is proposed for GSC in [5]. The analysis of a hybrid diversity combiner having gaussian errors and the decrease in average symbol rate performance compared to the ideal case is done by the author [11]. Expressions are obtained for the probability density function (pdf), cumulative distribution function (CDF), moment generating function (MGF) of the hybrid combiner (SC/MRC), and mean output SNR gain [11]. This paper reviews the already published result on the performance analysis of hybrid diversity combiner (SC/MRC) over Nakagami- m . We will consider generalized Nakagami- m channel and we review closed form expression for mean SNR gain and outage probability of hybrid combiner (SC/MRC). This paper considers the generalized equation in terms of the amount of fading (m).

1.1 Diversity Combining Techniques

Diversity approaches are used in fading channels to reduce the effect of fading [3]. It consists of numerous identical information bearing signals over various branches, and then we combine these branches to enhance the overall instantaneous or average received SNR [3].

For combining the different signal from different path having independent fading, following pure combining techniques are used [2]

- (a) Selection combining (SC)
- (b) Equal gain combining (EGC)
- (c) Maximal ratio combining (MRC).
- (a) Selection Combining (SC)

It is one of the simplest diversity approaches in which all the incoming signals from different paths are observed and the signal having maximum SNR is given to demodulator [2]. Therefore, SC is not a combining process but a selection process from the multiple received signals. However, obtaining SNR is hard because the selection is to be made in a small time. When the average power of noise is equal on each branch, the selection of the branch with the highest SNR is similar to select the branch with the highest received power [3, 12].

(b) Equal Gain Combining (EGC)

In this technique, we give equal weight coefficient to each signal or mostly unity, make them co-phased and after that, we merge or sum up each signal [2]. The performance of EGC is slightly inferior to the MRC. However, EGC is less complex compared to the MRC as the estimation of amplitude is not required [3].

(c) Maximal Ratio Combining (MRC)

In MRC, signals are initially co-phased, different weights are given and then summed. For maximizing the received SNR, the weights are selected proportional to the individual signal strength. The weights applied to the branches have to be provided according to the SNR. MRC is known as the optimal diversity approach to combat fading [3]. However, the disadvantage of MRC is complexity because it requires knowledge of all branch parameters like fading amplitudes, phase, and delay.

1.2 Mean SNR Gain Calculation for SC, EGC and MRC

(a) Selection combining (SC)

As we know that when we transmit a signal over wireless channel, it has some noise content which gets added in channel, hence [2, 12]

$$z(t) = \alpha x(t) + n(t)$$

where $n(t)$ is AWGN noise, $z(t)$ is the received envelope of the signal, $x(t)$ is transmitted signal, α is fading amplitude.

SNR of the received signal is given by [2]

$$\gamma = \frac{E[\alpha^2 x^2(t)]}{E[n^2(t)]} = \frac{\alpha^2 E_s}{N_0} \quad (1)$$

$$\begin{aligned} \bar{\gamma} &= \alpha^2 \frac{E_s}{N_0} \\ &= \beta \frac{E_s}{N_0} \end{aligned}$$

where $\bar{\gamma}$ is the average SNR, γ is the received SNR, β is the mean square fading amplitude, and E_s is the symbol energy. As we know that fading envelope for Rayleigh is given by [2]

$$p_\alpha(\alpha) = \frac{2\alpha}{\beta} e^{-\frac{\alpha^2}{\beta}}, \alpha \geq 0 \tag{2}$$

where β is the rms value of the collected voltage. By change of variable

$$p_\gamma(\gamma) = \frac{p_\alpha(\alpha)}{g'(\gamma)} \tag{3}$$

$$g'(\gamma) = 2\alpha \frac{E_s}{N_0} \tag{4}$$

Now from (1), we have

$$\alpha = \sqrt{\gamma \frac{N_0}{E_s}} \tag{5}$$

Putting this in Eq. (4), we get

$$g'(\gamma) = 2\sqrt{\frac{\gamma\bar{\gamma}}{\beta}} \tag{6}$$

Putting this in Eq. (3), we get [2]

$$p_\alpha = \frac{p_\alpha\left(\sqrt{\frac{\gamma N_0}{E_s}}\right)}{2\sqrt{\frac{\gamma\bar{\gamma}}{\beta}}} \tag{7}$$

Now from (2) we have

$$p_\gamma(\gamma) = \frac{2\sqrt{\frac{\gamma N_0}{E_s}} e^{-\left(\frac{\gamma N_0}{E_s} \frac{1}{\beta}\right)}}{2\sqrt{\frac{\gamma\bar{\gamma}}{\beta}}} \tag{8}$$

$$p_\gamma(\gamma) = \frac{e^{-\frac{\gamma}{\bar{\gamma}}}}{\bar{\gamma}}, \gamma \geq 0 \tag{9}$$

This is the required pdf of Rayleigh distribution.

Now, the probability of getting a signal having SNR lower than any threshold value γ_{th} is

$$P_\gamma[\gamma \leq \gamma_{th}] = \int_0^{\gamma_{th}} p_\gamma(\gamma) d\gamma \tag{10}$$

By using (9) in (10) and solving this, we will get [2]

$$\left(1 - e^{-\frac{\gamma_{th}}{\bar{\gamma}}}\right) \tag{11}$$

Now, clearly probability of M number of signal having SNR greater than γ_{th} is [2, 12]

$$P_\gamma[\gamma > \gamma_{th}] = 1 - \left(1 - e^{-\frac{\gamma_{th}}{\bar{\gamma}}}\right)^M$$

$$P_M(\gamma_{th}) = M \left(1 - e^{-\frac{\gamma_{th}}{\bar{\gamma}}}\right)^{M-1} \left[e^{-\frac{\gamma_{th}}{\bar{\gamma}}}\right] \frac{1}{\bar{\gamma}} \tag{12}$$

The mean SNR is given by [2]

$$\int_0^\infty \gamma_{th} P_M(\gamma_{th}) d\gamma_{th} \tag{13}$$

After substituting $p_M(\gamma_{th})$ from (12) in (13) and solving, we get [2, 12]

$$\frac{\gamma}{\bar{\gamma}} = \sum_{i=1}^M \frac{1}{i} \tag{14}$$

where $\frac{\gamma}{\bar{\gamma}}$ is mean SNR gain.

(b) Equal Gain Combining (EGC)

The envelope of the collected signal is given by [2]

$$y(t) = \sum_{i=1}^M y_i(t)$$

$$= \sum_{i=1}^M \alpha_i e^{j\varphi_i} x(t) + n_i(t) \tag{15}$$

where α_i is the amplitude of fading in i th path and φ_i is the phase of i th path and $n_i(t)$ is the AWGN noise.

Assuming that the noise $n_i(t)$ is mutually independent in each branch SNR at combine is [2, 12]

$$\gamma_{\text{EGC}} = \frac{E \left| \sum_{i=1}^M a_i \alpha_i e^{j\varphi_i} \right|^2}{N_0 \sum_{i=1}^M |a_i|^2} \tag{16}$$

After solving it, we will get [2, 12]

$$\frac{\gamma_{\text{EGC}}}{\bar{\gamma}} = 1 + (M - 1) \frac{\pi}{4} \tag{17}$$

where $\frac{\gamma_{\text{EGC}}}{\bar{\gamma}}$ is mean SNR gain.

(c) Maximal Ratio Combining (MRC)

The output signal of the i th diversity branch is represented as [2, 12]

$$y_i(t) = \alpha_i e^{j\varphi_i} x(t) + n_i(t) \quad \text{where } i = 1, 2, 3, \dots, M \tag{18}$$

Corresponding output of the M linear combining is given by [2, 12]

$$y(t) = \sum_{i=1}^M a_i y_i(t)$$

Using (18), we will get [2, 12]

$$= \sum_{i=1}^M a_i \alpha_i e^{j\varphi_i} x(t) + \sum_{i=1}^M a_i n_i(t)$$

$$(\text{SNR})_c = \frac{E \left[\left| x(t) \sum_{i=1}^M a_i \alpha_i e^{j\varphi_i} \right|^2 \right]}{E \left[\left| \sum_{i=1}^M (a_i n_i(t)) \right|^2 \right]} \tag{19}$$

After solving it, we will get [2, 12]

$$\frac{\gamma}{\bar{\gamma}} = M \tag{20}$$

where $\frac{\gamma}{\beta}$ is mean SNR gain.

1.3 Hybrid Diversity Combiner

A hybrid diversity combiner chooses the strongest signals from two or more than two branches and combines these selected signals coherently using a diversity approach like MRC or an EGC [12]. In maximum ratio combining (MRC), the chosen signals are combined with a weight proportional to the amplitude of the signal collected on respective branches, whereas in equal gain combining (EGC), the weights on each branch is the same [12].

Thus, a hybrid combiner is a two-stage processor, where the first stage chooses the L_c strongest signals from L signals (branches) and the other stage combines these by applying an MRC (or EGC) [12]. It becomes an MRC or EGC when all branches are picked at the first stage and becomes an SC (selection combining) when only one branch is picked [12]. The review expression for the mean output SNR is calculated below.

As we know that the pdf for output SNR Nakagami- m is given by

$$f_{\gamma}(\gamma) = \left(\frac{m}{\beta}\right)^m \frac{\gamma^{m-1}}{\Gamma(m)} e^{-\frac{m\gamma}{\beta}} \tag{21}$$

where m is the fading parameter, β is the rms value of the collected voltage. The joint pdf $p_{\gamma_{1:L}, \dots, \gamma_{L_c:L}}(\gamma_{1:L}, \dots, \gamma_{L_c:L})$ of the $(L_c \leq L)$ is written as [5]

$$L_c! \binom{L}{L_c} [p_{\gamma}(\gamma_{L_c:L})]^{L-L_c} \prod_{i=1}^{L_c} p_{\gamma}(\gamma_{i:L}) \tag{22}$$

where $\gamma_{1:L} \geq \gamma_{2:L} \geq \dots \gamma_{L_c:L}$, L is the number of branches available and L_c is the number of branches selected. The moment generating function (MGF) of combined SNR is given by [5, 12]

$$\begin{aligned} \text{SNR}_{\gamma_{\text{GSC}}} &= \sum_{i=1}^{L_c} \gamma_{1:i} \text{ is defined by} \\ M_{\gamma_{\text{GSC}}} &= E_{\text{GSC}}[e^{s\gamma_{\text{GSC}}}] \\ &= E_{\gamma_{1:L}, \gamma_{2:L}, \dots, \gamma_{L_c:L}} \left[e^{s \sum_{i=1}^{L_c} \gamma_{1:i}} \right] \end{aligned} \tag{23}$$

Putting (22) in (23), we will get [5]

$$\begin{aligned}
 M_{\gamma_{\text{GSC}}}(s) &= \int_0^\infty \int_{\gamma_{L_c:L}}^\infty \dots \int_{\gamma_{2:L}}^\infty p_{\gamma_{1:L}, \dots, \gamma_{L_c:L}}(\gamma_{1:L}, \dots, \gamma_{L_c:L}) e^{s \sum_{i=1}^{L_c} \gamma_{1:i}} d\gamma_{1:L} \dots d\gamma_{L_c:L} \\
 &\int_0^\infty \int_{\gamma_{L_c:L}}^\infty \dots \int_{\gamma_{2:L}}^\infty p_{\gamma_{1:L}, \dots, \gamma_{L_c:L}}(\gamma_{1:L}, \dots, \gamma_{L_c:L}) e^{s \sum_{i=1}^{L_c} \gamma_{1:i}} d\gamma_{1:L} \dots d\gamma_{L_c:L} \quad (24)
 \end{aligned}$$

Hence, the MGF of γ_{GSC} as provided in (24) can be obtained in terms of x_1 as [5]

$$\begin{aligned}
 M_{\gamma_{\text{GSC}}}(s) &= \int_0^\infty \dots \int_0^\infty p_{x_1 \dots x_L}(x_1 \dots x_L) \\
 &\cdot e^{s(x_1 + 2x_2 + \dots + L_c x_{L_c} + L_c x_{L_c+1} + \dots + L_c x_L)} dx_1 \dots dx_L \quad (25)
 \end{aligned}$$

i.e., $\gamma_{\text{GSC}} = x_1 + 2x_2 + \dots + L_c x_{L_c} + L_c x_{L_c+1} + \dots + L_c x_L$

As the x_1 's are independent, i.e., $p_{x_1 \dots x_L}(x_1 \dots x_L) = \prod_{i=1}^L P_{x_i}(x_i)$

We can put this integration in the required product form resulting in the equation provided below [5]

$$\int_0^\infty \dots \int_0^\infty \left[\prod_{i=1}^L P_{x_i}(x_i) \cdot e^{s x_1} e^{2s x_2} \dots e^{L_c s x_{L_c}} e^{L_c s x_{2+1}} \dots e^{L_c s x_L} \right] dx_1 \dots dx_L \quad (26)$$

Grouping terms of index l and partitioning the L -fold integral of (26) into a product of L one-dimensional integrals, we get [5]

$$\begin{aligned}
 &= \left[\int_0^\infty e^{s x_1} p_{x_1} dx_1 \right] \left[\int_0^\infty e^{2s x_2} p_{x_2}(x_2) dx_2 \right] \dots \\
 &\left[\int_0^\infty e^{L_c s x_{L_c}} P_{x_{L_c}}(x_{L_c}) dx_{L_c} \right] \dots \left[\int_0^\infty e^{L_c s x_L} p_{x_L}(x_L) dx_L \right] \quad (27)
 \end{aligned}$$

Now, calculating $p_{x_i}(x_i)$ with substituting (22) for $L_c = L$, we get

$$p_{x_i}(x_i) = \frac{i \left(\frac{m}{\beta}\right)^m (i x_i)^{(m-1)}}{\Gamma(m)} e^{\left(\frac{-m i x_i}{\beta}\right)} \quad (28)$$

Now, putting $p_{x_i}(x_i)$ from Eq. (28) into Eq. (27) for $i = 1$ to $L_c - 1$ we get For $i = 1$ we will get [5]

$$\int_0^\infty e^{J\omega x_1} \frac{\left(\frac{m}{\beta}\right)^m (x_1)^{(m-1)}}{\Gamma(m)} e^{\left(\frac{-mx_1}{\beta}\right)} dx_1 \tag{29}$$

Using Laplace transform, we get [13]

$$\begin{aligned} t^n e^{at} &= \frac{(n-1)!}{(s-a)^n} \text{ and putting } s = -s \\ &= \left(\frac{m}{\beta}\right)^m \frac{(m-1)!}{\Gamma(m)} \frac{1}{\left(\frac{m}{\beta} - s\right)^m} \end{aligned}$$

For $i = 2$

$$p_{x_i}(x_i) = \frac{2\left(\frac{m}{\beta}\right)^m (2x_2)^{(m-1)}}{\Gamma(m)} e^{\left(\frac{-2mx_2}{\beta}\right)}$$

Using (29), we get

$$\begin{aligned} &= \int_0^\infty 2e^{J\omega x_2} \frac{\left(\frac{m}{\beta}\right)^m (2x_2)^{(m-1)}}{\Gamma(m)} e^{\left(\frac{-2mx_2}{\beta}\right)} dx_2 \\ &= 2^m \left(\frac{m}{\beta}\right)^m \frac{(m-1)!}{\Gamma(m)} \frac{1}{\left(\frac{2m}{\beta} - s - s\right)^m} \end{aligned}$$

Similarly, for general case

$$= \prod_{i=1}^{L_c-1} \frac{(i)^m}{\Gamma(m)} \left(\frac{m}{\beta}\right)^m \frac{(m-1)!}{\left(\frac{im}{\beta} - s - (i-1)J\omega\right)^m} \tag{30}$$

Now, from L_c to L , we get

$$p_{x_i}(x_i) = \prod_{i=L_c}^L (i)^m \left(\frac{m}{\beta}\right)^m \frac{(m-1)!}{\Gamma(m)} \frac{1}{\left(\frac{im}{\beta} - s - ((L_c-1)J\omega)\right)^m} \tag{31}$$

Hence, substituting (31) and (30) in (27), we get required equation for MGF, i.e.,

$$M_{\gamma_{\text{GSC}}}(s) = \prod_{i=1}^{L_c-1} (i)^m \left(\frac{m}{\beta}\right)^m \frac{(m-1)!}{\Gamma(m)} \frac{1}{\left(\frac{im}{\beta} - si\right)^m}$$

$$\times \prod_{i=L_c}^L (i)^m \left(\frac{m}{\beta}\right)^m \frac{(m-1)!}{\Gamma(m)} \frac{1}{\left(\frac{im}{\beta} - sL_c\right)^m}$$

Now, taking L_N and differentiating w.r.t s , we get [12]

$$\sum_{i=1}^{L_c-1} \frac{mi}{\left(\frac{im}{\beta} - si\right)} + \sum_{i=L_c}^L \frac{mL_c}{\left(\frac{im}{\beta} - sL_c\right)}$$

Now, putting $s = 0$ and eliminating the common term, we get mean output SNR gain as [12],

$$= \left(1 + \sum_{i=L_c+1}^L \frac{1}{i}\right) \beta L_c \tag{32}$$

Now, we can observe from Eq. (32) that the mean SNR gain of a hybrid diversity combiner is independent of fading parameter m . This means that when we are going to use the hybrid combiner, then our mean output SNR gain will be independent of m .

1.4 Outage Probability of Hybrid Combiner (SC/MRC)

The outage probability is defined as the probability that the mean output SNR goes below a certain threshold value. From the previous analysis, we have an expression of moment generating function as [5, 12]

$$M_{\gamma\text{GSC}}(s) = \prod_{i=1}^{L_c-1} (i)^m \left(\frac{m}{\beta}\right)^m \frac{(m-1)!}{\Gamma(m)} \frac{1}{\left(\frac{im}{\beta} - si\right)^m} \times \prod_{i=L_c}^L (i)^m \left(\frac{m}{\beta}\right)^m \frac{(m-1)!}{\Gamma(m)} \frac{1}{\left(\frac{im}{\beta} - sL_c\right)^m}$$

Putting $s = -s$ and eliminating the common term, we get [5]

$$= \frac{[(m-1)!]^{L-1}}{\Gamma(m)} \frac{\binom{L}{L_c}}{\left(\frac{\beta}{m}\right)^{mL_c-m+1}} \left[\frac{1}{\left(1 + \frac{s\beta}{m}\right)^{m(L_c+1)}} + \sum_{i=0}^{L-L_c} \frac{(-m)^{mi} \binom{L-L_c}{i}}{\left(s + \frac{m}{\beta}\right)^{mL_c-m} \left(s + \frac{m+i}{\beta}\right)} \right]$$

So, the desired pdf can be found by taking inverse Laplace of the obtained expression which can be done by seeing a similar equation from [5]

$$\frac{[(m-1)!]^{L-1}}{\Gamma(m)} \binom{L}{L_c} \left[\frac{\gamma^{mL_c-m} e^{-\frac{m\gamma}{\beta}}}{\left(\frac{\beta}{m}\right)^{mL_c-m+1} (mL_c-m)!} + \frac{m}{\beta} \sum_{i=1}^{L-L_c} (-m)^{mL_c+mL-m} \binom{L-L_c}{i} \left(\frac{L_c}{i}\right)^{mL_c-m} e^{-\frac{m\gamma}{\beta}} \left(e^{\left(\frac{-i\gamma}{L_c\beta}\right)} - \sum_{k=0}^{mL_c-m-1} \frac{1}{k!} \left(\frac{-i\gamma}{L_c\beta}\right)^k \right) \right] \tag{33}$$

$$P_{\text{out}} = P_{\text{rob}}[\gamma_{\text{GSC}} \leq \gamma_{\text{th}}] = \int_0^{\gamma_{\text{th}}} P_{\gamma_{\text{GSC}}}(\gamma) d\gamma$$

Putting the value of the obtained result in the case of pdf in Eq. (33), we get outage by solving the integration using [12, 14]

$$P_{\text{out}}^{\text{GSC}} = \int_0^{\gamma_{\text{th}}} \frac{[(m-1)!]^{L-1}}{\Gamma(m)} \binom{L}{L_c} \left[\frac{\gamma^{mL_c-m} e^{-\frac{m\gamma}{\beta}}}{\left(\frac{\beta}{m}\right)^{mL_c-m+1} (mL_c-m)!} + \frac{m}{\beta} \sum_{i=1}^{L-L_c} (-m)^{mL_c+mL-m} \binom{L-L_c}{i} \left(\frac{L_c}{i}\right)^{mL_c-m} e^{-\frac{m\gamma}{\beta}} \left(e^{\left(\frac{-i\gamma}{L_c\beta}\right)} - \sum_{k=0}^{mL_c-m-1} \frac{1}{k!} \left(\frac{-i\gamma}{L_c\beta}\right)^k \right) \right] d\gamma \tag{34}$$

After dividing the entire equation into different parts and solving each part using the equation [13]

$$\int_0^u x^n e^{-\mu x} dx = \frac{n!}{\mu^{n+1}} - e^{-\mu u} \sum_{k=0}^n \frac{n!}{k!} \frac{u^k}{\mu^{n-k+1}}$$

we will get the equation for the outage probability of hybrid diversity combiner over Nakagami-*m* fading channels and as we know that after putting *m* = 1 in Nakagami-*m* distribution, we get Rayleigh distribution and so, if we put *m* = 1 in the equation below, we will get the same outage as of Rayleigh distribution.

$$= \frac{[(m-1)!]^{L-1}}{\Gamma(m)} \binom{L}{L_c} \left[-e^{-\frac{m\gamma_{\text{th}}}{\beta}} \sum_{i=0}^{mL_c-m} \frac{\left(\frac{m\gamma_{\text{th}}}{\beta}\right)^i}{i!} + \sum_{i=1}^{L-L_c} (-m)^{mL_c+mL-m} \binom{L-L_c}{i} m \left(\frac{L_c}{i}\right)^{mL_c-m} \left(\frac{1 - e^{-\left(m+\left(\frac{i}{L_c}\right)\left(\frac{\gamma_{\text{th}}}{\beta}\right)\right)}}{m + \frac{i}{L_c}} - \sum_{k=0}^{mL_c-m-1} \left(\frac{-i}{L_c}\right)^k \left(\frac{1}{m}\right)^k \left[1 - e^{-\frac{\gamma_{\text{th}} m}{\beta}} \sum_{p=0}^k \frac{\left(\frac{m\gamma_{\text{th}}}{\beta}\right)^p}{p!} \right] \right) \right] \tag{35}$$

If we put *m* = 1 in (35) we get outage as that of Rayleigh because if we put *m* = 1 in the distribution of Nakagami-*m* fading channel then it will become Rayleigh distribution [5, 12].

$$\begin{aligned}
 &= \binom{L}{L_c} \left[1 - e^{-\frac{\gamma_{th}}{\beta}} \sum_{i=0}^{L_c-1} \frac{\left(\frac{\gamma_{th}}{\beta}\right)^i}{i!} + \sum_{i=1}^{L-L_c} \binom{L-L_c}{i} \left(\frac{L_c}{i}\right)^{L_c-1} \right. \\
 &\quad \left. \left(\frac{\left[1 - e^{-\left(1+\frac{L}{L_c}\right)\left(\frac{\gamma_{th}}{\beta}\right)} \right]}{1 + \frac{i}{L_c}} \right) - \sum_{k=0}^{L_c-2} \binom{-i}{L_c}^k \left[1 - e^{-\frac{\gamma_{th}}{\beta}} \sum_{p=0}^k \frac{\left(\frac{\gamma_{th}}{\beta}\right)^p}{p!} \right] \right) \right] \quad (36)
 \end{aligned}$$

2 Numerical and Result Analysis

Figure 1 shows the mean SNR Gain of different diversity combining techniques based on the results already derived in [2]. We can observe that the SNR Gain of MRC is optimum compared to the other two. The mean SNR Gain of EGC is slightly inferior to the mean SNR Gain of MRC but better than that of SC [12]. Comparing all the three results after simulation, we can say that MRC combining is the optimal technique as we are giving different gains to different paths according to the need.

Figure 2 shows the mean SNR gain of hybrid combiner (SC/MRC) as already derived in [5, 12]. We can notice that as we increase the value of L_c , i.e., we are increasing the number of selected paths, then the performance of hybrid combiner increases. We can also notice that if the number of selected branches, i.e., L_c is 1,

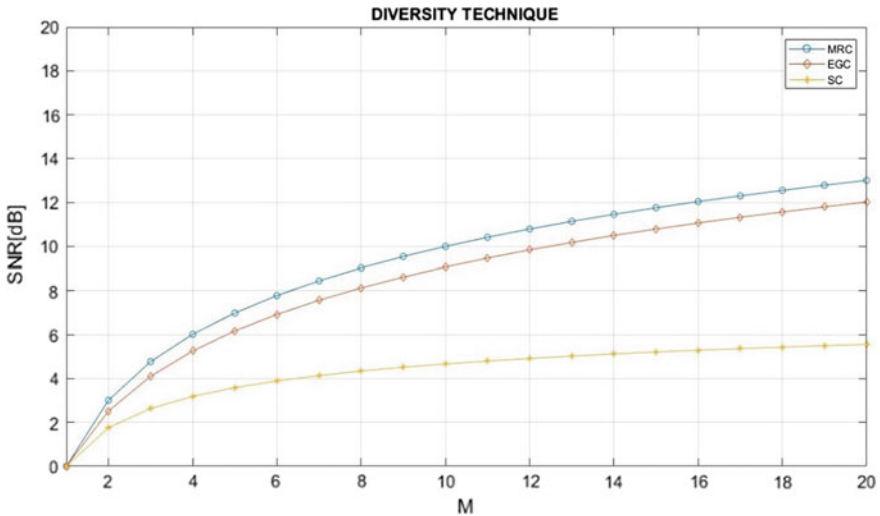


Fig. 1 Shows the mean SNR gain of SC, EGC, and MRC

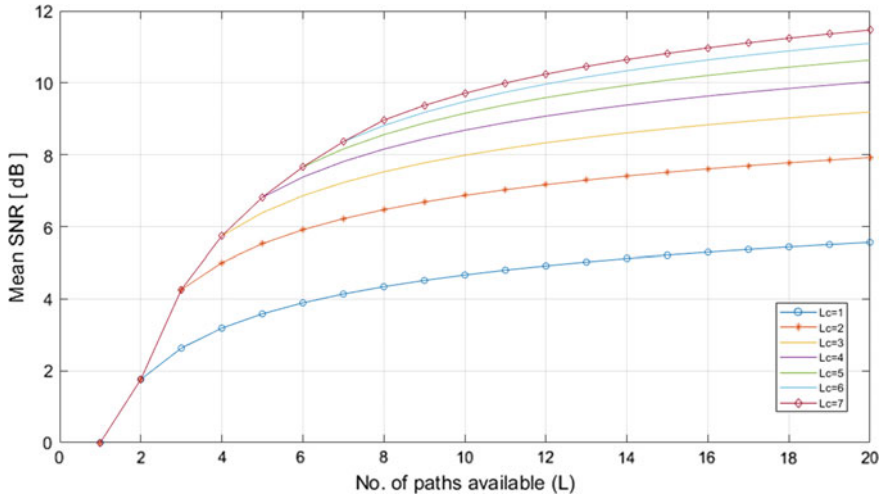


Fig. 2 Shows the mean SNR gain of hybrid combiner (SC/MRC) versus L (number of paths available)

then we are getting the same result as in case of selection combining (SC) because selecting one branch having maximum SNR is nothing but selection combining (SC).

Figure 3 shows the outage of hybrid combiner (SC/MRC) over Nakagami- m fading channels. As we can notice that the increase in the number of paths (L_c) leads to a better outage.

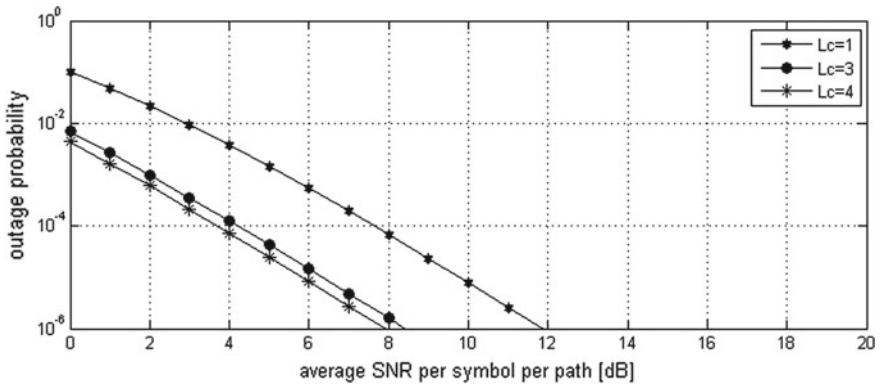


Fig. 3 Shows the outage probability of hybrid combiner (SC/MRC) having $L = 5$

3 Conclusion

This paper contains a detailed review of mean output SNR and the outage probability of hybrid diversity combiner (SC/MRC) over Nakagami- m fading channel. This review concludes that by applying a hybrid diversity combiner (SC/MRC) for Nakagami- m fading channel, our mean output SNR is independent of fading parameter m . It has better mean SNR gain from SC and EGC, but it will be inferior to the MRC as we increase the number of paths the performance of hybrid combiner (SC/MRC) improves. By using this technique, we can reduce the complexity of the system comparison to MRC with performance slightly inferior to MRC.

References

1. Khatalin S, Fonseka JP (2006) Capacity of correlated Nakagami- m fading channels with diversity combining techniques. *IEEE Trans Veh Technol* 55(1):142–150
2. Rappaport TS *Wireless communication, principles and practice*, 2nd edn. Prentice-Hall, India
3. Simon MK, Alouini M-S (2005) *Digital communication over fading channels*, 2nd edn. Wiley
4. Win MZ, Winters JH (1999) Analysis of hybrid selection/maximal-ratio combining in Rayleigh fading. *IEEE Trans Commun* 47(12)
5. Alouini MS, Simon MK (2000) An MGF-based performance analysis of generalized selection combining over Rayleigh fading channels. *IEEE Trans Commun* 48:401–415
6. Mallik RK, Win MZ (2002) Analysis of hybrid selection/maximal-ratio combining in correlated Nakagami- m fading. *IEEE Trans Commun* 50(8)
7. Roy Y, Chouinard JY, Mahmoud SA (1996) Selection diversity combining with multiple antennas for MM-wave indoor wireless channels. *IEEE J Sel Areas Commun* 14:674–682
8. Alouini MS, Simon MK (1999) Performance of coherent receiver with hybrid SC/MRC over Nakagami- m fading channels. *IEEE Trans Veh Technol* 48(4):1155–1164
9. Lombardo P, Fedele G, Rao MM (1999) MRC performance for binary signals in Nakagami fading with general branch correlation. *IEEE Trans Commun* 47(1):44–52
10. Alouini MS, Goldsmith A (1997, May) Capacity of Nakagami multipath fading channels. In: *Proceedings of IEEE Vehicular Technology Conference*, Phoenix, AZ, pp 358–362
11. Annamalai A, Tellambura C (2002) Analysis of hybrid selection/maximal ratio diversity combiners with gaussian errors. *IEEE Trans Wirel Commun* 1(3):498–512
12. Lal Chand Godara *Smart Antennas*. CRC Press
13. Gradshteyn IS, Ryzhik IM (2000) *Tables of integrals, series, and products*, 6th edn. Academic
14. Wolfram, *The Wolfram function site* (2015) Internet (online). <http://functions.wolfram.com>

Epileptic Seizure Detection Using Machine Learning Techniques



Akshay Sreekumar, A. N. Sasidhar Reddy, D. Udaya Ravikanth,
M. Chaitanya Chowdary, G. Nithin, and P. S. Sathidevi

Abstract Epilepsy is a neurological disorder, which causes seizures. Detection of epilepsy is carried out by analyzing EEG signals. Detecting epileptic seizures from long-term EEG data is a time consuming and tedious task, which requires vast clinical expertise. Most of the epilepsy detection algorithms available today are highly patient dependent. In this paper, an efficient and patient independent epileptic seizure detection algorithm based on machine learning is proposed. We have developed a method to classify seizure and non-seizure data using different machine learning algorithms. Time-domain, frequency-domain, and wavelet-domain features are used in this work. Feed-forward neural network, anomaly detection using multivariate Gaussian distribution and long short-term memory network are employed to classify seizure and non-seizure data. CHB-MIT database is used in this study. Long short-term memory network has given the highest seizure detection accuracy (97.4%) and the lowest false positive rate (7.88%).

A. Sreekumar (✉) · A. N. Sasidhar Reddy · D. Udaya Ravikanth · M. Chaitanya Chowdary ·
G. Nithin · P. S. Sathidevi
Department of Electronics and Communication Engineering, National Institute of Technology
Calicut, Kozhikode, Kerala 673601, India
e-mail: asktwoask@gmail.com

A. N. Sasidhar Reddy
e-mail: ansr2510@gmail.com

D. Udaya Ravikanth
e-mail: udayadara28@gmail.com

M. Chaitanya Chowdary
e-mail: chaitanyachowdarymovva@gmail.com

G. Nithin
e-mail: 2nithin.g@gmail.com

P. S. Sathidevi
e-mail: sathi@nitc.ac.in

Keywords Epilepsy · Seizure detection · Long short-term memory network · Anomaly detection · Multivariate Gaussian distribution · Feed-forward neural network · FNN · LSTM · EEG

1 Introduction

Epilepsy is a neurological disorder, which results in enduring predisposition to generate epileptic seizures. The epileptic seizure is a transient occurrence of symptoms due to abnormal and excessive neurological activity in the brain [1]. The epileptic seizure leads to unconsciousness of the patient thereby endangering his/her life during activities like driving, heavy machinery operation, etc. Doctors utilize the EEG signals of the patient to identify epileptic seizures. Hence, the detection of epilepsy in the EEG signals is an important task in its treatment. Detecting epileptic seizures from long-term EEG data is a time consuming and tedious task, which requires vast clinical expertise and is highly prone to manual errors. In addition, the presence of artefacts often leads to misinterpretation.

There has been a lot of work done on seizure detection, but most of them use patient-specific features, which cannot be generalized [2]. Hence, there is a need for robust patient independent algorithm that can detect seizures with high accuracy and minimum false positive rate.

The seizure detection involves feature extraction and binary classification of it into seizure and non-seizure. The important step in getting a good accuracy is selecting a set of key features, which can easily show the abnormalities in EEG during a seizure. A survey carried out by Alotaiby et al. [3] suggests that most of the detection and prediction algorithms used time- and wavelet-domain features. Algorithms which use multiple domains perform better than the algorithms which use single domain. In addition, they found that multi-channel EEG data yielded good results compared to single channel.

2 Methodology

2.1 EEG Database

The EEG data used in this study is from CHB-MIT database [4]. The data was collected at the Children's Hospital of Boston, on both males and females aged 1.5–23. The readings are sampled at 256 Hz with 16-bit resolution. All of the participants in the study are patients having drug-resistant epilepsy and were being observed in a hospital setting to judge candidacy for a neurosurgical intervention to prevent the seizures.

2.2 Feature Extraction from EEG

Several EEG features are extracted from time, frequency, and wavelet domains. The extracted features are given below:

2.2.1 Time Domain and Frequency-Domain Features

- Features based on statistical moments [5]: Mean, variance, skewness, and kurtosis.
- Features based on amplitude [5]: Root mean square amplitude, interquartile range.
- Features available in PyEEG library [6]: PyEEG is a Python function library to extract EEG features. It includes power spectral intensity, relative intensity ratio, Hjorth parameters, special entropy, singular value decomposition entropy, fisher information, Petrosian fractal dimension.

2.2.2 Wavelet Domain Features

Wavelet features are calculated from the wavelet coefficients of the decomposed EEG signal as mentioned in the paper [7]. However, instead of four-level discrete wavelet transform, we have used five-level discrete wavelet transform of EEG signal as shown in Fig. 1. The reason for doing five-level discrete wavelet transform is that the frequency bands of approximate and detailed coefficients closely match to the five major frequency bands of EEG signal, namely alpha (0.5–4 Hz), beta (4–8 Hz), gamma (8–15 Hz), theta (15–30 Hz), and delta (greater than 30 Hz). Here, the coefficients of A4, D4, D3, and D2 correspond to alpha, beta, gamma, and theta bands of EEG and D1, D0 together corresponds to delta band of EEG.

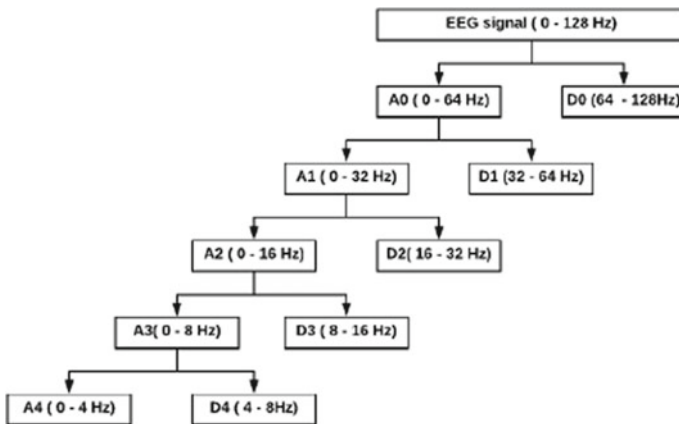


Fig. 1 Wavelet decomposition of EEG signal

The features calculated from coefficients are maximum, minimum, mean, variance, kurtosis, skewness, median, and spectral energies for each band.

2.3 Seizure Detection

2.3.1 Feed-Forward Neural Network

A feed-forward neural network is an artificial neural network wherein connections between the nodes do not form a cycle. We have used a one-dimensional feature vector formed using the above-mentioned features, calculated from 3 seconds (3 x 256 neurons) of EEG data as the input to the neural network.

2.3.2 Anomaly Detection using Multivariate Gaussian Distribution

In anomaly detection, we build a model using available data. We detect anomaly of a new data, which does not belong to the model.

Let the training set be $\{x^{(1)}, \dots, x^{(m)}\}$

$$p(x) = \prod_{i=1}^n p_1(x_i, \mu_i, \sigma_i^2) \sim N(\mu, \sigma) \tag{1}$$

where

$$\mu_j = (1/m) \sum_{i=1}^m x_j^i, \sigma_j^2 = (1/m) \sum_{i=1}^m (x_j^i - \mu_j)^2$$

We choose features x_i computed on the raw input that are indicative of anomalous examples. We then fix the parameters μ , and σ for features. Given a new example, we compute the probability of the anomaly $p(x)$ and declare it anomaly if $p(x) < \epsilon$.

The input to this algorithm is a feature vector. In this, we created a multivariate Gaussian distribution and trained its parameters, mean and variance, on non-seizure data. Then, we pass our seizure data to the model and get the corresponding probability value. We tune the threshold such that data samples in the seizure duration will have probability values less than the threshold.

2.3.3 Long Short-term Memory Network

In order to solve the problem of vanishing gradients in recurrent neural networks (RNN), we can use gated recurrent unit (GRU) architecture. In this, we have a memory cell and an update gate. Another architecture is long short-term memory (LSTM).It

is a powerful and general model of GRU. In this, we have a forget gate in addition. LSTM is the perfect recurrent neural network architecture that looks upon long-term dependencies. Since EEG data contains time dependency, we employed LSTM.

2.3.4 Deep Learning Techniques

- **Loss function:** Fine tuning the architecture will improve the accuracy of the network. In order to improve accuracy, we can change the cost function by giving more penalty for false detection. However, one must be careful while modifying the cost function. It must be converging and the values should not cause exploding or vanishing gradient problem. We have created and tuned our own weighted binary cross-entropy loss function.
- **Dropout:** Dropout is used to reduce the dependence of the network on any particular neuron. Using dropout randomly switches off some neurons with a probability and hence the weights are evenly distributed among all the neurons. This prevents overfitting of the data. This is a very important technique as without this, the network will cause irregular overfitting.
- **Batch normalization:** We usually normalize the data to a mean of 0 and variance of 1 before feeding to the input neurons. This is to improve the performance of the network. Consider doing this each time you feed this to a hidden layer. This considerably improves the performance and checks for exploding gradient problem before each hidden layer [8].
- **Adam optimizer cost function:** Instead of using conventional gradient descent, Adam optimizer cost function was used. This is superior to the gradient descent approach since it is faster owing to the combined benefits of adaptive gradient descent and root mean square propagation. Moreover, hyperparameters have intuitive interpretation and we cut off learning rate from the list of hyperparameters to tune, giving more degree of freedom towards orthogonal tuning.
- **Threshold variation:** The training threshold was 0.5 as the function was sigmoid. But we tried changing the testing threshold to various values. In LSTM network with all features, it was best suited to 0.5 while in LSTM without wavelet features, it was 0.4.

3 Results

3.1 *Training and Testing*

3.1.1 Training Size

We had initially started training on the entire 24 h for a patient. However, since the data was highly skewed, the algorithm failed. Hence, we cut short to portions where there was at least one seizure in the data.

3.1.2 Randomization

Two methods of training and testing were done. In the first method, the data taken was randomly arranged making it somewhat uncorrelated. More uncorrelated data meant more randomization and this decreased the performance. Hence, we did transfer learning with an hour long data. This method provided accuracy of 92.8%. But in real-life application, the data is sequential and hence when we tested the performance on sequential data and obtained accuracy of 97.4%.

3.1.3 Training and Test Accuracy

Initially, the training accuracy was low and hence the test accuracy. The training accuracy increased with epochs but above a certain value, the network started overfitting and the test accuracy was decreasing. A fine point of 500 epochs was found, but still, the accuracy was not sufficient enough. Tuning the hyper parameters of the network further increased the performance. The major outbreak has occurred when we changed the cost function. However, the test loss was not satisfactory due to some degree of overfitting. Hence, we divided the train set to 20% validation set and introduced dropout. This considerably reduced the test error.

Transfer learning: The data was trained one hour of a patient, initially for 500 epochs. Then, the learned neural network was transferred. However, in the next data sequence training to 500 epochs resulted in considerable degradation in the output as it started overfitting. Hence, we set the epochs to 200 for subsequent training. However, for a few patients whose data was considerably different from what was trained earlier, they required around 300–400 epochs and for those who had similar data needed only 50 epochs. This led to the problem of underfitting and overfitting. To avoid this, we made the epochs adaptably tunable for each patient. This was done by stopping at the point when the training and validation loss reached less than 1% error since training it further would lead to overfitting.

3.2 Detection Results

- Accuracy of seizure detection: It is the percentage ratio of number of correctly detected seizures to the number of actual seizures present.
- False positive rate: It is the percentage ratio of number of falsely detected non-seizures (as seizures) to the sum of the number of falsely detected non-seizures and actual seizures.

Table 1 shows the accuracy of seizure detection and false positive rate for different machine learning techniques. Initially, we have used time and frequency-domain features. Using these features as the inputs to FNN gave 74% accuracy. Adding wavelet features to it gave 84.5% accuracy. When we used LSTM with the wavelet features combined, the accuracy jumped to 97.4%. Training using wavelet features alone gave 87%. Therefore, the major contribution to accuracy was from wavelet features.

Figure 2 shows how the seizure detection accuracy is improving with the number of hours of data trained for the LSTM algorithm. Training and testing (first time) means the data is trained on the training set of one hour and the trained network is now tested on the test set. This trained network is transfer learned to the next hour and

Table 1 Comparison of performance parameters

Parameters	LSTM (without randomness)	LSTM (with randomness)	Anomaly detection	FNN
Seizure detection accuracy (%)	97.4	92.8	73	84.5
False positive rate (%)	7.88	3.2	72	7.8

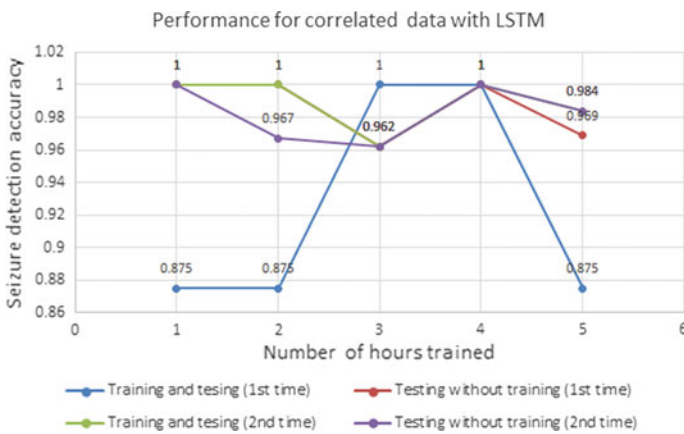


Fig. 2 Variation of seizure detection accuracy with the number of hours of data trained for LSTM without randomization

plotted. We have performed this for 5 h of data of five different patients. However, since we are applying transfer learning with one hour of data, the trained network will likely have a bias for the most recently trained data compared to the data trained in the beginning. To see this, we have plotted the accuracy of the final network on the test set without training as testing without training (first time). This entire procedure was repeated one more time to see the improvement in the accuracy.

The graph shows that the final ‘Testing without training (2nd time)’ gave 100% accuracy for the first patient, 96.7%, 96.2%, 100%, and 98.4% accuracy on the remaining patients, respectively. This shows that the accuracy is high and is patient independent.

4 Conclusion

We have used different machine learning algorithms such as feed-forward neural network (FNN), anomaly detection using multivariate Gaussian distribution, and long short-term memory network (LSTM) for the detection of epileptic seizures from EEG data of a patient. Anomaly detection algorithm gave us satisfactory results but the false positive rate was very high. FNN trained in our special architecture gave 84% accuracy but the training was too inefficient and highly computationally expensive. To capture the sequential data and to reduce complexity, LSTM architecture was used and it gave the best result with accuracy of 97.4% and false positive rate of 7.88%.

References

1. Fisher RS, Acevedo C, Arzimanoglou A, Bogacz A, Cross JH, Elger CE, Engel J Jr, Forsgren L, French JA, Glynn M, Hesdorffer DC (2014) ILAE official report: a practical clinical definition of epilepsy. *Epilepsia* 55(4):475–482
2. Vidyaratne LS, Iftekharruddin KM (2017) Real-time epileptic seizure detection using EEG. *IEEE Trans Neural Syst Rehabil Eng* 25(11):2146–2156
3. Alotaiby TN, Alshebeili SA, Alshawi T, Ahmad I, El-Samie FEA (2014) EEG seizure detection and prediction algorithms: a survey. *EURASIP J Adv Signal Process* 2014(1):183
4. <http://physionet.org/physiobank/database/chbmit/>
5. Boubchir L, Daachi B, Pangracious V (2017, July) A review of feature extraction for EEG epileptic seizure detection and classification. In: 2017 40th international conference on telecommunications and signal processing (TSP). IEEE, pp 456–460
6. Bao F, Li X, Zhang C (2011) PyEEG: an open source python module for EEG/MEG feature extraction. *Computational intelligence and neuroscience*
7. Hamad A, Houssein EH, Hassanien AE, Fahmy AA (2016, December) Feature extraction of epilepsy EEG using discrete wavelet transform. In: 2016 12th international computer engineering conference (ICENCO). IEEE, pp 190–195
8. Ioffe S, Szegedy C (2015) Batch normalization: Accelerating deep network training by reducing internal covariate shift. *arXiv preprint arXiv:1502.03167*

Comparative Analysis Among Various Soft Computing Classifiers for Nutrient Removal from Wastewater



Suresh Kumar and Surinder Deswal

Abstract The purpose of this study is to predict nutrient removal from wastewater by using different soft computing classifiers. A comparison of different classifiers, e.g., linear regression, nonlinear regression and artificial neural network (ANN) is done. ANN shows promising results as compared to linear and nonlinear regression. In this study, the data is collected from previous research papers. Out of the collected data, 75% is used to train the models and residual 25% is used for the validation of the models. The model accuracy is depending upon three evaluation parameters which are coefficient of determination (R^2), root mean square error (RMSE), and means absolute error (MAE). The result shows that the ANN model is more accurate to predict the nutrient removal from wastewater as compared to linear and nonlinear models.

Keywords Artificial neural network · Linear regression · Nonlinear regression · Nutrient removal

1 Introduction

Eutrophication is the process of over-enrichment of water with minerals and nutrients, which encourages excessive growth of algae that resulted in depletion of the oxygen content of water. Hence, eutrophication has become an indication of over polluted water bodies. Nitrogen and phosphorous are the main nutrients that cause eutrophication [1]. Water treatment by aquatic plants can be a solution for eutrophication. Wastewater treatment by aquatic plants getting popularity day by day in developing countries. It is a low-cost solution not only for domestic wastewater treatment but also for industrial wastewater treatment [2]. The usage of aquatic plant technologies

S. Kumar · S. Deswal (✉)
National Institute of Technology, Kurukshetra, Kurukshetra 136119, India

S. Kumar
e-mail: skdeswal21@gmail.com

© Springer Nature Singapore Pte Ltd. 2021
G. S. Hura et al. (eds.), *Advances in Communication and Computational Technology*, Lecture Notes in Electrical Engineering 668,
https://doi.org/10.1007/978-981-15-5341-7_70

927

is increasing gradually more as it is energy efficient and gives positive greenhouse results.

The aquatic plants can be categorized into three categories as free-floating, submerged and rooted plants. These systems have been proved very useful for onsite water treatment, and the production of biomass as a byproduct can provide benefits to the community after harvesting. These benefits can be in the form of biogas, biofertilizer, animal feed, compost, and fiber to make handicraft items.

The removal of nutrient (nitrogen and phosphorus) is achieved not only by plant uptake but also by bacteria present in the rhizosphere, adsorption by roots, and precipitation. The main pathways of nitrogen removal from the wastewater are conversion of ammonia into nitrite and then to nitrate through the nitrification process. In the absence of oxygen; nitrate again gets converted into nitrogen gas through the process of denitrification. The removal of nitrogen is achieved by direct adsorption by plants, denitrification, and nitrification processes, which is carried out by bacteria and ammonification [3], whereas the removal of phosphorus takes place by adsorption, plant uptake, and sedimentation process [3].

In this paper, the authors try to predict the value of nutrient removal from wastewater by using various soft computing techniques like multiple linear regression, multiple nonlinear regression, and ANN. Nowadays, soft computing techniques are getting popularity in the field of environmental engineering. Several researchers used these techniques in various fields and found reliable results [4, 5]. As reported by different researchers [4–6], in this paper also, the ANN classifier shows the most promising results as compared to linear and nonlinear regression.

2 Overview of Soft Computing Classifier

2.1 Artificial Neural Network

Artificial neural network (ANN) is a soft computing technique to analyze data. It is highly complex and nonlinear, inspired by the human brain system. It is used to model complex relations between input and output [7]. There are many types of ANN network applications, and the selection of the best depends on the nature of the work and data availability. The multilayer perceptron (MLP) is the most popular network used in the field of environmental hydraulics [8].

In this paper, an artificial neural network with backpropagation algorithm is used, which consist of three layers: input layer, hidden layer, and output layer. An input layer represents the input variables, the hidden layer helps the system to process data and finally, an output layer represents the outcome of the system [9].

The activation function used in this study (Eq. 1) as follows:

$$f(u_j) = \frac{1}{1 + e^{-u_j}} \quad (1)$$

2.2 Multiple Linear Regression

Multiple linear regression (MLR) is the simple and most commonly used regression technique to predict the values of a dependent variable. In this technique, there are two or more independent variables that help to predict the dependent variable. In this method, the model will be the best fit when the sum of squares of differences in actual values and predicted values is minimum [6].

The formula for multiple linear regression is as follows:

$$Y_i = \beta_i + \beta_1 x_{i1} + \beta_2 x_{i2} + \dots + \beta_p x_{ip} \quad (2)$$

where for $i = n$ observations:

Y_i = dependent variable, x_i = Independent variable, β_0 = Constant
 β_i = slope coefficient for independent variable.

2.3 Multiple Nonlinear Regression

As the name suggests the relationship between dependent and independent variables is of nonlinear nature.

The applied nonlinear regression model is given as:

$$Y_i = \beta_0 + \beta_1 x_1 + \beta_2 x_2 + \beta_3 x_3 + \beta_4 x_4 + \beta_5 x_5 + \beta_6 x_1^2 + \beta_7 x_2^2 + \beta_8 x_3^2 + \beta_9 x_4^2 + \beta_{10} x_5^2 \quad (3)$$

3 Performance Evaluation Criteria

To check the effectiveness of regression-based soft computing techniques, the following three parameters are used to evaluate the model performance:

1. Coefficient of determination (R^2)
2. Root mean square error (RMSE)
3. Mean absolute error (MAE)

All the above parameters are calculated using training and testing data sets. The formula of the above parameters as follows:

$$R^2 = \frac{(n \sum a_i p_i - \sum a_i \sum p_i)^2}{[n \sum (a_i)^2 - (\sum a_i)^2][n \sum (p_i)^2 - (\sum p_i)^2]} \tag{4}$$

$$RMSE = \sqrt{\frac{\sum_{i=1}^n (p_i - a_i)^2}{n}} \tag{5}$$

$$MAE = \frac{\sum_{i=1}^n |p_i - a_i|}{n} \tag{6}$$

where a is actual value; p is predicted value and n is the number of observations.

4 Data Set

A detailed study of literature has been conducted to get credible data and the same is collected from a number of resources like well-reputed journals and thesis [18–31]. There are about 44 number of data available on total nitrogen (TN) removal and 29 number of data available on total phosphorus (TP) removal (Table 1). Both types of data sets are divided into two separate parts: training (75%) and testing (25%). Tables 2 and 3 shows the features of training and testing data set, respectively, in which vegetation cover (VC), working water depth (D), hydraulic loading rate (HLR), hydraulic retention time (HRT), and initial concentration of total nitrogen (TN_{in}) and total phosphorous (TP_{in}) are considered as input parameters whereas removal rate of total nitrogen (R_{tn}), and total phosphorous (R_{tp}) are considered as output parameters.

The original data set is modified according to the requirement of the paper. The removal rate was calculated as

$$R = \frac{c_{in} - c_{out}}{c_{in}} \tag{7}$$

where c_{in} is the initial concentration of nutrient, and c_{out} is the final concentration of nutrient.

Hydraulic loading rate (HLR) is calculated, where it is not given: flow divided by surface area.

In case of batch study, HLR is calculated as

$$\frac{V}{A * HRT} \tag{8}$$

where V is vessel’s volume (m³), A is vessel’s surface area (m²) and HRT is in days. Vegetation cover is calculated as 1 for 100% coverage and 0 for control studies.

Table 1 Summary of studies for treatment of various water/wastewater types presenting references, plant species, vegetation cover, depth of water, HLR, HRT, and nutrient removal

References	Plant sp.	Veg cover (VC)	Depth (m)	HLR	HRT	TN in (mg/l)	TN out (mg/l)	Rtn $\frac{C_{in}-C_{out}}{C_{in}}$	TP in (mg/l)	TP out (mg/l)	Rtp $\frac{C_{in}-C_{out}}{C_{in}}$
[18]	Lpomnea aquatica	1	2	0.063	16	20	4.9	0.76	-	-	-
	Blank	0	1.1	0.063	16	20	8.9	0.56	-	-	-
	Lpomnea aquatica	1	1.1	0.125	8	31.96	19.52	0.39	-	-	-
	Blank	0	1.1	0.125	8	31.96	11.62	0.64	-	-	-
	Lpomnea aquatica	1	1.1	0.25	4	29.4	27	0.08	-	-	-
	Blank	0	1.1	0.25	4	29.4	22.8	0.22	-	-	-
	Lpomnea aquatica	1	1.1	0.375	2.7	29.4	26.7	0.09	-	-	-
	Blank	0	1.1	0.375	2.7	29.4	25.9	0.12	-	-	-
	Lpomnea aquatica	1	1.1	0.5	2	31.96	26.6	0.17	-	-	-
	Blank	0	1.1	0.5	2	31.96	25.9	0.19	-	-	-
	Lpomnea aquatica	1	1.1	0.625	1.6	20	19.2	0.04	-	-	-
	Blank	0	1.1	0.625	1.6	20	19.2	0.04	-	-	-
[19]	Cyperus sp.	1	0.35	0.115	2.7	31	10.3	0.67	23.8	9.1	0.62
	Miscatidium vlaceum	1	0.35	0.115	2.7	31	13.4	0.57	23.8	14.1	0.41

(continued)

Table 1 (continued)

References	Plant sp.	Veg cover (VC)	Depth (m)	HLR	HRT	TN in (mg/l)	TN out (mg/l)	R _{tn} $\frac{C_{in}-C_{out}}{C_{in}}$	TP in (mg/l)	TP out (mg/l)	R _{tp} $\frac{C_{in}-C_{out}}{C_{in}}$
[20]	Blank	0	0.35	0.115	2.7	31	14.9	0.52	23.8	13.3	0.44
	Oenathe javanica	0.56	0.48	0.014	35	18.32	1.59	0.91	0.8	0.34	0.58
	Oenathe javanica	1	0.38	0.0035	35	12.58	1.16	0.91	0.68	0.16	0.76
[22]	Blank	0	0.38	0.0035	35	12.58	4.35	0.65	0.68	0.45	0.34
	Lpomnea aquatica	0.14	1.8	0.16	7	5.15	1.96	0.62	0.97	0.36	0.63
	Lpomnea aquatica	0.14	1.8	0.22	5	5.15	2.29	0.56	0.97	0.43	0.56
[23]	Lpomnea aquatica	0.14	1.8	0.37	3	5.15	2.8	0.46	0.97	0.51	0.47
	Oenathe javanica	1	0.75	0.2	3	3.76	2.59	0.31	1.25	1.17	0.06
	Oenathe javanica	1	0.75	0.3	2	4.57	2.95	0.35	1.35	1.16	0.14
[24]	Oenathe javanica	1	0.75	0.6	1	7.94	2.86	0.64	1.54	1.34	0.13
	Cyperus sp.	1	0.32	0.03	7	90.2	38.9	0.57	34.85	16	0.54
	Colcasia esculenta	1	0.32	0.03	7	89.3	56.75	0.36	34.1	20	0.41
	Blank	0	0.32	0.03	7	88.85	83.6	0.06	31.5	31.05	0.01

(continued)

Table 1 (continued)

References	Plant sp.	Veg cover (VC)	Depth (m)	HLR	HRT	TN in (mg/l)	TN out (mg/l)	R _{tn} $\frac{C_{in}-C_{out}}{C_{in}}$	TP in (mg/l)	TP out (mg/l)	R _{tp} $\frac{C_{in}-C_{out}}{C_{in}}$
[25]	Lolium multiflorum	1	0.4	0.009	35	17	3.16	0.81	1.84	0.19	0.90
	Blank	0	0.4	0.009	35	17.4	5.36	0.69	2.16	0.62	0.71
[26]	Carex sp.	0.5	1.2	0.164	11	21.8	13.1	0.40	2.16	1.77	0.18
	Blank	0	1.2	0.164	11	21.8	19.5	0.11	2.16	1.9	0.12
[27]	Vetiveria zizanioides	0.55	0.5	0.104	7	38.4	19.4	0.49	5.2	4.1	0.21
	Vetiveria zizanioides	0.55	0.5	0.104	7	46.92	19.9	0.58	6.26	4.3	0.31
	Vetiveria zizanioides	0.55	0.5	0.145	5	38.4	23.5	0.39	5.2	4.5	0.13
	Vetiveria zizanioides	0.55	0.5	0.145	5	46.92	23	0.51	6.26	5.2	0.17
	Vetiveria zizanioides	0.55	0.5	0.242	3	38.4	30	0.22	5.2	4.4	0.15
	Vetiveria zizanioides	0.55	0.5	0.242	3	46.92	28.1	0.40	6.26	4.8	0.23
[28]	Canna sp. & juncus sp.	0.95	0.51	0.19	3	0.85	0.14	0.84	0.08	0.02	0.75
	Canna sp. & juncus sp.	0.95	0.51	0.19	3	1.88	0.79	0.58	0.22	0.12	0.45
[29]	cyperus sp.	1	0.43	0.242	5	58.5	16.1	0.72	-	-	-

(continued)

Table 1 (continued)

References	Plant sp.	Veg cover (VC)	Depth (m)	HLR	HRT	TN in (mg/l)	TN out (mg/l)	R _{tn} $\frac{C_{in}-C_{out}}{C_{in}}$	TP in (mg/l)	TP out (mg/l)	R _{tp} $\frac{C_{in}-C_{out}}{C_{in}}$
[30]	Miscanthium violaceum	1	0.43	0.242	5	58.5	17.9	0.69	-	-	-
	Blank	0	0.43	0.242	5	58.5	43.5	0.26	-	-	-
	Canna sp.	1	1.2	0.12	5	8.71	4.32	0.50	-	-	-
[31]	Blank	0	1.2	0.12	5	8.71	6.56	0.25	-	-	-
	Framites sp.	1	0.3	0.005	5	-	-	-	3.5	0.88	0.75
	Blank	0	0.3	0.005	5	-	-	-	3.5	2.07	0.41

Table 2 Summary of the data sets for total nitrogen

Variable	Training				Testing			
	Minimum	Maximum	Mean	Std. deviation	Minimum	Maximum	Mean	Std. deviation
Rtn	0.040	0.910	0.441	0.262	0.220	0.840	0.487	0.206
Veg cover	0.000	1.000	0.533	0.463	0.000	1.000	0.645	0.378
Depth (m)	0.320	2.000	0.885	0.493	0.430	1.200	0.610	0.294
HLR (m ³ /m ² /d)	0.004	0.625	0.204	0.191	0.120	0.242	0.193	0.052
HRT (days d)	1.000	35.000	9.991	11.370	3.000	5.000	4.273	1.009
TNin (mg/l)	3.760	90.200	28.040	22.454	0.850	58.500	33.299	23.617

Table 3 Summary of the data sets for total phosphorus

Variable	Training				Testing			
	Minimum	Maximum	Mean	Std. deviation	Minimum	Maximum	Mean	Std. deviation
Rtp	0.010	0.900	0.406	0.249	0.130	0.750	0.380	0.257
Veg cover	0.000	1.000	0.551	0.438	0.000	1.000	0.638	0.330
Depth (m)	0.320	1.800	0.719	0.522	0.300	0.510	0.453	0.094
HLR (m ³ /m ² /d)	0.004	0.600	0.136	0.147	0.005	0.242	0.146	0.094
HRT (d)	1.000	35.000	12.433	13.199	3.000	5.000	4.000	1.069
TPin (mg/l)	0.680	34.850	9.564	12.732	0.080	6.260	3.778	2.474

4.1 Characteristics of the Data Set Used in This Study

4.1.1 Data Set for Total Nitrogen

See Table 2.

4.1.2 Data Set for Total Phosphorus

See Table 3.

Table 4 Summary of performance evaluation parameters using different modeling techniques for total nitrogen data set

Modeling method	Training			Testing		
	R^2	RMSE	MAE	R^2	RMSE	MAE
Linear regression	0.601	0.1628	0.1314	0.101	0.2097	0.1638
Nonlinear regression	0.7540	0.1278	0.093	0.005	0.2634	0.1984
ANN	0.9651	0.0672	0.046	0.9150	0.06	0.0338

5 Results and Discussion

5.1 Result of ANN

In this paper, different MLP networks with a single hidden layer, and Log-Sigmoid as an activation function are used to predict nutrient reduction in wastewater.

5.1.1 Total Nitrogen Removal

Nitrogen is the main component found in domestic wastewater, agriculture land runoff, and effluent from various industries. It can exist in wastewater in various forms like ammonia, nitrite, nitrate, organic nitrogen. These forms act as a source or end product for each other depending on the oxygen present in wastewater. That's why total nitrogen is considered.

In this study, the values of learning rate, momentum, hidden layer, and number of iterations are tested by changing these model-specific parameters. The best results obtained from tuning of the MLP parameters: learning rate 0.2, momentum 0.2, hidden layer neurons 11, and number of iteration 3000 in case of total nitrogen removal. In the prediction of total nitrogen removal, MLP (4-11-1) showed the best prediction model because of the higher value of the coefficient of determination (R^2) and minimum values of errors (Table 4). Various evaluation parameters obtained from this model are $R^2 = 0.9651$, $RMSE = 0.0672$, $MAE = 0.046$; $R^2 = 0.9150$, $RMSE = 0.06$, $MAE = 0.0338$ for training data set and testing data set, respectively.

5.1.2 Total Phosphorus Removal

In the removal of total phosphorus, the values of learning rate, momentum, and the number of iterations are selected as 0.2, 0.2, and 3000, respectively, for both training and testing data set. The sensitivity of the model is checked by varying hidden layer neurons from 1 to 18 on both of the data sets. The best model to predict the total phosphorus removal is found by implementing MLP with 10 hidden layer neurons (4-10-1). The performance of the best MLP model is shown in Table 5. Various

Table 5 Summary of performance evaluation parameters using different modeling techniques for total phosphorus data set

Modeling method	Training			Testing		
	R^2	RMSE	MAE	R^2	RMSE	MAE
Linear regression	0.539	0.1652	0.1392	0.0254	0.3564	0.2687
Nonlinear regression	0.8493	0.0944	0.0706	0.0044	0.3271	0.2403
ANN	0.9602	0.0572	0.0446	0.9314	0.0703	0.0524

evaluation parameters obtained from this model are: $R^2 = 0.9602$, $RMSE = 0.0572$, $MAE = 0.0446$; $R^2 = 0.9314$, $RMSE = 0.0703$, $MAE = 0.0524$ for training data set and testing data set, respectively.

5.2 Result of Multiple Linear Regression

In case of total nitrogen removal, the following equation is the outcome of training data set after applying multiple linear regression.

$$\begin{aligned}
 Rtn = & 0.632 + 0.099 * VC - 0.031D - 0.744HLR \\
 & + 0.006HRT - 0.004 * TNin
 \end{aligned}
 \tag{9}$$

The parameters used for the performance evaluation are shown in Table 4. The values obtained are: $R^2 = 0.601$, $RMSE = 0.1628$, $MAE = 0.1314$ and $R^2 = 0.101$, $RMSE = 0.2097$, $MAE = 0.1638$ for training data set and testing data set, respectively.

In case of total phosphorus removal, the following equation is the outcome of training data set after applying multiple linear regression.

$$\begin{aligned}
 Rtp = & -0.275 + 0.224VC + 0.346D - 0.155HLR \\
 & + 0.018HRT + 0.011TPin
 \end{aligned}
 \tag{10}$$

The parameters used for the performance evaluation are shown in Table 5. The values obtained are: $R^2 = 0.539$, $RMSE = 0.1652$, $MAE = 0.1392$ and $R^2 = 0.0254$, $RMSE = 0.3564$, $MAE = 0.2687$ for training data set and testing set, respectively.

5.3 Result of Multiple Nonlinear Regression

In case of total nitrogen removal, the following equation is resulted from the training data set after applying multiple nonlinear regression

$$\begin{aligned}
 Rtn = & 1.12992 + 0.59477 * VC - 0.56417 * D - 2.70517 * HLR \\
 & - 0.01351 * HRT - 0.00330 * TNin + 0.51558 * VC^2 + 0.27216 * D^2 \\
 & + 2.91637 * HLR^2 + 0.00027 * HRT^2 - 0.00003 * TNin^2 \quad (11)
 \end{aligned}$$

The modeling results of multiple nonlinear regression are not as good as ANN. The performance of the model is shown in Table 4. The value of coefficient of determination (R^2) was far away from expectations and the errors were also high. Various evaluation parameters obtained from the model are: $R^2 = 0.7540$, RMSE = 0.1278, MEA = 0.093; and $R^2 = 0.005$, RMSE = 0.2634, MAE = 0.1984 for training data set and testing data set, respectively.

The following equation is derived from the training data set of total phosphorus.

$$\begin{aligned}
 Rtp = & 0.05734 + 0.17329 * VC - 1.16724 * D + 0.48498 * HLR \\
 & + 0.02418 * HRT + 0.04810 * TPin + 0.13887 * VC^2 + 0.71414 * D^2 \\
 & - 0.46378 * HRT^2 - 0.00008 * HRT^2 - 0.00127 * TPin^2 \quad (12)
 \end{aligned}$$

Various evaluation parameters obtained from the model are: $R^2 = 0.8493$, RMSE = 0.0944, MEA = 0.0706; and $R^2 = 0.0044$, RMSE = 0.3271, MAE = 0.2403 for training data set and testing data set, respectively.

5.4 Comparison of Models

The results of various computing techniques, e.g., ANN, multiple linear regression, and multiple nonlinear regression have been compared with each other. Figure 1 shows the scatter plots of total nitrogen for the trained data set. As you can see

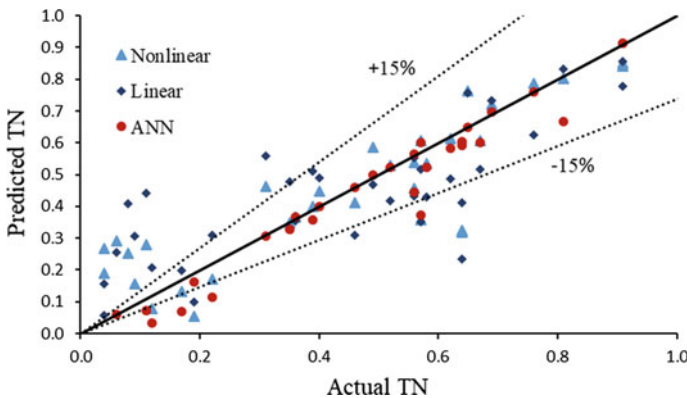


Fig. 1 Actual versus predicted values of total nitrogen by different modeling techniques with training data

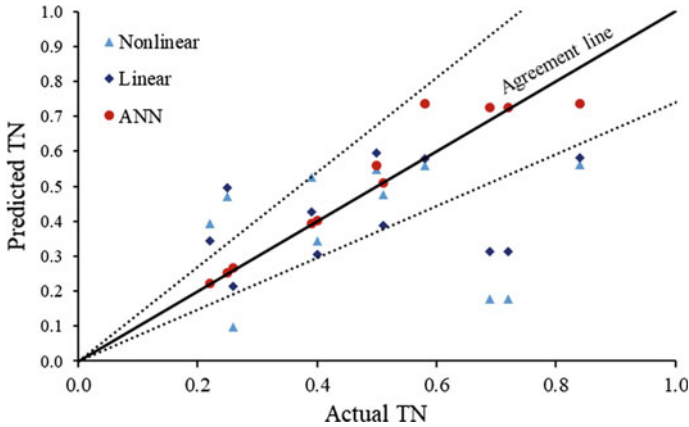


Fig. 2 Actual versus predicted values of total nitrogen by different modeling techniques with testing data

clearly from Fig. 1 that most of the predicted values of ANN model lie close to the line of perfect prediction and scatters within the range of $\pm 15\%$ of agreement line. However, predicted points plotted from linear and nonlinear regression models deviate at couple of points.

The results of the testing data of total nitrogen represented in the same way as training data in Fig. 2. Almost all the plots of ANN model are within $\pm 15\%$ of agreement line. Whereas plots of linear and nonlinear regression deviate at most of the points. So it is clear from both Figs. 1 and 2 that the prediction of ANN model is very close to the actual observed values. The values of various evaluation parameters are shown in Table 4. The prediction is done by ANN model on both training data ($R^2 = 0.9651$, RMSE = 0.0672, MAE = 0.046) and testing data ($R^2 = 0.9150$, RMSE = 0.06, MAE = 0.0338) is best, followed by nonlinear and linear regression models.

In case of total phosphorus removal, ANN model shows promising results as observed in case of total nitrogen removal. Figures 3 and 4 show the scatter plots of training and testing data set for total phosphorus removal. It is clearly shown that the prediction done by ANN model is well within $\pm 15\%$ of the agreement line, which confirms that the predictability of ANN model is more accurate than nonlinear and linear regression modeling (Table 5). The values of the performance evaluation parameters of ANN model are ($R^2 = 0.9602$, RMSE = 0.0572, MAE = 0.0446) for training data and ($R^2 = 0.9314$, RMSE = 0.0703, MAE = 0.0524) for testing data (Table 5). ANN model is more superior than linear and nonlinear regression models. The values of R^2 are on lower side and the values of errors are on higher side in case of linear and nonlinear regression models as compare to ANN.

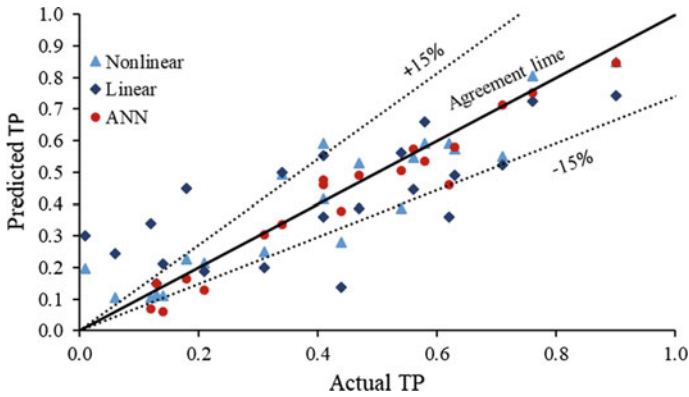


Fig. 3 Actual versus predicted values of total phosphorus by different modeling techniques with training data

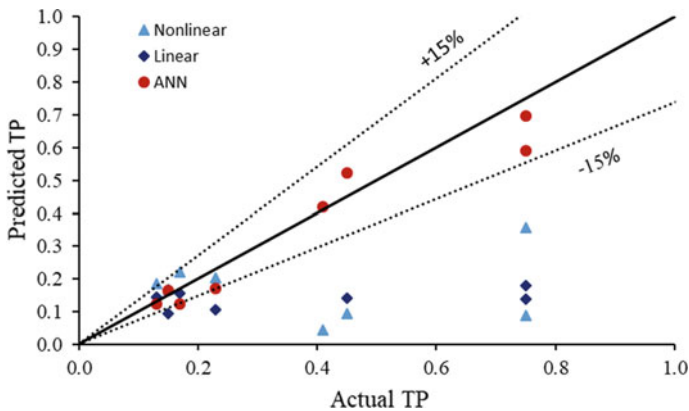


Fig. 4 Actual versus predicted values of total phosphorus by different modeling techniques with testing data

6 Application of Artificial Neural Network in the Field of Water and Wastewater Treatment

ANN has been found very useful in the past studies related to environmental engineering, to predict, control and monitoring problems, such as meteorology, soil pollution, air pollution, environmental impact assessment, environmental hydraulics, environmental geology, etc.

Some of the studies, where ANN used, are discussed as follows:

Akratos et al. [9] used ANN to predict orthophosphate and total phosphorus in a constructed wetland and found that the regression coefficient between predicted values and observed values is low ($R^2 = 0.43$). In another paper of the same researchers [10], the values of total nitrogen removal from water have been predicted and found regression coefficient (R^2) of 0.53.

Ozengin et al. [11] applied ANN computing technique for the estimation of total nitrogen and total phosphorus removal from water. The correlation coefficient between predicted values and observed values were as high as 0.9463 for total nitrogen and 0.9161 for total phosphorus.

Akratos et al. [12] used this technique to estimate the values of biochemical oxygen demand (BOD) and chemical oxygen demand (COD) and found the coefficient of determination, $R^2 = 0.52$ for BOD removal, and $R^2 = 0.44$ for COD removal.

Baxter et al. [13] developed a model for turbidity removal from water. When the predicted values were compared with field values, they obtained a high coefficient of determination $R^2 = 0.96$ and a low value of mean absolute error, $MAE = 0.08$ NTU.

Onkal-Engin et al. [14] used backpropagation based ANN model to determine the relationship between odor and BOD of the sewage. The correlation coefficients obtained from training and testing data sets were 0.98 and 0.91, respectively. The RMS errors were 0.04 for training data set and 0.07 for testing data set.

Yetilmezsoy and Sapci-Zengin [15] developed a three-layer ANN model (9:12:1) to predict chemical oxygen demand removal efficiency of a upflow anaerobic sludge blanket (UASB) reactor for treating cotton textile wastewater. They found that the ANN model prediction was satisfactory and the coefficient of correlation obtained was 0.82.

Karaca and Ozkaya [16] developed a model to control daily leachate flow rate. Backpropagation algorithm was used to develop a relationship between leachate flow rate and local meteorological data. The coefficient of determination (R^2) and mean squared error (MSE) obtained from this model were 0.847 and 0.00168, respectively.

Karul et al. [17] used a model with three-layer feedforward algorithm to predict the eutrophic process in three water bodies. They found the coefficient of correlation between 0.60 and 0.75.

So based on the above-discussed studies, it is evident that ANN is a strong statistical tool in learning the problems related to water and wastewater in the field of environmental engineering. ANNs gather their information by identifying the patterns and relationships in data and learn (or are implemented) through experience, not from programming. The behavior of a neural network is determined by the transfer functions of its neurons, by the learning rule, and by the structure itself. Due to these learning capabilities, ANN is implemented in this study and the results are encouraging and superior as compared to the other methods used.

7 Conclusion

Artificial neural network has been shown promising results to predict the nutrient removal (nitrogen and phosphorus) from wastewater by aquatic plants. In case of linear regression and nonlinear regression modeling, the values of performance evaluation parameters are significantly different and showing inferior capability in contrast to ANN modeling method. Coefficient of determination (R^2) values are significantly low in testing data set of linear as well as nonlinear regression as compared to ANN. The values of error are on higher side in both linear and nonlinear regression techniques. Comparing both of the regression techniques yield better results with nonlinear regression than linear regression, while ANN is found superior to the regression techniques.

References

1. Schindler DW (2006) Recent advances in the understanding and management of eutrophication. *Limnol Oceanogr* 51:356–363
2. Chen TY, Kao CM, Yeh TY, Chien HY, Chao AC (2006) Application of a constructed wetland for industrial wastewater treatment: a pilot-scale study. *Chemosphere* 64(3):497–502
3. Pavlineri N, Skoulikidis NT, Tsihrintzis VA (2017) Constructed floating wetlands: a review of research, design, operation and management aspects, and data meta-analysis. *Chem Eng J* 308:1120–1132
4. Kumar M, Tiwari NK, Ranjan S (2018) Prediction of oxygen mass transfer of plunging hollow jets using regression models. *ISH J Hydraul Eng* 5010:1–8
5. Taghi Sattari M, Yurekli K, Pal M (2012) Performance evaluation of artificial neural network approaches in forecasting reservoir inflow. *Appl Math Model* 36:2649–2657
6. Kumar M, Ranjan S, Tiwari NK (2018) Oxygen transfer study and modeling of plunging hollow jets. *Appl Water Sci* 8:121
7. Bishop, C.M.: *Neural networks: a pattern recognition perspective*. In: *Handbook of Neural Computation*, pp 1–23 (1996)
8. Govindaraju RS (2000) Artificial neural networks in hydrology II: hydrologic applications. *J Hydrol Eng* 5:124–137 Task Committee on Application of Artificial Neural Networks in Hydrology
9. Akratos CS, Papaspyros JNE, Tsihrintzis VA (2009) Artificial neural network use in orthophosphate and total phosphorus removal prediction in horizontal subsurface flow constructed wetlands. *Biosyst Eng* 102:190–201
10. Akratos CS, Papaspyros JNE, Tsihrintzis VA (2009) Total nitrogen and ammonia removal prediction in horizontal subsurface flow constructed wetlands: use of artificial neural networks and development of a design equation. *Bioresour Technol* 100:586–596
11. Ozengin N, Elmali A, Yonar T (2016) Application of artificial neural network in horizontal subsurface flow constructed wetland for nutrient removal prediction. *Appl Ecol Environ Res* 14:305–324
12. Akratos CS, Papaspyros JNE, Tsihrintzis VA (2008) An artificial neural network model and design equations for BOD and COD removal prediction in horizontal subsurface flow constructed wetlands. *Chem Eng J* 143:96–110
13. Baxter CW, Smith DW, Stanley SJ (2004) A comparison of artificial neural networks and multiple regression methods for the analysis of pilot-scale data. *J Environ Eng Sci* 3:S45–S58
14. Onkal-Engin G, Demir I, Engin SN (2005) Determination of the relationship between sewage odour and BOD by neural networks. *Environ Model Softw* 20:843–850

15. Yetilmezsoy K, Sapci-Zengin Z (2009) Stochastic modeling applications for the prediction of COD removal efficiency of UASB reactors treating diluted real cotton textile wastewater. *Stoch Environ Res Risk Assess* 23:13–26
16. Karaca F, Özkaya B (2006) NN-LEAP: a neural network-based model for controlling leachate flow-rate in a municipal solid waste landfill site. *Environ Model Softw* 21:1190–1197. <https://doi.org/10.1016/j.envsoft.2005.06.006>
17. Karul C, Soyupak S, Çilesiz AF, Akbay N, Germeç E (2000) Case studies on the use of neural networks in eutrophication modeling. *Ecol Modell* 134:145–152
18. Karnchanawong S, Sanjitt J (1995) Comparative study of domestic wastewater treatment efficiencies between facultative pond and water spinach pond. *Water Sci Technol* 32:263–270
19. Kyambadde J, Kansime F, Dalhammar G (2005) Nitrogen and phosphorus removal in substrate-free pilot constructed wetlands with horizontal surface flow in Uganda. *Water Air Soil Pollut* 165:37–59
20. Xin Z, Li X, Nielsen S, Yan Z, Zhou Y, Jia Y, Tang Y, Guo W, Sun Y (2012) Effect of stubble heights and treatment duration time on the performance of water dropwort floating treatment wetlands (FTWS). *Ecol Chem Eng S* 19:315–330
21. Zhou X, Wang G (2010) Nutrient concentration variations during *Oenanthe javanica* growth and decay in the ecological floating bed system. *J Environ Sci* 22:1710–1717
22. Li XN, Song HL, Li W, Lu XW, Nishimura O (2010) An integrated ecological floating-bed employing plant, freshwater clam and biofilm carrier for purification of eutrophic water. *Ecol Eng* 36:382–390
23. Yang Z, Zheng S, Chen J, Sun M (2008) Purification of nitrate-rich agricultural runoff by a hydroponic system. *Bioresour Technol* 99:8049–8053
24. Kansime F, Oryem-Origa H, Rukwago S (2005) Comparative assessment of the value of papyrus and cocoyams for the restoration of the Nakivubo wetland in Kampala, Uganda. *Phys Chem Earth* 30:698–705
25. Xian Q, Hu L, Chen H, Chang Z, Zou H (2010) Removal of nutrients and veterinary antibiotics from swine wastewater by a constructed macrophyte floating bed system. *J Environ Manag* 91:2657–2661
26. Van De Moortel AMK, Meers E, De Pauw N, Tack FMG (2010) Effects of vegetation, season and temperature on the removal of pollutants in experimental floating treatment wetlands. *Water Air Soil Pollut* 212:281–297
27. Boonsong K, Chansiri M (2008) Domestic wastewater treatment using vetiver grass cultivated with floating platform technique. *AU J Technol* 12:73–80
28. White SA, Cousins MM (2013) Floating treatment wetland aided remediation of nitrogen and phosphorus from simulated stormwater runoff. *Ecol Eng* 61:207–215
29. Kyambadde J, Kansime F, Gumaelius L, Dalhammar G (2004) A comparative study of *Cyperus papyrus* and *Miscanthidium violaceum*-based constructed wetlands for wastewater treatment in a tropical climate. *Water Res* 38:475–485
30. Sun L, Liu Y, Jin H (2009) Nitrogen removal from polluted river by enhanced floating bed grown canna. *Ecol Eng* 35:135–140
31. Sekiranda SBK, Kiwanuka S (1997) A study of nutrient removal efficiency of *Phragmites mauritianus* in experimental reactors in Uganda. *Hydrobiologia* 364(1):83–91

Automatic Keyphrase Extraction Using SVM



Ankit Guleria, Radhika Sood, and Pardeep Singh

Abstract The Internet has a plethora of text articles, and it has become a necessity to extract only the relevant information from all the sources. Automatic keyphrase extraction is an essential part of the process of information extraction as it is impossible to manually identify all the keyphrases in textual sources. Keyphrase extraction has thus become an indispensable component of contemporary world of Internet. Researchers have treated keyword extraction as a classification problem where the input candidate words are classified as keywords or non-keywords. The paper tries to address two major issues in keyphrase extraction process, namely candidate selection and extraction of relevant features. Noun phrases extracted using specified regular expressions are considered as candidate words. A supervised machine learning method based on statistical and linguistic features is proposed for keyword extraction using SVM. The experimental results compared with well-known methods, namely SingleRank, ExpandRank, baseline TF-IDF, and the latest work show considerable improvement over the previously achieved results.

Keywords Keyphrase extraction · Noun phrases · Feature extraction · SVM · Confusion matrix

A. Guleria (✉) · R. Sood · P. Singh
Department of Computer Science and Engineering, National Institute of Technology Hamirpur,
Hamirpur 177005, HP, India
e-mail: ankitguleria1@gmail.com

R. Sood
e-mail: radhikasood1006@gmail.com

P. Singh
e-mail: pardeep@nith.ac.in

1 Introduction

In today's era, tremendous information is available on the Web. Thousands of books, journals, articles, papers, etc., are published on a daily basis about a single topic. Whenever studying any topic, it is nearly impossible to read the complete documents. Therefore, an efficient information retrieval method is required to extract relevant information which generally involves extracting the index terms or keywords from the documents. Keywords are the smallest unit that plays a significant role in determining the main context of a given document. They can be used to easily identify the meaning of the entire document which can be easily exploited by various applications like text summarizer, topic detector, cataloger, etc.

Automatic keyphrase extraction is defined as “the automatic selection of important and topical phrases from the body of a document” [1]. The main goal of keyword extraction is to extract a set of phrases that help in grasping the central idea of the document without the need to read it. The readers of all kinds of articles whether academic, sports, business, social, etc., are benefited greatly from the automatically generated keywords. Keywords of a document are of great importance to search engines as they help in providing precise results of the queries. Having such a large importance, the topic automatic keyword extraction has received great attention in the recent years. Many automated keyword extraction systems have been introduced which are based on the following three approaches.

- **Statistical approach:** The statistical information of the words, such as word frequency, word co-occurrence, and term nesting statistics, is used to identify the keywords. This approach does not require any training data. The specified features are extracted for the document, and based on these obtained values, the keywords are listed.
- **Linguistic approach:** This approach includes usage of parts of speech such as nouns and adjectives in sentence semantics. Noun phrases are extracted and then further methods are used to weigh them to be identified as a keyword.
- **Machine learning-based approach:** A more sophisticated approach than the previous two which uses the concept of training a classifier using a dataset containing the documents along with their extracted keywords. This classifier is then used to predict the keywords of a document. Various techniques that can be used are support vector machine (SVM), Naive Bayes, etc.

Also, the keyword extraction methods can be classified as extractive or abstractive. The extractive methods directly extract keywords from the text, whereas the abstractive methods work similar to a human and generate keywords by using contextual knowledge of the text. These keywords generated by abstractive methods may not be directly present in the text and may be a combination of some words of the text.

The proposed ML method uses extractive approach to find and then classify the candidate words.

2 Literature Survey

Many supervised and unsupervised extractive approaches have been proposed till date.

The Kea System [2] firstly chooses the candidate phrases (maximum length three) by cleaning the input text and then identifying the candidate by removing stop-words and excluding proper nouns. Next, stemming is applied to get the final list of candidates. Secondly, selection of keyphrases is done on the basis of two features, namely term frequency-inverse document frequency (TF-IDF) and first occurrence. Discretization is then applied to convert features into nominal data which can be consumed by machine learning classifiers. Lastly, Naive Bayes is trained to build a classifier on the basis of these features.

The keyphrase extractor that Turney [1] suggested also works on a similar approach but uses candidate phrases of maximum length five. Features used for weighing the candidate keyphrases are frequency, relative length, first occurrence of phrase, number of words in phrase, etc. Decision tree is used to detect the keyphrases. The proposed algorithms in the above two approaches have ignored many other features such as part of speech and spread of word in the document.

Krulwich and Burkey [3] created an InformationFinder through “the extraction of semantically significant phrases.” The tasks which make it innovative are using heuristics such as considering words in italics or acronyms as keyphrases for learning rather than performing complex mathematical calculations on them and more importantly creating decision trees to determine user’s interest. Finally, the decision tree is transformed into a “boolean search query string.” The approach is unique but ignores the importance of various statistical and linguistic features.

Mihalcea and Tarau [4] proposed the unsupervised approach to find the keywords using a TextRank model defined by distance between co-occurrences of same word. The candidate words are limited by the use of only certain lexical units based on part of speech. The vertices or the candidate words are then ranked and the top T are said to be the extracted keywords. The model ranks the candidate words only on the basis of a single feature, and it seems that the accuracy can be improved by considering many other features such as frequency and part of speech [5].

Nguyen and Kan [6] proposed keyphrase extraction as an extension of Kea System for scientific articles by using morphological features found in scientific articles. The proposed model showed improvement over the baseline Kea System but does not consider spread of the word [7] as a feature.

Wan and Xiao [8] proposed a single document keyphrase extraction method using neighborhood knowledge whereby an expanded document is created by adding neighbor documents to the concerned document and then keywords are ranked using a graph utilizing both the local and global information in the neighbor documents. This model ignored the statistical and linguistic features of the words.

Kathait and Tiwari [9] proposed an unsupervised approach based on the extraction of noun phrases. The candidate words only contain adjectives and nouns. Firstly, individual words are scored using a scoring scheme such as TF-IDF, and secondly,

the n -grams or phrases are given scores equal to the sum of scores of individual words present in them. The top-ranked phrases are considered as the output keyphrases. The way in which co-occurrence is defined limits the efficiency of the approach.

3 Proposed Work

The proposed supervised keyphrase extraction scheme uses the DUC-2001 benchmark dataset that has 308 news articles [8]. The average length of the documents was 740 words. The methodology consists of four main tasks: (1) candidate selection, (2) feature extraction, (3) training SVM, and (4) prediction of keyphrases.

3.1 Candidate Selection

A set of words and phrases is extracted as candidate keyphrases using the regular expression [10].

$$\{(< \text{Adjective} > * < \text{Noun} > + < \text{Preposition} >)? < \text{Adjective} > * < \text{Noun} > +\}$$

Phrases following this pattern are noun phrases. Noun phrases are selected because nouns contain tremendous amount of information related to the document. Noun phrases can be better understood by knowing the most frequently occurring patterns in them, i.e., noun, adjective noun, noun and noun preposition noun.

All these phrases essentially contain noun as their component and hence are termed as noun phrases.

3.2 Feature Extraction

There are five features that we used to represent the candidate keyphrase which are explained in detail below:

POS sequences According to Hulth and Megyesi [5], keyphrases tend to have distinctive distribution of part of speech sequences, and hence, it is worth using them as a feature. This is done using POS tagging which identifies the individual word in candidate phrases as a common noun, proper noun, singular noun, plural noun, or an adjective, preposition, etc. These POS tags of the candidate then form a part of the feature list.

Position of Keyphrase The beginning part [11] and concluding part of a document typically contain more relevant information to the topic being addressed; thus, we

use parabolic and line position as a feature to rank the words such that the candidate words at the beginning and end of a document are assigned more weight.

- **Line position:** Line position ranks the candidate phrases in a way that the words at the beginning of the document have the maximum weight, which decreases linearly; it is least for a candidate word at the mid of the document and increases linearly thereafter such that a candidate word at the end of the document has the maximum weight again.
- **Parabolic position:** Parabolic position ranks or weighs the candidate words using a similar approach with difference that the weight of the candidate words decreases and increases according to the equation of a parabola instead of a line.

Spread of Keyphrase in Document The spread of the word in the document has been found as a beneficial feature in a closely related task of link generation [7]. A more important keyphrase has more standard deviation which implies it is widely spread in the text document and thus proves to be an essential feature. Hence, spread calculated using standard deviation of the candidate in the document forms a part of the feature list.

Frequency A more important word tends to occur repeatedly and as a result has higher frequency in the document [11]. Hence, we consider frequency as a feature in our proposed work.

Occurrences of candidates in the documents According to Louis and Gagnon [12], position-based features such as first and last occurrence have been found effective in keyword extraction. We used normalized position of first occurrence of the candidate and then extended this approach to use the normalized position of all occurrences of the candidate in the documents as part of the feature vector.

Values for these features are extracted for the selected candidate words. All these features are then stored as key value pairs for each candidate word.

3.3 *Training the SVM Classifier*

DUC-2001 dataset is split into training and testing data. The above-mentioned features for candidate words are extracted using the proposed regular expression. During training, the SVM classifier is provided with these features along with 1 or 0 indicating whether the candidate is a keyword or non-keyword, respectively. The ratio of sizes of keyword list and non-keyword list is adjusted to achieve the highest possible value of F-measure.

The SVM classifier used is linear SVC. Linear SVC is preferred over other classifiers as the data contains only two output classes and a large number of features. The aim of linear SVC is to find the “best-fit” hyperplane that categorizes the data into two classes, namely keyword (output class-1) and non-keyword (output class-0). SVC uses training data to find this hyperplane on the basis of output values provided along with the input feature set (Fig. 1).

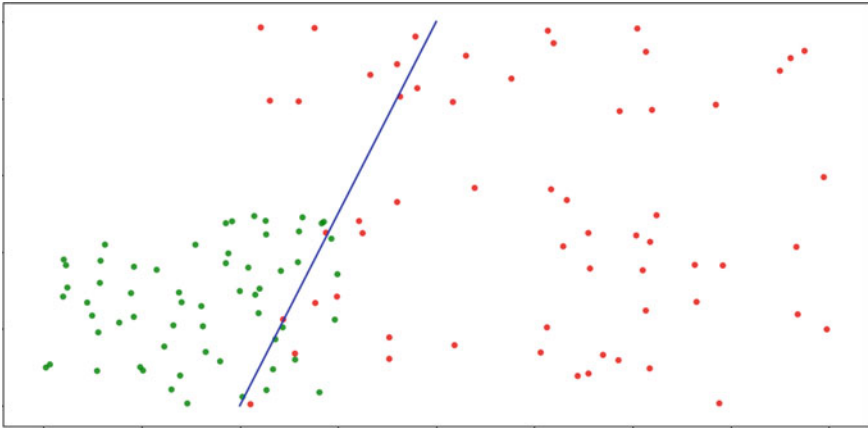


Fig. 1 Hyperplane separating two output classes in linear SVC

3.4 Prediction of Keyphrases

After training the SVM classifier, we test it by predicting the keyphrases from the testing data. The features of candidate words are again extracted and input to the trained model to classify them as a keyword or non-keyword. The resulting values of precision, recall, and F-measure are recorded (Fig. 2).

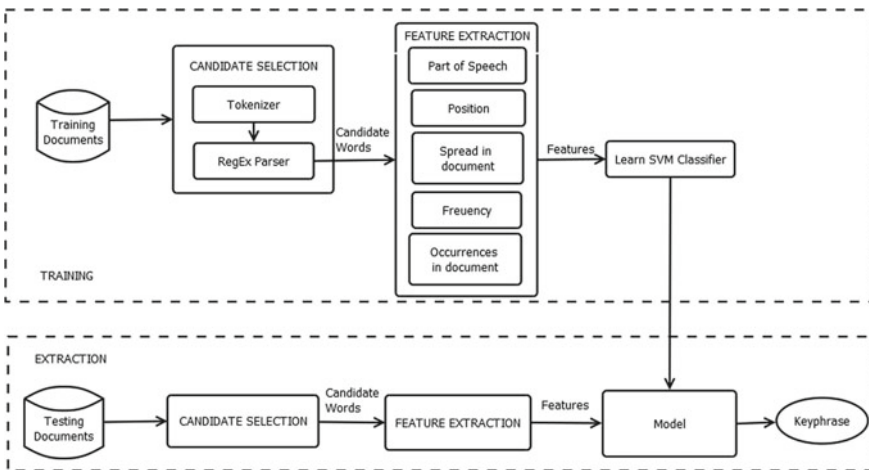


Fig. 2 Training and extraction process

4 Observations

The available dataset was split such that about 70% of the total scripts were used for training the classifier and remaining 30% data was used for testing the classifier. We plot confusion matrix during testing of the classifier and then describe the performance of our system in terms of the three standard metrics, i.e., precision, recall, and F-measure, calculated from this confusion matrix. Initially, there was a large imbalance in the values of both classes (one being the keyword and other being the non-keyword) of training data. Training the classifier using this data yields a high value of precision but a low recall, whereas completely balancing the values in both the classes yields a very high recall but a very low value of precision. Hence, we trained our classifier by restricting the values in non-keyword class to an optimal value such that we get the highest possible F-measure on the testing data. Firstly, we give a brief description of confusion matrix, precision, recall, and F-measure and then their respective values are achieved.

- Confusion matrix: It is a form of a table that is used to determine the performance of a classifier using a set of data having known true values. The four observations present in confusion matrix are true positives (TP), true negatives (TN), false positives (FP), and false negatives (FN).
- Precision: “Precision (also called positive predictive value) is the fraction of relevant instances among the retrieved instances”.

$$\text{Precision} = \frac{TP}{TP + FP} \quad (1)$$

- Recall: “In pattern classification, recall (also known as sensitivity) is the fraction of relevant instances that have been retrieved over the total amount of relevant instances”.

$$\text{Recall} = \frac{TP}{TP + FN} \quad (2)$$

- F-measure: In pattern classification, F-measure is calculated as the harmonic mean of precision and recall.

$$\text{F-measure} = \frac{2 * \text{Recall} * \text{Precision}}{\text{Recall} + \text{Precision}} \quad (3)$$

The values of precision, recall, and F-measure were recorded for the testing dataset when trained with different values of balance of classes.

Table 1 Observations for the completely balanced dataset

Precision	Recall	F-measure
12.9	81.35	22.2

Table 2 Observations for unbalanced dataset

Precision	Recall	F-measure
63.24	5.31	9.79

4.1 Completely Balanced Dataset

This dataset has 1600 samples for each class for training (Table 1).

We noted that recall was very high but precision was very low resulting in a low F-measure of 22.2%. This is because the classifier predicted a large number of false positives, i.e., a large no. of wrongly predicted keywords. The classifier assumes a lot of candidate words as keywords, a lot of them not actually being the keywords. Nonetheless, the actual keywords are correctly classified.

4.2 Unbalanced Dataset

Here, we did not impose any restriction on the size of non-keyword class in the training dataset, and there was a large imbalance in the size of two classes. The samples of keyword class were 1600, whereas those of non-keyword class were 31,187 (Table 2).

In this case, precision was very high, but recall became very low which again resulted in a very low F-measure of only 9.79%. The classifier is over-particular and does not assume many candidate words to be keywords. Therefore, misses a lot of keywords.

4.3 Optimally Balanced Dataset

We tried balancing the dataset to get the highest possible value of F-measure. This was achieved when there were 1600 samples corresponding to keyword class and 8400 samples corresponding to non-keyword class (Table 3).

Here, it is seen that F-measure is considerably high compared to the previous two cases (Fig. 3).

Table 3 Observations for optimally balanced dataset

Precision	Recall	F-measure
32.91	41.36	36.65

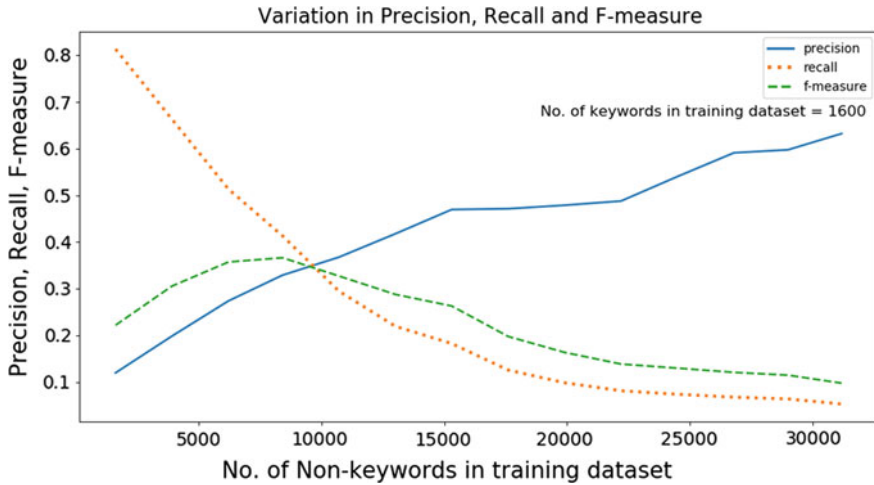


Fig. 3 Variations in precision, recall, and F-measure

5 Evaluation

For the evaluation of the effectiveness of our proposed system, we compared it to the previously achieved scores on DUC 2001 dataset. Three baseline methods used for comparison are TF-IDF, SingleRank, and ExpandRank. The score in TF-IDF baseline is the value of each word’s TF-IDF in the document. The SingleRank baseline model is based on graph ranking algorithm, wherein it firstly makes a graph for the document and secondly computes word scores from this graph. ExpandRank which was proposed by Wan and Xiao is a modification of SingleRank by including neighboring documents to create a graph using both local and global information and further computing score for each word [8].

The highest achieved precision, recall, and F-measure scores till date as also mentioned by Hasan and Ng [13] are 28.8, 35.4, 31.7, respectively. The scores as reported by Campos et al. in 2018 [14], though on a different dataset SemEval-2010, are 15.3, 10.3, and 12.3, respectively. The scores achieved using the proposed approach are considerably higher being 32.91, 41.36, and 36.65, respectively (Figs. 4, 5 and 6).

6 Conclusion

We have presented a supervised approach for keyword extraction. Noun phrases are selected as candidate words because majority of information of the document is contained in them. The paper also introduces five major features that affect the performance of the SVM classifier. The main finding is that the ratio of values in the

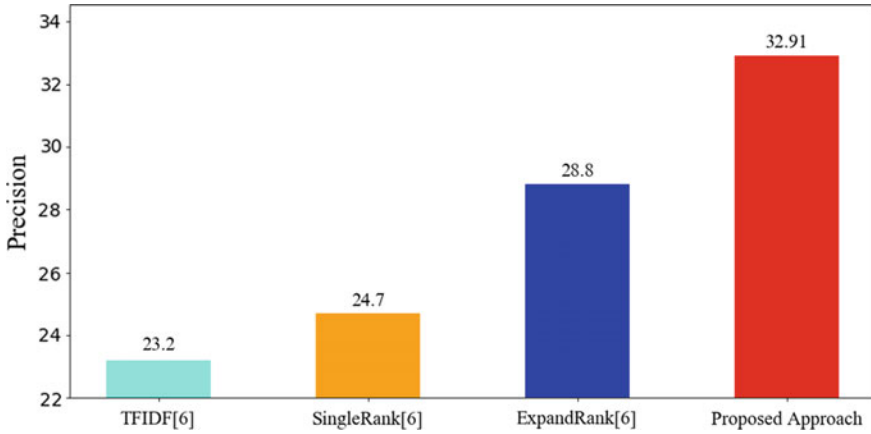


Fig. 4 Comparison of existing and achieved precision values

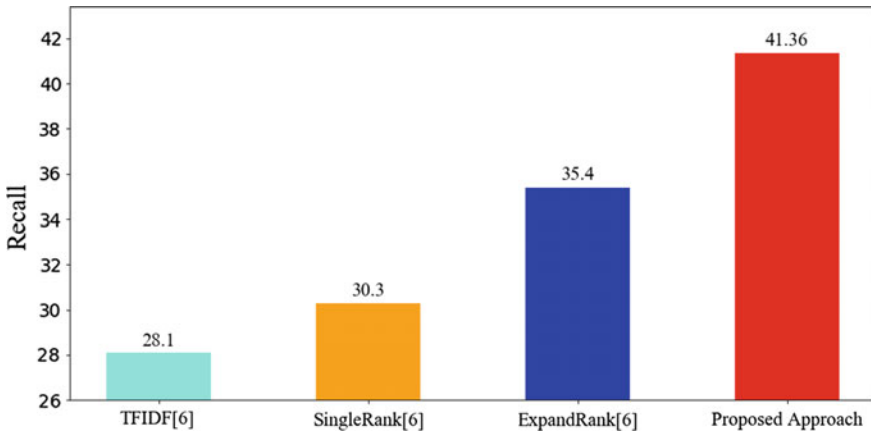


Fig. 5 Comparison of existing and achieved recall values

two classes of the training set greatly affects the precision and recall. Since F-measure is the harmonic mean of precision and recall, it is considered as the ultimate measure of performance. The optimal balance between the two classes yields a promisingly high value of F-measure. We also concluded that part of speech was the most essential feature since it increased the F-measure value to a great extent.

Although the values of F-measure attained are encouraging, there is a scope of improvement by incorporating more features that increase its value. The proposed model can also be extended to include more parts of speech such as adverbs in the regular expression used to extract candidate keyphrases.

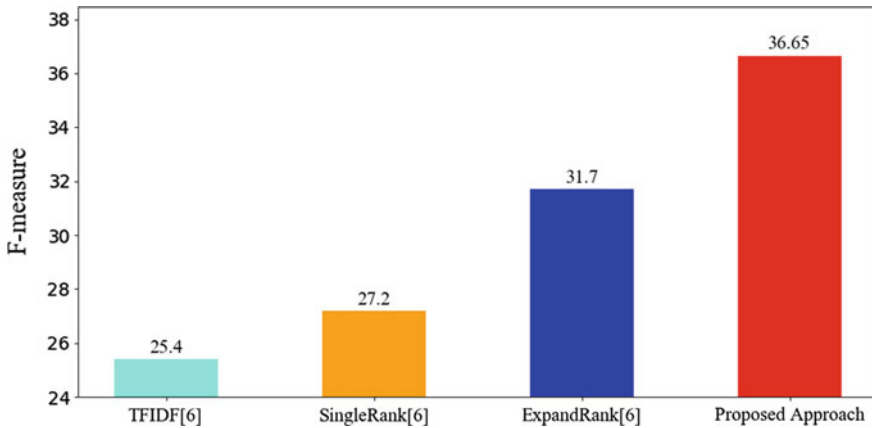


Fig. 6 Comparison of existing and achieved F-measure values

References

1. Turney PD (2000) Learning algorithms for keyphrase extraction. *Inf Retrieval* 2:303–336
2. Witten IH, Paynter GW, Frank E, Gutwin, C, Nevill-Manning CG (1999) KEA: practical automatic keyphrase extraction. In: *Proceedings of the fourth ACM conference on digital libraries (DL 1999)*. ACM, New York, USA, pp 254–255
3. Krulwich B, Burkey C (1996) Learning user information interests through the extraction of semantically significant phrases. In: Hearst M, Hirsh H (eds) *AAAI 1996 spring symposium on machine learning in information access*. AAAI Press, California
4. Mihalcea R, Tarau P (2004) TextRank: bringing order into text. In: *Proceedings of EMNLP 2004*. Association for Computational Linguistics, Barcelona, Spain, pp 404–411
5. Hulth A, Megyesi BB (2006) A study on automatically extracted keywords in text categorization. In: *Proceedings of the 21st international conference on computational linguistics and the 44th annual meeting of the association for computational linguistics (ACL-44)*. Association for Computational Linguistics, Stroudsburg, PA, USA, pp 537–544. <https://doi.org/10.3115/1220175.1220243>
6. Nguyen TD, Kan MY (2007) Keyphrase extraction in scientific publications. In: Goh DHL, Cao TH, Sølvsberg IT, Rasmussen E (eds) *Asian digital libraries. Looking back 10 years and forging new frontiers*. ICADL 2007. Lecture notes in computer science, vol 4822. Springer, Berlin
7. Hofmann K, Tsagkias M, Meij E, Rijke MD (2009) A comparative study of features for keyphrase extraction in scientific literature. In: *Proceedings of the 18th ACM conference on information and knowledge management, Hong Kong, China*
8. Wan X, Xiao J (2008) Single document keyphrase extraction using neighborhood knowledge. In: Cohn A (ed) *Proceedings of the 23rd national conference on artificial intelligence, (AAAI 2008)*, vol 2. AAAI Press, pp 855–860
9. Kathait SS, Tiwari S, Varshney A, Sharma A (2017) Unsupervised key-phrase extraction using noun phrases. *Int J Comput Appl* 162(1)
10. Jasmeen K, Gupta V (2010) Effective approaches for extraction of keywords. *Int J Comput Sci* 7(6):144
11. Campos R, Mangaravite V, Pasquali A, Jorge AM, Nunes C, Jatowt A (2018) A text feature based automatic keyword extraction method for single documents. In: Pasi G et al (eds) *ECIR 2018, LNCS 10772*. Springer, Berlin, pp 684–691

12. Jean-Louis L, Gagnon M, Charton E (2013) A knowledge-base oriented approach for automatic keyword extraction. *Computacion y Sistemas* 17(2):187–196 ISSN 1405-5546
13. Hasan KS, Ng V (2014) Automatic keyphrase extraction: a survey of the state of the art. In: *Proceedings of the 52nd annual meeting of the association for computational linguistics*. Baltimore, Maryland, USA, 23–25 June 2014, pp 1262–1273
14. Campos R, Mangaravite V, Pasquali A, Jorge AM, Nunes C, Jatowt A (2018) A text feature based automatic keyword extraction method for single documents. https://doi.org/10.1007/978-3-319-76941-7_63

Linearity Analysis of Line Tunneling Based TFET for High-Performance RF Applications



Neha Paras and Sudakar Singh Chauhan

Abstract In this work, in-line tunneling based dual metal double gate tunnel FET (DMDG-VTFET) is reported. A silicon epitaxial layer is present between the source and gate so as to align the carrier tunneling parallelly to the gate electric field. This proposed modulation in the design due to the introduction of silicon layer suppresses the parasitic tunneling paths which cause the depreciation of the subthreshold slope (SS). So, with this proposed device, a super-steep SS is achieved. The device parameters which are critical to the device characteristics are optimized such that the high-performance ON state current of 1.2 mA, low OFF state current nearly 3.53 fA and SS of 37 mV/decade are obtained. The reduction in SS of the device creates more room for the device scaling and makes it suitable for low-power and high switching speed applications. The accurate analysis of linearity of the device is also important hence linearity estimation of the device is done by investigating the linearity figures of merit such as VIP3, IMD3, IIP3, 1-dB compression point along with the temperature sensitivity analysis to get insight into the stability of the device in varying temperature environment.

Keywords TFET · Subthreshold slope · Linearity · Line tunneling

1 Introduction

The downscaling of MOSFETs gives benefits such as increased device density, current driving capability and cost savings. This continuous miniaturization introduced several disadvantages such as limited SS, subthreshold leakage and drain induced barrier lowering (DIBL) [1]. Due to the non-scalable SS behavior at room

N. Paras (✉) · S. S. Chauhan
Department of Electronics and Communication Engineering, NIT Kurukshetra, Kurukshetra, India
e-mail: neharao1993@gmail.com

S. S. Chauhan
e-mail: sudakar@nitkkr.ac.in

temperature, MOSFET fails in fulfilling the current low-power applications requirements. The concept of TFETs introduced in 1970s proved the capability of TFETs in providing SS below the thermal limit of 60 mV/dec. in case of MOSFETs which are based on classical mechanism of thermionic emission [2–5]. TFETs surmount the above-mentioned shortcomings by employing quantum tunneling mechanism based on the band to band tunneling (BTBT) of charge carriers. A prominent approach to improve I_{ON} significantly is by using compound semiconductor based TFETs. Various other techniques were proposed by different authors to enhance the functionality of TFETs [6–15]. However, they suffer from processing complexity due to mismatch of band edges, large SS causing high OFF state and ambipolar current [16–18]. An imminent issue in TFETs which still needs to be resolved is simultaneously optimizing the SS and ON to OFF current ratio (I_{ON}/I_{OFF}) owing to difficulty in minimizing the lateral tunneling components and high OFF state current. If with some modifications, the SS can be reduced and ON/OFF state current ratio is increased then high switching speed device can be obtained. So with this purpose, DMDG-VTFET having high- k gate dielectric material is proposed. The proposed device contains a thin silicon epitaxial layer sandwiched between the gate and source. This design increases the vertical tunnel current density and parasitic paths are minimized which helps in achieving a low SS and high ON to OFF current ratio. In addition to this, the metal electrodes present on a source named Tunnel Gate (TG) and drain named Auxiliary Gate (AG) are of different workfunction material so that the ON and OFF state currents can be controlled independently. Energy band profile of proposed device changes with change in tunnel gate workfunction. ON current is increased as the tunneling width is reduced with the help of TG. The AG is used to keep the OFF state current as low as possible.

Moreover, the linearity of a device has become a stringent requirement, especially for RF applications. As the temperature variations have shown to vary the analog as well as DC characteristics of the device, so it becomes important to understand the temperature effect on the linearity characteristics as well. In this work, the impact on the linearity behavior of the proposed device under different temperatures is accessed.

2 Device Description and Simulation Parameters

A 2D cross-sectional view of the silicon n-channel DMDG-VTFET is shown in Fig. 1. The doping concentration of source, channel and drain are: 10^{20} , 10^{16} and 10^{20} cm^{-3} , respectively. Silicon body (T_{si}) and gate oxide thickness (T_{ox}) are 10 and 2 nm. Length of channel (L_{ch}), tunnel gate (L_{tun}), and auxiliary gate length (L_{aux}) are 20, 10, and 20 nm. The work function on TG is 4.0 eV (Hafnium) and the AG is 4.3 eV (molybdenum). The device dimensions and simulation parameters of DMDG-VTFET are tabulated in Table 1. Doping concentration of source is not increased beyond 10^{20} cm^{-3} due to material solubility limits [19]. By optimizing the workfunctions of the dual gates, the ON state current, the OFF state current, and the threshold voltage (V_t) can be simultaneously optimized. The device simulation is

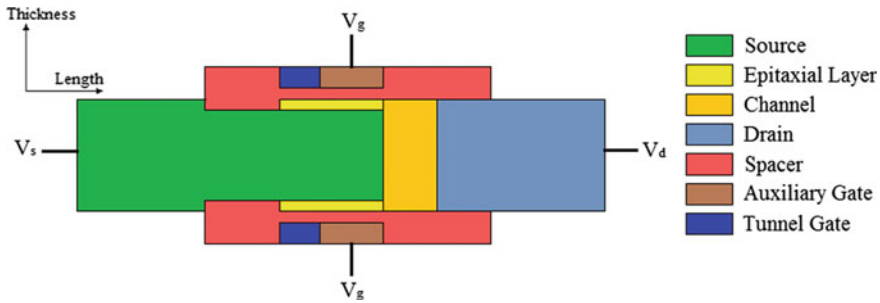


Fig. 1 Device design of DMDG-VTFET

Table 1 Device simulation parameters

Body thickness (T_{si})	10 nm
Epitaxial layer thickness	2 nm
Channel length (L_{ch})	20 nm
Source length (L_s)	80 nm
Drain length (L_d)	50 nm
Left spacer length (L_{ls}) (Source side)	20 nm
Right spacer length (L_{rs}) (Drain side)	40 nm
Tunnel gate length (L_{tg})	10 nm
Auxiliary gate length (L_{ag})	20 nm
Tunnel gate workfunction	4.0 eV
Auxiliary gate workfunction	4.3 eV

carried-out on Sentaurus TCAD 2D device simulator. The model parameters included in the physics section of the simulation were taken so as to include drift-diffusion, SRH recombination, dynamic nonlocal BTBT, Fermi-Dirac statistics, and effective intrinsic density bandgap narrowing [20].

3 Results and Discussion

The band diagram in ON state of the device ($V_{gs} = V_{ds} = 1$ V) and OFF state ($V_{gs} = 0$ V, $V_{ds} = 1$ V) is shown in Fig. 2.

As the V_{gs} is made more positive, the CB and VB of channel are lowered in energy which reduces barrier thickness at source-channel junction. Due to this, carriers get free energy state available to tunnel from source VB to channel CB which turns the device ON.

As seen in Fig. 3, the carrier generation in the proposed device is highly intense at the epi-layer. The tunnel path is orthogonal and below the gate in case of the proposed

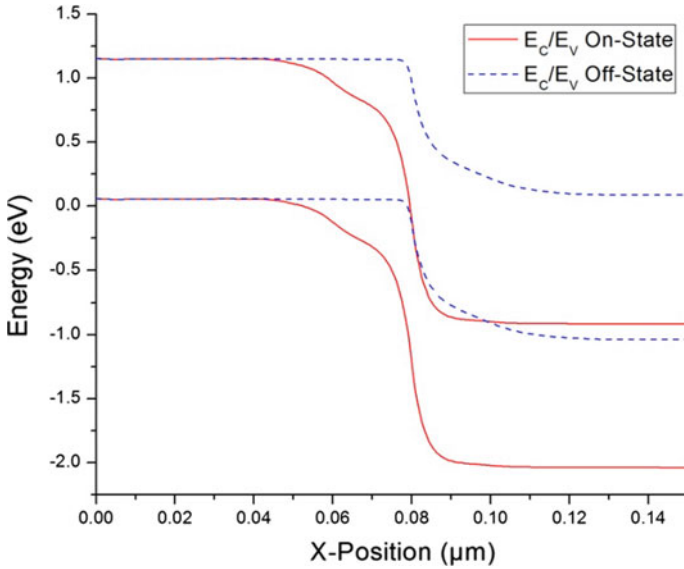


Fig. 2 Energy band diagram of the DMDG-VTFET

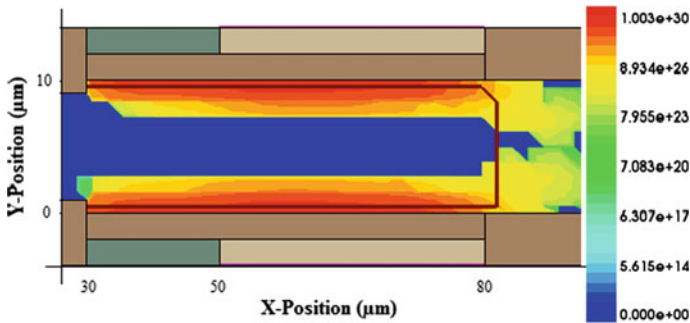


Fig. 3 Carrier generation for DMDG-VTFET

device. Because of this arrangement, the parasitic diagonal tunneling paths which degrade the SS are reduced thus improving the SS of the proposed device.

Figure 4 shows that OFF current varies as the temperature is increased from 250 to 400 K due to an increase in minority carrier concentration as thermally generated carriers are highly dependent on temperature as well as the SRH effect. The ON current does not vary much with a change in temperature due to dependency on BTBT rate which shows that the device has low sensitivity against temperature when in ON state. SS degrades with an increase in temperature due to its dependency on OFF current.

Fig. 4 Transfer characteristics at different temperatures

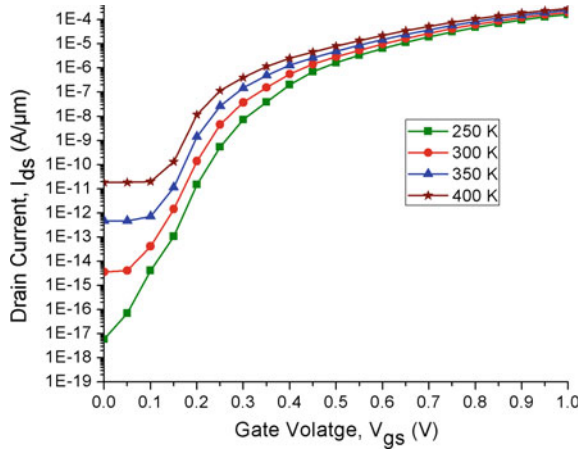


Figure 5 shows the transconductance of the proposed device at varying temperatures. Transconductance is the measure of the device’s potential to amplify the signal that is how well it can convert its input voltage into the current. With an increase in temperature, the peak of transconductance curve also increases signifying improved amplification capability of the device.

In RF applications, linearity becomes the fundamental requirement to ensure distortion-free system at high frequencies. The basic figures of merit to get insight into the linearity of the device are third-order derivative of transconductance (g_{m3}) second-order voltage intercept point (VIP2), third-order voltage intercept point (VIP3), third-order intermodulation intercept point (IIP3), third-order intermodulation distortion (IMD3) and 1-dB compression point which can be defined as below:

Fig. 5 Transconductance versus gate voltage at varying temperature

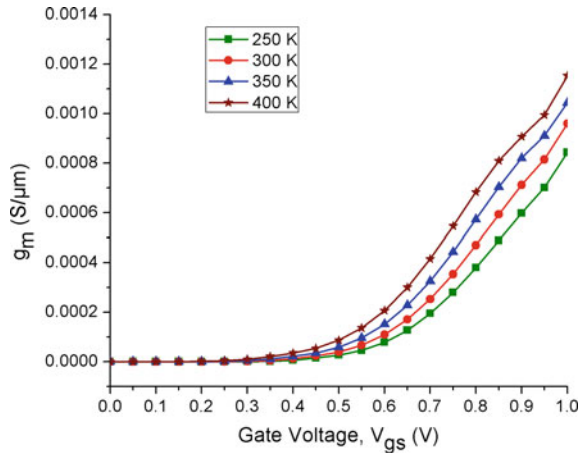
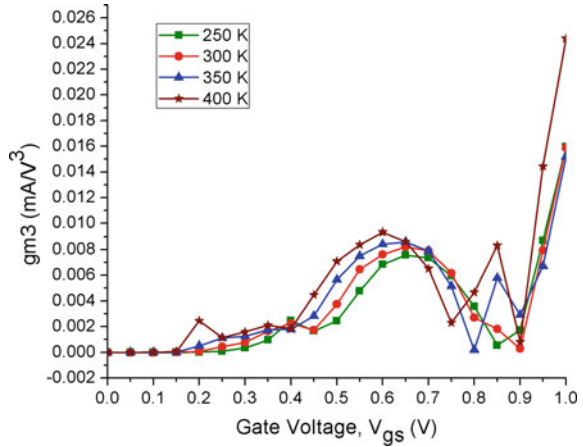


Fig. 6 3rd order transconductance variation with temperature



$$VIP2 = 4 \times \frac{g_{m1}}{g_{m2}} \tag{1}$$

$$VIP3 = \sqrt{24 \times \frac{g_{m1}}{g_{m3}}} \tag{2}$$

$$IIP3 = \frac{2}{3} \times \frac{g_{m1}}{g_{m3} \times R_s} \tag{3}$$

$$IMD3 = R_s [4.5 \times (VIP3^3) \times g_{m3}]^2 \tag{4}$$

$$1\text{-dB} = 0.22 \sqrt{\frac{g_{m1}}{g_{m2}}} \tag{5}$$

where $R_s = 50 \Omega$ is considered to match the internal impedance of antennas.

In Fig. 6, the variation in g_{m3} versus the gate voltage at varying temperatures is presented. g_{m3} is the zero cross-over point for the proposed device. It is observed that peak values of g_{m3} increase with an increase in temperature. This means that higher value of gate voltage will be required to maintain the linearity with an increase in temperature. The first-, second-, and third-order transconductance derivatives majorly control various other linearity parameters of a device.

VIP2/VIP3 represents the extrapolation of input voltage when the first and second/third-order harmonic voltages match. The third-order harmonics are cancelled by the device as the peak point is obtained at higher gate voltage. At higher temperatures, the peak in the VIP3 curve is low because of the dependency on g_{m1}/g_{m3} ratio. g_{m1} and g_{m3} are dominant non-linearity sources. High values of VIP2 and VIP3 are desirable to achieve high linearity and distortion-free system (Figs. 7 and 8).

Fig. 7 2nd order voltage intercept point (VIP2) at different temperatures

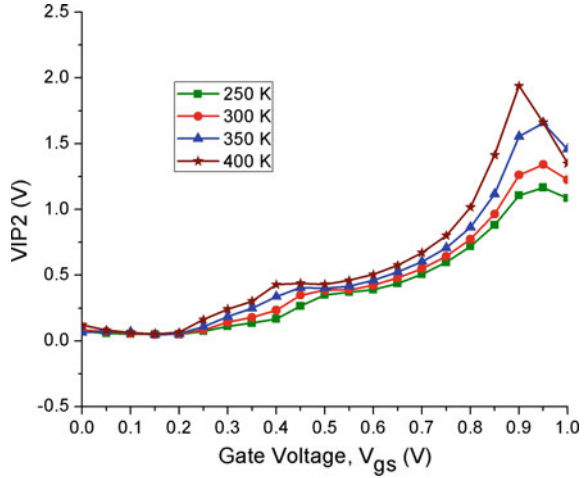
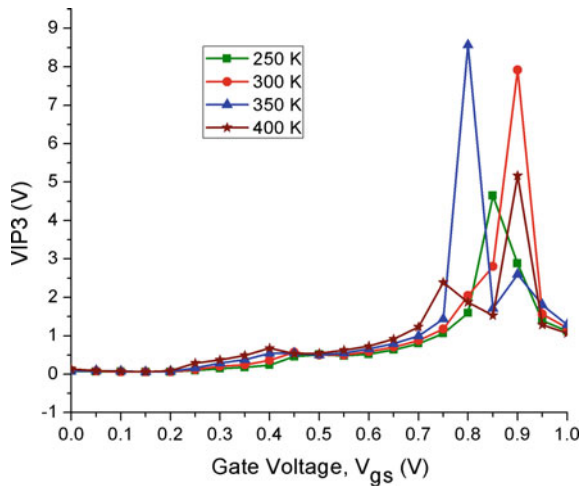


Fig. 8 3rd order voltage intercept point (VIP3) at different temperatures



IIP3 is another important parameter to understand the linearity of the device. When the 1st and 3rd harmonic power match then the extrapolation of input voltage at that point gives IIP3. Higher the value of IIP3, higher will be the linearity. Figure 9 shows the impact of temperature on IIP3 which indicates that IIP3 increases with gate voltage and temperature.

When 1st and 3rd order harmonic power matches then the extrapolation of intermodulation power indicates IMD3 and it should be as low as possible for better linearity. IMD3 depicts the linearity in static characteristics of the device. Figure 10 shows IMD3 characteristics where it is observable that rise of temperature at higher gate voltages does not cause any significant change in IMD3 showing the high linearity property of the device.

Fig. 9 3rd order intermodulation intercept point (IIP3) at different temperatures

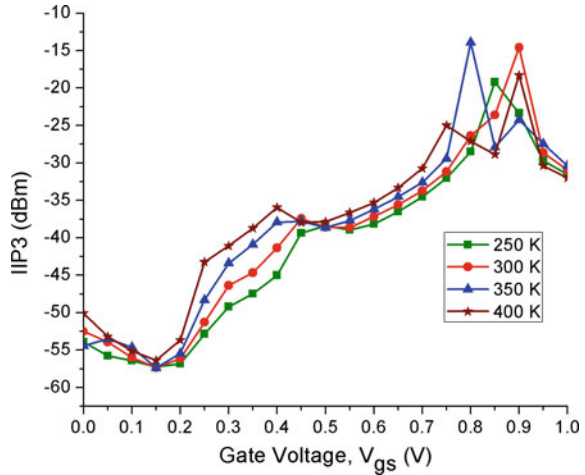
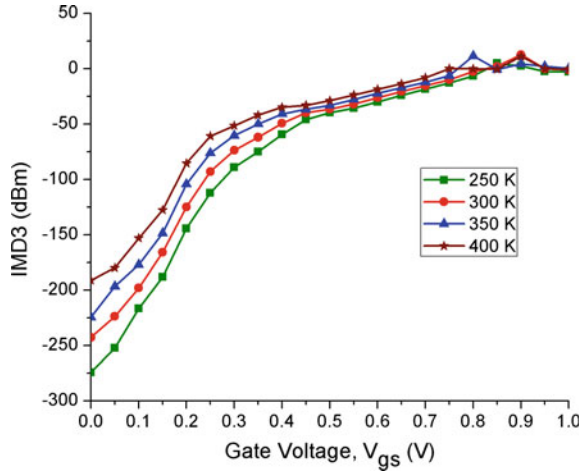
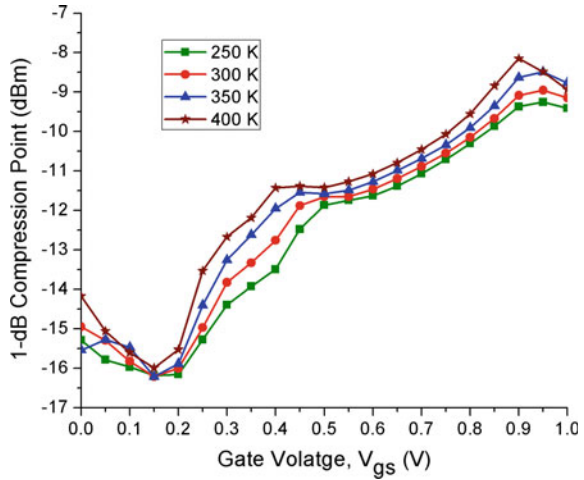


Fig. 10 3rd order intermodulation distortion (IMD3) at different temperatures



1-dB compression point shows the acceptability of device in terms of gain when high distortions are present in the system. The slope in the plot of output versus input gain depicts the gain of any system. The amplifier is said to be in saturation if the slope (gain) becomes flat. Figure 11 shows 1-dB compression point at varying temperatures. The curve shows that 1-dB compression point increases with rise in temperature but variation is very less at higher gate voltages.

Fig. 11 1-dB compression point at different temperatures



4 Conclusions

In this paper, novel DMDG-VTFET has been investigated and the influence of temperature on DC, analog/RF, and linearity is studied. The proposed TFET uses line (vertical) tunneling to achieve excellent I_{ON}/I_{OFF} ratio and SS which improves the switching capability of the device. I_{ON} , I_{OFF} , I_{ON}/I_{OFF} Ratio, transconductance value reported in this work makes the device suitable for prospect low-power applications. Further, the temperature variation is shown to have a significantly low impact on the device behavior when the device is in ON state. Results show that the high gate voltage can significantly reduce the effect of temperature on the device performance with superior linearity characteristics. Therefore, it can be concluded that the proposed device can be used for high switching speed RF applications with high linearity reliably at higher temperatures.

References

1. Ionescu AM, Riel H (2011) Tunnel field effect transistors as energy efficient electronic switches. Nature 479:329–337
2. Rahi SB, Asthana PK, Gupta S (2017) Heterogate junctionless tunnel field-effect transistor: future of low power devices. J Comput Electron 16(1):30–38
3. Paras N, Chauhan SS (2019) Temperature sensitivity analysis of vertical tunneling based dual metal Gate TFET on analog/RF FOMs. Appl Phys A Mater Sci Process 125(5):316
4. Jain P, Yadav C, Agarwal A, Chauhan YS (2017) Surface potential based modeling of charge, current, and capacitances in DGTTFET including mobile channel charge and ambipolar behaviour. Solid State Electron 134:74–81
5. Paras N, Chauhan SS (2019) Vertical tunneling based tunnel field effect transistor with work-function engineered hetero-gate to enhance DC characteristics. J Nanoelectron Optoelectron 14(1):50–53

6. Boucart K, Ionescu AM (2007) Double-gate tunnel FET with high-k gate dielectric. *IEEE Trans Electron Devices* 54(7):1725–1733
7. Colinge JP, Lee CW, Afzalian A, Akhavan ND, Yan R, Ferain I, Razavi P, O’Neill B, Blake A, White M, Kelleher AM, Mc Carthy B, Murphy R (2010) Nanowire transistors without junctions. *Nat Nanotechnol* 5(3):225–229
8. Park CH (2012) Electrical characteristics of 20-nm junctionless Si nanowire transistors. *Solid State Electron* 73:7–10
9. Seema, Chauhan SS (2018) Design of double gate vertical tunnel field effect transistor using HDB and its performance estimation. *Superlattices Microstruct* 117:1–8
10. Kumar MJ, Janardhanan S (2013) Doping-less tunnel field effect transistor: design and investigation. *IEEE Trans Electron Devices* 60(10):3285–3290
11. Wang Y, Zhang WH, Yu CH, Cao F (2016) Sandwich double gate vertical tunneling field-effect transistor. *Superlattices Microstruct* 93:138–143
12. Paras N, Chauhan SS (2019) Insights into the DC, RF/analog linearity performance of vertical tunneling based TFET for low-power applications. *Microelectron Eng* 216:111043
13. Wang X, Cho W, Baac HW, Seo D, Cho IH (2017) Optimization of double gate vertical channel tunneling field effect transistor (DVTFET) with dielectric sidewall. *J Semicond Technol Sci* 17(2):192–198
14. Chauhan SS (2018) A new design approach to improve DC, analog/RF and linearity metrics of Vertical TFET for RFIC design. *Superlattices Microstruct* 122:286–295
15. Rahi SB, Asthana P, Gupta S (2014) A simulation-based proposed high-k heterostructure AlGaAs/Si junctionless n-type tunnel FET. *J Semicond* 35(11):1140051–1140055
16. Narwal S, Chauhan SS (2019) Investigation of RF and linearity performance of electrode work-function engineered HDB vertical TFET. *Micro Nano Lett* 14(1):17–21
17. Li R, Lu Y, Zhou G, Liu Q, Chae SD, Vasen T, Hwang WS, Zhang Q, Fay P, Kosel T, Wistey M (2012) AlGaSb/InAs tunnel field-effect transistor with on-current of 78 $\mu\text{A}/\mu\text{m}$ at 05 V. *IEEE Electron Device Lett* 33(3):363–365
18. Lu Y, Zhou G, Li R, Liu Q, Zhang Q, Vasen T, Chae SD, Kosel T, Wistey M, Xing H, Seabaugh A, Fay P (2012) Performance of AlGaSb/InAs TFETs with gate electric field and tunneling direction aligned. *IEEE Electron Device Lett* 33(5):655–657
19. Schmid H, Bjrk MT, Knoch J, Karg S, Riel H, Riess W (2009) Doping limits of grown in situ doped silicon nanowires using phosphine. *Nano Lett* 5(4):820–826
20. Sentaurus Device User Guide. Synopsys Inc., Mountain View (2013)

Selection of Optimal Renewable Energy Resources Using TOPSIS-Z Methodology



Nisha Rathore, Kumar Debasis, and M. P. Singh

Abstract An innovation of Renewable Energy (RE) sources promises to bring down costs and starts to deliver a clean energy future without compromising reliability. Renewable energy resource selection comes under the domain of multi-criteria decision making (MCDM) problem as it includes multi-conflicting criteria, namely social, technological, environmental, economic, and political. MCDM methodologies are used in order to select preferred alternative resources because of the presence of complexities in energy planning and energy projects. This paper presents an integrated TOPSIS-Z MCDM method for the selection of optimal RE. The pairwise decision matrix is formed by the decision-makers (DM), which is represented in the Z-number, and weights are evaluated. TOPSIS is used to evaluate and rank suitable RE sources. To validate the efficacy of the proposed methodology, Spearman's Rank Correlation Coefficient (SRCC) is used and the proposed methodology is compared with various other MCDM methods such as ARAS, VIKOR, and COPRAS.

Keywords Renewable energy selection · MCDM tools · TFNs · Z-number · TOPSIS method

1 Introduction

The expeditious economic development and rising population lead to high demand for energy so energy becomes an essential part of the economic infrastructure. People's living standard is also enhanced by growing industrialization over the entire world

N. Rathore · K. Debasis (✉) · M. P. Singh
Department of Computer Science and Engineering, National Institute of Technology Patna, Patna,
Bihar 800005, India
e-mail: debasis.cse14@nitp.ac.in

N. Rathore
e-mail: nisha.rathor271@gmail.com

M. P. Singh
e-mail: mpps@nitp.ac.in

which leads to the growth of global demand for energy at an astonishing rate. The increasing demand for energy has been broadly met by fossil fuels—coal, mineral oil, and natural gases. The primary energy resources also lead to the emission of greenhouse gases, require high-maintenance, expensive in nature, and high preservation cost. Due to these issues, promoting a substitute for energy sources is demanding. One prominent category of alternative energy sources developed by scientists is non-primary sources of energy.

India fixed a goal in the Paris Agreement to achieve 40% of its total generated electricity that will be produced from RE sources by 2030 [1, 2]. Central Electricity Authority drafted a blueprint that 57% (275 GW) of the total generated electricity capacity will be produced from RE sources by 2027 [3]. In order to make a fruitful transformation from non-conventional resources to RE sources, thoughtful decision, careful energy planning, and optimal selection among a pool of alternative RE sources are required. The selection of RE is an MCDM problem as it incorporates various multiple-conflicting criteria that involve social, economic, political, technical, and environmental. MCDM techniques are effective methods to evaluate and prioritize the RE sources and finally select the most preferred alternative among available and feasible alternatives.

2 Literature Review

Numerous research works have already been done on MCDM approaches, implementing them in distinct fields of discipline such as supplier selection problem, renewable energy project selection, and various other alternative selection problems. San Cristóbal [4] proposed a methodology which is a combination of AHP and VIKOR method used to rank the alternatives among the various renewable energy resources in Spain. Abdolreza et al. [5] proposed an integrated methodology which is a combined form of AHP and COPRAS methodology to obtain the most preferred sustainable energy resource. Demirtas [6] and many other researchers [7, 8] used an AHP to select the best (most preferred) RE resource in the presence of various tangible and intangible criteria. Ali Zangeneh et al. [9] used an AHP methodology as an evaluation model for the prioritization and analysis of distributed generation (DG) automation in which renewable, as well as elementary sources based technologies, are considered in order to fulfill the rising demand for energy in Iran at the same time taking into account the issue of sustainable development.

But the prominent property of the MCDM problems is the involvement of uncertainty and vagueness in the sentiment of decision-makers, so to handle the uncertainty in the human's judgment; the concept of the fuzzy number and fuzzy set is used. The main limitation of Conventional AHP is that scores are given in the form of precise or crisp value which does not include the uncertainty and imprecise behavior of real-world selection problems so final ranking provided by original AHP may be erroneous because this method is unable to consider all the aspects of the problem. Turskis et al. [10] proposed ARAS methodology integrated with a fuzzy concept

to obtain a suitable site among a pool of alternatives for the logistics center. Wang et al. [11] performed an extent analysis principle on the fuzzy AHP and describes the application of FAHP. Heo et al. [12] presented a FAHP model with modified EA for the evaluation of various RE alternatives for the dissemination program. Tasri et al. [13] proposed fuzzy AHP in order to select the best resource among the available renewable energy resources in Indonesia. Wang et al. [14] presented an integrated FAHP-TOPSIS methodology for site selection in Vietnam to construct wind power plants for the generation of electricity.

Fuzzy numbers are able to handle the impression involved in the decisions, but it is incapable to include the certainty degree of information. So, Zadeh [15] proposed the Z-number concept to overcome the limitation of fuzzy numbers. Fuzzy numbers (restriction evaluation) with a degree of self-confidence (reliability of the judgment) are termed as Z-number which has more capability to express human thought appropriately as compared to fuzzy numbers. Kang et al. [16] proposed an MCDM methodology for the analysis of supplier selection problem using Z-number. This method is divided into two parts: first, Z-number is converted into fuzzy numbers using fuzzy expectation and then weights of the criteria for the supplier selection problem are evaluated using a genetic algorithm (GA). Chatterjee [17] proposes an integrated COPRAS-Z methodology to select the most preferred RE resources for India. Even though the concept of Z-number is successfully applied in various disciplines to solve complicated MCDM problems, but the application of Z-number in the field of selection of optimal RE resources is little and limited.

This paper proposes an integrated TOPSIS-Z methodology to find the optimal RE resource among various alternatives. Criteria are compared by decision-makers in the fuzzy environment using linguistic terms represented in Z-numbers which are needed to evaluate the weights of the criteria, then TOPSIS methodology is practiced to evaluate and prioritize the suitable alternative resources based on the relative closeness to the ideal solution value. To certify the capability and effectiveness of the proposed methodology, the method is compared with other MCDM methodologies such as ARAS, VIKOR, and COPRAS using Spearman's rank correlation coefficient.

3 Preliminaries

Definition 1: Triangular Fuzzy Number (TFN)

Fuzzy set theory was first introduced by Zadeh (1965) [14]. TFNs are more suitable to represent the expert's opinion as it is a set of three values (m_1, m_2, m_3) indicating the lowest, the most probable, and the greatest value $(m_1 \leq m_2 \leq m_3)$. The membership value of a TFN $\tilde{E} = (m_1, m_2, m_3)$ can be determined as:

$$\mu_{\tilde{E}}(x) = \begin{cases} 0, & x < m_1 \\ \frac{x-m_1}{m_2-m_1}, & m_1 \leq x \leq m_2 \\ \frac{m_3-x}{m_3-m_2}, & m_2 \leq x \leq m_3 \\ 0, & x \geq m_3 \end{cases} \quad (1)$$

Definition 2: Z-Number Concept [15] Zadeh introduced the concept of Z-number [15] to increase the reliability of real-world information by considering the degree of self-confidence along with the fuzzy numbers. It is defined as an ordered pair of fuzzy numbers: $Z = (\tilde{A}, \tilde{R})$ which determines the restriction value (\tilde{A}) of any real variable “X” and the measure of reliability (\tilde{R}) of fuzzy number \tilde{A} .

4 Proposed Methodology

An integrated TOPSIS-Z methodology is proposed to evaluate both the qualitative and quantitative criteria to retrieve their weights and then assess the alternatives to prioritize all the available alternatives and finally to get the most preferred alternative. The proposed methodology is divided into three main steps as shown in Fig. 1.

The proposed methodology comprises of three steps as follows:

Step 1: Identification of Criteria and Alternatives

This step determines the evaluation criteria and all the available RE resources that will be used in the process of decision-making and organize the decision hierarchy of criteria and alternatives along with their goal.

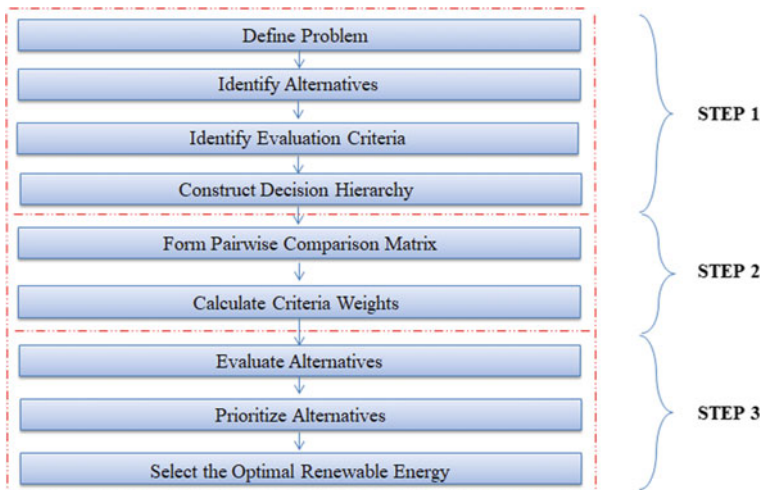


Fig. 1 Diagrammatic representation of the proposed methodology

Table 1 Linguistic terms of fuzzy restrictions and its reliability along with their TFN values

Fuzzy restrictions value			Fuzzy reliability	
Saaty scale	Definition	TFN scale	Definition	TFN scale
1	Equally important	(1, 1, 1)	Slightly Sure (SS)	(0.1, 0.1, 0.5)
3	Weakly important	(2, 3, 4)	Sure (S)	(0.1, 0.5, 0.8)
5	Fairly important	(4, 5, 6)	Very Sure (VS)	(0.5, 0.7, 1)
7	Strongly important	(6, 7, 8)	Extremely Sure (ES)	(0.7, 1, 1)
9	Absolutely important	(9, 9, 9)	(ES)	
2	The intermittent values between two adjacent scales	(1, 2, 3)		
4		(3, 4, 5)		
6		(5, 6, 7)		
8		(7, 8, 9)		

Step 2: Determining the Weights of the Criteria

- i. This step obtains the weights of evaluation criteria. Linguistic terms are used by the decision-maker to establish the pairwise comparison matrix in which each value is represented in Z-number. The codebook of related fuzzy restrictions [14] and its reliabilities for the criteria are shown in Table 1. The value of fuzzy restrictions and its reliability measures are expressed in the TFNs and to obtain the pairwise comparison information matrix of Z-numbers, $Y = [Z_{ij}]_{m \times m}$, where “m” is the number of criteria and “ Z_{ij} ” represents the estimated value of criterion “i” in criterion “j”, decision-maker has taken the corresponding value from this codebook.
 - ii. Fuzzy expectation concept is used to convert the Z-number present in the pairwise comparison matrix into fuzzy numbers to get the fuzzy pairwise decision matrix [18]. Initially, the centroid method is applied to convert the reliability part of a Z-number into a crisp value then weighted Z-number is evaluated by adding the weight of the reliability to the constraint \tilde{A} and finally irregular fuzzy number is transformed into regular FN.
 - iii. Normalize the pairwise fuzzy decision matrix to scale each criterion value in the equivalent measurement range as different criteria are represented in different units.
- Apply fuzzy arithmetic operations to sum up each row of the fuzzy comparison matrix [11] $\hat{Y} = (\tilde{y}_{ij})_{m \times m}$, where $\tilde{y}_{ij} = (m_{1ij}, m_{2ij}, m_{3ij})$, $\tilde{y}_{ij}^{-1} = (\frac{1}{m_{3ij}}, \frac{1}{m_{2ij}}, \frac{1}{m_{1ij}})$ for $i, j = 1, \dots, m$ & $i \neq j$.

$$V_i = \sum_{j=1}^m \tilde{y}_{ij} = \left(\sum_{j=1}^m m_{1ij}, \sum_{j=1}^m m_{2ij}, \sum_{j=1}^m m_{3ij} \right), \quad i = 1, \dots, m \quad (2)$$

- Normalize the above rows to get the fuzzy weights of the criteria [11].

$$= \left(\frac{\sum_{j=1}^m m_{1ij}}{\sum_{j=1}^m m_{1ij} + \sum_{k=1, k \neq i}^m \sum_{j=1}^m m_{3kj}}, \frac{\hat{W}_i = \frac{V_i}{\sum_{j=1}^m V_j}}{\sum_{j=1}^m m_{2ij}}, \frac{\sum_{j=1}^m m_{3ij}}{\sum_{j=1}^m m_{3ij} + \sum_{k=1, k \neq i}^m \sum_{j=1}^m m_{1kj}} \right) \tag{3}$$

where $i = 1, \dots, m$.

- iv. Apply the center of the area method to obtain the weights in crisp by defuzzifying the fuzzy weights [13].

$$\hat{W}_i = (m_{1i} + m_{2i} + m_{3i})/3, \quad i = 1, \dots, m. \tag{4}$$

The weights of the criteria in vector form is $W^T = [w_1, w_2, w_3, \dots, w_m]$.

Step 3: Assessment of Alternative Energies with TOPSIS

TOPSIS [19] method is used to evaluate and prioritize the available alternative energy resources. Alternatives are prioritized based on the relative closeness value C_i derived by the TOPSIS method. In this method, first positive ideal solution (PIS) and negative ideal solution (NIS) is calculated and then the distance of each alternative with the PIS and the NIS is determined. The basic concept of the TOPSIS method is a chosen (most preferred) alternative must have the shortest distance with the PIS and longest distance with the NIS which is determined with the help of relative closeness value. Relative closeness values decide the complex comparative capability of the viable alternatives which is directly proportional to the preference values of alternatives and weights of the criteria examined in the problem. RE resource having a higher value of relative closeness C_i is the best one.

5 Implementation

The proposed methodology is applied to the Cristobal data [4]. Cristobal uses this data to evaluate the available alternative resources with the help of the VIKOR method. The proposed TOPSIS-Z methodology is implemented in the following three steps:

Step 1: Implementation of the proposed method uses two categories of criteria namely benefit criteria and cost criteria. Benefit criteria are Power (C_{R1}) in kilowatt, Operating Hours (C_{R4}) in hours/year, useful life (C_{R5}) in years, and tons of emissions of CO₂ avoided/year (C_{R7}) in tCO₂/y. Cost criteria are Implementation Period (C_{R3}) in years, Investment Ratio (C_{R2}) in €/kilowatt, Operating and Maintaining Costs (C_{R6}) in $\text{€} \times 10^{-3}$ kilowatt hour.

Table 2 Preferred value of alternatives with respect to each criterion

Optimization direction	C_{R1}	C_{R2}	C_{R3}	C_{R4}	C_{R5}	C_{R6}	C_{R7}
	MAX _m	MIN _m	MIN _m	MAX _m	MAX _m	MIN _m	MAX _m
R_{S1}	5000	937	1	2350	20	1,470	1,929,936
R_{S2}	10,000	937	1	2350	20	1,470	3,216,560
R_{S3}	25,000	937	1	2350	20	1,510	9,649,680
R_{S4}	5000	1500	1.5	3100	25	1,450	472,812
R_{S5}	20,000	700	2	2000	25	0,700	255,490
R_{S6}	35,000	601	2.5	2000	25	0,600	255,490
R_{S7}	50,000	5000	2	2596	25	4,200	482,856
R_{S8}	5000	1803	1	7500	15	7,106	2,524,643
R_{S9}	5000	1803	1	7500	15	5,425	2,524,643
R_{S10}	5000	1803	1	7500	15	5,425	2,524,643
R_{S11}	5000	1803	1	7500	15	2,813	2,524,643
R_{S12}	56,000	856	1	7500	20	4,560	4,839,548
R_{S13}	2000	1503	1.5	7000	20	2,512	5,905,270

This paper considers 13 alternative RE projects which are: Wind power $P \leq 5$ MW (R_{S1}), Wind power $5 \leq P \leq 10$ MW (R_{S2}), Wind power $10 \leq P \leq 50$ MW (R_{S3}), Hydroelectric $P \leq 10$ MW (R_{S4}), Hydroelectric $10 \leq P \leq 25$ MW (R_{S5}), Hydroelectric $25 \leq P \leq 50$ MW (R_{S6}), Solar Thermo-electric $P \geq 10$ MW (R_{S7}), Biomass (energetic cultivation) $P \leq 5$ MW (R_{S8}), Biomass (forest and agricultural wastes) $P \leq 5$ MW (R_{S9}), Biomass (farming industrial wastes) $P \leq 5$ MW (R_{S10}), Biomass (forest industrial wastes) $P \leq 5$ MW (R_{S11}), Biomass (co-combustion in conventional central) $P \leq 5$ MW (R_{S12}), and Biofuels $P \leq 2$ MW (R_{S13}). Table 2 shows the preference value of alternatives with respect to each criterion. The decision hierarchy of criteria and alternatives along with its goal is shown in Fig. 2.

Step 2: Using Table 1, the paper defines a pairwise decision matrix as shown in Table 3. To calculate the relative importance of weights first, Z-number is transformed into TFNs by applying a fuzzy expectation concept to obtain a fuzzy decision matrix. Further, normalization of a Triangular Fuzzy decision matrix is done using Eqs. 2 and 3 and fuzzy weights are obtained then fuzzy weights are defuzzified using Eq. 4 in order to get the crisp weights and finally, priority weight vector $W = [0.307, 0.113, 0.025, 0.149, 0.161, 0.061, 0.202]$ is retrieved. Power (0.307) is the most important and implementation period (0.025) is the least important criterion in the optimal RE selection.

Step 3: TOPSIS method is applied in Table 2 and available alternative RE sources are evaluated. The normalized weighted decision matrix and the value of Q_i^+ , Q_i^- , and C_i are measured as shown in Table 4. In the last column of Table 4, the final rank of alternative RE is recorded. According to the relative closeness value C_i , the most preferred RE resource is R_{S12} .

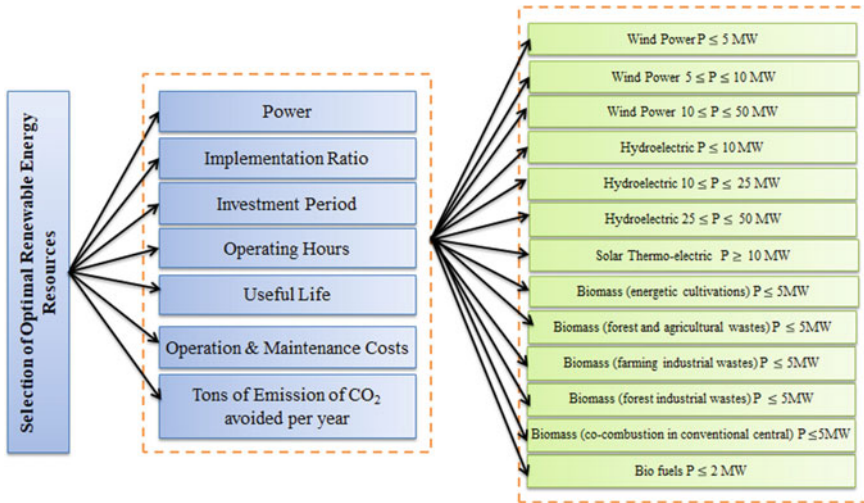


Fig. 2 A hierarchical structure of criteria and alternatives

6 Result Analysis

To justify the efficiency and efficacy of the proposed methodology that is TOPSIS-Z, evaluation and the performance ranking of feasible thirteen RE sources are done using relative closeness value and proposed methodology is compared by different MCDM methods namely ARAS, VIKOR, and COPRAS as shown in Table 5 using Spearman’s rank correlation coefficient (SRCC) [5]. The SRCC between the final ranking (Avg of each row) and the TOPSIS-Z, ARAS, VIKOR, COPRAS methods are 0.994, 0.994, 0.958, 0.994, respectively. As ARAS and COPRAS, the proposed method has a high SRCC value that is 0.994, hence validating the effectiveness and capability of the proposed method.

7 Conclusion and Future Scope

Different RE sources have relative merits and demerits and also the presence of multiple-conflicting criteria made the problem of selection of feasible RE sources complicated and sophisticated. This paper proposes an integrated (TOPSIS-Z) MCDM method for the selection of optimal RE. The uncertainty is ubiquitous in the real-world decision problems, so to handle the uncertainty, reliability is considered along with the TFN value to form the pairwise decision matrix, and weights are evaluated. TOPSIS is used to rank the available RE sources. To validate the efficacy of the proposed method SRCC is used. The proposed method that is TOPSIS-Z which handles the uncertainty by considering the reliability is compared with various

Table 3 Formation of pairwise decision matrix using Z-number

	C_{R1}	C_{R2}	C_{R3}	C_{R4}	C_{R5}	C_{R6}	C_{R7}
C_{R1}	[1, 1, 1], ES	[4, 5, 6], S	[9, 9, 9], S	[2, 3, 4], S	[4, 5, 6], S	[6, 7, 8], VS	[1, 1, 1], ES
C_{R2}	[1/6, 1/5, 1/4], S	[1, 1, 1], ES	[4, 5, 6], SS	[1/4, 1/3, 1/2], SS	[1/4, 1/3, 1/2], SS	[4, 5, 6], VS	[1/4, 1/3, 1/2], SS
C_{R3}	[1/9, 1/9, 1/9], S	[1/6, 1/5, 1/4], SS	[1, 1, 1], ES	[1/6, 1/5, 1/4], ES	[1/8, 1/7, 1/6], SS	[1/4, 1/3, 1/2], VS	[1/6, 1/5, 1/4], VS
C_{R4}	[1/4, 1/3, 1/2], S	[2, 3, 4], SS	[4, 5, 6], ES	[1, 1, 1], ES	[1, 1, 1], ES	[2, 3, 4], VS	[1/6, 1/5, 1/4], SS
C_{R5}	[1/6, 1/5, 1/4], S	[2, 3, 4], SS	[6, 7, 8], SS	[1, 1, 1], ES	[1, 1, 1], ES	[4, 5, 6], ES	[1/4, 1/3, 1/2], VS
C_{R6}	[1/8, 1/7, 1/6], VS	[1/6, 1/5, 1/4], VS	[2, 3, 4], VS	[1/4, 1/3, 1/2], VS	[1/6, 1/5, 1/4], ES	[1, 1, 1], ES	[1/6, 1/5, 1/4], SS
C_{R7}	[1, 1, 1], ES	[2, 3, 4], SS	[4, 5, 6], VS	[4, 5, 6], SS	[2, 3, 4], VS	[4, 5, 6], SS	[1, 1, 1], ES

Table 4 Outcome of analysis

	C_{R1}	C_{R2}	C_{R3}	C_{R4}	C_{R5}	C_{R6}	C_{R7}	Q_i^+	Q_i^-	C_i	R
R_{S1}	0.017	0.015	0.004	0.018	0.044	0.006	0.028	0.211	0.078	0.269	12
R_{S2}	0.034	0.015	0.004	0.018	0.044	0.006	0.047	0.187	0.089	0.323	7
R_{S3}	0.085	0.015	0.004	0.018	0.044	0.007	0.141	0.113	0.174	0.605	2
R_{S4}	0.017	0.024	0.007	0.024	0.055	0.006	0.006	0.222	0.069	0.236	13
R_{S5}	0.068	0.011	0.009	0.015	0.055	0.003	0.003	0.189	0.101	0.348	6
R_{S6}	0.119	0.009	0.012	0.015	0.055	0.002	0.003	0.161	0.139	0.463	4
R_{S7}	0.170	0.082	0.009	0.020	0.055	0.019	0.007	0.159	0.165	0.508	3
R_{S8}	0.017	0.029	0.004	0.058	0.033	0.033	0.037	0.207	0.076	0.270	11
R_{S9}	0.017	0.029	0.004	0.058	0.033	0.025	0.037	0.206	0.077	0.272	9
R_{S10}	0.017	0.029	0.004	0.058	0.033	0.025	0.037	0.206	0.077	0.272	9
R_{S11}	0.017	0.029	0.004	0.058	0.033	0.013	0.037	0.205	0.079	0.279	8
R_{S12}	0.190	0.014	0.004	0.058	0.044	0.021	0.070	0.073	0.212	0.742	1
R_{S13}	0.006	0.024	0.007	0.054	0.044	0.011	0.086	0.193	0.111	0.365	5

Table 5 Performance ranking obtained by using different MCDM methods

Different methodologies									
	ARAS		COPRAS		VIKOR		TOPSIS-Z		Final Rank
	Value	Rank	Value	Rank	Value	Rank	Value	Rank	
R_{S1}	0.051	12	35.20	12	0.951	13	0.270	12	12.25
R_{S2}	0.067	6	46.14	6	0.798	6	0.323	7	6.25
R_{S3}	0.135	2	91.43	2	0.262	2	0.606	2	2
R_{S4}	0.040	13	27.25	13	0.929	9	0.236	13	12
R_{S5}	0.067	7	42.86	7	0.775	5	0.348	6	6.25
R_{S6}	0.091	4	56.46	4	0.688	4	0.463	4	4
R_{S7}	0.095	3	63.42	3	0.666	3	0.508	3	3
R_{S8}	0.054	11	36.32	11	0.946	12	0.271	11	11.25
R_{S9}	0.055	9	36.88	9	0.935	10	0.273	9	9.25
R_{S10}	0.055	9	36.88	9	0.935	10	0.273	9	9.25
R_{S11}	0.056	8	38.08	8	0.917	8	0.279	8	8
R_{S12}	0.151	1	100.0	1	0.000	1	0.742	1	1
R_{S13}	0.079	5	53.40	5	0.823	7	0.365	5	5.5

other MCDM namely ARAS, VIKOR, COPRAS methods which don't consider the uncertainty involved in the decision-making process.

In the proposed methodology, to handle the uncertainty involved in the decisions made by the decision-maker, the Z-number concept is used which has more capacity to define the knowledge of human beings. Note that for the real applications, the idea

of Z-number has not been appraised. Hence, there is a need to transpose Z-number to a classic FN due to which there might be a possibility that some data will be lost. The comparison of different Z-number is an important and open issue, which is also an elementary issue to extend the applications of Z-number. So, in the future, a better or more significant method can be developed to deal with Z-number to further reduce the loss of data that is happening during Z-number conversion.

References

1. Kadian SK, Kesari JP, Mishra RS (2018) Hydraulic analysis and modelling of small hydro power: a case study of a plant at Gogripur, Karnal
2. Zhang W, Pan X (2016) Study on the demand of climate finance for developing countries based on submitted INDC. *Adv Clim Change Res* 7(1–2):99–104
3. Safi M (2016) India plans nearly 60% of electricity capacity from non-fossil fuels by 2027. *The Guardian*
4. San Cristóbal JR (2011) Multi-criteria decision-making in the selection of a renewable energy project in Spain: The Vikor method. *Renew Energy* 36(2):498–502
5. Yazdani-Chamzini A, Fouladgar MM, Zavadskas EK, Moini SHH (2013) Selecting the optimal renewable energy using multi criteria decision making. *J Bus Econ Manag* 14(5):957–978
6. Demirtas O (2013) Evaluating the best renewable energy technology for sustainable energy planning. *Int J Energy Econ Policy* 3(S):23–33
7. Amer M, Daim TU (2011) Selection of renewable energy technologies for a developing county: a case of Pakistan. *Energy Sustain Dev* 15(4):420–435
8. Wimpler C, Hejazi G, Fernandes EDO, Moreira C, Connors S (2015). Multi-criteria decision support methods for renewable energy systems on islands
9. Zangeneh A, Jadid S, Rahimi-Kian A (2009) A hierarchical decision making model for the prioritization of distributed generation technologies: a case study for Iran. *Energy Policy* 37(12):5752–5763
10. Turskis Z, Zavadskas EK (2010) A new fuzzy additive ratio assessment method (ARAS-F). Case study: The analysis of fuzzy multiple criteria in order to select the logistic center location. *Transport* 25(4):423–432
11. Wang YM, Luo Y, Hua Z (2008) On the extent analysis method for fuzzy AHP and its applications. *Eur J Oper Res* 186(2):735–747
12. Heo E, Kim J, Boo KJ (2010) Analysis of the assessment factors for renewable energy dissemination program evaluation using fuzzy AHP. *Renew Sustain Energy Rev* 14(8):2214–2220
13. Tasri A, Susilawati A (2014) Selection among renewable energy alternatives based on a fuzzy analytic hierarchy process in Indonesia. *Sustain Energy Technol Assessments* 7:34–44
14. Wang CN, Huang YF, Chai YC, Nguyen V (2018) A multi-criteria decision making (MCDM) for renewable energy plants location selection in Vietnam under a fuzzy environment. *Appl Sci* 8(11):2069
15. Zadeh LA (2011) A note on Z-numbers. *Inf Sci* 181(14):2923–2932
16. Kang B, Hu Y, Deng Y, Zhou D (2016) A new methodology of multicriteria decision-making in supplier selection based on-numbers. *Mathematical Problems in Engineering*, 2016
17. Chatterjee K, Kar S (2018) A multi-criteria decision making for renewable energy selection using Z-numbers in an uncertain environment. *Technol Econ Dev Econ* 24(2):739–764
18. Kang B, Wei D, Li Y, Deng Y (2012) A method of converting Z-number to classical fuzzy number. *J Inf Comput Sci* 9(3):703–709
19. Jadidi O, Firouzi F, Bagliery E (2010) TOPSIS method for supplier selection problem. *World Acad Sci Eng Technol* 47(11):956–958

Routing Algorithms for Hybrid Nodes in WSNs



Isha Pant and Shashi Kant Verma

Abstract The prominent criteria for the Wireless Sensor Network are a lifetime of the network, stability, and the energy parameter. To enhance these crucial parameters, the paper introduces Routing Algorithms for hybrid nodes in sensor networks ‘RA-HNW’ protocol having four forms of sensor nodes varying in energy and capacities to improve the stability and lifespan of the sensor networks. The simulations for the proposed RA-HNW is simulated in MATLAB 2018b. It is observed that using the functionalities and capabilities of the different types of nodes taken in the work, the stability of the proposed schema increases by 49.12% as compared to the DCHRP4, twice and thrice as compared to ETSSEP, TSEP, and SEP. The lifetime criteria also upgrade by 10.49% over DCHRP4 with level four heterogeneity, 15.85% over DCHRP, 19.65% over ETSSEP, and about 64.87% over TSEP. The proposed RA-HNW methodology is well suited for working in the fixed sink environment.

Keywords Heterogeneity · Routing techniques · Lifespan · Sensor networks

1 Introduction

Wireless sensor network addresses the use of sensors, more specifically the wirelessly connected form of sensors following a mechanism of one-time deployment. The area of WSN allows one the real-time aspect of monitoring of the physical sensing domains such as intelligent transport, healthcare, environmental aspects, and many more. WSN field works as a channel whose work is to connect the real world traits to the digital world. The general work of these networks is to pull together desired information from the subjected environment and convey that sensed data to the conducting unit known as the sink [1]. For using the capabilities of these network types in general

I. Pant (✉) · S. K. Verma
Department of Computer Science, GB Pant Institute of Engineering & Technology,
Pauri-Garhwal, India
e-mail: kkavyapant97@gmail.com

S. K. Verma
e-mail: skverma.gbpec@rediffmail.com

© Springer Nature Singapore Pte Ltd. 2021
G. S. Hura et al. (eds.), *Advances in Communication and Computational Technology*, Lecture Notes in Electrical Engineering 668,
https://doi.org/10.1007/978-981-15-5341-7_74

scenarios, designing protocols that can work upon different conditions is necessary. The aim for designing of a WSN protocol is to improve the common parameters such as increasing the total lifespan of the network, deploying of sensors in such a way that can increase the stability period criteria. The time when the first sensor node type dies in the sensor network is called its stability period in WSN. For the betterment of these parameters, clustering is the general approach being used. The process of clustering involves the assemblage of sensor nodes altogether into various clusters each having a leader, performing the operations of data transfer called as the cluster head. Main levels of performing clustering involve cluster creation, selection of CH, transferring of information to a central station [2]. Nodes other than the leader node are termed as the member node of the cluster. Homogeneous and Heterogeneous are the basic clustering methods, the former is associated with nodes having the same type of energy for all nodes and later one mainly have the varied type of energy of nodes. During the node deployment procedure, all nodes are deployed with the same energy in homogenous type, and in heterogeneous type, all nodes are dispersed with different energies in the sensing environment [3]. The class of homogeneous protocol constitutes of protocols like LEACH, HEED, etc. and a class of heterogeneous protocol comprises of protocols like SEP, TSEP, ETSSEP, DCHRP, etc.

The prominent type of heterogeneity based on resources is link heterogeneity, the computational heterogeneity and energetic heterogeneity focusing on different aspects of the sensor node [4]. The link type comprises of a node having a slight high bandwidth for sensing of the data, whereas in the computational heterogeneity form, a node contains extra memory and processing capabilities than the basic normal nodes [5]. Energetic heterogeneity involves replaceable battery type for heterogeneous sensor nodes (Fig. 1).

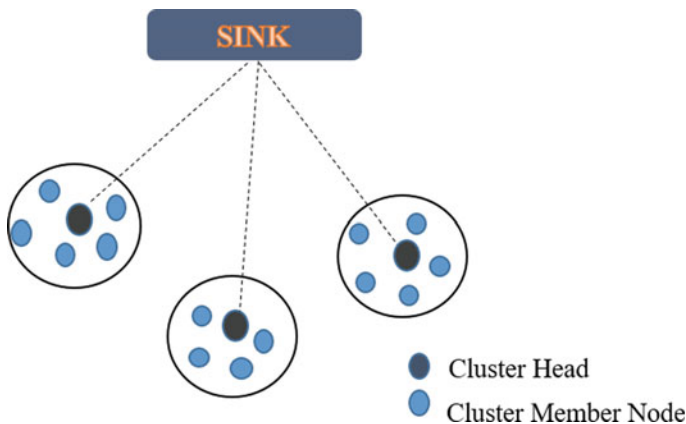


Fig. 1 Formation of Cluster

The rest paper is arranged accordingly. Associated work done is styled in Sect. 2 of the paper, Sect. 3 comprises of the proposed concept, Sect. 4 deals with the simulation and result part and Sect. 5 holds the conclusion of the proposed paper.

2 Related Work

This section embraces the literature review of various prevailing routing schemes and strategies used for homogeneous as well as heterogeneous WSNs.

LEACH protocol put forwarded by Heinzelman in 2000 is considered to be the very promising and oldest protocol in the family of the homogeneous protocol. Having similar energy levels of nodes, LEACH employs a mechanism that the selection of cluster heads among the similar types of nodes depends on the probability function. This protocol focuses on the adaptive clustering schema. Manjeshwar et al. in the year 2001 proposed the TEEN protocol mainly focusing on two different threshold types, the hard and soft threshold type [6]. The gain of the protocol is that it slightly eases the number of transmissions. Younset et al. in the year 2004 introduced HEED, improvement over basic LEACH protocol using the remaining energy in node concept [7]. The mentioned protocols for WSN are not fine-suited for the heterogeneous environment as it takes only the same energy type node.

Stable election SEP protocol is among the first protocol proposed for heterogeneous WSN environment having the characteristics of varied types of node dispersed in the sensor field, put forward in 2004 by Smaragdakis having two levels of nodes varying in energies [3]. Cluster Head is selected among nodes based on individual probability election criteria. It is fine-suited as it provides stability among nodes and an extended lifespan. SEP upgrades stability by 26% over LEACH using the heterogeneity of nodes.

Various protocols are put forwarded for the heterogeneous environment like DEEC, distributed energy-efficient clustering based on remaining and average energy between the nodes [8]. The advantage of the protocol is that it doesn't require former knowledge of energy among nodes. Kashaf proposed the TSEP Protocol as an advancement over the SEP by introducing a three-level heterogeneity mechanism. The basis of selecting the leader CH here is the threshold criteria [9]. The next enhancement on the heterogeneous type was given by Shekhar et al. in 2015 by proposing a new methodology ETSSEP, comprising of three levels of node heterogeneity and a reactive procedure of routing. Varying in energy type, the nodes are described as a normal node, advance node, and intermediate sensor nodes deployed in the field. By simulation, it is validated that it gave an enhancement in stability and lifespan among nodes by 33.5% and 37.70% over TSEP. Yasha et al. in 2017 proposed the DCHRP and in 2018 proposed the DCHRP4 protocol following the dual cluster head concept having prime CH and a secondary CH to divide work among themselves, DCHRP gives a stable increase in lifespan and the stability by an increase of 3.28% and 9.99% over ETSSEP, respectively [6].

3 Proposed Methodology

The proposed methodology 'RA-HNW' is grounded on the working of four forms of node dispersed in the sensor network field varying in energies. Put forwarded nodes diverge in computational capabilities as well as in energy levels. The nodes are centered on the link, computational and energetic heterogeneity criteria and named as normal type sensor nodes having modest computation capabilities, followed by advanced, intermediate, and supernodes having higher processing capabilities than each other. The normal nodes in the field will be having the least energy as compared to the super ones. The four nodes are given by α for normal, β for intermediate, γ for advanced and μ for supernodes.

The varying energy of normal nodes is denoted by E_{nor} , intermediate sensor node by E_{int} , advance nodes by E_{adv} , and highest capability supernode by E_{sup} . The use of the different types of nodes altogether reduces time consumption, provides better computational power. The supernode embedded with high energy senses the data for more time as compared to the other three nodes in the sensor network field. The energy of the proposed four forms of nodes is given as:

$$E_{nor} = E_o * (1 + \alpha) \quad (1)$$

for Normal sensor node,

$$E_{int} = E_o * (1 + \beta) \quad (2)$$

for Intermediate sensor node,

$$E_{adv} = E_o * (1 + \gamma) \quad (3)$$

for Advance sensor node,

$$E_{sup} = E_o * (1 + \mu) \quad (4)$$

for the most powerful, Supernodes.

The initial value of a node is 1.0 J for Supernode, 0.75 J for the Advance node, 0.5 J for Intermediate node, and 0.25 J for the normal node, this allocation of energy is done in the starting phase of node deployment.

CH election in every epoch is centered on the node having the utmost energy present. In our proposed work, every time the first cluster head will be a supernode having the highest-energy type of 1.0 J and greater processing abilities among others. Afterward, when the energy of the selected supernode gets diminished, the process for selecting the next CH follows the probability criteria. The CHs election procedure is of dynamic nature that is, any random node can be the leader based on probability. The probability of nodes is decided using certain formulas:

$$P_{\text{super}} = 1 - \frac{E_{\text{sup}} * (1 + \mu)}{N} \quad (5)$$

$$P_{\text{advance}} = 1 - \frac{E_{\text{sup}} * (1 + \gamma)}{N} \quad (6)$$

$$P_{\text{intermediate}} = 1 - \frac{E_{\text{int}} * (1 + \beta)}{N} \quad (7)$$

$$P_{\text{normal}} = 1 - \frac{E_{\text{nor}} * (1 + \alpha)}{N} \quad (8)$$

where P_{super} , P_{advance} , $P_{\text{intermediate}}$, P_{normal} are the probability function for the proposed work having four forms of nodes. Here E_{sup} , E_{adv} , E_{int} , E_{nor} , N , are initial energy of supernode, the initial energy of advance node, the initial energy of intermediate nodes, the initial energy of normal nodes, number of nodes, respectively. The total energy of the nodes in the network is given by:

$$E_{\text{tot}} = E_{\text{nor}} + E_{\text{int}} + E_{\text{adv}} + E_{\text{sup}} \quad (9)$$

3.1 Routing Algorithm

Nodes Setup and Proposed Network Initialization

- Step 1 While true
- Step 2 Follow steps CLH1= max (μ) for first cluster head selection from super nodes with max energy
- Step 3 Follow steps CLH2= max (α , β , γ) for selection of next CH among the remaining nodes
- Step 4 Allot task among the chosen leader heads
- Step 5 Calculate the total energy of nodes using (9)
- Step 6 Calculate Throughput using a number of packets being sent
- Step 7 Calculate the resources per iteration

The first leader head in a cluster gets selected from the high energy dispersed super node μ in the network field using procedure CLH1 = max (μ) where μ is the supernode, α , β , γ are the three remaining varying nodes and CLH is the cluster leader head of a particular cluster, then according to the energy left among the node, the next cluster head is selected from the remaining α , β , γ using CLH2 = max (α , β , γ), respectively. As soon as the energy of the nodes starts diminishing with time, the procedure starts the operation again beginning with the nodes remaining in the network. The sensor nodes stop sensing the values when all nodes are utilized according to their energy specification making the sensing nodes dying eventually

after completion of the desired tasks [10]. The process of sensing the data and gathering information increases due to the working of four forms of nodes in the sensing field altogether.

4 Result and Simulation

For evaluation of the proposed protocol, simulation is performed on MATLAB 2018a. Afterward, the performance of the proposed methodology is compared with the existing protocols such a SEP, TSEP, ETSSEP, DCHRP, and DCHRP4, respectively. For the simulation, firstly 15–300 distinct nodes are positioned in the sensor network field of dimension 100 * 100. We have stimulated by taking a lower number of nodes then going upwards to a higher number of the nodes to check the efficiency of the proposed schema. As described, the sensor field constitutes of four levels of nodes upgrades over each other in a relation to battery life and cost, making the system more favorable. Initially, energy during deployment is 0.5 J. The proposed RA-HNW Routing Algorithms for hybrid nodes in a wireless sensor network is better compared to other protocols in terms of different types of sensing nodes having different functionalities dispersed altogether working on the residual energy criteria of a node. The performance criteria are based on the total lifespan of the network, stability of nodes, and throughput.

Figure 2 displays the cluster formation using the distinct nodes in the sensing field. The varied color nodes depict the four forms of nodes in clusters randomly placed

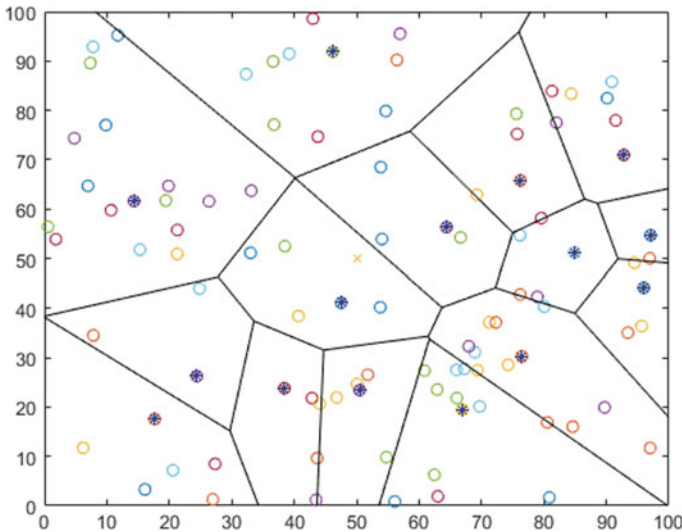


Fig. 2 Distribution of nodes according to energy levels

Table 1 Parameters for simulation

Parameter	Values
Network size	100 × 100 m ²
Number of nodes	15–300
Initial energy (E_0)	0.5 J
Packet	8 per iteration
Bandwidth	10 bit/s
E_{fs}	10 nJ/bit/m ²
E_{amp}	0.0025 Pj/bit/m ²
E_{DA}	5 nJ/bit/signal
α	0.25 J
β	0.50 J
γ	0.75 J
μ	1 J

in the sensor network field, each led by a cluster head. Parameter for simulation for the proposed methodology is defined in Table 1.

Figure 3 illustrates the alive nodes per round of the proposed protocol RA-HNW. In the proposed RA-HNW protocol, the first node is dying in 6430 rounds and the last node is dying in 8092 round, respectively.

Figure 4 displays the stability of various protocols. The stability period of SEP protocol is 974 rounds, TSEP Protocol is 2068 rounds, ETSSEP protocol is 2762

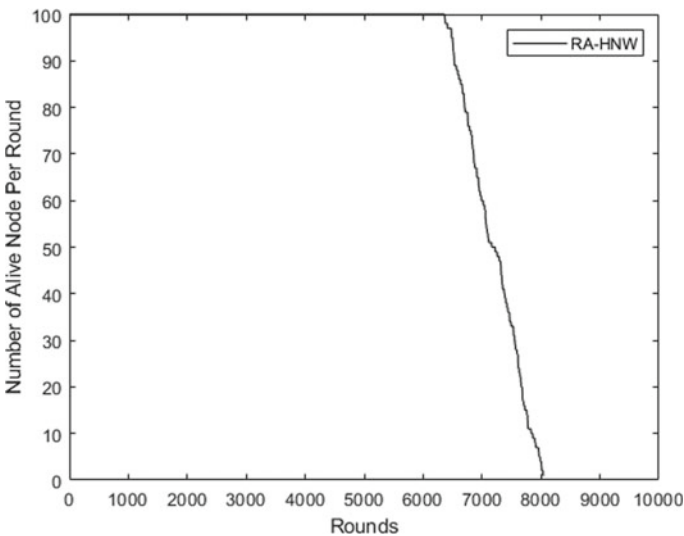


Fig. 3 Alive nodes per round in the network

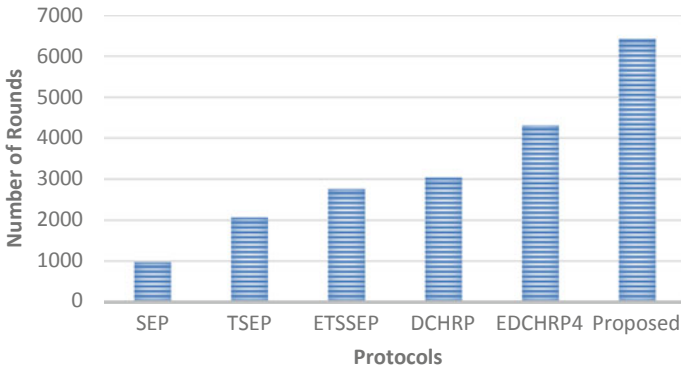


Fig. 4 Stability period of protocol with proposed RA-HNW

rounds, DCHRP protocol is 3038 rounds, DCHRP4 protocol is 4312 rounds and our proposed RA-HNW comes out to be 6430 rounds, respectively.

Figure 5 shows the lifespan of SEP, TSEP, ETSSEP, DCHRP, DCHRP4, and our proposed RA-HNW protocol. All nodes working die in SEP in 1667 rounds, in TSEP in 4908 rounds, in ETSSEP in 6763 rounds, in DCHRP in 6985 rounds, in DCHRP4 in 7324 rounds and our proposed RA-HNW in 8092, respectively.

Figure 6 throughput of various protocols such as SEP, ETSSEP, DCHRP4, and our proposed RA-HNW (Table 2).

The experiment is performed with a distinct number of nodes ranging from 15 nodes and going up to 300 nodes. The following figure shows the variation in network lifetime of the proposed protocol RA-HNW with a distinct number of nodes.

Figure 7 depicts the network lifetime of RA-HNW for different sensor nodes. The result redirects that for 15 nodes the lifespan of the network grows up sharply followed by a rise in lifespan for 25 nodes to 100 nodes and then goes down slightly

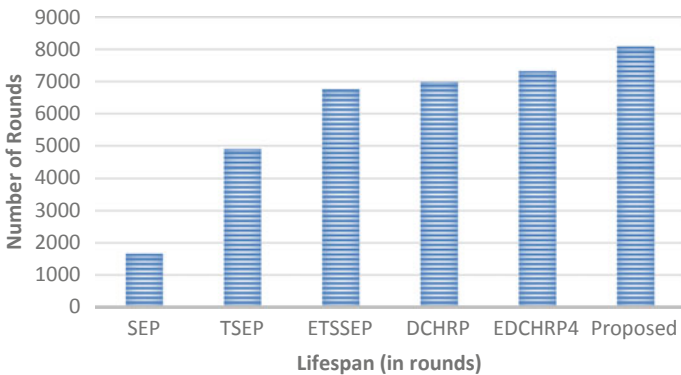


Fig. 5 Lifespan of protocol

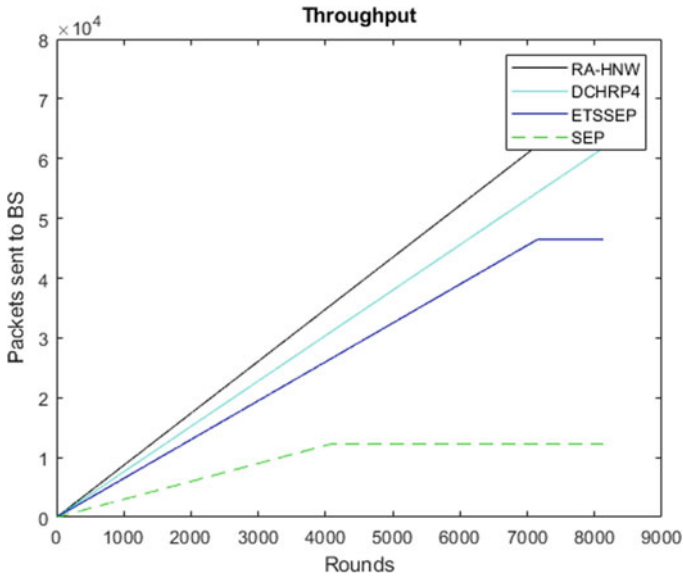


Fig. 6 Throughput of various protocol

Table 2 The comparison of protocols SEP, TSEP, ETSSEP, DCHRP, DCHRP4, and proposed RA-HNW

Protocols	Stable period	Instable period	Lifespan
SEP	974	693	1667
TSEP	2068	2840	4908
ETSSEP	2762	4001	6763
DCHRP	3038	3947	6985
DCHRP4	4312	3013	7325
RA-HNW	6430	1662	8092

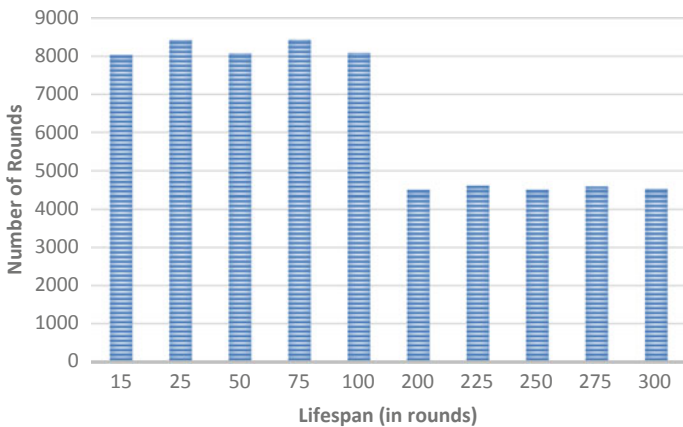


Fig. 7 Network lifetime of proposed DD-MAP with a distinct number of nodes

Table 3 Performance of proposed Protocol RA-HNW with a distinct number of nodes

Number of nodes	Stable period (rounds)	Lifespan
15	6361	8045
25	6768	8430
50	6387	8081
75	6748	8444
100	6430	8092
200	2761	4573
225	2593	4611
250	2761	4508
275	2578	4588
300	2757	4535

afterward. Here, it is observed that from 15 to 100 nodes lifetime is better according to the proposed methodology using a distinct type of nodes (Table 3).

5 Conclusion

In the proposed RA-HNW protocol, it is observed that using the distinction in the number of nodes varying in energy, the proposed schema works well in the WSN environment. The given methodology increases the stability by 49.12% as compared to DCHRP4 and twice and thrice as compared to protocols like ETSSEP, TSEP, and SEP. Using the node criteria, the lifespan of the sensor network also upgrades by 10.49%, 15.85%, 19.65%, and 64.87% over DCHRP4, DCHRP, ETSSEP, and TSEP.

References

1. Bandopadhyay S, Coyle E (2003) An energy efficient hierarchical clustering ALGO for WSN: In: Proceedings infocom
2. Heinzelman W, Balkrishnan H, Chandrakasan A (2000) Energy efficient comm protocol for wire-less sensor n/w system. In: Proceedings 33 annual Hawaii international conference, pp 4–7
3. Al-Karki N, Kamal AE (2004) Routing tech in wireless sensor n/w: a survey. IEEE wireless comm 11:6–28
4. Tan O, Korpeoglu I (2003) Power efficient data gathering & aggregation in WSN. In: SIG.MOD Record, vol 32, pp 66–71
5. Kashaf A, Javaid N, Khan ZA, Khan IA (2012) TSEP-Threshold sensitive stable election protocol. In: International 10th conference on frontier of IT, vol 164
6. Shekhar K, Verma SK, Kumar A (2015) Enhanced threshold sensitive SEP for heterogeneous wsns. Wirel Pers Comm 85:2643–2656

7. Timothy Shepard T (1996) Channel access schema for the large dense PKT radio N/W. In: Proceeding ACM-SIG.COMM
8. Aderohunmu F, Jeremiah D (2009) Enhanced SEP: enhanced stable election SEP for cluster heterogeneous WSNs. Dept. of Info Science, New Zealand
9. Mhatre V, Rosenberg C (2004) Homogenous v/s heterogenous cluster sensor n/w: a Comparative study. In: Proceedings IEEE
10. Bestavros A, Matta I, Smaragdakis G (2004) Stable SEP protocol for heterogeneous wsns. In: International workshop on actor & sensor n/w protocols & appl. SANPA

Extended Security in Heterogeneous Distributed SDN Architecture



Sugandhi Midha and Khushboo Tripathi

Abstract With the rapid growth in the network, a demand for more flexible and secure technology of network programmability is increasing. With the introduction of technology like SDN, a new platform for communication evolved which is free from traditional network barriers like vendor lock-ins, limited scope for innovation, buggy software, etc. No doubt, SDN has solved these problems but SDN security issues are of major concern. SDN security is the key research area that is gaining popularity. Our paper discusses SDN security challenges. In our experiments, we tried to depict the network performance and utilisation of resources in case of security attacks. With the aim of securing SDN in the case of heterogeneous distributed SDN controllers, we suggested a routing protocol that manages routing tasks where TLS security has been embedded in the header for OpenFlow packet. We simulated the system with our testbed of virtual machine with different attacks scripted in python.

Keywords Denial of service (DOS) · Openflow · Software defined network (SDN) · Ping of death · Flow rule · Transport layer security (TLS)

1 Traditional Networking and The SDN

With the accelerated growth in the number of computing devices that are connecting to the internet, a need for technology is arising which can manage the complexity of ongoing large-scale network. Cisco has estimated that today more than 25 billion devices are connected to the internet and looking at the rapid growth and usage these numbers will definitely rise to 50 billion by 2020 [1]. A solution to overcome this challenge has been mitigated by an emerging technology called the Software Defined Network (SDN). A separation of control function and data forwarding function has reduced the complexity of managing the growing network. Network function can be centralized on one controller or on several distributed controllers depending on the size of network. SDN offers several network control benefits which include:

S. Midha (✉) · K. Tripathi
ASET, Amity University, Gurgaon, India
e-mail: mailmetech@gmail.com

Support for Network Experimentation: In traditional networks, there was less possibility of innovation. Equipment vendors used to write the code. Network was considered to be a proprietary network and there were long delays to introduce new features. Due to support for heterogeneous network architecture in SDN, new features can be easily added. There are no vendor lock-ins.

Dynamic Adaption: In the case of network device failures, SDN reacts towards the changing environment and dynamically adapts to topology changes. No configuration changes are required by the network administrator.

Support for Add-on Features: Network functionality can be added into the network as per the requirements of the users without any delays that only network manufacturer will develop it.

Abstraction and Automation: Functionality of control plane is hidden from the data forwarding plane. Data forwarding plane merely transfers the packets. SDN offers us the flexibility to change the network devices' functionality via APIs.

Interoperability and Independence: Equipments from different vendors can communicate using open flow standards that support different services and independence to add features dynamically.

Saves Cost: In traditional networks, operating a network is expensive along with the cost to set it up. Decoupling data and control plane has broken the monopoly of proprietary network. It reduces network prices while also forces the vendors to compete on network prices (Fig. 1).

2 SDN Architecture Overview

In traditional networks, each network element acts as closed equipment. Software is bundled together on hardware elements. It works as per vendor-specific interfaces. This device was always over specified where many complex functions are baked on a single device. These elements with mostly 20+ million lines of code were more prone to cascading failure and other vulnerabilities.

An idea was to separate the control plane from the simple packet forwarding hardware. With the advent of SDN, this idea of decoupling control and data plane realized in the network world. SDN architecture is totally not a new concept. Decoupling is one of the key elements of MLPS (Multi-Protocol Label Switching) (Fig. 2).

SDN architecture is actually composed of three layers:

- Application Layer
- Control Layer
- Data Layer.

NBI corresponds to the Application and Control Plane interface and SBI corresponds to Data and Control Plane Interface.

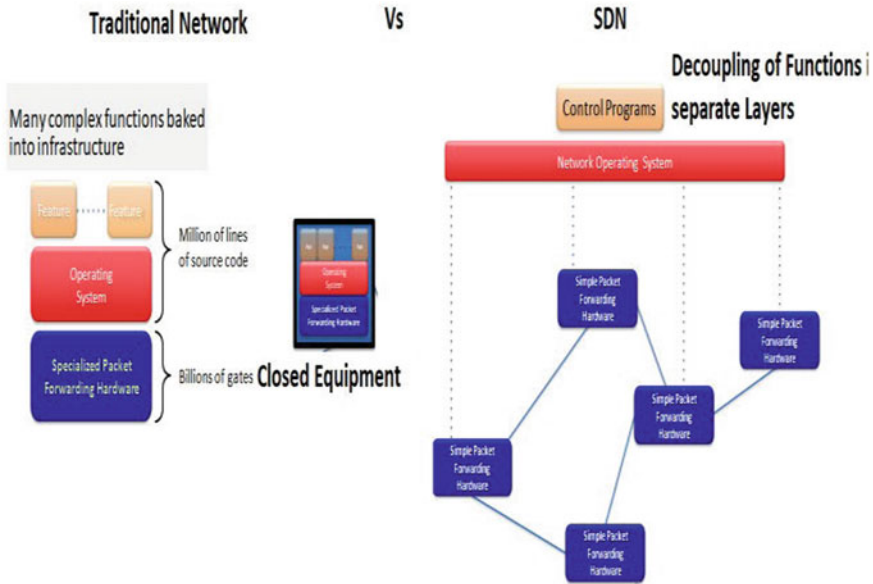


Fig. 1 Traditional network versus SDN

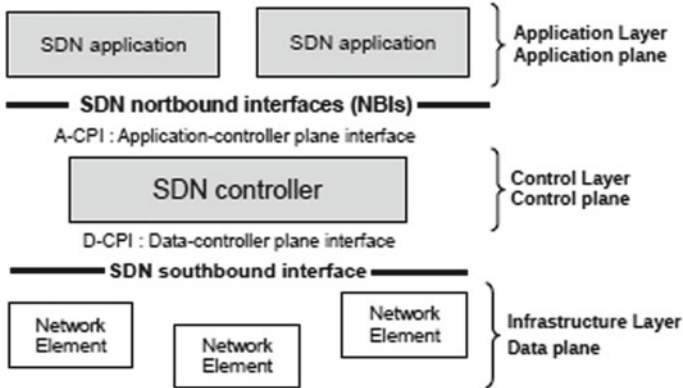
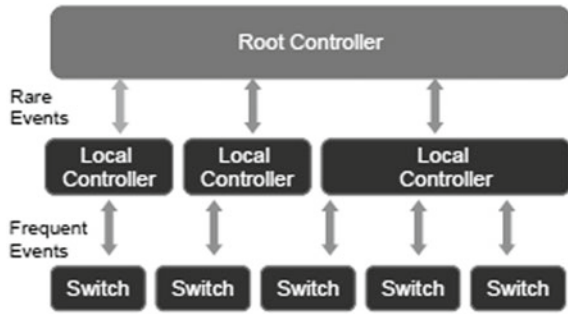


Fig. 2 SDN architecture [2]

The APIs are specified by ONF (Open Network Foundation). There is one central controller that installs routes and policies into network elements. Network controller is responsible for creating a flow table and managing the rules of flow.

SDN architecture performance is evaluated by analysing the forwarding speed and packet drop rate. But how far a single controller can handle the scalability. The author Jarschel et al. [3] proposed that the placement of multiple controllers is definitely going to have a positive impact on latency, fault discovery, and event propagation (Fig. 3).

Fig. 3 Distributed SDN architecture [3]



3 Tools and Services for SDN Deployment

SDN works intelligently by informing the network devices about the change in topology in case of device unavailability, device failure, traffic load change, etc. This dynamic knowledge and information of application context help to enhance network performance and services significantly.

SDN services are broadly categorized as:

Management and Monitoring: In SDN, interoperability between open flow (OF) and non-open flow network is a complex issue. Motivated by this problem, a legacy flow management solution is proposed [4]. Layer 1 of legacy flow management architecture is responsible for communication between open flow supported networks. Whereas, L2 is responsible for migrating the instructions from open flow to vendor-specific (legacy) network and vice versa (Fig. 4).

Slicing and Network Resource Allocation: Initially, the purpose Open Flow was created for experimentation of protocols and technology in an environment. This network was so efficient that it proved to be a significant test bed that does not have any adverse effect on the work environment. Later on, it has been analysed and

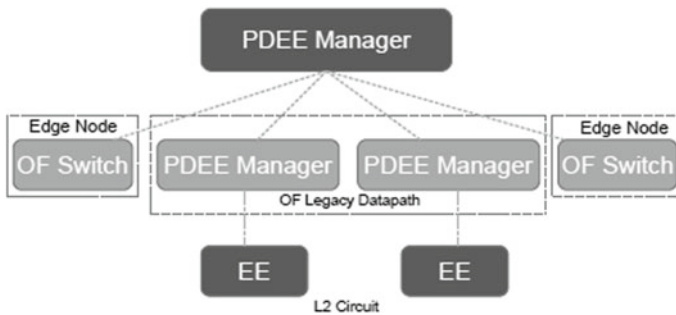


Fig. 4 Legacy network architecture of programmable distributed execution environment (PDEE) [4]

Table 1 Main components of open flow (OF) table [6]

Match fields	Priority	Counters	Instructions	Timeouts	Cookies
--------------	----------	----------	--------------	----------	---------

proposed that we can use this production test bed simultaneously for more than one experiment. The only thing which is required is slicing and distribution of network resources allocation in an efficient manner among different experiments. Flow Visor [5], has been designed specifically for this purpose.

Network Updates: A timely update that is provided by the SDN in case of topology change, load management, network fault, etc. has the potential to achieve network management efficiency.

Load Balancing: Another aspect that helps in managing and improving network efficiency is the availability of SDN Controller during peak traffic. The dynamic adaptability nature of SDN network makes it available and scalable during high traffic load. SDN load balancer helps to achieve this objective.

4 Open Flow Protocol

SDN and Open Flow are two words that are continuously used together in literature. Open Flow is one of the protocols that controls devices in SDN. There are several other protocols like Oplex, Lisp, NetConf, ForCES, etc. which can be used in SDN. But due to its flexibility, Open Flow is most popular for SDN southbound APIs.

SDN Controller set the flow entries in the flow table at network element via OF protocol. Network elements (NE) forwards the packets based on those entries. OF is responsible for communication process between controller and network elements.

Table 1 Field Description:

Match Fields: Consists of packets headers and ports.

Priority: Matching Precedence.

Counters: Updated when packets match occur.

Timeouts: Maximum amount of time a packet can be in network.

Cookie: Not used while processing packets (Fig. 5).

5 SDN Security

Open Flow (OF) does not typically implement security in the network. This is because Transport Layer Security (TLS) encryption is not mandatory. As this is an optional

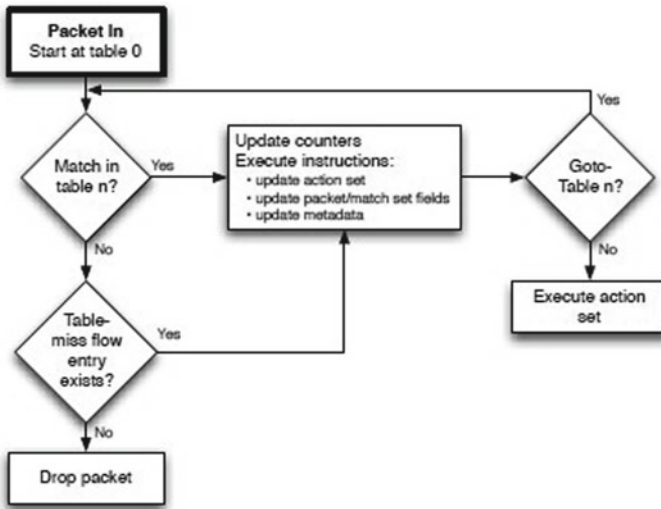


Fig. 5 Packet flow in open flow (OF) switch [6]

criterion to adopt TLS encryption, an attacker gets an opportunity to exploit this OF channel and can spoof network traffic on communication channels.

Various security challenges are:

Authentication and Accountability: Host authentication and identification is badly affected on the OF SDN.

Man in Middle Attack: An outside switch on the network may get connected to the controller by faking its identity.

Spoofing: SDN Controller is more prone to IP spoofing and ARP spoofing.

Denial of Service: An attacker will stop controller and switch from getting connected. SDN Controller is not able to service the authenticated service. Network performance is highly affected in this case as experimented by my simulation. This sometimes leads to ping of death of SDN Controller.

Figure 6 shows that 32 processes are running and CPU usage is 4%. And Fig. 7 shows that with a speed of 1 Gbps, Network Utilisation is nominal with 21 processes. And as soon as the network processes increase beyond a limit, it leads to ping of death as depicted in Fig. 8 and network controller stops replying.

6 Extended Identity Based Cryptography

Proposed approach DDOS defensive mechanism hosted in controller. A controller monitors the traffic passing to and from the open flow switches. It acts as a security

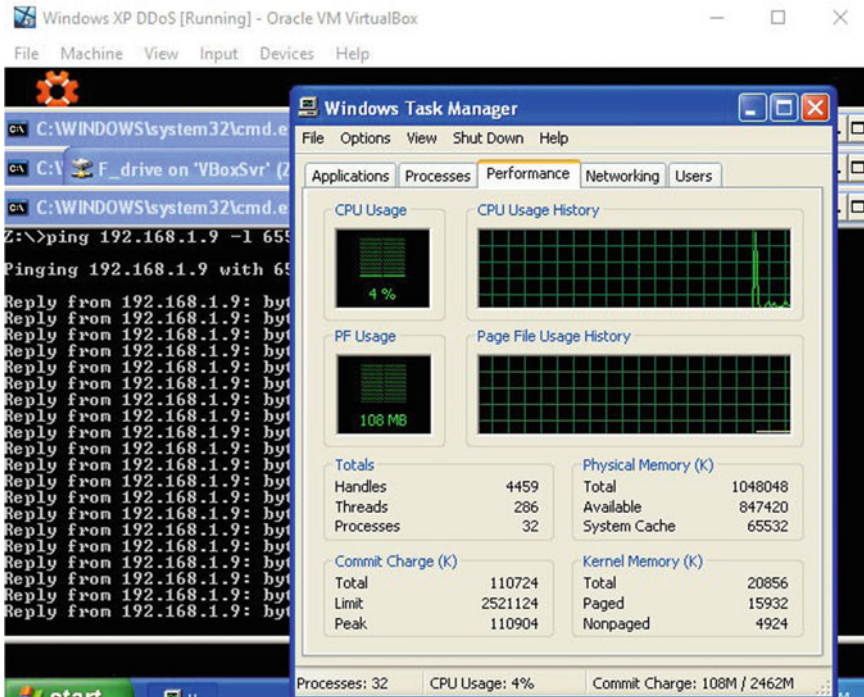


Fig. 6 Running: 32 processes, CPU usage: 4%

device to detect the threat at the network trust boundaries and supports preventive and defensive mechanisms. Content Oriented Network Architecture (CONA) finds the DDOS attack when the count of a particular context request exceeds a threshold. Our proposed defender algorithm for DDOS analyse the traffic rate against the prescribed predefined limit. DDOS is one of the catastrophic attacks which generates various other security threats on the network and is critical to handle.

Identity-based cryptography where we used Data Encryption Standard (DES) to support TLS in Open Flow which will protect the southbound security connections. This will ensure that no attacker adds malicious traffic on the network and cannot bring the network down. It also ensures that no tampering is possible on the data. As TLS is an optional mechanism in the Open Flow SDN because of the flexibility it offers to connect with any network. We are supporting TLS with the Open Flow to provide extended security. Figure 9 explains how DES is used to encrypt the text to secure the data so that any tampering with the data can be identified.

Figure 10 explains the complete flow of our algorithm. In the first step, the TLS support is provided by encrypting the packet and to prevent unauthorized user attacks like DOS, entropy is measured based on the type of network and flow of data. If the sender is in the legitimate, i.e. entropy is less than the defined threshold value, then another check is made by comparing the number of packets sent, i.e. count is less

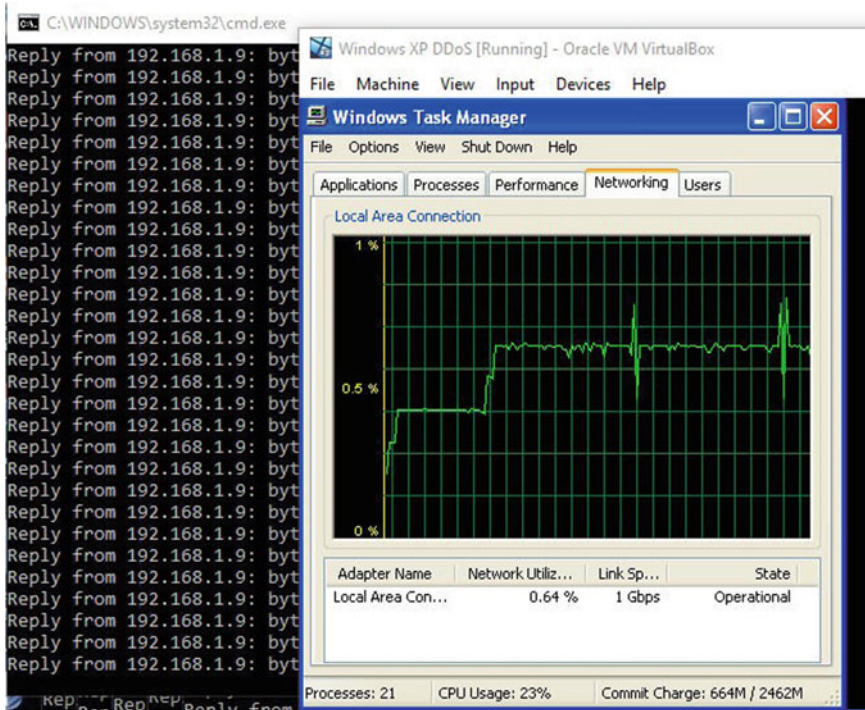


Fig. 7 Running: 21 processes, network usage: nominal

than 50 or not as per the capacity of the network. If the flow is more than the packets a network can handle then flow modifications become an important step to prevent from DOS.

7 Conclusion and Future Work

In this paper, we have proposed an extended TLS security with entropy parameters based on OpenFlow. We have built a virtual prototype system to simulate a real OpenFlow network. Experiments and their results show that network performance is highly underutilized in case of attacks. A measure has been taken to prevent the system from unauthorized users and to identify them. Another measure has been taken to detect any kind of tampering with the data with the support of DES.

For future work, there are many directions to explore to deal with fake IP. Our next set of experiments regarding this are in progress.

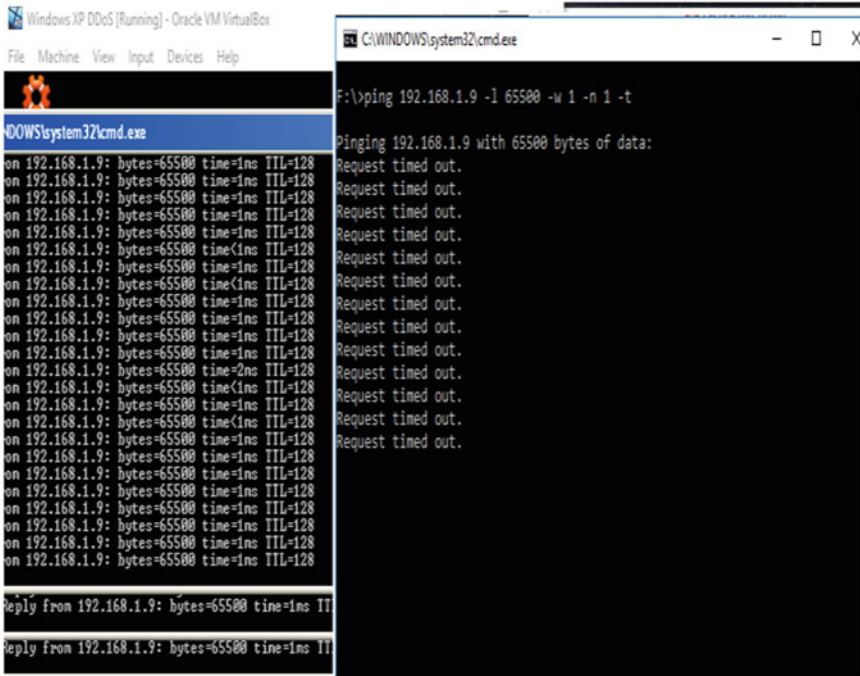


Fig. 8 Ping of death, denial of service

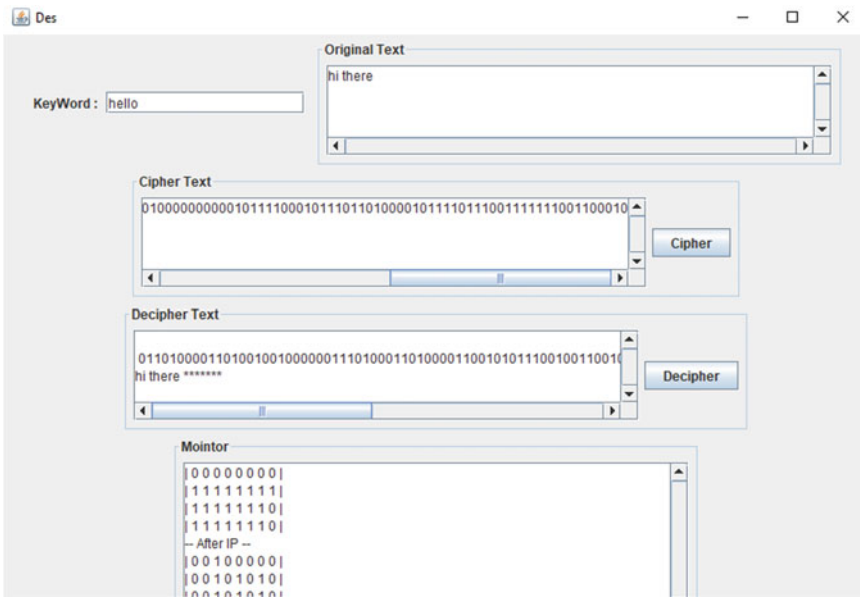
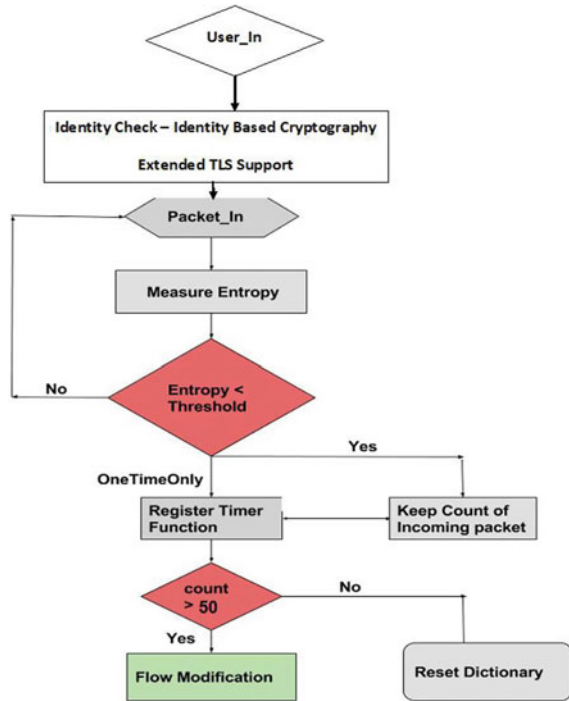


Fig. 9 Extended TLS support

Fig. 10 Defensive system flow



References

1. Santamaria CJG (2017) Management of a heterogeneous distributed architecture with the SDN. Networking and Internet Architecture [cs.NI], Universite de Reims Champagne Ardenne
2. Open Networking Foundation (2012) Software-defined networking: the new norm for networks. White Paper. <https://www.opennetworking.org/images/stories/downloads/sdn-resources/white-papers/wp-sdn-newnorm.pdf>, pp xvii, 14, 15, 53, 54
3. Jarschel M, Oechsner S, Schlosser D, Pries R, Goll S, Tran-Gia P (2011) Modeling and performance evaluation of an openflow architecture. In: Proceedings of the 23rd international teletraffic congress, ITC '11, pp 1–7, International Teletraffic Congress, pp 16, 55
4. Farias FNN, Salvatti JJ, Cerqueira E, Abelém AJG (2012) A proposal management of the legacy network environment using openflow control plane. In: NOMS. IEEE, pp 1143–1150, xvii, 29
5. Sherwood R, Chan M, Covington A, Gibb G, Flajslik M, Handigol N, Huang T-Y, Kazemian P, Kobayashi M, Naous J, Seetharaman S, Underhill D, Yabe T, Yap K-K, Yiakoumis Y, Zeng H, Appenzeller G, Johari R, McKeown N, Parulkar G (2010) Carving research slices out of your production networks with openflow. SIGCOMM Comput Commun Rev 40, 129–130, xvii, 31, 32, 39
6. Open Networking Foundation. “OpenFlow”, White Paper. <https://www.opennetworking.org/wp-content/uploads/.../openflow-switch-v1.5.1.pdf>
7. Hassas Yeganeh S, Ganjali Y (2012) Kandoo: a framework for efficient and scalable offloading of control applications. In: Proceedings of the first workshop on hot topics in software defined networks, HotSDN '12, New York, NY, USA, pp 19–24, ACM, pp xvii, 16, 17

8. Suh J, Choi H-g, Yoon W, You T, Kwon T, Choi Y (2010) Implementation of content-oriented networking architecture (CONA): a focus on DDOS countermeasure. In: 1st European NetFPGA developers workshop, p 34
9. Sherwood R, Gibb G, Yap KK, Appenzeller G, Casado M, McKeown N, Parulkar G (2009) Flowvisor: a network virtualization layer. OpenFlow Switch Consortium, Tech Rep
10. Yan Q, Yu FR (2015) Distributed denial of service attacks in software-defined networking with cloud computing. *IEEE Commun Mag*
11. Govindarajan K, Meng KC, Ong H (2013) A literature review on software-defined networking (SDN) research topics, challenges and solutions. In: IEEE fifth international conference on advanced computing (ICoAC)
12. Hakiria A, Gokhale A, Berthoua P, Schmidt DC, Thierry G (2014) Software-defined networking: challenges and research opportunities for future internet, vol 75, Part A, Elsevier, pp 453–471
13. Kreutz D, Ramos FM, Verissimo PE, Rothenberg CE, Azodolmolky S, Uhlig S (2014) Software-defined networking: a comprehensive survey. *Proc IEEE* 103(1):14–76
14. Kucminski A, Al-Jawad A, Shah P, Trestian R (2017) QoS-based routing over software defined networks. In: 2017 IEEE international symposium on broadband multimedia systems and broadcasting (BMSB)
15. Pisharody S, Natarajan J, Chowdhary A, Alshalan A (2017) A security policy analysis framework for distributed SDN-based cloud environments. *IEEE Trans Dependable Secure Comput* PP(99)
16. Ahmad I, Namal S, Ylianttila M, Gurtov A (2017) Analysis of deployment challenges of host identity protocol. *IEEE*
17. noxrep (2015) POX: OpenFlow Controller. [Online] https://www.opennetworking.org/wp-content/uploads/2014/10/Principles_and_Practices_for_Securing_Software_Defined_Networks_applied_to_OFv1.3.4_V1.0.pdf
18. Hengky “Hank” Susanto, Sing Lab. Introduction to SDN. www.cse.ust.hk/~kaichen/courses/spring2015/comp6611/.../SDN-presentation.pptx
19. Heller B, Handigol N, Jeyakumar V, McKeown N, Mazières D (2012) Where is the debugger for mySoftware-defined network? In: HotSDN
20. Hu Z, Wang M, Yan M, Yin Y (2015) A comprehensive security architecture for SDN. In: IEEE proceedings of 18th international conference on intelligence in next generation networks. *IEEE*
21. Shin S, Gu G (2013) Attacking software-defined networks: a first feasibility study. In: Proceedings of the second ACM SIGCOMM workshop on hot topics in software defined networking. *ACM*, pp 165–166
22. Al-Shaer E, Al-Haj S (2010) Flowchecker: configuration analysis and verification of federated openflow infrastructures. In: Proceedings of the 3rd ACM workshop on assurable and usable security configuration
23. Porras P, Shin S, Yegneswaran V, Fong M, Tyson M, Gu G (2012) A security enforcement kernel for OpenFlow networks. In: Proceedings of the first workshop on Hot topics in software defined networks. *ACM*, pp 121–126
24. Shin S, Gu G (2012) CloudWatcher: network security monitoring using OpenFlow in dynamic cloud networks (or: How to provide security monitoring as a service in clouds?). In: 20th IEEE international conference on network protocols (ICNP). *IEEE*, pp 1–6
25. Kordalewski D, Robere R (2012) A dynamic algorithm for loop detection in software defined networks
26. Khurshid A, Zhou W, Caesar M, Godfrey P (2012) Veriflow: verifying network-wide invariants in realtime. *ACM SIGCOMM Comput Commun Rev* 42(4):467–472
27. Yang H, Lam SS (2013) Real-time verification of network properties using atomic predicates. In: ICNP, the IEEE international conference on network protocols
28. Hu Z, Luo J (2015) Cracking network monitoring inDCNs with SDN. In: 2015 IEEE conference on computer communications, INFOCOM 2015, Hong Kong, China, 26 Apr–1 May 2015, pp 199–207

29. Chen F, Bruhadeshwar B, Liu AX (2011) Privacy preserving cross-domain network reachability quantification. In: 2011 19th IEEE International conference on network protocols (ICNP). IEEE, pp 155–164
30. Freedman MJ, Nissim K, Pinkas B (2004) Efficient private matching and set intersection. In: Advances in cryptology-EUROCRYPT 2004. Springer, pp 1–19
31. Chellani N, Tejpal P, Hari P, Neeralike V (2016) Enhancing security in OpenFlow. IEEE Proceedings
32. Abdullaziz OI, Chen Y-J, Wang L-C (2016) Lightweight authentication mechanism for software defined network using information hiding. IEEE
33. Mousavi SM, St Hilarie M (2015) Early detection of DDOS attacks against SDN controllers. IEEE
34. IBM Knowledge Center (2017) An overview of the SSL or TLS handshake. [online] Available at: http://www.ibm.com/support/knowledgecenter/en/SSFKSJ_7.1.0/com.ibm.mq.doc/sy10660_.htm. Accessed 7 Feb 2017
35. Lawal BH, Nuray AT (2018) Real-time detection and mitigation of distributed denial of service (DDOS) attacks in software defined networking (SDN). 978-1-5386-1501-0, ©2018 IEEE
36. Santos R, Souza D, Santo W, Ribeiro A, Moreno E (2019) Machine learning algorithms to detect DDOS attacks in SDN. Concurrency Computat Pract Exper. Wiley Ltd

Evaluation of SC-FDMA Physical Link Using USRP



Shweta Y. Kukade, M. S. Sutaone, and R. A. Patil

Abstract Single-Carrier Frequency Division Multiple-Access (SC-FDMA) is used in uplink data transmission in Long-Term Evaluation (LTE) due to its low Peak-to-Average Power Ratio (PAPR) properties. In this paper, SC-FDMA link has been modeled and proposed to design this link using LabVIEW. The real-time data transmission through the SC-FDMA link is carried out using Software Defined Radio (SDR) testbed which is implemented using Universal Software Radio Peripheral (USRP) devices. The data transmission and reception are carried out through SC-FDMA link and the performance evaluation is estimated for PAPR and Bit Error Rate (BER). The simulation results show that the PAPR and BER parameters of the proposed SC-FDMA link design are significantly lower than the OFDMA in downlink. Moreover, the simulation of BER with different modulation schemes is carried out for different Signal to Noise Ratio (SNR) values. The analysis of PAPR impacts the OFDMA waveform and benefits on SC-FDMA transmission link in any channel condition.

Keywords SC-FDMA · SDR · OFDM · PAPR · BER · USRP · FPGA

1 Introduction

LTE (Long-Term Evolution) and LTE-Advanced have made consistent efforts to enhance future cellular technologies in order to improve higher radio access data rates, spectral efficiency, power reduction, capacity, and coverage with reducing operating network costs. Therefore, Single-Carrier Frequency Division Multiple Access

S. Y. Kukade (✉) · M. S. Sutaone · R. A. Patil
Department of Electronics and Telecommunication, College of Engineering, Pune, India
e-mail: shweta.kukade08@gmail.com

M. S. Sutaone
e-mail: mssutaone@coep.ac.in

R. A. Patil
e-mail: rap@coep.ac.in

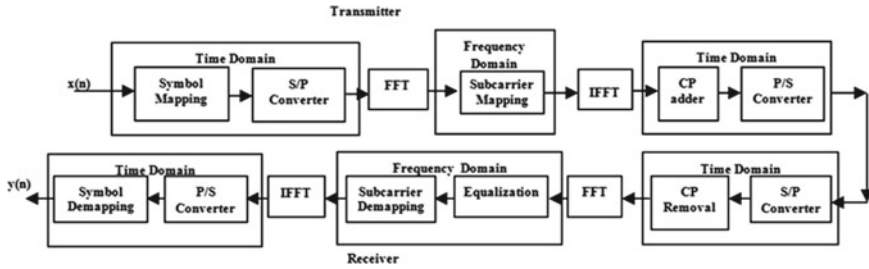


Fig. 1 SC-FDMA transmitter and receiver [1]

(SC-FDMA) is preferred as the multiple-access scheme for LTE uplink direction. The SC-FDMA and OFDMA are similar access schemes except for the additional operation of Discrete Fourier Transform (DFT) are performed on the modulated symbols in SC-FDMA. In this case, DFT converts the logic of the transmission to a large degree. The SC-FDMA transmitter and receiver components of the physical LTE link are explained in Fig. 1 [1]. The utilization of a guard interval appended at the beginning of each OFDM symbol is called a Cyclic Prefix (CP). It provides great robustness against multipath fading and the transmitter reduces the problem to Fast Fourier Transform (FFT) processing and scalar equalization per subcarrier at the receiver.

SC-FDMA has a lower PAPR than OFDMA which helps to save the mobile battery life for a long duration. Numerous papers are addressed different methods to lower down the PAPR of SC-FDMA. The different diversity techniques such as Space Time Frequency Block Codes (STFBC), Space Time Block Codes (STBC), and Space Frequency Block Codes (SFBC) are used in MIMO OFDMA and SC-FDMA systems to improve bit error rate and power [1]. The Raised Cosine (RC) and square root Raised Cosine filter with Absolute Exponential (AEXP) and Hyperbolic Tangent (HT) sigmoid transfer function companding methods are used in [2, 3]. In this technique, localized Discrete Cosine Transformed SC-FDMA (DCT-SC-FDMA) with RC filter shows significant improvement in BER and PAPR without increasing computational complexity and mortifying performance of the system. The Hadamard SC-FDMA scheme uses Hadamard transform that experience considerable reduction in PAPR and BER to produced pulse shaped SC-FDMA [4]. The circular QAM and rectangular QAM modulation schemes are simulated for SC-FDMA system in a different noisy environment [5], as a result, Symbol Error Rate (SER) is improved in circular QAM with less energy consumption. Also, the probabilistic pulse shaping and hybrid companding method with a discrete wavelet transform projected in [6, 7]. This method highlights the weighting windows with zero excess bandwidth at the output of DFT which is vigorous to channel estimation errors and gives better PAPR. In [8], the SC-FDMA performance is evaluated for Zero Forcing (ZF) and Minimum Mean Square Error (MMSE) method. The subcarrier mapping is carried out by localized and distributed mapping. The improved system performance is observed using MMSE method and localized distribution mode.

We addressed the graphical editing language used in LabVIEW software which replaces the text with graphical programming code. This module enables us to calculate PAPR and BER while transmitting and receiving the signal. Essentially, the OFDM has a high PAPR which is independent of Modulation and Coding Scheme (MCS). This is challenging for transmission in uplink because of limited power at the mobile terminal. Hence, transmit power will be inadequate by the linear range of power amplifiers due to the high value of PAPR. The essential backoff which reduces drastically both the average transmitted power and link-budget in the uplink. Therefore, this is very important for cell-edge users due to their large path loss. So having low PAPR is a large benefit for the mobile terminal in Uplink. Most of the wireless communication functions can be easily configured to Software Defined Radio (SDR) testbed using USRP and can be obtained in minimum cost, therefore hardware dependency is reduced [9, 10].

Several experimentations are carried out for real-time data analysis using USRP. The LTE-Advanced physical layer synchronization, framework, and USRP are implemented using LabVIEW for the dense wireless cells heterogeneous network in [11–13]. The result shows the extensive improvement of BER in the urban area of heterogeneous networks. The successful transmission and reception of the local radio stations are performed by using three different USRPs in [14]. The performance analysis of the coded and uncoded OFDM is carried out using SDR [15, 16]. In Coded OFDM, the convolution coding is used as forward error correction techniques which gives high data transfer rates and spectral efficiency. The effective spectrum sensing of 2.1 GHz frequency for LTE based system using LabVIEW platform is carried out using USRP 2920 [17]. This SDR based approach is highly applicable to practical testing environments at low cost. MATLAB is interfaced with USRP in [18] where SC-FDMA transmitter and receiver signal is simulated in MATLAB software and real-time signal transmission is performed using USRP. This implementation achieved transmission rate up to 5.184 Mbit/s in a noisy channel with different modulation schemes.

In this paper, we modeled the SC-FDMA link and proposed to design link using LabVIEW software. The finalization of the modulation scheme in SC-FDMA is carried out by simulating different modulation schemes in MATLAB. In the design of the SC-FDMA link, it brings out efforts to reduce PAPR, increase spectral efficiency, and increase the bit error rate performance. This reduces the spectral leakage into adjacent channels. This out-of-band reduction is reduced by padding with zeros to input signal, i.e., oversampling the original signal using localized subcarrier mapping. These oversampled signals are processed using a longer IFFT. This process reduces clipped oversampled signal and filtering the out-of-band radiation. The real-time experimentation of the designed link is carried using USRP testbed. In this experimentation, two USRPs are kept 1 m apart from each other. The transmitter USRP_{Tr} is considered as a User Equipment (UE) and receiver USRP_{Rx} is considered as a Base Station (BS). A series of data streams are transmitted through the USRP_{Tr} and received at the USRP_{Rx}. The PAPR and BER of the real-time received data are calculated theoretically and verified with LabVIEW software.

The paper is organized as follows: Functioning of SC-FDMA transmitter and receiver is described in Sect. 2, the system model is specified in Sect. 3, SC-FDMA link design is detailed in Sect. 4, experimental set up is explained in Sect. 5, results are discussed in Sect. 6 and the conclusion is drawn in Sect. 7 with future scope.

2 Overview of SC-FDMA Transmitter and Receiver

LTE downlink OFDMA and uplink SC-FDMA schemes are used for data transmission. SC-FDMA uses a linear combination of all data symbols which are modulated on to a given subcarrier and transmitted at the same time instance. The transmitted subcarriers signal carries a component of each modulated data symbol in each symbol period. In SC-FDMA, symbols are spread on a group of subcarriers. This is a single-carrier property of SC-FDMA which has a lower PAPR than the multicarrier transmission scheme of OFDMA. The spectral spreading radically reduced in SC-FDMA because of low PAPR than OFDMA. The block diagram of the SC-FDMA transmitter and receiver is shown in Fig. 1.

In Fig. 1, the input bitstream is mapped into modulation symbols, and grouped into symbol block of length M . This symbol block is converted in parallel for further process. The FFT operation is performed on each symbol block of M -QAM data. The zero padding is added to match the DFT size and the number of subcarriers. The output of zero-padded FFT symbols is mapped with Localized subcarriers. IFFT converts the signal into the time domain and CP is added to the transmitted block to avoid ISI. Finally, data blocks are converted into serial data for transmission. The reverse operation is performed at the receiver to get the original data stream.

In the formation of a wireless network, SDR has become more ubiquitous where software defines the transmitted waveform and received waveform to demodulate. Also, software signal processing is done by using Field Programmable Gate Array (FPGA) which offers great flexibility for wireless communication research and development. In this paper, NI USRP Rio is used as an SDR [19, 20]. The experimental model of USRP is shown in Fig. 4.

3 System Model

We consider a wireless communication system using two USRPs. The USRPTx is considered as a User Equipment (UE) and USRPRx is considered as a Base Station (BS). SC-FDMA link is designed in LabVIEW software to transmit the data in Up Link (UL) direction. A series of sample data stream is considered for modeling of SC-FDMA transmitter and receiver link.

3.1 SC-FDMA Transmitter

Symbol Mapping and S/P Converter

The input data stream is converted into a data block after passing it through serial to a parallel converter.

The data block of $\{A_p = [A_k[0], A_k[1], \dots, A_k[M - 1]]^T\}$ dimension M .

Where K is the index of an SC-FDMA symbol.

These data are grouped as $C_{(0,n)}$

$$C_{(0,n)} = \sum_{k=0}^M A_k \tag{1}$$

where M is the number of information bits is grouped.

Modulation and FFT

After modulation the signal becomes $\{C(0, n), C(1, n), \dots, C(M - 1, n)\}$. This modulated signal passed through FFT spreading

$$D(m) = \sum_{n=0}^{N-1} \left\{ c(n) \cdot e^{-\frac{j2\pi mn}{N}} \right\} \quad m \in 0, 1, \dots, N - 1 \tag{2}$$

where N is the total number of constellation mapped carriers.

Subcarrier Mapping Subcarrier Mapping has to be performed when the symbol block size ‘ m ’ is much smaller than IFFT size. In this paper, the localized subcarrier mapping is performed by considering ‘ m ’ symbol has ‘ L ’ frames.

$$d(m) = \sum_{L=0}^{N-1} D_{\text{mapping}}(L) e^{\frac{j2\pi mL}{N}} \tag{3}$$

$$d(m) = \sum_{k=0}^{k-1} D(k) e^{\frac{j2\pi k(L \times m - q)}{L \times k}} \tag{4}$$

For ‘ $q = 0$ ’ we find that $d(m \cdot L) = d_s(m)$ where $q = \text{no. of zeros to be added}$. Subcarrier Mapping in the time domain when ‘ $q \neq 0$ ’ we find that

$$(m \cdot L + q) = \frac{1}{L} \left(1 - e^{\frac{j2\pi q}{L}} \right) \cdot \frac{1}{M} \sum_{p=0}^{M-1} \frac{D_p}{1 - e^{j2\pi \left(\frac{m-p}{N} + \frac{q}{L \cdot M} \right)}} \tag{5}$$

Subcarrier Mapping in the frequency domain

$$d_i = [0, \dots, 0D_i[0]D_i[1], \dots, D_i[M - 1]0, \dots, 0]^T \tag{6}$$

IFFT

This signal is passed through IFFT to convert it into the time domain

$$I(k) = \frac{1}{N} \sum_{K=0}^{N-1} d(K)e^{-j2\pi Kn/N}, \quad n \in 0, 1, \dots, N - 1 \tag{7}$$

Cyclic Prefix

After adding the cyclic prefix the transmission blocks are given below.

$$I_{ci} = I_i[N - C], \dots, I_i[N - 1]I_i[0]I_i[1], \dots, I_i[N - 1]^T \tag{8}$$

where ‘C’ is the CP length.

3.2 SC-FDMA Receiver

The received SC-FDMA symbols are K [12]. The CP is included in the received symbol, given in Eq. (9)

$$[R^{cp}] = \begin{bmatrix} R_k^{cp}[0] \\ R_k^{cp}[1] \\ \vdots \\ R_k^{cp}[C - 2] \\ R_k^{cp}[C - 1] \\ R_k^{cp}[C] \\ \vdots \\ R_k^{cp}[N + C - 1] \end{bmatrix} = A \cdot \begin{bmatrix} h[0] \\ h[1] \\ \vdots \\ h[C - 1] \end{bmatrix} + \begin{bmatrix} S_k[0] \\ S_k[1] \\ \vdots \\ S_k[C - 2] \\ S_k[C - 1] \\ S_k[C] \\ \vdots \\ S_k[N + C - 1] \end{bmatrix} \tag{9}$$

After removing the CP and adding zeros to the channel matrix, the expression is given as (10)

$$\begin{bmatrix} R_k[0] \\ R_k[1] \\ \vdots \\ R_k[N-1] \end{bmatrix} = Q \cdot \begin{bmatrix} h[0] \\ h[1] \\ \vdots \\ h[C-1] \\ 0 \\ \vdots \\ 0 \end{bmatrix} + \begin{bmatrix} S_k[C] \\ S_k[C+1] \\ \vdots \\ S_k[N+C-1] \end{bmatrix} \tag{10}$$

Matrix Q is circulant and it is diagonal in the Fourier domain with diagonal elements given by FFT. So the expression can be written as (11)

$$\begin{bmatrix} R_k[0] \\ R_k[N-C+1] \\ \vdots \\ R_k[N-1] \end{bmatrix} = F^H \cdot \begin{bmatrix} X_k[0] & 0 & \dots & 0 \\ 0 & X_k[1] & \dots & 0 \\ \vdots & \ddots & \ddots & \vdots \\ 0 & 0 & \dots & X_k[N-1] \end{bmatrix} \cdot F \cdot \begin{bmatrix} h[0] \\ h[1] \\ \vdots \\ h[G-1] \\ 0 \\ \vdots \\ 0 \end{bmatrix} + \begin{bmatrix} S_k[N-C] \\ S_k[N-C+1] \\ \vdots \\ S_k[N+C-1] \end{bmatrix} \tag{11}$$

After applying the Fourier Transform, the received signal in the frequency domain is given as (12)

$$\begin{bmatrix} r_k[0] \\ \vdots \\ r_k[N-1] \end{bmatrix} = \begin{bmatrix} X_k[0] & 0 & \dots & 0 \\ 0 & X_k[1] & \dots & 0 \\ \vdots & \ddots & \ddots & \vdots \\ 0 & 0 & \dots & X_k[N-1] \end{bmatrix} \begin{bmatrix} H[0] \\ H[1] \\ \vdots \\ H[N-1] \end{bmatrix} + \begin{bmatrix} S_k[0] \\ \vdots \\ S_k[N-1] \end{bmatrix} \tag{12}$$

PAPR

In this paper, PAPR and BER are calculated. PAPR is the ratio of the square of the received power after IFFT to the mean power.

$$PAPR_{(m)} = \left\{ \frac{\max_{0 \leq m \leq NT} |x(m)|^2}{\frac{1}{NT} \cdot \int_0^{NT} |x(m)|^2 dt} \right\} \tag{13}$$

BER

$$BER = \left\{ \frac{\text{Error bits received}}{\text{No.of transmitted bits}} \right\} \tag{14}$$

4 SC-FDMA Link Design in LabVIEW

4.1 SC-FDMA Transmitter

The modeled SC-FDMA transmitter blocks are designed and simulated in LabVIEW software version 15. The complete design of SC-FDMA transmitter is shown in Fig. 2.

QAM Generator

The 16-QAM modulation scheme is used for the QAM generator. The QAM Generator Block includes ‘Bit Generator Block’, ‘QAM System Parameter Block’, and ‘Map Bit to Symbol Block’. A ‘Bit Generator Block’ generates a binary number using shift registers.

A ‘QAM System Parameter Block’ generates sample per symbol, symbol map, and bit per symbol. A ‘Map Bit To Symbol Block’, maps complex-valued QAM symbols to an output bitstream based on a user-specified symbol, respectively.

Subcarrier Mapping

Zero padding with localized subcarriers mapping is used to match the FFT size to an N -Subcarrier. In order to satisfy the Nyquist rate and fundamental frequency, the number of zeros has to be pad between positive and negative frequency. When the subcarriers are of even number, then ‘True’ value in IFFT is selected. Thus, the carriers are divided into two groups. One group of the carriers occupies positive frequency and another group of the carriers occupies negative frequency. The zeros are injected between to properly align the carriers relative to Nyquist rate. The

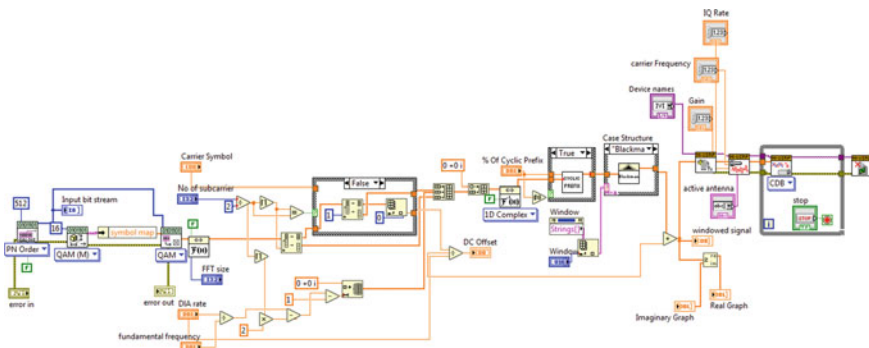


Fig. 2 SC-FDMA transmitter design in Labview

total number of padded zeros are $(f_s/f_o * \text{Subcarrier} - 1)$. When the subcarriers are odd numbers that imply ‘False’ in IFFT. In this case, one carrier is dropped and the first carrier symbol is placed at the dc offset. Finally, the positive frequency, zero paddings, and negative frequency are concatenated. The total number of padded zeros are $(f_s/f_o * \text{Subcarrier} - 1 - 1)$. The signal is oversampled by padding original signal with zeros and the out-of-band radiation reduced.

Cyclic Prefix

The split array ratio is used in the Cyclic Prefix. The original signal is multiplied with the ‘1-Input Cyclic Prefix value’ and given to the split array ratio. The second part of the split array ratio is taken at the output and then concatenated with the original signal. The Cyclic Prefix Accepts prefix between ‘0’ and ‘1’. ‘0’ indicates no change in the original input signal and ‘1’ indicates a symbol with 100% CP (Two Period original signal).

Windowing

Windowing reduces discontinuous signals driving to zero. The Ring Menu is used to add the desired window function and then DC offset is added to prevent distortion of the signal.

4.2 SC-FDMA Receiver

The modeled SC-FDMA receiver blocks are designed and simulated using LabVIEW software is shown in Fig. 3. The real-time transmitted bits trough USRP is received at the receiver and converted into parallel bits, a cyclic prefix is removed and converted into the frequency domain using FFT. For non-trivel channel received signal is dispersive. Channel equalizer equalizes the dispersive channel and then the subcarrier demapping is done. The data is converted into serial after IFFT. Thus, original data is recovered after doing the symbol demapping.

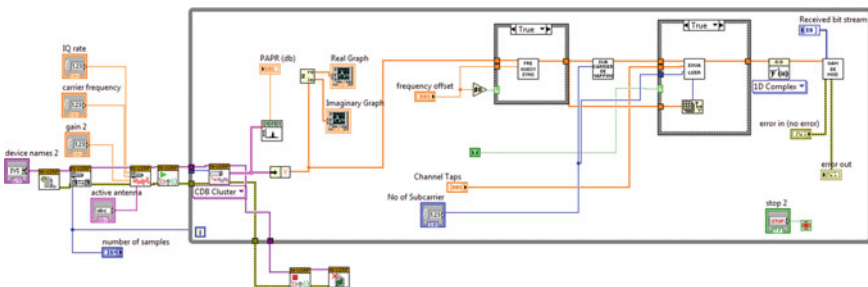


Fig. 3 SC-FDMA receiver design in LabVIEW

5 Experimental Setup

The real-time experimentation has performed using USRP testbed as shown in Fig. 4. In this experimental setup, two USRPs are used which are kept 1 m apart from each other. The transmitter USRP_{Tr} is considered as a UE and receiver USRP_{Rx} is considered as a BS. Each USRP has mounted with two antennas.

The data stream is transmitted through USRP_{Tr} and received at the USRP_{Rx} through SC-FDMA link. The LTE UL parameters are considered to simulate the link as shown in Table 1. USRP parameters are set for data transmission and reception shown in Table 2. These parameters are used to simulate the real-time data transmission in UL direction through USRP testbed.



Fig. 4 Experimental model

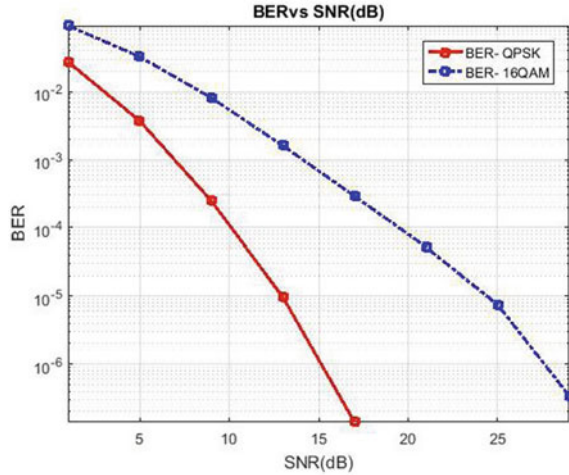
Table 1 Parameter setting for SC-FDMA

Parameter	Setting
Bandwidth	5 MHz
No. of subcarrier	324
FFT size	666
Fundamental frequency	1 kHz
DIA rating	7.8 MHz
Cyclic prefix	0.5
Windowing	Blackman

Table 2 Parameter setting of USRP

Parameter	Setting
IQ rate	1 MHz
Carrier frequency	500 MHz
Gain	30
Carrier	100 + 0i
No. of transmitting antenna	1
No. of receiving antenna	1

Fig. 5 SNR versus BER for different modulation schemes



6 Simulation Results

The proposed SC-FDMA link is designed and simulated using LabVIEW software. The 16-QAM modulation scheme is used in SC-FDMA transmitter. The selection of modulation scheme is based on estimated values BER for different modulation schemes, which are simulated in MATLAB software. For 10 dB SNR, the value of BER is 10^{-4} for QPSK and 10^{-2} for the 16-QAM modulation scheme shown in Fig. 5.

In real-time experimentation, the strings of data bits are transmitted through UE and received at the BS using USRP testbed. Table 2 shows USRP parameter settings. The transmitted bits string through SC-FDMA link at UE is “11111101000” and received bits string at BS is “10111101000” in UL direction. SC-FDMA link parameters are set for the 5 MHz Bandwidth shown in Table 1. For every transmission cycle, the BER and PAPR are calculated. The calculated BER is 10^{-1} . Also, the real and imaginary waveform of transmitted and received bits is observed. Transmitted waveforms are not the same as received waveforms because of two-bit errors shown in Figs. 6 and 7.

The estimated PAPR of the proposed SC-FDMA link design technique is 7.43825 dB which is lesser than the existing SC-FDMA link design technique [1, 6]. The comparison values are given in Fig. 8.

7 Conclusions and Future Work

In this paper, the SC-FDMA link is modeled and designed in LabVIEW. The effectiveness of the proposed system is investigated through simulation and implementation on

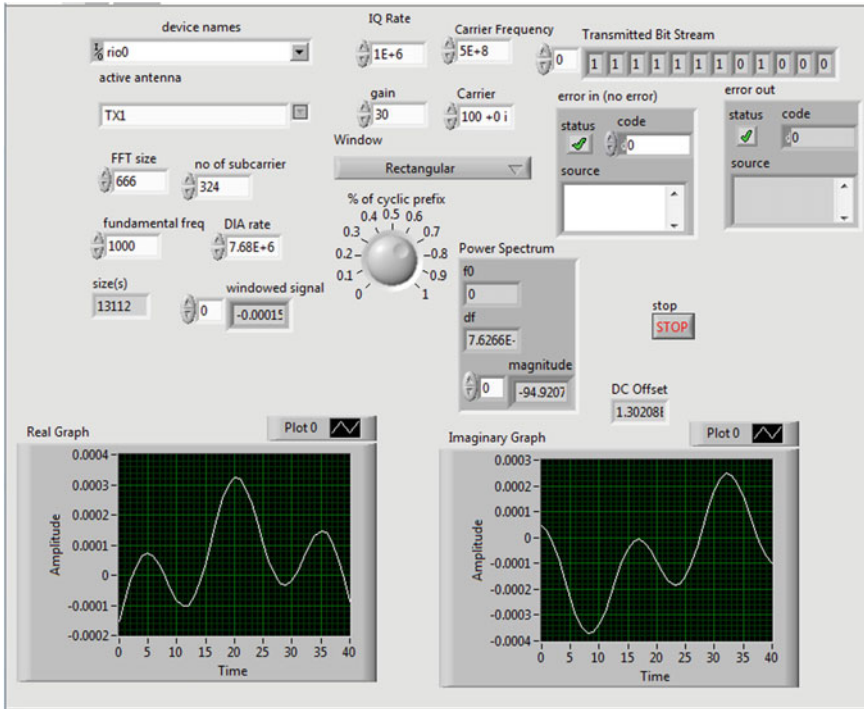


Fig. 6 Simulation result of transmitter

USRP testbed. The real-time data transmission through this link is carried out using SDR. As a result, PAPR for SC-FDMA is 20% lower than OFDM with selected 5 MHz BW. The simulation of SNR vs BER for different modulation schemes is performed. With 10 dB SNR, the BER is 10^{-4} for QPSK and 10^{-2} in the case of 16QAM which is significantly low.

SC-FDMA schemes of application work generally used in worldwide networks by operators like Verizon, AT&T, Vodafone, Idea, etc. It is most robust in multipath fading and has low PAPR than downlink OFDMA. It increases cell coverage capacity and spectral efficiency.

The work can be further extended for the development of scheduling algorithms for SC-FDMA to optimize the system performance. This will result in reducing the cost per bit transmitted over the radio interface, without causing an overhead on the computational complexity. It is most important to achieve fairness resource allocation and Quality of Service (QoS) among the UEs. At the same time try to utilize the resources assigned most efficiently as possible.

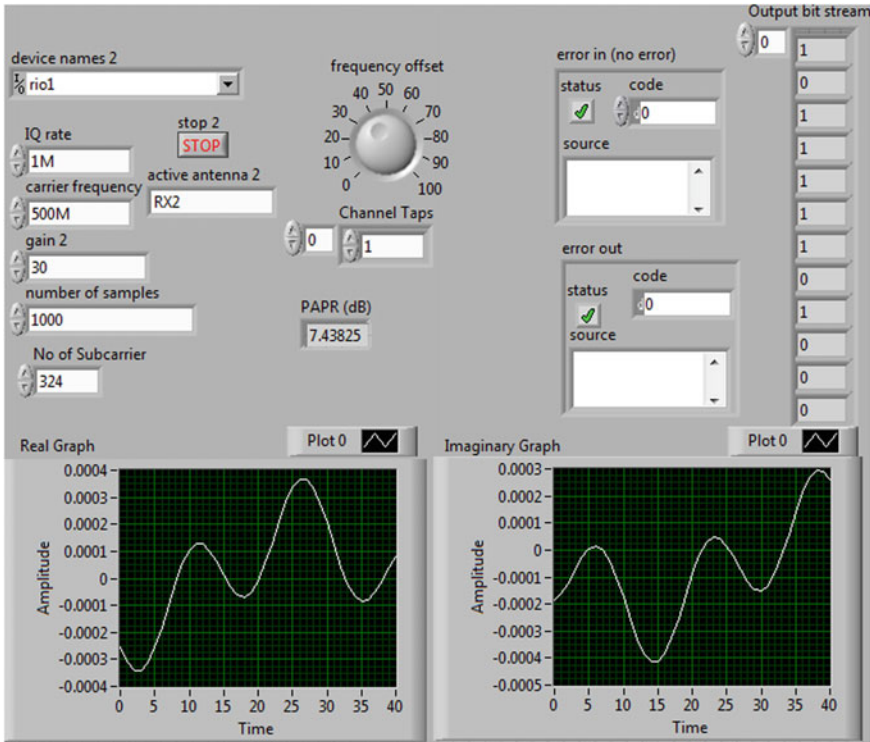


Fig. 7 Simulation result of receiver

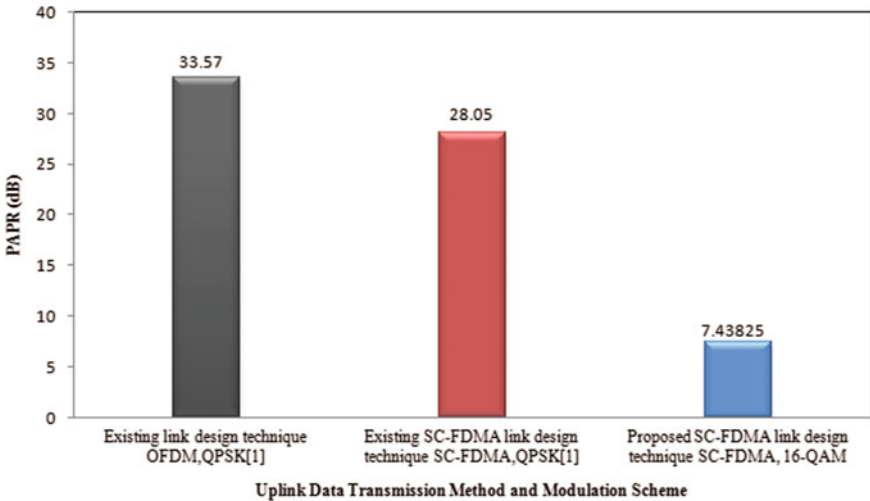


Fig. 8 PAPR comparison of the existing and proposed technique

References

1. Idris A, Farhana AN, Adiba H, Kassim M (2017) BER and PAPR analysis of MIMO OFDMA and SCFDMA system using different diversity techniques. In: 7th IEEE international conference on control system, computing and engineering (ICCSCE). <https://doi.org/10.1109/iccsce.2017.8284422>
2. Hossain MR, Ahmmed KT (2017) Efficient PAPR reduction in DCT-SCFDMA system based on absolute exponential companding technique with pulse shaping. *Wireless Pers Commun* 97(3):3449–3463. <https://doi.org/10.1007/s11277-017-4678-1>
3. Hossain MR, Ahmmed KT (2018) Non-linear companding based hybrid PAPR reduction approach for DCT-SCFDMA system. *IET Commun* 12(12):1468–1476. <https://doi.org/10.1049/iet-com.2017.0921>
4. Yeh H-G, Mutahir Abdul H (2015) Hadamard SCFDMA-A modified uplink transmission scheme with low PAPR and SER. In: Annual IEEE systems conference (SysCon) proceedings. <https://doi.org/10.1109/syscon.2015.7116834>
5. Sana AM, Hussein QM, Hameed MA, Saeed AT (2019) Performance analysis of circular 16-QAM constellation for single carrier-frequency division multiple access systems. *J Comput Theor Nanosci* 16(3):1019–1022. <https://doi.org/10.1166/jctn.2019.7991>
6. Ji J, Ren G, Zhang H (2015) PAPR reduction of SC-FDMA signals via probabilistic pulse shaping. *IEEE Trans Veh Technol* 64(9):3999–4008. <https://doi.org/10.1109/tvt.2014.2366598>
7. Al-Kamal FS, Hassan ES, El-Naby MA, Shawki F, El-Khamy SE, Dessouky MI, Sallam BM, Alshebeili SA, El-Samie FE (2015) An efficient transceiver scheme for sc-fdma systems based on discrete wavelet transform and discrete cosine transform. *Wirel Pers Commun* 83(4):3133–3155
8. Chisab RF, Shukla C (2014) Performance evaluation of 4G-LTE-SCFDMA scheme under SUI And ITU channel models. *Int J Eng Technol IJET-IJENS* 14(1):58–69. <https://doi.org/10.1109/s2019.2916937>
9. Hwang J-K, Li C-F, Chen C-M, Pan Y-W (2016) Cost effective software defined radio approach to cross-platform LTE vector signal analysis. In: IEEE symposium on computer applications & industrial electronics (ISCAIE). <https://doi.org/10.1109/fiscaie.2016.7575027>
10. Gouda ME, Moharam MH, Ragab MR, Anwar AM, Gouda AF (2016) USRP implementation of PTS technique for PAPR reduction in OFDM Using LABVIEW. *Adv Wirel Commun Netw* 2(2):15–24. <https://doi.org/10.11648/j.awcn.20160202.11>
11. Gupta R, Bachmann B, Kruppe A, Ford R, Rangan S, Kundargi N, Ekbal A, Rathi K, Asadi A, Mancuso V, Morelli A (2015) LabVIEW based software-defined physical/MAC layer architecture for prototyping dense LTE networks. <http://eprints.networks.imdea.org/id/eprint/1363>
12. Li P, Jia YJ, Chen F, He PH, Fan HF (2016) The synchronization design and implementation of LTE-advanced real-time test platform based on software defined radio. *Int J Smart Home* 10(5):149–158
13. Soni G, Verma C (2015) Performance investigation of LTE systems based on NI PXIe-5644R vector signal transceiver. In: Global conference on communication technologies (GCCT). doi:10.1109/gcct.2015.7342765
14. Sheybani E, Javidi G (2017) Integrating software defined radio with USRP. *Int J Interdisc Telecommun Networking* 9(3):1–9. <https://doi.org/10.4018/ijtn.2017070101>
15. Thakur A, Rattan M (2018) Implementation of convolution coded OFDM through different channel models on SDR platform. *Int J Inf Technol*. <https://doi.org/10.1007/s41870-018-0265-2>
16. Gökceli S, Alakoca H, Başaran ST, Kurt GK (2016) OFDMA-based network-coded cooperation: design and implementation using software-defined radio nodes. *EURASIP J Adv Sign Process* 2016(1). <https://doi.org/10.1186/s13634-016-0305-7>
17. Soni G, Megh G (2016) Experimental investigation of spectrum sensing for LTE frequency band based on USRP 2920/VST 5644. In: International conference on control, instrumentation,

- communication and computational technologies (ICCICCT). <https://doi.org/10.1109/iccicct.2016.7988062>
18. Jorgensen PB, Hansen TL, Sorensen TB, Berardinelli G (2011) Implementation of LTE SC-FDMA on the USRP2 software defined radio platform. In: IEEE Swedish communication technologies workshop (Swe-CTW). <https://doi.org/10.1109/swe-ctw.2011.6082485>
 19. Black BA (2014) Introduction to communication systems lab based learning with NI USRP and LabVIEW communications. Printed in Hungary, pp 1–154
 20. Une Introduction À La Radio Définie Par Logiciel avec NI LabVIEWet NI USRP Version 1.1—Q4 2013, pp 1–72

Real-Time Simulation and Analysis of Energy Storage System in Standalone PV-Based DC Microgrid



Prashant Singh and J. S. Lather

Abstract This paper presents a novel strategy for calculating Lead-Acid battery charging and discharging time with different cases for standalone PV-based DC microgrid systems. The strategy has been implemented for a PV module incorporating MPP tracker to control the Lead-Acid battery charging and discharging time. This technique allows for improved condition of Lead-Acid battery under charge and discharge cycles. In addition, a supercapacitor is connected to the proposed configuration. The supercapacitor charging time at constant solar irradiance is calculated and compared with Lead-Acid battery and further verified by Ragone Plot. The performance of the proposed strategy has been validated through implementation on OPAL-RT real-time simulator.

Keywords Battery energy storage (BES) · Supercapacitor (SC) · State of charge (SoC) · PV systems

1 Introduction

To meet extremely severe energy crisis, rising global power demand, and address immediate and long term environmental concerns, renewable energy sources (RESs) are considered as a replacement for conventional fossil fuel-based energy sources [1, 2]. Apart from the inherent advantages of such alternate energy resources, several infrastructure and operations-related financial concerns and technical control issues need to be addressed [1]. Intermittent and variable nature of renewable energy resources lead to demand mismatch and power quality issues, and thus demands for the incorporation of energy storage devices within the system [3]. The standalone PV systems with hybrid energy storage systems (battery, supercapacitor) are receiving steady exposure these days [4], thereby making the development of such multi-energy storage system a desirable solution for increasing power generation and lowering the cost of a standalone system [5]. Distinct power density versus energy density plot

P. Singh (✉) · J. S. Lather
EED, NIT Kurukshetra, Kurukshetra, India
e-mail: prs21017@gmail.com

© Springer Nature Singapore Pte Ltd. 2021
G. S. Hura et al. (eds.), *Advances in Communication and Computational Technology*, Lecture Notes in Electrical Engineering 668,
https://doi.org/10.1007/978-981-15-5341-7_77

1019

called Ragone Plot [6] for conventional to modern energy storage systems is as shown in Fig. 1, wherein it is evident that although batteries do have large energy density but admit low power densities. It means that batteries are not suitable to meet immediate load requirements. In contrast, supercapacitors admit large power densities but have a very low energy density, which renders them suitable to meet immediate low energy demands. Therefore, a hybrid energy storage system finds its place taking advantage of both high power and energy densities to address immediate as well as large energy requirements [7]. For improved performance, the battery and the supercapacitor are coupled in the proposed considered system.

Figure 2 presents the typical interconnections for standalone PV-based DC microgrid. It consists of PV, hybrid energy storage system (HESS), i.e., rechargeable battery, supercapacitor as well as an electronic charge controller.

Traditional charging controller incorporates maximum power point tracking (MPPT) which always enhances electricity generation and regulates battery charging by controlling battery charging status (SoC) to avoid excess charge and deep

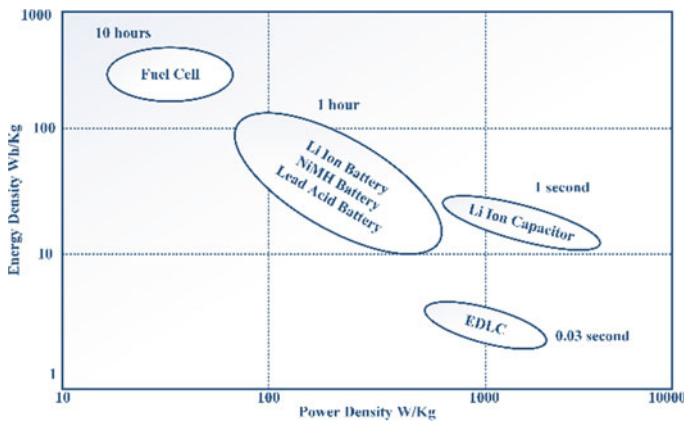


Fig. 1 Ragone plot [6]

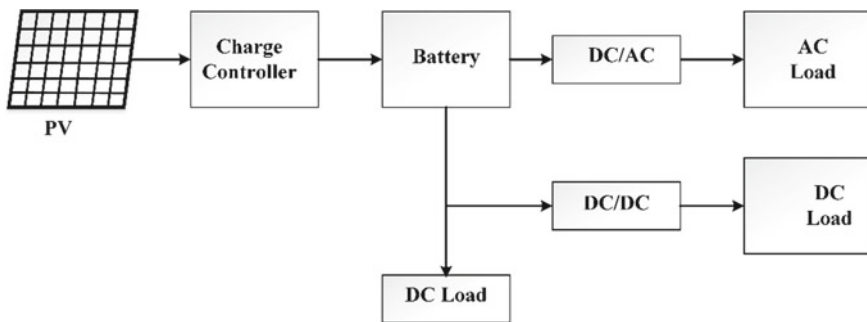


Fig. 2 Typical configuration of standalone PV-based DC microgrid

discharge [8]. Nonetheless, many life-limiting factors, which really increase battery efficiency degradation along with high C-rate, varying power exchange, deep discharge, and some other factors are not often taken into consideration in standard charge controllers. On such a local scale to better quantify the effects on the role of battery storage systems in the domestic energy balance is presented in [9]. In [10], a method has been developed to calculate the lifetime of lithium-ion batteries by incorporating electrochemical as well as thermal aged models. In [11] a genetic algorithm was presented to schedule each Li-ion battery charge/discharge rate with the aim of reducing energy exchange losses by minimizing the power in the PCC of the microgrid with the main grid. However, Li-ion batteries take more charging time as compared to Lead-Acid batteries. Therefore, Lead-Acid batteries are one of the popular energy storage systems used for the standalone PV power system suffering from short operational life, notwithstanding outstanding electrical features and lower initial costs [12, 13]. Comparison of different batteries charging time at various cases was presented [14, 15]. Most researchers have proposed that hybrid energy storage systems (HESSs) could boost the cycle lifespan of the battery by minimizing stresses during charge-discharge cycles [16]. Many such HESS require to remodel of the topologies of energy storage systems, particularly for remote locations from economic viability point of view. A smart HESSs plug and play systems resulting in improved life span of Lead-Acid battery in standalone PV power system by reducing variables like current volatility and surge current was proposed in [17]. An impressive report [18] on cost analysis of standalone PV system with Lead-Acid and Li-ion batteries observed that a framework with Lead-Acid battery would have been financially better value for money than that of a system with Li-ion battery. Keeping in view the high initial installation cost, [19] presenting a cost reduction for islanded mode alternatives in solar home system and remote area power supply system with better battery technologies. However, several literature were presented but did not discuss and compare battery and supercapacitor charging and discharging time with different cases, and besides this in several papers Li-ion battery is selected for storing energy. But, Li-ion batteries take more charging time as compared to Lead-Acid batteries.

This paper presents a study related to Lead-Acid battery and supercapacitor charging time with different cases in the standalone PV-based DC microgrid system. This work focuses on how to extend the battery lifetime without reaching a fully charging point reached on each battery, yet maximally utilizing solar energy by introducing a charging and discharging control system. These control systems are employed on every single battery in order to charge and discharge battery to its individual condition and limitation. The paper is organized as under Sect. 2 discusses the considered system configuration and its modeling with standalone PV-based DC microgrid. Section 3 details battery charge controller and its conditions. Real-time validation of the proposed charge control strategy on OPAL-RT is presented in Sect. 4, followed by conclusions and future directions in Sect. 5.

2 System Configuration and Modeling of Standalone PV-Based DC Microgrid

The considered standalone PV-based DC microgrid is as shown in Fig. 3, which comprises of PV array-based energy source assisted by battery and supercapacitor, charge controller, and loads.

2.1 PV System Modeling

PV effect is a fundamental physical mechanism that directly converts solar power into electric power. A PV cell is essentially a fundamental unit in systems with PV energy generation. The single-diode mathematical model can be used to simulate PV cells consisting of a photocurrent source I_L , a nonlinear diode, and R_S is series internal resistance as shown in Fig. 4. I-V Photovoltaic equation characteristics are given as [20].

$$I = I_L - I_o \left[\exp\left(\frac{V + IR_s}{\alpha}\right) - 1 \right] \tag{1}$$

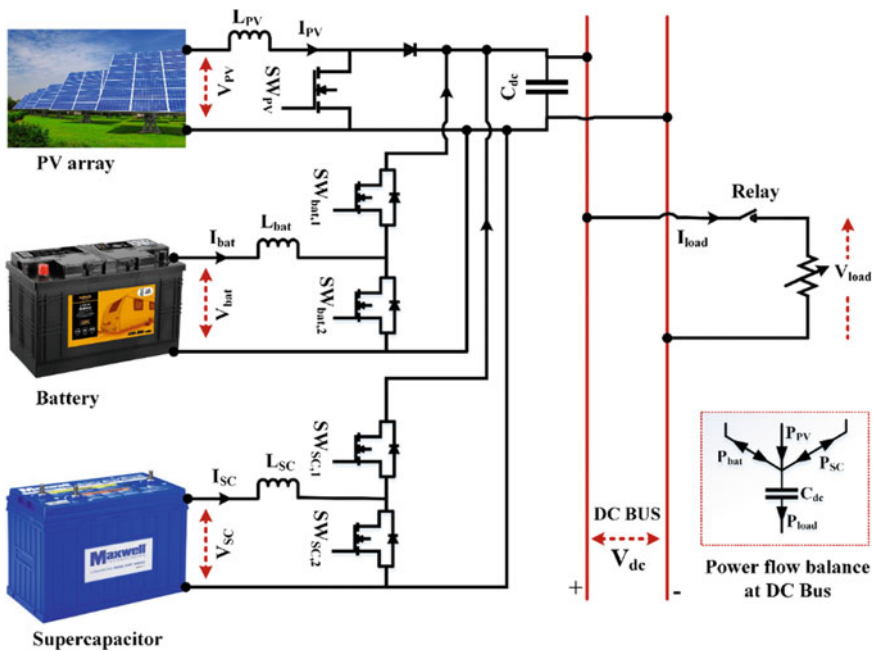
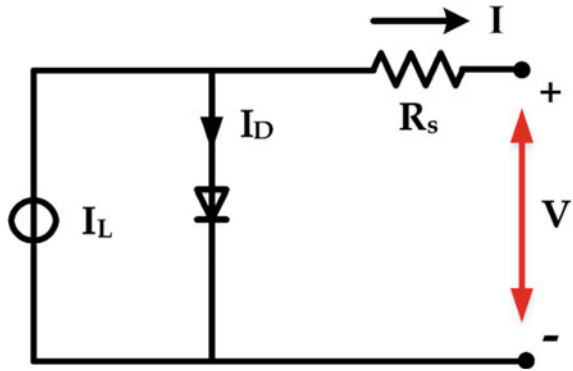


Fig. 3 Equivalent system configuration of considered standalone PV-based DC microgrid

Fig. 4 Single diode equivalent circuit of PV cell



here I_L is the light generated PV currents (A), I_D represents the module saturation current (A), I is the PV module output current (A), V is the PV output voltage (V), R_s is series resistance of PV cell and α is thermal voltage timing completion factor of PV cell (V).

2.2 Battery Modeling

The battery is modeled in series with a constant resistance used a simple controlled voltage source. The battery has been modeled using the following equation as just a nonlinear voltage source [21] (Fig. 5).

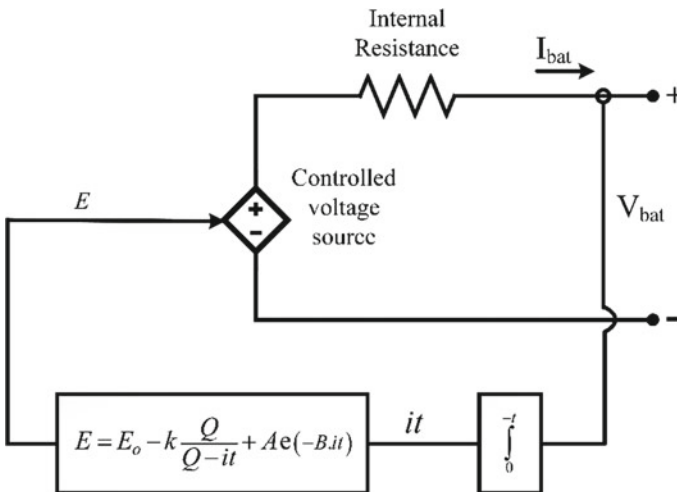


Fig. 5 Equivalent circuit of battery nonlinear model

$$V_{\text{bat}} = E_o - k \frac{Q}{Q - \int i dt} + A e^{B \int i dt} - i R_i \tag{2}$$

$$\% \text{ SoC} = \left(1 - \frac{1}{Q} \int i dt \right) * 100 \tag{3}$$

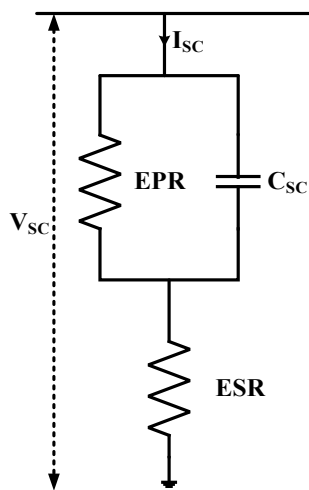
where V_{bat} , E_o and i is the nonlinear voltage (V), constant voltage (V) of battery, and battery current (A) and different parameters may also acquire from the configuration in [21].

2.3 Supercapacitor Modeling

SC is an electrostatic device that, owing to its construction functionality, i.e., the electrodynamic double layer, arrives with an enormous capability. Because its process is much like a capacitor, it could be relentlessly discharged/charged dissimilar most of the batteries showing deterioration ion with the increases in operation cycles. The super capacitor’s electrical equivalent circuit is seen in Fig. 6. Equivalent series resistance (ESR) and Equivalent parallel resistance (EPR) represent, respectively, the supercapacitor’s equivalent series and parallel resistance C_{eq} is the supercapacitor equivalent capacity [22].

$$\text{ESR} = \frac{\Delta V}{\Delta i} \tag{4}$$

Fig. 6 Equivalent RC circuit of supercapacitor



$$ESR = \frac{-(t_2 - t_1)}{\ln\left(\frac{V_2}{V_1}\right)c} \tag{5}$$

$$v_c = ESR \cdot i_c + \frac{1}{c} \int \left(i_c - \frac{e_c}{EPR}\right) d\tau + V_{c_init} \tag{6}$$

where V_1 , V_2 and C is the self-discharge voltage at t_1 , t_2 and rated capacitance, respectively.

3 Battery Charge Controller

The battery charge controller is configured with such a battery voltage level of 24 V and a current level of 5 A shown in Fig. 7. The function of the load controller is as follows: Unless the battery voltage exceeds 24 V, the battery becomes decoupled from PV system and even if the voltage goes down below 10 V, the PV system must be linked. And if the battery voltage around 10 and 24 V only connects the PV system to the battery. Taking into account the hysteresis relay, this logic is implemented. Whether the battery voltage is between 14 and 25 V, the regular load is linked to the battery other than the dump load. Battery charge controller conditional action charge diagram is shown in Table 1.

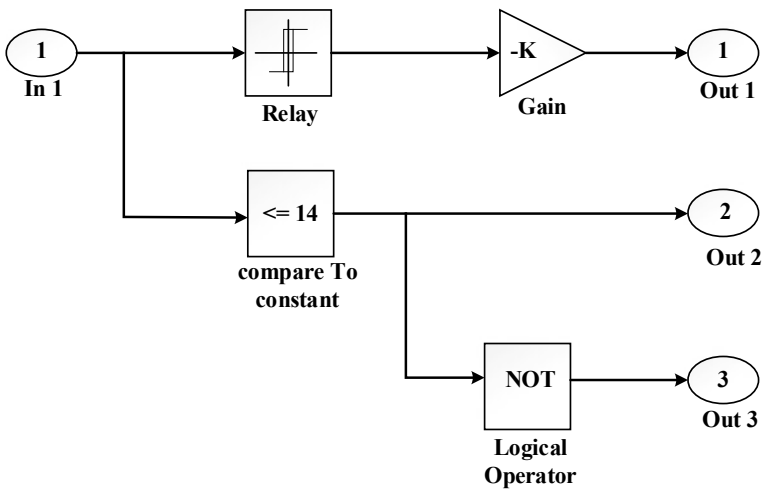


Fig. 7 Internal battery charge controller circuit diagram

Table 1 Battery charge controller condition chart

Condition	Action
PV power = Load battery SoC high	PV supplies load no battery charging
PV power = Load battery SoC low	PV supplies load no battery charging
PV power > Load battery SoC high	PV supplies load no battery charging
PV power > Load battery SoC low	PV supplies load PV charges battery
PV power < Load battery SoC high	PV supplies load battery supplies load
PV power < Load battery SoC Low	PV supplies load battery supplies load until minimum SoC reached then load disconnected
No PV power battery SoC high	Battery supplies load

4 Result and Discussion

In this section, the effectiveness of the proposed standalone PV-based DC microgrid is simulated in OPAL-RT real-time simulator (OP 5700 RTS) for 100*2000 and Test bed of OPAL-RT real-time simulator is shown in Fig. 8, including host (simulator), DB-37 connector, Bayonet Neill-Concelman (BNC) cables. The standalone PV-based DC microgrid nominal specifications are provided in Table 2.

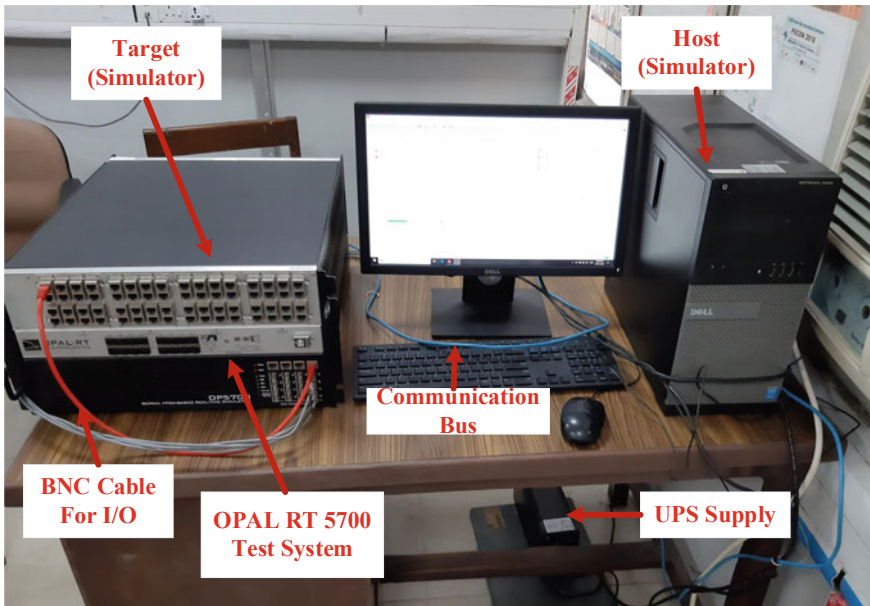


Fig. 8 OPAL-RT test bed for standalone PV-based DC microgrid

Table 2 Component rating of the standalone PV-based DC microgrid

Subsystem	Specifications
PV array at standard test condition	$V_{OC} = 22.2$ v, $I_{SC} = 7.96$ A, $V_M = 18.14$ v, $I_M = 7.44$ A
Battery (Lead-acid)	24 V, 165 Ah
Supercapacitor	5 F, 48 V
Battery charge controller	$L_{PV} = 8.64$, $L_{bat} = 1.4$, $L_{SC} = 1.24$ mH, $C = 440$ μ F, $R = 5$ Ω

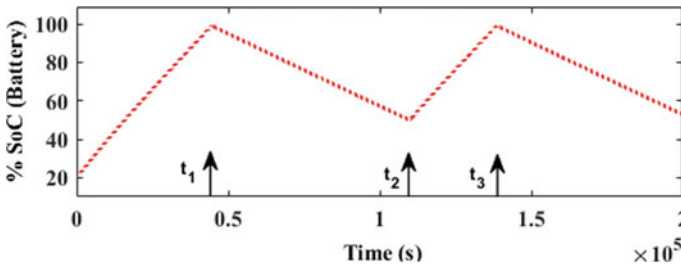


Fig. 9 Lead-acid battery SoC waveform (initial 20% SoC)

4.1 Case-1 at Standard Test Condition (1000 w/m² and 25 °C) with Lead-Acid Battery

4.1.1 Scenario (a)—with 20% SoC

Figure 9 shows the Lead-Acid battery SoC waveforms whereas load current and battery current waveforms are seen in Fig. 10. In this case Lead-Acid battery initial SoC is at 20%. From t_1 to t_2 instant battery SoC is decreasing, during this time battery is charging and load demand is fulfilled by PV. From t_2 to t_3 instant Lead-Acid battery SoC start increasing, and during this period battery is discharging means load demand is supplied by battery with PV.

4.1.2 Scenario (b)—with 50% SoC

Figures 11 and 12 demonstrate the Lead-Acid battery SoC, load current, and battery current waveforms. In this case Lead-Acid battery initial SoC is at 50%.

Figure 13 displays the comparison of batteries (Lead-Acid) charging time with different SoC and with different solar irradiance. At standard test condition with 20% initial SoC Lead-Acid battery holds 12.31 h to become full charge whereas with 50% initial SoC Lead-Acid battery takes 7.99 h to become full charge.

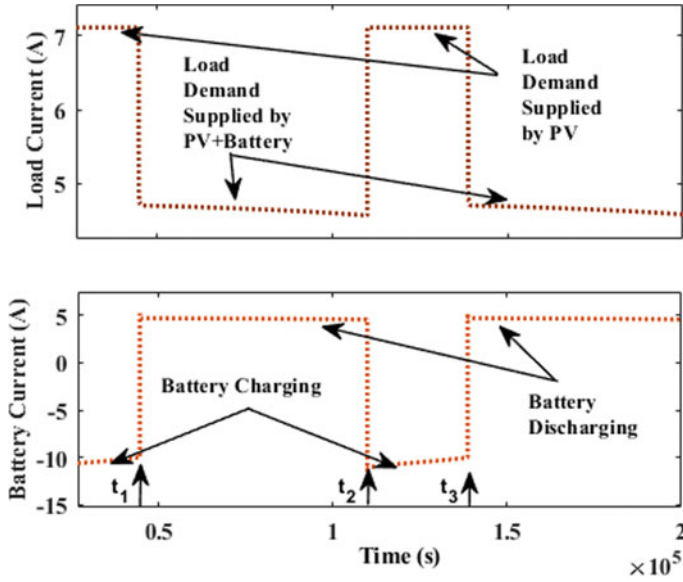


Fig. 10 Load current and battery current waveform (at constant solar Irradiance 1000 w/m² and with 20% SoC)

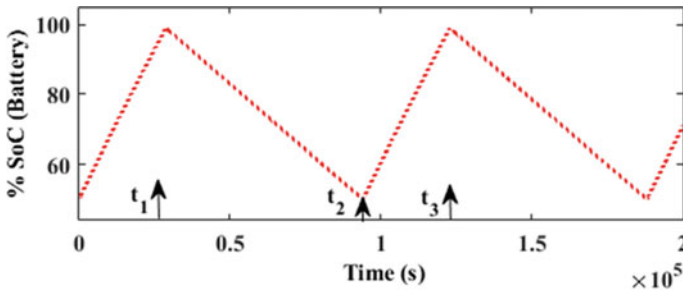


Fig. 11 Lead-acid battery SoC waveform (initial 50% SoC)

4.2 Case-2 at Standard Test Condition (1000 w/m² and 25 °C) with Supercapacitor

Figure 14 illustrates that the SC requires 6.54 s to fully charge at this time the voltage of the supercapacitor is 3.59 V and we can also see that the shape of the waveform charging and discharge is well reproduced by the simulation.

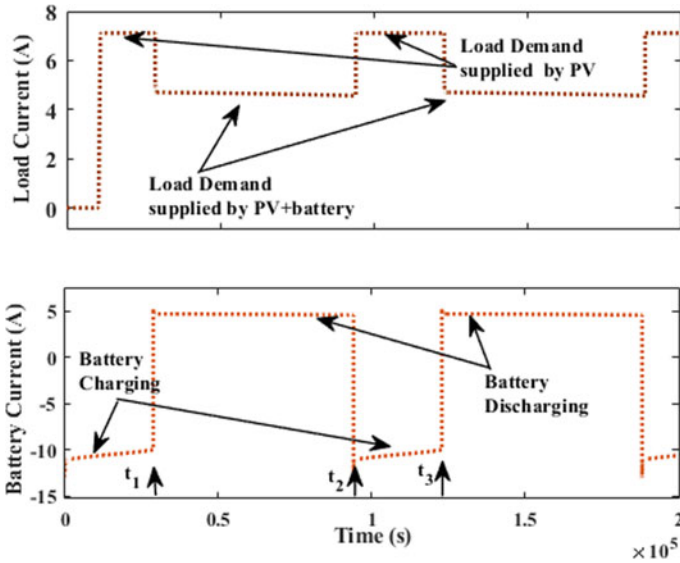


Fig. 12 Load current and battery current waveform (at constant solar Irradiance 1000 w/m² and with 50% SoC)

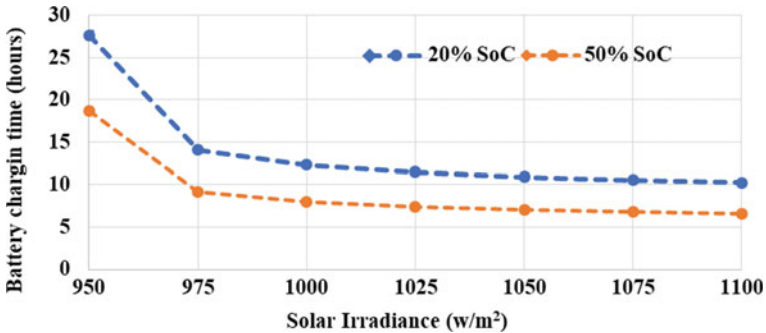


Fig. 13 Lead-acid battery charging time comparison with different SoC and at various solar irradiance

Figure 15 illustrates the SC charging time at constant solar irradiance, showing that the value of constant solar insolation increases the charging time of the supercapacitor decreases. Figure 15 also describes the increase in solar PV output voltage and power with regard to solar irradiance.

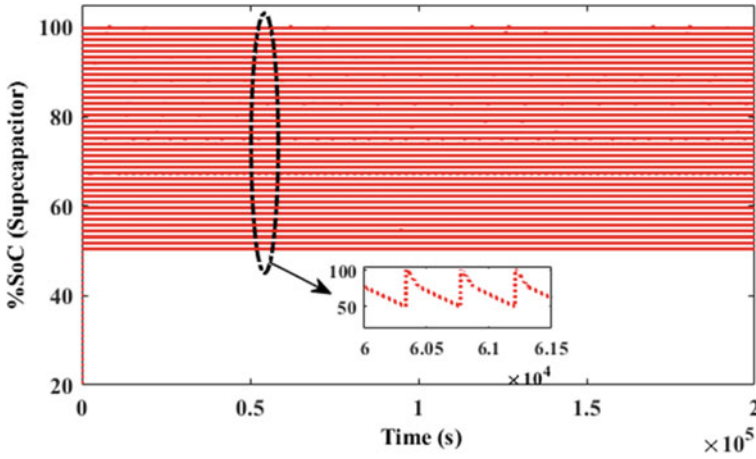


Fig. 14 SC charge-discharge waveforms

5 Conclusion

Analysis and comparison of Lead-Acid battery and SC charging time of standalone PV-based DC microgrid has been carried out and successfully validated through the OPAL-RT real-time simulator in this paper. Charging time taken by Lead-Acid battery (with different SoC and solar irradiance) and supercapacitor has also been verified through Ragone Plot. Comparative study between different types of batteries such as Li-ion battery, Nickel Cadmium (NiCd), and Nickel-Metal-Hydride (NiMH) batteries for solar home systems or standalone power supply system, with stability analysis, remains topic for future research.

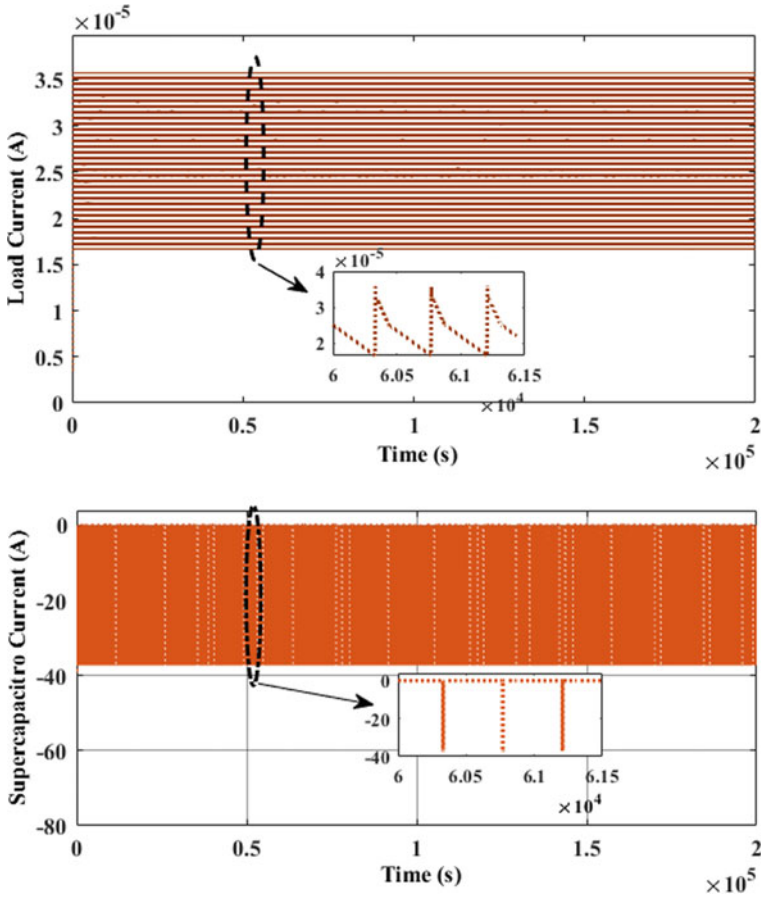


Fig. 15 Load current and SC current waveforms

Acknowledgements The authors express their heartfelt thanks to MHRD, Government of India for providing financial assistance during this research work.

References

1. Ehsan A, Yang Q (2018) Optimal integration and planning of renewable distributed generation in the power distribution networks: a review of analytical techniques. *Appl Energy* 210:44–59
2. Liu J, Luo W, Yang X, Wu L (2016) Robust model-based fault diagnosis for PEM fuel cell air-feed system. *IEEE Trans Ind Electron* 63:3261–3270
3. Nejabatkhah F, Li YW (2015) Overview of power management strategies of hybrid AC/DC microgrid. *IEEE Trans Power Electron* 30:7072–7089
4. Rekioua D, Bensmail S, Bettar N (2014) Development of hybrid photovoltaic-fuel cell system for stand-alone application. *Int J Hydrogen Energy* 39:1604–1611

5. Gahleitner G (2013) Hydrogen from renewable electricity: an international review of power-to-gas pilot plants for stationary applications. *Int J Hydrogen Energy* 38:2039–2061
6. Christen T, Carlen MW (2000) Theory of Ragone plots. *J Power Sources* 91:210–216
7. Mendis N, Muttaqi KM, Perera S (2014) Management of battery-supercapacitor hybrid energy storage and synchronous condenser for isolated operation of PMSG based variable-speed wind turbine generating systems. *IEEE Trans Smart Grid* 5:944–953
8. Bortolini M, Gamberi M, Graziani A (2014) Technical and economic design of photovoltaic and battery energy storage system. *Energy Convers Manag* 86:81–92
9. Reimuth A, Prasch M, Locherer V, Danner M, Mauser W (2019) Influence of different battery charging strategies on residual grid power flows and self-consumption rates at regional scale. *Appl Energy* 238:572–581
10. Ghorbanzadeh M, Astaneh M, Golzar F (2019) Long-term degradation based analysis for lithium-ion batteries in off-grid wind-battery renewable energy systems. *Energy* 166:1194–1206
11. Ruiz-Cortes M, Gonzalez-Romera E, Amaral-Lopes R, Romero-Cadaval E, Martins J, Milanese-Montero MI, Barrero-Gonzalez F (2019) Optimal charge/discharge scheduling of batteries in microgrids of prosumers. *IEEE Trans Energy Convers* 34:468–477
12. Luo X, Wang J, Dooner M, Clarke J (2015) Overview of current development in electrical energy storage technologies and the application potential in power system operation. *Appl Energy* 137:511–536
13. Greenleaf M, Dalchand O, Li H, Zheng JP (2015) A temperature-dependent study of sealed lead-acid batteries using physical equivalent circuit modeling with impedance spectra derived high current/power correction. *IEEE Trans Sustain Energy* 6:380–387
14. Pareek A, Singh P, Rao PN (2018) Analysis and comparison of charging time between battery and supercapacitor for 300 W stand-alone PV system. In: *Proceedings of 2018 international conference current trends towards converging technology, ICCTCT 2018*, pp 1–6
15. Singh P, Sujil A, Kumar P (2016) Analysis and comparison of batteries charging time for stand alone photovoltaic system. In: *2016 IEEE 6th international conference on power systems (ICPS)*. IEEE, pp 1–4
16. Kim Y, Raghunathan V, Raghunathan A (2017) Design and management of battery-supercapacitor hybrid electrical energy storage systems for regulation services. *IEEE Trans Multi-Scale Comput Syst* 3:12–24
17. Jing W, Lai CH, Ling DKX, Wong WSH, Wong MLD (2019) Battery lifetime enhancement via smart hybrid energy storage plug-in module in standalone photovoltaic power system. *J Energy Storage* 21:586–598
18. Anuphaphpharadorn S, Sukchai S, Sirisamphanwong C, Ketjoy N (2014) Comparison the economic analysis of the battery between lithium-ion and lead-acid in PV stand-alone application. *Energy Procedia* 56:352–358
19. Paul Ayeng'o S, Schirmer T, Kairies KP, Axelsen H, Uwe Sauer D (2018) Comparison of off-grid power supply systems using lead-acid and lithium-ion batteries. *Sol Energy* 162:140–152
20. Wang C, Nehrir MH (2008) Power management of a stand-alone wind/photovoltaic/fuel cell energy system. *IEEE Trans Energy Convers* 23:957–967
21. Tremblay O, Dessaint L-A, Dekkiche A-I (2007) A generic battery model for the dynamic simulation of hybrid electric vehicles. In: *2007 IEEE vehicle power and propulsion conference*. IEEE, pp 284–289
22. Cheng Z, Chen W, Li Q, Jiang Z, Yang Z (2010) Modeling and dynamic simulation of an efficient energy storage component-supercapacitor. In: *2010 Asia-Pacific power and energy engineering conference*. IEEE, pp 1–4

Intelligent Method for Detection of Coronary Artery Disease with Ensemble Approach



Luxmi Sapra, Jasminder Kaur Sandhu, and Nitin Goyal

Abstract Coronary artery is a major reason of health ailments all over the world. Its detection and management incurred huge amount of deaths across the nation. Heart disease can be diagnosed using various invasive and non-invasive methods. One of the effective methods for detection of coronary artery disease is coronary angiography, which is expensive and also has side effects. This further requires high level of technical expertise. Due to improvement in technology and low-cost storage devices, storage of huge amount of data becomes easy. Even health sector has been untouched. Machine learning methods are being used to analyze the collected data due to its capability to predict the diseases. In this work, machine learning methods are implemented in order to achieve low-cost, reproducible, non-invasive, rapid, and precise identification of heart disease. This paper adopted ensemble method with multiple classifiers to construct and validate the model. For experiment purpose, Z-Alizadesh Sani coronary artery disease dataset is used. The ensemble method of prediction outperforms the other disease prediction methods.

Keywords Ensemble method · Coronary artery disease · Non-invasive · Angiography

1 Introduction

Cardiovascular diseases are one of the foremost reasons of death and disability all over the country. Deaths due to these diseases are increasing day by day in every age group. These are basically the disease of heart and blood vessels. Coronary artery disease is a category of cardiovascular disease where the plaque is accumulated in heart vessels, interrupts the flow of blood, causes pain, and results into heart attack or even death [1–4]. The major causes of heart diseases are unhealthy lifestyle, lack of exercise, smoking, and unhealthy eating habits. Developing as well as developed

L. Sapra · J. K. Sandhu · N. Goyal (✉)
Chitkara University Institute of Engineering and Technology, Chitkara University, Rajpura,
Punjab, India
e-mail: nitin.goyal@chitkara.edu.in

© Springer Nature Singapore Pte Ltd. 2021
G. S. Hura et al. (eds.), *Advances in Communication and Computational Technology*, Lecture Notes in Electrical Engineering 668,
https://doi.org/10.1007/978-981-15-5341-7_78

1033

countries are spending large amount of its nation financial budget for detection and treatment of the disease. In spite of advancement in medical science, accurate diagnosis and treatment of the heart disease is still a challenging task because of the complexity of diagnosis and treatment methods, especially in resource poor settings. Accurate diagnosis and treatment of patients is necessary in order to save human life and also to reduce the risk of more severe disease [5–9]. Heart disease is prevented by adopting healthy life style and timely tracking off and treatment of the disease. There are many well-known invasive and non-invasive modalities available for identification of the disease [10]. Non-invasive methods include techniques such as ECG, echocardiogram, stress test, and so on. Sometimes the result of these modalities is inconclusive as well as requires time for assessment. So, coronary angiography is popular examining modality for disease identification. It is invasive, painful, and expensive as well as requires expensive clinical setup [11–14].

Due to improvement in technology and low-cost storage devices, storage of huge amount of data becomes easy. Even health sector has been untouched. Machine learning methods are being widely used to analyze the collected data due to its capability to predict the diseases. Researchers are seeking inexpensive, reproducible, fast, and computationally inexpensive methods for detection of heart disease. They are exploring machine learning methods such as support vector machine (SVM), K-nearest neighbor (KNN), artificial neural network (ANN), decision tree, logistic regression, and naive Bayes for identification of heart disease [15–20]. The paper focuses on various machine learning methodologies in order to identify the heart disease. For experiment purpose, Cleveland heart disease dataset and Alizeshani heart disease dataset available at University of California Irvine (UCI) machine learning repository are used.

Nowadays, healthcare sector is generating large amount of data related to patients, disease, clinical reports, physician notes, laboratory tests, and administrative data. The collected data is used by knowledge miners to extract useful patterns with the help of advanced computational intelligent methods results in low-cost healthcare services with reduced error, improved diagnostic methods.

2 Framework for Intelligent Coronary Artery Disease Prediction

The benchmark coronary artery disease dataset is collected from UCI machine learning repository available for research purpose. The Z-Alizadesh Sani coronary artery dataset contains 53 attributes and 303 records such as Age, Weight, Length, Gender, Body mass index, Diabetes Mellitus, Hypertension, Current smoker, EX-Smoker, Obesity, Airway disease, Thyroid, Chest pain, etc. The Cleveland data consists of 14 attributes and 303 instances. The features are Age, Gender, Chest pain type, Resting blood pressure on admission, Serum cholesterol, Fasting blood

sugar, Resting ECG outcome, Max heart rate achieved, Old peak, Slope, Number of fluoroscopy, Colored vessels, Reversible defect, and Outcome [21].

Data is preprocessed to apply predictive modeling using classification methods. The disease identification model is evaluated using performance measures such as accuracy, error rate, AUC, and F-measures. The experimental results exhibit that ensemble-based model which is a better approach with regard to reliability and predictivity of diagnosis. Table 1 shows the description of Z-Alizadesh Sani heart disease dataset.

The CAD dataset collected from UCI machine learning repository was preprocessed. Then, logistic regression, deep learning, decision tree, random forest, gradient boosted, and SVM learning algorithm were applied to identify the presence and absence of coronary artery disease. The performance measures to evaluate the recital of learning algorithms are recorded such as accuracy, error rate, AUC, and F-measure.

Accuracy parameter outputs the percentage of correctly identified patients keeping into consideration following the observations of people suffering from coronary artery disease and those who are not suffering from this disease. Error rate is the percentage of patients not suffering from coronary artery disease, identified as positive for disease, and patients who are suffering from disease and identified as negative for the diseases. Figure 1 shows the framework for intelligent coronary artery disease system.

3 Result Analysis

Table 2 presents the result on Z-Alizadesh Sani dataset having accuracy, error rate, F-measures, and AUC. Logistic regression achieves the prediction accuracy of 80%, deep learning-based model achieves the prediction accuracy of 78%, decision tree achieves the prediction accuracy of 69%, SVM achieves accuracy of 71%, and random forest achieves the prediction accuracy of 82%. The Ensemble-based model gradient boosted tree achieves highest prediction accuracy of 84%. Figure 2 presents the accuracy of classification methods.

In case of misclassification error rate, logistic regression achieves the error rate 20%, deep learning-based model achieves the error rate of 22%, decision tree achieves the error rate of 31%, random forest achieves the error rate of 18%, SVM achieves the error rate of 29%, and in case of gradient boosted tree, it achieves the lowest error rate of 16%. Figure 3 presents the misclassification error rate of classifiers. Figures 4 and 5 present the AUC and F-measure of prediction models.

Table 3 shows the experimental results on Cleveland heart disease dataset. Logistic regression achieves the prediction accuracy of 83%, deep learning achieves the prediction accuracy of 83%, and decision tree achieves the prediction accuracy of 74%. Random forest achieves the prediction accuracy of 77%, SVM achieves the prediction accuracy of 74%, and gradient boosted tree (the ensemble-based method) achieves the highest prediction accuracy of 84%. On the other hand, gradient boosted tree achieves the lowest error rate of 16%, and support vector machine has the highest

Table 1 Description of Z-Alizadesh Sani dataset

Attribute name	Type	Min	Max
Age	Integer	30.0	86.0
Weight	Integer	48.0	120
Length	Integer	140.0	188.0
Sex	Categorical	Male (176)	Female (127)
Body mass index	Real	18.11	40.9
Diabetes Mellitus	Integer	0.0	1.0
Hypertension	Integer	0.0	1.0
Current smoker	Integer	0.0	1.0
EX-smoker	Integer	0.0	1.0
Family history	Integer	0.0	1.0
Obesity	Categorical	Y (211)	N (92)
Chronic renal failure	Categorical	N (297)	Y(6)
Cerebrovascular accident	Categorical	N (298)	Y(5)
Airway disease	Categorical	N (292)	Y(11)
Thyroid disease	Categorical	N (296)	Y(7)
Congestive heart failure	Categorical	N (302)	Y(1)
Dyslipidemia	Categorical	N (191)	Y(112)
Blood pressure	Integer	90.0	190.0
Pulse rate	Integer	50.0	110.0
Edema	Integer	0.0	1.0
Weak peripheral pulse	Categorical	N (298)	Y(5)
Lung rales	Categorical	N (292)	Y(11)
Systolic murmur	Categorical	N (262)	Y(41)
Diastolic Murmur	Categorical	N (294)	Y(9)
Typical chest pain	Categorical	0.0	1.0
Dyspnea	Categorical	N (169)	Y (134)
Function class	Integer	0.0	3.0
Atypical	Categorical	N (210)	Y (93)
Nonanginal	Categorical	N (287)	Y(16)
Exertional chest pain	Categorical	N (303)	NA
Low threshold angina	Categorical	N (301)	Y{2)
Q wave	Integer	0.0	1.0
St elevation	Integer	0.0	1.0
St depression	Integer	0.0	1.0
Tinversion	Integer	0.0	1.0
left ventricular hypertrophy	Categorical	N (283)	Y(20)

(continued)

Table 1 (continued)

Attribute name	Type	Min	Max
Poor R wave regression	Categorical	N (294)	Y(9)
Bundle branch blocks	Categorical	N (282)	LBBB (13)
Fasting blood sugar	Integer	62.0	400.0
Creatine	Real	0.5	2.2
Triglyceride	Integer	37.0	1050.0
Low density lipoprotein	Integer	18.0	232.0
High density lipoprotein	Integer	15.0	111.0
Blood urea nitrogen	Integer	6.0	52.0
Erythrocyte sedimentation	Integer	1.0	90.0
Hemoglobin	Real	8.9	17.6
Potassium	Real	3.0	6.6
Sodium	Integer	128.0	156.0
White blood Cells	Integer	3700.0	18000.0
Lyniph	Integer	7.0	60.0
Neutrophil	Integer	32.0	89.0
Platelet	Integer	25.0	742.0
Ejection fraction	Integer	15.0	60.0
Regional wall motion abnormality	Integer	0.0	4.0
Valvular heart disease	Categorical	Mild (149)	N (116)
CAD	Categorical	Yes (216)	N (87)

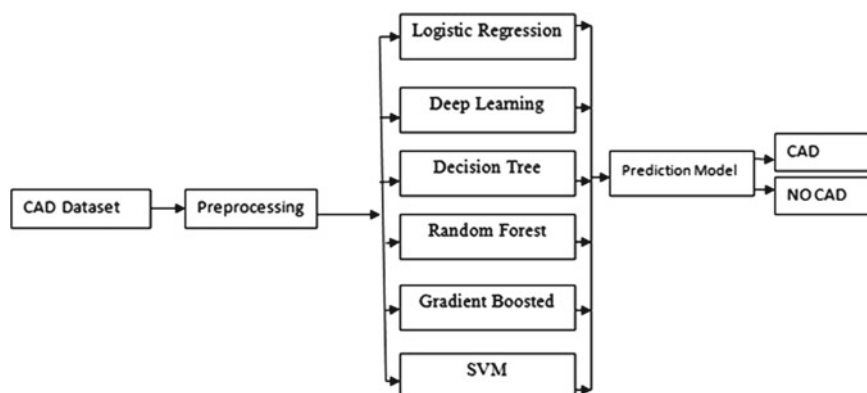
**Fig. 1** Framework for intelligent coronary artery disease system

Table 2 Accuracy/Error rate/F-measures/AUC of models on Z-Alizadesh Sani dataset

Model	Accuracy (%)	Error rate (%)	F-measure	AUC
Logistic regression	80	20	85	0.551
Deep learning	78	22	84	0.888
Decision tree	69	31	81	0.499
Random forest	82	18	88	0.923
Gradient boosted tree	84	16	89	0.881
Support vector machine	71	29	83	0.508

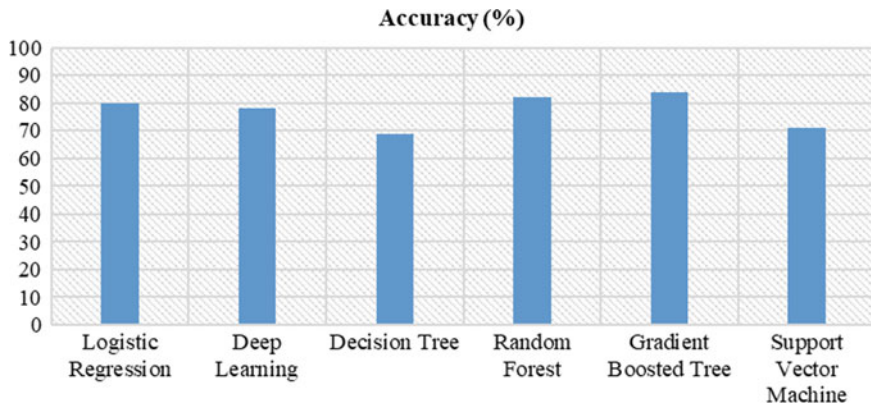


Fig. 2 Accuracy of models on Z-Alizadesh Sani dataset

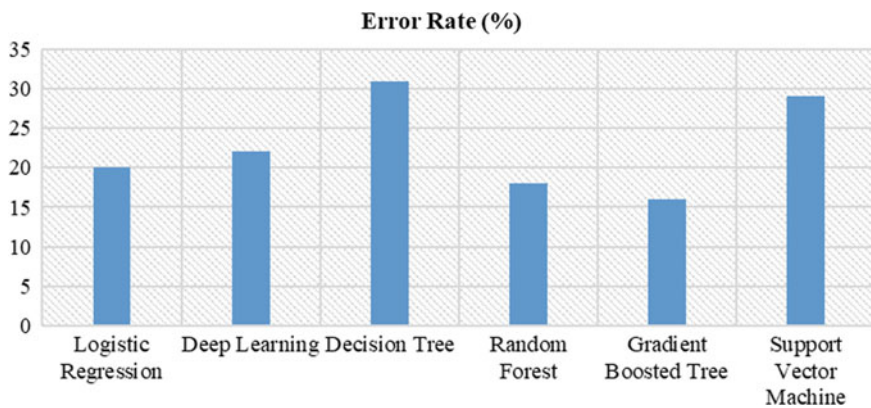


Fig. 3 Error rate of models on Z-Alizadesh Sani dataset

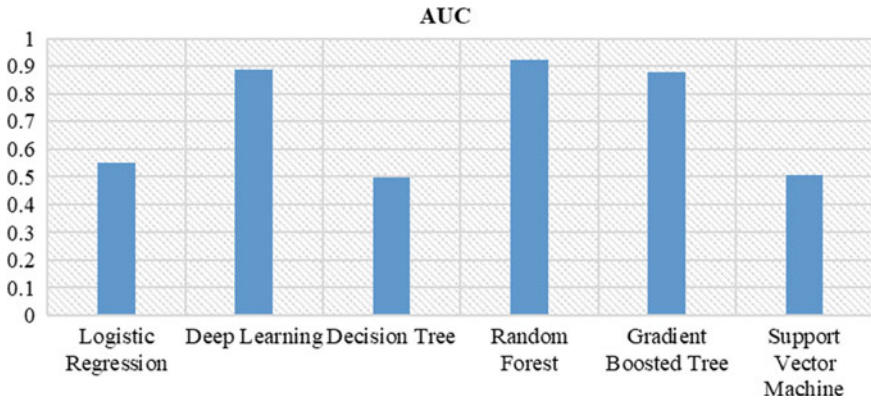


Fig. 4 AUC of models using Z-Alizadesh Sani dataset

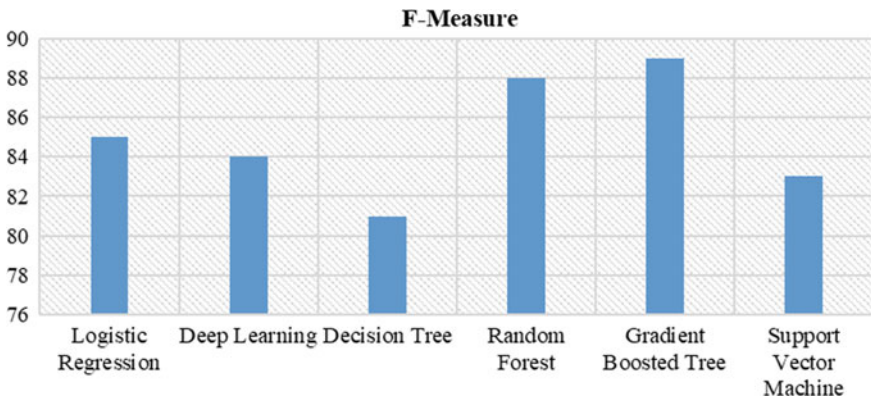


Fig. 5 F-measure of models using Z-Alizadesh Sani dataset

Table 3 Results on Cleveland heart disease dataset

Model	Accuracy (%)	Error rate (%)	AUC
Logistic regression	83	17	0.905
Deep learning	83	17	0.888
Decision tree	74	26	0.782
Random forest	77	23	0.893
Gradient boosted tree	84	16	0.905
Support vector machine	74	26	0.82

error rate of 26%. Logistic regression achieves the error rate of 17%, deep learning 17%, random forest 23%, respectively, (Figs. 6, 7 and 8).

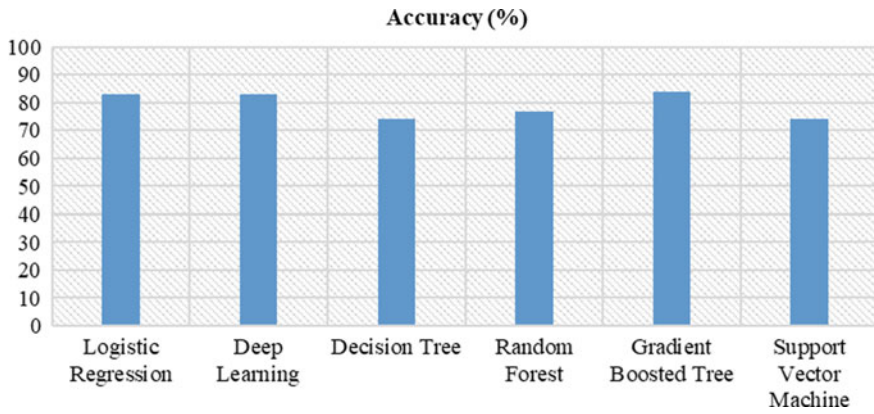


Fig. 6 Accuracy of models using Cleveland heart disease dataset

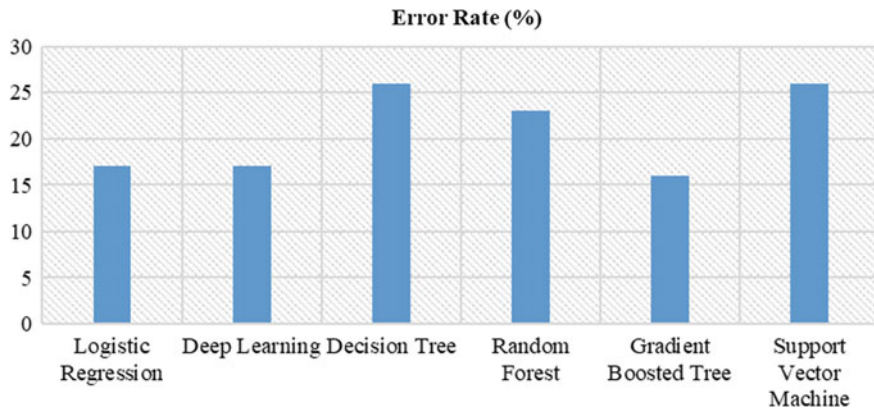


Fig. 7 Error rate of models using Cleveland heart disease dataset

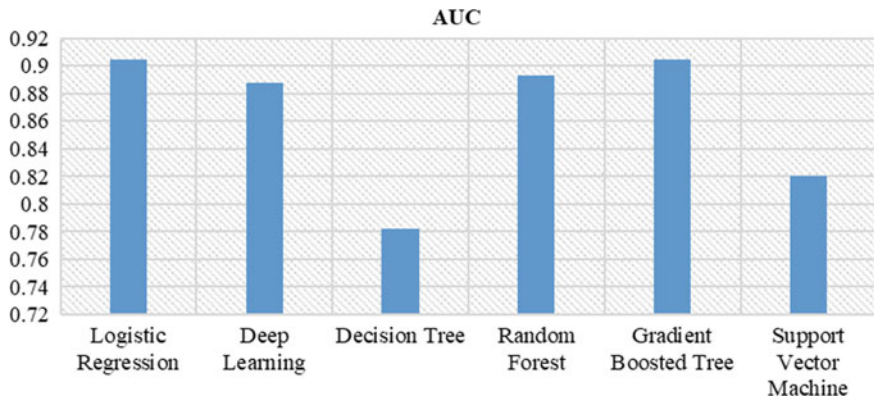


Fig. 8 AUC of models using Cleveland heart disease dataset

4 Conclusion

The experimental results using Z-Alizadesh Sani dataset and Cleveland datasets show that ensemble-based method is preferred as compared to other coronary artery disease detection models. The proposed model can be used to reduce cost of initial detection of coronary artery disease with low cost. The clinical parameters can be easily collected from hospitals, and results can be reproduced in a faster, more accurate, scalable, and reliable manner. It can serve an adjunct tool in clinical settings.

References

1. <http://www.who.int/mediacentre/factsheets/fs317/en/>
2. Terzic A, Waldman S (2011) Chronic diseases: the emerging pandemic. *Clin Transl Sci* 4(3):225–226. <https://doi.org/10.1111/j.1752-8062.2011.00295.x>
3. Reddy KS, Shah B, Varghese C, Ramadoss A (2005) Responding to the threat of chronic diseases in India. *The Lancet* 366(9498):1744–1749
4. Verma L, Srivastava S, Negi PC (2018) An intelligent noninvasive model for coronary artery disease detection. *Complex Intell Syst* 4(1):11–18
5. Wong ND (2014) Epidemiological studies of CHD and the evolution of preventive cardiology. *Nat Rev Cardiol* 11(5):276–289
6. Steele AJ, Denaxas SC, Shah AD, Hemingway H, Luscombe NM (2018) Machine learning models in electronic health records can outperform conventional survival models for predicting patient mortality in coronary artery disease. *PLoS ONE* 13(8):e0202344
7. Shameer K, Johnson KW, Glicksberg BS, Dudley JT, Sengupta PP (2018) Machine learning in cardiovascular medicine: are we there yet? *Heart* 104(14):1156–1164
8. Verma L, Srivastava S (2016) A data mining model for coronary artery disease detection using non-invasive clinical parameters. *Indian J Sci Technol* 9(48):1–6
9. Tiwaskar SA, Gosavi R, Dubey R, Jadhav S, Iyer K (2018) Comparison of prediction models for heart failure risk: a clinical perspective. In: 2018 Fourth international conference on computing communication control and automation (ICCUBEA). IEEE, pp 1–6
10. Verma L, Srivastava S, Negi PC (2016) A hybrid data mining model to predict coronary artery disease cases using non-invasive clinical data. *J Med Syst* 40(7):1–7
11. Takahashi N et al (2019) Computerized identification of early ischemic changes in acute stroke in noncontrast CT using deep learning. In: *Medical imaging 2019: computer-aided diagnosis*, vol 10950. International Society for Optics and Photonics
12. Alizadehsani R, Hosseini MJ, Sani ZA, Ghandeharioun A, Boghrati R (2012) Diagnosis of coronary artery disease using costsensitive algorithms. In: 2012 IEEE 12th international conference on data mining workshops (ICDMW). IEEE, pp 9–16
13. Arafat S, Dohrmann M, Skubic M (2005) Classification of coronary artery disease stress ECGs using uncertainty modeling. In: 2005 ICSC congress on computational intelligence methods and applications. IEEE, pp 4–pp)
14. Sandhu JK, Verma AK, Rana PS (2018) A data-driven framework for survivable wireless sensor networks. In: 2018 Eleventh international conference on contemporary computing (IC3). IEEE, pp 1–6
15. Ayatollahi H, Gholamhosseini L, Salehi M (2019) Predicting coronary artery disease: a comparison between two data mining algorithms. *BMC Public Health* 19(1):448
16. Dhanaseelan R, Sutha MJ (2018) Diagnosis of coronary artery disease using an efficient hash table based closed frequent itemsets mining. *Med Biol Eng Comput* 56(5):749–759

17. Alizadehsani R, Habibi J, Sani ZA, Mashayekhi H, Boghrati R, Ghandeharioun A, Bahadorian B (2012) Diagnosis of coronary artery disease using data mining based on lab data and echo features. *J Med Bioeng* 1(1)
18. Bouali H, Akaichi J (2014) Comparative study of different classification techniques: heart disease use case. In: 2014 13th International conference on machine learning and applications (ICMLA). IEEE, pp 482–486
19. Sandhu JK, Verma AK, Rana PS (2018) A novel framework for reliable network prediction of small-scale wireless sensor networks (SSWSNs). *Fundamenta Informaticae* 160(3):303–341
20. Acharya UR, Faust O, Sree V, Swapna G, Martis RJ, Kadri NA, Suri JS (2014) Linear and nonlinear analysis of normal and CAD-affected heart rate signals. *Comput Methods Prog Biomed* 113(1):55–68
21. <https://archive.ics.uci.edu/ml/datasets/Heart+Disease>

Competitive Study of Various Task-Scheduling Algorithm in Cloud Computing



Nishant Vaishla and Avtar Singh

Abstract Cloud computing is a newly emerged field, and it develops very quickly. In cloud computing, the focus is on delivering computing resources such as hardware and software to the end-user directly, no matter when and where. These services are charged from clients on the per-use bases. There is a need for a decent scheduling mechanism that can help in the appropriate use of the assets. There are various resources available on the cloud and needs an efficient algorithm for better utilization of resources. One way is task scheduling. In cloud environment, there are numerous tasks which are running on the cloud; if two tasks try to approach a common resource, then there may be a chance of deadlock, which leads to system failure and performance degradation. For the better experience of cloud resources and to eradicate the aforementioned situations, there is a need of proper mapping between tasks and resources. In this paper, we comprehensively survey the various existing scheduling algorithms and these algorithms are compared on the basis of various performance metrics which are important to consider for the proper utilization of the resource.

Keywords Task · Scheduling · Cloud computing

1 Introduction

Cloud computing is a newly introduced concept, which plays a significant role in the IT industries and in the government sectors. It provides various services related to computing. To access these services, high-speed Internet is needed and subscription must be taken to access them. The cloud services follow a pay-per-use policy, which helps in reducing the expenses of a business significantly. This cost reduction makes cloud computing an attractive and popular field among people [1]. The services

N. Vaishla (✉) · A. Singh
NIT Jalandhar, Jalandhar, Punjab, India
e-mail: nvaishla@gmail.com

A. Singh
e-mail: avtarz@gmail.com

provided by the cloud providers are: Software as a service (SaaS), include office 360, Google apps, Platform as a Service (PaaS) include Salesforce Heroku, AWS Elastic Beanstalk, Microsoft Azure, and Engine Yard, Infrastructure as a Service (IaaS) include Force.com, OpenShift, Apache Stratos, Amazon Web Services (AWS) [2].

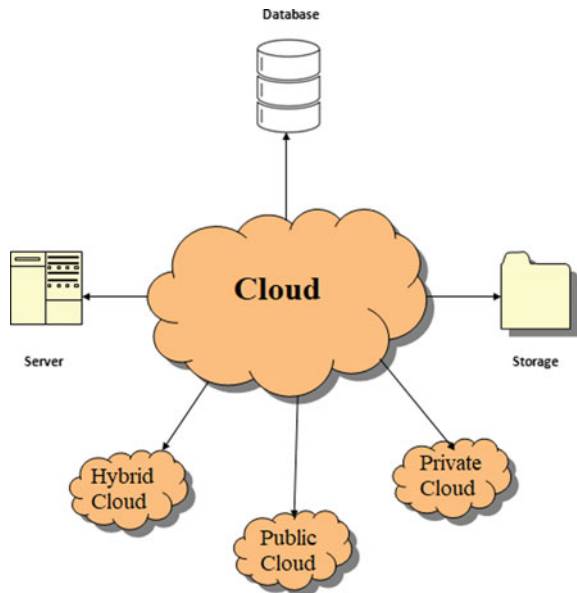
Many business applications like CRM, accounting, inventory, H.R management can be available as SaaS and IaaS. The demand expansion of resource allows scaling of business as and when required, any new features are automatically updated by cloud provider without the need for manual upgradation.

There are various resources present in the cloud and n numbers of tasks are running parallel. There is always a possibility that deadlock may occur. So it is necessary to maintain the availability of resources quality of service and avoid the situation of deadlock.

There are some performance factors on which these tasks are scheduled (Fig. 1).

Task scheduling is an important essential technique which helps in achieving better QoS in the context of cloud computing [3]. Task scheduling is the process in which the even distribution of tasks on the corresponding resource is done without disturbing the running task. The goal of scheduling is to improve performance and maintain resource usability [4]. Resource allocation and quality of service are the basic terms which are in the service-level agreement (SLA) between the customer and the service provider. So it is required to comparatively study all scheduling schemes to understand and classify them for further study [5]. In this, we study different scheduling algorithms based on some performance metrics. Cloud computing is a business focus service which aims to reduce the completion time and increase the

Fig. 1 Different type of cloud architecture



QoS. In this algorithm, the focus is on all the factors of QoS. In cloud computing, appropriate scheduling is required to increase the usability of resources which directly affect on the efficiency of the cloud environment [6]. To optimize the task-scheduling problem, there are many scheduling algorithms available, for example, minmin, max-min, FCFS, round robin, genetic algorithm, and PSO. The goal of these scheduling algorithms is to divide the workload among the resources and maximize resource utilization. But because task scheduling is an N-P hard problem, there is always a chance for a better solution. There are some more parameters which impact the task scheduling and the resource utilization, activity base costing, credit base scheduling, and energy efficient optimization method [7].

2 Type of Scheduling

Scheduling is a process by which the task is allocated to available resource in time. Task and resource are some basic terminologies. There are different types of scheduling such as static scheduling, dynamic scheduling centralized, hierarchical scheduling, distributed scheduling, on-preemptive scheduling, independent scheduling, workflow scheduling. Static scheduling—information seeing all resources just as all the task in an application is thought to be accessible when the application is scheduled. Dynamic scheduling—Tasks are available dynamically for scheduling after some time with no issue by the scheduler. Centralized scheduling—In this, resources have the higher priority and the scheduler know the resource state. Distributed scheduling—No central controlling is there for the resource. Multiple schedulers know the scheduling decision. Primitive scheduling—This allows each task to be disrupted during the execution and the task is able to migrate from one resource to another. Non-preemptive scheduling—resource are allowed to re-allocate until the current task finishes its execution. Independent scheduling—Task can be executed independently. Workflow scheduling—It flows the precedence order, i.e., new task cannot be started until its all parent are done. This shows the dependency of task on each other.

2.1 Overview of Task-Scheduling Technique

Resource allocation is one of the difficult tasks. Because of difficulties, important researchers attracted to it. How efficiently we allocate task is directly affecting the workflow and determining the cost and efficiency. Many new scholars come with a new algorithm to solve newly confronted problem. The detailed discussion on various scheduling techniques is given.

First Come First Serve

This is the simplest to understand this, the task comes in the queue and the task which come first is served first. It is an example of a static algorithm.

Round Robin

Round robin scheduling algorithm distributes task in a FIFO manner but for a limited amount of time called time slice. If the CPU time is complete and the task still remains, then the CPU has to preempt the task to next process which is present in the queue. The process which is preempted is placed to the last of the ready list. It is an example of a static algorithm.

Shortest Job First

Shortest job first flows the process in which it selects the smallest execution time for the next. The advantage of this scheduling algorithm has the minimum average waiting time among all algorithms. It is an example of a static algorithm.

PSO

Particle swarm optimization (PSO) is a population-based stochastic optimization technique developed by Dr. Eberhart and Dr. Kennedy in 1995, and it is based on the social behavior of bird flocking or fish schooling. PSO algorithm has many similarities which is shared with evolutionary computation techniques such as genetic algorithms (GA). PSO is an example of a dynamic algorithm.

Genetic Algorithm

It is an evolutionary algorithm and it always gives a better solution to a problem. The efficiency of genetic algorithm is dependent on the size of the population. Following the survival of fittest, i.e., ideal is selected most exceedingly awful is eliminated. It is a biological term which follows the following step.

Initialization

The initial population is selected randomly.

Selection

The goal is to find the individual with great fitness value.

Crossover

It is a genetic operator used to consolidate the genetic data of two parents to produce new offspring.

Mutation

The key though is to embed irregular genes in offspring to keep up the assorted variety in the population.

Max–Min

In this algorithm, choose the large task first and execute first which make the small task delay.

Min–Min

In this, short task is chosen by the algorithm to execute first which make the large task slower example of a static algorithm.

Ant Colony Optimization

It is a scheduling algorithm inspired by real ant as ant can find the minimum distance from their nest to food. All ants have a chemical known as pheromone. This chemical substance is spread while they search the food and path has more pheromone

means more ant travel through that path. This algorithm is considered as one of the best to allocate the task to the corresponding resource. It is an example of a dynamic algorithm.

Cuckoo Algorithm

It is a meta-heuristic algorithm inspired by the cuckoo bird. This bird never makes their own nest and they go to another birds nest to lay their eggs. This type of birds is called as brood parasite. In term of schedule, the egg represents the solution and cuckoo bird egg represents the new egg. It gives the new and better solution on the base of existence solution.

BAT Algorithm

It is a meta-heuristic algorithm inspired by a bat. It is developed in 2010 by Yang. It based on the echolocation action of bats. Echolocation is a highly sophisticated sense of hearing by this echo that bounced back help to determine the size of how fast the travel determines the size of the object distance forms them to object. BAT algorithm comes under dynamic algorithm.

Related Work

There are various schedulings present for task scheduling. Every algorithms has its own parameter and a different approach to handle the task on cloud Aujla and Ummat [8] Purposed algorithm is focused on the improvement of the existing algorithm use the result of two task-scheduling algorithm and give a hybrid cuckoo algorithm and the result produced by this hybrid algorithm is much better than the result produce by the traditional algorithm. The purposes of this algorithm are proper utilization of the resource and cut the energy utilization available in the cloud. Zheng et al. [9] in this parallel genetic algorithm is purpose which is better in term of performance and to reduce the unbalance distribution task problem on the cloud. it is easily implemented on networks of heterogeneous computers.

Tawfeek et al. [10] proposed ant colony algorithm based on ants that are having the capability to find their food from their nest in the best and the shortest path; this type of scheduling technique is adoptable and continuously improves according to

the environment and gives the best possible result. Khurma et al. [7] authors enhance the current round robin and after comparison between round robin and modified round robin on cloud sim, it finds that the modified round robin is efficient in term of average waiting time.

Zhang et al. [11], The author studies the impact of the improved min-max task-scheduling algorithm in the cloud. In enhancing min-max, the task is assigned with maximum execution time. Selvarani et al. [12] propose a better cost-based scheduling algorithm for a productive mapping of the task to the available resource. This scheduling algorithm divides all client tasks relying upon the priority of each task into three distinct records. This scheduling algorithm estimates resource cost, and it additionally improves the calculation ratio. Thomas et al. [13] cloud computing is a business-focused service. In this paper, the author uses a credit base job scheduling algorithm which reduces the completion time. In this task is classification done on bases of QoS. Then, the bases of task category suitable resource are allocated. The result comes after simulation with the other algorithm based on Berger model. Mrs. Selvarani et al. [14] author said when various task run simultaneously. And there are various different resource have a different cost. So this platform required an efficient mapping algorithm for the reduction of cost. So the task is grouped together according to the resource processing power.

Singh et al. [15] In this, earliest deadline first (EDF) in which the task has the short deadline, will execute first when scheduling is started then the searching starts in the queue for the closest process to its deadline and the matching task schedule next. Mathew et al. [16] This scheduling strategy has task-level scheduling and service-level scheduling. In task-level scheduling, the optimization of the task to the virtual machine is done and in service-level scheduling is done task to service, and this is done in the local cloud data center. It enhances efficiency in cost and time.

Kurdi et al. [17] The purpose scheduling algorithm is developed for providing the QoS in the private cloud; it is difficult to provide efficient task scheduling in private cloud comparatively to the public cloud. In this, author purposes a Hybrid Haizea Condor Scheduler (HHCS) which combines the advantage of Haizea and Condor, which provides a better addressing resource according to requirement. Zhong et al., [18] in cloud environment, the convergence of virtual machine is necessary to increase the efficiency of the server. The greedy particle swarm optimization (GPSO) is the purpose algorithm which solves this problem result improve the faster convergence rate proper load balancing and proper resource utilization.

Saleh et al. [19] authors purpose the algorithm for task scheduling for the large-scale data; the performance of PSO is decreased when the number of tasks is significant. So the propose of this algorithm is to improve the distribution number of a task and this is achieved by divide the task into batches in dynamically way. And the IPSO tries to map the final optimal solution to balance the load. This improves the makespan, and reduces the workload.

3 Scheduling Process

The scheduling is the process that divides into three steps; these are:

3.1 Resource Finding and Separating

Data center finds the resources available in the cloud system and gathers status information associated with them.

3.2 Resource Selection

Mark resource is selected on the bases of some certain parameters of resource and task. This is the deciding stage.

3.3 Task Submission

The task is a map of the target resource (Fig. 2).

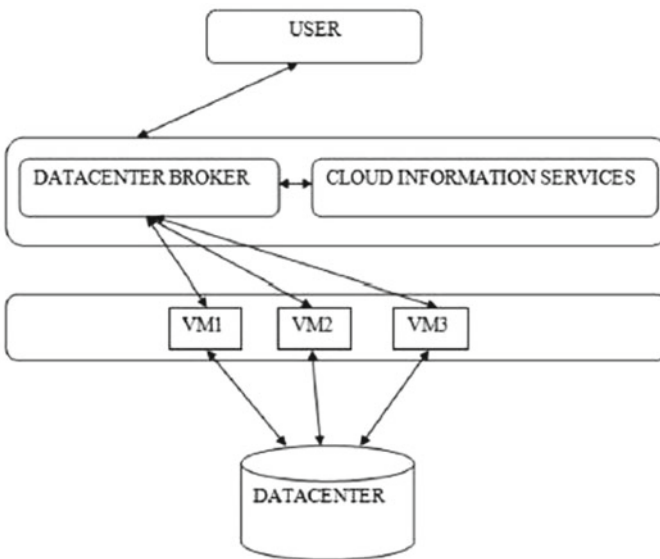


Fig. 2 Scheduling process model [14]

Algorithms	Objective	Scheduling method	Performance metric					Reduce energy consumption
			Memory utilization	Improve QoS	Reduce makespan	Resource utilization	Length and priority of the job	
Credit-based scheduling [13]	Reduce makespan and enhance the resource utilization	Credit base scheduling	No	No	Yes	Yes	No	No
Greedy base job scheduling [2]	To improve the QoS and reduce the makespan	Greedy base scheduling	Yes	Yes	No	Yes	No	No
Genetic [20]	Minimize inefficiencies maximize or productivity	Random selection	No	Yes	No	Yes	No	No
Ant colony optimization [21]	Minimize makespan	Selection base	No	Yes	No	Yes	No	No
Hybrid cuckoo algorithm [8]	Decrease energy consumption and increase resource utilization	Optimization based on genetic algorithm and cuckoo search algorithm	No	No	Yes	Yes	No	Yes
Min-min algorithm [22]	Maximize resource efficiency and reduce the makespan	A small task is allocated to the faster resource	No	No	No	Yes	Yes	No

(continued)

(continued)

Algorithms	Objective	Scheduling method	Performance metric					
			Memory utilization	Improve QoS	Reduce makespan	Resource utilization	Length and priority of the job	Reduce energy consumption
Priority-based earliest deadline first scheduling algorithm [23]	Decrease the makespan	Priority-based job scheduling	No	No	No	Yes	No	No
Heuristic-to based scheduling algorithm [24]	Reduce energy consumption	Based on swam optimization technique	Yes	No	Yes	Yes	No	No

4 Conclusion

Cloud computing rises day by day and faces new challenges. Scheduling of task and prediction of the resource is one of them. The traditional scheduling algorithm like FCFS, RR, etc., will not suitable to solve NP-hard scheduling problems. This paper focuses on the existing algorithm and technics are compared on the bases of various performance matrices and analysis.

In the future, we will focus on better resources utilization and resolve the deadlock problem by combining a particle swarm optimization and its policy. Further, this paper also helps future researchers to use this comparative study to develop a better scheduling algorithm for strengthening the cloud computing paradigm.

References

1. Arnav W, Thing D (2016) A survey of different scheduling algorithms in cloud computing. In 2nd international conference on advances in electrical, electronics, information, communication, and bio-informatics (AEEICB). IEEE
2. Li J, Feng L, Fang S (2014) A greedy-based job scheduling algorithm in cloud computing. *J Softw* 9(4):921–925
3. Qi C, Wei Z-B, Gong W-M (2009) An optimized algorithm for task scheduling based on activity-based costing in cloud computing. 3rd international conference on bioinformatics and biomedical engineering. IEEE
4. Arnav W, Thing D (2016) A survey of different scheduling algorithms in cloud computing. In: International conference on advances in electrical, electronics, information, communication, and bio-informatics (AEEICB). IEEE
5. Singh S, Chana I (2016) A survey on resource scheduling in cloud computing: issues and challenges. *J Grid Comput* 14(2):217–264
6. Zuo X, Zhang G, Tan W (2013) Self-adaptive learning PSO-based deadline constrained task scheduling for hybrid IaaS cloud. *IEEE Trans Autom Sci Eng* 11(2):564–573
7. Khurma RA, Al Harahsheh HEBA, Sharieh A (2018) Task scheduling algorithm in cloud computing based on modified round robin algorithm. *J Theor Appl Inf Technol* 96(17)
8. Aujla S, Ummat A (2015) Task scheduling in the cloud using the hybrid cuckoo algorithm. *Int J Comput Netw Appl (IJCNA)* 2(3):144–150
9. Zheng Z, Wang R, Zhong H, Zhang X (2011) An approach for cloud resource scheduling based on parallel genetic algorithm. In: 3rd International conference on computer research and development, vol 2. IEEE
10. Tawfeek MA, El-Sisi A, Keshk AE, Torkey FA (2013) Cloud task scheduling based on ant colony optimization. In: 8th International conference on computer engineering & systems (ICCES). IEEE
11. Zhang L, Tong W, Lu S (2014) Task scheduling of cloud computing based on improved CHC algorithm. In: 2014 International conference on audio, language and image processing. IEEE
12. Selvarani S, Sudha Sadhasivam G (2010) Improved cost-based algorithm for task scheduling in cloud computing. In: IEEE international conference on computational intelligence and computing research. IEEE
13. Thomas A, Krishnalal G, Raj VJ (2015) Credit based scheduling algorithm in cloud computing environment. *Procedia Comput Sci* 46:913–920
14. Salot Pinal (2013) A survey of various scheduling algorithm in cloud computing environment. *Int J Res Eng Technol* 2(2):131–135

15. Singh J, Patra BN, Singh SP (2011) An algorithm to reduce the time complexity of earliest deadline first scheduling algorithm in real-time system. *Int J Adv Comput Sci Appl (IJACSA)*
16. Mathew T, Sekaran KC, Jose J (2014) Study and analysis of various task scheduling algorithms in the cloud computing environment. In: *International conference on advances in computing, communications and informatics (ICACCI)*. IEEE
17. Kurdi H, Alotaibi ET (2014) A hybrid approach for scheduling virtual machines in private clouds. *Procedia Comput Sci* 249–256
18. Zhong Z, Chen K, Zhai X, Zhou S (2016) Virtual machine-based task scheduling algorithm in a cloud computing environment. *Tsinghua Sci Technol* 21(6):660–667
19. Saleh H, Nashaat H, Saber W, Harb HM (2019) IPSO task scheduling algorithm for large scale data in cloud computing environment. *IEEE Access* 7:5412–5420
20. Gupta S, Agarwal G, Kumar V (2013) An efficient and robust genetic algorithm for multiprocessor task scheduling. *Int J Comput Theor Eng* 5(2):377
21. Zhou S (2018) Cloud computing analysis and optimization based on map-reduce and improved ant colony optimization algorithm. In: *IEEE 9th international conference on software engineering and service science (ICSESS)*. IEEE
22. Bhoi U, Ramanuj PN (2013) Enhanced max-min task scheduling algorithm in cloud computing. *Int J Appl Inno Eng Manag (IJAIEM)* 2(4):259–264
23. Ghanbari S, Othman M (2012) A priority based job scheduling algorithm in cloud computing. *Procedia Eng* 50:778–785
24. Tareghian S, Bornae Z (2015) A new approach for scheduling jobs in cloud computing environment. *Fen Bilimleri Dergisi (CFD)* 36(3)

Internet of Things for Healthcare: Research Challenges and Future Prospects



Garima Verma and Shiva Prakash

Abstract In current scenario, there is a need of such a structure with related devices, individuals, time, spots, and frameworks, which is completely participated in what is called as Internet of things (IoT). This IoT combines the whole world with the PC-based system and around the end, it results in a greater efficiency, accuracy, and advantage for the customer. Security and assurance are the basic two factors for monitoring the health of any patient. A system is required for the blend of confirmation show with an essentialness capable access control instrument. IoT has emerged as one of the most trending domain in the present scenario. Health care is one of the leading research areas where people are moving to provide better solutions efficiently. This paper demonstrates a comprehensive and comparative study portraying the related work done by the current writers dependent on the wireless body zone systems (WBANs). Through this paper, different correlations between a several parameters and strategies of using various IoT devices related with healthcare frameworks are being furnished. Various research challenges of IoT healthcare domain have been also discussed. The comparative study presented here is based on various parameters like techniques used in healthcare frameworks, data collection techniques, etc.

Keywords Internet of things (IoT) · Smart hospital systems (SHS) · Internet of healthcare things (IoHT) · Lightweight break-glass access control systems (LiBAC) · Radio frequency identification (RFID)

1 Introduction

Internet of things has transformed into an authoritative segmented blocks in the progression of social protection monitoring system. The purpose of a powerful IoT

G. Verma (✉) · S. Prakash
Department of Information Technology and Computer Application, Madan Mohan Malaviya University of Technology, Gorakhpur, India
e-mail: garimaverma311016@gmail.com

S. Prakash
e-mail: shiva_pkec@yahoo.com

© Springer Nature Singapore Pte Ltd. 2021
G. S. Hura et al. (eds.), *Advances in Communication and Computational Technology*, Lecture Notes in Electrical Engineering 668,
https://doi.org/10.1007/978-981-15-5341-7_80

1055

therapeutic administrations system is to enhance progressing remote sensing of the patient prosperity condition, to foresee essential conditions of the patient, and for improving individual fulfillment. Conventional strategies for giving security cannot be straightforwardly executed in IoT, as a result, various models and correspondence stacks are included. Data and communication technologies (ICTs) are conveyed as a feature of medicinal data frameworks that must guarantee different critical security necessities together with honesty, secrecy, accessibility, non-disavowal, confirmation, approval, and responsibility to verify therapeutic effect of data without influencing the proficiency of administrations and protection of patients' information. In the current scenario, worldwide maturing and the commonly spreading of ceaseless sicknesses have transformed into a major concern [1]. Subsequently, it is the responsibility of human services industry to create healthcare-related advanced systems and various administrations by using the important data and information and communication technology (ICT) and then implementing them in home-related issues [2]. This paper is based on two basic fundamentals: (1) continuous observing and dissecting imperative signs to early recognize or anticipate hazardous antagonistic health issues; and (2) then, checking whether they are implementing the recommended solutions. In any case, with quickly maturing population, it has brought several difficulties in everybody's life. One audit assesses that about 25% of the grown-up populace do not hold fast to their endorsed medicine, which may prompt weakness results and expanded mortality [3]. Poor drug adherence is a noteworthy issue for many people and human services suppliers. Among other fields, the leading technologies are using smart devices like radio frequency identification (RFID) tags and smart mobile technologies.

Meanwhile, using the Internet of things (IoT), ICT was initiated with the twenty-first century [4, 5]. This review paper gives an idea about how IoT innovation gives the likelihood for associating sensors, actuators, or different gadgets to the healthcare-related framework and is considered as an empowering innovation to understand the vision of worldwide healthcare factors [6]. IoHT broadens the Internet into our regular day-to-day existences by remotely connecting different healthcare devices [7], and will bring major changes in the manner we behave and cooperate with savvy gadgets [8, 9]. Also the paper focuses on the emerging technologies related with healthcare devices using Internet of things.

2 Literature Review

The difficult problem that every patient, particularly who is surviving in remote regions found was unavailability of authorities and their treatment on fundamental conditions. This was having stunning results at the front line of people's contemplations about facilities and organizations. Nowadays, with the execution of new advances by using IoT devices for therapeutic administrations monitoring the system, these major problems have been organized to a big level. IoT helps to keep patients protected and strong, yet by improving how specialists pass on consideration as well.

Restorative administrations of IoT can similarly help getting duty and better satisfaction by empowering patients to contribute more vitality collaborating with their masters. The utilization of the Internet of things (IoT) in social protection is a colossal natural framework. Inside all around related social protection and e-Health picture, planned philosophies and favorable circumstances are searched for a vocation for the alleged Internet of Healthcare Things (IoHT) or Internet of Medical Things (IoMT).

Kevin Ashton immediately gave the possibility of IoT in the year 1999, and implied the IoT as exceptionally conspicuous having interoperability quality with radio-recurrence ID (RFID) advancement [10]. The fundamental engaging variable of this promising perspective is the coordination of a couple of progressions and courses of action. Conspicuous verification and following advancements, wired and remote sensor and actuator frameworks, improved correspondence shows (granted to the next-generation Internet), and scattered learning of sharp things are just the most appropriate [11]. The minor issues of IoT as the combination of Internet and the developing advances have been discussed about [12].

Shen [13] has thought about the e-Healthcare structure that basically involves three territories: body and area, correspondence and frameworks organization, and organization. The body zone space is described by different remote body district frameworks (WBANs), having each identification with a customer. Moved remote (e.g., cell frameworks, WiFi and WiMAX) interface WBAN gateways to the Internet and enables gainful shared data between the two WBANs [14]. In the organization space, a trusted master has an online server which is accountable for tolerating, recording, and separating customer prosperity related data [15].

The building of IoHT framework and the issues in the structure of IoHT gear and their coding parts [16] have been discussed. They have clarified the diverse application zones of IoHT, for instance, sharp urban zones, human administrations, agriculture, and the nano-scale applications [17]. In their paper, they have analyzed the front line of IoHT and presented the distinctive key mechanical drivers. Various mainstream ICT standards have been talked about [18], involving cloud computing, IoT, and the Big Data. It gave a broad cutting-edge survey of them and the combination between them. Next, they proposed an M2M framework dependent on a decentralized cloud design, general frameworks, and remote telemetry units (RTUs) for e-Health applications. The framework was worked for Big Data preparing of sensors in the manner that information can be amassed to create virtual sensors, and some estimation results were introduced. The patient's information security concerns were recognized [19] and their relating components were likewise found from the chosen writing. The survey told about the tracking of any patient's information by using various variations of cloud devices IBE and ABE. A lightweight break-glass access control system (LiBAC) structure was proposed [20] for supporting two distinct methods for encoding restorative records: quality-based access and break-glass. In common conditions, a helpful worker with a quality set satisfying the passage approach of a therapeutic record can disentangle and get to the data. In creating conditions, the break-glass frameworks avoid the passage way course of action of the therapeutic record to empower helpful access to the data by emergency remedial thought. LiBAC is the lightweight framework since relatively few calculations

are executed by devices in the human administrations. The limit and transmission overheads are extremely low. LiBAC is formally shown secure and safe model and expansive investigations are directed to demonstrate its viability.

The basic achievements of NDN design was used [21] for arranging and affirmation of NDN-based insightful prosperity IoT (NHealthIoT) structure. NHealthIoT uses unadulterated NDN- based M2M correspondence for getting and transmission of rough sensor data to the home server which can perceive the emergency social protection events using hidden Markov model. They widened the work procedures of normal formal philosophy model for affirming the rightness of NHealthIoT in the midst of the emergency. Furthermore, to endorse and to show the comfort of the NHealthIoT, they developed a thought model survey. The security highlights have been introduced [22] in every layer of IoT design with the emphasis on observation layer explicit to the IoT condition. The shortcoming of conventions has been evaluated and examined [23] for WMSNs-based human services application. The biometric has been presented [24] as the third confirmation factor, and another client unknown validation convention dependent on WMSNs is planned in order to evacuate the downsides of the convention [23]. Compared with past conventions, the new introduced convention upgrades security and performance of the healthcare devices. Nowadays, there are various types of variable devices for example fitness bands, heart-rate monitoring cuffs, etc., to monitor and control various types of diseases and providing required suggestions to them. IoT is one of the emerging fields which is constantly changing people's life to great extent by providing new healthcare techniques and also by giving various possible solutions to different problems.

3 Existing Methodologies

In Fig. 1, the biographer depicts the total human services structure and figures a situation wherein patient's well-being is being recorded and crucial parameters like BP, ECG, diabetes, and body pressure are verified by convenient restorative gadgets. The information that is verified are put away and investigated for other procedures, put away information are taken from various sensors. For example, pressure sensors, diabetes sensors, ECG sensors, and so forth. Contingent upon study and total figures can check out patients from different areas and respond as indicated by their need. The patients can likewise convey through a video spilling by Web-based amid a crisis case just as support the spouting of interconnected framework with by and large interoperability for a microwave get to (WiMAX), an Internet convention arrange and worldwide framework just as common doors and the entrance administration systems [25].

In Fig. 2, the system tells about the crucial indications of various factors that are working with the support of the WBAN and RFID tags. The body of the patient is connected with different sensors with the support of the WBAN device. The Client's body is being attached with different types of sensors like WSN, medical sensors, etc. The signals triggers in such a way that the patient's information is recorded in

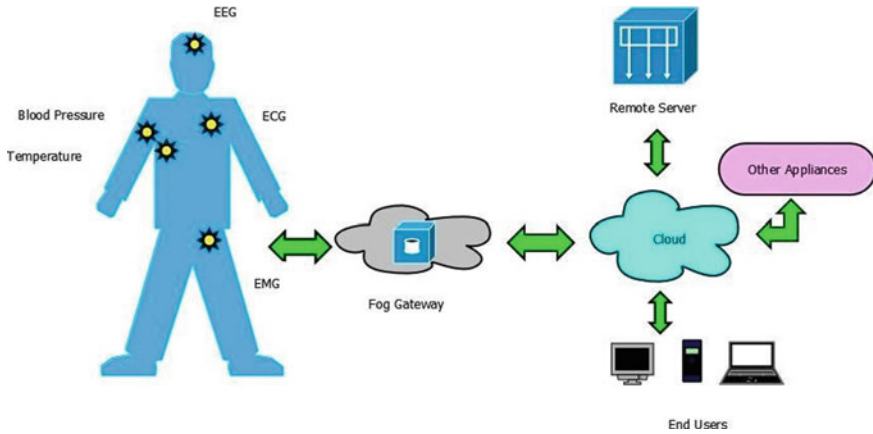


Fig. 1 Remote monitoring personal healthcare system

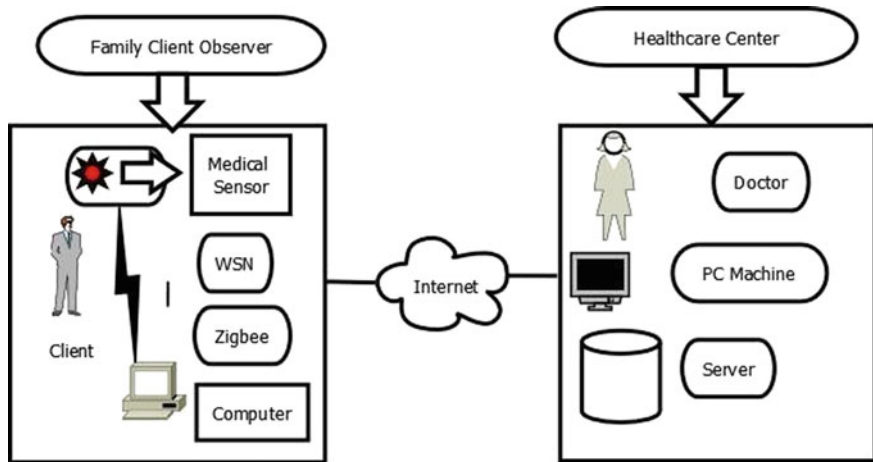


Fig. 2 IoT healthcare architecture

a rapid way on a system. The framework cannot guarantee the administration that is accommodated for 24 h that there would be a server issue [26].

The installed restorative gadget gets contributions from the client to coordinate the side effects with a pre-stacked indication document and endeavors to locate the coordinating malady for same. It performs tests recommended dependent on the pre-stacked side effect record to get the precise counterpart for the illness if the malady is not found by inspecting the side effects. In the event that the malady data is not discovered the framework includes the specialist with the given data, who will counsel the client, analyze the ailment and as needs be update the indication record and ailment document in the framework. The course server gets information and

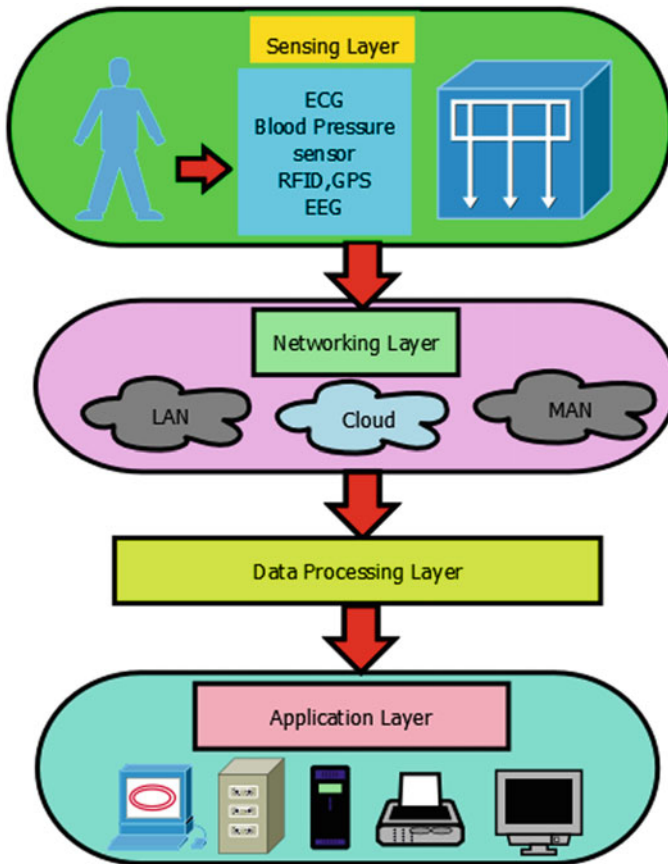


Fig. 3 Layers of IoT healthcare system

changes over into agreed arrangement and stores it in cloud for later investigation by the doctors. The innovation imagines a remote healthcare framework and for data social event, stockpiling and access every single records are watched for examination.

Figure 3 shows various architectural layers of how the processing of data is being done in the healthcare systems. Each layer has its own specific functions performing various operations like data gathering, data transmitting, storing, etc.

4 Comparative Study and Discussion

This section provides comparison of well-known IoT-based healthcare techniques and based on those techniques, the existing authors are developing new IoT-based devices. Data collection is a crucial step for developing any technique in the IoT-based

environment. Hence, a comparison chart is given below showing various paradigms of the literature review.

As Table 1 shows the various parameters on which the researchers are working upon and further studies are going on the related fields. Various data collection techniques are discussed in the given Table 1.

Table 1 Comparison of data collection techniques

Authors and their publication years	Parameters used	Data collection techniques	Advantages	Disadvantages
Tekieh and Rashemi [27], 2015	Accuracy	Survey uses electronic health record	Describes the merits of many different techniques hence in this, optimal approach can be selected for research	No new technique is suggested through this literature
Shahin et al. [28], 2014	Error rate accuracy is there	Electronic health record	It presents a case study to be implemented for practical applications	The specific environment is considered in which accuracy is an issue and can be further enhanced
Yang et al. [29], 2016	Accuracy	Rule-based approach	A Fast mechanism of data gathering is accomplished in this through a proposed mechanism	Accuracy can be further improved
Mdaghri et al. [30], 2016	Accuracy	Clinical decision support system	Data collection is done with accuracy	Missing values are not properly handled
Roy et al. [31], 2016	Correlation and accuracy	Correlation based and ratio analysis	Correlation is used hence specific information about health care is gathered efficiently	Missing values are not considered
Rao and Clarke [32], 2016	Prediction accuracy	An open data set	In this, graphical user interface(GUI) is used and hence better visualization	No missing values are there

Table 2 Distinction between RFID-enabled node and various sensor nodes

Reference of authors	Sensors used	Current sensors	RF nodes and recent consumption details	Features
D'Souza [33], 2008	TICC2420 used by the Telos B 802.15.4 Transceiver	Light, Temperature Humidity sensors	RX: 18.8 MA	They have great access control
Kunze [34], 2009	Altered M2M Device utilizing the TI CC2420 IEEE 802.15.4 handset	Use photoplethysmography (PPG) sensors	RX: 18.8 MA	They are machine dependent devices
Wei [35], 2008	XBEE IEEE 802.15.4 transceiver	Use Body Temperature, Heartbeat, EEG sensors	RX/TX: 40 MA	They have good sensing capabilities
Upcoming RFID tags	HT node transmitting sensors via RFID Gen 2 Interface	Acceleration, ECG sensors	RX/TX remains in fully passive mode: 0MA	They use RFID tags

As shown in Table 2, various authors have used different sensor technologies. There is a vast description given about RFID-enabled nodes and other sensor nodes in the table. Numerous current consumption details are also discussed in Table 2.

5 Strategies and Technologies

It has been explored the likelihood of decreasing overhead of DTLS by methods for 6LoWPAN header pressure, and present the first DTLS header pressure determination for 6LoWPAN [36]. A complete survey of modern necessities, correspondence, and enlisting for a bleeding edge u-Health systems has been shown. They analyzed new mechanical and particular examples and inspected how they address u-Health requirements [37]. The best in class ways to deal with planning productive and secure e-Health checking has been overviewed. In particular, they initially exhibited an exhaustive structure for cutting edge e-Health checking a framework by depicting, in detail, the whole observing life cycle. They have additionally featured the fundamental administration segments, with a specific spotlight on information gathering at patient side. To guarantee high proficiency of the proposed structure, we have introduced and broke down the key moves that should be illuminated so as to create productive and secure patient-driven observing framework [38].

At the end, they proposed an ensured IoT-based therapeutic administrations system using BSN, called BSN-care, which can successfully accomplish diverse

security essentials of a BSN-based social insurance system [39]. Giovanni Baldus built up a way to deal with keep up social insurance information of a patient gathered in various geographic areas [40]. The execution has displayed that the improved process could appreciate the security deficiencies of the thought and gives adaptability, productivity, and is legitimate for TMIS assurance in remote zones and low masses thickness [41]. Other research considers likewise present the fog enlisting structure in remedial organizations applications, which does not utilize the common focus focuses or brilliant door systems [33]. Another proposed show in the genuine RFID structure utilizing Omnikey smartcard per customer. Execution outcomes demonstrates that the proposed show rout in time unconventionality when separated from different other relative shows and it also requires less number of assignments [42].

5.1 Capacities of IoT Healthcare Components

A capacity variation has been portrayed by Muralidharan [43] as far as different areas are concerned as given:

- Location identifying: It uses various RFID names for different zones.
- Data congestion monitoring is used for the sharp area structure, where IoT performs the convincing control and the leading body of the area's traffic by using advancements, devices, and the system.
- Environmental checking: IoT helps in sharp condition, by enabling with sullyng control, disappointment figure and it triggers alarm under crisis for fitting circumstances.
- e-Healthcare monitoring: By the patient's progressing information, IoT can help in remote social protection watching.
- Remote area monitoring is done by IoT contraptions for devices control in emergency acknowledgment, threatening to theft and also for imperativeness protection.
- Ad hoc coordinator gives the patching up of the framework to outline a certain accessibility.

5.2 Security Attacks in Healthcare Devices

Jan et al. have discussed various security attacks and issues in detail. To this, they had talked about the making highlights and models in the Internet of things (IoT) with the objective of looking at their security suggestions. Second had gathered and investigated the assurance threats in the new setting, pointing out the issues that ought to be vanquished to ensure that the Internet of things transforms into a reality [44, 45] and the courses of action have been proposed for security attacks uncovered for electronics human administrations.

- Masquerade attack: [46] gave a productive, astute middleware game plan (that can be completed in a remote or wired contraption) to support data and system security in medicinal sensor systems.
- Attacks on wearable and implantable restorative gadgets: [47] proposed two potential safeguards against such assaults.
- Body-coupled correspondences (BCC): [48] has exhibited a methodology for abusing social connections that exist between individual clients to recognize clone assaults.
- Accountability and revocability assault: [49] has proposed a strategy that works to recognize and uncover the character of the key abuser.
- Data infusion assault: [14] An appropriated expectation-based secure and dependable (PSR) directing structure has been proposed which can be incorporated with a BAN steering convention for the betterment of last's dependability and avoid information infusion assaults amid information interchanges.

6 Research Challenges

This paper gives a general idea on various research challenges that many authors are facing. These challenges have mostly healthcare-related issues. The Internet of things (IoT) has considerably changed social insurance in a moderately short time. Most IoT initiatives are majorly unsuccessful due to several reasons. Cisco's review uncovered that completed tasks were just viewed as fruitful 26% of the time. Also, around 33% of respondents esteemed their completed activities fruitless. Along these lines, it is a noteworthy trouble for the specialists to take a shot at this test.

6.1 *Health Care Will Generate a Huge Amount of Data*

Probably, the most energizing social insurance IoT activities incorporate approaches to lessen crisis room holding up times, track resources and individuals that move all through clinics, and offer proactive alarms about restorative gadgets that may before long come up short. This is the ideal opportunity for associations to understand that choosing to utilize IoT innovation will probably make information stockpiling needs go up. Also, the well-being business must be especially mindful so as to treat persistent information from IoHT gadgets as per government and state guidelines. The surge of information made by the IoT devices and gadgets utilized in the human services industry could likewise cause unanticipated issues if associations are not prepared to deal with it appropriately and check its quality.

6.2 *Obsolete Infrastructure Hinders the Medical Industry*

Despite the fact that retrofitting can inhale new life into maturing foundation, really exploiting IoT is precarious if an office's framework is obsolete. Old foundation is a known issue in well-being care. When emergency clinics are in critical need of patched up framework, they likewise experience issues procuring the staff to make updates. Tech ability is in intense interest. Imminent competitors might not have any desire to handle old framework.

7 Conclusion

According to the discussed issues and comparative study which are perceived by any IoT system, it is still ought to be organized where the specialist on other region can analyze the consistency for patient's basic parameters through safe frameworks. A system ought to be organized so as to give an all out security against different ambushes, with access control for IoT-based human administrations. In last decades, the fast development of maturing populace has been a test to worldwide human services frameworks. Numerous counter attempts have been dynamically made in experiencing an emergency healthcare system rebuilding through the advancement of medicinal assets and expanding the utilization of home human services. This paper basically presents the various contributions of different authors and their respective works in the field of IoT. This paper will help in making a better comparative study and will help various new authors to develop and create a new scenario for the betterment and development of new healthcare-related technologies. The research is still going on in several fields related with the health care as there are many issues highlighted in the paper which have not been yet solved.

References

1. Department of Economic and Social Affairs of the United Nations (2009) World Population Ageing. United Nations New York, NY, USA
2. Koop CE et al (2008) Future delivery of health care: cybercare. *IEEE Eng Med Biol Mag* 27(6):29–38
3. Schuz B et al (2011) Medication beliefs predict medication adherence in older adults with multiple illnesses. *J Psychosom Res* 70(2):179–187
4. Ashton K (2009) 'Internet of Things' Thing, *RFID J* (Online). <http://www.rfidjournal.com/articles/view?4986>
5. Li S, Xu L, Wang X (2013) Compressed sensing signal and data acquisition in wireless sensor networks and Internet of Things. *IEEE Trans Ind Inf* 9(4):2177–2186
6. Welbourne E et al (2009) Building the Internet of Things using RFID: the RFID ecosystem experience. *IEEE Internet Comput* 13(3):48–55
7. Kortuem G, Kawsar F, Fitton D, Sundramoorthy V (2010) Smart objects as building blocks for the Internet of things. *IEEE Internet Comput* 14(1):44–51

8. Tozlu S, Senel M, Mao W, Keshavarzian A (2012) Wi-Fi enabled sensors for internet of things: a practical approach. *IEEE Commun Mag* 50(6):134–143
9. Jara AJ, Zamora-Izquierdo MA, Skarmeta AF (2013) Interconnection framework for mHealth and remote monitoring based on the Internet of Things. *IEEE J Sel Area Commun* 31(9):47–65
10. Shancang L, Li DX, Shanshan Z (2015) The web of things: a study. *Data Syst Front* 17(2):243–259
11. Atzori L, Lera A, Morabito G (2010) The internet of things: a survey. *Comput Netw* 54(15):2787–2805
12. Korteum G, Kawsar F, Fitton D, Sundramoorthy V (2010) Brilliant items as structure hinders for the Internet of Things. *IEEE Internet Comput* 1(51):44–51
13. Liang X, Barua M, Chen L, Lu R, Shen X, Li X, Luo HY (2012) Empowering inescapable human services through persistent remote wellbeing observing. *IEEE Wirel Commun* 19(6):10–18
14. Liang X, Xu L, Shen Q, Lu R, Lin X, Shen XS, Zhuang W (2012) Misusing expectation to empower secure and solid steering in remote body zone systems. In: *Procedures IEEE INFOCOM*, pp 388–396
15. Lu R, Lin X, Shen X (2013) Spoc: a protected and security saving shrewd figuring structure for portable social insurance crisis. *IEEE Trans Parallel Distrib Syst* 24(3):614–624
16. Gordana G, Mladen V, Nebojsa M, Dragan V, Igor R, Slavica T, Milutin R (2017) The IoT architectural framework, design issues and applications. *Wirel Pers Commun* 92(1):127–148
17. Bandyopadhyay D, Sen J (2011) Internet of Things: applications and challenges. *Wirel Pers Commun* 58(1):49–69
18. Suciú G, Suciú V, Martián A, Craciunescu R, Vulpe A, Marcu I, Halunga S, Fratu O (2016) Huge data, Internet of Things and cloud convergence—an architecture for secure e-health applications. *Diary Med Syst* 42(250)
19. Sajid A, Abbas H (2016) Information privacy in cloud-helped healthcare systems: state of the art and future challenges. *Diary Med Syst* 42(250)
20. Yang Y, Liu X, Deng RH (2017) Lightweight break-glass access control system for healthcare Internet-of-Things. *IEEE Trans Ind Inform* 1
21. Saxena D, Raychoudhary V (2017) Structure and verification of a NDN-based safety-critical application: a case study with smart medicinal services. *IEEE Trans Syst Man Cybern Syst* 1–15
22. Cvitic I, Vujic M, Husnjak S (2016) Classification of security risks in the IoT environment. In: *Proceedings of the 26th DAAAM international symposium on intelligent manufacturing and automation*, pp 731–740
23. He D, Kumar N, Chen J, Lee C, Chilamkurti N, Yeo SS (2015) Robust anonymous authentication protocol for health-care applications using wireless medical sensor networks
24. Muralidharan S, Roy A, Saxena N (2016) An exhaustive review on Internet of Things from Korea's perspective. *Remote Pers Commun* 90(3):1463–1486
25. Pang Z (2013) Technologies and architectures of the Internet-of-Things (IoT) for health and well-being. Ph.D. dissertation, Department of Electronics Systems, School of Information and Communication Technology, Royal Institute of Technology (KTH), Stockholm, Sweden
26. Shen Q, Liang X, Shen XS, Lin X (2014) Abusing geo dispersed mists for an e-wellbeing observing framework with least administration postponement and protection safeguarding. *IEEE J Biomed Wellbeing Inf* 18(2):430–439
27. Tekieh MH, Rashemi B (2015) Importance of data mining in healthcare. In: *Proceedings of 2015 IEEE/ACM international conference advances in social networks analysis and mining 2015—ASONAM'15*, pp 1057–1062
28. Shahin A, Moudani W, Chakik F, Khalil M (2014) Data mining in healthcare information systems case studies in Northern Lebanon. In: *2014 third international conference e-Technologies networks devices*, pp 151–155
29. Yang L, Li Z, Luo G (2016) MH-Arm: a multimode and high-value association rule mining technique for healthcare data analysis. In: *2016 international conference on computational science and computational intelligence*, no. 71432002, pp 122–127

30. Mdaghri ZA, El Yadari M, Benvoussef A, El Kenz A (2016) Study and analysis of data mining for healthcare. *IEEE*, pp 77–82
31. Roy S, Mondal S, Ekbal A, Desarkar MS (2016) CRDT: correlation ratio based decision tree model for healthcare data mining. In: 2016 IEEE 16th international conference on bioinformatics, bioengineering, pp 36–43
32. Rao AR, Clarke D (2016) A fully Integrated open-source toolkit for mining healthcare big-data: architecture and applications. In: Proceedings on 2016 IEEE international conference on healthcare informatics, ICHI 2016, pp 255–261
33. D'Souza M, Wark T, Ros M (2008) Wireless localization network for patient tracking. In: 2008 international conference on intelligent sensors, sensor networks and information processing, pp 79–84
34. Chandra-Sekaran AK, Dheenathayalan P, Weisser P, Kunze C, Stork W (2009) Empirical analysis and ranging using environment and mobility adaptive RSSI filter for patient localization during disaster management. In: International conference on networking and services (ICNS '09), pp 276–281
35. Xiaoguang Z, Wei L (2008) The research of network architecture in warehouse management system based on RFID and WSN integration. In: IEEE international conference on automation and logistics, pp 2556–2560
36. Touati F, Tabish R (2013) U-healthcare system: state-of-the-art review and challenges. *Diary Med Syst* 9949
37. Sawand A, Djahel S, Zhang Z, Abdesselam FN (2015) Toward energy-efficient and trustworthy eHealth monitoring system. *China Commun* 2(1):46–65
38. Gope P, Hwang T (2016) BSN-care: a secure and safe IoT-based modern healthcare system using body sensor network. *IEEE Sens J* 16(5):1368–1376
39. Bensallah M, Djeddou M, Drouiche K (2016) Dual cooperative RFID-telecare medicine information system, authentication. *Secur Commun Netw* 9(18):4924–4948
40. Gurjar AA, Sarnaik NA (2018) Heart attack detection by heartbeat sensing using Internet of Things: IoT. *IRJET* 5(3). p-ISSN: 2395-0072
41. Alamr AA, Kausar F (2016) A safe ECC-based RFID mutual authentication protocol for web of things. *J Supercomput* 1–14
42. Li L, Benton W (2006) Hospital technology and nurse staffing management decisions'. *J Oper Manage* 24(5):676–691
43. Ziegeldorf JH, Morchon OG, Wehrle K (2014) Protection in the Internet of Things: dangers and difficulties. *Secur Commun Netw* 7(12):2728–2742
44. Zeadally S, Jesus T, Zubair B (2016) Security attacks and solutions in electronic health (E-wellbeing) systems. *Diary Med Syst* 42(251):263
45. Bruce N, Sain M, Lee HJ (2014) A support middleware solution for e-healthcare system security. In: 16th international conference on advanced communication and technology
46. Li C, Raghunathan A, Jha NK (2011) Commandeering an insulin siphon: security assaults and safeguards for a diabetes treatment framework. In: Thirteenth IEEE international conference on e-Health networking applications and services, pp 150–156
47. Ren Y, Chen Y, Chuahy MC (2012) Social closeness based clone assault identification for versatile medicinal services framework. In: IEEE ninth international conference on mobile ad-hoc and sensor systems (MASS 2012), pp 191–199
48. Yu S, Ren K, Lou W, Li J (2009) Guarding against key abuse attacks in KP-ABE enabled broadcast systems. In: Worldwide conference on security and privacy in communication networks, pp 311–329
49. Garkoti G, Peddoju SK, Balasubramanian R (2014) Detection of insider attacks based on e-healthcare environment. In: International conference on information technology (ICIT2014), pp 195–200

An Animal Detection and Collision Avoidance System Using Deep Learning



Atri Saxena, Deepak Kumar Gupta, and Samayveer Singh

Abstract All over the world, injuries and deaths of wildlife and humans are increasing day by day due to the huge road accidents. Thus, animal–vehicle collision (AVC) has been a significant threat for road safety including wildlife species. A mitigation measure needs to be taken to reduce the number of collisions between vehicles and wildlife animals for the road safety and conservation of wildlife. This paper proposes a novel animal detection and collision avoidance system using object detection technique. The proposed method considers neural network architecture like SSD and faster R-CNN for detection of animals. In this work, a new dataset is developed by considering 25 classes of various animals which contains 31,774 images. Then, an animal detection model based on SSD and faster R-CNN object detection is designed. The achievement of the proposed and existing method is evaluated by considering the criteria namely mean average precision (mAP) and detection speed. The mAP and detection speed of the proposed method are 80.5% at 100 fps and 82.11% at 10 fps for SSD and faster R-CNN, respectively.

Keywords Deep learning · Object detection · CNN · SSD · Faster R-CNN

1 Introduction

When we search the word “animal–vehicle collision,” then we can find a lot of results and images related to the animal–vehicle collision on road. All these search results represent the issue of animal–vehicle collision (AVC). AVC not only causes danger to the animal but also causes damage to vehicles and even fatality for drivers and

A. Saxena (✉) · D. K. Gupta · S. Singh
Dr. B.R. Ambedkar, National Institute of Technology Jalandhar, Jalandhar, Punjab, India
e-mail: atrisaxena2@gmail.com

D. K. Gupta
e-mail: guptadk@nitj.ac.in

S. Singh
e-mail: samays@nitj.ac.in

passengers. AVC is a challenging issue especially in forest region where the national highway passes through the tiger reserves and wildlife reserves. In India, majorly 708,273 km² is a forest area, which is 21.54% of the total area of the country. Many highways like NH6 and NH7 pass through tiger reserve which results in tigers being killed by speeding cars [1]. Indian government also took steps to close the roads touching the national reserve area in the nighttime to avoid AVC [2].

The problem of AVC is a world problem and many official statistics demonstrate the severity of AVC. According to the data of Traffic Injury Research Foundation [3] from the year 2000 to 2014, the number of persons got killed in a motor vehicle collision with species of wildlife ranges from 20 to 45, similarly the number is 15–35 in case of a collision with large animals. Similarly, another study suggests the number of the person killed due to AVC in Canada is largest between 9:00 pm to midnight recorded from the year 2000–2014. There may be two causes behind this, first low visibility in the night and another may be driver getting exhausted. Studies have shown that exhausted drivers generally react slowly, pay less attention to the environment, and have impaired decision-making skills [4].

In the USA, the issue is severe; on an average 90% of animal–vehicle collision involves cases of 200 human deaths, 29,000 injuries, and \$1.1 billion in property damage annually [5]. In Washington State, the study of vehicle collisions with deer and elk on state and federal highways reports at least 14,969 deer and 415 elk death between 2000 and 2004 [6]. A similar situation exists in Europe, Africa, and Asia.

Many traditional solutions are being used such as fencing around the roads, crossing structures, and allowing animals to cross only at specific crossing points. Although these solutions work for some wild species, still this has certain disadvantages. Fencing around the roads will be breached by the animals soon after installation. Moreover, crossing structures are expensive and maintaining fences also costs millions of dollars.

For the well-being of the population of animals and the saving of all the lost property, measures must be taken. In order to provide the solution, simply asking drivers to focus more on the road to avoid animal collisions during driving is not enough. Vehicles are also expected to be smart enough to localize neighboring or approaching large animals so that the drivers or the intelligent system can take necessary steps. In this paper, the two methods for object detection namely, single shot multibox detector and faster region convolutional neural network (henceforth indicated as SSD and faster R-CNN, respectively) will be compared on animal detection problem. Broadly speaking, these two approaches are considered by the trade-off of data efficiency versus detection speed, as SSD can be utilized in real time, but SSD performs worst in detecting small objects [7]. Our results demonstrate that faster R-CNN can detect small objects and more accurate, while SSD is able to detect large object but problem in detecting the small object. These results demonstrate that autonomous vehicle considers accuracy and speed trade-off of detection of animals.

Organization of the paper is as follows. We begin this paper by introducing the background of CNN and object detection techniques in Sect. 2 and review the research work on animal detection in Sect. 2.2. In Sect. 3, we introduce dataset creation, which consists of different classes in different datasets. In Sect. 4, SSD and faster R-CNN

model results are briefly explained. In Sect. 4.4, the proposed model is compared with other existing models using different performance metrics. Finally, we concluded the work with useful remarks that also outline future work in Sect. 5.

2 Background and Literature Review

In this section, we will discuss the background of the CNN architecture which consists of convolutional filters, pooling layers like max-pooling and nonlinear functions. Also, the object detection techniques like SSD, you only look once (YOLO), and faster R-CNN in deep learning will be discussed. In the next subsection, the review of existing research work for the animal detection system will be discussed.

2.1 Background of Deep Learning and Object Detection Techniques

Deep learning has become popular in 2006 due to advancement in computation and labeled training data; many improvements are done in the architecture of the neural network. For the computer vision tasks, convolutional neural network (CNN) is used widely architecture [8, 9]. A CNN used in image classification transforms an input image of 3D to a vector of classification score. A sequence of layers is used to construct the structure of CNN, including convolutional layers, activation layers, pooling layers, and fully connected layers. The convolutional layer of CNN is a trainable 3D filter known as a feature map. Activation layer introduces nonlinearity to the transmitted data by reflecting the result of convolution into some range. CNN uses rectified linear Units (ReLU) to avoid gradient vanishing [10]. In the final layers, sigmoid or softmax layers is used, which restrains the output value into the range of [0, 1]. In a common CNN architecture, pooling layers are inserted in-between successive convolutional layers. Pooling operation such as max-pooling, L2-pooling, and average pooling helps to reduce the number of training parameters and control overfitting of the model [11].

In the final layers of CNN architecture, fully connected layers are added to adjust to entirely different visual tasks. In the fully connected layers, neurons nodes are connected to each other in the input volume. In final layers of fully connected layers, sigmoid or softmax activation functions are used. The whole network then can be trained by using some backpropagation algorithms namely stochastic gradient descent (SGD) or Adam with some loss method likely mean squared error or cross-entropy loss. From the introduction of deep learning, many researchers came up with different neural network architecture and CNN architecture that has been trained some standard dataset such as ImageNet. These architectures include AlexNet [9], VGG [12], Inception Net [13], and Res-Net [14] namely. These standard networks

such as VGG ranges from 11 to 19 CNN layer while ResNet architecture ranges from 50 to 152 layers. A standard approach for training deep learning model is to use publicly available weights of the pre-trained model such as VGG and ResNet; these networks can be retrained on our own limited dataset [15]. This approach is generally called as transfer learning and very common in computer vision task in deep learning [15].

CNN has demonstrated great success in computer vision classification tasks in which network is trained to output a single label for an image [9]. More than just recognition, object detection aims to localize each object in an appropriate position. The localization is represented by annotating a bounding box throughout the object [16]. Generally, object detection follows two approaches mainly. The object detection like faster R-CNN follows traditional pipeline using region proposal network (RPN) to generate region proposals first and then classifies each proposal into different object classes. Some other object detection technique like you only look once (YOLO) [17] and single shot multibox detector (SSD) [7] takes object detection as regression/classification-based framework. This framework is a one-step process based on mapping directly from image pixel to the bounding box coordinates and class probabilities. This regression/classification-based framework is faster in real use-case but not as accurate. Faster R-CNN breaks the bottleneck in the process of region proposal by generating candidate regions using CNN—the region proposal network (RPN) [18]. SSD adds a feature layer that produces a fixed set of detection prediction and probability score. These feature layers are CNN layers and decreasing size of the features helps with generating response maps for various object sizes. These layers have bigger receptive fields and this helps to detect a larger object.

Both the SSD uses static anchor boxes due to which it is faster but less accurate [19].

2.2 Literature Review

Before the widespread acceptance of deep learning, computer vision researchers advance a variety of techniques using the traditional machine learning algorithms for the automated detection of animals. In traditional machine learning, approach features are to be extracted manually, therefore, domain expert knowledge is required to recognize significant features for required classification task such as distinctive characteristic in animal species. The first complete animal detection system was done in 2013 using the template matching algorithm [20]. In template matching algorithm, a small part of the image is searched with a template image. In this paper, the author has created a dataset which contains the target image and template image, and then the target image is matched with the template image using the template matching algorithm. The template matching algorithm moves the template image across the target image and finds the normalized cross-correlation (NCC). The leading cause of this kind of approach is that detection is slow and also gives false results in different lighting conditions such as at night.

In 2014, Mammeri et al. [21] used the cascaded classifier for moose detection using the roadside cameras. This method assumed camera dispensed around the area of interest to detect the presence of moose. To detect moose, the cascaded classifier algorithm is used, and the algorithm is divided into two steps. In the first step, the input image is passed to the AdaBoost algorithm which is trained by LBP features. This first step generates region of interests (ROIs) which is passed to the second step with a set of ROIs containing moose and other alike objects. In the second stage, ROI from the first stage is processed by applying each ROI to an adapted version of HOG-SVM detector, where non-moose ROIs are rejected and moose ROIs are accepted. This system is two-step and the best speed of 52.8 ms achieved by LBP-AdaBoost algorithm.

Similarly in 2016, when convolutional neural networks (CNN) became famous and giving excellent results, many researchers started using the neural networks. Yousif et al. discussed human–animal detection using the camera-trap dataset [22]. In this, proposed model has two major components. First, back modeling and subtraction method are used, which detect the foreground objects (humans or animals) and generate the region proposals. The output of these regions proposals is inputted to the convolution neural network which classifies animal, human or false positive background. Then, a verification model takes input from region proposal and CNN to reduce the number of foreground objects. The significant advantage in this model is that speed increased due to use of CNN. However, still, it is a two-step process which takes time. The author has got a recall of 73.2% on HOG classifier with false alarm rate of 82.7%.

Kellenberger et al. in year 2017 discussed a model based on the deep learning object detection technique namely fast R-CNN [23]. It uses sliding window-based region proposal method to predict the region of interest (ROI). These ROIs are then classified by the CNN network and detect the animal in the image. But this animal detection system is slow due to region proposal method is slow in predicting the ROIs. For the evaluation, Kuzikus Wildlife images acquired by SAVMAP are used. The model is trained using the 224×224 images using gradient descent for 300 epochs at learning rate of 10⁻⁴. The author is able to achieve a recall of 0.60 but detection speed of 13 ms.

In 2017, Sharma et al. focused on the problem of Animal–vehicle collision and detecting cows and dogs mainly [24]. The histogram of oriented gradients (HOG) descriptor is used for detecting an object and extracting feature from the image. The image is divided into blocks of small cell, and HOG descriptor is then applied on these cells. The histogram is then accumulated on these normalized cell histograms to form a feature vector. Finally, the image goes to the cascaded classifiers for classification of the object. Cascading is the concatenation of the classifiers. These classifier outputs are taken and the window is considered as an object if and only if all layers of the cascade classifies as an object. There is also a method for distance calculation of the detected animal. However, this distance calculation depends on the height of the camera fixed. Using the HOG classifier, author can achieve accuracy of 82.5% with average processing time of 100 ms. The problem with this solution is that it cannot be extended to other countries as seen in countries like Australia, the collision of

kangaroo are high, in Saudi Arabia, collision cases of camel are high. Similar situation is in the USA and Russia. No effort has been made to detect animals during the night.

Schneider et al. in year 2018 used the modern deep learning object detection techniques, namely faster R-CNN and YOLO for detecting animals [25]. In this, author has used camera-trap images from Gold Standard Snapshot Serengeti (GSSS) dataset. For feature extraction, ResNet101 architecture is used which contains 101 convolutional layers. For the training weights of model trained on Common Object in Context 2017 dataset is used. The faster R-CNN and YOLO model are able to achieve an accuracy of 76.7% and 43.3%, respectively. There is no comparison found for detection speed.

All these approaches share the standard limitation of detecting only the presence of animal or not. These all use the two-step process which is slow and takes time to process. Now, due to the presence of data and computation, we can use object detection method which uses neural networks. These neural networks are single network which outputs multispecies detected in a single pass. So, the neural network is faster and more accurate than other methods.

3 Dataset Creation

We created our dataset containing following 25 species of animals: *camel, cheetah, pig, deer, elephant, fox, giraffe, horse, bear, dog, goat, jaguar, kangaroo, leopard, lion, ostrich, panda, sheep, rhinoceros, snake, tiger, zebra, cow, nilgai, and crocodile*. In this dataset, some species like cow, dog, horse, and sheep animal images are taken from PASCAL Visual Object Classes (VOC) dataset [26]. This dataset contains images and XML files. These XML files contain the class name and bounding box annotations. From Microsoft Common Objects in Context (COCO) dataset [27] we have taken species like dog, sheep, cow, horse, elephant, bear, zebra, and giraffe. This dataset contains the images and XML files which contains the annotation. Species like nilgai which does not found in any dataset are taken from the Internet and manually annotated. Rest of species of animals has taken from Open Image Dataset v4 [28]. A complete dataset with a set of images and XML files which contains the class name and annotation boxes is formed. This dataset contains approximately 31,774 images for training, as deep learning learns features automatically, so there is a requirement of a large amount of dataset. Each category concerns the different view of the animals such as side view, rear-view, and front-view at certain angles. For evaluation, testing data of required class is taken from PASCAL VOC [26], COCO [27], and Open Image Dataset [28] (Table 1; Fig. 1).

Table 1 Dataset used for training and evaluation

	Categories	Images
Training	25	31,774
Evaluation	25	6088



Fig. 1 Sample images for dataset

4 Experiment Results and Discussion

For this experiment, two models are built namely SSD and faster R-CNN. These two models will be compared to our dataset.

4.1 Performance Evaluation Metric

Four performance evaluation metrics namely precision, recall, mAP with Intersection over Union (IoU) > 0.5 and processing time are considered for evaluation. The IoU is calculated to measure the localization accuracy of the detected bounding box. Precision (P) is used to measure how relevant results are, while recall is to measure the number of the truly relevant result returned [29]. Precision defines show much percentage of your results are relevant the formula is shown in Eq. (1). Recall is defined as the percentage of total relevant results correctly classified as shown in Eq. (2).

$$\text{Precision} = \frac{\text{True Positive (TP)}}{\text{True Positive (TP)} + \text{False Positive (FP)}} \tag{1}$$

$$\text{Recall} = \frac{\text{True Positive (TP)}}{\text{True Positive (TP)} + \text{False Negative (FN)}} \tag{2}$$

where true positive (TP) indicates the number of animals successfully detected by the algorithm. False positive (FP) indicates the number of non-animal objects that are falsely detected as an animal. False negative (FN) indicates the number of animals that the algorithm did not recognize them as an animal.

The mean average precision (mAP) is the mean of average precision (AP) [29]. AP is defined as the weighted mean of precision achieved at each recall value. The weight is computed as the growth in recall from the previous. The calculation of AP is given by Eq. (3), where P_i and R_i are the sorted precision and recall at the i th index.

$$AP = \sum_i (R_i - R_{i-1}) / P_i \quad (3)$$

The mAP is defined in Eq. (4):

$$mAP = \frac{\sum_{q=1}^Q AP(q)}{Q} \quad (4)$$

where Q is the number of queries in the set and $AP(q)$ is the average precision (AP) for a given query, q .

4.2 SSD

In SSD, VGG16 is used as a backbone architecture and VGGNet shows significant improvement in image classification accuracy that can be achieved by increasing the depth from 8 to 16, or 16 to 19. The 16-layer network VGG16 has 13 convolutional layers, three fully connected layers, three max-pooling layers, and a softmax classification layer [12]. The VGGNet performs 3×3 convolutions and 2×2 pooling in all convolutional layers. VGG model trained on ImageNet dataset contains 14 million images with 1000 classes [30]. So, SSD model uses VGG16 weights as a pre-trained model, and more convolutional layers added which outputs bounding boxes with prediction probability. The weights of the final layers added after VGG were initialized using the Xavier initialization. After getting output from the final layer, non-max suppression is applied to suppress the non-max annotations for one object [7].

Loss Function For the training, there are two loss functions used one for localization and one for classification. For localization, smooth L1 loss is computed between the ground truth box and the predicted box and for classification, softmax loss is computed over multiple class confidence (c). The overall loss function is a weighted (α) sum of the localization loss (L_{loc}) and the confidence loss (L_{conf}) [18].

$$L(x, c, l, g) = \frac{1}{N} (L_{conf}(x, c) + \alpha L_{loc}(x, l, g)) \quad (5)$$

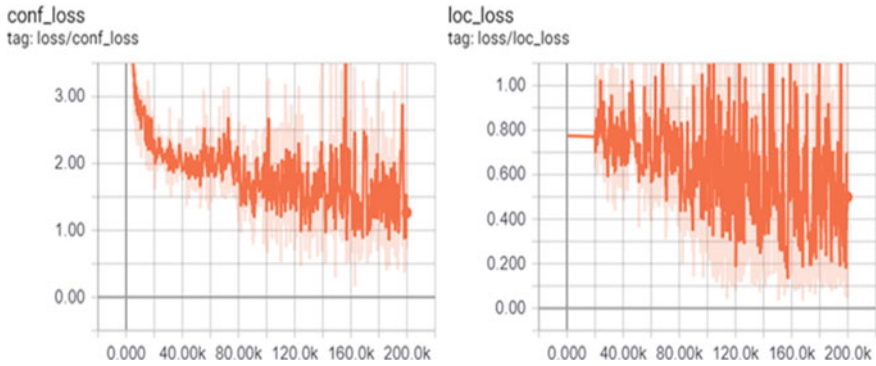


Fig. 2 Confidence and localization loss at runtime in TensorBoard

where

- N : Number of positive matches
- α : Weight of the localization loss
- c : Class confidence
- l : Predicted boxes
- g : Ground truth boxes

The loss value graph is recorded using the TensorBoard which records the loss value while training the network. The localization loss and confidence loss can be seen decreasing with respect to the number of iterations in Fig. 2 which results that the error is decreasing in our trained model.

Training The model has trained using the stochastic gradient descent with a momentum value of 0.9, with an initial learning rate of $1e-3$ and batch size of 16. After, 10,000 iterations, the batch size is decreased to 8 and trained more for 50,000 iterations so that the model can learn better. Again, the batch size is decreased to 4 and trained for 20,000 iterations, we can see a decrease in loss value. The model is trained by decaying batch size and learning rate. Concerning the configurations of the virtual machine on Google Cloud used in this research, they are:

- CPU: 12 vCPU
- Graphic Card: NVIDIA Tesla P100, 16 GB GDDR5
- RAM: 32 GB RAM
- Operating system: Linux (Ubuntu 16.04)

Results of SSD Figure 3 shows the mean average precision with respect to a different type of classes. We have considered 25 classes of different types of animal species. It is evident from Fig. 3 that sheep class has mAP of 0.45 since sheep has similar features to the goat class. So, a neural network might not be able to learn unique features from sheep and goat class. The main challenge of animal detection is animals depict similar features to each other, so becomes difficult to extract unique features from them.

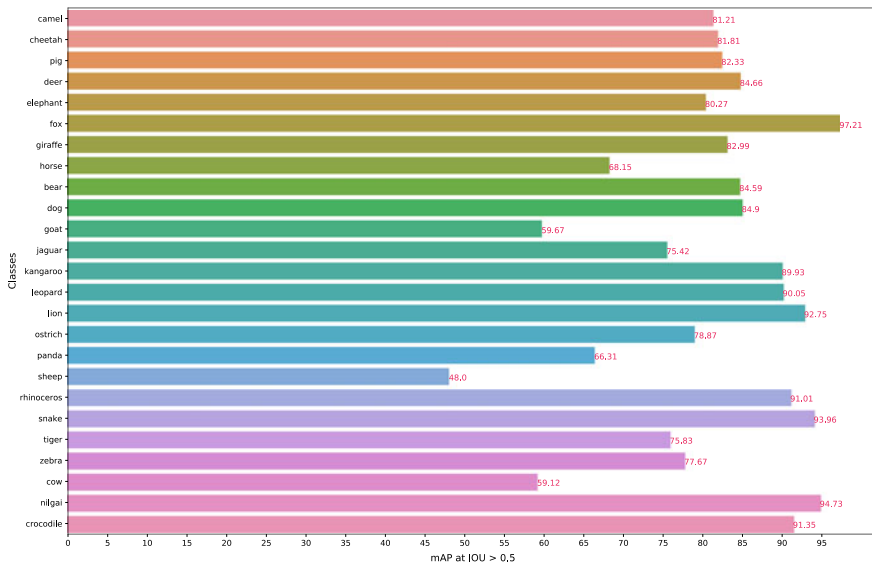


Fig. 3 Mean average precision value for each class on SSD model

4.3 Faster R-CNN

The region-based convolutional neural network (R-CNN) adopts CNN as a feature extractor. Faster R-CNN breaks the bottleneck in the process of region proposal by generating candidate regions using CNN—the region proposal network (RPN). RPN network time is reduced to an extent using CNN and made faster R-CNN detection to use in real time. ResNet101 is used as a backend feature extractor. ResNet stack residual block is of 3×3 convolutional layers. Except for the residual blocks, the ResNet architecture has an additional convolutional layer at the beginning and a global average pooling layer at the end.

Loss function For training RPNs, a binary class label to each anchor is assigned. For the RPN, we assign a positive label to the anchors with the highest Intersection over Union (IoU) or anchor that have IoU overlap higher than 0.7 with any ground truth boxes. For fast R-CNN, two loss values are computed for classification and bounding box regression. For classification, log loss is computed, and for bounding box regression, smooth L1 loss is computed. The loss value at the time of training can be seen in Fig. 4.

Training The model was trained using SGD optimizer with momentum of 0.9 and weight decay of 0.0005. The model was trained for 15 epochs with a batch size of 8 with an initial learning rate of 0.001. The configuration of the machine is same as for SSD model. The input image size to the model is 600×600 pixel.

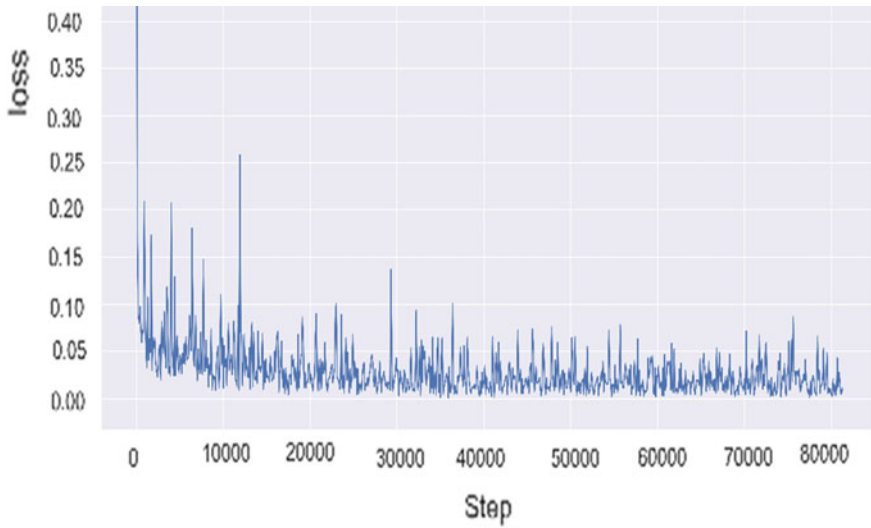


Fig. 4 Visualization of loss at time of training faster R-CNN

Results of Faster R-CNN Figure 5 shows the mean average precision with respect to different types of classes. We have considered 25 classes of different types of animal species. We can see faster R-CNN also getting problem in learning features as animals do not have unique features.

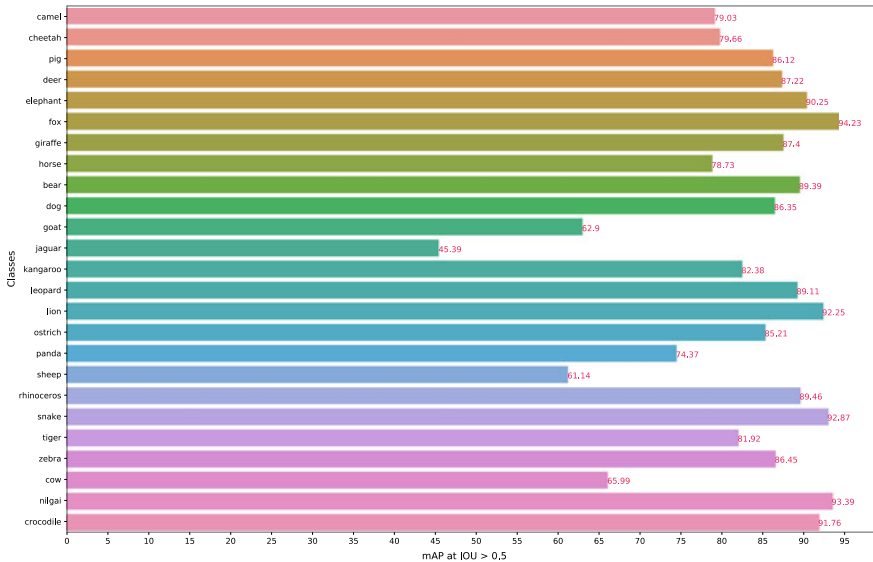


Fig. 5 Mean average precision value for each class on faster R-CNN model

4.4 Discussion

By applying state-of-the-art techniques of object detection, we demonstrated that the animal detection system can detect the animal in real time by using in autonomous vehicle with an onboard camera or roadside camera focused in a particular region. Previous studies and techniques which are used for ADS are using traditional machine learning model like HOG classifiers which learn features manually while deep learning solution learns features automatically. The two main challenge in ADS is that captured background is changing all the time with the movement of the vehicle and another difficulty is animals having common features such as horse, nilgai, and cow having similar shapes, size, and fur.

In Table 2, the proposed model is compared with the model in literature based on recall and detection speed. It can be clearly seen that the proposed model recall value is better and detection speed is also ten times better than the HOG model.

Both the animal detection SSD and faster R-CNN model are compared and found that SSD model is able to detect accurately if an object is not small. For, e.g., in Fig. 6, SSD shows poor performance in detecting the small image of the tiger and also false detected “tiger” as “fox” with a probability of 50%. While, on the other hand, faster R-CNN is able to detect all the tigers with a high probability of more than 97%.

Similarly, as shown in Fig. 7, all deer are not able to be detected properly while faster R-CNN model is able to detect all deer with a high probability. It has been observed that faster R-CNN model is more accurate but slow while the SSD model is fast but less accurate. So, it can be said that there are accuracy and speed trade-off between both the model.

Table 2 Comparison of the proposed model with model in the literature

Model	Recall (%)	Speed (ms)
HOG [23]	80.4	100
SSD	86.85	10
Faster R-CNN	88.34	90



a) Output from SSD model

b) Output from FRCNN model

Fig. 6 SSD false object detection on small objects

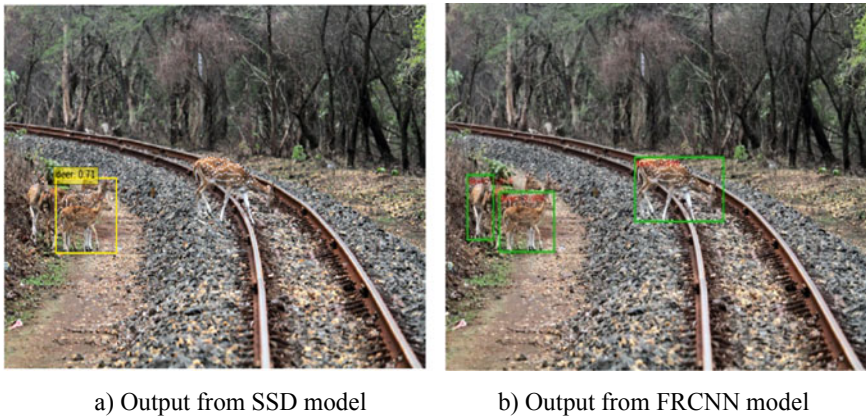


Fig. 7 SSD unable to detect animals

As deep learning requires a large amount of data, we tested the credibility of model on realistic sized data with on average 1200 images per class. This paper used techniques like data augmentation, dropout, and pre-trained model to prevent overfitting of the model. It has been also demonstrated that if the labeled data is approximately 1200 images, a reliable model can be created using faster R-CNN or SSD. We tested YOLO model on our data and it performed poorly with mAP of 60.2, likely due to limited data. The proposed model is also tested on detecting animals in night with only vehicle lighting condition as results can be seen in Figs. 8 and 9.

Considering the success of the out proposed faster R-CNN and SSD model, our method allows for future use in vehicle with an onboard camera and generates an alarm when detecting some animal on road. This model can be used to protect animals from crossing the boundary of wildlife sanctuary by populating cameras on the boundary of wildlife sanctuary if an animal will be detected, system will raise alarm [31]. With animal of various species, our model can be used all over the world like USA where deer vehicle collision is high and India where cow collision is high.

This model allows future possibilities, as it can be used to track animal with multiple cameras across the wildlife sanctuary. This model will also help to understand the nature of animals by taking snapshots of animals and understanding their behavior.

5 Conclusion

This has demonstrated the successful training of two models namely SSD and faster R-CNN. SSD which uses convolutional layers in decreasing form which will detect the object in certain regions. On the other hand, a very different technique which uses region proposal networks to output set of ROIs. These ROIs will be classified to



Fig. 8 Detected animal using the SSD

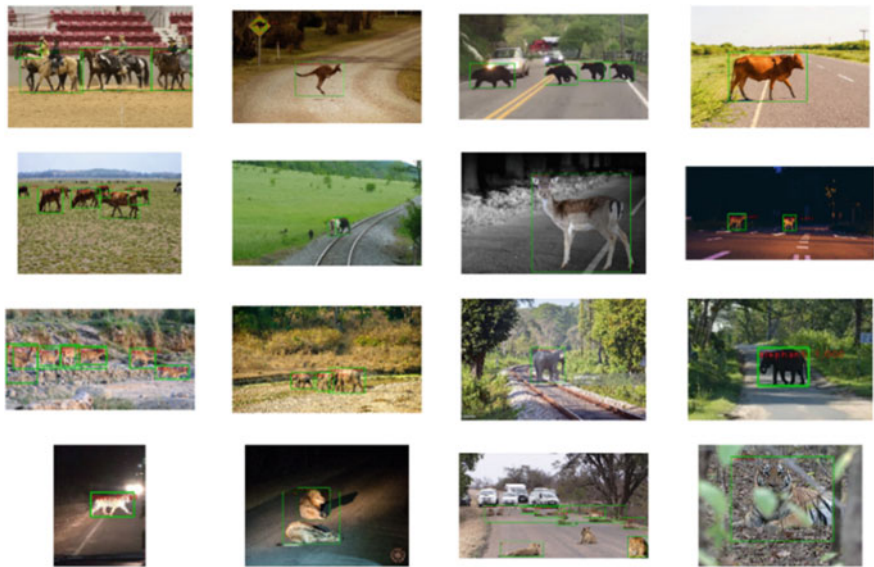


Fig. 9 Detected animals using the faster R-CNN model

detect the object. The results of both the model are compared with detection output. The proposed SSD model achieves the mAP of 80.5% with detection time of 10 ms, whereas faster R-CNN model achieves the mAP of 82.11% with detection time of 90 ms.

Applying the SSD and faster R-CNN model, a new framework for animal detection is obtained. Faster R-CNN performs slow as it needs to compute ROIs using the RPN while SSD is faster due to predefined anchor boxes parallel computation using CNN and it is a single network. But SSD model due to the predefined anchor boxes is not able to detect animals because of visibility issues due to long distance. On the other hand, faster R-CNN model due to RPN is able to detect the object which appears small from a large distance. So, it can be said that there is a trade-off between SSD and faster R-CNN in terms of speed and mAP accuracy.

Utilizing these proposed model, vehicle can autonomously identify, quantify, and localize individual species using the onboard camera, which helps lower the animal–vehicle collision rate. These findings show promising steps toward the animal–vehicle collision by using real-time animal detection system which can be used to lower animal–vehicle collision across the planet according to our understanding.

References

1. Vijay P. Two highways have cut six wildlife corridors in region. <https://timesofindia.indiatimes.com/home/environment/developmental-issues/Two-highways-have-cut-six-wildlife-corridors-in-region/articleshow/46268303.cms>. Last accessed 28 Feb 2019
2. Closing Highway to Night Traffic—A case study from Karnataka. <http://www.conservationindia.org/case-studies/closing-highways-to-night-traffic-a-case-study-from-karnataka>. Last accessed 10 Dec 2018
3. Wildlife-Vehicle Collisions: 2000–2014, TIRF Project, pp 2–3
4. Voelker R (2014) Reducing drowsy driving crashes. *J Am Med Assoc* 312(9):883
5. Huijser MP, McGowen PT, Fuller J, Hardy A, Kociolek A (2007) Wildlife-vehicle collision reduction study: Report to congress (No. FHWA-HRT-08-034)
6. Myers WL, Chang WY, Germaine SS, Vander Haegen WM, Owens TE (2008) An analysis of deer and elk-vehicle collision sites along state highways in Washington State. Publication WA-RD, 701
7. Liu W, Anguelov D, Erhan D, Szegedy C, Reed S, Fu CY, Berg AC (2016) SSD: single shot multibox detector. In: *European conference on computer vision*. Springer, Cham, pp 21–37
8. Fukushima K (1979) Neural network model for a mechanism of pattern recognition unaffected by shift in position-neocognitron. *Electron Commun Jpn* 62(10):11–18
9. Krizhevsky A, Sutskever I, Hinton GE (2012) Imagenet classification with deep convolutional neural networks. In: *Advances in neural information processing systems*, pp 1097–1105
10. Ding B, Qian H, Zhou J (2018) Activation functions and their characteristics in deep neural networks. In: *2018 Chinese control and decision conference (CCDC)*. IEEE, pp 1836–1841
11. Scherer D, Müller A, Behnke S (2010) Evaluation of pooling operations in convolutional architectures for object recognition. In: *International conference on artificial neural networks*. Springer, Berlin, pp 92–101
12. Simonyan K, Zisserman A (2014) Very deep convolutional networks for large-scale image recognition. arXiv preprint [arXiv:1409.1556](https://arxiv.org/abs/1409.1556)

13. Szegedy C, Liu W, Jia Y, Sermanet P, Reed S, Anguelov D, Erhan D, Vanhoucke V, Rabinovich A (2015) Going deeper with convolutions. In: Proceedings of the IEEE conference on computer vision and pattern recognition, pp 1–9
14. He K, Zhang X, Ren S, Sun J (2016) Deep residual learning for image recognition. In: Proceedings of the IEEE conference on computer vision and pattern recognition, pp 770–778
15. Pan SJ, Yang Q (2010) A survey on transfer learning. *IEEE Trans Knowl Discov Data Eng* 22(10)
16. Girshick R (2015) Fast R-CNN. In: Proceedings of the IEEE international conference on computer vision, pp. 1440–1448
17. Redmon J, Divvala S, Girshick R, Farhadi A (2016) You only look once: unified, real-time object detection. In: Proceedings of the IEEE conference on computer vision and pattern recognition, pp 779–788
18. Ren S, He K, Girshick R, Sun J (2015) Faster R-CNN: Towards real-time object detection with region proposal networks. In: Advances in neural information processing systems, pp 91–99
19. Zhao ZQ, Zheng P, Xu ST, Wu X (2019) Object detection with deep learning: a review. *IEEE Trans Neural Netw Learn Syst*
20. Parikh M, Patel M, Bhatt D (2013) Animal detection using template matching algorithm. *Int J Res Mod Eng Emerg Technol* 1(3):26–32
21. Mammeri A, Zhou D, Boukerche A, Almulla M (2014) An efficient animal detection system for smart cars using cascaded classifiers. In: 2014 IEEE international conference on communications (ICC). IEEE, pp 1854–1859
22. Yousif H, Yuan J, Kays R, He Z (2017) Fast human-animal detection from highly cluttered camera-trap images using joint background modeling and deep learning classification. In: 2017 IEEE international symposium on circuits and systems (ISCAS). IEEE, pp 1–4
23. Kellenberger B, Volpi M, Tuia D (2017) Fast animal detection in UAV images using convolutional neural networks. In: 2017 IEEE international geoscience and remote sensing symposium (IGARSS). IEEE, pp 866–869
24. Sharma SU, Shah DJ (2016) A practical animal detection and collision avoidance system using computer vision technique. *IEEE Access* 5:347–358
25. Schneider S, Taylor GW, Kremer S (2018) Deep learning object detection methods for ecological camera trap data. In: 2018 15th conference on computer and robot vision (CRV). IEEE, pp 321–328
26. Everingham M, Van Gool L, Williams CK, Winn J, Zisserman A (2007) The PASCAL visual object classes challenge 2007 (VOC2007) results
27. Lin TY, Maire M, Belongie S, Hays J, Perona P, Ramanan D, Dollár P, Zitnick CL (2014) Microsoft coco: common objects in context. In: European conference on computer vision. Springer, Cham, pp 740–755
28. Krasin I, Duerig T, Alldrin N, Ferrari V, Abu-El-Hajja S, Kuznetsova A, Rom H, Uijlings J, Popov S, Veit A, Belongie S (2017) Openimages: a public dataset for large-scale multi-label and multi-class image classification, 2, p 3. Dataset available from <https://github.com/openimages>
29. Everingham M, Van Gool L, Williams CK, Winn J, Zisserman A (2010) The pascal visual object classes (voc) challenge. *Int J Comput Vis* 88(2):303–338
30. Deng J, Dong W, Socher R, Li LJ, Li K, Fei-Fei L (2009) Imagenet: a large-scale hierarchical image database. In: 2009 IEEE conference on computer vision and pattern recognition. IEEE, pp 248–255
31. Cram RS (1999) Roadside deer warning method and system. U.S. Patent 5,939,987

Outcome Prediction of Patients for Different Stages of Sepsis Using Machine Learning Models



Pankaj Chaudhary, Deepak Kumar Gupta, and Samayveer Singh

Abstract Sepsis is a major challenge in the field of medical science. It affects over a million patients annually and also increases the mortality rate. Generally, sepsis condition is not identified easily. Thus, an intensive analysis of patients is required for identifying sepsis in the Intensive Care Unit (ICU). In this research work, an outcome prediction based machine learning models for identifying different stages of sepsis is proposed. Machine Learning (ML) models can help to predict the current stage of sepsis using existing clinical measurements like clinical laboratory test values and crucial signs in which patients are at high risk. We explore four ML models namely XGBoost, Random Forest, Logistic Regression, and Support Vector Machine by utilizing clinical laboratory values and vital signs. The performance evaluation of the proposed and existing techniques is performed by considering the same dataset. These models achieve an AUC (Area under the Curve) 0.95, 0.91, 0.76, and 0.93, respectively, for recognition of sepsis. Experimental results demonstrate that the XGBoost model with 10-fold cross-validation performs well than other models across all the performance metrics.

Keywords Sepsis · Machine learning · Medical science · Intensive care unit

1 Introduction

Sepsis is a fatal medical condition that usually occurs in patients of the ICU. It occurs when releases chemicals in human blood are not able to tackle the infection [1], and is one of the crucial causes of death in the ICU. As shown by the studies the

P. Chaudhary (✉) · D. K. Gupta · S. Singh
Dr. B.R, Ambedkar National Institute of Technology Jalandhar, Jalandhar, Punjab, India
e-mail: pankajchy037@gmail.com

D. K. Gupta
e-mail: guptadk@nitj.ac.in

S. Singh
e-mail: samays@nitj.ac.in

probability of occurrence is rising with every passing year. Sepsis caused an uncontrolled response of the immune system to tackle inflammations and its affects are tissue damage, organ dysfunction, and eventually death [2]. Recovery from sepsis is possible, but this needs careful selection of essential medicines and the timely administration of medication. It has already become a significant international health burden because of higher treatment costs, as well as hospitalization expenses. However, precise recognition of the risk associated with sepsis, and the selection of suitable antibiotics would play a major role in the depletion of mortality rate and cost among the patients in an ICU. Currently, existing screening methods such as the modified early warning system (MEWS) [3], systemic inflammatory response syndrome (SIRS) [4], sequential organ failure assessment score (SOFA score), etc., are not appropriate to recognize sepsis patients [5, 6]. Without timely treatment, sepsis can increase to the next level called septic shock, which has a hospital mortality rate greater than 40% [7]. Even though the death rate has decreased in recent years, the incidence of sepsis is increased rapidly in ICU, so that overall deaths are increasing. Sepsis is preventable if treated early. Identify sepsis as quickly as possible by using the data from past patients, it avoids the need for tools to have to experiment on new patients. Generally, electronic health records (EHR) data is considered for every measurement in a lab test and inform the patients if required. Using various ML models to analyze data of thousands of patients to identify important signs and symptoms that appear in patients with sepsis. Also needs to do is to figure out how to think about every signal in the context of every other signal in the human bodies. When a patient's body is septic it affects patient kidney it deteriorates your kidney capability to filter out creatinine, so creatinine level increases in patient's bodies. But there are numerous factors that can affect patient kidney ability to filter out creatinine. For example, if patient have chronic kidney disease patients are very likely to have high creatinine levels. So now ML models are having the ability to recognize the complex patterns within data and use those correlations for classification to figure out is your creatinine high because of sepsis or because of chronic kidney disease or numerous other factors that need to high creatinine levels. Every single signal that exists in the EHRs is important to think about every signal in the context of every other signal to identify signs and symptoms that occur more often in patients with sepsis and those without sepsis. Doctors sometimes find disease very late and that is the difference between life and death. Machine learning model provides doctors a much larger window to come in and intervene in order to prevent organ dysfunction and mortality. In many we might not need new measurements, the signs and symptoms were already present in the database. We use a machine learning model for discovering these signs and symptoms from the available database and learn something's that human eye unable to visualize. ML model learns much faster if it had a lot of patient's data available. Availability of abundant quantities of data improves the performance of the model. Various published epidemiological studies have already divulged the possibility of loss associated with sepsis. Significant number of studies have also confirmed that ML can recognize sepsis using the crucial clinical values [8]. There are many machine learning algorithms for binary classification and prediction applied to predict the most killer diseases like sepsis and its variant stages. In this

work, we employed the eXtreme Gradient Boosting (XGBoost), Logistic Regression (LR), Random Forest (RF), and Support Vector Machine (SVM) ML models to diagnose different stages of sepsis. Using the relevant clinical information that is obtained from sepsis patients during ICU period, we tend to train the ML models to calculate various useful metrics like sensitivity, specificity, and AUC in order to compare the performance of the models. In this study, XGBoost model attained highest AUC for the prediction of sepsis and also show the improvement of AUC over the existing methods in the literature.

The paper is organized as follows: In Sect. 2, we review the relevant existing research. In Sect. 3, we illustrate the experimental setup. In Sect. 4, we presents a machine learning model and proposed work and Sect. 5 discusses the results in comparison to existing works. Finally, Sect. 6 concludes the paper with some future recommendations.

2 Related Works

Use of routinely available physiological, pathology reports, biomedical signals, etc. are used to identify development of sepsis from one stage to another stage in an ICU [9]. Some studies mainly focused on the existing score-based system to identify patients with sepsis. These scores such as the SIRS, MEWS, Acute Physiology and Chronic Health Evaluation (APACHE) [10], Simplified Acute Physiology Score (SAPS), the Multiple Organ Dysfunction Score (MODS) [11], and SOFA [12]. In 2016, Mitchell et al. developed a LR model framework to distinguish non-ICU and ICU ward patients. In this research work, MIMIC-II database is used for the ICU patients. Their applied model attained an AUC of 73.9%, 56.2% for non-ICU, and ICU patients, respectively [13]. The recent research work mainly focused on ML techniques for detection of sepsis and related conditions. Several studies report that machine learning algorithm for sepsis prediction and detection reduced patient mortality and length of stay in an ICU. Desautels et al. proposed ML Insight method for the prediction of sepsis in 2016. MIMIC-III dataset was considered for this research. Desautels et al. compared the performance achieved by the proposed method to other existing manual scoring systems such as SOFA or SIRS. AUC score of 0.88 is achieved by using Insight method. This method is restricted to ICU patients and aged of patients are ≥ 15 years [14]. In 2018, Mao et al. proposed an ensemble boosting method to construct a sepsis prediction model by utilizing only six vital signs that are routinely checked and measured at medical facilities. Utilization of less number of vital signs reduced the cost and complexity of the model. Their model achieved an accuracy of 92% to classify patients with shock and no shock, and an accuracy of 96% achieved to predict the event 4 h before the onset of septic shock. Mao et al. achieved an AUC of 0.96 for the prediction of septic shock and an AUC of 0.85 for the prediction of severe sepsis. Further AUC of 0.92 for detection of sepsis and AUC of 0.87 for detection of severe sepsis [15]. In 2015, Guillen et al. in his research applied various ML models for the identification of early stages of sepsis.

For model training and evaluation purposed MIMIC-II database was used. 24 h' time period were considered for the observation of pathological samples. Samples collected 2 h before the occurrence of severe sepsis are considered as useful samples other than that are discarded. The data outside the 24 h's period are not considered for the model evaluation. Data imputation techniques were used to handle the missing clinical samples during the time period of 24 h. The model evaluation concluded that the SVM model performed better than logistic model trees. The SVM model achieved an AUC of 0.87 for the recognition of different stages of sepsis [16]. In 2018 Wang et al. proposed the fruit fly optimization algorithm that enhance the performance of existing kernel extreme learning machine (KELM) method for diagnosis of sepsis. Random Forest classifier is used for feature selection. The proposed method got 89.57% sensitivity, and 65.77% [17]. In 2018, Nemati et al. proposed a framework to predict sepsis using Artificial Intelligence methods. The proposed method is useful for identifying the patients who are at risk for sepsis and initiating appropriate treatment, prior to any clinical manifestations, would have a significant impact on the reduction of death rate and the cost burden of sepsis patients. The best performance achieved for predicting tSOFA 4 h in advance AUROC of 0.87 and sensitivity of 0.85 which was slightly higher than predicting tSepsis with AUROC of 0.85 [18]. Recently in 2019, Moor et al. demonstrated that Multi-task Gaussian process temporal adapter model to handle a non-uniform spaced time series data in early detection of sepsis [19].

3 Experimental Setup

In this section, we will discuss the dataset exploration, data cleaning, and data extraction and gold standards.

3.1 Dataset Exploration

This work uses the publically available “*Sepsis Skaraborg study*” dataset [20] collected between 2011 and 2012. A total of 1572 sepsis patients (only adults are considered) with an average age of 67.3 years were enrolled in this study (out of which 55.6% of whom were male patients and 44.4% were female patients) from an ICU or emergency ward. The data set includes comprehensive clinical data such as vital signs, appropriate medications, clinical measurements,, description of Sepsis-2 criteria, Sepsis-3 criteria hospital length of stay, survival data etc.

3.2 *Data Cleaning and Data Extraction*

The collected dataset were available in the form of xlsx file format. Dataset contain some categorical features like gender, age group, etc., we first convert categorical features into numeric features, because some model can handle only numeric features. We create dummy features for the transformation of categorical features into numeric features. After features transformation the next step of data processing is handling the missing values. We use data imputation technique to replace the missing measurement with another value by a simple average mean method. Missing data imputation improved the overall model performance. For more data exploration, we used a kernel density estimation [21] for outlier detection. Once the data is processed we split the sepsis dataset into train and test set in the ratio of 80:20 by using python ML library. After splitting process we train the ML model to predict onset sepsis.

3.3 *Gold Standards*

In this analysis, we followed the gold standard and new definitions of sepsis to train and test the dataset. ML model performance was tested on training and testing set according to various gold standards. SIRS (Systemic Inflammatory Response Syndrome), and SOFA (Sequential [Sepsis-related] Organ Failure Assessment) at least one of these gold standards satisfied to meet the definition of sepsis [22, 23]. In fact, we were concerned about the whole time series data of each patient's entry to observe the ICU patients.

Following features are considered for applying the ML techniques:

- 6 Vital signs: Respiratory Rate, Oxygen Saturation, Systolic Blood Pressure, Heart Rate, Temperature, Hemoglobin.
- 10 Lab test results: Leukocyte, Procalcitonin, Neutrophil-lymphocyte count ratio, White Blood Cell (WBC), C-reactive protein, Creatinine, Positive blood culture, P-lactate, Systemic inflammatory response syndrome, SOFA score.
- Location type: Emergency department or ICU.
- Progressive stages label preceding to septic shock: infection, inflammation, organ dysfunction, Bacterial sepsis, severe Bacterial sepsis/septic shock based on Sepsis-2 definition, and Bacterial sepsis based on new Sepsis-3 definition [24]: all are identified by machine learning experts system.

4 **Machine Learning Models Design**

In this section, we explore four binary classification model for performance comparison namely XGBoost, Random Forest, Logistic Regression, and SVM.

4.1 XGBoost (EXtreme GRAdient Boosting)

This study investigates the effectiveness of XGBoost model for the identification of sepsis. It is more efficient than the gradient boosting method. Boosting is an ensemble method in which every new model are added to correct the errors made by the previous models [25, 26]. It supports both the linear model solver and tree learning algorithms. XGBoost is faster than the other existing boosting implementations because it allows parallel computation on single machine. The main motivation of using XGBoost is the ability to fine-tune hyper-parameters and Built-in Cross-Validation to improve the performance of the model to predict the sepsis. Workflow analysis of the proposed method is demonstrated in Fig. 1. For cross-validation we select $k = 10$ and whole dataset is split into stratified bins of equal size, which was used to train and evaluate our models. Python Scikit-Learn library and XGBoost package [27] were used for the implementation of model.

Model evaluation. To use the XGBoost to classify sepsis disease, the minimum information we need to provide to the model are Input features, Target variable, Objective function, Number of iteration (Number of tree added to the model for classification), `n_estimators`, `learning_rate`, and `max_depth` of the tree. We try to change the value of parameters in order to achieve the optimal performance of the model. To train the model we split the data set into the ratio of 80:20, respectively,

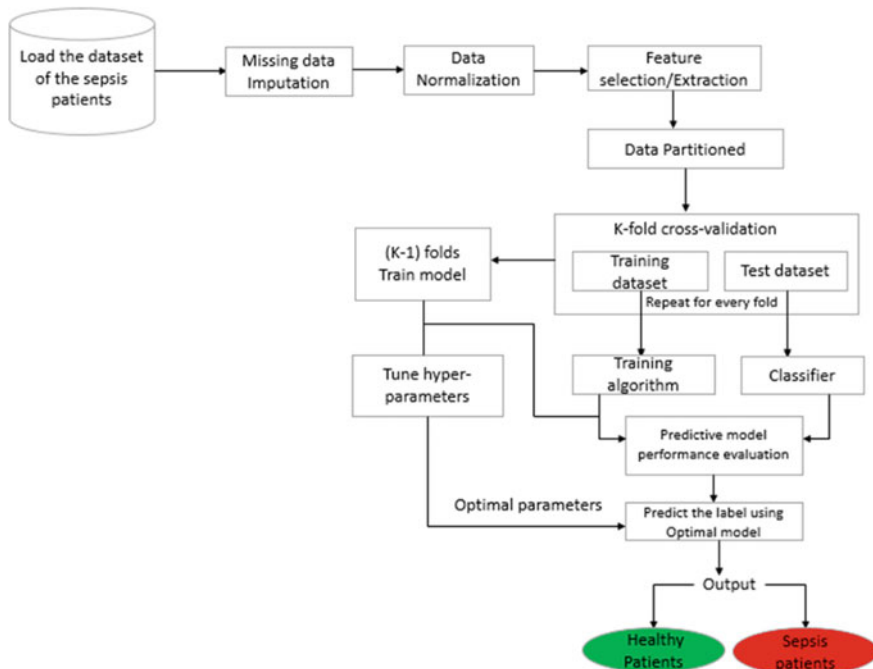


Fig. 1 Experimental workflow of model

and then applied 10-fold cross-validation and GridSearchCV to select the different parameter values to optimize the performance of the model.

Model specification. Distribution of train and test data set. To train the model, we need to optimize the function to get low test error. For optimization typically, we use: Log Loss for binary classification ($L1$), and mlog loss for multi-classification ($L2$) [27].

$$L1 = -\frac{1}{N} \sum_{i=1}^N (b_i \log(p_i) + (1 - b_i) \log(1 - p_i)) \quad (1)$$

In the above equation, b is denoted as the label and $p(b)$ is a predicted probability.

$$L2 = -\frac{1}{N} \sum_{i=1}^N \sum_{j=1}^M b_{i,j} \log(p_{i,j}) \quad (2)$$

In the above equation, N is the total number of samples and M is the total number of outcomes that are possible for a given situation.

4.2 Random Forest

This section outlines the details of a Random Forest (RF) [28] model. It is an ensemble ML method. With different initialization RF consist set of decision trees and trained in parallel manner. RF can be thought of as an extension to the decision tree base classifiers. The Random Forest ensemble classifier [29] has been used on many datasets spanning different environments and industries. The RF ensemble is preferred over other ensembles method because it is simple, can be easily parallelized, is comparatively strong to outliers, and noise, and it is comparatively faster than bagging or boosting techniques. RF Classifier being an ensemble algorithm tends to give a more accurate result because it works on the principle of weak estimators. Once all the weak estimators are merged it forms a strong estimator. Even though one or more decision trees are suffering from noise, the overall result could not be affected. The main reason behind choosing the RF model for prediction of sepsis are included: It runs efficiently on large dataset and model does not suffer from Underfitting. For the implementation of RF we first split our training and testing data set in the ratio of 80:20, respectively. Then, we import RandomForestClassifier from sklearn python library. We took $n_estimators = 20, 100, \text{ and } 200$, respectively, and change the other RF parameters during the model training to check the performance of the model.

4.3 *Logistic Regression*

Logistic Regression (LR) is a supervised machine learning classifier [29, 30]. It is a widely used technique for analyzing laboratory data. LR model is simple and highly interpretable and it is suitable for the baseline model to compare the results with other machine learning models. LR requires the dependent variable (target variable) should be in binary 0 or 1, to identify whether patients suffer from sepsis or not. For building an LR model in python, we import the linear model Logistic Regression package. To train the model we split the data set into the ratio of 80:20, respectively, and then applied 10-fold cross-validation technique and Grid Search CV to select the different parameter values to get the best performance of the model.

4.4 *Support Vector Machine*

This section outlines the implementation of a Support Vector Machine (SVM) [31] model. It is a classification method used to classify a patient into a new group. Our task is to identify patients with sepsis or patient without sepsis using SVM model. This method is suitable for binary classification problems, this means that 0 denote healthy patients and 1 denote patients with prone to sepsis or septic shock. Data of the different patients are similar, so performing linear SVM data separation is not efficient in this case. In this situation SVMs can efficiently perform a non-linear data separation with the use of the SVM kernel trick. Entire data separation problem mapped into multi-dimensional space. To minimize an error SVM generates optimal hyperplane in an iterative fashion. We Scikit-Learn python library for the implementation of SVM. We split train-test data in the ration of 80:20. To boost the performance of the model we applied the Gaussian Kernel method for the implementation of kernel SVM. For classification we select the two important parameters they are: First parameter is C: Inverse of the strength of regularization. As the value of 'C' increases the model gets overfit and the value of 'C' decreases the model get underfit. We select $C = 100$ for SVC (support vector classification) Second important parameter is γ : Gamma (used only for RBF kernel). As the value of ' γ ' increases the model gets overfit and the value of ' γ ' decreases the model underfit.

5 **Experimental Results and Discussions**

This section will introduce the performance analysis of the ML model that is trained for the identification of different sepsis conditions. Further, we will compare the performance of four binary classification models, namely XGBoost, RF, LR, and SVM based on the selected performance metrics.

5.1 Evaluation Metrics

In this section, we will discuss all the useful performance metrics to analyze the performance and predictive power of models. AUC curve (Area under the curve), accuracy, recall, and precision were computed to evaluate the models. Confusion matrix could be a helpful metric to explain the performance of a classification model on a set of test data. Confusion matrix table is divided into four parts such as True Positives (TP): Count total number of true positives values ($y_{\text{true}} = 1, y_{\text{pred}} = 1$) and True Negatives (TN): Compute number of true negatives values ($y_{\text{true}} = 0, y_{\text{pred}} = 0$) are the observations which were correctly predicted. The terms False Positives (FP): Count total number of false positives values ($y_{\text{true}} = 0, y_{\text{pred}} = 1$) and False Negatives (FN): Compute number of false negatives values ($y_{\text{true}} = 1, y_{\text{pred}} = 0$) can lead to confusion.

Recall (Sensitivity). Evaluate the percentage of patients that really had sepsis was properly diagnosed by the model.

$$\text{Recall} = \frac{\text{TP}}{\text{TP} + \text{FN}} \quad (3)$$

Specificity. Clinical test to correctly identify healthy patients.

$$\text{Specificity} = \frac{\text{TN}}{\text{TN} + \text{FP}} \quad (4)$$

AUROC (Area under the Receiver Operating Characteristics). ROC curve is a plot of the true positive rate (TPR) along with Y-axis against the false positive rate (FPR) along with X-axis. ROC indicates the probability curve and AUC quantify the separability. To select the AUC metric for a classification problem we need to know about the possible range of AUC that defines in the interval of [0, 1]. 100% TPR and 0% FPR indicate the perfect classifier, and ROC curve passes through the upper left corner of the square, and AUC values less than 0.5 indicate worthless classifier [34]. AUC is mainly used in the situation when accuracy misleads the classification problem, even we get 99% accuracy that doesn't mean the model is absolutely good for prediction of disease. In that case, AUC is considered good for the classification problem. Golden standard in the field of medicine indicates $\text{FPR} = 0$ and $\text{TPR} = 1$.

5.2 Results Summary

ML model was trained and tested on the sepsis patient's data set. This dataset contains a total of 1572 patients out of which 1257 patients were selected for the training dataset and 315 patients for test dataset. Out of four models the highest AUC achieved is 0.95 and lowest AUC achieved is 0.76, and the average AUC of 0.88 achieved for

the identification of the different levels of sepsis. The AUROC curve of each model is shown in Fig. 2.

XGBoost, RF, LR, and SVM models achieves AUC 0.95, 0.91, 0.76, and 0.93, respectively, for recognition of sepsis. We select linear kernel as well as Gaussian Kernel to build the SVM model for recognition of sepsis. We got an AUC of 0.76 and 0.93 for linear and Gaussian Kernel, respectively. Gaussian Kernel performed better on this dataset as compared to linear kernel for SVM model. We improved the prediction of sepsis by using ML models. Table 1 shows the results of different existing machine learning techniques in terms of their AUC for the identification of sepsis. The AUC value for the Desautels et al. (2016) [14], Guillen et al. (2015) [16], Balduino et al. [32], and Masino et al. (2019) [33] is 0.74, 0.87, 0.85, and 0.82 using Insight: 4 h, SVM, XGBoost, and RF, respectively (Fig. 3).

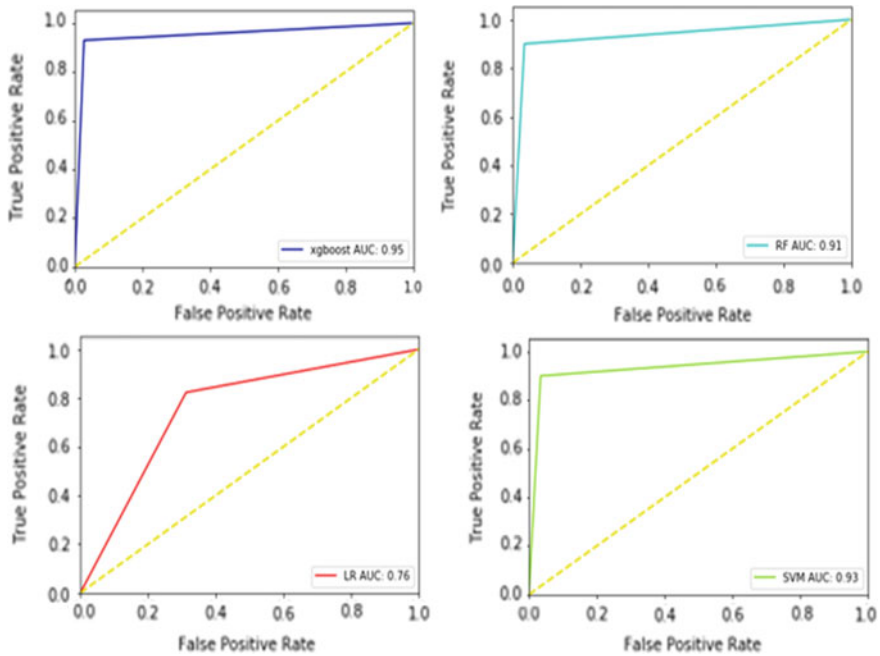


Fig. 2 ROC curve of XGBoost, RF, LR, and SVM

Table 1 Evaluation of performance of the model in terms of sensitivity, specificity, and AUC

Model	Sensitivity	Specificity	AUC
XGBoost	0.92	0.97	0.95
RF	0.88	0.94	0.91
LR	0.82	0.69	0.76
SVM	0.90	0.97	0.93

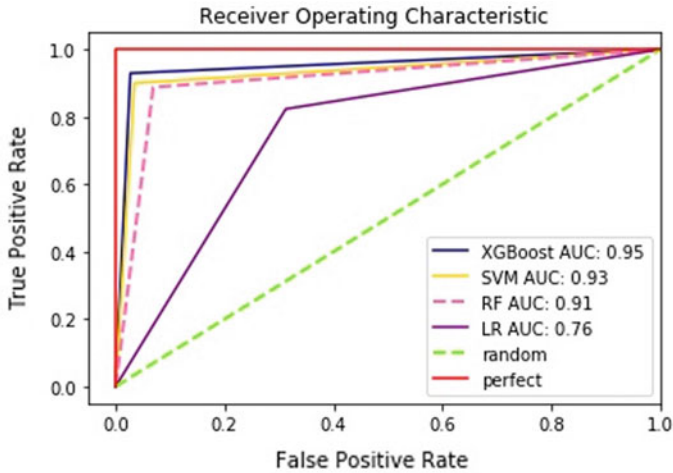


Fig. 3 ROC curve for all the four models for prediction of sepsis

Table 2 Results of the selected studies that applied the ML techniques to identify the sepsis

Paper	Data set	Method	AUC
Desautels et al. (2016) [14]	MIMIC-III	Insight: 4 h	0.74
Guillen et al. (2015) [16]	MIMIC-II	SVM	0.87
Balduino et al. (2018) [32]	Geisinger Healthcare System	XGBoost	0.85
Masino et al. (2019) [33]	Hospital of Philadelphia	RF	0.82

From Table 2, we see that the highest AUC value is 0.87 in [16] that is lower than our proposed work. However, it's tough to make a direct comparison as a dataset, and size of sample were used during this analysis are completely different.

6 Conclusion

In this research work, we have tested sepsis dataset using various ML model for accurate prediction of sepsis. First, we have used the imputation process to deal with missing data to improve the model performance then imputing using matrix factorization yields better predictive accuracy than imputing with simpler approaches like means. After that we used different packages to build models like XGBoost, LR, SVM, and RF. The XGBoost, Random Forest, Logistic Regression, and SVM ensemble model achieve 0.95, 0.91, 0.76, and 0.93 AUCROC for sepsis, respectively.

In summary, the result of XGBoost ensemble model improves the overall performance and delivers a more accurate classification as compared to other involved models in this study for the prediction of sepsis. The models presented in this work show promise in their ability to decrease morbidity and mortality rates resulting from septic shock and improve the outcome for sepsis patients.

The major limitations of this research work are the size of samples, so the work can be extended by using more data samples to improve the prediction of the sepsis. Another issue in this work is to focus on only the ICU in a single medical center and a limited period of time. In the future, researchers can collect more relevant laboratory specimens from multiple medical center databases to establish an error-free sepsis prediction model. We believe this model will be useful in the hospital environment to predict sepsis disease.

References

1. Novosad SA, Sapiano MR, Grigg C et al (2016) Vital signs: epidemiology of sepsis: prevalence of health care factors and opportunities for prevention. *MMWR Morb Mortal Wkly Rep* 65(33):864–869
2. van Wyk F, Khojandi A, Kamaleswaran R (2019) Improving prediction performance using hierarchical analysis of real-time data: a sepsis case study. *IEEE J Biomed Health Inf* 23(3):978–986
3. Subbe CP, Slater A, Menon D, Gemmell L (2006) Validation of physiological scoring systems in the accident and emergency department. *Emerg Med J* 23 (11):841–845
4. Lamping F, Jack T, Rübsamen N et al (2018) Development and validation of a diagnostic model for early differentiation of sepsis and non-infectious SIRS in critically ill children—a data-driven approach using machine-learning algorithms. *BMC Pediatrics* 18(1):1471–2431
5. Singer M, Deutschman CS, Seymour CW, Shankar-Hari M, Annane D, Bauer M et al (2016) The third international consensus definitions for sepsis and septic shock (Sepsis-3). *J Am Med Assoc* 315(8):801–810
6. Seymour CW, Liu VX, Iwashyna TJ, Brunkhorst FM, Rea TD, Scherag A et al (2016) Assessment of clinical criteria for sepsis: for the third international consensus definitions for sepsis and septic shock (Sepsis-3). *J Am Med Assoc* 315(8):762–774
7. Ho JC, Lee CH, Ghosh J (2014) Septic shock prediction for patients with missing data. In: *ACM transactions on management information systems (TMIS)* 5(1):1–1
8. Fleischmann C, Scherag A, Adhikari NK, Hartog CS, Tsaganos T, Schlattmann P, Angus DC, Reinhart K (2016) Assessment of global incidence and mortality of hospital-treated sepsis. Current estimates and limitations. *Am J Respir Crit Care Med* 193:259–272
9. Faisal M, Scally A, Richardson D, Beatson K, Howes R, Speed K, Mohammed MA (2018) Development and external validation of an automated computer aided risk score for predicting sepsis in emergency medical admissions using the patient's first electronically recorded vital signs and blood test results. *Crit Care Med* 46(4):612–618
10. Sadaka F, EthmaneAbouElMaali C, Cytron MA, Fowler K et al (2017) Predicting mortality of patients with sepsis: a comparison of apache ii and apache iii scoring systems. *J Clin Med Res* 9(11):907–910
11. Badrinath K, Shekhar M, Sreelakshmi M, Srinivasan M et al (2018) Comparison of various severity assessment scoring systems in patients with sepsis in a tertiary care teaching hospital. *Indian J Crit Care Med* 22(12):842–845
12. Vincent JL, Moreno R, Takala J, Willatts S, De Mendonca A, Bruining H et al (1996) The SOFA (Sepsis-related organ failure assessment) score to describe organ dysfunction/failure on

- behalf of the working group on sepsis-related problems of the European society of intensive care medicine. *Intensive Care Med* 22(7):707–710
13. Mitchell S, Schinkel K, Song Y, Wang Y (2016) Optimization of sepsis risk assessment for ward patients. In: 2016 IEEE systems and information engineering design symposium, pp 107–112. IEEE, Charlottesville
 14. Desautels T, Calvert J, Hoffman J et al (2016) Prediction of sepsis in the intensive care unit with minimal electronic health record data: a machine learning approach. *JMIR Med Inf* 4(3). <https://doi.org/10.2196/medinform.5909>
 15. Mao Q, Jay M, Hoffman JL, Calvert J, Barton C, Shimabukuro D, Shieh L, Chettipally U, Fletcher G, Kerem Y et al (2018) Multicentre validation of a sepsis prediction algorithm using only vital sign data in the emergency department, general ward and icu. *BMJopen* 8(1)
 16. Guillen J, Liu J et al (2015) Predictive models for severe sepsis in adult icu patients. *IEEE Systems and Information Engineering Design Symposium*, IEEE
 17. Wang X, Wang Z, Weng J, Wen C, Chen C, Wang X (2018) A new effective machine learning framework for sepsis diagnosis. *IEEE Access* 6:48300–48310
 18. Nemati S, Holder A, Razmi F, Stanley MD, Clifford GD, Buchman TG (2018) An interpretable machine learning model for accurate prediction of sepsis in the ICU. *Crit Care Med*, 46 (4), 547–553 (2018)
 19. Moor M, Horn M et al (2019) Early recognition of sepsis with Gaussian process temporal convolutional networks and dynamic time warping. In: *Proceedings of machine learning research XX*, pp 1–IX
 20. Sepsis biomarker study Homepage, <https://doi.org/10.5281/zenodo.823967>. Last accessed 7 Jan 2019
 21. Latecki LJ, Lazarevic A, Pokrajac D (2007) Outlier detection with kernel density functions. In: *Conference MLDM 2007, LNCS*, Springer, Leipzig, vol 4571, pp 61–75
 22. Fullerton JN, Thompson K, Shetty A, Iredell JR, Lander R, Myburgh JA, Finfer S (2017) New sepsis definition changes incidence of sepsis in the intensive care unit. *Crit Care Resuscitation* 19(1):9–13
 23. Barton C, Chettipally U, Zhou Y, Jiang Z, Lynn-Palevsky A et al (2019) Evaluation of a machine learning algorithm for up to 48-hour advance prediction of sepsis using six vital signs. *Comput Biol Med* 109:79–84
 24. Shankar Hari M, Harrison DA, Rubinfeld GD, Rowan K (2017) Epidemiology of sepsis and septic shock in critical care units: comparison between sepsis-2 and sepsis-3 populations using a national critical care database. *British J Anaesth* 119:626–636. <https://doi.org/10.1093/bja/aex234>
 25. Chen T, Guestrin C (2016) XGBoost: a scalable tree boosting system. *KDD 2016*, ACM, San Francisco
 26. Freund Y, Schapire RE (1999) A short introduction to boosting. *J Japanese Soc Artif Intell* 14(5):771–780
 27. XGBoost Python package homepage. <https://xgboost.readthedocs.io>. Last accessed 21 July 2019
 28. Breiman L (2001) Random forests. *Mach Learn* 45 (1):5–32
 29. Mitchell T (1997) *Machine learning*. McGraw-Hill
 30. Andrew Y, Jordan Ng (2002) On discriminative versus generative classifiers: a comparison of logistic regression and naive Bayes. In: *Dietterich TG, Becker S, Ghahramani Z (eds) Advances in NIPS 14*, MIT Press, Cambridge, pp 841–848
 31. Joachims T (1998) Text categorization with support vector machines: learning with many relevant features. In: *Proceedings of ECML-98, 10th European conference on machine learning*, Springer, Dortmund, pp 137–142. <https://doi.org/10.1007/bfb0026683>
 32. Balduino R, Bogle B, Hazard A (2019) Using machine learning to predict outcomes for sepsis patients: <https://medium.com/inside-machine-learning/using-machine-learning-to-predict-outcomes-for-sepsis-patients-cde5625ce9cb>. Last accessed 21 May 2019

33. Masino AJ, Harris MC, Forsyth D (2019) Machine learning models for early sepsis recognition in the neonatal intensive care unit using readily available electronic health record data. In PLoS ONE 14(2)
34. Cali C, Longobardi M (2015) Some mathematical properties of the ROC curve and their applications. *Ricerche mat* 64(2):391–402

Existence Result of HIV Model by Employing Mahgoub Adomian Decomposition Procedure



Yogesh Khandelwal, Pawan Chanchal, and Rachana Khandelwal

Abstract The Mahgoub Adomian Decomposition Procedure is scouted to offer an analytic outcome of a nonlinear differential equation for HIV contamination of $CD4^+$ T-cells. This procedure is implemented as a model for HIV contamination of $CD4^+$ T-cells. Numerical consequences display this procedure is straightforward and unique when implemented to system of nonlinear differential equations.

Keywords Mahgoub transform · Mahgoub Adomian Decomposition Procedure (MADP) · HIV infection · $CD4^+$ T-cells

1 Introduction

Human immunodeficiency virus (HIV) is one of the rarely and deadly diseases found in human all over the world. It is a type of virus called retrovirus, and if it is not treated at right time, it leads to acquired immunodeficiency syndrome (AIDS) [1], which eventually leads to deterioration of white cells present in the human body that may eventually lead to death. White cells help human body to fight against the disease. HIV minimizes the number of $CD4^+$ T-cells present in the human body. $CD4$ cells are subdivision of T cell that renders a vital aspect in the immune system, notably in the adaptive immune system [2]. They avail the exertion of other immune cells by acquitting $CD4^+$ T-cells cytokines [3].

In 1993, an ordinary differential equation (ODE) model of a cell-free viral spread of HIV in a well-mixed slot like bloodstream was anticipated by Perelson, Kirschner and De Boer. The model given by them consists of four parts: uninfected healthy $CD4^+$ T-cells, latently infected $CD4^+$ T-cells, actively infected $CD4^+$ T-cells and free virus [4]. Further, Culshaw and Ruan make things simpler by taking only three parts

Y. Khandelwal (✉) · R. Khandelwal
Department of Mathematics, Maharishi Arvind University, Jaipur, India
e-mail: yogeshmaths81@gmail.com

P. Chanchal
Department of Mathematics, Government Girls College, Ajmer, India

such that the healthy CD4⁺T-cells, infected CD4⁺T-cells and free virus [5]. These cells add up an indiscrete time delay to the model to illustrate the difference of time between infection of a CD4⁺T-cells and the secretion of viral particles on a cellular level also [6]. Present combination antiretroviral therapies are extensively applied to treat HIV. The development of the drugs which are powerful against HIV is a shining instance of how thoughtful the fundamentals of the genesis of HIV contamination have brought about the fast development of medication to fight the ailment. The concepts for the remedy of HIV infection have been developed concurrently because of big, randomized, clinically controlled trials and due to the growing know-how of the dynamics of HIV replication [7]. Voluntary medical male circumcision (VMMC) HIV prevention report [8] presented 230,000 new HIV infections have been found in 2017 as the 18.6 million VMMCs had previously anticipated. These data have been taken for interpretation into growing coverage of ART.

2 Preliminaries and Definition

2.1 Mahgoub Transform

A new procedure known as the Mahgoub transform [9–11] by the operator $M^\circ(\cdot)$ defined by the integral equation.

$$M^\circ[h(t)] = A(z) = z \int_0^\infty h(t)e^{-zt} dt. \quad t \geq 0 \quad \text{and} \quad k_1 \leq z \leq k_2 \quad (1)$$

2.2 Derivative of Mahgoub Transform

Let $A[z]$ be the Mahgoub transform of $M^\circ[h(t)] = A[z]$ subsequently [11],

- (i) $M^\circ[h'(t)] = zA(z) - zh(0)$.
- (ii) $M^\circ[h''(t)] = z^2A(z) - zh'(0) - z^2h(0)$.

3 Ally of Mahgoub Transform and Adomian Decomposition Procedure [12–16]

Presume the ordinary differential equation with preliminary condition given beneath

$$[Lh(t) + Rh(t) + Nh(t)] = [y(t)], \tag{2}$$

with the initial condition as followed

$$h(0) = a. \tag{3}$$

Here, L is invertible and first-order derivative, R is linear differential operator, N is the nonlinear term, and $y(t)$ is the source term. Implementing Mahgoub transform on both sides of the Eq. (2), we invade

$$M^\circ[Lh(t) + Rh(t) + Nh(t)] = M^\circ[y(t)], \tag{4}$$

Implementing the differentiation property of Mahgoub transform and taking the initial condition from Eq. (3).

$$zM^\circ[h(t)] - [h(0)] = M^\circ[y(t)] - M^\circ[Rh(t) + Nh(t)], \tag{5}$$

$$zM^\circ[h(t)] = [h(0)] + M^\circ[y(t)] - M^\circ[Rh(t) + Nh(t)], \tag{6}$$

$$M^\circ[h(t)] = \frac{a}{z} + \frac{1}{z}M^\circ[y(t)] - \frac{1}{z}M^\circ[Rh(t) + Nh(t)]. \tag{7}$$

Inverse of Mahgoub transform on both sides, we attain

$$[h(t)] = a + M^{\circ-1} \left\{ \frac{M^\circ}{z} [y(t)] - [Rh(t) + Nh(t)] \right\}. \tag{8}$$

Thus, the resolution can be embodied as an infinite series

$$h(t) = \sum_{n=0}^{\infty} h_n(t). \tag{9}$$

While the nonlinear term can be broke down as

$$Nh(t) = \sum_{n=0}^{\infty} A_n(h). \tag{10}$$

Where $A_n(h)$ are Adomian polynomials of h_0, h_1, h_2, \dots given by

$$A_n = \left[\frac{1}{n!} \frac{d^n}{d\hat{t}^n} Nh(\hat{t}) \right]_{\hat{t}=0}.$$

To get the value of A_n , we put a grouping parameter \hat{t} .
 Rewriting Eq. (8) with the help of Eq. (9), (10)

$$\sum_{n=0}^{\infty} h_n(t) = F(t) + M^{\circ-1} \left\{ \frac{M^{\circ}}{z} [y(t)] - \left[R \sum_{n=0}^{\infty} h_n(t) + \sum_{n=0}^{\infty} A_n(h) \right] \right\}, \tag{11}$$

Here, $F(t)$ is the term which is emerging from the source term and the given initial condition. On contrasting both sides of Eq. (10) and using standard Adomian decomposition procedure, we invade

$$h_0(t) = F(t), \tag{12}$$

$$h_1(t) = -M^{\circ-1} \left[\frac{M^{\circ}}{z} \{Ry_0(t) + A_0\} \right], \tag{13}$$

$$h_2(t) = -M^{\circ-1} \left[\frac{M^{\circ}}{z} \{Ry_1(t) + A_1\} \right], \tag{14}$$

Thus, the general solution can be penned as

$$h_{n+1}(t) = -M^{\circ-1} \left[\frac{M^{\circ}}{z} \{Ry_n(t) + A_n\} \right], \quad n \geq 0. \tag{15}$$

Again, implementing the Mahgoub transform on right hand side of Eq. (15) and then applying inverse of Mahgoub transform, we get n_0, n_1, n_2, \dots which is infinite series of form of the desired solution. The system of nonlinear differential equation of HIV infection model of [17] CD4⁺T-cells can be represented as in Eq. (16).

$$\left. \begin{aligned} \frac{dC}{dt} &= p - \alpha C + \dot{r}C \left(1 - \frac{C+O}{C_{\max}} \right) - \dot{\delta}CB \\ \frac{dO}{dt} &= \dot{\sigma}CB - \dot{\beta}O \\ \frac{dB}{dt} &= I\dot{\beta}O - \dot{\gamma}B - \dot{\delta}CB \end{aligned} \right\}, \tag{16}$$

with the initial conditions

$$C(0) = \epsilon_1 = 0.1, \quad O(0) = \epsilon_2 = 0 \quad \text{and} \quad B(0) = \epsilon_3 = 0.1. \tag{17}$$

Here, C = Healthy cells, O = Infected cells, B = Virus.

Here $C(t)$, $O(t)$ and $B(t)$ give the concentration of CD4⁺T-cells, infected CD4⁺T-cells by HIV and free HIV virus in the blood, respectively. α, β, γ Personify natural turnover rate of healthy CD4⁺T-cells, infected CD4⁺T-cells and death rate of HIV virus, respectively. $\delta > 0$ is the rate of infected cell. Also, P is the rate production of CD4⁺T-cells. \mathfrak{S} is the number of virus produced by infected CD4⁺T-cells. C_{\max} Give the information about the maximum population of CD4⁺T-cells. While $\left(1 - \frac{C+D}{C_{\max}} \right)$ describes the logistic growth of T-cells [17]. $\dot{\sigma}$ symbolize the rate of infected cells that became active. All the parameters that are chosen as

$$\begin{aligned} \dot{\alpha} &= 0.02, \dot{\beta} = 0.3, \dot{\gamma} = 2.4, \dot{\delta} = 0.0027, \\ p &= 0.1, I = 10, C_{\max} = 1500, \dot{\sigma} = 0.00, \dot{r} = 3. \end{aligned}$$

Equation (16) is rewritten as

$$\left. \begin{aligned} \frac{dC}{dt} &= p - \dot{\alpha}C + \dot{r}C \left(1 - \frac{C+O}{C_{\max}}\right) - \dot{\delta}CB \\ \frac{dO}{dt} &= \dot{\sigma}CB - \dot{\beta}O \\ \frac{dB}{dt} &= I\dot{\beta}O - \dot{\gamma}B - \dot{\delta}CB \end{aligned} \right\}. \tag{18}$$

Applying Mahgoub transform on both sides in the above equations

$$\begin{aligned} M^\circ \left\{ \frac{dC}{dt} \right\} &= M^\circ \left\{ p - \dot{\alpha}C + \dot{r}C \left(1 - \frac{C+O}{C_{\max}}\right) - \delta BC \right\}, \\ M^\circ \left\{ \frac{dC}{dt} \right\} &= \left\{ M^\circ(p) - M^\circ(\dot{\alpha}C) + M^\circ \left\{ \dot{r}C \left(1 - \frac{C+O}{C_{\max}}\right) \right\} \right. \\ &\quad \left. - M^\circ(\dot{\delta}BC) \right\}, \\ M^\circ \left\{ \frac{dC}{dt} \right\} &= M^\circ\{p\} - M^\circ\{\dot{\alpha}C\} + M^\circ\{\dot{r}C\} - M^\circ \left\{ \frac{\dot{r}C^2}{C_{\max}} \right\} \\ &\quad - M^\circ \left\{ \frac{\dot{r}CO}{C_{\max}} \right\} - M^\circ\{\dot{\delta}BC\} \end{aligned} \tag{19}$$

$$\begin{aligned} M^\circ \left\{ \frac{dO}{dt} \right\} &= M^\circ\{\dot{\sigma}BC - \dot{\beta}O\}, \\ M^\circ \left\{ \frac{dO}{dt} \right\} &= M^\circ\{\dot{\sigma}BC\} - M^\circ\{\dot{\beta}O\}. \end{aligned} \tag{20}$$

$$\begin{aligned} M^\circ \left\{ \frac{dB}{dt} \right\} &= M^\circ\{I\dot{\beta}O - \dot{\gamma}B - \dot{\delta}BC\}, \\ M^\circ \left\{ \frac{dB}{dt} \right\} &= M^\circ\{I\dot{\beta}O\} - M^\circ\{\dot{\gamma}B\} - M^\circ\{\dot{\delta}BC\}. \end{aligned} \tag{21}$$

Rewriting Eq. (19) by implementing properties of Mahgoub transform

$$\begin{aligned} h\{C(h)\} - C(0) &= pM^\circ\{1\} - \dot{\alpha}M^\circ\{C\} + \dot{r}M^\circ\{C\} \\ &\quad - \frac{\dot{r}}{C_{\max}}M^\circ\{C^2\} - \frac{\dot{r}}{C_{\max}}M^\circ\{CO\} - \dot{\delta}M^\circ\{BC\}, \\ h\{C(h)\} &= \epsilon_1 + p - \dot{\alpha}M^\circ\{C\} + \dot{r}M^\circ\{C\} - \frac{\dot{r}}{C_{\max}}M^\circ\{C^2\} \\ &\quad - \frac{\dot{r}}{C_{\max}}M^\circ\{CO\} - \dot{\delta}M^\circ\{BC\}, \end{aligned}$$

$$\begin{aligned}
 C(h) &= \frac{\epsilon_1}{h} + \frac{p}{h} - \frac{\dot{\alpha}}{h} M^\circ\{C\} + \frac{\dot{r}}{h} M^\circ\{C\} - \frac{\dot{r}}{h \cdot C_{\max}} M^\circ\{C^2\} \\
 &\quad - \frac{\dot{r}}{h \cdot C_{\max}} M^\circ\{CO\} - \frac{\dot{\delta}}{h} M^\circ\{BC\}, \\
 C(h) &= \frac{\epsilon_1}{h} + \frac{p}{h} - \frac{\dot{\alpha}}{h} M^\circ\{C\} + \frac{\dot{r}}{h} M^\circ\{C\} - \frac{\dot{r}}{h \cdot C_{\max}} M^\circ\{C^2\} \\
 &\quad - \frac{\dot{r}}{h \cdot C_{\max}} M^\circ\{CO\} - \frac{\dot{\delta}}{h} M^\circ\{BC\}, \tag{22}
 \end{aligned}$$

Rewriting Eq. (20) by implementing properties of Mahgoub transform, we arrive at

$$\begin{aligned}
 M^\circ\left\{\frac{dO}{dt}\right\} &= M^\circ\{\dot{\sigma}BC\} - M^\circ\{\dot{\beta}O\}, \\
 h\{O(h)\} - O(0) &= \dot{\sigma}M^\circ(BC) - \dot{\beta}M^\circ(O), \\
 h\{O(h)\} &= \epsilon_2 + \dot{\sigma}M^\circ(BC) - \dot{\beta}M^\circ(O), \\
 \{O(h)\} &= \frac{\epsilon_2}{h} + \frac{1}{h}[\dot{\sigma}M^\circ(BC) - \dot{\beta}M^\circ(O)], \\
 \{O(h)\} &= \frac{\epsilon_2}{h} + \frac{1}{h}\dot{\sigma}M^\circ(BC) - \frac{1}{h}\dot{\beta}M^\circ(O). \tag{23}
 \end{aligned}$$

Rewriting Eq. (21) by implementing properties of Mahgoub transform

$$\begin{aligned}
 h\{B(h)\} - B(0) &= I\dot{\beta}M^\circ(O) - \dot{\delta}M^\circ(BC) - \dot{\gamma}M^\circ(B), \\
 h\{B(h)\} &= \epsilon_3 + I\dot{\beta}M^\circ(O) - \dot{\delta}M^\circ(BC) - \dot{\gamma}M^\circ(B), \\
 \{B(h)\} &= \frac{\epsilon_3}{h} + \frac{1}{h}[I\dot{\beta}M^\circ(O) - \dot{\delta}M^\circ(BC) - \dot{\gamma}M^\circ(B)], \\
 \{B(h)\} &= \frac{\epsilon_3}{h} + \frac{1}{h}I\dot{\beta}M^\circ(O) - \frac{1}{h}\dot{\delta}M^\circ(BC) - \frac{1}{h}\dot{\gamma}M^\circ(B). \tag{24}
 \end{aligned}$$

Now, it was assumed that

$$\begin{aligned}
 E &= \sum_{n=0}^{\infty} E_n, \quad H = \sum_{n=0}^{\infty} C_n, \\
 I &= \sum_{n=0}^{\infty} O_n, \quad V = \sum_{n=0}^{\infty} B_n, \quad E = C^2, \\
 F &= CO, \quad G = BC.
 \end{aligned}$$

Putting the assumed values in Eq. (22)

$$\begin{aligned} \left\{ M^\circ \sum_{n=0}^\infty C_n \right\} &= \frac{\epsilon_1}{h} (+) \frac{p}{h} - \frac{\dot{\alpha}}{h} M^\circ \left\{ \sum_0^\infty C_n \right\} + \frac{\dot{r}}{h} M^\circ \left\{ \sum_0^\infty C_n \right\} \\ &\quad - \frac{1}{h} \frac{\dot{r}}{C_{\max}} M^\circ \left\{ \sum_0^\infty E_n \right\} - \frac{1}{h} \frac{\dot{r}}{C_{\max}} M^\circ \left\{ \sum_0^\infty F_n \right\} \\ &\quad - \frac{\dot{\delta}}{h} M^\circ \left\{ \sum_0^\infty G_n \right\}. \end{aligned} \tag{25}$$

Putting the assumed values in Eq. (23), then

$$\left\{ M^\circ \sum_{n=0}^\infty O_n \right\} = \frac{\epsilon_2}{h} + \frac{\dot{\sigma}}{h} M^\circ \left\{ \sum_0^\infty G_n \right\} - \frac{\dot{\beta}}{h} M^\circ \left\{ \sum_0^\infty O_n \right\}. \tag{26}$$

Putting the assumed values in Eq. (24), we obtained

$$\left\{ M^\circ \sum_{n=0}^\infty B_n \right\} = \frac{\epsilon_3}{h} + \frac{1}{h} I \dot{\beta} M^\circ \left\{ \sum_0^\infty O_n \right\} - \frac{\dot{\delta}}{h} M^\circ \left\{ \sum_0^\infty G_n \right\} - \frac{\dot{\gamma}}{h} M^\circ \left\{ \sum_0^\infty B_n \right\}. \tag{27}$$

Here, E_n, F_n, G_n are Adomian polynomials.

These are given by

$$\begin{aligned} E_0 &= C_0^2 \\ E_1 &= 2C_0C_1 \\ E_2 &= 2C_0C_2 + C_1^2 \\ E_3 &= 2C_0C_3 + 2C_1C_2 \\ E_4 &= 2C_0C_4 + 2C_1C_3 + C_2^2 \\ E_5 &= 2C_0C_5 + 2C_1C_4 + 2C_2C_3. \\ \\ F_0 &= C_0O_1 \\ F_1 &= C_1O_0 + C_0O_1 \\ F_2 &= C_2O_0 + C_1O_1 + C_0O_2 \\ F_3 &= C_3O_0 + C_2O_1 + C_1O_2 + C_0O_3 \\ F_4 &= C_4O_0 + C_3O_1 + C_2O_2 + C_1O_3 + C_0O_4 \\ F_5 &= C_5O_0 + C_4O_1 + C_3O_2 + C_2O_3 + C_1O_4 + C_0O_5. \\ \\ G_0 &= B_0C_0 \\ G_1 &= B_1C_0 + B_0C_1 \\ G_2 &= B_2C_0 + B_1C_1 + B_0C_2 \\ G_3 &= B_3C_0 + B_2C_1 + B_1C_2 + B_0C_3 \\ G_4 &= B_4C_0 + B_3C_1 + B_2C_2 + B_1C_3 + B_0C_4 \\ G_5 &= B_5C_0 + B_4C_1 + B_3C_2 + B_2C_3 + B_1C_4 + B_0C_5. \end{aligned}$$

Utilizing the above values in Eqs. (25), (26), (27), respectively, result from Eq. (25) was obtained

$$\begin{aligned}
 M^\circ\{C_0\} &= \frac{\epsilon_1}{h} + \frac{p}{h}, \\
 M^\circ\{C_1\} &= -\frac{\dot{\alpha}}{h}M^\circ\{C_0\} + \frac{\dot{r}}{h}M^\circ\{C_0\} - \frac{1}{h} \frac{\dot{r}}{C_{\max}}M^\circ\{E_0\} \\
 &\quad - \frac{1}{h} \frac{\dot{r}}{C_{\max}}M^\circ\{F_0\} - \frac{\dot{\delta}}{h}M^\circ\{G_0\}, \\
 M^\circ\{C_2\} &= -\frac{\dot{\alpha}}{h}M^\circ\{C_1\} + \frac{\dot{r}}{h}M^\circ\{C_1\} - \frac{1}{h} \frac{\dot{r}}{C_{\max}}M^\circ\{E_1\} \\
 &\quad - \frac{1}{h} \frac{\dot{r}}{C_{\max}}M^\circ\{F_1\} - \frac{\dot{\delta}}{h}M^\circ\{G_1\}, \\
 M^\circ\{C_{n+1}\} &= -\frac{\dot{\alpha}}{h}M^\circ\{C_n\} + \frac{\dot{r}}{h}M^\circ\{C_n\} - \frac{1}{h} \frac{\dot{r}}{C_{\max}}M^\circ\{E_n\} \\
 &\quad - \frac{1}{h} \frac{\dot{r}}{C_{\max}}M^\circ\{F_n\} - \frac{\dot{\delta}}{h}M^\circ\{G_n\}.
 \end{aligned} \tag{28}$$

From Eq. (26),

$$\begin{aligned}
 M^\circ\{O_0\} &= \frac{\epsilon_2}{h}, \\
 M^\circ\{O_1\} &= \frac{\dot{\sigma}}{h}M^\circ\{G_0\} - \frac{\dot{\beta}}{h}M^\circ\{O_0\}, \\
 M^\circ\{O_2\} &= \frac{\dot{\sigma}}{h}M^\circ\{G_1\} - \frac{\dot{\beta}}{h}M^\circ\{O_1\}, \\
 M^\circ\{O_{n+1}\} &= \frac{\dot{\sigma}}{h}M^\circ\{G_n\} - \frac{\dot{\beta}}{h}M^\circ\{O_n\}.
 \end{aligned} \tag{29}$$

Now, again obtaining the solution from Eq. (27)

$$\begin{aligned}
 M^\circ\{B_0\} &= \frac{\epsilon_3}{h}, \\
 M^\circ\{B_1\} &= \frac{I\dot{\beta}}{h}M^\circ\{O_0\} - \frac{\dot{\delta}}{h}M^\circ\{G_0\} - \frac{\dot{\gamma}}{h}M^\circ\{B_0\}, \\
 M^\circ\{B_{n+1}\} &= \frac{I\dot{\beta}}{h}M^\circ\{O_n\} - \frac{\dot{\delta}}{h}M^\circ\{G_n\} - \frac{\dot{\gamma}}{h}M^\circ\{B_n\}.
 \end{aligned} \tag{30}$$

4 Results

Consider the values of

$$C(0) = \epsilon_1 = 0.1, O(0) = \epsilon_2 = 0, B(0) = \epsilon_3 = 0.1$$

Applying Mahgoub inverse transform on both the sides of the above Eq. (28), (29), (30), we get

$$\begin{aligned} C(t) &= 0.1 + 0.3979521t + 0.59283t^2 + 0.5887185t^3 \\ &\quad + 0.438297t^4 + 0.2608635t^5 - 0.129196t^6. \\ O(t) &= 0.000024t + 0.000017276t^2 - 0.00000840519t^3 \\ &\quad - 0.000006147285t^4 - 0.000002835851t^5 + 0.000001152t^6. \\ B(t) &= 0.1 - 0.2407251t + 0.28792738t^2 + 0.2304143t^3 \\ &\quad + 0.138246t^4 - 0.0663524t^5 + 0.0265395t^6. \end{aligned}$$

$C(t)$, $O(t)$ and $B(t)$ give the concentration of $CD4^+$ T-cells, infected $CD4^+$ T-cells by HIV and free HIV virus in the blood.

5 Conclusion

This article concludes the solution of nonlinear ordinary differential equation of HIV model by Mahgoub Transform and Adomian decomposition procedure.

The outcome accomplished from this procedure was nearly equal to the exact solution of these nonlinear ordinary differential equations of HIV model. Results of this article infer that Mahgoub Adomian Decomposition Procedure is less complicated and efficacious tool for nonlinear ODE's of HIV model. Similar results were found when compared with the Kamal Transform Adomian Decomposition Method (KTADM) [18] and Natural Adomian Decomposition Method (NADM) [19]. Therefore, it was shown that the persuasiveness of Mahgoub Adomian Decomposition Procedure is valid.

References

1. Weiss RA (1993) How does HIV cause AIDS? Science 260(5112):1273–1279. <https://doi.org/10.1126/science.8493571>
2. Douek GC, Roederer M, Koup RA (2009) Emerging Concepts in the immune pathogenesis of AIDS. Annul Rev Med 60:471–484

3. Perelson AS, Chavez CC (1989) Modeling the interaction of the immune system with HIV. *Math Stat Approaches AIDS Epidemiology Lecture Notes Biomath* 83:350–370
4. Perelson AS, Kirschner DE, Boer RD (1993) Dynamics of HIV infection of CD4⁺T-cells. *Math Biosci* 114(1):81–125
5. Culshaw RV, Shigui R (2000) A delay differential equation model of HIV Infection of CD4⁺T-cells. *Math Biosci* 165(1):27–39
6. Senthilkumaran M, Joseph GA (2017) Stability analysis for fractional order differential equation model of HIV infection of CD4⁺T-Cells. *Int J Pure Appl Math* 109(9):221–228
7. Zhou X, Song X, Shi X (2008) A differential equation model of HIV infection of CD4⁺T-cells. *J Math Anal Appl* 342:1342–1355. <https://doi.org/10.1016/j.jmaa.2008.01.008>
8. WHO Progress Brief, Voluntary medical male circumcision for HIV prevention. WHO reference number: WHO/AF/CDS/HIV/03/2018
9. Khandelwal R, Khandelwal Y, Chanchal P (2018) Mahgoub deterioration method and its application in solving duo-combination of nonlinear PDE's. *Math J Interdisciplinary Sci* 7(1):37–44. <https://doi.org/10.15415/mjjs.2018.71006>
10. Mahgoub MMA (2017) The new integral transform mahgoub transform. *Adv Theor Appl Math* 11(4):391–398
11. Mahgoub MMA, Alshikh AA (2017) An application of new transform mahgoub transform to partial differential equations. *Math Theory Mod* 7(1):7–9
12. Adomian G (1993) Solving frontier problems of physics: the decomposition method. Springer, Berlin
13. Adomian G (1988) A review of the decomposition method in applied mathematics. *J Math Anal Appl* 135:501–544
14. Adomian G (1991) A review of the decomposition method and some recent results for nonlinear equations. *Comput Math Appl* 21(5):101–127
15. Dogan N (2012) Numerical treatment of the model for HIV infection of CD4⁺T-cells by using multistep laplace adomian decomposition method. *Discrete Dynamics Nat Soc* 11. <http://dx.doi.org/10.1155/2012/976352>
16. Ongun MY (2011) The laplace adomian decomposition method for solving a model for HIV infection of CD4⁺T-cells. *Math Comput Model* 53(5–6):597–603
17. Balamuralitharan S, Geetha V (2017) Analytical approach to solve the model for HIV infection of CD4⁺T-cells using LADM. *Int J Pure Appl Math* 113(11):243–251
18. Khandelwal Y, Kumawat P, Khandelwal R (2018) Analysis of HIV model by KTADM. *Math J Interdisciplinary Sci* 6(2):181–190(2018). <https://doi.org/10.15415/mjjs.2018.62013>
19. Khandelwal Y, Kumawat P, Khandelwal R (2018) A study of HIV model using NADM method. *Int J Manag Technol Eng* 8:909–915

Industry 4.0 Manufacturing Based on IoT, Cloud Computing, and Big Data: Manufacturing Purpose Scenario



Arun Kumar Rana and Sharad Sharma

Abstract Industry 4.0 is an energetic movement as of late offered by means of the German administration. The aim of the movement is the altering of modern assembling throughout digital technology and the abuse of possibilities of new innovations. Our nations pressed towards “Make in India” have taken comprehension of Industry 4.0 and ongoing it’s situating in this space. First shrewd processing plant—touching from mechanization to independence—where machines make conversation with one another is being laid down up in Bangalore at the Indian Institute of Science’s Centre for Product Design and Manufacturing with seed financing from the Boeing Corporation. An Industry 4.0 creation framework is in this manner adjustable and empowers individualized and modified items. This paper introduces the writing study on Internet of thing based assembling and arranging process in keen ventures. This paper gives an itemized depiction of things to come challenge, remote sensor observing, and efficient strategies over the IoT.

Keywords IoT · IIoT · 4.0 · Cloud computing · Big data

1 Introduction

An organization like Cisco, for example, expects in excess of 24 billion Internet-related gadgets by 2020; Morgan Stanley, regardless, predicts the utilization of 75 billion orchestrated contraptions by 2021 on the Internet of things [1]. With the consistent movement in advancements in IoT and its potential improvement, the Internet of things is quickly extending as an inescapable overall enlisting framework where everyone and everything will be related to the Internet [2, 3] (Fig. 1).

A. K. Rana (✉) · S. Sharma
Maharishi Markandeshwar (Deemed to be University), Mullana, Ambala, India
e-mail: ranaarun1.ece@piet.co.in

S. Sharma
e-mail: sharadpr123@rediffmail.com

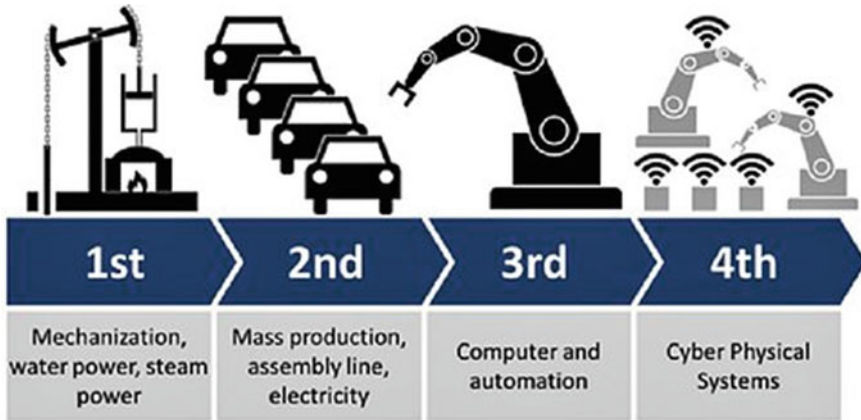


Fig. 1 4.0 generation with IoT

In the most recent years, the innovative advances of ITCs gave a lot of devices that transformed us into the Web, robots, automatons, the Internet of things, etc. Past this, things convey in an overall system: the Internet. This pattern will unquestionably discover its path additionally into mechanical generation, which will profit progressively from the advances in ICT and PC sciences [4]. The appearance of the IoT and services into the assembling condition is introducing a fourth modern insurgency: Industry 4.0. This new sort of industry depends on a model of smart enterprise, for example, Keen Factory [5]. The target of this examination was to dissect the oddity of the subject Industry 4.0 identified with the IoT through an orderly audit in the Web of the information base. Preceding Internet of things, there was a direct manual technique for dealing with machine/gadget interconnectivity. Be that as it may, with the progress in ongoing innovation, better methodologies need better associate for controlling machine stop save time, cost, and vitality, i.e., in the well-being segment, in farming, well-being, and for mechanization [6]. Web applications are a standout among the most common stages for data and administrations conveyed over the Internet today. As they are progressively utilized for basic administrations, Web applications become a well-known and profitable focus for security assaults in Industry 4.0 [7].

In Industry 4.0, ML is the main thrust for man-made brainpower (AI). The preferred standpoint ML frameworks are that it utilizes intelligent models, heuristic learning, information acquisitions, and choice trees for modern creation [7]. While Deloitte alludes to shrewd, associated producing as Industry 4.0, a few other regularly realized terms may point to a similar marvel [8]. These include Internet of everything

- a. Industrial Internet
- b. Manufacturing 4.0
- c. Connected enterprise
- d. Smart manufacturing
- e. Smart factory.



Fig. 2 Industrial Internet of things

Otherwise called the mechanical Web or Industry 4.0, IIoT uses the intensity of savvy machines and continuous examination to exploit the information that stupid machines have created in modern settings for a considerable length of time (Fig. 2).

2 Literature Review

In [9], a lead for upcoming investigation passion for the region of IoT, different pioneering patterns in IoT and its various uses we spoke to. Moreover, the inventor in [9] displayed a method for the future design of the Internet of things. They included an audit of ongoing advancements and furthermore displayed a focused plan for conceivable completing of things to come to IoT. The creators in [10] talked for upcoming difficulties in the Internet of things besides displaying the best in the class audit of ongoing uses of IoT innovation and the alternate points of view in scholastics and the modern network. Industry 4.0 alludes to the following phase in the advancement of the relationship and control of assembling forms Industry 4.0 really originates from a plan fund by the administration of German [11], which is said to be first made open amid the 2011 Hannover Fair [12]. The phrase was gotten with excitement by the overall manufacturing [13] and covers to some degree without ideal models like IIoT [14] and with different activities, for example, complete by the China 2025 [15]. As well, Industry 4.0 is truly for the association of sharp preparing plants [16], for consideration to run even more viable, their benefits and to unite enough edibility to acclimate to the age needs. Such a requirement for edibility is identified with how clients are dynamically mentioning things customization [17], which impacts progression and gathering at different stages. The thought acknowledges a significantly increasing broad application zone as the Industry 4.0 and covers control age and spread, social protection, produce, open division, transportation, and mining [18]. In France, the thought “Businesses du future” was exhibited as a focal point of things to go to the French present-day approach. It relies upon the interest of

manufacturing and skill and dependent on five sections: (1) cutting edge progresses included substance creating, fundamental plant, IoT, and extended reality, (2) at the bottom of the French associations, especially little to focus ones, to change in accordance with new developments, (3) expansive specialists' readiness, (4) bracing overall joint effort around present-day measures, and (5) headway of French industry of things to come [19]. The next near action in 2025 "Made in China" was introduced in 2015 [20]. It was begun by the China organization of Industry and Information Technology in investment with various authorities from the China Academy of Engineering. The main goal of this movement is to broadly refresh the Chinese business by delineation direct inspiration from Germany's Industry 4.0 thought and modifying it to China needs. The changed amassing should be progression driven. Kai et al. discussed smart health in the IoT. It is very different, think in the case of security in health care. It mainly works on the IoT is the Information and Communication Technology (ICT) industry. In this paper, the authors discussed security of health-care system. It follows the new strategy in the health of the IoT [30]. Zhao et al. "A Survey on the Internet of Things Security" The authors have discussed IoT, its application and usage in the future. In this paper, the authors proposed to find the solution to minimize the threat of IoT [31]. Skouby and Lynggaard introduced about smart home. Future smart home is as well as the security-related systems [32]. In future, device-to-device communications resolve the problems of vehicle-to-vehicle (V2V) transportations for traffic regulator and security uses [33]. In [34], different issues related to the health and farming were discussed. [35] discussed process for supervision massive IoT traffic in 5G networks.

3 Cyber-Physical System with 4.0

Cyber-physical system (CPS) jointly with the IoT, big data, cloud computing, and industrial wireless networks are the center innovations permitting the presentation of the fourth modern insurgency, Industry 4.0. Alongside the advances in new-age data advances, keen assembling is turning into the focal point of worldwide assembling change. An epic CPS engineering for the continuous perception of complex mechanical procedures is proposed. It basically considers the simulation innovative mainstay of Industry 4.0. Digital methods calculation, correspondence, and control are discrete exchanged and sensible [27]. A system characterized as must be innovations for overseeing interrelated frameworks among their processing abilities and physical resources [28] (Fig. 3).

A CPS is an arrangement of working together with IT components and intended to governor physical entities. Correspondence happens through an information foundation, for example, the Internet. Conventional implanted frameworks can be viewed as an exceptional instance of an independent CPS [29].

Figure 4 delineates IIoT from a CPS perspective. In the physical framework (left), the diverse current applications, for example, PA and FA, pursue a creation lifecycle (i.e., the cycle of getting ready, produce, transport, use, and reuse). During each

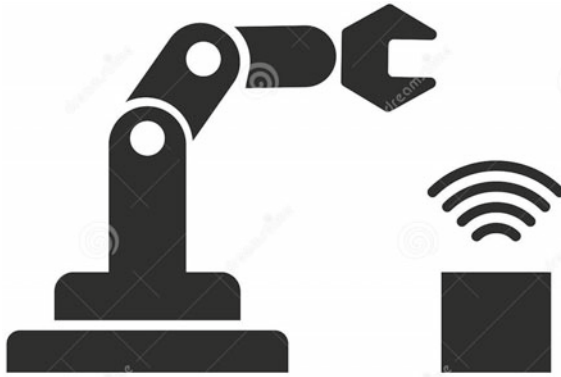


Fig. 3 CPS together with IoT, big data, and cloud computing

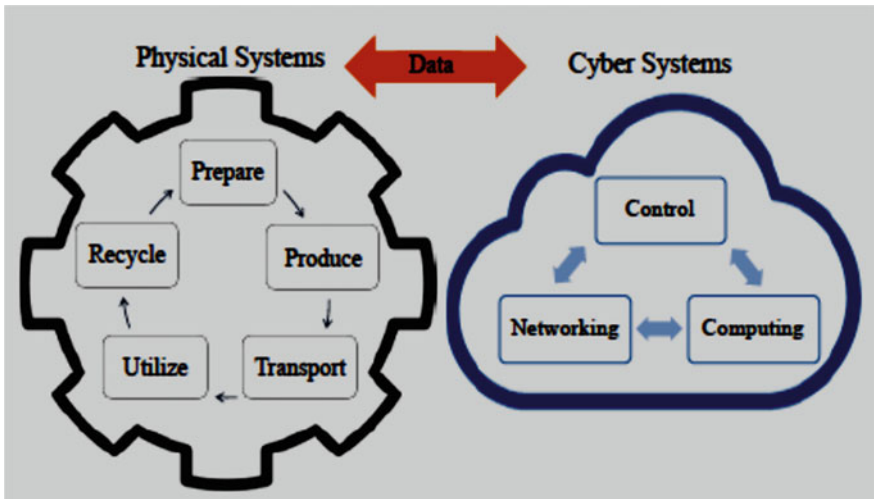


Fig. 4 IIoT from a CPS perspective [11]

progression in the creation of life cycle, a significant measure of information will be produced from various gadgets and gear. Control, systems administration, and processing frameworks assume significant jobs in the interconnection and reconciliation of parts and physical frameworks and perform observing and control, prompting efficient activity of physical frameworks.

4 Present Challenges

We are amidst the fourth modern transformation, or Industry 4.0 as its all the more usually known. Since the while sharp names have been used in the latest years in different mechanical fields, shrewd imprints are up 'til now a creating point that gathers responsibilities from traditional naming systems, IIoT, cloud/edge figuring, and sensor/actuator progressions. As Industry 4.0 keeps on changing the manner in which we interface with our general surroundings, new difficulties emerge. Here are the primary difficulties you may look not long from now:

4.1 Effect of Common Conditions

The circumstances of nature impudence splendid imprint task, so they should be viewed as while organizing and picking sharp name gear. The e-ink show is likely the most essential bit of the hardware, but current advancement has issues, for occurrence, with little and great temperatures.

4.2 Roughness

Shrewd imprints need to survive the fierce environments that are commonly existing in mechanical circumstances. Along these lines, clever imprints should suffer drops, a particular proportion of weight or outside impacts. It is extraordinary stress for the block of e-ink appears (Fig. 5).

4.3 Engendering of Interchanges Within the Sight of Metal

Numerous mechanical situations are described by the nearness of monstrous measures of metal that influence conventional electromagnetic remote interchanges and situating frameworks [20]. Subsequently, keen names need to endure the nearness of metal or utilize no electromagnetic based interchanges.

4.4 Resilience to Impedances and Sticking

Keen names depend on the reason that vigorous solid remote interchanges are accessible, so if correspondences are blocked or stuck (inadvertently or deliberately),



Fig. 5 Challenges of 4.0 with IoT

the framework must probably identify, recuperate, and give elective correspondence systems (e.g., reinforcement correspondence interfaces).

4.5 Adaptable Hardware Is Additionally

A rising era empowers printing sensors, transistors, and foldable shows on paper or plastic substrates. Completely printed frameworks still have certain exhibition confinements, yet they are as of now considering creating brilliant marks [23].

4.6 New Materials

By far most of the keen names depend on silicon materials, yet a rising subject is the advancement of electronic natural names. Such names can be created less expensive and with just a printer, be that as it may, as of composing, albeit some intriguing structures have been proposed [21], they cannot be as little as conventional silicon mark sand the reproducing ranges must be considered and improved [22].

4.7 Zero-Control Identification

So as to decrease the requirement for batteries and to evacuate vitality devouring hardware for recognizing items, a new era like brilliant skins, hipless RFID, and zero-control identification have advanced significantly in the last years [24, 25], so they could be connected to shrewd names sooner rather than later.

4.8 Human Variables/Ergonomics and Ease of Use Methods

So as to make a human-focused keen mark framework, the first step is to figure out who are the administrators, how, where, and what they are utilizing, and what they might want to use later on. The subsequent stage is to set pertinent and reasonable ease of use objectives for their UI. These targets incorporate, for instance, an opportunity to achieve the errand or the mistake resilience [26].

5 What Scenario Does the IoT and Industry 4.0 Pose for Manufacturers?

For upcoming days both Industry 4.0 and IoT request connecting together already free gadgets and frameworks, it is not astounding that a boss mutual concern is a security. As the pattern of utilizing keen gadgets builds, it will be more earnestly to follow breeches and deal with those gadgets. The business is moving rapidly to address these security concerns, merging new advancements with standard IT security advances like system security and encryption (Fig. 6).

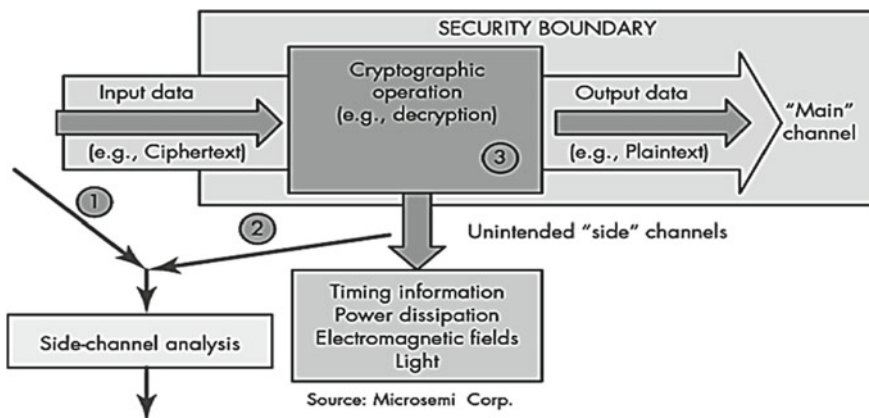


Fig. 6 IT security technologies like network security and encryption

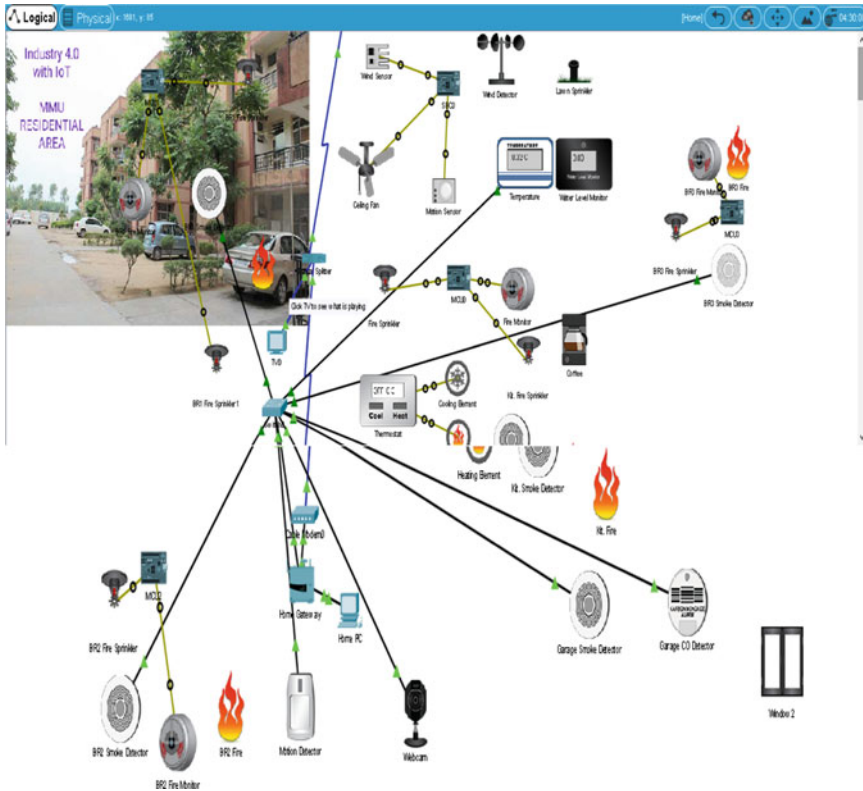


Fig. 7 IoT with 4.0 with DHCP secure protocol

For design residential area of MMU campus, we worked on cisco packet tracer 7.2.1 with dynamic host configure protocol (DHCP) protocol which provides the best security for the connected IoT sensor as shown in Fig. 7 and used for better accuracy in IP addressing for all connected device with gateway.

6 Research Objectives

- To develop new methods for providing quick data delivery for IoT and IIoT networks.
- To develop algorithm to provide strict security bounds for IoT and IIoT applications.
- To develop infrastructure to manage huge amounts of data, and build the IoT with IIoT applications that create a smarter, more connect world for 5G networks.

7 Conclusion

The word the primary target of this exploration is to break down the scholastic indications of advancement in subjects identified with the fourth mechanical insurgency in an efficient way and to give bits of knowledge into the past, present, and eventual fate of this theme. In this paper, the foundation and improvement of the Industry 4.0 idea are introduced. As the reconciliation of data innovation and task innovation develops, producers should evaluate where they are as well as where they wish to be—choices that will direct the kinds of data they should assemble, examine, and follow up on. By utilizing IoT with wireless sensor network innovation, different assembling assets are distinguished and their statuses could be then caught. It very well may be normal that the vast majority of the endeavors will present the Industry 4.0 components bit by bit and by structure on officially existing hardware and programming arrangements, in this manner not jeopardizing the strength of their generation. In this paper, we create a secured IoT environment with 4.0 revolution and in the future by creating full use of IoT with transmission protocol, cloud computing, and cyber-security technology, a variety of manufacturing resources is recognized and their statuses could be then captured.

References

1. Cloud and mobile network traffic forecast-visual networking index (VNI), Cisco (2015)
2. Danova T (2013) Morgan stanley: 75 billion devices will be connected to the internet of things by 2020. Business Insider
3. Khan R, Khan SU, Zaheer R, Khan S (2012) Future internet: the internet of things architecture, possible applications, and key challenges. In: Proceedings of frontiers of information technology (FIT), pp 257–260
4. Weyer S, Schmitt M, Ohmer M, Gorecky (2015) Towards industry 4.0-standardization as the crucial challenge for highly modular, multi-vendor production systems 48(3):579584
5. Veza I, Mladineo M, Gjeldum (2015) Managing innovative production network of smart factories. IFAC-Papers OnLine 48(3):555–56
6. Ayodeji, Gupta S (2018) Recent trends in IoT, its requisition with IoT built engineering: a review. Springer, Singapore, 20 Nov 2018. ISBN978-981-13-2553-3
7. Rana A, Ayodeji (2018) Survey of machine learning methods, what's more, their sensor and IoT applications for future world. Amity J Comput Scis (AJCS) 2(2). ISSN: 2456-6616
8. Vermesan O, Friess P, Guillemin P, Jubert IS, Mazura M, Harrison M, Eisenhauer M, Doody P (2011) Internet of things strategic research roadmap. In: Internet of things-global technological and societal trends, pp 9–52
9. Uckelmann D, Harrison M, Michahelles F (2011) An architectural approach towards the future internet of things, architecting the internet of things, Springer, Berlin, pp 1–24
10. Bandyopadhyay D, Sen J (2011) Internet of things: applications and challenges in technology and standardization. Wirel Personal Commun Springer 58(1):49–69
11. Industrie 4.0 project official web page. Available online: [https:// www.bmbf.de/de/zukunftsp-rojekt-industrie-4-0-848.html](https://www.bmbf.de/de/zukunftsp-rojekt-industrie-4-0-848.html). Accessed on 11 Mar 2018
12. Announcement of the Industrie 4.0 project in the 2011 Hannover Fair, 11 Mar 2018
13. Drath R, Horch A (2014) Industrie 4.0: Hit or Hype? IEEE Ind Electron Mag 8(2):56–58

14. Xu LD, He W, Li S (2014) Internet of things in industries: a survey. *IEEE Trans Industr Inf* 10(4):22332243
15. Center for Strategic and International Studies, “Made in China 2025”, 11 March 2018
16. Munera E, Poza-Lujan JL (2015) Posadas-Yagüe, J. L., Simo, J., Blanes, J. F., Albertos, P., “Control kernel in smart factory environments: Smart resources integration”, in Proceedings of the IEEE International Conference on Cyber Technology in Automation, Control, and Intelligent Systems (CYBER), Shenyang, China, June 2015
17. Xiong G et al (2018) From mind to products: towards social manufacturing and service. *IEEE/CAA J Automatica Sinica* 5(1):47–57
18. Industrial Internet Consortium, Industrial Internet Reference Architecture, Version 1.7 (2015)
19. Presentation at the French Embassy in Germany, “Industry of the future”. 2015. Available at. <http://www.ambafrance-de.org/Vorstellung-des-neuen-franzosischen-PlansIndustrie-du-Futur-in-der-Botschaft>. Last accessed: 24 Nov 2016
20. The State Council of the People’s Republic of China., Made in China 2025. 24 Nov 2016
21. Wagner J, Fischer R, Gunthner WA (2007) The influence of metal environment on the performance of UHF smart labels, in theory, experimental series and practice. In: Proceedings of the 1st annual RFID eurasia, Istanbul, Turkey, pp. 5–7 Sep 2007
22. Jakimovski P, Riedel T, Haddad A, Beigl M (2012) Design of a printed organic RFID circuit with an integrated sensor for smart labels. In: Proceedings of the international multi-conference on systems, Signals & Devices, Chemnitz, Germany, pp. 20–23 Mar 2012
23. Ferreira Chaves LW, Decker C (2010) A survey on organic smart labels for the internet-of-things. In: Proceedings of the international conference on networked sensing systems (INSS), Kassel, Germany, 15–18 June 2010
24. Bringans RD, Veres J (2016) Challenges and opportunities in flexible electronics. In: Proceedings of the IEEE international electron devices meeting, san francisco, United States, 3–7 Dec 2016
25. Cook BS, Le T, Palacios S, Traille A, Tentzeris MM (2013) Only skin deep: Inkjet-printed zero-power sensors for large-scale RFID-integrated smart skins. *IEEE Microwave Mag* 14(3):103–114
26. Cook BS, Vyas R, Kim S, Thai T, Le T, Traille A, Aubert H, Tentzeris MM (2014) RFID-Based sensors for zero-power autonomous wireless sensor networks. *IEEE Sens J* 14(8):2419–2431
27. Nadeem T (2013) Cyber-physical systems seminar. Old Dominion University, USA, Spring, Department of Computer Science
28. Lee J, Bagheri B, Kao H-A (2015) A Cyber-Physical systems architecture for industry 4.0-based manufacturing systems. *Manuf Lett* 3:18–23
29. Schoenthaler F, Augenstein D, Karle T (2015) Lisbon, Portugal. July 13, pp 1–8
30. Kai I K, Pang Z, Cong W (2013) Security and privacy mechanism for health internet of thing
31. Kai Zhao and Lina Ge (2013) Survey on the internet of things security. In: Ninth international conference on computational intelligence and security. pp 663–667
32. Skouby KE, Lynggaard P (2014) Smart home and smart city solutions enabled by 5G, IoT, AAI and CoT services. In: International conference on contemporary computing and informatics (IC3I). IEEE, pp 874–878
33. Militano L, Araniti G, Condoluci M, Farris I, Iera A (2015) Deviceto—device communications for 5G internet of things. *EAI Endorsed Trans Internet Things* 15(1):1–15
34. Al-Hamadi H, Chen R (2017) Trust-based decision making for health IoT systems. *IEEE Int Things J* 4(5):1408–1419
35. Marwat SNK, Mehmood Y, Khan A, Ahmed S, Hafeez A, Kamal T, Khan A (2018) Method for handling massive IoT traffic in 5G networks. *MDPI J*

Preprocessing Techniques for Colon Histopathology Images



Manju Dabass and Jyoti Dabass

Abstract The glandular morphology analysis done within the colon histopathological images is an imperative step for grade determination of colon cancer. But the manual segmentation is quite laborious as well as time-consuming. It also suffers from the subjectivity among pathologists. Thus, the rising computational pathology has escorted to the development of various automated methods for the gland segmentation task. However, automated gland segmentation remains an exigent task due to numerous factors like the need for high-level resolution for precise delineation of glandular boundaries, etc. Thus, in order to alleviate the development of automated gland segmentation techniques, various image enhancement techniques are applied on colon cancer images for preprocessing them in order to get an enhanced image in which all the critical elements are easily detectable. The enhancement results are analyzed based on both objective qualitative assessment as well as subjective assessment given in the form of scores by the pathologists. And thus based on the qualitative analysis, a new combined technique, i.e., colormap-enhanced image sharpening, is proposed in order to get an enhanced image in which all the critical elements are easily detectable. These techniques' results will thus help pathologists in better colon histopathology image analysis.

Keywords Colon cancer · Histopathology image analysis · Gland segmentation · Image enhancement

M. Dabass (✉) · J. Dabass
EECE Department, The NorthCap University, Gurugram, India
e-mail: manjurashi87@gmail.com

J. Dabass
e-mail: jyotidabas91@gmail.com

© Springer Nature Singapore Pte Ltd. 2021
G. S. Hura et al. (eds.), *Advances in Communication and Computational Technology*, Lecture Notes in Electrical Engineering 668,
https://doi.org/10.1007/978-981-15-5341-7_85

1121

1 Introduction

According to [1], colorectal cancer is among the top five cancers affecting the world population in which approximately 95% of all colorectal cancers are adenocarcinomas. The colorectal adenocarcinomas typically build up in the colon or rectum linings formulate the large intestine. It is characterized mainly by the glandular formations. There are four tissue components present in glands, i.e., epithelial nuclei, cytoplasm, lumen, and stroma (mainly blood vessels, nervous tissues, connective tissues, etc.). The stroma is not considered as a part of the gland while the epithelial cells enclose the cytoplasm and lumen and thus works as gland boundary. The benign, i.e., non-cancerous glands, as shown in Fig. 1a, are easily analyzed using the automated segmentation algorithms owing to significant variances in size, texture, staining, shape, and location of glands. But in the malignant, i.e., cancerous cases, the glandular objects are significantly different as compared to non-cancerous cases. Further for well-differentiated cases, more than 95% of the tumor is gland forming. On the other hand, for poorly differentiated cases, the typical glandular appearance is lost as shown in Fig. 1b. Hence, the glandular formation loss increases with the increase in cancer grading due to which glandular morphology is one of the critical factors in determining the cancer grade. Thus, the glandular histologic examination with hematoxylin and eosin stain is the clinical practice applied for differentiation assessment of cancer within the colorectal adenocarcinoma. Also, the degree of glandular formation is used by the pathologists for giving the final decision for the tumor's grade or degree of differentiation.

However, automated gland segmentation is still an exigent task due to various aspects [2] such as

1. To precisely delineate the glandular boundaries, there is a need for a high-resolution level.
2. There is variation in size and shapes of glands with the increase in cancer grade.
3. There exists the presence of poignant clustered substances in the tissue samples which make it pretty difficult for automatic segmentation techniques to split them into individual entities.

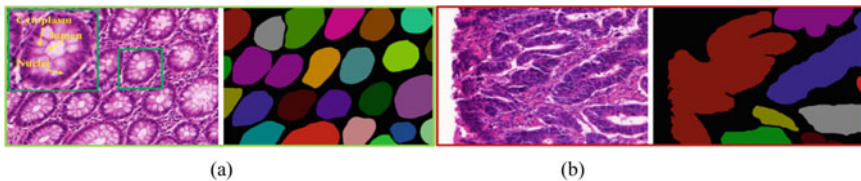


Fig. 1 Examples of gland segmentation challenge dataset **a** benign case with ground truth annotations and **b** malignant case with ground truth annotations [3]

Table 1 Enhancement techniques applied on various medical imaging modalities

Authors	Imaging modalities	Enhancement technique
Jeevaka et al. [6]	MRI images	Image sharpening
Reddy et al. [7]	Medical imaging	Histogram equalization
Sahu et al. [8]	Color retinal fundus	CLAHE
Cao et al. [9]	Medical imaging	Gamma correction
Duan et al. [10]	Mammograms	Image sharpening using unsharp masking
Hsu et al. [11]	Medical prostate cancer images	Color histogram equalization
Li et al. [12]	Medical images	CLAHE and unsharp masking
Ullah et al. [13]	MRI images	Histogram equalization
Mzoughi et al. [14]	MRI brain glioma tumor images	Histogram equalization
Dhal et al. [15]	Color retinal images	Histogram equalization with firefly algorithm
Clark et al. [16]	Radiology images	Image sharpening
Tiwari et al. [17]	Medical images	Adaptive histogram equalization with homomorphic filtering
Bhairannawar et al. [18]	Medical images	Adaptive histogram equalization in HSV space
Dabass et al. [19]	Mammograms	CLAHE

- The sole gland object output gives very limited information for diagnosis making. To increase the diagnostic making power, extra information is needed like uncertainty prediction and segmentation of additional histological components such as lumen, dense nuclei area, and artifacts.

Thus, to assist pathologists in giving an accurate diagnosis as well as assisting the research community to strengthen the automated segmentation techniques, we have assessed one of the preprocessing techniques, i.e., image enhancement in this paper.

The various image enhancement techniques used recently for enhancing various medical imaging modalities are summarized in Table 1.

2 Image Enhancement Techniques

The image enhancement techniques are those techniques which are applied to perk up the interpretability of the information content present in the images. These techniques are used to smoothen, emphasize, or sharpen specific features like contrast, luminance, brightness, etc., present in an image by in order to improve its visual perception. The various techniques applied for medical image analysis are explained in this section.

2.1 Image Sharpening

Image sharpness, in reality, is the contrast between the different colors present in it. The image sharpening amplifies the contrast along the edges where the different colors convene. Its main aim is to highlight very fine details present in an image and is particularly used for enhancement of images' high-frequency components. In this paper, the image sharpening is done using the unsharp masking method where first, a smoothed version of the original image is made to subtract from the original image and then it is added to the original image in order to tip the image balance toward the sharper content of the original image. Mathematically, this process is defined as

$$E(m, n) = O(m, n) + \alpha [O(m, n) - \overline{O}(m, n)] \quad (1)$$

where $O(m, n)$ is the original image, $\overline{O}(m, n)$ is the blurred or smoothed version of the original image, α is the weighting fraction, and $E(m, n)$ is the final enhanced sharpened resulted image.

In [5], the image sharpening technique is used for MRI images in order to enhance the tumor area as generally due to the noise, the MRI images come as hazy. Thus, by the sharpening technique usage, the tumor was easily and affectively detected as well as segmented from the MRI images.

2.2 Colormap Enhancement

In this technique, scaling by a constant factor is done for all pixels present in an image. Mathematically, this process can be defined as

$$E(m, n) = O(m, n) * K \quad (2)$$

where $O(m, n)$ is the original image, K is the scaling constant, and $E(m, n)$ is the final enhanced image.

It is applied for changing the contrast of the image in order to change the range of luminance values present in it.

2.3 Proposed Colormap-Enhanced Image Sharpening

In this technique, basically, the above two techniques are merged where first the image contrast is changed by applying the contrast adjustment technique and then the image sharpening technique is applied to the resultant image where the smoothed version is subtracted from the resultant image and scaled by a weighting fraction and then added to the resultant image. Thus, change in the range of luminance values and the

alignment of the image balance toward the sharper content present in the original image both are done in order to get a better enhanced image. Mathematically, this process is defined as

$$E(m, n) = [O(m, n) + \alpha \{O(m, n) - \overline{O}(m, n)\}] * K \quad (3)$$

where $O(m, n)$ is the original image, $\overline{O}(m, n)$ is the blurred or smoothed version of the original image, α is the weighting fraction, K is the scaling constant, and $E(m, n)$ is the final enhanced image.

2.4 Histogram Equalization

The histogram is a very prominent way to show the intensities summary present in an image. The technique of histogram equalization is applied for spreading out the gray levels present in an image in order to make them uniformly distributed across their range. It reassigns the pixels' brightness values based on the image histogram in order to make the histogram of the resultant image as flat as possible. This technique is applied for making the minor variations present within various regions to be seen adequately which earlier were appearing nearly uniform in the original image. This process can be defined as

$$S = T(R) \quad 0 \leq R \leq L - 1 \quad (4)$$

where R is denoting the intensities present in the original image, L is denoting the gray levels present in the original image, T is denoting the transformations (intensity mapping) applied, and S is denoting the output intensity levels produced for every pixel in the original image having the intensity R .

2.5 Contrast-Limited Adaptive Histogram Equalization (CLAHE)

This technique is used for the improvement of low contrast issue found in images by limiting the contrast enhancement, unlike the histogram equalization where noise also gets enhanced with the contrast enhancement. The contrast enhancement can be defined as the slope of the function relating the original image intensity with the desired resultant image intensities. Thus, contrast limitation can be performed by restraining the slope of this linking function. The contrast enhancement is unswervingly related to the histogram height at the intensity value. Thus, contrast limitation can be performed by stipulating the clip limit for the histogram height according to the contrast need.

2.6 Gamma Correction

This technique can be defined by the nonlinear power-law transformation, i.e.,

$$E(m, n) = [O(m, n)]^\gamma \quad (5)$$

where γ is the gamma constant and can take either integer or fraction value.

This nonlinearity must be compensated by using different values of γ in order to achieve the correct reproduction of intensity. In the case of color images, this is performed by either decomposing the color image into RGB components or HSV components. Each plane is transformed separately by choosing different values of γ and then after the transformations, all individual planes are merged back into one enhanced image.

3 Performance Analyzing Qualitative Matrices

For evaluating the quality of the resulted enhanced medical images, two criteria in the form of objective criteria and subjective criteria are used.

3.1 Objective Criteria

For evaluating the objective assessment, the following quantitative matrices are used:

- **Entropy:** It is a statistical measure of randomness which can be used to characterize the image texture. It gives the degree of information content present in images. For good enhancement techniques, the entropy value of enhanced image should remain near to the entropy value of the original image. It can be calculated as

$$E(\text{Image}) = - \sum_{k=0}^{l-1} p(k) \log_2 p(k) \quad (6)$$

Where $p(k)$ is the occurrence probability for the value of k in the image Image and $l = 2^q$ indicates the number of gray levels present in the image. Closer the entropy value to q indicates the high information content. For example, if the value of q is 8, then entropy value closer to this indicates high information content.

- **Mean square error or MSE:** It represents the cumulative square error between two images. If O is the original image and E is the enhanced image with both having physical size of $M \times N$, then MSE can be calculated as

$$\text{MSE} = \frac{\sum_{x=0}^{N-1} \sum_{y=0}^{M-1} \{O^2(x, y)\}}{\sum_{x=0}^{N-1} \sum_{y=0}^{M-1} \{O(x, y) - E(x, y)\}^2} \quad (7)$$

For having a high-quality enhanced image, the MSE should be low.

- **Peak signal-to-noise ratio (PSNR):** It is defined as a measure of peak error and can be calculated as:

$$\text{PSNR} = 10 \text{Log}_{10} \left(\frac{\text{Max}^2}{\text{MSE}} \right) \quad (7)$$

The high value of PSNR signifies that the enhanced image is of high quality.

The PSNR and MSE matrices estimate absolute errors.

- **Structure similarity index measure (SSIM):** It is an image quality assessing metric that is used for assessing the illustrative impact of the three distinctiveness of an image, i.e., luminance, contrast, and structure and is calculated as

$$\text{SSIM}(x, y) = \frac{(2\text{Mean}_x \cdot \text{Mean}_y + C_1)(2CV_{xy} + C_2)}{(\text{Mean}_x^2 + \text{Mean}_y^2 + C_1)(SD_x^2 + SD_y^2 + C_2)} \quad (8)$$

Where Mean_x and Mean_y are the local means, SD_x and SD_y are the standard deviations, and CV_{xy} is the cross-variance for images X and Y .

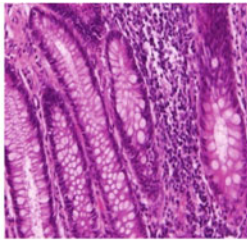
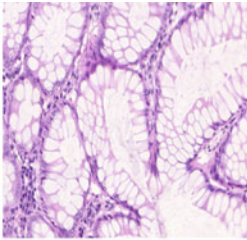
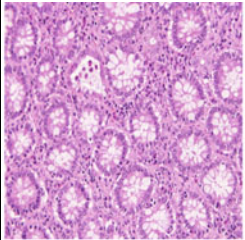
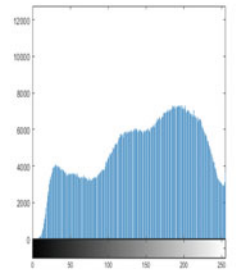
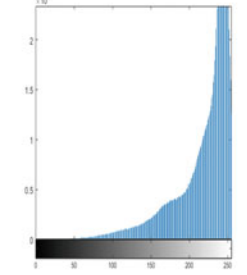
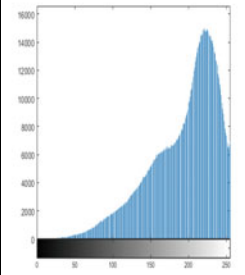
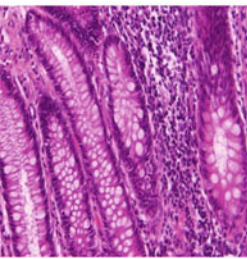
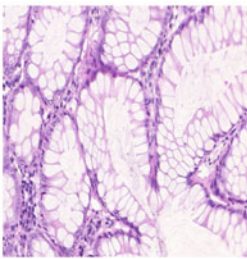
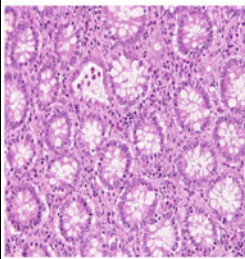
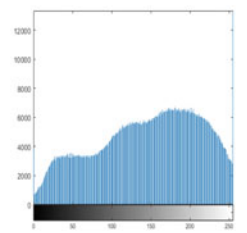
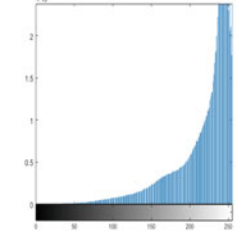
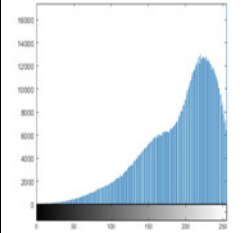
3.2 Subjective Criteria

In this, a team of pathologists gave scores for the enhanced images in the scale of 0–9 where 9 represents the best score, i.e., excellent fidelity and 0 represents the worst score, i.e., worst fidelity for the information content present in them which can be useful for accurately predicting cancer grade. It is shown as pathologists' score in the qualitative assessment metric given in Table 2.

4 Dataset

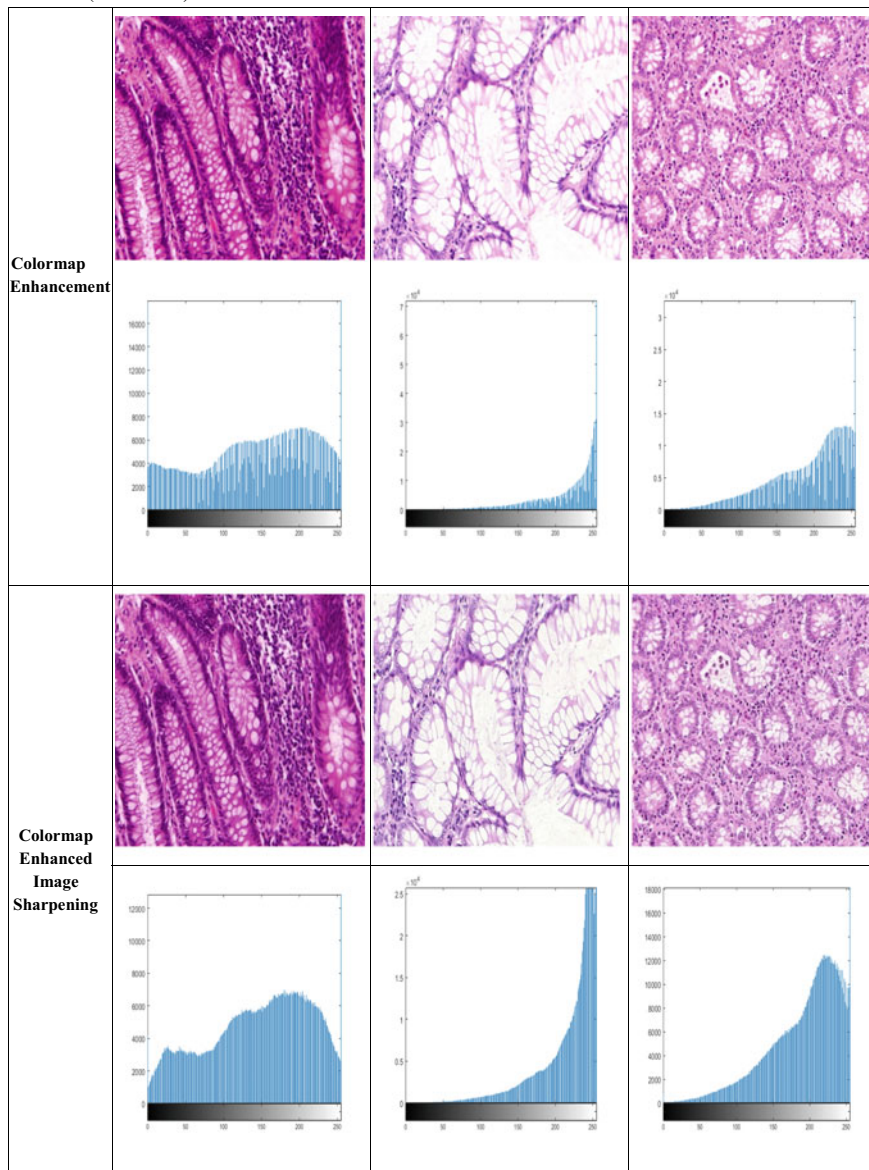
The implemented techniques are assessed on the database made available by the Gland Segmentation (GlaS) Challenge held in MICCAI 2015 [3] given at [4]. This dataset consists of 165 colon histopathology images mostly having a size of $775 \times 552 \times 3$. We also introduce blurring in each image in order to increase the size of the database to 330 images.

Table 2 Implementation results of various image enhancement techniques

Method	Image 1	Image 2	Image 3
Original			
			
Image Sharpening			
			

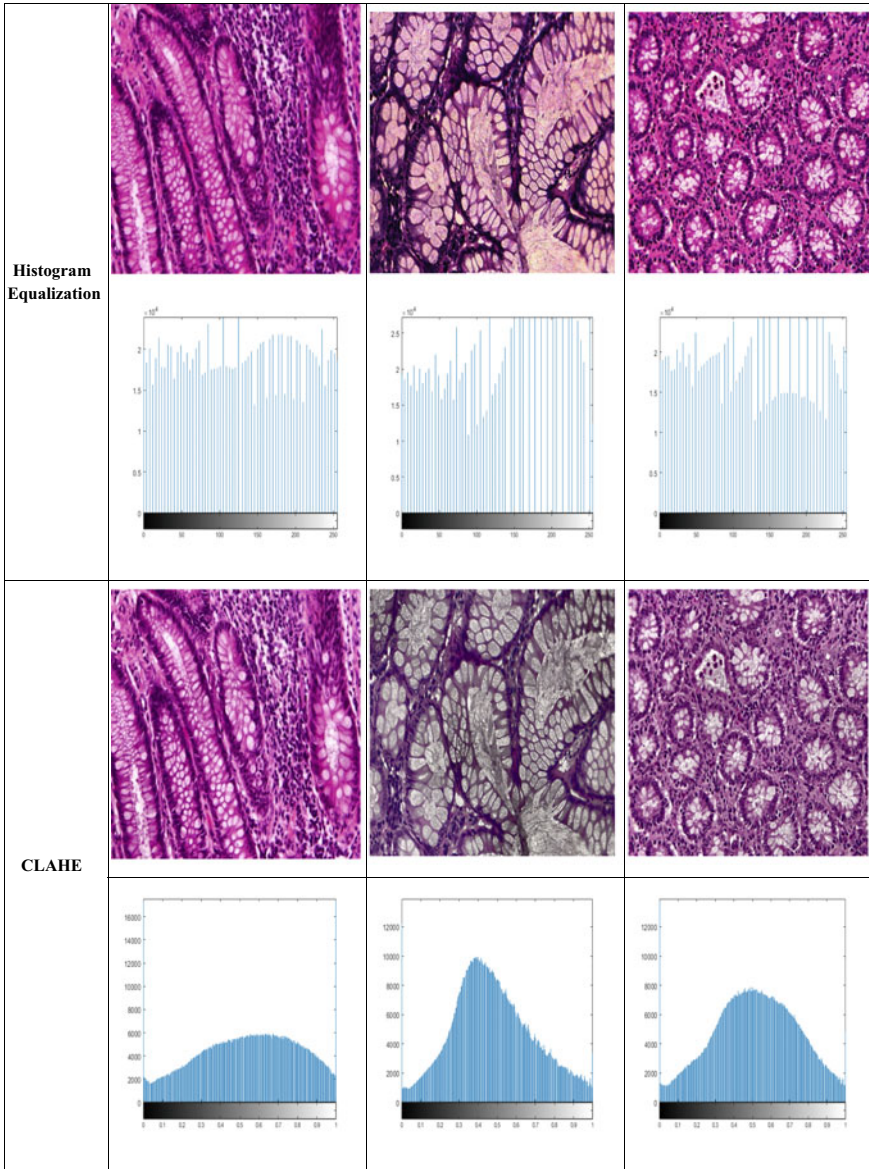
(continued)

Table 2 (continued)



(continued)

Table 2 (continued)



5 Experimental Setup

All the contrast enhancement techniques are implemented in MATLAB 2019a. The techniques are implemented as below:

5.1 *Image Sharpening*

Image sharpening is performed using the unsharp masking. Here, the input color image is first converted into LAB color space and then unsharp masking is applied to L channel only. And, in the end for producing output enhanced image, the LAB color space image is again converted into RGB color space.

5.2 *Colormap Enhancement*

It is performed by mapping the intensity values of the input image to new values in output image such that values between [bottom_in] and [top_in] map to values between [bottom_out] and [top_out]. In our experiment, we have taken [bottom_in] value as [0.1, 0.1, 0.8] and [top_in] as [0.9, 0.95, 0.95] for R, G, and B plane, respectively. Also, the [bottom_out] value is taken as zero and [top_out] value is taken as one. This technique enhances the contrast values in the output image.

5.3 *Proposed Colormap-Enhanced Image Sharpening*

In this technique, first the contrast is enhanced by mapping the intensity value of the input image to new values by taking lower values as [0, 0.3, 0] and top values as [1, 0.3, 1], i.e., saturating the intensity values in green plane only while keeping the original intensity values of red and blue plane. After this, the RGB image is converted into LAB space and image sharpening is performed on L channel using the unsharp masking. In the end, the LAB color space image is again converted to an RGB color image in order to produce an output image.

5.4 *Histogram Equalization*

In this technique, the colormap associated with the input image is transformed such that the histogram of the resultant image approximately matches the histogram hisgram, calculated by

$$\text{hisgram} = \text{one}(1, n) * \text{prod}(\text{size}(\text{input image } A))/n \quad (10)$$

then, the transformation T is chosen to minimize

$$|C_1(T(k)) - C_0(k)| \quad (11)$$

where C_0 is the cumulative histogram of the input image, i.e., A , and C_1 is the cumulative sum of the above-calculated hisgram values for all intensities k . Then, the histogram equalization uses the transformation $b = T(a)$ to map the gray levels present in input image colormap to the new values.

Here, we tried to match the output image histogram with a flat histogram with 64 bins.

5.5 Contrast-Limited Adaptive Histogram Equalization (CLAHE)

In this technique, first the RGB image is converted into LAB space. Then, the CLAHE is performed on the L channel by taking the tile size of $[4 \times 4]$ matrix, and contrast enhancement limit factor is 0.7. This contrast enhancement limit is used in order to prevent image over-saturation specifically in homogeneous areas which are characterized by a high peak in the histogram shown in a particular image tile as a result of its maximum pixels falling inside the same gray-level range. After this, the Rayleigh distribution is applied for creating a bell-shaped contrast transform function. In succession of this, exponential distribution is applied for creating a contrast transform function having a curved histogram. In the end, the LAB space image is converted to an RGB output image.

5.6 Gamma Correction in RGB Plane

In this technique, intensity values of an input RGB image are mapped into new colormap image by saturating the top 10% and bottom 10% intensity values of each plane along with keeping gamma value as 0.8 in order to weight the mapping toward the higher, i.e., brighter output values. The gamma value is used to specify the curve shape which defines the relationship between the intensity values in input and output image.

5.7 Gamma Correction in HSV Plane

In this technique, the input image is first converted into HSV space and then its intensity values are mapped into new colormap image by saturating the top 10% and bottom 10% intensity values of each plane along with keeping gamma value as 0.8. In the end, the HSV image is converted to an RGB output image.

6 Implementation Results

In order to scrutinize the effectiveness of different image enhancement techniques first, they were assessed for objective qualitative parameters like entropy, SSIM, PSNR, and MSE. And after that, the resulted images were sent to the pathologists in Dharamshila Narayana Hospital, New Delhi, for getting their score in the range of 0–9 where 9 was given to the excellent image and the decrease in score indicates the less image fidelity. The resulted images along with their resulting histogram plots are shown in Table 2 while the objective and subjective parameters are given in Table 3.

By the analysis of these techniques, we see that all the techniques like colormap enhancement, histogram equalization, and CLAHE are making the epithelial nuclei area darker and due to which the presence of cytoplasm was not coming clear along with the shape of the gland. On the other hand, the techniques like gamma correction in both of its form, i.e., whether applied on RGB or HSV plane is blurring the image and producing small circle like blocking artifacts at some places. Thus, these techniques are also not suited for histopathological image analysis. But the

Table 3 Qualitative evaluation of different image enhancement techniques

S. No.	Enhancement method	Entropy	MSE	PSNR	SSIM	Pathologist score ^a
1.	Image sharpening	7.2861	47.9766	32.9155	0.9864	8.8013
2.	Colormap enhancement	6.9183	149.9092	26.4179	0.9785	7.8675
3.	Colormap-enhanced image sharpening	7.6469	34.7820	36.4650	0.9886	8.8675
4.	Histogram equalization	5.9362	3674.4	13.8063	0.7916	5.7947
5.	CLAHE	6.7319	34,643	4.8086	0.0077	4.2052
6.	Gamma correction in RGB plane with $\gamma = 0.8$	7.4316	171.4274	25.9569	0.9629	7.7947
7.	Gamma correction in HSV Plane with $\gamma = 0.8$	7.1892	34,554	3.8190	0.0011	5.2052

Bold signifies that the highlighted technique is proposed in this paper and it is giving significantly better results in terms of the evaluation parameters

^aPathologist score is the mean score given by the team of pathologists of Dharamshila Narayana Superspeciality Hospital according to the critical information preservation and thus, become the deciding factor for choosing the appropriate enhancement technique

techniques like image sharpening and proposed colormap-enhanced image sharpening are giving better results in terms of increase in visibility of lumen, cytoplasm, and epithelial nuclei. Thus, these techniques can be used for image enhancement in histopathological image analysis. From the histogram plots of each image, it can be easily interpreted that image sharpening and contrast-enhanced image sharpening techniques are giving more uniform histogram plots along with coverage of all the available dynamic histogram range as compared to other techniques. In all other techniques, there is a sharp difference between low and high contrast value which is resulting in loss of information.

Also, from the qualitative analysis shown in Table 3, the above-mentioned results can be justified. From this table, it is easily interpreted that techniques like image sharpening and colormap enhancement are giving better results for colon histopathology images than techniques like histogram equalization, CLAHE, and gamma correction. Thus, taking these results into account, we have proposed colormap-enhanced image sharpening technique which is not only giving better visual results but also the qualitative evaluation results which are shown in bold letters in Table 3. All the qualitative parameters are evaluated for each of the 151 images and their individual values are represented in Figs. 2, 3, 4, and 5. In Table 3, the qualitative parameter values are given by taking mean of all the values coming for each of the 151 images.

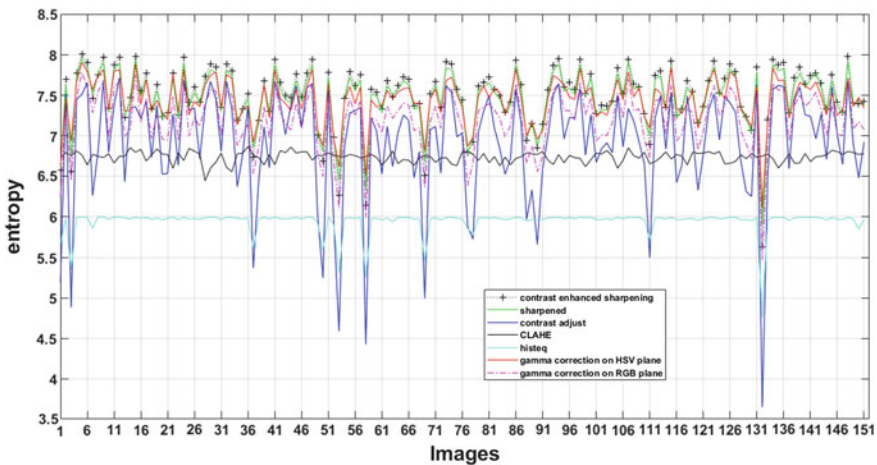


Fig. 2 Entropy values versus database images plot

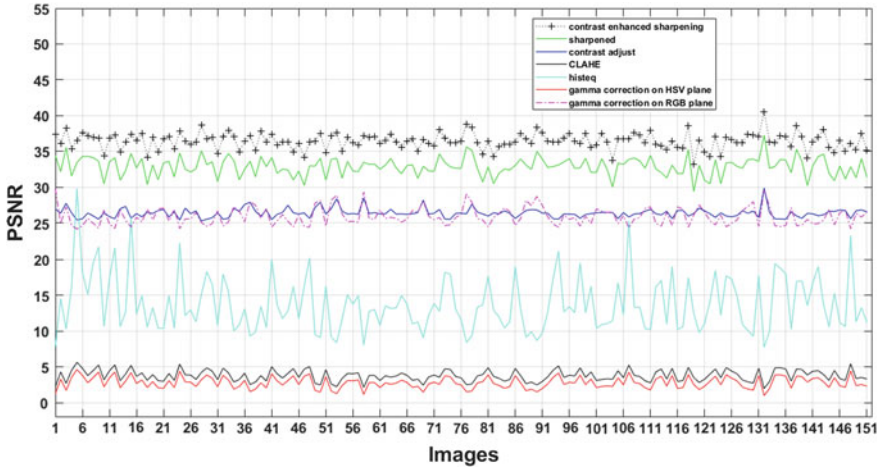


Fig. 3 PSNR values versus database images plot

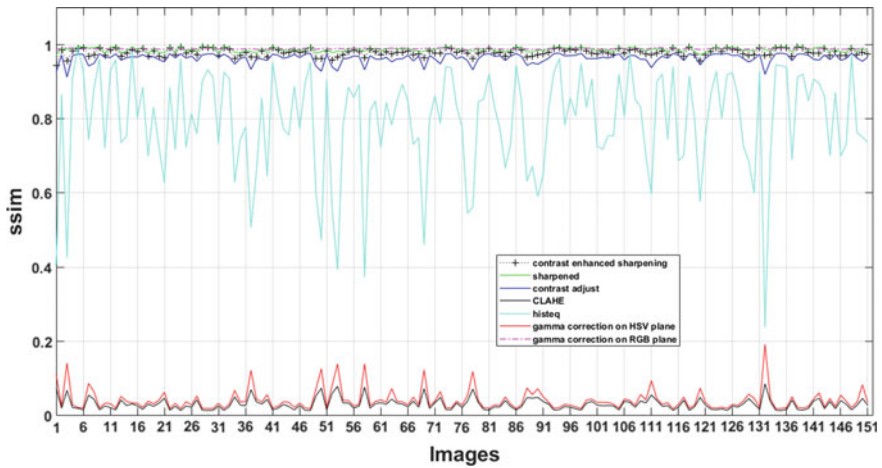


Fig. 4 SSIM values versus database images plot

7 Conclusion

The main rationale of the image enhancement techniques is to perk up the interpretability of the information content present in the images. These techniques emphasize specific features present in an image in order to improve its visual perception. These techniques are particularly application-specific. Thus, here, we are taking only some of the image enhancement techniques which are already used for various medical images such as magnetic resonance imaging (MRI), X-ray, and CT scans. As discussed earlier, for detecting and predicting cancer grades, there are some important

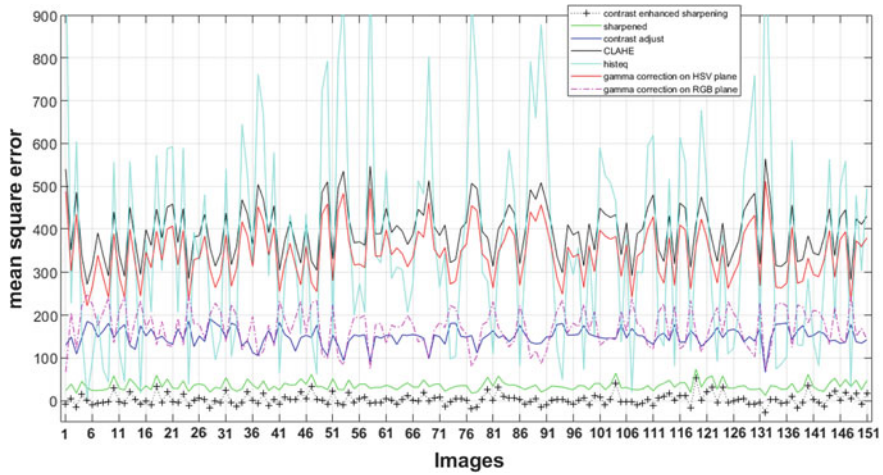


Fig. 5 Mean square error values versus database images plot

parts in the colon histopathological tissue samples like gland morphology, lumen, nuclei, etc. Thus, these techniques are applied and tested for their ability to highlight those areas.

In this paper, a total of seven image enhancement methods was applied to colon histopathology images. From these methods, six techniques were the classical techniques and when we applied them on our database, the objective results, as well as the subjective result in terms of pathologists' score, were coming best for image sharpening and colormap enhancement so we proposed a new technique by combining both these techniques in such a way so that the results will improve further. As only pathologists have to work on these techniques, their score is the most important deciding factor in determining the efficacy of the applied enhancement techniques, and thus, based on their score along with other objective qualitative measures, we can conclude that the proposed technique can be best suited for the histopathological image analysis. Also, this technique can be further used to increase the analytical as well as diagnostic accuracy of various applications like cancer classification [20, 21] and tumor segmentation [22].

Acknowledgements The authors are grateful to Dr. Hema Malini Aiyer, Head of Pathology, and Dr. Garima Rawat, Pathologist at Dharamshila Narayana Superspeciality Hospital, New Delhi, for their support to our research, and without their help, we will not be able to check the feasibility of the applied algorithm in the real-life scenario.

References

1. Fleming M, Ravula S, Tatishchev SF, Wang HL (2012) Colorectal carcinoma: Pathologic aspects. *J Gastrointest Oncol* 3(3):153
2. Gurcan MN, Boucheron L, Can A, Madabhushi A, Rajpoot N, Yener B (2009) Histopathological image analysis: a review. *IEEE Rev Biomed Eng* 2:147
3. Gonzalez RC, Woods, Richards E (2018) Image processing. *Digit Image Proc Intensity Trans Spatial Filtering*
4. Sirinukunwattana K, Pluim JP, Chen H, Qi X, Heng PA, Guo YB, Wang LY, Matuszewski BJ, Bruni E, Sanchez U, Böhm A (2017) Gland segmentation in colon histology images: the glas challenge contest. *Med Image Anal* 35:489–502
5. Warwick-QU image dataset description. <https://warwick.ac.uk/fac/sci/dcs/research/tia/glascontest/about/>
6. Jeevakala S (2018) Sharpening enhancement technique for MR images to enhance the segmentation. *Biomed Signal Process Control* 41:21–30
7. Reddy E, Reddy R (2018) Dynamic clipped histogram equalization technique for enhancing low contrast images. *Proc National Acad Sci India Sect A Phys Sci* 1–26
8. Sahu S, Singh AK, Ghreera SP, Elhoseny M (2019) An approach for de-noising and contrast enhancement of retinal fundus image using CLAHE. *Opt Laser Technol* 110:87–98
9. Cao G, Huang L, Tian H, Huang X, Wang Y, Zhi R (2018) Contrast enhancement of brightness-distorted images by improved adaptive gamma correction. *Comput Electr Eng* 66:569–582
10. Duan X, Mei Y, Wu S, Ling Q, Qin G, Ma J, Chen C, Qi H, Zhou L, Xu Y (2018) A multiscale contrast enhancement for mammogram using dynamic unsharp masking in Laplacian pyramid. In: *IEEE transactions on radiation and plasma medical sciences*
11. Hsu WY, Chou CY (2015) Medical image enhancement using modified color histogram equalization. *J Med Biol Eng* 35(5):580–584
12. Li L, Si Y, Jia Z (2018) Medical image enhancement based on CLAHE and unsharp masking in NSCT domain. *J Med Imaging Health Inf* 8(3):431–438
13. Ullah Z, Lee SH (2019) Magnetic resonance brain image contrast enhancement using histogram equalization techniques. *한국컴퓨터정보학회 학술발표논문집* 27(1):83–86
14. Mzoughi H, Njeh I, Slima MB, Hamida AB (2018) Histogram equalization-based techniques for contrast enhancement of MRI brain Glioma tumor images: Comparative study. In: *2018 4th International conference on advanced technologies for signal and image processing (ATSIP)*, pp. 1–6. IEEE
15. Dhal KG, Das S (2018) Colour retinal images enhancement using modified histogram equalisation methods and firefly algorithm. *Int J Biomed Eng Technol* 28(2):160–184
16. Clark JL, Wadhvani CP, Abramovitch K, Rice DD, Kattadiyil MT (2018) Effect of image sharpening on radiographic image quality. *J Prosthet Dent* 120(6):927–933
17. Tiwari M, Gupta B (2016) Brightness preserving contrast enhancement of medical images using adaptive gamma correction and homomorphic filtering. In: *2016 IEEE Students' conference on electrical, electronics and computer science (SCECS)*, pp 1–4. IEEE
18. Bhairannawar SS (2018) Efficient medical image enhancement technique using transform HSV space and adaptive histogram equalization. In: *Soft computing based medical image analysis academic press*, pp 51–60
19. Dabass J, Arora S, Vig R, Hanmandlu M (2019) Mammogram image enhancement using entropy and CLAHE based intuitionistic fuzzy method. In: *2019 6th International conference on signal processing and integrated networks (SPIN)*, IEEE, pp 24–29
20. Dabass M, Vashisth S, Vig R (2019) Review of classification techniques using deep learning for colorectal cancer imaging modalities. In: *2019 6th International conference on signal processing and integrated networks (SPIN) IEEE*, pp 105–110

21. Dabass M, Vig R, Vashisth S (2018) Five-grade cancer classification of colon histology images via deep learning. In: 2018 2nd international conference on communication and computing system (ICCCS), Taylor and Francis
22. Dabass M, Vig R, Vashisth S (2018) Review of histopathological image segmentation via current deep learning approaches. In: 2019 4th IEEE international conference on computing communication and automation (ICCCA)

Analysis of Energy Deposition in Hadrontherapy Using Monte Carlo Simulation Toolkit GEANT4



Nitika Sangwan, Summit Jalota, and Ashavani Kumar

Abstract This work focuses on one of the most important stages of hadrontherapy treatment planning. The simulation is performed using Monte Carlo (MC) Treatment Planning toolkit GEANT4 which is considered as the most accurate three-dimensional (3-D) dose calculation algorithm for studying Bragg peaks in tissue-equivalent material and dosimetric validation. In hadrontherapy, the study of a significant difference in the position of the Bragg peak is important to get realistic results. Proton therapy treatment planning involves a wider and sensitive range of parameters to be evaluated carefully from studying stopping power, linear energy transfer, the energy imparted to secondary particles and their range. The technical parameters from scanning, modification, accuracy and time also need to be assessed precisely as these vary from patient to patient depending on the health condition. All these parameters vary with Monte Carlo inputs and a slight variation in input generates different results, where, hadrontherapy treatment demands high precision. In this preliminary work, we studied one of the crucial factors ‘Step limit’ which shows the maximum ‘step size’ and limited by the accuracy and time factor of simulation. The simulation in GEANT4 is executed by activating suitable Physics Model ‘QGSP_BIC’ with default electromagnetic physics model `em_option_3` implemented in Geant4 taking proton as an incident particle with energies 70, 100 and 130 MeV. For simulation, the implemented step size is 0.5 and 0.05 mm step size. The step size value 0.05 mm is found superlative for simulation taking into account simulation time and accuracy.

Keywords GEANT4 · Proton therapy · Step size

N. Sangwan · A. Kumar (✉)
Department of Physics, National Institute of Technology Kurukshetra, Kurukshetra 136119,
Haryana, India
e-mail: ashavani@yahoo.com

S. Jalota
Department of Physics, DAV College, Jalandhar 144012, India

© Springer Nature Singapore Pte Ltd. 2021
G. S. Hura et al. (eds.), *Advances in Communication and Computational Technology*, Lecture Notes in Electrical Engineering 668,
https://doi.org/10.1007/978-981-15-5341-7_86

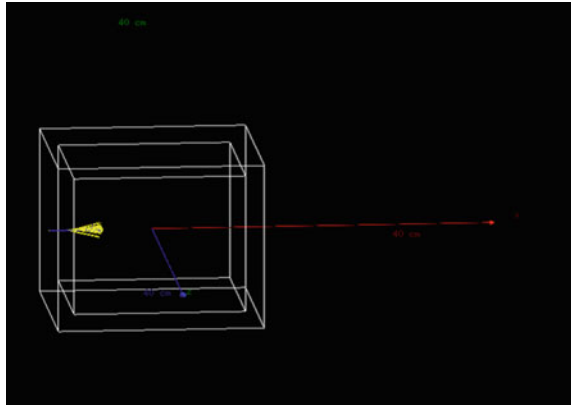
1139

1 Introduction

The cancer incidence and the fatality rate has grown rapidly across the world. Cancer burden has risen and case figures have been estimated up to 18.1 million and mortality up to 9.6 million according to the report produced by Global Cancer Incidence, Mortality and Prevalence GLOBOCAN 2018. In the future, incidence and mortality cases will increase by 63% and 71% respectively by the year 2040 [1, 2]. Cancer treatment has three main modalities, surgery, radiation therapy, and chemotherapy which can be used individually or with combination to others depending on cancer cell conditions and other factors related to the patient [3]. Radiation oncology modality for cancer treatment implicates the skillful use of radiation to treat affected cancer cells and was invented soon following the X-rays discovery in 1895 [4]. The use of charged particles is an emerging tool in radiation oncology due to localized energy deposition which results in the killing of cancer cells with less harmful effects on surrounding healthy tissues. Protons have excellent depth-dose and have slightly higher relative biological effectiveness (RBE) nearly 1.1 as compared to photons. The advantage of proton therapy over conventional therapy is finite, well-defined range of proton, and the higher value of RBE at the distal area of the Bragg curve [5]. The simulation codes play gold standard roles in broad areas of research and development and contributing to various areas of space science, accelerator design, nuclear physics, cosmic-ray, and medical physics. Monte Carlo codes-based simulation tools FLUKA, GATE, PHITS, TOPAS, LISE++, and GEANT4 provide flexible, accurate and easy to use ways to simulate particle transportation in matter accordance with the need of research problem [6]. The MC simulation advances to real-time monitoring systems to assure quality factors for radiation therapy and provides internal theoretical nuclear models for a precise explanation of all the secondary particles. In particle therapy, the range of particle, energy deposition, and energy distribution are of great importance for treatment [7]. The GEANT4 toolkit stands for Geometry and Tracking of the particle in the matter. The GEANT4 software is written in object-oriented language C++. The revolutionary object-oriented design of GEANT4 provides freedom for treatment planning by providing flexibility to decouple and modify predefined input parameters and physics models. The electromagnetic and hadronic processes are available for studying several particle interactions with a multiplicity of theoretical models. The linear energy transfer (LET) is one of the desirable quantities which play a key role in proton therapy treatment planning [8].

The step size sets the length of the tracking step. The cross-section remains fixed through the step. The simulation setup generates different results with the change of step length. The accuracy and time factor of the simulation is related to step size. The hadron therapy demands high precision, so the value of step size should be set with care to avoid harmful effects. This study represents the variation in the deposition of energy with two different step sizes 0.5 and 0.05 mm for proton energy 70, 100, and 130 MeV.

Fig. 1 Tissue equivalent cubic water phantom target with dimension 20 cm and incident radiation beam normal to target plane



2 Method of Simulation

2.1 Detector Geometry

The entire setup is constructed using predefined classes in GEANT4. The detector is constructed with the help of the Detector Construction class. The water phantom is used as the target material due to its equivalence of properties with living tissue. The parameters of water chemical formula, atomic weight, molecular mass, atomic value, ionization value, density, are defined in the NIST material list. Target water phantom is a cube having a dimension of 20 cm. The detector messenger class is used to define commands and to handle all detector geometry components. Proton beam is incident normal to the face of the water phantom (Fig. 1).

2.2 Physics Model

The selection of the best physics model according to the necessity of the problem is the most important task to get accurate results from the Monte Carlo simulation. In the simulation, we need to compromise between accuracy and computation time which may cause variation in spatial dose distribution, depth-dose curve and beam spot size. The selected physics model is defined in the Physics list class. Taking into account proton therapy clinical energy range (<250 MeV), three interactions that dominate in energy loss of proton within the matter for this energy range are; elastic, inelastic Coulomb scattering, and inelastic nuclear reactions [10]. Inelastic Coulomb scattering dominates over the other two reactions for defining particle range and dose distribution in longitudinal direction resulting in a high impact on the shape of the depth-dose curve. Elastic scattering gives rise to lateral straggling which directly shows effects on the beam spot size of the incident radiation beam. The third

interaction, inelastic nuclear reaction decreases the fluence of the projected radiation and affects the longitudinal dose distribution but contributes less due to low reaction cross-section. The QGSP_BIC model is recommended for simulation for medical application and is implemented in the code [9, 10] with the default electromagnetic process emstandard_option3.

2.3 Step Size Limit

Step size limit is one of the crucial factors related to the transportation of particles into the matter. In the MC simulation, it is assumed that cross-sections are almost invariant throughout the step. This applies the limitation on step length for reliable results. Step size limit for a particle with energy >1 MeV should be set so that the stopping range does not decrease more than ~20% during the one-step [10]. The computation time increases with a decrease in step size and vice-versa. One has to compromise between the accuracy and simulation time. In the present work, step size 0.5 and 0.05 mm are implemented for 3 sets of energies of proton particles 70, 100 and 130 MeV.

3 Results and Discussion

The simulation data shows with a decreasing step size smoother Bragg curve is obtained. It is cleared that energy deposition in the case of 0.05 mm step size is more localized and well-defined as compared to 0.5 mm. From computation time, this can be concluded that the smaller the step size more the time taken by CPU.

From Table 1 data, it can be verified that with an increase in particle energy, the projected range along with root means square (RMS) value increases and with decreasing step size the mean number of primary steps increases which results in

Table 1 Represents the range and run summary of 100,000 events incident with the clinical interested energy range for 0.5 and 0.05 mm step size

The energy of proton (MeV)	Step size (mm)	Projected range (cm)	RMS (mm)	Run summary (s)			Mean no. of primary steps
				User	Real	Sys	
70	0.05	4.09419	458.21	153.34	155.41	1.73	822.266
70	0.5	4.10933	465.485	15.575	16.35	0.61	87.1297
100	0.05	7.7437	855.266	302.63	305.12	2.07	1552.99
100	0.5	7.76483	860.903	89.88	70.72	0.65	160.318
130	0.05	12.3148	1327.18	444.1	447.27	2.57	2468.19
130	0.5	12.3401	1344.11	47.04	48.04	0.85	251.25

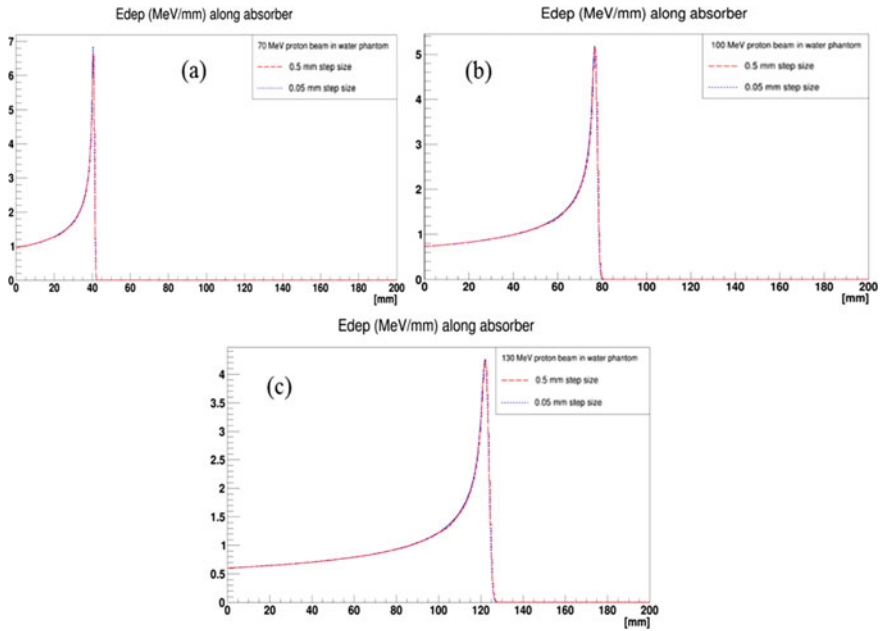


Fig. 2 **a** Energy deposition for the incident (70 MeV) proton particle. **b** Energy deposition for incident (100 MeV) proton particle. **c** Energy deposition for incident (130 MeV) proton particle, when step size 0.5 mm (red line) and 0.05 mm (blue line) are set respectively

increased run time. The localization of energy deposition is observed but at the expense of computational speed as shown in Fig. 2a–c.

The projected range and RMS values change slightly with a change in step size from 0.5 to 0.05 mm for the same incident energy and can be neglected as observed. The simulation time and mean number of steps changes almost about a factor of 10 with changing step size 0.5–0.05 mm. The considerable change in localization of energy deposition is detected. This can be verified from Fig. 2a–c in which fine localized line represents energy deposition for 0.05 mm and broad delocalized line for 0.5 mm step size which shows more uncertainty in energy deposition. Thus, accuracy tendency is associated with step size which is further connected with the time factor of simulation. Finally, one needs to compromise between these two factors, accuracy and time. One can settle to balance between these two major parameters of computation.

4 Conclusions

The comparative analysis of step size taking into account accuracy and simulation time is presented in the paper. The 'QGSP_BIC' Physics Model with default electromagnetic physics is implemented. The clinical range of proton beam 70, 100, and 130 MeV are incident on tissue-equivalent material for studying energy deposition finiteness in the form of Bragg curve. The step size 0.05 mm is found to give localized energy deposition at the expenses of simulation time and more uncertainty is observed with step size 0.5 mm as shown in Fig. 2a–c.

References

1. Ferlay J, Colombet M, Soerjomataram I, Mathers C, Parkin DM, Piñeros M, Znaor A, Bray F (2019) Estimating the global cancer incidence and mortality in 2018: GLOBOCAN sources and methods. *Int J Cancer* 144:1941–1953
2. World Health Organization. Global Health Observatory. Geneva: World Health Organization; 2018. <http://gco.iarc.fr/today/home>. Last accessed 20 Oct 2018
3. Jaffray DA, Gospodarowicz MK (2015) Radiation therapy for cancer. In: *Cancer: disease control priorities; the international bank for reconstruction and development/the world bank*, Washington, DC, USA, 239
4. Baskar R, Lee KA, Yeo R, Yeoh KW (2012) Cancer and radiation therapy: current advances and future directions. *Int J Med Sci* 9:193–199
5. Kozłowska WS, Böhlen TT, Cuccagna C, Ferrari A, Fracchiolla F, Magro G, Mairani A, Schwarz M, Vlachoudis V, Georg D (2019) FLUKA particle therapy tool for Monte Carlo independent calculation of scanned proton and carbon ion beam therapy. *Phys Med Biol* 64:075012
6. Sarrut D, Bardiès M, Bousson N, Freud N, Jan S, Létang JM, Loudos G, Maigne L, Marcatili S, Mauxion T, Papadimitroulas P (2014) A review of the use and potential of the GATE Monte Carlo simulation code for radiation therapy and dosimetry applications. *Med Phys* 41:064301
7. Dedes G, Pinto M, Dauvergne D, Freud N, Krimmer J, Létang JM, Ray C, Testa E (2014) Assessment and improvements of Geant4 hadronic models in the context of prompt-gamma hadrontherapy monitoring. *Phys Med Biol* 59:1747–1772
8. Ivanchenko V, Incerti S (2017) Geant4 standard and low energy electromagnetic libraries. *EPJ Web Conf* 142:01016
9. Tan HQ, Phua JH, Tan L, Ang KW, Lee J, Bettiol AA (2019) Geant4 simulation for commissioning of proton therapy centre. In: *World congress on medical physics and biomedical engineering*, Springer, Singapore, 583–587
10. Geant4 physics reference manual. Release: 10.4, https://geant4.web.cern.ch/support/user_documentation. Last accessed 11 Oct 2019

Impact of Optimized Value for Relative Humidity at Cathode in PEMFC for Improved Stack Performance



S. Dhanya, Varghese Paul, and Rani Thottungal

Abstract Proton Exchange Membrane Fuel Cells (PEMFC) is now emerging an eco-friendly solution of the future to conventional energy systems. The cell performance is influenced by various parameters such as operating temperature and also reactant pressure, flow rates, and relative humidity. Maintaining the critical parameters in required levels is very essential for ensuring efficient performance from the PEMFC system. This paper presents the effect of optimizing cathode Relative Humidity (RH_c) on stack performance. Here, the most popular optimization algorithms like Particle Swarm Optimization (PSO) and Simulated Annealing (SA) are used for finding the optimum value of RH_c . A performance evaluation between these algorithms is presented based on the voltage regulation obtained from the PEMFC stack for a PEMFC model in Simulink with intelligent controllers like fuzzy and neuro-fuzzy controllers.

Keywords Proton exchange membrane fuel cells (PEMFC) · Optimization · Particle swarm optimization · Simulated annealing

1 Introduction

Today, we are facing several environmental problems associated with the burning of fossil fuels which is emitting CO_2 leading to climatic change and greenhouse effect. Hence, we are forced to identify fuels that are safe for the environment. Fuel cells are a kind of green energy source. Among other fuel cell types available, Proton Exchange

S. Dhanya (✉)

Muthoot Institute of Technology and Science, Ernakulam, India
e-mail: dhanyasreedharan16@yahoo.co.in

V. Paul

Toch Institute of Science and Technology, Ernakulam, India
e-mail: vp.itcusat@gmail.com

R. Thottungal

Kumaraguru College of Technology, Coimbatore, India
e-mail: ranithottungal@yahoo.com

© Springer Nature Singapore Pte Ltd. 2021

G. S. Hura et al. (eds.), *Advances in Communication and Computational Technology*, Lecture Notes in Electrical Engineering 668,
https://doi.org/10.1007/978-981-15-5341-7_87

1145

Membrane Fuel Cells have very attractive features like fast response and low operating temperature requirements [1]. But there are few challenges that should be addressed to make them commercially viable [2]. These challenges are mainly related to cost and performance issues. When a PEMFC is operated, their behavior gets affected by the operating temperature, partial pressures of reactants, and humidity of membrane. Hence, it is very important that these input parameters are maintained in the correct range to ensure efficient operation. Development of computer-aided modeling and diagnostic techniques for investigating the characteristics of PEMFC stack are hot areas of research in the field of fuel cells [3].

Simulation and mathematical models are extremely important for PEMFC system development due to difficulty in experimentally characterizing their internal operation and the cost involved in replacing the damaged components. Within the fuel cell, tightly coupled electrochemical reactions, electrical and ionic conduction, and heat transfer happen simultaneously making their operation complex and nonlinear [4–6]. Mathematical model presented in [7] is used for performance study of PEMFC system and specifically on the effect of RH_c on stack performance.

2 PEMFC Operation

2.1 Dynamics Involved in PEMFC

Reversible open circuit voltage for Hydrogen Fuel cell, obtained by transferring two electrons with one water molecule is known as the Nernst voltage given in Eq. (1).

$$V_{\text{nernst}} = 1.229 - 0.85 \times 10^{-3}(T_{\text{fc}} - 298.15) + 4.3085 \times 10^{-5}T_{\text{fc}} \left[\ln(p_{H_2}) + \frac{1}{2} \ln(p_{O_2}) \right] \quad (1)$$

The fuel cell output voltage is reduced due to losses and the actual cell voltage is given as in Eq. (2).

$$V_{\text{stack}} = V_{\text{nernst}} - V_{\text{act}} - V_{\text{con}} - V_{\text{ohm}} \quad (2)$$

The activation loss of the fuel cell is associated with the speed of the reaction taking place on the electrode surface and is given in Eq. (3).

$$V_{\text{act}} = \left[\frac{RT}{4F\alpha c} \right] \times \ln\left(\frac{i}{ic}\right) + \left[\frac{RT}{2F\alpha c} \right] \times \ln\left(\frac{i}{ia}\right) \quad (3)$$

Electrons flowing through the electrodes and the interconnections create an electrical resistance which hinders the flow of ions in the membranes and results in a voltage drop called Ohmic Loss and can be expressed using the Eq. (4).

$$V_{ohm} = I_{fc} \times R \quad (4)$$

The rate of consumption of reactants at the electrode surfaces affects the fuel concentration and hence the fuel cell output voltage eventually leading to loss of voltage known as concentration loss. A reduction in the concentration of reactants due to failure to replenish (supply enough) reactant at the surface of the electrode results in mass transport loss or concentration loss and it is given in Eq. (5).

$$V_{con} = \left(i \times C_1 \times \frac{i}{i_{max}} \right)^{C2} \quad (5)$$

The stack voltage of a PEMFC depends on partial pressure of reactants—Oxygen (PO₂) and Hydrogen (PH₂) as given in Eq. (6) and (7).

$$P_{O_2} = RHC \times P_{sat_{H_2O}} \times \left\{ \left(\frac{1}{e^{\frac{4.192 \times T}{71.334}}} \right) \times \left(\frac{RHC \times P_{sat_{H_2O}}}{P_C} - 1 \right) \right\} \quad (6)$$

$$P_{H_2} = 0.5 \times \left(RHA \times P_{sat_{H_2O}} \times \frac{1}{e^{\frac{1.635 \times T}{71.334}}} \right) \times \frac{RHA \times P_{sat_{H_2O}}}{P_a} - 1 \quad (7)$$

Stack power and voltage depend deeply on membrane humidity. The air from the compressor has a humidity ratio given by Eq. (8).

$$\omega_{co} = \frac{M_v}{M_a} \cdot \frac{P_{vco}}{P_{aco}} \quad (8)$$

Here, M_a is the molar mass of dry air and M_v is molar mass of vapor. $P_{a,co}$ is partial pressure of dry air and $P_{v,co}$ is partial pressure of vapor. The air flow (ω_{co}) from compressor total of dry air flow ($\omega_{a,co}$) and vapor flow ($\omega_{v,co}$).

2.2 Effect of Membrane Humidity in PEMFC

Water management system maintains the humidity of the fuel cell membrane and simultaneously prevents the water from being accumulating at the electrodes. The dehydration or flooding of the membrane will result in an increase of polarization losses. Hence maintaining the optimum value of relative humidity in the membrane plays an important role in achieving the desired electrical performance from a PEMFC system. RH_c is estimated by an optimization process and it is validated against simulation results. To solve the optimization problem, the two standard and widely accepted optimization algorithms namely Particle Swarm Optimization (PSO) and Simulated Annealing (SA) optimization algorithms were used. Considering an initial set of parameters, the PEM fuel cell model compares previously

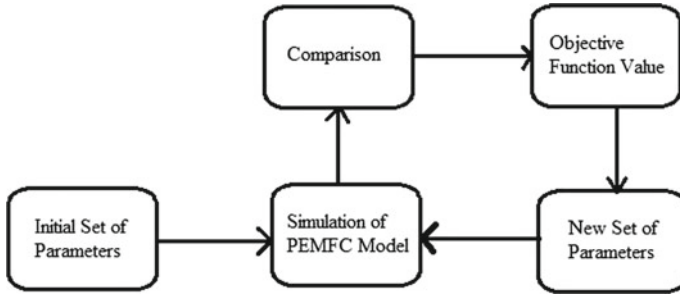


Fig. 1 Role of optimization in PEMFC

simulated waveforms and those having a current set of values, producing an error value (objective function). Role of optimization in PEMFC is shown in Fig. 1.

2.3 Optimizing Relative Humidity at Cathode

A study is performed to analyze the effect of varying RH_c on stack voltage and stack power and to understand the significance of RH_c on stack performance.

To predict the optimum RH_c of the fuel cell stack, the maximum power generated by the fuel cell stack is plotted as a function of the RH_c and operation temperatures. Figure 2: shows the effect of cathode relative humidity RH_c on stack power. Figure 2a gives the stack power at an operating temperature = 333 K (600 °C) and $RH_c = 0.5$ which is equal to 297 W. Figure 2b gives the stack power at an operating temperature

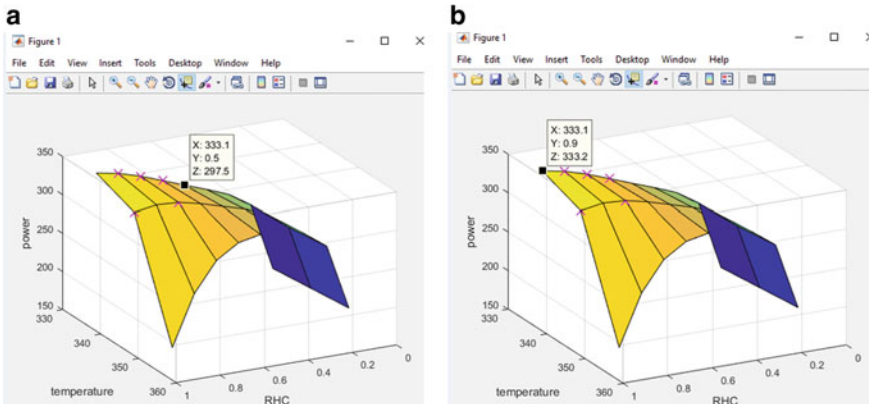


Fig. 2 a Power at $RH_c = 0.5$ and temperature = 333 K (600 °C). b Power at $RH_c = 0.9$ and temperature = 333 K (600 °C)

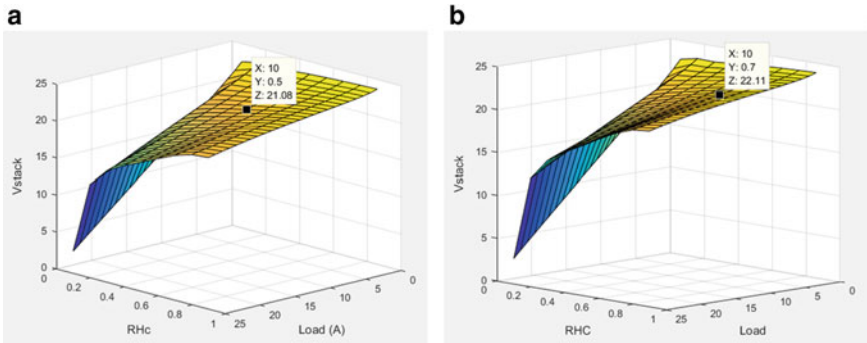


Fig. 3 a V_{stack} at $RH_c = 0.5$. b V_{stack} at $RH_c = 0.7$

= 333 K(600 °C) and $RH_c = 0.9$ which is equal to 333 W. These graphs show the effect of RH_c on the performance of the fuel cell stack.

Results in Fig. 3a, b shows the variation of stack voltage for different values of RH_c . The point marked in Fig. 3a gives the V_{stack} at 10A load at $RH_c = 0.5$ which is 21.06 V. Figure 3b shows V_{stack} with $RH_c = 0.7$ for the same load of 10A which is at 22.11 V. Value of RH_c plays an important role in stack performance.

3 Implementing Optimization Algorithm on PEMFC

3.1 Particle Swarm Optimization Algorithm

Particle swarm optimization, based on population and particle represents a solution for the problem and moving in the search space with a velocity based on its past best solution. Each particle is updated in very iteration using two “best” values. The first best solution it has achieved so far called pbest. Second “best” value is tracked by any particle in the population and is known as gbest. After getting the two best values, the particle updates the position and velocity.

3.2 Simulated Annealing Algorithm

The SA algorithm is a technique for random search based on the annealing process in metals wherein a metal cools and freezes into a minimum energy crystalline structure. SA avoids being trapped in a local minimum. The algorithm employs a random search that accepts changes that decrease the objective function f and also some changes that increase it. The latter can be accepted with a probability p . Its

flexibility and robustness as a global search method make it suitable for nonlinear systems like PEMFC [8].

4 Results and Conclusion

The simulation results in Fig. 4 shows the V-I curve from a 500 W PEMFC whose RH_c is optimized by PSO and SA. The optimized value of RH_c obtained using PSO was 0.86 and by SA was 0.72 and simulations were carried with both these values. The optimized value of RH_c obtained through Simulated Annealing showed a better stack performance than with Particle Swarm Optimization.

Table 1 shows the comparison of stack performance in terms of voltage regulation using different values of RH_c obtained from the two optimization algorithms. The stack performance was better with the value of $RH_c = 0.72$ obtained from SA.

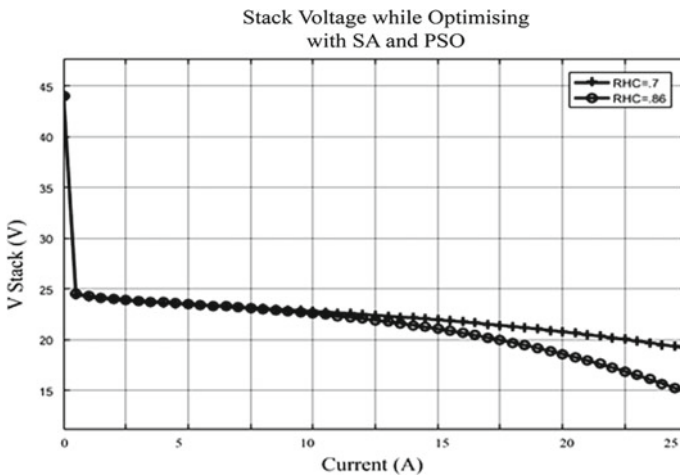


Fig. 4 V_{stack} with RH_c optimized by PSO and SA

Table 1 Voltage regulation using value of RH_c obtained from SA and PSO

Stack regulation (Vreg) without optimizing RH_c		Stack regulation (Vreg %) with optimized RH_c	
		Using SA	Using PSO
RH_c	Vreg (%)	RH_c (0.72)	RH_c (0.84)
0.5	47.65	34.72	80.32
0.7	43.89		
0.8	58.54		

Table 2 Voltage regulation using controllers

RH _c	Voltage regulation (%)		
	With fuzzy controller	With neuro-fuzzy controller	With fuzzy and neuro-fuzzy controller
Using PSO (RH _c = 0.86)	18.63	18.15	14.93
Using SA (RH _c = 0.72)	17.62	14.91	13.85

Stack performance was evaluated on PEMFC models implemented with fuzzy and neuro-fuzzy controllers [7] with both values of RH_c obtained from the two algorithms and results are tabulated in Table 2.

These can be used to develop various control strategies for regulating cathode pressure, flow rate and relative humidity to get desired electrical performance from PEMFC stack under the wide range of operating conditions.

References

1. Lee J-Y, Cha K-H, Lim T-W, Hur T (2011) Eco-efficiency of H₂ and fuel cell buses. *Int J Hydrog Energy* 36:1754–1765
2. DOE Fuel Cell Technologies Office (2015) 2014 Fuel Cells Technology Market Report Washington, D.C.
3. Amphlett JC, Bumert RM, Mann RF (1995) Performance modelling of the ballard mark IV solid polymer electrolyte fuel cell II: empirical model development. *J Electrochem Soc* 142:9–15
4. Pukrushpan JT (2003) modelling and control of fuel cell systems and fuel processors. Ph.D. Dissertation, University of Michigan, USA
5. Sousa JR, Gonzalez ER (2005) Mathematical modeling of polymer electrolyte fuel cells. *J Power Sources* 147:32–45
6. Daud WR, Rosli RE, Majlan EH, Hamid SA, Mohamed R, Husaini T (2017) PEM fuel cell system control: a review. *Renewable Energy* 1(113):620–638
7. Dhanya S, Thottungal R, Paul V, Hareendran SA (2019) Designing an intelligent controller for improving PEM fuel cell efficiency. In: *Asian conference on intelligent information and database systems*, Springer, Cham, pp 387–395
8. Lin L, Fei F (2012) The simulated annealing algorithm implemented by the MATLAB. *IJCSI Int J Comput Sci Issues* 9(6):2

Denoising, Edge Correction, and Enhancement of Breast Cancer Ultrasound Images



Jyoti Dabass and Manju Dabass

Abstract Mortality rate because of breast cancer diminishes to a large extent if the categorization of breast lesions as malignant or benign is done properly. But this process is quite complicated owing to erroneous detection of noisy pixels as false positives. It can be reduced by proper enhancement of cancer indicating features present in breast cancer ultrasound images. Therefore, the technique proposed for denoising, edge correction, and enhancement is pivoted around two drastic issues. The first issue is related to the blurring of important details because of improper noise suppression, whereas the second issue is associated with poor contrast between background tissues and masses in ultrasound images of breast cancer. In this paper, we propose an ensemble hybrid filter that restores the noisy ultrasound breast cancer images, corrects the edges of restored ultrasound images without getting degraded with additional Gaussian noise which degrades the ultrasound images during edge correction and finally enhances its visual quality. It uses Wiener filtering to remove a small amount of noise, fuzzy derivatives, and smoothing for edge preservation and intensification membership function along with contrast limited adaptive histogram equalization for enhancement. Experimental results are obtained to demonstrate the feasibility of the proposed approach. These results are also compared to traditional Wiener filter by numerical measures and visual inspection.

Keywords Contrast intensification operator · CLAHE (contrast limited adaptive histogram equalization) · Fuzzy logic · Gaussian filter · Optimization · Ultrasound images of breast cancer

J. Dabass (✉) · M. Dabass
EECE Department, The Northcap University, Gurugram, India
e-mail: [jyotidabas91@gmail.com](mailto: jyotidabas91@gmail.com)

M. Dabass
e-mail: [manjurashi87@gmail.com](mailto: manjurashi87@gmail.com)

© Springer Nature Singapore Pte Ltd. 2021
G. S. Hura et al. (eds.), *Advances in Communication and Computational Technology*, Lecture Notes in Electrical Engineering 668,
https://doi.org/10.1007/978-981-15-5341-7_88

1153

1 Introduction

Breast cancer is the most common cancer in India and accounts for 27% of all cancers in India. According to GLOBOCAN 2018, 144,937 new cases and 70,218 deaths were reported for breast cancer in India. The incidence rates in India begin to rise in the early thirties and peak at ages 50–64 years. Overall, 1 in 28 women is likely to develop breast cancer during her lifetime. In urban areas, 1 in 22 women develops breast cancer during her lifetime as compared to rural areas where 1 in 60 women develops breast cancer in her lifetime. Breast Cancer cannot be prevented but its early detection via mammography or breast cancer ultrasound images can lead to the likelihood of effective diagnosis and thus saving lives [1, 2].

Ultrasonography is an extensively used diagnostic method for early detection of breast cancer, due to its noninvasive nature, low charge, security, transportability, and competence of forming real-time imaging [3, 4]. Tactlessly, ultrasound images display a granular appearance called speckle, which damages visual appraisals. Hence, it becomes tough for a human to discriminate normal and pathological or abnormal tissue in diagnostic investigations. Also, Gaussian noise or Gaussian blur corrupts the ultrasound images making diagnosis difficult and error-prone [4]. Detection of abnormality in breast cancer ultrasound images becomes cumbersome due to low resolution and poor contrast. Simple denoising technique for medical image corrupted by Gaussian noise is the Weiner filter. The major drawback of the Weiner filter is that it leaves the noise pixels after filtering and is slow to apply [5, 6]. Also, by filtering edges get blurred and visual quality is affected. Various filtering algorithms have been proposed for denoising breast cancer ultrasound images which have been discussed in detail.

Perona Malik method is commonly used to denoise breast cancer ultrasound images but this method results in a locally optimal solution having the approximately same value of noise and edge gradient in the presence of large noise. So, for improving the efficiency of Perona Malik method in [7], the fuzzy logic-based method used PM method along with particle swarm optimization for finding a global optimal value. Also, they used diffusion coefficients and fuzzy logic denoising algorithm based on partial derivative and gradient differential operation for removing noise in highly corrupted ultrasound images. In [8], authors calculated wavelet coefficients using the wavelet transform and then applied sinusoidal membership function on the low-frequency coefficients of wavelet decomposition for converting spatial domain to fuzzy domain and soft thresholding denoising on high-frequency coefficients and finally index transform in order to get an enhanced image. In [9] Fuzzy logic is used to demarcate the corrupted pixels into homogeneous, detail, and edge-defined classes, and then a weighted averaging filter is used to differentiate edges along with noise.

To remove the nonlinear and speckle noise in breast cancer ultrasound images authors in [10] applied hybrid of median and diffusion filtering. It is followed by Otsu thresholding for extracting the region of interest and k means clustering for local thresholding to detect an abnormality. The limitation of their technique was

high run time. To overcome the limitation of high run time in removing speckle noise, the bilateral filter was proposed in [11]. In this, instead of applying the bilateral filter for Gaussian noise, the authors have applied the bilateral filter for speckle noise by replacing the intensity values of every pixel with a weighted average of intensity values from nearby pixels. This technique works well for a low quantity of speckle noise but its performance gets degraded when the noise increases.

In [12], the authors assessed despeckling filtering techniques in terms of edge and feature preservation. They applied the filtered results for segmenting malignant and benign tumors from ultrasound images. Out of 42 filters, they found DPAD despeckling filtering better for removing the speckle noise. In [13], authors found pre-processing essential for removing speckle noise and enhancing the contrast of the breast cancer ultrasound images. They observed that without enhancement, the canny operator was giving indistinguishable contours so they applied fuzzy-based enhancement techniques before fractal-based segmentation to get clear contours with less discontinuity.

In [14], the authors provided a review of denoising techniques for ultrasound images taking a better resolution, contrast enhancement, and edge preservation as a quality measure and found non-subsampled contourlet transform better. In [15], authors developed multi-gene genetic programming based intelligent estimator for removing multiplicative nature speckle noise which affects the visual quality. They found that by removing noise, ultrasound images get better resolution and contrast with the preservation of edges.

In [16], the authors applied the median filter and adaptive median filter for removing the speckle noise before segmenting the region of interest using the multi-fractal dimension. They found that pre-processing is essential for getting high classification accuracy. In [17], the authors applied histogram equalization and denoising for improving the contrast between background and tumor. Without pre-processing, poor quality and uneven distribution of echo make diagnosis difficult. So, they concluded that pre-processing helps in extracting ROI and clustering before classification to get better accuracy.

In [18], authors showed the effect of filtering on segmentation by applying morphology and non-local means on breast ultrasound images and got better segmentation with pre-processing. NLM filters classify patches as alike to a given filter having the same orientation and structure but similar patches with different orientations and similar structures do not have an effect on average. To rectify this limitation in [19], the authors assessed the orientation of the patch and modified it before applying RIBM for the weighted averaging process to get suitable regions.

In [20], authors applied non-local means for noise reduction and fuzzy logic for enhancement of breast ultrasound images before segmenting them using neutrosophic theory based on active contour to get better results. In [21], authors applied a hybrid denoising technique combining bilateral filtering, anisotropic filtering, and wavelet thresholding to get better segmentation and classification accuracy compared to other filters including lee filter.

From the literature review, it can be inferred that authors have mostly worked in removing speckle noise from breast cancer ultrasound images. Gaussian noise is

equally probable to affect the quality of breast cancer images. Very little work is done in removing Gaussian noise from breast ultrasound images. It can be deduced from the literature review that the noise removal process affects the visual quality. Also, edge correction of breast cancer ultrasound images introduces additional noise in the image which can be speckle, Gaussian, or additive white noise. And the presence of noise distorts the edges and affects the visual quality. To improve the visual quality, various fuzzy-based enhancement algorithms are proposed for breast cancer images. Usually, mammograms are of low contrast but after edge correction and denoising, visual quality of breast cancer ultrasound images gets affected. So, we have reviewed a few enhancement algorithms proposed for mammograms.

Fuzzy logic based on adaptive fuzzy contrast enhancement proposed in [22] overcomes the difficulties created due to the mammogram's fuzzy nature and low contrast between surroundings and breast cancer. It clears ill-defined borders that affect the detection of automated breast cancer. It normalizes the mammogram on the basis of grey level distribution for reducing the effects of various illuminations. Then it applies the adaptive fuzzy contrast enhancement to enhance the features of mammograms. It measures and enhances the local contrast using the local and global information to enhance details and to suppress the noise. It uses the maximum fuzzy entropy principle to do fuzzification. Finally, to transform the enhanced image of mammograms into the spatial domain, defuzzification is done. It increases the contours and texture structure and enhances the minute details of the features of mammograms. Fuzzy Rule-Based Enhancement anticipated in [23] is tested on both standard and medical images. It has better visual quality compared with a fuzzy INT operator due to SMRT (Sequence-based Mapped Real Transform Domain). It fuzzifies the grey level by dividing the image into non-overlapping blocks and SMRT matrix followed by calculation of histogram and SMRT matrix from the mean value of the block in order to modify the matrix and to apply the fuzzy rule. Finally, defuzzification is done by calculating inverse SMRT. These results are compared with the Fuzzy INT operator to attest to its effectiveness. Histogram clipping, invariant and crisp nature of clip limit (i.e. pre-defined value) made conventional histogram equalization-based techniques unsuitable for real applications.

So, in [24] FC-CLAHE (Fuzzy Clipped Contrast Limited Adaptive Histogram Equalization) was proposed. It generates a histogram and calculates contrast and entropy. It uses Fuzzy Inference System to select the fuzzy clipping enhancement parameter in order to get a clipped histogram. Finally, it checks the quality of redistributed clipped pixels and results in the fuzzy clipped contrast-enhanced image. If quality is not up to the mark, then it continues adjusting fuzzy rules and membership functions and inputting them to FIS until it gets the better-enhanced image. It provides better visual quality and high PSNR compared with traditional methods. To overcome the limitations of conventional methods in understanding mammary gland images, Intuitionist Fuzzy Sets (IFS) proposed in [25] uses membership function dependent on REFs (Restricted Equivalence Functions) to distinguish specific ROIs (Region of Interest). IFS demarcates the mammogram into the background and foreground area based on a threshold. To change the pixel plane to the membership

plane, IFS constructs the intuitionist fuzzification generator of foreground and background areas. Then it separately hyperbolizes the membership degrees of both areas. Normalization is performed to retransform the membership plane into a pixel plane in order to get the filtered image. Finally, it combines the enhanced image with the filtered image to get the enhanced image. It is efficient, simple, and uses only three parameters to enhance contrast and visual quality of abnormalities in a mammogram. It has a better mean Opinion Score, region of Interest, time expenditure, and visual quality compared with conventional methods. Since ambiguity and uncertainty are inevitably produced during the acquisition or transmission of mammogram and there is a possibility of noise affecting the image quality.

Current enhancement techniques increase the visual quality but degrade the edge information and fine details. Also, edge correction techniques lead to the introduction of noise. So, we proposed an algorithm that removes the Gaussian noise, corrects the edges without getting suffered from additional noise (Gaussian, speckle, or additive white noise) and enhances the contrast. First, the proposed technique looks for the presence of Gaussian noise. If Gaussian noise is present then it removes it using Weiner filter. Weiner filtering is capable of removing a small amount of noise but degrades the edges. After denoising, edges are corrected. Edge correction adds additional noise which cannot be removed well by Weiner filter. But the proposed technique is efficient in removing high density of speckle, Gaussian, and additive white noise. The proposed technique is applied for removing Gaussian noise, correction of edges, and removal of additional noise while correcting edges and improvement of the visual quality of breast cancer ultrasound images. Conventional denoising techniques were applicable either on colored or greyscale medical images but the proposed technique is efficient in working on both medical and colored images.

This paper is organized as follows: Sect. 2 discusses the proposed approach followed by results and discussions in Sect. 3. Section 4 draws a conclusion.

2 The Proposed Approach

Denoising and enhancement of breast cancer ultrasound images without degrading the fine details, structural information, and edges are the basic pre-processing steps for improving the detection accuracy of breast cancer [26]. In this paper, an image denoising scheme for removing Gaussian noise followed by edge correction, additional noise removal during edge correction coupled with the enhancement of fine details is proposed. It has two phases: first is detection tied with the filtering phase followed by edge correction and second is the contrast enhancement phase.

The procedure of the proposed filtering approach is discussed in Fig. 1. In this, first pixels of the input breast cancer ultrasound images are bifurcated into two categories namely noisy pixels corrupted with Gaussian noise and noise-free pixels. Noise-free pixels are left unchanged. For the noisy pixels, Weiner filter is applied. Weiner filter is able to remove a small amount of noise having a density of less than 1% but it corrupts the edges. For edge correction, edge correcting filter is used. In this first, $\Delta(u, v)$

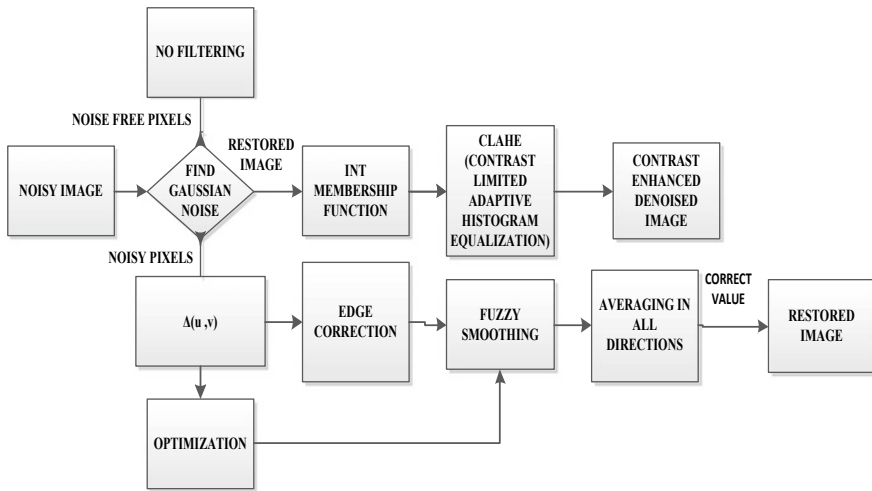


Fig. 1 The proposed filtering approach

detect edges in the direction of a pixel by calculating the difference in Luma values of neighbor and Luma value of the pixel. Using optimization spread of membership function ‘small’ is found. Optimization also affects the averaging of pixel values done in all possible directions using fuzzy smoothing to get the correction term. Finally, the correction value is added to the original pixel value. This restored image has low contrast. In order to enhance the contrast, image is fuzzified followed by modification of membership values according to INT membership function. Also, in order to get uniform distribution of grey levels, image intensity is changed using CLAHE (Contrast Limited Adaptive Histogram Equalization) with Rayleigh distribution and finally, we get the enhanced filtered image at the output. The proposed technique has the following phases which are discussed in detail.

2.1 Noise Description

Gaussian noise is a statistical noise having zero-mean Gaussian distribution which helps in reducing such noise by averaging pixel values in the local region. It has PDF (The Probability Density Function) equal to that of the normal distribution. The PDF P of a Gaussian random variable z represented by $P_G(z)$ is given by

$$P_G(z) = \frac{1}{\sigma\sqrt{2\pi}} e^{-\frac{(z-\mu)^2}{2\sigma^2}} \tag{1}$$

where z denotes grey level, μ is mean value and σ represents the standard deviation.

During the process of image acquisition, high temperature and poor illumination lead to Gaussian noise degrading the quality of the image. For an image J , the intensity value is denoted by J_{uv} where (uv) represents the pixel location of J . an image domain. When ultrasound image of breast cancer is degraded by additive noise (denoted by ρ_{uv}^K where K represents Gaussian and ρ implies noise at (uv) pixel location), all pixel get corrupted and then the degradation model for the noisy pixel E_{uv} can be written as

$$E_{uv} = J_{uv} + \rho_{uv}^K \quad (2)$$

where the value ρ_{uv}^K is taken from non- zero normal or Gaussian distribution. For expressing the efficiency of the proposed technique, we have used breast cancer ultrasound images with Gaussian noise density 0.001. While correcting the edges, a high density of Gaussian noise affected the breast cancer ultrasound images which is removed well by the proposed technique.

2.2 Fuzzy Filtering

It deals with removing Gaussian noise, edge correction, optimization, fuzzy smoothing and finally averaging in all possible directions to get the correct value. These phases are discussed in detail as follows. For the noise filtering, we used a Wiener filter which removes less density of noise (0.001) but disturbs the edges. So, we go for edge correction.

- (a) *Edge Correction*: This filter first detects and corrects the edges by calculating the difference in Luma values in possible eight directions. Consider a 3*3 block of pixels having (u, v) at the center. Here, the difference in the value of Luma ($\Delta(u, v)$) for an image K in all possible eight directions namely $N, E, W, S, NE, NW, SE, SW$ can be calculated using

$$\Delta N(u, v) = K(u, v - 1) - K(u, v) \quad (3)$$

$$\Delta S(u, v) = K(u, v + 1) - K(u, v) \quad (4)$$

$$\Delta NE(u, v) = K(u + 1, v - 1) - K(u, v) \quad (5)$$

and so on.

On combining the above three equations, we get an average filter that de-noises image without preserving the edges. Optimization reflecting dispersal of small membership function affects the amount of averaging and the correction term. For

preserving edges, we compare $\Delta(u, v)$ in a direction perpendicular to the correction term. E.g. for NE direction, we consider pixels along NW diagonal to determine $\Delta_{NE}(u, v)$ with $p1, p2, p3$ as diagonals using

$$p1 = \Delta_{NE}(u, v) \tag{6}$$

$$p2 = \Delta_{NE}(u - 1, v - 1) \tag{7}$$

$$p3 = \Delta_{NE}(u + 1, v + 1) \tag{8}$$

If the value of either two or three diagonal ($p1, p2, p3$) is small, then there is no edge in that direction. In this case, its correction value denoted by $\Delta_{NE}(u, v)$ is added to the final correction value. On the contrary, in the presence of an edge, only a small fraction of correction term is to be added to the final correction term. We denote the difference as small utilizing a fuzzy set with $M(d)$ representing the membership function and can be written as

$$M(d) = \begin{cases} 1 - \frac{|a|}{M_d}, & \text{if } 0 \leq |a| \leq M_d \\ 0 & \text{if } |a| > M_d \end{cases} \tag{9}$$

Here, M_d represents the minimum standard deviation of all 8*8 blocks of the image. Its selection depends on the optimization scheme. The term “ a ” is representing the x-axis. For taking all above three differences to be small, we define the fuzzy rules as

“If Δ_1 is small and Δ_2 is small and Δ_3 is small then $\Delta_m R(u, v)$ is small”

where $p1, p2, p3$ are $\Delta R(u, v)$ of the pixels perpendicular to $R \in \{S, N, E, W, SW, NW, NE, SE\}$. This rule is applied for all eight directions and $\Delta_M R(u, v)$ representing the membership function $\Delta R(u, v)$ is determined in a small fuzzy set.

- (b) *Optimization (Find M_d):* Instead of sampling the whole image, we take 8*8 blocks of image and calculate their standard deviation. Least deviation out of all blocks is considered for determining the variation in Luma values. This value is always less than the deviation in the case of edge. Finally, to reduce noise, we multiply the amplification factor b and standard deviation.

$$M_d = b * \text{standard deviation} \tag{10}$$

where b is determined according to noise level generally ranging from [3, 7] in order to control the level of smoothing

- (c) *Fuzzy Smoothing*: For fuzzy smoothing, if there is no edge in the direction then we add the difference of pixel value in a perpendicular direction to the final correction using $C_R(u, v)$ as the correction component and fraction of $\Delta R(u, v)$ in the direction R .

$$C_R(u, v) = \Delta_M R(u, v) * \Delta R(u, v) \quad (11)$$

To obtain the final correction term, we utilize the following fuzzy rules

$$"C_{Rpo} = \text{If } \Delta_M R(u, v) \text{ is small and } \Delta R(u, v) \text{ is positive then } C_{Rpo} \text{ is positive}" \quad (12)$$

$$"C_{Rne} = \text{If } \Delta_M R(u, v) \text{ is small and } \Delta R(u, v) \text{ is negative then } C_{Rne} \text{ is negative}" \quad (13)$$

- (d) *Averaging in all directions*: Finally, averaging is done by finding the difference between C_{Rpo} and C_{Rne} to get the correction term using expression given in [27–29] and written as

$$\Delta C(u, v) = \sum_{R \in \text{directions}} (C_{Rpo} - C_{Rne})/8 \quad (14)$$

where directions $\in \{S, N, E, W, SW, NW, NE, SE\}$. Finally, we achieve the correction, term with the help of direction who do not possess edges going through its perpendicular direction. This phase removes the additional noise including a high density of Gaussian noise which degrades the ultrasound images during edge correction.

2.3 Contrast Limited Fuzzy Based Adaptive Histogram Equalization

- (a) *Fuzzification using intensification MF*: It involves fuzzification of the image followed by modification of the membership values and finishing with defuzzification of image without affecting the brightness and naturalness of image. It first calculates the fuzzy matrix for the image of size $M \times N$ having intensity levels ranging from $[0, L - 1]$ with $L = 256$ for 8 bit image using

$$W = \bigcup_{g=1}^M \bigcup_{h=1}^N \frac{\mu_{gh}}{Y_{gh}} \quad (15)$$

where Y_{gh} = the intensity of gh th pixel and μ_{gh} (membership function) lies in the range of $[0, 1]$. To convert the spatial domain to fuzzy domain by making dark portions darker and bright portions brighter leaving others unmodified, it utilizes the INT membership function represented by $T(\mu_{gh})$ given in [30] using the expression

$$T(\mu_{gh}) = \begin{cases} 2\mu_{gh}^2 & \text{if } 0 \leq \mu_{gh} \leq 0.5 \\ 1 - 2[1 - \mu_{gh}]^2 & \text{if } 0.5 < \mu_{gh} \leq 1 \end{cases} \quad (16)$$

- (b) *Contrast Limited Adaptive Histogram Equalization (CLAHE)*: It changes the image intensity to enhance the contrast of the image. It works on small tiles rather than a global image. It increases the contrast so that the histogram of the output image resembles the specified histogram [31, 32]. To remove the artificially induced boundaries, bilinear interpolation combines the neighboring tiles. CLAHE is applied using

$$F = /I_{\text{maximum}} - I_{\text{minimum}}/ * F_c(I_{\text{input}}) + I_{\text{minimum}} \quad (17)$$

where I_{maximum} and I_{minimum} are maximum and minimum permissible intensity level, $F_c(I_{\text{input}})$ represent Cumulative probability distribution (CDF) for the input image J_{input} and I . presenting computed pixel value. For this, CDF ($F_c(I_{\text{input}})$) and Probability distribution function ($F_c(I_c)$) are represented using expressions

$$F_c(I_{\text{input}}) = \sum_{h=0}^c f_g(gh) \quad (18)$$

$$F_c(I_c) = \frac{m_c}{M} \quad (19)$$

where m_c represents pixel quantity having I_c intensity levels and M . notes total pixels. Finally, defuzzification represented as $T^{-1}(F(u, v))$ denoted by the term $\mathcal{G}(u, v)$ is applied using

$$G(u, v) = T^{-1}(F(u, v)) = \bigcup_{u=1}^M \bigcup_{v=1}^N F(u, v) * (L - 1) \quad (20)$$

where T^{-1} implies grey level. In this CLAHE with Rayleigh distribution is used which provides uniform intensity distribution. Also, the Rayleigh distribution works well for colored medical images.

3 Results and Discussions

Results and discussions deal with performance measures and simulation results.

3.1 Performance Measures

In the experiments, the proposed filter has been tested on a number of greyscale ultrasound images of breast cancer having ground truth to demonstrate its robustness and effectiveness. The database is given by Queen Sirikit Center for Breast Cancer of Thailand and the Department of Radiology of Thammasat University. Case-207-G1, Case-203-G1, Case-200-G1 is an image of Cyst. Case-170-G1 and Case-169-G1 denote Fibroadenoma [33]. While Case-22-G, Case-21-G, Case-19-G1, Case-16-G1, Case-15-G1, Case-11-G1 represents malignant solid mass.

Objective measures are taken into consideration for assessing the quality of the restored image as they can optimize the settings of the parameter by monitoring and adjusting the image quality and thus can be used to benchmark the systems of digital image processing. The quantitative metrics used to evaluate the performance of the proposed denoising technique is PSNR (Peak Signal to Noise Ratio), SSIM (Structural Similarity Index Measure), Entropy, MSE (Mean Square Error), AMBE (Absolute Mean Brightness Error), and RMSE (Root Mean Square Error). It is observed that the entropy of the output image should be greater than the input image. Lower entropy represents a loss of image details while high entropy suggests that the image is rich in detail. In the case of a noisy image, the value of entropy is high sometimes for it considers image noise as image details. If p_z is normalized histogram then entropy H as given in [34], can be represented using the expression

$$H = \sum_{z=1}^m p_z \log_2 p_z \tag{21}$$

PSNR is the ratio of maximum signal power and power of noise affecting the output signal. Let uv is image size, T is Dynamic range for pixel values, $K(x, y)$ is the noisy image and $Z(x, y)$ is a denoised image, R, E representing reference and enhanced image, respectively, then PSNR and MSE can be defined as given in Eqs. (22) and (23).

$$PSNE(R, E) = 10 \log_{10} \left(\frac{(T - 1)^2}{\text{Mean Square Error } (R, E)} \right) db \tag{22}$$

and

$$MSE (R, E) = \frac{1}{uv} \sum_{x=0}^{u-1} \sum_{y=0}^{v-1} [K(x, y) - Z(x, y)]^2 \tag{23}$$

In ultrasound images of breast cancer, the degree of contrast improvement achieved by an enhancement algorithm is derived by the fact that it should preserve brightness and originality. For a high degree of structural similarity, the value of SSIM = 1. Otherwise, its value always lies between zero and one. Let m_x, m_y our local mean s_x, s_y are a standard deviation and s_{xy} is cross-covariance for an image x,y with G_1 and G_2 as constants then SSIM can be mathematically derived as

$$SSIM = \frac{(2m_x m_y + G_1)(2s_{xy} + G_2)}{(m_x^2 + m_y^2 + G_1)(s_x^2 + s_y^2 + G_2)} \tag{24}$$

AMBE measures the absolute difference between input mean ($E(U)$) and output mean ($E(V)$). Its low value represents better brightness preservation. Let $E(.)$ denotes expected value or the statistical mean then for an input image U and output image V , AMBE is denoted as

$$AMBE = |E(U) - E(V)| \tag{25}$$

RMSE measures the difference between the values that are estimated and the values of the estimator. It is basically the standard deviation of mean square error. It can be measured by the expression

$$RMSE = \sqrt{MSE} \tag{26}$$

Tables 1 and 2 compare the objective performance of the proposed technique with the Weiner filter in terms of quantitative metrics. We have shown the noisy images which are achieved during edge correction. By fuzzy smoothing and averaging operation and averaging operation used in the proposed technique, high-density noise is removed effectively while the Weiner filter is not able to remove high-density noise. Table 1 compares the value of SSIM, RMSE, MSE, and PSNR obtained by the proposed technique with the Weiner filter. In case-169-U1, the proposed technique increased the PSNR from 14.0370 (using Weiner filter) to 24.8471 and SSIM from 0.2678 (with Weiner filter) to 0.8890. It reduces the value of RMSE from 50.6630 (Weiner) to 14.5944 and MSE value from 2.5667e + 03(with Weiner) to 212.9975. While in case-207, case-200, case-19 and case 15, the proposed techniques provide values of SSIM almost double as that obtained by Weiner filter and PSNR values about 1.5 times the value given by Weiner filter. It also reduces the values of RMSE and MSE to one third the values obtained using Weiner filtering and hence it can be used for denoising breast cancer ultrasound images corrupted with a high density of noise.

Table 2 shows the performance measures for enhancement. In the proposed technique we have used CLAHE with INT membership function for enhancing the

Table 1 Performance measures of the proposed method and Weiner filter for denoising

Image	SSIM Weiner	SSI prop.	RMSE Weiner	RMSE prop.	MSE Weiner	MSE prop.	PSNR Weiner	PSNR prop.
Case-207-U4.png	0.4805	0.9294	45.0695	11.2903	2.0313e + 03	127.4703	15.0532	27.0767
Case-203-U4.png	0.3845	0.8405	69.9749	19.8107	4.8965e + 03	392.4630	11.2320	22.1928
Case-200-U4.png	0.4757	0.9137	48.3708	11.3555	2.3397e + 03	128.9466	14.4391	27.0267
Case-170-G5.png	0.3158	0.8830	102.417	13.3018	1.0489e + 04	176.9374	7.9234	25.6526
Case-169-U1.png	0.2678	0.8890	50.6630	14.5944	2.5667e + 03	212.9975	14.0370	24.8471
Case-22-G-7-0.jpg	0.4268	0.8254	65.8623	16.9254	4.3378e + 03	286.4683	11.7581	23.5600
Case-21-D-24-0.jpg	0.4098	0.7736	70.7646	18.1518	5.0076e + 03	329.4894	2.9011	22.9524
Case-19-U-30-0.jpg	0.4402	0.8196	54.1950	16.4227	2.9371e + 03	269.7045	13.4516	23.8219
Case-16-G-4-0.jpg	0.5063	0.8423	50.4721	16.0945	2.5474e + 03	259.0345	14.0698	23.2379
Case-15-D-18-0.jpg	0.4207	0.8089	53.0801	17.5650	2.8175e + 03	308.5282	13.6322	23.2379
Case-11-D-14-0.jpg	0.4870	0.7124	54.1629	21.1714	2.9336e + 03	448.2296	13.4568	21.6158

Bold signifies the results obtained by proposed technique

Table 2 Performance measures of the proposed algorithm for enhancement compared with the traditional modified histogram equalization technique

Image	Input (H)	Noise (H)	HE with INT MF (H)	After filter (H)	After filter and enhance (H)	SNR Weiner	SNR Prop	AMBE HE with INT MF	AMBE Prop.
Case-207-U4.png	4.9496	1.0905	3.3048	4.9496	4.7832	1.5998	13.6090	1.6448	0.1664
Case-203-U4.png	5.8198	1.6351	4.2309	5.8036	5.9899	1.8043	12.7651	1.5889	0.1701
Case-200-U4.png	5.0046	1.1112	3.6995	5.0046	5.1692	1.7675	14.3334	1.3051	0.1646
Case-170-G5.png	6.0948	1.9677	4.7130	6.3777	6.0954	1.4070	19.1174	1.3818	0.0006
Case-169-U1.png	6.3304	1.5679	4.5530	6.3050	6.2829	2.0873	12.9205	1.7774	0.0475
Case-22-G-7-0.jpg	5.9889	1.7411	4.3099	5.9391	6.1563	2.0566	13.8400	1.6790	0.1674
Case-21-D-24-0.jpg	6.0483	2.4191	4.4454	5.9844	6.3712	11.1345	14.7505	1.6029	0.3229
Case-19-U-300.jpg	5.7636	1.8415	4.0645	5.6757	5.9216	2.5796	12.8440	1.6991	0.1580
Case-16-G-4-0.jpg	5.4324	1.7842	3.8537	5.3767	5.6355	2.4461	12.3556	1.5787	0.2031
Case-15-D-18-0.jpg	6.1433	2.0499	4.4853	6.0982	6.2006	2.5002	12.1587	1.6580	0.0573
Case-11-D-14-0.jpg	5.5844	2.5870	3.9207	5.5731	5.6400	3.4835	11.6702	1.6637	0.0556

Bold signifies the results obtained by proposed technique

restored image. We have applied traditional histogram equalization (HE) with INT membership function (MF) on the image restored by fuzzy filtering for comparison purposes of enhancement block in terms of entropy and AMBE. Table 2 also compares the SNR values of the proposed technique with the Wiener filter. The proposed technique gives high entropy which shows no loss of information. The value of AMBE is low in the case of the proposed technique which shows its better ability in edge preservation. While in the case of Wiener filter, entropy is low and the value of AMBE is large. For example, in case-21, the proposed technique increases the SNR from 11.1345 using the Wiener filter to 14.7505. The value of AMBE is reduced to one fifth compared with Histogram equalization with intensification MF. The value of entropy (H) is 6.3712 in the case of the proposed technique compared with 4.4454 using Histogram equalization with intensification MF. It can be observed that by filtering block we get entropy as 5.9844 which is low in comparison with a proposed technique that emphasis both filtering and enhancement have an effective role in improving the quality of the image. In case-203, case-15, case-11, and case-22, the proposed approach shows its remarkable efficiency compared with the traditional method.

3.2 Simulation Results

Figures 2, 3, 4, 5, 6, 7, 8, 9, 10, 11, and 12 represent 11 different ultrasound images of breast cancer. In each Fig. 4 images are shown. The first image is the original image with a very low density of noise (0.001). This noise is removed by Weiner filter but edges get affected so, we have used edge correction technique. While correcting the

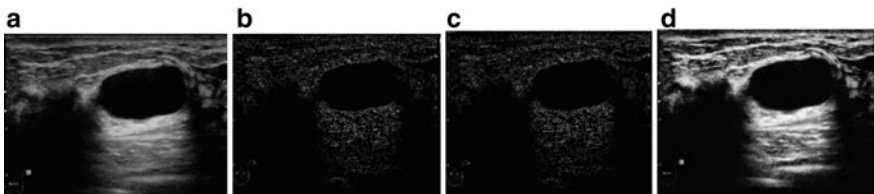


Fig. 2 a Case-207-U4.png (Cyst) b noisy image c Weiner filter d proposed technique

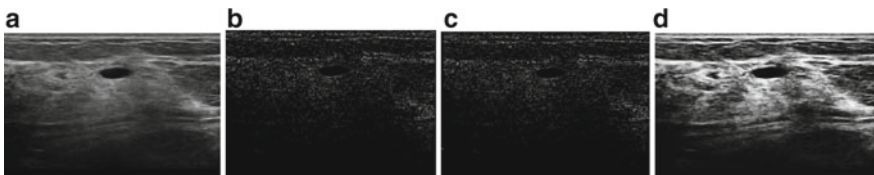


Fig. 3 a Case-200-U4.png (Cyst) b noisy image c Weiner filter d proposed technique

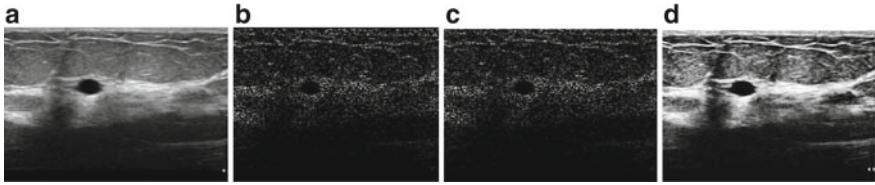


Fig. 4 a Case-203-U4.png (Cyst) b noisy image c Wiener filter d proposed technique

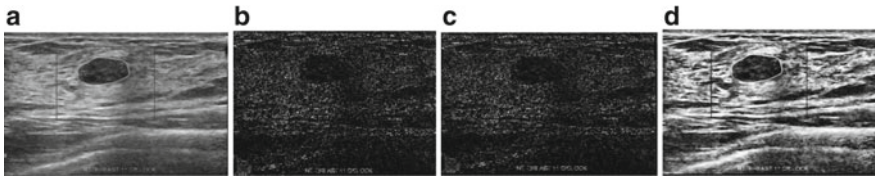


Fig. 5 a Case-170-G5.png (Fibroadenoma) b noisy image c Wiener filter d proposed technique

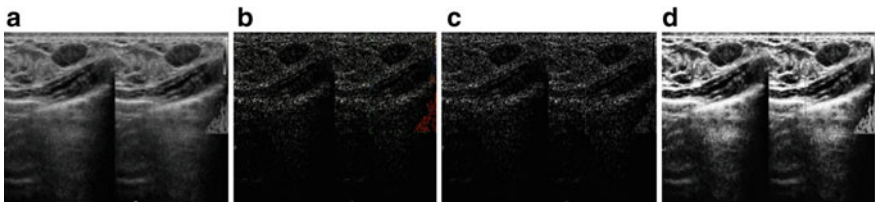


Fig. 6 a Case-169-U1.png (Fibroadenoma) b noisy image c Wiener filter d proposed technique

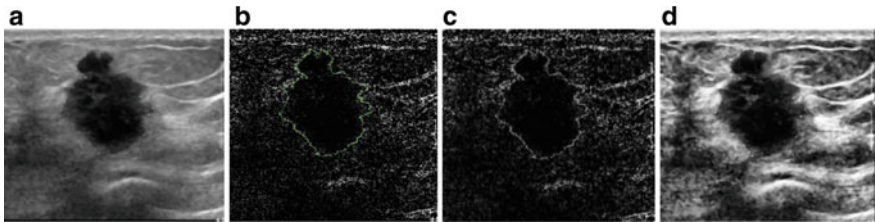


Fig. 7 a Case-22-G-7-0.jpg (malignant solid mass) b noisy image c Wiener filter d proposed technique

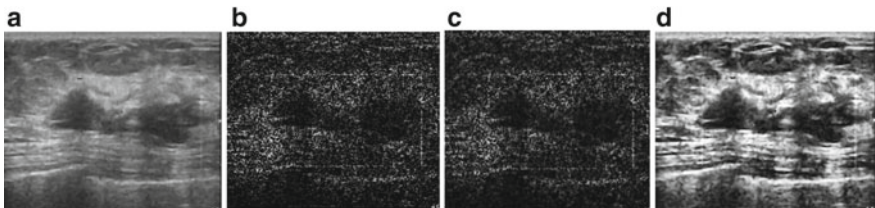


Fig. 8 a Case-21-D-24-0.jpg (malignant solid mass) b noisy image c Wiener filter d proposed technique

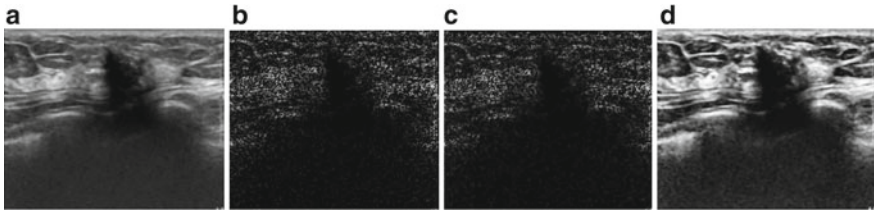


Fig. 9 a Case-19-U-30-0.jpg (malignant solid mass) b noisy image c Wiener filter d proposed technique

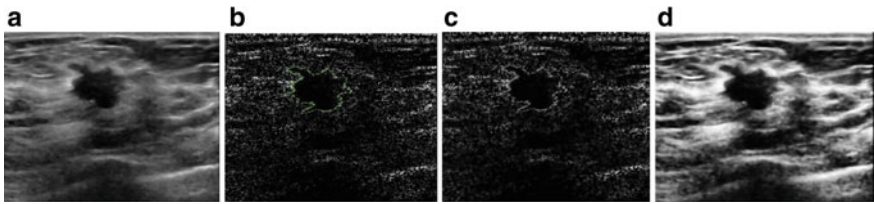


Fig. 10 a Case-16-G-4-0.jpg (malignant solid mass) b noisy image c Wiener filter d proposed technique

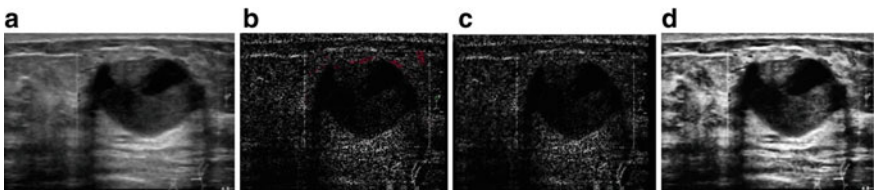


Fig. 11 a Case-15-D-18-0.jpg(malignant solid mass) b noisy image c Wiener filter d proposed technique

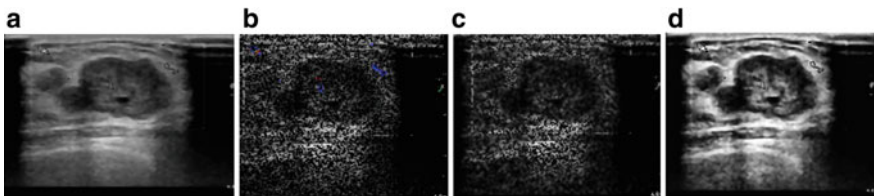


Fig. 12 a Case-11-D-14-0.jpg (malignant solid mass) b noisy image c Wiener filter d proposed technique

edges, a high density of noise affects breast cancer ultrasound images. The second image is of high-level Gaussian noise obtained during edge correction to show the effectiveness of the proposed technique in dealing with severe noise. The third image shows the result obtained by the proposed technique and finally, the last image

represents the results obtained after applying the Weiner filter. Results of simulation show a marked improvement in the visual quality of image corrupted with a high density of Gaussian noise compared with traditional Weiner filter.

From the results, one can see that the proposed technique is able to remove the low-density noise, and is able to correct the edges along with additional noise which affected the breast cancer ultrasound images while correcting edges. Whereas Weiner filter could remove a very low density of noise (0.001) but could not remove the high density of Gaussian noise. Also, the proposed technique provides high contrast and better visual quality. We have also applied histogram equalization with INT membership function on the edge corrected image.

But this technique was not giving good results compared to CLAHE with INT membership function so we didn't use this technique in the proposed method. In CLAHE with INT membership function, we focused on improving the visual quality and in getting uniform intensity distribution of grey levels. The main hitch of the proposed technique is that in CLAHE, instead of using a uniform distribution, we have used Rayleigh distribution keeping other parameters as default. The significance of using Rayleigh distribution is that Rayleigh distribution can work equally well even in the case of colored medical images. While CLAHE having uniform distribution sometimes changes the color of medical images.

Figures 2, 3, 4, 5, 6, 7, 8, 9, 10, 11, and 12 (a) Input Image (b) Noisy image having a random high density of noise (c) Results of Weiner filter applied on noisy image (d) Results obtained after applying the proposed technique on different images of ultrasound breast cancer.

4 Conclusions

This paper proposed an enhanced fuzzy filter for removing additive noise from the medical image. It preserves edges using the fuzzy difference in different directions. Fuzzy rules are formulated based on the local neighborhood of pixel using different membership functions like negative, positive, and small. Then optimization based on a current image is allowed for few iterations of noise reduction on given image simulation results show high visual quality coupled with high values of PSNR, SSIM, entropy, and low value of AMBE. Fuzzy filtering works well for both normal and Gaussian noise. The smoothing process is intensified by tuning the amplification factor without degrading edges. Compared with other filters, Fuzzy logic provides better quality. After restoring the image, enhancement operation improves the visual quality of the image which helps in extracting features and thus aid in the computer-aided diagnosis of breast cancer. The proposed techniques exhibit high noise immunity without degrading the edges and blurring the fine details. In the future, we can come up with a multi-fuzzy filter that deals with all types of noise and adaptively enhances the medical images.

References

1. Bray F, Ferlay J, Soerjomataram I, Siegel RL, Torre LA, Jemal A (2018) Global cancer statistics 2018: GLOBOCAN estimates of incidence and mortality worldwide for 36 cancers in 185 countries. *CA: a cancer journal for clinicians* 68(6):394–424
2. Ferlay J, Colombet M, Soerjomataram I, Mathers C, Parkin DM, Piñeros M, Znaor A, Bray F (2019) Estimating global cancer incidence and mortality in 2018: GLOBOCAN sources and methods. *Int J Cancer* 144(8):1941–1953
3. Zhang E, Seiler S, Chen M, Lu W, Gu X (2019) BIRADS features-oriented semi-supervised deep learning for breast ultrasound computer-aided diagnosis. *arXiv preprint arXiv:1904.01076*
4. Leal AS, Paiva HM (2019) A new wavelet family for speckle noise reduction in medical ultrasound images. *Measurement* 140:572–581
5. Joseph AM, John MG, Dhas AS (2017) Mammogram image denoising filters: a comparative study. In: 2017 Conference on emerging devices and smart systems (ICEDSS), pp 184–189. IEEE
6. Gupta S, Chauhan RC, Sexana SC (2004) A wavelet-based statistical approach for speckle reduction in medical ultrasound images. *Med Biol Eng Compu* 42(2):189–192
7. Shi S, Yan S, Wang Y, Li Y (2014) Medical ultrasound image denoising based on fuzzy logic. In: 2014 Fifth international conference on intelligent systems design and engineering applications, pp 611–614. IEEE
8. Wen H, Qi W (2015) Enhancement and denoising method of medical ultrasound image based on wavelet analysis and fuzzy theory. In: 2015 Seventh international conference on measuring technology and mechatronics automation, pp 448–452. IEEE
9. Kala R, Deepa P (2017) Removal of rician noise in MRI images using the bilateral filter by a fuzzy trapezoidal membership function. In: 2017 4th International conference on advanced computing and communication systems (ICACCS). IEEE
10. Joshi S, Kulkarni RK (2019) Medical image enhancement using hybrid techniques for accurate anomaly detection and malignancy predication. In: the third international congress on information and communication technology, pp 951–961, Springer, Singapore
11. Gupta A, Bhateja V, Srivastava A, Gupta A (2019) Suppression of speckle noise in ultrasound images using a bilateral filter. In: Information and communication technology for intelligent systems, pp 735–741, Springer, Singapore
12. Virmani J, Agarwal R (2019) Assessment of despeckles filtering algorithms for segmentation of breast tumors from ultrasound images. *Biocybernetics Biomed Eng* 39(1):100–121
13. Zhuang Z, Lei N, Raj ANJ, Qiu S (2019) Application of fractal theory and fuzzy enhancement in ultrasound image segmentation. *Med Biol Eng Compu* 57(3):623–632
14. Joel T, Sivakumar R (2018) An extensive review of despeckling of medical ultrasound images using various transformation techniques. *Appl Acoust* 138:18–27
15. Javed SG, Majid A, Lee YS (2018) Developing a bio-inspired multi-gene genetic programming based intelligent estimator to reduce speckle noise from ultrasound images. *Multimedia Tools Appl* 77(12):15657–15675
16. Mohammed MA, Al-Khateeb B, Rashid AN, Ibrahim DA, Ghani MKA, Mostafa SA (2018) Neural network and multi-fractal dimension feature for breast cancer classification from ultrasound images. *Comput Electr Eng* 70:871–882
17. Fang Z, Zhang W, Ma H (2019) Breast cancer classification with ultrasound images based on SLIC. *arXiv preprint arXiv:1904.11322*
18. Adabi S, Ghavami S, Bayat M, Fatemi M, Alizad A (2019) A two-fold enhancement of ultrasound vessel images using a non-local based restoration and morphological filtering. In: Medical imaging 2019: ultrasonic imaging and tomography, international society for optics and photonics, vol 10955, p 1095506
19. Prabusankarlal KM, Manavalan R, Sivaranjani R (2018) An optimized non-local means filter using automated clustering based pre-classification through gap statistics for speckle reduction in breast ultrasound images. *Appl Comput Inf* 14(1):48–54

20. Lotfollahi M, Gity M, Ye JY, Far AM (2018) Segmentation of breast ultrasound images based on active contours using neutrosophic theory. *J Med Ultrasonics* 45(2):205–212
21. Hermawati FA, Tjandrasa H, Suciati N (2018) Hybrid speckle noise reduction method for abdominal circumference segmentation of fetal ultrasound images. *Int J Electr Comput Eng* 8(3):2088–8708
22. Cheng HD, Xu H (2002) A novel fuzzy logic approach to mammogram contrast enhancement. *Inf Sci* 148(1–4):167–184
23. Jaya VL, Gopikakumari R (2015) Fuzzy rule-based enhancement in the SMRT domain for low contrast images. *Procedia Comput Sci* 46:1747–1753
24. Jenifer S, Parasuraman S, Kadirvelu A (2016) Contrast enhancement and brightness preserving of digital mammograms using fuzzy clipped contrast-limited adaptive histogram equalization algorithm. *Appl Soft Comput* 42:167–177
25. Deng H, Deng W, Sun X, Liu M, Ye C, Zhou X (2016) Mammogram enhancement using intuitionistic fuzzy sets. *IEEE Trans Biomed Eng* 64(8):1803–1814
26. Quintanilla-Dominguez J, Ojeda-Magaña B, Cortina-Januchs MG, Ruelas R, Vega-Corona A, Andina D (2011) Image segmentation by fuzzy and possibilistic clustering algorithms for the identification of microcalcifications. *Scientia Iranica* 18(3):580–589
27. Van De Ville D, Nachtegael M, Van der Weken D, Kerre EE, Philips W, Lemahieu I (2003) Noise reduction by fuzzy image filtering. *IEEE Trans Fuzzy Syst* 11(4):429–436
28. Zhu Y, Li H, Jiang H (2017) Fuzzy logic-based filter for removing additive and impulsive noise from color images. *Sensing Imaging* 18(1):3
29. Jayasree M, Narayanan NK (2017) A novel fuzzy filter for mixed impulse gaussian noise from color images. In: *Proceedings of the international conference on signal, networks, computing, and systems*, Springer, New Delhi, 53–59
30. Chaira T, Ray AK (2009) *Fuzzy image processing and applications with MATLAB*. CRC Press
31. Kharel N, Alsadoon A, Prasad PWC Elchouemi A (2017) Early diagnosis of breast cancer using contrast limited adaptive histogram equalization (CLAHE) and morphology methods. In: *2017 8th International conference on information and communication systems (ICICS)*, pp 120–124. IEEE
32. Sunny S, Gandhi MI (2018) An efficient citrus canker detection method based on contrast limited adaptive histogram equalization enhancement. *Int J Appl Eng Res* 13(1):809–815
33. Rodtook A, Makhanov, SS (2013) Multi-feature gradient vector flow snakes for adaptive segmentation of the ultrasound images of breast cancer. *J Vis Commun Image Represent* 24(8):1414–1430
34. Rani VMK, Dhenakaran SS (2019) Classification of ultrasound breast cancer tumor images using neural learning and predicting the tumor growth rate. *Multimedia Tools Appl* 1–19

U-FIN: Unsupervised Feature Integration Approach for Salient Object Detection



Vivek Kumar Singh and Nitin Kumar

Abstract Salient object detection is a challenging research field in computer vision. The existing saliency detection methods generally focus on finding feature maps for saliency computation. However, the combination of these feature maps significantly improves salient region(s) detection. In this paper, we propose a novel feature integration approach called U-FIN in which final saliency map is obtained by a weighted combination of individual feature maps. The proposed approach works in three phases *viz.* (i) artifact reference (AR) map generation (ii) weight learning and (iii) final saliency map computation. Firstly, AR map is produced using majority voting on the individual feature maps extracted from the input image. Secondly, linear regression is employed for weight learning which is used in the next phase. Finally, the individual feature maps are linearly combined using weights learned in the second phase to generate the final saliency map. Extensive experiments are conducted on two benchmark datasets, i.e., ASD and ECSSD to validate the proposed feature integration approach. The performance is measured in terms of precision, recall, receiver operating characteristic (ROC) curve, F-measure and area under the curve (AUC). Extensive experiments demonstrate the superiority of the proposed U-FIN approach against nine state-of-the-art saliency methods on ASD dataset and comparable on ECSSD dataset with the best performing methods.

Keywords Combine · Linear regression · Majority voting · Artifact reference map

1 Introduction

The phenomenon of the human visual system is simulated in salient object detection. Salient object detection approach rapidly extracts more relevant information in a scene. It attempts to locate visually more prominent and conspicuous objects/regions

V. Kumar Singh (✉) · N. Kumar
National Institute of Technology Uttarakhand, Srinagar (Garhwal), Uttarakhand, India
e-mail: vivek.kumarsingh@nituk.ac.in

N. Kumar
e-mail: nitin@nituk.ac.in

© Springer Nature Singapore Pte Ltd. 2021
G. S. Hura et al. (eds.), *Advances in Communication and Computational Technology*, Lecture Notes in Electrical Engineering 668,
https://doi.org/10.1007/978-981-15-5341-7_89

1173

in an image. Saliency detection is a more attractive and challenging research area in various fields such as neuroscience, psychology and computer vision. Salient object detection devoted to compute a saliency map [9] that highlights most significant part(s) in an image. It has also been deemed as preprocessing step to rectify the computational time in variety of visual applications such as object detection [20], video summarization [15], visual tracking [32] and image classification [26].

In the last decade, a number of saliency detection methods have been investigated to achieve efficient performance in a robust manner. However, this problem is still challenging specifically on complex images. Salient object detection (SOD) methods are broadly divided into two categories [30] (a) bottom-up and (b) top-down methods based on the way in which visual cues are explored. Bottom-up saliency detection methods [5, 9] exploit various low-level visual cues, i.e., color, intensity, texture and contrast, while top-down methods [17] entail training model and prior knowledge for computing saliency value of image elements. Typically, a single feature is not sufficient to capture salient object in an efficient and robust manner, e.g., frequency-tuned (FT) SOD [1], and hierarchical contrast (HC) [3] methods are single feature methods. In both these methods, contrast feature is employed for finding the saliency map, which is not appropriate for complex structure images. Besides, many saliency methods exploit multiple features and heuristic features combination approaches for saliency analysis such as linear [9] and nonlinear [8].

Learning-based feature integration methods were introduced by Liu et al. [13] who fused three novel visual feature maps, i.e., (a) color spatial distribution, (b) surround histogram and (c) center-multi-scale contrast using a weight vector. This is a supervised learning method, and weights are learnt using conditional random field (CRF). Feature integration approach defines the role of each feature in the saliency computation. Hence, the performance of these kinds of methods mainly depends upon the weights which are used for combination of individual features maps. A simple approach can be to linearly combine all the features with equal weights, but the performance may be poor due to the fact that all the features may not equally highlight salient regions. Another approach can be to derive single weight vector for all the natural images similar to Liu et al. [13]. The performance may again be poor due to the diverse characteristics of natural images. Based on the above discussion, we have made an attempt to alleviate the problem of feature combination approach by deriving image-dependent weights in an unsupervised manner.

Here, we propose an unsupervised feature integration (U-FIN) approach which derives image-dependent weights by using unsupervised method. The feature integration approach has three phases: (i) artifact reference (AR) map generation (ii) weight learning and (ii) final saliency map computation. Firstly, AR map is produced using majority voting on the individual feature maps extracted from the input image. Secondly, linear regression (LR) is employed for learning weight. Finally, the individual feature maps are linearly combined to generate the final saliency map. In this paper, our contribution is twofold:

1. A novel feature integration approach is proposed which derives weights in an unsupervised manner using linear regression.
2. Extensive validation is performed on two publicly available datasets to exhibit the better performance of the proposed approach.

2 Related Work

In the last few years, numerous saliency detection methods have been developed, and fabulous performance has been achieved. The early saliency computation work was prompted by capturing the visual attention process of human visual system (HVS). First computational on salient object detection was proposed by Itti et al. [9] in which feature integration theory [22] with biologically plausible visual attention system [10] was explored to generate saliency map. Itti et al. [9] proposed model extract various contrast feature maps, namely orientation, luminance and color based on center-surround approach across multiple scales, and after that normalize all the features and aggregate for generating the saliency map. A number of methods have extended Itti et al. [9] work in different disciplines such as Walther et al. [23] had extended it to highlight proto-object and Han et al. [7] extended it with Markov random field (MRF) and region growing approach to identify salient objects. The center-surround contrast has been extensively used either locally or globally in many existing saliency detection methods since it clearly highlights salient region from their surrounds regions. The center-surround mechanism is studied across variety of visual features, *viz.* color, shape and texture [14]. Zhang et al. [29] measures saliency based on information theory where the uniqueness is represented using self-information of local image features. Seo and Milanfar [21] proposed saliency method in which local regression kernels-based self-resemblance is utilized for saliency estimation. Rahtu et al. [19] proposed saliency method that integrates saliency measures obtained by jointly consideration of a statistical framework and local feature contrast with a conditional random field (CRF). Murray et al. computed weighted center-surround maps and applied inverse wavelet transform (IWT) for generation of saliency map.

Furthermore, global knowledge of visuals has been exploited in different directions to compute saliency map. Context-aware saliency detection approach proposed by Goferman et al. [5] which incorporates local center-surround difference along the global distinctive few visual organization principles and color feature to compute saliency map. The statistical information of image has been exploited to build foreground/background model which assigns saliency value to image elements based on posterior probability of foreground model to background model [30]. Li et al. [12] learnt the prior information for saliency estimation. In [11], saliency is analyzed in the frequency domain that which part of the frequency spectrum significantly contributed to saliency estimation. Additionally, many saliency detection methods decomposed the image into regions by applying either segmentation or clustering approach. Such participation of images is helpful for incorporating global knowledge at region level [3]. Ren et al. [20] proposed effective region-based

saliency computation approach that decomposed input image into the perceptually and semantically meaningful regions, and saliency of each region is measured based on spatial compactness using Gaussian mixture model (GMM). Furthermore, Fang et al. [4] suggested an approach in which discriminative subspaces are learnt for image saliency computation. Zeng et al. [28] proposed saliency estimation based on an unsupervised game-theoretic approach which does not depend on labeled training data.

Recently, deep learning-based methods have been proposed that influence performance greatly, but performance of these models entirely depends on large number of training data for optimizing network learnable parameters which increase computational time. Wang et al. [25] suggested saliency measure approach in which two deep neural network (DNNs) are trained to extract local features and global search, respectively. Context-based DNN is suggested by Zhao et al. [31] that constructs multi-context DNN with the consideration of local and global context. Pan et al. [18] proposed various saliency estimation approaches using convolutional neural networks (CNN) which greatly reduce computational cost. Guan et al. [6] proposed edge-aware CNN in which global contextual knowledge is combined along with the low-level edge features for saliency measure. Wang et al. [24] exploited recurrent fully convolutional networks (RFCNs) that incorporated saliency priors to generate saliency map.

3 Proposed Approach

In this section, we illustrate the framework of the proposed model in which features are integrated using a three-phase approach, i.e., (i) artifact reference map generation (ii) weight learning using linear regression and (iii) final saliency map generation.

In the first phase, more than one visually distinguishing feature maps are extracted from an image. In this proposed model, we have employed three features maps, *viz.* color spatial distribution, multi-scale contrast and center-surround histogram as suggested by Liu et al. [13]. A Gaussian image pyramid is employed for multi-scale contrasts which are linearly added to derive multi-scale contrast feature map. This is local feature that perseveres high-contrast boundaries (i.e., edges) while suppressing homogeneous regions. The center-surround histogram is regional features which significantly highlight salient object that is distinctive with its surroundings. This feature is calculated with the consideration of surroundings for salient object and measures the distinctiveness as the distance between histograms of RGB color of salient object and its surroundings. The global information of image is captured using color spatial distribution. Larger a color is scattered in the image, then it is less likely to be contained by salient object. Hence, the global spatial distribution of a certain color is utilized to compute saliency of regions. The spatial distribution of color can be calculated as spatial variance of the color. The Gaussian mixture model (GMM) is used statistically to describe all colors of image and assign all color belongingness probability to each pixel. Then, variance of each color is computed,

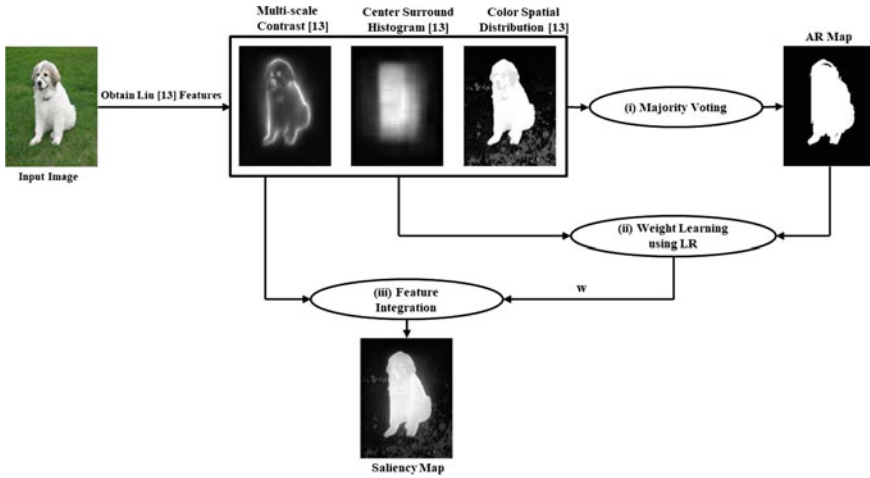


Fig. 1 A schematic representation of the proposed approach. Several features like color spatial distribution, center-surround histogram and multi-scale contrast are extracted using Liu [13] saliency method

and using these variances, color spatial distribution is calculated. Further, the color spatial distribution is refined by image center weight. These features are integrated into various disciplines such as linear summation and weighted linear summation. All these feature maps are combined using majority voting, and the resultant labeled map is termed as artifact reference (AR) map.

In phase two, linear regression (LR) is employed to learn the weights for combining initial feature maps. The AR map is used as the target map. Thus, instead of using human-annotated map of an image, our approach uses the estimated AR map. Hence, the proposed approach entails unsupervised learning mechanism and presents a novel unsupervised learning-based feature integration approach which learns integration weights for each image. In phase three, a final saliency map is found by combining the initial feature maps with corresponding weights learnt in the previous phase.

The architecture of the proposed feature integration approach is delineated in Fig. 1. First, the saliency method [13] is utilized to extract various features from the given input image. These features are incorporated with majority of vote process to obtain AR map. Further, features and AR map are fed into LR, and a set of weights (w) are learnt. Afterward, the features are linearly combined using w to generate final saliency map S . Next, we provide the mathematical formulation of the proposed approach.

3.1 Artifact Reference (AR) Map Generation

The feature maps of an image are obtained using Liu et al. [13] method. These feature maps are represented as a set of features $\mathbf{F} = \{\mathbf{F}_1, \mathbf{F}_2, \dots, \mathbf{F}_N\}$ where N is the number of feature maps. \mathbf{F} is transformed into a set of classified map in which pixel value is either 0 or 1. Suppose \mathbf{C}_i is the classified map corresponding to feature \mathbf{F}_i . Thus, all the classified map can be represented as $\mathbf{C} = \{\mathbf{C}_1, \mathbf{C}_2, \dots, \mathbf{C}_N\}$. The classified map is obtained using adaptive thresholding as suggested by Achanta et al. [1] where the threshold (T_i) for i -th feature map (\mathbf{F}_i) is computed as follows:

$$T_i = \frac{2}{I_w \times I_h} \sum_{x=1}^{I_w} \sum_{y=1}^{I_h} \mathbf{F}_i(x, y) \quad i = 1, 2, \dots, N \quad (1)$$

where I_w and I_h are width and height of the input image. Hence, classified map \mathbf{C}_i corresponding to feature \mathbf{F}_i is computed as follows:

$$\mathbf{C}_i(x, y) = \begin{cases} 1 & \text{if } \mathbf{F}_i(x, y) \geq T_i \\ 0 & \text{otherwise} \end{cases} \quad (2)$$

Here, (x, y) represents the location of the pixel under consideration such that $1 \leq x \leq I_w$ and $1 \leq y \leq I_h$.

Hence, the classified maps thus contain only two values, i.e., 1 and 0 where 1 denotes salient region and 0 denotes background region in a given image. Therefore, the classified map is annotated map which partitions the input image pixels into two parts. Further, we use these classified maps for generating artifact reference map. Since these classified maps have class labels, we apply the majority vote scheme to obtain a artifact reference map which is act like human annotation map in a better manner. To find the artifact reference map \mathbf{AR} for the input image, the following equation is used:

$$\mathbf{AR}(x, y) = \begin{cases} 1 & \text{if } \sum_{i=1}^N \mathbf{C}_i(x, y) > N/2 \\ 0 & \text{otherwise} \end{cases} \quad (3)$$

For proper working of the above equation, N must be an odd number. In this research work, we have chosen $N = 3$.

3.2 Weight Learning Using Linear Regression

Linear regression using gradient descent learns image-dependent weights for combination of various feature maps of an image. Each pixel value is described with the help of a set of features (i.e., color spatial distribution, multi-scale contrast and center-

surround histogram) given in Liu et al. [13] as a feature vector $\mathbf{x} = \{x_1, x_2, \dots, x_N\}$ where N is the number of features. Hence, the i -th feature of an image \mathbf{I} is represented as $\mathbf{A}_i = \{x_1(i), x_2(i), \dots, x_p(i)\}$, $i = 1, 2, \dots, N$, where $\mathbf{A}_i \in \mathbb{R}^p$ and $p = I_w \times I_h$. The set of features $\mathbf{A} = \{\mathbf{A}_1, \mathbf{A}_2, \dots, \mathbf{A}_N\}$, where $\mathbf{A} \in \mathbb{R}^{p \times N}$ and corresponding artifact reference (AR) map $\mathbf{Y} = \{y_1, y_2, \dots, y_p\}$, where $\mathbf{Y} \in \mathbb{R}^p$. The proposed linear regression is mathematically defined as follows:

$$\Phi : (\mathbb{R}^N | \mathbf{w}) \rightarrow \mathbb{R} \tag{4}$$

where $\mathbf{w} = \{w_1, w_2, \dots, w_{N+1}\}$ is set of image-dependent weights. Initially, \mathbf{w} is set to zero and is gradually adjusted during learning in order to reduce error between combined features output and the AR map. Consequently, the linear regression is obtained fitted weights which is further used from features combination task. The linear regression predicts pixel-wise output and is denoted as \hat{y}_j for j -th pixel in the given image and mathematically represented as:

$$\hat{y}_j = \Phi(\mathbf{x}_j | \mathbf{w}) \tag{5}$$

$$\Phi(\mathbf{x}_j | \mathbf{w}) = \sum_{\substack{i=1 \\ x_i \in \mathbf{x}_j}}^N w_i x_i + w_{N+1} \tag{6}$$

The linear regression predicts saliency map for an image as follows:

$$\Phi(\mathbf{A} | \mathbf{w}) = \{\Phi(\mathbf{x}_1 | \mathbf{w}), \Phi(\mathbf{x}_2 | \mathbf{w}), \dots, \Phi(\mathbf{x}_p | \mathbf{w})\} \tag{7}$$

$$\hat{\mathbf{Y}} = \Phi(\mathbf{A} | \mathbf{w}) \tag{8}$$

where $\hat{\mathbf{Y}}$ is predicted saliency map of the given image. Linear regression is utilized mean square error cost function between predicted saliency map $\hat{\mathbf{Y}}$ and AR map \mathbf{Y} to evaluate goodness of weights. The cost function $L(\mathbf{x}_j | \mathbf{w})$ gives the error between j -th pixel predicted output and its artifact reference value as given in Eq. 9:

$$L(\mathbf{x}_j | \mathbf{w}) = (y_j - \Phi(\mathbf{x}_j | \mathbf{w}))^2 \tag{9}$$

$$L(\mathbf{x}_j | \mathbf{w}) = (y_j - \hat{y}_j)^2 \tag{10}$$

Similarly, we can define the cost function for an input images as follows:

$$L(\mathbf{A} | \mathbf{w}) = \frac{1}{p} \sum_{j=1}^p (y_j - \hat{y}_j)^2 \tag{11}$$

Thus, our objective is to minimize the cost function $L(\mathbf{A} | \mathbf{w})$ whose solution is obtained using gradient descent algorithm.

3.3 Final Saliency Map Generation

The weight vector \mathbf{w} learnt for a specific image is used to integrate extracted features. The set of features \mathbf{A} and learnt weights are incorporated to compute final saliency map as weighted linear combination of features as follows:

$$\mathbf{S} = \sum_{i=1}^N w_i \mathbf{A}_i + w_{N+1} \quad (12)$$

Thereafter, the saliency map \mathbf{S} is normalized in the range of [0, 1] as follows:

$$\mathbf{S} = \frac{\mathbf{S} - \theta_{\min}(\mathbf{S})}{\theta_{\max}(\mathbf{S}) - \theta_{\min}(\mathbf{S})} \quad (13)$$

where θ_{\max} and θ_{\min} are operators which find maximum and minimum value from the input matrix, respectively.

4 Experimental Setup and Results

In this section, we discuss the experimental outcomes to analyze of the proposed feature integration approach across various state-of-the-art methods on two publicly available salient object datasets, i.e., ASD [1] and ECSSD [27]. ASD dataset is widely used dataset which contains 1000 natural images with variety of salient object from the MSRA-5000 saliency detection dataset [13]. ECSSD [27] dataset consists of 1000 images which shows diversity in terms of semantics and complexity constructed from the Web resources. The human annotations (i.e., ground truth labels) are obtained using five observers. Further illustrating the superiority of the proposed feature integration approach, its performance is compared with nine state-of-the-art saliency detection methods *viz.* Liu [13], SUN [29], SeR [21], CA [5], SEG [19], SIM [16], SP [12], SSD [11], LDS [4]. The validation is conducted in two different aspects: qualitative and quantitative.

The quantitative study is carried out with five performance measures, i.e., recall, precision, receiver operating characteristics (ROC), F-measure and area under the ROC curve(AUC), for validation of the proposed feature integration approach. Precision and recall are calculated by inferring an overlapped region of saliency map (\mathbf{S}) with human annotation, i.e., ground truth (\mathbf{G}). The strength of saliency methods as predicted salient regions are likely salient is depicted by precision. However, recall reveals the strength of methods in the form of completeness of real salient regions.

Besides, F-measure is illustrated as a weighted combination of precision and recall for comprehensive validation. All these metrics are mathematically represented as follows [2]:

$$\text{Precision} = \frac{|\mathbf{B} \cap \mathbf{G}|}{|\mathbf{B}|} \quad (14)$$

$$\text{Recall} = \frac{|\mathbf{B} \cap \mathbf{G}|}{|\mathbf{G}|} \quad (15)$$

$$F_{\beta} = \frac{(1 + \beta^2)\text{Precision} \times \text{Recall}}{\beta^2\text{Precision} + \text{Recall}} \quad (16)$$

where \mathbf{B} is a binary map corresponding to saliency map \mathbf{S} which is generated with the help of an adaptive threshold as reported in [1]. The operator $|\cdot|$ is used to find sum of ones in the binary map in the enclosed binary labeled matrix. The β is fixed with 0.3 during all the experiments as suggested in [1] to more emphasize on precision than recall. Further, ROC is delineated using false positive rate (FPR) and true positive rate (TPR) where false positive rate (FPR) and true positive rate (TPR) on the x-axis and y-axis in the plot, respectively. The TPR and FPR are computed using a sequence of thresholds which are varied between the range of [0, 1] with equal steps and formulated as follows [2]:

$$\text{TPR} = \frac{|\mathbf{B} \cap \mathbf{G}|}{|\mathbf{G}|} \quad (17)$$

$$\text{FPR} = \frac{|\mathbf{B} \cap \mathbf{N}|}{|\mathbf{N}|} \quad (18)$$

Another most widely used metric AUC is determined as the area covered beneath the ROC curve. The experimental parameters such as learning rate ($\alpha = 0.03$) and number of iterations ($I = 25$) which are used in LR for weight leaning are set empirically.

4.1 Performance Comparison with State-of-the-art Methods

We compare the proposed approach against nine state-of-the-art saliency methods qualitatively and quantitatively to illustrate the effectiveness of the proposed approach. Figure 2 demonstrates the qualitative performances of the proposed model and the compared well-performing state-of-the-art saliency methods. The columns (from left to right) show the first-third and fourth-sixth input images from ASD [1] and ECSSD [27] datasets, respectively.

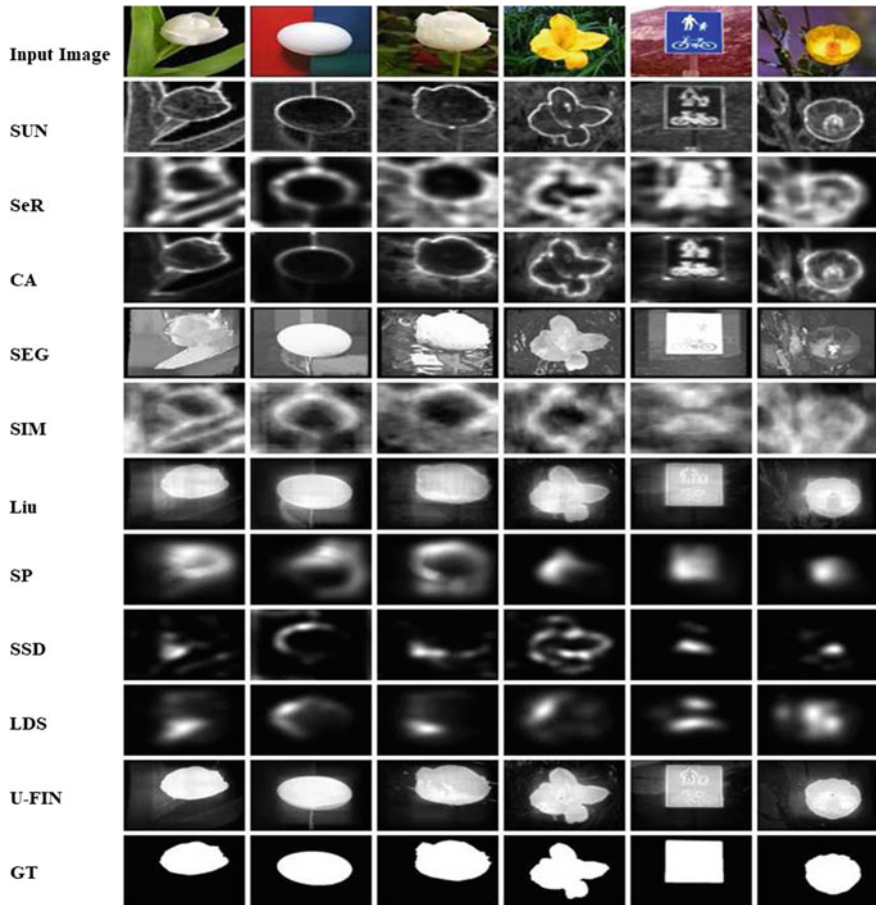


Fig. 2 Visual results of the proposed U-FIN approach with compared nine state-of-the-art methods on ASD [1] and ECSSD [27] datasets

These images represent different scenes such as single object, object near to image boundary and complex background. One can observe that some saliency methods such as SP [12], SSD [11], LDS [4], SIM [16] and SeR [21] fail to capture entire object even on simple image, e.g., fifth column. SUN [29] clearly detects the edge of object but fails to suppress background and highlights region inside object. However, Liu [13] and SEG [19] deliver better results on simple images, e.g., second and fifth columns, while fail to suppress background on complex structure images, e.g., first and sixth columns. In contrast, the proposed approach U-FIN performs uniformly on each of these images and clearly suppresses background in comparison with the second good performing saliency method, i.e., Liu [13] as shown in the first, third and sixth columns.

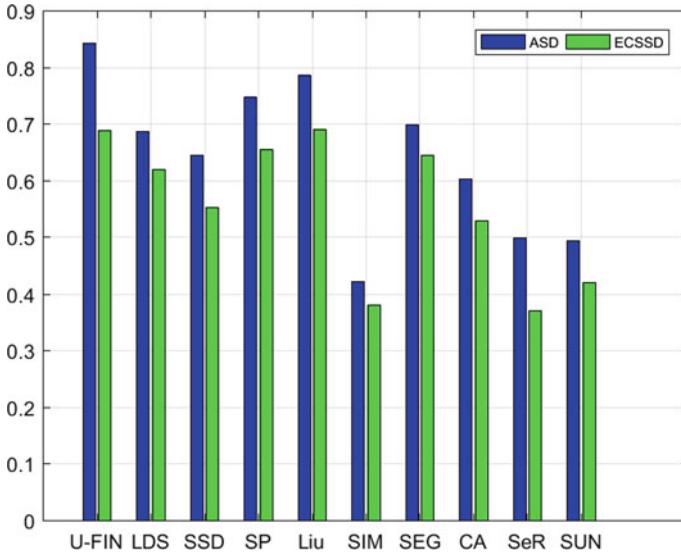


Fig. 3 Precision scores of the proposed U-FIN approach with compared nine state-of-the-art methods on ASD [1] and ECSSD [27] datasets

The quantitative analysis of the proposed U-FIN approach with compared state-of-the-art saliency detection methods in terms of *Precision*, *Recall*, *F-measure*, *AUC* and *ROC curve* is shown in Figs. 3, 4, 5, 6 and 7, respectively. It can be readily observed that on ASD [1] dataset, U-FIN outperforms compared state-of-the-art saliency detection methods. However, SIM [16] and SUN [29] are the worst performers in terms of F-measure, recall, precision, AUC and ROC curve, respectively. On ECSSD [27] dataset, U-FIN outperforms the other compared methods in terms of F-measures and equally performs with Liu [13] in terms of AUC and ROC curve. The proposed approach performs better than Liu et al. [13] in terms of recall, but LDS [4] is the best among the compared methods. In terms of precision, Liu [13] performs best, while the proposed method is comparable with the top performer.

4.2 Computational Time

The computational times of the proposed feature integration approach along with the compared saliency methods on the ASD [1] dataset are reported in Fig. 8. The dataset contains images whose size is 400×300 . The execution timings have been obtained on a desktop PC that configured with the following specification: Intel(R)Core(TM)i7-4770 CPU@3.40GHz. As shown in Fig. 8, the proposed feature

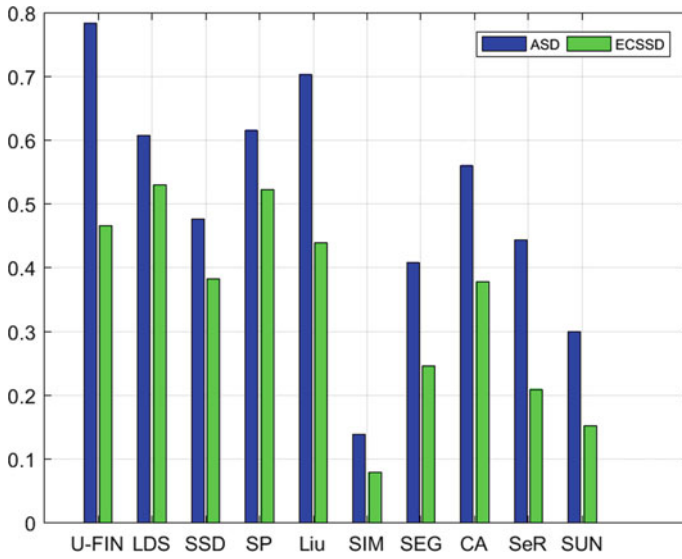


Fig. 4 Recall scores of the proposed U-FIN approach with compared nine state-of-the-art methods on ASD [1] and ECSSD [27] datasets

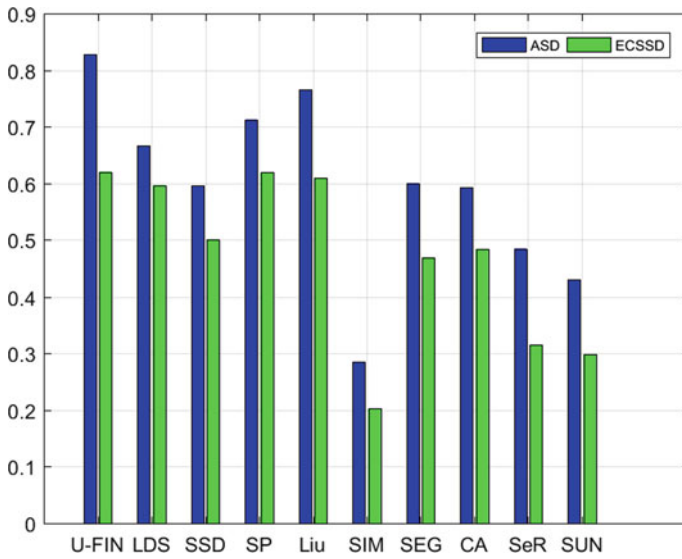


Fig. 5 F-measure scores the proposed U-FIN approach with compared nine state-of-the-art methods on ASD [1] and ECSSD [27] datasets

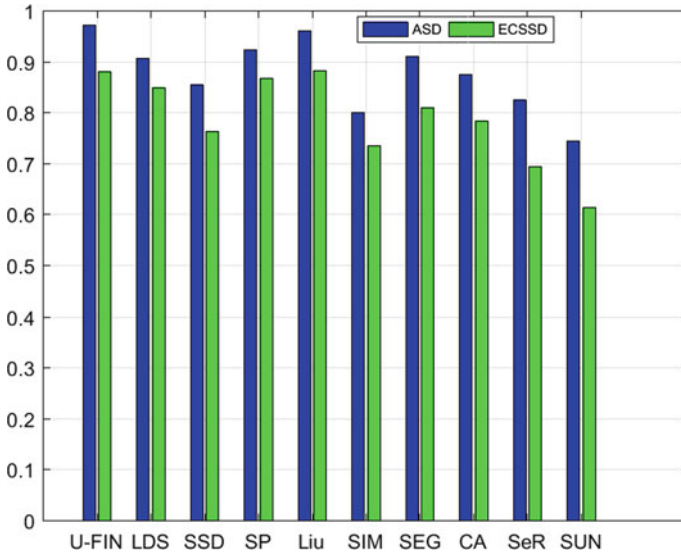


Fig. 6 AUC scores of the proposed U-FIN approach with compared nine state-of-the-art methods on ASD [1] and ECSSD [27] datasets

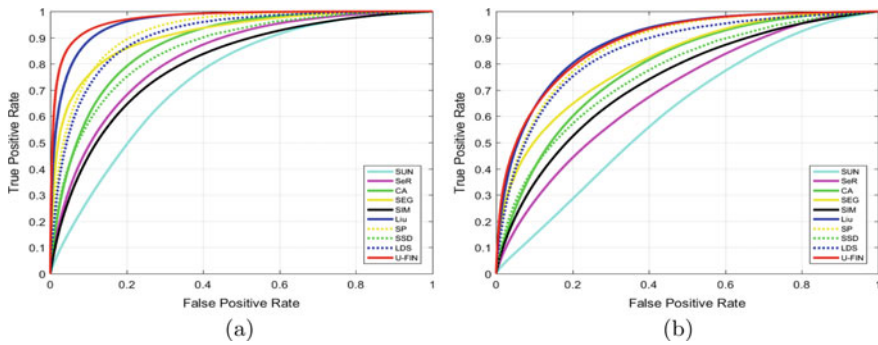


Fig. 7 ROC on the two widely used datasets: **a** ASD [1], **b** ECSSD [27]

integration approach is faster than CA [5], while SSD [11], LDS [4], SP [12], SeR [21] and SIM [16] are better than the proposed feature integration approach, and from other, it is comparable. Although the proposed method is computationally more expensive than several methods, the same can be mitigated with the improvement noticed in performance.

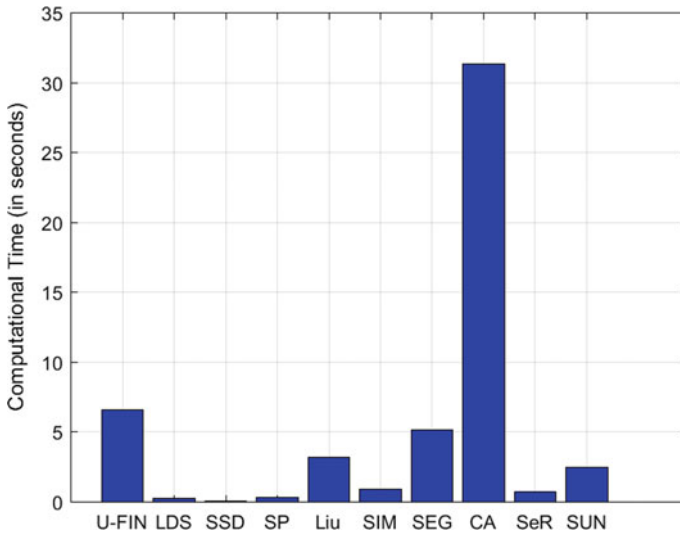


Fig. 8 Computational time analysis of the proposed U-FIN approach with compared nine state-of-the-art methods on ASD [1] dataset

5 Conclusion and Future Work

In this paper, we have presented a novel feature integration approach U-FIN in which image-dependent weights are learnt using linear integration of features extracted from the input image in an unsupervised manner. Initially, artifact reference (AR) map is produced from a set of features extracted from the image. This map assists in leaning the appropriate weights to combine specific image features. Further, linear regression (LR) model is built using gradient descent to learn weights for specific image features. Finally, these weights are used to linearly combine features to generate final saliency map. A comprehensive evaluation has been shown on two publicly available benchmark datasets, i.e., ASD and ECSSD, that show the effectiveness of the proposed U-FIN approach. It is also found that U-FIN is superior than nine state-of-the-art saliency methods on ASD dataset and comparable on ECSSD dataset. In our future work, we will extend the current feature integration approach with the selection of efficient feature maps and alternative feature integration approach(s).

References

1. Achanta R, Hemami S, Estrada F, Süsstrunk S (2009) Frequency-tuned salient region detection. In: IEEE international conference on computer vision and pattern recognition (CVPR 2009), No. conf, pp 1597–1604
2. Borji A, Cheng MM, Jiang H, Li J (2015) Salient object detection: a benchmark. *IEEE Trans Image Process* 24(12):5706–5722

3. Cheng MM (2011) Global contrast based salient region detection. In: Conference on computer vision and pattern recognition (CVPR), IEEE, pp 409–416
4. Fang S, Li J, Tian Y, Huang T, Chen X (2017) Learning discriminative subspaces on random contrasts for image saliency analysis. *IEEE Trans Neural Netw Learn Syst* 28(5):1095
5. Goferman S (2010) Context-aware saliency detection. In: Proceedings of IEEE conference computer vision and pattern recognition, pp 2376–2383
6. Guan W, Wang T, Qi J, Zhang L, Lu H (2018) Edge-aware convolution neural network based salient object detection. *IEEE Signal Processing Letters* 26(1):114–118
7. Han J, Ngan K, Li M, Zhang HJ (2006) Unsupervised extraction of visual attention objects in color images. *IEEE Transactions on Circuits and Systems for Video Technology* 16(1):141–145
8. Harel, J., Koch, C., Perona, P.: Graph-based visual saliency. In: Advances in neural information processing systems. pp. 545–552 (2007)
9. Itti L, Koch C, Niebur E (1998) A model of saliency-based visual attention for rapid scene analysis. *IEEE Transactions on Pattern Analysis & Machine Intelligence* 11:1254–1259
10. Koch C, Ullman S (1987) Shifts in selective visual attention: towards the underlying neural circuitry. *Matters of intelligence*. Springer, Berlin, pp 115–141
11. Li J, Duan LY, Chen X, Huang T, Tian Y (2015) Finding the secret of image saliency in the frequency domain. *IEEE Trans Pattern Anal Mach Intell* 37(12):2428–2440
12. Li J, Tian Y, Huang T (2014) Visual saliency with statistical priors. *Int J Comput Vis* 107(3):239–253
13. Liu T, Yuan Z, Sun J, Wang J, Zheng N, Tang X, Shum H (2011) Learning to detect a salient object. *IEEE Trans Pattern Anal Mach Intell* 33(2):353
14. Ma YF, Zhang HJ (2003) Contrast-based image attention analysis by using fuzzy growing. In: Proceedings of the eleventh ACM international conference on Multimedia. ACM, pp 374–381
15. Marat S, Guironnet M, Pellerin D (2007) Video summarization using a visual attention model. In: 2007 15th European signal processing conference. IEEE, pp 1784–1788
16. Murray N, Vanrell M, Otazu X, Parraga CA (2011) Saliency estimation using a non-parametric low-level vision model. In: 2011 IEEE conference on computer vision and pattern recognition (cvpr). IEEE, pp 433–440
17. Oliva A, Torralba A, Castelhana MS, Henderson JM (2003) Top-down control of visual attention in object detection. In: Proceedings 2003 international conference on image processing (Cat. No. 03CH37429), vol 1. IEEE, pp 1–253
18. Pan H, Wang B, Jiang H (2015) Deep learning for object saliency detection and image segmentation. arXiv preprint [arXiv:1505.01173](https://arxiv.org/abs/1505.01173)
19. Rahtu E, Kannala J, Salo M, Heikkilä J (2010) Segmenting salient objects from images and videos. In: Computer vision–ECCV 2010. Springer, pp 366–379
20. Ren Z, Gao S, Chia LT, Tsang IWH (2013) Region-based saliency detection and its application in object recognition. *IEEE Trans Circ Syst Video Technol* 24(5):769–779
21. Seo HJ, Milanfar P (2009) Static and space-time visual saliency detection by self-resemblance. *J Vis* 9(12):15–15
22. Treisman AM, Gelade G (1980) A feature-integration theory of attention. *Cogn Psychol* 12(1):97–136
23. Walther D, Koch C (2006) Modeling attention to salient proto-objects. *Neural Netw* 19(9):1395–1407
24. Wang L, Wang L, Lu H, Zhang P, Ruan X (2019) Salient object detection with recurrent fully convolutional networks. *IEEE Trans Pattern Anal Mach Intell* 41(7):1734
25. Wang L, Lu H, Ruan X, Yang MH (2015) Deep networks for saliency detection via local estimation and global search. In: Proceedings of the IEEE conference on computer vision and pattern recognition, pp 3183–3192
26. Wang Q, Lin J, Yuan Y (2016) Salient band selection for hyperspectral image classification via manifold ranking. *IEEE Trans Neural Netw Learn Syst* 27(6):1279–1289
27. Yan Q, Xu L, Shi J, Jia J (2013) Hierarchical saliency detection. In: Proceedings of the IEEE conference on computer vision and pattern recognition, pp 1155–1162

28. Zeng Y, Feng M, Lu H, Yang G, Borji A (2018) An unsupervised game-theoretic approach to saliency detection. *IEEE Trans Image Process* 27(9):4545–4554
29. Zhang L, Tong MH, Marks TK, Shan H, Cottrell GW (2008) Sun: a bayesian framework for saliency using natural statistics. *J Vis* 8(7):32–32
30. Zhang W, Wu QJ, Wang G, Yin H (2010) An adaptive computational model for salient object detection. *IEEE Transactions on Multimedia* 12(4):300–316
31. Zhao R, Ouyang W, Li H, Wang X (2015) Saliency detection by multi-context deep learning. In: *Proceedings of the IEEE conference on computer vision and pattern recognition*, pp 1265–1274
32. Zhou T, He X, Xie K, Fu K, Zhang J, Yang J (2015) Robust visual tracking via efficient manifold ranking with low-dimensional compressive features. *Pattern Recogn* 48(8):2459–2473

Input Image-Based Dictionary Formation in Super-Resolution for Online Image Streaming



Garima Pandey and Umesh Ghanekar

Abstract Real-time images are very much desirable in different real-life applications such as defense, medical, satellite, tv, Internet. Construction of relevant dictionary for the training of computer during the prediction of high-resolution image from low-resolution images in real-time requires high mathematical computations. This paper presents a new way of dictionary formation for learning-based super-resolution of real-time streaming of images. Here, the dictionary is formed with help of images that are similar to the input image in terms of structural similarity score. It helps in reducing memory requirement for the dictionary formation. Further, to speed up the process, a technique based on similarity score is proposed for updating of the dictionary. This involves the comparison of current image in the input sequence with the present reference image that was used for dictionary formation. Efficacy of the algorithm is shown through extensive simulations.

Keywords Sparse representation · Learning-based SISR · Online images

1 Introduction

In the world of technology, stipulation of high-quality images and videos for online applications is growing exponentially. High-resolution (HR) images are mostly required for either increasing the pictorial representation of images for human perception or for better understanding and information extraction by computers for automatic sagacity of machines. Accessibility of HR images is not an easy task due to the limitations of optical hardware imaging systems and sensors. One of the economical and propitious processes is to opt for software method like super-resolution

G. Pandey (✉) · U. Ghanekar
Department of Electronics and Communication Engineering,
National Institute of Technology, Kurukshetra, India
e-mail: garima_6160006@nitkkr.ac.in

U. Ghanekar
e-mail: ugnitk@nitkkr.ac.in

© Springer Nature Singapore Pte Ltd. 2021
G. S. Hura et al. (eds.), *Advances in Communication and Computational Technology*, Lecture Notes in Electrical Engineering 668,
https://doi.org/10.1007/978-981-15-5341-7_90

1189

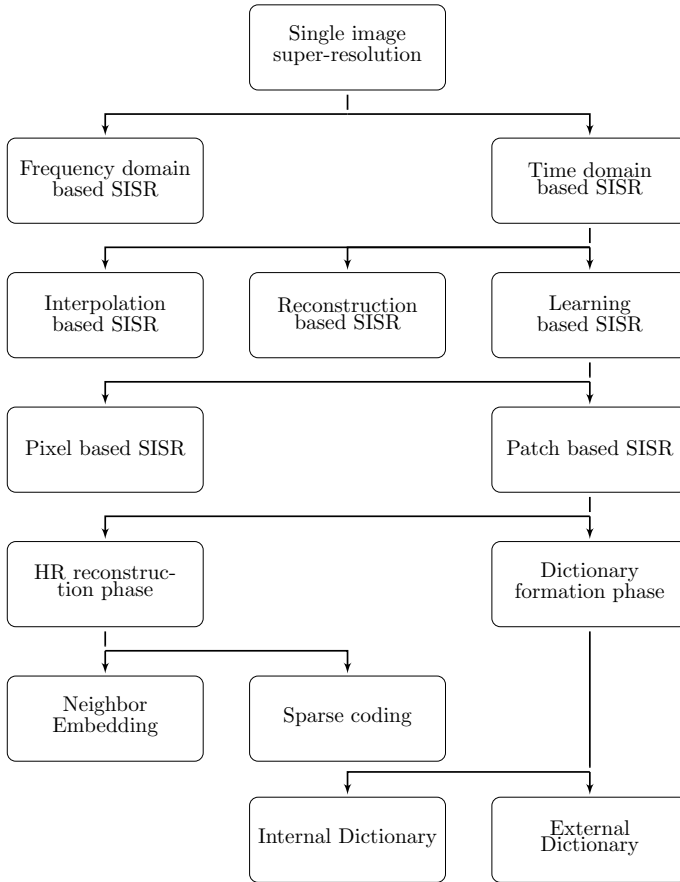


Fig. 1 Classification of existing SISR processes

(SR), instead of hardware improvements [1]. SR is one of the straightaway methods of increasing the resolution of low-resolution (LR) images by predicting the missing information. Since in SR process more than one HR image can be estimated from the same input image/images during reconstruction process, it is an ill-posed inverse process. Basic classification of existing SR processes [2, 3] is shown in Fig. 1. Along with images, SR process is also used in videos [4–6] which consist of image frames related to each other in terms of context contained in it. Additional benefits of SR are that it can be used with existing imaging system and are suitable for both offline and online applications.

In current time, learning-based techniques [7–14] are more prevalent in the field of super-resolution. It helps in capturing the probable co-occurrence of prior information between input LR and original HR image patches for HR image reconstruction. In this process, SR techniques mainly consist of two steps. In first step, machine is

trained by forming a dictionary/dictionaries and then, with the help of this dictionary/dictionaries along with input image, the HR image is estimated in second step. In this process, dictionary formation can be based on outside images, i.e., external dictionary formation, or the input image itself, i.e., internal dictionary formation. Normally, external dictionary is independent of input LR image and thus requires large memory space for its storage and increases the time complexity of the system. Dictionary size can be reduced by forming it with the help of images which are similar to input LR image.

In online processing of images, input image-dependent external dictionary formation is a very exhaustive and time-consuming process, and, image-independent external dictionary formation results in a huge dictionary size and poor performance. Thus, this research paper focuses on a variant of learning-based SISR technique for images streaming in real time. It involves input image-based external dictionary formation. Here, a new concept of updating the existing external dictionary has been introduced which involves comparing of the present input image in the streamline with the previously used reference image for the formation of dictionary. It uses the statistical parameters like structural similarity for comparing the input LR images. This helps in reducing the time complexity by lessing the updating of dictionary for very separate image. At the same time, since dictionary formation is dependent on input image, it requires less memory and has maximum textural variations with the minimum number of images in the training process.

Layout of rest of the paper is as follows. Section 2 consists the degradation model and problem formulation. Section 3 explains the algorithm proposed in this paper. Section 4 discusses the experimental setup, results, and comparison with some of the existing SISR algorithms. At last, conclusion is drawn in Sect. 5.

2 Degradation Model and Problem Formulation

First step for any SISR reconstruction is to formulate a degradation model for mathematical modeling of the SISR process.

2.1 Degradation Model for Mathematical Modeling

Images captured by the existing image acquisition system are normally of low quality due to the application of different degradation factors like rotation, mis-focuss, and noise addition. A simple observation model [1, 2] including degradation factors like rotation, averaging, downscaling, and noise addition is shown in Fig. 2.

Relationship shown in Fig. 2, between original HR image, i.e., H , and acquired LR image, i.e., L , is modeled mathematically in Eq. 1.

$$L = RADH + N \tag{1}$$

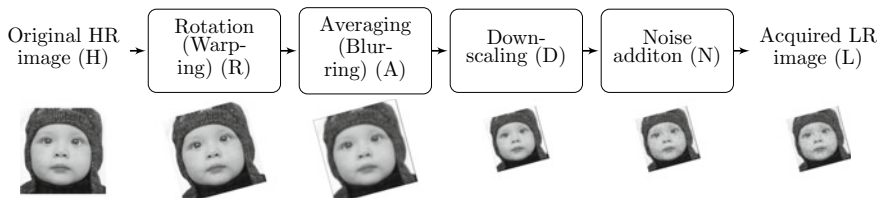


Fig. 2 Observation model for different degradation factors

Generally, only blurring and down-sampling are considered for SISR techniques evaluation. Thus, Eq. 1 is minimized to Eq. 2 by removing the rotation and noise addition factors.

$$L = ADH \tag{2}$$

2.2 Learning-Based SISR

Equation 2 discussed in 2.1 can be solved as optimization equation as shown in Eq. 3.

$$\min_H \|ADH - L\| \tag{3}$$

A general diagram showing the basics of learning-based SISR is given by Fig. 3. In learning-based techniques, machine is trained, which is further used for HR image reconstruction. Since SISR is an ill-posed inverse problem, image priors are used to restrict the possible solutions. It is incorporated in the mathematical equation in form of regularizer. Generalized solution is shown by Eq. 4. In this equation, λ is the Lagrangian multiplier and $\theta(O)$ is the prior.

$$\min_H \|ADH - L\|_2^2 + \lambda \cdot \theta(O) \tag{4}$$

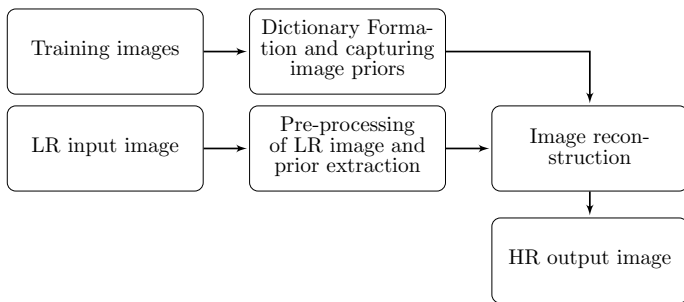


Fig. 3 Block diagram for SISR using image priors

2.2.1 Basic Concepts of Sparse Representation

Dictionary formation can be more compact by using of sparse representation of patch pairs instead of complete HR-LR patch pairs. Over-complete external dictionary E consisting of k atoms can be used to obtain co-occurrence priors. Here, a HR patch p_h and p_l can be represented with the help of sparse dictionary in the form of Eqs. 5 and 6, respectively.

$$p_h = E\beta_0 \quad \text{where } \beta_0 \text{ is a vector with few non zeros values} \quad (5)$$

$$p_l = Lp_h \quad \text{where } L \text{ is a projection matrix} \quad (6)$$

In this paper, sparse coding proposed in paper [7] is used for dictionary formation and HR image reconstruction.

3 The Proposed Algorithm

Learning-based SISR consists of two main steps for image reconstruction. Firstly, a dictionary is created for training of machine and secondly, HR image is created by optimizing a minimization equation. This method is for online streaming images on a machine. In this, an input image-based over-complete dictionary is formed. A generalized process is explained here.

1. For the input LR image, ten most similar images are taken from the image database that is used for training of machine. For similarity calculation, structural similarity index (SSIM) [15] is considered, which is given by Eq. 7. In this paper, training dataset consists of 100 images taken from [16], comprising LR-HR pairs.

$$\text{SSIM}(i, j) = \frac{(2\mu_i\mu_j + v_1)}{(\mu_i^2 + \mu_j^2 + v_1)} \quad (7)$$

2. The 3×3 overlapping patches from the selected LR and HR images are formed to form D_l and D_h as given in paper [7].
3. Here, dictionary is dependent on input images. Dictionary is updated for a better performance. For updating the dictionary, the present input LR image, i.e., q th, streaming in queue is compared with the previous reference image that was used for dictionary formation previously, i.e., (q_p) , on the basis of SSIM score given by Eq. 7. If the difference between score value of q th and (q_p) is less than threshold, i.e., t_h , then previously formed dictionary will be used for HR image reconstruction, and when the score value is greater than t_h , again dictionary formation will be done according to the process explained in point 3.
4. Once the dictionary is formed, HR image is reconstructed as explained in [7].

4 Experimental Results and Comparison

Usefulness of the method proposed in this paper is proved by performing experiments for images like Leena, Butterfly, Baby and Hat, which are taken from set5 and set14 [17], shown in Fig. 4. Peak signal-to-noise ratio (PSNR) and SSIM are used for quantitative comparisons, which are given by Eqs. 8 and 7, respectively.

$$\text{PSNR} = 10 \log_{10} \left(\frac{(\text{Maximum Pixel Value})^2}{\text{Mean Square Value}} \right) \quad (8)$$

Validation of the proposed algorithm is done for a LR image that is obtained by averaging a HR image by 3×3 block and down-sampling the obtained image by a factor of 3. All the experiments are performed on the luminance component, that is obtained by changing the format of image from 'RGB' to 'YCbCr'. Threshold value t_h is kept 0.05 for all the experiments. Experimental results, in terms of PSNR (dB) and SSIM, are shown in Table 1. Techniques used for comparison are bicubic interpolation, neighbor embedding (NE) [18], sparse coding (SC) [7], adaptive group-based sparse domain selection (AGBSDS) [14].



Fig. 4 Test images (from left to right): pepper, Plant, leena, butterfly

Table 1 Experimental results of different SISR techniques in terms of PSNR (dB) and SSIM for $D = 3$

Techniques	Images				Measuring parameters
	Pepper	Plant	Lenna	Butterfly	
Bicubic interpolation	22.72	25.25	21.20	26.95	PSNR
	0.78001	0.7355	0.7993	0.8035	SSIM
NE [18]	24.66	27.01	24.10	28.91	PSNR
	0.8134	0.8098	0.8386	0.8276	SSIM
SC [7]	27.00	28.36	26.94	28.99	PSNR
	0.8377	0.8432	0.8619	0.8605	SSIM
AGBSDS [14]	27.01	27.26	27.09	29.04	PSNR
	0.8404	0.8490	0.8704	0.8656	SSIM
Proposed method	27.35	27.36	27.03	29.37	PSNR
	0.8429	0.8507	0.8742	0.8661	SSIM



Fig. 5 Pictorial representation of different SISR techniques on 'Butterfly' (from top to bottom and left to right): LR input image, Bicubic interpolation, NE [18], SC [7], AGBSDS [14], Proposed method, original HR image

Figure 5 shows the pictorial representation of the HR images obtained by different techniques, along with LR image and original HR image. A zoomed area of 'Butterfly' image is used for visual comparison. Quantitative comparison shown in Table 4 and qualitative visual comparison shown in Fig. 5 confirm the superiority of the proposed method with a few other methods used in the present study. The proposed method works well for online images and is efficient in producing corresponding HR image for input LR image.

5 Conclusion

This paper consists of a learning-based SISR algorithm for online applications. Here, an external dictionary based on input images has been formed. It uses sparse coding for dictionary formation and HR image reconstruction. Here, during the streaming of images, dictionary is updated when the input image differs from the present reference image by a threshold value. SSIM is used for comparing the input images, which results in the global capturing of features. Input image-based dictionary formation helps in reducing the memory requirement and thus speed up the process. The efficacy of the proposed method is shown by the experimental results.

References

1. Park SC, Park MK, Kang MG (2003) Super-resolution image reconstruction: a technical overview. *IEEE Sign Process Mag* 3(20):21–36
2. Pandey G, Ghanekar U (2018) A compendious study of super-resolution techniques by single image. *Optik* 166:147–160. <https://doi.org/10.1016/j.ijleo.2018.03.103>
3. Pandey G, Ghanekar U (2019) Classification of priors and regularization techniques appurtenant to single image super-resolution. *Visual Comput.* <https://doi.org/10.1007/s00371-019-01729-z>
4. Kim SY, Bindu P (2016) Realizing real-time deep learning-based super-resolution applications on integrated GPUs. In: 15th IEEE international conference on machine learning and applications (ICMLA). <https://doi.org/10.1109/ICMLA.2016.0122>
5. Caballero J, Ledig C, Aitken A, Acosta A, Totz J, Wang Z, Shi W (2017) Real-Time video super-resolution with spatio-temporal networks and motion compensation. In: IEEE conference on computer vision and pattern recognition (CVPR). <https://doi.org/10.1109/CVPR.2017.304>
6. Hu J, Li H, Li Y (2014) Real time super resolution reconstruction for video stream based on GPU. In: IEEE international conference on orange technologies, pp 9–12
7. Yang J, Wright J, Huang TS, Ma Y (2010) Image super-resolution via sparse representation. *IEEE Trans Image Process* 19(11):2861–2873. <https://doi.org/10.1109/tip.2010.2050625>
8. Yang J, Wang Z, Lin Z, Cohen S, Huang T (2012) Coupled dictionary training for image super-resolution. *IEEE Trans Image Process* 21(8):3467–3478. <https://doi.org/10.1109/tip.2012.2192127>
9. Ahmed J, Shah MA (2016) Single image super-resolution by directionally structured coupled dictionary learning. *EURASIP J Image Video Process* 1(1). <https://doi.org/10.1186/s13640-016-0141-6>
10. Choi JS, Kim M (2017) Single image super-resolution using global regression based on multiple local linear mappings. *IEEE Trans Image Process* 3(26):1300–1314
11. Xu K, Wang X, Yang X, He S, Zhang Q, Huang T, Yin B, Wei X, Lau RWH (2018) Efficient image super-resolution integration. *Vis Comput* 34(6):1065–1076. <https://doi.org/10.1007/s00371-018-1554-2>
12. Wang Z, Liu D, Yang J, Han W, Huang T (2015) Deep networks for image super-resolution with sparse prior. In: 2015 IEEE international conference on computer vision. <https://doi.org/10.1109/iccv.2015.50>
13. Nam Y, Mun J, Jang Y, Kim J (2019) Single image super-resolution with self-similarity. In: IEEE international conference on consumer electronics (ICCE). <https://doi.org/10.1109/ICCE.2019.8662051>
14. Mikaeli E, Aghagolzadeh A, Azghani M (2018) Single image super resolution via adaptive group-based sparse domain selection. In: Iranian conference on electrical engineering (ICEE). <https://doi.org/10.1109/ICEE.2018.8472489>
15. Wang Z, Bovik A, Sheikh H, Simoncelli E (2004) Image quality assessment: from error visibility to structural similarity. *IEEE Trans Image Process* 4(13):600–612
16. Berkeley dataset. <https://www2.eecs.berkeley.edu>
17. Timofte R, De V, Gool LV (2013) Anchored neighborhood regression for fast example-based super-resolution. In: 2013 IEEE international conference on computer vision. <https://doi.org/10.1109/iccv.2013.241>
18. Chang H, Yeung DY, Xiong Y (2004) Super-resolution through neighbor embedding. In: Proceedings of the 2004 IEEE computer society conference on computer vision and pattern recognition (CVPR). <https://doi.org/10.1109/cvpr.2004.1315043>

Feature Selection Using Genetic Algorithm for Cancer Prediction System



Rupali, Rupali Verma, Rohit Handa, and Veena Puri

Abstract In healthcare sector, cancer is one of the most threatening and fast-growing diseases. The early diagnosis of this disease is very important as the success rate of its treatment depends upon how early and accurately it is diagnosed. The machine learning algorithms are helpful in detection and prediction of diseases. To improve efficiency of these algorithms, optimal features need to be selected. So, this research work uses genetic algorithm to select optimal features before applying k-nearest neighbor (KNN) and weighted k-nearest neighbor (WKNN) on Wisconsin Breast Cancer Prognosis dataset extracted from UCI repository. This approach helps in early prediction and the results show that WKNN performed better with 86.44% accuracy than KNN which gives 83.05% accuracy.

Keywords Genetic algorithm · Classification · K-nearest neighbor

1 Introduction

In recent years, the scope of data mining and machine learning has increased in the healthcare sector. These algorithms are widely used due to their ability to process huge datasets and extract meaningful insights from it. These insights provide vital information to make early diagnosis and predictions about various diseases which helps in providing proper treatment and care in advance.

Nowadays, cancer is emerging as a very fatal disease especially breast cancer which has higher possibility of recurrence. Breast cancer occurs when there is a type of mutation in cell or when cells in breast tissue involve unnecessary splitting and developing uncontrollably. It most probably occurs in middle-aged women and if not detected at initial stage, then it can increase uncontrollably, even leading to death.

Rupali (✉) · R. Verma · R. Handa
Punjab Engineering College (Deemed to be University), Chandigarh, India
e-mail: rupalibansal07@gmail.com

V. Puri
Centre for Systems Biology and Bioinformatics, Panjab University, Chandigarh, India

In 2017, about 252,710 cases of breast cancer are diagnosed among US women, out of which 40,610 died due to late diagnosis [1]. Therefore, it becomes critical to detect this disease as early as possible and with high accuracy. For this, advanced technologies like data mining and machine learning are used. Earlier these algorithms are only useful for cancer detection and diagnosis but now recent systems mainly focus on prediction and prognosis of cancer.

Data mining and machine learning uses advance models to make predictions by processing information from huge datasets which are beyond the scope of human capabilities. These algorithms have been used in detection and prediction of various diseases which includes diabetes [2], skin cancer [3], colon cancer [4], arrhythmia [5], breast cancer [6–10], heart disease [11], etc. The results of these studies show that the new emerging algorithms of data mining and machine learning can become a predictive tool for early detection and prediction of breast cancer.

The research work focuses on improving the accuracy of early prediction of breast cancer. Out of different feature selection methods [12], genetic algorithm is used with different mutation operators; k-nearest neighbor (KNN) and weighted KNN (WKNN) are used for classification. Based on the results, a comparative analysis of both the classification techniques is presented that showed WKNN performed better than traditional KNN algorithm. The dataset used in this study is Wisconsin Breast Cancer Prognosis dataset obtained from UCI machine learning repository.

The remaining part of paper is organized as follows: Section 2 presents review of work done in this field, Sect. 3 presents description of phases involved in proposed work, Sect. 4 represents the performance analysis of implementation and results, and finally, conclusion of the paper is drawn in Sect. 5.

2 Literature Review

Sakri et al. [9] have studied the performance of three algorithms Naive Bayes, k-nearest neighbor (KNN), and reduced error pruning tree (REP-Tree) with and without feature selection algorithm on Wisconsin Breast Cancer Prognostic Dataset. Particle swarm optimization algorithm (PSO) was used for feature selection algorithm. The results showed that with feature selection, performance of all algorithms was improved and Naive Bayes outperforms with accuracy 81.3% than REPTree (80%) and KNN (75%).

Mittal et al. [7] have studied the performance of KNN and k-means algorithm for the diagnosis on the breast cancer and cervical dataset. The study concluded that KNN performs better only for one value of k than k-means algorithm which is $k = 21$ close to square root of number of training data.

Pawlovsky et al. [8] have used genetic algorithm for selecting important components to increase the accuracy of KNN algorithm on UCI breast cancer prognosis dataset. The study used different mutation and crossover probabilities in genetic algorithm. The results indicate that by using only 16 components, the accuracy of KNN increases from 76 to 79%.

Walid Cherif [13] has used k-means clustering algorithm and reliability coefficients with k-nearest neighbor (KNN) algorithm. The results indicate that f-measure for the proposed approach was 94.1% which exceeds other approaches SVM (89.7%), Naive Bayes (92.2%), and KNN (91.1%). Artificial neural networks slightly performed better with 95.6% f-measure but time consumption was almost 2.2 times the proposed algorithm.

Kumari et al. [6] have studied three classifiers SVM, linear regression, and k-nearest neighbor (KNN) algorithm for prediction of breast cancer. To select most favorable features, Pearson's correlation coefficient was used. The outcome of study indicates that the KNN ($k = 10$) algorithm with accuracy 99.28% outperforms SVM and linear regression.

Ivancakova et al. [14] have used different classifier algorithms SVM, KNN, random forests, Naive Bayes, neural network, and C4.5 algorithm on breast cancer diagnosis dataset. The methodology applied was CRISP-DM. The author has used the under-sampling method for balancing the dataset and the results indicate that approach achieved highest accuracy with SVM-97.66%, random forest-97.37%, and C4.5-96.61%.

Amrane et al. [15] have used k-nearest neighbor (KNN) and Naive Bayes for prediction of breast cancer. The approach used value of $k = 3$ in KNN algorithm. The study indicates that k-nearest neighbor algorithm has performed better with accuracy 97.51% with lower error rate than Naive Bayes (96.19%).

Sharma et al. [10] have studied logistic regression, nearest neighbor, support vector machines using breast cancer diagnosis and prognosis dataset. The results showed that in case of diagnosis dataset, linear regression outperforms and in case of prognosis, SVM outperforms.

Irfan et al. [16] have used genetic algorithm with k-means to reduce time and to increase performance of algorithm. The results showed that by using genetic algorithm, time and number of iterations required for clustering using k-means were reduced and performance was increased.

Asri et al. [17] have studied the support vector machine (SVM), Naive Bayes (NB), decision tree (C4.5), and KNN for early prediction of breast cancer on WEKA tool. The results showed that SVM has best accuracy of 97.13%.

Al-Rajab et al. [4] have proposed three phase approach for cancer dataset. In first phase, different feature selection approaches were implemented out of which particle swarm optimization (PSO) performed better than other approaches. In next phase, SVM approach outperforms other classification algorithms without feature selection. In last phase, PSO with SVM outperforms other combinations of approaches. The results concluded that feature selection plays significant role before performing classification algorithms.

Ayyad et al. [18] have proposed modified version of k-nearest neighbor algorithm in two ways smallest modified KNN (SMKNN) and largest modified KNN (LMKNN) on gene expression cancer datasets. Before implementing these algorithms, optimal features are selected by information gain feature selection algorithm. The results indicated that the proposed technique achieved better results when compared with other standard techniques.

Zhang et al. [19] have proposed a new sigmoid weighted weighted KNN-based on sigmoid (WKS) classification algorithm performed on different UCI datasets. The algorithm WKS works on idea of AdaBoost algorithm which changes values of weight according to sigmoid function in training phase. The results showed that proposed WKS algorithm performed better than traditional KNN algorithm.

3 Proposed Work

The proposed work consists of several phases as depicted in Fig. 1. Initially, dataset is preprocessed and then feature selection using genetic algorithm with different mutation operators is performed. The selected features are fed to the KNN and WKNN classifiers. In the last phase, results of classifiers are analyzed.

The main phases are import dataset, data preprocessing, feature selection, classification, and performance evaluation. Description of these phases is given below:

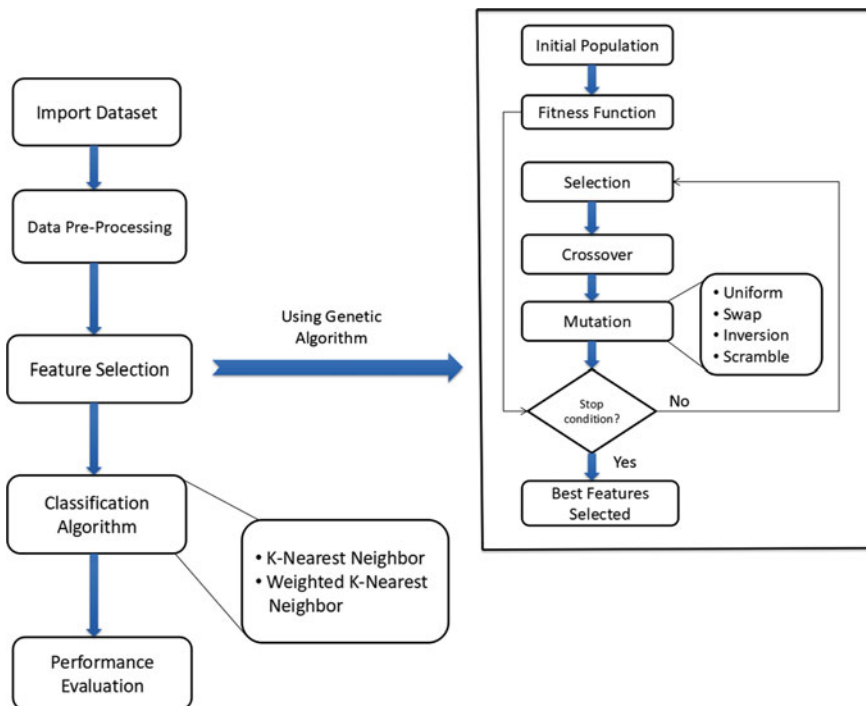


Fig. 1 Proposed work

Fig. 2 Attributes of dataset

S No.	Attribute
1	ID Number
2	Outcome (N = Non-Recur, R = Recur)
3	Time (recurrence time if field 2 = R, disease-free time if field 2 = N)
4 : 33	Mean, standard error, and "worst" or largest of 10 features :- radius, texture, perimeter, area, smoothness, compactness, concavity, concave points, symmetry and fractal dimension resulting in 30 features.
34	Tumor Size
35	Lymph Node Status

3.1 Import Dataset

The study uses Wisconsin Breast Cancer Prognosis Dataset obtained from UCI repository database [20]. The dataset contains 198 instances and 35 attributes description of which are given in Fig. 2. It contains one output variable which has 151 non-recur and 47 recur cases. There are four missing values in lymph node status attribute. This raw dataset is imported into RStudio.

3.2 Data Preprocessing

The dataset must contain appropriate values as it directly affects the prediction results of algorithms. So, initially, preprocessing is done to remove the missing values from dataset and further normalization [4] is done to use values of dataset on common scale by using min-max formula using (1):

$$X_{norm} = \frac{X - X_{min}}{X_{max} - X_{min}} \tag{1}$$

3.3 Feature Selection

To eliminate redundant and insignificant features, genetic algorithm (GA) is applied to choose appropriate features and reduces dimensionality of dataset. In this study, the genetic algorithm uses different mutation operators to have diversity in population and avoid local minima.

Genetic Algorithm: The structural outline of GA is illustrated in Fig. 1 and detailed description is given below:

Fig. 3 Genetic parameters

Parameter	Method or Value
Population Size	50
No. of Generations	10
Selection Method	Tournament
Crossover Function	Single point
Crossover Probability	0.8
Mutation Probability	0.1
Elite Count	2

1. **Initial Population:** The algorithm starts with initializing population that provide encoded solutions. In this study, genetic algorithm initializes population randomly in form of binary chromosomes. The number of attributes (33, 2 attributes are excluded ID and class label) represents length of chromosome. The binary bits 0 and 1 represent exclusion and inclusion of features, respectively.
2. **Fitness Function:** This function is used to evaluate the fitness of each member of population. On basis of fitness values, best-fitted members will be used to reproduce using selection, crossover, and mutation operators. In this research work, the RStudio is used for implementation. In RStudio, three functions rfGA, caretGA, and treebagGA are available out of which rfGA function is used in this work as it takes less time to run genetic algorithm than others. rfGA internally uses random forest algorithm. The smallest fitness of member is picked as best solution by GA. After evaluating fitness values, new population is created by using efficient selection, crossover, and mutation methods. Figure 3 summarizes the GA parameters utilized in this study. In order to determine these parameters, proper analysis is carried out by altering one parameter at a time while keeping other values constant.
3. **Selection:** After evaluating fitness function, selection operator is used for reproduction. The commonly used methods are Roulette wheel selection, tournament selection, rank selection, and hierarchical selection. The study uses tournament selection to choose best chromosome. In this method, any k number of chromosomes is taken and tournament is used to select the fitted chromosome. The value $k = 3$ is considered in this work.
4. **Crossover:** Crossover operator is used to create new chromosomes from existing one by exchanging the part of their chromosomes known as genes. Most common types of chromosomes used are uniform, single-point, two-point crossover. In this study, single-point crossover is used.
5. **Mutation:** This operator provides diversity in search space and avoid local minima by making changes in genes of population. This work uses different mutation operators described below:
 - (a) **Uniform:** Uniform operator randomly selects one position of chromosome and changes the value of gene from 0 to 1 and 1 to 0 as shown in Fig. 4.

Fig. 4 Uniform mutation

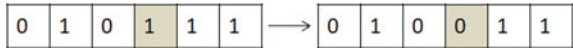


Fig. 5 Inversion mutation

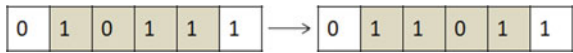


Fig. 6 Swap mutation

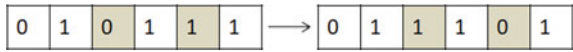


Fig. 7 Scramble mutation



- (b) **Inversion:** Inversion operator takes two positions of genes randomly and invert the values of whole string between these positions as shown in Fig. 5.
 - (c) **Swap:** Swap operator chooses two positions of genes randomly and exchanges the values of these genes as shown in Fig. 6.
 - (d) **Scramble:** Like inversion operator, scramble operator selects two positions of genes and the values between these positions are randomly shuffled as shown in Fig. 7.
6. **Elitism:** Elitism ensures that best-fitted members will be passed to next generation. To balance diversity and avoid over-fitting problem, small value of elitism is used. In our implementation, value of elite is 2 means best two fitted chromosomes will be copied to next generation.
 7. **Termination:** When best solution is obtained or number of generations is reached, termination condition is satisfied. The study uses ten number of generations.

3.4 Classification

After feature selection phase, k-nearest neighbor (KNN), and weighted KNN (WKNN) algorithms are used for classification. The detailed description of algorithms is given below:

K-Nearest Neighbor (KNN): KNN is simple, non-parametric and lazy learning algorithm which provides high predictive power. The algorithm finds k closest neighbors by using different distance metrics and then classify new instance into class with majority voting. There is no proper training phase in KNN, and all is done in testing phase. Generally, KNN uses only odd values of k if number of classes is 2. In this work, first divide the dataset into training and testing part in the ratio of 70:30 and then perform KNN. The pseudo code of KNN is presented in Table 1.

Weighted K-Nearest Neighbor (WKNN): Weighted KNN is the extension of k-nearest neighbor algorithm. This algorithm classifies data by using weighted majority

Table 1 Pseudo code of KNN algorithm

<p>Input :-</p> <ul style="list-style-type: none"> - Input training data of n samples $S=\{x_i, a_i\}$ where x_i is sample, a_i is class label and $i=1$ to n. - Input testing data of m samples $T=\{y_j\}$ where y_m is test sample and $j=1$ to m. <p>Output :- Classify testing data as non-recur and recur.</p> <p>KNN(x, y, a) for each sample $y \in T$ do { initialize odd values of k from 1 to 50 compute distance between testing sample and all training samples using Euclidean distance formula (2):-</p> $d(x_i, y) = \sqrt{\sum_{i=1}^t (y_t - x_t)^2} \quad \text{where } t = \text{no. of attributes} \quad (2)$ <p>sort the distances in ascending order select k nearest samples from training data with k minimum distances denoted by $Z=\{x_k, a_k\}$ return class of testing sample using majority voting from selected a_k class labels }</p>
--

voting. The main problem in KNN is that it is very sensitive to k value. KNN uses only odd values for even number of classes. But WKNN uses both odd and even values which results in improving the efficiency of algorithm. WKNN depends on weights rather than only distance value for which different kernels is used. The study uses following kernels [21] to compute weights:

1. Gaussian = $\frac{\sqrt{1} \exp(-D^2)}{2\pi \cdot \frac{2}{2}}$
2. Triangular = $(1 - |D|) \cdot I(|D| \leq 1)$
3. Rectangular = $\frac{1}{2} I(|D| \leq 1)$
4. Inversion(Inv) = $\frac{1}{|D|}$
5. Epanechnikov = $\frac{3}{4}(1 - D^2) \cdot I(|D| \leq 1)$.

Initially, divide the dataset into training and testing part in the ratio of 70:30 and then performs WKNN. The pseudo code of WKNN is presented in Table 2.

3.5 Performance Evaluation

In this phase, the performance of KNN and WKNN algorithm is evaluated and comparative analysis is done by using metrics accuracy, sensitivity, specificity, positive predicted value, negative predicted value, error rate, and f-measure.

Table 2 Pseudo code of weighted KNN algorithm

```

Input :-
    - Input training data of n samples  $S=\{x_i, a_i\}$  where  $x_i$  is sample,  $a_i$  is class label and  $i= 1$  to  $n$ .
    - Input testing data of m samples  $T=\{y_j\}$  where  $y_j$  is test sample and  $j=1$  to  $m$ .

Output :- Classify testing data as non-recur and recur.

WKNN(x, y, a)
for each sample  $y \in T$  do
{
initialize value of  $k$  from 1 to 50
compute distance between testing sample and all training samples using Euclidean distance formula (3):-


$$d(x,y) = \sqrt{\sum_{i=1}^t (y_i - x_i)^2} \quad \text{where } t = \text{no. of attributes} \quad (3)$$


sort the distances in ascending order
standardize the distance of  $k$ -nearest neighbors with distance of  $(k+1)$  neighbor using formula (4):-


$$D_l = d(x_l, y) = \frac{d(x_l, y)}{d(x, x_{k+1})} \quad \text{where } l = 1 \text{ to } k \quad (4)$$


compute weights with kernel functions applied on distances  $D_l$  by using  $w_l = K(D_l)$ 
return class of testing sample by using weighted majority voting of summed kernel densities of  $k$ -nearest neighbors
}
    
```

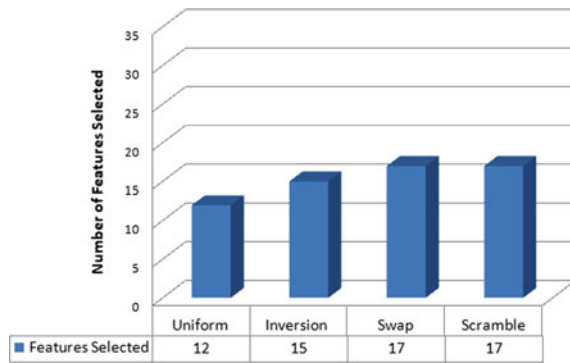
4 Implementation and Results

For implementation, an open source integrated development environment (IDE) RStudio is used where R programming can be used. This tool provides advantage of utilizing inbuilt packages which enable parallel execution of code. For example, the proposed work uses caret package where gafs function uses parallel execution of genetic algorithm.

The study uses breast cancer dataset which contains 35 features out of which two features ID number and class variable are removed for preprocessing. After preprocessing the dataset, genetic algorithm is implemented by using parameter values listed in Fig. 3. Figure 8 displays different number of features selected for different mutation operators. It shows that uniform operator selects the minimum number of features whereas swap and scramble operators select the maximum number of features.

When relevant features are selected, classification algorithms, KNN and WKNN are performed. Firstly, data is divided into training and testing part in ratio of 70:30.

Fig. 8 Number of features selected by using different mutation operators in genetic algorithm



In KNN, k-nearest samples from training data are selected when new sample of testing data is to be classified based on Euclidean distance. Further, classify samples of testing data using majority voting. In this, values of $k = 1-50$ are considered and finally, for k value which has highest accuracy of prediction is chosen. In WKNN, the model is trained using different kernels on training data. The kernel and k value which has minimum classification error are selected. The kernel and k values selected for uniform, inversion, swap, and scramble operators using WKNN are shown in Figs. 9, 10, 11 and 12, respectively. By using selected kernel and k values, testing part is done to measure accuracy of model.

Finally, the performance of both classification models KNN and WKNN is analyzed by using confusion matrix which contains results, namely true positive (TP), true negative (TN), false positive (FP), and false negative (FN) resulting in various metrics given in Fig. 13.

The results and comparison analysis of classifiers KNN and WKNN are shown in Table 3. In this analysis, the evaluation of three metrics accuracy, sensitivity, and specificity is performed.

Fig. 9 Best kernel and k value for testing data using WKNN for uniform operator

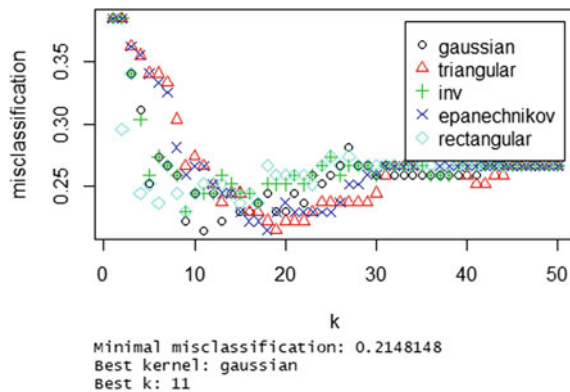


Fig. 10 Best kernel and k value for testing data using WKNN for inversion operator

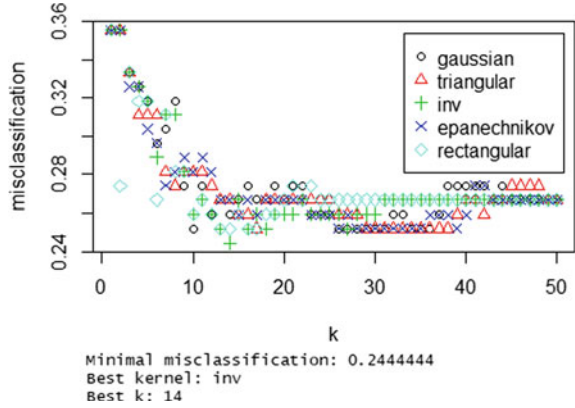


Fig. 11 Best kernel and k value for testing data using WKNN for swap operator

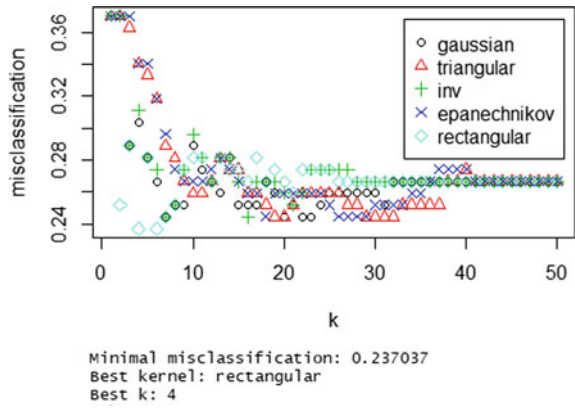
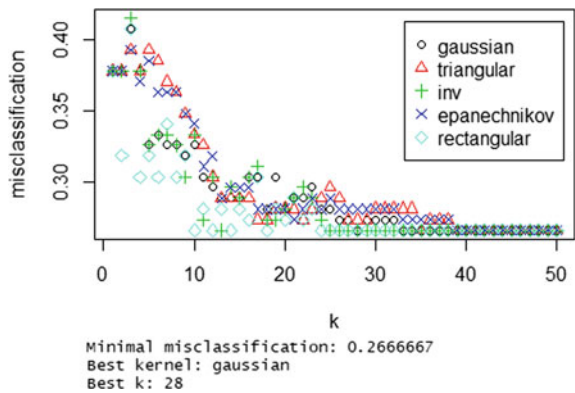


Fig. 12 Best kernel and k value for testing data using WKNN for scramble operator



$$Accuracy = \frac{TP + TN}{TP + FN + FP + TN}$$

$$Sensitivity (Recall) = \frac{TP}{TP + FN}$$

$$Specificity = \frac{TN}{FP + TN}$$

$$Positive Predicted Value (Precision) = \frac{TP}{TP + FP}$$

$$Negative Predicted Value = \frac{TN}{TN + FN}$$

$$F - Measure = 2 * \frac{Precision * Recall}{Precision + Recall}$$

$$Error Rate = \frac{FP + FN}{TP + TN + FP + FN}$$

Fig. 13 Performance metrics**Table 3** Evaluation metrics of KNN and WKNN

Mutation operator	Metric	KNN (K)	WKNN (W)	Gain (W-K)
Uniform	Accuracy	0.8305	0.8644	0.0339
	Sensitivity	0.8333	0.8868	0.0535
	Specificity	0.8000	0.6667	–
Inversion	Accuracy	0.8136	0.8305	0.0169
	Sensitivity	0.8571	0.8545	–
	Specificity	0.6000	0.5000	–
Swap	Accuracy	0.8305	0.8644	0.0339
	Sensitivity	0.8333	0.9020	0.0687
	Specificity	0.8000	0.6250	–
Scramble	Accuracy	0.7966	0.8475	0.0509
	Sensitivity	0.8269	0.8448	0.0179
	Specificity	0.5714	1.0000	0.4286

The evaluation metrics shown in Table 3 indicates that WKNN has higher accuracy as compared to KNN for all the mutation operators. It has highest accuracy of 86.44% for uniform and swap operator. WKNN has highest sensitivity of 90.2% for swap operator. It has higher sensitivity compared to KNN for uniform, swap, and scramble operators but has lower value for inversion operator. WKNN has lower specificity as compared to KNN for uniform, inversion, and swap operator with minimum value of 50% for inversion operator. Further, the graphical representations of achieved results of KNN and WKNN are depicted in Fig. 14.

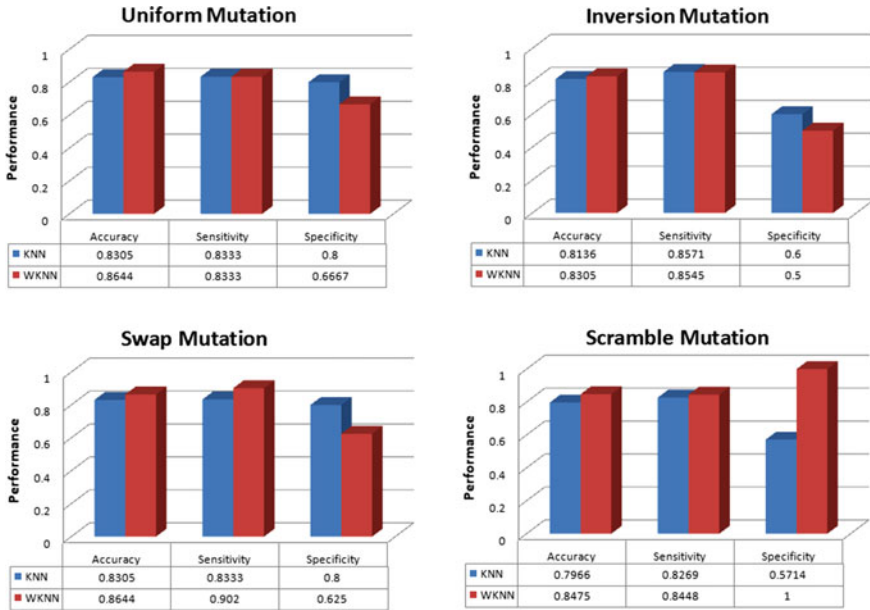


Fig. 14 Comparison of performance metrics of KNN and WKNN for all mutation operators

The detailed statistics of KNN and WKNN with all mutation operators are illustrated in Table 4, with various performance metrics.

The evaluation metrics in Table 4 depicts that WKNN has higher precision value as compared to KNN for inversion and scramble operators. It also showed that WKNN has lower error rate than KNN for all mutation operators. The classifier WKNN has lower negative predicted value for inversion and scramble operators.

The average f-measure for WKNN has higher value when compared to KNN for all operators.

Table 4 Detailed statistics of KNN and WKNN for all mutation operators

Metric	Classifier	Mutation operators			
		Uniform	Inversion	Swap	Scramble
Positive-predicted value (precision)	KNN	0.9783	0.9130	0.9783	0.9348
	WKNN	0.9592	0.9592	0.9388	1.0000
Negative-predicted value	KNN	0.3077	0.4615	0.3077	0.3077
	WKNN	0.4000	0.2000	0.5000	0.1000
Error rate	KNN	0.1695	0.1864	0.1695	0.2034
	WKNN	0.1356	0.1695	0.1395	0.1525
F-measure	KNN	0.8999	0.8841	0.8999	0.8775
	WKNN	0.9215	0.9038	0.9200	0.9158

Further, the graphical representation of performance metrics of KNN and WKNN with all mutation operators is depicted in Figs. 15 and 16, respectively. The graph shows the comparison analysis of all performance metrics between all mutation operators with KNN and WKNN.

The comparative analysis presented in Fig. 15 shows that KNN with uniform and swap operator performs better than inversion and scramble operators. Similarly, Fig. 16 depicts that WKNN gives better results with uniform and swap operators.

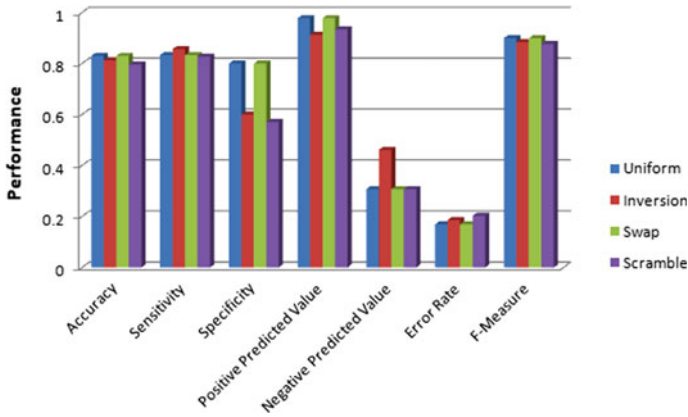


Fig. 15 Performance comparison of KNN with all mutation operators

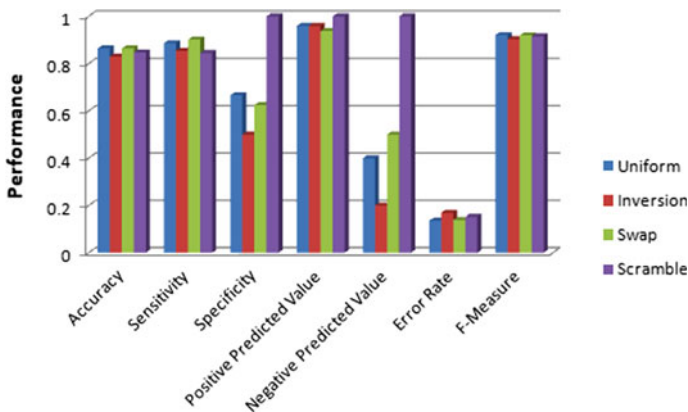


Fig. 16 Performance comparison of WKNN with all mutation operators

5 Conclusion

In healthcare domain, there is need to propose a system for early detection and prediction which can be developed by using machine learning algorithms with high accuracy so that proper treatment can be taken on time. In this work, the study has implemented genetic algorithm with different mutation operators, KNN, and weighted KNN algorithm in order to diagnose breast cancer. This work initially used genetic algorithm to select optimal features and further KNN algorithm is used for classification. In KNN, choosing value of k is very tricky and wrong value can decline efficiency of algorithm. Generally, KNN uses only odd values of k for binary classification. Further, when weighted KNN is implemented with different kernels and k values, the results showed that it has significantly performed better than KNN algorithm. To conclude, by selecting significant features, choosing appropriate value of k and classifying on the basis of weights enhance the performance of traditional KNN algorithm.

References

1. <https://www.cancer.org/research/cancer-facts-statistics/breast-cancer-facts-figures.html>. Accessed 07 Nov 2018
2. Bhatia K, Syal R (2017) Predictive analysis using hybrid clustering in diabetes diagnosis. In: 2017 Recent developments in control, automation and power engineering (RDCAPE), pp 447–452. IEEE
3. Srividya T, Arulmozhi V (2018) Feature selection classification of skin cancer using genetic algorithm. In: 2018 3rd International conference on communication and electronics systems (ICCES), pp 412–417. IEEE
4. Al-Rajab M, Lu J, Xu Q (2017) Examining applying high performance genetic data feature selection and classification algorithms for colon cancer diagnosis. *Comput Methods Programs Biomed* 146:11–24
5. Jung WH, Lee SG (2017) An arrhythmia classification method in utilizing the weighted knn and the fitness rule. *IRBM* 38(3):138–148
6. Kumari M, Singh V (2018) Breast cancer prediction system. *Procedia Comput Sci* 132:371–376
7. Mittal, K, Aggarwal G, Mahajan P, Performance study of k-nearest neighbor classifier and k-means clustering for predicting the diagnostic accuracy. *Int J Inf Technol* 1–6
8. Pawlovsky AP, Matsuhashi H, Orozco P, Montoya Y, Bustamante J, Mayorga P, Chavez G, Druzgalski C, Zeljkovic V, Valdez J (2017) The use of a novel genetic algorithm in component selection for a knn method for breast cancer prognosis. In: IEEE global medical engineering physics exchanges/pan american health care exchanges, pp 1–5
9. Sakri S, Rashid NA, Zain ZM (2018) Particle swarm optimization feature selection for breast cancer recurrence prediction. *IEEE Access*
10. Sharma A, Kulshrestha S, Daniel S (2017) Machine learning approaches for breast cancer diagnosis and prognosis. In: 2017 International conference on soft computing and its engineering applications (icSoftComp), pp 1–5. IEEE (2017)
11. Pawlovsky AP (2018) An ensemble based on distances for a knn method for heart disease diagnosis. In: 2018 International conference on electronics, information, and communication (ICEIC). pp. 1–4. IEEE (2018)
12. Jain D, Singh V (2018) Feature selection and classification systems for chronic disease prediction: a review. *Egyptian Inf J* 19(3):179–189

13. Cherif W (2018) Optimization of k-nn algorithm by clustering and reliability coefficients: application to breast-cancer diagnosis. *Procedia Comput Sci* 127:293–299
14. Ivančáková J, Babič, F, Butka P (2018) Comparison of different machine learning methods on wisconsin dataset. In: 2018 IEEE 16th World symposium on applied machine intelligence and informatics (SAMI), pp 000173–000178. IEEE
15. Amrane M, Oukid S, Gagaoua I, EnsarI T (2018) Breast cancer classification using machine learning. In: 2018 Electric electronics, computer science, biomedical engineerings' meeting (EBBT), pp 1–4. IEEE
16. Irfan S, Dwivedi G, Ghosh S (2017) Optimization of k-means clustering using genetic algorithm. In: 2017 International conference on computing and communication technologies for smart nation (IC3TSN), pp 156–161. IEEE
17. Asri H, Mousannif H, Al Moatassime H, Noel T (2016) Using machine learning algorithms for breast cancer risk prediction and diagnosis. *Procedia Comput Sci* 83:1064–1069
18. Ayyad SM, Saleh AI, Labib LM (2019) Gene expression cancer classification using modified k-nearest neighbors technique. *Biosystems* 176:41–51
19. Zhang M, Qi M, Sun K, Niu Y, Shi L (2017) A new classification algorithm wks based on weight. In: 2017 IEEE 19th international conference on e-health networking, applications and services (Healthcom), pp 1–4. IEEE
20. Uci breast cancer prognosis dataset. <https://archive.ics.uci.edu/ml/machine-learning-databases/breast-cancer-wisconsin/>. Accessed 27 Nov 2018
21. Hechenbichler K, Schliep K (2004) Weighted k-nearest-neighbor techniques and ordinal classification

A Hybrid Approach for Diabetes Prediction and Risk Analysis Using Data Mining



Bhavna, Rupali Verma, Rohit Handa, and Veena Puri

Abstract With the increase in patients suffering from diabetes, early detection and prediction of diabetes are the major area of concern. In this study, we propose a hybrid model using data mining techniques to analyze the available data to predict the occurrence of diabetes. This model is a combination of cluster and class-based approach which uses K-means and weighted K-means for clustering and logistic regression for classification. K-means is a simple and widely used technique, but it is highly sensitive toward initial centroids and outliers which further affect the prediction accuracy of logistic regression. The aim is to determine a way to improve the initial centroid selection for K-means and retain maximum original dataset to enhance the performance of logistic regression. Results show that accuracy of the classification model using K-means and weighted K-means is 96.97% and 97.84%, respectively. Further, using the classification results, this paper analyzes the risk associated with diabetic and non-diabetic patients.

Keywords Data mining · K-means clustering · Weighted K-means clustering · Logistic regression

1 Introduction

With the ever-increasing data in every field, specifically in healthcare sector, there is a need to utilize the obtained information in a productive way. Focusing on usage and advantages of various technologies and their applications, they can result in refined patient data analysis and better overall healthcare predictions. These technologies and platforms can provide provisions for improved solutions, individual health plans and development of clinical support systems.

Bhavna (✉) · R. Verma · R. Handa
Punjab Engineering College (Deemed to be University), Chandigarh, India
e-mail: bansal.bhavna14@gmail.com

V. Puri
Centre for Systems Biology and Bioinformatics, Panjab University, Chandigarh, India

Nowadays, there has been an extensive increase in the number of diabetic patients. According to WHO report, about 69 million people in India were diagnosed with diabetes in 2015 [1]. It is estimated that this count will rise to 98 million by the end of 2030. Diabetes is caused due to high rise in blood sugar level. The most common types of diabetes are Type 1, Type 2 and gestational diabetes [2]. Type 1 diabetes is caused when the human body is not able to generate sufficient amount of insulin. In type 2 diabetes, the body is unable to make proper use of produced insulin. Gestational diabetes develops in pregnant women and in most cases goes away after the birth of baby, but they are highly prone to type 2 later on. In order to identify the high risk patients, advanced technologies can be used. The emerging technologies play a pivotal role in addressing these challenges, and data mining proves to be an appropriate field.

Data mining analyzes the data to obtain connections and find patterns within the data, and using them, predictions can be made or the recent trends can be uncovered and analyzed [3]. They are broadly categorized into predictive and descriptive techniques. The predictive techniques have been implemented to obtain the results regarding breast cancer, heart disease and diabetes to analyze the current status and make future predictions regarding the occurrence of disease, early detection and preventable patient deaths.

This research paper focuses on improving the accuracy of diabetes prediction model. With a median-based approach for initial centroid selection, K-means and weighted K-means (WKM) are used to cluster the instances based on the similarity between them and are classified using logistic regression. Based on the results, a comparative study of both the techniques is presented, and risk associated with non-diabetic and diabetic patients is analyzed. This paper consists of different sections as mentioned: Sect. 2 comprises the work related to disease prediction methods. Section 3 gives an insight of the proposed work. Section 4 presents the results obtained. Section 5 provides a comparative study of the existing work and the proposed model followed by conclusions in Sect. 6.

2 Related Work

Recently, more efforts have been made to improve the accuracy of prediction. Several techniques have been used to obtain better classification and prediction results. Some of the existing works have been discussed in this section.

Priyadarshini et al. [4] proposed a hybrid algorithm for the classification of the diabetic and non-diabetic patients using K-means algorithm and the gravitation search algorithm. GSA is the optimization-based algorithm where the classification is done based on the best available centroid. It identifies the true positive and true negative class. K-mean rather than taking the random classifier uses optimized centroid for the classification purpose. The performance given by the hybrid technique is the best for the given training and testing set.

Rabindra et al. [5] proposed a process of SDI as spatial data infrastructure for the sharing of geospatial big data. This SDI has been integrated to the cloud-based architecture to build a combined process of cloud-SDI. This paper studied various malaria vector-borne disease for the state of Maharashtra and also used lossless data compression on the data for the easy sharing globally with efficient way.

Archana et al. [6] presented a comparative study of the performance of K-means clustering by varying the distance metrics. Results showed that performance of clustering using K-means is affected by the selection of distance metrics and Euclidean distance metric provides the better result than the others.

Sandeep et al. [7] presented a hybrid approach for diabetes prediction where K-means is used for dimensionality reduction and classification is done using support vector machine. The initial centroids for K-means are obtained by partitioning the dataset and choosing a centroid from each partition. Results showed that this hybrid approach achieved an accuracy of 92%. Another hybrid approach used K-means clustering. Further, data was classified using SVM [8]. The results showed that the combination of K-means and SVM produces promising results and use of optimization techniques can further enhance the performance of the model. Wenqian et al. [9] proposed a hybrid approach implementing K-means for data reduction and classified PIMA Indian diabetes dataset using J48 decision tree. The correctly clustered 532 instances obtained from K-means were used to obtain the decision tree. Results showed that the accuracy of prediction model came out to be 90.04%. Kanika et al. [10] proposed an optimized hierarchical clustering method which aimed at reducing the computation cost. Genetic algorithm and SVM were also used for feature selection and classification, respectively. PIMA Indians diabetes dataset was used, and the accuracy was improved by 1.351%. Isaac et al. [11] compared the accuracy obtained by implementing K-means algorithm and decision tree. Results showed that both the techniques resulted in high accuracy, but statistical results show that K-means algorithm has higher performance than decision tree.

De Amorim et al. [12] presented a comparative study of different feature weighing methods for K-means clustering. A discussion of the nine most innovative techniques to assign weights to feature for K-means is presented out of which six algorithms were implemented using dataset with and without noise. Further, eight key characteristics were discussed which were used to provide a detailed comparison of the algorithms. Meng et al. [13] presented a comparison of the performance of three different classifiers by using diabetes dataset consisting of 12 attributes. The three models, logistic regression, ANN and decision tree were evaluated based on accuracy and a few more parameters. Experimental results showed that the decision tree and artificial neural network came out to be the best and worst classifiers among the three models. Ambika et al. [14] presented a comparative analysis of various machine learning techniques by listing the pros and cons of each and comparing their accuracy and other performance parameters. The techniques, namely decision tree, ANN, random forest, KNN, Naive Bayes, logistic regression and SVM, have been implemented using the PIMA diabetes dataset. The experimental results showed that logistic regression provides the best accuracy as compared to other algorithms.

Liu [15] implemented logistic regression to classify the dataset using a combination of features. Varying the set of selected attributes affected the performance of classifier. Results showed that logistic regression proved to be an easy and efficient way. Sun et al. [16] used a combination of logistic regression, random forest algorithm to identify different genes of breast cancer on micro array dataset. The prediction accuracy rates were analyzed by varying the threshold value. Top 20 genes were recognized that are expected to influence the development of breast cancer, and a maximum accuracy obtained was 95.57%.

Han Wu et al. [17] also proposed a model that implemented K-means algorithm, logistic regression using WEKA toolkit to predict type 2 diabetes. The main aim was to enhance the accuracy and implement the model using various datasets. This model produced satisfying results and was less time consuming. Accuracy of the proposed model was 3.04% more than the existing ones.

3 Proposed Work

The proposed model consists of several stages as shown in Fig. 1. Firstly, the data is preprocessed and used to find the initial cluster centers using median-based approach. Then, using the obtained initial centroids, data is clustered into two clusters. The

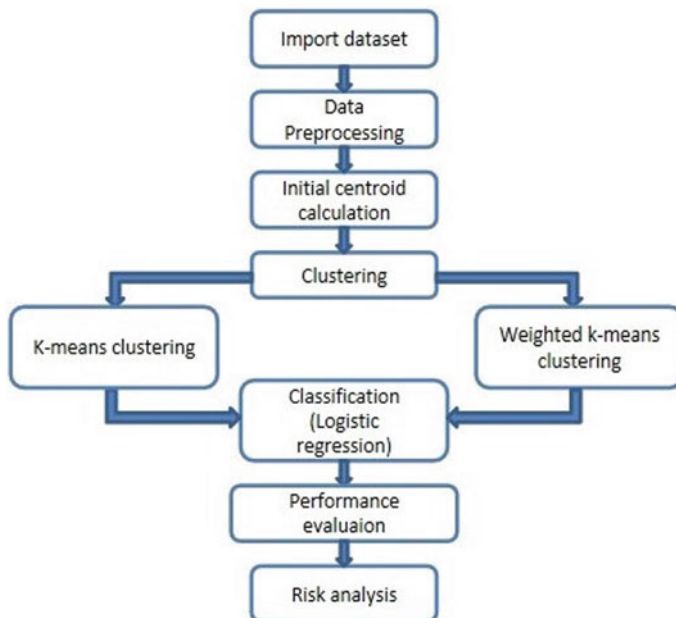


Fig. 1 Design of proposed model

S.No.	Attributes	Type
1	Number of times pregnant	Numeric
2	Plasma glucose concentration	Numeric
3	Diastolic blood pressure (mm Hg)	Numeric
4	Triceps skin fold thickness (mm)	Numeric
5	2-Hour serum insulin (μ U/ml)	Numeric
6	Body mass index (weight in kg/(height in m) ²)	Numeric
7	Diabetes pedigree function	Numeric
8	Age (years)	Numeric
9	Class variable (0 or 1)	Numeric

Fig. 2 Dataset description

incorrectly clustered data items are removed and the rest are fed to the classifier. In the final stage, results of classifier are used to analyze risk associated with the patients.

3.1 Dataset

The PIMA Indian diabetes dataset contains data of 768 female patients from Phoenix, Arizona, the USA extracted from online repository [18]. It consists of eight attributes and one output variable. Out of 768 patients, 500 tested negative, whereas 268 tested positive for diabetes. The attributes of the dataset used are shown in Fig. 2.

The last attribute indicates whether the patient is non-diabetic(0) or diabetic(1). Sample of dataset used is shown in Fig. 3.

3.2 Data Preprocessing

The dataset quality is of utmost importance as it directly affects the results of prediction. So, initially, the dataset is preprocessed to replace the incorrect or missing values.

S.No.	Pregnancies	Glucose	BloodPressure	SkinThickness	Insulin	BMI	PedigreeFunction	Age	Outcome
1	6	148	72	35	0	33.6	0.627	50	1
2	1	85	66	29	0	26.6	0.351	31	0
3	8	183	64	0	0	23.3	0.672	32	1
4	1	89	66	23	94	28.1	0.167	21	0
5	0	137	40	35	168	43.1	2.288	33	1

Fig. 3 Sample of dataset

The PIMA Indian diabetes dataset contains incorrect values for some attributes like blood pressure and BMI. These attribute values cannot be zero and were replaced by the column median. Further, each data value (x) was normalized [17] using (1).

$$x = \frac{x - \text{mean}}{\text{standard deviation}} \quad (1)$$

The preprocessed data is further divided into training and testing set.

3.3 Initial Centroid Calculation

The K-means algorithm starts by choosing random initial centroids, and after several iterations, it obtains the final cluster centers. These initial centroids play a vital role in K-means clustering. Selection of initial centroids can lead to more precise final cluster centers, thus improving the accuracy of clustering.

In the proposed work, initial centroids are selected as shown in Fig. 4.

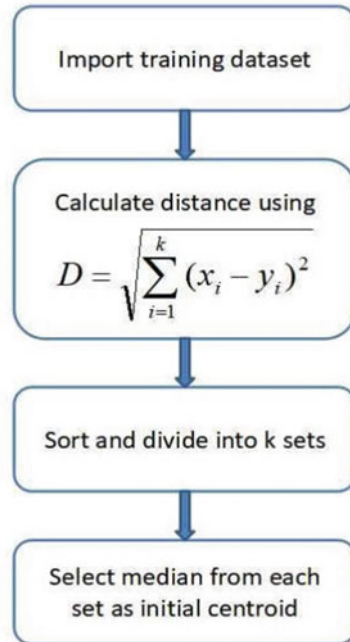
The distance of each data value is calculated from origin using (2).

$$D_{xy} = \sqrt{\sum_{k=1}^m (x_{ik} - y_{jk})^2} \quad (2)$$

where D_{xy} is the distance between x and y and m is the total number of attributes for each instance.

The dataset is sorted according to the distance, and based on the number of clusters required, the sorted dataset is divided into k sets. Since the class variable has two values (non-diabetic-0 and diabetic-1), value of k is assigned to 2. The median of each set is selected as an initial centroid. Selection of median value diminishes the effect of outliers and returns a unique value.

Fig. 4 Initial centroid selection



3.4 K-means Clustering

K-means clustering is a popular unsupervised approach where the observations are partitioned into predefined number of clusters based upon the similarity between them. The clusters formed follow the below-mentioned properties:

1. $S_{i=1}^k C_i = N$

where N = Number of observations and k = Number of clusters

2. $C_k \cap C_{k'} = \emptyset \forall k \neq k'$

In the second step, K-means clustering is applied on training dataset with specific initial centroids as shown in Fig. 5. The correctly clustered data is collected and fed to the logistic regression algorithm, and the incorrectly clustered data is discarded so that the model is trained with more accurate data values.

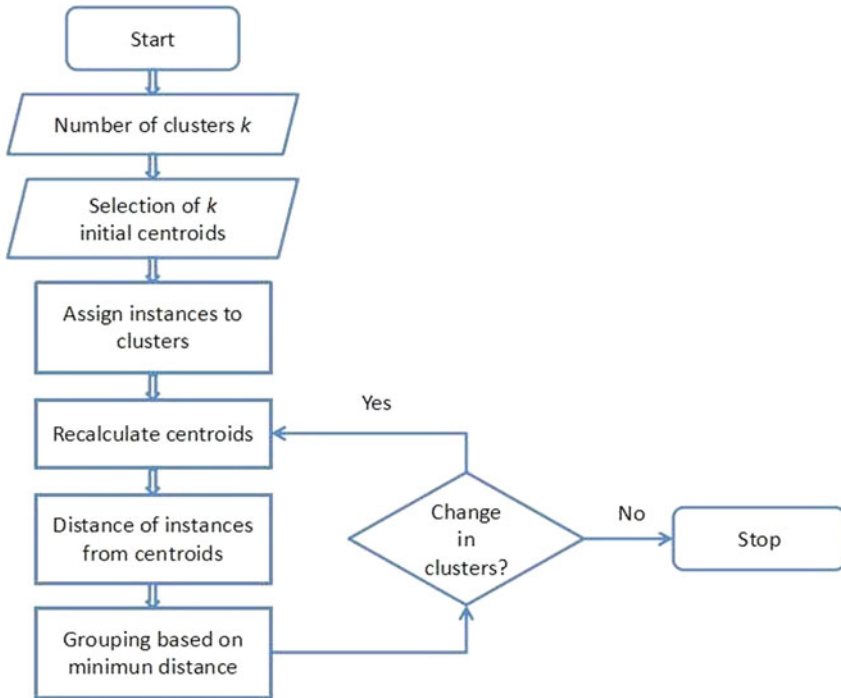


Fig. 5 Flowchart of K-means clustering

3.5 Weighted K-means Clustering

This approach is an extension of K-means clustering where the weights are assigned to individual features based on their importance [12]. The features assigned more weights will have more effect on figuring out the cluster to which the observation belongs. Initially, a random weight is assigned to each feature. Then, the feature weights are calculated automatically each time the clusters are obtained and distances are calculated. The objective is to minimize the Eq. (3).

$$W(C, P, w) = \sum_{k=1}^K \sum_{i \in C_k} \sum_{v \in V} w_v d(y_{iv}, p_{kv}) \quad (3)$$

where w_v is the weight of feature v where $v \in V$ (set of features) for a dataset y having k number of clusters C_k and centroids P_k .

This process continues till the algorithm converges as shown in Fig. 6. The final weights obtained indicate the importance of each feature.

Then, the correctly clustered observations are used to train the classifier.

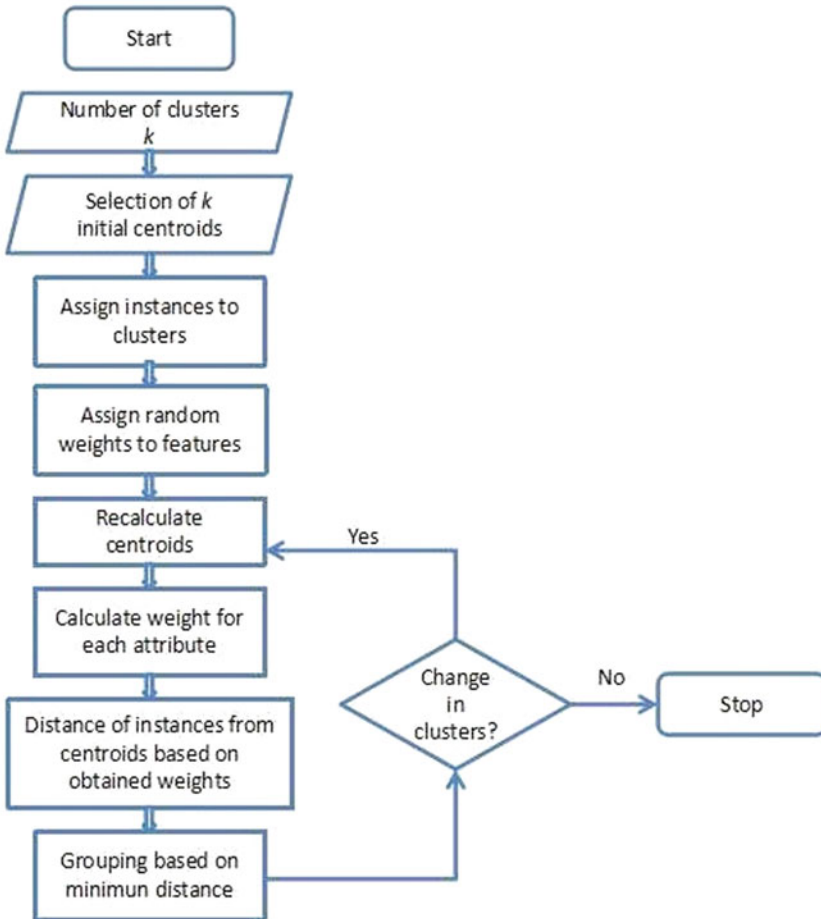


Fig. 6 Flowchart of WKM clustering

3.6 Logistic Regression

Regression comes into use when there is a need to establish a relation between the independent variables that determine the output and the dependent variable. It maps data values to predefined categories. There are several types of regression techniques, but the commonly used are linear and logistic regression. Linear regression produces a continuous outcome which can also fall outside the range 0–1 and is not suitable for binary classification as shown in Fig. 7, whereas logistic regression is a predictive analysis technique mostly used for classification where the output is either 0 or 1. It can also be used for multinomial classification with or without ordering.

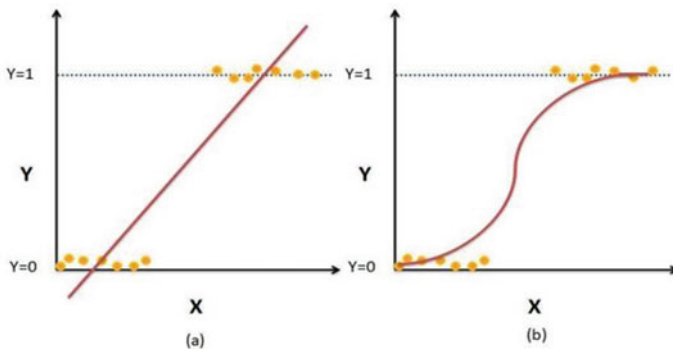


Fig. 7 (a) Linear regression and (b) logistic regression

Logistic regression initially produces a continuous outcome but makes use of sigmoid function. This function returns a probability value which can be mapped to two or more discrete classes. Further, this value is mapped based on the threshold value, which is normally set to 0.5 but may vary for imbalanced dataset.

In the proposed model, the correctly clustered data values are used to train the logistic model considering all the attributes of the dataset. The probability for each data value is calculated using (4).

$$P(t) = \frac{1}{1 + e^{-t}} \tag{4}$$

$t = A_0 + A_1 X_1 + \dots + A_n X_n$ where A_i denotes the model’s parameters, X_i refers to the input parameters, and $P(t)$ is the calculated probability. Based on threshold value ($th = 0.5$), the probability obtained is mapped to binary outcome (0 or 1). The ones having probability greater than 0.5 are marked as diabetic, whereas those having probability value less than 0.5 are considered non-diabetic.

3.7 Risk Analysis

Risk analysis basically refers to analyzing the outcomes of previous observations and based on that predicting the chances or risk probability for new ones. Based on the results of hybrid model, risk analysis is performed for non-diabetic and diabetic patients.

4 Results

The model is implemented using R tool. It provides a convenient and more user-friendly interface to implement and study the experimental results.

The dataset containing eight different attributes and an outcome variable is imported. The outcome variable is eliminated, and the remaining data is pre-processed, and then, it is divided into training and testing set in the ratio of 70:30. Further, using the median-based approach, two initial centroids are obtained based on which data is clustered into two clusters using K-means and WKM clustering. Since, the initial centers were defined, and this reduced the effect of outliers on the formation of final clusters and increased the number of instances that are clustered correctly. The clusters obtained are shown in Fig. 8. The cluster having data points marked in green refers to non-diabetic patients cluster, and the one in red indicates the diabetic cluster. Further, these data values were used for classification of instances using logistic regression.

4.1 Performance Parameters

To measure the performance of the model, several evaluation parameters are used which are obtained using confusion matrix. The confusion matrix is a combination of actual and predicted values which are used to measure the performance of the model. The performance parameter is calculated as shown in Fig. 9. Accuracy is the ratio of correctly predicted instances to total number of instances. The accuracy obtained for the proposed model using K-means and WKM clustering is 96.97% and 97.84%, respectively.

Kappa coefficient is an evaluation parameter to measure homogeneity of the given model. Its value ranges from 0 to 1. The value closer to 0 means that there is less agreement between the actual and predicted outcomes, whereas value closer to 1 means that there is more resemblance between the actual and predicted values.

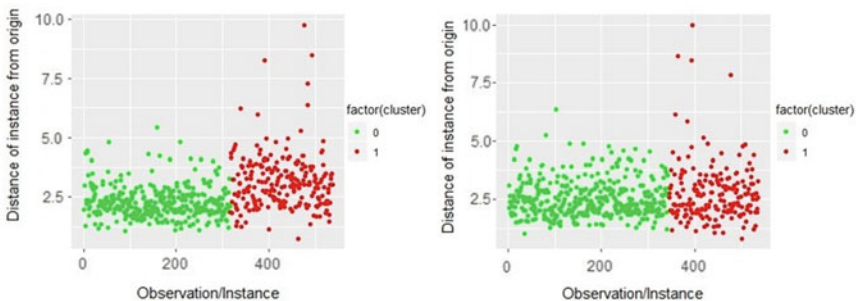


Fig. 8 Clusters obtained using K-means and WKM clustering

Fig. 9 Various performance parameters

$$\text{Accuracy} = \frac{TP + TN}{TP + TN + FP + FN}$$

$$\text{Recall} = \frac{TP}{TP + FN}$$

$$\text{Precision} = \frac{TP}{TP + FP}$$

$$\text{Specificity} = \frac{TN}{TN + FP}$$

$$\text{F-score} = 2 * \frac{\text{precision} * \text{recall}}{\text{precision} + \text{recall}}$$

$$1 - \frac{p_o - p_e}{1 - p_e} \quad (5)$$

where

$$p_o = \frac{TP + TN}{N}$$

and

$$p_e = \frac{[(TP + FN) * (TP + FP) * (TN + FN)]}{N}$$

The results obtained for the prediction of diabetes using the proposed model in R studio are shown in Fig. 10. The confusion matrix shown in the screenshot is used to calculate the value of various performance metrics.

Table 1 summarizes the values obtained for different performance metrics. It is observed that WKM and logistic regression perform better than K-means and logistic regression in terms of all parameters except for specificity.

The ROC curve is useful for visualizing the performance of binary classifier. For every classification threshold, it plots the true positive rate against false positive rate to provide a performance overview of the classifier. The ROC curve obtained for the proposed model is shown in Figs. 11 and 12. Area under the curve is obtained from ROC curve. Higher the value, more the accuracy of the model. The values obtained for the classifier using K-means and WKM clustering are 0.9712 and 0.9775, respectively.

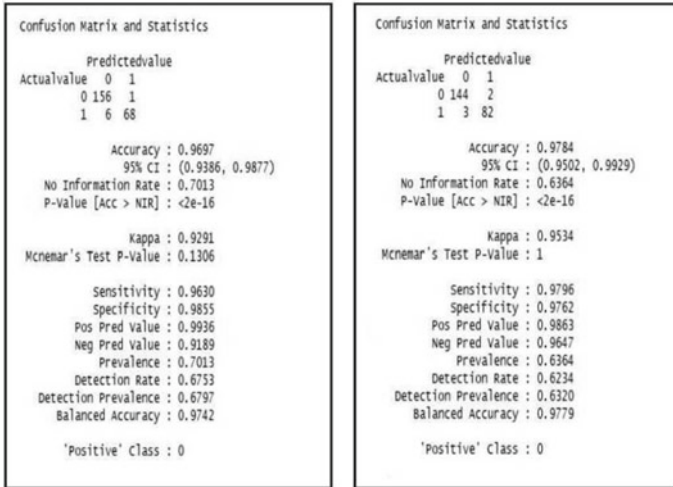


Fig. 10 Results of classifier using K-means and WKM clustering

Table 1 Performance measure indices of proposed work

Performance metric	Proposed work (K-means and logistic regression)	Proposed work (WKM and logistic regression)
Accuracy	0.9697	0.9784
Recall	0.9630	0.9796
Precision	0.9629	0.9795
Specificity	0.9855	0.9762
F score	0.9629	0.9795
Kappa	0.9291	0.9534

Fig. 11 ROC curve using K-means, logistic regression

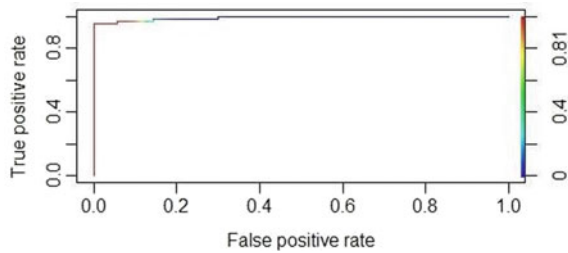


Fig. 12 ROC curve using WKM, logistic regression

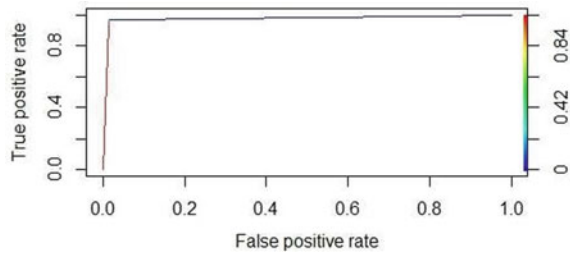
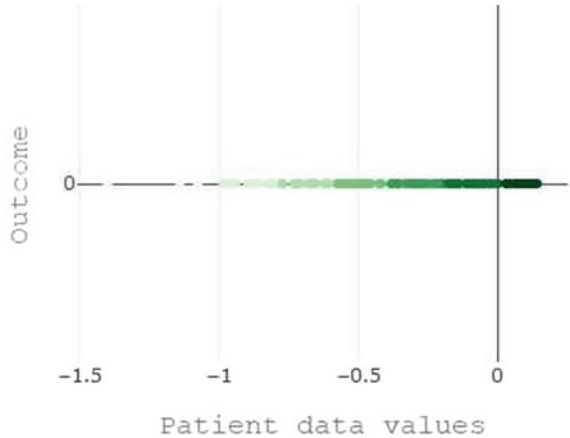


Fig. 13 Risk analysis of non-diabetic patients



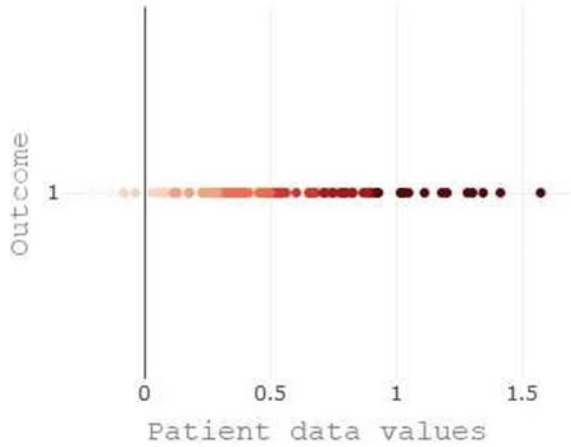
4.2 Risk Analysis

Based on the results obtained from classification, risk analysis for both non-diabetic and diabetic patients is performed. The screenshot of plots obtained is shown in Figs. 13 and 14.

In case of non-diabetic patients, the data values that lie close to zero as shown in Fig. 13 have a high probability of having diabetes in the future, whereas the ones that lie far away have low probability of having diabetes. This analysis can be helpful to patients having high risk as they can take necessary precautions to avoid the disease.

In case of diabetic patients, the ones that lie near zero as shown in Fig. 14 can take necessary precautions to control their sugar level, and the ones that lie far away are at a high risk and need to take immediate measures to control the blood sugar level since it can prove to be fatal.

Fig. 14 Risk analysis of diabetic patients



5 Discussion

The experimental results in Table 2 show that using the proposed model, the number of correctly clustered instances increased as compared to existing work. Weqian et al. [9] and Mustafa et al. [19] implemented standard K-means algorithm, whereas Han wu et al. [17] implemented K-means with different seed values.

These approaches selected centroids based on local optima and were affected by outliers. Using the median-based approach for initial centroid calculation in the proposed work, improved the percentage of correctly clustered instances obtained after clustering.

Table 3 summarizes the value of different performance parameters obtained by researchers for diabetes prediction on the PIMA Indian diabetes dataset. The comparison shows that the proposed model performed better than the existing work in terms of various parameters like accuracy, precision, recall and specificity.

The model proposed by Han Wu et al. [17] has accuracy closest to the proposed model. So, a comparative analysis of the models is shown in Fig. 15 considering

Table 2 Comparison of clustering results

Author	Correctly clustered instances (%)
Wenqian et al. [9]	69.27
Mustafa et al. [19]	74.21
Han Wu et al. [17]	76.69
Our proposed model (using K-means)	80.07
Our proposed model (using WKM)	84.72

Table 3 Comparison of different models

Author	Methodology	Accuracy (%)	Precision (%)	Recall (%)	Specificity (%)
Proposed model	WKM, logistic regression	97.84	97.95	97.96	97.62
Proposed model	K-means, logistic regression	96.97	96.29	96.30	98.55
Han Wu et al. [17]	K-means, ogistic regression	95.42	95.4	95.4	–
Wenqian et al. [9]	K-means, Decision tree	90.04	–	87.27	91.28
Patil et al. [20]	K-means, C4.5	92.38	–	90.38	93.29
Purushottam et al. [21]	C4.5	81.27	–	–	–
Deepti et al. [22]	Naive bayes SVM Decision tree	76.30 65.10 73.82	75.90 42.40 73.50	76.30 65.10 73.80	– – –

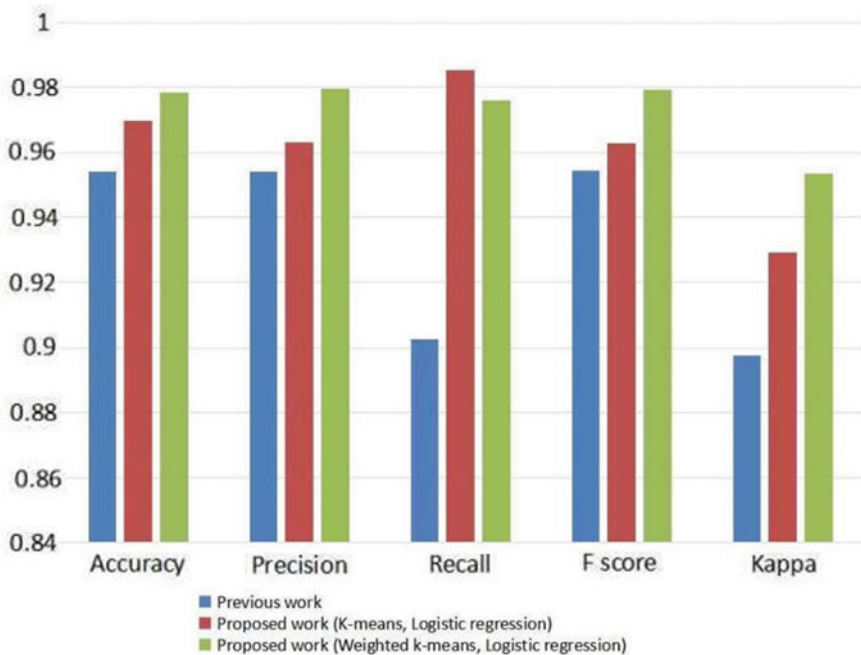


Fig. 15 Comparative analysis using various performance parameters

several quality measures. The figure clearly illustrates that the proposed model performs better in terms of all parameters.

6 Conclusion

With the increasing demand of predictive analysis in the medical field, the aim is to propose an efficient model for diagnosing and predicting the occurrence of diabetes based on several parameters. The proposed model is a combination of cluster and class-based techniques. Though K-means clustering is an efficient technique to obtain clusters based on similarity between the instances, but it is sensitive toward the selection of initial centroids. Here, we presented a median-based method for the selection of initial centers to reduce the effect of outliers and further enhance the performance of the classifier. Further, K-means and WKM have been applied for clustering and classification of instances is done using logistic regression. Experimental results showed that about 80% and 84% of the original data is retained after K-means and WKM clustering, respectively, which is fed to classifier. Accuracy obtained for classification using K-means and WKM in combination with logistic regression is 96.97% and 97.84%, respectively. The model with WKM performs slightly better than the one using K-means for clustering. Further, the risk associated with diabetic and non-diabetic patients is analyzed using results of classifier which can be helpful to the patients and medication can be prescribed accordingly.

The current research focused on hybridization of K-means and logistic regression for diabetes prediction based on eight different parameters. In the future, focus can be laid on using several other combinations of clustering and classification approaches for disease prediction on a larger dataset having more number of attributes. Different feature weighing approaches can also be used to enhance the process of clustering.

References

1. Diabetes patients in india. <https://www.indiatoday.in/education-today/gk-current-affairs/story/98-million-indians-diabetes-2030-prevention-1394158-2018-11-22>. Accessed: 25 Nov 2018
2. Information about diabetes. <https://www.niddk.nih.gov/health-information/diabetes/overview/what-is-diabetes>. Accessed: 06 Oct 2018
3. Kavakiotis I, Tsave O, Salifoglou A, Maglaveras N, Vlahavas I, Chouvarda I (2017) Machine learning and data mining methods in diabetes research. *Comput Struct Biotechnol J* 15:104–116
4. Priyadarshini R, Barik RK, Dash N, Mishra BK, Misra R (2017) A hybrid GSA-K-mean classifier algorithm to predict diabetes mellitus. *Int J Appl Metaheuristic Comput (IJAMC)* 8(4):99–112
5. Barik RK, Dubey H, Mankodiya K, Sasane SA, Misra C (2019) Geofog4health: a fog-based sdi framework for geospatial health big data analysis. *J Ambient Intell Humaniz Comput* 10(2):551–567
6. Singh A, Yadav A, Rana A (2013) K-means with three different distance metrics. *Int J Comput Appl* 67(10)

7. Kaur S, Kalra S (2016) Disease prediction using hybrid K-means and support vector machine. In: 2016 1st India international conference on information processing (IICIP), pp 1–6. IEEE
8. Osman AH, Aljahdali HM (2017) Diabetes disease diagnosis method based on feature extraction using k-SVM. *Int J Adv Comput Sci Appl* 8(1)
9. Chen W, Chen S, Zhang H, Wu T (2017) A hybrid prediction model for type 2 diabetes using K-means and decision tree. In: 2017 8th IEEE International conference on software engineering and service science (ICSESS), pp 386–390. IEEE
10. Bhatia K, Syal R (2017) Predictive analysis using hybrid clustering in diabetes diagnosis. In: 2017 Recent developments in control, automation and power engineering (RDCAPE), pp 447–452. IEEE
11. Isaac LD, Sureshkumar C (2018) Diagnosis prognosis and prevention of breast cancer based on present scenario of human life. In: 2018 International conference on communication information and computing technology (ICCICT), pp. 1–7. IEEE
12. De Amorim RC, Mirkin B (2012) Minkowski metric, feature weighting and anomalous cluster initializing in K-means clustering. *Pattern Recogn* 45(3):1061–1075
13. Meng XH, Huang YX, Rao DP, Zhang Q, Liu Q (2013) Comparison of three data mining models for predicting diabetes or prediabetes by risk factors. *Kaohsiung J Med Sci* 29(2):93–99
14. Choudhury A, Gupta D (2019) A survey on medical diagnosis of diabetes using machine learning techniques. In: *Recent developments in machine learning and data analytics*, pp 67–78. Springer, Berlin
15. Liu L (2018) Research on logistic regression algorithm of breast cancer diagnose data by machine learning. In: 2018 International conference on robots an intelligent system (ICRIS), pp 157–160. IEEE
16. Sun M, Ding T, Tang XQ, Yu K (2018) An efficient mixed-model for screening differentially expressed genes of breast cancer based on lr-rf. In: *IEEE/ACM transactions on computational biology and bioinformatics*
17. Wu H, Yang S, Huang Z, He J, Wang X (2018) Type 2 diabetes mellitus prediction model based on data mining. *Inf Med Unlocked* 10:100–107
18. Dataset. <https://www.kaggle.com/uciml/pima-indians-diabetes-database>. Accessed 12 Nov 2018
19. Kadhms MS, Ghindawi IW, Mhawi DE (2018) An accurate diabetes prediction system based on K-means clustering and proposed classification approach. *Int J Appl Eng Res* 13(6):4038–4041
20. Patil BM, Joshi RC, Toshniwal D (2010) Hybrid prediction model for type-2 diabetic patients. *Expert Syst Appl* 37(12):8102–8108
21. Saxena K, Sharma R et al (2015) Diabetes mellitus prediction system evaluation using c4.5 rules and partial tree. In: 2015 4th International conference on reliability, infocom technologies and optimization (ICRITO) (trends and future directions) pp 1–6. IEEE
22. Sisodia D, Sisodia DS (2018) Prediction of diabetes using classification algorithms. *Procedia Comput Sci* 132:1578–1585

Performance Analysis of Classification Methods for Cardio Vascular Disease (CVD)



N. Komal Kumar , R. Lakshmi Tulasi, and D. Vigneswari 

Abstract Cardio Vascular Diseases (CVD) are a cluster of diseases of blood vessels and heart, which ranges from a small blood clot to severe heart failure. Machine learning classifiers help to forecast the plausibility of patients subjected to Cardio Vascular Disease (CVD) by analyzing various medical parameters such as heart rate, Cholesterol level, HbA1c, weight, ECG results. This paper focuses on the performance of various machine learning classifiers based on accuracy and execution time over a CVD dataset in predicting Cardio Vascular Disease (CVD). RandomForest, J48, Hoeffding tree, Logistic Model Trees (LMT), and RandomTree classifiers were used in the prediction. In the analysis, Hoeffding tree classifier achieved high accuracy of 85.1852% and execution time of 0.17 s in predicting patients subjected to CVD than the other classifiers under analysis.

Keywords RandomForest · J48 · Hoeffding tree · Logistic model tree · RandomTree · TPR · FPR · Accuracy

N. Komal Kumar (✉)

Department of Computer Science and Engineering, St. Peter's Institute of Higher Education and Research, Avadi, Chennai, India

e-mail: komalkumarnapa@gmail.com

R. Lakshmi Tulasi

Department of Computer Science and Engineering, R.V.R & J.C College of Engineering, Guntur, India

e-mail: rtulasi.2002@gmail.com

D. Vigneswari

Department of Information Technology, KCG College of Technology, Karapakkam, Chennai, India

e-mail: vigneswari121192@gmail.com

© Springer Nature Singapore Pte Ltd. 2021

G. S. Hura et al. (eds.), *Advances in Communication and Computational*

Technology, Lecture Notes in Electrical Engineering 668,

https://doi.org/10.1007/978-981-15-5341-7_93

1231

1 Introduction

Cardio Vascular Diseases are the disorders of blood vessels and heart; they include rheumatic heart disease, peripheral heart disease, cerebrovascular disease, coronary heart disease, congenital heart disease, and deep vein thrombosis. Rheumatic heart disease damages the muscles and valves of the heart caused by streptococcal bacteria. Peripheral arterial heart disease is the disease of blood vessels in arms and legs. Congenital heart disease deals with the malformation of heart structure from birth. Cerebrovascular is the disease of the blood vessel connecting to the brain. According to the heart disease and stroke statistics, 2017 cardiovascular disease (CVD) listed as an underlying cause for death in US [1]. About 2200 die due to Cardio Vascular Diseases every day. The main factors causing heart diseases are Coronary Heart Disease (CHD), hypertension, and stroke. Heart attacks and strokes are mainly caused by a blockage of blood that flows to the brain or heart. The reason for the blockage is the growth of fatty deposits in the inner walls of the blood vessels. Strokes are caused by the leakage in the blood vessels which carries blood to heart. The causes of the strokes and heart attacks are due to the use of tobacco, hypertension, diabetes, consumption of alcohol, and hyperlipidaemia. Terminating tobacco and alcohol use, reducing salt in the diet can reduce the risks of Cardio Vascular Diseases. The common symptoms include difficulty in vision, speaking, and understanding, confusion, numbness of the leg, arms, and face. Recent advancement helps to predict Cardio Vascular Disease at early stages and the factors affecting it. Data mining classifiers help to reveal the hidden information by analyzing the medical parameters and provides the solution efficiently.

2 Related Study

Cardio Vascular Disease has several factors such as smoking, Physical Inactivity, Nutrition, Obesity, level of cholesterol in the blood, High BP, and even Diabetes Mellitus. According to the statistics [1] about 2200 die due to heart-related diseases every day, 9.1% of middle age have been diagnosed suffering from Diabetes Mellitus, 30.4% of the population lack physical activity, 37.7% are obese, and 39.7% of middle age has a cholesterol level of 200 mg/dL. Irene Marzona et al. [2] has predicted the model that the patients with diabetics have higher CV risk. Medical Practitioner suggests that every individual according to their congenital characteristics may have previous atherosclerosis diseases; these characteristics will try to erupt when the environment becomes favorable for them. The explosions of these are caused mainly due to two reasons, one is improper dietary plan, smoking, alcohol consumption, etc., and another reason is the intake of Oral Anti-diabetic Drugs (OAD) for the treatment of Diabetics Mellitus. Even the patient with N-3 fatty acid is subject to Cardio Vascular risk factors [3]. The study of High-Low risk of cardiovascular risk was presented

in [4]. The data mining techniques can also be applied to software [5]. The performance comparison of various classifiers such as C4.5 and Naïve Bayes is presented in [6]. Machine learning classifier analysis for Diabetes Mellitus (DM) prediction was presented in [7], where the machine learning classifiers such as REP tree, decision tree, and Logistic Model Tree (LMT) were subjected to a dataset of the patients who suffer from Diabetes Mellitus. A multimodel-based ensemble technique for chronic kidney disease prediction was proposed in [8], which involves hybrid classifiers for patient disease classification. An optimized random forest machine learning classifier was proposed in [9], where a GA-ORF classifier is used for predicting patients with Diabetes Mellitus. Further, machine learning classifiers [10] can be applied to a medical dataset for optimized and accurate outcomes that can help the medical practitioner to take preventive actions.

3 Methodologies

The analysis was conducted by using data set [11] from the University of California at Irvin (UCI) which includes 13 attributes classified into two classes “present” and “absent”. The implementation process starts with feature selection data preprocessing technique, the preprocessed observations are fed to ML classifiers such as Random-Forest, J48, Hoeffding tree, LMT, and RandomTree using WEKA tool. True Positive (TP), False Positive (FP), True Negative (TN), and False Negative values obtained from the confusion matrix were used in the calculation of accuracy of the classifiers. The framework for predicting cardiovascular disease is represented in Fig. 1.

Ho [12] proposed random forest or Random Decision Forest in 1995, uses multiple learning classifiers such as decision trees to predict the solution. Taking the average of the majority of votes can do prediction. J48 is a java implementation of C4.5 [13] classifier, the decision trees created by this classifier can be used for classification hence the name statistical classifier. C4.5 uses training data for classification. The classifier works as follows. An attribute is chosen at each node, which effectively splits the set of samples into subsets. The splitting is based upon the information gain. Hoeffding tree [14] or VFDT (Very Fast Decision Trees) is the standard decision tree classifier for data stream classification. VFDT uses the hoeffding bound to decide the minimum number of arriving instances. Logistic Model Tree or LMT [15, 16] is a classification model for supervised learning, which combines logistic regression and decision tree. Logistic regression deals with linear regression models used in the olden days. These linear regression models [14] are combined with the decision tree learning classifiers for classification. Random Trees or Decision tree [17] is the simplest classification mechanism created to classify the variable based upon certain conditions.

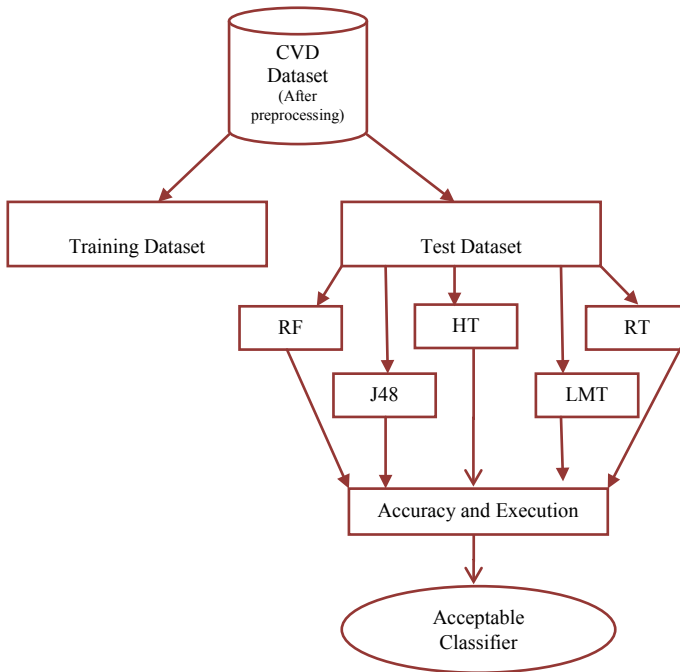


Fig. 1 Framework

4 Experimental Analysis and Findings

The data set comprises of 75 attributes with 1550 observations. After data preprocessing, the 13 attributes such as age, gender, blood pressure, ECG results, pain in chest, cholesterol, blood sugar, angina, old peak value, the slope, no of major vessels colored by fluoroscopy (value = 0–3), thal (3-normal, 6-fixed defect, 7-reversible defect) and attribute class (present, absent) comprising of 270 observations which are the major cause of CVD. A split criterion is used to divide the dataset into 60% as training and 40% as test. The training set is used to build the classifiers model which validates the test set. The satisfaction is obtained from both training and test sets. In order to find the conclusions of the analysis, these classifiers are tested on the basis of several statistics and models. First, we started to apply various statistics approaches [18, 19] like finding its MAR (Mean Absolute Error), Percentage of RAR (Relative Absolute Error), RMSER (Root Mean Squared Error), percentage of RRSER (Root Relative Squared Error). Second, we followed to perceive the characteristics models, calculating performance metrics such as true positive, false positive, true negative and false negative values (Table 1), Precision, ROC (Receiver Operating Characteristics), Recall [20], Precision-Recall Curve (PRC) [20], represented in Table 2. Finally, we calculate the accuracy (CCI), inaccuracy (ICI), and model building time that are

Table 1 Confusion matrix of RandomForest, J48, Hoeffding tree, LMT and RandomTree

Classifier	TP	TN	FP	FN
RandomForest	47	4	18	39
J48	48	3	14	43
Hoeffding tree	45	6	10	47
LMT	45	6	12	45
RandomTree	42	9	25	32

Table 2 Classifiers with their true positive rate, false positive rate, precision, recall, ROC, PRC

Classifier	True positive rate	False positive rate	Precision	Recall	ROC	PRC
RandomForest	0.796	0.191	0.820	0.796	0.916	0.905
J48	0.843	0.147	0.859	0.843	0.842	0.801
Hoeffding tree	0.852	0.145	0.854	0.852	0.917	0.919
LMT	0.833	0.162	0.838	0.833	0.926	0.927
RandomTree	0.685	0.300	0.708	0.685	0.692	0.637

Note Weighted average of class a and class b are taken into consideration

Table 3 Classifiers with their accuracy, inaccuracy and execution time (s) to build the model

Classifier	CCI (%)	ICI (%)	Exec time (s)
RandomForest	79.6296	20.3704	1.03
J48	84.2593	15.7407	0.19
Hoeffding tree	85.1852	14.8148	0.17
LMT	83.3333	16.6667	1.4
RandomTree	68.5185	31.74815	0.06

represented in Table 3. Both, statistics and characteristics models are together used in obtaining the feasible classifier by comparing the accuracy and the execution time.

General confusion matrix [21] is denoted as TP—True Positive, FP—False Positive (Type I Error), FN—False Negative (Type II Error) [22], TN—True Negative, respectively [23, 24].

The comparison of the TPR, FPR, Precision, Recall, ROC, and PRC values of RandomForest, J48, Hoeffding tree, LMT and RandomTree classifiers is represented in Fig. 2. Accuracy and inaccuracy of RandomForest, J48, Hoeffding tree, LMT and RandomTree classifiers are shown in Fig. 3. The execution time (sec) of RandomForest, J48, Hoeffding tree, LMT, and RandomTree classifiers are shown in Fig. 4 respectively.

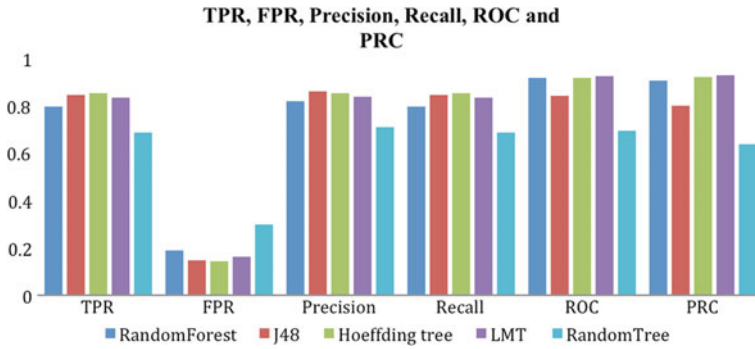


Fig. 2 Parameter values

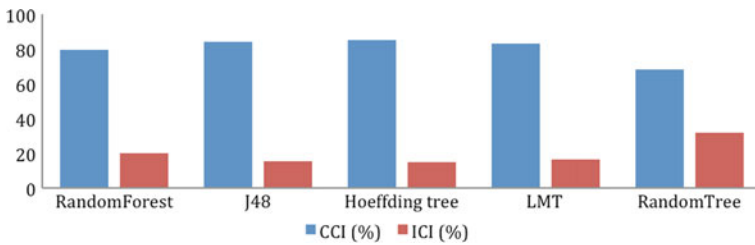


Fig. 3 Accuracy and inaccuracy

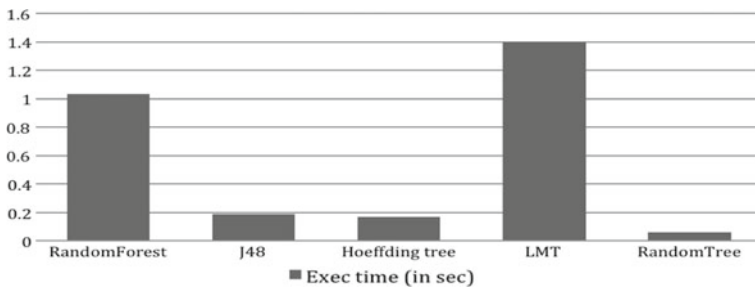


Fig. 4 Execution time (s)

5 Conclusion and Future Outlook

This paper focuses on performance analysis of ML classifiers such as Random-Forest, J48, Hoeffding tree, Logistic Model Trees (LMT), and RandomTree were analyzed in predicting Cardio Vascular Disease (CVD) in this study. The accuracy of the classifiers was calculated based on the True Positive (TP), False Positive (FP), True Negative (TN), and False Negative (FN) values from the confusion matrix [21]. In the analysis, the Hoeffding tree classifier achieved high accuracy of

85.1852% and a model building time (execution) of 0.17 s which is greater than the RandomTree machine learning classifier with 68.5185% accuracy. Applying hybrid machine learning classifiers on a real-time datasets can do further exploration.

Acknowledgements The authors are grateful to the authorities and management of St. Peter's Institute of Higher Education and Research, Chennai, India, RVR & JC College of Engineering, India, and KCG College of Technology, Chennai, India, who greatly motivated and assisted in the research.

References

1. Benjamin EJ, Blaha MJ, Chiuve SE, Cushman M, Das SR, Deo R, De ferranti SD, Floyd J, Fornage M, Gillespie C, Isasi CR, Jimenez MC, Jordan LC, Judd SE, Lackland D, Lichtman JH, Lisabeth L, Liu S, Longenecker CT, Mackey RH, Matsushita K, Mozaffarian D, Mussolino ME, Nasir K, Neumar RW, Palaniappan L, Pandey DK, Thiagarajan RR, Reeves MJ, Ritchey M, Rodriguez CJ, Roth GA, Rosamond WD, Sasson C, Towfighi A, Tsao CW, Turner MB, Virani SS, Voeks JH, Willey JZ, Wilkins JT, Wu JH, Alger HM, Wong SS, Muntner P (2017) Heart disease and stroke statistics-2017 Update: a report from the American Heart Association. *Circulation* 135:e146–603
2. Marzona I, Avanzini F, Lucisano G et al (2017) *Acta Diabetol* 54:123
3. Roncaglioni MC, Tombesi M, Avanzini F, Barlera S, Caimi V, Longoni P, Marzona I et al (2013) n-3 fatty acids in patients with multiple cardiovascular risk factors. *N Engl J Med* 368(19):1800
4. Marzona I, Avanzini F, Lucisano G, Tettamanti M, Baviera M, Nicolucci A, Roncaglioni MC (2017) Are all people with diabetes and cardiovascular risk factors or microvascular complications at very high risk? Findings from the Risk and Prevention Study. *Acta Diabetol* 54(2):123–131
5. Kumar P, Wahid A (2015) Performance evaluation of data mining techniques for predicting software reliability. *World Acad Sci Eng Tech* 9(8):2041–2048
6. Anshul G, Rajni M (2012) Performance comparison of naive bayes and J48 classification classifiers. *Int J Appl Eng Res* 7(11):281–297
7. Vigneswari D, Komal Kumar N, Ganesh Raj V, Gugan A, Vikash SR (2009) Machine learning tree classifiers in predicting diabetes mellitus. In: *IEEE-2019 5th International conference on advanced computing and communication systems*, pp 84–87. <https://doi.org/10.1109/icaccs.2019.8728388>
8. Komal Kumar N, Lakshmi Tulasi R, Vigneswari D (2019) An ensemble multi-model technique for predicting chronic kidney disease. *Int J Electr Comput Eng* 9(2):1321–1326. <https://doi.org/10.11591/ijece.v9i2.pp1321-1326>
9. Komal Kumar N, Vigneswari D, Vamsi Krishna M, Phanindra Reddy GV (2018) An optimized random forest classifier for diabetes mellitus. In: Abraham A, Dutta P, Mandal J, Bhattacharya A, Dutta S. (eds) *Emerging technologies in data mining and information security. Advances in intelligent systems and computing*. Vol 813, no 67. https://doi.org/10.1007/978-981-13-1498-8_67
10. Komal Kumar N, Vigneswari D, Kavya M, Ramya K, Lakshmi Druthi T (2018) Predicting non-small cell lung cancer: a machine learning paradigm. *J Comput Theoretical Nanoscience*. 5(6/7):2055–2058. <https://doi.org/10.1166/jctn.2018.7406>
11. <https://archive.ics.uci.edu/ml/machinelearningdatabases/statlog/heart/>
12. Ho TK (1995) Random Decision Forests. In: *Proceedings of the 3rd international conference on document analysis and recognition*. Montreal 278–282
13. Quinlan JR (1993) *C4.5: Programs for machine learning*. Morgan Kaufmann Publishers

14. <https://samoaincubator.apache.org/documentation/Vertical-Hoeffding-Tree-Classifier.html>
15. Landwehr N, Hall M, Frank E (2005) Logistic model trees. *Mach Learn* 59:161. <https://doi.org/10.1007/s10994-005-0466-3>
16. Kumar NK, Sindhu GS, Prashanthi DK, Sulthana AS (2020) Analysis and prediction of cardiovascular disease using machine learning classifiers. In 2020 6th International Conference on Advanced Computing and Communication Systems (ICACCS), pp 15–21. IEEE
17. Utgoff PE (1989) Incremental induction of decision trees. *Mach Learn* 4(2):161–186. <https://doi.org/10.1023/A:1022699900025>
18. Dodge Y (2006) *The oxford dictionary of statistical terms*, Oxford University Press. ISBN 0-19-920613-9
19. Romijn J-W (2014) *Philosophy of statistics*. Stanford Encyclopedia of Philosophy
20. Bradley A (1997) The use of the area under the ROC curve in the evaluation of machine learning classifiers. *Pattern Recogn* 30:1145–1159
21. Stehman SV (1997) Selecting and interpreting measures of thematic classification accuracy. *Remote Sensing of Envir* 62(1):77–89. [https://doi.org/10.1016/s0034-4257\(97\)00083-7](https://doi.org/10.1016/s0034-4257(97)00083-7)
22. Thron C, Hernandez N (2019) ‘Statistics Gone on Holiday’: misinterpretations of hypothesis tests propagated by internet resources. *J Soc Sci Humanit* 5(3)
23. Komal Kumar N, Vigneswari D, Roopa Devi BAS (2018) MSO—MLP diagnostic approach for detecting DENV serotypes. *Int J Pure Appl Math* 118(5):1–6
24. Komal Kumar N, Vigneswari D (2019) Hepatitis-infectious disease prediction using classification algorithms. *Res J Pharm Technol* 12(8) 3720–3725

Secure Data Deduplication (SD^2eDup) in Cloud Computing: Threats, Techniques and Challenges



Basappa B. Kodada and Demian Antony D'Mello

Abstract Storage is the most important service provided by cloud computing technology helps many individuals from managing in-house storage infrastructure. To provide the availability of data at any time and anywhere, the cloud service provider will store the redundant copy of data in the cloud storage server. This will leads to the waste of storage space by duplicating the user's data in the cloud. The data deduplication technique has attracted many cloud vendors to increase the storage space by deleting the same copy of data from the cloud storage server and reduce the storage cost for cloud users. The data deduplication comes with many security issues due to its exploration of metadata stored in the cloud. To deal with these security issues, many secure data deduplication techniques have been proposed. Hence, in this article, we present the taxonomy on the classification of data deduplication techniques for general data. And we discuss the secure data deduplication along with different security threat models during data deduplication process. In this article, we also discuss the various existing secure data deduplication schemes proposed by researchers and present in taxonomy. Finally, we identify some of the open research challenges and present for future research direction in the big data era.

Keywords Cloud computing · Data security · Cloud security · Deduplication · Secure deduplication · Taxonomy of cloud security · Big data · Big data security

1 Introduction

Cloud computing allows a huge amount of data to be stored in a centralized storage server and allow users to access it at any time and anywhere based on their demand. The increasing of its popularity and cost-effective [1], many organizations are plan-

B. B. Kodada (✉)

A J Institute of Engineering and Technology Mangalore, VTU Belagavi, Belgaum, India
e-mail: basappabk@gmail.com

D. Antony D'Mello

Canara Engineering College Mangalore, VTU Belagavi, Belgaum, India
e-mail: demianantony@gmail.com

© Springer Nature Singapore Pte Ltd. 2021

G. S. Hura et al. (eds.), *Advances in Communication and Computational Technology*, Lecture Notes in Electrical Engineering 668,
https://doi.org/10.1007/978-981-15-5341-7_94

1239

ning to move from the private storage system to the cloud storage system. Because storage service provided by the cloud is one of the most widely used by users and organizations and have greatly benefited from it since they can store huge amount of data without upgrading to their hardware [2]. Nowadays, cloud storage services are provided by many local and global cloud service providers (CSP) and most of the social media, software application, users and organizations use these services to store their huge amount of data which is being generated from them. Hence, the cloud computing has become the most important which has significantly changed the big data management system for small and medium scale industry due to its scalability, reliability and on-demand services wherever and whenever needs with negligible cost. The applications of cloud computing have been used in health care sector, the author of [3, 4] has presented the article of cloud computing application toward the health care sector and analyzing the special data by spatial data infrastructure model named as cloud ganga [102]. The author also presented the cloud architecture for big data analytic technique for spatial data in [5].

The big data are being generated from small scale, medium scale industries, social media and stored in the cloud storage server. The growth of data has become 8.4 ZB by 2018 and will reach 15.3 ZB per year by 2020 [6] and 90% of traffic will be coming from cloud data center [6]. That means the huge amount of duplicated data may present in the cloud storage server. These duplicate data might be backup of user's data, but it eats a lot of storage space. In this regard, the lot of duplicated copy of data is being generated from cloud users, CSP, social media which basically leads to the waste of storage space in the cloud. Because many times, the same data being uploaded to cloud storage server by many users which consume more storage space, more bandwidth, more computing power leads to environmental pollution due to its computational power requirements to manage the huge amount of data in a different data center located at a different geographical location. Hence, it is very essential that duplicated copies of data must be eliminated from the cloud which increases the utilization of storage space by 30%. So CSP performs the deduplication process in order to eliminate the same copies of data stored in the cloud storage server. It is a challenging task to delete the redundant copies of data stored and is stored to the cloud storage server. The data deduplication is a process of increasing the storage space by eliminating the redundant copies of data stored in cloud storage. That means, only one copy of data will be kept in cloud storage even if such data is owned by the same or multiple users.

1.1 Literature Survey

There are many survey papers on data deduplication technique only for general data. The author of [7] presented the deduplication technique for multimedia data in cloud computing and has classified the deduplication technique based on multimedia like type, level, inline and postline processing, client and server side, single and cross-user deduplication techniques. Fue et al. presented a classification of data deduplication

techniques based on functionalities and operational aspects in [8] and author of [9] has identified the deduplication techniques based on the level of data like file level and block level (fixed length, variable length). The author of [10] has classified the data deduplication based on system design by referring classification of deduplication defined by [11]. The author further classified deduplication techniques into six key decisions: granularity, locality, timings, indexing, algorithms and scope. Most of all previous work has been focused on analysis and efficiency on data deduplication without caring for the data security because deduplication and cryptographic algorithms are opposed to each other [12]. The author of this paper has described detail survey on various techniques for secure data deduplication by considering all threats during data-in-transit and data-at-rest in the deduplication process.

1.2 Scope and Contribution

This survey presents an overview of cloud computing and its importance in providing storage service for users. This article is mainly focused on secure data deduplication in cloud computing through which CSP and users will be benefited in terms of storage space utilization at an affordable cost. We discuss the different deduplication techniques for general data and present their taxonomy based on computational resources and geographical location. We extend this article by exploring security threat models during data deduplication process. We also present the existing mechanisms to provide security during data deduplication in cloud computing at various levels. We finally give some insights into the open research challenges of secure data deduplication in big data era.

1.3 Organization

The remaining part of this article is organized as follows: Sect. 2 describes and presents the secure data deduplication and taxonomy on data deduplication classifications. The existing security schemes for data deduplication is resented in Sect. 3. Section 4 discusses some of the open research challenges for future research direction in cloud computing and finally, we conclude the article in Sect. 5.

2 Secure Data Deduplication (SD^2eDup) in Cloud Computing

Duplicated copies of data are being generated from different users, organizations and CSP to backup of data for availability purpose. Basically, if we have an important file and would not like to lose it, then the copy of the file will be stored in different

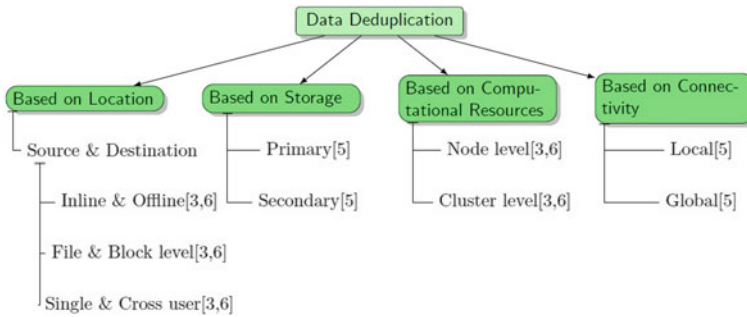


Fig. 1 Taxonomy of data deduplication techniques

locations and due to this duplicated data will be generated in the cloud. Hence, it is very essential to eliminate the redundant copies of data is being stored in the cloud storage server. The process of deleting the same copy of data stored in a single cloud or multi-cloud called data deduplication [13] improves the storage efficiency, increase the storage space and reduce storage cost. That is why, the data deduplication has attracted many CSP to improve the storage space utilization and attracting the many users by reducing the storage cost. The recent studies show that the data deduplication in the cloud can reduce the 50% storage cost in the standard file system and by up to 90–95% for backup application [14]. The data deduplication is usually performed by three entities: Cloud user who is data owner, CSP is a storage service provider to outsource the user data and third party who is trusted the party to trust on related computation. We know that the data can be text, numbers and multimedia, and we classify the deduplication based on computational resources and presents in taxonomy which is shown in Fig. 1.

2.1 Classification

Generally, we know that duplicate copy of data will be stored in the memory (primary or secondary) by the user at the source side or destination side. Hence, the data deduplication has to be done at source or destination. But many researchers have classified the deduplication techniques based on the general opinion, system design and architecture. In this paper, we classify the data deduplication techniques based on system resources and location of data being stored and duplicated. The taxonomy on the classification of data deduplication is shown in Fig. 1.

2.1.1 Based on Storage

The data deduplication techniques can be applied on either primary storage or secondary storage [6].

- **Primary Storage:** The primary storage-based deduplication executes on main memory to delete the redundant copies of data being stored in main memory because the primary storage consists of flash drives on storage area network where data are used to store on a daily basis which includes structured and unstructured data [9].
- **Secondary Storage:** All data are stored on a secondary storage device, the deduplication techniques have been applied to the data stored on secondary storage [9]. First, the data has to bring back to primary memory to verify the existence of duplication.

2.1.2 Based on Computational Resources

To improve the throughput and efficiency of data, deduplication can be applied on the node level or cluster level.

- **Node Level:** Instead the central deduplication, data can be distributed over node level and improves the throughput of deduplication [7, 10]. Data deduplication is identified by the computational resources of a single node, but it does not improve the throughput much. It will have the same cost as a local node.
- **Cluster Level:** The set of nodes can improve the throughput of the deduplication process on large scale data set. So distributed system needs to define the special routing mechanism to route data to the clustering nodes where several computational resources of nodes will be used to identify the data duplication which improves its efficiency and throughput as well [7, 10].

2.1.3 Based on Connectivity

Deduplication can also be categorized based on connectivity where cloud data are distributed to locally and globally connected nodes to eliminate the duplicated copies of data

- **Local Connectivity:** The data deduplication is done at local area network where local computers are connected to each other. In this process, the data has to be distributed to nodes in local connectivity to identify the duplicated copies of data with the help of parallelism and indexing techniques [9].
- **Global Connectivity:** The common data elimination is done in the distributed environment, i.e., across multiple data set at globally connected nodes. It is also known as multi-node deduplication globally [9]. The data are sent to the cluster connected globally to identify the existence of the common file and eliminate it.

2.1.4 Based on Location

Data deduplication can be done based on the location of data is being generated. That mean data is being generated at both source and destination side. So data deduplication can be done at either source side or destination side by deleting common copies of data

- **Source and Destination Side:** Data deduplication is performed at a source or client side before sending into cloud storage server. Using this technique fewer data can be sent over the network, so that network traffic will be reduced. The index data component has to bring into the source side to compare the similarity. The problem in this is, the index data can tamper. Because the data deduplication is performed after data arrives at the destination point. Data deduplication at destination side, the data management is done at the server side, which is why, the popular vendors like Amazon S3, Microsoft DepSky, Google Dropbox, etc., perform the destination side deduplication.

The data deduplication can be done before and after storing into system memory. The deduplication can be performed before storing into system memory called inline data deduplication [7], in which the first object comparison hash catalog has to bring into system memory to verify the existence of the same data. This technique uses more system resources [2]. The data deduplication is performed after writing into system memory is called offline (post processing) data deduplication [7]. It does not require the heavy utilization of computational resources. The disadvantage of this technique is that all duplicates data must be written into the storage system first, then verifying the same copy of data. Hence, data deduplication is at source and destination side with the help of these techniques can be done in file level or block level [7, 10]. By generating the hash code of files or blocks or checksum of data will be compared with the existing index of hash code and verify the same data existed or not.

2.2 Merits of Data Deduplication

The deduplication of data in cloud computing has many benefits and advantages for the CSP, infrastructure and the users as well. This paper highlight some of the merits of data deduplication in cloud computing.

- **Storage Efficiency:** The Data deduplication process will improve and increase the storage space for the users by deleting a redundant copy of data, so that storage space will be available to store more data.
- **Profitability:** By eliminating same copies of data in the cloud storage server, the storage space at cloud will be increased due to this availability of storage space will also be increased and more users will use the storage space and from this CSP will be benefited and profited.

- **Network Bandwidth utilization:** The only one copy is going to be stored in storage server and reference pointers or links to the actual data will be created for duplicated data, the duplicated data need not be transmitted to store in the storage server. This deduplication helps in reducing network bandwidth usage which improves network bandwidth utilization.
- **Energy consumption efficiency:** Nowadays, the huge amount of data is being generated from smart devices and social media and being stored in the cloud storage server. To maintain these servers, lots of computational resources are required. By deleting the duplicated copy of data from the server will have fewer data to maintain and energy consumed by the server will also be reduced. Hence, by deduplication, the energy consumption will be optimized and also the performance of data maintenance will be increased.
- **Green Computing:** The huge amount of data is being generated and stored in different data centers located in different geographical location. To maintain these data centers, a lot of cooling systems are required. From these cooling systems, the lots of carbon copy are generated which leads to the environment pollution. The deduplication process will reduce environmental pollution, because of fewer data in the data center which requires less cooling systems.

2.3 Security Threats

Nowadays, many users and organizations outsource their data into the cloud storage server. The outsourcing data is owned by the data owner, but once the data is outsourced to the cloud storage server, the data owner will lose physical control on his own data. The CSP will have full control over user data. Hence, many organizations are having fairness of adopting cloud storage due to its security and privacy issues. The data deduplication technique also faces sever and various security threats that means deduplication itself may become the security threat to the adversaries because deduplication and cryptographic algorithms are opposed to each other [12]. The security threat model during deduplication can be categorized as insider, outsider and network threats, its anatomy is shown in Fig. 2.

- **Insider Threat:** The adversaries might be within the cloud environment and could be a malicious employee who has the access privileges on the storage server and cloud network. This malicious employee may exploit the storage server while the process in deduplication of data. Because, during the deduplication process, all kinds of information will bring into the open environment, in such a situation, the malicious employee may exploit the process or may help an outsider to exploit it. Or just for curiosity, the employee may look into all information, which will lead to violation of data privacy and other security-related issues. It is very essential and important to consider these security issues like data breaches during data deduplication in cloud computing as shown in Fig. 2.

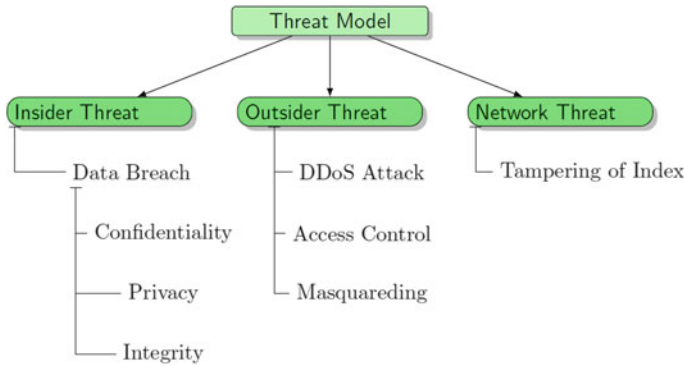


Fig. 2 Anatomy of security threat model during data deduplication

- **Outsider Threat:** There is some eavesdropper who will be interested in just harming the system resources. So the eavesdropper will try to gain the access to the resources during data deduplication at various levels or will try to break or exploit the deduplication process itself by DoS attack and masquerading.
- **Network Threat:** During deduplication at client side, the CSP has to send indexed data to the client for verifying the existence of redundant copy of data in cloud before uploading it into cloud storage server. The index information has to send through the network and the eavesdropper can perform various network attacks on index information during data deduplication.

3 Existing Deduplication Schemes

Many individual organizations are moving toward cloud to outsource their data due to its on-demand and availability characteristics. Once the data is outsourced to cloud, the data owner will lose the physical control on data and will be controlled by CSP. In practically, CSP is not trusted entity. So data owner may encrypt the data before outsourcing into cloud to meet the confidentiality and privacy of data. Presently, the convention encryption techniques are being used to provide the data confidentiality and privacy. The data deduplication process will be very difficult using these techniques. Because data owner encrypts their data with different secret keys and then outsource the unique ciphertext to the cloud even though the same data might present in the cloud storage server. The uniqueness of ciphertext will become very difficult for the deduplication server. With respect to this issue, the message level encryption is considered [12]. The message level encryption technique has four deterministic algorithms, namely encryption, decryption, key generation and

tag generation. The key generation algorithm will generate the secret key based on outsourcing content for encryption and decryption. This message level encryption technique has been classified into two categories: client-side encryption and server-side encryption [12].

The author of [15] proposed a theoretical message level encryption called message locked encryption (MLE). This is basically considered as convergent encryption (CE) algorithm. It has four different variants like CE, HCE1, HCE2 and RCF [12]. The key is generated from its own contents, the adversaries can mount a brute force and dictionary attack. Hence, this scheme does not provide much data security during deduplication. The author of [16, 17] has presented a client-side encryption technique without revealing about the outsourcing data to cloud storage. The client-side encryptions are suffered from offline and online brute force attack, the [18] proposed server-side encryption for data deduplication called DupLESS. In this scheme, the key is obtained from the key server and is generated from pseudo-random function (PRF) protocols and the key server is separated from cloud storage. In this, the key server plays a vital role to resist the dictionary and brute force attack.

It is a single point of connection to get key, there is a possibility of failure in key server and some data owners may not like, to avoid this problem, the author of [18] presents multiserver-aided DupLESS which allows the data owner to generate the keys from multiple key servers. The author of [19] proposed server-side data duplication schema over the encrypted data which allows CSP to control on outsourced data and prevents the data leakages in cloud.

During deduplication in the client side, the hash code of data is being verified to identify the duplicated copy data is stored in a cloud storage server or not. With the knowledge of the hash code, an attacker can get the ownership of the data stored in the cloud by showing the hash code of data to CSP. This will be one of security threat in client-side deduplication. To overcome this issue, proof of ownership is introduced [12]. The author of [20, 21] proposed MHT-based PoW in which CSP can challenge the client to prove its ownership on the data stored in the cloud storage server. Later, the Kaniche and Launt [22] also proposed a PoW schema over the encrypted data with the help of CE to achieve the confidentiality on data.

In data deduplication, data integrity is also an important security issue in the cloud storage server. [23] has proposed proof of storage with deduplication (POSD) in which auditor can verify the integrity of data stored in the cloud storage server. The author of [24] has identified the security weakness of weak key on the POSD proposed by [23] and proposed a new schema called e-POSD which enhance the security by minimizing the client load on key generation. The existing mechanisms for secure data deduplication are presented in taxonomy which are shown in Fig. 3.

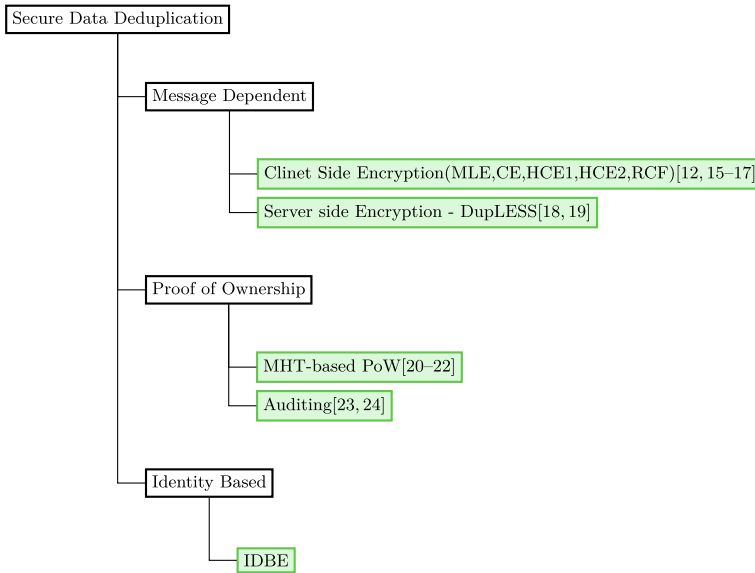


Fig. 3 Taxonomy of existing mechanisms on secure data deduplication

4 Open Research Challenges in Cloud Computing W.R.T. Deduplication

Duplicated copies of data are being generated from different users, organizations and CSP to backup of data for availability purpose that will leads to increase in the storage consumption and storage cost. Consider the scenario presented conceptual diagram of data duplication as shown in Fig. 4, the cloud user1 (CU1), cloud user2 (CU2), cloud user4 (CU4) and cloud user5 (CU5) have the same data to outsource into the cloud storage server. The CU1, CU2, CU3 and CU4 will encrypt their data by using individual secret key before uploading into the storage server to maintain the confidentiality, then upload it on to the storage server. Due to the encryption of same data with different secret key, the same data will be stored in cloud storage server and consumes the lot of storage space and also increase the storage cost and maintenance cost. It is very essential to avoid the duplication of data of different users in the cloud storage server that will improve the optimum usage of storage server and reduces the storage cost as well as maintenance cost. The some of the research challenges are listed below w.r.t the security during data deduplication process.

- Data Access Control:** Whenever a new user would like to upload the data into the cloud will be denied by CSP if it has the same copy in cloud storage. Now CSP has to give access permission to a new user for the data which is owned by someone else. Another case is that, if the owner of data stored in cloud storage requests for deleting or updating the contents of the file, in such cases, the revoked

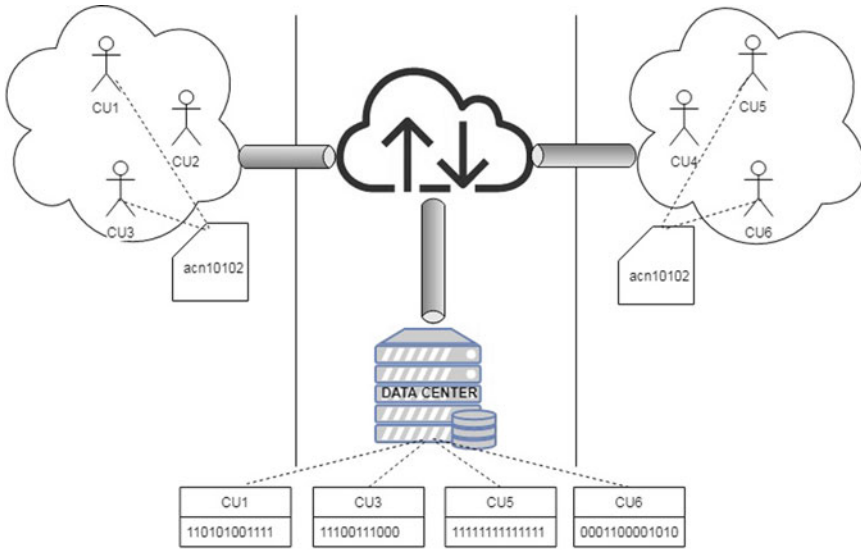


Fig. 4 Conceptual diagram of data duplication

users will be prevented from access of data. Hence, this one of the major security issues during data deduplication.

- Privacy of data:** Nowadays, the ownership of data is dynamically updated in cloud storage during deduplication process, the confidentiality and privacy of such data will be exposed by a CSP to users who would like to upload the same data to the cloud. Hence, the privacy of data during data deduplication has to be improved.
- Semantically Secure Deduplication:** The semantic encryption schema enables the user to have the privacy on their data stored in cloud storage by generating the independent ciphertext. This may make the deduplication process impossible due to independent ciphertext generated by the users for the same files.

5 Conclusion

Data deduplication has attracted many cloud service providers like Amazon, Google dropbox, etc., from which both CSP and users will be benefited. The secure data deduplication in cloud computing is a very important scheme for increasing the storage space of cloud and preserving the data confidentiality, privacy and other security of cloud data. In this article, we discussed the security concerns and classified different deduplication methods for general data which helps in eliminating the same copy of data. We also presented a security threat model during data deduplication at both source and destination side. In this article, the existing mechanisms to provide

the security to user data during data deduplication are presented. And finally, we gave some insights into the open research challenges for future research direction where security issues on data can still improve during the deduplication process in the cloud.

Our future work is to provide data deduplication in a multi-cloud environment by using lightweight cryptosystem.

References

1. Goswami V, Patra SS, Mund GB (2012) Performance analysis of cloud with queue-dependent virtual machines. In 2012 1st International conference on recent advances in information technology (RAIT). IEEE, pp 357–362
2. Yan Z, Zhang L, Ding W, Zheng Q (2017) Heterogeneous data storage management with deduplication in cloud computing. *IEEE Transactions Big Data*
3. Patra SS, Barik RK (2015) Dynamic dedicated server allocation for service oriented multi-agent data intensive architecture in biomedical and geospatial cloud. In: *Cloud technology: concepts, methodologies, tools, and applications*. IGI Global, pp 2262–2273
4. Barik RK (2019) Cloudganga: cloud computing based SDI model for ganga river basin management in India. In: *Geospatial intelligence: concepts, methodologies, tools, and applications*. IGI Global, pp 278–297
5. Barik RK, Dubey H, Mankodiya K (2017) SOA-FOG: secure service-oriented edge computing architecture for smart health big data analytics. In 2017 IEEE global conference on signal and information processing (GlobalSIP). IEEE, pp 477–481
6. Cisco (2015) CISCO global cloud index (2015–2020). Accessed 3 Jan 2018
7. Rashid F, Miri A (2018) Deduplication practices for multimedia data in the cloud. In: *Guide to big data applications*. Springer, Berlin, pp 245–271
8. Zhou Y, Feng D, Xia W, Fu M, Huang F, Zhang Y, Li C (2015) Secdep: a user-aware efficient fine-grained secure deduplication scheme with multi-level key management. In: 2015 31st Symposium on mass storage systems and technologies (MSST). IEEE, pp 1–14
9. Kaur R, Chana I, Bhattacharya J (2017) Data deduplication techniques for efficient cloud storage management: a systematic review. *J Supercomput*, pp 1–51
10. Paulo J, Pereira J (2014) A survey and classification of storage deduplication systems. *ACM Comput Surv (CSUR)* 47(1):11
11. Mandagere N, Zhou P, Smith MA, Uttamchandani S (2008) Demystifying data deduplication. In: *Proceedings of the ACM/IFIP/USENIX middleware'08 conference companion*. ACM, pp 12–17
12. Shin Y, Koo D, Hur J (2017) A survey of secure data deduplication schemes for cloud storage systems. *ACM Comput Surv (CSUR)* 49(4):74
13. Definition on Data Deduplication (2009) Accessed 1 Jan 2018
14. Meyer DT, Bolosky WJ (2012) A study of practical deduplication. *ACM Trans Storage (TOS)* 7(4):14
15. Bellare M, Keelveedhi S, Ristenpart T (2013) Message-locked encryption and secure deduplication. In: *Annual international conference on the theory and applications of cryptographic techniques*. Springer, pp 296–312
16. Bellare M, Keelveedhi S (2015) Interactive message-locked encryption and secure deduplication. In: *IACR international workshop on public key cryptography*. Springer, pp 516–538
17. Liu J, Asokan N, Pinkas B (2011) Secure deduplication of encrypted data without additional independent servers. In: *Proceedings of the 22nd ACM SIGSAC conference on computer and communications security*. ACM, pp 874–885

18. Bellare M, Keelveedhi S, Ristenpart T (2013) Dupless: server-aided encryption for deduplicated storage. IACR Cryptol ePrint Arch 2013:429
19. Hur J, Koo D, Shin Y, Kang K (2016) Secure data deduplication with dynamic ownership management in cloud storage. IEEE Trans Knowled Data Eng 28(11):3113–3125
20. Merkle RC (1989) A certified digital signature. In: Conference on the theory and application of cryptology. Springer, pp 218–238
21. Halevi S, Harnik D, Pinkas B, Shulman-Peleg A (2011) Proofs of ownership in remote storage systems. In: Proceedings of the 18th ACM conference on computer and communications security. ACM, pp 491–500
22. Kaaniche N, Laurent M (2014) A secure client side deduplication scheme in cloud storage environments. In: 2014 6th International conference on new technologies, mobility and security (NTMS). IEEE, pp 1–7
23. Zheng Q, Xu S (2012) Secure and efficient proof of storage with deduplication. In: Proceedings of the second ACM conference on data and application security and privacy. ACM, pp 1–12
24. Shin YJ, Hur J, Kim K (2012) Security weakness in the proof of storage with deduplication. IACR Cryptol ePrint Arch 2012:554

Analyzing Ensemble Methods for Software Fault Prediction



Nitin, Kuldeep Kumar, and Santosh Singh Rathore

Abstract Prediction of software faults using different machine learning techniques has been reported earlier by many researchers. However, these individual techniques suffered from performance problems as the software fault dataset changes. In the last few years, ensemble-based approaches gained popularity in the software fault prediction because of their improved performance over the single-fault prediction techniques. Motivated by this reason, an experimental study is performed on ensemble methods for predicting whether a software contains fault or not. The study includes random forest, bagging, random subspace, and boosting as ensemble methods, and decision trees, logistic regression, and k-nearest neighbors as base learning algorithms for the ensembles. The experiments are conducted on 15 software fault datasets corresponding to the Eclipse project and PROMISE Software Engineering repository. We evaluated the results using precision, accuracy, recall, and ROC-AUC score. Additionally, we performed the Friedman statistical test to see whether the performance difference of ensemble methods is statistically significant or not. We also performed the Wilcoxon signed-rank test for the paired samples to check which of the two techniques have performance differences.

Keywords Software fault prediction · Ensemble methods · Statistical test

Nitin (✉) · K. Kumar

Department of Computer Science and Engineering, Dr. B R Ambedkar National Institute of Technology Jalandhar, Jalandhar, Punjab, India
e-mail: nitin13695@gmail.com

K. Kumar

e-mail: kuldeepgargkkr@gmail.com

S. S. Rathore

Atal Bihari Vajpayee Indian Institute of Information Technology and Management, Gwalior, India
e-mail: santoshs@iiitm.ac.in

© Springer Nature Singapore Pte Ltd. 2021

G. S. Hura et al. (eds.), *Advances in Communication and Computational Technology*, Lecture Notes in Electrical Engineering 668,
https://doi.org/10.1007/978-981-15-5341-7_95

1253

1 Introduction

To ensure a fault-free operation of the software system, it needs to be completely tested. However, testing a software completely is not possible due to various constraints such as testing cost, time, and project budget [1]. Therefore, identifying which software modules is likely to be faulty before the testing phase will help in efficiently utilizing the resources. It is because now the limited resources can be optimally allocated to the fault-prone modules. Software fault prediction is used to detect such fault-prone modules. It is performed before the testing phase. It reduces the unnecessary effort that is needed in the testing phase to find the faulty modules. The software fault prediction model is generally constructed using the fault dataset from the previous releases of similar software projects, and later it is applied to the currently underdevelopment software. Many researchers earlier explored different machine learning techniques such as decision trees, support vector machines, and naive Bayes classifiers [2] for software fault prediction. However, these individual techniques suffered from performance problems as the software fault dataset changes.

In recent years, some researchers evaluated ensemble methods for software fault prediction [3, 4]. These studies showed that ensemble methods performed better than single-fault prediction techniques. Motivated by this reason, we perform an experimental study on the ensemble methods for the binary classification of software modules that is whether the software module contains fault or not. The experiments are conducted on 15 software fault datasets, out of which five datasets correspond to different versions of Eclipse software and 10 datasets are from the PROMISE Software Engineering repository. The results of the experiments are evaluated using four metrics: precision, accuracy, recall, and area under the receiver operating characteristic curve (ROC-AUC) score. Further, for each performance measure, we performed the Friedman statistical test to see whether the performance difference of ensemble methods is statistically significant or not. After applying the Friedman test, we also performed the Wilcoxon signed-rank test for the paired samples to check which of the two techniques have significant performance differences.

The paper is organized as follows. Related work is presented in Sect. 2. In Sect. 3, the used ensemble methods are discussed. Section 4 discusses the experimental setup and results. Section 5 concludes the paper.

2 Related Work

In recent years, software fault prediction has become one of the most important research areas in software engineering due to its great contribution in improving software quality. In this section, previous works done by researchers in the software fault prediction have been presented. Based on the existing literature, it is

found that ensemble-based approaches gained popularity in software fault prediction because of their improved performance in comparison with individual machine learning techniques.

Tao et al. [5] conducted a comparative study of ensemble methods with the context of software defect prediction. The used ensemble methods were random subspace, bagging, random forest, boosting, stacking, and voting. The datasets used were PC1, PC2, PC3, PC4, KC1, KC2, KC3, CM1, JM1, KC4, MC1, MC2, MW1, and PC5 from NASA data repository. From experimental analysis, it was concluded that ensemble methods achieved better performance over a single classifier.

Huda et al. [6] proposed an ensemble model for software fault prediction, which focused on the class imbalance problem in the software fault datasets. They reported that different oversampling techniques have been used by the researchers to build an ensemble model that can reduce low minority samples in the software fault data. They presented a model that used a combination of three oversampling techniques namely majority voted minority oversampling technique, fuzzy-based feature instance recovery, and random oversampling to build an ensemble model. The datasets used were from the PROMISE repository. The results showed that the ensemble oversampling technique has reduced the false-negative rate and performed better than standard classification techniques and identified the faulty components more accurately.

Osman et al. [7] performed hyper-parameter optimization to improve bug prediction accuracy. The authors investigated whether by optimizing the hyper-parameters of a machine learning model improves its performance or not. The used techniques were k-nearest neighbors and support vector machines and used datasets were from different versions of Eclipse software, namely Eclipse JDT core, MYLYN, Equinox, LUCENE, and Eclipse PDE UI. The results of the experiments showed that hyper-parameter optimization should be performed before using a machine learning model.

Shanthini et al. [8] analyzed the effect of the ensemble model build with the help of the bagging technique for software fault prediction. They worked on the class- and package-level metrics. The ensemble technique used was bagging with the base learner as support vector machines. The datasets used were Eclipse package-level dataset and NASA KC1 dataset. To evaluate the performance of the classifier, AUC-ROC and PR curves are used. Results showed that better performance is given by a bagged SVM classifier. In future work, the authors suggested building the ensemble by using other machine learning algorithms such as neural networks and genetic algorithms.

Alsaedi et al. [9] performed a study on supervised machine learning techniques and ensemble techniques for software fault prediction. The ensemble techniques used were bagging and boosting. The base learners used were decision tree, support vector machines, random forest, and logistic regression. The datasets used were PC1, PC2, PC3, PC4, PC5, MC1, MC2, MW1, JM1, KC3 from the NASA data repository. Accuracy, F-score and ROC-AUC score were used as performance measures. From experimental analysis, it was concluded that random forest, AdaBoost with random forest, and bagging with decision tree performed well.

Chubato et al. [10] compared two ensemble techniques and realized their performance improvement when combined with feature selection and data balancing. The ensemble techniques used were bagging and boosting. The performance measures used were accuracy and ROC-AUC score. The datasets used were ar1, ar4, JM1, KC2, MC1, MW1, PC3, and PC4 from the NASA repository. Their results showed performance improvement when ensemble techniques were combined with feature selection and data balancing.

The conclusions from the above literature review showed that ensemble methods help in obtaining better performance than individual fault prediction techniques. However, very few works have been done in software fault prediction with ensemble methods. Thus, this paper presents an experimental study on four different ensemble techniques.

3 Ensemble Methods for Software Fault Prediction

Ensemble methods generate several intermediate models and combine them to produce the final output with the aim of improved results. Generally, ensemble methods produce better results than single machine learning techniques due to the reason that the ensemble method utilizes a group of weak learners, each having the expertise for a sub-region of the input data to form a strong learner and thus increasing the accuracy of the prediction model. In this study, we have used four ensemble techniques, which are discussed as follows. Chang and Ma gave a detailed description of these techniques [11].

3.1 Bagging

Bagging stands for bootstrap aggregating. It is an ensemble technique proposed by Breiman Leo in 1996. In the bagging algorithm, in the first step, multiple models are created. For each model, the dataset is generated by randomly selecting the training examples from the original training dataset, and then training each model using some base learning algorithm. There is a chance that some training examples are selected more than once and some may not be selected even once. Finally, the results of the models are combined by averaging for majority voting for classification.

3.2 Boosting

Boosting is an ensemble method proposed by Freund and Schapire in 1997. It is a sequential method. Initially, all the instances in the training dataset are assigned equal weights which mean that all the instances have equal probability to appear in

the training dataset of a model. Then, the first model is built by randomly selecting the instances from the original training dataset. After the model is trained, it is tested on the original training dataset and then the misclassified instances by the first model are assigned higher weights to increase their chances to be selected in the next iteration. This process is repeated until we reach some specified models that we have to build. Finally, their results are combined with majority voting.

3.3 Random Subspace

It is an ensemble method proposed by Tin Kam Ho. Like bagging, in this method also the random selection is done, but instead of instances, it is of features. For each model, the training dataset is created by randomly selecting the subset of features. Each model is trained using some base learning algorithm. Finally, the results are combined by majority voting. This method is used when the size of the training dataset is small in comparison with the numbers of features because the relative training size increases. Also, it is used when there are redundant features because a better classifier is obtained in the subspace of features instead of the original feature space.

3.4 Random Forest

Random forest proposed by Breiman is an ensemble method which is also known as decision forest. Each model in the forest is constructed using the decision tree as a base learning algorithm. For each model, the tree is constructed in two steps. In the first step, at each node, a subset of features is selected randomly to split on. In the second step, the feature at the node is selected which is performing the best split. Finally, after building the specified number of trees in the forest, their result is combined by means of majority voting.

4 Experimental Methodology and Results

This section describes the experimental methodology used for the analysis. Further, this section provides the details of software fault datasets used in the experimentation. Performance evaluation measures, base learning techniques, experimental methodology, and the results of the experimental analysis are discussed thereafter.

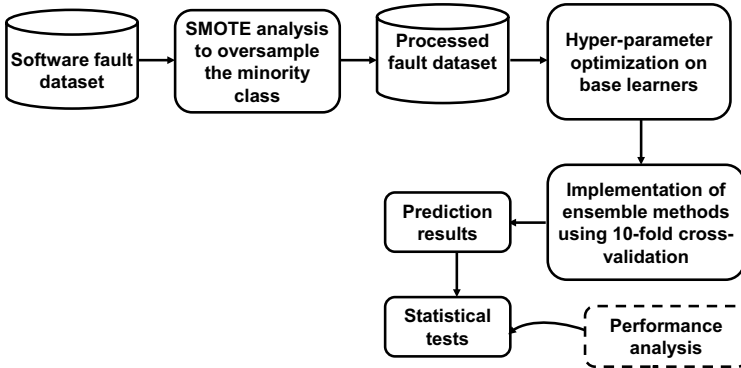


Fig. 1 Overview of the experimental methodology

4.1 Experimental Methodology

Figure 1 gives an overview of the experimental methodology used in the presented work. It consists of four major steps. In the first step, we preprocess the original software fault dataset to remove the imbalance problem. Since, in the fault dataset, representation of minority class values (faulty modules) is lesser than the representation of majority class values (non-faulty), therefore, we perform oversampling analysis on minority class values (SMOTE) to make the dataset balanced. In the second step, we perform hyper-parameter optimization of the base learners on the processed fault dataset. This step will result in the optimized parameter values for each used base learner. In the third step, we build the ensemble method-based fault prediction models. We use a tenfold cross-validation scheme to handle the prediction biasing due to the partition of the dataset into training and testing parts. The used cross-validation scheme initially partition fault dataset into ten parts: use 9 parts as training data and the rest one part as testing data. This process is repeated ten times and results are averaged. The last step is the evaluation of prediction results to validate the performance of the ensemble method-based fault prediction models.

4.2 Software Fault Dataset

Out of 15 datasets used in this paper, five datasets correspond to the Eclipse project¹ and 10 datasets correspond to the PROMISE Software Engineering repository.² Eclipse is an integrated development environment (IDE) used in software development and is the most widely used Java IDE. PROMISE Software Engineering repository contains a group of open datasets and tools that are available publicly

¹ Available at: “<http://bug.inf.usi.ch/download.php>”.

² Available at: “<http://tunedit.org/repo/PROMISE/DefectPrediction>”.

to help researchers in building predictive software models. The used software fault datasets from Eclipse software are Equinox framework, Eclipse JDT core, Mylyn, Eclipse PDE UI, Lucene and from PROMISE repository are ar1, kc1, mc2, mw1, pc2, ar3, ar4, ar5, pc3, ar6.

Independent variables corresponding to the software fault datasets are coupling between objects (CBO), fan in, fan out, depth of inheritance tree (DIT), lack of cohesion methods (LCOM), number of children (NOC), number of attributes, number of attributes inherited, number of lines of code, number of methods, number of methods inherited, number of private attributes, number of private methods, number of public attributes, number of public methods, response for classes (RFC), weighted methods for class (WMC). The dependent variable is bug, which is either true or false, true means that the software module is faulty and false means the module is not faulty.

4.3 Performance Evaluation Measures

We have used four performance measures to evaluate the ensemble methods. The used performance measures are precision, accuracy, recall, and ROC-AUC score. Some common terms used to find performance measures are discussed below.

True Positive (TP). Observation is predicted to be positive and actually is positive.

False Negatives (FN). Observation is predicted to be negative and actually is positive.

True Negatives (TN). Observation is predicted to be negative and actually is negative.

False Positive (FP). Observation is predicted to be positive and actually is negative.

The used performance measures are:

Accuracy. It is the ratio of correctly predicted observation to the total number of observations. It means how often the classifier is correct. It is calculated as $(TP + TN)/\text{total numbers of observations}$.

Precision. It is the ratio of correctly predicted positive observations to the total predicted positive observations. It means when the classifier predicts yes, how often it is correct. It is calculated as $TP/\text{predicted yes}$.

Recall. It is the ratio of correctly predicted yes to all the observations in actual class yes. It means when it is actually yes, how often the classifier predicts it yes. It is calculated as $TP/\text{actual yes}$.

ROC-AUC score. It computes the area under the receiver operating characteristic curve from prediction scores. ROC is a probability curve and AUC represents the degree of separability which tells how much the model is able to differentiate the classes. Higher the area under the curve, the good is the model in differentiating the classes.

4.4 Base Learning Techniques

Decision Tree. It is a flowchart-like structure where each internal node best divides the data to classify a target variable. The tree contains a root node, internal nodes, and leaves, which denotes the class labels. Each branch of the tree represents some decisions. Now given a new instance, it is classified by traversing the tree from the root node to leaves according to the values of its features.

K-Nearest Neighbors. It is a machine learning technique that uses all the instances in the dataset to classify a new instance. It basically computes the distance of a new instance with all the instances in the dataset by using some distance functions such as Euclidean distance, Manhattan distance, Minkowski distance. A new query is classified by seeing which class in the k-nearest neighbors has the majority. The class which is having the majority is assigned to it.

Logistic Regression. It is a machine learning algorithm that is used for classification problems and based on the concept of probability. It computes the probability of an event occurrence. It uses logit score to compute the probability of occurrence of classes. The logit score is passed into the logistic function to get the probability of each target class. If we pass the logit through logistic function, then it calculates the probability of both the classes. Later the target class with high probability is considered as the predicted class for the given activity.

4.5 Experimental Setup

We have done our experimentation using Python language. We have used python's *sklearn* library³ to implement and evaluate the ensemble techniques. First of all, we have applied the synthetic minority oversampling technique (SMOTE) to the datasets to oversample the minority class because most of the datasets are imbalanced. Then, we have performed hyper-parameter optimization to find the best hyper-parameters for the individual techniques using grid search cross-validation. Then, the base learners with optimized hyper-parameters are used with ensemble techniques as a base learner. Thereafter, we evaluated the ensemble techniques with the performance measures using cross-validation. At the last, using real statistics tool in excel, we performed the Friedman statistical test⁴ for each performance measure to check whether the performance difference of ensemble methods is statistically significant or not. We further performed the Wilcoxon signed-rank test⁵ for the paired samples to check which of the two ensemble techniques differ from each other.

³Scikit-learn, "Machine Learning in Python, <https://scikit-learn.org/stable/>".

⁴Friedman Statistical Test, "<http://www.real-statistics.com/anova-repeated-measures/friedman-test/>".

⁵Wilcoxon Signed Rank Test, "<http://www.real-statistics.com/non-parametric-tests/wilcoxon-signed-ranks-test/>".

4.6 Results and Analysis

The Friedman test is a statistical test that is used for checking whether there is a statistical difference between several related samples or not. The Wilcoxon test is a statistical test that compares two paired groups and checks whether these groups are statistically different or not. In this section, we discuss the results of the Friedman test on all the performance measures (i.e., precision, accuracy, recall, and ROC-AUC score). Also, the results of the Wilcoxon test are discussed for the performance measures for which the techniques have performance differences.

Tables 1, 2, 3, and 4 present the results of accuracy, precision, recall, and ROC-AUC performance measures of all the techniques corresponding to all the datasets. For each technique, we have taken the result of the best-performing base learner, means out of the three used base learners for ensemble methods (i.e., decision trees, logistic regression, and k-nearest neighbors), whoever is performing best, the results of that base learner is taken.

We have performed Friedman test on the accuracy, precision, recall, and ROC-AUC results observed in Tables 1, 2, 3, and 4, respectively. The results of the Friedman test are shown in Table 5. From the results, we conclude that in case of accuracy and precision, there are no statistically significant performance differences among the ensemble techniques. It is because the p-value is greater than the alpha value. But, in the case of recall and ROC-AUC score, since the p-value is smaller than the alpha value (i.e., 0.05), there are statistically significant performance differences among the techniques.

Table 1 Accuracy results of ensemble techniques

Dataset	Bagging	Boosting	Random subspace	Random forest
Eclipse JDT Core	0.91	0.92	0.89	0.89
Eclipse PDE UI	0.90	0.92	0.90	0.90
Equinox	0.79	0.74	0.77	0.80
Lucene	0.93	0.96	0.92	0.94
Mylyn	0.89	0.91	0.91	0.91
AR1	0.92	0.92	0.90	0.89
KC1	0.71	0.71	0.62	0.72
MC2	0.76	0.81	0.79	0.76
MW1	0.93	0.94	0.95	0.94
PC2	0.99	0.99	0.99	0.99
AR3	0.88	0.86	0.90	0.85
AR4	0.85	0.89	0.84	0.84
AR5	0.90	0.92	0.92	0.89
PC3	0.92	0.93	0.92	0.92
AR6	0.85	0.85	0.90	0.88

Table 2 Precision results of ensemble techniques

Dataset	Bagging	Boosting	Random subspace	Random forest
Eclipse JDT Core	0.89	0.91	0.89	0.90
Eclipse PDE UI	0.90	0.92	0.89	0.90
Equinox	0.77	0.71	0.72	0.80
Lucene	0.93	0.96	0.92	0.95
Mylyn	0.90	0.91	0.89	0.91
AR1	0.89	0.88	0.89	0.89
KC1	0.67	0.69	0.68	0.76
MC2	0.79	0.84	0.81	0.79
MW1	0.90	0.91	0.92	0.92
PC2	0.99	0.99	0.99	0.99
AR3	0.89	0.90	0.85	0.86
AR4	0.84	0.85	0.84	0.82
AR5	0.90	0.90	0.94	0.90
PC3	0.92	0.93	0.92	0.92
AR6	0.90	0.92	0.91	0.90

Table 3 Recall results of ensemble techniques

Dataset	Bagging	Boosting	Random subspace	Random forest
Eclipse JDT Core	0.94	0.92	0.90	0.92
Eclipse PDE UI	0.94	0.91	0.90	0.89
Equinox	0.82	0.80	0.79	0.84
Lucene	0.96	0.96	0.93	0.96
Mylyn	0.96	0.91	0.91	0.95
AR1	1.00	0.94	0.92	0.98
KC1	0.73	0.66	0.65	0.70
MC2	0.78	0.79	0.75	0.70
MW1	0.97	0.96	0.98	0.95
PC2	0.99	0.99	0.99	0.99
AR3	0.96	0.96	0.78	0.87
AR4	0.89	0.92	0.90	0.87
AR5	0.96	0.96	0.88	0.96
PC3	0.94	0.94	0.93	0.94
AR6	0.89	0.87	0.83	0.84

Table 4 ROC-AUC score results of ensemble techniques

Dataset	Bagging	Boosting	Random subspace	Random forest
Eclipse JDT Core	0.95	0.97	0.95	0.95
Eclipse PDE UI	0.96	0.96	0.96	0.96
Equinox	0.83	0.85	0.81	0.87
Lucene	0.97	0.99	0.98	0.98
Mylyn	0.96	0.96	0.95	0.96
AR1	0.96	0.96	0.95	0.96
KC1	0.82	0.74	0.76	0.83
MC2	0.87	0.9	0.88	0.85
MW1	0.98	0.97	0.97	0.98
PC2	0.99	0.99	0.99	0.99
AR3	0.94	0.94	0.93	0.94
AR4	0.93	0.96	0.91	0.91
AR5	0.96	0.95	0.94	0.95
PC3	0.97	0.97	0.97	0.97
AR6	0.95	0.9	0.92	0.92

Table 5 Friedman test results on the accuracy, precision, and recall

	Accuracy	Precision	Recall	ROC-AUC score
Alpha	0.05	0.05	0.05	0.05
Q-stat	5.225	7.68595	17.136	8.234694
Df	3	3	3	3
p-value	0.156044	0.052968	0.000663	0.041402

Because there is a performance difference among the ensemble techniques in case of recall and ROC-AUC score, we have also applied the Wilcoxon test on Table 3 (recall results) and Table 4 (ROC-AUC score results) to check which of the two techniques differ from each other. The results of the Wilcoxon test are shown in Tables 6 and 7 for recall and ROC-AUC score, respectively.

From the results of the Wilcoxon test on recall in Table 6, we observed that the performance of bagging is differing with boosting, random subspace, and also with random forest. Also, there is a performance difference between boosting and random forest, and between random subspace and random forest. As there are performance differences between the techniques, so we have compared the ensemble techniques with each other. In order to compare the techniques, we have taken the mean from all the datasets for each technique. The mean values of bagging, boosting, random forest, and random subspace are 0.9153, 0.8993, 0.8693, and 0.8906, respectively, which are shown in Fig. 2. From Fig. 2, we concluded that bagging is performing best

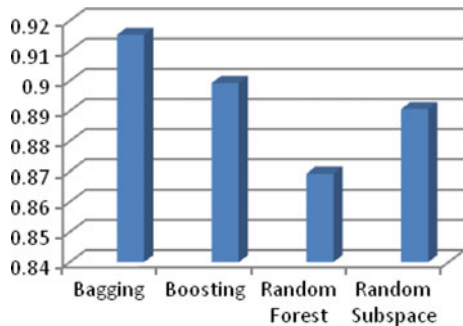
Table 6 Wilcoxon test results on recall

Treatment	<i>p</i> -norm	<i>p</i> -exact	Result
Bagging versus boosting	0.059006	0.048828	Significantly different
Bagging versus random forest	0.003121	0.001221	Significantly different
Bagging versus random subspace	0.012353	0.006836	Significantly different
Boosting versus random forest	0.007745182	0.004638672	Significantly different
Boosting versus random subspace	0.609368	0.625000	Significantly not different
Random subspace versus random forest	0.109159	0.104004	Significantly different

Table 7 Wilcoxon test results on ROC-AUC score

Technique	<i>p</i> -norm	<i>p</i> -exact	Result
Bagging versus boosting	0.811892	0.820313	Significantly not different
Bagging versus random forest	0.027717	0.024414	Significantly different
Bagging versus random subspace	0.669815	0.687500	Significantly not different
Boosting versus random forest	0.116056	0.123047	Significantly not different
Boosting versus random subspace	1.000000	0.945313	Significantly different
Random subspace versus random forest	0.103011	0.109375	Significantly not different

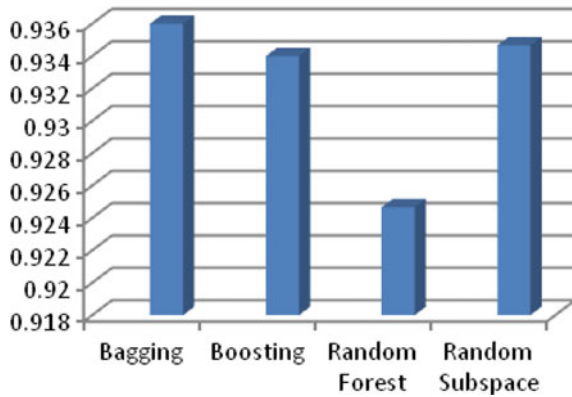
Fig. 2 Recall results for ensemble techniques



among all the ensemble techniques. The lowest performance is achieved by random forest. Boosting and random subspace performed relatively similar.

From the results of the Wilcoxon test on the ROC-AUC score in Table 7, we observed that there is a performance difference between bagging and random forest, and also between boosting and random subspace. Similar to recall, in the case of ROC-AUC score, we have also performance differences between the techniques, so we have compared the ensemble techniques with each other. The results are shown in Fig. 3. The results showed that bagging is performing best among the techniques and random forest achieved the least performance.

Fig. 3 ROC-AUC score results for ensemble techniques



4.7 Comparative Evaluation

Table 8 shows the comparison of our results with the previous work [9, 10]. We have compared our results with previous work using datasets, techniques, and performance measures that matched with their works. To compare the techniques, we have taken the mean of their performances from the matched datasets. In the case of Alsaeedi and Khan [9], the performance measures that matched are accuracy, ROC-AUC score, the datasets that matched are PC3 and MC2, and the techniques that matched are bagging, boosting, and random forest.

From the table, it can be observed that our presented techniques performed better for both the performance measures and yielded better results. In the case of Chubato et al. [10], the performance measures that matched are accuracy and ROC-AUC score,

Table 8 Comparison evaluation

Author	Datasets used	Performance measure	Ensemble method used		
			Bagging	Boosting	Random forest
Alsaeedi and Khan [9]	PC3, MC2	Accuracy	0.79	0.77	0.76
		ROC-AUC score	0.67	0.67	0.62
Our results		Accuracy	0.84	0.87	0.84
		ROC-AUC score	0.92	0.93	0.91
Chubato et al. [10]	AR1, AR4 MW1, PC3,	Accuracy	0.84	0.84	NA
		ROC-AUC score	0.90	0.89	NA
Our results		Accuracy	0.90	0.92	NA
		ROC-AUC score	0.96	0.96	NA

the techniques that matched are bagging and boosting, the datasets that matched are MW1, PC3, AR1, and AR4. From the table, it can be concluded that our presented work produced a better performance for both the performance measures. In the case of accuracy, we achieved an improvement of 6% and 8% for bagging and boosting techniques, respectively. Similarly, for ROC-AUC measure, we achieved 6% and 7% improvement for bagging and boosting techniques, respectively

5 Conclusions and Discussion

In this paper, we performed an evaluation of four ensemble techniques namely random subspace, bagging, boosting, and random forest for the software fault prediction. We used three different learning techniques, namely decision tree, k-nearest neighbors, and logistic regression, as base learners to the ensemble method. Four performance measures were used which are precision, accuracy, recall, and ROC-AUC score. The experiments were conducted on 15 software fault datasets corresponding to the Eclipse project and PROMISE Software Engineering repository. For each performance measure, we performed Friedman statistical test to see whether the difference in the performance of ensemble techniques is statistically significant or not. Results of the Friedman test showed that there was a statistically significant performance difference between the techniques for the recall and ROC-AUC score performance measures. However, for accuracy and precision measures, no statistically significant difference has been found between techniques. We have performed the Wilcoxon test on the performance measures for which we have found performance differences between the ensemble techniques. The results of the Wilcoxon test on recall showed that the performance of bagging was statistically significantly different from boosting, random subspace, and random forest. Additionally, a performance difference between boosting and random forest and between random subspace and the random forest has also been found. For the ROC-AUC score, the results of the Wilcoxon test showed that there was a performance difference between bagging and random forest and also between boosting and random subspace. Also, bagging is performing best and random forest performed least among all the techniques in case of recall and ROC-AUC score as the performance measures.

References

1. Hall T et al (2012) A systematic literature review on fault prediction performance in software engineering. <https://doi.org/10.1109/TSE.2011.103>
2. Rathore SS, Kumar S (2019) A study on software fault prediction techniques. *Artif Intell Rev*. <https://doi.org/10.1007/s10462-017-9563-5>
3. Rathore SS, Kumar S (2017) Linear and non-linear heterogeneous ensemble methods to predict the number of faults in software systems. *Knowl-Based Syst* 119:232–256. <https://doi.org/10.1016/j.knsys.2016.12.017>

4. Tong H et al (2018) Software defect prediction using stacked denoising autoencoders and two-stage ensemble learning. *Inf Softw Technol* 96:94–111. <https://doi.org/10.1016/j.infsof.2017.11.008>
5. Wang T et al.: Software defect prediction based on classifiers ensemble. *J Inf Comput Sci* 8(16):4241–4254 (2011)
6. Huda S et al (2018) An ensemble oversampling model for class imbalance problem in software defect prediction. *IEEE Access* 6:24184–24195. <https://doi.org/10.1109/ACCESS.2018.2817572>
7. Osman H et al (2017) Hyperparameter optimization to improve bug prediction accuracy. In: *MaLTesQuE 2017—IEEE international workshop on machine learning techniques for software quality evaluation, co-located with SANER 2017*. pp 33–38 IEEE (2017). <https://doi.org/10.1109/MALTESQUE.2017.7882014>
8. Shanthini A, Chandrasekaran RM (2014) Analyzing the effect of bagged ensemble approach for software fault prediction in class level and package level metrics. In: *International conference on information communication and embedded systems (ICICES2014)*, pp 1–5. IEEE <https://doi.org/10.1109/ICICES.2014.7033809>
9. Alsaeedi A, Khan MZ (2019) Software defect prediction using supervised machine learning and ensemble techniques: a comparative study. *J Softw Eng Appl* 12(05):85–100. <https://doi.org/10.4236/jsea.2019.125007>
10. Yohannese CW et al (2017) Ensembles based combined learning for improved software fault prediction: a comparative study. In: *Proceedings of the 2017 12th international conference on intelligent systems and knowledge engineering, ISKE 2017*. <https://doi.org/10.1109/ISKE.2017.8258836>
11. Zhang C, Ma Y (2012) Ensemble machine learning: methods and applications. <https://doi.org/10.1007/9781441993267>

Porting of eChronos RTOS on RISC-V Architecture



Shubhendra Pal Singhal, M. Sridevi, N. Sathya Narayanan,
and M. J. Shankar Raman

Abstract eChronos is a formally verified real-time operating system (RTOS) designed for embedded microcontrollers. eChronos was targeted for tightly constrained devices without memory management units. Currently, eChronos is available on proprietary designs like ARM, PowerPC, and Intel architectures. eChronos is adopted in safety critical systems like aircraft control system and medical implant devices. eChronos is one of the very few system softwares not been ported to RISC-V. RISC-V is an open-source instruction set architecture (ISA) that enables a new era of processor development. Many standard operating systems, software toolchain has migrated to the RISC-V architecture. According to the latest trends [1], RISC-V is replacing many proprietary chips. As a secure RTOS, it is attractive to port on an open-source ISA. SHAKTI and PicoRV32 are some of the proven open-source RISC-V designs available. Now having a secure RTOS on an open-source hardware design, designed based on an open-source ISA makes it more interesting. In addition to this, the current architectures supported by eChronos are all proprietary designs [2], and porting eChronos to the RISC-V architecture increases the secure system development as a whole. This paper presents an idea of porting eChronos on a chip which is open-source and effective, thus reducing the cost of embedded systems. Designing a open-source system that is completely open-source reduces the overall cost, increased the security, and can be critically reviewed. This paper explores the design and architecture aspect involved in porting eChronos to RISC-V. The authors

S. P. Singhal (✉) · M. Sridevi

Department of Computer Science and Engineering, National Institute of Technology,
Tiruchirappalli, India

e-mail: shubhendrapalsinghal@gmail.com

M. Sridevi

e-mail: msridevi@nitt.edu

N. Sathya Narayanan · M. J. Shankar Raman

Department of Computer Science and Engineering, Indian Institute of Technology, Madras,
Chennai, India

e-mail: sathya281@gmail.com

M. J. Shankar Raman

e-mail: mjsraman@gmail.com

© Springer Nature Singapore Pte Ltd. 2021

G. S. Hura et al. (eds.), *Advances in Communication and Computational*

Technology, Lecture Notes in Electrical Engineering 668,

https://doi.org/10.1007/978-981-15-5341-7_96

have successfully ported eChronos to RISC-V architecture and verified it on spike [3]. The port of RISC-V to eChronos is made available open-source by authors [4]. Along with that, the safe removal of architectural dependencies and subsequent changes in eChronos is also analyzed.

Keywords eChronos · Porting · Real-time operating systems · RISC-V · SHAKTI

1 Introduction

Porting is the process of converting the software for the another architecture. A software has many exceptions and forms of programming specific to the architecture like memory or register allocation. To be able to run such executable file, we need porting. There are many OS porting techniques available in the literature [5] that follow trial and error approach. In this paper, we have used the hit and trial approach for porting eChronos on an open-source architecture RISC-V [6, 7].

1.1 eChronos

The eChronos RTOS is a real-time operating system (RTOS) [8]. It is intended for tightly resource-constrained devices without memory management units and virtual memory support. Also, RTOS code base is designed to be highly modular so that only the minimal amount of code necessary is ever compiled into a given system image [8]. The eChronos RTOS is highly configurable and functional as shown in Fig. 1 [9].

1.2 RISC-V

RISC-V is an open-source hardware ISA based on reduced instruction set computer (RISC) principles. RISC-V is a layered and extensible open-source ISA which means that it can support the implementation of well-defined extensions for a given application. RISC-V offers a very flexible usage of instruction set which adds to up to RISC-V becoming more popular [10]. RISC-V is modular and flexible, which reduces the effort to develop the ancillary software for a specific processor.

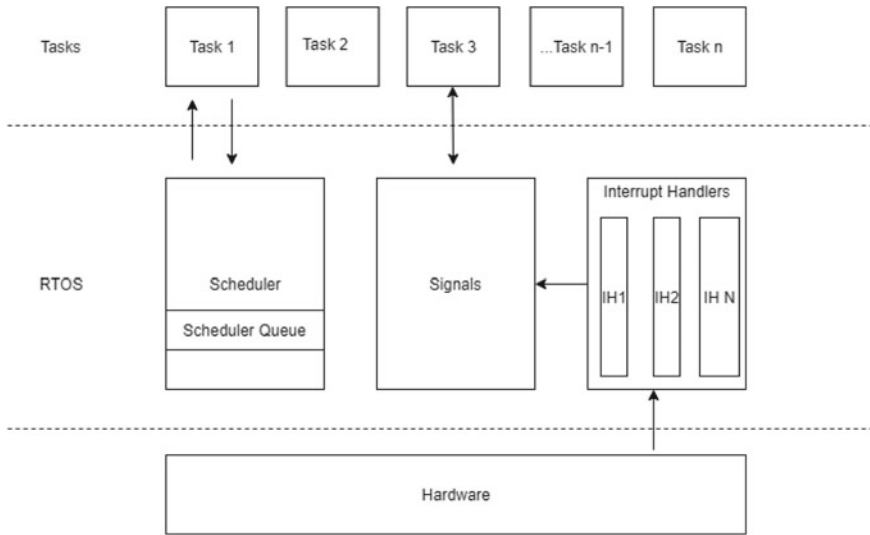


Fig. 1 eChronos RTOS functionality

1.3 Porting an Operating System

Porting of OS is a time-consuming process as it involves changes to big and complex programs. Porting every specific program seems to be a bit irrational. So the solution to such a complex problem is the modern-day compilers, which translates the high-level language program to a platform-independent code unlike the traditional compilers translating the code directly to the machine code. The intermediate language can then execute all programs, and it gets translated into a sequence of machine code by a code generator to create an executable file. The use of intermediate code enhances the portability of the compiler, because only the machine-dependent code (the interpreter or the code generator) of the compiler needs to be ported instead of porting the program itself. The remaining part of the code in the compiler can be treated as an intermediate code and then processed by the ported code interpreter. This reduces design efforts, because the machine-independent code just needs to be developed only once to create a portable intermediate code. An interpreter is less complex to code, and it follows a certain algorithm avoiding the need to be specifically ported for every single program [11]. A software can be compiled and linked from source code for various operating systems and architectures. Real-time operating system files are all architecture-dependent. A small mistake in port files will lead to an easy system crash. [3, 5].

2 Porting eChronos

The subsequent sections explain the stepwise process involved in the porting of eChronos for RISC-V architecture.

2.1 Prerequisites for Porting eChronos on RISC-V

The following are the prerequisites

1. A Linux operating system running on personal computer with 4 GB RAM.
2. A GNU-based environment that has all necessary software packages mentioned in [12].

2.2 Platform Setup for eChronos

The following steps need to be done to run eChronos on an emulator,

Installation of RISC-V emulator Follow the following steps that are listed below for the installation of RISC-V tools [13–15]:

1. **The following packages are required for the RISC-V tools:**
 autoconf automake autotools-dev curl libmpc-dev libmpfr-dev libgmp-dev
 libusb-1.0-0-dev gawk build-essential bison flex texinfo gperf libtool patchutils
 bc zlib1g-dev device-tree-compiler pkg-config
 libglib2.0-dev zlib1g-dev libpixman-1-dev
2. **Set up a directory for the RISC-V tools, and the RISC-V environment variable, which we refer to in future steps.**
 mkdir RISC-V
 cd RISC-V
 export RISC-V = {PWD}
3. **Get the RISC-V tools**
 cd RISC-V
 git clone <https://github.com/RISC-V/RISC-V-git>
 cd RISC-V-tools
 git submodule update --init --recursive
4. **Get RISC-V qemu sources, and build them:**
 cd RISC-V/RISC-V-tools
 git clone <https://github.com/heshamelmatary/RISC-V-qemu.git>
 cd RISC-V-qemu
 git checkout sfence git submodule update --init dtc
 ./configure --target-list = RISC-V64-softmmu,RISC-V32-softmmu --prefix =
 RISC-V make -j8 && make install

5. Build the 64-bit toolchain

```
cd RISC-V/RISC-V-tools
sed -i 's/build project RISC-V-gnu-toolchain --prefix = $RISC-V/build project
RISC-V-gnu-toolchain --prefix = RISC-V --with-arch = rv64imafdc --with-abi
= lp64'
./build.sh
```

6. Installation of eChronos

Download and install the eChronos [10].

3 eChronos System Design

Figure 2 shows the system diagram of eChronos. The following steps explain Fig. 2 [2] that help eChronos produce an executable file (of the test program) [8]:

1. Ensure that there is no break in the packages installed earlier and the dependencies are installed properly. A yml file is created for the purpose of testing the version of the dependencies installed and whether they are suitable for running eChronos or not? For example, running 3.4 version of python needs to be verified.
2. /x.py build packages execute x.py file which uses the skeleton of the system as a reference for the order of installation. The following output files will be produced by x.py:

- a. release/prj - <version>.zip
- b. release/ <rtos - foo> - <version>.zip
- c. release/ <build - name> - <version>.zip

3. If the installation shows any error related to traceback like Traceback (most recent call last):

File “prj/app/prj.py”, line 1293, in start sys.exit(main()), then the installation or dependencies are not installed properly. Follow the earlier steps again properly.

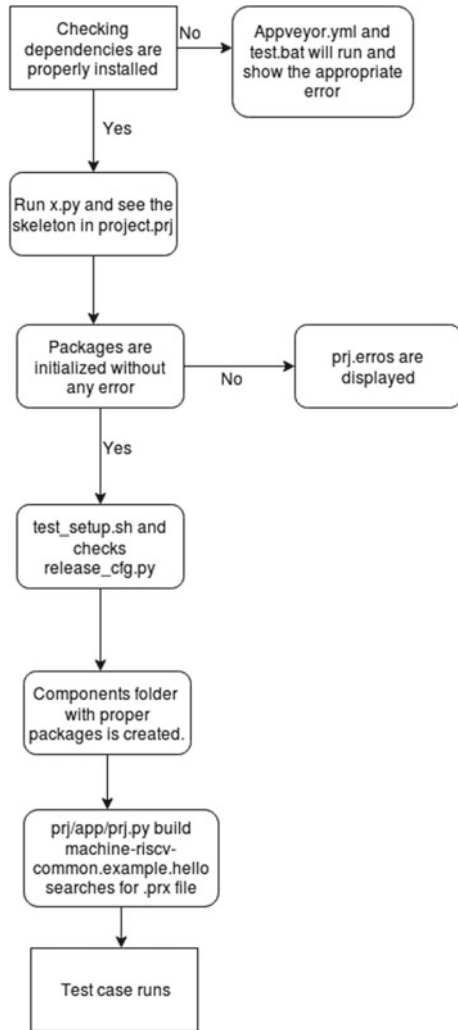
4. After prj errors are removed, we have to ensure that the class standard cfg.py should contain the RISC-V architecture. Simultaneously, spike [12] emulator is installed. The test setup.sh script downloads the package eChronos from Github. It contains travis to ensure that if package is missing then the alternative can be downloaded, i.e., the posix version [8].

5. Components folder:

Api-conditions, context-switch-RISC-V, docs, error, interrupt-event-RISC-V, message-queue, rigel, rigel.py, stack-RISC-V, task, timer-RISC-V are the necessary components that will be created once the script runs properly.

6. After ensuring a proper installation of eChronos, we test our sample program. prj/app/prj.py build <example name> command runs the test case on eChronos RTOS and produces the binary file which can be tested on spike.
7. The block “Test case runs” is explained in detail in Sect. 4.1.

Fig. 2 Flow diagram of eChronos



3.1 Challenges Encountered in Porting

Porting requires the understanding of the flow of data and the subsequent changes in the system related to architecture. As eChronos is architecture-dependent, there were many changes pertaining to specificity of the architecture like: General architecture similar to 8086 consists of extra data segment by default; but in case of RISC-V architecture, it has to be declared explicitly. The default edata (extra data segment) initialization is missing from RISC-V architecture so the edata declaration had to be

removed from every file in eChronos [4]. Likewise, there were some architecture-dependent terms which had to be modified, so as to provide support to eChronos for RISC-V.

4 Stepwise Porting of eChronos on RISC-V

eChronos initially could run only one program(test case), i.e., concurrency of task A and task B. eChronos could not run any generic program like “Hello World”. Porting eChronos on RISC-V thus became difficult because RISC-V cannot support the execution of concurrent programs. So porting eChronos on RISC-V meant that we have to change the test case to a generic one which RISC-V can support. Thus, eChronos was first changed to support generic programs like “Hello World” and then the subsequent execution of its exe file on the RISC-V could intimate whether eChronos is ported successfully or not.

4.1 Changing Test Case in eChronos

Hit and trial method of porting The components section of eChronos consists of libraries like mutex, context switching, and other concurrency supportive packages which are not used by our sample program. We removed all the unnecessary packages and removed their declarations from all the files like x.py core configuration, prj.py file because “build packages” command would take unnecessary time executing irrelevant packages otherwise.

After ensuring correct set of packages like rigel, api-conditions, errors, doc, we try to modify the test case. Test case has only one external dependency, i.e., print statement. “printf” could used as one of the options but then gcc support for eChronos needs to be ensured which leads to multiple dependency issues and these issues might be difficult to track. Also, we need to port eChronos with minimal set of library dependencies, and thus, we configured the print function [1] by using write() command of stdio library which is comparatively a less complex function than printf function of gcc. Thus, a test program with least dependency is programmed, and now, we have to produce its executable file to ensure that every interlinked package is working properly. This implies that if its executable file is generated, then removal of unnecessary packages was a success plus the test case is running properly on eChronos else we have to again solve the package error and keep on trying (hit and trial). Further, if risc-v linker along with this executable file generates a system dump (which executes properly on spike too), then eChronos is successfully ported on RISC-V.

Initialization of packages The main principle of porting is to understand what lines of code to modify in accordance with the architecture and what dependencies need to be taken into consideration. In this case, the prj tool written in python is

the initial script which initializes all the packages present and creates the required directories. When `prj` tools runs in eChronos, `project.prj` is the skeleton file which runs `x.py` file. It states all the dependencies of packages that are required by the system to function properly. There are many components like errors and api-conditions which are addressed by eChronos and needs to be initialized. `x.py` helps in initialization of these packages.

`./x.py build packages`

The command `./x.py` will initialize the packages that are mentioned in skeleton of your system in `x.py` file. For instance: For RISC-V, `rigel` is the system name which has packages like error and test case mentioned in `x.py` file, which helps in initial creation of sub-directories. This helps to create the build structure in a modular fashion where every module consists of `.exe` files of different packages initialized in `x.py` file.

Running an application on eChronos `prj/app/prj.py build machine-RISC-V-common.example.hello` is the command that runs the test case by first creating an `exe` file of the test case. After creating `.exe` files of packages using `build` command, we run test case using these packages. This `exe` file created by OS is architecture-dependent and may raise some errors if OS files are corrupted or not ported correctly.

Test case is stored in the `hello.c` file, and `machine-RISC-V-common.example.hello.prx` consists of skeleton of how the test case should run as shown in Fig. 3. It consists of the modules names which need to be executed in the sequential order. This command searches for `.prx` file which contains all the files to be used for running your program stored in the system.

We will illustrate this using our model `rigel`.

- (1) `prx` file instructs the system to compile `debug.c` in generic folder, `hello.c` in generic folder, `default-linker.py` in RISC-V folder and `build.py` as mentioned in `machine-RISC-V-common.example.hello.prx` file.
- (2) `RISC-V.default-linker` means that we should go to the RISC-V folder and run `default-linker.py` file. One thing must remembered that only `.c`, `.py`, and other high-level language files can run in the `.prx` file.

Data flow of a running application This section tries to explain the data flow in eChronos, when a test case run. The file “`debug.h`” consists of initialization of function: `debug print` and `debug.c` consist of its declaration. The `hello.c`, i.e., the test case uses `debug.h` as its header file and uses the function `debug print` to print “Hello world”. This requires the compilation of header files.

- (1) `build.py` file takes the system files, and some other helper files like `debug.h` to compile, assemble, and run your `hello.c` file in generic folder.
- (2) `hello.c` file just wants to print “Hello World”. So for printing the command `printf` is not used, rather we have created the `debug.c` file where the `print` command has been declared. `printf` command is not used because it is a part of `gcc` library which is yet not ported to RISC-V. So a generic `print` statement is declared in `debug` file.
- (3) The compilation of all libraries is over. `Rigel` model along with its components is built, and the libraries used in the test case are also compiled. Only proper linking

```

<system>

    <modules>

        <module name="machine-riscv-common.build"/>

        <module name="riscv.default-linker"/>

        <module name="generic.debug"/>

        <module name="generic.hello"/>

    </modules>

</system>

```

Fig. 3 Machine-riscv-common.example.hello.prx

of all these files is left. The linker file default.ld is created where the linking occurs according to RISC-V architecture. Linker file of different architectures was referred while making default.ld. This linker file assumed “edata” one of the variables to be declared by default but RISC-V does not support any default declarations. So we changed “edata = null” and linking errors were solved. Thus, all the compiled files were linked.

4.2 Running Test Case on Spike(RISC-V Emulator)

As soon as you hit the first command, the out folder is created with rtos- <system-name> folder. Continuing further, if the second command runs with no error, then the system image will be created in the <program-name> folder. This, then needs to be executed on your respective architecture as in our case it is on spike, RISC-V emulator [11, 12].

5 Results

Running the system dump of `hello.c` file gave an output: “Hello World” assuming the starting address of execution of program was 10,000 on the architecture. RISC-V emulator [11] has been designed in such a way that the address for the program needs to be specified above 10,000 only. But it is just a design issue which will not be of any problem in the real chip SHAKTI [6]. This indicates that the executable file produced by eChronos successfully ran on spike (RISC-V emulator). The output of sample program on eChronos is available (open source) [1].

Additions of any critical programs will be just a further extension of ported Hello World program provided the RISC-V supports that functionality of the program. Supposedly, a program which needs to determine the shortest path needs to be ported on RISC-V using eChronos. Program would consist of the same logic but instead of using gcc functions we will be using generic functions as seen with `print` in `debug.h`. This ensures a safe porting technique with no dependency on outer (alien) packages. Thus, eChronos is ported for RISC-V, for the base program `hello world`. Any additions to eChronos will be an extended version of the ported `hello.c` file with some extra headers files (declaring some predefined functions).

6 Conclusion

eChronos real-time operating system is ported to the RISC-V architecture and successfully executed on spike. The sample program `hello.c` has only one external dependency, i.e., `print`. This is the base-level porting for RISC-V that can be used as a reference for further adaptability of complex programs. Extensive porting of libraries in eChronos can be done by modifying the files in the same way as the sample program file.

References

1. Singhal SP (2019) Porting and testing on risc-v. <https://github.com/singhalshubh/Porting-and-Testing-on-RISCV>, (Online; last accessed 3 Jan 2019)
2. Andronick J, Lewis C, Morgan C (2015) Controlled owicki-gries concurrency: reasoning about the preemptible echronos embedded operating system. MARS 10–24. <https://doi.org/10.4204/EPTCS.196.2>, <https://arxiv.org/abs/1511.04170>
3. RIOT-OS: Family:arm.riot-os (2017), <https://github.com/RIOTOS/RIOT/wiki/Family:-ARM>, (Online; last accessed 7 Jan 2019)
4. Holothurion (2019) Porting. <https://en.wikipedia.org/wiki/Porting>, (Online; last accessed 23 July 2019)
5. Marcondes H, Hoeller AS, Wanner LF, Frohlich AA (2018) Operating systems portability: 8 bits and beyond. In: 2006 IEEE conference on emerging technologies and factory automation, vol 50, pp 124–130. IEEE <https://doi.org/10.1109/ETFA.2006.355371>, (Online; last accessed 23 Dec 2018)

6. Gala N, Menon A, Bodduna R, Madhusudan GS, Kamakoti V (2016) Shakti processors: an open-source hardware initiative. In: 29th International conference on VLSI design and 2016 15th international conference on embedded systems (VLSID), Kolkata, India, IEEE. <https://doi.org/10.1109/VLSID.2016.130>, (Online; last accessed 13 Dec 2018)
7. RISC-V: risc-v-gnu-toolchain (2017), <https://github.com/riscv/riscv-gnutoolchain>, (Online; last accessed 4 Apr 2019)
8. eChronos RTOS: the echronos real-time operating system (2017), <https://github.com/echronos/echronos>, (Online; last accessed 4 Apr 2019)
9. Andronick J (2018) echronos rtos. <https://ts.data61.csiro.au/projects/TS/echronos/>, (Online; last accessed 30 Dec 2018)
10. Bradbury A (2019) The future of operating systems on risc-v. <https://www.infoq.com/presentations/risc-v-future/>, (Online; last accessed 24 May 2019)
11. Johnson D (2017) Porting hyperkernel to the arm architecture. Tech. rep. University of Washington-CSE. <https://pdfs.semanticscholar.org/bb86/ea6a08c9b8c09a600367785b27aceff710d.pdf>, (Online; last accessed 2 Jan 2019)
12. Keller B (2013) Risc-v, spike, and the rocket core. <http://wwwinst.eecs.berkeley.edu/cs250/fa13/handouts/lab2-riscv.pdf>, (Online; last accessed 27 Dec 2018)
13. Waterman A, Lee Y, Patterson DA, Asanovic K (2016) The risc-v instruction set manual, volume i: base user-level isa. Tech. rep. UCB/EECS-2011- 62, EECS Department, University of California, Berkeley (May 2016). <https://www2.eecs.berkeley.edu/Pubs/TechRpts/2011/EECS-2011-62.pdf>, (Online; last accessed 27 May 2019)
14. Waterman A, Lee Y, Avizienis R, Cook H, Patterson DA, Asanovic K (2013) The riscv instruction set. <http://www.hotchips.org/wpcontent/uploads/hcarchives/hc25/HC25-posters/HC25.26.p70-RISC-VWaterman-UCB.pdf>
15. Kanter D (2016) Risc-v offers simple-modular isa. Tech. rep. The Linley Group MICROPROCESSOR. <https://riscv.org/2016/04/risc-v-offers-simplemodular-isa/>, (Online; last accessed 3 Jan 2019)

Development of Multi-band MIMO Antenna with Defected Ground Structure



Shrenik S. Sarade and Sachin D. Ruikar

Abstract This paper presents the proposed design of a multi-band MIMO antenna for the Wi-Max technology having a frequency range is 2–11 GHz. The MIMO antenna was designed by using two rectangular patches having width 19.76 mm and length 15.67 mm with defected ground structure. The inset feed method is used in phase for the exciting the antenna. This antenna has resonated on multiple bands with the enhancement of specifications like VSWR, return loss, efficiency, gain, and directivity. The Directivity and Gain of MIMO antenna have obtained 6.09 dB and 6.03 dB, respectively. Also, the efficiency of the MIMO antenna is 99.06%. This MIMO antenna is provided better return loss and VSWR for higher efficiency. The objective of this paper is providing a novel approach with multi-band operation by using the defective ground.

Keywords Microstrip patch antenna · Wi-Max · VSWR · Return loss · MIMO · DGS

1 Introduction

Wi-Max is a broadband technology, similar to Wi-Fi. This is operated on digital communication, which is also known as “metropolitan area networks”. Wi-Max has an operating range of signal up to 50 km for fixed devices, and 5–15 km for movable devices (mobile) [1].

The wireless communications industry is growing tremendously. Therefore, require to design the microstrip patch antenna for proper communication. This antenna plays a very important role in wireless communication. MIMO antenna is mostly used in the wireless technology for enhancement of the capacity of channels

S. S. Sarade (✉) · S. D. Ruikar
Walchand College of Engineering, Sangli, Maharashtra, India
e-mail: shreniks2k7@gmail.com

S. D. Ruikar
e-mail: sachin.ruikar@walchandsangli.ac.in

and the strength of the signal. MIMO antenna is consisting of multiple antennas used at the transmitting side and receiving side. MIMO based wireless technology which integrates the multiple antennas within mobile devices. The use of the MIMO antenna in communication technology can increase the data rate by providing multimedia and real-time video connectivity for the mobile user [2].

MIMO antenna, which is small, compact, reasonable and easy to fabrication, which is required to design in the wireless systems for the higher frequency. The MIMO antenna consists of two or more radiating patches on a single substrate. Therefore, isolation between the patches is making the effect on antenna parameters [3–5]. The MIMO antenna was designed for the enhancement of the return loss, VSWR, gain, efficiency, and isolation [6–8].

There are so many techniques of energy feeding methods available to energize the radiating patch. Here, in this paper, the inset feed techniques are used to energize the radiating patch [9]. The efficiency and isolation of the antenna are improved by using the defect in ground structure (DGS). Therefore, which affects on the effective capacitance and inductance of the ground structure, due to that affects on the current distribution in ground plane [10–12]. In this paper, the MIMO antenna is designed for the multi-band operation for the Wi-Max band by using the DGS. This antenna resonates on the 3, 4, 6.3, 6.9, 7, and 9.2 GHz frequency. The parameter of the antenna, i.e., return loss, gain, VSWR, and efficiency are enhanced.

2 Literature Survey

The following research paper suggests the literature survey.

Chen et al. [3] have proposed a compact size MIMO antenna, which successively reduces the size of the antenna. Also, enhance the isolation between the antennas by using the Meander strip connected to the ground [3].

Bansod and Niture [4] has designed a circular patch antenna with providing two-port orthogonal feed. Therefore, these techniques have improved bandwidth and isolation. Besides, this antenna proposed for the multi-band operation [4].

El Bakouch et al. [5] has investigated a MIMO antenna for WLAN, Wi-Max, and Hiper LAN/2 applications. This MIMO antenna results in a large broad bandwidth with good isolation between the radiating elements [5].

Kavitha and Rajan [6], has designed a MIMO antenna with dual bowtie shape by providing slots in each patch that operates on the dual-band by using the microstrip feed line with circular polarization. This antenna structure is simple and easy to fabricate [6].

Suzanefi et al. [7] have to investigate a dipole MIMO antenna with omnidirectional radiation pattern. When the operating frequency is changed, then the size of the antenna is changed. It works on the enhancement of parameters like VSWR, Return loss [7].

Yussuf and Paker [9] in this paper, a wideband MIMO antenna has investigated for a wireless technology that operates on the LTE and Wi-Fi band. The designed MIMO antenna contains a single patch with 4-port. Therefore, the bandwidth, return loss and isolation are improved [9].

Chaudhari and Gupta [10], has a proposed MIMO antenna that operates on the multi-band with higher isolation. In addition, various isolation improvement techniques, i.e., Metamaterials, DGS, parasitic elements are explained [10].

Kishore et al. [11] have designed multi-band circularly polarized antenna. The T-shaped patch designed with the defected ground structure for the improvement of the bandwidth. The proposed antenna use for GPS, Wi-Max and short-range communication [11].

Zhang et al. [13], has designed a small size MIMO antenna that operates on the dual-band for 5G smartphone application, which consists of four radiating patches. Therefore, the reflection coefficient and isolation have improved [13].

Wen et al. [8], has proposed a compact MIMO antenna, which operates on the two different frequencies for the Bluetooth/Wi-Fi band in the smartwatch application. High isolation has achieved for the operating frequency band [8].

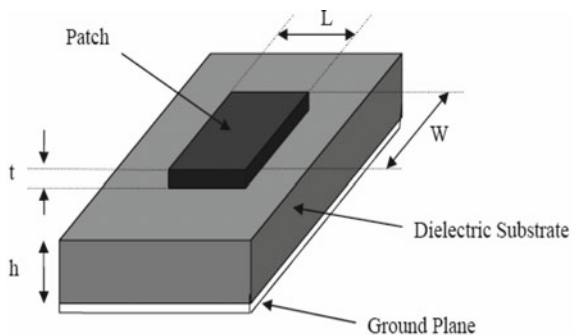
Shoaib et al. [12] has proposed a compact MIMO antenna consist of 8 * 8 structures for the smartwatches and dongles used for the 5G devices. This antenna was designed for the enhancement of gain and efficiency [12].

Zhao and Ren [14], has designed a compact size MIMO antenna, which consists of eight elements for the 5G mobile application. The proposed antenna has enhanced isolation and efficiency [14].

3 Design of MIMO Antenna

The printed antenna is shown in Fig. 1 was designed by using the following parameter. The square, rectangular, circular, triangular, and elliptical shapes are mostly used for radiation patch [15, 16]. For a rectangular patch, the substrate height (h) is selected from

Fig. 1 Simple structure of MSA



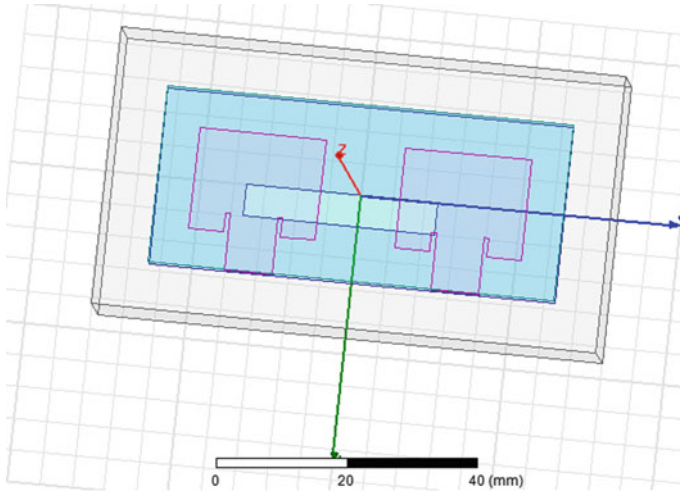


Fig. 2 Top side of MIMO antenna

$$0.003\lambda_0 \leq h \leq 0.05\lambda_0$$

and having dielectric constant (ϵ_r) is selected from range $2.2 \leq \epsilon_r \leq 12$. The width and length of the patch and ground plane are calculated by using transmission line model.

In this paper, the MIMO antenna has been designed by using HFSS software, which contains two rectangular patches as shown in Fig. 2.

This antenna is designed, which contains two radiating patches with the dimension of length 15.67 mm and width 19.76 mm. The FR4 substrate is used for the design of an antenna having length 27.67 mm, width 63.52 mm, and height 2 mm. The RF energy is provided to a radiating patch by using the inset feed method. The spacing between the two patches is [2].

The length L_p and width W_p of the radiating patch is computed by using the following equation [15, 17].

$$\text{Width}(W_p) = \frac{1}{2f_r\sqrt{\mu_0\epsilon_0}}\sqrt{\frac{2}{\epsilon_r + 1}} \tag{1}$$

$$\Delta L = 0.412h \frac{(\epsilon_{\text{reff}} + 0.3)\left(\frac{W_p}{h} + 0.264\right)}{(\epsilon_{\text{reff}} - 0.258)\left(\frac{W_p}{h} + 0.8\right)} \tag{2}$$

$$L_{\text{eff}} = L_p + 2\Delta L \tag{3}$$

$$f_r = \frac{1}{2L_p\sqrt{\epsilon_r}\sqrt{\mu_0\epsilon_0}} \quad (4)$$

$$\epsilon_{\text{reff}} = \frac{\epsilon_r + 1}{2} + \frac{\epsilon_r - 1}{2} \left[1 + 12 \frac{h}{W_p} \right]^{-1/2} \quad (5)$$

where

W_p = Width of Patch

L_p = Length of Patch

The length L_g and width W_g of the ground plane is computed by using the following equation.

$$L_g = L_p + 6h \quad (6)$$

$$W_g = W_p + 6h \quad (7)$$

where

L_g = Length of Ground

W_g = Width of Ground

Feed line length and width for inset feed is calculated by using the following formula.

$$\text{Feed line length}(L_f) = \frac{\lambda_g}{4} \quad (8)$$

where,

$$\text{Guided wavelength}(\lambda_g) = \frac{\lambda_0}{4}$$

The minimum width of the inset feed line required to excite the patch antenna is given by,

$$W_f = \frac{2h}{\pi} \times \left[\frac{377\pi}{2Z_0\sqrt{\epsilon_r}} - 0.7 - \ln \left(\frac{2 \times 377\pi}{2Z_0\sqrt{\epsilon_r}} + 1 \right) \right] + \frac{2h}{\pi} \times \left[\frac{(\epsilon_r - 1)}{2\epsilon_r} \left(\ln \left(\frac{377\pi}{2Z_0\sqrt{\epsilon_r}} - 1 \right) - \frac{0.6}{\epsilon_r} \right) \right] \quad (9)$$

where

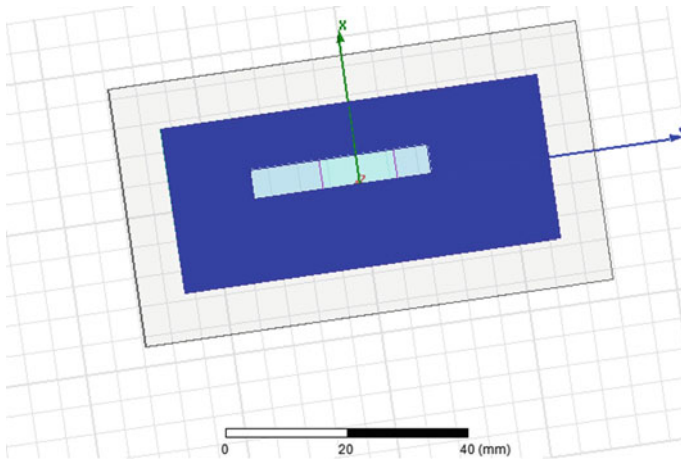


Fig. 3 Ground plane of designed antenna

$$\text{Characteristics Impedance} = Z_0 = 50\Omega$$

The ground plane of the antenna with DGS as shown in Fig. 3. The rectangular slot cut with length 5 mm and width 30 mm is provided in the ground plane. This DGS technique is used for the improvement of isolation and efficiency [2, 11, 17].

4 Design Flowchart

The flowchart shown in Fig. 4 indicates the design step of antenna.

5 Result and Analysis

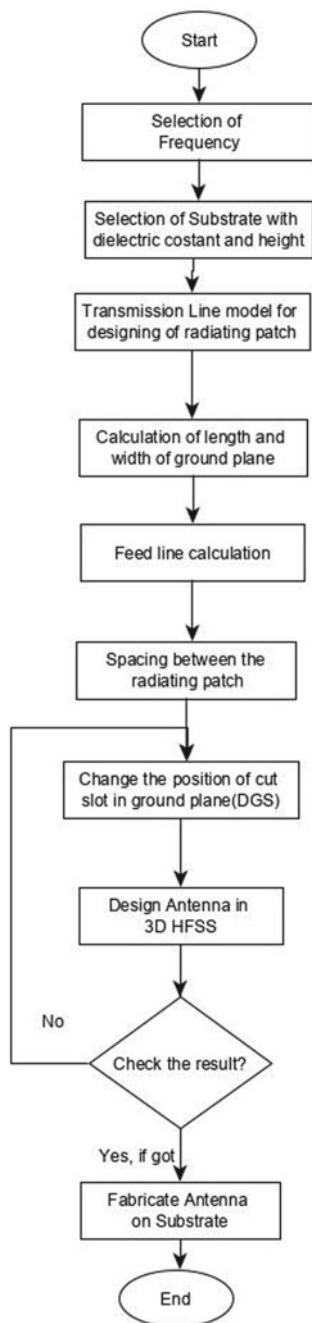
The MIMO antenna, which designed in HFSS software shown in Fig. 2. After completion of the simulation, the return loss of S(1, 1) as shown in Fig. 5, as well as values in Table 1 and the return loss of S(2, 2) as shown in Fig. 6, as well as values in Table 2. All values obtained are less than -10 dB.

The Gain (G) and the Directivity (D) of antenna have shown in Figs. 7 and 8 respectively. Table 3 shows the values of gain and directivity.

The radiation pattern of the antenna as shown in Fig. 9.

The VSWR 1 and VSWR2 of MIMO antenna as shown in Figs. 10 and 11 respectively. The VSWR absolute value as shown in Tables 4 and 5. The VSWR values obtained is less than 3.

Fig. 4 Design flowchart of antenna



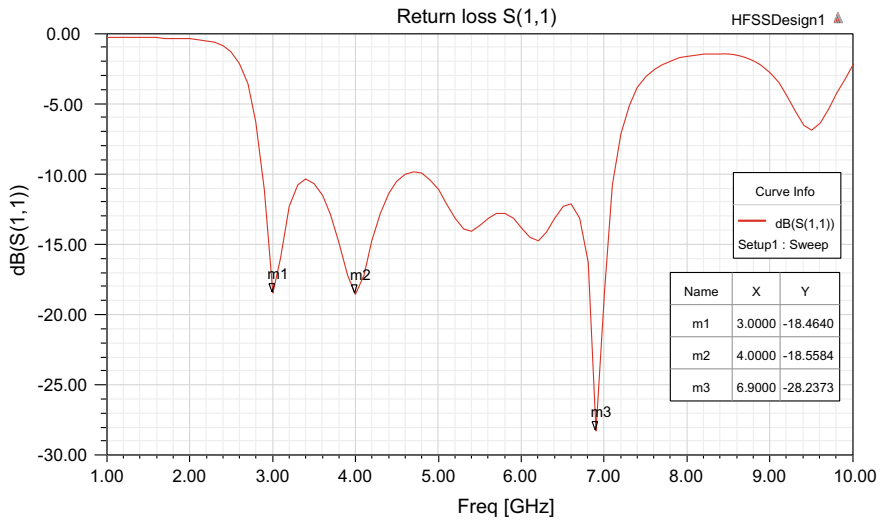


Fig. 5 Return loss S(1,1)

Table 1 Return loss S(1,1) values verses frequency

Name	Frequency in GHz	Return loss (dB)
m1	3.00	-18.46
m2	4.00	-18.55
m3	6.9	-28.23

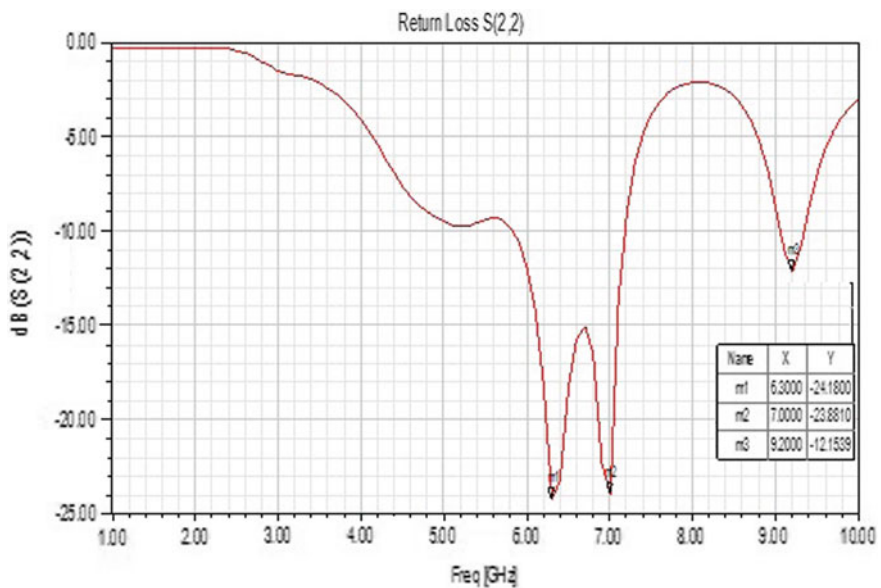


Fig. 6 Return loss S(2,2)

Table 2 Return loss S(2,2) values versus frequency

Name	Frequency in GHz	Return loss (dB)
m1	6.3	-24.18
m2	7.00	-23.88
m3	9.20	-12.15

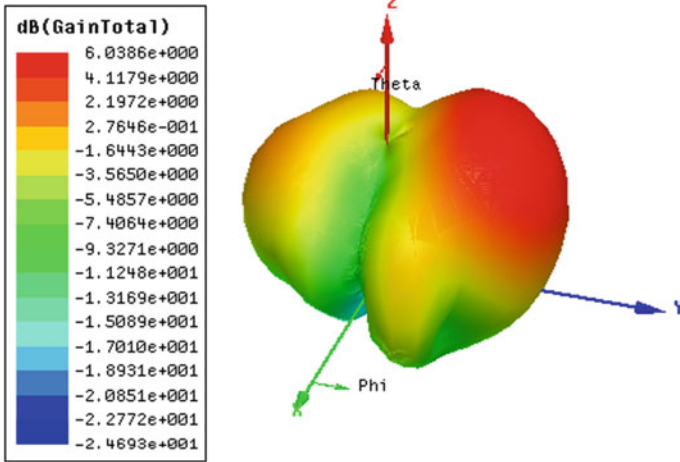


Fig. 7 Gain (*G*) in dB

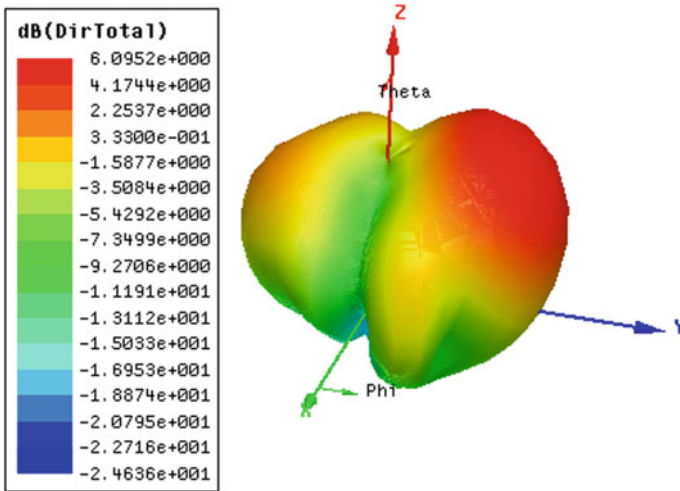


Fig. 8 Directivity (*D*) in dB

Table 3 Gain And directivity measured value

Parameter	Value (dB)
Gain	6.03
Directivity	6.095

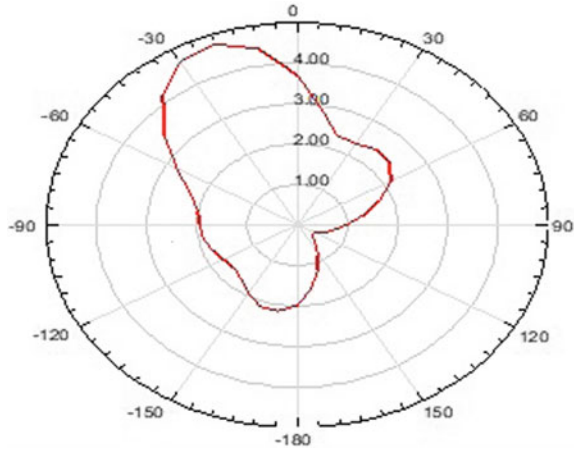


Fig. 9 Pattern of MIMO Antenna

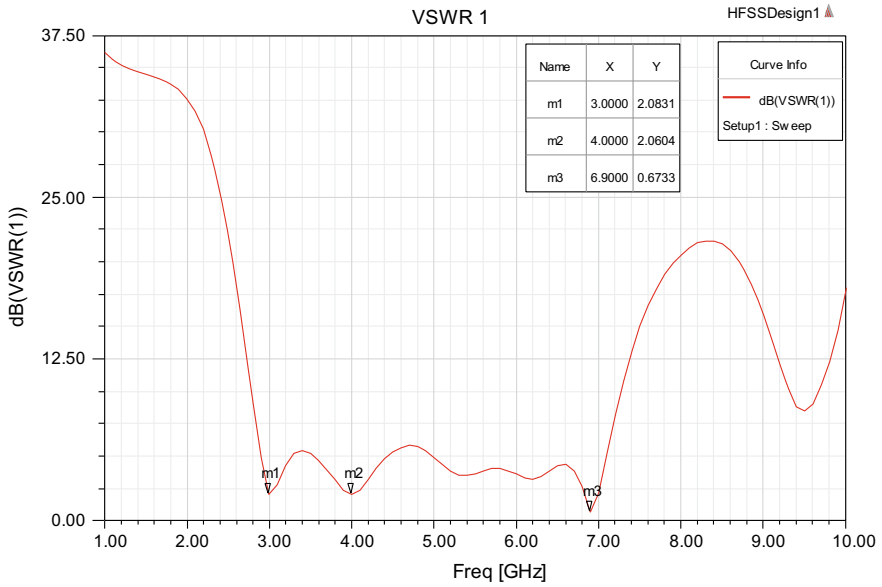


Fig. 10 VSWR of antenna 1

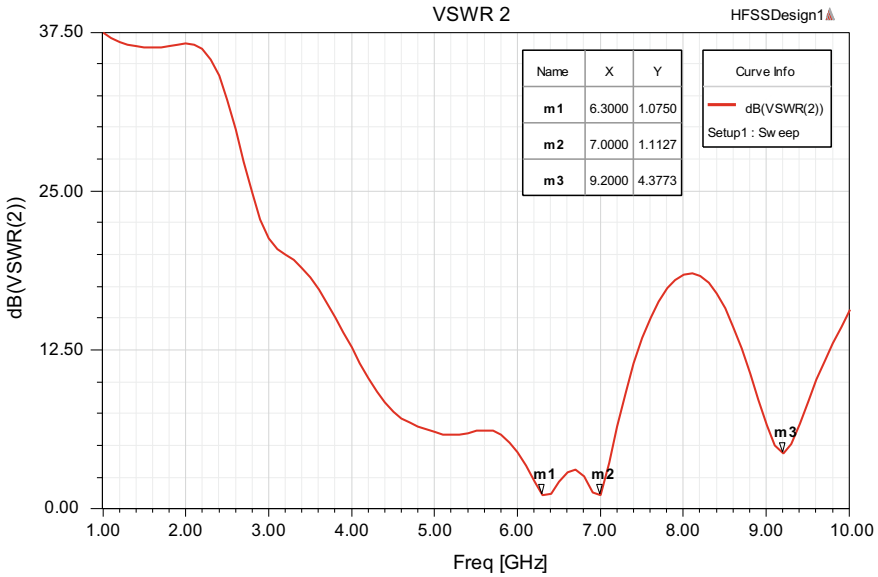


Fig. 11 VSWR of antenna 2

Table 4 VSWR 1 values versus frequency

Name	Frequency in GHz	VSWR	Absolute value
m1	3.00	2.08	1.61
m2	4.00	2.06	1.60
m3	6.90	0.67	1.16

Table 5 VSWR 2 values versus frequency

Name	Frequency in GHz	VSWR	Absolute value
m1	6.30	1.07	1.27
m2	7.00	1.11	1.29
m3	9.20	4.37	2.73

The isolation $S(1, 2)$ and $S(2, 1)$ as shown in Figs. 12 and 13, respectively, and corresponding values are shown in Tables 6 and 7. The isolation values are obtained which is less than -8 dB.

The Energy flow diagram of the antenna has shown in Fig. 14.

Radiating antenna with a radiating beam has shown in Fig. 15.

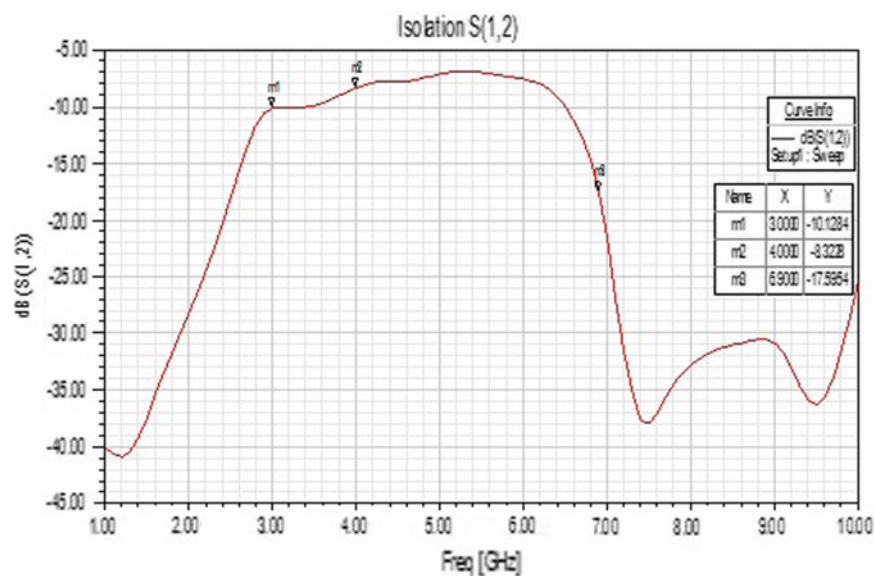


Fig. 12 Isolation S(1,2)

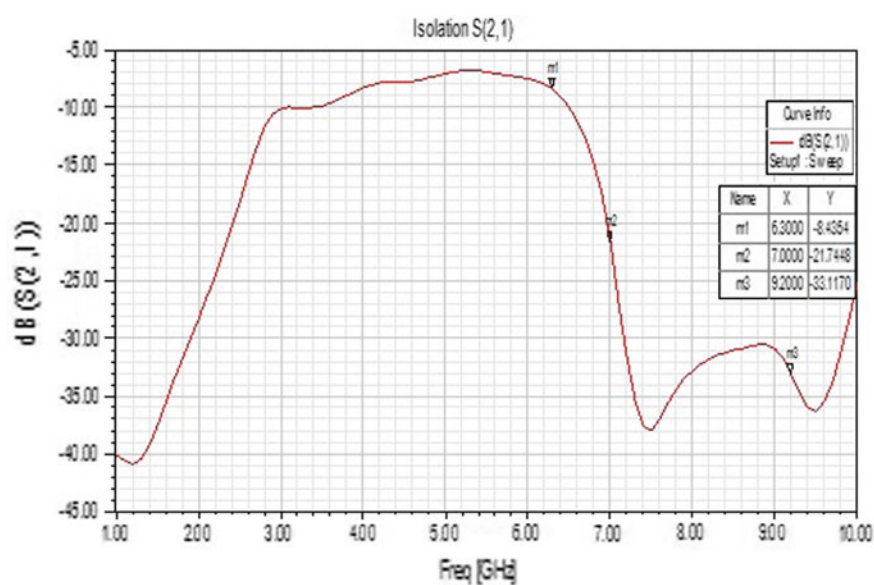


Fig. 13 Isolation S(2,1)

Table 6 Isolation values

Frequency (GHz)	S(1,2) in dB
3.00	-10.12
4.00	-8.32
6.90	-17.59

Table 7 Isolation values

Frequency (GHz)	S(1,2) in dB
6.30	-8.43
7.00	-21.74
9.20	-33.11

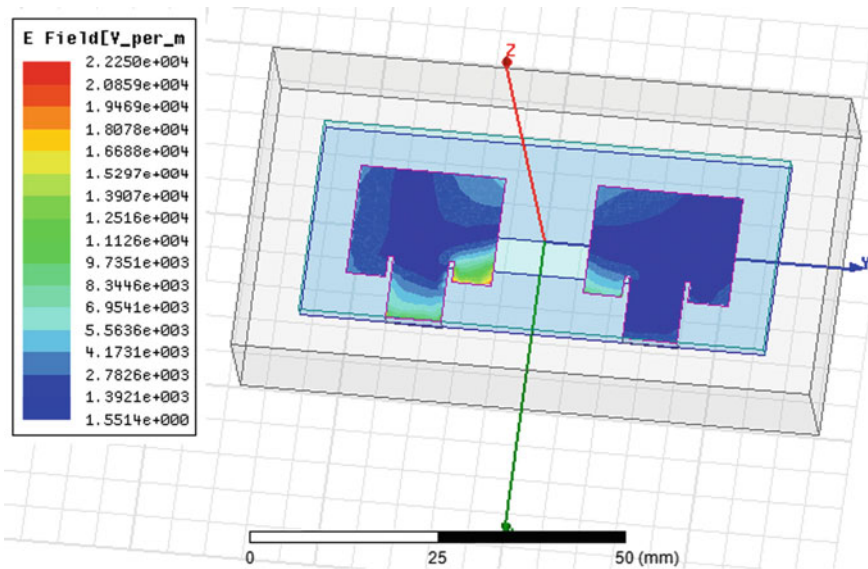


Fig. 14 Energy flow diagram

6 Conclusion

In this paper, the MIMO antenna is designed for the Wi-Max application by using HFSS simulation software. The MIMO antenna is designed which contains the two radiating patch of the same length and width with inset feeding. The simulating results obtained for various bands. Return loss $S(1, 1)$ has obtained -18.45 dB for 3 GHz, -18.56 dB for 4 GHz and -28.23 dB for 6.9 GHz and the return loss $S(2, 2)$ has obtained -24.18 dB for 6.3 GHz, -23.88 dB for 7 GHz and -12.15 dB for 9.2 GHz. The VSWR 1 has obtained 2.08 dB for 3 GHz, 2.06 dB for 4 GHz and 0.67 dB for 6.9 GHz and VSWR 2 has obtained 1.07 dB for 6.3 GHz, 1.11 dB 7 GHz

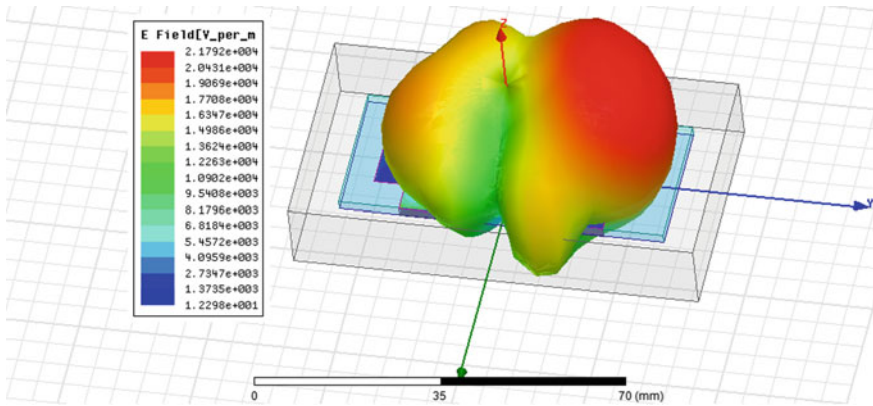


Fig. 15 Radiation pattern with antenna

and 4.33 dB for 9.2 GHz. The VSWR values for resonating frequency is in between the 1 and 3, hence it is the perfectly matched antenna. The Directivity and Gain of MIMO antenna have obtained 6.09 dB and 6.03 dB, respectively. The efficiency of the MIMO antenna is 99.06%. This MIMO antenna has provided better return loss and VSWR for higher efficiency.

References

1. Prakash G, Pal S, Wimax technology and its applications. *Int J Eng Res Appl (IJERA)*
2. Sharawi MS, Printed MIMO antenna engineering book. Artech house antennas and propagation library, ISBN 13: 978-1-60807-681-9
3. Chen W-S, Chi Y, Chang F-S (2014) Compact WiMAX MIMO antenna design for laptop applications. In: *Proceedings of ISAP 2014, Taiwan, IEEE paper, Dec 2–5*
4. Bansod BH, Niture D (2015) Compact two port MIMO microstrip antenna for 4G applications. In: *ICIP-2015 IEEE paper. 978-1-4673-7758-4/15*
5. El bakouchi RJ, Brunet M, Razban T, Ghammaz A (2015) Broadband MIMO antenna for HiperLAN/2, WLAN, and WiMAX applications with highisolation. *IJMWTC, Cambridge University Press and the European Microwave Association*
6. Kavitha K, Rajan SP (2016) Design of dual band MIMO antenna for Wlan/Wimax application. (*IJRECT-2016*)
7. Suzanzeffi, Hadi I, Ciksadan, Thussyadiyah RAH, Sholihin (2019) MIMO printed dipole antenna for Wimax network usage application. In: *IOP conference series: IOP Publishing, J Phys Conf Series*
8. Wen D, Hao Y, Wang H, Zhou H (2018) Design of a MIMO antenna with high isolation for smartwatch applications using the theory of characteristic modes. *IEEE Trans 0018–926X (c)*
9. Yussuf AA, Paker S (2017) Design of wideband MIMO antenna for wireless applications. In: *IEEE paper, 978-1-5090-6494-6/17*
10. Chaudhari A, Gupta RK (2018) Isolation enhancement in multi-band and wideband MIMO antenna systems: A review. In: *4th ICECILZCODE—EQUINOX*
11. Kishore N, Prakash A, VS. Tripathi (2016) Multiband microstrip patch antenna with defected ground structure for its applications. *microwave and optical technology letters. /https://doi.org/10.1002/mop.30151*

12. Shoaib N, Shoaib S, Khattak RY, Shoaib I, Chen X, Perwaiz A (2018) MIMO antennas for smart 5G devices. *IEEE Access*. <https://doi.org/10.1109/ACCESS.2018.2876763>
13. Zhang W, Weng Z, Wang L (2018) Design of a dual-band MIMO Antenna for 5G “smartphone application”. *IEEE*, 978-1-5386-1851-6/18
14. Zhao A, Ren Z (2018) Size reduction of self-isolated MIMO antenna system for 5G mobile phone applications. *IEEE*. <https://doi.org/10.1109/LAWP.2018.2883428>
15. Balanis CA, *Antenna theory analysis and design*. Wiley, Inc., Publication
16. Kraus JD, *Antenna and wave propagation*. Tata Mcgraw-Hill Edition
17. Kumar G, Ray KP, *Broadband microstrip antennas, Artech house antennas and propagation library*

Reliability Evaluation of Environmentally Affected Mobile Ad Hoc Wireless Networks



N. Padmavathy

Abstract Mobile ad hoc network due to its inherent capabilities received a significant researcher's attention recently. Wireless networks like mobile ad hoc networks are application-specific, infrastructure-less, short-duration networks with many features like arbitrary or dynamic topology, homogeneity/heterogeneity, self-organizing, decentralization, high flexibility, routing, etc. The main purpose of mobile ad hoc networking is to extend its short-duration services for specific applications into the realm of autonomous, mobile, wireless domains, where the mobile nodes form the network topology in an arbitrary fashion. The vulnerabilities in a wireless environment, viz., temperature, noise, pressure, magnetic effects, have significant impact on the connectivity. Connectivity is related to node mobility, link formation and hence failure of either one or both results in connectivity loss. When connectivity is lost, the network becomes unreliable. In this paper, a comprehensive review of the effects of wireless environment on mobile ad hoc network reliability is proposed. From the results, it is understandable that in the absence of noise the network is highly reliable and as the environmental noise increases, the reliability falls down by 32%.

Keywords Arbitrary topology · Geometric random graph · Infrastructure-less networks · Mobile ad hoc networks · Multi-hop · Network reliability

1 Introduction

Communication is a purposeful activity of exchanging information between living organisms or artificial devices using various technical or natural means. A communication network consists of two or more nodes (computers/devices) that are linked for the purpose of transfer or exchange of information which may be either a wired

N. Padmavathy (✉)

Vishnu Institute of Technology, Bhimavaram, AP, India

e-mail: padmavathy.n@vishnu.edu.in

network or wireless network. A network connected through cables and telephone lines is a wired network, whereas a network that is linked via RF, satellites or IR waves is wireless network.

Among different types of the networks, infrastructure-less wireless networks (wireless sensor networks (WSNs) and mobile ad hoc networks (MANETs)) are considered here in this paper for reliability evaluation. In infrastructure-less wireless networks, the nodes are wirelessly connected and are auto-configurable networks with scarce resource. Moreover, these networks are inadequate in terms of traditional protocols and networking algorithms. In MANET, the nodes move continuously in any direction with the capability of path configuration periodically. The formation and deletion of link depend on the mobility of the nodes [1]. The temporary communication link among the nodes within its deployment area (undesirable areas) [2] defines connectivity.

The networks' wireless topology may change rapidly and unpredictably such that network may operate in an arbitrary fashion. The routes between nodes in an ad hoc network may include multi-hops. Each node will be able to communicate directly (single-hop communication) with any other node that resides within its transmission range. For indirect communication with destination nodes, there is a need of intermediate nodes (multi-hop communication [3]). Ad hoc wireless networks inherit the traditional problems of wireless communications and wireless networking [4] as listed below.

1. The wireless medium has neither outright, nor promptly discernible limits outside of which stations are recognized to be unable to organize network frames.
2. The channel is unprotected from outside signals.
3. The wireless medium is notably much less dependable than wired media.
4. The channel has time-varying and asymmetric propagation properties.
5. Hidden-terminal and exposed-terminal phenomena may occur.

To the above-mentioned problems, the multi-hop nature and the lack of fixed infrastructure add a number of characteristics, complexities and design constraints that are specific to ad hoc networking [5–7]. All these problems pose direct effect on the performance of the MNs. Points 2 and 3 indeed mean that the channel or the medium is prone to noise which further has impact on the nodes, due to which the nodes may fail leading to a decrease in reliability. In other words, due to the failure of the network components (nodes and links), the network reliability reduces [8].

The authors of this paper previously have contributed over the past decade on evaluation of connectivity-based network reliability considering non-capacitated [9], capacitated [10], path reliability [11], interference [12], link reliability models (binary [9] and propagation-based [13]), mobility models [14], fading models [15], node failures [16] and node distribution [17]. But, all the above-mentioned contributions [9–17] have failed to consider environmental noise.

This paper mainly emphasizes on the connectivity of network considering environmental noise in order to estimate the reliability of the network. Therefore, the authors of this paper have evaluated the reliability of the MANETs considering the environmental noise. It is been depicted that environmental noise has significant

impact on the reliability of the network. To improve the readability of the paper, the paper has been organized in the following way. Section 2 elaborates on the assumptions considered for the reliability evaluation. The reliability evaluation methodology along with the proposed algorithm is provided in Sect. 3 and Sect. 4 provides a detailed simulation result.

2 Assumptions

1. The network is homogeneous and operational at the start of the mission time.
2. The node movement follows RWPM with zero pause time, uniformly distributed node velocity (V_{\min} , V_{\max}) and direction $(0, 2\phi)$.
3. Every node has the same transmission range (r_j), and every node pair within the transmission range is considered to be connected.
4. Times-to-failure of nodes are assumed to fail due to environmental parameters, viz., noise (EP), and the failure follows Weibull distribution with scale parameter (β) and shape parameter (θ).
5. Failures of node are statistically independent, and once a node fails, it is in the same state for rest of the time.
6. All links are bidirectional without any constraint on their load-carrying capacity.
7. The creation and destruction of the link depend on the distance (d_{ij}) between the nodes and the transmission range (r_j).

3 The Methodology

3.1 Network Model

At any instant of mission duration, MANET can be represented as a fixed geometric random undirected graph $G = (U, L, K)$ consisting of a set of U number of vertices, a set of L number of edges and a set of KU terminals. Both node and links can fail. However, time-to-failure of nodes follow a known distribution as explained in assumption # 4.

The successful communication between the nodes in K is a random event with a probability $R_G(\tau)$ given that the all nodes in K must be active. Therefore, the network reliability is defined of the product of the reliability of (s, t) pair and the reliability of the network with perfect (s, t) node pair. Therefore, the reliability of the network uses factoring theorem [9] to be mathematically expressed as (1) by noting that the failure of designated nodes will certainly lead to network failure.

$$R'_G(\tau) = \left(\prod_{u_i \in K \subseteq U} R_{u_i}(\tau) \right) R_{(G|K)}(\tau) \quad (1)$$

Therefore, (1) can be utilized to compute the reliability of MANET at a particular instant of mission duration in our MCS.

3.2 Network Model

Each environmentally affected node u_i has an operational probability and is defined as in (2)

$$Pr(u_i(\tau)) = e^{\left[\frac{-(EP+\tau)}{\theta}\right]^\beta} \quad (2)$$

where

$$u_i(\tau) = \begin{cases} 1 & \text{if node}_i \text{ is operational at time } \tau \\ 0 & \text{Otherwise} \end{cases} \quad (3)$$

Each node u_i has an operational probability R_{u_i} [9] and is defined as given in (4)

$$R_{u_i}(\tau) = \begin{cases} Pr(u_i(\tau)) & \text{if node}_i \text{ is operational at time } \tau \\ 0 & \text{Otherwise} \end{cases} \quad (4)$$

The status of the links, $L_{ij}(\tau)$, [9] between a pair of nodes (u_i, u_j) is determined by Euclidian distance, $d_{ij}(\tau)$, between them at time, ' τ ', and transmission range, r_i , of the nodes, i.e.,

$$L_{ij}(\tau) = \begin{cases} 1 & \text{if } d_{ij}(\tau) \leq r_i \text{ (or } r_j) \\ 0 & \text{Otherwise} \end{cases} \quad (5)$$

where

$$d_{ij}(\tau) = \left((x_j(\tau) - x_i(\tau))^2 + (y_j(\tau) - y_i(\tau))^2 \right)^{1/2} \quad (6)$$

Therefore, at time ' τ ', the network can be represented by an adjacency matrix [9], $A(\tau)$ of size $|U_1 \times U_1|$, with its elements, $L_{ij}(\tau)$. This matrix is utilized to determine the connectivity [18, 19] between the (s, t) pairs, where connectivity $C_q(\tau)$ is defined as in (7)

$$C_q(\tau) = \begin{cases} 1 & \text{if } K \subseteq U \text{ nodes are connected at time } \tau \\ 0 & \text{Otherwise} \end{cases} \quad (7)$$

3.3 Node Mobility Model

The node movements are modeled using random-based synthetic mobility model as it mimics the real-time movements of the nodes. Location change, node speed and direction change are the characteristics that had direct impact on the movement of the MNs at time instant. The study using the node movements according to RWPM has been discussed in detail in several literatures [9, 20–23]. Thus, the mathematical equation used for computing the new locations is as given in (8).

$$\begin{aligned} x_i(\tau + \Delta \tau) &= x_i(\tau) + \Delta \tau v_i(\tau) \cos \phi_i(\tau) \\ y_i(\tau + \Delta \tau) &= y_i(\tau) + \Delta \tau v_i(\tau) \sin \phi_i(\tau) \end{aligned} \tag{8}$$

The reliability $R_G(\tau)$ of MANET KU is defined as functions of time by averaging the results for simulation run at each incremental time (τ) of the total mission duration (9). That is, (9) indicates the ratio of the product of the node reliability of any two nodes of a network over entire duration of the mission time over the total number of simulation runs.

$$R_G(\tau) = \frac{\left(\prod_{u_i \in K \subseteq U} R_{u_i}(\tau)\right) \sum_{q=1}^Q C_q(\tau)}{Q} \tag{9}$$

3.4 Algorithm for Computing MANET Reliability

Based on the descriptions and discussions done in earlier sections, an algorithm is developed to compute reliability of the MANET. The algorithm starts with the network conversion, wherein the network that has perfect KU nodes as per (1) is considered. The next task is connectivity check, and this process is repeated for every $\Delta \tau$ till the specified mission time has been reached. It may be noted that every $\Delta \tau$ is one complete iteration of ‘ Q ’ numbers of iterations in our simulation study. The MC simulation-based algorithm is as follows:

Step 1: Initialize network parameters ($U, A, t_{Mission}$), node parameters (parameter of time-to-failure pdf (θ, β), (V_{min}, V_{max}), ($0, 2$), r_j , (X_i, Y_i)), $q = 1, C_q(\tau) = 0, EP$ (environmental noise).

Step 2: Initialize $R'_G(\tau) = \left(\prod_{u_i \in K} R_{u_i}(\tau)\right)$.

Step 3: Simulate the node status using (2).

Step 4: Simulate the link status using (5) after computing the Euclidean distance (6).

Step 5: Check for connectivity of nodes KU of the network at time τ . If network is connected, then increment the $C_q(\tau)$ and set $\tau = \tau + \Delta \tau$.

Step 6: Simulate the mobility of the nodes according to *RWPM*, and compute the new node positions at every time increments using (8). Repeat step 3 through step 5 if $\tau \leq t_{\text{Mission}}$.

Step 7: Repeat *step 2* to *step 6* for q number of simulation runs.

Step 8: Compute network reliability as per (9).

The algorithm has been implemented using MATLAB® 2009a on a Windows® XP run on a Pentium dual processor @1.60 GHz speed. MATLAB is being used in simulating the concept demonstration for problem solving on the specified example defined in subsequent section.

4 Simulation Results

The proposed algorithm is applied on the study considered in [1, 9] to evaluate the reliability of the MANET. The impact of EP on the movement of the radios is additionally considered in this paper.

The simulation study on the reliability evaluation of the MANET has been conducted considering a network size (NS) (9–100 nodes) placed in simulation boundary (NCA) (say 8-by-8 sq. miles to 20-by-20 sq. miles) with node transmission range (TR) up to 8 miles. It may be noted that, at the start of the mission time i.e., at 0th hour the network nodes are fully operational and at the end of the mission time i.e., at 72nd hour the nodes may be operational or fails. Network's performance on the basis of the effect of EP (0 dB to 1.5 dB) subjected to different scenario conditions has been analyzed. In this paper, it is assumed that natural noise exists in the environment. The following session describes the effect of different scenario metrics (NCA, NS, TR) [24] on the reliability metrics 2TR under the influence of environmental noise. Initially, the network is considered to be free from the environmental noise, i.e., $EP = 0$. Later, the environmental parameter is increased up to 1.5 dB in steps of 0.5 dB.

4.1 Simulated Network Topology

Network topology is the arrangement of the entities (links and nodes) of a network. Essentially, it is the topological structure of a network which may be depicted physically or logically. For the study taken, many network structures are generated through simulation as observed through Figs. 1, 2, 3, 4 and 5 that no two topologies are alike, and only few of the simulated topologies are shown below. This segment gives an understanding of the topology changes depending on different scenario metrics with and without noise effect at different time instants. Figure 1a, b shows the changing topology in the absence of noise ($EP = 0.0$ dB) and in the presence of noise ($EP = 0.5$ dB), respectively, for the parameters considered in this study.

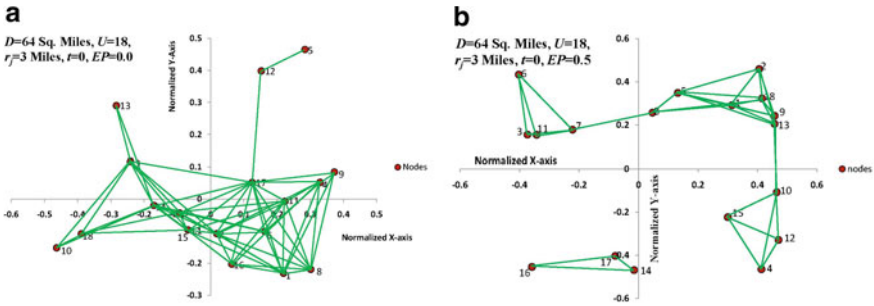


Fig. 1 Network topology with $D = 64$ miles², $U = 18$, $r_j = 3$ miles, $t = 0$: **a** $EP = 0$ and **b** $EP = 0.5$

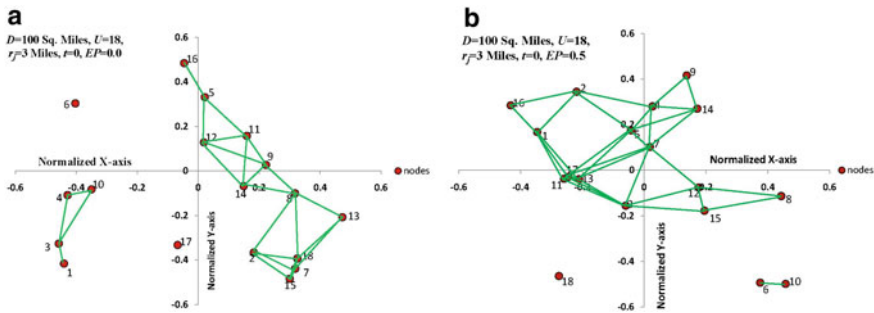


Fig. 2 Network topology with $D = 100$ miles², $U = 18$, $r_j = 3$ miles, $t = 0$: **a** $EP = 0$ and **b** $EP = 0.5$

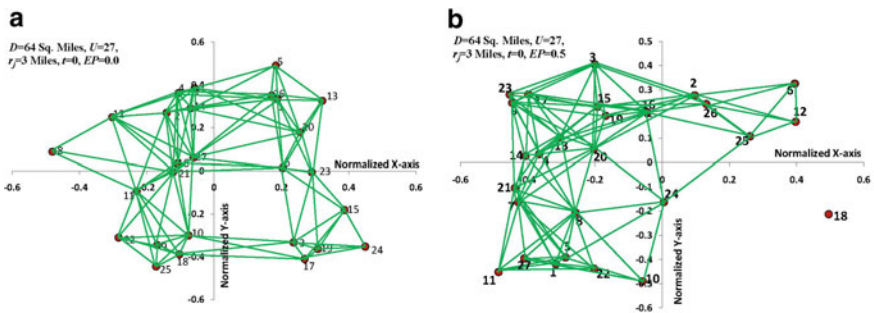


Fig. 3 Network topology with $D = 64$ miles², $U = 27$, $r_j = 3$ miles, $t = 0$: **a** $EP = 0$ and **b** $EP = 0.5$

There is loss of connectivity between the mobile nodes when the environmental noise increases though all other simulation parameters are maintained constant as shown in Fig. 1b. That is, the network connectivity is good (Fig. 1a) in the absence of noise and subsequently in the presence of noise the established connectivity breaks

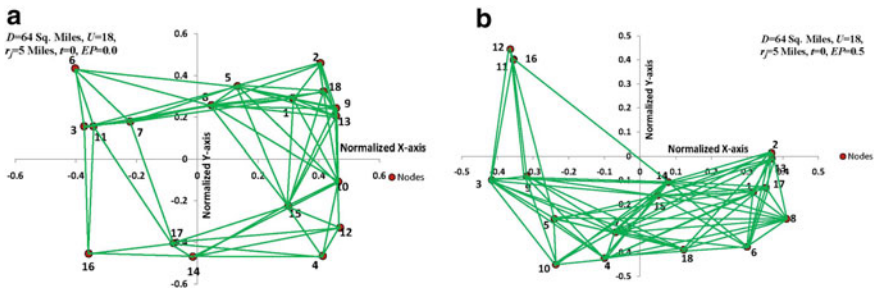


Fig. 4 Network topology with $D = 64$ miles², $U = 18$, $r_j = 5$ miles, $t = 0$: **a** $EP = 0$ and **b** $EP = 0.5$

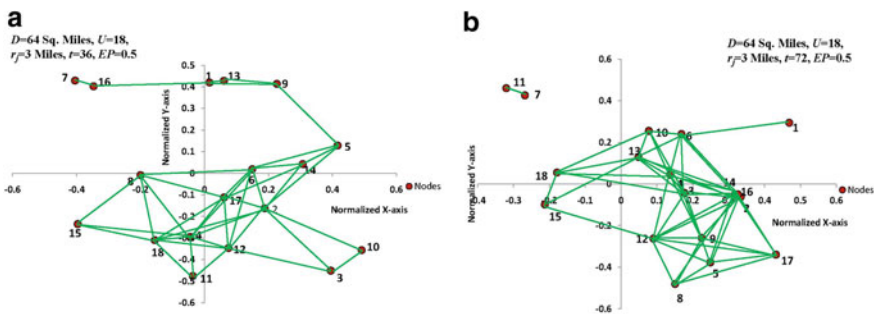


Fig. 5 Network topology with $D = 64$ miles², $U = 18$, $r_j = 3$ miles, $t = 36$: **a** $EP = 0$ and **b** $EP = 0.5$

(Fig. 1b). Clusters are predominantly visible in large number when the environmental noise is high. Figure 2a, b indicates that the probability of the network connectivity is very small and hence has direct impact on the network reliability.

As the coverage area increases (say $D = 10$ -by- 10 sq. miles) with a fixed node size (say 18 nodes), due to mobility the distance between the nodes exceeds the node transmission range and hence link formation fails. The simulated topologies depict the occurrence of isolation nodes which may be either the source node (see Fig. 2a; node 1 is isolated) or the destination nodes (see Fig. 2b; node 18 is isolated), though these nodes are active at the start of the mission time. Not only source node or destination node is isolated, sometimes the intermediate nodes are also isolated. Figure 2b clearly shows the isolation of the intermediate nodes (node 6 and node 10). However, the connectivity can be improved by allowing same number of nodes to move in a smaller area (see Fig. 3a, b) or increase the transmission range of the mobile nodes (see Fig. 4a, b). Though the number of nodes is increased, the environmental noise still has a significant effect on the reliability as shown in Fig. 3b because of the isolated (s-t) pair nodes. Similarly, studies have been done for different network sizes and different transmission ranges in the absence of noise ($EP = 0.0$) and in the presence of noise ($EP = 0.5$) as shown in Figs. 3 and 4.

Figure 5a, b depicts the change in topology of the MANET at different time instants for changing environmental condition during a single iteration. The topologies depicted here show the probability of successfully connected network, though few nodes seem to be active but isolated (see Fig. 5b). As mission time increases, the node may also become inactive because of the statistical distribution considered. If node is inactive, connectivity between the nodes will be lost. It was also observed that if the node fails at a particular instant of time it remains in the same state for the rest of the mission time (topology not shown here).

4.2 Effect of Environmental Noise on Network Reliability

The effect of environmental noise on network reliability with varying network coverage area has been studied and performed with coverage area ranging from 64 to 400 sq. miles and environmental noise ranging from 0.0 to 1.5 dB. The reliability (2TR) of the network decreases with increasing network coverage area and environmental noise as shown in Figs. 6 and 7. Because the non-existence of link (the distance between the nodes is so large) for small number of nodes (though active) of a network is deployed in large simulation boundary, the connectivity is lost. Similarly, when the noise in environment is high, the connectivity between nodes is lost. In the absence of environmental noise, the network is reliable with a reliability of 0.6944 and further the reliability decreases by 68% in the presence of high environmental noise (1.5 dB). A fall in reliability implies that the network is not suitable for the specific application in the presence of high noise.

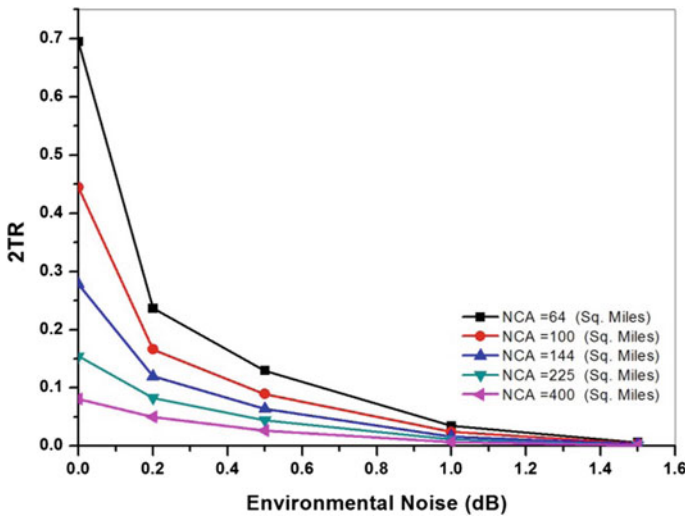


Fig. 6 Effect of EP on 2TR with changing NCA

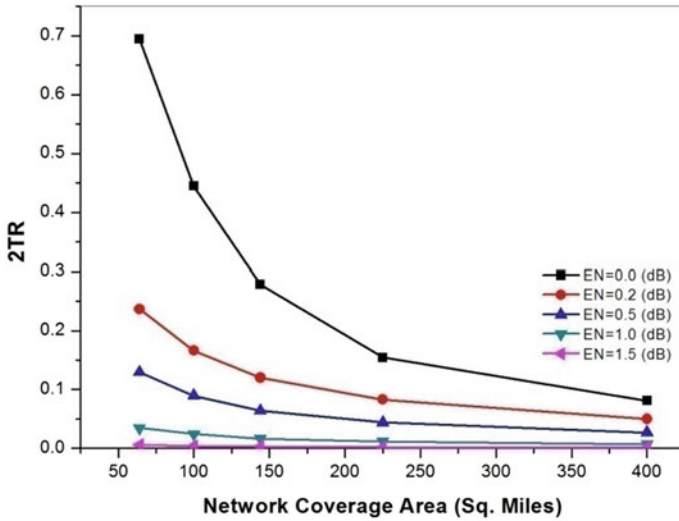


Fig. 7 Effect of NCA on 2TR in noisy environment

Figure 8 clearly depicts that an increase in the environmental noise causes a decrease in the reliability of the network, and Fig. 9 depicts the performance of MANET in a noisy environment for different network sizes. Here, the network size is varied between 9 and 100 and environmental noise is also varied up to 1.5 dB to study the effect on network reliability. An effect similar to the one seen in earlier

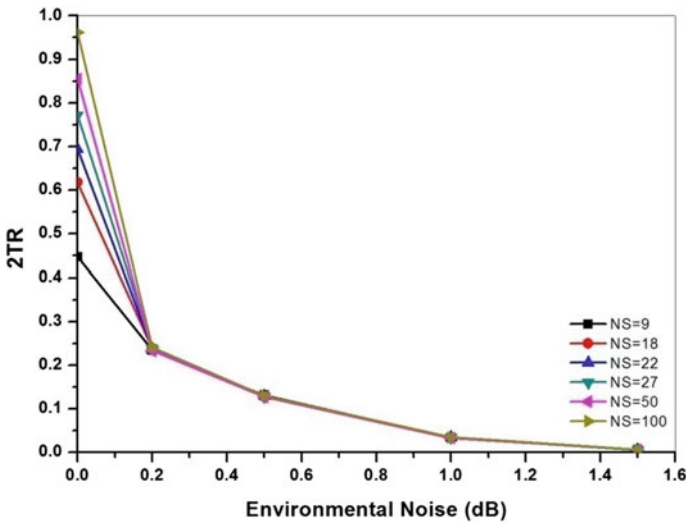


Fig. 8 Effect of EP on 2TR with changing NS

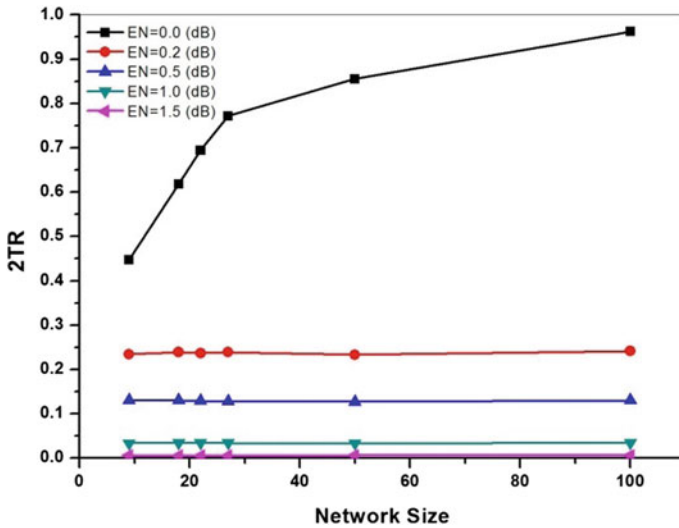


Fig. 9 Effect of NS on 2TR in noisy environment

cases can also be seen here. With increasing environmental noise, the network is almost unreliable and the values decrease by more than 45%.

The evaluation of 2TR is performed by considering environmental noise and transmission range ranging from 1 mile to 8 miles while keeping the other parameters such as network coverage area and network size as constant. As the transmission range increases, the reliability also increases while reliability decreases with increasing environmental noise. These variations are shown in Figs. 10 and 11, respectively.

With varying scenario metrics (NCA, NS, TR), it can be observed that the network reliability decreases or increases. Figure 11 depicts that larger the transmission range, each node covers a large area, and hence more mobile nodes fall within the vicinity of each other, thus increasing the link connectivity. Figures 11 and 12 clearly show that in the absence of noise the 2TR is high (0.9575 when TR = 5 miles) and is almost stable beyond 5 miles (0.8513 for NS of 27 nodes). This implies that it would be optimum enough to consider nodes that can transmit or receive at a range of 5 miles. The simulation results show that for the given example with NS = 18, NCA = 64 sq. miles and TR = 3miles, the obtained reliability is 0.6944 which is quite low. The designer can improve the reliability of the network (say up to maximum of R_i^2) by considering optimum parameters that would cover a simulation area with large number of nodes with the best transmission range. In other words, the network reliability can be improved by increasing either the number of nodes in the network or transmission range of the node when the coverage area is small.

When nodes are environmentally affected, Figs. 6, 8 and 10 depict a drastic decrease in reliability. A noise of 0.2 dB has a monotonic impact on the reliability that decreases by about 32% when compared with the case of noise-free nodes. However, the reliability under influence of noise can be increased to 0.6855 (approximately

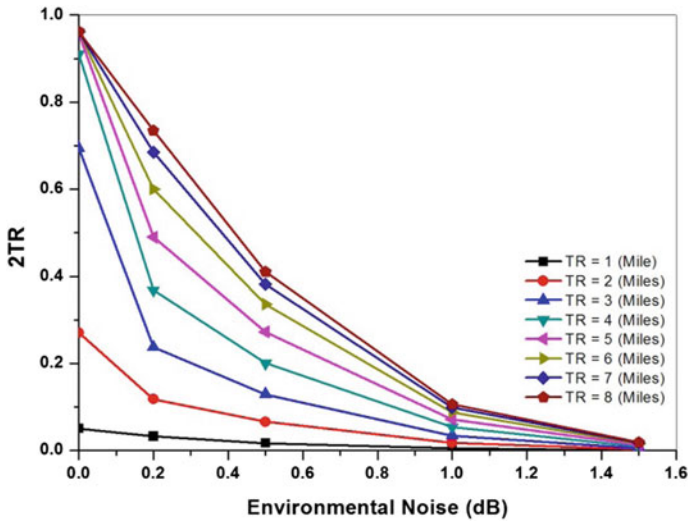


Fig. 10 Effect of EP on 2TR with changing TR

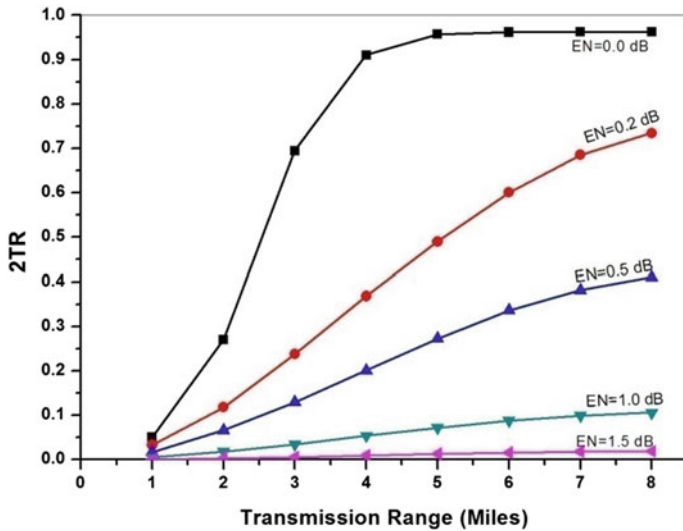


Fig. 11 Effect of TR on 2TR in noisy environment

to 0.6944) by increasing the transmission range to 7 miles or can achieve higher reliability (say 0.7340) by decreasing the coverage area to 50 sq. miles or still lesser (plot for $D = 50$ sq. miles has not been provided).

5 Conclusion

Nowadays, every application (military, disaster management, health care, etc.) needs a reliable communication. Hence, reliability plays a vital role in mobile ad hoc network. For the analysis of reliability, modeling of network has been done by using geometric random graph. The mobility of node is governed by random waypoint mobility model (RWPM). The nodes are subjected to environmental noise (noise is assumed to be present in the environment), and hence the simulation studies of the effect of environmental noise on network reliability have been considered. The reliability of the MANET varies in accordance with the scenario metrics (network coverage area, network size, transmission range) and environmental noise. From the results, it is understandable that in the absence of noise the network is highly reliable. Moreover as the environmental noise increases, the reliability falls down by 32%. The reliability can be improved by considering large network size or transmission range.

References

1. Cook JL, Ramirez-Marquez JE (2007) Two-terminal reliability analyses for a mobile ad hoc wireless network. *Reliab Eng Syst Safety* 92(6):821–829
2. Zhao X, You Z, Wan H (2013) A novel two-terminal reliability analysis for MANET. *J Appl Math* 2013(216186):9
3. Bruno R, Conti M, Enrico G (2005) Mesh networks: commodity multihop ad hoc networks. *IEEE Commun Mag* 43(3):123–131
4. IEEE P802.11/D10, Jan 14 1999
5. Corson MS, Macker JP, Cernicione JH (1999) Internet-based mobile ad hoc networking. *IEEE Internet Comput* 3(4):63–70
6. Chiasserini CF, Rao RR (1999) Pulsed battery discharge in communication devices. In the proceedings of the fifth annual ACM/IEEE international conference on mobile computing and networking (MOBICOM_99), pp. 88–95
7. Ankur OB, Prabhakar LR (2013) MANET: history, challenges and applications. *Int J Appl Innov Eng Manag* 2(9)
8. Abdullah K, Smith AE (2006) Network reliability optimization, chapter 26, handbook of optimization in telecommunication, Springer Science+Business Media, pp 735–760
9. Chaturvedi SK, Padmavathy N (2013) The influence of scenario metrics on network reliability on mobile ad hoc networks. *Int J Performability Eng* 9(1):61–74
10. Padmavathy N, Chaturvedi SK (2015) Reliability evaluation of capacitated mobile ad hoc network using log-normal shadowing propagation model. *Int J Reliab Saf* 9(1):70–89
11. Venkata SB, Padmavathy N (2017) A systematic approach for analyzing hop count and path reliability of mobile ad hoc networks. In: International conference on advances in computing, communications and informatics (ICACCI), pp 155–160
12. VenkateswaraRao Ch, Padmavathy N, Chaturvedi SK (2017) Reliability evaluation of mobile ad hoc networks with and without interference. *IEEE 7th International Advance Computing Conference*, 233–238, 2017
13. Padmavathy N, Chaturvedi SK (2013) Evaluation of mobile ad hoc network reliability using propagation based link reliability model. *Reliab Eng Syst Saf* 11(5)1–9
14. Padmavathy N, Chaturvedi SK (2015) Reliability evaluation of mobile ad hoc network: with and without mobility considerations. *PROCEDIA Comput Sci* 46:1126–1139

15. Padmavathy N, Chaturvedi SK (2016) A systematic approach for evaluating the reliability metrics of MANET in shadow fading environment using monte carlo simulation. *Inte J Performability Eng* 12(3):265–282
16. Padmavathy N, Teja JRC, Chaturvedi SK (2017) Performance evaluation of mobile ad hoc network using monte carlo simulation with failed nodes. In: *Second international conference on electrical, computer and communication technologies (ICECCT)*, Coimbatore, pp. 1–6
17. Padmavathy N, Anusha K (2018) *Dynamic reliability evaluation framework for mobile ad-hoc network with non-stationary node distribution*. Commun Comput Syst CRC Press Taylor and Francis
18. Deo N (1974) *Graph theory with application to engineering and computer science*”, englewood cliffs. Prentice-Hall, NJ
19. Kubat P (1989) Estimation of reliability for communication/computer networks—simulation/analytic approach. *IEEE Trans Commun* 37(9):927–933
20. Padmavathy N, Sanjay K, Chaturvedi (2016) *Mobile ad hoc networks: reliability measures and evaluation*. LAMBERT Academic Publishing
21. Chaturvedi SK, Padmavathy N (2017) *Mobile ad hoc network reliability: an imperative research challenge*, chapter 4 *advances in reliability and system engineering*. Springer International Publishing, pp 87–119
22. Camp T, Boleng J, Davies V (2002) A Survey of mobility models for ad hoc network. Res 1–21. <http://toilers.mines.edu>
23. Christian B (2001) Mobility modeling in wireless networks: categorization, smooth movement, and border effects. *Mobile Comput Commun Rev* 5(3):55–67
24. Subbarao MW (1999) *Ad Hoc networking critical features and performance metrics*, NIST Group, pp 1–11

Design of Tunable Miniaturized Frequency Selective Surface Based on Miura-Ori Pattern



Sailabala Soren and Ashwin Kothari

Abstract In this paper, a foldable miniaturized higher-order FSS with a tunable characteristic which acts as the band-stop filter is studied. The miniaturized configuration is achieved by bending the arms of the rotated cross-shaped structure. The proposed parallelogram facet is reduced by 75% as compared to the facet of the rotated cross-shaped structure. The proposed Miura-ori pattern design demonstrates the most stable angular performance at large angles of incidence and the frequency deviation obtained is 0% when the angles of incidence (θ) are varied from 0° to 60° at different TE and TM polarization. The folding and unfolding in the FSS structure occur due to the variation of different folding angles $\alpha = 0^\circ, 30^\circ, 60^\circ$. This causes the interaction between the incident waves and the movement of the interface of the foldable FSS which results into shift of the resonant frequency up to 20% as per the desired performance. Thus, the kinematics deformation makes the design tunable. The proposed structure of FSS is simulated in HFSS 15.0. The corresponding higher-order transfer function of the twisted and foldable FSS is obtained from the MATLAB R2014a using the HFSS simulation data. The simulation results are presented which shows the viability of the proposed design.

Keywords Frequency selective surface · Miura-Ori fold · Scattering parameters · Origami · Tunable filters · Polylactic acid

1 Introduction

A frequency selective surface (FSS) is an assembly of identical conducting elements arranged in two-dimensional array on a dielectric substrate. The arrangement of each unit cell should be in a periodic manner. The periodic structures are excited in two methods: by an incident wave or by connecting generators to individual elements [1].

S. Soren (✉) · A. Kothari
Electronics and Communication Engineering Department,
Visvesvaraya National Institute of Technology, Nagpur 440010, India
e-mail: sailabala.soren67@gmail.com

© Springer Nature Singapore Pte Ltd. 2021
G. S. Hura et al. (eds.), *Advances in Communication and Computational Technology*, Lecture Notes in Electrical Engineering 668,
https://doi.org/10.1007/978-981-15-5341-7_99

1311

The FSS exhibits different scattering parameters to illustrate the filtering behavior which is highly dependent on the geometrical structure of the element, substrate thickness, periodicity, relative permittivity of the dielectric substrate, the polarization of incident wave, and inter-element spacing. The proper selection of these mentioned properties results in enhanced filtering characteristics due to the occurrence of the matching between the frequency of the plane wave and the resonant frequency of the elements in FSS. The applications of FSS can be often found in antenna radar domes, cellular communication system, resonant beam, radars, spatial filters, and electromagnetic band-gap material. Theoretically, the FSS is a periodic surface with infinite elements. But practically, it is limited in size. Generally, the desired result is achieved by including a large number of elements which is around 400 [18]. Unlike classical filter, FSS deals with the angle of incidence of the wave and polarization along with the frequency of the signal. According to researchers, the sensitivity of the FSS to the various oblique angles of incidence can be reduced by miniaturizing the area of the unit cell keeping the size of the arms unchanged and also the resonant frequency.

Various FSS designs have been proposed for miniaturization. The convoluted technique [2, 3], lumped reactive element [4], and fractal geometry [5] are used to optimize the design of FSS for reduction in the size of unit cell. Complementary structures have been applied to improve the miniaturization [6–8]. The 2.5D ultra-miniaturized FSS is one of the versatilities found in recent research [9].

Mathematics and the philosophy behind origami art have a good impact on the architecture framework as it is useful for innovative designs and deployable systems used in transportation, such as rocket and foldable origami-style solar panels. It is expected that the entire complex system can be regulated with a basic motion. In this phase, the most feasible approach is selected for FSS tuning. The proposed Miura-ori model has a single control parameter that determines the angle of the folding state and therefore the strength of the resonance. Such motion should not disturb the periodicity of the system. A 3D mechanically tunable FSS with a flat square slot having incident angle stability up to 45° and tunability from 2.4 to 4 GHz [10]. An active FSS used as a tunable low-frequency radar broadband absorber with a frequency range between 2 and 11.3 GHz controlled by p-i-n diodes is studied in [11]. An electronically switchable FSS used as a spatial filter with square loop aperture geometry controlled by four p-i-n diodes and wave polarization insensitivity up to $\pm 45^\circ$. The FSS designed by circular loops connected through varactor diodes having a tunability range of 363% for band-stop application is discussed in [12]. The FSS can also be tuned by using special types of the substrate like liquid crystals [13–15] and ferrites [16] achieving 15–20% shift in resonant frequency.

The lead idea in this project is to embed a miniaturized pattern in a foldable FSS-based origami art structure. The proposed FSS structure is insensitive to large angles of incidence and to both TE and TM polarization. The resonance frequency can be changed with a single control parameter of the Miura-ori pattern. The difference of resonance frequency is the result of a change in the direction of the conductive elements owing to variability in the folding angle. The tunability is therefore accomplished in a specific band. First, an incurved cross-shaped structure is used to design

an FSS array that shows stable performance for different incident angles and polarizations. The second is to create a geometrical structure based on the Miura-ori fold, which allows the FSS to be tailored to one control variable (folding angle: α). The shifting of the folding angle takes the system from smooth to highly folded. In order to demonstrate the effectiveness of the system, the simulated tunable FSS experiment is carried out in HFSS 15.0.

2 Design of FSS Structure

The unit cell is designed consisting of four parallelogram facets and each cell is assembled periodically. Each facet is made of a biodegradable plastic, i.e., polylactic acid (PLA) material. The facet is arranged in such a way that it is foldable. The accumulation of all the unit cells is aligned in x - and y -directions. The angle α determines the folding state of paper for the surface. When α is 0° , the structure appears as a 2D FSS. But when the angle α becomes more than 0° the proposed model develops height giving rise to a 3D FSS structure where height is in z -direction. To be more precise the lengths of P_x and P_y will change when α is increased or decreased as shown in Fig. 3. The lengths P_x and P_y are different for various unit cell structures. The variation in P_x and P_y affects the orientation of the locations of the metallic patches. The proposed design of facet, unit cell, and array of unit cell are shown in Fig. 2a, b, c, respectively. The arrays of metallic patches are aligned on top of the dielectric substrate as shown in Fig. 2c. The angle (β) determines the angle between two sides of the facets. The sheet becomes parallel to the plane (flat), when $\alpha = 0_0$. When the value of α changes from 0 to 60° , the lengths of P_x and P_y vary correspondingly but the value of angle β remains constant. The value of β is 45_0 . These expressions are represented in (1) and (2) [17].

$$P_x = 2x\cos(\phi) \quad (1)$$

$$P_y = 2y(\sin(\phi)\cos(\beta) + \cos(\phi)\cos(\alpha)\cos(\beta)) \quad (2)$$

where, $\phi = \tan^{-1}[1/\tan(\beta)\cos(\alpha)]$.

Foldable design is evolved without tearing the surface of the sheet. The dielectric substrate used for simulation is PLA having a thickness of 0.76 mm. PLA filament is widely thought of as an aesthetic material best used for rapid prototyping. The permittivity of the dielectric and loss tangent are 2.3 and 0.07, respectively. The dimension of the overall facet is $30 \times 20.21 \text{ mm}^2$. The symmetric structure is considered to reduce the dependency on polarization. In the first step of the modification process as shown in Fig. 1, the crossed shaped reference design [1] is converted to rotated crossed shaped structure aiming for miniaturization. After incurring the arms of rotated cross-shaped element, the area of the unit cell is reduced up to 75% as shown in Fig. 2a.

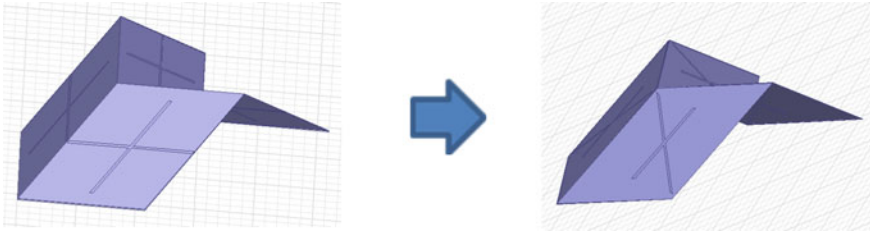


Fig. 1 First modification of unit cell from cross-shaped to rotated cross-shaped

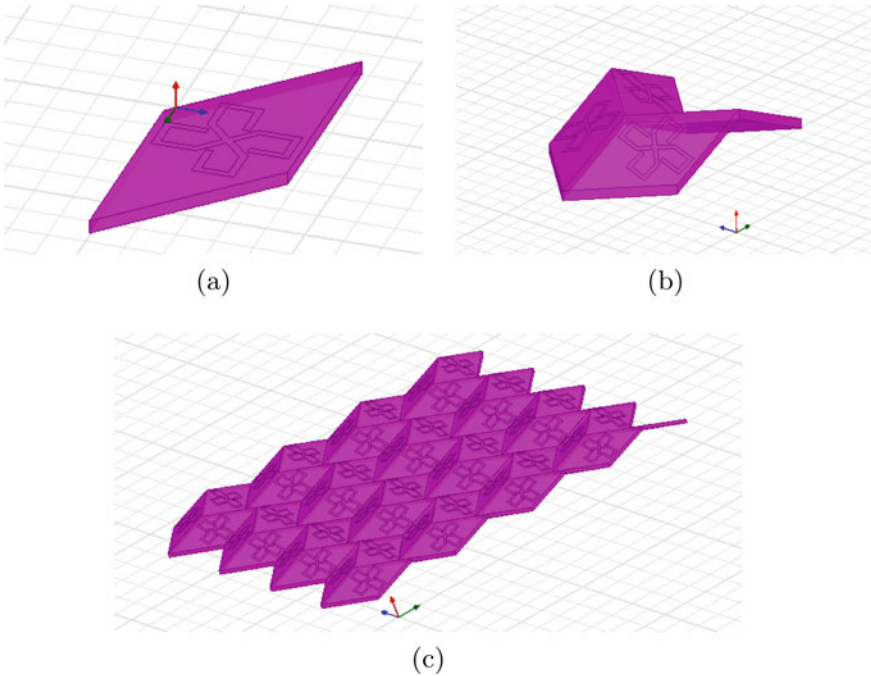


Fig. 2 **a** Facet, **b** unit cell of proposed FSS, **c** array design of proposed tunable FSS

The angle of rotation of the cross structure conducting element is 45° . Each arm is twisted by 90° inside for all the facets of the unit cell as shown in Fig. 2a as per the second modification and the proposed unit cell of FSS is shown in Fig. 2b. The size of the rotated cross-shaped FSS is $39.68 \times 28.05 \text{ mm}^2$. The length of arm (l) remains unchanged before and after the modification process as shown in Fig. 4 [1]. The substrate used here is the same as before. The areas of unit cells before and after modification process are compared. The area of the proposed unit cell is reduced by 75% after modification process. The size of facet for the resonant frequency of stop-band filter corresponds to $1.313\lambda_0 \times 0.928\lambda_0$, where λ_0 is free-space wavelength. The significance of miniaturization is to reduce the dependency of FSS on the angle of incidence (Fig. 3).

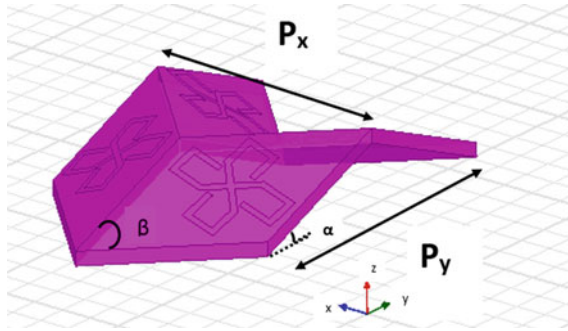


Fig. 3 Geometry of rotated cross-shaped unit cell before proposed miniaturized unit cell

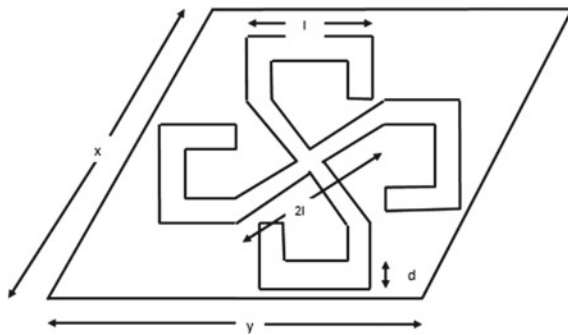


Fig. 4 Dimension of proposed unit cell

Table 1 Geometrical parameters of proposed design

Parameter	x (mm)	y (mm)	d (mm)	l (mm)
Value	30	30	1	5

The structure is designed symmetrically to both x - and y -axes to eliminate polarization sensitivity. The geometrical parameter of incurred rotated cross structure shaped FSS is shown in Table 1. An optimized filtering characteristic is aimed at the beginning of the process of designing. Therefore, miniaturization is done by incurring rotated crossed structure keeping the length same as shown in Fig. 2b at the resonant frequency 9.4 GHz.

The sides of these crossed shape structures are rotated inside with 45° keeping the arms identical in lengths and then incurred with 90° . The strategy of the design is formed symmetrical in both x - and y -axes to make the FSS design miniaturized and polarization insensitive. The proposed unit cells are arranged in a chevron pattern for incorporating the tunability in the FSS design. Since the folding and unfolding are done for the required operation, the inter-element spacing does not affect the result

much. Still, the periodicity (B) needs to be maintained to eliminate the grating lobes [18] so that the following condition should be satisfied.

$$B < \frac{\lambda_0}{1 + \sin(\theta_0)} \tag{3}$$

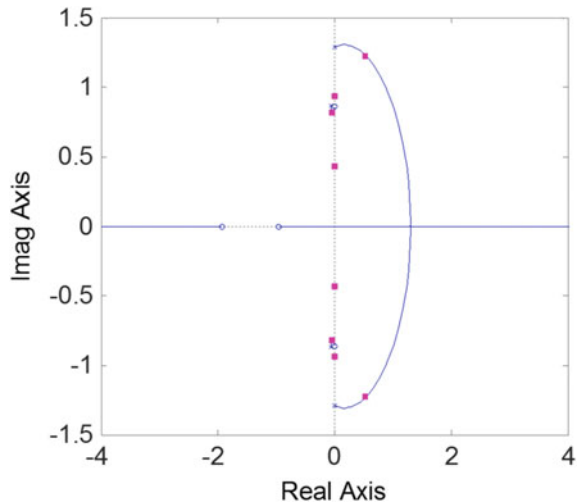
where λ_0 is the wavelength and θ_0 is the angle of incidence. For 60° angle of incidence, the periodicity should be less than 12.24 mm.

The optimal transfer function is obtained with MATLAB using data solution of S_{21} of proposed FSS (imaginary and real parts of S_{21} , amplitude, and phase of S_{21}). S_{21} is showing the transmission coefficient which can be collected from the result of simulation of the proposed design. The improved band-stop filter is analyzed by determining the transfer function (4).

Using MATLAB code, the optimal transfer function is obtained by changing the degree from 5 to 8. It is observed from the simulation of MATLAB that when the number of poles and zeros are 8, the most optimal transfer function (4) of the FSS is achieved. The curves obtained from HFSS analysis and MATLAB results are compared and it is found that both curves are similar in nature as shown in Fig. 6. Resultant band-stop filter characteristics are estimated by observing the location of poles and zeroes as shown in Fig. 5.

$$\frac{-0.2861s^8 - 0.8233s^7 - 1.036s^6 - 1.488s^5 - 1.223s^4 - 0.7818s^3 - 0.5421s^2 - 0.09735s - 0.06447}{s^8 + 0.1297s^7 + 3.489s^6 + 0.3541s^5 + 4.001s^4 + 0.2508s^3 + 1.731s^2 + 0.0355s + 0.2031} \tag{4}$$

Fig. 5 Location of poles and zeros of estimated transfer function



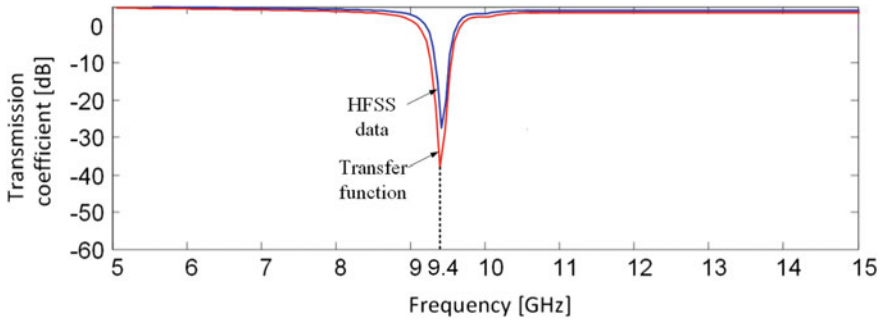


Fig. 6 HFSS analysis and evaluated transfer function comparison

3 Simulation Results

The demanding characteristics of band-stop spatial FSS are to obtain flat pass band gain near 0 dB over wide range and to obtain sharp roll-off at the cutting edges. These specified features are expected from miniaturized model even if the angle of incidence is high. The proposed new design accomplishes the mentioned characteristics with a good precision. When the angle of incidence wave is 0°, -3 dB bandwidth of the band-stop filter is acquired between 8.9 and 10.41 GHz. From the simulation results, it is confirmed that even if the polarization are TE and TM, the transmission coefficient is unaffected and stable and also the bandwidth is also wider in proposed FSS. Excitation of FSS is considered due to different angle of oblique incident waves (0°, 15°, 30°, 45°, and 60°). The newly designed foldable FSS gives a stable performance at various incident wave angles and linear polarization. When FSS with larger unit cell size is being illuminated by plane wave with oblique incidence the sensitivity of the FSS structure to the angle of incidence is increased as a result the frequency deviation becomes more which is compared in Figs. 7 and 8.

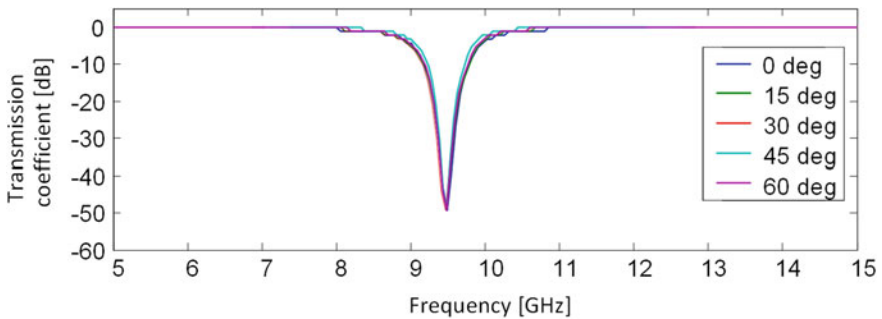


Fig. 7 Plot of transmission coefficient of proposed FSS under different, normal, and oblique angles of incidence

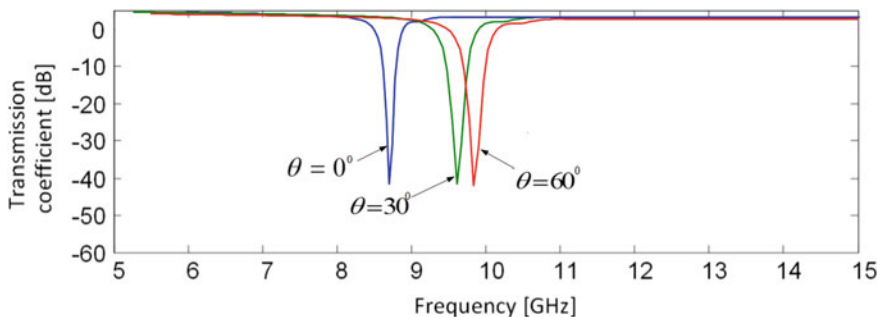


Fig. 8 Plot of transmission coefficient of FSS before modification

The deviation in resonant frequency is around 0% when the resonance frequency at a various angle of incidence is compared with the resonance frequency at normal incidence. Compared to the resonance frequency which is 9.4 GHz, it is observed that the relative deviation in case of crossed shaped structure is 1.29% for TE polarization at the angle of 60° incident wave. The less frequency deviation means less sensitivity to the incident wave angles. This design with biodegradable plastic substrate is showing a good result. It is observed by implementing the following equation [18] on the data obtained from simulation result.

$$\Delta f = \frac{F_r - F_{ang}}{F_r} \times 100 \tag{5}$$

where, Δf is relative frequency deviation, F_r is resonance frequency, and F_{ang} is frequency at different angle of incidence.

During the filtering process when the FSS is in excited state the current paths are observed. The current path is visible along the vertical arms in case of TE mode. The current is distributed along the horizontal path at 9.4GHz in case of TM mode. Figure 9 represents the current distribution for TE and TM polarization. Even though the linear polarization is different the resonance zero frequency is obtained around 9.4GHz till 60° angle of incidence.

Simulation of the second modification is as shown in Fig. 4, with ANSYS HFSS 15.0 the resonant frequency is obtained at 9.4 GHz. Bandwidth utilization has been increased in this design segment where each facet consists of incurved rotated crossed structure shape metallic patch. The later FSS has a single layer, as shown in the chart. Figure 2c indicates notch features of the filter. At different angles (0°, 30°, and 60°) the electromagnetic waves are reflected on the FSS. The operational frequency is 9.4GHz for usual occurrence. The folding and unfolding of FSS can be depicted by Poisson’s ratio as follows.

$$\sigma = -\frac{\epsilon_l}{\epsilon_s} = -\tan(2\alpha) \tag{6}$$

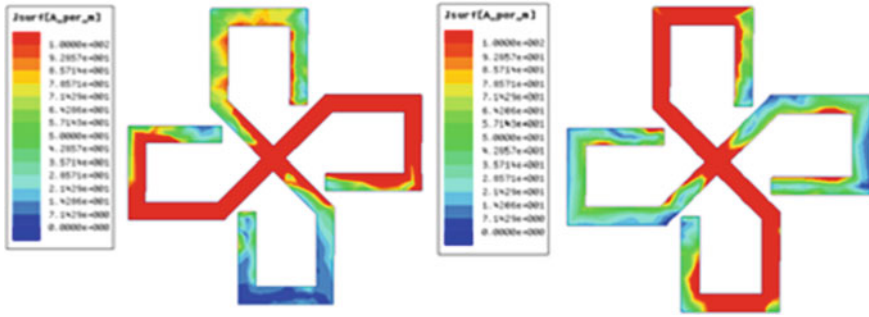


Fig. 9 Simulated surface current distribution under **a** TM mode and **b** TE mode of proposed FSS at resonant frequency

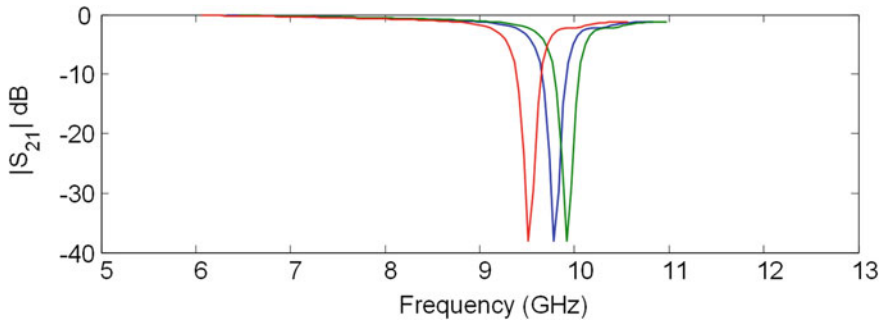


Fig. 10 Simulated transmission coefficient at $\theta = 0^\circ$ of the proposed FSS design when $\alpha = 0^\circ$ (red), 30° (blue), and 60° (green)

where α —folding angle, ϵ_l —transverse contraction strain and ϵ_s —longitudinal extension strain. In different folding angles, $0^\circ, 30^\circ$, and 60° are observed transmitting functions of this FSS system. With natural and oblique incidence to 60° , the FSS irradiates through EM waves. As Fig. 10 indicates the resonance frequency at $\alpha = 30^\circ$ is observed at approximately 9.4 GHz at the normal angle of incidence. Customizing the folding angle (α) should control the FSS.

After changing the folding angle around $\alpha = 60^\circ$ the resonance frequency is switched near to 10 GHz as shown in Fig. 11. When the folding angle (α) deviations take place from 0° to 60° , a shift of 20% occurs in resonance frequency relatively. If the single control parameter, i.e., α , is modified, the controllable FSS changes in an exact frequency band. Such treatments should be carried out across a broad spectrum. Because of the contact between the conduction components and the interaction with the incident waves at different angles, the target position creates a resonance frequency. The groundbreaking aspects of this architecture are that FSS is only operated by a single variable. The frequency shifts by increasing the α folding angle is calculated by:

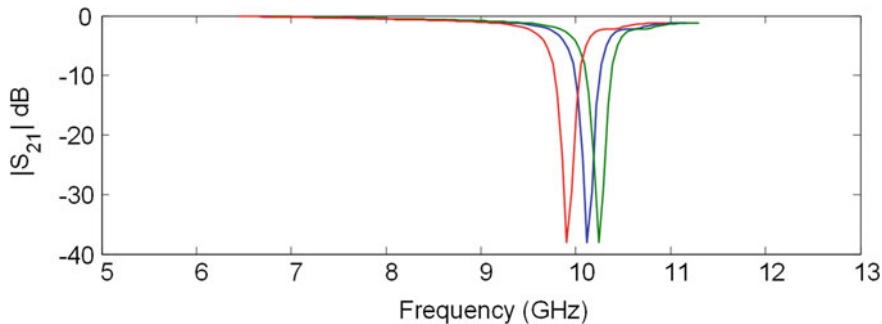
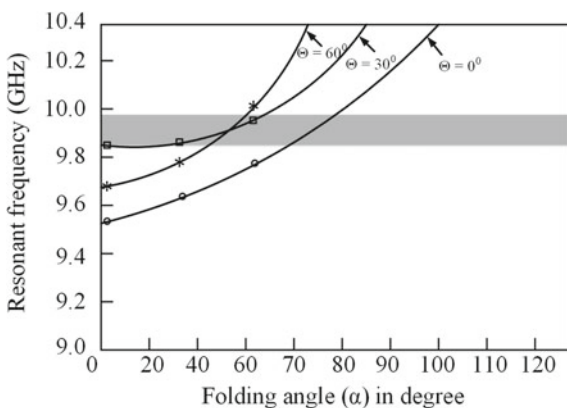


Fig. 11 Simulated transmission coefficient at $\theta = 30^\circ$ of the proposed FSS design when $\alpha = 0^\circ$ (red), 30° (blue), and 60° (green)

Fig. 12 Different folding angle versus simulated resonant frequency



$$\frac{\Delta f}{f_{\text{mid}}} = -\frac{f_{\alpha_1} - f_{\alpha_2}}{0.5|f_{\alpha_1} + f_{\alpha_2}|} \tag{7}$$

where Δf is change in frequency when α varies from α_1 to α_2 , f_{mid} is middle position in frequency band between f_{α_1} and f_{α_2} . A graph is plotted to summarize the tuning result as shown in Fig. 12 at a different folding angle. It is observed that within a shared band of frequency spectrum the change in folding angle α causes a considerable shift in resonant frequency. This shared band is displayed in gray color as shown in Fig. 12. The folding pattern and dimensions of conducting elements are highly responsible for shift in resonance frequency.

4 Conclusion

In X-band implementations, both the proposed FSS architecture is miniaturized and adapted to band-stop properties. With each facet of the unit cell, the rotated cross-shaped structure can be bent without alteration of the arm length of the structure.

The proposed new feature has two benefits: for a specified resonance frequency and tuning capacity, the size of the engineered aspect of the unit cell is 75% reduced. Increased filtering properties improve performance stability, while the incidence angle is sufficiently large in the various types of linear polarization. This system has the advanced filters that achieve the required sharp roll-off at the stop band and strong flattop at the pass band below 0 dB, using only 0% resonant frequency gap in different angles of incidence, foldable, and miniaturized devices. In order to achieve tunability with the required resonant frequency of FSS, any miniaturized part will be arranged in chevron pattern by varying only one control variable (α). The suggested FSS indicates that the resonance frequency ranges from 0° to 60° in a 20% change from folding angle (α). Miniaturization is therefore built into the origami system, which exhibits tuning and provides a stable performance at the optimal level of incidences and polarizations, simulated and tested in HFSS 15.0. This is why PLA is known as the substratum and the requisite measurement of the folding duration is done to insure that production is feasible in the future. The object is the proposed FSS model with a 3D printer.

References

1. Munk BA (2000) Frequency selective surfaces: theory and design. Wiley, New York
2. Yong WY et al (2018) Flexible convoluted ring shaped FSS for X-band screening application. *IEEE Access* 6:11657–11665
3. Liu N, Sheng X, Zhang C, Fan J, Guo D (2017) A design method for synthesizing miniaturized FSS using lumped reactive components. *IEEE Trans Electromagn Compat* 60(2):536–539
4. Neto VPS, Duarte MJ, Albuquerque MRML, D'Assunção AG (2015) Analysis and design of fractal-like circular patch elements for miniaturized and stable FSSs. In: SBMO/IEEE MTT-S international microwave and optoelectronics conference (IMOC). Porto de Galinhas, pp 1–4
5. Hu X, Zhou X, Wu L, Zhou L, Yin W (2009) A miniaturized dual-band frequency selective surface (FSS) with closed loop and its complementary pattern. *IEEE Antennas Wirel Propag Lett* 8:1374–1377
6. Soren S, Kothari A (2019) Miura-Ori fold based tunable bandstop frequency selective surface for Ku band applications. In: 2019 2nd IEEE international conference on computing, power and communication technologies (GUCON-2019), New Delhi, India
7. Soren S, Kothari A, Design of Miura-Ori fold based tunable and miniaturized band-stop frequency selective surface. Dissertation submitted to Visvesvaraya National Institute of Technology, Nagpur
8. Wei PS, Chiu CN, Wu TL (2018) Design and analysis of an ultraminiaturized frequency selective surface with two arbitrary stopbands. *IEEE Trans Electromagn Compat* 61(5):1447–1456
9. Ferreira D, Cuiñas I, Caldeirinha RFS, Fernandes TR (2017) 3-D mechanically tunable square slot FSS. *IEEE Trans Antennas Propag* 65(1):242–250 Jan
10. Li J et al (2016) Design of a tunable low-frequency and broadband radar absorber based on active frequency selective surface. *IEEE Antennas Wirel Propag Lett* 15:774–777
11. Ghosh S, Srivastava KV (2018) Broadband polarization-insensitive tunable frequency selective surface for wideband shielding. *IEEE Trans Electromagn Compat* 60(1):166–172 Feb
12. Mias C (2005) Varactor-tunable frequency selective surface with resistive-lumped-element biasing grids. *IEEE Microw Wirel Compon Lett* 15(9):570–572
13. Hu W et al (2007) Liquid crystal tunable mm wave frequency selective surface. *IEEE Microw Wirel Compon Lett* 17(9):667–669

14. Lima AD, Parker EA, Langley RJ (1994) Tunable frequency selective surface using liquid substrates. *Electron Lett* 30(4):281–282
15. Bossard JA et al (2008) Tunable frequency selective surfaces and negative-zero-positive index metamaterials based on liquid crystals. *IEEE Trans Antennas Propag* 56(5):1308–1320 May
16. Chang TK, Langley RJ, Parker EA (1994) Frequency selective surfaces on biased ferrite substrates. *Electron Lett* 30(15):1193–1194
17. Fuchi K, Tang J, Crowgey B, Diaz AR, Rothwell EJ, Ouedraogo RO (2012) Origami tunable frequency selective surfaces. *IEEE Antennas Wirel Propag Lett* 11:473–475
18. Kocakaya A, Çakir G (2018) Novel angular-independent higher order band-stop frequency selective surface for X-band applications. *IET Microw Antennas Propag* 12(1):15–22

Vulnerability Assessment, Risk, and Challenges Associated with Automated Vehicles Based on Artificial Intelligence



Aditya Raj Singh, Harbhajan Singh , and Abhineet Anand 

Abstract Artificial intelligence is the future of technology and due to the presence of artificial intelligence in the vehicle industry the growth rate has increased exponentially. With this enormous growth in the technology, various vulnerabilities also emerged that are generally neglected by the manufacturers during the manufacturing stage. The vulnerabilities are not only from the manufacturer's side but also it can be from the developer's side who is developing the hardware for Internet connectivity and also the software which is being used to operate the hardware which will ultimately control the vehicle. These vulnerabilities can prove to be a hacker's paradise that is looking to infiltrate into a system like this and it will make things complicated as human lives will be at risk. This paper deals with a discussion on various security features and challenges that are emerging with the development of this technology. The paper also discusses the various risk associated with the vulnerabilities of automated vehicles and it also discuss the possible security and safety measures that can be opted to produce a safe automated vehicle. This paper also discusses the security models that are implemented by various manufacturers of the automated vehicles and it also measures the precision of those security models. The paper also deals with various intrusion detection and prevention methodologies that can be followed to control the attack on the target machine.

Keywords Self-driving vehicles · Driverless vehicles · Robotic land vehicles · Vehicles · Cyber-physical systems · Cybersecurity · Network security · Intrusion detection

A. R. Singh · H. Singh (✉)
Galgotias University, Gr. Noida, India
e-mail: abhaysingh4660@gmail.com

A. R. Singh
e-mail: adityarajsingh77@gmail.com

A. Anand
Chitkara University Institute of Engineering and Technology, Chitkara University, Chandigarh, Punjab, India
e-mail: Abhineet.anand@chitkara.edu.in

1 Introduction

Automated vehicles are connected in a network which is commonly known as vehicular ad hoc networks (VANET) that are based on the principle of ad hoc networks. An ad hoc network is a type of network in which there is no fixed topology that is to be followed by the connected nodes, which means that the connected nodes or the vehicles have a dynamic topology in which vehicles get connected and leave the network according to their desire and they do not have to follow a static topology. This type of network is much more advantageous as compared to a centralized network in which all the functioning is maintained by a single controlling unit. But the network is not purely centralized but it is partially centralized as the dynamic networks themselves are under control of a centralized network which keeps the record of the dynamic networks with the help of Internet. This tendency of the network makes way for the loopholes in the security of the structure as an intruder can pretend to be a vehicle by using a pseudo-vehicular identity and can mislead other vehicles of the network to perform some malicious activity. So vulnerability assessment becomes a crucial point that has to be covered while developing technology of this nature.

Automation of vehicles attracted humans for a long time. Automation of vehicles was first shown in fictional movies as a concept which would be broadly implemented in the future. But today this idea is under implementation and the world is looking forward to it [1]. The automated vehicle uses software that works on the observations that they get from the surroundings with the help of various sensors that are placed at different points of the vehicle so that the vehicle can cover every aspect that should be taken into account while driving the vehicle. The decision-making and observing tendency is achieved through artificial intelligence which is explained in the upcoming sections. Precise location calculation is achieved with the help of GPS trackers that are placed on the vehicle at appropriate positions so that the vehicle can identify its location concerning other automated vehicles that are connected in the ad hoc network and can also know the location of other vehicles that are nearby. Involvement of the ad hoc networks and the Internet makes it easy for intruders and attackers to infiltrate into the network.

Artificial intelligence has made it possible for the vehicles to distinguish and recognize the behavior and objects like humans, vehicles, and various traffic signals and symbols. Due to this tendency of automated vehicles, they overshadow the human capabilities in some aspects of driving. Further, this paper describes how artificial intelligence is responsible for this emerging growth of technology and also numerous security issues that are faced by this type of technology when they are exposed to the environment.

2 Automated Vehicles

A type of vehicle of any size in which no human interaction is required for safely operating the vehicle in any environment in which it is intended to work appropriately is an automated vehicle. Automation of a vehicle is achieved through GPS, software running on the vehicles that provides the control of the vehicle by managing the physical components of the vehicle, sensors which observe the environment in which the vehicle has to be operated, Internet connectivity using an ad hoc network so that the vehicles should not be connected in a centralized manner but instead they are connected in a dynamic topological network so that any vehicle can join with any network and leave it according to its requirements without affecting any other vehicle in the network.

Automation of vehicles is categorized into five major levels depending upon the capabilities that the vehicle upholds concerning the controls of the vehicle that are mentioned in Table 1. These five levels broadly cover the controlling of vehicles from a little automation to full automation of the vehicles. The zero-level vehicles are those in which no automation is achieved and the vehicle remains in the old school form. The first-level vehicles are an advanced version of zero-level vehicles in which automation is achieved up to some extent but not entirely which means that some of the control goes into the hands of the vehicle but they require major control of the vehicle to be performed by the human driver who is operating the vehicle. The advanced first-level vehicles are categorized as second-level vehicles in these vehicles the characteristics of the first-level and zero-level vehicles are kept intact while advancement is made in controls. In this type of vehicles, the steering

Table 1 Autonomy of automated vehicles

Levels	Capability
Zero	This level is one in which the control of the vehicle is entirely in the hands of the driver sitting in the vehicle
One	This level is one in which the control of the vehicle is not entirely in the hands of the driver sitting in the vehicle but some of the features of the vehicle are automatically performed by the vehicle itself
Two	This level is one in which the control of the steering of the vehicle and the accelerator are performed by the vehicle, moreover, the vehicle is also capable of collecting data related to the driving environment and it allows the driver to sit back and let the vehicle control itself just like the autopilot mode of an airplane
Three	In this level, the advancement is done in an auto-driving mode where in any case the driver thinks that he needs to intervene in the situation the control of the vehicle goes into the hands of the driver
Four	This level is one in which the vehicle can control not only the driving part but also it can take decisions based on the security that has to be followed appropriately while driving but this is limited to only a few scenarios
Five	This level is more advanced than level four where the vehicle takes full control of driving and safety in every situation

and acceleration of the vehicle are managed by the vehicle itself which provides it with the tendency to turn and fluctuation of the speed of the vehicle according to it. When further modifications are done in the driverless mode of second-level vehicles then they are characterized in level three automated vehicles. Level three automated vehicles are capable of providing the control of the vehicle to the driver whenever the driver feels that he need to intervene in a situation. Another level of automation is when the vehicle gets the control of driving aspects as well as decision-making tendencies then those types of vehicles come under the fourth level of automation of vehicles. When maximum advancement is made in fourth level automated vehicles where the full control goes into the hands of the vehicle and no involvement of human is required then they are termed as level five automated vehicles.

Figure 1 shows the connectivity among various automated vehicles with the help of different technologies. Following technologies are used in the vehicles to achieve automation of level five autonomous vehicles [2]:

- **RADAR:** Radars sends and receive radio waves around the automated vehicle to observe the surroundings and it precisely spots other vehicles that are present in the surrounding. Radars are reliable as they do not get affected by fog, rain or snow.
- **LIDAR:** LIDAR's are fixed on the top of automated vehicles to detect light and it also helps in range calculation. LIDAR's transmits millions of laser beams every second, to measure the bounce back the time taken by the lasers, this collected data is then used for building a virtual 3D map which is easier for a computer to understand than compared to a normal 2D camera image.
- **Deep Learning:** It is a very important artificial intelligence tool that is used for training the automated vehicle to do the functions like detection of lanes, identification of other objects like cars, bikes, trucks, traffic signals, etc.

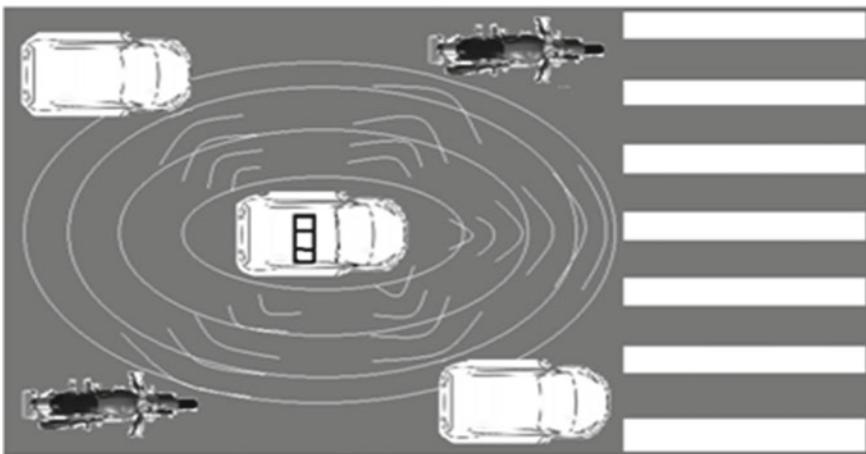


Fig. 1 Connectivity among automated vehicles through radar, lidar, and cameras

- **Cameras:** Cameras are used for spotting entities like lane lines on highways, road signals, road signs, and other vehicles like cars, bikes, cycles, trucks, buses, etc. With the help of better machine vision, cameras can be utilized for recognizing various other entities.

3 Artificial Intelligence

Artificial intelligence is the ability of a computer program or a machine to think, learn, and make decisions similar to humans. Artificial intelligence enables algorithm and machines to do what human desire. Machine learning and deep learning concepts are utilized to train the artificial intelligence-based automated vehicles. Numerous programs are fed with a massive amount of data that is analyzed and processed by the computer, robot or software that results in thinking logically and performing human actions, on behalf of it, or computer command. Artificial intelligence enables the vehicle to manage, make sense of, and respond quickly to the real-world data inputs from hundreds of different sensors receiving information from the surrounding environment.

The automotive industry has joined the race to reach higher-level autonomous driving capabilities. There are many challenges that are being faced but artificial intelligence has taken the automotive industry by storm at a very high level to drive the development of level four and level five autonomous vehicles as given in Table 1. However, the benefits of level four and level five autonomous driving vehicle's capabilities are, particularly, with regards to fewer accidents and life-long mobility, which means that every aspect of driving experience will change with the implementation of artificial intelligence to the vehicles. Artificial intelligence-based systems are broadly categorized into two types:

- Infotainment human-machine interface, which comprises speech recognition, gesture recognition, eye tracking, driver monitoring, virtual assistance, and natural language interfaces.
- Advanced driver assistance systems (ADAS) and autonomous vehicles, which includes camera-based machine vision systems, radar-based detection units, driver condition evaluation, and sensor fusion control units.

4 Working of Autonomous Vehicles Based on Artificial Intelligence

The working of artificial intelligence-based automated vehicles comprises of the following three components those are as follows (Fig. 2):

- In-vehicles data collections and communication systems,
- Autonomous driving platform,

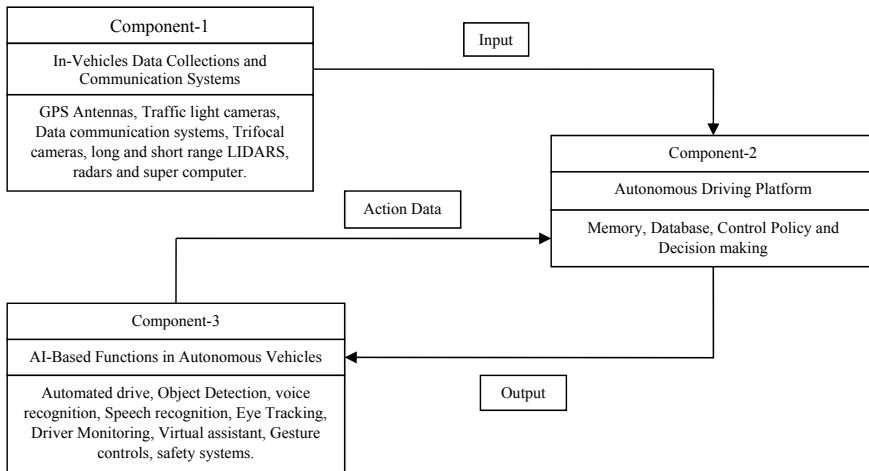


Fig. 2 Data flow in autonomous vehicles (artificial intelligence perception cycle)

- AI-based functions in autonomous vehicles.

Automation of the vehicle is achieved by performing the following three major steps [3]:

- Generation of data for autonomous vehicles,
- Testing of the autonomous vehicle,
- Training of autonomous vehicles.

A. Generation of Data for the Autonomous Vehicles

This is the first step for achieving automation in the vehicles. In this process, four cameras are installed on the vehicle in which automation has to be achieved, two cameras are placed at the top center of the vehicle, one of which is for a front view while the second camera is for back view and other two cameras are placed on each side of the car. They recorded the steering wheel's data and capture the steering angles. Installation of GPS, Radars, LIDAR's, and sensors also takes place. After all, the installation of various types of observing equipment is finished then these equipment become capable of generating the data for observation. These data are stored in a CSV file for observation.

B. Training of Autonomous Vehicles

The data and images captured from equipment that is installed on the vehicles are randomly shifted and rotated and then fed into the neural network. Based on these input data, the neural network gives the output as a single value, the steering angle. With the help of input data, the neural network decides by what angle the car must be steered. Again this output value is compared with the steering data collected from human driving to compute the error in the convolutional neural network's decision.

C. Testing of Autonomous Vehicles

- After training the automated vehicle successfully the testing of autonomous vehicles is done taking the perspective of the front view camera and the rearview camera. Then the camera’s inputs are fed to the neural network, the neural network outputs the steering angle values and these values are fed into the autonomous vehicles. An autonomous vehicles simulator follows the server-client architecture. In which server will be the simulator and the client would be the convolutional neural network. The simulator inputs the images, further analyzed by the programming language and outputs the steering angle. The simulator receives the data and turns the car accordingly. And this whole process goes on and on iteratively or cyclically.

5 Vulnerability Assessment of Automated Vehicles

Security is an essential element of any automated device so is it for an automated vehicle as it would be functioning in an environment where it can affect the masses. The connectivity of the automated vehicle to the Internet and the ad hoc networks is one of the major trouble-causing issues as these types of networks are broadly exposed to numerous vulnerabilities [4]. These factors can be exploited by an attacker who can use them for fulfilling his malicious intentions. Numerous attacks can be performed on these types of networks and they can be categorized into various sections that are explained in Table 2.

The attacks can target the vulnerabilities that are present in the network like a data packet that is containing the information related to the device control and

Table 2 Classification of attacks based on vulnerable sections of automated vehicles

Category of associated attack	Effects
Attack on network	<ul style="list-style-type: none"> • Causes problems in authentication • Causes unavailability • Compromised integrity
Attack on timings	<ul style="list-style-type: none"> • Response timing loses synchronization
Attack on application	<ul style="list-style-type: none"> • Loss of reliability • Causes unavailability • Compromised integrity • Compromised confidentiality
Social attacks	<ul style="list-style-type: none"> • Compromises all security components
An attack based on monitoring	<ul style="list-style-type: none"> • Causes problems in authentication • Causes loss of anonymity

device location is traveling through a network that does not end to end encrypted can be under a spoofing attack in which the attacker can get access to the data packet's information which he can modify using various exploitation techniques [5]. Since in an ad hoc network vehicles can join or leave the network at any point of time so an attacker can use a pseudo-identity of a vehicle and can get into the network to cause malfunctioning to the vehicular network and the connected vehicles. Further, the vehicle's response time can be altered by the attacker to delay the information that is to be conveyed to other devices that are present in the ad hoc network. Another point of vulnerability can be in authentication phase as it can be under de-authentication attack in which the vehicle would be removed from the ad hoc network forcefully, and when the vehicle will try to connect to the network, then it would not be allowed to pass through the authentication phase which will cause the automated vehicle to function improperly as connection with other automated vehicles is a necessity for automated vehicles. Another problem with the authentication phase can be that an intruder with the false identity after getting into the network can send a large amount of data into the network which will cause network instability, as a result, the vehicles connected to the network will start working abruptly and no more vehicles would be allowed to join the network which can cause complications in the surrounding in which the vehicle is operating. Another vulnerable section can be the software running on the automated vehicle, an attacker can install malicious software on the victim vehicle to take the control of the vehicle or he can use some payload to get the access of the victim vehicle. The exploitation methodology can vary but the outcome would be same, i.e., the control of the vehicle will go into the hands of the attacker which will use the vehicle to perform some malicious activity. Another point of attack can be the GPS connectivity of the automated vehicle as GPS is required by the vehicle to calculate the location of the automated vehicle along with the location of known local vehicles. Further, various attacks that are possible on automated vehicles are mentioned in Table 3 along with their brief information.

6 Risk Assessment

The nature of risks associated with automated vehicles differs hugely as compared to the non-automated vehicles but some of the risks associated are quite the same. The idea of automation is being adopted in order to achieve precision in driving as humans can get distracted while driving the vehicles but this does not mean that automated vehicles are perfect in nature, instead, there are lots of technologies associated with an unmanned vehicle and any technical failure in any of the component of the vehicle can be disastrous [36]. There are chances of fault in manned vehicles and unmanned vehicles; it is certain that when any of the two will face an accident then both of them can cause loss of life or can cause serious damage to the environment. But there is one fact that if a fault occurs in an automated vehicle and it loses its control then it can be more disastrous as compared to manned vehicles. This does not mean that severe accidents cannot be caused by manned vehicles but there are very few chances

Table 3 Possible attacks that can be implemented on automated vehicles

Attack name	About the attack	References
Masquerade attack	In this type of attack, an illegitimate entity acquires the identity of a known autonomous vehicle and tries pretending to be that legitimate entity	[6–11]
Fuzz testing attack	In this type of attack, a large number of messages are generated and sent in the network which comprises of various vehicles to activate the instructions as done in the brute force methodology	[12]
Message flooding attack (DOS)	In this type of attack, a large amount of data is flooded in the network to cause a problem in the vehicular network. This data is generally false and illegitimate and affects the vehicle functioning by stopping it	[13–21]
Malware	In this type of attack, malicious software is injected into the victim vehicle which is used later to control the vehicle remotely	[14, 22–25]
Replay attack	In this type of attack, a previously obtained information of the vehicle is repeated in the later period for malicious intention	[9, 11, 26–28]
Sybil attack	In this type of attack, various false vehicular entities are created in a network to perform malicious activity	[21, 29, 30]
GPS spoofing	In this type of attack, a false GPS signal is produced and sent to take control of the vehicle whose navigation depends on the GPS signals	[31]
Location spoofing	In this type of attack, false coordinates of a vehicle is transmitted which shows the false location of a vehicle that is connected in a network	[32]
Isolation attack	In this type of attack, all the data coming in and out of the vehicle is dropped as a result the vehicle becomes isolated	[9]
Timing attack	In this type of attack, the data timeslots of vehicles are modified to perform malicious activities	[33]

(continued)

Table 3 (continued)

Attack name	About the attack	References
GPS jamming	This attack is the first attack of hacking the GPS which is later followed by GPS masquerading. In this type of attack, the GPS signals that are produced by a vehicle in a vehicular network are jammed. This attack is very much similar to de-authentication attack	[31]
Packet duplication	In this type of attack, network messages are sent on a large scale to exhaust the bandwidth of the network or it is performed to make the network work on a lot of data which will result in a lot of data processing	[29, 30, 34]
Sensory channel attack	In this type of attack, a false environment is portrayed in front of the sensors of the vehicle to mislead them so that they can be used to fulfill a malicious task	[24, 35]
Selective forwarding	In this type of attack, data is transmitted to selective vehicles of the network only	[29, 30, 34]

that manned vehicle driver will show such type of actions. There are also cases when GPS directs to a passage that can be of greater risk as in some cases when there is a road which is under construction or it has gone through some calamity than the path according to the satellite would be appropriate for the automated vehicle but humans taking such risk can be neglected for safety reasons [37]. Another risk associated with automated vehicles is the risk of the market value for the automated car manufacturer as if an unmanned vehicle of a particular company suffers a serious malfunctioning then the market value of that company can go down which could be of great loss for the manufacturing company. Further, there is a risk of maintaining the cybersecurity of the automated vehicle as it is open to the Internet and various types of attacks that are mentioned in the previous section can take place in the automated vehicle.

7 Challenges Associated with Automated Vehicles

On looking at various features of the automated vehicles they appear to be fascinating but there are lots of challenges that are faced in implementing the automation in the vehicles, some of the challenges are mentioned in Table 4. The size of the bandwidth is one of the serious challenges that are faced during the implementation of automation in vehicles as the size of the bandwidth is restricted that causes delay in the message delivery to the other vehicles that are connected to the network [38]. The integrity of the transmitted data is another issue as the data packet can be altered before it reaches

Table 4 Challenges faced by automated vehicles

Challenges needed to be overcome	Difficulties faced
Bandwidth restriction	Bandwidth causes a delay in the message delivery, network issues like congestion, the signal becomes less reliable
Intruders and hackers	Vulnerability in security architecture, various attacks, loss of privacy
Computation of the associated key values and their management	Lack of proper encryption methodologies and algorithms, distribution of the computed keys and their maintenance becomes very difficult
Maintaining the originality of the transmitted data	Data sent can be altered and modified which can cause devastating results
Lack of centralization	Any unknown vehicle can join into the network

the required recipient vehicle in the network. The network itself is a huge issue as it lacks centralization which results in the connectivity of vehicles at any point which causes the chance for an attacker to get the control of the network and the automated vehicle. Another challenge that is faced by the automated car manufacturers is the price of the automated vehicle as lots of expensive technology is installed in an automated vehicle so it cannot be made available to most of the common masses but can be made available to only luxury class.

8 Intrusion Prevention System Based on Authentication Factor

Automated vehicles while traveling transmit a beacon message in every specific period which comprises of information related to the automated vehicle like the speed of the vehicle, time, and GPS location information of the automated vehicle. This information from the beacon message can be used along with certain other information to authenticate the vehicular node that wants to get into the vehicular network. The proposed model for intrusion prevention is based on the concept of the beacon messages that are transmitted by the on-board unit (OBU) that are installed in the automated vehicle and the road side units (RSU) along with IEEE 802.11p standard for vehicular networks. The proposed model states that the beacon messages are split into its different components from which GPS information is used for calculating the distance between the vehicular node that is requesting for connectivity and the nearest vehicular node of that network. The distance (DR) is computed using Eq. (1).

$$DR = \sqrt{(X_2 - X_1)^2 + (Y_2 - Y_1)^2} \tag{1}$$

The computed distance between the two vehicles is then used for the implementation of IEEE 802.11p standard according to which the vehicular node can get into the network, if the distance between the two nodes is less than or equal to 1000 m, then the time (TR) is calculated which is relative. Time is computed in a relative manner which provides the information that the vehicles are coming toward each other or they are going away from each other as this information is very necessary to compute the time the vehicular node will get to transmit the request frame for getting connectivity in the network. If the two vehicles are coming toward each other than the time for packet transmission they will have would be lesser than compared to the vehicles that are going away from each other within the range of 1000 m. The relative time between the two vehicles is computed using Eq. (2).

$$TR = \frac{D}{S_R} \quad (2)$$

If the packet transmission time between the two vehicles is lesser than or equal to the relative time, then the authentication packet size of the vehicular node is compared with the standard packet size of the predefined organization vehicle authentication packets if the packet matches with any of the organization standard packet then authentication is granted or else authentication is denied.

Algorithm 1: Authentication of a node in the vehicular network

```

1: Input: Beacon messages from the OBU and RSU.
2: for the two vehicular nodes do
3: Compute DR between OBU and RSU using equation (1)
4: for DR <=1000 meters do
5: compute the relative between the vehicles using equation (2)
6:   if packet_transmission_time <= TR then
7:     if packet_size == SPS then
8:       Auth=1;
9:     else
10:      Auth=0;
11:    end if
12:  end if
13: end for
14: end for
15: Output: Authentication managed

```

9 Conclusion

This paper covers various vulnerabilities of automated vehicles along with the numerous types of attacks that an unmanned vehicle can go through in a detailed manner along with the working of automated vehicles based on artificial intelligence. This paper also describes various challenges along with the risks that are faced during the implementation of automation in the vehicles. This paper helps understand the working of automated vehicles and it also provides a broad overview of loopholes that can be exploited by an attacker. In the future, this work can be extended to provide an assessment of more security vulnerabilities in automated vehicles which in turn can be used to reduce the risks and can also be used to overcome some of the challenges associated with automated vehicles.

References

1. La Torre GD, Rad P, Choo KR, La Torre GD, Rad P, Choo KR (2018) Driverless vehicle security: challenges and future research opportunities. *Futur Gener Comput Syst* 2018:1–51
2. Robotics WM (2017) Autonomous guided vehicles
3. Shi W, Baker M, Li X, Yu H (2017) Algorithm and hardware implementation for visual perception system in the autonomous vehicle: a survey. *Integr VLSI J* 59(July):148–156
4. Talwar R, Koury A (2017) Artificial intelligence—the next frontier in IT security? *Netw Secur* 2017(4):14–17
5. Questions F, Summary C (2015) Cyber-physical attacks on implants and vehicles
6. Martinelli F, Mercaido F, Nardone V, Santone A (2017) Car hacking identification through fuzzy logic algorithms. In: 2017 IEEE international conference on fuzzy systems (FUZZ-IEEE), pp 1–7
7. Cho K, Shin KG (2016) Fingerprinting electronic control units for vehicle intrusion detection. In: 25th USENIX security symposium, pp 911–927
8. Narayanan SN, Mittal S, Joshi A (2016) OBD secure alert: an anomaly detection system for vehicles. In: IEEE workshop on smart service systems (SmartSys 2016), pp 1–6
9. Boudguiga A, Chiron P, Boulanger A, Klaudel W (2016) A Simple intrusion detection method for controller area network. In: IEEE ICC 2016 communication and information systems security symposium a, pp 1–7
10. Michael M, Asaj N (2011) Entropy-based anomaly detection for in-vehicle networks. In: IEEE intelligent vehicles symposium (IV)4:1110–1115
11. Ansari MR, Miller WT, She C, Yu Q (2017) A low-cost masquerade and replay attack detection method for CAN in automobiles. In: 2017 IEEE international symposium on circuits and systems (ISCAS), pp 7–10
12. Koscher K et al (2010) Experimental security analysis of a modern automobile. In: 2010 IEEE symposium on security and privacy, pp 447–462
13. Alheeti KMA, Gruebler A, McDonald-maier KD (2015) An intrusion detection system against malicious attacks on the communication network of driverless cars. In: IEEE 12th consumer communications and networking conference (CCNC), pp 916–921
14. Vuong TP, Loukas G, Gan D (2015) Performance evaluation of cyber-physical intrusion detection on a robotic vehicle. In: IEEE international conference on computer and information technology; ubiquitous computing and communications; dependable, autonomic and secure computing; pervasive intelligence and computing, pp 2106–2113
15. Song HM, Kim HR, Kim HK (2016) Intrusion detection system based on the analysis of network. In: 2016 International conference on information networking (ICOIN), pp 63–68

16. Vuong TP, Loukas G, Gan D, Bezemskij A (2015) Decision tree-based detection of denial of service and command injection attacks on robotic vehicles. In: IEEE International workshop on information forensics and security (WIFS), pp 1–6
17. Subba B, Biswas S, Karmakar S (2017) A game theory based multi layered intrusion detection framework for VANET. *Futur Gener Comput Syst* 82(2018):12–28
18. Alheeti KMA, Gruebler A, Alheeti KMA, Gruebler A, Mcdonald-maier K (2017) Using discriminant analysis to detect intrusions in external communication of self-driving vehicles. *Digit Commun Netw* 3(3):180–187
19. Alheeti KMA, Mcdonald-maier K (2016) Hybrid intrusion detection in connected self-driving vehicles. In: 22nd International conference on automation and computing (ICAC), pp 1–6
20. Vuong T, Filippopolitis A, Loukas G, Gan D (2014) Physical indicators of cyber attacks against a rescue robot. In: The fourth international workshop on pervasive networks for emergency management, pp 338–343
21. Alheeti KMA, Mcdonald-maier K (2016) An intelligent intrusion detection scheme for self-driving vehicles based on magnetometer sensors. In: International conference for students on applied engineering (ICSAE), pp 1–4
22. Mitchell R, Chen I (2014) Adaptive intrusion detection of malicious unmanned air vehicles using behavior rule specifications. *IEEE Trans Syst MAN Cybern Syst* 44(5):593–604
23. Moosbrugger P, Rozier KY, Schumann J (2017) R2U2: monitoring and diagnosis of security threats for unmanned aerial systems. *Form Methods Syst Des* 51(1):31–61
24. Brien EO, Muller D (2014) Unmanned aerial vehicle security using recursive parameter estimation. In: International Conference on Unmanned Aircraft Systems (ICUAS), pp 692–702
25. Mitchell R, Tech V, Chen I, Tech V (2012) Specification based intrusion detection for unmanned aircraft systems. In: The first ACM MobiHoc workshop on airborne networks and communications, pp 31–35
26. Bezemskij A, Loukas G, Gan D, Anthony RJ (2017) Detecting cyber-physical threats in an autonomous robotic vehicle using bayesian networks. In: IEEE international conference on internet of things (iThings) and IEEE green computing and communications (GreenCom) and IEEE cyber, physical and social computing (CPSCom) and IEEE smart data (SmartData), pp 98–103
27. Larson UE, Nilsson DK, Jonsson E (2008) An approach to specification-based attack detection for in-vehicle networks. In: IEEE Intelligent Vehicles Symposium, pp 220–225
28. Marchetti M, Stabili D (2017) Anomaly detection of CAN bus messages through analysis of ID sequences. In: IEEE intelligent vehicles symposium (IV)4:1577–1583
29. Sedjelmaci H, Senouci SM (2015) An accurate and efficient collaborative intrusion detection framework to secure vehicular networks q. *Comput Electr Eng* 43(2015):33–47
30. Sedjelmaci H, Senouci SM, Ansari N (2016) Intrusion detection and ejection framework against lethal attacks in UAV-aided networks: a bayesian game-theoretic methodology. *IEEE Trans Intell Transp Syst* 1–11
31. Sedjelmaci H, Senouci SM, Ansari N (2017) A hierarchical detection and response system to enhance security against lethal cyber-attacks in UAV networks. *IEEE Trans Syst MAN, Cybern Syst* 48(9):1–13
32. Kong S, Member S, Jun S (2017) Cooperative positioning technique with decentralized malicious vehicle detection. *IEEE Trans Intell Transp Syst* 3(2018):1–13
33. Chuang M, Lee J (2013) TEAM: Trust-extended authentication mechanism for vehicular ad hoc networks. *IEEE Syst J* 8(3):1–10
34. Sedjelmaci H, Senouci SM (2014) A new intrusion detection framework for vehicular networks. In: IEEE ICC 2014—Ad-hoc and sensor networking symposium, pp 538–543
35. Bezemskij A, Loukas G, Anthony RJ, Gan D (2016) Behaviour-based anomaly detection of cyber-physical attacks on a robotic vehicle. In: 15th International conference on ubiquitous computing and communications and 2016 8th international symposium on cyberspace and security, pp 61–68
36. Bogumil V, Vlasov V (2018) Analysis of the main risks in the development and implementation of unmanned vehicles of urban passenger transport. *Transp Res Procedia* 36(2018):63–67

37. Hengstler M, Enkel E, Duelli S (2016) Applied artificial intelligence and trust—the case of autonomous vehicles and medical assistance devices. *Technol Forecast Soc Chang* 105(2016):105–120
38. Braun T, Benjamin CM, Fung F (2018) Security and privacy challenges in smart cities. *Sustain Cities Soc* 39:499–507

A Review to Forest Fires and Its Detection Techniques Using Wireless Sensor Network



Roopali Dogra, Shalli Rani, and Bisham Sharma

Abstract Recently reported technological growth in wireless sensor network (WSN) has extended its application in various disastrous applications. One of the most concerned issues is the forest fires occurring across the globe. Every year thousands of hectares of forest are burnt in the forest fires occurring due to one or the other reasons. Although numerous attempts have been made for the detection of forest fires at the earliest, there is still scope for the utilization of optimum technique for the same. This paper aims to report a review of taxonomy of some of the significant forest fire detection techniques encountered in the literature so far. Moreover, scenario of the forest fires prevailing in India is also discussed. In this paper, the comprehensive tabular study of the state-of-art techniques is given which will help in the appropriate selection of methods to be employed for the real-time detection of forest fire.

Keywords Wireless sensor network · Forest fire detection · Routing protocols · Forest fire causes · Early detection

1 Introduction

One of the prominent environmental problems is the forest fire that mostly leads to the number of dangerous catastrophes that further disgruntled human lives. Retrospectively, historical data and meteorological factors were taken into consideration

R. Dogra · S. Rani (✉)

Chitkara University Institute of Engineering and Technology, Chitkara University, Rajpura, Punjab, India

e-mail: shalli.rani@chitkara.edu.in

R. Dogra

e-mail: Roopali.dogra@chikara.edu.in

B. Sharma

Department of Computer Science and Engineering, Chitkara University School of Engineering and Technology, Chitkara University, Chandigarh, Himachal Pradesh, India

e-mail: bhisham.sharma@chitkarauniversity.edu.in

© Springer Nature Singapore Pte Ltd. 2021

G. S. Hura et al. (eds.), *Advances in Communication and Computational*

Technology, Lecture Notes in Electrical Engineering 668,

https://doi.org/10.1007/978-981-15-5341-7_101

1339

for the estimation of probability of danger caused by fire [1]. The forest fires are a global occurrence that happens throughout the year in different parts of the world. However, a number of fires are not reported on a common platform to keep an eye on the global status of forest fire suffering countries [2]. Extinguishing the forest fires normally costs billions of dollars to the victim nation [3].

Forest not only brings ecological balance to the earth but also helps in many different ways to the corresponding nation. It is quite unfortunate that the fires caused in forests are mostly discovered when they are spreading over the large area, which makes it possible for human being to have a control over it. Consequently, devastating loss and irreparable damage are caused to the particular atmosphere as 30% of the carbon dioxide is generated from the atmosphere [4]. Other than causing eventual loss to the forest resources, the long-term adverse effects are also seen due to the forest fires that may include the devastation of flora and fauna [5].

The remote areas, abandoned/unmanaged areas filled with trees, and region with dry leaves act as a fuel to cause forest fire. In addition to this, human actions may cause forest fires that include smoking or barbeque parties, the temperature rise in the hot weather and sometimes the piece of glass that makes the sunlight focusing on the single point causing it to catch a fire. Such fire at the initial stage is termed as 'surface fire'; however, as soon as it catches the other trees and leading to the high flames of fire it is termed as 'crown fire.' At this stage, it becomes quite difficult to control fire and it lasts for a long time causing heavy damage to the forest resources.

The amount of land being destroyed due to the forest fire is in millions of hectares. It is quite unfortunate to know that the carbon dioxide released due to the forest fire is more as compared to that of automobile traffic. Early detection of forest fires could reduce the amount of loss that would have occurred in the case of fire. To make the things easier to understand, the following example can be considered. Let us suppose for an instance of fire, 1 min of fire, 1 cup of water is required, for next minute, i.e., for two minutes, 1000 L of water are required and 10 min of fire make the requirement of water to be 10,000 L [4]. Therefore, it is imperative to detect fire as early as possible to minimize the loss that would be caused by the forest fire.

1.1 The Scenario of Forest Fire in India

In accordance with the report of the Food and Agricultural Organization (FAO) [4], the humans contribute to 80% of total forest fires. The harms caused by the forest fires are much more than the harms caused due to the insects causing damage to the woods. India is the seventh-largest country in terms of area it owns. The total forest covers it owns around 7 lacs square km covering almost 21% area of the country. The fires affect much of the forest cover. The forest fires occur in tropical and subtropical areas. Dry deciduous forests and manufactured plantations are mostly victim of forest fire [1].

As shown in Fig. 1, in the year 2017 the forest fires are enhanced to the tremendous amount, i.e., 35,888, which is much more than what it was in the year 2011 [2]. In

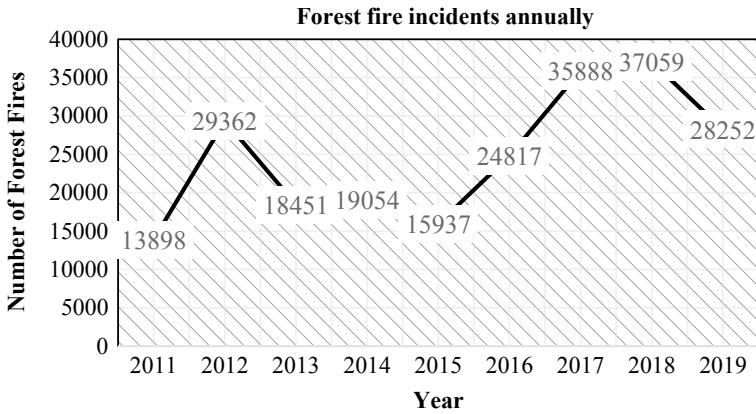


Fig. 1 Scenario of forest fire in India [1]

the British time, the first time the negative effect of forest fire was reported. It was reported that one-half to three-quarters of mature trees in plains was hollowed due to the forest fires. That caused heavy damage to the forest resources in India [4]. It is not only India; in fact many countries across the globe suffering from forest fires. The status of forest fires in world can be studied from [5]. It is important to note that the virtues of forest fires are the growth of plants that contain many nutrients. The negative effects still overcome positive effects. The hard rules have not been implemented; therefore, appropriate strategies are needed to be devised to protect our environment, human health, biodiversity. Forest fire policies need to be cemented and need to be grounded [6].

1.2 The Different Genres of Forest Fires and Their Causes The Scenario of Forest Fire in India

Forest fires are caused by the three essential elements act altogether; these elements or sources are fuel, air, and some ignition source. The classification of the forest fire causing factors can be done as follows and also shown in Fig. 2 [7].

Natural

There are some natural reasons, which are not in the control of human beings. For example, whenever there is lightning hitting in dry areas where the availability of grass and logs is at higher magnitude, the chances of fire in those areas become maximum. Whenever there is high-temperature weather, under those circumstances, the needles, peel are dried down and become favorite to forest fires. Sometimes, such fires are caused in no man’s land, and in those scenarios, the bacterial breathing becomes responsible as it emits enough energy that causes fire. The term ‘ghost

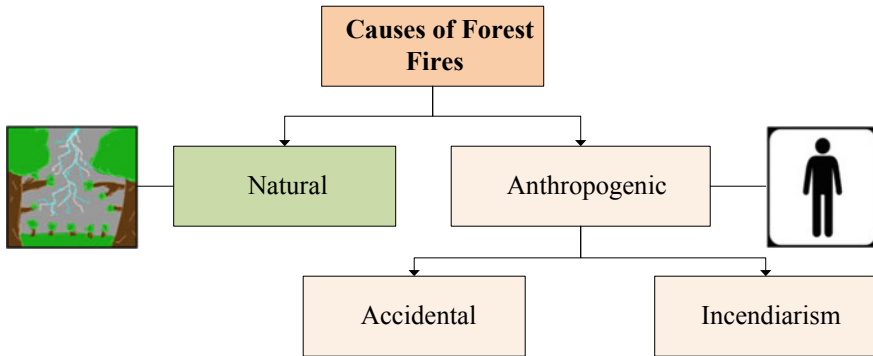


Fig. 2 Causes of forest fires

fire' is used for such generated fires. In addition to these circumstances, when two quartzite stones hit each other and create a spark that may contribute in causing fire. The important thing here that is to be noticed is the fact that chances of such fires are very few.

Anthropogenic

The anthropogenic component of forest fire includes the 'accidental and incendiarism' reasons that result in causing the fires in the forest. These factors are discussed as follows.

Accidental

Mostly, the human activities cause forest fires and the surprising fact is that it is due to more than 80% of the total causes for forest fire that is responsible for forest fires, and they are categorized under accidental forest fires [2]. These are discussed as follows.

- (a) In some scenarios, when cigarette or a *bidi* is thrown into the forest, the crown fires are resulted.
- (b) Railways contribute to forest fires due to their locomotive engines; however, such incidents are very low due to the replacement of such engines with diesel engines.
- (c) To avail the lights in the dark nights, the part of wooden is burnt that leads to the forest fires in the worst-case scenarios.
- (d) The farmers burn the old residue of crop to plant new seeds for new cultivation that also results in forest fires.
- (e) In India, people burn tendu leaves to have enhancement in the production of tendu leaves.
- (f) Charcoal making and alcohol extraction are the others prominent reasons of causing fires in forest.
- (g) Fires from the transformers installed nearby to the forest lead to the forest fires in some adverse scenarios.

- (h) There are some religious beliefs that prompt the residents to light fire in some portion of the forest that sometimes expands in uncontrolled fashion.

Incendiarism

Incendiarism can be a reason for forest fires in some locations where forest offenders can light trees to hide illegal felling and other forest crimes. Forest fires are also induced by hunters and poachers to promote the killing of wild animals. Frustrated villagers burn forests/plants unless their real requirements for grasslands, fuel, wood, and other liberties are met. Often land grabbers/innovationists deliberately burn forest regions adjacent to their planted lands and orchards to illegally expand their holdings in public forest fields.

2 Existing Forest Fire Detection Techniques

The detection of forest fire is one of the essential concerns that every other nation is experiencing. Although the huge number of attempts have been reported to detect the fires to the earliest, the control on the crown fires is still not acceptable in consideration of the damage that is being caused by these fires. The techniques for forest fire detection have been briefly discussed as follows.

2.1 Wireless Sensor Network (WSN)

Wireless sensor network (WSN) is the network constructed from the various nodes deployed in mostly remote areas to sense the surrounding and the gathered data is forwarded to the sink [8–10]. Since its development, the WSN has been playing a significant role in handling the remote and attended area monitoring through its various applications [11, 12]. The routing of the data packets sensed from the different environment helps in uplifting the quality of monitoring the target area. It is the sink from where the alarm signals are sent to the user or the rescue team for the necessary steps to douse the fire. The various essential methods have been discussed that helps in dousing the fire at the earliest.

The sensor nodes that are deployed have four main components: battery, micro-controller, transceiver, and sensing device [13]. The one thing that bothers the user while employing WSN is the limited battery of the sensor nodes which cannot be replaced once its exhausted [14]. Therefore, the efficient utilization of these sensor nodes becomes one of the primitive tasks for the users working toward forest fire detection [15].

Once these sensor nodes are deployed, they connect to each other. These sensor nodes have sensing device that can have different sensors, namely temperature, moisture, vibrational, etc. It entirely depends upon the application for which the WSN is

made to work. In forest fire detection, it is the temperature sensor that is used and in case of an event that crosses the upper limit to the predefined hard threshold for the temperature; subsequently, an alarm is generated [16].

These sensor nodes communicate wirelessly with some wireless technology like Zigbee with IEEE Standard of 802.15.4 [17–22]. Many countries have started to utilize the sensor nodes for the detection of forest fires so as the damage could be minimized.

The devastation caused by the forest fires is of great magnitude and that too occurring all over the world [23].

The numerous studies have been reported so far that have been utilized WSN for the forest fire detection. Some of the extensive reviews that are reported for deciding upon any selected suitable technique are discussed as follows.

In [24], Bahrepour et al. reviewed the crucial aspects that demonstrate the fire detection for different regions like residential or commercial areas. Shahid et al. in [25] presented the features of outlier detection techniques for WSNs that too targeting the harsh environment. Alkhatib et al. in [26] discussed various methods that help in detecting the forest fire.

Comparative analysis of forest fire detection methods in WSN

We have devised a Table 2 that incorporates different methods that cover forest fire. Further, their key findings and research gap are also highlighted.

2.2 Satellite-Based Systems

In the modern technological world, the satellites have also been used for the detection of forest fires. These satellites are Earth-orbiting satellites and in addition, some air floating device has been also used for the detection of forest fire. Advanced very high-resolution radiometer (AVHRR) [27] and the MODerate resolution Imaging Spectroradiometer (MODIS) gathered images for the forest fire detection [28, 29]. But the most unfortunate fact about using these satellites is that the images are delivered after two days which would be an unacceptable delay to deal with crown fires. Furthermore, while these satellites are put into practice, the weather conditions can disturb the image capturing by the satellites [30].

2.3 Optical Sensor and Digital Camera

In modern technology, various sensors are available for fire detection. The optical, automated early recognition and warning of forest fires are developed due to the production of huge number of sensors for the same purpose of fire detection. Various sensors are employed in terrestrial systems [31] that are mentioned as follows.

Table 1 Table captions should be placed above the tables

Metrics	Satellite System	Optical Cameras	WSN
Detection latency	Very long	Long	Small
Information related to fire behavior	Yes	–	Yes
Fire localizing accuracy	Medium	Medium	High
Efficiency	Low	Medium	High
Repetition of faulty alarm	Low	Medium	Medium

- (a) Many applications use video camera that recognizes the smoke in a day and fire at night.
- (b) Thermal imaging camera that depicts the flow of heat from the present sources.
- (c) IR spectrometers helps in the identification of spectral components of smoke.

2.4 Comparative Analysis and Discussion

Among the aforementioned methods, the WSN has left an everlasting impression on the early detection of forest fires as given in Table 1. The sensor nodes are cheap and readily available in the market to use for the harsh environment monitoring. The methods involving ‘satellites’ and ‘optical sensor and digital cameras’ have the following shortcomings over the WSN.

- (a) There is comparatively larger delay in case of delivering critical information to the rescue team in case of employing satellites and digital cameras; however, WSN performs the same task by consuming very little of time.
- (b) The methods employing WSNs are more robust as compared to the competitive methods.
- (c) The most striking feature for using WSNs is the least cost incurred for fire detection in forest as compared to the other methods.

3 Management of Forest Fires

The management of forest fires is done in four ways [32]. These ways have been shown in Fig. 3. Firstly, the prevention of forest fires is done by taking control on the activities nearby to the forest prone areas. Secondly, there are different mitigation processes shown in Fig. 3, that are important to consider to control the number of forest fires. Thirdly, it is essential to create early warning for the forest fires occurring in the fire-prone areas. Lastly, the preparation needs to be intact to deal with the crown fires. It is the responsibility of every citizen to follows the laws laid down by the forest ministry. Moreover, it is also important to be aware of the mischievous activities that might bring havoc to the natural resources of any nation. Prevention of throwing

Table 2 Methods of forest fire detection in heterogeneous WSN

Study reference	Name of technique	Method used	Key findings	Research gap
Yu et al. (2005) [33]	Neural Network Method	<ul style="list-style-type: none"> Collected data by CH is then forwarded to sink and hence to manager node Data processing and network processing, neural network is applied in context of forest fires 	<ul style="list-style-type: none"> Average communication load is reduced on nodes with the proposed method The threshold factor is varied for inspecting behavior of communication load at different values of threshold 	<ul style="list-style-type: none"> The selection of CH is inefficient as it only considers energy and node density factor The approach is not suitable for large area network, as the hotspot problem will counter the network performance
Zhang et al. (2008) [34]	Zigbee-based WSN	<ul style="list-style-type: none"> Employed Zigbee-based WSN CC2430 chip is used to design the hardware circuitry 	<ul style="list-style-type: none"> Information regarding temperature and humidity can be collected from any part of the network at any given time 	<ul style="list-style-type: none"> The concern of energy consumption, location of nodes, and requirement of synchronization question the reliability of the proposed system
Hefeeda et al. (2009) [35]	Distributed k-Coverage algorithm	<ul style="list-style-type: none"> It employs Fire Weather Index (FWI) to model the fire detection system by investigating its (FWI) different parameters 	<ul style="list-style-type: none"> Activate near-optimal number of sensors 	<ul style="list-style-type: none"> The selection of CH is done only based on remaining energy which can be improved further
Aslan et al. (2012) [23]	A general forest fire detection framework	<ul style="list-style-type: none"> Develops its own custom simulator using C# and Microsoft Visual Studio 2008 development environment 	<ul style="list-style-type: none"> Focuses on efficient energy consumption along with the earliest detection of forest fire 	<ul style="list-style-type: none"> Remaining energy is considered for CH selection but the distance and node density factors are not taken into consideration

(continued)

Table 2 (continued)

Study reference	Name of technique	Method used	Key findings	Research gap
Koga et al. (2014) [36]	Improved Maximize Unsafe Path routing protocol (MUP)	<ul style="list-style-type: none"> The priority fire detection data is selected, and thereafter parent election is done for a node to whom data is to be forwarded 	<ul style="list-style-type: none"> Improves MUP by decreasing dropped rate and end-to-end delay of high priority data 	<ul style="list-style-type: none"> Multi-hop transmission among nodes will exert burden on relaying nodes that eventually lead to energy-hole problem
MA et al. (2018) [37]	Sybil detection method	<ul style="list-style-type: none"> RSSI-based and Residual energy-based Sybil attack detection techniques are used False negative alerts are avoided 	<ul style="list-style-type: none"> High stability period and network lifetime are achieved by the proposed technique as compared to LEACH, SEP, and PASCCC 	<ul style="list-style-type: none"> There is computational complexity in CH selection. Overheads are too many that lead to energy consumption

any inflammable material in the forest mitigating the dry leaves and helps the ruling government bodies to declare early warning timely are some of the important tasks that are to be valued.

4 Conclusion and Future Scope

Forest fires are one of the important concerns that every other country with significant forest resources is experiencing. In this paper, different scenarios of forest fires are briefly discussed while pointing out the reasons and the prevention measures to avoid the forest fires. Moreover, we have statistically discussed the forest fires prevailing in India and the role of WSN and different attempts made in WSN to detect forest fires are discussed. It is observed through the reported study that the forest fires still seek a lot of significant serious attention to avoid heavy damage to natural resources or human resources at big magnitude. In future, this study will be taken into consideration to frame an effective measure to avoid the forest fires and also the actions that should be taken to put control on fires before it spreads all across the lands. Moreover, in future, a framework can be generated that regulates the local body around the forest area, so as the forest resources could be saved from fire caused due to any reason.

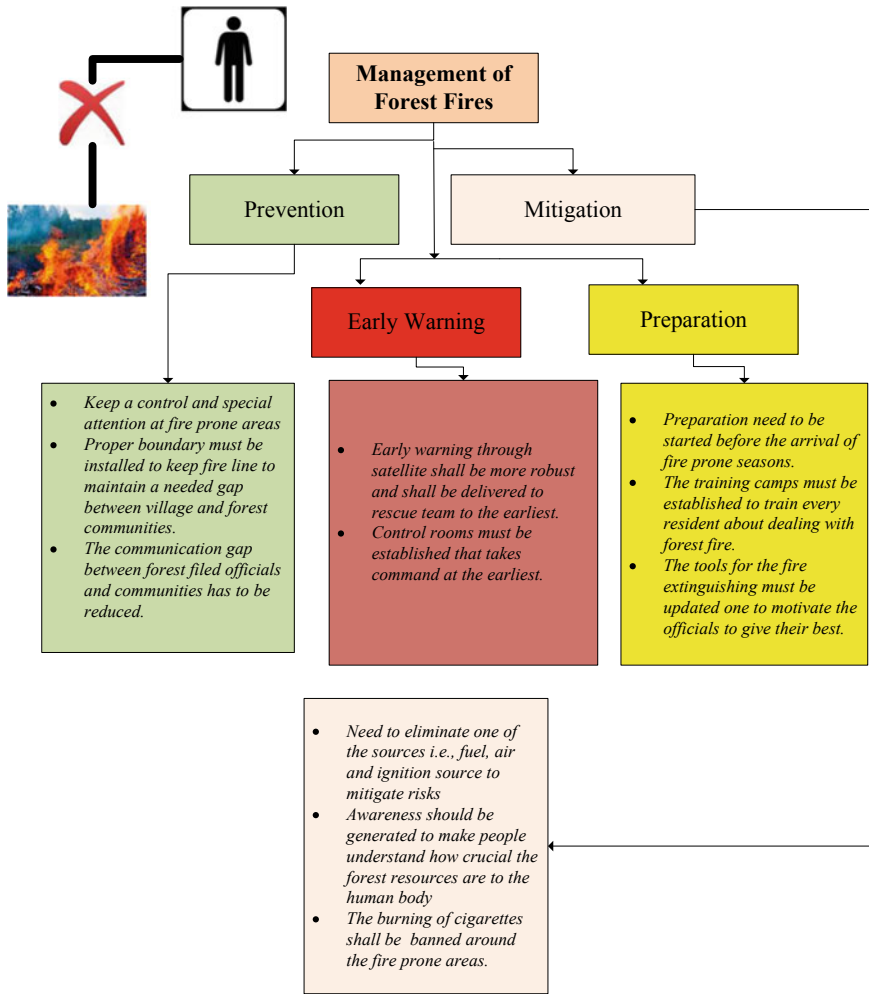


Fig. 3 Management of forest fires

References

1. Vasudeva SP (2018) Disastrous Forest Fires: Management and Control. Indian J Public Adm 64:237–253
2. What is the status of Forest fires in India? In: FACTLY. <https://factly.in/what-is-the-status-of-forest-fires-in-india/>. Accessed 2 Oct 2019
3. Keenan RJ, Reams GA, Achard F, de Freitas JV, Grainger A, Lindquist E (2015) Dynamics of global forest area: Results from the FAO global forest resources assessment 2015. For Ecol Manag 352:9–20
4. Bahuguna VK, Upadhyay A (2002) Forest fires in India: policy initiatives for community participation. Int For Rev 4:122–127
5. List of wildfires. Wikipedia (2019)

6. Joseph S, Anitha K, Murthy MSR (2009) Forest fire in India: a review of the knowledge base. *J For Res* 14:127–134
7. Certini G (2005) Effects of fire on properties of forest soils: a review. *Oecologia* 143:1–10
8. Verma S, Sood N, Sharma AK (2019) Genetic Algorithm-based Optimized Cluster Head selection for single and multiple data sinks in Heterogeneous Wireless Sensor Network. *Appl Soft Comput* 105788
9. Ammari HM, Gomes N, Grosky WI, Jacques M, Maxim B, Yoon D (2012) Review of applications of wireless sensor networks. *Wirel Sens Netw Curr Status Future Trends* 1
10. Ahmed A, Bakar KA, Channa MI, Khan AW, Haseeb K (2017) Energy-aware and secure routing with trust for disaster response wireless sensor network. *Peer-Peer Netw Appl* 10:216–237
11. Djurišić MP, Tafa Z, Dimić G, Milutinović V (2012) A survey of military applications of wireless sensor networks. In: *Embedded Computing (MECO), 2012 Mediterranean Conference on*. IEEE, pp 196–199
12. Akkaya K, Younis M (2005) A survey on routing protocols for wireless sensor networks. *Ad Hoc Netw* 3:325–349
13. Al-Karaki JN, Kamal AE (2004) Routing techniques in wireless sensor networks: a survey. *IEEE Wirel Commun* 11:6–28
14. Verma S, Sood N, Sharma AK (2018) Design of a novel routing architecture for harsh environment monitoring in heterogeneous WSN. *IET Wirel Sens Syst*
15. Verma S, Sood N, Sharma AK (2019) QoS provisioning-based routing protocols using multiple data sink in IoT-based WSN. *Mod Phys Lett A* 1950235
16. Dubey V, Kumar P, Chauhan N (2019) Forest Fire Detection System Using IoT and Artificial Neural Network. In: *International Conference on Innovative Computing and Communications*. Springer, pp 323–337
17. Mohapatra S, Khilar PM (2016) Forest fire monitoring and detection of faulty nodes using wireless sensor network. In: *Region 10 Conference (TENCON)*. IEEE, pp 3232–3236
18. Verma S, Sood N, Sharma AK (2019) A novelistic approach for energy efficient routing using single and multiple data sinks in heterogeneous wireless sensor network. *Peer–Peer Netw Appl* 1–27
19. Pant D, Verma S, Dhuliya P (2017) A study on disaster detection and management using WSN in Himalayan region of Uttarakhand. In: *2017 3rd International conference on advances in computing, communication & automation (ICACCA)(Fall)*. IEEE, pp 1–6
20. Alami HE, Najid A (2017) Routing-Gi: routing technique to enhance energy efficiency in WSNs. *Int J Ad Hoc Ubiquitous Comput* 25:241–251
21. Granger JE (1984) Fire in forest. In: *Ecological effects of fire in South African ecosystems*. Springer, pp 177–197
22. Javaid N, Waseem M, Khan ZA, Qasim U, Latif K, Javaid A (2013) ACH: Away cluster heads scheme for energy efficient clustering protocols in WSNs. In: *Electronics, Communications and Photonics Conference (SIEPC), 2013 Saudi International*. IEEE, pp 1–4
23. Aslan YE, Korpeoglu I, Ulusoy Ö (2012) A framework for use of wireless sensor networks in forest fire detection and monitoring. *Comput Environ Urban Syst* 36:614–625
24. Bahrepour M, Meratnia N, Havinga PJ (2008) Automatic fire detection: A survey from wireless sensor network perspective. *Pervasive Syst Group Univeristy Twente*
25. Shahid N, Naqvi IH, Qaisar SB (2015) Characteristics and classification of outlier detection techniques for wireless sensor networks in harsh environments: a survey. *Artif Intell Rev* 43:193–228
26. Alkhatib AA (2014) A review on forest fire detection techniques. *Int J Distrib Sens Netw* 10:597368
27. Stowe LL, Jacobowitz H, Ohring G, Knapp KR, Nalli NR (2002) The advanced very high resolution radiometer (AVHRR) Pathfinder Atmosphere (PATMOS) climate dataset: Initial analyses and evaluations. *J Clim* 15:1243–1260
28. Justice CO, Townshend JRG, Vermote EF, Masuoka E, Wolfe RE, Saleous N, Roy DP, Morisette JT (2002) An overview of MODIS Land data processing and product status. *Remote Sens Environ* 83:3–15

29. Nakau K, Fukuda M, Kushida K, Hayasaka H, Kimura K, Tani H (2006) Forest fire detection based on MODIS satellite imagery, and Comparison of NOAA satellite imagery with fire fighters' Information. In: IARC/JAXA Terrestrial Team Workshop, pp 18–23
30. Aslan Y (2010) A framework for the use of wireless sensor networks in the forest fire detection and monitoring. Dep Comput Eng Inst Eng Sci Bilkent Univ (MS thesis)
31. Robert S, Józef P, Ryszard S (2013) EUFOFINET: european collaboration to improve preparation and response to wildfires and forest fires in Europe. *Bezp Tech Pożarnicza* 32
32. Devadevan V, Sankaranarayanan S (2019) Forest fire information system using wireless sensor network. In: *Environmental Information Systems: Concepts, Methodologies, Tools, and Applications*. IGI Global, pp 894–911
33. Yu L, Wang N, Meng X (2005) Real-time forest fire detection with wireless sensor networks. In: *Proceedings. 2005 International Conference on Wireless Communications, Networking and Mobile Computing, 2005*. IEEE, pp 1214–1217
34. Zhang J, Li W, Han N, Kan J (2008) Forest fire detection system based on a ZigBee wireless sensor network. *Front For China* 3:369–374
35. Hefeeda M, Bagheri M (2009) Forest fire modeling and early detection using wireless sensor networks. *Ad Hoc Sens Wirel Netw* 7:169–224
36. Koga T, Toyoda K, Sasase I (2014) Priority based routing for forest fire monitoring in wireless sensor network. *J Telecommun Inf Technol* 90–97
37. Jan MA, Nanda P, He X, Liu RP (2015) A sybil attack detection scheme for a centralized clustering-based hierarchical network. In: *2015 IEEE Trustcom/BigDataSE/ISPA*. IEEE, pp 318–325

The Need for Virtualization: When and Why Virtualization Took Over Physical Servers



Abhineet Anand, Amit Chaudhary, and M. Arvindhan

Abstract In early days, industries used physical role-based servers but as they were hard to scale according to the load they are getting and it was hard to manage the infrastructure; if any server is failed, then the service that corresponds to that server also gets down and a plausible solution to all these problems was solved by virtualization. Different researchers have been contributing and showing their effort to make this worth in the past. In this work, the server has been deployed and Datadog tool has been used to record different parameters to check the performance. Different parameters which have been considered are CPU utilization, disk usage, disk latency, memory breakdown. The aim of this work is to show how servers are reacting when the servers are at full load and when the load is lesser. Further, the virtualized environment also provides advanced features like load management on servers in real time and it also enables the organization to make their environment more efficient and robust with more efficient backups and security.

Keywords Cloud computing · Virtualization · Datacenter · Performance · Response time · Resource utilization

1 Introduction

Today many people know that the most efficient way of getting max performance from an infrastructure is by virtualization as it provides efficiency and redundancy at many levels but only a few knows that why all major organizations moved to

A. Anand
Chitkara University, Mohali, India
e-mail: abhineet.mnnit@gmail.com

A. Chaudhary · M. Arvindhan (✉)
Galgotias University, Gr. Noida, India
e-mail: saroarvindmster@gmail.com

A. Chaudhary
e-mail: amit2cha@gmail.com

virtualization from using physical servers in their datacenters and why is it more efficient, convenient, and better choice to run all servers on virtualized computing fabric rather than deploying everything on physical servers [1].

2 About Virtualization

Virtualization is a technology that takes an application, guest shell, or cloud storage away from real hardware or software. The main use of virtualization is server virtualization, which uses hypervisor software to simulate the existing hardware. It includes the memory, I/O, and network traffic of the CPU in terms of politics. Now all the communication with the actual hardware is done through that hardware's software emulation, and sometimes the host OS will have no concept on virtualized hardware. The reliability of this virtualization framework is not equal to the efficiency of OS running on real hardware, and the principle of virtualization works because most guest operating systems and applications do not need the complete use of the corresponding hardware. It allows for greater versatility, power, autonomy, and more productive use of true hardware by eliminating reliance on a given platform of hardware. The idea of virtualization now applies and extends to devices, networks, data, and desktops [2].

2.1 History of Virtualization

As many say that virtualization started from 1972 by IBM in its mainframe on VM/370 as an advanced function and a Type-I code; but the truth is that it goes at least 8 years before that, and the idea of virtualization came in a research by IBM Cambridge Scientific Center in 1964 as System/360 Model 40 and then in 1967, all this aligned with IBM system/360 Model 67 with also start of new technology dynamic address translation (DAT) which basically acted as the base technology for virtualization of memory. Later by 1968 when IBM started to provide all this technology as CP/CMS as type-III code without any service or support. Now then IBM announced its IBM System/370 in 1970. Virtualization was not part of it, and later in 1972, when IBM announced advance function for its System/370, it was called VM/370; but at this time all virtualization was only focused on mainframe systems to make them more secure and to make them more efficient [2, 3].

2.2 The Rise of Virtualization in Commercial Marketplace

At this time, the virtualization was limited to mainframe computing field but as the time continues researchers realized that virtualization can be a great boon for the

field of datacenters, servers, and normal computing environment as typically these systems are being under or overused at a given piece of time. By 2001, the first major program for virtualization or a hypervisor came in market by many different brands like Connectix, VMware, Egenera Inc., and Virtutech in collaboration with AMD. At this point, the race of bringing virtualization came into the place, and by 2003, first open-source hypervisor came which was named as Xen; at this point, Microsoft also came into market with Microsoft Virtual PC, by the real use of virtualization started by 2006 [4, 5]. Now these companies started to make solutions for enterprise server virtualization environment, and it was first done by product name virtual iron from virtual iron software later which have been bought by oracle. At this point, people started to realize why it was better to use virtualization by 2009 [5, 6].

3 Comparative Study

In his paper, Richard Scroggins (2013) describes that trends in virtualization are constantly changing. As the technology recovers and improvements are made, there are more solutions that can be introduced for management and more cost-saving initiatives for virtualization. The Web site The VMware Corporation's virtualize your IT systems give you some insight into the functionality of using the VMware software, which is just one of the choices for virtualization. The usability of VMware's ESX and Esxi looks off when compared to other hypervisors such as Hyper V or KVM. (Virtualize Your IT Infrastructure 2012) [7].

Connor (2004) makes the case that the virtualization of servers moves from the smaller leagues to the mainstream and that the introduction rate is increasing steadily. Spiegel (2006) made the case that there are market benefits in application and application virtualization. "Database virtualization is the new hipster name for cloud-based processing. Instead of installing applications on desktops; however, applications are installed for safe remote access in a server farm. Virtualization of servers enables you to take various physical servers and build its same number of physical servers, or "machines," on a single computer server-client [8].

Hassell (2007) offers us a review of his abstract article when he states, "virtualization, shifting from actual, physical technology to virtual hardware, has also been one of the" last huge things "in IT. Envision a world where the terms of economics-purpose operating system are replaced by a much smaller, purpose-specific architecture that only exists to run a single component are becoming simpler. I think that is where the future lies, but we should not expect the market to change overnight. (Matt Prigge-InfoWorld). According to all of these people, the shift to virtualization from physical infrastructure has been a major move in the industry. At present, virtualization is very popular and commonly used, as well as very significant [9].

4 Why Major Industries Went for Virtualized Environment

Virtualization helps to regain control of the organization's infrastructure. Virtualization allows the organization to view and manage the organization's computing resources in a way that offers more flexibility; since the organization is not restricted by the accomplishment, location, or physical package among virtualization, the organization has a logical rather than physical view of the data, compute power, luggage compartment capacity, and other resources. By gaining greater control of the organization's infrastructure, the organization can improve cost management [10].

1. Cost reductions are a primary driver for the initial implementation of virtualization. Virtualization's current value is its capacity to:
 - Reduce operating costs.
2. (A) Simplify to less systems by virtualization.
 (B) Simplifying network management.
 (C) Recapture by the reduction of floor space.
3. Improve service responsiveness.
 - (A) Improve the performance of the program, network, and application.
 - (B) In order to make better financial decisions, process additional information in real time.
 - (C) Fast delivery of new products online.
4. Supervise accessibility in a 24/7 world.
 - (a) Boost efficiency and resilience.
 - (b) Handle and secure data without regard to their availability.
5. Enthusiastically adapt to the peaks of the business.
 - (a) Provide resources efficiently where they are most needed.
 - (b) Render anywhere, everywhere, information available.

By reducing administration costs and increasing the utilization of assets, the organization can experience a rapid return on investment (ROI) with virtualization. In adding up, by virtualizing assets and facilitating migration or failover to other physical devices or locations, the organization can improve system availability and help reduce the price tag and complexity of disaster revival solutions.

Virtualization facilitates the pooling of information that can be efficiently handled through a company center to meet better-evolving business needs. Virtualization offers a stable platform and shared network to improve access to resources and knowledge to encourage business operations.

Virtualization technologies are being actively embraced by businesses of all sizes to assist with:

1. **Simple form of infrastructure**—Virtualization can help control network expansion by installing safely operating virtual servers and computing in a common

hardware environment. Virtualization helps not only to combine servers, but also to host servers as new devices are deployed. Virtual development restructuring can enable you to increase server utilization rates from 5 to 15% to more than 70%, which helps to improve ROI. Furthermore, with a common management platform and tools, a streamlined infrastructure can help to reduce management costs.

2. **Rapid application deployment**—Virtualization can help to activate quick infrastructure provision (e.g., minutes versus days). It can allow developers to speed up the development and delivery of software, boost collaboration, and increase network access. Project and test conditions can gain significant benefits from virtualization by building and reorganizing guest operating systems (OS) with ease and versatility. For instance, in a shared development platform where applications can reside in logically separate operating system environments; but on communal hardware, you can use dynamic logical partitions (LPARs) in power. Partitions can be dynamically extended for the load test and when the test is done, it can be dynamically contracted. Therefore, you can maximize your investment in your environment and make changes quickly based on business demands and priorities.
3. **Business resiliency**—In order to encourage replication and reconstruction, virtualization can help IT administrators secure and isolate throughput and software data on virtual servers and storage systems. This increased strength can provide more flexibility for IT administrators to maintain a high-availability network when conducting planned maintenance and configuring solutions for low-cost disaster preparedness. Virtualization systems address many conventional backup issues by decoupling the relations between the operating system (with the program and data) and the corresponding hardware.
4. **Managing a virtualized infrastructure**—Several different companies offer the right framework for system management and specific technologies to benefit both virtual and external devices. IT managers should discuss all of their infrastructure's configuration, deployment, reporting, task management, and external administrative functions in a clear and standard manner. This can help to improve the detection of issues, improve performance, and reduce costs of administration.

Virtualization enables the enterprise to freely mix and match technologies to handle heterogeneous decentralized resources through increasing management solutions. This added freedom provides the ability to reduce switching costs, add versatility and option independence, and mask uncertainty. Never having to handle each device or resource individually, but handling them in virtual form allows for substantial improvements in use and expenditure.

Virtualization facilitates faster maintenance, greater reliability, and better problem-solving. Because you can now create virtual machines by trying to copy a disk from a specific prototype to a production disk, this improves the client operating system's stability and longevity. Admins used to install operating systems with various disk controllers, different network cards, etc., on hardware compatibility platforms in the past, which increased the difficulty of the software stack and the devices

being installed. Because one of the key virtualization benefits is to preserve the actual hardware used, it offers a comprehensive set of virtual hardware frameworks that are accessible to the guest operating system.

5 Implementation

5.1 Softwares and Hardwares Used

1. Physical server specifications
 - (a) CPU— $2 \times$ Xeon E5450
 - (b) RAM—48 GB DDR2 ECC 5300R
 - (c) MOBO—SuperMicro X7DCL-3
 - (d) HDD—2X Seagate Constellation (Raid 1)
 - (e) OS—Centos 7 minimal
 - (f) Webserver—Apache
 - (g) Major Role—Webserver, MySQL server (MariaDB)
2. CentOS Web Panel (CWP): Web hosting panel is used for quick and easy management of servers without the effort to use SSH console every time.
3. Putty: Open-Source SSH and Telnet Client.
4. Datadog: Software for modern monitoring and analytics.
5. Apache Webserver and MySQL server.

5.2 Process

Setting up the test environment is started by installation CentOS 7 on the physical server and using an SSH client to access and configure it as a webserver. It is a common industry practice to use headless servers which are servers without a monitor. For metrics, Datadog was used which is a monitoring software to generate the performance metrics. Putty is a commonly used SSH client which is used to access the server for configuration of the server (Fig. 1).

CWP stands for centos web panel which provides a Gui-based dashboard which helps to control the services that are being installed on the server as shown in Fig. 2.

This is a custom script to request http request from the server on different services its running, and we used to simulate the workload on the server as discussed in Figs. 3 and 4.

The analysis includes CPU utilization, disk usage, disk latency, memory breakdown and MySQL and Apache statistics. The load is at its peak from 4:00 pm to 7:00 pm. From the above images of Datadog metrics, we can conclude that this server is only being used for a certain role and this server is highly inefficient as its

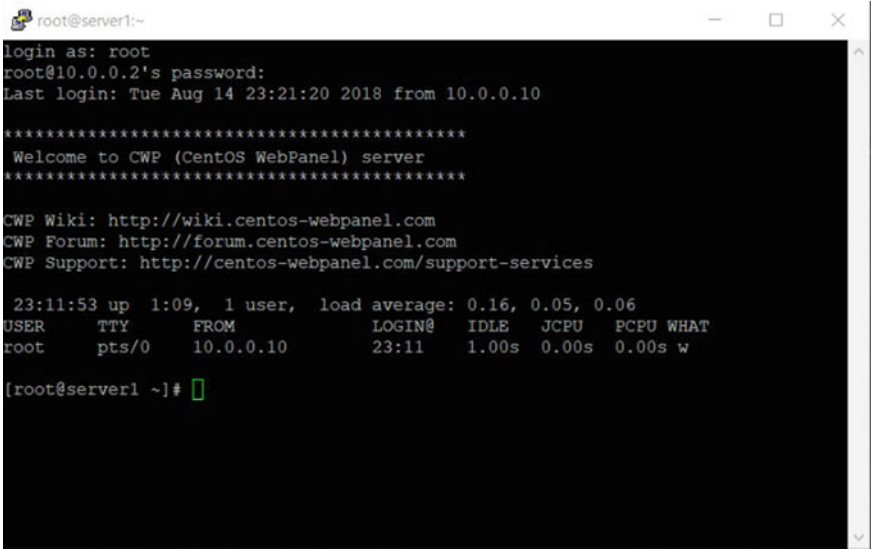


Fig. 1 Accessing the server

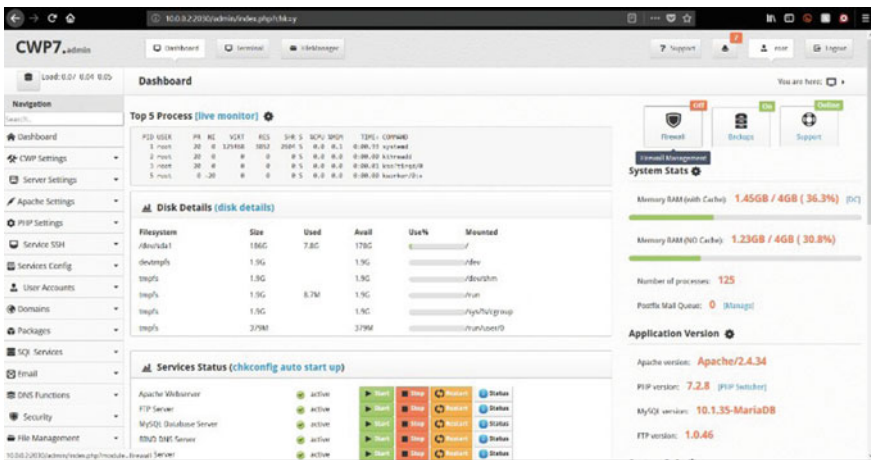


Fig. 2 Managing server using CWP

wasting power 24×7 and the workload is on its peak only for a few hours, which can be solved if we virtualized the server on a pool and a custom rule can be also created to make the server configuration better when the server observes the peak of its workload and decreases it back again.

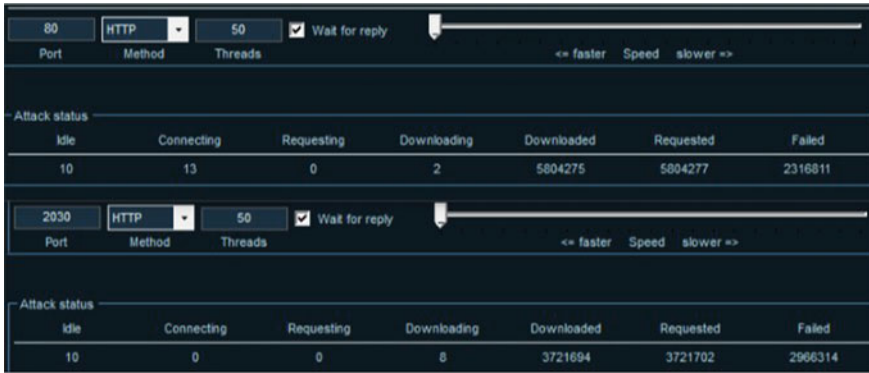


Fig. 3 Managing server using CWP

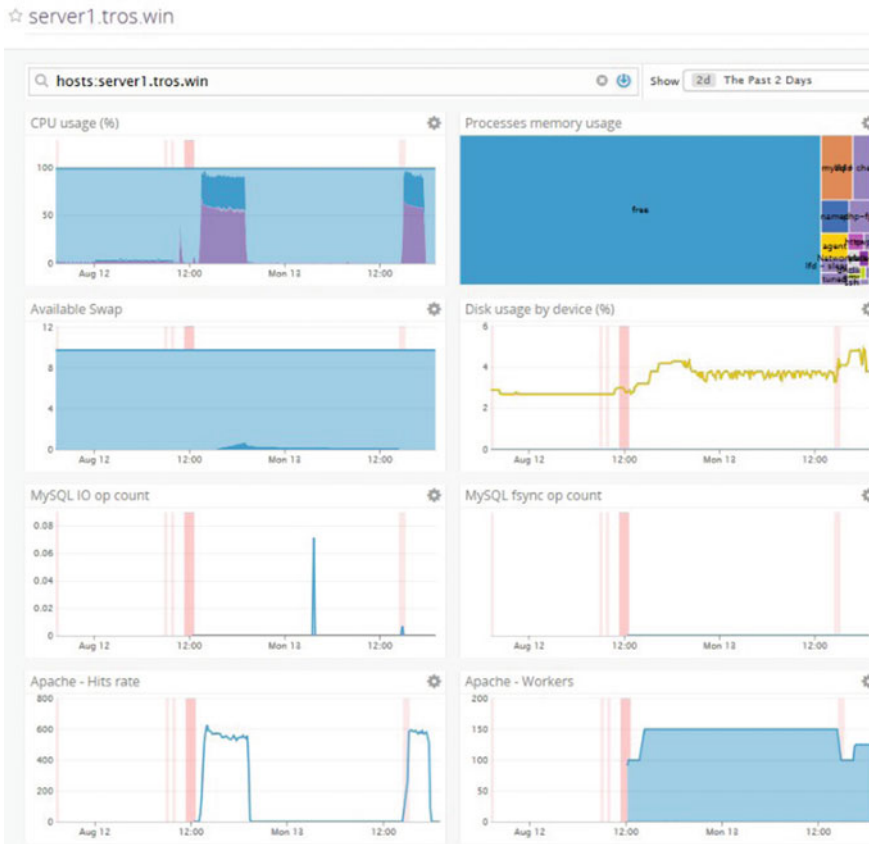


Fig. 4 24 h metrics of physical server on Datadog

6 Result

What was observed from this study is that in enterprise environment, this server would be running many role-based servers 24×7 and doing its work; but when its workload was on its peak, this server was not able to handle all the workload which this server was requested because it was too much for its capacity, and as the role of this server was limited to a few roles, this was wasting power. For an enterprise environment, the most important thing is performance–watt ratio for them, and as this server was used only a few hours a day and wasting power all other time, so servers like this are very inefficient; hence, this all was changed when virtualization came into the loop. By virtualizing the environment, we can keep this server at minimum configuration, and at the time when this server expects heavy workload, the configuration of the server can be cranked up so the server performs maximum on the performance–watt ratio. The virtualized environment also provides advanced features like load management on servers in real time, and it also enables the organization to make their environment more efficient and robust with more efficient backups and security.

References

1. All trademarks are owned by their respected owners we have used name of products which are owned by many different organizations and hold their rights
2. CWP, Apache Webserver, MySQL server, putty are freeware and used according to their License
3. IBM 40 years anniversary talk on virtualization
4. DataDog is property of datadoghq.com and is used under educational license
5. (2012) Virtualization technology literature review. *Global J Comput Sci Technol Interdisciplinary*, Volume 13, Issue 1, Version 1.0 (2013), Publisher: Global Journals Inc. (USA) Online ISSN: 0975-4172 & Print ISSN: 0975-4350
6. Singh S, Anand A, Tiwari R (2018) Optimization of data centres for heat management. *Adv Intell Syst Comput* 624:1025–1032
7. Connor D (2004) Server virtualization is on the rise. *Netw World* 21(49):25–25, 28. Retrieved from <http://search.proquest.com/docview/215981425?account-tid=27965>
8. Virtualization technology literature review (Volume 13 Issue 1 Version 1.0 Year 2013) by Richard Scroggins
9. Using IBM Virtualization to Manage Cost and Efficiency <http://www.redbooks.ibm.com/abstracts/redp4527.html>
10. <https://searchservervirtualization.techtarget.com/definition/virtualization>

A Comparative Analysis on Online Handwritten Strokes Classification Using Online Learning



Charanjeet, Sukhdeep Singh, and Anuj Sharma

Abstract The online handwriting recognition is recognition of handwritten data through the machine using a digital pen. The online learning includes training of the classifier with test data and the test data becomes part of a training model for next test data. We have done a novel study first in this direction to experiment online learning with online handwritten strokes. The experimentation carried out with benchmarked datasets as unipen and online handwritten Gurmukhi script strokes including 12,477 and 26,572 samples, respectively. The tool used in experimentation is Libol which includes all the state of art algorithms for online learning. The results indicate that online learning could be a suitable choice for online handwriting recognition. The online learning is popular today for its use with large data and less computation time. The present study could be benefited for online handwriting recognition like applications in online learning environments.

Keywords Online handwriting recognition · Classification · Machine learning · Online learning

1 Introduction

The recent advances in online handwriting recognition resulted in reliable real-time applications. Alignment and different structures of handwritten strokes need special attention in the recognition process. Some of the geometrical properties as aspect ratio, position, size, slants, and retraces of strokes are common examples of align-

Charanjeet · A. Sharma
Department of Computer Science and Applications, Panjab University,
Chandigarh 160014, India
e-mail: charan@pu.ac.in

S. Singh (✉)
D.M College, Moga, India
e-mail: sukha13@gmail.com
URL: <https://sites.google.com/site/sransingh13/>

© Springer Nature Singapore Pte Ltd. 2021
G. S. Hura et al. (eds.), *Advances in Communication and Computational Technology*, Lecture Notes in Electrical Engineering 668,
https://doi.org/10.1007/978-981-15-5341-7_103

1361

ments and variability. The variations in handwriting exist from one writer to another writer as well as happen in individual handwriting. As dataset includes multiple records of a character class, the variations among same class records are challenging in view to see a high degree of similarities. Also, the shape of a character does have variations subject to a position in a word. Some of the handwritten strokes appear similar, although the difference in their writing order, directionality, and positions. Handwriting styles could be constrained and unconstrained. Writers handedness offer special variations as left/right handed directions that could have multiple challenges geometrically. The situational factors also result in variations of handwriting. The text was written in haste or stressed or slowly do have multiple variations for the same writers. In addition, the handedness to record digital handwriting results in a variation of handwriting. The dependency of handwriting is writer based and independent of writers. The writer-based is writer dependent and the other is writer independent. The handwriting known to system prior recognition is writer dependent, otherwise writer independent. Writer-dependent system has better accuracy, but not suitable for unknown handwriting. Therefore, the writer independent system is more complex in comparison with writer dependent and advised for real-life use. The detailed study regarding handwriting recognition is available in the literature [3–6]. Handwriting recognition is a popular application of pattern recognition and machine learning.

Machine learning includes two types of training data as batch-based and online. If the system is trained in batch mode and used for test data prediction. In the case of online learning, data is trained as it comes and tested simultaneously. The online learning is an important part of machine learning and a very useful technique in large scale data applications. The nature of online learning algorithms is influenced by artificial intelligence, statistics, and machine learning. A rich set of online learning algorithms can be witnessed in the state-of-art study in this area. The online learning refers to understand the data as it comes and classifies parallelly, this continuously improves the training system with new data and helps in making system more reliable. This makes online learning an integral part of real-life use and overcomes the disadvantages of traditional batch-based learning. The details of online learning are available in the literature [7, 8].

One of the motivations behind online handwritten strokes with online learning is their behavior in common. This could be more meaningful if unknown scripts strokes are understood in real life where training data is not available or for unknown writers for common scripts strokes. This paper is an effort in this direction to use the rich properties of both online handwriting and online learning. We have included five sections in this paper including this first section as an introduction. The second section presents selected literature for online handwriting and online learning. Section three discusses features of handwriting strokes and problem formulation in online learning and the common techniques. The experiments are discussed in section four using benchmarked datasets and discuss the outcome of experiments. Section 5 presents the conclusion of the proposed study.

2 Previous Work

The online handwritten strokes and online learning do have rich literature but these both used together have not been observed. In the mid-seventies, digitizer tablets were available in which resistive technique and analog to digital conversion techniques were used. It was possible to measure the pen tip using these tablets. The established flow to recognize online handwriting include: data collection, preprocessing, feature computation, segmentation, recognition, and post-processing [9, 10]. These components are most of the time used in the same sequence as the output of one component becomes the input to the next component. The data is captured in the first step and this data is referred to as capturing of input handwritten stroke. These collected handwritten strokes include noise in the form of irregular sizes or missing points of trajectories, such noise removed in the preprocessing stage. The features are computed in the next stage and this step provides concrete information about writing trajectories as features make handwritten data points more meaningful and helpful in recognition or post-processing stages. Also, segmentation is performed in many cases where writing strokes need to be broken in subparts so that small trajectories could be attended easily. The next stage is recognition where the outcome of the handwritten stroke is found in terms of labels assigned. The last step is post-processing which includes recognized strokes to verify further or used for any linguistic information. The literature of all these steps has been discussed many times in the past [6, 11].

In online learning, it has been observed that research carried out in the last fifteen years, although the first algorithm by Rosenblatt for classification was in the 1960s [12]. An approximate large margin algorithm was based on a p - norm margin of linearly separable data [13]. The other algorithm called relaxed online maximum margin was proposed that repeatedly chooses the hyperplane for previously seen examples. This technique achieved by minimizing the length of weight vector subject to linear constraints [14]. Ultraconservative online algorithms for multi-class problems studied which include updation of only the prototypes attained similar scores higher than the score of correct label prototype. This technique was called margin infused relaxed algorithm [15]. A second-order perceptron algorithm was developed as an extension of classical perceptron where second-order data was considered [16]. An online passive-aggressive algorithm was developed for multi-classes including three cases as hard margin, soft margin linear, and soft margin quadratically [17]. Multi-class confidence weighted algorithm proposed where multivariate distribution with mean and covariance matrix was used [18]. A technique using Gaussian weight distribution by trading off velocity constraints with a function [19]. A double update online algorithm was developed where fixed weights for misclassified examples were used with weights of existing support vectors [20]. An exact soft confidence weighted algorithm was developed which includes large margin training, confidence weighting, handle non-separable data, and adaptive margin [21]. This algorithm resulted in better results than earlier algorithms. An adaptive regularization weights technique was developed that combines large margin training, confidence weighting, and capacity to handle

non-separable multi-class data [22]. An online passive-aggressive active learning technique was developed to handle multi-class data where a Bernoulli random variable is computed based on smoothing parameter and prediction margin [23]. A large scale online learning using two algorithms as Fourier online gradient descent and Nystrom online gradient descent was applied to approximate large kernel machines [24]. A study for comparing linear and kernel classification presents the key features of using linear kernel machines [25]. Implementation of linear online kernels has been performed for popular techniques and their comparison is done [7].

3 Online Learning Machines and Handwritten Strokes Features

In the online setting, a learning algorithm works in a sequential manner for each observation to predicts an outcome. This outcome results in to accept or reject the decision. After the prediction is done, it gets feedback indicating the correct outcome and online algorithm may modify its prediction mechanism to higher the correct prediction chances based on subsequent modifications. The common abbreviations are presented in Table 1.

The data is represented as $(x_1, y_1), (x_2, y_2), \dots, (x_n, y_n)$ in vector R^n , where x_t are data points and corresponding y_t are targets. The corresponding targets are unique labels as $y_t \in \{-1, +1\}$. An instance on round t is represented as x_t and its example is (x_t, y_t) . The decisions are based on sign function as $sign(w^T \cdot x)$, where w is the

Table 1 Symbol descriptions

Notations	Definitions
\mathbf{w}	weight vector
\mathbf{X}	$\mathbf{x}_1, \mathbf{x}_2, \dots, \mathbf{x}_t$
y	The true class label
μ_t	Mean vector
Σ_t	Covariance matrix
m_t	Mean margin
v_t	Margin variance
α_t	Optimal value of the Lagrange multiplier
C	Aggressiveness parameter
ϕ	Probability required for the updated distribution on the current instance
r	The value of $r \in (0, +\infty)$
l_t	Loss function of t th interation
$\ \cdot\ $	Euclidean norm

weight vector as $w \in R^n$. The magnitude as $|w \cdot x|$ is the degree of confidence in prediction. The common hinge loss is computed in each round of training as:

$$\ell(w; (x, y)) = \begin{cases} 0 & y(w \cdot x) \geq 1 \\ 1 - y(w \cdot x) & \text{otherwise} \end{cases} \tag{1}$$

and the loss suffered in round t is termed as $\ell_t = \ell(w_t; (x_t, y_t))$. This makes sum of squared loss as $\sum_{t=1}^T \ell_t^2$, where T is the total round of sequences. The general method used for deriving online update rule is to define the new weight vector w_{t+1} as the solution to the following projection problem:

$$\begin{aligned} w_{t+1} = \operatorname{argmin}_w & \| w - w_t \|^2 \\ \text{s.t. } & L_\gamma(w; (x, y)) = 0 \end{aligned} \tag{2}$$

The Lagrangian of the above problem is:

$$\mathcal{L}(w, \alpha) = \| w - w_t \|^2 + \alpha(\gamma - y_t \langle w, x_t \rangle) \tag{3}$$

where $\alpha \geq 0$ is Lagrangian multiplier. On simple differentiating of \mathcal{L} with respect to w , we find:

$$w = w_t + \alpha y_t x_t \tag{4}$$

This is the update step, where α is:

$$\alpha = L_\gamma(w; (x_t, y_t)) / \|x_t\|^2 \tag{5}$$

The details of above are available in [8].

3.1 Online Learning

Some of the selected online learning with better results are discussed here with their update step and upper bounds of errors. We have used data where soft margin minimizations are required and data is multi-class in nature. Therefore, we have studied the techniques that solve these two conditions of data as soft margin constraint and multi-label classes. These algorithms are first-order and second-order learning methods. The first order mainly includes classical method of working as discussed above and second order includes weight vector follows Gaussian distribution with mean vector $\mu \in R^d$ and covariance matrix $\Sigma \in R^{d \times d}$. We have done experiments including both first order and second order. For multi-class, update rule common equation in first order is:

$$w_{t+1,i} = w_{t,i} + \alpha_{t,i} x_t \tag{6}$$

Here, t is the current iteration round and the value of α is subject to technique used. In online gradient descent method [26], the value of α calculated as:

$$\alpha_{t,i} = \begin{cases} -1/\sqrt{t} & i = \operatorname{argmax}_{j=1}^k w_{i,j} \cdot x_t \\ 1/\sqrt{t} & i = y_t \\ 0 & \text{otherwise} \end{cases} \tag{7}$$

The other algorithm as passive-aggressive [17] for squared loss is:

$$\alpha_{t,i} = \begin{cases} -\frac{\ell(w_t;(x_t,y_t))}{2\|x_t\|^2 + \frac{1}{2C}} & i = \operatorname{argmax}_{j=1}^k w_{i,j} \cdot x_t \\ \frac{\ell(w_t;(x_t,y_t))}{2\|x_t\|^2 + \frac{1}{2C}} & i = y_t \\ 0 & \text{otherwise} \end{cases} \tag{8}$$

In case of multi-class using second order, confidence weighted learning [18] includes the following update rule as in Eq. 9.

$$\begin{aligned} \mu_{t+1} &= \mu_t + \alpha_t \Sigma_t \Delta \psi_t, \\ \Sigma_{t+1} &= \Sigma_t - \beta_t \Sigma_t \Delta \psi_t \Delta \psi_t^T \Sigma_t, \\ m_t &= \mu_t^T \Delta \psi_t, v_t = \Delta \psi_t^T \Sigma_t \Delta \psi_t \\ \alpha_t &= \max\{0, \frac{-(1 + 2\phi m_t) + \sqrt{(1 + 2\phi m_t)^2 - 8\phi(m_t - \phi v_t)}}{4\phi v_t}\} \\ \beta_t &= \frac{1}{1/(2\alpha_t \phi) + v_t} \end{aligned} \tag{9}$$

Here, ψ is label dependent feature. An algorithm adaptive regularization of weights was proposed [22] include as in Eq. 10.

$$\begin{aligned} \mu_{t+1} &= \mu_t + \alpha_t \Sigma_t \Delta \psi_t, \\ \Sigma_{t+1} &= \Sigma_t - \beta_t \Sigma_t \Delta \psi_t \Delta \psi_t^T \Sigma_t, \\ \text{where, } \Delta \psi_t &= \psi(x_t, y_t) - \psi(x_t, \tilde{y}_t), \tilde{y}_t = \operatorname{argmax}_{i=1, i \neq y_t}^k (\mu_i \cdot x_t) \\ m_t &= \mu_t^T \Delta \psi_t, v_t = \Delta \psi_t^T \Sigma_t \Delta \psi_t \\ \alpha_t &= \max\{0, 1 - m_t \beta_t\} \\ \beta_t &= \frac{1}{r + v_t} \end{aligned} \tag{10}$$

The other development in this area by introducing soft confidence weighted technique for squared loss [21] include as in Eq. 11.

$$\begin{aligned}
 \mu_{t+1,r_t} &= \mu_{t,r_t} + \alpha_t y_t \Sigma_t x_t, \mu_{t+1,s_t} = \mu_{t,s_t} - \alpha_t y_t \Sigma_t x_t \\
 \Sigma_{t+1} &= \Sigma_t - \beta_t \Sigma_t x_t^T x_t \Sigma_t, \\
 \text{where, } \alpha_t &= \max\left\{0, \frac{-(2m_t \rho_t + \phi^2 m_t v_t + \gamma_t)}{2\rho_t^2 + \rho_t v_t \phi^2}\right\}, \beta_t = \frac{\alpha_t \phi}{\sqrt{2u_t + v_t \alpha_t \phi}} \\
 \gamma_t &= \phi \sqrt{\phi^2 m_t^2 v_t^2 + 8\rho_t v_t (\rho_t + v_t \phi^2)}, \rho_t = 2v_t + \frac{1}{2C} \\
 u_t &= \frac{1}{8}(-\alpha_t v_t \phi + \sqrt{\alpha_t^2 v_t^2 \phi^2 + 8v_t})^2, v_t = x_t^T \Sigma_t x_t m_t \\
 \phi &= \Phi^{-1}(\eta), \psi = 1 + \frac{\phi^2}{2}
 \end{aligned}
 \tag{11}$$

The details of above-mentioned update steps for respective algorithms are available in [7] in addition to their individual references.

3.2 Handwritten Strokes Features

Online handwriting data is a sequence of pen coordinates in two dimensions. The data input to the online kernel machine needs to be in a more meaningful form as a set of features. These features better present the nature of handwritten strokes and results in more accuracy as compared to data in raw format. There are two categories of features in handwriting as low-level and high-level features. In handwriting strokes, we consider low-level features existence inside a stroke, whereas high-level features depend on multiple strokes. High-level features mainly include features among one or more strokes and low-level features include features inside a single stroke. Some of the common low-level features inside a stroke are directions, positions, slope, area, slant, etc. The high-level features are distance, writing directions between strokes, etc. The computational complexity of a classification problem can also be reduced if suitable features are selected. Each script result in a different set of features and the same set of features is not suitable for different scripts. In addition, a common method to compute features is not possible in view to see the complex nature of handwritten strokes. Also, computed features must vary to an acceptable level, such that feature must be available in different writer’s data. Also, these features should be measurable through algorithms. In the present study, we have used a common high-level feature technique as a chain code. The chain code technique includes computation of directions between trajectories sequential points. The two adjacent points make one direction chain code and this applies to other points of handwritten stroke trajectory. These computed directions from the handwritten stroke result in a string as chain code feature vector. The scope of directions and their use has been studied in past for handwritten strokes [6, 27].

4 Experimental Results

The online learning performance has experimented with benchmarked datasets as unipen and online handwritten Gurmukhi strokes [11, 28]. The unipen dataset includes 10 classes of digits written for online handwriting environment from multiple writers. The online handwritten Gurmukhi strokes dataset include 62 classes and written in an online handwriting environment contributed by 100 writers. The datasets as unipen and online handwritten Gurmukhi strokes used in our experiments include 12,477 and 26,572 samples of data for respective 10 and 62 classes. The tool used to execute online linear kernel is Libol [7], a benchmarked MATLAB-based tool includes all mentioned techniques in Sect. 3 on online learning. We have conducted experiments for online performance and studied results for mistake rate, support vectors, and execution time. This way we are able to understand that how online learning performs for different techniques and their accuracy could be studied for respective classes. Table 1 presents the outcome for different algorithms for both datasets used and information for mistake rate, support vectors with execution time. The total features used for both the datasets per sample is 37. These features are computed based on the dominant point feature extraction technique as discussed in literature [29]. The five techniques experiment for both datasets as online gradient (OGD), passive aggressive 2 (PA2), confidence weighted (CW), adaptive regularization of weights (AROW), and soft confidence weighted 2 (SCW 2). The other techniques mentioned in Libol also used but results are not better than these five common techniques. We find that the techniques as adaptive regularization of weights and soft confidence weighted learning results in low mistake rates as compared to other techniques. The number of support vectors is observed in soft confidence weighted learning is less as compared to other techniques. Also, the CPU time is less for soft confidence weighted learning as compared to other techniques. This is interesting to observe for online handwritten Gurmukhi strokes dataset as it includes 62 classes and complex nature of handwritten strokes. The mistake rates for this dataset shows that online learning could be promising techniques in the real-life environment as mistake rate reduces with more number of data addition. This shows how online handwriting is adapted by the system for classification in the online environment. This helps to understand the sensitive data points in classification. As stated earlier, online handwritten data include a number of variations and its complexities increase with unknown writers, online learning could overcome such issues as such online learning are suitable for large data and new environments. The accuracy of online learning could be improved with the selection of suitable features and adaptability of data with more samples (Tables 2 and 3).

Table 2 Online learning performance for Gurmukhi dataset (26,572 samples, 62 classes)

Technique	Mistake rate	Support vector updates	Time (s)
OGD	0.535± 0.002	14,326.7± 56.4	1.270 ± 0.097
PA2	0.586 ± 0.002	22,180.9 ± 44.5	1.549 ± 0.360
CW	0.403 ± 0.001	14,431.2 ± 43.5	2.057 ± 0.105
AROW	0.382 ± 0.010	20,349.8 ± 405.7	2.180 ± 0.107
SCW2	0.348 ± 0.004	11,951.8 ± 106.5	2.066 ± 0.119

Table 3 Online learning performance for unipen dataset (12,477 samples, 10 classes)

Technique	Mistake rate	Support vector updates	Time (s)
OGD	0.596 ± 0.004	7476.5 ± 56.2	0.553 ± 0.034
PA2	0.681 ± 0.003	11,908.8 ± 27.6	0.609 ± 0.033
CW	0.497 ± 0.003	9121.3 ± 41.8	1.102 ± 0.036
AROW	0.378 ± 0.010	11,737.5 ± 244.4	1.088 ± 0.032
SCW2	0.398 ± 0.007	5758.1 ± 90.8	0.950 ± 0.026

5 Conclusion

We present a comparative analysis of online handwritten data in the online learning environment. In this study, we show how online learning algorithms are responded with online handwritten data. This study helps us in classification to understand the responsive data points in classification. The data which is online handwritten in nature include a number of variations and its complexity differs from the writer to writer. Therefore, it could be suitable technique in recognition of continuous handwritten data.

References

1. Cortes C, Vapnik V (1995) Support-vector networks. *Mach Learn* 20(3):273–297
2. Kao W, Chung K, Sun C, Lin C (2004) Decomposition methods for linear support vector machines. *Neural Comput* 16:1689–1704
3. Plamondon R, Srihari N (2000) Online and offline handwriting recognition: a comprehensive survey. *IEEE Trans Pattern Anal Mach Intell* 22(1):63–84
4. Tappert CC, Suen CY, Wakahara T (1990) The state of the art in online handwriting recognition. *IEEE Trans Pattern Anal Mach Intell* 12(8):787–808
5. Casey RG, Lecolinet E (1996) A survey of methods and strategies in character segmentation. *IEEE Trans Pattern Anal Mach Intell* 18(7):690–706
6. Sharma A (2009) Online handwritten gurmukhi character recognition. Thapar University
7. Hoi SC, Wang J, Zhao P (2014) Libol: a library for online learning algorithms. *J Mach Learn Res* 15:495–499. <http://LIBOL.stevenhoi.org>
8. Crammer S, Online learning of complex categorical problems. Hebrew University

9. Jaeger S, Manke S, Reichert J, Waibel A (2001) Online handwriting recognition: the npen++ recognizer. *Int J Doc Anal Recogn* 3(3):169–180
10. Suen CY, Koerich AL, Sabourin R (2003) Lexicon-driven hmm decoding for large vocabulary handwriting recognition with multiple character models. *Int J Doc Anal Recogn* 6(2):126–144
11. Singh S, Sharma A, Chhabra I (2016) Online handwritten gurmukhi strokes dataset based on minimal set of words. *ACM Trans Asian Low Resour Lang Inf Process* 16(1):1–20
12. Rosenblatt F (1958) The perceptron: a probabilistic model for information storage and organization in the brain. *Psych Rev* 7:551–585
13. Gentile C (2001) A new approximate maximal margin classification algorithm. *J Mach Learn Res* 2:213–242
14. Li Y, Long PM (2002) The relaxed online maximum margin algorithm. *Mach Learn* 46(1–3):361–387
15. Crammer K, Singer Y (2003) Ultraconservative online algorithms for multiclass problems. *J Mach Learn Res* 3:951–991
16. Cesa-Bianchi N, Conconi A, Gentile C (2005) A second-order perceptron algorithm. *SIAM J Comput* 34(3):640–668
17. Crammer K, Dekel O, Keshet J, Shalev-Shwartz S, Singer Y (2006) Online passive aggressive algorithms. *J Mach Learn Res* 7:551–585
18. Crammer K, Dredze M, Kulesza A (2009) Multi-class confidence weighted algorithms. In: *Proceedings of EMNLP*, pp 496–504
19. Crammer K, Lee DD (2010) Learning via gaussian herding. In: *Proceedings of NIPS*, pp 451–459
20. Zhao P, Hoi SCH, Jin R (2011) Double updating online learning. *J Mach Learn Res* 12:1587–1615
21. Wang J, Hoi CHS, Exact soft confidence-weighted learning. In: *Proceedings of ICML*
22. Crammer K, Kulesza A, Dredze M (2013) Adaptive regularization of weight vectors. *Mach Learn* 91(2):155–187
23. Lu J, Zhao P, Steven CH (2016) Online passive-aggressive active learning. *Mach Learn* 103:141–187
24. Lu J, Hoi SC, Wang J, Zhao P, Liu ZY (2016) Large scale online kernel learning. *J Mach Learn Res* 17(1):1613–55
25. Huang HY, Lin CJ, Linear and kernel classification: when to use which? In: *SIAM international conference on data mining*
26. Zinkevich M (2003) Online convex programming and generalized infinitesimal gradient ascent. In: *Proceedings of ICML*, pp 928–936
27. Yimei D, Fumitika K, Yasuji M, Malayappan S (2000) Slant estimation for handwritten words by directionally reined chain code. In: *Proceedings of IWFHR*, pp 53–62
28. Vuurpijl LL, Niels R, van M, Schomaker L, Ratzlai E (2004) Verifying the unipen devset. In: *Proceedings of IWFHR*, pp 586–591
29. Singh S, Sharma A, Chhabra I (2017) A dominant points based feature extraction approach to recognize online handwritten strokes. *Int J Doc Anal Recogn (IJ DAR)* 20(1):37–58

Segmentation of Noisy Mammograms Using Hybrid Techniques



Jyoti Dabass and Manju Dabass

Abstract Breast cancer is the most routinely identified carcinoma among women in India, and it is one of the foremost causes of cancer death in women. Radiologists prefer mammograms for visualizing breast cancer. Different types of noises including Gaussian noise and salt-and-pepper noise affect the mammograms leading to inaccurate classification. Mammograms consist of numerous artifacts too, which depressingly affect the finding of breast cancer. The existence of pectoral muscles makes anomaly finding a cumbersome task. The recognition of glandular tissue in mammograms is vital in assessing asymmetry between left and right breasts and in conjecturing the radiation risk associated with screening. Thus, the proposed method focuses on improving the segmentation accuracy of noisy mammograms. It involves preprocessing which includes denoising using a pretrained convolutional neural network, artifacts removal using thresholding, and modified region growing and enhancement using two-stage adaptive histogram equalization along with segmentation of mammogram images into sections conforming to different densities using K-means clustering. The projected method has been confirmed on the Mini-MIAS database with ground truth provided by expert radiologists. The results illustrate that the proposed method is competent in eradicating noise and pectoral muscles without degrading quality and contrast and in fragmenting different denoised mammograms into different mammographic densities with high accuracy.

Keywords Breast cancer · Region growing · Image segmentation · Mammograms · Denoising using the convolutional neural network · K-means clustering · Mini-MIAS database · Pectoral muscles

J. Dabass (✉) · M. Dabass
EECE Department, The Northcap University, Gurugram, India
e-mail: [jyotidabas91@gmail.com](mailto: jyotidabas91@gmail.com)

M. Dabass
e-mail: [manjurashi87@gmail.com](mailto: manjurashi87@gmail.com)

© Springer Nature Singapore Pte Ltd. 2021
G. S. Hura et al. (eds.), *Advances in Communication and Computational Technology*, Lecture Notes in Electrical Engineering 668,
https://doi.org/10.1007/978-981-15-5341-7_104

1371

1 Introduction

According to GLOBOCON 2018 reports, breast cancer is one of the most frequently identified carcinoma in the huge mass of countries (154 of 183). It is the major reason for cancer-related demises in about 100 countries, i.e., 15%. Worldwide, there are about 2.1 million women who are diagnosed with cancer in 2018 making a record of one in four cancer cases in females. Most of the breast cancer-related demise cases are from Fiji, while Melanesia shows utmost mortality [3]. It is also anticipated that by 2025 there will be about 19.3 million new cancer cases [4, 25]. Furthermore, in the case of developing countries like India, the mortality rate is high because of the massive population, unawareness of patients' regarding the cancer symptoms and coming for treatment when the problems get critical or it gets too late. Also, in rural areas, medical specialists and experts are less which makes early exposure of breast cancer a difficult task. In order to abridge the transience frequency and to increase the treatment likelihood medical support systems using medical data and information technology can be a great answer as it can succor in early detection of abnormalities by satirizing the doctor's reasoning and concluding symptoms. The accuracy and efficacy of the medical support system are augmented by providing the exact region of interest. The mining region of interest is a thought-provoking task in preprocessing because the occurrence of pectoral muscles stimulates the exposure of anomaly [17].

Also, mammogram gets affected by different types of noises comprising salt-and-pepper, Gaussian, and speckle noise during image acquisition which affects the accurate classification of mammograms. Additionally, a lot of uncertainties are present in mammograms because of poor illumination. Most of the structures which are essential to determine the degree of carcinoma are not perceptible properly which can sometimes lead to delay in the treatment of breast cancer patients. In order to get a better quality of mammograms, it is imperative to denoise the mammograms. By denoising, mammograms are renovated into a form that is apt for further processing [6].

Furthermore, the amount of fibrous or glandular tissues appearing on woman mammograms and called breast density affects the radiologist's propensity to detect breast cancer. Sometimes, tumorous lump and calcifications that can be associated with breast cancer appear as white on a mammogram. It becomes difficult to detect cancer in case of dense breast tissue. Also, high tissue density makes it difficult to find out the vicissitudes that may indicate cancer [18].

The BIRADS classification system is mostly used for the classification of breast density. According to the American college of radiology, the BIRADS cataloging system is helpful in segmenting breast region into different densities which helps in early detection of breast cancer. There are four classes as per the BIRAD classification. BIRAD type I and type II classes are early stages of benign phases as breast cysts and breast Lipomas. BIRAD type III has numerous fibrous tissues and symbolizes probable benign stage, and BIRAD type IV deals with malignant stage or skeptical anomaly. BIRAD classification rules are applied to the publicly available

mini-MIAS database. This database is established on the basis of BIRAD classification and categorizes the breast density into three classes: dense glandular, fatty glandular, and fatty [5].

In order to support the radiologists in early and precise identification of breast cancer, the proposed method dedicated to denoising mammograms, breast part extraction, and muscle part deletion, enhancement of mammograms and segmentation of mammograms into distinct densities. The draft of the paper is as trails. Section 1 offers the topic trailed by the related work in Sect. 2. Section 3 provides the proposed techniques which are followed by Sect. 4 dealing with conclusion.

2 Related Work

This section analyzes the literature related to image denoising, image segmentation, pectoral muscle segment and breast density segmentation under the following heads.

2.1 Image Denoising

During the process of mammogram image transmission and acquisition, it gets affected by noise. Image denoising is the process that denoises the mammograms by removing the Gaussian noise without affecting the information content required for finding the presence of carcinoma. Gaussian noise basically follows the Gaussian distribution function and it is evenly distributed over the image. Different types of filtering techniques are proposed for removing Gaussian noise from the mammograms. In [9], a residual learning approach is used to denoise medical images. While in [2] deep neural networks were used for removing noise from the medical images. Table 1 reviews the denoising techniques for removing the Gaussian noise. Most of the techniques used for removing Gaussian noise are based on a convolutional neural network as they are easy to train.

Table 1 Methods for denoising mammograms

S. No.	Author and year	Methods used
1	Ghosh et al. 2020 [6]	Deep convolutional denoising auto-encoders based on multi-norm loss function minimization
2	Lee et al. 2019 [12]	The non-local means denoising algorithm
3	Marrocco et al. 2018 [15]	Generalized transformation, Convolutional neural networks.
4	Singh et a. (2019), [31]	Deep convolutional neural network

Table 2 Methods for segmenting the pectoral muscle

S. No.	Author and year	Methods followed
1	Shen et al. 2018 [28]	Polynomial curve fitting, genetic process, and morphological medley algorithm
2	Pavan et al. 2018 [22]	Active contour to segment pectoral muscles and Hough transform to detect edges
3	Yin et al. 2019 [36]	Fitting and rough contour, Iterative threshold
4	Shinde and Rao 2019 [29]	k-means clustering, thresholding and region growing

2.2 Image Segmentation

Image segmentation means manual, automatic or semi-automatic dissection of mammograms in order to find the region of interest. Manual segmentation is subjective and tedious but accurate [20]. In the case of the automatic segmentation results are objective in nature but there are chances of error in this because of noise and other imaging artifacts. Most of the commonly used automated segmentation techniques comprise graph and region based-based methods [23, 33, 35], level set-based [34] and active contour-based [13]. In the present scenario, there is no standard segmentation that can work perfectly for all datasets. These days researchers have started exploring deep learning techniques like convolutional neural networks for mammogram image segmentation [11, 24].

2.3 Pectoral Muscle Segment

Pectoral muscle (PM) is a tissue with high density. It has somewhat the same features as that of fibro-glandular tissues which make its impulsive exposure a difficult task [22]. So, in order to detect breast cancer in the early stages, it becomes essential to remove the pectoral muscles. Table 2 reviews the methods utilized for segmenting pectoral muscles.

2.4 Breast Density Segmentation

Breast cancer is mostly found in the fibro-glandular part of breast tissue which looks bright on mammograms and called as breast density. This breast density consists of fibrous connective tissues, lobular elements, and ducts. Breast density plays a crucial role in analyzing the mammogram images. Breast density is a significant aspect of the elucidation of mammograms. While analyzing the mammograms, radiologists look for fibro-glandular and fatty tissues of the breast region. This assessment is subjective in nature and varies from one radiologist to another [26]. Therefore it becomes

Table 3 Methods for breast density segmentation

S. No.	Author and year	Methods used
1	Kallenberg et al. 2016 [10]	Sparse autoencoder, deep convolutional network
2	Mohamed et al. 2018 [16]	Convolutional neural network (CNN)-based model
3	Oliver et al. 2015 [19]	Supervised pixel-based classification and exploiting morphological and textural features
4	Pavan et al. 2016 [21]	Fuzzy c means clustering
5	Salman and Ali (2019) [27]	Median filter, k-means clustering, region growing

essential to fragment breast density in order to get early and accurate exposure of breast cancer. Table 3 reviews the breast density segmentation methods.

3 Proposed Technique

The proposed approach comprises of five stages which involves denoising of mammograms, deletion of background, removal of pectoral muscles, and enhancement of mammogram image and finally segmentation of enhanced mammogram into regions of different breast densities. These approaches are applied to a publicly available mini-MIAS database consisting of 322 mammograms having a size of 1024*1024 pixels. These approaches are discussed below in detail.

3.1 Denoising Mammograms

Mammogram image corrupted with Gaussian noise having a variance of 0.01 is provided as the input. Because of the presence of noise, the segmentation of pectoral muscles and breast density becomes a cumbersome task. In order to remove the Gaussian noise, a pretrained feedforward Denoising is performed using a convolutional neural network [1].

A Convolutional Neural Network (CNN) [8, 38] resembles a typical multilateral network comprising one or more additional layers which are followed by one or more fully connected layers. The structural design of a CNN [7, 30] helps in availing the benefits of a 2D arrangement of an input image. Local networks and weights supervised by certain pooling methods affecting translation-invariant features help in achieving this. Moreover, CNN needs a few parameters than fully associated networks with the same size as hidden units. They are simple to train that's why predominately used for regression and classification. In [14], for image Denoising, CNN was used and it was emphasized that CNN has improved power representation compared to the MRF model. The DnCNN [37] contains 59 layers including batch normalization, convolution, and regression output layers. Moreover,

it offers favorable outcomes when used for numerous traditional denoising tasks. This model is efficient in removing speckle, salt and pepper, and Gaussian noise. The proposed technique used DnCNN for removing the Gaussian noise present in improved mammogram images.

3.2 Removal of Background

In this phase, the background of the mammogram images is removed. For this purpose, first mammogram images are converted into binarized form by using thresholding with threshold value 0.1 which helps in extracting breast profile. For threshold values up to 0.7, the proposed technique shows good results. After that, in order to extract the largest blob or pectoral muscles, binarized connected components are rearranged in order from highest to lowest.

3.3 Removal of Pectoral Muscle

In the third step, a modified region growing method is used to remove the pectoral muscle. For the segmentation seeded region growing method segments the mammograms either on the basis of the assortment of seed point or selected pixel location value. This seed point can be chosen either adaptively or manually. In this paper, the seed point is selected automatically taking the help of the orientation of mammography. This technique is useful in regulating the pixels which are near to the seed point. It examines the next pixels and takes the decision whether it can be merged into the region or not. This procedure is continued for extracting the whole region of interest.

3.4 Enhancement of Image

In the fourth phase, two-stage adaptive histogram equalization techniques are applied to improve visual quality. For the two-stage adaptive histogram equalization, we have applied contrast limited adaptive histogram equalization twice in order to get better visual quality. In the first stage, we used uniform distribution and in the second stage, we used Rayleigh distribution keeping other parameters as default. It helps in improving the image contrast with uniform distribution. The enhanced image devoid of noise, artifacts and pectoral muscles is provided to k-means clustering for dissection centered on breast density. K-means clustering segments the enhanced mammogram image into regions of different density.

3.5 K-means Clustering

The fifth phase is k-means clustering in which repetitive alteration is practiced in order to get an ultimate result. In this, the first no of cluster z and dataset are given as input. This dataset comprises features of all data points. The algorithm twitches with original estimates for the k centroids which can be either randomly created or unpredictably chosen from the dataset. The process then reiterates between two phases.

- *Consignment of data:* In this stage, on the basis of squared Euclidean distance, each centroid makes outlines of clusters by dispensing to its nearest centroid.
- *Updating of Centroid:* In this stage, the centroids are computed. This step carries on until the mean of all data points distributed to that centroid's cluster is trans-fixed. This phase of reiteration amid steps one and two endures until a stopping benchmark is encountered.
- *Selection of k :* For finding the number of clusters and relating its outcome, a user is required to run k-means clustering algorithm for a range of k values.

Algorithm phases involved in segmentation mammograms using k mean clustering For segmenting the mammogram images into areas of diverse densities k-means clustering follows a few steps which are discussed as follows.

- Let us consider an image ' I ' with member labels denoted by ml . Consider $p = 1$ to M , $q = 1$ to N , C_s be cluster centroid, Di_{pqk} be the distance between p th row, q th column and k th cluster centroid, T_m is the extreme number of iterations, DM be matrix distance between input image I and cluster centroids, ml_{pq} be label of p th row and q th column pixel of the input image, $C_s(k)$ with $k = 1$ to k ., be k cluster centers.
- Set $EPS = 1E-5$, NC (No. of clusters) = 4, C_s as randomly initialized value and $T_m = 50$. While $T < T_m$ ($T_m = T+1$) and $CMS > EPS$ then $DM = \text{find_distance}(I, C_s)$, $ml = \text{cluster_labeling } Di_{pqk}$, $C_s = \text{update_cluster_centroid}(ml)$ $CMS = \max(\text{abs}(pC_s - C_s))$, where pC_s signifies the previous iteration cluster centroid.

This classification is finished in a supervised manner taking the expert radiologists' ground truth as reference. The proposed method is competent in segmenting the noisy mammograms into different densities with accuracy.

3.6 Results and Discussions

The anticipated method is applied to publicly available mini-MIAS [32] databases having 322 images. This dataset includes all categories of images such as dense glandular, fatty and glandular images.

Figure 1 shows the results achieved by the proposed algorithm. Figure 1a shows the input image corrupted with Gaussian noise having a variance of 0.01. Noisy

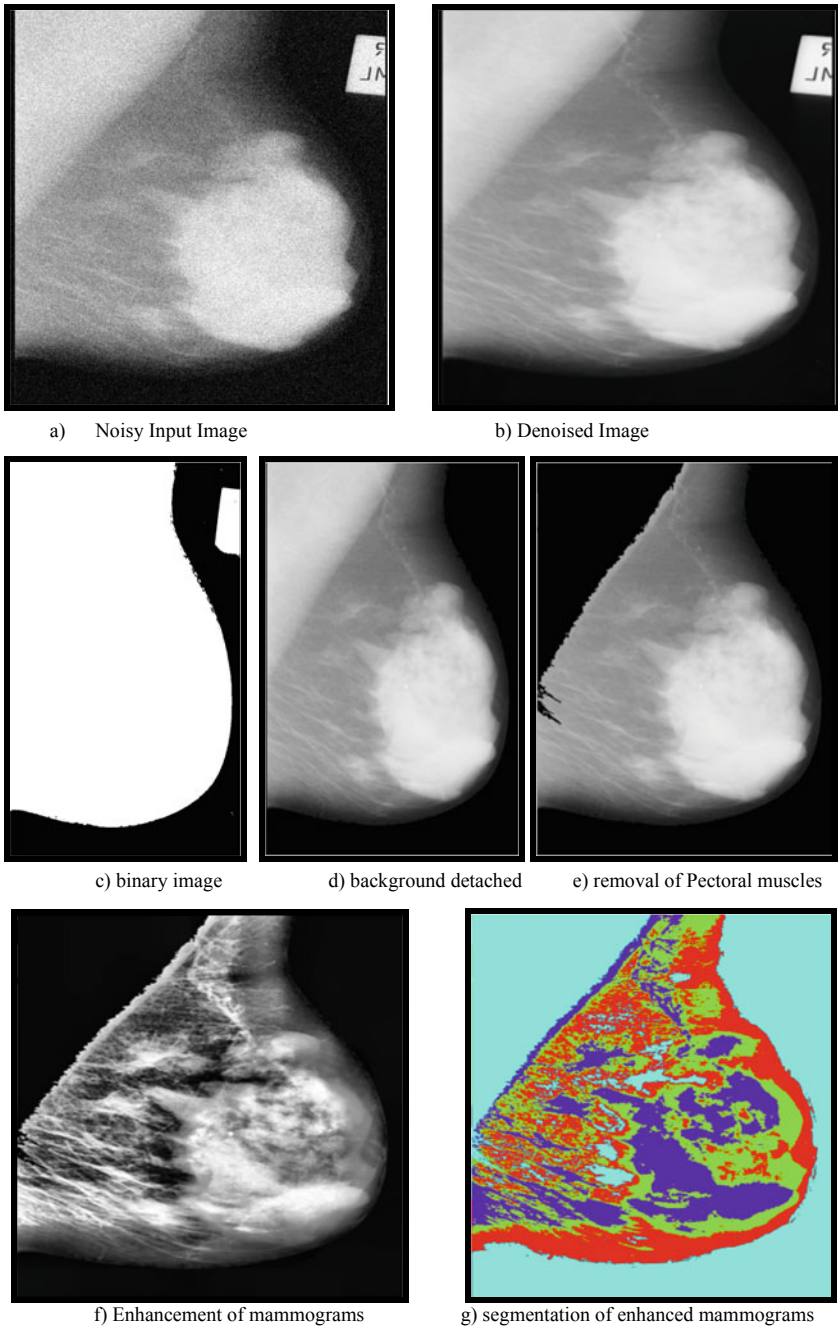


Fig. 1 Mammogram attained after denoising, pectoral muscle deletion, enhancement and dissection **a** input mammogram image corrupted with Gaussian noise **b** denoised image **c** binary image with threshold value 0.1 **d** after deleting the background **e** after removing the pectoral muscles **f** enhanced image **g** segmented image

mammograms are denoised using a pretrained feedforward convolutional neural network. This pretrained network implements a residual learning technique for predicting residual image. Figure 1b shows the denoised mammogram image. Denoised mammogram images contain labels and pectoral muscles which can affect the segmentation accuracy. So, after denoising, binarization is applied with threshold 0.1 to remove the artifacts. After this in order to extract the largest blob, all the associated components are rearranged from biggest to minutest in size. Then for obtaining the original breast profile, the original image is multiplied with the blob. The region growing technique helps in removing the pectoral muscles. Figure 1c displays the binary image having 0.1 as the threshold value. Figure 1d represents the image attained after eradicating the background.

After the automatic selection of seed point, The proposed method applies an adaptive region growing which helps in removing the pectoral muscles. On the basis of image alignment, a conventional grouping of seed points is reformed. This reformation helps in automatic selection of seed point which aids in removing the pectoral muscles using an adapted region growing process. The mini-MIAS database comprises right-oriented or left-oriented images. So, the seed point will be either right topmost or left topmost first non-zero pixel. For finding the orientation of the image, the first image is divided into half and then non-zero pixels are counted. In the case of right-oriented, the right part has more pixels while in case of left-oriented then the left part comprises more pixels. Figure 1e displays the image which is obtained after removing the pectoral muscles from the mammograms. For improving the visual quality of the image, two-stage adaptive histogram equalization is applied. Figure 1f demonstrates the enhanced image with better visual excellence.

The basic aim of the proposed segmentation process is to find the effects of k-means clustering in dispersing the mammogram images into different densities (glandular, adipose, etc. as given by Wolfe for different density patterns). These patterns are considered as diverse density regions by radiologists in analyzing the mammogram. The segmentation results authenticate functionally credible breast density segmentation. Figure 1g shows the segmented image with different mammographic breast densities.

As per the assessment of radiologists, segmentation can result in different sections. This section may include breast edge, purely adipose tissue, adipose tissue having curvilinear strands of fibrous tissues dense tissues with non-homogeneous structures, comparatively dense tissues having glandular tissue or fibrotic stromal tissue and highly dense tissues. Table 4 shows the segmentation accurateness achieved in the case of three- category classification.

The results achieved by the proposed method are compared with the results provided by radiologists. There was a strong resemblance between both results in segmenting mammograms into regions of different densities. It can be deduced from

Table 4 Accuracy results obtained by automatic region segmentation

Segmentation precision	Breast edge (%)	Dense	Fatty (%)
	94.8	98.75	95.8

the results that for darker images, the density of the classified texture will be lower. On the basis of ground truth provided by radiologists, images are analyzed both qualitatively and quantitatively. The algorithm was applied to publicly available mini-MIAS database considering 321 mammogram images from it. For assessing the segmentation qualitatively, a highly expert screening radiologist was pleaded to scale the segmentation results into four categories: satisfactory, very satisfactory, poor or good. Out of 321 images, 4 images were ranked as good, 8 were rated as acceptable and 309 images were found as very satisfactory. The proposed algorithm is able to segment the mammogram into three classes with segmentation accuracy as follows: 98.75% for dense, 95.8% for fatty and 94.8% for breast edge respectively.

4 Conclusion

This paper proposes the technique for improving the segmentation accuracy of noisy mammograms. For this, first input mammograms corrupted with Gaussian noise are denoised using a pretrained convolutional neural network. This network removes noise by calculating the difference between the latent clean image and noisy image. It is then followed by thresholding for background suppression and modified region growing for removing pectoral muscles. Two-stage adaptive histogram equalization is applied to denoised mammograms free of artifacts in order to increase the visual quality. Preprocessed mammograms are then segmented into different mammographic densities. The proposed technique delivers high accuracy in segmenting the breast density and its results match with the segmentation results provided by radiologists. The proposed approach shows a good example of the texture-based segmentation of breast density.

References

1. Agarwal R et al (2019) Automatic mass detection in mammograms using deep convolutional neural networks. *J Med Imaging*. <https://doi.org/10.1117/1.jmi.6.3.031409>
2. Asante-Mensah MG, Cichocki A (2019) Medical image de-noising using deep networks. In: IEEE international conference on data mining workshops, ICDMW. <https://doi.org/10.1109/ICDMW.2018.00052>
3. Bray F et al (2018) Global cancer statistics 2018: GLOBOCAN estimates of incidence and mortality worldwide for 36 cancers in 185 countries. *CA Cancer J Clin*. <https://doi.org/10.3322/caac.21492>
4. Bray F et al (2013) Global estimates of cancer prevalence for 27 sites in the adult population in 2008. *Int J Cancer*. <https://doi.org/10.1002/ijc.27711>
5. Gandomkar Z et al (2019) BI-RADS density categorization using deep neural networks. Presented at the. <https://doi.org/10.1117/12.2513185>
6. Ghosh SK et al (2020) Restoration of mammograms by using deep convolutional denoising auto-encoders. Presented at the. https://doi.org/10.1007/978-981-13-8676-3_38

7. Gu S et al (2014) Weighted nuclear norm minimization with application to image denoising. In: Proceedings of the IEEE computer society conference on computer vision and pattern recognition. <https://doi.org/10.1109/CVPR.2014.366>
8. Jain V, Seung HS (2009) Natural image denoising with convolutional networks. In: Advances in neural information processing systems 21—proceedings of the 2008 conference
9. Jifara W et al (2019) Medical image denoising using convolutional neural network: a residual learning approach. *J. Supercomput.* <https://doi.org/10.1007/s11227-017-2080-0>
10. Kallenberg M et al (2016) Unsupervised deep learning applied to breast density segmentation and mammographic risk scoring. *IEEE Trans Med Imaging.* <https://doi.org/10.1109/TMI.2016.2532122>
11. Krizhevsky A et al (2012) ImageNet classification with deep convolutional neural networks. In: Advances in neural information processing systems
12. Lee S et al (2019) Noise removal in medical mammography images using fast non-local means denoising algorithm for early breast cancer detection: a phantom study. *Optik (Stuttg).* <https://doi.org/10.1016/j.ijleo.2018.11.167>
13. Liu Z et al (2013) A robust region-based active contour model with point classification for ultrasound breast lesion segmentation. In: Medical imaging 2013: computer-aided diagnosis. <https://doi.org/10.1117/12.2006164>
14. Mao XJ et al (2016) Image restoration using very deep convolutional encoder-decoder networks with symmetric skip connections. *Adv Neural Inf Proces Syst*
15. Marrocco C et al (2018) Mammogram denoising to improve the calcification detection performance of convolutional nets. Presented at the. <https://doi.org/10.1117/12.2318069>
16. Mohamed AA et al (2018) A deep learning method for classifying mammographic breast density categories. *Med Phys.* <https://doi.org/10.1002/mp.12683>
17. Mughal B et al (2018) Removal of pectoral muscle based on topographic map and shape-shifting silhouette. *BMC Cancer.* <https://doi.org/10.1186/s12885-018-4638-5>
18. Oiwa M et al (2019) Can quantitative evaluation of mammographic breast density, “volumetric measurement”, predict the masking risk with dense breast tissue? Investigation by comparison with subjective visual estimation by Japanese radiologists. *Breast Cancer.* <https://doi.org/10.1007/s12282-018-0930-0>
19. Oliver A et al (2015) Breast density analysis using an automatic density segmentation algorithm. *J Digit Imaging.* <https://doi.org/10.1007/s10278-015-9777-5>
20. Parmar C et al (2014) Robust radiomics feature quantification using semiautomatic volumetric segmentation. *PLoS ONE.* <https://doi.org/10.1371/journal.pone.0102107>
21. Pavan ALM, de Oliveira M, Alvarez M, Sampaio AJM, Trindade AP, Duarte SB, de Pina DR (2016) Breast tissue segmentation by fuzzy C-means. *Phys Medica* 32:336
22. Pavan ALM et al (2019) Automatic identification and extraction of pectoral muscle in digital mammography. In: IFMBE Proceedings. https://doi.org/10.1007/978-981-10-9035-6_27
23. Peng J et al (2015) 3D liver segmentation using multiple region appearances and graph cuts. *Med Phys.* <https://doi.org/10.1118/1.4934834>
24. Pereira S et al (2016) Brain tumor segmentation using convolutional neural networks in MRI images. *IEEE Trans Med Imaging.* <https://doi.org/10.1109/TMI.2016.2538465>
25. Release P (2013) Latest world cancer statistics global cancer burden rises to 14:1 million new cases in 2012: marked increase in breast cancers must be addressed
26. Saidin N, Sakim HAM, Ngah UK, Shuaib IL (2012) Segmentation of breast regions in mammogram based on density: a review. *Int J Comput Sci Issues* 9(4): 104
27. Salman NH, Ali SIM (2019) Mammograms segmentation and extraction for breast cancer regions based on region growing. *Baghdad Coll Econ Sci Univ* 57:448–460
28. Shen R et al (2018) Automatic pectoral muscle region segmentation in mammograms using genetic algorithm and morphological selection. *J Digit Imaging.* <https://doi.org/10.1007/s10278-018-0068-9>
29. Shinde V, Thirumala Rao B (2019) Novel approach to segment the pectoral muscle in the mammograms. *Adv Intell Syst Comput* https://doi.org/10.1007/978-981-13-0617-4_22

30. Simonyan K, Zisserman A (2014) Very deep convolutional networks for large-scale image recognition. In: International conference for learning representations
31. Singh G et al (2019) Deep convolution neural network based denoiser for mammographic images. Presented at the https://doi.org/10.1007/978-981-13-9939-8_16
32. Suckling J et al (1994) The mammographic image analysis society digital mammogram database. *Expert Medica Int Congr Ser*
33. Sun C et al (2017) Automatic segmentation of liver tumors from multiphase contrast-enhanced CT images based on FCNs. *Artif Intell Med.* <https://doi.org/10.1016/j.artmed.2017.03.008>
34. Suzuki K et al (2010) CT liver volumetry using geodesic active contour segmentation with a level-set algorithm. In: *Medical Imaging 2010: Computer-Aided Diagnosis.* <https://doi.org/10.1117/12.843950>
35. Wu W et al (2016) Automatic liver segmentation on volumetric CT images using supervoxel-based graph cuts. *Comput Math Methods Med.* <https://doi.org/10.1155/2016/9093721>
36. Yin K et al (2019) A robust method for segmenting pectoral muscle in mediolateral oblique (MLO) mammograms. *Int J Comput Assist Radiol Surg.* <https://doi.org/10.1007/s11548-018-1867-7>
37. Zhang K et al (2017) Beyond a Gaussian denoiser: residual learning of deep CNN for image denoising. *IEEE Trans Image Process.* <https://doi.org/10.1109/TIP.2017.2662206>
38. Zhang XP (2001) Thresholding neural network for adaptive noise reduction. *IEEE Trans Neural Networks.* <https://doi.org/10.1109/72.925559>

An Empirical Comparison of Generative Adversarial Network (GAN) Measures



Pradnyawant Kokate, Amit D. Joshi, and P. S. Tamizharasan

Abstract Generative adversarial network (GAN) is the most potent unsupervised learning generative model in deep learning. Though numerous impressive results have been published in computer vision tasks, it is still complex to compare and validate the performance of GAN algorithms. In this work, the review of quantitative evaluation measures of GAN is done with the performance of Frechet inception distance (FID) and the inception score (IS). Evaluations of several recently proposed GAN approaches are based on these two metrics. These evaluations demonstrate an evident variation in their performance based on key factors like training model and hyperparameters such as dimensions of the latent space, learning rate, and gradient penalty. This work discovers the proper dimension of latent space and compares FID and IS that are implemented for evaluation of generated data distribution. FID and IS are the best metrics for evaluating generated data distribution. This work gives an emphasis on appropriate dimension of the latent space and compares these two metrics concerning the improved GAN models. The experimental analysis shows that FID gives better performance compared to IS. NS-GAN and LS-GAN perform more precise. The generator generates better results for 10-dimensional latent spaces, which are not really distinct from the consequence of the normal 100-dimensions. It is recommended to use LS-GAN for better performance and understanding of algorithms.

Keywords Generative adversarial network · GAN metrics · Frechet inception distance · Inception score

P. Kokate (✉) · A. D. Joshi
Department of Computer Engineering and IT, College of Engineering, Pune, MS, India
e-mail: kokatepb17.comp@coep.ac.in

A. D. Joshi
e-mail: adj.comp@coep.ac.in

P. S. Tamizharasan
Department of Computer Science, Birla Institute of Technology & Science (BITS), Pilani, Dubai Campus, Dubai, UAE
e-mail: tamizharasan@dubai.bits-pilani.ac.in

1 Introduction

GAN generates photo-realistic images which are indistinguishable from original images [1]. The new process for training generative models is a generative model (G) which synthesizes the data and a discriminative model (D) which tries to distinguish properties in data to identify fake samples (samples created by the discriminator). The generator is expected to generate unique and different samples each time. Hence, it is supplied with random noise. G tries to generate fake data (which seems like real) and D tries to identify (given both real and fake data) which is artificial and which is original. When D can authenticate the fake data, G incurs loss corresponding to the mistakes it made and it trains itself using it. Likewise, when G can fool D , D provokes the loss and uses it to train itself. This extraordinary ability has powered numerous real-world applications which range from visual recognition to image manipulation and video prediction [2–4]. Several GAN variants have been proposed for such real-world applications that usually produce more realistic and diverse samples with satisfying training stability [5, 6]. GAN are analyzed extensively in the past several years. Besides producing incredibly plausible images, their evaluation remains mainly qualitative, quite often resorting to manual inspection of the visual fidelity of generated images. This evaluation is time consuming, subjective, and possibly misleading. Thinking about the inherent limitations of qualitative evaluations, proper quantitative metrics are crucial for the development of GAN to steer the design of much better models.

The main goal of this work is to conduct detailed comparative analysis of GAN evaluation metrics IS and FID. After analysis this can be used in practice. In this work, unconditional generative adversarial network is used with unlabeled data. The analysis is performed using recently proposed improved GAN training methods like MM-GAN, NS-GAN, BEGAN, DRAGAN, LS-GAN, WGAN, and WGAN-GP.

The contents of this paper are organized as literature review in Sect. 2, experimental analysis and results in Sect. 3 followed by conclusion and future scope in Sect. 4.

2 Literature Review

This section gives an overview of present evaluation methods that are generally implemented along with different metrics. The emphasis is given on the evaluation of GAN models to achieve diversity and quality. Of the diversity aspect, we evaluate GAN's capability to generate diverse fake samples capturing various modes in the actual distribution; and by the quality perspective, we evaluate GAN's ability to generate realistic looking data samples.

2.1 GAN

GAN is composed of a generative network (G) that generates data samples with the same distribution as the real data (x), (D) that distinguishes $G(z) = x$ from each other. The block schematic of GAN is shown in Fig. 1. In this case, the creation network can be expressed as playing the minimum maximal game and the loss function [1].

$$\min G \max D(D, G) = E_{x \sim p_d} [\log(D(x))] + E_{z \sim p_z} [\log(1 - D(G(z)))]$$

DC-GAN The most notable of the various approaches proposed to conquer the problems of GAN include instability and mode collapse. DC-GAN is a convolutional neural network (CNN) with excellent performance in image mapping learning neural networks and various GAN discovered after that are all based on the structure of DC-GAN. DC-GAN is one of the most productive network designs for GAN. It mostly composed of convolution layers without any max pooling or fully connected layers. It employs convolutional stride and transposed convolution for the downsampling and the upsampling [5].

NS-GAN Since the data generated at the initial steps of learning are much different from the actual data, the discriminative network shows excellent results. Then, the term $\log(1 - D(G(z)))$ is close to 0 and the generative network is not able to provide an adequately large slope to be learned GAN non-saturating training to maximize the $\log(D(G(z)))$ rather than minimizing $\log(1 - D(G(z)))$. Goodfellow et al. proposed the NS-GAN. As a result of this research, in the early stage of learning, we can get quick results [1]. The NS loss function is given as follows.

$$L_D^{\text{GAN-NS}} = E_{x \sim p} [\log(D(x))] + E_{\hat{x} \sim p_g} [\log(D(\hat{x}))],$$

$$L_G^{\text{GAN-NS}} = E_{\hat{x} \sim p} [\log(D(\hat{x}))]$$

LS-GAN The GAN discriminator (D) classifies actual images from the generated data samples. In practice, the discriminator generally performs reasonably well. In the GAN, sigmoid cross-entropy function is used as the loss function of the discriminator

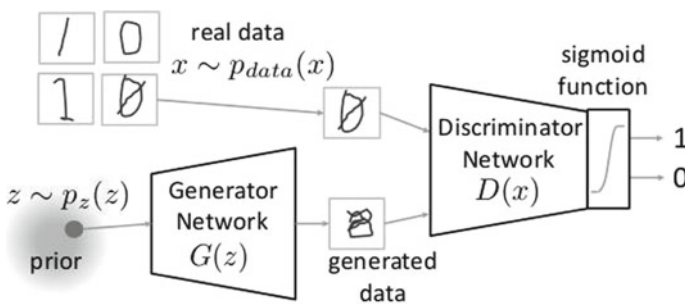


Fig. 1 Generative adversarial network

function. If the generated data is classified as actual data, no matter how far the generated data are from the actual data. This causes a problem that the learning does not proceed any further in the generative network. To solve this problem, least-squares loss function is used to disrupt the generated data away from the actual data. Least squares help to improve the stability of learning by making it more accessible [7]. Its value function is as follows.

$$L_D^{LS-GAN} = E_{x \sim p_d} [(x - 1)^2] + E_{\hat{x} \sim p_g} [D(\hat{x})^2],$$

$$L_G^{LS-GAN} = E_{\hat{x} \sim p} [(D(\hat{x}) - 1)^2]$$

WGAN Neither KL-divergence nor JS-divergence may give the ideal way to learn the capability. Martin et al. proposed EM distance or known as Wasserstein1 [8]. The physical idea of EM distance is to determine the quantity of work you need to spend to transfer the distribution to a different one. This gives the positive value with symmetric shape.

$$L_D^{WGAN} = E_{x \sim p_d} [D(x)] + E_{\hat{x} \sim p_g} [D(\hat{x})],$$

$$L_G^{WGAN} = E_{\hat{x} \sim p_g} [D(\hat{x})]$$

WGAN-GP In WGAN, it takes a long time to converge when the threshold value of the weight constraint is substantial. On the contrast, if the threshold value is small, the problem of slope disappearing occurs that complicates the process of optimization. Gulrajani et al. solved this problem with the Wasserstein GAN-gradient penalty (WGAN-GP) that applies a constraint and limits the slope of the discriminator output for the input [9]. The value function of the generation network is the same as that of WGAN and the discrimination network is as follows in the form of a slope penalty added to the value function of WGAN.

$$L_D^{WGAN-GP} = L_D^{WGAN} \lambda E_{\hat{x} \sim p} [\|D(\alpha x + (1 - \alpha \hat{x}))\|_2 - 1],$$

$$L_G^{WGAN-GP} = L_G^{WGAN}$$

DRAGAN In the learning process, if the slope of the discriminant function around the actual data is vast, the mode collapse occurs, leading the generation network to a single output. Kodali et al. proposed a deep regret analytic GAN (DRAGAN) that normalizes the discrimination network and limits the slope in the data space, thereby improving learning speed and stability [10]. The value function is expressed by the following equation, including inclination penalty in the GAN discrimination network.

$$L_D^{DRAGAN} = L_D^{GAN} + \lambda E_{x \sim p_d} + N(0, c) \left[(\|\nabla D(\hat{x})\|_2 - 1)^2 \right],$$

$$L_G^{DRAGAN} = L_G^{GAN}$$

where λ is a parameter controlling the strength of the penalty.

BEGAN The boundary equilibrium GAN (BEGAN) proposed by Berthelot et al. is based on the energy-based GAN [11]. The energy-based GAN was proposed by Zhao et al. [12]. The Wasserstein distance of the auto-encoder loss distribution is used to compute the value function.

$$L_D^{\text{BEGAN}} = E_{x \sim p_d} [\|x - \text{AE}(x)\|_1] - k_t E_{\hat{x} \sim p_g} [\|\hat{x} - \text{AE}(\hat{x})\|_1],$$

$$L_G^{\text{BEGAN}} = E_{\hat{x} \sim p_g} [\|\hat{x} - \text{AE}(\hat{x})\|_1]$$

Here, AE is an auto-encoder, and k_t [0, 1] is a parameter for controlling the degree of emphasis on generation data.

2.2 GAN Evaluation Measures

This subsection gives an overview of present evaluation methods which are generally implemented along with different metrics. The emphasis is given on the evaluation of GAN models to achieve diversity and quality. Of the diversity aspect, we evaluate GANs capability to generate diverse fake samples capturing various modes in the actual distribution; and by the quality perspective, we evaluate GANs ability to generate realistic looking data samples. Borji et al. proposed a detailed summary of different GAN evaluation measures [13].

Visual Inspection GANs are generative machines that may generate samples directly; therefore, professionals often appraise GANs by visually inspecting samples that can be produced. One easy method is to visualize a batch of samples generated by GANs and to evaluate their attributes by researchers. This practice is employed in several research works [1, 5]. Even though they claimed the top left model be the best, it had been slightly biased. It is generally tough to get a reasonable judgment according to visual inspection. Unluckily, these manual works suffer from reduced scalability and higher subjectivity. Unconscious bias at the theoretical analysis is unavoidable, such as when investigators report only their best outcomes that lead to unfair comparisons for a variety of GAN. An observer could likely miss mode collapse and do not evaluate diversity. Although to get a simple dataset like the MNIST, it is easy for an individual viewer to see the missing digits by inspecting a succession of samples in much more realistic configurations where a GAN is trained on data with thousands of modes. An individual observer would hardly detect the missing version by manual review. Thus, we clearly demand an excellent statistical assessment method.

Inception Score The generated samples would distinguishably look like some real thing, e.g., buckets or cows. This means that the samples look real and we can generate samples of items in our dataset. For this, we already have computer vision classifiers that can classify an image as belonging to a class. It is known as inception network,

which is one of those classifiers. Moreover, our classifier should be confident that what it sees is an item it recognizes. The generated samples should be varied and include ideally all the classes that were represented in the original dataset. This point is also highly desirable because our samples should be representative of the given dataset. One most commonly used metric taking this method is using inception score [14].

Frechet Inception Distance Heusel et al. proposed classification-based technique using Frechet inception distance [15]. Rather than working with the class label distribution, the FID uses a specific layer of inception net to compare embedding of the actual and the data that is generated. The Frechet distance between these two Gaussians is known as Wasserstein-2 space. It is used to measure the quality of generated data samples.

2.3 Training Challenges

Training GAN models is complex. Following are the main issues associated with training GAN.

Mode Collapse Mode collapse is a state where some of the modes (classes) are not alone outlined in the generated samples. To put it differently, the mode has collapsed even though the actual data distribution has support for those samples. Be aware that mode collapse can occur even if the network has converged. This work discusses inter-class mode collapse throughout the explanation of IS and intra-class mode collapse while discussing the FID.

Slow Convergence This is a big issue with GAN and unsupervised settings where commonly the rate of convergence and available computer systems are the principal constraints. Unlike with supervised learning, available labeled data is normally the first obstacle.

Failure to Learn Here, we discuss exceptional circumstances where modes (possible data samples) which should not have support (should not exist), do this occurs when the GAN over generalizes and learns things that should not exist based on the real data. Mode collapse and failure to learn can sometimes most naively be resolved by re-initializing the algorithm that makes the algorithm weaker. This list gives us broadly two key measures speed and quality. These two measures are quite alike as much of training is eventually focused on closing the gap between the real distribution and the generated distribution faster. So how do we resolve this? When it comes to GAN training, there are several techniques that help to improve the training method. This is exactly the same way as with any other machine learning algorithm. In this work, some training techniques are discovered.

3 Experiments and Results

Experiments are performed using recently proposed improved GAN training models like MM-GAN, NS-GAN, BEGAN, DRAGAN, LS-GAN, WGAN, and WGAN-GP. The values of GAN measures are obtained and compared with respect to parameters such as latent space dimension, structure of GAN, and various datasets.

3.1 Experimental Setup

All experiments are performed in Python language using a deep learning library Tensorflow by Google with Nvidia GeForce GTX TITAN X GPU of 64 GB RAM. The packages like Tensorflow and Keras are used as back end. The datasets used for these experiments include Fashion-MNIST, CIFAR-10, CelebFaces Attributes Dataset (CelebA), and MNIST.

3.2 Measures

Inception Score Inception model includes 1000 classes and 1.2 million of images [16]. CNN model is pre-trained by ImageNet and outputs a probability vector belonging to 1000 classes each [17]. This is due to the wide use of transfer learning and fine tuning.

$$I(G) = \exp(E_{\hat{x} \sim p_g} KL(p(y|\hat{x}) \| p(y)))$$

where $(p(y|x))$ is the conditional class distribution and $p(y)$ marginal class distribution. IS can have a value between 1 and 1000, but usually has a value near 2 [18].

Frechet Inception Distance The measure FID developed by Heusel et al. measures the difference between two normal distributions. A smaller value of FID represents a better quality of a model. It is calculated as follows.

$$FID = \|m - m_\omega\|_2^2 + T_r(C + C_\omega - 2(CC_\omega)^{1/2})$$

where (m, C) and (m, C_ω) mean and covariance are the distribution of generated data samples and the actual data. FID is the ratio of two distributions. Since the difference between actual and generated distribution is calculated, it can be a large value.

3.3 Methods

In order to estimate the appropriate latent space dimension, this work has considered the size of latent space dimensions as 1, 2, 3, 10, 50, and 100. The different types of generative adversarial networks like MM-GAN, NS-GAN, BEGAN, DRAGAN, LS-GAN, WGAN, and WGAN-GP are considered for each size. Although all GAN learning conditions cannot be the same. After the learning of the GAN, the IS and FID values of the generated data are measured, this experiment was repeated three times.

GAN Training The training process includes training of the discriminator and generator separately for each iteration. The discriminator network is to classify between real example x and fake example x^* . It also computes the classification errors and backpropagate the total error to update the discriminator weights and biases to minimize the classification errors. The generator network uses a new random noise vector z to synthesize a fake example x^* . The generator network uses a discriminator network to classify the x^* . It also computes the classification error and backpropagate the error to update the generator weights and biases to maximize the discriminator's error.

3.4 Comparison of Results

Table 1 shows the average FID for various datasets, latent space dimensions, and GAN models. The least significant value in bold indicates the optimal value for each model with respect to the latent space dimension.

FID and IS In Table 1, FID has the largest value in the 1, 2, and 3 latent space dimensions, especially in CelebA except for Cifar-10. It cannot confirm the trend that FID value of the data increases with dimension except Cifar-10. However, the FID value does not have the smallest value in the 1, 2, and 3 dimensions, as shown in Table 1. FID is more superior than IS. Figure 2 shows the quality of images generated in 1, 2, and 3 dimensions. In most of the models and datasets, the FID value decreases sharply from 10 to 100 dimensions. There are many cases in which the least value is obtained in 10 dimension.

Table 2 shows the average IS for various datasets, latent space dimensions, and GAN models. The most significant value in bold indicates the optimal value for each model with respect to latent space dimensions 1, 2, 3, 10, 50, and 100.

Latent Space Dimension In most of the models, FID values are rapidly decreased up to 10 dimension. As shown in Table 1, there are no significant changes in 10 or more dimensions. The values in 50 and 100 dimensions are not significantly smaller than in 10 dimension. Figures 2 and 3 show the gray-scale images of MNIST and

Table 1 Average FID for various datasets, latent space dimensions, and GAN

Data	Model	1	2	3	10	50	100
MNIST	GAN-MM	316.36	33.56	17.10	4.96	5.46	5.28
	GAN-NS	186.43	29.60	14.21	4.93	4.93	4.90
	LS-GAN	166.79	26.67	13.96	4.79	4.99	4.98
	WGAN	142.57	65.88	44.43	25.77	27.25	24.35
	WGAN-GP	176.28	92.97	45.21	18.94	20.94	17.67
	DRAGAN	221.04	44.64	22.68	8.46	6.94	8.36
	BEGAN	136.32	49.18	25.35	23.11	18.79	19.70
Fashion	GAN-MM	366.01	65.25	38.10	17.27	16.31	17.59
	GAN-NS	232.19	68.34	37.46	15.94	15.87	15.80
	LS-GAN	311.81	71.72	39.33	16.28	15.28	15.53
	WGAN	177.42	95.01	75.55	61.83	67.35	66.73
	WGAN-GP	197.58	93.35	54.78	36.22	28.88	30.12
	DRAGAN	255.11	87.64	42.76	23.49	22.91	27.28
	BEGAN	164.90	71.91	41.00	36.94	35.61	33.25
Cifar-10	GAN-MM	477.09	220.43	161.25	96.46	87.21	85.29
	GAN-NS	320.36	197.49	150.07	88.46	91.08	83.20
	LS-GAN	326.35	205.98	160.87	86.03	85.81	89.41
	WGAN	270.79	178.49	157.73	130.27	148.65	144.60
	WGAN-GP	360.58	318.33	226.03	207.80	179.99	192.14
	DRAGAN	332.29	222.52	182.41	117.88	101.53	102.44
	BEGAN	361.71	236.29	186.26	117.88	152.20	117.06
CelebA	GAN-MM	459.98	319.80	414.02	60.96	72.69	88.90
	GAN-NS	376.76	160.36	94.71	51.21	46.23	53.26
	LS-GAN	430.22	299.40	112.83	57.68	61.40	54.17
	WGAN	319.16	160.55	113.88	77.91	76.51	78.49
	WGAN-GP	442.79	379.45	323.68	212.01	118.12	103.28
	DRAGAN	436.35	168.98	167.05	72.52	62.81	63.33
	BEGAN	290.72	190.59	119.51	67.23	69.93	68.37

Fashion-MNIST datasets give good results in 2D. However, in Figs. 4 and 5, the more complex color images of Cifar-10 and CelebA datasets are used. The images generated in the dimension less than 10 dimensions are not perfect. It is confirmed that this produce data similar to the actual data in 10 dimension or higher. In many studies, the size of the latent space is typically used as 100 dimension. These studies confirmed that 10 dimension is sufficient. It reduces the amount of space and time required for computations.

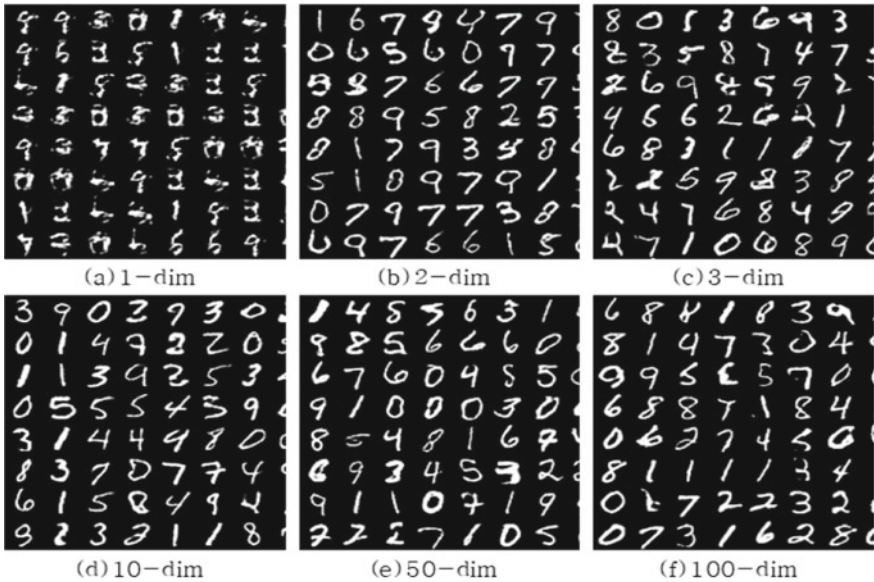


Fig. 2 Generated images of MNIST dataset with LS-GAN for different latent space dimensions

GAN Comparison It is difficult to keep the experimental conditions same to decide the best GAN model [19]. According to the FID results of this work, NS-GAN is evaluated as a good model with MNIST and Fashion-MNIST datasets.

LS-GAN performs better with Cifar-10 and CelebA datasets. As a result of comparing performance of the models in the 10 dimension, NS-GAN and LS-GAN show stable performance in both gray-scale and color images. The WGAN, which gained much attention, shows low performance with the gray-scale images. WGAN-GP showed low performance with color images. Therefore, it is recommended to use LS-GAN, which is considered to be better in performance and easy to understand algorithms.

4 Conclusion

This work focused on performance evaluation of GAN including NS-GAN, BE-GAN, DRAGAN, LS-GAN, WGAN, and WGAN-GP. The latent space dimension used as the input of the GAN is divided by 1, 2, 3, 10, 50, and 100. The appropriate dimension size is estimated. Evaluation of proper latest space dimension is carried out with performance improvement up to 1, 2, 3, and 10 dimensions. Thereafter, the performance was maintained at 10, 50, and 100 dimensions. However, in the WGAN-GP, unlike other models, the CelebA dataset has shown continuous performance improvement in the 10, 50, and 100 latent space dimensions. WGAN has shown

Table 2 Average IS for various datasets, latent space dimensions, and GAN

Data	Model	1	2	3	10	50	100
MNIST	GAN-MM	1.15	2.17	2.17	2.19	2.18	2.19
	GAN-NS	1.76	2.22	2.18	2.20	2.20	2.19
	LS-GAN	1.82	2.15	2.29	2.19	2.17	2.18
	WGAN	1.92	2.14	2.15	2.31	2.23	2.23
	WGAN-GP	1.92	2.27	2.22	2.19	2.20	2.22
	DRAGAN	1.68	2.13	2.25	2.19	2.19	2.18
	BEGAN	1.90	2.26	2.17	2.21	2.26	2.26
Fashion	GAN-MM	1.51	4.02	4.07	4.43	4.33	4.35
	GAN-NS	2.46	4.11	4.31	4.43	4.37	4.40
	LS-GAN	1.36	4.04	4.39	4.32	4.33	4.34
	WGAN	3.19	3.61	3.91	3.89	3.79	3.77
	WGAN-GP	2.74	3.65	4.03	4.20	4.28	4.24
	DRAGAN	2.32	3.72	4.04	4.42	4.02	4.05
	BEGAN	2.82	3.82	4.26	4.25	4.02	4.05
Cifar-10	GAN-MM	1.01	2.46	3.15	4.57	5.12	5.29
	GAN-NS	2.13	2.82	3.27	4.92	4.67	5.19
	LS-GAN	1.72	2.85	3.05	4.70	5.04	4.83
	WGAN	2.34	2.95	3.09	3.10	2.69	2.85
	WGAN-GP	1.67	1.89	2.18	2.21	2.38	2.49
	DRAGAN	1.90	2.67	2.80	3.79	4.28	4.16
	BEGAN	1.62	2.40	2.92	4.32	3.62	4.26
CelebA	GAN-MM	1.58	1.52	1.01	2.13	2.20	2.43
	GAN-NS	2.58	2.02	2.15	2.37	2.19	2.25
	LS-GAN	2.05	2.24	2.03	2.23	2.90	2.24
	WGAN	2.77	2.25	2.39	2.27	2.24	2.26
	WGAN-GP	1.72	2.47	2.55	3.03	2.65	2.45
	DRAGAN	2.21	2.00	2.58	2.21	2.21	2.24
	BEGAN	1.47	2.35	2.12	2.15	2.21	2.21

poor performance in gray-scale images and WGAN-GP has shown low performance in color images. In the first dimension, dimensions IS shows a better measure for evaluating the performance over FID. It is recommended to use LS-GAN, which is considered to be better in performance and easy to understand algorithms. Future research can be done that compares the structure of generative adversarial networks, learning rate, batch normalization, and dropout ratio using various parameters.

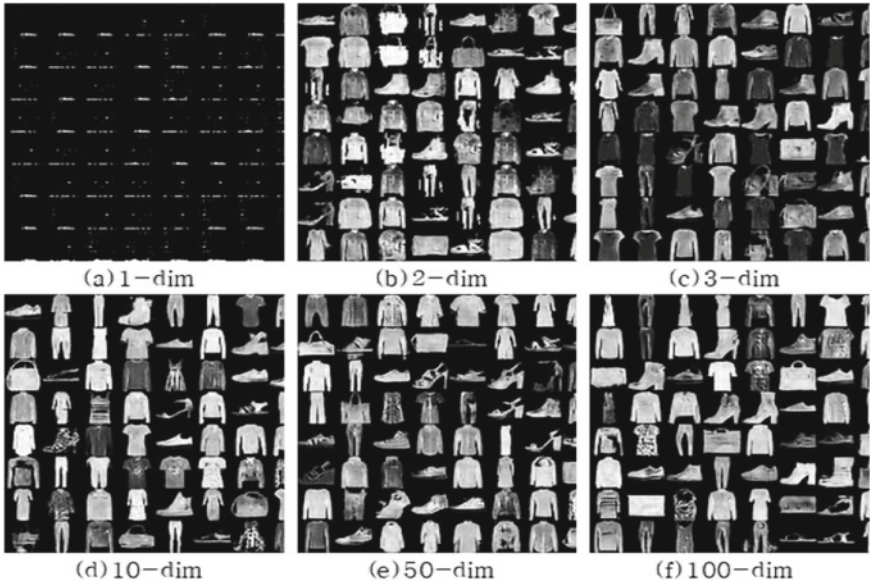


Fig. 3 Generated images of Fashion-MNIST dataset with LS-GAN for different latent space dimensions

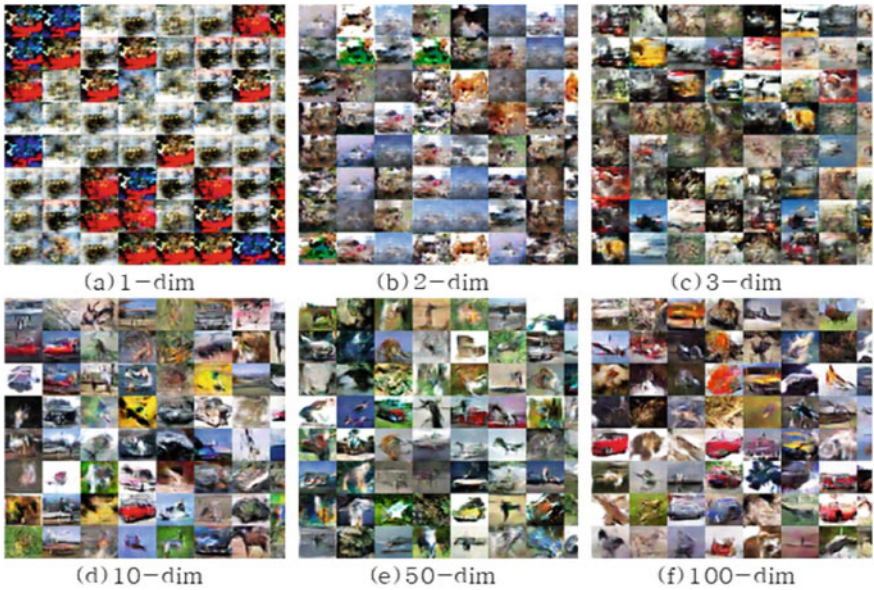


Fig. 4 Generated images of Cifar-10 dataset with NS-GAN for different latent space dimensions



Fig. 5 Generated images of CelebA dataset with NS-GAN for different latent space

References

1. Goodfellow IJ, Pouget-Abadie J, Mirza M, Xu B, Warde-Farley D, Ozair S, Courville A, Bengio Y (2014) Generative adversarial nets. In: Proceedings of the advances in neural information processing systems, pp 2672–2680
2. Wang H, Weng C, Yuan J (2017) Visual pattern discovery and recognition. Springer
3. Zhu JY, Park T, Isola P, Efros AA (2017) Unpaired image-to-image translation using cycle-consistent adversarial networks. In: Proceedings of the IEEE international conference on computer vision, pp 2223–2232
4. Mathieu M, Couprie C, LeCun Y (2015) Deep multi-scale video prediction beyond mean square error. arXiv preprint [arXiv:1511.05440](https://arxiv.org/abs/1511.05440)
5. Radford A, Metz L, Chintala S (2015) Unsupervised representation learning with deep convolutional generative adversarial networks. arXiv preprint [arXiv:1511.06434](https://arxiv.org/abs/1511.06434)
6. Jin Y, Zhang J, Li M, Tian Y, Zhu H, Fang Z (2017) Towards the automatic anime characters creation with generative adversarial networks. arXiv preprint [arXiv:1708.05509](https://arxiv.org/abs/1708.05509)
7. Mao X, Li Q, Xie H, Lau RY, Wang Z, Smolley SP (2017) Least squares generative adversarial networks. In: Proceedings of the IEEE international conference on computer vision, pp 2794–2802
8. Arjovsky M, Chintala S, Bottou L (2017) Wasserstein gan. arXiv preprint [arXiv:1701.07875](https://arxiv.org/abs/1701.07875)
9. Gulrajani I, Ahmed F, Arjovsky M, Dumoulin V, Courville AC (2017) Improved training of Wasserstein gans. In: Advances in neural information processing systems, pp 5767–5777
10. Kodali N, Abernethy J, Hays J, Kira Z (2017) How to train your DRAGAN. 2(4). arXiv preprint [arXiv:1705.07215](https://arxiv.org/abs/1705.07215)
11. Berthelot D, Schumm T, Began ML (2017) Boundary equilibrium generative adversarial networks. arXiv preprint [arXiv:1703.10717](https://arxiv.org/abs/1703.10717)
12. Zhao J, Mathieu M, LeCun Y (2016) Energy-based generative adversarial network. arXiv preprint [arXiv:1609.03126](https://arxiv.org/abs/1609.03126)

13. Borji A (2019) Pros and cons of gan evaluation measures. *Comput Vis Image Underst* 179:41–65
14. Salimans T, Goodfellow I, Zaremba W, Cheung V, Radford A, Chen X (2016) Improved techniques for training gans. In: *Advances in neural information processing systems*, pp 2234–2242
15. Heusel M, Ramsauer H, Unterthiner T, Nessler B, Hochreiter S (2017) Gans trained by a two time-scale update rule converge to a local nash equilibrium. In: *Advances in neural information processing systems*, pp 6626–6637
16. Szegedy C, Vanhoucke V, Ioffe S, Shlens J, Wojna Z (2016) Rethinking the inception architecture for computer vision. In: *Proceedings of the IEEE conference on computer vision and pattern recognition*, pp 2818–2826
17. Deng J, Dong W, Socher R, Li LJ, Li K, Fei-Fei L (2009) Imagenet: a large-scale hierarchical image database. In: *2009 IEEE conference on computer vision and pattern recognition*, pp 248–255
18. Barratt S, Sharma R (2018) A note on the inception score. arXiv preprint [arXiv:1801.01973](https://arxiv.org/abs/1801.01973)
19. Lucic M, Kurach K, Michalski M, Gelly S, Bousquet O (2018) Are gans created equal? a large-scale study. In: *Advances in neural information processing systems*, pp 700–709

The Fusion of Local and Global Descriptors in Face Recognition Application



Ali Mohammed Sahan  and Ali Sami Al-Itbi 

Abstract In a complex process like face recognition, the type of the features embedded in human face plays a dominant role in the recognition process. The global features describe the whole face image, while the local features are used to describe the local areas in the face. Therefore, combining these features together in the same feature vectors leads to provide attractive features, which have the ability to distinguishing between similar face images. In this paper, we propose a combined local and global face recognition technique. The local features are captured using radon transform descriptor, while the global features are provided using Chebyshev–Fourier moments. Extensive experiments have been performed on four different face databases, namely JAFFE, FERET, YALE, and UMIST, to evaluate the accuracy of the suggested approach under different face variations. Results of these experiments indicate that the presented technique achieved high recognition accuracy in the presence of illumination, pose, and facial expression variations.

Keywords Local descriptor · Global descriptor · Face recognition · Radon transform · Chebyshev–Fourier moments

1 Introduction

Face recognition is an important field in the biometric domain, because it has a large number of applications such as content-based indexing, different authentication and identity purposes, access control, video retrieval control, video; therefore, face recognition received high attention by the researchers. Hence, different face recognition methods have been existed. Face recognition operation suffers from different challenges like illumination, facial expression, age, and pose variations

A. M. Sahan · A. S. Al-Itbi (✉)
IT Department, Technical College of Management, Middle Technical University, Baghdad, Iraq
e-mail: ali.sami@mtu.edu.iq

A. M. Sahan
e-mail: dralimohammed2@gmail.com

[1, 2]. The existing human face recognition methods can be classified into four types [3], which are local feature extraction methods, global feature extraction methods, and combined local and global feature extraction methods. The global methods focus on the complete image of the face. Therefore, they are more robust against the variations that affected the entire face image like illumination. However, the accuracy of these methods is affected by facial expression variations. On the other hand, the local feature extraction methods capture the local details in the face image. The principal advantage of these methods is that they are not much affected by irrelevant information in the face image such as background, shoulders, and hair. However, the disadvantage of these methods is that they are affected by environmental conditions and unpredictability of face appearance [4]. Face recognition process in the human visual system uses both local and global features [5]. The local features are used to recognize the finer details of the face image, while global features are used to recognize the complete face image. Combined face recognition methods stimulate the human perception in face recognition problem. The main advantage of these methods is that they exploit the best characteristics of both local and global feature extraction descriptors. Yu et al. [5] analyse the robustness of both local and global features in the face recognition system. The global features are extracted using two-dimensional Fourier transform, while Gabor wavelet is utilized to provide local features. Singh et al. [6] propose a face recognition approach that uses both local and global features based on wavelet moments. The same author in [7] presents combined global and local features. The global features are derived by ZMs, whereas the local features are captured by scale-invariant feature transform (SIFT). The traits of ZMs and SIFT are exploited to construct robust descriptor against pose, illumination, and expression variations. Ruba and Murugesan [8] presented a combination of global and local features by using linear discriminant analysis (LDA) to capture global features and locality preserving projections (LPP) to extract local features. Fang et al. [9] proposed the fusion of global PCA features and Haar wavelet-based local features for face verification. Zhou et al. [10] used a discrete cosine transform (DCT) to derive both global and local facial features. The low-to-mid-frequency subset of the two-dimensional DCT coefficients of a face image is extracted as the facial global feature, while the facial local features are extracted from several subset images such as eyes, nose, and forehead. In [11], global features are extracted using Fourier transform while the local features are derived using Gabor wavelet. Sahan et al. [12] proposed global and local face recognition method. In this method, the vectors of face features consist of the global features extracted by Zernike moments and local features provided by radon transform. Nguyen et al. [13] proposed a method to improve the security of face recognition system by combining the deep image features with presentation attack detection extracted using support vector machine.

Singaravelan and Murugan [14] presented global and local face recognition method. The global features are provided by a linear discriminant analysis, while the local features are extracted by locality preserving projection.

In this article, we introduce an effective face recognition system that combines global and local features; the global features are provided by Chebyshev–Fourier moments, while the local features are extracted by radon transform. Extensive

experiments are performed to evaluate the performance of the proposed approach against facial expressions, pose, and illumination variations. Extensive experiments are conducted on four different face databases, namely JAFFE, FERET, UMIST, and YALE.

The rest of the paper has been organized as follows: Sect. 2 provides an overview of Chebyshev–Fourier moments. The radon transform is explained in Sect. 3. Section 4 describes the utilized similarity measures. Section 5 presents the proposed technique. The databases used are presented in Sect. 6. Details of experimental results are given in Sect. 7. Section 8 concludes the paper.

2 Chebyshev–Fourier Moments

Chebyshev–Fourier moment was early introduced by [15] as a special case of Jacobi–Fourier moments with high capability of image reconstruction and better noise sensitivity. The Chebyshev–Fourier moments are used in different applications such as representation of printed characters [16], action recognition [17], image focus measure [18], image description [19], target recognition in SAR images [20], and image fusion [21]. The two-dimensional Chebyshev moments of order p with repetition q of image intensity function are [22–26]:

$$f(x, y) = \sum_{p=0}^{M-1} \sum_{q=0}^{M-1} \text{ch}_{pq} a_p(x) a_q(y) \tag{1}$$

where the coefficient ch_{pq} are the Chebyshev moments which satisfy the orthogonal property, with

$$P(i, M) = \frac{M(M^2 - 1)(M^2 - 2^2) \dots (M^2 - i^2)}{2n + 1} = 0, \dots, M - 1 \tag{2}$$

To make it suitable for image analysis:

$$\text{ch}_{pq} = \frac{1}{\rho(p, M)\rho(q, M)} \sum_{x=0}^{M-1} \sum_{y=0}^{M-1} a_p(x) a_q(y) f(x, y) \quad p, q = 0, 1, \dots, M - 1 \tag{3}$$

where

$$\rho(p, M) = \frac{M \left(1 - \frac{1^2}{M^2}\right) \left(1 - \frac{2^2}{M^2}\right) \dots \left(1 - \frac{p^2}{M^2}\right)}{2p + 1} \tag{4}$$

And the scaled Chebyshev polynomials $t_p(x)$ are computed using the following recurrence relation:

$$a_0(x_0) = 1 \tag{5}$$

$$a_1(X) = \frac{2X + 1 - M}{M} \tag{6}$$

$$a_p(x) = \frac{(2p - 1)a_1(x)a_{p-1}(x) - (p - 1)\left\{1 - \frac{(p-1)^2}{M^2}\right\}a_{p-2}(x)}{p}, p > 1 \tag{7}$$

3 Radon Transform

Radon transform has an inherent trait. Hence, it has the ability to provide the directional details of images [27]; therefore, radon transform is used as an active descriptor in a different nondestructive special testing. Radon transform converts the image components into peaks by computing the image projections at different angles. Each projection derived computes multiple line integrals of the intensities along with a set of parallel beams. The general equation of the 2D radon transform can be defined as [28]

$$R(x, \theta)[f(i, j)] = \int_{-\infty}^{\infty} \int_{-\infty}^{\infty} f(i, j)\delta(x - x \cos \theta - y \sin \theta)dx dy \tag{8}$$

where $\delta(\cdot)$ is the delta function with value, not equal zero only for argument equal 0, $\theta \in [0, \pi]$ is the angle of incidence of the beams, and x is the perpendicular distance of the beam from the origin and can be computed as follows:

$$x = i \cos \theta + j \sin \theta, \quad x \in [-\infty, \infty] \tag{9}$$

The discrete approximation of 1 can be defined as:

$$R(x, \theta) = \sum_{i=0}^{M-1} \sum_{j=0}^{N-1} f(i, j)\delta(x - i \cos \theta - j \sin \theta) \tag{10}$$

Figure 1 illustrates the radon transform of an image.

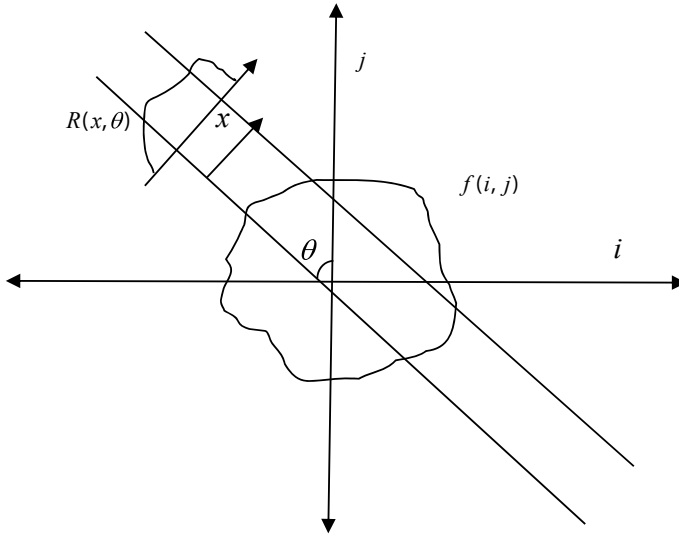


Fig. 1 Radon transform of an image

4 Distance Measure

In the stage of classification, we have considered the cosine distance similarity measure. The cosine distance similarity measure evaluates the similarity between two feature vectors in an angular direction [29]. It estimates the angle between feature vectors. The lower the angular separation refers to little similarity. The utilized distance measure can be expressed as:

$$d = \frac{\sum_{i=0}^{N-1} (F_i(T) \times F_i(D))}{\sqrt{\sum_{i=0}^{N-1} (F_i(T)^2)} \sqrt{\sum_{i=0}^{N-1} (F_i(D)^2)}} \tag{11}$$

5 Proposed Technique

The proposed technique exploits the advantages of fusion, and both local and global features ensure good distinguishing between different face images. Chebyshev–Fourier moment descriptor has been used to provide global features, while the radon transform descriptor has been used to extract local features. The resulted radon transform coefficients are converted into histogram bins, to reduce the complexity

of the classification stage. Cosine similarity measure is used to compute the difference between training and query face images. The following steps summarize the proposed technique:

1. Extract the global feature of the face image by using Chebyshev–Fourier moment descriptor.
2. Compute the radon transform coefficients of the face image, which represent the local features.
3. Compute the histogram bins of radon transform coefficients.
4. Construct the feature vector by combining the result features in the steps 1 and 3.
5. Estimate the difference between the query and training face images using the cosine similarity measure.
6. Classify the query face image into recognized or unrecognized.

Figure 2 presents the block diagram of the proposed technique.

The novelty of the proposed technique is that we have combined two distinct descriptors, namely radon transform (provides local features) and Chebyshev moments (provides global features); also, the proposed technique has been evaluated

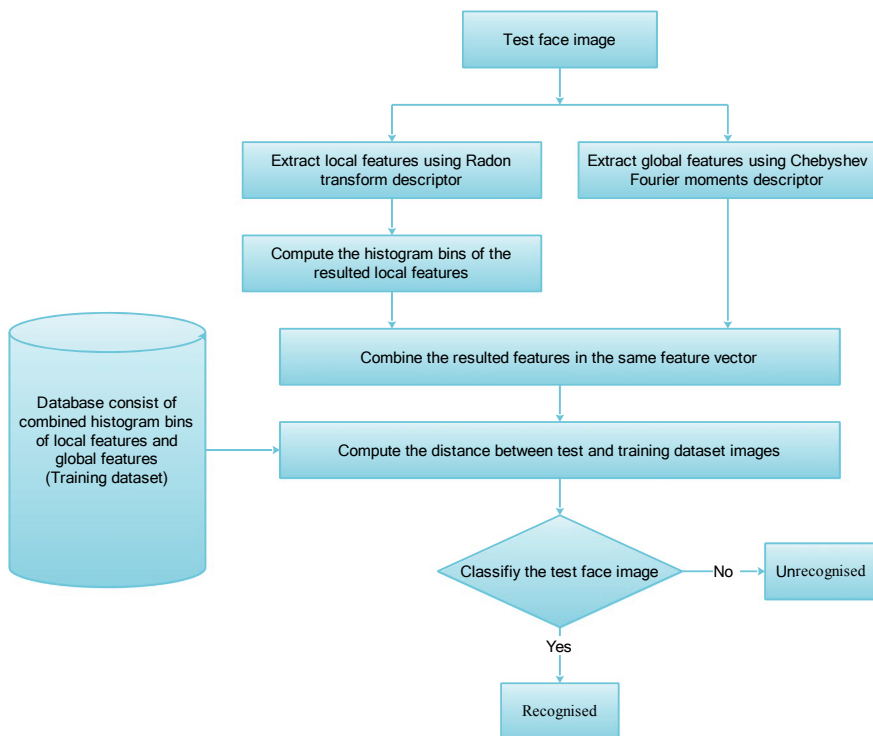


Fig. 2 Proposed technique’s block diagram

under most important challenges in face recognition problem such as illumination, facial expression, and pose variations using three standard face databases. Furthermore, each descriptor has been assessed alone under the same conditions which applied on the proposed technique.

6 Description of the Utilized Databases

The used four standard databases are explained as below:

- (a) *YALE database*: It consists of 15 individuals. Each individual has 11 samples representing different facial expression variations; therefore, the total database images are 165 with a size of 243×320 pixels. The images in this database exhibit significant changes in illumination and different facial expressions.
- (b) *JAFFE database*: It includes 213 images for 10 female individuals. The database contains 7 facial expression variations, which are surprise, fear, disgust, anger, happiness, sadness, and neutral. Each individual is represented by 2 or 4 images with a size of 256×256 pixels.
- (c) *FERET database*: It includes 1196 individuals represented by several 256×384 pixel greyscale images. The database contains facial expression, illumination, pose, ageing, etc. Here, in our experiments, we consider pose and facial expression variation. The evaluation protocol of FERET database consists of five probe sets, namely *fa*, *fb*, *fc*, *dup I*, and *dup II*. The images in *fa* are used for training. The *fb* and *fc* sets contain images with facial expression and illumination variations, respectively, while the sets in *dup I* and *dup II* include images with an ageing variation.
- (d) *UMIST database*: It includes 20 subjects with different pose angle variations. Each subject is presented by different pose 220×220 pixel images. A few images from the above databases are shown in Fig. 3.

7 Experimental Analysis

We perform different experiments using the above-mentioned databases to investigate the accuracy of the proposed technique under different variations. We convert all images to the size 64×64 pixels to reduce the computation time of the experiments.

7.1 Facial Expression Variation Evaluation

In this section, we conduct two experiments to assess the robustness of the suggested technique against facial expression variation using two different standard face databases. The first experiment is performed using JAFFE database, while the second



Fig. 3 Some samples from utilized databases: first row (JAFFE), second row (UMIST), third row (YALE), and fourth row (FERET)

experiment is performed on FERET database. In the first experiment, the test images are selected by taking three images representing normal expression of each individual as training, while the remaining facial expression taken for testing. In the second experiment, two sets of FERET database are used, which are *fa* and *fb*. The first set represents frontal images utilized for training, while the second set includes images with facial expression utilized for training. Tables 1 and 2 present the results of the first and second experiments, respectively. As observed in Tables 1 and 2, the recognition rate of the proposed technique is higher than the recognition rates of all the comparable techniques. The recognition rate gained using global features is less

Table 1 Results of facial expression variation evaluation (first experiment)

Method	Recognition rate (%)
Chebyshev–Fourier moment descriptor	96.9
Radon transform descriptor	97.8
Proposed technique	98.8

Table 2 Results of facial expression variation evaluation (second experiment)

Method	Recognition rate (%)
Chebyshev–Fourier moments	93.3
Radon transform descriptor	94.1
Proposed technique	96.0

Table 3 Results of pose variation experiment

Method	Recognition rate (%)
Chebyshev–Fourier moment descriptor	97.2
Radon transform descriptor	98.2
Proposed technique	99.4

than the recognition rates provided by local features. This is because of the fact that the global feature extraction techniques are sensitive to facial expression variation, while the local feature extraction techniques like radon transform are not. Therefore, radon transform descriptor is robust against facial expression variation.

7.2 Pose Variation Evaluation

The impact of pose variation on the accuracy of the proposed technique is investigated by carrying out an experiment using UMIST database. In this experiment, the training set includes a random selection of 11 face images of each person, while the remaining utilized for testing. Results of this experiment are presented in Tables 3. The results refer that the accuracy of the suggested technique is better than the accuracy of its counterparts (Chebyshev–Fourier moment and radon transform descriptors). Moreover, the local feature extraction descriptor (radon transform) is better than the global feature descriptor (Chebyshev–Fourier moments). This is because the performance of global descriptor is affected by some occluded areas in the face image caused by pose angle.

7.3 Illumination Variation Evaluation

In this section, we evaluate the effect of illumination variation on the accuracy of the suggested technique. For this purpose, two experiments on YALE database are conducted. The data set of the first experiment consisted of four images selected randomly for each person while remaining utilized for testing. The data set of the second experiment consists of one normal face image for each person for training, while remaining utilized for testing. As presented in Tables 4 and 5, the recognition rates achieved using the suggested technique outperform the recognition rates

Table 4 Illumination variation evaluation (first experiment)

Method	Recognition rate (%)
Chebyshev–Fourier moments	93.5
Radon transform descriptor	91.4
Proposed technique	97.1

Table 5 Illumination variation evaluation (second experiment)

Method	Recognition rate (%)
Chebyshev–Fourier moments	92.1
Radon transform descriptor	90.3
Proposed technique	95.0

achieved using radon transform descriptor and Chebyshev–Fourier moments. Moreover, the recognition rate achieved using Chebyshev moment descriptor is better than that achieved using radon transform descriptor; this is because the illumination variation affects the whole face image and causes global distortion.

8 Conclusions

The local and global features in the face image are complementary to each other in the recognition processes. The local features reflect the finer details, while the global features represent the general information about the face image. In a complex application like face recognition, one type of features is not sufficient to represent the image of a human face with high accuracy. In this paper, a combined technique using local and global features is presented to achieve an accurate distinction between the face images. The radon transform is used as the local descriptor, which captures the local variation in the image. The global features are extracted using Chebyshev–Fourier moments. Results of the extensive experiments carried out on four standard databases, which are JAFFE, FERET, UMIST, and YALE, refer that the presented technique is robust against most of face recognition challenges like illumination, pose, and facial expression variations.

The results of the experimental analysis are summarized as follows:

- The proposed face recognition technique achieves high accuracy under illumination, pose, and facial expression variations.
- Combining local and global features provided by utilizing radon transform and Chebyshev–Fourier moments, respectively, leads to provide distinct features having the ability to achieve a high recognition rate in the face recognition system. Moreover, the proposed combined features perform much better than their individual counterparts.
- The performance of radon transform descriptor is better than the performance of Chebyshev–Fourier moment descriptor in facial expression variation.
- In the presence of pose variation, which causes local distortion in some areas of the face image, the accuracy of radon transform descriptor is better than the accuracy of Chebyshev–Fourier moment descriptor.
- The recognition rate achieved using Chebyshev–Fourier moment descriptor is better than that achieved using radon transform descriptor; this is because the illumination variation affects the whole face image and causes global distortion.

References

1. Sharif M, Naz F, Yasin M, Shahid MA, Rehman A (2017) Face recognition: a survey. *J Eng Sci Technol Rev* 10(2):166–177
2. Heisele B, Ho P, Poggio T (2001) Face recognition with support vector machines: global versus component-based approach. In: *Proceedings 8th IEEE international conference on computer vision (ICCV 2001)*, Vancouver, vol 2, pp 688–694
3. Zhao W, Chellappa R, Rosenfeld A, Phillips PJ (2003) Face recognition: a literature survey. *ACM Comput Surv* 35(4):399–458
4. Farajzadeh N, Faez K, Pan G (2010) Study on the performance of moments as invariant descriptors for practical face recognition systems. *IET Comp Vis* 4(4):272–285
5. Su Y, Shan S, Chen X, Gao W (2009) Hierarchical ensemble of global and local classifiers for face recognition. *IEEE Trans Image Process* 18(8):1885–1895
6. Singh C, Sahan AM (2012) Face recognition using complex wavelet moments. *Optics Laser Technol* 47:256–267
7. Singh C, Walia E, Mittal N (2012) Fusion of zernike moments and SIFT features for improved face recognition. In: *International conference on recent advances and future trend in IT*, Patiala, Punjab, India, 21–23 Mar 2012. *Proceedings published in Int J Comput Appl* (6):26–31
8. Soundar R, Karuppasamy M (2010) Preserving global and local information—a combined approach for recognising face images. *IET Comp Vis* 4(3):173–182
9. Fang Y, Tan T, Wang Y (2002) Fusion of global and local features for face verification. In: *Proceedings of the IEEE conference on pattern recognition* vol 2, pp 382–385
10. Zhou D, Yang X, Peng N, Wang Y (2006) Improved-LDA based face recognition using both facial global and local information. *Pattern Recogn Lett* 27:536–543
11. Ojala T, Pietikäinen M, Maenpää T (2002) Multiresolution gray-scale and rotation invariant texture classification with local binary patterns. *IEEE Trans Pattern Anal Mach Intell* 24(7):971–987
12. Sahan AM, Oudah KZ, Majed A (2015) Face recognition using zernike moments and Radon transform. *Int J Modern Trends Eng Res (IJMTER)* 2(11)
13. Nguyen DT, Pham TD, Lee MB, Park KR (2019) Visible-light camera sensor-based presentation attack detection for face recognition by combining spatial and temporal information. *Sensors* 19(2):410
14. Singaravelan S, Murugan D (2019) Robust automatic visual method for determining facial angles from profile view images. *Media Cult Publ Relat* 10(1):6–18
15. Ping Z, Wu R, Sheng Y (2002) Image description with Chebyshev Fourier moments. *J Opt Soc Am A* 19(9):1748–1754
16. Saharia S, Bora PK, Saikia DK (2004) A comparative study on discrete orthonormal chebyshev moments and legendre moments for representation of printed characters. In: *ICVGIP 2004*, pp 491–496
17. Alhamzah KH, Wang T (2014) Action recognition and identity using chebyshev moments. *Int J Comput Eng Appl* 8(2)
18. Yap PT, Raveendran P (2004) Image focus measure based on chebyshev moments. *IEE Proc Vis Image Signal Process* 151(2)
19. Ping Z, Wu R, Sheng Y (2002) Image description with Chebyshev Fourier moments. *J Opt Soc Am A* 19(9)
20. Bolourchi P, Demirel H, Uysal S (2017) Target recognition in SAR images using radial chebyshev moments. *Signal Image Video Process* 11(6):1033–1040
21. Omar Z, Mitianoudis N, Stathaki T (2010) Two-dimensional chebyshev polynomials for image fusion. In: *Picture coding symposium (PCS)*, pp 426–429
22. Mukundan R, Ong SH, Lee PA (2001) Discrete versus continuous orthogonal moments in image analysis. In: *International conference on imaging science systems and technology*, pp 23–29
23. Mukundan R, Ong SH, Lee PA (2001) Image analysis by tchebichef moments. *IEEE Trans Image Process* 10:1357–1364

24. Teh CH, Chin RT (1986) On digital approximation of moment invariants. In: CVIP, vol 33, pp 318–326
25. Mukundan R, Ong SH, Lee PA (2000) Discrete orthogonal moment features using chebyshev polynomials. *Image Vis Comput. NewZealand*, 20–25 Nov 2000
26. Athilakshmi R, Amitabh W (2014) An efficient method for shape-based object classification using radial chebyshev moment on square transform. *Australian J Basic Appl Sci. AENSI Publisher*
27. Biswas S, Biswas A (2012) Face recognition algorithms based on transformed shape features. In: *International conference on imaging for crime detection and prevention*
28. Magli E, Olmo G, Lo Presti L (1999) Pattern recognition by means of the Radon transform and the continuous wavelet transform. *Signal Process* 73:277–289
29. Ye J (2011) Cosine similarity measures for intuitionistic fuzzy sets and their applications. *Math Comput Model* 53:91–97

ANFIS-Based Reactive Strategy for uRLLC and eMBB Traffic Multiplexing in 5G New Radio



Naveen Kumar and Anwar Ahmad

Abstract Ultra-reliable low-latency communications (uRLLC) and enhanced mobile broadband (eMBB) traffics are needed to be supported expeditiously in the emerging 5G networks. To achieve ultra-reliability as high as $1 - 10^{-7}$ in uRLLC, ongoing eMBB packets should be stopped instantly, which results in reduced quality of services (QoS) of eMBB services. This difficulty, known as co-existence problem, is a serious concern in 5G cellular networks and requires a proper mechanism to protect the ongoing services. This paper introduces ANFIS-based reactive strategy for a flexible frame structure that can provide high priority to the uRLLC traffic while ensuring the reliability to other eMBB traffic in the 5G cellular network scenario. Proposed flexible frame structure approach can be a possible solution to the co-existence problem by providing improved QoS for eMBB and reduced delay for uRLLC. The experimental results prove that the proposed approach contributes to the critical advancement for forecasting performance in accordance with the error analysis results.

Keywords 5G · uRLLC · eMBB · ANFIS

1 Introduction

As multi-scenario has become a major feature of fifth generation (5G) cellular networks. A modern air interface in 5G, known as new radio (NR) has been introduced by Third Generation Partnership Project (3GPP) to bring out completely new features and technologies [1]. With enhanced mobile broadband (eMBB) and ultra-reliable low-latency (uRLLC) scenarios, 5G will face acceleratory requirements and challenges with diverse services [2]. On one hand, eMBB traffic such as virtual

N. Kumar (✉) · A. Ahmad
Jamia Millia Islamia, New Delhi, India
e-mail: newnky1991@gmail.com

A. Ahmad
e-mail: aahmad4@jmi.ac.in

reality, real-time traffic alerts, 4 K video streaming, etc., require bandwidth as high as 100 MHz with few milliseconds latency. On the other hand, uRLLC services such as wireless industrial automation, real-time vehicle to vehicle communication, smart grid, automatic drive, etc., require extremely low latency, on the order of tens to hundreds of μSec with ultra-high reliability (99.999%) [3]. Various performance requirements, such as heavy connectivity, low latency, high reliability, energy efficiency, have been acquainted with adapt to these new service requirements.

eMBB, an extension of 4G wireless standard, is defined by larger payloads as well as design stimulation pattern that stays static over a larger time interval, so that maximum data rate can be achieved while guaranteeing an average reliability on the order of 10^{-3} . While in uRLLC, transmission of small payloads with low latency and very high reliability from a limited set of terminals is required, which become active due to patterns specified by exterior events. However, due to the spectrum limitations it becomes quit challenging for uRLLC and eMBB both the applications, to co-exist in the same carrier. At the point when there is a service request, the packet must be transmitted immediately by the base station, regardless of whether it is in scheduling period or in middle of the eMBB transmission, which will lead to degraded eMBB services. This problem commonly referred as co-existence problem is critical issue to non-uRLLC traffic and requires immediate solutions to protect the ongoing traffic. In one approach, adopted by 3GPP-NR, a preemptive indicator is used, which consists of the time and frequency information of the interruption to provide users data about lost packets. Furthermore, part of code-blocks affected due to uRLLC can be retransmitted. However, efficiency will decrease if frequent uRLLC transmissions occur, as it will lead to more preemptive indicator transmissions. Due to the fact that uRLLC transmissions are much less as compared to eMBB transmissions, a combination of scheduling can be employed to ensure available resources' predictability instead of keeping the resources idle [4].

For uRLLC and eMBB traffic multiplexing in 5G, Esswie et al. [5] proposed null space-based spatial preemptive scheduler, which seeks for cross-objective optimization where the critical uRLLC quality of service is guaranteed while providing maximum capacity to the eMBB traffic. Anand et al. [6] designed an optimal joint scheduler, which uses an iterative gradient scheduler for eMBB services to anticipate the likely losses from uRLLC services, and uRLLC demand scheduler that is oblivious to channel conditions of eMBB traffic, utility functions and allocation decision of the eMBB scheduler. Another approach by Elsenvi et al. [7] introduced conditional value at risk (CVaR)-based risk measurement for eMBB traffic. Recently, an approach based on machine learning (ML) was exploited by [8] where random forest decision algorithm was used for flexible transmission time interval (TTI) scheduling for each service. However, besides providing strong ability of generalization, the time cost of ML classifiers is relatively high [9].

Compared to traditional methods ANFIS-based approach provides advanced prospects and possibilities. In this work, ANFIS-based flexible framework scheme, where ultra-low latency for uRLLC can always be guaranteed while maintaining QoS of eMBB. Compared to classical methods used for traffic control in 5G NR, proposed

flexible frame structure-based approach shows robustness toward the co-existence problem.

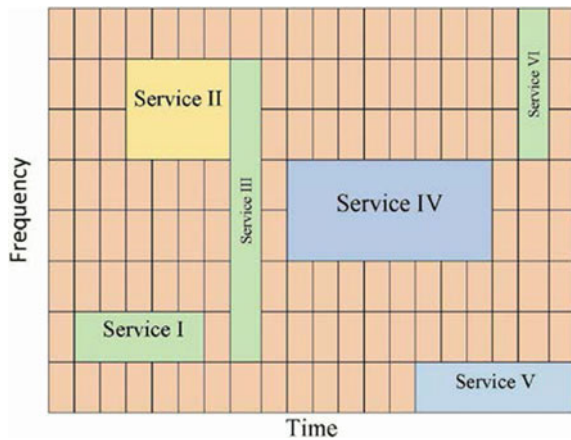
Remaining of the paper is organized as follow, Sect. 2 provides system model and problem formulation where a multi-user system is considered with two service types—eMBB and uRLLC. uRLLC services are assigned higher priority. Then, Sect. 3 introduces a detailed machine learning-based reactive strategy is for the solution. Performance evaluation results are discussed in Sect. 4 and finally Sect. 5 concludes the paper.

2 System Model and Problem Formulation

Fifth generation new radio (NR) technology is standardized by 3GPP in which many proposals and issues related to physical layer protocols as well as radio frequency are investigated [10, 11]. 3GPP-NR has a flexible and wide range of bandwidth for orthogonal frequency division multiplexing framework. To provide flexible transmission time interval (TTI), resource blocks (RB) are considered where RBs determine the length and frequency of flexible TTI. Figure 1 provides the basic idea of the resource blocks where one square grid represents one RB (i.e., 0.125 ms-time axis and 180 kHz-frequency axis) and entire area represents all resources available.

Mostly, larger TTI is chosen for eMBB traffic and shorter TTI for uTLLC traffic. Figure 2 illustrates a scenario where, for the eMBB service, transport block consisting of three sequentially mapped code-blocks, is transmitted. However, problem arises when uRLLC service is initiated in the middle of eMBB service. To achieve low latency some of the symbols in the eMBB code-block are immediately replaced by uRLLC code-blocks. While the flexible frame structure may ease the problem, a more feasible solution is required for the practical implementation due to randomness and uncertainty of uRLLC services.

Fig. 1 Resource allocation using flexible TTI



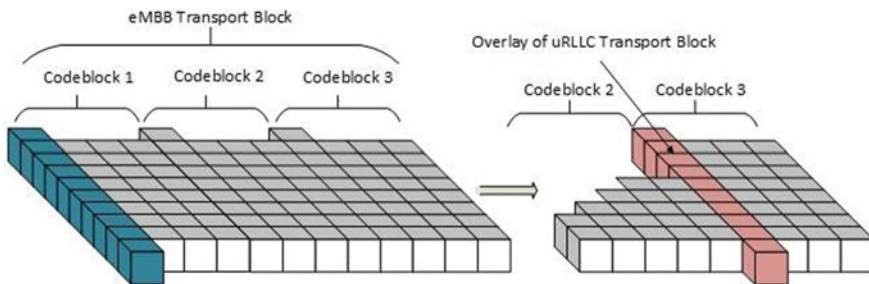


Fig. 2 Illustration of scheduling of uRLLC packet into eMBB packet at the symbol level

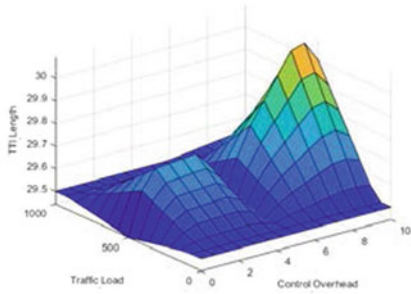
Coincidentally, artificial intelligence (AI) provides the potential solutions by learning with variations, classifying the issues and interacting with the environment. Therefore, cellular network traffic in 5G can leverage the idea of cognitive radio [12, 13] and interact with traffic conditions of various 5G services using AI. Various multi-disciplinary approaches such as machine learning (ML), optimization theory, game theory, control theory, and metaheuristics [14] have been evolve in AI. Among them, ML belongs to one of the most crucial field in AI.

3 Reactive Strategy for uRLLC-eMBB Traffic Multiplexing

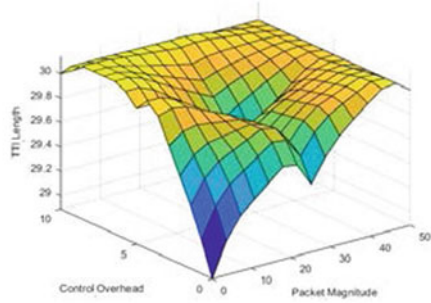
In this paper, based on adaptive neuro-fuzzy inference system (ANFIS), a new reactive strategy is proposed to provide flexible frame structure with higher priority for uRLLC traffic while ensuring the QoS for eMBB traffic. Based on the frame structure, each time the system is flexibly schedules to satisfy QoS. However, it is not easy to choose the transmission frame length in frequency and time domain, as it involves various influencing factors. The work done in [5] concluded that transmission and queuing delay play a major role in achieving the low latency and are highly correlated with packet size and rate of packet arrival. In this paper, four parameters: eMBB-uRLLC service ratio, traffic load, control overhead, and packet magnitude are considered in fuzzy environment to decide the frame structure. The relationship of these four factors with the frame can be observed from surface plots as illustrated in Fig. 3.

Service Ratio The ratio of eMBB and uRLLC services reflects traffic density. When there are no available resources, uRLLC traffic can occupy eMBB resources. Generally, eMBB traffic requires high bandwidth as compared to uRLLC traffic. Higher bandwidth with larger TTI can be provided to eMBB traffic if the service ratio is high.

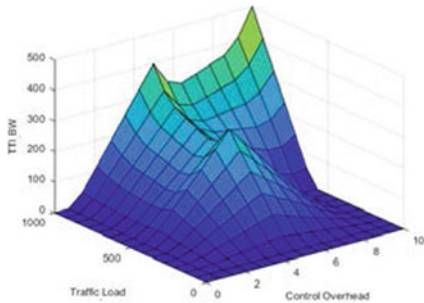
Traffic Load Taking TTI length directly proportional to the traffic load is feasible; however, this approach will lead to queuing delay due to increased TTI length with increased traffic load.



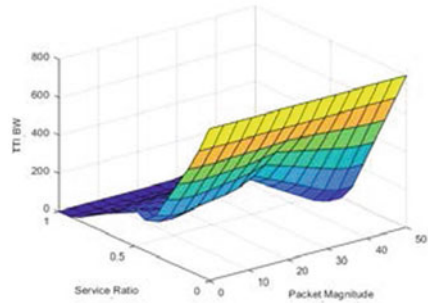
(a) Time frame of TTI vs Traffic load & control overhead.



(b) Time frame of TTI vs control overhead & packet magnitude.



(c) TTI bandwidth vs traffic load & control overhead.



(d) TTI bandwidth vs service ratio & packet magnitude

Fig. 3 Surface rule-view of fuzzy inference system

Control Overhead Transmission delay can be reduced by using short TTI length but it will result in decreased spectral efficiency due to higher control overhead requirements. Control overhead also depends on the signal to interference plus noise ratio (SINR). Poor channel quality will result in larger control overhead requirement.

Packet Magnitude Due to the impact of transmission time, increased data packets lead to delay in the service. However, increased packet magnitude overcomes the effect of control overhead on delay. Therefore, packet magnitude of same service can vary to completely explore the influential factors.

Based on above factors, a data set, composed of 1000 sets of data, is generated through Sugano-based fuzzy inference system (FIS). Each of which contains four eigenvalues described above representing the input, along with frame structure in terms of frequency and time, as the output. Furthermore, as shown in Fig. 4, neural network structure is developed using ANFIS in MATLAB, where first layer, the input layer shows four inputs discussed above.

First layer fuzzification layer, each node represents membership function

$$O_{1,i} = \mu_{A_i}(x) \tag{1}$$

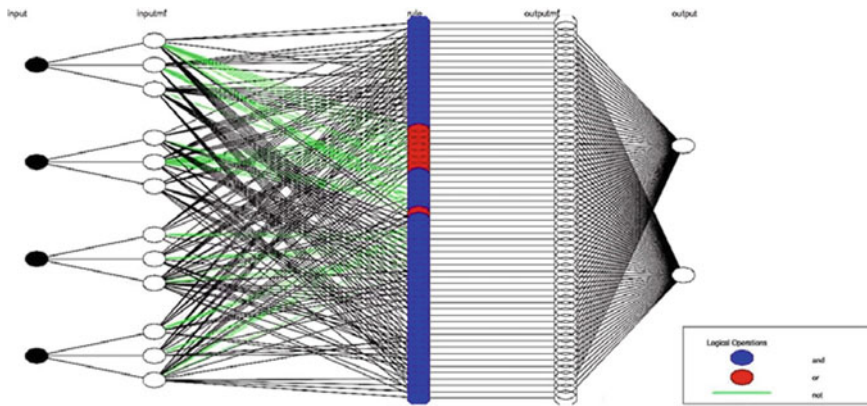


Fig. 4 Structure of ANFIS in MATLAB

where $O_{1,i}$ denotes the output of the i node, and $\mu_{A_i}(x)$ is Gaussian membership function.

Second layer is rule layer, where 80 rules, designed in FIS are represented by 80 neurons.

$$O_{2,i} = w_i = \mu_{A_i}(x) \times \mu_{B_i}(x), \quad \text{for } i = 1, 2 \tag{2}$$

where $O_{2,i}$ represents the output result in this layer, w_i denotes the weight of the i th rule.

Third layer is normalization layer.

$$O_{3,i} = w_i = \frac{w_i}{w_1 + w_2}, \quad \text{for } i = 1, 2 \tag{3}$$

Next, layer four is defuzzification layer.

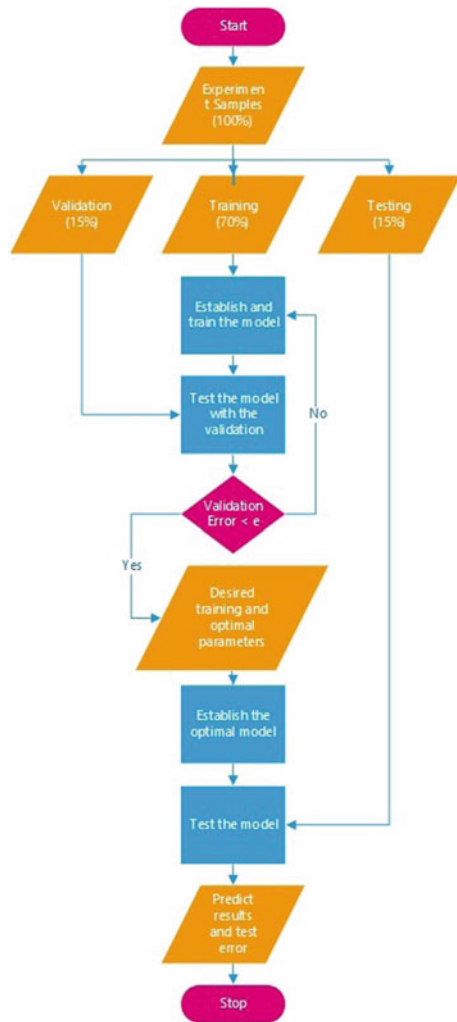
$$O_{4,i} = w_i f_i = w_i(p_i x + q_i y + r_i), \quad \text{for } i = 1, 2 \tag{4}$$

Finally, in the output layer, two nodes represent two outputs, i.e., flexible length of the TTI on time and frequency axis.

$$O_{5,i} = \sum_i w_i f_i = \frac{\sum_i w_i f_i}{\sum_i w_i} \quad \text{for } i = 1, 2 \tag{5}$$

MATLAB toolbox-nnstart is used to train the ANFIS model. Weight between the two neurons is first determined by backpropagation algorithm, and Levenberg–Marquardt (LM) algorithm is used to train the network. According to the certain proportion training, validation and testing data of the experimental samples are

Fig. 5 Model structure of input and output and curve fitting



selected and the built model is trained and tested. Then, after performing the validation to determine the requirements the model is optimized, tested and the results are predicted and the errors are analyzed (Fig. 5).

4 Results and Discussion

Figure 6 shows the normalized error histogram, where it can be observed that the difference between targets and outcomes is slightly less, representing the predicted values are approaching to the target values.

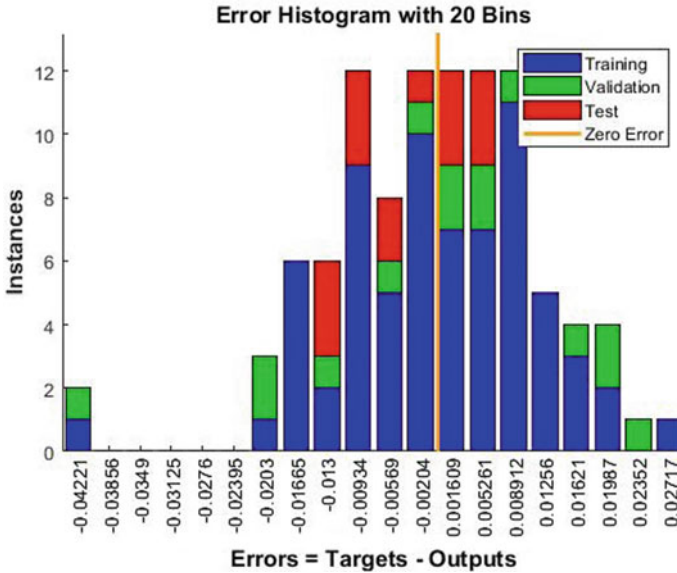


Fig. 6 Error histogram

Next, the target and calculated output values are computed as shown in Fig. 7 where out of 1000 trials data set, 70% of total trials (700) are used for training, 15% (150) of the total trials are used for validation and 15% (150) of the total trials are used for testing.

The model is trained in nntoolbox and mean square error (MSE) is calculated according to the LM algorithm. The results of training, validation and testing data are consisting of the foremost results. The best performance obtained is 0.000096424 at 318 epoch, as indicated in Fig. 8 by the MSE plot.

5 Conclusion

Due to the unavailability of the standard/reference data set, in this paper, four important factors were taken and based on their effects on the uRLLC-eMBB traffic and Sugano-based FIS was used to generate data in the MATLAB. Then, ANFIS-based approach was proposed to generate flexible frame structure for eMBB and uRLLC traffic in 5G-NR. The data obtained from FIS was used for training and testing. The parameter MSE was used for predicting the performance of proposed approach. The analysis shows that flexible frame structure can easily solve the co-existence problem, maintaining short delay for uRLLC traffic while providing high QoS for

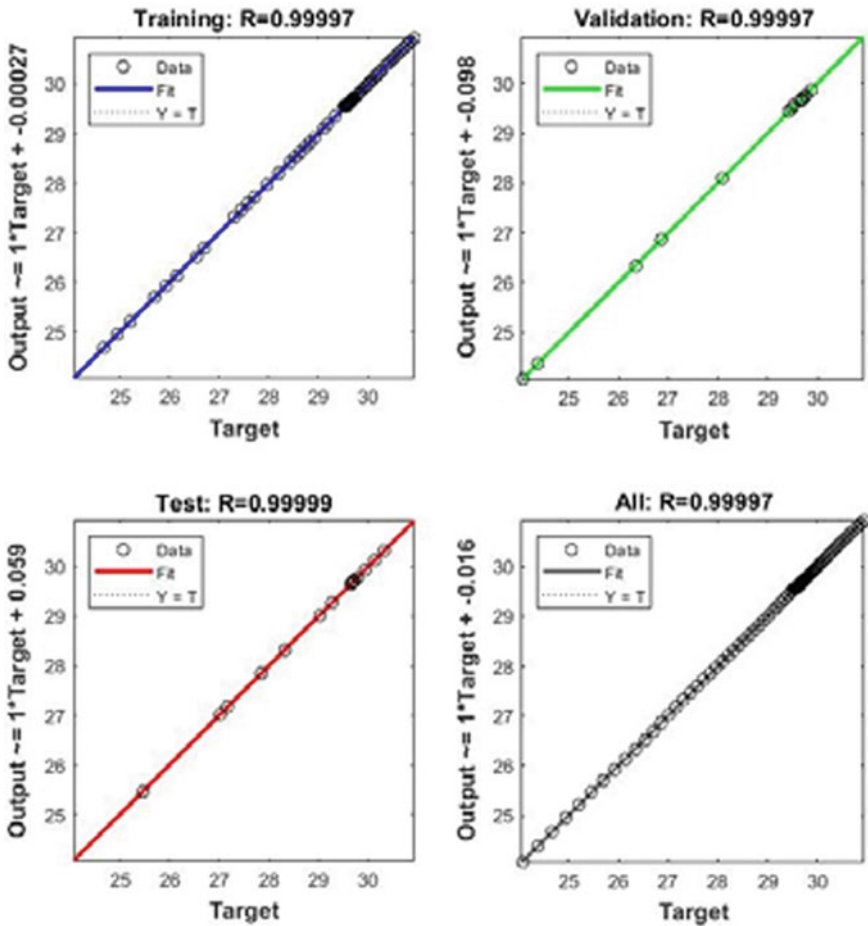


Fig. 7 Structure of model control training data

eMBB traffic. Future work can consider real-time data set and employ more advanced machine learning-based methods, also can provide a detailed study to recover eMBB capacity.

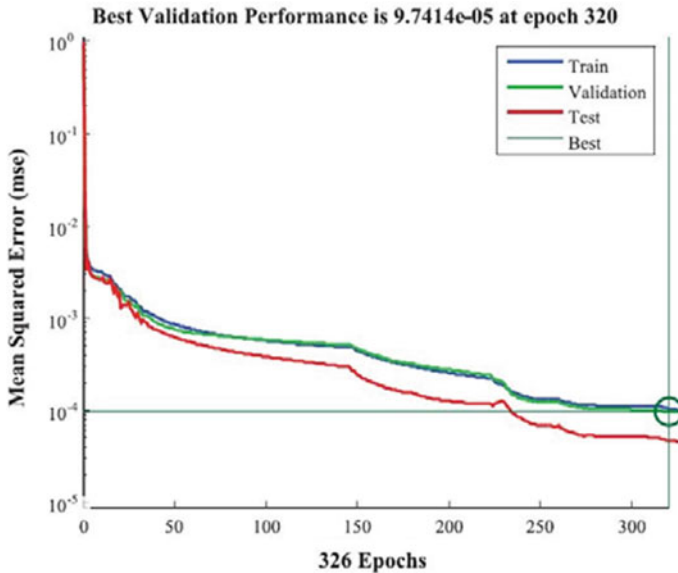


Fig. 8 Structure of ANFIS in MATLAB

References

- (2017) 5G; study on scenarios and requirements for next generation access technologies (3GPP, TR 38.913, Version 14.2.0, Release 14), Ref: DTR/TSGR-0038913ve20. https://www.etsi.org/deliver/etsi_tr/138900_138999/138913/14.02.00_60/tr_138913v140200p.pdf
- Shafi M et al (2017) 5G: a tutorial overview of standards, trials, challenges, deployment, and practice. *IEEE J Sel Areas Commun* 35(6):1201–1221
- Tafazolli R (2015) IET 5G radio technology seminar. In: Exploring technical challenges in the emerging 5G ecosystem, London, UK. <https://doi.org/10.1049/ic.2015.0027>
- Gupta A, Jha RK (2015) A survey of 5G network: architecture and emerging technologies. In: Recent advances in software defined networking for 5G networks. *IEEE Access* 3:1206–1232. <https://doi.org/10.1109/ACCESS.2015.2461602>
- Esswie AA, Pedersen KI (2018) Opportunistic spatial preemptive scheduling for uRLLC and eMBB coexistence in multi-user 5G networks. *IEEE Access* 6:38451–38463
- Anand A, Veciana GD, Shakkottai S (2018) Joint scheduling of uRLLC and eMBB traffic in 5G wireless networks. In: *IEEE conference on computer communications*, Honolulu, HI, USA. <https://doi.org/10.1109/INFOCOM.2018.8486430>
- Alsenwi M, Tran NH, Bennis M, Bairangi AK, Hong CS (2019) eMBB-uRLLC resource slicing: a risk-sensitive approach. *IEEE Commun Lett* 23(4):740–743
- Zhang J, Xu X, Zhang K, Zhang B, Tao X, Zhang P (2019) Machine learning based flexible transmission time interval scheduling for eMBB and uRLLC coexistence scenario. In: *IEEE Access Spec Sect Artif Intell Phys Layer Wirel Commun* 7:65811–65820
- Jiang C, Zhang H, Ren Y, Han Z (2016) Machine learning paradigms for next generation wireless networks. *IEEE Wirel Commun* 16. ISSN 1536-1284
- Chih-Lin I, et al. (2016) New paradigm of 5G wireless internet. *IEEE J Sel Areas Commun* 34(3):474–482

11. Pérez-Romero J, Sallent O, Ferrus R, Agusti R (2016) Knowledge-based 5G radio access network planning and optimization. In: Proceedings of international symposium of wireless communication systems, pp 359–365
12. Mitola J, Maguire GQ (1999) Cognitive radio: making software radios more personal. *IEEE Pers Commun* 6(4):13–18
13. Otani T, Toubé H, Kimura T, Furutani M (2017) Application of AI to mobile network operation. *ITU J ICT Discov* (1):1–7
14. Qadir J et al (2015) Artificial intelligence enabled networking. *IEEE Access* 3:3079–3082

Lexicon-Based Sentiment Analysis



Kavleen Kour, Jaspreet Kour, and Parminder Singh

Abstract The sentiment analysis is an emerging field of natural language processing which is based on human–computer interaction, information retrieval and distilling sentiments from the ever-increasing online social data. It involves identifying the words or phrases in the underlying text express positive, negative or neutral attitude. The objective of this paper is to extract the editorial text of a leading newspaper and classify the sentiments expressed at different levels, namely paragraph level, sentence level and word level into positive, negative or neutral.

Keywords Natural language processing · Sentiment analysis · Lexicon based

1 Introduction

The human beings communicates with each other through different ways such as speech, text and sign language. Natural language like other types of data needs to be understood and analyzed. Natural language processing abbreviated as NLP is the manipulation of natural language by using computers through software. It is a way by which computers can bring out meaning from human language which enables their human–computer interaction to have various real-time applications like speech recognition, stemming, entity recognition, sentiment analysis, machine translation to name a few.

Sentiment analysis is an approach to NLP which identifies the emotion expressed in a text. Sentiment analysis is an area of research that finds human opinions, responses, feedback and emotions toward various products, people, facilities, activities, etc [1]. It is a hot topic of research in the field of NLP and machine learning. Sentiment analysis is also known by other names as opinion mining, emotion AI

K. Kour (✉) · P. Singh
GNDEC, Ludhiana, Punjab, India
e-mail: kavleenkour99@gmail.com

J. Kour
Galgotias College of Engineering and Technology, Greater Noida, UP, India

opinion extraction, subjectivity analysis and review mining. SA is used to gather insight from unstructured data obtained from various sources into meaningful and subjective information. Since the information/data available over the Internet is exponentially growing, large chunk of text is available publically or privately in the form of social media content such as reviews, blogs, micro blogs, comments and discussion forums. This available data can be used for various commercial and non-commercial applications as the opinions expressed in data. Automated sentiment analysis is the need of the hour as today we are having huge volume of opinion data freely available. The research in SA would not have been possible without this huge chunk of data. Today, SA is an important part of the social media research.

There are various areas where sentiment analysis is in use, the foremost being the branding. In today's world, the companies and their promoters are keen to know the value of their product or brand in public. Earlier people use to ask the opinions from the friends, elders or known people but now with the advancement in technology they read the reviews and comments of various users available freely on the Internet and make decision accordingly. Marketers also look forward to the information shared by their potential users. It also help the companies in knowing the credibility of the brand, reputation crisis, etc. SA gauges the attitude of the company along with that of competitors which can be used to find the strength and weakness of one's company as well as others. The product developer team uses sentiment analysis to find the strength and flaws of the product launched. Early feedback helps in bringing necessary changes in the product. Nowadays, people share the views and discuss new products, events, news on social media. Using SA consumer behavior and market track can be studied and future decisions can be made. Users who voluntarily pass information can be used to understand market trends. SA can also be used for human resource-related issues. Organizations use SA to measure employer satisfaction and track the response of their employers to various policies to maintain a friendly and healthy environment. It is also a useful tool for workforce analysis. Prediction analysis is another application of SA, wherein candidate expectations are known by the leaders before elections [2].

SA can be done at three different levels, namely document level, sentence level, entity or aspect level. In the document level, the task is to classify the opinion of whole document where it is assumed that the document express opinion on a single entity. In sentence level, each sentence in a text is positive, negative or neutral. In this level there are two steps: the first is subjective classification of a sentence and the other is objective classification. The sentence which presents factual information is called objective sentence, on the other hand, the sentence expressing emotions, feelings, views are called subjective sentence. The second step of sentence level classification is expressing sentence as positive or negative or neutral. Finding out the particular aspect of the service offered or the product launched is taken care of in aspect level SA.

There are various challenges involved in the developing automatic sentiment analysis. As anyone is free to express opinions without disclosing the identity and place where he belongs to, it leads to opinion spamming. Some people post fake reviews and comments to discredit certain products and services. There have been reports of

some companies who are commercially involved in the business of fake reviews for fake clients. Sentiment lexicon suffers from several issues like same word expresses opposite meaning in different contexts and applications. Some sentiment words may not be expressing any sentiment; on the contrary, from words without sentiments, opinion can be inferred.

The sentiment techniques can be broadly classified into three categories namely machine learning-based approach, lexicon-based approach and hybrid approach. Machine learning-based SA can be further subdivided into supervised and unsupervised learning techniques. In supervised learning, the data is divided into training and testing set. The classifier learns the distinct characteristic of the training set and a model is developed. This model is fit on the test set to check the performance of the classifier. Naive Bayes is the simplest and first choice to be used as a classifier. The other classifiers in the category of supervised learning are maximum entropy classifier, support vector machine (SVM), neural network, etc. The application of deep learning approaches to finance research has received a great deal of attention [3]. Sometimes there is difficulty in obtaining the labeled training data, in such cases, unsupervised learning methods are used. Also, machine learning-based classifiers work with acceptable accuracy when sufficiently large text as given as input. Lexicon-based approach is very common because of its accessibility and economy. It has poor recognition of affect when linguistic rules are involved. For example, it can correctly classify the sentence “today was a happy day” as being happy, it is likely to fail on a sentence like “today wasn’t a happy day at all” [4].

2 Literature Review

The challenge in sentiment analysis is not only to find out the sentiment behind the word but also to understand the sentiment of the reader, his pre-specified notions about the product [5]. This includes detecting sentiment at various levels of text granularities; finding out the sentiments of the person reading a text; obtaining the opinion of various aspects of the product, etc. The author in this paper also addresses the challenges of lexicons created by individuals at various levels.

The detailed study of lexicons and dataset used for SA is done in [6]. Sentiment lexicon is a repository of words labeled as positive negative and neutral. This paper discusses different labeling schemes and trends underlying research in lexicon generation. Also, it shows how datasets and lexicons for one language can be transferred to a new language. In [7], lexicon-based approach is applied to BBC news dataset and news is classified as business, entertainment, sports, technical and politics. Document level analysis is done on the basis of score generation. SA on news dataset helps users to read the news of their corresponding interests, thereby customizing their news feed. Machine learning-based approach is considered in [8] for sentiment analysis of popular blogging platform Twitter. Naive Bayes classifier is used for categorizing of polarity of English tweets. The classification of text in the form of tweets

is very useful for business interpretations, product management, political campaigns, etc.

The classification is done in [9] based on document level using support vector machine. A new algorithm has been proposed where in parts of speech is used to enhance the accuracy on the movie reviews dataset. The analysis of election sentiments using two popular machine learning algorithms, Naïve Bayes and support vector machine, is done in [10]. They authors have done comparison between sentiment lexicons (W-WSD, SentiWordNet, TextBlob) so that the best can be utilized for sentiment analysis. The authors in paper [11] extract the subjective review information as the object of the study and perfect the emotional dictionary of the social security theme. A model of emotional analysis is built which helps government in grasping the public opinion and knowing the feelings of the people from different levels of society.

The performance analysis of sentiments using machine learning techniques is elaborated in [12]. The authors in [13] describe the sentiment classifier approach based on various features and discuss the tools available for sentiment analysis. The effect of tweets over the rise and fall in stock prices of Samsung Electronics limited is available in [14] along with the strategy to predict the fluctuation in stock price.

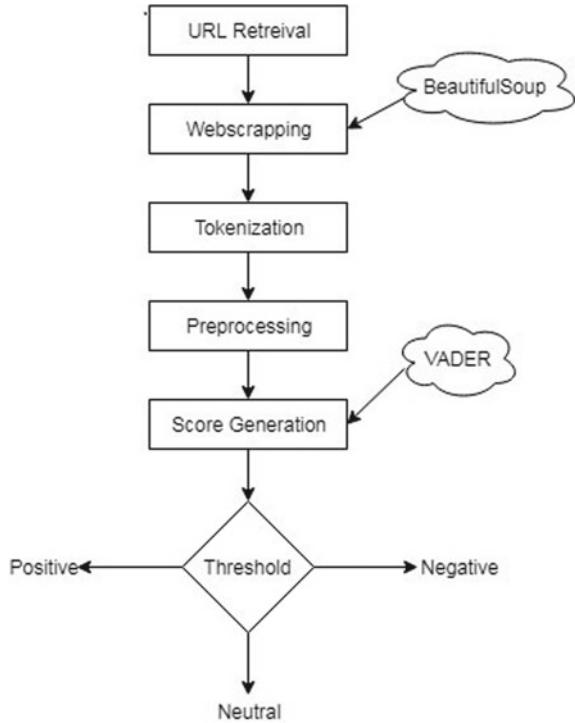
3 Proposed Work

The dictionary-based approach has been used for sentiment analysis of news article using VADER. An overview of the steps involved in sentiment analysis is shown by the flowchart in Fig. 1.

The steps involved are as follows:

- Retrieve URL of the Web site: For fetching the HTML page of the Web site, we use requests library/package of python.
- Web scrapping: Extracting content from URL: HTML page of the desired Web site obtained in first step is not in structured form. BeautifulSoup, a Python library is used for HTML parsing. It provides methods for extracting information contained within HTML tags. The desired text for analyzing here is the first paragraph of the retrieved Web page.
- Tokenization: The text obtained from step 2 is a paragraph which needs to be segmented into individual words. The splitting of text into words is referred to as tokenization. Tokens or words are separated by white space and are input to the next step.
- Pre-processing: This step involves removal of some words from the text which are called as stop words. These words do not carry meaning and do not confer semantic values. There is a list of core English stop words in NLTK though additional words can be added to the list. After this process, we get a list of filtered words.
- Sentiment analysis at three different levels: The sentiments can be measured at various levels in a text, namely paragraph level, sentence level and word level.

Fig. 1 Flowchart of the proposed sentiment analysis



- A document may contain a single or multiple paragraphs which may be expressing positive, negative or neutral opinion. The first paragraph of the retrieved Web site is considered for analysis. Valence Aware Dictionary and sEntiment Reasoner (VADER) is a lexicon and rule-based sentiment analysis tool that is used to classify sentiments expressed in the text available on the Internet in the form of reviews comments or feedback, etc. VADER uses sentiment lexicon which is a list of lexical features (e.g., words) which are generally labeled according to their semantic orientation as positive, negative or neutral. Compound score is generated by the weighted sum of positive, negative and neutral score. The paragraph is finally classified based on the compound score.
- Next for more detailed analysis, for each sentence of the paragraph, a sentiment score is generated. The paragraph is broken down into individual sentences. Sentiment analysis using VADER is done for each sentence and score is generated. The sentence is classified based on the compound score obtained for particular sentence.
- The in-depth and exhaustive analysis is done at word level in the next step. VADER is capable of classifying the words into positive negative and neutral words along with the intensity of the underlying sentiment. The sentence is fragmented into individual words. The stop words are removed from the list of words. The filtered text after tokenization and pre-processing is used in this

The idea of designating an individual as a terrorist, as the latest amendments to the Unlawful Activities [Prevention] Act propose to do, may appear innocuous. However, designating an individual as a terrorist raises serious constitutional questions and has the potential for misuse. The practice of designating individuals under anti-terrorism laws, prevalent in several countries, is seen as being necessary because banned groups tend to change their names and continue to operate. However, there is no set procedure for designating an individual a terrorist. Parliament must consider whether an individual can be called a 'terrorist' prior to conviction in a court of law. The absence of a judicial determination may render the provision vulnerable to invalidation. There ought to be a distinction between an individual and an organisation, as the former enjoys the right to life and liberty. The likely adverse consequences of a terrorist tag may be worse for individuals than for organisations.

Fig. 2 Extracted paragraph

step for sentiment analysis. The sentiment score is generated for each word in the filtered list. Also, the words in the filtered text are classified into positive negative and neutral words based on threshold.

4 Result

In this section, details of the dataset used and various experiments performed are discussed.

4.1 Dataset

The dataset used for analysis in this work is the paragraph of leading Indian newspaper titled 'The Hindu' dated July 29, 2019 [15]. It is an editorial article regarding Unlawful Activities Act and terrorism. The first paragraph scrapped in this work is shown in Fig. 2.

4.2 Experimental Results

- Paragraph Level
The news article having a sentiment score of 0 is considered as neutral, with a score of +1 as positive and score of -1 as negative. As seen in Fig. 3 the first paragraph has been classified as negative with a compound score of -0.9732.
- Sentence Level
The snapshot of the sentences in the paragraph with their respective scores is shown in Fig. 4. It has been observed that most of the sentences are neutral along with one sentence classified as positive and two sentences as negative.

The idea of designating an individual as a terrorist, as the latest amendments to the Unlawful Activities (Prevention) Act propose to do, may appear innocuous. However, designating an individual as a terrorist raises serious constitutional questions and has the potential for misuse. The practice of designating individuals under anti-terrorism laws, prevalent in several countries, is seen as being necessary because banned groups tend to change their names and continue to operate. However, there is no set procedure for designating an individual a terrorist. Parliament must consider whether an individual can be called a 'terrorist' prior to conviction in a court of law. The absence of a judicial determination may render the provision vulnerable to invalidation. There ought to be a distinction between an individual and an organisation, as the former enjoys the right to life and liberty. The likely adverse consequences of a terrorist tag may be worse for individuals than for organisations.

compound: -0.9732, neg: 0.188, neu: 0.758, pos: 0.054, <FreqDist with 77 samples and 91 outcomes>

Fig. 3 Paragraph level SA

The idea of designating an individual as a terrorist, as the latest amendments to the Unlawful Activities (Prevention) Act propose to do, may appear innocuous.
compound: -0.6908, neg: 0.17, neu: 0.83, pos: 0.0,
 However, designating an individual as a terrorist raises serious constitutional questions and has the potential for misuse.
compound: -0.7184, neg: 0.3, neu: 0.7, pos: 0.0,
 The practice of designating individuals under anti-terrorism laws, prevalent in several countries, is seen as being necessary because banned groups tend to change their names and continue to operate.
compound: -0.4588, neg: 0.097, neu: 0.903, pos: 0.0,
 However, there is no set procedure for designating an individual a terrorist.
compound: -0.7845, neg: 0.434, neu: 0.566, pos: 0.0,
 Parliament must consider whether an individual can be called a 'terrorist' prior to conviction in a court of law.
compound: 0.0, neg: 0.0, neu: 1.0, pos: 0.0,

Fig. 4 Sentence level SA

- Word Level

The result of a word-level classification is shown in Fig. 5 where each word (except stop words) has been classified into positive, negative or neutral based on the score.

4.3 Word Cloud

Word cloud generators work on the principle of breaking the text into words and count the frequency of their appearance in the text. Further font point size is attached to the words based on the number of times a word appears in the text. Word cloud is effective means of showing responses obtained from surveys and helps in preliminary analysis and validation of previous findings. It displays the keywords, provides emotion connection and is engaging. Word cloud adds clarity in the text which helps in communicating the data results effectively. It is used by politicians to share political pulse, educators to convey important issues, Q researchers for communicating qualitative data, marketers to highlight customer needs and nonprofit organizations to collect and share sentiments.

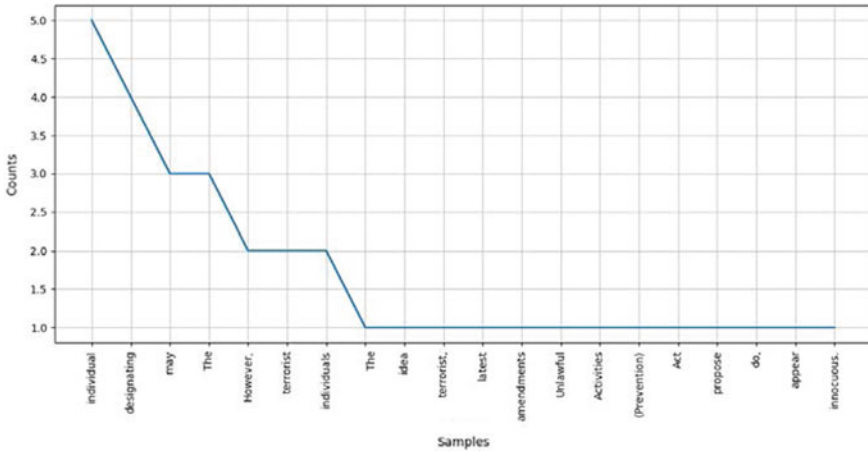


Fig. 7 Frequency distribution of filtered text

5 Conclusion and Future Scope

Sentiment analysis can be explored in many directions. In this paper, we defined the polarity (i.e., positive or negative or neutral sentiment) of the news article by observing the scores obtained using VADER. The structural level at which sentiment analysis is performed is entirely driven by the requirements and the type of text to be processed. For tweets or very short texts, document level sentiment analysis is a good choice. However, if profiling sentiment around a specific aspect or feature of a brand, product or organization is to be done, and then sentence level or entity level analysis is considered. The experimentation in this work includes sentiment analysis at paragraph, sentence and word level. Future work in the area of sentiment analysis will be based on developing machine learning as well as hybrid approach-based classifier.

References

1. Liu B (2012) Sentiment analysis and opinion mining. Morgan & Claypool, San Rafael, CA
2. Kaur H, Mangat V, Nidhi N (2017) A survey of sentiment analysis techniques. In: International conference on I-SMAC (IoT in Social, Mobile, Analytics and Cloud), pp 921–925
3. Souma W, Vodenska I, Aoyama H (2019) Enhanced news sentiment analysis using deep learning methods. J Comput Soc Sci 1–14
4. Cambria E, Das D, Bandyopadhyay S, Feraco A (2017) Affective computing and sentiment analysis. In: Das D, Cambria E (eds) A practical guide to sentiment analysis. Springer Publication
5. Mohammad MS (2017) Challenges in sentiment analysis. https://doi.org/10.1007/978-3-319-55394-8_4

6. Joshi A, Ahire S, Bhattacharyya P (2017) Sentiment resources: lexicons and datasets. In: Das D, Cambria E (eds) *A practical guide to sentiment analysis*. Springer Publication
7. Taj S, Shaikh BB, Meghji AF (2019) Sentiment analysis of news articles: a lexicon based approach. In: *International conference on computing, mathematics and engineering technologies-iCoMET*, Pakistan
8. Wagh B, Shinde JV, Kale PA (2017) A Twitter sentiment analysis using NLTK and machine learning techniques. *Int J Emerg Res Manag Technol* 6(12). ISSN 2278-9359
9. Mouthami K, Nirmala KD (2013) Sentiment analysis and classification based on textual reviews. In: *International conference on information communication and embedded systems (ICICES)*, Chennai, India, pp 271–276
10. Hasan A, Moin S, Karim A, Shamshirband S (2018) Machine learning-based sentiment analysis for Twitter accounts. *Math Comput Appl* 23(1):11
11. Zhang X, Li C (2017) The research of sentiment analysis of microblog based on data mining exemplified by basic endowment insurance. In: *International conference on signal processing, communication and computing*. <https://doi.org/10.1371/journal.pone.0191163>
12. Gautam G, Yadav D (2014) Sentiment analysis of Twitter data using machine learning approaches and semantic analysis. In: *7th international conference on contemporary computing*, Noida, India, pp 437–442
13. D'Andrea A, Ferri F, Grifoni P, Guzzo T (2015) Approaches, tools and applications for sentiment analysis implementation. *Int J Comput Appl* 125(3). ISSN 0975-8887
14. Bakshi R, Kaur N, Kaur R, Kaur G (2016) Opinion mining and sentiment analysis. In: *3rd international conference on computing for sustainable global development*, New Delhi, India, pp 452–455
15. <https://www.thehindu.com/opinion/editorial/>

Early Prediction of Childhood Obesity Using Machine Learning Techniques



Kakali Chatterjee, Upendra Jha, Priya Kumari, and Dhatri Chatterjee

Abstract The aim of this research work is the early prediction of childhood obesity after the age of three years from available clinical records of patients. Nowadays, child obesity is a highlighted research area as excessive body fat harmfully affects a child's health. Obese children have more risk of suffering from health problems such as heart diseases, type 2 diabetes, cancer, and osteoarthritis in their adulthood. Thus, early prediction of childhood obesity is essential for fat and overweight babies. In this paper, we have proposed a prediction model for this purpose. Analyses of three different machine learning methods: SVM, KNN, and ANN for establishing accuracy in the prediction model have been done. From the result analysis, it can be established that a prediction model based on machine learning techniques can be used to predict obesity in children after the age of two years.

Keywords Obesity · Prevention · Machine learning techniques

1 Introduction

Obesity is a common problem in child healthcare. It may occur due to excessive food intake, lack of physical activity, genetic susceptibility, endocrine disorders, etc. It can result in many diseases including heart diseases, high blood pressure, diabetes, some

K. Chatterjee (✉) · U. Jha · P. Kumari
Computer Science and Engineering Department, National Institute of Technology Patna, Patna,
Bihar 800005, India
e-mail: kakali@nitp.ac.in

U. Jha
e-mail: upendrajha97@gmail.com

P. Kumari
e-mail: priyapatna148@gmail.com

D. Chatterjee
Gitam Institute of Medical Science and Research, Visakhapatnam, India
e-mail: dhatri2012@gmail.com

types of cancers, gall stones, osteoarthritis, and breathing problems from a very early age [1]. Hence prevention is a better approach than treatment since the treatment of the aforementioned conditions is more expensive and time-consuming. Early age prediction of obesity is needed because if the symptoms of obesity or obesity itself can be predicted at an early age, then it will decrease the chance of diseases caused by obesity.

Children with a high BMI (Body Mass Index) at a very low age and those with a faster increase in BMI between the ages of 8–12 years have increased risk factors for cardiovascular morbidity and vascular diseases [2]. The chances of obesity in some individuals increase in a short period due to the unhealthy lifestyle of the family or the child. There are many obesity conditions that are especially critical in childhood. Due to childhood obesity, psychological distress [2] and complications from associated conditions like high blood sugar can arise. In adulthood it may increase the risk of heart diseases, diabetes, and premature mortality [3].

The risk of adult obesity is at least doubled in the case of obese children relative to non-obese children [3]. Many research works have been proposed in the literature. Some of them proposed clinical prediction models [4], machine learning techniques [5–7], and decision tree based approaches [8–10]. High body mass index (BMI) in childhood is related to increased risk of cardiovascular disease (CVD), type 2 diabetes mellitus (T2DM), and premature death [3]. The regression models used modifiable predictors like maternal pregnancy BMI, paternal BMI, and non-modifiable risk predictors such as birth weight, weight gain, sex [10], etc. The frequency of obesity has been increased in the world from 1975 to 2017 [11]. Recent reviews of Butler et al. [12] show that there is an established guideline for risk threshold for these prediction models where prediction is more important than treatment in this case.

Hence in this paper, we have proposed a prediction model of early childhood obesity using machine learning techniques such as Support Vector Machine (SVM), k-Nearest Neighbor (KNN), Artificial neural network (ANN). These algorithms have been applied on a standard dataset for performance evaluation and the highest accuracy obtained 97.77% using the KNN algorithm. Our major contributions are:

- We design and implement a prediction model for early childhood obesity detection and also find the best features for this early prediction model.
- This model has been experimented using real-world data for accuracy checking and the result shows that performance is acceptable.
- This model performance is also compared with other existing models to establish its performance. We have selected and prioritized the attributes on the basis of information gain. Hence the accuracy percentage has been improved from other models.

The rest of the paper is organized as follows: Childhood obesity risk is discussed in Sect. 2. Section 3 presents the proposed prediction model. The implementation Result and Performance Analysis is explained in Sect. 4 and Conclusion are discussed in Sect. 5.

2 Childhood Obesity Prevalence and Risk

As an essential survival mechanism, human body is equipped with the ability to store excess energy in adipose tissue as triglycerides which is released when required as free fatty acids. Any imbalance in the levels of energy intake, energy utilization, which are regulated by the neuroendocrine and metabolic systems, or a combination of both energy intake and utilization results in a state of excess adipose tissue which is termed as obesity [13].

Obesity is associated with 50–100% increase in the risk of death from systemic causes compared to normal-weight individuals and hence corresponds to an increased mortality rate despite it being a preventable disease [1]. Obesity in children has been observed to show ‘tracking’ with age as basal metabolic rate and physical activity usually decreases with age and they tend to become obese adults [2]. Hence, an early prediction and employment of a suitable prevention strategy would be considered beneficial. Underlying aetiology maybe environmental factors like dietary composition, amount and frequency of meals, lack of physical activity, and genetic susceptibility. Other causes include endocrinal disorders, hypothalamic causes, drugs, genetic syndromes, single-gene mutations and eating disorders [14–16]. Environmental factors account for 95% of the cases [2] increased consumption of energy-dense food, including fats and rapidly absorbed sugars, larger quantity of meal, frequent meals and irregular eating habits promote obesity. Sedentary lifestyle is also known to promote obesity [2].

Sleep deprivation has been suggested to be a factor for obesity [4]. Heritability of body weight has been supported by studies that state that adopted kids resemble their biological parents and biological siblings more closely than their adoptive parents [5]. Twin studies also support genetic influence [6]. Genetic obesity, which is relatively uncommon, has been studied in rodents. It is attributed to a number of distinct single-gene mutations in their genome, causing increased appetite and decreased energy utilization. Normal variant of *ob* gene causes the production of peptide leptin from adipose cells which acts on the hypothalamus and is responsible for decreased appetite and increased energy utilization and a mutation in the aforementioned gene results in severe obesity [7]. Administration of leptin in such genetically obese *ob/ob* mouse has led to a decrease in body weight [8]. A similar course is seen in the mutation of *db* gene which affects leptin receptor and results in obesity. Mutations in *ob* gene, which is also present in humans have been described in several families with morbid early onset obesity [9]. Single-gene mutations in genes encoding for POMC, MC4R, PC-1, AgRP are also known to cause obesity [1]. Endocrinal causes include Cushing’s syndrome, hypothyroidism in which obesity occurs along with other specific symptoms of the respective diseases. Genetic syndromes with proven inheritance like Prader–Willi, Bardet–Biedl syndrome also present with obesity. Insults on central nervous system in cases of trauma, tumor, infection, surgery may result in rapid onset of obesity [3]. A recent study has suggested that a rapid weight gain during infancy may be a risk factor for childhood obesity [11] Gut microbiota may have a possible role [1] as it can determine the metabolic potential.

The most widely used method to determine obesity is the calculation of body mass index. BMI more than 85th percentile for age is considered as overweight and BMI more than 95th percentile is considered obese. Weight for height more than 120% is considered obese [3]. Waist circumference is an important parameter as intra-abdominal and upper body fat is strongly linked with complications of obesity like insulin resistance, hypertension, hyperlipidemia, and hypoandrogenism [1].

Other parameters include skinfold thickness and densitometry. According to the Framingham study, obesity is an independent risk factor for cardiovascular disease [11]. It leads to hyperlipidemia, hypertension, coronary artery disease, and stroke. Obesity is associated with insulin resistance and hence may present as type 2 diabetes mellitus. It is also associated with increased androgen production leading to a polycystic ovarian syndrome in women. Restricted respiratory movements may occur due to chest wall obesity and in severe cases, ‘obesity hypoventilation syndrome’ may occur. Obese children are more likely to have slipped femoral epiphyses, flat feet, and early onset osteoarthritis [3]. Obesity is also associated with fatty liver disease and cholecystitis. There is an increased risk of several types of cancer including cancer of colon, pancreas, liver, gall bladder, ovaries [10]. Acanthosis nigricans (hyperpigmented patches on the neck, axilla) occurs due to the associated raised insulin level. Psychological trauma due to stigmatization may result in low self-esteem or depression.

3 Proposed Prediction Model

The main objective of this proposed model shown in Fig. 1 is to build an intelligent obesity prediction model that predicts obesity accurately before the age of five years, using data collected prior to the fifth birthday. This model has three units. First one is Dataset Collection Unit. Second one is Data Preprocessing and Normalization Unit and third one is machine learning unit. It will run in two phases training and testing phase. After several training and testing processes, the learned model will be prepared.

3.1 Dataset Collection Unit

We first gather data from CHICA system [17]. This clinical decision support system is mainly nine years of collection of clinical information from four different health centers. In this data set, 167 attributes were present with 7519 patient records. From this database we have selected 11 attributes to predict obesity. Attribute selection is mainly performed through information gain calculation. Now we have collected data of these attributes from a hospital database where only children aged 3–5 years are considered. The total no of children data is 200 having both rural and urban backgrounds. This database contains child data of age, gender, weight, height, birth

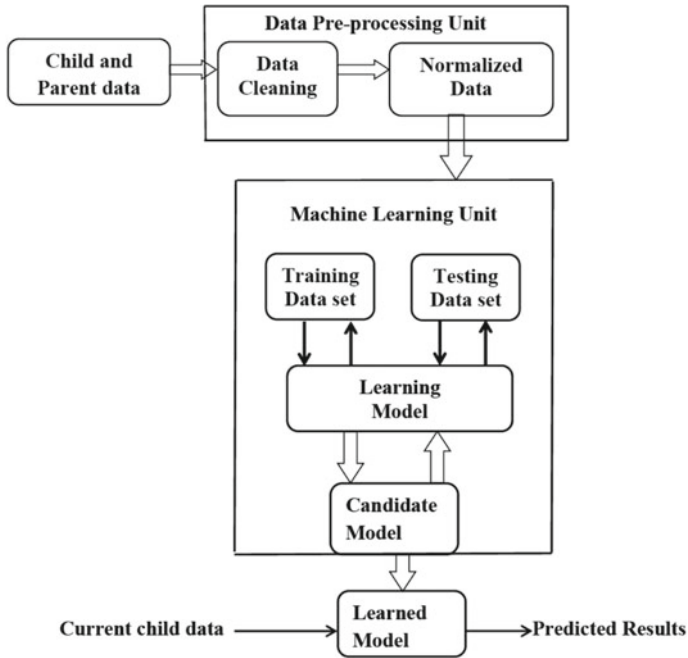


Fig. 1 Proposed model

weight, physical activity, school hours, food habits, parental data, etc. To develop this system 11 input attributes are used in Table 1.

Table 1 Details of attributes for prediction model

No.	Attribute	Description
1	Age	Numerical values of ages of children from age of 2 years to 5 years
2	Gender	Boy child as 0 and girl child as 1
3	Weight	Weights of children as a numerical value
4	Height	Height is also considered as a numerical value
5	BMI	Weight in kg/(height in meters) ²
6	Food habit	Healthy food taken by a child is considered as 1 and unhealthy food is considered as 0
7	Mother obesity	An obese mother is considered as 1 and not obese is considered as 0
8	Father obesity	An obese father is considered as 1 and not obese is considered as 0
9	Physical activity	For outdoor games, it is considered as 1 and for indoor games it is considered as 0
10	Infant weight	Birth weight (Numerical value is considered)
11	Sleeping duration	Time in mins

3.2 Dataset Preprocessing Unit

The function of this unit is to transform raw data into an understandable format. Real-time data is incomplete, inconsistent, and contain many errors. Hence Data preprocessing is essential to resolve in completeness, inconsistency issues of dataset. We used Data Preprocessing for this purpose and also checked whether any missing values are there or not. Dataset preprocessing algorithm is giving below:

Algorithm 1: Dataset Preprocessing

- 1: Importing the libraries (import numpy as np, import pandas as pd, import matplotlib.pyplot as plt)
- 2: Importing the dataset (dataset = pd.readcsv('training_data_set.csv'))
- 3: Checking out the missing values (data.isnull().sum())
- 4: Seeing the categorical values (from sklearn.preprocessing import LabelEncoder encoder = LabelEncoder())
- 5: Splitting data in training and testing dataset (from sklearn.model selection import train_test_split)

After this processing, we get the normalized data which is considered as an input of the next section.

3.3 Classification and Decision Unit

This unit mainly involves in data classification and decision purposes. After completing two phases of work dataset collection and dataset preprocessing, we analyzed our dataset and found that our problem can be solved with supervised learning techniques.

Therefore, we have applied three machine learning algorithms namely Support Vector Machine (SVM), K-Nearest Neighbors (KNN), and Artificial Neural Network (ANN). The standard SVM algorithm builds a binary classifier to construct a hyper-plane separating class members from non-members in the input space. K-Nearest Neighbors is a simple algorithm that stores all available cases and classifies new cases based on a similarity measure (e.g., distance functions) [9]. Also ANN can actually learn from observing data sets. Thus these algorithms are used for learning purposes. The classification that is involved in our problem is binary classification, as either a child will be obese or not obese. The performance of these classification algorithms is measured in the form of accuracy, Precision, and recall. Accuracy is defined as the ratio of correctly predicted samples from the total samples. Precision Value is the ratio of correctly predicted positive samples to the total predicted positive samples. Recall is the ratio of correctly predicted positive samples to all samples in actual class.

Precision and recall are used for prediction purposes with current data set. To measure the prediction performance of classifiers, sensitivity, and specificity values

are used. Sensitivities refer to the true positive rate or recall rate which is defined as risk class [7]. Specificities measure the proportion of true negatives which is defined as normal class. In this work, we have considered higher priority for sensitivities than specificities because it is important to predict a risk case so that the medical practitioner can plan appropriate treatments.

4 Result and Performance Analysis

To evaluate the performance of our prediction model, we conduct experiments with real-world data. Firstly data collected from CHICA system [17]. This clinical decision support system is mainly nine years collection of clinical information from four different health centers. In this data set, 167 attributes were present with 7519 records. From this data set, we have selected the most sensitive 11 attributes which we used in our model. We calculate information gain of every attribute using its entropy. After the calculation of individual information gain, we prioritize the attributes with higher information gain.

Records of those selected attributes (11 attributes) are used for training model. We use SVM, KNN, and ANN classifiers for this purpose. This model is implemented using the data mining tool Weka 3.8. To check the performance of our prediction model, we have created a new data set with our collected real-world data. The dataset consists of 222 records and 11 attributes. This is used as testing data test. SVM, KNN, and ANN models are implemented for performance evolution and results are shown in Table 2.

Table 2 shows that, the accuracy increases when KNN model is used. But the highest accuracy is achieved by using ANN classifier. Performance is also measured in terms of Sensitivity and Specificity. Recall is also referred to as Sensitivity. It has been observed that Specificity is increased from 85 to 92% when ANN model is used. Also Sensitivity is increased from 94 to 97% when ANN model is used. It means that ANN can classify risk cases better than normal classes. Hence the proposed prediction model achieved 96% accuracy while predicting it. This is more desirable for our prediction model.

In Table 3, Mean Absolute Error (MAE), Root Mean Squared Error (RMSE), Relative Absolute Error (RAE), Root Relative Squared Error (RRSE) of three different algorithms are shown. MAE and RMSE mainly show the difference between actual and prediction value. Here MAE is lesser than RMSE. If the sample size increases,

Table 2 Implementation results

Algorithm	Accuracy (%)	Precision (%)	Recall (%)	Specificity (%)
SVM	91.90	93.46	94.70	85.91
KNN	94.14	94.80	96.68	88.73
ANN	96.81	96.73	97.36	92.85

Table 3 Error calculation results of three algorithms

Algorithm	Correlation coefficient	MAE	RMSE	RAE	RRSE
SVM	0.8122	0.081	0.284	18.67	61.04
KNN	0.9639	0.059	0.200	13.57	42.97
ANN	0.9135	0.071	0.199	16.38	42.37

Table 4 Comparison with other works

Work	Method used	Accuracy (%)	Specificity (%)	Sensitivity (%)
[1]	RF	86	85	84
[7]	KNN	88.62	91.30	64.71
[7]	SVM	90.54	88.24	86.96
This work	SVM	91.90	85.91	94.70
This work	KNN	94.14	88.73	97.36

RMSE will be greater than MAE. The other two metrics are “relative”, so those can be used for measuring accuracy. The classifier which produces bigger correlation value with smaller error estimation is preferable for this prediction model. Hence ANN can be considered for more accurate results of our prediction model.

This model is compared with the existing models [1, 7]. In this work [1], different machine learning algorithms such as RT (Random Tree), RF (Random Forest), NB (Naive Bayes), BN (BayesNet) are applied on CHICA data set to predict childhood obesity after age of two years. From the analysis of that work, it has been found that highest accuracy (86%) is achieved by using Random Forest. The second work [7] is mainly prediction of obesity using Publicly Available Genetic Profiles with own dataset. Here highest accuracy has been achieved by using SVM classifier. In our model KNN classifier gives the highest accuracy.

The result of Table 4 shows that sensitivities are lower than the corresponding specificities for above-mentioned classifiers in existing approaches. This means that normal cases can be classified better than risk ones by these tested models. In our work, SVM and KNN show higher sensitivity than specificity. This shows that these classifiers can predict more risk classes than normal classes. This result is promising because predicting risk classes is more important than normal classes so that the medical practitioner can plan appropriate treatments. Hence our model is a better model in comparison to other models.

5 Conclusion

This paper proposed a model to predict obesity accurately after the third birthday of a child as an early prediction of childhood obesity is essential for fat and overweight babies. To predict obesity more accurately, data mining classification techniques SVM, KNN, and ANN are used. Different attributes are identified during feature selection and data capturing module is used to capture the data of those selected features. After preparing the raw dataset, Data Preprocessing has been performed. This process results in a new dataset which is used in the machine learning unit for classification and decision purpose. The result shows that the model can predict more risk classes so that the medical practitioner can plan appropriate treatments. Performance analysis shows that this model's prediction accuracy is comparably better than existing models.

References

1. Dugan TM, Mukhopadhyay S, Carroll A, Downs S (2015) Machine learning techniques for prediction of early childhood obesity. *Applied Clin Inform* 6(3):506–520
2. Magarey AM, Daniels LA, Boulton TJ, Cockington RA(2003) Predicting obesity in early adulthood from childhood and parental obesity. *Int J Obes* 27(4):505–515
3. Albu-Shamah A, Zhan J (2013) Towards obesity causes, prevalence and prevention. In: 2013 International conference on social computing. IEEE, pp 852–857
4. Rolland-Cachera MF, Deheeger M, Maillot M, Bellisle F (2006) Early adiposity rebound: causes and consequences for obesity in children and adults. *Int J Obes* 30(S4):S11
5. Zhang S, Tjortjis C, Zeng X, Qiao H, Buchan I, Keane J (2009) Comparing data mining methods with logistic regression in childhood obesity prediction. *Inform Syst Front* 11(4):449–460
6. Yu W, Liu T, Valdez R, Gwinn M, Khoury MJ (2010) Application of support vector machine modeling for prediction of common diseases: the case of diabetes and pre-diabetes. *BMC Med Inform Decis Making* 10(1):16
7. Montañez CAC, Fergus P, Hussain A, Al-Jumeily D (2017) Machine learning approaches for the prediction of obesity using publicly available genetic profiles. In: International joint conference on neural networks (IJCNN). IEEE, pp 2743–2750
8. Devi ChJ, Reddy BSP, Kumar KV, Reddy BM, Nayak NR (2012) Ann approach for weather prediction using back propagation. *Int J Eng Trends Technol* 3(1):19–23
9. Kotsiantis SB, Zaharakis I, Pintelas P (2007) Supervised machine learning: a review of classification techniques. *Emerg Artif Intell Appl Comput Eng* 160:3–24
10. Weng SF, Redsell SA, Nathan D, Swift JA, Yang M, Glazebrook C (2013) Estimating overweight risk in childhood from predictors during infancy. *Pediatrics* 132(2): e414–e421
11. (2017) UNICEF, world health organization, world bank group: joint child malnutrition estimates: levels and trends. WHO, Geneva
12. Butler EM, Derraik JG, Taylor RW, Cutfield WS (2018) Prediction models for early childhood obesity: applicability and existing issues. *Hormon Res Paediatr* 90(6):358–367
13. Steur M, Smit HA, Schipper CMA, Scholtens S, van de Kerkhof M, de Jongste JC, Haveman-Nies A, Brunekreef B, Wijga AH (2010) Predicting the risk of newborn children to become overweight later in childhood. In: 3rd European public health conference, Amsterdam, The Netherlands, p 66

14. Beccuti G, Pannain S (2011) Sleep and obesity. *Curr Opin Clin Nutr Metab Care* 14(4)
15. DiBaise JK, Zhang H, Crowell MD, Krajmalnik-Brown R, Decker GA, Rittmann BE (2008) Gut microbiota and its possible relationship with obesity. *Mayo Clin Proc (Rev)* 83(4):460–469
16. Stettler S, Kumanyika SK, Katz SH, Zemel BS, Stallings VA (2003) Rapid weight gain during infancy and obesity in young adulthood in a cohort of African Americans. *Am J Clin Nutr* 77(6):1374–1378
17. Anand V, Biondich PG, Liu GC, Rosenman MB, Downs SM (2004) Child health improvement through computer automation: the CHICA system. In: *Medinfo*, pp 187–191

A Review on Automatic Epilepsy Detection from EEG Signals



Satyender, Sanjeev Kumar Dhull, and Krishna Kant Singh

Abstract Epilepsy is a well-known neurological disorder which affects moreover 2% of the World's population. Irregular excessive neuronal activities to the human brain cause epileptic seizures onset. Electroencephalograph (EEG) signals are mostly examined for the detection of epileptic seizure onsets. But an EEG signal consists of a huge amount of complicated information and it is very difficult to analyze it manually. Over the decades, a lot of research has been focused on the development of automated epilepsy diagnosis systems. These systems are dependent on sophisticated feature captureization and classification techniques. The paper aims to present a generalized review and performance comparison of the work reported over a decade in the area of automated epilepsy diagnosis systems that will help future researchers lead a better direction.

Keywords Electroencephalogram (EEG) · Epilepsy · Feature extraction · Classifier

1 Introduction

Epilepsy is among the commonly existing neurological infirmity and is described as an unexpected change in the usual electrical activities in some parts of the brain or in the entire brain. These abnormal responses in the brain are called epileptic seizures [1]. A normal brain produces low amplitude electrical pulses but if a person is suffering from epilepsy then these pulses are produced in excessive amounts and

Satyender (✉) · S. K. Dhull
Guru Jambheshwar University of Science and Technology, Hisar, India
e-mail: jaglan86@gmail.com

S. K. Dhull
e-mail: sanjeevdhull2011@yahoo.co.in

K. K. Singh
GL Bajaj Institute of Technology and Management, Greater Noida, India
e-mail: krishnaiitr2011@gmail.com

are not easily controllable. The diagnosis of seizures is not easily predictable and if it is ignored, then it may lead to the death of the patient. According to a recent study, epilepsy affects around 6–10 million people in India, and less than half are treated [2].

Electroencephalogram (EEG) is a method of recording the electrical signals of the brain developed by cortical neurons. As per international standards, 10–20 electrodes are located around the scalp of the person to record the brain signals which are produced by the cerebral cortex nerve cells [3]. Neurologists generally use EEG signals for detection and diagnoses of epileptic seizures. Analyzing the EEG signals visually or manually requires a lot of time and neurological knowledge, making the epilepsy detection process tedious, difficult and may sometimes result in incorrect diagnoses. So, a lot of research has been done to propose computer-based automatic EEG epilepsy detection systems. Such a system must be able to classify the epileptic seizure signal from non-epileptic signals with more accuracy and in less time.

To automatize the seizure detection from an EEG signal, various machine learning approaches have been proposed by various researchers. Machine learning methods are more fast, accurate, and consistent in performance compared to manual labelling [4–9]. The machine learning approach is basically based on training a classifier with a repository of existing data consisting of both, epilepsy seizure signals and normal signals. A typical automated diagnosis system for epilepsy detection generally consists of following modules: EEG signal pre-processing, feature extraction and feature selection and finally classification of extracted features as normal, seizure or non-seizure. The performance efficiency of a typical automated epilepsy seizure detection technique is dependent on the type of classifier used, as well as on the features that are inputted to that classifier. Figure 1 presents a typical approach of detecting epileptic seizures for single-channel dataset, for example, the University of Bonn dataset. Similarly, Fig. 2 provides a general framework of epilepsy seizure detection for a multichannel dataset, for example, CHB-MIT dataset. These datasets are discussed in detail in the next section.

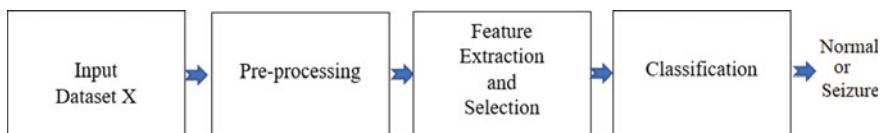


Fig. 1 Common approach to detect epilepsy seizure for single-channel dataset

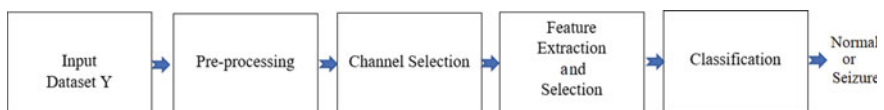


Fig. 2 Schematic illustration of the general approach to detect epilepsy seizure for multichannel dataset

The objective of this literature is to present an advanced review of the methods and techniques used for designing these modules. The remaining part of this paper is organized as follows: Sect. 2 focused on the various freely available standard seizure and non-seizure EEG signal datasets. Section 3 briefly summarizes various pre-processing and feature extraction techniques available in the literature. Section 4 studies various classification techniques used in the literature. Finally, the conclusion is given in Sect. 5.

2 EEG Dataset

In literature, many standard datasets for epileptic EEG signals and non-epileptic EEG signals have been utilized by authors for their research work. Online access is available for all such datasets; some are freely accessible and some have paid access. Two well-known datasets are being discussed, in this paper, that have free access online, and these are the University of Bonn dataset and CHB-MIT dataset. The details of these datasets are given below:

(i) University of Bonn dataset

The above-mentioned EEG dataset was recorded at the University of Bonn, Germany acquired by Andrzejak et al. [10]. This dataset comprises five sets A, B, C, D and E of EEG signal, where every set encompasses 100 single-channel EEG fragments of 23.6 s, which are sampled at a rate of 173.61 Hz, thus giving a total of 4097 samples per set. The spectral bandwidth for all sets ranges between 0.5 and 85 Hz. All the recordings were made using the same 128 channel amplifier system. Set A and B comprises of information gathered from five healthy volunteers with eyes open and closed, separately, utilizing the standardized surface EEG recordings. Sets C, D and E were obtained from five epileptic patients experiencing pre-surgical epilepsy diagnosis. Set C and set D were recorded during epilepsy free interval and set E was recorded during the occurrence of epileptic seizures. More information about this dataset can be gathered from [10]. The authors in papers [4, 6, 12, 13, 16–20] have utilized the University of Bonn dataset for their research work. Table 1 depicts a summary for the University of Bonn dataset and Fig. 3 presents waveforms of typical signals from set A to set E. As can be observed from Fig. 3 the amplitude of set E (ictal with seizure) is much greater than the amplitude of other sets.

(ii) CHB-MIT Dataset

It is also one of the commonly used datasets. This dataset is also referred to as the EEG PhysioNet dataset. It was acquired at Boston Children's Hospital [11], consisting of multichannel EEG signals that were recorded from 23 paediatric patients (5 males and 18 females) suffering from intractable epilepsy. The paediatric patients were reported to be between age 1.5 and 22 years.

The data was recorded for 23 channels using the international Federation of clinical neurophysiology standard of 10–20 electrode placement. Each channel data was

Table 1 Detail of University of Bonn dataset

	Set A	Set B	Set C	Set D	Set E
Patient's condition	Conscious and eyes open (normal)	Conscious and eyes closed (normal)	Seizure-free (inter-ictal)	Seizure-free (inter-ictal)	Seizure activity(ictal)
Type of electrode	Surface	Surface	Intra-cranial	Intra-cranial	Intra-cranial
Placement of electrode	International 10–20 system	International 10–20 system	Opposite to epileptogenic zone	Within epileptogenic zone	Within epileptogenic zone

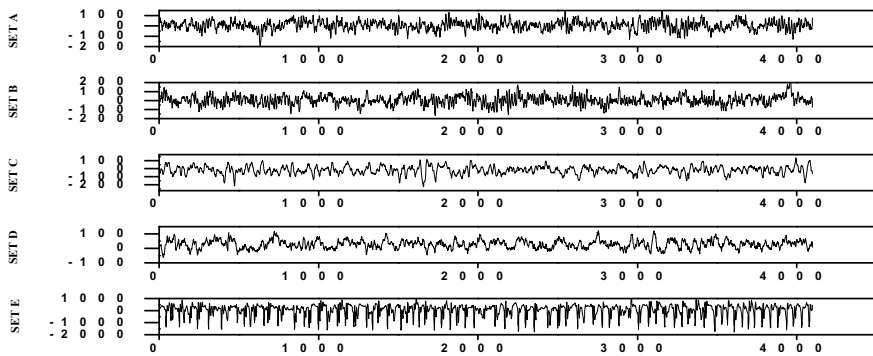


Fig. 3 Single channel Bonn dataset typical EEG signal from set A, B, C, D and E

digitized at a sampling rate of 256 Hz with 16-bit resolution. While recording clinical experts manually annotated the beginning and end of each seizure, and classified the EEG signals as epileptic seizures and non-seizures. The acquired dataset was 916 h long and consisted of a total of 198 identified seizures. The shortest duration seizure lasts for 6 s and the longest duration seizure lasts for 752 s with an average seizure duration of 72 s. The authors in papers [7, 8, 27–31] have utilized CHB-MIT dataset for their research work. Table 2 further gives detailed insight into the CHB-MIT dataset. Figure 4 plots a typical multichannel CHB-MIT dataset signal.

3 Pre-processing Techniques and Feature Extraction Methods

Pre-processing is a process of removing unwanted artifacts and noise from raw EEG signal that is collected directly from the scalp. These artifacts/noise may be present either because of blinking eyes, muscle movements, head motion during the record

Table 2 CHB-MIT dataset detailed description

Identification No.	Patient gender	Patient age	Seizure events ($T_{\min} - T_{\max}$) in seconds	Total seizure time in seconds	Total seizure-free time in seconds
1	F	11	7 (28–102)	449	23,475
2	M	11	3 (10–83)	175	7983
3	F	14	7 (48–70)	409	24,791
4	M	22	4 (50–117)	382	37,976
5	F	7	5 (97–121)	563	17,437
6	F	1.5	9 (13–21)	147	93,051
7	F	14.5	3 (87–144)	328	32,208
8	M	3.5	5 (135–265)	924	17,076
9	F	10	4 (63–80)	280	34,218
10	M	3	7 (36–90)	454	50,008
11	F	12	3 (23–753)	809	9249
13	F	3	12 (18–71)	547	28,253
14	F	9	8 (15–42)	117	25,023
15	M	16	20 (31–205)	2012	48,420
16	F	7	10 (7–15)	94	21,506
17	F	12	3 (89–116)	296	10,528
18	F	18	6 (31–69)	323	19,951
19	F	19	3 (78–82)	239	10,307
20	F	6	8 (30–50)	302	19,732
21	F	13	4 (13–82)	203	13,587
22	F	9	3 (59–75)	207	10,593
23	F	6	7 (21–114)	431	31,823
24			16 (17–71)	527	42,673

of the data, any problem in the channel/electrode, or any connectivity issue. Pre-processing thus may be utilized not just for artifacts removal but also for improving the Signal to Noise ratio and spatial resolution. Digital filters have been used by most of the authors in the pre-processing step.

In [12] EEG sample data is filtered through a 50 Hz IIR notch filter to eliminate AC power supply noise. In [13] the raw EEG signal is made to pass from a band-pass filter having a lower cut-off frequency of 0.53 Hz and higher cut-off frequency of 40 Hz for the removal of artifacts and noise. In [14] seventh order Chebyshev IIR filter is utilized. In [15] the EEG signal is de-noised by passing it through an FIR low-pass filter designed using Hamming with cut-off frequency at 60 Hz.

For an EEG prediction model to accurately classify between epileptic and non-epileptic signals, feature extraction is a very crucial step. Feature extraction is required because of the non-linear, stochastic and non-stationary behaviour of the

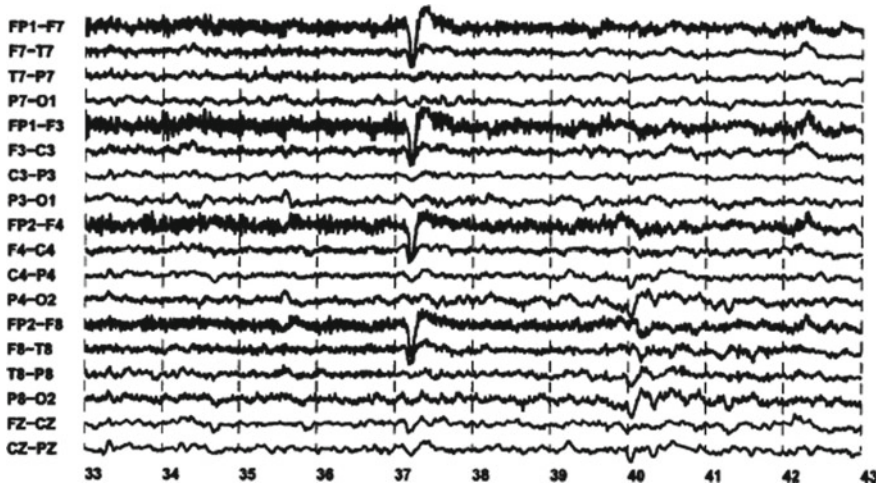


Fig. 4 Multichannel CHB-MIT dataset typical signal

EEG signal [6]. A good feature extraction technique must minimize the resources required for accurate classification of the signal as well as the loss of valuable information. The feature extraction process basically converts the raw signal information into a set of mathematical descriptors so that a better understanding of the complex data can be gained. Feature extraction is followed by a feature selection that aims to select the most relevant features and removes redundant features. Although there exist a number of feature selection algorithms in the literature, however Independent Component Analysis (ICA) [14] and Principal Component Analysis (PCA) [18] being the most popular.

The feature extraction techniques used in EEG signals analysis model are either time-based [2–14, 23], frequency-based [5, 12, 14, 23] or time-frequency based [4, 5, 16–18, 20, 21, 23–25, 27]. The most popular being the time-frequency analysis since it is able to provide both time and frequency information of the signal simultaneously. Time-domain features are obtained by analyzing the EEG signal as a function of time. Examples of typical features of time-domain include mean, median, standard deviation, kurtosis, amplitude, etc. Likely frequency-domain features are extracted by analyzing EEG data as a function of frequency. Various techniques like Fourier Transform are used for frequency-domain feature extraction. These features are related to spectral information of EEG signals. Examples of such features include spectral flux, power spectrum, spectral centroid, spectral entropy, etc. In the time-frequency domain both time-domain as well as frequency-domain features are extracted simultaneously. Discrete Wavelet Transform (DWT) is the most popular time-frequency domain based feature extraction technique.

In [4] authors have proposed a unique feature extraction technique based on Stockwell-transform (ST). It is a joint time-frequency analysis technique that is applicable to non-stationary signals. Such technique is more noise-robust, able to

retain the absolute phase of the individual frequency component and provide more information with less features. After performing S-transform, two features namely, energy and standard deviation are extracted for both seizure and seizure-free EEG signals. In [12] the cross-bispectrum values for three EEG channels are computed to determine various linear (average, maximum and minimum) and non-linear features in EEG data. In [13], for feature extraction EEG signals are sampled twice and plotted as vertical bars. Then a feature called visibility height is computed for the three adjoining neighbours from the top of the referenced bar. Then four various types of entropy are computed to reduce the dimension of data. In [14] after pre-processing the EEG signal, Wavelet Analysis also known as DWT is used for feature extraction. DWT is a time-frequency analysis method used for analyses of non-stationary signals. In this technique the signal is passed through a set of consecutive low-pass and high-pass filters to decompose the signal into set of five sub-bands. Thus, decomposing the initial signal into a set of coefficients that describe the frequency content. But to lower the spectrum usage and time complexities authors in this paper have used only the lowest frequency sub-band for feature extraction. The feature extracted from these identified sub-bands helps in further classification of data. In [15] authors have extracted thirteen features like min amplitude, max amplitude, Entropy, Mean, Median, Standard Deviation, etc. belonging to time, frequency as well as both domains. In [16] also authors have utilized DWT for feature extraction. After DWT decomposition, the sub-bands of EEG signals are discretized using Equal Frequency Discretization (EFD) technique. EFD technique helps to compute the probability density for all sub-band of each EEG segment. Thus, providing the probability densities of both healthy EEG dataset and epilepsy patient EEG dataset. In [17] Local Mean Decomposition (LMD) is utilized that iteratively transforms raw EEG data into a set of product functions (PFs) where a PF is generated by multiplying envelope signal with a frequency modulated signal. This technique has got the advantage of high processing speed along with low computational complexity. From each PF three time-domain features namely maximum amplitude, minimum amplitude, average absolute value, and three frequency-domain features namely maximum power spectral density, skewness, kurtosis are extracted. The authors have further computed the Fractal Dimension (FD), Renyi Entropy (RE) and Hurst exponent for EEG dataset to form a nine-dimensional feature vector. In [18] for feature extraction authors have utilized Daubechies Wavelet order 4 (DB4). Then for the dimensionality reduction, PCA is applied to the extracted data. PCA reduces the data to lower dimensional space by modifying the signal into the new Principal Components (PCs). This is done to reduce the complexity in both space and time. In [19] authors have proposed a Discrete Cosine Transform (DCT) based 3-level multi-rate filter bank that extracts alpha, beta, gamma, delta and theta brain rhythms. Delta brain rhythms are modelled using fractional Brownian motion (fBm) process and the other four brain rhythms namely alpha, beta, gamma and theta are modelled using fractional Gaussian noise (fGn) process. Autoregressive Moving Average (ARMA) model and Hurst exponent (H value) together constitute the extracted feature vector. In [20] Daubechies 4 (DB4) wavelet transform (WT) of the EEG signal is computed to produce wavelet coefficients. Then, phase-space reconstruction (PSR) is computed

for the wavelet coefficients of both normal and epileptic EEG signals. Then, in the third step Euclidean Distance (ED), the distance between the origin and the wavelet coefficients plotted in PSR, is calculated. These EDs form the initial feature vector.

4 Classification

An automated epilepsy diagnosis system must be able to accurately classify the EEG signals as epileptic and non-epileptic signal. In this regard many machine learning-based classification algorithms have been proposed in the literature. These algorithms usually train the system using either supervised, unsupervised or semi-supervised learning bypassing the selected features of the relevant class of the training data; and then the trained system performance is evaluated using different parameters for predicting the class of testing data. Although in literature there exists so many machine learning-based classification algorithms that classify the EEG signal as an epileptic class and non-epileptic class but the most popular being Support Vector Machine (SVM) [12, 13, 17, 21, 25, 26], K-nearest neighbour (KNN) [17, 18, 27, 30, 31], Linear Discriminant Analysis (LDA) [17] and Random forest (RF) [8, 13].

SVM is a very commonly used supervised learning-based classifier. It works by a creating hyperplane or set of hyperplanes in a multi-dimensional space that will separate data into various classes linearly. For a two-dimensional space, the hyperplane reduces to a line. The vectors that define the hyperplane are termed as support vector. This algorithm has got good generalization properties but the poor speed of execution. LDA is also one of the most commonly used supervised learning-based pattern reduction and dimensionality reduction algorithms. Like SVM this technique also separates the data into different classes using hyperplanes. In this algorithm, the first separability between different classes is computed which is termed as a between-class variance. Then it calculates within-class variance, i.e. the distance between the mean of the class and the individual samples of the class. Then creates a low-dimensional space that will maximize the between-class variance and minimize the within-class variance. KNN is also a very simple, popular and supervised based learning algorithm. The basic idea behind this is to first make the system learn through training data and as the new instance comes, it is assigned the class that is closest among the k -neighbours. The performance of the algorithm is very much dependent on k value. Greater k value reduces the effect of noise and increases the processing time. Random forest (RF) is a simple, flexible and easy to use machine learning algorithm. RF is also a supervised learning algorithm that works by creating an ensemble of decision trees. As a new instance comes, the class of this instance is decided by travelling from the root node of the tree to its leaf. At each node end, the successor may be chosen if there is a need to split the input space data. For the design of more efficient classifiers, future work can be done in the direction of using various optimization algorithms that have been explored in other applications [32–35].

The performance of a classifier is very much dependent on the characteristics/features of the data that is being inputted. Thus, if the extracted features are

not relevant then the classification algorithm may not be able to accurately identify the class of the data. Also, the performance of a classifier is evaluated by using a number of performance measures/parameters that include classification accuracy, false alarm rate, specificity, sensitivity, latency and Receiving Operating Characteristic (ROC). The performance measures that are being accessed also depends on the dataset that is being used. Authors that have used the University of Bonn dataset have evaluated the accuracy, sensitivity, specificity, confusion matrix, and ROC as the performance parameters, with accuracy and confusion matrix being the most common and widely used performance measure. Table 3 presents the comparison of accuracy level achieved through different classifiers inputting different extracted features. In literature, as briefed in Table 4, it is also found that some researchers have computed the classification accuracy by considering different cases that constitute a different combination of sets (from A to D) with set E from the University of Bonn dataset. For the CHB-MIT dataset apart from performance parameters evaluated for the University of Bonn dataset, two more parameters namely latency and false alarm rate are also evaluated. Table 5 briefs the literature work of different performance parameters evaluated and their experimental values for the CHB-MIT database.

5 Conclusion

This paper presents a review of the automatic epilepsy detection system that is able to classify EEG signals as epileptic or non-epileptic. A brief literature survey of the automated epilepsy detection system with a focus on its modules such as pre-processing, feature extraction and selection, and finally classification is been given. Two most commonly used and freely available datasets, i.e. University of Bonn dataset and CHB-MIT dataset are also discussed. The findings of different authors in terms of different performance parameters have also been summarized and compared. This review will give a clear birds-eye view of the recent advancements and techniques to the upcoming researchers in this field.

Table 3 Comparison of accuracy level of different classifiers designed for University of Bonn dataset

Researchers	Year	Feature Extraction Technique	Classifier	Accuracy
Orhan et al. [16]	2011	DWT + Equal Frequency Discretization (EFD) + Probability density	Mean square error (MSE)	82.5%
Leeet al. [20]	2014	Wavelet transform (WT) + Phase-space reconstruction (PSR) + Euclidean distance (ED)	Neural network with weighted fuzzy membership functions (NEWFM)	98.17%
Lasefr et al. [14]	2017	DWT	SVM	96%
			ANN	98%
Zhang et al. [17]	2017	Local mean decomposition (LMD)	BPNN	98.10%
			KNN	98.87%
			LDA	98.47%
			SVM	98.40%
			GA-SVM	100%
Jiang et al. [5]	2017	Wavelet packet decomposition (WPD) Short time-frequency transform (STFT) Kernel principal component analysis (KPCA)	S-TL-SSL-TSK A-TL-SSL-TSK	Above 95% in all cases
Rahmawati et al. [18]	2017	DWT + PCA	KNN	99.83%
Tiwari et al. [21]	2017	Key points detection + Local binary patterns (LBPs) computation	SVM	99.89%
Saini et al. [15]	2018	Standard mathematical formulas	ANN	99%
			PSO-ANN	99.3%
Mahmoodian et al. [12]	2019	Cross-bispectrum Analysis	SVM	96.84%

Table 4 Accuracy comparison of classifier used for University of Bonn dataset with different dataset combinations

Researchers/Year	Methodology	Dataset	Accuracy	No. of features
Kaleem et al. [22]	Empirical mode decomposition modified peak selection (EMD-MPS) + 1-NN classifier + 10-fold cross validation	A and E AB and CD ABCD and E	100% 99% 98.2%	4
Peker et al. [23]	Dual-tree complex wavelet transformation + Complex-valued neural network			5
	DTCWT + CVANN-1 + 10-fold cross validation	A-E	100	
	DTCWT + CVANN-2 + 10-fold cross validation		99.5	
	DTCWT + CVANN-3 + 10-fold cross validation		100	
	DTCWT + CVANN-3 + 10-fold cross validation	A, D, E	99.3	
	DTCWT + CVANN-3 + 10-fold cross validation	AB-CD-E	98.23	
Alsharabi et al. [24]	DWT-based shannon entropy feed-forward neural network (FFNN)	A-E	100	1
Zhang et al. (2017) [17]	Local mean decomposition (LMD) + GA-SVM	A-E	100	9
		D-E	98.10	
		ABCD-E	98.87	
		A-D-E	98.47	
		AB-CD-E	98.40	
Sharma et. al. [26]	Analytic time-frequency flexible wavelet transform (ATF-FWT) + Fractal dimension (FD) least squares SVM classifier	A-E	100	7
		B-E	100	16
		C-E	99	17
		D-E	98.50	17
		AB-E	100	17
		CD-E	98.67	16
		AB-CD	92.50	17
		ABCD-E	99.20	16
Zeng et al. [13]	Entropy of visibility heights of hierarchical neighbours (EVHHN) + 4 different classifiers (i) SVM (ii) Least squares SVM (iii) KNN (iv) RF	A-E	100	4
			100	
			100	
			100	
			100	

(continued)

Table 4 (continued)

Researchers/Year	Methodology	Dataset	Accuracy	No. of features
	(i) SVM (ii) Least squares SVM (iii) KNN (iv) RF	AB-E	99.67 99.67 99.67 99.67	
	(i) SVM (ii) Least squares SVM (iii) KNN (iv) RF	C-E	98 98.50 97.3 97.25	
	(i) SVM (ii) Least squares SVM (iii) KNN (iv) RF	CD-E	97.67 98.37 97.63 97.20	

Table 5 Performance comparison of different techniques used for CHB-MIT dataset

Researchers/Year	Technology/Method/Algorithm used	Dataset/Parameters used	Experimental values
Samiee et al. [29]	Sparse rational decomposition and the local gabor binary patterns (LGBP)	Average sensitivity Rate of false alarms per hour	91.13% 0.35
Abhijit et al. [27]	Empirical wavelet transform (EWT) + Random forest classifier	Average sensitivity Specificity Accuracy	97.91% 99.57% 99.41%
Shanir et al. [30]	Morphological attribute extraction method based on the local binary pattern (LBP) operator + K-nearest neighbour classifier	Mean accuracy Mean specificity Average false detection Sensitivity	99.7% 99.8% 0.47/h 99.2%
Solaija et al. [7]	Dynamic mode decomposition (DMD) + RUS boost classifier + Post processing step	Sensitivity Specificity	0.87 0.99
Wu et al. [8]	Mixed seizure finding algorithm by combining cEEG-based and aEEG-based seizure finding algorithm + Random forest classifier	Accuracy (AC) Specificity (SP) Sensitivity based on the event (SE) False positive ratio based on the event (FPRE)	99.36% 82.98% 99.41% 0.57 times/h
Bashivan et al. [31]	Spectral features (using STFT), spatial features (using Multi-scale 3D-CNN), temporal features (using bidirectional GRU) + Deep neural network (DNN) classifier	Sensitivity False positive rate	89.4% 0.5/h
Fan et al. [28]	Recurrence network (RN) based multivariate seizure detection	Sensitivity Latency	98% 6 s

References

1. Pachori RB, Patidar S (2014) Epileptic seizure classification in EEG signals using second-order difference plot of intrinsic mode functions. *Comput Methods Programs Biomed* 113:494–502
2. Megiddo I, Colson A, Chisholm D, Dua T, Nandi A, Laxminarayan R (2016) Health and economic benefits of public financing of epilepsy treatment in India: an agent-based simulation model. *Epilepsia* 57:464–474
3. Paul Y (2018) Various epileptic seizure detection techniques using biomedical signals: a review. *Brain Inform* 5
4. Chatterjee S, Choudhury NR, Bose R (2017) Detection of epileptic seizure and seizure-free EEG signals employing generalised S-transform. *IET Sci Meas Technol* 11:847–855
5. Jiang Y, Wu D, Deng Z et al (2017) Seizure classification from EEG signals using transfer learning, semi-supervised learning and TSK fuzzy system. *IEEE Trans Neural Syst Rehabil Engg* 25(12):2270–2284
6. Jiang Z, Chung F, Wang S (2019) Recognition of multiclass epileptic EEG signals based on knowledge and label space inductive transfer. *IEEE Trans Neural Syst Rehabil Eng* 27(4):630–642
7. Saleem S, Hassan SA, Kamboh AM et al (2018) Dynamic mode decomposition based epileptic seizure detection from scalp EEG. *IEEE Access* 6:38683–38692
8. Wu D, Wang Z, Jiang L et al (2019) Automatic epileptic seizures joint detection algorithm based on improved multi-domain feature of cEEG and spike feature of aEEG. *IEEE Access* 7:41551–41564
9. Alickovic E, Kevric J, Subasi A (2018) Performance evaluation of empirical mode decomposition, discrete wavelet transform, and wavelet packed decomposition for automated epileptic seizure detection and prediction. *Biomed Signal Process Control* 39:94–102
10. Andrzejak RG, Lehnertz K, Mormann F et al (2001) Indications of nonlinear deterministic and finite-dimensional structures in time series of brain electrical activity: dependence on recording region and brain state. *Phys Rev E Stat Phys Plasmas Fluids Relat Interdiscip Top* 64(8)
11. Goldberger AL et al (2000) Physiobank, physiotookit, and physionet: components of a new research resource for complex physiologic signals. *Circulation* 101(23):e215–e220
12. Mahmoodian N, Boese A, Friebe M, Haddadnia J (2019) Epileptic seizure detection using cross-bispectrum of electroencephalogram signal. *Seizure* 66:4–11
13. Zeng M, Zhao CY, Meng QH (2019) Detecting seizures from EEG signals using the entropy of visibility heights of hierarchical neighbours. *IEEE Access* 7:7889–7896
14. Lasefr Z, Ayyalasomayajula SSVNR, Elleithy K (2017) Epilepsy seizure detection using EEG signals. In: 2017 IEEE 8th annual ubiquitous computing, electronics and mobile communication conference (UEMCON), pp 162–167
15. Saini J, Dutta M (2018) Epilepsy classification using optimized artificial neural network. *Neurol Res* 40:982–994
16. Orhan U, Hekim M, Ozer M, Provaznik I (2011) Epilepsy diagnosis using probability density functions of EEG signals. In: 2011 international symposium on innovations in intelligent systems and applications, pp 626–630
17. Zhang T, Chen W (2017) LMD based features for the automatic seizure detection of EEG signals using SVM. *IEEE Trans Neural Syst Rehabil Eng* 25(8):1100–1108
18. Rahmawati D, Ucn R, Sarno R (2017) Classify epilepsy and normal electroencephalogram (EEG) signal using wavelet transform and K-nearest neighbour. In: 2017 3rd international conference on science in information technology (ICSITech), pp 110–114
19. Gupta A, Singh P, Karlekar M (2018) A novel signal modeling approach for classification of seizure and seizure-free EEG signals. *IEEE Trans Neural Syst Rehabil Eng* 26:925–935
20. Lee SH, Lim JS, Kim JK et al (2014) Classification of normal and epileptic seizure EEG signals using wavelet transform, phase-space reconstruction, and euclidean distance. *Comput Methods Programs Biomed* 116:10–25

21. Tiwari AK, Pachori RB, Kanhangad V, Panigrahi BK (2017) Automated diagnosis of epilepsy using key-point-based local binary pattern of EEG signals. *IEEE J Biomed Heal Inform* 21:888–896
22. Kaleem M, Guergachi A, Krishnan S (2013) EEG seizure detection and epilepsy diagnosis using a novel variation of empirical mode decomposition. In: 2013 35th annual international conference of the IEEE engineering in medicine and biology society (EMBS), pp 4314–4317
23. Peker M, Sen B, Delen D (2016) A novel method for automated diagnosis of epilepsy using complex-valued classifiers. *IEEE J Biomed Heal Inform* 20:108–118
24. Alsharabi K, Ibrahim S, Djemal R, Alsuwailem A (2016) A DWT-entropy-ANN based architecture for epilepsy diagnosis using EEG signals. In: 2016 2nd international conference on advanced technologies for signal and image processing (ATSIP), pp 288–291
25. Yuan Y, Xun G, Jia K, Zhang A (2019) A multi-view deep learning framework for EEG seizure detection. *IEEE J Biomed Heal Inform* 23:83–94
26. Sharma M, Pachori RB, Rajendra Acharya U (2017) A new approach to characterize epileptic seizures using analytic time-frequency flexible wavelet transform and fractal dimension. *Pattern Recogn Lett* 94:172–179
27. Abhijit B, Ram BP (2017) A multivariate approach for patient-specific EEG seizure detection using empirical wavelet transform. *IEEE Trans Biomed Eng* 64:2003–2015
28. Fan M, Chou CA (2019) Detecting abnormal pattern of epileptic seizures via temporal synchronization of EEG signals. *IEEE Trans Biomed Eng* 66:601–608
29. Samiee K, Kovács P, Gabbouj M (2017) Epileptic seizure detection in long-term EEG records using sparse rational decomposition and local gabor binary patterns feature extraction. *Knowl Based Syst* 118:228–240
30. Shanir PPM, Khan KA, Khan YU et al (2018) Automatic seizure detection based on morphological features using one-dimensional local binary pattern on long-term EEG. *Clin EEG Neurosci* 49:351–362
31. Bashivan P, Rish I, Yeasin M, Codella N (2019) Learning representations from EEG with deep recurrent-convolutional neural networks. *IEEE Int Conf Consum Electron*
32. Rathore NS, Singh VP, Phuc BDH (2019) A modified controller design based on symbiotic organisms search optimization for desalination system. *J Water Supply Res Tech Aqua* 68(5):337–345
33. Rathore NS, Singh VP (2019) Whale optimization algorithm based controller design for reverse osmosis desalination plants. *Int J Intell Eng Inf* 7(1):77–88
34. Rathore NS, Singh VP, Kumar B (2018) Controller design for DOHA water treatment plant using grey wolf optimization. *J Intell Fuzzy Syst* 35(5):5329–5336
35. Singh VP, Prakash T, Rathore NS, Chauhan DPS, Singh SP (2016) Multilevel thresholding with membrane computing inspired TLBO. *Int J AI Tools* 25(6)

Energy Aware Resource Efficient-(EARE) Server Consolidation Framework for Cloud Datacenter



Deepika Saxena and Ashutosh Kumar Singh

Abstract Cloud datacenter offers economic and elastic computing benefits to the customers, where on-demand virtual machine (VM) allocation plays a significant role. Inefficient VM placement leads to resource wastage and high power consumption that raises the requirement of server consolidation. The feasibly optimal placement of VMs with the objectives of minimum power consumption and maximum resource utilization is the key to server consolidation. Though many multi-objective VM placement schemes are available in the literature, it mostly works on weighted sum approaches that transforms multi-objective problem (where some objectives maximize and others minimize) into single objective to give optimized solution. Hence, the existing approaches do not correctly justify the multi-objective VM placement problem. To provide correct solution of multi-objective and multi-constrained VM allocation problem, this work presents GA based evolutionary server consolidation framework by applying rank based non-dominated sorting for multiple objectives to generate pareto-optimal solution. It enables maximum resource utilization and minimum power consumption to accomplish effective server consolidation. The VM placement is done using genetic algorithm (GA) which encodes VM allocation information into chromosomes. The performance evaluation of the proposed work is carried out by execution of numerous experiments in simulated datacenter environment. The experimental outcome reveals that the proposed VM allocation framework improves resource utilization upto 38.54, 41.67, and 44.8% and minimize power consumption upto 11.32, 12, and 13.7% over random, best-fit, and first-fit heuristic-based approaches.

Keywords Cloud computing · VM allocation · Genetic algorithm · Resource utilization · Power consumption

Supported by NIT Kurukshetra.

D. Saxena (✉) · A. K. Singh
Department of Computer Applications, NIT Kurukshetra, Kurukshetra, India
e-mail: 13deepikasaxena@gmail.com

A. K. Singh
e-mail: ashutosh@nitkr.ac.in

© Springer Nature Singapore Pte Ltd. 2021
G. S. Hura et al. (eds.), *Advances in Communication and Computational Technology*, Lecture Notes in Electrical Engineering 668,
https://doi.org/10.1007/978-981-15-5341-7_111

1455

1 Introduction

Cloud computing has emerged as an indispensable ubiquitous computing paradigm across the world. The minimum investment and maximum elasticity features of cloud computing have allured research, academia, and business organization, etc. In order to satisfy the resource demand of users, large number of servers and cooling devices are installed at cloud datacenter, and consequently, power consumption has increased [14]. Though cloud service providers apply multiplexing to enhance elasticity of resources (CPU, memory, bandwidth, etc.) and reduce power consumption, server consolidation greatly depends on VM allocation strategy. Due to over-commitment of resources by cloud users, virtual machines are allocated with demanded capacity of resources. These resources are never utilized completely, and consequently, resources get waste [2]. Most of the time, excess number of servers are in operational mode that results into under utilization of resources and extravagant energy consumption.

To minimize power consumption and bring effective utilization of resources, consolidation of servers is an essential requirement. The near-optimal VM placement on physical machines (PMs) leads to effective server consolidation. The resource allocation manager has to satisfy certain mandatory constraints before VM placement, like resource (CPU, memory) capacity constraints [6, 9, 10]. That is why server consolidation through optimal VM allocation is multi-dimensional and multi-constrained optimization problem. In this paper, we consider all these challenges while consolidating VMs at cloud datacenter. Firstly, we assign VMs to randomly selected PMs such that they satisfy all the constraints and then optimize the VM allocations by applying multi-objective evolutionary optimization approach, i.e., non-dominated sorting-based genetic algorithm NSGA-II technique [4]. During optimization, VM migration [3] occurs from more power consuming physical machine to other physical machine with lesser power consumption. The proposed VM placement method applies rank-based sorting according to both the objectives and selects the non-dominated solution which gives feasibly optimal VM placement.

1.1 Our Contribution

- A novel multi-objective VM placement framework is proposed based on GA-based evolutionary optimization and non-dominated sorting approach.
- We have encoded VM placement information as genetic chromosome followed by selection of feasibly optimal VM allocation based on ranking-based fitness evaluation.
- The resource utilization has increased, and power consumption has reduced substantially as compared to related approaches.

The rest of the paper is organized as follows: Sect. 2 discusses the related work, followed by problem formulation in Sect. 3. Section 4 entails proposed NSGA-II based VM allocation framework. Section 5 pertains to discuss experiment and results, and finally, Sect. 6 presents conclusive remarks and future scope of the proposed work.

2 Related Work

Goudarzi et al. presented SLA-driven resource management specifically for reduction of SLA-violation and electrical energy consumption including cooling devices and CPU utilization at cloud datacenters in [6]. In this approach, a set of decentralized decision managers (power and cooling managers) generated constraints and worked in cooperation to make hierarchical decision for VM management so as to reduce the operational cost of datacenter.

Dynamic resource allocation and VM placement were presented by [19] and Yu et al. [20]. These were stochastic approaches which worked on single solution only and optimized it for optimal VM placement. Online VM placement for raising cloud provider's revenue was proposed in [21].

The evolutionary optimization algorithms have wide range of applications [7, 11–13, 16, 17] which supported the fact that evolutionary optimization in VM placement could allow enhanced consolidation of servers.

For instance, Sharma et al. [14] proposed HGAPSO algorithm by combining genetic algorithm (GA) and particle swarm optimization (PSO) to allocate VMs on servers with minimum resource wastage and SLA violation. GA helped in migration of VM from source server to target server and PSO assisted GA in selecting optimal target server by allowing VM placement from non-energy-efficient to energy-efficient server. Euclidean distance was applied to find multi-objective VM placement solution. This approach generated single point solution rather than pareto front. This work consumed extra computation time and space due to application of PSO.

Multi-objective genetic algorithm for resource prediction and allocation was proposed in [18, 20] addressing CPU and memory utilization of VMs and PMs and overall energy consumption of datacenter. The GA algorithm predicted resource usage before VM was allocated to PM. Then, VM placement algorithm was applied to maximize resource utilization and minimize energy consumption. To find multi-objective VM placement solution, weighted sum approach was applied, which was the major limitation of the work as for multi-objective problem, it generated a single solution rather than pareto-front. Dabbagh et al. [2] proposed energy-efficient VM prediction and migration for overcommitted clouds. For energy efficiency, the idea was to deploy new VMs and migrating VMs to the already running PMs that satisfied overload threshold constraints rather than to start new PM.

Recently, Singh et al. [15] presented secure and energy aware load balancing (SEA-LB) framework for load balancing at datacenter, including minimization of side channel attacks. To provide security to each user, resource sharing and resource utilization was minimized. In reality, every VM does not carry enough confidential

data that requires strong security, and therefore, security is not the priority of every VM while load balancing. Moreover, they ignored the role of VM migration that is essential for real world balancing VMs on PMs.

3 System Model

Consider a datacenter having m physical machines (PMs) and n number of virtual machines (VMs). This scenario can be represented as physical machines $S \in P_1, P_2, \dots, P_m$ and virtual machines $V \in v_1, v_2, \dots, v_n$ owned by p users as shown in Fig. 1. The problem is how to consolidate server by applying optimal resource allocation during VM placement on servers so as to reduce resource wastage yet avoid overloading, SLA violation, and enable minimum power consumption.

To efficiently handle this problem, GA-based multi-objective VM allocation framework is developed, and ranking-based non-dominated sorting is applied to find 'pareto-optimal' solution, in which no objective can improve without degrading the other objective(s). Mathematically, the problem can be stated as:

$$\sum_{i=1}^m P_i = \text{Min} \sum_{i=1}^m \text{Pow} + \text{Max} \sum_{i=1}^m \text{RU} \quad (1)$$

where Pow and RU are power consumption and resource utilization, respectively. The resources include processing element (PE), CPU, and memory usage by VM; however, it could extend upto any number and type of resources. A VM allocation is feasible only if it satisfies the following constraints:

$$\sum_{j=1}^n v_j^r \times \beta_{ji} \leq P_j^r \quad \forall i \in 1, 2, \dots, m, r \in \text{PE, CPU, Memory} \quad (2)$$

Energy (or power) consumption and resource utilization model are stated as.

3.1 Energy Consumption Model

The energy consumption for a server can be formulated as Pow_i for i th server and total power consumption Pow_{dc} for time-interval $[t_1, t_2]$ as depicted in Eq. 3 and 4.

$$\text{Pow}_i = ([\text{Pow}_i^{\max} - \text{Pow}_i^{\min}] \times \text{RU}_{\text{cpu}} + \text{Pow}_i^{\text{idle}}) \quad (3)$$

$$\text{Pow}_{\text{dc}} = \int_{t_1}^{t_2} \left(\sum_{i=1}^m \text{Pow}_i \right) \quad (4)$$

where $\text{Pow}_i^{\text{max}}$, $\text{Pow}_i^{\text{min}}$, and $\text{Pow}_i^{\text{idle}}$ are maximum, minimum, and idle power consumption for i th server.

3.2 Resource Utilization Model

: We consider three different resource usage PE, CPU, and memory, though we can extend the model to any number of resources. Assume P_i^{cpu} , P_i^{memory} , and P_i^{PE} are CPU, memory, and processing element with capacity of i th server. If P_i is ON, then $\alpha_i = 1$, means one or more VMs are hosted by server, otherwise $\alpha_i = 0$. Let β represents mapping of VMs having vector size n to PMs of size m . If server P_i hosts v_j , then $\beta_{ji} = 1$, otherwise $\beta_{ji} = 0$. For VM v_j , CPU, memory, and PE utilization are represented as v_j^{cpu} , v_j^{memory} , and v_j^{PE} , respectively, as shown in Eq. (5):

$$\text{RU}_{\text{dc}} = \int_{t_1}^{t_2} \left(\frac{\text{RU}_{\text{dc}}^{\text{cpu}} + \text{RU}_{\text{dc}}^{\text{memory}} + \text{RU}_{\text{dc}}^{\text{PE}}}{|N| \times \sum_{i=1}^P \alpha_i} \right) \quad (5)$$

$$\text{RU}_i^r = \frac{\sum_{j=1}^n \beta_{ji} \times v_j^r}{S_i^r} \quad \forall i \in 1, 2, \dots, m, r \in \text{PE, CPU, Memory} \quad (6)$$

4 Proposed NSGA-II Based Server Consolidation Framework

The proposed server consolidation framework consists of four phases, namely initialization (I), fitness evaluation (F), crossover followed by mutation (C/M), and selection (S) as shown in Fig. 1. Initialize N random VM allocations as Λ_i represents i th VM placement ($i \leq N$) encoded as chromosomes. To evaluate fitness of each chromosome, compute cost function $\eta(f_{\Lambda_i}^{\text{Pow}}, f_{\Lambda_i}^{\text{RU}})$ where $f_{\Lambda_i}^{\text{Pow}}$ and $f_{\Lambda_i}^{\text{RU}}$ are cost associated to energy consumption and resource utilization, respectively. The cost functions $f_{\Lambda_i}^{\text{Pow}}$ and $f_{\Lambda_i}^{\text{RU}}$ are evaluated by computing Eqs. 4 and 5. Then, one-point crossover and mutation operations are applied to explore the entire search space for better solution by migrating VMs from less energy-efficient server to selected server having better energy efficiency. The resultant solutions may be infeasible with respect to VM allocation constraints, which are turned into feasible solutions by re-arranging the infeasible VM placement. Further, the fitness of updated solutions are

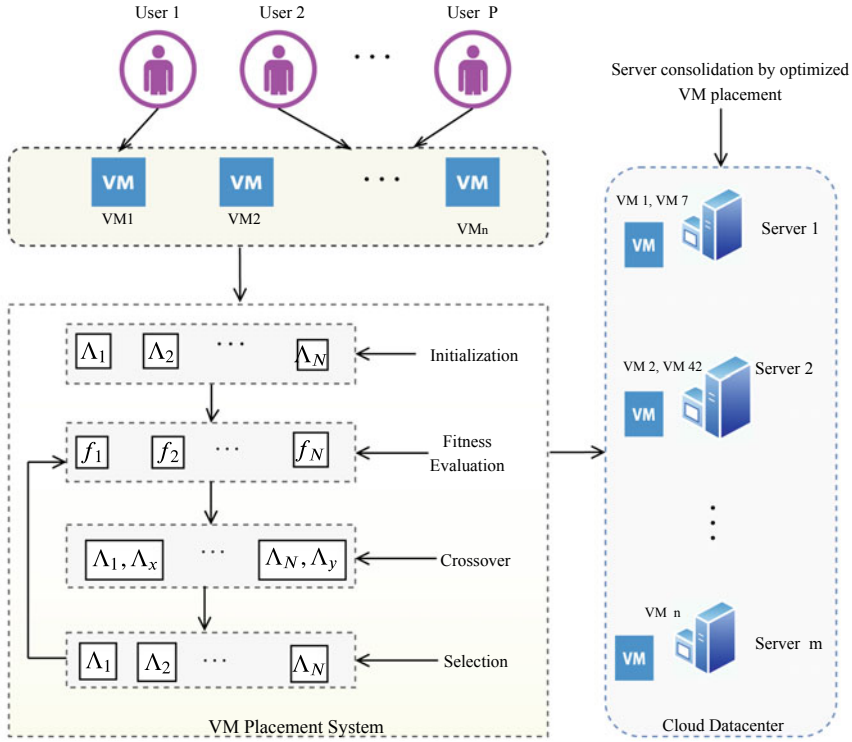


Fig. 1 Proposed NSGA-II based server consolidation framework

evaluated, and selection is done by applying multi-objective non-dominating sorting (NSGA-II) algorithm to replace the least fit solution by better ones. The operational summarized algorithm for proposed work is given in Algorithm 1.

4.1 Time Complexity

The time complexity of Algorithm 1 is as follows: Line 1 initializes N random solutions which consumes $O(1)$ time. Lines 2–14 have nested loops where lines 5–12 shows inner loop which updates N solutions by using crossover and mutation operations and consumes $O(N)$ time units. Line 4 applies non-dominated sorting that depends on number of objectives (o) and size of solutions(N), and its complexity comes out to be $O(oN^2)$. Outer loop iterates ($Gmax$) times. Therefore, the total time complexity can be computed as $O(ob \times N \times N \times m \times n \times Gmax) \rightarrow O(oN^2mn(Gmax))$.

Algorithm 1 Proposed NSGA-II based Server consolidation algorithm:

```

1: Initialize  $N$  random VM allocations  $(\Lambda_1, \Lambda_2, \dots, \Lambda_N)$ .
2: for  $g = 1, 2, \dots, Gmax$  do
3:    $[Pow, RU] = \eta(\Lambda^g)$ 
4:    $[\Lambda_{non-dominatedsorted}(NDS) = NSGA(\Lambda^g)], \Lambda_{best} \leftarrow \Lambda_{NDS}[0]$ 
5:   for each  $i=(1,2,\dots,N)$  do
6:      $rn = random(1, N)$ ,  $cross\_point = random(1, P)$ , where  $P$  is randomly generated crossover-point.
7:      $Cr_1 = [\Lambda_i(1 : cross\_point), \Lambda_{rn}(cross\_point + 1 : P)]$ 
8:      $Cr_2 = [\Lambda_{rn}(1 : cross\_point), \Lambda_i(cross\_point + 1 : P)]$ 
9:      $Cr = [Cr, \mu(Cr_1), \mu(Cr_2)]$ 
10:     $VM^{feasible} = Feasible\ VM\ Allocation(C)$ 
11:     $[Pow, RU] = \eta(VM^{feasible})$ 
12:  end for
13:   $\Lambda^g = [\Lambda^g, Cr], [\Lambda^{g+1} = NSGA(\Lambda^g)]$ 
14: end for

```

5 Performance Evaluation

5.1 Experimental Set Up

The simulation experiments are executed on a server machine assembled with two Intel® Xeon® Silver 4114 CP. The computation machine is deployed with 64-bit Ubuntu 16.04 LTS, having main memory of 128 GB. We set up datacenter environment in Python version-3 with three different types of server and four types of VMs configuration. The resource characteristics like MIPS, memory, and power consumption (P_{max}, P_{min}) are taken from real IBM [8] and Dell [5] server configuration as given in Table 1. Furthermore, the experimental VM configuration are inspired from the VM instances from Amazon Web site [1] as shown in Table 2.

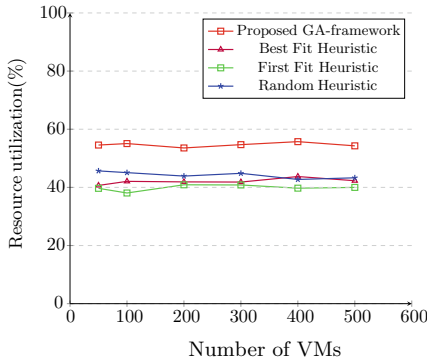
The experiments were executed with 50 VMs on 30 servers, 100 VMs on 60 servers, 200, 300, 400, and 500 VMs on 120, 180, 240, and 300 servers, respectively. Each experiment was executed for 20 times, and mean value of the obtained results is reported in the article. In the observed simulation, it is to be noted that resource utilization is closer to 56% for almost every combination of VMs and servers while

Table 1 Server configuration

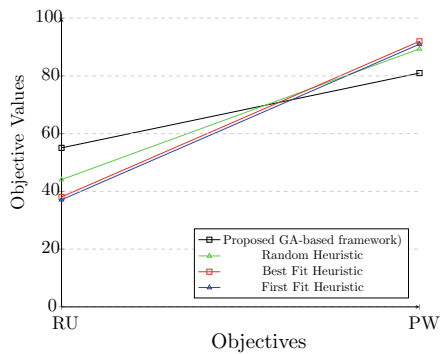
Server type	PE	MIPS	RAM (GB)	Secondary storage (GB)	P_{max}	P_{min}	P_{idle}
ProLiantM110G5XEON3075	2	2660	4	160	135	93.7	93.7
IBMX3250Xeonx3480	4	3067	8	250	113	42.3	42.3
IBM3550Xeonx5675	12	3067	16	500	222	58.4	58.4

Table 2 VM configuration

VM type	PE	MIPS	RAM (GB)	Secondary storage (GB)
VM_{Small}	1	500	0.5	40
VM_{Medium}	2	1000	1	60
VM_{Large}	3	1500	2	80
$VM_{Extra\ large}$	4	2000	3	100



(a) Resource Utilization



(b) Pareto-Front for 100 VMs

Fig. 2 Comparison of proposed GA-based framework and other approaches

Table 3 Power consumption (W) for different number of VMs request

VMs (PMs)	Proposed	Random	Best-fit	First-fit
50 (30)	3.90E+03	4.01E+03	4.92E+03	4.52E+03
100 (60)	7.07E+03	7.99E+03	7.78E+03	7.61E+04
200 (120)	1.55E+04	1.61E+04	1.58E+04	1.91E+04
300 (180)	2.42E+04	2.41E+04	2.44E+04	2.52E+04
400 (240)	3.21E+04	3.62E+04	3.65E+04	3.58E+04
500 (300)	4.01E+04	4.20E+04	4.23E+04	4.43E+04

power consumption is increasing from 50 to 500 VMs with increase in number of active servers.

The comparative resource utilization and pareto-front for 100 VMs which depicts contradictory behavior of two objectives are shown in Fig. 2. The comparative power consumption is given in Table 3 where proposed GA scales down power consumption by 11.32, 12, and 13.7% over random, best-fit, and first-fit heuristic-based VM allocations as given in Table 3.

6 Conclusion

This paper presented GA-based server consolidation framework to provide non-dominated pareto-optimal solution for multi-objective VM placement. There is substantial power consumption, and resource utilization is improved during VM placement. Evidently, the results show superiority of proposed work compared to random, first-fit, and best-fit heuristic approaches.

In future, the proposed VM placement strategy can be extended with more objectives like security, trust, and reliability-based VM allocation scheme. In addition, the load balancing of resources can be extended to scheduling of user's applications on VMs.

References

1. Amazon. Amazon ec2 instances. [online]. <https://aws.amazon.com/ec2/instance-types/> (1999)
2. Dabbagh M, Hamdaoui B, Guizani M, Rayes A (2016) An energy-efficient VM prediction and migration framework for overcommitted clouds. *IEEE Trans Cloud Comput* 6(4):955–966
3. Dadrwal A, Nehra S, Khan AA, Dua M (2018) Checkpoint based live migration of virtual machine. In: 2018 International conference on communication and signal processing (ICCSP). IEEE, pp 1083–1086 (2018)
4. Deb K, Pratap A, Agarwal S, Meyarivan T (2002) A fast and elitist multiobjective genetic algorithm: Nsga-ii. *IEEE Trans Evol Comput* 6(2):182–197
5. Dell. Power model. [online]. <https://www.dell.com/systems/power/hardware/> (1999)
6. Goudarzi H, Pedram M (2015) Hierarchical sla-driven resource management for peak power-aware and energy-efficient operation of a cloud datacenter. *IEEE Trans Cloud Comput* 4(2):222–236
7. Goyal J, Varma K, Maheshwari N, Dua M (2017) Load optimization by activity monitoring: push notifications for user device multiplicity. In: 2017 International conference on communication and signal processing (ICCSP). IEEE, pp 0231–0235 (2017)
8. IBM. Power model. [online]. <https://www.ibm.com/> (1999)
9. Li JQ, Pan QK, Liang YC (2010) An effective hybrid tabu search algorithm for multi-objective flexible job-shop scheduling problems. *Comput Ind Eng* 59(4):647–662
10. Liu C, Shen C, Li S, Wang S (2014) A new evolutionary multi-objective algorithm to virtual machine placement in virtualized data center. In: 2014 IEEE 5th international conference on software engineering and service science. IEEE, pp 272–275
11. Prakash T, Singh VP, Mohanty SR (2019) Cyber-attack resilient design of wide-area pss considering practical communication constraints. *IEEE Syst J*
12. Prakash T, Singh VP, Mohanty SR (2019) A synchrophasor measurement based wide-area power system stabilizer design for inter-area oscillation damping considering variable time-delays. *Int J Electr Pow Energy Syst* 105:131–141
13. Prakash T, Singh V, Singh SP, Mohanty S (2018) Economic load dispatch problem: quasi-oppositional self-learning tlbo algorithm. *Energy Syst* 9(2):415–438
14. Sharma NK, Reddy GRM (2016) Multi-objective energy efficient virtual machines allocation at the cloud data center. *IEEE Trans Serv Comput* 12(1):158–171
15. Singh A, Kumar J (2019) Secure and energy aware load balancing framework for cloud data centre networks. *Electron Lett* 55(9):540–541
16. Singh SP, Prakash T, Singh V, Babu MG (2017) Analytic hierarchy process based automatic generation control of multi-area interconnected power system using jaya algorithm. *Eng Appl Artif Intell* 60:35–44

17. Singh V, Prakash T, Rathore NS, Singh Chauhan DP, Singh SP (2016) Multilevel thresholding with membrane computing inspired tibo. *Int J Artif Intell Tools* 25(06):1650030
18. Tseng FH, Wang X, Chou LD, Chao HC, Leung VC (2017) Dynamic resource prediction and allocation for cloud data center using the multiobjective genetic algorithm. *IEEE Syst J* 12(2):1688–1699
19. Xiao Z, Song W, Chen Q (2012) Dynamic resource allocation using virtual machines for cloud computing environment. *IEEE Trans Parallel Distrib Syst* 24(6):1107–1117
20. Yu L, Chen L, Cai Z, Shen H, Liang Y, Pan Y (2016) Stochastic load balancing for virtual resource management in datacenters. *IEEE Trans Cloud Comput*
21. Zhao L, Lu L, Jin Z, Yu C (2015) Online virtual machine placement for increasing cloud provider's revenue. *IEEE Trans Serv Comput* 10(2):273–285

Ambient Environment Monitoring and Air–Sound Pollution Analyzer on Wi-Fi Network



Rahul, O. P. Sahu, and Gaurav Verma

Abstract This paper focuses on the monitoring of air pollution, sound level, and ambient environment on small-scale areas such as home supplies and organization, etc., or rural area-based cost-effective and user-friendly with software-based metering infrastructure. It is an integrated system that monitors air pollution and AQI-based upon NAMP, sound level, ambient temperature, and smoke concentration in an environment with high level of accuracy. A dedicated VI panel is designed and developed to analyze AQI with and without temperature compensation. It involves the use of various gas sensors for sensing various gases that acquire through NI my-RIO DAQ module via Wi-Fi standard FPGA technology. It has a no. of smart features such as data logging, alert mechanism, and comparison of accuracy of AQI with and without temperature compensation. The whole setup is linked to a virtual panel for monitoring the parameters and checks the status of air quality index, sound level, and different gases concentration using LabVIEW software.

Keywords Air quality index · AQI calculator · Wireless data acquisition · Air and sound quality monitoring

1 Introduction

The monitoring of environmental air pollution is a familiar topic and of research interest in the field of public health studies and environmental analysis. Air pollution could be described as the existence of toxic chemicals or compounds in the atmosphere, at such a level that causes a health risk. The origin of pollution varies from

Rahul (✉) · O. P. Sahu · G. Verma
NIT Kurukshetra, Kurukshetra, India
e-mail: rahulsheoran2050@gmail.com

O. P. Sahu
e-mail: ops_nitk@yahoo.co.in

G. Verma
e-mail: gaurav@nitkk.acin

small burning of plastic and natural sources such as volcanic activities to bulk emission from engines of automobiles and industrial exertion [1–3]. Air pollution will not only affect the animal and human health but it will affect the entire environment [2]. Different geographical conditions, global climate changes, and the environmental variations not only affect the human health but also cause cardiovascular and respiratory disease, cancers, and detrimental changes to the quality of life. Air quality is very crucial directly as we have to breathe the air around us. People living in industrial areas cities should be more concerned, since we are exposed to large amount of pollutants coming from industries, automobile traffic, commercial, and from many other sources [4]. Exposure of air pollution to population should be the deciding factor for air quality monitoring systems. A large number of contaminants such as nitrogen oxide, carbon monoxide (CO), ammonia, sulfur dioxide (SO₂), and total suspended particles PM₁₀ and PM_{2.5} are released as a result of combusted fossil fuels and common pollutant in most developing and developed countries, from industrial processing plants (coal, oil, cement, metal, wood, copper, electric power plants, etc. [4].

For reporting day-to-day air quality with respect to human health and the environment, air quality index (AQI) is used. Higher air quality index signifies increased air pollution and serious warnings to health of humans [5].

AQI calculations target major air pollutants that include: particulate matter, ground-level ozone, ammonia, lead, sulfur dioxide (SO₂), nitrogen dioxide (NO₂), and carbon monoxide (CO) [6].

The most common studies involve air quality monitoring and air pollution monitoring using wireless sensor network [7–9]. These studies that have been carried out by different health agencies, environmental agencies, and researchers in the field of environmental, public, and global health across the globe focus on indoor or outdoor air pollutant as well as ambient air pollution [10, 11]. The main aim of this studies lies in the fact that the errors occurring due to temperature in the semiconductor sensors have been tried to reduce with the help of calibration chart provided by the sensor manufacturer to get the best optimum result along with the monitoring of surrounding parameter such as temperature, smoke level, and sound level.

The main objective of this work is to design multi-sensor gas sensor module for monitoring air pollutants such as CO, NH₃, PM_{2.5}, and estimation of air pollutants in PPM level and air quality index on the guidelines of National Air Monitoring Program (NAMP) along with sound level and smoke concentration, and different mechanisms are proposed such as temperature compensation method for multi-gas pollutant sensor and warning alert mechanism for air and sound pollution for better estimation of AQI. In this work, wireless data acquisition system is implemented for monitoring of multiple parameters such as air pollutants, sound pollution level and ambient temperature and smoke level concentration in the environment. This paper also includes design and development of ambient environment monitoring and air sound pollution analyzer software with GUI for displaying of different concentration of gases, sound level, and AQI, testing the working performance on a continuous time scale and analysis of pollution level in different places of the city or campus.

2 Proposed System Architecture

The architecture of the proposed system developed using pc-based VI network technology and system hardware required components including multi-sensor unit, DAQ system interfacing circuits, and testing software used for the monitoring, analysis, and measuring the environmental air and sound pollution, analyzing and quantifying the same. Figure 1 shows the proposed model of air pollution and ambient environment monitoring panel system architecture with integrated hardware and software components.

The proposed system is wirelessly enabled data acquisition for monitoring the different gases concentration. The aim of the system is to determine the air quality index according to the standards and suggest the corrective actions that need to be taken. The hardware and software components consist of different gas sensors for monitoring different parameters, data acquisition system, and LabVIEW platform. Data acquisition hardware is connected to the computer over Wi-Fi interfacing such that user interface on pc is running LabVIEW software to monitor the hardware which communicates directly with user.

There are six AQI categories, namely good, satisfactory, moderately polluted, poor, very poor, and severe based on the guidelines of National Air Monitoring Program (NAMP). A sub-index is calculated for each of these pollutants based on the measured ambient concentrations, corresponding standards and likely health impact, The worst sub-index reflects overall AQI. The AQI values and corresponding ambient concentrations (health breakpoints) as well as correlated likely health impacts for the identified eight pollutants are shown in Tables 1 and 2 as follows.

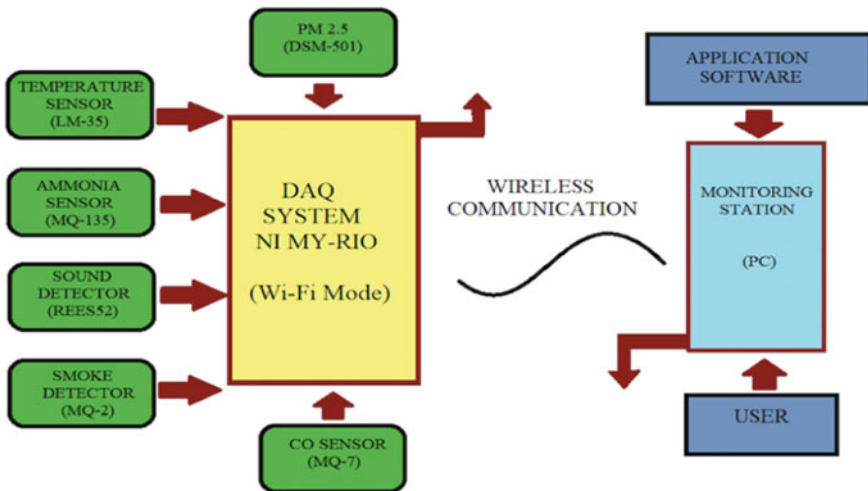


Fig. 1 Proposed architecture of air quality and ambient environment monitoring

Table 1 AQI values

AQI Category, Pollutants and Health Breakpoints								
AQI Category (Range)	PM ₁₀ 24-hr	PM _{2.5} 24-hr	NO ₂ 24-hr	O ₃ 8-hr	CO 8-hr (mg/m ³)	SO ₂ 24-hr	NH ₃ 24-hr	Pb 24-hr
Good (0-50)	0-50	0-30	0-40	0-50	0-1.0	0-40	0-200	0-0.5
Satisfactory (51-100)	51-100	31-60	41-80	51-100	1.1-2.0	41-80	201-400	0.5 – 1.0
Moderately polluted (101-200)	101-250	61-90	81-180	101-168	2.1- 10	81-380	401-800	1.1-2.0
Poor (201-300)	251-350	91-120	181-280	169-208	10-17	381-800	801-1200	2.1-3.0
Very poor (301-400)	351-430	121-250	281-400	209-748*	17-34	801-1600	1200-1800	3.1-3.5
Severe (401-500)	430 +	250+	400+	748+*	34+	1600+	1800+	3.5+

Table 2 Health impacts of pollutants

AQI	Associated health impacts
Good (0–50)	Minimal impact
Satisfactory (51–100)	May cause minor breathing discomfort to sensitive people
Moderately polluted (101–200)	May cause breathing discomfort to people with lung disease, such as asthma, and discomfort to people with heart disease, children and older adults
Poor (201–300)	May cause breathing discomfort to people prolonged exposure and discomfort to people with heart disease
Very poor (301–400)	May cause respiratory illness to the people on prolonged exposure. Effect may be more pronounced in people with lung and heart disease
Severe (401–500)	May cause respiratory impact even on healthy people, and serious health impacts on people with lung/heart disease. The health impacts may be experienced even during light physical activity

In order to calculate AQI, out of these 8 pollutants concentration, concentrations of minimum three pollutants are required; one of them should be PM₁₀ or PM_{2.5}

2.1 System Hardware

System hardware consists of multiple sensors connected to wireless data acquisition system and Wi-Fi-enabled unit for acquiring data and analyzing data using suitable program. The important hardware components used in the proposed model design are

- Air pollution sensor module
- Ambient environment sensor module
- Sound detector
- Wireless data acquisition module
- Computing and monitoring station

Air Pollution Sensor Module

It consists of a number of smart semiconductor gas sensors on recent gas sensing technology for monitoring of air pollutants in gaseous or solid form such as ammonia, carbon monoxide, and PM_{2.5}. Semiconductor gas sensors undergo either oxidation or reduction when a gas comes into contact with a metal oxide surface. One of the advantages of semiconductor sensors is their flexibility in sensor design for a particular application [12].

The sensors used for monitoring of air pollution are:

Carbon Monoxide Gas Sensor (MQ-7)

Sensitive material of MQ7 gas sensor is SnO₂ (tin oxide) which detects carbon monoxide present in the atmosphere. It has lower conductivity in clean air. The sensor's conductivity gets higher along with the rising of CO gas concentration.

Ammonia Gas Sensor (MQ-135)

The MQ-135 gas sensor is used for sensing of gases like ammonia nitrogen, oxygen, alcohols, aromatic compounds, sulfide, and smoke. With the rising level of gas concentration of target gas explosive gas, the sensor's conductivity increases along with the rising levels signal of gas concentration. Change of conductivity is converted into output signal using a simple electronic circuit.

Dust Sensor DSM 501A (PM 2.5)

The PM_{2.5} sensor uses a light scattering laser sensor for PM_{2.5} measurements. Laser light beam is beamed onto particles within the sensor's measuring chamber, and this light is then irradiated in all directions from these particles. A photometer detector then measures all of this scattered light, and from this concentration of particles within the chamber can be calculated. Using this, the sensor can detect near-microscopic particles ranging from 1 to 10 μm. To ensure a constant flow of air through the measuring chamber, the sensor is equipped with a small fan.

Now, the required equations to calculate the PPM from the sensitivity characteristics provided by manufacturer [13] are

$$\log(R_s/R_o) = m \log(\text{ppm}) + c$$

$$\text{PPM} = (R_s/R_o * 10 - c)1/m$$

$$\text{PPM} = ((V_B/ V_C - 1) * R_L/R_o * 10 - c)1/m$$

where

V_B Voltage of the battery.

V_C Output voltage given by the sensor.

R_L 10 k Ω .

R_o Sensor resistance in the clean air.

The resistance obtained using the voltage output of the sensor requires the calculation of R_o , i.e., the resistance of the sensor in clean air, to calculate the resistance in clean air, we have taken 1000 samples and taken the average values of the 1000 values.

Using the above method, the values calculated of different resistance are:

R_o for MQ-135: 53.0857

R_o for MQ-7: 119.0364

R_o for MQ-2: 23.2768

Ambient Environment Sensor Module

It consists of a number of smart semiconductor gas sensors on recent gas sensing technology for monitoring of ambient environment in gaseous form such as smoke and temperature.

Smoke sensor (MQ-2)

Sensitive material of MQ-2 gas sensor is SnO_2 . The sensor's conductivity increases along with the gas concentration rising. It uses simple electric circuit; output signal is produced corresponding to change of conductivity due to change in gas concentration. MQ-2 gas sensor has higher sensitivity to LPG, propane, and hydrogen, but can also be used for methane and other combustible steam which makes it suitable for different applications.

Temperature Sensor (LM-35)

It is used for sensing the environment temperature using 5 V DC power supply and gives analog output in the form of voltage. By using temperature sensitivity graph, i.e., 10 mV/ $^{\circ}\text{C}$ directly converts voltage to temperature value. The sensor circuitry is sealed and not subject to oxidation. With an electrical output corresponding to the temperature (in $^{\circ}\text{C}$), the LM35 an integrated circuit sensor can be used to measure temperature.

Sound Detection Module

The sound sensor module is generally used for detecting sound intensity. This module can be used for various applications such as security, switch, and monitoring. It uses

a microphone which supplies the input to an amplifier, peak detector, and buffer. Output signal voltage is processed whenever the sensor detects a sound, which is sent to a microcontroller that performs necessary processing.

Data Acquisition System

Data acquisition (DAQ) device interfaces the physical parameters to the digital computation. It has many functions and cheaper in terms of cost than other device such as PLC and SCADA system. Data acquisition is the process to obtain analog signals from physical parameter that is converted to digital signals. Simultaneously, the analog signals are conditioned by convenient signal conditioner [14]. A PC-based data acquisition system can be configured to deal with the dynamic requirements of the user. To transform standard computer into a user-defined control or measurement unit, a PC-based DAQ system is used as a combination of hardware and flexible software. Also, data acquisition is the method of sampling signal from data, that measure real-time system and changing the resulting samples of data into digital equivalent which can be changed by computer. In this project, NI myRIO-1900 data acquisition card is used which take the data from the sensors directly in the form of the voltage signals. The advantage of using this NI my-RIO DAQ card is that data can be transferred easily through Wi-Fi-enabled or through serial communication able to LabVIEW software [14].

Computing and Displaying Platform

The data gathered from the different sensors is shown either on a Wi-Fi-enabled PC or a laptop with wireless connectivity. The pc acts as a platform for displaying the AQI and ambient environment analysis and the corresponding suggestions for the user to understand in simple terms. The LabVIEW software is installed along With NI myRIO-1900 in the PC for running of the system [14, 15].

3 AEM-ASPA Code Design and Implementation

Ambient environment monitoring-air sound pollution analyzer (AEM-ASPA) is an integrated software that performs all the function of wireless acquisition of data from system hardware, processing, and analyzing of environment measured data for better estimation of air quality index, sound index, and ambient condition monitoring. It has many smart features and data logging capabilities with a versatile user interface. It is implemented a virtual instrument with block diagram code and front panel for user interaction.

Figure 2 shows the functional block diagram code of the software. The figure shown is divided into the following modules.

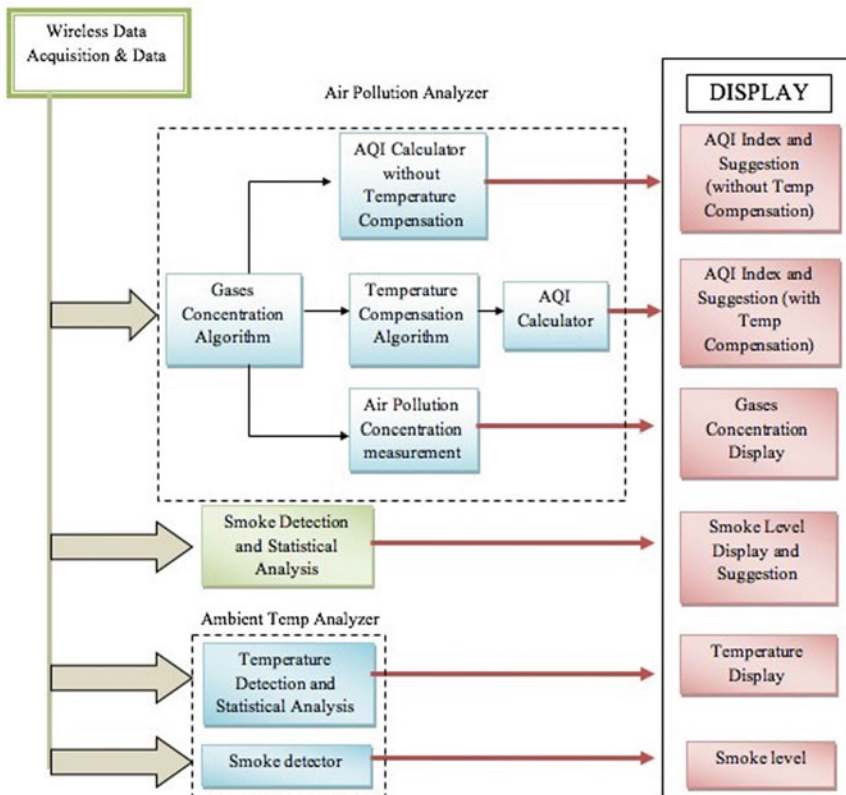


Fig. 2 Functional block diagram code of software

3.1 Temperature Compensation

With an increase in temperature, the conductivity as well as the number of carriers of the semiconductor material increases, which leads to an increase in conductivity of the material and hence resistance decreases. Ambient temperature variation causes drift in sensor characteristics. There is variation in the nominal value of sensor resistance in clean air if ambient temperature changes from calibrated temperature.

There is a change in sensitivity of the sensor to gas concentration if ambient temperature changes. So, to remove the effect of temperature variations on the gas sensor output, the temperature characteristics curves of the gas sensors from datasheet are used to derive temperature models for gas sensors to compensate temperature errors as

$$\text{Sensor true value} = \text{Sensor measured value} - \text{Errors due to temperature.}$$

Piecewise Linearization

From the sensitivity characteristics, the curve is nonlinear so we cannot use the least squares linear fitting, so for nonlinear curve piecewise linearization is performed [16].

Consider a general nonlinear function $f(x)$ of a single variable x ; $f(x)$ is a continuous function, and x is within the interval $[a_0, a_m]$.

Denote a_k ($k = 0, 1, 2, \dots, m$) as the breakpoints of (x) , $a_0 < a_1 < a_2 \dots < a_m$, $f(x)$ can then be approximately linearized over the interval $[a_0, a_m]$ as

$$(f(x)) = \sum_{k=1}^m f(a_k)t_k \tag{1}$$

$$x = \sum_{k=1}^m (a_k)t_k, \quad t_0 \leq y_0 \tag{2}$$

$$\sum_{k=1}^m (t_k) = 1, \quad \sum_{k=1}^{m-1} (y_k) = 1,$$

where $y_k \in \{0, 1\}$, $t_k \geq 0, k = 0, 1, \dots, m - 1$.

The mathematical equation obtained from the piecewise linearization using the sensitivity characteristics of the sensors is shown in Table 3.

Polynomial Curve Fitting

The exact value of Rs/Ro from the sensitivity characteristic is by using the polynomial curve fitting for this MATLAB software is used to determine the polynomial equation that best fits the curve.

Polynomial models for curves is described as

Table 3 Mathematical equations from the sensitivity curves

Temp in (°C)	MQ-135	MQ-7
	$Y \equiv MX + C$	$Y \equiv MX + C$
-10 to 0	$M_1 = -0.03, C_1 = 1.4$	$M_1 = -0.03, C_1 = 1.25$
0 to 5	$M_2 = -0.03, C_2 = 1.4$	$M_2 = -0.025, C_2 = 1.25$
5 to 10	$M_3 = -0.02, C_3 = 1.35$	$M_3 = -0.02, C_3 = 1.25$
10 to 15	$M_4 = -0.02, C_4 = 1.35$	$M_4 = -0.019, C_4 = 1.19$
15 to 20	$M_5 = -0.01, C_5 = 1.2$	$M_5 = -0.0125, C_5 = 1.1$
20 to 22	$M_6 = -0.0125, C_6 = 1.25$	$M_6 = -0.0125, C_6 = 1.1$
22 to 30	$M_7 = -3.12 * 10^{(-3)}, C_7 = 1.0437$	$M_7 = -2.24 * 10^{(-3)}, C_7 = 0.94$
30 to 40	$M_8 = -2 * 10^{(-3)}, C_8 = 1.01$	$M_8 = -2.1 * 10^{(-3)}, C_8 = 0.91$
40 to 50	$M_9 = -3 * 10^{(-3)}, C_9 = 1.05$	$M_9 = -2 * 10^{(-3)}, C_9 = 0.89$

Table 4 Mathematical coefficient from curve fitting

Sensor	P_1	P_2	P_3	P_4
MQ-135	$-1.7821 e^{-06}$	0.002676	0.033654	1.25
MQ-7	$-1.821 e^{-06}$	0.000374	-0.02284	1.24

$$y = \sum_{k=1}^{m-1} y_i x^{n+1-i} \tag{3}$$

where $n + 1$ is the order of the polynomial, n -degree of the polynomial, and $1 \leq n \leq 9$ [17].

In this project, polynomials are presented with respect to their degree. For example, a cubic polynomial is specified by

$$Y = P_1x^3 + P_2x^2 + P_3x + P_4,$$

where Y is relative change in resistance (R_s/R_o), x is temperature variation from the standard level, and $x = (t - t_{25})$ for temperature range of -10 to 50 degree.

The value of polynomial coefficient obtained using the curve fitting is shown in Table 4.

By comparing the above two methods and choosing the best method that has less error, the temperature compensation is done.

4 Analysis of Measurement Results

In this section, the proposed system is implemented inside the NIT Jalandhar campus at different locations and different concentration of smoke level, sound level, and air pollutants are compared at different locations. The improvement in air quality index is also compared with temperature compensation and without temperature compensation.

Figure 3 shows the front panel of the LabVIEW software indicating different parameters and gases concentration comparison with and without temperature compensation, sound level along with suggestions, average AQI as well as instantaneous AQI along with the suggestions, the system can be programmed for 24 hour monitoring as well as for continuous monitoring.

The red line denotes the AQI with the temperature compensation and white without temperature compensation. As observed from the graphs, the AQI with temperature compensation is within the satisfactory limit with a value of 64.8334, the AQI without temperature compensation is also showing the AQI satisfactory with a value of 56.6242 which is near to good instead of satisfactory due to temperature effect. The error in the AQI values is 12.66% within a temperature range of 30–34 °C. The percentage error of 12.66% is compensated which was accruing due to temperature

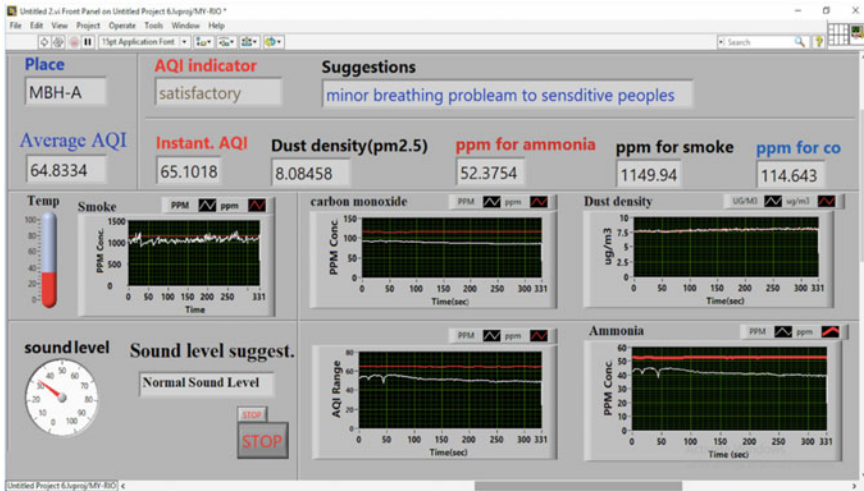


Fig. 3 Virtual panel for ambient environment and pollution analyzer

effect on the semiconductor. The temperature range varies from 30 to 34 °C. During the working of the system, the smoke level and the sound level were found to be 1149.94 ppm and 33 db which were normal and the corresponding suggestion was also displayed.

The three different conditions and the change in AQI values at different level of temperatures varying from 30 to 34 °C (MBH-A), 25 to 27 °C (MBH-B) and 31 to 35 °C (Hostel-6) as well as sound and smoke level are shown in bar graph.

The % improvement in AQI at different places is shown in Fig. 5.

The three different conditions and the change in AQI values as well as sound and smoke level are shown in Figs. 4, 5, 6 and 7.

As we can observe from the above figures that if the contributing factor to the air pollution is PM2.5, then the effect of temperature is negligible. The parameter comparison of the AQI with ambient environment conditions is given in Table 5.

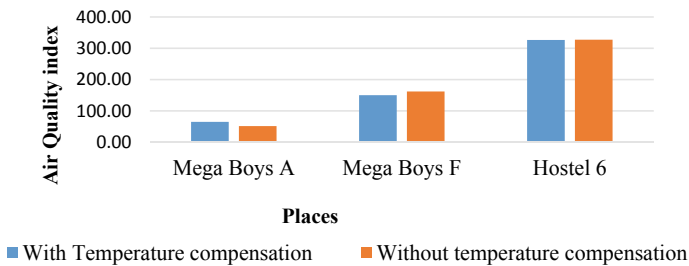


Fig. 4 AQI at different places

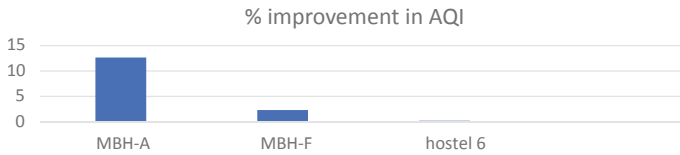


Fig. 5 AQI improvement with temperature compensation

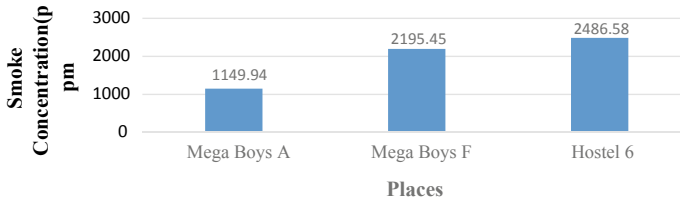


Fig. 6 Smoke concentration at different places

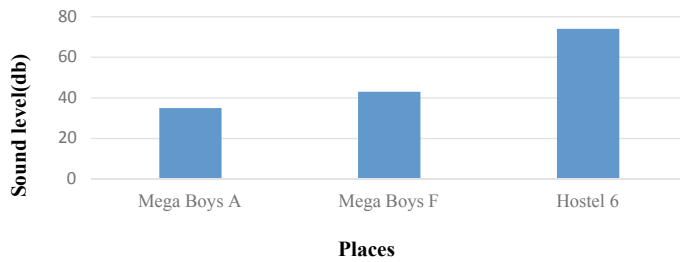


Fig. 7 Sound level at different places

Table 5 Parameter comparison

Place	AQI	Temp. variation (°C)	Smoke conc. (ppm)	Sound level (db)
Mega boys A	64.83	30–34	1149.94	35
Mega boys F	150.10	25–27	2195.45	43
Hostel 6	326.66	31–35	2486.58	74

The effect of temperature on the conductivity of the sensors is compensated and % improvement in AQI. Based upon test results, the estimated improvement in AQI varies from 12.33 to 2.4% depending upon temperature and the contributing gas. In this system, the Pre-calibrated data provided by the sensor manufacturer is used for temperature compensation.

5 Conclusion

In this paper, an end-to-end system for ambient real-time air quality monitoring and sound pollution along with smoke concentration is presented. The system has two main components, the multi-gas monitoring stations and AEM-ASPA code design and implementation. The prototype is placed at different locations inside the NIT Jalandhar campus and data is collected and analyzed. With a backend server using GPRS communications, the monitoring stations communicate in an M2M fashion. The data gathered from the different sensors is shown either on a Wi-Fi-enabled PC or a laptop with wireless connectivity. The pc acts as a platform for displaying the AQI and ambient environment analysis and the corresponding suggestions for the user to understand in simple terms. The LabVIEW software is installed along With NI myRIO-1900 in the PC for running of the system. This model can be modified for future uses by connecting the system to Internet in order to determine the pollution of that location from anywhere in the world. A number of such systems can be implemented in the different locations of a city or campus and can be connected to each other with the help of IoT so that a complete monitoring and air pollution map generation of a city or campus can be done from a remote location and corrective steps can be taken to control the air pollution before it reaches the alarming level. More number of sensors can be connected to monitor the different remaining pollutants which will increase the accuracy of the AQI.

References

1. (2012) 7 million premature deaths annually linked to air pollution. World Health Organisation
2. <http://elte.prompt.hu/sites/default/files/tananyagok/AtmosphericChemistry/ch13.html>. Last accessed 2017/04/11
3. World Health Organization (WHO) (1999) Monitoring ambient air quality for health impact assessment. WHO Regional Publications. European Series, No. 85
4. <https://www.epa.gov/air-quality-management-process/managing-air-quality-ambientair-monitoring>. Last accessed 2017/04/11
5. http://www.arthapedia.in/index.php?title=National_Air_Quality_Index. Last accessed 2017/04/11
6. <https://blissair.com/what-is-pm-2-5.htm>. Last accessed 2017/04/11
7. Postolache OA, Dias Pereira JM, Silva Girao PMB (2009) Smart sensors network for air quality monitoring applications. *IEEE Trans Instrum Meas* 58(9):3253–3262
8. Ando B, Baglio S, Graziani S, Pitrone N (2009) Models for air quality management and assessment. *IEEE Trans Syst Man Cybern Part C Appl Rev* 30(3):358–363
9. Tsujita W, Ishida H, Moriizumi T (2004) Dynamic gas sensor network for air pollution monitoring and its auto-calibration. *Sensors* 1:56–59
10. Khedo KK, Perseedoss R, Mungur A (2010) A wireless sensor network air pollution monitoring system. *Int J Wirel Mob Netw (IJWMN)* 2(2):31–45
11. Ando B, Cammarata G, Fichera A, Graziani S, Pitrone N (1999) A procedure for the optimization of air quality monitoring networks. *IEEE Trans Syst Man Cybern Part C Appl Rev* 29(1):157–163
12. Jaimini U, Banerjee T, Romine W, Thirunarayan K, Sheth A, Kalra M (2017) Investigation of an indoor air quality sensor for asthma management in children. *IEEE Sens Lett* 1(2):1–4

13. Hu K, Sivaraman V, Luxan BG, Rahman A (2016) Design and evaluation of a metropolitan air pollution sensing system. *IEEE Sens J* 16(5):1448–1459
14. <http://www.ni.com/white-paper/10700/en/>. Last accessed 2017/04/11
15. <http://www.ni.com/pdf/manuals/376047c.pdf>. Last accessed 2017/04/11
16. Shaban KB, Kadri A, Rezk E (2016) Urban air pollution monitoring system with forecasting models. *IEEE Sens J* 16(8):2598–2606
17. <https://www.mathworks.com/products/curvefitting.html>. Last accessed 2017/04/11

Modified Decision Tree Learning for Cost-Sensitive Credit Card Fraud Detection Model



Sudhansu R. Lenka, Rabindra K. Barik, Sudhashu S. Patra,
and Vinay P. Singh

Abstract Credit card fraudulent transactions are cost-sensitive in nature, where the cost differs in each misclassification transaction. Generally, the classification methods do not work on the cost factor. It considers a constant cost factor for each misclassification. In this paper, it proposes a modified instance-based cost-sensitive decision tree algorithm which reflects on different cost factor for each misclassified transactions. In the proposed algorithm, it implements different instance-based costs into the cost-based impurity measure as well as cost-based pruning approach. Experimentally, it shows that the proposed algorithm performs better in terms of cost savings as compared against classical decision tree algorithms. Additionally, it observes that the smaller trees are generated in minimum computational time.

Keywords Cost-sensitive classification · Credit card · Fraud detection · Decision tree

1 Introduction

Classification model normally considers all the misclassified instances with an equal cost. Cost-insensitive learning approaches mainly aim to reduce the probability of misclassification and the same cost is considered for each incorrect prediction [1, 2].

S. R. Lenka (✉)

Department of CSE, Trident Academy of Technology, Bhubaneswar, India

e-mail: sudhansulenka2000@gmail.com

R. K. Barik

School of Computer Engineering, KIIT Deemed to Be University, Bhubaneswar, India

e-mail: rabindra.mnnit@gmail.com

S. S. Patra

School of Computer Applications, KIIT Deemed to Be University, Bhubaneswar, India

e-mail: sudhanshupatra@gmail.com

V. P. Singh

Malaviya National Institute of Technology, Jaipur, India

e-mail: vinaymnnit@gmail.com

© Springer Nature Singapore Pte Ltd. 2021

G. S. Hura et al. (eds.), *Advances in Communication and Computational*

Technology, Lecture Notes in Electrical Engineering 668,

https://doi.org/10.1007/978-981-15-5341-7_113

Most of the researchers work on equal costs for each misclassification or a constant heterogeneous misclassification costs. In the financial application system, accuracy is not the only goal of the model, cost factor must be taken into account. Cost-sensitive learning is one of the important issues in the field of Machine Learning (ML) community. Objective of those cost-sensitive classifiers is to reduce the total misclassification cost [3]. Thus, implementing cost-sensitive methods in credit card Fraud Detection System (FDS) helps to get a large amount of financial gain. In financial applications, the cost-sensitive classifiers assign different costs to misclassified instances. For example, False Positive (FP) transaction is penalized with an administrative cost and in case of False Negative (FN) the financial institutions have to face heavy penalty and the cost depends upon the amount of transaction [4]. In FDS, the fraudulent transactions are treated as positive instances whereas the legitimate transactions are treated as negative instances.

The classifiers following cost-sensitive approaches assign a constant cost to each misclassification [2, 3, 5]. But, these class-dependent approaches are not applicable to many real-world applications. In case of *FDS*, it has focused on instance-based cost-sensitive classifiers, where misclassification costs vary with instances [3]. In instance-based approaches, the cost may be assigned to the instances in either before, after, or during the training phase [6]. In the proposed work, it considers the cost during the training phase.

The credit card transactions are highly skewed towards the negative class instances. So, the methods like cost-based rejection-sampling [7] and cost-based over-sampling [3, 8] were used to re-weight the training sets according to their costs. In the rejection-sampling approach a subset of instances is selected by randomly picking each instance from the training set based on the misclassification cost of the instance. Similarly, in over-sampling approach a new dataset is created by replicating each instance n times, where n denotes the value of the misclassification cost of that instance. In this paper, it has proposed a new Modified Cost-Sensitive Decision Tree (MCSDT) algorithm which has included the instance-based cost-sensitive approach. In the proposed algorithm, it has used instance-based cost-sensitive impurity measure and cost-based pruning technique as defined in [9]. It has also evaluated the proposed MCSDT algorithm using credit card transactions. The results have shown that the proposed algorithm has performed better than traditional decision tree algorithms. Additionally, the proposed method has also built smaller trees as compared to traditional decision tree.

The classification model for the *FDS* can be built either by employing a single classifier or ensemble of multiple classifiers [10]. The rest of this article is organized as follows. In Sect. 2, it presents the traditional evaluation measures of classification algorithms and the instance-based cost-sensitive evaluation approach of credit card transactions. In Sect. 3, it explains an instance-based cost-sensitive decision tree algorithm. In Sect. 4, it implements the cost-sensitive impurity measures and cost-sensitive pruning techniques on the proposed decision tree. The experimental analysis and results have presented in Sect. 5. Finally, Sect. 6 includes the conclusion of the article.

2 Instance-Based Cost-Sensitive Evaluation Parameter

In this section, it highlights the background details of instance-based cost-sensitive classification. It elaborates on the traditional evaluation measures and cost-sensitive evaluation approaches on the fraud detection model.

2.1 Traditional Evaluation Measures

In A binary classification model aims to predict the class label y_i for a given set of instances S and each instance i is characterized by n features, i.e. $S = \{(x_i, y_i \mid x_i \in R^n \wedge y_i = \{0,1\})\}$, where $i = 1 \dots N$. The objective of the classifier $k(S)$ is to identify the class p_i of each instance i belong to S and it contains N instances.

In order to access the performance of a fraud detection model, it is needed to determine the number of misclassified instances. The error or the misclassification in the model is defined as:

$$\text{Err}(k(S)) = 1 - \frac{1}{N} \sum_{i=1}^N I(y_i = p_i) \tag{1}$$

where $I[\cdot]$ is an indicator function, defined as

$$I(y_i = p_i) = \begin{cases} 1 & \text{if } y_i = p_i \\ 0 & \text{if } y_i \neq p_i \end{cases} \tag{2}$$

Accuracy is the reciprocal of error, i.e.

$$\text{Acc}(k(S)) = 1 - \text{Err}(k(S)) \tag{3}$$

Including these statistics, other measures need to be evaluated for which a reference to the confusion matrix (shown in Table 1) is needed. Those statistic measures are:

$$\text{Recall} = \frac{\text{TP}}{\text{TP} + \text{FN}} \tag{4}$$

Table 1 Confusion matrix

	Actual positive $y_i = 1$	Actual negative $y_i = 0$
Predicted positive $p_i = 1$	True positive (TP)	False positive (FP)
Predicted negative $p_i = 0$	True positive (FN)	True negative (TN)

$$\text{Precision} = \frac{\text{TP}}{\text{TP} + \text{FP}} \tag{5}$$

$$\text{F}_1 \text{ Score} = \frac{2 \cdot \text{Precision} \cdot \text{recall}}{\text{Precision} + \text{recall}} \tag{6}$$

where TP and TN are true positive and true negative respectively. These measures are mostly used to evaluate the performance of the classification algorithms [10, 11]. But, these measures may not be a suitable approach while evaluating the fraud detection model.

2.2 Cost-Sensitive Evaluation of Credit Card Transactions

In fraud detection model, predicting a fraudulent transaction as genuine (i.e. in case of FN) should be more costly than misclassifying a genuine transaction as fraud (i.e. in case FP). Taking costs into consideration different costs are assigned to misclassified transactions. Table 2 shows the cost matrix for each transaction i . It contains costs that are associated with two correct predictions, true positive ($C_{\text{TP}i}$), true negative ($C_{\text{TN}i}$) and the costs associated with incorrect predictions, false positives ($C_{\text{FP}i}$), false negatives ($C_{\text{FN}i}$). As proposed in [11], the costs associated with both false positives and true positives is the administrative cost (i.e. $C_{\text{FP}i} = C_{\text{TP}i} = C_a$). The administrative cost is the cost of predicting the transactions and contacting the card owners. But in case of false negative transactions, the cost is assumed to be hundred times C_a , i.e. $C_{\text{FN}i} = 100 C_a$. But in real scenarios the amount of losses due to fraudulent transactions may vary from few dollars to millions of dollars, so it is impractical of assuming a fixed cost for FN transactions. So, the cost of FN equals to the amount of transaction [4] (i.e. $C_{\text{FN}i} = \text{Amt}_i$). The costs of each transaction are depicted in Table 2.

For instance-based cost-sensitive approaches, each instance x_i of the set S are converted to augmented feature vector, $x_i^* = [x_i, C_{\text{TP}i}, C_{\text{FP}i}, C_{\text{FN}i}, C_{\text{TN}i}]$ and the class label y_i . According to [4, 12], using the cost matrix the cost of each transaction is defined as:

$$C(k(x_i^*)) = y_i(p_i C_a + (1 - p_i)\text{Amt}_i) + (1 - y_i)p_i C_a \tag{7}$$

Table 2 Credit card transactions cost matrix

	Actual positive $y_i = 1$	Actual negative $y_i = 0$
Predicted positive $p_i = 1$	$C_{\text{TP}i} = C_a$	$C_{\text{FP}i} = C_a$
Predicted negative $p_i = 0$	$C_{\text{FN}i} = \text{Amt}_i$	$C_{\text{TN}i} = 0$

where y_i and p_i represent the actual and predicted class labels of the instance i respectively.

The total cost of the set S is defined as:

$$C_{\text{total}}(k(S)) = \sum_{i=1}^N C(k(x_i^*)) \tag{8}$$

After defining the cost factors into the detection model k , it has needed to examine the performance of the algorithm. Through cost savings, it can find the improvement in the costs and through which it can evaluate the performance of the algorithm [13]. To evaluate the savings it needs to compute the cost of predicting each instance as the class with minimum lowest cost [13], is defined as:

$$C_{\text{low}}(k(S)) = \min\{C(k_0(S)), C(k_1(S))\} \tag{9}$$

where $k_0(S)$ and $k_1(S)$ are the detection models that predict each instance in S to the negative and positive classes respectively. Then, the savings are computed by comparing the overall cost (8) with the lowest cost (9).

$$\text{Savings}(k(S)) = \frac{C_{\text{total}}(k(S)) - C_{\text{low}}(k(S))}{C_{\text{low}}(k(S))} \tag{10}$$

A standard way to associate instance-based costs into the fraud detection model is to resample the training instances according to the cost value. It involves two approaches either by cost-based rejection-sampling [7], or over-sampling [3] (already discussed in Section-1). In rejection-sampling approach, a random subset is created by randomly selecting the instances from S and each instance i is selected with probability $w_i/\max_{i \dots N} \{w_i\}$, where w_i is the expected misclassification cost of instance i , defined as:

$$w_i = y_i \cdot C_{\text{FN}_i} + (1 - y_i) \cdot C_{\text{FP}_i} \tag{11}$$

In case of over-sampling approach, the class distribution gets balanced in constructing a new set S_0 by replicating w_i times each instance i . But, this approach increases the training complexity since $\text{abs}(S_0) \gg \text{abs}(S)$ and it also may cause over-fitting [14]. But, both these approaches use only the misclassification costs of the cost matrix, i.e. they compute part of the cost matrix.

3 Decision Trees

Decision Trees (DT) outperformed other algorithms with low computational cost, easy interpretation and overall better performance in case of a dataset with large

number of attributes and instances [15]. In this section, it has presented a new modified decision tree algorithm.

3.1 Construction of Modified Decision Tree Algorithm

Let S be the training set with N instances and the instance is categorized by n attributes $\{A_1, A_2, \dots, A_n\}$. Each attribute A_i contains k values $\{A_{i1}, A_{i2}, \dots, A_{ik}\}$. The training set is also associated with the class labels $Y = \{y_1, y_2, \dots, y_m\}$.

Removal of noisy instances Initially, it has compared the prior probability, $P(y_i)$ for each class, $y_i \in S$ and the conditional probability $P(A_{ij}|y_i)$ for each attribute value in S . For each training instance $x_i \in S$ with class y_i , the posterior probability is computed as:

$$P\left(\frac{y_i}{x_i}\right) = \frac{P\left(\frac{x_i}{y_i}\right)P(y_i)}{P(x_i)} \quad (12)$$

In (12), $P(x_i)$ is constant for each class y_i , so it needs to compute only $P(x_i|y_i) \cdot P(y_i)$ where $P(y_i) = |y_{i,s}|/|S|$ and $P(x_i|y_i) = \prod_{j=1}^n P(A_{ij}/y_j)$. The class y_i with the maximum posterior probability, $P(y_i|x_i)$ is considered as the final label for the training instance x_i . Then, it eliminates all the incorrect classified (noisy) instances from the training set S . The removal of these noisy training instances may reduce the chance of over-fitting and increase the accuracy level of the DT classifier. Algorithm 1 represents the detailed procedure for the removal of noisy samples.

Algorithm 1 Pseudocode of the removal of noisy instances

Input: $S = \{x_i, y_i\}_1^N$

Output: Training dataset S without noise

- 1: for all class $y_i \in S$ do
- 2: compute prior probability, $P(y_i)$
- 3: end for
- 4: for all attribute $A_{ij} \in S$ do
- 5: compute conditional probability, $P(A_{ij}|y_i)$
- 6: end for
- 7: for all training instance $x_i \in S$ do
- 8: compute posterior probability, $P(y_i|x_i)$
- 9: if x_i is incorrectly classified then
- 10: $S \leftarrow S - x_i$
- 11: end if
- 12: end for

Splitting rule In DT, the splitting rules are associated with each level in the form of node and it is represented as (A_j, V_j) . The rule split the set S into two sets S_l and S_r according to the values of (A_j) and (V_j) .

$$S_l = \{x_i^* | x_i^* \in S \wedge A_{ij} \leq V_j\} \quad (13)$$

and

$$S_r = \{x_i^* | x_i^* \in S \wedge A_{ij} > V_j\} \quad (14)$$

where A_j is the j th attribute which is represented in the form of vector $A_j = [A_{j1}, A_{j2}, \dots, A_{jN}]$ and V_j is the value which is defined as $\min(A_j) \leq V_j \leq \max(A_j)$. The tree is built by considering all the possible V_j for each attribute A_j and select the rule (A_j, V_j) that maximizes the splitting rule. Based on the best splitting criteria, the training dataset is partitioned into subsets and the procedure is repeated for each subset, until the stopping criteria are satisfied. Then, it computes the number of positive samples in each set as:

$$S_1 = \{x_i^* | x_i^* \in S \wedge y_i = 1\} \quad (15)$$

and the percentage of positive samples is computed as:

$$P_1 = \frac{|S_l|}{|S|} \quad (16)$$

Using entropy the impurity of each leaf node is computed as:

$$I_e(P_1) = P_1 \log(P_1) - (1 - P_1) \log(1 - P_1) \quad (17)$$

Finally, using the rule (A_j, V_j) the gain is computed as:

$$\text{Gain}(A_j, V_j) = I_e(P_1) - \frac{|S_l|}{|S|} I(p_1^l) - \frac{|S_r|}{|S|} I(p_1^r) \quad (18)$$

Similarly, the gain is computed for all the possible splitting rules and it selects the splitting attribute that generates maximal gain as the root node of the tree.

$$(\text{best}_A, \text{best}_V) = \arg \max_{(A_j, V_j)} \text{Gain}(A_j, V_j) \quad (19)$$

which split the set S into S_l and S_r . After splitting, each set is added to the leaf node and the algorithm continues recursively for each leaf node until the stopping criteria are satisfied. Algorithm 2 represents the pseudocode of the proposed decision tree.

3.2 Pruning of the Decision Tree

After execution of Algorithm 2, there may be the possibility that a large tree may be generated and it may over fits the training data. So to overcome such issues, pruning techniques are widely used [16]. The pruning technique is used to eliminate those branches that have no contribution towards the accuracy of the tree.

Normally, pruning techniques are implemented on a fully grown tree and recursively eliminate the nodes if that leads to lower error rate Err of the tree. Cost-sensitive pruning technique is most widely used and it was originally proposed by Brieman [16]. This technique is evaluated successively if the deduction of a node reduces the error rate Err of a Tree in the set S . The cost-sensitive pruning technique is defined as:

$$\text{PC} = \frac{\text{Err}(\text{EN}(\text{Tree}, \text{node}), S) - \text{Err}(\text{Tree}, S)}{|\text{Tree}| - |\text{EN}(\text{Tree}, \text{node})|} \quad (20)$$

where $\text{EN}(\text{Tree}, \text{node})$ is the function used to remove nodes from Tree and generates a new Tree. $\text{Err}()$ function computes the error rate of the Tree in the set S . At each iteration, the error rate of the current tree is compared considering each node.

Algorithm 2: Pseudocode of the tree build function

Input: S , Training data after removal of noisy instances
Output: Tree, Decision tree

- 1: $\text{Tree} = \varphi$
- 2: if $\text{Stopping}(S, \text{Tree}) = \text{true}$ then
- 3: return Tree
- 4: end if
- 5: for all attribute j do
- 6: for all possible thresholds m do
- 7: $\text{Gains}(j, m) = \text{GAIN}(A_j, V_{jm}, S)$
- 8: end for
- 9: end for
- 10: $(j^*, v^*) = \text{argmax}_{j,m} \text{Gains}$
- 11: $S_l = \{x_i^* \mid x_i^* \in S \wedge A_{ij^*} \leq v^*\}$
- 12: $S_r = \{x_i^* \mid x_i^* \in S \wedge A_{ij^*} > v^*\}$
- 13: $\text{Tree} = \text{Build the splitting attribute as the root node}$
- 14: $\text{Tree} = \text{Add arc to the root node for each split predicate and label}$
- 15: for all arc do
- 16: $\text{TreeGrow}(S_l)$
- 17: $\text{TreeGrow}(S_r)$
- 18: end for
- 19: return Tree

4 Instance-Based Modified Cost-Sensitive Decision Trees

Most of the ML algorithms mainly work on to improve performance of the model. But, it is not effective if the misclassification costs are different [3]. This encourages many researchers to work on cost-sensitive aspects [17–20] and each of them focused on class-dependent costs. However, in case of a fraud detection system the cost of false positives should not be the same as that of false negatives, so the cost factor should be instance-dependent rather than class-dependent.

In this section it has implemented costs into the DT by using cost-based impurity measures and pruning techniques [9].

4.1 Cost-Based Impurity Measures

In credit card, fraud detection model minimizing costs has got more importance than minimizing the misclassification rate. So, the splitting rule must be evaluated not only on accuracy but also cost-wise.

In the proposed work, a cost-based impurity measure is used to classify all the instances either as fraudulent using k_1 or as genuine using k_0 model. It evaluates the splitting rule in the form of lowest cost:

$$I_c = \min\{(C(k_0(S)), C(k_1(S)))\} \quad (21)$$

Similarly, all the instances of the set S are classified based on the lowest cost as:

$$k(S) = \begin{cases} 0 & \text{if } C(k_0(s)) \leq (k_1(S)) \\ 1 & \text{otherwise} \end{cases} \quad (22)$$

Finally, using this impurity measure the cost-based gain is computed considering the splitting rule (A_j, V_j) (as shown in Eq. 18).

4.2 Cost-Based Pruning

After building the tree, a cost-based pruning technique is used by replacing the misclassification rate Err in Eq. 20 with the cost, i.e. Err is replaced with $C(k(S))$.

$$PC_c = \frac{C(k(S)) - C(k^*(S))}{|\text{Tree}| - |\text{EB}(\text{Tree}, \text{node})|} \quad (23)$$

where, k^* is the classifier without the selected node $\text{EB}(\text{Tree}, \text{node})$.

Table 3 Description of the datasets

Set	#Instances	#Fraud	% of fraud
Total	2,84,807	492	0.172
Training (t)	1,99,365	301	0.151
Testing	85,442	191	0.002
Under-sampling (u)	602	301	50.42
Rejection-sampled (r)	1,97,119	295	0.148
Over-sampled (o)	2,93,881	418	0.142

5 Experimental Analysis

This section includes the dataset to be used to evaluate the instance-based cost-sensitive proposed MCSDT algorithm (discussed in Sect. 4) and the comparison is made with the classical decision tree (DT).

5.1 Dataset

The dataset [21], used here is provided by a European company, that contains transactions occurred during two days of September 2013. In which out of 284,807 total transactions 492 records are fraudulent. In the entire dataset only 0.172% of the total transactions are fraudulent. The total financial loss due to fraudulent transactions is 60,127.97 Euros.

The entire dataset is partitioned into training and testing sets. It has taken 70% of the transactions as training set and the remaining 30% as testing. The algorithms underperforms when the class distribution is highly skewed towards one of the classes [15], so under-sampling approach is used to make the class distribution balanced. It has been proved that under-sampling is the best approach to overcome the imbalanced issue [22]. Additionally, it has worked on cost-based rejection-sampling and cost-based over-sampling methods on the training data. The test data must be kept unchanged in order to reflect the actual class distribution. Table 3 shows the description of different datasets. The credit card transactions are cost-sensitive because the cost of misclassifying a fraud is significantly much more than the cost when a false alarm is generated [3].

5.2 Results

In this section, it has highlighted the performance of the proposed MCSDT algorithm by comparing it with classical decision tree. Different decision trees are evaluated

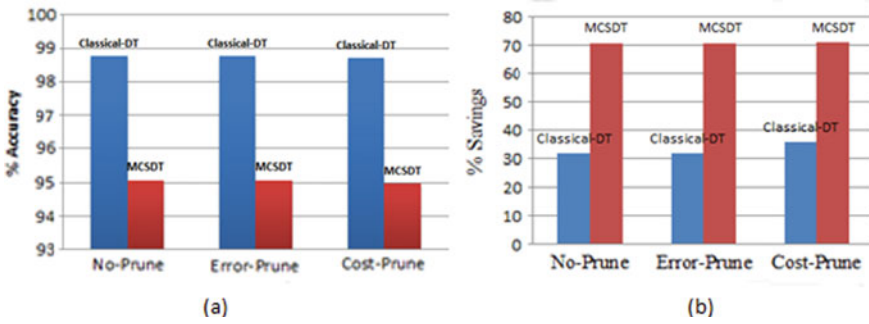


Fig. 1 **a** Results of the savings in both classical DT and MCSDT algorithms. **b** Results of accuracy in both classical DT and MCSDT algorithms where MCSDT algorithms show better savings than DT taking $C_a = 2.50$ Euros. But, the same difference is not observable in case of accuracy

using no pruning technique (*np*), with error-based pruning (*ep*) and also with cost-based pruning (*cp*) technique. The decision trees are formed using Gini impurity metrics, using pruning and no pruning approach defined in (20). The trees are also generated using cost-based pruning technique (23). Similarly, the MCSDT is also constructed taking both the pruning approaches as well as the cost-based impurity measure (21). All these algorithms (i.e. classical DT and MCSDT) are trained using the training (*t*), under-sampling (*u*), cost-proportionate rejection-sampling (*r*), and the cost-proportionate over-sampling (*o*) datasets. Initially, it has compared with the proposed algorithm with the classical DT using only the training set. The results are shown in Fig. 1 which shows that the MCSDT algorithm achieves better savings than DT. The savings are evaluated by taking the C_a equals to 2.50 Euros. But the same results it didn't achieve in case of accuracy or F1Score. The reason is in the proposed MCSDT algorithm, it has focused on improving the savings, not on accuracy or F1Score. Both the algorithms have shown slight improvement in savings in case of cost-based pruning.

Similarly, it compares MCSDT algorithm with the classical DT using all the training sets. The comparison results are presented in Table 4. Moreover, the overall savings of both the decision trees (i.e. DT and MCSDT) are shown in Fig. 2a, by averaging the results of both cost-sensitive and classical DT algorithms. In all the datasets, MCSDT algorithm achieves better savings than the classical decision tree algorithms except the under-sampling set. Finally, algorithms are analyzed by considering the tree size and training time. For the datasets, the MCSDT algorithm generates significantly smaller trees as a result reduces the training time. The results are shown in Table 5. The MCSDT algorithm not only achieve better results in terms of savings but also it takes less training time than classical DT. Figure 2b, c shows the overall tree size and training time in minutes by averaging the results of classifier DT and the cost-sensitive algorithms, respectively.

Table 4 Results of the DT and MCSDT using no pruning (*np*), with error-based pruning (*ep*) and cost-based pruning (*cp*). The algorithms are trained on different training sets

Set	Algorithm	% Sav	% Acc	F ₁ Score
<i>t</i>	DT _{<i>np</i>}	31.76	98.76	0.4458
	DT _{<i>ep</i>}	31.76	98.76	0.4458
	DT _{<i>cp</i>}	35.89	98.71	0.4590
	MCSDT _{<i>np</i>}	70.85	95.07	0.2529
	MCSDT _{<i>ep</i>}	70.85	95.07	0.2529
	MCSDT _{<i>cp</i>}	71.16	94.98	0.2522
<i>u</i>	DT _{<i>np</i>}	52.39	85.52	0.1502
	DT _{<i>ep</i>}	52.39	85.52	0.1502
	DT _{<i>cp</i>}	70.26	92.67	0.2333
	MCSDT _{<i>np</i>}	12.46	69.34	0.0761
	MCSDT _{<i>ep</i>}	14.98	70.31	0.0741
	MCSDT _{<i>cp</i>}	15.01	70.31	0.0743
<i>r</i>	DT _{<i>np</i>}	34.39	98.70	0.4321
	DT _{<i>ep</i>}	34.39	98.70	0.4321
	DT _{<i>cp</i>}	38.99	98.64	0.4478
	MCSDT _{<i>np</i>}	70.85	95.07	0.2529
	MCSDT _{<i>ep</i>}	70.85	95.07	0.2529
	MCSDT _{<i>cp</i>}	71.09	94.94	0.2515
<i>o</i>	DT _{<i>np</i>}	31.72	98.77	0.4495
	DT _{<i>ep</i>}	31.72	98.77	0.4495
	DT _{<i>cp</i>}	37.35	98.68	0.4575
	MCSDT _{<i>np</i>}	70.84	95.06	0.2529
	MCSDT _{<i>ep</i>}	70.84	95.06	0.2529
	MCSDT _{<i>cp</i>}	71.09	94.94	0.2515

6 Conclusion

In order to maximize the financial gain of the company, most of the algorithms are cost-sensitive in nature. In this paper, it introduces an instance-based cost-sensitive decision tree algorithm on credit card transactions. It experimentally shows that the proposed algorithm achieves better results in terms of savings by comparing with classical decision tree algorithms. In the proposed algorithm, it implements the cost factor to each instance using both the cost-based impurity metric and cost-based pruning criteria. Moreover, the proposed algorithm generates significantly smaller trees and the training time is much less as compared to traditional decision trees. So, it concludes that the proposed algorithm performs better results in terms of cost savings and builds smaller trees in a small fraction of time as compared with the existing instance-based cost-sensitive techniques.

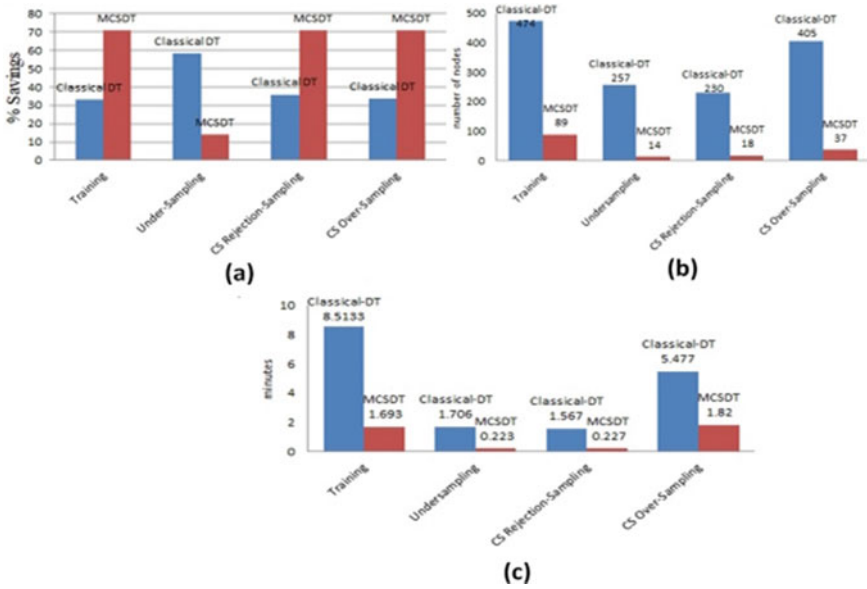


Fig. 2 a Average savings of DT and MCSDT estimated taking different datasets. b Average tree size (No. of nodes) of classical decision trees and MCSDT algorithms. c Average training time (in minutes) of classical decision trees and MCSDT algorithms

Table 5 Training time and the tree size of the classical DT and MCSDT, using different training sets

Set	Algorithm	Node	Time	Avg (node)
<i>t</i>	DT _{np}	488	2.45	474
	DT _{ep}	488	3.90	
	DT _{cp}	446	19.19	
<i>t</i>	MCSDT _{np}	89	1.47	89
	MCSDT _{ep}	88	1.87	
	MCSDT _{cp}	89	1.74	
<i>u</i>	DT _{np}	308	1.10	257
	DT _{ep}	308	1.43	
	DT _{cp}	153	2.59	
<i>u</i>	MCSDT _{np}	14	0.20	14
	MCSDT _{ep}	14	0.23	
	MCSDT _{cp}	14	0.24	
<i>r</i>	DT _{np}	268	0.98	230
	DT _{ep}	268	1.24	
	DT _{cp}	153	2.48	

(continued)

Table 5 (continued)

Set	Algorithm	Node	Time	Avg (node)
<i>r</i>	MCSDT _{np}	18	0.22	18
	MCSDT _{ep}	18	0.23	
	MCSDT _{cp}	18	0.23	
<i>o</i>	DT _{np}	425	2.30	405
	DT _{ep}	425	3.98	
	DT _{cp}	364	10.15	
<i>o</i>	MCSDT _{np}	37	1.58	37
	MCSDT _{ep}	37	1.90	
	MCSDT _{cp}	37	1.98	

References

- Iranmehar A, Masnadi-Shirazi H, Vasconcelos N (2019) Cost-sensitive support vector machines. *Neurocomputing* 343:50–64
- Min F, Liu FL, Wen LY, Zhang ZH (2019) Tri-partition cost-sensitive active learning through kNN. *Soft Comput* 23(5):1557–1572
- Elkan C (2004) The foundations of cost-sensitive learning. In: International joint conference on artificial intelligence, vol 17. Lawrence Erlbaum Associates Ltd, pp 973–978
- Ngai EW, Hu Y, Wong Y, Chen Y, Sun X (2011) The application of data mining techniques in financial fraud detection: a classification framework and an academic review of literature. *Decis Support Syst* 50(3):559–569
- Kim J, Choi K, Kim G, Suh Y (2012) Classification cost: an empirical comparison among traditional classifier, cost-sensitive classifier, and metacost. *Expert Syst Appl* 39(4):4013–4019
- Wang T (2013) Efficient techniques for cost-sensitive learning with multiple cost considerations. Ph.D. thesis
- Zadrozny B, Langford J, Abe N (2003) Cost-sensitive learning by cost-proportionate example weighting. In: Third IEEE international conference on data mining (ICDM 2003). IEEE, pp 435–442
- Yang W, Zhang Y, Ye K, Li L, Xu CZ (2019) FFD: a federated learning based method for credit card fraud detection. In: International conference on big data. Springer, pp 18–32
- Bahnsen AC, Aouada D, Ottersten B (2015) Example-dependent cost-sensitive decision trees. *Expert Syst Appl* 42(19):6609–6619
- Bolton RJ, Hand DJ (2002) Statistical fraud detection: a review. *Stat Sci* 235–249
- Hand DJ, Whitrow C, Adams NM, Juszczak P, Weston D (2008) Performance criteria for plastic card fraud detection tools. *J Oper Res Soc* 59(7):956–962
- Bahnsen AC, Stojanovic A, Aouada D, Ottersten B (2013) Cost sensitive credit card fraud detection using bayes minimum risk. In: Proceedings-2013 12th international conference on machine learning and applications (ICMLA 2013), vol 1. IEEE Computer Society, pp 333–338
- Bahnsen AC, Aouada D, Ottersten B (2014) Example-dependent cost-sensitive logistic regression for credit scoring. In: 2014 13th international conference on machine learning and applications (ICMLA). IEEE, pp 263–269
- Drummond C, Holte RC et al (2003) C4.5, class imbalance, and cost sensitivity: why under-sampling beats over-sampling. In: Workshop on learning from imbalanced datasets II, vol 11. Citeseer, pp 1–8
- Trevor H, Robert T, Friedman JH (2009) The elements of statistical learning: data mining, inference, and prediction
- Breiman L, Friedman J, Olshen R, Stone C (1984) Classification and regression trees. Chapman y hall, Wadsworth International Group, Monterey, CA

17. Draper BA, Brodley CE, Utgoff PE (1994) Goal-directed classification using linear machine decision trees. *IEEE Trans Pattern Anal Mach Intell* 16(9):888–893
18. Ling CX, Yang Q, Wang J, Zhang S (2004) Decision trees with minimal costs. In: *Proceedings of the twenty-first international conference on machine learning*. ACM, p 69
19. Ting KM (2002) An instance-weighting method to induce cost-sensitive trees. *IEEE Trans Knowl Data Eng* 14(3):659–665
20. Vadera S (2010) CSNL: a cost-sensitive non-linear decision tree algorithm. *ACM Trans Knowl Discov Data (TKDD)* 4(2):6
21. Pozzolo AD, Caelen O, Johnson RA, Bontempi G (2015) Calibrating probability with under-sampling for unbalanced classification. In: *2015 IEEE symposium series on computational intelligence*. IEEE, pp 159–166
22. Van Hulse J, Khoshgoftaar TM, Napolitano A (2007) Experimental perspectives on learning from imbalanced data. In: *Proceedings of the 24th international conference on machine learning*. ACM, pp 935–942

Doha Water Treatment Plant: Interval Modeling and Its Reduced-Order Modeling



V. P. Singh 

Abstract Parameter variations can effectively be defined by interval systems. Due to this, several systems are modeled as interval systems. In this work, Doha water treatment plant is modeled as interval system. Then, reduced-order modeling is also proposed for such interval modeled Doha water treatment plant. Firstly, for obtaining the interval system of Doha water treatment plant, uncertainty is considered in all coefficients of systems. Secondly, reduced-order modeling for interval model obtained is proposed by minimizing error in between time moments and Markov parameters. For minimization, Jaya algorithm is utilized due to being simple in implementation. It is established from the results obtained that the reduced-order model is effectively approximating the system.

Keywords Doha system · Interval system · Jaya algorithm · Modeling · Optimization

1 Introduction

While defining a mathematical model for any physical system, a nominal model is generally preferred. This is done due to simplicity in analysis, simpler controller design, etc. But, the main limitation with these nominal models is that these can operate in the vicinity of certain operating point only. If the operating point is shifted, then, the performance of such systems degrades considerably. Other problems with nominal models are that these cannot handle parameter variations, sensor noises, etc. However, taking interval model for such physical systems can be overcome by these limitations.

In interval model of any physical systems, the system parameters are considered to be variable within certain boundaries. Recently, a few engineering systems are modeled as interval systems. Some examples are oblique wing aircraft, cold rolling mill, etc. [1].

V. P. Singh (✉)
Department of Electrical Engineering, MNIT, Jaipur, India
e-mail: vinaymnnit@gmail.com

© Springer Nature Singapore Pte Ltd. 2021
G. S. Hura et al. (eds.), *Advances in Communication and Computational Technology*, Lecture Notes in Electrical Engineering 668,
https://doi.org/10.1007/978-981-15-5341-7_114

1495

In the literature, to address the problem of freshwater scarcity, many systems are proposed. These systems generally employ desalination for purifying the saline water. The reverse osmosis (RO) technique is generally preferred for desalination. For desalination, many systems are proposed in the literature. Some examples are Doha RO plant [2, 3], Riverol-Pilipovik (RP) water treatment plant [4, 5], Chaabene water treatment plant [6], etc.

When considering the mathematical models of systems proposed in the literature, generally interacting multi-input-multi-output (MIMO) models are obtained. The Doha RO system has two manipulated variables (input-pressure and input-pH) and two controlled variables (output-flux and output-conductivity). Similarly, RP RO system has two manipulated variables (pressure and pH) and two controlled variables (flux and conductivity). In same manner, Chaabene RO system [6] also has two manipulated variables (angular speed of pump and reject valve aperture), and two controlled variables (flux and conductivity).

In this contribution, an interval system for Doha water treatment plant is developed. Additionally, reduced-order model is proposed for derived interval system. For deriving the interval system, fixed amount of uncertainty in every coefficient of transfer function of Doha water treatment plant is considered. For obtaining the reduced-order model of interval model developed, an error in between time moments and Markov parameters is minimized. This minimization is accomplished with the help of Jaya algorithm [7]. The advantage of employing Jaya algorithm for minimization is that simulation becomes easier. The results in terms of step response are plotted for the derived model. The obtained results suggest that the methodology adopted for reduced-order modeling produces good approximation of the considered system.

The remaining article is organized as follows. The description of Doha water treatment plant is given in Sect. 2. Section 3 deals with interval modeling. The Jaya algorithm is discussed in Sect. 4. Section 5 provides the reduction procedure for interval system. Sections 6 and 7 produce discussion of results and conclusion carried out.

2 Doha Water Treatment Plant

The Doha reverse osmosis (RO) plant is designed at Kuwait Institute for scientific research [8]. Figure 1 shows the pilot plant structure of Doha RO desalination system.

The whole plant can be segregated into four main compartments: (i) pre-treatment compartment, (ii) high-pressure pump compartment, (iii) membrane compartment, and (iv) post-treatment compartment. The seawater is first treated to remove dissolved impurities in pre-treatment compartment. Then, the pressure of pre-treated water is raised in high-pressure pump compartment. Next, the pressurized water is fed to membrane compartment. In membrane compartment, the freshwater passes through the membranes while saline water is rejected. The freshwater available after

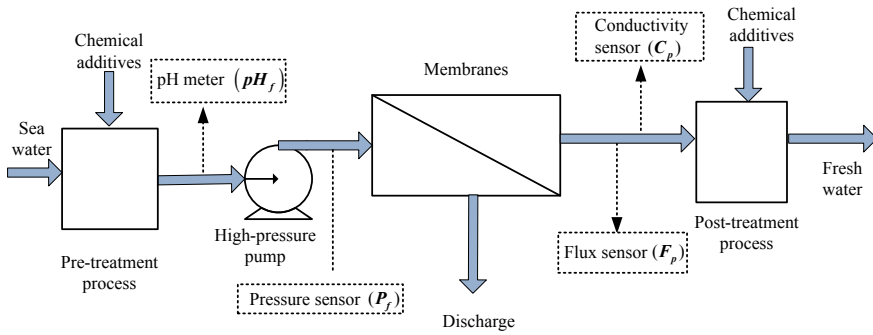


Fig. 1 Pictorial representation of Doha RO system

membrane compartment is post-treated in post-treatment compartment to make it suitable for particular application. All the four compartments are shown in Fig. 1.

The mathematical model of Doha RO system proposed in the literature has two manipulated variables and two controlled variables. The manipulated variables are input-pH and input-pressure; however, the controlled variables are output-flux and output-conductivity.

The mathematical model proposed for the Doha RO system is basically two-input-two-output (TITO) system. The transfer function of TITO system describing the Doha RO is given as:

$$\begin{bmatrix} Y_1(s) \\ Y_2(s) \end{bmatrix} = \begin{bmatrix} h_{p11}(s) & h_{p12}(s) \\ h_{p21}(s) & h_{p22}(s) \end{bmatrix} \begin{bmatrix} R_1(s) \\ R_2(s) \end{bmatrix} \tag{1}$$

where $Y_1 = F_p$ (gpm), $Y_2 = C_p$ (μ S/cm), $R_1 = P_f$ (psig), and $R_2 = \text{pH}_f$ are, respectively, flux, conductivity, pressure, and pH.

The descriptions of $h_{p11}(s)$, $h_{p12}(s)$, $h_{p21}(s)$, and $h_{p22}(s)$ are represented as

$$h_{p11}(s) = \frac{0.002(0.056s + 1)}{0.003s^2 + 0.1s + 1} \tag{2}$$

$$h_{p12}(s) = 0 \tag{3}$$

$$h_{p21}(s) = \frac{-0.51(0.35s + 1)}{0.213s^2 + 0.7s + 1} \tag{4}$$

$$h_{p22}(s) = \frac{-57(0.32s + 1)}{0.6s^2 + 1.8s + 1} \tag{5}$$

3 Derivation of Interval System for Doha RO System

A simple interval system for Doha RO system is proposed in this work. This is done by considering 10% uncertainty in every coefficient of transfer functions given in (2–5), respectively. Interval transfer functions for (2–5)

$$h_{p11}(s) = \frac{[0.1008, 0.1232]s + [1.8, 2.2]}{[2.7, 3.3]s^2 + [90, 110]s + [900, 1100]} \quad (6)$$

$$h_{p12}(s) = 0 \quad (7)$$

$$h_{p21}(s) = \frac{-[160.65, 196.35]s - [459, 561]}{[191.7, 234.3]s^2 + [630, 770]s + [900, 1100]} \quad (8)$$

$$h_{p22}(s) = \frac{-[1641.6, 2006.4]s - [5130, 6270]}{[54, 66]s^2 + [162, 198]s + [90, 110]} \quad (9)$$

by considering 10% deviation in every coefficient of transfer functions.

4 Jaya Algorithm

Recently, Jaya algorithm [9] is proposed in the literature. It is also one of the population-based optimization algorithms [10–19]. The main feature of Jaya algorithm is its simplicity. Additionally, Jaya algorithm does not have algorithm-specific parameters which further make it easy for implementation. Only two common-control parameters, i.e., population size and number of iterations, are necessary while obtaining the solution using Jaya algorithm. Owing to these advantages, Jaya algorithm is applied to many engineering problems [20–22].

While obtaining the optimal solution for a given objective function, Jaya algorithm focuses to move solutions toward best solutions and simultaneously moving them away from the worst solution.

Suppose, the total population is denoted as Y_{ij} where $i = 1, 2, \dots, M$ and $j = 1, 2, \dots, N$. The variables M and N define a number of candidates in the population and number of decision variables involved in the given objective function. The best and worst candidates can be represented as $Y_{1,j}^{\text{Best}}$ and $Y_{1,j}^{\text{Worst}}$. In Jaya algorithm, the solution is updated as:

$$Y_{i,j}^{\text{new}} = Y_{i,j} + \alpha(Y_{1,j}^{\text{Best}} - |Y_{i,j}|) - \beta(Y_{1,j}^{\text{Worst}} - |Y_{i,j}|) \quad (10)$$

where $Y_{i,j}^{\text{new}}$ denotes new solution for $Y_{i,j}$. The variables α and β are chosen randomly from the range [0, 1]. The symbol $|\cdot|$ represents the absolute value. The factor $(Y_{1,j}^{\text{Best}} - |Y_{i,j}|)$ represents the movement toward the best candidate; however, the

movement from the worst solution is represented by the factor $-(Y_{1,j}^{Worst} - |Y_{i,j}|)$. However, α and β show the degree of movement toward the best solution or away from the worst solution. In next iteration, $Y_{i,j}^{new}$ will be considered if it has better fitness value otherwise it is discarded. This process is repeated until the satisfactory solution is obtained.

5 Model Order Reduction

The reduced-order modeling of transfer functions presented in (6–9) is accomplished using the technique presented in [23]. For details, [23] can be referred. In this technique, error in terms of time moments and Markov parameters is minimized along with matching of first time moments.

6 Results and Discussion

For explaining the procedure, reduced-order model of nominal transfer function obtained by considering the upper bounds of transfer function (6) is obtained. The nominal transfer function for upper bounds of transfer function (6) can be written as

$$h(s) = \frac{0.1232 s + 2.2}{3.3 s^2 + 110 s + 1100} \tag{11}$$

For (11), first-order model represented as

$$H(s) = \frac{n_0}{d_1 s + d_0} \tag{12}$$

can be obtained.

After application of technique presented in [23], the fitness function given as

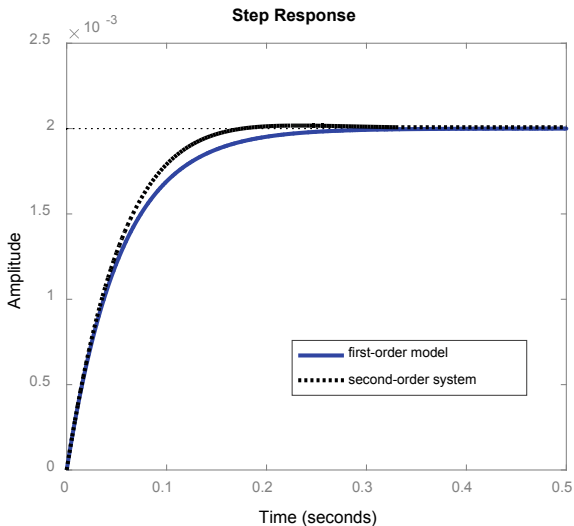
$$J = \left(1 - \frac{3.3 n_0}{0.1232 d_1} \right)^2 \tag{13}$$

has to be minimized provided

$$n_0 = 2.2 d_0 / 1100 \tag{14}$$

in order to match the first time moments and to minimize the errors between first Markov parameters. After minimization using Jaya algorithm, the first-order model obtained is

Fig. 2 Step responses



$$H(s) = \frac{0.1715}{4.593 s + 85.74} \tag{15}$$

The step response of first-order model (15) and second-order system (11) is shown in Fig. 2. The steady state of the model is exactly matching to the steady state of the system. It is clearly evident from Fig. 2 that model is efficiently approximating the system. Hence, the reduced-order modeling presented can efficiently be applied for reducing the interval systems.

7 Conclusion

In this paper, one interval system for Doha water treatment plant is proposed. Also, reduced-order model is proposed for interval system. The interval system for Doha water treatment plant is obtained by considering fixed amount of uncertainty in every coefficient of transfer function of Doha water treatment plant. After the development of interval system, the reduced-order model is derived by minimizing error constituted in terms of time moments and Markov parameters. The error constituted is minimized using Jaya algorithm. Jaya algorithm is applied due to being simple in implementation. The obtained model is successfully approximating the system. The future line of research of work proposed is possible developments of other interval models by considering other sets of uncertainty in the system coefficients. Another future line of research is the development of interval models for interval system using other existing techniques of model reduction of interval systems [24–27].

Acknowledgements The work is sponsored by TEQIP-III and MNIT Jaipur, India (F(15) TEQIP-III/MNITJ/2019/911).

References

1. Choudhary AK, Nagar SK (2018) Order reduction in z-domain for interval system using an arithmetic operator
2. Rathore NS, Singh V, Kumar B (2018) Controller design for Doha water treatment plant using grey wolf optimization
3. Rathore N, Chauhan D, Singh V (2015) Luus-Jaakola optimization procedure for PID controller tuning in reverse osmosis system. In: International conference on electrical, electronics, and robotics (IRAJ-IACEER 2015)
4. Rathore NS, Singh V, Phuc BDH (2019) A modified controller design based on symbiotic organisms search optimization for desalination system
5. Riverol C, Pilipovik V (2005) Mathematical modeling of perfect decoupled control system and its application: a reverse osmosis desalination industrial-scale unit
6. Chaabene AB, Sellami A (2013) A novel control of a reverse osmosis desalination system powered by photovoltaic generator. In: 2013 international conference on electrical engineering and software applications (ICEESA). IEEE, pp 1–6
7. Rao RV, Saroj A (2017) A self-adaptive multi-population based Jaya algorithm for engineering optimization
8. Alatiqi I, Ghabris A, Ebrahim S (1989) System identification and control of reverse osmosis desalination
9. Rao R (2016) Jaya: a simple and new optimization algorithm for solving constrained and unconstrained optimization problems
10. Singh SP, Prakash T, Singh VP (2019) Coordinated tuning of controller-parameters using symbiotic organisms search algorithm for frequency regulation of multi-area wind integrated power system
11. Prakash T, Singh VP, Mohanty SR (2019) A synchrophasor measurement based wide-area power system stabilizer design for inter-area oscillation damping considering variable time-delays
12. Rathore NS, Singh V (2019) Whale optimisation algorithm-based controller design for reverse osmosis desalination plants
13. Prakash T, Singh V, Patnana N (2019) Gray wolf optimization-based controller design for two-tank system. In: Applications of artificial intelligence techniques in engineering. Springer, pp 501–507
14. Prakash T, Singh V, Singh SP, Mohanty S (2018) Economic load dispatch problem: quasi-oppositional self-learning TLBO algorithm
15. Rathore NS, Singh V (2018) Design of optimal PID controller for the reverse osmosis using teacher-learner-based-optimization
16. Singh V (2017) Sine cosine algorithm based reduction of higher order continuous systems. In: 2017 international conference on intelligent sustainable systems (ICISS). IEEE, pp 649–653
17. Shrivastava S, Singh VP, Dohare R, Singh SP, Chauhan DPS (2016) PID tuning for position control of DC servo-motor using TLBO. In: National conference on process, automation and control. National Institute of Technology, Jaipur
18. Singh V, Prakash T, Rathore NS, Chauhan DPS, Singh SP (2016) Multilevel thresholding with membrane computing inspired TLBO
19. Prakash T, Singh VP, Mohanty SR (2018) A novel binary whale optimization algorithm-based optimal placement of phasor measurement units. In: Handbook of research on power and energy system optimization. IGI Global, pp 115–138

20. Singh SP, Prakash T, Singh V, Babu MG (2017) Analytic hierarchy process based automatic generation control of multi-area interconnected power system using Jaya algorithm
21. Prakash T, Singh V, Singh S, Mohanty S (2017) Binary Jaya algorithm based optimal placement of phasor measurement units for power system observability
22. Prakash T, Singh VP (2018) A novel membrane computing inspired Jaya algorithm based automatic generation control of multi-area interconnected power system
23. Singh S, Singh V, Singh V (2019) Analytic hierarchy process based approximation of high-order continuous systems using TLBO algorithm
24. Bokam J, Singh V, Raw S (2017) Comments on large scale interval system modelling using routh approximants
25. Singh V, Chauhan D, Singh S, Prakash T (2017) On time moments and markov parameters of continuous interval systems
26. Singh V, Chandra D (2012) Model reduction of discrete interval system using clustering of poles
27. Singh VP, Chandra D (2012) Reduction of discrete interval systems based on pole clustering and improved Padé approximation: a computer-aided approach

Extreme Event Forecasting Using Machine Learning Models



Manish Kumar, Deepak Kumar Gupta, and Samayveer Singh

Abstract Extreme event forecasting helps in predicting the user demands during the peak travel times. The application of extreme event forecasting lies in predicting an increased demand for resources and hence can aid in effective resource allocation. The statistical approaches are used for the analysis of time series forecasting but for extreme events, it becomes difficult to predict the actual nature by using only the historical data. These methods alone are not sufficient to accurately predict user demands. Time series forecasting techniques along with machine learning algorithms are used to perform the extreme event forecasting. Here, in the paper, we have created the ensemble of two machine learning models, viz. recurrent neural networks (RNN) and Bayesian neural networks which remove the anomaly and improve the accuracy. Automatic feature extraction module long short-term memory (LSTM) has been used to extract the features. The proposed model enhances the accuracy by an extensive margin.

Keywords Recurrent neural network · Long short-term memory · Bayesian neural network · Mean absolute error · Anomaly detection

1 Introduction

Extreme events are peak travel time such as holidays, sporting events, and weather conditions. These events affect the normal flow of the time series data. For example, the data of rainfall prediction depends on the months during which rainfall occurred

M. Kumar (✉) · D. K. Gupta · S. Singh
Dr. B. R. Ambedkar, National Institute of Technology Jalandhar, Jalandhar, Punjab, India
e-mail: manishkumar123.mk4256@gmail.com

D. K. Gupta
e-mail: guptadk@nitj.ac.in

S. Singh
e-mail: samays@nitj.ac.in

(i.e., June–September). These are the high variance periods that affect the predictions. Next, it depends on the areas, for example, the areas of Meghalaya which are adversely affected by the rainfall [1]. So, extreme events are not easy to predict. There are various methods to predict these events from the past. The classical methods like random R forecast package have been dealing with it.

The extreme events aid a type of error in the series as a spike in it. These spikes affect the regular patterns of the series. The series is then analyzed by using various methods, and the methods used depend on various factors [2].

Some of the fields where extreme events are predicted such as Cabs services like Uber Technologies and Ola services. The regular trips they do some times are affected by these extreme events like holidays and rainfall. The most vulnerable date is New Year Eve. Uber is mostly affected by these events. Therefore, we have collected the data from Uber running in New York City. The data collected is transformed into time series and this time series is analyzed by using machine learning models. Extreme events are the irregularities in the time series. These time series display unusual behavior and affect the prediction. Firstly, we are required to detect these anomalies [3]. Then, proper methods are used to predict these events. The previous year's data is collected and this data is analyzed by using machine learning models. These models are chosen wisely so that these models increase the accuracy of prediction. At hand are three conditions for selecting a machine learning model used for time series:

- A number of time series,
- Size of time series,
- Correlation among the time series. If overhead three criteria are lofty then the model might be the correct choice, else traditional time series methodology might work finest.

1.1 Recurrent Neural Network

The recurrent neural networks (RNN) are the most powerful type of neural networks because they have internal memory.

The applications of RNN are image captioning, reading handwriting, etc. When we train RNN with sentences, they generate similar results. They have shown amazing results with catboats, image captioning, and machine translation.

Feedforward is not good for these tasks because the neural network needs a fixed size input and it gives a fixed size output [4]. They do not capture the sequences or the time series information nor they account for the memory. Now, this makes them very unsuitable for lots of tasks that involve time series data. The RNN, on the other hand, captures information about the sequences or the time series data and can take variable size inputs and can give variable size outputs (Fig. 1).

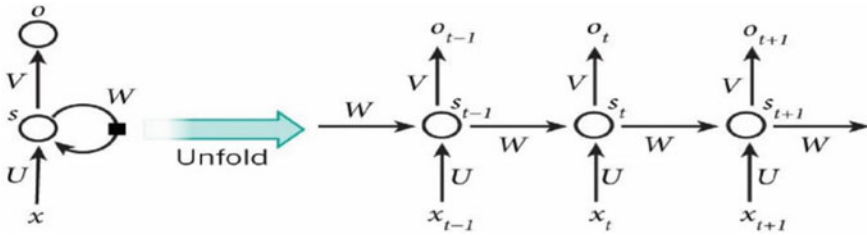


Fig. 1 Recurrent neural network [4]

1.2 Long Short-Term Memory (LSTM)

LSTM also is known as long short-term memory is a special kind of RNN network, which can be used to determine dependencies over a period of time. LSTM has a chain-like structure similar to recurrent neural network but the repeating unit is different in structure. The problem of vanishing gradient is also solved by LSTM and gives us much better accuracy than RNN [5].

LSTM is made up of three gates and one cell state. Cell state acts as a conveyor belt which extends straight down to the entire chain having little or no linear interactions. These gates and cell gates are additional interactions. The forget gate takes the old state and the input and multiplies it with the respective weights. Then, we pass it through a sigmoid activation and the same with the input gates and output gates. Each gate has a different set of weights [6] (Fig. 2).

2 Related Work

The field of EVT presents the time series analysis. The classical methods like autoregression were used to analyze the series, but with the improvement of technology and science, there came the field of machine learning which has changed the world. Machine learning and AI have revolutionized the world. This field has

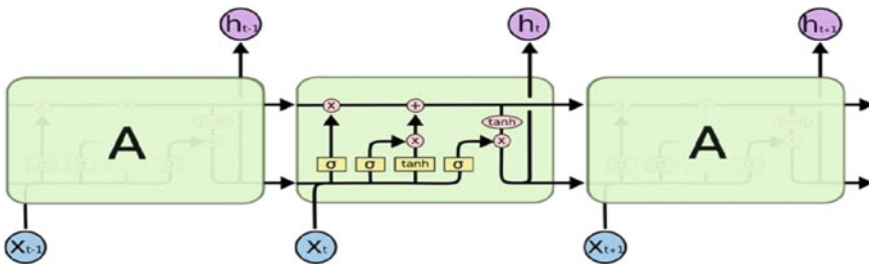


Fig. 2 LSTM recurrent neural network [5]

provided various new techniques to handle the continuously occurring activities in this universe. Today science has changed every sphere of life, and the comfort provided to us is the legacy of machine learning. One such is in the area of prediction [7]. The prediction is a technique that helps in predicting the near future by using the previous year's data. The forecasting can be done in any area like rainfall, weather, and such an area is the cabs like Uber and Ola. The brief review of the literature is presented below:

Laptev et al. [1] discussed extreme events and the various types of extreme events. They also provide various types of classical methods used to handle extreme events by using the random R forecast package. The technique proposed by them is based on machine learning models, i.e., recurrent neural network and Bayesian learning. So, we get an idea of the basic concepts of RNN and Bayesian learning. These models are well generalized to the M3 public data set. The MC dropout method used is to stop the overgrowing of the tree. Also, it explains the uncertainty misspecification. We got the idea of time series analysis and the types of times series, how to stationary the time series.

Yosinski et al. [2] discussed the neural network model applicable to time series information set. The network build is the LSTM model which is explained in the paper. We learned about this model by using this data set of Uber. The implementation of the LSTM model is learned by us. The encoder–decoder model is used for the feature extraction of the time series data set. The author explained about the Bayesian neural network and its introduction in brief [8]. The author also ponders some light on the classical and statistical models like average used for calculation of error in the results. Also, we learned about the uncertainty estimation by using a probabilistic approach to the later allocation of the data set.

Ogunmolu et al. [3] discussed various methods by which the problem of pattern recognition can be solved. The author described the machine learning methodology using LSTM and support vector machine learning models. The methodology used helps in the estimation of patterns in the series. The classification problem of handwritten text prediction and other prediction problems like stock market prediction can be solved by using the LSTM technique. The author applied this technique to find the next pattern in the series by using the previous value stored in the LSTM cell. The text classification and handwritten character recognition can be done by using the LSTM method. The results show that regression problems can have much accuracy using the LSTM model as compared to the classification problem. The data set used is taken from the kaggle and implemented in colab environment. The comparisons are made by using this technique between classification and regression. The author has taken the 45,000 rows of the data set comprising the series taken from different cities of London. The methodology of time series prediction using classical methods like R forecast is not been able to predict the actual nature of the data set.

3 Experimentation Setup

3.1 Data set Exploration

The data set used is the Uber data set collected from the Uber trips completed in New York City. For the prediction of Uber trips, we made use of a data set of daily trips among different cities, including additional features, i.e., weather information and city-level information. The aim is to forecast the next day demand from a fixed window of past observations. The data set has the following properties:

- The data set consists of 27,457 rows in total and the columns include city id, no. of trips, no. of vehicles, and date of the trips.
- The data set is prepared in excel having a size of 740 Kb.
- The data contains many missing values and the date was in different formats, which is later on prepared into a single format by using data preprocessing for the missing information, we use the technique, which consolidates time pattern relapse with an autoregressive model and uses a stepwise strategy to choose the slacks to use for the autoregressive procedure.

In the wake of filling in all the missing information, the quantity of records is 24,348. Our decision was because of the need for a settled data set with transient reliance. We have time arrangement for every US advertise, 54 altogether, a number that develops to 108 on the off chance that we think of one as time arrangement for each kind (ordinary and natural). The informational collection is then isolated into a preparation data set and testing data set by utilizing the technique for cross-approval in which testing information is 20 and 80% are preparing information [9] (Fig. 3).

The time series above shows the no. of trips taken by the Uber during the period from January 2015 to September 2015.

```
[ ] dataset.head()
C>
   Number  Date  Trips  veh
0  B00013  01-01-15    26   17
1  B00014  01-01-15    45   24
2  B00029  01-01-15   731   36
3  B00053  01-01-15    10    9
4  B00095  01-01-15   814   62

[ ] dataset.info()
C>
<class 'pandas.core.frame.DataFrame'>
RangeIndex: 25007 entries, 0 to 25006
Data columns (total 4 columns):
Number      25007 non-null object
Date        25007 non-null object
Trips       25007 non-null int64
veh         25007 non-null int64
dtypes: int64(2), object(2)
memory usage: 781.5+ KB
```

Fig. 3 Uber data set in the working environment

3.2 Encoder–Decoder Model

The architecture of the encoder–decoder LSTM is shown above. The system contains two noteworthy segments: (i) the encoder–decoder structure which catches the characteristic example through the time arrangement, i.e., is found out through prepreparing stage, plus (ii) a forecast system which takes contribution on or after the took in installing after encoder–decoder, just as some possible outside highlights toward managing the expectation. Firstly, the time series data is given to autoencoder which analyzes the series. The series is generally multivariate which generates multiple features by using the variables of the time series. The extra features which are not required are neglected and only required features are kept. These features are then concatenated by using the average method. After this, model uses these features for the prediction and the results are analyzed (Fig. 4).

4 Results and Discussion

The section describes the time series analysis of the daily trips of the Uber. The section consists of three sets of results. Firstly, we will perform the time sequence examination of the data set. The time sequence plotting of the data set is done by using the matplotlib function of the Python library. Secondly that we will implement the test for checking the stationarity of the time series. The analysis like the augmented Dickey–Fuller test, autocorrelation (ACF), and partial autocorrelation function (PACF) is used for checking the stationarity of the instance series data [10]. Lastly, we will evaluate the accuracy of the models used for prediction. The results are evaluated by using a reasonable volume data set of everyday trips.

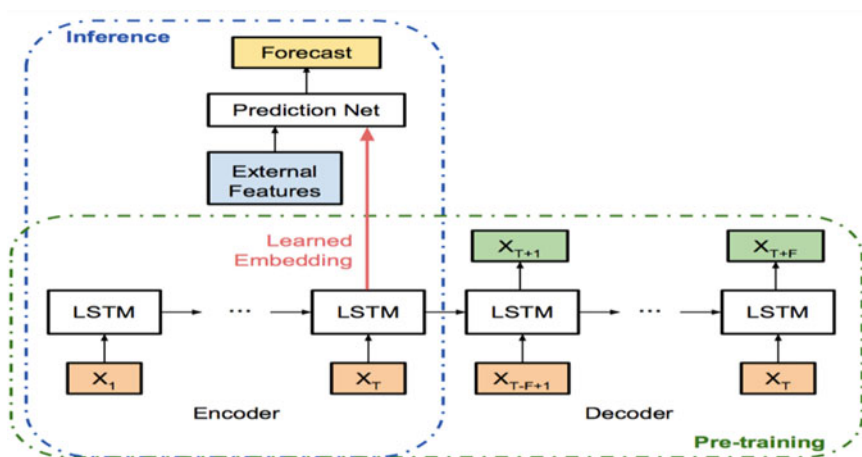


Fig. 4 Encoder–decoder LSTM model [6]

4.1 Time Series Analysis

The data is selected for nine months, spanning from January 2015 to September 2015. Data is resampled on a daily basis. The data set is then made for time series examination by using stationarity methods of time sequence. These methods of time series analysis help in analyzing the patterns generated. It gives us an indication of the type of time series by focusing on trends, seasonality, and pattern. The time series if follows some trend then taken for other tests like seasonality. We can notice a couple of things which you should be familiar with if you are used to analyzing time series:

- We observe a clear upwards trend
- Mean and variance increase through time
- We also observe spikes which may be caused by external events (holidays and weather).

Stationarity could be checked with an augmented Dickey–Fuller test or a KPSS test as shown in Fig. 5. Running the model prints the test estimation of $-1.149e+01$. The more negative this estimation, the practically certain we are to reject the invalid theory (we have a stationary data set). As part of the field, we get an investigate table to help choose the ADF estimation. We can see that the estimation of -1 is more than the estimation of -3.449 at 1%. This suggests we cannot reject the invalid hypothesis with a significance level of under 1% (for instance, a low probability that the result is a quantifiable mishap). Rejecting the invalid theory suggests that the strategy has

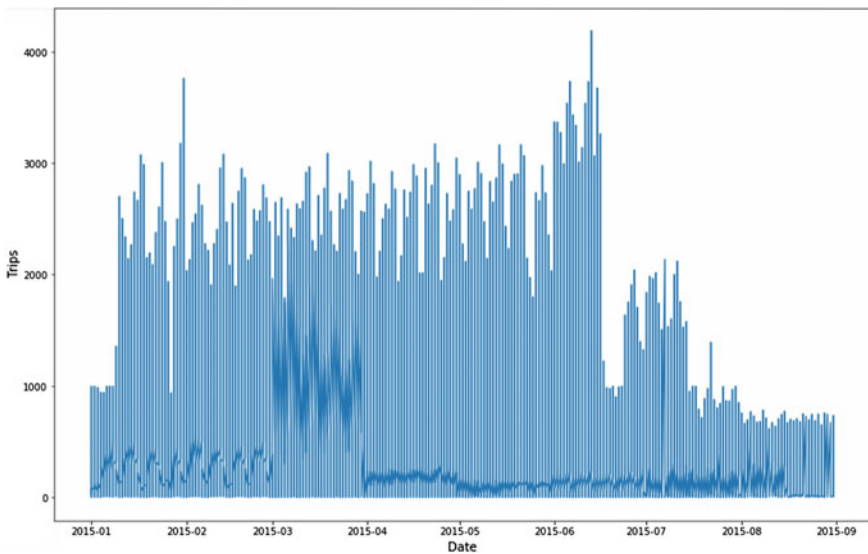


Fig. 5 Shows the time series plot of the no. of trips of Uber

no unit root, and in this manner that the time course of action is stationary or does not have a time structure [11] (Fig. 6).

Autocorrelation plots like ACF and PACF help in choosing the association between the plans. These plots are pulled in to find the estimation of the P and Q factors. These components are then used for the foreseeing of the model (Fig. 7).

The characteristics are given to the model and after that, the model anticipates the characteristics for the next years. The plots decided are showed up in Fig. 8. The surveyed estimation of P and Q is controlled by using that where the game plan starting zero worth that value is considered as P and Q regard in ACF and PACF plots independently. As showed up underneath, the game plan of autocorrelation limit contacts the 0 at 1 and the course of action of inadequate autocorrelation work in like manner contacts the zero at 1 [12].

```
from statsmodels.tsa.stattools import adfuller
print('Results of Dickey Fuller Test:')
dftest = adfuller(indexedDataset.iloc[:,0].values, autolag='AIC')
dfoutput = pd.Series(dftest[0:4], index = ["Test Statistic", "p-value", "#lags used", "no. of observations used"])
for key,value in dftest[4].items():
    dfoutput["Critical Value (%s)"%key] = value
print(dfoutput)

Results of Dickey Fuller Test:
Test Statistic      -1.149080e+01
p-value             4.741831e-21
#lags used          4.800000e+01
no. of observations used  2.495800e+04
Critical Value (1%)  -3.430612e+00
Critical Value (5%)  -2.861656e+00
Critical Value (10%) -2.566832e+00
dtype: float64
```

Fig. 6 Shows the results of the Dickey–Fuller test

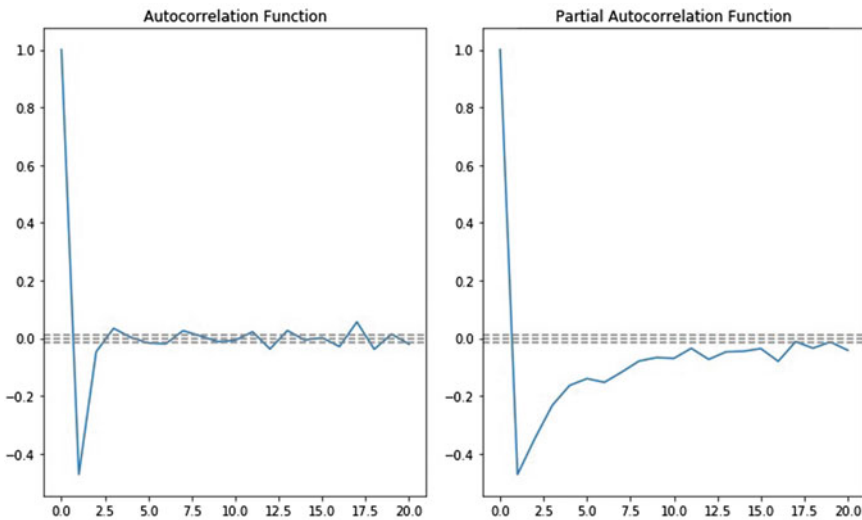


Fig. 7 Shows the ACF and PACF values calculated for time series

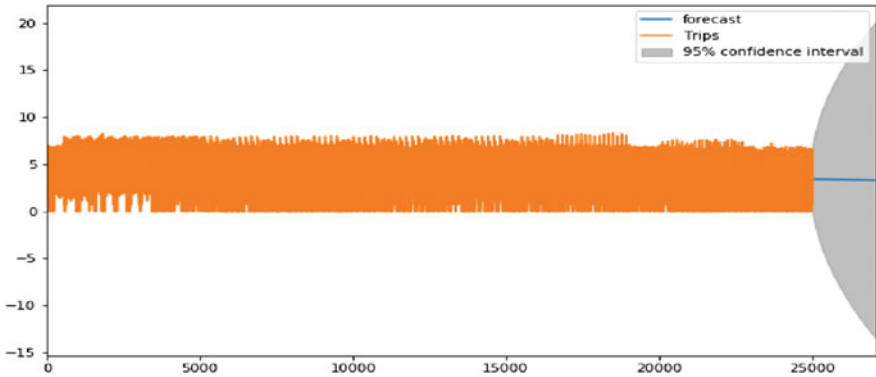


Fig. 8 Forecasted value for the Uber trips with a 95% confidence interval

Table 1 Accuracy of various machine learning models on Uber data set

Model used	Data set	Accuracy
SVM	Uber data set	63.57
Last day	Uber data set	54.38
LSTM	Uber data set	79.886
KNN	Uber data set	81.17
Ensemble	Uber data set	81.83

4.2 The Models Prediction

Table 1 below shows the prediction values calculated by applying different types of models to the Uber data set. There is a huge difference between the values of accuracy calculated by the different types of data sets.

The values calculated by using simple models like last day which calculates the prediction for the next day trips by using only the previous day value shows the difference [13]. The last day model is not suitable for the prediction of the Uber data set. The model uses only the previous value to predict the next value [14]. The other models like LSTM and ensemble are much better than the last day model. The values of these models are 81.17% and 81.71%, respectively. The ensemble models which use the mean values of the models show much accuracy as compared to the rest of the models.

Table 2 MAEs of various models are calculated

Model Used	Data set	Method	MAEs
SVM	Uber data set	Classical method	36.43
Last day	Uber data set	Statistical method	45.62
LSTM	Uber data set	Classical method	20.134
KNN	Uber data set	Backpropagation	18.8317
Ensemble	Uber data set	LSTM and MC dropout	18.1742

4.3 Error Rate (MAEs)

The MAEs value is calculated by using this formula:

$$\text{MAE} = 1/N \times \sum |\hat{y} - y_t| \quad (4.1)$$

The MAEs value calculated for various models is revealed in Table 2. These standards are intended by using the Uber Data set. The accuracy has been improved by using machine learning techniques. The mean absolute error helps in determining the model. This parameter measures the error rate of models. The models like last day and SVM have more errors as compared to other models applied. These models are thus not efficient for the prediction of Uber trips. The models like LSTM, KNN, and ensemble have less error rate of 20%, 18%, and 18.17%, respectively. Thus, these models are efficient in predicting the no. of trips of Uber.

As shown above, the MAE's value is very high for simple models like last day model. The model described above was trained by using no. of time series with no. of data points. Also, the uncertainty is predicted by using the formula of coefficient of variation which is:

$$C_v = \frac{\sigma}{\mu} \quad (4.2)$$

So, by using this formula, we can predict that one of the most vulnerable holidays to predict is the holiday of Christmas.

5 Conclusion

Time series forecasting by using relatively recent methods of machine learning has shown greater improvement from the earlier method (i.e., classical models). Extreme events are more difficult to predict during high variance periods.

The models proposed by us, i.e., LSTM model for the recurrent neural network is an ensemble method that works quite well for the data set of Uber. The method proposed shows 81.83% accuracy with error rate as low as possible from the earlier classical methods and also from statistical methods [15].

The MAE values show great improvement with accuracy improvement of 4–5% and the error rate much lower in value with 4.78%.

These methods of machine learning help in predicting the Uber trips during the high variance period like the New Year. The data collected from the New York City trips of Uber generalizes well to our model.

The MC dropout technique used for uncertainty estimation has shown great improvement in the accuracy of 95% uncertainty coverage.

Based on the results drawn in the previous chapter, the following conclusions have been identified:

- The ensemble generated above for the time series data can best generalize this data.
- The classical methods (i.e., random R forecast package) are not really fit for the time series prediction [16].
- The multivariate time series data can be generalized with deep learning models (i.e., recurrent neural network and Bayesian neural network).
- The Uber data set is applicable to the model and state-of-the-art methods.
- The error rate of the prediction is decreased by using the ensemble of RNN and the Bayesian method of deep learning.
- There is much improvement inaccuracy in predicting the model by far 10% improvement from the classical methods.

6 Future Work

Some interesting challenges were identified while carrying out this paperwork, which could be further considered for future work: utilizing the uncertainty information of the neural network debugging and continuing the analyses in the period of high variance and errors.

- Time series analyses have become easy by using these methods and further research can be done for providing better methods based on deep learning models [17].
- The ensemble model can be applied to other extreme events like pollution control and rainfall prediction.
- The exogenous variable can be interpolated by using the heterogeneous time series.

References

1. Home JD, Manzenreiter W (2004) Accounting for mega-events. *Int Rev Sociol Sport* 39(2):187–203
2. Hyndman RJ, Khandakar Y (2008) Automatic time series forecasting: the forecast package for R. *J Stat Softw* 26(3):1–22
3. Hochreiter S, Schmidhuber J (1997) Long short-term memory. *Neural Comput* 9(8):1735–1780
4. Assaad M, Bone R, Cardot H (2008) A new boosting algorithm for improved timeseries forecasting with recurrent neural networks. *Inform Fusion* 9(1):41–55
5. Ogunmolu OP, Gu X, Jiang SB, Gans NR (2016) Nonlinear systems identification using deep dynamic neural networks. arXiv preprint [arXiv:1610.01439](https://arxiv.org/abs/1610.01439)
6. Laptev N, Yosinski J, Li E, Smyl S (2017) Time-series extreme event forecasting with neural networks at Uber. In: International conference on machine learning
7. Kendall A, Gal Y (2017) What uncertainties do we need in Bayesian deep learning for computer vision? arXiv preprint [arXiv:1703.04977](https://arxiv.org/abs/1703.04977)
8. Goodfellow J, Shlens J, Szegedy C (2014) Explaining and harnessing adversarial examples. In: International conference on learning representations
9. Wei WWS (1994) Time series analysis. Addison-Wesley Publ, Reading
10. Opitz T (2016) Modeling asymptotically independent spatial extremes based on Laplace random fields. *Spat Stat* 16:1–18
11. Fortunato M, Blundell C, Vinyals O (2017) Bayesian recurrent neural networks. arXiv preprint [arXiv:1704.02798](https://arxiv.org/abs/1704.02798)
12. Gal Y, Hron J, Kendall A (2017) Concrete dropout. arXiv preprint [arXiv:1705.07832](https://arxiv.org/abs/1705.07832)
13. Gal Y, Ghahramani Z (2016) Dropout as a Bayesian approximation: representing model uncertainty in deep learning. In: Proceedings of the 33rd international conference on machine learning, pp 1050–1059
14. Paisley J, Blei D, Jordan M (2012) Variational Bayesian inference with stochastic search. In: Proceedings of the 29th international conference on machine learning, pp 1367–137
15. Kingma DP, Welling M (2014) Auto-encoding variational bayes. In: The international conference on learning representations
16. Hernandez-Lobato JM, Adams R (2015) Probabilistic backpropagation for scalable learning of bayesian neural networks. In: Proceedings of the 32nd international conference on machine learning, pp 1861–1869
17. Blundell C, Cornebise J, Kavukcuoglu K, Wierstra D (2015) Weight uncertainty in neural networks. In: Proceedings of the 32nd international conference on machine learning, pp 1613–1622

Enhancing Mist Assisted Cloud Computing Toward Secure and Scalable Architecture for Smart Healthcare



Arijit Dutta, Chinmaya Misra, Rabindra K. Barik, and Sushruta Mishra

Abstract Exponential growth and enormous development have made faster and seamless communication possible in the field of information and communication technology between several devices amongst each other. New technological innovations brought up new opportunities over several disciplines such as individual well-being and customized healthcare services. Internet-of-Healthcare Things (IoHT) improved consistently and developed in a steady manner. However, according to unstructured and critical healthcare data nature, higher Quality of Service (QoS) is considered a major challenge over designing such systems for providing faster responses and data-specific complicated analytics services. Considering the mentioned issues, this particular paper aims to provide agenda of a five-layered heterogeneous model with IoHT framework based on cloud, fog, and mist along with the capability of routing offline/batch mode data and efficiently handling either instantaneously or real-time.

Keywords Cloud · Fog computing · Mist computing · Healthcare · Information processing · IoT

A. Dutta (✉) · S. Mishra
School of Computer Engineering, KIIT Deemed to Be University, Bhubaneswar, India
e-mail: arijit1995@gmail.com

S. Mishra
e-mail: mishra.sushruta@gmail.com

C. Misra · R. K. Barik
School of Computer Application, KIIT Deemed to Be University, Bhubaneswar, India
e-mail: cmisra@yahoo.com

R. K. Barik
e-mail: rabindra.mnnit@gmail.com

1 Introduction

Internet of Things (IoT) is considered as a substantial part of development over medical information management systems and healthcare systems. IoT over the medical domain is a network of devices that are capable of collection and data exchange among the device network. To conduct medical treatment, different types of sensors, disease diagnosis devices, disease screening tools, and other devices are integrated together for performing primary activities of IoT. Application of IoT in healthcare domain enhances real-time screening, alerting, tracking, helps in ensuring patient safety constraints and increasing the chance of safety as well. FMRI, multi-dimensional image data of ultrasound report, along with structured and unstructured electronic health records, data from wearable sensors are generated continuously. Huge amount of data from these sources in several different formats is combined together in real-time is referred to as big data [1]. Big Data Analytics involves monitoring of these data for extracting relevant knowledge, the discovery of necessary information, and understanding relevant patterns. IoT devices include limited speed and CPU efficiency. However, medical big data comprises complex and large electronic datasets and these datasets are difficult to analyze with existing software and hardware tools. Therefore, organizations prefer to deploy cloud computing services to rely on its storing, processing, and decision-making capabilities. Cloud computing offers customized storing, processing of data, and analysis of the data as per user's requirements [2].

Cloud computing service usage in healthcare improves QoS as well as it helps to reduce medical expenditure over a significant amount. The healthcare organizations share several medical records such as prescriptions, MRI test results, X-ray reports, and doctor availability, references over cloud sharing space so that the details can be accessed from any location by any authorized personnel at any time [3]. Moreover, cloud computing services provide other benefits such as better accessibility, elastic resources, and better storage capabilities over lower expenditure. Besides, there exists some security and privacy issues, latency, real-time computation delay over sensitive healthcare data. In terms of medical emergency, time is a crucial factor for data processing and computation, uploading data to centralized cloud from distant cloud, department personnel or physician could cause delay. There exists a mild chance of network failure or cloud data centre failure as well. To handle these issues, a distributed architecture is incorporated eight known as fog computing. Fog computing includes low-power embedding of computers capable of local computation of data to user or cloud [4]. Fog nodes are known as faster gateways to integrate all clients and fog computing architecture supports simultaneous cloud linking. These fog nodes are capable of filtering out unstructured data and can identify appropriate data that needs further analysis over cloud. This process can be achieved in fog computing within lesser bandwidth consumption; apart from this feature, fog computing can handle security and privacy issues during sensitive medical data processing. This framework can prevent unauthorized data usage by enabling limited data access considering user's requirements [5].

Fog computing has the capability of leveraging increased analysis of real-world data regarding disease and handling other location-based problems as well. Geospatial health data are heterogeneous data in nature could lead to challenges of migrating within existing healthcare facilities and its interoperability as well. Mist and fog computing are considered to be the most robust and emerging solutions combined together. This feature can provide low-power nodes with enhanced throughput, reduced latency near the edge of several systems at the client-side. Mist computing needs lesser cloud storage and lesser transmission power over long-term analysis data. Fog computing is part of successful healthcare organizations and smart cities. Mist computing environment comprises of low-power gateways with enhancing throughput, reduced latency closer to client-side edge nodes [6]. Consequently, cloud storage has reduced to increase throughput over other factors; additionally, reduction in required transmission power can affect overall efficiency. Therefore, geospatial health data should be processed at the edge nodes using proposed secure Mist-based architecture [7].

2 Internet-of-Healthcare Things Framework

Most of the developments are made over the IoHT framework along with integrating IoT technology over healthcare systems. In this section, we performed a survey over different aspects of IoT based on healthcare industries with descriptions of several existing applications, platforms, network models, industrial trends, and architectures. Existing network architectures, platforms, applications, research trends can facilitate over healthcare solutions in the context of IoT. In addition, IoT trends in research activities over healthcare domain were examined to highlight how IoT can adhere to several issues in healthcare services such as care of elderly patients, pediatric care, private care, chronic disease diagnosis, fitness management and monitoring. IoT pinpointed some research problems as well as displaying the security challenges and requirements [8, 9]. Over a short discussion, the researchers provided a collaborative and intelligent security model and appropriate ways over anomaly detection. The conducted survey provided regulations over the world for healthcare stakeholders in order to incorporate IoT healthcare technologies to ensure sustainability in the long run and some e-health and IoT policies accordingly. Moreover, IoT enabled customized and patient-related healthcare systems known as Personalized Healthcare Systems (PHS). The researchers tried to identify the diversity and breadth of existing PHS enabled with IoT. The underpinned major technologies and their sophisticated applications are mentioned along with case study over healthcare and future research directions are provided in the study.

Based on survey of IoT based e-healthcare systems, the viewpoint of conventional clinic-dependent treatment is transformed towards patient-dependent treatment. The researchers' opined some major difficulties of IoT based e-healthcare systems and they provided comprehensive plan about a multi-layered e-healthcare ecosystem along with other applications such as e-medicine, alert systems, assisted

well-being, and population monitoring. The researchers have provided a comprehensive summary of requirements of future healthcare, deployment scenarios, and several fog computing-based processing activities. The study provided current fog-based framework flaws and also suggested some major recommendations to revise the identified flaws for reliable IoT solutions. They performed a systematic survey on existing technologies emphasizing fog computing usage in healthcare IoT system field [10]. In order to increase reliability in IoT architecture for healthcare; fog computing is combined for building smarter e-healthcare gateways and demonstrated about the capability of being suited to pervasiveness. The researchers have implemented a prototype of such system along with detailed fog assisted demonstration with cloud computing for warning and health monitoring processes [11].

Additionally, related works on IoT healthcare include anomaly detection, cardiac arrhythmia management systems, smart rehabilitation systems, emergency medical services and smart healthcare systems, do-it-yourself solutions focusing on patient-based treatment facility development, body sensor network-based healthcare systems, and self-aware early warning systems. Based on huge amount of data, processing and storage requirements increased with big data volume as well [12]. Seamless integration of remote health monitoring techniques such as sensor analytics, visualization, and others should be performed simultaneously and major challenges are pointed out over clinical practices. Incorporation of three-layered cloud-based framework in IoT and cloud computing integration are more popular in domain of healthcare for several innovations. Moreover, network layers are designed considering internet connectivity should be seamless and the possibility of high bandwidth consumption [13].

Application-dependent client, service layer along with SimpleDB and logic layer exists in the mentioned architecture. A multi-layered architecture includes IoT devices coupled with the implementation of physiological sensors for cardiac patients monitoring remotely. Cloud Health IIoT (Healthcare Industrial IoT) framework was proposed for transmitting healthcare data with security in cloud for accessing through healthcare personnel [14]. The data can be evaluated via an IoT driven ECG-based patient monitoring application.

3 Proposed Framework and Ecosystem

The implementation of IoT over large-scale could result in several connected devices. Therefore, most of the connected devices should be within a designated processing capacity and resources; however, huge data and unstructured data are being generated from these devices should need efficient data type specific processing [15]. Centralization of the cloud-based IoT framework schema requires effective solution; however, private cloud dependent processing is separated from this processing from latency and high power consumption tendency. These tendencies can be solved based on a certain extent with the introduction of a fog computing layer. The proposed fog computing assisted IoT framework with intelligent gateways is considered as an

approach in order to boost up the reliability factor, efficient energy consumption, and improvement in the performance of the IoT framework.

However, there are some Quality of Service (QoS) issues existing in the transmission of sensitive data and therefore, there is no requisition of several variants of data (such as loss sensitive and delay-sensitive) processing in all the layers of the framework. One of the most effective solutions can be considered in these issues handling; to put an allowance to the different data handling for high demand on time data processing privileges over different layers [16, 24]. This custom can be implemented over the proposed framework considering five different layers such as perception activity layer, mist computing layer, fog computing layer, cloud computing layer, and application layer. Introduction of the excess layer as mist computing layer to the existing fog computing architecture can reduce data storage at the mist nodes and can control data transmission by IoT devices over rule-based data pre-processing. The data volume restrictions can entirely help with lesser power consumption of IoT devices, reducing latency (speeding up transmission and processing), and computational improvements of the framework.

Therefore, proposed IoHT ecosystem is suitable for handling required data selection over data transmission policies over disparate data sources for latency minimization. The proposed framework can ensure optimal resource allocation and utilization over delegation of processes and delivering the processes with lesser load [7, 17, 18]. Minimization of transmission delay is guaranteed with appropriate load balancing and favorable data-sensitive data resource allocation is assured for priority-based data collection and transmission.

Interoperable ecosystem consists of diverse devices in terms of their functionalities and applications; the back-end systems are important for successful architecture designing of IoHT proposed framework. The framework will be able to ensure continuous data flow along with appropriate and precise decision-making. Moreover, theoretical conceptual design of the proposed IoHT concept is shown as in Fig. 1. On the basis of the conceptual diagram, several healthcare stakeholders will be at the lowest stage such as healthcare organizations, patients, professionals, applications, and information exchange [19]. Outer layer includes the user interactive and super responsive modules with limited amount of analytical capabilities. Coming towards the inner circles in the diagram, the analytics capabilities will be increased with latency and data storage increasing gradually. Therefore, time delay-sensitive data collection and transmission for real-time should be ensured along with big data transmission; the proposed architecture is designed to adopt layer-related data collection and transmission policies as well.

4 Network Architecture

IoHT proposed framework architecture where five layers are shown as perception activity layer, mist computing layer, fog computing layer, cloud computing layer, and application layer. Individual layers out of them are designed and depicted with the

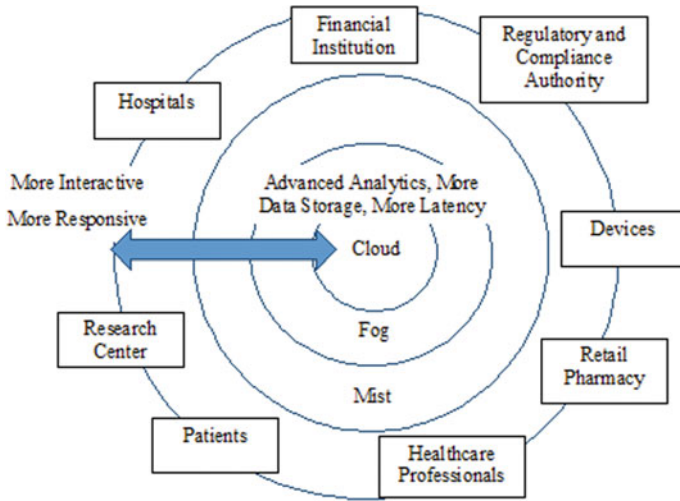


Fig. 1 Proposed IoHT framework

help of pre-defined functionalities. These are related to IoHT proposed framework’s data transmission, collection and processing pipeline [20]. Figure 2 provides a block diagram about the individual layers’ functionalities.

APPLICATION LAYER					
CLOUD LAYER	 BIG DATA ANALYTICS	 DATA STORAGE	 MACHINE LEARNING	 LOAD BALANCE	
FOG LAYER	 DATA FUSION	 DATA STORAGE	 DATA FILTER	 DATA ANALYTICS	 DATA COMPRESS
MIST LAYER	 RULE BASED PREPROCESSING		 DATA TRANSMISSION		
PERCEPTION LAYER	 DATA SENSING		 DATA TRANSMISSION		

Fig. 2 Proposed IoHT framework functionality

The perception activity layer is considered as the lowest layer of the IoHT proposed framework architecture. This particular layer is part of recognizing physical objects; the layer is responsible for perceiving contextual healthcare data from nearby devices. Perception layer could collect data instantaneously, over real-time or over short interval time. The collected data should be measured and obtained from individual patients and from devices such as sensors, embedded systems, RFID readers, tags, and diagnostic devices, clinical and medical devices, screening devices, and other data acquisition devices [21, 22].

In order to process time-based critical data, the mist computing layer has been incorporated into the model. The mist computing layer is situated inside the network fabric which facilitates it to work on the most outer edge of the network with the use of various sensors and data controllers. The layer is designed to work on simple rules-based pre-processing of the data collected from the sensors like aggregations, filtering, and fusion [23, 24].

The main driving force which makes the process of development of IoT devices is the need for processing data as it is being collected in order to detect anomalies, improvise necessary activities and provide real-time alerts for the same. This makes the system to be of high responsiveness as well as have minimal latency in data transfer. To achieve this goal use of centralized model of cloud system uses high latency in their framework. Thus, the decentralizing of the system and making the—processes distributed among various layers helps in the reduction of the latency [2, 20]. The cloud layer of the architecture is able to establish a connection among the perception layer, the application layer and the fog layer. Aggregation of the healthcare data collected is stored in the cloud data storage layer for long-term availability and data analysis. Data collected from other non-sensor locations such as e-prescription, eHR and eMR are also integrated into the layer seamlessly. The cloud layer is able to perform various data analytics methodology on the data being stored [7, 22]. Machine learning, rule-based processing, data mining are some of the processes performed on the data. However, it is to be noted that delegation of proper computing loads towards the fog layer of the system and using the cloud layer for time and resource expensive operations will help in the increase of the systems performance factor.

The topmost application layer of the IoHT proposed framework helps in establishing a connection between the users and the framework reflecting the social and economic benefits. With the help of the user interface the stakeholders are able to receive all the healthcare applications are required [2, 4, 23]. The layer also helps in provision of access rights with privileges from the cloud layer or the fog layer of the architecture directly to the consumers and other developers of the application.

5 Model Description

The model has been designed so as to effectively switch between the sleep mode and the busy mode. When the system is working in sleep mode, the fog assisted data management and processing layer sleeps for a fixed interval of time. The system

wakes up after the sleep interval and checks if there are any packets of data which needs to be transmitted. If no packets are ready for transmission the system would adjust the sleep interval and go back to sleep mode. Each time the system wakes up it would check for packets to be transmitted [18, 24]. The sleep interval is made to vary from time to time, however, the standard protocol would be twice the previous sleep interval.

The proposed model has been designed to work in batch as sleep mode and busy mode. There is a small changeover time between the busy and sleep modes. Let us consider two values a and b which are, respectively, described as minimum number of packets in the buffer queue required to start the fog service and the capacity of the batch. Upon completion of transferring of packets, the system changes into sleep mode. The sleep timer described as β is exponentially distributed. The fog assisted data management and processing layer wakes up when there are some non-transferred packets [7, 24]. If the intermediate packets are less than j number of packets where $0 \leq j \leq a - 2$, the system goes into sleep mode. If there are $a - 1$ number of packets the system will wait for some time and then start in busy mode. This is known as changeover time denoted as α which is exponentially distributed.

6 Performance Analysis of Framework

The proposed framework makes use of a queuing system $\{(i, j) | 0 \leq i \leq N, j = 0, 1\} \cup \{(a - 1, 2)\}$ where i denotes the size of intermediate buffer and j indicated the state of the fog processor. The state of $(i, 0)$ denotes i number of packets and sleep state of DMPL module. The state of $(i, 1)$ denotes i number of packets and busy state of DMPL module. The state of $(a - 1, 2)$ denotes $a - 1$ number of packets and waiting state of DMPL module. The equations are derived as follows:

$$\lambda P_{i,0} = \lambda \psi (1 \leq i \leq a - 2) P_{i-1,0} + \mu P_{i,1}, 0 \leq i \leq a - 2, \tag{1}$$

$$(\lambda + \beta) P_{i,0} = \lambda P_{i-1,0} + \alpha \psi (i = a - 1) P_{a-1,2}, a - 1 \leq i \leq N - 1, \tag{2}$$

$$\beta P_{N,0} = \lambda P_{N-1,0}, \tag{3}$$

$$(\lambda + \mu) P_{0,1} = \lambda P_{a-1,2} + \mu \sum_{s=a}^b P_{s,1} + \beta \sum_{s=a}^b P_{s,0}, \tag{4}$$

7 Performance Measuring Factors

In order to measure the performance of the framework, the average number of packets in buffer (L_q), average waiting time for the packets in the buffer (W_q) and probability of blocking (PBL) are measured. It is given by the following equation:

$$L_q = \sum_{i=1}^N i P_{i,0} + \sum_{i=1}^N i P_{i,1} + (a - 1) P_{a-1,2}$$

The PBL is denoted as $PBL = P_{N,0} + P_{N,1}$.

(L_q) in the buffer is calculated by Little's rule as $W_q = L_q/\lambda'$ where $\lambda' = \lambda(1 - PBL)$.

Figure 3 the impact of L_q with the variation in the values of a and b is shown. The L_q is seen to first decrease then increase exponentially with the increase of time. The value of L_q will increase with increase of a value. However, a constant λ is seen with the decrease in buffer length with increase in b which shown in Fig. 3.

In Fig. 4 above the impact of L_q on λ and μ is shown. With a constant μ the value of L_q decreases as λ increases. The framework has been implemented with the help of Raspberry Pi, Arduino Mega and Pocket Beagle. The CPU load for the three boards has been shown in the following figure below. The arrival rate of packet is 10 per second. The batch size has been considered as 3 and a maximum limit of 7 is taken.

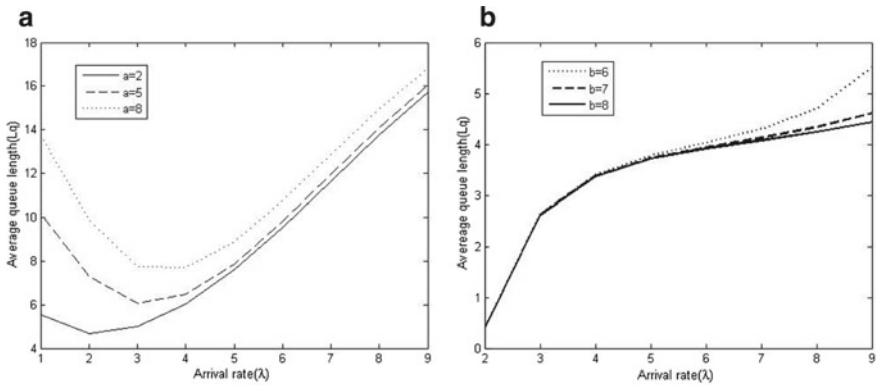
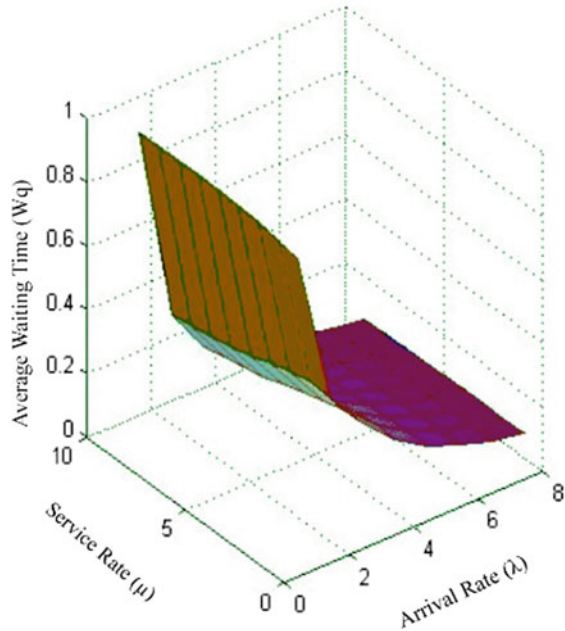


Fig. 3 Effect of λ on waiting time with varying a b Effect of λ on L_q with varying b

Fig. 4 Effect of λ and μ on W_q



8 Conclusions

From the above research it can be concluded that the framework has been designed to be able to work on an energy-efficient environment with the implementation of fog assisted IoT devices. The model different QoS factors of L_q , W_q and PBL have been calculated based on sleep window. The proposed model discusses the fog assisted IoT enables health monitoring system with delay tolerance. In future, the framework can be redesigned for cost optimization factors. The consideration of internal sleep timer and change over time helps in a more precise analysis of the framework. The research work proposes a heterogeneous model of cloud-based IoHT framework which is integrated with fog and mist computing technology. The various layers are able to simultaneously manage data from different sensors. Simulation results show the proposed framework has been able to achieve a low latency and drop rate in packets. The result shows the implementation of the system in real-world healthcare domain. Extensive machine learning techniques can be implemented in the system to make it more robust and effective. The system can stand to be a stepping stone in next-generation IoHT-based healthcare system development.

References

1. Atzori L, Iera A, Morabito G (2010) The internet of things: a survey. *Comput Netw* 54(15):2787–2805
2. Baker SB, Xiang W, Atkinson I (2017) Internet of things for smart healthcare: technologies, challenges, and opportunities. *IEEE Access* 5:26521–26544
3. Botta A, De Donato W, Persico V, Pescapé A (2016) Integration of cloud computing and internet of things: a survey. *Future Gener Comput Syst* 56:684–700
4. Bishop CM (1995) *Neural networks for pattern recognition*. Oxford University Press, Oxford
5. Borthakur D, Dubey H, Constant N, Mahler L, Mankodiya K (2017) Smart fog: fog computing framework for unsupervised clustering analytics in wearable internet of things. In: 2017 5th IEEE global conference on signal and information processing. IEEE, p 15
6. Dastjerdi AV, Gupta H, Calheiros RN, Ghosh SK, Buyya R (2016) Fog computing: principles, architectures, and applications. In: *Internet of things*. Morgan Kaufmann, pp 61–75
7. Barik RK, Misra C, Lenka RK, Dubey H, Mankodiya K (2019) Hybrid mist-cloud systems for large scale geospatial big data analytics and processing: opportunities and challenges. *Arab J Geosci* 12(2):32
8. Bonomi F, Milito R, Zhu J, Addepalli S (2012) Fog computing and its role in the internet of things. In: *Proceedings of the first edition of the MCC workshop on mobile cloud computing*. ACM, p 13–16
9. Gope P, Hwang T (2015) BSN-care: a secure IoT-based modern healthcare system using body sensor network. *IEEE Sens J* 16(5):1368–1376
10. Liyanage M, Chang C, Srirama SN (2016) MEPAAS: mobile-embedded platform as a service for distributing fog computing to edge nodes. In: 2016 17th international conference on parallel and distributed computing, applications and technologies (PDCAT). IEEE, pp 73–80
11. Chiang M, Zhang T (2006) Fog and IoT: an overview of research opportunities. *IEEE Internet Things J* 3(6):854–864. <https://doi.org/10.1109/JIOT.2016.2584538>
12. Manogaran G, Thota C, Kumar MV (2016) Meta cloud data storage architecture for big data security in cloud computing. *Procedia Comput Sci* 87:128–133
13. Orsini G, Bade D, Lamersdorf W (2015) Computing at the mobile edge: designing elastic android applications for computation offloading. In: 2015 8th IFIP wireless and mobile networking conference (WMNC). IEEE, pp 112–119
14. Barik RK (2017) Cloud Ganga: cloud computing based SDI model for Ganga River basin management in India. *Int J Agric Environ Inform Syst (IAEIS)* 8(4):54–71
15. Barik R, Dubey H, Lenka RK, Mankodiya K, Pratik T, Sharma S (2017) Mistgis: optimizing geospatial data analysis using mist computing. In: *International conference on computing analytics and networking (ICCAN 2017)*. Springer
16. Bera S, Misra S, Rodrigues JJ (2015) Cloud computing applications for smart grid: a survey. *IEEE Trans Parallel Distrib Syst* 26(5):1477–1494
17. Varshney P, Simmhan Y (2017) Demystifying fog computing: characterizing architectures, applications and abstractions. In: 2017 IEEE 1st international conference on fog and edge computing (ICFEC). IEEE, pp 115–124
18. Barik RK, Dubey H, Mankodiya K, Sasane SA, Misra C (2019) GeoFog4Health: a fog-based SDI framework for geospatial health big data analysis. *J Ambient Intell Humanized Comput* 10(2):551–567
19. Yi S, Li C, Li Q (2015) A survey of fog computing: concepts, applications and issues. In: *Proceedings of the 2015 workshop on mobile big data*. ACM, pp 37–42
20. Yue P, Zhou H, Gong J, Hu L (2013) Geoprocessing in cloud computing platforms—a comparative analysis. *Int J Digit Earth* 6(4):404–425
21. Chen Z, Chen N, Yang C, Di L (2012) Cloud computing enabled web processing service for earth observation data processing. *IEEE J Sel Top Appl Earth Obs Remote Sens* 5(6):1637–1649

22. Barik RK, Dubey H, Samaddar AB, Gupta RD, Ray PK (2016) FogGIS: fog computing for geospatial big data analytics. In: 2016 IEEE Uttar Pradesh section international conference on electrical, computer and electronics engineering (UPCON), pp 613–618
23. Barik R, Dubey H, Sasane S, Misra C, Constant N, Mankodiya K (2017) Fog2Fog: augmenting scalability in fog computing for health GIS systems. In: 2017 IEEE/ACM international conference on connected health: applications, systems and engineering technologies (CHASE), pp 241–242

Analysis of YouTube Channel Analytics and Affiliate Marketing with Operating System



Kanika Singhal  and Abhineet Anand 

Abstract Operating system is the heart and soul of any computer system. It is solely responsible for the communication between user and hardware. Many important functions of computer system are assigned to the operating system. It not only helps to perform the assigned task but also plays an important role in management. Affiliate marketing is going through a major change in this era. The opportunities are increasing and so is the scope of affiliate marketing. In this paper, we will describe how the different operating systems help to improve the performance of affiliate marketing mechanism. It will also analyze the performance of affiliate marketing under different operating system conditions.

Keywords Affiliate marketing · Operating system · Time sharing-performance

1 Introduction

Affiliate marketing is the performance-based earning mechanism through different Web sites or an affiliate program. The process involves the commission per buy concept. The person joining the affiliate program is known as affiliate. The affiliate can join the affiliate program of any Web site running their own program or can link to Cuelink, which links all the affiliate programs under one roof and make the process simple. One such method of operating the affiliate marketing is by a YouTube channel [1]. Once you create your own YouTube channel, the videos can be used to generate revenue through affiliate marketing. For example, if you post a video on your channel that is related to the review of a particular product, you can mention the affiliate link of that product in the description box of the video. The viewers viewing

K. Singhal (✉)

Galgotias College of Engineering and Technology, Greater Noida, India
e-mail: kanikasinghal28@gmail.com

A. Anand

Chitkara University Institute of Engineering and Technology, Chitkara University, Rajpura,
Punjab, India
e-mail: abhineet.anand@chitkara.edu.in; abhineet.mnnt@gmail.com

© Springer Nature Singapore Pte Ltd. 2021

G. S. Hura et al. (eds.), *Advances in Communication and Computational Technology*, Lecture Notes in Electrical Engineering 668,
https://doi.org/10.1007/978-981-15-5341-7_117

1527

the video may click on the affiliate link and buy the product. The commission will be added to your account.

The analytics of the channel includes the overview which subcategorizes views, watch time (in minutes), subscribers and the estimated revenue. Top videos in the last 28 days and the real-time activity of last 48 h are also visible in the overview section as shown in Fig. 1.

The reach section of YouTube analytics includes the impressions, impressions click-through rate, views and unique viewers viewing the videos. It also includes the traffic source type of the videos being viewed as shown in Fig. 2.

The engagement includes the watch time in minutes and the average view duration as shown in Fig. 3.

The audience section includes the unique viewers watching the video, average views per viewer, and the subscribers of the channel as shown in Fig. 4.

The revenue includes the estimated revenue of the channel, estimated monetized playbacks, and playback-based CPM as shown in Fig. 5.

Improvement of YouTube analytics can lead to more views on the channel and this can serve as a base for affiliate marketing [2]. More views on the channel mean more people are viewing the videos on your channel and there will be more chances of click on the affiliate link in the description box.

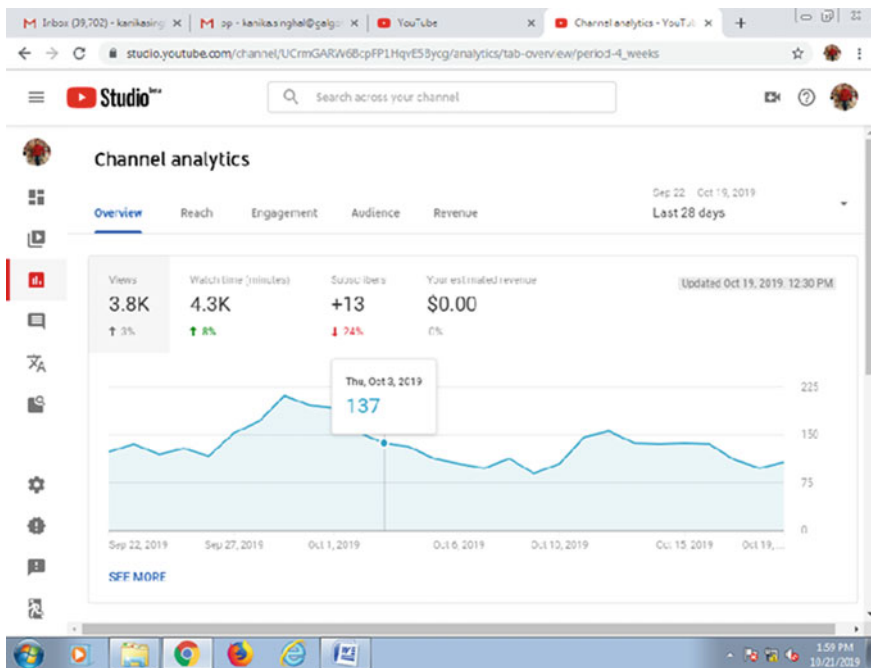


Fig. 1 Overview section of YouTube analytics

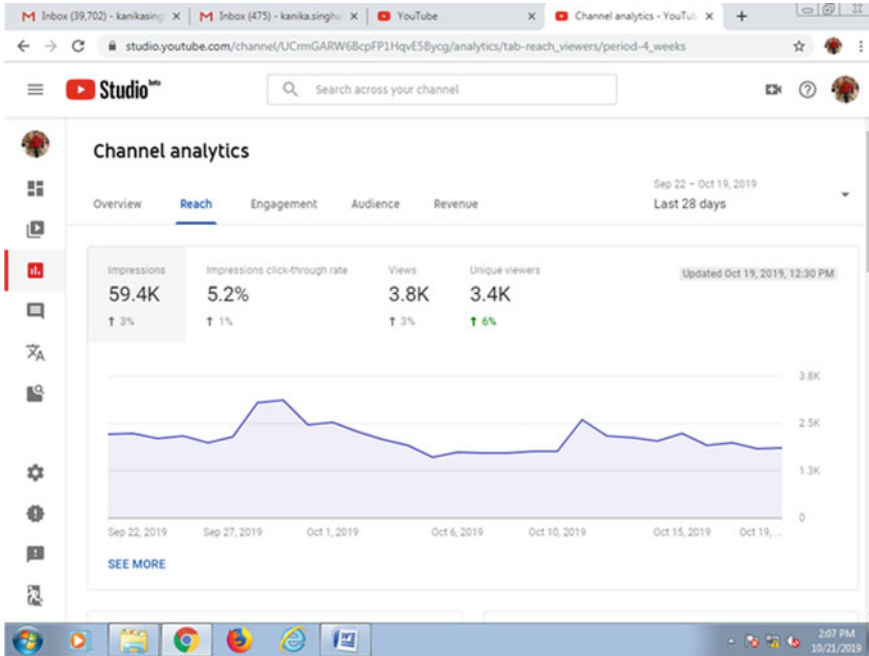


Fig. 2 Reach of the YouTube analytics

2 Linkage of YouTube and Affiliate Marketing

The YouTube channel consists of various analytics such as overview, revenue, reach, engagement, and audience. These all analytical factors have their further subcategorization. The YouTube channel can be directly linked to affiliate marketing in a simple manner. If there will be more views on the YouTube channel video, definitely there will be high chances of people clicking on affiliate link [3]. The traffic will be more driven to that videos, improving the analytics of the channel and there will be high chances of customer buying the product. Both factors will lead to a high commission rate. The flow chart is shown in Fig. 6.

2.1 Linkage of YouTube Analytics with Different Operating Systems

Operating system plays a key role in the functioning of a computer system. Management of resources is an arduous task [4]. It acts both as a resource manager and a resource allocator. The mechanism of affiliate marketing can be linked to different operating systems in the following manner.

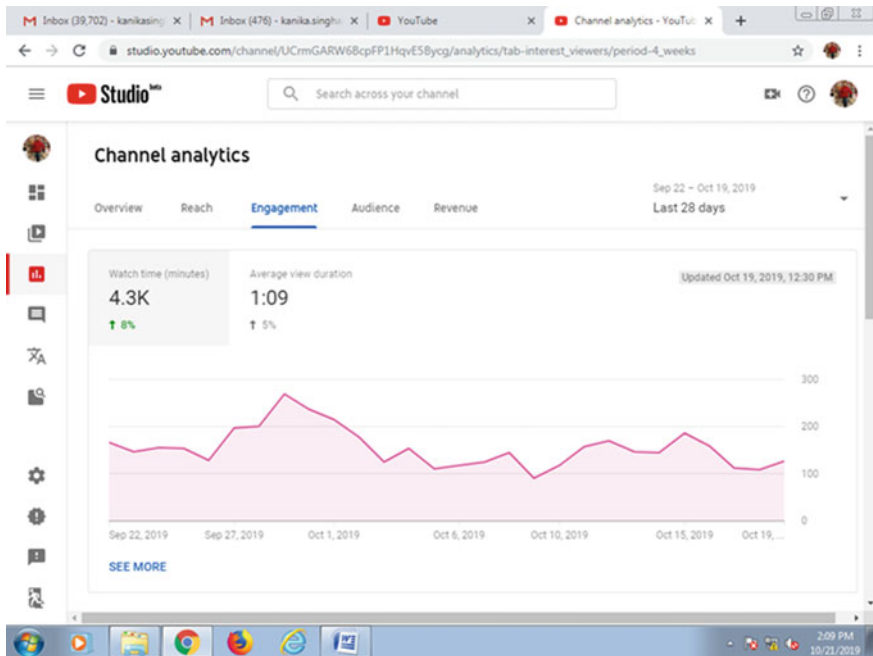


Fig. 3 Engagement section of YouTube analytics

Real-Time Operating System In view of the performance of the video capture of real-time activity of the video is a must. Real-time operating system focuses on the time constraint of the activity. The analytics of the YouTube channel also focuses on the real-time activity constraint very clearly. The real-time activity of last 48 h is shown on the YouTube analytics page which clearly shows which videos are most viewed. The most viewed videos are listed in the top videos as shown in Fig. 7.

Batch Operating System The speed of processing is a very important factor in any computer system. If the tasks are run individually as a standalone unit, the speed of the system will be definitely slow. The bandwidth will be wasted and the CPU processing cycles are also compromised. The better way is to group the similar tasks in one batch and execute it in one go without any interruption. Batch operating system does the same thing [5]. It groups the similar tasks in one cluster and executes the cluster. CPU processing time and memory cycles both are saved by this method. The YouTube channel also groups the same structure videos in one cluster known as playlist and videos can be directly viewed by opening that playlist as shown in Fig. 8.

Time Sharing Operating System Time sharing operating system allows the users to use a particular computer system from various locations at the same time. Whenever a video is posted on the YouTube channel, the views keep on increasing every minute depending on the popularity of the video. The users from different states and even

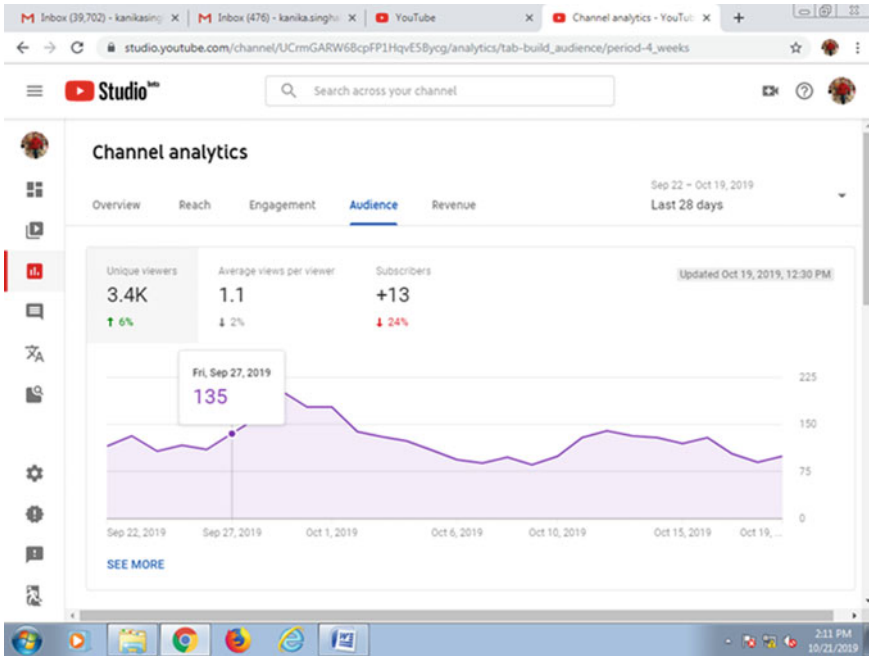


Fig. 4 Audience section of YouTube analytics

different countries can view the same video at the same time without any problem [6]. The viewer will get an immediate response. Time sharing concept is definitely applied to the YouTube analytics. The reliability of the system increases, and data communication is done easily.

Distributed Operating System The computer system will work more efficiently if the task is distributed among various processors rather than assigning it to a single processor. Distributing the load will increase the speed of processing and resource sharing will also be improved. The YouTube channel analytics follow the same pattern. Different tasks are assigned to different processors. The views on the video, the updating of real-time activity, and the processing on the video all go hand in hand. The tasks can be completed within the prescribed time frame. Better service to the customer is also provided along with the reduction in burden on the single processor.

Multitasking Operating System Multitasking is a very important mechanism in a computer system. The performance of the system will be enhanced if the editing of the video, posting the video on the channel, searching something on the Internet to improve the quality of the video, and video processing all go hand in hand [7]. This could be accomplished with the help of multitasking operating system. It allows multiple tasks to be carried at a time without interruption.

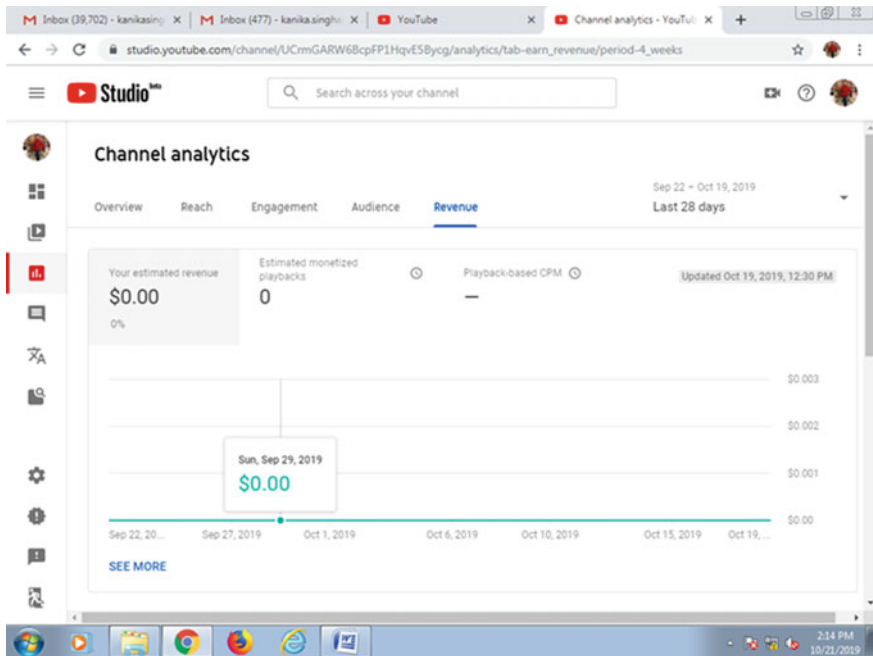


Fig. 5 Revenue section of YouTube analytics

2.2 Linkage of Affiliate Marketing with Different Operating Systems

Real-Time Operating System Affiliate marketing allows the commission to be transferred into the affiliate account only if something is bought from the affiliate link. The money is calculated according to the payout of the item bought. The payout of every item is different. As the real-time operating system focuses on real-time activity of the video with the time constraint of 48 h, it gives a description of the most viewed video [8]. The affiliate link in the most viewed videos will be automatically clicked more and that will generate the revenue for sure. Better is the respond time, better is the revenue generated.

Batch Operating System The videos are grouped into a batch and can be grouped into a playlist. When a person views a particular video, it might be possible that he develops an interest in other videos of the playlist and clicks on the affiliate link present in these videos and buy something. Forming a batch can be an advantage here because if the viewer buys something influenced by the particular product, the revenue can be generated.

Time Sharing Operating System When more viewers can watch the same video from different locations at the same time, there will be high chances of increased

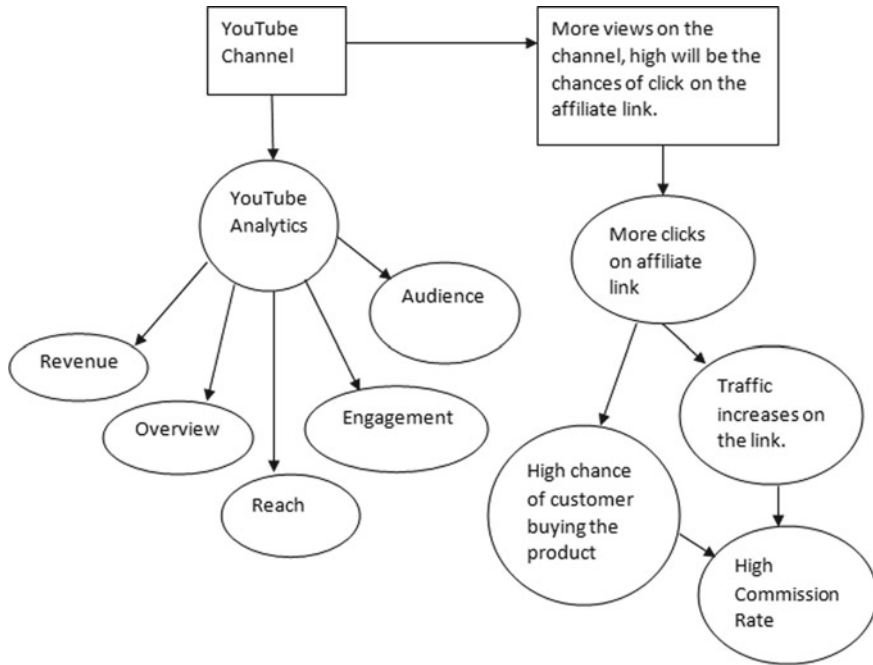


Fig. 6 Linkage of YouTube and affiliate marketing

traffic on your YouTube channel. High traffic will lead to high views on the videos, which will automatically bring more clicks to the affiliate link. Ultimately, the generation of revenue will happen.

Distributed Operating System When the load is distributed among different processors, the speed of the task will increase. Increased speed means more videos will be viewed in the same time. More videos will be viewed means there will be high chances of people watching your videos and buying something from your affiliate link [9]. This will automatically lead to the generation of revenue from the affiliate marketing strategy.

Multitasking Operating system When the user can carry out different tasks simultaneously, the affiliate marketing strategy also improves. Posting of the video and formation of affiliate link can be done in the same time frame. The affiliate link can be created by Cuelink or any other online Web site that offers the affiliate program. The different tasks going hand in hand increase the speed of processing and decrease the time latency. The tasks can be done without any time gap in a proficient manner.

The linkage of affiliate marketing with different operating system is shown in Fig. 9.

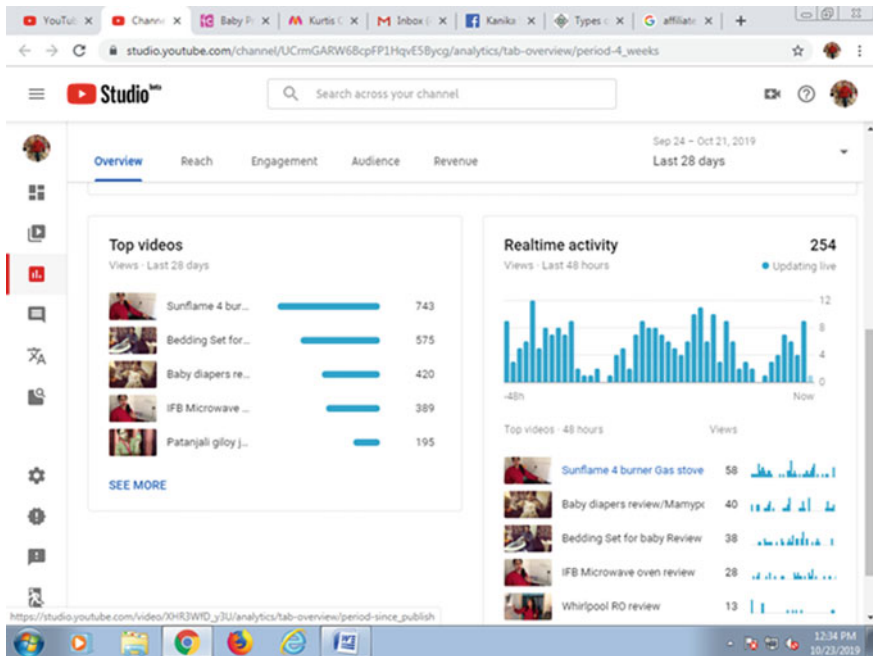


Fig. 7 Real-time activity on YouTube channel

3 Work Analysis

The different operating systems play different roles in YouTube analytics and affiliate marketing. The functions and analysis are based on several factors.

Real-time operating system depicts the real-time activity of the videos running on the channel. The real-time activity gives an estimate of the top videos on the channel. Once we know the famous videos, there are high chances that the affiliate link in these videos will be clicked more and it might be possible that some revenue be generated from the affiliate link present in such videos.

Batch operating system plays an important role both in YouTube analytics and affiliate marketing. The cluster formation is very important. It diverts more traffic to the source. Once the user views the playlist on the YouTube channel, it might be possible that he/she get interested in some other video in the playlist. Creating playlist or we can say batch plays a prominent role here [10]. It can become a source of revenue generation for the user.

Time sharing operating system shares the time slot between the different users at different locations. Different users are watching the same video from their place. If a particular video is watched more or getting popular, many users can watch the video at the same time due to time sharing operating system. More users mean more click on the affiliate link and it increases the chances of revenue generation for the user.

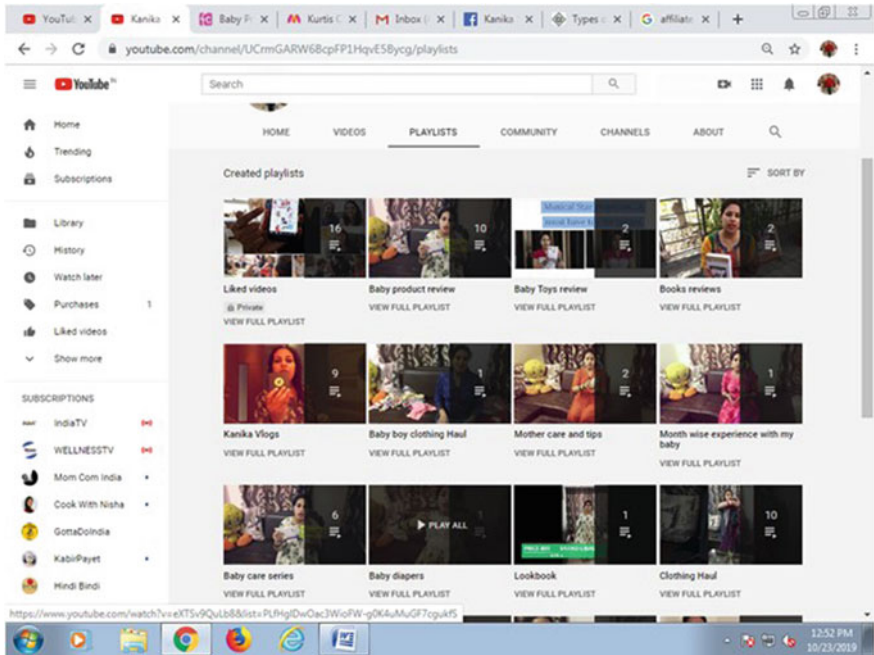


Fig. 8 Playlist as cluster on YouTube channel

Distributed operating system relates more to the server-side rather than the front end. Rather than putting the complete load on one processor, distribution of work will surely enhance the performance of the system. The performance of the system will automatically enhance the YouTube analytics and affiliate marketing phenomenon.

Multitasking operating system allows different tasks to be carried out simultaneously at the same time. Simultaneous tasks improve the YouTube analytics of the system. The tasks can be carried out with a faster pace and with a high speed of processing. Affiliate marketing mechanism also gets enhanced by the multitasking environment [11]. The affiliate links can be generated with a faster pace and at the same time, the same product affiliate link can be generated from another Web site, improving the efficiency of affiliate marketing.

The impact of different operating systems on YouTube analytics and affiliate marketing is shown in Table 1.

4 Conclusion

Affiliate marketing and YouTube analytics can be definitely linked with operating system. Different operating systems have different impact on YouTube analytics and affiliate marketing depending on different criteria and factors [12]. Affiliate

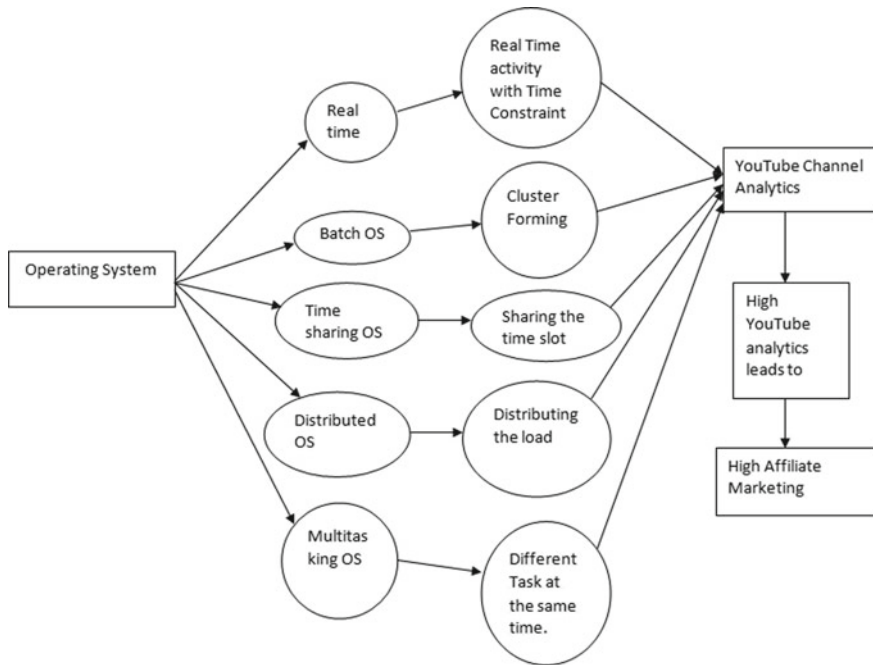


Fig. 9 Linkage of affiliate marketing with different operating systems

Table 1 Impact of different operating system with YouTube analytics and affiliate marketing

Operating system	YouTube analytics	Affiliate marketing	YouTube analytics + affiliate marketing
Real-time OS	High	High	High
Batch OS	High	Low	High
Time sharing OS	Low	High	High
Distributed OS	Low	Low	Low
Multitasking OS	High	High	High

marketing is growing at a very rapid pace. Linking of YouTube channel to affiliate marketing is very advantageous. Diverting traffic to the YouTube video and generation of revenue from the affiliate link depend on many unknown factors and still remain a great challenge which is to be explored in the coming times.

References

1. AdChoices (2018) Adchoices. <http://youradchoices.com/>
2. AdAge (2016) FTC cracking down on social influencers' labeling of paid promotions. <http://adage.com/article/digital/ftc-cracking-social-influencers-labeling-promotions/305345/>
3. FTC (2016) Lord & Taylor settles FTC charges it deceived consumers through paid article in an online fashion magazine and paid instagram posts by 50 "fashion influencers". <https://www.ftc.gov/news-events/press-releases/2016/03/lord-taylor-settles-ftc-charges-it-deceived-consumers-through>
4. Fair L (2016) FTC challenges influencer campaign for Warner Bros.' Shadow of Mordor game. <https://www.ftc.gov/news-events/blogs/business-blog/2016/07/ftc-challenges-influencer-campaign-warner-bros-shadow-mordor>
5. FTC (2018) The FTC's endorsement guides: what people are asking. <https://www.ftc.gov/tips-advice/business-center/guidance/ftcs-endorsement-guides-what-people-are-asking>
6. Chachra N, Savage S, Voelker GM (2015) Affiliate crookies: characterizing affiliate marketing abuse. In: Proceedings of the 2015 ACM conference on internet measurement conference. ACM, pp 41–47
7. McCoy D, Pitsillidis A, Grant J, Weaver N, Kreibich C, Krebs B, Voelker G, Savage S, Levchenko K (2012) Pharmaleaks: understanding the business of online pharmaceutical affiliate programs. In: Presented as part of the 21st USENIX security symposium (USENIX Security 12). Bellevue, WA. USENIX, pp 1–16. [Online]. Available <https://www.usenix.org/conference/usenixsecurity12/technical-sessions/presentation/mccoy>
8. Kanich C, Weaver N, McCoy D, Halvorson T, Kreibich C, Levchenko K, Paxson V, Voelker GM, Savage S (2011) Show me the money: characterizing spam-advertised revenue. In: USENIX security symposium, pp 15–15
9. Leskovec J, Faloutsos C (2006) Sampling from large graphs. In: Proceedings of the 12th ACM SIGKDD international conference on knowledge discovery and data mining. ACM, pp 631–636
10. Zhou J, Li Y, Adhikari VK, Zhang Z-L (2011) Counting YouTube videos via random prefix sampling. In: Proceedings of the 2011 ACM SIGCOMM conference on internet measurement conference, ser. IMC'11. ACM, New York, NY, pp 371–380. [Online]. Available <http://doi.acm.org/10.1145/2068816.2068851>
11. Gilbert E, Bakhshi S, Chang S, Terveen L (2013) "I need to try this?": a statistical overview of pinterest. In: Proceedings of the SIGCHI conference on human factors in computing systems, ser. CHI'13. ACM, New York, NY, pp 2427–2436. [Online]. Available <http://doi.acm.org/10.1145/2470654.2481336>
12. Google (2018) Add YouTube functionality to your app. <https://developers.google.com/youtube/v3/>